Cover Picture



Tapas Kumar Maji, Kazuhiro Uemura, Ho-Chol Chang, Ryotaro Matsuda, and Susumu Kitagawa*

To expand or shrink are properties of the new pillared-layer porous coordination polymers shown in the cover picture. These features show that coordination polymers are much softer than generally believed. The adsorption selectivity exhibited by these new zeolite-like materials arises from a simple change in the organic-pillar module, and may find applications in molecular separation techniques. For more information see the Communication by S. Kitagawa et al. on page 3269 ff.

Contents

Angewandte EarlyView

The following Communications are available online (in Wiley InterScience). You can find them, as well as forthcoming Reviews, Highlights, and Essays, at www.angewandte.org, under Early View.

F. Turcu, A. Schulte, G. Hartwich, W. Schuhmann:*
Label-Free Electrochemical Recognition of DNA Hybridization by Means of Modulation of the Feedback Current in SECM
DOI: 10.1002/anie.200454228
Published online: June 9, 2004

S. J. George, A. Ajayaghosh, P. Jonkheijm, A. P. H. J. Schenning, E. W. Meijer:*
Coiled-Coil Gel Nanostructures of Oligo(*p*-phenylenevinylene)s: Gelation-Induced Helix Transition in a Higher-Order Supramolecular Self-Assembly of a Rigid π-Conjugated System
DOI: 10.1002/anie.200453874
Published online: June 4, 2004

Articles judged by the referees or the editor as being either very important or very urgent are immediately edited, proof-read, and electronically published once the manuscript has arrived in the editorial office in its final form. As long as there is no page number available these articles should be cited in the following manner:

Author(s), *Angew. Chem. Int. Ed.*, online publication date, DOI.

Meeting Reviews

Ordered Porous Nanoarchitectures with Specific Functions ——— **3216 – 3217** *N. Hüsing*

Books

Bioactive Natural Products ——— **3218** Atta-ur-Rahman *reviewed by F. von Nussbaum*

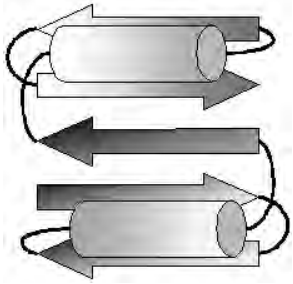
Fundamental World of Quantum Chemistry ——— **3219** Erkki J. Brändas, Eugene S. Kryachko *reviewed by M. Reiher*

Highlights

Protein Design

A. Tramontano* ——— **3222 – 3223**

A Brighter Future for Protein Design



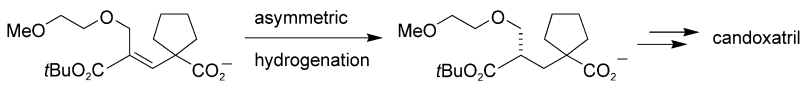
A deeper understanding of the sequence–structure relationship in proteins has resulted from research in the field of protein design. Recent success in designing a protein with a topology not yet observed in nature (see picture) increases our confidence in computational biology and should open the road to the engineering of molecular machines with specified properties and functions.

Essays

Industrial Chemistry

J. M. Hawkins,*
T. J. N. Watson ——— **3224 – 3228**

Asymmetric Catalysis in the Pharmaceutical Industry

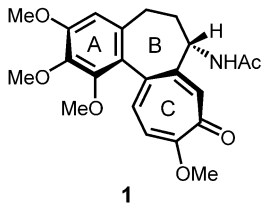


The best catalyst from a chemical perspective is not necessarily the best catalyst from an overall economic perspective. In competing approaches to candoxatril the most selective catalyst for the asymmetric hydrogenation (see scheme) was not the one ultimately chosen. The constraints of the pharmaceutical industry are discussed with regard to the application of asymmetric catalysis to the large-scale synthesis of drug candidates and commercial drugs.

 © 2004 Wiley-VCH Verlag GmbH & Co. KGaA, Weinheim

Reviews

The tubulin-binding alkaloid colchicine (**1**), isolated from the meadow saffron, is an antimitotic agent with a great pharmaceutical potential. Only a few other natural products have proved to be such a challenge to synthetic chemists for half a century. The comparative analysis of the often fascinating synthetic strategies reveals why this seemingly simple structure still belongs to the "difficult targets".



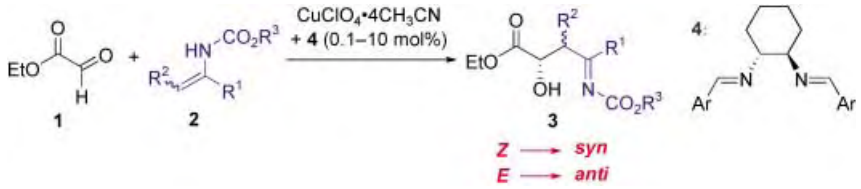
1

Natural Products Synthesis

T. Graening,
H.-G. Schmalz* ——— **3230 – 3256**

Total Syntheses of Colchicine in Comparison: A Journey through 50 Years of Synthetic Organic Chemistry

Communications

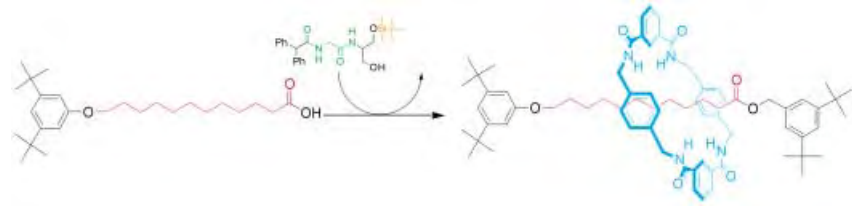


The remarkably selective addition of enecarbamates **2** to ethyl glyoxylate (**1**) in the presence of a copper–diimine catalyst (0.1 mol%) gives the corresponding imines **3** in high yields with excellent enantioselectivities. A concerted aza-ene-type reaction mechanism was proposed to explain the stereochemical outcome.

Addition Reactions

R. Matsubara, Y. Nakamura,
S. Kobayashi* ——— **3258 – 3260**

Highly Diastereo- and Enantioselective Reactions of Enecarbamates with Ethyl Glyoxylate To Give Optically Active *syn* and *anti* α-Alkyl-β-Hydroxy Imines and Ketones



Sew simple: How can you put a molecular bead on a thread when no recognition elements exist between them? A mechanically interlocking auxiliary assembles the macrocycle around a template, controlled submolecular translation moves the ring over the desired substrate and, finally, cleavage of the auxiliary leaves an apparently "impossible" rotaxane (see scheme).

Molecular Shuttles

J. S. Hannam, S. M. Lacy, D. A. Leigh,*
C. G. Saiz, A. M. Z. Slawin,
S. G. Stitchell ——— **3260 – 3264**

Controlled Submolecular Translational Motion in Synthesis: A Mechanically Interlocking Auxiliary

For the USA and Canada:
ANGEWANDTE CHEMIE International Edition (ISSN 1433-7851) is published weekly by Wiley-VCH PO Box 191161, D 69451 Weinheim, Germany. Air freight and mailing in the USA by Publications Expediting Inc. 200 Meacham Ave., Elmont, NY 11003. Periodicals postage paid at Jamaica NY 11431. US POSTMASTER: send address changes to *Angewandte Chemie*, Wiley-VCH, 111 River Street, Hoboken, NJ 07030. Annual subscription price for institutions: Europe € 3430.00/3118.00; outside Europe US$ 4499.00/4090.00 (valid for print and electronic/print or electronic delivery); for individuals who are personal members of a national chemical society, or whose institution already subscribes, or who are retired or self-employed consultants, print only: Europe € 248.00/outside Europe US$ 378.00. Postage and handling charges included. All Wiley-VCH prices are exclusive VAT.

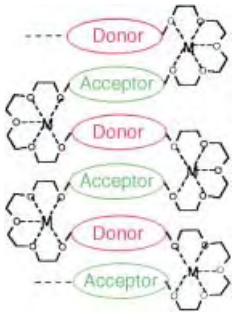
 © 2004 Wiley-VCH Verlag GmbH & Co. KGaA, Weinheim

Contents

Folded Polymers

S. Ghosh,
S. Ramakrishnan* ——— 3264 – 3268

Aromatic Donor–Acceptor Charge-Transfer and Metal-Ion-Complexation-Assisted Folding of a Synthetic Polymer

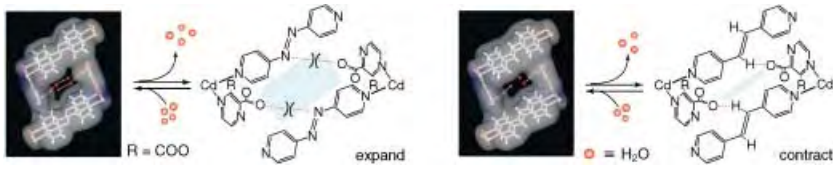


Designer folds: The interplay of three design elements (aromatic donor–acceptor charge-transfer complexation, solvophobic effect, and metal-ion complexation) guided the preparation of a folded structure (see picture) in a synthetic macromolecule. Evidence for this is provided by UV/Vis and ^{1}H NMR spectroscopy.

Microporous Materials

T. K. Maji, K. Uemura, H.-C. Chang,
R. Matsuda, S. Kitagawa* — 3269 – 3272

Expanding and Shrinking Porous Modulation Based on Pillared-Layer Coordination Polymers Showing Selective Guest Adsorption



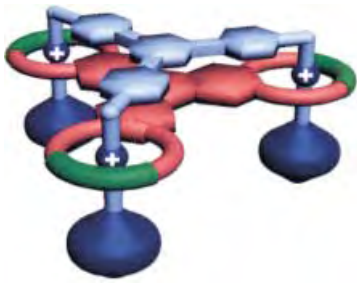
Rationally designed and synthesized, two novel pillar-layered 3D microporous frameworks $\{[Cd(pzdc)(azpy)]\cdot 2H_2O\}_n$ (**1**, left) and $\{[Cd(pzdc)(bpee)]\cdot 1.5H_2O\}_n$ (**2**, right) have high thermal stability and highly selective adsorption properties. Removal of guest water molecules results in the expansion of **1** but the contraction of **2**.

Mechanically Interlocked Compounds

J. D. Badjić, S. J. Cantrill, R. H. Grubbs,*
E. N. Guidry, R. Orenes,
J. F. Stoddart* ——— 3273 – 3278

The Exclusivity of Multivalency in Dynamic Covalent Processes

Less is more: It is much less efficient to synthesize both components of a multivalent recognition site separately than it is to use one multivalent component to act as a template for the catalytically orchestrated construction of the other component, as demonstrated by the formation of the mechanically interlocked, triply threaded molecular bundle shown. The situation is reminiscent of nature.



Template Synthesis

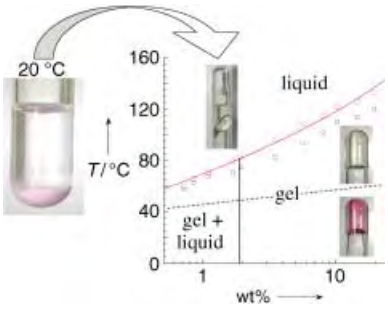
M. Numata, K. Sugiyasu, T. Hasegawa,
S. Shinkai* ——— 3279 – 3283

Sol–Gel Reaction Using DNA as a Template: An Attempt Toward Transcription of DNA into Inorganic Materials



The topologically different structures in plasmid DNA can be successfully transcribed into silica structures by using the DNA as a template for sol–gel polycondensation of tetraethoxysilane after treatment by two cation-exchange steps (see scheme). These findings imply that the different ordered silica structures can be created from the same template through its higher-order conformational changes.

 © 2004 Wiley-VCH Verlag GmbH & Co. KGaA, Weinheim



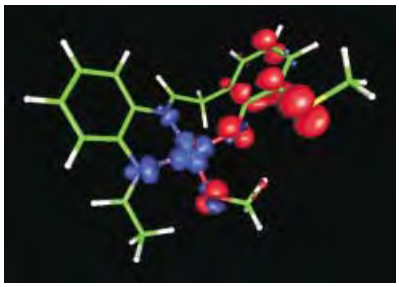
Polyfunctional gels: Thermoreversible switchable gels with tunable magnetic, optical, and rheological properties are obtained from a modified spin-crossover polymeric precursor and alkane solvents (see picture). The iron triazole polymer which acts as the gelator, undergoes a spin crossover that is accompanied by a change in the color of the gel. The transfer of spin-crossover properties from solid materials into gels offers a route to new applications.

Spin Crossover in Gels

O. Roubeau, A. Colin, V. Schmitt, R. Clérac* ——— **3283 – 3286**

Thermoreversible Gels as Magneto-Optical Switches

Ab initio calculations were used for the rational design of efficient alcohol oxidation catalysts that mimic the enzyme galactose oxidase. Different ligand substitutions were explored based on natural (copper, depicted) and alternative (rhodium) metal redox centers. The calculated turnover rate for the most efficient copper-based biomimetic compound is greater than that of the natural enzyme.



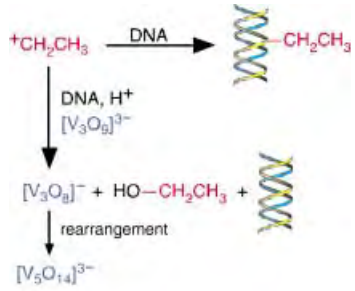
Computer Chemistry

L. Guidoni, K. Spiegel, M. Zumstein, U. Röthlisberger* ——— **3286 – 3289**

Green Oxidation Catalysts: Computational Design of High-Efficiency Models of Galactose Oxidase

---

Intercepting Carcinogens: The cancer-preventing properties of inorganic species, such as selenium and vanadium, are well known, but mechanistic understanding is scant. It is shown that inorganic oxo species (e.g., $[SeO_4]^{2-}$, $[VO_4]^{3-}$) can prevent DNA alkylation as well as detoxify alkylating agents by promoting hydrolysis to relatively harmless alcohols (see scheme).



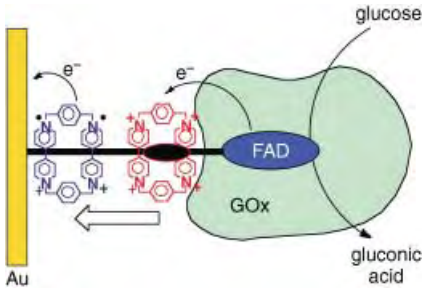
Cancer Prevention

E. E. Hamilton, J. J. Wilker* **3290 – 3292**

Inorganic Oxo Compounds React with Alkylating Agents: Implications for DNA Damage

---

Shuttle of electrons: A redox-active bisbipyridinium cyclophane stoppered by the enzyme glucose oxidase (GOx) in a rotaxane configuration on a molecular wire linked to a gold electrode (see picture) leads to the effective electrical contacting of the biocatalyst that oxidizes glucose at −0.4 V (versus saturated calomel electrode).



Nanotechnology

E. Katz, L. Sheeney-Haj-Ichia, I. Willner* ——— **3292 – 3300**

Electrical Contacting of Glucose Oxidase in a Redox-Active Rotaxane Configuration

 © 2004 Wiley-VCH Verlag GmbH & Co. KGaA, Weinheim

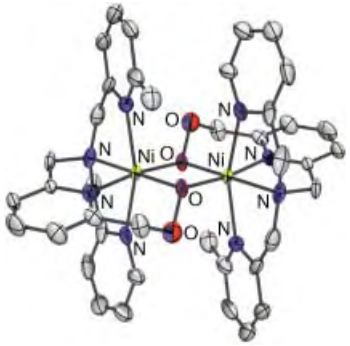
Contents

Reaction Intermediates

J. Cho, H. Furutachi, S. Fujinami, M. Suzuki* ——— **3300 – 3303**

A Bis(μ-alkylperoxo)dinickel(II) Complex as a Reaction Intermediate for the Oxidation of the Methyl Groups of the Me_2-tpa Ligand to Carboxylate and Alkoxide Ligands

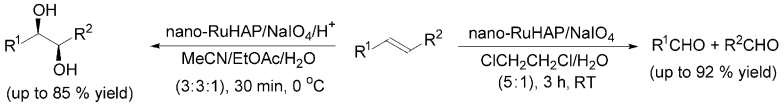
A radical approach: The reaction of $[Ni_2(OH)_2(Me_2\text{-tpa})_2]^{2+}$ with H_2O_2 resulted in the peroxidation of a methyl group of the Me_2-tpa ligand to produce a bis(μ-alkylperoxo)dinickel(II) complex (see ORTEP diagram) as a reaction intermediate for further oxidation to carboxylato and alkoxo complexes $[Ni(Me_1\text{-tpa-COO})]^+$ and $[Ni_2(Me_1\text{-tpa-CH}_2O)_2]^{2+}$. Me_2-tpa = bis[(6-methyl-2-pyridyl)methyl][(2-pyridyl)methyl]amine.



Supported Catalysts

C.-M. Ho, W.-Y. Yu,* C.-M. Che* ——— **3303 – 3307**

Ruthenium Nanoparticles Supported on Hydroxyapatite as an Efficient and Recyclable Catalyst for *cis*-Dihydroxylation and Oxidative Cleavage of Alkenes

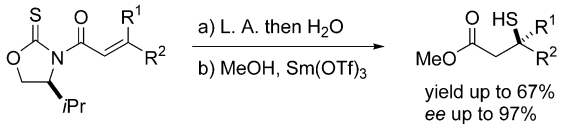


Impregnation of hydroxyapatite with colloidal ruthenium results in the formation of a catalyst that effects *cis*-dihydroxylation and oxidative cleavage of alkenes to their respective *cis*-1,2-diols and carbonyl products in good to excellent yields (see scheme). The supported ruthenium catalyst can be easily recycled and reused for consecutive reaction runs without significant deterioration of the catalytic activities. R^1, R^2 = H, alkyl, aryl.

Asymmetric Synthesis

C. Palomo,* M. Oiarbide, F. Dias, R. López, A. Linden ——— **3307 – 3310**

Construction of C–S Bonds with a Quaternary Stereocenter through a Formal Michael Reaction: Asymmetric Synthesis of Tertiary Thiols

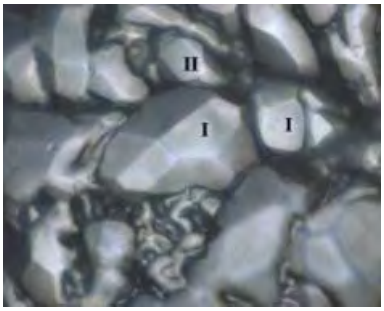


Quaternary stereocenters that bear a sulfur substituent can be created with nearly perfect stereocontrol through an intramolecular Michael-type process. Lewis acids (L.A.) accelerate the intramolecular sulfur-atom transfer from the oxazolidine-2-thione functionality to the β carbon atom of the β,β-disubstituted enoyl moiety, whereas the chirality of the oxazolidine-2-thione portion controls reaction stereochemistry (see scheme).

Kinetics versus Thermodynamics

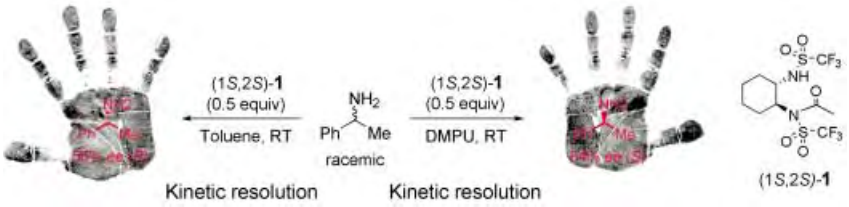
J. M. Schicks,* J. A. Ripmeester ——— **3310 – 3313**

The Coexistence of Two Different Methane Hydrate Phases under Moderate Pressure and Temperature Conditions: Kinetic versus Thermodynamic Products



The unexpected coexistence of structure I (s I) and structure II (s II) methane hydrates under conditions where only s I hydrates should be stable (see picture) suggests that the initial product is determined by kinetics. The state of coexistence as well as the transformation of the kinetic product into the thermodynamically stable s I hydrate was documented by microscopic visual observation as well as Raman spectroscopy.

 © 2004 Wiley-VCH Verlag GmbH & Co. KGaA, Weinheim



Solvents lend a hand: Changing the polarity of the reaction solvent from 1,3-dimethyltetrahydropyrimidin-2-one (DMPU) to toluene reverses the stereoselectivity observed in the acetylation of amines with (1*S*,2*S*)-**1** (see scheme). Optimizing the reaction conditions led to an unprecedented 90% *ee* (*S*) in DMPU at −20°C with a 33% conversion.

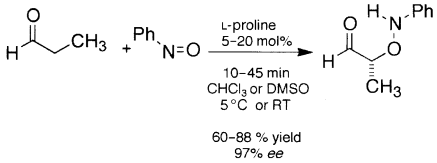
Enantiomeric Synthesis

S. Arseniyadis, A. Valleix, A. Wagner,* C. Mioskowski* ——— **3314 – 3317**

Kinetic Resolution of Amines: A Highly Enantioselective and Chemoselective Acetylating Agent with a Unique Solvent-Induced Reversal of Stereoselectivity

---

The evolution of homochirality from simple organic molecules can perhaps be modeled on the proline-mediated aminoxylation of aldehydes (see scheme). The observed accelerating reaction rate combined with an amplification of the enantiomeric excess of the product is attributed to an autoinductive reaction mediated by an adduct of proline and the product.

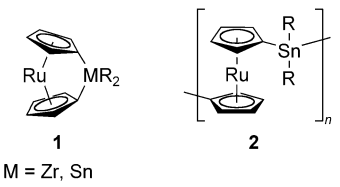


Asymmetric Amplification

S. P. Mathew, H. Iwamura, D. G. Blackmond* ——— **3317 – 3321**

Amplification of Enantiomeric Excess in a Proline-Mediated Reaction

---



Strained, ring-tilted [1]ruthenocenophanes **1** have been prepared for the first time. Ring-opening polymerization (ROP) of an example of **1** with a Sn bridge affords a novel, bimetallic, high-molecular-weight polyruthenocenylstannane **2** (R = mesityl).

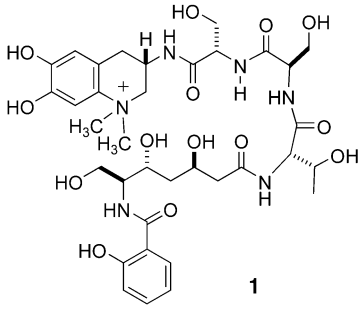
Bimetallic Polymers

U. Vogel, A. J. Lough, I. Manners* ——— **3321 – 3325**

Isolation of [1]Ruthenocenophanes: Synthesis of Polyruthenocenylstannanes by Ring-Opening Polymerization

---

A postulated biogenesis forms the basis for a synthetic route to the natural product anachelin H (**1**). Key steps include a tellurium-mediated, oxidative aza annulation and a Claisen condensation under mild conditions. Experiments with a model substrate indicate that it is likely that a catechol oxidase-type enzyme is involved in the biosynthesis of the anachelin chromophore.



Biomimetic Synthesis

K. Gademann,* Y. Bethuel ——— **3327 – 3329**

A Biomimetic Route to the Peptide Alkaloid Anachelin

 © 2004 Wiley-VCH Verlag GmbH & Co. KGaA, Weinheim

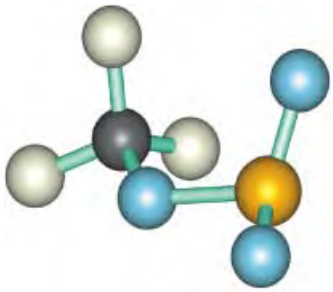
Contents

Atmospheric Chemistry

S. von Ahsen,*
J. S. Francisco ——— 3330 – 3333

The Trifluoromethoxy Sulfuryl Radical, $CF_3OSO_2^{\bullet}$

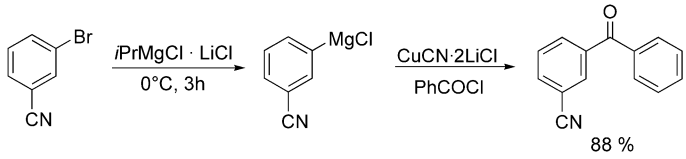
A radical with great implications: Matrix-isolated CF_3O radicals interact with SO_2 yielding $CF_3OSO_2^{\bullet}$ (see picture) when the matrix is annealed at 35 K. The new radical was characterized spectroscopically and studied by DFT calculations. $CF_3OSO_2^{\bullet}$ may have significant impact on atmospheric processes.



Grignard Reactions

A. Krasovskiy, P. Knochel* — 3333 – 3336

A LiCl-Mediated Br/Mg Exchange Reaction for the Preparation of Functionalized Aryl- and Heteroarylmagnesium Compounds from Organic Bromides

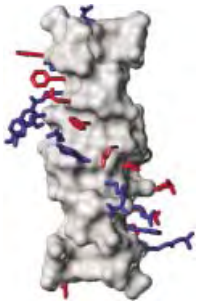


A wide range of aryl and heteroaryl bromides, which are usually sluggish in exchange reactions, are readily converted into the corresponding Grignard reagents by means of a Br/Mg exchange reaction triggered by *i*PrMgCl·LiCl (see scheme). These Grignard intermediates react with electrophiles in good yields.

DNA Modification

S. Jäger, M. Famulok* ——— 3337 – 3340

Generation and Enzymatic Amplification of High-Density Functionalized DNA Double Strands



Up to eight modifications could be incorporated into a DNA heteroduplex (see picture) by introducing different sets of 2′-deoxynucleotide derivatives through DNA polymerase mediated primer extension. All four natural nucleobases in each strand were substituted with different base-modified analogues. PCR conditions are described that allow the direct amplification of fully functionalized DNA double strands.

Communications labeled with this symbol have been judged by two referees as being "very important papers".

The issues for June 2004 appeared online on the following dates
Issue 21: May 12. · Issue 22: May 19. · Issue 23: June 1. · Issue 24: June 9.

Sources

Product and Company Directory

You can start the entry for your company in "Sources" in any issue of *Angewandte Chemie*.

If you would like more information, please do not hesitate to contact us.

Wiley-VCH Verlag – Advertising Department
Tel.: 0 62 01 - 60 65 65
Fax: 0 62 01 - 60 65 50
E-Mail: MSchulz@wiley-vch.de

Service

Keywords ——— *3342*
Authors ——— *3343*
Sources ——— *A41*
Preview ——— *3345*

Apology

In the Communication "Block-Selected Molecular Recognition and Formation of Polypseudorotaxanes between Poly(propylene oxide)-Poly(ethylene oxide)-Poly(propylene oxide) Triblock Copolymers and α-Cyclodextrin" by J. Li, X. Ni, and K. Leong (*Angew. Chem. Int. Ed.* **2003**, *42*, 69–72), the authors neglected to cross-reference their thematically related full article in *J. Am. Chem. Soc.* **2003**, *125*, 1788–1795 by J. Li, X. Ni, Z. Zhou, and K. Leong. The later full article reported the strong evidence for the formation of the triblock copolymer architectures, as well as details of the preparation and characterization of the polypseudorotaxanes. The authors apologize for this oversight.

Industrial Pharmaceutical Biotechnolgy



2002. XII, 381 pages, 16 figures, 53 tables. Hardcover.
ISBN 3-527-29995-5
€ 149.- /£ 105.- /US$ 195.-

HEINRICH KLEFENZ, Bornheim, Germany

10630402_kn

Features

- Covers genomics, proteomics, cytomics, structural and functional biology.
- Shows networks and multi-gene traits at the molecular, genetic, biochemical, cellular and organismal levels.
- Describes nature technologies that are used in industry.
- Is interesting for everyone who wants to know what is really applied.
- Helps to get an overview on real processes.

This book is the ideal source of information for scientists and engineers in research and development, for decision-makers in biotech, pharma and chemical corporations, as well as for research institutes, but also for founders of biotech companies and people working for venture capital corporations.

"... a useful introduction... provides a significant amount of insight and useful information about a thriving scientific area in which there exist few comprehensive texts."
SIM News

Register now for the free
WILEY-VCH Newsletter!
www.wiley-vch.de/home/pas

WILEY-VCH • P.O. Box 10 11 61 • D-69451 Weinheim, Germany
Fax: +49 (0) 62 01 - 60 61 84
e-mail: service@wiley-vch.de • http://www.wiley-vch.de

WILEY-VCH

 © 2004 Wiley-VCH Verlag GmbH & Co. KGaA, Weinheim



Ordered Porous Nanoarchitectures with Specific Functions**

Nicola Hüsing

Porosity—or "the nothing", as it was recently termed—is an important and integral part of the architectural design of zeolites and related mesoscopically organized materials, such as MCM-41 and SBA-15.[1,2] Although these materials can be very different in terms of pore size, wall structure (amorphous or crystalline), chemical composition, and synthesis, the introduction of the desired (multi)functionality for possible applications, for example, through the incorporation of guest species in the pores, on the walls, or as an integral part of the pore walls, remains one of the key challenges. The growing interest in this field can be seen in the fact that more and more researchers—not only from classical solid-state science, which is typically related to zeolite chemistry, but also from areas of soft-materials chemistry, such as sol-gel chemistry, organic and polymer chemistry, supramolecular chemistry, and even biochemistry—are working on these materials.[3] This high interdisciplinarity and the growing interest in this research field were taken into account by Frank Marlow (MPI Mülheim, Germany) in the organization of the EURESCO conference on guest-functionalized molecular-sieve systems, not only through the invitation of well-known scientists from several different scientific areas, but also through the opportunity given to young scientists from Eastern European countries to participate at this meeting.

The main focus of the conference was on the functionalization of molecular sieves by the incorporation of guest species. Molecular-sieve systems can be composed of a large variety of materials, from aluminosilicates and pure silicates, inorganic phosphates, and inorganic–organic hybrids to purely carbon-based materials, to mention but a few. Many of these types of materials were represented in the various oral and poster presentations. Not only because of this variety, many different options exist for the functionalization of molecular-sieve systems (Figure 1). Topics such as the inclusion of molecules or guest entities, such as dyes and biomolecules, by adsorption into a preformed porous matrix from solution or the gas phase were discussed, as well as the in situ incorporation of noncovalently included functionalities during the synthesis of the host matrix. The latter approach is complex, as the active entity should also act as a template molecule so that the periodic pore structure is not disturbed. An alternative approach presented by D. Wöhrle (Bremen, Germany) is stepwise synthesis within a preformed porous host matrix, for example, of a dye molecule. This method, also termed "ship-in-a-bottle synthesis", is especially attractive, as it allows the incorporation of large molecules, such as dyes, which can not be diffused into the matrix because of size restrictions. An additional advantage is that leaching of the active molecule is thus prevented.[4]

Another approach is based on condensation reactions of functional entities with the host matrix. This method is called grafting if carried out in two steps or true co-condensation if carried out in a single step. Some presentations covered the possibility of the post-treatment of preformed matrices through the grafting of functional molecules. Elegant approaches are based on true in situ co-condensation reactions well known from sol-gel science. A highlight in this area are the so-called periodic mesoporous organosilicas (PMOs), as was clear from the discussions after the talk of H. Garcia (Valencia, Spain) on co-condensation reactions of bifunctional, bridged organosilanes with tetraethoxysilanes to form a hybrid material with periodically arranged pores in which the organic functionality is an integral part of the pore walls of the porous material.[5] One focal point of the discussion, which was led by M. Froeba (Giessen, Germany), was the difference between this type of material and "typical" hybrid sol-gel materials, for example, in terms of the acidity of the corresponding silanols. In connection with this point, the question arose as to whether the term PMO truly classifies the uniqueness and significance of these systems.

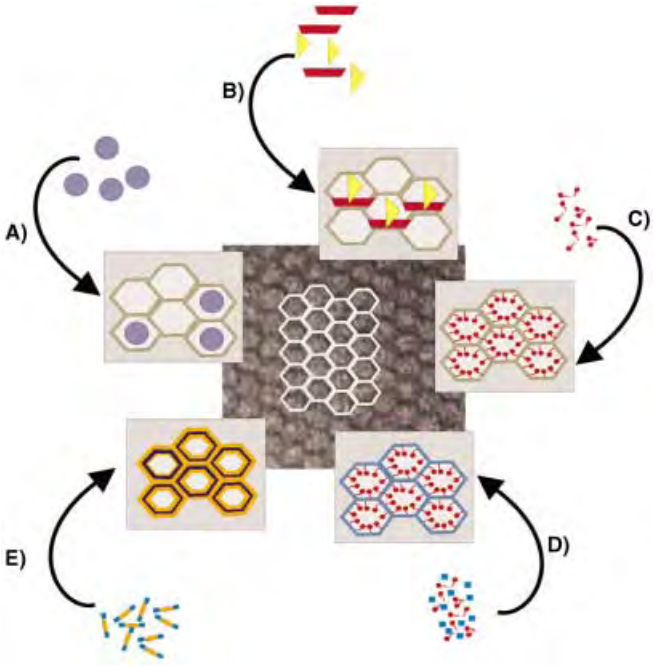


Figure 1. Inclusion of guest species in a molecular sieve, in this case hexagonal MCM-41: A) inclusion by treatment of a preformed matrix with a gas or liquid; B) ship-in-a-bottle synthesis; C) grafting of functional entities through covalent bonding in a post-treatment step; D) co-condensation reactions of network-forming and functionalizing molecules; E) bridged silanes in the synthesis of PMOs.

[*] N. Hüsing
Technische Universität Wien (Austria)
E-mail: nhuesing@mail.zserv.tuwien.ac.at

[**] EURESCO Conference on Zeolite Molecular Sieves: Euroconference on Guest-Functionalised Molecular Sieve Systems, Hattingen (Germany), March 20–25, 2004.Organized by Dr. Frank Marlow.

 © 2004 Wiley-VCH Verlag GmbH & Co. KGaA, Weinheim DOI: 10.1002/anie.200460497

In addition to the scientific presentations, a lot of time was allocated during the conference for general discussions, many of which were particularly fruitful because of the diverse research areas represented by the scientists present. Not only was the uniqueness of PMOs analyzed, but also other issues, such as the very important question as to whether periodicity of the pores is actually necessary for later applications. Many porous sol–gel materials can be utilized in similar or the same applications as the corresponding microporous zeolites or mesoporous molecular sieves, for example, in separations, in catalysis, or as a support for active species.[6] In both cases (that is, whether a system is arranged periodically or not), an activity enhancement can be found, for example, for dyes or biomolecules, or in certain catalytic applications (P. Wright (St. Andrews, UK), D. Wöhrle). C. Sanchez showed an intelligent combination of sol–gel and surfactant solution chemistry, which yieled mesoporous materials in a wide variety of chemical compositions and nanostructures. The establishment of efficient communication pathways between the different scientific disciplines is indispensable for efficient research in this area in the future. For some applications, such as those that require excellent reproducibility in the synthesis, alignment, or preferential orientation of guest molecules within the pores, an ordered arrangement of the pore channels has some distinct advantages. For dye molecules in particular, an ordered arrangement can lead to specific properties, such as frequency doubling or optical switching. F. Laeri (Darmstadt, Germany) presented one potential application in zeolite-based lasing systems.

It was evident from all presentations that the characterization techniques necessary for a thorough investigation of the structure and properties of these molecular-sieve systems must be highly advanced and again interdisciplinary. Depending on the type of host–guest system, optical, electrical, or magnetic techniques may be required (F. Tihay (Rueil-Malmaison, France), B. Weckhuysen, (Utrecht, The Netherlands)). The art of generating and evaluating aesthetic transmission and scanning electron microscopy images in the characterization of periodically arranged materials was impressively demonstrated by O. Terasaki (Stockholm, Sweden). An inspiring example of the characterization of porous materials was provided by C. Bräuchle (München, Germany), who showed that single-molecule spectroscopy is a useful tool for the analysis not only of the architectural features of the channel systems of porous substances, but also of the orientation of dye molecules within the channels (Figure 2).[7]

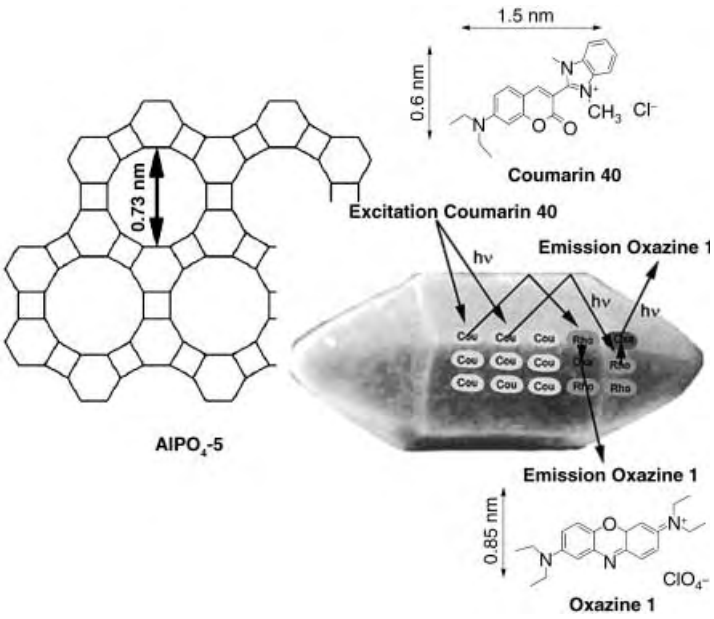


Figure 2. Energy transfer by different dye molecules aligned in the channel system of an aluminophosphate ($AlPO_4$-5; with the kind permission of D. Wöhrle, Bremen).

Technologically important questions were also addressed, such as the fabrication of molecular-sieve systems in morphologies other than powders, for example, as zeolite membranes (J. Caro (Hannover, Germany)). Films are quite easy to prepare from systems with larger pores and amorphous pore walls, such as M41S-type molecular sieves. However, in the case of a one-dimensional channel system the pores are always aligned parallel to the substrate. The alignment of mesoporous channels in thin films vertical to the substrate surface by applying external fields (T. Bein (München, Germany)) and the fabrication of zeolitic architectures as shape-selective membranes are areas still in their infancy. The first zeolite membranes for hydrophilic pervaporation are ready to enter the market. However, for shape-selective applications, the reliability and performance of the corresponding membranes must still be improved.

Although zeolites and molecular-sieving systems of different types have been known for quite some time, true large-scale commercial applications for these materials are still rare. To broaden the prospects for these materials, new fields and interdisciplinary networking have to be established. The EURESCO conference was a big step forward in this direction, bringing together scientists from different fields in a scientifically stimulating environment. It was clearly shown that zeolites and related molecular sieves are not only aesthetic materials, but that emerging fields for ordered host systems can be found in catalysis and nanotechnology, for example, in enantioselective catalysis, sensors, solid lasers, intelligent switches, membranes, waveguides, and solar cells, by combining the know-how and expertise from the various disciplines. The next EURESCO conference of this series will be organized by M. Lindén and held in Helsinki (Finland).

[1] C. S. Cundy, P. A. Cox, *Chem. Rev.* **2003**, *103*, 663.
[2] J. Y. Ying, C. P. Mehnert, M. S. Wong, *Angew. Chem.* **1999**, *111*, 58; *Angew. Chem. Int. Ed.* **1999**, *38*, 56.
[3] M. E. Davis, *Nature* **2002**, *417*, 813.
[4] A. Corma, H. Garcia, *Eur. J. Inorg. Chem.* **2004**, *6*, 1143.
[5] G. Kickelbick, *Angew. Chem.* **2004**, *116*, 3164; *Angew. Chem. Int. Ed.* **2004**, *43*, 3102.
[6] F. Ribot, C. Sanchez, *Comments Inorg. Chem.* **1999**, *20*, 327.
[7] M. Ganschow, C. Hellriegel, E. Kneuper, M. Wark, C. Thiel, G. Schulz-Ekloff, C. Bräuchle, D. Wöhrle, *Adv. Funct. Mater.* **2004**, *14*, 269.

 © 2004 Wiley-VCH Verlag GmbH & Co. KGaA, Weinheim

Protein Design

A Brighter Future for Protein Design**

*Anna Tramontano**

Keywords:
computational biology · protein design · protein folding · structure elucidation

Deciphering the code that relates protein sequence to structure is one of the major goals of computational biology, but unfortunately also a very elusive one. If the code were known, we could infer the structure of proteins from their sequences (direct folding problem or structure prediction) and design sequences able to adopt predetermined folds (inverse folding problem or protein design).

The solution of the direct folding problem would allow us to gain structural information on the multitude of proteins of known sequence and to infer, and interfere with, their molecular function. The successful design of novel proteins would have important practical implications and would open the road to biotechnological, nanotechnological, and therapeutic applications, and an equally profound theoretical significance by allowing hypotheses on protein sequence and structure relationships to be formulated and tested.

Historically, protein design comes in three flavors:[1] redesign of the sequence of a known protein, insertion of a novel function into a given protein scaffold, and design of a sequence that adopts a novel, not yet observed, topology or fold. Each of these approaches aims at answering different but related questions.

Naturally occurring protein sequences are presumably selected for stability, solubility, function, compartmentalization, kinetics behavior, avoidance of undesired conformation, etc. Redesigning the sequence of a known protein can help understanding the relative weight of these factors and their role in shaping natural sequences and the extent to which evolution has sampled the protein sequence space.[2] The second approach permits engineering of useful reagents, but might also help to unravel the properties of functional sites and to explicitly address the issue of molecular specificity.[3] Finally, the design of a completely novel fold can facilitate the identification of the properties that make a fold physically realizable, as it is clear that evolution did not have the opportunity to sample all the available fold space. Ideally, this would allow us to compile a catalogue of feasible and unfeasible topologies, to try and discriminate between them and therefore understand the fundamental rules of "foldability".

Whereas the first two routes have delivered good results in some cases, the last strategy was, until now, less successful. Hence the recent successful automatic design of a novel protein reported by Baker and co-workers[4] represents a landmark in computational structural biology and raises our hopes to gain further understanding in the elusive protein folding problem.

Protein design started in the 1980s on the basis of a rather optimistic view of the problem: Although a given sequence is known to adopt a unique three-dimensional structure, the same fold is shared by several sequences.[5] This degeneracy of the sequence–structure relationship was taken to imply that designing a sequence that folds into a given structure could be easier than predicting the unique structure adopted by a given amino acid sequence. Nevertheless, the route to success has been harder than expected; in a few cases the designed proteins had some proteinlike properties, such as cooperative unfolding and the expected circular dichroism spectra, but they resembled more a molten globule than a native folded protein.[6–8]

Indeed these attempts highlight one of the major differences between the direct and inverse folding problem. Whereas it is relatively easy to measure the correctness of a structure prediction, and therefore methods can be compared, combined, and improved with a stepwise approach, it is much more difficult to verify how close to success a designed fold is, given the difficulty of characterizing almost native structures. Even though the number of acceptable solutions for designing a protein is larger than that for predicting a structure, the extent of success of the former can only be assessed if one of the solutions is correctly and precisely identified.

The contribution by Baker and coworkers to the field is a landmark for several reasons. The design produced a protein sufficiently nativelike to be amenable to X-ray crystallographic analysis. The procedure used was automatic, apparently general, and based on essentially the same model of protein forces used in the Rosetta structure-prediction method developed by the same group.[9] This makes us confident that the reported success is not fortuitous, but represents a real step ahead in our understanding of protein folding, incidentally not the first coming from this research group!

[*] Prof. A. Tramontano
Department of Biochemical Sciences
"A. Rossi Fanelli"
Universitá "La Sapienza"
P. le A. Moro, 00185 Roma (Italy)
Fax: (+39) 06-4440-062
E-mail: anna.tramontano@uniroma1.it

[**] I wish to express my gratitude to David Baker and Gautam Dantas for kindly providing us with Figure 1. Support by the CNR "Progetto Finalizzato Genetica Molecolare" and by the Ministero della Sanità is gratefully acknowledged.

 © 2004 Wiley-VCH Verlag GmbH & Co. KGaA, Weinheim DOI: 10.1002/anie.200301738

The initial step of the method is the selection of a set of distance constraints defining the desired fold. They were used to generate several initial conformations by assembling fragments of proteins of known structure. Sequence optimization for each of the starting structures was performed with Monte Carlo simulations and essentially the same energy function of the Rosetta method. Subsequent cycles of sequence and structure optimization led to the final sequence–structure pair named Top7. The biophysical characterization of the synthesized protein showed that Top7 was soluble, monomeric, stable, and that it underwent two-state cooperative unfolding. Its high-resolution crystal structure showed an impressive similarity with the designed model, only deviating in two short exposed turns (Figure 1).

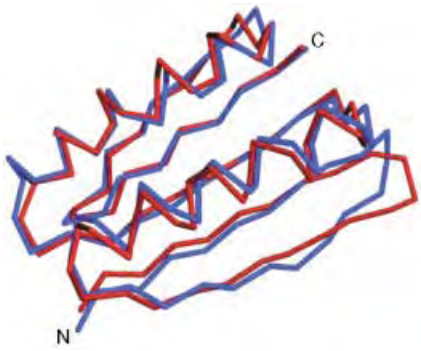


Figure 1. Cα superposition of the designed (blue) and X-ray crystallographically determined (red) structure of Top7. (Courtesy of David Baker and Gautam Dantas, Department of Biochemistry, University of Washington, USA)

As mentioned before, the success of the design has several theoretical implications. First, it confirmed the power of the approach of generating several models at the atomic level by using known subfragments, an approach that has also led to notable success in protein-structure prediction.[10] It also highlighted the usefulness of simultaneous optimization of sequence and structure. Furthermore, it confirmed one of the conclusions derived from protein-structure-prediction experiments: A correct model can be identified more easily at the atomic level, after extensive optimization of side-chain packing, than at any of the intermediate steps of the process.[10]

Interestingly, none of the aspects deemed to be responsible for past failures were taken into account in the procedure of Baker and co-workers; no attempt was made to destabilize alternative putative folds, neither was the kinetics of folding taken into account in the design. The authors attribute the higher accuracy of their design with respect to their predictions to the possibility of changing the sequence during the design procedure and to the lack of functional constraints in the designed protein.

On the one hand, the possibility of changing the sequence, and therefore alter the energy landscape can at least partially compensate for the limited accuracy of the available force fields in searching the complex, vast, and rugged conformational space of proteins. On the other, the active sites of proteins are most likely suboptimal in terms of their structure, because they need to satisfy functional and dynamic constraints; therefore a prediction of their conformation on the basis of energy optimization can be misleading. However, there have been several cases in which active sites have been successfully inserted into known proteins. Top7 has a free energy of unfolding of 13.2 kcal mol^{-1}, higher than that of most proteins of similar size, and therefore it would not be surprising if a functional site could, indeed, be accommodated in the designed scaffold, thus opening the road to the engineering of tailored molecular machines.

Published Online: May 14, 2004

[1] C. Sander, *Trends Biotechnol.* **1994**, *12*, 163–167.
[2] D. T. Jones, *Protein Sci.* **1994**, *3*, 567–574; B. I. Dahiyat, C. A. Sarisky, S. L. Mayo, *J. Mol. Biol.* **1997**, *273*, 789–796; R. B. Hill, D. P. Raleigh, A. Lombardi, W. F. DeGrado, *Acc. Chem. Res.* **2000**, *33*, 745–754; M. Mutter, G. Tuchscherer, *Cell. Mol. Life Sci.* **1997**, *53*, 851–863; S. Dalal, L. Regan, *Protein Sci.* **2000**, *9*, 1651–1659; A. E. Keating, V. N. Malashkevich, B. Tidor, P. S. Kim, *Proc. Natl. Acad. Sci. USA* **2001**, *98*, 14825–14830; L. L. Looger, H. W. Hellinga, *J. Mol. Biol.* **2001**, *307*, 429–445; S. A. Marshall, S. L. Mayo, *J. Mol. Biol.* **2001**, *305*, 619–631; J. Mendes, R. Guerois, L. Serrano, *Curr. Opin. Struct. Biol.* **2002**, *12*, 441–446; A. Jaramillo, L. Wernisch, S. Hery, S. J. Wodak, *Proc. Natl. Acad. Sci. USA* **2002**, *99*, 13554–13559; G. Dantas, B. Kuhlman, D. Callender, M. Wong, D. Baker, *J. Mol. Biol.* **2003**, *332*, 449–460.
[3] M. Szardenings, B. Vasel, H. J. Hecht, J. Collins, D. Schomburg, *Protein Eng.* **1995**, *8*, 45–52; A. L. Pinto, H. W. Hellinga, J. P. Caradonna, *Proc. Natl. Acad. Sci. USA* **1997**, *94*, 5562–5567; A. Skerra, *Biochim. Biophys. Acta* **2000**, *1482*, 337–350; J. Reina, E. Lacroix, S. D. Hobson, G. Fernandez-Ballester, V. Rybin, M. S. Schwab, L. Serrano, C. Gonzalez, *Nat. Struct. Biol.* **2002**, *9*, 621–627; O. Maglio, F. Nastri, V. Pavone, A. Lombardi, W. F. DeGrado, *Proc. Natl. Acad. Sci. USA* **2003**, *100*, 3772–3777.
[4] B. Kuhlman, G. Dantas, G. C. Ireton, G. Varani, B. L. Stoddard, D. Baker, *Science* **2003**, *302*, 1364–1368.
[5] C. Sander, *Biochem. Soc. Symp.* **1990**, *57*, 25–33.
[6] A. N. Fedorov, D. A. Dolgikh, V. V. Chemeris, B. K. Chernov, A. V. Finkelstein, A. A. Schulga, Yu. B. Alakhov, M. P. Kirpichnikov, O. B. Ptitsyn *J. Mol. Biol.* **1992**, *225*, 927–931.
[7] T. Kortemme, M. Ramirez-Alvarado, L. Serrano, *Science* **1998**, *281* 253.
[8] A. Pessi, E. Bianchi, A. Crameri, S. Venturini, A. Tramontano, M. Sollazzo, *Nature* **1993**, *362*, 367–369.
[9] K. T. Simons, R. Bonneau, I. Ruczinski, D. Baker, *Proteins* **1999**, *Suppl. 3*, 171–176.
[10] A. Tramontano, V. Morea, *Proteins* **2003**, *Suppl. 6*, 352–368.

 © 2004 Wiley-VCH Verlag GmbH & Co. KGaA, Weinheim

Industrial Chemistry

Asymmetric Catalysis in the Pharmaceutical Industry

Joel M. Hawkins and Timothy J. N. Watson*

Keywords:
asymmetric catalysis · chiral auxiliaries · freedom to operate · hydrogenation · industrial processes

In principle, asymmetric catalysis is the best method to introduce stereochemistry into pharmaceutically active molecules. In practice, other techniques are often used. This Essay addresses this dichotomy by presenting asymmetric catalysis from the perspective of the pharmaceutical industry. Herein we characterize the constraints of the industry for the application of asymmetric catalysis to the large-scale synthesis of drug candidates and commercial drugs by providing supporting examples from Pfizer's portfolio. The industrial constraints derive from economic considerations, including an analysis of the total transformation, the speed to implement a process, freedom to operate, and process robustness. Freedom to operate has become a significant issue in recent years.[1]

For the synthesis of chiral drug candidates and commercial products, either commercially available starting materials (the preregulatory raw materials which proceed the regulated steps of a drug synthesis) can be purchased with the required stereocenters incorporated, or the stereocenters can be introduced during the synthesis. Chiral-pool sources are in the former category by definition. Listed in decreasing order of tonnage production, these sources include carbohydrates, α-amino acids, terpenes, hydroxy acids, and alkaloids.[2] If not supplied by nature, stereocenters can be established by resolution, the use of a chiral auxiliary, or asymmetric catalysis.[3]

[*] Dr. J. M. Hawkins, Dr. T. J. N. Watson
Pfizer Global Research and Development
Groton, Connecticut 06340 (USA)
Fax: (+1) 860-441-3788
E-mail: joel_m_hawkins@groton.pfizer.com

Resolution is commonly used instead of asymmetric synthesis for large-scale chemistry, and some excellent new methodologies have been developed recently. These include the use of phase diagrams (which make the selection of a resolving agent more of a science than an art),[4] the use of resolving-agent families (which can provide remarkable results),[5] and automation to mechanize the remaining empirical aspects of developing a resolution. In addition to crystallization-based resolutions, chromatographic methods have become much more accessible for large-scale resolutions through the use of continuous chromatography or simulated moving bed (SMB) processes. For example, tetralone intermediate **1** in the synthesis of the antidepressant sertraline (**2**) can be resolved by continuous chromatography,[6] thus providing an alternative to the classical resolution of racemic sertraline with mandelic acid at the end of the synthesis.[7] As shown schematically in Figure 1, the SMB involves a series of columns of a chiral stationary phase which are connected so that the output of each column can be switched between the input of the adjacent column and either of two effluent streams. These outputs can be switched to simulate a moving bed (the chiral stationary phase), thus generating a continuous process whereby racemic **1** is fed into the system and the enantiomers are separated into two effluent streams. In an ideal case, the undesired enantiomer can be recycled through a racemization unit so that all of the racemate can be converted into the desired isomer. In cases where continuous chromatography positions a resolution earlier in a synthesis, plant capacity can be utilized more efficiently.[8] Thus, the design of efficient chiral-recognition mechanisms is important not only for asymmetric synthesis, but also for resolutions in which chiral stationary phases are used for continuous chromatography.

Chiral auxiliaries provide another alternative to asymmetric catalysis. In principle, chiral auxiliaries suffer from the disadvantages that additional steps are required for attaching and cleaving the chiral auxiliary, and that a stoichiometric by-product is formed which needs to be separated after the auxiliary is cleaved.[9] Even so, chiral auxiliaries can be useful for the stereoselective synthesis of pharmaceutical intermediates on a large scale. For example, a chiral-auxiliary-based aldol reaction provided control of both relative and absolute stereochemistry in the multikilogram synthesis of **3**, an intermediate in the process to prepare the LTB_4-receptor antagonist **4** (Scheme 1).[10] For this large-scale Evans aldol reaction, a titanium- rather than a boron-based process was used to avoid pyrophoric intermediates and exothermic quenches. The stoichiometry of TMEDA was increased and NMP was added to give good stereoselectivity with 1 equivalent of the expensive aldehyde component.[10]

The control of stereochemistry by the use of a minute amount of an asymmetric catalyst offers clear advantages. However, to be economical an asymmetric catalyst must fit the desired transformation: One does not want to have to add steps to a synthesis to run a particular key step. Scheme 2 shows an alternative route to tetralone **1** in which a chiral-oxazaborolidine-catalyzed reduction is used.[11] The key reduction is preceded by a protection step and followed by activation, displacement, and cyclization steps, so that a total of five steps are required to prepare (*S*)-**1**.

 © 2004 Wiley-VCH Verlag GmbH & Co. KGaA, Weinheim DOI: 10.1002/anie.200330072

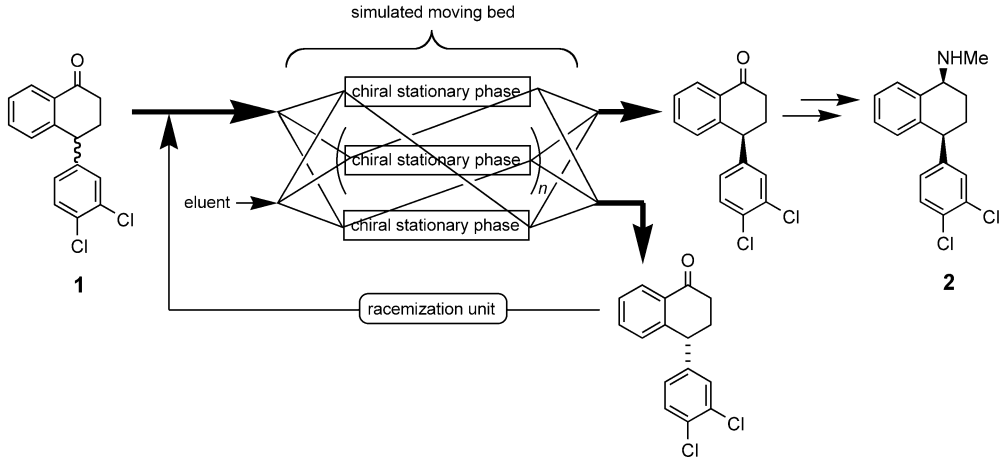
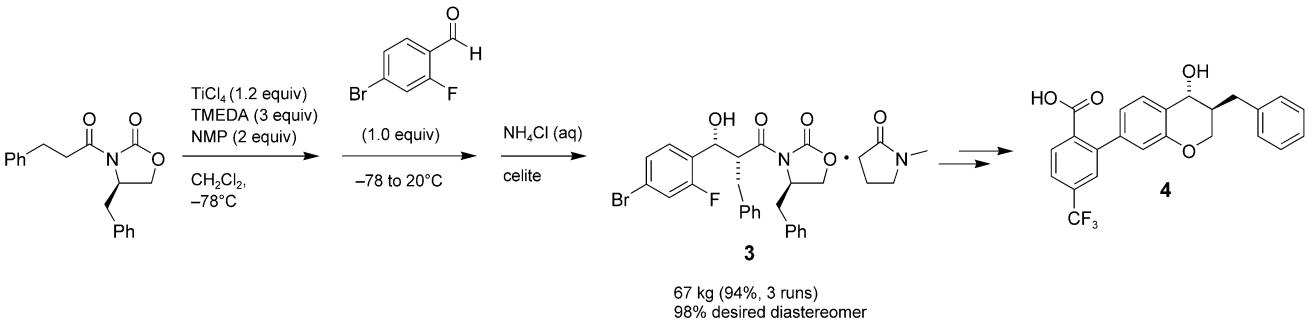


Figure 1. Schematic depiction of a continuous chromatographic resolution of tetralone intermediate **1** in the synthesis of sertraline (**2**).



Scheme 1. Chiral-auxiliary-based titanium aldol synthesis of intermediate **3** in the process to prepare LTB_4-receptor antagonist **4**. TMEDA = *N*,*N*,*N*′,*N*′-tetramethylethylenediamine, NMP = *N*-methyl-2-pyrrolidone.

In contrast, the racemate (±)-**1** can be made in one step from 1-naphthol[12] and resolved by SMB. Routes in which a racemate can be prepared inexpensively and resolved efficiently are often more economical than routes in which the use of an asymmetric catalyst requires additional synthetic steps.[13]

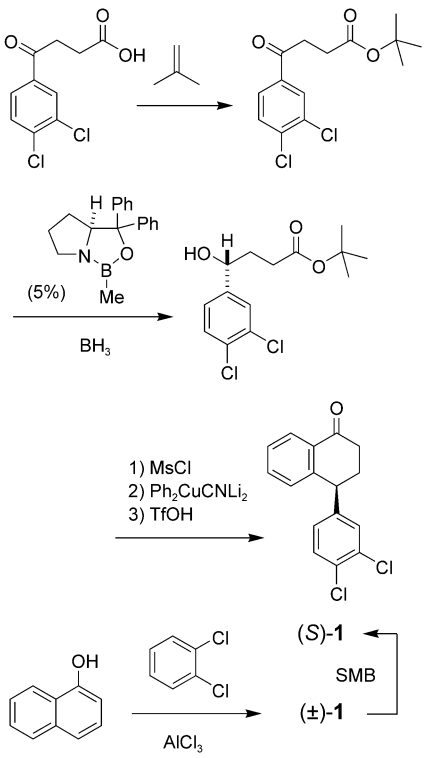
Scheme 3 shows a more natural fit for asymmetric catalysis, whereby a chiral-oxazaborolidine-catalyzed reduction of ketone **5** controls the configuration α to the thiazole ring in antidiabetic **6**.[14] In this case, the asymmetric reduction fits in the synthetic progression starting with thiazole formation by using symmetrical 1,4-dibromodiacetyl. After reduction, the second bromine substituent provides for the introduction of the amine side chain.

The economics of asymmetric catalysis involve not only the principle transformation as discussed above, but also the required stoichiometric reagents. For example, for asymmetric catalytic aldol reactions,[15] the enolate source can range in complexity from the ketone itself, an ideal case, to ketene silyl acetals of thioesters, which demand extra steps for reagent preparation, are air sensitive, and have stench issues associated with them (Scheme 4). These factors can influence the relative economics of chiral-auxiliary-based and asymmetric-catalyst-based aldol processes. Similarly, asymmetric catalytic oxidations require stoichiometric oxidants ranging in complexity and molecular weight from O_2 itself to ferricyanide (Scheme 5). The more complex and higher-molecular-weight enolate sources and oxidants also have more complex and higher-molecular-weight stoichiometric by-products that need to be separated from the desired product and disposed of, which adds to the overall cost of the process. Catalytic asymmetric reductions with H_2 are ideal in terms of reagent simplicity and the absence of stoichiometric by-products.

Three additional economic factors are derived from the important industrial constraints of the speed to implement a process, freedom to operate, and process robustness. The earlier an asymmetric catalytic process can be implemented during the development of a drug candidate, the greater the chance that the asymmetric catalytic chemistry will be applied on a commercial scale, as the first successful route to a drug candidate often gains momentum. Raw materials are procured on an ever larger scale for a route with a proven track record as the amount of drug substance required for toxicological and clinical studies grows. The profiles of trace impurities (which depend most on the later steps of a synthesis) become qualified in toxicological studies by using early bulk drug prepared by early synthetic routes. New routes must meet these specifications or else be qualified by additional studies.

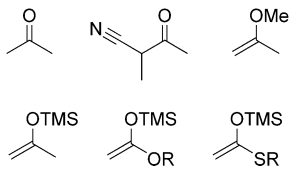
Furthermore, the final solid form of the drug substance (including particle size, habit, and polymorph) can depend on trace impurities or residual solvents

 © 2004 Wiley-VCH Verlag GmbH & Co. KGaA, Weinheim

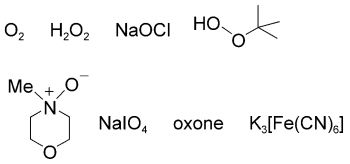


Scheme 2. Syntheses of sertraline tetralone (*S*)-**1** by using asymmetric catalysis and (±)-**1** by using a Friedel–Crafts arylation. Ms = methanesulfonyl, Tf = trifluoromethanesulfonyl.

from the final synthetic steps. Thus, an asymmetric catalyst that can prove its chemical and economic viability early in the development process has the greatest chance of being incorporated in the ultimate synthesis, especially if it is used in a late synthetic step. (The early steps used to prepare the regulatory raw material can be changed more readily later in development.) Establishing the economic viability of a catalyst early in development requires that any royalties and freedom-to-operate issues be clearly defined and resolved early in the development process. This is facilitated by simple rather than complex business



Scheme 4. Progression of increasing complexity of enolate sources for asymmetric catalytic aldol reactions.



Scheme 5. Progression of increasing complexity and molecular weight of stoichiometric oxidants.

arrangements, as discussed further below.[16]

The cost of an asymmetric catalyst can be broken into three components, the chiral ligand, the metal if present, and any royalties. Asymmetric ligands range in complexity from simple derivatives of cheap chiral-pool molecules to complex species that require multistep syntheses. Complexity not only adds cost, it also impedes the rapid availability of the ligand in sufficient quantity to meet the needs of bulk-drug production.[17] Simple ligands can be sourced more rapidly and can be incorporated into a synthetic route early in the development process with greater confidence. Metal costs can be quite variable over time, as precious-metal prices depend on geopolitical events well beyond the chemist's control. For example, the price of palladium escalated rapidly in 2000 (Figure 2).[18] Low catalyst loadings for precious-metal-based systems mitigate this risk. Royalties, if present, add the third component to the cost of an asymmetric catalyst. Like the cost and availability of ligands and precious metals, uncertainties in royalty costs add risk to a synthesis: risk that will often be avoided by choosing an alternative route. The sum of these three costs, the ligand, the metal, and royalties, add to the cost of a route based on asymmetric catalysis. If these costs are too high, an alternative route will be used.

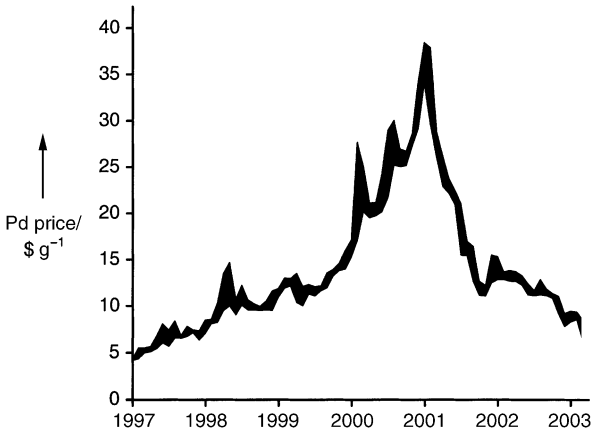
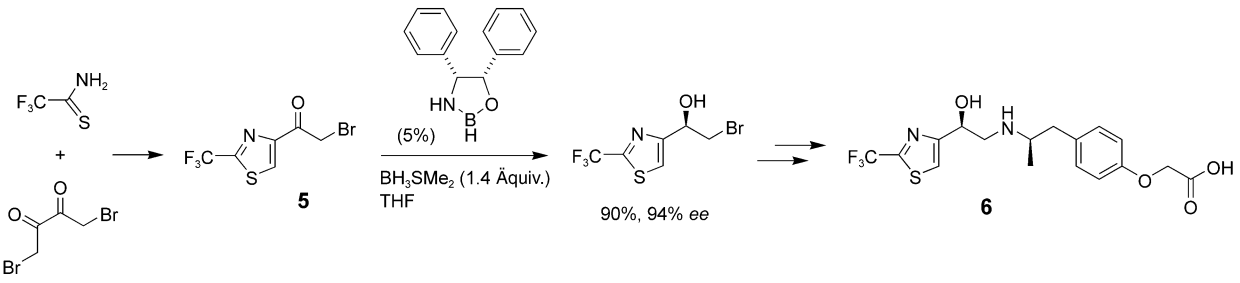


Figure 2. Cost of palladium from January 1997 to March 2003 (monthly ranges in US$ g^{-1}, London).

Freedom to operate is a key distinguishing feature between asymmetric catalysts. To base the commercial synthesis of a drug on a particular chemical process, a company needs to have freedom to operate the process both internally and externally with multiple out-



Scheme 3. Application of oxazaborolidine-catalyzed asymmetric reduction in the synthesis of the antidiabetic **6**.

 © 2004 Wiley-VCH Verlag GmbH & Co. KGaA, Weinheim

sourcing partners. Any limitation to a sole source imposes unacceptable risk. To avoid uncertainties regarding freedom to operate and royalty costs, and to lower the total cost of a catalytic step, a catalyst that is published in the literature and not patented will be far more likely to be used for large-scale drug synthesis than a catalyst that is patented and has licensing constraints or high royalties. This distinction is far more important than small differences in enantioselectivity.

Process robustness is also key. To be ultimately useful, a catalytic step must scale up predictably from laboratory to pilot plant to production. Furthermore it must work every time on scale, as each large-scale batch is critical to the development of a drug candidate. Robustness is often at odds with catalyst loading. At a very low catalyst loading a process may work in the laboratory and may work on a larger scale under ideal conditions, but it will be more susceptible to variations typical of pilot-plant and production operations. For example, variations in the amount of residual solvent brought in with the starting materials from the previous step, variations in the quality of recycled solvent in production, increased cycle times on a larger scale, and trace amounts of air or moisture all pose risk to catalyst activity or enantioselectivity. Whereas all of these parameters are controlled within the limits of GMP (good manufacturing practice), if they must be very tightly controlled to assure catalyst performance it would add too much cost. A further consideration is whether or not a catalytic process can be restarted by adding more of the catalyst if the catalyst dies. If not, this adds considerable risk.

The issues of freedom to operate and process robustness are illustrated by the competing approaches to candoxatril (**7**) based on asymmetric hydrogenation.[19–21] To avoid classical resolution of acid **8**, Challenger et al. developed the asymmetric hydrogenation of alkene **9** (Scheme 6).[19] Although the enantioselectivity was good when a Ru–binap catalyst was used (94% *ee*), competing isomerization of **9** to **10** led to a significant decrease in the yield. Burk et al. showed that Rh–Me-duphos gave very high enantioselectivity (>99% *ee*) and high yield (95%) without any olefin isomerization, and they demonstrated this process on a 12-kg scale.[20] They explored substrate-to-catalyst (S/C) ratios of 100:1 to 10000:1 and described the "delicate balance between hydrogen pressure, temperature, and S/C ratio … to provide the most economically attractive process," choosing 3500:1 for the 12-kg run. Although Rh–Me-duphos gave excellent yield and selectivity, it was not chosen to prepare the two metric tons of candoxatril required for phase-III clinical trials. As described by Bulliard et al., "Access to a reasonably priced ligand which would be readily available on large scale (up to 10 kg) was a key issue. Patents were also a concern, and we needed to have the right to use the catalyst in-house."[21] For these reasons, they applied a Ru–MeO-biphep catalyst for the large-scale asymmetric hydrogenation of **9**, working in 231-kg batches in a 4000-L reactor. Olefin isomerization was attenuated by switching the solvent from methanol/water to THF/water, and purity specifications were met by recrystallization.[22] Thus, freedom-to-operate and royalty issues drove the choice to use a less-selective catalyst, and chemical means were found to effectively work with this catalyst on a large scale.

Tremendous new asymmetric catalysts which offer phenomenal scope and selectivities are being developed in laboratories around the world. They will be used by the pharmaceutical industry on a large scale when they meet the corresponding economic constraints. These are best met by inexpensive and readily available catalysts that can be implemented rapidly. The cost and speed of implementation encompass the total cost of the catalyst (the ligand, metal, and any royalties), the breadth of its availability, and any licensing constraints. The catalyst must efficiently fit the desired synthetic transformation, and the overall transformation must minimize stoichiometric by-products. Low catalyst loadings minimize ligand and metal costs, yet this must be balanced with process robustness and throughput. Publishing rather than patenting catalysts will assure that the best catalyst from a chemical perspective will also be the best catalyst from an overall economic perspective. *These* catalysts will be used to prepare pharmaceutically active chiral molecules on a large scale, the reason that many catalysts were developed and their development funded in the first place.

Received: August 29, 2003 [E30072]

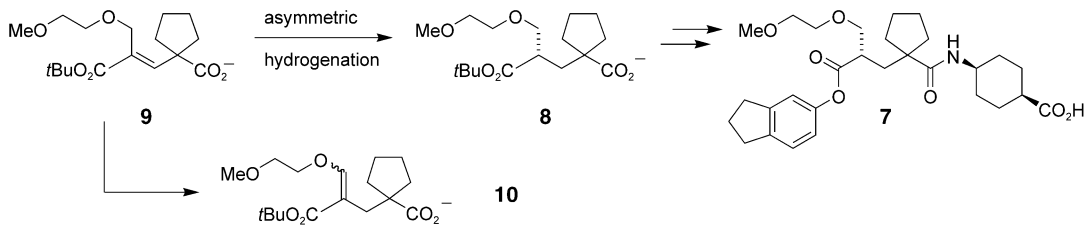
[1] As early as 1997, the increased tendency to patent synthetic methodology was noted to be "creating a complex legal maze for the chemical industry." D. B. Collum in *1997 Yearbook of Science and the Future* (Ed.: D. Calhoun), Encyclopedia Britannica, Chicago, **1996**, p. 284.

[2] M. K. O'Brien, B. Vanasse, *Curr. Opin. Drug Discovery Dev.* **2000**, *3*, 793.

[3] For a detailed analysis illustrated with many examples including the use of enzymes, see reference [2].

[4] A. Collet, *Angew. Chem.* **1998**, *110*, 3429; *Angew. Chem. Int. Ed.* **1998**, *37*, 3239.

[5] T. Vries, H. Wynberg, E. van Echten, J. Koek, W. ten Hoeve, R. M. Kellogg, Q. M. Broxterman, A. Minnaard, B. Kaptein, S. van der Sluis, L. Hulshof, J. Kooistra, *Angew. Chem.* **1998**, *110*, 2491; *Angew. Chem. Int. Ed.* **1998**, *37*, 2349.



Scheme 6. Asymmetric hydrogenation approach to candoxatril (**7**).

 © 2004 Wiley-VCH Verlag GmbH & Co. KGaA, Weinheim

[6] O. Dapremont, F. Geiser, T. Zhang, S. S. Guhan, R. M. Guinn, G. J. Quallich, US Pat. 6444854, **2002**.
[7] W. M. Welch, A. R. Kraska, R. Sarges, B. K. Koe, *J. Med. Chem.* **1984**, *27*, 1508.
[8] In favorable cases, the benefits of continuous chromatography outweigh the capital expense for specialty equipment, which can be operated internally or at a specialist company.
[9] Stoichiometric chiral ligands (chiral mediators) do not require attachment and cleavage steps and in an optimized case can be recycled in the same reaction vessel by in situ regeneration of the active species: A. Choudhury, J. R. Moore, M. E. Pierce, J. M. Fortunak, I. Valvis, P. N. Confalone, *Org. Process Res. Dev.* **2003**, *7*, 324.
[10] A. Piscopio, J. M. Hawkins, S. Caron, S. E. Kelly, J. W. Raggon, M. J. Castaldi, R. W. Dugger, S. G. Ruggeri, US. Pat 6096906, **2000**.
[11] G. J. Quallich, T. M. Woodall, *Tetrahedron* **1992**, *48*, 10239.
[12] I. B. Repinskaya, K. Y. Koltunov, *Sib. Khim. Zh.* **1993**, *3*, 73.
[13] For other multistep routes to sertraline tetralone (*S*)-**1** by using asymmetric catalysis, see: E. J. Corey, T. G. Gant, *Tetrahedron Lett.* **1994**, *35*, 5373; M. Lautens, T. Rovis, *J. Org. Chem.* **1997**, *62*, 5246; H. M. L. Davies, D. G. Stafford, T. Hansen, *Org. Lett.* **1999**, *1*, 233.
[14] G. J. Quallich, PCT Int. Appl. WO 9502585, 1995.
[15] T. D. Machajewski, C.-H. Wong, *Angew. Chem.* **2000**, *112*, 1406; *Angew. Chem. Int. Ed.* **2000**, *39*, 1352.
[16] For a comparison of the classical royalty model (where the license fee is based on the projected added value of the catalyst) and the "all-inclusive" model (where the price of the chiral catalyst contains the IP licensing costs as a simple per-kilogram-of-catalyst fee), see: M. Thommen, *sp*^{2} **2003**, April issue, 26.
[17] For example, the scarce supply and expense of binap prompted Merck chemists to develop a simple and efficient synthesis of binap: D. Cai, J. F. Payack, D. R. Bender, D. L. Hughes, T. R. Verhoeven, P. J. Reider, *J. Org. Chem.* **1994**, *59*, 7180.
[18] Palladium prices from http://www.kitco.com/charts/historicalpalladium.html. We thank Dr. Don Zeng of Heraeus for pointing out this internet reference.
[19] S. Challenger, A. Derrick, C. P. Mason, T. V. Silk, *Tetrahedron Lett.* **1999**, *40*, 2187.
[20] M. J. Burk, F. Bienewald, S. Challenger, A. Derrick, J. A. Ramsden, *J. Org. Chem.* **1999**, *64*, 3290.
[21] M. Bulliard, B. Laboue, J. Lastennet, S. Roussiasse, *Org. Process Res. Dev.* **2001**, *5*, 438.
[22] Crystallization of the product of an asymmetric catalytic reaction, a step often included to enhance the optical purity, can contribute to the robustness of the process (for example, in the case of varying selectivity), provided that the optical purity does not drop below the eutectic composition.

 © 2004 Wiley-VCH Verlag GmbH & Co. KGaA, Weinheim

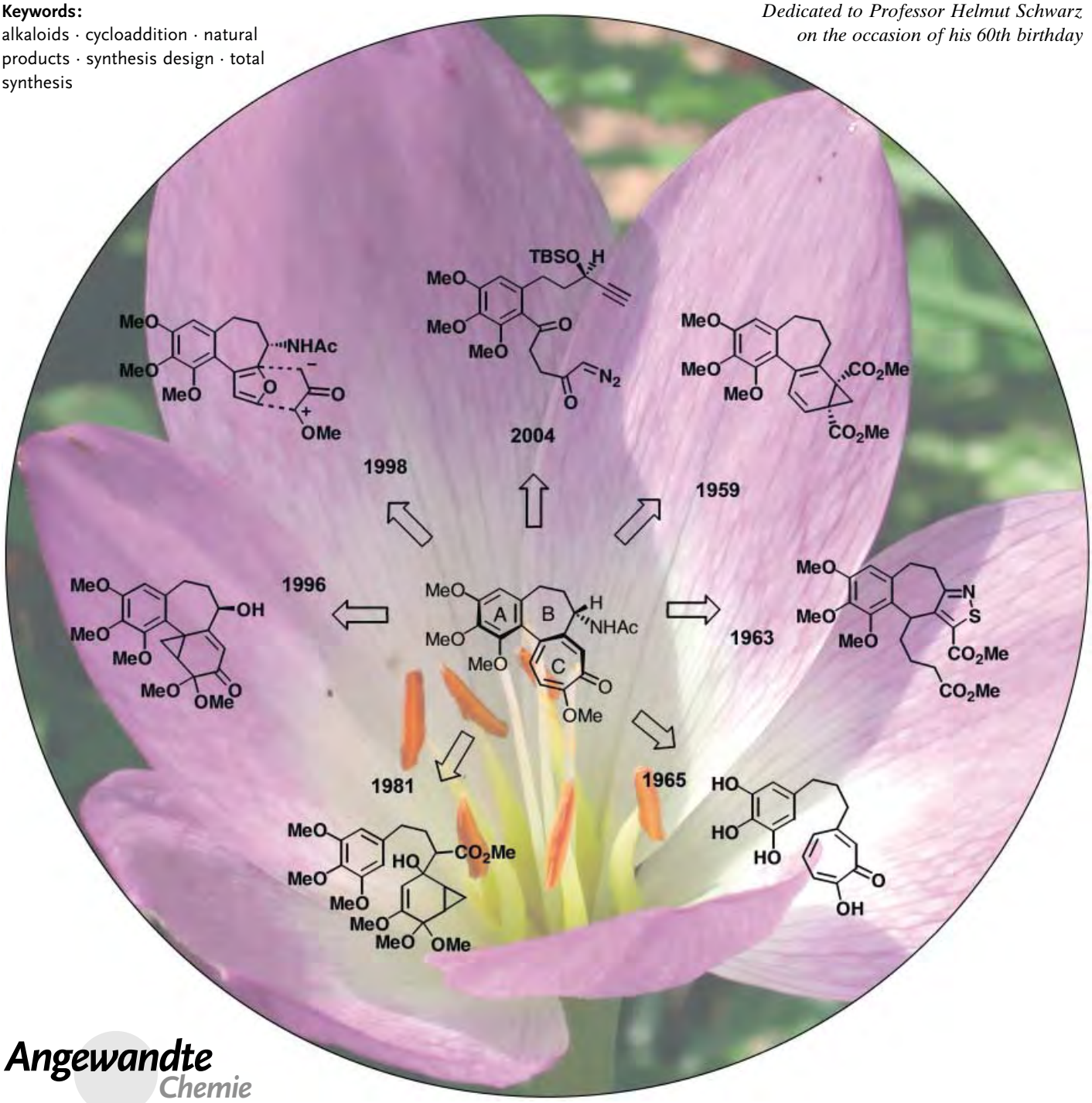
Natural Products Synthesis

Total Syntheses of Colchicine in Comparison: A Journey through 50 Years of Synthetic Organic Chemistry

*Timm Graening and Hans-Günther Schmalz**

Keywords:
alkaloids · cycloaddition · natural products · synthesis design · total synthesis

Dedicated to Professor Helmut Schwarz on the occasion of his 60th birthday



© 2004 Wiley-VCH Verlag GmbH & Co. KGaA, Weinheim
DOI: 10.1002/anie.200300615

Colchicine, the major alkaloid of the meadow saffron, is one of the most prominent natural products and, like other tubulin-binding natural products (e.g. taxol and the epothilones), exhibits great pharmaceutical potential. The first syntheses in the late 1950s were milestones in natural product synthesis. But even today this structurally supposedly simple molecule poses a challenge to synthetic chemists. Only in the last years have syntheses been developed that are efficient enough to provide novel structurally modified colchicine analogues. The comparative examination of all known colchicine total syntheses undertaken in this Review not only reveals the tremendous progress in synthetic organic methodology over the past decades, but also shows how the unique synthetic problems posed by this molecule can be solved in an exceptionally creative manner. Only a few target molecules have been synthesized in such multifaceted ways.

From the Contents

1. Structure Elucidation and Biosynthesis 3231

2. The Colchicine/Tubulin Interaction 3233

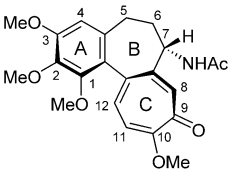
3. Target Structure and Classification of the Total Syntheses 3234

4. Colchicine Total Syntheses 3235

5. Summary 3253

1. Structure Elucidation and Biosynthesis

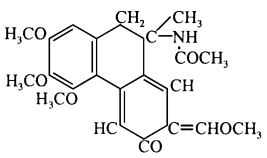
Colchicine (**1**) is the main alkaloid of the poisonous plant meadow saffron (*Colchicum autumnale* L.),[1] a common plant of European and North African origin that flowers in autumn on a leafless stalk (Figure 1). Despite its alternative name, autumn crocus, it belongs to the family Liliaceae.



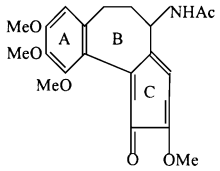
1 (–)-(a*R*,7*S*)-colchicine

The name *Colchicum* is derived from Colchis, a region east of the Black Sea that is known in Greek mythology as the home of the Golden Fleece and the notorious poisoner Medea. Besides their use as a poison, the active ingredients of the *Colchicum* species belong to the oldest known drugs and have been used for more than 2000 years in the treatment of acute gout.[2]

Colchicine (**1**) was first isolated in 1820 by Pelletier and Caventou,[3] the same natural scientists who had previously isolated the important natural products strychnine, brucine, and quinine. Several aspects of this unusual alkaloid have challenged chemists in the past. In fact, the elucidation of the chemical structure and the biosynthesis of colchicine represent historic achievements in natural product chemistry. Despite considerable efforts, the structure remained uncertain for a long time. After investigations by Zeisel (1883–1913), which led to the development of a method for the determination of methoxy groups,[4] Windaus (1910–1924) made some more specific structural proposals, which were erroneously based on a phenanthrene ring system (**2**).[5]



2 (Windaus, 1924)



3 (Dewar, 1945)

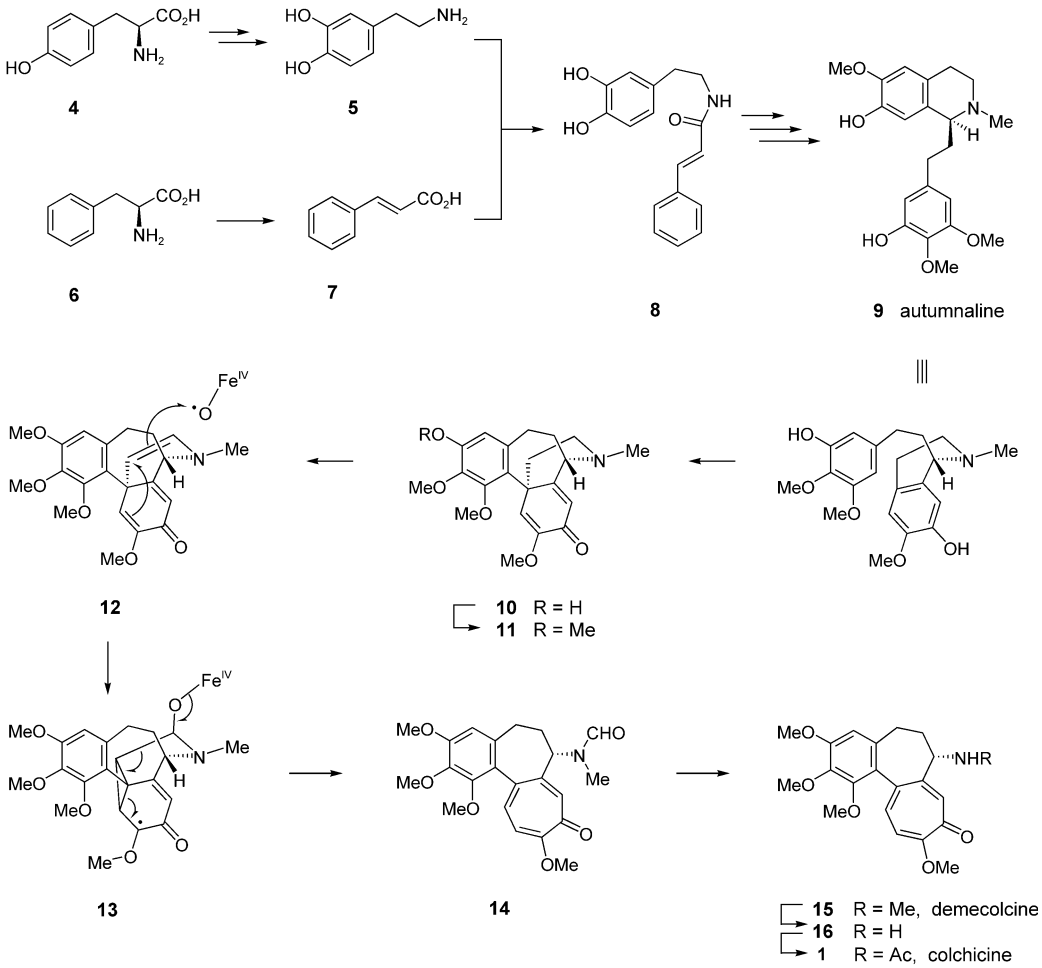
The key to the elucidation of the colchicine structure was the correct interpretation of the experimental data concerning ring C of the tricyclic skeleton. Significant progress was made by Dewar in 1945, who assumed that ring C was a cycloheptatrienolone with aromatic character (**3**).[6a] Together with his structural proposal for stipitatic acid in the same year, this hypothesis marked the starting point of the chemistry of tropolones, the term coined by Dewar for this class of compounds.[6b] The correct structure of colchicine was confirmed in 1952 by means of X-ray crystal-structure analysis,[7]



Figure 1. Meadow saffron (*colchicum autumnale* L.).[1f]

[*] Dipl.-Chem. T. Graening, Prof. Dr. H.-G. Schmalz
Institut für Organische Chemie
Universität zu Köln
Greinstrasse 4, 50939 Köln (Germany)
Fax: (+49) 221-470-3064
E-mail: schmalz@uni-koeln.de

 DOI: 10.1002/anie.200300615 © 2004 Wiley-VCH Verlag GmbH & Co. KGaA, Weinheim



Scheme 1. Colchicine biosynthesis.

and the absolute configuration was proven by chemical degradation.[8]

The biosynthesis of colchicine was puzzling in the beginning, because the unusual ring system did not show any clear relationship to other types of plant alkaloids. Many different hypotheses were put forward before the groups of Leete and, in particular, Battersby proposed the currently accepted biosynthetic route based on a large number of labeling and incorporation experiments.[9] This pathway involves a *para*/*para* phenol coupling of autumnaline (**9**, Scheme 1).

The cyclization product **10** is then methylated and dehydrogenated enzymatically to the enamine **12**, before a subsequent skeletal rearrangement takes place to form the tropolone ring. It is assumed that this process (**12**→**13**→**14**) is triggered by a cytochrome P450-dependent oxidation. The final steps involve deformylation to give demecolcine (**15**), followed by demethylation and acetylation to give colchicine (**1**).



Hans-Günther Schmalz, born in 1957, studied chemistry at Johann Wolfgang Goethe-University, Frankfurt (Germany), where he obtained his Ph.D. in 1985 with Prof. G. Quinkert. After a postdoctoral stay at Princeton University with Prof. M. F. Semmelhack, he returned to Frankfurt in 1988 and completed his Habilitation in 1993. In 1994 he became Professor at the Technical University Berlin, and in 1999 he moved to the University of Cologne. His research interests lie in organic synthesis, from organometallic methodology to the stereoselective total synthesis of bioactive natural products and analogues.



Timm Graening, born in 1971 in Flensburg (Germany), studied chemistry at the Christian-Albrechts-Universität Kiel and joined the group of Prof. Schmalz at the University of Cologne in 2000. In his doctoral thesis he is currently working on the total synthesis of colchicine.

 © 2004 Wiley-VCH Verlag GmbH & Co. KGaA, Weinheim

2. The Colchicine/Tubulin Interaction

Colchicine (**1**) is an important bioactive compound used in the treatment of a broad variety of diseases and still remains the sole drug for the therapy of acute gout and familial Mediterranean fever.[10] Moreover, colchicine acts as an antimitotic agent by binding to tubulin (Figure 2). Tubulin is

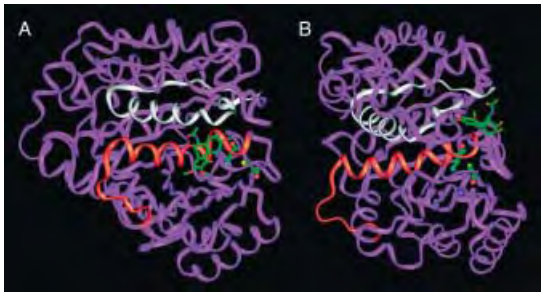


Figure 2. Electron crystallographic structure of the αβ-tubulin dimer with two alternative binding modes for colchicine (A and B) as found by molecular modeling.[18]

a globular protein and was formerly known as colchicine-binding protein.[11] In the presence of guanosine triphosphate (GTP), tubulin forms heterodimers consisting of an α and a β subunit. These α,β-dimers assemble in a helical fashion into polymeric tubes, the so-called microtubules (Figure 3).[12]



Figure 3. Model for the assembly of αβ-tubulin dimers to microtubules.

These long protein fibers, which consist of 12 to 13 protofilaments with an alternating linear arrangement of α- and β-tubulin units, exist in dynamic equilibrium with the tubulin dimer. Microtubules are polar structures with a faster-growing (+) and a less-dynamic (−) terminus. They have an outer diameter of 24 nm and form a hollow cylinder with a diameter of approximately 15 nm. The microtubules are responsible for several important functions within the cell: Besides mechanically stabilizing cellular structures, they serve as "highways" for transport and signal processes. Most importantly, however, they form the mitotic spindle during cell division (Figure 4).

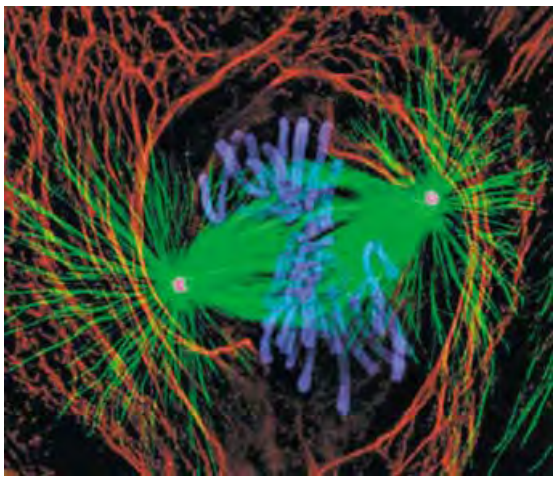
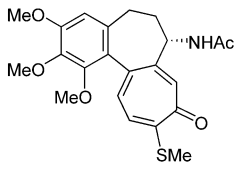


Figure 4. Fluorescence microscopy image of the spindle apparatus of a cell during the process of mitosis in the metaphase. The microtubules are marked green and the chromosomes are colored blue.

At this point colchicine exerts its dramatic effect: By binding to the tubulin dimer, it distorts the tubulin/microtubule equilibrium in such a manner that mitosis is arrested in the metaphase. In fact, several so-called spindle poisons exert their influence at this very stage, making this a very successful approach for cancer chemotherapy. Whereas colchicine and vinblastine induce depolymerization of microtubules, other drugs such as taxol and the epothilones effect their stabilization.[13] Therefore such compounds can be used to selectively damage the rapidly proliferating cancer cells. However, the general toxicity of colchicine has hampered its use in cancer chemotherapy so far. A large number of colchicine analogues have been prepared in the past from the natural product itself, with the aim of developing new antitumor agents, and some QSAR (quantitative structure–activity relationship) studies have been performed.[14] Nevertheless, the general toxicity could hardly be suppressed. For example, thiocolchicine (**17**)[15] and demecolcine (**15**),[16] which show a comparable activity and enjoy medical application, exhibit a slightly lower toxicity.



17 thiocolchicine

As a result of the success of taxol in the treatment of mammalian and ovarian cancer, molecules that interact with the colchicine-binding site of tubulin have regained pharmaceutical interest. According to the National Cancer Institute, they are considered as important lead structures for the development of new antitumor agents.[17] So far, a major obstacle in the identification of more-active colchicine derivatives was the difficulty in accessing colchicine and its structural analogues by means of total synthesis. Also, the rational design of new colchicine-related drugs is

 © 2004 Wiley-VCH Verlag GmbH & Co. KGaA, Weinheim

complicated by the fact that the binding site and the mechanism leading to the destabilization of microtubules are not yet fully understood.[18] Unquestionably, colchicine binds in a temperature-dependent and irreversible manner to a high-affinity binding site at the β-tubulin subunit, inducing a partial unfolding at the carboxy terminus.[19] It is assumed that this change in the secondary structure affects the regions of the protein dimer that are essential for microtubule formation. Different opinions have been put forward concerning the conformational changes of colchicine itself during its interaction with the protein.[20] Nevertheless, it has been clearly demonstrated that the helical twist inherent to the colchicine ring skeleton, seems to be of prime importance for effective binding. The molecule contains a stereocenter at C7 as well as an a*R*-configured chiral axis defined by the pivot bond joining rings A and C (Figure 5).[21] Berg et al. were able

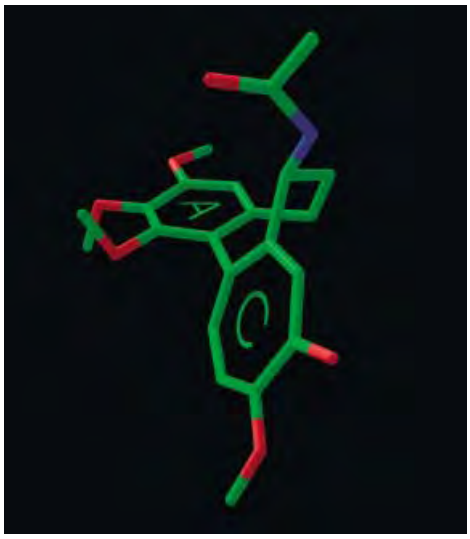
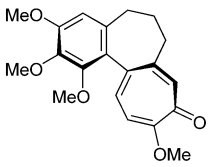
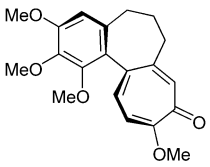


Figure 5. Stereostructure of colchicine.

to separate the atropisomers of desacetamidocolchicine (a*R*-**18**, a*S*-**18**) and were able to demonstrate that only the a*R* enantiomer binds to tubulin.[22]



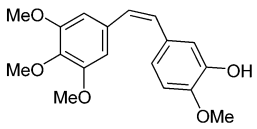
a*R*-**18**



a*S*-**18**

During the search for new drugs, a series of compounds were discovered by chance which also interact with the colchicine-binding site of tubulin. Some of them exhibit a great pharmacological potential. Combretastatin A4 (**19**), for instance, is a highly promising antitumor agent which recently passed phase I clinical trials.[23]

To study the interaction of colchicine analogues with tubulin in more detail, an efficient and flexible total synthetic

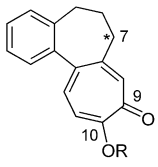


19 combretastatin A4

access would be required. A deeper understanding of the complex phenomena could ultimately lead to a rational design of new drugs derived from colchicine as a lead structure.

3. Target Structure and Classification of the Total Syntheses

In the 1950s, colchicine was considered as a milestone in natural product synthesis, and the first syntheses from the laboratories of Eschenmoser and van Tamelen in 1959 were highly recognized masterpieces of synthetic chemistry,[24–26] a field that was rapidly developing at this time. By today's standards of synthetic chemistry—highly complex natural products containing novel and often sensitive structural elements are synthesized in the laboratory only a few years after their discovery—the small molecule colchicine (**1**) appears to be a rather simple target at first glance.[27] For that reason, it is remarkable that its synthesis still poses a problem, despite all the modern methodology available. Since the early syntheses of Eschenmoser and co-workers and van Tamelen and co-workers, new approaches towards colchicine have been brought forward continuously, in most cases following fundamentally different strategies.[28–37] However, only in recent years have syntheses been developed that show a satisfying overall efficiency.[38–40] The reason for the difficulties inherent to the target structure does not result from a lack of general methods for the synthesis of tropolones. Also, stereocontrol does not pose too much of a problem, because the configuration of the chiral axis is thermodynamically predetermined by the stereogenic center at C7. The main difficulty actually lies in the regioselective construction of the highly oxidized ring C within the unusual 6,7,7-membered ring system **20**.



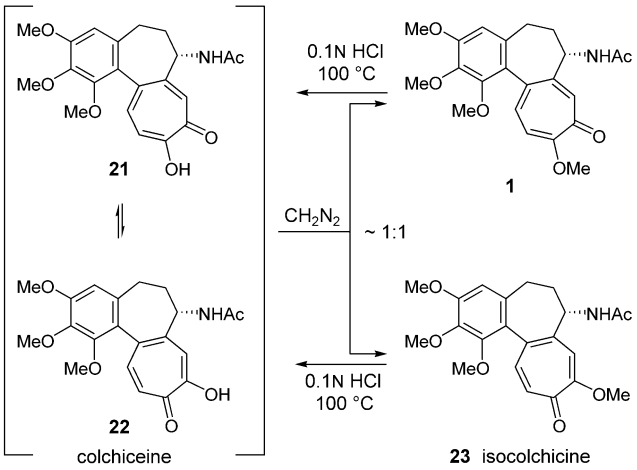
20

The tropolone ring C is deeply embedded within the molecular architecture by the neighborhood of the stereocenter, the direct connection to the benzenoid ring, and its annulation to the seven-membered ring B. Therefore, its generation forms an integral part of any synthetic strategy. During many investigations directed towards the total synthesis of colchicine, it became clear that in this context standard methods for tropolone formation either gave bad yields or were complicated by regioselectivity problems. Also the introduction of tropolone derivatives as ring C building blocks has hitherto been disadvantageous.[30,32,33,41] Thus, specific methodology for the construction of annulated tropolones is a precondition for any efficient total synthesis.

 © 2004 Wiley-VCH Verlag GmbH & Co. KGaA, Weinheim

The chemistry of the parent tropolone and simple tropone and tropolone derivatives has been studied extensively since the 1950s.[42] Tropolones exist in a tautomeric equilibrium and behave similarly to phenols with respect to aromatic substitution. Their acidity ($pK_a = 7$) is inbetween those of phenols and carboxylic acids. The carbonyl group shows little ketone character and should rather be considered as part of a vinylogous carboxylic acid. The aromatic character of tropolone, which was a matter of intense debate in the past, should not be overemphasized.

The free tropolone derived from **1** is named colchiceine. It is a prominent colchicine precursor, which exists in a tautomeric equilibrium (**21**/**22**) and can be easily converted into colchicine by treatment with diazomethane (Scheme 2).



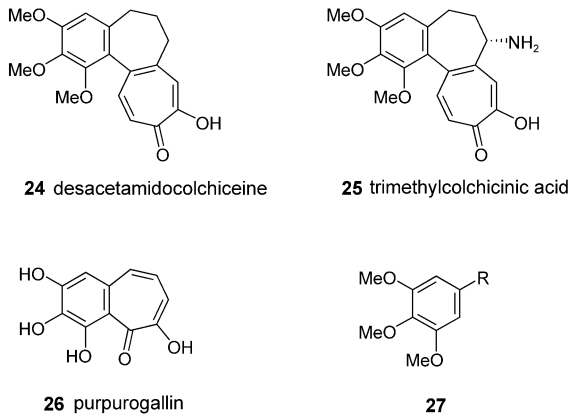
Scheme 2. Interconversion of colchiceine (**22**), colchicine (**1**), and isocolchicine (**23**).

Actually, a 1:1 mixture of colchicine (**1**) and isocolchicine (**23**) is formed, which can be separated by chromatography. The undesired isomer can then be recycled by cleavage of the methyl ether upon heating with dilute hydrochloric acid.[43]

Besides colchiceine (**21**/**22**), other important intermediate molecules that have been reached in formal total syntheses are desacetamidocolchiceine (**24**) and the advanced colchicine precursor trimethylcolchicinic acid (**25**), both of which had been converted into the target compound **1** during the early syntheses (Scheme 3). As a readily available starting material, purpurogallin (**26**) was used in several syntheses, and the majority of the other syntheses started from a symmetric C5-substituted pyrogallol trimethyl ether of type **27**.

To give an overview of the various synthetic approaches towards colchicine, including formal total syntheses, it is advantageous to classify them according to the cyclization strategies used in the construction of the 6,7,7-membered ring system (Scheme 4).

Monotopic cyclization strategies involving the formation of strategic bonds in ring B or C (AC→ABC or AB→ABC, respectively) make up the majority of the early syntheses. In these systems, however, the crucial ring-closing reactions



Scheme 3. Important colchicine intermediates and starting materials.

proceed with only low to moderate yields. A second major group encompasses strategies that exploit five- or six-membered cyclic precursors for the construction of the crucial tropolone ring C (ABC′→ABC, AB′C′→ABC, AC′→ABC). A common feature of most of these syntheses is the preparation of the seven-membered ring by a ring enlargement of a norcarane precursor. Following this concept, some fascinating transformations for the construction of ring C in a highly oxidized form, or even as the complete tropolone ring, have been designed. The greatest retrosynthetic simplification of the fundamental *ortho*-condensed ring system corresponds to an intramolecular cycloaddition strategy (A→ABC). Ideally, both seven-membered rings B and C are formed simultaneously with the correct placement of the oxygen functions in ring C.

The different strategies developed for the total synthesis of **1** in the course of the past 50 years are presented in the following sections, with an emphasis on the overall synthetic scheme.[44] The order of the syntheses is not strictly chronological. Instead, the conceptually different synthetic routes are organized according to the progress that they contributed to the solution of key synthetic problems.

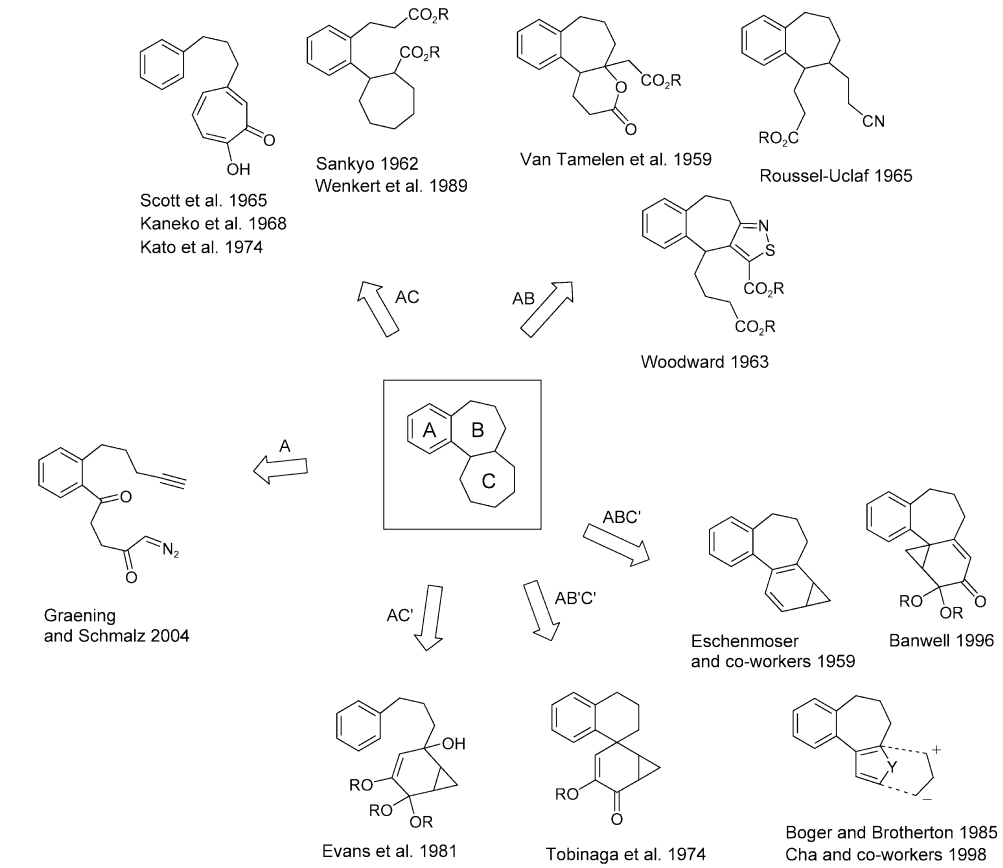
4. Colchicine Total Syntheses

4.1. The Scott Synthesis of Desacetamidocolchiceine through Oxidative Coupling

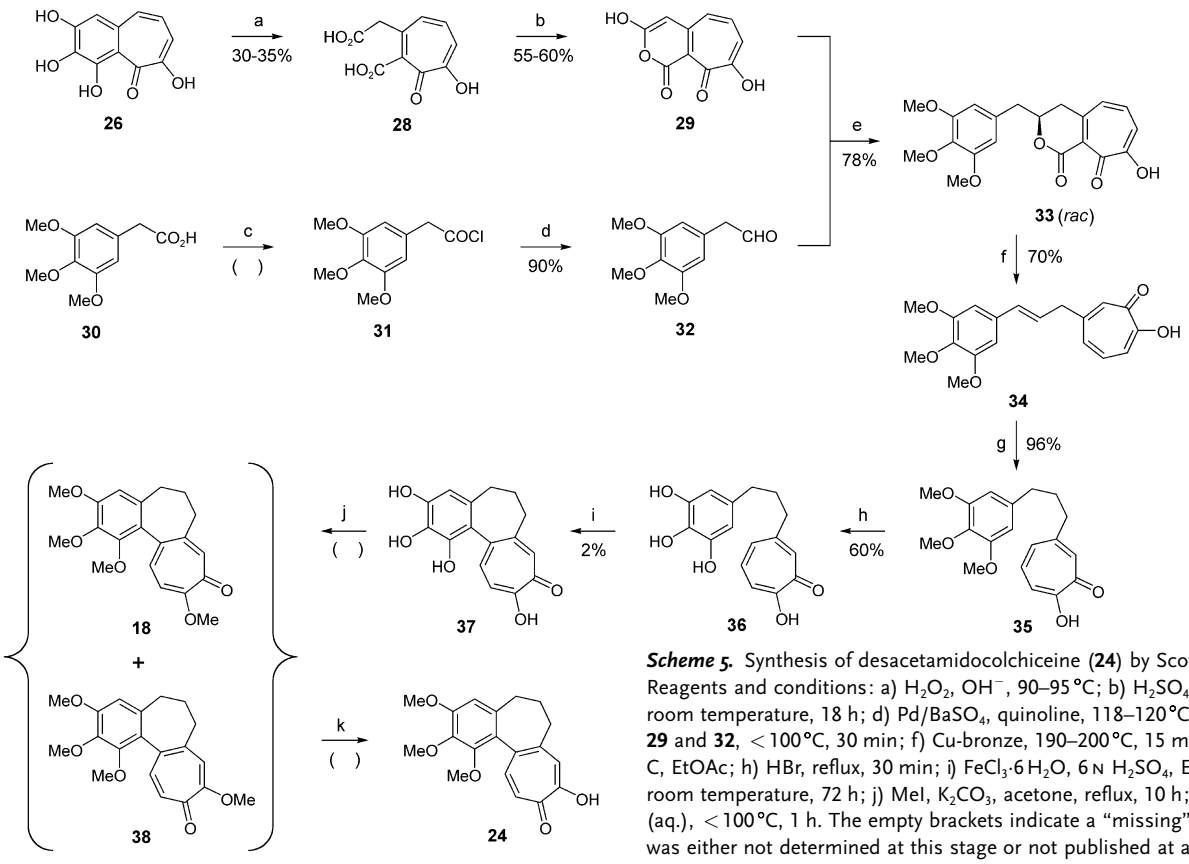
The synthesis reported by Scott et al. in 1965 started from a tropolone derivative as the ring C building block and followed the strategy A + C→AC→ABC (Scheme 5).[30] This synthesis is based on an earlier biosynthetic hypothesis postulating the formation of ring B by oxidative phenol–tropolone coupling.[45]

The tropolone part was derived from purpurogallin (**26**) from which the anhydride **29** was synthesized by oxidative degradation of the electron-rich benzene ring followed by dehydration. By condensation of **29** with the aldehyde **32**, prepared from the acid chloride **30** in a Rosenmund reduction, the lactone *rac*-**33** was obtained under elimination

 © 2004 Wiley-VCH Verlag GmbH & Co. KGaA, Weinheim



Scheme 4. Retrosynthetic classification of colchicine syntheses.



Scheme 5. Synthesis of desacetamidocolchiceine (**24**) by Scott et al. Reagents and conditions: a) H_2O_2, OH^-, 90–95 °C; b) H_2SO_4; c) $(COCl)_2$, room temperature, 18 h; d) $Pd/BaSO_4$, quinoline, 118–120 °C, 5 h; e) neat **29** and **32**, < 100 °C, 30 min; f) Cu-bronze, 190–200 °C, 15 min; g) H_2, Pd/C, EtOAc; h) HBr, reflux, 30 min; i) $FeCl_3 \cdot 6H_2O$, 6 N H_2SO_4, EtOH, $CHCl_3$, room temperature, 72 h; j) MeI, K_2CO_3, acetone, reflux, 10 h; k) H_2SO_4 (aq.), < 100 °C, 1 h. The empty brackets indicate a "missing" yield, which was either not determined at this stage or not published at all.

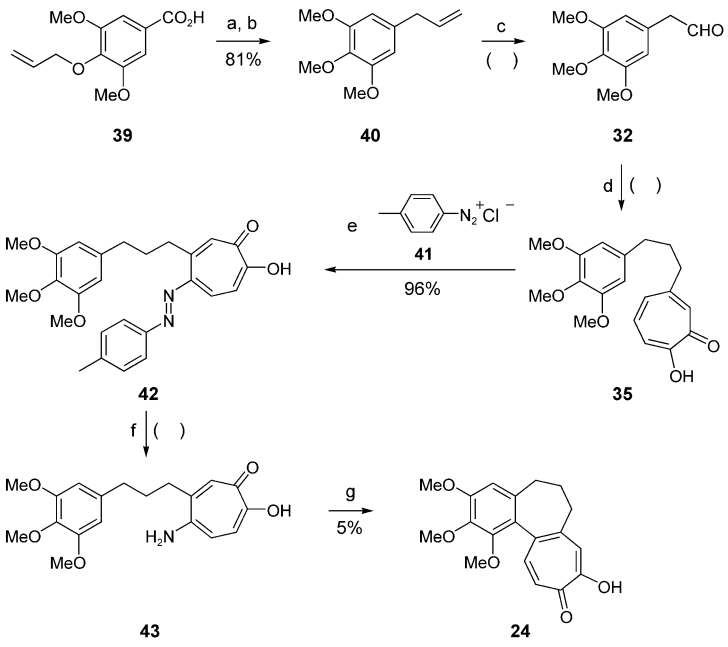
 © 2004 Wiley-VCH Verlag GmbH & Co. KGaA, Weinheim

of CO_2. After elimination/decarboxylation and subsequent hydrogenation of the C–C double bond in **34** (which proceeds smoothly in the presence of the tropolone moiety), the secocolchicine intermediate **35** was obtained in good yield. To prepare for the projected key coupling reaction, the methyl ether groups were cleaved to give the free pyrogallol derivative **36**. Various reaction conditions for the crucial coupling (**36**→**37**) were tested, and it was found that the reaction product was overoxidized under the initially chosen conditions. Eventually, a two-phase oxidation system consisting of $FeCl_3$ in H_2SO_4 (6 N) and ethanol in chloroform was used, and the tricyclic product **37** was isolated in 2% yield after preparative paper chromatography under an inert atmosphere. After methylation, the obtained mixture of **18** and **38** was hydrolyzed to desacetamidocolchiceine (**24**), which had been previously converted into (±)-colchicine (*rac*-**1**) by Eschenmoser and co-workers (see Section 4.2.).[25]

Despite the straightforward strategy, the success of the Scott synthesis is diminished by the extremely low yield of the key step. However, the problems associated with this putative biomimetic transformation are in agreement with the fact that the colchicine biosynthesis does not involve a phenol/tropolone coupling, as was recognized later.

4.1.1. The Kaneko Variant of the Scott Synthesis

Kaneko et al. addressed the improvement of the key step in the Scott synthesis. Except for alternative preparation of the aldehyde **32** through decarboxylative Claisen rearrangement and ozonolysis, the seco intermediate **35** was prepared by following the scheme of Scott et al. (Scheme 6).[32]

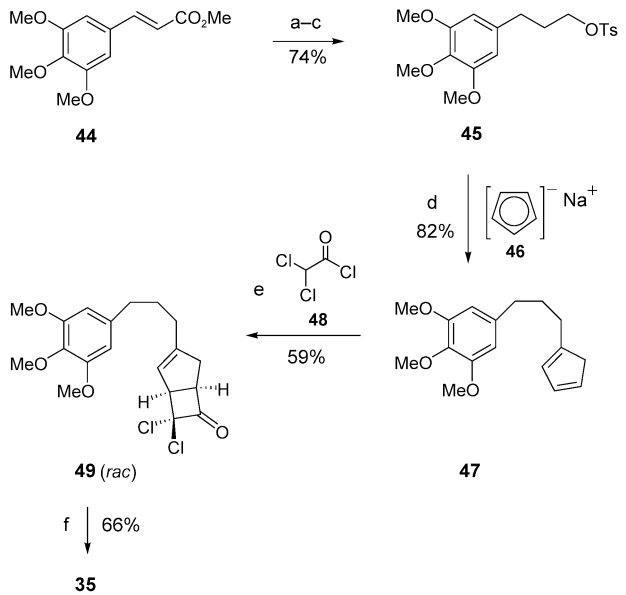


Scheme 6. Synthesis of desacetamidocolchiceine (**24**) by Kaneko et al. Reagents and conditions: a) *N*,*N*-dimethylaniline, reflux, 10 h; b) Me_2SO_4, aqueous NaOH, MeOH, reflux, 3 h; c) O_3, EtOAc, 30–40 min; then H_2, Pd/C, 25 °C; d) reference [30]; e) $NaNO_2$, HCl, H_2O, *p*-toluidine, 0 °C (→**41**); then **35**, aqueous NaOH, 2–10 °C, 50 min; f) H_2, Pd/C, MeOH, room temperature, 1.5 h; g) isoamylnitrite, conc. H_2SO_4, dioxane, 7–10 °C; then Cu powder, dioxane, room temperature, 24 h.

Azo coupling of **35** and subsequent hydrogenation afforded the aminotropolone **43**, which after diazotization directly gave rise to desacetamidocolchiceine (**24**) in a Pschorr cyclization. Unfortunately the yield did not exceed 5%.

4.1.2. The Kato Variant of the Scott Synthesis

An alternative access to the seco intermediate **35** was reported by Kato et al.[33] For the synthesis of the tropolone ring, these authors used the solvolysis of the cyclopentadiene/dichloroketene adduct *rac*-**49** following the Stevens and Bartlett protocol for tropolone synthesis (Scheme 7).[46]



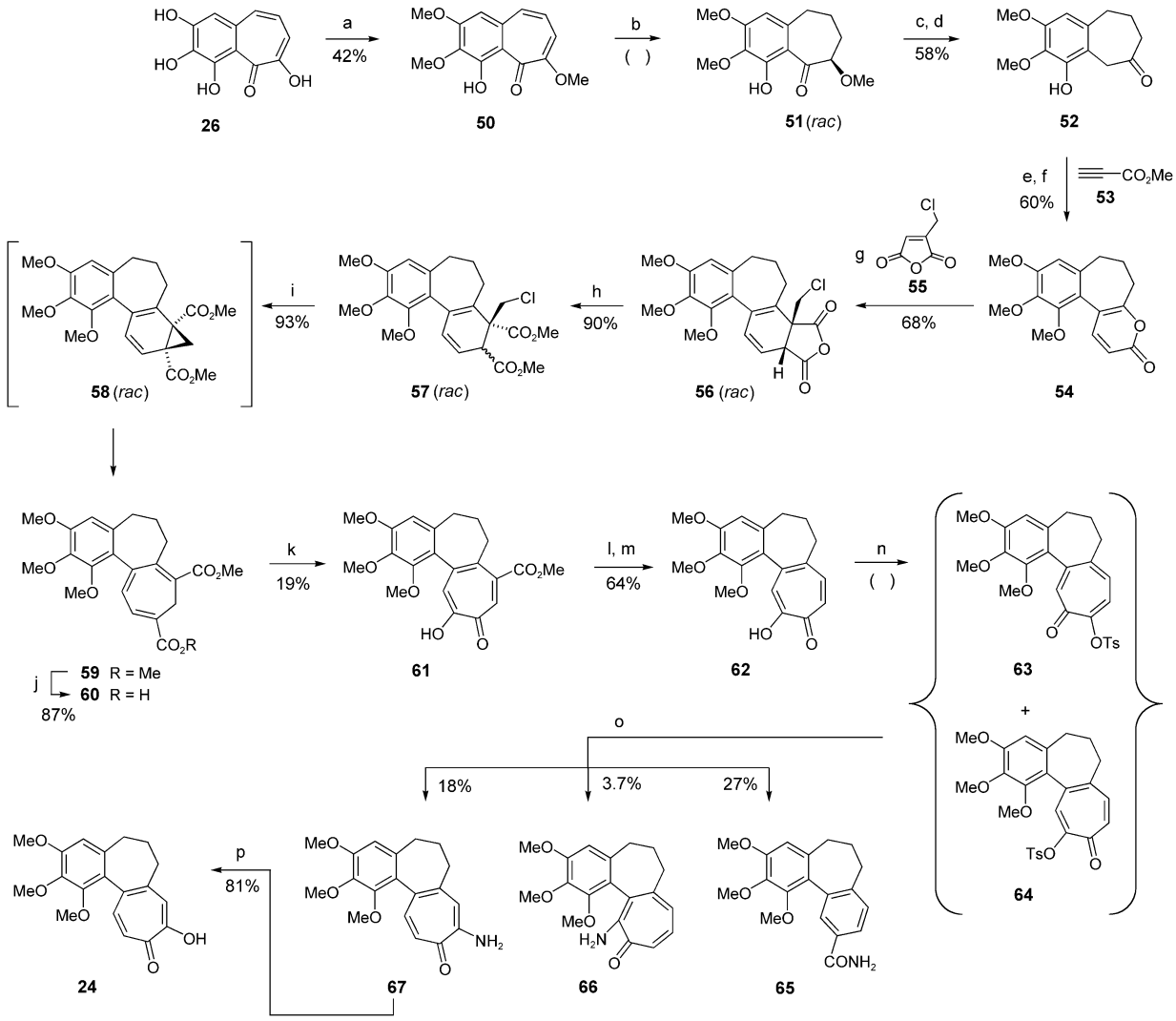
Scheme 7. Synthesis of secodesacetamidocolchiceine (**35**) by Kato et al. Reagents and conditions: a) H_2 (1 atm), Pd/C, MeOH, room temperature; b) $LiAlH_4$, Et_2O, 0 °C, 4 h, →RT, 14 h; c) TsCl, pyridine, 0 °C, 2 h; d) NaH, cyclopentadiene, THF, 0 °C, then **45**, 3 h; e) **48**, NEt_3, *n*-hexane, 5 h; f) KOAc, H_2O, HOAc, reflux, 2 days. Ts = *para*-toluenesulfonyl.

The cyclopentadiene precursor **47** was prepared from the tosylate **45** by nucleophilic substitution with sodium cyclopentadienyl (**46**) and concomitant double-bond isomerization. Attempts by Kato et al. to increase the yield of the Pschorr reaction described by Kaneko (**43**→**24**) were not successful.

4.2. The Pioneering Eschenmoser Synthesis

The first successful total synthesis of colchicine (**1**), a seminal work by Eschenmoser and co-workers, was reported in 1959.[25] As in the synthesis by Scott et al. discussed before, purpurogallin (**26**) was used as starting material, but in a completely different strategy, that is, as an AB building block (Scheme 8). Therefore, the chosen strategy required

© 2004 Wiley-VCH Verlag GmbH & Co. KGaA, Weinheim

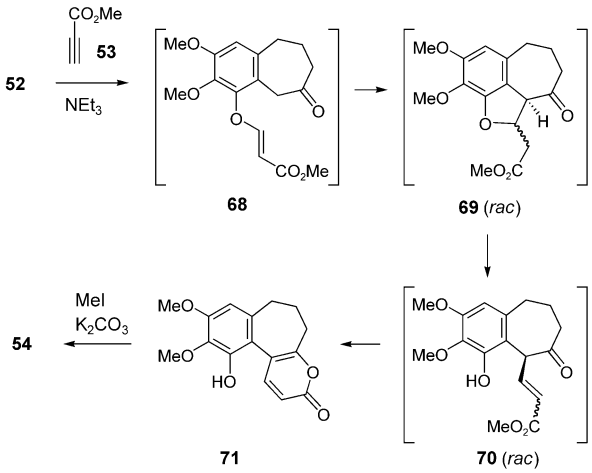


Scheme 8. Synthesis of desacetamidocolchiceine (**24**) by Eschenmoser and co-workers. Reagents and conditions: a) Me_2SO_4, NaOH, H_2O, 0 °C, 3 h → RT, 7 h; b) H_2, Pd, THF, 45 °C, 7.5 h; c) $LiAlH_4$, Et_2O, 0 °C, 2.5 h; d) H_3PO_4, EtOH, 60–70 °C, 1 h 15 min; e) **53**, NEt_3, benzene, *tert*-amylalcohol, reflux, 45 min; f) MeI, K_2CO_3, acetone, room temperature, 18 h; g) **55**, 175 °C, 1 h 40 min; h) H_2SO_4, MeOH, reflux, 40 min; then CH_2N_2; i) KO*t*Bu, *t*BuOH, benzene, room temperature, 2 h 45 min; j) NaOH, H_2O, MeOH, reflux, 30 min; k) OsO_4, pyridine, Et_2O, room temperature, 10 h; then $KClO_3$, $NaHCO_3$, MeOH, 100 °C, 2.5 h; l) NaOH, H_2O, reflux, 30 min; m) powdered quartz glass, 260–270 °C, 9 min; n) TsCl, pyridine, room temperature, 14 h; o) NH_3, EtOH, 90–95 °C, 15 h; p) aqueous KOH, EtOH, 130 °C, 22 h.

the development of a suitable method for the annulation of the tropolone ring C.

The tropolone ring of trimethylpurpurogallin **50** was reduced, and the product *rac*-**51** was used to prepare the dimethoxybenzosuberone **52**. The free phenol functionality proved to be of importance as several attempts to alkylate the corresponding trimethoxybenzosuberone had failed. As shown in Scheme 9, the free phenol function first undergoes a Michael addition to the electrophilic propyne ester **53** (**52** → **68**). In a second (intramolecular) Michael addition, the tricyclic ketoester *rac*-**69** is formed. Subsequent β elimination of the phenol group and cyclization then leads to the isolated product **71**.

The pyrone **54** obtained after methylation of **71** was then heated with chloromethylmaleic anhydride (**55**) to give the Diels–Alder adduct *rac*-**56** (Scheme 8), which served as starting point for the following key transformation, that is, a



Scheme 9. Intermediates involved in the preparation of the α-pyrone **54** from **52** according to Eschenmoser.

 © 2004 Wiley-VCH Verlag GmbH & Co. KGaA, Weinheim

norcaradiene–tropilidene valence tautomerization. Starting from the diester *rac*-**57**, treatment with base led to regioselective formation of the norcaradiene derivative *rac*-**58**, which immediately furnished the tropilidene diester **59** by electrocyclic ring opening. The sterically less-hindered ester group was selectively hydrolyzed, before oxidation with OsO_4 afforded the tropolone **61** under decarboxylation. Further decarboxylation gave the product **62**, a regioisomer of the targeted tropolone. The required conversion of **62** into desacetamidocolchiceine (**24**) oxygenated at C9 and C10, relied on the findings of Nozoe et al.[47] Initially, an isomeric mixture of tosylates **63** and **64** was prepared. Ammonolysis then resulted in a tele-substitution, which again afforded a mixture from which the aminotropone **67** was separated and finally converted into desacetamidocolchiceine (**24**) by saponification. This compound was utilized as a relay product, as it could be prepared in four steps from natural colchicine according to a private communication of R. B. Woodward to Albert Eschenmoser (even though at the time Woodward was a competitor in the race for the first synthesis of colchicine).

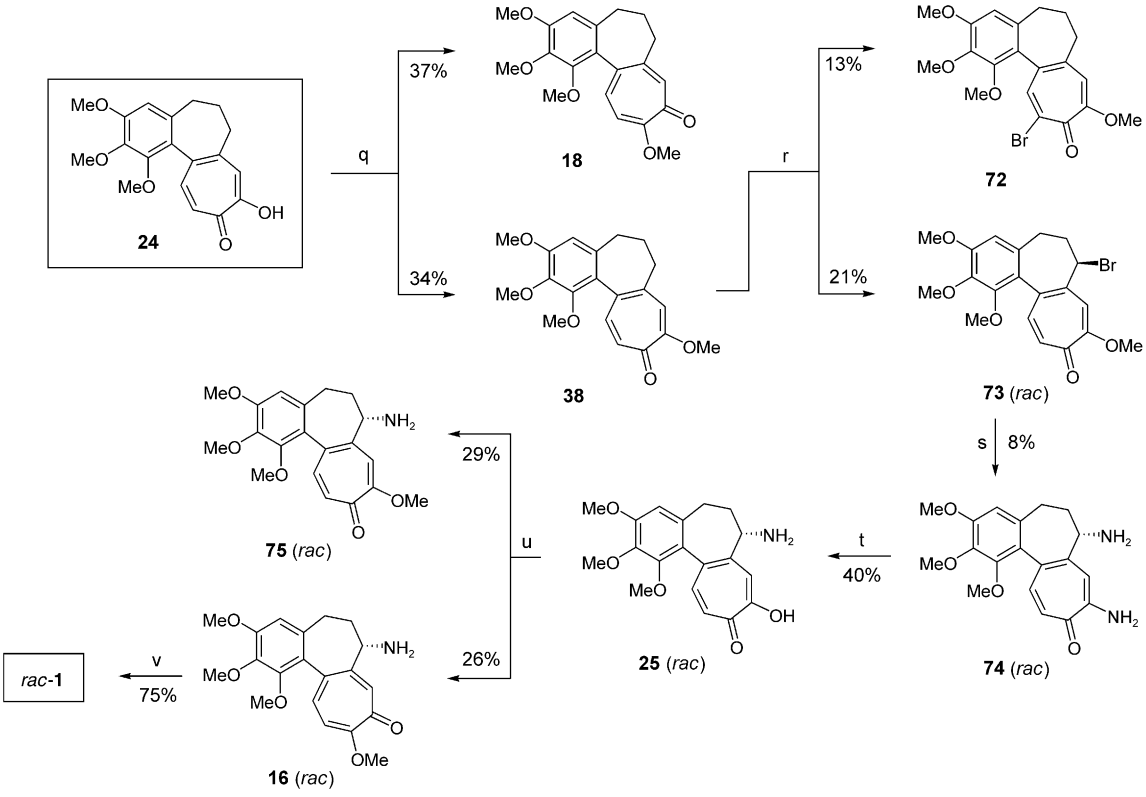
Methylation of **24** led to a mixture of the regioisomers **18** and **38** (Scheme 10). From these regioisomers, only the isocolchicide **38** was a suitable substrate for radical bromination at C7 because of the better stabilization of the radical intermediate. Ammonolysis of the bromination product *rac*-**73** afforded the diamino compound *rac*-**74**, but only in low yield. After remethylation of the hydrolysis product *rac*-**25** and chromatographic separation of the resulting regioisomers, acetylation of *rac*-**16** finally gave racemic colchicine (*rac*-**1**), which had previously been separated into the enantiomers.[48]

The Eschenmoser synthesis opened a highly efficient access to the colchicine ring scaffold with an unsaturated ring C (**59**). In spite of that, the inherent difficulties posed by the target structure became apparent: both the regioselective placement of the oxygen functionalities at C9 and C10 of the tropolone ring and the introduction of the acetamido group at C7 required many additional steps and proceeded with rather low yield and selectivity.

4.3. The van Tamelen Synthesis

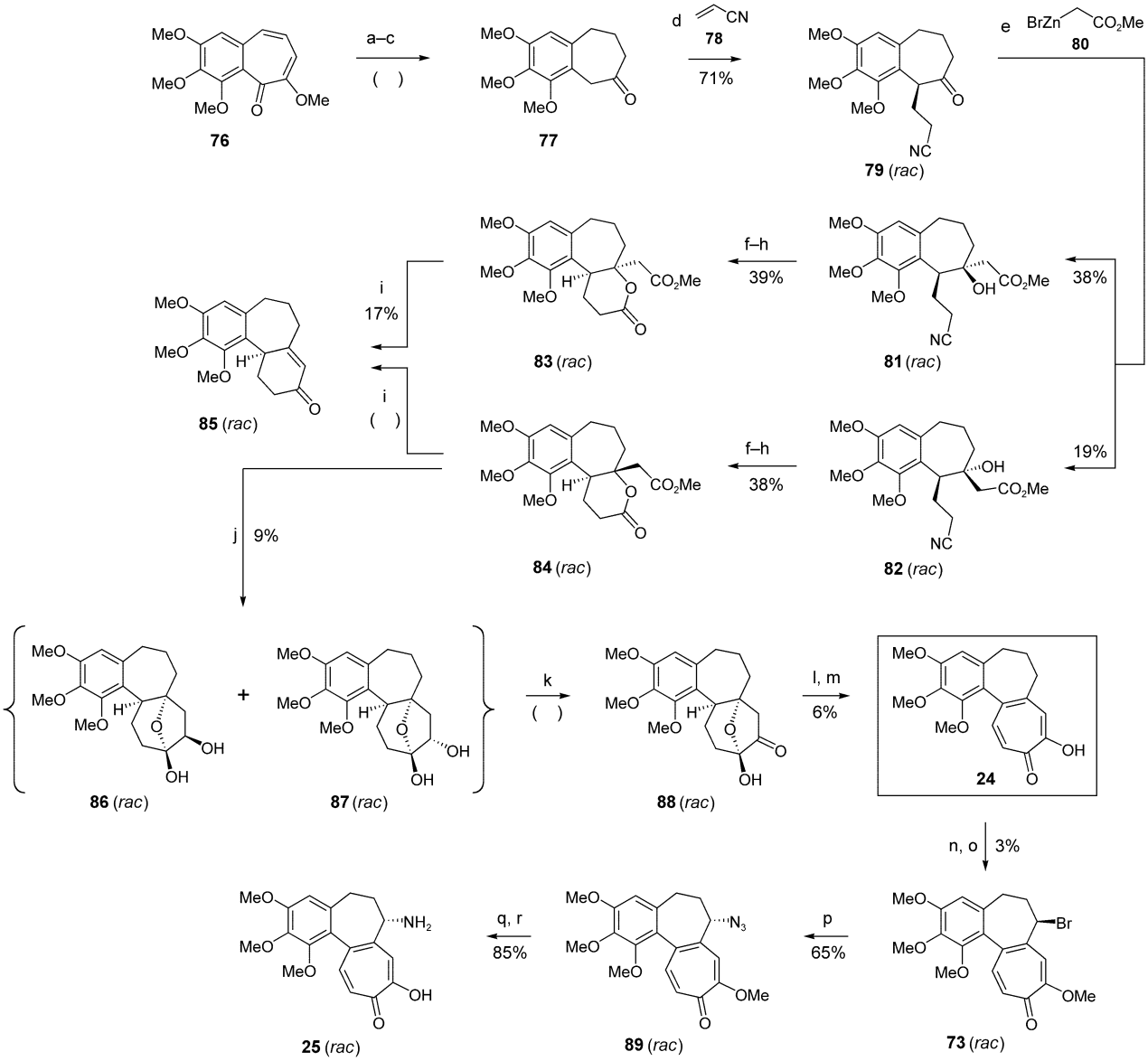
Also in 1959, van Tamelen et al. reported a total synthesis of colchicine which in part followed the same pathway as the strategy Eschenmoser.[26] However, it differs with respect to the central step for the construction of ring C (Scheme 11).

The synthesis started with the preparation of the ketone **77** from tetramethylpurpurogallin (**76**) in analogy to the synthesis discussed above. The alkylation of the reluctant substrate trimethoxybenzosuberone **77** could successfully be realized by using acrylamide (**78**) as a Michael acceptor. In a Reformatsky reaction, the Michael adduct *rac*-**79** was transformed into the diastereomeric products *rac*-**81** and *rac*-**82**, which were separated by chromatography and fractional crystallization. These isomers were separately transformed



Scheme 10. Completion of the synthesis of (±)-colchicine (*rac*-**1**) by Eschenmoser et al. utilizing the relay compound **24**. Reagents and conditions: q) CH_2N_2, Et_2O, MeOH, 0 °C, 1 h; r) NBS, benzoyl peroxide, CCl_4, *hν*, reflux, 18 min; s) NH_3, EtOH, H_2O, 95–100 °C, 15 h; t) aqueous KOH, EtOH, 130 °C, 23 h; u) CH_2N_2, Et_2O, CH_2Cl_2, MeOH, 0 °C, 30 min; v) Ac_2O, pyridine, 100 °C, 15 min. NBS = *N*-bromosuccinimide.

 © 2004 Wiley-VCH Verlag GmbH & Co. KGaA, Weinheim



Scheme 11. Synthesis of (±)-trimethylcolchicinic acid (*rac*-**25**) by van Tamelen et al. utilizing the relay compound **24**. Reagents and conditions: a) $LiAlH_4$; b) Zn, H_2SO_4; c) H_2, Pd/C; d) **78**, KO*t*Bu, MeCN, *t*BuOH, room temperature, 9 h; e) Zn, I_2, methyl bromoacetate, benzene, reflux, 3 h; f) KOH, MeOH/H_2O, reflux, 21 h; g) DCC, pyridine, room temperature, 2 days; h) CH_2N_2, MeOH, Et_2O; i) Na, xylene, reflux, 4 h; j) Na, liquid NH_3, 20 min; k) $Cu(OAc)_2$, MeOH, reflux, 3 h; l) $TsOH{\cdot}H_2O$, benzene, 5.5 h; m) NBS, $CHCl_3$, reflux, 1 h, 15 min; n) CH_2N_2, MeOH; o) NBS, CCl_4, *hν*, reflux, 23 min, →RT, 1 h; p) NaN_3, MeOH, 90–95 °C, 27 h; q) H_2 (1 atm), Pd/C, MeOH, room temperature; r) HCl (aqueous, 1 N), reflux, 2 h.

into the corresponding lactone esters *rac*-**83** and *rac*-**84**. In this case, the lactone acts as an internal protecting group. During the subsequent acyloin condensation, deprotonation of the hydroxy group had to be suppressed to avoid base catalysis of the competing Dieckmann condensation. Under classical conditions for the acyloin condensation, both lactones afforded exclusively the cyclohexenone *rac*-**85** derived from the Dieckmann condensation product. With sodium in liquid ammonia, only the minor lactone isomer *rac*-**84** was converted, to give the condensation products *rac*-**86** and *rac*-**87** in 9% yield.

This mixture of hemiketals was oxidized to give *rac*-**88** and an acid-catalyzed opening of the oxa bridge followed by further oxidation of the resulting dihydrotropolone with NBS afforded desacetamidocolchiceine (**24**). Again, the colchiceine derivative **24** was used as a relay compound and was brominated at C7 by the method of Eschenmoser to give *rac*-**73**. In contrast to the direct ammonolysis, the introduction of the amino function *via* the azide *rac*-**89** proceeded in good yield. Hydrogenation of the azide function and cleavage of the tropolone methyl ether were also carried out in excellent yield to give trimethylcolchicinic acid (*rac*-**25**).

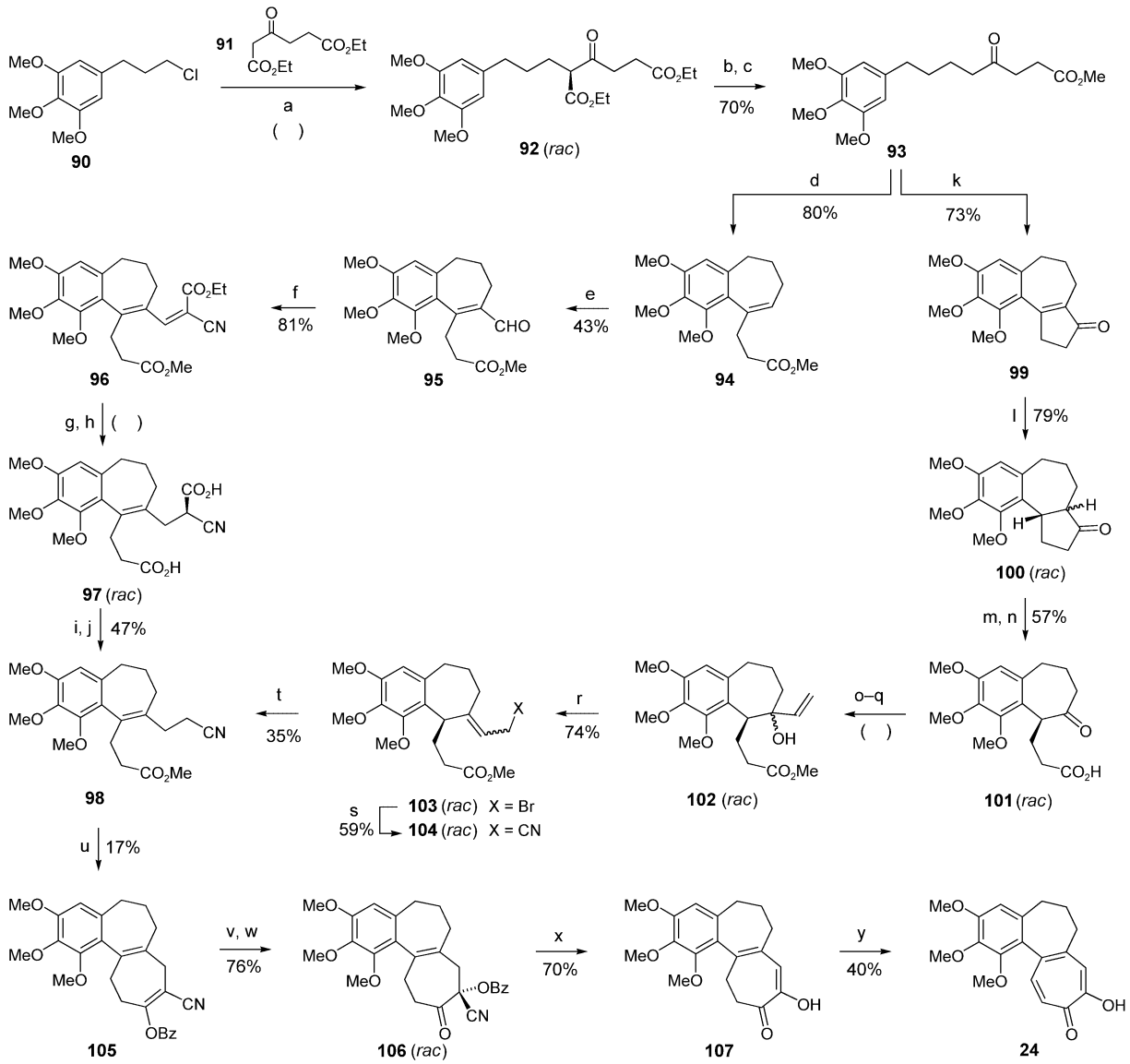
Although the synthesis addressed the problem of selective oxygenation at C9 and C10, the construction of ring C, on the other hand, could only be accomplished in very low yields both in the key reaction (acyloin condensation) and the subsequent oxidation steps.

 © 2004 Wiley-VCH Verlag GmbH & Co. KGaA, Weinheim

4.4. The Roussel–Uclaf Synthesis

The Roussel–Uclaf synthesis of desacetamidocolchiceine (**24**) (Scheme 12) reported in 1965 by Toromanoff and co-workers strategically resembles the approach of van Tamelen and co-workers, but brought about improvements with respect to the critical points mentioned above.[31] Ring B was condensed to the aromatic ring A in a Friedel–Crafts-type cyclization (A→AB→ABC).

The synthesis started with the preparation of the ketoester **93** from which either of the Friedel–Crafts products **94** or **99** could be obtained under Brønsted acidic conditions. Both compounds were converted into the cyanoester **98** in satisfying yields, either in a six-step sequence from **94** or in nine steps from **99**. The use of the cyanoester rather than the corresponding diester was of advantage because it guaranteed the formation of the Dieckmann condensation product in a regioselective manner. The product of this key reaction was isolated as the enolbenzoate **105** in only 17% yield. The free enolate anion derived from **105** was oxygenated at the α position and subsequently transformed into the dihydrotropolone **107**, which had already been used as an intermedi-



Scheme 12. Roussel–Uclaf synthesis of desacetamidocolchiceine (**24**). Reagents and conditions: a) **91**, Na, benzene, reflux, 6 h, →RT, 14 h; b) NaOH, MeOH/H_2O; then aqueous HCl; c) CH_2N_2, CH_2Cl_2; d) TsOH, benzene, reflux, 16 h; e) *N*-methylformanilide, $POCl_3$, 55–60°C, 4 h; f) ethyl cyanoacetate, piperidine, HOAc, benzene, reflux, 20 h; g) H_2 (1 atm), PtO_2, EtOH, room temperature, 1 h; h) KOH, MeOH, room temperature, 17 h; i) 180–200°C; j) CH_2N_2, CH_2Cl_2; k) 85% H_3PO_4, 50°C, 16 h; l) Na, NH_3, THF, −70°C, 1 h 35 min; m) NaOEt, EtOH, isoamylnitrite, 0°C, 1 h 20 min; then HOAc; n) pyruvic acid, HOAc/H_2O, <100°C, 2 h; o) C_2H_2, Na, liquid NH_3, −70°C, 2.5 h; then addition of *rac*-**101**, THF, −40°C, 5.5 h; p) H_2 1 atm, Pd/$CaCO_3$, pyridine, DMF, room temperature; q) CH_2N_2; r) PBr_3, $CHCl_3$/ligroin, −20→−10°C, 5 h; s) CuCN, DMSO, 50°C, 25 h; t) 2,4-dinitrobenzenesulfonic acid, benzene, reflux, 2 h; u) K, toluene, reflux, 2 h; then BzCl, pyridine, 10°C, →RT, 2 h; v) KOH, MeOH/H_2O, room temperature, 16 h; w) Na, benzene, reflux, 15 h; then benzoyl peroxide, room temperature, 14 h; x) aqueous $NaHCO_3$, EtOH/H_2O, reflux, 10 min; y) NBS, reference [26]. DMF = *N*,*N*-dimethylformamide; DMSO = dimethyl sulfoxide; Bz = Benzoyl.

 © 2004 Wiley-VCH Verlag GmbH & Co. KGaA, Weinheim

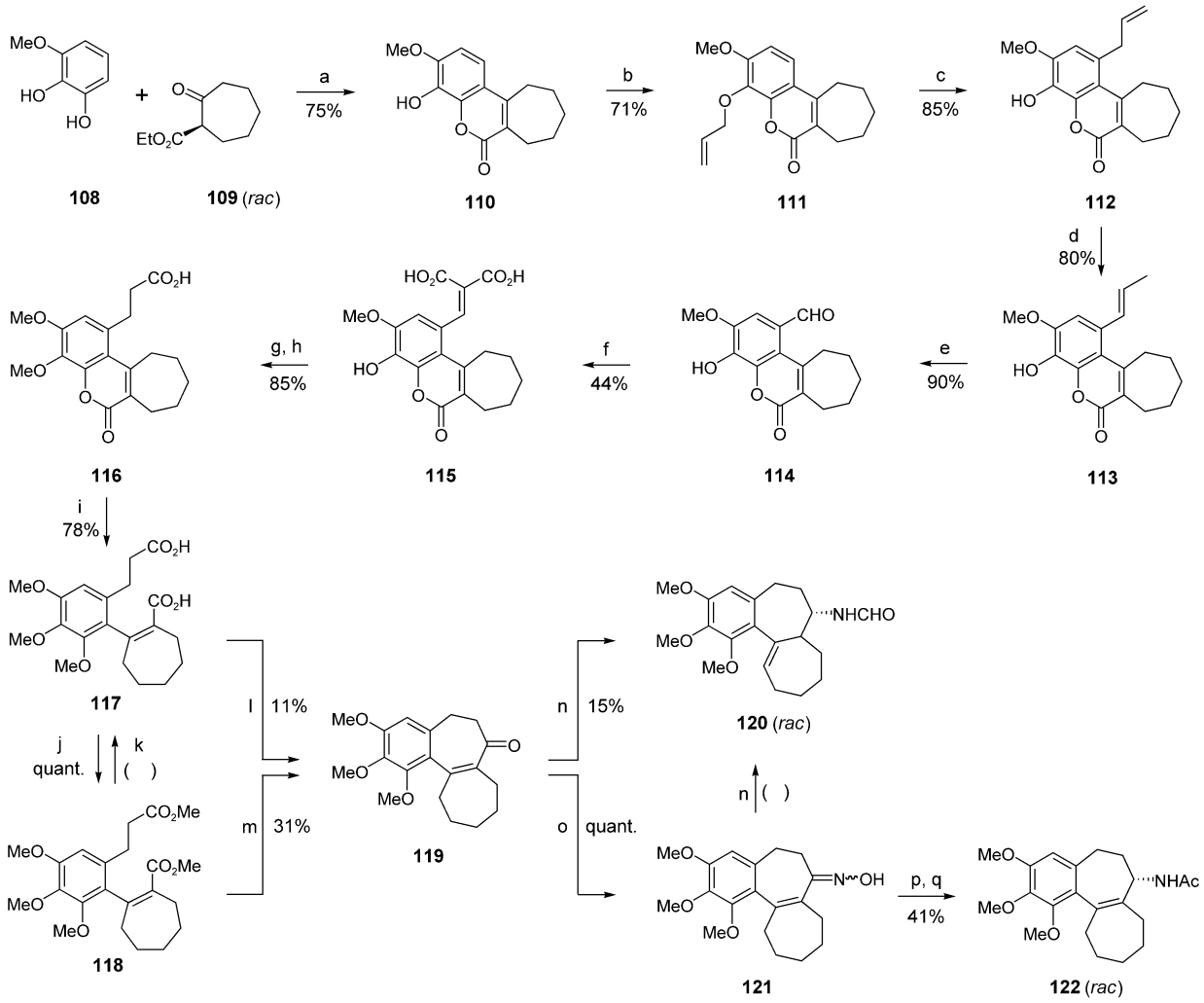
ate by van Tamelen et al. The oxidation of **107** to desacetamidocolchiceine (**24**) with NBS completed the formal total synthesis of **1**.

All in all, the selective construction of the C9, C10 oxygenated tropolone was improved. Nevertheless, selective functionalization at C-7 had still not been implemented.

4.5. The Sankyo Synthesis

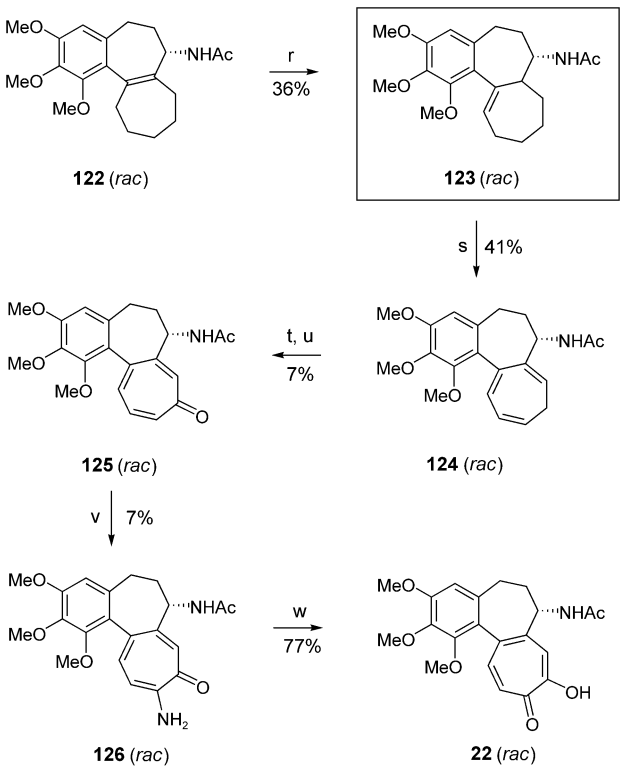
The problem of the selective functionalization at C7 was addressed in the Sankyo synthesis of colchiceine (**22**) reported by Nakamura et al. in 1962 (Schemes 13 and 14).[28] In this synthesis, the amino group was introduced prior to the oxidation of ring C to a tropolone. The strategy was actually based on previous works of Boekelheide et al.[24c] and focused on the functionalization of C7 by formation of the strategic C6–C7 bond in ring B (AC→ABC).

As shown in Scheme 13, pyrogallol mono(methyl ether) **108** was first treated with the suberone *rac*-**109** in a Pechmann condensation to give the coumarin **110**. The seven-membered ring later serves as a precursor for ring C. The coumarin also contains a carbonyl function, which is later required for the cyclization of ring B. The free phenol functionality was transformed into an allyl ether (**111**) and subsequent Claisen rearrangement (→**112**) allowed the selective introduction of a side chain for the projected construction of ring B. The propanoic acid side chain was established in five subsequent steps. Hydrolysis of the coumarin **116** afforded the dicarboxylic acid **117.** Methylation provided the diester **118**, which proved to be a better starting material than **117** for the crucial cyclization step (decarboxylative Dieckmann condensation). The product of this cyclization (**119**) already contains the complete 6,7,7-membered carbocyclic scaffold. To introduce the nitrogen function at C7, a Leuckart–Wallach reaction was used to give the formamide *rac*-**120** with a concomitant shift



Scheme 13. Sankyo synthesis of the colchicine intermediate *rac*-**122**. Reagents and conditions: a) $MeSO_3H$, room temperature, 20 h; b) allyl bromide, K_2CO_3, NaI, $MeOH/H_2O$, reflux, 16 h; c) *N*,*N*-dimethylaniline, reflux, 6 h; d) KOH, MeOH, 110–120 °C, 6 h; e) O_3, CH_2Cl_2, −60 °C, 1 h; f) malonic acid, pyridine, aniline, 50 °C, 22 h; g) H_2, Pd/C, MeOH, 1 h; h) 180 °C, 1 mm Hg, 8 h; i) Me_2SO_4, KOH, <100 °C, 3 h, →RT, 14 h; j) CH_2N_2, $MeOH/Et_2O$, room temperature, 1 h; k) KOH, $MeOH/H_2O$, reflux, 2 h; l) KOAc, Ac_2O, reflux, 2 h, →138 °C, 20 h; m) KO*t*Bu, *t*BuOH, xylene, 139 °C, 20 h; n) HCO_2H, $CO(NH_2)_2$, 110→180 °C over 6 h; o) $NH_2OH{\cdot}HCl$, pyridine, EtOH, reflux, 20 h; p) $LiAlH_4$, THF, reflux, 6 h; q) Ac_2O, pyridine, room temperature, 12 h.

 © 2004 Wiley-VCH Verlag GmbH & Co. KGaA, Weinheim

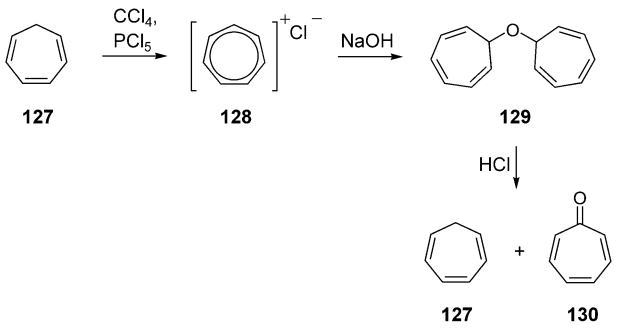


Scheme 14. Completion of the Sankyo synthesis of (±)-colchiceine (*rac*-**22**). Reagents and conditions: r) $BF_3{\cdot}OEt_2$, benzene, room temperature, 60 h; s) NBS, CCl_4, reflux, 5 min; then collidine 160–180 °C, 2 h; t) PCl_5, CCl_4, room temperature, 24 h; u) aqueous NaOH, 0 °C; then conc. HCl, room temperature, 3 days; v) $N_2H_4{\cdot}H_2O$, EtOH, reflux, 7.5 h; w) aqueous NaOH

of the C–C double bond. Alternatively, the corresponding oxime **121** was reduced and the resulting amine subsequently converted into the acetamide *rac*-**122**.

The synthesis was completed by using either synthetic *rac*-**123**, which was available by $BF_3{\cdot}OEt_2$-mediated double-bond isomerization of *rac*-**122** (Scheme 14), or enantiomerically pure material obtained from natural colchicine as a relay compound. The cycloheptene *rac*-**123** was converted into the tropilidene *rac*-**124** in a bromination/dehydrobromination sequence. As the direct oxidation of *rac*-**124** to the tropone *rac*-**125** was not viable with the various methods tried, a fairly wasteful deviation had to be made. The Nozoe method for tropone synthesis via a ditropyl ether that was applied is illustrated in Scheme 15.[49] First, an intermediate tropylium salt **128** was generated by hydride abstraction from cycloheptatriene (**127**). Reaction with NaOH then gave a ditropyl ether **129**, which upon treatment with concentrated HCl disproportionated to afford a mixture of the starting tropilidene (**127**) and the oxidation product, tropone (**130**).

The corresponding reaction of *rac*-**124** afforded the desired tropone *rac*-**125**, albeit in a disappointing low yield (Scheme 14). One can suspect that not only the desired colchicide *rac*-**125** but also regioisomeric products were formed in this step. Without further purification, crude *rac*-**125** was treated with hydrazine, presumably again with the formation of a mixture of regioisomers, from which colchiceineamide *rac*-**126** could be isolated in pure form (again in very low yield). Saponification of the aminotropone finally furnished (±)-colchiceine (*rac*-**22**).



Scheme 15. Tropone synthesis via a ditropyl ether.

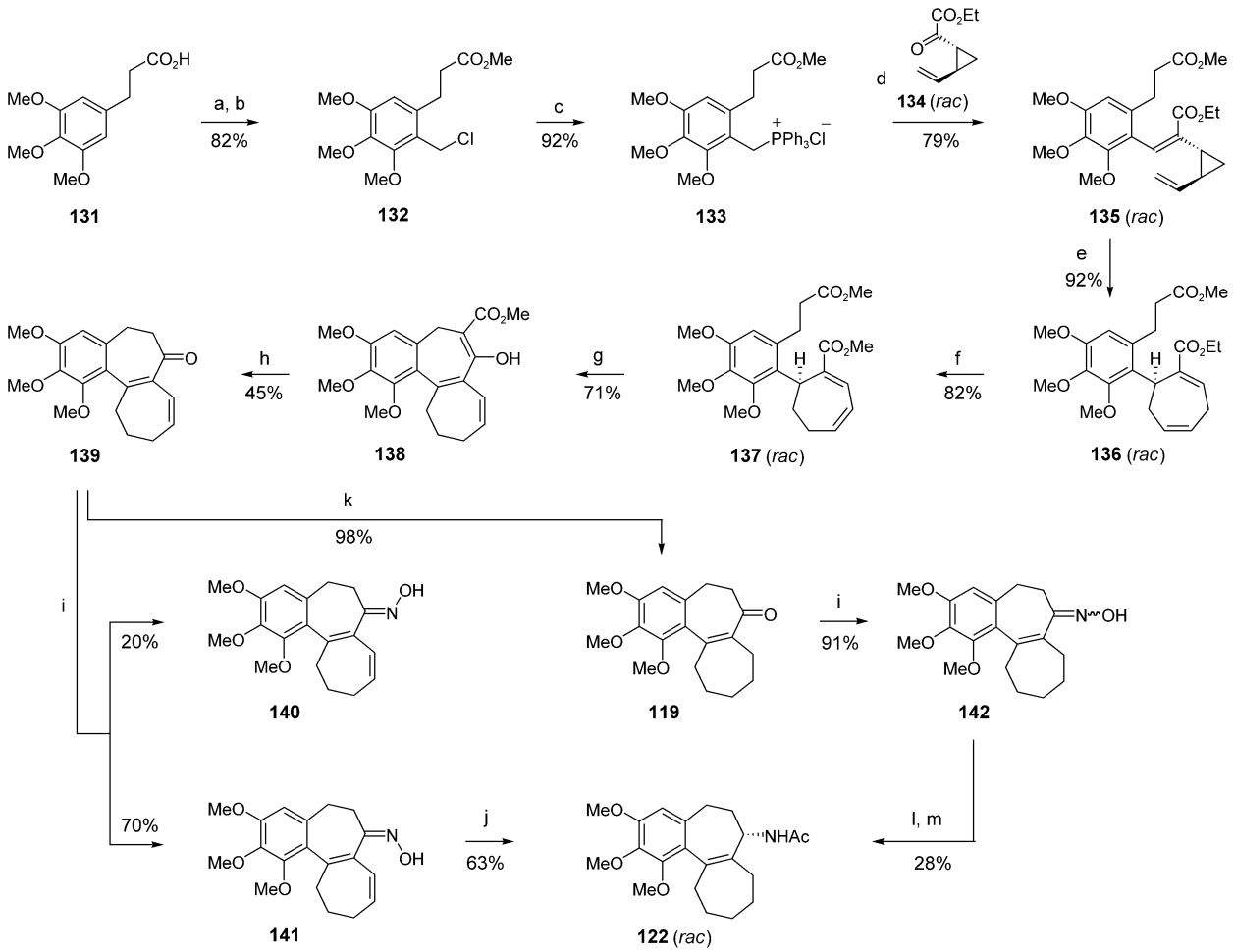
4.5.1. *Synthesis of an Advanced Colchicine Intermediate by Wenkert et al.*

Wenkert et al. reported an alternative synthesis of the key intermediates **119** and *rac*-**122**, which had already occurred in the Sankyo synthesis.[37] The Wenkert approach differs from the Sankyo synthesis mainly in the way that the Dieckmann condensation precursor, that is, the diester *rac*-**137**, is prepared (Scheme 16). For the construction of the seven-membered ring C, a divinylcyclopropane rearrangement was applied.

The hydrocinnamic acid **131** was used as starting material. The precursor *rac*-**135** required for the cyclization of ring C was prepared by a Wittig reaction from *rac*-**134** and the phosphorane obtained from **133**. The subsequent [3,3] sigmatropic rearrangement proceeded in high yield, and the diester *rac*-**137** was obtained after a shift of the remote C–C double bond in *rac*-**136** and subsequent esterification. Further conversion into the ketone **139** by Dieckmann condensation and demethoxycarbonylation was achieved in a yield comparable to that of the analogous transformation described by Nakamura (32%). The diastereomeric oximes **140** and **141** obtained from the ketone **139** could be separated, and the major *Z* isomer **141** was transformed into the acetamide *rac*-**122** by catalytic hydrogenation with concomitant *N*-acetylation. As a second point of overlap with the Sankyo synthesis, the key intermediate **119** was reached by catalytic hydrogenation of **139**. Reduction of the corresponding oxime mixture (**142**) with lithium aluminum hydride followed by acetylation also provided *rac*-**122**. At this stage the synthetic study was concluded, constituting a formal total synthesis of racemic colchicine.

Both the synthesis of Wenkert (Scheme 16) and the Sankyo synthesis (Schemes 13 and 14) provided an improved solution for the problem of C7 functionalization. While focusing on this problem, regioselectivity in the construction of the tropolone ring C was strategically neglected, and the overall efficiency of the synthetic schemes was spoiled by substantial losses of material during the completely unselective introduction of functionality in ring C following the strategy of Nakamura et al.

 © 2004 Wiley-VCH Verlag GmbH & Co. KGaA, Weinheim



Scheme 16. Synthesis of colchicine intermediates **119** and *rac*-**122** by Wenkert et al. Reagents and conditions: a) Me_2SO_4, K_2CO_3, acetone, reflux, 2 h; b) $MeOCH_2Cl$, $CHCl_3$/HOAc, 20 °C 18 h; c) PPh_3, benzene, reflux, 24 h; d) LDA, THF, −10 °C, →20 °C, 3 h, then *rac*-**134**, THF, −10 °C, →RT, 3 h; e) xylene, reflux, 24 h; f) NaOMe, MeOH, reflux, 12 h; then CH_2N_2, Et_2O; g) NaOMe, xylene, reflux, 12 h; h) 5% HCl, HOAc, H_2O, dioxane, reflux, 4 h; i) NH_2OH·HCl, pyridine, EtOH, reflux, 2 h; j) H_2, Pd/C, Ac_2O; k) H_2 (3 atm), Pd/C, EtOAc, room temperature, 2 h; l) $LiAlH_4$, THF, reflux, 12 h; m) Ac_2O, pyridine, room temperature, 16 h. LDA = lithium diisopropylamide.

4.6. Synthesis of Desacetamidocolchiceine through [4+3] Cycloaddition by Boger and Brotherton

In contrast to the approaches discussed above, Boger and Brotherton developed a very direct entry to annulated tropone structures by means of a cycloaddition strategy ABC′→ABC (Scheme 17).[36]

The cycloaddition of the Eschenmoser α-pyrone **54** and the cyclopropenone ketal **143** gave either the Diels–Alder product *rac*-**144** (which could not be converted into the desired tropone) or the [4+3] cycloaddition product *rac*-**146**, depending on the reaction conditions chosen. Upon heating, the cyclopropenone ketal **143** is in thermal equilibrium with a reactive open chain species, which according to Boger is best described as a nucleophilic delocalized vinyl carbene (**150**/**151**; Scheme 18).

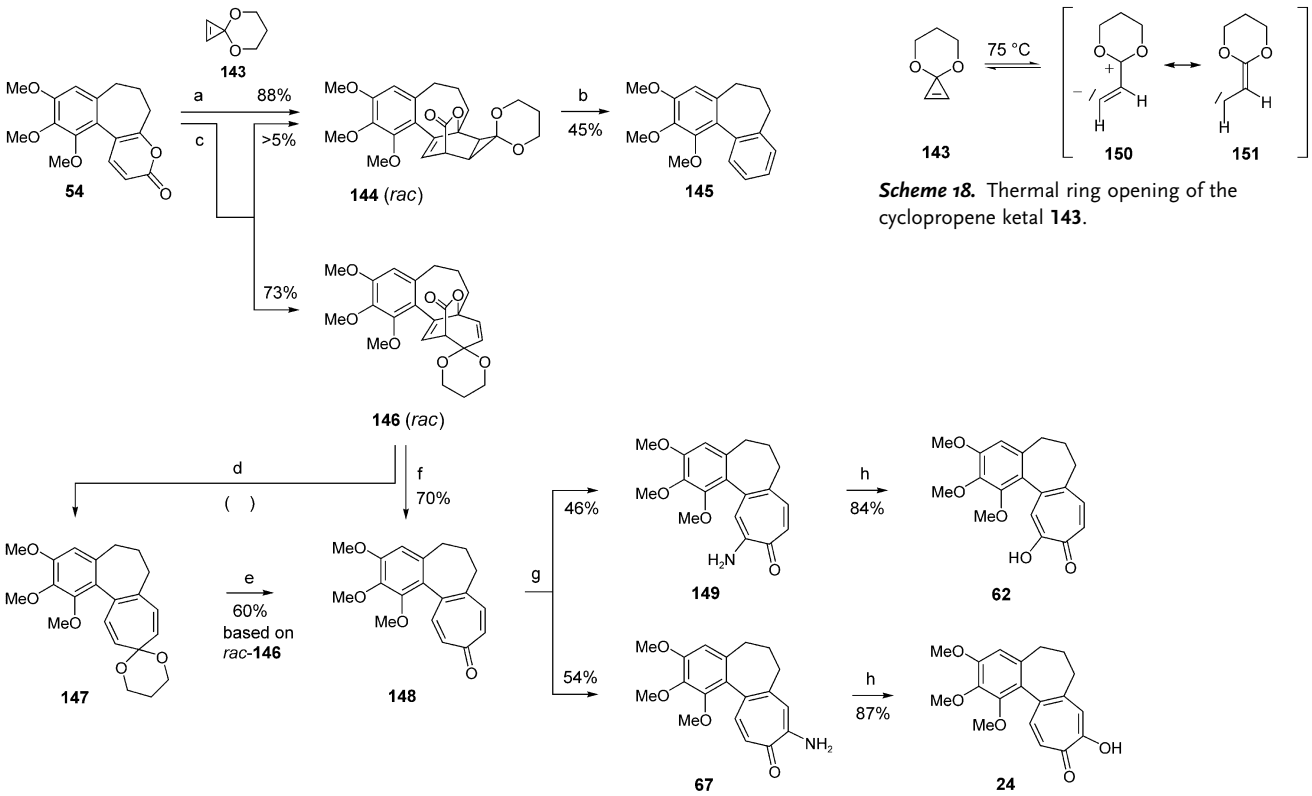
The [4+3] cycloaddition product **146** could easily be transformed into the tropone **148** in good yield through a retro-Diels–Alder decarboxylation and subsequent hydrolysis of the ketal function (Scheme 17). A one-pot procedure was used to increase the yield to 70% (*rac*-**146**→**148**). α Functionalization of **148** with hydrazine according to Nozoe et al. afforded the regioisomeric aminotropones **149** and **67**, which could be separately converted into the regioisomeric tropolones **62** and **24** (desacetamidocolchiceine), respectively, by saponification.

The sequence elaborated by Boger (**54**→**24**) greatly abbreviates the Eschenmoser synthesis. Although the route was very efficient, the unselective α oxygenation of the tropone intermediate **148** still remained a strategic drawback.

4.7. Synthesis of Desacetamidoisocolchicine by Skeletal Rearrangement According to Tobinaga and Co-workers

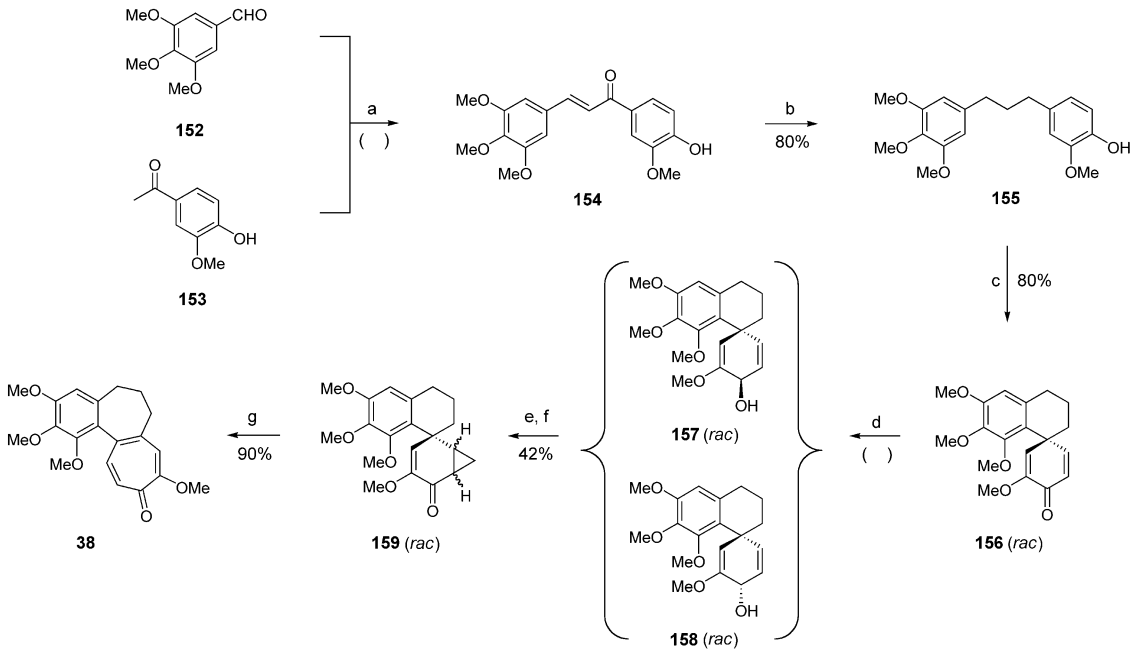
A rather striking strategy, completely different to all previous approaches, was described by Tobinaga and co-workers (Scheme 19).[34] Their synthesis of desacetamidoiso-

 © 2004 Wiley-VCH Verlag GmbH & Co. KGaA, Weinheim



Scheme 18. Thermal ring opening of the cyclopropene ketal **143**.

Scheme 17. Synthesis of desacetamidocolchiceine (**24**) by Boger and Brotherton. Reagents and conditions: a) **143**, 6.2 kbar, 25 °C, 5 days, b) mesitylene, 200 °C, 50 min; c) **143**, benzene, 75 °C, 36 h; d) 200 °C, 2 min; e) HOAc, H_2O, THF, 25 °C, 5 min; f) HOAc, H_2O, THF, 100 °C, 3.5 h; g) $N_2H_4 \cdot H_2O$, EtOH, 0→25 °C, 4.5 h; h) KOH (aqueous, 2 N), EtOH, 100–110 °C, 21 h.



Scheme 19. Synthesis of desacetamidoisocolchicine (**38**) by Tobinaga and co-workers Reagents and conditions: a) condensation, no conditions given; b) catalytic hydrogenation, no conditions given; c) anodic oxidation, HBF_4, MeCN, 20 min; d) $NaBH_4$; e) CH_2I_2, Zn/Cu couple; f) Jones oxidation; g) Ac_2O, H_2SO_4, room temperature.

 © 2004 Wiley-VCH Verlag GmbH & Co. KGaA, Weinheim

colchicine (**38**) along the lines of a rearrangement strategy AC′→AB′C′→ABC is based, like the Scott synthesis, on a false hypothesis concerning the biosynthesis of colchicine.[50]

The synthesis started from the simple aromatic compounds **152** and **153**. The chalcone **154** prepared from these simple building blocks was hydrogenated and the intermediate **155** was cyclized in an electrochemical oxidation to the spirocyclic dienone *rac*-**156**. Reduction with sodium borohydride afforded a mixture of the diastereomeric alcohols *rac*-**157** and *rac*-**158**, which was transformed into the cyclopropane derivative *rac*-**159** by Simmons–Smith cyclopropanation and subsequent Jones oxidation. Although the stereostructure of *rac*-**159** remained unknown, treatment with an Ac_2O/H_2SO_4 mixture directly gave rise to **38**. Evidently, the opening of the cyclopropane ring in *rac*-**159** was accompanied by a migration of the aryl residue followed by dehydration to give the tropolone methyl ether **38** (migration of the alkyl residue would have resulted in the formation of a regioisomeric tropolone).

This single operation served to unfold the complete 6,7,7-membered ring skeleton establishing the tropolone ring C with the desired oxidation state. Furthermore, the desired regioisomer of the tropolone methyl ether required for the C7 functionalization according to Eschenmoser was generated selectively. Nevertheless, both the synthesis of Boger and Brotherton and the synthesis of Tobinaga and co-workers are inefficient, as they rely on this low-yielding and non-stereoselective introduction of the amido functionality.

4.8. The Evans Synthesis of (±)-Trimethylcolchicinic Acid

Inspired by the interesting work of Tobinaga and coworkers, Evans et al. reported a synthesis of the Eschenmoser intermediate **38** in 1978 in which they further investigated the rearrangement transformation.[35a] Three years later, the Evans group came up with a very convincing total synthesis of trimethylcolchicinic acid following a AC′→ABC strategy in which the problems of the construction of the tropolone ring and the introduction of C7 functionality were equally well-addressed (Scheme 20).[35b]

The main innovation was that the precursor *rac*-**167** for the key transformation, that is, the skeletal rearrangement, only contains rings A and C′. Intermediate *rac*-**167** was prepared in a convergent fashion and in high yield from the cyclohexenone derivative *rac*-**163** and the arylbutanoate **165**. The synthesis of *rac*-**163** started with the electrochemical oxidation of trimethoxybenzene **160** to give **161**, which was selectively hydrolyzed to the quinone monoketal **162**. Subsequent methylenation with dimethylsulphoxonium methylide afforded *rac*-**163**. The arylbutanoate **165** in turn was obtained by chain elongation of the trimethoxycinnamate **44**. Coupling of the ester enolate derived from **165** with the building block *rac*-**163** afforded a mixture of diastereomers (*rac*-**166**), which was directly hydrolyzed to give the cyclization precursor *rac*-**167**.

The subsequent key transformation was performed with very high yield in a one-pot procedure or, alternatively, via *rac*-**168** under milder conditions. The rearrangement proceeded in analogy to the transformation designed by Tobinaga et al., with the difference that the presence of the additional ester function resulted in the formation of **169** as well as the expected product *rac*-**170**. The mixture of these isomeric products was treated with DDQ to give a 3:7 mixture of the heptafulvene **171** and the desired tropolone methyl ether *rac*-**172**. These two oxidation products were separated, and it was found that they can be readily equilibrated back to the initial 3:7 mixture. Hydrolysis of the ester and decarboxylation of *rac*-**172** gave rise to the Eschenmoser intermediate **38**. For the conclusion of the formal total synthesis, the isomeric mixture **171**/*rac*-**172** was converted in a three-step sequence into the advanced colchicine precursor *rac*-**25** by hydrolysis of the ester, Curtius degradation, and demethylation.

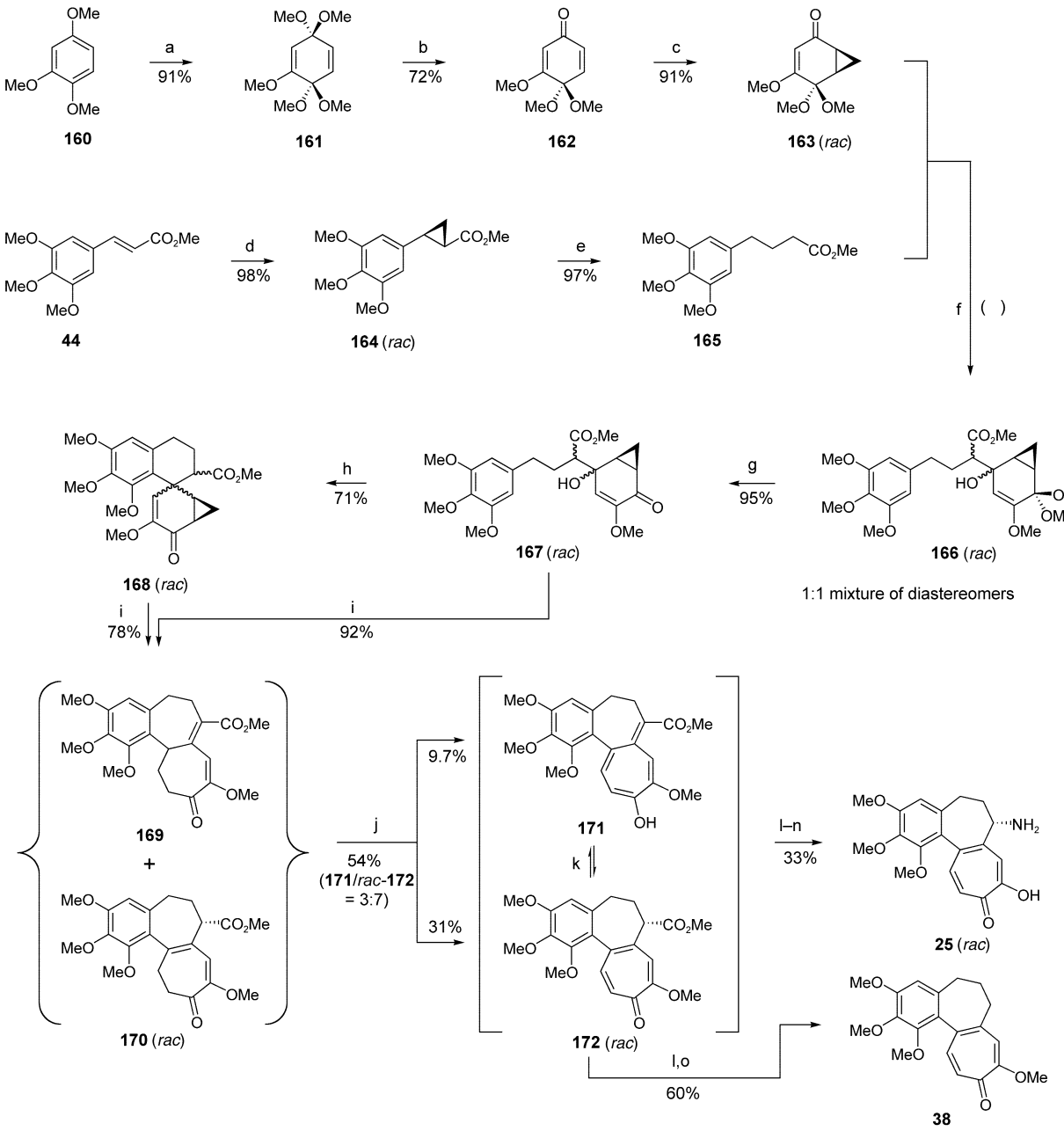
In conclusion, the synthesis of Evans et al. provided an outstanding solution for the construction of the unusual 6,7,7-membered ring system and included the selective functionalization of both rings C and B. The unsatisfactory yield for the generation of the tropolone remained a shortcoming in this synthesis. Also, the development of an enantioselective variant seemed extremely difficult owing to the facile equilibration of **172** and its isomer **171**.

4.9. The Woodward Synthesis

One of the most innovative studies in the field of colchicine synthesis was presented by Woodward in 1963 as a Harvey Lecture.[29] A remarkable feature of his synthesis was the implementation of the nitrogen functionality at C7 as an integral part of the synthetic strategy. The crucial role in the very straightforward synthetic concept was played by the isothiazole ring, a heterocycle first described in the course of this synthesis. It served as a masked amino function and acted as platform for the cyclization of rings B and C (Scheme 21).

The disubstituted isothiazole **174** was obtained by treatment of the β-aminocrotonate **173** with thiophosgene. Photobromination and reaction with triphenylphosphane afforded the phosphonium salt **175**, which was used for the Wittig olefination of trimethoxybenzaldehyde **152**. After reduction of the C–C double bond with diimine (the isothiazole sulphur atom precluded the use of catalytic hydrogenation) and conversion of the ester into an aldehyde, the resulting intermediate **177** was subjected to a second Wittig reaction with the phosphorane **178**. Saponification and isomerization of the *Z*/*E* mixture of isomers afforded the *E*,*E*-dienecarboxylic acid **179** as a pure stereoisomer. Cyclization to form ring B was achieved in a Friedel–Crafts-type alkylation, and subsequent reduction with diimine afforded *rac*-**181**. In the following step, the heterocycle was lithiated at the unsubstituted position and carboxylated with CO_2. The corresponding diester *rac*-**182** then served as a precursor for the cyclization of ring C in a Dieckmann condensation. Subsequent decarboxylation gave the tetracyclic ketone *rac*-**183**. C10 was functionalized by Woodward's method for the introduction of a 1,3-dithiane. For this purpose, the position

 © 2004 Wiley-VCH Verlag GmbH & Co. KGaA, Weinheim

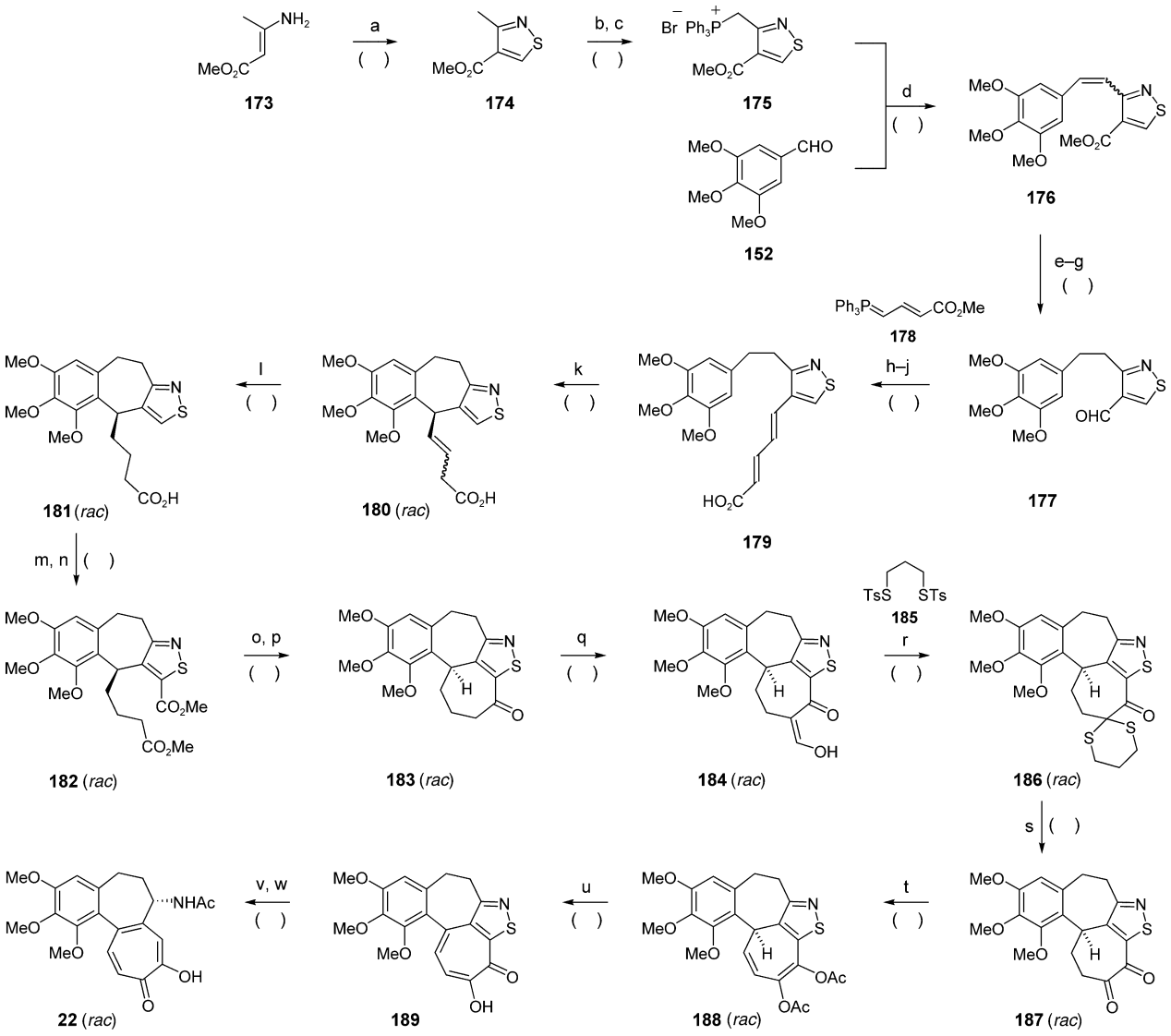


Scheme 20. Synthesis of (±)-trimethylcolchicinic acid (*rac*-**25**) by Evans et al. Reagents and conditions: a) KOH, MeOH, anodic oxidation, 0°C, 25 h; b) $(CO_2H)_2$, THF/H_2O, room temperature, 12 min; c) $Me_3S(O)I$, NaH, DMSO, 0°C, 15 min, →RT, 30 min, then **162**, DMSO, room temperature, 2 h; d) CH_2N_2, $Pd(OAc)_2$, Et_2O/CH_2Cl_2, 0°C, 15 min; e) H_2 (51 psi), Pd/C, MeOH; f) **165**, LDA, THF, −78°C, 35 min, then *rac*-**163**, →0°C, 30 min; g) aqueous $(CO_2H)_2$, THF, room temperature, 5 h; h) CF_3CO_2H, room temperature, 20 min; i) CF_3CO_2H, reflux, 35 min; j) DDQ, benzene, reflux, 18 h; k) $CDCl_3$, room temperature, 24 h, equilibration to a 3:7 mixture of **171**/*rac*-**172**; l) NaH, MeOH/H_2O, 75°C, 45 min; m) $(PhO)_2P(O)N_3$, NEt_3, *t*BuOH, reflux, 17 h; n) HCl (aqueous, 3 N), 110°C, 90 min; o) 180°C, 1–2 min. DDQ = 2,3-dichloro-5,6-dicyano-1,4-benzoquinone.

α to the carbonyl group of *rac*-**183** was first activated by formylation (→*rac*-**184**) before reaction with the bisthiotosylate **185** gave rise to the dithiane *rac*-**186**. Hydrolysis of *rac*-**186** afforded the α-diketone *rac*-**187**, which was converted into the dienol diacetate *rac*-**188**. Remarkably, a spontaneous aerial oxidation under basic conditions yielded the desired tropolone **189**. To liberate the amino function, desulphurization was performed with Raney nickel, and (±)-colchiceine (*rac*-**22**) was obtained after acetylation.

Although this synthesis is 40 years old, it demonstrates how selectivity problems can be overcome in a masterly fashion with conceptual creativity. Unfortunately, Woodward did not report yields in his publication, so that the overall efficiency and any possible obstacles cannot be judged.

 © 2004 Wiley-VCH Verlag GmbH & Co. KGaA, Weinheim



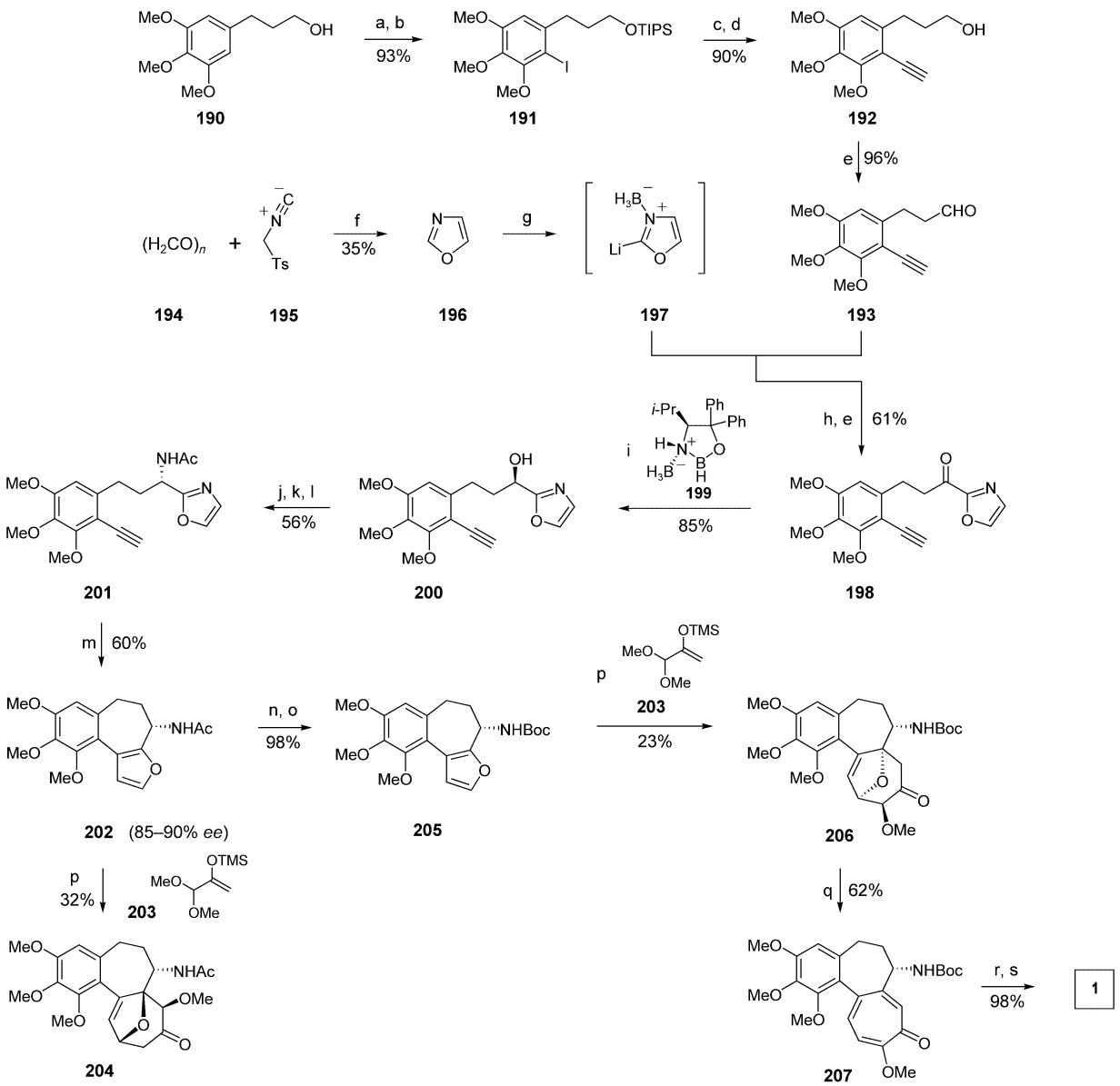
Scheme 21. Synthesis of (±)-colchiceine (*rac*-**22**) by Woodward et al. Reagents and conditions: a) $CSCl_2$, NEt_3, Et_2O; b) NBS, CCl_4, $h\nu$; c) PPh_3; d) NaOMe; then **152**; e) N_2H_4, H_2O_2, Cu^{II}; f) $LiAlH_4$; g) MnO_2; h) Wittig olefination; i) NaOH aq.; j) I_2, $h\nu$; k) 70% $HClO_4$, 60°C; l) N_2H_4, H_2O_2, Cu^{II}; m) *o*-lithiobiphenyl, THF; then CO_2; n) esterification; o) NaH, dioxane; p) HOAc, H_2SO_4, heating; q) NaH, HCO_2Et, EtOH, THF; r) **185**, KOAc, *i*PrOH, reflux; s) $Hg(OAc)_2$, aqueous $HClO_4$, HOAc, heating; t) Ac_2O, pyridine; u) NaOH, air; v) Raney Ni, aqueous NaOH; w) Ac_2O, pyridine; then aqueous NaOH.

4.10. The Cha Synthesis of (−)-Colchicine by Oxyallyl [4+3] Cycloaddition

In a much more recent synthesis, Cha et al. also made intensive use of heterocyclic chemistry. The annulated furan **202** was used as the central intermediate for a cycloaddition, corresponding to the general ABC′→ABC strategy (Scheme 22).[39]

The starting material, alcohol **190**, was first protected, then iodinated, coupled with TMS-acetylene in a Sonogashira coupling, and finally desilylated (deprotected) to give **192**. A subsequent Swern oxidation afforded the aldehyde **193** in high overall yield. Oxazole (**196**), which was prepared by condensation of TosMIC (**195**) with formaldehyde, served as the second building block. Compound **196** was first converted into the borane adduct to assure regioselective lithiation and to avoid cleavage of the heterocycle. The product obtained from the reaction of the intermediate **197** with the aldehyde **193** was directly oxidized under Swern conditions, and the resulting ketone **198** was enantioselectively reduced to the alcohol **200** with the (*S*)-diphenylvalinol-derived oxazaborolidine **199** following the Itsuno protocol. The transformation to **201** was carried out through Mitsunobu reaction with DPPA as an azide source, Staudinger reduction to the amine, and *N*-acetylation. Upon heating of **201**, the furan **202** was formed in an intramolecular Diels–Alder/retro-Diels–Alder reaction cascade under extrusion of HCN. Whereas the following key step, the cycloaddition of **202** with an oxyallyl

 © 2004 Wiley-VCH Verlag GmbH & Co. KGaA, Weinheim



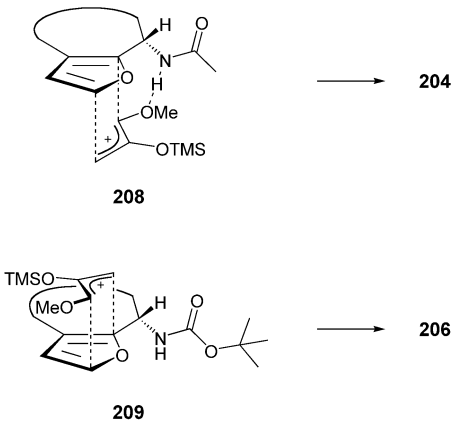
Scheme 22. Synthesis of (−)-colchicine (**1**) by Cha and co-workers. Reagents and conditions: a) TIPSOTf, 2,6-lutidine, CH_2Cl_2, 0 °C, →RT, 5 h; b) I_2, $Ag(CF_3CO_2)$, $NaHCO_3$, $CHCl_3$, 3 h; c) HC≡CTMS, $[Pd(PPh_3)_2Cl_2]$, CuI, Et_2NH, DMSO, 90 °C, 20 h; d) TBAF, THF, 0 °C, →RT, 7 h; e) $(COCl)_2$, DMSO, CH_2Cl_2, −78 °C, 1 h 15 min; then NEt_3, −78→0 °C; f) $(CH_2O)_n$, **195**, K_2CO_3, DMSO, room temperature, 5 h; then KOH, ethylene glycol, room temperature, 5 h; g) BH_3·THF, THF, room temperature, 1 h; then *t*BuLi, −78 °C, 40 min; h) THF, −78 °C, 3 h; i) BH_3·THF, (*S*)-(−)-diphenylvalinol, THF, −78 °C, 20 min, →RT; then **198**, THF, 6 h; j) $(PhO)_2P(O)N_3$, PPh_3, DIAD, THF, room temperature, 12 h; k) PPh_3, H_2O, THF, room temperature, 50 h; l) Ac_2O, NEt_3, DMAP, Et_2O, room temperature, 7 h; m) *o*-dichlorobenzene, reflux, 66 h; n) Boc_2O, NEt_3, DMAP, CH_2Cl_2, 35 °C, 10 h; o) LiOH, THF, 12 h; p) **203**, TMSOTf, $EtNO_2$, −78 °C, 1 h, →−60 °C, 12 h; q) TMSOTf, NEt_3, CH_2Cl_2, 0 °C, 2 h; r) HCl (1 N), Et_2O, room temperature, 1 h; s) Ac_2O, NEt_3, DMAP, Et_2O, 25 °C, 10 h. TIPS = triisopropylsilyl; Tf = trifluoromethanesulfonyl; TMS = trimethylsilyl; TBAF = tetra-*n*-butylammonium fluoride; Boc = *tert*-butoxycarbonyl; DIAD = diisopropylazodicarboxylate; DMAP = 4-dimethylaminopyridine.

generated from **203**, afforded the undesired regioisomer **204**, the analogous [4+3] cycloaddition of the Boc-protected compound **205** proceeded with the reversed regioselectivity. However, the desired product **206** was obtained in a mere 23% yield.

As an explanation for the observed selectivity, the authors assumed a participation of a hydrogen bond in the case of **202** as a substrate (structure **208** in Scheme 23). By changing the *N*-protecting group to Boc (**202**→**205**), such a hydrogen bond does not seem to play a role and steric interactions dominate the selectivity (structure **209**).

The use of related oxa-bridged [4+3]-cycloadducts was introduced by Föhlisch et al. as a generally applicable method for tropone synthesis.[51] The oxygen bridge of **206** was removed by treatment with TMSOTf/NEt_3 to furnish the tropolone **207** with the correctly placed methyl ether func-

 © 2004 Wiley-VCH Verlag GmbH & Co. KGaA, Weinheim



Scheme 23. Influence of the amide function on the regio- and stereoselectivity of the cycloadditions to give **204** and **206**.

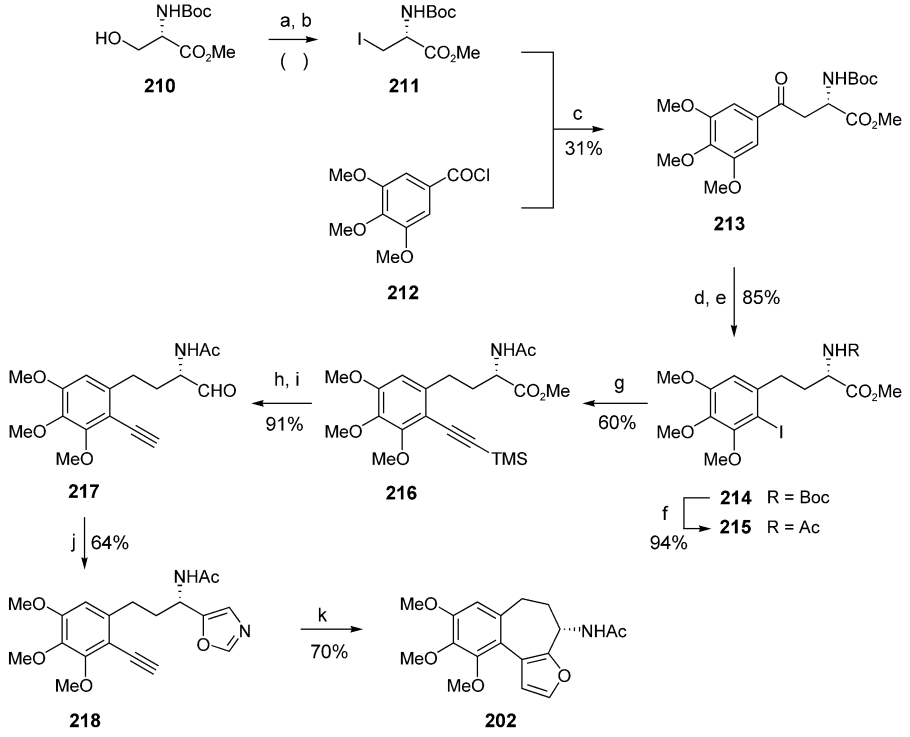
tionality (Scheme 22). After *N*-deprotection and renewed acetylation, colchicine (**1**) was obtained (ca. 90% *ee*).

Thus nonracemic colchicine was synthesized in a relatively short reaction sequence. The strength of this synthesis lies in the highly efficient preparation of the key intermediate **202**. However, the overall scheme is stained by the low yield of the key cycloaddition (**205**→**206**, 23%, 45% with respect to 50% recovered starting material).

Cha and co-workers also reported another method for the preparation of the advanced furan intermediate **202** in which they exploited the chiral pool (Scheme 24).[39b] The protected L-serine derivative **210** was converted into the iodide **211**, and its organozinc derivative was treated with the acid chloride **212** in a Pd-catalyzed coupling. The resulting aryl ketone **213** was converted into **214** by benzylic hydrogenation and subsequent iodination at the arene nucleus. A Sonogashira coupling of the acetamide **215** followed by desilylation and reduction with DIBAH afforded the aldehyde **217**. The oxazole **218**, prepared from the aldehyde with TosMIC (**195**), was heated at reflux in *ortho*-dichlorobenzene to yield the same furan **202** previously obtained from the isomeric oxazole **201**.

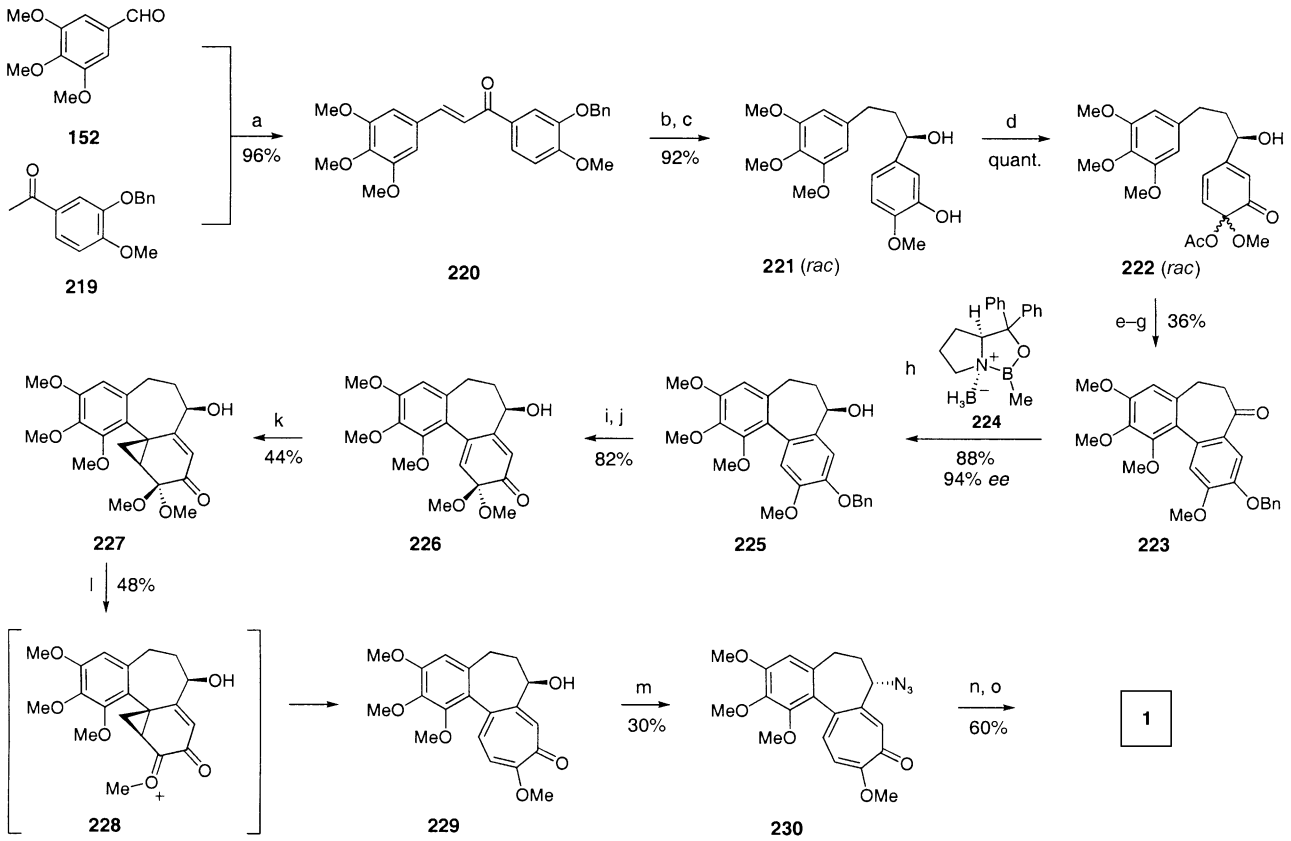
4.11. The Banwell Synthesis of (−)-Colchicine by Biomimetic Ring Enlargement

Another efficient enantioselective synthesis, which is strategically related to the syntheses of Tobinaga and co-workers and Evans et al. and follows the AC′→ABC′→ABC ring enlargement strategy, was reported by Banwell in 1996 (Scheme 25).[38] This synthesis was the culmination of comprehensive efforts by Banwell et al.[38,41,52] and was also guided by the biosynthesis of the natural product, which according to our current knowledge (Scheme 1) does, indeed, proceed



Scheme 24. Alternative route to the colchicine intermediate **202** according to Cha and co-workers. Reagents and conditions: a) MsCl, no further details given; b) NaI, no further details given; c) **211**, Zn/Cu couple, benzene, ultrasound, room temperature, 3 h; then $[Pd(PPh_3)_2Cl_2]$, **212**, ultrasound, 2 h; d) H_2 (60 psi), Pd/C, EtOH, H_2O, 22 h; e) I_2, $Ag(CF_3CO_2)$, $NaHCO_3$, $CHCl_3$, 0 °C, 2 h; f) CF_3CO_2H, Et_2O, room temperature, 3 h; then Ac_2O, NEt_3, DMAP, Et_2O, 10 h; g) HC≡CTMS, $[Pd(PPh_3)_2Cl_2]$, CuI, Et_2NH, DMSO, 90 °C, 15 h; h) K_2CO_3, MeOH, room temperature, 11 h; i) DIBAH, CH_2Cl_2, −78 °C, 1 h; j) TosMIC, K_2CO_3, MeOH, reflux, 1 h; then KOH, reflux, 3 h; k) *o*-dichlorobenzene, reflux, 40 h. Ms = methanesulfonyl; DIBAH = diisobutylaluminum hydride; TosMIC = toluenesulfonylmethylisocyanide.

 © 2004 Wiley-VCH Verlag GmbH & Co. KGaA, Weinheim



Scheme 25. Banwell synthesis of (−)-colchicine (**1**). Reagents and conditions: a) NaOH, MeOH, room temperature, 48 h; b) H_2, Pd/C, EtOAc, 15 °C, 10 h; c) $NaBH_4$, THF/MeOH, 15 °C, 1.5 h; d) $Pb(OAc)_4$, molecular sieves (3 Å), CH_2Cl_2, 15 °C, 1 h; e) CF_3CO_2H, molecular sieves (3 Å), THF/benzene, 0 °C, 1 h; f) BnBr, K_2CO_3, MeCN, 82 °C, 4 h; g) NMO, TPAP, molecular sieves (4 Å), CH_2Cl_2, 15 °C, 43 h; h) **224**, THF, 15 °C, 6 h; i) H_2, Pd/C, EtOAc, 15 °C, 9 h; j) $Tl(NO_3)_3$, MeOH, −20 °C, 30 min; k) $Me_3S(O)I$, NaH, DMSO, 15 °C, 7 h; l) CF_3CO_2H, CH_2Cl_2, 15 °C, 3 h; m) $Zn(N_3)_2{\cdot}Py_2$, DIAD, PPh_3, THF, 15 °C, 38 h; n) PPh_3, H_2O, THF, 15 °C, 63 h; o) Ac_2O, pyridine, 15 °C, 15 min. NMO = *N*-methylmorpholine-*N*-oxide; TPAP = tetra-*n*-propylammonium perruthenate.

through ring enlargement of a norcarane intermediate as a precursor for ring C.

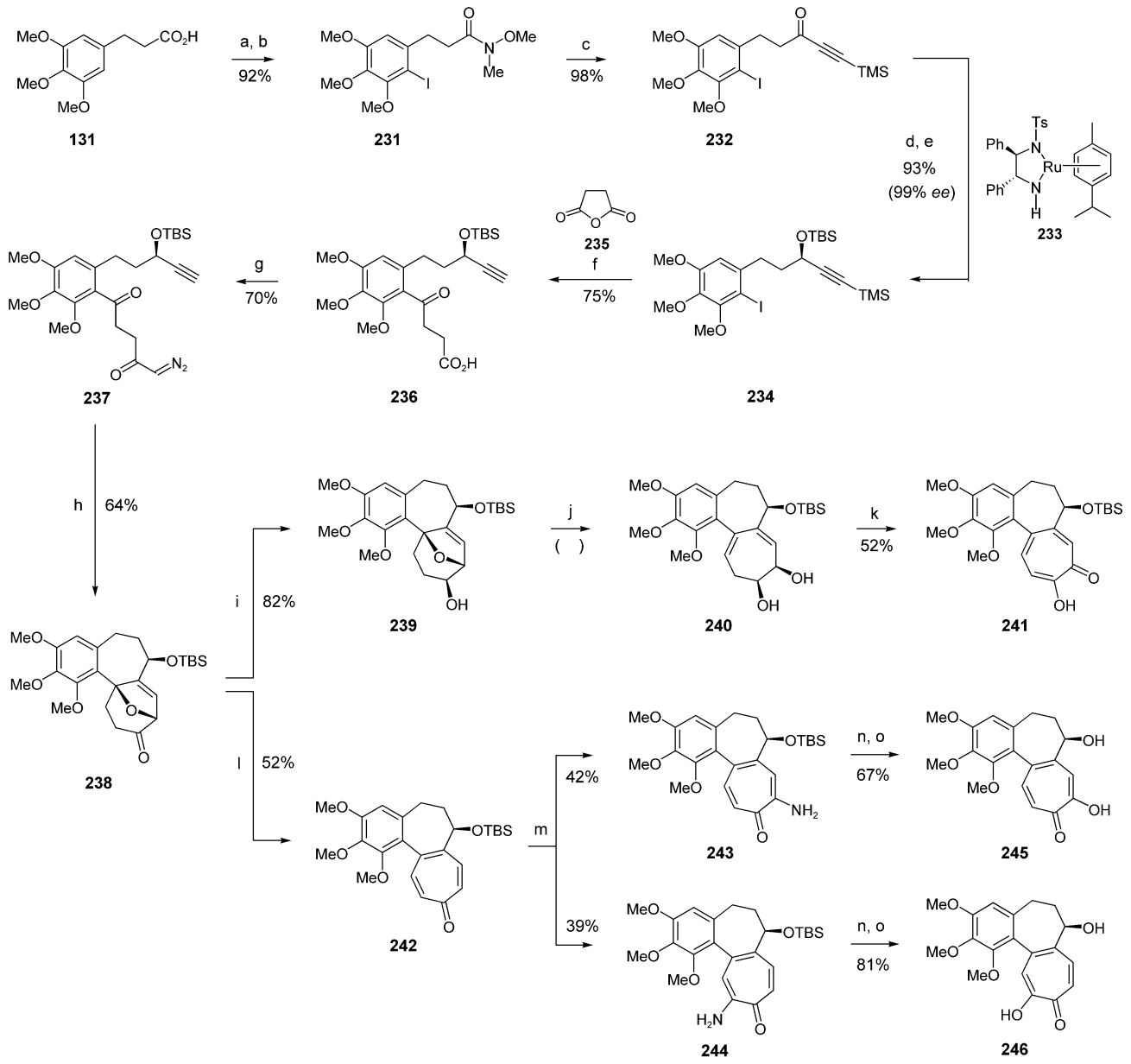
Starting from the easily obtainable chalcone **220**, the stepwise reduction of the C–C double bond and the keto group under cleavage of the benzyl ether afforded the racemic diaryl propanol *rac*-**221**. Wessely oxidation gave rise to the cyclohexadienone *rac*-**222**, which was converted into the aryl ketone **223** by cationic cyclization, benzylation of the resulting phenol, and oxidation of the alcohol. Enantioselective reduction of the ketone **223** with stoichiometric quantities of the CBS reagent **224** afforded **225** (94 % *ee*). Cleavage of the benzyl ether was followed by a renewed oxidation of the phenol, in this case with $Tl(NO_3)_3$ according to the procedure of Taylor and McKillop. Methylenation of **226** with dimethylsulphoxonium methylide gave the cyclopropane **227** in only moderate yield. The ring enlargement to establish the 6,7,7-membered ring system (→**229**) was achieved by treatment of **227** with CF_3CO_2H. Along these lines, the tropolone ring C was delivered with the correct oxidation state and arrangement of the oxygen functions as found in the target structure. Unexpectedly, the S_N2-type conversion of the OH function of **229** into a nitrogen functionality was rather difficult. At first an azido group was introduced by Mitsunobu reaction. The product **230** was obtained in only low yield, and partial racemization occurred during the subsequent Staudinger reduction. From the resulting amine, the natural product **1** was obtained with only 81 % *ee* after acetylation.

In summary, the synthetic problem was solved by Banwell in a relatively short sequence of rather simple transformations. Even the rather low yields of some steps do not distort the beautiful overall scheme.

4.12. Our Synthesis of an Advanced Colchicine Intermediate Exploiting a Rh-Catalyzed Cyclization Cascade

Our conceptually very direct approach towards colchicin (**1**) is based on a retrosynthetic analysis in which the oxa-bridged key intermediate **238** is traced back to the open-chain cyclization-precursor **237** (A→ABC).[40,53] This strategy was designed in analogy to the benzotropolone synthesis of Friedrichsen and Plüg.[54] The crucial step, a Rh-catalyzed cyclization cascade (**237**→**238**), not only generated the 6,7,7-membered ring system, but also installed the oxygen substituents correctly at C9 and C10 in the newly formed ring C (Scheme 26).

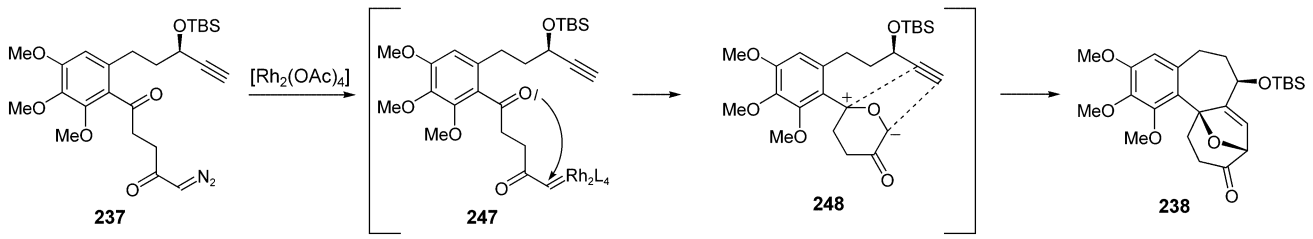
 © 2004 Wiley-VCH Verlag GmbH & Co. KGaA, Weinheim



Scheme 26. Synthesis of the advanced colchicine intermediates **241** and **245** according to Graening and Schmalz. Reagents and conditions: a) $(COCl)_2$, CH_2Cl_2, 0 °C→RT, 12 h; then NHMeOMe·HCl, pyridine, CH_2Cl_2, 0 °C, 1 h; b) $Ag(CF_3CO_2)$, I_2, $CHCl_3$, room temperature, 4 h; c) LiC≡C-TMS, THF, −78 °C, →−10 °C, 45 min; d) **233** (1 mol %), *i*PrOH, 16 h; e) TBSCl, imidazole, DMF, room temperature, 18 h; f) *i*PrMgCl, THF, −25 °C, 4.5 h; then **235**, THF, −40 °C, 30 min; then K_2CO_3, MeOH, room temperature, 3 h; g) *i*BuOCOCl, NEt_3, THF/Et_2O, −20→−15 °C; then CH_2N_2, Et_2O, −5 °C, 16 h; h) $[Rh_2(OAc)_4]$, toluene, reflux, 4 h; i) L-selectride, THF, −78 °C, 3 h; j) TMSOTf, NEt_3, CH_2Cl_2, −50→−10 °C, 1 h; then K_2CO_3, MeOH, 0 °C, 45 min; k) DMSO, $(CF_3CO)_2O$, CH_2Cl_2, −60 °C, 1.5 h; then NEt_3, −60 °C, 1.5 h; l) Et_2AlCl, CH_2Cl_2, −78→0 °C, 2.5 h; m) $NH_2N_2·H_2O$, EtOH, 0 °C→RT, 4.5 h; n) TBAF, THF, 0 °C, 45 min; o) 2 N KOH, EtOH, 110 °C, 16 h. TBS = *tert*-butyldimethylsilyl.

The bifunctional Weinreb amide **231** was prepared from hydrocinnamic acid **131** and treated with lithium trimethylsilylacetylide to give the alkynone **232**. This compound proved to be an excellent substrate for enantioselective transfer hydrogenation according to Noyori. In the presence of the Ru complex **233** as a catalyst, the corresponding propargylic alcohol was obtained in essentially enantiomerically pure form and was subsequently silylated to give the protected derivative **234** in 93 % yield (two steps). Acylation to give the ketocarboxylic acid **236** was achieved utilizing a protocol of Knochel for iodine–magnesium exchange and reaction of the resulting Grignard intermediate with succinic anhydride (**235**). An advantage of this method was that deprotonation at the propargylic position, which was observed with the stronger base *n*BuLi, could be inhibited. Treatment of the α-diazoketone **237** (obtained from **236**) with catalytic $[Rh_2(OAc)_4]$ in refluxing toluene gave the tetracyclic key intermediate **238** with complete diastereoselectivity.

 © 2004 Wiley-VCH Verlag GmbH & Co. KGaA, Weinheim

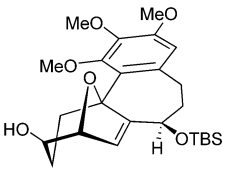


Scheme 27. Rh-Catalyzed cyclization cascade to the key intermediate **238**.

The mechanism and scope of related transformations introduced by Ibata[55a] were investigated in detail by Padwa et al.[55b] As shown in Scheme 27 the cyclization cascade is initiated by the generation of an electrophilic rhodium carbene **247**, which is then attacked by the adjacent Lewis basic carbonyl group to form a reactive carbonyl ylide **248**. The ylide is trapped in another intramolecular reaction step, a 1,3-dipolar cycloaddition with the tethered alkyne unit.

The cycloaddition product **238** formed in 64 % yield has a rather rigid ring system in which the benzylic C–O bond is aligned with the π system of the aromatic ring. Therefore, a selective cleavage of the oxa bridge should be feasible by exploiting stereoelectronic effects.

In fact, the alcohol **239**, prepared from **238** by reduction with L-selectride, is readily converted into the dienediol **240** upon treatment with $TMSOTf/NEt_3$ and immediate hydrolysis of the primarily formed bis(silyl ether) (to avoid isomerization by a sigmatropic [1,5] H-shift). Oxidation of **240** with $DMSO/(CF_3CO_2)_2O$ then immediately gave rise to the stable tropolone **241**. An alternative route for the conversion of the key intermediate **238** into a tropolone started with its Lewis acid mediated dehydration to the tropone **242**. Following a similar protocol as applied by Boger, treatment of **242** with hydrazine resulted in the formation of the two regioisomeric aminotropones **243** and **244**, which were easily separable. From these, the two regioisomeric tropolones **245** and **246**, respectively, were accessible by desilylation and alkaline hydrolysis. As **241** and **245** can be converted into the Banwell intermediate **229**, their formation completes a formal total synthesis of colchicine (**1**). Furthermore, the alternative route via the tropone **242** opens an easy entry to the pseudo-colchicine series starting from **246**.



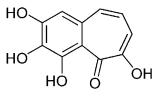
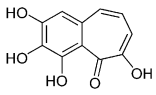
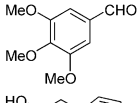
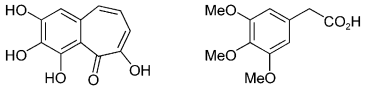
239

With a 12 % overall yield for the conversion of the simple starting material **131** into the advanced colchicine precursor **241**, our synthesis represents a highly efficient approach towards colchicinoid structures (Scheme 26). The strategy should be flexible enough to allow the synthesis of modified analogues. However, this has to be demonstrated in the future.

5. Summary

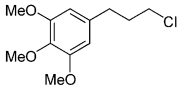
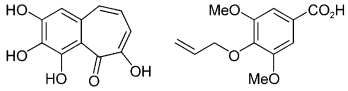
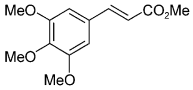
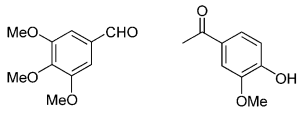
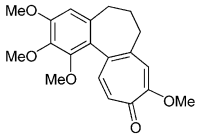
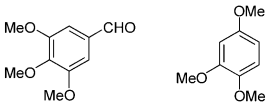
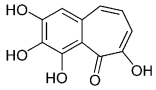
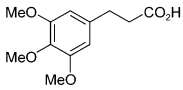
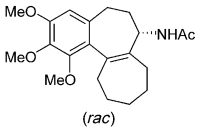
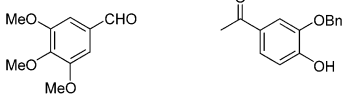
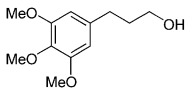
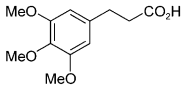
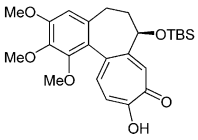
Over the past 50 years, colchicine has challenged synthetic chemists like only few other target molecules. The synthetic efforts of many research groups have culminated in fascinating and very diverse synthetic solutions (Table 1). These studies led to the development of novel tropolone syntheses and served to scrutinize the methodology for the synthesis of seven-membered rings in general. Although the early syntheses represent cultural achievements of highest merit, their

Table 1: Summary of colchicine syntheses.[a]

Authors	Year	Starting compound	Target	Number of steps	Yield [%]
Eschenmoser and co-workers	1959		(±)-colchicine (*rac*-**1**)	22	0.00006
van Tamelen et al.	1959		Trimethylcolchicinic acid (*rac*-**25**)	18	0.0005
Nakamura et al.	1962		(±)-colchiceine (*rac*-**21**)	20	0.0007[b]
Woodward	1963		(±)-colchiceine (*rac*-**21**)	23	–[c]
Scott et al.	1965		desacetamidocolchiceine (**24**)	11	0.1

 © 2004 Wiley-VCH Verlag GmbH & Co. KGaA, Weinheim

Table 1: (Continued)

Authors	Year	Starting compound	Target	Number of steps	Yield [%]
Toromanoff and co-workers	1965		desacetamidocolchiceine (**24**)	15[d]	0.3[d]
Kaneko et al.	1968		desacetamidocolchiceine (**24**)	11	0.5[e]
Kato et al.	1974		desacetamidocolchiceine (**24**)	9	~1
Tobinaga and co-workers	1974			7	24
Evans et al.	1984		trimethylcolchicinic acid (*rac*-**25**)	12	5
Boger and Brotherton	1985		desacetamidocolchiceine (**24**)	10[f]	3.5[f]
Wenkert et al.	1989		 (*rac*)	10	6.3
Banwell	1996		(−)-colchicine (**1**) ~81% *ee*	15	0.9
Cha and co-workers	1998		(−)-colchicine (**1**) ~90% *ee*	18	1.9
Graening and Schmalz	2004			11	12

[a] The overall yields and the number of steps, as a matter of interpretation, should only be taken for the purposes of comparison. [b] For the racemic series. [c] No yields were reported. [d] For the shorter and more efficient route via **94**. [e] Based on the yields for **26**→**35** reported by Scott et al. [f] Based on the preparation of pyrone **54** reported by Eschenmoser and co-workers.

overall efficiency, of course, cannot meet modern standards. As the comparative analysis of the many syntheses reveals, solutions for the problem have only slowly evolved and colchicine must still be considered as a difficult target molecule. Notwithstanding the powerful arsenal of modern synthetic technology, even today synthetic chemists require a high level of creativity and the ability to integrate subtle structural and reactivity aspects to tame such a recalcitrant target structure.

Like other tubulin-binding molecules such as taxol and the epothilones, colchicine enjoys a great interest from medicinal research and has experienced a renaissance in the last few years. To explore its pharmaceutical potential further as a lead structure, flexible synthetic schemes must be developed that allow a diversity-oriented synthesis of structural analogues of colchicine. Only the most recent syntheses come within reach of the efficiency and flexibility levels required for such purposes. Consequently, it can be expected that colchicine will remain an important synthetic target and challenge further creativity in synthetic chemistry.

Received: June 13, 2003 [A615]
Published Online: April 19, 2004

[1] For reviews of the chemistry of colchicine, see: a) J. W. Cook, J. D. Loudon in *The Alkaloids*, *Vol. 2* (Eds.: R. H. F. Manske, H. L. Holmes), Academic Press, New York, **1952**, p. 261; b) W. C. Wildman in *The Alkaloids*, *Vol. 6* (Ed.: R. H. F. Manske), Academic Press, New York, **1960**, p. 247; c) A. Brossi in *The Alkaloids*, *Vol. 23* (Ed.: A. Brossi), Academic Press, Orlando, **1984**, p. 1; d) W. C. Wildman in *The Chemisry of the Alkaloids* (Ed.: S. W. Pelletier), Van Nostrand-Reinhold,

New York, **1970**, chap. 8; e) O. Boyé, A. Brossi in *The Alkaloids, Vol. 41* (Eds.: A. Brossi, G. A. Cordell), Academic Press, San Diego, **1992**, p. 125; f) The picture of the meadow saffron was taken from: B. Besler, *Hortus Eystettensis*, Eichstätt, **1613**..

[2] a) C. Bryan, *The Papyrus Ebers*, Appleton, New York, **1931**; b) P. Dioscorides, *De Materia Medica*, **78 A.D**.

[3] P. J. Pelletier, J. B. Caventou, *Ann. Chim. Phys.* **1820**, *14*, 69.

[4] a) S. Zeisel, *Monatsh. Chem.* **1883**, *4*, 162; b) S. Zeisel, *Monatsh. Chem.* **1886**, *7*, 557; c) S. Zeisel, K. R. von Stockert, *Monatsh. Chem.* **1913**, *34*, 1339.

[5] A. Windaus, *Justus Liebigs Ann. Chem.* **1924**, *439*, 59.

[6] a) M. J. S. Dewar, *Nature* **1945**, *155*, 141; b) M. J. S. Dewar, *Nature* **1945**, *155*, 50.

[7] M. V. King, J. L. De Vries, R. Pepinsky, *Acta Crystallogr. Sect. B* **1952**, *5*, 437.

[8] H. Corrodi, E. Hardegger, *Helv. Chim. Acta* **1955**, *38*, 2030.

[9] a) E. Leete, P. E. Nemeth, *J. Am. Chem. Soc.* **1961**, *83*, 2192; b) E. Leete, *Tetrahedron Lett.* **1965**, 333; c) E. McDonald, R. Ramage, R. N. Woodhouse, E. W. Underhill, L. R. Wetter, A. R. Battersby, *J. Chem. Soc. Perkin Trans. 1* **1998**, 2979; c) A. C. Barker, D. R. Julian, R. Ramage, R. N. Woodhouse, G. Hardy, E. McDonald, A. R. Battersby, *J. Chem. Soc. Perkin Trans. 1* **1998**, 2989; d) R. N. Woodhouse, E. McDonald, R. Ramage, A. R. Battersby, *J. Chem. Soc. Perkin Trans. 1* **1998**, 2995; e) P. W. Sheldrake, K. E. Suckling, R. N. Woodhouse, A. J. Murtagh, R. B. Herbert, A. C. Barker, J. Staunton, A. R. Battersby, *J. Chem. Soc. Perkin Trans. 1* **1998**, 3003 and earlier works in this journal.

[10] C. Le Hello in *The Alkaloids*, *Vol. 53* (Ed.: G. A. Cordell), Academic Press, San Diego, **2000**, chap. 5.

[11] For a structure determination of the αβ-tubulin dimer by electron crystallography, see: E. Nogales, S. G. Wolf, K. H. Downing, *Nature* **1998**, *391*, 199.

[12] For an overview of the structure and dynamics of microtubules, see: a) P. Dustin, *Microtubules*, 2nd ed., Springer, Berlin, **1984**; b) R. H. Wade, A. A. Hyman, *Curr. Opin. Cell Biol.* **1997**, *9*, 12; c) S. Guha, B. Bhattacharyya, *Curr. Sci.* **1997**, *73*, 351.

[13] For an overview of tubulin as a target for anticancer drugs and agents that interact with the mitotic spindle, see: A. Jordan, J. A. Hadfield, N. J. Lawrence, A. T. McGown, *Med. Res. Rev.* **1998**, *18*, 259.

[14] S.-X. Zhang, J. Feng, S.-C. Kuo, A. Brossi, E. Hamel, A. Tropsha, K.-H. Lee, *J. Med. Chem.* **2000**, *43*, 167, and references therein. During these investigations, active compounds were designed, which are, however, structurally unrelated to colchicine.

[15] a) L. Velluz, G. Müller, *Bull. Soc. Chim. Fr.* **1954**, 755; b) L. Velluz, G. Müller, *Bull. Soc. Chim. Fr.* **1954**, 1072.

[16] a) A. C. Banerjee, B. Bhattacharyya, *FEBS Lett.* **1979**, *99*, 333; b) A. S. Sherpinskaya, V. I. Gelfand, B. P. Kopnin, *Biochim. Biophys. Acta* **1981**, *673*, 86.

[17] See, for example: L. M. Leoni, E. Hamel, D. Genini, H. Shih, C. J. Carrera, H. B. Cottam, D. A. Carson, *J. Natl. Cancer Inst.* **2000**, *92*, 217.

[18] R. Bai, D. G. Covell, X.-F. Pei, J. B. Ewelli, N. Y. Nguyeni, A. Brossi, E. Hamel, *J. Biol. Chem.* **2000**, *275*, 40443, and references therein.

[19] J. M. Andreu, S. N. Timasheff, *Biochemistry* **1982**, *21*, 6465.

[20] a) H. W. Detrich III, R. C. Williams, Jr., T. L. Macdonald, L. Wilson, D. Puett, *Biochemistry* **1981**, *20*, 5999; b) B. Bhattacharyya, J. Wolff, *J. Biol. Chem.* **1984**, *259*, 11836; c) R. P. Rava, S. B. Hastie, J. C. Myslik, *J. Am. Chem. Soc.* **1987**, *109*, 2202; d) W. A. Donaldson, *Tetrahedron* **1988**, *44*, 7409.

[21] Until the correction in 1999, the stereochemical descriptor of the chiral axis had been erroneously assigned as a*S*: a) U. Berg, H. Bladh, *Helv. Chim. Acta* **1999**, *82*, 323; b) K.-H. Lee, A. Brossi, *Helv. Chim. Acta* **1999**, *82*, 1223.

[22] U. Berg, J. Deinum, P. Lincoln, J. Kvassman, *Bioorg. Chem.* **1991**, *19*, 53.

[23] a) D. J. Chaplin, G. R. Pettit, S. A. Hill, *Anticancer Res.* **1999**, *19*, 189; b) M. C. Bibby, *Drugs Future* **2002**, *27*, 475.

[24] For earlier work in colchicine synthesis, see: a) H. Rapoport, A. R. Williams, M. E. Cisney, *J. Am. Chem. Soc.* **1951**, *73*, 1414; b) J. W. Cook, J. Jack, J. D. Loudon, G. L. Buchanan, J. MacMillan, *J. Chem. Soc.* **1951**, 1397; c) V. Boekelheide, F. C. Pennington, *J. Am. Chem. Soc.* **1952**, *74*, 1558; d) H. J. E. Loewenthal, *J. Chem. Soc.* **1953**, 3962; e) H. J. E. Loewenthal, *J. Chem. Soc.* **1958**, 1367; f) C. D. Gutsche, F. A. Fleming, *J. Am. Chem. Soc.* **1954**, *76*, 1771; g) H. J. E. Loewenthal, P. Rana, *Proc. Chem. Soc. London* **1958**, 114.

[25] a) J. Schreiber, W. Leimgruber, M. Pesaro, P. Schudel, A. Eschenmoser, *Angew. Chem.* **1959**, *71*, 637; b) J. Schreiber, W. Leimgruber, M. Pesaro, P. Schudel, A. Eschenmoser, *Helv. Chim. Acta* **1961**, *44*, 540.

[26] a) E. E. van Tamelen, T. A. Spencer, Jr., D. S. Allen, Jr., R. L. Ovis, *J. Am. Chem. Soc.* **1959**, *81*, 6341; b) E. E. van Tamelen, T. A. Spencer, Jr., D. S. Allen, Jr., R. L. Ovis, *Tetrahedron* **1961**, 8.

[27] K. C. Nicolaou, S. A. Snyder, *Classics in Total Synthesis II: More Targets, Strategies, Methods*, Wiley-VCH, **2003**.

[28] a) T. Nakamura, Y. Murase, R. Hayashi, Y. Endo, *Chem. Pharm. Bull.* **1962**, *10*, 281; b) G. Sunugawa, T. Nakamura, J. Nakazawa, *Chem. Pharm. Bull.* **1962**, *10*, 291; c) T. Nakamura, *Chem. Pharm. Bull.* **1962**, *10*, 299.

[29] R. B. Woodward, *The Harvey Lecture Series* **1963**, *59*, 31.

[30] a) A. I. Scott, F. McCapra, R. L. Buchanan, A. C. Day, D. W. Young, *Tetrahedron* **1965**, *21*, 3605.

[31] J. Martel, E. Toromanoff, C. Huynh, *J. Org. Chem.* **1965**, *30*, 1752.

[32] S.-i. Kaneko, M. Matsui, *Agric. Biol. Chem.* **1968**, *32*, 995.

[33] M. Kato, F. Kido, M.-D. Wu, A. Yoshikoshi, *Bull. Chem. Soc. Jpn.* **1974**, *47*, 1516.

[34] E. Kotani, F. Miyazaki, S. Tobinaga, *J. Chem. Soc. Chem. Commun.* **1974**, 300.

[35] a) D. A. Evans, D. J. Hart, P. M. Koelsch, *J. Am. Chem. Soc.* **1978**, *100*, 4593; b) D. A. Evans, S. P. Tanis, D. J. Hart, *J. Am. Chem. Soc.* **1981**, *103*, 5813.

[36] a) D. L. Boger, C. E. Brotherton, *J. Org. Chem.* **1985**, *50*, 3425; b) D. L. Boger, C. E. Brotherton, *J. Am. Chem. Soc.* **1986**, *108*, 6713.

[37] E. Wenkert, H.-S. Kim in *Studies in Natural Products Chemistry (Part B), Vol. 3* (Ed.: Atta-ur-Rahman), Elsevier, Amsterdam, **1989**, p. 287.

[38] M. G. Banwell, *Pure Appl. Chem.* **1996**, *68*, 539.

[39] a) J. C. Lee, S.-j. Jin, J. Cha, *J. Org. Chem.* **1998**, *63*, 2804; b) J. C. Lee, S.-j. Jin, J. Cha, *Tetrahedron* **2000**, *56*, 10175.

[40] a) T. Graening, W. Friedrichsen, J. Lex, H.-G. Schmalz, *Angew. Chem.* **2002**, *114*, 1594; *Angew. Chem. Int. Ed.* **2002**, *41*, 1524; b) T. Graening, H.-G. Schmalz, unpublished results.

[41] For the synthesis of secocolchicine, see: M. G. Banwell, J. N. Lambert, G. L. Gravatt, *J. Chem. Soc. Perkin Trans. 1* **1993**, 2817.

[42] For reviews on tropolone chemistry, see: a) P. L. Pauson, *Chem. Rev.* **1955**, *55*, 9; b) T. Nozoe in *Non-Benzenoid Aromatic Compounds* (Ed.: D. Ginsburg), Interscience, New York, **1959**, p. 339; c) D. Lloyd, *Carbocyclic Non-Benzenoid Aromatic Compounds*, Elsevier, Amsterdam, **1966**; d) T. Nozoe, *Pure Appl. Chem.* **1971**, *28*, 239; e) F. Pietra, *Chem. Rev.* **1973**, *73*, 293; f) F. Pietra, *Acc. Chem. Res.* **1979**, *12*, 132; see also: g) M. G. Banwell, *Aust. J. Chem.* **1991**, *44*, 1.

[43] M. Sorkin, *Helv. Chim. Acta* **1946**, *29*, 246.

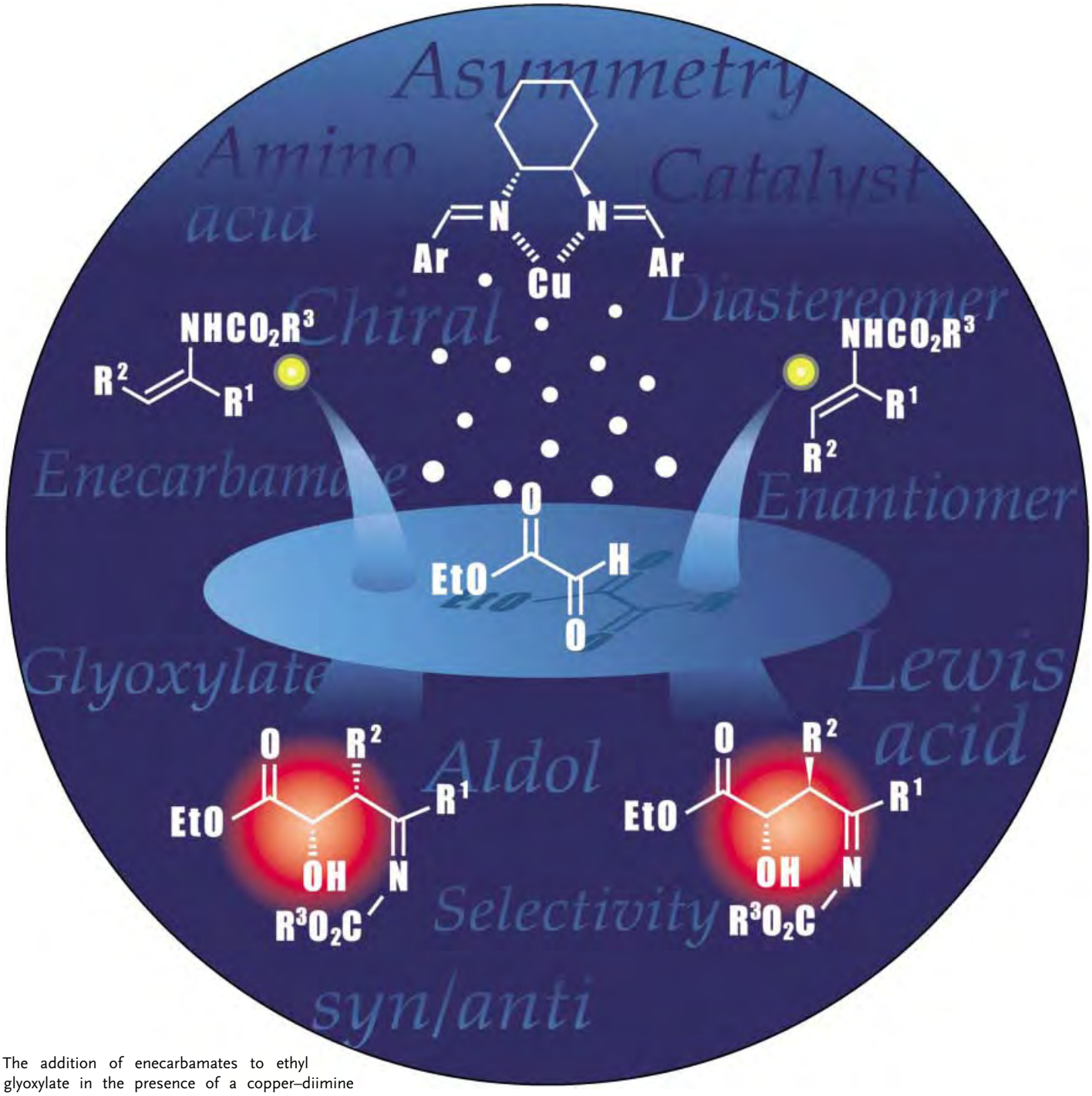
[44] For graphical compilations of colchicine syntheses, see: a) N. Anand, J. S. Bindra, S. Ranganathan, *Art in Organic Synthesis*, Holden-Day, San Francisco, **1970**, p. 103; b) S. Ito in *Natural Products Chemistry*, *Vol. 2* (Eds.: K. Nakanishi, T. Goto, S. Ito, S.

 © 2004 Wiley-VCH Verlag GmbH & Co. KGaA, Weinheim

Natori, S. Nozoe), Kodansha, Tokyo, Academic Press, New York, **1975**, p. 349; c) G. Quinkert, *Synform* **1990**, *8*, 207; for a textbook discussion of some early syntheses, see: d) I. Fleming, *Selected Organic Syntheses*, Wiley, London, **1973**, p. 183.
[45] A. I. Scott, *Nature* **1960**, *186*, 556.
[46] For a review, see: W. T. Brady, *Synthesis* **1971**, *3*, 415.
[47] T. Nozoe, T. Seto, T. Sato, *Proc. Jpn. Acad.* **1954**, *30*, 473.
[48] Separation into the enantiomers via trimethylcolchicinic acid (*rac*-**25**): H. Corrodi, E. Hardegger, *Helv. Chim. Acta* **1957**, *40*, 193.
[49] T. Ikemi, T. Nozoe, H. Sugiyama, *Chem. Ind.* **1960**, 932.
[50] R. Robinson, *The Structural Relations of Natural Products*, Claredon, Oxford, **1954**, p. 46.
[51] B. Föhlisch, S. Sendelbach, H. Bauer, *Liebigs Ann. Chem.* **1987**, 1.
[52] For a synthesis of the colchicine framework, see: a) M. G. Banwell, M. Berak, D. C. R. Hockless, *J. Chem. Soc. Perkin Trans. 1* **1996**, 2217; for a synthesis of desacetamidoisocolchicine, see: b) M. G. Banwell, J. N. Lambert, M. Corbett, R. J. Greenwood, J. L. Gulbis, M. F. Mackay, *J. Chem. Soc. Perkin Trans. 1* **1992**, 1415; for a synthesis of (±)-colchicine, see: c) M. G. Banwell, J. N. Lambert, M. Mackay, R. J. Greenwood, *J. Chem. Soc. Chem. Commun.* **1992**, 974.
[53] The intention to apply a similar strategy was published after our disclosure[40a]: M. C. McMills, D. L. Wright, R. M. Weekly, *Synth. Commun.* **2002**, *32*, 2417.
[54] C. Plüg, W. Friedrichsen, *Tetrahedron Lett.* **1992**, *33*, 7509–7510.
[55] a) K. Ueda, T. Ibata, M. Takebayashi, *Bull. Chem. Soc. Jpn.* **1972**, *45*, 2779; b) A. Padwa, M. D. Weingarten, *Chem. Rev.* **1996**, *96*, 223, and references therein.

 © 2004 Wiley-VCH Verlag GmbH & Co. KGaA, Weinheim

Communications



The addition of enecarbamates to ethyl glyoxylate in the presence of a copper–diimine catalyst gives the corresponding imines in high yields with excellent enantioselectivities. Whereas *E* enecarbamates give *anti* adducts, *syn* adducts are obtained from *Z* enecarbamates. On the following pages, Kobayashi and co-workers describe this novel reaction and propose a concerted aza-ene-type reaction mechanism to explain the remarkable stereochemical outcome.

DOI: 10.1002/anie.200460165
© 2004 Wiley-VCH Verlag GmbH & Co. KGaA, Weinheim

Addition Reactions

Highly Diastereo- and Enantioselective Reactions of Enecarbamates with Ethyl Glyoxylate To Give Optically Active *syn* and *anti* α-Alkyl-β-Hydroxy Imines and Ketones**

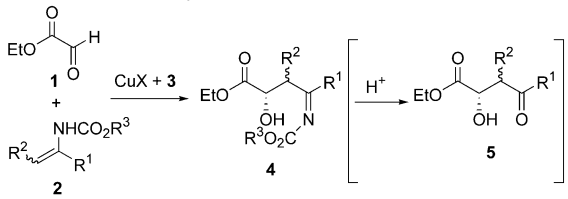
*Ryosuke Matsubara, Yoshitaka Nakamura, and Shū Kobayashi**

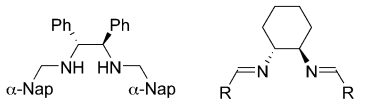
Control of the absolute configuration of two adjacent stereogenic centers that include alkyl and hydroxy groups is among the most important reactions for the synthesis of many biologically active compounds.[1] For the relative stereochemistry issue (*syn*/*anti*), aldol,[2] allylation,[3] and related reactions via six-membered transition states are powerful tools, and diastereoselective reactions with chiral auxiliaries have opened the way to optically active compounds. For asymmetric catalysis, on the other hand, Mukaiyama-type reactions of silicon reagents with chiral Lewis acids have been investigated extensively.[4] However, the reactions proceed via acyclic transition states to afford *syn* adducts in most cases, and control of the relative stereochemistry by geometrical isomers is difficult.

We recently investigated the use of enamides and enecarbamates as nucleophiles.[5] In spite of their importance in organic chemistry, examples of nucleophilic additions of enamides or enecarbamates are few,[6] whereas there are many reports on the use of enamines as nucleophiles.[7] Herein we report the first highly diastereo- and enantioselective addition reaction of enecarbamates with ethyl glyoxylate. This reaction proceeds smoothly in the presence of a Cu^{I}–chiral diimine complex, and α-monosubstituted enecarbamates provide the corresponding adducts stereospecifically; that is, *syn* products are obtained from *Z* enecarbamates and *anti* products are obtained from *E* enecarbamates with high diastereo- and enantioselectivities.

Initially, the reaction of ethyl glyoxylate (**1**), which was freshly distilled from a commercially available polymer-form solution in toluene, with enecarbamate **2a**[8] was investigated in the presence of various chiral Lewis acids. It was found that some Lewis acids were effective and afforded the corresponding imine-type adducts **4** in high yields. For determining the *ee* values of the products, **4** was converted into the corresponding ketones **5**.[9] Although some copper salts worked well in this reaction, Cu^{II}–diamine complexes,[10] which gave excellent results in Mannich-type reactions of *N*-acylimino esters with enamides and enecarbamates,[5] afforded the product with moderate enantioselectivity (Table 1, entry 1). On the other hand, it was revealed that much higher enantioselectivities were obtained when Cu^{I}–diimine complexes[11] were used (Table 1, entries 4 and 5). Among several chiral imines tested, Cu^{I}–diimine ligand **3c** gave the highest enantioselelctivity (97% *ee*). Furthermore, lower loading of the catalyst (2 mol%) gave the same level of reactivity and selectivity (96% yield, 95% *ee*; Table 1, entry 6).

Table 1: Catalyzed reactions of ethyl glyoxylate (**1**) with enecarbamate **2a** (R^1 = Ph, R^2 = H, R^3 = Bn).[a]





Entry	Ligand	CuX	Yield [%][b]	*ee* [%][c]
1	**3a**	$Cu(OTf)_2$	93	55[d]
2	**3b**	$Cu(OTf)_2$	65	70[d]
3	**3a**	$CuClO_4 \cdot 4CH_3CN$	90	35[d]
4	**3b**	$CuClO_4 \cdot 4CH_3CN$	94	93
5	**3c**	$CuClO_4 \cdot 4CH_3CN$	93	97
6[e]	**3c**	$CuClO_4 \cdot 4CH_3CN$	96	95

[a] All reactions were performed in CH_2Cl_2 at 0°C for 1 h in the presence of CuX (10 mol%) and **3**. [b] Yield of isolated **5a**. [c] Determined by HPLC (see Supporting Information). [d] The absolute configuration is *R*. [e] Catalyst: 2 mol%. Tf = trifluoromethanesulfonyl.

We then examined several other enecarbamates, and the results are summarized in Table 2. α-Unsubstituted enecarbamates **2b–e** reacted smoothly to afford the desired adducts in high yields with excellent enantioselectivities (Table 2, entries 1–4). For the reactions with α-substituted enecarbamates, remarkable results were obtained. The reactions proceeded stereospecifically: *E* enecarbamates gave *anti* adducts, whereas *Z* enecarbamates produced *syn* adducts with both excellent diastereo- and enantioselectivities in most cases. These selectivities are in contrast to Lewis acid catalyzed asymmetric aldol-type reactions of silicon enolates with aldehydes, which give mostly *syn* adducts, regardless of the geometry of the enolates.[4,12] The asymmetric reactions discussed herein also proceeded smoothly in the presence of 0.1 mol% of the Cu^{I} catalyst. Moreover, it was found that under the same conditions as those shown in Table 1, entry 5, comparable yield and enantioselectivity were obtained when using an undistilled polymer-form ethyl glyoxylate solution in

[*] R. Matsubara, Y. Nakamura, Prof. Dr. S. Kobayashi
Graduate School of Pharmaceutical Sciences
The University of Tokyo
Hongo, Bunkyo-ku, Tokyo 113-0033 (Japan)
Fax: (+81) 3-5684-0634
E-mail: skobayas@mol.f.u-tokyo.ac.jp

[**] This work was partially supported by CREST, SORT, and ERATO, Japan Science Technology Agency (JST), and a Grand-in-Aid for Scientific Research from Japan Society for the Promotion of Sciences (JSPS). R.M. is grateful for a JSPS fellowship for Japanese Junior Scientists.

Supporting information for this article is available on the WWW under http://www.angewandte.org or from the author.

 © 2004 Wiley-VCH Verlag GmbH & Co. KGaA, Weinheim DOI: 10.1002/anie.200460165

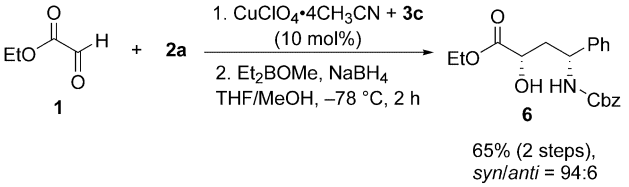
Table 2: Cu^{I}–**3c**-catalyzed reactions of **1** with **2** (R^3 = Bn).[a]

Entry	2	5	Yield [%][b]	*syn*/*anti*[c]	*ee* [%][d]
1	**2b** (R^1 = PMP, R^2 = H)	**5b**	94	–	93
2	**2c** (R^1 = PCP, R^2 = H)	**5c**	97	–	97
3	**2d** (R^1 = PMeP, R^2 = H)	**5d**	quant	–	96
4	**2e** (R^1 = 2-Nap, R^2 = H)	**5e**	91	–	96
5	(*E*)-**2f** (R^1 = Ph, R^2 = Me)	**5f**	83	1:99	98
6[e,f]	(*E*)-**2f**	**5f**	95	1:99	98
7	(*Z*)-**2f**	**5f**	82	98:2	98
8[f]	(*Z*)-**2f**	**5f**	96	98:2	98
9	(*E*)-**2g** (R^1 = PMP, R^2 = Me)	**5g**	96	2:98	98
10	(*Z*)-**2g**	**5g**	97	98:2	98
11	(*E*)-**2h** (R^1 = PMP, R^2 = Me)[g]	**5g**	82	3:97	96
12	(*Z*)-**2h**[g]	**5g**	96	99:1	98
13	(*E*)-**2i** (R^1 = PCP, R^2 = Me)	**5i**	85	2:98	98
14	(*Z*)-**2i**	**5i**	79	99:1	98
15	(*E*)-**2j** (R^1 = Ph, R^2 = Et)[h]	**5j**	58	1:99	98
16	(*Z*)-**2j**	**5j**	92	99:1	98
17[e]	(*E*)-**2k** (R^1 = Et, R^2 = Me)	**5k**	83	3:97[i]	97
18[e]	(*Z*)-**2k**	**5k**	89	92:8[i]	98
19	**2l** (R^1, R^2 = $-(CH_2)_4-$)	**5l**	85	16:84[i]	94

[a] All reactions were performed in CH_2Cl_2 at 0°C in the presence of the catalyst (10 mol%, unless otherwise noted). Reaction time was 0.5–2 h in most cases. [b] Yield of isolated product. [c] Determined by HPLC. [d] Major diastereomer, *ee* value determined by HPLC (see Supporting Information). [e] −20°C. [f] Catalyst: 0.1 mol%. [g] R^3 = Et. [h] **1** (1.0 equiv) and **2** (2.0 equiv). [i] Determined by NMR analysis. PMP = *p*-methoxyphenyl, PCP = *p*-chlorophenyl; PMeP = *p*-methylphenyl; 2-Nap = 2-naphthyl.

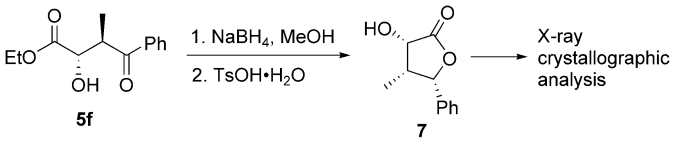
toluene, which indicates that the Cu^{I}–diimine complex both depolymerizes the glyoxylate as well as catalyzes the following asymmetric addition reaction.[13]

The reactions with enecarbamates are more atom economical than those with enolates; the initial imine-type products **4** contain all the atoms that compose both substrates (ethyl glyoxylate and enecarbamates). After the enecarbamate addition, the following diastereoselective reduction was conducted in the same pot to afford *N*-Cbz-protected α-hydroxy-γ-amino acid ester **6** with high selectivity (Scheme 1).[14] For *anti*-**5f** (d.r. = 99:1), the reduction of the



Scheme 1. Conversion into *N*-Cbz α-hydroxy γ-amino acid ester **6**. Cbz = benzyloxycarbonyl.

ketone moiety with $NaBH_4$ followed by cyclization gave lactone **7** as a diastereomeric mixture (Scheme 2).[15] One diastereomer of **7** was obtained as a crystalline compound, which was characterized by X-ray crystallography.[16] From the knowledge of the relative configuration of **7**, the relative configuration of **5f** was determined.



Scheme 2. Determination of the relative configuration of **5f**.

The fact that α-monosubstituted enecarbamates provided products stereospecifically led us to propose a concerted aza-ene-type reaction mechanism outlined in Figure 1.[17,18] This

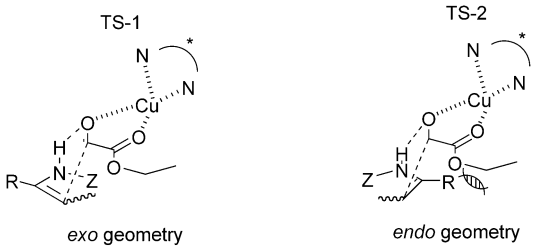


Figure 1. Proposed transition-state models.

proposed mechanism does not contradict the result that the reaction of *N*-methylated enecarbamate **2m** with ethyl glyoxylate gave no adduct with almost all the starting materials left unconverted. TS-1 should be a predominant transition state since the other candidate, TS-2, has unfavourable steric interaction between the bulky R group of the enecarbamate and the ester group of ethyl glyoxylate and/or the bulky copper catalyst. The TS-1 model would account for the stereochemical outcome of the reaction.



2m

In summary, novel highly enantioselective copper–diimine-catalyzed addition reactions of enecarbamates with ethyl glyoxylate have been developed. It was demonstrated that high yields and high enantioselectivities were obtained, even when using 0.1 mol% of the catalyst. α-Monosubstituted enecarbamates also reacted with glyoxylate stereospecifically to give the corresponding adducts in high yields with excellent diastereo- and enantioselectivities. Further investigations into the precise mechanism of this reaction as well as the use of enecarbamates as nucleophiles in other reactions are in progress.

Received: March 31, 2004 [Z460165]
Published Online: May 17, 2004

Keywords: asymmetric catalysis · aza-ene reaction · copper · N ligands · synthetic methods

[1] For recent examples, see: T. Wakabayashi, K. Mori, S. Kobayashi, *J. Am. Chem. Soc.* **2001**, *123*, 1372, and references therein.
[2] Reviews: a) C. H. Heathcock in *Comprehensive Organic Synthesis, Vol. 2* (Ed.: B. M. Trost), Pergamon, Oxford, **1991**, p. 181; b) R. Mahrwald, *Chem. Rev.* **1999**, *99*, 1095; c) E. M. Carreira in *Modern Carbonyl Chemistry* (Ed.: J. Otera), Wiley-VCH, Weinheim, **2000**, p. 227.

 © 2004 Wiley-VCH Verlag GmbH & Co. KGaA, Weinheim

[3] Reviews: a) Y. Yamamoto, N. Asao, *Chem. Rev.* **1993**, *93*, 2207; b) S. E. Denmark, N. G. Almstead in *Modern Carbonyl Chemistry* (Ed.: J. Otera), Wiley-VCH, Weinheim, **2000**, p. 299.
[4] E. M. Carreira in *Comprehensive Asymmetric Catalysis* (Eds.: E. N. Jacobsen, A. Pfaltz, H. Yamamoto), Springer, Berlin, **1999**, p. 998.
[5] R. Matsubara, Y. Nakamura, S. Kobayashi, *Angew. Chem.* **2004**, *116*, 1711; *Angew. Chem. Int. Ed.* **2004**, *43*, 1679.
[6] a) T. Shono, Y. Matsumura, K. Tsubata, Y. Sugihara, S. Yamane, T. Kanazawa, T. Aoki, *J. Am. Chem. Soc.* **1982**, *104*, 6697; b) L. Eberson, M. Malmberg, K. Nyberg, *Acta. Chem. Scand.* **1984**, *38*, 391; c) for the use of a diene in Diels–Alder reactions, see: P. J. Jessup, C. B. Petty, J. Roos, L. E. Overman, *Org. Synth.* **1980**, *59*, 1; d) O. Meth-Cohn, K. T. Westwood, *J. Chem. Soc. Perkin Trans. 1* **1984**, 1173; e) M. Chigr, H. Fillion, A. Rougny, *Tetrahedron Lett.* **1987**, *28*, 4529; f) P. Wipf, X. Wang, *Tetrahedron Lett.* **2000**, *41*, 8747.
[7] a) Y. Hayashi, K. Otaka, N. Saito, K. Narasaka, *Bull. Chem. Soc. Jpn.* **1991**, *64*, 2122; b) for asymmetric synthesis with chiral auxiliaries, see: T. Schrader, R. Kober, W. Steglich, *Synthesis* **1986**, 372; c) J. d'Angelo, D. Desmaële, F. Dumas, A. Guingant, *Tetrahedron: Asymmetry* **1992**, *3*, 459; d) K. Hervouet, A. Guingant, *Tetrahedron: Asymmetry* **1996**, *7*, 421; e) A. Zarghi, M. R. Naimi-Jamal, S. A. Webb, S. Balalaie, M. R. Saidi, J. Ipaktschi, *Eur. J. Org. Chem.* **1998**, 197; f) J. Christoffers, A. Mann, *Chem. Eur. J.* **2001**, *7*, 1014.
[8] Enecarbamates are readily prepared (see Supporting Information).
[9] The absolute configuration of **5a** was determined by the comparison of HPLC retention time: P. Herold, A. F. Indolese, M. Studer, H. P. Jalett, U. Siegrist, H. U. Blaser, *Tetrahedron* **2000**, *56*, 6497; the absolute configuration of **5f** was also determined by the Mosher esterification method (see Supporting Information).
[10] S. Kobayashi, R. Matsubara, Y. Nakamura, H. Kitagawa, M. Sugiura, *J. Am. Chem. Soc.* **2003**, *125*, 2507.
[11] Z. Li, K. R. Conser, E. N. Jacobsen, *J. Am. Chem. Soc.* **1993**, *115*, 5326.
[12] For Mukaiyama-type catalytic asymmetric aldol reactions of glyoxylates, see: a) K. Mikami, S. Matsukawa, *J. Am. Chem. Soc.* **1993**, *115*, 7039; b) K. Mikami, S. Matsukawa, *J. Am. Chem. Soc.* **1994**, *116*, 4077; c) D. A. Evans, D. W. C. MacMillan, K. R. Campos, *J. Am. Chem. Soc.* **1997**, *119*, 10859; d) D. A. Evans, C. E. Masse, J. Wu, *Org. Lett.* **2002**, *4*, 3375.
[13] The Cu^{II}–box catalyst is known to have the same activity for depolymerization of ethyl glyoxylate; see: D. A. Evans, S. W. Tregay, C. S. Burgey, N. A. Paras, T. Vojkovsky, *J. Am. Chem. Soc.* **2000**, *122*, 7936.
[14] K.-M. Chen, G. E. Hardtmann, K. Prasad, O. Repic, M. J. Shapiro, *Tetrahedron Lett.* **1987**, *28*, 155.
[15] S. Kanemasa, N. Nakagawa, H. Suga, O. Tsuge, *Bull. Chem. Soc. Jpn.* **1989**, *62*, 171.
[16] See also Supporting Information.
[17] A cncerted aza-ene-type reaction was proposed for the Michael reaction with a chiral enamine: a) L. Ambroise, D. Desmaële, J. Mahuteau, J. d'Angelo, *Tetrahedron Lett.* **1994**, *35*, 9705; b) M. J. Lucero, K. N. Houk, *J. Am. Chem. Soc.* **1997**, *119*, 826; c) S. Bahmanyar, K. N. Houk, *J. Am. Chem. Soc.* **2001**, *123*, 11273.
[18] The reactions with imines did not proceed stereospecifically; see reference [5].

 © 2004 Wiley-VCH Verlag GmbH & Co. KGaA, Weinheim

Molecular Shuttles

Controlled Submolecular Translational Motion in Synthesis: A Mechanically Interlocking Auxiliary**

Jeffrey S. Hannam, Stephen M. Lacy, David A. Leigh, Carlos G. Saiz, Alexandra M. Z. Slawin, and Sheila G. Stitchell*

In memory of Norma A. Stoddart

As well as being prototypical design elements for various types of molecular machines,[1–5] rotaxanes (molecules in which one or more rings are held on one or more threads by bulky stoppers[6]) often dramatically change the properties of their components (including solubility,[7] fluorescence,[8] electroluminescence,[9] and membrane transport[10]) and can protect encapsulated regions of threaded substrates from chemical attack[11] and degradation.[12] Interestingly, since they are molecular compounds—not supramolecular[13] complexes (i.e., the atoms cannot be separated without breaking covalent bonds)—rotaxane architectures also, in principle, circumvent patents that only claim derivatives that branch out from a principal structure through continuous sequences of covalent bonds. Despite such attractive characteristics, practical exploitation of the property-changing and patent-breaking features of rotaxanes have been slow to develop. This is probably because most efficient strategies for rotaxane synthesis require specific recognition elements to be built into each noncovalently linked unit,[14,15] thus limiting the types of chemical structures that can be interlocked. In other words, up to now it has not been possible to make a mechanically interlocked derivative of any particular pharmaceutical, dye, chromophore, catalyst, or reagent that one might choose. Herein we describe a practical rotaxane synthesis that has the potential to be more general than previous methods because it does not depend on a strong recognition motif existing between the ultimately interlocked components. A synthetic auxiliary is used to mechanically interlock a macrocycle around a suitable template, followed by translation of the ring to a position over the desired substrate and, finally, cleavage of the auxiliary to leave a rotaxane (e.g. **1**) with no designed noncovalent interactions

[*] J. S. Hannam, Dr. S. M. Lacy, Prof. D. A. Leigh, Dr. S. G. Stitchell
School of Chemistry
University of Edinburgh
The King's Buildings, West Mains Road, Edinburgh EH9 3JJ (UK)
Fax: (+44) 131-667-9085
E-mail: david.leigh@ed.ac.uk

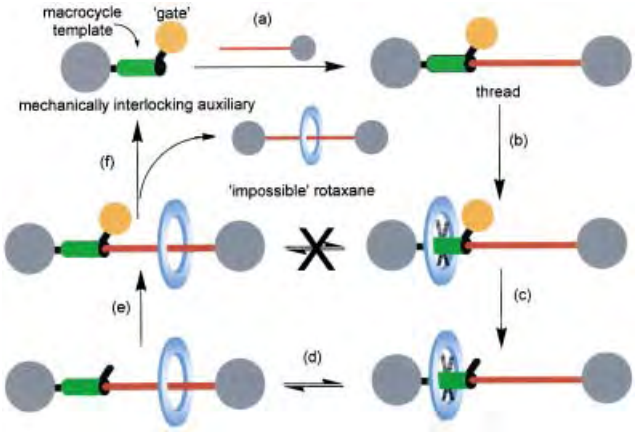
Dr. C. G. Saiz, Dr. A. M. Z. Slawin
Department of Chemistry
University of St. Andrews
St Andrews, Fife KY16 9AJ (UK)

[**] This work was carried out through the support of the EU Future and Emerging Technologies program MechMol and the EPSRC.

Supporting information for this article is available on the WWW under http://www.angewandte.org or from the author.

 © 2004 Wiley-VCH Verlag GmbH & Co. KGaA, Weinheim DOI: 10.1002/anie.200353606

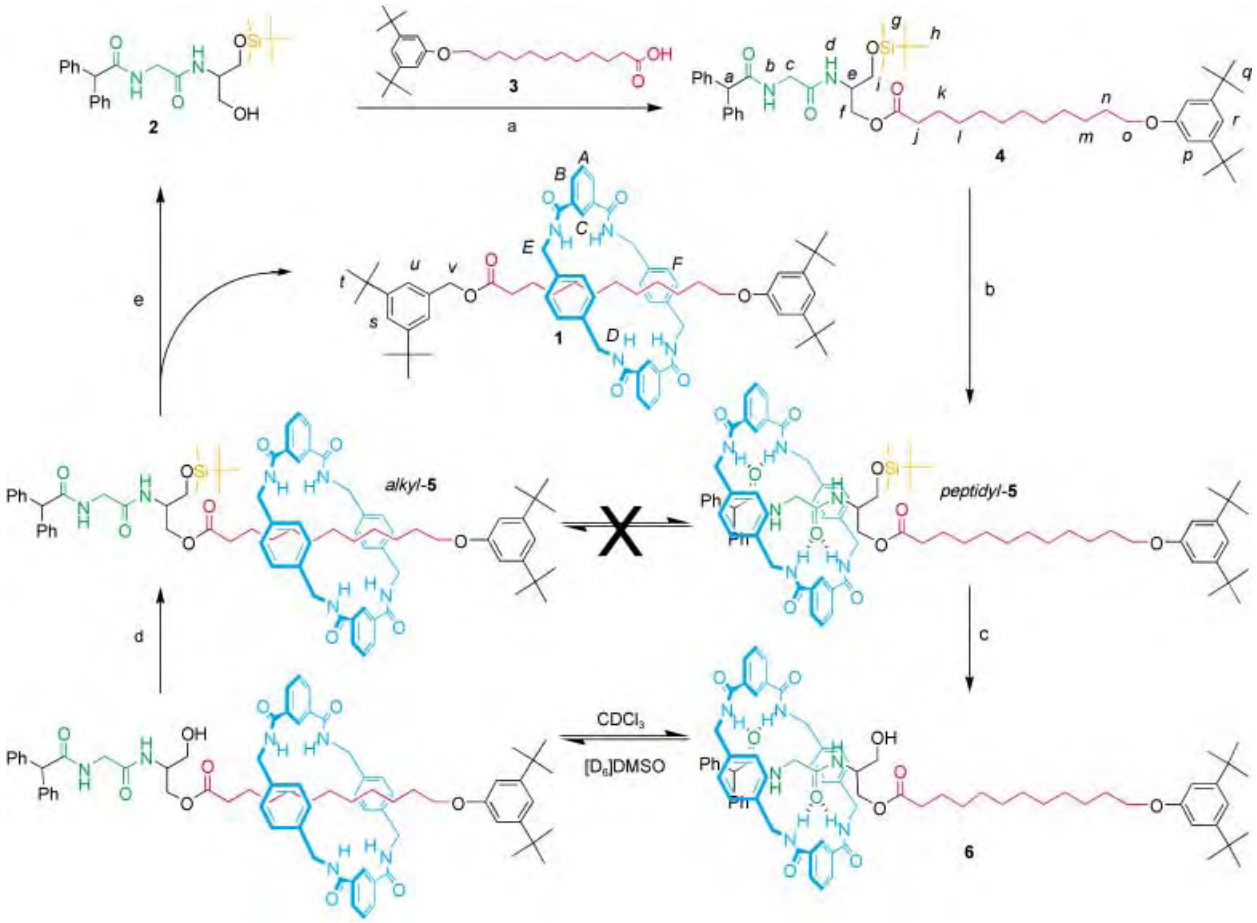
between macrocycle and thread (Scheme 1). As well as providing a synthetic route to otherwise difficult or impossible to obtain structures, a consequence of such unnatural geometries upon molecular fragments is seen in the X-ray crystal structure of rotaxane **1**, which features the first example of an NH amide to *alkyl* O ester hydrogen bond.



Scheme 1. Schematic preparation of a rotaxane that is otherwise difficult or impossible to obtain by using a mechanically interlocking auxiliary. a) Attach substrate to auxiliary; b) formation of rotaxane about template; c) open gate; d) shuttle macrocycle from template to substrate; e) close gate; f) cleave auxiliary.

Switching of the position of a macrocycle between nonequivalent sites in a rotaxane can be achieved by using a variety of stimuli in bistable "molecular shuttles".[1,6] In one such system, a benzylic amide macrocycle is assembled around a glycine-containing peptide template through intercomponent hydrogen bonding in nonpolar solvents.[11,16,17] The macrocycle can be subsequently decomplexed from the peptide by changing to a highly polar medium, which solvates the peptide and macrocycle hydrogen-bonding sites more strongly than they bind to each other.[18,19] We decided to investigate whether this solvent effect could be used to move the macrocycle from its template site to a desired substrate during synthesis, thus providing a means to a "mechanically interlocking auxiliary" (Scheme 2).[20]

The mechanically interlocking auxiliary, **2**, consists of an *N*-stoppered glycine residue and a monosilylated serinol derivative. The role of the serinol is twofold: the free hydroxy group provides a site for the attachment of a carboxylic acid-terminated substrate (and eventual cleavage of the auxiliary) through an ester linkage, while the bulky *tert*-butyldimethylsilyl ether acts as a closed "gate" through which the macro-



Scheme 2. Synthesis of rotaxane **1**. a) 1-(3-dimethylaminopropyl)-3-ethyl-carbodiimide hydrochloride, 4-dimethylaminopyridine (4-DMAP), CH_2Cl_2, 87%; b) isophthaloyl dichloride, *p*-xylylenediamine, Et_3N, $CHCl_3$, 25%; c) tetrabutylammonium fluoride, THF, 95%; d) *tert*-butyldimethylsilyl chloride, imidazole, 4-DMAP, DMSO, 85%; e) di-*tert*-butylbenzyl alcohol, potassium *tert*-butoxide (5 mol%), 78%. Full experimental procedures can be found in the Supporting Information.

 © 2004 Wiley-VCH Verlag GmbH & Co. KGaA, Weinheim

cycle cannot pass. Coupling of **2** to the dodecanoic acid **3** gave the composite thread **4**, which was subjected to standard[16–19] hydrogen-bond-directed rotaxane-forming conditions to give the [2]rotaxane *peptidyl*-**5**.[21] Since the xylylene rings of the macrocycle shield the encapsulated region of the thread, the position of the macrocycle in the rotaxane could be unambiguously determined by comparing the nuclear magnetic resonance (NMR) chemical shifts of the thread and rotaxane protons. The ^{1}H NMR spectra in $CDCl_3$ (Figure 1 a and b) and

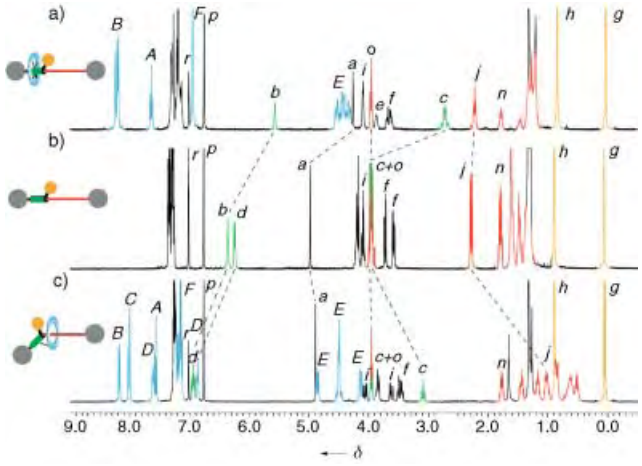


Figure 1. 400 MHz ^{1}H NMR spectra of a) *peptidyl*-**5**, b) **4**, and c) *alkyl*-**5** in $CDCl_3$ at 298 K. The color coding and lettering correspond to the assignments shown in Scheme 2.

[D_6]DMSO (Figure 2 a and b) shows that the closed gate means the macrocycle resides solely on the peptide station in both solvents (for example, the rotaxane H_c glycine protons are shielded by $\delta = -1.26$ ppm in $CDCl_3$ and by $\delta = -1.30$ ppm in [D_6]DMSO with respect to H_c in the thread).

Cleavage of the silyl group of *peptidyl*-**5** with tetrabutylammonium fluoride afforded [2]rotaxane **6**. In **6**, the macrocycle can move through the open gate to get to either the peptide or substrate side of the thread and ^{1}H NMR spectroscopy confirms that its location is determined by the nature of the solvent. Accordingly, **6** was dissolved in anhydrous DMSO and the silyl ether reattached with *tert*-butyldimethylsilyl chloride.[22] A new rotaxane was isolated in 85% yield together with <2% of *peptidyl*-**5**. ^{1}H NMR spectroscopy confirms the new rotaxane to be *alkyl*-**5**, a translational diastereoisomer (identical covalent connectivity but a different spatial arrangement[23]) of *peptidyl*-**5** with the macrocycle locked on the alkyl-chain side of the closed gate, irrespective of the solvent the rotaxane is dissolved in (Figure 1 c and Figure 2 c).[24]

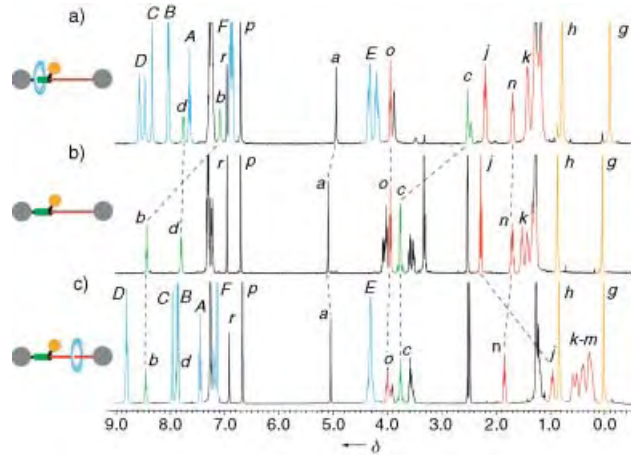


Figure 2. 400 MHz ^{1}H NMR spectra of a) *peptidyl*-**5**, b) **4**, and c) *alkyl*-**5** in [D_6]DMSO at 298 K.

Since there are no strong binding interactions between the macrocycle and thread in *alkyl*-**5**, maintenance of the rotaxane architecture whilst cleaving the mechanically interlocking auxiliary requires a reaction that does not permit unstoppering at any stage.[25] Transesterification with di-*tert*-butylbenzyl alcohol in the presence of catalytic potassium *tert*-butoxide,[26] afforded the desired [2]rotaxane **1** in 78% yield with complete recovery of the regenerated auxiliary and no evidence of any accompanying dethreading.[27] The shielding of all the alkyl chain protons, as revealed in the ^{1}H NMR spectrum of **1** (Figure 3), indicates that the macrocycle is delocalized over the entire length of the substrate, although the greater shielding of H_j indicates that it spends more time nearer the ester end of the molecule in $CDCl_3$.

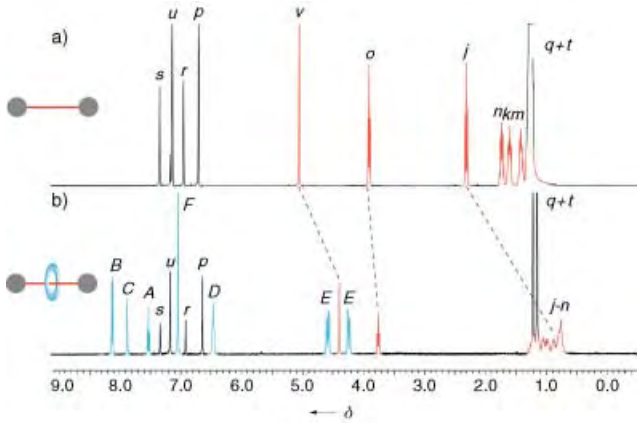


Figure 3. 400 MHz ^{1}H NMR spectra of a) thread and b) rotaxane **1** in $CDCl_3$ at 298 K.

Small single crystals of the rotaxane suitable for X-ray crystallography with a synchrotron source were obtained by slow evaporation of a solution of **1** in acetonitrile. The X-ray crystal structure (Figure 4) confirms the interlocked nature of the rotaxane and shows a remarkable consequence of forcing such unnatural spatial arrangements on submolecular fragments. Although ester groups are normally poor hydrogen-bonding groups,[28] the ester in the thread is the best acceptor available to the macrocycle amide hydrogen-bond donors. Accordingly, the rotaxane exhibits not only a rare[29] example of a solid-state hydrogen bond from the NH group of an amide to an acyl–O atom of an ester but also what appears to be a genuine hydrogen bond from the NH group of an amide to an alkyl–O atom of an ester, which is long (2.60 Å) but

 © 2004 Wiley-VCH Verlag GmbH & Co. KGaA, Weinheim

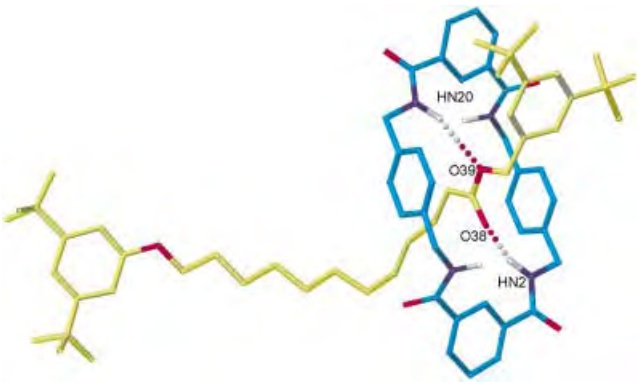


Figure 4. *X*-ray crystal structure of rotaxane **1**. Intramolecular hydrogen-bond lengths (Å) and angles: O38-HN2 1.89, 161.9°; O39-HN20 2.60, 162.2°. Carbon atoms of the macrocycle are shown in blue and those of the thread in yellow; oxygen atoms are red, nitrogen atoms dark blue and amide hydrogen atoms white. Non-amide hydrogen atoms are omitted for clarity. CCDC-127612 contains the supplementary crystallographic data for this paper. These data can be obtained free of charge via www.ccdc.cam.ac.uk/conts/retrieving.html (or from the Cambridge Crystallographic Data Centre, 12, Union Road, Cambridge CB2 1EZ, UK; fax: (+44) 1223-336-033; or deposit@ccdc.cam.ac.uk).

directional (162.2° is a typical NH···O hydrogen bond angle[30]) to a lone pair of an sp^3-hybridized orbital of an oxygen atom, in what is presumably a very weak interaction.

In conclusion, we have synthesized rotaxane **1**, whose components bear no formal mutual recognition elements through the first example of controlled submolecular translational motion in organic synthesis. In principle, there is no reason why mechanically interlocking auxiliary strategies should not work with other molecular-shuttle systems, including those based on cyclodextrins, which already have US FDA approval for use in the pharmaceutical and food industries. In our laboratories the approach is currently being used to prepare mechanically interlocked analogues of substrates that are unavailable by conventional synthetic methods and to modify the physical and chemical properties of a range of pharmaceuticals, dyes, reagents, catalysts, and components for molecular electronics.

Received: December 22, 2003 [Z53606]

Keywords: molecular machines · molecular shuttles · rotaxanes · submolecular motion · synthetic auxiliary

[1] V. Balzani, A. Credi, F. M. Raymo, J. F. Stoddart, *Angew. Chem.* **2000**, *112*, 3484–3530; *Angew. Chem. Int. Ed.* **2000**, *39*, 3348–3391.

[2] C. P. Collier, E. W. Wong, M. Bělohradský, F. M. Raymo, J. F. Stoddart, P. J. Kuekes, R. S. Williams, J. R. Heath, *Science* **1999**, *285*, 391–394.

[3] A. M. Brouwer, C. Frochot, F. G. Gatti, D. A. Leigh, L. Mottier, F. Paolucci, S. Roffia, G. W. H. Wurpel, *Science* **2001**, *291*, 2124–2128.

[4] M. C. Jiménez, C. Dietrich-Buchecker, J.-P. Sauvage, *Angew. Chem.* **2000**, *112*, 3422–3425; *Angew. Chem. Int. Ed.* **2000**, *39*, 3284–3287.

[5] P. Thordarson, E. J. A. Bijsterveld, A. E. Rowan, R. J. M. Nolte, *Nature* **2003**, *424*, 915–918.

[6] *Molecular Catenanes Rotaxanes and Knots*: *A Journey Through the World of Molecular Topology* (Eds.: J.-P. Sauvage, C. Dietrich-Buchecker), Wiley-VCH, Weinheim, **1999**.

[7] A. G. Johnston, D. A. Leigh, A. Murphy, J. P. Smart, M. D. Deegan, *J. Am. Chem. Soc.* **1996**, *118*, 10662–10663.

[8] S. Anderson, H. L. Anderson, *Angew. Chem.* **1996**, *108*, 2075–2078; *Angew. Chem. Int. Ed. Engl.* **1996**, *35*, 1956–1959.

[9] F. Cacialli, J. S. Wilson, J. J. Michels, C. Daniel, C. Silva, R. H. Friend, N. Severin, P. Samori, J. P. Rabe, M. J. O'Connell, P. N. Taylor, H. L. Anderson, *Nat. Mater.* **2002**, *1*, 160–164.

[10] V. Dvornikovs, B. E. House, M. Kaetzel, J. R. Dedman, D. B. Smithrud, *J. Am. Chem. Soc.* **2003**, *125*, 8290–8301.

[11] D. A. Leigh, A. Murphy, J. P. Smart, A. M. Z. Slawin, *Angew. Chem.* **1997**, *109*, 752–756; *Angew. Chem. Int. Ed. Engl.* **1997**, *36*, 728–732.

[12] M. R. Craig, M. G. Hutchings, T. D. W. Claridge, H. L. Anderson, *Angew. Chem.* **2000**, *112*, 1105–1108; *Angew. Chem. Int. Ed.* **2001**, *40*, 1071–1074.

[13] Within the context of a recent book and paper (V. Balzani, A. Credi, M. Venturi, *Chem. Eur. J.* **2002**, *8*, 5524–5532; V. Balzani, A. Credi, M. Venturi, *Molecular Devices and Machines—A Journey into the Nanoworld*, Wiley-VCH, Weinheim, **2003**) it was proposed that the term "supramolecular" be expanded from Lehn's original definition of "chemistry beyond the molecule" (i.e., assemblies of two or more molecules or ions held together by noncovalent forces) to include large molecules (e.g., dendrimers, rotaxanes, proteins etc.) which feature functional intramolecular interactions or photophysics. In our view such a revision is unwarranted. When scientific language evolves it needs to retain a precise definition to remain useful (e.g., "acid" to "Lewis acid" or "Brønsted acid"). Consider as a contrary example the term "self-assembly", which has acquired such an imprecise meaning over recent years that it now conveys virtually nothing as a descriptor. In its currently accepted definition, "supramolecular"—by analogy to the term "molecular"—refers to how the atoms in a structure are held together, not their photophysical properties. It distinguishes molecules from clusters of molecules, for example pseudorotaxanes (host–guest complexes in which the components are free to exchange between bound and unbound species) and rotaxanes (molecules in which the components cannot exchange with outside systems without breaking covalent bonds). It does not matter that their properties can be similar or that bond energies sometimes make it difficult to distinguish between molecular and supramolecular species, just as the timescale-dependent inversion of asymmetric nitrogen atoms does not confer on the term "chirality" any less clear a meaning. Language—especially scientific language—needs to be precise; subject areas, for example, "supramolecular chemistry" or "organometallic catalysis", on the other hand, should be as broad and inclusive as possible, and have always happily encompassed chemistry not technically suggested by their titles (J.-M. Lehn, *Supramolecular Chemistry: Concepts and Perspectives*, Wiley-VCH, Weinheim, **1995**, p. 90).

[14] In addition to the rotaxane-forming methods based on specific templates for metal-ion coordination, aromatic stacking and hydrogen bonding,[6] cyclodextrins (S. A. Nepogodiev, J. F. Stoddart, *Chem. Rev.* **1998**, *98*, 1959–1976), and certain cyclophanes[12] can form rotaxanes of a broad range of substrates through general hydrophobic binding. The trapping of phenolate anions by amide macrocycles can also produce rotaxanes with no recognition elements (C. Seel, F. Vögtle, *Chem. Eur. J.* **2000**, *6*, 21–24; R. Shukla, M. J. Deetz, B. D. Smith, *Chem. Commun.* **2000**, 2397–2398), but requires a specific template in the stopper and is apparently of limited generality (C. A. Schalley, G. Silva, C. F. Nising, P. Linnartz, *Helv. Chim. Acta* **2002**, *85*, 1578–1596).

 © 2004 Wiley-VCH Verlag GmbH & Co. KGaA, Weinheim

[15] The earliest rotaxane syntheses produced rotaxanes without attractive interactions between the subunits but were carried out under "statistical" conditions, which only generates rotaxanes in low yields (I. T. Harrison, S. Harrison, *J. Am. Chem. Soc.* **1967**, *89*, 5723 – 5724). Other routes to rotaxanes without noncovalent recognition elements between macrocycle and thread have been developed based on covalent bond-directed methods (G. Schill, H. Zollenkopf, *Justus Liebigs Ann. Chem.* **1969**, *721*, 53; K. Hiratani, J.-I. Suga, Y. Nagawa, H. Houjou, H. Tokuhisa, M. Numata, K. Watanabe, *Tetrahedron Lett.* **2002**, *43*, 5747 – 5750).
[16] M. Asakawa, G. Brancato, M. Fanti, D. A. Leigh, T. Shimizu, A. M. Z. Slawin, J. K. Y. Wong, F. Zerbetto, S. Zhang, *J. Am. Chem. Soc.* **2002**, *124*, 2939 – 2950.
[17] G. Brancato, F. Coutrot, D. A. Leigh, A. Murphy, J. K. Y. Wong, F. Zerbetto, *Proc. Natl. Acad. Sci. USA* **2002**, *99*, 4967 – 4971.
[18] A. S. Lane, D. A. Leigh, A. Murphy, *J. Am. Chem. Soc.* **1997**, *119*, 11092 – 11093.
[19] T. Da Ros, D. M. Guldi, A. F. Morales, D. A. Leigh, M. Prato, R. Turco, *Org. Lett.* **2003**, *5*, 689 – 691.
[20] Since hydrogen bonding of the DMSO to the peptide and macrocycle provides much of the driving force for displacement of the macrocycle from the template, this switching strategy should be largely independent of the nature of the substrate.
[21] The prefix refers to the position of the macrocycle on the thread.
[22] Silyl ether protections of hydroxyl groups are routinely performed in DMF but DMSO is equally efficacious, a key requirement for the gate functionality with the chosen method of shuttling.
[23] J. O. Jeppesen, J. Perkins, J. Becher, J. F. Stoddart, *Angew. Chem.* **2001**, *113*, 1256 – 1261; *Angew. Chem. Int. Ed.* **2001**, *40*, 1216 – 1221.
[24] One (but not both) of the glycyl H_c protons of *alkyl*-**5** is shielded by $\delta = 1.02$ ppm in $CDCl_3$, which indicates that the macrocycle is able to hydrogen bond to the peptide despite being locked on the substrate side of the silyl ether gate.
[25] For examples of postassembly stopper-substitution reactions in rotaxanes see a) S. J. Rowan, S. J. Cantrill, J. F. Stoddart, *Org. Lett.* **1999**, *1*, 129 – 132; b) S. J. Rowan, J. F. Stoddart, *J. Am. Chem. Soc.* **2000**, *122*, 164 – 165; c) S. J. Rowan, S. J. Cantrill, J. F. Stoddart, A. J. P. White, D. J. Williams, *Org. Lett.* **2000**, *2*, 759 – 762; d) D. W. Zehnder, D. B. Smithrud, *Org. Lett.* **2001**, *3*, 2485 – 2487; e) S. H. Chiu, S. J. Rowan, S. J. Cantrill, J. F. Stoddart, A. J. P. White, D. L. Williams, *Chem. Eur. J.* **2002**, *8*, 5170 – 5183.
[26] M. G. Stanton, M. R. Gagné, *J. Am. Chem. Soc.* **1997**, *119*, 5075 – 5076.
[27] The *tert*-butyloxy group is too small to act as a stopper, but tertiary alkoxides are unreactive towards esters and so *t*BuOK provides a means of generating low concentrations of the reactive stopper primary alkoxide in situ.
[28] F. G. Gatti, D. A. Leigh, S. A. Nepogodiev, A. M. Z. Slawin, S. J. Teat, J. K. Y. Wong, *J. Am. Chem. Soc.* **2001**, *123*, 5983 – 5989.
[29] There are fewer than 30 examples of amide–ester hydrogen bonds in the Cambridge Crystallographic Database and all are from the NH group to the ester carbonyl oxygen atom (C. Alemán, J. J. Navas, S. Muñoz-Guerra, *J. Phys. Chem.* **1995**, *99*, 17653 – 17661 and ref. [28]).
[30] G. A. Jeffrey, *An Introduction to Hydrogen Bonding*, Oxford University Press, Oxford, **1997**.

 © 2004 Wiley-VCH Verlag GmbH & Co. KGaA, Weinheim

Folded Polymers

Aromatic Donor–Acceptor Charge-Transfer and Metal-Ion-Complexation-Assisted Folding of a Synthetic Polymer**

*Suhrit Ghosh and S. Ramakrishnan**

Synthetic polymers typically adopt a random-coil conformation in solution primarily driven by the tendency to maximize entropy. Generation of well-defined secondary structures in synthetic polymers, therefore, will need to include specific intrachain intersegment interactions that will provide adequate enthalpic contribution to overcome this entropic penalty associated with the formation of well-ordered conformations.[1] The motivation to generate synthetic polymers with a precisely controlled conformation stems from the desire to emulate the elegance of nature on the one hand, while at the same time from the expectation that this will enable one to bridge the gap between the molecular and the macroscopic scales in terms of the evolution of structural order. The term "foldamer"[2] is used to describe synthetic polymers that can be made to adopt well-defined conformations in solution, such as a helix, by inclusion of specific intrachain interactions, such as hydrogen bonding, steric and/or bond-angle constraints along the backbone, solvophobic interactions, etc.[3] Although several examples of synthetic polymers that adopt helical conformations in solutions are known, for example, poly(trityl methacrylate)s,[4] polyisocyanates,[5] *cis*-poly(acetylene)s,[6] polyisocyanides,[7] and poly(1,3-phenylene ethynylene)s,[8] most of these deal with relatively stiff chains that have very limited conformational degrees of freedom as a result of steric and/or bond-angle constraints. There are, however, only very few examples of relatively flexible systems that have been made to adopt a well-defined conformation in solution. Iverson and co-workers[9] described one such system in a series of elegant papers in which they demonstrated the possibility of forming folded structures in specifically designed oligomers by virtue of specific intrachain aromatic donor–acceptor charge-transfer interactions aided by solvophobic effects. Thus far, most studies on flexible foldamers have dealt only with precisely defined oligomers,[10] and to the best our knowledge there are no reports on analogous polymeric systems.[10c] Thus, in an effort to explore directed folding in truly flexible synthetic polymers, we designed and synthesized a segmented donor–acceptor polyimide **3**, which contains three design elements

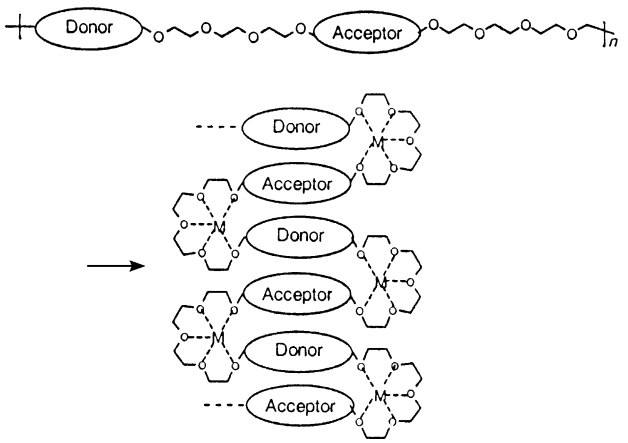
[*] S. Ghosh, Prof. S. Ramakrishnan
Department of Inorganic and Physical Chemistry
Indian Institute of Science
Bangalore 560012 (India)
Fax: (+80) 2360-0683
E-mail: raman@ipc.iisc.ernet.in

[**] We thank the DST, New Delhi, and 3M India Ltd, for their financial support.

Supporting information for this article is available on the WWW under http://www.angewandte.org or from the author.

 © 2004 Wiley-VCH Verlag GmbH & Co. KGaA, Weinheim DOI: 10.1002/anie.200453860

that could induce folding in tandem under appropriate conditions. The three design elements are: 1) alternate placement of aromatic donor and acceptor units that could form an intrachain donor–acceptor charge transfer complex, analogous to the Iverson systems, 2) a hexa(ethylene oxide) linking segment that could impart a solvophobic driving force to folding, and 3) the alkali-metal-ion complexation ability of the flexible oligoethylene oxide segment that could further assist in the formation of folded structures by restricting the conformational freedom of the loop, which in turn should further aid the formation of the donor–acceptor charge-transfer complex.[11] A schematic representation of such a folded structure is shown in Scheme 1.



Scheme 1. The folding process.

Polymer **3** was prepared through standard polyimide synthesis methodology from diamine **1** (which contains the appropriate naphthalene (donor) and oligoethylene oxide moieties) and pyromellitic dianhydride (**2**; Scheme 2). The diamine **1** was synthesized in several steps from 1,5-dihydroxynaphthalene.[12] The polymer was structurally characterized by ^{1}H and ^{13}C NMR spectroscopy and elemental analysis, and its molecular weight was determined to be about 17000 (M_n, PDI ~ 2.0) by GPC in THF, using a triple detector system. The ^{1}H NMR spectrum (Figure 3) clearly shows the presence of the naphthalene protons (3 sets, $\delta = 6.7$–7.6 ppm) and a single signal for the pyromellitic diimide protons ($\delta =$ 7.9 ppm), in addition to the oligoethylene oxide proton signals in the aliphatic region (not shown). The polymer was readily solution-cast to give bright red films, which clearly suggests the formation of a strong charge-transfer complex in the solid state.[13]

The formation of intrachain charge-transfer complex between the adjacent donor and acceptor units not only provides the driving force for the formation of the anticipated folded structure but also serves as a spectroscopic probe to examine the formation of such a structure. The UV/Vis absorption spectrum of the polymer in chloroform ($c =$ 0.23 mM) is shown in Figure 1. The charge-transfer absorption band is clearly visible at 450 nm, which is well separated from the other absorption bands owing to the individual donor and acceptor units. For comparison, the absorption spectrum of a mixture of model donor and acceptor molecules,[14] at the same concentration as that of the polymer (considering the repeat unit), is also shown in Figure 1. It is clear from the significantly larger charge-transfer absorbance (see inset in Figure 1) that linking of the donor and acceptor units in an alternating fashion along the polymer backbone enhances the formation of the charge-transfer complex.[15] Confirmation that such a complex is indeed formed intramolecularly (intrachain) was obtained by dilution experiments (in the range 0.7–0.06 mM), which shows the expected Beer–Lambert law dependence (inset in Figure 1).

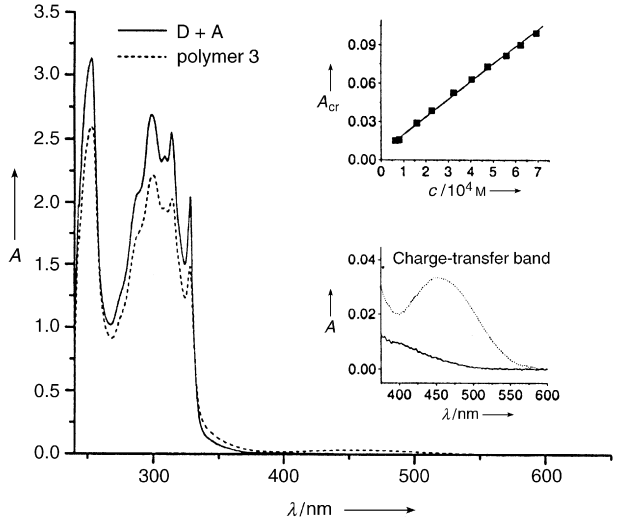
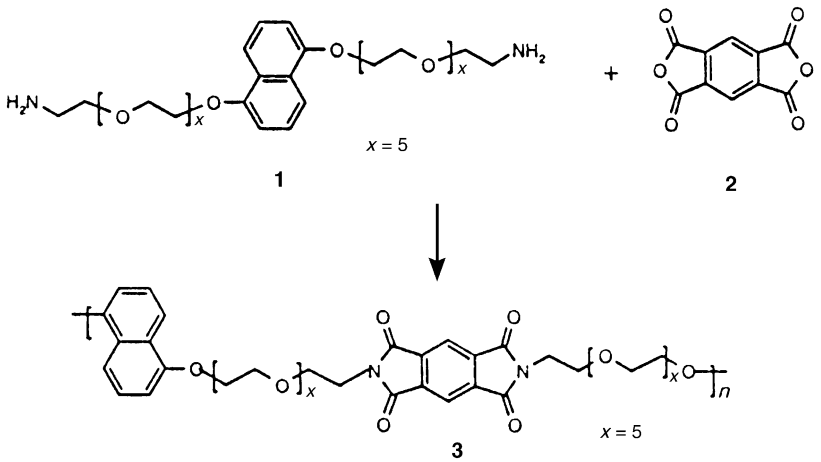


Figure 1. Comparison of UV/Vis spectra of polymer **3** and a mixture of analogous model donor and acceptor compounds in chloroform. Insets: bottom: expanded region of the charge-transfer band; top: variation of charge-transfer absorbance with concentration. D = donor, A = acceptor.



Scheme 2. Synthesis of the polymer **3**.

 © 2004 Wiley-VCH Verlag GmbH & Co. KGaA, Weinheim

To examine whether the difference in solubility characteristics between the aromatic units and the oligoethylene oxide loop can be utilized to induce folding (solvophobic effect), we carried out a solvent titration experiment in chloroform/methanol. A noticeable increase in the charge-transfer absorption band intensity with increasing methanol composition is evident from Figure 2. A plot of the concentration-corrected normalized absorbance as a function of solvent composition (inset in Figure 2) shows a small initial decrease in the intensity before the onset of the increase. The initial decrease is ascribed to possible destabilization of the donor–acceptor charge-transfer complex in polar solvents,[16] which is later overcome by the solvent-induced conformational transition of the polymer chain, which apparently forces closer contacts between the donor and acceptor units.[17] An increase in the methanol content beyond a certain value makes the solution visibly cloudy owing to the onset of precipitation. This was also seen from a second abrupt rise in the apparent absorbance (not shown) as a result of scattering losses arising from precipitation. To further confirm that the first increase in the charge-transfer absorbance, prior to precipitation, is indeed due to solvent-induced enhancement in the intrachain charge-transfer complex formation, dilution experiments maintaining the solvent composition as that just prior to precipitation (43% v/v CH_3OH in $CHCl_3$) were done, which again exhibited the expected Beer–Lambert dependence.

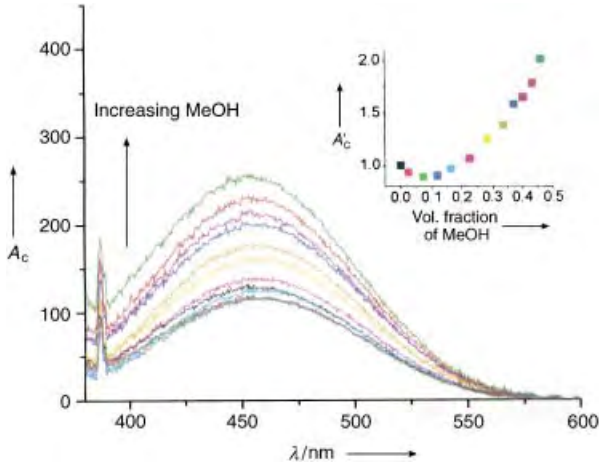


Figure 2. Variation of UV/Vis spectra of polymer **3** in chloroform with increasing amounts of methanol. The inset shows the variation of normalized concentration-corrected charge-transfer absorbance (A_c') as a function of methanol volume fraction. A_c = concentration-corrected absorbance.

^{1}H NMR spectroscopic studies of the polymer provide further unequivocal evidence for the formation of an intrachain donor–acceptor charge-transfer complex. First, it is observed that signal for the acceptor proton ($\delta = 7.9$ ppm) undergoes a considerable upfield shift upon the formation of the charge-transfer complex; the signals for the donor protons also undergo a similar but smaller upfield shift.[18] In Figure 3, we compare the ^{1}H NMR spectra of a mixture of donor and acceptor model compounds (D+A)[14] with that of the polymer **3**; it is clearly evident that the chemical shift of the acceptor proton in the latter case is significantly shifted upfield relative to the former, reconfirming the greater propensity for the polymer to form a charge-transfer complex. In the presence of a polar solvent such as acetonitrile (50% v/v CH_3CN in $CDCl_3$), a further upfield shift of signal for the aromatic acceptor proton[19] is seen, and this we ascribe to the solvophobic effect, which was earlier seen in the absorption spectra as well. More importantly, in the presence of an alkali-metal ion, the formation of the charge-transfer complex is further enhanced, as is evident from the variation of the NMR spectrum as a function of increasing amounts of metal ions, such as K^+ (Figure 4).

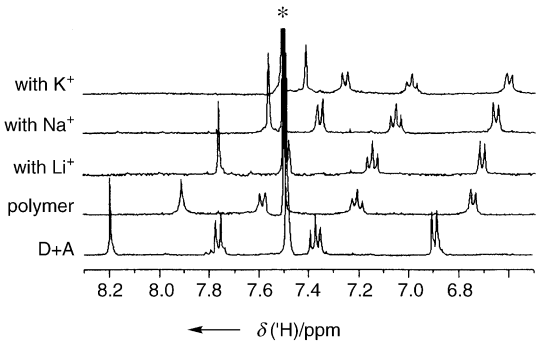


Figure 3. The aromatic region of the ^{1}H NMR spectra of polymer **3** in the presence of various alkali-metal ions (ca. ninefold excess) in $CDCl_3/CH_3CN$ (1:1 v/v). For comparison, the spectrum of an equimolar mixture of model compounds (D+A) is also given. The peak indicated with the ⋆ is due to the solvent.

It is apparent from Figure 4 that the signal for the acceptor proton undergoes the most significant upfield shift, which

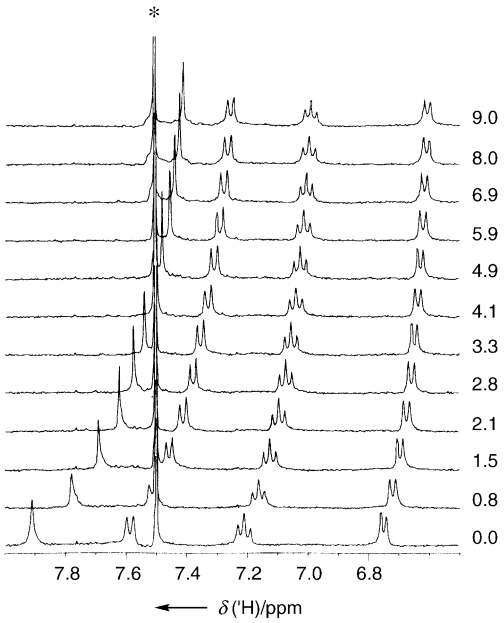


Figure 4. Variation of the aromatic region of the ^{1}H NMR spectra of polymer **3** with increasing amounts of KSCN in $CH_3CN/CDCl_3$ (50% v/v). The numbers on the right represent the mole equivalents of the salt with respect to the polymer repeat unit. The peak indicated with the ⋆ is due to the solvent.

 © 2004 Wiley-VCH Verlag GmbH & Co. KGaA, Weinheim

appears to level off at higher concentrations of K^+ ions. Similar changes in the spectrum are also seen in the presence of both Li^+ and Na^+ ions, but the extent of the change is smaller. In Figure 3, the aromatic region of the spectra in the presence of an excess of different alkali-metal ions (approximately ninefold excess) is compared and clearly reflects these differences. In Figure 5, the variation in the chemical shift of

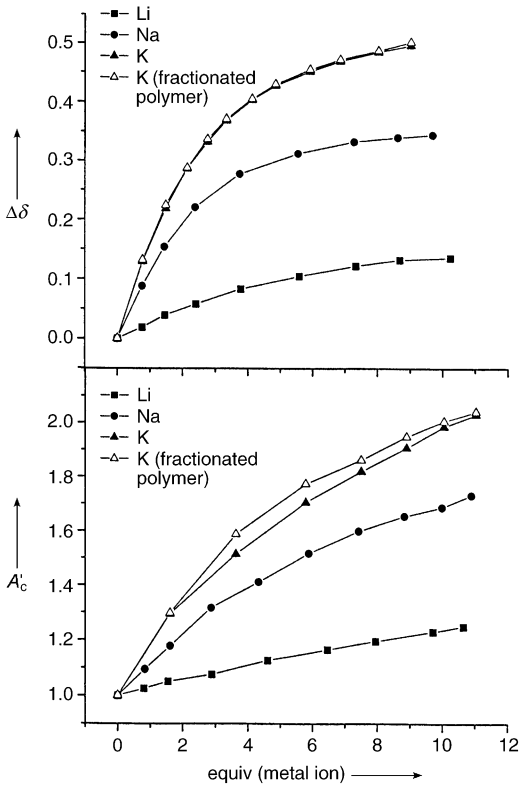


Figure 5. The change in chemical shift ($\Delta\delta$) of the acceptor proton of polymer **3** (top) and charge-transfer absorbance (bottom) as a function of different alkali-metal ion concentrations. The open symbols represent changes observed in the high-molecular-weight fractionated sample. A_c' = normalized concentration-corrected charge-transfer absorbance.

the acceptor proton as a function of the metal-ion concentration for various metal ions, along with a similar comparison of the absorbance of the charge-transfer band in the absorption spectra, is presented. It is clear from this comparison that the extent of variation in both the spectral methods is largest for K^+ followed by Na^+ and Li^+. The variation in chemical shift was used as an indicator of the extent of metal-ion complexation to calculate the apparent association constant K to be 85, 356, and 299 mol^{-1} for Li^+, Na^+, and K^+, respectively.[20] Importantly, the enhanced charge-transfer complex formation in the presence of alkali-metal ions, and the apparent ionic size-dependant complexation ability of the hexaethylene oxide loop, is clear evidence in support of the hypothesis that the aromatic charge-transfer interactions are indeed occurring between adjacent donor and acceptor units along the polymer chain. The changes in the aliphatic region of the NMR spectra in the presence of the metal ion helps to reconfirm that the complexation of the hexaethylene oxide loop indeed occurs with the metal ion, as seen from the considerable downfield shift of several of the signals for the methylene protons along with an enhanced discrimination between the different types of methylene units.[21] In an effort to see if the molecular weight of the polymer has any effect on the folding, the nascent polymer was fractionated and the high-molecular-weight fraction ($M_n = 52\,000$, PDI = 1.2) was used to carry out two representative experiments. The variations in the ^1H NMR and the UV/Vis spectra as a function of K^+ ion concentration was monitored and found to be similar to those exhibited by the nascent polymer (see Figure 5). This helped to confirm that the molecular weight has very little effect on the folding process, at least in the range investigated.

In conclusion, we have demonstrated that by proper design, flexible synthetic macromolecules can be made to fold under the influence of relatively weak intrachain intersegment interactions, such as charge-transfer complex formation, assisted in tandem by solvophobic effects and metal-ion complexation of a flexible oligoethylene oxide loop—leading to a stacking of aromatic donor and acceptor segments enveloped by the relatively hydrophilic oligoethylene oxide loops that wrap around suitable metal ions by coordination (as depicted in Scheme 1). The maximum probability of such a folded state is seen when all the three effects are present at the same time, which occurs in a relatively polar medium in the presence of an alkali-metal ion. The number of stacked donor and acceptor units, which would be a truer reflection of the extent of folding, remains a difficult question that needs further investigations. Preliminary studies of model compounds of the type donor–oligoethylene oxide acceptor (DA) and analogous DAD and ADA, clearly suggest that the stacking exceeds simple pairing of the donor and acceptor units. Further studies are currently underway to probe this aspect in greater detail with possible inclusion of chirality, which will enable the use of CD methods as a probe for the extent of stacking.

Experimental Section

Polymer **3** was prepared from the diamine **1** and pyromellitic dianhydride **2** under standard polyimide preparation conditions, using *m*-cresol as a solvent during the first step at 80 °C, followed by a polyimidization step at a higher temperature (185 °C), which was done under continuous azeotropic (toluene) removal of water.[12] The polymer formed was purified by repeated reprecipitation from chloroform/methanol. A high-molecular-weight fraction was separated by fractionation with chloroform/methanol, and independently studied to assess the role of molecular weight. Dry and purified solvents were used in all the NMR and UV/Vis spectroscopic experiments. The NMR studies were carried out on a Bruker 400 MHz NMR machine and the UV/Vis spectra were measured on an Hitachi spectrometer. The alkali-metal salts were purified by recrystallization before use. For NMR complexation studies, 1.5 mL of the polymer solution was prepared in 1:1 $CDCl_3/CH_3CN$ (concentration range 1–3 mM) (solution A). A calculated amount of the appropriate alkali-metal salt (≈20–25 equiv with respect to the polymer repeat unit) was added to 0.9 mL of solution A (solution B). Solution A (0.6 mL) was then taken in an NMR tube and titrated with solution B (in 20–100 μL steps), which resulted in a series of solutions

 © 2004 Wiley-VCH Verlag GmbH & Co. KGaA, Weinheim

with a fixed polymer concentration but varying amounts of the alkali-metal salts. The UV/Vis studies were also carried out in a similar manner, maintaining a fixed polymer concentration of 1 mM, in the same solvent mixture. In the solvent titration experiment, the polymer solution in chloroform was diluted in steps with a measured volume of methanol and the charge-transfer band intensity was monitored. The spectra were then corrected to adjust for the decreasing polymer concentration with dilution. The NMR studies were also done similarly, and the peak positions were monitored with varying composition.

Received: January 27, 2004 [Z53860]

Keywords: charge transfer · donor–acceptor systems · polymers · solvophobic effect · supramolecular chemistry

[1] M. Muthukumar, C. K. Ober, E. L. Thomas, *Science* **1977**, *277*, 1225.
[2] S. H. Gellman, *Acc. Chem. Res.* **1998**, *31*, 173.
[3] a) D. J. Hill, M. J. Mio, R. B. Prince, T. S. Huges, J. S. Moore, *Chem. Rev.* **2001**, *101*, 3893; b) C. Schmuck, *Angew. Chem.* **2003**, *115*, 2552; *Angew. Chem. Int. Ed.* **2003**, *42*, 2448.
[4] T. Nakano, Y. Okamoto, *Chem. Rev.* **2001**, *101*, 4013.
[5] M. M. Green, J. W. Park, T. Sato, A. Teramoto, S, Lifson, R. L. B. Selinger, J. V. Selinger, *Angew. Chem.* **1999**, *111*, 3328; *Angew. Chem. Int. Ed.* **1999**, *38*, 3138.
[6] K. Maeda, S. Okada, E. Yashima, Y. Okamoto, *J. Polym. Sci., Part A: Polym. Chem.* **2001**, *39*, 3180.
[7] J. J. L. M. Cornelissen, A. E. Rowan, R. J. M. Nolte, N. A. J. M. Sommerdijk, *Chem. Rev.* **2001**, *101*, 4039.
[8] J. C. Nelson, J. G. Saven, J. S. Moore, P. G. Wolynes, *Science* **1997**, *277*, 1793; a more recent report describes an elegant way to crosslink photochemically the helical conformation in high molecular weight poly(1,3-phenylene ethynylene)s: R. S. Hecht, A. Khan, *Angew. Chem.* **2003**, *115*, 6203; *Angew. Chem. Int. Ed.* **2003**, *42*, 6021.
[9] a) R. S Lokey, B. L. Iverson, *Nature* **1995**, *375*, 303; b) J. Q. Nguyen, B. L. Iverson, *J. Am. Chem. Soc.* **1999**, *121*, 2639; c) A. J. Zych, B. L. Iverson, *J. Am. Chem. Soc.* **2000**, *122*, 8898; d) G. J. Gabriel, B. L. Iverson, *J. Am. Chem. Soc.* **2002**, *124*, 15174.
[10] For well-defined oligomers containing perylene units linked by oligoethylene glycol units, see: a) W. Wang, L-S. Li, G. Helms, H-H. Zhou, A. D. Q. Li, *J. Am. Chem. Soc.* **2003**, *125*, 1120; b) A. D. Q. Li, W. Wang, L-Q. Wang, *Chem. Eur. J.* **2003**, *9*, 4594; c) for a postulated self-assembly in similar polymeric systems containing perylene bisimide units linked through flexible spacers, see:E. E. Neuteboom, S. C. J. Meskers, E. W. Meijer, R. A. J. Janssen, *Macromol. Chem. Phys.* **2004**, 205, 217.
[11] Early comprehensive studies on podands clearly demonstrated the possibility of open-chain analogues of crown ethers to complex with metal ions and generate folded structures. Several workers exploited such metal-ion-induced folding to modulate photophysical behavior in small molecules. For comprehensive reviews, see: a) F. Vogtle, E. Weber, *Angew. Chem.* **1979**, *91*, 813; *Angew. Chem. Int. Ed. Engl.* **1979**, *18*, 753; b) H. G. Lohr, F. Vogtle, *Acc. Chem. Res.* **1985**, *18*, 65; for examples of photophysical studies, see: c) H. G. Lohr, F. Vogtle, *Chem. Ber.* **1985**, *118*, 914; d) A. Ajayaghosh, E. Arunkumar, J. Daub, *Angew. Chem.* **2002**, *114*, 1844; *Angew. Chem. Int. Ed.* **2002**, *41*, 1766; e) Y. Suzuku, T. Morozumi, H. Nakamura, M. Shimomura, T. Hayashita, R. A. Bartsh, *J. Phys. Chem. B* **1998**, *102*, 7910; f) B. Tummler, G. Maass, F. Vogtle, H. Sieger, U. Heimann, E. Weber, *J. Am. Chem. Soc.* **1979**, *101*, 2588.
[12] Experimental details regarding the synthesis and characterization of the monomer and the polymer are available in the Supporting Information.
[13] In contrast, the homopolyimide, which is devoid of the naphthalene unit, prepared from simple amine terminated oligoethylene glycol and pyromellitic dianhydride, is white in colour.
[14] 1,5-Dimethoxynaphthalene was used as the model donor and the pyromellitic diimide prepared from pyromellitic dianhydride with 2-[2-(2-methoxyethoxy)ethoxy]ethylene amine was used as the model acceptor.
[15] For examples of small molecule systems in which enhanced charge-transfer complexation results from linking of the donor and acceptor units, see: a) N. C Yang, Y. Gaoni, *J. Am. Chem. Soc.* **1964**, *86*, 5022; b) J. W. Verhoeven, I. P. Drikx, T. J. Deboer, *Tetrahedron Lett.* **1966**, *7*, 439; c) D. Kost, N. Peor, G. Sod-Moriah, Y. Sharabi, D. T. Durocher, M. Raban, *J. Org. Chem.* **2002**, *67*, 6938.
[16] a) R. Forster in *Organic Charge-Transfer Complex*, Academic Press, London, **1969**; b) M. S. Cubberley, B. L. Iverson, *J. Am. Chem. Soc.* **2001**, *123*, 7560.
[17] A similar variation in the chemical shift of the acceptor protons, going through a maximum with increasing solvent polarity was noticed, which confirms the initial decrease prior to the increase in the apparent association constant. Detailed NMR spectral evolution as a function of solvent composition is included in the Supporting Information.
[18] Similar upfield shifts of the signals for the donor and acceptor protons upon charge-transfer complex formation was previously reported, and may be ascribed to the perturbation of the aromatic ring current causing a shielding effect: a) Y. Nakamura, S. Minami, K. Iizuka, J. Nishimura, *Angew. Chem.* **2003**, *115*, 3266; *Angew. Chem. Int. Ed.* **2003**, *42*, 3158; see also reference [9c].
[19] The chemical shift value of the acceptor proton in pure $CDCl_3$ is 8.07 ppm as compared to 7.9 ppm in $CDCl_3/CH_3CN$ (1:1 v/v). In contrast, there was no change in the chemical shifts in the case of a mixture of the model compounds at the same concentration.
[20] The program EQNMR version 2.10 was used to calculate the *K* values from the variation of the chemical shift of the acceptor proton. (Freeware developed by M. J. Hynes, Chemistry Department, University College, Galway, Ireland). It is evident that the association constant does not directly parallel the extent of change seen in either the charge-transfer absorbance or the chemical shift. It may be reasoned that the extent of change experienced by the donor and acceptor units (both in their NMR and UV/Vis spectra), owing to metal-ion complexation by the loop, would greatly depend on the final geometry of the donor–acceptor complex. Thus, formation of a strong complex with the metal ion need not necessarily bring the donor and acceptor units in the optimum geometry for most effective charge-transfer interaction. Further studies are currently being done on model conor–acceptor oligomers to gain better insight into these aspects.
[21] The maximum change is noticed for the methylene protons of the central region of the loop, which move downfield, whereas the methylene protons immediately adjacent to the chromophores move slightly upfield with K^+ and Na^+ and change little in the case of Li^+. A similar variation was reported by Vogtle and co-workers in the case of podands (see reference [11a]). All the spectral variations are included in the Supporting Information.

 © 2004 Wiley-VCH Verlag GmbH & Co. KGaA, Weinheim

Microporous Materials

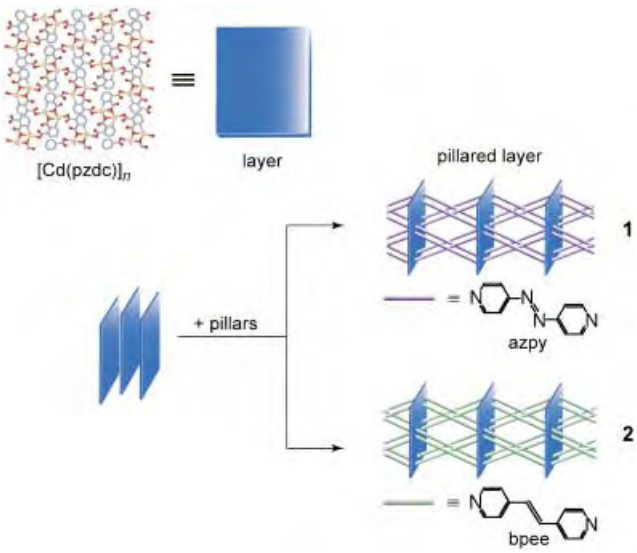
Expanding and Shrinking Porous Modulation Based on Pillared-Layer Coordination Polymers Showing Selective Guest Adsorption**

*Tapas Kumar Maji, Kazuhiro Uemura, Ho-Chol Chang, Ryotaro Matsuda, and Susumu Kitagawa**

The design and construction of coordination polymers are of great interest due to their intriguing new structural topologies and potential application as functional materials.[1–5] Their microporous frameworks have a large surface area, which is relevant for storage of large quantities of natural gas or hydrogen, and this is becoming a new field of research.[6–12] In addition, it has been shown that these frameworks display unique dynamic behavior, that is, crystal-to-crystal or crystal-to-amorphous transformations, which are characteristic of metal–organic motifs. Therefore, their selective-sorption profiles are fascinating,[13–18] and pave the way for practical applications such as specific sensing and separation of gas molecules. Recently, several coordination polymers that exhibit selective gas adsorption were reported; $\{Er_2(PDA)_3\}_n$ (PDA = $OOCCH_2PhCH_2COO$) selectively adsorbs CO_2 but not Ar or N_2,[10] while $\{Mn(HCO_2)_2\}_n$ adsorbs H_2 and CO_2 but not N_2.[12] This selectivity is attributed to the fact that the apertures of the channels are smaller than the molecules attempting pass through them.

For the rational construction of porous frameworks with controlled channel dimensions, the "pillared-layer" motif has so far been employed, because simple modification of the pillars can control not only the channel size but also chemical functionality.[19–21] Here, we selected $\{Cd(pzdc)\}_n$ (pzdc = pyrazine-2,3-dicarboxylate) as a layer, and py-N=N-py (azpy)/py-CH=CH-py (bpee; py is pyridine) as pillar ligands, and obtained similar prototype structures, $\{[Cd(pzdc)(azpy)]\cdot 2H_2O\}_n$ (**1**) and $\{[Cd(pzdc)(bpee)]\cdot 1.5H_2O\}_n$ (**2**; Scheme 1). Despite the slight difference in the spacer groups (-N=N-/-CH=CH-) found between azpy and bpee, the observed adsorption/desorption behavior of **1** and **2** were distinct. We show them in detail below.

The crystal structures of **1** and **2** were determined by X-ray crystallography as shown in Figure 1. In **1**, each Cd^{II} center is hexacoordinated, residing in a distorted octahedral environment, surrounded by three oxygen atoms, one nitrogen atom in the equatorial position from one of possibly three



Scheme 1. Simplified representation of the network topology of complex **1** and **2**. The second carboxy group on each pzdc ligand has been omitted for clarity.

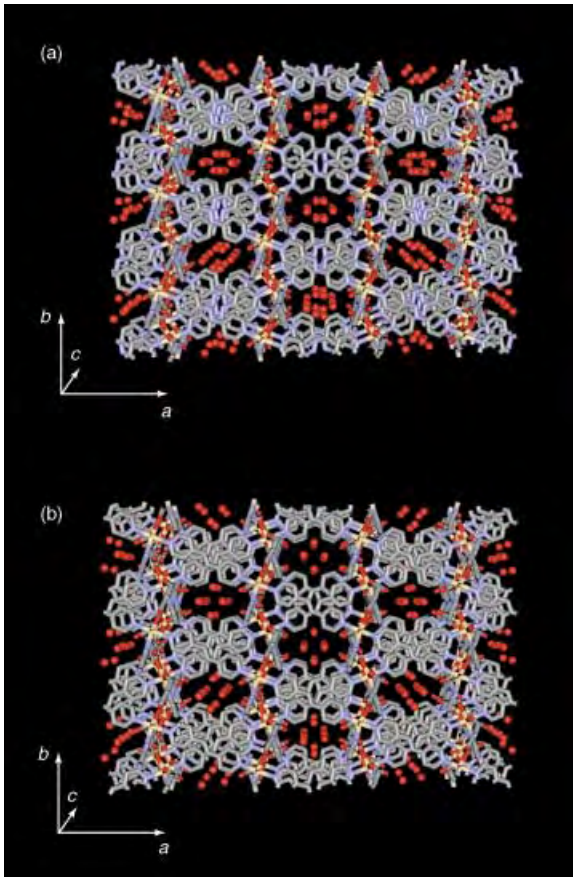


Figure 1. Crystal structures of a) $\{[Cd(pzdc)(azpy)]\cdot 2H_2O\}_n$, **1**, and b) $\{[Cd(pzdc)(bpee)]\cdot 1.5H_2O\}_n$, **2**, along the *c* axis. Hydrogen atoms are omitted for clarity.

[*] Dr. T. K. Maji, K. Uemura, Dr. H.-C. Chang, R. Matsuda, Prof. Dr. S. Kitagawa
Department of Synthetic Chemistry and Biological Chemistry
Graduate School of Engineering
Kyoto University
Katsura, Nishigyo-ku, Kyoto 615-8510 (Japan)
Fax: (+81) 75-383-2732
E-mail: kitagawa@sbchem.kyoto-u.ac.jp

[**] This work was supported by Core Research for Evolutional Science and Technology (CREST), and by the Japan Science and Technology Corporation (JST). Dr. T. K. Maji is grateful to JSPS for postdoctoral fellowship.

Supporting information for this article is available on the WWW under http://www.angewandte.org or from the author.

 DOI: 10.1002/anie.200453923 © 2004 Wiley-VCH Verlag GmbH & Co. KGaA, Weinheim

different pzdc ligand and two nitrogen atoms from the two azpy ligands ligated in axial positions to give a CdO_3N_3 chromophore. Each pzdc ligand is coordinated to three Cd^{II} centers through three oxygen and one nitrogen atoms, forming a 2D corrugated layer, $\{Cd(pzdc)\}_n$, in the *bc* plane. $\{Cd_2(\mu\text{-}O)_2\}$ units ($\angle Cd^{II}\text{-}O\text{-}Cd^{II} = 111.7(2)°$, $Cd^{II}\cdots Cd^{II} = 3.883(1)$ Å) in the layers are pillared with the axial coordination of azpy, forming a 3D network. An interesting aspect of the structure is that azpy ligands connect the layers in a criss-cross fashion, which facilitates the formation of π–π interactions (C···C = 3.71–4.89 Å, dihedral angle = 0.3–1.7°) among the pyridine planes. Such a criss-cross pattern resembles topologically the α-polonium net, a topology that has been generated via $\{M(CN)_2\}$ sheets linked by pyrazine ligands.[22]

The framework has interlayer spaces (volume of the void $V_{void} = 20.3\,\%$),[23] affording 1D microchannels along the *c* axis with window dimensions of 3.5×6.1 Å^2 (Figure 1a).[24] Each pore is surrounded by four perpendicular pyridine planes and two internal panels of pzdc plane, and filled with four water molecules. In the channel walls two oxygen atoms of the carboxylate moiety in pzdc protrude, thus allowing hydrogen-bonding interactions with water (w) molecules (C=O···O(w) = 2.66(3) Å). Moreover, the four water molecules are hydrogen bonded to each other (O(w)···O(w′)) = 2.40(3) Å, 3.03(2) Å).

The unit cell parameters of **2** are very close to those of **1** and structure determination reveals that they are isostructural. In **2**, the corrugated $\{Cd(pzdc)\}_n$ layers in the *bc* plane are pillared through axial coordination of bpee in a criss-cross fashion, thus forming a 3D network. Compound **2** also contains 1D channels along the *c* axis with window dimensions of 3.5×4.5 Å^2 ($V_{void} = 19.3\,\%$; Figure 1b) and each pore is occupied by three water molecules. The water molecules form hydrogen bonds with protruding carboxylate moieties of pzdc ligands (C=O···O(w) = 2.68(4) Å).

To examine the thermal stability of these porous networks, thermal gravimetric (TG) analyses and X-ray powder diffraction pattern (XRPD) measurements were carried out. The TG curve of **1** and **2** indicates the release of guest water molecules up to 105 °C for **1** and 100 °C for **2** to give their dehydrated forms, **1a** and **2a**, respectively. At 265 °C for **1** and 260 °C for **2**, the ligand molecules start to be released. No chemical decomposition was observed between the dehydration and ligand-release temperatures. Figure 2 shows the observed XRPD patterns of **1, 1a**, **2**, and **2a**. XRPD patterns of **1a** and **2a** show sharp diffraction peaks indicating that the porous framework is maintained even without guest molecules. XRPD shifts of the (200) reflections demonstrate the elongated (or shrunken) *a* axes. In the process of "**1**→**1a**", the peak (200) at 7.50° for **1** moves to 7.40° for **1a**, exhibiting a slight increase in the interlayer distance (Figure 2b). Whereas, in the process of "**2**→**2a**", the peak (200) at 7.28° for **2** slightly moves to the higher angle 7.34° in dehydrated **2a** indicating that slight decrease in the inter-layer distance (Figure 2e).

It is worth mentioning that we succeeded in obtaining single crystals of guest-free **1a** by heating **1** at 130 °C for 30 minutes to completely remove the water molecules. The

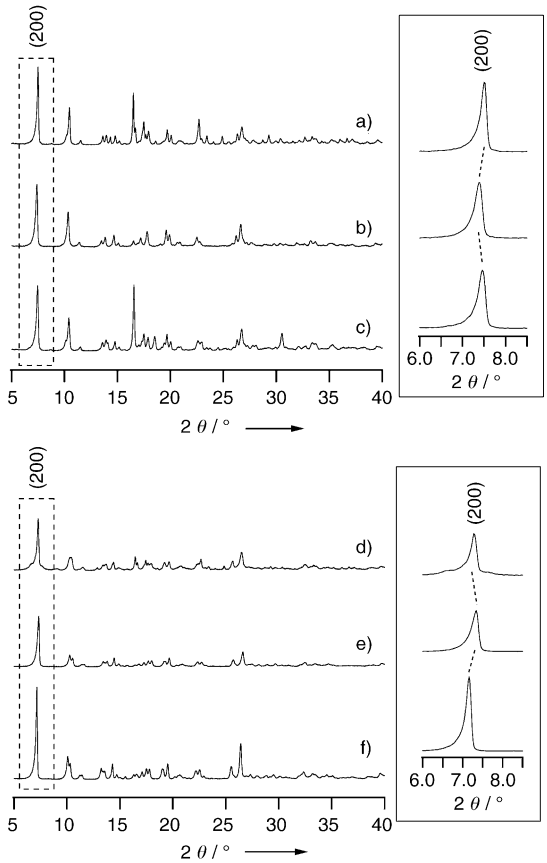


Figure 2. Powder XRD pattern of a) as-synthesized **1**, b) drying of **1** in vacuo at 130 °C for 30 minutes (**1a**), c) **1a** exposed to H_2O, d) as-synthesized **2**, e) drying **2** in vacuo at 130 °C for 30 minutes (**2a**), f) **2a** exposed to H_2O. (inset; enlarged view of the 200 peak position in hydrated, dehydrated, and rehydrated state.)

structure determination of **1a** shows that the crystal system and space group remain the same as those of **1**, but there is a significant increase in the cell volume. **1a** is isostructural to **1**, the only difference being the distance between the pendant oxygen atom of pzdc and the nitrogen atom of azpy; C=O(2)···N=N (azpy) = 4.57(1) Å (**1**) and C=O(2)···N=N (azpy) = 4.721(8) Å (**1a**; Figure 3a and b). Moreover, V_{void} = 21.2 % of the total crystal volume for **1a**, with effective dimensions of the pore size being 3.7×6.4 Å^2, which is larger than the original **1** ($V_{void} = 20.3\,\%$, 3.5×6.1 Å^2), thus indicating that **1a** has expanded relative to **1**. This expansion is attributed to lone pair–lone pair electronic repulsion from the pendant oxygen atom of the carboxylate and nitrogen atom of the azo group. In contrast, the interlayer distance of **2** decreases upon the removal of water molecules. In case of **2** the pendant oxygen (O2) atoms are in close contact with ethylene hydrogen atoms (C-O(2)···HC=CH (bpee) = 3.46 Å; Figure 3c), and after dehydration of **2** to give **2a** the C–O(2)···HC=CH hydrogen-bonding interaction results in a more closely packed structure, which is responsible for the shrinking.[25] These results coincide with the results of XPRD. Thus, the different phenomena of adsorption/desorption, expanding and shrinking, have been realized in **1** and **2**, respectively (Scheme 2). In both **1a** and **2a**, the original

 © 2004 Wiley-VCH Verlag GmbH & Co. KGaA, Weinheim

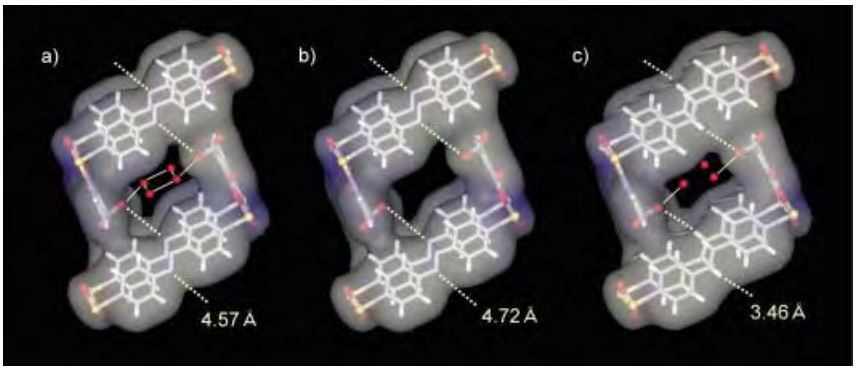
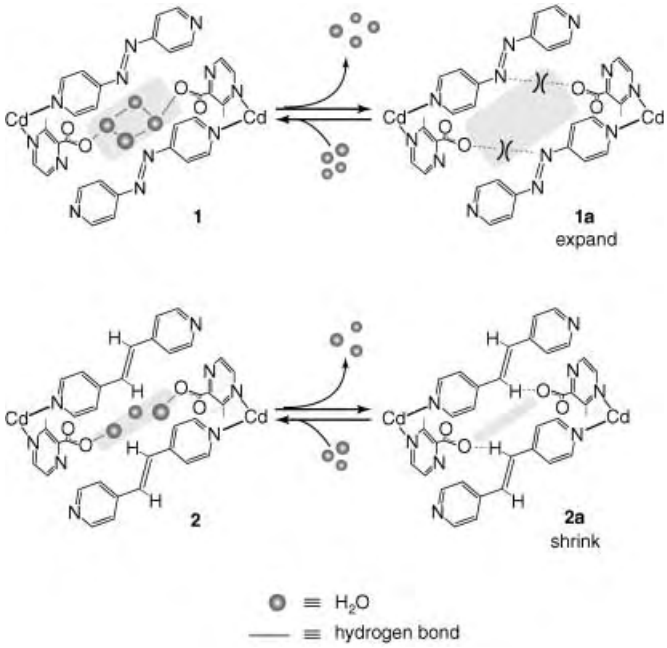


Figure 3. Views of pores in a) **1**, b) **1a**, and c) **2**, along the *c* axis. In **1** and **2**, water molecules are accommodated by hydrogen bonds.



Scheme 2. Schematic diagram of expansion and shrinking of complex **1** and **2**.

framework completely reformed when exposed to water vapor for several hours (Figure 2c and f).

Based on well-defined **1a** and **2a**, the adsorption isotherms for N_2, H_2O, MeOH, EtOH, THF, and Me_2CO were measured. The adsorption isotherm of N_2 (surface area; 16.3 $Å^2$)[26,27] at 77 K for both **1a** and **2a** reveals only surface adsorption occurs, indicating that N_2 molecules cannot diffuse into the channel at low temperature (77 K; see Supporting Information). On the other hand, at 298 K, H_2O (10.5 $Å^2$), MeOH (18.0 $Å^2$), EtOH (23.1 $Å^2$), THF (28.7 $Å^2$), and Me_2CO (26.8 $Å^2$) can diffuse into the micropores of **1a**, irrespective of whether or not it is similar in size to N_2 (Figure 4), and all the adsorption profiles show hysteretic adsorption (see Supporting Information). The amount of adsorption was calculated by using the Langmuir analysis and which shows that for every Cd atom, 1.62 of H_2O, 1.11 of MeOH, 0.28 of EtOH, 0.62 of THF, and 0.44 of Me_2CO molecules can be adsorbed.

The adsorption properties of **2a** were also studied (Figure 4); the adsorption of molecules per Cd atom calculated from the Langmuir analysis is as follows: 1.12 for H_2O, 0.72 for MeOH, 0.08 for EtOH, 0.02 for THF, and 0.04 for Me_2CO. It is note worthy that **2a** adsorbs selectively; H_2O and MeOH are adsorbed, whereas EtOH, THF and Me_2CO molecules are not. As it is the larger molecules that are not adsorbed, it is clear that this selectivity arises from the size of the channel windows in **2a**, that is the channel windows are smaller than the adsorbates.[12]

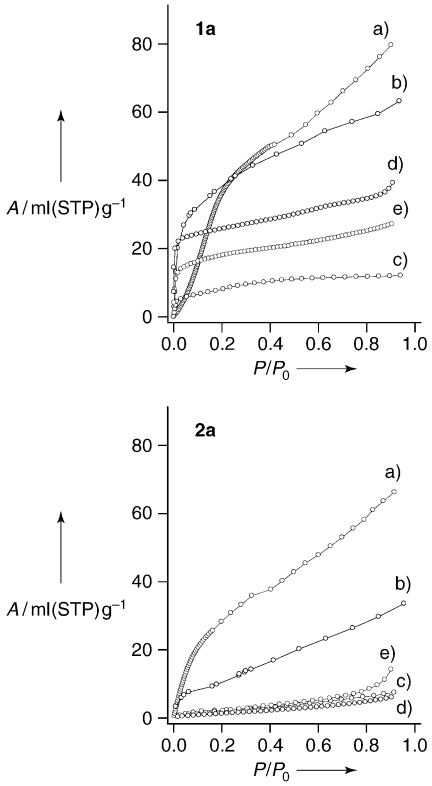


Figure 4. Isotherm for a) H_2O, b) MeOH, c) EtOH, d) THF, e) Me_2CO vapor adsorption, *A*, at 298 K of **1a** (top) and **2a** (bottom). P_0 is the saturated vapor pressure at 298 K; 3.17 kPa (H_2O), 16.94 kPa (MeOH), 7.87 kPa (EtOH), 23.45 kPa (THF), and 30.59 kPa (Me_2CO). STP is standard temperature and pressure.

In conclusion, we have synthesized new pillared-layer porous coordination polymers with different properties: the ability to expand or shrink, and by doing so we have shown that the coordination polymer is much softer than generally believed. **2a** selectively adsorbs H_2O and MeOH, which is due to the small aperture of the channels. The adsorption selectivity exhibited by these new zeolite-like materials arises from a simple change in the organic pillar module, and may well find useful applications in molecular separation techniques.

 © 2004 Wiley-VCH Verlag GmbH & Co. KGaA, Weinheim

Experimental Section

Synthesis of **1:** An aqueous solution of $Cd(NO_3)_2 \cdot 4H_2O$ (2 mL, 0.5 mmol; 0.154 g, in 50 mL) was slowly and carefully layered to a solution of azpy (2 mL, 0.5 mmol, 0.92 g) and Na_2pzdc (0.5 mmol, 0.107 g) in MeOH/H_2O (1:1; 50 mL). Dark red diamond-shaped crystals were obtained after one week. The crystals were separated and washed with a methanol/water (1:1) mixture and dried. Yield 80%.

Synthesis of **2:** An aqueous solution of $Cd(ClO_4)_2 \cdot$hydrate (2 mL, 0.5 mmol; 0.156 g, in 50 mL) was slowly and carefully layered to a solution of bpee (2 mL, 0.5 mmol, 0.91 g) and Na_2pzdc (0.5 mmol, 0.107 g) in MeOH/H_2O (1:1; 50 mL). Colorless square crystals were obtained after one month. The crystals were separated and washed with a methanol/water (1:1) mixture and dried. Yield 60%.

X-ray structure determination for **1**, **1a**, and **2**: Measurements were recorded on a Rigaku mercury CCD diffractometer with graphite monochromated $Mo_{K\alpha}$ radiation ($\lambda = 0.71069$ Å) and a CCD two-dimensional detector. All the structures were solved by direct methods by using SIR97 program and expanded by using Fourier techniques. For all compounds, the non-hydrogen atoms were refined anisotropically and all hydrogen atoms were placed in the ideal positions. Crystal data of **1**: $CdC_{16}H_{10}N_6O_6$, $M_r = 494.71$, Monoclinic, Space group $C2/c$ (no. 15); $a = 25.02(7)$, $b = 11.44(2)$, $c = 13.78(2)$ Å, $\beta = 104.58(4)°$, $V = 3817(14)$ Å^3, $Z = 8$, $\rho_{calc} = 1.722$ g cm^{-3}, $\mu(Mo_{K\alpha}) = 1.191$ mm^{-1}, $F(000) = 1952$, $T = 253$ K; $\lambda(Mo_{K\alpha}) = 0.71069$ Å, $\theta_{max} = 29.5°$, Total data = 16580, Unique data = 5155, $R_{int} = 0.065$, Observed data [$I > 2\sigma(I)$] = 3096, $R = 0.0398$, $R_w = 0.0845$. Crystal data of **1a**: $CdC_{16}H_{10}N_6O_4$, $M_r = 462.70$, Monoclinic, Space group = $C2/c$ (no. 15), $a = 25.09(3)$, $b = 11.472(3)$, $c = 13.762(6)$ Å, $\beta = 102.94(2)°$, $V = 3861(5)$ Å^3, $Z = 8$, $\rho_{calc} = 1.592$ g cm^{-3}, $\mu(Mo_{K\alpha}) = 1.167$ mm^{-1}, $F(000) = 1824$, , $T = 323$ K; $\lambda(Mo_{K\alpha}) = 0.71069$ Å, $\theta_{max} = 30.6°$, Total data = 16620, Unique data = 5150, $R_{int} = 0.025$, Observed data [$I > 2\sigma(I)$] = 3809, $R = 0.0390$, $R_w = 0.0616$. Crystal data of **2**: $CdC_{18}H_{12}N_4O_{5.5}$, $M_r = 484.73$, Monoclinic, Space group = $C2/c$ (no. 15), $a = 25.650(10)$, $b = 11.215(5)$, $c = 13.983(9)$ Å, $\beta = 105.60(10)°$, $V = 3874(4)$ Å^3, $Z = 8$, $\rho_{calc} = 1.662$ g cm^{-3}, $\mu(Mo_{K\alpha}) = 1.167$ mm^{-1}, $F(000) = 1920$, $T = 193$ K, $\lambda(Mo_{K\alpha}) = 0.71069$ Å, $\theta_{max} = 31.6°$, Total data = 19172, Unique Data = 5620, $R_{int} = 0.058$, Observed data [$I > 2\sigma(I)$] = 1733, $R = 0.0773$, $R_w = 0.1257$. The oxygen atoms O5, O6 of water molecules in case of **1** and **2** were refined isotropically. In case of **1** the oxygen atom O6 was found in the final stage, and thus its atom position was isotropically refined under rigid condition. CCDC-230071 (**1**), CCDC-230072 (**2**), and CCDC-230073 (**1a**) contain the supplementary crystallographic data for this paper. These data can be obtained free of charge via www.ccdc.cam.ac.uk/conts/retrieving.html (or from the Cambridge Crystallographic Data Centre, 12 Union Road, Cambridge CB21EZ, UK; fax: (+44) 1223-336-033; or deposit@ccdc.cam.ac.uk).

Gas adsorption measurement: The sorption isotherm measurements for N_2, O_2 gases and solvents H_2O, MeOH, EtOH were carried out at 77 K and 298 K respectively by using an automatic volumetric adsorption apparatus (BELSORP 18; BEL inc). A known weight (150–200 mg) of the as-synthesized sample was placed in the quartz tube, then, prior to measurements, the sample was dried under high vacuum at 403 K for 5 h to remove the solvated water molecules. The adsorbate was placed into the sample tube, then the change of the pressure was monitored and the degree of adsorption was determined by the decrease of the pressure at the equilibrium state.

Received: February 4, 2004 [Z53923]
Published Online: May 12, 2004

[1] O. M. Yaghi, H. Li, C. Davis, D. Richardson, T. L. Groy, *Acc. Chem. Res.* **1998**, *31*, 474.
[2] S. Kitagawa, M. Kondo, *Bull. Chem. Soc. Jpn.* **1998**, *71*, 1739.
[3] P. J. Hagrman, D. Hagrman, J. Zubieta, *Angew. Chem.* **1999**, *111*, 2798; *Angew. Chem. Int. Ed.* **1999**, *38*, 2638.
[4] B. Moulton, M. J. Zaworotko, *Chem. Rev.* **2001**, *101*, 1629.
[5] C. Janiak, *Dalton Trans.* **2003**, 2781.
[6] P. J. Langley, J. Hulliger, *Chem. Soc. Rev.* **1999**, *28*, 279.
[7] O. M. Yaghi, H. Li, *J. Am. Chem. Soc.* **1996**, *118*, 295.
[8] J. S. Seo, D. Whang, H. Lee, S. I. Jun, J. Oh, Y. J. Jeon, K. Kim, *Nature* **2000**, *404*, 982.
[9] M. Eddaoudi, J. Kim, N. Rosi, D. Vodak, J. Wachter, M. O'Keeffe, O. M. Yaghi, *Science* **2002**, *295*, 469; N. L. Rosi, J. Eckert, M. Eddaoudi, D. T. Vodak, J. Kim, M, O'Keefe, O. M. Yaghi, *Science* **2003**, *300*, 1127.
[10] L. Pan, K. M. Adams, H. E. Hernandez, X. Wang, C. Zheng, Y. Hattori, K. Kaneko, *J. Am. Chem. Soc.* **2003**, *125*, 3062.
[11] R. Kitaura, S. Kitagawa, Y. Kubota, T. C. Kobayashi, K. Kindo, Y. Mita, A. Matsuo, M. Kobayashi, H.-C. Chang, T. C. Ozawa, M. Suzuki, M. Sakata, M. Takata, *Science* **2002**, *298*, 2358.
[12] D. N. Dybtsev, H. Chun, S. H. Yoon, D. Kim, K. Kim, *J. Am. Chem. Soc.* **2004**, *126*, 32.
[13] E. J. Cussen, J. B. Claridge, M. J. Rosseinsky, C. J. Kepert, *J. Am. Chem. Soc.* **2002**, *124*, 9574.
[14] K. Uemura, S. Kitagawa, M. Kondo, K. Fukui, R. Kitaura, H.-C. Chang, T. Mizutani, *Chem. Eur. J.* **2002**, *8*, 3586.
[15] K. Biradha, Y. Hongo, M. Fujita, *Angew. Chem.* **2002**, *114*, 3545; *Angew. Chem. Int. Ed.* **2002**, *41*, 3395.
[16] S. K. Makinen, N. J. Melcer, M. Parvez, G. K. H. Shimizu, *Chem. Eur. J.* **2001**, *7*, 5176.
[17] D. Maspoch, D. Ruiz-molina, K. Wurst, N. Domingo, M. Cavallini, F. Biscarini, J. Tejada, C. Rovira, A. J. Veciana, *Nat. Mater.* **2003**, *2*, 190.
[18] D. V. Soldatov, J. A. Ripmeester, S. I. Shergina, I. E. Sokolov, A. S. Zanina, S. A. Gromilov, Y. A. Dyadin, *J. Am. Chem. Soc.* **1999**, *121*, 4179.
[19] M. Kondo, T. Okubo, A. Asami, S.-I. Noro, T. Yoshitomi, S. Kitagawa, T. Ishii, H. Matsuzaka, K. Seki, *Angew. Chem.* **1999**, *111*, 190; *Angew. Chem. Int. Ed.* **1999**, *38*, 140.
[20] G. Alberti, E. Brunet, C. Dionigi, O. Juanes, M. J. d. L. Mata, J. C. RodrIguez-Ubis, R. Vivani, *Angew. Chem.* **1999**, *111*, 3548; *Angew. Chem. Int. Ed.* **1999**, *38*, 3351.
[21] R. Kitaura, K. Fujimoto, S.-i. Noro, M. Kondo, S. Kitagawa, *Angew. Chem.* **2002**, *114*, 141; *Angew. Chem. Int. Ed.* **2002**, *41*, 133.
[22] B. F. Abrahams, M. J. Hardie, B. F. Hoskins, R. Robson, E. E. Sutherland, *J. Chem. Soc. Chem. Commun.* **1994**, 1049.
[23] A. L. Spek, PLATON, The University of Utrecht, Utrecht, The Netherlands, **1999**.
[24] The size is measured by considering van der Waals radii for constituting atoms. Hereafter, all the size-estimation of pore is made in this way.
[25] S. S. Kuduva, D. C. Craig, A. Nangia, G. R. Desiraju, *J. Am. Chem. Soc.* **1999**, *121*, 1936.
[26] Molecular area is calculated from liquid density, assuming spherical symmetry and a hexagonal close packing. The equation and values are in reference [24].
[27] C. E. Webster, R. S. Drago, M. C. Zerner, *J. Am. Chem. Soc.* **1998**, *120*, 5509.

Keywords: adsorption · cadmium · coordination polymers · host–guest systems · microporous materials

 © 2004 Wiley-VCH Verlag GmbH & Co. KGaA, Weinheim

Mechanically Interlocked Compounds

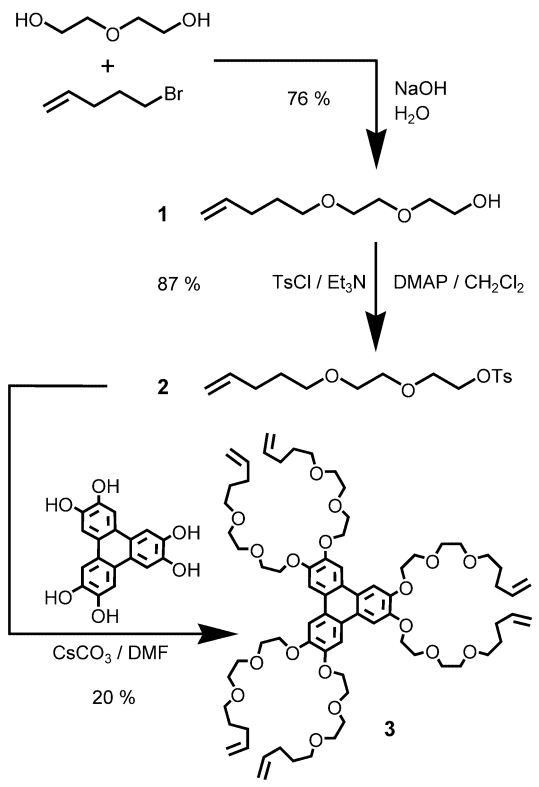
The Exclusivity of Multivalency in Dynamic Covalent Processes**

Jovica D. Badjić, Stuart J. Cantrill, Robert H. Grubbs, Erin N. Guidry, Raul Orenes, and J. Fraser Stoddart**

Nature's reliance on multivalency[1] as a means[2] of compensating for weak monovalent protein–ligand interactions is now a widely accepted phenomenon[3] which controls a panoply of biological events and whose delicate manipulations could have far-reaching therapeutic implications. In recent times, the physical basis of multivalency effects, based on a thermodynamic model combined with computational studies, has been explored rigorously[4] and a comprehensive thermodynamic investigation of the calcium–EDTA interactions has been reported.[5] Since thermodynamics seem, by and large,[6] to rule the roost as far as multivalency is concerned, it occurred to us that it should be the perfect phenomenon to probe using the concept of dynamic covalent chemistry.[7] Herein we describe a situation in which the concept works in the exclusive context of the phenomenon; that is, dynamic covalent chemistry can be achieved in a highly efficient manner using multivalent ligands, but fails altogether when no ligand or a monovalent counterpart is employed.

As a part of some on-going research to probe multivalency in artificial systems[8] exhibiting molecular recognition, we have recently uncovered a compelling example[9] of multivalency between a tritopic receptor, in which three benzo[24]crown-8 rings are fused onto a triphenylene core, and a trifurcated trication, wherein three dibenzylammonium ions are linked 1,3,5 to a central benzenoid core: the outcome is an extremely stable ($K_a > 10^7\ mol\,L^{-1}$ in CH_2Cl_2) triply threaded, two-component superbundle. This observation led subsequently to the template-directed synthesis[10] of a prototype[11] of an artificial molecular machine,[12] namely, a mechanically interlocked, triply threaded, molecular bundle by kinetically controlled post-assembly covalent modification. The advent of dynamic covalent chemistry[7] has, however, opened up an attractive alternative route[13] to mechanically interlocked molecules which relies upon the thermodynamically controlled strict self-assembly of their covalently linked components proceeding in unison with mechanical bond formation under the guidance of the templation provided by noncovalent interactions. In particular, it has been shown that 1) the reversible ring-closing metathesis (RCM) reaction and 2) the ring-opening, ring-closing metathesis (RORCM) reaction, also operating under equilibrium control, are both mediated by functional-group-tolerant ruthenium–alkylidene catalysts[14] and can be used[15] in the thermodynamically controlled synthesis of catenanes and rotaxanes.[16] In the specific knowledge that [2]rotaxanes[17] and [3]catenanes,[18] where the supramolecular assistance[19] for their formation comes from the interaction[20] of $CH_2NH_2^+CH_2$ ion centers, either by developing olefinic crown ether analogues containing 24-membered rings or with dibenzo[24]crown-8, we decided to explore the possibility that the multivalency effect can be exploited during RCM and RORCM. We demonstrate that it can be exploited in a convincing manner: multivalency flourishes in situations where monovalency falters.

As outlined in Schemes 1 and 2, respectively, we have prepared the triphenylene hexa-olefin **3** and the trifurcated trisammonium salt [**5**-H_3][PF_6]$_3$ by standard protocols (see the Experimental Section). Their ^{1}H NMR spectra, recorded in CD_3CN and $CDCl_3$, respectively, are reproduced in Figure 1 a and b, respectively. When a solution of **3** (15 mM) in CD_2Cl_2 at

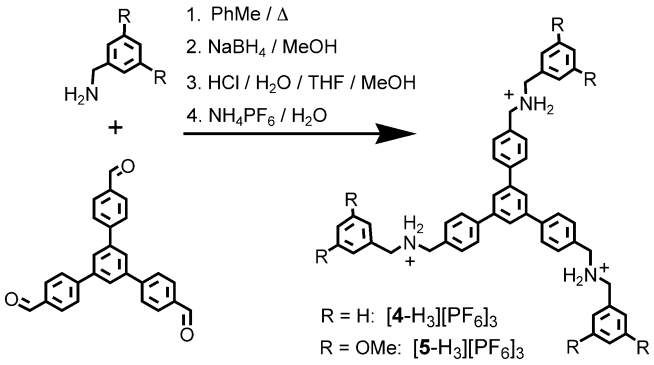


Scheme 1. Synthesis of the hexa-olefin **3**. DMAP = 4-dimethylaminopyridine, DMF = dimethylformamide, Ts = toluene-4-sulfonyl.

[*] Prof. R. H. Grubbs, E. N. Guidry
Arnold and Mabel Beckman Laboratory of Chemical Synthesis
Division of Chemistry and Chemical Engineering
California Institute of Technology
Pasadena, CA 91125 (USA)
Fax: (+1) 626-564-9297
E-mail: rhg@caltech.edu
Dr. J. D. Badjić, Dr. S. J. Cantrill, R. Orenes, Prof. J. F. Stoddart
California NanoSystems Institute and
Department of Chemistry and Biochemistry
University of California, Los Angeles
405 Hilgard Avenue, Los Angeles, CA 90095 (USA)
Fax: (+1) 310-206-1843
E-mail: stoddart@chem.ucla.edu

[**] We thank the National Science Foundation (CHE 0317170) for funding this research which is also supported in part by equipment grants (CHE 9974928 and CHE 0092036) from the National Science Foundation. We also thank the Office of Naval Research for support through its MURI program.

 DOI: 10.1002/anie.200453963 © 2004 Wiley-VCH Verlag GmbH & Co. KGaA, Weinheim



Scheme 2. Syntheses of the trisammonium tris(hexafluorophosphate) salts [**4**-H_3][PF_6]$_3$ and [**5**-H_3][PF_6]$_3$. THF = Tetrahydrofuran

40 °C is treated with [$(PCy_3)_2(Cl)_2Ru$=CHPh] (1.6 mM, 11 mol %), a complex mixture of products is formed, as indicated by thin layer chromatography and ^{1}H NMR spectroscopy. A very similar outcome emerged when a mixture of **3** (15 mM) with the monovalent bis-3,5-dimethoxybenzylammonium hexafluorophosphate[17] (45 mM) was treated under exactly the same reaction conditions with the same ruthenium–alkylidene catalyst. Thus, both without and with a monovalent template, little or none of the desired crown ether analogue **7**, or the anticipated[4] rotaxane, are formed. The reasons for these observations could relate to the myriad of potential products that could be formed by different intramolecular RCM reactions. Also, amplification by the monovalent template to give a [4]rotaxane would incur a considerable entropy loss which most likely would swamp a very small enthalpic gain.

When a mixture (each 15 mM in CD_2Cl_2 at 40 °C) of **3** and [**5**-H_3][PF_6]$_3$ was subjected to a RCM reaction using [$(PCy_3)_2(Cl)_2Ru$=CHPh] (1.6 mM, 11 mol %), the ^{1}H NMR spectrum recorded after 4 h revealed a complex array of well-defined resonances. With the aid of 2D NMR (^{1}H-^{1}H COSY) experiments, almost all the resonances could be assigned to an isomeric mixture of [**6**-H_3][PF_6]$_3$ containing C=C double bonds with both *E* and *Z* configurations. The formation (Scheme 3) of the mechanically interlocked molecular "bundle" [**6**-H_3][PF_6]$_3$ with averaged quasi C_{3v} symmetry is consistent with the ^{1}H NMR spectroscopic data (see Figure 1c). The methylene protons H_d and H_e on the carbon atoms adjacent to the secondary dialkylammonium centers in [**6**-H_3][PF_6]$_3$ resonate as broad multiplets centered on $\delta = 4.63$ and 4.74 ppm: these "same" protons resonate as sharp singlets at $\delta = 4.20$ and 4.29 ppm in [**5**-H_3][PF_6]$_3$. The downfield shifts and the multiplicities exhibited by H_d and H_e in [**6**-H_3][PF_6]$_3$ are diagnostic of their having been threaded by benzo[24]-crown-6 rings, that is, they demonstrate the interlocked nature of the "two" components in [**6**-H_3]$^{3+}$. Furthermore, the resonances of the aromatic core protons H_a and H_h at $\delta =$ 7.72 and 7.44 ppm, respectively, in the "two" components within [**6**-H_3]$^{3+}$ are shifted significantly upfield relative (Figure 1a and b) to the chemical shifts ($\delta = 7.96$ and 7.88 ppm, respectively) of the analogous protons in the individual components—namely [**5**-H_3]$^{3+}$ and **3**, respectively—which indicates π-π stacking of the central aromatic cores of the components with respect to one another. The

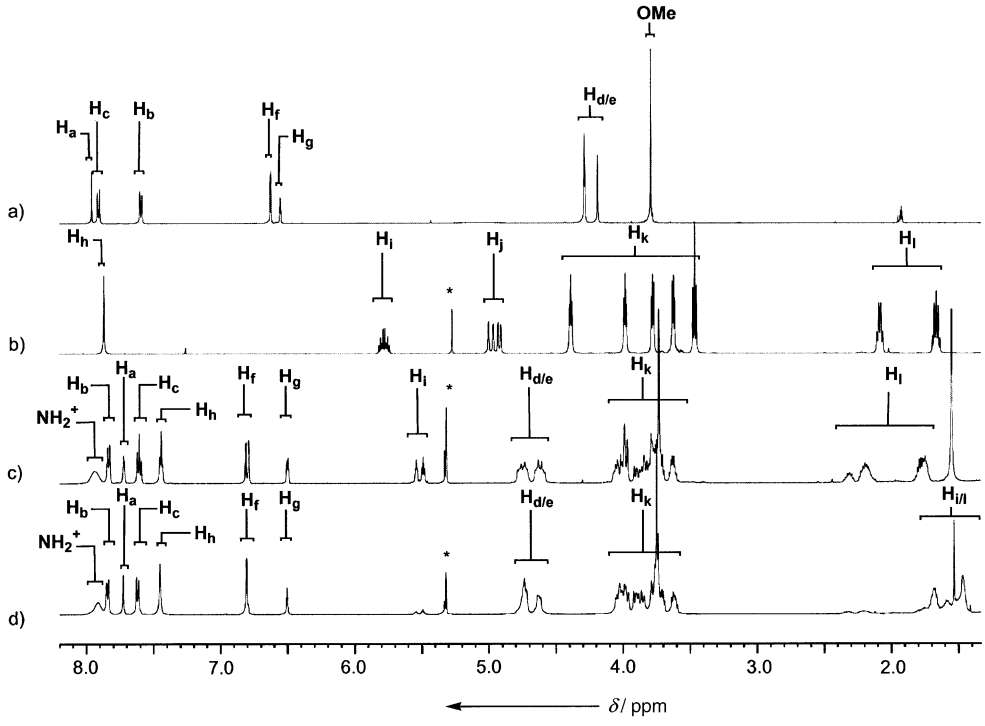
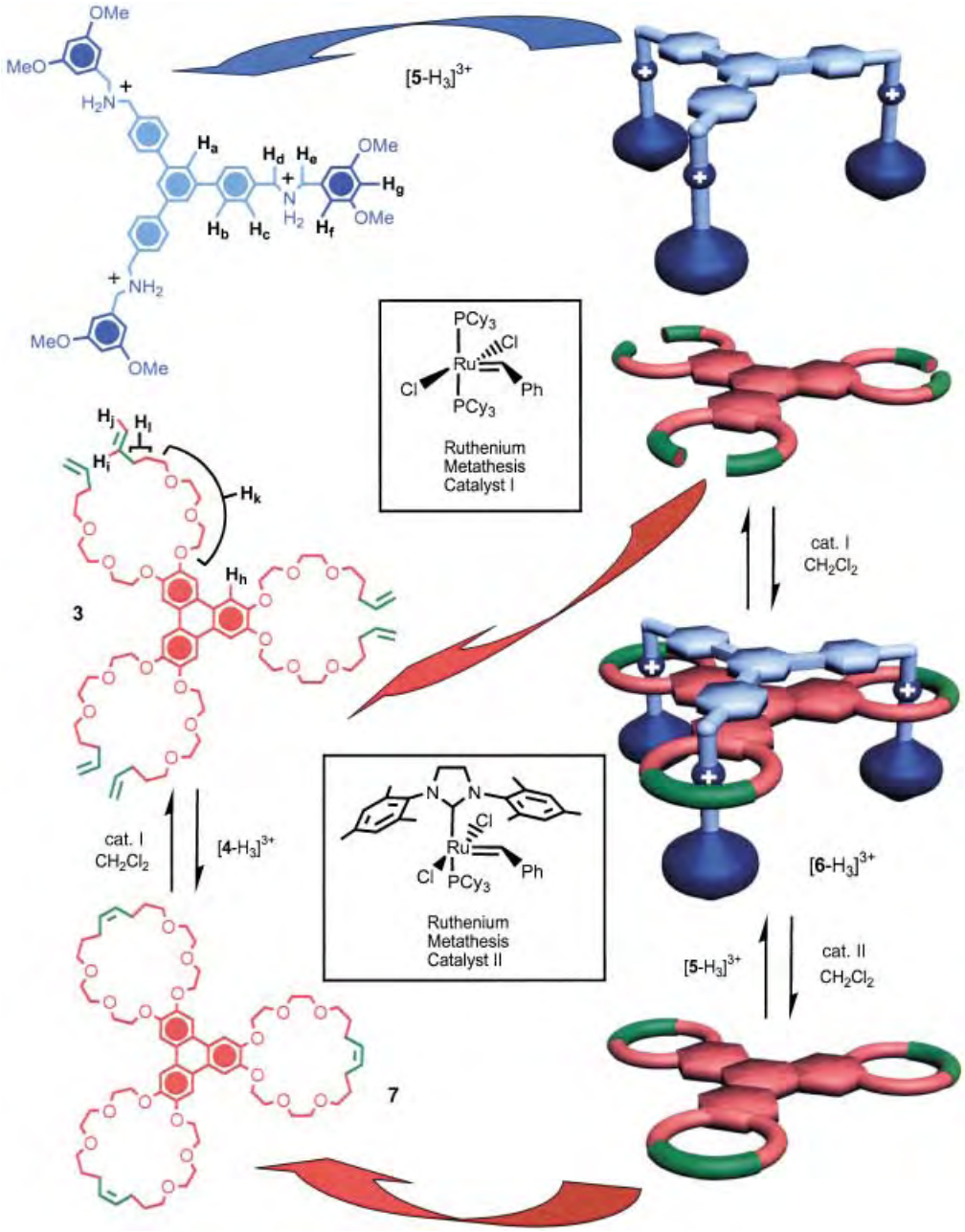


Figure 1. The ^{1}H NMR spectra (500 MHz, 298 K) of a) the trifurcated trisammonium salt [**5**-H_3][PF_6]$_3$ (15 mM in CD_3CN), b) the hexa-olefin **3** (15 mM in $CDCl_3$), c) the mechanically interlocked "bundle" [**6**-H_3][PF_6]$_3$ (15 mM in CD_2Cl_2), and d) the hydrogenated [**6**-H_3][PF_6]$_3$ (15 mM in CD_2Cl_2). Asterisk = residual solvent.

 © 2004 Wiley-VCH Verlag GmbH & Co. KGaA, Weinheim



Scheme 3. The efficient preparation of the mechanically interlocked "bundle" [**6**-H_3][PF_6]$_3$ as a mixture of isomers containing C=C bonds with both *E* and *Z* configurations can be achieved through either a ring-closing metathesis (RCM) reaction starting from an equimolar mixture (each 15 mM in CH_2Cl_2 at 40 °C) of the trifurcated trisammonium salt [**5**-H_3][PF_6]$_3$ and hexa-olefin **3** using the functional group tolerant [$(PCy_3)_2(Cl)_2Ru$=CHPh] (1.6 mM, 11 mol%) catalyst or ring-closing ring-opening metathesis (RORCM) reaction starting from an equimolar mixture (each 16 mM in CH_2Cl_2 at 25 °C) of the trifurcated trisammonium salt [**5**-H_3][PF_6]$_3$ and triscrown **7** using the catalyst [$(IMesH_2)(PCy_3)(Cl)_2Ru$=CHPh] (2.35 mM, 15 mol%). The synthesis of the triscrown **7** is shown on the left side. A triply threaded two component "superbundle" is assembled from an equimolar mixture (25 mM each in CH_2Cl_2 at 40 °C) of **3** and the trifurcated trisammonium tris(hexafluorophosphate) salt [**4**-H_3][PF_6]$_3$ containing [$(PCy_3)_2(Cl)_2Ru$=CHPh] (1.6 mM, 6 mol%) as the catalyst. The 1:1 complex formed as a result of this RCM reaction was then treated with a slight excess (>3 equiv) of Et_3N to deprotonate the [**4**-H_3]$^{3+}$ component and so release[9] the tris(crown ether) **7** as a mixture of isomers where the C=C bonds in the macrorings have either *E* or *Z* configurations.

almost quantitative production[21] of [**6**-H_3][PF_6]$_3$ is presumably the result of the build-up of cooperative binding interactions, which result from the three productive RCM reactions that lead to the statistical and cluster effects[8] associated with the multivalency that characterizes the thermodynamically stable product. Hydrogenation (H_2/PtO_2) of all the (*E*/*Z*) olefinic bonds present in [**6**-H_3][PF_6]$_3$ yielded (72%) a mechanically interlocked bundle with averaged C_{3v} symmetry as evidenced (Figure 1d) by ^{1}H NMR spectroscopy. The "resonance" at $\delta = 5.53$ ppm for the olefinic protons H_i in [**6**-H_3][PF_6]$_3$ disappears and is replaced by a signal centered on $\delta = 1.57$ ppm for protons

 © 2004 Wiley-VCH Verlag GmbH & Co. KGaA, Weinheim

associated with CH_2 groups located in the middle of polymethylene chains.

We have also discovered that it is possible to assemble [**6**-H_3][PF_6]$_3$ directly from the situation (Scheme 3) wherein both components—that is, [**5**-H_3]$^{3+}$ and **7**—are already preformed. The tris(crown ether) **7** was synthesized by, first of all, constructing a triply threaded two-component "superbundle" from an equimolar mixture (25 mM each in CH_2Cl_2 at 40 °C) of **3** and the trifurcated trisammonium tris(hexafluorophosphate)[9] salt [**4**-H_3][PF_6]$_3$ containing [(PCy_3)$_2$(Cl)$_2$Ru=CHPh] (1.6 mM, 6 mol %) as the catalyst. The 1:1 complex formed as a result of this RCM reaction was then treated with a slight excess (> 3 equiv) of Et_3N to deprotonate the [**4**-H_3]$^{3+}$ component and so release[9] the tris(crown ether) **7** as a mixture of isomers in which the C=C bonds in the macrorings have either *E* or *Z* configurations. The "compound" was isolated in 69 % yield following chromatography. Hydrogenation (H_2/PtO_2) of the C=C bonds in **7** afforded a *pure* saturated tris(crown ether) which was fully characterized by ^{1}H NMR spectroscopy and mass spectrometry. Next, a solution of [**5**-H_3]$^{3+}$ and **7**—each 16 mM in CD_2Cl_2—was prepared and an ^{1}H NMR spectrum was recorded (Figure 2).

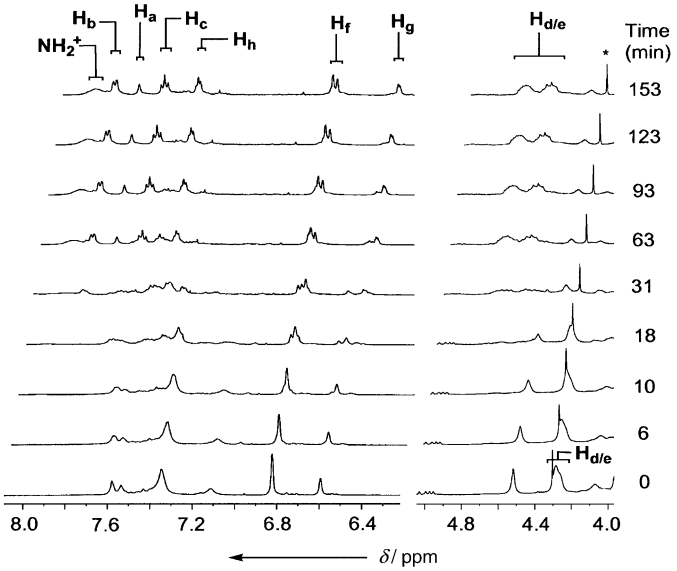


Figure 2. Partial ^{1}H NMR spectra (500 MHz, CD_2Cl_2, 16 mM each, 298 K) of an equimolar mixture of [**5**-H_3][PF_6]$_3$ and **7**, before (0 min) and after (6–153 min) addition of the catalyst [($IMesH_2$)(PCy_3)(Cl)$_2$Ru=CHPh] (2.35 mM, 15 mol %), which shows the exclusive formation (> 95 %) of the mechanically interlocked "bundle" [**6**-H_3][PF_6]$_3$ with time in a series of RORCM reactions. Asterisk = residual solvent.

It revealed that, even though the two components do *not* form a supramolecular bundle, an RORCM reaction does take place upon addition of [($IMesH_2$)(PCy_3)(Cl)$_2$Ru=CHPh] (2.3 mM, 15 mol %) as the catalyst.[22] The equilibration process was followed (Figure 2) by ^{1}H NMR spectroscopy: equilibrium was attained in about 150 minutes to give a 95 % yield of the mechanically interlocked two-component "bundle" [**6**-H_3][PF_6]$_3$ which was also characterized by mass spectrometry. Hence, an RCM reaction has been employed, using a template, to make a component—namely, the tris(crown ether) **7**—for use subsequently in a successful RORCM reaction, using another template, to make a "bundle" incorporating that component.

Since the multivalency effect[1–6] is primarily a thermodynamic phenomenon, it seems entirely reasonable that multivalent sites between two or more components can be created spontaneously in situ by dynamic covalent chemistry,[7] a concept wherein reactivity is expressed in a thermodynamic context. The results reported here, together with those already described in the literature,[9,10] demonstrate that it is much less efficient to synthesize both components of a multivalent recognition site separately than it is to use one multivalent component to act as a template for the catalytically orchestrated construction of the other component. The situation is reminiscent of nature which frequently uses enzymes, in conjugation with self-assembly processes, to build up large and functional molecular structures. We foresee developments in polymer chemistry where the dynamic interplay between molecular recognition and the reversible formation of covalent (and mechanical) bonds using suitable catalysts will lead to the efficient production of high-molecular-weight polymers just as rich in information content as are many biopolymers.

Experimental Section

1: A solution of diethylene glycol (71 g, 0.67 mol), 5-bromo-1-pentene (10 g, 0.17 mol) in H_2O containing NaOH (13.4 g, 0.33 mol) was heated at 80 °C for 24 h. A standard work-up procedure gave a crude product, which was purified by column chromatography (SiO_2:hexanes/Et_2O, 1:1), to yield **1** as a colorless oil (11.7 g, 76 %). ^{1}H NMR (500 MHz, $CDCl_3$): $\delta = 1.64$ (m, 2H), 2.05 (m, 2H), 3.42 (m, 2H), 3.61 (m, 8H), 4.94 (m, 2H), 5.74 ppm (m, 1H); ^{13}C NMR (125 MHz, $CDCl_3$): $\delta = 28.5$, 30.0, 61.5, 70.0, 70.2, 70.6, 72.4, 114.6, 138.0 ppm.

2: Compound **1** (3.0 g, 17.0 mmol), Et_3N (8.6 g, 85.0 mmol), and a few crystals of DMAP were dissolved in dry CH_2Cl_2 (50 mL) and a solution of TsCl (7.0 g, 36.0 mmol) in dry CH_2Cl_2 (100 mL) was added over 2 h. The reaction mixture was stirred overnight before being subjected to a standard work-up procedure. Column chromatography (SiO_2, hexanes/Et_2O, 1:1) of the crude product afforded **2** as a pale yellow oil (4.9 g, 87 %). ^{1}H NMR (500 MHz, $CDCl_3$): $\delta = 1.63$ (m, 2H), 2.06 (m, 2H), 2.42 (s, 3H), 3.41 (t, $J = 7$ Hz, 2H), 3.48 (m, 2H), 3.55 (m, 2H), 3.67 (t, $J = 5$ Hz, 2H), 4.14 (t, $J = 5$ Hz, 2H), 4.94 (m, 2H), 5.77 (m, 1H), 7.31 (d, $J = 8$ Hz, 2H), 7.77 ppm (d, $J = 8$ Hz, 2H); ^{13}C NMR (125 MHz, $CDCl_3$): $\delta = 21.5$, 28.6, 30.1, 68.5, 69.1, 69.9, 70.6, 70.7, 114.6, 127.8, 129.7, 132.9, 138.1, 144.7 ppm. HRMS (EI): *m/z* found: 329.1425, calcd for $C_{14}H_{25}O_5S$: 329.1423 [M+H]$^+$.

3: An oven-dried 1 L three-necked, round-bottomed flask, equipped with a stirrer bar, a gas-inlet tube, a dropping funnel, and a condenser, was purged with Ar for 10 min and then filled with anhydrous DMF (150 mL). Cs_2CO_3 (10.1 g, 31.0 mmol) was added to the flask and the white suspension stirred vigorously with heating at 100 °C. The dropping funnel was charged with a solution of 2,3,6,7,10,11-hexahydroxytriphenylene (500 mg, 1.6 mmol) and **2** (4.1 g, 12.4 mmol) in anhydrous DMF (250 mL) and this solution was added dropwise over 24 h to the suspension, which was then heated at 100 °C for another 3 days. On cooling the reaction mixture down to room temperature, the suspension was filtered off and the residue was washed with $CHCl_3$ (250 mL). The filtrate and $CHCl_3$ washings were concentrated under reduced pressure. The resulting dark tar was dissolved in $CHCl_3$ (200 mL) and washed with 10 % aqueous K_2CO_3 (2 × 150 mL) and finally with brine (150 mL). The

 © 2004 Wiley-VCH Verlag GmbH & Co. KGaA, Weinheim

organic layer was dried (Na_2SO_4), filtered, and concentrated under reduced pressure to afford a crude product which was subjected to column chromatography (SiO_2, hexanes/EtOAc, 4:6) to yield **3** as a yellow oil (400 mg, 20%); ^{1}H NMR (500 MHz, $CDCl_3$): $\delta = 1.66$ (m, 12H), 2.08 (m, 12H), 3.46 (t, $J = 7$ Hz, 12H), 3.62 (t, $J = 5$ Hz, 12H), 3.78 (t, $J = 5$ Hz, 12H), 3.98 (t, $J = 5$ Hz, 12H), 4.39 (t, $J = 5$ Hz, 12H), 4.95 (m, 12H), 5.77 (m, 6H), 7.87 ppm (s, 6H); ^{13}C NMR (125 MHz, $CDCl_3$): $\delta = 28.6$, 30.1, 69.1, 69.8, 70.1, 70.6, 70.8, 107.9, 114.6, 123.8, 138.1, 148.6 ppm. HRMS (MALDI): *m/z* found: 1283.7393, calcd for $C_{72}H_{108}O_{18}Na$: 1283.7428 $[M+Na]^+$.

[**4**-H_3][PF_6]$_3$: The synthesis of this trisammonium tris(hexafluorophosphate) salt has been reported previously.[9]

[**5**-H_3][PF_6]$_3$: A mixture of 1,3,5-tris(*p*-formylphenyl)benzene (1.0 g, 2.6 mmol) and 3,5-dimethoxybenzylamine (1.3 g, 7.7 mmol) in PhMe (150 mL) was heated under reflux for 24 h and the H_2O was collected in a Dean–Stark apparatus. The solution was allowed to cool down to room temperature and the solvent was evaporated under reduced pressure to give the trisimine as a yellow oil (2.1 g, 99%). This oil was dissolved in dry THF (60 mL) and dry MeOH (25 mL). After the portionwise addition of $NaBH_4$ (600 mg, 15.8 mmol), the reaction mixture was left to stir overnight. 5 M HCl (200 mL) was then added to the reaction mixture, which was concentrated to a residue that was partitioned between aqueous 2 M NaOH solution (100 mL) and CH_2Cl_2 (150 mL). The aqueous layer was then extracted further with CH_2Cl_2 (100 mL). The combined organic extracts were washed with H_2O (100 mL) and then dried (Na_2SO_4). Filtration, followed by solvent evaporation, gave the crude product which was subjected to column chromatography (SiO_2, hexanes/Et_2O, 1:1) to afford the trisamine as a pale yellow oil (1.0 g, 46%). ^{1}H NMR (500 MHz, $CDCl_3$): $\delta = 3.84$ (s, 6H), 3.85 (s, 18H), 3.93 (s, 6H), 6.44 (t, $J = 2$ Hz, 3H), 6.60 (d, $J = 2$ Hz, 6H), 7.51 (d, $J = 8$ Hz, 6H), 7.73 (d, $J = 8$ Hz, 6H), 7.84 ppm (s, 3H). This oil was dissolved in THF/MeOH (30 mL, 25:5) and concentrated 12 M HCl (30 drops) was added. The reaction mixture was stirred for 6 h and then filtered. The resulting white solid was dissolved in hot MeOH/H_2O and saturated aqueous NH_4PF_6 solution was added. The resulting suspension was extracted with $MeNO_2$ (50 mL). The $MeNO_2$ extract was washed with H_2O (4 × 70 mL), dried (Na_2SO_4), filtered, and the solvent was removed under reduced pressure to give [**5**-H_3][PF_6]$_3$ as a white solid (1.2 g, 79%). ^{1}H NMR (500 MHz, CD_3CN): $\delta = 3.79$ (s, 18H), 4.19 (s, 6H), 4.29 (s, 6H), 6.55 (t, $J = 2$ Hz, 3H), 6.62 (d, $J = 2$ Hz, 6H), 7.59 (d, $J = 8$ Hz, 6H), 7.90 (d, $J = 8$ Hz, 6H), 7.96 ppm (s, 3H); ^{13}C NMR (125 MHz, CD_3CN): $\delta = 50.9$, 51.4, 55.1, 100.9, 107.7, 117.2, 125.2, 127.7, 130.1, 130.7, 132.5, 141.3, 141.4, 161.2 ppm. HRMS (ESI): *m/z* found: 844.4312, calcd for $C_{54}H_{58}O_6N_3$: 844.4320 $[M-2H-3PF_6]^+$.

[**6**-H_3][PF_6]$_3$: A solution of **3** (58 mg, 0.046 mmol) and [**5**-H_3][PF_6]$_3$ (59 mg, 0.046 mmol) in anhydrous CH_2Cl_2 (3.0 mL) was purged with Ar for 10 min. The catalyst [$(PCy_3)_2(Cl)_2Ru$=CHPh] (4 mg, 0.005 mmol) was added under a dry Ar atmosphere and the reaction mixture heated at 40 °C for 4 h. The solvent was evaporated off under reduced pressure and the crude product subjected to column chromatography (SiO_2, CH_2Cl_2/$MeNO_2$, 8:2) to yield [**6**-H_3][PF_6]$_3$ as a white solid (70 mg, 62%) and as a mixture of isomers. ^{1}H NMR (500 MHz, CD_2Cl_2): $\delta = 1.77$ (m, 12H), 2.10–2.40 (m, 12H), 3.60–4.10 (m, 60H), 3.73 (s, 18H), 4.60 (m, 6H), 4.74 (m, 6H), 5.47–5.55 (m, 6H), 6.50 (m, 3H), 6.80 (m, 6H), 7.44 (m, 6H), 7.60 (m, 6H), 7.72 (br s, 3H), 7.83 (d, $J = 7$ Hz, 6H), 7.95 ppm (br s, 6H); MS (MALDI-TOF): *m/z* (%): 2313.9 $[M-PF_6]^+$ (10), 2166.5 $[M-H-2PF_6]^+$ (40), 2020.7 $[M-2H-3PF_6]^+$ (57). To complete the characterization of this mechanically interlocked "bundle", PtO_2 (5.4 mg) was added to a solution of [**6**-H_3][PF_6]$_3$ (48 mg, 0.020 mmol) in anhydrous THF (8 mL) and the reaction mixture was stirred under H_2 for 4 h. The solvent was then removed under reduced pressure and the crude product purified by column chromatography (SiO_2, CH_2Cl_2/$MeNO_2$, 8:2) to yield the fully characterized derivative of [**6**-H_3][PF_6]$_3$ as a white solid (35 mg, 72%). ^{1}H NMR (500 MHz, CD_2Cl_2): $\delta = 1.40$–1.70 (m, 36H), 3.50–4.15 (m, 60H), 3.74 (s, 18H), 4.71 (m, 6H), 4.80 (m, 6H), 6.47 (br t, 3H), 6.79 (d, $J = 2$ Hz, 6H), 7.47 (s, 6H), 7.58 (d, $J = 8$ Hz, 6H), 7.71 (s, 3H), 7.83 (d, $J = 8$ Hz, 6H), 7.96 ppm (br s, 6H); ^{13}C NMR (125 MHz, CD_2Cl_2): $\delta = 25.7$, 27.9, 29.6, 51.9, 52.8, 55.3, 67.9, 70.7, 71.2, 72.1, 73.0, 100.5, 104.4, 106.0, 120.5, 123.1, 125.8, 129.0, 129.6, 133.8, 136.5, 138.1, 145.9, 161.2 ppm; MS (MALDI): *m/z* (%): 2319.0 $[M-PF_6]^+$ (5), 2174.1 $[M-2PF_6]^+$ (40), 2028.1 $[M-H-3PF_6]^+$ (100). HRMS (ESI): *m/z* found: 1087.5990, calcd for $C_{120}H_{162}O_{24}N_3PF_6$: 1087.5606 $[M-2PF_6]^{2+}$.

7: A solution of **3** (96 mg, 0.076 mmol) and [**4**-H_3][PF_6]$_3$ (84 mg, 0.076 mmol) in anhydrous CH_2Cl_2 (3 mL) was purged with argon for 10 min. The catalyst [$(PCy_3)_2(Cl)_2Ru$=CHPh] (4 mg, 0.005 mmol) was added under a dry Ar atmosphere and the reaction mixture heated at 40 °C for 4 h. The solvent was evaporated off under reduced pressure and several drops of Et_3N added, followed by CH_2Cl_2 (5 mL). The solvent was once again removed under reduced pressure and the crude product subjected to column chromatography (SiO_2, CH_2Cl_2/MeOH, gradient from 10:0 to 8:2) to yield **7** as a white solid (62 mg, 69%) as a mixture of isomers. ^{1}H NMR (500 MHz, CD_2Cl_2): $\delta = 1.61$ (m, 12H), 2.02–2.17 (m, 12H), 3.47 (m, 12H), 3.51 (m, 12H), 3.76 (m, 12H), 3.97 (m, 12H), 4.37 (m, 12H), 5.31–5.40 (m, 6H), 7.88 ppm (s, 6H). HRMS (MALDI): *m/z* found: 1199.6463, calcd for $C_{66}H_{96}O_{18}Na$: 1199.6489 $[M+Na]^+$. To complete the characterization of this tris(crown ether), PtO_2 (5.4 mg) was added to a solution of **7** (50 mg, 0.020 mmol) in anhydrous THF (8 mL), and the reaction mixture was stirred under H_2 for 5 h. The solvent was then removed under reduced pressure and the crude product was subjected to column chromatography (SiO_2, CH_2Cl_2/MeOH, 95:5) to yield the *pure* fully characterized hydrogenated derivative of **7** as an off-white solid (38 mg, 75%). ^{1}H NMR (500 MHz, CD_2Cl_2): $\delta = 1.20$–1.70 (m, 36H), 3.46 (t, $J = 6$ Hz, 12H), 3.60 (t, $J = 5$ Hz, 12H), 3.75 (t, $J = 5$ Hz, 12H), 3.97 (t, $J = 5$ Hz, 12H), 4.39 (t, $J = 5$ Hz, 12H), 7.92 ppm (s, 6H); ^{13}C NMR (125 MHz, CD_2Cl_2): $\delta = 25.5$, 28.4, 29.2, 69.7, 70.2, 70.5, 71.1, 71.2, 108.7, 124.1, 148.9 ppm; HRMS (MALDI): *m/z* found: 1205.7015, calcd for $C_{66}H_{102}O_{18}Na$: 1205.6958 $[M+Na]^+$.

"Magic ring" synthesis of [**6**-H_3][PF_6]$_3$: Catalyst [$(IMesH_2)(PCy_3)(Cl)_2Ru$=CHPh] (1.0 mg dissolved in CD_2Cl_2, 15 mol%) was added to a solution of the tris(crown ether) **7** (9.6 mg, 0.008 mmol) and the trisammonium salt [**5**-H_3][PF_6]$_3$ (10.5 mg, 0.008 mmol) in CD_2Cl_2 (0.5 mL) under a dry Ar atmosphere. The reaction to give [**6**-H_3][PF_6]$_3$ was followed (Figure 2) by ^{1}H NMR spectroscopy at 298 K.

Received: February 6, 2004 [Z53963]

Keywords: metathesis · molecular recognition · NMR spectroscopy · supramolecular chemistry

[1] a) R. T. Lee, Y. C. Lee, *Glycoconjugate J.* **2000**, *17*, 543–551; b) J. J. Lundquist, E. J. Toone, *Chem. Rev.* **2002**, *102*, 555–578; c) S. L. Tobey, E. V. Anslyn, *J. Am. Chem. Soc.* **2003**, *125*, 10963–10970; d) G. Ercolani, *J. Am. Chem. Soc.* **2003**, *125*, 16097–16103.

[2] With a few provisos, the adage "many a mickle makes a muckle", comes to mind; for some key articles relating the multivalency effects, see: a) E. J. Gordon, W. J. Sanders, L. L. Kiessling, *Nature* **1998**, *392*, 30–31; b) J. Rao, J. Lahiri, L. Isaacs, R. M. Weiss, G. M. Whitesides, *Science* **1998**, *280*, 708–711; c) P. I. Kitov, J. M. Sadawska, G. Mulvey, G. D. Armstrong, H. Ling, N. S. Pannu, R. J. Read, D. R. Bundle, *Nature* **2000**, *403*, 669–672; d) J. E. Gestwicki, C. W. Cairo, L. E. Strong, K. A. Oetjen, L. L. Kiessling, *J. Am. Chem. Soc.* **2002**, *124*, 14922–14933; e) E. K. Woller, E. D. Walter, J. R. Morgan, D. J. Singel, M. J. Cloninger, *J. Am. Chem. Soc.* **2003**, *125*, 8820–8826.

[3] a) R. T. Lee, Y. C. Lee, *Acc. Chem. Res.* **1995**, *28*, 321–327; b) K. Drickamer, *Nat. Struct. Biol.* **1995**, *2*, 437–439; c) J. M. Rini, *Annu. Rev. Biophys. Biomol. Struct.* **1995**, *24*, 551–557; d) R. Roy, *Polym. News* **1996**, *21*, 226–232; e) W. I. Weiss, K.

 © 2004 Wiley-VCH Verlag GmbH & Co. KGaA, Weinheim

Drickamer, *Annu. Rev. Biochem.* **1996**, *65*, 441 – 473; f) N. Jayaraman, S. A. Nepogodiev, J. F. Stoddart, *Chem. Eur. J.* **1997**, *3*, 1193 – 1199; g) L. L. Kiessling, J. E. Gestwicki, L. E. Strong, *Curr. Opin. Chem. Biol.* **2000**, *4*, 696 – 703; h) N. Rockendorf, T. H. Lindhorst, *Top. Curr. Chem.* **2001**, *217*, 201 – 238; i) W. B. Turnbull, J. F. Stoddart, *Rev. Mol. Biotechnol.* **2002**, *90*, 231 – 255; j) M. Dubber, J. M. J. Fréchet, *Bioconjugate Chem.* **2003**, *14*, 239 – 246.

[4] P. I. Kitov, D. R. Bundle, *J. Am. Chem. Soc.* **2003**, *125*, 16271 – 16284.

[5] T. Christensen, D. M. Gooden, J. E. Kung, E. J. Toone, *J. Am. Chem. Soc.* **2003**, *125*, 7357 – 7366.

[6] A recent study carried out on the high-avidity, reversible low-affinity multivalent interactions of the lectin XL35 with the jelly coat proteins surrounding oocytes in *Xenopus laevis* shows that they require a very long time to reach equilibrium, so long in fact that the partners do not attain true equilibrium on the timescale of the biological event, namely polyspermy, yet are such that their metastable mode of interaction is probably more than enough to guarantee an insurmountable physical block to polyspermy; see a) E. Arranz-Plaza, A. S. Tracy, A. Siriwardena, J. M. Pierce, G.-J. Boons, *J. Am. Chem. Soc.* **2002**, *124*, 13035 – 13046; in the strict self-assembly of a triply threaded two-component superbundle, starting from a tritopic receptor in which three benzo[24]crown-8 macrorings are fused onto a triphenylene core and a trifurcated trication wherein three bipyridinium units are linked 1,3,5 to a central benzenoid core, it transpires that the rapid formation of a doubly threaded two-component complex is followed by an extremely slow conversion (a week at 253 K in CD_3COCD_3 to reach equilibrium) of this kinetically controlled product into a thermodynamically controlled one—namely, a triply threaded two-component superbundle; see: b) J. D. Badjić, S. J. Cantrill, J. F. Stoddart, *J. Am. Chem. Soc.* **2004**, *126*, 2288 – 2289.

[7] a) P. A. Brady, R. P. Bonar-Law, S. J. Rowan, C. J. Suckling, J. K. M. Sanders, *Chem. Commun.* **1996**, 319 – 320; b) P. A. Brady, J. K. M. Sanders, *Chem. Soc. Rev.* **1997**, *26*, 327 – 336; c) J.-M. Lehn, *Chem. Eur. J.* **1999**, *5*, 2455 – 2463; d) J. K. M. Sanders, *Pure Appl. Chem.* **2000**, *72*, 2265 – 2274; e) L. M. Greig, D. Philp, *Chem. Soc. Rev.* **2001**, *30*, 287 – 302; f) S. J. Rowan, S. J. Cantrill, G. R. L. Cousins, J. K. M. Sanders, J. F. Stoddart, *Angew. Chem.* **2002**, *114*, 938 – 993; *Angew. Chem. Int. Ed.* **2002**, *41*, 899 – 952.

[8] a) D. A. Fulton, S. J. Cantrill, J. F. Stoddart, *J. Org. Chem.* **2002**, *67*, 7968 – 7981; b) J. N. Lowe, D. A. Fulton, S.-H. Chiu, A. M. Elizarov, S. J. Cantrill, S. J. Rowan, J. F. Stoddart, *J. Org. Chem.*, in press; see also: c) H. W. Gibson, N. Yamaguchi, L. Hamilton, J. W. Jones, *J. Am. Chem. Soc.* **2002**, *124*, 4653 – 4665.

[9] a) M. C. T. Fyfe, J. N. Lowe, J. F. Stoddart, D. J. Williams, *Org. Lett.* **2000**, *2*, 1221 – 1224; b) V. Balzani, M. Clemente-Leon, A. Credi, J. N. Lowe, J. D. Badjić, J. F. Stoddart, D. J. Williams, *Chem. Eur. J.* **2003**, *9*, 5348 – 5360.

[10] J. D. Badjić, V. Balzani, A. Credi, J. N. Lowe, S. Silvi, J. F. Stoddart, *Chem. Eur. J.* **2004**, *10*, 1926 – 1935.

[11] This prototype has been developed yet further in the incrementally staged-design, bottom-up construction, extensive characterization, and chemically driven operation of a two-component molecular machine that behaves like a nanoscale elevator; see: J. D. Badjić, V. Balzani, A. Credi, S. Silvi, J. F. Stoddart, *Science* **2004**, *303*, 1845 – 1849.

[12] a) V. Balzani, A. Credi, F. M. Raymo, J. F. Stoddart, *Angew. Chem.* **2000**, *112*, 3484 – 3530; *Angew. Chem. Int. Ed.* **2000**, *39*, 3348 – 3391; b) V. Balzani, A. Credi, M. Venturi in *Molecular Devices and Machines—A Journey into the Nano World*, Wiley-VCH, Weinheim, **2003**.

[13] A recent communication of dynamic chiral crown ether complexes during cyclic acetal formation lists a selection of the various reaction types which can be carried out under thermodynamic control, to create dynamic combinatorial libraries, from which selected products can often be amplified with a specific template; see: B. Fuchs, A. Nelson, A. Star, J. F. Stoddart, S. Vidal, *Angew. Chem.* **2003**, *115*, 4352 – 4356; *Angew. Chem. Int. Ed.* **2003**, *42*, 4220 – 4224.

[14] T. M. Trnka, R. H. Grubbs, *Acc. Chem. Res.* **2001**, *34*, 18 – 29.

[15] For an example of a [2]catenane synthesis employing RORCM and operating under thermodynamic control, see: a) T. J. Kidd, D. A. Leigh, A. J. Wilson, *J. Am. Chem. Soc.* **1999**, *121*, 1599 – 1600; for examples of [2]catenanes utilizing RCM, see: b) D. G. Hamilton, N. Feeder, S. J. Teat, J. K. M. Sanders, *New J. Chem.* **1998**, *22*, 1019 – 1021; c) M. Weck, B. Mohr, J.-P. Sauvage, R. H. Grubbs, *J. Org. Chem.* **1999**, *64*, 5463 – 5471; d) P. Mobian, J.-M. Kern, J.-P. Sauvage, *J. Am. Chem. Soc.* **2003**, *125*, 2016 – 2017; for examples of [2]rotaxane syntheses using RCM, see: e) J. A. Wisner, P. D. Beer, M. G. B. Drew, M. R. Sambrook, *J. Am. Chem. Soc.* **2002**, *124*, 12469 – 12476; f) J. S. Hannam, T. J. Kidd, D. A. Leigh, A. J. Wilson, *Org. Lett.* **2003**, *5*, 1907 – 1910; g) R. G. E. Coumans, J. A. A. W. Elemans, P. Thordarson, R. J. M. Nolte, A. E. Rowan, *Angew. Chem.* **2003**, *115*, 674 – 678; *Angew. Chem. Int. Ed.* **2003**, *42*, 650 – 653.

[16] Olefin metathesis, catalyzed by Ru^{II} complexes developed at CALTECH, have found wide application in, for example, the reversible covalent capture of supramolecular assemblies; see: a) T. D. Clark, K. Kobayashi, M. R. Ghadiri, *Chem. Eur. J.* **1999**, *5*, 782 – 792; b) F. Cardullo, M. Crego Calama, B. H. M. Snellink-Ruël, J.-L. Weidmann, A. Bielejewska, R. Fokkens, N. M. M. Nibbering, P. Timmerman, D. N. Reinhoudt, *Chem. Commun.* **2000**, 367 – 368; c) M. O. Vysotsky, M. Bolte, I. Thondorf, V. Böhmer, *Chem. Eur. J.* **2003**, *9*, 3375 – 3382; for the cross-linking of dendrimer hosts employed as monomolecular imprinting systems, see: d) E. Mertz, S. C. Zimmerman, *J. Am. Chem. Soc.* **2003**, *125*, 3424 – 3425.

[17] A. F. M. Kilbinger, S. J. Cantrill, A. W. Waltman, M. W. Day, R. H. Grubbs, *Angew. Chem.* **2003**, *115*, 3403 – 3407; *Angew. Chem. Int. Ed.* **2003**, *42*, 3281 – 3285.

[18] H. Iwamoto, K. Itoh, H. Nagamiya, Y. Fukuzawa, *Tetrahedron Lett.* **2003**, *44*, 5773 – 5776.

[19] M. C. T. Fyfe, J. F. Stoddart, *Acc. Chem. Res.* **1997**, *30*, 393 – 401.

[20] a) A. G. Kolchinski, D. H. Busch, N. W. Alcock, *J. Chem. Soc. Chem. Commun.* **1995**, 1289 – 1291; b) P. R. Ashton, P. J. Campbell, E. J. T. Chrystal, P. T. Glink, S. Menzer, D. Philp, N. Spencer, J. F. Stoddart, P. A. Tasker, D. J. Williams, *Angew. Chem.* **1995**, *107*, 1997 – 2001; *Angew. Chem. Int. Ed. Engl.* **1995**, *34*, 1865 – 1869; c) P. R. Ashton, E. J. T. Chrystal, P. T. Glink, S. Menzer, C. Schiavo, N. Spencer, J. F. Stoddart, P. A. Tasker, A. J. P. White, D. J. Williams, *Chem. Eur. J.* **1996**, *2*, 709 – 728.

[21] When the reaction is followed by ^{1}H NMR spectroscopy, one *major* product, namely $[\mathbf{6}\text{-}H_3][PF_6]_3$, is formed with high conversion (> 95 %) from the starting materials, namely, **3** and $[\mathbf{5}\text{-}H_3][PF_6]_3$. The yield of 62 % recorded in the Experimental Section is considerably lower because of the loss of $[\mathbf{6}\text{-}H_3][PF_6]_3$ during silica gel chromatography.

[22] $IMesH_2$ = 1,3-dimesityl-4,5-dihydroimidazol-2-ylidene; see: M. Scholl, S. Ding, C. W. Lee, R. H. Grubbs, *Org. Lett.* **1999**, *1*, 953 – 956.

 © 2004 Wiley-VCH Verlag GmbH & Co. KGaA, Weinheim

Template Synthesis

Sol–Gel Reaction Using DNA as a Template: An Attempt Toward Transcription of DNA into Inorganic Materials

*Munenori Numata, Kazunori Sugiyasu, Teruaki Hasegawa, and Seiji Shinkai**

The creation of nanosized inorganic superstructures is a challenging research target not only from a purely scientific viewpoint, in an attempt to make artificial fossils, but also from its great potential for application, such as for catalysts, nanowires, circuits, molecular containers, and complicated patterning, which are regarded to be indispensable tools for nanotechnology.[1] However, an essential difference in the research approaches exists between "organic" and "inorganic" materials: that is, a diversity of supramolecular structures can be created by the self-assembly of designed "organic" building blocks, whereas it seems very difficult or nearly impossible to create supramolecular "inorganic" materials in a diverse and regulated fashion because of their inability to self-assemble. Accordingly, the sole solution to overcome this difficulty in designing supramolecular "inorganic" materials is to use an appropriate "organic" template with diverse and well-regulated shapes onto which "inorganic" materials can be deposited by utilizing some specific interaction.

Recently, we and other research groups have demonstrated that organogel fibers, which are formed from the self-assembly of low-molecular-weight compounds, act as excellent templates for the creation of silica fibers by sol–gel polycondensation of tetraethoxysilane (TEOS).[2] Very interestingly, it was shown that sol–gel polycondensation of gelated TEOS solutions affords novel silica materials with lamellar,[2a,b] linear fiber,[2c,d] or helical[2e–h] structures as a result of their supramolecular structures acting as a template containing a hollow center during the TEOS polycondensation process. One may now propose, therefore, that the unique superstructures constructed in the organogels are readily transcribed into the silica structures: this means that superstructures of organic assemblies that are temporarily formed by noncovalent interactions could be permanently fixed as inorganic materials.

Biomolecules exhibit various unique higher-order structures, so they should act as fascinating templates to create such inorganic superstructures. In fact, it has been demonstrated by several research groups that protein cages,[3] biolipid cylinders,[4] multicellular superstructures,[5] and collagen fibers[6] can be utilized as templates for the direct deposition of silica or other metal clusters. Among these biomolecules, DNA is one of the most attractive templates because its double-stranded structure has a well-regulated micrometer length and uniform 2-nm diameter which cannot be prepared by artificial polymers or low-molecular-weight gels. Furthermore, one can find several topologically different higher-order DNA structures in the native DNA system. For example, plasmid DNA, produced by *Escherichica coli*, adopts a coiled-coil structure with a well-regulated length and width under appropriate biological conditions, and the morphology can be readily changed to the closed circular structure by chemical or enzymatic treatment. It thus occurred to us that if plasmid DNA could be used as a template for sol–gel polycondensation, it would give unique silica structures reflecting the higher-order structures of DNA. Herein we report several novel findings related to this research aim: 1) plasmid DNA can be solublilized into organic solvents by appropriate modification with cationic surfactants, 2) when the overall charge of the DNA–surfactant complex is positive, it can act as an active template for the sol–gel reaction, and 3) the topologically different structures in plasmid DNA can be successfully transcribed into resultant silica structures. These findings imply that the different higher-order silica structures could be created from the same DNA template through its higher-order conformational change.

To use DNA as a template we had to overcome two problems which arise from the mismatching properties between DNA and TEOS. Firstly, it is known that when sol–gel polycondensation is carried out in neutral or alkaline media, the propagating silica species are considered to be anionic. Hence, only a molecular assembly having a cationic surface can act as the template to adsorb the anionic silica particles. Since DNA itself is an anionic polymer, one must transform the "anionic" to a "cationic" species. Secondly, TEOS is soluble in organic solvents, whereas DNA itself is soluble virtually only in water, hence some appropriate solvent system which can dissolve both components had to be found. One potential solution to overcome these problems is to dissolve DNA in an organic solvent by replacing the sodium counterions with cationic amphiphiles.[7] One might expect that the resultant DNA–amphiphile complex would gain not only moderate solubility in organic solvents but also the ability to adsorb the anionic silica particles. Previously, we mixed DNA with an excess amount of *n*-octyl-1,8-diammonium dibromide (**1**) with the expectation that one ammonium cation would form an ion pair with one phosphate anion and the resultant DNA–**1** complex would become overall positively charged because of the presence of another ammonium cation. The analysis of the obtained precipitate revealed, however, that the two ammonium groups form ion pairs with the two phosphate groups in an intramolecular manner and the resultant precipitate is apparently neutral (Figure 1a). This failure brought forth an alternative idea, that is, provided that intermolecular ion-pair formation proceeds in preference to an intramolecular one, it follows that the second cationic group should remain without forming an ion pair with the

[*] Dr. M. Numata, K. Sugiyasu, Dr. T. Hasegawa, Prof. S. Shinkai
Department of Chemistry and Biochemistry
Graduate School of Engineering
Kyushu University
Fukuoka 812–8581 (Japan)
Fax: (+81) 92-642-3611
E-mail: seijitcm@mbox.nc.kyushu-u.ac.jp

Supporting information for this article is available on the WWW under http://www.angewandte.org or from the author.

 DOI: 10.1002/anie.200454009 © 2004 Wiley-VCH Verlag GmbH & Co. KGaA, Weinheim

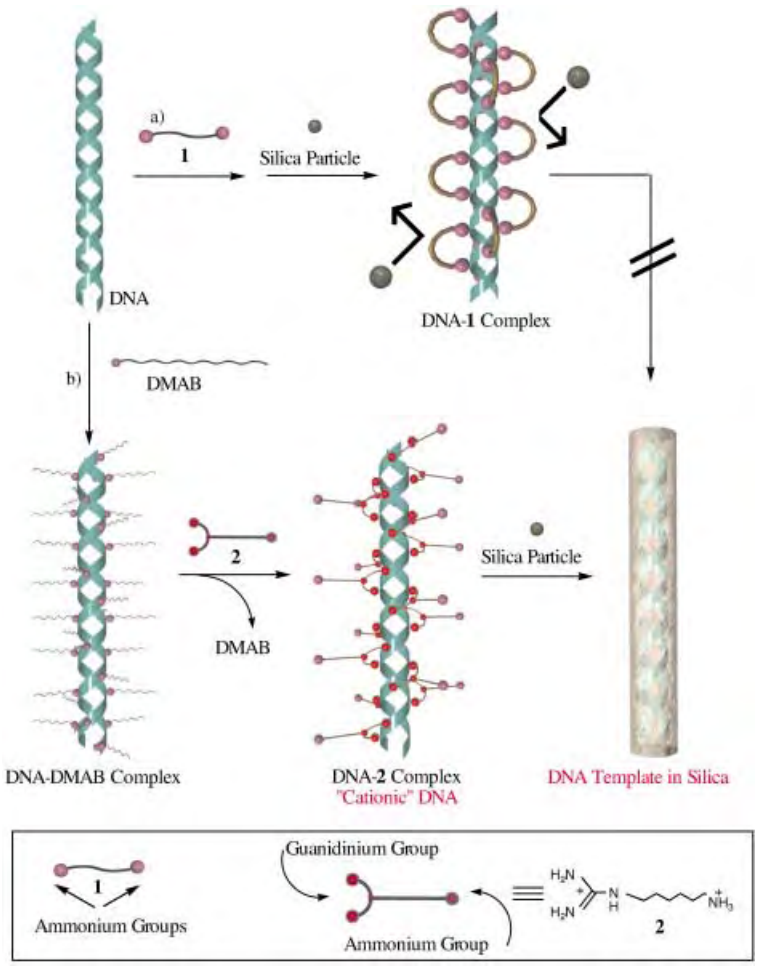


Figure 1. Schematic representation of the transformation of the DNA surface. See text for details.

phosphate group. We thus designed **2** bearing one ammonium group and one guanidinium group with the expectation that intermolecular formation of an ion pair with the guanidinium group would proceed in preference to an intramolecular one with the ammonium group (Figure 1b). By utilizing this strategy we have found that DNA can act as a new "cationic" template for sol–gel transcription and the resultant silica materials transcribe the higher-order structures of DNA very precisely.

Firstly, we prepared the plasmid DNA–amphiphile complex by mixing DNA and cationic didodecyldimethylammonium bromide (DMAB) according to the reported method.[7] The plasmid DNA aqueous solution (45.0 μL, 0.67 μg μL^{-1}) containing 10 mM Tris-HCl (Tris = tris(hydroxymethyl)aminomethane) and 1.0 mM ethylenediamine tetraacetate (EDTA) was added to the DMAB solution (100 mM, 15.0 μL) and the mixture was stirred at room temperature. The resultant white precipitate was collected by centrifugation (9000 rpm, 50 min) and washed with distilled water several times. Freeze-dry treatment of this sample afforded a white powder. The product (DNA–DMAB complex) was easily solubilized into a mixture of chloroform and methanol (3:1, v/v). The CD and UV/Vis spectra of the thus obtained DNA–DMAB complex are shown in Figure 2a, b, respectively (the final concentration was adjusted to 1.0 mM/base). The CD spectrum shows a positive Cotton effect at 280 nm and a negative Cotton effect at 260 nm. A peak at around 260–300 nm is evident in the UV/Vis spectrum which is attributed to DNA bases. These spectral features observed in organic solution are similar to those observed in aqueous solution.[8] The spectral similarities indicate that the prepared plasmid DNA–DMAB complex maintains the morphology similar to that in aqueous solution. For the subsequent experiments we employed a 1.0 mM chloroform:methanol (3:1, v/v) solution as a stock solution.

Secondly, we carried out sol–gel polycondensation using the DNA–DMAB complex as a template. Water (6.3 μL), benzylamine (5.0 μL), and TEOS (10.0 μL) were added sequentially to the DNA–DMAB solution (500 μL). After mixing, the resultant solution was left at room temperature for three days. Although this is the procedure frequently employed to create superstructures of silica materials using an organogel as a template, we could not observe any specific silica structure by SEM or TEM. This result shows that the DNA–DMAB complex, expected to be neutral overall, cannot act as a template. Taking this observation into consideration, we added **2**, which has the ammonium group at one end and the guanidinium group at the other end. It is well-known that the guanidinium group is complementary to the phosphate group and the interaction is much stronger than that with the ammonium group. One can

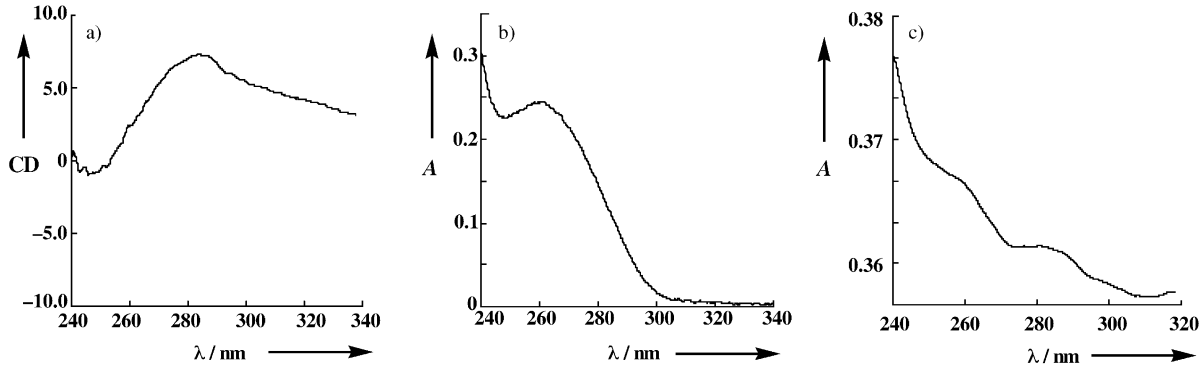


Figure 2. a) CD spectrum and b) UV/Vis spectrum of the DNA–DMAB complex ($CHCl_3$:MeOH (3:1, v/v)), 1.0 mM/base, 5.0 mM, 25 °C; c) UV/Vis spectrum of the obtained silica.

 © 2004 Wiley-VCH Verlag GmbH & Co. KGaA, Weinheim

thus expect that: 1) when **2** is added to the DNA–DMAB complex solution, the DMAB is exchanged with **2** because of the stronger guanidinium–phosphate interaction, 2) the resultant DNA–**2** complex becomes "cationic" overall (Figure 1b), and 3) the oligomeric silica particles should be adsorbed to the DNA–**2** complex, because of the silica–ammonium electrostatic interaction. To test this intriguing hypothesis, we carried out in situ cation exchange by mixing the DNA–DMAB complex (500 μL, chloroform:methanol (3:1 v/v)) with **2** (5 μL, 100 mM, one equivalent/base) in methanol. This cation exchange proceeded without the formation of any precipitate, unless a very high DNA concentration was used with an excess amount of **2**. Then, we carried out sol–gel polycondensation using the resultant DNA–**2** complex as a template according to the general procedure. The obtained silica was analyzed after washing it with distilled water and methanol. Figure 2c shows the UV/Vis spectrum of the resultant silica composite. The spectrum is somewhat broadened, but the basic spectral features of the DNA–**2** solution (Figure 2b) are evident, thus indicating that DNA is incorporated into the silica.

To obtain further evidence that the DNA really acted as a template to create this silica structure, we analyzed the composite by SEM and TEM. Figure 3 shows the SEM images

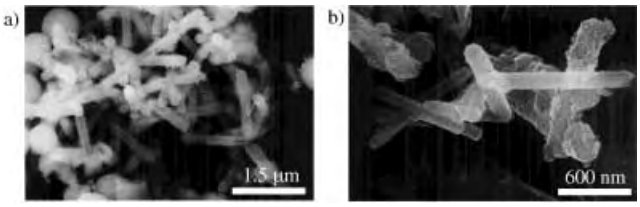


Figure 3. SEM pictures of the rodlike silica obtained.

of the obtained silica composite: the unique, rodlike silica structures of uniform length (ca. 1 μm) can be observed. It is well-known that plasmid DNA adopts a coiled-coil (super-coil) structure under the appropriate pH conditions or salt concentrations. In a separate study with TEM analysis, we confirmed that the DNA–**2** complex mostly exists in the coiled-coil structure in solution and the length is estimated to be about 800 nm (not shown). This structural similarity between the DNA–**2** complex and the observed silica composite supports the view that the DNA–**2** complex acted as a template during the polycondensation reaction of TEOS. In addition, many small spherical silica particles around the rodlike silica can also be recognized (Figure 3a). Formation of these spherical silica particles is explained as follows: DMAB, which is dissociated from the first DNA–DMAB complex by exchange with **2**, forms the spherical aggregates (micelles), which act as templates for formation of these spherical silica particles. As a reference experiment, we carried out sol–gel polycondensation in the presence of only DMAB as well as with a mixture of DMAB and **1** under the same reaction conditions. As expected, formation of similar spherical silica particles was recognized by both SEM and TEM.

To observe the inner structure of the silica composite we used TEM, which usually gives higher resolution and more useful information than SEM. Figure 4 shows the TEM images of the obtained silica composite, in which uniform rodlike silica structures (Figure 4a) can be recognized. The

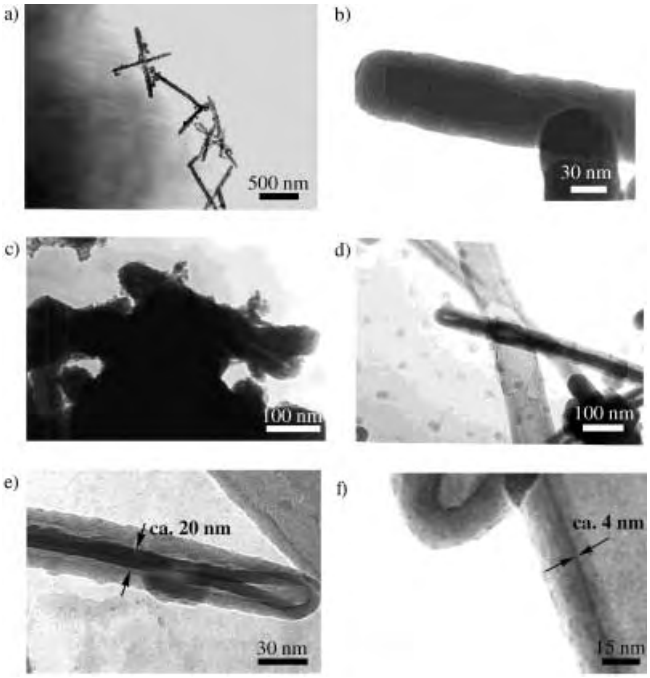


Figure 4. TEM pictures of a) the rodlike silica, b) close-up image of the inner hollow of the rodlike silica, c) rodlike silica after calcination, d) silica structures obtained from the partial coiled-coil template, e) close-up image of the core silica obtained from the partial coiled-coil template, and f) close-up image of the silica obtained from the DNA dulplex template.

presence of a hollow with a diameter of approximately 10 nm inside the silica rods is confirmed (Figure 4b). The diameter is very close to that of the plasmid DNA–**2** complex in solution (ca. 7 nm). The hollow structure of the silica rods can be recognized even after calcination (Figure 4c). These findings unambiguously support the view that the plasmid DNA–**2** (super-coil structure) complex works as an efficient template for the formation of these rodlike silica composites (Figure 5a).

Conformational relaxation of the coiled-coil structure in plasmid DNA may be induced by extraction into organic solution with a surfactant, thus giving rise to a morphological change into a partial coiled-coil DNA. One may expect, therefore, that if these transformed DNA morphologies were also useful as templates, several new silica structures could be created. Furthermore, it is expected that the silica particles are predominantly adsorbed onto the surface of the partial coiled-coil DNA–**2** complex, because such relaxation exposes the anionic charges of the DNA on the surface and exchange with **2** can occur more preferably. If this is the case, one can obtain the TEM pictures in which the template–silica interface is more deeply stained by silica particles (Figure 5b). Actually, we observed several silica rods in which the

 © 2004 Wiley-VCH Verlag GmbH & Co. KGaA, Weinheim

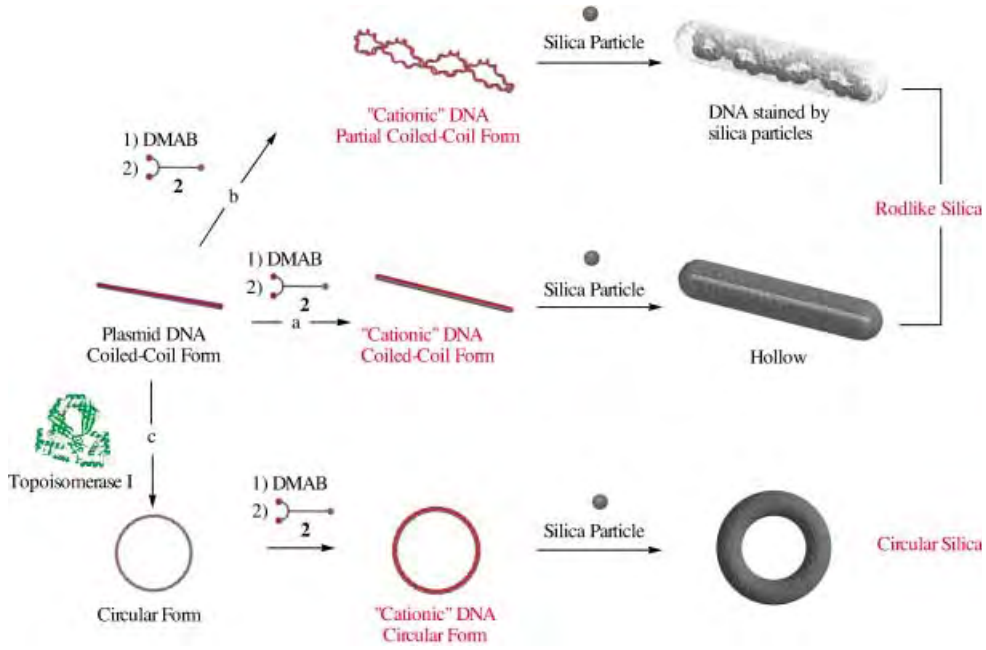


Figure 5. Formation of the different ordered silica structures created from the same template through conformational changes.

morphological pattern of partial coiled-coil DNA is shadowed more darkly than the outer surface (Figures 4d,e and 5b). It should be noticed that these silica rods commonly include hairpin or internal loop DNA templates. Very interestingly, even the structure created from the template effect of one double-stranded DNA can be found (Figure 4f): the diameter of the smallest silica-stained fiber is approximately 4 nm, which can be regarded as the template effect arising from one DNA double strand (2 nm diameter).

It is known that relaxation of the coiled-coil structure finally results in the circular form. This fact further stimulated us to utilize the circular DNA structure as a template for sol–gel polycondensation, with the expectation that the circular-shaped silica would be obtained (Figure 5c). Topoisomerase I is an enzyme that is able to induce such relaxation of the coiled-coil structure.[9] The relaxation process by topoisomerase I is known to proceed almost quantitatively under mild conditions. Accordingly, we first treated plasmid DNA with topoisomerase I for 1 h at 37 °C under the conventional reaction conditions.[9] The topological change from the coiled-coil structure to the circular one was confirmed by the gel mobility shift assay (see the Supporting Information). Then, the sol–gel polycondensation reaction was carried out using the resultant circular plasmid DNA after extraction into the organic phase with DMAB followed by cation exchange with **2** according to the same procedure as above. Figure 6 shows SEM and TEM images of the obtained silica composite. Many toroidal-shaped silica structures with diameters of 500–800 nm (center to center) can be observed (Figure 6a): these values are very reasonable, provided that plasmid DNA adopts the circular form. The central cavity can be also recognized in the close-up picture (Figure 6b). Figure 6c and d show TEM images of the same silica composite before and after calcination, respectively. The similar toroidal silica structure can also be recognized in these TEM images. The

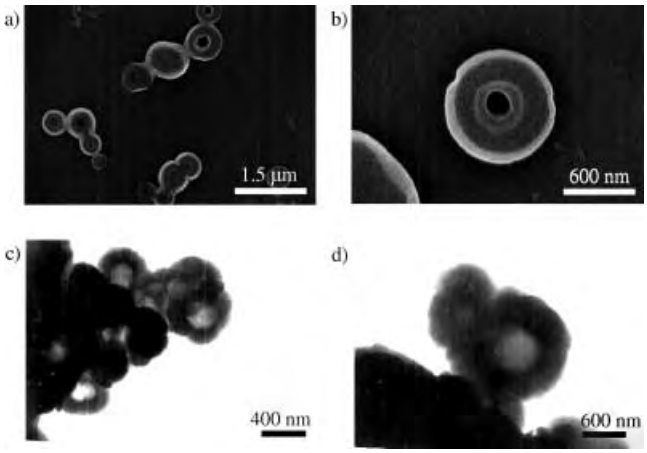


Figure 6. a) SEM picture of the circular silica, b) close-up SEM image of the circular silica, c) TEM picture of the circular silica, and d) TEM picture of the circular silica after calcination.

results clearly support the view that circular plasmid DNA acted as the template for creating the toroidal silica structure.

In conclusion, we have demonstrated that plasmid DNA can act as an attractive, new template for sol–gel polycondensation of TEOS after treatment by two cation-exchange steps. The obtained silica structures are drastically changed and reflect the conformationally transformed template structures. To the best of our knowledge, this is the first study showing that DNA can work as a template for sol–gel polycondensation. We believe that this is the first step to immobilize the memory of DNA on an inorganic material, as in the formation of fossils. We are now planning to apply the present concept to more complicated but sophisticated templating systems using the rationally designed natural DNA and artificial DNA structures.

 © 2004 Wiley-VCH Verlag GmbH & Co. KGaA, Weinheim

Experimental Section

2: *N*-(6-Aminohexyl)carbonic acid *tert*-butyl ester (0.30 g, 1.72 mmol) and triethylamine (240 μL, 1.72 mmol) were dissolved in MeOH (30 mL). *O*-methylisourea hydrogensulfate (0.36 g) was added to this mixture and the resultant solution was stirred at room temperature. The MeOH was removed under reduced pressure after 12 h. The reaction mixture was subjected to column chromatography using $CHCl_3$:MeOH (3:1, v/v) as eluant. After removing the solvent, a colorless oil was obtained (170 mg). The product obtained (100 mg, 0.3 mmol) was then dissolved in dried CH_2Cl_2. Trifluoroacetic acid (TFA, 50 μL, 2.5 equiv) was added to this solution and the mixture was stirred at room temperature. After 6 h, the solvent and exces TFA were removed under reduced pressure to give **2** as a colorless oil. TEM and SEM observations were carried out on a JEOL TEM-2010 (accelerate voltage 120 kV) and Hitachi S-5000, respectively. CD and UV/Vis spectroscopic studies were performed on a JASCO J-720WI and SHIMADZU UV-2500PC, respectively.

Received: February 13, 2004 [Z54009]

Keywords: DNA · nanocomposites · silicates · sol–gel processes · template synthesis

[1] For recent reviews, see a) N. K. Raman, M. T. Anderson, C. J. Brinker, *Chem. Mater.* **1996**, *8*, 1682; b) S. Mann, S. L. Burkett, S. A. Davis, C. E. Fowler, N. H. Mendelson, S. D. Sims, D. Walsh, N. T. Whilton, *Chem. Mater.* **1997**, *9*, 2300; c) L. A. Estroff, A. D. Hamilton, *Chem. Mater.* **2001**, *13*, 3227; d) S. A. Davis, M. Breulmann, K. H. Rhodes, B. Zhang, S. Mann, *Chem. Mater.* **2001**, *13*, 3218; e) R. A. Caruso, M. Antonietti, *Chem. Mater.* **2001**, *13*, 3272; f) C. Sanchez, G. J. A. A. Soler-Illia, F. Ribot, T. Lalot, C. R. Mayer, V. Cabuil, *Chem. Mater.* **2001**, *13*, 3061; g) G. Soler-lllia, C. Sanchez, B. Lebeau, J. Patarin, *Chem. Rev.* **2002**, *102*, 4093; h) C. Sanchez, G. Soler-lllia, F. Ribot, D. Grosso, *C. R. Acad. Sci. Ser. IIc* **2003**, *8*, 109.

[2] a) J. H. Jung, Y. Ono, S. Shinkai, *Langmuir* **2000**, *16*, 1643; b) J. H. Jung, Y. Ono, S. Shinkai, *J. Chem. Soc. Perkin Trans. 2* **1999**, *1289*; c) Y. Ono, K. Nakashima, M. Sano, Y. Kanekiyo, K. Inoue, J. Hojo, S. Shinkai, *Chem. Commun.* **1998**, 1477; d) Y. Ono, Y. Kanekiyo, K. Inoue, J. Hojo, S. Shinkai, *Chem. Lett.* **1999**, 23; e) Y. Ono, K. Nakashima, M. Sano, J. Hojo, S. Shinkai, *Chem. Lett.* **1999**, 1119; f) J. H. Jung, Y. Ono, S. Shinkai, *Angew. Chem.* **2000**, *112*, 1931; *Angew. Chem. Int. Ed.* **2000**, *39*, 1862; g) J. H. Jung, Y. Ono, K. Hanabusa, S. Shinkai, *J. Am. Chem. Soc.* **2000**, *122*, 4520; h) K. Sugiyasu, S. Tamaru, M. Takeuchi, D. Berthier, I. Huc, R. Oda, S. Shinkai, *Chem. Commun.* **2002**, 1212.

[3] a) K. K. W. Wong, T. Douglas, S. Gider, D. D. Awshalom, S. Mann, *Chem. Mater.* **1998**, *10*, 279; b) D. J. van Unen, J. F. J. Engbersen, D. N. Reinhoudt, *Biotechnol. Bioeng.* **2001**, *75*, 154.

[4] a) D. D. Archibald, S. Mann, *Nature* **1993**, *364*, 430; b) S. Baral, P. Schoen, *Chem. Mater.* **1993**, *5*, 145.

[5] S. A. Davis, S. L. Burkett, N. H. Mendelson, S. Mann, *Nature* **1997**, *385*, 420.

[6] Y. Ono, Y. Kanekiyo, K. Inoue, J. Hojo, M. Nango, S. Shinkai, *Chem. Lett.* **1999**, 475.

[7] a) K. Tanaka, Y. Okahata, *J. Am. Chem. Soc.* **1996**, *118*, 10679; b) H. Nakayama, H. Ohno, Y. Okahata, *Chem. Commun.* **2001**, 2300.

[8] G. Chirico, L. Lunelli, G. Baldini, *Biophys. Chem.* **1990**, *38*, 201.

[9] a) A. M. Ferro, N. P. Higgins, B. M. Olivera, *J. Biol. Chem.* **1983**, *258*, 6000; b) A. M. Ferro, B. M. Olivera, *J. Biol. Chem.* **1984**, *259*, 547.

 © 2004 Wiley-VCH Verlag GmbH & Co. KGaA, Weinheim

Spin Crossover in Gels

Thermoreversible Gels as Magneto-Optical Switches**

*Olivier Roubeau, Annie Colin, Véronique Schmitt, and Rodolphe Clérac**

The discovery of solid materials with appealing physical properties is mostly stimulated by their "potential" applications in nanotechnologies, molecular electronics, or quantum computing.[1] To achieve these objectives, the limiting step is often the transfer of bulk properties to technologically convenient systems (films, nanocomposites, fibers, gels).[2] In the past 20 years, spin-crossover (SC) materials have attracted considerable interest for their applicability as information storage, sensors, or display devices.[3] In particular, polymeric chains of iron(II) bridged by triazole ligands display abrupt spin-crossovers making of these materials optical and magnetic switches.[4] Moreover, their SC temperature can be adjusted to around ambient temperature by choosing suitable counteranions and triazole substituents.[4] Nevertheless, only a few prototypes using films of solid particles embedded in polymer matrices have been developed, but none has ever been used industrially. An alternative to these films consists in incorporating SC entities into soft-matter phases, such as gels. Herein, we describe physical gels exhibiting magnetic and optical properties originating from SC precursors. This system illustrates a route for processing SC solids into physical gels as carried out, for example with photofunctional[5] and biocompatible organogels.[6]

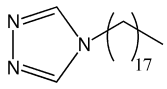
Among the spin-crossover Fe^{II}/triazole materials, we have focused on the solid precursor of formula $[Fe^{II}(C_{18}trz)_3](ptol)_2{\cdot}2H_2O$ (**1**, ptol = *para*-tolylsulfonate; $C_{18}trz$ = 4-octadecyl-1,2,4-triazole). This SC material presents two interesting features: it contains ptol anions inducing a spin-crossover around room temperature[7] and it contains triazole ligands functionalized by long alkyl chains which are typically introduced to obtain gelator or mesogenic molecules.[8] Compound **1** can be easily obtained by reaction of aqueous solutions of $[Fe(ptol)_2]{\cdot}6H_2O$ with ethanolic solutions of $C_{18}trz$ (Scheme 1).[9] As shown in Scheme 2 (top), the

[*] Dr. O. Roubeau, Dr. V. Schmitt, Dr. R. Clérac
Centre de Recherche Paul Pascal/CNRS-UPR 8641
115 avenue du Dr. A. Schweitzer
33600 Pessac (France)
Fax: (+33) 5-5684-5600
E-mail: clerac@crpp-bordeaux.cnrs.fr
Dr. A. Colin
Rhodia Laboratoire du Futur, CNRS-FRE 2771
Bat B de L'Institut Européen de Chimie et Biologie
2 rue Robert Escarpit, 33607 Pessac Cedex (France)

[**] The authors thank Hassan Saadaoui for AFM images, Marie-France Achard and Florent Carn. Financial support from the CNRS, the University Bordeaux 1, and the Région Aquitaine are gratefully acknowledged.

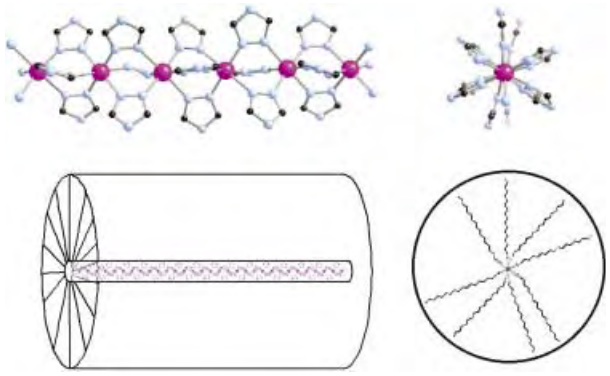
Supporting information for this article is available on the WWW under http://www.angewandte.org or from the author.

 DOI: 10.1002/anie.200454050 © 2004 Wiley-VCH Verlag GmbH & Co. KGaA, Weinheim



Scheme 1. 4-octadecyl-1,2,4-triazole ligand (C_{18}trz).

obtained material has a linear polymeric structure, with triazole units or substituted triazole rings in an eclipsed arrangement around the Fe^{II} metal ions.[10] The Fe chains in **1** can thus be viewed as anisotropic rodlike species with organic pendent arms (see Scheme 2, bottom). In the solid state, this polymeric material has a thermal magnetic and thermochromic crossover from a purple diamagnetic solid (low-spin, $S=0$, absorption band at about 550 nm) at room temperature to a colorless paramagnetic solid (high-spin, $S=2$, absorption band at about 820 nm) at higher temperature. The crossover temperature, T_{SC}, depends on whether the sample is hydrated ($T_{SC}=47\,°C$) or dehydrated ($T_{SC}=7\,°C$). This difference is usually attributed to a solvent effect on the ligand-field strength around the Fe^{II} centers.[11] A small fraction of the iron ions remains in the high-spin state over the whole temperature range. It is accepted that these ions are the Fe^{II} units at chain ends, and amount here to 2% of the sample (based on the residual magnetism observed below 200 K), thus indicating an average mean chain length of approximately 33 nm in the solid (taking a value of 3.3 Å as an approximate Fe–Fe separation[10]).



Scheme 2. Top: schematic representation of the polymeric structure of $[Fe^{II}(Rtrz)_3]_n^{2n+}$ chains (R groups have been removed for clarity; purple Fe, cyan N, and black C). Bottom: schematic view of the cylindrical anisotropic rod formed by polymeric chains bearing long alkyl groups.

This solid precursor is only slightly soluble in alkane solvents, for example, decane, dodecane or cyclohexane. However, heating heterogeneous mixtures of various compositions (1.9 to 35, 1 to 30, and 1 to 20 wt% of **1** to decane, dodecane, and cyclohexane, respectively) above 140 °C yields monophasic viscous liquids. At these temperatures, the liquid phases are colorless and transparent. Cooling the system back to room temperature does not produce any solid precipitation and a homogeneous purple gel is obtained (see Supporting Information).[12] We have studied the temperature/composition pseudo-phase diagram of the system **1**/decane in more detail. At any concentration, the starting mixture is heterogeneous (e.g. solid + decane) at room temperature. Upon heating, jelly domains start to appear around 50–60 °C, and an isotropic viscous liquid is obtained above T_{melt}. Upon cooling, a homogeneous gel forms at T_{gel} below T_{melt}. This hysteresis feature at the gel–liquid transition is commonly observed for gels of low-molecular-mass gelators.[13] Below a threshold concentration of solid (1.9 wt% of **1** in decane), biphasic mixtures of gel-like aggregates and decane are obtained. Above 35 wt% of **1** in decane, the mixture remains in the form of a heterogeneous "pasty solid". The characteristic temperatures, T_{melt} and T_{gel} are given on the pseudo-phase diagram of Figure 1. The gel/liquid phase transition can be

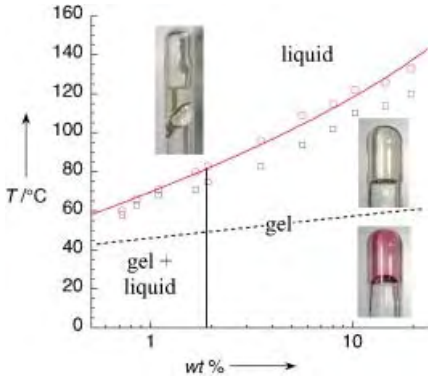


Figure 1. Temperature–composition pseudo-phase diagram for the binary **1**/decane system. Red points are data obtained upon warming, blue points are data obtained on cooling and determined by the inverted tube test. The red full line is the fit obtained with the ideal solution model (see text). The dashed line represents the spin-crossover temperature T_{SC} of the gels and the black vertical line represents the frontier between the homogeneous gel domain and the biphasic region.

considered as a dissolution process.[8] For an ideal solution, the molar concentration C can be expressed as follows Equation (1).

$$ln\,C(T_{melt}) = -\Delta H_{melt}/R\,T_{melt} + constant \qquad (1)$$

Experimentally, fitting of the T versus $wt\,\%$ semi-log plot displayed in Figure 1 confirms this typical behavior. Hence the exothermic heat of association or melting enthalpy, ΔH_{melt}, has been estimated as approximately 55 kJ mol^{-1}, in good agreement with melting enthalpies of organogels with interactions between long alkyl chains.[13] By analogy with these organogels, the gel formation may result from a precipitation of small aggregates.[14] Indeed atomic force microscopy (AFM) reveals the presence of anisotropic aggregates in the gels with an average size of 150 nm in length and about 10 nm in diameter (Figure 2). This result indicates that the gels are not formed from individual chains of the solid precursor but from bundles of them. To probe the solvent–aggregates interaction, thermogravimetric experiments (see Supporting Information) have been performed. The solvent loss from the hybrid gels occurs at the boiling temperature of the pure solvents. Therefore, the interaction between solvent and gelator aggregates is weak. This feature and the thermoreversibility of the gel–liquid transition are characteristic of the physical nature of the formed gels.

 © 2004 Wiley-VCH Verlag GmbH & Co. KGaA, Weinheim

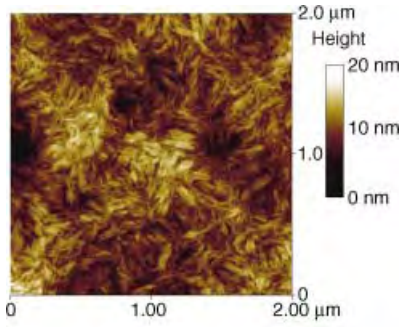


Figure 2. Tapping mode AFM image of a **1**/decane gel (3.5 wt%) on highly oriented pyrolytic graphite measured with a multimode Nanoscope III from Digital Instruments.

By analogy with the precursor material, the purple color of the transparent gels indicates that at least some of the Fe^{II} ions are in their low-spin state at room temperature. As observed during the gelation, the gels turn colorless above about 45 °C indicative that only iron(II) centers in the high-spin configuration are present. This optical signature of a spin crossover and the detection of typical IR bands[15] confirm the presence of the Fe^{II}/triazole polymeric chains in the gel. The spin-crossover process has been monitored and yields a reproducible peak in differential scanning calorimetry (DSC) and a sharp increase of the magnetization at this temperature (corresponding to the dashed line in Figure 1). Typical behavior of a **1**/decane gel (5 wt%) is depicted in Figure 3.

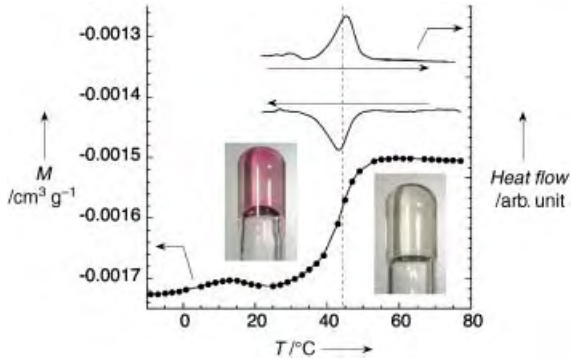


Figure 3. Temperature dependence of the massic magnetic moment (M) at 1000 Oe and DSC thermograms (inset; 5 °C min^{-1}) of a 5 wt% **1**/decane gel. The dotted line corresponds to the spin-crossover temperature (T_{SC} = 44 °C) deduced from DSC and magnetic measurements. The anomalies observed on the magnetic moment curve below 25 °C correspond to the solid–liquid first-order transition in pure decane.

The jump in magnetization of 2.3×10^{-4} emu g^{-1}, centered around 44 °C, corresponds well to what is expected for 72% of the Fe^{II} centers going from a diamagnetic to a paramagnetic state. Taking into account that the terminal iron ions remain in the high-spin state, a comparison with the solid (in which 98% of Fe^{II} undergoes a spin-crossover) suggests that the chain length may be reduced in the gel. Nevertheless, polymeric chains of **1** have been incorporated into gels and still present SC properties, which makes these gels thermochromic and magnetic switches.

All the gels can be cut into pieces and present a jelly-like behavior. Preliminary rheological measurements on **1**/decane gels, in the linear regime at low stress (0.1 to 5 Pa), show a visco-elastic behavior dominated by the elastic component, as expected for a gel (G' about one order of magnitude higher than G''). G' was found to increase slightly with the frequency, in particular below 1 Hz, while two broad modes of relaxation were observed for G'', one centered around 10^{-4} Hz, and one at frequencies higher than 10 Hz (not shown). This behavior is reproducible in homogenous gels of various compositions, either freshly prepared or after several months. The order of magnitude of G' depends on the concentration of precursor material and ranges from about 30 Pa (2 wt%) to around 900 Pa (15 wt%). Moreover, flow experiments show that the gel is shear-thinning, which suggests an orientation of the anisotropic aggregates under controlled shears. In addition, after applying such high shears, recovery of the original visco-elastic behavior would indicate a thixotropic nature for these gels.

Studying these SC gels, one main drawback has been found. As shown in Figure 4, large solid particles of a few

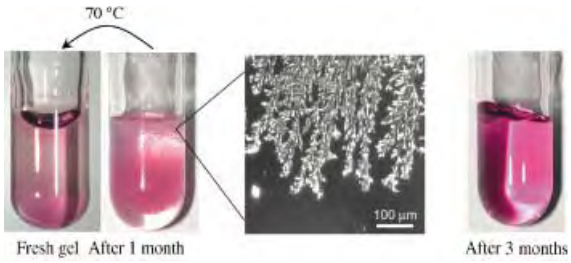


Figure 4. Demixion-crystallization process in gel of **1**/decane (left), with the observation of the large crystallites through crossed analyzers-polarizers (center). Typical stable homogeneous **1**/$CHCl_3$/decane gel (solvent mixture: 28/72 wt%; right).

hundreds of micrometers slowly form within the gel (over days to weeks depending on the preparation conditions). These particles can take the form of starlike aggregates, cross-linked fibers, and even cubic crystals (depending of the conditions). The homogeneous gel can be regenerated easily as the particles disappear upon warming above T_{melt} and cooling down below T_{gel}. Such a demixion-crystallization process is the sign of the gel metastability at room temperature and results from the weak solubility of the precursor solids in alkanes. Since chloroform is a good solvent for these precursors, we have used $CHCl_3$/alkane mixtures (10/90 to 30/70 wt%) in which the gelation occurs spontaneously at room temperature. The resulting gels are homogeneous and stable for at least over five months. In addition, the use of solvent mixtures has allowed tuning of the T_{gel} and T_{melt} temperatures between 20 and 120 °C. This ability to tune the gel–liquid transition temperatures also makes the formulation processes of this system easier.

In conclusion, the known polymeric Fe^{II}/triazole system has been modified by functionalizing the triazole ligands with

 © 2004 Wiley-VCH Verlag GmbH & Co. KGaA, Weinheim

long alkyl chains. Dissolving these new SC materials in organic solvents, we have been able to obtain hybrid gels and to study their thermo-reversible magnetic (at T_{SC} diamagnetic metal ions become paramagnetic), optical (at T_{SC} the transparent purple gel becomes colorless), and rheological (at T_{melt} the thixotropic gel converts into liquid) properties. We have shown that T_{melt} can be tuned using mixtures of solvents. Moreover, preliminary results indicate that T_{SC} is also adjustable by changing the counteranions of the SC precursor.[16] These gels illustrate successfully the strategy of transferring the unusual physical properties of solids into a soft-matter phase and open a new route to design polyfunctional materials.

Received: February 18, 2004 [Z54050]

Keywords: gels · iron · magneto-optical properties · polymers · spin-crossover

[1] a) M. N. Leuenberger, D. Loss, *Nature* **2001**, *410*, 789; b) D. Gatteschi, R. Sessoli, *Angew. Chem.* **2003**, *115*, 278; *Angew. Chem. Int. Ed.* **2003**, *42*, 268; c) E. Coronado, J. R. Galán-Mascarós, C. Gómez-García, V. Laukhin, *Nature* **2000**, *408*, 447.

[2] a) B. Vigolo, A. Pénicaud, C. Coulon, C. Sauder, R. Pailler, C. Journet, P. Bernier, P. Poulin, *Science* **2000**, *290*, 1331; b) T. Coradin, J. Larionova, A. A. Smith, G. Rogez, R. Clérac, C. Guérin, G. Blondin, R. E. P. Winpenny, C. Sanchez, T. Mallah, *Adv. Mater.* **2002**, *14*, 896; c) A. Cornia, A. C. Fabretti, M. Pacchioni, L. Zobbi, D. Bonacchi, A. Caneschi, D. Gatteschi, R. Biagi, U. Del Pennino, V. De Renzi, L. Gurevich, H. S. J. Van der Zant, *Angew. Chem.* **2003**, *115*, 1683; *Angew. Chem. Int. Ed.* **2003**, *42*, 1645; d) M. Antonietti, G. A. Ozin, *Chem. Eur. J.* **2004**, *10*, 28.

[3] a) O. Kahn, J. Kröber, C. Jay, *Adv. Mater.* **1992**, *4*, 718; b) R. N. Muller, L. Vander Elst, S. Laurent, *J. Am. Chem. Soc.* **2003**, *125*, 8405.

[4] O. Kahn, C. Jay Martinez, *Science* **1998**, *279*, 44.

[5] K. Sugiyasu, N. Fijita, S. Shinkaï, *Angew. Chem.* **2004**, *116*, 1249; *Angew. Chem. Int. Ed.* **2004**, *43*, 1229, and references therein.

[6] K. J. C. van Bommel, C. van der Pol, I. Muizebelt, A. Friggeri, A. Heeres, A. Meetsma, B. L. Feringa, J. van Esch, *Angew. Chem.* **2004**, *116*, 1695; *Angew. Chem. Int. Ed.* **2004**, *43*, 1663, and references therein.

[7] F. Armand, C. Badoux, P. Bonville, A. Ruaudel-Texier, O. Kahn, *Langmuir* **1995**, *11*, 3467.

[8] P. Terech, R. G. Weiss, *Chem. Rev.* **1997**, *97*, 3133.

[9] O. Roubeau, J. M. Alcazar Gomez, E. Balksus, J. J. A. Kolnaar, J. G. Haasnoot, J. Reedijk, *New J. Chem.* **2001**, *25*, 144.

[10] a) A. Michalowicz, J. Moscovici, O. Kahn, *J. Phys. IV* **1997**, *C2*, 633; b) M. Verelst, L. Sommier, P. Lecante, A. Mosset, O. Kahn, *Chem. Mater.* **1998**, *10*, 980.

[11] a) P. Gütlich, A. Hauser, H. Spiering, *Angew. Chem.* **1994**, *106*, 2109; *Angew. Chem. Int. Ed. Engl.* **1994**, *33*, 2024; b) O. Roubeau, J. G. Haasnoot, E. Codjovi, F. Varret, J. Reedijk, *Chem. Mater.* **2002**, *14*, 2559.

[12] Note that the pure ligand 4-octadecyl-1,2,4-triazole does not gelify alkane solvents, while gels are also obtained starting from SC solids having other lengths of alkyl substituents (C_{13} and C_{16}) on the triazole rings.

[13] F. Placin, J.-P. Desvergne, J.-C. Lassègues, *Chem. Mater.* **2001**, *13*, 117, and references therein.

[14] M. Lescanne, A. Colin, O. Mondain-Monval, F. Fagès, J.-L. Pozzo, *Langmuir* **2003**, *19*, 2013.

[15] When the triazole ligand is in a local C_{2v} symmetry (case of a 1,2-bridging coordination mode), the intensity of ring torsion vibration modes is weak compared to their intensities in a non-C_{2v} case, as for example, in the pure 1*H*-1,2,4-triazole. In our case in the gel spectra, these vibration bands at approximately 670 cm^{-1} are very weak confirming the local C_{2v} symmetry.

[16] 5 wt% of $[Fe^{II}(C_{18}trz)_3](X)_2 \cdot 2H_2O$ in decane forms upon warming purple and colorless gels in which $X^- = Cl^-$ or $[BF_4]^-$. Their T_{SC} values are above and below room temperature, approximately 80 °C and −20 °C, respectively.

 © 2004 Wiley-VCH Verlag GmbH & Co. KGaA, Weinheim

Computer Chemistry

Green Oxidation Catalysts: Computational Design of High-Efficiency Models of Galactose Oxidase**

*Leonardo Guidoni, Katrin Spiegel, Martin Zumstein, and Ursula Röthlisberger**

The metalloenzyme galactose oxidase (GOase) is a highly efficient catalyst for the two-electron oxidation of a broad variety of primary alcohols. This enzyme is capable of catalytic oxidations in water, making direct use of the molecular oxygen of the air. Even polyalcohols are converted, in a highly regio and stereoselective way, into the corresponding aldehydes. This elegant synthetic route stands out against the stoichiometric alternatives of the same reaction as performed by traditional inorganic oxidants. Not surprisingly, GOase thus constitutes a highly attractive target for the development of biomimetic strategies aimed at the design of environmentally friendly, green oxidation catalysts.[1] During the last years, this enzyme has inspired a variety of groups to design synthetic analogues. Although different classes of spectroscopic,[2] structural[3] and even functional[4–9] models of GOase have been characterized, none of them is as yet able to compete with the natural enzyme in terms of catalytic efficiency. For the few existing functional models, rates of turnover lie still approximately four orders of magnitude

[*] Dr. L. Guidoni, K. Spiegel,[+] M. Zumstein, Prof. Dr. U. Röthlisberger
Institut de chimie moléculaire et biologique
Ecole polytechnique fédérale de Lausanne—BCH—LCBC
1015 Lausanne (Switzerland)
Fax: (+41) 21-693-0320
E-mail: ursula.roethlisberger@epfl.ch

[+] Present address:
Statistical and Biological Physics Sector
International School for Advanced Studies
Via Beirut, 4 34014, Trieste (Italy)

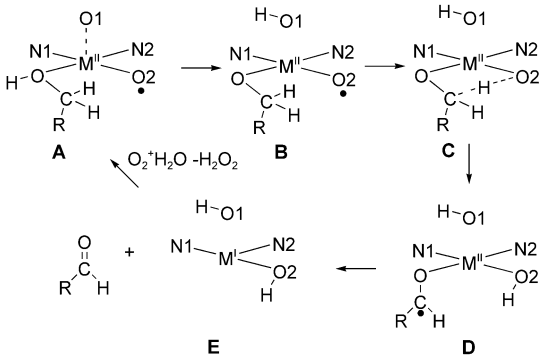
[**] We are grateful to the Swiss Center for Scientific Computing (Large User Project Grant 2002–2003) for providing computational resources. We thank Prof. H. Grützmacher for stimulating discussions and comments to the manuscript.

Supporting information for this article is available on the WWW under http://www.angewandte.org or from the author.

 © 2004 Wiley-VCH Verlag GmbH & Co. KGaA, Weinheim DOI: 10.1002/anie.200454081

below that of the natural target (around 0.5 s^{-1} [10] versus 800 s^{-1} for GOase[11]).

How does the enzyme achieve this remarkable proficiency and in which way do the synthetic analogues differ from their natural counterpart? Numerous investigations have contributed to a basic understanding of the enzymatic mechanism of action. [11–14] These studies have confirmed that GOase applies an intricate type of radical chemistry in which the metal ion serves as a one-electron redox center whereas the second electron is provided by a protein radical site. The enzyme contains a copper ion in an approximately square-pyramidal coordination environment with two nitrogen and two oxygen equatorial donor atoms (originating from His581, His496, Tyr272 and the substrate) with an additional oxygen atom from an axial ligand (Tyr495) as depicted in Scheme 1. As a

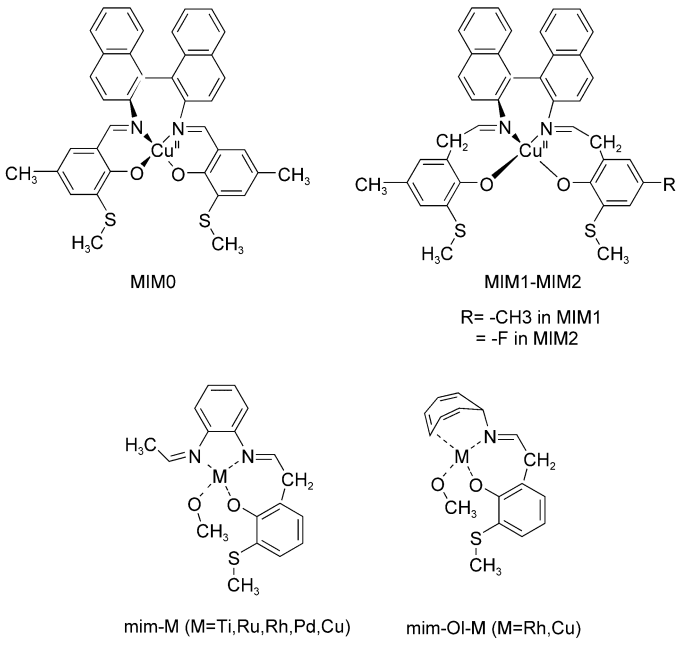


Scheme 1. Simplified reaction mechanisms of GOase and its models.

peculiar feature, the equatorial Tyr272 shows an unusual covalent linkage to Cys228. In the active form, the unpaired spin of a copper(II) ion is antiferromagnetically coupled to a tyrosyl radical, thus forming an EPR-silent, open-shell singlet complex.[15,16] As a first step of the catalytic process (**A**→**B**), an alcoholate is formed through the deprotonation of the substrate by the axial tyrosinate ligand acting as a general base. In the next reaction step (**B**→**C**), a hydrogen atom is abstracted from the substrate to the equatorial tyrosyl radical (**C**→**D**) and subsequently (or quasi simultaneously) the copper center is reduced to Cu^{I} by a single-electron transfer from the ketyl radical (**D**→**E**). The weakly bound newly formed aldehyde is replaced by dioxygen and the catalytic cycle is closed by recovering the initial copper oxidation state under concomitant reduction of O_2 to H_2O_2 (**E**→**A**). Measurements of the kinetic isotope effect reveal that the H-abstraction step is rate-limiting for substrates that are more difficult to oxidize.[13]

Notwithstanding the fact that the recently developed functional models of GOase apparently reproduce the overall features of the natural reaction (e.g., an EPR-silent active form and a kinetic isotope effect of similar magnitude[4]) they fail to rival the natural activity.

A number of recent quantum-chemical investigations have aimed at a full atomistic characterization of the enzymatic reaction mechanism, thereby complementing the available experimental data.[16–19] We have recently performed a mechanistic analysis of the functional biomimetic compound developed by Wang et al.[4] (MIM0 in Scheme 2)[18] in direct comparison with its natural target.[17] This study identified the delocalization of the unpaired spin density during the rate-determining H-abstraction step (Scheme 1,



Scheme 2. Full (MIM- top) and minimal (mim- bottom) computational models used in our calculations.

C→**D**) as the crucial determinant for the efficiency of the process. Specifically, due to a different orientation of the equatorial tyrosyl ligand (in MIM0 the equatorial ring system is essentially in plane with the copper coordination plane, whereas in GOase it is almost perpendicular) the spin delocalization in the transition state is greatly reduced in the synthetic compound. A second relevant difference concerns the product release step (Scheme 1, **D**→**E**). In the case of MIM0 the copper centre loses one of its nitrogen ligands to adopt a competing conformation in which the phenolate-binaphtyl moiety is fully planar and thus stabilized by hyperconjugation. Consequently, the newly formed aldehyde is strongly bound and cannot be released as easily as in the case of GOase, in which it is only marginally coordinated to the copper ion. These crucial factors identified in our previous study, namely: 1) efficient spin delocalization in the rate-determining transition state; 2) stabilization of the copper coordination sphere in the product-release step can now be used as a guideline for the design of modified synthetic models with increased activity. Herein, in particular, we probe the effects of alternative metal centers, ligand modifications, and group substitutions, with the aim of designing more efficient compounds with accessible synthetic strategies.

Ligand Modifications: We designed two new biomimetic models derived from MIM0 (see Scheme 2): in MIM1, we introduced an additional CH_2-group between the phenolate and the binaphtyl moiety to break the extended conjugated system and to introduce more flexibility for an optimal orientation of the equatorial ring. In MIM2, we also

 © 2004 Wiley-VCH Verlag GmbH & Co. KGaA, Weinheim

introduced a fluorine atom in the *para* position of the critical equatorial ring to enhance the spin delocalization from the copper center and the substrate towards the equatorial ligand.[18]

As intended, the enhanced flexibility introduced by the additional -CH_2 group leads to a different orientation of the aromatic ring of the equatorial phenolate ligand. In the reactant geometries (Scheme 1 **B**) the aromatic ring moves significantly out of the coordination plane, with an angle between the aromatic ring system and the copper plane ranging from 55° to 83° (with respect to 21° for MIM0) thus approaching the orientation of the natural system of 71°. Consequently, at the transition state (Scheme 1 **C**), the unpaired spin density of the ketyl radical is partially delocalized to the equatorial tyrosyl. This enhanced delocalization of the unpaired spin density in the transition state has indeed a distinct effect on the activation barrier.[18] The enzymatic activation barrier has been estimated from experimental turnover rates to be about 14 kcal mol^{-1}.[11] Within our computational framework,[*] we previously obtained an activation barrier for GOase and MIM0 of 16 and 21 kcal mol^{-1}, respectively.[18] The structural modifications introduced in the design of MIM1 and MIM2 are able to reduce the activation barrier significantly resulting in values as low as 13.8 kcal mol^{-1} for the case of MIM2, that is, a value even lower than that for the natural enzyme (Table 1). The expected turn over rates for MIM1 and MIM2 are 150 s^{-1} and 4000 s^{-1}, respectively, therefore up to five orders of magnitude higher than the one of the original compound MIM0.

Table 1: Activation barriers for GOase and its models.

Catalyst	GOase	MIM0	MIM1	MIM2	mim-Cu	mim-Ol-Cu	mim-Rh	mim-Ol-Rh
Activation barrier [kcal mol^{-1}]	16.0	21.0	15.7	13.8	15.8	14.1	22.9	21.4

For a more complete scan of optimal modified ligand systems and possible metal substitutions, we also developed a smaller computational model that is able to catch the essential features of MIM1 and MIM2 at a lower computational cost. To this purpose, we investigated the H-abstraction step of the minimal compound mim-Cu (see Scheme 2), and found excellent similarity to MIM1 in terms of geometry and activation energy as shown in Table 1. The axial ligand seems, therefore, not to be important for H-abstraction and matter only for the protonation/deprotonation steps. The robustness of our scaffold against ligand substitutions has been further investigated by replacing the phenylamine-*N*-ethylidene with a seven membered olefine ring (mim-Ol-Cu in Scheme 2). Again, in this case, the calculated activation barrier turns out to be insensitive to this substitution.

Alternative Metals: With the aim of investigating whether these catalytic properties are unique to copper, we also explored the possibility of using alternative metal centers. From the experimental point of view, the search for alternative transition metal centers in functional models of GOase has so far been limited to Zn^{II},[8] however, with inferior turnover rates (0.02 s^{-1} for Cu^{II} vs 0.003 s^{-1} for Zn^{II}). As a further alternative, herein, we concentrate our studies on compounds based on the Rh^{I}/Rh^{II} center (mim-Rh and mim-Ol-Rh in Scheme 2).[+]

The calculated activation barrier for mim-Rh and mim-Ol-Rh are 22.7 and 21.4 kcal mol^{-1}, respectively, that is, essentially competitive with the one of the copper-containing compound MIM0 (21.0 kcal mol^{-1}). A comparative study of the hydrogen abstraction step in mim-Cu and mim-Rh reveals that although the activation energies are roughly comparable, qualitative differences are present in the electronic structure of the two enzyme mimetics at the transition state. The total integrated spin density is reported as a function of the reaction coordinate in Figure 1 a. These data show that in the case of mim-Rh the electron transfer from the ketyl species to the rhodium ion occurs before hydrogen abstraction (i.e., formally corresponding to a transferred H^+) and not after as in mim-Cu, MIM0, MIM1, and MIM2. At the mim-Rh transition state, the unpaired electron is shared between the substrate and the metal center, in contrast to what occurs in mim-Cu, in which the electron is localized on the substrate and on the equatorial ligand. This difference suggests that, whereas for the copper-based mimetic the reaction is enhanced by improving spin delocalization (to the equatorial ligand), in the case of rhodium a tailoring of the metal redox properties appears to be an apt procedure to lower the rate-limiting barrier.

In summary, we have illustrated how the rational design of modifications of enzyme mimetic compounds can significantly improve their catalytic efficiency, reaching and even surpassing the one of the natural target. Furthermore, other metals, such as rhodium, could replace copper as the redox center, which may result in activation barriers comparable to those found in existing copper-based compounds.

Experimental Section

Methods: Density functional theory calculations were carried out by using the programs CPMD (www.cpmd.org)[20] and ADF[21] with the BLYP exchange correlation functional.[22,23] Geometries were converged up to a residual nuclear gradient of 0.001 atomic units. In CPMD calculations, the Kohn–Sham orbitals were expanded in plane waves with an energy cutoff of 80 Ry, which has been shown to be

[*] The calculations presented here refer to $\Delta U^{\neq}$ which should be a good approximation of $\Delta F^{\neq}$ in the case of a unimolecular reaction with only very minor structural rearrangements.

[+] Preliminary screening within the simplified class of models mim-M (Scheme 2) has also been performed on the series of transition metals M = Ti, Ru, Rh, Pd that were selected because of their similarity to copper in terms of chemical properties (such as redox potential, coordination geometry and ionic radii). The ruthenium and titanium oxidation states involved in the catalytic cycle were Ru^{III}/Ru^{II} and Ti^{IV}/Ti^{III} respectively. Metal-binding energies are reported in the Supporting Information. Whereas Ti favors geometries with an enhanced coordination number, Ru and Pd appear both as valuable alternatives to Rh as reactive centers.

 © 2004 Wiley-VCH Verlag GmbH & Co. KGaA, Weinheim

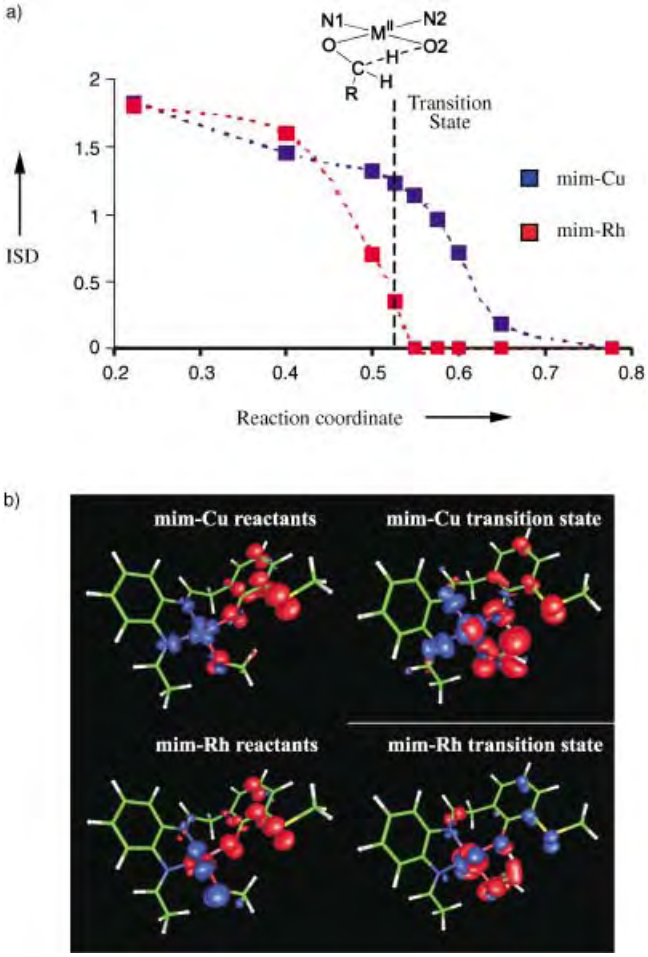


Figure 1. Hydrogen-abstraction step in copper- and rhodium-based models. a) The values of the integrated spin densitiy (ISD) indicate the number of unpaired electrons along the reaction coordinate. Whereas in the case of copper, the electron transfer from the substrate is not completed at the transition state, in the case of rhodium it occurs before hydrogen abstraction. This fact is reflected in the spatial distribution of the unpaired spin density on the substrate radical (b). In mim-Cu (top) the negative charge that accumulates on the substrate during the hydrogen-abstraction step is efficiently delocalized over the phenolate ligand. This stabilizing delocalization is lacking in the case of mim-Rh (bottom).

sufficiently accurate for these compounds.[17] In ADF calculations we used DZP (H, N, O) and TZP (Cu, Ti, Ru, Rh, Pd) basis sets. The transition states of the hydrogen abstraction step have been localized in CPMD by using the three-point constraint described by Ensing et al.[24] on atoms C, H, and O2 (Scheme 1).

Supporting Information includes: the calculated binding energies for mim-M, the coordinates of the fully optimized equilibrium and transition state geometries of mim-Rh and mim-Cu.

Received: February 23, 2004
Revised: April 13, 2004 [Z54081]

Keywords: ab initio calculations · alcohols · biomimetic synthesis · oxidation · transition metals

[1] R. A. Sheldon, I. W. C. E. Arends, G. J. Ten Brink, A. Dijksman, *Acc. Chem. Res.* **2002**, *35*, 774–781.
[2] M. A. Halcrow, L. M. L. Chia, X. M. Liu, E. J. L. McInnes, L. J. Yellowlees, F. E. Mabbs, I. J. Scowen, M. McPartlin, J. E. Davies, *J. Chem. Soc. Dalton Trans.* **1999**, 1753–1762.
[3] Y. Shimazaki, S. Huth, A. Odani, O. Yamauchi, *Angew. Chem.* **2000**, *112*, 1732–1735; *Angew. Chem. Int. Ed.* **2000**, *39*, 1666–1669.
[4] Y. Wang, J. L. DuBois, B. Hedman, K. O. Hodgson, T. D. Stack, *Science* **1998**, *279*, 537–540.
[5] R. Pratt, T. D. P. Stack, *J. Am. Chem. Soc.* **2003**, *125*, 8716–8717.
[6] P. Chaudhuri, M. Hess, U. Flörke, K. Wieghardt, *Angew. Chem.* **1998**, *110*, 2340–2343; *Angew. Chem. Int. Ed.* **1998**, *37*, 2217–2220.
[7] S. Itoh, M. Taki, S. Takayama, S. Nagatomo, T. Kitagawa, N. Sakurada, R. Arakawa, S. Fukuzumi, *Angew. Chem.* **1999**, *111*, 2944–2946; *Angew. Chem. Int. Ed.* **1999**, *38*, 2774–2776.
[8] P. Chaudhuri, M. Hess, J. Muller, K. Hildenbrand, E. Bill, T. Weyhermuller, K. Wieghardt, *J. Am. Chem. Soc.* **1999**, *121*, 9599–9610.
[9] F. Thomas, G. Gellon, I. G. Luneau, E. Saint-Aman, J. L. Pierre, *Angew. Chem.* **2002**, *114*, 3173–3176; *Angew. Chem. Int. Ed.* **2002**, *41*, 3047–3050.
[10] P. Chaudhuri, M. Hess, T. Weyhermüller, K. Wieghardt, *Angew. Chem.* **1999**, *111*, 1165–1168; *Angew. Chem. Int. Ed.* **1999**, *38*, 1095–1098.
[11] R. M. Wachter, B. P. Branchaud, *Biochim. Biophys. Acta* **1998**, *1384*, 43–54.
[12] A. J. Baron, C. Stevens, C. Wilmot, K. D. Seneviratne, V. Blakeley, D. M. Dooley, S. E. V. Phillips, P. Knowles, M. J. Mc. Pherson, *J. Biol. Chem.* **1994**, *269*, 25095–25105.
[13] M. M. Whittaker, D. P. Ballou, J. W. Whittaker, *Biochemistry* **1998**, *37*, 8426–8436.
[14] J. W. Whittaker, *Chem. Rev.* **2003**, *103*, 2347–2363.
[15] J. Müller, T. Weyhermüller, E. Bill, P. Hildebrandt, L. Ould-Moussa, T. Glaser, K. Wieghardt, *Angew. Chem.* **1998**, *110*, 637–640; *Angew. Chem. Int. Ed.* **1998**, *37*, 616–619.
[16] F. Himo, L. A. Eriksson, F. Maseras, P. E. M. Siegbahn, *J. Am. Chem. Soc.* **2000**, *122*, 8031–8036.
[17] U. Rothlisberger, P. Carloni, *Int. J. Quantum Chem.* **1999**, *73*, 209–218.
[18] U. Rothlisberger, P. Carloni, K. Doclo, M. Parrinello, *J. Biol. Inorg. Chem.* **2000**, *5*, 236–250.
[19] L. Guidoni, P. Maurer, S. Piana, U. Rothlisberger, *Quant. Struct. Act. Relat.* **2002**, *21*, 173–181.
[20] CPMD V3.7 Copyright IBM Corp 1990–2003, Copyright MPI fuer Festkoerperforschung Stuttgart, **1997**.
[21] G. T. Velde, F. M. Bickelhaupt, E. J. Baerends, C. F. Guerra, S. J. A. Van Gisbergen, J. G. Snijders, T. Ziegler, *J. Comput. Chem.* **2001**, *22*, 931–967.
[22] A. D. Becke, *Phys. Rev. A* **1988**, *38*, 3098–3100.
[23] C. L. Lee, W. Yang, R. G. Parr, *Phys. Rev. B* **1988**, *37*, 785–789.
[24] B. Ensing, E. J. Meijer, P. E. Blochl, E. J. Baerends, *J. Phys. Chem. A* **2001**, *105*, 3300–3310.

 © 2004 Wiley-VCH Verlag GmbH & Co. KGaA, Weinheim

Cancer Prevention

Inorganic Oxo Compounds React with Alkylating Agents: Implications for DNA Damage**

*Elizabeth E. Hamilton and Jonathan J. Wilker**

The cancer-preventing properties of selenium have been long known and are more potent than any other normal component of the human diet.[1–4] For example, patients taking selenium-supplemented brewer's yeast experienced significant reductions of colorectal, lung, and prostate cancer incidences as well as cancer related mortality.[5] Rat model studies have shown that the toxicity of food-borne alkylating toxins, such as diethylnitrosamine or methylnitrosourea, can be minimized by addition of various forms of selenium (e.g., Na_2SeO_3, Na_2SeO_4) to the diet.[6–8] Similar work with the vanadium compounds $VOSO_4$, $NaVO_3$, and Na_3VO_4 has also demonstrated the ability to prevent cancer induced by alkylating carcinogens.[9–11] The potential for dietary inorganic species to have significant impact on cancer prevention is illustrated by the "Selenium and Vitamin E Chemoprevention Trial" (SELECT).[12,13] In this ongoing trial sponsored by the National Cancer Institute, over 30000 males at risk for development of prostate cancer are having their diets supplemented with selenium alone, vitamin E alone, both selenium and vitamin E, or a placebo.[12,13] Despite this great promise of preventing cancer with inorganic species, no significant mechanistic data are available to explain the activity.[1–4] Indeed the scope of which inorganic compounds prevent cancer has not been explored fully.

The toxicity of food- and tobacco-borne carcinogens is often derived from activation into DNA-damaging alkylating agents. Diethylnitrosamine, for example, is enzymatically oxidized, undergoes subsequent decomposition, and yields the potent alkylating agent ethyl diazonium ($[C_2H_5N_2]^+$).[14] This alkylating toxin then reacts with nucleophilic sites of DNA (e.g., guanine N^7, thymine O^4) to give ethylated DNA. Unable to base-pair properly, this damaged DNA yields genomic mutations after replication. We wonder if the presence of alternate nucleophiles may allow for mitigation of this DNA alkylation. Under aqueous conditions, both selenium[15] and vanadium[16–18] exhibit tendencies to form anionic oxo species (e.g., $[SeO_4]^{2-}$, $[VO_4]^{3-}$). Perhaps these oxo compounds can consume electrophilic alkylating toxins, thereby minimizing DNA damage. By testing a hypothesis of inhibiting DNA damage, we present results to indicate that select inorganic compounds can both prevent alkylation of DNA and detoxify alkylating agents.

A modified assay for the observation of DNA alkylation[19] was used in which supercoiled pUC19 DNA was treated with the common alkylating toxin diethyl sulfate ($(C_2H_5O)_2SO_2$).[20] Base alkylation renders the sugar–base glycosidic bond susceptible to hydrolysis.[19] After alkylation, the DNA was hydrolyzed to release ethylated bases (e.g., N^7-ethylguanine) and create abasic sites. Endonuclease cleavage of DNA specifically at abasic sites then transformed the supercoiled DNA into nicked (one cleavage event) and linear (two or more cleavages) forms. Gel electrophoresis was used to separate and identify each form of the DNA (supercoiled, nicked, linear) thereby providing observation of DNA alkylation. Figure 1a shows the gel of a typical experiment (pH 7) containing DNA (lane 1) and various controls of DNA + enzyme (lane 2), DNA + Na_2SeO_4 (lane 3), DNA + Na_2SeO_4 + enzyme (lane 4), and DNA + $(C_2H_5O)_2SO_2$ (lane 5). In lane 6 is a reaction of DNA + $(C_2H_5O)_2SO_2$ + enzyme in which the supercoiled DNA form was consumed by alkylation and the subsequent digest. Lanes 7–12 show similar alkylation reactions with increasing concentrations of Na_2SeO_4 added to DNA + $(C_2H_5O)_2SO_2$ + enzyme. The Na_2SeO_4:$(C_2H_5O)_2SO_2$ ratios, ranging from 0.01 up to 10, are provided in Figure 1a. As can be seen, especially in lanes 11 and 12, addition of Na_2SeO_4 preserved the unalkylated, supercoiled DNA. Analogous experiments were performed in which the effects of the vanadium salt Na_3VO_4 upon DNA alkylation were examined (Figure 1b). Similar to that seen with the selenium compound, Na_3VO_4 maintained a portion of DNA in the unalkylated, supercoiled form. Control experiments demonstrated that neither Na_2SeO_4 nor Na_3VO_4 inhibited activity of the enzyme (data not shown). From these results, we conclude that both Na_2SeO_4 and Na_3VO_4 prevent DNA-alkylation damage in a concentration-dependent manner.

Inspection of the gels in Figure 1 reveals that the abilities of Na_2SeO_4 and Na_3VO_4 to prevent DNA alkylation are not identical. From digital-imaging quantification of the bands in lanes 6 and 11 we find that, with 1:1 ratios of inorganic:alkylating agent, Na_2SeO_4 preserved 6.7% of DNA unalkylated whereas Na_3VO_4 protected 40%.[20] Perhaps higher charge density of the $[VO_4]^{3-}$ ion, relative to the $[SeO_4]^{2-}$ ion, affords greater nucleophilicity and consequently an enhanced ability to react with electrophilic alkylating agents. Interestingly, cancer-prevention trials in rats are often performed by administering Na_2SeO_4 at 4 ppm in drinking water[6] whereas Na_3VO_4 is dosed lower at 0.5 ppm.[9,10]

Such differences in preventing DNA alkylation by these two compounds led us to examine an array of inorganic salts, all at pH 7 and in a background of 150 mM $MgCl_2$ to prevent simple cationic shielding of DNA nucleophilicity.[20–22] The following compounds prevented DNA alkylation at inorganic:alkylating agent ratios of 10 or less: $NaHCO_3$, Na_2CO_3, $NaNO_2$, Na_3PO_4, Na_2HPO_4, NaH_2PO_4, $Na(OOCCH_3)$, $NaIO_3$, Na_2MoO_4, $Na_2S_2O_4$, Na_2SeO_3, Na_2SeO_4, $NaVO_3$, Na_3VO_4, and $[(C_4H_9)_4N]_3(V_3O_9)\cdot 0.5\,H_2O$.[23] No protection of DNA was found from NaCl, NaBr, NaI, $NaNO_3$, KCl, KBr,

[*] E. E. Hamilton, Prof. J. J. Wilker
Department of Chemistry
Purdue University
West Lafayette, IN 47907-2084 (USA)
Fax: (+1) 765-494-0239
E-mail: wilker@purdue.edu

[**] This work was funded by the Cancer Research and Prevention Foundation. Additional support was provided to J.J.W. by an Alfred P. Sloan Foundation Research Fellowship.

Supporting information for this article is available on the WWW under http://www.angewandte.org or from the author.

 © 2004 Wiley-VCH Verlag GmbH & Co. KGaA, Weinheim DOI: 10.1002/anie.200353363

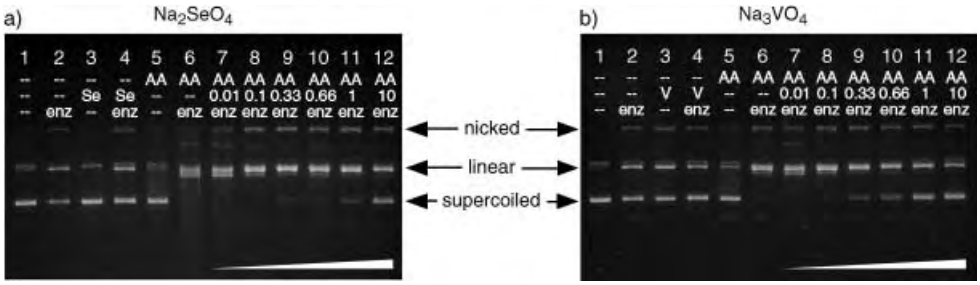


Figure 1. Agarose gels showing the ability of a) Na_2SeO_4 and b) Na_3VO_4 to prevent DNA alkylation damage. As described in the text and Supporting Information, an endonuclease enzyme-based assay was used to visualize alkylation. The presence of supercoiled pUC19 DNA (e.g., lane 1) indicates a lack of alkylation, whereas loss of this fast moving band demonstrates alkylation (e.g., lane 6). Where applicable, presence of the alkylating agent $(C_2H_5O)_2SO_2$ ("AA"), enzyme ("enz"), and inorganic compounds Na_2SeO_4 ("Se") or Na_3VO_4 ("V") are indicated atop each lane. All reactions were run at pH 7 with a DNA concentration of 150 μM in nucleotides. The $(C_2H_5O)_2SO_2$ concentration was 1.5 mM and the salts Na_2SeO_4 and Na_3VO_4 were at 1.5 mM unless stated otherwise. The numbers provided in lanes 7–12 (e.g., 0.1, 10) are ratios of concentrations for inorganic salts:alkylating agent. The ramps correspond to increasing concentrations of Na_2SeO_4 or Na_3VO_4. In lanes 7–12, higher concentrations of Na_2SeO_4 or Na_3VO_4 can be seen to maintain greater amounts of unalkylated DNA.[20]

KI, KNO_3, $MgCl_2$, $Mg(NO_3)_2$, $CaCl_2$, $Ca(NO_3)_2$, $CoCl_2$, $Co(NO_3)_2$, $MnCl_2$, $NiCl_2$, and $Ni(NO_3)_2$. Many other salts examined (e.g., $VOSO_4$, $FeCl_3$) were not soluble at pH 7, thereby yielding data not directly comparable with those described above.[20] The trend arising from these results appears to be that nucleophiles, in the form of anionic oxo species (e.g., $[CO_3]^{2-}$, $[MoO_4]^{2-}$, $[NO_2]^-$, $[VO_4]^{3-}$), are needed to prevent alkylation of DNA. By contrast, non-oxo compounds (e.g., NaCl, $NiCl_2$) provide no protection against DNA damage.

To understand the nature of these detoxification processes, we turn to model reactions between alkylating agents and inorganic compounds. The high activity of $[VO_4]^{3-}$ for preventing DNA alkylation brought our focus to vanadate chemistry. Although aqueous speciation of vanadates is exceedingly complex, with multiple species often coexisting in one solution (e.g., $[H_2VO_4]^-$, $[H_2V_2O_7]^{2-}$, $[V_4O_{12}]^{4-}$, $[V_5O_{15}]^{5-}$),[16–18] use of acetonitrile as a solvent simplifies the system, thereby permitting chemical insights on reactivity.[23] Detailed speciation data are available for the $[V_3O_9]^{3-}$ ion, prepared as the $[(C_4H_9)_4N]^+$ salt, and provide a suitable starting point for model reactions.[23] Figure 2 shows the ^{1}H NMR spectrum of a 1:1 reaction between $[(C_4H_9)_4N]_3(V_3O_9)\cdot 0.5\,H_2O$ and $(C_2H_5O)_2SO_2$ in which this vanadate transformed the alkylating toxin into relatively harmless ethanol. Spectral identification of the ethanol reaction product was confirmed by spiking the ^{1}H NMR reaction solution with a genuine sample as well as gas chromatography–mass spectrometry. Control experiments with $(C_2H_5O)_2SO_2$ alone did not produce ethanol. The proton source for ethanol formation may be adventitious water in the solvent or from the crystal lattice of $[(C_4H_9)_4N]_3(V_3O_9)\cdot 0.5\,H_2O$.[23] The predominant vanadium-containing product of this detoxification reaction was identified by ^{51}V NMR to be $[V_5O_{14}]^{3-}$.[20,24] A 3:1 reaction of $(C_2H_5O)_2SO_2$:$[(C_4H_9)_4N]_3(V_3O_9)\cdot 0.5\,H_2O$ yielded $[V_5O_{14}]^{3-}$ initially, which then transformed to $[V_{12}O_{32}]^{4-}$.[20,25] When viewed as oligomers of metavanadate ($[VO_3]^-$), the starting trimeric $[V_3O_9]^{3-}$ ion (i.e., $([VO_3]^-)_3$) yielded products deficient in oxygen (i.e., $[V_5O_{14}]^{3-}$ versus $[V_5O_{15}]^{5-}$ and $[V_{12}O_{32}]^{4-}$ versus $[V_{12}O_{36}]^{12-}$) along with oxygen-containing ethanol. Thus the detoxifying transformation of an alkylating agent into an alcohol requires an inorganic oxide source.

This transformation appears to be a general phenomenon given that we found a variety of alkylating agents (e.g., C_2H_5Br, C_2H_5I, $C_2H_5OSO_2CF_3$, $(C_2H_5O)_2SO_2$) all reacted with an assortment of vanadates (e.g., $[V_3O_9]^{3-}$,[23] $[HV_4O_{12}]^{3-}$,[26] $[V_5O_{14}]^{3-}$,[24] $[V_{10}O_{26}]^{4-}$,[27] $[H_3V_{10}O_{28}]^{3-}$[28]) to yield ethanol. When the selenium compound Ag_2SeO_4 was treated with the alkylating agents C_2H_5Br or C_2H_5I, ethanol was produced. Note that the phosphate $[(C_4H_9)_4N](H_2PO_4)$ did react with various alkylating agents, but an alcohol product was never released. Facile interconversion between different oxo species (e.g., $[V_5O_{14}]^{3-} \rightleftharpoons [V_{12}O_{32}]^{4-}$) may be the key to producing ethanol and preventing cancer. For aqueous phosphate, by contrast, mononuclear species predominate.[29] The 1:1 reaction between $(C_2H_5O)_2SO_2$ and $[(C_4H_9)_4N]_3(V_3O_9)\cdot 0.5\,H_2O$ (50 mM each) was approximately 75% complete after

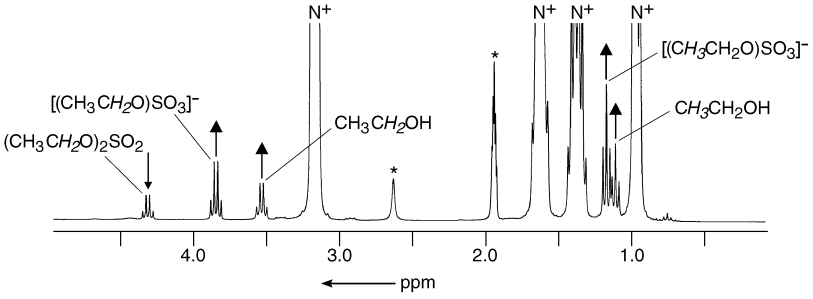


Figure 2. The ^{1}H NMR spectrum of a 1:1 detoxification reaction, in progress, between the alkylating agent $(C_2H_5O)_2SO_2$ and vanadate $[(C_4H_9)_4N]_3(V_3O_9)\cdot 0.5\,H_2O$ in distilled CD_3CN. Arrows indicate the changes associated with the consumption of the starting material $(C_2H_5O)_2SO_2$ and formation of the products $[(C_2H_5O)SO_3]^-$ and ethanol. Water and CHD_2CN are marked with a "*". The $[(C_4H_9)_4N]^+$ counterion is designated "N^+". The methyl resonance of $(C_2H_5O)_2SO_2$ at $\delta = 1.36$ ppm is obscured by those of $[(C_4H_9)_4N]^+$.

 © 2004 Wiley-VCH Verlag GmbH & Co. KGaA, Weinheim

20 minutes. Analogous reactions showed the following kinetic trend of reactivity: $[V_3O_9]^{3-} > [HV_4O_{12}]^{3-} > [V_5O_{14}]^{3-} \gg [V_{10}O_{26}]^{4-} \gg [H_3V_{10}O_{28}]^{3-}$. Again, charge density seems to dictate the ability to consume alkylating toxins.

Herein we have shown that inorganic oxo compounds can prevent DNA alkylation damage and that oxo compounds detoxify alkylating agents by oxide transfer. Although these reactions do not necessarily demonstrate processes occurring in cells, they do serve to illustrate interactions that are possible. These reactions raise the intriguing possibility that the inorganic compounds known to prevent cancer do so by a "carcinogen interception" mechanism in which oxo species consume the toxin, thereby preventing DNA damage. We present these results, propose a mechanism for minimizing DNA damage with inorganic compounds, and suggest that further work be done to understand this promising avenue of preventing cancer.

Received: November 19, 2003
Revised: March 8, 2004 [Z53363]

Keywords: antitumor agents · bioinorganic chemistry · DNA alkylation · DNA damage · vanadium

[1] G. F. Combs, W. P. Gray, *Pharmacol. Ther.* **1998**, *79*, 179–192.
[2] H. E. Ganther, *Carcinogenesis* **1999**, *20*, 1657–1666.
[3] C. Ip, *J. Nutr.* **1998**, *128*, 1845–1854.
[4] Y. S. Kim, J. Milner, *Nutr. Cancer* **2001**, *40*, 50–54.
[5] L. C. Clark, G. F. Combs, B. W. Turnbull, E. H. Slate, D. K. Chalker, J. Chow, L. S. Davis, R. A. Glover, G. F. Graham, E. G. Gross, A. Krongrad, J. L. Lesher, H. K. Park, B. B. Sanders, C. L. Smith, J. R. Taylor, *J. Am. Med. Assoc.* **1996**, *276*, 1957–1963.
[6] C. Thirunavukkarasu, D. Sakthisekaran, *J. Cell. Biochem.* **2003**, *88*, 578–588.
[7] J. W. Finley, C. Ip, D. J. Lisk, C. D. Davis, K. J. Hintze, P. D. Whanger, *J. Agric. Food Chem.* **2001**, *49*, 2679–2683.
[8] C. Ip, H. Ganther, *Carcinogenesis* **1988**, *9*, 1481–1484.
[9] A. Bishayee, M. Chatterjee, *Br. J. Cancer* **1995**, *71*, 1214–1220.
[10] A. Bishayee, S. Banik, A. Mandal, P. Marimuthu, M. Chatterjee, *Int. J. Oncol.* **1997**, *10*, 413–423.
[11] H. J. Thompson, N. D. Chasteen, L. D. Meeker, *Carcinogenesis* **1984**, *5*, 849–851.
[12] E. A. Klein, S. M. Lippman, I. M. Thompson, P. J. Goodman, D. Albanes, P. R. Taylor, C. Coltman, *World J. Urol.* **2003**, *21*, 21–27.
[13] R. W. Pak, V. J. Lanteri, J. R. Scheuch, I. S. Sawczuk, *Integr. Cancer Ther.* **2002**, *1*, 338–344.
[14] J. A. Swenberg, D. G. Hoel, P. N. Magee, *Cancer Res.* **1991**, *51*, 6409–6414.
[15] H. Robberecht, R. V. Grieken, *Talanta* **1982**, *25*, 823–844.
[16] D. C. Crans, C. D. Rithner, L. A. Theisen, *J. Am. Chem. Soc.* **1990**, *112*, 2901–2908.
[17] E. Heath, O. W. Howarth, *J. Chem. Soc. Dalton Trans.* **1981**, 1105–1110.
[18] L. Pettersson, B. Hedman, I. Andersson, N. Ingri, *Chem. Scr.* **1983**, *22*, 254–264.
[19] N. R. Drinkwater, E. C. Miller, J. A. Miller, *Biochemistry* **1980**, *19*, 5087–5092.
[20] See Supporting Information.
[21] W. J. Bodell, *Chem. Res. Toxicol.* **1999**, *12*, 965–970.
[22] R. L. Wurdeman, B. Gold, *Chem. Res. Toxicol.* **1988**, *1*, 146–147.
[23] E. E. Hamilton, P. E. Fanwick, J. J. Wilker, *J. Am. Chem. Soc.* **2002**, *124*, 78–82.
[24] V. W. Day, W. G. Klemperer, O. M. Yaghi, *J. Am. Chem. Soc.* **1989**, *111*, 4518–4519.
[25] V. W. Day, W. G. Klemperer, O. M. Yaghi, *J. Am. Chem. Soc.* **1989**, *111*, 5959–5961.
[26] J. Fuchs, S. Mahjour, J. Pickardt, *Angew. Chem.* **1976**, *88*, 385; *Angew. Chem. Int. Ed. Engl.* **1976**, *15*, 374–375.
[27] A. Bino, S. Cohen, C. Heitner-Wirguin, *Inorg. Chem.* **1982**, *21*, 429–431.
[28] V. W. Day, W. G. Klemperer, D. J. Maltbie, *J. Am. Chem. Soc.* **1987**, *109*, 2991–3002.
[29] F. A. J. Armstrong in *Analytical Chemistry of Phosphorus Compounds* (Ed.: M. Halmann), Wiley-Interscience, New York, **1972**, pp. 743–769.

 © 2004 Wiley-VCH Verlag GmbH & Co. KGaA, Weinheim

Nanotechnology

Electrical Contacting of Glucose Oxidase in a Redox-Active Rotaxane Configuration**

*Eugenii Katz, Laila Sheeney-Haj-Ichia, and Itamar Willner**

Dedicated to Professor Mordecai Rabinovitz on the occasion of his 70th birthday

The electrical contacting of redox enzymes such as glucose oxidase, with electrodes is of fundamental importance for the development of amperometric biosensors[1] and biofuel cells.[2] The tethering of redox-active units to the enzyme[3] or the immobilization of the biocatalysts in redox-active polymers[4] have been reported as means of establishing electrical communication between the redox centers of enzymes and electrodes.

Recently, our laboratory reported the surface reconstitution of apo-proteins (e.g. apo-glucose oxidase (apo-GOx)) on cofactor-functionalized monolayers associated with electrodes as a general method to establish electrical communication between redox sites in proteins and electrodes. The reconstitution of apo-GOx on a relay-functionalized flavin adenine dinucleotide (FAD) monolayer (e.g. pyrroloquinoline quinone (PQQ) linked to FAD),[5] or on FAD-functionalized Au nanoparticles,[6] or on FAD-functionalized carbon nanotubes[7] proved to be effective means of bringing the redox enzyme into electrical contact with the electrodes, and unprecedented high electron-transfer turnover rates were observed.

One of the challenges is the electrochemical activation of the biocatalyzed oxidation or reduction of a substrate at the

[*] Dr. E. Katz, L. Sheeney-Haj-Ichia, Prof. I. Willner
Institute of Chemistry, The Hebrew University of Jerusalem
Jerusalem 91904 (Israel)
Fax: (+972) 2-652-7715
E-mail: willnea@vms.huji.ac.il

[**] This research (No. 101/00) is supported by the Israel Science Foundation.

 © 2004 Wiley-VCH Verlag GmbH & Co. KGaA, Weinheim DOI: 10.1002/anie.200353455

lowest possible positive or negative potential, respectively, close to the thermodynamic potential of the respective enzyme. This feature is significant for biosensor devices in order to eliminate nonspecific redox processes under applied overpotentials, and of key importance in developing biocatalytic electrodes for biofuel-cell elements to extract maximum electrical power.

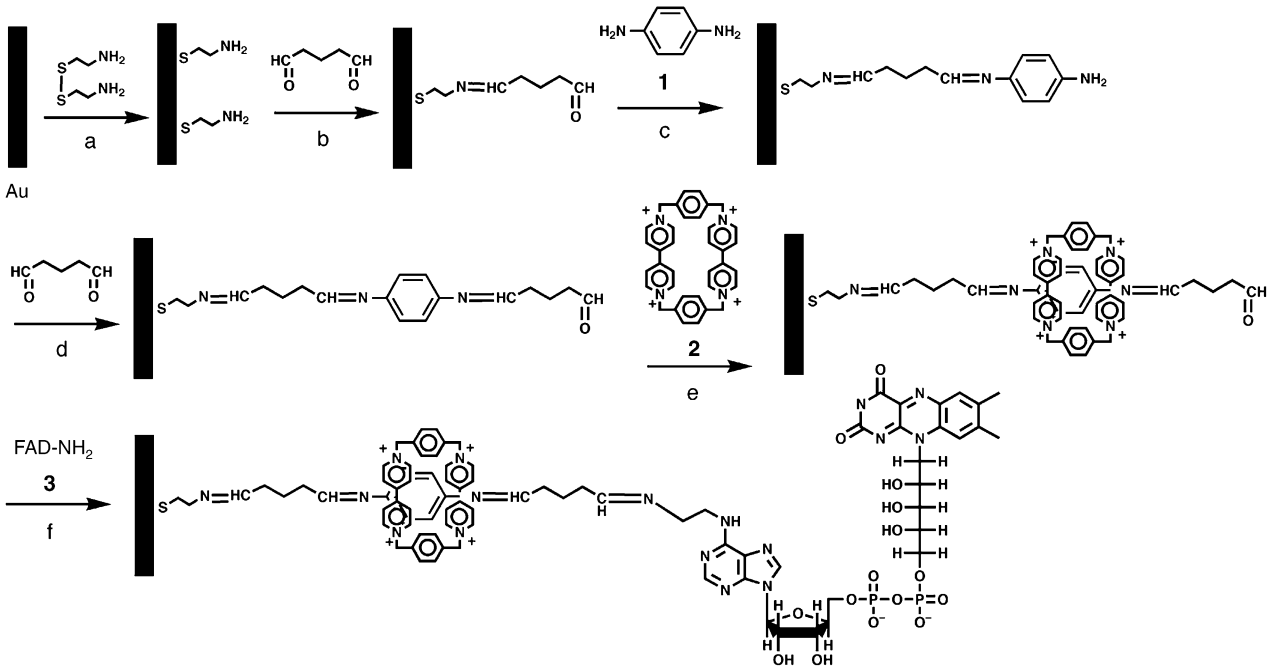
Rotaxanes are interesting supramolecular structures[8] and redox-active rotaxanes on surfaces have been used to assemble molecular electronic[9] and optoelectronic[10] devices. Herein we report the first glucose oxidase (GOx)-reconstituted FAD-stoppered redox-active rotaxane on a Au electrode. The reconstituted GOx is brought into electrical contact with the electrode by the redox-active rotaxane which operates as an electron-transfer mediator to allow the effective bioelectrocatalytic oxidation of glucose at -0.4 V versus SCE (saturated calomel electrode)—a value that is very close to the thermodynamic redox potential of the FAD cofactor ($E° = -0.51$ V versus SCE at pH 8.0).[11]

Scheme 1 outlines the assembly of the rotaxane system on a gold electrode. Cystamine was self-assembled as a monolayer on a Au electrode (step a). The functionalized electrode was then treated with glutaric dialdehyde (step b) and the resulting monolayer was treated with 1,4-diaminobenzene (**1**; step c) to yield the iminophenylamino-functionalized monolayer. The monolayer was further treated with glutaric dialdehyde (step d) and then with the electron acceptor cyclobis(paraquat-*p*-phenylene) (**2**; step e) to yield the supramolecular donor–acceptor complex with the diiminobenzene electron-donating unit. The resulting supramolecular structure was then stoppered with N^6-(2-aminoethyl)-FAD (**3**; step f) to generate the rotaxane structure consisting of **2** threaded onto the stoppered wire. Subsequently, apo-GOx was reconstituted on the FAD cofactor to generate the electrically contacted enzyme assembly (Scheme 2).

Stepwise modification of the electrode thus yields amino-functionalized surfaces after self-assembly of cystamine (step a) and after the covalent attachment of 1,4-diaminobenzene (step c), whereas the reactions with glutaric dialdehyde (steps b and d) result in the surface amino groups being blocked. The stepwise appearance and disappearance of the surface amino groups and the surface coverage of these groups were probed by electrochemical assay of the PQQ redox units immobilized on the amino functionalities.[12] The cyclic voltammograms of the PQQ-treated electrodes (not shown) demonstrate similar loading of the PQQ units (ca. 1×10^{-10} mol cm^{-2}) on the two amino-terminated monolayer structures generated upon the stepwise assembly of the system. The low limit of the concentration of the amino groups on the surface (ca. 1×10^{-10} mol cm^{-2}) generated after modification steps a and c, could be derived from the cyclic voltammograms of PQQ. On the other hand, attempts to induce a reaction between PQQ and the surfaces whose amino groups are blocked by glutaric dialdehyde did not yield any redox response of PQQ. These experiments confirmed the quantitative formation of the surface structures outlined in Scheme 1.

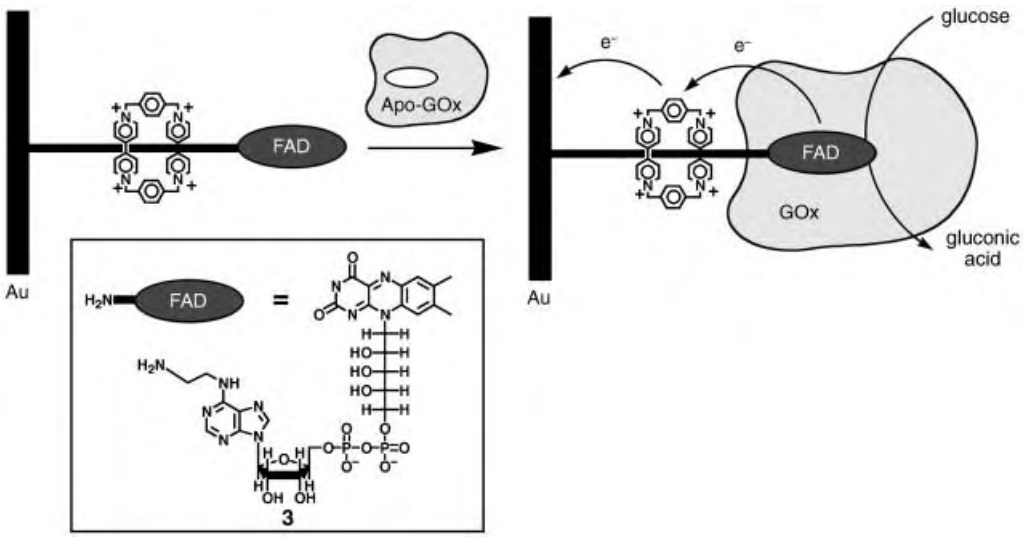
The amounts of surface-bound molecular components after each step of the electrode modification (ca. 1×10^{-10} mol cm^{-2}) were also calculated from quartz crystal microbalance (QCM) measurements performed upon the assembly of the monolayer on a Au–quartz piezoelectric crystal following a similar synthetic strategy. Formation of the supramolecular donor–acceptor complex between the redox-active rotaxane **2** and the diiminobenzene electron-donating units on the electrode surface was probed at various bulk concentrations of **2** by a chronocoulometric technique by means of Equation (1):[13]

$$Q = 2nFAD^{1/2}c\pi^{-1/2}t^{1/2} + Q_{dl} + nFA\Gamma_2 \quad (1)$$



Scheme 1. Assembly of interlocked rotaxane redox units on a molecular string.

 © 2004 Wiley-VCH Verlag GmbH & Co. KGaA, Weinheim



Scheme 2. The reconstitution of apo-GOx on the FAD–redox rotaxane molecular wire and the mechanism of the bioelectrocatalytic oxidation of glucose.

in which n is the number of electrons per molecule of **2** ($n=2$), F is the Faraday constant ($C\,equiv^{-1}$), A is the electrode area (cm^2), D is the diffusion coefficient ($cm^2\,s^{-1}$), c is the bulk concentration of **2** ($mol\,cm^{-3}$), Q_{dl} is the capacitance charge (C), and $nFA\Gamma_2$ is the charge associated with the reduction of the redox-active rotaxane **2** bound to the electron-donating sites on the surface; Γ_2 corresponds to the surface coverage of **2** ($mol\,cm^{-2}$).

Figure 1 A shows the chronocoulometric transients of the diiminobenzene-functionalized Au electrode in the absence of **2** (curve a) and in the presence of **2** at different bulk concentrations (curves b–d). The capacitance charge, Q_{dl}, was derived from the chronocoulometric transient measurement in the absence of the redox-rotaxane **2** by the extrapolation of its linear part to $t=0$. The sum of Q_{dl} and $nFA\Gamma_2$ was derived from the chronocoulometric transients for each bulk concentration of **2** by the extrapolation of their linear parts to $t=0$. As Q_{dl} and the surface coverages were known, the equilibrium Γ_2 values of the surface-bound **2** at variable bulk concentrations were calculated[13] (Figure 1 B). From this curve we were able to derive the association constant for the interaction between the acceptor **2** and the diimine donor sites to be approximately $K_a = 1\times10^4\,M^{-1}$. We then selected a bulk concentration of 0.3 mM for **2** to stopper the rotaxane with **3**. Under these conditions, about 80% of the diiminobenzene electron-donating units are associated with **2** in the rotaxane structure through the donor–acceptor complex. The surface coverage of **2** on the molecular wire is estimated to be approximately $0.8\times10^{-10}\,mol\,cm^{-2}$ and that of the cofactor-stopper approximately $1\times10^{-10}\,mol\,cm^{-2}$.

Microgravimetric quartz crystal microbalance (QCM) measurements provide a further means for following the association of **2** with the diiminobenzene-functionalized surface. The formation of the electron donor–acceptor complex of rotaxane **2** with the diiminobenzene moieties on the QCM surface is anticipated to cause a mass change (Δm) that

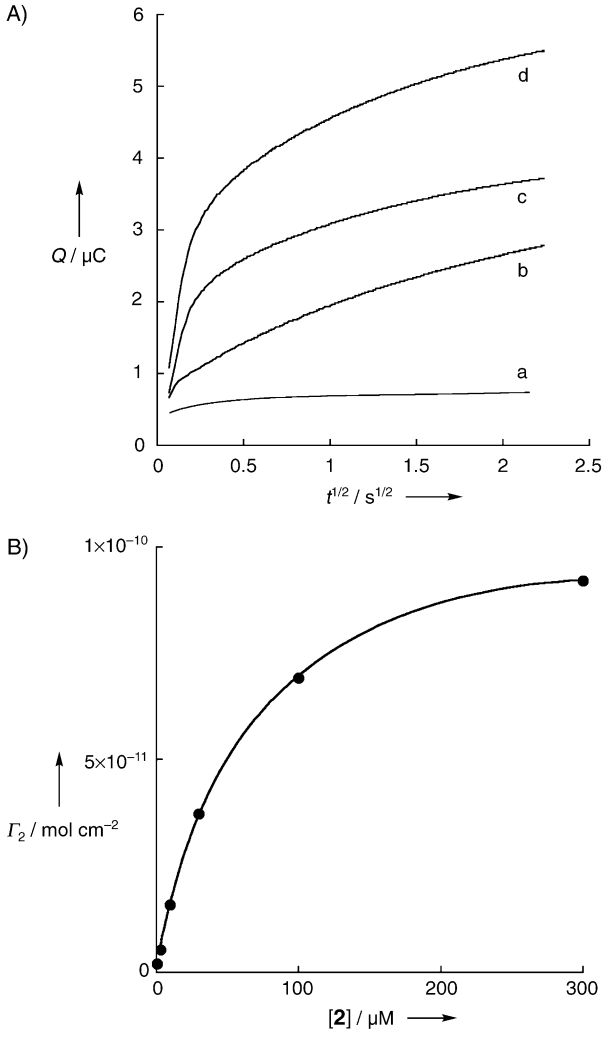


Figure 1. A) Chronocoulometric traces measured on the diiminobenzene-functionalized Au electrode upon application of a potential step from −0.35 to −0.50 V in the presence of **2** at various concentrations in the bulk solution in phosphate buffer (0.1 M, pH 8.0) under Ar: a) 0 μM, b) 10 μM, c) 30 μM, d) 100 μM. B) Variation of surface concentration of **2** (Γ_2) upon variation of its bulk concentration [**2**].

 © 2004 Wiley-VCH Verlag GmbH & Co. KGaA, Weinheim

results in a frequency change (Δf) of the crystal according to the Sauerbrey equation [Eq. (2)]. (f_0 is the base frequency of

$$\Delta f = -2 f_0 \Delta m / A(\rho_q \mu_q)^{1/2} \quad (2)$$

the crystal, ρ_q is the quartz density (2.648 g cm^{-3}), μ_q is the shear modulus of the crystal (2.947×10^{11} dyn cm^{-2} for AT-cut quartz), and A is the surface area).[14]

A gold surface associated with the quartz crystal was modified with the diiminobenzene monolayer by the same procedure that was used for modification of the regular Au electrode. Figure 2A shows the time-dependent frequency change of the modified quartz crystal upon stepwise increase of the concentration of **2** in the solution. Interaction of the monolayer-modified quartz crystal with **2** results in a frequency decrease which implies a mass increase on the crystal. A time-dependent decrease of the crystal frequency is observed, and the frequency stabilizes to a constant Δf value which represents the equilibrium binding of **2** to the surface. As the bulk concentration of **2** increases, the Δf values increase; Figure 2B shows the steady-state values of Δf at various bulk concentrations of **2**. The Δf values were translated to the Δm values by using Equation (2), and then the respective surface-coverage values Γ_2 were derived (e.g. Γ_2 values of 3.8×10^{-11}, 6.9×10^{-11} and 9.2×10^{-11} mol cm^{-2} were obtained when the bulk concentrations of **2** were 30, 100 and 300 μM, respectively). The Γ_2 values derived from the microgravimetric measurements are similar to those obtained by the chronocoulometric technique. Thus, the association constant $K_a = 1 \times 10^4$ M^{-1} was confirmed by the QCM measurements. Importantly, the addition of **2** to a bare or cysteamine-modified quartz crystal did not result in any frequency changes of the quartz crystal, implying that no nonspecific adsorption occurred on the surface in the absence of the diiminobenzene electron-donating sites.

The formation of the supramolecular complex between the diiminobenzene π-donor moiety and the cyclobis(paraquat-*p*-phenylene) (**2**) π acceptor (Scheme 3) was further supported by UV/Vis absorbance and ^{1}H NMR spectroscopy experiments in solution. The addition of *p*-dipropyliminobenzene (**4**), as a model compound for the diiminobenzene unit in the monolayer structure, to a solution of **2** in acetone gave rise to a charge-transfer band at $\lambda_{max} = 608$ nm ($\varepsilon = 270$ M^{-1} cm^{-1}), Figure 3. We monitored the changes in the charge-transfer band upon variation of the concentration of **4** with respect to **2**, which allowed us to determine the association constant for the formation of the supramolecular complex between the two species. The association constant $K_a = 1.23 \times 10^4$ M^{-1} was derived from computer fitting of the

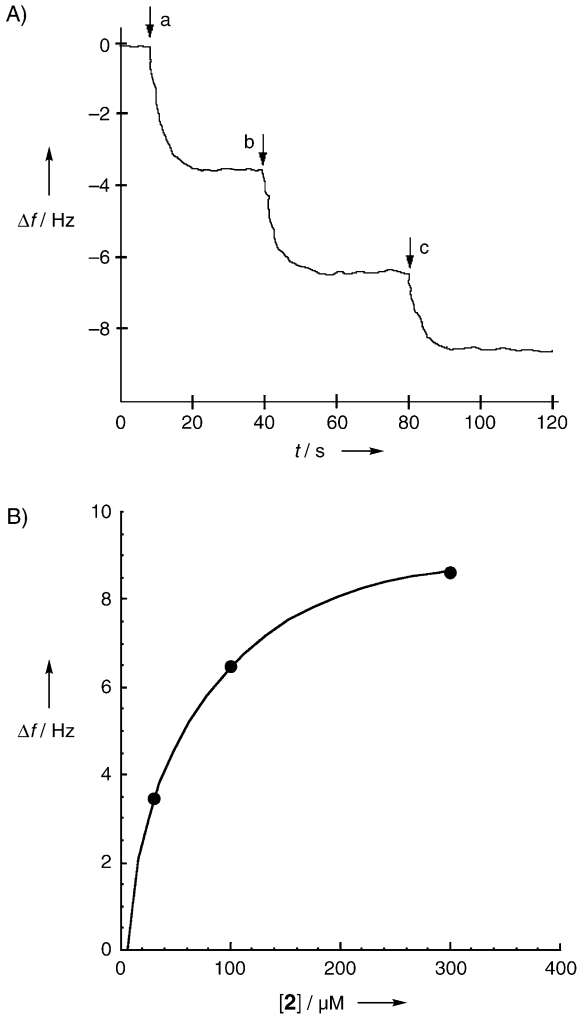
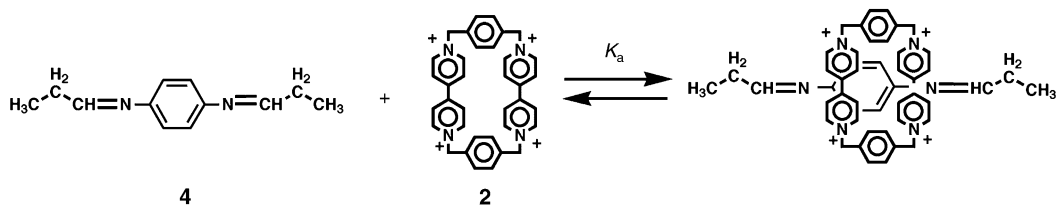


Figure 2. A) Time-dependent frequency changes of the diiminobenzene-functionalized Au/quartz crystal in the presence of **2** at different bulk concentrations in phosphate buffer (0.1 M, pH 8.0): a) 30 μM, b) 100 μM, c) 300 μM. B) Variation of the QCM frequency (Δf)with varying bulk concentrations of **2**.

experimental absorbance values (Figure 3, inset) to the absorbance expressed by Equation (3):[15]

$$A = l\varepsilon K_a [\mathbf{2}] [\mathbf{4}]/(1 + K [\mathbf{4}]) \quad (3)$$

(A is the absorbance of the charge-transfer complex measured at $\lambda_{max} = 608$ nm, l is the optical path length ($l = 1$ cm), ε is the molar absorptivity of the charge-transfer complex, K_a is the equilibrium constant for the formation of the complex,



4 **2**

Scheme 3. Threading of the cyclophane **2** onto the model diimine compound **4** wire in solution.

 © 2004 Wiley-VCH Verlag GmbH & Co. KGaA, Weinheim

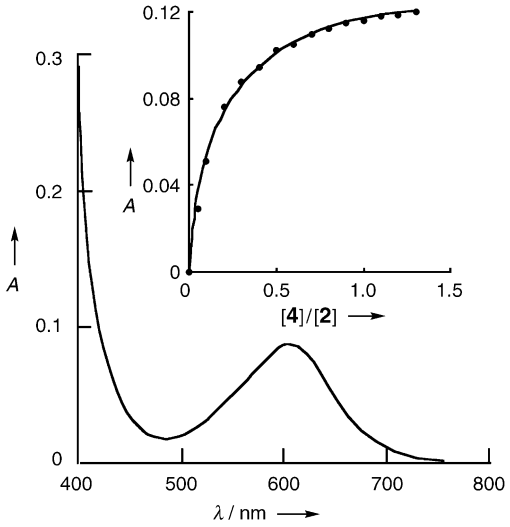


Figure 3. Absorption spectrum of cyclophane **2** (0.5 mM in acetone) in the presence of *p*-dipropyliminobenzene (**4**) (0.15 mM in acetone). Inset: Variation of the absorbance of the charge-transfer complex at $\lambda_{max} = 608$ nm, as a function of the molar ratio of **4** to **2**. The solid line represents computer fitting of the experimental points to Equation (3) using $K_a = 1.23 \times 10^4\ M^{-1}$ and $\varepsilon = 270\ M^{-1}\,cm^{-1}$.

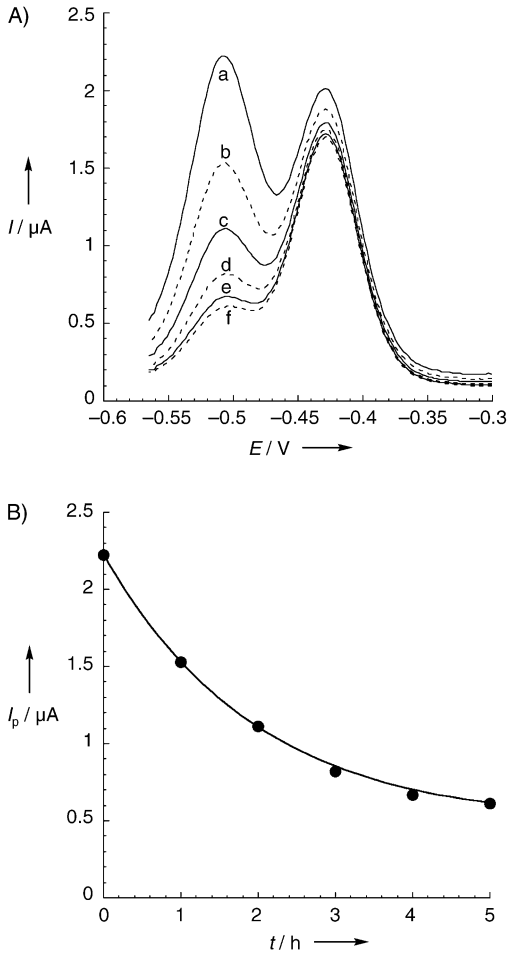


Figure 4. A) Differential pulse voltammograms of the **2**–FAD-functionalized Au electrode upon its reconstitution with apo-GOx, 1 mg mL^{-1}: a) 0 h, b) 1 h, c) 2 h, d) 3 h, e) 4 h, f) 5 h. DPVs were recorded in phosphate buffer (0.1 M, pH 8.0) under Ar, versus SCE . B) Decrease of the FAD peak upon the reconstitution process.

and [**2**] and [**4**] are the concentrations of the materials **2** and **4**, respectively.) Interestingly, despite the structural differences between the diimine moiety in the monolayer configuration and the model compound **4** in solution, and despite the fact that the association constants for the supramolecular complex of the monolayer assembly and the solute molecular units are determined in different solvents (water and acetone, respectively), very similar association constant values were deduced for the two structures.

The small difference between the potentials of FAD ($E° = -0.51$ V at pH 8) and **2** ($E° = -0.43$ V) did not allow the characterization of the redox components by cyclic voltammetry on the modified electrode. Thus, differential pulse voltammograms (DPVs) were recorded to observe the separate electrochemical responses of FAD and the interlocked redox units **2** (Figure 4A, curve a). As the two redox components FAD[11] and **2**[15] show two-electron-transfer processes, the peaks observed in the DPVs directly relate to the amount of surface-confined molecules. The surface coverage of **2** in the modified layer was estimated to be $\approx 0.8 \times 10^{-10}$ mol cm^{-2} and that of the FAD cofactor stopper $\approx 1 \times 10^{-10}$ mol cm^{-2}.[16]

Figure 4A curves b–f, show the time-dependent changes in the DPVs of the rotaxane-functionalized monolayer electrode upon the reconstitution of apo-GOx on the FAD stopper units. The peak corresponding to the FAD units decreases owing to the insulation of the FAD cofactor upon its reconstitution into the protein, whereas the peak for the complexed **2** is almost unaffected. The surface coverage of the reconstituted GOx ($\approx 2 \times 10^{-12}$ mol cm^{-2}) was derived from QCM measurements. The kinetics of reconstitution of the FAD monolayer into the apo-GOx (Figure 4B) is similar to that observed for other apo-GOx reconstitution systems.[17] The blocking of the FAD electrochemical response upon reconstitution with apo-GOx is not surprising and has been previously observed in other related systems.[5,17] In the free rotaxane–FAD monolayer configuration, the observed redox responses of **2** and FAD are due to the flexibility of the molecular spacer that provides short electron-transfer distances for both components. Upon reconstitution, the monolayer is rigidified and the FAD unit is shielded by the protein backbone thus preventing its direct electrical communication with the electrode.

From the redox potentials of the cyclophane **2** and the FAD units, one may conclude that vectorial electron transfer could be mediated by **2** provided that FAD exists in its biocatalytically generated reduced state. Figure 5A shows the cyclic voltammograms of the reconstituted enzyme electrode with the rotaxane-mediator structure in the presence of variable concentrations of glucose. Electrocatalytic anodic currents corresponding to bioelectrocatalyzed oxidation of glucose are observed at around −0.4 V versus SCE. The current increases as the concentration of glucose is elevated (Figure 5B). A control experiment reveals that the reconstitution of apo-GOx on a FAD monolayer that lacks the

 © 2004 Wiley-VCH Verlag GmbH & Co. KGaA, Weinheim

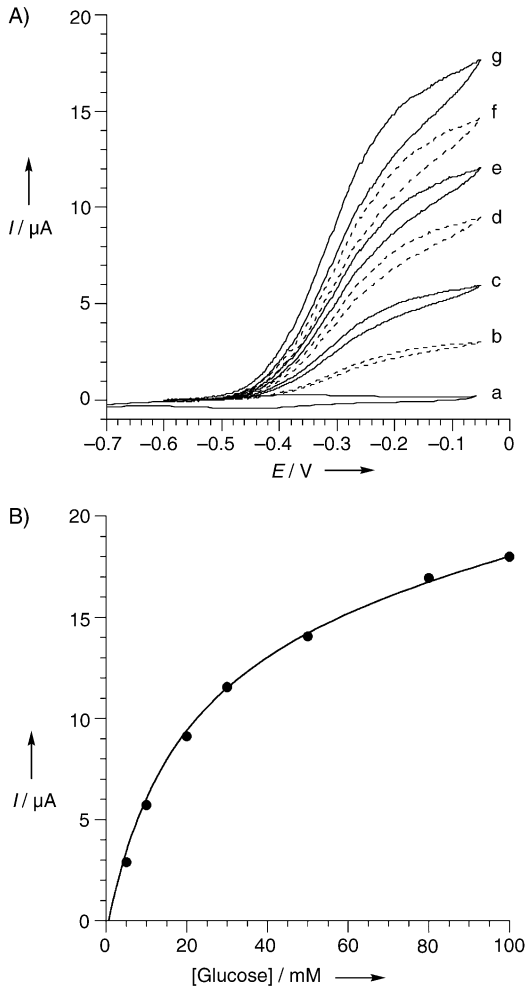


Figure 5. A) Cyclic voltammograms of the GOx-reconstituted electrode at different concentrations of glucose: a) 0 mM, b) 5 mM, c) 10 mM, d) 20 mM, e) 30 mM, f) 50 mM, g) 80 mM. Data were recorded in phosphate buffer (0.1 M, pH 8.0) under Ar. B) Calibration plot for glucose derived from the cyclic voltammograms at −0.1 V.

complex **2** does not yield an electrically contacted enzyme interface, although the biocatalyst is in a structurally active configuration.[18] These results clearly indicate that the monolayer-interlocked **2** acts as an electron-transfer mediator that transports the electrons from the FAD cofactor to the electrode surface. Knowing the surface coverage of the enzyme and the maximum current that is extracted from the system, we calculate an electron-transfer turnover rate of approximately 400 s^{-1}.

The effective electrical contact between the enzyme and the electrode in the rotaxane configuration may be attributed to two factors: 1) The electron-transfer mediator **2** is a two-electron relay, thus complementing the redox features of the FAD cofactor which also involves the transfer of two electrons. 2) The electron-relay **2** loses its electron acceptor properties after accepting the electrons from the FAD cofactor. As a result, the original donor–acceptor complex is perturbed and the reduced relay is free to move on the "molecular wire". This facilitates the transport of electrons to the electrode, resulting in the efficient bioelectrocatalyzed oxidation of glucose.

The dynamic shuttling of the bipyridinium cyclophane **2** on the molecular wire upon its reduction and reoxidation was confirmed by chronoamperometric experiments. The time-dependent current ($I(t)$) generated upon the reduction or the oxidation of a surface-confined redox species is given by Equation (4), in which k_{et} is the rate constant for the electron

$$I(t) = k_{et}\, Q \exp(-k_{et}\, t) \qquad (4)$$

transfer between the redox species and the electrode, and Q is the charge associated with the reduction (or oxidation) of the redox species linked to the electrode.[19]

Previous studies indicate[20] that the interfacial electron-transfer rate constant is controlled by the distance separating the redox unit and the electrode surface. Indeed, several studies[9e,21] have monitored dynamic and structural changes of redox-active components associated with electrodes by following the electron-transfer rate constants at the conductive supports. We have applied the chronoamperometric technique to follow the dynamic shuttling of **2** on the functional molecular wire and to prove that this shuttling occurs upon the mediated bioelectrocatalytic activation of the enzyme. Figure 6A shows the current transient observed upon application of an oxidation potential step on the glucose oxidase-stoppered–rotaxane electrode from −0.45 V to −0.39 V in the absence of glucose. Under these conditions, the cyclophane **2** initially exists in its reduced state and its oxidation proceeds when the potential step is applied. The current transient follows a monoexponential kinetics (Figure 6A, inset) and the derived rate constant and surface coverage of the cyclophane units correspond to $k_{et} = 1100\ s^{-1}$ and 0.8×10^{-10} mol cm^2, respectively. Figure 6B shows the current transient observed upon application of a potential step from −0.39 V to −0.45 V, again in the absence of glucose. Under these conditions, the cyclophane **2** exists in its oxidized state and is reduced to the respective biradical when the potential step is applied. The kinetic analysis (Figure 6B, inset) of the current transient indicates an interfacial electron-transfer rate constant that corresponds to $k_{et} = 80\ s^{-1}$. Thus, reduction of the cyclophane proceeds with a substantially lower electron-transfer rate constant than the oxidation process. This is consistent with the fact that the oxidized cyclophane is localized on the π-donor site by π-donor–acceptor interactions (even though the electrode is negatively charged), and the spatial separation of the redox-active cyclophane **2** from the electrode results in the slow electron-transfer rate. Reduction of the cyclophane unit results in the dissociation of the supramolecular complex on the wire. As the electrode is negatively charged, the positively charged reduced cyclophane is attracted to the electrode and the resulting short distance with respect to the electrode leads to fast electron transfer upon oxidation of the reduced cyclophane.

The position of the cyclophane on the molecular wire upon bioelectrocatalyzed oxidation of glucose by the functionalized enzyme-stoppered–rotaxane assembly was also confirmed by chronoamperometry. Figure 7 shows the current

 © 2004 Wiley-VCH Verlag GmbH & Co. KGaA, Weinheim

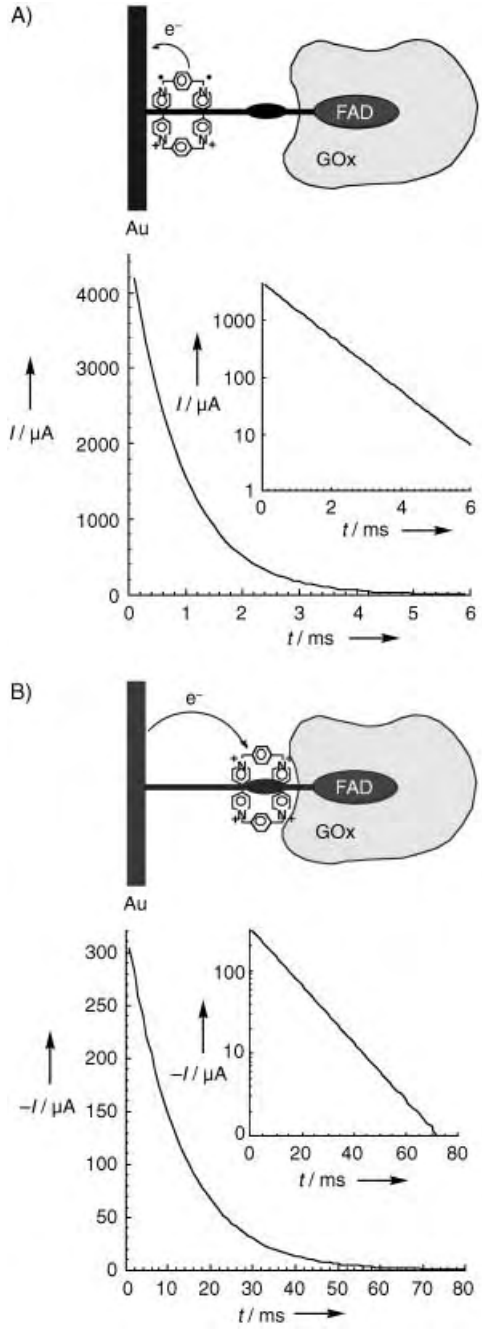


Figure 6. Current transients observed upon application of a potential step; A) from −0.45 to −0.39 V on the enzyme-stoppered–rotaxane electrode (pre-biased at −0.45 V for 10 s). Inset: Kinetic analysis of the current transient curve. B) From −0.39 to −0.45 V on the enzyme-stoppered–rotaxane electrode (pre-biased at −0.39 V for 10 s); Inset: Kinetic analysis of the current transient. All data were recorded in phosphate buffer (0.1 M, pH 8.0) under Ar in the absence of glucose.

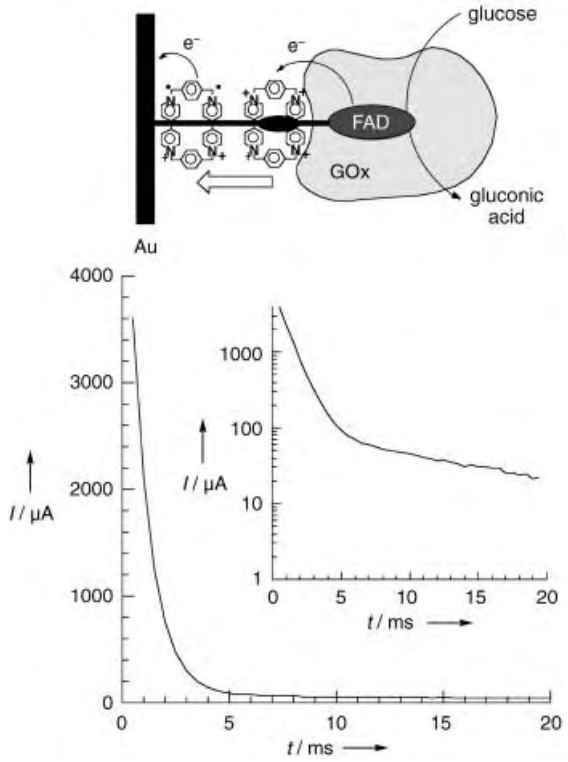


Figure 7. Current transient observed upon the application of a potential step from the open-circuit potential to −0.39 V in the presence of a glucose solution (80 mM) in phosphate buffer (0.1 M, pH 8.0) under Ar. Inset: Kinetic analysis of the experimental current transient curve.

transient upon application of the oxidative step from the open circuit potential to −0.39 V in the presence of glucose (80 mM). This potential step leads to the oxidized form of **2**; the current implies that under the open-circuit conditions the cyclophane exists in its reduced state. The inset in Figure 7 shows the kinetic analysis of the current transient; a fast exponential electron-transfer process is observed (k_{et} = 1100 s^{-1}) followed by a slow nonexponential current tail. The fast electron-transfer rate constant is characteristic of the oxidation of the reduced biradical cyclophane that is in close proximity to the electrode. The slow current transient is attributed to the electrocatalytic anodic current that is developed in the system. These results confirm the functions of the rotaxane as an electron-transfer shuttle in the activation of the enzyme. Under open-circuit conditions, oxidation of glucose leads to reduction of the rotaxane **2** located on the π-donor site and this results in the displacement of the reduced biradical cyclophane to a position that is close to the electrode. The oxidation of the reduced cyclophane reorganizes **2** on the π-donor site leading to the cyclic electrocatalytic activation of the enzyme.

In conclusion, the present study has demonstrated a novel method for the electrical contacting of a redox enzyme by using a rotaxane electron relay interlocked on a molecular wire connecting the enzyme to the electrode. Besides the fundamental interest of the study in establishing a new supramolecular configuration for the bioelectrocatalytic activation of enzymes, the fact that the bioelectrocatalyzed oxidation of glucose by glucose oxidase is activated at a redox potential of around −0.4 V has important practical implications. The nano-structured electrode reveals the lowest possible potential for the oxidation of glucose and thus represents the optimal electrode configuration (anode) for a glucose-based biofuel-cell element. The incorporation and

 © 2004 Wiley-VCH Verlag GmbH & Co. KGaA, Weinheim

examination of this electrode in biofuel cells is underway in our laboratory.

Experimental Section

Chemicals: Apo-glucose oxidase (apo-GOx) was prepared by a modification[5b] of a reported method.[22] N^6-(2-Aminoethyl)-flavin adenine dinucleotide (N^6-(2-aminoethyl)-FAD)[23] and cyclobis(paraquat-*p*-phenylene) (**2**)[24] were synthesized and purified as described before. *p*-Dipropyliminobenzene (**4**) was prepared by stirring a mixture of propionic aldehyde (15 mL) and 1,4-diaminobenzene (4.65 g) in dichloromethane (50 mL) overnight at room temperature. The solvent was then evaporated, and the product was recrystallized from ethanol (~80%); ^{1}H NMR (300 MHz; $CDCl_3$): $\delta = 1.2$–1.5 (t, $J = 25$ Hz, 6H), 1.7–1.9 (m, 4H), 6.8–7.1 (m, 4H), 6.1–6.5 ppm (m, 2H). All other chemicals, including pyrroloquinoline quinone (PQQ), 2,2′-dithio-bis(ethaneamine) (cystamine), 4-(2-hydroxyethyl)-piperazine-1-ethanesulfonic acid sodium salt (HEPES), 1-ethyl-3-(3-dimethylaminopropyl)-carbodiimide (EDC), glutaric dialdehyde, β-D-(+)-glucose, and ferrocene monocarboxylic acid, were purchased from Sigma–Aldrich and used as supplied. Ultrapure water (Seralpur Pro 90 CN) was used in all experiments.

Modification of Electrodes: Au electrodes (0.5 mm diameter Au wire, geometrical area ≈0.24 cm^2, roughness factor ≈1.2) were used for modifications. The Au electrodes were cleaned and modified with a self-assembled cysteamine monolayer as described before.[12] The cysteamine monolayer-functionalized electrodes were treated with glutaric dialdehyde (10% v/v) for 20 min. This and all other modification steps were performed in phosphate buffer (0.1M, pH 8.0). After each modification step the electrodes were rinsed with water. The aldehyde-functionalized electrodes were treated with *p*-phenylenediamine (10 mM) for 20 min. The *p*-phenylenediamine-functionalized electrodes were again treated with glutaric dialdehyde (10% v/v) for 20 min to yield diiminobenzene groups on the molecular wire. To analyze the appearance and disappearance of surface amino groups during the modification steps, sample electrodes after each modification step were treated with PQQ (1 mM, in 0.1M HEPES-buffer, pH 7.2) in the presence of EDC (1 mM) for 2 h. The PQQ units covalently attached to the amino groups were assayed by cyclic voltammetry.[12] The electrodes functionalized with the diiminobenzene groups were treated with different bulk concentrations of the rotaxane **2** to generate donor–acceptor complexes under equilibrium. The complex formation was probed by chronocoulometry upon the potential step from −0.35 V to −0.5 V. Surface concentration of the redox complex for each bulk concentration of **2** was derived from the chronocoulometric transients.[13] The electrode containing the surface donor–acceptor complex in equilibrium with **2** (0.3 mM) was further treated with N^6-(2-aminoethyl)-FAD (1 mM) for 20 min to generate a stopper on the molecular string. The resulting **2**–FAD-functionalized electrode was treated with apo-GOx (1 mg mL^{-1}). The process was analyzed by differential pulse voltammetry. After 6 h the reconstitution process was completed and the electrode was rinsed of the excess nonreconstituted apo-GOx. The bioelectrocatalytic oxidation of glucose by the reconstituted GOx-electrode was analyzed by cyclic voltammetry. The real surface area of the Au electrode accessible for the electrochemical reactions was found by the chronocoulometric method by using the Cottrell equation.[25] The measurements performed in the presence of $[Fe(CN)_6]^{3-}$ on a bare Au electrode and the diiminobenzene-functionalized Au electrode show that the electrochemically accessible electrode area is not affected by the formation of the monolayer. All modification steps were repeated on a QCM electrode to perform microgravimetric analyses of the components bound to the surface.

Electrochemical and microgravimetric measurements: A conventional three-electrode cell, consisting of the modified Au working electrode, a glassy carbon auxiliary electrode isolated by a glass frit, and a saturated calomel reference electrode (SCE) connected to the working volume with a Luggin capillary was used for the electrochemical measurements. All potentials are reported with respect to the SCE. Argon bubbling was used to remove oxygen from the solutions in the electrochemical cell, unless otherwise stated. The cell was placed in a grounded Faraday cage. Cyclic voltammetry, differential pulse voltammetry, and chronocoulometry were performed on an electrochemical analyzer composed of a potentiostat/galvanostat (EG&G model 283) connected to a computer (EG&G software no. 270/250). A QCM analyzer (Fluke 164T multifunction counter, 1.3 GHz, TCXO) and quartz crystals (AT-cut, 9 MHz, Seiko) sandwiched between two Au electrodes (area 0.196 cm^2, roughness factor ≈3.2) were employed for the microgravimetric analyses in air and in the liquid phase using a flow-cell. The QCM crystals were calibrated by electropolymerization of aniline in H_2SO_4 (0.1M) and Na_2SO_4 (0.5M) electrolyte solution, followed by coulometric assay of the resulting polyaniline film and relating the crystal frequency changes to the electrochemically derived polymer mass.

Received: December 3, 2003
Revised: March 22, 2004 [Z53455]

Keywords: biosensors · electron transfer · enzymes · molecular devices · monolayers

[1] a) E. Katz, A. N. Shipway, I. Willner in *Encyclopedia of Electrochemistry*, *Vol. 9* (Eds.: G. S. Wilson, A. J. Bard, M. Stratmann), Wiley-VCH, Weinheim, **2002**, chap. 17, pp. 559–626; b) I. Willner, E. Katz, *Angew. Chem.* **2000**, *112*, 1230–1269; *Angew. Chem. Int. Ed.* **2000**, *39*, 1180–1218; c) A. Heller, *Acc. Chem. Res.* **1990**, *23*, 128–134; d) F. A. Armstrong, G. S. Wilson, *Electrochim. Acta* **2000**, *45*, 2623–2645.

[2] a) E. Katz, A. N. Shipway, I. Willner in *Handbook of Fuel Cells—Fundamentals, Technology, Applications*, *Vol. 1*, *Part 4* (Eds.: W. Vielstich, H. Gasteiger, A. Lamm), Wiley, New York, **2003**, chap. 21, pp. 355–381; b) E. Katz, I. Willner, A. B. Kotlyar, *J. Electroanal. Chem.* **1999**, *479*, 64–68; c) E. Katz, I. Willner, *J. Am. Chem. Soc.* **2003**, *125*, 6803–6813; d) N. Mano, F. Mao, A. Heller, *J. Am. Chem. Soc.* **2003**, *125*, 6588–6594.

[3] a) Y. Degani, A. Heller, *J. Phys. Chem.* **1987**, *91*, 1285–1289; b) W. Schuhmann, T. J. Ohara, H.-L. Schmidt, A. Heller, *J. Am. Chem. Soc.* **1991**, *113*, 1394–1397; c) I. Willner, A. Riklin, B. Shoham, D. Rivenzon, E. Katz, *Adv. Mater.* **1993**, *5*, 912–915.

[4] a) A. Heller, *J. Phys. Chem.* **1992**, *96*, 3579–3587; b) H. Bu, S. R. Mikkelsen, A. M. English, *Anal. Chem.* **1995**, *67*, 4071–4076.

[5] a) I. Willner, V. Heleg-Shabtai, R. Blonder, E. Katz, G. Tao, A. F. Bückmann, A. Heller, *J. Am. Chem. Soc.* **1996**, *118*, 10321–10322; b) E. Katz, A. Riklin, V. Heleg-Shabtai, I. Willner, A. F. Bückmann, *Anal. Chim. Acta* **1999**, *385*, 45–58.

[6] Y. Xiao, F. Patolsky, E. Katz, J. F. Hainfeld, I. Willner, *Science* **2003**, *299*, 1877–1881.

[7] F. Patolsky, Y. Weizmann, I. Willner, *Angew. Chem.* **2004**, *116*, 2165–2169; *Angew. Chem. Int. Ed.* **2004**, *43*, 2113–2117.

[8] a) R. A. Bissell, E. Cordova, A. E. Kaifer, J. F. Stoddart, *Nature* **1994**, *369*, 133–137; b) M. C. T. Fyfe, J. F. Stoddart, *Acc. Chem. Res.* **1997**, *30*, 393–401; c) H. R. Tseng, S. A. Vignon, J. F. Stoddart, *Angew. Chem.* **2003**, *115*, 1529–1533; *Angew. Chem. Int. Ed.* **2003**, *42*, 1491–1495; d) S. J. Rowan, J. F. Stoddart, *Polym. Adv. Technol.* **2002**, *13*, 777–787; e) S. J. Rowan, S. J. Cantrill, G. R. L. Cousins, J. K. M. Sanders, J. F. Stoddart, *Angew. Chem.* **2002**, *114*, 1528–1531; *Angew. Chem. Int. Ed.* **2002**, *41*, 898–952.

[9] a) M. Lahav, A. N. Shipway, I. Willner, *J. Chem. Soc. Perkin Trans. 2* **1999**, *9*, 1925–1931; b) A. B. Kharitonov, A. N. Shipway, I. Willner, *Anal. Chem.* **1999**, *71*, 5441–5443; c) I. Willner, V. Pardo-Yissar, E. Katz, K. T. Ranjit, *J. Electroanal. Chem.* **2001**, *497*, 172–177; d) C. P. Collier, E. W. Wong, M. Belohradsky,

 © 2004 Wiley-VCH Verlag GmbH & Co. KGaA, Weinheim

F. M. Raymo, J. F. Stoddart, P. J. Kuekes, R. S. Williams, J. R. Heath, *Science* **1999**, *285*, 391 – 394; e) Y. Luo, C. P. Collier, J. O. Jeppesen, K. A. Nielsen, E. Delonno, G. Ho, J. Perkins, H. R. Tseng, T. Yamamoto, J. F. Stoddart, J. R. Heath, *ChemPhysChem* **2002**, *3*, 519 – 525.

[10] a) L. Sheeney-Haj-Ichia, I. Willner, *J. Phys. Chem. B* **2002**, *106*, 13094 – 13097; b) M. Asakawa, P. R. Ashton, V. Balzani, C. L. Brown, A. Credi, O. A. Matthews, S. P. Newton, F. M. Raymo, A. N. Shipway, N. Spencer, A. Quick, J. F. Stoddart, A. J. P. White, D. J. Williams, *Chem. Eur. J.* **1999**, *5*, 860 – 875; c) P. R. Ashton, V. Balzani, O. Kocian, L. Prodi, N. Spencer, J. F. Stoddart, *J. Am. Chem. Soc.* **1998**, *120*, 11190 – 11191.

[11] a) P. J. Elving, J. E. O'Reilly, C. O. Schmakel in *Methods of Biochemical Analysis*, *Vol. 21* (Ed.: D. Click), Interscience, New York, **1973**; b) G. Dryhurst, *Electrochemistry of Biological Molecules*, Academic Press, New York, **1977**.

[12] a) E. Katz, D. D. Schlereth, H.-L. Schmidt, *J. Electroanal. Chem.* **1994**, *367*, 59 – 70; b) E. Katz, D. D. Schlereth, H.-L. Schmidt, A. J. J. Olsthoorn, *J. Electroanal. Chem.* **1994**, *368*, 165 – 171.

[13] a) F. C. Anson, *Anal. Chem.* **1966**, *38*, 54 – 57; b) A. B. Steel, T. M. Herne, M. J. Tarlov, *Anal. Chem.* **1998**, *70*, 4670 – 4677.

[14] D. A. Buttry, M. D. Ward, *Chem. Rev.* **1992**, *92*, 1355 – 1379.

[15] A. R. Bernardo, J. F. Stoddart, A. E. Kaifer, *J. Am. Chem. Soc.* **1992**, *114*, 10624 – 10631.

[16] The surface coverages cannot be directly derived from the DPVs; they were derived from a cyclic voltammogram recorded at pH 9.5 at which the FAD potential is negatively shifted ($\delta E°/\delta pH \approx 30\ mV\,pH^{-1}$ at $pH > 7$) relative to the pH-independent potential of **2,** to provide separate waves for both redox components in the cyclic voltammogram.

[17] M. Zayats, E. Katz, I. Willner, *J. Am. Chem. Soc.* **2002**, *124*, 14724 – 14735.

[18] The GOx-reconstituted electrode, which lacks the interlocked rotaxane-mediator and thus does not show bioelectrocatalytic oxidation of glucose, was activated in the presence of the diffusional electron-transfer mediator, ferrocene monocarboxylic acid (0.5 mM). Therefore, the reconstituted GOx exists on the surface in the biocatalytically active state.

[19] a) R. J. Forster, L. R. Faulkner, *Anal. Chem.* **1995**, *67*, 1232 – 1239; b) R. J. Forster, *Langmuir* **1995**, *11*, 2247 – 2255; c) R. J. Forster, *Anal. Chem.* **1996**, *68*, 3143 – 3150; d) R. J. Forster, *Analyst* **1996**, *121*, 733 – 741.

[20] E. Katz, I. Willner, *Langmuir* **1997**, *13*, 3364 – 3373.

[21] V. Pardo-Yissar, E. Katz, I. Willner, A. B. Kotlyar, C. Sanders, H. Lill, *Faraday Discuss.* **2000**, *116*, 119 – 134.

[22] D. L. Morris, R. T. Buckler, *Methods Enzymol.* **1983**, 92, 413 – 417.

[23] A. F. Bückmann, V. Wray, A. Stocker in *Methods in Enzymology: Vitamins and Coenzymes, Vol. 280, Part 1* (Ed.: B. B. McCormick), Academic Press, Orlando, **1997**, p. 360.

[24] M. Asakawa, W. Dehaen, G. Labbe, S. Menzer, J. Nouwen, F. M. Raymo, J. F. Stoddart, D. J. Williams, *Org. Chem.* **1996**, *61*, 9591 – 9595.

[25] A. J. Bard, L. R. Faulkner, *Electrochemical Methods: Fundamentals and Applications*, Wiley, New York, **1980**.

 © 2004 Wiley-VCH Verlag GmbH & Co. KGaA, Weinheim

Reaction Intermediates

A Bis(μ-alkylperoxo)dinickel(II) Complex as a Reaction Intermediate for the Oxidation of the Methyl Groups of the Me_2-tpa Ligand to Carboxylate and Alkoxide Ligands**

*Jaeheung Cho, Hideki Furutachi, Shuhei Fujinami, and Masatatsu Suzuki**

Aliphatic C–H bond functionalization by various metal-active oxygen species M_m/O_n such as superoxo, peroxo, high-valent oxo-metal complexes, etc. is of great importance for understanding the reaction mechanisms of metalloenzymes and utilizing metal complexes as oxidation catalysts.[1–4] In some cases, aliphatic C–H bond functionalization starts from hydrogen abstraction, and the resulting alkyl radicals undergo a variety of subsequent reactions.[5–7] For example, a bis(μ-alkylperoxo)dicopper(II) complex was suggested as an intermediate in the reaction of a copper(I) complex, $[Cu(i\mathrm{Pr}_3\text{-tacn})]^+$,[8] with O_2 in the presence of 2,4-*tert*-butylphenol.[5] Very recently, an alkylperoxopalladium(II) complex was also reported which was produced from the reaction of a hydroperoxopalladium(II) complex in the presence of a copper(II) complex as a catalyst.[6] Although various transition-metal–alkylperoxo complexes are known,[9] the alkylperoxo complexes generated as reaction intermediates are limited. Previously, we found that the reaction of $[Ni_2(OH)_2(Me_3\text{-tpa})_2]^{2+}$ with H_2O_2 generates a bis(μ-oxo)dinickel(III) complex, $[Ni_2(O)_2(Me_3\text{-tpa})_2]^{2+}$, and a bis(μ-superoxo)dinickel(II) complex, $[Ni_2(O_2)_2(Me_3\text{-tpa})_2]^{2+}$.[10] The decomposition of $[Ni_2(O)_2(Me_3\text{-tpa})_2]^{2+}$ and $[Ni_2(O_2)_2(Me_3\text{-tpa})_2]^{2+}$ under O_2 caused the oxidative conversion of a methyl group of the Me_3-tpa ligand to give carboxylate and alkoxide ligands. Furthermore, the carboxylate ligand has been shown to be not derived from the autoxidation of the alkoxide ligand, and some other reaction pathways have been suggested. Herein, we report the formation, structural characterization, and reactivity of a novel bis(μ-alkylperoxo)dinickel(II) complex as a reaction intermediate in the oxidative conversion of the methyl groups of the Me_2-tpa ligand into carboxylate and alkoxide ligands; this nickel complex is the first example of a structurally characterized dinuclear transition-metal complex with bridging alkylperoxides, although a crystal structure of a main-group-metal complex with a bis(μ-alkylperoxo)Zn^{II}_2 core was reported very recently.[11]

[*] J. Cho, H. Furutachi, Prof. S. Fujinami, Prof. M. Suzuki
Department of Chemistry, Faculty of Science
Kanazawa University
Kakuma-machi, Kanazawa 920-1192 (Japan)
Fax: (+81) 76-264-5742
E-mail: suzuki@cacheibm.s.kanazawa-u.ac.jp

[**] Me_2-tpa = bis[(6-methyl-2-pyridyl)methyl][(2-pyridyl)methyl]amine. Financial support of this research by the Ministry of Education, Science, and Culture (Grant-in-Aid for Scientific Research to M.S.) is gratefully acknowledged.

Supporting information for this article is available on the WWW under http://www.angewandte.org or from the author.

 © 2004 Wiley-VCH Verlag GmbH & Co. KGaA, Weinheim DOI: 10.1002/anie.200353637

The reaction of a solution of the bis(μ-hydroxo)dinickel(II) complex $[Ni_2(OH)_2(Me_2\text{-tpa})_2]^{2+}$ (**1**)[12] in acetonitrile with excess hydrogen peroxide at −40 °C showed a rapid color change from sky blue to dark green. The positive ESI-TOF mass spectrum of the solution diluted with acetone at −78 °C suggested the formation of a monomeric superoxonickel(II) species,[13] $[\{Ni(O_2)(Me_2\text{-tpa})\}^+]$ (**2**; *m*/*z* 408.1078, 100 %), a bis(μ-alkylperoxo)dinickel(II) species, $[\{Ni_2(Me_1\text{-tpa-}CH_2OO)_2\}^{2+}]$ (**3**; see below), and a (μ-superoxo)(μ-alkylperoxo)dinickel(II) species, $[\{Ni_2(O_2)(Me_2\text{-tpa})(Me_1\text{-tpa-}CH_2OO)\}^{2+}]$ together with some unidentified minor species (see Supporting Information). The formation of such a monomeric superoxonickel(II) species **2** was also observed for the Me_3-tpa system in solution by ESI-TOF MS measurements, although the isolated species is a dimeric bis(μ-superoxo)Ni_2^{II}.[10] The formation of **2** implies the presence of a bis(μ-oxo)dinickel(III) species that can oxidize excess hydrogen peroxide into superoxide to generate **2**, as found for the Me_3-tpa system.[10] For the Me_3-tpa system, the superoxo species was shown to regenerate a bis(μ-oxo)dinickel(III) species by the disproportionation of the superoxo ligands, with evolution of dioxygen. The resulting bis(μ-oxo)dinickel(III) species is responsible for the abstraction of a hydrogen atom from the methyl group. The ESI-TOF mass spectrum revealed that **2** is unstable, and warming the solution at −20 °C resulted in decomposition to generate a bis(μ-alkylperoxo)dinickel(II) complex, $[Ni_2(Me_1\text{-tpa-}CH_2OO)_2]X_2$ (X = BPh_4 (**3**-$(BPh_4)_2$) or ClO_4 (**3**-$(ClO_4)_2$)).

The X-ray diffraction study of **3**-$(BPh_4)_2$ revealed that the complex has a $Ni_2(\mu\text{-OOR})_2$ core in which one of the methyl groups of each Me_2-tpa ligand is oxidized to a ligand-based peroxide and the resulting two peroxides link two nickel(II) ions (Figure 1). The peroxides seem to be stabilized by the formation of the six-membered chelate rings (Ni1-O1-O2-C7-C6-N2) and bridges. The O1−O2 bond length of 1.458(4) Å is in the range of those of transition-metal–alkylperoxo complexes (1.36–1.52 Å).[4,6,9] Complex **3** is a novel example of a structurally characterized reaction intermediate isolated during the oxidation reaction. The ESI-TOF mass spectrum of **3** in MeCN showed a signal at *m*/*z* 407.1008 (100 %), indicating that the dimeric structure remains intact (see Supporting Information).

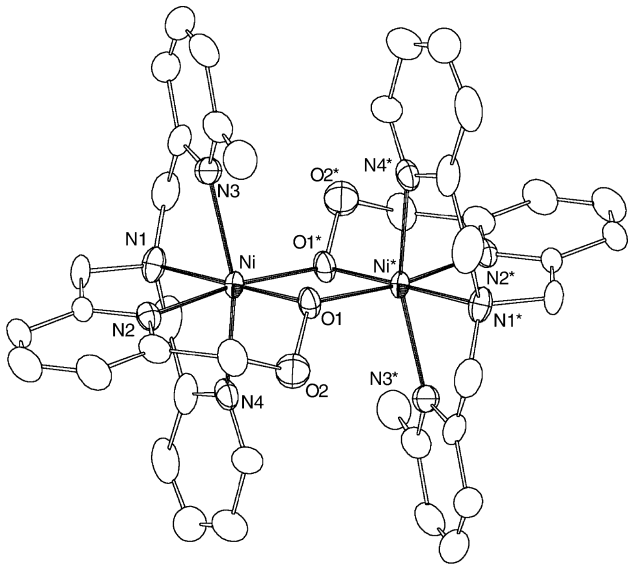
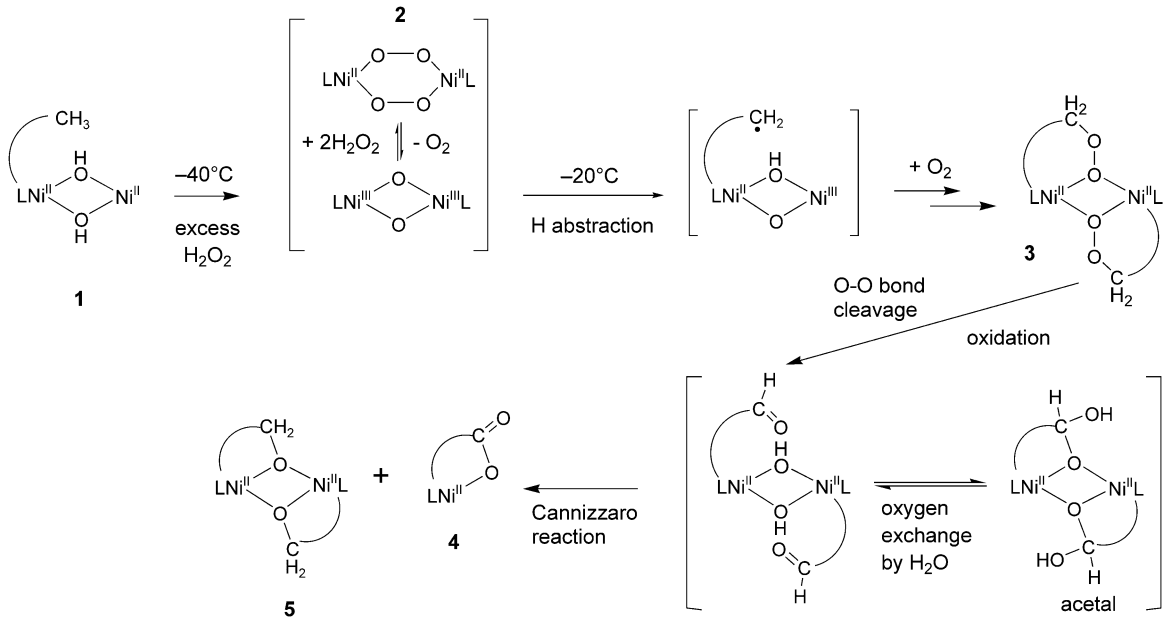


Figure 1. ORTEP diagram (50% probability) of the $[Ni_2(Me_1\text{-tpa-}CH_2OO)_2]^{2+}$ cation in **3**-$(BPh_4)_2$. Hydrogen atoms are omitted for clarity. Selected bond lengths [Å] and angles [°]: Ni1-O1 1.993(2), Ni1-O1* 2.048(2), Ni1-N1 2.065(3), Ni1-N2 2.031(3), Ni1-N3 2.166(3), Ni1-N4 2.198(3), O1-O2 1.458(4), O1-Ni1-O1* 83.72(10), Ni1-O1-O2 108.3(2).

The oxygen source of the alkylperoxo groups in **3** was identified by isotope-labeling experiments (see Supporting Information). The ESI-TOF mass spectrum of a sample prepared by the reaction of **1** with $H_2{}^{18}O_2$ while bubbling $^{16}O_2$ through the solution revealed the formation of only ^{16}O-alkylperoxo species, whereas the reaction under N_2 (i.e. in the absence of $^{16}O_2$) gave ^{18}O-alkylperoxo species. In the latter reaction, $^{18}O_2$ may be generated by the disproportionation of the ^{18}O-superoxo species and/or the disproportionation of $H_2{}^{18}O_2$. Furthermore, only the ^{16}O-alkylperoxo species was obtained by the reaction with $H_2{}^{16}O_2$ in the presence of $H_2{}^{18}O$ under N_2. These results clearly indicate that the two oxygen atoms of the alkylperoxo ligand come from exogenous dioxygen. Although the detailed mechanism of formation of **3** is not clear at present, the reaction may involve the abstraction of a hydrogen atom from a methyl group by a bis(μ-oxo)dinickel(III) species as found for $[Ni_2(O)_2(Me_3\text{-tpa})_2]^{2+}$[10] (although not identified in this study) to generate a ligand-based radical (Me_1-tpa-$CH_2^{\bullet}$), which reacts with exogenous dioxygen to afford a peroxyl radical species (Me_1-tpa-$CH_2OO^{\bullet}$). The resulting peroxyl radical species seems to be converted into the alkylperoxo species through unidentified reaction pathway(s). Further studies are necessary for clarifying this point.

A solid sample of **3** is relatively stable at room temperature, whereas the ESI-TOF mass spectrum in a dry DMF/MeCN mixture showed that decomposition occurs within 1 hour at room temperature, and **3** is converted into a ligand-based carboxylato complex $[\{Ni(Me_1\text{-tpa-COO})(dmf)\}^+]$ (**4**·dmf; *m*/*z* 478.1380, 100 %) and a ligand-based alkoxo complex $[\{Ni_2(Me_1\text{-tpa-}CH_2O)_2\}^{2+}]$ (**5**; *m*/*z* 391.1125, 20 %) together with some unidentified species (see Supporting Information).[14] The carboxylato complex **4** was isolated as $[Ni(Me_1\text{-tpa-COO})(H_2O)]ClO_4$ (**4**-$H_2O{\cdot}ClO_4$) (see Experimental Section and Supporting Information). The formation of both Me_1-tpa-COO^- and Me_1-tpa-CH_2OH was also confirmed by a ligand-recovery experiment after the decomposition of **3**-$(ClO_4)_2{\cdot}H_2O$ in DMF under Ar; the yields of Me_1-tpa-COO^- and Me_1-tpa-CH_2OH are approximately 62 % and 37 %, respectively (see Supporting Information). It was also found that the decomposition of **3** containing Me_1-tpa-$CH_2{}^{16}O{}^{16}O^-$ in the presence of $H_2{}^{18}O$ under N_2 gave a mixture of ^{16}O-^{16}O, ^{16}O-^{18}O, and ^{18}O-^{18}O carboxylato species **4** (see Supporting Information), and the same is true for the formation of the alkoxo complex **5**. Decomposition under $^{18}O_2$ in the presence of $H_2{}^{16}O$, however, gave only ^{16}O-^{16}O carboxylato species. These results indicate that there is some reactive species that reacts with water molecules during the conversion of **3** into **4** and **5**. One possible reaction pathway for the formation of Me_1-tpa-COO^- and Me_1-tpa-CH_2OH involves the following steps: (Scheme 1): 1) the peroxide

 © 2004 Wiley-VCH Verlag GmbH & Co. KGaA, Weinheim



Scheme 1. Possible pathway for the formation of carboxylate and alkoxide ligands.

ligand can be converted into a ligand-based aldehyde by either homolysis or heterolysis of the O–O bond, 2) the oxygen atom of the aldehyde can be exchanged through the formation of an acetal, 3) disproportionation of the aldehyde may give a carboxylate and an alkoxide through the Cannizzaro reaction and/or the aldehyde can be oxidized by an additional alkylperoxo ligand. Insertion of oxygen into the alkoxo ligand of **5** from water strongly supports the disproportionation of the aldehyde by the Cannizzaro reaction. The presence of a larger amount of the carboxylate ligand than the alkoxide ligand probably suggests that some other side reaction(s) take(s) place at the same time. As mentioned before, such oxidation of a methyl group into carboxylate has also been observed for the decomposition of $[Ni_2(O)_2(Me_3\text{-tpa})_2]^{2+}$ and $[Ni_2(O_2)_2(Me_3\text{-tpa})_2]^{2+}$ under O_2,[10] during which ligand-based alkylperoxo species such as **3** seem to be common intermediates for the conversion into the corresponding carboxylato complexes. Further studies into a detailed conversion mechanism are in progress.

In conclusion, we have succeeded in the isolation and structural characterization of bis(μ-alkylperoxo)dinickel(II) complex **3** derived from the reaction of the bis(μ-hydroxo)-dinickel(II) complex **1** with H_2O_2 and O_2 through the formation of the Me_1-tpa-$CH_2^{\bullet}$ and Me_1-tpa-$CH_2OO^{\bullet}$ radicals. Subsequent decomposition of **3** afforded the carboxylato complex **4** and the alkoxo complex **5**. Thus, such an alkylperoxo species seems to be a common intermediate for the oxidation of a methyl group of the supporting ligand into carboxylate and alkoxide ligands in the present type of nickel complexes.

Experimental Section

1-$(ClO_4)_2\cdot 3H_2O$: nBu$_4$NOH in methanol (1M; 175 μL, 0.5 mmol) was added to a stirred mixture of $Ni(ClO_4)_2\cdot 6H_2O$ (183 mg, 0.5 mmol) and Me_2-tpa (159 mg, 0.5 mmol) in methanol (20 mL) in a Schlenk tube under N_2. The resulting solution was allowed to stand overnight at 0 °C to afford **1** as sky blue crystals. FTIR (KBr): $\tilde{\nu}=1604, 1577, 1484, 1457, 1353, 1105, 786, 624\ cm^{-1}$; UV/Vis (DMF): λ_{max} (ε) = 610 nm (23); ESI-TOF MS (MeCN): m/z (%): 393.1167 (100) $[\{Ni_2(OH)_2(Me_2\text{-tpa})_2\}^{2+}]$; elemental analysis (%) calcd for $C_{40}H_{52}N_8Cl_2Ni_2O_{13}$: C 46.14, H 5.03, N 10.76; found: C 46.20, H 4.70, N 10.82. X-ray crystallographically suitable crystals were obtained by the addition of $NaBPh_4$ (see Supporting Information).

3-$(BPh_4)_2$: Aqueous H_2O_2 (30%; 550 μL, 5 mmol) was added to a rapidly stirred solution of **1** (52 mg, 0.05 mmol) in MeCN (20 mL) at −40 °C under O_2. The resulting solution was allowed to stand overnight, to which a solution of $NaBPh_4$ (68 mg, 0.2 mmol) in acetonitrile (2 mL) was added. The resulting solution was left for 1 day at −20 °C to give **3**-$(BPh_4)_2$ as brown crystals (35 mg, 48%) suitable for X-ray crystallography. FTIR (KBr): $\tilde{\nu}=1604, 1577, 1353, 1162, 705, 613\ cm^{-1}$; UV/Vis (reflectance): $\lambda_{max}=\sim 398$ (shoulder), 545, ~630 (shoulder), 780, 1035 nm; ESI-TOF MS (DMF/MeCN): m/z (%): 407.1023 (100) $[\{Ni_2(Me_1\text{-tpa-}CH_2OO)_2\}^{2+}]$ and 480.1537 (20) $[\{Ni(Me_1\text{-tpa-}CH_2OO)\}^{+}$ + DMF]; elemental analysis (%) calcd for $C_{88}H_{82}N_8O_4B_2Ni_2$: C 72.66, H 5.68, N 7.70; found: C 72.84, H 5.73, N 7.88.

4-$H_2O\cdot ClO_4$: An excess amount of H_2O_2 (30%; 550 μL, 5 mmol) was added to a rapidly stirred suspension of **1** (52 mg, 0.05 mmol) in EtOH at room temperature. The resulting dark green suspension was allowed to stand for 1 day, without stirring, to give a blue solution, from which blue crystals of **4** were obtained. FTIR (KBr): $\tilde{\nu}=1635, 1606, 1577, 1457, 1444, 1392, 1284, 1103, 887, 775, 624\ cm^{-1}$; UV/Vis (DMF): λ_{max} (ε) = 570 (15), 790 (14), 942 nm (32); ESI-TOF MS (DMF/MeCN): m/z (%): 478.1376 (100) $[\{Ni(Me_1\text{-tpa-COO})\}^{+}$ + DMF]; elemental analysis (%) calcd for $C_{20}H_{21}N_4ClNiO_7$: C 45.88, H 4.04, N 10.70; found: C 45.42, H 4.03, N 10.74.

Crystal data for **3**-$(BPh_4)_2$: $C_{88}H_{82}N_8B_2Ni_2O_4$, triclinic, $P\bar{1}$, $Z=1$, $a=10.234(1)$, $b=14.009(2)$, $c=14.080(1)$ Å, $\alpha=68.931(10)$, $\beta=73.92(1)$, $\gamma=84.43(1)°$, $V=1810.0(3)$ Å^3, $\rho_{calcd}=1.334\ g\,cm^{-1}$, $0.25\times 0.18\times 0.08$ mm, $T=-150$ °C, $F_{000}=764.00$, $\mu(Mo_{K\alpha})=5.80\ cm^{-1}$, Rigaku Mercury CCD diffractometer, $Mo_{K\alpha}$ ($\lambda=0.71070$ Å), ω scan, 14484 measured, 5723 independent reflections ($I>3.00\sigma(I)$), 469 parameters; structure solution with direct methods[15] and successive Fourier technique.[16] All calculations were performed with the teXsan[17] crystallographic software package of the Molecular Structure Corporation. All non-hydrogen atoms were refined with anisotropic displacement parameters. Hydrogen atoms were placed

 © 2004 Wiley-VCH Verlag GmbH & Co. KGaA, Weinheim

geometrically. They were included, but not refined against $|F|$, to yield R (Rw) = 0.0562 (0.0786); largest residual electron densities 1.44/−0.71 (GOF = 1.387). CCDC-226793 contains the supplementary crystallographic data for this paper. These data can be obtained free of charge via www.ccdc.cam.ac.uk/conts/retrieving.html (or from the Cambridge Crystallographic Data Centre, 12, Union Road, Cambridge CB21EZ, UK; fax: (+44) 1223-336-033; or deposit@ccdc.cam.ac.uk).

Received: December 30, 2003 [Z53637]

Keywords: nickel · oxidation · peroxides · reaction mechanisms

[1] J. M. Mayer, *Biomimetic Oxidations Catalyzed by Transition Metal Complexes* (Ed.: B. Meunier), Imperial College Press, London, **2000**, pp. 1–44.
[2] a) L. Que, Jr, R. Y. N. Ho, *Chem. Rev.* **1996**, *96*, 2607; b) L. Que, Jr, W. B. Tolman, *Angew. Chem.* **2002**, *114*, 1160; *Angew. Chem. Int. Ed.* **2002**, *41*, 1114; c) J.-U. Rohde, M. R. Bukowski, L. Que, Jr, *Curr. Opin. Chem. Biol.* **2003**, *7*, 674.
[3] a) E. I. Solomon, T. C. Brunold, M. I. Davis, J. N. Kemsley, S.-K. Lee, N. Lehnert, F. Neese, A. J. Skulan, Y.-S. Yang, J. Zhou, *Chem. Rev.* **2000**, *100*, 235; b) J. J. Girerd, F. Banse, A. J. Simaan, *Struct. Bonding (Berlin)* **2000**, *97*, 145.
[4] a) S. Hikichi, M. Akita, Y. Moro-oka, *Coord. Chem. Rev.* **2000**, *198*, 61; b) M. Akita, S. Hikichi, *Bull. Chem. Soc. Jpn.* **2002**, *75*, 1657.
[5] J. A. Halfen, V. G. Young, Jr, W. B. Tolman, *Inorg. Chem.* **1998**, *37*, 210.
[6] M. Kujime, S. Hikichi, M. Akita, *Chem. Lett.* **2003**, *32*, 486.
[7] K. Haas, H. Dialer, H. Piotrowski, J. Schapp, W. Beck, *Angew. Chem.* **2002**, *114*, 1969; *Angew. Chem. Int. Ed.* **2002**, *41*, 1879.
[8] iPr$_3$-tacn = 1,4,7-triisopropyl-1,4,7-triazacyclononane; Me$_2$-tpa = bis[(6-methyl-2-pyridyl)methyl][(2-pyridyl)methyl]amine; Me$_3$-tpa = tris[(6-methyl-2-pyridyl)methyl]amine.
[9] a) N. Kitajima, T. Katayama, K. Fujisawa, Y. Iwata, Y. Moro-oka, *J. Am. Chem. Soc.* **1993**, *115*, 7872; b) H. Komatsuzaki, N. Sakamoto, M. Satoh, S. Hikichi, M. Akita, Y. Moro-oka, *Inorg. Chem.* **1998**, *37*, 6554; c) S. Hikichi, H. Komatsuzaki, M. Akita, Y. Moro-oka, *J. Am. Chem. Soc.* **1998**, *120*, 4699; d) M. Bonchio, S. Calloni, F. D. Furia, G. Licini, G. Modena, S. Moro, W. A. Nugent, *J. Am. Chem. Soc.* **1997**, *119*, 6935; e) F. A. Chavez, P. K. Mascharak, *Acc. Chem. Res*, **2000**, *33*, 539; e) P. Chen, K. Fujisawa, E. I. Solomon, *J. Am. Chem. Soc.* **2000**, *122*, 10177.
[10] K. Shiren, S. Ogo, S. Fujinami, H. Hayashi, M. Suzuki, A. Uehara, Y. Watanabe, Y. Moro-oka, *J. Am. Chem. Soc.* **2000**, *122*, 254.
[11] J. Lewinski, Z. Ochal, E. Bojarski, E. Tratkiewicz, I. Justyniak, J. Lipkowski, *Angew. Chem.* **2003**, *115*, 4791; *Angew. Chem. Int. Ed.* **2003**, *42*, 4643.
[12] The crystal data and ORTEP diagram for **1** are given in the Supporting Information.
[13] Although there is a possibility of a peroxonickel(III) species as an alternative formulation, it is not clear which is correct at present.
[14] Surprisingly, it was found that the thermal decomposition of **3** was very slow in the presence of a small amount of water (> 2 days).
[15] SIR92: A. Altomare, G. Cascarano, C. Giacovazzo, A. Guagliardi, M. C. Burla, G. Polidori, M. Camalli, *J. Appl. Crystallogr.* **1994**, *27*, 435.
[16] DIRDIF94: P. T. Beurskens, G. Admiraal, G. Beurskens, W. P. Bosman, R. de Gelder, R. Israel, J. M. M. Smits, The DIRDIF-94 program system, Technical Report of the Crystallography Laboratory, University of Nijmegen, The Netherlands, **1994**.
[17] teXsan: Crystal Structure Analysis Package, Molecular Structure Corporation, **1985** & **1999**.

 © 2004 Wiley-VCH Verlag GmbH & Co. KGaA, Weinheim

Supported Catalysts

Ruthenium Nanoparticles Supported on Hydroxyapatite as an Efficient and Recyclable Catalyst for *cis*-Dihydroxylation and Oxidative Cleavage of Alkenes**

Chi-Ming Ho, Wing-Yiu Yu, and Chi-Ming Che**

The development of osmium-catalyzed alkene dihydroxylation and its asymmetric variants represents an important milestone in modern organic synthesis.[1] While this technology has been widely applied to the synthesis of pharmaceuticals and fine chemicals, the high cost and possible product contamination by toxic osmium metal have restricted its use for large-scale reactions in industry. Currently, there is considerable interest in the search for alternative metal catalysts for alkene dihydroxylations.[2] Ruthenium and its complexes, being isoelectronic to its osmium counterparts, are well-known for their catalytic activities for oxidative transformations.[3,4] And indeed, $RuCl_3{\cdot}xH_2O$ has been demonstrated to catalyze *cis*-dihydroxylation[5] and oxidative cleavage[6] of alkenes.

Application of nanosized metal particles as catalysts for organic transformations is an area of growing interest.[7,9a] Because of its high surface area and high density of active sites, nanosized metal particles exhibit superior catalytic activities compared with the corresponding bulk materials. Herein, we report that ruthenium nanoparticles immobilized on hydroxyapatite[8] are an effective catalyst for *cis*-dihydroxylation and oxidative cleavage of alkenes. With ethyl *trans*-cinnamate as substrate, the supported catalyst has been recycled for successive *cis*-dihydroxylation reactions without significant deterioration of catalytic activities. Prior to this work, there are no precedent examples in the literature of recyclable ruthenium catalysts for *cis*-dihydroxylation and oxidative cleavage of alkenes.[9,10]

One approach to obtain supported catalysts with well-defined metal particles is to immobilize metal colloids onto solid supports.[7] Based on the Fiévet's protocol,[11a] stable ruthenium colloids can be prepared by the reduction of $RuCl_3{\cdot}xH_2O$ (0.32 mmol) in 1,2-propanediol (100 mL) in the presence of sodium acetate (1 mmol) at 150 °C. Reduction of

[*] Dr. C.-M. Ho, Dr. W.-Y. Yu, Prof. Dr. C.-M. Che
Department of Chemistry and
Open Laboratory of Chemical Biology
Institute of Molecular Technology for Drug Discovery and Synthesis
The University of Hong Kong
Pokfulam Road, Hong Kong (China)
Fax: (+852) 2857-1586
E-mail: cmche@hku.hk

[**] This work is supported by the Areas of Excellence Scheme established under the University Grants Committee of the Hong Kong Special Administrative Region, China (AoE/P-10/01), The University of Hong Kong (University Development Fund), and the Hong Kong Rearch Grants Council (HKU 7384/02P).

Supporting information for this article is available on the WWW under http://www.angewandte.org or from the author.

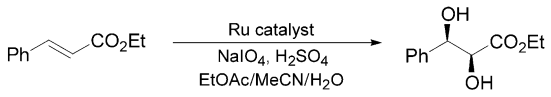
 DOI: 10.1002/anie.200453703 © 2004 Wiley-VCH Verlag GmbH & Co. KGaA, Weinheim

the Ru^{3+} salt was considered complete upon the disappearance of the band at about 400 nm in the corresponding UV/Vis spectrum (see Supporting Information). The ruthenium colloid (3.2 mM) prepared in this manner exhibited excellent stability against agglomeration since no precipitation of metal powder was evident upon standing the colloidal solution at room temperature for 7 days. Successful immobilization of the ruthenium nanoparticles was achieved by treating the colloidal solution with calcium hydroxyapatite (0.4 g) and H_2O (50 mL) for 24 h. [12] Ruthenium nanoparticles that were grafted onto hydroxyapatite (nano-RuHAP) were obtained as a dark-grey solid after centrifugation, washing with deionized water, and drying under vacuum at 110 °C overnight. By means of inductively coupled plasma mass spectrometry ICPMS, the Ru content of nano-RuHAP was determined to be 5 wt % (0.5 mmol g^{-1}) and the Ca:P molar ratio was 1.66; the latter agrees with the reported value of 1.67,[10d] thus indicating no significant exchange of the constituent Ca^{2+} ions. Attempts to immobilize the ruthenium nanoparticles on some common inorganic supports such as silica gel and alumina were not successful, since the resulting materials contained < 0.1 wt % Ru based on ICP analysis.

The powder X-ray diffraction (XRD) pattern [Philips PW1830 (2 kW), $Cu_{K\alpha}$, 40 kV, 40 mA, 25 °C] of nano-RuHAP showed prominent peaks at $2\theta = 25.90°$, 31.85°, 32.25°, 32.95° and 49.55°, which are indexed to the [002], [211], [112], [300], and [213] reflections of the hexagonal crystal system of hydroxyapatite (JCPDS card no: 09-0432), respectively (see Supporting Information). It should be noted that free hydroxyapatite (i.e., without Ru particles) exhibits an almost identical XRD pattern, thus indicating that the crystallinity of hydroxyapatite was retained after immobilization of ruthenium nanoparticles. The TEM image of nano-RuHAP shows randomly dispersed particles, and energy-dispersive X-ray (EDX) and selected-area electron diffraction (SAED) analyses confirmed that the particles corresponded to ruthenium with an average diameter of about 4 nm. X-ray photoelectron spectroscopy (XPS) analysis of the freshly prepared nano-RuHAP catalyst revealed the binding energy of Ru $3p_{3/2}$ at 462.7 eV (see Supporting Information). This value is slightly larger than the reported value (462 eV) for a bulk ruthenium metal.[13] There is a small increase in the surface area of nano-RuHAP (25 $m^2 g^{-1}$) compared to its parent hydroxyapatite (17 $m^2 g^{-1}$) as determined by the N_2 adsorption isotherms. This is accounted for by the physical adsorption of ruthenium nanoparticles on the solid support.

The nano-RuHAP catalyst was tested for *cis*-dihydroxylation of ethyl *trans*-cinnamate.[5a] In the presence of nano-RuHAP (1 mol % Ru), ethyl *trans*-cinnamate (2 mmol) was treated with $NaIO_4$ (3.0 mmol) and H_2SO_4 (20 mol %) in EtOAc/MeCN/H_2O (3:3:1 v/v) at 0 °C for 30 min with complete substrate consumption. After workup and chromatographic purification, (±)-*threo*-ethyl 2,3-dihydroxy-3-phenylpropanoate was isolated in 70 % yield, and benzaldehyde (18 %) and benzoic acid (6 %) were obtained as minor products (Table 1, entry 1). By centrifugation, the supported ruthenium catalyst was recovered and was used for the second, third, and fourth runs under identical reaction conditions. No apparent loss of catalytic activity was observed, and the product, *cis*-diol, was isolated in 80, 82, and 66 % yields (entries 2–4, respectively). A total product turnover of 298 was attained over four consecutive runs. No alkene conversion to *cis*-diol or any oxidized products was detected in the absence of the nano-RuHAP catalyst. It is noteworthy that when the ethyl *trans*-cinnamate (2 mmol) oxidation was performed by using commercially available ruthenium metal powder (1 mol % Ru) as catalyst [reaction conditions: $NaIO_4$ (1.5 equiv) and H_2SO_4 (20 mol %) in an EtOAc/MeCN/H_2O mixture (3:3:1)], neither *cis*-1,2-diol nor benzaldehyde was obtained, and the starting alkene was recovered quantitatively.

Table 1: Nano-RuHAP-catalyzed *cis*-dihydroxylation of ethyl *trans*-cinnamate.[a]



Entry	Catalyst	Reaction run	Yield [%][b]
1	nano-RuHAP	first	70
2		second	80
3		third	82
4		fourth	66
5[c]	nano-RuHAP		67
6	RuHAP[d]	first	80
7[e]		second	50

[a] Reaction conditions: ethyl *trans*-cinnamate (2 mmol), nano-RuHAP (40 mg, 1 mol %), $NaIO_4$ (1.5 equiv) and H_2SO_4 (20 mol %) in EtOAc-MeCN-H_2O 3:3:1 at 0 °C, time = 30 min. [b] Yield of isolated product based on complete alkene consumption. [c] Ethyl *trans*-cinnamate (10 mmol). [d] Kaneda's catalyst, see reference [12]. [e] Conversion = 80 %.

The nano-RuHAP-catalyzed protocol is equally effective on a larger scale. For example, the reaction of ethyl *trans*-cinnamate (10 mmol) in the presence of nano-RuHAP (0.2 mol %) gave the corresponding *cis*-1,2-diol in 67 % isolated yield (product turnover = 330; Table 1, entry 5).

During our catalyst recycling study, we observed about 20–30 % weight loss of the nano-RuHAP catalyst after each reaction run. The observed weight loss was attributed to slow dissolution of the HAP support in the acidic reaction medium. After centrifugation, the supernatant solution was subject to ICPMS, and the Ru content in solution was measured to be < 5 ppm. Both recovered and freshly prepared catalysts exhibited similar TEM images (i.e., metal particles with an average diameter ca. 4 nm). By XPS analysis, the binding energy of Ru $3p_{3/2}$ of the recovered catalyst was found to be 463.3 eV, which is different from the 462.7 eV value found for the freshly prepared catalyst sample (see Supporting Information). Similar SAED patterns of the ruthenium particles were obtained for the recovered and the freshly prepared catalysts, thus revealing that the crystal packing structure of the metal particles did not exhibit any significant changes after the oxidation reaction (see Supporting Information).

Previously Kaneda and co-workers reported that an Ru^{3+}-exchanged hydroxyapatite, prepared by treating hydroxyapatite with methanolic $RuCl_3$, is an efficient heterogeneous catalyst for aerobic alcohol oxidations.[10d] In the work presented herein, we found that Kaneda's catalyst is also

 © 2004 Wiley-VCH Verlag GmbH & Co. KGaA, Weinheim

effective for dihydroxylation of ethyl *trans*-cinnamate under the reaction conditions: alkene (2 mmol), Ru (1 mol%), $NaIO_4$ (3.0 mmol), H_2SO_4 (20 mol%) in EtOAc-MeCN-H_2O (3:3:1) at 0°C for 30 min, and (±)-*threo*-ethyl 2,3-dihydroxy-3-phenylpropanoate was isolated in 80% yield (Table 1, entry 6). However, when the recovered Kaneda's catalyst (by centrifugation) was subjected to a second reaction run, a mixture of *cis*-1,2-diol (50%) and benzaldehyde (28%) was obtained (Table 1, entry 7).

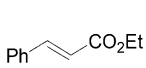
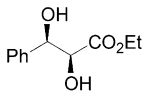
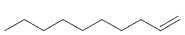
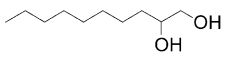
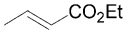
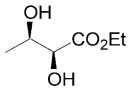
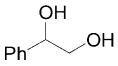
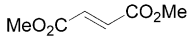
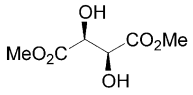
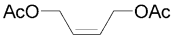
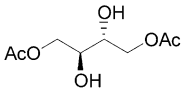
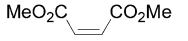
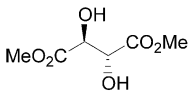
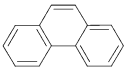
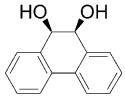
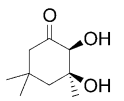
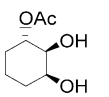
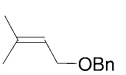
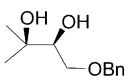
Dihydroxylations of other alkenes were examined by using the nano-RuHAP-catalyzed protocol, and the results are depicted in Table 2; a family of α,β-unsaturated alkenes, including ethyl crotonate, dimethyl fumarate, dimethyl maleate, and isophorone can be converted into their corresponding *cis*-1,2-diols in 65, 53, 50, and 64% isolated yields, respectively (Table 2, entries 2–5). The lower yields obtained for the dihydroxylations of dimethyl fumarate and dimethyl maleate are probably due to the high aqueous solubility of the *cis*-diol products. Under the Ru-catalyzed conditions, oxidation of 1-dodecene and styrene gave the respective dodecene glycol (75%) and styrene glycol (85%) in good yields (entries 6 and 7). Likewise, dihydroxylation of 1,2-disubstituted alkenes such as 1,4-diacetoxy-*cis*-but-2-ene and phenanthrene afforded the corresponding *cis*-1,2-diols in 61 and 60% yields (entries 8 and 9). With 1-acetoxy-2-cyclohexene as substrate, the Ru-catalyzed dihydroxylation furnished 1-acetoxy-2,3-*cis*-dihydroxycyclohexane in 75% yield (entry 10) with the *anti*-isomer being the major product (*anti*:*syn* = 9:1). Yet, the catalytic dihydroxylation of trisubstituted alkenes such as (3-benzloxy)-1-methylbut-1-ene appeared to be less effective, and the corresponding *cis*-1,2-diol was obtained in only 45% yield (entry 11).

Further to alkene dihydroxylation, we examined the catalytic activity of nano-RuHAP for oxidative cleavage of alkenes, which is also a synthetically useful transformation.[14] With *trans*-stilbene as the model substrate, treatment of the alkene (0.5 mmol) with $NaIO_4$ (1 mmol) and nano-RuHAP (4 mol% Ru) in a 1,2-dichloroethane-H_2O (5:1 v/v) at room temperature for 2 h gave benzaldehyde in 81% yield based on capillary GC analysis (Table 3, entry 1). The catalyst was recycled for repetitive *trans*-stilbene oxidations, and benzaldehyde was formed in comparable yields: 75% (2nd run), 71% (3rd run) and 72% (4th run). No significant weight loss of the catalyst was observed under the reaction conditions for the oxidative C=C cleavage reactions.

Oxidative cleavages of other stilbene derivatives such as *cis*-stilbene and 1-methyl-1,2-diphenylethylene under the nano-RuHAP catalyzed conditions also proceeded efficiently, and the carbonyl products were produced in excellent yields (>85%, Table 3 entries 2 and 3). Styrene, α-methylstyrene, and *trans*-β-methylstyrene were found to undergo oxidative cleavage by using the "nano-RuHAP + $NaIO_4$" protocol, and benzaldehyde was obtained in 66–92% yield (entries 4–6). When dihydronaphthalene was employed as substrate, the corresponding dicarbonyl product was isolated in 86% yield with 76% substrate conversion (entry 7). Likewise, cyclic aliphatic alkenes such as norbornene, cyclohexene, 1-*tert*-butyldimethylsiloxy-2-cyclohexene, and cyclooctene were found to undergo effective C=C bond cleavage to afford the corresponding dicarbonyl products in 51–87% yields (Table 3, entries 8–11). Catalytic oxidative C=C bond cleavage was also achieved for linear aliphatic alkenes such as methyl oleate and 1-dodecene, giving the corresponding carbonyl products in about 80% yields, albeit with 10–20% substrate conversion (entries 12 and 13).

However, α,β-unsaturated alkenes such as chalcone are poor substrates for the "nano-RuHAP + $NaIO_4$" protocol, and only 23% substrate conversion was attained with benzaldehyde (16%) and benzoic acid (14%) being formed after one day of reaction. In this work, we found that the use

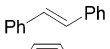
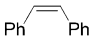
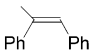
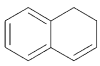
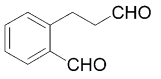
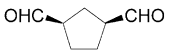
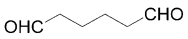
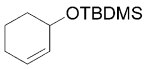
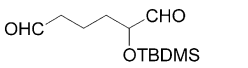
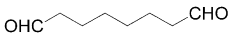
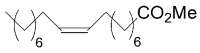
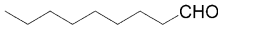
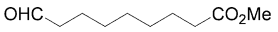
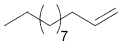
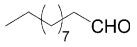
Table 2: Nano-RuHAP-catalyzed *cis*-dihydroxylation of alkenes.[a]

Entry	Alkene	Product	Yield [%][b]	Entry	Alkene	Product	Yield [%][b]
1			70	6			75
2			65	7			85
3			53	8			61
4[c]			50	9[d]			60
5			64	10			75 (*anti*:*syn* = 9:1)
				11			45

[a] Reaction conditions: alkene (2 mmol), nano-RuHAP (40 mg, 1 mol%), $NaIO_4$ (1.5 equiv) and H_2SO_4 (20 mol%) in EtOAc/MeCN/H_2O (3:3:1 v/v) at 0°C, reaction time = 30 min. [b] Isolated yield based on complete alkene consumption. [c] Reaction time = 10 min. [d] Reaction time = 40 min.

 © 2004 Wiley-VCH Verlag GmbH & Co. KGaA, Weinheim

Table 3: Nano-RuHAP catalyzed oxidative cleavage of alkenes.[a]

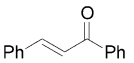
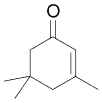
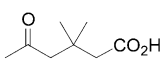
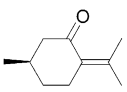
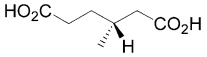
Entry	Alkene	*t* [h]	Product	Yield [%][b]
1		2	PhCHO	81[c]
2		2	PhCHO	85[c]
3		3	PhCHO	85
			PhCOMe	89
4		2	PhCHO	66
5		3	PhCOMe	92
6		3	PhCHO	90
7		3		86[d,e]
8		3		72[d]
9		3		51[d]
10		3		79[d,f]
11		3		87[d]
12		12		84[g]
				79
13		12		82[h]

[a] Reaction conditions: alkene (0.5 mmol), nano-RuHAP (40 mg, 4 mol%), $NaIO_4$ (1 mmol), in $ClCH_2CH_2Cl/H_2O$ (5:1 v/v) at room temperature, and the products were identified and quantified by GC analysis. [b] Yield based on complete alkene consumption. [c] Yield based on 2 equiv of benzaldehyde formed. [d] Yield of isolated product. [e] 76% conversion. [f] 48% conversion. [g] 16% conversion. [h] 12% conversion.

of a "nano-RuHAP + oxone" protocol[6a,15,16] would effect oxidative cleavage of α,β-unsaturated alkenes (Table 4). When chalcone (0.5 mmol) was treated with oxone (1.25 mmol) and nano-RuHAP (4 mol%) in a $NaHCO_3$ buffered $MeCN/H_2O$ (1.5:1 v/v) at room temperature for 4 h, benzaldehyde and benzoic acid were produced in 67 and 72% yields, respectively (Table 4, entry 1). Facile oxidative cleavages of isophorone and (+)-pulegone were also observed when using nano-RuHAP as catalyst and oxone as oxidant (entries 2 and 3). Notably, oxidative cleavage of C≡C bonds was also achieved using the "nano-RuHAP + Oxone" protocol. For example, when alkynes such as 1-phenyl-1-propyne were subjected to the Ru-catalyzed conditions, benzoic acid was produced in 82% yield (entry 4). Results for the catalytic oxidation of other alkenes are given in the Supporting Information.

In summary, a heterogeneous catalyst was prepared by grafting ruthenium nanoparticles onto hydroxyapatite. The supported Ru nanoparticle catalyst exhibited excellent activities for dihydroxylation and oxidative cleavage of alkenes, and the catalyst can be recycled for repeated uses. Considering that preparation of the supported catalyst involves easy chemical manipulation and the lower toxicity of ruthenium compared to OsO_4, the application of the ruthenium nanoparticles-based catalyst to other catalytic transformations are being pursued.

Table 4: Nano-RuHAP-catalyzed oxidative cleavage of α,β-unsaturated alkenes.[a]

Entry	Alkene	*t* [h]	Product	Yield [%][b]
1		4	PhCHO	67
			$PhCO_2H$	72
2		7		85
3		3		84
4[c]		2	$PhCO_2H$	82

[a] Reaction conditions: alkene (0.5 mmol), nano-RuHAP (40 mg, 4 mol%), oxone (2.5 equiv) and $NaHCO_3$ (7.7 equiv) in $MeCN-H_2O$ 1.5:1 at RT. [b] Yield of isolated product based on complete alkene consumption. [c] Oxone (4 equiv) and $NaHCO_3$ (12 equiv).

Received: January 9, 2004
Revised: March 31, 2004 [Z53703]

Keywords: alkenes · heterogeneous catalysis · nanostructures · ruthenium · solid-phase synthesis

[1] a) R. A. Johnson, K. B. Sharpless in *Catalytic Asymmetric Synthesis* (Ed.: I. Ojima), 2nd ed., VCH, New York, **2000**; b) H. C. Kolb, M. S. VanNieuwenhze, K. B. Sharpless, *Chem. Rev.* **1994**, *94*, 2483.

[2] Recent examples on alkene dihydroxylations using Fe and Mn catalysts: a) K. Chen, M. Costas, J. Kim, A. K. Tipton, L. Que Jr., *J. Am. Chem. Soc.* **2002**, *124*, 3026; b) M. Costas, A. K. Tipton, K. Chen, D.-H. Jo, L. Que Jr., *J. Am. Chem. Soc.* **2001**, *123*, 6722; c) K. Chen, L. Que Jr., *Angew. Chem.* **1999**, *111*, 2365; *Angew. Chem. Int. Ed.* **1999**, *38*, 2227; d) D. E. De Vos, S. de Wildeman, B. F. Sels, P. J. Grobet, P. A. Jacobs, *Angew. Chem.* **1999**, *111*, 1033; *Angew. Chem. Int. Ed.* **1999**, *38*, 980.

[3] For reviews on ruthenium-catalyzed organic oxidations, see: a) S.-I. Murahashi, N. Komiya in *Biomimetic Oxidations Catalyzed by Transition Metal Complexes* (Ed.: B. Meunier), Imperial College Press, London, **2000**, p. 563; b) J. L. McLain, J. Lee, J. T. Groves in *Biomimetic Oxidations Catalyzed by Transition Metal Complexes* (Ed.: B. Meunier), Imperial College Press, London, **2000**, p. 91; c) S. V. Ley, J. Norman, W. P. Griffith, S. P. Marsden, *Synthesis* **1994**, 639; d) W. P. Griffith, *Chem. Soc. Rev.* **1992**, *21*, 179.

 © 2004 Wiley-VCH Verlag GmbH & Co. KGaA, Weinheim

[4] Selected works by us on stereo- and enantioselective ruthenium-catalyzed oxidative transformations: see: a) J.-L. Liang, S.-X. Yuan, J.-S. Huang, W.-Y. Yu, C.-M. Che, *Angew. Chem.* **2002**, *114*, 3615; *Angew. Chem. Int. Ed.* **2002**, *41*, 3465; b) R. Zhang, W.-Y. Yu, H.-Z. Sun, W.-S. Liu, C.-M. Che, *Chem. Eur. J.* **2002**, *8*, 2495; c) R. Zhang, W.-Y. Yu, K.-Y. Wong, C.-M. Che, *J. Org. Chem.* **2001**, *66*, 8145; d) C.-M. Che, W.-Y. Yu, P.-M. Chan, W.-C. Cheng, S.-M. Peng, K.-C. Lau, W.-K. Li, *J. Am. Chem. Soc.* **2000**, *122*, 11380; e) W.-Y. Yu, C.-M. Che, *Pure Appl. Chem.* **1999**, *71*, 281; f) R. Zhang, W.-Y. Yu, T.-S. Lai, C.-M. Che, *Chem. Commun.* **1999**, 1791; g) W.-H. Fung, W.-Y. Yu, C.-M. Che, *J. Org. Chem.* **1998**, *63*, 2873.

[5] a) B. Plietker, M. Niggemann, *Org. Lett.* **2003**, *5*, 3353; b) T. K.-M. Shing, E. K.-W. Tam, *Tetrahedron Lett.* **1999**, *40*, 2179; c) T. K.-M. Shing, V. W.-F. Tai, E. K.-W. Tam, I. H.-F. Chung, Q. Jiang, *Chem. Eur. J.* **1996**, *2*, 50; d) T. K.-M. Shing, V. W.-F. Tai, E. K.-W. Tam, *Angew. Chem.* **1994**, *106*, 2408; *Angew. Chem. Int. Ed. Engl.* **1994**, *33*, 2312.

[6] a) D. Yang, C. Zhang, *J. Org. Chem.* **2001**, *66*, 4814; b) P. H. J. Carlsen, T. Katsuki, V. S. Martin, K. B. Sharpless, *J. Org. Chem.* **1981**, *46*, 3936.

[7] a) M. Moreno-Mañas, R. Pleixats, *Acc. Chem. Res.* **2003**, *36*, 638; b) A. Roucoux, J. Schulz, H. Patin, *Chem. Rev.* **2002**, *102*, 3757; c) D. Horn, J. Rieger, *Angew. Chem.* **2001**, *113*, 4460; *Angew. Chem. Int. Ed.* **2001**, *40*, 4330; d) H. Bönnemann, R. M. Richards, *Eur. J. Inorg. Chem.* **2001**, 2455; e) C. N. R. Rao, G. U. Kulkarni, P. J. Thomas, P. P. Edwards, *Chem. Soc. Rev.* **2000**, *29*, 27; f) B. F. G. Johnson, *Coord. Chem. Rev.* **1999**, *190–192*, 1269; g) J. S. Bradley in *Clusters and Colloids: from Theory to Application* (Ed.: G. Schmid), VCH, Weiheim, **1994**, p. 459; h) L. N. Lewis, *Chem. Rev.* **1993**, *93*, 2693; i) G. Schmid, *Chem. Rev.* **1992**, *92*, 1709.

[8] a) J. C. Elliot, *Structure and Chemistry of the Apatites and Other Calcium Orthophosphate*s, Elsevier, Amsterdam, **1994**; b) S. Sugiyama, T. Minami, H. Hayashi, M. Tanaka, N. Shigemoto, J. B. Moffat, *J. Chem. Soc. Faraday Trans.* **1996**, *92*, 293.

[9] Earlier examples of recyclable osmium catalysts for alkene dihydroxylations: a) K. Lee, Y.-H. Kim, S. B. Han, H. Kang, S. Park, W. S. Seo, J. T. Park, B. Kim, S. Chang, *J. Am. Chem. Soc.* **2003**, *125*, 6844; b) B. M. Choudary, N. S. Chowdari, M. L. Kantam, K. V. Raghavan, *J. Am. Chem. Soc.* **2001**, *123*, 9220; c) S. Kobayashi, M. Endo, S. Nagayama, *J. Am. Chem. Soc.* **1999**, *121*, 11229; d) C. Bolm, A. Gerlach, *Eur. J. Org. Chem.* **1998**, *1*, 21; e) P. Salvadori, D. Pini, A. Petri, *Synlett* **1999**, 1181; f) D. J. Gravert, K. D. Janda, *Chem. Rev.* **1997**, *97*, 489.

[10] Selected examples of heterogeneous ruthenium catalysts for organic oxidations, see: a) B.-Z. Zhan, M. A. White, T.-K. Sham, J. A. Pincock, R. J. Doucet, K. V. R. Rao, K. N. Robertson, T. S. Cameron, *J. Am. Chem. Soc.* **2003**, *125*, 2195; b) K. Yamaguchi, N. Mizuno, *Angew. Chem.* **2002**, *114*, 4720; *Angew. Chem. Int. Ed.* **2002**, *41*, 4538; c) W.-H. Cheung, W.-Y. Yu, W.-P. Yip, N.-Y. Zhu, C.-M. Che, *J. Org. Chem.* **2002**, *67*, 7716; d) K. Yamaguchi, K. Mori, T. Mizugaki, K. Ebitani, K. Kaneda, *J. Am. Chem. Soc.* **2000**, *122*, 7144; e) X.-Q. Yu, J.-S. Huang, W.-Y. Yu, C.-M. Che, *J. Am. Chem. Soc.* **2000**, *122*, 5337; f) T. Matsushita, K. Ebitani, K. Kaneda, *Chem. Commun.* **1999**, 265; g) K. Kaneda, T. Yamashita, T. Matsushita, K. Ebitani, *J. Org. Chem.* **1998**, *63*, 1750; h) A. Bleloch, B. F. G. Johnson, S. V. Ley, A. J. Price, D. S. Shephard, A. W. Thomas, *Chem. Commun.* **1999**, 1907; i) C.-J. Liu, W.-Y. Yu, S.-G. Li, C.-M. Che, *J. Org. Chem.* **1998**, *63*, 7364.

[11] For methods to prepare ruthenium colloids, see: a) G. Viau, R. Brayner, L. Poul, N. Chakroune, E. Lacaze, F. Fiévet-Vincent, F. Fiévet, *Chem. Mater.* **2003**, *15*, 486; b) I. Balint, A. Miyzaki, K.-I. Aika, *J. Catal.* **2002**, *207*, 66; c) A. Miyazaki, I. Balint, K.-I. Aika, Y. Nakano, *J. Catal.* **2001**, *204*, 364; d) S. Gao, J. Zhang, Y.-F. Zhu, C.-M. Che, *New J. Chem.*, **2000**, *24*, 739.

[12] E. Hayek, H. Newesely, *Inorg. Synth.* **1963**, *7*, 63.

[13] J. F. Moulder, W. F. Stickle, P. E. Sobol, K. D. Bomben in *Handbook of X-ray Photoelectron Spectroscopy* (Eds.: J. Chastain, R. C. King, Jr.), Physical Electronics, Eden Prairie, **1995**.

[14] a) D. G. Lee, T. Chen in *Comprehensive Organic Synthesis* (Eds.: B. M. Trost, I. Fleming, S. V. Ley), 1st ed., Pergamon, Oxford, **1991**, chap. 3.8, p. 541; b) R. Criegee, *Angew. Chem.* **1975**, *87*, 765; *Angew. Chem. Int. Ed. Engl.* **1975**, *14*, 745.

[15] B. R. Travis, R. S. Narayan, B. Borhan, *J. Am. Chem. Soc.* **2002**, *124*, 3824.

[16] Oxone is a mixture of 2 $KHSO_5 \cdot KHSO_4 \cdot K_2SO_4$.

 © 2004 Wiley-VCH Verlag GmbH & Co. KGaA, Weinheim

Asymmetric Synthesis

Construction of C–S Bonds with a Quaternary Stereocenter through a Formal Michael Reaction: Asymmetric Synthesis of Tertiary Thiols**

Claudio Palomo, Mikel Oiarbide, Flavia Dias, Rosa López, and Anthony Linden*

There are several reactions for the asymmetric construction of C–S bonds, often with excellent results in terms of efficiency and selectivity.[1,2] Among them, the Michael reaction, that is, the conjugate addition of nucleophiles to electron-deficient olefins,[3] has received special attention. This approach is very attractive not only because of the availability of a broad range of Michael acceptors and the suitability of the simultaneous formation of both a new C–S bond and a stereocenter, but also because the conjugate addition step provides a reactive species that may be trapped by electrophiles leading to tandem processes of significant synthetic value. Several approaches have been documented for diastereo-[4] and enantiocontrol[5,6] in the conjugate addition of sulfur-based nucleophiles to Michael acceptors. To the best of our knowledge, however, construction of quaternary C–S systems[7] through this reaction remains essentially unexplored within

[*] Prof. Dr. C. Palomo, Prof. Dr. M. Oiarbide, F. Dias, Dr. R. López
Departamento de Química Orgánica I
Facultad de Química
Universidad del País Vasco
Apdo. 1072, 20080 San Sebastián (Spain)
Fax: (+34) 943-212-236
E-mail: qoppanic@sc.ehu.es

Dr. A. Linden[+]
Organisch-chemisches Institut
Universität Zürich
Winterthurerstrasse 190, 8057 Zürich (Switzerland)

[+] crystal structure analysis

[**] We thank The University of the Basque Country (EHU/UPV) and Ministerio de Ciencia y Tecnología (Spain) for financial support. A Ramón y Cajal grant to R.L. from Ministerio de Educación Cultura y Deporte and a predoctoral grant to F.D. from EHU/UPV are acknowledged.

Supporting information for this article is available on the WWW under http://www.angewandte.org or from the author.

 DOI: 10.1002/anie.200453889 © 2004 Wiley-VCH Verlag GmbH & Co. KGaA, Weinheim

the asymmetric endeavor.[8] There are three conceptual restraints that may be invoked for this omission: a) the attenuated reactivity of β,β-disubstituted Michael acceptors;[9] b) the inherent difficulty in controlling π-facial diastereo- and enantioselectivity in these substrates;[8] and c) virtual thermodynamic equilibration of the stereoisomeric products through an addition–elimination mechanism,[10] which makes kinetic stereocontrol rather challenging. Yet, the asymmetric construction of quaternary stereocenters, particularly from β,β-disubstituted Michael acceptors, is a very difficult synthetic task.[11,12]

Our hypothesis was that the above restraints might be counterbalanced if an intramolecular version of the Michael-type approach could be implemented (Figure 1). In this

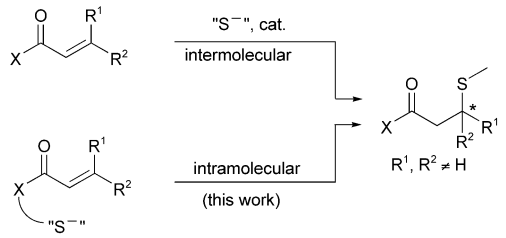
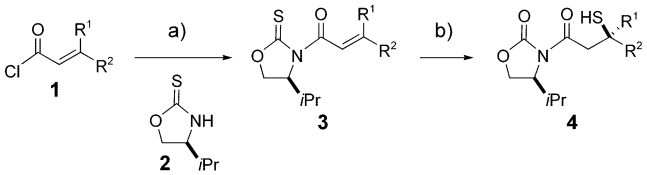


Figure 1. Intermolecular and intramolecular variants of the Michael-type addition of sulfur nucleophiles to enoyl systems as a route to C–S bonds with a quaternary stereocenter.

instance, the favorable entropy usually associated with an intramolecular process might help to solve the reactivity problem, whilst at the same time, a sufficiently high π-facial discrimination could also be exerted because of the intramolecular nature of the chirality transfer.

To validate this hypothesis, we have formulated the approach outlined in Scheme 1 on the basis of previous



Scheme 1. Preparation of Michael acceptors **3** and their intramolecular reaction leading to tertiary thiols **4**. Conditions: a) NaH, THF, −78 °C. b) $BF_3{\cdot}Et_2O$ then H_2O.

observations made in our laboratory.[13,14] Accordingly, several β,β-disubstituted *N*-enoyl oxazolidine-2-thiones, **3**, were prepared from **1** and **2**, and their intramolecular reaction in the presence of Lewis acids[15] examined, whereby the chiral oxazolidine-2-thione moiety was expected to act not only as the controller of the reaction stereochemistry but also as the sulfur transfer reagent. We were pleased to find that tertiary thiols **4** were indeed formed with good to excellent yields and, most significantly, with high diastereoselectivity under the action of an appropriate Lewis acid. The most satisfactory results in terms of both reactivity and stereoselectivity were obtained with $BF_3{\cdot}Et_2O$. Among the Lewis acids tested,[16] $SnCl_4$ also led to a clean reaction, but longer reaction times and in general lower diastereoselectivities were obtained. For a variety of substrates examined (Table 1) the diastereoselectivity of the reactions carried out at −30 °C ranged from

Table 1: $BF_3{\cdot}Et_2O$-promoted intramolecular Michael-type addition of sulfur in β,β-disubstituted enoyl systems **3** leading to tertiary thiols **4**.[a]

Compound	R^1	R^2	*T* [°C]	*t* [h]	d.r.[b]	Yield [%][c]
3a	Me	Ph	−78	13	n.d.	<40
			−30	9	>99:1	80
			25	52	86:14	n.d.
3b		4-MeC_6H_4	−30	7	97:3	77
			25	5	73:27	89[d]
3c		4-ClC_6H_4	−30	9	92:8	72
			25	5	90:10	90[d]
3d		4-BrC_6H_4	−30	72	98:2	76
			25	24	96:4	42
3e		4-$MeOC_6H_4$	−30	7	52:48	65
3f		3-$MeOC_6H_4$	−30	120	93:7	83
3g		4-CNC_6H_4	−30	36	92:8	73[e]
3h		4-$NO_2C_6H_4$	−30	12	91:9	70
3i	Et	Ph	−30	10	98:2	77
3j	*n*Bu	Ph	−30	15	96:4	68

[a] Reactions conducted at 0.5 mmol scale and 0.1 M substrate concentration. Ratio of **3**:$BF_3{\cdot}OEt_2$ 1:2. For details, see Supporting Information. [b] Determined by ^1H and/or ^{13}C NMR spectroscopy. [c] Yields of isolated compound after purification by column chromatography. [d] Yield of crude product. [e] Reaction performed at 0.2 mmol scale.

very high to essentially perfect, while even at 25 °C diastereoselectivity remained high in some instances (compounds **3c**,**d**). Curiously, whilst the β-4-methoxyphenyl substituted enoyl derivative **3e** brought about almost no diastereoselection, the enoyl compound **3f** bearing the 3-methoxyphenyl substituent showed quite good diastereoselectivity. On the other hand, from comparison of the results with substrates **3a**, **3i**, and **3j**, it appears that the size of the "small" substituent at the β position does not influence selectivity very much and high d.r. values are regularly observed.

The assigned configuration for the adducts was established by a single-crystal X-ray crystallographic analysis of the *p*-nitrobenzoyl derivative **5**,[17] and by assuming a uniform reaction mechanism. In this respect, the sense of the asymmetric induction can be explained by assuming a preferential attack of sulfur on the *Si* face of the enoyl β carbon atom with no interference of the *i*Pr group (model **A**), Figure 2.

In an effort to add some insight into the reaction mechanism, several substrates with variable *E*/*Z* composi-

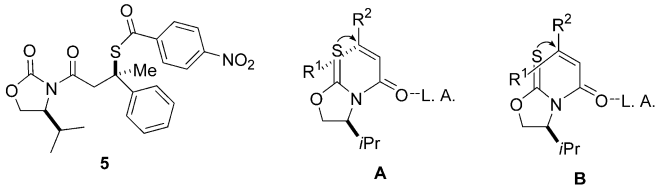


Figure 2. The attacking trajectories of sulfur onto (**A**) the *Si* face and (**B**) the *Re* face of the enoyl β-carbon, showing the distal and proximal alignments, respectively, of *i*Pr group and (R^1R^2C=C) moiety, and structure of **5**.

 © 2004 Wiley-VCH Verlag GmbH & Co. KGaA, Weinheim

tions were prepared[18] and the outcomes of their reactions were examined. Strikingly, it was found that the reaction diastereoselectivity was essentially the same regardless of the *E*/*Z* composition of the starting enoyl substrate **3**,[19] Table 2.

Table 2: Reaction diastereoselectivities obtained from substrates **3** of variable *E*/*Z* compositions.[a]

Compound	R^1	R^2	Substrate **3** *E*/*Z* ratio[b]	Product **4** d.r.[b]
3d	Me	4-BrC_6H_4	100:0	92:8
			30:70	92:8
3g	Me	4-CNC_6H_4	100:0	92:8
			83:13	92:8
3j	*n*Bu	Ph	100:0	96:4
			50:50	96:4
			0:100	96:4

[a] Reactions conducted at 0.5 mmol scale and 0.1 M substrate concentration. Ratio of **3**:BF_3·OEt_2 1:2. [b] Determined by 500 MHz ^{1}H NMR spectroscopy.

The same behavior was also observed for substrate **6** (Figure 3), which bears a structurally different oxazolidine-2-thione auxiliary.[20] These results show that products with very high diastereomeric purity may be accessible from

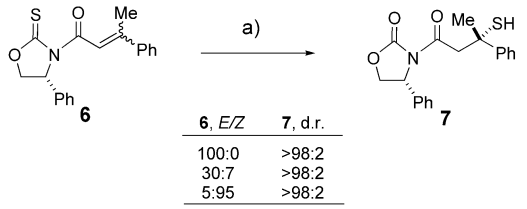
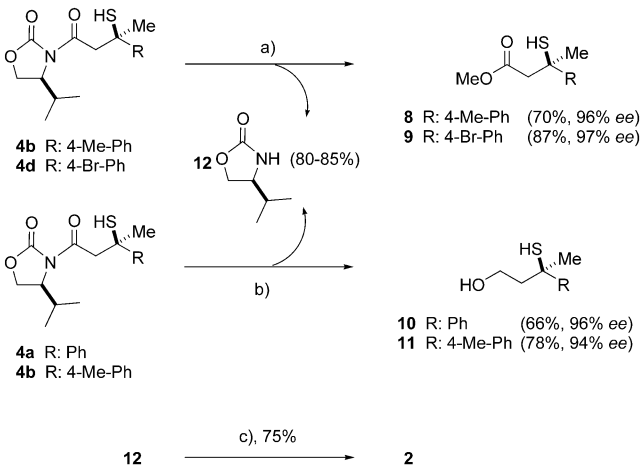


Figure 3. Uniform diastereoselectivity sense and level regardless of the *E*/*Z* composition of substrate **6**. Conditions: a) BF_3·Et_2O, −30 °C then H_2O.

configurationally nonhomogeneous β,β-disubstituted Michael acceptors, a feature that is of practical interest.[21]

Although at the present time we do not have a rational explanation for the above observations,[22] the excellent diastereoselectivity attained in these reactions is also of particular interest, since treatment of the thiol adducts such as **4b** and **4d** with $Sm(OTf)_3$ (Tf = trifluromethanesulfonyl) in MeOH[23] provides the β,β-disubstituted β-sulfanyl carboxylic esters **8** and **9**, respectively. Likewise, treatment of **4a** and **4b** with $NaBH_4$[24] leads to the corresponding 1,3-hydroxythiols **10**[25] and **11**. In each case, the oxazolidinone **12** is produced and can be transformed into the oxazolidine-2-thione **2** for reuse by treatment with Laweson's reagent (Scheme 2).

In conclusion, it has been shown that β,β-disubstituted *N*-enoyl oxazolidine-2-thiones react upon the action of Lewis acids through a highly stereoselective intramolecular Michael-type process. This transformation allows for the construction of C–S bonds with a quaternary stereocenter and results in the formation of functionalized tertiary sulfanyls in very high enantioselectivity. Further studies are underway to clarify the mechanism of this reaction.



Scheme 2. Elaboration of adducts into enantiopure sulfanyl-bearing esters and alcohols bearing a quaternary stereocenter, and recycling of the chiral auxiliary. Conditions: a) $Sm(OTf)_3$, MeOH, RT; b) $NaBH_4$, THF/H_2O. c) Lawesson's reagent, 1,4-Dioxane, reflux.

Experimental Section

General Procedure: BF_3·Et_2O (1.0 mmol, 0.127 mL) was added dropwise by syringe to a solution of the corresponding *N*-enoyl oxazolidine-2-thione (**3**; 0.5 mmol) in methylene chloride (8 mL) under a nitrogen atmosphere at −30 °C (bath temperature) or at the corresponding temperature (see Table 1). The resulting mixture was stirred at the same temperature until signals corresponding to starting material were no longer visible in the ^{1}H NMR spectra of the extracted samples. The mixture was then poured into a saturated solution of sodium bicarbonate (20 mL) and the layers were separated. The organic layer was washed with brine (50 mL), dried over $MgSO_4$, and the solvent evaporated under reduced pressure. The crude material was purified by silica gel chromatography by using a mixture of ethyl acetate and hexane (10:90) as eluent.

Received: January 30, 2004 [Z53889]

Keywords: asymmetric synthesis · chirality · Lewis acids · Michael addition · thiols

[1] For an updated account on the synthesis of thiols, sulfides, and derivatives, see: D. J. Procter, *J. Chem. Soc. Perkin Trans. 1* **2001**, 335–354 and previous review articles in the series.
[2] For a review on metal-catalyzed C–S bond formation, see: T. Kondo, T. Mitsudo, *Chem. Rev.* **2000**, *100*, 3205–3220.
[3] P. Perlmutter, *Conjugate Addition Reactions in Organic Synthesis*, Pergamon, Oxford, **1992**.
[4] For recent examples, see: a) D. F. Taber, G. J. Gorski, L. M. Liable-Sands, A. L. Rheingold, *Tetrahedron Lett.* **1997**, *38*, 6317–6318; b) O. Miyata, T. Shinada, I. Ninomiya, T. Naito, *Tetrahedron* **1997**, *53*, 2421–2438; c) C.-H. Lin, K.-S. Yang, J.-P. Pan, K. Chen, *Tetrahedron Lett.* **2000**, *41*, 6815–6819; d) M. Node, K. Nishide, Y. Shigeta, H. Shiraki, K. Obata, *J. Am. Chem. Soc.* **2000**, *122*, 1927–1936; e) K. Nishide, S.-i. Ohsugi, H. Shiraki, H. Tamakita, M. Node, *Org. Lett.* **2001**, *3*, 3121–3124.
[5] For some recent examples, see: a) E. Emori, T. Arai, H. Sasai, M. Shibasaki, *J. Am. Chem. Soc.* **1998**, *120*, 4043–4044; b) M. Saito, M. Nakajima, S. Hashimoto, *Tetrahedron* **2000**, *56*, 9589–9594; c) V. A. Castelli, A. D. Cort, L. Mandolini, D. N. Reinhoudt, D. L. Schiaffino, *Chem. Eur. J.* **2000**, *6*, 1193–1198; d) M. Saito, M. Nakajima, S. Hashimoto, *Chem. Commun.* **2000**, 1851–1852;

 © 2004 Wiley-VCH Verlag GmbH & Co. KGaA, Weinheim

e) S. Kobayashi, C. Ogawa, M. Kawamura, M. Sugiura, *Synlett* **2001**, 983 – 985; f) P. McDaid, Y. Chen, L. Deng, *Angew. Chem.* **2002**, *114*, 348 – 350; *Angew. Chem. Int. Ed.* **2002**, *41*, 338 – 340; g) K. Nishimura, K. Tomioka, *J. Org. Chem.* **2002**, *67*, 431 – 434; h) N. Prabagaran, G. Sundararajan, *Tetrahedron: Asymmetry* **2002**, *13*, 1053 – 1058.

[6] Reviews on catalytic enantioselective Michael additions: a) N. Krause, A. Hoffmann-Röder, *Synthesis* **2001**, 171 – 196; b) M. P. Sibi, S. Manyem, *Tetrahedron* **2000**, *56*, 8033 – 8061.

[7] For the synthesis of quaternary C–S systems other than thiols asymmetrically, see: Sulfoxides: a) D. A. Evans, G. C. Andews, *Acc. Chem. Res.* **1974**, *7*, 147 – 155; sulfones from rearrangement of chiral sulfinates: b) K. Hiroi, M. Yamamoto, Y. Kurihara, H. Yonezawa, *Tetrahedron Lett.* **1990**, *31*, 2619 – 2622; sulfides from rearrangement of sulfur ylides: c) X. Zhang, Z. Qu, Z. Ma, W. Shi, X. Jin, J. Wang, *J. Org. Chem.* **2002**, *67*, 5621 – 5625; sulfides from rearrangement of allyl xanthates: d) M. S. Chambers, E. J. Thomas, D. J. Williams, *J. Chem. Soc. Chem. Commun.* **1987**, 1228 – 1230.

[8] The preparation of a tertiary arylsulfide is described in reference [5a] (53% yield and 85% *ee*); another one in reference [5b] (43% yield and 10% *ee*).

[9] M. E. Jung in *Comprehensive Organic Synthesis*, *Vol. 4* (Eds.: B. M. Trost, I. Fleming, M. F. Semmelhack), Pergamon, Oxford, **1991**, p. 17.

[10] a) J. A. Marshall, S. L. Crooks, B. S. DeHoff, *J. Org. Chem.* **1988**, *53*, 1616 – 1623; b) J. A. Marshall, M. W. Andersen, *J. Org. Chem.* **1992**, *57*, 2766 – 2768.

[11] Reviews: a) K. Fuji, *Chem. Rev.* **1993**, *93*, 2037 – 2066; b) E. J. Corey, A. Guzman-Perez, *Angew. Chem.* **1998**, *110*, 402 – 415; *Angew. Chem. Int. Ed.* **1998**, *37*, 388 – 401; c) J. Christoffers, A. Mann, *Angew. Chem.* **2001**, *113*, 4725 – 4732; *Angew. Chem. Int. Ed.* **2001**, *40*, 4591 – 4597; d) I. Denissova, L. Barriault, *Tetrahedron* **2003**, *59*, 10105 – 10146.

[12] The use of Michael addition reactions in the construction of quaternary stereocenters: J. Christoffers, A. Baro, *Angew. Chem.* **2003**, *115*, 1726 – 1728; *Angew. Chem. Int. Ed.* **2003**, *42*, 1688 – 1690.

[13] C. Palomo, M. Oiarbide, F. Dias, A. Ortiz, A. Linden, *J. Am. Chem. Soc.* **2001**, *123*, 5602 – 5603.

[14] For further development by others, see: T. Kataoka, H. Kinoshita, S. Kinoshita, T. Osamura, S. Watanabe, T. Iwamura, O. Muraoka, G. Tanabe, *Angew. Chem.* **2003**, *115*, 2995 – 2997; *Angew. Chem. Int. Ed.* **2003**, *42*, 2889 – 2891.

[15] For Lewis acid-assisted cyclization of *N*-enoyl thioureas leading to 1,3-thiazines, see: M. Dzurilla, P. Kutschy, P. Kristan, *Synthesis* **1985**, 933 – 934.

[16] While the treatment with $SnCl_2$ led to the recovery of unreacted **3**, the reaction with other Lewis acids such as $TiCl_4$, $Sm(OTf)_3$, $AlCl_3$, $AlEt_2Cl$, BCl_3, and BBr_3 led to variable quantities of undesired side products.

[17] CCDC-228804 contains the supplementary crystallographic data for this paper. These data can be obtained free of charge via www.ccdc.cam.ac.uk/conts/retrieving.html (or from the Cambridge Crystallographic Data Centre, 12 Union Road, Cambridge CB21EZ, UK; fax: (+44) 1223-336-033; or deposit@ccdc.cam.ac.uk).

[18] Mixtures of different *E*/*Z* composition were obtained by either column chromatography- or recrystallization-driven enrichment of the original *E*/*Z* mixture. See Supporting Information for details.

[19] For example, it has been described recently that the conjugate addition of lithium thiophenolate to an *E* and *Z* mixture of a cyclic enone gives exclusively one diastereomeric addition product. T. J. Houghton, C. Soongyu, V. H. Rawal, *Org. Lett.* **2001**, *3*, 3615 – 3617.

[20] Note for this case it is the opposite configuration of both the auxiliary and the resulting tertiary sulfanyl. Also, see reference [25].

[21] The synthesis of β,β-disubstituted Michael acceptors with either solely *E* or solely *Z* configuration is, in general, not so straightforward. For further information, see, for instance, N. Zhu, D. G. Hall, *J. Org. Chem.* **2003**, *68*, 6066 – 6069, and references therein.

[22] There are two possible rationales: kinetic production of the observed diastereomer through any reaction pathway involving a common intermediate reachable from both *E*- and *Z*-configured enoyl derivatives, and thermodynamic equilibration of the formed diastereomeric products before final hydrolysis. Among the possible pathways for the first rationale would be the virtual *E*/*Z* isomerization of the substrate under the reaction conditions. After analysis by NMR spectroscopy of aliquots taken for a set of reactions at times corresponding to different degrees of reaction conversion, however, no detectable *E*/*Z* isomerization could be observed, and this possibility can be ruled out.

[23] a) E. Lee, E. J. Jeong, E. J. Kang, L. T. Sung, S. K. Hong, *J. Am. Chem. Soc.* **2001**, *123*, 10131 – 10132; b) A. Ortiz, L. Quintero, H. Hernandez, S. Maldonado, G. Mendoza, S. Bernés, *Tetrahedron Lett.* **2003**, *44*, 1129 – 1132.

[24] M. Prashad, D. Har, H.-Y. Kim, O. Repic, *Tetrahedron Lett.* **1998**, *39*, 7067 – 7070.

[25] The enantiomer of **10** is obtained in $\geq$97% *ee* from the reduction of **7** under otherwise identical conditions.

 © 2004 Wiley-VCH Verlag GmbH & Co. KGaA, Weinheim

Kinetics versus Thermodynamics

The Coexistence of Two Different Methane Hydrate Phases under Moderate Pressure and Temperature Conditions: Kinetic versus Thermodynamic Products**

Judith M. Schicks and John A. Ripmeester*

Clathrate hydrates are nonstoichiometric crystalline icelike solids comprising a three-dimensional framework in which water molecules are hydrogen-bonded so as to form well-defined cavities that contain gas molecules. The empty framework is unstable with respect to ice but is stabilized by a minimum degree of occupancy of the cavities.

[*] Dr. J. M. Schicks
GeoForschungsZentrum Potsdam Telegrafenberg
14473 Potsdam (Germany)
Fax: (+49) 331-288-1436
E-mail: schick@gfz-potsdam.de

Dr. J. A. Ripmeester
Ripmeester Steacie Institute for Molecular Science National Research Council Ottawa Canada

[**] The Geotechnologien program of BMBF and DFG provided funding of this work through the Research Grant G0555A. This is publication no. GEOTECH-61 of the Geotechnologien program.

 © 2004 Wiley-VCH Verlag GmbH & Co. KGaA, Weinheim DOI: 10.1002/anie.200453898

There are three known gas hydrate structures capable of holding light hydrocarbons (Table 1): structure I, structure II and structure H. Small guests such as Ar, Kr, O_2, and N_2 form structure II hydrates with both large and small cages being

Table 1: Number of cavies per unit cell for the different gas hydrate structures.[8]

Structure	Cavities				
	5^{12}	$5^{12}6^2$	$5^{12}6^4$	$4^35^66^3$	$5^{12}6^8$
Structure I	2	6	–	–	–
Structure II	16	–	8	–	–
Structure H	3	–	–	2	1

filled. Slightly larger guests such as methane, CO_2 and ethane form structure I hydrates, with partial filling of the small cavity, and larger molecules such as propane and isobutane form structure II hydrates with the small cavities being empty. Even larger molecules such as neohexane form structure H hydrates in the presence of an aiding gas such as methane. However, when more than one guest is present, the relationship between structure and size is not straightforward, as guests that individually form structure I hydrates sometimes together form structure II hydrates when present in certain proportions. This was documented many years ago for the guest pairs H_2S/CH_3Br, H_2S/CH_3CHF_2, H_2S/COS, and more recently for ethane/methane.[1]

Guests such as methane and carbon dioxide are not known to form structure II hydrates under moderate pressure and temperature conditions ($P \leq 100$ MPa and $T \leq +20$ °C), either individually or in combination, and it is generally accepted that structure I hydrate is the thermodynamically stable phase for these guests. Hence, natural gas hydrate as well as synthetic methane hydrate—grown under conditions close to those in nature—are known to be structure I.

Although all theoretical and experimental considerations lead to the conclusion that the formation of structure II methane hydrate is unlikely under conditions encountered in nature, in this study it is shown that the coexistence of structure I and structure II methane hydrate is possible under moderate conditions. Herein, we present the results of Raman spectroscopic investigations on methane hydrate, synthesised in a pressure range between 3.0 MPa and 9.0 MPa and at temperatures between +1.5 °C and +12 °C. Euhedral crystals of methane hydrate were grown under conditions close to the dissociation curve at constant pressure and temperature in a small pressure cell with a window suitable for optical and Raman observation. Figure 1 shows a microscopic photograph of the crystals.

Analysis of the crystals by Raman spectroscopy gave some rather unexpected results. It is known that the vibrational frequency of a C–H symmetric stretch for methane can be correlated with the size of the cage—vibrational frequencies for small cavities are shifted to higher frequencies than those for methane molecules in large cavities according to the Pimentel–Charles "tight-cage–loose-cage model" as recently elaborated by Subramanian and Sloan.[3,4] Since the ratios of large to small cavities for structure I and structure II hydrates

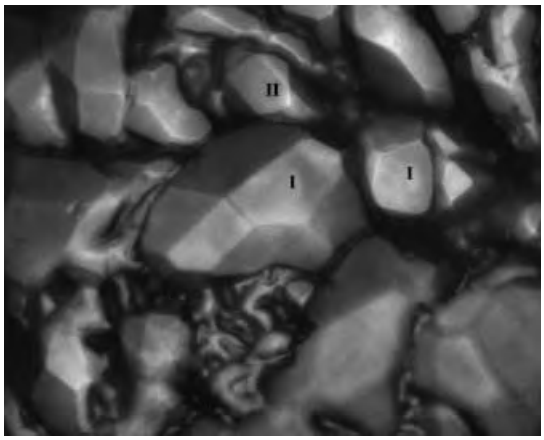


Figure 1. Coexistence of structure I (s I) and structure II (s II) methane hydrates. The width of the photographed area is 420 μm.

are 3:1 and 1:2, respectively, the relative peak areas in the experimental spectra should be good indicators of the structure. It turns out that the ratio of the Raman bands for most of the crystals is close to 3:1 (Figure 2a), thus indicating the presence of structure I, as expected for methane hydrate. Nevertheless, the Raman spectra of a few crystals (Figure 2b) give spectra with peak intensities 1:2, indicating the presence of structure II hydrate.

Raman spectra of encaged CH_4 similar to those in Figure 2b have been published by Subramanian and Sloan for mixed methane/hydrocarbon structure II hydrates.[4]

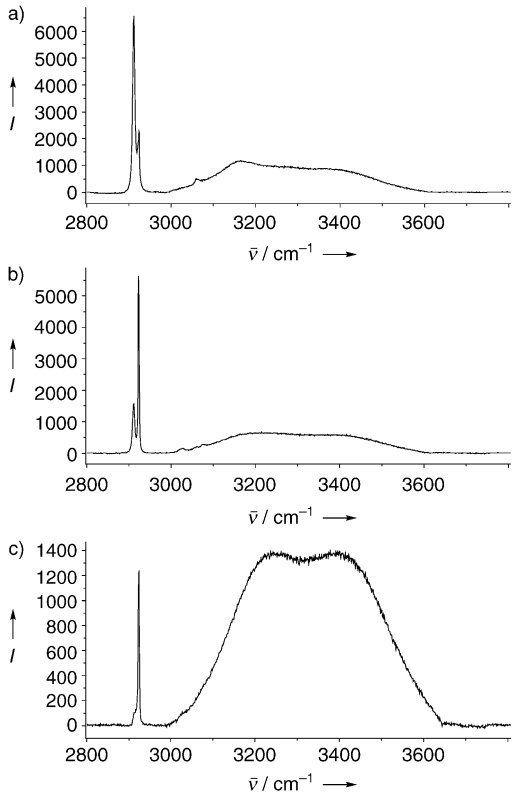


Figure 2. Raman spectra of structure I and structure II hydrates. *I* is intensity, arbitrary units.

 © 2004 Wiley-VCH Verlag GmbH & Co. KGaA, Weinheim

Raman spectra for pure structure II methane hydrate have also been described by Chou et al., for samples that were converted from structure I hydrate by applying high pressure (> 100 MPa), and these also look similar to the spectrum shown in Figure 2c.[5] Chou and co-workers verified their results evincing the presence of structure II methane hydrate with X-ray diffraction data. Our Raman spectra of the CH_4 bands prove that there are at least two different phases of methane hydrate that coexist in a pressure range between 3 MPa and 9 MPa and a temperature range of between 1.5 °C and 12 °C. The two different Raman spectra for the structure II methane hydrate are probably caused by different degrees of saturation of the large cages with methane. We want to point out that the experimental setup permits a selective analysis of the separate phases. This is described in more detail in the Experimental Section.

It is clear that structure II methane hydrate is less stable than structure I methane hydrate under these conditions: if the conditions are changed, for instance, to lower temperature at constant pressure, or to higher pressure at constant temperature, the structure II crystals transform. First the crystals become less well-defined and develop characteristic micrometer-sized specks. A rounding of the crystals, reminiscent of a melting process, is followed by a transformation into a fine-grained hydrate mass. These processes are documented in Figure 3a–e. This exothermic transformation process—beginning with the structure II crystals—induces a recrystallization of the entire hydrate phase until a new steady state is reached. All of the hydrate phase has a fine-grained texture before new well-defined crystals start to grow again.

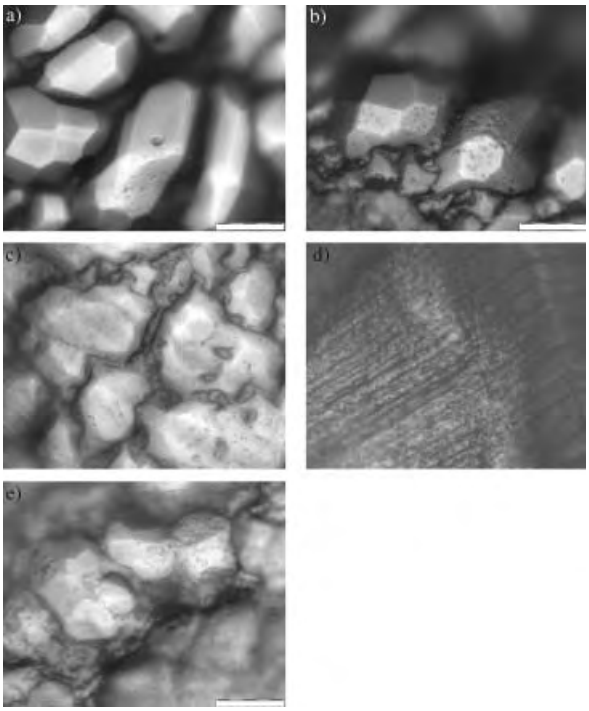


Figure 3. Transformation of structure II into structure I methane hydrates. The width of the photographed area is 420 μm, the length of the bars in a,b,e) are 100 μm.

Raman spectroscopic measurements (shown in Figure 4a–d) on these hydrates during the change in morphology show a loss of the structure II character: the intensity of the methane band at 2904 cm^{-1} (large cavities) increases, while

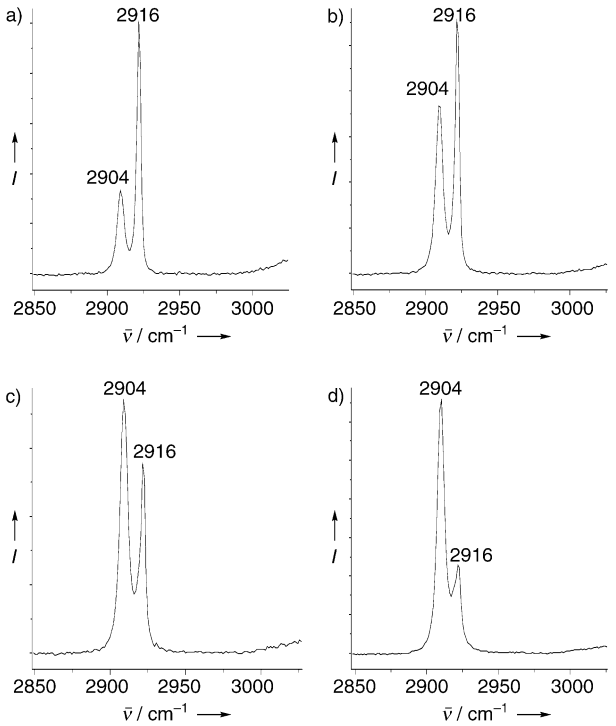


Figure 4. Raman spectra of the transformation of structure II methane hydrates into structure I methane hydrates.

the intensity of the methane band at 2916 cm^{-1} (small cavities) decreases. Finally, structure II methane hydrate can no longer be detected by Raman spectroscopy.

Up to now the reason for the formation of structure II methane hydrate under the conditions mentioned above is unexplained. Subramanian and Sloan observed in their real-time-monitoring Raman spectra the transformation of dissolved CH_4 to CH_4 in the large and small cages of structure I methane hydrate.[6] In the initial stages of hydrate formation the ratio of large cages to small cages was 0.5, which corresponds well with ratio of large cages to small cages of structure II clathrate hydrates. Subramanian and Sloan assumed that the formation of the large cavity is the rate-limiting factor in the formation of structure I methane hydrate. The time dependency of the occupancy ratio does change with time, which is consistent with a slow transformation of structure II into structure I and it is almost complete after 5000 s. Staykova et al. observed the transient formation of structure II CO_2 hydrates during the growth of pure CO_2 hydrates on grains of ice.[7] The ^{129}Xe NMR experiments of Moudrakovski et al., who determined the cage-occupancy ratio as a function of time during the early stages of formation and growth of hydrate, also observed a predominance of small cages at an earlier part of the reaction, thus indicating a major role for the small cavities.[8] We also note that a structure II hydrate of Xe, prepared from

 © 2004 Wiley-VCH Verlag GmbH & Co. KGaA, Weinheim

structure II THF hydrate, proved to be quite fragile, as it is converted into more stable hydrates within minutes.[9] In these various studies the presence of large numbers of guest molecules in small cages at early stages of the hydrate growth process suggests that structure II hydrate may be the kinetically favored structure as it contains the small cage as the major building block for the structure II framework.

In summary, Raman spectroscopic investigations of the formation of synthetic methane hydrate show some remarkable features: methane hydrate crystals of very different composition have been identified. Raman spectra showing cage occupancy ratios for methane in large and small cavities were either 3:1 or 1:2, respectively, for different crystals. These in situ measurements were made in a pressure cell at temperatures between −15 °C and +15 °C and at a pressures ranging from 3.0 to 9.0 MPa. The observation of structure I and structure II hydrates under conditions where only structure I hydrate should be stable, suggests that the initial product is determined by kinetics, with structure II hydrate appearing as a metastable phase. The state of coexistence as well as the transformation of the kinetic product to the thermodynamically stable structure I of methane hydrate was documented by microscopic visual observation as well as Raman spectroscopy.

Experimental Section

The main component of the experimental setup was a pressure cell (Figure 5), which can be used in a temperature range between −27 °C and +80 °C. The temperature of the sample cell was controlled by a thermostat and the temperature was determined with a precision of ±0.1 °C. The applicable pressure range was between 0.1 and 10.0 MPa. A pressure controller was used to adjust the sample pressure with a precision of 2% relative pressure. The small sample volume (0.393 cm^3) and the all-around cooling of the sample prevented interference from temperature gradients. With a gas flow rate of 1 mL min^{-1}, it took 17 s for the incoming gas flow to pass the cell body and to enter the void space of the cell; this time is sufficient to allow the gas to attain the cell temperature. The presence of a quartz window permitted the analysis of the phases by Raman Spectroscopy, and allowed the observation and recording of microscopic photodocumentation of formation and decomposition processes. It is worth noting that this experimental setup permits one to focus a laser beam on a precise point, for example, the surface of a hydrate crystal, and to have a precise definition of the analyzed volume thus assuring that only the selected segment is analyzed.

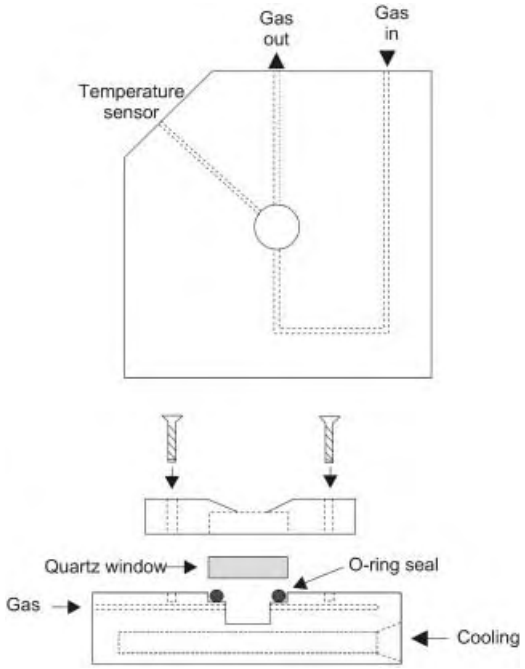


Figure 5. Sketch of the pressure cell.

The experiments were carried out by using the following procedure: pure degassed water (150 μL) was placed in the sample cell. The cell was carefully sealed and flushed with the appropriate gas before pressurization. The system was cooled down as rapidly as possible until hydrates were formed. The system was then warmed at a constant pressure to melt most of the hydrate. When only a few crystals remained, the temperature was lowered to 0.3 °C and the euhedral crystals of gas hydrate grew under steady-state conditions.

Received: February 2, 2004
Revised: April 14, 2004 [Z53898]

Keywords: gas hydrate · kinetics · raman spectroscopy · thermodynamics

[1] M. von Stackelberg, W. Z. Jahns, *Elektrochem. Z.* **1954**, *58*, 162.
[2] E. D. Sloan, Jr., *Clathrate Hydrates of Natural Gases*, 2nd ed., Marcel Dekker, New York, **1998.**
[3] G. C. Pimentel, S. W. Charles, *Pure Appl. Chem.* **1963**, *35*, 111.
[4] S. Subramanian, E. D. Sloan, *J. Phys. Chem. B* **2002**, *106*, 4348–4355.
[5] I-M. Chou, A. Sharma, R. C. Burrus, J. Shu, H-K. Mao, R. J. Hemley, A. F. Goncharov, L. A. Stern, S. H. Kirby, *Proc. Natl. Acad. Sci. USA* **2000**, *97*, *25*, 13484–13487.
[6] S. Subramanian, E. D. Sloan, *Fluid Phase Equilib.* **1999**, *158–160*, 813–820.
[7] D. K. Staykova, W. F. Kuhs, A. N. Salamantin, T. Hansen, *J. Phys. Chem.* **2003**, *107*, 10299–10311.
[8] I. L. Moudrakovski, A. A. Sanchez, C. I. Ratcliffe, J. A. Ripmeester, *J. Phys. Chem. B* **2001**, *105*, 12338–12347.
[9] I. L. Moudrakovski, C. I. Ratcliffe, J. A. Ripmeester, *Angew. Chem.* **2001**, *113*, 4008; *Angew. Chem. Int. Ed.* **2001**, *40*, 3890.

 © 2004 Wiley-VCH Verlag GmbH & Co. KGaA, Weinheim

Enantiomeric Synthesis

Kinetic Resolution of Amines: A Highly Enantioselective and Chemoselective Acetylating Agent with a Unique Solvent-Induced Reversal of Stereoselectivity**

Stellios Arseniyadis, Alain Valleix, Alain Wagner, and Charles Mioskowski**

Despite the development of some effective enzymatic processes,[1] racemate resolution through a nonenzymatic, enantioselective acylation pathway has become the focus of tremendous work over the past few years and remains a valuable alternative for the preparation of optically active compounds.[2] In addition, the development of new reagents capable of reacting specifically with either enantiomer by simply modifying the experimental conditions introduces a new challenge.[3]

In the early 1990s, Evans et al.[4] and Vedejs and Chen[5] reported the first examples of nonenzymatic kinetic resolution of secondary alcohols using stoichiometric amounts of chiral acylating agents that allowed the resolution of a broad family of racemic substrates with useful levels of enantioselection (selectivity factor, $s \geq 10$).[6] Soon after, Vedejs et al.,[7] Oriyama et al.,[8] Fuji and co-workers,[9] Miller et al.,[10] Ruble and Fu,[11] and Spivey et al.[12] described some of the first effective chiral acylation catalysts for the kinetic resolution of alcohols.

Amines are another important family of substrates.[13] While their kinetic resolution by enzymatic processes has been studied intensively, little attention has been given to nonenzymatic kinetic resolution. Therefore, over recent years, the design of nonenzymatic alternatives has been the focus of many research efforts, and substantial progress has been made.

In 1998, Murakami and co-workers[14] were the first to report an example of kinetic enantioselective N-acetylation using chiral 2-acetylamino-2′-diacetylamino-1,1′-binaphthyl. However, the levels of selectivity were moderate. Hence, by variation of the reaction conditions, the kinetic resolution of various amines to give products with up to 48% *ee* was achieved using 0.25 equivalents of chiral reagent at room temperature.[15]

[*] Dr. S. Arseniyadis, Dr. A. Wagner, Dr. C. Mioskowski
Laboratoire de Synthèse Bioorganique
UMR 7514 du CNRS, Faculté de Pharmacie
74 route du Rhin, 67400 Illkirch (France)
Fax: (+33) 3-9024-4306
E-mail: mioskow@aspirine.u-strasbg.fr

A. Valleix, Dr. C. Mioskowski
CEA Saclay, Service des molecules marquées
91191 Gif sur Yvette (France)

[**] We thank Rhodia for financial support to S.A., as well as Dr. A. De Cian and Dr. N. Gruber for their helpful collaborations in the collection of the X-ray crystallographic data.

Supporting information for this article is available on the WWW under http://www.angewandte.org or from the author.

Atkinson and co-workers[16] also contributed to the development of a nonenzymatic process for the kinetic resolution of amines by developing an enantioselective acylating agent derived from 3-(*N*,*N*-diacylamino)quinazolin-4(3*H*)-ones (DAQs).

Recently, Ie and Fu reported the first effective nonenzymatic kinetic resolution of amines using planar-chiral 4-dimethylaminopyridine (DMAP) derivatives.[17] The stereoselective acylation of a family of racemic amines to give products with up to 91% *ee* at −78 °C (at 12.5% conversion) was achieved using 0.125 equivalents of pre-formed acylpyridinium salts derived from the chiral catalyst.[18] Building on these results, Fu and co-workers developed a catalytic system[19] that allowed the kinetic resolution of various benzylic amines with moderate to good selectivities ($11 \leq s \leq 27$). For example, the kinetic resolution of (±)-1-phenylethylamine was described to give products with 79% *ee* using 10 mol% of the chiral catalyst at −50 °C but with only 35% conversion (3.5 turnovers).[20]

Herein, we describe a new and highly enantioselective acetylating agent for the kinetic resolution of primary amines. This reagent allows, to our knowledge, the highest levels of selectivity at room temperature and 50% conversion. Moreover, it exhibits a unique solvent-induced reversal of stereoselectivity that enables us to selectively acetylate one or the other stereoisomer with the same reagent by simply changing the reaction conditions.

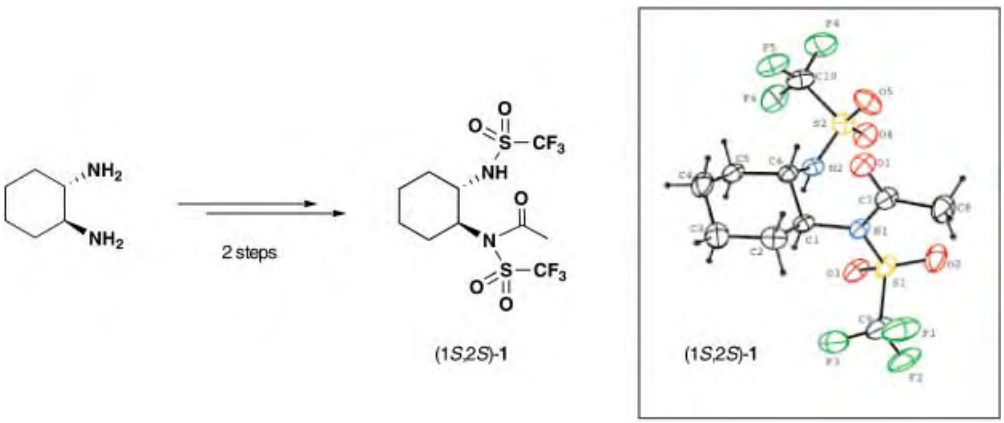
For the construction of our new reagent we used *trans*-1,2-diaminocyclohexane as a chiral scaffold, as it has been a very efficient core structure in many reagents and catalysts.[21] Both amino groups were converted into their corresponding trifluoromethanesulfonamide derivatives to confer good leaving-group ability to the nitrogen atoms. Monoacetylation of the bissulfonamide was then readily performed by addition of one equivalent of acetyl chloride in a 76% overall yield from commercially available (1*S*,2*S*)-diaminocyclohexane. The molecular structure was confirmed by single-crystal X-ray determination (Scheme 1).

The *N*-acetylsulfonamide can be classified as an "active ester". As expected, the *N*-acetyl-1,2-bis(trifluoromethanesulfonamide, (1*S*,2*S*)-**1**, reacted at room temperature with benzylamine to yield *N*-acetylbenzylamine in a quantitative yield.

It is noteworthy that while this product reacts with amines, it proved to be stable when dissolved in ethanol. This chemoselectivity was further demonstrated by the quantitative exclusive N-acetylation of 5-amino-1-pentanol. Moreover, this reagent proved to be insensitive to hydrolysis and could be kept on the bench top for several months without any noticeable loss of activity.

We chose to initiate our study with the reaction of reagent (1*S*,2*S*)-**1** on (±)-1-phenylethylamine. The enantioselective N-acetylations were performed using 0.5 mol equivalent of chiral (1*S*,2*S*)-**1** (unless otherwise specified). In a preliminary experiment, a good chemical yield and a promising level of selectivity were observed. Indeed, complete conversion of the starting material into the *N*-acetylated product with 58% *ee* ($s = 7$) was obtained in toluene at room temperature, as determined by high-performance liquid chromatography

 © 2004 Wiley-VCH Verlag GmbH & Co. KGaA, Weinheim DOI: 10.1002/anie.200453956



Scheme 1. Synthesis of (1*S*,2*S*)-**1** and its structure as determined by X-ray crystallographic analysis.

(HPLC) analysis using a column with a chiral stationary phase (Chiracel OD, *n*-pentane/ethanol 98/2). In addition, the chiral auxiliary was recovered in a yield of over 90% and could be reused. This result compares favorably with those described by Fu and Murakami.

A thorough investigation of this reaction was then undertaken. First, we examined the effect of the solvent on the selectivity of the reaction (Table 1). A wide-ranging study of solvents established that both the rate and the enantioselectivity of the acetylation are highly solvent-dependent; however, no correlation could be made between the reaction time and the *ee* value obtained. Hence, while three hours were needed to reach total conversion with 40% *ee* in dichloromethane (entry 6), total conversion was reached in dimethyl sulfoxide (DMSO) after one hour of stirring and the optical yield was considerably higher (60% *ee*; entry 12). It was noted that solvents having low relative permittivity such as toluene, chloroform, 1,4-dioxane, cyclohexane, THF, dichloromethane, and ethyl acetate led to preferential acetylation of the *R* enantiomer (entries 1–7), while dipolar nonprotic solvents such as DMSO, *N*,*N*-dimethylformamide (DMF), *N*,*N*-dimethylacetamide (DMAc), *N*-methylpyrrolidone (NMP), *N*,*N*,*N*',*N*'-tetramethylurea (TMU), hexamethylphosphoramide (HMPA), and 1,3-dimethyltetrahydro-2-pyrimidinone (DMPU) induced both a reversal of the reaction stereochemistry, thus leading to the *S* enantiomer, and a significant rise in the stereoselectivity (entries 10–18). Finally, dipolar protic solvents such as *N*-methylformamide (NMF) and methanol also induced a reversal of the stereoselectivity; however, the *ee* values were lower (entries 8 and 9).[22]

Table 1: Influence of the solvent on enantioselectivity using (1*S*,2*S*)-**1** as the acylating agent.



Entry	*t* [h][a]	Solvent	ε_t[b]	*ee* [%][c]	*s*
1	2	toluene	2.38	58 (*R*[d])	6.6
2	2	$CHCl_3$	4.81	56 (*R*)	6.1
3	2	1,4-dioxane	2.21	50 (*R*)	4.8
4	2	cyclohexane	2.02	46 (*R*)	4.2
5	3	THF	7.58	42 (*R*)	3.6
6	3	CH_2Cl_2	8.93	40 (*R*)	3.4
7	1	EtOAc	6.02	18 (*R*)	1.7
8	1	NMF	18.24	34 (*S*)	2.8
9	1	MeOH	32.66	38 (*S*)	3.2
10	1	acetone	20.56	30 (*S*)	2.4
11	1	CH_3CN	35.94	35 (*S*)	2.8
12	1	DMSO	46.45	60 (*S*)	7.2
13	3	DMF	36.71	72 (*S*)	13.1
14	3	DMAc	37.78	72 (*S*)	13.1
15	3	NMP	32.2	74 (*S*)	14.6
16	3	TMU	23.6	78 (*S*)	19.0
17	3	HMPA	29.6	84 (*S*)	30.3
18	3	DMPU	36.12	84 (*S*)	30.3

[a] The reaction was run until (1*S*,2*S*)-**1** disappeared, unless otherwise stated. [b] Relative permittivity of the pure liquid at 24°C. [c] The enantiomeric excess was determined by high-performance liquid chromatography (HPLC) analysis using a column with a chiral stationary phase. [d] The absolute configuration of the acetylated enantiomer was assigned by comparison with an authentic standard.

DMPU was the solvent of choice for the kinetic resolution of (±)-1-phenylethylamine, as the product was obtained in 84% *ee* in this solvent system ($s = 30$; entry 18). This is a remarkable result given that it is obtained at room temperature with only two equivalents of amine relative to the amount of chiral (1*S*,2*S*)-**1**. Moreover, to the best of our knowledge, this is the first example of a process in this field that displays a marked solvent-induced reversal of enantioselectivity.

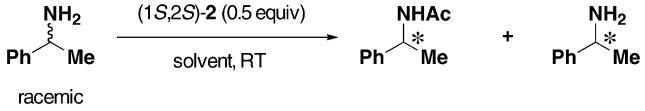
A ^{1}H NMR study of (1*S*,2*S*)-**1** revealed a shift of the free sulfonamide NH resonance according to the nature of the solvent. Hence, in [D_8]toluene this proton signal appeared at $\delta = 4.3$ ppm, whereas in CD_2Cl_2, CD_3CN, and [D_6]DMSO, it appeared at $\delta = 5.0$, 6.7, and 9.7 ppm, respectively. This downfield shift is typical for acidic protons since their acidity is increased because of the effect of solvation in bipolar solvents.

We propose that the acetylation of the amine proceeds through two different mechanisms which depend on the polarity of the solvent. Hence, strong hydrogen bonding with the acidic sulfonamide guides the attack of the amine in bipolar solvents, while only steric interactions govern the selectivity in nonbipolar solvents. To support this hypothesis

 © 2004 Wiley-VCH Verlag GmbH & Co. KGaA, Weinheim

we prepared the *N*-methylsulfonyl analogue (1*S*,2*S*)-**2** and treated it with (±)-1-phenylethylamine at room temperature employing exactly the same conditions as used for (1*S*,2*S*)-**1** (Table 2). As expected, no reversal of stereoselectivity was

Table 2: Influence of the solvent on the enantioselectivity with (1*S*,2*S*)-**2** as the acylating agent.



Entry	*t* [h][a]	Solvent	*ee* [%][b]	*ee* [%][c]
1	1	DMPU	40 (*R*[d])	84 (*S*)
2	1	DMF	20 (*R*)	72 (*S*)
3	1	DMSO	12 (*R*)	60 (*S*)
4	1	1,4-dioxane	50 (*R*)	50 (*R*)
5	1	CCl_4	60 (*R*)	50 (*R*)
6	1	toluene	64 (*R*)	58 (*R*)

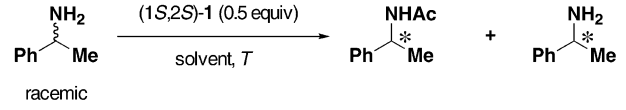
[a] The reaction was run until (1*S*,2*S*)-**2** disappeared, unless otherwise stated. [b] The enantiomeric excess was determined by HPLC analysis on a column with a chiral stationary phase. [c] The enantiomeric excess was obtained using (1S,2S)-**1**. [d] The absolute configuration of the acetylated enantiomer was assigned by comparison with an authentic standard.

observed in bipolar solvents (entries 1–3), while enantioselection increased in nonbipolar solvents (entries 5–6). Hence, we have demonstrated the key role of the free sulfonamide in bipolar–nonprotic solvents.

Next, we examined the possibility of increasing the selectivity by lowering the temperature of the reaction (Table 3). Decreasing the temperature to below 0 °C induced a slight increase in the *ee* values when carrying out the reaction in the four solvents given in Table 3, thus demonstrating that the selectivity of the reaction is also temperature-dependent.

Finally, increasing the amine/acetylating reagent ratio should, in principle, also increase the selectivity. Under otherwise identical conditions, we observed an increase in the enantioselectivity from 86 to 90% when using three equivalents of amines relative to (1*S*,2*S*)-**1** instead of two (entries 4 and 5; Table 3).

Table 3: Influence of the temperature on enantioselectivity using (1*S*,2*S*)-**1** as the acylating agent.



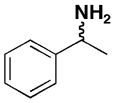
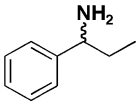
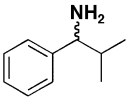
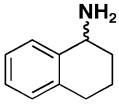
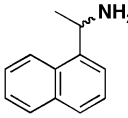
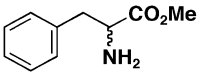
Entry	*T* [°C]	Solvent	*ee* [%][a]	*s*
1	−10	DMAc	74 (*S*[b])	14.6
2	−20	DMF	77 (*S*)	17.7
3	−20	NMP	78 (*S*)	19.0
4	−20	DMPU	86 (*S*)	36.7
5	−20	DMPU	90[c] (*S*)	29.4

[a] The enantiomeric excess was determined by HPLC analysis on a column with a chiral stationary phase. [b] The absolute configuration of the acetylated enantiomer was assigned by comparison with an authentic standard. [c] Using three equivalents of amine versus (1*S*,2*S*)-**1**.

After optimization of the reaction conditions we achieved the stereoselective acetylation of various alkyl amines with good selectivities (Table 4).

Table 4: Kinetic resolution of various amines using (1*S*,2*S*)-**1** as the acylating agent.



Entry	Amine	*ee*[a] [%]
1		90[b]
2		86
3		72
4		69
5		73
6		80

[a] The enantiomeric excess was determined by HPLC analysis using a chiral phase column. [b] All reactions led to 33% yield after 24 h at −20 °C.

Increasing the steric hindrance of the alkyl group of the alkyl amine from a methyl group (entry 1) to an isopropyl group (entry 3) resulted in a decrease in the enantioselectivity from 90 to 72% *ee*. Acetylation of the more rigid (±)-1,2,3,4-tetrahydro-1-naphthylamine gave a product with 69% *ee* (entry 4). Surprisingly, increasing the bulkiness of the aromatic unit did not result in an increase in the selectivity; acetylation of (±)-1-naphthylethylamine afforded a product with 73% *ee* (entry 5). Finally, (±)-phenylalanine methyl ester proved to be a good substrate, with the corresponding acetamide derivative being obtained with 80% *ee* (entry 6).

In summary, we have demonstrated that *N*-acetyl-1,2-bis(trifluoromethanesulfonamide), (1*S*,2*S*)-**1**, can serve as an highly effective reagent for the kinetic resolution of amines to give products with an unprecedented 84% *ee* at room temperature using two equivalents of amine and up to 90% *ee* using three equivalents of amine at −20 °C. In addition, a unique solvent-induced reversal of stereoselectivity was observed, which can be rationalized on the basis of two different mechanistic pathways depending on the polarity of the solvent. Ongoing efforts are focused on both improving the reaction enantioselectivity by tuning chiral reagent (1*S*,2*S*)-**1** and increasing its scope.

 © 2004 Wiley-VCH Verlag GmbH & Co. KGaA, Weinheim

Experimental Section

1: Freshly distilled acetyl chloride (1.88 mL, 2.64 mmol) was added dropwise by syringe to a stirred solution of 1,2-bis(trifluoromethanesulfonamido)cyclohexane (Aldrich; 1.00 g, 2.64 mmol), and triethylamine (5.50 mL, 3.96 mmol) in diethyl ether (20 mL) at −20 °C. The mixture was stirred for 3 h at 0 °C, after which time the solvent was removed under reduced pressure. The resulting residue was purified by flash chromatography on silica gel (ethyl acetate/*n*-hexane 1/9) to afford the desired product as a white solid in 85 % yield. m.p. 111 °C; $[\alpha]_D^{20} = +17.46°$ ($c = 1.5$; $CHCl_3$); ^1H NMR (300 MHz, $CDCl_3$): $\delta =$ 1.10–1.60 (m, 3H), 1.70–2.00 (m, 3H), 2.05–2.35 (m, 1H), 2.35–2.60 (m, 1H), 2.52 (s, 3H), 3.60–4.05 (m, 1H), 4.10–4.60 (m, 1H), 5.04 ppm (d, $J = 10$ Hz, 1H); ^{13}C NMR (75 MHz, $CDCl_3$): $\delta = 24.4$, 25.5, 26.8, 29.1, 35.4, 54.5, 66.9, 119.4, 119.5, 170.0 ppm; FT-IR (CsI): $\tilde{\nu} = 3296$, 3221, 2947, 2868, 1737, 1716, 1456, 1385, 1233, 1200, 1131, 1071, 1016, 971, 942, 918, 896, 737, 611, 532 cm^{-1}; MS (IC/NH_3): *m*/*z* 438 $[M+NH_4]^+$.

General procedure for enantioselective acetylation of secondary alkyl amines: The racemic amine (0.36 mmol) was added dropwise by syringe to a stirred solution of chiral acetylating agent (0.12 mmol) in the chosen solvent/temperature system. The mixture was stirred at the same temperature and the reaction was followed by thin layer chromatography analysis (ethyl acetate/*n*-hexane 2/8). Once complete conversion of the reagent was observed, the solvent was removed by distillation under reduced pressure. The resulting residue was then purified by flash chromatography on silica gel (ethyl acetate/*n*-hexane 1/1) and analyzed by high-performance liquid chromatography (HPLC) on a chiral stationary phase.

Received: February 6, 2004 [Z53956]

Keywords: acylation · enantioselectivity · kinetic resolution · solvent effects

[1] U. T. Bornscheuer, R. J. Kazlauskas, *Hydrolases in Organic Synthesis. Regio- and Stereoselective Biotransformations*, Wiley-VCH, Weinheim, **1999**.
[2] a) A. C. Spivey, A. Maddaford, A. Redgrave, *Org. Prep. Proced. Int.* **2000**, *32*, 331; b) S. M. Roberts, *J. Chem. Soc. Perkin Trans. 1* **1999**, 1.
[3] G. Zanoni, F. Castronovo, M. Franzini, G. Vidari, E. Giannini, *Chem. Soc. Rev.* **2003**, *32*, 115.
[4] D. A. Evans, J. C. Anderson, M. K. Taylor, *Tetrahedron Lett.* **1993**, *34*, 5563.
[5] E. Vedejs, X. Chen, *J. Am. Chem. Soc.* **1996**, *118*, 1809.
[6] Selectivity factor $s =$ (rate of fast-reacting enantiomer)/(rate of slow-reacting enantiomer); for a review of kinetic resolution, see: H. B. Kagan, J. C. Fiaud, *Top. Stereochem.* **1998**, *18*, 249.
[7] E. Vedejs, O. Daugulis, S. T. Diver, *J. Org. Chem.* **1996**, *61*, 430.
[8] T. Oriyama, Y. Hori, K. Imai, R. Sasaki, *Tetrahedron Lett.* **1996**, *37*, 8543.
[9] T. Kawabata, M. Nagato, K. Takasu, K. Fuji, *J. Am. Chem. Soc.* **1997**, *119*, 3169.
[10] a) S. J. Miller, G. T. Copeland, N. Papaioannou, T. E. Horstmann, E. M. Ruel, *J. Am. Chem. Soc.* **1998**, *120*, 1629; b) E. R. Jarvo, G. T. Copeland, N. Papaioannou, P. J. Bonitatebus, S. J. Miller, *J. Am. Chem. Soc.* **1999**, *121*, 11638.
[11] a) J. C. Ruble, G. C. Fu, *J. Org. Chem.* **1996**, *61*, 7230; b) J. C. Ruble, H. A. Latham, G. C. Fu, *J. Am. Chem. Soc.* **1997**, *119*, 1492; c) B. Tao, J. C. Ruble, D. A. Hoic, G. C. Fu, *J. Am. Chem. Soc.* **1999**, *121*, 5091; d) S. Bellemin-Laponnaz, J. Tweddell, J. C. Ruble, F. M. Breitling, G. C. Fu, *Chem. Commun.* **2000**, 1009; e) J. C. Ruble, J. Tweddell, G. C. Fu, *J. Org. Chem.* **1998**, *63*, 2794; f) G. C. Fu, *Acc. Chem. Res.* **2000**, *33*, 412.
[12] a) A. C. Spivey, T. Fekner, S. E. Spey, *J. Org. Chem.* **2000**, *65*, 3154; b) A. C. Spivey, A. Maddaford, T. Fekner, A. J. Redgrave, C. S. Frampton, *J. Chem. Soc. Perkin Trans. 1* **2000**, 3460; c) A. C. Spivey, F. Zhu, M. B. Mitchell, S. G. Davey, R. L. Jarvest, *J. Org. Chem.* **2003**, *68*, 7379.
[13] Besides displaying various biological activities, enantiopure amines are widely used as reagents in asymmetric synthesis, for example, see: E. Juaristi, J. L. Leon-Romo, A. Reyes, J. Escalante, *Tetrahedron: Asymmetry* **1999**, *10*, 2441.
[14] K. Kondo, T. Kurosaki, Y. Murakami, *Synlett* **1998**, 725.
[15] The kinetic resolution of (±)-1-naphthylethylamine was obtained with up to 48 % *ee* using 0.25 equivalents of chiral reagent at room temperature. This *ee* value corresponds to a selectivity factor (*s*) of 3 at 25 % conversion.
[16] A. G. Al-Sehemi, R. S. Atkinson, J. Fawcett, D. R. Russell, *Tetrahedron Lett.* **2000**, *41*, 2239.
[17] Y. Ie, G. C. Fu, *Chem. Commun.* **2000**, 119.
[18] Under these reaction conditions, Fu and co-workers achieved the kinetic resolution of (±)-1 phenylethylamine with 87 % *ee*.
[19] S. Arai, S. Bellemin-Laponnaz, G. C. Fu, *Angew. Chem.* **2001**, *113*, 667; *Angew. Chem. Int. Ed.* **2001**, *40*, 234.
[20] This *ee* value corresponds to a selectivity factor (*s*) of 13 at 35 % conversion.
[21] For a review on chiral 1,2-diamines, see: D. Lucet, T. Le Gall, C. Mioskowski, *Angew. Chem.* **1998**, *110*, 2724; *Angew. Chem. Int. Ed.* **1998**, *37*, 2580.
[22] For a review on solvents and solvent effects, see: C. Reichardt, *Solvents and Solvent Effects in Organic Chemistry*, 3rd ed., Wiley–VCH, Weinheim, Germany, **2002**.

 © 2004 Wiley-VCH Verlag GmbH & Co. KGaA, Weinheim

Asymmetric Amplification

Amplification of Enantiomeric Excess in a Proline-Mediated Reaction**

*Suju P. Mathew, Hiroshi Iwamura, and Donna G. Blackmond**

The origin of homochirality has intrigued scientists ever since the biological importance of L-amino acids and D-sugars was first recognized. Although a theoretical basis for the evolution

[*] Dr. S. P. Mathew, Prof. D. G. Blackmond
Department of Chemistry, Imperial College
London SW7 2AZ (United Kingdom)
Fax: (+44) 207-594-8504
E-mail: d.blackmond@imperial.ac.uk

H. Iwamura
Mitsubishi Pharma Corporation
14 Sunayama, Hasaki-machi, Ibaraki 314-0255 (Japan)

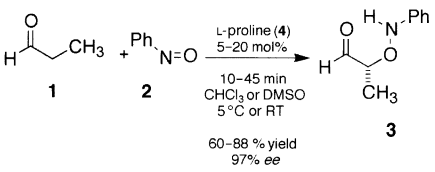
[**] We are grateful to the Department of Chemistry, University of Hull, where parts of the experimental work was carried out. Stimulating discussions with Dr. B. G. Cox and Dr. D. L. Lathbury (AstraZeneca) and Prof. Peter Beak (Illinois), technical assistance with NMR experiments from Mrs. B. Worthington (Hull), and funding from EPSRC/DTI/LINK and Mitsubishi Pharma are gratefully acknowledged.

Supporting information for this article is available on the WWW under http://www.angewandte.org or from the author.

 DOI: 10.1002/anie.200453997 © 2004 Wiley-VCH Verlag GmbH & Co. KGaA, Weinheim

of high optical activity from a minute initial imbalance of enantiomers was suggested more than half a century ago,[1] experimental proof of such a concept eluded scientists until a remarkable report by Soai and co-workers in 1995.[2] The Soai reaction offered the first, and to date the only, example of an asymmetric autocatalytic reaction employing a catalyst with a very *low* enantiomeric excess and ultimately yielding the catalyst with a very *high* enantiomeric excess catalyst as product. While the Soai reaction serves as a mechanistic model[3] for the evolution of homochirality, the dialkylzinc chemistry involved in the reaction is unlikely to have been of importance in an aqueous prebiotic environment. Therefore speculation has continued concerning the types of transformations that might have been directly responsible for the development of high optical activity in biological systems. The area of amino acid catalysis may hold significant clues to the evolution of prebiotic chemistry. That prebiotic building blocks such as sugars can be formed asymmetrically from such reactions has recently led to speculation about the evolution of biological homochirality through such routes.[4] We report herein a proline-mediated reaction exhibiting an accelerating reaction rate and an amplified, temporally increasing enantiomeric excess of the product. Thus, catalysis with amino acids is implicated in an autoinductive, selectivity-enhancing process, providing the first general chemical strategy for the evolution of biological homochirality from a purely organic origin.

The growing field of asymmetric aminocatalysis[5] makes use of biomimetic strategies via enamine and iminium intermediate species common to class I aldolase and ketoacid decarboxylase enzymes. The proline-catalyzed intramolecular Hajos–Parrish–Eder–Sauer–Wiechert reaction was the first example employing a similar strategy in organic synthesis.[6,7] More recently, this approach has been successfully expanded by several groups, beginning with the first report by List, Barbas, and Lerner[8] which demonstrated the proline-catalyzed direct asymmetric intermolecular aldol reaction. A recent addition to this rapidly growing list of aminocatalytic transformations was offered by two independent and nearly simultaneous reports of the proline-catalyzed α-aminoxylation of aldehydes shown in Equation (1).[9,10] Both studies



(1)

noted good yields and high *ee* values with 5–20 mol % catalyst in reaction times measured on the order of tens of minutes. This finding was all the more notable given the dramatically lower activity of other proline-catalyzed reactions; for example, completion of the aldol reaction between acetone and isobutyraldehyde required 48 h at 30 mol % catalyst.[10] Most, recently the scope of this reaction was widened to include ketone substrates, which also exhibited rapid reaction times.[11]

Intrigued by these reports, which imply a fundamental mechanistic difference between the reaction shown in Equation (1) and other proline-catalyzed transformations, we undertook continuous monitoring of reaction progress by reaction calorimetry, a kinetic approach that we have developed over the past several years as a mechanistic probe of multistep reactions.[12,13] We observed, quite unexpectedly, that the rate of the reaction in Equation (1) *rose* steadily throughout the course of the reaction (Figure 1). A

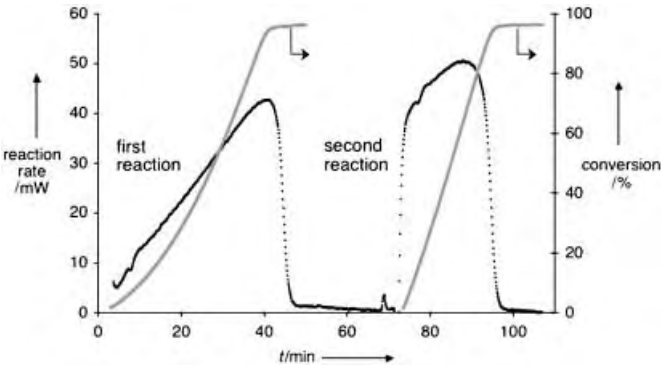


Figure 1. Reaction rate (filled black circles, corresponding to the left axis) and percent conversion (shaded grey line, corresponding to the right axis) versus time for a one-pot, two-consecutive-reaction sequence of the reaction shown in Equation (1) ($CHCl_3$ solvent, 278 K). Initial concentrations of aldehyde **1** and L-proline **4** were 2.07 and 0.07 M, respectively. First reaction: 0.26 M PhNO; second reaction: 0.24 M PhNO.

plot of conversion versus time accordingly showed the hyperbolic shape indicative of an accelerating reaction rate. This behavior suggests a process whereby the catalyst is improving over time, as in autocatalytic or autoinductive reactions, in which the reaction product either is itself a catalyst or promotes the formation of a more effective catalyst. Addition of the reaction product to fresh reagents gave no discernible heat flow signal, indicating that the effect is not due simply to an autocatalytic reaction. However, as shown in Figure 1, when a second dose of reagents was added to the crude reaction mixture containing the original proline catalyst and the product of the first reaction, the initial rate at the outset of this second reaction was as high as that at the end of the first. These experiments indicate that the rising rate is not due to substrate inhibition and suggest that the reaction is mediated by a proline-product adduct that forms over the course of the reaction and serves as an improved catalyst for the reaction. Enantioselective autoinductive reactions have been reported previously,[14,15] including the report by Danda et al.[14] of an organocatalytic hydrocyanation of a substituted benzaldehyde.

Amplification of the enantiomeric excess of the product is a key feature of a chemical rationalization of the evolution of biological homochirality. Considerable discussion has ensued over the past several years about whether proline-catalyzed reactions exhibit such nonlinear effects, since the Hajos–Parrish reaction was cited in the context of Kagan's mathematical models for nonlinear effects.[16] The more recent

 © 2004 Wiley-VCH Verlag GmbH & Co. KGaA, Weinheim

observation by List and co-workers of a strictly linear relationship between the catalyst and the *ee* value of the product in both inter- and intramolecular aldol transformations,[17] however, has generally been taken to infer that amino acid catalysis is unlikely to be involved in processes resulting in amplification of enantiomeric excess.[18] We were intrigued to find, therefore, that when the reaction shown in Equation (1) was carried out with non-enantiopure proline, the enantiomeric excess of the product was *higher* than that expected for a linear relationship (Figure 2) and that enantiomeric excess *rose* over the course of the reaction (Figure 3).[19] Rate acceleration and continuous improvement of enantiomeric excess are requisite characteristics for chemical models of the evolution of homochirality from precursors of low optical activity.

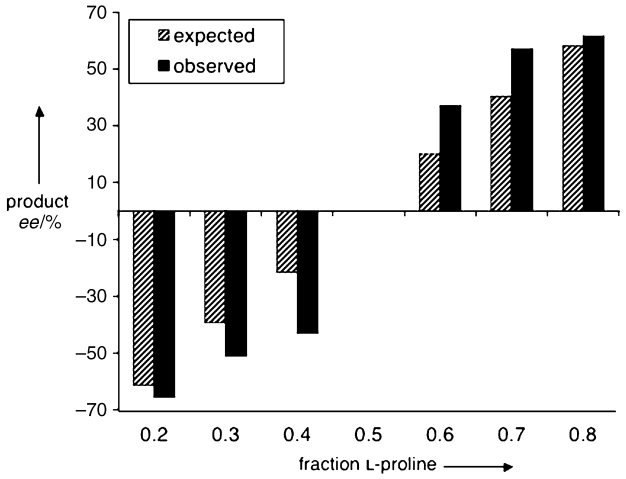


Figure 2. Final enantiomeric excess of the product as a function of the fraction of L-proline in the reaction shown in Equation (1) carried out using mixtures of D- and L-proline. Initial concentrations of aldehyde **1**, nitrosobenzene **2**, and total (L + D)-proline **4** were 2.07, 0.7, and 0.07 M, respectively ($CHCl_3$ solvent, 278 K). Conversions were greater than 90%.

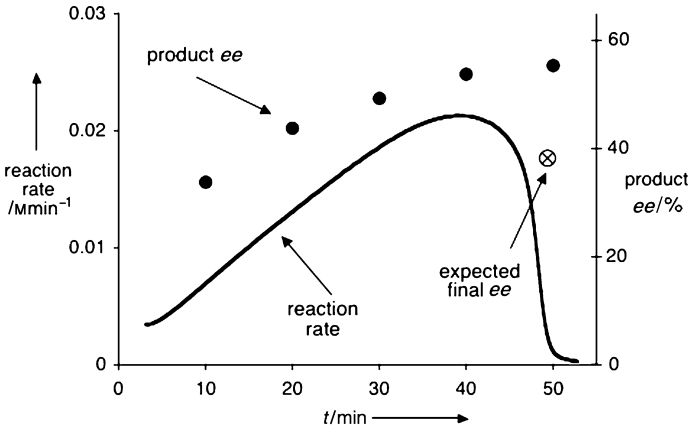
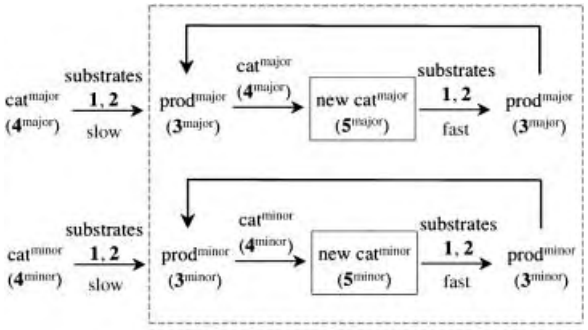


Figure 3. Reaction rate and enantiomeric excess of the product of the reaction of Scheme 1 carried out with a mixture of L- and D-proline with 40% *ee* (L). Reaction conditions: 278 K, total proline concentration (L + D): 0.071 M, nitrosobenzene: 0.70 M, propionaldehyde: 1.95 M.

Kagan and co-workers provided the first explanations of the phenomenon of nonlinear product enantioselectivity,[16] and variations on these models have been proposed for both catalytic[20,21] and autocatalytic reactions.[3] Scheme 1 outlines



Scheme 1. General mechanism for the product-induced kinetic amplification of enantiomeric excess.

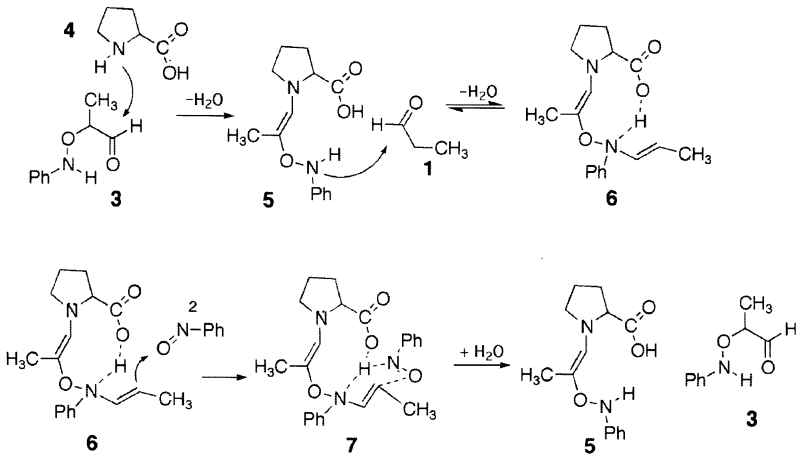
a general mechanism for a product-induced reaction in which both rate and selectivity improve over time for the case in which one enantiomer of the original catalyst **4** is present in excess concentration relative to the other (noted as the "major" and "minor" species, respectively). The first molecules of reaction product **3** are formed through the less-reactive pathways shown outside the dashed lines, after which the reaction is dominated by the manifold shown inside the dashed lines. Within this manifold, product **3** associates reversibly with the original catalyst **4** to form the new catalytic species **5**, which exhibits higher catalytic activity than **4**. As the concentration of **3** increases with increasing turnover, a larger fraction of both hands of the original catalyst **4** is driven toward further formation of **5**, resulting in increased reaction rate. If the mismatched catalyst-product "cross-reaction" rates ($\mathbf{3}^{maj}$–$\mathbf{4}^{min}$ and $\mathbf{4}^{maj}$–$\mathbf{3}^{min}$) are suppressed relative to those of the matched reaction, the enantiomeric excess of the improved catalyst **5** will be higher than that of **4** and will increase over time. Accordingly, the enantiomeric excess of the product **3** will increase over time and will be amplified relative to that of the original catalyst **4**.

The process described in Scheme 1 is kinetic. The enantiomeric excess of the product **3** will rise until the formation of new catalyst **5** has reached equilibrium, after which the *ee* value will slowly erode back to the linear relationship. In agreement with this, we found that reactions carried out with lower concentrations of proline, which take longer to reach completion, exhibited milder ultimate asymmetric amplification. However, it is important to note that such erosion of enantiomeric excess is predicted only for a *closed* system such as that occurring in reaction vials in the laboratory. In an *open* system, in which catalyst and product fluxes can exist across the system boundaries,[22] the chemical propagation mechanism described in Scheme 1 would permit enantiomeric excess to continue to rise. Kinetic amplification of enantiomeric excess as observed in the present studies could be sustained, requiring only that

 © 2004 Wiley-VCH Verlag GmbH & Co. KGaA, Weinheim

the process of equilibration between the original catalyst **4** and the product **3** to form the improved catalyst **5** is slower than the **5**-catalyzed formation of product **3** from substrates.

We may now relate the model shown in Scheme 1 to the chemistry of the reaction in Equation (1) to suggest a structure for the improved catalyst **5** and to rationalize its higher activity. The key to the effectiveness of this system lies in the fact that the reaction product **3** is multifunctional; it is both an aldehyde and an amine. Scheme 2 suggests that



Scheme 2. Proposed mechanism for product induction in the reaction shown in [Eq. (1)].

proline **4** may attack the carbonyl group of the reaction product **3** to form the new catalyst **5**. This reaction is virtually irreversible on the reaction timescale, since product racemization was not observed. This species **5** is a special amine bearing an α-oxygen atom with lone pairs of electrons. The "alpha effect"[23] describes the unexpectedly high activity of such a nitrogen nucleophile, thought to be due in part to stabilization of the transition state by the lone pair on the oxygen α to the nucleophilic atom. Thus **5** may be a highly efficient competitor to proline for nucleophilic attack on propionaldehyde, forming a new enamine, **6**. This enamine may be competent to attack PhNO, forming a transition state such as **7** by interaction with the carboxylic acid proton as a Brønsted acid cocatalyst. This leads to the formation of product **3** and regeneration of the improved catalyst **5**.

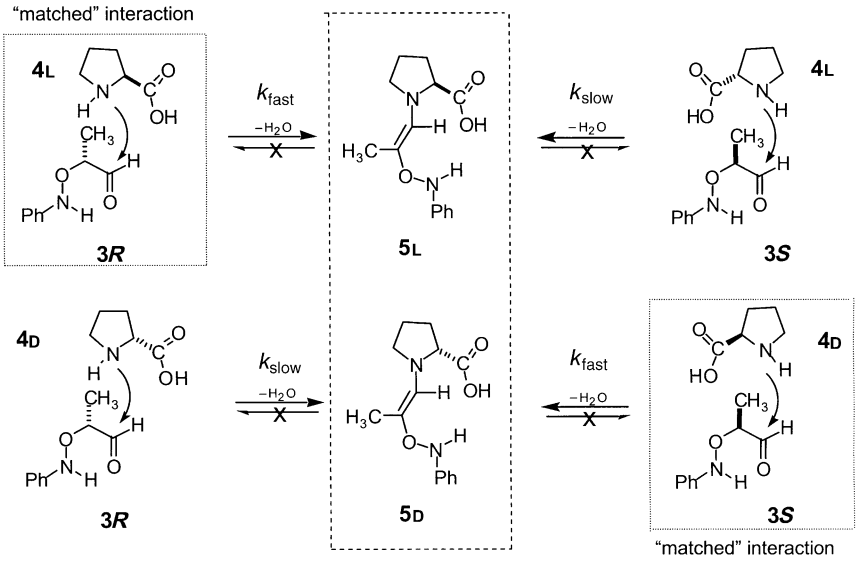
The observed asymmetric amplification is rationalized as a kinetic resolution of the proline in the reaction with product **3** to form **5**, as shown in Scheme 3. The "matched" reactions **4**L–**3*R*** and **4**D–**3*S*** dominate the enantiopure cases. If we assume that the *E* enamine is the stable product from either the "matched" or "mismatched" interaction, we can see that this competitive process alters the enantiomeric excess of species **5** relative to that of the original proline **4**. This case is more complex than in a simple first-order kinetic resolution because the selectivity factor k_{rel} will be a function of the temporally changing product concentration, as shown in Equation (2):

$$\frac{d[\mathbf{4_L}]}{d[\mathbf{4_D}]} = k_{rel}\frac{[\mathbf{4_L}]}{[\mathbf{4_D}]} \quad k_{rel} = \frac{k_{fast}[\mathbf{3}\boldsymbol{R}] + k_{slow}[\mathbf{3}\boldsymbol{S}]}{k_{fast}[\mathbf{3}\boldsymbol{S}] + k_{slow}[\mathbf{3}\boldsymbol{R}]} \tag{2}$$

We observed that extended room temperature preequilibration of proline with excess propionaldehyde in $CHCl_3$ produces a clear solution, as compared to the cloudy suspension normally observed after mixing for shorter times or at lower temperatures. The reaction exhibits considerably lower activity following this preequilibration, resulting in less than 10% conversion into **3** after 1 h[13] and giving linear behavior in product enantioselectivity. This suggests that new catalyst **5** cannot form as readily when the concentration of free proline is low, and under such conditions the initial reaction is directed toward the slower proline-catalyzed pathway.

The product **3** may also be capable of condensing with itself, and, in fact, it has been suggested that the products of this reaction exist in oligomeric form.[10] Preliminary ^{1}H NMR studies of the crude reaction product mixture reveal complex spectra.[13] In the case of reactions carried out with non-enantiopure **4**, the formation of higher-order species could further skew the enantiomeric excess of the improved catalyst species **5** relative to **4**, resulting in either enhancement or suppression of the nonlinear effect, depending on the relative rates at which different species react in such condensation reactions.

The nucleophilic nitrogen atom of product **3** might also attack propionaldehyde directly. Since the reaction was found not to be autocatalytic, the enamine thus formed cannot be



Scheme 3. Proposed kinetic resolution in the formation of **5** through the interaction of proline **4** with the reaction product **3**.

 © 2004 Wiley-VCH Verlag GmbH & Co. KGaA, Weinheim

competent to react with **2** to form a further molecule of product **3**; the lack of a Brønsted acid function as an intramolecular cocatalyst may compromise its effectiveness.[24] This argument leads naturally to speculation about the potential for truly autocatalytic systems based on similar chemistry. For example, reactions of aldehydic or keto acids with a nitrogen-containing electrophile might yield an amine nucleophile capable of reproducing itself. Investigations along these lines are ongoing in our laboratories.

The experimental observation of an unexpectedly high, accelerating reaction rate and an amplified, temporally increasing enantiomeric excess of product in the proline-mediated aminoxylation of aldehydes is consistent with a mechanistic model for a selectivity-enhancing autoinductive process as given in Schemes 1–3. This represents the first example of a purely organic reaction exhibiting characteristics that are key to a chemical rationalization of the evolution of biological homochirality. A full kinetic model of these experimental results will be published separately.

Received: February 11, 2004 [Z53997]

Keywords: asymmetric amplification · asymmetric catalysis · autocatalysis · chirality · kinetics

[1] a) F. C. Frank, *Biochim. Biophys. Acta* **1953**, *11*, 459; b) M. Calvin, *Chemical Evolution*, Oxford University Press, Oxford, **1969**.
[2] For the first publications, see: a) K. Soai, T. Shibata, H. Morioka, K. Choji, *Nature* **1995**, *378*, 767; b) T. Shibata, K. Choji, T. Hayase, Y. Aizu, K. Soai, *Chem. Commun.* **1996**, 1235; c) T. Shibata, H. Morioka, T. Hayase, K. Choji, K. Soai, *J. Am. Chem. Soc.* **1996**, *118*, 471; for a recent review, see: K. Soai, I. Sato, *Chirality* **2002**, *14*, 548.
[3] a) D. G. Blackmond, C. R. McMillan, S. Ramdeehul, A. Schorm, J. M. Brown, *J. Am. Chem. Soc.* **2001**, *123*, 10103; b) D. G. Blackmond, *Adv. Synth. Catal.* **2002**, *344*, 156; c) F. G. Buono, D. G. Blackmond, *J. Am. Chem. Soc.* **2003**, *125*, 8978; d) F. G. Buono, H. Iwamura, D. G. Blackmond, *Angew. Chem.* **2004**, *116*, 2151; *Angew. Chem. Int. Ed.* **2004**, *43*, 2099; e) I. D. Gridnev, J. M. Serafimov, H. Quiney, J. M. Brown, *Org. Biomol. Chem.* **2003**, *1*, 3811.
[4] S. Pizzarello, A. L. Weber, *Science* **2004**, *303*, 1151.
[5] a) B. List, *Synlett* **2001**, *1675*; b) B. List, *Tetrahedron* **2002**, *58*, 5573; c) E. R. Jarvo, S. J. Miller, *Tetrahedron* **2002**, *58*, 2481; d) S. France, D. J. Geurin, S. J. Miller, T. Lectka, *Chem. Rev.* **2003**, *103*, 2985.
[6] U. Eder, G. Sauer, R. Wiechert, *Angew. Chem.* **1971**, *83*, 492; *Angew. Chem. Int. Ed. Engl.* **1971**, *10*, 496.
[7] Z. G. Hajos, D. R. Parrish, *J. Org. Chem.* **1974**, *39*, 1615.
[8] B. List, R. A. Lerner, C. F. Barbas, *J. Am. Chem. Soc.* **2000**, *122*, 2395.
[9] G. Zhong, *Angew. Chem.* **2003**, *115*, 4379; *Angew. Chem. Int. Ed.* **2003**, *42*, 4247.
[10] S. Brown, M. Brochu, C. J. Sinz, D. W. C. MacMillan, *J. Am. Chem. Soc.* **2003**, *125*, 10808.
[11] a) A. Bøgevig, H. Sundén, A. Córdova, *Angew. Chem.* **2004**, *116*, 1129; *Angew. Chem. Int. Ed.* **2004**, *43*, 1109; b) Y. Hayashi, J. Yamaguchi, T. Sumiya, M. Shoji, *Angew. Chem. Int. Ed.* **2004**, *116*, 1602; *Angew. Chem. Int. Ed.* **2004**, *43*, 1112.
[12] a) T. Rosner, A. Pfaltz, D. G. Blackmond, *J. Am. Chem. Soc.* **2001**, *123*, 4621; a) U. K. Singh, E. R. Strieter, D. G. Blackmond, S. L. Buchwald, *J. Am. Chem. Soc.* **2002**, *124*, 14104; c) E. R. Strieter, D. G. Blackmond, S. L. Buchwald, *J. Am. Chem. Soc.* **2003**, *125*, 13978; d) L. P. C. N. Nielsen, C. P. Stevenson, D. G. Blackmond, E. N. Jacobsen, *J. Am. Chem. Soc.* **2004**, *126*, 1360.
[13] See Supporting Information for further details.
[14] H. Danda, H. Nishikawa, K. Otaka, *J. Org. Chem.* **1991**, *56*, 6740.
[15] A. H. Alberts, H. Wynberg, *J. Am. Chem. Soc.* **1989**, *111*, 7265.
[16] C. Puchot, O. Samuel, E. Duñach, S. Zhao, C. Agami, H. B. Kagan, *J. Am. Chem. Soc.* **1986**, *108*, 2353.
[17] L. Hoang, S. Bahmanyar, K. N. Houk, B. List, *J. Am. Chem. Soc.* **2003**, *125*, 16.
[18] For example, no asymmetric amplification in product enantioselectivity was observed in the recent study cited in reference [4], which implicated amino acids as prebiotic catalysts.
[19] Asymmetric amplification distinguishes this reaction from the organocatalytic example of autoinduction reported by Danda et al.[14] in which a linear relationship with enantiomeric excess was observed in cases in which the product was not added to the reaction mixture.
[20] M. Kitamura, S. Suga, H. Oka, R. Noyori, *J. Am. Chem. Soc.* **1998**, *120*, 9800.
[21] D. G. Blackmond, *Acc. Chem. Res.* **2000**, *33*, 402.
[22] C. J. Welch, *Chirality* **2001** *14*, 425.
[23] J. O. Edwards, R. G. Pearson, *J. Am. Chem. Soc.* **1962**, *84*, 16.
[24] S. Bahmanyar, K. N. Houk, *J. Am. Chem. Soc.* **2001**, *123*, 11273.

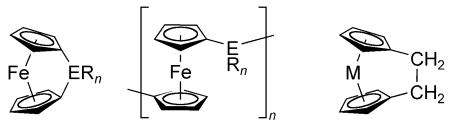
 © 2004 Wiley-VCH Verlag GmbH & Co. KGaA, Weinheim

Bimetallic Polymers

Isolation of [1]Ruthenocenophanes: Synthesis of Polyruthenocenylstannanes by Ring-Opening Polymerization**

*Ulf Vogel, Alan J. Lough, and Ian Manners**

Strained [1]ferrocenophanes **1**[1] have attracted considerable attention over the past decade because of their interesting structures and reactivity and their ability[2] to function as precursors of high-molecular-weight polyferrocenes through ring-opening polymerization (ROP). Studies of the unusual properties of the resulting metallopolymers **2**[3] as well as



1 **2** **3**

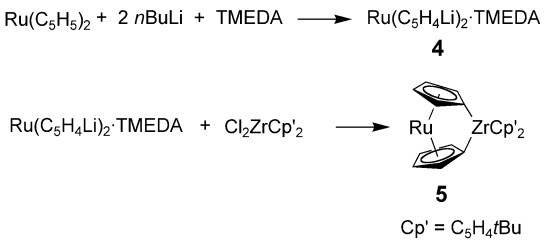
[*] Dr. U. Vogel, Dr. A. J. Lough, Prof. Dr. I. Manners
Dept. of Chemistry, University of Toronto
80 St. George Street, Toronto, M5S 3H6, Ontario (Canada)
Fax: (+1) 416-978-6157
E-mail: imanners@chem.utoronto.ca

[**] We thank the NSERC and the DAAD exchange program for financial support of this work. U.V. is grateful for a research fellowship granted by the Deutsche Forschungsgemeinschaft. We also thank K. T. Kim and S. Fournier for thermal analysis measurements.

 DOI: 10.1002/anie.200454022 © 2004 Wiley-VCH Verlag GmbH & Co. KGaA, Weinheim

fundamental interest in strained organometallic rings,[4] have inspired the synthesis and study of a range of new [1]ferrocenophanes **1** with either main-group[5] or d- or f-block elements[6] in the bridge. A feature of these strained molecules is the presence of a tilting of the cyclopentadienyl rings which can result in a dihedral angle of up to 32°. The expansion of this chemistry to allow the incorporation of other metals into analogous strained organometallic monomers is of considerable interest but has been much slower to develop. Rare examples of strained and potentially polymerizable species studied to date include silicon-bridged bis(benzene)chromium complexes,[7] [2]cobaltocenophanes,[8] and [2]ruthenocenophanes **3** (M = Ru) with a CH_2CH_2 bridge.[9] In the latter case, the species were shown to exhibit a significantly higher ring tilt and degree of strain than their iron analogues, as a result of the larger size of the ruthenium atom which forces the Cp rings further apart.[9,10] Herein we report the first examples of [1]ruthenocenophanes together with preliminary studies of their ROP behavior.

Attempts to synthesize silicon-bridged [1]ruthenocenophanes by reaction of the *N*,*N*,*N*′,*N*′-tetramethylethylenediamine (TMEDA) adduct of dilithiated ruthenocene $Ru(C_5H_4Li)_2$·TMEDA (**4**) with Cl_2SiMe_2 have been reported to result in the formation of dimeric and oligomeric species.[11,12] Introduction of larger elements such as zirconium or tin as the bridging atoms might be expected to lead to less-strained and therefore more-stable [1]ruthenocenophanes. We attempted to prepare the zirconium-bridged [1]ruthenocenophane by the reaction of **4** with $[Cl_2ZrCp'_2]$ (Cp′ = C_5H_4tBu) in Et_2O at low temperature. Recrystallization of the crude reaction product from hexanes at −55 °C afforded **5** as a pale yellow powder in 35 % yield (Scheme 1).



Scheme 1. Synthesis of **4** and **5**.

The identity of **5** was confirmed by ^{1}H NMR and ^{13}C NMR spectroscopy, and by mass spectrometry. The ^{1}H NMR spectrum indicates a ring-strained structure with a set of two pseudotriplets at $\delta = 4.52$ and 4.86 ppm, which we assigned to the α and β H atoms of the Cp ring bound to ruthenium. The ^{13}C NMR spectrum shows an unusual downfield shift for the signal of the *ipso*-C atom of the ruthenocene Cp ring at $\delta = 162.5$ ppm. The same is observed for the analogous iron compound **1** ($ER_n = ZrCp'_2$),[6a] in which the corresponding shift is $\delta = 159.0$ ppm. For strained [1]ferrocenophanes the signals for the *ipso*-Cp carbon atoms are usually shifted upfield relative to those for unstrained compounds.

To probe the structure of **5**, an X-ray crystal structure determination of a single crystal grown from hexanes at −30 °C was conducted (Figure 1).[13] As expected from the

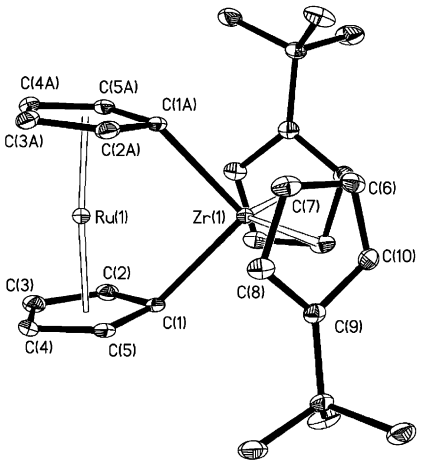


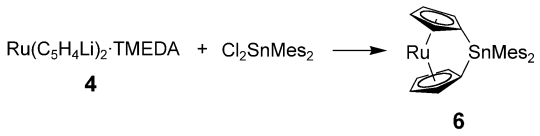
Figure 1. Structure of **5** in the solid state, hydrogen atoms are omitted for clarity. Selected bond lengths [pm] and angles [°]: Ru(1)···Zr(1) 295.04(4), Ru(1)-C(1) 214.6(2), Ru(1)-C(2) 216.9(3), Ru(1)-C(3) 221.3(3), Ru(1)-C(4) 221.0(4), Ru(1)-C(5) 215.5(2), Zr(1)-C(1) 214.6(2), Zr(1)-C(6) 249.5(2), Zr(1)-C(7) 252.9(2), Zr(1)-C(8) 258.5(2), Zr(1)-C(9) 262.5(2), Zr(1)-C(10) 254.0(2); C(1)-Zr(1)-C(1A) 92.3(1).

larger size of the ruthenium atom in comparison to the iron atom, **5** shows more strain than the corresponding iron compound **1** ($ER_n = ZrCp'_2$). The tilt angle α for **5** is 10.4°, which is significantly greater than for the analogous iron compound (6°),[6a] but the increase in tilt is not as high as expected when compared with **3**[10]. Another feature indicating the strain in **5** is the $Cp_{centroid}$-Ru-$Cp_{centroid}$ angle θ which is 175° as opposed to 177.3° in **1** ($ER_n = ZrCp'_2$). The angle β between the planes of the Cp rings and the Zr–C(1) bond is 41°, which is slightly larger than in **1** ($ER_n = ZrCp'_2$, 40.1°).[6a] The constrained geometry in **5** forces the Ru atom and the Zr atom into close contact. The Ru–Zr distance is 295.04(4) pm, close to distances found for Ru–Zr single bonds ($[Cp_2Zr\{Ru(CO)_2Cp\}_2]$: Zr–Ru = 293.8(1), 294.9(1) pm;[14] $[Cp_2Zr\{Ru(CO)_2Cp\}Ot$Bu]: Zr–Ru = 291.0(1) pm).[15] The electronic nature of this interaction is currently under theoretical investigation.

To determine if **5** can be polymerized thermally, a DSC (differential scanning calorimetry) experiment was carried out. It showed a melt endotherm at 188 °C; a ROP exotherm could not be detected. On heating the monomer to 200 °C in a sealed tube for 4 days, only unconverted starting material was recovered. Compound **5** is also unreactive towards anionic initiators such as MeLi.

Tin-bridged [1]ferrocenophanes can be isolated with bulky substituents and are sufficiently strained to undergo ROP.[5b] To synthesize a tin-bridged [1]ruthenocenophane, **4** was treated with Cl_2SnMes_2 at low temperature in Et_2O. A ^{1}H NMR spectrum of the crude reaction mixture showed broad peaks owing to the formation of presumably oligomeric material. However, signals attributable to the tin-bridged [1]ruthenocenophane **6** could also be detected in the mixture. When the reaction was carried out in THF instead of Et_2O, **6** was formed as the main product. Extraction of the crude reaction mixture with hexanes and repeated recrystallizations from Et_2O led to the isolation of **6** in 13 % yield (Scheme 2).[16]

 © 2004 Wiley-VCH Verlag GmbH & Co. KGaA, Weinheim



Scheme 2. Synthesis of **6** (Mes = 2,4,6-trimethylphenyl).

The identity of **6** was confirmed by NMR and UV/Vis spectroscopy and mass spectrometry. Signals attributable to the α and β H atoms of the Cp ring are detected in the ^{1}H NMR spectrum at $\delta = 5.03$ and 4.30 ppm, respectively. At $\delta = 0.73$ ppm the separation of these signals ($\Delta\delta_{Cp}$) is larger than in the analogous iron compound **1** ($ER_n = SnMes_2$), for which $\Delta\delta_{Cp}$ is 0.13 ppm.[5b] This increasing separation has been attributed to an increased tilt angle α in several other cases, but in this study we could not confirm this trend. On the contrary, we found that in some cases $\Delta\delta_{Cp}$ decreases with increasing α: The [2]ruthenocenophane **3** (M = Ru, $\alpha = 29.6(5)°$) shows a separation of 0.38 ppm for the hydrogen atoms of the Cp ring,[12] whereas for the analogous [2]ferrocenophane **3** (M = Fe, $\alpha = 21.6(5)°$)[17] this value increases to $\delta = 0.88$ ppm.[12] The same can be observed for **5** (**5**: $\Delta\delta_{Cp} = 0.34$ ppm; **1** ($ER_n = ZrCp'_2$): $\Delta\delta_{Cp} = 0.37$ ppm). The shift of the ^{13}C NMR signal for the Cp *ipso*-carbon atom of **6** ($\delta = 31.8$ ppm) seems to follow the usual trend: The signal is shifted upfield relative to that for the corresponding iron complex **1** ($ER_n = SnMes_2$, $\delta = 38.2$ ppm).

Also indicating the strain in **6** is the UV/Vis spectrum in CH_2Cl_2 (Figure 2) which shows a band at 363 nm ($\varepsilon_{max} =$ 436 L mol^{-1} cm^{-1}). For comparison, ruthenocene shows an absorption band at 322 nm, which can be resolved into two bands when measured at 77 K (339 nm, $\varepsilon_{max} = 120$ L mol^{-1} cm^{-1} and 308 nm, $\varepsilon_{max} = 160$ L mol^{-1} cm^{-1}). These bands have been assigned to the $^1A_{1g} \rightarrow {}^1E_{1g}$ and $^1A_{1g} \rightarrow {}^1E_{2g}$ transitions, respectively.[18] For strained ferrocenophanes it has been shown that the longer wavelength band is red-shifted and the absorption coefficient of this band increases with the amount of ring tilt.[5,19] Compound **5** only shows a weak shoulder in the same wavelength region. This behavior is also observed for [1]ruthenocenophanes.

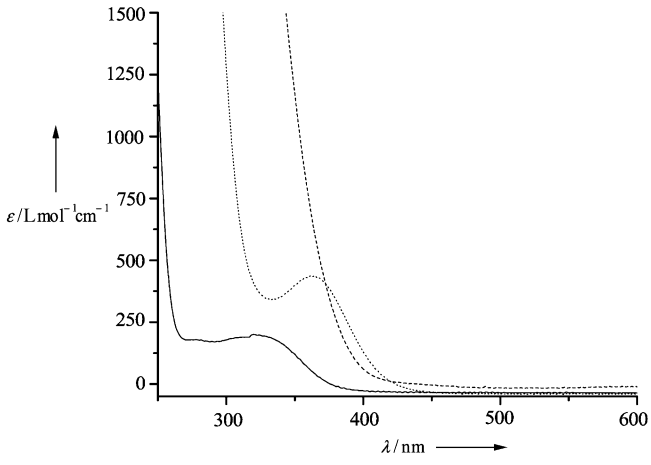


Figure 2. UV/Vis spectra of ruthenocene (——), **5** (••••), and **6** (- - - -) in CH_2Cl_2.

To determine the solid-state structure of **6** an X-ray diffraction study was carried out on single crystals grown from nBu$_2$O (Figure 3).[13] Complex **6** is isostructural with **1** ($ER_n =$ $SnMes_2$) and crystallizes in the space group $P2_1/c$ with three independent molecules (designated **6^{I}**, **6^{II}**, **6^{III}**) in the asymmetric unit. The three molecules mainly differ in the rotation of the mesityl groups around the Sn–C bond. The tilt angles α are 20.9(3), 20.2(3), and 20.8(4)°, which are significantly higher than in **1** ($ER_n = SnMes_2$, $\alpha = 15.3(2)$, 14.5(2), and 15.7(3)°).[5b] The β angles (**6^{I}** 34.7, 35.5; **6^{II}** 35.7, 35.6; **6^{III}** 35.6, 35.3°) are comparable to **1** ($ER_n = SnMes_2$, $\alpha = 35.3(2)$). As expected, the angle θ between the Cp-ring centroids and the central Ru atom in **6** ($\theta = 164.3$, 164.9, and 164.5°) is smaller than in the analogous iron compound **1** ($ER_n = SnMes_2$, $\theta =$ 167.5(2), 168.0(2), and 167.3(2)°) and therefore also indicates the higher strain in **6**. The average Sn–C bond lengths (Sn–C_{Mes}: 216.9(7) pm; Sn–C_{Cp}: 219.3(7) pm) are consistent with values typically found for such bonds. As in the case of **5**, the Ru and the bridging Sn atom are forced into close contact with the distance Ru–Sn being 299.63(7), 299.36(7), and 299.26(8) pm. These distances are longer than the values normally found for Ru–Sn single bonds,[20] but shorter than the long distances in $[Ru_6C(CO)_{16}SnCl_3]_2^-$ in which a five-coordinate tin atom asymmetrically bridges two ruthenium atoms (Ru–Sn = 314.0(2), 258.1(3), 310.2(2), and 258.3(3) pm).[21] Based on these findings an interaction between the two elements cannot be ruled out.

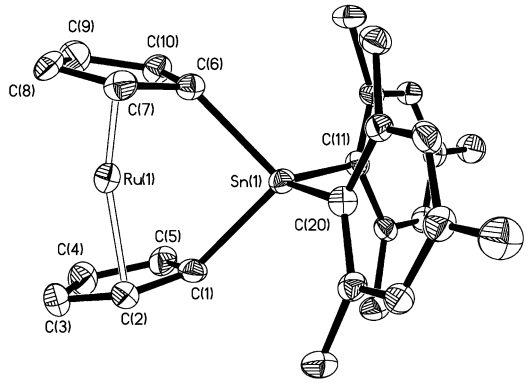
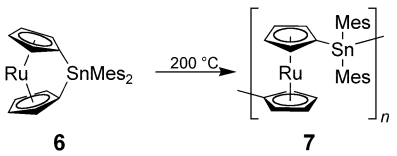


Figure 3. Structure of **6** in the solid state. Only one of the three independent molecules in the unit cell is depicted, hydrogen atoms are omitted for clarity. Selected bond lengths [pm] and angles [°]: Ru(1)···Sn(1) 299.63(7), Ru(1)-C(1) 213.0(6), Ru(1)-C(2) 215.0(7), Ru(1)-C(3) 221.3(8), Ru(1)-C(4) 221.4(7), Ru(1)-C(5) 215.2(6), Ru(1)-C(6) 215.5(6), Ru(1)-C(7) 215.4(7), Ru(1)-C(8) 221.5(7), Ru(1)-C(9) 220.8(8), Ru(1)-C(10) 214.6(7), Sn(1)-C(1) 219.7(6), Sn(1)-C(6) 218.1(6), Sn(1)-C(11) 217.0(6), Sn(1)-C(20) 217.4(6), C(1)-Sn(1)-C(6) 91.2(2), C(11)-Sn(1)-C(20) 116.7(2).

A DSC study of **6** showed no melt transition, but a ROP exotherm was detected at 181 °C. On heating **6** in a sealed tube at 200 °C for 4.5 h, the polymeric material **7** was obtained after precipitation from THF into methanol (Scheme 3). The structure of **7** was confirmed by NMR spectroscopy. The ^{1}H NMR spectrum of **7** shows peaks for the H atoms of the Cp

 © 2004 Wiley-VCH Verlag GmbH & Co. KGaA, Weinheim



6 7

Scheme 3. Ring-opening polymerization of **6**.

ring as well as the mesityl ligands, which are typically broad as expected for a polymer. The most prominent feature of the ^{13}C NMR spectrum of **7** is the signal for the Cp *ipso*-carbon atom at $\delta = 76.9$ ppm, which shows a significant downfield shift relative to that of the monomer **6** ($\delta = 31.8$ ppm). GPC analysis in THF versus polystyrene standards showed the material to be of high molecular weight with a relatively broad molecular-weight distribution ($M_n = 2.7 \cdot 10^5$, $M_w/M_n = 2.28$). The polymer **7** is stable to air, moderately soluble in organic solvents such as toluene, CH_2Cl_2 and THF, and insoluble in hexanes and methanol. DSC analysis showed a glass transition temperature (T_g) of 221 °C. Thermogravimetric analysis of **7** showed decomposition starting at 270 °C. The ceramic yield at 900 °C was 32 %.

Further studies of the reactivity of **5** and **6** are in progress. Current work is also focused on the synthesis of other examples of [1]ruthenocenophanes with different bridging elements and the study of the properties of the resulting ring-opened polymers, which should differ substantially from those based on ferrocene.

Experimental Section

4: TMEDA (4.12 mL, 27.3 mmol) and *n*BuLi (1.6 M solution in hexanes, 21.2 mL, 33.9 mmol) were added to a suspension/solution of ruthenocene (3.11 g, 13.5 mmol) in hexanes (100 mL), and the mixture was stirred at room temperature for 60 h. The resulting light yellow precipitate was collected by filtration, washed with hexanes until the washings were colorless, and dried in vacuo (4.05 g, 84 %). The solid should be stored at −30 °C.

5: Solid $[Cl_2ZrCp'_2]$[22] (1.32 g, 3.26 mmol) was added to a suspension of **4** (1.17 g, 3.26 mmol) in Et_2O (50 mL) at −70 °C. The solution was allowed to warm to room temperature overnight and the solvent was then removed in vacuo. Extraction with hot hexanes, filtration, and concentration of the resulting solution yielded **5** as a pale yellow powder (650 mg, 35 %) on storage at −55 °C. ^1H NMR (300 MHz, C_6D_6, 25 °C): $\delta = 5.92$ (t, $^3J(H,H) = 5.1$ Hz, 4H; Cp*t*Bu), 5.33 (t, $^3J(H,H) = 5.1$ Hz, 4H; Cp*t*Bu), 4.86 (t, $^3J(H,H) = 3$ Hz, 4H; Cp), 4.52 (t, $^3J(H,H) = 3$ Hz, 4H; Cp), 1.31 ppm (s, 18H; *t*Bu); ^{13}C NMR (75 MHz, C_6D_6, 25 °C): $\delta = 162.5$ (s; *ipso* CpRu), 138.3 (s; *ipso*-CpZr), 104.8 (s; CpZr), 104.6 (s; CpZr), 87.1 (s; CpRu), 74.4 (s; CpRu), 33.3 (s; $C(CH_3)_3$), 33.2 ppm (s; $C(CH_3)_3$); MS: *m*/*z* (%): 562 (100) [M^+], 547 (15) [M^+-CH_3], 506 (25) [$M^+-C_4H_8$], 232 (56) [$RuCp_2^+$]; UV/Vis (CH_2Cl_2): λ_{max} (ε) = 310 nm (shoulder); elemental analysis: calcd for $C_{28}H_{34}RuZr$ (%): C 59.75, H 6.09; found: C 59.58, H 6.32.

6: Compound **4** (1.0 g, 2.78 mmol) in THF (6 mL) was added to a suspension of finely ground Cl_2SnMes_2[23] (1.3 g, 3.04 mmol) in THF (2 mL) at −70 °C. The mixture was stirred at low temperature for 4 h and then allowed to slowly reach −30 °C. The solution was taken out of the cold bath, and the solvent removed in vacuo. Extraction of the residue with hexanes (50 mL) and removal of the solvent gave a crude product, which was repeatedly recrystallized from Et_2O to give **6** as a pale yellow powder (210 mg, 13 %). ^1H NMR (300 MHz, C_6D_6, 25 °C): $\delta = 6.79$ (s, $^4J(^{117/119}Sn,^1H) = 22.0$ Hz, 4H; *m*-H), 5.03 (t, $^3J(H,H) = 2.4$ Hz, 4H; Cp), 4.30 (t, $^3J(H,H) = 2.4$ Hz, 4H; Cp), 2.75 (s, $^4J(^{117/119}Sn,^1H) = 6.9$ Hz, 12H; *o*-CH_3), 2.14 ppm (s, 6H; *p*-CH_3); ^{13}C NMR (100.5 MHz, C_6D_6, 25 °C): $\delta = 145.7$ (s, $^2J(^{117/119}Sn,^{13}C) = 42$ Hz; *o*-Mes), 139.6 (s, $^4J(^{117/119}Sn,^{13}C) = 11$ Hz; *p*-Mes), 136.8 (s, $^1J(^{119}Sn,^{13}C) = 406$ Hz, $^1J(^{117}Sn,^{13}C) = 392$ Hz; *ipso*-Mes), 129.4 (s, $^3J(^{119}Sn,^{13}C) = 50$ Hz, $^3J(^{117}Sn,^{13}C) = 48$ Hz; *m*-Mes), 79.8 (s, $^3J(^{117/119}Sn,^{13}C) = 34$ Hz, Cp), 77.9 (s, $^2J(^{117/119}Sn,^{13}C) = 49$ Hz; Cp), 31.8 (s, $^1J(^{119}Sn,^{13}C) = 398$ Hz, $^1J(^{117}Sn,^{13}C) = 380$ Hz; *ipso* Cp), 25.6 (s, $^3J(^{119}Sn,^{13}C) = 42$ Hz, $^3J(^{117}Sn,^{13}C) = 40$ Hz; *o*-CH_3), 21.4 ppm (s, $^5J(^{117/119}Sn,^{13}C) = 7$ Hz; *p*-CH_3); ^{119}Sn NMR (111.8 MHz, C_6D_6, 25 °C) $\delta = -112.5$ ppm; MS: *m*/*z*:(%) 586 (6) [M^+], 467 (23) [M^+−Mes], 349 (100) [$M^+-2Mes+H$], 232 (48) [$RuCp_2^+$]; UV/Vis (CH_2Cl_2): λ_{max} (ε) = 363 nm (436 L mol^{-1} cm^{-1}); elemental analysis: calcd for $C_{28}H_{30}RuSn$ (%): C 57.36, H 5.16; found: C 57.21, H 5.51.

7: **6** (130 mg, 0.22 mmol) was sealed in an evacuated tube and heated to 200 °C for 4.5 h. The crude polymer was purified by repeated precipitation from THF into methanol to yield **7** as a white powder, which was dried in vacuo (59 mg, 45 %). ^1H NMR (300 MHz, C_6D_6, 25 °C): $\delta = 6.72$ (s, 4H; *m*-H), 4.71 (s, 4H; Cp), 4.65 (s, 4H; Cp), 2.37 (s, 12H; *o*-CH_3), 2.12 ppm (s, 6H; *p*-CH_3); ^{13}C NMR (100.5 MHz, C_6D_6, 25 °C): $\delta = 144.5$ (s, $^2J(^{117/119}Sn,^{13}C) = 33$ Hz; *o*-Mes), 141.6 (s; *ipso*-Mes) 138.2 (s; *p*-Mes), 129.0 (s; *m*-Mes), 77.9 (s; Cp), 76.9 (s; *ipso*-Cp), 75.2 (s, $J(^{117/119}Sn,^{13}C) = 36$ Hz; Cp), 26.9 (s, $^3J(^{117/119}Sn,^{13}C) = 32$ Hz; *o*-CH_3), 21.5 ppm (s; *p*-CH_3); ^{119}Sn NMR (111.8 MHz, C_6D_6, 25 °C): $\delta = -133.0$ ppm; GPC (THF, versus polystyrene): $M_n = 2.7 \times 10^5$, $M_w/M_n = 2.28$; elemental analysis: calcd for $C_{28}H_{30}RuSn$ (%): C 57.36, H 5.16; found: C 57.67, H 5.38.

Received: February 13, 2004 [Z54022]

Keywords: cyclopentadienyl ligands · ring-opening polymerization · ruthenium · stannanes · strained molecules

[1] a) M. Herberhold, *Angew. Chem.* **1995**, *107*, 1985; *Angew. Chem. Int. Ed. Engl.* **1995**, *34*, 1837; b) H. Braunschweig, F. M. Breitling, E. Gullo, M. Kraft, *J. Organomet. Chem.* **2003**, *680*, 31.

[2] D. A. Foucher, B. Z. Tang, I. Manners, *J. Am. Chem. Soc.* **1992**, *114*, 6246.

[3] a) I. Manners, *Chem. Commun.* **1999**, 857; b) I. Manners, *Science* **2001**, *294*, 1664.

[4] a) J. C. Green, *Chem. Soc. Rev.* **1998**, *27*, 263; b) A. Berenbaum, F. Jäkle, A. J. Lough, I. Manners, *Organometallics* **2002**, *21*, 2359; c) A. Berenbaum, H. Braunschweig, R. Dirk, U. Englert, J. C. Green, F. Jäkle, A. J. Lough, I. Manners, *J. Am. Chem. Soc.* **2000**, *122*, 5765; d) T. Mizuta, Y. Imamura, K. Miyoshi, *J. Am. Chem. Soc.* **2003**, *125*, 2068.

[5] a) A. G. Osborne, R. H. Whiteley, *J. Organomet. Chem.* **1980**, *193*, 345; b) F. Jäkle, R. Rulkens, G. Zech, D. A. Foucher, A. J. Lough, I. Manners, *Chem. Eur. J.* **1998**, *4*, 2117; c) H. K. Sharma, F. Cervantes-Lee, J. S. Mahmoud, K. H. Pannell, *Organometallics* **1999**, *18*, 399; d) T. Baumgartner, F. Jäkle, R. Rulkens, G. Zech, A. J. Lough, I. Manners, *J. Am. Chem. Soc.* **2002**, *124*, 10062; e) M. Herberhold, F. Hertel, W. Milius, B. Wrackmeyer, *J. Organomet. Chem.* **1999**, *582*, 352; f) R. Rulkens, D. P. Gates, D. Balaishis, J. K. Pudelski, D. F. McIntosh, A. J. Lough, I. Manners, *J. Am. Chem. Soc.* **1997**, *119*, 10976; g) H. Braunschweig, R. Dirk, M. Müller, P. Nguyen, R. Resendes, D. P. Gates, I. Manners, *Angew. Chem.* **1997**, *109*, 2433; *Angew. Chem. Int. Ed. Engl.* **1997**, *36*, 2338; h) W. Uhl, I. Hahn, A. Jantschak, T. Spies, *J. Organomet. Chem.* **2001**, *637*, 300.

[6] a) R. Broussier, A. Da Rold, B. Gautheron, Y. Dromzee, Y. Jeannin, *Inorg. Chem.* **1990**, *29*, 1817; b) A. Bucaille, T. Le Borgne, M. Ephritikhine, J. C. Daran, *Organometallics* **2000**, *19*, 4912.

 © 2004 Wiley-VCH Verlag GmbH & Co. KGaA, Weinheim

[7] a) C. Elschenbroich, J. Hurley, B. Metz, W. Massa, G. Baum, *Organometallics* **1990**, *9*, 889; b) K. C. Hultzsch, J. M. Nelson, A. J. Lough, I. Manners, *Organometallics* **1995**, *14*, 5496.
[8] a) M. J. Drewitt, S. Barlow, D. O'Hare, J. M. Nelson, P. Nguyen, I. Manners, *Chem. Commun.* **1996**, 2153; b) S. Fox, J. P. Dunne, M. Tacke, D. Schmitz, R. Dronskowski, *Eur. J. Inorg. Chem.* **2002**, 3039.
[9] J. M. Nelson, A. J. Lough, I. Manners, *Angew. Chem.* **1994**, *106*, 1019; *Angew. Chem. Int. Ed. Engl.* **1994**, *33*, 989.
[10] For **3** the difference in the tilt angle α between the planes of the Cp ligands for the Ru and Fe species is 8°. (**3** (M = Ru): $\alpha = 29.6(5)°$, **3** (M = Fe): $\alpha = 21.6(5)°$); see references [9] and [17].
[11] U. Vogel, J. M. Nelson, I. Manners, unpublished results.
[12] M. Herberhold, T. Bärtl, *Z. Naturforsch. B* **1995**, *50*, 1692.
[13] Crystallographic data for $C_{28}H_{34}RuZr$ (**5**): monoclinic $C2/c$, $a = 19.0368(4)$, $b = 9.5493(4)$, $c = 15.1497(4)$ Å, $\beta = 124.306(2)°$, $V = 2274.9(1)$ Å^3, $Z = 4$, $\mu = 1.135$ mm^{-1}, $\rho_{calcd} = 1.643$ Mg m^{-3}, 150(1) K, Nonius Kappa-CCD diffractometer using graphite-monochromated $Mo_{K\alpha}$ radiation ($\lambda = 0.71073$ Å), pale yellow crystal ($0.30 \times 0.22 \times 0.16$ mm^3). Of 9615 reflections collected ($5.1 \le 2\theta \le 55.0°$), 2617 were independent ($R_{int} = 0.0296$), and 2279 were observed with $F_o \ge 4\sigma(F_o)$. Solution and refinement with SHELXTL-PC v6.12, non-hydrogen atoms were refined with anisotropic parameters, hydrogen atoms were refined on calculated positions using a riding model, $R1 = 0.0256$, $wR2 = 0.0628$, ($R1 = \Sigma(F_o - F_c)/\Sigma F_o$ observed data, $wR2 = \{\Sigma[w(F_o^2 - F_c^2)^2]/\Sigma[w(F_o^2)^2]\}^{1/2}$ for all data), GOF = 1.102, $\Delta\rho_{max} = 0.896$ e Å^{-3}. Crystallographic data for $C_{28}H_{30}RuSn$ (**6**): monoclinic $P2_1/c$, $a = 17.8377(4)$, $b = 12.4501(3)$, $c = 31.9136(7)$ Å, $\beta = 93.826(1)°$, $V = 7071.6(3)$ Å^3, $Z = 12$, $\mu = 1.712$ mm^{-1}, $\rho_{calcd} = 1.652$ Mg m^{-3}, 150(1) K, Nonius Kappa-CCD diffractometer using graphite-monochromated $Mo_{K\alpha}$ radiation ($\lambda = 0.71073$ Å), pale yellow crystal ($0.26 \times 0.26 \times 0.03$ mm^3). Of 36931 reflections collected ($5.1 \le 2\theta \le 55.0°$) 16057 were independent $R_{int} = 0.0657$, and 10129 were observed with $F_o \ge 4\sigma(F_o)$. Solution and refinement as for **5**, $R1 = 0.0557$, $wR2 = 0.1296$, ($R1 = \Sigma(F_o - F_c)/\Sigma F_o$ observed data, $wR2 = \{\Sigma[w(F_o^2 - F_c^2)^2]/\Sigma[w(F_o^2)^2]\}^{1/2}$ for all data), GOF = 1.015, $\Delta\rho_{max} = 1.47$ e Å^{-3}. CCDC-231377 (**6**) and -231378 (**5**) contain the supplementary crystallographic data for this paper. These data can be obtained free of charge via www.ccdc.cam.ac.uk/conts/retrieving.html (or from the Cambridge Crystallographic Data Centre, 12, Union Road, Cambridge CB2 1EZ, UK; fax: (+44) 1223-336-033; or deposit@ccdc.cam.ac.uk).
[14] C. P. Casey, R. F. Jordan, A. L. Rheingold, *Organometallics* **1984**, *3*, 504.
[15] C. P. Casey, R. F. Jordan, A. L. Rheingold, *J. Am. Chem. Soc.* **1983**, *105*, 665.
[16] Although the ^{1}H NMR spectrum of the crude reaction mixture showed the formation of **6** in approximately 40% yield, the purification of the compound was difficult owing to the similar solubilities of **6** and the by-products.
[17] a) J. M. Nelson, H. Rengel, I. Manners, *J. Am. Chem. Soc.* **1993**, *115*, 7035; b) J. M. Nelson, P. Nguyen, R. Peterson, H. Rengel, P. M. Macdonald, A. J. Lough, I. Manners, N. P. Raju, J. E. Greedon, S. Barlow, D. O'Hare, *Chem. Eur. J.* **1997**, *3*, 573.
[18] Y. S. Sohn, D. N. Hendrickson, H. B. Gray, *J. Am. Chem. Soc.* **1971**, *93*, 3603.
[19] a) J. K. Pudelski, D. A. Foucher, C. H. Honeyman, A. J. Lough, I. Manners, S. Barlow, D. O'Hare, *Organometallics* **1995**, *14*, 2470; b) S. Barlow, M. J. Drewitt, T. Dijkstra, J. C. Green, D. O'Hare, C. Whittingham, H. H. Wynn, D. P. Gates, I. Manners, J. M. Nelson, J. K. Pudelski, *Organometallics* **1998**, *17*, 2113.
[20] The average bond length of 119 Ru–Sn bonds found in a CSD database search was 266(6) pm.
[21] S. Hermans, B. F. G. Johnson, *Chem. Commun.* **2000**, 1955.
[22] R. A. Howie, G. P. McQuillan, D. W. Thompson, G. A. Lock, *J. Organomet. Chem.* **1986**, *303*, 213.
[23] F. Jäkle, I. Manners, *Organometallics* **1999**, *18*, 2628.

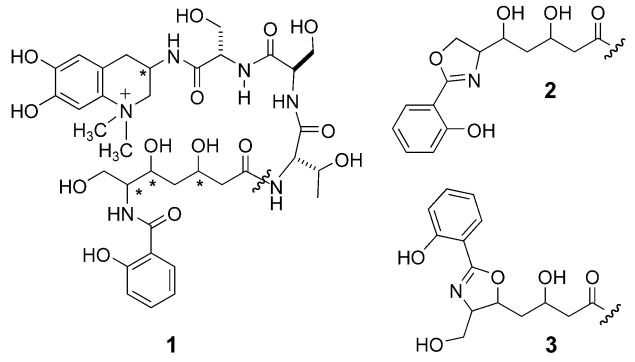
 © 2004 Wiley-VCH Verlag GmbH & Co. KGaA, Weinheim

Biomimetic Synthesis

A Biomimetic Route to the Peptide Alkaloid Anachelin**

Karl Gademann and Yann Bethuel*

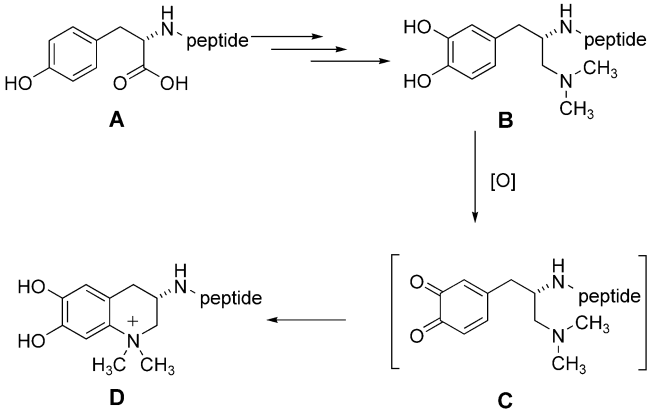
The acquisition and storage of iron is a central challenge for virtually all life forms due to its low bioavailability. Although cyanobacteria are one of the most successful life forms on earth, the molecular mechanism of iron acquisition by cyanobacteria remains largely unknown. Recently, the first complex secondary metabolites were isolated from *Anabaena cylindric*a.[1] These compounds were postulated to have biological activity as ligands for Fe (siderophores). While Budzikiewicz et al. isolated mixtures of anachelin H (**1**) and anachelin-1 (**2**),[1] Murakami et al. described the isolation and determination of the constitution of **2** and anachelin-2 (**3**).[2]



1 **2** **3**

These compounds are composed of a fascinating blend of alkaloid, peptide, and polyketide building blocks. In particular, they contain structurally interesting fragments such as the rare tetrahydroquinolinium ring, which contains a quaternary N atom, as well as a polyhydroxylated ε-amino acid.[3] The biological activity and the mode of action of compounds **1**–**3** as siderophores are not yet established. In addition, the absolute and relative configuration of the four stereogenic centers was not determined. Since these questions can be addressed by total synthesis, we chose anachelin H as the subject for our synthetic studies.[4]

We propose the following hypothetical transformations for the biogenesis of the unique tetrahydroquinolinium chromophore (Scheme 1): It is reasonable to assume that peptide **A** containing a C-terminal tyrosine residue could serve as precursor. Oxidation to dihydroxyphenylalanine, subsequent reductive amination, and methylation would



Scheme 1. A biogenetic hypothesis for the formation of the anachelin chromophore **D**. The key intermediate **B** could be formed from the tyrosine peptide **A**. Subsequent oxidation to the *ortho*-quinone **C** and spontaneous intramolecular aza annulation would result in formation of the chromophore **D**.

result in the dopamine derivative **B**. This key precursor could then be transformed by enzymatic oxidation into the *ortho*-quinone **C**, which would react by spontaneous aza annulation to generate the anachelin chromophore **D**.[5]

In order to evaluate this biogenetic hypothesis in the chemical laboratory, we chose the transformation **B**→**D** as the key step of our biomimetic strategy.[6] The starting material L-DOPA (**4**) was Boc-protected using standard reagents (Scheme 2). Activation via the mixed anhydride and subsequent transformation with dimethylamine in THF gave Boc-L-DOPA-dimethylamide (**5**) as a crystalline solid.[7] A three-step sequence[8] (deprotection using trifluoroacetic acid, borane reduction, and Boc protection) resulted in the air-sensitive Boc-protected diamine **6**, the low yield of which is attributed to problems in the isolation and purification. The key intermediate **7** analogous to **B** in Scheme 1 was obtained after Boc removal and coupling with a serine derivative in good yield. After testing different oxidants, we found that the oxidative aza annulation of **7** using dianisyltellurium oxide[9] gave the desired cyclization product in 80% yield. Again, this compound is not stable on silica gel. Thus the hydroxy groups were protected as benzyl ethers, and the resulting quaternary ammonium salt **8** was isolated after flash chromatography. Cleavage of the N-terminal protecting group and coupling with the protected dipeptide derivative Boc-Thr-Ser-OH, which is readily available in four steps,[6] gave, after removal of the Boc group of **9**, fragment **10**.

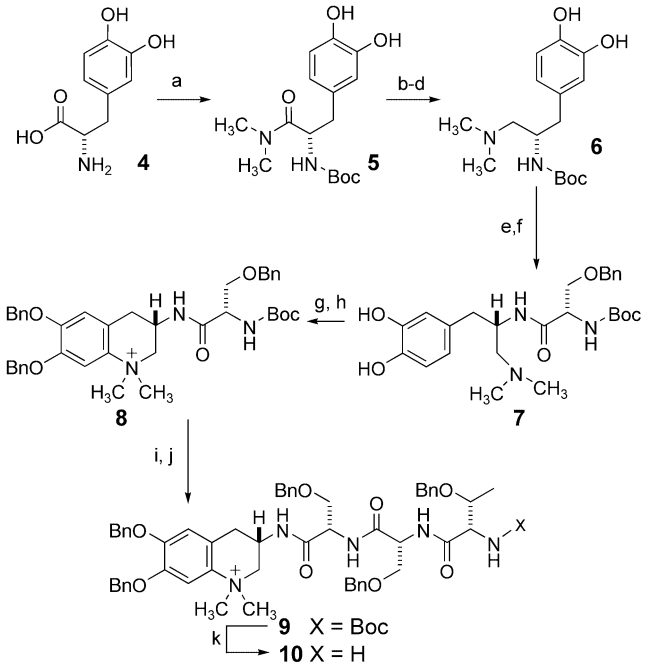
The unknown relative and absolute configuration of the ε-amino acid forced us to choose a flexible strategy for the construction of the aldol skeleton. Through biomimetic C_2-homologation by means of a crossed Claisen condensation and subsequent reduction of the β-keto ester, we can prepare all the possible isomers in good yields and few steps. Our

[*] Dr. K. Gademann, Y. Bethuel
Laboratorium für Organische Chemie
Eidgenössische Technische Hochschule Zürich
ETH Hönggerberg, 8093 Zürich (Switzerland)
Fax: (+41) 1-632-1328
E-mail: gademann@org.chem.ethz.ch

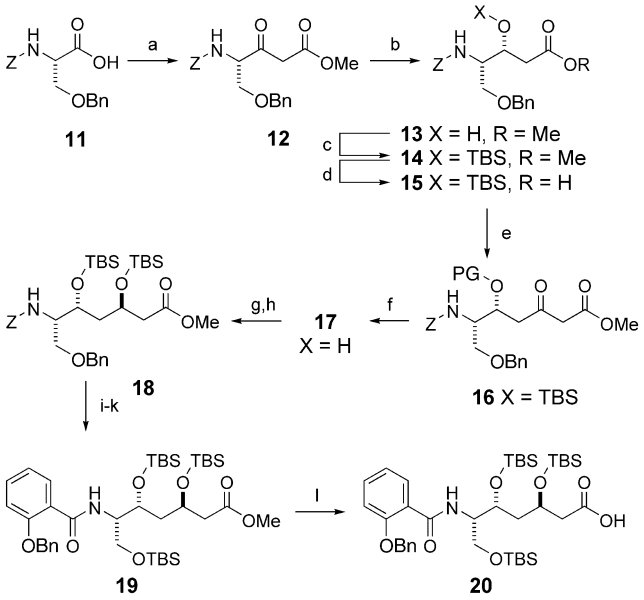
[**] K.G. thanks Prof. Dr. E. M. Carreira for generous financial support, as well as the Roche Research Foundation and the Schweizerischer Nationalfonds.

Supporting information for this article is available on the WWW under http://www.angewandte.org or from the author.

 DOI: 10.1002/anie.200453909 © 2004 Wiley-VCH Verlag GmbH & Co. KGaA, Weinheim



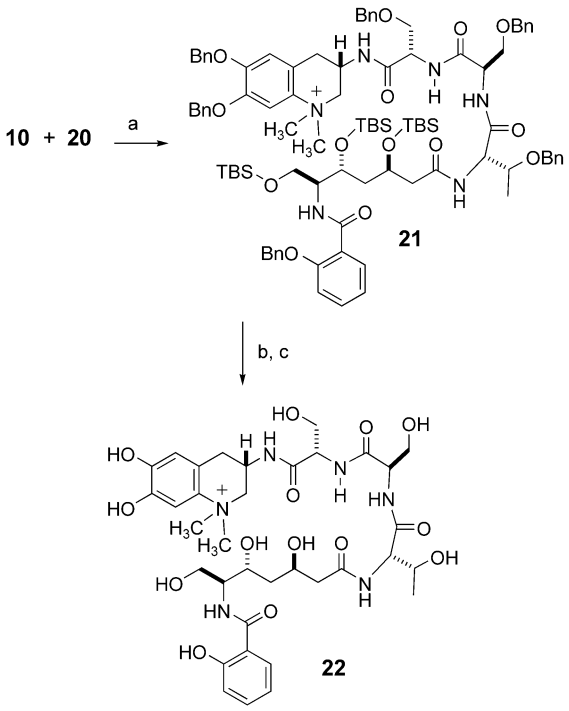
Scheme 2. a) 1. Boc_2O, dioxane, aq. NaOH, 2. *i*BuOCOCl, THF, 3. $HN(CH_3)_2$, 61%; b) TFA, CH_2Cl_2; c) BH_3·THF; d) Boc_2O, dioxane, aq. NaOH, (16% over three steps starting from **5**); e) TFA, CH_2Cl_2, quant.; f) Boc-L-Ser(OBn)-OH, EDC, HOBt, 58%; g) dianisyltellurium oxide, CH_2Cl_2, 80%; h) BnBr, Cs_2CO_3, acetone, 85%; i) TFA, CH_2Cl_2, quant.; j) Boc-L-Thr(OBn)-D-Ser(OBn)-OH, EDC, HOBt, 73%; k) TFA, CH_2Cl_2, quant. Abbreviations: Boc = butoxycarbonyl, DOPA = 3,4-dihydroxyphenylalanine, EDC = *N*-ethyl-*N*′-(dimethylaminopropyl)carbodiimide hydrochloride, HOBt = 1-hydroxybenztriazole, TFA = CF_3CO_2H.



Scheme 3. a) 1. CDI, THF, 2. $KO_2CCH_2CO_2Me$, $MgCl_2$, 71%; b) $NaBH_4$, MeOH, Et_2O, −60°C, 90%, then separation of the diastereoisomers, 48%; c) TBSOTf, 2,6-lutidine, CH_2Cl_2, 78%; d) NaOH, MeOH, THF, 54%; e) 1. CDI, THF, 2. $KO_2CCH_2CO_2Me$, $MgCl_2$; f) TBAF (1 M in THF), 60% (over two steps starting from **15**); g) $Me_4NB(OAc)_3H$, AcOH, CH_3CN (d.r. > 95:5); h) TBSOTf, 2,6-lutidine, CH_2Cl_2, 75% (over two steps from **17**); i) Pd/C, H_2, MeOH; j) EDC, HOBt, 2-BnO-salicylic acid, $CHCl_3$; k) TBSCl, imidazole, DMAP, DMF, 70% (over three steps from **18**); l) NaOH, MeOH, THF, quant. Abbreviations: CDI = carbonyldiimidazole, DMAP = 4-*N*,*N*-dimethylaminopyridine, PG = protecting group, TBAF = tetrabutylammonium fluoride, TBS = *tert*-butyldimethylsilyl, Tf = triflate.

synthesis started with the protected serine derivative **11**, which, after activation to the imidazolide, was allowed to react using the procedure of Masamune et al. with monomethylpotassium malonate in the presence of $MgCl_2$[10] (Scheme 3). The resulting β-keto ester **12** was deliberately reduced with low selectivity using $NaBH_4$ in order to produce both isomers.[11] The secondary hydroxy group in **13** was protected (→**14**) and the methyl ester saponified. This reaction called for careful optimization of the reaction conditions, as major amounts of the corresponding γ-lactam were isolated as a side product. The carboxylic acid **15** was again homologated to **16** using a Claisen condensation, and the silyl group was cleaved. A stereoselective 1,3-*anti* reduction of the hydroxyketoester following the Evans protocol[12] and subsequent TBS protection gave **18** in 75% yield. Hydrogenolytic cleavage of the benzyl protecting groups, coupling to the salicylic acid derivative, and TBS protection resulted in **19** (70% yield over three steps); the methyl ester was easily hydrolyzed at this time to give **20**.

Fragments **10** and **20** were then coupled using EDC to the protected anachelin H derivative **21** (Scheme 4) The benzyl groups were cleaved hydrogenolytically in acidic medium (MeOH, AcOH). Since the use of TBAF resulted only in partial deprotection of the TBS-protected secondary hydroxy groups, the reagent of choice proved to be 1% HCl in MeOH, and the completely deprotected peptide alkaloid **22** was isolated.

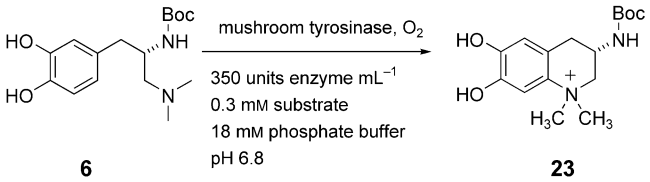


Scheme 4. a) EDC, HOBt, $CHCl_3$, 63%; b) Pd/C, H_2, MeOH, AcOH; c) 1% conc. aq. HCl in MeOH (45% over two steps).

 © 2004 Wiley-VCH Verlag GmbH & Co. KGaA, Weinheim

Both the exact mass of compound **22** as well as the fragmentation pattern in the mass spectrum are identical to those of an authentic sample of anachelin H (**1**);[13] however, the ^{1}H NMR spectra of **1** and **22** display minor differences. This indicates that compound **22** could be a diastereoisomer of anachelin H (**1**). The synthetic route shown here allows for the preparation of all possible fifteen diastereoisomers of **22** and thus should lead the determination of the absolute and relative configuration of anachelin H (**1**).

In addition, our synthesis described herein delivers intermediates that serve in the further evaluation of our biogenetic hypothesis. For example, the postulated cascade **B**→**D** in Scheme 1 can be corroborated by biochemical experiments. While one can assume that in this transformation **C** spontaneously reacts to give **D**, we postulate that an enzyme in the class of catechol oxidases catalyzes the oxidation of **B** to **C**. Therefore, we decided to test this hypothesis using an intermediate of our synthesis. We chose diamine **6** as model substrate, which was transformed in 18 mM phosphate buffer at pH 6.8 with commercially available tyrosinase (catechol oxidase, EC 1.14.18.1) isolated from mushrooms (Scheme 5). Interestingly, the formation of the



Scheme 5. Catalytic oxidation of diamine **6** with O_2 and catechol oxidase.

cyclization product **23** could be observed by UV spectroscopy at 305 nm![14] This biochemical experiment corroborates our postulated biogenesis and indeed suggests that a catechol oxidase is likely involved in the biosynthesis of the anachelin chromophore.

We present in this communication a biomimetic strategy for the preparation of the peptide alkaloid anachelin featuring a Te-mediated oxidative aza annulation as well as Claisen condensations under mild conditions as key steps. This route also delivers substrates, by which our biogenetic hypothesis can be corroborated. For example, we were able to show that the enzyme tyrosinase catalyses the cyclization of a key model substrate of the biogenetic hypothesis. This experiment suggests that a catechol oxidase could be involved in the biosynthesis of anachelin. Additional experiments concerning the biosynthesis, the configuration of anachelin, and the mechanism of iron acquisition of *A. cylindrica* are being pursued in our laboratory and will be reported in due course.

Received: February 3, 2004 [Z53909]

Keywords: alkaloids · biomimetic syntheses · natural products · peptides · polyketides

[1] H. Beiderbeck, K. Taraz, H. Budzikiewicz, A. E. Walsby, *Z. Naturforsch. C* **2000**, *55*, 681–687; H. Beiderbeck, Dissertation, Universität Köln, Germany, **2000**.
[2] Y. Itou, S. Okada, M. Murakami, *Tetrahedron* **2001**, *57*, 9093–9099. This group did not isolate anachelin H (**1**), but instead two esters isomeric to **1** of the salicylic acid with C(5)-O and C(7)-O of the ε-amino acid of anachelin.
[3] This amino acid is only to be found in the peptide antibiotic galantin. Isolation: J. Shoji, R. Sakazaki, Y. Wakisaka, K. Koizumi, M. Mayama, S. Matsuura, *J. Antibiot.* **1975**, *28*, 122–125; First synthesis: N. Sakai, Y. Ohfune, *J. Am. Chem. Soc.* **1992**, *114*, 998–1010.
[4] Compound **2** can be transformed by hydrolysis of the oxazoline ring into **1** (see [1]). Therefore, we assume that anachelin H is the more stable compound in the extracellular aquatic environment of *A. cylindri*ca.
[5] The transformation **B**→**C** is analogous to the biosynthesis of *cyclo*-DOPA starting from L-DOPA, important intermediates in the biogenesis of betanidin and the melanins.
[6] Experimental procedures and analytical data of all new compounds are reported in the Supporting Information and can be obtained from http://www.angewandte.org or from the corresponding author.
[7] We did not observe acylation of the aromatic hydroxy groups, as no corresponding by-products could be isolated.
[8] The Boc group is not stable under the conditions of the borane reduction.
[9] S. V. Ley, C. A. Meerholz, D. H. R. Barton, *Tetrahedron* **1981**, *37*, 213–223; for a related application, see J. Clews, C. J. Cooksey, P. J. Garratt, E. J. Land, C. A. Ramsden P. A. Riley, *J. Chem. Soc. Perkin Trans. 1* **2000**, 4306–4315.
[10] D. W. Brooks, L. D.-L. Lu, S. Masamune, *Angew. Chem.* **1979**, *91*, 76–78; *Angew. Chem. Int. Ed. Engl.* **1979**, *18*, 72–74; T. S. Mansour, C. A. Evans, *Synth. Commun.* **1990**, *20*, 773–781.
[11] The diastereoisomers were separated by crystallization. The relative configuration of **13** was assigned after derivatization to the N,O-acetal using the method of Joullié: B. D. Harris, M. M. Joullié, *Tetrahedron* **1988**, *44*, 3489–3500.
[12] D. A. Evans, K. T. Chapman, E. M. Carreira, *J. Am. Chem. Soc.* **1988**, *110*, 3560–3578.
[13] We thank Prof. Dr. H. Budzikiewicz for an authentic sample of natural anachelin H.
[14] A reference sample of **23** was prepared by chemical oxidation of **6** using dianisyltellurium oxide and characterized: (UV: λ_{max} = 284 nm, $\varepsilon = 3960\,M^{-1}s^{-1}$, shoulder at $\lambda = 305$ nm, $\varepsilon = 850\,M^{-1}s^{-1}$).

 © 2004 Wiley-VCH Verlag GmbH & Co. KGaA, Weinheim

Atmospheric Chemistry

The Trifluoromethoxy Sulfuryl Radical, $CF_3OSO_2^{\bullet}$**

Stefan von Ahsen and Joseph S. Francisco*

Sulfur oxides like SO_2 and SO_3 play a major role in the chemistry of the atmosphere such as in the production of acid rain and smog. In addition, the heterogeneous chemistry of H_2SO_4 in stratospheric clouds is a topical research area in atmospheric chemistry. Much is known about the conversion of SO_2 into H_2SO_4 in homogeneous oxidation reactions in the atmosphere. However, little is known about the interaction of SO_x species with CF_3O_y radicals in the atmosphere. Since chlorofluorocarbons (CFCs) cause ozone depletion in the stratosphere, these materials are being replaced by alternatives such as hydrofluorocarbons (HFCs) and hydrofluoroethers (HFEs). Both CFCs and their replacements are known to be sources of CF_3 and CF_3O_y radicals.[1] It is commonly accepted that the main fate of CF_3O radicals is their reaction with NO or CH_4.[2] While methane is present in the lower atmosphere with a mixing ratio of around 1800 ppb (parts per billion, molecules per 10^9 molecules) and NO reaches only concentrations of around 1 ppb, the reaction of $CF_3O^{\bullet}$ with nitrogen monoxide is roughly 2000 times faster than its reaction with methane.[3,4] A coupling between the chemistry of CF_3O_y and SO_x in atmospheric processes has not been addressed in the literature although the SO_2 mixing ratio ranges from 1 to 1000 ppb depending on the air quality and is hence not too far away from the methane concentration.[3,4] To our knowledge no kinetic data for the reaction of $CF_3O^{\bullet}$ with SO_2 have been published. We present here the first direct spectroscopic identification of the CF_3OSO_2 radical isolated in an inert-gas matrix generated by reaction of CF_3O radicals with SO_2. Thus we demonstrate the existence of the first link between $C_nF_mO_y$ species and SO_x in the atmosphere.

[*] Dr. S. von Ahsen
Bergische Universität Wuppertal
Fachbereich C/Anorganische Chemie
42097 Wuppertal (Germany)
Fax: (+49) 202-439-3052
E-mail: von.ahsen@freenet.de
Prof. Dr. J. S. Francisco
Department of Chemistry, Earth and Atmospheric Sciences
Purdue University
1393 H. C. Brown Building
West Lafayette, IN 47907 (USA)

[**] This work was supported by the Deutsche Forschungsgemeinschaft and the Fonds der Chemischen Industrie. J.S.F. thanks the Alexander von Humboldt Foundation for a research award for senior U.S. scientists. The experiments were carried out in the laboratories of Prof. Dr. H. Willner at the Universities of Duisburg (Germany) and Wuppertal (Germany). We want to express special thanks for his support and for helpful discussions.

Supporting information for this article is available on the WWW under http://www.angewandte.org or from the author.

A gas mixture of $CF_3OC(O)OOCF_3$, SO_2, and Ar (1:10:1000) was thermolyzed under low pressure and subsequently quenched as an inert-gas matrix. The first reaction step corresponds to the thermal decay of the peroxide [Eq. (1)], which is also observed in the absence of SO_2.[5]

$$CF_3OC(O)OOCF_3 \rightarrow 2\,CF_3O^{\bullet}+CO_2 \quad (1)$$

In the IR spectra of the thermolysis products isolated in matrix the absorptions of $CF_3O^{\bullet}$ are present in addition to the bands of SO_2, CO_2, and COF_2 and weak absorptions of a previously unknown species. The absorptions of the unidentified compound strongly increase when the matrix is annealed at 35 K while the $CF_3O^{\bullet}$ absorptions[5] disappear. Hence, in the matrix and in the gas phase or during the condensation process CF_3O radicals react. Due to the lack of IR bands of CF_3OOCF_3 in the product spectrum, recombination of CF_3O radicals can be ruled out. Neither the formation of $FSO_2^{\bullet}$ was observed, as no IR absorption in the typical S–F stretching region occurs, nor the generation of COF_2 was detected during annealing. Hence, the transfer of fluorine from $CF_3O^{\bullet}$ to SO_2 can be excluded. The fluorophosgene present in the matrix was formed during the thermolysis by secondary reactions of $CF_3O^{\bullet}$ with the walls of the reaction vessel. Finally only an interaction of $CF_3O^{\bullet}$ with SO_2 according to Equation (2) is consistent with the observations.

$$CF_3O^{\bullet}+SO_2\ (+M) \rightarrow CF_3OSO_2^{\bullet}\ (+M) \quad (2)$$

Although it is reasonable to assume that the new species is $CF_3OSO_2^{\bullet}$, and the recorded IR spectrum is reproduced by quantum chemical calculation very well (see below), we needed additional experimental proof of the existence of the new radical. For this purpose the annealed and recooled (16 K) product matrix, which does not contain any CF_3O radicals, was irradiated with UV light ($\lambda > 280$ nm). While the absorptions of the new formed compound disappear, fluorophosgene and SO_2 form in the photochemical reaction. The fluorine atoms that presumably form are not detectable by IR spectroscopy. An explanation is that UV light induces the back-reaction of CF_3OSO_2 formation, and the resulting CF_3O radicals are photolyzed to give COF_2 and fluorine atoms in a second step. Since CF_3O photolysis with light of $\lambda > 280$ nm is known to be slow,[5] a more favored way to fluorophosgene and $F^{\bullet}$ formation is that excited CF_3OSO_2 dissociates into SO_2 and excited $CF_3O^{\bullet}$, which subsequently decays into COF_2 and $F^{\bullet}$, yielding a net reaction according to Equation (3).

$$CF_3OSO_2^{\bullet}+h\nu \rightarrow SO_2+COF_2+F^{\bullet} \quad (3)$$

The formation of SO_3 and $CF_3^{\bullet}$ was not observed. This is in contrast to the behavior of the CF_3OCO radical, which mainly photodissociates into CO_2 and $CF_3^{\bullet}$.[6] In the case of $CF_3OCO^{\bullet}$, generation of CO_2 and $CF_3^{\bullet}$ is an exothermic process, while the dissociation of $CF_3OSO_2^{\bullet}$ into $CF_3^{\bullet}$ and SO_3 is calculated to be endothermic. It is interesting to note that also no formation of $FSO_2^{\bullet}$ (from $F^{\bullet}+SO_2$) was detected, and the FSO_2 radical remains—to our knowledge—undiscovered.

 © 2004 Wiley-VCH Verlag GmbH & Co. KGaA, Weinheim DOI: 10.1002/anie.200453925

A difference IR spectrum from before and after photolysis of the matrix is shown in Figure 1. The absorptions of the photolabile compound, which decrease in the course of the photolysis, are depicted with positive extinction values while

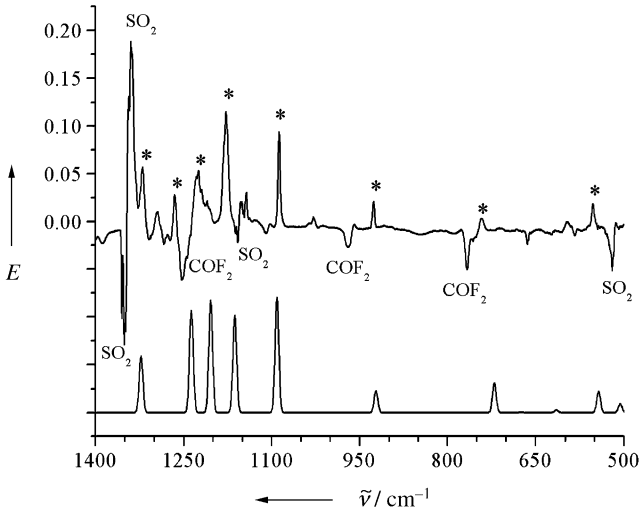


Figure 1. IR spectrum of the thermolysis products of a CF_3O-C(O)$OOCF_3$/SO_2/Ar mixture isolated as a matrix after annealing (upper trace). The depicted spectrum is the difference before and after irradiation of the reaction products with UV light. The bands that disappear on irradiation point upwards; the bands corresponding to the photolysis products point downwards. Those assigned to $CF_3OSO_2^{\bullet}$ are marked with an asterisk (*).The simulated IR spectrum (lower trace) is down shifted by 0.2 absorbance units.

those of the photolysis products correspond to negative bands. In the region of the SO_2 stretching frequencies around 1350 and 1150 cm^{-1} incompensation occurs, but the net production of SO_2 is evident from the increasing intensity of the SO_2 deformation band. The bands assigned to $CF_3OSO_2^{\bullet}$ are marked with an asterisk (*). Nevertheless, some absorptions that also vanish upon UV photolysis are not due to $CF_3OSO_2^{\bullet}$ as they did not clearly grow during the preceding annealing period. The origin of these bands remains unclear.

We observed 11 absorption bands that increase during annealing of the thermolysis product matrix and vanish upon UV irradiation of the matrix. In Table 1 the assignment of these bands to the CF_3OSO_2 radical and the description of the IR modes are listed. The mode descriptions are based on the calculated data and can be only approximate due to strong vibrational coupling.

According to the calculations $CF_3OSO_2^{\bullet}$ exhibits C_1 symmetry (close to C_s), and all 18 fundamentals are IR active. The normal modes can roughly be described as seven stretching, nine deformation (five from the CF_3O unit, three from the SO_2 unit, and one COS angle deformation), and two torsion modes. In addition, the IR spectrum confirms the connectivity to be CF_3OSO_2; an isomer like CF_3OOSO would display an O–O stretching absorption (expected between 800 and 900 cm^{-1}) and an unusual high frequency of the S=O stretching mode, both of which were not found experimentally. The use of isotopically labeled $S^{18}O_2$ resulted in isotopic shifts of the observed absorptions that are in agreement with

Table 1: Vibrational data of CF_3OSO_2 isolated in SO_2-doped Ar matrix.

Argon matrix		B3LYP/6-311++G(3df,3pd)		B3LYP/6-31+G(d)		Description (approx.)[a]
$\tilde{\nu}$ [cm^{-1}]	$I_{rel.}$[b]	$\tilde{\nu}$ [cm^{-1}]	I [km mol^{-1}]	$\tilde{\nu}$ [cm^{-1}]	I [km mol^{-1}]	
1325	40	1322	176	1251	349	$\nu_a(SO_2)$
1266	55	1237	320	1223	190	$\nu_a(CF_3)$
1227	50	1204	351	1201	401	$\nu_a(CF_3)$
1178	100	1163	304	1168	474	$\nu_s(CF_3)$/ $\nu_s(SO_2)$/ ν(CO)
1087	87	1091	360	1046	183	$\nu_s(SO_2)$/ ν(CO)/ $\nu_s(CF_3)$
926	26	922	69	908	35	$\nu_s(CF_3)$/ ν(CO)
741	13	720	92	693	77	ν(OS)
		674	1.0	658	0.48	$\delta(CF_3)$/ δ(COS)
		615	7.5	602	6.9	$\delta(CF_3)$
553	22	543	67	522	72	$\delta(CF_3)$/ $\gamma(SO_3)$[c]
514	[d]	506	28	478	28	$\delta(SO_2)$
470	8	464	24	444	26	$\delta(SO_2)$/ $\delta(CF_3)$
417	4	410	15	400	21	$\rho(CF_3)$
321[e]	1	313	1.6	292	2.0	$\delta(SO_2)$
		303	3.0	279	4.3	$\rho(CF_3)$
		147	0.65	140	0.93	δ(COS)/ $\rho(CF_3)$
		79	0.47	70	0.42	τ(FCOS)/ $\tau(COSO_2)$
		49	0.55	40	0.69	$\tau(COSO_2)$/ τ(FCOS)

[a] Vibration types: ν = stretching, δ,ρ = deformation; τ = torsion, γ = out-of-plane. [b] Relative integrated intensities. [c] Although the OSO_2 group is not planar, the S atom moves nearly perpendicular to the plain of the three O atoms. [d] Overlapping with $\delta(SO_2)$. [e] From a F-IR spectrum not shown here.

values predicted by DFT calculations. The assignment involves only one isomer of $CF_3OSO_2^{\bullet}$, although the appearance of two torsional modes may indicate the existence of more than one rotamer. In the calculations the dihedral angle β(FCOS) leads, if varied from +180° to −180° during relaxed scans, to three identical minimum-energy structures, each with one fluorine atom of the CF_3 group nearly *trans* to the O–S bond. The calculated energy barrier is 5.9 kJ mol^{-1}. The COSO dihedral angle was varied from −180° (a C_s configuration with a CF_3-O-S(O)-O structure and all oxygen atoms in the symmetry plane) to +180°. Two minima were found with C_1 symmetry, identical energy, and structure, which describe two enantiomeric forms of the radical. In all calculations the two terminally bound oxygen atoms at the sulfur atom avoid becoming symmetry-equivalent, forcing the radical into C_1 symmetry instead of C_s. Hence, $CF_3OSO_2^{\bullet}$ should exist only in one distinguishable isomeric form.

The calculated structure (B3LYP/6-311++G(3df,3pd)) of one enantiomer is shown in Figure 2. The C–F, C–O, and S=O bond lengths are in the expected range. The length of the O–S single bond, 1.686 Å, is also not unusual. The C-O-S angle is calculated to be 120.4°. Some structural parameters and calculated charges and spin densities are listed in Table 2.

 © 2004 Wiley-VCH Verlag GmbH & Co. KGaA, Weinheim

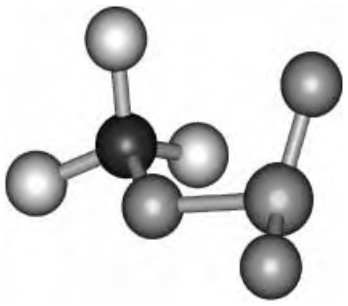


Figure 2. Calculated [B3LYP/6-311++G(3df,3pd)] structure of $CF_3OSO_2^{\bullet}$.

Table 2: Calculated [B3LYP/6-311++G(3df,3pd)] structural parameters and properties of $CF_3OSO_2^{\bullet}$.

Coordinate		Property[a]	
r(O–S) [Å]	1.686	q(S) [e]	+0.81
r(C–O) [Å]	1.380	q(O) [e]	−0.66
r(C–F) [Å]	1.327	q(F) [e]	−0.41
	1.336		−0.42
	1.324		−0.40
r(S=O) [Å]	1.437	q(=O) [e]	−0.34
	1.441		−0.34
α(COS) [°]	120.4	q(C) [e]	+1.76
α(FCO) [°]	111.7		
	111.6		
	106.9	ρ_s(S) [a.u.]	0.47
α(OS=O) [°]	102.6	ρ_s(=O) [a.u.]	0.22
	109.0		0.22
β(FCOS) [°]	164.1	ρ_s(O) [a.u.]	0.11
β(COS=O) [°]	175.9		
Symmetry: C_1		ΔE_{diss}[b] [kJ mol^{-1}]	+71.9
		ΔH_{diss}[b] [kJ mol^{-1}]	+63.4
		ΔG_{diss}[b] [kJ mol^{-1}]	+13.9

[a] r = bond length, q = charge, ρ_s = spin density. [b] Dissociation: $CF_3OSO_2^{\bullet} \rightarrow CF_3O^{\bullet} + SO_2$.

The calculated spin density distribution, which indicates the delocalization of the unpaired electron within the complete SO_2 moiety, corresponds to about 0.47 atomic units (a.u.) on the S atom, 0.22 a.u. on each of the double-bonded O atoms, and about 0.1 a.u. on the bridging O atom. This results are in agreement with published data from a previous ESR experiment, in which a spectrum was assigned to CF_3OSO_2 radicals proposed to arise from $CF_3OS(O)_2Cl$ and $(CH_3)_3Si$ radicals by Cl atom abstraction in toluene at low temperatures.[7]

A relaxed-scan calculation on the S–O distance at the B3LYP/6-31+G(d) level of theory results in an anharmonic potential, which is roughly described by a Morse function. The potential has a depth of 51.2 kJ mol^{-1}; with the expanded basis set 6-311++G(3df,3pd) the potential depth increases to 71.9 kJ mol^{-1}. At higher levels of theory (including more polarization and diffuse functions) the O–S bond strength and the dissociation enthalpy (dissociation into CF_3O and SO_2) increase. For the formation of $CF_3OSO_2^{\bullet}$ according to Equation (2) at standard conditions the following thermodynamic values were calculated: $\Delta H_B = -63.4$ kJ mol^{-1} and $\Delta G_B = -13.9$ kJ mol^{-1}. The negative free enthalpy value indicates a spontaneous generation of the trifluoromethoxy sulfuryl radical from $CF_3O^{\bullet}$ and sulfur dioxide not only in the matrix but also in the atmosphere.

Based on the now-proven existence of $CF_3OSO_2^{\bullet}$ further reaction pathways for $C_nF_mO_y$ radicals as well as for SO_2 must exist. In analogy to the reactions of the related CF_3OCO radical,[6,8–10] conversion of the sulfuryl radical into a peroxy radical [Eq. (4)] should be the most important reaction of the CF_3OSO_2 radical.

$$CF_3OSO_2^{\bullet} + O_2\ (+M) \rightarrow CF_3OS(O)_2OO^{\bullet}\ (+M) \qquad (4)$$

In general, peroxy radicals are reduced by trace gases in the atmosphere such as NO to yield the corresponding oxy radicals. In addition, the conversion of SO_2 (S^{IV}) into a sulfur species with sulfur in the +6 oxidation state by the reaction of CF_3O radicals may, in principle, enhance or accelerate H_2SO_4 production from SO_2.

The CF_3OSO_2 radical may also be an intermediate in the formation of $CF_3OS(O)_2X$ compounds, where X = OH, halogen, or OR. These compounds include some very stable and very acidic species. Hence, the CF_3OSO_2 radical may contribute to the formation of superacids in the atmosphere. Up until now the occurrence of superacids in the atmosphere and the possible consequences have not been considered. Therefore future work must address the impact of fluorocarbon sulfur compounds on atmospheric chemistry.

Experimental Section

$CF_3OC(O)OOCF_3$ was prepared as a by-product of the synthesis of $CF_3OC(O)OOC(O)OCF_3$ described in the literature.[9] Dry SO_2 was prepared by reaction of commercial $SOCl_2$ (99%, Merck, Darmstadt, Germany) with MgO powder (>98%, Riedel de Haen, Seelze, Germany) in fivefold excess at room temperature over two days. For the isotopic labeling, a mixture of $S^{16}O_2$, $S^{18}O^{16}O$, and $S^{18}O_2$ was prepared by hydrolysis of SCl_2 with $H_2{}^{16}O/H_2{}^{18}O$ mixture (where elemental sulfur and HCl are formed as well). All compounds were purified by trap-to-trap condensation in a glass vacuum line. The matrix experiments used a gas mixture of $CF_3OC(O)OOCF_3$, SO_2, and argon (99.9999%, Messer-Griesheim, Krefeld, Germany) (1:10:1000), which was prepared and stored in a stainless-steel vacuum line which was connected to the thermolysis nozzle by a stainless-steel capillary. The thermolysis device was mounted directly in front of the matrix support and held under high vacuum. The nozzle was heated to 633 K while the matrix support was cooled to 16 K. In a typical experiment 1 mmol of the mixture was deposited in 15 min. The sample was then annealed to 35 K for 5 min and recooled to 16 K. Photolysis experiments were carried out with a 150-W Xe high-pressure lamp (AMKO, Tornesch, Germany) in combination with cut-off filters (Schott, Mainz, Germany) with an irradiation time of 2 min. Details of the matrix apparatus are given elsewhere.[11]

IR spectra were recorded with a FT-IR spectrometer (IFS66v/S, Bruker, Ettlingen, Germany) with an apodized resolution of 0.5 cm^{-1}, and 64 scans were coadded. For measurements in the middle-IR range a KBr beamsplitter, a KBr window, and a DTGS detector were used; in the far-IR range a Ge-covered 6-μm Mylar foil beamsplitter, a PE window, and a DTGS detector were used. UV spectra were recorded with a Lambda 900 spectrometer (Perkin-Elmer, Norwalk CT, USA) with a step size of 1 nm (1 s integration time, slid width 1 nm) and the use of a quartz cable optic (Hellma, Jena, Germany). All spectra were detected in reflection.

 © 2004 Wiley-VCH Verlag GmbH & Co. KGaA, Weinheim

All calculations were performed using the Gaussian98 software package.[12] For accurate structures, energies, and vibrational frequencies the density functional[13] method B3LYP[14,15] with a 6-311++G(3df,3dp) basis set was used. Relaxed-scan calculations along one internal coordinate were conducted using the smaller 6-31+G(d) basis set and the minimum-energy structures were checked by geometry optimization calculations using the larger basis set. The simulation of the IR spectrum of CF_3OSO_2 is based on the calculated [B3LYP/6-311++G(3df,3dp)] band positions and intensities. A Gaussian band shape with a full width at half-maximum of 10 cm^{-1} was applied. The results of the relaxed-scan calculations are found in Figures S1–S4 in the Supporting Information.

Received: February 4, 2004 [Z53925]

Keywords: atmospheric chemistry · density functional calculations · IR spectroscopy · matrix isolation · radicals

[1] J. S. Francisco, M. M. Maricq, *Adv. Photochem.* **1995**, *21*, 79.
[2] J. S. Francisco, M. M. Maricq, *Acc. Chem. Res.* **1996**, *29*, 391.
[3] E. Uherek, *Atmospheric trace gas mixing ratios,* Max Planck Institut für Chemie, Mainz, Germany, **2004** (www.atmosphere.mpg.de/enid/25i.html, **2004**).
[4] Kinetic data from various studies: NIST webbook (http://kinetics.nist.gov) and references therein.
[5] G. A. Argüello, H. Willner, *J. Phys. Chem. A* **2001**, *105*, 3466.
[6] S. von Ahsen, J. Hufen, H. Willner, J. S. Francisco, *Chem. Eur. J.* **2001**, *8*, 1189.
[7] C. Chatgilialoglu, D. Griller, S. Rossini, *J. Org. Chem.* **1989**, *54*, 2734.
[8] F. E. Malanca, G. A. Argüello, E. H. Staricco, *J. Photochem. Photobiol. A: Chem.* **1997**, *103*, 19.
[9] G. A. Argüello, H. Willner, F. E. Malanca, *Inorg. Chem.* **2000**, *39*, 1195.
[10] M. A. Burgos Paci, G. A. Argüello, P. García, H. Willner, *Int. J. Chem. Kinet.* **2003**, *35*, 15.
[11] H. Schnöckel, H. Willner in *Infrared and Raman Spectroscopy. Methods and Applications* (Ed.: B. Schrader), VCH, Weinheim, **1994**, p. 297.
[12] M. J. Frisch, G. W. Trucks, H. B. Schlegel, G. E. Scuseria, M. A. Robb, J. R. Cheeseman, V. G. Zakrzewski, J. J. A. Montgomery, R. E. Stratmann, J. C. Burant, S. Dapprich, J. M. Millam, A. D. Daniels, K. N. Kudin, M. C. Strain, O. Farkas, J. Tomasi, V. Barone, M. Cossi, R. Cammi, B. Mennucci, C. Pomelli, C. Adamo, S. Clifford, J. Ochterski, G. A. Petersson, P. Y. Ayala, Q. Cui, K. Morokuma, D. K. Malick, A. D. Rabuck, K. Raghavachari, J. B. Foresman, J. Cioslowski, J. V. Ortiz, B. B. Stefanov, G. Liu, A. Liashenko, P. Piskorz, I. Komaromi, R. Gomperts, R. L. Martin, D. J. Fox, T. Keith, M. A. Al-Laham, C. Y. Peng, A. Nanayakkara, C. Gonzalez, M. Challacombe, P. M. W. Gill, B. Johnson, W. Chen, M. W. Wong, J. L. Andres, C. Gonzalez, M. Head-Gordon, E. S. Replogle, J. A. Pople, *GAUSSIAN 98 Rev. A.5*, Gaussian Inc., Pittsburgh PA, **1998**.
[13] W. Kohn, L. J. Sham, *Phys. Rev.* **1965**, *140*, 1133.
[14] A. D. Becke, *Phys. Rev. A* **1988**, *38*, 3098.
[15] A. D. Becke, *J. Chem. Phys.* **1993**, *98*, 5648.

 © 2004 Wiley-VCH Verlag GmbH & Co. KGaA, Weinheim

Grignard Reactions

A LiCl-Mediated Br/Mg Exchange Reaction for the Preparation of Functionalized Aryl- and Heteroarylmagnesium Compounds from Organic Bromides**

*Arkady Krasovskiy and Paul Knochel**

Dedicated to Professor Friedrich Bickelhaupt

Polyfunctionalized organometallic reagents are ubiquitous intermediates in modern organic chemistry.[1] One of the best methods for preparing these reagents is the halogen–metal exchange reaction.[1,2] Whereas Br/Li exchange is fast and occurs at low temperatures, the corresponding Br/Mg exchange[3] is considerably slower, which limits its synthetic application for several reasons: 1) The exchange requires higher reaction temperatures and is therefore not compatible with many functional groups; 2) The slow Br/Mg exchange especially for electron-rich aromatic bromides is in competition with the elimination of HBr from the alkyl bromide also produced during the reaction (usually isopropyl bromide) and therefore results in low yields. A catalyzed version of the Br/Mg exchange reaction would be a highly desirable process.

Recently we found that I/Zn exchange can be converted into a catalytic reaction by the addition of [Li(acac)] (10 mol%, acac = acetylacetonato) to an aryl iodide and $i\mathrm{Pr}_2\mathrm{Zn}$.[4] Encouraged by these results, we have examined the effect of salt additives on the rate of Br/Mg exchange.[3] We chose the electron-rich and therefore unreactive 4-bromoanisole (**1a**) and treated it with *i*PrMgCl (1.05 equiv; 1M in THF) in the presence of several lithium salts. A slow Br/Mg exchange occurred in the absence of additives, leading to only 18% conversion after 68 h at room temperature (entry 1, Table 1). Whereas the addition of LiBF_4 resulted in several products (entry 2), the addition of LiBr, LiI, and LiClO_4 gave minor improvements (38–40% conversion; entries 3–5). On the other hand, the addition of LiCl (1 equiv) led to a spectacular rate increase and 70% conversion (entry 6). The addition of smaller amounts of LiCl resulted in lower conversion (entries 7 and 8), whereas larger quantities did not lead to further rate increases (entries 9 and 10). When a

[*] Dr. A. Krasovskiy, Prof. Dr. P. Knochel
Ludwig Maximilians-Universität München
Department Chemie
Butenandtstrasse 5–13, Haus F
81377 München (Germany)
Fax: (+49) 89-2180-77680
E-mail: paul.knochel@cup.uni-muenchen.de

[**] We thank the Fonds der Chemischen Industrie and Merck Research Laboratories (MSD) for financial support. We also thank V. Malakhov for performing some preliminary experiments as well as Chemetall GmbH (Frankfurt), Wacker Chemie GmbH (München), BASF AG (Ludwigshafen), and Bayer-Chemicals AG for generous gifts of chemicals.

Supporting information for this article is available on the WWW under http://www.angewandte.org or from the author.

 DOI: 10.1002/anie.200454084 © 2004 Wiley-VCH Verlag GmbH & Co. KGaA, Weinheim

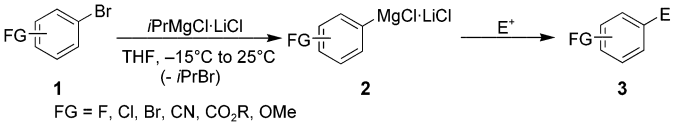
Table 1: Effect of the addition of lithium salts on the formation of 4-methoxyphenylmagnesium chloride at 25 °C after a reaction time of 68 h (1 M solution in THF).

Entry	Additive	Equiv.	Conv. [%][a]
1	–	–	18
2	$LiBF_4$	1.0	5
3	LiBr	1.0	40
4	LiI	1.0	38
5	$LiClO_4$	1.0	38
6	LiCl	1.0	70
7	LiCl	0.25	22
8	LiCl	0.5	43
9	LiCl	1.5	73
10	LiCl	2.0	74
11	LiCl	1.0	84[b]

[a] The conversion of the reaction was determined by GC analysis of reaction aliquots; precision ±2%. [b] The concentration of *i*PrMgCl·LiCl was 2.22 M.

more concentrated solution of *i*PrMgCl·LiCl (2.22 M) was used, 84% conversion was achieved (entry 11).[5] Trapping of **2a** with benzaldehyde furnished the benzhydryl alcohol **3a** in 70% yield (entry 1 of Table 2). Analogous results were obtained with other aryl- and heteroarylmagnesium derivatives (Scheme 1).

Herein we describe the preparation of functionalized arylmagnesium compounds of type **2** using the new reagent

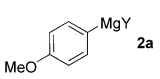
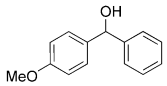
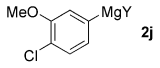
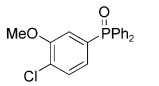
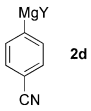
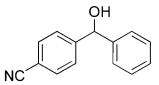
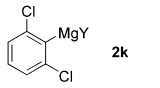
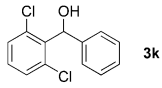
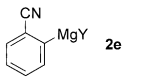
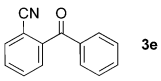
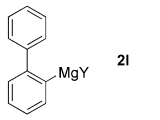
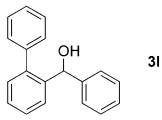
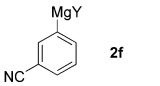
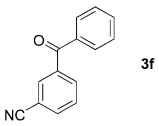
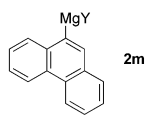
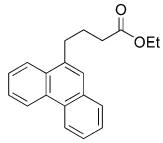
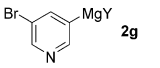
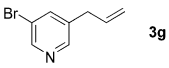
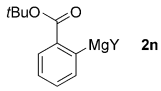
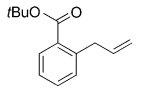
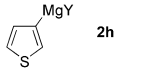
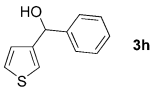
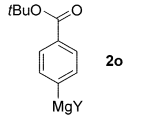
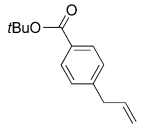
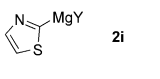
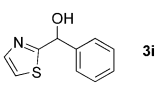
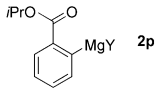
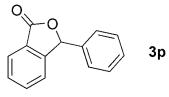


Scheme 1. Preparation of functionalized arylmagnesium reagents.

*i*PrMgCl·LiCl, which was made by adding *i*PrCl to Mg turnings and LiCl (*i*PrCl/Mg/LiCl = 1:1.1:1) in THF. Alternatively, the reagent can be prepared by addition of a solution of *i*PrMgCl in THF to LiCl. This reagent was used for the preparation of a range of aryl- and heteroarylmagnesium derivatives (**2a**–**p**) starting from the corresponding bromides. After the reaction with electrophiles (E^+), the expected products (**3a**–**p**) were isolated in good to excellent yields (Scheme 1 and Table 2).

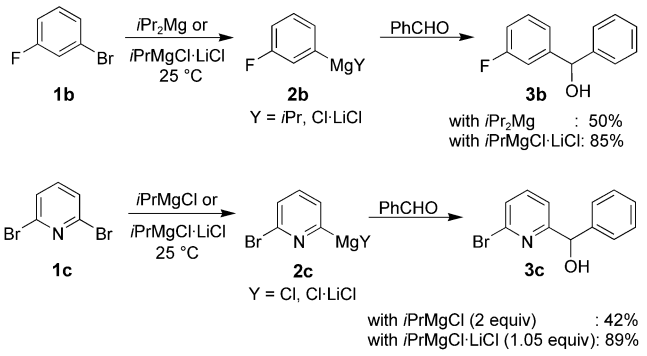
Thus, the previously reported reaction of 1-bromo-3-fluorobenzene (**1b**)[6a] with iPr_2Mg (1.1 equiv, RT, 3 h) provided the corresponding Grignard reagent **2b** with moderate conversion, and after the subsequent reaction with PhCHO the alcohol **3b** was obtained in only 50% yield (Scheme 2). When we conducted the reaction with *i*PrMgCl·LiCl, the alcohol **3b** was obtained in 85% yield. Similarly, the reaction of 2,6-dibromopyridine (**1c**) with *i*PrMgCl (2 equiv) was reported to afford the alcohol **3c** in 42% yield.[6f] By using *i*PrMgCl·LiCl (1.05 equiv), we have now obtained **3c** in 89% yield (Scheme 2).

Table 2: Preparation and reaction of functionalized Grignard reagents of type **2** using *i*PrMgCl·LiCl.

Entry	Grignard reagent[a]	Electrophile	Product	Yield[b]	Entry	Grignard reagent[a]	Electrophile	Product	Yield[b]
1	 **2a**	PhCHO	 **3a**	70	8	 **2j**	$ClPPh_2$	 **3j**	85[d]
2	 **2d**	PhCHO	 **3d**	81	9	 **2k**	PhCHO	 **3k**	83
3	 **2e**	PhCOCl	 **3e**	87[c]	10	 **2l**	PhCHO	 **3l**	90
4	 **2f**	PhCOCl	 **3f**	88[c]	11	 **2m**	$I(CH_2)_3CO_2Et$	 **3m**	81[c]
5	 **2g**	allyl bromide	 **3g**	93[c]	12	 **2n**	allyl bromide	 **3n**	82[c]
6	 **2h**	PhCHO	 **3h**	90	13	 **2o**	allyl bromide	 **3o**	88[c]
7	 **2i**	PhCHO	 **3i**	87	14	 **2p**	PhCHO	 **3p**	80[e]

[a] Y = Cl·LiCl. [b] Yield of isolated analytically pure product. [c] The Grignard reagent was transmetalated with CuCN·2 LiCl before reaction with an electrophile. [d] The reaction mixture was worked up oxidatively with aq. H_2O_2. [e] The exchange reaction was conducted in THF/DMPU (1:3).

 © 2004 Wiley-VCH Verlag GmbH & Co. KGaA, Weinheim

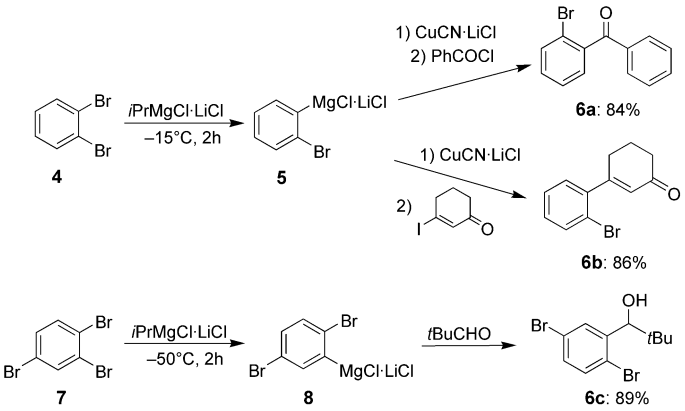


Scheme 2. Br/Mg exchange reactions with various magnesium reagents.

The presence of an electron-withdrawing group considerably increases the exchange rate, and 4-cyanophenylmagnesium chloride (**2d**) was formed within 2 h at 0 °C (> 95% conversion) when *i*PrMgCl·LiCl was employed. In contrast, with *i*PrMgCl a conversion of only 50% was reached. The addition of PhCHO led to the alcohol **3d** in 81% yield (entry 2). The position of the substituent on the aromatic ring is not important, and both 2-cyano- and 3-cyanophenylmagnesium chloride **2e**,**f** were readily prepared and benzoylated in the presence of CuCN·2 LiCl (0.2 equiv; entries 3 and 4). The inductive effect of the cyano group accelerates further the formation of **2e** (1 h, 0 °C) relative to that of **2f** (3 h, 0 °C). Similar reactivity was observed for 5-bromo-3-pyridylmagnesium chloride (**2g**; prepared at −10 °C within 15 min, > 95% conversion). The copper-catalyzed allylation of **2g** led to pyridine **3g** in 93% yield. Other heterocyclic systems such as 3-bromothiophene and 2-bromothiazole reacted smoothly with *i*PrMgCl·LiCl at room temperature furnishing **2h** and **2i**, respectively.[7] After reaction with PhCHO the corresponding alcohols **3h** and **3i**[8] were obtained in yields of 87% and 90%, respectively (Table 2, entries 6 and 7). Aryl bromides bearing electron-donating substituents undergo the Br/Mg exchange only slowly with *i*PrMgCl. The *i*PrMgCl·LiCl reagent was used in an expeditive preparation of the methoxy-substituted Grignard compound **2j**. Reaction with Ph_2PCl provided, after oxidative workup, the phosphane oxide **3j** in 85% yield (entry 8). Similarly, sterically hindered 2,6-dichlorophenylmagnesium chloride (**2k**) was prepared from the corresponding bromide (25 °C, 1 h), and its reaction with PhCHO furnished the alcohol **3k** in 83% yield (entry 9). Various unfunctionalized aromatic Grignard compounds such as **2l** and **2m** can be prepared in high yields as well. Interestingly, the copper derivative of **2m** underwent a smooth cross-coupling with $I(CH_2)_3CO_2Et$ furnishing phenanthrene **3m** in 81% yield (entry 11).[9]

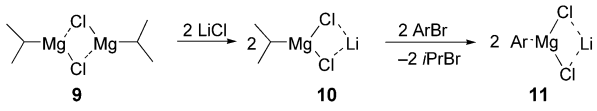
We have also examined the formation of a Grignard reagent bearing an ester functionality. Preliminary results have shown that the presence of LiCl enhances the reactivity of *i*PrMgCl, making the competitive addition to the ester carbonyl group a serious side reaction. However, a *tert*-butyl ester is compatible with the Br/Mg exchange reaction. The copper-catalyzed allylation gave the desired esters **3n** and **3o** in 82% and 88% yields, respectively (entries 12 and 13). Moreover, when a THF/DMPU (1:3; DMPU = 1,3-dimethyltetrahydro-2(1*H*)-pyrimidinone) mixture was used, 2-isopropyl bromobenzoate could serve as a substrate. The resulting Grignard reagent **2p** (−10 °C, 3 h) then reacted with PhCHO leading to lactone **3p** in 80% yield (entry 14).

Only a few reports are available on the preparation of *ortho*-bromophenylmagnesium halides from 1,2-dibromobenzene (**4**).[10] Oshima et al. have reported that lithium tributylmagnesiate (Bu_3MgLi) leads to the formation of benzyne by means of 1,2-elimination and not to *ortho*-bromophenylmagnesium halide (**5**).[6c] The generation of this Grignard reagent can be achieved conveniently with *i*PrMgCl·LiCl. Thus, the reaction of **4** with *i*PrMgCl·LiCl was complete within 2 h at −15 °C and led to the Grignard reagent **5**.[11] After transmetalation with CuCN·2 LiCl,[9] reactions with PhCOCl and 3-iodo-2-cyclohexen-1-one furnished the products **6a** and **6b** in yields of 84% and 86%, respectively. Also unsymmetrical 1,2,4-tribromobenzene (**7**) reacted with *i*PrMgCl·LiCl by means of a highly regioselective Br/Mg exchange to provide exclusively the Grignard reagent **8**,[11] which after reaction with pivalaldehyde gave alcohol **6c**[12] in 89% yield (Scheme 3).



Scheme 3. Selective Br/Mg exchanges of polybromides.

The necessity of using the stoichiometric complex *i*PrMgCl·LiCl leads us to postulate that the addition of LiCl breaks the polymeric aggregates **9** of *i*PrMgCl, producing the reactive complex **10** (Scheme 4).[13] The magnesiate character



Scheme 4. Catalysis of the Br/Mg exchange reaction with LiCl.

of **10** [$iPrMgCl_2^-Li^+$] may be responsible for the enhanced reactivity of this reagent. Interestingly, the magnesiate character of the resulting organometallic complexes **11** is similar to that of a dimeric or oligomeric magnesium reagent prepared in the absence of LiCl (standard Grignard reagent) but the former display higher reactivity towards electrophiles.

 © 2004 Wiley-VCH Verlag GmbH & Co. KGaA, Weinheim

In conclusion, we have shown that *i*PrMgCl·LiCl can be used for the simple, high-yielding preparation of a broad range of functionalized aryl- and heteroarylmagnesium reagents starting from cheap and readily available aryl bromides.[14] All reactions proceed within a convenient range of temperatures (−15 °C–RT) and can be extended to the large-scale preparation of Grignard reagents. We have demonstrated for the first time the promoter effect of LiCl in the Br/Mg exchange reaction. Extensions of this work are currently underway in our laboratories.

Experimental Section

1) Preparation of the reagent *i*PrMgCl·LiCl: Magnesium turnings (110 mmol) and anhydrous LiCl (100 mmol) were placed in an Ar-flushed flask, and THF (50 mL) was added. A solution of *i*PrCl (100 mmol) in THF (50 mL) was slowly added at room temperature. The reaction started within a few minutes. After the addition, the reaction mixture was stirred for 12 h at room temperature. The gray solution of *i*PrMgCl·LiCl was cannulated into another Ar-filled flask and removed in this way from excess magnesium. *i*PrMgCl·LiCl was obtained in a yield of ca. 95–98 %.

2) Typical procedure (**3g**): A dry and argon-flushed 10-mL flask equipped with a magnetic stirrer and a septum was charged with *i*PrMgCl·LiCl (1 mL, 1.05 M in THF, 1.05 mmol). The reaction mixture was cooled to −15 °C, and 3,5-dibromopyridine (237 mg, 1.0 mmol) was added in one portion. The reaction temperature was increased to −10 °C, and the Br/Mg exchange was complete after 15 min (checked by GC analysis of reaction aliquots, the conversion was more than 98 %). Allyl bromide (133 mg, 1.1 mmol) was added, followed by addition of one drop of CuCN·2 LiCl (a 1.0 M solution in THF was used, ca. 0.02 mmol, 0.02 equiv). The reaction mixture was stirred for 1 h at 0 °C and was then quenched with saturated aqueous NH_4Cl solution (2 mL). The aqueous phase was extracted with ether (3 × 4 mL), dried with Na_2SO_4, and concentrated in vacuo. The crude residue was purified by flash chromatography (CH_2Cl_2) yielding 3-allyl-5-bromopyridine (**3g**; 184 mg, 93 %) as a colorless oil.

Received: February 23, 2004 [Z54084]
Published Online: May 26, 2004

Keywords: C–C coupling · copper · cross-coupling · Grignard reaction · heterocycles

[1] A. Boudier, L. O. Bromm, M. Lotz, P. Knochel, *Angew. Chem.* **2000**, *112*, 4584; *Angew. Chem. Int. Ed.* **2000**, *39*, 4414.

[2] a) W. F. Bailey, J. J. Patricia, *J. Organomet. Chem.* **1988**, *352*, 1; b) W. F. Bailey, E. R. Punzalan, *J. Org. Chem.* **1990**, *55*, 5404; c) W. F. Bailey, J. D. Brubaker, K. P. Jordan, *J. Organomet. Chem.* **2003**, *681*, 210; d) E. Negishi, D. R. Swanson, C. J. Rousset, *J. Org. Chem.* **1990**, *55*, 5406; e) G. Boche, M. Schimeczek, J. Cioslowski, P. Piskorz, *Eur. J. Org. Chem.* **1998**, 1851; f) H. J. Reich, M. J. Bevan, B. O. Gudmundsson, C. L. Puckett, *Angew. Chem.* **2002**, *114*, 3586; *Angew. Chem. Int. Ed.* **2002**, *41*, 3436; g) C. E. Tucker, T. N. Majid, P. Knochel, *J. Am. Chem. Soc.* **1992**, *114*, 3983; h) R. W. Hoffmann, P. G. Nell, R. Leo, K. Harms, *Chem. Eur. J.* **2000**, *6*, 3359; i) R. W. Hoffmann, B. Holzer, O. Knopff, K. Harms, *Angew. Chem.* **2000**, *112*, 3206; *Angew. Chem. Int. Ed.* **2000**, *39*, 3072.

[3] a) L. Boymond, M. Rottländer, G. Cahiez, P. Knochel, *Angew. Chem.* **1998**, *110*, 1801; *Angew. Chem. Int. Ed.* **1998**, *37*, 1701; b) A. E. Jensen, W. Dohle, I. Sapountzis, D. M. Lindsay, V. A. Vu, P. Knochel, *Synthesis* **2002**, 565; c) P. Knochel, W. Dohle, N. Gommermann, F. F. Kneisel, F. Kopp, T. Korn, I. Sapountzis, V. A. Vu, *Angew. Chem.* **2003**, *115*, 4438; *Angew. Chem. Int. Ed.* **2003**, *42*, 4302.

[4] F. F. Kneisel, M. Dochnahl, P. Knochel, *Angew. Chem.* **2004**, *116*, 1032; *Angew. Chem. Int. Ed.* **2004**, *43*, 1017.

[5] Interestingly, we have noticed that the addition of LiO*t*Bu (1 equiv, 1 M solution) resulted in 92 % conversion under the same reaction conditions. However, the reagent *i*PrMgCl·LiO*t*Bu seems to be of less general use than *i*PrMgCl·LiCl. See also: a) J. J. Farkas, S. J. Stoudt, E. M. Hanawalt, A. D. Pajerski, H. G. J. Richey, *Organometallics* **2004**, *23*, 423; b) E. M. Hanawalt, J. J. Farkas, H. G. J. Richey, *Organometallics* **2004**, *23*, 416.

[6] a) M. Abarbri, F. Dehmel, P. Knochel, *Tetrahedron Lett.* **1999**, *40*, 7449; for the synthesis of arylmagnesium species starting from aryl bromides using lithium organomagnesiates for the Br/Mg exchange reaction, see: b) K. Kitagawa, A. Inoue, H. Shinokubo, K. Oshima, *Angew. Chem.* **2000**, *112*, 2594; *Angew. Chem. Int. Ed.* **2000**, *39*, 2481; c) A. Inoue, K. Kitagawa, H. Shinokubo, K. Oshima, *J. Org. Chem.* **2001**, *66*, 4333; d) A. Inoue, K. Kitagawa, H. Shinokubo, K. Oshima, *Tetrahedron* **2000**, *56*, 9601; e) F. Trécourt, G. Breton, V. Bonnet, F. Mongin, F. Marsais, G. Queguiner, *Tetrahedron Lett.* **1999**, *40*, 4339; f) F. Trécourt, G. Breton, V. Bonnet, F. Mongin, F. Marsais, G. Quéguiner, *Tetrahedron* **2000**, *56*, 1349.

[7] We treated 2-bromo-, 3-bromopyridine, and 2-bromothiophene with *i*PrMgCl·LiCl and obtained ca. 15–20 % better yields than the analogous reactions with $BuMe_2MgLi$.[6c]

[8] Previous exchange conditions required both an excess of iPr_2Mg and of PhCHO (> 2 equiv).[6a]

[9] P. Knochel, M. C. P. Yeh, S. C. Berk, J. Talbert, *J. Org. Chem.* **1988**, *53*, 2390.

[10] Y. Van der Winkel, O. S. Akkerman, F. Bickelhaupt, *Main Group Met. Chem.* **1988**, *11*, 91.

[11] The half-lives of magnesium reagents **5** and **8** at −10 °C are 24 h and 12 h, respectively.

[12] The regioselective formation of Grignard reagent **8** was proved by quenching with water, which led to the formation of 1,4-dibromobenzene in quantitative yield.

[13] The heterometallic organomagnesium complex RMgBr·LiBr·3 THF (R = $(Me_3Si)_3C$) has been structurally characterized: N. H. Buttrees, C. Eaborn, M. N. A. E-Khely, P. B. Hitchcock, J. D. Smith, K. Tavakkoli, *J. Chem. Soc. Dalton Trans.* **1988**, 381.

[14] A patent application has been filed.

 © 2004 Wiley-VCH Verlag GmbH & Co. KGaA, Weinheim

DNA Modification

Generation and Enzymatic Amplification of High-Density Functionalized DNA Double Strands**

*Stefan Jäger and Michael Famulok**

Dedicated to Professor Julius Rebek, Jr. on the occasion of his 60th birthday

The specific pairing of DNA bases in double-stranded DNA (dsDNA) provides an intriguing rationale for the straightforward generation of molecular assemblies on the nanometer scale and has led to growing interest in the exploitation of DNA for nanotechnology, material science, computing, and biotechnology purposes.[1] The application of conventional DNA molecules for these purposes by utilization of simple Watson–Crick pairing has already led to considerable progress in the generation of an impressive variety of topological two- and three-dimensional geometries, nanomechanical devices, and supramolecular assemblies.[2] In addition, DNA exhibits unique template properties which allows for its enzymatic replication and amplification by DNA polymerases and enables the development of sensors based on nucleic acids, therapeutics, and catalysts by in vitro evolution.[3]

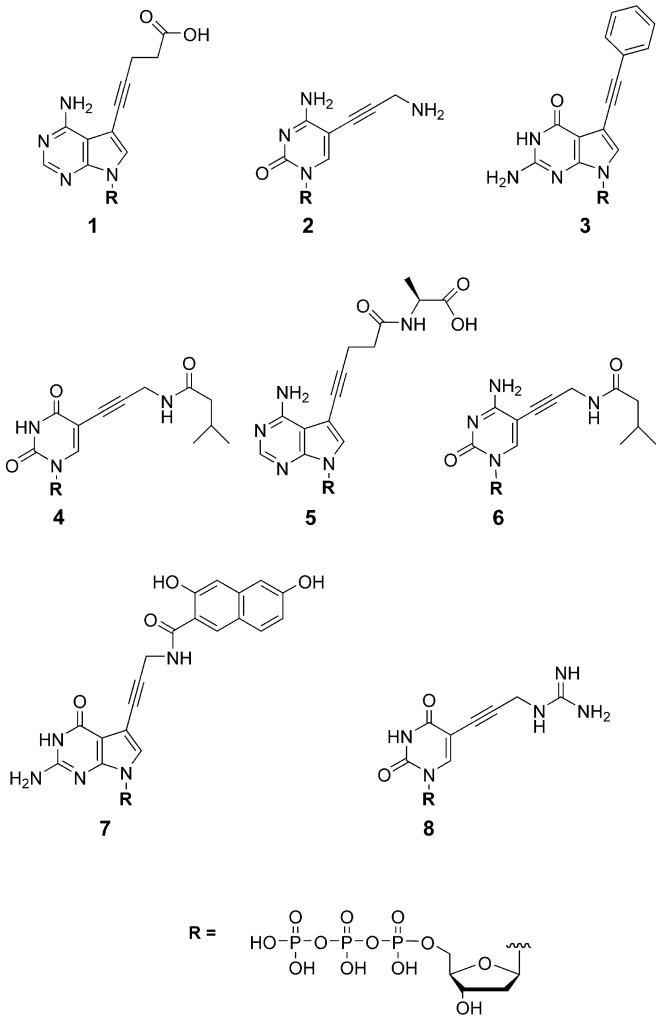
The scope of applications of dsDNA in nanotechnology would be greatly expanded if DNA molecules could be modified in a base-specific fashion with additional chemical functionalities that could be employed for other functions and interactions apart from Watson–Crick pairing. For maximal flexibility, it would be important to develop strategies that allow for the modification of as many base positions as possible within a given DNA strand without interfering with base pairing. To achieve replication and amplification of such nanostructured systems DNA polymerases that tolerate a broad range of substrates and templates would have to be generated by in vitro evolution.[4] Alternatively, reaction conditions would have to be found that enable enzymes to process unnatural templates and monomers that are usually not replicated. This would open up the possibility to synthesize longer DNA constructs (>100 bp) which are usually inaccessible synthetically. As a consequence, a larger sequence space of functionalized DNA molecules, including amplifiable libraries for in vitro selection experiments, could be generated faster and more easily.

[*] Dipl. Chem. S. Jäger, Prof. Dr. M. Famulok
Kekulé-Institut für Organische Chemie und Biochemie
Universität Bonn
Gerhard-Domagk-Strasse 1, 53121 Bonn (Germany)
Fax: (+49) 228-735-388
E-mail: m.famulok@uni-bonn.de

[**] This work was supported by the Deutsche Forschungsgemeinschaft (SFB 624) and by the Fonds der Chemischen Industrie. We thank A. Marx, G. Rasched, O. Thum, and S. Brakmann for helpful discussions.

Supporting information for this article is available on the WWW under http://www.angewandte.org or from the author.

A series of chemically modified 2′-deoxynucleoside triphosphates has already been synthesized, and the template-directed enzymatic polymerization of up to two different modified nucleotides was achieved by primer extension or polymerase chain reaction (PCR).[5,6] Single-stranded high-density functionalized DNA (fDNA) in which every base is modified with additional functionality can be generated by enzymatic primer extension of base-modified deoxynucleoside triphosphates (dNTPs) using conventional DNA as a template.[7,8] Single-stranded fDNAs containing residues **1**–**3** and **8** (Scheme 1) can in turn serve as templates in PCR



Scheme 1. Chemical structures of base-modified 2′-deoxynucleoside-5′-*O*-triphosphates.

reactions with natural nucleotides.[7] However, the utilization of a high-density fDNA template for the enzymatic synthesis of the corresponding fDNA counterstrand has so far been unsuccessful. For this to occur, the polymerase would not only have to recognize the functionalized DNA strand as a template, but would also have to be able to incorporate modified bases—according to the directions of the template—opposite a certain base modification. The ability to do so would not only allow for the straightforward synthesis of

 DOI: 10.1002/anie.200453926 © 2004 Wiley-VCH Verlag GmbH & Co. KGaA, Weinheim

fDNA double strands and their enzymatic amplification, but would also enable the introduction of even further chemical diversity into the counterstrand. Consequently, both strands could be decorated with different chemical groups sequence-specifically. Functionalized dsDNA modified at high density in such a way would enable the directed assembly of completely novel supramolecular structures which could not be accessed using conventional dsDNA.

Herein we describe the first example of an enzymatically synthesized fDNA double strand in which all four nucleobases in each strand are substituted with various base analogues, thus allowing the introduction of up to eight different modifications into one dsDNA. The dNTP derivatives used (Scheme 1) cover a broad range of different functionalities, such as aromatic (**3**, **7**), basic (**2**, **8**), acidic (**1**, **5**), and lipophilic residues (**4**, **6**).[9] Furthermore, we have established a screen to identify and optimize conditions that enable the direct amplification of fully modified fDNA by PCR.

We synthesized a fully functionalized fDNA template enzymatically under similar conditions as described before from a 79 nucleotide 5′-biotinylated DNA template **M79** using dNTPs **1**–**4**.[7,10] The dNTPs **1**–**4** proved to be good substrates for the Vent(exo-), and Pwo DNA polymerase and replaced their natural counterparts sequence specifically (data not shown). We then tested whether **fM79** could serve as a template in standard primer extensions in the presence of dNTPs **1–4** using Pwo DNA polymerase.

As shown in Figure 1 a, full-length double-stranded fDNA could be obtained (lane 5), whereas omitting one of the four modified dNTPs resulted in premature termination of the counterstrand synthesis (lanes 1–4). A primer extension using nonfunctionalized **M79** template in the presence of natural dNTPs served as a size marker (lane M). Figure 1 b shows the same set of experiments, but this time a new set of modified dNTPs **5**–**8** (Scheme 1) was used that bear chemical functionalities different from those in the **fM79** template modified with **1**–**4**. Again, the full-length primer extension product was obtained (lane 10). This product represents the first example of a high-density functionalized dsDNA in which each strand contains a different set of modifications in one fDNA double strand. Furthermore, these data show that Pwo DNA polymerase not only accepts a high-density functionalized DNA single strand as a template, but is also capable of template-directed incorporation of all four modified dNTPs opposite a modified base.

We next investigated whether the conditions under which primer extension could be achieved would also allow for amplification of double-stranded fDNA under PCR conditions. PCR amplification under standard buffer conditions with the **fM79** template and the modified dNTPs **1**–**4** did not result in amplification of product with the desired length (Figure 2 b, lane 1a). Therefore, we tested different concen-

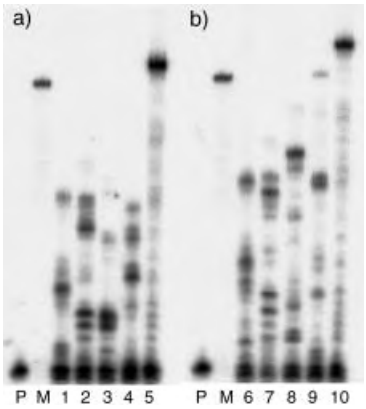


Figure 1. Primer extension experiments with ^{32}P-labeled primer **P5**′ and template **fM79**, modified dNTPs, and Pwo polymerase, with analysis by gel electrophoresis (8% denaturing polyacrylamide). a) Lanes: P: primer; M: primer extension with four natural dNTPs and **M79** as template; 1: reactions with modified nucleotides **2**–**4**; 2: **1**, **3**, and **4**; 3: **1**, **2**, and **4**; 4: **1**–**3**; 5: **1**–**4**. b) Lanes P: primer; M: primer extension with four natural dNTPs and **M79** as template; 6: **6**–**8**; 7: **5**, **7**, and **8**; 8: **5**, **6**, and **8**; 9: **5**–**7**; 10: **5**–**8**.

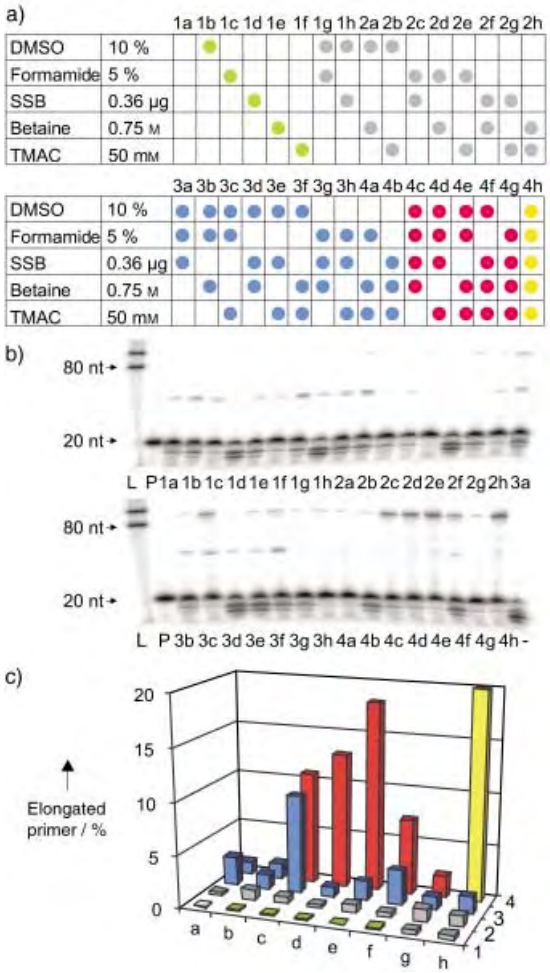


Figure 2. Combinatorial screen of 32 different buffer conditions for the PCR. The PCR experiments included ^{32}P-labeled primer **P5**′, dNTPs **1**–**4**, and template **fM79.** Lane numbers 1a–4h refer to the different combinations of additives. The PCR products were analyzed by gel electrophoresis (10% denaturing polyacrylamide). a) Reaction buffers. Dots indicate the presence of the respective additive in the PCR buffer. b) Lanes L: length marker; P: primer; 1a–4h: PCR reactions with the respective buffer conditions (a); (−): control without template. c) Quantification of the PCR products by PhosphorImaging as the percentage of the total radioactivity.

 © 2004 Wiley-VCH Verlag GmbH & Co. KGaA, Weinheim

trations of various additives, such as tetramethylammonium chloride (TMAC), dimethyl sulfoxide (DMSO), formamide, *E. coli* single-strand binding protein (SSB), and betaine, which are known to have a positive effect on PCR reactions using the highly thermostable Pwo DNA polymerase. No significant improvement was observed when either of these components was added to the PCR reactions alone (Figure 2b, lanes 1b-f).

We performed a combinatorial screen of all possible permutations of combinations of the five additives to investigate the possibility that combinations of these additives would improve PCR amplification. Figure 2a shows all the various compositions of additives. The quantified results are presented in Figure 2b and c. As a positive control of polymerase activity we tested the same buffer conditions using natural dNTPs as the monomer source (see Supporting Information).

Indeed, considerable amounts of full-length high-density functionalized dsDNA PCR products could be obtained with certain combinations of at least three different additives, although in the "three-component-set" (Figure 2, 3a–4b, blue dots) only combination 3c led to significant amplification. Combinations of four different components significantly improved the amount of PCR product, except for 4f and 4g (Figure 2) in which either DMSO or formamide were omitted. Addition of all five components (4h) did not significantly improve the results obtained with combination 4e, which led to the best result in the "four-component set" (4c–4g, red dots). The amount of high-density modified dsDNA obtained corresponds to about 30% of the amount obtained in the control experiment in which the natural dNTPs were used exclusively with the same number of cycles (see Supporting Information). These data thus allow the conditions to be defined that enable PCR amplification of high-density functionalized double-stranded fDNA using functionalized dNTPs as the only monomer source.

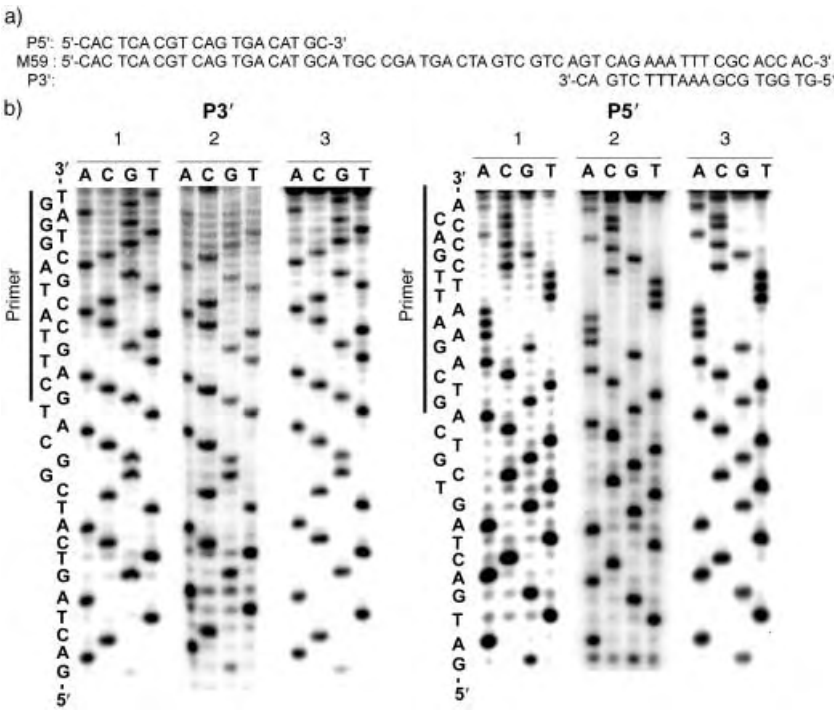


Figure 3. Autoradiograms of the Sanger dideoxy sequencing reaction with T7 DNA polymerase. a) Sequencing primers **P3′**, **P5′**, and template **M59**. b) 1. Sequencing of the original template **M59**; 2. sequencing of fully functionalized DNA **fM59**, which was generated by PCR with modified dNTPs **1**–**4**. 3. Sequencing of a PCR product derived from **fM59** as a template and natural dNTPs. Sequences were read in both directions with primers **P3′** and **P5′**. The sequencing patterns from the original template **M59** (1), the direct sequencing of fDNA **fM59** (2), and of the natural PCR product derived from functionalized **fM59** as template (3) are indistinguishable.

To investigate the accuracy of the incorporation of the modified nucleotides and the PCR amplification of fDNA under conditions 4e (Figure 2) with Pwo DNA polymerase we synthesized a fully modified double-stranded fDNA in 20 PCR cycles from a DNA template **M59** (Figure 3a) and dNTPs **1**–**4** (Scheme 1). The strands were separated (see Supporting Information) and sequenced using T7 DNA polymerase by the dideoxy method developed by Sanger (Figure 3b, 2). To verify that the additional bands did not originate from mis-incorporation of modified nucleotides we amplified the modified template **fM59** with natural dNTPs and sequenced the resulting natural dsDNA (Figure 3b, 3). As a control we also amplified and sequenced the original template **M59** (Figure 3b, 1). Comparison of the sequencing patterns shows that the sequence information is conserved during PCR amplification with **1**–**4** and that the incorporation of the modified nucleotides is sequence-specific within the accuracy of a sequencing reaction. Interestingly, similar to Pwo polymerase, T7 DNA polymerase is also able to read modified DNA strands correctly.

Furthermore, we examined whether the high-density modification of a dsDNA affects the conformation relative to that obtained with the corresponding nonmodified dsDNA. Indeed, comparison of the CD spectra of both species revealed that a natural dsDNA version of **M59** showed a typical B-DNA spectrum (Figure 4, ▲), while functionalized double-stranded DNA of the same sequence **fM59** (Figure 4, □) showed the same inversion of the CD spectrum as observed originally for Z-DNA under the same conditions.[11] A similar inversion of the CD spectra was observed by Brakmann and Löbermann when all the pyrimidine residues of one strand were substituted with fluorescently labeled analogues.[6] However, the wavelengths observed in the CD spectra of fDNA **fM59** are significantly shifted compared to those with unmodified Z-DNA motifs, which might be a result of the altered polarizability of the nucleobases. Similar wavelength shifts were found in short DNA duplexes that contained sporadic alkinyl-modified purines and pyrimidines.[12] The CD spectra obtained in this study showed more similarity to B-DNA, in contrast to the fully modified

 © 2004 Wiley-VCH Verlag GmbH & Co. KGaA, Weinheim

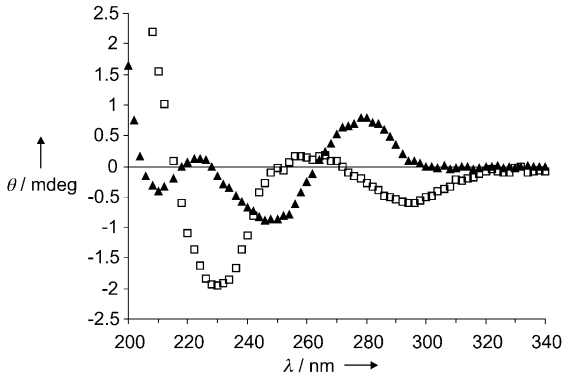


Figure 4. CD spectra of natural, unmodified dsDNA **M59** (▲) and dsDNA **fM59** fully modified with dNTPs **1**–**4** (□).

sequence investigated here, which suggests that the conformation of the fully modified dsDNA changes from a right-handed B-type to a left-handed Z-type DNA.

Interestingly, the visualization and quantification of the double-stranded fDNA products shown in Figure 2b necessitated the use of a radiolabeled primer because these products could only be slightly stained with ethidium bromide. Presumably, the presence of the modifications at the 5-position of the pyrimidines and at the 7-position of the purines not only leads to a conformational change but also to sterically hindering intercalation.

In conclusion, this study demonstrates for the first time that high-density DNA double strands can be generated enzymatically in a template-directed fashion and can be amplified by PCR under certain conditions. Remarkably, a natural DNA polymerase is capable of selecting the correct base-modified nucleoside triphosphate opposite a modification in the template and of catalyzing its incorporation into the growing counterstrand. The incorporation of chemical functionalities into a DNA double strand at high-density with nanoscale resolution opens up the possibility to program higher-order dsDNA architectures, assembled through base pairing, with additional functionalities. Thus, this approach offers significant potential to facilitate the construction of complex nanoscale objects and materials based on DNA.

Received: February 4, 2004 [Z53926]
Published Online: May 26, 2004

Keywords: DNA replication · nanostructures · polymerase chain reaction · polymerases

[1] N. C. Seeman, *Angew. Chem.* **1998**, *110*, 3408 – 3428; *Angew. Chem. Int. Ed.* **1998**, *37*, 3220 – 3238.
[2] a) N. C. Seeman, *Nature* **2003**, *421*, 427 – 431; b) W. M. Shih, J. D. Quispe, G. F. Joyce, *Nature* **2004**, *427*, 618 – 621; c) N. C. Seeman, *Biochemistry* **2003**, *42*, 7259 – 7269; d) N. C. Seeman, *Chem. Biol.* **2003**, *10*, 1151 – 1159; e) N. C. Seeman, *Trends Biotechnol.* **1999**, *17*, 437 – 443; f) L. H. Eckardt, K. Naumann, W. M. Pankau, M. Rein, M. Schweitzer, N. Windhab, G. von Kiedrowski, *Nature* **2002**, *420*, 286; g) A. Csaki, G. Maubach, D. Born, J. Reichert, W. Fritzsche, *Single Mol.* **2002**, *3*, 275 – 280; h) C. A. Mirkin, *Inorg. Chem.* **2000**, *39*, 2258 – 2272; i) C. M. Niemeyer, *Angew. Chem.* **2001**, *113*, 4254 – 4387; *Angew. Chem. Int. Ed.* **2001**, *40*, 4128 – 4158; j) C. M. Niemeyer, M. Adler, *Angew. Chem.* **2002**, *114*, 3933 – 3937; *Angew. Chem. Int. Ed.* **2002**, *41*, 3779 – 3783.
[3] a) T. Hermann, D. J. Patel, *Science* **2000**, *287*, 820 – 825; b) M. Famulok, M. Blind, G. Mayer, *Chem. Biol.* **2001**, *8*, 931 – 939; c) C. K. O'Sullivan, *Anal. Bioanal. Chem.* **2002**, *372*, 44 – 48; d) S. Verma, S. Jäger, O. Thum, M. Famulok, *Chem. Rec.* **2003**, *3*, 51 – 60; e) M. Famulok, A. Jenne, *Top. Curr. Chem.* **1999**, *202*, 101 – 131.
[4] a) F. J. Ghadessy, J. L. Ong, P. Holliger, *Proc. Natl. Acad. Sci.* USA **2001**, *98*, 4552 – 4557; b) J. L. Jestin, P. Kristensen, G. Winter, *Angew. Chem.* **1999**, *111*, 1196 – 1200; *Angew. Chem. Int. Ed.* **1999**, *38*, 1124 – 1127; c) M. Fa, A. Radeghieri, A. A. Henry, F. E. Romesberg, *J. Am. Chem. Soc.* **2004**, *126*, 1748 – 1754.
[5] a) K. Sakthivel, C. F. Barbas III, *Angew. Chem.* **1998**, *110*, 2998 – 3001; *Angew. Chem. Int. Ed.* **1998**, *37*, 2872 – 2875; b) D. M. Perrin, T. Garestier, C. Hélène, *Nucleosides Nucleotides* **1999**, *18*, 377 – 391; c) S. E. Lee, A. Sidorov, T. Gourlain, N. Mignet, S. J. Thorpe, J. A. Brazier, M. J. Dickman, D. P. Hornby, J. A. Grasby, D. M. Williams, *Nucleic Acids Res.* **2001**, *29*, 1565 – 1573; d) T. Gourlain, A. Sidorov, N. Mignet, S. J. Thorpe, S. E. Lee, J. A. Grasby, D. M. Williams, *Nucleic Acids Res.* **2001**, *29*, 1898 – 1905; e) H. A. Held, S. A. Benner, *Nucleic Acids Res.* **2002**, *30*, 3857 – 3869; f) D. Summerer, A. Marx, *Angew. Chem.* **2001**, *113*, 3806 – 3808; *Angew. Chem. Int. Ed.* **2001**, *40*, 3693 – 3695; g) M. M. Masud, A. Ozaki-Nakamura, M. Kuwahara, H. Ozaki, H. Sawai, *ChemBioChem* **2003**, *4*, 584 – 588; h) J. C. Chaput, J. W. Szostak, *J. Am. Chem. Soc.* **2003**, *125*, 9274 – 9275.
[6] S. Brakmann, S. Löbermann, *Angew. Chem.* **2001**, *113*, 1473 – 1476; *Angew. Chem. Int. Ed.* **2001**, *40*, 1427 – 1429.
[7] O. Thum, S. Jäger, M. Famulok, *Angew. Chem.* **2001**, *113*, 4112 – 4115; *Angew. Chem. Int. Ed.* **2001**, *40*, 3990 – 3993.
[8] M. A. Augustin, W. Ankenbauer, B. Angerer, *J. Biotechnol.* **2001**, *86*, 289 – 301.
[9] The synthesis of the nucleotides **1**–**6** and **8** will be published elsewhere. Nucleotide **7** was purchased from Perkin–Elmer.
[10] Further information on the synthesis of **fM79**, primer extension assay, PCR conditions, screening, and sequencing reactions can be found in the Supporting Information.
[11] F. M. Pohl, T. M. Jovin, *J. Mol. Biol.* **1972**, *67*, 375 – 396.
[12] J. L. He, F. Seela, *Nucleic Acids Res.* **2002**, *30*, 5485 – 5496.

 © 2004 Wiley-VCH Verlag GmbH & Co. KGaA, Weinheim

Cover Picture

Shannon S. Stahl*



Environmentally friendly chemistry is often inspired by nature itself. This principle is portrayed in the cover picture depicting recent advances in the palladium-catalyzed selective oxidation of organic molecules with molecular oxygen. In the Review on pp. 3400 ff., S. S. Stahl outlines the mechanistic principles and diversity of applications of "Palladium Oxidase Catalysis". These catalytic reactions are reminiscent of enzymatic oxidases in which independent dioxygen reduction and substrate oxidation steps are coupled in a sequential, two-stage mechanism.

Contents

Angewandte EarlyView

The following Communications are available online (in Wiley InterScience). You can find them, as well as forthcoming Reviews, Highlights, and Essays, at www.angewandte.org, under Early View.

P. Wang, A. Fichera, K. Kumar, D. A. Tirrell:*
Alternative Translations of a Single RNA Message: An Identity Switch of (2*S*,3*R*)-4,4,4-Trifluorovaline between Valine and Isoleucine Codons
DOI: 10.1002/anie.200454036
Published online: June 21, 2004

A. Pfitzner, M. F. Bräu, J. Zweck, G. Brunklaus, H. Eckert*:*
Phosphorus Nanorods—Two Allotropic Modifications of a Long-Known Element
DOI: 10.1002/anie.200460244
Published online: June 17, 2004

Z. Deng, C. Mao:*
Molecular Lithography with DNA Nanostructures
DOI: 10.1002/anie.200460257
Published online: June 17, 2004

Articles judged by the referees or the editor as being either very important or very urgent are immediately edited, proof-read, and electronically published once the manuscript has arrived in the editorial office in its final form. As long as there is no page number available these articles should be cited in the following manner:

Author(s), *Angew. Chem. Int. Ed.*, online publication date, DOI.

Obituary

S. Chandrasekhar (1930–2004): Discotic Liquid Crystals ——— **3360** *P E. Cladis, B. R. Ratna and R. Shashidar*

Books

Photochromism ——— **3362** Heinz Dürr, Henri Bouas-Laurent *reviewed by K. Uchida*

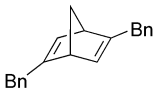
Affinity, that Elusive Dream ——— **3362** Mi Gyung Kim *reviewed by S. Tomic, P. M. Vauthelin*

Highlights

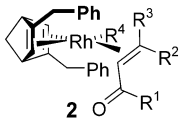
Ligand Design

F. Glorius* ——— **3364 – 3366**

Chiral Olefin Ligands—New "Spectators" in Asymmetric Catalysis



1

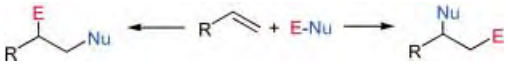


2

Bidentate chiral olefin ligands such as **1** (shown with its catalytically active Rh complex **2**) have been applied successfully in asymmetric catalysis recently. New coordination geometries are possible with this class of ligands, and the electronic character of the olefin ligand can be varied over a wide range, leading to catalysts with increased stability, selectivity, and catalytic activity.

 © 2004 Wiley-VCH Verlag GmbH & Co. KGaA, Weinheim

Reviews

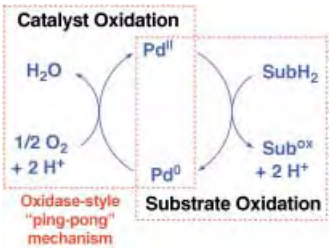


It was the 19th century when Markovnikov set out his rules for the regioselectivity of addition reactions to C—C multiple bonds. Despite the traditional view, it is often possible nowadays to direct the regioselectivity of such reactions towards the Markovnikov or anti-Markovnikov products by using transition-metal catalysts (see picture). In this Review, recent progress in the selective functionalization of alkenes and alkynes is described.

Addition to C–C Multiple Bonds

M. Beller, J. Seayad, A. Tillack, H. Jiao ——— **3368 – 3398**

Catalytic Markovnikov and anti-Markovnikov Functionalization of Alkenes and Alkynes: Recent Developments and Trends



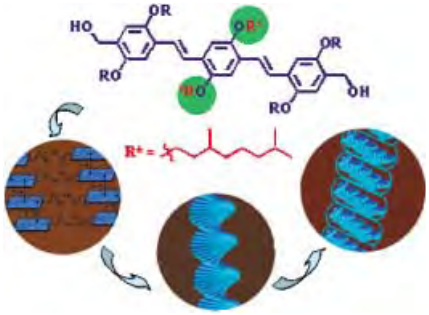
A long-term goal of synthetic and catalytic chemistry for several decades has been the selective oxidation of organic chemicals with molecular oxygen. This goal is rapidly becoming a reality with the development of new "palladium oxidase" reactions. New catalysts exhibit improved stability and activity and they utilize oxidatively stable ligands that modulate reaction selectivity.

Catalytic Oxidations

S. S. Stahl* ——— **3400 – 3420**

Palladium Oxidase Catalysis: Selective Oxidation of Organic Chemicals by Direct Dioxygen-Coupled Turnover

Communications



Left-handed-helical nanoropes are formed from higher-order self-assemblies of chiral aggregates during the gelation of a rigid π-conjugated oligo(*p*-phenylenevinylene) with remote chiral handles (see picture; R = $C_{12}H_{25}$). The concentration- and temperature-dependent CD-signal changes observed for these assemblies are indicative of a helix transition. This process is reminiscent of the folding and unfolding of helical biological macromolecules.

Helical Nanostructures

S. J. George, A. Ajayaghosh,* P. Jonkheijm, A. P. H. J. Schenning, E. W. Meijer ——— **3422 – 3425**

Coiled-Coil Gel Nanostructures of Oligo(*p*-phenylenevinylene)s: Gelation-Induced Helix Transition in a Higher-Order Supramolecular Self-Assembly of a Rigid π-Conjugated System

For the USA and Canada:
ANGEWANDTE CHEMIE International Edition (ISSN 1433-7851) is published weekly by Wiley-VCH PO Box 191161, D 69451 Weinheim, Germany. Air freight and mailing in the USA by Publications Expediting Inc. 200 Meacham Ave., Elmont, NY 11003. Periodicals postage paid at Jamaica NY 11431. US POSTMASTER: send address changes to *Angewandte Chemie*, Wiley-VCH, 111 River Street, Hoboken, NJ 07030. Annual subscription price for institutions: Europe € 3430.00/3118.00; outside Europe US$ 4499.00/4090.00 (valid for print and electronic/print or electronic delivery); for individuals who are personal members of a national chemical society, or whose institution already subscribes, or who are retired or self-employed consultants, print only: Europe € 248.00/outside Europe US$ 378.00. Postage and handling charges included. All Wiley-VCH prices are exclusive VAT.

 © 2004 Wiley-VCH Verlag GmbH & Co. KGaA, Weinheim

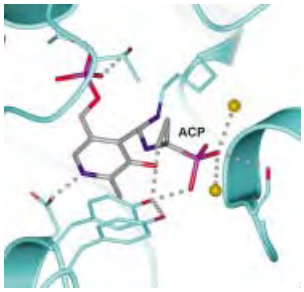
Contents

Enzymatic Mechanisms

S. Karthikeyan, Z. Zhao, C.-I. Kao, Q. Zhou, Z. Tao, H. Zhang,* H.-w. Liu* ——— **3425 – 3429**

Structural Analysis of 1-Aminocyclopropane-1-Carboxylate Deaminase: Observation of an Aminyl Intermediate and Identification of Tyr294 as the Active-Site Nucleophile

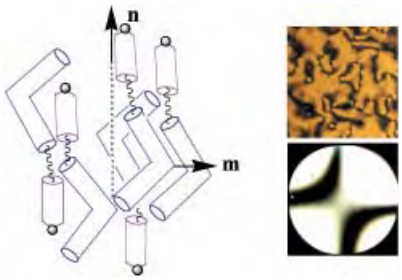
Finding an angle of attack: Structural studies of 1-aminocyclopropane-1-carboxylate (ACC) deaminase complexed with the tight-binding inhibitor 1-aminocyclopropanephosphonate (ACP, see picture) revealed the existence of an aminyl adduct intermediate. The crystal structure of the enzyme and mutation studies suggest that the ring cleavage of ACC is initiated by nucleophilic attack by Tyr294.



Liquid Crystals

C. V. Yelamaggad, S. Krishna Prasad,* G. G. Nair, I. S. Shashikala, D. S. Shankar Rao, C. V. Lobo, S. Chandrasekhar ——— **3429 – 3432**

A Low-Molar-Mass, Monodispersive, Bent-Rod Dimer Exhibiting Biaxial Nematic and Smectic A Phases

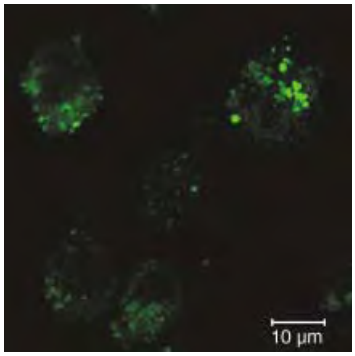


A "peelable banana" is formed when a bent-core molecule is linked to a rodlike mesogen through a flexible aliphatic spacer. This is an appropriate description of this novel low-molar-mass organic system, which displays a transition from a biaxial nematic (N_b) phase to a biaxial smectic A phase. The illustration gives a schematic representation of the dimeric molecules in the N_b phase as well as the corresponding textural and conoscopic patterns obtained.

Fluorescent Amino Acids

M.-P. Brun, L. Bischoff, C. Garbay* ——— **3432 – 3436**

A Very Short Route to Enantiomerically Pure Coumarin-Bearing Fluorescent Amino Acids



No bulkier than a tryptophan or a tyrosine residue are the fluorescent coumaryl amino acids described. These building blocks can be synthesized rapidly with high enantiomeric purity and introduced readily into a peptidic sequence. Their fluorescence properties allow, for example, the investigation of the cellular localization of labeled peptides through confocal fluorescence microscopy (see picture).

Magnetism in Clusters

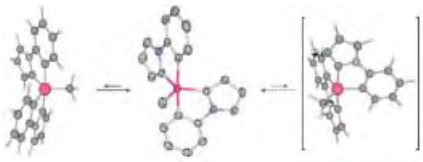
K. Hegetschweiler,* B. Morgenstern, J. Zubieta,* P. J. Hagrman, N. Lima, R. Sessoli,* F. Totti ——— **3436 – 3439**

Strong Ferromagnetic Interactions in $[V_8O_{14}(H_{-2}taci)_2]$: An Unprecedented Large Spin Ground State for a Vanadyl Cluster



Tactics with taci: Strong ferromagnetic interactions (up to $\approx 150\ cm^{-1}$) and an $S = 3$ ground state have been observed in the octanuclear vanadyl cluster $[V_8O_{14}(H_{-2}taci)_2]$ (taci = 1,3,5-triamino-1,3,5-trideoxy-*cis*-inositol; see structure: V yellow, O red, N blue, C black) where the polydentate taci ligand forces some of the coordination polyhedra into a mutually orthogonal arrangement. Ab initio DFT calculations confirm the magnetostructural analysis.

 © 2004 Wiley-VCH Verlag GmbH & Co. KGaA, Weinheim

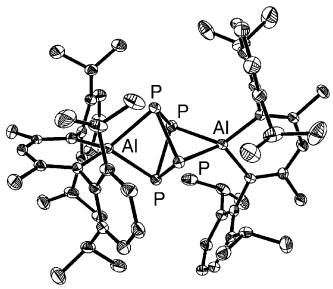


Molecule with three faces: Two of the three possible configurations that a stable silicate with five carbon substituents can adopt have been observed by NMR spectroscopy and shown to be in dynamic equilibrium through a Berry pseudorotation. The thermodynamics and kinetics of their exchange are in good agreement with calculations. The major configuration (from the crystal structure of the nBu$_4$N$^+$ salt) is shown in the center of the picture.

Pentaorganosilicate Pseudorotamers

E. P. A. Couzijn, M. Schakel, F. J. J. de Kanter, A. W. Ehlers, M. Lutz, A. L. Spek, K. Lammertsma* ——— **3440 – 3442**

Dynamic Configurational Isomerism of a Stable Pentaorganosilicate

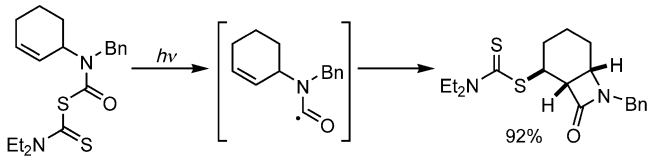


A whiter shade of PAl: The reaction of LAl^I with white phosphorus yields the first main-group complex [(LAl)$_2$P$_4$] (L = HC(CMeNAr)$_2$, Ar = 2,6-iPr$_2$C$_6$H$_3$) containing the {P$_4$}$^{4-}$ moiety, in which two P–P edges of the P$_4$ tetrahedron are opened and each is bridged by a LAl moiety (see structure). The results are supported by quantum chemical calculations.

Phosphorous Compounds

Y. Peng, H. Fan, H. Zhu, H. W. Roesky,* J. Magull, C. E. Hughes —— **3443 – 3445**

[{HC(CMeNAr)$_2$}$_2$Al$_2$P$_4$] (Ar = 2,6-iPr$_2$C$_6$H$_3$): A Reduction to a Formal {P$_4$}$^{4-}$ Charged Species

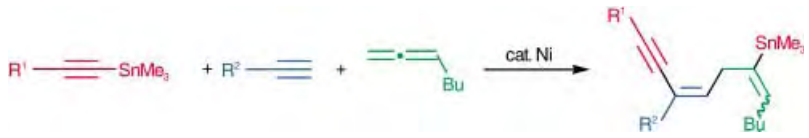


Oxygen or nitrogen? Radical chemists overwhelmingly choose to work with xanthates rather than dithiocarbamates, yet the latter offer a distinct advantage in the case of a new method for generating carbamoyl radicals. Functionalized lactams of various ring sizes can be prepared in an operationally simple procedure involving irradiation or heating in the presence of a radical initiator (see scheme).

Radical Reactions

R. S. Grainger,* P. Innocenti ——— **3445 – 3448**

Dithiocarbamate Group Transfer Cyclization Reactions of Carbamoyl Radicals under "Tin-Free" Conditions



Alkynes and 1,2-dienes insert into the carbon–tin bond of alkynylstannanes to afford various stannyldienynes in the presence of a nickel catalyst (see scheme). This is the first example of a transition-metal-catalyzed tandem carbometalation of two different carbon–carbon unsaturated bonds.

C–C Coupling Reactions

E. Shirakawa,* Y. Yamamoto, Y. Nakao, S. Oda, T. Tsuchimoto, T. Hiyama* ——— **3448 – 3451**

Nickel-Catalyzed Tandem Carbostannylation of Alkynes and 1,2-Dienes with Alkynylstannanes

 © 2004 Wiley-VCH Verlag GmbH & Co. KGaA, Weinheim

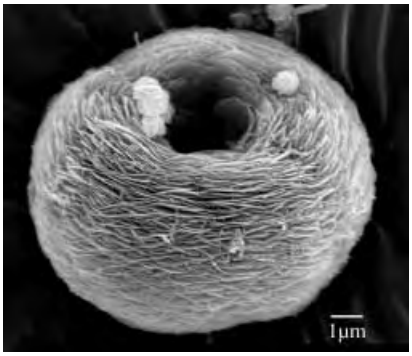
Contents

Nanostructures

G. Hu, D. Ma,* L. Liu, M. Cheng, X. Bao* ——— **3452 – 3456**

In Situ Assembly of Zeolitic Building Blocks into High-Order Structures

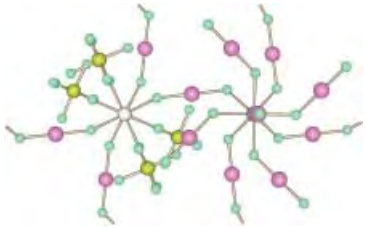
Zeolitic hierarchical structures with complex morphologies, such as the peony-shaped superstructure illustrated in the picture, are synthesized in a one-pot dual-template assembly reaction. One template acts as the structural directing agent to construct the microporous building block (zeolite), and a second template is employed to assemble these building blocks into a superlattice.



Noble-Gas Compounds

M. Tramšek,* P. Benkič, B. Žemva* ——— **3456 – 3458**

The First Compound Containing a Metal Center in a Homoleptic Environment of XeF_2 Molecules

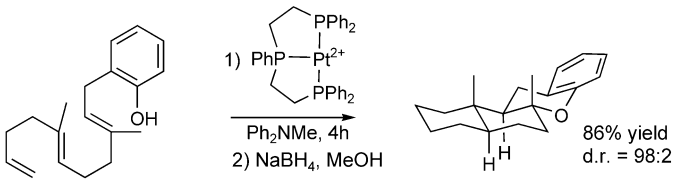


Wrapped in a cloak of noble-gas fluoride: Coordination compounds with XeF_2 as a ligand on the metal center are more abundant than considered in the past. The structure of the coordination compound $Ca_2(XeF_2)_9(AsF_6)_4$ is reported. For the first time one calcium center is found to be coordinated only with XeF_2 molecules (a homoleptic center), while the other calcium center is coordinated with XeF_2 and $[AsF_6]^-$ as ligands (see structure; As yellow, Ca gray, F green, Xe magenta).

Cyclizations

J. H. Koh, M. R. Gagné* ——— **3459 – 3461**

Pd^{II}- and Pt^{II}-Mediated Polycyclization Reactions of 1,5- and 1,6-Dienes: Evidence in Support of Carbocation Intermediates



1 **2**

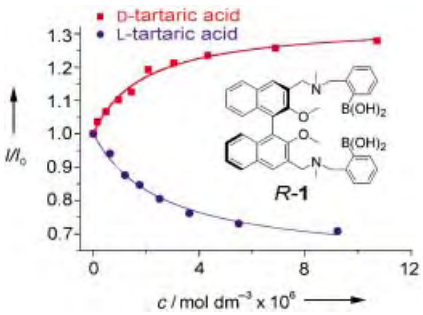
Pincer-ligated Pd^{II} and Pt^{II} dicationic complexes efficiently generate cations from 1,5- and 1,6-dienes. These transient cations can be selectively trapped with heteroatoms, alkenes, and through pinacol rearrangements. For example, trienylphenol **1** is converted into tetracyclic **2** in high yield and diastereomeric ratio (see scheme).

Enantioselective Sensors

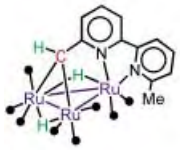
J. Zhao, T. M. Fyles, T. D. James* ——— **3461 – 3464**

Chiral Binol–Bisboronic Acid as Fluorescence Sensor for Sugar Acids

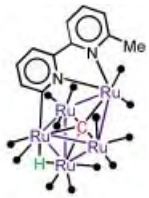
A novel fluorescence response to enantiomeric analytes was observed for binol–bisboronic acid sensors (*R*- or *S*-**1**): One enantiomer of the analyte enhances and the other enantiomer diminishes the fluorescence of **1**. So, the fluorescence intensity of *R*-**1** was enhanced by D-tartaric acid and diminished by L-tartaric acid (see scheme). These changes are mirrored by the *S* sensor.



 © 2004 Wiley-VCH Verlag GmbH & Co. KGaA, Weinheim



1



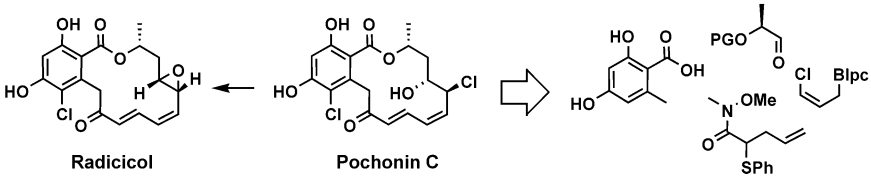
2

Activation of one C–C and three C–H bonds associated with a methyl group attached to an organic fragment has been achieved. Two compounds, which arise from the activation of two (**1**) and three C–H bonds of a methyl group of 6,6′-dimethyl-2,2′-bipyridine (Me_2bipy), and pentanuclear cluster **2**, which contains a carbide ligand arising from a methyl group of Me_2bipy, were isolated from reactions of $[Ru_3(CO)_{12}]$ with Me_2bipy. ● = CO.

C–H/C–C Activation

J. A. Cabeza,* I. da Silva, I. del Río, L. Martínez-Méndez, D. Miguel, V. Riera ——— 3464 – 3467

Activation of All Bonds of a Methyl Group Attached to an Organic Fragment

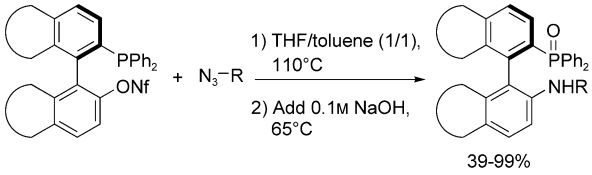


Back to its origins: Pochonin C was synthesized in 11 steps from the four fragments shown in the scheme. This asymmetric synthesis and the conversion of pochonin C into radicicol defines the configuration at the center bearing the chlorine atom as *S*. Ipc = isopenocampheyl, PG = protecting group.

Natural Products Synthesis

S. Barluenga, P. Lopez, E. Moulin, N. Winssinger* ——— 3467 – 3470

Modular Asymmetric Synthesis of Pochonin C



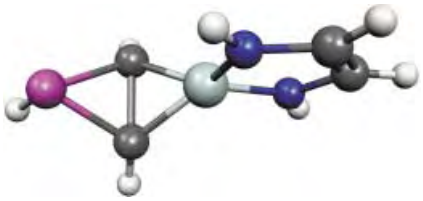
An intramolecular S_NAr reaction makes the synthesis of enantiopure MAP(O)-type P,N ligands in high yields possible (see scheme) and demonstrates that the synthetic potential of the 85-year-old Staudinger reaction between phosphanes and azides is still far from being exhausted. Nf = nonafluorobutanesulfonate.

Bidentate P,N Ligands

P. N. M. Botman, O. David, A. Amore, J. Dinkelaar, M. T. Vlaar, K. Goubitz, J. Fraanje, H. Schenk, H. Hiemstra,* J. H. van Maarseveen* ——— 3471 – 3473

A Staudinger Approach towards Binol-Derived MAP-Type Bidentate P,N Ligands

Thermally stable silylene Si{1,2-$(NCH_2tBu)_2C_6H_4$} reacts with 1*H*-phosphirenes to give the first isolated 2,3-dihydro-1,3-phosphasiletes, a unique type of zwitterion, and 1,2-dihydro-1,2-phosphasiletes. The novel 2-phospha-4-silabicyclo[1.1.0]butane (see picture) is a reactive intermediate in the reaction, whose course can be tuned by changing the substituents.



Phosphorus Heterocycles

J. C. Slootweg, F. J. J. de Kanter, M. Schakel, A. W. Ehlers, B. Gehrhus, M. Lutz, A. M. Mills, A. L. Spek, K. Lammertsma* ——— 3474 – 3477

2-Phospha-4-silabicyclo[1.1.0]butane as a Reactive Intermediate

 © 2004 Wiley-VCH Verlag GmbH & Co. KGaA, Weinheim

Contents

Protein Structures

Y.-S. Jung, M. Sharma, M. Zweckstetter* ——— 3479 – 3481

Simultaneous Assignment and Structure Determination of Protein Backbones by Using NMR Dipolar Couplings

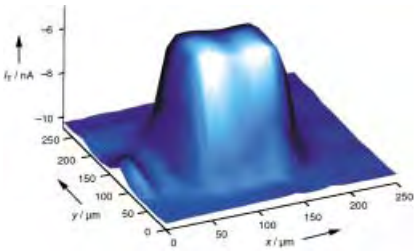


Running on automatic: Folds for proteins up to around 125 residues can be achieved rapidly and without manual intervention by integration of bioinformatics tools with NMR spectroscopy in dilute liquid-crystalline phases (see picture). Data intensive and time-consuming assignment of backbone resonances prior to structure determination is not required any more. This greatly accelerates structure determination of proteins by NMR spectroscopy.

Scanning Probe Techniques

F. Turcu, A. Schulte, G. Hartwich, W. Schuhmann* ——— 3482 – 3485

Label-Free Electrochemical Recognition of DNA Hybridization by Means of Modulation of the Feedback Current in SECM



Stranded on the surface: The modulation of the amperometric feedback current in scanning electrochemical microscopy (SECM) through coulomb interactions between the phosphate groups of immobilized oligonucleotides and a freely diffusing, negatively charged redox mediator is used for imaging DNA spots (see picture) and establishing a simple and efficient label-free electrochemical detection of complementary hybridization on DNA microarrays.

Polyoxometalates

F. Hussain, B. S. Bassil, L.-H. Bi, M. Reicke, U. Kortz* ——— 3485 – 3488

Structural Control on the Nanomolecular Scale: Self-Assembly of the Polyoxotungstate Wheel $[\{\beta\text{-}Ti_2SiW_{10}O_{39}\}_4]^{24-}$

Wheel meet again: The titanium(IV) substituted $[\{\beta\text{-}Ti_2SiW_{10}O_{39}\}_4]^{24-}$ (**1**) consists of four β-Keggin moieties that are linked via Ti-O-Ti bonds leading to a cyclic arrangement (see picture; red WO_6, green TiO_6, and blue SiO_4). The wheels stack to give a tunnel-like structure. Synthesis of **1** is from the dilacunary precursor $[\gamma\text{-}SiW_{10}O_{36}]^{8-}$ and gives insights into the mechanism of formation of polyoxoanion assemblies.



Communications labeled with this symbol have been judged by two referees as being "very important papers".

Deadline for recruitment adverts

31/2004	July 22	Publication date:	August 6
32/2004	July 29	Publication date:	August 13

Angewandte Chemie International Edition
Advertising Sales Department:
Marion Schulz
Phone: 0 62 01 – 60 65 65
Fax: 0 62 01 – 60 65 50
E-Mail: MSchulz@wiley-vch.de

Place an advert in the printed version and have it made available online for 1 month, free of charge!

Service

Keywords ——— 3492

Authors ——— 3493

Angewandte's Sister Journals ——— 3490 – 3491

Preview ——— 3495

S. Chandrasekhar (1930–2004): Discotic Liquid Crystals

Sivaramakrishna Chandrasekhar, inventor and discoverer of discotic liquid crystals, renowned educator and tireless advocate, for over four decades, of liquid-crystal sciences and technologies, died March 8, 2004 in Bangalore, India. He was born 73 years earlier to a large family distinguished in both science and public service. Convinced that major research advances arise from interactions among scientists from many different cultures, he organized several Liquid Crystal Conferences in Bangalore, chaired four biennial International Liquid Crystal Conferences and set up bilateral scientific collaborations between India and many countries. In 1992, he co-founded the International Liquid Crystal Society and was its first president. In 1998, along with George W. Gray, Nobel Laureate Pierre-Gilles de Gennes, and Alfred Saupe, he was elected one of its first Honored Members.



S. Chandrasekhar

Chandrasekhar is best known for his prediction, discovery, and elucidation of a new class of liquid crystals where disc-shaped molecules stack in liquid columns.[1] This discovery opened an entirely new area of research, which has since led to a host of applications ranging from legibility films for giant LCDs, clearly legible in large public spaces, to hybrid nano-chips. Research interest in discotics has recently surged with the recognition that some liquid-crystal phases exhibited by bent-core molecules (banana liquid crystals) could be columnar and polar.[2] Chandrasekhar's book, *Liquid Crystals*, a universally acclaimed classic,[3] elegantly presents the beautiful and complex world of liquid crystals to all students, beginning and "experienced".

We are grateful to Professor Chandrasekhar's widow, Ila, for the following biographical details. While many of us knew him as Chandra, Ila called him Chander: "Chander was born in Calcutta, India, on August 6, 1930. His father, R. B. S. Sivaramakrishnan, was Accountant General in both colonial and independent India. His mother, Sitalakshmi, a beautiful woman, was the younger sister of Nobel Laureate C. V. Raman. Chander was the fourth of five brothers. Only the oldest is alive today. His second brother, A. S. Natarajan, worked for Tatas, a well-known industrial house. The third brother was S. Ramaseshan, a widely known crystallographer and materials scientist. The fifth, S. Pancharatnam[4] died young while at Oxford. The 1983 Nobel Laureate, astrophysicist Subrahmanyan Chandrasekhar, was a first cousin.

Chander was educated at a well-known Catholic institution, Loyola College, Madras. He received a D.Sc. from Nagpur University while working with C. V. Raman at the Raman Research Institute. He obtained a second Ph.D. from Cambridge University. Post-doctoral work was with Kathleen Lonsdale at University College, London, and Lawrence Bragg at the Royal Institution, London. He returned to India in 1961 as the first Head of the Department of Physics of the University of Mysore. There, on the heels of Charles Frank's seminal paper,[5] he began working on liquid crystals.

Chander was deeply interested in classical Indian as well as western music and sang well, a talent inherited from his mother. He was also interested in theater, painting, and sculpture. But he always put his research before anything else in life."

In 1971, Chandra moved his group from Mysore to found the liquid-crystal laboratory at the Raman Research Institute, Bangalore, soon recognized as a world-class research center. In 1991, to help build the high-tech enterprises emerging from India's important research base, he founded a new Center for Liquid Crystal Research in Bangalore. Chandra was proud of the pioneering work of his group, especially on pressure effects on liquid-crystal phase transitions[6] and their discovery of the optical analogue of the Borrman effect.[7]

Just as his research contributions are too numerous to mention here, so are the many honors conferred on him for his research and teaching. Most recent of these include the Royal Medal of the Royal Society of London for his discovery of discotics and his book, and the Niels Bohr UNESCO Gold Medal for his outstanding contributions to the development of liquid crystals, the advancement of science in developing countries, and the teaching of physics (1998). Chandra was a gentle, friendly, and caring man devoted to his family, friends and fellow researchers. Our hearts go out to his wife, two children, and two grand-children. He will be remembered with great affection and respect well into the future as his rich legacy to liquid-crystal research continues to flourish. Life is the word.

Patricia E. Cladis
Advanced Liquid Crystal Technologies, Summit, NJ (USA)
Banahalli R. Ratna
Naval Res. Labs, Washington, DC (USA)
Ranganathan Shashidar
GEO-CENTERS, Washington, DC (USA)

Photo by Ila Chandrasekhar

[1] S. Chandrasekhar, B. K. Sadashiva, K. A. Suresh, *Pramana* **1977**, *9*, 471.
[2] See for example: H. Pleiner, H. R. Brand, P. E. Cladis, *Mol. Cryst. Liq. Cryst.* **2003**, *396*, 169.
[3] S. Chandrasekhar, *Liquid Crystals*, Cambridge University Press, **1977/1992/1994**.
[4] S. Pancharatnam, *Proc. Indian Acad. Sci. A* **1956**, *44*, 247.
[5] F. C. Frank, *Discuss. Faraday Soc.* **1958**, *25*, 19. Much later, F. C. Frank, S. Chandrasekhar, *J. Phys. (Paris)* **1980**, *41*, 1285 deduced tilted columns from their study of discotic defects.
[6] S. Chandrasekhar, S. Ramaseshan, A. S. Reshamwala, B. K. Sadashiva, R. Shashidhar, V. Surendranath, *Pramana* **1975**, *Suppl. 1*, 117.
[7] R. Nityananda, U. D. Kini, S. Chandrasekhar, K. A. Suresh, *Pramana* **1975**, *Suppl. 1*, 325.

 © 2004 Wiley-VCH Verlag GmbH & Co. KGaA, Weinheim DOI: 10.1002/anie.200460918

Ligand Design

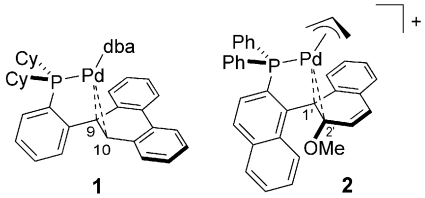
Chiral Olefin Ligands—New "Spectators" in Asymmetric Catalysis**

*Frank Glorius**

Keywords:
alkene ligands · asymmetric catalysis · homogeneous catalysis · ligand design

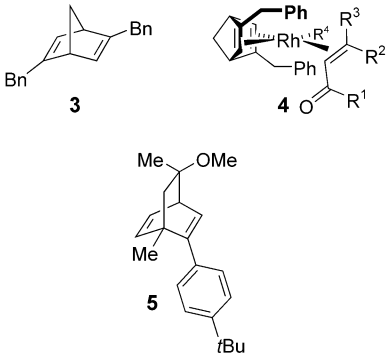
Since the preparation of Zeise's salt ($K[PtCl_3(C_2H_4)]$) in 1827, transition-metal complexes of η^2-bonded olefins have become ubiquitous in organometallic chemistry.[1] In catalysis, olefin ligands mostly dissociate from the metal or undergo chemical conversion. The alternative role of olefins as "spectator" ligands[2] that stay on the metal during catalysis and influence the metal's catalytic properties is underutilized. The application of olefins as π-acids in cross-coupling reactions of two $C(sp^3)$ centers is a significant exception.[3] In these reactions an acceptor-substituted olefin ligand binds to and removes electron density from the metal center and thereby facilitates the otherwise difficult reductive elimination step. More recently, new olefin spectator ligands with exciting properties have been identified which will eventually lead to a reappraisal of olefin ligands in catalysis.

Considerable attention has been attracted by two ligands each consisting of a phosphane donor and an aromatic system. The structural analysis of their palladium complexes revealed that the supposedly monodentate phosphane ligands can bind in a bidentate fashion.[4–6] In Pd^0 complex **1** of an electron-rich phosphane ligand, which was successfully used in the Suzuki cross-coupling of sterically hindered substrates, the C^9–C^{10} double bond of the phenanthrene moiety coordinates to Pd (Scheme 1).[4] Similarly, in cationic Pd^{II} complex **2** of the mop ligand[7] the methoxy-substituted $C^{1'}$–$C^{2'}$ double bond also binds to the metal.[5a,b] Whereas in the first case the effect of double-bond coordination on the catalytic activity is unclear, the latter complexation has been evoked to explain the stereochemical memory effect exhibited by the mop ligand in Pd-catalyzed allylic alkylations.[5b,c]



Scheme 1. Unusual bidentate binding mode of "monodentate" phosphane ligands. Cy = cyclohexyl, dba = dibenzylideneacetone.

Chiral η^2-bonded olefin "spectator" ligands have not played a major role in asymmetric catalysis,[8] in part, because of the facile dissociation of these ligands from the metal. However, as a consequence of chelation, dienes with the proper geometry can form intriguingly stable complexes. Independently, Hayashi et al. and Carreira et al. have developed new chiral diene ligands **3**[9] and **5**,[10] respectively, and used them successfully in asymmetric catalysis, interestingly, in reactions of double bonds (Scheme 2). This important pioneering work demonstrates the sufficient stability of olefin metal complexes for asymmetric catalysis.



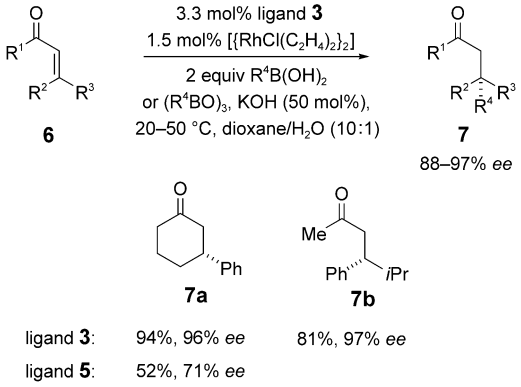
Scheme 2. Diene ligands **3** and **5** as well the Rh complex **4** derived from **3** and thought to be catalytically active.

The C_2-symmetrical [2.2.1]bicycloheptadiene **3** was synthesized in nine steps, and the key transformation was an efficient [Pd(mop)]-catalyzed asymmetric hydrosilylation of norbornadiene (> 99 % *ee*).[9] The catalytic potential of the in situ generated rhodium complex of **3** was demonstrated convincingly in the asymmetric conjugate addition of organoboron reagents to α,β-unsaturated ketones and esters (Scheme 3).[9,11,12] For a wide range of substrates like cyclic and linear enones **6** as well as aryl- and alkenylboron reagents good yields and high enantioselectivities were obtained, generally above 90 % *ee*. Moreover, the activity exhibited by the diene-derived complex is unrivaled by that of any known chiral rhodium catalyst. Because of this enhanced catalytic activity, less reactive transmetalation reagents, for example, an otherwise nearly inert organostannane, can be used efficiently. The observed stereoinduction presumably results from the preferred formation of complex **4**, in which steric repulsion between the enone carbonyl

[*] Dr. F. Glorius
Max-Planck-Institut für Kohlenforschung
Kaiser-Wilhelm-Platz 1
45470 Mülheim an der Ruhr (Germany)
Fax: (+49) 208-306-2994
E-mail: glorius@mpi-muelheim.mpg.de

[**] I thank Prof. A. Fürstner for generous support and constant encouragement and the BMBF and the Fonds der Chemischen Industrie for financial support (Liebig scholarship).

 © 2004 Wiley-VCH Verlag GmbH & Co. KGaA, Weinheim DOI: 10.1002/anie.200301752



Scheme 3. Rh-catalyzed conjugate addition of boronic acids to enones.

moiety and the benzyl groups of the diene ligand is avoided (Scheme 2).

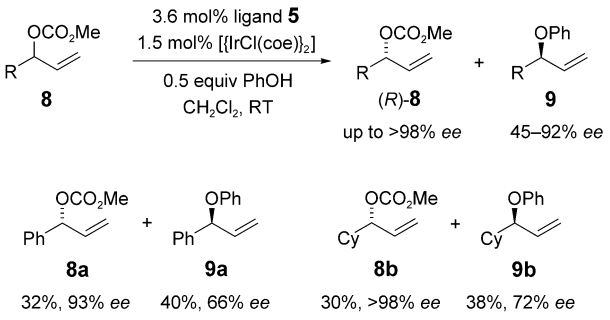
In an Ir-catalyzed allylic substitution, Carreira and co-workers discovered remarkable differences in reactivity between catalysts derived from several olefin ligands.[10,13,14] Whereas cyclooctadiene- and [2.2.2]bicyclooctadiene-derived catalysts led to complete reaction in 24 h, norbornadiene (> 96 h) and cyclooctene (coe) gave much less reactive and completely inactive catalysts, respectively. Consequently, a versatile synthesis for chiral and nonracemic [2.2.2]bicyclooctadiene **5** was developed. Both enantiomers of C_1-symmetrical **5** can be readily synthesized in only four steps from inexpensive ($< \$100\,kg^{-1}$) (*R*)- or (*S*)-carvone. The ligand can easily be made with different aryl groups, since the aryl moiety is introduced in the last step of the synthesis.

Ligand **5** was applied successfully in the Ir-catalyzed kinetic resolution of a broad range of aryl- and alkyl-substituted allylic carbonates **8** by allylic substitution (Scheme 4).[10] With 0.5 equivalents of PhOH as the nucleophile, allylic carbonates of high *ee* were obtained together with phenyl ethers **9** in varying enantiomeric purity. The selectivity factors for this transformation are generally between 5 and 15. Different degrees of unfavorable steric interactions between the carbonate enantiomers **8** and the Ir catalyst during the oxidative addition step presumably account for the preferred conversion of (*S*)-**8** to the observed product (*S*)-**9**.

In a comparative experiment, ligand **5** was submitted to the Rh-catalyzed conjugate addition (Scheme 3).[10] It was found that the yields and enantioselectivities of the products were much lower than those obtained with ligand **3**. Thus, it seems that the [2.2.1] and [2.2.2]bicyclic ligands complement one other, each best suited for particular metals and reactions.

These recent developments have opened the door to an exciting new class of chiral ligands. The application of stable double-bond ligands with new geometries and electronic properties should result in catalysts with increased stability, selectivity, and catalytic activity. Furthermore, the electronic character of olefin ligands can be varied over a wide range, such that catalysts can be fine-tuned for a specific application. Thus, bidentate ligands consisting of an alkene unit and another coordination element, as indicated by complexes **1**, **2**, and **4** and the Ir complex of **5**, should become a valuable class of ligands with new catalytic properties.

Published Online: June 9, 2004



Scheme 4. Ir-catalyzed kinetic resolution of allylic carbonates with phenol as the nucleophile.

[1] For reviews, see: a) *Comprehensive Organometallic Chemistry* (Eds.: E. W. Abel, F. G. A. Stone, G. Wilkinson), Pergamon, Oxford, **1995**; b) *Applied Homogeneous Catalysis with Organometallic Compounds* (Ed.: B. Cornils, W. A. Herrmann), Wiley, New York, **2002**; c) R. H. Crabtree, *The Organometallic Chemistry of Transition Metals, Wiley, New York*, **001**; d) L. S. Hegedus, *Transition Metals in the Synthesis of Complex Organic Molecules*, University Science Books, Sausalito, **1999**.

[2] Definitions of the term "spectator" ligand can be found in references [1c] and [1d].

[3] a) T. Yamamoto, A. Yamamoto, S. Ikeda, *J. Am. Chem. Soc.* **1971**, *93*, 3350; b) R. Sustmann, J. Lau, M. Zipp, *Tetrahedron Lett.* **1986**, *27*, 5207; c) R. Giovannini, T. Stüdemann, G. Dussin, P. Knochel, *Angew. Chem.* **1998**, *110*, 2512; *Angew. Chem. Int. Ed.* **1998**, *37*, 2387; d) A. E. Jensen, P. Knochel, *J. Org. Chem.* **2002**, *67*, 79, and references therein; e) A. Yamamoto, *J. Organomet. Chem.* **2002**, *653*, 5, and references therein.

[4] J. Yin, M. P. Rainka, X.-X. Zhang, S. L. Buchwald, *J. Am. Chem. Soc.* **2002**, *124*, 1162.

[5] a) P. Kočovský, Š. Vyskočil, I. Císařová, J. Sejbal, I. Tišlerová, M. Smrcina, G. C. Lloyd-Jones, S. C. Stephen, C. P. Butts, M. Murray, V. Langer, *J. Am. Chem. Soc.* **1999**, *121*, 7714; For a profound analysis of the effect of bidentate coordination on the memory effect in allylic alkylations, see: b) G. C. Lloyd-Jones, S. C. Stephen, M. Murray, C. P. Butts, Š. Vyskočil, P. Kočovský, *Chem. Eur. J.* **2000**, *6*, 4348; see also: c) T. Hayashi, M. Kawatsura, Y. Uozumi, *J. Am. Chem. Soc.* **1998**, *120*, 1681.

[6] For hemilabile olefin complexes, see: C. S. Slone, D. A. Weinberger, C. A. Mirkin, *Prog. Inorg. Chem.* **1999**, *48*, 233.

[7] The ligand mop (or MeO-mop) is 2-(diphenylphosphanyl)-2′-methoxy-1,1′-binaphthalene; see: T. Hayashi, *Acc. Chem. Res.* **2000**, *33*, 354.

[8] a) *Comprehensive Asymmetric Catalysis* (Eds.: E. N. Jacobsen, A. Pfaltz, H. Yamamoto), Springer, Berlin, **1999**; b) *Catalytic Asymmetric Synthesis* (Ed.: I. Ojima), VCH, Weinheim, **2000**.

[9] T. Hayashi, K. Ueyama, N. Tokunaga, K. Yoshida, *J. Am. Chem. Soc.* **2003**, *125*, 11508.

[10] C. Fischer, C. Defieber, T. Suzuki, E. M. Carreira, *J. Am. Chem. Soc.* **2004**, *126*, 1628.

[11] For reviews on conjugate addition, see: a) N. Krause, A. Hoffmann-Röder, *Synthesis* **2001**, 171; b) M. Kanai, M.

 © 2004 Wiley-VCH Verlag GmbH & Co. KGaA, Weinheim

Shibasaki in *Catalytic Asymmetric Synthesis* (Ed.: I. Ojima), VCH, Weinheim, **2000**, p. 569; c) K. Tomioka, Y. Nagaoka in *Comprehensive Asymmetric Catalysis* (Eds.: E. N. Jacobsen, A. Pfaltz, H. Yamamoto), Springer, Berlin, **1999**, p. 1105.

[12] For a review on rhodium-catalyzed conjugate additions, see: a) T. Hayashi, K. Yamasaki, *Chem. Rev.* **2003**, *103*, 2829; see also: b) Y. Takaya, M. Ogasawara, T. Hayashi, M. Sakai, N. Miyaura, *J. Am. Chem. Soc.* **1998**, *120*, 5579; c) T. Hayashi, M. Takahashi, Y. Takaya, M. Ogasawara, *J. Am. Chem. Soc.* **2002**, *124*, 5052.

[13] For reviews on allylic alkylations, see: a) B. M. Trost, C. B. Lee in *Catalytic Asymmetric Synthesis* (Ed.: I. Ojima), VCH, Weinheim, **2000**, p. 593; b) A. Pfaltz, M. Lautens in *Comprehensive Asymmetric Catalysis* (Eds.: E. N. Jacobsen, A. Pfaltz, H. Yamamoto), Springer, Berlin, **1999**, p. 833; c) B. M. Trost, D. L. van Vranken, *Chem. Rev.* **1996**, *96*, 395.

[14] For allylic alkylations with phenols, see: a) F. Lopez, T. Ohmura, J. F. Hartwig, *J. Am. Chem. Soc.* **2003**, *125*, 3426; b) B. M. Trost, F. D. Toste, *J. Am. Chem. Soc.* **1998**, *120*, 815; c) B. M. Trost, H.-C. Tsui, F. D. Toste, *J. Am. Chem. Soc.* **2000**, *122*, 3534; For allylic alkylations with Ir, see ref. [14a] and: d) R. Takeuchi, M. Kashio, *J. Am. Chem. Soc.* **1998**, *120*, 8647; e) B. Bartels, C. Garcia-Yebra, F. Rominger, G. Helmchen, *Eur. J. Inorg. Chem.* **2002**, 2569, and references therein.

BE ON THE BALL!



0186_0010_vi

The new free **WILEY-VCH Alerting Service** makes time-consuming random finds a thing of the past!

Register now for the free WILEY-VCH Alerting Service

Now you can be supplied per e-mail regularly with information tailored precisely to your needs and interests. Just fill out the registration form at *www.wiley-vch.de/home/pas* for e-mails with news on the latest WILEY-VCH publications in your field. Added benefit: general info on important developments and services at WILEY-VCH.

Be on the ball so you'll be in the know!

www.wiley-vch.de

Addition to C–C Multiple Bonds

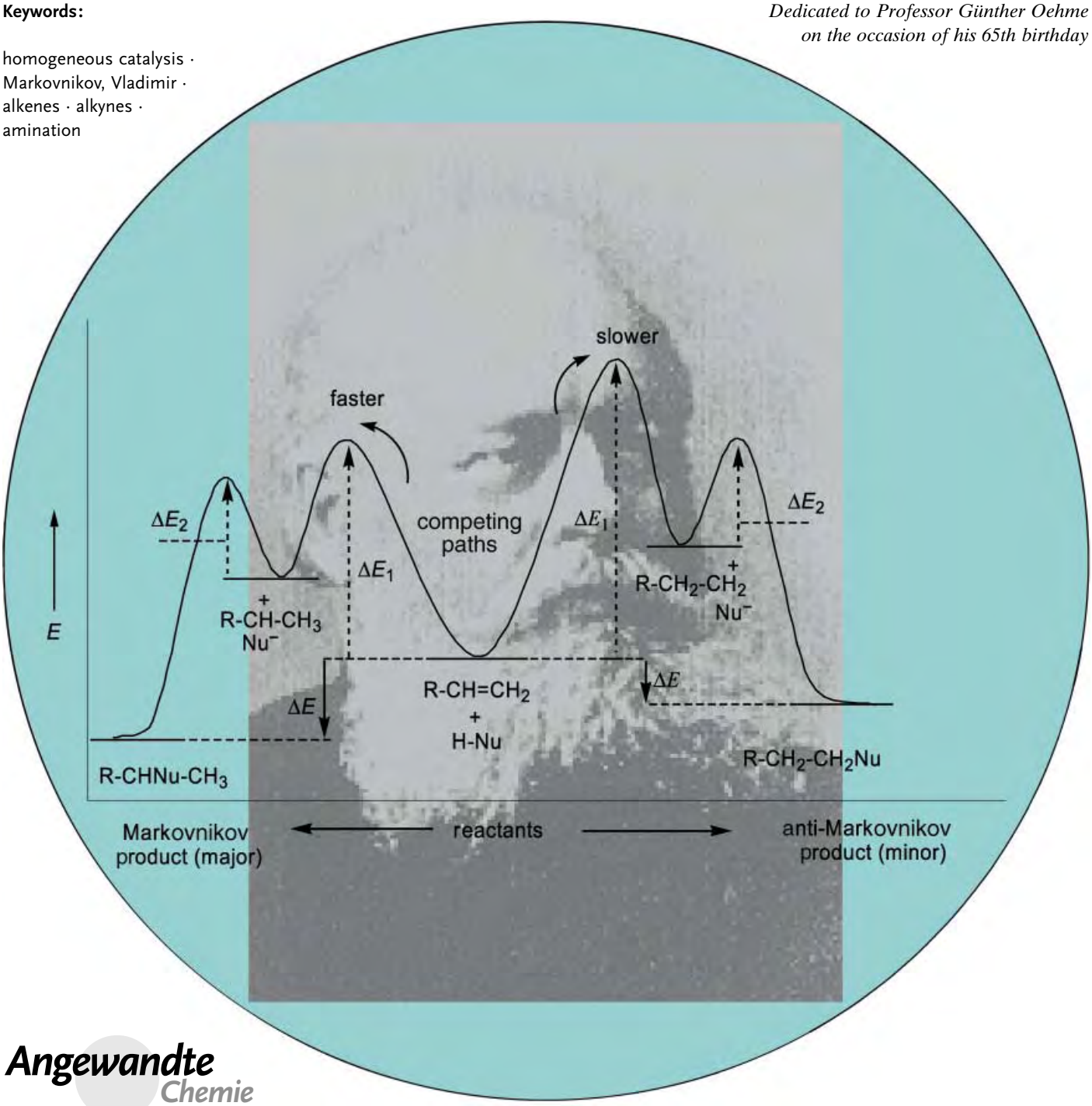
Catalytic Markovnikov and anti-Markovnikov Functionalization of Alkenes and Alkynes: Recent Developments and Trends**

Matthias Beller, Jayasree Seayad, Annegret Tillack, and Haijun Jiao*

Keywords:

homogeneous catalysis · Markovnikov, Vladimir · alkenes · alkynes · amination

Dedicated to Professor Günther Oehme on the occasion of his 65th birthday



© 2004 Wiley-VCH Verlag GmbH & Co. KGaA, Weinheim
DOI: 10.1002/anie.200300616

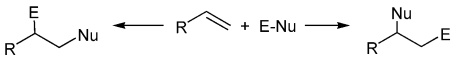
The regioselective functionalization of terminal alkenes and alkynes is of utmost importance for the synthesis of a wide variety of organic products. Based on the original observation by Vladimir Markovnikov—the pioneer of this field of research—in the 19th century, the possible regioisomeric products are classified as Markovnikov or anti-Markovnikov products. Contrary to traditional belief, it is nowadays possible to control the regiochemistry of various additions of nucleophiles to alkenes and alkynes by applying different transition-metal catalysts. Recent developments in this area of selective functionalization of alkenes and alkynes are reviewed.

From the Contents

1. Introduction	3369
2. Carbonylations	3372
3. Hydrocyanation	3381
4. Hydroamination	3384
5. Reactions of O-Nucleophiles	3387
6. Miscellaneous	3391

1. Introduction

The most generally and extensively used chemical transformation of carbon–carbon multiple bonds is the addition of E–Nu (E = H, BR_2, Si, Hg, Sn, etc.; Nu = halogen, CN, CHO, OH, CO, COOR, NR_2, etc.) across the multiple bond. Such addition reactions are perfectly suited to fulfil today's need for "green chemistry"[1] because the atom economy[2] or atom efficiency[3] could be 100%. Due to the availability and price of starting materials, a significant number of industrially important processes involve such reactions. The refinement of ubiquitous olefins exemplified by C–C bond forming reactions, for example, hydroformylation, hydrocarboxylation, hydrocyanation, are prime examples for this type of reaction. The addition of E–Nu to an unsymmetrical olefin can lead to two isomeric products (Scheme 1).



Scheme 1. Functionalization reactions of olefins.



Vladimir V. Markovnikov
1838–1904

In general, most of the electrophilic addition reactions in which E = H follow the Markovnikov Rule, which states: "*When a hydrocarbon of unsymmetrical structure combines with a halogen hydroacid, the halogen adds itself to the less hydrogenated carbon atom, that is, to the carbon atom which is more under the influence of other carbon atoms*"[4][+] In the H–Nu addition reaction with nonfunctionalized aliphatic olefins, the first step is the formation of a carbocation intermediate, which then combines rapidly with the nucleophile. For unsymmetrical alkenes, there are two possible carbocation intermediates generated from two competing protonation paths. An energy diagram for the competing reaction pathways for this two-step addition mechanism is shown in Figure 1. Here, the first reaction is the rate-determining step, which also determines the regioselectivity of the product. The

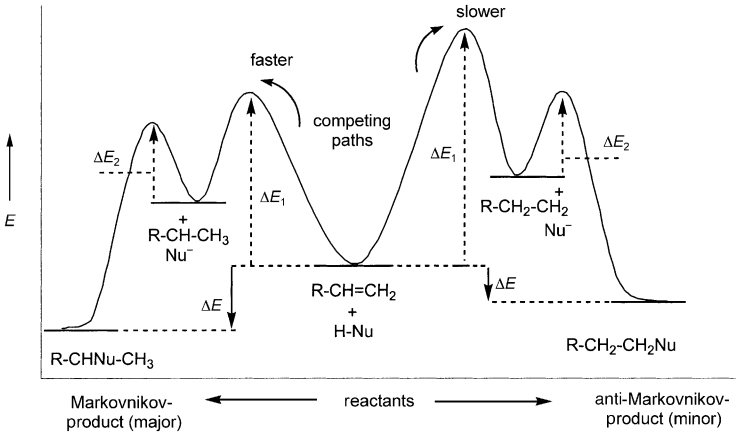


Figure 1. Energy diagram of the addition of H–Nu to olefins.

difference of the relative rate of the two paths and the relative stability of the carbocation intermediates reveal Markovnikov's rule. For example, the more stable secondary carbocation ($R(CH_3)CH^+$) forms with a lower activation barrier (ΔE_1) of protonation than the less-stable primary carbocation ($RCH_2CH_2^+$), and thus the formation of the former is faster compared to the latter. In addition, the final addition product formed from the more-stable carbocation is more stable than that formed from the less-stable carbocation. Therefore, the rate and regioselectivity of the reaction are determined by the energies of the possible transition states and hence by the stability of the relevant carbocations; the regioselectivity is a kinetically and thermodynamically controlled process.

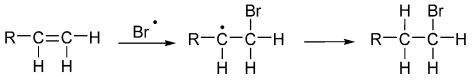
[*] Prof. Dr. M. Beller, Dr. J. Seayad, Dr. A. Tillack, Dr. H. Jiao
Leibniz-Institut für Organische Katalyse (IfOK)
an der Universität Rostock e.V.
Buchbinderstrasse 5–6, 18055 Rostock (Germany)
Fax: (+49) 381-466-9324
E-mail: matthias.beller@ifok.uni-rostock.de

[**] Together with all co-workers of the IfOK we are thankful to him for more than 36 years of work in the institute and we have a deep respect for his achievements.

[+] "*Wenn ein unsymmetrisch constituirter Kohlenwasserstoff sich mit einer Haloidwasserstoffsäure verbindet, so addirt sich das Haloid an das weniger hydrogenisirte Kohlenstoffatom, d. h. zu dem Kohlenstoff, welcher sich mehr unter dem Einflusse anderer Kohlenstoffe befindet.*"

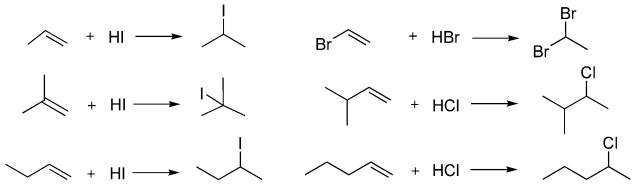
DOI: 10.1002/anie.200300616
© 2004 Wiley-VCH Verlag GmbH & Co. KGaA, Weinheim

Despite the generality, there are exceptions to this rule. For instance, the addition of H–Nu to olefins that contain strongly electron-withdrawing groups preferentially form the anti-Markovnikov product. In this case, the addition occurs primarily as a nucleophilic attack on the "activated" olefin (Michael addition). Hence, the obtained anti-Markovnikov selectivity is due to the increased stability of the in situ formed α carbanion. Other exceptions to the Markovnikov rule often include free-radical additions. As shown by the free-radical addition of HBr to terminal aliphatic olefins, the observed anti-Markovnikov selectivity seems to be mainly sterically determined (Scheme 2).



Scheme 2. Free-radical addition of HBr to olefins.

In this context it is interesting to know that Markovnikov developed his rule by studying in detail the reaction of HX (X = I, Br, Cl) with propylene, butenes, pentenes, and vinylbromide (Scheme 3).



Scheme 3. Markovnikov addition of hydrogen halides to olefins.

Although the original Markovnikov rule is limited to the addition of hydrogen halides, clearly this rule can be used in a much wider context. When $E \neq H$, a more general statement nowadays is "*When adding (a polar compound) to the double bond of unsymmetrical alkenes, the initial electrophile prefers to add to the primary (1°) carbon the most, the secondary (2°) carbon next, and the tertiary (3°) carbon least.*"[5] Thus, in the case of hydroboration, hydrosilylation, hydrostannation, etc., in which H is the nucleophile, a formal anti-Markovnikov product is formed.

Despite the apparent simplicity of addition reactions to olefins or alkynes, it is still an important challenge to control the regioselectivity of such processes. Often the control of the regioselectivity is as difficult as the control of the stereoselectivity of the formed stereogenic center in the Markovnikov product. Even now in some reactions it is not possible to obtain the desired regioselectivity at all. Examples include the anti-Markovnikov addition of amines, alcohols, and water to simple aliphatic olefins, which are of significant industrial interest. When considering the control of selectivity, it is important to note that both potential products (linear and branched ones) are of value in organic synthesis, but for different applications. While the branched Markovnikov products are often intermediates on a smaller scale in organic synthesis and for natural-product synthesis, they are also valuable for the fine-chemical industry, for example, as intermediates for pharmaceuticals and agrochemicals. In these cases, benzylic products, which arise from the addition to styrenes, are especially useful building blocks. Apart from the direction of regioselectivity, the control of stereochemistry is an important issue for these reactions.



Matthias Beller, born 1962 in Gudensberg (Germany), obtained his doctorate in 1989 with Prof. L. F. Tietze. After his postdoctoral studies (Liebig scholarship) with Prof. K. B. Sharpless in 1990 at MIT (USA), he rose to the position of project leader in Central Research at Hoechst AG, Frankfurt (Germany). From 1996 to 1998 he was Associate Professor of Inorganic Chemistry at the TU, Munich and since June 1998 he has been Professor and Director of the Leibniz Institute of Organic Catalysis (IfOK) at the Univerität Rostock. His research topics cover the development of practical catalytic methodologies.



Annegret Tillack, born 1949 in Bad Wilsnack (Germany), studied chemistry at the University of Rostock and obtained her doctorate in 1977 under the supervision of Prof. G. Schott for her work on organosilicon chemistry. She then moved to IfOK, Rostock. Since 1998 she has been a project leader in the group of Prof. M. Beller.



Jayasree Seayad was born in Kerala, India. She worked as a research fellow (CSIR, India) at the Homogeneous Catalysis Division, National Chemical Laboratory, Pune, India for her doctoral thesis and was awarded her PhD in 2000 from the University of Pune. From 2002 to 2003 she was a postdoctoral fellow in the group of Prof. M. Beller. Her research interests include C_1 chemistry, transition-metal catalysis, and amination chemistry.



Haijun Jiao, born 1963 in Shanxi (China), received his Ph.D. in 1995 at the University of Erlangen-Nürnberg with Professor Paul von R. Schleyer for studies on aromaticity. He was a fellow of DFG (Erlangen) and CNRS (Rennes). Since 2002 he has been working in the Leibniz Institute of Organic Catalysis, and his research interests are development and application of theoretical methods in catalytic reactions and metallorganic chemistry.

 © 2004 Wiley-VCH Verlag GmbH & Co. KGaA, Weinheim

Regarding production volume, the nonchiral anti-Markovnikov products are, by far, more important for the chemical industry. Every year linear aliphatic aldehydes, alcohols, and amines are produced in multimillion tonne scale as bulk-chemical intermediates. Due to the comparably low price of these products the corresponding production processes must be highly efficient (product yields $>95\%$, low catalyst costs, high space–time yield, etc.). Somewhat paradoxically, anti-Markovnikov selectivities $\gg 95\%$ for aliphatic olefins are often undesirable for industrial purposes because a "small" amount of the branched isomer is also needed as commercial product.

In the area of bulk chemicals, recent interest has also focused on the so-called anti-Markovnikov functionalization of internal aliphatic olefins. Olefin mixtures that contain major amounts of internal double bonds represent an economically attractive feedstock, which can be transformed predominantly to linear products by domino isomerization-selective functionalization reactions.[6] This interesting type of reaction is studied mainly with regard to hydroformylation (see Section 2.1).

In addition to the traditional polar additions that obey the Markovnikov rule, the advancements in organometallic chemistry and catalysis led to the development of a variety of regioselective addition reactions mediated by transition-metal catalysts; the control of selectivity is not simply explained by the stability of the carbocation intermediate. For example, the latest density functional theory (DFT) computation for hydroformylation, which involves the conversion of terminal olefins and syngas ($H_2 + CO$) directly to the corresponding linear and branched aldehydes, shows that the regioselectivity of the unmodified cobalt catalyst $[CoH(CO)_4]$ is determined by the higher stability of the linear (primary) alkyl cobalt tetracarbonyl complex $[CoR(CO)_4]$ with respect to the branched (secondary) isomer.[7] This difference in energy comes from the steric interaction between the alkyl group and the equatorial CO ligands. Neither the stability of the alkyl cobalt tricarbonyl complex $[CoR(CO)_3]$, nor the activation barrier of the carbonylation step ($[RCo(CO)_4 \rightarrow [RCOCo(CO)_3]$) determines the regioselectivity. For hydroformylation reactions with the phosphane-modified rhodium catalyst $[RhH(CO)(PPh_3)_2]$, the situation becomes more complicated due to the equatorial–equatorial (eq–eq) and equatorial–apical (eq–ax) isomers on the basis of the phosphane ligands. Therefore, two reaction paths (eq–eq and eq–ax) are possible, and each path can lead to both the linear and branched products. The potential-energy surface on the basis of theoretical computations is shown in Figure 2.[8] One can see that the ea adduct is more stable than the ee isomer by 1.0 kcal mol^{-1}, which indicates that the former is more favored thermodynamically and more populated than the latter under those reaction conditions. On the basis of the calculated barriers that lead to the linear and branched Rh-alkyl products, the linear product from ea adduct is exothermic, while the branched isomer is endothermic, the large energy difference identifies the linear isomer as the only product. On the other hand, ee adduct produces primarily the branched product favored kinetically, but gives also the linear product due to the small difference in activation barrier. In addition, the linear product is more stable than the branched isomer. Thus, the observed regioselectivity may be rationalized in terms of the stability of the possible olefin adducts and the small difference in the competing transition states.

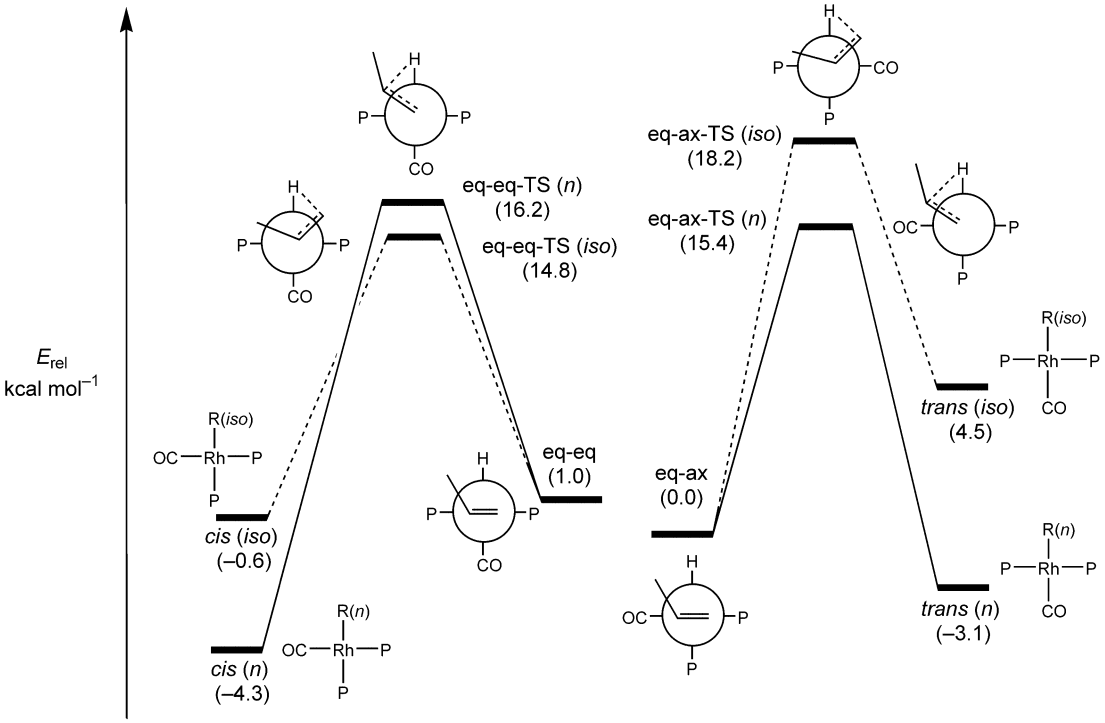


Figure 2. Potential-energy surface for the regioselective Rh–H insertion into CH_3–CH=CH_2 (on the basis of the most stable reactants, transition states and products).

 © 2004 Wiley-VCH Verlag GmbH & Co. KGaA, Weinheim

In addition, the regioselectivity in catalytic reactions can be determined by many other factors under the individual reaction conditions, for example, the structure of the intermediate of the active catalyst. One example to be emphasized in the case of aromatic olefins is the increased stability of the intermediate that leads to the branched product through a η^3-benzyl interaction. Such a case has been reported recently by Hartwig and co-workers in a set of reactions between anilines and styrenes or vinylnaphthalene.[9] On the basis of an NMR spectroscopic study, the branched ethylnaphthyl palladium complex has been identified, isolated, and characterized (by X-ray crystallography) as an active intermediate.[9a] The obtained structure shows an η^3 coordination between the terminal protonated vinylnaphthalene and palladium center. The subsequent nucleophilic attack of aniline at the internal carbon atom leads to the Markovnikov addition product.

The aim of this review is to describe recent developments in the area of transition-metal-catalyzed intermolecular addition reactions to olefins or alkynes with special focus on the control of regioselectivity. In the last few decades there has been no general review on this topic. However, the present interest in the area is demonstrated by more than 150 publications since 2000 that use the term Markovnikov and/or anti-Markovnikov. Because of the general importance of this topic, this review focuses on direct reactions with a proton as the electrophile. We have structured the text according to the different addition reactions.

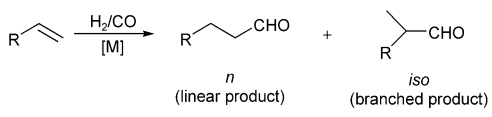
2. Carbonylations

In the area of carbonylations the terms Markovnikov and anti-Markovnikov are in general not used with regard to regioselectivity. Typically, the obtained regioselectivity is called *n*/*iso* or linear/branched selectivity because the addition of a formyl, carboxyl, or ester group to a double bond is not a classic case of a polar addition reaction to an olefin or alkyne. Nevertheless, we have included these transformations in this review because of their similarities to other polar addition reactions, for example, hydrocyanation, and because of the scientific and industrial importance of carbonylation processes.

2.1. Hydroformylation

Hydroformylation is the reaction of alkenes or alkynes with CO and H_2 in the presence of transition-metal catalysts resulting in the formal addition of H–CHO across the multiple bond (Scheme 4).

This process is perhaps the most important and well-investigated homogeneously catalyzed industrial reaction, particularly with regard to the regioselectivity. Due to the

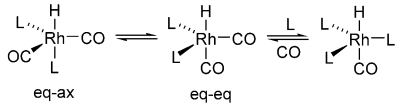


Scheme 4. Hydroformylation of olefins. [M] is catalyst.

commercial interest in linear plasticizer alcohols, the aliphatic anti-Markovnikov *n*-aldehydes are the most desired products. A number of excellent reviews[10] have recently discussed the various features of hydroformylation reactions. The most important examples relevant to the control of regioselectivity of the reaction are described here.

Modified or unmodified cobalt and rhodium carbonyls constitute common hydroformylation catalysts, which form the corresponding hydridometalcarbonyl complexes as the active species. In either case, the regioselectivity is strongly influenced by added ligands, the temperature of the reaction, and the partial pressure of CO. The *n*:*iso* ratio is found to decrease with increase in temperature for almost all olefins except for certain functionalized and some internal olefins.[11] Hence, modern oxo plants that use a rhodium-based catalyst operate at temperatures below 125 °C to prevent ligand degradation and to maintain a high *n*:*iso* ratio. At high CO pressures and low temperature, the rate of isomerization of acyl metalcarbonyl species decreases thereby leading to high *n*:*iso* ratios with terminal olefins. For industrial cobalt based oxo processes it is known as a rule of thumb that the *n*-butyraldehyde (from propene) is found to increase by 0.5 kg/100 kg of alkene per 10 bar rise in pressure.[12]

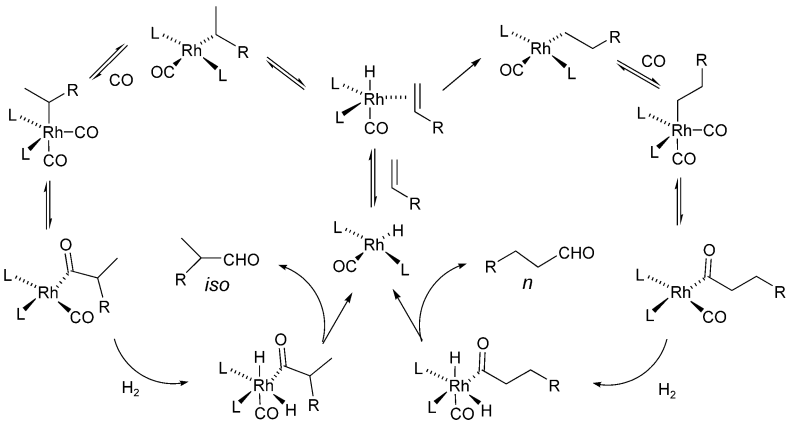
In the case of phosphane-modified rhodium-based oxo catalysts, the key features that determine the regiochemistry are 1) the number of coordinated phosphorus ligands (L), 2) the reaction temperature and the partial pressure of CO, 3) the electronic and steric properties of the ligands, and 4) the stereochemistry at the Rh center. In the hydroformylation of olefins with $[RhH(CO)L_3]$ ($L = PPh_3$), the highest linear-aldehyde selectivity is achieved at the highest attainable concentrations of L.[13] Thus, in the hydroformylation of 1-hexene, an increase in PPh_3:Rh from 3:1 to 955:1 results in an increase in *n*-heptanal selectivity from 62 % to 86 %.[14] At higher concentrations of L, the major catalytic species is of the type $[RhHCOL_3]$ and at lower concentrations, the complex $[RhH(CO)_2L_2]$ predominates (Scheme 5).[10a,15]



Scheme 5. Equilibrium of rhodium bis- and trisphosphane complexes (eq–ax = equatorial–axial; eq–eq = diequatorial coordination).

Relative concentrations of these diphosphane and triphosphane species, which form the corresponding alkene hydride complexes, strongly influence the regioselectivity of the reaction. Higher concentrations of the alkene diphosphane species lead to higher linear-aldehyde selectivity and higher concentrations of the alkene monophosphane complex give an increased amount of the branched aldehyde. The regioselectivity of the aldehyde formation is principally determined by the step that converts the five coordinate $[RhH(alkene)(CO)_nL_m]$ (n, $m = 1$ or 2) complex into either a linear or branched four coordinate $[Rh(alkyl)(CO)_nL_m]$ complex (Scheme 6), the relative concentrations of which are also controlled by the concentration of L. The square-

 © 2004 Wiley-VCH Verlag GmbH & Co. KGaA, Weinheim



Scheme 6. Simplified catalytic cycle for hydroformylation of olefins.

planar alkyl rhodium complexes can undergo β-hydride elimination, leading to isomerization, or can react with CO to form complexes of the type $[Rh(alkyl)(CO)_2L_2]$. Deuteroformylation studies with 1-hexene[16] and styrene[17] have shown that at moderate temperatures and high CO pressures, the insertion step is irreversible for linear alkyl rhodium species. On the other hand, the branched alkyl complex may favor β-hydride elimination, thereby resulting in the partial isomerization of the branched alkyl to linear alkyl complex.

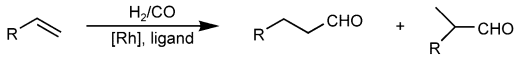
$[RhH(CO)_2L_2]$ ($L = PPh_3$) complexes are found to exist as two rapidly equilibrating isomeric structures in which the phosphane ligands coordinate either in an eq–eq and an eq–ax fashion (Scheme 5).[10a,15] In some cases, a correlation between the eq–eq:eq–ax ratio and the *n*:*iso* ratio has been observed, with the diequitorial complexes leading to a higher selectivitiy of the linear products, the reasons for which are unclear yet. This effect is more evident for bidentate ligands in which a wider bite angle leads to a higher proportion of diequatorial hydride complexes and higher *n*:*iso* ratios. For instance, when the bite angle of diphosphane increases from 78° (dppe, **1**) to 107° (*trans*-dppm-cyp, **2**) to 112° (bisbi, **3**), the *n*:*iso* ratio increases from 1 to 5–8 to 25 (Table 1).[18] However, 2,5-dppm-nor (**4**), which has a wide natural-bite angle (126°) gave only lower *n*:*iso* ratio (2.6) because of its inability to form stable chelates.

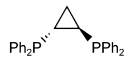
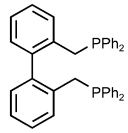
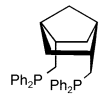
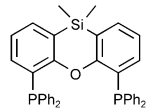
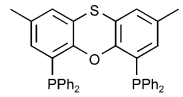
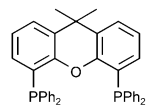
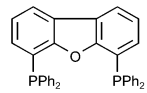
Van Leeuwen and co-workers[10a,19] studied in detail the effect of bite angle on the regioselectivity in the rhodium-catalyzed hydroformylation reaction of terminal olefins with a series of xanthane-based diphosphanes (the so-called xantphos family). It was observed that the bite angle can be increased stepwise from 102° to 131° by changing the bridge group, X (e.g., $Si(CH_3)_2$ (**5**), S (**6**), $C(CH_3)_2$ (**7**), bond (**8**)) in position 10 of the xanthane ring without a significant variation in the steric and electronic properties of the ligands. For example in the hydroformylation of 1-octene the regioselectivity increased up to 98% for *n*-aldehyde at 40°C with the optimal ligand. A comparison of these xantphos ligands revealed a regular increase in selectivity with an increase in bite angle up to the point at which the calculated bite angle has increased to such an extent that chelation is no longer possible. A further comparison of these ligands with 2,2′-bis(diphenylphosphinomethyl)-1,1′-biphenyl (bisbi) showed that the rigidity of the ligand backbone is essential for maintaining high regioselectivity, even at elevated temperatures.

More recently, it was also demonstrated that dibenzophospholyl- and phenoxaphosphanyl-substituted xanthane ligands[20] **9** and **10** (Scheme 7) provide high selectivity in the hydroformylation of 1-octene (*n*:*iso* up to 68:1). These ligands exhibit high activity and selectivity in the hydroformylation of internal double bonds (*trans*-2- and -4-octenes) to give linear aldehydes with selectivities up to 90 and 86%, respectively. A study at our laboratory showed that NAPHOS-type ligands, especially those with electron-withdrawing groups at the *meta* position of the phenyl rings, for example, ligands **11** and **12**, also induce excellent selectivities for the reaction of a variety of internal double bonds to give linear aldehydes. 2-Butene and 4-octene are converted into *n*-pentanal and *n*-nonanal with selectivities of up to 95 and 70%, respectively.[21]

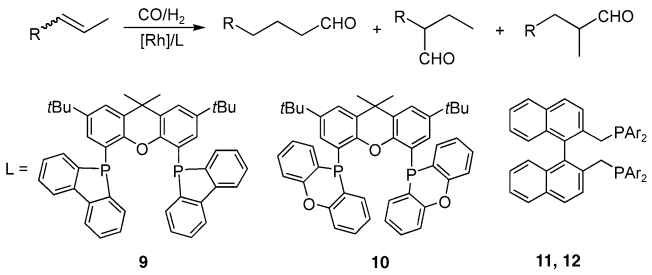
Rhodium complexes immobilized by means of a xanthene-based ligand, *N*-(3-trimethoxysilane-*n*-propyl)-4,5-bis-(diphenylphosphanyl)-phenoxazine (siloxantphos, **13**) are

Table 1: Correlation between the bite angle and the *n*/*iso* selectivity for different diphosphane ligands ($R = C_6H_{14}$).

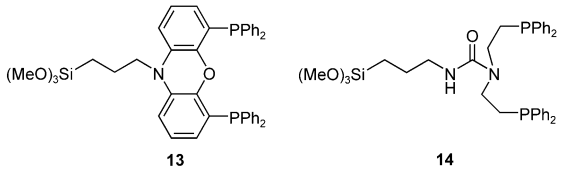


Ligand		Bite angle [°]	*n*/*iso*
dppe (**1**)		78	1
trans-dppm-cyp (**2**)		107	5–8
bisbi (**3**)		112	25
2,5-dppm-nor (**4**)		126	2.6
$Si(CH_3)_2$ sixantphos (**5**)		108.7	34.6
thixantphos (**6**)		109.4	50
xantphos (**7**)		111.7	52.2
dpfphos (**8**)		131	3.4

 © 2004 Wiley-VCH Verlag GmbH & Co. KGaA, Weinheim



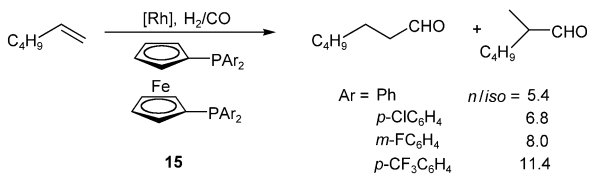
Scheme 7. Ligands used for the hydroformylation of internal olefins. **11**: Ar = 3,5-bis(trifluoromethyl)phenyl; **12**: Ar = 3,5-difluorophenyl.



found to give regioselectivities similar to those of the corresponding homogeneous systems.[22] In this case, as previously observed, a large bite angle (108°) is necessary for achieving high regioselectivities. The application of **13** to 1-octene gives an *n*:*iso* ratio of 40:1, which is 15 times higher than that obtained with a similar catalyst that contained the ligand *N*-(3-triethoxysilane-*n*-propyl)-*N*′,*N*′-bis[2-(diphenylphosphanyl)ethyl]urea **14** (bite angle: 93°).

In addition to immobilized ligands, phosphane-containing dendrimers were applied to the hydroformylation of simple olefins, such as 1-octene. The use of diphenylphosphane-functionalized oligomeric silsesquioxane dendrimers resulted in a high regioselectivity for the linear aldehyde (*n*:*iso* = 14:1). The "positive dendritic effect" on the selectivity is explained by the formation of a constrained bidentate ligand as in bisbi or xantphos.[23]

Apart from the bite angle, the electronic properties of the ligand also influence the regioselectivity of hydroformylation reactions. In general, less basic triarylphosphanes lead to higher *n*:*iso* ratios with respect to their more basic counterparts.[24] In the case of bidentate ferrocene-based ligands that vary only electronically but not sterically, it is found that as the ligand becomes less basic the *n*:*iso* ratio increases (Scheme 8).[25] This is mainly because, as the basicity of the ligand decreases, the branched alkyl species becomes more prone to β-hydride elimination. The increased electrophilicity of the rhodium center leads to higher reactivity of the alkyl

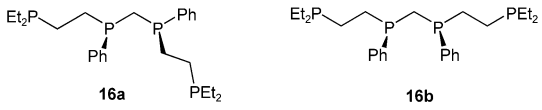


Scheme 8. Hydroformylation of 1-hexene by using substituted dppf ligands.

rhodium species toward CO dissociation and β-hydrogen elimination.

Casey and co-workers found that the ee:ea isomer ratio increases with decreasing phosphane basicity, which leads to a further increase in the *n*:*iso* ratio.[26] In addition, the presence of electron-withdrawing groups on the phosphane groups in the equatorial positions leads to high *n*:*iso* ratios, while electron-withdrawing substituents on phosphanes in the apical position leads to low *n*:*iso* ratios.[27] This may not be a purely electronic effect, but a mixture of steric and electronic effects, because ee and ea coordinating diphosphanes considerably differ with respect to their steric properties. An increase in the ee:ea isomer ratio with decreasing basicity of the ligands is also observed in the case of substituted thixanthphos ligands in which steric differences are minimal.[28] Surprisingly, the selectivity of the linear aldehyde remained, in this case, almost the same, thus indicating no influence of electronic effects on regioslectivity. For instance, in the case of 1-octene the selectivity for the linear aldehyde in the presence of different ligands is 92–93%. Apparently, in the case of less basic ligands, the linear alkyl rhodium species is mainly converted into the linear aldehyde, while the branched alkyl rhodium species generates some 2-octene by β-hydrogen elimination. It is concluded that for this catalytic system, the *n*:*iso* ratio is determined mainly by the steric constraints, not by the phosphane basicity and ee:ea isomer ratio.

Homo-bimetallic cationic norbornadiene rhodium complexes of the type $[Rh_2(nbd)_2L](BF_4)_2$ that contain racemic and meso diastereomers of an electron-rich dinucleating tetraphosphane ligand (L) **16a** or **16b** are found to give an

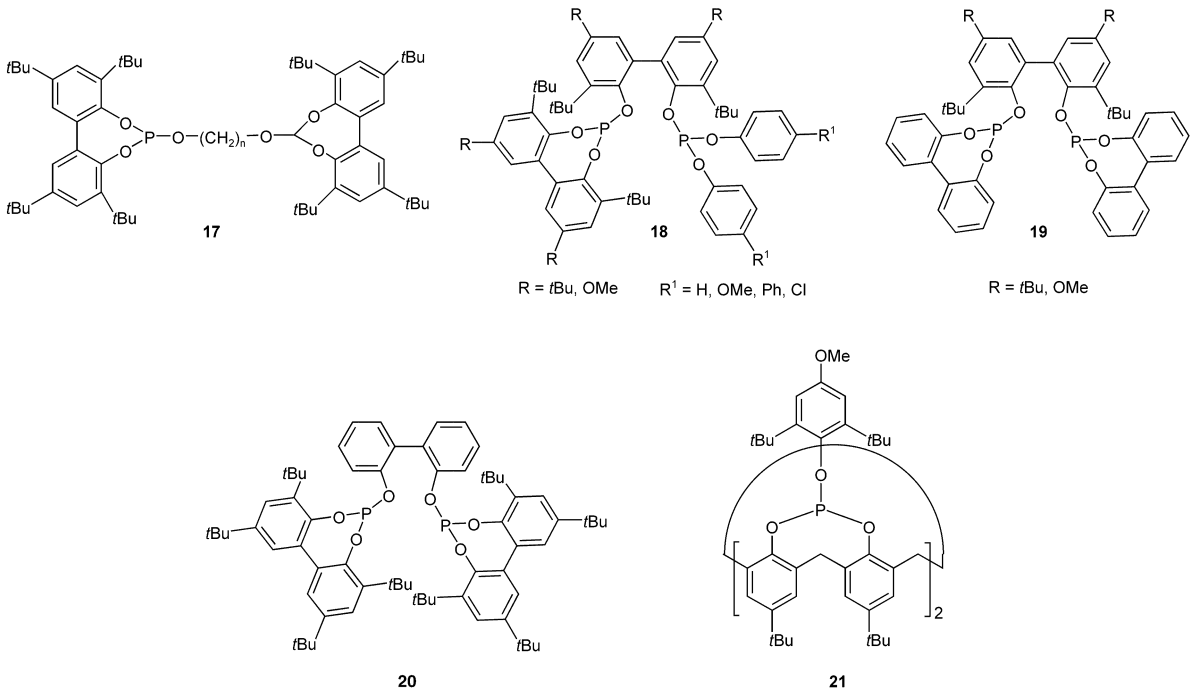


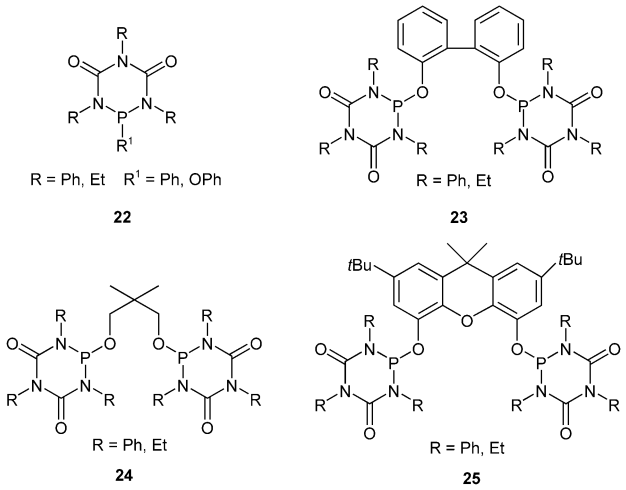
n:*iso* ratio up to 30:1 in the case of 1-hexene hydroformylation.[29] It is proposed that the mechanism of the reaction involves an intramolecular hydride transfer between the two rhodium centers.

Bulky diphosphite ligands **17**–**21** are known to effect the regioselective hydroformylation of propene,[30] 1-octene,[31] and a variety of functionalized terminal olefins to give the corresponding linear aldehydes.[32] It is found that a bulky and diequatorially coordinating diphosphite is required to obtain high regioselectivity for linear aldehydes, while flexible diphosphites or ea coordinating diphosphites lead to enhanced formation of the branched aldehyde. Chelating diphosphites with a *p*-*tert*-butylcalix[4]arene backbone lead to surprisingly high regioselectivity for *n*-nonanal (99.5%), though with low catalytic activity.[33] By varying the two *tert*-butyl substitutents on the ligand with isopropyl and methyl groups, higher activity can be achieved while the *n*/*iso* selectivity remaines high (96.4% and 92.4%, respectively).

Monodentate and bidentate diamide ligands derived from 1,3,5-trisubstituted biuret derivatives **22**–**25** leads to very

 © 2004 Wiley-VCH Verlag GmbH & Co. KGaA, Weinheim





bulky and π-acidic ligands thereby combining the properties of phosphanes and phosphites with respect to the hydroformylation of terminal olefins.[34] In the hydroformylation of 1-octene, high activity but only moderate selectivity (up to 61 % *n*-nonanal) is obtained by using a monodentate ligand, though it exclusively forms a hydride complex in which the phosphorus ligands are coordinated in the equatorial plane.[35] Bidentate biuret ligands, which form stable catalysts of the type $[RhH(CO)_2L{-}L]$ show improved selectivity (up to 86 % *n*-nonanal) compared to the monodentate ligands.

More recently, somewhat similar aryl sulfonylamino phosphanes have been applied resulting in moderate selectivity for the hydroformylation of 1-hexene.[36]

In addition to the reaction conditions, catalysts, and ligands, the substrate also has a strong influence on the regioselectivity of hydroformylation reactions. Clearly, terminal olefins that have sterically demanding substituents favor the linear aldehyde. Aryl olefins[37] and functionalized olefins[38] that contain electron withdrawing groups (e.g., vinyl acetate, vinyl phthalimide, acrylic esters, fluoro-substituted olefins) favor the formation of branched aldehydes. In general here the branched alkyl rhodium complex is thermodynamically more stable than the linear alkyl rhodium complex.[39] For example in the case of aryl olefins the formation of a stable π-benzyl complex is favored.[40]

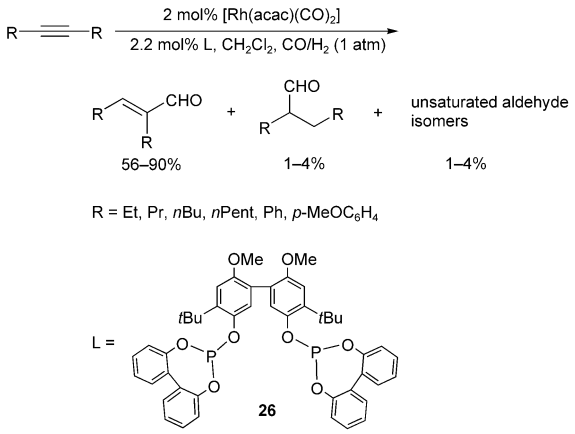
Compared to the hydroformylation of olefins the corresponding reaction of alkynes is less interesting. In general alkynes should give α,β-unsaturated aldehydes as products. Only a few studies have been performed recently.[41] Most catalysts suffer from low selectivity and/or low yield of the unsaturated aldehydes, mainly because the formation of the corresponding saturated aldehydes. The hydroformylation of symmetrical alkynes is rather simpler; Buchwald and coworkers reported an effective catalyst composed of $[Rh(acac)(CO)_2]$ and a diphosphite ligand (**26**), which worked under mild conditions (Scheme 9).[42]

2.2. Hydroaminomethylation

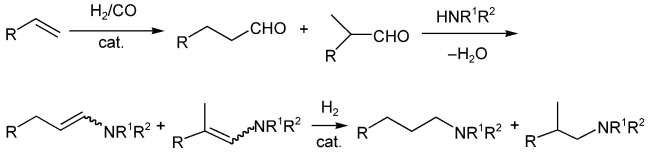
Hydroformylation of olefins in the presence of ammonia or an amine leads to an overall addition of $H{-}CH_2NR_2$ group across the double bond (Scheme 10). This elegant one-pot synthesis of amines is called hydroaminomethylation and involves an initial hydroformylation reaction of the olefin followed by condensation of the resulting aldehyde with an amine to form an enamine or imine, which on hydrogenation leads to the final amine product.[43]

The catalysts used initially for this reaction were iron carbonyl and cobalt carbonyl complexes, whereas more

 © 2004 Wiley-VCH Verlag GmbH & Co. KGaA, Weinheim



Scheme 9. Hydroformylation of symmetric alkynes to α,β-unsaturated aldehydes.



Scheme 10. Hydroaminomethylation of olefins.

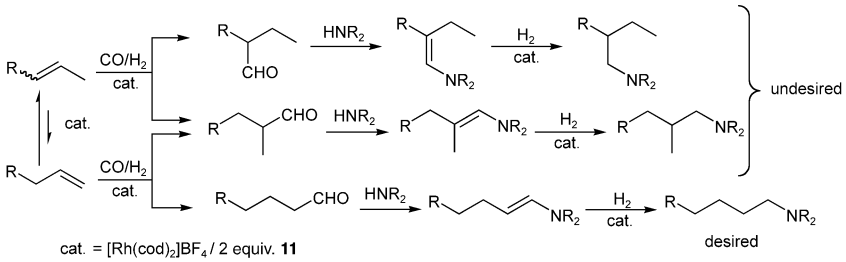
efficient rhodium complexes have been developed in recent decades. Clearly, the regioselectivity of the overall hydroaminomethylation reaction is determined in the initial hydroformylation step. However, the presence of basic amines that may coordinate strongly at the Rh center, results in lower *n*:*iso* ratios than those of similar hydroformylation reactions. For instance, aliphatic terminal olefins such as 1-octene, 1-dodecene, 1-tetradecene, 1-hexadecene, and 1-octadecene are hydroaminomethylated with morpholine by using a $[\{RhCl(cod)\}_2]$ catalyst to form mixtures of the corresponding linear and branched amines.[44] On the other hand, in the presence of phosphane ligands, for example, xantphos derivatives, highly regioselective and efficient hydroaminomethylations are achieved.[45] Good *n*:*iso* ratios (up to 10:1) have been observed for the hydroaminomethylation of the functionalized olefin 3,3-dimethylpent-4-ene-2-one with secondary amines by using phosphane-free rhodium catalysts. In general, high selectivity of the linear product is obtained in hydroaminomethylations with 1,1-disubstituted olefins due to steric hindrance.

A rhodium complex catalyst $[Rh_2(\mu\text{-}S\mathit{t}Bu)_2(CO)_2(PPh_3)_2]$ with a bulky sulfur bridge is reported to give high regioselectivity in favor of linear amines. An *n*:*iso* ratio of 40:1 is observed in the hydroaminomethylation of 1-octene with diethylamine at 80 °C.[46] The less-bulky Rh^I-2-ethylhexanoate also showed selective formation of the corresponding linear amine from 1-dodecene and dimethylamine, though in low yield.[47] The hydroaminomethylation of lower α-olefins (propene, 1-butene and 1-pentene) with ammonia by using a biphasic dual-metal catalyst system consisting of complexes of rhodium and iridium with water-soluble phosphanes (130 °C, 120 bar; $CO:H_2 = 1:5$) leads to the corresponding primary amines with high selectivity (up to 90 %).[48] Though the regioselectivity towards the linear primary amine with TPPTS as ligand is low (tppts = tris sodium salt of *meta* trisulfonated triphenylphosphane; *n*:*iso* = 76:24 to 87:13), up to 99 % selectivity in favor of the linear isomer has been achieved in the presence of binas (sulfonated 2,2′-bis[(diphenylphosphanyl)methyl]-1,1′-binaphthyl) as the ligand.

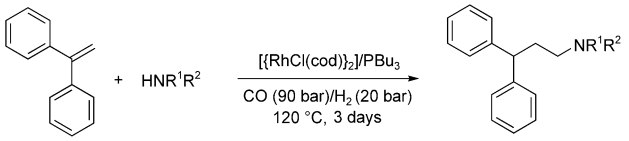
More recently, even the selective synthesis of linear amines from aliphatic olefins with internal double bonds or olefin mixtures has been achieved by hydroaminomethylation with 2,2′-bis[di(3,5-trifluoromethylphenyl)phosphinomethyl]-1,1′-binaphthyl (iphos) as a ligand in the presence of cationic Rh complexes. To obtain the desired linear products, a fast isomerization of the internal double bonds should occur (Scheme 11). Olefins such as 2-butene (94 %), 2-pentene (82 %), 2-hexene (76 %), 3-hexene (68 %), and 1-octene (90 %) form the corresponding linear amines by hydroaminomethylation with secondary and primary amines in selectivities of 53–90 %.[6]

Vinyl arenes such as styrene and vinylnaphthalene are hydroaminomethylated with various primary and secondary amines by using $[\{RhCl(cod)\}_2]$[49] or $[Rh^+(cod)(\eta^6\text{-}PhBPh_3)^-]$[50] as the catalyst to form the corresponding branched amines (*n*:*iso* up to 1:16; yield = 81–99 %) as the major products. This regiochemistry is in agreement with simple hydroformylation of styrene. However, the hydroaminomethylation of 1,1-diphenylethene forms the corresponding linear amines (68–76 % yields) with $[\{RhCl(cod)\}_2]/PBu_3$ as catalyst. Here, the linear amines are selectively formed due to the steric bulk offered by the aryl groups (Scheme 12).[51]

In the same way, methallyl chloride reacts with secondary amines to form the corresponding linear 1,4-diamines (67–79 %).[52] Due to the steric hindrance, functionalization of the



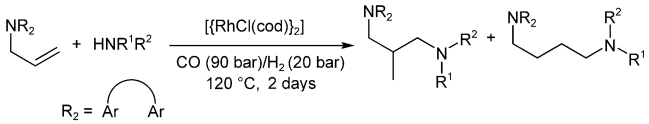
Scheme 11. Selective hydroaminomethylation of internal double bonds (R = H, alkyl, **11**).



Scheme 12. Hydroaminomethylation of 1,1-diphenylethene.

 © 2004 Wiley-VCH Verlag GmbH & Co. KGaA, Weinheim

α-C atom and formation of 1,3-diamines is not observed. Various *N*-allylic and *N*-methallylic compounds[53] are hydroaminomethylated to γ- and δ-aminofunctionalized phenothiazine, iminodibenzyl, carbazol, and pyrazole derivatives (Scheme 13). Often mixtures of Markovnikov and anti-

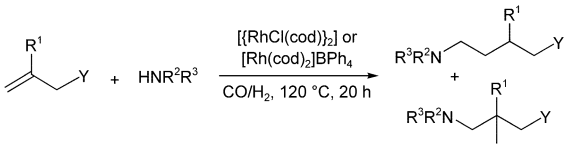


Scheme 13. Hydroaminomethylation of *N*-allylic amines.

Markovnikov products are obtained. For instance, *N*-allylphenothiazene is hydroaminomethylated in the presence of cyclic and acyclic aliphatic primary or secondary amines to form the corresponding secondary or tertiary diamines with slight preference to the *iso* isomer. However, when *N*-methylaniline or benzylamine are used, the corresponding linear 1,4-diamines are formed exclusively. Similarly, *N*-allyliminodibenzyl, *N*-allylcarbazole, and *N*-allylpyrazole react with various aliphatic and aromatic secondary amines to form the corresponding 1,3- and 1,4-diamines in good yields. While in the case of *N*-allyliminodibenzyl, generation of the *n*-isomer is preferred, in the case of *N*-allylcarbazole and *N*-allylpyrazole the *iso*-isomers are preferably formed.

In a similar way to that of *N*-allylic amines, silyl-substituted vinylic amines are also reported to produce β- or γ-diamines, by hydroaminomethylation with different amines.[54] The carbonylation occurs preferentially at the β position due to the steric hindrance of the silyl group and the product is obtained in 46–98% yield.[55]

Heterofunctionalized amines such as γ- and δ-amino-ethers, amines and silanes, are easily synthesized by one-pot hydroaminomethylation of the corresponding allylic compounds (Scheme 14).[56] Formation of the *iso* product (56–

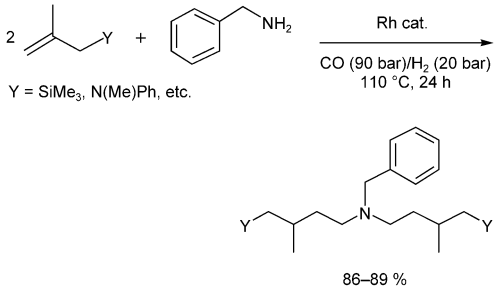


Y = OEt, Me_3Si, NH(Ac), N(Et)Ac, N(Me)Ph, piperidyl, etc.

Scheme 14. Hydroaminomethylation of heterofunctionalized allylic compounds.

69%) is observed only when R^1 is H. Moderate to good regioselectivities (60–95%) in favor of the linear isomer are achieved in most cases, though the reaction rates are relatively low (turn over frequency, TOF, $\approx 5\ h^{-1}$).

Multiple alkylation reactions of primary amines or ammonia by hydroaminomethylation have been used for producing symmetrical, unsymmetrical secondary and tertiary amines.[57] Otherwise these products are formed by multiple stepwise procedures.[58] For instance, the dialkylation of ammonia with styrene gave up to 99% yield with an *iso*,*iso*:*iso*,*n* ratio of 14:1.[59,60] In a similar reaction to that of ammonia, primary amines are symmetrically dialkylated with two equivalents olefin by using rhodium catalysts such as $[Rh(cod)_2]BPh_4$ and $[\{RhCl(cod)\}_2]$ (Scheme 15; cod is cyclo-

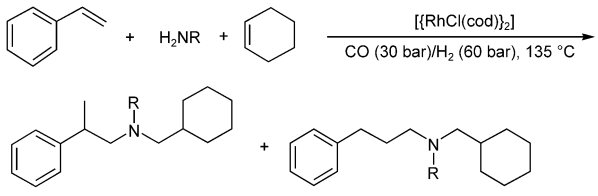


Scheme 15. Dialkylation of benzylamine.

octadiene).[56] When two equivalents of styrene are used as olefin, tertiary amines with mediocre *iso* selectivity (*iso*,*iso*:*iso*,*n* = 2:1) are formed in good yield (80%). However, the application of equivalent amounts of styrene and benzylamine resulted in the exclusive formation of the secondary amine with high *iso* selectivity (82% yield).

Dialkylation of secondary diamines such as piperazine also gives *iso*,*iso*-diamine as the major product (*n*:*iso* = 1:5 with 90% overall yield) with styrene as the olefin, while exclusive formation of the *n*-isomer is observed when α-methylstyrene is the olefin, with almost quantitative yield. Again in the former case the selectivity is controlled by the stability of the intermediate benzylic rhodium complex, while in the latter case the regioselectivity is determined by steric factors. Unsymmetrical dialkylation can be easily carried out with two different olefins that undergo initial hydroformylation with different reaction rates. For example, mixed dialkylation of *n*-butylamine (*n*:*iso* = 1:6) and benzylamine (*n*:*iso* = 1:27) with styrene and cyclohexene produced the corresponding unsymmetrical tertiary *iso*- and *n*-amines in 54–56% yield. Since the hydroformylation of styrene is much faster compared to cyclohexene, the in situ generated secondary amine mainly arises from the reaction of styrene. The resulting amine reacts then with the slow-forming hydroformylation product of cyclohexene (Scheme 16).[59]

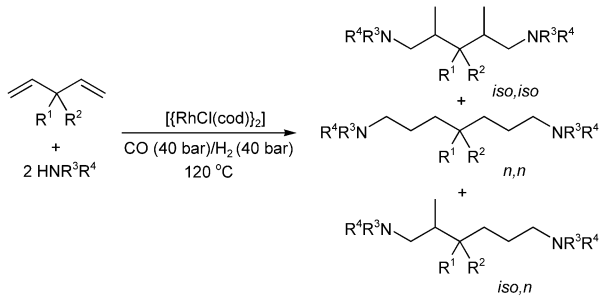
α,ω-Diamines with long aliphatic chains separating the two amino functions can also be synthesized by carbonylative bishydroaminomethylation of the corresponding α,ω-diole-



Scheme 16. Mixed dialkylation of amines.

 © 2004 Wiley-VCH Verlag GmbH & Co. KGaA, Weinheim

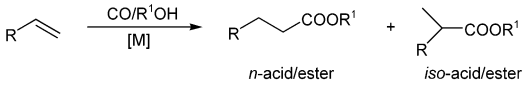
fins together with suitable amines (Scheme 17).[61] Problems of regioselectivity are circumvented by introducing bulky groups in the vicinity of the double bond. Thus, the two methyl groups of 3,3-dimethylpenta-1,4-diene effect an exclusive formation of the *n*,*n*-isomer.



Scheme 17. Bishydroaminomethylation of α,ω-diolefins.

2.3. Hydrocarboxylation and Hydroesterification

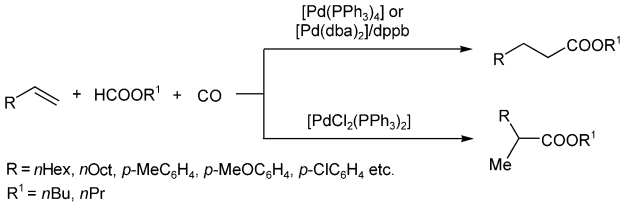
Similar to hydroformylation reactions, the hydrocarboxylation or hydroesterification of olefins can also be controlled to form linear or branched carboxylic acids/esters preferentially (Scheme 18).



Scheme 18. Hydrocarboxylation ($R^1 = H$) or hydroesterification (R^1 = alkyl, aryl) of olefins.

Standard carbonylation catalysts such as $[Co_2(CO)_8]$ and $[Ni(CO)_4]$ have been used industrially to prepare mixtures of fatty acids/esters from olefins.[62] In addition, the use of palladium and platinum compounds, along with Sn or Ge salts, was described many years ago as catalysts for the carbonylation of aliphatic olefins (C_2–C_{14}) to form the corresponding linear carboxylic acids or esters in good yields (65–85%) albeit at high pressure (300 bar).[62,63] Later on, different catalysts based on Pd, Pt, and Rh were found to be more attractive for organic synthesis because of their better performances under milder reaction conditions.[64] Hence, $PdCl_2$ with PPh_3,[65] or with $CuCl_2/HCl/O_2$[66] forms an efficient catalyst for the hydrocarboxylation of aliphatic olefins at lower CO pressure (1–54 bar). The latter catalyst system is particularly selective towards branched carboxylic acids and esters,[67,68] while in the former system the *n*:*iso* ratio is mainly controlled by changes in reaction parameters, such as concentration of PPh_3, water, and CO partial pressure.

Olefins react also with formate esters and CO in the presence of Pd^{II} or Pd^0 compounds, $CuCl_2$, O_2, and HCl to form the carboxylic acid esters (Scheme 19).[69] Indeed, the carbonyl group of the product ester is derived from CO, not from the formate ester.[70] An interesting feature of this reaction is the use of a palladium complex in an appropriate



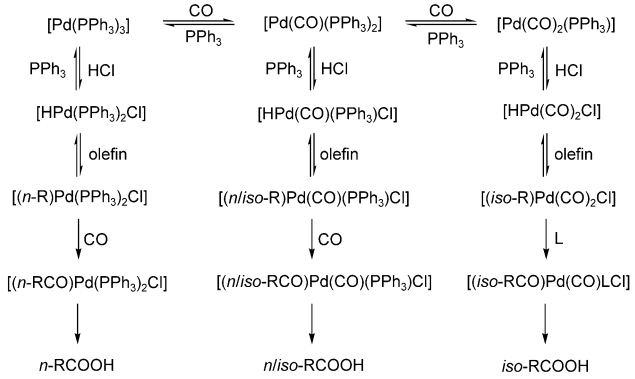
Scheme 19. Regioselective carbonylation of olefins by using formate esters.

oxidation state and an added ligand enabling one to prepare linear or branched chain esters in a regioselective manner. Thus, palladium(0) complexes such as $[Pd(PPh_3)_4]$ or $[Pd(dba)_2]$ (dba = dibenzylidene acetone)in the presence of 1,4-bis(diphenyl phosphino)butane (dppb), catalyze the reaction of alkenes and formate esters to give linear carboxylic esters as the major product, while the branched chain isomer is the principal ester obtained by using $[PdCl_2(PPh_3)_2]$ as the catalyst.[69] Similarly, $Pd(OAc)_2$/dppb in the presence of formic or oxalic acids under CO atmosphere provided regioselective formation of straight chain acids for a number of mono and disubstituted olefins.[71]

In the case of carbonylation of vinylarenes, monosphosphane palladium complexes mainly lead to the formation of branched carboxylic acids or esters. Clearly, the special thermodynamic stability of the transition-metal benzyl complex is the main factor that governs the regioselectivity of this functionalization process. For instance, $PdCl_2$[72] and $[PdCl_2(PPh_3)_2]$[73] along with 10% HCl in ethanol catalyze the carbonylation of styrene to ethyl-2-phenyl propionate with 95% yields. Hydrocarboxylation and hydroesterification (alkoxycarbonylation) of 4-methylstyrene with $PdCl_2/CuCl_2$/HCl as the catalyst system in the presence of PPh_3 as a ligand, gave the corresponding branched aryl propionic acid and ester[74] in 93% regioselectivity. Cationic palladium complexes formed in situ from $Pd(OAc)_2$, a monophosphane, and TsOH efficiently catalyze the methoxycarbonylation of styrene to give in high regioselectivity (up to 96%) the branched product methyl 2-phenylpropionate.[75] A detailed study on the hydroesterification of styrene with the above catalyst system shows that the regioselectivity towards methyl 2-phenylpropionate increases with a decrease in the basicity of phosphane ligands as well as steric bulk around the palladium center and polarity of the reaction medium.[76] Noskov et al.[77] also studied the hydrocarboxylation of styrene with $[PdCl_2(PPh_3)_2]/PPh_3$ as the catalyst. With this catalyst system, a temperature-dependent regioselectivity pattern was observed: increased formation of 3-phenylpropionic acid (linear isomer) was obtained at higher temperatures. This trend is explained in terms of the difference in the energy of activation for the formation of linear and branched isomers. In the case of the linear isomer, the energy of activation is calculated to be 80 kJ mol^{-1} higher than that of the branched isomer. The use of excess amounts of PPh_3, synthesis gas instead of pure CO[78] and $SnCl_2$ as co-catalysts also helps to increase the linear isomer selectivity. The observed regioselectivity is explained with the help of three different {Pd–H} species as the active catalyst initiating

 © 2004 Wiley-VCH Verlag GmbH & Co. KGaA, Weinheim

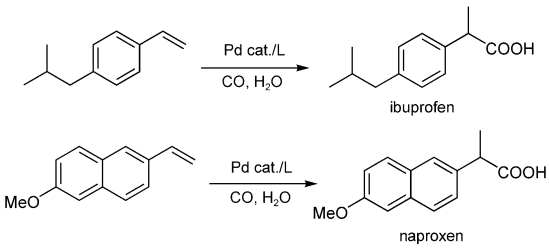
different catalytic cycles. It is proposed that the monocarbonyl species, $[Pd(CO)(PPh_3)_2]$, produces both the isomers, while the double carbonyl, $[Pd(CO)_2(PPh_3)]$, and the $[Pd(PPh_3)_3]$ species form branched and linear products, respectively (Scheme 20).[77d]



Scheme 20. Different reaction pathways in the palladium catalyzed hydrocarboxylation of olefins.

Interestingly, the selectivity pattern for the hydrocarboxylation or alkoxycarbonylation of styrenes is reversed towards the linear carboxylic acid/ester[79] by using bidentate phosphane ligands $Ph_2P(CH_2)_nPPh_2$ ($n = 1$–10), instead of monophosphanes. As discussed above in case of monophosphane complexes,[80] the branched benzyl complex is more stable than the linear complex since it is stabilized by π-benzylic interaction of phenyl group with palladium and hence favoring the branched product. On the other hand with diphosphane palladium complexes, the branched structure is less favorable because of a steric interaction between the alkyl moiety and the chelate ligand. In addition, the chelate coordination of the phosphane increases the hydridic character of the {Pd–H} complex. Both these effects together promote the anti-Markovnikov addition in the latter case. Thus, the carbonylation of styrene, with $PdCl_2$ in the presence of 1,4-bis(diphenylphosphino)butane (dppb) as the ligand gave a selectivity of 68% to ethyl 3-phenylpropionate (48% yield).[80] Due to the increased steric bulk at the double bond, the carbonylation of α-methylstyrene by using $PdCl_2$ and (*R*,*R*)-2,3-*O*-isopropylidene-dihydroxy-1,4-bis(diphenylphosphino)butane ((−)-diop) gave exclusively the straight chain ester.[81]

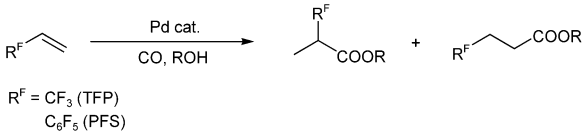
An industrially important application of the hydrocarboxylation of vinyl aromatics is the production of 2-arylpropionic acids, especially ibuprofen and naproxen, which are pharmaceutically important nonsteroidal analgesics (Scheme 21). Many companies, such as Nippon Petrochemicals Company,[82] Ethyl Corporation,[83] Montedison,[84] Albermarle, and others, have patented their own processes for the production of ibuprofen from *p*-isobutylstyrene and naproxen from 2-vinyl-6-methoxynaphthalene. In a process described by Nippon Petrochemicals Company Ltd., *p*-isobutylstyrene is carbonylated in a biphasic system consisting of 10% aqueous HCl and toluene as the organic phase in the presence



Scheme 21. Synthesis of ibuprofen and naproxen by hydrocarboxylation.

of $[PdCl_2(PPh_3)_2]$ forming ibuprofen (with 89% selectivity).[85] Similarly the methyl ester of ibuprofen is prepared by using methanol as the reaction medium in 89% selectivity in the presence of $CuCl_2$ as co-catalyst. The catalyst system consisting of $PdCl_2$, $CuCl_2$, HCl and O_2 in the presence of a chiral ligand *R*-(−)- or (*S*)-(+)-1,1′-binaphthyl-2-2′-diyl hydrogenphosphate (bnppa) give 84% and 91% ee for *S*-ibuprofen and *S*-naproxen respectively, though the catalytic activity is poor (ca. 0.39 h^{-1}).[86] Palladium complexes such as $[PdCl_2(PPh_3)_2]$, and [Pd(pyridine-2-carboxyate)(OTs)(PPh_3)] or Pd/C and PPh_3 along with promoters such as TsOH and LiCl are found to be highly active for the carbonylation of vinyl aromatic compounds to 2-arylpropionic acids.[87] These catalyst systems offer branched acid selectivities up to 99.8% at 115 °C and 54 bar CO.

The hydrocarboxylation and alkoxycarbonylation of fluorinated olefins (Scheme 22) such as 3,3,3-trifluoropropene



Scheme 22. Hydrocaboxylation of fluorinated olefins.

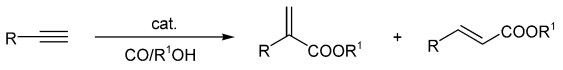
(TFP) and pentafluorostyrene (PFS) leads to the formation of fluorinated acid derivatives, which might be useful intermediates for organic synthesis. Different regioisomers are obtained depending on the type of catalyst applied. Either linear or branched products can be obtained in high yields with high regioselectivities.[39,88] For example, 4,4,4-trifluorobutyric acid is obtained in 93% yield and 99% regioselectivity by using a $[PdCl_2(dppf)]/SnCl_2$ catalyst in the hydrocarboxylation of TFP at 115 °C and 100 bar CO, while ethyl 2-methyl-3,3,3-trifluoropropionate is obtained in 96% yield with 79% regioselectivity in the hydroesterification of TFP by using $[PdCl_2(PPh_3)_2]$ as the catalyst. Similarly, 3-(pentafluorophenyl)propionic acid is obtained in 93% with 99% regioselectivity in hydrocarboxylation of PFS catalyzed by $[PdCl_2(dppf)]$ or $[PdCl_2(dppb)]$ and methyl-2-(pentafluorophenyl)propionate is obtained in 89% yield with 95% regioselectivity in the hydroesterification of PFS catalyzed by $[PdCl_2(PPh_3)_2]$. Based on these observations the authors have proposed that the hydrocarboxylations of TFP and PFS may involve (hydroxycarbonyl)palladium(II) intermediates

 © 2004 Wiley-VCH Verlag GmbH & Co. KGaA, Weinheim

while the hydroesterification of TFP and PFS proceeds via alkylpalladium(II) and acylpalladium(II) intermediates, which explains the observed regioselectivity pattern. However, it is more likely that the type of ligand (monodentate versus bidentate) determines the selectivity similar to the carbonylation reactions of aromatic olefins.

As discussed above palladium-based catalysts have been mainly applied for hydroxycarbonylation reaction. However, other metal-based catalysts have been proven also active for these transformations. A recent example includes the use of rhodium catalysts for the hydroxycarbonylation of aliphatic olefins in the presence of formic acid at higher temperature (>160 °C).[89] In general moderate selectivitiy for the anti-Markovnikov product is reported.

Even though for the carbonylation of acetylene (the simplest alkyne) is efficiently carried out on commercial scale, a similar process for higher alkynes remained underdeveloped because of problems associated with controlling the regioselectivity and because of the price and availability of other alkynes. In the last decade attention has been focused on the development of catalysts consisting of complexes of nickel, palladium, and platinum with different phosphane ligands.[90] Here, a major goal has been the development of chemo- and regioselective carbonylation catalysts for application to higher alkynes for the selective synthesis of certain fine chemicals and pharmaceuticals or their intermediates. Nowadays mainly palladium and platinum catalysts allow the carbonylation of terminal alkynes (Scheme 23) to proceed under milder operating conditions (1 to 60 bar, 50–100 °C) with higher rates compared to those applied in the original Reppe process.



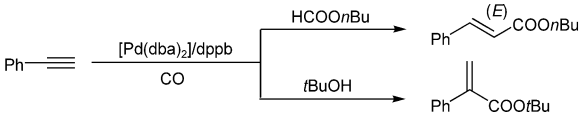
Scheme 23. Carbonylations of alkynes.

As an example Knifton has reported that $[PdCl_2(p\text{-}MeC_6H_4)_3P)_2]/SnCl_2$ and $[PdCl_2(Me_2PPh)_2]/SnCl_2$ catalyze the carbonylation of 1-alkynes under mild conditions with high selectivity (up to 96 %) to give the linear α,β-unsaturated carboxylic acid esters.[91] Similarly, Pt-based catalyst systems $[PtCl_2(PPh_3)_2]/SnCl_2$ and $[PtH(SnCl_3)(PPh_3)_2]$ are found to be active for the carbonylation of terminal as well as internal acetylenes, the product distribution being dependent on the catalyst system used.[92] For example, in case of 1-octyne, the branched ester methyl 2-methyleneoctanoate is selectively formed with $[PtH(SnCl_3)(PPh_3)_2]$ as the catalyst (59 % yield), while $[PtCl_2(PPh_3)_2]$ combined with $SnCl_2$ gave higher yields to the linear ester (*n*:*iso* = 1.2:1). The reasons for this selectivity difference are not fully understood.

In a similar way to that of olefins, carbonylation of alkynes are also reported with formic acid or oxalic acid in the presence of a catalytic amount of $Pd(OAc)_2$ and phosphanes at 8 bar of CO and 110 °C, to produce the corresponding α,β-unsaturated carboxylic acids in 60–90 % yields.[93] The most suitable ligands under these conditions are PPh_3 and dppb. Surprisingly, in some cases the use of a mixture of the two ligands, dppb and PPh_3, significantly improved the yields. The regioselectivity of products is approximately 90:10 in favor of the branched acid when R is phenyl or a straight chain alkyl groups. Due to steric reasons, the linear acid is favored when R is *t*Bu, and is the exclusive product when R is $SiMe_3$. The hydrocarboxylation of alkynes with formic acid or oxalic acid is also achieved by using a heterogeneous catalyst (Pd/C) in the presence of dppb and PPh_3. The catalytic activity of the heterogeneous and homogeneous systems is similar. It might be concluded that similar to other Pd-catalyzed carbonylation[87c] and coupling reactions[94] an initial leaching of palladium from the support takes place. At the end of the reaction most of the palladium is deposited on the support again.

In addition to advancements in the area of Pd- and Pt-based catalyst systems, some progress is also reported regarding Ni catalysts. Alper and co-workers have demonstrated that phase-transfer catalysis is beneficial for the Ni-catalyzed carbonylation of alkynes. For instance, the carbonylation of phenyl acetylene using $[Ni(CN)_2]$ and cetyltrimethylammonium bromide (CTAB) as the phase-transfer agent in the presence of an aqueous base yielded atropic acid as the only product (yield = 35–62 %). The application of the same catalytic system to diynes gave unsaturated diacids in good yields. Similarly, the direct regioselective hydrocarboxylation of alkynes to saturated carboxylic acids is achieved by using cobalt chloride, potassium cyanide, or nickel cyanide, under phase-transfer conditions with polyethylene glycol (PEG-400) as the phase-transfer agent. Under these conditions, branched saturated acids are formed as the major products (43–65 %).[95]

As discussed in the section on olefin carbonylation, a related method to the hydrocarboxylation reaction is the hydroesterification reaction. Alcohols instead of water are used as nucleophiles to trap the intermediate transition metal acyl complex. In general, the regioselective preferences are not influenced by the nucleophile. Hence, similar selectivities are observed. An exception is the hydroesterification of alkynes with formate esters (Scheme 24). In the presence of



Scheme 24. Alkoxycarbonylation of phenyl acetylene with alcohols and formate esters.

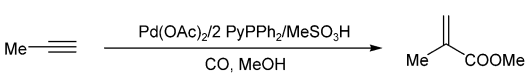
$[Pd(dba)_2]$/dppb as the catalyst at 80 bar and 100 °C the regioselective formation of *trans*-α,β-unsaturated esters is observed. For instance, phenyl acetylene in the presence of *n*-butyl formate afforded of *trans*-*n*-butyl cinnamate (yield 31 %) regiospecifically.[96,97] However, when the same reaction is carried out in the presence of tertiary butanol instead of the formate ester, the *tert*-butyl ester of atropic acid is obtained with a yield of 56 %, and none of the isomeric cinnamate ester is detected.[90] The fundamental difference between the regiochemistry of the alkyne to alcohol and alkyne to formate

 © 2004 Wiley-VCH Verlag GmbH & Co. KGaA, Weinheim

ester reactions is proposed to be due to the involvement of a {Pd-COOR} mechanism in the former and a {Pd-H} mechanism in the latter reaction.

Torri et al.[98] demonstrated that the aminocarbonylation of various terminal acetylenes proceeds regioselectively to the branched amides in the presence of a catalytic amount of organic iodides or ammonium iodides and palladium complexes such as $[PdCl_2(PPh_3)_2]$, $[PdCl_2(dppb)]$ or $Pd(OAc)_2$/$4\,PPh_3$. The resulting 2-substituted acrylamides are formed in high regioselectivity and good yields under mild conditions (5 bar, 120 °C). In another study, Miura and co-workers have reported the alkoxycarbonylation of terminal acetylenes in the presence of $[Pd(PPh_3)_4]$, or $Pd(OAc)_2$/dppf by using weakly acidic 3- or 4-substituted phenols as nucleophiles.[99] Again the branched products (2-substituted 2-propenoate aryl esters) are formed preferentially in good yield (up to 95%) along with traces of the corresponding 3-substituted isomer. Similar results for the hydroesterification of alkynes in butanol are obtained by using a catalyst system consisting of $[Pd(dba)_2]$, $4\,PPh_3$, pyridine carboxylic acid and *p*-toluenesulfonic acid. The resulting 2-substituted propenoic acid butyl esters are obtained in good selectivity and yield at 1 bar of CO.[100] Thus, for the hydroesterification of phenyl acetylene a maximum regioselectivity of 89% towards the butyl ester of atropic acid is achieved. Not surprisingly the alkoxycarbonylation of alkynes in the presence of chiral alcohols gave chiral 2-arylpropenoic esters in good yields.[101] As an example, phenyl acetylene is readily carbonylated to (1*R*,2*S*,5*R*)-menthyl 2-phenylpropenoate (88% yield) at 100 °C and 10 bar of CO with the $[Pd(dba)_2]$/$4\,PPh_3$/TsOH catalyst system.

From the standpoint of application it is important to note that with all of these catalysts, the reaction rates are poor, and catalyst productivities are not sufficient for larger-scale industrial applications. More recently, a class of highly efficient homogeneous cationic palladium catalysts has been developed for the alkoxycarbonylation of alkynes by Drent et al.[102] The cationic catalyst system not only allows the rapid carbonylation of acetylene but also of higher alkynes. Special emphasis has been given to study the alkoxycarbonylation of propyne as a promising reaction for the production of the bulk monomer methyl methacrylate (MMA). The methoxycarbonylation of propyne had a very-high turnover frequency ($TOF = 50\,000\ h^{-1}$) and a selectivity of 98.9–99.95% to MMA, thereby allowing a cost-effective single-step process for MMA product (Scheme 25). Unfortunately, until today no industrial process has been realized, most likely due to feedstock costs.



Scheme 25. Methoxycarbonylation of propyne. (Py = 2-pyridyl)

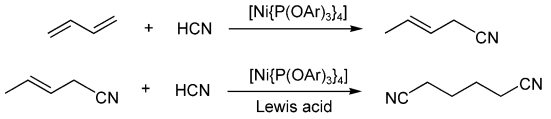
The essential feature of the Drent catalyst is the combination of 2-pyridylphosphanes with a palladium(II) species and acidic promoters having weakly coordinating anions. The structure of the pyridylphosphane has a dramatic effect on the catalytic activity as well as the selectivity. It was demonstrated that a variation of the position of a methyl substituent attached to the pyridine ring resulted in significant changes in the regiospecificity of the catalyst. Whereas, substitution at the 4 position of the 2-pyridyl group has virtually no effect, it is remarkable that the introduction of the methyl substitutent at the 6 position of the 2-pyridyl group raises the regioselectivity to 99.95% with retention of the high overall catalytic activity. This implies that formation of methyl crotonate is suppressed by a factor of 20 compared to that observed with the unsubstituted ligand. The same catalyst system also showed high activity for the alkoxycarbonylation of aryl alkynes giving the branched ester products, which are interesting intermediates for the production of optically active 2-arylpropionic acids by enantioselective hydrogenation. A TOF of $20\,000\ h^{-1}$ and 99.9% selectivity to the branched product methyl 2-phenylpropenoate is reported for the hydroesterification of phenyl acetylene with $Pd(OAc)_2$ as the catalyst precursor along with (6-methyl-2-pyridyl)diphenylphosphane as the ligand.[103] Similarly, the hydrocarboxylation of phenyl acetylene by using $Pd(OAc)_2$/2-pyridylphosphane as catalyst gave a TOF of $3000\ h^{-1}$ and >98% selectivity to the branched unsaturated acid (2-phenylpropenoic acid) at 30 bar and 50 °C.[104] In addition, the carbonylation of 6-methoxy-2-naphthylethyne resulted in the formation of 2-(6-methoxy-2-naphthyl)propenoic acid, a naproxen precursor, at 10 bar of CO, though with a low reaction rate. More recently, Reetz and co-workers described a modified ligand for the Drent system. They reported $Pd(OAc)_2$ along with 2-pyrimidylphosphanes[105] to give TOFs in the range of $7000\ h^{-1}$ for the carbonylation of different alkynes with >97% selectivity to the branched products.

3. Hydrocyanation

The transition-metal catalyzed addition of hydrogen cyanide to olefins and alkynes offers a direct pathway for the synthesis of a variety of nitriles. Ni, Co, and Pd complexes are generally used as catalysts for this conversion. Cobalt carbonyl catalysts gave rise to Markovnikov nitriles as the major product by the addition of HCN to olefins, at comparably high temperatures (120–140 °C).[106] For example, olefins such as propylene, 1-butene (65% conversion), 2-butene (9%), 1-octene (13%) and styrene (50%) are sluggishly converted into the corresponding branched nitriles by using dicobalt octacarbonyl either in presence or absence of triphenylphosphane. Major attention has been paid to the hydrocyanation of 1,3-dienes, especially 1,3-butadiene due to the importance of this reaction for the production of nylon monomers.[107] In the presence of cobalt carbonyl catalysts, 1,3-dienes react with HCN giving mainly the 1,4-addition products. 1,3-Butadiene (60% conversion) formed a mixture of 3-pentenenitrile (60%), 2-methyl-3-butenenitrile (8%), 4-pentenenitriles (7%), 2-methylglutaronitrile (20%) and 2,3-dimethylsuccinonitrile (5%). Isoprene formed 4-methyl-3-pentene nitrile (67%) and 3-methyl-3-pentenenitrile (33%) with a total conversion of 40%.

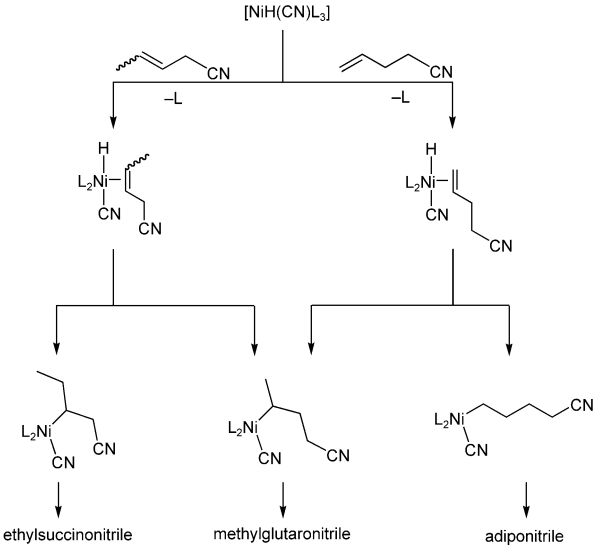
 © 2004 Wiley-VCH Verlag GmbH & Co. KGaA, Weinheim

A more efficient anti-Markovnikov hydrocyanation of olefins is realized by the use of zerovalent triarylphosphite nickel complexes as catalysts.[108] For this reaction, the most important industrial example is the DuPont adiponitrile process. In this two-step process (Scheme 26), 1,3-butadiene



Scheme 26. Adiponitrile synthesis by DuPont.

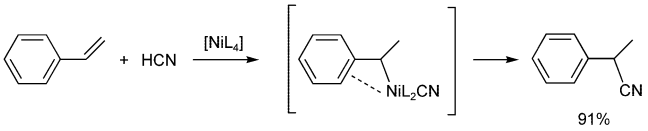
is hydrocyanated, in the presence of a triarylphosphite nickel complex and a Lewis acid promoter, to give adiponitrile with good selectivity.[109] In the initial step of this process, monohydrocyanation of 1,3-butadiene to 3-pentenenitrile (70%) and 2-methyl-3-butenenitrile (30%) occurs in the presence of a [NiL_4] catalyst [L_x = P (O-Ar)$_3$ (x = 3, 4; Ar = Ph, 2-, 3- or 4-tolyl)]. In the second step, a Lewis acid promoter, such as $ZnCl_2$ or BPh_3, is added to the NiL_4 catalyst effecting the concurrent isomerization of 3-pentenenitrile to 4-pentenenitrile and the selective anti-Markovnikov addition of HCN to 4-pentenenitrile to give adiponitrile in high yield and selectivity (83–96%). Nevertheless, 2-methylglutaronitrile and ethylsuccinonitrile are formed as by-products. The reaction proceeds through the formation of relatively stable π-allylnickel cyanide intermediates, which participate in the successive carbon–carbon coupling and play a key role in determining the regioselectivity of the reaction (Scheme 27). The catalyst loses its activity in the presence of an excess HCN owing to its irreversible oxidation, which is also promoted by Lewis acids. Hence maintaining a low HCN concentration in the process is crucial for optimal catalytic activity.



Scheme 27. Regioselective addition of Ni hydride complexes to pentenenitriles.

Major improvements in both catalytic efficiency and adiponitrile selectivity are realized by adding Lewis acid co-catalysts.[110] Lewis acids, such as $AlCl_3$ and $ZnCl_2$, accelerate the rate of hydrocyanation by coordinating with the lone pair on the cyanide nitrogen atom and hence increase the concentrations of the active species and the rate-determining carbon–carbon coupling reaction. Olefin isomerization is also promoted. The selectivity is mainly determined by the steric bulk of the Lewis acid used, for example, the hydrocyanation of 3-pentenenitrile by using a NiL_4 catalyst (L = P (O-*p*-tolyl)$_3$) at 50 °C gives 96% selectivity for the linear product in the presence of BPh_3, 82% with $ZnCl_2$ and 50% with $AlCl_3$.[110b] Under similar conditions, other conjugated and nonconjugated dienes, such as 1,3- and 1,5-hexadienes, and cyanoolefins, such as butenenitriles (*n*:*iso* = 2), 2-methyl-3-butenenitriles (*n*:*iso* = 16) form the corresponding linear dinitriles as the major products.

A variety of other functionalized and nonfunctionalized olefins can be hydrocyanated by using the [Ni{P(O-*o*-tolyl)$_3$}$_4$] catalyst. In the case of aliphatic olefins, the anti-Markovnikov nitrile (linear isomer) is formed as the major product, while in the case of aryl olefins the Markovnikov product (branched isomer) predominates.[107b] For instance, propylene gives *n*-butyronitrile and *iso*-butyronitrile in a 70:30 ratio. 1-Hexene gives a similar distribution of linear and branched nitriles in addition to traces of 2-ethylvaleronitrile, which is formed by isomerization of 1- to 2-hexene followed by HCN addition. Isobutene forms 3-methylbutyronitrile as the only product owing to the steric crowding at the *tert*-butylnickel cyanide center. The reaction with trimethylsilylethylene or trifluromethylethylene affords the corresponding linear nitriles. On the other hand, the use of styrene in this reaction favors the formation of the branched nitrile (91%) over the linear (9%) isomer owing to the unusual stabilization of the branched benzylnickel complex (Scheme 28).[110a] As in the case of



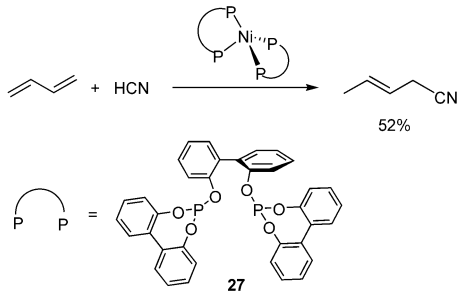
Scheme 28. Nickel catalyzed hydrocyanation of styrene.

adiponitrile process, for aliphatic or aromatic olefins, the addition of aryl boranes increases the amount of the anti-Markovnikov products significantly. For example, for the reaction of 1-hexene in the presence of B(*p*-tolyl)$_3$, the yield of the linear heptanenitrile increased from 67% to 91%. For the reaction of styrene, there is an increase in the linear product (3-phenylpropionitrile) from 9% to 14% and in the case of 4-pentenenitrile there is an increase in the linear product from 77 to 99% when B(*p*-tolyl)$_3$ is the promoter.[107]

As with boron-based Lewis acids, the addition of copper(I) salts is known to provide an increase in the linear selectivity. For instance 3-pentenenitrile is obtained with 90% regioselectivity by the hydrocyanation of 1,3-butadiene.[111] In the case of isoprene 100% regioselectivity towards 1,4-addition is observed under similar conditions.[112]

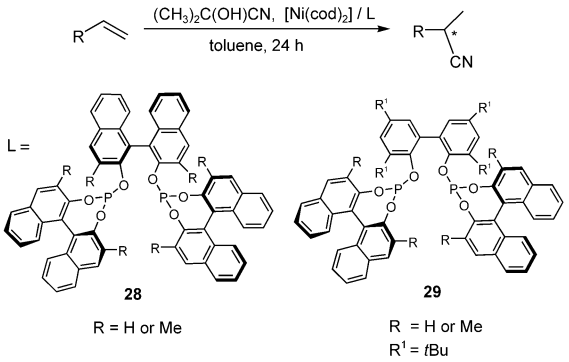
 © 2004 Wiley-VCH Verlag GmbH & Co. KGaA, Weinheim

The Ni^0 complex of a diphosphite ligand **27** derived from 2,2′-dihydroxybiphenyl forms a highly stable catalyst for hydrocyanation of 1,3-butadiene, though the selectivity to 3-pentenenitrile (52%) is relatively low (Scheme 29).[113]



Scheme 29. Stable Ni^0 diphosphite catalyst for the hydrocyantion of butadiene. (Turn over number, TON = 1430).

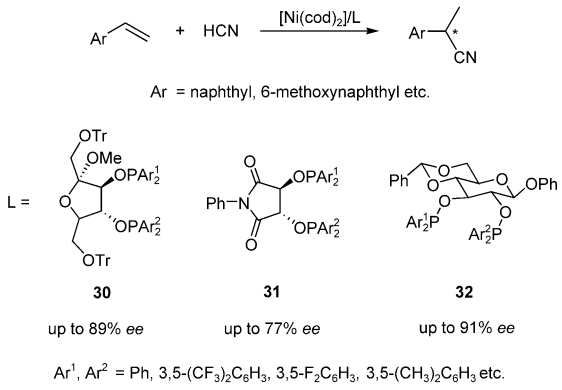
Recently, chiral aryl diphosphite ligands derived from 2,2′-binaphthol are found to be useful for the Ni^0-catalyzed enantioselective hydrocyanation of styrenes (up to 94% regioselectivity; up to 65% *ee*) and vinyl acetate (83% regioselectivity; 73% *ee*) by using acetone cyanohydrine as the cyanating agent (Scheme 30).[114] Again, the branched



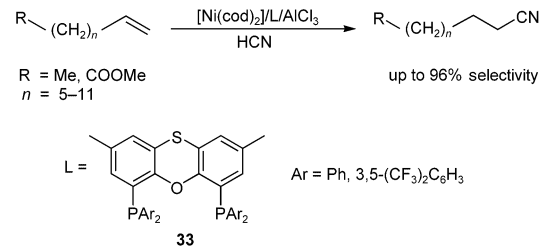
Scheme 30. Enantioselective hydrocyanation of olefins by using chiral diphosphite ligands **28** and **29**.

nitriles are formed due to the thermodynamically stabilized branched benzyl nickel complex. Earlier RajanBabu et al. described the reaction of vinylarenes with HCN in the presence of Ni^0 complexes of sugar-based diarylphosphinites. As shown in Scheme 31, the branched nitriles are formed exclusively with high enantioselectivities.[115]

More recently, Vogt and co-workers reported the hydrocyanation of different terminal olefines and ω-unsaturated fatty acid esters by using chelating xantphos-type diphosphanes.[116] For instance, in the presence of $[Ni(cod)_2]$, $AlCl_3$, and thixantphos ligands, which have a rigid backbone and large natural bite angles, 1-octene (up to 96%) and methyl 9-dec-1-enoate (up to 75%) form the corresponding terminal nitriles, selectively (Scheme 32). As expected, styrene gave predominantly the branched nitrile, with an excellent regioselectivity of > 99% when the substituted thixantphos ligands

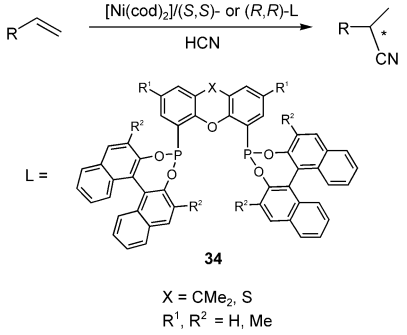


Scheme 31. Regio- and stereoselective hydrocyanation of vinylarenes by using different diarylphosphinite ligands **30**–**32**. (Tr = triphenylmethyl).



Scheme 32. Selective hydrocyanation of terminal olefins by using thixantphos ligands.

was used with $[Ni(cod)_2]$.[117] Higher activity of the nickel complexes is observed when the ligand has electron withdrawing substituents (e.g. when $R = CF_3$; 90% yield of the branched nitrile). Similarly, Ni^0 complexes of homochiral xantphos-type diphosphonite ligands with 2,2′-binaphthol substituents are found to be effective for the addition of HCN to vinylarenes to form the branched nitrile as the major product with regioselectivities in the range of 99% (up to 80% *ee*; Scheme 33).[118]



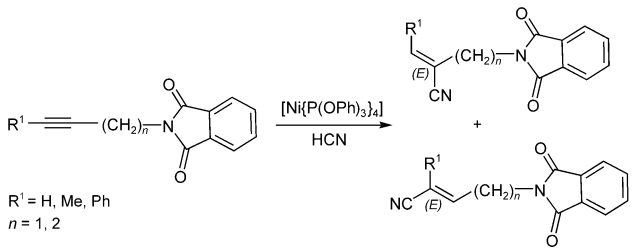
Scheme 33. Asymmetric hydrocyanation of vinylarenes by using homochiral xantphos diphosphonite ligands.

The addition of HCN to straight chain terminal alkynes such as 1-hexyne with nickeltetrakistriphenylphosphite lead predominantly to the branched chain nitrile, whereas the reaction of bulky 3,3-dimethylbut-1-yne forms predominantly

 © 2004 Wiley-VCH Verlag GmbH & Co. KGaA, Weinheim

the linear nitrile, thus indicating the significance of steric effects on regioselectivity.[119] Similar reactions of silylalkynes containing bulky *tert*-butyldimethylsilyl (*n*:*iso* = up to 98:2), triphenylsilyl (only the *n*- product) and trimethylsilyl (up to 80:20) groups also showed the preferential formation of the linear nitrile in case of sterically hindered substituents on one side of the alkyne.[120]

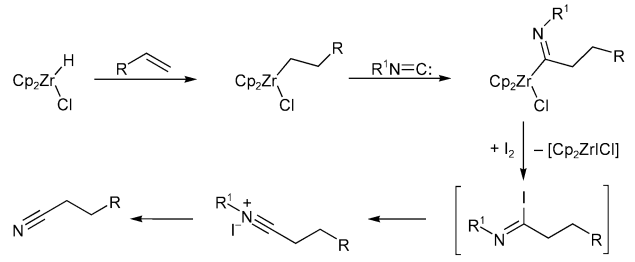
As demonstrated in Scheme 34, phthalimido-substituted alkynes react with HCN in the presence of nickeltetrakis-



Scheme 34. Hydrocyanation of phthalimido-substituted alkynes.

triphenylphosphite yielding predominantly branched nitriles (Markovnikov:anti-Markovnikov ratio up to 9:1).[121] Acetylenes, for example, phenyl acetylene (up to 98%), 4-phenylbut-1-yne (95%), 1-phenylprop-1-yne (63%), 1-phenylbut-1-yne (61%), 1-ethynylcyclohexanol (85%) can be hydrocyanated selectively to the corresponding saturated nitriles by using $[Co(CN)_5]^{3-}$ and H_2[122] or $[Ni(CN)_4]^{2-}$ in the presence of excess cyanide ions, and $NaBH_4$ or Zn in ethylene glycol or water as the source of hydrogen atoms.[123]

Finally it is worth mentioning that Buchwald and Lamaire have developed an indirect method for the regiospecific anti-Markovnikov hydrocyanation of olefins and alkynes that involves stoichiometric hydrozirconation of the olefin followed by reaction of the resulting product with isocyanides (Scheme 35).[124] This method is applicable to simple aliphatic

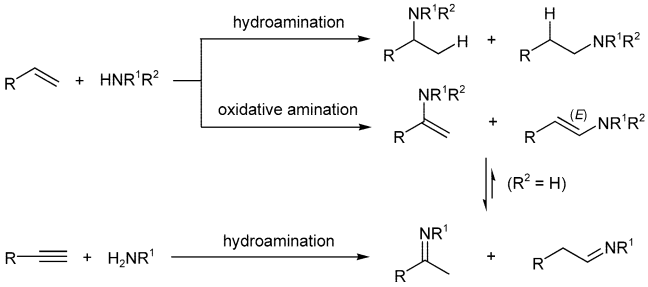


Scheme 35. Regiospecific anti-Markovnikov hydrocyanation of olefins and alkynes.

olefins and alkynes. For instance, olefins such as 1-octene, 2-octene, 1-dodecene, and 3,3-dimethylbut-1-ene, form the corresponding linear nitriles in 65–84% yields. However, styrene gives the linear and branched nitriles in low selectivity (ratio of 2.6:1). Alkynes such as 1-decyne and 3-(*tert*-butyldimethylsiloxy)prop-1-yne form the corresponding linear unsaturated nitriles in 55–90% yield.

4. Hydroamination

Amination of unsaturated systems can take place either as hydroamination, which constitutes the formal addition of an N–H bond across the C–C multiple bond, or as an oxidative amination reaction (Scheme 36). In principle these methods



Scheme 36. Possible amination products from olefins and alkynes.

offer a promising route to a variety of amines, enamines and imines.[125]

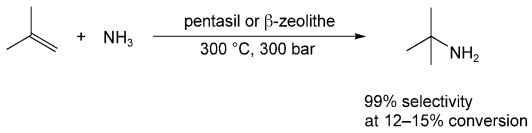
Unfortunately the direct nucleophilic addition of amines across C-C multiple bonds is hampered by several thermodynamic and kinetic barriers:[125g,126]

- Attack of the amine nitrogen atom that bears the lone pair on electron-rich non-activated multiple bonds leads to electrostatic repulsion.
- A [2+2]-cycloaddition of the N–H bond to the alkene is forbidden by the high energy difference between π (C=C) and σ (N–H) orbitals.
- Because of the highly negative reaction entropy, the reaction is not favored at high temperatures.
- The hydroamination reaction is only slightly exothermic or even thermoneutral.[125h]

However, the direct nucleophilic addition of amines proceeds easily with electron-deficient (activated) π-systems containing neighboring functional groups, such as keto, ester, nitrile, sulfoxide, and nitro, which leads to the formation of the anti-Markovnikov products,[127] though the presence of an additional catalyst is found to be advantageous in some cases. Clearly, the stabilization of the initially formed carbanion determines the regiochemistry.

Although a general transformation of nonfunctionalized olefins to amines is still an important challenge in the field of catalysis, in special cases catalysts such as Brønsted acids, Lewis acids, alkali metals, transition metals, lanthanide complexes, and actinide complexes permit successful hydroamination reactions. In the presence of Brønsted acid or Lewis acid catalysts (e.g. zeolites), aliphatic as well as most of the aromatic olefins react with amines, usually forming the Markovnikov product due to the higher stability of the intermediate carbocation. For example, propene[128] and isobutene[129] react with ammonia in the presence of zeolites to form isopropylamine (90–100% selectivity) and *tert*-butylamine (up to 99% selectivity) respectively. BASF has commercialized a *tert*-butylamine process based on this reaction (Scheme 37).[130]

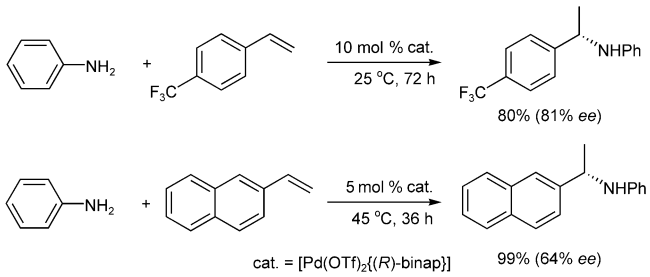
 © 2004 Wiley-VCH Verlag GmbH & Co. KGaA, Weinheim



Scheme 37. BASF *tert*-butylamine process.

In the presence of alkali-metal catalysts, short-chain aliphatic olefins predominantly form the Markovnikov hydroamination products, though in general in low yield. For example, in the presence of metallic sodium or metal amides ($CsNH_2/NaNH_2$) as catalysts, the amination of propene with ammonia or *n*-butylamine yields isopropylamine (82% yield) and *n*-butylisopropylamine (36% conversion), respectively, as the major products.[131] Similarly, isobutene reacts with ammonia in the presence of Na to form *tert*-butylamine regioselectively with (32% yield). The regioselectivity arises from the increased stability of the primary carbanion compared to the corresponding secondary carbanion.

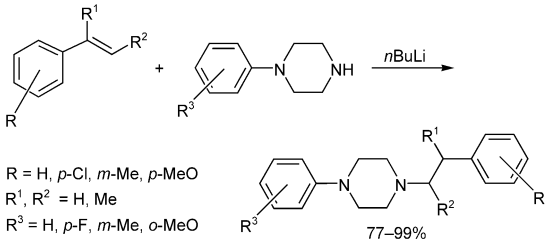
The formation of Markovnikov hydroamination products is also achieved on treating styrenes with anilines in the presence of a Rh catalyst $[\{RhCl(PEt_3)_2\}_2]$ and lithium anilide,[132] or a catalyst system consisting of $[Pd(PR_3)_2(NCMe)(H_2O)](TfO)_2$, $[Pd(PPh_3)_4]$ or Pd-$(OC(O)CF_3)_2$/dppf and triflic acid (> 99% yields).[133] In the latter case, Hartwig and co-workers demonstrated that when chiral phosphane ligands are used, for example, binap, benzylic amines are obtained with good *ee* values.[9] For instance, the reaction of aniline with trifluoromethylstyrene or with vinylnaphthalene catalyzed by $[Pd(OSO_2CF_3)_2\{(R)$-binap$\}]$ at 25 °C formed the addition products in quantitative yields, and with 81% and 64% enantioselectivity, respectively (Scheme 38).[9] The observed selectivity is determined by a η^3-



Scheme 38. Asymmetric hydroamination of vinylarenes with aniline.

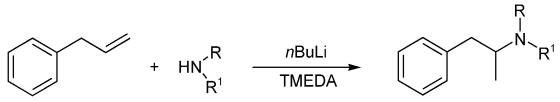
coordination between the terminal protonated vinylnaphthalene and palladium center. Clearly, this method is a milestone in the development of asymmetric catalytic amination reactions. Unfortunately, so far, catalyst productivities are relatively low and the reaction seems to be limited with respect to the starting materials.

Aryl olefins form anti-Markovnikov hydroamination products in the presence of base catalysts. The increased stability of the benzylic anion compared to the corresponding linear carbanion determines the regioselectivity of the reaction. For instance, in the presence of Na or *n*BuLi as precatalysts, primary amines, such as methyl, *n*-propyl, *n*-butyl, *n*-pentyl, and cyclohexylamines as well as benzylamine and 2-phenylethylamine add to styrene forming the corresponding linear secondary and tertiary amines in variable yields (10–70%).[134] Secondary amines also add to styrene in the presence of catalytic amounts of *n*-BuLi or Na_2Np (Np = naphthalene) to give the anti-Markovnikov products in good yields. For example, diethyl, di-*n*-propyl, and di-*n*-nonylamines (41–70% yields), piperidine (88% yield), and aziridine (72–90% yield) are found to react with styrene efficiently affording the corresponding β-phenethylamines.[131,135] Functionalized amines, such as *N*-arylpiperazines, add to styrenes in the presence of *n*BuLi catalyst forming pharmaceutically interesting 1-(aryl-4-phenylethyl)-piperazines in excellent yields (77–99%; Scheme 39).[136]



Scheme 39. Base-catalyzed hydroamination of styrenes with N-arylpiperazines.

Knochel and co-workers showed that aniline can also be added to styrene by using CsOH (120 °C) as a catalyst to form the corresponding anti-Markovnikov secondary amine in 70% yield.[137] A recent study has shown that KO*t*Bu forms a particularly suitable catalyst for this reaction. For instance, *N*-(2-phenethyl)aniline is formed up to 99% yield and > 99.9% selectivity by the reaction of styrene and aniline in the presence of 10 mol% of KO*t*Bu in THF at 120 °C.[138] Substituted styrenes can also be hydroaminated with various amines. For instance, piperidine reacts with α-methylstyrene or α-phenylstyrene in the presence of *n*BuLi giving the corresponding linear amines in 71 and 82% yield, respectively.[134a] Aziridine (in the presence of metallic Na)[135] or *N*-(4-fluorophenyl)piperazine (in the presence of *n*BuLi)[136] react with 4-methoxystyrene providing the anti-Markovnikov hydroamination products in yields of 47 and 77%, respectively. Diethylamine (Na_2Np),[139] 1-phenylpiperazine (*n*BuLi)[136] and aniline (KO*t*Bu)[138] add to α- and β-methyl styrenes to form the corresponding β-phenethylamines in 34–86% yield. Amphetamines are accessible by a base-catalyzed domino-isomerization-hydroamination reaction of 3-phenylpropene (Scheme 40).[140]

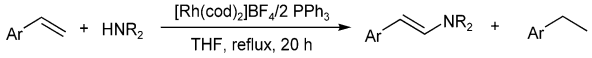


Scheme 40. Base-catalyzed domino-isomerization-hydroamination of allylbenzene.

 © 2004 Wiley-VCH Verlag GmbH & Co. KGaA, Weinheim

For instance, allylbenzene reacts with various primary (*n*-butylamine, benzylamine, aniline) and secondary amines (piperidine, morpholine, *n*-butyl(methyl)amine) in the presence of catalytic amounts of *n*BuLi forming up to 89% of the corresponding 2-aminosubstituted arylalkane with >99% selectivity. In the case of aniline, a mixture of *n*BuLi and KO*t*Bu has to be used as the catalyst. These reactions proceed through a base-catalyzed fast isomerization of 3-phenylpropene to the thermodynamically more stable β-methylstyrene, which further undergoes hydroamination. Again the regiochemistry of the attack of the amine is determined by the stability of the intermediate carbanion. Similarly, 4-phenyl-1-butene reacts with piperidine forming *N*-2-(1-phenyl)butylpiperidine in 59% yield.

Studies at our laboratory showed that cationic rhodium complexes of the type $[RhL_4]X$ (L = olefin or phosphane, X = BF_4^-) catalyze the regiospecific intermolecular oxidative amination of unfunctionalized olefins with secondary amines to form the corresponding anti-Markovnikov enamines (Scheme 41).[125c,141] For example, $[Rh(cod)_2]BF_4$ in the

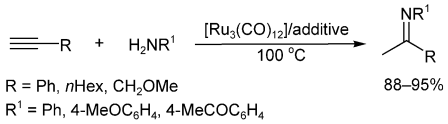


Scheme 41. Anti-Markovnikov oxidative amination of styrenes.

presence of monodentate phosphane ligands catalyzes the reaction between styrene and piperidine or morpholine to form *N*-(2-phenylethenyl)piperidine or *N*-(2-phenylethenyl)-morpholine (74% yield). In the latter case, the formation of *N*-(2-phenylethyl)morpholine, the anti-Markovnikov hydroamination product, is also observed though in lower yields.[142] This was the first example of a transition-metal catalyzed anti-Markovnikov hydroamination of a not strongly activated olefin. Very recently, Hartwig and co-workers[143] performed this reaction by using a similar catalyst system in the presence of chelating ligands such as the xantphos family, which resulted in increased yields of the hydroamination products.[10a,19]. Previous to this, we described that 2-vinylpyridine, an activated olefin, reacted with piperidine in the presence of $[Rh(cod)_2]BF_4/2\,PPh_3$ catalyst to form *N*-[2-(2-pyridyl)ethyl]piperidine (53% yield) along with the intermolecular anti-Markovnikov oxidative amination product *N*-[2-(2′-pyridyl)ethenyl]piperidine (47% yield).[144]

Transformation of simple aliphatic olefins to anti-Markovnikov amines is basically not known and rather tricky compared to their aryl counterparts. Hence, functionalization of olefins with anti-Markovnikov regioselectivity has been viewed for decades as one of the major challenges of catalysis.[145] In a special example, the reactivity of aliphatic olefins is shown to be reversed towards the anti-Markovnikov products by using electrophilic nitrogen radicals.[125k]

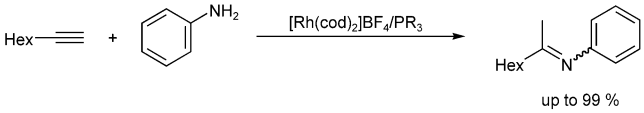
The intermolecular hydroamination of aromatic acetylenes with secondary amines occurs regiospecifically forming the corresponding allylic amines in good to high yields in the presence of $[Pd(PPh_3)_4]$ and benzoic acid. [146] For example, 1-phenyl-1-propyne reacts with dibenzylamine in dioxane at 100 °C to give the corresponding allylamine (98% yield). Similarly, the reaction between 1-phenyl-1-propyne and primary amines such as benzylamine and aniline affords the corresponding 2:1 adducts in good yields (72–82%). Wakatsuki and co-workers introduced a $[Ru_3(CO)_{12}]$/additive (NH_4PF_6 or HBF_4/OEt_2) catalyst system furnishing efficiently the conversion of terminal phenyl acetylenes with anilines into the corresponding Markovnikov imines in high yields (88–95%; Scheme 42).[147] Even in the absence of any



Scheme 42. Hydroamination of phenyl acetylenes with anilines.

additives, $[Ru_3(CO)_{12}]$ is found to be active for the hydroamination of alkynes with *N*-methylaniline forming *N*-methyl-*N*-(α-styryl)amines in high yields (76–88%).[148]

A recent study by us demonstrated that aliphatic alkynes can also be hydroaminated to the corresponding imine. For example, 1-octyne react with aniline in the presence of a cationic rhodium catalyst $[Rh(cod)_2]BF_4/2\,PCy_3$, at room temperature. The regioselective formation of *N*-(2-octylidene)aniline is observed (Scheme 43).[149]

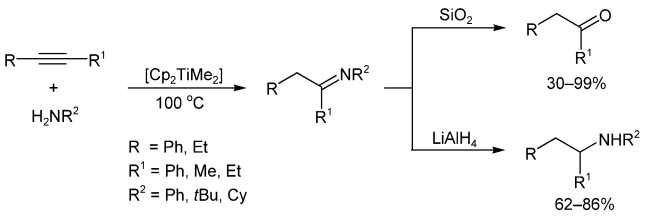


Scheme 43. Amination of 1-octyne by using cationic rhodium complexes. Cy = cyclohexyl.

Apparently, in all these aminations of alkynes with late-transition-metal catalysts, electronic factors govern the regioselective attack of the nucleophile at the internal C atom.

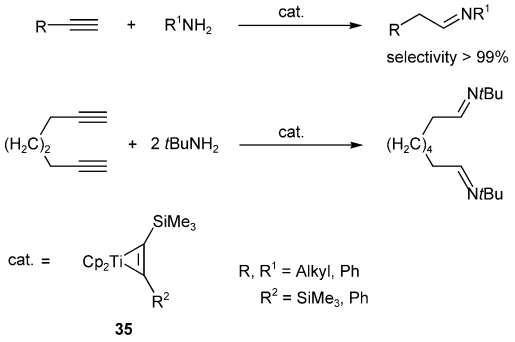
An alternative method for the hydroamination of alkynes uses easily available titanium and zirconium complexes. Important progress in the intermolecular hydroamination of alkynes with titanium complexes was realized initially by the groups of Bergmann,[150] and Doye.[151] While Bergmann and co-workers developed [Cp(ArNH)(py)Ti=NAr] and used it for the reaction of 2,6-dimethylaniline and diphenyl acetylene, the Doye group described a general method for the hydroamination of various internal alkynes (e.g., phenyl acetylene, 1-phenyl-1-propyne, 1-phenyl-1-butyne, 1-phenyl-1-pentyne) by using dimethyltitanocene, $[Cp_2TiMe_2]$, as catalyst, followed by reduction or hydrolysis, which leads to the regioselective formation of the corresponding internal amines (up to 79% yield) or ketones (up to 99% yield) (Scheme 44).

More recently, we found that titanocene alkyne complexes of the type $[Cp_2Ti(\eta^2\text{-}Me_3SiC_2R)]$ (R = $SiMe_3$, Ph)[152] catalyze the anti-Markovnikov hydroamination of different aliphatic alkynes (e.g. 1-hexyne, 1-octyne, 1-decyne) and phenyl acetylene with primary amines with high regioselec-



Scheme 44. Hydroamination of alkynes followed by reduction or hydrolysis.

tivity (> 99 %) and in high yields (84–98 %).[153] Interestingly, in the presence of an excess of amine (amine/alkyne = 4:1) the dihydroamination of diynes, for example, 1,7-octadiyne, proceeds smoothly, both triple bonds react selectively with anti-Markovnikov regiochemistry affording the 1,8-bisimines (92 % yield; Scheme 45). Theoretical calculations demon-



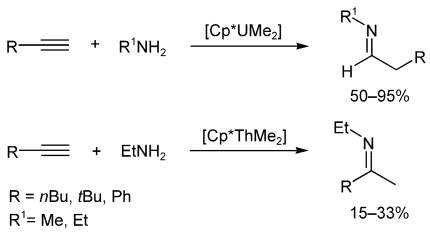
Scheme 45. Hydroamination of alkynes in the presence of $[Cp_2Ti(\eta^2\text{-}Me_3SiC_2R^2)]$.

strated that the observed anti-Markovnikov selectivity is determined by steric interactions of the alkyne with ligands on the titanium center in the corresponding alkyne titanium-π-complex.[154]

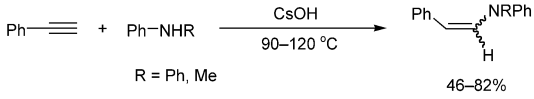
Odom and co-workers demonstrated that titanium amido complexes, such as $[Ti(NMe_2)_4]$ and $[Ti(NMe_2)_2(dpma)]$ (dpma is di(pyrrolyl-α-methyl)-methylamine), are also effective precatalysts for the hydroamination of terminal alkynes, such as 1-hexyne (anti-M:M = 1: > 50), and phenyl acetylene (anti-M:M = 1: > 100) with primary amines to form Markovnikov imines with high regioselectivity.[155]

Organolanthanides (e.g. $[Me_2Si(C_5Me_4)NdCH(TMS)_2]$) catalyze the regioselective hydroamination of internal alkynes with primary amines in good yield (85–91 %).[156] In addition, it is known that the organouranium complex $[Cp^*_2UMe_2]$ (Cp^* is C_5Me_5) catalyzes the formation of anti-Markovnikov imines (50–95 % yield) by the reaction of terminal aliphatic alkynes (1-hexyne) and aromatic alkynes (phenyl acetylene). However, the similar reaction but with $[Cp^*_2ThMe_2]$ as catalyst completely reverses the regioselectivity (Scheme 46).[157]

In the area of base-catalyzed aminations of alkynes, it is worth mentioning that Knochel and co-workers[137,158] showed that phenyl acetylene reacts with anilines (Scheme 47) and various heterocyclic amines such as *N*-methylaniline, pyrrole,



Scheme 46. Hydroamination of alkynes in the presence of organoactinides.



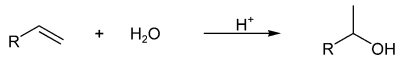
Scheme 47. Hydroamination of phenyl acetylene with anilines.

imidazole, indole, and benzimidazole in the presence of catalytic amounts of CsOH in *N*-methylpyrrolidone at 90–120 °C leading to the corresponding anti-Markovnikov enamines (46–83 % yield).

5. Reactions of O-Nucleophiles[159]

5.1. Hydration

Hydration, the addition of H_2O to multiple bonds, is in principle one of the most useful methods for functionalizing olefins and alkynes. However, this apparently simple transformation is scarcely realized with organometallic catalysts. On the other hand it is well known that terminal olefins react with water in the presence of acidic catalysts to form the corresponding branched alcohols (Scheme 48).



Scheme 48. Hydration of olefins.

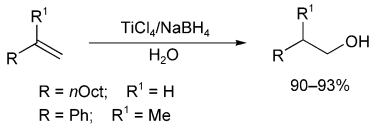
In accordance with the Markovnikov rule, secondary and tertiary alcohols are formed. On a larger scale mainly two variants of the hydration reaction are used. In the indirect process, the reaction takes place in liquid-phase in two steps. Initially the olefin reacts with sulfuric acid to form mono- and dialkylsulfates, which, after dilution with water, are hydrolyzed to the corresponding alcohol. In the direct process hydration occurs in the gas phase in the presence of solid phosphoric acids,[160] zeolites,[161] ion exchangers,[162] or heteropoly acids[163] as catalysts. Since the reaction is exothermic and is accompanied by a reduction in volume, the alcohol formation is favored by high pressures and low temperatures. An industrial example of the direct hydration is the preparation of isopropyl alcohol from propene. In addition, 2-butanol is formed from a mixture of 1-butene and 2-butene (raffinate II) and most importantly *tert*-butanol from isobutene.[164a]

 © 2004 Wiley-VCH Verlag GmbH & Co. KGaA, Weinheim

Recently, Hölderich and co-workers described the formation of 2-phenylethanol from styrene in the presence of zeolites under UV irradiation. Although the yield of the product is low due to polymerization side reactions, this is an interesting example for achieving anti-Markovnikov selectivity. It is presumed that the first reaction step of this transformation is the oxidation of styrene by singlett oxygen.[165]

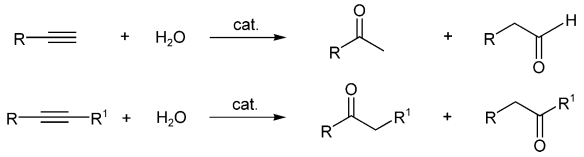
More specifically, olefins can be hydrated by the use of an oxymercuration reaction followed by in situ treatment with $NaBH_4$ to give the Markovnikov hydration products under mild reaction conditions. For instance, 2-methyl-1-butene treated with mercuric acetate followed by reaction with $NaBH_4$ gave 2-methyl-2-butanol in 90% yield.[164b]

While no direct anti-Markovnikov hydration of non-activated olefins exists, the linear alcohols can be obtained by treatment of terminal alkenes with a 1:2 mixture of $TiCl_4$ and $NaBH_4$ in 1,2-dimethoxyethane followed by the addition of water (Scheme 49).[166]



Scheme 49. Reaction of olefins with $TiCl_4/NaBH_4$.

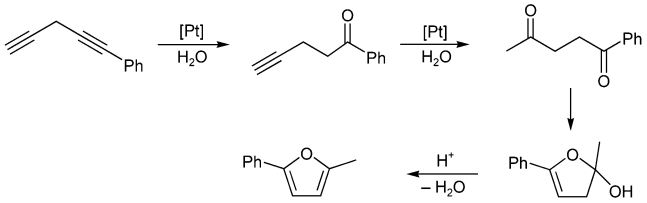
Hydration of alkynes is more easily achieved, and thus has been studied more intensively. In general, in this reaction the corresponding ketones are formed by electronic control. Nevertheless there are some exceptions known that give the aldehyde product preferentially (see below). The reaction is classically carried out under dilute acidic conditions with mercury ion salts as catalyst. In the case of terminal alkynes (RC≡CH), methyl ketones are formed exclusively by the Markovnikov addition, but with internal alkynes ($RC{\equiv}CR^1$) both ketone isomers are usually formed (Scheme 50). When



Scheme 50. Hydration of alkynes.

R is primary and R^1 is secondary or tertiary, the carbonyl group is formed preferentially next to the secondary or tertiary carbon atom.[167]

Further studies showed that other metal complexes, such as those of Cu^{I}, Ag^{I}, Pd^{II}, Ru^{III}, Rh^{III},[168] Os^{II}, Pt^{II}, Au^{III},[169] and Fe^{III}[170] are also useful as catalysts for this conversion. Pt^{II} salts such as $[\{PtCl_2(C_2H_4)\}_2]$, PtX_2 (X = Cl, Br, I) have been shown to be promising catalysts for the hydration of several non-activated alkynes. Unsymmetrical alkynes form both possible ketones with a bias favoring the more hindered side. For instance, 1-heptyne is hydrated to 2-heptanone in 93% yield.[171] 2-Hexyne forms 3-hexanone (65%) and 2-hexanone (35%); 4,4-dimethyl-3-pentanone (61–78%) and 4,4-dimethyl-2-pentanone (24–39% are formed from 4,4-dimethyl-2-pentyne.[172] Regioselective reactions take place when the platinum moiety is forced aside from the alkyne center by steric factors creating a partial cationic center at the distal carbon atom at which the water molecule attacks. Blum and co-workers[173] found that complexes generated from $PtCl_4$ and CO are efficient catalysts for the hydration of various aliphatic and aromatic acetylenes both under homogeneous conditions in wet THF and under phase transfer conditions in $(CHCl_2)_2/H_2O$ in the presence of Aliquat 336. Under these conditions, terminal alkynes such as phenyl acetylene and 5-phenylpent-1-yne follow Markovnikov's rule and yield ketones in up to 95% yield. Alkylarylacetylenes, such as 1-phenylprop-1-yne and 1-phenylbut-1-yne, yield mixtures of ketones among which those that have a carbonyl group adjacent to the aliphatic moieties predominate (up to 68% yield). Asymmetrical diarylacetylenes with bulky substituents exclusively form ketones with the carbonyl groups away from the bulky moieties. Thus, $2\text{-}MeC_6H_4C{\equiv}CPh$ and $2\text{-}BrC_6H_4C{\equiv}CPh$ form only $2\text{-}MeC_6H_4CH_2COPh$ and $2\text{-}BrC_6H_4CH_2COPh$ respectively. Diynes and triynes undergo stepwise hydration followed by an intramolecular condensation (Scheme 51).



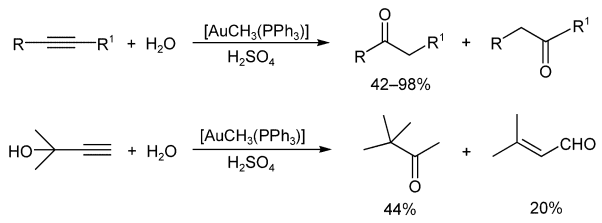
Scheme 51. Hydration of diynes followed by an intramolecular condensation.

More recently, it has been shown that *cis*-$[PtCl_2(tppts)_2]$ (tppts is $P(m\text{-}C_6H_4SO_3Na)_3$) in water is an effective catalyst for the room temperature hydration of the water-soluble alkynes, for example, 4-pentyn-1-ol and 3-pentyn-1-ol. Interestingly, both hydration reactions lead to 5-hydroxy-2-pentone regioselectively. Hydration of 4-pentyne-1-ol occurs by a 5-exo-dig mechanism (Markovnikov product), while hydration of 3-pentyn-1-ol occurs through a 5-endo-dig mechanism (anti-Markovnikov product).[174]

In 2002, a gold-based catalyst system consisting of $[AuCH_3(PPh_3)]$/acid in methanol was found to catalyze the hydration of various alkynes to form the corresponding Markovnikov hydration products (Scheme 52). Propargylic alcohols also react smoothly, but form mixtures of methyl ketones and α,β-unsaturated aldehydes (anti-Markovnikov addition followed by dehydration).[175]

The anti-Markovnikov addition of water to terminal alkynes to form aldehydes by using different Ru-based catalyst systems has been reported recently.[176] As catalyst, either a mixture of $RuCl_2$ and phosphane $(P(C_6H_5)_2(C_6F_5)$ or tppts)[176a] or an indenyl ruthenium(II) complex $[Ru(\eta^5\text{-}C_9H_7)Cl(PPh_3)_2]$[176c] or cyclopentadienyl ruthenium com-

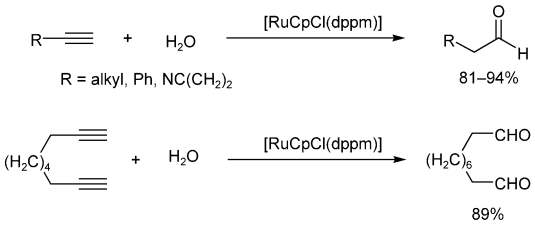
 © 2004 Wiley-VCH Verlag GmbH & Co. KGaA, Weinheim



R = *n*-alkyl, Ph, (*o*-, *m*- or *p*-)$MeOC_6H_4$, (*o*- or *p*-)ClC_6H_4, $NC(CH_2)_3$, $Cl(CH_2)_3$
R^1 = H, Ph, Me, *n*Pr

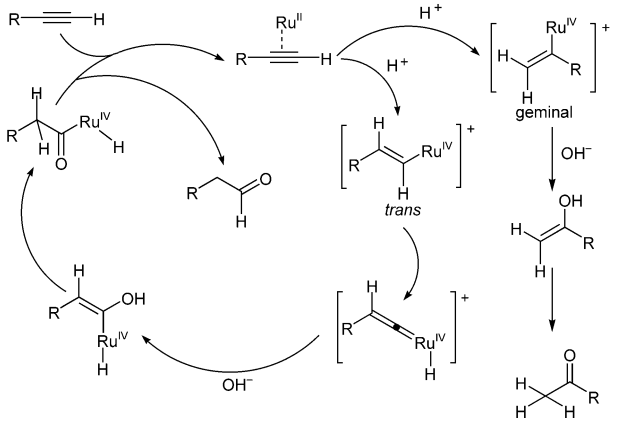
Scheme 52. Au^I-catalyzed hydration of alkynes.

plexes of the type $[RuCpCl(PR_3)_2]$ and [RuCpCl(P–P)],[176b] in which R is Ph or Me and P–P is a diphosphane such as bis(diphenylphosphanyl)methane (dppm), 1,2-bis(diphenylphosphanyl)ethane (dppe), 1,3-bis(diphenylphosphanyl)propane (dppp), 1,4-bis(diphenylphosphanyl)butane(dppb), 1,2-bis(di-4-sulfonatophenylphosphanyl)benzenetetrasodium (dppbts), bis(dimethylphosphanyl)methane (dmpm) or 1,2-bis(diethylphosphanyl)ethane (depe) is used. Among the different catalysts, the latter system is highly active and allows regiospecific formation of aldehydes. For instance, the hydration of various terminal alkynes such as 1-hexyne (>99%), 1-octyne (93%), 1-dodecyne (94%), *tert*-butylacetylene (81%), phenyl acetylene (90%), 3-phenylprop-1-yne (93%) in 2-propanol (solvent) results in the formation of the corresponding aldehydes in good to excellent yields by using [RhCpCl(dppm)] as catalyst at 100°C. In addition, 1,9-decadiyne formed the corresponding dialdehyde (89%) and 5-cyanopent-1-yne gave 5-cyanopentanal (88%; Scheme 53).



Scheme 53. [RuCpCl(dppm)]-catalyzed anti-Markovnikov hydration of terminal alkynes.

Grotjahn et al. reported that in the presence of a phosphanylimidazole Ru catalyst the hydration of *tert*-butylacetylene occurs, giving yields in excess of 90%.[177] Advantages claimed for this catalyst compared to the above described Ru^{II} catalysts include a lack of inhibition by nitriles, and tolerance of acid-sensitive propargylic ether substituents. Experimental and theoretical studies on the mechanism of the Ru-catalyzed hydration indicate that the key step in the catalytic cycle is the protonation of the η^2-alkyne Ru complex rather than its tautomerization to a Ru^{II}-vinylidene complex (Scheme 54).[178] The vinyl complex undergoes an α-hydride transfer to form a hydrido-Ru^{IV}-vinylidene intermediate, which is very reactive. The empty π-orbital at the α-C atom easily accepts the nucleophilic attack by hydroxide ion, since

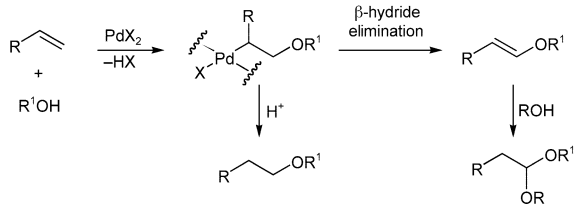


Scheme 54. The catalytic cycle of alkyne hydration.

the back donation from Ru^{IV} is small. The resulting (α-hydroxyvinyl)ruthenium complex isomerizes instantaneously to the acyl form, which is followed by reductive elimination of the aldehyde. Thus, the anti-Markovnikov selectivity originates from the initial protonation step. If the proton is attached to the terminal carbon, the next reaction step of the resulting vinyl complex may be the attack by OH^-, resulting in the formation of the ketone (Scheme 54).

5.2. Hydroalkoxylation

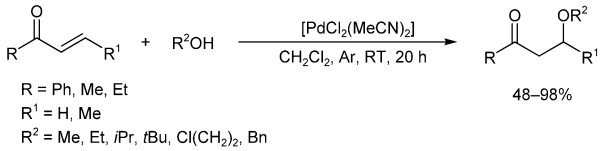
The addition of alcohols or phenols across multiple bonds leads to the corresponding ethers. As usual when acid-catalyzed, the reaction gives preferentially the corresponding Markovnikov products. For substrates that are more susceptible to nucleophilic attack (polyhalo olefins, Michael acceptors), the reaction is carried out in basic media leading to the anti-Markovnikov products due to the better stabilization of the linear carbanion. Reactions of olefins with alcohols in the presence of Pd salts leads to the corresponding acetals[179] or ethers (Scheme 55). When applied to nonfunctionalized



Scheme 55. Pd^{II}-catalyzed addition of alcohols to olefins.

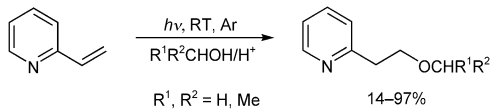
aliphatic olefins, this reaction is a variation of the well-known Wacker process and the palladium catalyst has to be reoxidized from Pd^0 to the active Pd^{II} species.[180] However, activated olefins such as vinyl ketones give the corresponding hydroalkoxylated products in the presence of catalytic amounts of $[PdCl_2(MeCN)_2]$ in high yields (up to 98%) (Scheme 56).[181]

 © 2004 Wiley-VCH Verlag GmbH & Co. KGaA, Weinheim



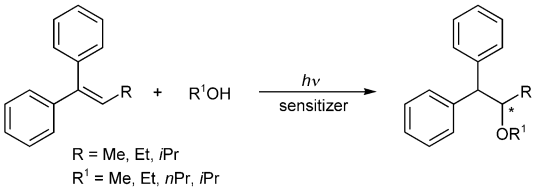
Scheme 56. Pd^{II}-catalyzed hydroalkoxylation of α,β-unsaturated olefins.

An unusual olefin alkoxylation reaction was reported by Ishida et al..[182] They discovered that the photochemical alkoxylation of 2-vinylpyridine in acidic methanol afforded 2-(2-pyridyl)ethyl methyl ether in high yield (up to 97%; Scheme 57). It is suggested that a photoinduced intramolecular charge transfer from the pyridinium ion moiety into the vinyl group initiates the regioselective nucleophilic addition of the alcohol. A somewhat similar photochemical anti-Markovnikov addition of methanol to 1,1-diphenylpropene is effected in the presence of 9,10-dicyanoanthracene, which acts as a sensitizer in polar solvents.[183]



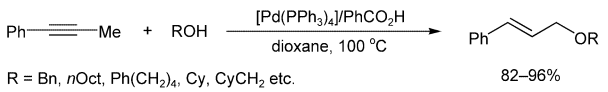
Scheme 57. The photochemical anti-Markovnikov hydroalkoxylation of 2-vinylpyridine.

Interestingly, the photochemical enantioselective addition of alcohols to 1,1-diphenyl-1-alkenes to form the chiral adducts in up to >99% yield and 33% *ee* occurs in the presence of a variety of optically active dialkylnaphthalene(-di)carboxylates as chiral sensitizers (Scheme 58).[184]



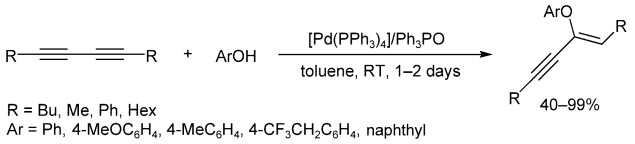
Scheme 58. Enantioselective addition of alcohols to 1,1-diphenyl-1-alkenes.

There have been a few investigations of hydroalkoxylation reactions of alkynes. An example is shown in Scheme 59. In this example, the reaction of 1-phenylprop-1-yne with various primary and secondary alcohols proceeds in the presence of catalytic amounts of $[Pd(PPh_3)_4]$ and benzoic acid. The corresponding cinnamyl ethers are obtained in good to excellent yields (82–96%; Scheme 59).[185]



Scheme 59. Pd-catalyzed hydroalkoxylation of alkynes.

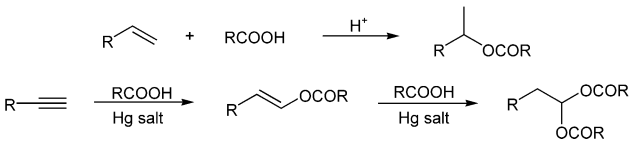
The mechanism of this reaction is similar to the hydroamination of alkynes, in which the reaction proceeds by the palladium/benzoic acid-catalyzed isomerization of the alkyne to the allene, followed by the addition of alcohols to the π-allylpalladium intermediate formed by the hydropalladation of the resulting allene. Acidic alcohols undergo regioselective trans addition to conjugated diynes in the presence of a Pd^0 catalyst to form the corresponding monohydroalkoxylated product (Scheme 60).[186] For instance, phenol adds to 5,7-dodecadiyne in the presence of $[Pd(PPh_3)_4]/Ph_3PO$ to form the hydroalkoxylated product in 92% yield.



Scheme 60. Hydroalkoxylation of diynes.

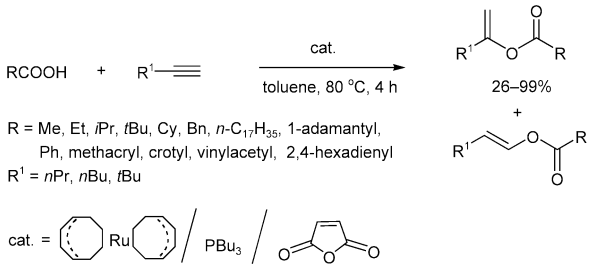
5.3. Addition of Carboxylic Acids to Olefins and Alkynes (Hydroacyloxylation)

The acid-catalyzed addition of carboxylic acids to olefins leads to the corresponding Markovnikov-type carboxylic esters. This transformation is reminiscent of the industrial reaction of olefins and sulfuric acid (see Section 5.1.). Clearly, the regioselectivity is determined by the thermodynamic stability of the secondary or tertiary carbocation. When treated with carboxylic acid, alkynes give enol esters or acylals. These reactions are usually catalyzed by mercuric salts (Scheme 61).[164b]

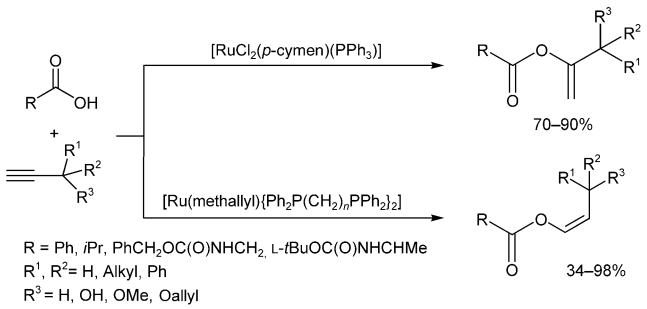


Scheme 61. Addition of carboxylic acids to olefins and alkynes.

By the mid-1980s, it had been shown that Ru complexes form particularly suitable catalysts for the addition of carboxylic acids to alkynes. A variety of saturated and unsaturated carboxylic acids as well as aromatic carboxylic acids are found to react with terminal acetylenes in the presence of bis(η^5-cyclooctadienyl)ruthenium/trialkylphosphane/maleic anhydride as the catalytic system resulting in high yields and regioselectivity to give the corresponding Markovnikov enol esters (Scheme 62).[187] For instance, in the reaction of 1-hexyne with acetic acid, 1-hexen-2-yl acetate is formed in up to 93% yield and up to 94% selectivity. The addition of 3-butenoic acid to 1-pentyne proceeds with lower selectivity giving 1-penten-2-yl 3-butenoate and its isomer in 40% and 26% yields, respectively. On the other hand, propargyl alcohol derivatives react with a large excess of

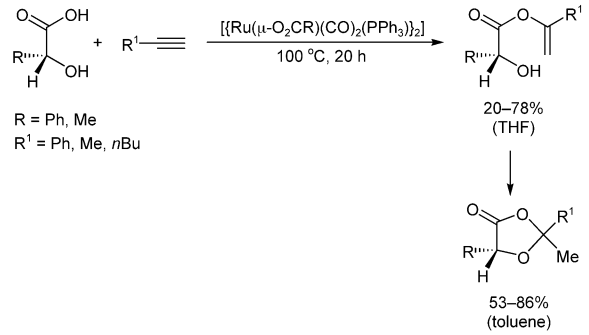


Scheme 62. Regioselective addition of carboxylic acids to alkynes. Bn = benzyl.



Scheme 64. Regioselective addition of carboxylic acids to alkynes.

acetic acid in the presence of bis(η^5-cyclooctadienyl)ruthenium/PCy_3/maleic anydride forming the corresponding Markovnikov addition products in good yields (up to 70%) and high regioselectivity (up to 99%).[188] The regioselective formation of 2-(benzoyloxy)propene results from the addition of benzoic acid to propyne in the presence of the trigonal-bipyramidal Rh^I-monohydrides $[RhH(PP_3)]$ and $[RhH(NP_3)]$ ($PP_3 = P(CH_2CH_2PPh_2)_3$, $NP_3 = N(CH_2CH_2PPh_2)_3$).[189] A variety of isopropenyl esters can be synthesized by the direct regioselective addition of *N*-protected amino acids to propyne by using $[RuCl_2(p\text{-cymene})(PPh_3)]$ as catalyst.[190] Similarly, α-hydroxy acids add to terminal alkynes in the presence of $[\{Ru(\mu\text{-}O_2CR)(CO)_2(PPh_3)\}_2]$, affording the corresponding Markovnikov α-hydroxy enol esters (up to 78% yield) or their cyclization products 1,3-dioxolan-4-ones (up to 86% yield) selectively (Scheme 63).[191]



Scheme 63. Addition of α-hydroxy acids to alkynes.

In the presence of $[Ru_3(CO)_{12}]$ or $[\{Ru(O_2CCH_3)(CO)_2\}_n]$ as catalyst aliphatic and aromatic carboxylic acids add to mono- and disubstituted alkynes yielding vinyl esters.[192] In the case of the addition of benzoic acid to phenyl acetylene, the anti-Markovnikov isomer, β-(benzyloxy)styrene, is mainly formed (77%).

Ruthenium phosphane complexes of the type $[RuCl_2(arene)(PR_3)]$ and $[Ru(\eta^2\text{-}O_2CH)(CO)_2(PR_3)\}_2]$ are efficient catalysts for the Markovnikov addition of carboxylic acids to terminal aliphatic and aromatic alkynes.[193] The regioselectivity of the addition is reversed towards anti-Markovnikov addition of carboxylic acids by modifying the active Ru^{II} center by the coordination of a chelating diphosphane and labile allylic ligands as in $[Ru(methallyl)_2(Ph_2P(CH_2)_nPPh_2)]$ (Scheme 64).[194] The use of $[Ru(methallyl)_2(dppb)]$ leads to the formation of (*Z*)-hex-1-en-1-yl benzoate in 95% yield and 98% selectivity or (*Z*)-styryl benzoate in 92–97% yield and 96–98% selectivity by the anti-Markovnikov *trans*-addition of benzoic acid to 1-hexyne and phenyl acetylene, respectively. In addition, a variety of (*Z*)-2-(trimethylsilyl)(alk-1-en-1-yl) esters are selectively (formed 34–96% yield, up to 100% selectivity) by the addition of various aliphatic and aromatic carboxylic acids to trimethylsilylacetylenes in the presence of $[Ru(2\text{-methylallyl})_2(Ph_2P(CH_2)_2PPh_2)]$ as catalyst. In the case of propargylic alcohols[195] and ethers[196] the use of dppe as the ligand is essential to achieve similar anti-Markovnikov *trans*-addition. This may be because the $\{Ru(Ph_2PCH_2CH_2PPh_2)\}$ moiety allows an interaction of the metal center with both the triple bond and the oxygen atom of the functional group of the propargylic compound so that the approach of the carboxylate to the C1 atom of the triple bond is favored. This is not the case with a $\{(Ph_2P(CH_2)_4PPh_2)Ru\}$ complex, which has a distorted planarity.

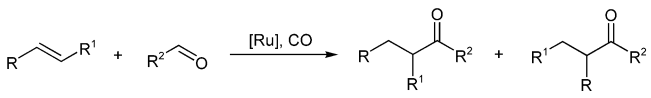
Recently Goossen et al.[197] observed that the addition of benzoic acid to 1-hexyne by using a catalyst system consisting of $[\{RuCl_2(p\text{-cumene})\}_2]$ and a monophosphane proceeds efficiently with high regioselectivity towards the Markovnikov product (97%) in the presence of an inorganic base (e.g., Na_2CO_3). On the other hand the *Z* anti-Markovnikov product (98–99%) is obtained in the presence of organic bases such as (4-dimethylamino)pyridine (DMAP), which acts as a coordinating ligand to the metal center. More recently, ruthenium complexes with carbene ligands have been used for the addition of carboxylic acids to 1-alkynes.[198] The selectivity of the addition to phenyl acetylene is dependent on the acidity of the added carboxylic acid. At decreasing pK_a a change in regioselectivity from Markovnikov to anti-Markovnikov addition is observed.[199]

6. Miscellaneous

6.1. Hydroacylation

Hydroacylation is the addition of an aldehyde across multiple bonds to form ketones by the activation of carbonyl C–H bond (Scheme 65). Among others,[200] zerovalent Ru complexes such as $[Ru_3(CO)_{12}]$, $[Ru(cod)_2]$, and [Ru(cod)(cot)] (cot is cyclooctatetraene) have been employed as catalysts for the addition of various aromatic and heteroaromatic aldehydes to olefins (40–54% yield).[201] Often these

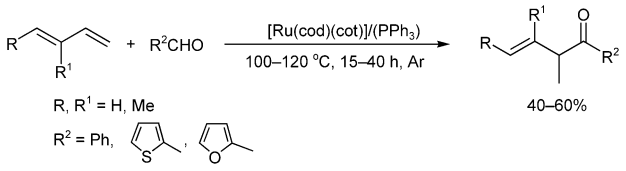
 © 2004 Wiley-VCH Verlag GmbH & Co. KGaA, Weinheim



Scheme 65. Hydroacylation of olefins.

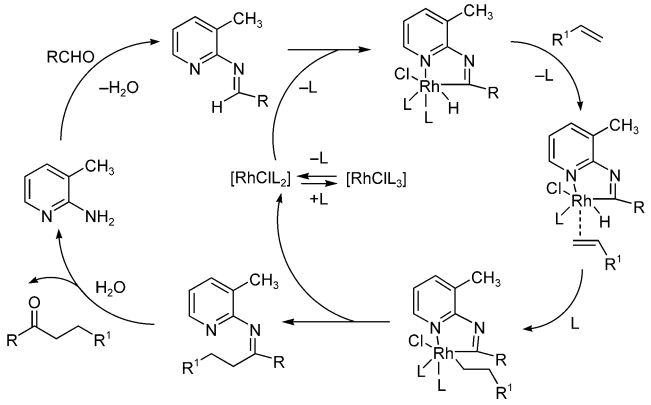
reactions are performed at high temperature (180–200 °C) under a slight CO pressure to suppress aldehyde decarbonylation as a side-reaction.

Typically, terminal olefins form both linear and branched adducts, for example, 1-hexene gave a ratio of the linear to branched product of 3:1. 1,3-Dienes, such as isoprene and *trans*-1,3-pentadiene, are hydroacylated to the corresponding β,γ-unsaturated ketones (40–60 % yield) with [Ru(cod)(cot)]/PR_3 as the catalyst (Scheme 66).[202] Interestingly, no hydroacylation reaction occurred with *cis*-1,3-pentadiene, which strongly suggests an (η^3-allyl)ruthenium species as a key intermediate in the reaction mechanism.



Scheme 66. Hydroacylation of 1,3-dienes.

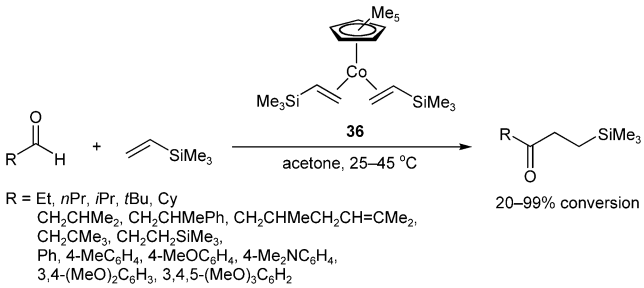
Various heteroaromatic aldehydes such as pyridine carboxaldehyde, thiophene carboxaldehyde and furfural derivatives add to 1-pentene in the presence of $[RhCl(PPh_3)_3]$/2-amino-3-picoline as the catalyst system[203a] and $[Cp_2ZrCl_2]$ or $[Cp_2TiCl_2]$ as additives[203b] to afford the corresponding linear ketones (32–92 % yield). In this reaction, aldimines are supposed to be the key intermediates (Scheme 67), which



Scheme 67. Proposed mechanism of the rhodium-catalyzed hydroacylation.

allow for a more facile C–H activation through cyclometallation. It was found that the addition of benzoic acid considerably improves the hydroacylation reactivity, probably because it simply catalyzes the condensation step to form the aldimine.[204] The same rhodium catalyst system is also applied for the hydroacylation of various olefins to ketones under solvent free conditions in the presence of microwave radiation (up to 95 % yield).[205]

Brookhart and co-workers reported an interesting intermolecular hydroacylation of vinylsilanes with various aromatic and aliphatic aldehydes by using a bisolefin cobalt(I) complex **36**, (Scheme 68) forming the corresponding anti-Markovnikov ketones exclusively (up to 99 % conversion) under mild conditions.[206]

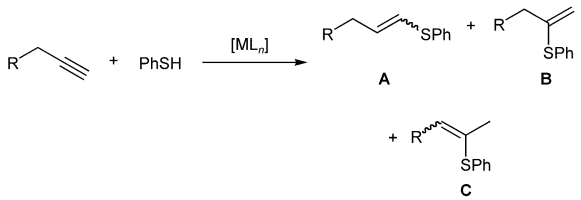


Scheme 68. Intermolecular cobalt-catalyzed hydroacylation of vinylsilanes.

Very recently a new catalytic asymmetric reductive coupling between aldehydes and alkynes was reported by Jamison and co-workers.[207] In the presence of 10 mol % $[Ni(cod)_2]$, 20 mol % neomenthyldiphenylphosphane, and 200 mol % of BEt_3, different trisubstituted allylic alcohols are produced. With 1-aryl-2-alkylalkynes, the acyl group adds selectively to the 2-position of the alkyne.

6.2. Hydrothiolation

Thiols have been reported to add to double and triple bonds in the presence of free-radical initiators to form the anti-Markovnikov adducts.[208] In the presence of base catalysts, Michael type substrates react with a similar orientation through a nucleophilic mechanism. Apart from that various transition metal complexes catalyze the hydrothiolation of alkynes forming either the Markovnikov or anti-Markovnikov product depending on the catalyst used (Scheme 69).



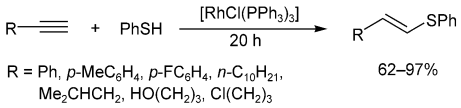
Scheme 69. Transition-metal catalyzed hydrothiolation of alkynes.

In general, palladium catalysts form the Markovnikov products more selectively. Thus, in the presence of $Pd(OAc)_2$, thiophenol adds to alkynes giving the corresponding vinylic sulfides with Markovnikov selectivity in moderate to good

 © 2004 Wiley-VCH Verlag GmbH & Co. KGaA, Weinheim

yields (29–87%).[209] The possible active catalyst here is a polymeric palladium sulfide species $[\{Pd(SPh)\}_n]$ which undergoes regioselective thiopalladation of alkynes to the corresponding vinylic palladium intermediate followed by protonation forming the Markovnikov type vinylic sulfide **B**. When $[PdCl_2(PhCN)_2]$ is used as the catalyst, a novel Markovnikov addition and sequential double-bond isomerization occur, forming the corresponding internal vinylic sulfides of the type **C** (Scheme 69).[210] For instance, terminal alkynes such as 1-octyne, 5-methyl-1-hexyne, benzylacetylene, and 5-cyanopentyne selectively form 2-(phenylthio)-2-octene (66%), 2-(phenylthio)-5-methyl-2-hexene (77%) 2-(phenylthio)-2-methylstyrene (70%), and 2-(phenylthio)-5-cyano-2-pentene (63%), respectively, in good yields. However, under these conditions, hydrothiolation of propargyldimethylamine provides only the Markovnikov product regioselectively (69% yield), thus indicating that the presence of the basic amino group inhibits the double-bond isomerization entirely. Phenyl acetylene, which does not have a propargylic proton also forms the Markovnikov addition product selectively (68% yield). The active catalyst in this case is a complex of the type $[PdCl(SPh)L_n]$, which is found to catalyze the thiol addition-isomerization reaction as well as the double bond isomerization in the Markovnikov addition products of thiols and alkynes independently.

In contrast to the palladium catalysts, $[RhCl(PPh_3)_3]$ leads to regio- and stereoselective addition of thiols to alkynes to form only the *E* isomer of the corresponding anti-Markovnikov type vinylic sulfide in good yields (Scheme 70).[210] This

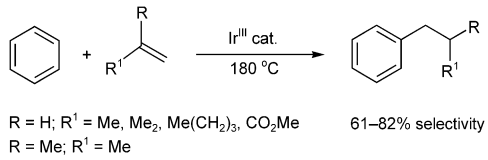


Scheme 70. $[RhCl(PPh_3)_3]$-catalyzed regio- and steroselective hydrothiolation of acetylenes.

reaction is proposed to proceed through the formation of $[RhH(SPh)ClL_n]$ which may undergo stereoselective insertion of the alkyne to the Rh–H bond resulting in a *trans* vinylrhodium intermediate, followed by the reductive elimination of the anti-Markovnikov adduct in the presence of the thiol.

6.3. Hydroarylation

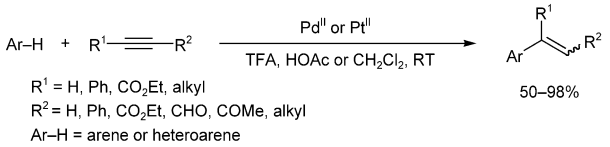
Hydroarylation of olefins catalyzed by Lewis and Brønsted acids (Friedel–Crafts alkylation of aromatic compounds) follows the Markovnikov rule producing mainly the branched alkylbenzenes.[211] However, recent developments in the area of C–H activation reactions of aromatics by using transition-metal complexes have lead to the regio- and stereoselective addition of arenes to olefins and alkynes. For instance, the binuclear Ir^{III} complex $[\{Ir(acac)_3\}_2]$ is shown to catalyze the addition of benzene to various terminal olefins, for example, propylene (61%), *iso*-butene (82%), 1-hexene (69%) and methyl acrylate (68%) to form the corresponding linear-alkyl benzene derivatives with good selectivity (Scheme 71).[212]



Scheme 71. Addition of benzene to aliphatic olefins.

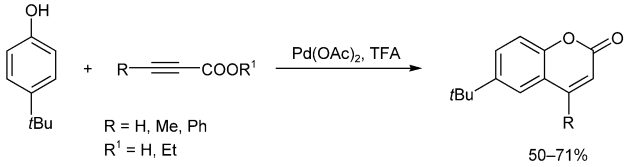
With norbornene as olefin, a catalytic asymmetric alkylation of phenol is achieved in the presence of ferrocenylphosphane iridium complexes (low *ee* values). Due to the symmetric nature of the olefin no problems with regioselectivity occurred.[213]

Arenes and heteroarenes also add regio- and stereoselectively to terminal and internal alkynes in the presence of cationic Pd or Pt complexes in trifluoroacetic acid, affording the thermodynamically less favorable *cis*-arylalkenes (Scheme 72) predominantly.[214]



Scheme 72. Palladium- or platinum-catalyzed hydroarylation of alkynes.

The reaction of electron-rich arenes with electron poor alkynes affords products in good yields, indicating the reaction is electrophilic in nature. The nature of the substituents on the alkyne has a considerable effect on the regiochemistry of the products. For instance, alkynes conjugated to electron withdrawing groups such as CHO, CO_2H, COMe, or CO_2Et act as good acceptors of aryl nucleophiles and provide β-aryl substituted alkenes exclusively and *cis*-alkenes predominantly. The reaction of the alkynes conjugated to a phenyl group affords 1-arylalkenes, the Markovnikov-type adduct, selectively. A similar reaction of phenol with alkynoate forms coumarins, which result from the addition of the phenol to the alkyne followed by cyclization through ester exchange (Scheme 73).[215]



Scheme 73. Formation of coumarins by hydroarylation–cyclization.

© 2004 Wiley-VCH Verlag GmbH & Co. KGaA, Weinheim

Conclusions

Although more than 130 years old, the question of regioselective functionalizations of olefins (and alkynes) continues to be an important subject for organic synthesis and catalysis. Clearly, efficient and highly regioselective transformations of olefins and alkynes constitute prime examples of green chemistry because of the 100% atom economy of these reactions. Due to the availability of the feedstock, functionalization reactions of unsaturated compounds are of utmost interest not only on small laboratory scale, but also for a number of industrial fine and bulk chemical processes. Important examples include the well-known Markovnikov amination and hydroxylation reactions of aliphatic olefins.

Major advances have been made in a number of functionalization reactions by the introduction of tailor-made transition-metal complexes. There are examples of reactions that are known in which one catalyst gives highly selectively the Markovnikov isomer whereas another catalyst the anti-Markovnikov product. Such a control of selectivity is an important basis for futher innovations in organic synthesis. However, on paper, apparently simple transformations, for example, the anti-Markovnikov hydroxylation of terminal aliphatic olefins are still not possible. For this reaction during the last decades, virtually no progress has been made. Clearly, more research is needed in this direction, not only because it is important for practical applications but it is also scientifically fascinating.

Our work in the area of selective anti-Markovnikov functionalizations was supported by grants from the Deutsche Forschungsgemeinschaft, the state of Mecklenburg–Western Pomerania, the Bundesministerium für Bildung und Forschung (BMBF) and the Fonds der Chemischen Industrie (FCI). We thank Degussa AG (Oxeno Olefinchemie GmbH) for funding in the area of hydroformylation reactions. Analytical support from Prof. Dr. M. Michalik, Dr. W. Baumann, Dr. C. Fischer, S. Buchholz, B. Harzfeld, R. Jesse, and H. Baudisch is gratefully acknowledged. We thank all co-workers named in the reference section for their excellent work and C. Mewes for her technical support. We also acknowledge the help of Cathleen Buch with the drawings.

Received: June 16, 2003 [A616]

[1] *Green chemistry: Challenging Perspectives* (Eds.: P. Tundo, P. T. Anastas), Oxford Science, Oxford, **1999**.
[2] a) B. M. Trost, *Acc. Chem. Res.* **2002**, *35*, 695; b) B. M. Trost, *Angew. Chem.* **1995**, *107*, 285; *Angew. Chem. Int. Ed. Engl.* **1995**, *34*, 259.
[3] R. A. Sheldon, *Chem. Tech.* **1994**, 38.
[4] a) V. V. Markownikow, *Ann. Chem. Pharm.* **1870**, *153*, 228; b) V. V. Markownikow, *C. R. Hebd. Seances Acad. Sci.* **1875**, *85*, 668.
[5] E. E. Gooch, *J. Chem. Educ.* **2001**, *78*, 1358.
[6] A. Seayad, M. Ahmed, H. Klein, R. Jackstell, T. Gross, M. Beller, *Science* **2002**, *297*, 1676.
[7] C.-F. Huo, Y.-W. Li, M. Beller, H. Jiao, *Organometallics* **2003**, *22*, 4665.
[8] S. A. Decker, T. R. Cundari, *J. Organomet. Chem.* **2001**, *635*, 132.
[9] a) U. Nettekoven, J. F. Hartwig, *J. Am. Chem. Soc.* **2002**, *124*, 1166; b) M. Kawatsura, J. F. Hartwig, *J. Am. Chem. Soc.* **2000**, *122*, 9546.
[10] a) P. W. N. M. van Leeuwen, P. C. J. Kamer, J. N. H. Reek, P. Dierkes, *Chem. Rev.* **2000**, *100*, 2741; b) B. Breit, W. Seiche, *Synthesis* **2001**, 1; c) F. Ungváry, *Coord. Chem. Rev.* **2001**, *218*, 1; c) P. W. N. M. van Leeuwen, C. P. Casey, G. T. Whiteker in *Rhodium Catalyzed Hydroformylation* (Eds.: P. W. N. M. van Leeuwen, C. Claver), Kluwer Academic Publishers, Dordrecht, **2000**; d) C. D. Frohning, C. W. Kohlpaintner in *Applied Homogeneous Catalysis with Organometallic Compounds*, 2nd ed. (Eds.: B. Cornils, W. A. Herrmann), Wiley-VCH, Weinheim, **2002**.
[11] J. Falbe, N. Huppes, *Brennst.-Chem.* **1967**, *48*, 46.
[12] a) C. Hewlett (Halcon Int. Inc.), DE 2441502, **1974**; b) C. Hewlett (Halcon Int. Inc.), DE 2462444, **1974**.
[13] a) C. K. Brown, G. Wilkinson, *J. Chem. Soc. A* **1970**, 2753; b) C. K. Brown, G. Wilkinson, *Tetrahedron Lett.* **1969**, 1725; c) R. L. Pruett, J. A. Smith, *J. Org. Chem.* **1969**, *34*, 327.
[14] O. R. Hughes, J. D. Unruh, *J. Mol. Catal.* **1981**, *12*, 71.
[15] J. M. Brown, A. G. Kent, *J. Chem. Soc. Perkin Trans. 2* **1987**, 1597.
[16] C. P. Casey, L. M. Petrovich, *J. Am. Chem. Soc.* **1995**, *117*, 6007.
[17] R. Lazzaroni, R. Settambolo, G. Uccello-Barretta, A. Caiazzo, S. Scamuzzi, *J. Mol. Catal. A* **1999**, *143*, 123.
[18] C. P. Casey, G. T. Whiteker, M. G. Melville, L. M. Petrovich, J. A. Gavney, D. R. Powell, *J. Am. Chem. Soc.* **1992**, *114*, 5535.
[19] M. Kranenburg, Y. E. M. van der Burgt, P. C. J. Kamer, P. W. N. M. van Leeuwen, *Organometallics* **1995**, *14*, 3081.
[20] L. A. van der Veen, P. C. J. Kamer, P. W. N. M. van Leeuwen, *Angew. Chem.* **1999**, *111*, 349; *Angew. Chem. Int. Ed.* **1999**, *38*, 336.
[21] H. Klein, R. Jackstell, K.-D. Wiese, C. Borgmann, M. Beller, *Angew. Chem.* **2001**, *113*, 3505; *Angew. Chem. Int. Ed.* **2001**, *40*, 3408.
[22] a) A. J. Sandee, L. A. van der Veen, J. N. H. Reek, P. C. J. Kamer, M. Lutz, A. L. Spek, P. W. N. M. van Leeuwen, *Angew. Chem.* **1999**, *111*, 3428; *Angew. Chem. Int. Ed.* **1999**, *38*, 3231; b) A. J. Sandee, R. S. Ubale, M. Makkee, J. N. H. Reek, P. C. J. Kamer, J. A. Moulijn, P. W. N. M. van Leeuwen, *Adv. Synth. Catal.* **2001**, *343*, 201.
[23] L. Ropartz, K. J. Haxton, D. F. Forster, R. E. Morris, A. M. Z. Slawin, D. J. Cole-Hamilton, *J. Chem. Soc. Dalton Trans.* **2002**, 4323.
[24] W. R. Moser, C. J. Papile, D. A. Brannon, R. A. Duwell, S. J. Weininger, *J. Mol. Catal.* **1987**, *41*, 271.
[25] J. D. Unruh, J. R. Christenson, *J. Mol. Catal.* **1982**, *14*, 19.
[26] C. P. Casey, G. T. Whiteker, M. G. Melville, L. M. Petrovich, J. A. Gavney, D. R. Powell, *J. Am. Chem. Soc.* **1992**, *114*, 5535.
[27] C. P. Casey, E. L. Paulsen, E. W. Beuttenmueller, B. R. Proft, L. M. Petrovich, B. A. Matter, D. R. Powell, *J. Am. Chem. Soc.* **1997**, *119*, 11817.
[28] L. A. van der Veen, M. D. K. Boele, F. R. Bregman, P. C. J. Kamer, P. W. N. M. van Leeuwen, K. Goubitz, J. Fraanje, H. Schenk, C. Bo, *J. Am. Chem. Soc.* **1998**, *120*, 11616.
[29] a) M. E. Broussard, B. Juma, S. G. Train, W. J. Peng, S. A. Laneman, G. G. Stanley, *Science* **1993**, *260*, 1784; b) G. Süss-Fink, *Angew. Chem.* **1994**, *106*, 71; *Angew. Chem. Int. Ed. Engl.* **1994**, *33*, 67.
[30] E. Billig, A. G. Abatjoglou, D. R. Bryant, US 4769498, **1992**.
[31] A. van Rooy, P. C. J. Kamer, P. W. N. M. van Leeuwen, K. Goubitz, J. Fraanje, N. Veldman, A. L. Spek, *Organometallics* **1996**, *15*, 835.
[32] G. D. Cuny, S. L. Buchwald, *J. Am. Chem. Soc.* **1993**, *115*, 2066.

 © 2004 Wiley-VCH Verlag GmbH & Co. KGaA, Weinheim

[33] R. Paciello, L. Siggel, M. Röper, *Angew. Chem.* **1999**, *111*, 2045; *Angew. Chem. Int. Ed.* **1999**, *38*, 1920.
[34] S. C. van der Slot, P. C. J. Kamer, P. W. N. M. van Leeuwen, J. Fraanje, K. Goubitz, M. Lutz, A. L. Spek, *Organometallics* **2000**, *19*, 2504.
[35] S. C. van der Slot, P. C. J. Kamer, P. W. N. M. van Leeuwen, J. A. Iggo, B. T. Heaton, *Organometallics* **2001**, *20*, 430.
[36] M. P. Magee, H.-Q. Li, O. Morgan, W. H. Hersh, *J. Chem. Soc. Dalton Trans.* **2003**, 387.
[37] a) M. Dieguez, O. Pamies, A. Ruiz, C. Claver, *New J. Chem.* **2002**, *26*, 827; b) M. Dieguez, A. Ruiz, C. Claver, *J. Org. Chem.* **2002**, *67*, 3796; c) M. Dieguez, O. Pamies, A. Ruiz, S. Castillon, C. Claver, *Chem. Eur. J.* **2001**, *7*, 3086; d) M. Dieguez, O. Pamies, A. Ruiz, S. Castillon, C. Claver, *Chem. Commun.* **2000**, 1607; e) H. K. Reinius, A. O. J. Krause, *Catal. Lett.* **2000**, *70*, 149; f) S. Deerenberg, P. C. J. Kamer, M. M. van der Pereira, P. W. N. M. van Leeuwen, *Organometallics* **2000**, *19*, 2065; g) M. Dieguez, M. M. van der Pereira, A. M. Masdeu-Bulto, C. Claver, J. C. Bayon, *J. Mol. Catal. A* **1999**, *143*, 111; h) J. H. Feng, M. Garland, *Organometallics* **1999**, *18*, 417; i) K. Nozaki, N. Sakai, T. Nanno, T. Higashijima, S. Mano, T. Horiuchi, H. Takaya, *J. Am. Chem. Soc.* **1997**, *119*, 4413; j) B. Breit, *Chem. Commun.* **1996**, 2071.
[38] a) P. Meessen, D. Vogt, W. Keim, *J. Organomet. Chem.* **1998**, *551*, 165; b) G. Fremy, E. Monflier, J. F. Carpentier, Y. Castanet, A. Mortreux, *J. Catal.* **1996**, *162*, 339; c) K. Nozaki, H. Takaya, T. Hiyama, *Top. Catal.* **1997**, *4*, 175; d) C. Basoli, C. Botteghi, M. A. Cabras, G. Chelucci, M. Marchetti, *J. Organomet. Chem.* **1995**, *488*, C20; e) M. P. Doyle, M. S. Shanklin, M. V. Zlokazov, *Synlett* **1994**, 615; f) T. V. RajanBabu, T. A. Ayers, *Tetrahedron Lett.* **1994**, *35*, 4295; g) C. Botteghi, S. Paganelli, A. Schionato, M. Marchetti, *Chirality* **1991**, *3*, 355.
[39] I. Ojima, *Chem. Rev.* **1988**, *88*, 1011.
[40] M. Tanaka, Y. Watanabe, T. Mitsudo, Y. Takegami, *Bull. Chem. Soc. Jpn.* **1974**, *47*, 1698.
[41] Y. Ishii, K. Miyashita, K. Kamita, M. Hidai, *J. Am. Chem. Soc.* **1997**, *119*, 6448.
[42] J. R. Johnson, G. D. Cuny, S. L. Buchwald, *Angew. Chem.* **1995**, *107*, 1877; *Angew. Chem. Int. Ed. Engl.* **1995**, *34*, 1760.
[43] P. Eilbracht, L. Bärfacker, C. Buss, C. Hollmann, B. E. Kitsos-Rzychon, C. L. Kranemann, T. Rische, R. Roggenbuck, A. Schmidt, *Chem. Rev.* **1999**, *99*, 3329.
[44] T. Rische, P. Eilbracht, *Synthesis* **1997**, *11*, 1331.
[45] A. Moballigh, A. Seayad, R. Jackstell, M. Beller, *J. Am. Chem. Soc.* **2003**, *125*, 10311.
[46] a) T. Baig, J. Molinier, P. Kalck, *J. Organomet. Chem.* **1993**, *454*, 219; b) T. Baig, P. Kalck, *J. Chem. Soc. Chem. Commun.* **1992**, 1373.
[47] G. Diekhaus, D. Kampmann, C. Kniep, T. Müller, J. Walter, J. Weber (Hoechst AG), DE 4334809, **1993** [*Chem. Abstr.* **1995**, *122*, 314160g].
[48] B. Zimmermann, J. Herwig, M. Beller, *Angew. Chem.* **1999**, *111*, 2515; *Angew. Chem. Int. Ed.* **1999**, *38*, 2372.
[49] T. Rische, P. Eilbracht, *Tetrahedron* **1999**, *55*, 7841.
[50] Y.-S. Lin, B. El Ali, H. Alper, *Tetrahedron Lett.* **2001**, *42*, 2423.
[51] T. Rische, P. Eilbracht, *Tetrahedron* **1999**, *55*, 1915.
[52] T. Rische, P. Eilbracht, *Tetrahedron* **1999**, *55*, 3917.
[53] T. Rische, K.-S. Müller, P. Eilbracht, *Tetrahedron* **1999**, *55*, 9801.
[54] a) F. Rohet, C. Rubat, P. Coudert, *Chem. Pharm. Bull.* **1996**, *44*, 980; b) L. D. Wise, I. C. Pattison, D. E. Butler, *J. Med. Chem.* **1985**, *28*, 1811.
[55] L. Bärfacker, T. Rische, P. Eilbracht, *Tetrahedron* **1999**, *55*, 7177.
[56] T. Rische, L. Bärfacker, P. Eilbracht, *Eur. J. Org. Chem.* **1999**, 653.
[57] a) J. Berthoux, Y. Chevallier, J.-P. Martinaud (Rhone-Progil), US 4096150, **1978**; b) R. M. Laine (SRI Int.), US 4292242, **1981**; c) Y. Yanagi, K. Yoneyama, H. Omori (Mitsubishi Petrochem. Co.), US 4448996, **1984**; d) J. F. Knifton, D. C. Alexander (Texaco Inc.), US 4543411, **1985**; e) E. E. McEntire, K. Square Pa, J. F. Knifton (Texaco, Inc.), US 4705898, **1987**.
[58] a) O. Mitsunobu in *Comprehensive Organic Synthesis*, *Vol. 6* (Ed.: B. M. Trost), Pergamon, Oxford, **1991**, p. 65; b) C. M. Marson, A. D. Holson in *Comprehensive Organic Functional Group Transformations 2* (Eds.: A. R. Katritzky, O. Meth-Cohn, C. W. Rees), Pergamon, Cambridge, **1995**, p. 297.
[59] T. Rische, B. Kitsos-Rzychon, P. Eilbracht, *Tetrahedron* **1998**, *54*, 2723.
[60] a) A. T. Larson (DuPont), US 2497310, **1950** [*Chem. Abstr.* **1950**, *44*, 4489h]; b) A. Striegler, J. Weber, *J. Prakt. Chem.* **1965**, *29*, 281.
[61] C. L. Kranemann, P. Eilbracht, *Synthesis* **1998**, 71.
[62] E. L. Jenner, R. V. Lindesey, Jr., (DuPont), US 2876254, **1959**.
[63] J. F. Knifton, *J. Org. Chem.* **1976**, *41*, 2885.
[64] M. Beller, B. Cornils, C. D. Frohning, C. W. Kohlpaintner, *J. Mol. Catal. A* **1995**, *104*, 17.
[65] D. M. Fenton, *J. Org. Chem.* **1973**, *38*, 3192.
[66] H. Alper, J. B. Woell, B. Despeyroux, D. J. H. Smith, *J. Chem. Soc. Chem. Commun.* **1983**, 1270.
[67] S. Toda, M. Miyamoto, H. Kinoshita, K. Inomata, *Bull. Chem. Soc. Jpn.* **1991**, *64*, 3600.
[68] F. Bertoux, Y. Castanet, E. Civade, E. Monflier, A. Mortreux, *Catal. Lett.* **1998**, *54*, 199.
[69] M. Mlekuz, F. Joo, H. Alper, *Organometallics* **1987**, *6*, 1591.
[70] L. J. B. Lin, H. Alper, *J. Chem. Soc. Chem. Commun.* **1989**, 248.
[71] B. El Ali, H. Alper, *J. Mol. Catal.* **1992**, *77*, 7.
[72] a) J. Tsuji, *Adv. Org. Chem.* **1969**, *6*, 150; b) J. Tsuji, *Acc. Chem. Res.* **1969**, *2*, 144; c) J. Tsuji, M. Morikawa, J. Kiji, *Tetrahedron Lett.* **1963**, 1437.
[73] K. Bittler, N. V. Kutepow, D. Neubauer, H. Reis, *Angew. Chem.* **1968**, *80*, 352; *Angew. Chem. Int. Ed. Engl.* **1968**, *7*, 329.
[74] J.-Y. Yoon, E. J. Jang, K. H. Lee, J. S. Lee, *J. Mol. Catal. A* **1997**, *118*, 181.
[75] S. Oi, M. Nomura, T. Aiko, Y. Inoue, *J. Mol. Catal. A* **1997**, *115*, 289.
[76] a) A. Seayad, A. A. Kelkar, L. Toniolo, R. V. Chaudhari, *J. Mol. Catal. A* **2000**, *151*, 47; b) A. Seayad, A. A. Kelkar, L. Toniolo, R. V. Chaudhari, *Ind. Eng. Chem. Res.* **1998**, *37*, 2180; c) A. Seayad, J. Seayad, K. Damodaran, L. Toniolo, R. V. Chaudhari, *J. Organomet. Chem.* **2000**, *601*, 100.
[77] a) Y. G. Noskov, M. I. Terekhova, E. S. Petrov, *Kinet. Catal.* **1989**, *30*, 204; b) Y. G. Noskov, N. A. Novikov, M. I. Terekhova, E. S. Petrov, *Kinet. Catal.* **1991**, *32*, 291; c) Y. G. Noskov, M. I. Terekhova, E. S. Petrov, *Kinet. Catal.* **1993**, *34*, 898; d) Y. G. Noskov, E. S. Petrov, *Kinet. Catal.* **1993**, *34*, 902; e) Y. G. Noskov, E. S. Petrov, *Kinet. Catal.* **1994**, *35*, 672; f) Y. G. Noskov, E. S. Petrov, *Kinet. Catal.* **1997**, *38*, 520.
[78] A. D. Karpyuk, S. Starosel'skaya, E. S. Petrov, I. P. Beletskaya, *Izv. Akad. Nauk. SSSR*, *Izv. Akad. Nauk SSSR Ser. Khim.* **1986**, *1*, 218.
[79] Y. Sugi, K. Bando, S. Shin, *Chem. Ind.* **1975**, 397.
[80] Y. Sugi, K. Bando, *Chem. Lett.* **1976**, 727.
[81] G. Consiglio, M. Marchetti, *Chimia* **1976**, *30*, 26.
[82] a) I. Shimizu, R. Hirano, Y. Matsumura, H. Nomura, K. Uchida, A. Satao, US 4694100, **1985**; b) I. Shimizu, R. Hirano, Y. Matsumura, H. Nomura, K. Uchida, A. Sato, (Nippon), US 4694100, **1987**; c) I. Shimizu, Y. Matsumura, Y. Tokumoto, K. Uchida (Nippon), US 5097061, **1992**; d) I. Shimizu, Y. Matsumura, Y. Tokumoto, K. Uchida (Nippon), US 5260477, **1993**.
[83] a) T.-C. Wu (Ethyl Corp.), US 5254720, **1992**; b) T.-C. Wu (Ethyl Corp.), US 5315026, **1994**; c) T.-C. Wu (Ethyl Corp.), US 5315028, **1994**.

 © 2004 Wiley-VCH Verlag GmbH & Co. KGaA, Weinheim

[84] a) G. Cometti, G. P. Chiusoli, US 4439618, **1984**; b) G. Cometti, G. P. Chiusoli, EP 0074866 A1, **1983**.
[85] a) I. Shimizu, R. Hirano, Y. Matsumura, Y. Tokumoto, K. Uchida, US 5260477, **1985**; b) Y. Tokumoto, I. Shimizu, S. Inue, US 5166419, **1990**; c) T. Manimaran, T.-C. Wu, F. M. Orihuela, US 5315027, **1993**.
[86] H. Alper, H. Hamel, *J. Am. Chem. Soc.* **1990**, *112*, 2803.
[87] a) A. Seayad, S. Jayasree, R. V. Chaudhari, *Org. Lett.* **1999**, *1*, 459; b) A. Seayad, S. Jayasree, R. V. Chaudhari, *Catal. Lett.* **1999**, *61*, 99; c) S. Jayasree, A. Seayad, R. V. Chaudhari, *Chem. Commun.* **1999**, 1067; d) S. Jayasree, A. Seayad, R. V. Chaudhari, *Org. Lett.* **2000**, *2*, 203; e) S. Jayasree, A. Seayad, R. V. Chaudhari, *Chem. Commun.* **2000**, 1239.
[88] T. Fuchikami, K. Ohishi, I. Ojima, *J. Org. Chem.* **1983**, *48*, 3803.
[89] J.-P. Simonato, *J. Mol. Catal. A* **2003**, *197*, 61.
[90] a) I. Amer, H. Alper, *J. Organomet. Chem.* **1990**, *383*, 573; b) B. El Ali, H. Alper, *J. Mol. Catal.* **1991**, *67*, 29; c) A. Scrivanti, R. Chinellato, U. Matteoli, *J. Mol. Catal.* **1993**, *84*, L141.
[91] J. F. Knifton, *J. Mol. Catal.* **1977**, *2*, 293.
[92] Y. Tsuji, T. Kondo, Y. Watanabe, *J. Mol. Catal.* **1987**, *40*, 295.
[93] D. Zargarian, H. Alper, *Organometallics* **1993**, *12*, 712.
[94] a) F. Y. Zhao, B. M. Bhanage, M. Shirai, M. Arai, *Chem. Eur. J.* **2000**, *6*, 843; b) K. Köhler, M. Wagner, L. Djakovitch, *Catal. Today* **2001**, *66*, 101.
[95] J. T. Lee, H. Alper, *Tetrahedron Lett.* **1991**, *32*, 1769.
[96] H. Alper, M. Saldana-Maldonado, L. J. B. Lin, *J. Mol. Catal.* **1988**, *49*, L27.
[97] B. El Ali, H. Alper, *J. Mol. Catal. A* **1995**, *96*, 197.
[98] S. Torri, H. Okumoto, M. Sadakane, L. H. Xu, *Chem. Lett.* **1991**, 1673.
[99] K. Itoh, M. Miura, M. Nomura, *Tetrahedron Lett.* **1992**, *33*, 5369.
[100] a) Y. Kushino, K. Itoh, M. Nomura, *J. Mol. Catal.* **1994**, *89*, 151; b) S. Jayasree, A. Seayad, S. P. Gupte, R. V. Chaudhari, *Catal. Lett.* **1999**, *58*, 213.
[101] A. L. Monteiro, V. R. Lando, V. Gasparini, *Synth. Commun.* **1997**, *27*, 3605.
[102] a) E. Drent, P. Arnoldy, P. H. M. Budzelaar, *J. Organomet. Chem.* **1994**, *475*, 57; b) E. Drent (Shell Research BV), EP 271145A2, **1988**; c) E. Drent, P. H. M. Budzelaar, W. W. Jager (Shell Oil Corp.), US 5099062, **1992**.
[103] a) E. Drent, P. H. M. Budzelaar, W. W. Jager, J. Stapersma (Shell Oil Corp.), US 5166116, **1992**; b) E. Drent, P. H. M. Budzelaar, W. W. Jager, J. Stapersma (Shell Oil Corp.), US 5179225, **1993**; c) E. Drent, P. H. M. Budzelaar (Shell Oil Corp.), US 5103043, **1992**; d) E. Drent, P. H. M. Budzelaar (Shell Oil Corp.), US 5028576, **1991**; e) E. Drent, P. H. M. Budzelaar, W. W. Jager (Shell Oil Corp.), US 5158921, **1992**; f) E. Drent, P. H. M. Budzelaar, W. W. Jager (Shell Oil Corp.), US 5177253, **1993**.
[104] A. Scrivanti, U. Matteoli, *Tetrahedron Lett.* **1995**, *36*, 9015.
[105] M. T. Reetz, R. Demuth, R. Goddard, *Tetrahedron Lett.* **1998**, *39*, 7089.
[106] a) P. Arthur, B. G. Pratt, US 2666748, **1954**; b) P. Arthur, D. C. England, B. G. Pratt, G. M. Whitman, *J. Am. Chem. Soc.* **1954**, *76*, 5364.
[107] a) *Chem. Eng. News* **1971**, *49*, 30; b) C. A. Tolman, R. J. Mckinney, W. C. Seidel, J. D. Druliner, W. R. Stevens, *Adv. Catal.* **1985**, *33*, 1; c) R. J. McKinney in *Homogeneous Catalysis* (Ed.: G. W. Parshall), Wiley, New York, **1992**, p. 42.
[108] W. C. Drinkard, Jr., R. J. Kassal, US 3496217, **1970**.
[109] C. A. Tolman, *J. Chem. Educ.* **1986**, *63*, 199.
[110] a) C. A. Tolman, W. C. Seidel, J. D. Druliner, P. J. Domaille, *Organometallics* **1984**, *3*, 33; b) R. J. McKinney, W. A. Nugent, *Organometallics* **1989**, *8*, 2871.
[111] a) E. Puentes, I. Mamalis, A. F. Noels, A. J. Hubert, P. Teyssie, D. Y. Waddan, *J. Catal.* **1983**, *82*, 365; b) I. Mamalis, A. F. Noels, E. Puentes, R. Warin, P. Teyssie, A. J. Hubert, J. Grandjean, R. Hubin, D. Y. Waddan, *J. Catal.* **1986**, *102*, 357.
[112] E. Puentes, A. F. Noels, R. Warin, A. J. Hubert, P. Teyssié, D. Y. Waddan, *J. Mol. Catal.* **1985**, *31*, 183.
[113] M. J. Baker, K. N. Harrison, A. G. Orpen, P. G. Pringle, G. Shaw, *J. Chem. Soc. Chem. Commun.* **1991**, 803.
[114] M. Yan, Q.-Y. Xu, A. S. C. Chan, *Tetrahedron: Asymmetry* **2000**, *11*, 845.
[115] a) T. V. RajanBabu, A. L. Casalnuovo, *J. Am. Chem. Soc.* **1992**, *114*, 6265; b) A. L. Casalnuovo, T. V. RajanBabu, T. A. Ayers, T. H. Warren, *J. Am. Chem. Soc.* **1994**, *116*, 9869; c) T. V. RajanBabu, A. L. Casalnuovo, *J. Am. Chem. Soc.* **1996**, *118*, 6325.
[116] W. Goertz, P. C. J. Kamer, P. W. N. M. van Leeuwen, D. Vogt, *Chem. Commun.* **1997**, 1521.
[117] a) M. Kranenburg, P. C. J. Kamer, P. W. N. M. van Leeuwen, D. Vogt, W. Keim, *J. Chem. Soc. Chem. Commun.* **1995**, 2177; b) W. Goertz, W. Keim, D. Vogt, U. Englert, M. D. K. Boele, L. A. van der Veen, P. C. J. Kamer, P. W. N. M. van Leeuwen, *J. Chem. Soc. Dalton Trans.* **1998**, 2981.
[118] W. Goertz, P. C. J. Kamer, P. W. N. M. van Leeuwen, D. Vogt, *Chem. Eur. J.* **2001**, *7*, 1614.
[119] W. R. Jackson, C. G. Lovel, *Aust. J. Chem.* **1983**, *36*, 1975.
[120] N. J. Fitzmaurice, W. R. Jackson, P. Perlmutter, *J. Organomet. Chem.* **1985**, *285*, 375.
[121] W. R. Jackson, P. Perlmutter, A. J. Smallridge, *Tetrahedron Lett.* **1988**, *29*, 1983.
[122] a) T. Funabiki, Y. Yamazaki, K. Tarama, *J. Chem. Soc. Chem. Commun.* **1973**, 63; b) T. Funabiki, Y. Yamazaki, H. Sato, S. Yoshida, *J. Chem. Soc. Perkin Trans. 2* **1983**, 1915.
[123] a) T. Funabiki, Y. Yamazaki, *J. Chem. Soc. Chem. Commun.* **1979**, 1110; b) T. Funabiki, H. Sato, N. Tanaka, Y. Yamazaki, S. Yoshida, *J. Mol. Catal.* **1990**, *62*, 157.
[124] S. L. Buchwald, S. J. Lamaire, *Tetrahedron Lett.* **1987**, *28*, 295.
[125] For leading reviews see; a) I. Bytschkov, S. Doye, *Eur. J. Org. Chem.* **2003**, 935; b) F. Pohlki, S. Doye, *Chem. Soc. Rev.* **2003**, *32*, 104; c) M. Beller, C. Breindl, M. Eichberger, C. G. Hartung, J. Seayad, O. Thiel, A. Tillack, H. Trauthwein, *Synlett* **2002**, 1579; d) J. Seayad, A. Tillack, C. G. Hartung, M. Beller, *Adv. Synth. Catal.* **2002**, *344*, 795; e) J. J. Brunet, D. Neibecker in *Catalytic Heterofunctionalization from Hydroamination to Hydrozirconation* (Eds.: A. Togni, H. Grützmacher), Wiley-VCH, Weinheim, **2001**, p. 98; f) M. Nobis, B. Drießen-Hölscher, *Angew. Chem.* **2001**, *113*, 4105; *Angew. Chem. Int. Ed.* **2001**, *40*, 3983; g) E. Haak, S. Doye, *Chem. Unserer Zeit* **1999**, *33*, 296; h) T. E. Müller, M. Beller, *Chem. Rev.* **1998**, *98*, 675; i) T. E. Müller, M. Beller in *Transition Metals for Organic Synthesis*, *Vol. 2* (Eds.: M. Beller, C. Bolm), Wiley-VCH, Weinheim, **1998**, p. 16; j) J. J. Brunet, D. Neibecker, F. Niedercorn, *J. Mol. Catal.* **1989**, *49*, 235; k) M. B. Gasc, A. Lattes, J. J. Perie, *Tetrahedron* **1983**, *39*, 703.
[126] D. Steinborn, R. Taube, *Z. Chem.* **1986**, *26*, 349.
[127] a) J. March, *Advanced Organic Chemistry*, 3rd ed., Wiley, New York, **1991**, p. 711, and references therein; b) J. J. Bozel, L. S. Hegedus, S. Louis, *J. Org. Chem.* **1981**, *46*, 2561; c) M. Kawatsura, J. F. Hartwig, *Organometallics* **2001**, *20*, 1960.
[128] a) J. O. H. Peterson, H. S. Fales, US 4307250, **1981**; b) H. S. Fales, J. O. H. Peterson, EP 39618, **1981**; c) J. O. H. Peterson, H. S. Fales, US 4375002, **1983**; d) W. J. Ambs, M. Deeba, J. F. Ferguson, EP 101921, **1984**; e) M. Deeba, M. E. Ford, T. A. Johnson, *J. Chem. Soc. Chem. Commun.* **1987**, 562; e) M. Deeba, M. E. Ford, *J. Org. Chem.* **1988**, *53*, 4594.
[129] a) V. Taglieber, W. Hölderich, R. Kummer, W. D. Mross, G. Saladin, US 4929758, **1990**; b) M. Tabata, N. Mizuno, M. Iwamoto, *Chem. Lett.* **1991**, 1027; c) N. Mizuno, M. Tabata, T. Uematsu, M. Iwamoto, *J. Catal.* **1994**, *146*, 249.

 © 2004 Wiley-VCH Verlag GmbH & Co. KGaA, Weinheim

[130] a) W. F. Hölderich, *Catal. Today* **2000**, *62*, 115; b) U. Dingerdissen, K. Eller, R. Kummer, H. J. Lützel, P. Stops, J. Herrmann (BASF AG), WO 97/07088, **1995**; c) A. Chauvel, B. Delmon, W. F. Hölderich, *Appl. Catal. A* **1994**, *115*, 173; d) W. F. Hölderich, V. Taglieber, H. Pohl, R. Kummer, K. G. Baur (BASF AG), DE 36342747, **1987**.

[131] a) B. W. Howk, E. L. Little, S. L. Scott, G. M. Whitman, *J. Am. Chem. Soc.* **1954**, *76*, 1899; b) G. P. Pez, J. E. Galle, *Pure Appl. Chem.* **1985**, *57*, 1917.

[132] J. J. Brunet, D. Neibecker, K. Philippot, *Tetrahedron Lett.* **1994**, *35*, 3877.

[133] a) K. Li, P. N. Horton, M. B. Hursthouse, K. K. Hii, *J. Organomet. Chem.* **2003**, *665*, 250; b) Ref. 9b.

[134] a) R. J. Schlott, J. C. Falk, K. W. Narducy, *J. Org. Chem.* **1972**, *37*, 4243; b) R. Wegler, G. Pieper, *Chem. Ber.* **1950**, *83*, 1.

[135] R. K. Razdam, *Chem. Commun.* **1969**, 770.

[136] M. Beller, C. Breindl, *Tetrahedron* **1998**, *54*, 6359.

[137] D. Tzalis, C. Koradin, P. Knochel, *Tetrahedron Lett.* **1999**, *40*, 6193.

[138] a) M. Beller, C. Breindl, T. H. Riermeier, M. Eichberger, H. Trauthwein, *Angew. Chem.* **1998**, *110*, 3571; *Angew. Chem. Int. Ed.* **1998**, *37*, 3389; b) M. Beller, C. Breindl, T. H. Riermeier, A. Tillack, *J. Org. Chem.* **2001**, *66*, 1403.

[139] a) T. Fujita, K. Suga, S. Watanabe, *Aust. J. Chem.* **1974**, *27*, 531; b) T. Fujita, K. Suga, S. Watanabe, *Chem. Ind.* **1973**, 231.

[140] C. G. Hartung, C. Breindl, A. Tillack, M. Beller, *Tetrahedron* **2000**, *56*, 5157.

[141] a) M. Beller, M. Eichberger, H. Trauthwein, *Angew. Chem.* **1997**, *109*, 2306; *Angew. Chem. Int. Ed. Engl.* **1997**, *36*, 2225; b) A. Tillack, H. Trauthwein, C. G. Hartung, M. Eichberger, S. Pitter, A. Jansen, M. Beller, *Monatsh. Chem.* **2000**, *131*, 1327; c) M. Beller, O. R. Thiel, H. Trauthwein, C. G. Hartung, *Chem. Eur. J.* **2000**, *6*, 2513.

[142] M. Beller, H. Trauthwein, M. Eichberger, C. Breindl, J. Herwig, T. E. Müller, O. R. Thiel, *Chem. Eur. J.* **1999**, *5*, 1306.

[143] M. Utsunomiya, R. Kuwano, M. Kawatsura, J. F. Hartwig, *J. Am. Chem. Soc.* **2003**, *125*, 5608.

[144] M. Beller, H. Trauthwein, M. Eichberger, C. Breindl, T. E. Müller, *Eur. J. Inorg. Chem.* **1999**, 1121.

[145] J. Haggin, *Chem. Eng. News* **1993**, *71*(23), 23.

[146] a) I. Kadota, A. Shibuya, L. M. Lutete, Y. Yamamoto, *J. Org. Chem.* **1999**, *64*, 4570; b) T. Shimada, Y. Yamamoto, *J. Am. Chem. Soc.* **2002**, *124*, 12670.

[147] M. Tokunaga, M. Eckert, Y. Wakatsuki, *Angew. Chem.* **1999**, *111*, 3417; *Angew. Chem. Int. Ed.* **1999**, *38*, 3222.

[148] Y. Uchimaru, *Chem. Commun.* **1999**, 1133.

[149] C. G. Hartung, A. Tillack, H. Trauthwein, M. Beller, *J. Org. Chem.* **2001**, *66*, 6339.

[150] a) J. S. Johnson, R. G. Bergman, *J. Am. Chem. Soc.* **2001**, *123*, 2923; b) B. Straub, R. G. Bergman, *Angew. Chem.* **2001**, *113*, 4768; *Angew. Chem. Int. Ed.* **2001**, *40*, 4632.

[151] a) E. Haak, I. Bytschkov, S. Doye, *Angew. Chem.* **1999**, *111*, 3584; *Angew. Chem. Int. Ed.* **1999**, *38*, 3389; b) E. Haak, H. Siebeneicher, S. Doye, *Org. Lett.* **2000**, *2*, 1935; c) I. Bytschkov, S. Doye, *Eur. J. Org. Chem.* **2001**, 4411; d) F. Pohlki, S. Doye, *Angew. Chem.* **2001**, *113*, 2361; *Angew. Chem. Int. Ed.* **2001**, *40*, 2305; e) A. Heutling, S. Doye, *J. Org. Chem.* **2002**, *67*, 1961.

[152] U. Rosenthal, V. V. Burlakov, P. Arndt, W. Baumann, A. Spannenberg, *Organometallics* **2003**, *22*, 884; the so-called Rosenthal catalysts are commercially available from Fluka.

[153] A. Tillack, I. Garcia Castro, C. G. Hartung, M. Beller, *Angew. Chem.* **2002**, *114*, 2646; *Angew. Chem. Int. Ed.* **2002**, *41*, 2541.

[154] A. Tillack, H. Jiao, I. Garcia Castro, C. G. Hartung, M. Beller, *Chem. Eur. J.* **2004**, *10*, 2409.

[155] a) Y. Shi, C. Hall, J. T. Ciszewski, C. Cao, A. L. Odom, *Chem. Commun.* **2003**, 586; b) T.-G. Ong, G. P. A. Yap, D. S. Richeson, *Organometallics* **2002**, *21*, 2839; c) Y. Shi, J. T. Ciszewski, A. L. Odom, *Organometallics* **2001**, *20*, 3967; d) C. Cao, J. T. Ciszewski, A. L. Odom, *Organometallics* **2001**, *20*, 5011.

[156] a) Y. Li, T. J. Marks, *J. Am. Chem. Soc.* **1998**, *120*, 1757; b) Y. Li, T. J. Marks, *Organometallics* **1996**, *15*, 3770.

[157] T. Straub, A. Haskel, T. G. Neyroud, M. Kapon, M. Botoshansky, M. S. Eisen, *Organometallics* **2001**, *20*, 5017.

[158] A. Rodriguez, C. Koradin, W. Dohle, P. Knochel, *Angew. Chem.* **2000**, *112*, 2607; *Angew. Chem. Int. Ed.* **2000**, *39*, 2488.

[159] K. Tani, Y. Kataoka in *Catalytic Heterofunctionalization from Hydroamination to Hydrozirconation* (Eds.: A. Togni, H. Grützmacher), Wiley-VCH, Weinheim, **2001**, p. 171.

[160] a) H. Lansink-Rotgerink, H. Hocker, S. Wieland, S. Seebald, H. Riedemann (Degussa AG), EP 798040A1, **1997** [*Chem. Abstr.* **1997**, *127*, 294945]; b) M. Kuge, I. Yanai (Japan Gasoline Co., Ltd., Japan), JP 51045562, **1976** [*Chem. Abstr.* **1977**, *86*, 155191].

[161] a) S. Faramawy, *Pet. Sci. Technol.* **1998**, *16*, 811; b) K. Eguchi, T. Tokai, Y. Kimura, H. Arai, *Chem. Lett.* **1986**, 567.

[162] a) M. A. Harmer, Q. Sun, *Appl. Catal. A* **2001**, *221*, 45; b) W. F. Hölderich, *Stud. Surf. Sci. Catal.* **1993**, *75*, 127; c) I. N. Amor, *Appl. Catal.* **1991**, *78*, 141; d) H. Momose, K. Kusumoto, Y. Izumi, Y. Mizutani, *J. Catal.* **1982**, *77*, 554.

[163] I. V. Kozhevnikov, *Chem. Rev.* **1998**, *98*, 171.

[164] a) *Ullmann's Encyclopedia of Industrial Chemistry*, 6th ed., *Vol. 2*, Wiley-VCH, Weinheim, **2003**, p. 27; b) J. March, *Advanced Organic Chemistry*, 3rd ed., Wiley, New York, **1991**, p. 681 and p. 686, and references therein.

[165] M. Steilemann, J. N. Armor, W. F. Hölderich, *Chem. Commun.* **1999**, 697.

[166] S. Kano, Y. Tanaka, S. Hibino, *J. Chem. Soc. Chem. Commun.* **1980**, 414.

[167] M. Bassetti, B. Floris, *J. Chem. Soc. Perkin Trans. 2* **1988**, 227.

[168] J. Blum, H. Huminer, H. Alper, *J. Mol. Catal.* **1992**, *75*, 153.

[169] Y. Fukuda, K. Utimoto, *J. Org. Chem.* **1991**, *56*, 3729.

[170] J. P. Damiano, M. Postel, *J. Organomet. Chem.* **1996**, *522*, 303.

[171] W. Hiscox, P. W. Jennings, *Organometallics* **1990**, *9*, 1997.

[172] J. W. Hartman, W. C. Hiscox, P. W. Jennings, *J. Org. Chem.* **1993**, *58*, 7613.

[173] W. Baidossi, M. Lahav, J. Blum, *J. Org. Chem.* **1997**, *62*, 669.

[174] L. W. Francisco, D. A. Moreno, J. D. Atwood, *Organometallics* **2001**, *20*, 4237.

[175] E. Mizushima, K. Sato, T. Hayashi, M. Tanaka, *Angew. Chem.* **2002**, *114*, 4745; *Angew. Chem. Int. Ed.* **2002**, *41*, 4563.

[176] a) M. Tokunaga, Y. Wakatsuki, *Angew. Chem.* **1998**, *110*, 3024; *Angew. Chem. Int. Ed.* **1998**, *37*, 2867; b) J.-H. Teles, *Chem. Unserer Zeit* **1999**, *33*, 58; c) T. Suzuki, M. Tokunaga, Y. Wakatsuki, *Org. Lett.* **2001**, *3*, 735; d) P. Alverez, M. Bassetti, J. Gimeno, G. Mancini, *Tetrahedron Lett.* **2001**, *42*, 8467.

[177] D. B. Grotjahn, C. D. Incarvito, A. L. Rheingold, *Angew. Chem.* **2001**, *113*, 4002; *Angew. Chem. Int. Ed.* **2001**, *40*, 3884.

[178] M. Tokunaga, T. Suzuki, N. Koga, T. Fukushima, A. Horiuchi, Y. Wakatsuki, *J. Am. Chem. Soc.* **2001**, *123*, 11917.

[179] T. Hosokawa, T. Ohta, S. Kanayama, S.-I. Murahashi, *J. Org. Chem.* **1987**, *52*, 1758.

[180] R. Jira in *Applied Homogeneous Catalysis with Organometallic Compounds*, 2nd ed., *Vol. 1* (Eds.: B. Cornils, W. A. Herrmann), Wiley-VCH, Weinheim, **2002**, p. 386.

[181] T. Hosokawa, T. Shinohara, Y. Ooka, S.-I. Murahashi, *Chem. Lett.* **1989**, 2001.

[182] A. Ishida, T. Uesugi, S. Takamuku, *Bull. Chem. Soc. Jpn.* **1993**, *66*, 1580.

[183] K. Mizuno, I, Nakanishi, N. Ichinose, Y. Otsuji, *Chem. Lett.* **1989**, 1095.

[184] a) Y. Inoue, T. Okano, N. Yamasaki, A. Tai, *J. Chem. Soc. Chem. Commun.* **1993**, 718; b) S. Asaoka, T. Kitazawa, T. Wada, Y. Inoue, *J. Am. Chem. Soc.* **1999**, *121*, 8486.

 © 2004 Wiley-VCH Verlag GmbH & Co. KGaA, Weinheim

[185] I. Kadota, L. M. Lutete, A. Shibuya, Y. Yamamoto, *Tetrahedron Lett.* **2001**, *42*, 6207.
[186] D. H. Camaho, S. Saito, Y. Yamamoto, *Tetrahedron Lett.* **2002**, *43*, 1085.
[187] a) T. Mitsudo, Y. Hori, Y. Watanabe, *J. Org. Chem.* **1985**, *50*, 1566; b) T. Mitsudo, Y. Hori, Y. Yamakawa, Y. Watanabe, *Tetrahedron Lett.* **1986**, *27*, 2125; c) T. Mitsudo, Y. Hori, Y. Yamakawa, Y. Watanabe, *J. Org. Chem.* **1987**, *52*, 2230.
[188] Y. Hori, T. Mitsudo, Y. Watanabe, *J. Organomet. Chem.* **1987**, *321*, 397.
[189] C. Bianchini, A. Meli, M. Peruzzuni, F. Zanobini, *Organometallics* **1990**, *9*, 1155.
[190] C. Ruppin, P. H. Dixneuf, *Tetrahedron Lett.* **1988**, *29*, 5365.
[191] M. Neveux, B. Seiller, F. Hagedorn, C. Bruneau, P. H. Dixneuf, *J. Organomet. Chem.* **1993**, *451*, 133.
[192] a) M. Rotem, Y. Shvo, *Organometallics* **1983**, *2*, 1689; b) M. Rotem, Y. Shvo, *J. Organomet. Chem.* **1993**, *448*, 189.
[193] a) C. Ruppin, P. H. Dixneuf, *Tetrahedron Lett.* **1986**, *27*, 6323; b) C. Ruppin, P. H. Dixneuf, S. Lécolier, *Tetrahedron Lett.* **1988**, *29*, 5365; c) C. Bruneau, M. Neveux, Z. Kabouche, P. H. Dixneuf, *Synlett* **1991**, 755; d) C. Bruneau, P. H. Dixneuf, *Chem. Commun.* **1997**, 507.
[194] a) H. Doucet, J. Höfer, C. Bruneau, P. H. Dixneuf, *J. Chem. Soc. Chem. Commun.* **1993**, 850; b) H. Doucet, B. Martin-Vaca, C. Bruneau, P. H. Dixneuf, *J. Org. Chem.* **1995**, *60*, 7247; c) H. Doucet, C. Bruneau, P. H. Dixneuf, *Synlett* **1997**, 807.
[195] M. Picquet, C. Bruneau, P. H. Dixneuf, *Chem. Commun.* **1997**, 1201.
[196] H. Doucet, N. Derrien, Z. Kabouche, C. Bruneau, P. H. Dixneuf, *J. Organomet. Chem.* **1997**, *551*, 151.
[197] L. J. Gooßen, J. Paetzold, D. Koley, *Chem. Commun.* **2003**, 706.
[198] K. Melis, D. de Vos, P. Jacobs, F. Verpoort, *J. Organomet. Chem.* **2003**, *671*, 131.
[199] K. Melis, F. Verpoort, *J. Mol. Catal. A* **2003**, *194*, 39.
[200] a) M. Tanaka, M. Imai, Y. Yamamoto, K. Tanaka, M. Shimowatari, S. Nagumo, N. Kawahara, H. Suemune, *Org. Lett.* **2003**, *5*, 1365; b) K. Takai, S. Sakamoto, T. Isshiki, *Org. Lett.* **2003**, *5*, 653.
[201] a) T. Kondo, Y. Tsuji, Y. Watanabe, *Tetrahedron Lett.* **1987**, *28*, 6229; b) T. Kondo, M. Akazome, Y. Tsuji, Y. Watanabe, *J. Org. Chem.* **1990**, *55*, 1286.
[202] T. Kondo, N. Hiraishi, Y. Morisaki, K. Wada, Y. Watanabe, T.-A. Mitsudo, *Organometallics* **1998**, *17*, 2131.
[203] a) C.-H. Jun, H. Lee, J.-B. Hong, *J. Org. Chem.* **1997**, *62*, 1200; b) C.-H. Jun, D.-Y. Lee, J.-B. Hong, *Tetrahedron Lett.* **1997**, *38*, 6673.
[204] C.-H. Jun, D.-Y. Lee, H. Lee, J.-B. Hong, *Angew. Chem.* **2000**, *112*, 3214; *Angew. Chem. Int. Ed.* **2000**, *39*, 3070.
[205] C.-H. Jun, J.-H. Chung, D.-Y. Lee, A. Loupy, J.-B. Hong, *Tetrahedron Lett.* **2001**, *42*, 4803.
[206] a) C. P. Lenges, M. Brookhart, *J. Am. Chem. Soc.* **1997**, *119*, 3165; b) C. P. Lenges, P. S. White, M. Brookhart, *J. Am. Chem. Soc.* **1998**, *120*, 6965.
[207] K. M. Miller, W.-S. Huang, T. F. Jamison, *J. Am. Chem. Soc.* **2003**, *125*, 3442.
[208] a) K. Griesbaum, *Angew. Chem.* **1970**, *82*, 276; *Angew. Chem. Int. Ed. Engl.* **1970**, *9*, 273; b) M. E. Peach in *The Chemistry of the Thiol Group*, *Vol. 2* (Ed.: S. Patai), Wiley, London, **1974**.
[209] a) H. Kuniyasu, A. Ogawa, K. Sato, I. Ryu, N. Kambe, N. Sonoda, *J. Am. Chem. Soc.* **1992**, *114*, 5902; b) H. Kuniyasu, A. Ogawa, K. Sato, I. Ryu, N. Sonoda, *Tetrahedron Lett.* **1992**, *33*, 5525; c) A. Ogawa, A. Kudo, T. Hirao, *Tetrahedron Lett.* **1998**, *39*, 5213.
[210] A. Ogawa, T. Ikeda, K. Kimura, T. Hirao, *J. Am. Chem. Soc.* **1999**, *121*, 5108.
[211] J. March, *Advanced Organic Chemistry*, 3rd ed., Wiley, New York, **1991**, p. 479, and references therein.
[212] a) T. Matsumoto, D. J. Taube, R. A. Periana, H. Taube, H. Yoshida, *J. Am. Chem. Soc.* **2000**, *122*, 7414; b) R. A. Periana, X. Y. Liu, G. Bhalla, *Chem. Commun.* **2002**, 3000.
[213] R. Dorta, A. Togni, *Chem. Commun.* **2003**, 760.
[214] a) C. Jia, W. Lu, J. Oyamada, T. Kitamura, K. Matsuda, M. Irie, Y. Fujiwara, *J. Am. Chem. Soc.* **2000**, *122*, 7252; b) W. Lu, C. Jia, T. Kitamura, Y. Fujiwara, *Org. Lett.* **2000**, *2*, 2917; c) W. Lu, C. Jia, T. Kitamura, Y. Fujiwara, *Acc. Chem. Res.* **2001**, *34*, 633.
[215] C. Jia, D. Piao, J. Oyamada, W. Lu, T. Kitamura, Y. Fujiwara, *Science* **2000**, *287*, 1992.

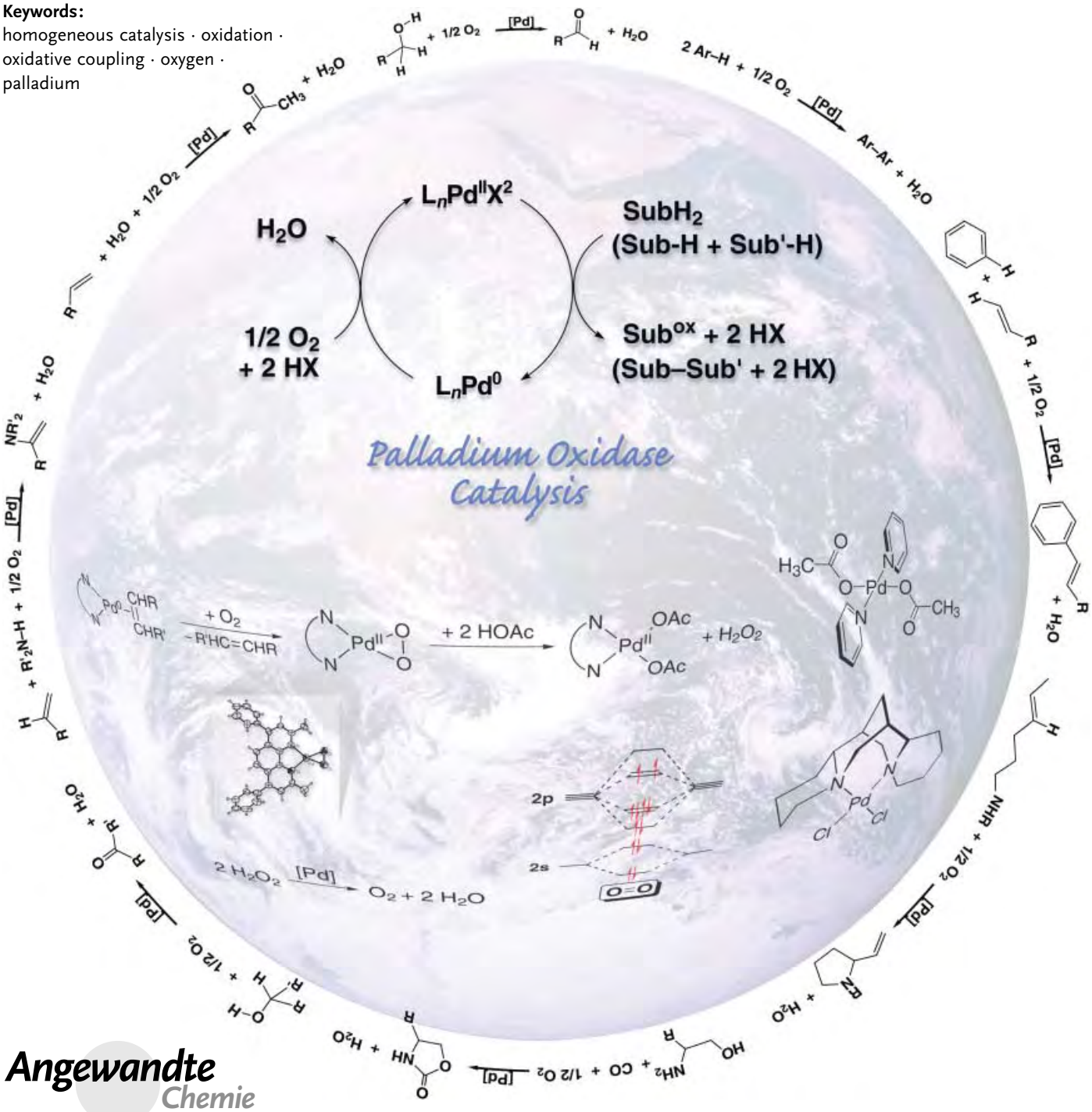
 © 2004 Wiley-VCH Verlag GmbH & Co. KGaA, Weinheim

Catalytic Oxidations

Palladium Oxidase Catalysis: Selective Oxidation of Organic Chemicals by Direct Dioxygen-Coupled Turnover

*Shannon S. Stahl**

Keywords:
homogeneous catalysis · oxidation · oxidative coupling · oxygen · palladium



 © 2004 Wiley-VCH Verlag GmbH & Co. KGaA, Weinheim DOI: 10.1002/anie.200300630

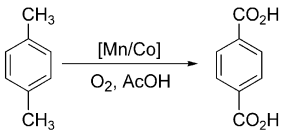
Selective aerobic oxidation of organic molecules is a fundamental and practical challenge in modern chemistry. Effective solutions to this problem must overcome the intrinsic reactivity and selectivity challenges posed by the chemistry of molecular oxygen, and they must find application in diverse classes of oxidation reactions. Palladium oxidase catalysis combines the versatility of Pd^{II}-mediated oxidation of organic substrates with dioxygen-coupled oxidation of the reduced palladium catalyst to enable a broad range of selective aerobic oxidation reactions. Recent developments revealed that cocatalysts (e.g. Cu^{II}, polyoxometalates, and benzoquinone) are not essential for efficient oxidation of Pd^{0} by molecular oxygen. Oxidatively stable ligands play an important role in these reactions by minimizing catalyst decomposition, promoting the direct reaction between palladium and dioxygen, modulating organic substrate reactivity and permitting asymmetric catalysis.

From the Contents

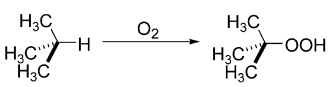
1. Introduction 3401
2. Palladium Oxidases: Reactions and Catalyst Systems 3403
3. Mechanistic Aspects of Catalyst Oxidation by Molecular Oxygen 3404
4. Alcohol Oxidation 3405
5. Oxidation of Alkenes 3408
6. Oxidative C–C Coupling Reactions with Non-Alkene Substrates 3413
7. Synthesis of Hydrogen Peroxide 3414
8. Miscellaneous Palladium Oxidase Reactions 3414
9. Summary and Outlook 3416

1. Introduction

Petroleum feedstocks serve as the primary source (>90%) of the world's industrial organic chemicals, ranging from pharmaceuticals and agrochemicals to large-scale commodity products.[1] Petroleum primarily consists of reduced hydrocarbons, and their selective oxidation chemistry remains one of the foremost challenges in the chemical industry. This challenge has increased in recent decades with the recognition that many of the best selective oxidants, for example, chlorine and transition-metal oxides, produce environmentally hazardous by-products. The economic and environmental advantages of molecular oxygen as a chemical oxidant are readily apparent; however, uncatalyzed reactions between dioxygen and organic substrates generally result in combustion. Aerobic oxidation reactions in industry often proceed by radical autoxidation, but these methods are inherently limited to substrates that undergo selective radical chemistry, such as autoxidation of tertiary or benzylic C–H bonds [Eq. (1,2)]. Consequently, widespread use of molecular oxygen in chemical synthesis will require the development of general catalytic strategies that are compatible with broad classes of substrates and oxidative transformations.



(1)



(2)

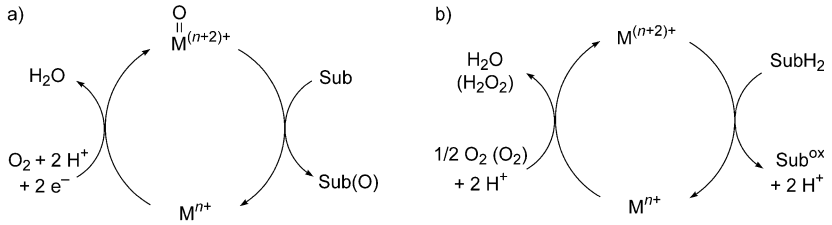
Metalloenzymes that catalyze selective aerobic oxidation reactions provide an important framework for the design of new catalysts, and the contributions of numerous groups within the biological and chemical communities have provided much insight into the activation and use of molecular oxygen in selective oxidation. Two distinct classes of such enzymes have been characterized, oxygenases and oxidases, which differ with respect to the fate of the oxygen atoms from dioxygen (Scheme 1). Oxygenases effect oxygen-atom transfer from dioxygen to the substrate (Scheme 1a), whereas oxidases simply use molecular oxygen as an electron/proton acceptor in substrate oxidation. In the latter case, the oxygen atoms are released as water or hydrogen peroxide (Scheme 1b). This mechanistic distinction has important implications for the development of new aerobic oxidation methods.

Atom-transfer oxidation reactions, that is, oxygenase mimics, are well-known and are among the most successful methods in asymmetric catalysis.[2] Molecular oxygen is seldom used in these reactions.[3] Instead, various dioxygen surrogates are used, typically two-electron oxidants such as iodosylbenzene, amine *N*-oxides, alkyl and acyl peroxides, and hydrogen peroxide.

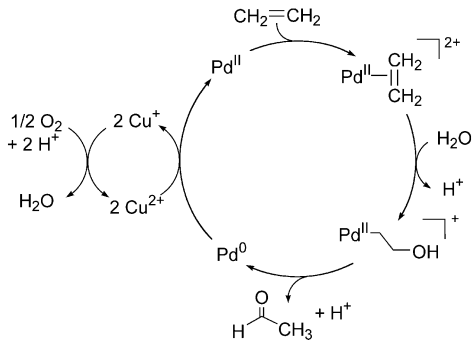
"Chemical oxidase" methods represent an attractive alternative strategy for the development of new aerobic oxidation methods, in part because many desirable oxidation reactions, such as alcohol oxidation, olefin aziridination, and alkane dehydrogenation, do not involve oxygen-atom transfer. Indeed, the oxidase strategy formally permits any

[*] Prof. S. S. Stahl
Department of Chemistry, University of Wisconsin-Madison
1101 University Avenue, Madison, WI 53706 (USA)
Fax: (+1) 608-262-6143
E-mail: stahl@chem.wisc.edu

 DOI: 10.1002/anie.200300630 © 2004 Wiley-VCH Verlag GmbH & Co. KGaA, Weinheim



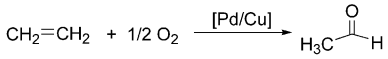
Scheme 1. Simplified catalytic cycles of metalloenzyme-catalyzed aerobic oxidation. In the *oxygenase* pathway (a), the substrate oxidation involves oxygen-atom transfer from molecular oxygen, often via a high-valent metal–oxygen intermediate. The *oxidase* pathway (b) simply utilizes molecular oxygen as a two-electron/two-proton acceptor in the oxidation of the substrate; no oxygen-atom transfer to the substrate occurs.



Scheme 2. Catalytic mechanism for the Wacker process.

oxidation reaction to be coupled to dioxygen reduction, provided that the catalyst can mediate both key steps in the catalytic cycle: 1) selective oxidation of the organic substrate by the oxidized catalyst and 2) efficient dioxygen-coupled reoxidation of the reduced catalyst (Scheme 1b).

Several palladium-catalyzed transformations fit this reactivity pattern, most notably the Wacker process [Eq. (3)],



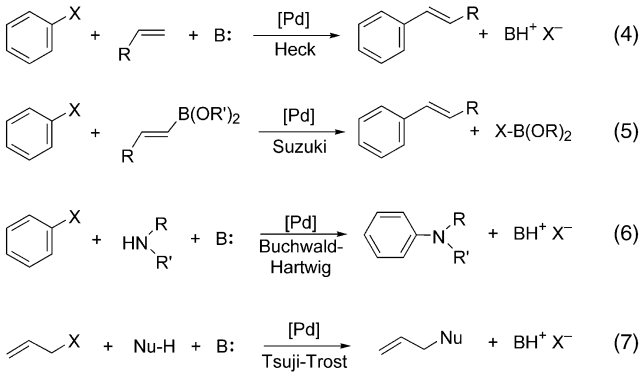
(3)

which has been used in industry for more than 40 years.[4] Although the stoichiometry of this reaction appears to reflect oxygen-atom transfer, water supplies the oxygen atom in the acetaldehyde product and dioxygen simply regenerates the palladium(II) catalyst through the intermediacy of a copper cocatalyst (Scheme 2). Despite this well-established precedent, the diversity of palladium-catalyzed oxidation reactions that undergo efficient dioxygen-coupled turnover has been relatively limited.

Palladium is perhaps the most active and versatile transition metal employed in organic synthesis, catalyzing both oxidative and nonoxidative transformations.[5,6] Prominent examples include the Wacker process [Eq. (3), oxidative] and numerous cross-coupling reactions between nucleophilic and electrophilic partners [Eqs. (4)–(7), nonoxidative].[7] The latter nonoxidative catalytic transformations are among the most efficient carbon–carbon and carbon–heteroatom bond-forming reactions in organic chemistry. The



Shannon Stahl obtained his BS degree in chemistry from the University of Illinois at Urbana-Champaign (1992) and his PhD at the California Institute of Technology (1997) with Prof. John Bercaw, where his thesis work focused on mechanistic organometallic chemistry. Subsequently, he conducted postdoctoral research in bioinorganic enzymology with Prof. Stephen Lippard at the Massachusetts Institute of Technology (NSF Postdoctoral Fellowship, 1997–1999). In 1999, he joined the faculty at the University of Wisconsin-Madison. His research is focused on metal-catalyzed reactions for organic chemistry.

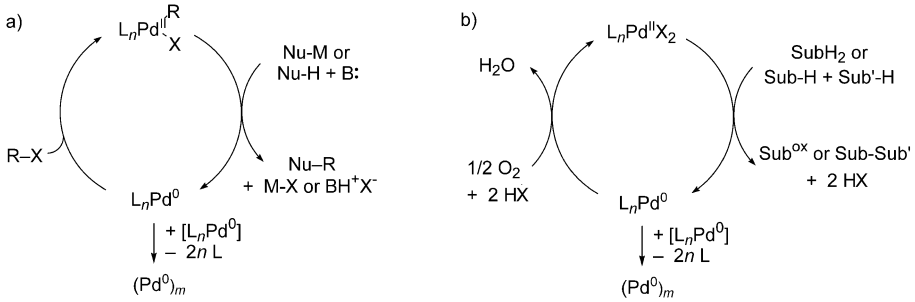


reduced attention to oxidation reactions possibly reflects the added complexity that arises from the need for a stoichiometric oxidant to regenerate the active catalyst. In most palladium-catalyzed oxidation reactions, stoichiometric oxidants such as copper(II) salts, benzoquinone, and alkyl hydroperoxides must be used because molecular oxygen is not an effective oxidant.

A persistent problem in both oxidative and nonoxidative palladium catalysis is decomposition of the homogeneous catalysts into inactive bulk metal (Scheme 3). The dramatic success of palladium-catalyzed cross-coupling reactions reflects, in part, the utility of phosphanes and other soft donor ligands to stabilize palladium(0). These ligands also serve to promote reactions between palladium(0) and substrates, such as the oxidative addition of an aryl halide (Scheme 3a). Dramatic ligand effects have been observed, and certain palladium/ligand combinations allow more than 1 000 000 catalytic turnovers.[7c] Unfortunately, similar success has not been achieved in oxidation catalysis. Most common ligands decompose rapidly under oxidizing reaction conditions, and therefore palladium oxidation chemistry has been dominated by the use of simple palladium salts and their solvates such as palladium acetate, palladium chloride, and $[(CH_3CN)_2PdCl_2]$.[5]

This Review surveys the development of homogeneous palladium-catalyzed oxidation reactions that undergo direct dioxygen-coupled catalytic turnover without a redox-active cocatalyst. These results promise a significant increase in the scope of aerobic oxidation reactions. In many of these reactions, the identification of oxidatively stable organic

 © 2004 Wiley-VCH Verlag GmbH & Co. KGaA, Weinheim



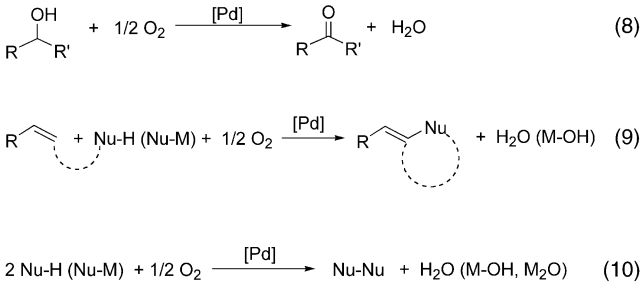
Scheme 3. Simplified catalytic cycles of palladium-catalyzed cross-coupling (a) and oxidation (b) reactions.

ligands plays an important role in the reaction success. Palladium-mediated oxidation reactions that use stoichiometric palladium, palladium(II)/cocatalyst systems, palladium colloids, and heterogeneous catalysts will be cited in certain cases, but numerous excellent monographs and reviews of these topics are available elsewhere.[4b,5,6,8,9]

2. Palladium Oxidases: Reactions and Catalyst Systems

Direct dioxygen-coupled turnover significantly enhances the appeal of palladium-catalyzed oxidation reactions by lowering cost, increasing net atom efficiency, facilitating product isolation, and, in many cases, improving reaction selectivity. During the past 10 years, the scope of these reactions has expanded considerably. The most prominent reaction classes developed to date consist of alcohol oxidation, that is, dehydrogenation [Eq. (8)], and oxidative couplings between substrates such as alkenes and various carbon and heteroatom nucleophiles [Eq. (9,10)].

Both intra- and intermolecular examples of oxidative coupling reactions have been described, and a broad range of nucleophiles have been used, including alcohols, amides, aryl boronic acids, aryl tin reagents, and even unactivated aryl C–H bonds. Oxidative coupling reactions are attractive because, in many cases, they enable the use of less-functionalized (and therefore less expensive and more readily available) substrates relative to nonoxidative cross-coupling reactions, for example, alkenes and arenes versus alkenyl and aryl halides. These reactions may also display complementary reactivity and selectivity patterns based on switching the electronic character of the substrate (i.e., from an electrophile to a nucleophile). Although oxidation reactions of this type were recognized quite early,[10] the requirement for stoichiometric palladium(II) or cooxidants significantly limited their development relative to the corresponding cross-coupling reactions.



During the past 10 years, numerous effective palladium catalyst systems have been developed for aerobic oxidation reactions (Table 1). These catalysts, which require no redox-active cocatalyst, range from simple palladium salts dissolved in an appropriate polar, coordinating solvent to more recently

Table 1: Representative palladium oxidase catalyst systems.

Entry	Catalysts	Oxidations	References
1[a]	$Pd(OAc)_2$/DMSO ± anionic bases	alcohol oxidation (allylic and benzylic)	[32]
		intramolecular hetero- and carbocyclization of alkenes	[33, 35–37]
		dehydrosilylation of silyl enol ethers (Saegusa Oxidation)	[34]
		oxidative C–C bond cleavage of tertiary alcohols	[95]
2	$Pd(OAc)_2$/pyridine	alcohol oxidation (primary, secondary, allylic and benzylic)	[24]
		intramolecular hetero- and carbocyclization of alkenes	[41, 49, 76]
		intermolecular O–C and C–C coupling reactions with alkenes	[56, 96]
		oxidative C–C bond cleavage of tertiary alcohols	[94–96]
3	$Pd(OAc)_2/NEt_3$	alcohol oxidation (primary, secondary, and benzylic)	[53a]
		intermolecular oxidative amination of alkenes	[60]
4[b]	$[LPd(OAc)_2]$ (biphasic solvents)	synthesis of hydrogen peroxide coupled to alcohol (primary, secondary, and benzylic) or carbon monoxide oxidation	[19]
5[c]	$[LPd(OAc)_2]$, NaOAc (aqueous)	alcohol oxidation (primary, secondary, allylic, and benzylic)	[23]
		intermolecular oxygenation of alkenes	[22]
6[d]	PdX_2/(−)-sparteine	alcohol oxidation (secondary, benzylic, allylic)	[49, 50]
		intramolecular heterocyclization of alkenes	[49c]

[a] DMSO = dimethyl sulfoxide. [b] L = bathocuproine (2,9-dimethyl-4,7-diphenyl-1,10-phenanthroline) (see Scheme 4). [c] L = phenS* = bathophenanthroline disulfonate (4,7-diaryl-1,10-phenanthroline; aryl = $C_6H_4SO_3^-$; see also structure **5** in Section 4.4). [d] X = Cl, OAc, O_2CCF_3.

 © 2004 Wiley-VCH Verlag GmbH & Co. KGaA, Weinheim

developed, well-defined palladium–ligand complexes. Nitrogen-based ligands represent a common theme among the latter catalysts (Table 1, entries 2–6), but phosphane- and NHC-ligated (NHC = N-heterocyclic carbene) complexes have also been reported (see Sections 4.1, 4.6, 6, and 7). Many of these catalyst systems promote several different oxidative transformations, displaying versatility reminiscent of palladium cross-coupling catalysts. In addition to the homogeneous mononuclear catalysts described herein, palladium clusters, colloids, and heterogeneous catalysts have also been shown to undergo direct dioxygen-coupled turnover, in most cases to catalyze alcohol oxidation.[9]

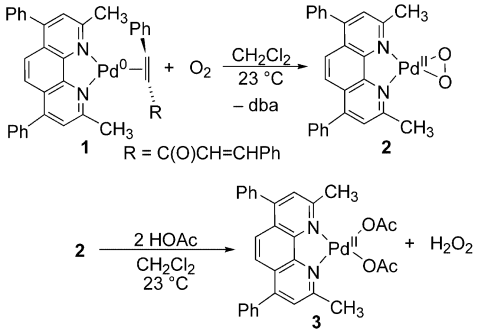
3. Mechanistic Aspects of Catalyst Oxidation by Molecular Oxygen

Efficient reoxidation of the catalyst is critical for the success of palladium-catalyzed oxidation reactions. Under many conditions, molecular oxygen is thermodynamically capable of oxidizing reduced palladium. However, in the absence of cocatalysts, direct aerobic oxidation of palladium often cannot compete kinetically with aggregation of the catalyst into inactive bulk metal (see Scheme 3b). In several early studies, this problem was addressed by conducting the reaction at elevated oxygen pressures (20–50 atm);[11] however, these conditions render the reaction operationally less appealing and unsafe owing to explosion hazards.[11c]

Direct reaction between palladium(0) and molecular oxygen was first observed by Wilke and co-workers in 1967 in the preparation of $[(Ph_3P)_2Pd(\eta^2\text{-}O_2)]$ from $[(Ph_3P)_4Pd]$ under an aerobic atmosphere in benzene.[12] Solutions of the η^2-peroxo complex form triphenylphosphane oxide over time. Additional peroxopalladium(II) complexes stabilized by soft phosphane or isonitrile ligands were reported shortly thereafter.[13] At the time of these reports, research attention was focused on the reactivity of the peroxo ligand with substrates in oxygen-atom-transfer reactions. Although some atom-transfer reactivity was observed,[12,14] these adducts proved to be nearly inert toward broad classes of important substrates, such as olefins and sulfides. Unlike their early-transition-metal counterparts, these peroxo complexes exhibit *nucleophilic* character, and their chemistry is dominated by reactions with electrophiles, including SO_2, CO_2, and Brønsted acids.[14]

In these early reactivity studies of peroxopalladium(II) complexes, no attention was paid to the characterization of the reaction between palladium(0) and molecular oxygen. Recently, Stahl and co-workers prepared a bathocuproine (bc)-coordinated palladium(0) complex (Scheme 4; cf. Table 1, entry 4) to investigate mechanistic features of its aerobic oxidation to palladium(II).[15] The dibenzylideneacetone adduct of $[(bc)Pd^0]$, **1**, reacts readily with molecular oxygen at room temperature to produce an η^2-peroxopalladium complex, **2**, formally oxidizing the palladium by two electrons. The reaction proceeds through an associative substitution mechanism, analogous to alkene-exchange reactions at palladium(0).[16] This pathway contrasts other oxidative addition reactions (e.g., aryl halides) that proceed through dissociative pathways.[17] Further studies will be necessary to address the mechanistic role of the electronic spin state on the reaction between singlet d^{10} palladium(0) and triplet molecular oxygen.

Palladium(II)-mediated oxidation of substrates such as alcohols formally reduces the metal by two electrons and releases two protons into solution. With $Pd(OAc)_2$ as the catalyst, these proton equivalents will be present in the form of acetic acid (Scheme 3b). Indeed, $[(bc)PdO_2]$ undergoes rapid protonolysis in the presence of 2 equivalents of acetic acid to generate $[(bc)Pd(OAc)_2]$ (**3**) and hydrogen peroxide (Scheme 4).[15,18] As noted by Muzart,[8g] the proton source



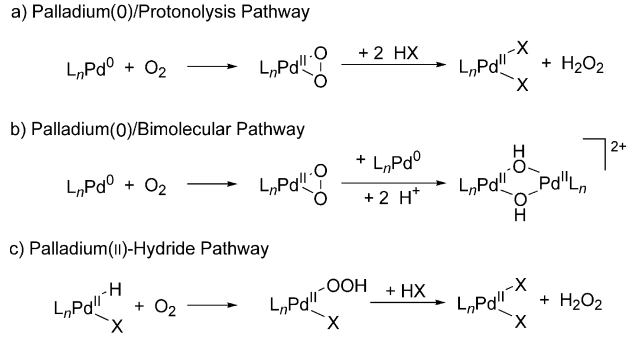
Scheme 4. Aerobic oxidation sequence characterized for the conversion of bathocuproine-coordinated palladium(0) into palladium(II) (dba = dibenzylideneacetone).

may change depending on the catalytic reaction conditions. When the reaction is conducted in the presence of base, the substrate itself (e.g., ROH) may supply the proton equivalents.

The absolute rates of the reactions in Scheme 4 indicate that this sequence is kinetically competent to operate in the palladium oxidase reactions reported by Bianchi, Bortolo, and co-workers at Enichem,[19] who used a bathocuproine-coordinated palladium catalyst for the production of hydrogen peroxide under biphasic conditions.[20] Hydrogen peroxide is not detected in other palladium oxidase reactions, suggesting that either an alternative catalyst oxidation sequence is operating or that hydrogen peroxide reacts further under catalytic conditions. These considerations will be addressed in Section 4.2.

Two other mechanisms have been proposed for catalyst oxidation by molecular oxygen (Scheme 5), and despite the evidence described above supporting path a, data from catalytic reactions often cannot exclude the other proposals. Path b parallels the well-characterized aerobic oxidation reactions of isoelectronic copper(I) complexes[21] whereby the initial dioxygen adduct reacts with another reduced metal species to yield 2 equivalents of oxidized catalyst. This mechanism, which was proposed based on kinetic data supporting a binuclear resting state during the catalytic reaction,[22b,23a] does not accommodate reactions that yield hydrogen peroxide. According to path c, palladium hydride intermediates, which arise during the oxidation of organic substrates, could react directly with molecular oxygen through insertion into the Pd–H bond to produce hydro-

 © 2004 Wiley-VCH Verlag GmbH & Co. KGaA, Weinheim



Scheme 5. Mechanistic proposals for aerobic catalyst oxidation in direct dioxygen-coupled palladium oxidation reactions.

peroxopalladium(II) species.[8c,24b] No direct evidence for this pathway exists, but similar reactivity has been reported for other late-transition-metal hydrides, including cobalt, rhodium, iridium, and platinum.[25] Subsequent protonolysis of the hydroperoxide releases hydrogen peroxide in a manner analogous to path a. If path c is correct, palladium remains in the +2 oxidation state throughout the catalytic cycle, and the use of relatively hard nitrogen donor ligands might favor this pathway by stabilizing the higher oxidation state. Further work will be needed to exclude or support these proposed mechanisms and to determine if one mechanism is universal to all systems.

4. Alcohol Oxidation

The conversion of alcohols into carbonyl compounds is an important transformation for laboratory and industrial chemistry, and catalytic methods for aerobic oxidation have received considerable attention.[23c,26] Homogeneous palladium catalysts are particularly effective for the oxidation of alcohols [Eq. (8)], and the overall reaction conforms to a two-stage palladium oxidase cycle outlined in Scheme 3b ($SubH_2 = RR'CHOH$, $Sub^{ox} = RR'CO$). The sections below highlight synthetic and mechanistic advances in direct dioxygen-coupled methods for the palladium-catalyzed oxidation of alcohols. A survey of various homogeneous and heterogeneous palladium-catalyzed alcohol oxidation reactions (not limited to aerobic conditions), including a discussion of the scope and limitations of the various methods, was published recently.[8g]

4.1. Early Developments

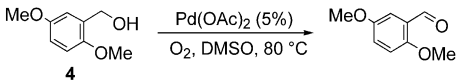
Stoichiometric alcohol oxidation by palladium(II) can be traced to the work of Berzelius in 1828,[27] but nearly 140 years elapsed before efficient dioxygen-coupled catalytic turnover was achieved by employing catalyst mixtures of palladium and copper salts in neat alcohol as the solvent and substrate.[28] In 1977, Blackburn and Schwartz reported the first example of palladium-catalyzed alcohol oxidation that underwent dioxygen-coupled turnover in the absence of a cocatalyst.[29] The aerobic oxidation of secondary alcohols proceeds with a $PdCl_2$(1%)/NaOAc(5%) catalyst mixture in ethylene carbonate at ambient temperatures and 1 atm of oxygen pressure. The rate of these relatively slow reactions, 1–2 turnovers h^{-1} ($TO\,h^{-1}$), is independent of oxygen pressure; however, palladium metal precipitation can be avoided if the reaction is conducted at 3 atm of oxygen pressure.

Over the next 20 years, relatively little work in this area was reported.[30,31] In the course of studying allylic alkylation reactions, Echavarren and co-workers discovered that $[Pd(dba)_2]$(10%)/PPh_3(30%) catalyzes the oxidation of allylic alcohols in toluene under an air atmosphere. Modest yields were generally obtained (38–56%, 90% for cinnamyl alcohol).[30] Later, Muzart and co-workers reported the $PdCl_2$-catalyzed oxidation of indanol (51% yield) in refluxing hexane under an air atmosphere[31] with the phase-transfer catalyst andogen 464 (10%) and Na_2CO_3 (2 equiv).

4.2. The $Pd(OAc)_2$/DMSO Catalyst System

The past five years have seen numerous significant advances in the development and understanding of palladium-catalyzed aerobic alcohol oxidation. The first significant breakthrough was reported by Peterson and Larock, who employed the $Pd(OAc)_2$(5%)/DMSO(solvent) (Table 1, entry 1) catalyst system for the oxidation of a wide range of benzylic and allylic alcohols with molecular oxygen (1 atm) as the sole oxidant.[32] The reactions are relatively slow ($\leq 1\,TO\,h^{-1}$), but the corresponding carbonyl compounds are produced in moderate to excellent yields (42–95%). Other palladium sources ($PdCl_2$, $Pd(OCCF_3)_2$, $[Pd(dba)_2]$) were significantly less effective than $Pd(OAc)_2$, and different solvents (CH_3CN, DMSO/H_2O mixture) also led to lower yields. Anionic bases such as $NaHCO_3$ and K_2CO_3 (2 equiv) significantly enhance the reaction rate and product yield for secondary alcohol substrates.

The $Pd(OAc)_2$/DMSO catalyst system was developed independently by the groups of Larock and Hiemstra for the aerobic oxidative heterocyclization of alkene substrates, and similar conditions have been employed for a variety of other substrate oxidations (see Section 5.3).[33–37] Despite this broad synthetic utility, little was known about the catalytic mechanism until Stahl and co-workers recently reported a mechanistic study of the aerobic oxidation of benzylic alcohol **4** [Eq. (11)].[38] Kinetic studies indicate that oxidation of



4 (11)

palladium(0) is the turnover-limiting step. The presence of a palladium(0) resting state is detrimental to catalyst stability because decomposition of the catalyst into bulk metal (rate $\propto [Pd^0]^2$) is more sensitive to the steady-state palladium(0) concentration than is the catalyst reoxidation (rate $\propto [Pd^0]$) (see Scheme 3).

No hydrogen peroxide is detected in this reaction, and manometry studies indicate that 1 equivalent of oxygen yields 2 equivalents of product. Although these results may suggest

 © 2004 Wiley-VCH Verlag GmbH & Co. KGaA, Weinheim

a palladium(0) oxidation mechanism in which no hydrogen peroxide is produced (path b, Scheme 5), control experiments reveal that hydrogen peroxide undergoes rapid disproportionation under catalytic conditions [Eq. (12)]. This result also

$$H_2O_2 \xrightarrow{[Pd]} H_2O + 1/2\ O_2 \qquad (12)$$

indicates that hydrogen peroxide, a stronger oxidant than molecular oxygen, is not kinetically competent to serve as an oxidant during catalysis.

Further control experiments reveal that DMSO does not undergo redox chemistry during the reaction, and therefore, the favorable characteristics of DMSO as the solvent appear to reflect its metal-coordinating ability. Both sulfur- and oxygen-bound DMSO-palladium complexes have been characterized.[39] The relatively soft coordination sphere provided by sulfur donation may explain, in part, why $Pd(OAc)_2$ in DMSO is currently the only catalyst system among this class of reactions (Table 1) for which aerobic oxidation of the catalyst is turnover-limiting.

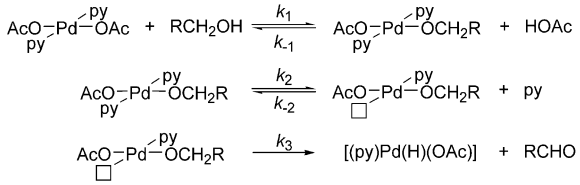
4.3. The $Pd(OAc)_2$/Pyridine Catalyst System

Nearly concurrent with the report of the $Pd(OAc)_2$/DMSO system,[32] Uemura and co-workers reported what remains one of the most versatile and operationally simple catalyst systems for the aerobic oxidation of alcohols: $Pd(OAc)_2$(5%)/pyridine(20%)/MS3A (MS3A = 3-Å molecular sieves) in toluene (80°C) (Table 1, entry 2).[24] All major classes of alcohols (primary, secondary, benzylic, and allylic) are oxidized under these conditions, generally in good-to-excellent yields (80–100%). Substrates bearing alkene functionality, especially allylic alcohols, require the use of excess pyridine (500 mol%) to prevent palladium metal precipitation, which may be accelerated by complexation of the alkene to palladium. Several alcohol-protecting groups are compatible with the reaction conditions, including tetrahydropyranyl, *tert*-butyldimethylsilyl, and benzyl ethers. Alcohols bearing vicinal heteroatom functionality (amines, ethers) appear to be ineffective substrates, possibly reflecting substrate chelation.

Other palladium sources, including $PdCl_2$, $[(CH_3CN)_2PdCl_2]$, $Pd(O_2CCF_3)_2$, $[Pd(dba)_2]$, and $[Pd(PPh_3)_4]$, proved to be ineffective in these reactions. Seven different pyridine derivatives were investigated, but none performed better than pyridine itself. Notably, use of the chelating ligand 2,2′-bipyridine significantly inhibited the reaction. The origin of the beneficial effect of molecular sieves in these reactions is not fully understood, but the authors proposed that they serve to facilitate disproportionation of hydrogen peroxide, which if present may inhibit palladium alkoxide formation.[40]

In conjunction with the application of this catalyst system to other palladium oxidase reactions (see Section 5.3),[41] Steinhoff and Stahl reported a mechanistic study of $Pd(OAc)_2$/pyridine-catalyzed aerobic oxidation of benzyl alcohol.[42] In contrast to the $Pd(OAc)_2$/DMSO reaction, but similar to the other palladium catalyst systems that employ nitrogen ligands (see Table 1), this catalytic reaction features a palladium(II) resting state with turnover-limiting oxidation of the alcohol substrate. This observation, together with the 10–100-fold higher turnover rates relative to the $Pd(OAc)_2$/DMSO system, implies that pyridine significantly enhances the rate of palladium(0) oxidation by molecular oxygen. The alternative proposal by Uemura and co-workers, that palladium remains in the +2 oxidation state throughout the catalytic cycle (path c, Scheme 5), presently cannot be excluded.[24b]

The role of pyridine is not entirely favorable. Kinetic studies indicate that $[(py)_2Pd(OAc)_2]$ reacts with the alcohol in a preequilibrium step to produce the palladium(II) alkoxide (k_1, Scheme 6). Coordinated acetate serves as an internal base

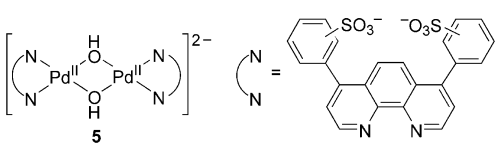


Scheme 6. Mechanistic sequence for palladium(II)-mediated alcohol oxidation by the $[(py)_2Pd(OAc)_2]$ catalyst system.

in this step. Subsequently, one of the two pyridine ligands must dissociate (k_2) prior to rate-limiting β-hydride elimination of the alkoxide ligand (k_3). The maximum initial rates in this reaction are observed with the addition of only 1 equivalent of pyridine relative to palladium,[42] explaining why bidentate ligands strongly inhibit the reaction under these conditions.[24b] At low pyridine concentrations (pyridine/palladium < 2:1), catalyst precipitation is observed during the course of the reaction. Thus, even under conditions in which substrate oxidation is turnover-limiting, the competition of catalyst oxidation versus decomposition (Scheme 3b) is critical to the success of the reaction. The reported use of 20 mol% pyridine in synthetic reactions[24b] represents a balance between optimizing the turnover rates and catalyst stability.

4.4. The $Pd(OAc)_2$/Bathophenanthroline Disulfonate (PhenS*) Catalyst System

In 2000, Sheldon and co-workers reported the first example of direct dioxygen-coupled alcohol oxidation in aqueous solution.[23a] This advance offers potential advantages with respect to product isolation and should be considerably safer under aerobic reaction conditions. The optimized (pre-) catalyst is $[(PhenS^*)Pd(OAc)_2]$ (Table 1, entry 5). Upon dissolution in water, this complex forms the dimer **5**, which



5

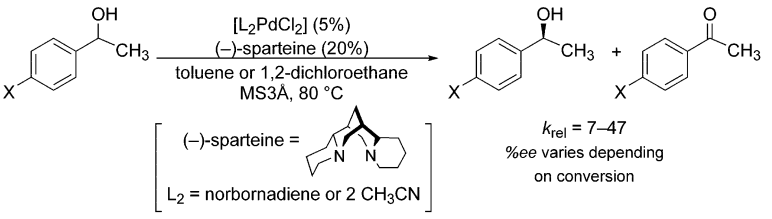
 © 2004 Wiley-VCH Verlag GmbH & Co. KGaA, Weinheim

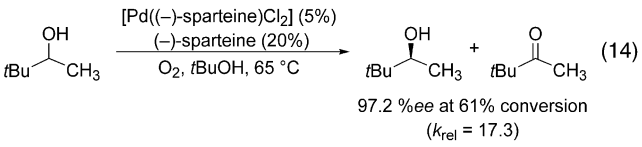
is the resting state during catalysis. The reaction conditions are: catalyst (0.2–0.5 mol%), NaOAc (10%), 30 bar air pressure, 100 °C. The advantages of operating in aqueous solution are partially offset by the requirement for elevated pressures and the limited water solubility of many organic substrates, but overall the reactions are remarkably effective. Catalytic rates (up to 100 TO h^{-1}) and turnover numbers (200–400) are significantly higher than those reported for previous catalyst systems.

As with the $Pd(OAc)_2$/pyridine system, all general classes of alcohol substrates are oxidized under these conditions, and aliphatic alcohols generally undergo more rapid turnover than the less-electron-rich benzylic and allylic alcohols.[23c,d] Aliphatic primary alcohols are converted into carboxylic acids under the reaction conditions, but in the presence of 2% 2,2,6,6-tetramethylpiperidinyl-1-oxy (TEMPO) (4 equiv relative to palladium), the reaction can be stopped after oxidation into the aldehyde. Amine, sulfide, and polyether functionalities present in the alcohol substrate appear to inhibit turnover by coordination to palladium. Studies of substrate and catalyst electronic effects together with kinetic investigations clearly support turnover-limiting substrate oxidation by palladium(II). The beneficial effect of sodium acetate can be traced to its promotion of dioxygen-coupled oxidation of the catalyst. The use of non-coordinating anions, such as perchlorate, tetrafluoroborate, or triflate, result in rapid palladium black deposition.[23c] Similar beneficial effects of anionic ligands have been observed in the oxidative addition of aryl halides to palladium(0).[43]

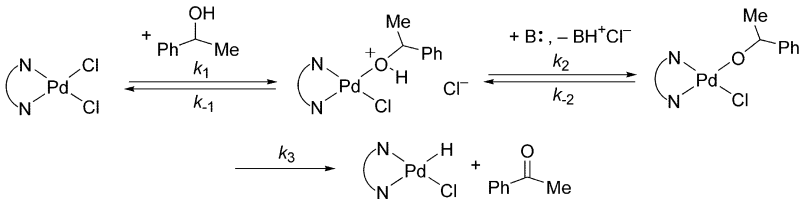
4.5. The $PdCl_2$/(−)-Sparteine Catalyst System

The catalyst systems outlined above highlight the ability of organic ligands to promote dioxygen-coupled catalytic turnover and introduce the possibility of asymmetric catalysis. Relatively few enantioselective palladium-catalyzed oxidation reactions have been reported,[44,45b–e,46–51] and until recently, molecular oxygen was seldom used as the stoichiometric oxidant.[45b–e,46,49,50,51] The recent development of aerobic oxidative kinetic resolution of secondary alcohols, reported independently by the groups of Sigman and Stoltz, represents a significant advance.[49a,50a] The catalyst consists of [((−)-sparteine)$PdCl_2$] (5%) together with excess (−)-sparteine (20%). The chiral palladium complex itself is inactive in the absence of exogenous ligand. This reaction is particularly effective for aryl-[49a,b,50a,50c] and *tert*-butyl-substituted[50d] ethanol derivatives ([Eq. (13,14)]; Table 1, entry 6). *tert*-Butanol appears to be a particularly effective solvent[50d] or additive[49b] in these reactions.





Mechanistic studies by Sigman and co-workers determined that the excess (−)-sparteine serves as an exogenous base to promote the formation of the palladium alkoxide intermediate, which undergoes subsequent β-hydride elimination to yield the ketone product (Scheme 7).[50b,e] The chirality of both the catalyst and the base influences the reaction stereoselectivity, and changes in (−)-sparteine concentration affect the stereoselectivity of the reaction by altering the identity of the rate-limiting step in the reaction. At low concentrations of (−)-sparteine, relatively little discrimination between the enantiomeric alcohols ($k_{rel} = 7.6$) reflects rate-limiting deprotonation of the coordinated alcohol (k_2, Scheme 7). At high concentrations of (−)-sparteine, rate-limiting β-hydride elimination (k_3) yields significantly higher selectivities ($k_{rel} = 25$). Kinetic resolution can even be achieved with achiral palladium catalysts if (−)-sparteine is present as a chiral exogenous base.[50c] Selectivities are somewhat lower than with the chiral catalyst/chiral base combination, but this strategy represents an important consideration for the future development of asymmetric reactions. Alternatively, achiral exogenous bases can also be used in combination with the chiral catalyst. For example, anionic bases such as Cs_2CO_3[49b,50f] significantly enhance reaction rates, while maintaining good stereoselectivities.



Scheme 7. Mechanistic sequence for palladium(II)-mediated alcohol oxidation by the [((−)-sparteine)$PdCl_2$] catalyst system.

Limited access to the (+)-sparteine isomer presently limits the generality of this methodology. However, a readily accessible (+)-sparteine analogue was synthesized recently, and moderate selectivities were obtained in the oxidative kinetic resolution reaction.[51] The development of new chiral ligands for palladium-catalyzed aerobic oxidation reactions represents an important target for future research.

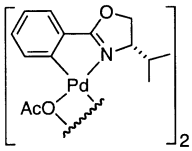
4.6. Additional Catalyst Systems for Aerobic Alcohol Oxidation

Several new catalysts have been reported recently that continue to extend the scope and utility of direct-dioxygen-coupled alcohol oxidation. Hallman and

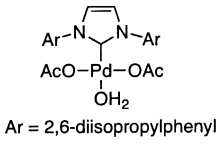
 © 2004 Wiley-VCH Verlag GmbH & Co. KGaA, Weinheim

Moberg demonstrated that cyclometallated catalyst **6** (5%), in combination with pyridine (20%), catalyzes the oxidation of *sec*-phenethyl alcohol and 1- and 2-octanol in toluene under an air atmosphere.[52] The oxidation of racemic *sec*-phenethyl alcohol displayed no significant resolution with this chiral catalyst.

Sigman and co-workers reported two significant advances in catalyst development.[53] First, $Pd(OAc)_2$(3%)/triethylamine(6%) is an effective alternative to the $Pd(OAc)_2$/pyridine catalyst system and allows alcohol oxidation reactions to be conducted at room temperature.[53a] Triethylamine is not fully coordinated at room temperature, and an equilibrium between free $Pd(OAc)_2$, $[(Et_3N)Pd(OAc)_2]$, and $[(Et_3N)_2Pd(OAc)_2]$ is observed by ^{1}H NMR spectroscopy, whereas 2 equivalents of pyridine are fully coordinated under the same conditions. The differences in coordination equilibria for the two ligands probably accounts for their different activities. Allylic alcohols represent challenging substrates, but primary and secondary aliphatic and benzylic alcohols are oxidized readily. Very recently, Sigman and co-workers reported an N-heterocyclic carbene coordinated catalyst **7** that successfully oxidizes alcohols at quite low catalyst loadings (0.1–0.5 mol%).[53b] The catalyst is most effective in the presence of catalytic quantities of acetic acid (2%). At slightly higher acetic acid concentrations (5%), the oxygen atmosphere can be replaced with air with only a slight increase in reaction times. A crystal structure of the precatalyst **7** reveals hydrogen-bonding interactions between the



6



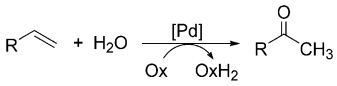
7

acetate and water ligands, supporting earlier hypotheses that acetate can serve as an internal base to facilitate the formation of a palladium alkoxide intermediate.[42,50b] Preliminary kinetic studies revealed that substrate oxidation, specifically β-hydride elimination, is the turnover-limiting step in the cycle.

Alternative reaction media, including ionic liquids[54] and fluorous biphasic systems,[24c] have also been investigated. Moreover, numerous heterogeneous catalysts have been developed that operate effectively with oxygen as the sole oxidant.[9] For certain applications, these catalyst systems offer practical advantages over the homogeneous systems described above.

5. Oxidation of Alkenes

The aerobic oxidation of alkenes is the earliest example of "palladium oxidase" catalysis. Stoichiometric palladium(II)-mediated conversion of ethylene into acetaldehyde was first observed in 1894,[55] but more than 60 years elapsed before researchers at Wacker-Chemie discovered that copper salts could be used in combination with $PdCl_2$ to achieve dioxygen-coupled turnover [Eq. (3)].[4a] The Wacker process has played a major role in the chemical industry for several decades. In synthetic organic chemistry, the most extensive application of this chemistry has been in the conversion of terminal alkenes into methyl ketones [Eq. (15)].[8b,d,f] In most cases, however,

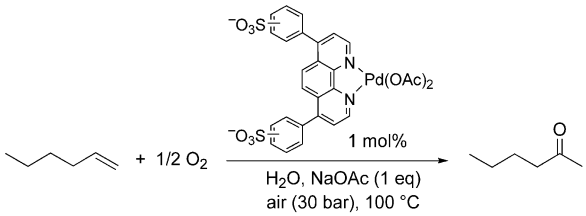


(15)

molecular oxygen is not used as the stoichiometric oxidant in these reactions. Similarly, the extension of this reactivity to the use of nucleophiles other than water has faced considerable difficulty. The sections below highlight recent progress in the development of efficient aerobic oxidative coupling reactions between alkenes and carbon and heteroatom nucleophiles. Both inter- and intramolecular reactions have been developed.

5.1. Intermolecular Oxidation of Alkenes: Carbon–Heteroatom Bond Formation

Sheldon and co-workers first developed their $Pd(OAc)_2$/PhenS* catalyst system (Table 1, entry 5) for the oxidation of terminal alkenes into methyl ketones in aqueous solution [Eq. (16)].[22] The reaction conditions avoid the use of

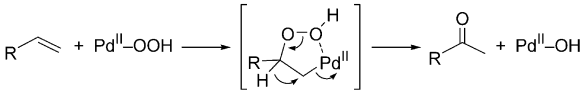


(16)

cocatalysts and high chloride concentrations that cause the traditional Wacker conditions to be highly corrosive. The mechanistic features are very similar to those described above for alcohol oxidation: substrate oxidation by palladium(II) is turnover-limiting, and kinetic studies are consistent with the same hydroxo-bridged palladium(II) dimer **5** as the catalyst resting state (see Section 4.4). Sodium acetate added to the reaction mixture helps to prevent palladium metal deposition. Although this system alleviates the need for chloride, substrate solubility for higher alkenes remains a challenge.

The $Pd(OAc)_2$/pyridine catalyst system is also successful for the conversion of terminal alkenes into methyl ketones.[56] In this case, the reactions are conducted in a solvent mixture of toluene and *n*-propanol. Water is not present at the start of these reactions, and the authors proposed an alternative mechanism in which a palladium hydroperoxide species undergoes oxygen-atom transfer to a coordinated alkene (Scheme 8). This mechanism reflects an "oxygenase" rather than "oxidase" mechanism and has been proposed in other palladium-catalyzed alkene oxidation reactions that employ

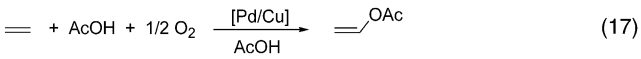
 © 2004 Wiley-VCH Verlag GmbH & Co. KGaA, Weinheim



Scheme 8. Oxygen-atom transfer pathway for methyl ketone formation from terminal alkenes.

alkyl peroxides or hydrogen peroxide as the oxidant.[57] In the aerobic reaction, the primary alcohol is required as a cosubstrate to reduce palladium(II) to palladium(0).

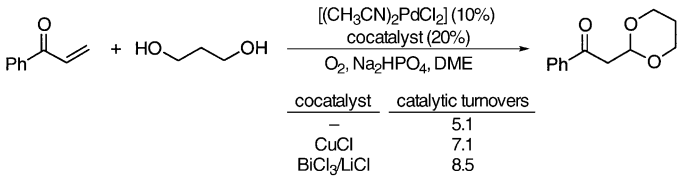
The use of nucleophiles other than water in palladium-catalyzed aerobic oxidation of alkenes has met with little success. The most successful examples are nucleophiles that also serve as the solvent, for example, acetic acid and primary alcohols [e.g., Eq. (17)].[4b,5] Reactions conducted with



(17)

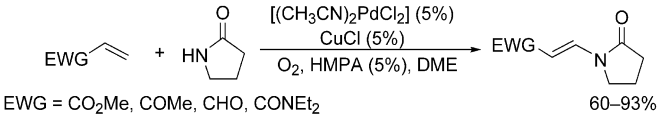
approximately equal amounts of the alkene and a carbon or heteroatom nucleophile generally require stoichiometric quantities of palladium or the secondary oxidant, often copper(II).

Hosokawa, Murahashi, and co-workers described a series of aerobic intermolecular oxy- and aminopalladation reactions with electron-deficient alkenes.[8c,58,59] The alcohols and amine-derived nucleophiles (amides and carbamates) attack the alkenes at the terminal position, resulting in a net oxidative conjugate addition [Eq. (18,19)] (HMPA = hexamethylphosphoramide, EWG = electron-withdrawing group).



cocatalyst	catalytic turnovers
–	5.1
CuCl	7.1
$BiCl_3$/LiCl	8.5

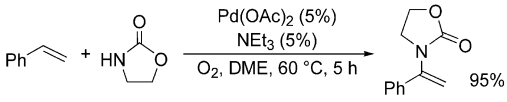
(18)



EWG = CO_2Me, COMe, CHO, $CONEt_2$ 60–93%

(19)

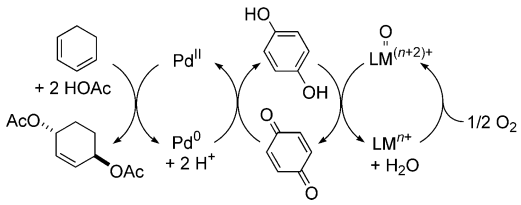
Stoichiometric or cocatalytic copper salts are typically required, but in a few cases, several turnovers can be achieved in the absence of a cocatalyst. More recently, Stahl and co-workers reported the intermolecular oxidative amination of styrene with various nitrogen nucleophiles, including pyrrolidinone, oxazolidinone, phthalimide, and *p*-toluenesulfonamide.[60] In these reactions, the regioselectivity of addition to styrene is subject to catalyst control; $[(CH_3CN)_2PdCl_2]$ promotes anti-Markovnikov addition, but $[(NEt_3)_2PdCl_2]$ leads to the Markovnikov product. In most of the reactions, a catalytic quantity of $CuCl_2$ (5%) was used, but a copper-free catalyst system was also discovered (5% $Pd(OAc)_2$/5% NEt_3) that affords Markovnikov oxidative amination in nearly quantitative yield [Eq. (20)]. The mechanistic origin of this regiocontrol continues to be studied, but the results suggest an



(20)

important role for a Brønsted base in the mechanism. These reactions provide important leads for the ongoing development of efficient aerobic oxidative coupling of alkenes and heteroatom nucleophiles.

Bäckvall and co-workers have conducted extensive studies of palladium(II)-mediated oxidative 1,4-addition of nucleophiles to conjugated dienes. Benzoquinone is the most common stoichiometric oxidant in these reactions, but they have also developed multistep coupled catalytic systems that utilize molecular oxygen as the terminal oxidant (Scheme 9).[61] A similar cocatalytic strategy provides access



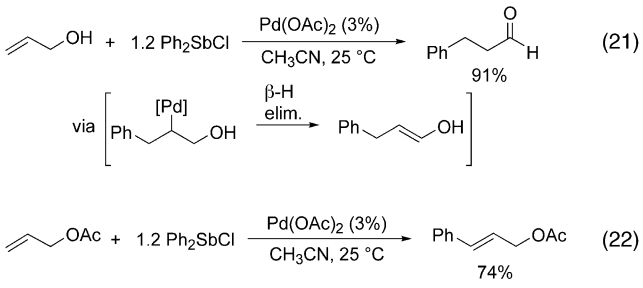
Scheme 9. Multistep, coupled catalytic system for the aerobic 1,4-oxidation of dienes.

to chloride-free Wacker oxidation conditions for the conversion of terminal alkenes into methyl ketones.[61b,62] The coordination of benzoquinone to palladium in these reactions has been exploited to achieve asymmetric 1,4-diacetoxylation of 2-phenyl-1,3-cyclohexadiene by using chiral benzoquinone derivatives.[46] Although these reactions do not correspond to the direct dioxygen-coupled reactions emphasized in this Review, they represent rare examples of ligand-based asymmetric induction in palladium oxidation catalysis.

5.2. Intermolecular Oxidation of Alkenes: Carbon–Carbon Bond Formation

Palladium(II)-mediated oxidative coupling reactions between alkenes and a variety of carbon nucleophiles have been studied for several decades.[10,63] However, the requirement for stoichiometric palladium(II) or copper(II) renders them considerably less appealing than the corresponding nonoxidative cross-coupling reactions with alkenyl and aryl halides. The first examples of aerobic catalytic turnover have appeared only recently.[64] Uemura and co-workers observed that diphenylantimony chloride undergoes clean oxidative phenyl transfer to olefins, catalyzed by palladium acetate in air [Eq. (21,22)].[65] Measurement of the oxygen consumption

 © 2004 Wiley-VCH Verlag GmbH & Co. KGaA, Weinheim

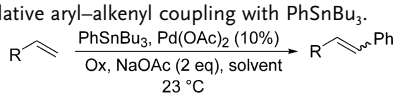


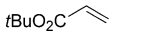
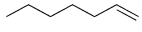
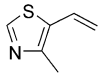
(21)

(22)

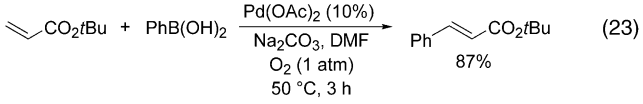
revealed a 1:1 ratio with respect to the product. The form of the reduced oxygen species was not identified, but the authors speculate that the antimony by-product reacts with a peroxide equivalent. Other aryl metal chlorides, including Ph_2TlCl, Ph_3SnCl, and Ph_2TeCl_2, were not successful in this reaction. Subsequently, Jung and co-workers described the use of aryl stannanes[66] in oxidative cross-coupling reactions with alkenes (Table 2). These reaction conditions proved more

Table 2: Oxidative aryl–alkenyl coupling with $PhSnBu_3$.



Entry	Olefin	Oxidant	
		$CuCl_2$ (3 equiv, THF)	O_2 (1 atm, DMF)
1		96% (1 h)	74% (12 h)
2		0%	82%
3		0%	51%

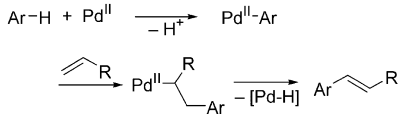
versatile than those reported previously with copper(II) salts as the oxidant.[63i] In several cases, olefins that did not react in the presence of copper formed the desired product in moderate to good yields under aerobic conditions (e.g., Table 2, entries 2 and 3). Chlorinated by-products observed in reactions with $CuCl_2$ could be avoided. Lower yields were obtained when the reactions were conducted under air rather than a pure oxygen atmosphere. Recently aryl boronic acids and boronic esters [Eq. (23)] also proved to be successful



(23)

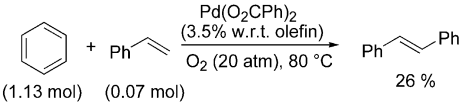
nucleophiles.[67] This reaction is insensitive to the electron density on the olefin, as good yields (73–90%) were obtained for a series of olefins ranging from *tert*-butyl acrylate to *n*-butyl vinyl ether.

The mechanism of these oxidative coupling reactions has not been studied in detail, but the most likely pathway involves aryl transfer to palladium(II), followed by olefin insertion and β-hydride elimination. The oxidized catalyst then may be regenerated according to the pathways outlined above (Section 3). In principle, similar reaction products may be formed by accessing the aryl palladium(II) intermediate through arene C–H activation (Scheme 10).



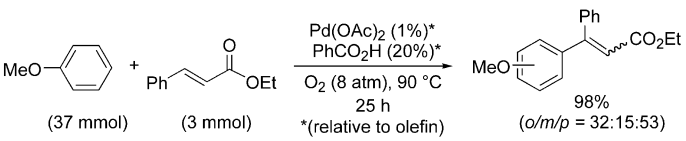
Scheme 10. Arene–olefin coupling via palladium(II)-mediated C–H activation.

In the late 1960s, Fujiwara and Moritani established that $PdCl_2$ promotes the formation of stilbene from styrene and benzene in a solvent mixture of acetic acid and dry benzene.[10a] In the intervening 35 years, palladium(II)-mediated C–H activation and functionalization reactions have been studied extensively,[68] and numerous palladium-catalyzed arene–olefin coupling reactions have been developed by using various stoichiometric oxidants, including silver(I),[69a,b,d] copper(II)/$\pm O_2$,[69b–d,f,g] $PhCO_3tBu$,[69e,h] benzoquinone/$\pm$ tBuOOH,[69i,j] and polyoxometallate/O_2.[69k] Most significant for the present discussion are several reports of palladium-catalyzed oxidative coupling of arenes (typically benzene) and alkenes in which molecular oxygen serves as the sole oxidant.[70,71,72b] Palladium carboxylates are the most effective catalysts. In the first report of this reactivity [Eq. (24)],[70]



(24)

Shue observed that the catalyst activity correlates inversely with the basicity of the carboxylate, that is, $Pd(O_2CPh)_2 > Pd(O_2CMe)_2 > Pd(O_2CEt)_2$. Furthermore, higher catalytic activities are observed when the oxidative coupling of benzene and ethylene is conducted with acetic acid as a cosolvent, but under these conditions, a significant quantity of vinyl acetate by-product is formed.[72b,c] These results are consistent with the proposal by Fujiwara that arene C–H activation proceeds by an electrophilic mechanism, possibly involving a cationic $[Pd(O_2CR)]^+$ fragment.[68d] Very recently, Jacobs and co-workers reported high catalytic activity in the reaction between simple arenes (benzene, toluene, and anisole) with electron-deficient alkenes [Eq. (25)].[71] After



(25)

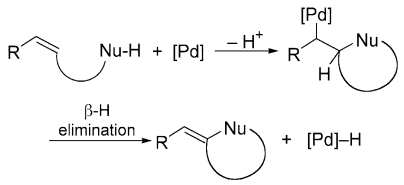
investigating a number of redox-active cocatalysts such as $Co(OAc)_2$ and $Mn(OAc)_3$, the authors determined that efficient turnover could be obtained simply by adding

 © 2004 Wiley-VCH Verlag GmbH & Co. KGaA, Weinheim

catalytic quantities of benzoic acid to the reaction. In situ formation of a palladium benzoate species was detected by ^{1}H NMR spectroscopy, and this more-electrophilic palladium species presumably facilitates rate-limiting C–H activation, as suggested by a primary kinetic isotope effect of 2.1 (toluene/[D_8]toluene). In the reaction between anisole and ethyl *trans*-cinnamate, turnover numbers of up to 762 with a turnover frequency of 73 h^{-1} could be obtained.

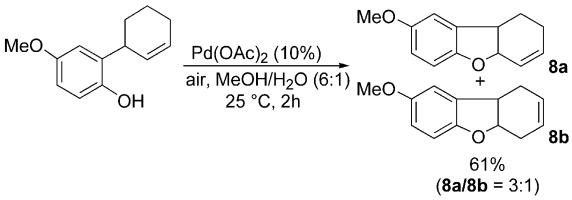
5.3. Intramolecular Oxidation of Alkenes: Oxidative Hetero- and Carbocyclization Reactions

Electrophile-promoted cyclizations of alkenes bearing pendant nucleophiles find extensive use in synthetic organic chemistry,[73] and palladium(II) reagents have been widely used in such reactions (Scheme 11).[74] If the reaction terminates in β-hydride elimination from an alkyl palladium(II) intermediate, a secondary oxidant must be used to ensure catalysis. Efficient dioxygen-coupled catalysis in these reactions has advanced significantly in the past 10 years. In many cases, the successful catalyst systems are very similar or identical to those described above for alcohol oxidation.

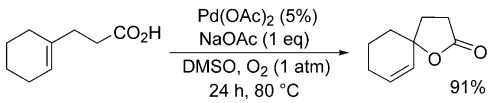


Scheme 11. Palladium-mediated oxidative cyclization of alkene substrates.

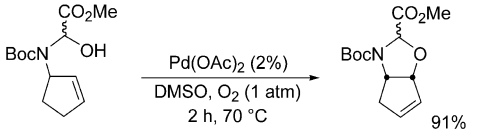
The oxidative cyclization of allyl phenols, reported by Hosokawa et al., is the earliest example of direct dioxygen-coupled oxidative heterocyclization [Eq. (26)].[45a] $Pd(OAc)_2$ and $PdCl_2$/NaOAc (1:16) catalyze these reactions without a cocatalyst in a methanol/water solvent mixture. These reactions continued to be explored in subsequent years, but most applications used copper(II) salts or benzoquinone as the stoichiometric oxidant. In the early 1990s, however, the groups of Larock[33] and Hiemstra[35] independently discovered that $Pd(OAc)_2$ in DMSO promotes the aerobic oxidative cyclization of a variety of alkene substrates [Eq. (27–29a)]. The inclusion of a copper(II) salt in the reaction had no beneficial effect and often hindered the reaction.[33a,35a,36a] The reactions were particularly suited for the preparation of five- and six-membered heterocycles, and nucleophiles that underwent effective cyclization included carboxylic acids,[33a,36b] aliphatic alcohols[35a,c,36a] and phenols,[33c] carbamoyl- and tosyl-protected amines,[33b,35b,36a,36b] carboxamides,[35b] and stabilized carbanions such as malonate derivatives[36c] and silyl enol ethers.[37] $Pd(OAc)_2$ was the preferred catalyst in most cases, but [$Pd(dba)_2$] and $PdCl_2$ were also used. Furthermore, anionic bases such as NaOAc and $KHCO_3$ often improved the reaction selectivity or yield. A pure oxygen atmosphere was generally required; however, the catalytic 6-*endo* cyclization of *o*-allylic phenols to yield chromene structures [Eq. (30)] proceeded successfully in air.[33c] In the 1,4-oxidation of cyclohexadienes [Eq. (31)], deprotonation of the carboxylic acid additive led to a switch in the product stereochemistry from *cis* to *trans*.[36b]



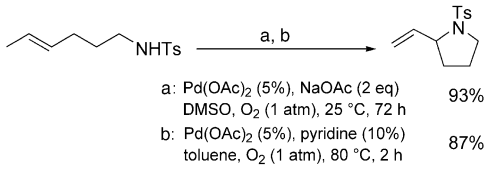
(26)



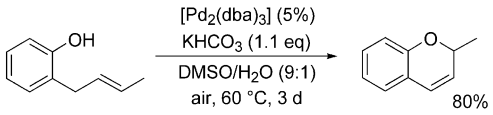
(27)



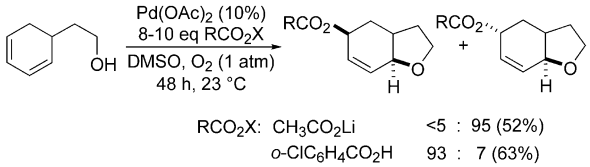
(28)



(29)

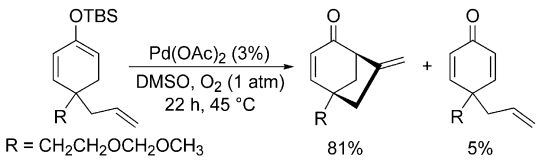


(30)



(31)

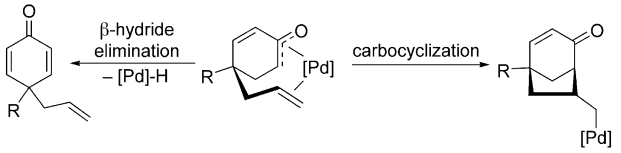
Toyota and Ihara have developed a number of aerobic oxidative carbocylization reactions with silyl enol ether substrates [Eq. (32); TBS = *tert*-butyldimethylsilyl]. Use of



(32)

 © 2004 Wiley-VCH Verlag GmbH & Co. KGaA, Weinheim

TBS rather than a TMS protecting group hinders the formation of the dehydrosilylation by-product that arises from from β-hydride elimination (Scheme 12). The authors speculate[37f] that the bulky TBS group may hinder the



Scheme 12. Alternate fates of the oxo-π-allyl palladium(II) intermediate in the oxidative carbocyclization of silyl enol ether substrates.

formation of the oxo-π-allyl intermediate, thus causing a change in mechanism to backside attack of the silyl enol ether on the coordinated alkene. This methodology has been applied to the total synthesis of several biologically active terpenoid natural products (Figure 1).[37a–d,h]

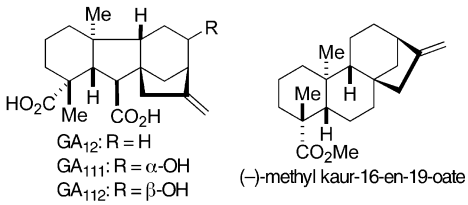
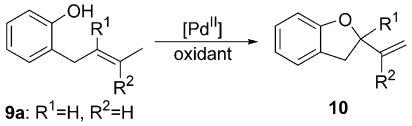


Figure 1. Diterpenoid natural products for which a palladium-catalyzed oxidative carbocyclization step was applied in their total synthesis.

Hiemstra and co-workers reported that DMSO-stabilized palladium clusters isolated from the oxidative cyclization reaction mixtures can be reused in subsequent reactions.[35c] This result contrasts the formation of inactive palladium black in the $Pd(OAc)_2$/DMSO-mediated oxidation of alcohols.[38] The substrate dependence on catalyst stability suggests that the alkene substrate may assist DMSO in stabilizing the palladium(0) clusters to prevent aggregation into inactive bulk metal, or the alkene substrate may facilitate the aerobic oxidation of colloidal palladium. The data cannot distinguish whether the clusters themselves serve as the catalyst, or if active mononuclear palladium(II) is generated by oxidation-induced dissociation from the clusters.[75]

The $Pd(OAc)_2$/pyridine catalyst system is also successful in oxidative cyclization reactions, and the first application was described by Stahl and co-workers in the oxidative cyclization of alkenyl sulfonamides to generate pyrrolidine and pyrroline products [Eq. (29b)].[41] A carbamate nucleophile was also successful, but a longer reaction time was required. The $Pd(OAc)_2$/pyridine catalyst system proved to be more robust than the DMSO system. The precipitation of palladium metal was not observed, and very high activities were attained at low catalyst loadings (70 TO h^{-1} at 0.2% $Pd(OAc)_2$/0.4% pyridine). Stoltz and co-workers subsequently extended this reactivity to substrates with several other types of nucleophiles.[49c] Palladium trifluoroacetate proved to be significantly more active than $Pd(OAc)_2$, and the use of 2 equivalents of Na_2CO_3 further enhanced the reactions. The allyl phenol derivative **9b** produces the cyclized product **10** [Eq. (33)] in

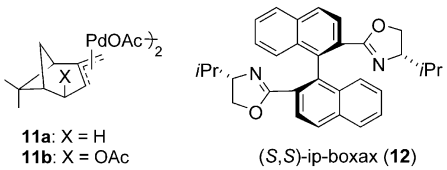


(33)

9a: R^1=H, R^2=H
9b: R^1=Me, R^2=H
9c: R^1=Me, R^2=Me

10

76% yield in 24 h with $Pd(OAc)_2$ (5%) as the catalyst, whereas with $Pd(O_2CCF_3)_2$ (5%) and 2 equivalents of Na_2CO_3, the product is obtained in 95% yield in 20 minutes under otherwise identical conditions (20% pyridine, 3-Å molecular sieves, 1 atm O_2, 80 °C in toluene). This insight permitted the development of an asymmetric oxidative cyclization of **9b** by employing [((−)-sparteine)$Pd(O_2CCF_3)_2$] (10%) as the catalyst (Table 1, entry 6). This reaction exhibits similar characteristics to the aforementioned alcohol oxidation reactions. Excess (−)-sparteine (100 mol%) is required to achieve high levels of enantioselectivity, and use of the bidentate (−)-sparteine ligand significantly lowers the catalytic activity relative to the pyridine system. Examples of asymmetric palladium-catalyzed oxidative cyclizations are quite rare,[45b–e,47–49] and allyl phenol substrates **9a–c** were the subject of investigation in all but one case (Table 3).[48]



11a: X = H
11b: X = OAc

(*S*,*S*)-ip-boxax (**12**)

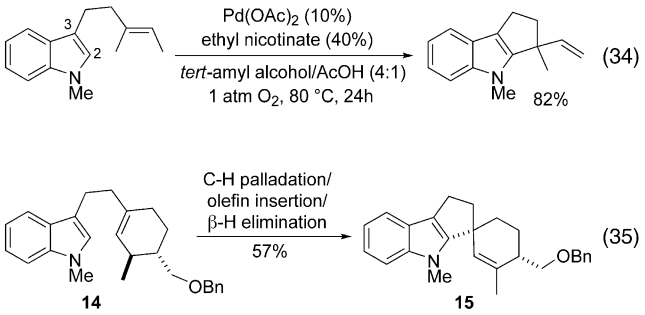
Ferreira and Stoltz recently reported the aerobic oxidative cyclization of various alkene-substituted indoles that lead to the formation of fused five-membered rings [Eq. (34,35)].[76]

Table 3: Examples of asymmetric palladium-catalyzed oxidative heterocyclization of allylphenol derivatives **9**.

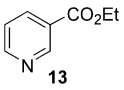
Entry	Catalyst, [Pd^{II}]	Oxidant (solvent)	Substrate	Configuration (yield [%]/*ee* [%])	References
1	[(η^3-pinene)Pd(OAc)]$_2$ (**11a**; 10 mol%)	$Cu(OAc)_2$ (10 mol%), O_2 (MeOH)	**9a**	*S* (67/18)	[45b]
2	[(η^3-acetoxypinene)Pd(OAc)]$_2$ (**11b**; 10 mol%)	$Cu(OAc)_2$ (10 mol%), O_2 (MeOH)	**9a**	*R* (49/18)	[45c]
3	$Pd(O_2CCF_3)_2$/(*S*,*S*)-ip-boxax (**12**) (10/20 mol%)	Benzoquinone (4 equiv) (MeOH)	**9c**	*S* (91/97)	[47]
4	[(sp)$Pd(O_2CCF_3)_2$]/sp/$Ca(OH)_2$[a] (10/100/200 mol%)	O_2 (toluene)	**9b**	*R* (87/81)	[49c]

[a] sp = (−)-sparteine.

 © 2004 Wiley-VCH Verlag GmbH & Co. KGaA, Weinheim

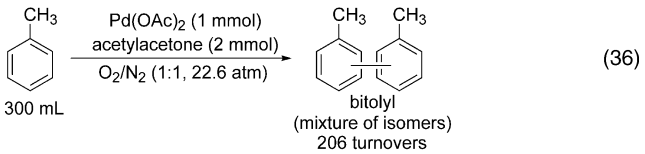


Ethyl nicotinate (**13**) proved superior to pyridine and several other substituted pyridines as a ligand in the reaction. The use of acetic acid as a cosolvent plays an important role in preventing the oxidative decomposition of the indoles. The C–C coupling can occur at either C2 or C3, depending on the site from which the alkene is appended. The use of substrate **14** permitted the authors to assess the mechanistic course of the reaction [Eq. (35)], possibilities of which include nucleophilic attack of the indole on a coordinated alkene or palladation of the indole C–H bond followed by alkene insertion. The observed stereochemistry of the product **15** favors the latter pathway.



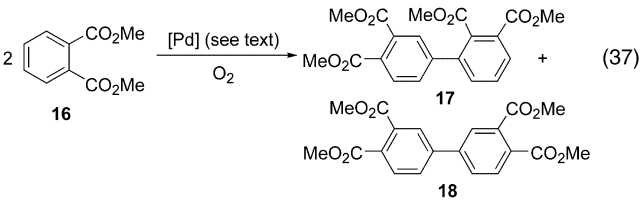
6. Oxidative C–C Coupling Reactions with Non-Alkene Substrates

Oxidative C–C coupling reactions between alkenes and aryl nucleophiles (Section 5.2) often generate by-products from the oxidative homocoupling of the aryl nucleophiles. In the absence of alkenes, the reaction can be optimized for the formation of biaryl products. This reactivity was first recognized by van Helden and Verberg in the oxidative homocoupling of arenes with stoichiometric $PdCl_2$ and sodium acetate.[77] Davidson and Triggs[78] and, later, Yoshimoto and Itatani identified conditions that employed catalytic quantities of $Pd(OAc)_2$ under high pressures of molecular oxygen (9–50 atm) [Eq. (36)].[79,80] The initial protocol,[78] which used



acetic acid as the solvent, led to significant quantities of phenyl acetate as the by-product, especially when lithium acetate was added to the reaction mixture.[78a,c] This product was shown to arise from a radical chain side reaction. The yields of the biaryl products improved when the reaction was conducted in neat arene and were enhanced further by adding catalytic quantities of acetylacetone to the reaction [Eq. (36)].[79] The reaction was compatible with arenes bearing ester, trifluoromethyl, chloro, fluoro, and nitro substituents, but amino, cyano, and anhydride groups completely inhibited the reaction.

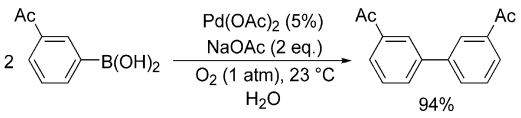
Control of the product regioselectivity represents a key challenge in these reactions. Electrophilic C–H activation by palladium(II) is sensitive to electronic factors of the substrate, although the effects vary with the reaction conditions and the palladium source.[79d,81] But overall, the electronic dependence of these reactions is substantially smaller than in other electrophilic aromatic substitution reactions. For instance, the palladation of toluene occurs competitively at the *meta* and *para* positions, and in some cases, *meta* substitution is favored.[81] Steric effects, on the other hand, play a significant role, and attack at the *ortho* position is significantly inhibited. Several strategies may be considered to overcome this intrinsic limitation. Chelate effects have been used extensively to enhance the regioselectivity of aromatic metallation, typically to the *ortho* position;[68e,69i,82] however, this approach has not yet been applied to aerobic palladium-mediated oxidation reactions. Alternatively, catalyst control over regioselectivity can be envisioned, but early results indicated that polar solvents and traditional ligands, such as triphenylphosphane, pyridine, bipyridine, and cyclooctadiene, inhibit the oxidative coupling of aromatics.[79b] The use of phenanthroline (phen) as a ligand, however, was later shown to have an important effect on the oxidative coupling of dimethyl phthalate (**16**)[83] to tetramethyl 3,4,3′,4′-biphenyltetracarboxylate (**18**), an important intermediate in the production of polyimide films. Under conditions similar to those outlined above for the oxidative coupling of toluene [Eq. (36)], **16** generates a mixture of isomeric products, primarily **17** and **18** (≈3:2) [Eq. (37)]. By employing [(phen)$Pd(OAc)_2$] as the



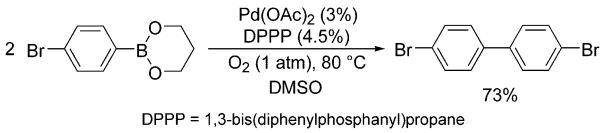
catalyst under a partial oxygen pressure of 1 atm (20 atm 95:5 N_2/O_2, 200 °C) the selectivity shifts to favor **18** (**17**/**18** = 1:9). These reactions must be carried out to relatively low conversion (< 25 %) to avoid substantial formation of trimers and higher oligomers.

By far the most effective approach to achieve regioselective control in the synthesis of biaryl products is palladium(0)-catalyzed cross-coupling of aryl halides with aryl boronic acids, aryl stannanes, and related organometallic derivatives.[84] The oxidative corollary to these methods is the palladium(II)-mediated coupling of two nucleophilic aryl reagents [Eq. (10)], and recently a number of these oxidative coupling reactions were achieved with molecular oxygen as the sole oxidant for palladium [Eq. (38,39)]. To date, success has been limited to oxidative dimerization reactions in which 2 equivalents of the aryl group are transferred through transmetallation to palladium(II) followed by reductive elimination of the symmetrical biaryl product. Effective nucleo-

 © 2004 Wiley-VCH Verlag GmbH & Co. KGaA, Weinheim

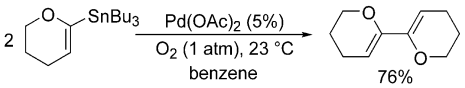


(38)



(39)

philes include aryl boronic acids[85] and esters,[86] aryl stannanes,[87] aryl zinc iodides,[88] and aryl bismuthanes,[89] and reactions have been conducted in solvents ranging from benzene to DMF to water. The compatibility of these reactions with halide substitution on the arene [Eq. (39)] suggests that if palladium(0) is formed in the reaction, it reacts more rapidly with oxygen than with the carbon–halogen bond. The homocoupling of vinyl organometallic reagents to produce symmetrical conjugated dienes is also successful under these reaction conditions [Eq. (40)].[85d,87b] Several of



(40)

the reactions proved to be more successful when a phosphane-ligated palladium catalyst was employed in the reaction;[85c,86,87a] however, it is not known how rapidly the ligand undergoes oxidative degradation.

7. Synthesis of Hydrogen Peroxide

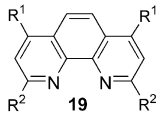
Hydrogen peroxide is a versatile oxidant that has found widespread industrial use for a variety of applications, ranging from chemical synthesis and pulp and paper bleaching to precious-metal extractions from ores.[90] Currently, the industrial production of hydrogen peroxide is based on the anthraquinone process, a two-stage process consisting of sequential autoxidation and reduction of 2-alkylanthrahydroquinone derivatives. The development of an alternative, direct route to hydrogen peroxide [Eq. (41,42)] has been of

$$O_2 + H_2 \xrightarrow{cat.} H_2O_2 \quad (41)$$

$$O_2 + CO + H_2 \xrightarrow{cat.} H_2O_2 + CO_2 \quad (42)$$

long-standing interest, but doing so requires the combination of oxygen and the reductant (e.g., H_2 or CO) within a single reactor. Nevertheless, this possibility was demonstrated in 1979 by Ermakov and co-workers, who employed triphenylphosphane/$Pd(OAc)_2$ combinations to generate hydrogen peroxide from oxygen and water in the presence of carbon monoxide. The yield was limited by the instability of triphenylphosphane under these oxidizing conditions,[91b] but this work subsequently led to the use of catalysts ligated by triaryl arsines. These catalysts are more oxidatively robust and up to 87 turnovers were obtained.[19] The use of biphasic conditions was essential to minimize contact between hydrogen peroxide and the catalyst, thereby limiting disproportionation [Eq. (12)].

Researchers at Enichem recently employed aromatic diimine ligands (**19**; ligand/Pd = 4:1), especially bathocuproine (R^1 = Ph, R^2 = Me), in this reaction and obtained



R^1 = H; R^2 = H, Me, Bu, Ph, Cl
R^1 = Ph; R^2 = Me

significantly higher turnover numbers (> 900 after 3 h) and catalytic activities (up to 630 TO h^{-1}).[19] The substitution pattern on the ligand is critical: too much steric bulk in R^2 (R^2 = Bu, Ph) results in precipitation of palladium metal, whereas no substituent in this position (R^2 = H) leads to the formation of inactive oligomeric palladium species. Optimal conditions consist of a biphasic solvent mixture of toluene, *tert*-butanol, and water (35:25:40) and a gas pressure of 70 atm (O_2/CO ≈ 64:6) at 70 °C. Chlorinated solvents (trichlorobenzene, 1,2-dichloroethane) in the organic phase promote faster initial rates, but irreversible catalyst deactivation occurs by reduction of the organic chloride in the presence of carbon monoxide [Eq. (43)]. The hydrochloric

$$RCl + CO + H_2O \xrightarrow{cat.} RH + HCl + CO_2 \quad (43)$$

acid produced in the latter reaction inhibits catalysis, even at low concentrations (Cl/Pd = 4:1). When the reaction is conducted in toluene, however, addition of a controlled amount of chloride anion (Cl/Pd = 1:1) helps to prevent palladium-metal precipitation. Catalytic quantities of a strong acid (CF_3CO_2H, $C_7F_{15}CO_2H$, *p*-Tol-SO_3H; acid/Pd ≈ 40:1) are also used in the reaction, the anion of which exchanges with acetate and coordinates only weakly to palladium. More-hydrophobic anions facilitate the partitioning of the catalyst into the organic phase.

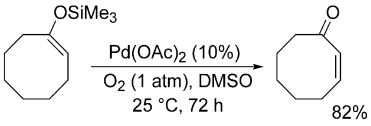
The catalytic mechanism is consistent with a palladium oxidase sequence (Scheme 3b; $SubH_2 = CO + H_2O$). Palladium(II) is reduced by carbon monoxide and water to yield carbon dioxide and 2 equivalents of H^+. Subsequent aerobic oxidation of the reduced catalyst to produce hydrogen peroxide could proceed by either of two possible pathways (Scheme 5, path a or c). Consistent with this proposal, primary and secondary alcohols can replace carbon monoxide and water as the reductant in this reaction [Eq. (44)].[19e]

$$O_2 + RR'CHOH \xrightarrow{cat.} H_2O_2 + RR'CO \quad (44)$$

8. Miscellaneous Palladium Oxidase Reactions

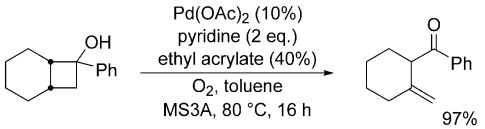
The conversion of aldehydes and ketones into α,β-unsaturated carbonyl compounds is an important transforma-

tion in organic synthesis.[92] Silyl enol ethers, which may be prepared regioselectively from the corresponding carbonyl compounds, undergo dehydrosilylation to the α,β-unsaturated carbonyl compound in the presence of stoichiometric amounts of $Pd(OAc)_2$. The original protocol reported by Saegusa and co-workers[93] demonstrated that palladium loading could be lowered to 0.5 equivalents when benzoquinone (0.5 equiv) was also included in the reaction. The only truly catalytic version of this reaction was developed by Larock and co-workers and is carried out under the $Pd(OAc)_2$/DMSO catalyst conditions [Eq. (45)].[34]

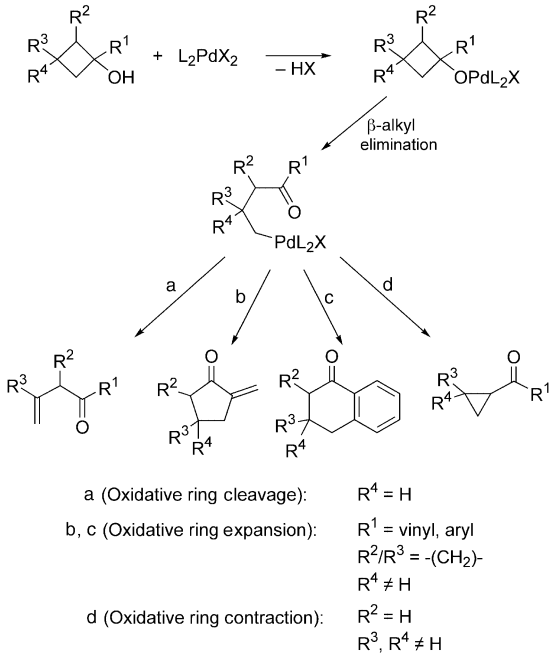


(45)

Uemura and co-workers recently employed their $Pd(OAc)_2$/pyridine catalyst system in the oxidative ring cleavage of tertiary cyclobutanols [Eq. (46)].[94] Upon formation of the palladium-alkoxide intermediate, β-alkyl elimination opens the cyclobutane ring and leads to the formation of a new palladium–carbon bond. Subsequent β-hydride elimination yields the ring-cleavage product (Scheme 13a).



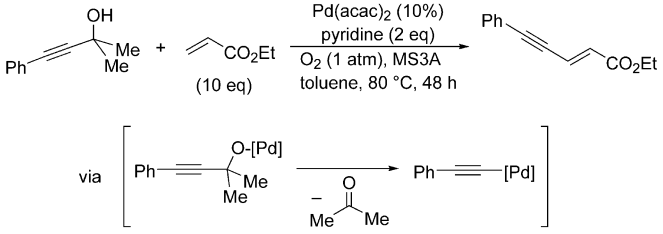
(46)



Scheme 13. Palladium-catalyzed oxidative transformations of *tert*-cyclobutanols.

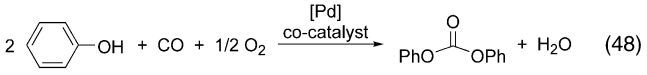
Depending on the substitution elsewhere on the cyclobutane ring, the alkylpalladium(II) intermediate can also undergo ring-expansion or -contraction reactions (Scheme 13b–d). Related ring-opening reactions of hydroxycyclopropanes have also been developed.[95]

Tertiary propargylic alcohols serve as a source of alkynyl anion in the palladium-catalyzed oxidative alkynylation of alkenes.[96] An alkynyl palladium(II) intermediate, generated by C_{sp}–C_{sp^3} β-alkyl elimination from a palladium alkoxide species [Eq. (47)], can undergo insertion of an alkene to produce the conjugated enyne product.



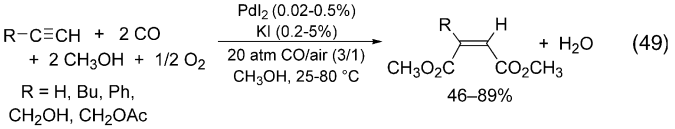
(47)

Oxidative carbonylation reactions constitute an important class of palladium(II)-mediated transformations. Considerable industrial attention has focused on the development of a direct catalytic route to the synthesis of diphenyl carbonate [Eq. (48)] to avoid the use of highly toxic phosgene.[97]

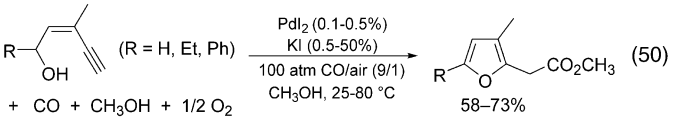


(48)

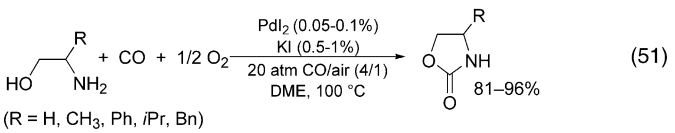
Benzoquinone and a variety of metal oxidants and cocatalysts have been employed in these reactions to promote catalytic turnover. Recently, a number of oxidative carbonylation reactions, including urea and carbamate syntheses and inter- and intramolecular coupling reactions between carbon monoxide and alkynes, have been achieved with a catalyst consisting of PdI_2 and cocatalytic iodide [Eq. (49–51)].[98] In



(49)



(50)



(51)

 © 2004 Wiley-VCH Verlag GmbH & Co. KGaA, Weinheim

these reactions, the iodide may serve a redox role in addition to a role as an anionic ligand. The authors proposed that iodide is oxidized under the aerobic reaction conditions to iodine, and the latter serves as the oxidant for palladium(0) [Eq. (52,53)].

$$2\,HI + {}^{1}/_{2}\,O_2 \rightarrow I_2 + H_2O \quad (52)$$

$$[Pd^0] + I_2 \rightarrow [PdI_2] \quad (53)$$

9. Summary and Outlook

Palladium-mediated oxidation of organic chemicals can trace its heritage back nearly two centuries,[27] but the commercial development of the Wacker process in the late 1950s initiated most of the research activity in this field. As the chemical industry retains its dependence on petroleum-derived feedstocks, the demand for improved selective oxidation reactions will continue to grow. Palladium oxidase reactions, with their use of molecular oxygen as the stoichiometric oxidant and the broad scope of their synthetic transformations, can have a significant impact on the future of oxidation chemistry.

The majority of palladium-mediated oxidation reactions still require stoichiometric amounts of palladium or a terminal oxidant other than molecular oxygen, and the factors underlying these limitations are not fully understood. The ongoing elucidation of mechanistic principles will play an important role in guiding the development of new catalysts and catalytic reactions. The use of organic ligands and well-defined palladium coordination complexes in these reactions presents numerous new opportunities in this chemistry. As described above, ligands can have a significant effect on the catalyst lifetime and activity. Moreover, the use of these catalysts introduces new prospects for reagent-controlled selectivity in palladium oxidation reactions, including controlled regioselectivity and asymmetric catalysis. The identification of effective new ligands and catalysts represents an important future research objective. In summary, the results highlighted in this Review demonstrate that the selective oxidation of organic chemicals with molecular oxygen is no longer a long-term target, but has become a practical research enterprise.

Addendum

Since the submission of this manuscript, numerous additional papers have appeared in this area of research. Tsuji and co-workers have functionalized pyridine in the 3-position with bulky dendritic aryl substituents (e.g., 2,3,4,5-tetraphenylphenyl), and the use of these pyridine derivatives greatly suppresses palladium black formation in the $Pd(OAc)_2$-catalyzed aerobic oxidation of secondary alcohols (see Section 4.3).[99] The increased catalyst stability permits the use of air rather than pure molecular oxygen, and 1480 catalytic turnovers were achieved in the oxidation of 1-phenylethanol. Sheldon and co-workers have investigated solvent and ligand steric effects in their aqueous alcohol oxidation system (see Section 4.4).[100] Substantially higher catalytic activity is observed when bathophenanthroline disulfonate (PhenS*) is replaced as a ligand with 2,9-dimethylphenanthroline and the reaction is conducted in a 1:1 mixture of water and dimethyl sulfoxide. The methyl substituents appear to promote dissociation of the dimer, **5**, into the active monomeric form of the catalyst. Larger substituents, such as phenyl and *sec*-butyl, are not as effective as methyl groups in promoting higher activity. Turnover frequencies of $>1500\ h^{-1}$ were observed under optimal conditions. Stoltz and co-workers reported that air can replace pure oxygen in the [((−)-sparteine)$PdCl_2$]-catalyzed oxidative kinetic resolution of secondary alcohols when chloroform is used as the solvent (see Section 4.5).[101] The same group has prepared and structurally characterized a (−)-sparteine-coordinated palladium alkoxide complex that provides insight into the origin of stereoselectivity in these reactions.[102] A key result in this study is that (–)-sparteine operates as a C_1- rather than a C_2-symmetric ligand. The oxidative kinetic resolution of secondary alcohols has also been applied synthetically.[103] Moberg and co-workers have also investigated pyridine-derived palladacycles as catalysts for aerobic oxidation of 1-phenylethanol under air.[104] These catalyst are more active than the oxazoline-derived pallacycle **6** (see Section 4.6), but overall these catalysts remain less active that the simple $Pd(OAc)_2$/pyridine system.

Larhed and co-workers have described the aerobic oxidative coupling of aryl boronic acids with acrylate esters (see Section 5.2, [Eq. (23)]).[105] Optimized conditions employ 2,9-dimethylphenanthroline/$Pd(OAc)_2$ (1–2 mol%) as the catalyst in combination with a stoichiometric quantity of *N*-methylmorpholine as a base. The utility of such oxidative Heck reactions is demonstrated by a recent synthetic application in which traditional Heck cross-coupling conditions were unsuccessful.[106] Two recent examples of aerobic oxidative cyclization have been reported (see Section 5.3). Tius and co-workers employed the $Pd(OAc)_2$/DMSO catalyst system in an oxidative Nazarov-type cyclization.[107] With $[(CH_3CN)_2PdCl_2]$ as the catalyst, a nonoxidative cyclization takes place with the same substrates. The difference between these reactions appears to arise from the role of acetate as a base under catalytic conditions. $PdCl_2$ catalyzes the cyclization of β-hydroxyenones, formally an intramolecular oxidative conjugate addition, to yield dihydropyranones.[108] A copper cocatalyst is used under optimized conditions, but good yields can also be obtained in the absence of a cocatalyst, if base is present (10 mol% Na_2HPO_4). Finally, Gabriele, Costa, and co-workers have extended the utility of their PdI_2/KI catalyst system (see Section 8) in a series of new aerobic oxidative carbonylation reactions with alkyne substrates.[109]

Research in the author's laboratory has been supported by the National Science Foundation (CAREER, CHE-0094344), the National Institutes of Health (RO1 GM67173-01), and the Petroleum Research Fund of the American Chemical Society. I gratefully acknowledge additional support from the following agencies: the Research Corporation (Innovation Recognition

Award), the Dreyfus Foundation (New Faculty and Teacher-Scholar Awards), the Dow Chemical Company (Innovation Recognition Award), and 3M (Untenured Faculty Award). I appreciate the significant editorial assistance on the manuscript from Natia Anastasi, Jodie Brice, and Jeff Johnson.

Received: August 29, 2003 [A630]

[1] K. Weissermel, H.-J. Arpe, *Industrial Organic Chemistry*, 3rd ed., VCH, New York, **1997**.

[2] See, for example: a) R. A. Johnson, K. B. Sharpless in *Catalytic Asymmetric Synthesis*, 2nd ed. (Ed.: I. Ojima), Wiley-VCH, New York, **2000**, pp. 231–285; b) E. N. Jacobsen in *Comprehensive Organometallic Chemistry II*, *Vol. 12* (Eds.: G. Wilkinson, F. G. A. Stone, E. W. Abel, L. S. Hegedus), Pergamon, New York, **1995**, pp. 1097–1135; c) T. Katsuki in reference [2a], pp. 287–325; d) R. A. Johnson, K. B. Sharpless in reference [2a], pp. 357–398; e) H. B. Kagan in reference [2a], pp. 327–356.

[3] For leading references, see: a) *Oxygenases and Model Systems* (Ed.: T. Funabiki), Kluwer, Boston, **1997**; b) J. T. Groves, R. Quinn, *J. Am. Chem. Soc.* **1985**, *107*, 5790–5792; c) R. Neumann, M. Dahan, *Nature* **1997**, *388*, 353–355; d) C. Döbler, G. M. Mehltretter, U. Sundermeier, M. Beller, *J. Am. Chem. Soc.* **2000**, *122*, 10289–10297.

[4] a) J. Smidt, W. Hafner, R. Jira, J. Sedlmeier, R. Sieber, R. Rüttinger, H. Kojer, *Angew. Chem.* **1959**, *71*, 176–182; b) R. Jira in *Applied Homogeneous Catalysis with Organometallic Compounds*, *Vol. 1*, 2nd ed. (Eds.: B. Cornils, W. A. Herrmann), Wiley-VCH, Weinheim, **2002**, pp. 386–405; c) I. I. Moiseev, M. N. Vargaftik in reference [4b], pp. 406–412.

[5] P. M. Henry, *Palladium Catalyzed Oxidation of Hydrocarbons*, Kluwer, Boston, **1980**.

[6] J. Tsuji, *Palladium Reagents and Catalysts*, Wiley, New York, **1995**.

[7] For leading references, see: a) *Metal-catalyzed Cross-coupling Reactions* (Eds.: F. Diederich, P. J. Stang), Wiley-VCH, New York, **1998**; b) *Transition Metals for Organic Synthesis: Building Blocks and Fine Chemicals*, *Vol. I, II* (Eds.: M. Beller, C. Bolm), Wiley-VCH, New York, **1998**; c) I. P. Beletskaya, A. V. Cheprakov, *Chem. Rev.* **2000**, *100*, 3009–3066.

[8] a) J.-E. Bäckvall, *Acc. Chem. Res.* **1983**, *16*, 335–342; b) J. Tsuji, *Synthesis* **1984**, 369–384; c) T. Hosokawa, S.-I. Murahashi, *Acc. Chem. Res.* **1990**, *23*, 49–54; d) J. Tsuji in *Comprehensive Organic Synthesis*, *Vol. 7* (Eds.: B. M. Trost, I. Fleming), Pergamon, New York, **1991**, pp. 449–468; e) A. Heumann, K.-J. Jens, M. Réglier, *Prog. Inorg. Chem.* **1994**, *42*, 483–576; f) J. M. Takacs, X.-t. Jiang, *Curr. Org. Chem.* **2003**, *7*, 369–396; g) J. Muzart, *Tetrahedron* **2003**, *59*, 5789–5816.

[9] For leading references on colloidal and heterogeneous palladium-catalyzed oxidations, see: a) M. N. Vargaftik, V. P. Zagorodnikov, I. P. Stolarov, I. I. Moiseev, D. I. Kochubey, V. A. Likholobov, A. L. Chuvilin, K. I. Zamaraev, *J. Mol. Catal.* **1989**, *53*, 315–348; b) K. Kaneda, M. Fujii, K. Morioka, *J. Org. Chem.* **1996**, *61*, 4502–4503; c) K. Kaneda, Y. Fujie, K. Ebitani, *Tetrahedron Lett.* **1997**, *38*, 9023–9026; d) K. Ebitani, Y. Fujie, K. Kaneda, *Langmuir* **1999**, *15*, 3557–3562; e) T. Nishimura, N. Kakiuchi, M. Inoue, S. Uemura, *Chem. Commun.* **2000**, 1245–1246; f) N. Kakiuchi, Y. Maeda, T. Nishimura, S. Uemura, *J. Org. Chem.* **2001**, *66*, 6620–6625; g) K. Mori, K. Yamaguchi, T. Hara, T. Mizugaki, K. Ebitani, K. Kaneda, *J. Am. Chem. Soc.* **2002**, *124*, 11572–11573; h) G. Kovtun, T. Kameneva, S. Hladyi, M. Starchevsky, Y. Pazdersky, I. Stolarov, M. Vargaftik, I. Moiseev, *Adv. Synth. Catal.* **2002**, *344*, 957–964; i) K.-M. Choi, T. Akita, T. Mizugaki, K. Ebitani, K. Kaneda, *New J. Chem.* **2003**, *27*, 324–328; j) Y. Uozumi, R. Nakao, *Angew. Chem.* **2003**, *115*, 204–207; *Angew. Chem. Int. Ed.* **2003**, *42*, 194–197.

[10] a) I. Moritani, Y. Fujiwara, *Tetrahedron Lett.* **1967**, *8*, 1119–1122; b) R. F. Heck, *J. Am. Chem. Soc.* **1968**, *90*, 5518–5526.

[11] a) J. M. Davidson, C. Triggs, *Chem. Ind.* **1967**, 1361; b) M. O. Unger, R. A. Fouty, *J. Org. Chem.* **1969**, *34*, 18–21; c) H. Itatani, H. Yoshimoto, *Chem. Ind.* **1971**, 674–675.

[12] G. Wilke, H. Schott, P. Heimbach, *Angew. Chem.* **1967**, *79*, 62; *Angew. Chem. Int. Ed. Engl.* **1967**, *6*, 92–93.

[13] a) J. S. Valentine, *Chem. Rev.* **1973**, *73*, 235–245; b) T. Yoshida, S. Otsuka, *J. Am. Chem. Soc.* **1977**, *99*, 2134–2140; c) S. Otsuka, A. Nakamura, Y. Tatsuno, M. Miki, *J. Am. Chem. Soc.* **1972**, *94*, 3761–3767; d) S. Otsuka, A. Nakamura, Y. Tatsuno, *J. Am. Chem. Soc.* **1969**, *91*, 6994–6999; e) T. Yoshida, K. Tatsumi, M. Matsumoto, K. Nakatsu, A. Nakamura, T. Fueno, S. Otsuka, *Nouv. J. Chim.* **1979**, *3*, 761–774.

[14] R. A. Sheldon, J. K. Kochi, *Metal-Catalyzed Oxidations of Organic Compounds*, Academic Press, New York, **1981**.

[15] S. S. Stahl, J. L. Thorman, R. C. Nelson, M. A. Kozee, *J. Am. Chem. Soc.* **2001**, *123*, 7188–7189.

[16] a) R. van Asselt, C. J. Elsevier, W. J. J. Smeets, A. L. Spek, *Inorg. Chem.* **1994**, *33*, 1521–1531; b) S. M. Reid, J. T. Mague, M. J. Fink, *J. Organomet. Chem.* **2000**, *616*, 10–18; c) S. S. Stahl, J. L. Thorman, N. de Silva, I. A. Guzei, R. W. Clark, *J. Am. Chem. Soc.* **2003**, *125*, 12–13.

[17] a) M. Portnoy, D. Milstein, *Organometallics* **1993**, *12*, 1665–1673; b) C. Amatore, A. Jutand, *Coord. Chem. Rev.* **1998**, *178–180*, 511–528; c) L. M. Alcazar-Roman, J. F. Hartwig, A. L. Rheingold, L. M. Liable-Sands, I. A. Guzei, *J. Am. Chem. Soc.* **2000**, *122*, 4618–4630; d) A. K. de K. Lewis, S. Caddick, F. G. N. Cloke, N. C. Billingham, P. B. Hitchcock, J. Leonard, *J. Am. Chem. Soc.* **2003**, *125*, 10066–10073.

[18] For other studies of peroxopalladium(II) protonolysis, see: a) S. Muto, H. Ogata, Y. Kamiya, *Chem. Lett.* **1975**, 809–812; b) S. Muto, Y. Kamiya, *Bull. Chem. Soc. Jpn.* **1976**, *49*, 2587–2589; c) S. Muto, K. Tasaka, Y. Kamiya, *Bull. Chem. Soc. Jpn.* **1977**, *50*, 2493–2494.

[19] a) D. A. Bianchi, R. N. Bortolo, R. N. D'Aloisio, M. N. Ricci, S. C. Soattini (Enichem S.p.A.), EP0-808-796A1, **1997**; b) D. Bianchi, R. Bortolo, R. D'Aloisio, M. Ricci, *Angew. Chem.* **1999**, *111*, 734–736; *Angew. Chem. Int. Ed.* **1999**, *38*, 706–708; c) D. Bianchi, R. Bortolo, R. D'Aloisio, M. Ricci, *J. Mol. Catal. A* **1999**, *150*, 87–94; d) D. Bianchi, R. Bortolo, R. D'Aloisio, C. Querci, M. Ricci, *Stud. Surf. Sci. Catal.* **1999**, *126*, 481–484; e) R. Bortolo, D. Bianchi, R. D'Aloisio, C. Querci, M. Ricci, *J. Mol. Catal. A* **2000**, *153*, 25–29.

[20] W. R. Thiel, *Angew. Chem.* **1999**, *111*, 3349–3351; *Angew. Chem. Int. Ed.* **1999**, *38*, 3157–3158.

[21] a) K. D. Karlin, S. Kaderli, A. D. Zuberbühler, *Acc. Chem. Res.* **1997**, *30*, 139–147; b) W. B. Tolman, *Acc. Chem. Res.* **1997**, *30*, 227–237; c) V. Mahadevan, R. J. M. K. Gebbink, T. D. P. Stack, *Curr. Opin. Chem. Biol.* **2000**, *4*, 228–234; d) E. I. Solomon, P. Chen, M. Metz, S.-K. Lee, A. E. Palmer, *Angew. Chem.* **2001**, *113*, 4702–4724; *Angew. Chem. Int. Ed.* **2001**, *40*, 4570–4590.

[22] a) G.-J. ten Brink, I. W. C. E. Arends, G. Papadogianakis, R. A. Sheldon, *Chem. Commun.* **1998**, 2359–2360; b) G.-J. ten Brink, I. W. C. E. Arends, G. Papadogianakis, R. A. Sheldon, *Appl. Catal. A* **2000**, *194–195*, 435–442.

[23] a) G.-J. ten Brink, I. W. C. E. Arends, R. A. Sheldon, *Science* **2000**, *287*, 1636–1639; b) R. A. Sheldon, I. W. C. E. Arends, G.-J. ten Brink, A. Dijksman, *Acc. Chem. Res.* **2002**, *35*, 774–781; c) G.-J. ten Brink, I. W. C. E. Arends, R. A. Sheldon, *Adv. Synth. Catal.* **2002**, *344*, 355–369; d) G.-J. ten Brink, I. W. C. E. Arends, M. Hoogenraad, G. Verspui, R. A. Sheldon, *Adv. Synth. Catal.* **2003**, *345*, 497–505.

 © 2004 Wiley-VCH Verlag GmbH & Co. KGaA, Weinheim

[24] a) T. Nishimura, T. Onoue, K. Ohe, S. Uemura, *Tetrahedron Lett.* **1998**, *39*, 6011 – 6014; b) T. Nishimura, T. Onoue, K. Ohe, S. Uemura, *J. Org. Chem.* **1999**, *64*, 6750 – 6755; c) T. Nishimura, Y. Maeda, N. Kakiuchi, S. Uemura, *J. Chem. Soc. Perkin Trans. 1* **2000**, 4301 – 4305.

[25] a) J. H. Bayston, R. N. Beale, N. K. King, M. E. Winfield, *Aust. J. Chem.* **1963**, *16*, 954 – 968; b) J. H. Bayston, M. E. Winfield, *J. Catal.* **1964**, *3*, 123 – 128; c) H. L. Roberts, W. R. Symes, *J. Chem. Soc. A* **1968**, 1450 – 1453; d) L. E. Johnston, J. A. Page, *Can. J. Chem.* **1969**, *47*, 4241 – 4246; e) R. D. Gillard, B. T. Heaton, D. H. Vaughan, *J. Chem. Soc. A* **1970**, 3126 – 3130; f) J. F. Endicott, C.-L. Wong, T. Inoue, P. Natarajan, *Inorg. Chem.* **1979**, *18*, 450 – 454; g) M. T. Atlay, M. Preece, G. Strukul, B. R. James, *Can. J. Chem.* **1983**, *61*, 1332 – 1338; h) D. D. Wick, K. I. Goldberg, *J. Am. Chem. Soc.* **1999**, *121*, 11900 – 11901.

[26] a) I. E. Markó, P. R. Giles, M. Tsukazaki, S. M. Brown, C. J. Urch in *Transition Metals for Organic Synthesis: Building Blocks and Fine Chemicals*, *Vol. II* (Eds.: M. Beller, C. Bolm), Wiley-VCH, New York, **1998**, pp. 350 – 360; b) R. A. Sheldon, I. W. C. E. Arends, A. Dijksman, *Catal. Today* **2000**, *57*, 157 – 166.

[27] J. J. Berzelius, *Ann. Phys. Chem.* **1828**, *13*, 435 – 488.

[28] W. G. Lloyd, *J. Org. Chem.* **1967**, *32*, 2816 – 2819.

[29] T. F. Blackburn, J. Schwartz, *J. Chem. Soc. Chem. Commun.* **1977**, 157 – 158; Correction: T. F. Blackburn, J. Schwartz, *J. Chem. Soc. Chem. Commun.* **1978**, 632.

[30] E. Gómez-Bengoa, P. Noheda, A. M. Echavarren, *Tetrahedron Lett.* **1994**, *35*, 7097 – 7098.

[31] S. Aït-Mohand, F. Hénin, J. Muzart, *Tetrahedron Lett.* **1995**, *36*, 2473 – 2476.

[32] K. P. Peterson, R. C. Larock, *J. Org. Chem.* **1998**, *63*, 3185 – 3189.

[33] a) R. C. Larock, T. R. Hightower, *J. Org. Chem.* **1993**, *58*, 5298 – 5300; b) R. C. Larock, T. R. Hightower, L. A. Hasvold, K. P. Peterson, *J. Org. Chem.* **1996**, *61*, 3584 – 3585; c) R. C. Larock, L. Wei, T. R. Hightower, *Synlett* **1998**, 522 – 524.

[34] R. C. Larock, T. R. Hightower, G. A. Kraus, P. Hahn, D. Zheng, *Tetrahedron Lett.* **1995**, *36*, 2423 – 2426.

[35] a) R. A. T. M. van Benthem, H. Hiemstra, J. J. Michels, W. N. Speckamp, *J. Chem. Soc. Chem. Commun.* **1994**, 357 – 359; b) R. A. T. M. van Benthem, H. Hiemstra, G. R. Longarela, W. N. Speckamp, *Tetrahedron Lett.* **1994**, *35*, 9281 – 9284; c) R. A. T. M. van Benthem, H. Hiemstra, P. W. N. M. van - Leeuwen, J. W. Geus, W. N. Speckamp, *Angew. Chem.* **1995**, *107*, 500 – 503; *Angew. Chem. Int. Ed. Engl.* **1995**, *34*, 457 – 460.

[36] a) M. Rönn, J.-E. Bäckvall, P. G. Andersson, *Tetrahedron Lett.* **1995**, *36*, 7749 – 7752; b) M. Rönn, P. G. Andersson, J.-E. Bäckvall, *Acta Chem. Scand.* **1997**, *51*, 773 – 777; c) M. Rönn, P. G. Andersson, J.-E. Bäckvall, *Tetrahedron Lett.* **1997**, *38*, 3603 – 3606.

[37] a) M. Toyota, T. Wada, K. Fukumoto, M. Ihara, *J. Am. Chem. Soc.* **1998**, *120*, 4916 – 4925; b) M. Toyota, M. Rudyanto, M. Ihara, *Tetrahedron Lett.* **2000**, *41*, 8929 – 8932; c) M. Toyota, T. Odashima, T. Wada, M. Ihara, *J. Am. Chem. Soc.* **2000**, *122*, 9036 – 9037; d) M. Toyota, T. Wada, M. Ihara, *J. Org. Chem.* **2000**, *65*, 4565 – 4570; e) M. Toyota, A. Ilangovan, R. Okamoto, T. Masaki, M. Arakawa, M. Ihara, *Org. Lett.* **2002**, *4*, 4293 – 4296; f) M. Toyota, M. Ihara, *Synlett* **2002**, 1211 – 1222; g) M. Toyota, M. Rudyanto, M. Ihara, *J. Org. Chem.* **2002**, *67*, 3374 – 3386; h) M. Toyota, M. Sasaki, M. Ihara, *Org. Lett.* **2003**, *5*, 1193 – 1195.

[38] B. A. Steinhoff, S. R. Fix, S. S. Stahl, *J. Am. Chem. Soc.* **2002**, *124*, 766 – 767.

[39] a) B. B. Wayland, R. F. Schramm, *Inorg. Chem.* **1969**, *8*, 971 – 976; b) D. P. Bancroft, F. A. Cotton, M. Verbruggen, *Acta Crystallogr. Sect. C* **1989**, *45*, 1289 – 1292; c) A. I. Stash, T. I. Perepelkova, S. V. Kravtsova, Y. G. Noskov, I. P. Romm, *Russ. J. Coord. Chem.* **1998**, *24*, 36 – 39.

[40] This proposal is not consistent with observations in our own laboratory, which suggest that hydrogen peroxide disproportionation is slower in the *presence* of molecular sieves: B. A. Steinhoff, S. S. Stahl, unpublished results.

[41] S. R. Fix, J. L. Brice, S. S. Stahl, *Angew. Chem.* **2002**, *114*, 172 – 174; *Angew. Chem. Int. Ed.* **2002**, *41*, 164 – 166.

[42] B. A. Steinhoff, S. S. Stahl, *Org. Lett.* **2002**, *4*, 4179 – 4181.

[43] a) C. Amatore, A. Jutand, *J. Organomet. Chem.* **1999**, *576*, 254 – 278; b) C. Amatore, A. Jutand, A. Suarez, *J. Am. Chem. Soc.* **1993**, *115*, 9531 – 9541; c) L. M. Alcazar-Roman, J. F. Hartwig, *J. Am. Chem. Soc.* **2001**, *123*, 12905 – 12906.

[44] a) A. El-Qisairi, O. Hamed, P. M. Henry, *J. Org. Chem.* **1998**, *63*, 2790 – 2791; b) O. Hamed, P. M. Henry, *Organometallics* **1998**, *17*, 5184 – 5189; c) A. El-Qisairi, P. M. Henry, *J. Organomet. Chem.* **2000**, *603*, 50 – 60; d) A. K. El-Qisairi, H. A. Qaseer, P. M. Henry, *J. Organomet. Chem.* **2002**, *656*, 168 – 176; e) A. K. El-Qisairi, H. A. Qaseer, G. Katsigras, P. Lorenzi, U. Trivedi, S. Tracz, A. Hartman, J. A. Miller, P. M. Henry, *Org. Lett.* **2003**, *5*, 439 – 441.

[45] a) T. Hosokawa, S. Miyagi, S.-I. Murahashi, A. Sonoda, *J. Org. Chem.* **1978**, *43*, 2752 – 2757; b) T. Hosokawa, T. Uno, S. Inui, S.-I. Murahashi, *J. Am. Chem. Soc.* **1981**, *103*, 2318 – 2323; c) T. Hosokawa, Y. Imada, S. I. Murahashi, *Bull. Chem. Soc. Jpn.* **1985**, *58*, 3282 – 3290; d) T. Hosokawa, C. Okuda, S.-I. Murahashi, *J. Org. Chem.* **1985**, *50*, 1282 – 1287; e) T. Hosokawa, T. Kono, T. Shinohara, S.-I. Murahashi, *J. Organomet. Chem.* **1989**, *370*, C13 – C16.

[46] a) A. Thorarensen, A. Palmgren, K. Itami, J.-E. Bäckvall, *Tetrahedron Lett.* **1997**, *38*, 8541 – 8544; b) K. Itami, A. Palmgren, A. Thorarensen, J.-E. Bäckvall, *J. Org. Chem.* **1998**, *63*, 6466 – 6471; c) H. K. Cotton, R. C. Verboom, L. Johansson, B. J. Plietker, J.-E. Bäckvall, *Organometallics* **2002**, *21*, 3367 – 3375.

[47] a) Y. Uozumi, K. Kato, T. Hayashi, *J. Am. Chem. Soc.* **1997**, *119*, 5063 – 5064; b) Y. Uozumi, K. Kato, T. Hayashi, *J. Org. Chem.* **1998**, *63*, 5071 – 5075; c) Y. Uozumi, H. Kyota, K. Kato, M. Ogasawara, T. Hayashi, *J. Org. Chem.* **1999**, *64*, 1620 – 1625.

[48] M. A. Arai, M. Kuraishi, T. Arai, H. Sasai, *J. Am. Chem. Soc.* **2001**, *123*, 2907 – 2908.

[49] a) E. M. Ferreira, B. M. Stoltz, *J. Am. Chem. Soc.* **2001**, *123*, 7725 – 7726; b) J. T. Bagdanoff, E. M. Ferreira, B. M. Stoltz, *Org. Lett.* **2003**, *5*, 835 – 837; c) R. M. Trend, Y. K. Ramtohul, E. M. Ferreira, B. M. Stoltz, *Angew. Chem.* **2003**, *115*, 2998 – 3001; *Angew. Chem. Int. Ed.* **2003**, *42*, 2892 – 2895.

[50] a) D. R. Jensen, J. S. Pugsley, M. S. Sigman, *J. Am. Chem. Soc.* **2001**, *123*, 7475 – 7476; b) J. A. Mueller, D. R. Jensen, M. S. Sigman, *J. Am. Chem. Soc.* **2002**, *124*, 8202 – 8203; c) D. R. Jensen, M. S. Sigman, *Org. Lett.* **2003**, *5*, 63 – 65; d) S. K. Mandal, D. R. Jensen, J. S. Pugsley, M. S. Sigman, *J. Org. Chem.* **2003**, *68*, 4600 – 4603; e) J. A. Mueller, M. S. Sigman, *J. Am. Chem. Soc.* **2003**, *125*, 7005 – 7013; f) S. K. Mandal, M. S. Sigman, *J. Org. Chem.* **2003**, *68*, 7535 – 7537.

[51] M. J. Dearden, C. R. Firkin, J.-P. R. Hermet, P. O'Brien, *J. Am. Chem. Soc.* **2002**, *124*, 11870 – 11871.

[52] K. Hallman, C. Moberg, *Adv. Synth. Catal.* **2001**, *343*, 260 – 263.

[53] a) M. J. Schultz, C. C. Park, M. S. Sigman, *Chem. Commun.* **2002**, 3034 – 3035; b) D. R. Jensen, M. J. Schultz, J. A. Mueller, M. S. Sigman, *Angew. Chem.* **2003**, *115*, 3940 – 3943; *Angew. Chem. Int. Ed.* **2003**, *42*, 3810 – 3813.

[54] K. R. Seddon, A. Stark, *Green Chem.* **2002**, *4*, 119 – 123.

[55] F. C. Phillips, *Am. Chem. J.* **1894**, *16*, 255 – 277.

[56] T. Nishimura, N. Kakiuchi, T. Onoue, K. Ohe, S. Uemura, *J. Chem. Soc. Perkin Trans. 1* **2000**, 1915 – 1918.

[57] a) M. Roussel, H. Mimoun, *J. Org. Chem.* **1980**, *45*, 5387 – 5390; b) H. Mimoun, R. Charpentier, A. Mitschler, J. Fischer, R. Weiss, *J. Am. Chem. Soc.* **1980**, *102*, 1047 – 1054; c) H. Mimoun,

Angew. Chem. **1982**, *94*, 750 – 766; *Angew. Chem. Int. Ed. Engl.* **1982**, *21*, 734 – 750.

[58] a) T. Hosokawa, T. Ohta, S.-I. Murahashi, *J. Chem. Soc. Chem. Commun.* **1983**, 848 – 849; b) T. Hosokawa, T. Ohta, S. Kanayama, S.-I. Murahashi, *J. Org. Chem.* **1987**, *52*, 1758 – 1764; c) T. Hosokawa, Y. Ataka, S.-I. Murahashi, *Bull. Chem. Soc. Jpn.* **1990**, *63*, 166 – 169; d) see also: W. G. Lloyd, B. J. Luberoff, *J. Org. Chem.* **1969**, *34*, 3949 – 3952.

[59] a) T. Hosokawa, M. Takano, Y. Kuroki, S.-I. Murahashi, *Tetrahedron Lett.* **1992**, *33*, 6643 – 6646; b) See also: F. Ragaini, T. Longo, S. Cenini, *J. Mol. Catal. A* **1996**, *110*, L171 – L175.

[60] V. I. Timokhin, N. R. Anastasi, S. S. Stahl, *J. Am. Chem. Soc.* **2003**, *125*, 12996 – 12997.

[61] a) J.-E. Bäckvall, A. K. Awasthi, Z. D. Renko, *J. Am. Chem. Soc.* **1987**, *109*, 4750 – 4752; b) J.-E. Bäckvall, R. B. Hopkins, H. Grennberg, M. M. Mader, A. K. Awasthi, *J. Am. Chem. Soc.* **1990**, *112*, 5160 – 5166; c) H. Grennberg, A. Gogoll, J.-E. Bäckvall, *J. Org. Chem.* **1991**, *56*, 5808 – 5811; d) H. Grennberg, S. Faizon, J.-E. Bäckvall, *Angew. Chem.* **1993**, *105*, 269 – 271; *Angew. Chem. Int. Ed. Engl.* **1993**, *32*, 263 – 264; e) K. Bergstad, H. Grennberg, J.-E. Bäckvall, *Organometallics* **1998**, *17*, 45 – 50; f) J. Wöltinger, J.-E. Bäckvall, Á. Zsigmond, *Chem. Eur. J.* **1999**, *5*, 1460 – 1467.

[62] J. E. Bäckvall, R. B. Hopkins, *Tetrahedron Lett.* **1988**, *29*, 2885 – 2888.

[63] A variety of different nucleophiles have been used; see the following for selected early and recent examples: organomercury reagents: a) reference [10a]; b) R. F. Heck, *J. Am. Chem. Soc.* **1971**, *93*, 6896 – 6901; aryl amines, -phosphanes, -arsanes, -stibanes, and -bismuthane: c) R. Asano, I. Moritani, Y. Fujiwara, S. Teranishi, *Bull. Chem. Soc. Jpn.* **1973**, *46*, 2910 – 2911; d) C. S. Cho, S. Motofusa, K. Ohe, S. Uemura, *Bull. Chem. Soc. Jpn.* **1996**, *69*, 2341 – 2348; alkyl lithium: e) S. Murahashi, M. Yamamura, N. Mita, *J. Org. Chem.* **1977**, *42*, 2870 – 2874. organomagnesium: f) N.-T. Luong-Thi, H. Riviere, *J. Chem. Soc. Chem. Commun.* **1978**, 918 – 919; aryl stannanes: g) H. Oda, M. Morishita, K. Fugami, H. Sano, M. Kosugi, *Chem. Lett.* **1996**, 811 – 812; h) K. Fugami, S. Hagiwara, H. Oda, M. Kosugi, *Synlett* **1998**, 477 – 478; i) K. Hirabayashi, J. Ando, Y. Nishihara, A. Mori, T. Hiyama, *Synlett* **1999**, 99 – 101; aryl and vinyl boronic acids and esters: j) X. Du, M. Suguro, K. Hirabayashi, A. Mori, T. Nishikata, N. Hagiwara, K. Kawata, T. Okeda, H. F. Wang, K. Fugami, M. Kosugi, *Org. Lett.* **2001**, *3*, 3313 – 3316; aryl and alkenyl silanols: k) K. Hirabayashi, Y. Nishihara, A. Mori, T. Hiyama, *Tetrahedron Lett.* **1998**, *39*, 7893 – 7896; l) K. Hirabayashi, J. Ando, J. Kawashima, Y. Nishihara, A. Mori, T. Hiyama, *Bull. Chem. Soc. Jpn.* **2000**, *73*, 1409 – 1417; m) K. Hirabayashi, T. Kondo, F. Toriyama, Y. Nishihara, A. Mori, *Bull. Chem. Soc. Jpn.* **2000**, *73*, 749 – 750; aryl phosphonic acids: n) A. Inoue, H. Shinokubo, K. Oshima, *J. Am. Chem. Soc.* **2003**, *125*, 1484 – 1485.

[64] K. Matoba, S. Motofusa, C. S. Cho, K. Ohe, S. Uemura, *J. Organomet. Chem.* **1999**, *574*, 3 – 10.

[65] T. Ohe, T. Tanaka, M. Kuroda, C. S. Cho, K. Ohe, S. Uemura, *Bull. Chem. Soc. Jpn.* **1999**, *72*, 1851 – 1855.

[66] J. P. Parrish, Y. C. Jung, S. I. Shin, K. W. Jung, *J. Org. Chem.* **2002**, *67*, 7127 – 7130.

[67] Y. C. Jung, R. K. Mishra, C. H. Yoon, K. W. Jung, *Org. Lett.* **2003**, *5*, 2231 – 2234.

[68] For reviews most pertinent to the present discussion, see: a) A. E. Shilov, G. B. Shul'pin, *Chem. Rev.* **1997**, *97*, 2879 – 2932; b) S. S. Stahl, J. A. Labinger, J. E. Bercaw, *Angew. Chem.* **1998**, *110*, 2298 – 2311; *Angew. Chem. Int. Ed.* **1998**, *37*, 2181 – 2192; c) A. Sen, *Acc. Chem. Res.* **1998**, *31*, 550 – 557; d) C. Jia, T. Kitamura, Y. Fujiwara, *Acc. Chem. Res.* **2001**, *34*, 633 – 639; Correction: C. Jia, T. Kitamura, Y. Fujiwara, *Acc. Chem. Res.* **2001**, *34*, 844; e) V. Ritleng, C. Sirlin, M. Pfeffer, *Chem. Rev.* **2002**, *102*, 1731 – 1769.

[69] For representative examples, see: a) Y. Fujiwara, I. Moritani, M. Matsuda, S. Teranishi, *Tetrahedron Lett.* **1968**, 3863 – 3865; b) Y. Fujiwara, I. Moritani, S. Danno, R. Asano, S. Teranishi, *J. Am. Chem. Soc.* **1969**, *91*, 7166 – 7169; c) O. Maruyama, M. Yoshidomi, Y. Fujiwara, H. Taniguchi, *Chem. Lett.* **1979**, 1229 – 1230; d) T. Itahara, M. Ikeda, T. Sakakibara, *J. Chem. Soc. Perkin Trans. 1* **1983**, 1361 – 1363; e) J. Tsuji, H. Nagashima, *Tetrahedron* **1984**, *40*, 2699 – 2702; f) M. Miura, T. Tsuda, T. Satoh, M. Nomura, *Chem. Lett.* **1997**, 1103 – 1104; g) M. Miura, T. Tsuda, T. Satoh, S. Pivsa-Art, M. Nomura, *J. Org. Chem.* **1998**, *63*, 5211 – 5215; h) K. Mikami, M. Hatano, M. Terada, *Chem. Lett.* **1999**, 55 – 56; i) C. Jia, W. Lu, T. Kitamura, Y. Fujiwara, *Org. Lett.* **1999**, *1*, 2097 – 2100; j) M. D. K. Boele, G. P. F. van Strijdonck, A. H. M. de Vries, P. C. J. Kamer, J. G. de Vries, P. W. N. M. van Leeuwen, *J. Am. Chem. Soc.* **2002**, *124*, 1586 – 1587; k) T. Yokota, M. Tani, S. Sakaguchi, Y. Ishii, *J. Am. Chem. Soc.* **2003**, *125*, 1476 – 1477.

[70] a) R. S. Shue, *J. Chem. Soc. Chem. Commun.* **1971**, 1510 – 1511; b) R. S. Shue, *J. Catal.* **1972**, *26*, 112 – 117; c) R. S. Shue (Phillips Petroleum Co.), US 3,775,511, **1973**.

[71] M. Dams, D. E. De Vos, S. Celen, P. A. Jacobs, *Angew. Chem.* **2003**, *115*, 3636 – 3639; *Angew. Chem. Int. Ed.* **2003**, *42*, 3512 – 3515.

[72] a) H. Weissman, X. Song, D. Milstein, *J. Am. Chem. Soc.* **2001**, *123*, 337 – 338; b) T. Matsumoto, H. Yoshida, *Chem. Lett.* **2000**, 1064 – 1065; c) T. Matsumoto, R. A. Periana, D. J. Taube, H. Yoshida, *J. Catal.* **2002**, *206*, 272 – 280.

[73] For recent reviews, see: a) N. Petragnani, H. A. Stefani, C. J. Valduga, *Tetrahedron* **2001**, *57*, 1411 – 1448; b) M. Frederickson, R. Grigg, *Org. Prep. Proced. Int.* **1997**, *29*, 33 – 62; c) M. Frederickson, R. Grigg, *Org. Prep. Proced. Int.* **1997**, *29*, 63 – 115.

[74] See, for example: a) L. S. Hegedus, *J. Mol. Catal.* **1983**, *19*, 201 – 211; b) L. S. Hegedus, *Angew. Chem.* **1988**, *100*, 1147 – 1161; *Angew. Chem. Int. Ed. Engl.* **1988**, *27*, 1113 – 1126.

[75] Evidence for the formation of mononuclear complexes has been obtained in "heterogeneous" palladium-catalyzed cross-coupling reactions: a) I. W. Davies, L. Matty, D. L. Hughes, P. J. Reider, *J. Am. Chem. Soc.* **2001**, *123*, 10139 – 10140; b) A. Biffis, M. Zecca, M. Basato, *J. Mol. Catal. A* **2001**, *173*, 249 – 274.

[76] E. M. Ferreira, B. M. Stoltz, *J. Am. Chem. Soc.* **2003**, *125*, 9578 – 9579.

[77] R. van Helden, G. Verberg, *Recl. Trav. Chim. Pays-Bas* **1965**, *84*, 1263 – 1273.

[78] a) J. M. Davidson, C. Triggs, *Chem. Ind.* **1966**, 457; b) reference [11a]; c) J. M. Davidson, C. Triggs, *J. Chem. Soc. A* **1968**, 1324 – 1330.

[79] a) reference [11c]; b) H. Iataaki, H. Yoshimoto, *J. Org. Chem.* **1973**, *38*, 76 – 79; c) H. Yoshimoto, H. Itatani, *Bull. Chem. Soc. Jpn.* **1973**, *46*, 2490 – 2492; d) H. Yoshimoto, H. Itatani, *J. Catal.* **1973**, *31*, 8 – 12; e) M. Kashima, H. Yoshimoto, H. Itatani, *J. Catal.* **1973**, *29*, 92 – 98.

[80] A number of cocatalytic (especially Pd/Cu and Pd/polyoxometallate) methods for the oxidative coupling of arenes have been developed; for leading references, see: a) G. U. Mennenga, A. I. Rudenkov, K. I. Matveev, I. V. Kozhevnikov, *React. Kinet. Catal. Lett.* **1976**, *5*, 401 – 406; b) A. I. Rudenkov, G. U. Mennenga, L. N. Rachkovskaya, K. I. Matveev, I. V. Kozhevnikov, *Kinet. Katal.* **1977**, *18*, 915 – 920; c) V. E. Tarabanko, I. V. Kozhevnikov, K. I. Matveev, *React. Kinet. Catal. Lett.* **1978**, *8*, 77 – 79; d) A. K. Yatsimirsky, S. A. Deiko, A. D. Ryabov, *Tetrahedron* **1983**, *39*, 2381 – 2392; e) S. H. Lee, K. H. Lee, J. S. Lee, J. D. Jung, J. S. Shim, *J. Mol. Catal. A* **1997**, *115*, 241 – 246; f) M. Okamoto, T. Yamaji, *Chem. Lett.* **2001**, 212 – 213;

 © 2004 Wiley-VCH Verlag GmbH & Co. KGaA, Weinheim

g) S. Mukhopadhyay, G. Rothenberg, G. Lando, K. Agbaria, M. Kazanci, Y. Sasson, *Adv. Synth. Catal.* **2001**, *343*, 455 – 459; h) T. Yokota, S. Sakaguchi, Y. Ishii, *Adv. Synth. Catal.* **2002**, *344*, 849 – 854; i) M. Okamoto, M. Watanabe, T. Yamaji, *J. Organomet. Chem.* **2002**, *664*, 59 – 65.

[81] See also: a) reference [11b]; b) Y. Fujiwara, R. Asano, I. Moritani, S. Teranishi, *J. Org. Chem.* **1976**, *41*, 1681 – 1683; c) L. J. Ackerman, J. P. Sadighi, D. M. Kurtz, J. A. Labinger, J. E. Bercaw, *Organometallics* **2003**, *22*, 3884 – 3890.

[82] S. Murai in *Activation of Unreactive Bonds and Organic Synthesis* (Ed.: S. Murai), Springer, Berlin, **1999**, pp. 47 – 79.

[83] a) H. Itatani, A. Shiotani, A. Yokota, (Ube Industries, Ltd., Japan), US 4,292,435, **1981**; b) H. Itatani, A. Shiotani, A. Yokota, (Ube Industries, Ltd., Japan), US 4,338,456, **1982**; c) A. Shiotani, M. Yoshikiyo, H. Itatani, *J. Mol. Catal.* **1983**, *18*, 23 – 31; d) A. Shiotani, H. Itatani, T. Inagaki, *J. Mol. Catal.* **1986**, *34*, 57 – 66.

[84] For leading references, see: a) reference [7a]; b) A. F. Littke, G. C. Fu, *Angew. Chem.* **2002**, *114*, 4350 – 4386; *Angew. Chem. Int. Ed.* **2002**, *41*, 4176 – 4211.

[85] a) M. Moreno-Mañas, M. Pérez, R. Pleixats, *J. Org. Chem.* **1996**, *61*, 2346 – 2351; b) K. A. Smith, E. M. Campi, W. R. Jackson, S. Marcuccio, C. G. M. Naeslund, G. B. Deacon, *Synlett* **1997**, 131 – 132; c) M. S. Wong, X. L. Zhang, *Tetrahedron Lett.* **2001**, *42*, 4087 – 4089; d) J. P. Parrish, Y. C. Jung, R. J. Floyd, K. W. Jung, *Tetrahedron Lett.* **2002**, *43*, 7899 – 7902.

[86] H. Yoshida, Y. Yamaryo, J. Ohshita, A. Kunai, *Tetrahedron Lett.* **2003**, *44*, 1541 – 1544.

[87] a) E. Shirakawa, Y. Murota, Y. Nakao, T. Hiyama, *Synlett* **1997**, 1143 – 1144; b) L. Alcaraz, R. J. K. Taylor, *Synlett* **1997**, 791 – 792.

[88] K. M. Hossain, T. Kameyama, T. Shibata, K. Takagi, *Bull. Chem. Soc. Jpn.* **2001**, *74*, 2415 – 2420.

[89] T. Ohe, T. Tanaka, M. Kuroda, C. S. Cho, K. Ohe, S. Uemura, *Bull. Chem. Soc. Jpn.* **1999**, *72*, 1851 – 1855.

[90] C. W. Jones, *Applications of Hydrogen Peroxide and Derivatives*, Royal Society of Chemistry, Cambridge, **1999**.

[91] a) V. N. Zudin, V. A. Likholobov, Y. I. Ermakov, *Kinet. Katal.* **1977**, *18*, 921 – 926; b) V. N. Zudin, V. A. Likholobov, Y. I. Ermakov, *Kinet. Katal.* **1979**, *20*, 1599 – 1600.

[92] R. C. Larock, *Comprehensive Organic Transformations*, 2nd ed., Wiley-VCH, New York, **1999**, pp. 251 – 256.

[93] Y. Ito, T. Hirao, T. Saegusa, *J. Org. Chem.* **1978**, *43*, 1011 – 1013.

[94] a) T. Nishimura, K. Ohe, S. Uemura, *J. Am. Chem. Soc.* **1999**, *121*, 2645 – 2646; b) T. Nishimura, K. Ohe, S. Uemura, *J. Org. Chem.* **2001**, *66*, 1455 – 1465.

[95] S.-B. Park, J. K. Cha, *Org. Lett.* **2000**, *2*, 147 – 149.

[96] T. Nishimura, H. Araki, Y. Maeda, S. Uemura, *Org. Lett.* **2003**, *5*, 2997 – 2999.

[97] For a discussion of synthetic and industrial applications of oxidative carbonylation, see: a) H. M. Colquhoun, D. J. Thompson, M. V. Twigg, *Carbonylation: Direct Synthesis of Carbonyl Compounds*, Plenum, New York, **1991**; b) A. Klausener, J.-D. Jentsch in reference [4b], pp. 164–182; c) M. Beller, A. M. Tafesh in reference [4b], pp. 182–194.

[98] a) G. P. Chiusoli, M. Costa, S. Reverberi, *Synthesis* **1989**, 262 – 265; b) B. Gabriele, M. Costa, G. Salerno, G. P. Chiusoli, *J. Chem. Soc. Chem. Commun.* **1992**, 1007 – 1008; c) B. Gabriele, M. Costa, G. Salerno, G. P. Chiusoli, *J. Chem. Soc. Chem. Commun.* **1994**, 1429 – 1430; d) B. Gabriele, M. Costa, G. Salerno, G. P. Chiusoli, *J. Chem. Soc. Perkin Trans. 1* **1994**, 83 – 87; e) A. Bonardi, M. Costa, B. Gabriele, G. Salerno, G. P. Chiusoli, *Tetrahedron Lett.* **1995**, *36*, 7495 – 7498; f) B. Gabriele, G. Salerno, F. De Pascali, G. T. Sciano, M. Costa, G. P. Chiusoli, *Tetrahedron Lett.* **1997**, *38*, 6877 – 6880; g) B. Gabriele, G. Salerno, F. De Pascali, M. Costa, G. P. Chiusoli, *J. Chem. Soc. Perkin Trans. 1* **1997**, 147 – 154; h) A. Bacchi, G. P. Chiusoli, M. Costa, C. Sani, B. Gabriele, G. Salerno, *J. Organomet. Chem.* **1998**, *562*, 35 – 43; i) A. Fazio, B. Gabriele, G. Salerno, S. Destri, *Tetrahedron* **1999**, *55*, 485 – 502; j) B. Gabriele, G. Salerno, D. Brindisi, M. Costa, G. P. Chiusoli, *Org. Lett.* **2000**, *2*, 625 – 627; k) B. Gabriele, G. Salerno, F. De Pascali, M. Costa, G. P. Chiusoli, *J. Organomet. Chem.* **2000**, *593–594*, 409 – 415; l) A. Bacchi, M. Costa, B. Gabriele, G. Pelizzi, G. Salerno, *J. Org. Chem.* **2002**, *67*, 4450 – 4457; m) B. Gabriele, G. Salerno, A. Fazio, F. B. Campana, *Chem. Commun.* **2002**, 1408 – 1409; n) B. Gabriele, L. Veltri, G. Salerno, M. Costa, G. P. Chiusoli, *Eur. J. Org. Chem.* **2003**, 1722 – 1728; o) B. Gabriele, R. Mancuso, G. Salerno, M. Costa, *Chem. Commun.* **2003**, 486 – 487; p) B. Gabriele, R. Mancuso, G. Salerno, M. Costa, *J. Org. Chem.* **2003**, *68*, 601 – 604.

[99] T. Iwasawa, M. Tokunaga, Y. Obora, Y. Tsuji, *J. Am. Chem. Soc.* **2004**, *126*, ASAP article.

[100] G.-J. ten Brink, I. W. C. E. Arends, M. Hoogenraad, G. Verspui, R. A. Sheldon, *Adv. Synth. Catal.* **2003**, *345*, 1341 – 1352

[101] J. T. Bagdanoff, B. M. Stoltz, *Angew. Chem.* **2004**, *116*, 357 – 361; *Angew. Chem. Int. Ed.* **2004**, *43*, 353 – 357.

[102] R. M. Trend, B. M. Stoltz, *J. Am. Chem. Soc.* **2004**, *126*, 4482 – 4483.

[103] a) I. S. Ali, A. Sudalai, *Tetrahedron Lett.* **2002**, *43*, 5435 – 5436; b) D. D. Caspi, D. C. Ebner, J. T. Bagdanoff, B. M. Stoltz, *Adv. Synth. Catal.* **2004**, *346*, 185 – 189.

[104] S. Paavola, K. Zetterberg, T. Privalov, I. Csöregh, C. Moberg, *Adv. Synth. Catal.* **2004**, *346*, 237 – 244.

[105] M. M. S. Andappan, P. Nilsson, M. Larhed, *Chem. Commun.* **2004**, 218 – 219.

[106] B. Furman, M. Dziedzic, *Tetrahedron Lett.* **2003**, *44*, 8249 – 8252

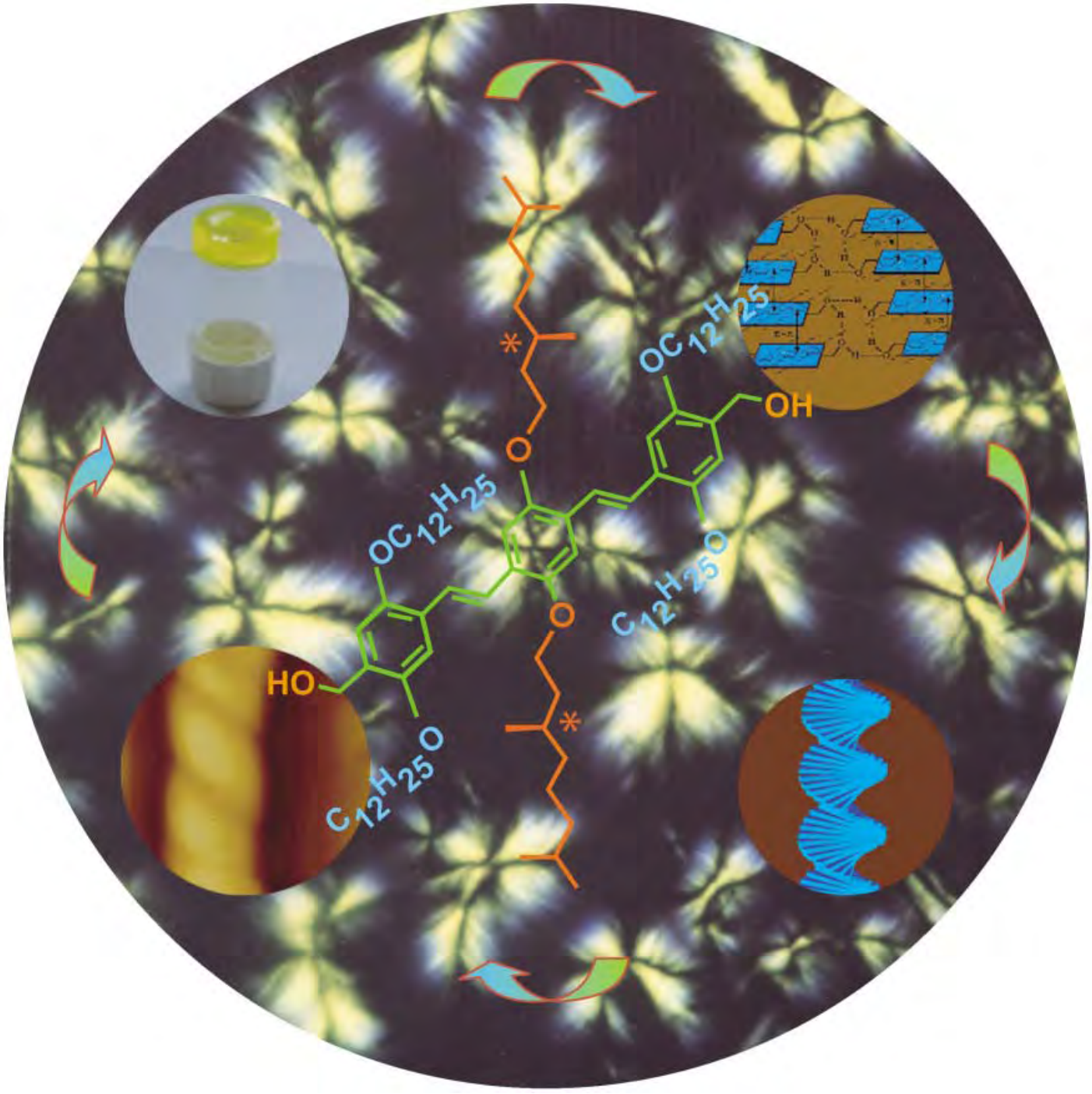
[107] C. Bee, E. Leclerc, M. A. Tius, *Org. Lett.* **2003**, *5*, 4927 – 4930.

[108] M. Reiter, S. Ropp, V. Gouverneur, *Org. Lett.* **2004**, *6*, 91 – 94.

[109] a) B. Gabriele, G. Salerno, M. Costa, G. P. Chiusoli, *J. Organomet. Chem.* **2003**, *687*, 219 – 228; b) B. Gabriele, G. Salerno, P. Plastina, M. Costa, A. Crispini, *Adv. Synth. Catal.* **2004**, *346*, 351 – 358; c) A. Bacchi, M. Costa, N. Della Cà, M. Fabbricatore, A. Fazio, B. Gabriele, C. Nasi, G. Salerno, *Eur. J. Org. Chem.* **2004**, 574 – 585; d) M. Costa, N. Della Cà, B. Gabriele, C. Massera, G. Salerno, M. Soliani, *J. Org. Chem.* **2004**, *69*, 2469 – 2477.

 © 2004 Wiley-VCH Verlag GmbH & Co. KGaA, Weinheim

Communications



In the following article A. Ajayaghosh and co-workers describe the hierarchical growth of left-handed-helical nanostructures of chiral oligo(*p*-phenylenevinylene)s (OPVs) and the associated CD-signal transition. (The birefringent fibrous four-arm brush patterns of a fluorescent chiral OPV gel are shown in the background.)

DOI: 10.1002/anie.200453874
© 2004 Wiley-VCH Verlag GmbH & Co. KGaA, Weinheim

Helical Nanostructures

Coiled-Coil Gel Nanostructures of Oligo(*p*-phenylenevinylene)s: Gelation-Induced Helix Transition in a Higher-Order Supramolecular Self-Assembly of a Rigid π-Conjugated System**

Subi J. George, Ayyappanpillai Ajayaghosh, Pascal Jonkheijm, Albertus P. H. J. Schenning, and E. W. Meijer*

Dedicated to Professor C. N. R. Rao on the occasion of his 70th birthday

The intriguing phenomenon of the supramolecular assembly of biological molecules into helical nanostructures, such as the DNA double helix, the collagen triple helix, and the α coiled-coil of myosin, has always fascinated scientists. With the help of noncovalent forces, such as hydrogen bonding, π stacking, and van der Waals interactions, chemists have been able to design a variety of aesthetically appealing helical supramolecular assemblies.[1,2] In this context, the control of the supramolecular organization of π-conjugated systems into helices of nanoscopic dimensions is of the utmost importance, as the resulting structures could find application in the emerging area of supramolecular electronics because of their unique optical and electronic properties.[3]

The spontaneous self-assembly of organic molecules to form gels is a method for creating nanoscopic and mesoscopic structures.[4] In particular, the gelation of chiral molecules to form helical morphologies has received considerable attention.[5–8] Recently, through a serendipitous observation, we showed the gelation of functionalized oligo(*p*-phenylenevinylene)s (OPVs) and their application in light harvesting.[9] Herein we report an interesting case of a gelation-assisted helix transition during the hierarchical self-assembly of a rigid π-conjugated system to form coiled-coil helical ropes. The gelation-induced helix formation in the present case is promoted by a pair of remote chiral handles and assisted by weak hydrogen-bonding motifs and long hydrocarbon chains, thus allowing the molecules sufficient freedom to undergo self-assembly.

Three different OPVs with remote chiral handles, **C-OPV1**, **C-OPV2**, and **C-OPV3** (Figure 1), were prepared by a

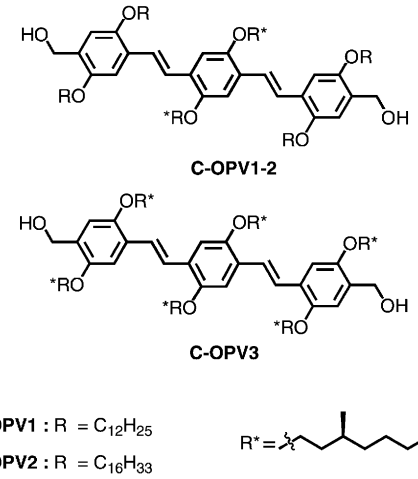


Figure 1. Structures of chiral OPV derivatives.

reported procedure and fully characterized.[9,10] **C-OPV2**, with hexadecyl side chains, was most able to form stable aggregates in solution (as evident from optical studies).[10] **C-OPV1**, with dodecyl side chains, was found to be a better gelator than **C-OPV2**, and formed a yellow fluorescent gel in nonpolar solvents, such as dodecane, heptane, and cyclohexane (critical gelator concentration in dodecane: 6.4×10^{-3} M). However, **C-OPV3**, which is substituted with six chiral side chains, failed to form a gel in any of the solvents. Optical polarizing microscopy (OPM) revealed that **C-OPV1** forms birefringent fibrous four-arm brushes when cooled from the isotropic dodecane solution, whereas neat **C-OPV1** and **C-OPV2** crystallize into spherulite textures when cooled from the isotropic melt.[10] Field emission scanning electron microscope (FESEM) images of **C-OPV1** from a dilute solution in dodecane (9×10^{-5} M) showed left-handed helical fibers of 20–50 nm in diameter and a few micrometers in length with a uniform helical pitch of approximately 150 nm (Figure 2a).[11] However, the FESEM image of **C-OPV1** (partially gelled) from a more concentrated solution in dodecane (5×10^{-4} M) showed the formation of left-handed coiled-coil ropelike structures of 50–100 nm in diameter with an average pitch of 330 nm. These ropelike structures are formed by the twisting together of several helical fibers (Figure 2b). AFM analysis of the **C-OPV1** gel from dodecane (6.5×10^{-3} M) clearly showed the formation of entangled left-handed-helical coiled-coil fibers of 50–100 nm in diameter (Figure 3b). Careful analysis of a single fiber showed the morphology of a left-handed coiled-coil rope of approximately 90 nm in width and 11 nm in height in which the pitch of each helix has an angle of about 40° with respect to the main fiber axis (Figure 3c). These observations point towards a hierarchical self-organization of

[*] S. J. George, Prof. Dr. A. Ajayaghosh
Photosciences and Photonics Division
Regional Research Laboratory, CSIR
Trivandrum-695019 (India)
Fax: (+91) 471-2490-186
E-mail: aajayaghosh@rediffmail.com
P. Jonkheijm, Dr. A. P. H. J. Schenning, Prof. Dr. E. W. Meijer
Laboratory of Macromolecular and Organic Chemistry
Eindhoven University of Technology
P.O. Box 513, 5600 MB Eindhoven (The Netherlands)

[**] We thank Dr. Toshimi Shimizu and Masaki Kogiso of the Nanoarchitectonics Research Center, AIST, Tsukuba, Japan for the FESEM pictures and Prof. René Janssen of the TU/e, Eindhoven for useful discussions. Financial support from the Department of Science and Technology, New Delhi (SR/S5/OC-31/2003 under invited category) and a research fellowship from the CSIR to S.J.G. are gratefully acknowledged. The Meijer research group acknowledges the Council for Chemical Sciences of the Netherlands Organization for Science Research (CW-NWO). This is contribution number RRLT-PPD-179.

Supporting information for this article is available on the WWW under http://www.angewandte.org or from the author.

 © 2004 Wiley-VCH Verlag GmbH & Co. KGaA, Weinheim DOI: 10.1002/anie.200453874

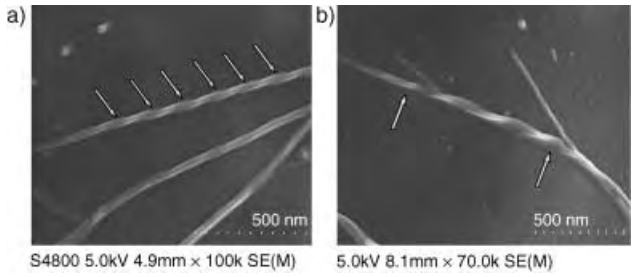


Figure 2. Helical morphology of **C-OPV1** self-assembly from a solution in dodecane: a) FESEM image of left-handed-helical fibers (9×10^{-5} M) and b) FESEM image showing the formation of a coiled-coil rope (5×10^{-4} M).

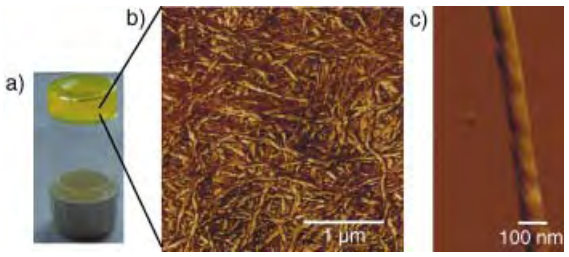


Figure 3. Physical appearance and AFM images of the **C-OPV1** gel from a solution in dodecane (6×10^{-3} M): a) photograph of the gel; b) dense network of helical fibers; c) single left-handed coiled-coil rope.

the **C-OPV1** into coiled-coil aggregates of nanometer dimensions.

UV/Vis absorption, fluorescence emission, and circular dichroism (CD) experiments were performed on **C-OPV1** to obtain better insight into the self-assembly of chiral OPVs. The absorption and emission properties of **C-OPV1** in chloroform are typical of molecularly dissolved OPVs.[10] The absence of a CD signal in chloroform suggests that **C-OPV1** is not aggregated in chloroform (Figure 4a, inset). However, the CD spectrum of **C-OPV1** in dodecane (5.3×10^{-4} M) showed a vibronic shoulder at 470 nm and 25 °C. The fluorescence spectrum of **C-OPV1** in dodecane (5.3×10^{-4} M, 1-mm cuvette, with front-face geometry to minimize the inner filter effect) at 25 °C showed peaks at 450 nm and 480 nm, and a shoulder at 525 nm. Upon cooling, the intensity of these bands decreased and their relative ratios changed with the formation of an additional red-shifted peak at 570 nm. These changes are characteristic of the formation of aggregates of OPVs as a result of cooperative hydrogen-bonding and π-stacking interactions. CD experiments in dodecane (**C-OPV1**: 5.3×10^{-4} M) revealed a strong bisignated Cotton effect at the position of the π–π* band, with a zero crossing close to the absorption maximum (400 nm), thus indicating the transfer of chiral information to the self-assembled chromophores in a helical sense (Figure 4a). The exciton-coupled bisignated negative couplet in the CD spectra is a signature of the left-handed-helical assembly of OPVs. Thus, these results are in agreement with those of the FESEM and AFM analyses, in which left-handed helicity was also found.

Concentration- and temperature-dependent CD measurements of **C-OPV1** in dodecane have provided insight into the hierarchical helical self-assembly and helix transition during the gelation of the molecules. The changes in the CD spectrum in the concentration range 8.8×10^{-5} M–5.3×10^{-4} M at 20 °C are shown in Figure 4a ($g_{381nm}=6.8\times10^{-4}$–$5.2\times10^{-3}$). Up to a concentration of 2.7×10^{-4} M, the CD spectrum of **C-**

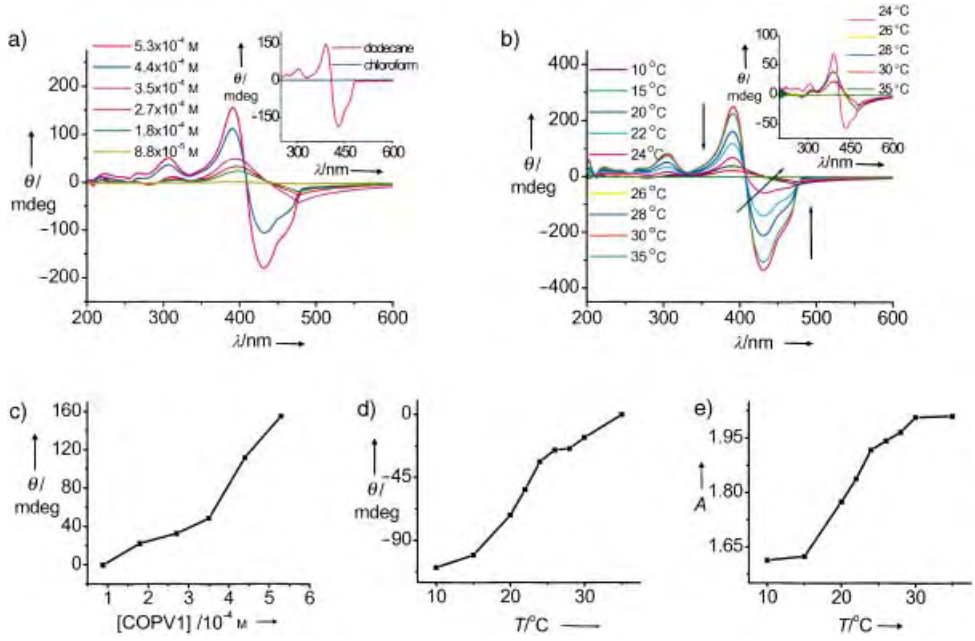


Figure 4. Concentration and temperature dependence of the CD spectrum of **C-OPV1** in dodecane: CD spectra of **C-OPV1** at different a) concentrations ($T=293$ K, $l=1$ mm) and b) temperatures ($c=5.3\times10^{-4}$ M, $l=1$ mm). c) Concentration-dependent transition of the intensity of the CD signal of **C-OPV1** monitored at 391 nm; d) melting-transition plot of CD intensity at 470 nm; e) melting-transition curve of the absorbance of **C-OPV1** at 405 nm. The inset in (a) shows the CD spectra of **C-OPV1** in dodecane and chloroform ($c=5.3\times10^{-4}$ M, $l=1$ mm); the inset in (b) shows the same CD spectra as in the main plot at different temperatures, but just within the range 24–35 °C.

 © 2004 Wiley-VCH Verlag GmbH & Co. KGaA, Weinheim

OPV1 in dodecane showed a bisignated signal with a negative first Cotton effect followed by a second positive Cotton effect, with a zero crossing at about 440 nm; this value does not correspond to the absorption maximum of the chromophore. Surprisingly, above a concentration of 3.5×10^{-4} M, a sharp transition was observed in the CD spectrum from one bisignated signal to a different bisignated signal.[12] The zero crossing of the new CD signal now occurred exactly at the absorption maximum (400 nm), which is indicative of a true exciton-coupled spectrum. A study of temperature dependence at a concentration of 5.3×10^{-4} M in dodecane revealed a decrease in the intensity of the CD signal up to a temperature of 24 °C, but the zero-crossing point remained the same (Figure 4b). However, at 26 °C a sharp transition of the intense exciton-coupled CD signal to a weak bisignated signal with a shift of the zero crossing from 400 nm to 440 nm was observed (Figure 4b, inset). The intensity of the signal continued to decrease until it reached the baseline at 35 °C. The plots in Figure 4c–e clearly show two transitions during the concentration- and temperature-dependent changes in circular dichroism and UV/Vis absorption. The occurrence of a two-stage transition was further supported by temperature-dependent fluorescence measurements, which showed a higher melting transition of 27 °C for a sample that was 40 times more dilute (1.24×10^{-5} M).[10] The complementary nature of the concentration- and temperature-dependent transitions of the CD signals indicates that a similar pathway via same chiral intermediate is involved during the formation and breaking down of the supramolecular assembly.

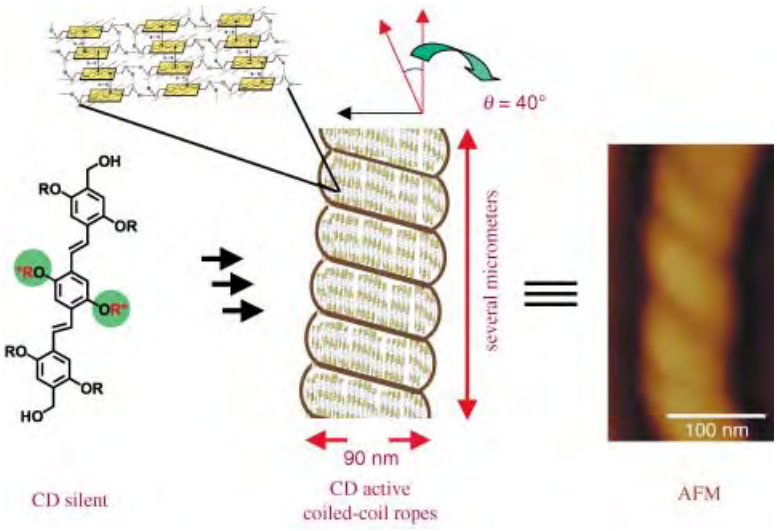


Figure 5. Schematic representation of the hierarchical self-assembly of **C-OPV1** into helical coiled-coil gel nanostructures. A magnified AFM image of the coiled-coil rope is shown on the right.

The characteristic transition described above for the CD, UV/Vis absorption, and fluorescence signals of **C-OPV1** is a unique observation associated with the gelation of chiral OPVs. During the gelation of **C-OPV1**, several hierarchical levels of supramolecular assemblies could be possible. In the initial levels, the molecules organize to form left-handed chiral aggregates, which are helical as indicated by the weak bisignated CD signal. At higher concentrations, these initial chiral assemblies grow further into helical fibers and coiled-coil ropes, thus resulting in a strong exciton-coupled CD signal. The helical packing of **C-OPV1** to form the left-handed coiled-coil rope, in which it is postulated that hydrogen-bonding and π-stacking interactions play an important role, is represented with the observed AFM image in Figure 5.[13] When the results of the CD and microscopic analyses are considered together, it is evident that the hierarchical growth of the coiled-coil structures evolves through two distinct chiral assemblies. At higher temperatures, denaturing of the coiled-coil gel assemblies occurs via intermediate chiral states, and the helical self-assembly ultimately collapses into isotropic single molecules for which no CD signals are observed.

In conclusion, we have shown the hierarchical helical growth of coiled-coil nanostructures during the gelation of rigid π-conjugated systems. Although a few reports on helical self-assemblies of OPVs have appeared,[14] to the best of our knowledge this is the first example of a gelation-induced CD-signal change. The unusual transition observed in the CD signal is indicative of a helix transition during the hierarchical evolution of ropelike nanostructures via intermediate chiral assemblies and is reminiscent of the multistate folding and unfolding of the helical assemblies of biological macromolecules.

Received: January 28, 2004 [Z53874]
Published Online: June 4, 2004

Keywords: helical structures · nanostructures · organogels self-assembly · supramolecular chemistry

[1] For recent reviews, see: a) A. E. Rowan, R. J. M. Nolte, *Angew. Chem.* **1998**, *110*, 71–73; *Angew. Chem. Int. Ed.* **1998**, *37*, 63–68; b) C. Schmuck, *Angew. Chem.* **2003**, *115*, 2552–2556; *Angew. Chem. Int. Ed.* **2003**, *42*, 2448–2452.

[2] For helical nanostructures, see: a) J. C. Nelson, J. G. Saven, J. S. Moore, P. G. Wolynes, *Science* **1997**, *277*, 1793–1796; b) J. J. L. M. Cornelissen, M. Fisher, N. A. J. M. Sommerdijk, R. J. M. Nolte, *Science* **1998**, *280*, 1427; c) H. Engelkamp, S. Middelbeek, R. J. M. Nolte, *Science* **1999**, *284*, 785–788; d) R. Oda, M. Schmutz, S. J. Candau, F. C. MacKintosh, *Nature* **1999**, *399*, 566–569; e) J. H. K. K. Hirschberg, L. Brunsveld, A. Ramzi, J. A. J. M. Vekemans, R. P. Sijbesma, E. W. Meijer, *Nature* **2000**, *407*, 167–170; f) V. Berl, I. Huc, R. G. Khoury, M. J. Krische, J.-M. Lehn, *Nature* **2000**, *407*, 720–723; g) E. R. Zubarev, M. U. Pralle, E. D. Sone, S. I. Stupp, *J. Am. Chem. Soc.* **2001**, *123*, 4105–4106; h) E. D. Sone, E. R. Zubarev, S. I. Stupp, *Angew. Chem.* **2002**, *114*, 1785–1788; *Angew. Chem. Int. Ed.* **2002**, *41*, 1706–1709; i) H. Fenniri, B.-L. Deng, A. E. Ribbe, *J. Am. Chem. Soc.* **2002**, *124*, 11064–11072; j) T. Giorgi, S. Lena, P. Mariani, M. A. Cremonini, S. Masiero, S. Pieraccini, J. P. Rabe, P. Samori, G. P. Spada, G. Gottarelli, *J. Am. Chem. Soc.* **2003**, *125*, 14741–14749; k) R. Iwaura, K. Yoshida, M. Masuda, M. O.

 © 2004 Wiley-VCH Verlag GmbH & Co. KGaA, Weinheim

Kameyama, M. Yoshida, T. Shimizu, *Angew. Chem.* **2003**, *115*, 1039 – 1042; *Angew. Chem. Int. Ed.* **2003**, *42*, 1009 – 1012.

[3] a) F. S. Schoonbeek, J. van Esch, B. Wegewijs, D. B. A. Rep, M. P. de Haas, T. M. Klapwijk, R. M. Kellogg, B. L. Feringa, *Angew. Chem.* **1999**, *111*, 1486 – 1489; *Angew. Chem. Int. Ed.* **1999**, *38*, 1393 – 1397; b) F. Würthner, C. Thalacker, A. Sautter, *Adv. Mater.* **1999**, *11*, 754 – 758; c) F. Würthner, C. Thalacker, A. Sautter, W. Schärtl, W. Ibach, O. Hollricher, *Chem. Eur. J.* **2000**, *6*, 3871 – 3886; d) R. B. Prins, L. Brunsveld, E. W. Meijer, J. S. Moore, *Angew. Chem.* **2000**, *112*, 234 – 236; *Angew. Chem. Int. Ed.* **2000**, *39*, 228 – 230; e) E. W. Meijer, A. P. H. J. Schenning, *Nature* **2002**, *419*, 353; f) V. Percec, M. Glodde, T. K. Bera, Y. Miura, I. Shiyanovskaya, K. D. Singer, V. S. K. Balagurusamy, P. A. Heiney, I. Schnell, A. Rapp, H.-W. Spiess, S. D. Hudson, H. Duan, *Nature* **2002**, *419*, 384 – 387; g) F. Würthner, S. Yao, U. Beginn, *Angew. Chem.* **2003**, *115*, 3373 – 3375; *Angew. Chem. Int. Ed.* **2003**, *42*, 3247 – 3250.

[4] a) P. Terech, R. G. Weiss, *Chem. Rev.* **1997**, *97*, 3133 – 3159; b) J. H. van Esch, B. L. Feringa, *Angew. Chem.* **2000**, *112*, 2351 – 2354; *Angew. Chem. Int. Ed.* **2000**, *39*, 2263 – 2266; c) K. J. C. van Bommel, A. Friggeri, S. Shinkai, *Angew. Chem.* **2003**, *115*, 1010 – 1030; *Angew. Chem. Int. Ed.* **2003**, *42*, 980 – 999.

[5] For cholesterol-based helical gels, see: a) Y.-C. Lin, B. Kachar, R. G. Weiss, *J. Am. Chem. Soc.* **1989**, *111*, 5542 – 5551; b) J. H. Jung, Y. Ono, S. Shinkai, *Angew. Chem.* **2000**, *112*, 1931 – 1933; *Angew. Chem. Int. Ed.* **2000**, *39*, 1862 – 1865; c) J. H. Jung, H. Kobayashi, M. Masuda, T. Shimizu, S. Shinkai, *J. Am. Chem. Soc.* **2001**, *123*, 8785 – 8789.

[6] For cyclohexane-based helical gels, see: a) K. Hanabusa, M. Yamada, M. Kimura, H. Shirai, *Angew. Chem.* **1996**, *108*, 2086 – 2088; *Angew. Chem. Int. Ed. Engl.* **1996**, *35*, 1949 – 1951; b) J. van Esch, F. Schoonbeek, M. de Loos, H. Kooijman, A. L. Spek, R. M. Kellog, B. L. Feringa, *Chem. Eur. J.* **1999**, *5*, 937 – 950.

[7] For carbohydrate-based helical gels, see: a) R. J. H. Hafkamp, M. C. Feiters, R. J. M. Nolte, *J. Org. Chem.* **1999**, *64*, 412 – 426; b) J. H. Jung, G. John, M. Masuda, K. Yoshida, S. Shinkai, T. Shimizu, *Langmuir* **2001**, *17*, 7229 – 7232; c) A. Friggeri, O. Gronwald, K. J. C. van Bommel, S. Shinkai, D. N. Reinhoudt, *J. Am. Chem. Soc.* **2002**, *124*, 10754 – 10758; d) S. Kawano, S. Tamaru, N. Fujita, S. Shinkai, *Chem. Eur. J.* **2004**, *10*, 343 – 351.

[8] For miscellaneous helical gels, see: a) R. Oda, I. Huc, S. J. Candau, *Angew. Chem.* **1998**, *110*, 2835 – 2838; *Angew. Chem. Int. Ed.* **1998**, *37*, 2689 – 2691; b) U. Maitra, V. K. Potluri, N. M. Sangeetha, P. Babu, A. R. Raju, *Tetrahedron: Asymmetry* **2001**, *12*, 477 – 480; c) J. J. van Gorp, J. A. J. M. Vekemans, E. W. Meijer, *J. Am. Chem. Soc.* **2002**, *124*, 14759 – 14769; d) W.-D. Jang, D.-L. Jiang, T. Aida, *J. Am. Chem. Soc.* **2000**, *122*, 3232 – 3233.

[9] a) A. Ajayaghosh, S. J. George, *J. Am. Chem. Soc.* **2001**, *123*, 5148 – 5149; b) A. Ajayaghosh, S. J. George, V. K. Praveen, *Angew. Chem.* **2003**, *115*, 346 – 349; *Angew. Chem. Int. Ed.* **2003**, *42*, 332 – 335.

[10] See Supporting Information.

[11] Exposure of the **C-OPV1** self-assembly to high-magnification FESEM conditions causes deformation of the helical fibers. The disappearance of the helicity of some of the fibers in Figure 2a is a result of this problem. However, a low-magnification image of the densely populated fibers showed uniform left-handed helicity in all fibers.

[12] The minimum concentration required for gelation in a 1-mm cuvette is much lower than that in a 1-cm cuvette or vial. Thus, the CD spectra recorded at concentrations above 3.5×10^{-4} M at 293 K correspond to the gel state. The contribution from linear dichroism (LD) in the gel state is negligibly small, as turning of the sample had no effect on the type of Cotton effect observed.

[13] The postulated chromophore arrangement in Figure 5 is based on a fluorescence polarization experiment on an OPV gel, which showed packing of the OPV units perpendicular to the fiber axis.

[14] a) A. P. H. J. Schenning, P. Jonkheijm, E. Peeters, E. W. Meijer, *J. Am. Chem. Soc.* **2001**, *123*, 409 – 416; b) A. P. H. J. Schenning, J. v. Herrikhuyzen, P. Jonkheijm, Z. Chen, F. Würthner, E. W. Meijer, *J. Am. Chem. Soc.* **2002**, *124*, 10252 – 10253; c) P. Jonkheim, F. J. M. Hoeben, R. Kleppinger, J. V. Herrikhuyzen, A. P. H. J. Schenning, E. W. Meijer, *J. Am. Chem. Soc.* **2003**, *125*, 15941 – 15949; d) P. Jonkheijm, A. Miura, M. Zdanowska, F. J. M. Hoeben, S. De Feyter, A. P. H. J. Schenning, F. C. De Schryver, E. W. Meijer, *Angew. Chem.* **2004**, *116*, 76 – 80; *Angew. Chem. Int. Ed.* **2004**, *43*, 74 – 78.

 © 2004 Wiley-VCH Verlag GmbH & Co. KGaA, Weinheim

Enzymatic Mechanisms

Structural Analysis of 1-Aminocyclopropane-1-Carboxylate Deaminase: Observation of an Aminyl Intermediate and Identification of Tyr294 as the Active-Site Nucleophile**

Subramanian Karthikeyan, Zongbao Zhao, Chai-lin Kao, Qingxian Zhou, Zhihua Tao, Hong Zhang, and Hung-wen Liu**

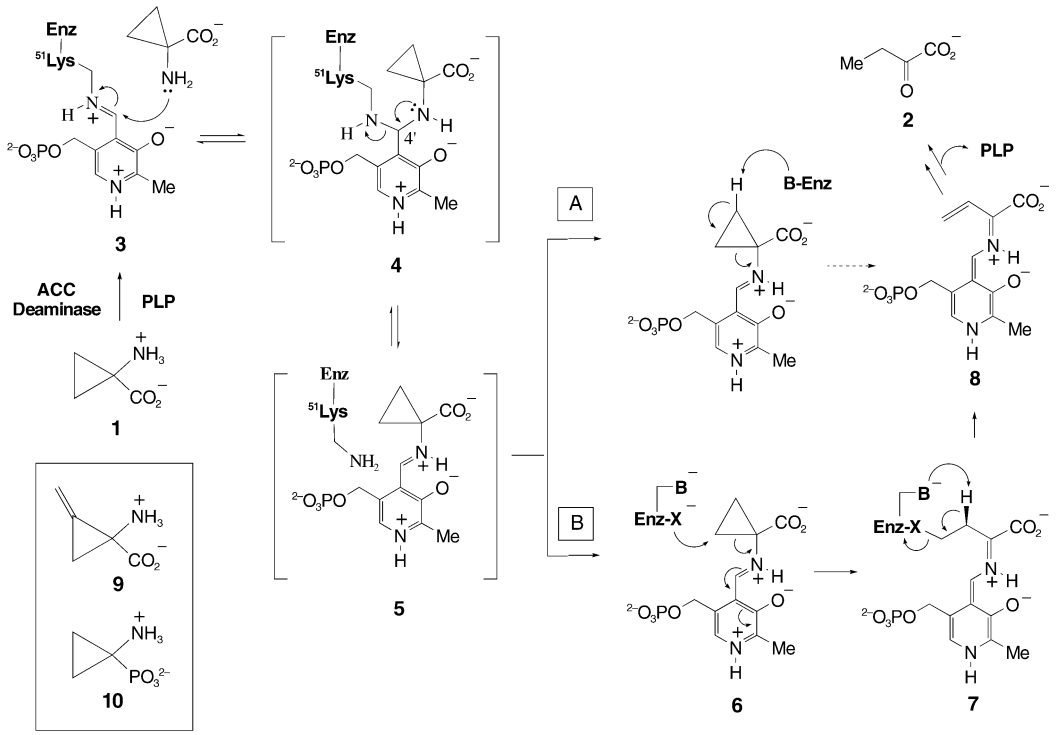
Dedicated to Professor Christopher Walsh on the occasion of his 60th birthday

1-Aminocyclopropane-1-carboxylate (ACC) deaminase is a pyridoxal phosphate (PLP)-linked enzyme that catalyzes the conversion of ACC (**1**) into α-ketobutyrate (**2**) and ammonia (Scheme 1).[1] In most other PLP-dependent reactions the formation of an α-carbanionic intermediate is the initiating event,[2] but the ring cleavage catalyzed by ACC deaminase

[*] Dr. Z. Zhao,[+] Dr. C.-l. Kao, Z. Tao, Prof. Dr. H.-w. Liu
Department of Biochemistry
University of Texas Southwestern Medical Center
Dallas, TX 75390-9038 (USA)
Fax: (+1) 214-648-9099
E-mail: h.w.liu@mail.utexas.edu
Dr. S. Karthikeyan, Q. Zhou, Prof. Dr. H. Zhang
Division of Medicinal Chemistry
College of Pharmacy
and Department of Chemistry and Biochemistry
University of Texas
Austin, TX 78712 (USA)
Fax: (+1) 612-626-7541
E-mail: zhang@chop.swmed.edu
[+] Current address:
Dalian Institute of Chemical Physics
Dalian 116023 (P.R. China)

[**] The authors gratefully acknowledge financial support provided by the National Institutes of Health (Grant no. GM40541 to H.-w.L., and no. GM63689 to H.Z.). We also thank Dr. Howard Robinson at Brookhaven National Laboratory for helping to collect the diffraction data.

 DOI: 10.1002/anie.200453353 © 2004 Wiley-VCH Verlag GmbH & Co. KGaA, Weinheim



Scheme 1. Proposed mechanisms of ACC deaminase. Enz = enzyme, X^- = nucleophile, B^- = base.

cannot proceed through such an intermediate because ACC does not have an abstractable α-H atom. An early study in which the α-anion equivalent of the vinylglycyl-PLP aldimine **8** was shown to be an intermediate in ACC fragmentation suggested two possible mechanisms for the ring scission.[3,4] As depicted in Scheme 1, the reaction could involve a direct β-proton abstraction that initiates cyclopropane cleavage (Route A), or it might proceed by a nucleophilic addition that opens the ring, followed by β-proton abstraction to give **8** (Route B). We recently synthesized 1-amino-2-methylenecyclopropane-1-carboxylic acid (**9**), which has a more electrophilic ring than ACC, as a tool for studying the mechanism of this unusual reaction. We found **9** to be a better substrate than ACC for the enzyme.[5–7] This result strongly suggests that Route B is the reaction course. This conclusion is strengthened by the fact that compound **9** irreversibly inhibits ACC deaminase and the inactivation can be rationalized by a mechanism analogous to Route B.[6,7]

Various labeling and mutagenesis results implicated one of the two active-site residues (Ser78 or Lys51) as the nucleophile (Enz-X^-) that attacks the cyclopropane ring and initiates the fragmentation of ACC as shown in Scheme 1 (Route B).[7] Although the crystal structure of the enzyme from the yeast *Hansenula saturnus* without substrate/product (or their analogues) in the active site had been solved when the structural study described herein was initiated,[8] little mechanistic information could be deduced from this crystal structure. To gain more insight into this intriguing coenzyme B_6 dependent reaction, we determined the crystal structure of the *Pseudomonas* ACC deaminase in a complex with a known tight-binding inhibitor, 1-aminocyclopropanephosphonate (ACP; **10**).[9] We report herein our structural results along with mutagenesis data, which together provide strong evidence that Tyr294 is the active-site nucleophile involved in the ring-cleavage step.

Early attempts to determine the three-dimensional structure of the *Pseudomonas* ACC deaminase were unsuccessful.[8] However, we were able to crystallize this protein in the presence of ACP (**10**) and solve the structure of the ACP–protein binary complex.[10] The electron density map showed that the PLP coenzyme is covalently attached to Lys51 at C-4′, as in the holoenzyme (data not shown). To our surprise, there is also a covalent bond between the C-4′ atom of PLP and the amino group of ACP (Figure 1A). Such an aminyl adduct (**4**) has long been proposed as an intermediate that occurs during the interchange between the internal aldimine (formed by PLP and the Lys anchor; **3**) and the external aldimine (formed by PLP and the substrate; **5**) in PLP-dependent catalysis. However, proof of the existence of this adduct has been elusive because of the transient nature of this intermediate.[11] Direct observation of this species was achieved only recently in a structural study of histidinol phosphate aminotransferase.[12] Our detection of the aminyl adduct shown in Figure 1A is only the second example of the direct observation of such an intermediate. It is conceivable that the tight binding of ACP[9] is partially a result of the trapping of the PLP coenzyme in the middle of the Schiff base exchange process.

The structure shown in Figure 1A not only reveals a generally undetected intermediate of the PLP-dependent reaction but also sheds new light on the catalytic mechanism of ACC deaminase. Ser78, which was previously thought to be the nucleophile (Enz-X^- in Route B) involved in the ring-opening process or the base (Enz-B^- in Route B) responsible

 © 2004 Wiley-VCH Verlag GmbH & Co. KGaA, Weinheim

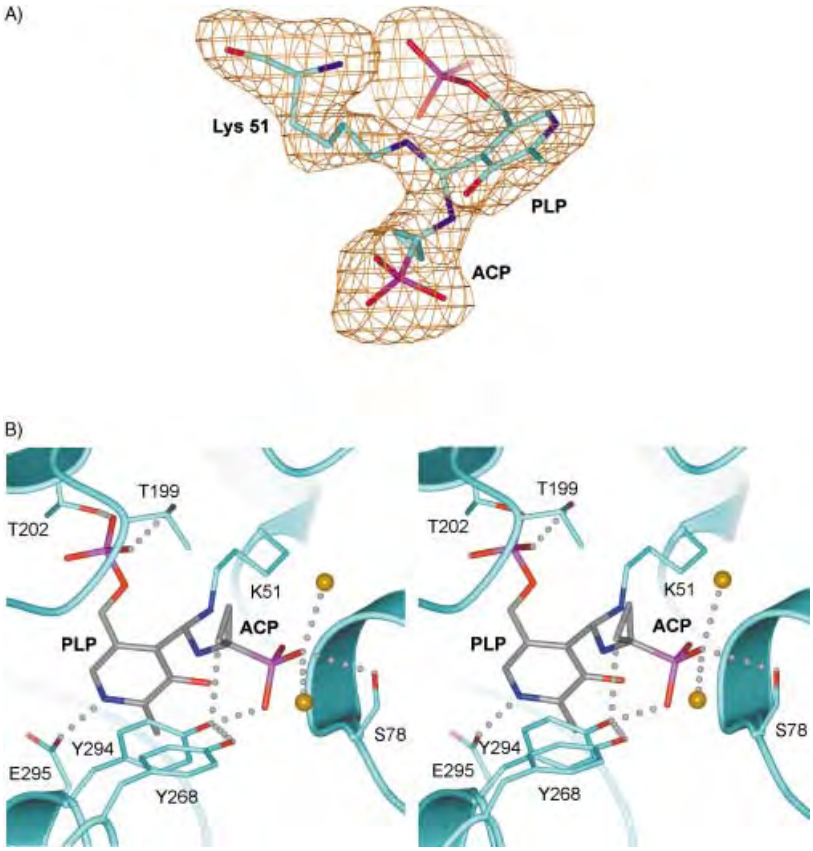


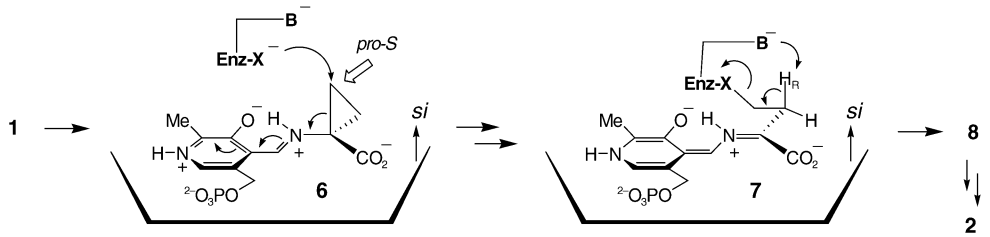
Figure 1. The active site of ACC deaminase in the ACP complex. A) The F_o-F_c difference electron densities for Lys51, PLP, and bound ACP (**10**), which show the existence of the aminyl intermediate. The map is contoured at 3 σ. B) Stereoview in which the interactions between bound ACP, PLP, and surrounding protein atoms are shown. Hydrogen bonds and close van der Waals interactions (over a distance $\leq$ 3.5 Å) are indicated by dotted lines. The two active-site water molecules are shown as yellow balls.

for the subsequent β-H abstraction,[7] was found to be distanced from the cyclopropyl ring but within H-bonding range (3.01 Å) of the phosphonate group of **10** (Figure 1B). This result suggests that Ser78 plays a primary role in substrate binding instead of directly participating in the chemical transformation. Accordingly, the large decrease in the activity caused by S78A mutation (to around 2.3% of the wild-type activity) observed in a previous experiment[7] should be attributed to a low affinity of the substrate for the active site.

Our second important observation is that Lys51, which anchors the PLP coenzyme in the active site and is a likely candidate for the attacking nucleophile in the ring-opening step,[7] is found in proximity (3.53 Å) to the pro-*S* carbon atom, rather than the pro-*R* carbon atom, of ACP (**10**) in the aminyl structure (Figure 1B).[13] The relative orientation of Lys51 is inconsistent with its proposed role as a nucleophile in catalysis because the ACC-deaminase-catalyzed ring cleavage of **1** occurs exclusively between the α-C atom and the pro-*S* β-CH_2 group of **1** (see **6** in Scheme 2).[13,14] Clearly, the previously deduced functions of both Ser78 and Lys51 in the ring-cleavage event need to be reevaluated.

Tyr294, which is hydrogen bonded to Tyr268, lies adjacent to the pro-*R* carbon atom of ACP. The 2.98 Å gap between the hydroxy oxygen atom of Tyr294 and the pro-*R* carbon atom of ACP (**10**) puts Tyr294 within reach of the cyclopropane ring (Figure 1B). This tyrosine residue is strictly conserved among the more than twenty ACC deaminase homologues known so far. It is therefore highly probable that Tyr294 is the elusive nucleophile whose addition to the pro-*S* β-CH_2 group of **1** induces ring opening. The reactivity of Tyr294 may be enhanced by hydrogen bonding to Tyr268, which is only 2.84 Å away. The catalytically more relevant structure **5** was recently observed by Ose et al. in a complex of the yeast ACC deaminase K51T mutant and ACC (**1**)[15] in which a two-phenol relay system (Y269 and Y295 in the yeast enzyme) exists that involves a similar juxtaposition of residues to that shown in Figure 1B. Comparison of the active site structure of the *Pseudomonas* enzyme (see Figure 1B) with structure **5** of the yeast enzyme[15] reveals little difference in the protein backbone and a shift of about 1 Å on the part of PLP–ACC adduct. The Tyr295 residue of the yeast enzyme is also found in proximity to the cyclopropane ring and could easily perform the proposed nucleophilic role.

To test this hypothesis, the Y294F mutant of the *Pseudomonas* enzyme was prepared. The mutant protein was determined to exhibit chromatographic behavior and spectral properties identical to those of the wild-type enzyme. However, no turnover by the mutant was detected with the lactate dehydrogenase/reduced nicotinamide-adenine dinucleotide



Scheme 2. Stereochemical course of ACC-deaminase-catalyzed ring opening and β-deprotonation.

 © 2004 Wiley-VCH Verlag GmbH & Co. KGaA, Weinheim

(NADH) assay.[4,16] A subsequent large-scale incubation in which ACC (**1**, 17 mM) was mixed with Y294F protein (60 μM) in potassium phosphate buffer (650 μL) prepared in D_2O (pD 8.0) led to no product formation, as assessed by ^1H NMR spectroscopy after 24 h. In contrast, the control reaction with wild-type enzyme (5 μM) resulted in complete conversion of **1** into **2** in 2 h. The inability of the Y294F mutant to process ACC provides strong support for the assigned role of Tyr294 in catalysis.[17] As we expected, Y268F mutation also caused the loss of more than 98% of the wild-type activity.[18] Ose et al. have reported the crystal structure of the yeast ACC deaminase Y295F mutant complexed with ACC, which revealed that the bound ACC adopts a very different, nonproductive conformation in the mutant complex.[15] This result suggests that, in addition to its proposed catalytic role, the Tyr294 residue of the *Pseudomonas* enzyme (or Tyr295 in the yeast enzyme) may help to correctly position the bound substrate in the active site.

Since the hydroxy group of Tyr295 is near the amino group (3.48 Å) of ACC in the yeast enzyme complex, Ose et al. proposed that this tyrosine residue plays a role in facilitating the formation of the external aldimine **5**. In fact, the authors favored Route A as the mechanism for the yeast enzyme and assigned Lys51, whose side chain orientation could only be deduced by modeling, as the base responsible for abstraction of the β proton.[15] This interpretation clearly differs from ours and warrants additional comment. A ring-opening mechanism initiated by deprotonation is inconsistent with the results obtained from studies of 2-methylene-ACC (**9**).[6,7] Such a mechanism is also thermodynamically unfavorable because the cyclopropane ring hydrogen atoms are not acidic. In contrast, the cyclopropane ring of ACC is readily susceptible to nucleophilic attack because of activation by the electron-withdrawing 1-carboxylate group and the imine moiety of the Schiff base.[19] The fact that Tyr294 is positioned close to the β-C atom of ACC/ACP makes it an ideal candidate to assume the role of the attacking nucleophile. Moreover, a ring opening initiated by a direct β-proton abstraction is inconsistent with the pro-*R* stereospecificity determined for this β-C–H bond cleavage event (see **7** in Scheme 2),[20] since it is the pro-*S* hydrogen atom, not the pro-*R* hydrogen atom, at the pro-*S* β-C atom (in **10**) is more accessible to the proposed base, Lys51, in the enzyme–ACP (**10**) complex (Figure 1B).

In summary, structural studies of ACC deaminase complexed with the tight-binding inhibitor ACP (**10**) revealed the presence of an aminyl adduct formed by the PLP cofactor and ACP in a rare example of the capture of a transient intermediate during enzymatic turnover. Both Ser78 and Lys51 are oriented away from the pro-*S* β-C atom of the ring cleavage site (in **1**), which casts doubt on the previously proposed functions of these two residues. Most significantly, the crystal structure reveals that Tyr294, which has not been implicated as a key residue in this reaction, is probably the nucleophile involved in the cyclopropane ring opening step. This assignment is further corroborated by the finding that the Y294F mutant is totally inactive with regard to ACC turnover. These results, coupled with the observations of Ose et al.,[15] provide strong evidence in support of the hypothesis that the ring cleavage of ACC is initiated by nucleophilic addition and thus establish an unprecedented role of coenzyme B_6 in catalysis.[21] Our ongoing investigation into the structures of this enzyme in complexes with other ligands may provide additional mechanistic insight into this unusual coenzyme B_6 dependent reaction.

Received: November 18, 2003
Revised: March 12, 2004 [Z53353]

Keywords: enzyme catalysis · enzymes · proteins · reaction mechanisms · structure elucidation

[1] M. Honma, T. Shimomura, *Agric. Biol. Chem.* **1978**, *42*, 1825–1831.
[2] A. E. Evangelopoulos, *Chemical and Biological Aspects of Vitamin B_6 Catalysis*, Alan R. Liss, New York, **1984**.
[3] M. Honma, T. Shimomura, K. Shiraishi, A. Ichihara, S. Sakamura, *Agric. Biol. Chem.* **1979**, *43*, 1677–1679.
[4] C. T. Walsh, R. A. Pascal, Jr., M. Johnston, R. Raines, D. Dikshit, A. Krantz, M. Honma, *Biochemistry* **1981**, *20*, 7509–7519.
[5] H.-w. Liu, *Pure Appl. Chem.* **1998**, *70*, 9–16.
[6] K. Li, W. Du, N. L. S. Que, H.-w. Liu, *J. Am. Chem. Soc.* **1996**, *118*, 8763–8764.
[7] Z. Zhao, H. Chen, K. Li, W. Du, S. He, H.-w. Liu, *Biochemistry* **2003**, *42*, 2089–2103.
[8] M. Yao, H. Sugimoto, A. Horiuchi, A. Nakagawa, S. Wakatsuki, D. Yokoi, T. Murakami, M. Honma, I. Tanaka, *J. Biol. Chem.* **2000**, *275*, 34557–34565.
[9] M. D. Erion, C. T. Walsh, *Biochemistry* **1987**, *26*, 3417–3425.
[10] The protein crystals were grown in a buffer containing 10% isopropanol and 20% poly(ethylene glycol) 4000 in 0.1M 2-[4-(2-hydroxyethyl)-1-piperazinyl]ethanesulfonic acid (pH 7.5), and in the presence of ACP (**10**; 5 mM). The X-ray diffraction data were collected at beamline X12C, National Synchrotron Light Source, at Brookhaven National Laboratory. The crystals diffract to give results with a 2.5-Å resolution and belong to the space group $P2_12_12_1$, with cell dimensions of $a = 67.76$, $b = 68.59$, and $c = 350.91$ Å. The complex structure has been refined to $R = 0.202$ and $R_{free} = 0.244$. The initial phases were solved by the molecular replacement method with the yeast enzyme structure[8] as the search model. The accession code of this enzyme complex in the Protein Data Bank is 1RQX.
[11] For studies in which the presence of a transient aminal adduct is implied, see: a) C. S. Federiuk, J. A. Shafer, *J. Biol. Chem.* **1983**, *22*, 5372–5378; b) J. F. Kirsch, G. Eichele, G. C. Ford, M. G. Vincent, J. N. Jansonius, H. Gehring, P. Christen, *J. Mol. Biol.* **1984**, *174*, 497–525; c) Y. M. Torchinsky in *Vitamin B_6 Pyridoxal Phosphate, Chemical, Biochemical, and Medical Aspects*, Part B (Eds.: D. Dolphin, R. Poulson, O. Avramovic), Wiley-Interscience, New York, **1986**, pp. 163–221.
[12] J. Sivaraman, Y. Li, R. Larocque, J. D. Schrag, M. Cygler, A. Matte, *J. Mol. Biol.* **2001**, *311*, 761–776.
[13] The pro-*R* carbon atom in the cyclopropane ring of ACP (**10**) is equivalent to the pro-*S* atom in ACC (**1**) as a result of a change in the priority assignment of the substituents.
[14] R. K. Hill, S. R. Prakash, R. Wiesendanger, W. Angst, B. Martinoni, D. Arigoni, H.-w. Liu, C. T. Walsh, *J. Am. Chem. Soc.* **1984**, *106*, 795–796.
[15] T. Ose, A. Fujino, M. Yao, N. Watanabe, M. Honma, I. Tanaka, *J. Biol. Chem.* **2003**, *278*, 41069–41076.
[16] Interestingly, enzyme activity is higher when the reaction is run in the buffer system used for crystallization than when a plain potassium phosphate buffer is used.

 © 2004 Wiley-VCH Verlag GmbH & Co. KGaA, Weinheim

[17] Tyrosine can act as a nucleophile in enzyme catalysis, for example, in tyrosine kinase reactions. For examples involving enzymes other than kinases, see: a) J. A. Mancini, R. J. Waugh, J. A. Thompson, J. F. Evans, M. Belley, R. Zamboni, R. C. Murphy, *Arch. Biochem. Biophys.* **1998**, *354*, 117–124; b) J. C. Gebler, D. E. Trimbur, R. A. J. Warren, R. Aebersold, M. Namchuk, S. G. Withers, *Biochemistry* **1995**, *34*, 14547–14553.

[18] The Y268F mutant protein was characterized and assayed by the procedures described for Y294F. The mutant retained less than 2% of the wild-type activity. While both tyrosine residues are important for catalysis, Tyr294 is a more likely candidate for the nucleophile for two reasons: Tyr294 is closer than Tyr268 to the cyclopropane ring, and all enzymatic activity is lost when Tyr294 is mutated to phenylalanine.

[19] Examples of cyclopropane-ring activation in enzyme catalysis can be found in a few reviews: C. J. Suckling, *Angew. Chem.* **1988**, *100*, 555–570; *Angew. Chem. Int. Ed. Engl.* **1988**, *27*, 537–552; J. Salaün, *Top. Curr. Chem.* **2000**, *207*, 1–67.

[20] H.-w. Liu, R. Auchus, C. T. Walsh, *J. Am. Chem. Soc.* **1984**, *106*, 5335–5348.

[21] There are many examples in which the PLP coenzyme promotes nucleophilic addition at the β-carbon atom of the substrate–PLP complex. However, the reaction is always initiated by an α-deprotonation step, which occurs prior to the nucleophilic addition at the β-position. Such an α-deprotonation is not possible for ACC deaminase since ACC (**1**) has no α-H atom. In fact, the nucleophilic addition is the initiation step in the ACC-deaminase-catalyzed reaction, a mechanism that is unprecedented in coenzyme B_6 dependent enzymes.

[+]

 © 2004 Wiley-VCH Verlag GmbH & Co. KGaA, Weinheim

Liquid Crystals

A Low-Molar-Mass, Monodispersive, Bent-Rod Dimer Exhibiting Biaxial Nematic and Smectic A Phases

Channabasaveshwar V. Yelamaggad, Subbarao Krishna Prasad, Geetha G. Nair, Indudhara Swamy Shashikala, Doddamane S. Shankar Rao, Chetan V. Lobo, and Sivaramakrishna Chandrasekhar*[+]

In memory of V. N. Raja

Liquid crystal (LC) phases are a unique state of matter. Apart from their importance in life sciences, they have been used as novel media in many practical applications.[1,2] Of the variety of thermotropic LC phases known, the simplest but most exploited phase in display device technology is the optically uniaxial nematic (N_u) phase, in which the constituent rodlike molecules, on average, orient about a common axis called the director **n** (Figure 1a). In contrast, one of the most sought after phases in thermotropic LCs is the biaxial nematic (N_b) phase, in which there is, additionally, a correlation of the molecules in a direction **m** perpendicular to the prime director **n** (Figure 1b). Chandrasekhar et al.[3] were the first to observe this phase, which is yet to be universally accepted.[4] Designing a molecular structure for realizing a N_b phase is not a trivial task, necessitating careful molecular engineering. Nonetheless, several different classes of LCs have been realized[4–8] in which the shape biaxiality[9] of the rodlike or disclike entity is optimized by breaking the shape symmetry. Another phase, the smectic A (SmA) phase, generally has a uniaxial character (Figure 1c), although the possibility of a biaxial smectic A (SmA_b) phase in which the molecules are along the layer normal, but have an additional director **m** in the plane of the layers, was pointed out.[10] Brand et al.[11] developed this idea and proposed a SmA_b phase whose symmetry depends on the type of constituent molecules: D_{2h} if the molecules are boardlike (Figure 1d) and C_{2v} if they are bent-core or banana-shaped molecules (Figure 1e,f). The phase will be SmA_{AP} if the bent-core molecules are randomly oriented within the smectic layer (Figure 1g) The SmA_b phase was first observed in a polymeric system[12] and

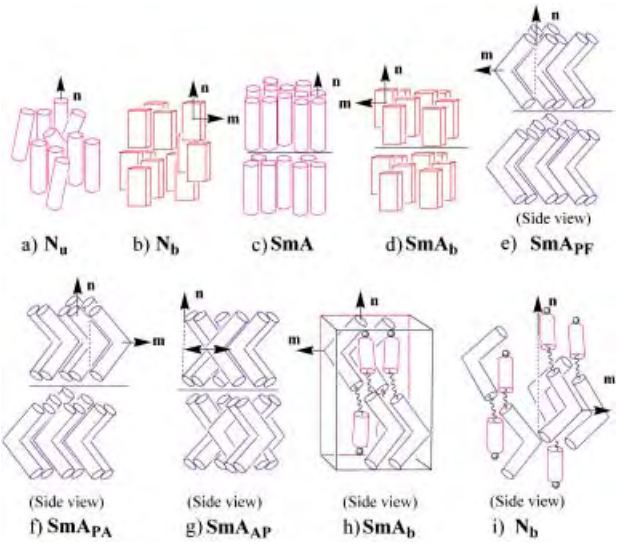


Figure 1. Structural representation of a) the N_u phase formed by conventional rodlike mesogens; b) the N_b phase in which the constituent molecules are boardlike; c) the SmA phase with $D_{\infty h}$ symmetry formed by rodlike molecules; d) the SmA_b phase with the local D_{2h} symmetry built up by boardlike mesogens; e) the SmA_{PF} phase (C_{2v} symmetry) formed by bent-core molecules having a common bent direction; f) the SmA_{PA} phase in which the bent direction of molecules in the neighboring layer alternates; g) the SmA_{AP} phase formed by bent-core molecules with a random orientation of molecules; h) a quartet structure for the SmA_b phase with D_{2h} symmetry, in which a pair of nonsymmetric dimeric molecules in the plane of the paper have their **m** director antiparallel to the pair below that plane; and i) the dimeric molecules in the N_b phase, which is based on ideas of the frustrated spin gas model.

[*] Dr. C. V. Yelamaggad, Dr. S. Krishna Prasad, Dr. G. G. Nair, I. S. Shashikala, Dr. D. S. Shankar Rao, C. V. Lobo, Prof. S. Chandrasekhar[+]
Centre for Liquid Crystal Research
Jalahalli, Bangalore-560 013 (India)
Fax: (+91) 80-2838-2044
E-mail: skprasad1@yahoo.com

[+] Deceased.

Supporting information for this article is available on the WWW under http://www.angewandte.org or from the author.

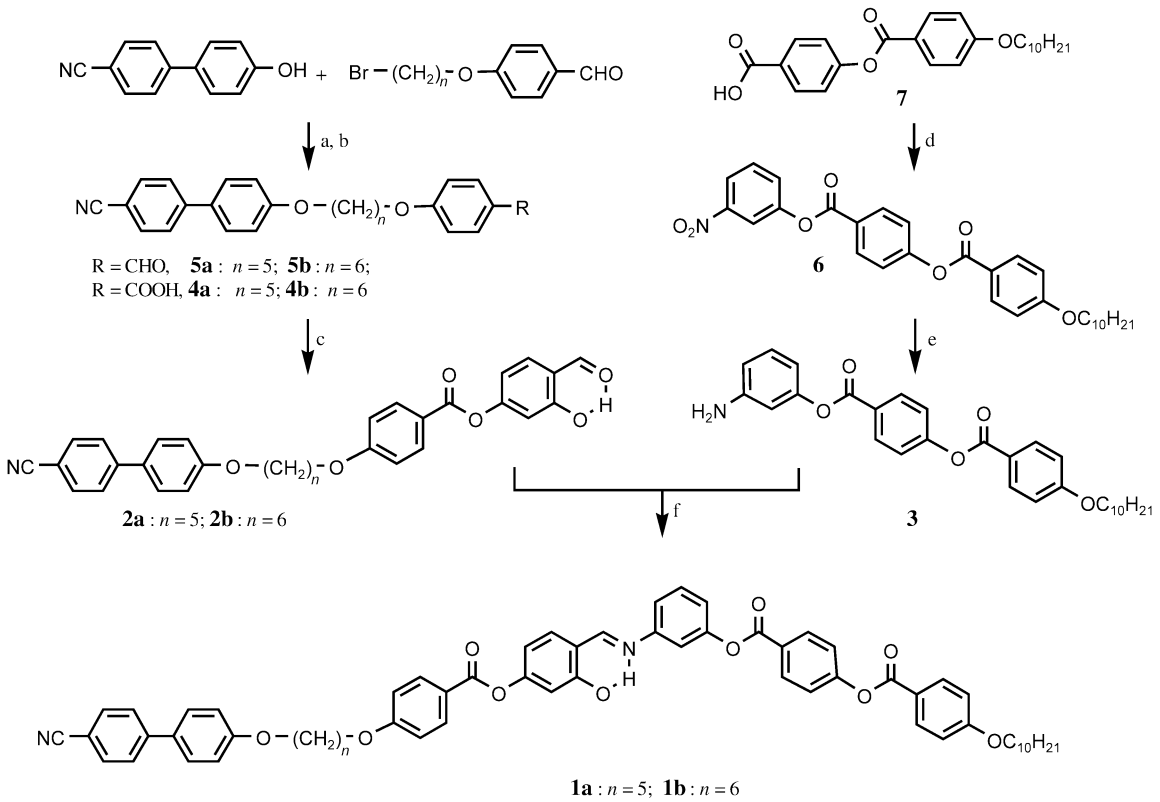
 DOI: 10.1002/anie.200453908 © 2004 Wiley-VCH Verlag GmbH & Co. KGaA, Weinheim

subsequently in a mixture of rodlike and bent-core molecules,[13] pure bent-core molecules,[14] and a metallomesogen mixed with 2,4,7-trinitrofluorenone (TNF).[15] The nematic–smectic A transition (N–SmA) is perhaps the most exhaustively studied, but is still the least understood with quite a few open questions.[16] Investigations on the N_b–SmA_b transition that could answer some of these questions have thus far been limited to a report on a side chain LC polymer[12] in which the authors mentioned the difficulties of working with polymeric material. Thus the need arises to observe such a transition in a low-molecular-weight system. Here we report the first example of a low-molar-mass system displaying a N_b–SmA_b transition, as evidenced by textural pattern, in-plane birefringence, conoscopic, calorimetric, electro-optical switching, and X-ray studies.

In view of the fact that bent-core molecules have strong shape biaxiality,[17,18] we introduced a new molecular engineering concept in which the shape biaxiality of a rodlike mesogen is enhanced by covalently linking the mesogen linearly to a bent-core molecule through a flexible polymethylene spacer to form nonsymmetrical dimers.[19,20] Additional support for this idea came from the results of the frustrated spin-gas model.[21] Thus we produced linear dimers consisting of a cyanobiphenyl unit—that is, a rodlike molecule known to exhibit the nematic phase—covalently attached to a salicylaldimine-based, unsymmetrical, banana-shaped molecule that generally supports the formation of smectic phases through a central flexible spacer containing an odd or even number of methylene units.

The synthesis of the unique dimers **1a** and **1b**, which contain a pentamethylene and a hexamethylene spacer, respectively, is depicted in Scheme 1 (see the Supporting Information for data on **1a** and **1b**). Owing to the presence of the terminal polar group and the asymmetric structure, the molecule can be regarded as a "peelable banana" in which the top (with the stalk) can be differentiated from the bottom. This new structural feature is the important factor in stabilizing the mesomorphic sequence observed for **1b** (see below).

Contrary to our expectations, dimer **1a** is non-liquid crystalline, perhaps due to the stiffer conformation of the spacer. On the other hand, three mesophases could be detected for **1b** by polarizing microscopy, calorimetry, and X-ray investigations. The lowest temperature mesophase (M) was found to be uniaxial with a layered structure but with some unusual textures. Detailed characterization is underway to establish the nature of this phase. From preliminary microscopic observations the other two phases could easily be identified as nematic (N) and smectic (Sm) phases, respectively. First, we will discuss the characterization of the Sm phase. The X-ray measurements were carried out by placing **1b** in a Lindemann capillary tube and aligning it in the



Scheme 1. Synthesis of the nonsymmetrical, bent-rod dimers **1a** and **1b**. a) K_2CO_3, DMF, 80 °C, 12 h; b) **5a** or **5b**, Jones's reagent (CrO_3, H_2SO_4, H_2O); c) 2,4-dihydroxybenzaldehyde, DCC, DMAP, CH_2Cl_2, RT, 2 h; d) 3-nitrophenol, DCC, DMAP, CH_2Cl_2, RT, 4 h; e) H_2/Pd–C (10%), EtOH, 16 h; f) abs. EtOH, AcOH (one drop), reflux, 2 h. DCC = *N*,*N*′-dicyclohexylcarbodiimide, DMAP = 4-dimethylaminopyridine. Phase transition temperatures and transition enthalpies: **1a**: Cr 141.7 °C (35.8 J g^{-1}) I. **1b**: I 162.1 °C (0.4 J g^{-1}) N_b 135.6 °C (0.1 J g^{-1}) SmA_b 119.2 °C M 105.5 °C (49.6 J g^{-1}) Cr. (Cr crystalline, I isotropic, M uniaxial smectic, N nematic, Sm smectic).

 © 2004 Wiley-VCH Verlag GmbH & Co. KGaA, Weinheim

presence of a magnetic field (≈2 T) by cooling it from the isotropic (I) phase through the N phase. The X-ray diffraction pattern collected using a two-dimensional imaging plate showed a pair of small-angle reflections and a pair of wide-angle diffuse arcs orthogonal to the small-angle ones (Figure 2a). The extracted spacing of the low-angle reflection (see the Supporting Information) is comparable to the length of the molecule in its most extended configuration, showing that the phase is SmA.

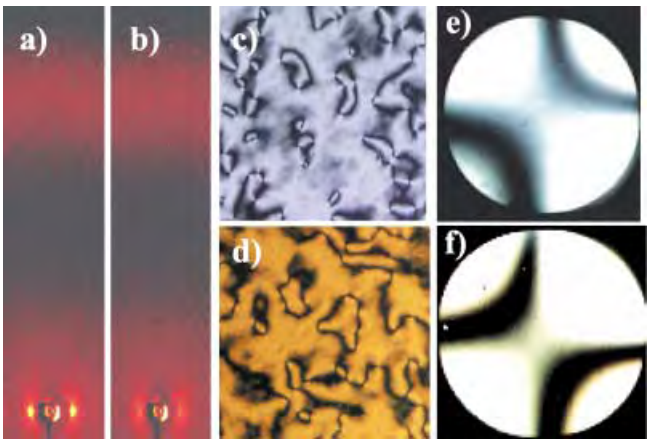


Figure 2. The X-ray (a, b), textural (c, d), and conoscopic (e, f) patterns obtained for the SmA_b (a, c, e) and N_b phases (b, d, f). The texture consists of only 1/2 strength disclinations and isogyres in the conoscopic pattern are well separated.

In the optical studies, with the substrates treated for planar configuration of the molecules, a focal conic texture was observed. However, even glass plates treated with octadecyltriethoxysilane failed to produce a perfectly homeotropically aligned sample. Instead a low-birefringence schlieren texture consisting of exclusively two-brush disclinations (strength $S = \pm 1/2$, Figure 2c) was seen, which has some important implications. Firstly, it rules out the phase being a SmC phase. The $\pm 1/2$ defects have been predicted[11] as well as observed for the SmA_b/SmA_p phase.[12–15] However, the ordering of the bent-core molecules in a layer such that their "arrow" directions are uniformly oriented would result in a polar layer (Figure 1e) with an electric polarization parallel to the in-plane director **m**. Since **m** is polar, such a structure will not support the formation of $\pm 1/2$ defects. But if the direction of **m** alternates between adjacent layers (Figure 1f), it can exhibit a two-brush schlieren pattern and the structure would be antiferroelectric in character. However, the absence of any switching upon the application of square-wave as well as triangular-wave, low-frequency (1–10 Hz) fields rules out the antiferroelectric structure. The optical biaxiality of the phase was evidenced by conoscopic studies on a homeotropically aligned sample in which the molecules are uniformly oriented with the director **n** normal to the substrate. Application of a 1-kHz sine wave, in-plane electric field (70 V magnitude) to this sample aligned the director **m**. The conoscopic pattern obtained shows clear separation of the isogyres (Figure 2e), a characteristic feature of biaxial phases. Two other aspects that need to be mentioned are the strong intensity fluctuations and the formation of a striped texture (see the Supporting Information), both features being reported for the SmA_b/SmA_p phase.[14,15] All these points unambiguously prove that this phase is the SmA_b. Quantitative measurements of the in-plane birefringence (Δm) using a tilting plate compensator yielded a value of 0.013 at ≈10 °C away from the transition to the N phase.

When the sample was taken between either untreated or polyimide-coated, unrubbed plates, the N phase showed the typical schlieren texture, except that the pattern consisted entirely of two-brush disclinations (Figure 2d), which is an indication of biaxiality.[6] This is supported by the topological considerations of Mermin[22] and recent computer simulations.[23] To ensure that the biaxiality was not introduced by the glass surfaces, we examined the textures formed in both the N and SmA_b phases in a free-standing film. Again only $S = \pm 1/2$ spontaneous defects were observed (see the Supporting Information). The conoscopic observations carried out in the N phase as described above showed clear separation of the isogyres (Figure 2f), confirming the biaxiality of the phase, although Δm is only 0.005. The X-ray pattern (Figure 2b) obtained in this phase was identical to that in the SmA_b phase, except that the width of the reflections was more indicative of a lack of positional order along any direction. Furthermore, samples taken between kapton sheets that were coated with a polyimide solution and unidirectionally rubbed also yielded essentially similar patterns in both the SmA_b and N_b phases.

As discussed earlier, two apparent forms of molecular packing for SmA_b having ferroelectric and antiferroelectric arrangements of the dimers are similar to the structures shown in Figures 1e and 1f. However, the observation of the $S = \pm 1/2$ defects and the absence of any antiferroelectric-like electric switching signal rules out these structures. (Even with moderately high fields we did not observe any switching. However, the presence of a cyano group adds a new dimension to the problem, namely, that higher fields result in Freedericksz transition. Therefore, measurements at higher fields were not possible.) Although a packing of the molecules such that the **m** director of the neighboring molecules lies in the molecular plane, but points randomly to the left or to the right (Figure 1g), can explain the observed features, it is not efficient from the point of view of excluded volume. The quartet structure[14] (Figure 1h) in which four dimers form a group is a possibility since this structure, as an entity, has D_{2h} symmetry and accounts for all the features observed for the SmA_b phase. The quartet model can also be used to explain a nonpolar N_b phase, in which the quartets are arranged in such a fashion as to loose the one-dimensional positional order of the smectic phase, leading to the appearance of the N_b phase. For the N_b phase, the problem of excluded volume mentioned above does not place any serious restrictions on the packing of the molecules. Hence, the structure shown in Figure 1i is more probable than the quartet structure. Furthermore, from a molecular point of view, the appearance of the N_b phase in a system of bent-core molecule of the type we have synthesized can be explained on the basis of the quite successful frustrated spin gas model developed by Berker and Walker.[21]

 © 2004 Wiley-VCH Verlag GmbH & Co. KGaA, Weinheim

In summary, we report the first occurrence of the N_b–SmA_b phase transition in a low-molecular-weight LC system. This was achieved by a careful design of the constituent molecules that incorporates covalently linking a bent-core molecule to a rodlike mesogen through a flexible spacer. Realization of a biaxial nematic phase in a low-molar-mass system is significant since it opens up the possibility of fabricating new types of liquid crystal display devices. A device employing such a material is attractive as the switching of the in-plane **m** director is expected to be much faster than the switching of the **n** director.

Received: February 3, 2004 [Z53908]

Keywords: biaxial phases · liquid crystals · mesogens · phase transitions

[1] S. Chandrasekhar, *Liquid Crystals*, Cambridge University Press, Cambridge, **1992**.
[2] P. G. de Gennes, J. Prost, *The Physics of Liquid Crystals*, Clarendon, Oxford, **1993**.
[3] S. Chandrasekhar, B. K. Sadashiva, B. R. Ratna, V. N. Raja, *Pramana* **1988**, *30*, L-491.
[4] G. R. Luckhurst, *Thin Solid Films* **2001**, *393*, 40.
[5] K. Praefcke, B. Kohne, B. Gundogan, D. Singer, D. Demus, S. Diele, G. Pelzl, U. Bakowsky, *Mol. Cryst. Liq. Cryst.* **1991**, *198*, 393.
[6] S. Chandrasekhar, G. G. Nair, D. S. Shankar Rao, S. Krishna Prasad, K. Praefcke, D. Blunk, *Liq. Cryst.* **1998**, *24*, 67; S. Chandrasekhar, G. G. Nair, D. S. Shankar Rao, S. Krishna Prasad, K. Praefcke, D. Blunk, *Curr. Sci.* **1998**, *75*, 1042.
[7] J. Li, V. Percec, C. Rosenblatt, O. D. Lavrentovich, *Europhys. Lett.* **1994**, *25*, 199.
[8] a) B. R. Acharya, A. Primak, T. J. Dingemans, E. T. Samulski, S. Kumar, *Pramana* **2003**, *61*, 231; b) L. Omnes, B. A. Timimi, T. Gelbrich, M. B. Hursthouse, G. R. Luckhurst, D. W. Bruce, *Chem. Commun.* **2001**, 2248; c) R. W. Date, D. W. Bruce, *J. Am. Chem. Soc.* **2003**, *125*, 9012.
[9] Based on considerations of symmetry, a feature required to realize biaxial phases is molecular biaxiality. This could be due to the molecules having biaxial correlations or to their shape biaxiality. Here we consider only the latter.
[10] W. L. McMillan, *Phys. Rev. A* **1973**, *8*, 1921.
[11] H. R. Brand, P. E. Cladis, H. Pleiner, *Macromolecules* **1992**, *25*, 7223.
[12] H. F. Leube, H. Finkelmann, *Makromol. Chem.* **1991**, *192*, 1317.
[13] R. Pratibha , N. V. Madhusudana, B. K. Sadashiva, *Science* **2000**, *288*, 2184.
[14] K. J. K. Semmler, T. J. Dingemans, E. T. Samulski, *Liq. Cryst.* **1998**, *24*, 799; A. Eremin, S. Diele, G. Pelzl, H. Nadasi, W. Weissflog, J. Salfetnikova, H. Kresse, *Phys. Rev. E* **2001**, *64*, 051701; B. K. Sadashiva, R. A. Reddy, R. Pratibha, N. V. Madhusudana, *J. Mater. Chem.* **2002**, *12*, 943.
[15] T. Hegmann, J. Kain, S. Diele, G. Pelzl, C. Tschierske, *Angew. Chem.* **2001**, *113*, 911; *Angew. Chem. Int. Ed.* **2001**, *40*, 887.
[16] P. Barois in *Physical Properties of Liquid Crystals*, (Eds.: G. W. Gray, V. Vill, H.-W. Spiess, D. Demus, J. W. Goodby), Wiley-VCH, Weinheim, **1999**.
[17] T. Niori, T. Sekine, J. Watanabe, T. Furukawa, H. Takezoe, *J. Mater. Chem.* **1996**, *6*, 1231.
[18] a) D. M. Walba, E. Korblova, R. Shao, J. E. Maclennan, D. R. Link, M. A. Glaser, N. A. Clark, *Science* **2000**, *288*, 2181; b) T. C. Lubensky, *Science* **2000**, *288*, 2146.
[19] Several monodispersive cyclic compounds formed by combining a banana-shaped unit and a rodlike moiety have been reported to form uniaxial nematic and smectic mesophases: A. Godt, S. Duda, O. Unsal, J. Thiel, A. Harter, M. Roos, C. Tschierske, S. Diele, *Chem. Eur. J.* **2002**, *8*, 5094.
[20] "Liquid Crystal Dimers and Oligomers": C. T. Imrie, G. R. Luckhurst in *Handbook of Liquid Crystals*, *Vol. 2B* (Eds.: D. Demus, J. W. Goodby, G. W. Gray, H.-W. Spiess, V. Vill), Wiley-VCH, Weinheim, **1998**, chap. X.
[21] A. N. Berker, J. S. Walker, *Phys. Rev. Lett.* **1981**, *47*, 1469.
[22] N. D. Mermin, *Rev. Mod. Phys.* **1979**, *51*, 591.
[23] C. Chiccoli, I. Feruli, O. D. Lavrentovich, P. Pasini, S. V. Shiyanovskii, C. Zannoni, *Phys. Rev. E* **2002**, *66*, 030701.

 © 2004 Wiley-VCH Verlag GmbH & Co. KGaA, Weinheim

Fluorescent Amino Acids

A Very Short Route to Enantiomerically Pure Coumarin-Bearing Fluorescent Amino Acids**

*Marie-Priscille Brun, Laurent Bischoff, and Christiane Garbay**

Fluorescent derivatives of biologically active peptides are useful experimental tools for studying biological structure and function[1] and for visualizing intracellular processes or molecular interactions.[2] To achieve adequate detection of peptide fluorescence, the monitored peptide must either include a natural fluorescent amino acid, such as tyrosine (Tyr) or tryptophan (Trp), or must be labeled with extrinsic or intrinsic probes.[3] Since C- and N-terminal domains are often important interactive sites, the incorporation of the fluorescent label into the peptide at a well-chosen position is critical to avoiding changes in the conformational and biological characteristics of the parent peptide.[4a] The use of an amino acid as a fluorescent chromophore[4] offers at least two advantages: first, peptides containing this amino acid can be synthesized by solid-phase peptide synthesis (SPPS); and second, since both ends of these peptides are free, other residues may be attached to improve solubility or lability.[5] In addition to the excitation and emission properties of a

[*] M.-P. Brun, Prof. Dr. C. Garbay
Laboratoire de Pharmacochimie Moléculaire et Cellulaire
INSERM U648 CNRS FRE 2718, UFR Biomedicale
45, Rue des Saints Pères, 75270 Paris Cedex 06 (France)
Fax : (+33) 142-864-082
E-mail: christiane.garbay@univ-paris5.fr
Prof. Dr. L. Bischoff
IRCOF, UPRES-A 6014, INSA
B.P. 08, 76131 Mont-St-Aignan Cedex (France)

[**] This research was supported by "La Ligue Nationale contre le Cancer". We thank Dr. Veronique Gigoux for assistance in the preparation of cell cultures and Dr. Nicolae Ghinea for confocal microscopy studies.

Supporting information for this article is available on the WWW under http://www.angewandte.org or from the author.

 © 2004 Wiley-VCH Verlag GmbH & Co. KGaA, Weinheim DOI: 10.1002/anie.200454116

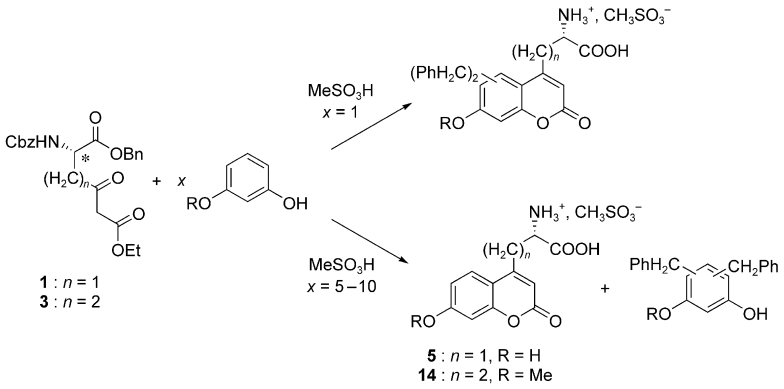
fluorescent amino acid its steric hindrance must also be considered. Thus, augmenting the conjugation in an amino acid increases its fluorescence-emission properties. On the other hand, however, such increased conjugation (as in the case of polycycles) gives rise to more steric hindrance, associated with lowered coupling yields. Furthermore, since a higher chemical stability is expected if the fluorophore is linked to the amino acids by a side-chain carbon–carbon bond, we have focused on developing small and sensitive fluorescent coumaryl amino acids that could be incorporated efficiently into peptides in place of Tyr or Trp.

Coumarins are interesting fluorescent molecules due to their relatively high quantum yields, low bleaching, reasonable stability, and relative ease of synthesis. They have been used extensively to label amines, thiols, and acids,[6] thereby providing useful experimental tools.[7] To date, enantioselective synthesis of amino acids,[8] especially coumaryl amino acids, has been carried out by diastereoselective alkylation of chiral glycine equivalents. For example, the chiral auxiliaries of Oppolzer et al.[9] and Williams[10] were used for the synthesis of L-(6,7-dimethoxycoumar-4-yl)alanine and L-(7-methoxycoumar-4-yl)alanine (Mca, (*S*)-**6**), respectively.[4c,d] These methods produced optically pure amino acids, but they required multiple steps and the amino acids were obtained in poor global yields. Herein we report a more rapid, cheap, and versatile synthesis of coumaryl amino acids that led to coumaryl alanines and coumaryl ethylglycines in either a two- or a three-step process.

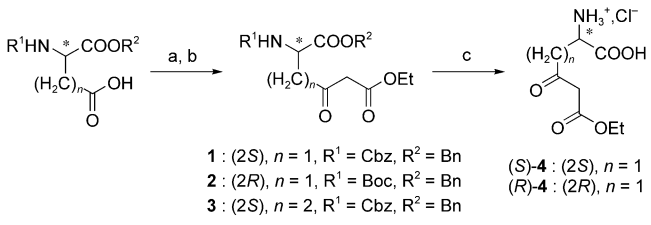
Protected aspartic (Asp) and glutamic acids (Glu) were used as chiral starting materials,[11] thus avoiding high-cost chiral auxiliaries. They were transformed into side-chain β-ketoesters (which we had chosen as coupling partners for the condensation with phenols to obtain the coumarin moiety[12]) by using the procedure of Masamune et al.[13] (Scheme 1). Pure β-ketoesters **1**–**3** were obtained in good yields after silica-gel column chromatography.

Coumarins have been synthesized by many pathways, including von Pechmann, Perkin, Knoevenagel, Reformatsky, and Wittig reactions.[14] The von Pechmann reaction is one of the simplest and most straightforward methods. It involves a phenol condensation with a β-ketoester in the presence of a variety of Brønsted[14a,15] and Lewis acids.[12,16] We chose the von Pechmann condensation in methanesulfonic acid (MSA).[15] This condensation, carried out in the presence of 25 equivalents of MSA, proceeded smoothly and resulted in the complete dissolution of starting material and the complete conversion of the β-ketoester. Reaction times depended on the substituents on the phenol ring: the greater the number of electron-donating groups, the shorter the reaction time.

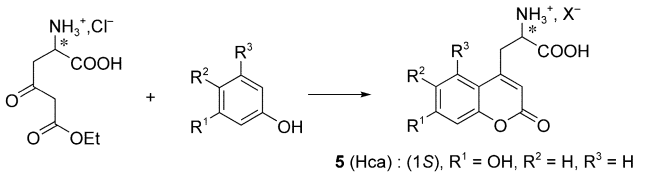
Since OCO–benzyl and NCO_2–benzyl bonds are not stable under these conditions, running the reaction in the presence of one equivalent of resorcinol produced polybenzylated coumarins. This could be avoided by using a large excess of the resorcinol derivative, which acts as a scavenger for the benzyl cations (Scheme 2). This allowed the formation of compounds **5** and **14** in only one, direct step. For expensive resorcinols, we first deprotected both amine and carboxy groups to avoid side reactions (step c in Scheme 1). The deprotected aspartic acid derived β-ketoester, (*S*)- or (*R*)-**4**, was then treated with various polysubstituted phenols in the presence of MSA to give compounds **5**–**13** (Scheme 3). Hydrogenolytic conditions used for Asp are unsuitable for



Scheme 2. General synthesis of coumaryl amino acids.



Scheme 1. Synthesis of amino acid derived β-ketoesters. a) Carbonyldiimidazole, THF, room temperature; b) magnesium salt of monoethyl malonic acid, THF, 0 °C and 12 h at room temperature, 50–80%; c) H_2, Pd/C 10%, HCl, AcOEt/EtOH, room temperature, 90–100% (and for **2**, 1:1 TFA:$CHCl_3$ at 0 °C and 1 h at room temperature). TFA = trifluoroacetic acid, Cbz = benzyloxycarbonyl, Boc = *tert*-butoxycarbonyl, Bn = benzyl.

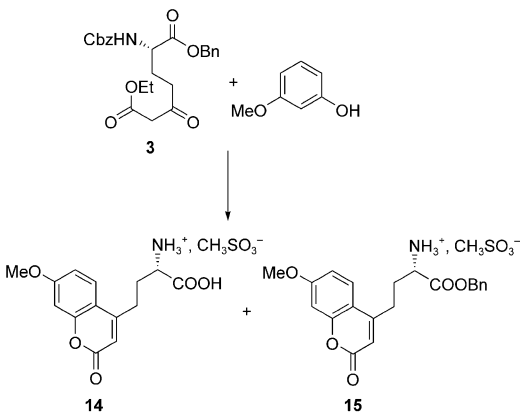


5 (Hca) : (1*S*), R^1 = OH, R^2 = H, R^3 = H
(*S*)-**6** (Mca) : (1*S*), R^1 = OMe, R^2 = H, R^3 = H
(*R*)-**6** : (1*R*), R^1 = OMe, R^2 = H, R^3 = H
7 : (1*S*), R^1 = OMe, R^2 = OMe, R^3 = H
8 : (1*S*), R^1 = OH, R^2 = Cl, R^3 = H
9 : (1*S*), R^1 = OEt, R^2 = H, R^3 = H
10 : (1*S*), R^1 = OMe, R^2 = H, R^3 = OH
11 : (1*S*), R^1 = OH, R^2 = H, R^3 = OMe
12 : (1*S*), R^1 = OMe, R^2 = H, R^3 = OMe
13 : (1*S*), R^1 = OH, R^2 = H, R^3 = OH

Scheme 3. Synthesis of aspartic acid derived coumaryl amino acids. MSA (25 equiv), 0 °C, then room temperature, 2–4 h, 16% (**8**) to 71% (**6**); $X^- = CH_3SO_3^-$ ((*S*)-**6**) or $CF_3CO_2^-$ in case of purification by semi-preparative HPLC on a Kromasil C_8 column (A (H_2O+0.1% TFA) and B (70:30 CH_3CN:H_2O+0.09% TFA), with an appropriate linear gradient of B).

 © 2004 Wiley-VCH Verlag GmbH & Co. KGaA, Weinheim

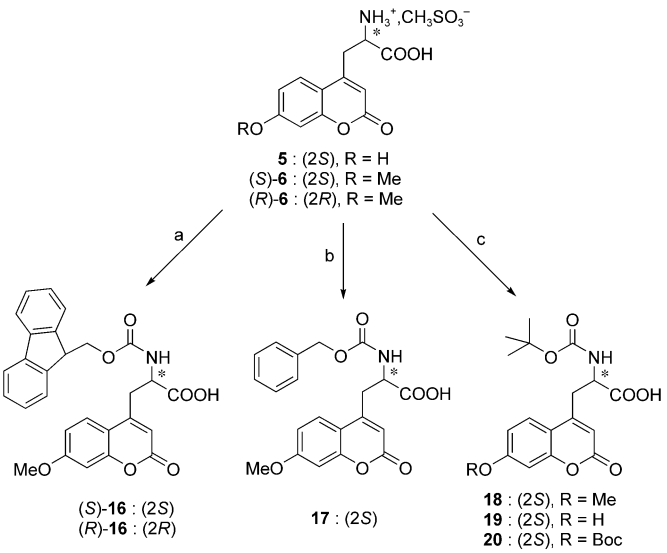
Glu.[17] Therefore, coumarin formation was conducted on the still-protected β-ketoester **3** with a large excess of 3-methoxyphenol (Scheme 4), which led to two products. In one product, compound **14**, the amine and acid functionalities were



Scheme 4. Synthesis of glutamic acid derived coumaryl amino acids. 3-Methoxyphenol (10 equiv), MSA (25 equiv), 0 °C then room temperature, 2 h, 60% (ratio **14**:**15** = 62:38).

deprotected, whereas the other, compound **15**, still bore the benzyl ester group. Coumaryl amino acids in which the amino group was protected with a widely used protecting group, such as Fmoc ((*S*)- and (*R*)-**16**), Cbz (**17**), or Boc (**18**–**20**), were also synthesized (Scheme 5).

Since a stereogenic carbon atom is present in these amino acids, we measured optical rotation (Table 1) and also determined the enantiomeric purity of one of the compounds. We assumed that the other compounds would exhibit the same sensitivity towards racemization, given that the most probable source of racemization should be the earlier formation of the β-ketoester in a slightly alkaline medium. To verify the optical purity, the amino groups of (*S*)- and (*R*)-**6** were protected with an Fmoc group and the compounds coupled with *tert*-butylalaninate. The purity of the corresponding diastereomeric products **21** and **22** was examined by



Scheme 5. Synthesis of *N*-protected coumaryl amino acids. a) 10% $NaHCO_3$ at 0 °C, FmocCl at 0 °C, 1:1 dioxane:H_2O, 1 h at 0 °C then 2 h at room temperature, 80% ((*S*)-**16**) and 70% ((*R*)-**16**); b) NaOH at 0 °C, CbzCl at 0 °C, 1:1 dioxane:H_2O, 1 h at room temperature, 91%; c) Boc_2O at 0 °C, 1:1 dioxane:5% $NaHCO_3$, 1 h at 0 °C then 3 h at room temperature, 84% (**18**) and 75% (**19** and **20**). Fmoc = 9-fluorenylmethoxycarbonyl.

using appropriate HPLC isocratic conditions (Figure 1). In the case of **21**, only one diastereomer could be detected. For **22**, a diastereomeric ratio of 98:2 was observed for the crude reaction mixture. We can conclude that no racemization occurred during the β-ketoester formation, in the course of the cyclization, or during the protection and coupling processes (BOP (= benzotriazol-1-yloxytris(dimethylamino)-phosphonium hexafluorophosphate)/DIEA (= *N*,*N*-diisopropylethylamine)). These observations suggest that the *N*-protected amino acids obtained can be incorporated by SPPS into peptides without risk of racemization.

Absorption and fluorescence wavelength maxima, extinction coefficients, and fluorescence quantum yields (QY) were measured for each compound (Figure 2, Table 1). The optical

Table 1: Physicochemical properties of coumaryl amino acids.[a]

		n	R^1	R^2	R^3	Yield [%]	$[\alpha]_D^{20}$[a]	$\lambda_{Abs.}$ [nm][b]	$\lambda_{Em.}$ [nm][b]	ε [cm^{-1} M^{-1}][c]	QY[d]
Trp	–	–	–	–	–	–	–	278[18a]	352[18a]	5300[18a]	0.12[18b]
Tyr	–	–	–	–	–	–	–	274[18a]	303[18a]	1400[18a]	0.13[18b]
5	(2*S*)	1	OH	H	H	47	8.4	329	464	9000	0.49
(*S*)-**6**	(2*S*)	1	OMe	H	H	71	12.9	324	383	12000	0.18
(*R*)-**6**	(2*R*)	1	OMe	H	H	70	−12.1	323	386	14000	0.15
7	(2*S*)	1	OMe	OMe	H	45	n.d.[e]	345	423	12000	0.60
8	(2*S*)	1	OH	Cl	H	16	3.2	331	465	10300	0.54
9	(2*S*)	1	OEt	H	H	39	15.7	325	387	13300	0.17
10	(2*S*)	1	OMe	H	OH	36	n.d.[e]	329	421	6800	0.50
11	(2*S*)	1	OH	H	OMe	18	10.1	323	421	12700	0.18
12	(2*S*)	1	OMe	H	OMe	34	12.0	324	419	11500	0.39
13	(2*S*)	1	OH	H	OH	48	13.2	327	463	11800	n.d.[e]
14	(2*S*)	2	OMe	H	H	37	19.4	321	380	12500	0.21
15	(2*S*)	2	OMe	H	H	23	n.d.[e]	322	381	14600	0.17

[a] Determined in 1 N HCl. [b] Determined in 95% ethanol. [c] Extinction coefficient. [d] Quantum yield using quinine sulfate in sulfuric acid as a standard reference. [e] Not determined.

 © 2004 Wiley-VCH Verlag GmbH & Co. KGaA, Weinheim

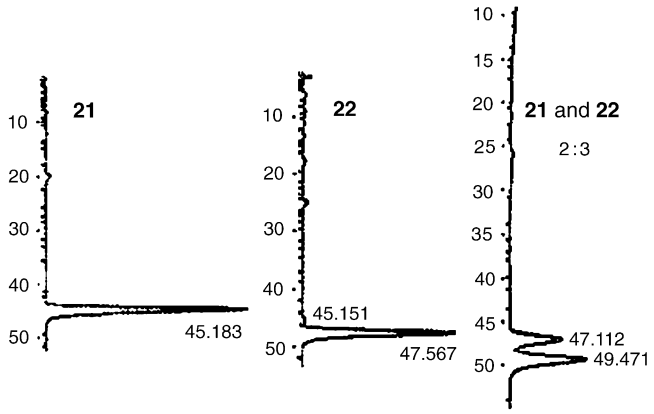


Figure 1. HPLC chromatograms of diastereoisomers **21** and **22**. HPLC isocratic conditions on a Vydac C_{18} column (38% A (H_2O + 0.1% TFA) and 62% B (3:1:1 CH_3CN:EtOH:MeOH)).

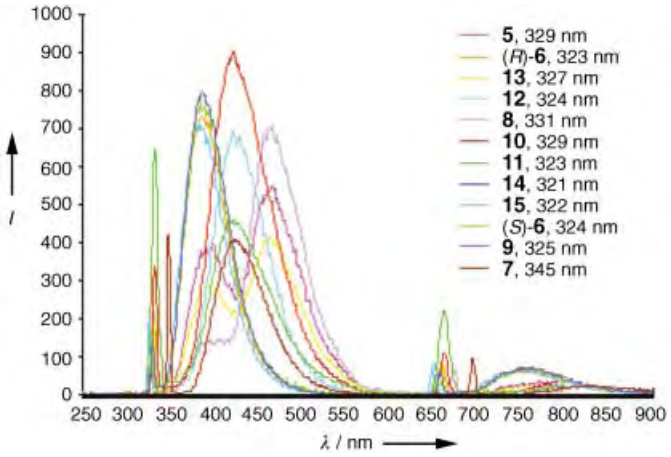


Figure 2. Fluorescence properties of the coumaryl amino acids **5**–**15**.

properties of the natural fluorescent amino acids Trp and Tyr were included for comparison. The novel coumaryl amino acids **5**–**14** had higher wavelength values and higher absorption values than Trp or Tyr, and they displayed higher quantum yields than Trp or Tyr, especially in the case of compounds **5**, **7**, **8**, **10** and **12**, with values ranking from 0.39 to 0.60 versus 0.12 and 0.13 for Trp and Tyr, respectively. These characteristics make compounds **5**–**14** good fluorophores for biological studies.

The use of such fluorescent amino acids in SPPS was validated by adding *N*-Fmoc-protected (*S*)-**6** (Mca) to the C-terminal end of penetratin, a 16 amino acid peptide corresponding to the third helix of the homeodomain of the Antennapedia protein (to give peptide 1, see Experimental Section).[19] To investigate whether the coumaryl amino acid could be used in biological studies, compound **5** (Hca) was added to the N-terminal end of penetratin (to give peptide 2, see Experimental Section). After incubation of this peptide in HeLa cells, we visualized its internalization by confocal microscopy (Figure 3), thus validating the use of coumaryl

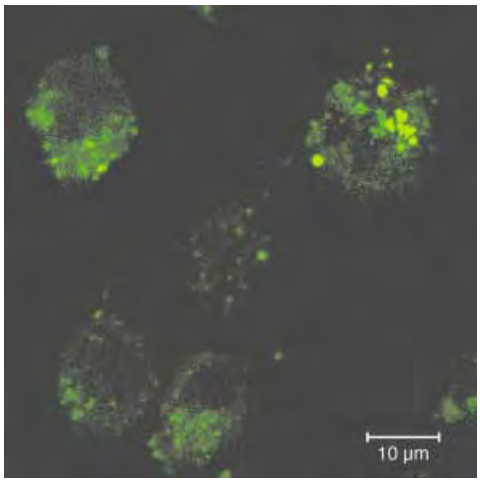


Figure 3. Peptide visualization using confocal microscopy. HeLa cells grown in DMEM (= Dulbecco's minimum essential medium) were treated with 10 μM peptide 2. After 2 h incubation at 37 °C, the cells were washed with PBS (= phosphate-buffered saline), fixed with 3% PFA (= paraformaldehyde) for 20 min at room temperature and mounted for examination. Images were obtained with a Zeiss LSM510 confocal scanning microscope using an argon ion laser set at 488 nm.

amino acids as intrinsic fluorescent labels.

peptide 1 H_2N–RQIKIWFQNRRMKWKK–Mca–COOH
peptide 2 H_2N–Hca-RQIKIWFQNRRMKWKK–COOH

In conclusion, we have developed an extremely direct synthesis of optically pure fluorescent amino acids, starting from inexpensive chiral materials. Our synthesis represents a useful tool in the preparation of coumaryl amino acids, which can be easily incorporated into peptides and used in biological studies. Potential applications of these molecules include the wide range of investigating cellular processes and other aspects of biological mechanism and function.

Experimental Section

Synthesis of peptides 1 and 2: SPPS by using small-scale Fmoc chemistry on a HMP (= 4-hydroxymethylphenoxy) resin, DCC/HOBt coupling method (BOP/HOBt/DIEA for Hca), removal of Fmoc groups with piperidine (20% in NMP), resin cleavage with TFA/TIPS/H_2O (9.5:0.25:0.25 in volume) and HPLC semipreparative purification on a Vydac C_{18} column (A (H_2O+0.1% TFA) and B (70:30 CH_3CN:H_2O+0.09% TFA), using a linear gradient of B from 10 to 90% in 30 min). DCC = *N*,*N*′-dicyclohexylcarbodiimide, HOBt = 1-hydroxybenzotriazole, NMP = *N*-methylpyrrolidinone, TIPS = triisopropylsilane.

See Supporting Information for detailed reaction conditions and compound characterization.

Received: February 26, 2004 [Z54116]

Keywords: amino acids · coumarin · cyclization · fluorescent probes · solid-phase synthesis

[1] a) C. G. Bradshaw, K. Ceszkowski, G. Turcatti, I. J. Beresford, A. Chollet, *J. Med. Chem.* **1994**, *37*, 1991–1995; b) J.-M. Soleilhac, F. Cornille, L. Martin, C. Lenoir, M.-C. Fournié-Zaluski, B. P. Roques, *Anal. Biochem.* **1996**, *241*, 120–127.

 © 2004 Wiley-VCH Verlag GmbH & Co. KGaA, Weinheim

[2] a) G. Turcatti, H. Vogel, A. Chollet, *Biochemistry* **1995**, *34*, 3972 – 3980; b) M. R. Tota, C. D. Strader, *J. Biol. Chem.* **1990**, *265*, 16891 – 16897; c) D. J. Cowley, A. J. Schulze, *J. Pept. Res.* **1997**, *49*, 444 – 454.
[3] a) T. Licher, E. Kellner, H. Lill, *FEBS Lett.* **1998**, *431*, 419 – 422; b) G. Drin, M. Mazel, P. Clair, D. Mathieu, M. Kaczorek, J. Temsamani, *Eur. J. Biochem.* **2001**, *268*, 1304 – 1314; c) G. Jin, X. Huang, R. Black, M. Wolfson, C. Rauch, H. McGregor, G. Ellestad, R. Cowling, *Anal. Biochem.* **2002**, *302*, 269 – 275; d) E. H. Pap, T. B. Dansen, K. W. Wirtz, *Trends Cell Biol.* **2001**, *11*, 10 – 12.
[4] a) H. Mihara, S. Lee, Y. Shimohigashi, H. Aoyagi, T. Kato, N. Izumiya, T. Costa, *FEBS Lett.* **1985**, *193*, 35 – 38; b) M. Taki, T. Hohsaka, H. Murakami, K. Taira, M. Sisido, *FEBS Lett.* **2001**, *507*, 35 – 38; c) F. A. Bennett, D. J. Barlow, A. N. O. Dodoo, R. C. Hider, A. B. Lansley, M. J. Lawrence, C. Marriott, S. S. Bansal, *Tetrahedron Lett.* **1997**, *38*, 7449 – 7452; d) P. Kele, G. Sui, Q. Huo, R. M. Leblanc, *Tetrahedron Asymmetry* **2000**, *11*, 4959 – 4963.
[5] W. Wang, T. C. Liang, *Biochem. Biophys. Res. Commun.* **1994**, *201*, 835 – 840.
[6] a) H. Wendt, C. Berger, A. Baici, R. M. Thomas, H. R. Bosshard, *Biochemistry* **1995**, *34*, 4097 – 4107; b) J. H. Wolf, J. Korf, *J. Pharm. Biomed. Anal.* **1992**, *11*, 99 – 107.
[7] a) R. O'Kennedy in *Coumarins*, Wiley, New York, **1997**; b) R. M. Christie, *Rev. Prog. Color. Relat. Top.* **1993**, *23*, 1.
[8] a) R. O. Duthaler, *Tetrahedron* **1994**, *50*, 1539 – 1650; b) R. M. Williams, *Aldrichimica Acta* **1992**, *25*, 11 – 25.
[9] W. Oppolzer, A. J. Kingma, G. Poli, *Tetrahedron Lett.* **1989**, *30*, 6009.
[10] W. Zhai, *Tetrahedron* **1988**, *44*, 5425 – 5430.
[11] R. M. Adlington, J. E. Baldwin, D. Catterick, G. J. Pritchard, *J. Chem. Soc. Perkin Trans. 1* **2001**, 668 – 679.
[12] S. P. Chavan, K. Shivasankar, R. Sivappa, R. Kale, *Tetrahedron Lett.* **2002**, *43*, 8583 – 8586.
[13] D. W. Brooks, L. D. Lu, S. Masamune, *Angew. Chem.* **1979**, *91*, 76 – 77; *Angew. Chem. Int. Ed. Engl.* **1979**, *18*, 72 – 74.
[14] a) H. von Pechmann, C. Duisberg, *Ber. Dtsch. Chem. Ges.* **1883**, *16*, 2119; b) J. R. Johnson, *Org. React.* **1942**, *1*, 210; c) G. Brufola, F. Fringuelli, O. Piermatti, F. Pizzo, *Heterocycles* **1996**, *43*, 127; d) R. L. Shriner, *Org. React.* **1942**, *1*, 1; e) I. Yavari, R. Hekmat-Shoar, A. Zonouzi, *Tetrahedron Lett.* **1998**, *39*, 2391.
[15] W. C. Sun, K. R. Gee, R. P. Haugland, *Bioorg. Med. Chem. Lett.* **1998**, *8*, 3107 – 3110.
[16] D. S. Bose, A. P. Rudradas, M. H. Babu, *Tetrahedron Lett.* **2002**, *43*, 9195 – 9197.
[17] M. P. Brun, A. S. Martin, C. Garbay, L. Bischoff, *Tetrahedron Lett.* **2003**, *44*, 7011 – 7013.
[18] a) G. D. Fasman in *Handbook of Biochemistry and Molecular Biology*, *Proteins*, *Vol. I*, CRC, Boca Raton, FL, **1976**, pp. 183 – 203; b) R. Chen, *J. Res. Natl. Bur. Stand. Sect. A* **1976**, *76*, 593 – 606.
[19] L. Theodore, D. Derossi, G. Chassaing, B. Llir, M. Kubes, P. Jordan, H. Chneiweiss, P. Godement, A. Prochiantz, *J. Neurosci.* **1995**, *15*, 7158 – 7167.

 © 2004 Wiley-VCH Verlag GmbH & Co. KGaA, Weinheim

Magnetism in Clusters

Strong Ferromagnetic Interactions in $[V_8O_{14}(H_{-2}taci)_2]$: An Unprecedented Large Spin Ground State for a Vanadyl Cluster**

Kaspar Hegetschweiler, Bernd Morgenstern, Jon Zubieta,* Pamela J. Hagrman, Nicola Lima, Roberta Sessoli,* and Federico Totti*

The control of the spin of the ground state in molecular clusters behaving like single molecule magnets (SMM) has been an important challenge in coordination chemistry. The spin value is a critical parameter because the barrier for the orientation of the magnetization depends on the square of it.[1,2] The most common strategies exploit antiferromagnetic interactions both in hetero-spin clusters, such as the archetypal SMM, $[Mn_{12}O_{12}(CH_3COO)_{16}(H_2O)_4]$,[3–5] and in particular spin topologies, such as the propeller structure of Fe_4 clusters.[6,7] Ferromagnetic interactions are relatively rare in molecular clusters, and often encountered in very symmetric structures, where the orthogonality of the magnetic orbitals is more easily controlled.[8,9] In low-symmetry environments the sign of the magnetic interaction is, in general, easily predictable for paramagnetic centers with one unpaired electron.[10] Magneto-structural correlations are well established, for instance, for oxo-bridged $\{VO^{2+}\}$ fragments[11] and ferromagnetic interactions have been observed when the d_{xy} magnetic orbitals are orthogonal to each other, where a local reference system with the x and y axis pointing towards the oxo-bridging ligands is considered. The J values usually do not exceed $-10\ cm^{-1}$,[12] the Hamiltonian being defined as $\mathscr{H} =$

[*] N. Lima, Prof. R. Sessoli, Dr. F. Totti
Department of Chemistry & INSTM (UdR Firenze)
Università degli Studi di Firenze
Via della Lastruccia 5, 50019 Sesto Fiorentino (Italy)
Fax: (+39) 055-457-3372
E-mail: roberta.sessoli@unifi.it

Prof. J. Zubieta, Dr. P. J. Hagrman
Department of Chemistry
Syracuse University
Syracuse, NY 13244 (USA)
Fax: (+1) 315-443-4070
E-mail: jazubiet@mailbox.syr.edu

Prof. K. Hegetschweiler, Dr. B. Morgenstern
Universität des Saarlandes
Anorganische Chemie
Postfach 15 11 50, 66041 Saarbrücken (Germany)
Fax: (+49) 681-302-2663
E-mail: hegetschweiler@mx.uni-saarland.de

[**] 1,3,5-Triamino-1,3,5-trideoxy-*cis*-inositol, a Ligand with a Remarkable Versatility for Metal Ions, Part 12. R.S. acknowledges the financial support of Italian MIUR and CNR, German DFG (SPP1137), and EC network MOLNANOMAG(contract Nos. HPRN-CT-1999–00012). K.H. thanks the Syracuse University and the Universität des Saarlandes for a visiting scholarship at Syracuse. taci = 1,3,5-Triamino-1,3,5-trideoxy-*cis*-inositol. Part 11: ref. [21].

Supporting information for this article is available on the WWW under http://www.angewandte.org or from the author.

 © 2004 Wiley-VCH Verlag GmbH & Co. KGaA, Weinheim DOI: 10.1002/anie.200454130

$\sum_{i<j} J_{ij}\mathbf{S}_i\mathbf{S}_j$. In spite of the very rich chemistry of V^{IV} oxo clusters,[13,14] where the nuclearity can be as high as 20,[15] to date only singlet ground states, or $S = 1/2$ for odd nuclearity clusters, have been reported.

Herein we exploit the ability of the ligand 1,3,5-triamino-1,3,5-trideoxy-*cis*-inositol (taci) to multiple-bind metal ions[16,17] to obtain an octanuclear vanadyl cluster, $[V_8O_{14}(H_{-2}taci)_2]$ (**1**; Figure 1).[18–20] This complex is the first

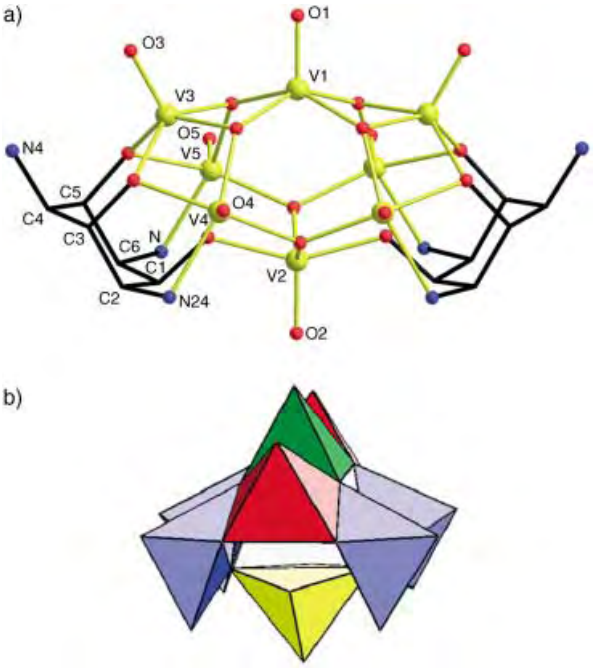


Figure 1. Molecular structure of $[V_8O_{14}(H_{-2}taci)_2]$.[19,20] a) Ball-and stick-representation. V yellow, O red, N blue. b) Polyhedral representation of the $\{V_8O_{20}N_4\}$ core rotated by 90°. The color scheme highlights the idealized C_{2v} symmetry of the cluster exploited in the analysis of the magnetic properties (the colors indicate symmetry related units). Averaged interatomic distances [Å] (215 K), values at 90 K are given in parentheses: V=O 1.621 (1.622), V-μ_3O 1.946 (1.939), V-μ_2O_{alkoxo} 2.019 (2.010), V2-O12 1.987 (1.981), V4/5-O12 2.433 (2.420) V-N 2.141 (2.130).

example where four metal cations are bonded simultaneously to one single taci molecule. The peculiar chelating properties of the ligand enforces a mutually orthogonal orientation of the V–$O_{terminal}$ vectors in the subsequent V5 V3 V4 array. This structural feature is unique in vanadium(IV)-oxo clusters and is a prerequisite for significant ferromagnetic interactions.

Of note is that the $[V_8O_{14}(H_{-2}taci)_2]$ aggregate was only obtained hydrothermally by using an excess of vanadium(V) as starting material.[18] If an excess of taci was allowed to react with $[VO]^{2+}_{(aq)}$, formation of a mononuclear bis(taci) complex $[V(taci)_2]^{4+}$ with exclusive binding of V^{IV} to six alkoxo groups was observed.[21]

Figure 2 illustrates the temperature dependence of the ratio of the magnetization and the applied field, labeled as χ_M, in the form $\chi_M T$ versus T.[22] The room temperature value is 2.62 emu K mol^{-1}, slightly smaller than the values of 2.94 emu K mol^{-1} expected for eight uncorrelated spins $S =$

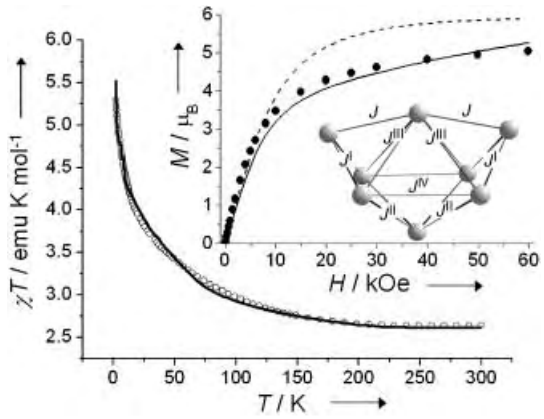


Figure 2. Temperature dependence of the $\chi_M T$ product of **1**.[23] —— calculated values with the best fit parameters (see text), ○ data points. Inset: the field dependence of the magnetization at 2.0 K, ----- simulation taking into account the spin-levels spectrum obtained from the best fit (see text), —— as above with $D(S=3) = 1.3$ cm^{-1}, ● data points. The labeling of the coupling constants is also shown.

1/2 with $g = 1.98$, thus suggesting the presence of antiferromagnetic (AF) interactions. The χT product decreases slightly on lowering the temperature with a broad minimum around 250 K and at lower temperature it steadily increases reaching the value of 5.52 emu K mol^{-1} at 2.1 K. This value is very close to that expected for an $S = 3$ ground state, $\chi_M T = 5.88$ emu K mol^{-1} for $g = 1.98$. This behavior is typical of a ferrimagnetic spin arrangement. The magnetization has been measured as a function of the field at three different temperatures: 2 K, 5 K, and 10 K. The highest measured value is 27930 emu mol^{-1}: this value is between the $S = 3$ (33175 emu mol^{-1}) and $S = 2$ (22117 emu mol^{-1}) saturation magnetization.

To rationalize the magnetic behavior an idealized C_{2v} symmetry, with five different coupling constants, is used in the HDVV spin Hamiltonian [Eq. (1)] where the labeling of the spin is the same as the vanadium atoms in Figure 1a and primes have been added for symmetry related atoms, and the exchange coupling scheme is shown in the inset of Figure 2.

$$\begin{aligned}\hat{\mathbf{H}} = {} & J(\mathbf{S}_1\mathbf{S}_3 + \mathbf{S}_1\mathbf{S}_{3'}) + J^{I}(\mathbf{S}_3\mathbf{S}_4 + \mathbf{S}_3\mathbf{S}_5 + \mathbf{S}_{3'}\mathbf{S}_{4'} + \mathbf{S}_{3'}\mathbf{S}_{5'}) \\ & + J^{II}(\mathbf{S}_2\mathbf{S}_4 + \mathbf{S}_2\mathbf{S}_5 + \mathbf{S}_2\mathbf{S}_{4'} + \mathbf{S}_2\mathbf{S}_{5'}) \\ & + J^{III}(\mathbf{S}_1\mathbf{S}_4 + \mathbf{S}_1\mathbf{S}_5 + \mathbf{S}_1\mathbf{S}_{4'} + \mathbf{S}_1\mathbf{S}_{5'}) + J^{IV}(\mathbf{S}_4\mathbf{S}_{5'} + \mathbf{S}_5\mathbf{S}_{4'})\end{aligned} \quad (1)$$

Even if five J values represent the smallest set of parameters able to take into account the different bridges in **1**, this choice leads inevitably to over-parameterization problems so that different fitting sets with very close agreement factors, R, are expected. Given that V1 and V3(V3′) are doubly μ_3-oxo bridged and arranged in a slightly bent *syn*-orthogonal[11] fashion, which gives rise to strong antiferromagnetic interactions, we can discard those sets for which the J is found to be ferromagnetic. J^I is associated to a μ_3-oxo and a μ-alkoxo bridge with an unprecedented quasi-orthogonality of the V=O bonds (80.26° (V3–V4) and 78.60° (V3–V5)) where the two bridging oxygen atoms occupy a basal position. The geometry can be described as that of two truncated octahedrons sharing one of the missing faces (see Figure 1b).

 © 2004 Wiley-VCH Verlag GmbH & Co. KGaA, Weinheim

The V–V separation (2.95 Å (V3–V4), 2.97 Å (V3–V5)) is comparable to that observed for the strongly antiferromagnetic pairs V1–V3(V3′)(2.86 Å) but the orthogonality imposed by the taci ligand is expected to lead to a sizeable ferromagnetic J^{I} coupling. The quasi-orthogonality of the V=O bonds is also observed in the pairs described by J^{II} and J^{III}, which are both mediated by a single μ_3-oxo bridge. Ferromagnetic values for the two exchange constants are expected on the basis of the quasi-orthogonality of V=O directions. The last exchange constant, J^{IV}, is eventually related to a vertex-sharing bridge where the V=O groups are almost parallel (orthogonal–orthogonal interaction geometry with $\varphi = 2.1°$).[11] A moderate antiferromagnetic interaction is therefore expected. Negligible magnetic interactions have been assumed to be present between V4 and V5 since the V4–O12 and V5–O12 separations are 2.42 Å and 2.44 Å, respectively. With these assumptions the parameters range, for $R = 1.5\cdot10^{-5}$, in the following intervals: $390 < J < 440$, $-150 < J^{I} < -140$, $-60 < J^{II} < -44$, $-60 < J^{III} < -40$, $48 < J^{IV} < 50$.

To overcome the problem of over-parameterization and obtain reliable magnetochemical information on the unconventional bridging modes encountered in **1** we performed quantum mechanical calculations based on the density functional theory (DFT) in the B3LYP broken-symmetry[23] framework. The X-ray structure has been used throughout the calculations. Gaussian type LanL2DZ basis set with LanL2 effective potential was used for the vanadium atoms while D95(d) basis sets were used for the N, O, and H atoms. The NWChem 4.1 package[24] was employed. To date, few attempts have been made to compute the exchange coupling constants on magnetic clusters containing more than two transition-metal atoms without any approximation of the X-ray structure.[25] To calculate the five exchange coupling constants, we computed five broken-symmetry states BS1–BS5 (see Table 1). BS6 and BS7 have been computed to check the validity of the assumption of a C_{2v} symmetry and the consistency of the calculations. In a C_{2v} SH, BS6, and BS7 should be degenerate with BS1: the 3 BS states have been found to be degenerate on the order of few cm^{-1}. The average energy has then been used for BS1. The degeneracy with BS2 has to be considered fortuitous. In general, the number of possible BS states that can be computed (and the energy differences from which the J_{ij} values are obtained) exceed the number of SH parameters to be computed leading to a system of equations that contains more equations than parameters. One common solution of this problem is to choose only one subset of equations for computing the J_{ij} values.[25,26] Nevertheless, as shown by Bencini and Totti,[26] such an approach can give misleading values of the exchange coupling parameters J_{ij}, whenever a close agreement between the expected and the computed $\langle\hat{S}^2\rangle$ value is not found. It is important to stress that in our case, the computed $\langle\hat{S}^2\rangle$ values are in a good agreement with those expected. This result suggests that the choice of one subset of equations, in our case five of the possible 435 energy differences (Table S1 of the Supporting Information), can be fairly accurate, a feature which is also confirmed by the computed degeneracy between BS1, BS6, and BS7. It should be noted that BS4 with M_s (eigenvalue of **Z**) equal to 3, is the determinant with the lowest energy. The solution of the system of five equations and five parameters leads to the following values: $J = 723.6\ cm^{-1}$, $J^{I} = -113.4\ cm^{-1}$, $J^{II} = -74.8\ cm^{-1}$, $J^{III} = -74.9\ cm^{-1}$, $J^{IV} = 36.9\ cm^{-1}$. As expected, a very strong antiferromagnetic J and ferromagnetic J^{I}, J^{II}, and J^{III} couplings have been found. J^{IV} is also antiferromagnetic in character. To verify that the computed magnetic structure corresponds to the experimental data, we tried to fit the $\chi_M T$ curve imposing as starting values the computed J values. The fitting procedure has given the following values: $J = 430\ cm^{-1}$, $J^{I} = -153\ cm^{-1}$, $J^{II} = -72\ cm^{-1}$, $J^{III} = -75\ cm^{-1}$, $J^{IV} = 56\ cm^{-1}$, and $R = 1.7\times10^{-4}$, and the calculated curve is shown in Figure 2. The fitted J values are in a fairly good agreement with the computed ones, with the exception of J, which appears to be significantly overestimated as already observed for strong antiferromagnetic couplings.[26] Nevertheless, the picture of the magnetic structure given by the DFT calculations seems to be reliable and of significant assistance in the fitting procedure of the experimental data and, therefore, to be reasonably close to a meaningful magnetochemical solution.

If we look at the low-energy spectrum (not shown) of the spin states of the cluster, computed with the best fit J values, we see that the $S = 3$ ground state is separated only by $2.89\ cm^{-1}$ from the first $S = 2$ excited state. The first $S = 1$ and $S = 0$ are found at, respectively, $8.76\ cm^{-1}$ and $9.22\ cm^{-1}$. Of course the ferromagnetic $S = 4$ state is very high in energy, because it can only be attained by violating the strong antiferromagnetic interaction J. The existence of a group of levels close to the ground state is a direct consequence of the antiferromagnetic nature of J^{IV}, which is in competition with the parallel orientation of the spin of the two halves of the cluster.

We have taken into account these low-lying spin states to reproduce the magnetization curve of the inset of Figure 2. The calculated curve is, however, very different from the experimental one. The data can only give a reasonably fit assuming that the ground spin state is subject to zero-field splitting (ZFS). The ZFS has only been introduced in the ground $S = 3$ multiplet and the curve of Figure 2 has been obtained

Table 1: Determinants, computed expectation values of $\langle\hat{S}^2\rangle$ (theoretical values in parenthesis and self-consistent-field energies (a.u.) for the high-spin (HS) and seven broken symmetry (BS) states. Only determinants with positive M_s values are reported.

BS state	M_s	$\langle\hat{S}^2\rangle$[a]	SCF Energy
HS: $\lvert\,1/2\ 1/2\ 1/2\ 1/2\ 1/2\ 1/2\ 1/2\ 1/2\rangle$	$M_s = \pm4$	20.11 (20.00)	−2878.378318
BS1: $\lvert\,1/2\ \overline{1/2}\ 1/2\ 1/2\ \overline{1/2}\ 1/2\ \overline{1/2}\ 1/2\rangle$	$M_s = \pm0$	4.06 (4.00)	−2878.380549
BS2: $\lvert\,1/2\ \overline{1/2}\ \overline{1/2}\ 1/2\ 1/2\ \overline{1/2}\ 1/2\ 1/2\rangle$	$M_s = \pm1$	4.70 (5.00)	−2878.379965
BS3: $\lvert\,1/2\ 1/2\ \overline{1/2}\ 1/2\ 1/2\ \overline{1/2}\ 1/2\ 1/2\rangle$	$M_s = \pm2$	8.05 (8.00)	−2878.380581
BS4: $\lvert\,\overline{1/2}\ 1/2\ 1/2\ 1/2\ 1/2\ 1/2\ 1/2\ 1/2\rangle$	$M_s = \pm3$	13.06 (13.00)	−2878.381274
BS5: $\lvert\,\overline{1/2}\ 1/2\ \overline{1/2}\ 1/2\ 1/2\ \overline{1/2}\ 1/2\ 1/2\rangle$	$M_s = \pm1$	5.11 (5.00)	−2878.376602
BS6: $\lvert\,\overline{1/2}\ \overline{1/2}\ 1/2\ 1/2\ \overline{1/2}\ 1/2\ 1/2\ \overline{1/2}\rangle$	$M_s = \pm0$	4.05 (4.00)	−2878.380570
BS7: $\lvert\,1/2\ \overline{1/2}\ \overline{1/2}\ 1/2\ \overline{1/2}\ \overline{1/2}\ 1/2\ \overline{1/2}\rangle$	$M_s = \pm1$	4.98 (5.00)	−2878.380516

 © 2004 Wiley-VCH Verlag GmbH & Co. KGaA, Weinheim

with $D = 1.3\ cm^{-1}$ and $g = 1.98$. The positive value of D implies an easy-plane type anisotropy and therefore is consistent with the absence of out-of-phase ac susceptibility in zero field.[2]

Even if an SMM based on ferromagnetically coupled $S = 1/2$ spins is still lacking, a significant high-spin ground state has been achieved thanks to the use of a multidentate ligand that forces the V^{IV} coordination polyhedra into an unprecedented orthogonal closed packed motif. This situation is the result of a remarkable improvement in the control of the magnetic properties by the use of tailored ligands. A method that combines ab initio calculations with simulations based on the spin Hamiltonian approach has been shown to be crucial for the proper description of complex magnetic structures.

Received: February 27, 2004 [Z54130]

Keywords: cluster compounds · density functional calculations · magnetic properties · N,O ligands · vanadium

[1] J. Villain, F. Hartman-Boutron, R. Sessoli, A. Rettori, *Europhys. Lett.* **1994**, *27*, 159.
[2] D. Gatteschi, R. Sessoli, *Angew. Chem.* **2003**, *115*, 278; *Angew. Chem. Int. Ed.* **2003**, *42*, 268.
[3] R. Sessoli, H. L. Tsai, A. R. Schake, S. Wang, J. B. Vincent, K. Folting, D. Gatteschi, G. Christou, D. N. Hendrickson, *J. Am. Chem. Soc.* **1993**, *115*, 1804.
[4] N. Regnault, T. Jolicoeur, R. Sessoli, D. Gatteschi, M. Verdaguer, *Phys. Rev. B* **2002**, *66*, 054409.
[5] C. Raghu, I. Rudra, D. Sen, S. Ramasesha, *Phys. Rev. B* **2001**, *64*, 4419.
[6] A. L. Barra, A. Caneschi, A. Cornia, F. F. De Biani, D. Gatteschi, C. Sangregorio, R. Sessoli, L. Sorace, *J. Am. Chem. Soc.* **1999**, *121*, 5302.
[7] R. W. Saalfrank, I. Bernt, M. M. Chowdhry, F. Hampel, G. B. M. Vaughan, *Chem. Eur. J.* **2001**, *7*, 2765.
[8] J. Larionova, M. Gross, M. Pilkington, H. Andres, H. Stoeckli-Evans, H. U. Güdel, S. Decurtins, *Angew. Chem.* **2000**, *112*, 1667; *Angew. Chem. Int. Ed.* **2000**, *39*, 1605.
[9] V. Marvaud, C. Decroix, A. Scuiller, C. Guyard-Duhayon, J. Vaissermann, F. Gonnet, M. Verdaguer, *Chem. Eur. J.* **2003**, *9*, 1677.
[10] W. A. Hatfield, *Inorg. Chem.* **1983**, *22*, 833.
[11] W. Plass, *Inorg. Chem.* **1997**, *36*, 2200.
[12] W. Plass, *Angew. Chem.* **1996**, *108*, 699; *Angew. Chem. Int. Ed. Engl.* **1996**, *35*, 627.
[13] a) A. Müller, F. Peters, M. T. Pope, D. Gatteschi, *Chem. Rev.* **1998**, *98*, 239. b) R. E. P. Winpenny, *Adv. Inorg. Chem.* **2001**, *52*, 1; c) L. Cronin, *Comprehensiv Coordation Chemistry II*, *Vol. 7*, (Eds.: J. A. McCleverty, T. J. Meyer), Elsevier, Amsterdam, **2004**, p. 1.
[14] a) C. J. Warren, J. T. Rijssenbeek, D. J. Rose, R. C. Haushalter, J. Zubieta, *Polyhedron* **1998**, *17*, 2599. b) R. P. Bontchev, J. Do, A. J. Jacobson, *Angew. Chem.* **1999**, *111*, 2063; *Angew. Chem. Int. Ed.* **1999**, *38*, 1937.
[15] A. Müller, M. Koop, H. Bögge, M. Schmidtmann, F. Peters, P. Kögerler, *Chem. Commun.* **1999**, 1885.
[16] a) K. Hegetschweiler, M. Ghisletta, T. F. Fässler, R. Nesper, *Angew. Chem.* **1993**, *105*, 1514; *Angew. Chem. Int. Ed. Engl.* **1993**, *32*, 1426; b) N. Ouali, J.-P. Rivera, D. Chapon, P. Delangle, C. Piguet, *Inorg. Chem.* **2004**, *43*, 1517.
[17] K. Hegetschweiler, *Chem. Soc. Rev.* **1999**, *28*, 239.
[18] K. Hegetschweiler, R. C. Finn, R. S. Rarig Junior, J. Sander, S. Steinhauser, M. Wörle, J. Zubieta, *Inorg. Chim. Acta* **2002**, *337*, 39.
[19] Crystal data for **1**·7 H_2O: $C_{12}H_{40}N_6O_{27}V_8$ ($M_r = 1108.02$), tetragonal, space group $I4_1/a$; $a = 16.160(2)$, $c = 24.179(5)$ Å, $V = 6314.2(17)$ Å^3, $Z = 8$, $T = 215(2)$ K, $\rho_{calcd} = 2.331\ g\,cm^{-3}$, $\mu(Mo_{K\alpha}) = 2.377\ mm^{-1}$, refl. 19634 collected, 2488 unique ($R_{int} = 0.0616$), 1952 observed [$I > 2\sigma(I)$]. 255 parameters refined with $R = 0.0363$ [$I > 2\sigma(I)$], $wR_2 = 0.979$ [all data], $GOF = 1.055$; residual electron density: $+0.573$, $-0.444\ e\,Å^{-3}$. SHELX-97 program set for structure solution (direct methods) and refinement (full-matrix least-squares on F^2). The positions of hydrogen atoms were calculated (riding model). An additional data set was recorded at 90(2) K (see supporting information). CCDC-232009 (90 K) and CCDC-232010 (215 K) contains the supplementary crystallographic data for this paper. These data can be obtained free of charge via www.ccdc.cam.ac.uk/conts/retrieving.html (or from the Cambridge Crystallographic Data Centre, 12 Union Road, Cambridge CB2 1EZ, UK; fax: (+44) 1223-336-033; or deposit@ccdc.cam.ac.uk).
[20] Bond-valence calculations confirmed the exclusive presence of V^{IV}: The valences are 4.05 (V1), 4.03 (V2), 4.03 (V3), 3.99 (V4), 3.97 (V5); see N. E. Brese, M. O'Keeffe, *Acta Crystallogr. Sect. B* **1991**, *47*, 192.
[21] B. Morgenstern, S. Steinhauser, K. Hegetschweiler, E. Garribba, G. Micera, D. Sanna, L. Nagy, *Inorg. Chem.* **2004**, *43*, 3116.
[22] The dc magnetization and ac susceptibility (not shown) on microcrystalline powder samples have been recorded using a Cryogenic S600 SQUID magnetometer, with applied fields of 10000, 1000, and 100 Oe upon decreasing temperature to avoid saturation effects. The diamagnetic contributions of the sample were estimated from Pascal's constants and subtracted from the data.
[23] a) L. Noodleman, J. G. J. Norman, *J. Chem. Phys.* **1979**, *70*,4903; b) L. Noodleman, *J. Chem. Phys.* **1981**, *74*, 5737.
[24] T. P. Straatsma, E. Apra', T. L. Windus, M. Dupuis, E. J. Bylaska, W. de Jong, S. Hirata, D. M. A. Smith, M. Hackler, L. Pollack, R. Harrison, J. Nieplocha, V. M. Tipparaju Krishnan, E. Brown, G. Cisneros, G. Fann, H. Fruchtl, J. Garza, K. Hirao, R. Kendall, J. Nichols, K. Tsemekhman, M. Valiev, K. Wolinski, J. Anchell, D. Bernholdt, P. Borowski, T. Clark, D. Clerc, H. Dachsel, M.,Deegan, K. Dyall, D. Elwood, E. Glendening, M. Gutowski, A. Hess, J. Jaffe, B. Johnson, J. Ju, R. Kobayashi, R. Kutteh, Z. Lin, R. Littlefield, X. Long, B. Meng, T. Nakajima, S. Niu, M. Rosing, G. Sandrone, M. Stave, H. Taylor, G., Thomas, J. van Lenthe, A. Wong, Z. Zhang, NWChem, A Computational Chemistry Package for Parallel Computers, v. 4.5, Pacific Northwest National Laboratory, Richland, Washington, USA, **2003**; R. A. Kendall, E. Apra, D. E. Bernholdt, E. J. Bylaska, M. Dupuis, G. I. Fann, R. J. Harrison, J. L. Ju, J. A. Nichols, J. Nieplocha, T. P. Straatsma, T. L. Windus, A. T. Wong, *Comput. Phys. Commun.* **2000**, *128*, 260. See references therein for the effective core potentials LanL2DZ and D95(d) basis sets, and for the B3LYP functional.
[25] a) D. N. Hendrickson, G. Christou, E. A. Schmitt, E. Libby, J. S. Bashkin, S. Wang, H.-L. Tsai, J. B. vincent, P. D. W. Boyd, J. C. Huffman, K. Folting, Q. Li, W. E. Streib, *J. Am. Chem. Soc.* **1992**, *114*, 2455; b) R. A. Torres, T. Lovell, L. Noodleman, D. A. Case, *J. Am. Chem. Soc.* **2003**, *125*, 1923; c) T. A. O'Brien, E. R. Davidson, *Int. J. Quantum Chem.* **2003**, *92*, 294.
[26] A. Bencini, F. Totti, *Int. J. Quantum Chem.* accepted for publication.

 © 2004 Wiley-VCH Verlag GmbH & Co. KGaA, Weinheim

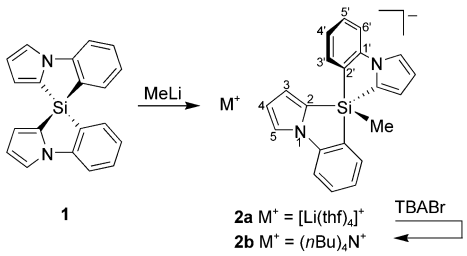
Pentaorganosilicate Pseudorotamers

Dynamic Configurational Isomerism of a Stable Pentaorganosilicate**

*Erik P. A. Couzijn, Marius Schakel, Frans J. J. de Kanter, Andreas W. Ehlers, Martin Lutz, Anthony L. Spek, and Koop Lammertsma**

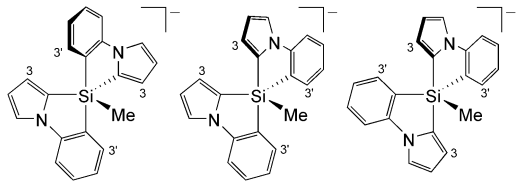
Stable silicates with five carbon substituents are extremely rare.[1] These pentacoordinate anions often have a trigonal-bipyramidal geometry with three equatorial and two apical sites that should make them prone to configurational isomerism in which the substituent sites interchange. Such a process is known as the Berry pseudorotation mechanism.[2] However, pseudorotamers other than the energetically preferred species have seldom been observed,[3] even among the more accessible neutral phosphoranes.[4] Insight into the thermodynamics of this type of isomerism is even more scarce,[4c,d] and nonexistent for the silicates. Here we report a new, stable pentaorganosilicate of which different configurational isomers coexist in solution, and present thermodynamic and kinetic data on their interconversion.

The starting material bis(1-phenylpyrrole-2,2′-diyl)silane (**1**) was synthesized in 53% yield (white crystals from ethyl acetate; m.p. 276°C (decomp)) from 2′-bromo-1-phenylpyrrole in diethyl ether by treatment with 2 equivalents of butyllithium (0°C) and 0.5 equivalents $SiCl_4$ (reflux).[5] Reaction of **1** with methyllithium in THF at −78°C afforded a pale yellow solution of lithium silicate **2a** (Scheme 1), as indicated by the upfield shift of the ^{29}Si NMR signal from $\delta = -35$ to −131 ppm. The NMR spectra were recorded at −50°C to minimize signal broadening (see below). Compound **2a** was fully characterized by ^{1}H NMR, ^{13}C NMR, HMQC, and HMBC spectroscopic measurements. The silicate anion can potentially adopt three configurations **I**–**III**,[6] which differ in the orientation of the bidentate substituents. The ^{1}H and ^{13}C NMR spectra revealed twofold symmetry, while the 2D NOESY[7] spectrum showed correlations between H3′ and H3



1 **2a** $M^+ = [Li(thf)_4]^+$ **2b** $M^+ = (n\text{Bu})_4N^+$

Scheme 1. Synthetic route to silicate salts **2a** and **2b**.



Δ-**I** Δ-**II** Δ-**III**

as well as between H3′ and the methyl group. Only geometry **I** is compatible with these observations (Table 1). Furthermore, the $J_{C2,Si}$ value of 86 Hz is similar to that of a typical Si(sp^2)–C(sp^2) bond,[8a] while the $J_{C2',Si}$ value of 30 Hz is much smaller than that of a Si(sp^3)–C(sp^2) bond (64–70 Hz)[8b] and reflects the small silicon s character of the apical bonds.

Table 1: H···H distances [Å] for the pseudorotamers of **2** calculated with B3LYP/6-31G(d).

	H3···H3′	H3···Me[b]	H3′···Me[b]
I	2.69	4.31–4.76	2.60–3.30
II[a]	6.05 eq–eq	4.41–4.79 eq	4.02–4.42 eq
	6.82 ap–ap	3.11–3.64 ap	2.51–3.07 ap
III	2.66	2.85–3.57	4.03–4.49

[a] Equatorial(eq) and apical (ap) H3 (H3′) interactions are listed separately. [b] Minimum and maximum distances, depending on the rotation of the methyl group.

Ion exchange with tetrabutylammonium bromide (TBABr) in THF enabled near-quantitative isolation of silicate **2b** as a moisture-sensitive white solid (m.p. > 160°C (decomp)). Studies by NMR spectroscopy in DMF gave results comparable to those of **2a**. X-ray crystal-structure determination of **2b** (from DMF) confirmed the geometry (Figure 1).[9] The centrosymmetric crystal contained Δ-**I** and Λ-**I** in a 1:1 ratio.[10] The trigonal-bipyramidal coordination environment around the pentacoordinate silicon atom is distorted by 16% towards square-pyramidal along the Berry pseudorotation coordinate.[11] The observed bond lengths are in good accordance with those of previously reported pentaorganosilicates,[1c,d,12] the apical Si–C bonds being distinctly longer than the equatorial bonds. There are no close contacts with the ammonium cation, which is disordered in one butyl chain.

We expected the apical-site preferences of the phenyl and pyrrole moieties to be very similar. This led us to the presumption that minor quantities of conformers **II** and **III**

[*] E. P. A. Couzijn, Dr. M. Schakel, Dr. F. J. J. de Kanter, Dr. A. W. Ehlers, Prof. Dr. K. Lammertsma
Department of Chemistry, Faculty of Sciences
Vrije Universiteit, De Boelelaan 1083
1081 HV Amsterdam (The Netherlands)
Fax: (+31) 20-44-47488
E-mail: lammert@chem.vu.nl
Dr. M. Lutz, Prof. Dr. A. L. Spek
Bijvoet Center for Biomolecular Research,
Crystal and Structural Chemistry
Utrecht University, Padualaan 8
3584 CH Utrecht (The Netherlands)

[**] This work was supported by the Netherlands Foundation for Chemical Sciences (CW) with financial aid from the Netherlands Organization for Scientific Research (NWO). We thank Prof. G. W. Klumpp for helpful discussions and J. W. H. Peeters of the University of Amsterdam for exact mass determinations.

Supporting information for this article is available on the WWW under http://www.angewandte.org or from the author.

 © 2004 Wiley-VCH Verlag GmbH & Co. KGaA, Weinheim DOI: 10.1002/anie.200353006

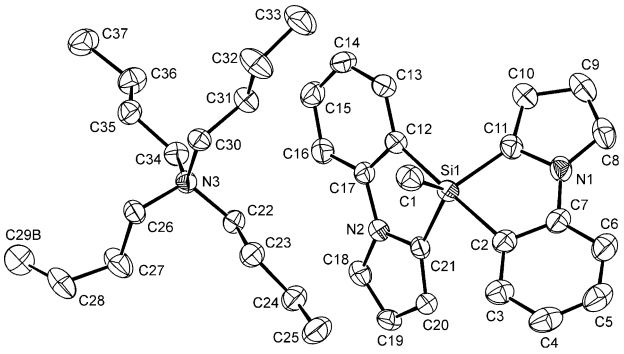


Figure 1. Displacement ellipsoid plot (50% probability) of **2b**. Hydrogen atoms are omitted for clarity. Only the major conformation of the disordered *n*-butyl group is shown. Selected bond lengths [Å] and angles [°]: Si-C1 1.903(2), Si-C2 2.024(2), Si-C11 1.909(2), Si-C12 2.026(2), Si-C21 1.9093(19); C1-Si-C2 93.95(9), C1-Si-C11 118.51(9), C1-Si-C12 93.31(9), C1-Si-C21 117.25(9), C2-Si-C11 82.97(9), C2-Si-C12 172.72(8), C2-Si-C21 92.92(8), C11-Si-C12 94.03(8), C11-Si-C21 124.23(8), C12-Si-C21 83.26(8)

might be present in solution. By using a concentrated solution of **2a**, an additional ^{13}C resonance was found in the NMR spectrum at $\delta = 9.3$ ppm, which was correlated to a methyl ^1H signal at $\delta = 0.36$ ppm with an intensity of 6% relative to the main silicate. The ^{29}Si INEPT spectrum also revealed a small but distinct extra signal at $\delta = -128$ ppm. We subsequently applied $^1H,^{29}Si$ ge-HMQC as a very sensitive 2D NMR technique[13] to detect and characterize the silicates. The spectra not only showed the methyl and pyrrole groups of the minor silicate (Figure 2), but even suggested a third pyrrole-

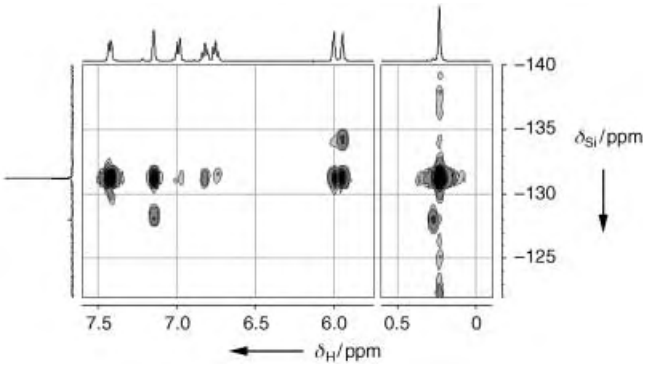


Figure 2. $^1H,^{29}Si$ ge-HMQC spectrum of 0.33 M **2a** (THF/C_6D_6, −50 °C; optimized for $J = 2.25$ Hz; ^1H and ^{29}Si INEPT spectra are displayed along the axes)

containing silicate at $\delta = -134$ ppm in an even smaller amount. Unfortunately, no distinctly resolved proton signals could be associated with the latter compound.[15]

If the minor silicate at $\delta = -128$ ppm is indeed **II** or **III**, it should be able to interchange with **I** by Berry pseudorotation. Barriers for such processes are generally about 9–14 kcal mol^{-1},[14,1a] which can be readily overcome at room temperature and thus lead to line broadening and coalescence phenomena. Indeed, the extra ^{29}Si correlations vanished at 25 °C and reappeared upon cooling again to −50 °C. Similar behavior was observed for a solution of **2b** in DMF. Exchange was also indicated by broadening of various ^{13}C resonances at 25 °C, particularly that for the methyl carbon atom; the aromatic signals narrowed again at 90 °C. The extra ^1H signal also disappeared at room temperature, but the main resonance of the methyl protons resonance of pseudorotamer **I** did not broaden significantly. This is a consequence of its abundance, as confirmed by dynamic NMR simulations. Hence, we carried out ^1H magnetization-transfer experiments[16] at −25 °C, at which temperature both methyl signals are still separated, thus indicating that exchange is slow on the NMR timescale. Substantial magnetization transfer indeed occurred from the major ($\delta_H = 0.32$ ppm, **I**) to the minor ($\delta_H = 0.36$ ppm) resonance on increasing the mixing time from 10 ms to 0.5 s. This unequivocally demonstrates interchange between **I** ($\delta_{Si} = -131$ ppm) and the minor silicate ($\delta_{Si} = -128$ ppm).

Thermodynamic and kinetic parameters for the exchange process were determined by lineshape analysis for the methyl regions of 13 ^1H NMR spectra in the temperature range from −36 to 0 °C. A plot of $\ln K$ versus temperature displayed excellent linear behavior and gave an energy difference between the pseudorotamers of $\Delta G_{258} = 1.66(6)$ kcal mol^{-1}. The Eyring plot gave an activation barrier of $\Delta G^{\ddagger}_{258} = 15.5(5)$ kcal mol^{-1} for pseudorotation of the major to the minor isomer. These values are in very good agreement with B3LYP/6-31G(d) calculations,[17] which indicated that **I** is more stable than **II** (+1.8 kcal mol^{-1}), with an overall barrier of 15.0 kcal mol^{-1} (**I**→**III**→**II**). On this basis we assign configuration **II** to the silicate with a ^{29}Si NMR resonance at $\delta = -128$ ppm. The similar temperature behavior of the $^1H,^{29}Si$ correlation at $\delta = -134$ ppm makes us speculate that it might originate from the third pseudorotamer. The calculated relative energy of **III** (+2.6 kcal mol^{-1}) would be consistent with a rather low abundance, since its pseudorotation barrier is also modest (12.1 kcal mol^{-1}).

In conclusion, silicate pseudorotamers have been observed in dynamic equilibrium for the first time. This allowed the determination of the thermodynamics and kinetics of the Berry pseudorotation mechanism involved. The reported pentaorganosilicate also gives more insight into the stabilizing factors of these very rare anions.

Experimental Section

1: *n*-Butyllithium (16 mmol) was added slowly to a solution of 1-(2′-bromophenyl)pyrrole (8 mmol) in diethyl ether (15 mL) at 0 °C. The yellow solution was treated with tetrachlorosilane (4 mmol), and the resulting suspension was heated at reflux for 4 h. Acidic aqueous workup, extraction, and evaporation of the solvent afforded crude **1**, which was recrystallized from ethyl acetate in 52% yield. M.p. 275.7–279.6 °C (minor decomp); ^1H NMR ($CDCl_3$): $\delta = 7.54$ (dd, 2H, $^3J_{H,H} = 2.6$, $^4J_{H,H} = 0.9$ Hz, H5), 7.47 (td, 2H, $^3J_{H,H} = 7.6$, $^4J_{H,H} = 1.3$ Hz, H5′), 7.41–7.40 (m, 4H, H6′/H3′), 7.07 (td, 2H, $^3J_{H,H} = 7.2$, $^2J_{H,H} = 0.9$ Hz, H4′), 6.58 (dd, 2H, $^3J_{H,H} = 3.3$, $^4J_{H,H} = 0.9$ Hz, H3), 6.46 ppm (t, 2H, $^3J_{H,H} = 3.0$ Hz, H4); $^{13}C\{^1H\}$ NMR ($CDCl_3$): $\delta = 148.8$ (C1′), 135.2 (C3′), 132.2 (C5′), 124.8 (C4′), 124.4 (C2′), 123.8 (C2), 120.7 (C3), 119.2 (C5), 114.5 (C4), 111.8 ppm (C6′); $^{29}Si\{^1H\}$ INEPT NMR ($CDCl_3$, $^3J_{H,Si} = 4.5$ Hz, 4H): $\delta = -35$ ppm; HR FAB-MS: found: 311.1009; calcd for $C_{20}H_{15}N_2Si$ $[M+H]^+$: 311.1005.

 © 2004 Wiley-VCH Verlag GmbH & Co. KGaA, Weinheim

2a: Methyllithium (0.144 mmol) was added to a solution of **1** (0.138 mmol) in THF (1.0 mL) at −78 °C. After stirring the mixture for 30 min, the pale yellow solution of **2a** was warmed to room temperature. ^{1}H NMR (THF/[D$_8$]THF, −50 °C): $\delta = 7.51$ (d, 2H, $^3J_{H,H} = 6.4$ Hz, H3′), 7.25 (s, 2H, H5), 7.10 (d, 2H, $^3J_{H,H} = 7.6$ Hz, H6′), 6.92 (t, 2H, $^3J_{H,H} = 7.0$ Hz, H5′), 6.85 (t, 2H, $^3J_{H,H} = 6.9$ Hz, H4′), 6.08 (d, 2H, $^3J_{H,H} = 2.4$ Hz, H3), 6.04 (t, 2H, $^3J_{H,H} = 2.6$ Hz, H4), 0.32 ppm (s, 3H, $^2J_{H,Si} = 7$ Hz, Me); ^{13}C{^{1}H} NMR (THF/[D$_8$]THF, −50 °C): $\delta =$ 155.6 (C2′, $^1J_{C,Si} = 30$ Hz), 144.8 (C1′), 139.2 (C2, $^1J_{C,Si} = 86$ Hz), 132.7 (C3′), 123.9 (C5′), 121.6 (C4′), 118.7 (C3), 113.1 (C5), 110.1 (C4), 108.7 (C6′), 6.1 ppm (Me, $^1J_{C,Si} = 64$ Hz); ^{29}Si{^{1}H} INEPT NMR ($^2J_{H,Si} =$ 7.0 Hz, 3H, THF/[D$_8$]THF, −50 °C): $\delta = -131$ ppm ($^1J_{Si,C2} = 86$ Hz, $^1J_{SiMe} = 64$ Hz, $^1J_{Si,C2'} = 30$ Hz).

2b: A slightly warmed solution of tetrabutylammonium bromide (0.138 mmol) in THF (1.0 mL) was added to a solution of **2a** in THF at −78 °C. The resulting white suspension was warmed to room temperature, precipitated by centrifugation, washed with THF, and dried under vacuum. This afforded **2b** as a white powder in 94% yield, which could be recrystallized from DMF; m.p. > 160 °C (decomp); ^{1}H NMR (DMF/[D$_7$]DMF, −50 °C): $\delta = 7.51$ (s, 2H, H5), 7.49 (d, 2H, $^3J_{H,H} = 6.8$ Hz, H3′), 7.28 (d, 2H, $^3J_{H,H} = 7.6$ Hz, H6′), 6.95 (t, 2H, $^3J_{H,H} = 6.8$ Hz, H5′), 6.88 (t, 2H, $^3J_{H,H} = 6.9$ Hz, H4′), 6.08 (s, 4H, H3/H4), 1.66 (br s, 8H, NCH$_2$*C*H$_2$), 1.29 (m, 8H, C*H*$_2$CH$_3$), 0.89 (t, 12H, $^3J_{H,H} = 7.3$ Hz, CH$_2$C*H*$_3$), 0.29 ppm (s, 3H, Me), NC*H*$_2$ is buried under the solvent peak; ^{13}C{^{1}H} NMR (DMF/[D$_7$]DMF, −50 °C): $\delta = 156.0$ (C2′), 145.6 (C1′), 139.6 (C2), 133.4 (C3′), 125.3 (C5′), 122.9 (C4′), 119.8 (C3), 115.3 (C5), 111.5 (C4), 110.3 (C6′), 58.4 (N*C*H$_2$), 24.1 (NCH$_2$*C*H$_2$), 20.3 (*C*H$_2$CH$_3$), 14.2 (CH$_2$*C*H$_3$), 7.3 ppm (Me); ^{29}Si{^{1}H} INEPT NMR ($^2J_{H,Si} = 7.0$ Hz, 3H, DMF/[D$_7$]DMF, −50 °C): $\delta = -131$ ppm; HR FAB-MS: found 326.1240; calcd for $C_{21}H_{18}N_2Si$ $[M+H]^+$: 326.1239.

Received: October 2, 2003
Revised: March 18, 2004 [Z53006]

Keywords: density functional calculations · hypervalent compounds · isomers · NMR spectroscopy · silicon

[1] a) A. H. J. F. de Keijzer, F. J. J. de Kanter, M. Schakel, R. F. Schmitz, G. W. Klumpp, *Angew. Chem.* **1996**, *108*, 1183 – 1184; *Angew. Chem. Int. Ed. Engl.* **1996**, *35*, 1127 – 1128; b) A. H. J. F. de Keijzer, F. J. J. de Kanter, M. Schakel, V. P. Osinga, G. W. Klumpp, *J. Organomet. Chem.* **1997**, *548*, 1, 29 – 32; c) S. Deerenberg, M. Schakel, A. H. J. F. de Keijzer, M. Kranenburg, M. Lutz, A. L. Spek, K. Lammertsma, *Chem. Commun.* **2002**, 348 – 349; d) D. Ballweg, X. Liu, I. A. Guzei, R. West, *Silicon Chem.* **2002**, *1*, 57 – 60.

[2] R. S. Berry, *J. Chem. Phys.* **1960**, *32*, 933 – 938.

[3] a) M. Pülm, R. Willeke, R. Tacke in *Organosilicon Chemistry IV—From Molecules to Materials* (Eds.: N. Auner, J. Weis), Wiley-VCH, Weinheim, **2000**, pp. 478 – 488; b) D. Kost, I. Kalikhman, S. Krivonos, R. Bertermann, C. Burschka, R. E. Neugebauer, M. Pülm, R. Willeke, R. Tacke, *Organometallics* **2000**, *19*, 1083 – 1095.

[4] a) D. Hellwinkel, W. Krapp, *Chem. Ber.* **1979**, *112*, 292 – 297; b) S. Kojima, K. Kajiyama, M. Nakamoto, K. Akiba, *J. Am. Chem. Soc.* **1996**, *118*, 12866 – 12867; c) O. Lösking, H. Willner, H. Oberhammer, J. Grobe, D. L. Van, *Inorg. Chem.* **1992**, *31*, 3423 – 3427; d) S. Matsukawa, K. Kajiyama, S. Kojima, S. Furuta, Y. Yamamoto, K. Akiba, *Angew. Chem.* **2002**, *114*, 4912 – 4916; *Angew. Chem. Int. Ed.* **2002**, *41*, 4718 – 4722, and references therein.

[5] Analogous to: G. W. H. Cheeseman, S. G. Greenberg, *J. Organomet. Chem.* **1979**, *166*, 139 – 152.

[6] Only pseudorotamers **I**, **II**, and **III** are identified as minima in calculations with B3LYP/6–31G(d).

[7] R. Wagner, S. Berger, *J. Magn. Reson. Ser. A* **1996**, *123*, 119 – 121.

[8] a) A. G. Brook, M. A. Brook in *Advances in Organometallic Chemistry*, *Vol. 39* (Eds.: F. G. A. Stone, R. West), Academic Press, New York, **1996**, pp. 71 – 158; b) G. C. Levy, D. M. White, J. D. Cargioli, *J. Magn. Reson.* **1972**, *8*, 280 – 283.

[9] Crystal data for **2b**: $[C_{16}H_{36}N][C_{21}H_{17}N_2Si]$, $M_r = 567.91$, colorless block, $0.24 \times 0.15 \times 0.15$ mm, monoclinic, space group $P2_1/c$ (no. 14), $a = 11.0900(2)$, $b = 18.5217(3)$, $c = 19.5505(3)$ Å, $\beta =$ 122.1753(12)°, $V = 3399.05(10)$ Å^3, $Z = 4$, $\rho_{exptl} = 1.110$ g cm^{-3}, $\mu = 0.097$ mm^{-1}. 35804 reflections were measured on a Nonius KappaCCD diffractometer with rotating anode ($\lambda = 0.71073$ Å) at 150(2) K up to a resolution of $(\sin\theta/\lambda)_{max} = 0.60$ Å^{-1}; 5991 reflections were unique ($R_{int} = 0.067$); an absorption correction was not considered necessary. The structure was solved with direct methods (SHELXS-97)[18] and refined with SHELXL-97[19] against F^2 of all reflections. Non-hydrogen atoms were refined freely with anisotropic displacement parameters; H atoms were refined as rigid groups. One *n*-butyl group was refined with a disorder model. 381 refined parameters, 14 restraints. *R* values $[I > 2\sigma(I)]$: $R1 = 0.0504$, $wR2 = 0.1231$. *R* values (all data): $R1 = 0.0726$, $wR2 = 0.1357$. GOF = 1.029. Residual electron density between −0.25 and 0.37 e Å^{-3}. Molecular illustration, structure checking, and calculations were performed with the PLATON package.[20]

[10] Δ (Λ) denotes a positive (negative) helicity of the spirocyclic system.

[11] Assuming a *trans* basal angle of 150°; see R. R. Holmes, *Prog. Inorg. Chem.* **1984**, *32*, 119 – 235.

[12] A. Kolomeitsev, G. Bissky, E. Lork, V. Movchun, E. Rusanov, P. Kirsch, G.-V. Röschenthaler, *Chem. Commun.* **1999**, 1017 – 1018.

[13] S. Provera, S. Davalli, G. H. Raza, S. Contini, C. Marchioro, *Magn. Reson. Chem.* **2001**, *39*, 38 – 42.

[14] C. Chuit, R. J. P. Corriu, C. Reye, J. C. Young, *Chem. Rev.* **1993**, *93*, 1371 – 1448, and references therein.

[15] Identification of the third silicate is hampered by its low abundance, the absence of resolved ^{1}H signals, and the inherent NMR insensitivity of C and Si nuclei.

[16] a) S. Forsen, R. A. Hoffman, *J. Chem. Phys.* **1963**, *39*, 2892 – 2901; b) J. Stonehouse, P. Adell, J. Keeler, A. J. Shaka, *J. Am. Chem. Soc.* **1994**, *116*, 6037 – 6038; c) K. Stott, J. Stonehouse, J. Keeler, T. L. Hwang, A. J. Shaka, *J. Am. Chem. Soc.* **1995**, *117*, 4199 – 4200.

[17] Gaussian 98 (Revision A.7), M. J. Frisch, G. W. Trucks, H. B. Schlegel, G. E. Scuseria, M. A. Robb, J. R. Cheeseman, V. G. Zakrzewski, J. A. Montgomery, R. E. Stratmann, J. C. Burant, S. Dapprich, J. M. Millam, A. D. Daniels, K. N. Kudin, M. C. Strain, O. Farkas, J. Tomasi, V. Barone, M. Cossi, R. Cammi, B. Mennucci, C. Pomelli, C. Adamo, S. Clifford, J. Ochterski, G. A. Petersson, P. Y. Ayala, Q. Cui, K. Morokuma, D. K. Malick, A. D. Rabuck, K. Raghavachari, J. B. Foresman, J. Cioslowski, J. V. Ortiz, B. B. Stefanov, G. Liu, A. Liashenko, P. Piskorz, I. Komaromi, R. Gomperts, R. L. Martin, D. J. Fox, T. Keith, M. A. Al-Laham, C. Y. Peng, A. Nanayakkara, C. Gonzalez, M. Challacombe, P. M. W. Gill, B. G. Johnson, W. Chen, M. W. Wong, J. L. Andres, M. Head-Gordon, E. S. Replogle, J. A. Pople, Gaussian, Inc., Pittsburgh, PA, **1998**.

[18] G. M. Sheldrick, SHELXS-97, University of Göttingen, Germany, **1997.**

[19] G. M. Sheldrick, SHELXL-97, University of Göttingen, Germany, **1997.**

[20] A. L. Spek, *J. Appl. Crystallogr.* **2003**, *36*, 7 – 13.

 © 2004 Wiley-VCH Verlag GmbH & Co. KGaA, Weinheim

Phosphorous Compounds

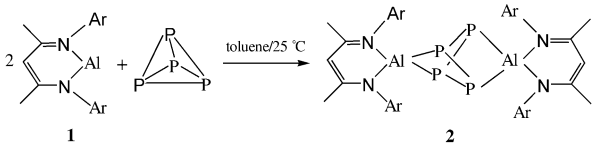
$[\{HC(CMeNAr)_2\}_2Al_2P_4]$ (Ar = 2,6-*i*Pr$_2$C$_6$H$_3$): A Reduction to a Formal $\{P_4\}^{4-}$ Charged Species**

Ying Peng, Hongjun Fan, Hongping Zhu, Herbert W. Roesky, Jörg Magull, and Colan E. Hughes*

The chemistry of white phosphorus has generated much interest over the past decades owing to its unique tetrahedral structure and variable bonding situation. Organophosphorus compounds can be used as reagents[1] and as ligands for innumerable complexes in catalytic processes.[2] The reactions of transition-metal complexes with white phosphorus have been extensively studied and have resulted in a large variety of P_x ligands with unpredictable structures.[3] Among them, only one compound $[Cp^*_2(CO)_2Co_2P_4]$ ($Cp^* = C_5Me_5$)[4] with a $\{P_4\}^{4-}$ species is reported. However, the reactions of the P_4 molecule with main-group complexes are limited to a few examples, $[(AlCp^*)_6P_4]$,[5a] $[(GaR)_3P_4]$ ($R = (SiMe_3)_3C$),[5b] and $[Ga_2P_4tBu_6]$.[5c]

[LAl^I] (**1**) (L = HC(CMeNAr)$_2$, Ar = 2,6-*i*Pr$_2$C$_6$H$_3$)[6] with its nonbonding lone pair of electrons at aluminum indicates a singlet carbene-like character. It could be used in carbene-type reactions, as a Lewis base and moreover as a reducing reagent, which may show unprecedented chemical reactions. To our knowledge, the study of the chemical behavior of **1** is limited so far to coupling reactions.[7,8] Compounds containing the heavy elements of Group 13 and 15 are used as models in bonding theory[9] and as precursors for semiconducting materials.[10] Herein we report the reaction of **1** with white phosphorus to yield the first main-group complex of composition $[(LAl)_2P_4]$ (**2**) containing the $\{P_4\}^{4-}$ species.

Treatment of two equivalents of **1** with white phosphorus at room temperature leads to **2** in good yield (Scheme 1). In contrast, the reaction of the tetrahedral aluminum(I) compound $[(AlCp^*)_4]$ with white phosphorus gave the electron-deficient cage compound $[(AlCp^*)_6P_4]$,[5a] which consists of two face-sharing heterocubanes with two opposing corners unoccupied, and four P atoms from the complete cleavage of the P_4 molecule. Therefore we treated **1** with P_4 in a 4:1 ratio to explore the possibility of complete cleavage of all P–P bonds, however we obtained **2** and residual **1**, based on the results of ^{1}H and ^{31}P NMR spectroscopic investigations. Clearly the bulky ligand L prevents the arrangement of a larger number of LAl moieties around the P atoms. When the reaction was carried out in a ratio of 1:1 between **1** and P_4, **2** and residual P_4 together with some byproducts were obtained, again based on the results of ^{1}H and ^{31}P NMR spectroscopic investigations. Compound **2** is air sensitive and decomposes at 145 °C. **2** is sparingly soluble in pentane and hexane, however readily soluble in benzene, toluene, and diethyl ether. In $CDCl_3$ we observed the decomposition of **2**.



1 2

Scheme 1. The synthesis of **2**. Ar = 2,6-*i*Pr$_2$C$_6$H$_3$.

Compound **2** was characterized by ^{1}H, ^{13}C, and ^{31}P NMR spectroscopy using [D$_6$]benzene as the solvent, and by EI mass spectrometry and elemental analysis. The EI mass spectrum shows the molecular ion of **2**. The ^{31}P NMR spectrum of **2** ($\delta = 78.6$ ppm) has a very different chemical shift compared to that of the free P_4 molecule ($\delta = -519$ ppm). No resonance signals were observed in C_6D_6 solution for the ^{27}Al NMR spectrum of **2**, thus measurement in the solid state was carried out and signals in a range of 50–120 ppm were found which are comparable to those for four-coordinate Al^{III} compounds, and much different from the resonance for [LAl^I] (**1**) (590 ± 40 ppm, $\upsilon_{1/2} = 30\,000$ Hz).[7] In the ^{1}H NMR pattern of **2**, just one set of resonances for the ligands L is detected indicating that the two ligands are in the same chemical environment. The X-ray single-crystal structural analysis confirms the composition of **2** (Figure 1). Compound **2** crystallizes in the orthorhombic space group $P2_12_12_1$ with one molecule of pentane. As shown in Figure 1,[11] compound **2** contains an $\{Al_2P_4\}$ core, and the four-membered P_4 ring is attached to two LAl moieties. The Al–P bond length (av. 2.37 Å) of **2** is in the range of those in $[(AlCp^*)_6P_4]$ (2.31–2.42 Å).[5a] The P–P bond length (av. 2.29 Å) is slightly longer than that in $[Cp^*_2(CO)_2Co_2P_4]$ (av. 2.23 Å).[4] The distances between P(1)···P(3) and P(2)···P(4) in **2** (3.049(2) and 3.063(2) Å) are distinctly longer than those in $[Cp^*_2(CO)_2Co_2P_4]$ (2.560(2), 2.597(2) Å),[4] and indicate the complete cleavage of two P–P bonds within the P_4 molecule. The Al–N bond length (av. 1.90 Å) is in the range of those aluminum derivatives bearing the ligand L.[12] The average P-Al-P bond angle is 80.27°.

DFT calculation with RI-BP86/TZVP within TURBOMOLE[13,14] was carried out to investigate the electronic structure of **2**. The calculated Mulliken charges on the P atom (−0.22) show a significant charge transfer from the Al atoms to P_4, which indicates the formation of an ionic Al–P bond. The bond order (shared electrons between two P atoms) of P–P bonds (0.01) supports the complete cleavage of the P(1)–P(3) and P(2)–P(4) bonds. The calculated binding energy ($(E_{(LM)_2-P_4} - 2*E_{L-M} - E_{P_4})/2.0$) (36.4 kcal mol^{-1}) shows the strong interaction between P_4 and the Al atoms. (In the

[*] Y. Peng, H. Zhu, Prof. Dr. H. W. Roesky, Prof. Dr. J. Magull
Institut für Anorganische Chemie
Universität Göttingen
Tammannstrasse 4, 37077 Göttingen (Germany)
Fax: (+49) 551-39-3373
E-mail: hroesky@gwdg.de
H. Fan
Labor für Physikalische und Theoretische Chemie
Universität Siegen, 57068 Siegen (Germany)
Dr. C. E. Hughes
Max-Planck-Institut für Biophysikalische Chemie
37077 Göttingen (Germany)

[**] This work was supported by the Deutsche Forschungsgemeinschaft and the Fonds der Chemischen Industrie.

Supporting information for this article is available on the WWW under http://www.angewandte.org or from the author.

 DOI: 10.1002/anie.200353406 © 2004 Wiley-VCH Verlag GmbH & Co. KGaA, Weinheim

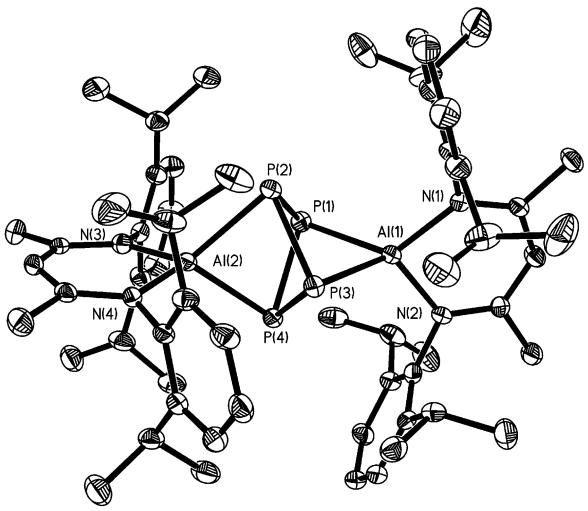


Figure 1. The crystal structure of **2**. The hydrogen atoms and cocrystallized pentane are omitted for clarity. Selected bond lengths [Å] and angles [°]: Al(1)-P(1) 2.377(2), Al(1)-P(3) 2.359(2), Al(2)-P(2) 2.387(2), Al(2)-P(4) 2.360(2), P(1)-P(2) 2.287(2), P(1)-P(4) 2.292(2), P(2)-P(3) 2.284(2), P(3)-P(4) 2.295(2), P(1)···P(3) 3.049(2), P(2)···P(4) 3.063(2), Al(1)-N(1) 1.897(5), Al(1)-N(2) 1.912(5), Al(2)-N(3) 1.901(5), Al(2)-N(4) 1.909(5); P(3)-Al(1)-P(1) 80.16(7), P(4)-Al(2)-P(2) 80.37(7), P(2)-P(1)-P(4) 83.98(7), P(3)-P(2)-P(1) 83.69(8), P(2)-P(3)-P(4) 83.96(8), P(1)-P(4)-P(3) 83.34(8), P(2)-P(1)-Al(1) 81.64(8), P(4)-P(1)-Al(1) 77.60(7), P(2)-P(3)-Al(1) 82.07(8), P(4)-P(3)-Al(1) 77.91(7), P(3)-P(2)-Al(2) 77.84(7), P(1)-P(2)-Al(2) 81.02(7), P(1)-P(4)-Al(2) 81.50(7), P(3)-P(4)-Al(2) 78.19(7).

above calculation the P atoms are the P atoms of the coordinated P–P edge.)

In the uncoordinated P_4 molecule the P–P bonds are about 2.21 Å. Herein we use PH_2–PH_2 as an example to study how much the P–P bond loses energy during its extension.[15] The energy curve of PH_2–PH_2 for the P–P separation (1.7 to 3.6 Å) is given in the Supporting Information. It shows that near the minimum the curve is quite flat. At r(P–P) > 3.0 Å, most of the bond energy is lost and the bond order is about zero. Thus, both the charge calculation and the P–P bond analysis support an ionic Al–P_4 bond for **2**. Therefore, in **2**, the P_4 unit is carrying formally four negative charges.

In summary, the reaction of LAl[1] (**1**) with white phosphorus yields the first main-group complex $[(LAl)_2P_4]$ (**2**) containing the $\{P_4\}^{4-}$ moiety, in which two P–P edges of the P_4 tetrahedron are opened and each is bridged by a LAl moiety.

Experimental Section

2: Toluene (30 mL) was added to a mixture of **1** (0.445 g, 1 mmol) and P_4 (0.062 g, 0.5 mmol). The resulting solution was stirred at room temperature for one week. After removal of the solvent, the residue was recrystallized from a mixture of hexane and pentane at room temperature to afford red crystals (0.40 g, 79 %). M.p. 145 °C dec; EI-MS: *m/z* (%) 1012 (30) [M^+], 429 (100) [LAl-Me]. ^{1}H NMR (500.13 MHz, C_6D_6): δ = 7.15–7.02 (m, 12H, Ar-H), 5.03 (s, 2H, γ-H), 3.61 (sept, J = 6.8 Hz, 8H, C*H*Me$_2$), 1.70 (s, 12H, Me), 1.15 (d, J = 6.8 Hz, 24H, CH*Me*$_2$), 1.13 ppm (d, J = 6.8 Hz, 24H, CH*Me*$_2$); ^{13}C NMR (125.77 MHz, C_6D_6): δ = 169.97 (*C*N), 143.94, 142.07, 124.14 (Ar), 97.79 (γ-C), 29.26 (*C*HMe$_2$), 25.43(CH*Me*$_2$), 24.57 (CH*Me*$_2$), 23.86 ppm (Me); ^{31}P NMR (121.5 MHz, C_6D_6): δ = 78.6 ppm; ^{27}Al NMR (600 MHz, 26 KHz, MAS, $AlCl_3$): δ = 50–120 ppm (MAS = magic-angle spinning). elemental analysis calcd (%) for $C_{63}H_{94}Al_2N_4P_4$ (1085.26): C 69.72, H 8.73, N 5.16; found C 69.88, H 8.12, N 5.76.

Received: November 26, 2003
Revised: March 4, 2004 [Z53406]

Keywords: aluminum · charge transfer · N ligands · phosphorus · structure elucidation

[1] H.-J. Cristau, *Chem. Rev.* **1994**, *94*, 1299–1313.
[2] G. O. Spessard, G. L. Miessler, *Organometallic Chemistry*, Prentice Hall, Upper Saddle River, NJ, **1996**, p. 131.
[3] Reviews: a) M. Ehses, A. Romerosa, M. Peruzzini, *Top. Curr. Chem.* **2002**, *220*, 108–140; b) O. J. Scherer, *Angew. Chem.* **1990**, *102*, 1137–1155; *Angew. Chem. Int. Ed. Engl.* **1990**, *29*, 1104–1122; c) M. Scheer, E. Herrmann, *Z. Chem.* **1990**, *29*, 41–55; d) O. J. Scherer in *Multiple Bonds and Low Coordination in Phosphorus Chemistry* (Eds.: M. Regitz, O. J. Scherer), Thieme, Stuttgart, **1990**, chap. 3; e) K. H. Whitmire, *Adv. Organomet. Chem.* **1998**, *42*, 1–145; f) O. J. Scherer, *Acc. Chem. Res.* **1999**, *32*, 751–762.
[4] O. J. Scherer, M. Swarowsky, G. Wolmershäuser, *Organometallics* **1989**, *8*, 841–842.
[5] a) C. Dohmeier, H. Schnöckel, C. Robl, U. Schneider, R. Ahlrichs, *Angew. Chem.* **1994**, *106*, 225–226; *Angew. Chem. Int. Ed. Engl.* **1994**, *33*, 199–200; b) W. Uhl, M. Benter, *Chem. Commun.* **1999**, 771–772; c) M. B. Power, A. R. Barron, *Angew. Chem.* **1991**, *103*, 1403–1404; *Angew. Chem. Int. Ed. Engl.* **1991**, *30*, 1353–1354.
[6] C. Cui, H. W. Roesky, H.-G. Schmidt, M. Noltemeyer, H. Hao, F. Cimpoesu, *Angew. Chem.* **2000**, *112*, 4444–4446; *Angew. Chem. Int. Ed.* **2000**, *39*, 4274–4276.
[7] C. Cui, S. Köpke, R. Herbst-Irmer, H. W. Roesky, M. Noltemeyer, H.-G. Schmidt, B. Wrackmeyer, *J. Am. Chem. Soc.* **2001**, *123*, 9091–9098.
[8] C. Cui, H. W. Roesky, H.-G. Schmidt, M. Noltemeyer, *Angew. Chem.* **2000**, *112*, 4705–4707; *Angew. Chem. Int. Ed.* **2000**, *39*, 4531–4533.
[9] M. A. Petrie, P. P. Power, *Inorg. Chem.* **1993**, *32*, 1309–1312, and references therein.
[10] A. H. Cowley, R. A. Jones, *Angew. Chem.* **1989**, *101*, 1235–1242; *Angew. Chem. Int. Ed. Engl.* **1989**, *28*, 1208–1215.
[11] Crystal data for **2**·pentane: $C_{63}H_{94}Al_2N_4P_4$, M_r = 1085.26, orthorhombic, space group $P2_12_12_1$, a = 13.8751(7), b = 14.3627(8), c = 31.8580(16) Å, $\alpha = \beta = \gamma = 90°$, V = 6348.8(6) Å^3, Z = 4, ρ_{calcd} = 1.135 Mg m^{-3}, $F(000)$ = 2344, λ = 0.71073 Å, T = 133(2) K, μ = 0.186 mm^{-1}; $1.28 \le \theta \le 22.63°$; of 25400 reflections collected, 8387 were independent (R(int) = 0.0983). The R values are $R1$ = 0.0618 and $wR2$ = 0.1372 ($I > 2\sigma(I)$); The Flack value is −0.17(14); max./min. residual electron density: 0.491/−0.410 e Å^{-3}. All non-hydrogen atoms were refined anisotropically except for the pentane carbon atoms. All hydrogen atoms were included at geometrically calculated positions and refined using a riding model. CCDC-224941 (**2**) contains the supplementary crystallographic data for this paper. These data can be obtained free of charge via www.ccdc.cam.ac.uk/conts/retrieving.html (or from the Cambridge Crystallographic Data Centre, 12 Union Road, Cambridge CB2 1EZ, UK; fax: (+44) 1223-336-033; or deposit@ccdc.cam.ac.uk).
[12] C. Cui, H. W. Roesky, H. Hao, H.-G. Schmidt, M. Noltemeyer, *Angew. Chem.* **2000**, *112*, 1885–1887; *Angew. Chem. Int. Ed.* **2000**, *39*, 1815–1817.

 © 2004 Wiley-VCH Verlag GmbH & Co. KGaA, Weinheim

[13] R. Ahlrichs, M. Bär, H.-P. Baron, R. Bauernschmitt, S. Böcker, P. Deglmann, M. Ehrig, K. Eichkorn, S. Elliott, F. Furche, F. Haase, M. Häser, H. Horn, C. Hättig, C. Huber, U. Huniar, M. Katannek, A. Köhn, C. Kölmel, M. Kollwitz, K. May, C. Ochsenfeld, H. Öhm, A. Schäfer, U. Schneider, M. Sie, TURBOMOLE 5.5, University of Karlsruhe, Germany, **2002**.
[14] J. P. Perdew, *Phys. Rev. B* **1986**, *33*, 8822 – 8824.
[15] The calculation was done on the accurate level RI-MP2/TZVPP in TURBOMOLE.

 © 2004 Wiley-VCH Verlag GmbH & Co. KGaA, Weinheim

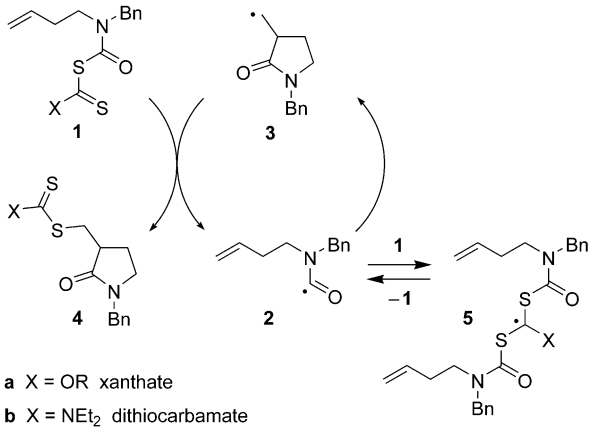
Radical Reactions

Dithiocarbamate Group Transfer Cyclization Reactions of Carbamoyl Radicals under "Tin-Free" Conditions**

Richard S. Grainger and Paolo Innocenti*

The use of radical reactions in modern organic synthesis is now well-established.[1] Despite the many well-documented advantages of free-radical chain reactions in organic chemistry, the majority of examples still rely on the use of tributyltin hydride in stoichiometric amounts, and a major area of current research is the development of processes which seek to either alleviate the problems associated with toxic tin residues, or remove the need for tin completely.[2] Among these methods, the group transfer chemistry of xanthates, extensively developed by Zard and co-workers, is one of the most powerful.[3] Xanthate precursors to acyl,[4] alkoxycarbonyl,[5] and a variety of other carbon-centered[6] and nitrogen-centered[7] radicals have been reported, and found numerous applications in synthesis.[5,8] However, group transfer of xanthates from carbamoyl radical precursors has not been described. Herein we describe the difficulties associated with using xanthates as carbamoyl radical precursors, and report a solution based on replacing the classical xanthate with a dithiocarbamate group.

Carbamoyl radicals, or aminoacyl radicals, offer a useful means to introduce an amide functional group into an organic molecule through a nonclassical disconnection. A number of elegant methods for the generation of carbamoyl radicals are known.[9] Faced with a problematic carbamoyl radical cyclization in the course of a recent synthetic endeavor, we considered that xanthate chemistry would offer a potential solution. The principle is outlined in Scheme 1: radical cyclization of carbamoyl radical **2** should lead to the alkyl radical **3**, which after addition to the carbon–sulfur double bond of a carbamoyl xanthate **1a** and fragmentation of the resulting carbon-centered radical gives the desired lactam **4a** along with the initial radical **2**, which can continue the chain process. An alternative reaction pathway available to carbamoyl radical **2** is addition to the radical precursor **1** to give the intermediate radical **5**. However, this process is fast and reversible as **5** will fragment back to **1** and **2**.[10] The continuous regeneration of carbamoyl radical **2** by this degenerate pathway means it should be capable of undergoing cyclizations which would not otherwise compete favorably with premature reduction of **2** under conditions used for tin hydride (or other hydrogen atom abstraction).[9d,g–l]



Scheme 1. Group transfer radical cyclization of carbamoyl radicals.

A survey of the literature showed that carbamoyl xanthates have been proposed as intermediates in the reaction between readily prepared carbamoyl chlorides and xanthate salts, which ultimately affords the corresponding S-substituted thiocarbamates upon loss of carbon oxysulfide.[11] Aware of this behavior, we investigated the possibility that the reaction could be stopped at the carbamoyl xanthate stage by choosing appropriate conditions. However, despite extensive variations of temperature, solvent, xanthate salt (R = ethyl, neopentyl), leaving group,[12] and stoichiometry we were unable to isolate the desired carbamoyl xanthate **1a** in anything other than small amounts (< 10% yield). All the conditions tried invariably gave a complex mixture of compounds (e.g. compounds **1a**, **6**–**9** in the reaction shown in Scheme 2);[13] formation of S-substituted thiocarbamates was not observed in our experiments. Incorporation of an electron-withdrawing group (phenylsulfonyl) on the nitrogen atom in place of the benzyl group also failed to alleviate this problem.[9g,14] Frustratingly, the desired cyclization of **1a** to the expected pyrrolidinone **4a** is readily achieved in 67% yield simply upon irradiation of a refluxing toluene solution of **1a** using a halogen or tungsten lamp, but the overall process remains untenable in the absence of an efficient method for the preparation of **1a**.

[*] Dr. R. S. Grainger, P. Innocenti
Department of Chemistry
King's College London
Strand
London WC2R 2LS (UK)
Fax: (+44) 20-7848-2810
E-mail: richard.grainger@kcl.ac.uk

[**] We thank King's College London for funding this work, and AstraZeneca and Pfizer for additional financial support.

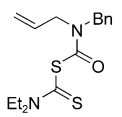
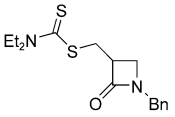
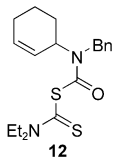
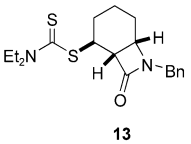
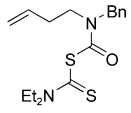
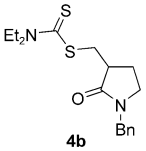
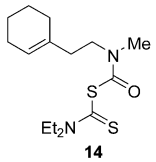
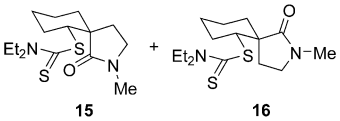
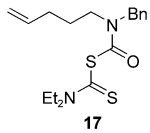
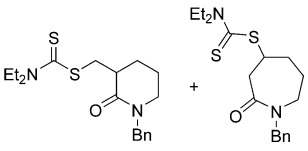
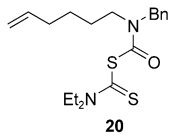
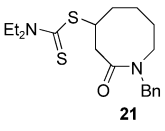
Supporting information for this article is available on the WWW under http://www.angewandte.org or from the author.

 DOI: 10.1002/anie.200453600 © 2004 Wiley-VCH Verlag GmbH & Co. KGaA, Weinheim

In a search for a "xanthate-like" radical precursor, our attention turned to the corresponding *N*,*N*-dialkyl dithiocarbamates. Apart from aromatic amines, such compounds were described in a patent as unstable to heat.[15] In fact, the desired dithiocarbamate **1b** can be prepared in high yield (>95%) from the corresponding carbamoyl chloride **6** by treatment with commercially available sodium diethyldithiocarbamate trihydrate, without any of the problems known from the corresponding xanthates (Scheme 2). More importantly, *N*,*N*-dialkyldithiocarbamates substitute for xanthates in group transfer radical cyclization reactions of carbamoyl radicals. Two methods can be used to initiate the radical process. The first simply involves irradiation with visible light using a 500-W halogen lamp. The second uses commercially available dilauroyl peroxide (DLP) as an initiator, added portionwise. The desired cyclization of **1b** to **4b** can be achieved in up to 96% yield (Table 1, entry 3).

The results of the cyclization of a selection of dithiocarbamates to the corresponding cyclic amides are shown in Table 1.[16] A range of ring sizes can be achieved with this chemistry. As has been previously demonstrated by others,[9d,e,i–l] carbamoyl radicals efficiently cyclize to form four-membered rings (Table 1, entries 1 and 2). In the case of β lactam **13**, a single diastereomeric adduct is formed, the configuration of which has been proven by X-ray crystallography. The stereochemical outcome is consistent with group transfer to the intermediate cyclohexyl radical occurring on the less hindered convex face of the [4.2.0]bicyclic ring system. Five-membered rings are also formed with complete regioselectivity and in good to excellent yields through the 5-*exo-trig* radical cyclization mode (Table 1, entries 3 and 4). The orientation of the resulting dithiocarbamate group in the spirobycyclic γ lactams **15** and **16** relative to the heterocycle has been tentatively assigned on the basis of NOESY experiments.[17]

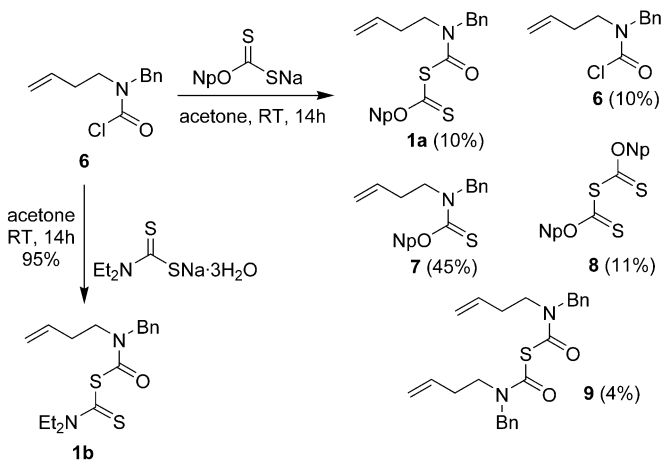
Table 1: Carbamoyl radical cyclization reactions through dithiocarbamate group transfer.[a]

Entry	Radical precursor	Lactam product(s)[b]	Method	Yield [%]
1	 **10**	 **11**	A	70
2	 **12**	 **13**	A	92
3	 **1b**	 **4b**	A B	96 80
4	 **14**	 **15** **16**	A	78 (**15**:**16** 1:5)
5	 **17**	 **18** **19**	A B	65 (**18**:**19** 8.4:1) 58 (**18**:**19** 5.6:1)
6	 **20**	 **21**	C	37

[a] Reaction conditions: A: *hν*, cyclohexane, reflux; B: DLP, cyclohexane, reflux; C: DLP, chlorobenzene, reflux. [b] Details on the synthesis of the lactams along with analytical data are given in the Supporting Information.

Six-membered rings are also readily obtained using this chemistry, with a small amount of the seven-membered ring lactam **19** formed in addition to the expected product **18** (Table 1, entry 5). Lactam **19** presumably arises through a 7-*endo-trig* pathway, although ring expansion of the alkyl radical arising from the 6-*exo-trig* pathway through 3-*exo-trig* cyclization onto the amide carbonyl group followed by cyclopropyloxy radical fragmentation prior to group transfer cannot be excluded.[9d]

We are not aware of any reports of the cyclization of carbamoyl radicals being used to form ring sizes larger than



Scheme 2. Reaction of carbamoyl chlorides with xanthate and dithiocarbamate salts. Np = neopentyl.

 © 2004 Wiley-VCH Verlag GmbH & Co. KGaA, Weinheim

six. The formation of an eight-membered ring using this chemistry is therefore notable (Table 1, entry 6). Although the yield is only moderate, there are relatively few reports of direct formation of an eight-membered ring in the radical chemistry literature.[18] The use of a higher-boiling solvent was found to be beneficial in this case.

The replacement of a xanthate with an *N*,*N*-dialkyl dithiocarbamate in the above process is notable and has little precedent in the literature: work on controlled radical polymerization has shown that dithiocarbamates only undergo radical group transfer reactions if an electron-withdrawing group is placed on the nitrogen atom.[19,20] In the present case, even though the carbon–sulfur double bond in *N*,*N*-dialkyl dithiocarbamate **1b** is more electron rich than in xanthate **1a**, efficient group transfer to the nucleophilic alkyl radical **3** is still observed.

In conclusion, *N*,*N*-diethyldithiocarbamates are ideal substitutes for xanthates in a new method for generating carbamoyl radicals undergoing efficient group transfer to both primary and secondary alkyl radicals after cyclization. The overall process is simple to carry out, requires no special precautions, and has a number of advantages over existing radical methodologies: the lack of toxic tin hydrides, the mild and safe method for initiating the radical chain process, the functionalization of the final radical which can lead to further useful chemical transformations,[21] and the nonreliance on slow (syringe pump) addition and high-dilution techniques. We are currently extending this work to include other radical acceptors, asymmetric variants, and applications in target-directed synthesis.

Experimental Section

Representative procedure for the preparation of carbamoyl diethyldithiocarbamates from secondary amines:

Pyridine (10.1 mmol) was added dropwise to a solution of triphosgene (2.9 mmol) in toluene (70 mL); the resulting suspension was treated with a solution of the secondary amine (7.8 mmol) in toluene (10 mL). The reaction was stirred overnight at room temperature, quenched with saturated aqueous $NaHCO_3$, and extracted with Et_2O. The organic layer was washed with 0.3 M HCl, water and brine, and dried over $MgSO_4$. The solvent was removed under reduced pressure to give the crude carbamoyl chloride which was used directly in the next step.

A solution of the crude carbamoyl chloride (ca. 6.6 mmol) in acetone (45 mL) was treated with sodium diethyldithiocarbamate trihydrate (26.2 mmol). The reaction was stirred overnight at room temperature, quenched with saturated aqueous $NaHCO_3$, and extracted with Et_2O. The organic layer was washed with water and brine, and dried over $MgSO_4$. The solvent was removed under reduced pressure to give the crude carbamoyl diethyldithiocarbamate, which in most cases was sufficiently pure to be used directly in the cyclization reactions.

Representative procedure for the photomediated cyclization (method A): Carbamoyl dithiocarbamate (0.8 mmol) was dissolved in cyclohexane (8 mL) and oxygen was removed from the resulting solution using a nitrogen stream for ca. 15 min. The solution was irradiated with a 500-W halogen or tungsten lamp that generated sufficient heat to bring the solvent to reflux. The reaction progress was monitored by thin-layer chromatography (TLC). After the reaction was complete (1–8 h) the solvent was removed under reduced pressure and the crude was purified by column chromatography.

Representative procedure for the DLP-induced cyclization (method B): Carbamoyl dithiocarbamate (0.4 mmol) was dissolved in cyclohexane (4 mL) and oxygen was removed from the resulting solution using a nitrogen stream for ca. 15 min. The solvent was heated to reflux and DLP (0.04 mmol) was added to the boiling solution. The reaction progress was monitored by TLC and fresh portions of initiator were added every 1.5–2 h. After the reaction was complete (2–10 h) the solvent was removed under reduced pressure and the crude was purified by column chromatography.

Received: December 22, 2003
Revised: May 7, 2004 [Z53600]

Keywords: cyclization · group transfer · lactams · radical reactions · synthetic methods

[1] a) B. Giese, *Radicals in Organic Synthesis: Formation of Carbon–Carbon Bonds, Pergamon, Oxford*, **986**; b) W. B. Motherwell, D. Crich, *Free Radical Chain Reactions in Organic Synthesis, Academic Press, London*, **992**; c) D. P. Curran, N. A. Porter, B. Giese, *Stereochemistry of Radical Reactions, VCH, Weinheim*, **996**; d) *Radicals in Organic Synthesis, Vol. 1–2* (Eds.: P. Renaud, M. P. Sibi), Wiley-VCH, Weinheim, **2001**.

[2] a) P. A. Baguley, J. C. Walton, *Angew. Chem.* **1998**, *110*, 3272; *Angew. Chem. Int. Ed.* **1998**, *37*, 3072; b) A. Studer, S. Amrein, *Synthesis* **2002**, 835.

[3] S. Z. Zard, *Angew. Chem.* **1997**, *109*, 724; *Angew. Chem. Int. Ed. Engl.* **1997**, *36*, 672, and references therein.

[4] a) D. H. R. Barton, M. V. George, M. Tomoeda, *J. Chem. Soc.* **1962**, 1967; b) P. Delduc, C. Tailhan, S. Z. Zard, *J. Chem. Soc. Chem. Commun.* **1988**, 308.

[5] J. E. Forbes, R. N. Saicic, S. Z. Zard, *Tetrahedron* **1999**, *55*, 3791.

[6] a) J. Axon, L. Boiteau, J. Boivin, J. E. Forbes, S. Z. Zard, *Tetrahedron Lett.* **1994**, *35*, 1719; b) J. E. Forbes, C. Tailhan, S. Z. Zard, *Tetrahedron Lett.* **1990**, *31*, 2565; c) J. E. Forbes, S. Z. Zard, *Tetrahedron* **1993**, *49*, 8257; d) F. Bertrand, V. Pevere, B. Quiclet-Sire, S. Z. Zard, *Org. Lett.* **2001**, *3*, 1069; e) F. Gagosz, S. Z. Zard, *Org. Lett.* **2002**, *4*, 4345; f) F. Gagosz, S. Z. Zard, *Org. Lett.* **2003**, *5*, 2655; g) G. Ouvry, B. Quiclet-Sire, S. Z. Zard, *Org. Lett.* **2003**, *5*, 2907.

[7] a) A. C. Callier-Dublanchet, B. Quiclet-Sire, S. Z. Zard, *Tetrahedron Lett.* **1997**, *38*, 2463; b) F. Gagosz, C. Moutrille, S. Z. Zard, *Org. Lett.* **2002**, *4*, 2707; for reviews on nitrogen-centered radicals, see: c) S. Z. Zard, *Synlett* **1996**, 1148; d) A. G. Fallis, I. M. Brinza, *Tetrahedron* **1997**, *53*, 17543.

[8] a) L. Boiteau, J. Boivin, A. Liard, B. Quiclet-Sire, S. Z. Zard, *Angew. Chem.* **1998**, *110*, 1197; *Angew. Chem. Int. Ed.* **1998**, *37*, 1128; b) X. Hoang-Cong, B. Quiclet-Sire, S. Z. Zard, *Tetrahedron Lett.* **1999**, *40*, 2125; c) C. Kalaï, E. Tate, S. Z. Zard, *Chem. Commun.* **2002**, 1430; d) L. D. Miranda, S. Z. Zard, *Org. Lett.* **2002**, *4*, 1135; e) A. C. Vargas, B. Quiclet-Sire, S. Z. Zard, *Org. Lett.* **2003**, *5*, 3717.

[9] a) F. Minisci, A. Citterio, E. Vismara, C. Giordano, *Tetrahedron* **1985**, *41*, 4157; b) F. Minisci, F. Fontana, F. Coppa, Y. M. Yan, *J. Org. Chem.* **1995**, *60*, 5430; c) F. Minisci, F. Recupero, C. Punta, C. Gambarotti, F. Antonietti, F. Fontana, G. F. Pedulli, *Chem. Commun.* **2002**, 2496; d) G. B. Gill, G. Pattenden, S. J. Reynolds, *J. Chem. Soc. Perkin Trans. 1* **1994**, 369; e) G. Pattenden, S. J. Reynolds, *J. Chem. Soc. Perkin Trans. 1* **1994**, 379; f) M. Sakamoto, M. Takahashi, T. Fujita, T. Nishio, I. Iida, S. Watanabe, *J. Org. Chem.* **1995**, *60*, 4682; g) J. H. Rigby, D. M. Danca, J. H. Horner, *Tetrahedron Lett.* **1998**, *39*, 8413; h) G. E. Keck, M. C. Grier, *Synlett* **1999**, 1657; i) L. V. Jackson, J. C. Walton, *Chem. Commun.* **2000**, 2327; j) A. F. Bella, L. V.

 © 2004 Wiley-VCH Verlag GmbH & Co. KGaA, Weinheim

Jackson, J. C. Walton, *Org. Biomol. Chem.* **2004**, *2*, 421; k) E. M. Scanlan, J. C. Walton, *Chem. Commun.* **2002**, 2086; l) E. M. Scanlan, A. M. Z. Slawin, J. C. Walton, *Org. Biomol. Chem.* **2004**, *2*, 716; m) S. Fujiwara, Y. Shimizu, T. Shin-ike, N. Kambe, *Org. Lett.* **2001**, *3*, 2085; n) R. Leardini, A. Tundo, G. Zanardi, *J. Chem. Soc. Perkin Trans. 1* **1981**, 3164; o) for a review on acyl radicals and related radicals, see: C. Chatgilialoglu, D. Crich, M. Komatsu, I. Ryu, *Chem. Rev.* **1999**, *99*, 1991.

[10] Additions of tin radicals and a range of other carbon-centered radicals to thiocarbonyl groups are regarded as fast compared to other competitive processes; see for example refs. [3,5]. For alternative reaction modes of xanthates and thiourethanes in the Barton–McCombie reaction, see: J. U. Rhee, B. I. Bliss, T. V. RajanBabu, *J. Am. Chem. Soc.* **2003**, *125*, 1492.

[11] J. J. D'Amico, T. Schafer, *Phosphorus, Phosphorus Sulfur Silicon Relat. Elem.* **1980**, *8*, 301.

[12] R. A. Batey, C. Yoshina-Ishii, S. D. Taylor, V. Santhakumar, *Tetrahedron Lett.* **1999**, *40*, 2669.

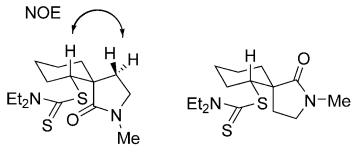
[13] The formation of products analogous to **8** and **9** has been observed by Zard in his preparation of acyl radical precursors. In his case careful control of the stoichiometry (xanthate salt):(acid chloride) together with the correct order of addition was sufficient to ensure good yields of the radical precursor. See ref. [3].

[14] The incorporation of a Cbz group in place of the benzyl group could not be achieved. Keck has reported an example of a carbamoyl xanthate where the nitrogen atom is part of an oxazolidinone ring; see ref. [9h].

[15] I. Williams (DuPont de Nemours), US 2171420, **1939**.

[16] All dithiocarbamate radical precursors were prepared in $>80\%$ yield from the corresponding secondary amine in a two-step procedure (see Experimental Section), with the exception of **14** which was prepared from the corresponding tertiary dimethylamine.

[17] The coupling constants for the proton on the carbon atom adjacent to the sulfur atom in both **15** and **16** are consistent with an equatorial arrangement of the dithiocarbamate group on the cyclohexane ring. This proton shows a NOE interaction to one of the pyrrolidinone ring hydrogen atoms in the case of **15**, whereas no NOE interaction is observed to either of these hydrogen atoms in the case of **16**.



[18] For notable examples involving xanthates, see: a) J. H. Udding, J. P. M. Giesselink, H. Hiemstra, W. N. Speckamp, *J. Org. Chem.* **1994**, *59*, 6671; b) E. Bacqué, F. Pautrat, S. Z. Zard, *Org. Lett.* **2003**, *5*, 325; for a review on free-radical methods for the synthesis of medium-size rings, see: c) L. Yet, *Tetrahedron* **1999**, *55*, 9349.

[19] M. Destarac, D. Charmot, X. Franck, S. Z. Zard, *Macromol. Rapid Commun.* **2000**, *21*, 1035.

[20] For a radical-mediated synthesis of tertiary alkyl dithiocarbamates, see: a) G. Bouhadir, N. Legrand, B. Quiclet-Sire, S. Z. Zard, *Tetrahedron Lett.* **1999**, *40*, 277; b) S. H. Thang, Y. K. Chong, R. T. A. Mayadunne, G. Moad, E. Rizzardo, *Tetrahedron Lett.* **1999**, *40*, 2435.

[21] Representative functional group transformations of dithiocarbamates: a) T. Hayashi, K. Sasaoka, T. Oishi, *J. Chem. Soc. Chem. Commun.* **1990**, 1362; b) M. A. Ali, L. Hough, A. C. Richardson, *Carbohydr. Res.* **1991**, *216*, 271; c) J. Eames, S. Warren, *J. Chem. Soc. Perkin Trans. 1* **1999**, 2783.

 © 2004 Wiley-VCH Verlag GmbH & Co. KGaA, Weinheim

C–C Coupling Reactions

Nickel-Catalyzed Tandem Carbostannylation of Alkynes and 1,2-Dienes with Alkynylstannanes**

Eiji Shirakawa, Youko Yamamoto, Yoshiaki Nakao, Shinichi Oda, Teruhisa Tsuchimoto, and Tamejiro Hiyama**

Carbometalation of carbon–carbon unsaturated bonds affords versatile synthetic reagents that have a newly formed carbon–carbon bond and a carbon–metal bond, which can be used for further construction of carbon frameworks.[1] In particular, a series of transition-metal-catalyzed carbostannylations[2] of alkynes,[3] 1,3-dienes[4] and 1,2-dienes[5] provides us with various substituted organostannanes, which are converted into a variety of conjugated and nonconjugated olefinic compounds through carbon–carbon bond forming reactions such as the Kosugi–Migita–Stille coupling.[6] The high chemoselectivity and mild reactivity of organostannanes make the sequence of carbostannylation and subsequent carbon–carbon bond-forming reactions an attractive synthetic strategy. Herein, we report an example of a tandem carbostannylation reaction,[7] namely, sequential insertion of two different carbon–carbon unsaturated bonds into a tin–alkynyl carbon bond.[8]

Treatment of trimethyl(phenylethynyl)tin (**1a**, 0.10 mmol) with 1-octyne (**2a**, 0.60 mmol) and 1,2-heptadiene (**3**, 0.30 mmol) in the presence of [Ni(cod)$_2$] (5.0 μmol) and [2-(dimethylamino)phenyl]diphenylphosphane (pn, 5.0 μmol; dibutyl ether, 50 °C, 24 h) gave rise to tandem alkynylstannylation to give a 98:2 mixture[9] of (3*Z*,6*Z*)-3-hexyl-1-phenyl-6-(trimethylstannyl)undeca-3,6-dien-1-yne (**4a**) and (3*Z*,6*E*)-

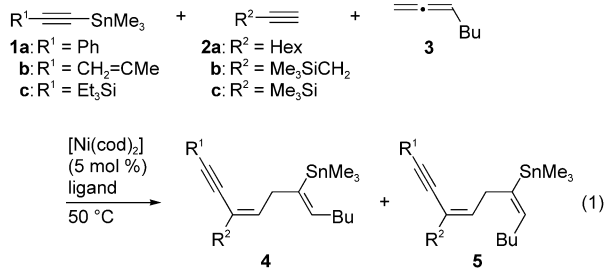
[*] Prof. Dr. E. Shirakawa,[+] Y. Yamamoto, Dr. T. Tsuchimoto
Graduate School of Materials Science
Japan Advanced Institute of Science and Technology
Asahidai, Tatsunokuchi, Ishikawa 923-1292 (Japan)
E-mail: shirakawa@kuchem.kyoto-u.ac.jp
Y. Nakao, S. Oda, Prof. Dr. T. Hiyama
Department of Material Chemistry
Graduate School of Engineering
Kyoto University
Nishigyo-ku, Kyoto 615-8510 (Japan)
Fax: (+81) 75-383-2445
E-mail: thiyama@npc05.kuic.kyoto-u.ac.jp
[+] Present address:
Department of Chemistry
Graduate School of Science
Kyoto University
Sakyo-ku, Kyoto 606-8502 (Japan)
Fax: (+81) 75-753-3988

[**] Financial support by Grant-in-Aid for Scientific Research on Priority Areas (A) "Exploitation of Multi-Element Cyclic Molecules" (to ES and TH) and COE Research on Elements Science, No. 12CE2005 (to TH) and on United Approach to New Material Science (to TH) from the Ministry of Education, Culture, Sports, Science and Technology, Japan is highly acknowledged.

Supporting information for this article is available on the WWW under http://www.angewandte.org or from the author.

 © 2004 Wiley-VCH Verlag GmbH & Co. KGaA, Weinheim DOI: 10.1002/anie.200353649

Table 1: Nickel-catalyzed tandem alkynylstannylation of alkynes and 1,2-heptadiene.[a]



Entry	R^1	R^2	Cond.[b]	t [h]	Yield [%][c]	**4**:**5**[c]	Product(s)
1	Ph (**1a**)	Hex (**2a**)	A	24	56	98:2	**4a**, **5a**
			B	24	73	4:96	**4a**, **5a**
			C	24	55	1:>99	**5a**
2[d]	Ph (**1′a**)	Hex (**2a**)	A	24	33	82:18	**4′a**, **5′a**
			B	24	49	1:>99	**5′a**
			C	49	12	1:>99	**5′a**
3	Ph (**1a**)	Me_3SiCH_2 (**2b**)	A	24	49	96:4	**4b**, **5b**
			B	24	59	12:88	**4b**, **5b**
			C	24	35	14:86	**4b**, **5b**
4	Ph (**1a**)	Me_3Si (**2c**)	A	6	5	>99:1	**4c**
			B	8	31	10:90	**4c**, **5c**
			C	6	31	7:93	**4c**, **5c**
5	$CH_2=CMe$ (**1b**)	Hex (**2a**)	A	4.5	44	>99:1	**4d**
			B	6	67	6:94	**4d**, **5d**
			C	24	31	9:91	**4d**, **5d**
6	Et_3Si (**1c**)	Hex (**2a**)	A	10	61	51:49	**4e**, **5e**
			B	9	60	5:95	**4e**, **5e**
			C	8	57	8:92	**4e**, **5e**

[a] The reaction was carried out in solvent (0.15 mL) with an alkynylstannane (0.10 mmol), an alkyne (0.60 mmol) and 1,2-heptadiene (0.30 mmol) in the presence of $[Ni(cod)_2]$ (5.0 μmol) and a ligand. [b] Ligand and solvent for Conditions A: pn (5.0 μmol), dibutyl ether; B: ttpp (10 μmol), toluene; C: dpp (5.0 μmol), THF. [c] Determined by ^{119}Sn NMR spectroscopy with Me_4Sn (Bu_4Sn for entry 2) as an internal standard. [d] Tributyl(phenylethynyl)tin was used instead of the trimethylstannyl analogue.

isomer **5a** in 56% yield [Eq. (1) and entry 1 of Table 1].[10] Screening of effective ligands led us to find that tris[*p*-(trifluoromethyl)phenyl]phosphane (ttpp) and 2-(diphenylphosphanyl)pyridine (dpp) gave the products in comparable yields[11] (entry 1 of Table 1) but in preference for **5a** over **4a** for conditions B and C (see Figure 1). Worthy of note is that **4a** or **5a** is generated in each case with selectivities higher than 96% out of 48 possible isomers.

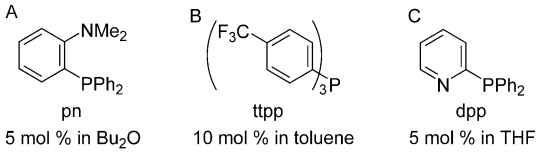
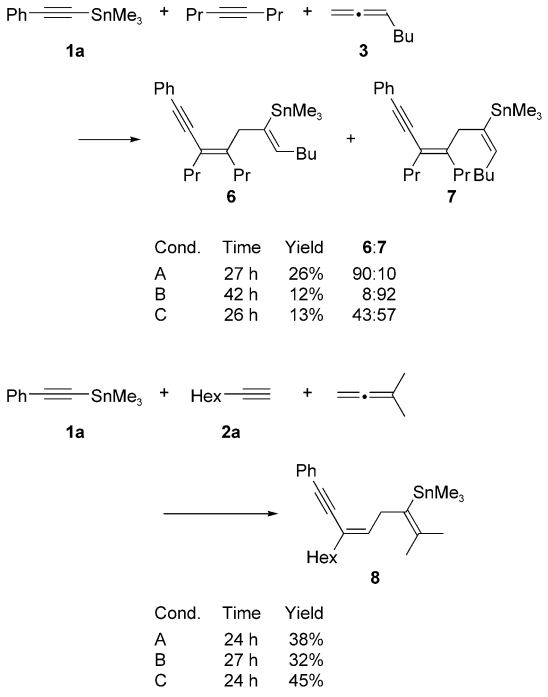


Figure 1. Ligands and solvents used in the tandem alkynylstannylation for conditions A, B, and C.

The tandem alkynylstannylation conditions A (pn in dibutyl ether), B (ttpp in toluene) or C (dpp in THF) were applied to various alkynylstannanes, alkynes and 1,2-heptadiene (entries 2–6 of Table 1). Tributylstannyl(phenyl)acetylene (**1′a**) also participated in the reaction (entry 2) but less efficiently. Similarly, stannyldienynes **4** and **5** that have a trimethylsilylmethyl or trimethylsilyl substituent were prepared (entries 3 and 4). Enynyl- and silylethynylstannanes also gave the corresponding trienynes and dienynes, respectively (entries 5 and 6). In addition to terminal alkynes and a monosubstituted allene, an internal alkyne and a 1,1-disubstituted allene reacted, albeit with much lower yields (Scheme 1).

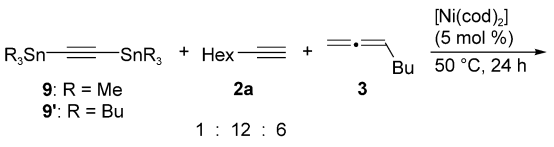
Tandem alkynylstannylation of bis(trimethylstannyl)acetylene **9** with **2a** and **3** gave 1:2:2 adducts **10** predominantly, whereas bis(tributylstannyl) analogue **9′** gave a mixture of 1:1:1 adducts **11′** [Eq. (2)]. The stereochemical preferences change depending on whether conditions A or B are used, as before. Thus, the size of trialkylstannyl groups effectively controls the ratio of **10**:**11** or **10′**:**11′**.

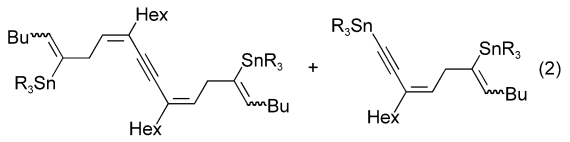
Some pieces of evidence are available to contribute towards a discussion of the mechanism of the tandem reaction. An oxidative adduct of tributyl(phenylethynyl)-tin (**1′a**) to a Ni^0–pn complex was observed by ^{31}P NMR and



Scheme 1. Tandem alkynylstannylation by using an internal alkyne or a 1,1-disubstituted allene. Reagents and conditions are the same as those in Table 1.

 © 2004 Wiley-VCH Verlag GmbH & Co. KGaA, Weinheim



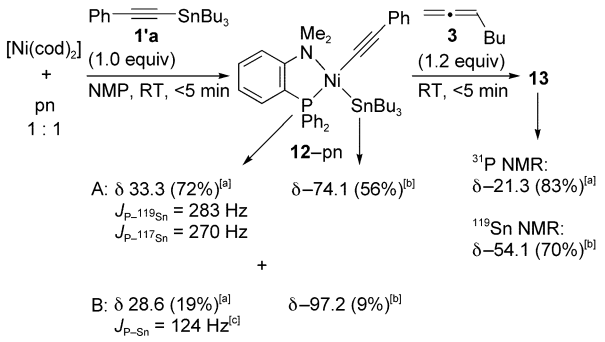


10a or **10'a**: 5*Z*,8*Z*,12*Z*,15*Z*
10b or **10'b**: 5*Z*,8*Z*,12*Z*,15*E*
10c or **10'c**: 5*E*,8*Z*,12*Z*,15*E*

11a or **11'a**: 3*Z*,6*Z*
11b or **11'b**: 3*Z*,6*E*

R	Cond.	Yield	**10a** or **10'a**	**10b** or **10'b**	**10c** or **10'c**	**11a** or **11'a**	**11b** or **11'b**
Me (**9**)	A	34%	84	16	<1	<1	<1
	B	58%	<1	6	56	4	34
Bu (**9'**)	A	42%	11	11	<1	62	16
	B	58%	<1	<1	<1	<1	>99

^{119}Sn NMR spectroscopies (Scheme 2),[12,13] while the reaction of [Ni(cod)$_2$]–pn with trimethylstannyl analogue **1a** gave a complex mixture. On treatment of **1′a** with [Ni(cod)$_2$]

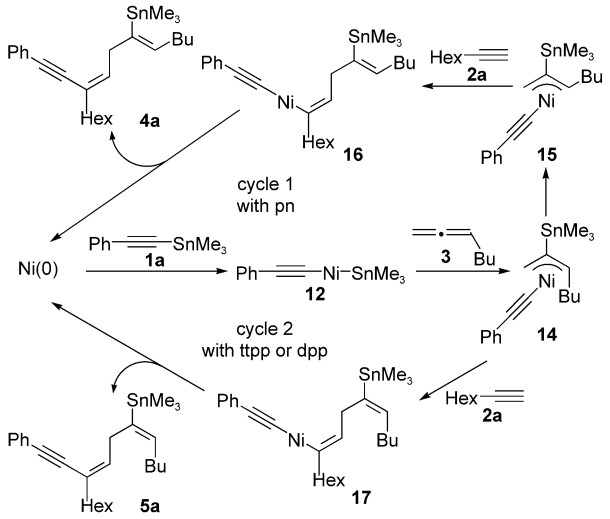


Scheme 2. Oxidative addition of an alkynylstannane to a nickel(0)–pn complex and the subsequent reactions traced by ^{31}P NMR and ^{119}Sn NMR spectroscopies: [a] Percentage of integral with respect to all of the observed peaks; [b] Yield based on **1′a** (determined by ^{119}Sn NMR spectroscopy with Bu_4Sn as an internal standard); [c] $J_{P-^{119}Sn}$ and $J_{P-^{117}Sn}$ were not resolved.

(1.0 equiv) and pn (1.0 equiv) in *N*-methylpyrrolidone (NMP)[14] in an NMR tube, two sets (**12**–pn A and **12**–pn B) of distinct signals were observed both in ^{31}P NMR and ^{119}Sn NMR spectra. Although the observed J_{P-Sn} values in both sets A and B indicate that a Sn–Ni σ bond is formed *cis* to the P atom,[15] thus suggesting structure **12**–pn shown in Scheme 2, we do not understand why two sets of peaks were observed. Both of these sets did not change on addition of alkyne **2a** (1.0 equiv) but did so smoothly with 1,2-diene **3** (1.2 equiv) to give **13**,[16] which lacks Sn–P coupling, thus showing that the insertion of **3** took place at the Ni–Sn bond of **12**–pn.[17] All attempts to obtain **4′a** or any other carbostannylation products by the reaction of **13** with **2a** were unsuccessful.

A survey of side products in the tandem alkynylstannylation of **1a**, **2a**, and **3** also provided information on the reaction order. Formation of any alkyne-alkynylstannylation product was not observed to any extent under conditions A, B, or C,[18] whereas a small amount of an allene-alkynylstannylation product was isolated under conditions A and B.[19] The results clearly show that 1,2-diene **3** rather than alkyne **2a** reacts with **12**–pn.

With the above data in hand, cycles 1 and 2 (see Scheme 3) may rationally explain the formation of tandem alkynylstannylation products **4a** and **5a** from the reaction of **1a** with **2a** and **3**. The catalytic cycles start with oxidative addition of **1a** to a nickel(0) complex. When oxidative adduct **12** undergoes insertion of **3** in a manner similar to acylstannane-nickel(0) oxidative adducts,[20] **3** should insert into the Ni–Sn bond of **12** in a direction such to avoid steric repulsion of the Bu substituent to give an (*E*)-σ-allylnickel complex,[21] which is prone to isomerize into the more stable *anti*-π-allyl complex **14**. Alkyne **2a** should then insert into the bond between the nickel atom and the nonsubstituted allyl carbon atom of **14** or the corresponding *syn*-isomer **15**.[22,23] The stereoselectivity of the tandem alkynylstannylation products should be determined by the relative rate of insertion of **2a** into the Ni–C bond of **14** and *anti–syn* isomerization from **14** to **15**, depending on ligand pn, ttpp or dpp. Reductive elimination from **16** or **17** should finally afford **4a** or **5a**, respectively.[24]



Scheme 3. Plausible catalytic cycles that start with oxidative addition of an alkynylstannane to a nickel(0) complex.

In conclusion, we have disclosed the first example of transition-metal-catalyzed tandem carbostannylation of two different carbon–carbon unsaturated bonds. Nickel catalysts assemble alkynylstannanes, alkynes and 1,2-dienes into alkenylstannanes having a dienyne structure that is otherwise hard to access by a direct route. Studies on the details of the mechanism as well as application of the reaction to other substrates are in progress.

 © 2004 Wiley-VCH Verlag GmbH & Co. KGaA, Weinheim

Experimental Section

Tandem alkynylstannylation of alkynes and 1,2-dienes, general procedure: 1,2-Diene (0.30 mmol) and an alkyne (0.60 mmol) were added to a solution that contained an alkynylstannane (0.10 mmol), $[Ni(cod)_2]$ (1.4 mg, 5.1 μmol) and a ligand (pn: 1.5 mg, 4.9 μmol; ttpp: 4.7 mg, 10 μmol; dpp: 1.3 mg, 4.9 μmol) in a solvent (dibutyl ether, toluene, or THF: 0.15 mL), and the resulting mixture was stirred at 50 °C. After the time specified (see Table 1 and Scheme 1 for specific details), the mixture was diluted with diethyl ether and filtered through a pad of florisil. The crude product was analyzed by ^{119}Sn NMR spectroscopy with Me_4Sn (Bu_4Sn for the reaction of tributyl(phenylethynyl)tin) as an internal standard.

Received: December 30, 2003
Revised: April 21, 2004 [Z53649]

Keywords: C–C coupling · metalation · multicomponent reactions · nickel · tin

[1] P. Knochel in *Comprehensive Organic Synthesis*, *Vol. 4* (Eds.: B. M. Trost, I. Fleming, M. F. Semmelhack), Pergamon, New York, **1991**, chap. 4.4, pp. 865–911.

[2] For accounts, see: a) E. Shirakawa, T. Hiyama, *Bull. Chem. Soc. Jpn.* **2002**, *75*, 1435–1450; b) E. Shirakawa, T. Hiyama, *J. Organomet. Chem.* **2002**, *653*, 114–121.

[3] a) E. Shirakawa, H. Yoshida, T. Kurahashi, Y. Nakao, T. Hiyama, *J. Am. Chem. Soc.* **1998**, *120*, 2975–2976; b) E. Shirakawa, K. Yamasaki, H. Yoshida, T. Hiyama, *J. Am. Chem. Soc.* **1999**, *121*, 10221–10222; c) E. Shirakawa, H. Yoshida, Y. Nakao, T. Hiyama, *Org. Lett.* **2000**, *2*, 2209–2211; d) H. Yoshida, E. Shirakawa, T. Kurahashi, Y. Nakao, T. Hiyama, *Organometallics* **2000**, *19*, 5671–5678; e) H. Yoshida, Y. Honda, E. Shirakawa, T. Hiyama, *Chem. Commun.* **2001**, 1880–1881; f) E. Shirakawa, Y. Yamamoto, Y. Nakao, T. Tsuchimoto, T. Hiyama, *Chem. Commun.* **2001**, 1926–1927.

[4] E. Shirakawa, Y. Nakao, H. Yoshida, T. Hiyama, *J. Am. Chem. Soc.* **2000**, *122*, 9030–9031.

[5] a) E. Shirakawa, Y. Nakao, T. Hiyama, *Chem. Commun.* **2001**, 263–264; b) E. Shirakawa, Y. Nakao, T. Tsuchimoto, T. Hiyama, *Chem. Commun.* **2002**, 1962–1963.

[6] For an account on the cross-coupling reaction by using carbostannylation products, see reference [2b]. For a review of the palladium-catalyzed coupling of organostannanes with organic electrophiles, see: K. Fugami, M. Kosugi, *Top. Curr. Chem.* **2002**, *219*, 87–130, and references therein.

[7] We have already reported the dimerization–carbostannylation of alkynes, in which two molecules of alkynes insert into a carbon–tin bond: a) E. Shirakawa, H. Yoshida, Y. Nakao, T. Hiyama, *J. Am. Chem. Soc.* **1999**, *121*, 4290–4291; b) H. Yoshida, E. Shirakawa, Y. Nakao, Y. Honda, T. Hiyama, *Bull. Chem. Soc. Jpn.* **2001**, *74*, 637–647.

[8] For nickel-catalyzed multicomponent coupling reactions, see: a) J. Montgomery, *Acc. Chem. Res.* **2000**, *33*, 467–473; b) S. Ikeda, *Acc. Chem. Res.* **2000**, *33*, 511–519.

[9] Configuration of two double bonds in the tandem alkynylstannylation products was determined by NMR spectroscopic studies on coupling constants ($^3J_{Sn-H}$ and $^3J_{Sn-C}$) and NOE. For details, see Supporting Information.

[10] Unless otherwise noted, the yields and the ratio of isomers were determined by ^{119}Sn NMR spectroscopy with Me_4Sn or Bu_4Sn as an internal standard.

[11] The isolated yield of **4a** and **5a** after purification with reversed phase chromatography (octadecylsilyl, ODS) followed by gel-permeation chromatography (GPC) under conditions A or B (Figure 1) was 50% (88:12) or 63% (2:98), respectively, obtained from independent experiments from those shown in Table 1, entry 1.

[12] $[(Ph_3P)_2Ni(C{\equiv}CPh)(SnMe_3)]$ is reportedly obtained, but in an analytically impure form, see: B. Cetinkaya, M. F. Lappert, J. McMeeking, D. E. Palmer, *J. Chem. Soc. Dalton Trans.* **1973**, 1202–1208.

[13] Density functional study shows that $HC{\equiv}CSnH_3$ can oxidatively add to $[Ni(PH_3)_2]$, see: T. Matsubara, K. Hirao, *Organometallics* **2002**, *21*, 4482–4489.

[14] Oxidative adduct **12**–pn was observed also in dibutyl ether, THF, [D$_6$]benzene or DMF but in a purity less than 50%. NMP as a solvent for the Ni–pn-catalyzed reaction of **1a** with **2a** and **3** was found to be as efficient as dibutyl ether in the yield and stereoselectivity.

[15] The $J_{P-Sn(cis)}$ of oxidative adduct of **1′a** to a palladium–iminophosphane or dppp complex is reported to be 21 or 29 Hz, respectively, whereas the $J_{P-Sn(trans)}$ of the dppp complex is 1479/1411 Hz. See, E. Shirakawa, H. Yoshida, T. Hiyama, *Tetrahedron Lett.* **1997**, *38*, 5177–5180. The $J_{P-^{119}Sn(cis)}$ and $J_{P-^{119}Sn(trans)}$ of a similar complex, $[(dppe)Pd(SnMe_2Cl)(C{\equiv}CMe)]$, prepared by successive transmetalation of the corresponding dichloro complex, are reported to be 183 and 2392 Hz. See, C. Stader, B. Wrackmeyer, *J. Organomet. Chem.* **1985**, *295*, C11–C15.

[16] Complex **12-pn** reacted with **3** also in the presence of **2a** (1.0 equiv) to give **13**.

[17] We could not obtain further information on the structure of complex **13**: its short lifetime and insufficient purity in addition to low availability of deuterated NMP do not allow us to gain meaningful ^{13}C and ^{1}H NMR spectra.

[18] The reaction of **1a** with **2a** in the absence of **3** under conditions A or B gave (*Z*)-2-hexyl-4-phenyl-1-trimethylstannylbut-1-en-3-yne in 13% or 6% yield, respectively. For the nickel-catalyzed alkynylstannylation of alkynes, see reference [3b].

[19] (*Z*)-4-Trimethylstannyl-1-phenylnon-4-en-1-yne or 3-butyl-5-phenyl-2-trimethylstannylpent-1-en-4-yne was generated in 6% yield under conditions A or B, respectively. For the nickel-catalyzed alkynylstannylation of 1,2-dienes, see reference [5b].

[20] In the nickel-catalyzed acylstannylation of 1,2-dienes, oxidative adducts of acylstannanes to nickel(0) complexes are considered to accept insertion of 1,2-dienes at the Ni–Sn bonds in the direction that affords σ-allylnickel complexes. See reference [5a].

[21] Intermediary σ-allylnickel complexes, which should be involved in cycle 1 and 2, are omitted from Scheme 3 for clarity.

[22] The regioselection should be reasonable, as terminal alkynes are considered to insert into a π-allylnickel complex at a less substituted carbon in the nickel-catalyzed three-component coupling of allyl chlorides, alkynes, and alkynylstannanes, see: a) S. Ikeda, D.-M. Cui, Y. Sato, *J. Org. Chem.* **1994**, *59*, 6877–6878; b) D.-M. Cui, T. Tsuzuki, K. Miyake, S. Ikeda, Y. Sato, *Tetrahedron* **1998**, *54*, 1063–1072.

[23] When allylnickel complexes fail to accept insertion of **2a**, alkynylstannylation products of **3** should be generated through reductive elimination.

[24] Oxidative cyclization of **2a** and **3** with a nickel(0) complex followed by the reaction with **1a** may be an alternative mechanism, but no evidence is currently available. See reference [7].

 © 2004 Wiley-VCH Verlag GmbH & Co. KGaA, Weinheim

Nanostructures

In Situ Assembly of Zeolitic Building Blocks into High-Order Structures**

Gang Hu, Ding Ma, Lin Liu, Mojie Cheng, and Xinhe Bao**

The construction of inorganic architectures with hierarchically complex structures and optimized properties for specific applications is a current objective in materials chemistry.[1–3] These highly organized materials, including metal and metal oxides,[4] bio-minerals,[5] and micro- and mesoporous materials,[6–9] have great potential as agents in medical (e.g. controlled drug delivery), optical, electronic, and magnetic applications. Besides methods that involve molecular cross-linking[10] or antibody–antigen recognition,[11] most high order inorganic frameworks are synthesized through so-called template-assisted processes with building blocks such as nanosized particles generated either beforehand or in situ.

Although classified under template-assisted processes, many different approaches are involved in such constructions. Examples include guided growth within confined geometries,[12] monodisperse polymer sphere templating,[5b,6b,7,13] polydimethylsilane stamp patterning,[4c,8] aligned polyurethane film matrixing,[9] and pseudomorphic self-templating transformations.[14] Interestingly, although different in concept, most templates employed in the synthesis are hard templates such as polymer spheres, organic moulds, macro- or mesoporous materials,[15] bacteria,[6a] and diatom shells.[16] Very few cases of simple processes that employ soft or dual-soft templates to build complex multilevel structures from a functional basic unit have been reported. Herein we describe a feasible and facile one-pot approach, which first employs a small HMI (hexamethyleneimine) template to generate the sheetlike building block of microporous MCM-22 zeolite, then a supramolecular surfactant acts as a co-template to assist the assembly of these building blocks in situ into superstructures.

[*] G. Hu, Dr. D. Ma, L. Liu, Prof. M. Cheng, Prof. X. Bao
State Key Laboratory of Catalysis
Dalian Institute of Chemical Physics
Chinese Academy of Sciences
Dalian 116023 (China)
Fax: (+86) 411-8469-4447
E-mail: xhbao@dicp.ac.cn
Dr. D. Ma
School of Chemistry, University of Bristol
Bristol, BS8 1TS (UK)
Fax: (+44) 117-9290-509
E-mail: ding.ma@bristol.ac.uk

[**] Financial support (2003CB615806, G1999022406) from the National Natural Science Foundation and the Ministry of Science and Technology of the People's Republic of China is gratefully acknowledged. We also thank Dr. M. Li and Dr. D. Walsh for kind help in composing the paper and Dr. A. Kulak for technical expertise.

Supporting information for this article is available on the WWW under http://www.angewandte.org or from the author.

Zeolite MCM-22 is a microporous material composed of interconnected $\{4^3 5^6 6^3 [4^3]\}$ building units that form two independent pore systems: two-dimensional 10-ring intralayer channels, and 12-ring interlayer supercages with depths of 18.2 Å, both of which are accessible through 10-ring apertures.[17] This makes MCM-22 a promising catalyst for many processes and particularly for hydrocarbon conversion reactions.[18] Although other morphologies such as spheres have been reported for MCM-22 crystals,[19] the more common morphology of MCM-22 consists of sheetlike discs or aggregates of several cross-linked discs of 2–5 μm in diameter and 10–40 nm in thickness (see Supporting Information).[20,21]

However, when nonionic surfactants were added to the system doughnutlike products with different morphologies and surface patterns were obtained. For example, the sample M20 was synthesized with the addition of $C_{16}H_{33}(OC_2H_4)_{20}OH$ at 160 °C. The dominant product (> 85 % yield) was spherical with a diameter of around 8–10 μm and with a scaled surface pattern (Figure 1 a, b).

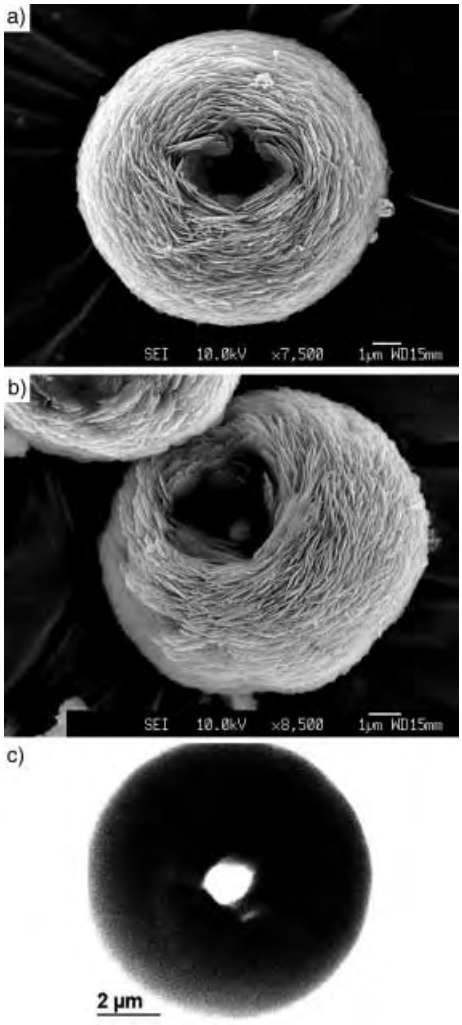


Figure 1. a), b) FESEM pictures, and c) TEM picture of the sample M20 (synthesized at 160 °C in the presence of $C_{16}H_{33}(OC_2H_4)_{20}OH$). Scale-like patterns and holes can be observed on the spheres in a) and b); c) shows a channel penetrating the sphere.

 © 2004 Wiley-VCH Verlag GmbH & Co. KGaA, Weinheim DOI: 10.1002/anie.200453777

Furthermore, small holes (≈1.5–2 μm according to TEM) were found at the center of the spherical structures. The TEM image of the top surface of one such particle (Figure 1c) revealed that these holes are actually channels that penetrate through the centers of the particles to form doughnutlike structures. FESEM (field emission scanning electron microscopy) measurements of samples prepared in the absence of nonionic surfactants show that the doughnuts are composed of individual sheets (see Supporting Information). However, at this stage, we were unable to conclude whether or not these scales consisted of MCM-22 as the influence of the added nonionic surfactants on the crystal structure of the products was unclear.

XRD studies of the "doughnuts" before and after calcination (Figure 2a, I and II, respectively) reveal both sharp and broad peaks that are consistent with the diffraction peaks of zeolite MCM-22.[17,20] Peaks at $2\theta = 6.5$ and 7.2° in Figure 2aI corresponding to (002) and (100) peaks, respectively, are clearly discerned. After calcination, these two peaks overlap owing to the structural contraction along the *c* axis. Furthermore, broad peaks within the range 18–25° split and become more defined (Figure 2aII). These XRD details are characteristic of MCM-22 and confirm that the building blocks constructing the giant doughnut-shaped structures are indeed zeolite MCM-22. The nonionic surfactants, which are not involved in the crystallization process of the individual scales of MCM-22 sheets, are instead involved in the self-assembly into super-structures. Importantly, samples prepared in the absence of nonionic surfactants consist of normal random oriented MCM-22 discs (see Supporting Information).

Figure 2bI shows the ^{13}C cross-polarization/magic-angle spinning (CP/MAS) NMR spectrum of the sample MN (which was synthesized in the absence of surfactant). When compared with the standard ^{13}C NMR spectrum of HMI which displays three signals at $\delta = 51.5$, 34, and 29.5 ppm (see Supporting Information), the three peaks in the spectrum of MN at $\delta \approx 55$, 47, and 26.5 ppm can be assigned to signals arising from C1, C1, and C2/C3 (Figure 2b), respectively, of HMI molecules within the zeolitic channels.[21] The two signals for C1 are attributed to HMI template molecules residing in two distinct inter- and intralayer void spaces of MCM-22; the strong interactions between HMI molecules and the zeolite framework account for the different chemical shifts for C1.[21]

Two additional peaks appear in the NMR spectrum of the sample M20 (synthesized in the presence of surfactant), one at $\delta \approx 28$ ppm and the other at $\delta \approx 53.5$ ppm (Figure 2bII) although the sample was repeatedly washed with deionized water before NMR measurements. When compared with the ^{13}C NMR spectrum of the surfactant $C_{16}H_{33}(OC_2H_4)_{20}OH$ (see Supporting Information), we see that the signal at $\delta =$ 28 ppm in Figure 2bII arises from the carbon atoms in the alkyl chain $C_{16}H_{33}$-, whereas the signal at $\delta \approx 53.5$ ppm can be assigned to the carbon atoms in the oxyethylene groups $(OC_2H_4)_{20}$. The former peak overlaps with that of the C2/C3 atoms of HMI to result in a more intense peak at $\delta \approx 28$ ppm. The shift in the signals arising from pure surfactant molecules and those incorporated into the MCM-22 superstructure are

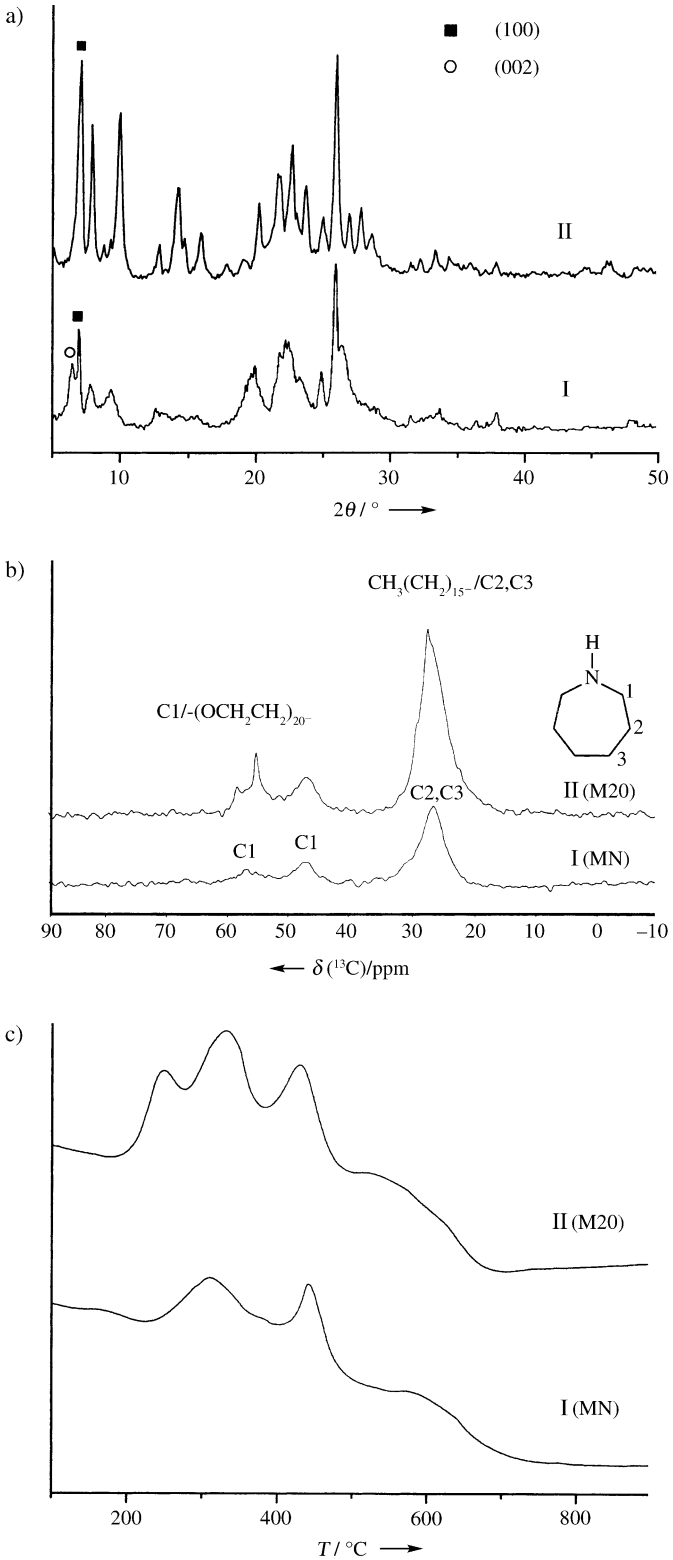


Figure 2. a) XRD patterns of sample M20: I) before and II) after calcination. The disappearance of the (002) peak and the increased intensity of the peaks at 18–28° are characteristic of the zeolite MCM-22; b) ^{13}C CP/MAS NMR spectra: I) MN (prepared in the absence of surfactant) and II) M20; the signal from incorporated oxyethylene groups is seen at $\delta = 53.5$ ppm; (c) DTA curves of synthesized samples I) MN and II) M20; the new peak at about 250 °C arises from oxyethylene carbon species.

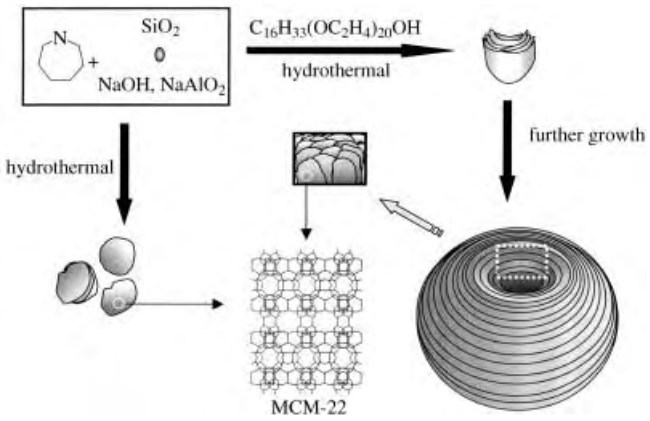
 © 2004 Wiley-VCH Verlag GmbH & Co. KGaA, Weinheim

again attributed to strong interactions of the nonionic surfactant with the MCM-22 discs. This result suggests that the nonionic surfactant remains between the adjacent discs of individual MCM-22 discs and contributes to the assembly of the MCM-22 sheets into the "doughnuts". In other words, the strong interactions between the surfactant molecules and MCM-22 building-block discs are the driving force for the formation of the zeolitic superstructure.

To determine whether the nonionic surfactant had taken part in the assembly of the doughnutlike superstructure, further investigations by DTA (differential thermal analysis) were undertaken as shown in Figure 2c. For the standard MCM-22 sample, the weight loss in the range of 220–520 °C is mainly attributed to the removal of the organic template HMI from the framework.[21] Two peaks were observed when MN (the sample prepared without the addition of surfactants) was analyzed; these peaks arise from the presence of template HMI molecules (Figure 2c I) inside the zeolitic channels. For sample M20, the peak at about 250 °C on the DTA curve (Figure 2c II) is characteristic of the removal of oxyethylene carbon species. Again, this confirms that the second template (i.e. the surfactant $C_{16}H_{33}(OC_2H_4)_{20}OH$) does participate in the assembly of MCM-22 discs to form high-order superstructures.

An investigation throughout the duration of the growing process aided us in understanding the assembly mechanism of the doughnutlike superstructures. After the gelation of slurrylike reactants (normally after 2–3 days in a hydrothermal bomb at 160 °C), partially crystallized intermediates, which are occasionally found as by-products (about 5-20 %) in the final product, were sometimes observed (see Supporting Information). These intermediates are thin, oriented MCM-22 discs aggregated together which then form rolls probably owing to the larger surface tension on the side with nonionic surfactant micelles. This stress imbalance probably arises from the strong interaction between MCM-22 crystallites and surfactant micelles.

A clearer description of this process is illustrated in Scheme 1. In a typical synthetic procedure for MCM-22, the mixture of $NaAlO_2$, H_2O, HMI, and silica sol produces a milky slurry. With further hydrothermal reaction, single or aggregated MCM-22 discs with MWW topology crystallize from the system. If a nonionic surfactant (e.g. $C_{16}H_{33}(OC_2H_4)_{20}OH$) is added to the slurry with vigorous stirring before the hydrothermal crystallization process, a synergic effect of HMI and $C_{16}H_{33}(OC_2H_4)_{20}OH$ combines both the growth of MCM-22 discs and the self-assembly in situ of disclike MCM-22 building blocks in a one-pot reaction. However, the presence of a possible intermediate state of the product suggests that the formation of the doughnutlike superstructure through the growth of MCM-22 discs and the assembly of these zeolitic building blocks is likely to occur by a sequential process instead of a one-step procedure. Under these conditions, the formation of doughnutlike structures is probably geometrically more favorable than the normal flat discs.



Scheme 1. With the addition of nonionic surfactant, rolled MCM-22 building blocks crystallize in the system and assemble in situ into doughnutlike superstructures. Without the addition of surfactant, MCM-22 discs do not form macrostructured spherical products.

During the study, we also noticed that products with different morphologies could be obtained upon variation of the crystallization temperature. Taking M20 for example, when the system was heated at 150 °C uniform spherical superstructures were synthesized with an average diameter of 8–12 μm (see Supporting Information). XRD analysis confirmed that the superstructures consisted of building blocks with MWW topology (MCM-22). However, high resolution SEM pictures show that the MCM-22 discs assembled in a much more compact manner at 150 °C (Figure 3a) than at 160 °C (Figure 3b).

Besides $C_{16}H_{33}(OC_2H_4)_{20}OH$, other nonionic surfactants such as $C_{16}H_{33}(OC_2H_4)_{10}OH$ and $H(OC_2H_4)_{20}(OC_3H_6)_{70}(OC_2H_4)_{20}OH$ (P123) that have different numbers of oxyethylene groups as well as different molecular sizes were employed in the synthesis. SEM pictures show remarkable morphological differences of the two samples obtained at 150 °C when compared with that of M20. The surface of the M10 superstructure (prepared in the presence of $C_{16}H_{33}(OC_2H_4)_{10}OH$) was more coarse and scale-like fragments on the surfaces were observed among the particles (Figure 3c). Sample MP (with the addition of P123) consisted of spheres with a similar average diameter of about 8–12 μm. However, Figure 3e shows that the linear patterns on the MP surfaces are thicker and more compact than those on the M10 and M20 surfaces. When the crystallization temperatures were increased to 160 °C, a much less compact assembly was observed by SEM analysis of samples M10 (Figure 3d) and MP (Figure 3f). For $C_{16}H_{33}(OC_2H_4)_{10}OH$, which has a smaller polyoxyethylene group, the MCM-22 discs were only poorly aggregated and no doughnutlike superstructures were observed by SEM for the sample synthesized at 160 °C (Figure 3d). However, in this case a peony-like superstructure resulted in which there was no penetrating hole in the center. Owing to the larger polyoxyethylene groups in P123 and $C_{16}H_{33}(OC_2H_4)_{20}OH$, the interactions between nanoscale MCM-22 building blocks and surfactant molecules (in the *z* direction) were still strong enough for the discs to assemble into large spherical superstructures, though in a relatively less compact manner at 160 °C. XRD results of samples M10 and MP at 150 and 160 °C both confirmed that these products were still constructed of zeolite MCM-22. ^{13}C CP/MAS NMR and DTA studies gave similar results for M20.

 © 2004 Wiley-VCH Verlag GmbH & Co. KGaA, Weinheim

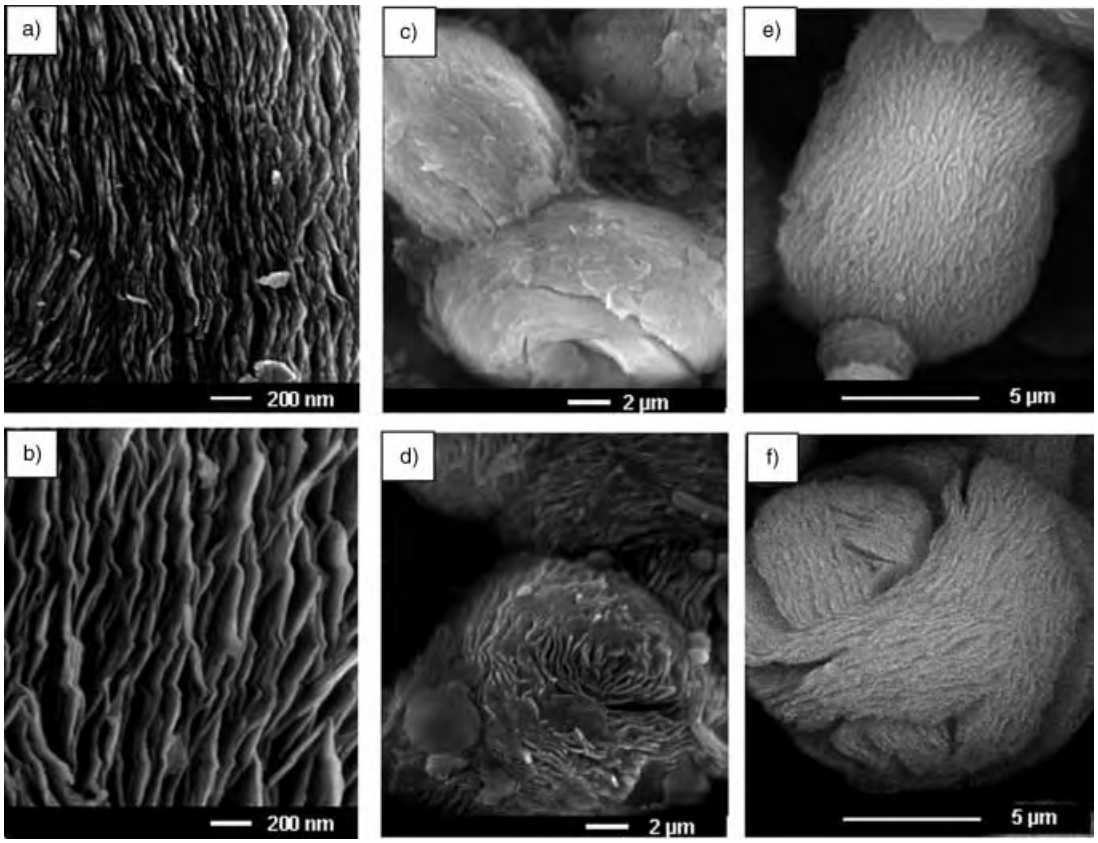


Figure 3. FESEM pictures of samples synthesized with different surfactants at different temperatures. a), c), and e) show samples M20, M10, and MP, respectively, at 150 °C; b), d), and f) are SEM pictures of the respective samples crystallized at 160 °C. The MCM-22 building blocks are arranged in a more compact manner at lower temperature and with increasing numbers of oxyethylene groups.

It is likely that the repeating oxyethylene units in the surfactant molecules play an important role in the assembly process. The interactions of these hydrophilic groups with the aluminosilicates appear to be the driving force behind the assembly of the zeolitic units into superstructures. With more hydrophilic oxyethylene units in the surfactant molecules, the interactions become stronger and so the zeolitic discs are assembled more tightly. This is possibly the reason why MP superstructures have more compact surface linear patterns than those of M20 and M10 superstructures. It is not quite clear why the discs combined less compactly with increased reaction temperatures, but a possible explanation is that higher temperatures are not favorable for the surfactants to form "liquid-crystal" micelles in the mixture and thus the capacity of the surfactants to assemble is weakened. Another factor may be that the polyoxyethylene chains in nonionic surfactant molecules are not stable and decompose at higher temperatures, which might also account for the less compact arrangement of the discs in the samples obtained at higher temperatures.

In conclusion, we have shown that high-order superstructures with nanoscale zeolitic building units can be synthesized through the synergic dual-template method by a one-pot reaction, which opens a new way to construct hierarchical macrostructures using functional inorganic units as building blocks.

Experimental Section

Reagents were used as received without further purification: silica sol (25 wt %), hexamethyleneimine (HMI), sodium aluminate, sodium hydroxide, deionized water and nonionic surfactants. Three nonionic surfactants were used: $C_{16}H_{33}(OC_2H_4)_{10}OH$, $C_{16}H_{33}(OC_2H_4)_{20}OH$, and $H(OC_2H_4)_{20}(OC_3H_6)_{70}(OC_2H_4)_{20}OH$ (P123). A typical synthetic procedure for different MCM-22 samples follows:

Sodium aluminate (1 g) and sodium hydroxide (0.2 g) were dissolved in deionized water (135 mL), and HMI (10.3 g) was added dropwise to the stirred mixture. Then, either $C_{16}H_{33}(OC_2H_4)_{20}OH$ (1.0 g) or $C_{16}H_{33}(OC_2H_4)_{10}OH$ (1.0 g) or P123 (2.0 g) was dissolved in silica sol (100.2 g) and added to the above mixture with vigorous stirring. After stirring for 5 h at room temperature, the slurry was transferred into a stainless-steel hydrothermal bomb lined with teflon and heated at 150 °C or 160 °C for 4–6 days. The final products (labeled M20, M10, and MP, respectively) were washed repeatedly with cold and hot deionized water and then dried at 80 °C. Calcination of the synthesized products was carried out in air at 540 °C for 10 h. For comparison, a normal MCM-22 sample (MN) was also synthesized in the same way but without the addition of surfactant. The products were characterized by X-ray powder diffraction (XRD, Rigaku Dmax/rb diffractometer with $Cu_{K\alpha}$ radiation, $\lambda = 0.1542$ nm, 40 kV, 100 mA), electron microscopy (Hitachi HB600 and JEOL 6300F FEGSEM), nuclear magnetic resonance spectroscopy (NMR, Bruker DRX-400 with BBO MAS probe and 4-mm ZrO_2 rotors; ^{13}C CP/MAS NMR spectra were recorded at 100.62 MHz with a 2500-μs contact time, a 4-s recycle delay, and a 4-kHz spinning rate), and differential thermal analysis (DTA, Perkin-Elmer DTA1700) studies.

Received: January 19, 2004 [Z53777]

 © 2004 Wiley-VCH Verlag GmbH & Co. KGaA, Weinheim

Keywords: nanostructures · self-assembly · surfactants · template synthesis · zeolites

[1] S. Mann, G. A. Ozin, *Nature* **1996**, *382*, 313.
[2] I. Dierking, *Adv. Mater.* **2003**, *15*, 152.
[3] A. Stein, *Adv. Mater.* **2003**, *15*, 763.
[4] a) O. D. Velev, P. M. Tessier, A. M. Lenhoff, E. W. Kaler, *Nature* **1999**, *401*, 548; b) A. Imhof, D. J. Pine, *Nature* **1997**, *389*, 948; c) P. Yang, T. Deng, D. Zhao, P. Feng, D. Pine, B. F. Chmelka, G. M. Whitesides, G. D. Stucky, *Science* **1998**, *282*, 2244; d) Z. Yang, Z. Niu, Y. Lu, Z. Hu, C. C. Han, *Angew. Chem.* **2003**, *115*, 1987; *Angew. Chem. Int. Ed.* **2003**, *42*, 1943.
[5] a) W. Shenton, D. Pum, U. B. Sleytr, S. Mann, *Nature* **1997**, *389*, 585; b) B. T. Holland, C. F. Blanford, A. Stein, *Science* **1998**, *281*, 538.
[6] a) S. A. Davis, S. L Burkett, N. H. Mendeison, S. Mann, *Nature* **1997**, *385*, 420; b) K. H. Rhodes, S. A. Davis, F. Caruso, B. Zhang, S. Mann, *Chem. Mater.* **2000**, *12*, 2832.
[7] B. T. Holland, L. Abrams, A. Stein, *J. Am. Chem. Soc.* **1999**, *121*, 4308.
[8] L. Huang, Z. Wang, J. Sun, L. Miao, Q. Li, Y. Yan, D. Zhao, *J. Am. Chem. Soc.* **2000**, *122*, 3530.
[9] J. S. Lee, Y. J. Lee, E. L. Tae, Y. S. Park, K. B. Yoon, *Science* **2003**, *301*, 818.
[10] R. P. Andres, J. D. Bielefeld, J. I. Henderson, D. B. Janes, V. R. Kolagunta, C. P. Kubiak, W. Mahoney, R. G. Osifchin, *Science* **1996**, *273*, 1690.
[11] W. Shenton, S. A. Davis, S. Mann, *Adv. Mater.* **1999**, *11*, 449.
[12] M. Trau, N. Yao, E. Kim, Y. Xia, G. M. Whitesides, I. A. Aksay, *Nature* **1997**, *390*, 694.
[13] X. D. Wang, W. L. Yang, Y. Tang, Y. J. Wang, S. K. Fu, Z. Gao, *Chem. Commun.* **2000**, 2161; A. Dong, Y. Wang, Y. Tang, Y. Zhang, N. Ren, Z. Gao, *Adv. Mater.* **2002**, *14*, 1506.
[14] T. Martin, A. Galarneau, F. Di Renzo, F. Fajula, D. Plee, *Angew. Chem.* **2002**, *114*, 2702; *Angew. Chem. Int. Ed.* **2002**, *41*, 2590.
[15] C. Z. Yu, J. Fan, B. Z. Tian, D. Y. Zhao, *Adv. Mater.* **2002**, *14*, 1742.
[16] M. W. Anderson, S. M. Holmes, N. Hanif, C. S. Cundy, *Angew. Chem.* **2000**, *112*, 2819; *Angew. Chem. Int. Ed.* **2000**, *39*, 2707.
[17] M. E. Leonowicz, J. A. Lawton, S. L. Lawton, M. K. Rubin, *Science* **1994**, *264*, 1910; G. J. Kennedy, S. L. Lawton, M. K. Rubin, *J. Am. Chem. Soc.* **1994**, *116*, 11 000; S. L. Lawton, M. E. Leonowicz, R. D. Partridge, P. Chu, M. E. Rubin, *Microporous Mesoporous Mater.* **1998**, *23*, 109.
[18] D. Ma, Y. Shu, X. Han, X. liu, Y. Xu, X. Bao, *J. Phys. Chem. B* **2001**, *105*, 1170.
[19] a) A. Marques, J. Monteiro, H. O. Pastore, *Microporous Mesoporous Mater.* **1999**, *32*, 131; b) M. Cheng, G. Hu, D. Tan, X. Bao, *Microporous Mesoporous Mater.* **2001**, *50*, 69; c) A. Corma, C. Corell, J. Perez-Pariente, *Zeolites* **1995**, *15*, 2. Attempts to repeat the experiments reported in reference [19a] yield only disclike products (see Supporting Information) instead of the spherical products reported. In other works,[19c] some spherical MCM-22 aggregates were occasionally observed, although the main products were small thin plates. To the best of our knowledge, no other relevant work had ever been reported before. An inadvertent introduction of organic materials into the system may have led to the false phenomena in the above reports and the poor reproducibility encountered afterwards.
[20] a) I. Mochida, S. Eguchi, M. Hironaka, S. Nagao, K. Sakanishi, D. D. Whitehurst, *Zeolites* **1997**, *18*, 142; b) I. Güray, J. Warzywoda, N. Baç, A. Sacco, Jr., *Microporous Mesoporous Mater.* **1999**, *31*, 241.
[21] S. L. Lawton, A. S. Fung, G. J. Kennedy, L. B. Alemany, C. D. Chang, G. H. Hatzikos, D. N. Lissy, M. K. Rubin, H.-K. C. Timken, S. Steuernagel, D. E. Wossner, *J. Phys. Chem.* **1996**, *100*, 3788.

 © 2004 Wiley-VCH Verlag GmbH & Co. KGaA, Weinheim

Noble-Gas Compounds

The First Compound Containing a Metal Center in a Homoleptic Environment of XeF_2 Molecules**

Melita Tramšek, Primož Benkič, and Boris Žemva**

Since Bartlett and co-workers reported that XeF_2 can act as ligand for Ag^I,[1] several coordination compounds with metal ions coordinated by XeF_2 have been prepared.[2,3] Metal centers in all the compounds of this type are coordinated simultaneously by XeF_2 molecules and $[AF_6]^-$ ions (A = As, Sb, P). The important feature of the compound described herein, $Ca_2(XeF_2)_9(AsF_6)_4$, is that for the first time one calcium center is coordinated to XeF_2 molecules only (a homoleptic center) while the second is coordinated to XeF_2 molecules and $[AsF_6]^-$ ions.

The reaction between $Ca(AsF_6)_2$ and XeF_2, in anhydrous HF (aHF) as a solvent, yields two compounds: $[Ca(XeF_2)_n](AsF_6)_2$; $n = 4$ and 2.5.[2] Which compound is formed depends on the mole ratio of the reactants (n corresponds the mole ratio between XeF_2 and Ca). Noted that an excess of XeF_2 is necessary ($n > 4$) in order to obtain pure $[Ca(XeF_2)_4](AsF_6)_2$, free of $[Ca(XeF_2)_{2.5}](AsF_6)_2$. We believe that at lower concentrations of XeF_2 ($n < 4$), there is always also some HF coordinated to the Ca^{2+} ion, this being lost as the solvent is removed.

In the present study a very high concentration of XeF_2 ($n > 20$) was employed to create the reaction conditions for the preparation of a possible homoleptic compound with XeF_2. A new coordination compound $Ca_2(XeF_2)_9(AsF_6)_4$ was isolated. It is clear that, with increased XeF_2 concentration, the number of XeF_2 molecules coordinated to the Ca^{2+} center will increase. The most important point is probably the mass action effect of the increased XeF_2 concentration. This effect increases the likelihood that the Ca^{2+} ion will be coordinated by XeF_2 rather than HF. As the solvent HF is removed this mass action effect is even greater.

There are two crystallographically different Ca atoms in the $Ca_2(XeF_2)_9(AsF_6)_4$ structure. Ca1 atoms (Figure 1) are in a homoleptic environment of nine XeF_2 molecules. Eight of the XeF_2 molecules donate fluorine atoms to the apexes of an Archimedean antiprism, while the ninth fluorine atom is from the $Xe3F_2$ molecule and caps one rectangular face of the antiprism. The four XeF_2 molecules that form the non-capped face of the antiprism bridge Ca1 atoms to Ca2 atoms. The coordination sphere of the Ca2 atom is also an Archimedean

[*] Dr. M. Tramšek, Dr. P. Benkič, Dr. B. Žemva
Jožef Stefan Institute
Jamova 39, SI-1000 Ljubljana (Slovenia)
Fax: (+386) 1423-21-25
E-mail: melita.tramsek@ijs.si
boris.zemva@ijs.si

[**] The authors acknowledge the financial support of the Ministry of Education, Science and Sport of the Republic of Slovenia. They are also grateful to Dr. M. Ponikvar for the chemical analyses.

 © 2004 Wiley-VCH Verlag GmbH & Co. KGaA, Weinheim DOI: 10.1002/anie.200453802

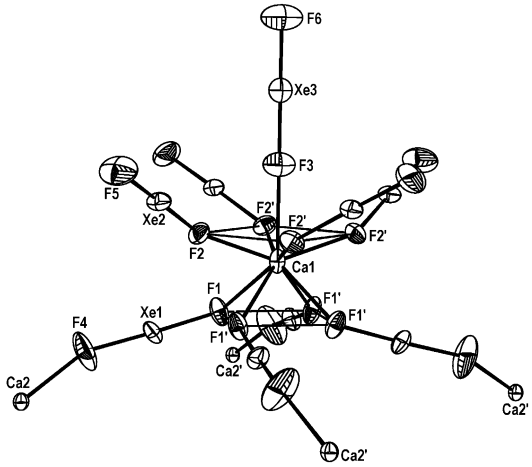


Figure 1. Coordination of the Ca1 center in $Ca_2(XeF_2)_9(AsF_6)_4$ (thermal ellipsoids set at 50% probability). Selected bond lengths [pm]: Ca1-F1 247.4(7), Ca1-F2 231.2(6), Ca1-F3 265.8(18) Xe1-F1 198.7(7), Xe1-F4 197.8(9), Xe2-F2 205.8(7), Xe2-F5 194.3(9), Xe3-F3 201.3(17), Xe3-F6 197(2)

antiprism, this time composed of fluorine atoms from four monodentate $[AsF_6]^-$ units and four bridging XeF_2 molecules (Figure 2). In this way two Ca1 atoms and two Ca2 atoms are

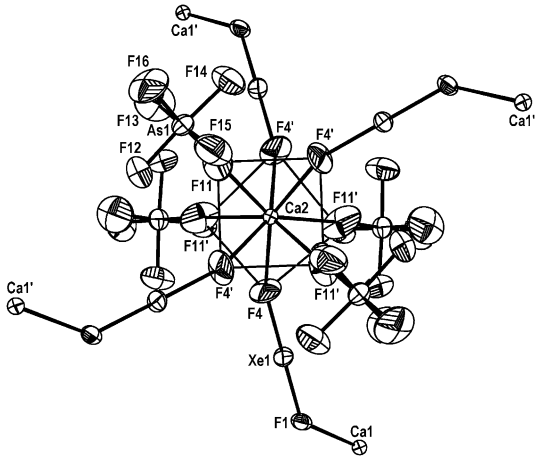


Figure 2. Coordination of the Ca2 center in $Ca_2(XeF_2)_9(AsF_6)_4$ (thermal ellipsoids set at 50% probability). Selected bond lengths [pm]: Ca2-F4 232.9(8), Ca2-F11 227.7(10), As1-F11 170.9(9), As1-F12 170.3(9), As1-F13 168.8(11), As1-F14 169.9(9), As1-F15 168.7(10), As1-F16 167.9(9).

connected by XeF_2 molecules to form sixteen-member rings (Figure 3), which are further connected into wavy layers. Between the layers, stacked down the *c* axis, there are several electrostatic interactions between negatively charged fluorine atoms from $[AsF_6]^-$ units and positively charged Xe from nonbridging $Xe2F_2$ and $Xe3F_2$ molecules. These interactions hold the layers together. There are six close Xe2···F(As) contacts in the range 314.7 to 368.2 pm, while the Xe3 atom is surrounded by twelve fluorine atoms at distances between 340.8 and 379.9 pm. The Xe3 atom lies between four $[AsF_6]^-$ units with triangular faces oriented towards the Xe3 atoms. In

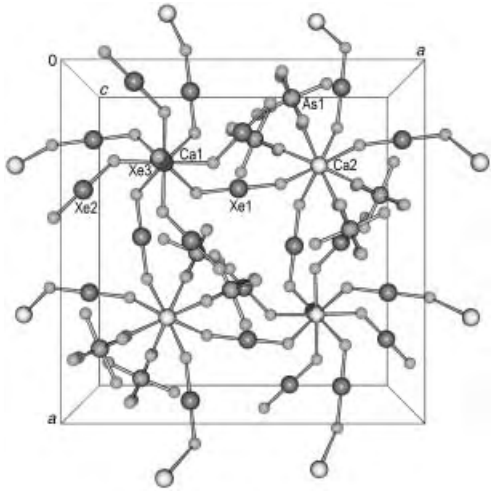


Figure 3. Position of the sixteen-member ring in the unit cell of $Ca_2(XeF_2)_9(AsF_6)_4$.

this way the free electron pairs at the Xe3 atoms are anchored between $[AsF_6]^-$ which is reflected in a longer Ca–F(Xe3) bond (265.8(18) pm) compared to the other Ca–F(Xe) bonds in the structure (231.2(6) to 247.4(7) pm).

With respect to the different environments of the calcium atoms in the structure, the formula of the compound can be written as a salt: $[Ca(XeF_2)_5(XeF_2)_{4/2}]^{2+}[Ca(AsF_6)_4(XeF_2)_{4/2}]^{2-}$. This formulation emphasizes that, in aHF solutions of $Ca(AsF_6)_2$ with a large amount of XeF_2, calcium cations are fully surrounded by XeF_2 molecules. The $[AsF_6]^-$ ions are bulky, therefore, by grouping only linear XeF_2 molecules around one calcium cation, an energetically and sterically preferred arrangement is achieved. For the crystal packing, it is important that XeF_2 is able to bridge two calcium cations, which is less likely with more acidic cations, such as, magnesium cations[3] where more covalent character in the M–F bond is expected (electron affinity of Mg^{2+} is 15.04 eV, for Ca^{2+} it is 11.87 eV[4]). This situation means that the Lewis basicity of the fluorine atoms in the XeF_2 molecule strongly depends on the cation to which XeF_2 is already coordinated. The XeF_2 molecules, in this compound, favor the formation of a crystal-structure network, in which there are monodentate $[AsF_6]^-$ groups compensating for the overall charge of the network.

There is no significant difference between the Ca–F(Xe) and Ca–F(As) separations. Although the latter is shorter than the former (see Figure 2), owing to the electrostatic attraction of oppositely charged $[AsF_6]^-$ ion and Ca^{2+} ion, higher Lewis basicities are expected for the fluorine atoms from XeF_2 molecules. This situation is evident from the elongation of the bridging Xe–F bonds and the contraction of the terminal Xe–F bonds, while the As–F11 bridging distance (170.9(9) pm) does not show significant elongation compared to the terminal As–F bonds (ranging from 167.9 to 170.3 pm).

The high polarizability of xenon usually results in the Raman active modes of xenon fluorides and their coordination compounds having intense Xe–F stretching modes. Modes involving Ca–F and As–F vibrations are usually far less intense. The intense bands in the Raman spectrum of

 © 2004 Wiley-VCH Verlag GmbH & Co. KGaA, Weinheim

$Ca_2(XeF_2)_9(AsF_6)_4$ at 548 cm^{-1} and 533 cm^{-1} can therefore be confidently attributed to Xe–F stretching modes.

According to the Rundle model of XeF_2[5] which proposes three-center molecular orbitals, and as a result of the high polarizability of XeF_2, charge from the XeF_2 molecule is transferred towards the calcium cation and it accumulates at the bridging fluorine atom giving the coordinated XeF_2 molecule some F^-XeF^+ character. This situation is also evident from the Raman spectroscopy. In free XeF_2 the totally symmetric (ν_1) stretching mode is at 497 cm^{-1},[6] where charge at fluorine ligands of 0.5 e_0 is expected.[7] When XeF_2 is coordinated to metal ion it is distorted and the band at 497 cm^{-1} is replaced by two bands. The band at higher frequency is labeled as the short-bond Xe–F stretch (at 548 cm^{-1}) and that at lower frequency is labeled as the long-bond Xe–F stretch (this band is much weaker and it is probably hidden in the band at 466 cm^{-1}). The bridging XeF_2 unit might be expected to exhibit a symmetric XeF_2 stretch at approximately 497 cm^{-1} but as can be seen from the Raman data (see Experimental Section), the observed band at 533 cm^{-1} is most likely to be associated with this vibration. The enhancement of this stretching frequency is probably a consequence of the XeF_2 molecule being anchored between two Ca^{2+} ions, and therefore more energy is required for the symmetric stretching mode.

The remaining question is whether it is possible to prepare a compound in which all the metal centers will be homoleptic and coordinated only to XeF_2 molecules. Reactions in the system $M(AF_6)_2$ with a weak Lewis acid AF_5 (e.g. A = P, V) and a medium strong Lewis base M, coupled with a large excess of XeF_2 (XeF_2: $M(AF_6)_2 > 20$), in HF as solvent, will give the answer.

Experimental Section

The bulk of the product for chemical analysis and Raman spectroscopy was synthesized by the reaction of $Ca(AsF_6)_2$ (0.603 g, 1.44 mmol) and excess XeF_2 (4.105 g, 24.2 mmol) in anhydrous HF (aHF) as solvent. Both solid reagents were weighed directly into a FEP (tetrafluoroethylene-hexafluoropropylene copolymer) reaction vessel inside a dry box. After the solvent (aHF) was added, the reaction was allowed to proceed for 24 h. A crystalline white solid (1.717 g, calcd: 1.699 g) was isolated by pumping off the solvent and excess XeF_2 on a vacuum line.

Chemical analysis: free and total fluoride ion contents were determined by using an ion-selective electrode.[8,9] Calcium was determined by complexometric titration.[10] $[AsF_6]^-$ was determined gravimetrically by precipitation with tetraphenylarsonium chloride.[11] Arsenic was determined potentiometrically.[12] Calcd (%) for $Ca_2(XeF_2)_9(AsF_6)_4$: F_{total} 33.8, F_{free} 14.5, As 12.7, Ca 3.4, $[AsF_6]^-$ 32.0; found: F_{total}, 33.5, F_{free} 14.4, As 13.1, Ca 3.4, $[AsF_6]^-$ 32.3.

Raman spectrum: 690 (2.0), 591 (0.4), 548 (8.0), 533 (10.0), 491 (0.4), 466 (0.9), 377 (0.4), 368 cm^{-1} (0.4).

Crystals with composition $Ca_2(XeF_2)_9(AsF_6)_4$ were prepared in a T-shaped reaction vessel constructed from large (16 mm i.d.) and smaller (4 mm i.d.) FEP tubes joined at right angles and equipped with a Teflon valve. $Ca(AsF_6)_2$ (0.080 g, 0.19 mmol) and XeF_2 (0.653 g, 3.86 mmol) were weighed in the dry box, aHF was added and the solution decanted into the narrower arm of the reaction vessel. After several days of crystallization with a small temperature gradient, (6 K) crystals were obtained in the narrower tube and were isolated by pumping off the solvent on a vacuum line. Crystals were immersed in perfluorinated oil in the dry box. A suitable crystal was selected under the microscope and transferred into a cold nitrogen stream at the diffractometer.

Crystallographic data for $Ca_2(XeF_2)_9(AsF_6)_4$: $M_r(As_4Ca_2F_{42}Xe_9) = 2359.54$, crystal dimensions ca. $0.2 \times 0.15 \times 0.1$ mm, tetragonal, $a = 1396.94(6)$, $c = 2207.69(14)$ pm, $V = 4.3082(4)$ nm^3, $\rho_{calcd} = 3.638$ $g\,cm^{-1}$, space group $P4/ncc$, $Z = 4$, $Mo_{K\alpha}$ radiation ($\lambda = 71.073$ pm), $\mu(Mo_{K\alpha}) = 10.462$ mm^{-1}, $F(000) = 4144$, $T = 200(1)$ K, no. of measured reflections 20346, of 2636 independent reflections, 2440 were considered with $I > 2\sigma(I)$, $R_{int} = 0.0595$. Data were collected on a Rigaku AFC7 diffractometer coupled with Mercury CCD area detector, ω and φ scans, multiscan absorption correction ($T_{min} = 0.176$, $T_{max} = 0.350$). Program used: Rigaku CrystalClear,[13] SIR92,[14] SHELXL-97.[15] Structure was solved by direct methods and full-matrix least-square refinement (133 parameters) of F^2 against all independent reflections was performed. Final R indices $R1 = 0.0780$ (all), $R1 = 0.0704$ [for $I > 2\sigma(I)$], $wR = 0.1391$ (all), $wR = 0.1342$ [for $I > 2\sigma(I)$], residual electron density 2614 and -2999 $e_0\,nm^{-3}$. Further details on the crystal structure investigations may be obtained from the Fachinformationszentrum Karlsruhe, 76344 Eggenstein-Leopoldshafen, Germany (fax: (+49) 7247-808-666; e-mail: crysdata@fiz-karlsruhe.de), on quoting the depository number CSD-413643.

Received: January 20, 2004 [Z53802]

Keywords: calcium · coordination compounds · homoleptic compounds · Lewis acids · xenon difluoride

[1] R. Hagiwara, F. Hollander, C. Maines, N. Bartlett, *Eur. J. Solid State Inorg. Chem.* **1991**, *28*, 855–866.
[2] P. Benkič, M. Tramšek, B. Žemva, *Solid State Sci.* **2002**, *4*, 1425–1434, and references therein.
[3] M. Tramšek, P. Benkič, B. Žemva, *Inorg. Chem.* **2004**, *43*, 699–703, and references therein.
[4] R. G. Pearson, *Inorg. Chem.* **1988**, *27*, 734–740.
[5] R. E. Rundle, *J. Am. Chem. Soc.* **1963**, *85*, 112–113.
[6] P. A. Agron, G. M. Begun, H. A. Levy, A. A. Mason, C. G. Jones, D. F. Smith, *Science* **1963**, *139*, 842–844.
[7] J. Jortner, E. G. Wilson, C. A. Rice, *J. Am. Chem. Soc.* **1963**, *85*, 814–815.
[8] M. Ponikvar, B. Žemva, J. F. Liebman, *J. Fluorine Chem.* **2003**, *123*, 217–220.
[9] M. Ponikvar, B. Sedej, B. Pihlar, B. Žemva, *Anal. Chim. Acta* **2000**, *418*, 113–118.
[10] R. Pribil, *Applied Complexometry*, Pergamon, Oxford, **1982**, p. 200.
[11] H. M. Dess, R. W. Parry, G. L. Vidale, *J. Am. Chem. Soc.*, **1956**, *78* 5730–5734.
[12] M. Ponikvar, B. Pihlar, B. Žemva, *J. Fluorine Chem.* **2003**, *122*, 215–217.
[13] CrystalClear: Rigaku Corporation, Woodlands, Texas, USA, **1999**.
[14] A. Altomare, G. Cascarano, C. Giacovazzo, A. Guagliardi, *J. Appl. Crystallogr.* **1993**, *26*, 343–350.
[15] G. M. Sheldrick, SHELXL-97, University of Göttingen, Germany, **1997**.

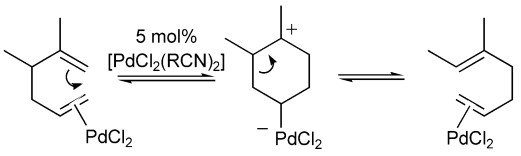
 © 2004 Wiley-VCH Verlag GmbH & Co. KGaA, Weinheim

Cyclizations

Pd^{II}- and Pt^{II}-Mediated Polycyclization Reactions of 1,5- and 1,6-Dienes: Evidence in Support of Carbocation Intermediates**

*Jeong Hwan Koh and Michel R. Gagné**

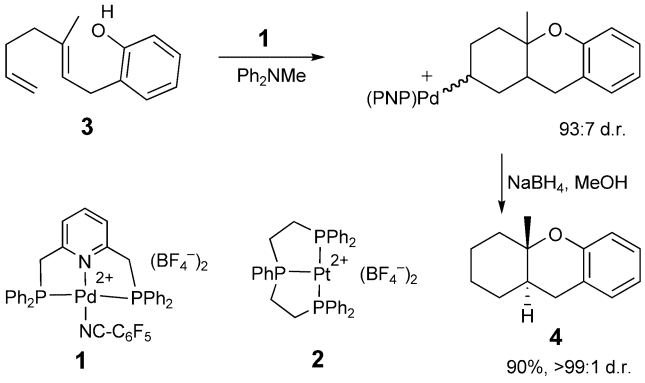
Biomimetic polyolefin cascade reactions[1,2] represent some of the most challenging problems in reaction design, and their products are ubiquitous in the natural world.[3] Since the Brønsted–Lewis acids (BLAs) of Yamamoto et al. are the only known synthetic catalysts for asymmetric catalytic initiation of cation–olefin cyclizations,[4,5] we became interested in an alternative C–C bond-forming cascade wherein activation of a terminal alkene occurs with an electrophilic Pd^{II} source. Although this process is uncommon, it is precedented in the catalysis of the Cope rearrangement with $[PdCl_2(RCN)_2]$ [Eq. (1)] by Overman et al.[6] Fragmentation of a cationic intermediate in the opposite regiodirection was proposed to generate a new diene and a Pd^{II} complex. More recently, Widenhoefer et al.[7] and Toyota, Ihara et al.[8] demonstrated that nucleophilic enols lead to carbocyclic products by β-hydride elimination[9] or protonation.[10]



(1)

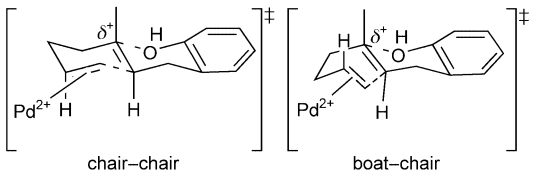
Although substituent effects[11] and stereochemical studies[6c] support a cationic and cyclic intermediate, respectively, the exact nature of this intermediate is unclear, and direct evidence for this cation is lacking.[12] We therefore initiated a plan that first gathered evidence supporting the intermediacy of the carbocyclic cation, while also determining whether it could function as a point for initiating new metal-mediated reactivity. The key to our pursuit was a recent report by Vitagliano et al. of a dicationic Pt complex of a pyridyl bisphosphane pincer ligand $[Pt(PNP)](BF_4)_2$ (PNP = 2,6-bis(diphenylphosphanylmethyl)pyridine) that catalyzes the dimerization of ethylene and 2-methyl-2-butene.[13,14] Intermolecular nucleophilic addition of 2-methyl-2-butene to coordinated ethylene was proposed, with turnover by a sequence of 1,2-hydride shifts. Most importantly, β-hydride elimination did not occur, since no open *cis* coordination sites were available, and this suggests that this complex might be capable of initiating cation formation while preserving the stereochemistry of the M–C bond.

Our first approach to trapping the putative cation utilized the Pd analogue of the Vitagliano complex **1** and dienylphenol **3**. Unlike direct Brønsted acid[4] and Hg^{II}[15] activation/polycyclization, Pd^{II} prefers to coordinate and activate the least substituted alkene,[16] ensuring activation at the terminus. As shown in Scheme 1, the isolable C_6F_5CN adduct[17] efficiently (1 h, RT, CH_2Cl_2) converted **3** to a new metal-containing product devoid of alkene resonances (^{1}H NMR spectroscopy) as a 93:7 mixture of isomers according to ^{31}P NMR spectroscopy. This compound is stable up to 100 °C, though demetalation with $NaBH_4$ at room temperature rapidly[14b] yielded tricycle **4** in 90 % yield (two steps) and d.r. > 99:1.[18]



Scheme 1. Phenol trapping of an intermediate cation and reductive cleavage of the stable Pd alkyl complex.

Since a single diastereomer was observable in the crude demetalation product, we surmised that the isomer mixture for the Pd alkyl complex must result from epimers at the metal-containing stereocenter, a situation suggestive of competing chair–chair and boat–chair transition states,[19] each with a degree of concertedness in the C–C/C–O bond-forming event, that is, a free carbocation is not likely formed [cf. Eq. (1)].[1,20] Pincer complex $[Pt(PPP)](BF_4)_2$ (**2**, PPP = bis(2-diphenylphosphanylethyl)phenylphosphane),[21] derived from commercially available triphos, provided the intermediate alkyl complex with a slightly higher diastereoselectivity (96:4), and **4** in similarly high yield (87 %) and selectivity (> 99:1).



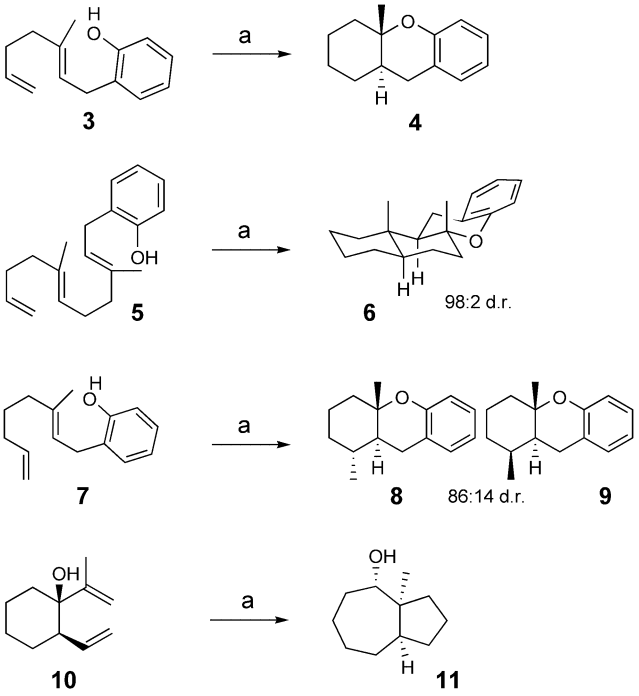
[*] J. H. Koh, Prof. M. R. Gagné
Department of Chemistry
University of North Carolina at Chapel Hill
Chapel Hill, NC 27599-3290 (USA)
Fax: (+1) 919-962-6342
E-mail: mgagne@unc.edu

[**] This work was supported by the NIH (GM-60578); we also thank Dr. Cheryl Mascarenhas and Ms. Claire Catteral for related experiments. M.R.G. is a Camille Dreyfus Teacher Scholar.

Supporting information for this article is available on the WWW under http://www.angewandte.org or from the author.

 DOI: 10.1002/anie.200453913 © 2004 Wiley-VCH Verlag GmbH & Co. KGaA, Weinheim

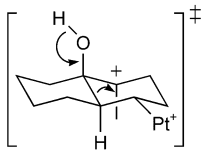
To explore the possibility of cascading the putative cation in a polycyclization reaction,[1] we examined the reaction of trienylphenol **5** with **2** (Scheme 2). As before, cyclization was rapid (4 h), and ^{31}P NMR analysis of the resulting Pt alkyl complex indicated that the product was formed with d.r. ≈ 95%. Treatment with $NaBH_4$ provided tetracyclic **6** as a 96:3:1 mixture of diastereomers (GC), which was isolated as a 98:2 mixture of diastereomers after chromatography (86% yield). Catalyst **1** provided the Pd alkyl complex as a 77:11:8:4 mixture of diastereomers, which simplified to 80:5:minors after treatment with $NaBH_4$; the major diastereomer purified to 98:2 (77% yield).



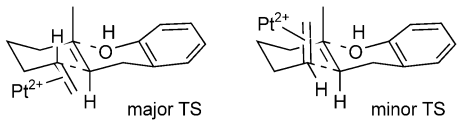
Scheme 2. Interception of cations generated with **2**. Compound **8** was characterized by X-ray crystallography. a: 1) **2**, 1.05 equiv Ph_2NMe, CH_2Cl_2, RT, 1–4 h; 2) $NaBH_4$, MeOH.

Compound **7**, wherein the activated alkene is positioned 6-*exo* to the forming six-membered ring, reacted with **2** to provide a stable Pt alkyl complex as an 86:14 mixture of isomers; reductive cleavage yielded **8** and **9** in the same ratio (Scheme 2, 83% yield). Crystals of the major stereoisomer grew from the oil, and X-ray crystallography confirmed the relative configuration shown in Scheme 2.[22] The major isomer apparently results from a chairlike transition state that places the activated alkene in a pseudo-equatorial orientation. The minor isomer **9** also contained a *trans* ring junction, but a Me···Me NOE suggested a 1,3-diaxial disposition arising from a pseudo-axial position in the putative transition state. The stereo-electronic reasons for this outcome may be related to the pseudo-axial preference of oxonium initiators in polyolefin cascades.[1,23,24] Complex **1** provided **8** with a 78:22 preference (85% yield).

The efficiency of the above cation-trapping experiments prompted us to examine other processes that would support a carbocation intermediate. The reaction of **10** with **2** yielded a new ketone-containing organometallic product that was free of alkene resonances. Reductive removal of the carbocycle ($NaBH_4$) provided *cis*-fused bicyclic alcohol **11** (Scheme 2, 90%, d.r. > 95:5). This reaction is most succinctly explained by cyclogeneration of a carbocation, ring-expanding/contracting pinacol rearrangement (**A**),[25] and Pt–C and C=O reduction. Mechanistic analysis followed from Prins-initiated formation of cations[26] which similarly rearrange to provide *cis*-fused bicyclic ketones. Complex **1** also provided **11** in high yield (93%) and diastereoselectivity (d.r. > 95:5).



The pincer-ligated complexes **1** and **2** uniquely provide a solution to the notion of trapping/cascading the putative intermediate obtained from electrophilic carbocyclization of 1,5- and 1,6-dienes. The variety of trapping reactions (heteroatom addition, cation–olefin, and pinacol rearrangement) are individually consistent with a cationic intermediate, but taken together provide a compelling case for Overman's proposal that cyclization-induced rearrangements proceed through carbenium ion intermediates. Furthermore, the data indicate that 1,5-dienes do not represent a boundary condition for electrophilic carbocyclization/cation generation; other diene arrangements can participate.



Received: February 3, 2004 [Z53913]

Keywords: carbocations · carbocycles · cyclization · palladium · platinum

[1] P. A. Bartlett in *Asymmetric Synthesis*, *Vol. 3* (Ed.: J. D. Morrison), Academic Press, New York, **1984**, p. 341.
[2] K. U. Wendt, G. E. Schultz, E. J. Corey, D. R. Liu, *Angew. Chem.* **2000**, *112*, 2930; *Angew. Chem. Int. Ed.* **2000**, *39*, 2812.
[3] B. M. Fraga, *Nat. Prod. Rep.* **2003**, *20*, 392.
[4] See for example: a) K. Ishihara, H. Ishibashi, H. Yamamoto, *J. Am. Chem. Soc.* **2002**, *124*, 3647; b) S. Nakamura, K. Ishihara, H. Yamamoto, *J. Am. Chem. Soc.* **2000**, *122*, 8131.
[5] Catalytic antibodies show some asymmetric tendencies: J. Hasserodt, K. D. Janda, R. A. Lerner, *J. Am. Chem. Soc.* **2000**, *122*, 40.
[6] a) L. E. Overman, F. M. Knoll, *J. Am. Chem. Soc.* **1980**, *102*, 865; b) L. E. Overman, *Angew. Chem.* **1984**, *96*, 565; *Angew. Chem. Int. Ed. Engl.* **1984**, *23*, 579; c) L. E. Overman, E. J. Jacobsen, *J. Am. Chem. Soc.* **1982**, *104*, 7225.
[7] a) T. Pei, X. Wang, R. A. Widenhoefer, *J. Am. Chem. Soc.* **2003**, *125*, 648; b) X. Wang, T. Pei, X. Han, R. A. Widenhoefer, *Org. Lett.* **2003**, *5*, 2699; c) T. Pei, R. A. Widenhoefer, *Chem. Commun.* **2002**, 650; d) T. Pei, R. A. Widenhoefer, *J. Am. Chem. Soc.* **2001**, *123*, 11290.
[8] M. Toyota, M. Rudyanto, M. Ihara, *J. Org. Chem.* **2002**, *67*, 3374.

 © 2004 Wiley-VCH Verlag GmbH & Co. KGaA, Weinheim

[9] In certain instances cyclohexene products were also observed: L. E. Overman, A. F. Renaldo, *Tetrahedron Lett.* **1983**, *24*, 2235.
[10] X. Wang, R. A. Widenhoefer, *Chem. Commun.* **2004**, 660.
[11] L. E. Overman, A. F. Renaldo, *J. Am. Chem. Soc.* **1990**, *112*, 3945.
[12] For a review of 1,6-diene carbocyclization mechanisms, see: G. C. Lloyd-Jones, *Org. Biomol. Chem.* **2003**, *1*, 215.
[13] C. Hahn, M. E. Cucciolito, A. Vitagliano, *J. Am. Chem. Soc.* **2002**, *124*, 9038.
[14] Vitagliano et al. have extensively documented the addition of weak heteronucleophiles to $[Pd(PNP)]^{2+}$- and $[Pt(PNP)]^{2+}$-activated alkenes: a) C. Hahn, P. Morvillo, E. Herdtweck, A. Vitagliano, *Organometallics* **2002**, *21*, 1807; b) C. Hahn, P. Morvillo, A. Vitagliano, *Eur. J. Inorg. Chem.* **2001**, 419; c) C. Hahn, A. Vitagliano, F. Giordano, R. Taube, *Organometallics* **1998**, *17*, 2060.
[15] M. Nishizawa, H. Takenaka, Y. Hayashi, *J. Org. Chem.* **1986**, *51*, 806.
[16] a) L. S. Hegedus in *Comprehensive Organic Synthesis*, *Vol. 4* (Ed.: B. M. Trost), Pergamon Press, **1991**, p. 571; b) L. S. Hegedus in *Transition Metals in the Synthesis of Complex Organic Molecules*, University Science Books, Mill Valley, California, **1994**, p. 199.
[17] J. J. Becker, L. J. V. Orden, P. S. White, M. R. Gagné, *Org. Lett.* **2002**, 727.
[18] The benzylic CH groups are diagnostic: $\Delta\delta = 0.78$ ppm for *cis*, and $\Delta\delta = 0.15$ ppm for *trans*. M. Palucki, J. P. Wolfe, S. L. Buchwald, *J. Am. Chem. Soc.* **1996**, *118*, 10333.
[19] This information would necessarily be lost if β-hydride elimination or β-fragmentation [Eq. (1)] were operative.
[20] a) G. Stork, A. W. Burghstahler, *J. Am. Chem. Soc.* **1955**, *77*, 5068; b) A. Eschenmoser, L. Ruzicka, O. Jeger, D. Arigoni, *Helv. Chim. Acta* **1955**, *38*, 1890–1904.
[21] The dication was generated in situ from $[PtI_2(PPP)]$ and $AgBF_4$.
[22] CCDC-230057 contains the supplementary crystallographic data for this paper. These data can be obtained free of charge via www.ccdc.cam.ac.uk/conts/retrieving.html (or from the Cambridge Crystallographic Data Centre, 12, Union Road, Cambridge CB21EZ, UK; fax: (+44) 1223-336-033; or deposit@ccdc.cam.ac.uk).
[23] W. S. Johnson, A. van der Gen, J. J. Swoboda, *J. Am. Chem. Soc.* **1967**, *89*, 170.
[24] For a recent example, see: J. R. Seiders II, L. Wang, P. E. Floreancig, *J. Am. Chem. Soc.* **2003**, *125*, 2406.
[25] D. J. Coveney in *Comprehensive Organic Synthesis*, *Vol. 3* (Ed.: G. Pattenden), Pergamon, New York, **1991**, p. 777.
[26] a) L. E. Overman, J. P. Wolfe, *J. Org. Chem.* **2002**, *67*, 6421; b) L. E. Overman, *Acc. Chem. Res.* **1992**, *25*, 352.

 © 2004 Wiley-VCH Verlag GmbH & Co. KGaA, Weinheim

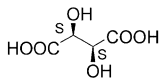
Enantioselective Sensors

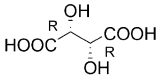
Chiral Binol–Bisboronic Acid as Fluorescence Sensor for Sugar Acids**

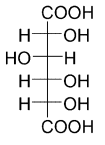
*Jianzhang Zhao, Thomas M. Fyles, and Tony D. James**

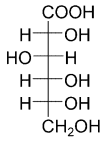
The chemistry of saccharides is of paramount importance to a wealth of biological functions within nature. By providing the building blocks for processes ranging from the production of metabolic energy to tissue recognition, saccharides have found themselves to be the focus of a vast body of research aimed at understanding and mimicking their specific role and function at a cellular level.[1] Unsurprisingly the ability to derive synthetic receptors with the capacity to selectively detect specific saccharides (and related molecules) and signal their presence by altering the optical signature has captured the attention of supramolecular chemists.[2–16]

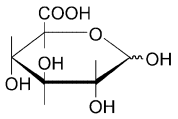
Binol is an important chiral building block and has been widely used in asymmetric catalysis,[17,18] and for enantioselective fluorescence sensors bearing a variety of recognition elements.[19–30] In early work, a binol-based bisboronic acid (**1**) was used to recognize the enantiomers of monosaccharides, such as D/L-glucose, -fructose, and -galactose.[2,14,15] Recently

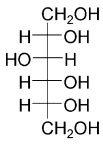

D-tartaric acid

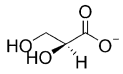

L-tartaric acid

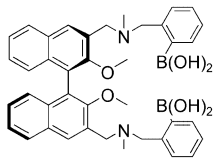

D-glucaric acid


D-gluconic acid


D-glucuronic acid


D-sorbitol


L-glycerate


R-**1**

[*] Dr. J. Zhao, Dr. T. D. James
Department of Chemistry
University of Bath
Bath, BA2 7AY (UK)
Fax: (+44) 1225-386-231
E-mail: t.d.james@bath.ac.uk
Professor T. M. Fyles
Department of Chemistry
University of Victoria
Victoria, BC, V8W 3V6 (Canada)

[**] TDJ and JZ wish to acknowledge the University of Bath and Beckman-Coulter for support. We also wish to acknowledge the help of the EPSRC National Mass Spectrometry Service in Swansea.

Supporting information for this article is available on the WWW under http://www.angewandte.org or from the author.

 DOI: 10.1002/anie.200454033 © 2004 Wiley-VCH Verlag GmbH & Co. KGaA, Weinheim

Houston and Gray demonstrated that racemic tartaric acid and other α-hydroxy acids can bind with the racemic form of **1**.[31] The binding constant reported for tartaric acid ($1.41 \times 10^3\,M^{-1}$ at pH 7.77) is comparable to the strengths of interactions with monosaccharides.[2,14,15] Boronic-acid-based fluorescence sensors for tartaric acid,[32] D-glucuronate,[33,34] and D-glucarate[35] have been reported, as has a boronic-acid-based colorimetric indicator-displacement assay for the determination of the enantiomeric excess of α-hydroxy acids.[36] Hydrogen-bonding receptors for the binding of tartaric acid[37] and the chiral discrimination of hydroxy carboxylates[38] and tartaric acid[39,40] are also known.

In order to develop improved fluorescent chiral discriminating systems, we investigated the interaction of the two chiral forms of sensor **1** (*R* and *S*) with a range of sugar acids over a range of pH values. The results for titrations of *R*-**1** and *S*-**1** with D- and L-tartaric acid are given in Figure 1.

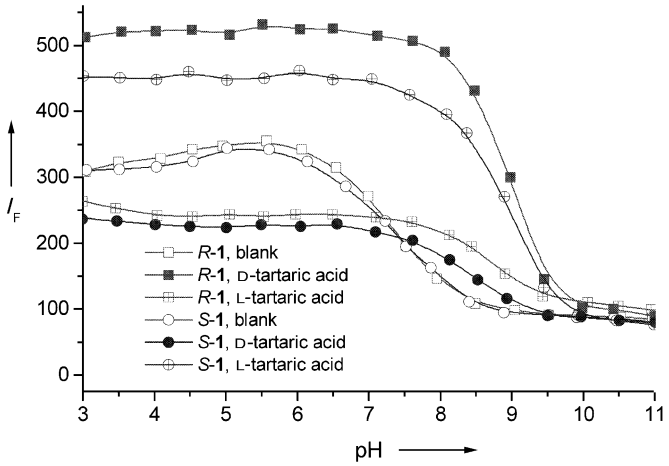


Figure 1. Fluorescence intensity–pH profiles for titrations of *R*- and *S*-**1** with D- or L-tartaric acid. 5.0×10^{-6} mol dm^{-3} **1** in 0.05 mol dm^{-3} NaCl solution (52.1% methanol in water), c(D-tartaric acid) = c(L-tartaric acid) = 0.02 mol dm^{-3}, λ_{ex} = 289, λ_{em} = 358 nm, 23 °C.

The recognition of D- and L- tartaric acid by sensor **1** (*R* or *S*) is strongly pH dependent. The fluorescence enhancement for the complexes formed by either *R*- or *S*-**1** at pH 8.3 is expected.[2,14,15] Remarkably, at pH 5.6 the fluorescence of *S*-**1** is *enhanced* by the presence of L-tartaric acid, but for *R*-**1** with the same analyte, the fluorescence is *diminished* relative to that of the free bisboronic acid. Conversely, the fluorescence of the sensor *R*-**1** is *enhanced* by the presence of D-tartaric acid, but for S-**1** with D-tartaric acid, the fluorescence is *diminished* relative to that of the free bisboronic acid. The fluorescence of the binol moiety can be enantioselectively diminished (via a non-emissive exiplex, or by charge-transfer between the analyte and the sensor),[19–21] or enantioselectively enhanced (usually by photoinduced electron transfer (PET)).[2,14,15,19,27,29] However, previous reports of chiral discrimination were based solely on a different *extent* of the spectral change in a single sense (either enhanced or diminished),[19] rather than on the *sense* of the change.

Fluorescence intensity–pH profiles for titrations with all four saccharides (glucaric acid, gluconic acid, glucuronic acid, and sorbitol) showed that they were bound by *R*/*S*-**1**. However, only D-gluconic acid showed the same type of behavior as the tartrates: at pH 5.6 the signal of the D-gluconate complex with *S*-**1** was augmented relative to that of the starting bisboronate whereas for *R*-**1** the signal was diminished. This implies that the normal PET quenching that gives rise to the fluorescence changes must be mediated by geometrical changes in individual sensor–analyte complexes.[19,41] Static quenching within a complex is more likely than dynamic quenching, both on these steric grounds, and because the effect occurs at very low analyte concentration due to the high binding constants (see below).[19,41]

Binding constants were determined at pH 5.6 and 8.3 where a 1:1 binding isotherm was fit to the normalized fluorescence (I/I_0) as function of added substrate (Figure 2, Table 1).[42] The values for the tartaric acid complexes at pH 8.3 are of the same order of magnitude as those reported for the racemic system,[31] but at pH 5.6 the apparent

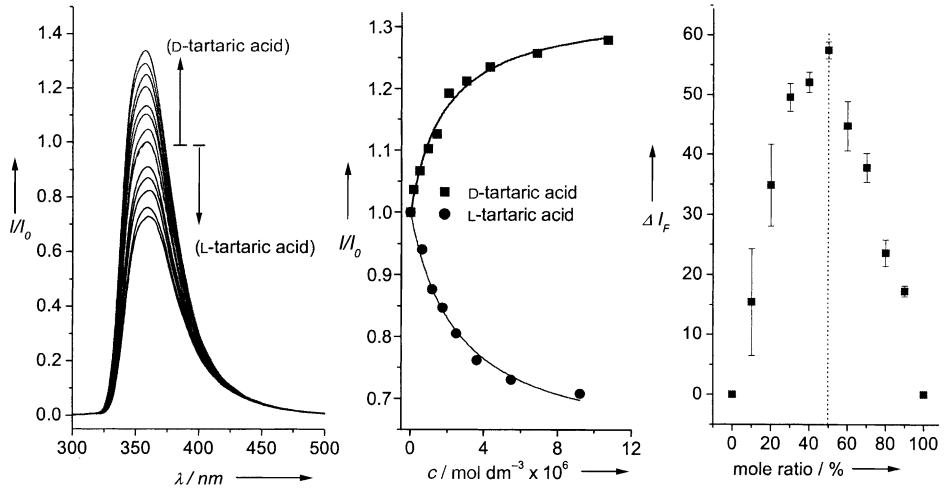


Figure 2. Chiral discrimination of D- and L-tartaric acid by *R*-**1** at pH 5.6. c(**1**) = 5.0×10^{-6} mol dm^{-3}, pH 5.6 in 0.05 mol dm^{-3} NaCl (52.1% methanol in water), λ_{ex} = 289 nm, 22 °C. The pH was kept at 5.6 with NaOH/HCl. Left: emission spectra. Center: normalized emission intensity as a function of the concentration of added tartaric acid. Lines represent the fit of a 1:1 binding isotherm. Right: Job plot of *R*-**1** with D-tartaric acid at a constant total concentration c(D-tartaric acid) + c(*R*-**1**) of 5.0×10^{-6} mol dm^{-3}; λ_{em} = 358 nm.

 © 2004 Wiley-VCH Verlag GmbH & Co. KGaA, Weinheim

Table 1: Logarithm of 1:1 stability constants *K*, fluorescence enhancement *F* on binding, and response enantioselectivity of sensors *R*-**1** and *S*-**1**.[a]

Analyte	pH	lg *K*		*F*		Response selectivity[b]
		R-**1**	*S*-**1**	*R*-**1**	*S*-**1**	*R*:*S*
D-tartaric acid	5.6	5.72 ± 0.12	5.42 ± 0.16	1.39 ± 0.04	0.53 ± 0.01	(5.2 ± 2.5):1
	8.3	3.71 ± 0.06	2.21 ± 0.12	3.09 ± 0.11	1.37 ± 0.04	(71 ± 23):1
L-tartaric acid	5.6	5.59 ± 0.12	5.44 ± 0.10	0.62 ± 0.05	1.47 ± 0.01	1:(3.3 ± 1.2)
	8.3	2.02 ± 0.12	3.37 ± 0.06	1.37 ± 0.02	2.59 ± 0.06	1:(42 ± 13)
D-gluconic acid	5.6	4.45 ± 0.18	5.42 ± 0.26	0.81 ± 0.01	1.22 ± 0.01	1:(14 ± 5)
	8.3	3.61 ± 0.06	4.38 ± 0.08	2.31 ± 0.04	3.10 ± 0.14	1:(8 ± 2)
D-glucaric acid	8.3	4.47 ± 0.14	4.11 ± 0.06	2.32 ± 0.11	3.08 ± 0.10	(1.7 ± 0.6):1
D-glucuronic acid	8.3	3.52 ± 0.14	3.55 ± 0.14	3.43 ± 0.05	2.63 ± 0.03	(1.2 ± 0.6):1
D-sorbitol[c]	8.3	4.13 ± 0.06	4.16 ± 0.04	3.23 ± 0.01	2.91 ± 0.01	(1.0 ± 0.2):1

[a] 5.0×10^{-6} mol dm^{-3} *R*-**1** or *S*-**1** in 0.05 mol dm^{-3} NaCl solution (52.1% methanol in water), $\lambda_{ex}=289$, $\lambda_{em}=358$ nm, (23 ± 1) °C. Constants determined by fitting a 1:1 binding model to I/I_0. Errors reported are two standard deviations (95% confidence limit); $r^2>0.99$ in all cases. [b] Response selectivity = $(K(R)\,F(R))/(K(S)\,F(S))$. [c] Values determined from a sequential 1:1 plus 2:1 binding model. $\lg K_2$(*R*-**1**) = 1.80 ± 0.10, F = 1.6 ± 0.02; $\lg K_2$(*S*-**1**) = 1.71 ± 0.08, F = 1.59 ± 0.02.

constants are about 100-fold greater. This is presumably due to nitrogen protonation which would provide an adjacent positive charge to stabilize the boronate. Table 1 also reports a derived response-selectivity factor: the product of the chiral selectivity of binding (K_R/K_S) and the chiral selectivity of the fluorescence enhancement ($F(R)/F(S)$). The overall range is large—ranging from indiscriminate (with D-sorbitol) up to an approximately 50-fold difference between *R*- and *S*-**1** with the tartaric acids at pH 8.3.

The opposing effect of enantiomeric D- and L-tartaric acid on the fluorescence of *R*- and *S*-**1** allows the system to be used to determine the enantiomeric excess of a D/L tartaric acid mixture (Figure 3). The data can be related to the relative

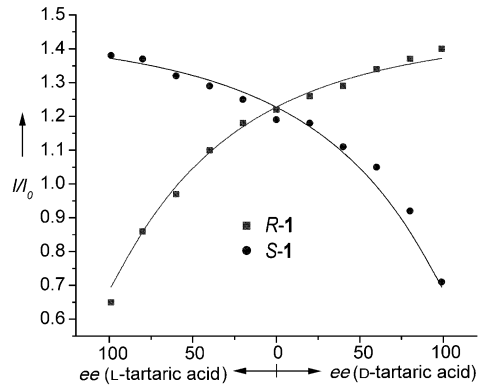


Figure 3. Relative fluorescence changes for *R*- and *S*-**1** in mixtures of D- and L-tartaric acid. c(*R*-**1**) or c(*S*-**1**) = 5×10^{-6} mol dm^{-3}, c(D-tartaric acid) + c(L-tartaric acid) = 0.01 mol dm^{-3}, pH 5.6 in 0.05 mol dm^{-3} NaCl (52.1% methanol in water), $\lambda_{ex}=289$, $\lambda^{em}=358$ nm, 22 °C.

binding constants for the diasteromeric complexes and to the enhancement factors for the fluorescence of these complexes. A model that considers only 1:1 complexes cannot reproduce the shape of the curves. However, at the total tartaric acid concentration used for Figure 3, the extent of 2:1 binding is significant (see Supporting Information). We therefore considered a model of mixed 1:1 and 2:1 complexes in which the properties of the enantiomeric components were assumed to be equal.

In this model, there are four binding constants and four enhancement factors. Some of these parameters are known independently (Table 1) and likely values for the enhancement factors for the 2:1 complexes are evident from the titrations done to high concentration. The model was fit to the combined data of Figure 3 to refine these eight parameters and to produce the curves shown. The values determined by this method are: $\lg K_1(R_L)=\lg K_1(S_D)=5.33\pm0.1$, $\lg K_1(R_D)=\lg K_1(S_L)=5.84\pm0.1$, $\lg K_2(R_{L_2})=\lg K_2(S_{D_2})=0.9\pm0.2$ and $\lg K_2(R_{D_2})=\lg K_2(S_{L_2})=1.2\pm0.2$; $F_1(R_L)=F_1(S_D)=0.63\pm0.03$, $F_1(R_D)=F_1(S_L)=1.42\pm0.02$, $F_2(R_{L_2})=F_2(S_{D_2})=1.2\pm0.3$ and $F_2(R_{D_2})=F_2(S_{L_2})=1.2\pm0.3$ ($K_1(R_D)$ is the binding constant for the 1:1 complex of *R*-**1** and D-tartaric acid; $F_2(R_{L_2})$ is the enhancement factor for the 1:2 complex of *R*-**1** and L-tartaric acid). The same values correctly reproduce the individual titration curves (see Supporting Information). A further confirmation of the model is that the 1:1 binding constants and enhancement factors determined from Figure 3 data agree within the experimental uncertainty with the independently determined values for the same complexes in Table 1.

The data in Table 1 are consistent with the structural proposals of previous work in which "bridging" of the two boronic acid sites by the bound substrate led to stable 1:1 complexes.[2,14,15] Binding of L-glycerate by **1** (*R* or *S*) was not observed presumably because this substrate lacks a second binding site for bridging. Similarly, the cyclic substrate D-glucuronic acid has smaller binding constants than the linear D-glucaric acid. Linear saccharic acids can adjust to be complementary to the binding requirement of the sensor, and therefore show generally higher binding constants. The chiral discrimination in binding is independent of the chiral discrimination in fluorescence enhancement. The former varies to a larger extent (up to about 25-fold) than does the latter (up to about 3-fold), so the most significant factor determining the overall response selectivity is the binding selectivity. Geometrical differences thus play a larger role in substrate recognition than they do in the photophysical processes that lead to the signal.

In summary, our study shows that the binol-based sensor **1** can selectively bind a range of saccharic acids, and that binding with some analytes is highly enantioselective. Moreover, a novel fluorescence response to enantiomeric analytes has been observed. We believe that these results will offer new ideas for the analysis of these metabolic intermediates with synthetic fluorescence sensors. Our future work will focus on the design of binol-based sensors with enhanced

 © 2004 Wiley-VCH Verlag GmbH & Co. KGaA, Weinheim

binding selectivity towards sugar acids, in the expectation that these will lead to even higher response selectivities.

Received: February 16, 2004
Revised: April 6, 2004 [Z54033]

Keywords: boronic acids · chiral recognition · fluorescence sensors · sugar acids · tartaric acid

[1] S. Hurtley, R. Service, P. Szuromi, *Science* **2001**, *291*, 2337.
[2] T. D. James, S. Shinkai, *Top. Curr. Chem.* **2002**, *218*, 159.
[3] A. P. Davis, R. S. Wareham, *Angew. Chem.* **1999**, *111*, 3160; *Angew. Chem. Int. Ed.* **1999**, *38*, 2978.
[4] A. P. de Silva, H. Q. N. Gunaratne, T. Gunnlaugsson, A. J. M. Huxley, C. P. McCoy, J. T. Rademacher, T. E. Rice, *Chem. Rev.* **1997**, *97*, 1515.
[5] M. Granda-Valdes, R. Badia, G. Pina-Luis, M. E. Diaz-Garcia, *Quim. Anal.* **2000**, *19*, 38.
[6] W. Wang, X. Gao, B. Wang, *Curr. Org. Chem.* **2002**, *6*, 1285.
[7] S. Striegler, *Curr. Org. Chem.* **2003**, *7*, 81.
[8] W. Yang, H. He, D. G. Drueckhammer, *Angew. Chem.* **2001**, *113*, 1764; Angew. *Chem. Int. Ed.* **2001**, *40*, 1714.
[9] Z. Zhong, E. V. Anslyn, *J. Am. Chem. Soc.* **2002**, *124*, 9014.
[10] A. J. Tong, A. Yamauchi, T. Hayashita, Z. Y. Zhang, B. D. Smith, N. Teramae, *Anal. Chem.* **2001**, *73*, 1530.
[11] N. DiCesare, J. R. Lakowicz, *Chem. Commun.* **2001**, 2022.
[12] H. Cao, D. I. Diaz, N. DiCesare, J. R. Lakowicz, M. D. Heagy, *Org. Lett.* **2002**, *4*, 1503.
[13] H. Eggert, J. Frederiksen, C. Morin, J. C. Norrild, *J. Org. Chem.* **1999**, *64*, 3846.
[14] T. D. James, K. R. A. S. Sandanayake, S. Shinkai, *Angew. Chem.* **1996**, *108*, 2038; *Angew. Chem. Int. Ed. Engl.* **1996**, *35*, 1911.
[15] T. D. James, K. R. A. S. Sandanayake, S. Shinkai, *Nature* **1995**, *374*, 345.
[16] J. T. Suri, D. B. Cordes, F. E. Cappuccio, R. A. Wessling, B. Singaram, *Langmuir* **2003**, *19*, 5145.
[17] S. Matsunaga, T. Ohshima, M. Shibasaki, *Adv. Synth. Catal.* **2002**, *344*, 3.
[18] Y. Chen, S. Yekta, A. K. Yudin, *Chem. Rev.* **2003**, *103*, 3155.
[19] L. Pu, *Chem. Rev.* **2004**, *104*, 1687.
[20] M. Irie, T. Yorozu, K. Hayashi, *J. Am. Chem. Soc.* **1978**, *100*, 2236.
[21] T. Yorozu, K. Hayashi, M. Irie, *J. Am. Chem. Soc.* **1981**, *103*, 5480.
[22] D. Avinir, E. Wellner, M. Ottolenghi, *J. Am. Chem. Soc.* **1989**, *111*, 2001.
[23] V. J. Pugh, Q.-S. Hu, L. Pu, *Angew. Chem.* **2000**, *112*, 3784; Angew. *Chem. Int. Ed.* **2000**, *39*, 3638.
[24] G. Beer, K. Rurack, J. Daub, *Chem. Commun.* **2001**, 1138.
[25] L.-Z. Gong, Q.-S. Hu, L. Pu, *J. Org. Chem.* **2001**, *66*, 2358.
[26] V. J. Pugh, Q.-S. Hu, X. Zuo, F. D. Lewis, L. Pu, *J. Org. Chem.* **2001**, *66*, 6136.
[27] J. Lin, Q.-S. Hu, M.-H. Xu, L. Pu, *J. Am. Chem. Soc.* **2002**, *124*, 2088.
[28] S. J. Lee, W. Lin, *J. Am. Chem. Soc.* **2002**, *124*, 4554.
[29] J. Lin, H.-C. Zhang, L. Pu, *Org. Lett.* **2002**, *4*, 3297.
[30] J. Lin, Z.-B. Li, H.-C. Zhang, L. Pu, *Tetrahedron Lett.* **2004**, *45*, 103.
[31] C. W. Gray, T. A. Houston, *J. Org. Chem.* **2002**, *67*, 5426.
[32] J. J. Lavigne, E. V. Anslyn, *Angew. Chem.* **1999**, *111*, 3903; *Angew. Chem. Int. Ed.* **1999**, *38*, 3666.
[33] M. Takeuchi, M. Yamamoto, S. Shinkai, *Chem. Commun.* **1997**, 1731.
[34] M. Yamamoto, M. Takeuchi, S. Shinkai, *Tetrahedron* **1998**, *54*, 3125.
[35] W. Yang, J. Yan, H. Fang, B. Wang, *Chem. Commun.* **2003**, 792.
[36] J. Zhu, E. V. Anslyn, *J. Am. Chem. Soc.* **2004**, *126*, 3676.
[37] S. Goswami, K. Ghosh, R. Mukherjee, *Tetrahedron* **2001**, *57*, 4987.
[38] A. Tejeda, A. I. Oliva, L. Simon, M. Grande, M. Caballero, J. R. Moran, *Tetrahedron Lett.* **2000**, *41*, 4563.
[39] J. V. Hernandez, M. Almaraz, C. Raposo, M. Martin, A. Lithgow, M. Crego, C. Cabellero, J. R. Moran, *Tetrahedron Lett.* **1998**, *39*, 7401.
[40] F. Garcia-Tellado, J. Albert, A. D. Hamilton, *J. Chem. Soc. Chem. Commun.* **1991**, 1761.
[41] J. R. Lakowicz, *Principles of Fluorescence Spectroscopy*, Kluwer Academic, New York, **1999**.
[42] At low concentrations, the binding of the saccharides in Table 1 occurs with a 1:1 stoichiometry. This is implied by the excellent fits of the model, and is more directly demonstrated by the Job plot given in Figure 2 (right) for the *R*-**1** plus D-tartrate system. However, at higher concentrations (> millimolar), all systems show some deviation from the expectations of a strict 1:1 binding model. The sorbitol system clearly indicates that these deviations are due to 2:1 complexes. For further discussion see the Supporting Information.

 © 2004 Wiley-VCH Verlag GmbH & Co. KGaA, Weinheim

C–H/C–C Activation

Activation of All Bonds of a Methyl Group Attached to an Organic Fragment**

Javier A. Cabeza, Iván da Silva, Ignacio del Río, Lorena Martínez-Méndez, Daniel Miguel, and Víctor Riera*

Activation of C–H[1] and C–C[2] bonds promoted by transition-metal complexes has increasingly attracted the attention of researchers over the last two decades. The use of these processes in chemoselective organic synthesis[1–3] with atom economy[4] is the final goal of this intense research activity. In the case of sp^3 carbon atoms, examples of C–H bond activation by oxidative addition processes in solution are still scarce,[1,3] and the number of processes in which C–C bonds are activated is even smaller.[2,3] Therefore, the search

[*] Prof. Dr. J. A. Cabeza, I. da Silva, Prof. Dr. I. del Río, L. Martínez-Méndez, Prof. Dr. V. Riera
Departamento de Química Orgánica e Inorgánica
Instituto de Química Organometálica "Enrique Moles"
Universidad de Oviedo-CSIC, 33071 Oviedo (Spain)
Fax: (+34) 985-103446
E-mail: jac@fq.uniovi.es
Prof. Dr. D. Miguel
Departamento de Química Inorgánica
Facultad de Ciencias
Universidad de Valladolid, 47005 Valladolid (Spain)

[**] This work has been supported by the Spanish MCyT (projects BQU2002-02623 to J.A.C. and BQU2002-03414 to D.M.) and the Government of Principado de Asturias (project PR01-GE-7 to V.R.).

Supporting information for this article is available on the WWW under http://www.angewandte.org or from the author.

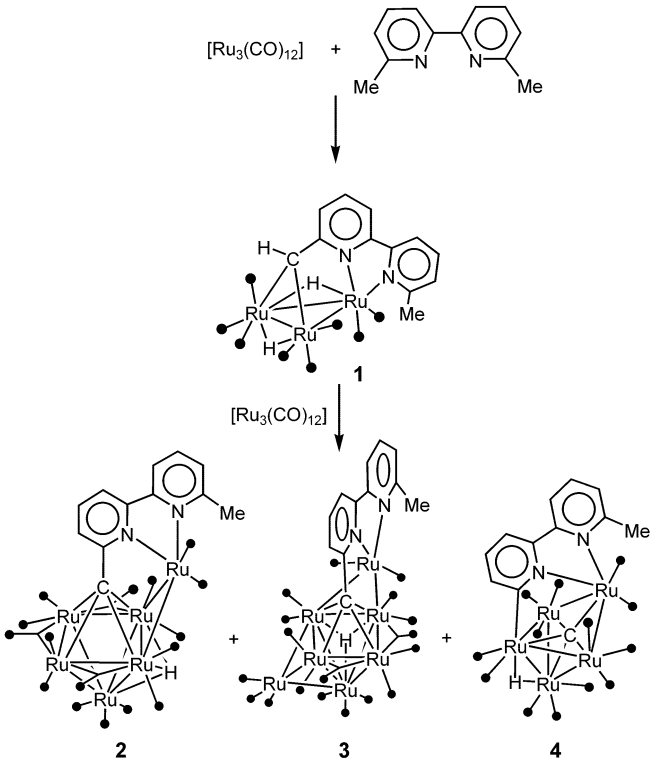
 © 2004 Wiley-VCH Verlag GmbH & Co. KGaA, Weinheim DOI: 10.1002/anie.200454066

for new systems capable of activating C–H and C–C bonds involving sp^3 carbon atoms under mild conditions and understanding the factors that control such processes are currently highly active research fields.

During our study of the reactivity of transition metal carbonyl compounds with 2-aminopyridines in solution we discovered that $[Ru_3(CO)_{12}]$ can promote the oxidative addition of both N–H bonds of the amino group and transform it into a μ_4-imido fragment.[5] Such an uncommon reaction prompted us to attempt the activation of the methyl C–H bonds of a series of 2-methylpyridines under analogous conditions.

We now report the transformation of an organic methyl group into bridging methylene, carbyne, and carbide ligands by using $[Ru_3(CO)_{12}]$ as the transition metal complex promoter and 6,6′-dimethyl-2,2′-bipyridine (Me_2bipy) as the organic precursor.

The trinuclear cluster $[Ru_3(\mu\text{-}H)_2(\mu_3\text{-}HCbipyMe)(CO)_8]$ (**1**) was prepared by treating $[Ru_3(CO)_{12}]$ with 2.5 equivalents of Me_2bipy in THF at reflux temperature (Scheme 1). Its X-ray structure (Figure 1) shows that a bridging HCbipyMe ligand is attached to three ruthenium atoms in such a way that the CH fragment spans an Ru–Ru edge and the bipy fragment chelates the remaining Ru atom. The cluster shell is completed by eight terminal CO ligands and two edge-bridging hydride ligands.[6]



Scheme 1. Synthesis of **1**–**4** from $[Ru_3(CO)_{12}]$ and 6,6′-dimethyl-2,2′-bipyridine. ● = CO.

The reaction of $[Ru_3(CO)_{12}]$ with bipy has been reported to give $[Ru_3(bipy)(\mu\text{-}CO)_2(CO)_8]$, in which the bipy ligand chelates a ruthenium atom.[7] Careful inspection of its X-ray structure reveals that such a structure would not be possible for Me_2bipy, because there is not enough room to accommodate the methyl groups without their interacting with the carbonyl ligands. Thus, in the reaction of $[Ru_3(CO)_{12}]$ with Me_2bipy, chelation of the ligand should be accompanied by the release of at least three CO ligands. The unsaturation of the thus-formed intermediate (46e) would promote the activation of a methyl C–H bond. However, such a monohydrido nonacarbonyl intermediate has not been observed, probably because it is thermodynamically less stable than **1**, which arises from a double C–H activation process. As no reaction was observed between 2,6-dimethylpyridine and $[Ru_3(CO)_{12}]$ in refluxing chlorobenzene, it is clear that the chelating ability of Me_2bipy is probably the driving force for the metalation of one of its methyl groups. A related chelation-assisted approach, but with mononuclear complexes, was used to activate methyl C–H and C–C bonds of appropriate bidentate ligands.[8] There are very few published reports describing the oxidative addition of two C–H bonds of a methyl group to a metal fragment, and none of them deals with organic methyl groups, but with methyl groups already attached to metal atoms.[9] The activation of both methylene C–H bonds of a metal-bound ethyl group has also been reported.[10]

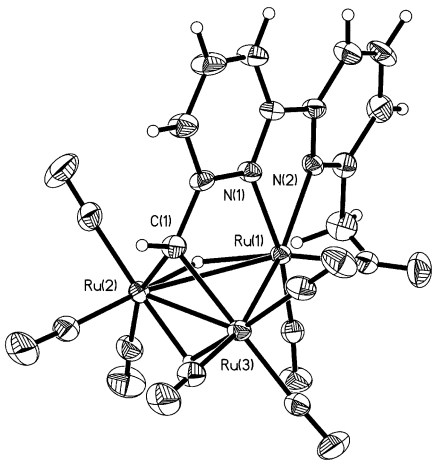


Figure 1. Molecular structure of **1**.

The compounds $[Ru_6(\mu_3\text{-}H)(\mu_5\text{-}CbipyMe)(\mu\text{-}CO)_3(CO)_{13}]$ (**2**), $[Ru_7(\mu_3\text{-}H)(\mu_5\text{-}CbipyMe)(\mu\text{-}CO)_2(CO)_{16}]$ (**3**), and $[Ru_5(\mu\text{-}H)(\mu_5\text{-}C)(\mu\text{-}bipyMe)(CO)_{13}]$ (**4**; Scheme 1) were prepared by heating equimolar amounts of **1** and $[Ru_3(CO)_{12}]$ in chlorobenzene under reflux. In addition, these clusters were also obtained in similar yields when $[Ru_3(CO)_{12}]$ was treated with Me_2bipy in a 2:1 ratio in refluxing chlorobenzene. Their structures were determined by single-crystal X-ray diffraction.[6]

Compounds **2** and **3** contain a carbyne-type carbon atom that was originally bound to three hydrogen atoms in Me_2bipy. The structure of hexanuclear **2** (Figure 2a) is comparable to that of $[Ru_6(\mu\text{-}H)_3(\mu_5\text{-}NpyC_6H_4)(\mu\text{-}CO)_3(CO)_{13}]$,[5] in which the ligand $NpyC_6H_4$ is attached to the metal skeleton in the same way as the CbipyMe ligand in **2**, but with exchanged positions of an N and a C atom. The structure of heptanuclear cluster **3** (Figure 2b) is reminiscent

 © 2004 Wiley-VCH Verlag GmbH & Co. KGaA, Weinheim

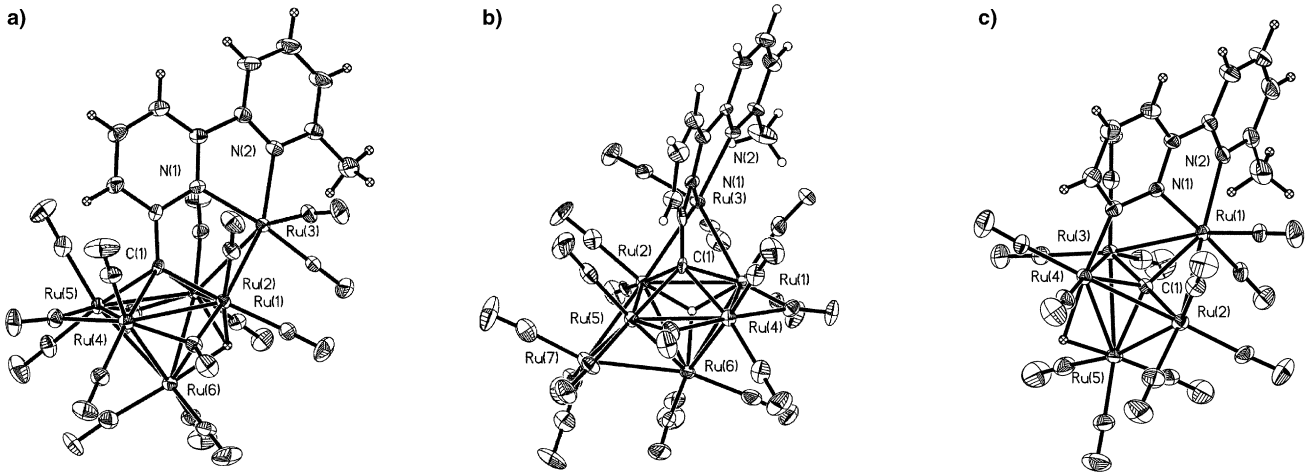


Figure 2. Molecular structures of **2** (a), **3** (b), and **4** (c).

of that of **2**, but now an additional Ru atom caps a triangular face of the square-pyramidal fragment of the metal skeleton.

Activation of the three C–H bonds of a metal-bound methyl group has been reported.[11] However, to our knowledge, the oxidative addition of all three C–H bonds of an organic methyl group is unprecedented. Carbyne ligands bridging four metal atoms are also scarce,[9a,b,12] and none of them arose from an organic methyl group.

The structure of **4** (Figure 2c) clearly shows the presence of a carbide ligand surrounded by five Ru atoms in a distorted trigonal-bipyramidal environment and a bipyMe ligand attached to a Ru atom through both N atoms and to another Ru atom through the carbon atom which was originally bound to the activated methyl group. The cluster shell is completed by 13 CO ligands and a bridging hydride ligand. Many transition-metal clusters containing carbide ligands have been reported, but no such ligands arose from an organic methyl group. A few C–C bond-activation reactions involving methyl groups have been reported,[2,8,13] but the products contain methyl groups that do not undergo further C–H activation.

Clearly **1** is an intermediate in the synthesis of **2**–**4**. We have checked that the hexanuclear complex **2** is not transformed into a mixture of **3** and **4** when it is heated in refluxing chlorobenzene. Therefore, the formation of **2**–**4** should take place through the condensation of compound **1** with $[Ru_n(CO)_m]$ ($n = 1$, 3) species, which are available in hot solutions of $[Ru_3(CO)_{12}]$.

In conclusion, we have described the ruthenium-cluster-mediated transformation of an organic methyl group into a carbide ligand. Such a process involves the unprecedented activation of all bonds (three C–H and one C–C) associated with the carbon atom of an organic methyl group. In addition, **1**–**3** are unique examples of activation of two and three C–H bonds of an organic methyl group.

Received: February 22, 2004 [Z54066]

Keywords: C–C activation · C–H activation · cluster compounds · N ligands · ruthenium

[1] Selected reviews on C–H bond activation: a) J. A. Labinger, J. E. Bercaw, *Nature* **2002**, *417*, 507; b) B. A. Arndtsen, R. G. Bergman, T. A. Mobley, T. H. Peterson, *Acc. Chem. Res.* **1995**, *28*, 154; c) A. E. Shilov, G. B. Shul'pin, *Chem. Rev.* **1997**, *97*, 2879; d) W. D. Jones in *Topics in Organometallic Chemistry: Activation of Unreactive Bonds and Organic Synthesis* (Ed.: S. Murai), Springer, Heidelberg, **1999**, p. 9; e) G. Dyker, *Angew. Chem.* **1999**, *111*, 1808; *Angew. Chem. Int. Ed.* **1999**, *38*, 1699; f) Y. Guari, S. Sabo-Etienne, B. Chaudret, *Eur. J. Inorg. Chem.* **1999**, 1047.

[2] Selected reviews on C–C bond activation: a) B. Rybtchinski, D. Milstein, *Angew. Chem.* **1999**, *111*, 918; *Angew. Chem. Int. Ed.* **1999**, *38*, 870; b) M. Murakami, Y. Ito in *Topics in Organometallic Chemistry: Activation of Unreactive Bonds and Organic Synthesis* (Ed.: S. Murai), Springer, Heidelberg, **1999**, p. 97.

[3] See, for example: a) C. Jia, T. Kitamura, Y. Fujiwara, *Acc. Chem. Res.* **2001**, *34*, 633; b) C.-H. Jun, C. W. Moon, D.-Y. Lee, *Chem. Eur. J.* **2002**, *8*, 2423; c) A. E. Shilov, G. B. Shul'pin, *Activation and Catalytic Reactions of Saturated Hydrocarbons in the Presence of Metal Complexes*, Kluwer, Dordrecht, **2000**; d) A. Sen, *Acc. Chem. Res.* **1998**, *31*, 550; e) F. Kakiuchi, S. Murai in *Topics in Organometallic Chemistry: Activation of Unreactive Bonds and Organic Synthesis* (Ed.: S. Murai), Springer, Heidelberg, **1999**, p. 47.

[4] B. M. Trost, *Angew. Chem.* **1995**, *107*, 285; *Angew. Chem. Int. Ed. Engl.* **1995**, *34*, 259.

[5] a) J. A. Cabeza, I. del Río, P. García-Alvarez, V. Riera, M. Suárez, S. García-Granda, *Dalton Trans.* **2003**, 2808; b) J. A. Cabeza, I. del Río, V. Riera, M. Suárez, S. García-Granda, *Organometallics* **2004**, *23*, 1107.

[6] Data for **1**: $C_{20}H_{12}N_2O_8Ru_3$, $M_r = 711.53$, crystal dimensions $0.19 \times 0.10 \times 0.05$ mm, triclinic, space group $P\bar{1}$, $a = 8.159(1)$, $b = 10.953(2)$, $c = 13.132(2)$ Å, $\alpha = 91.752(3)$, $\beta = 98.785(3)$, $\gamma = 95.719(3)°$, $V = 1152.8(3)$ Å^3, $Z = 2$, $\rho_{calcd} = 2.050$ g cm^{-3}, $F(000) = 684$, $\mu = 1.988$ mm^{-1}, 3293 independent reflections, $R_1 = 0.0269$, $wR_2 = 0.0514$ (all data). Data for **2**: $C_{28}H_{10}N_2O_{16}Ru_6$, $M_r = 1236.80$, crystal dimensions $0.14 \times 0.12 \times 0.08$ mm, monoclinic, space group $P2_1/c$, $a = 10.306(3)$, $b = 30.631(8)$, $c = 10.826(3)$ Å, $\beta = 94.188(4)$, $V = 3409(1)$ Å^3, $Z = 4$, $\rho_{calcd} = 2.410$ g cm^{-3}, $F(000) = 2336$, $\mu = 2.667$ mm^{-1}, 4811 independent reflections, $R_1 = 0.0304$, $wR_2 = 0.0656$ (all data). Data for **3**: $C_{30}H_{10}N_2O_{18}Ru_7$, $M_r = 1393.89$, crystal dimensions $0.24 \times 0.21 \times 0.11$ mm, orthorhombic, space group $Pna2_1$, $a = 30.505(12)$, $b = 11.815(5)$, $c = 10.394(4)$ Å, $V = 3746(3)$ Å^3, $Z = 4$, $\rho_{calcd} = 2.472$ g cm^{-3}, $F(000) = 2624$, $\mu = 2.825$ mm^{-1}, 4152

 © 2004 Wiley-VCH Verlag GmbH & Co. KGaA, Weinheim

independent reflections, $R_1 = 0.0315$, $wR_2 = 0.0650$ (all data). Data for **4**: $C_{25}H_{10}N_2O_{13}Ru_5$, $M_r = 1051.70$, crystal dimensions $0.19 \times 0.12 \times 0.06$ mm, triclinic, space group $P\bar{1}$, $a = 10.282(2)$, $b = 10.895(2)$, $c = 13.508(2)$ Å, $\alpha = 89.939(3)$, $\beta = 89.194(3)$, $\gamma = 89.532(3)°$, $V = 1513.0(4)$ Å^3, $Z = 2$, $\rho_{calcd} = 2.309$ g cm^{-3}, $F(000) = 996$, $\mu = 2.506$ mm^{-1}, 4268 independent reflections, $R_1 = 0.0293$, $wR_2 = 0.0763$ (all data). CCDC-231373 (**1**), CCDC-231374 (**2**), CCDC-231375 (**3**), and CCDC-231376 (**4**) contain the supplementary crystallographic data for this paper. These data can be obtained free of charge via www.ccdc.cam.ac.uk/conts/retrieving.html (or from the Cambridge Crystallographic Data Centre, 12 Union Road, Cambridge CB21EZ, UK; fax: (+44) 1223-336-033; or deposit@ccdc.cam.uk).

[7] a) T. Venäläinen, J. Pursiainen, T. A. Pakkanen, *J. Chem. Soc. Chem. Commun.* **1985**, 1348; b) M. I. Bruce, M. G. Humphrey, M. R. Snow, E. R. T. Tiekink, R. C. Wallis, *J. Organomet. Chem.* **1986**, *314*, 311.

[8] M. Gandelman, L. J. W. Shimon, D. Milstein, *Chem. Eur. J.* **2003**, *9*, 4295, and references therein.

[9] See, for example: a) A. Herzog, H. W. Roesky, F. Jager, A. Steiner, M. Noltemeyer, *Organometallics* **1996**, *15*, 909; b) A. Herzog, H. W. Roesky, Z. Zak, M. Noltemeyer, *Angew. Chem.* **1994**, *106*, 1052; *Angew. Chem. Int. Ed. Engl.* **1994**, *33*, 967; c) R. Andrés, P. Gómez-Sal, E. de Jesús, A. Martín, M. Mena, C. Yélamos, *Angew. Chem.* **1997**, *109*, 72; *Angew. Chem. Int. Ed. Engl.* **1997**, *36*, 115; d) R. Andrés, M. V. Galakhov, A. Martín, M. Mena, C. Santamaría, *J. Chem. Soc. Chem. Commun.* **1995**, 551; e) D. S. Richeson, S.-H. Hsu, N. H. Fredd, G. Van Duyne, K. H. Theopold, *J. Am. Chem. Soc.* **1986**, *108*, 8273.

[10] R. Andrés, M. V. Galakhov, A. Martín, M. Mena, C. Santamaría, *Organometallics* **1994**, *13*, 2159.

[11] a) J. E. Kickham, F. Guérin, J. C. Stewart, D. W. Stephan, *Angew. Chem.* **2000**, *112*, 3406; *Angew. Chem. Int. Ed.* **2000**, *39*, 3263; b) J. E. Kickham, F. Guérin, J. C. Stewart, E. Urbanska, D. W. Stephan, *Organometallics* **2001**, *20*, 1175.

[12] For relevant examples of complexes containing μ_4-carbyne ligands, see a) M. J. Fernández, B. F. G. Johnson, J. Lewis, P. R. Raithby, *Acta Crystallogr. Sect. B* **1978**, *34*, 3086; b) M. Miekuz, P. Bougeard, R. Faggiani, C. J. L. Lock, M. J. McGlinchey, G. Jaouen, *Organometallics* **1985**, *4*, 2046; c) J. S. Bradley, G. B. Ansell, E. W. Hill, *J. Am. Chem. Soc.* **1979**, *101*, 7417; d) S. Haak, A. Neels, H. Stoeckli-Evans, G. Süss-Fink, *Inorg. Chem. Commun.* **1999**, *2*, 60; e) J. Wang, A. M. Crespi, M. Sabat, S. Harris, C. Woodcock, D. F. Shriver, *Inorg. Chem.* **1989**, *28*, 697; f) O. Steigelmann, P. Bissinger, H. Schmidbaur, *Z. Naturforsch. B* **1993**, *48*, 72; g) F. Sherbaum, B. Huber, G. Müller, H. Schmidbaur, *Angew. Chem.* **1988**, *100*, 1600; *Angew. Chem. Int. Ed. Engl.* **1988**, *27*, 1542; h) H. Adams, L. V. Y. Guio, M. J. Morris, S. E. Spey, *J. Chem. Soc. Dalton Trans.* **2002**, 2907; i) D. L. Davies, J. C. Jeffery, D. Miguel, P. Sherwood, F. G. A. Stone, *J. Chem. Soc. Chem. Commun.* **1987**, 454.

[13] a) R. M. Gauvin, H. Rozenberg, L. J. W. Shimon, D. Milstein, *Organometallics* **2001**, *20*, 1719; b) M. Gandelman, A. Vigalok, L. J. W. Shimon, D. Milstein, *Organometallics* **1997**, *16*, 3981; c) B. Rybtchinski, S. Oevers, M. Montag, A. Vigalok, H. Rozenberg, J. M. L. Martin, D. Milstein, *J. Am. Chem. Soc.* **2001**, *123*, 9064; d) R. F. R. Jazzar, S. A. Macgregor, M. F. Mahon, S. P. Richards, M. K. Whittlesey, *J. Am. Chem. Soc.* **2002**, *124*, 4944.

 © 2004 Wiley-VCH Verlag GmbH & Co. KGaA, Weinheim

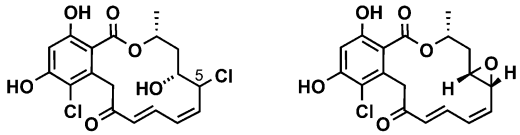
Natural Products Synthesis

Modular Asymmetric Synthesis of Pochonin C**

*Sofia Barluenga, Pilar Lopez, Emilie Moulin, and Nicolas Winssinger**

Dedicated to Professor Jean-Marie Lehn on the occasion of his 65th birthday

Pochonin C was isolated from a high-throughput screening program aimed at discovering novel antiviral agents against Herpes Simplex Virus (HSV).[1] Pochonin C (Scheme 1)



1: pochonin C **2**: radicicol (monorden)

Scheme 1. Structure of pochonin C (**1**) and radicicol (**2**).

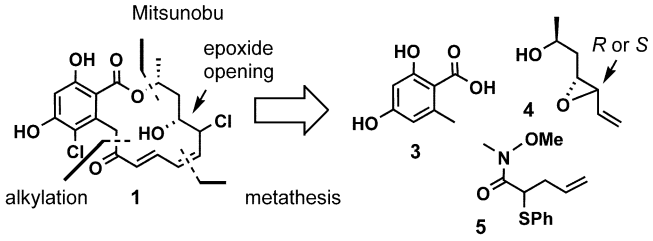
belongs to a family of six related macrolides (pochonins A–F) but attracted our attention by having the highest selectivity index (Tox_{50}/IC_{50}) against HSV amongst the pochonins and by being closely related to radicicol (also known as monorden),[2–4] a potent HSP90 inhibitor.[5] In fact, Hellwig et al. suggest that a formal ring opening of radicicol yields the chlorohydrin functionality of pochonin C. Nevertheless, the stereochemistry of C5 bearing the chlorine atom in pochonin C remains undefined. Although an HCl-promoted ring opening of radicicol has been described in the literature,[6] the two products have not been compared. Herein, we report the total synthesis of pochonin C and its conversion into radicicol.

The important therapeutic potential of HSP90 inhibition[7] and the structural relationship of pochonin C to radicicol motivated us to develop a synthesis that would be sufficiently concise to allow it to be mostly performed in a combinatorial fashion. A major criterion in such analysis is the commercial availability or ease of preparation of the fragments. Inspired by the previous work in the area,[8,9] we reasoned that the molecule could be disconnected into three fragments as shown in Scheme 2; both possible diastereoisomers of the C5 chlorine center would stem from the *cis*- or *trans*-epoxide moiety **4**. Given that ring-closing metathesis (RCM) of the conjugated diene could lead to four different products (12-

[*] Dr. S. Barluenga, Dr. P. Lopez, E. Moulin, Prof. N. Winssinger
Institut de Science et d'Ingénierie Supramoleculaires
Université Louis Pasteur
8 allée Gaspard Monge, 67000 Strasbourg (France)
Fax: (+33) 3-9024-5112
E-mail: winssinger@isis.u-strasbg.fr

[**] A Marie Curie Fellowship to S.B. (Grant no.: HPMF-CT-2002-01968) and Fellowships from the CNRS to P.L. and E.M. are gratefully acknowledged.

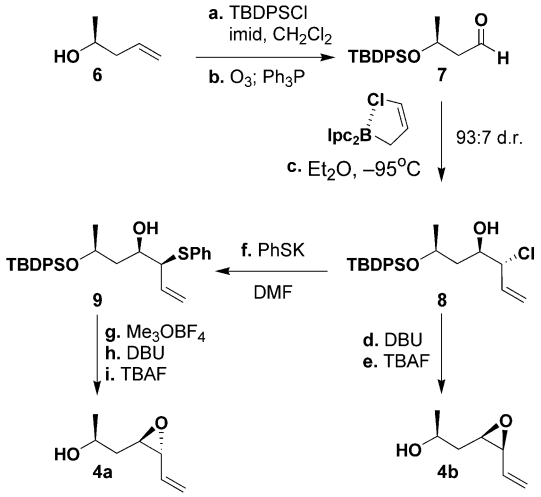
 DOI: 10.1002/anie.200454108 © 2004 Wiley-VCH Verlag GmbH & Co. KGaA, Weinheim



Scheme 2. Retrosynthetic disconections of pochonin C (**1**).

versus 14-membered ring and *cis*/*trans* isomers), it was reasoned that keeping the α,β-conjugated olefin masked as a thioether could prevent undesired cyclization to the 12-membered ring. The second element of control in the RCM was thought to be the timing of epoxide opening (before or after the RCM), which would offer some flexibility over the conformational organization of the open-chain system.

Both the *cis* and *trans* epoxides, **4a** and **b**, were accessed by a divergent strategy based on inversion of one of the epoxide stereocenters (Scheme 3). Thus, silyl protection of



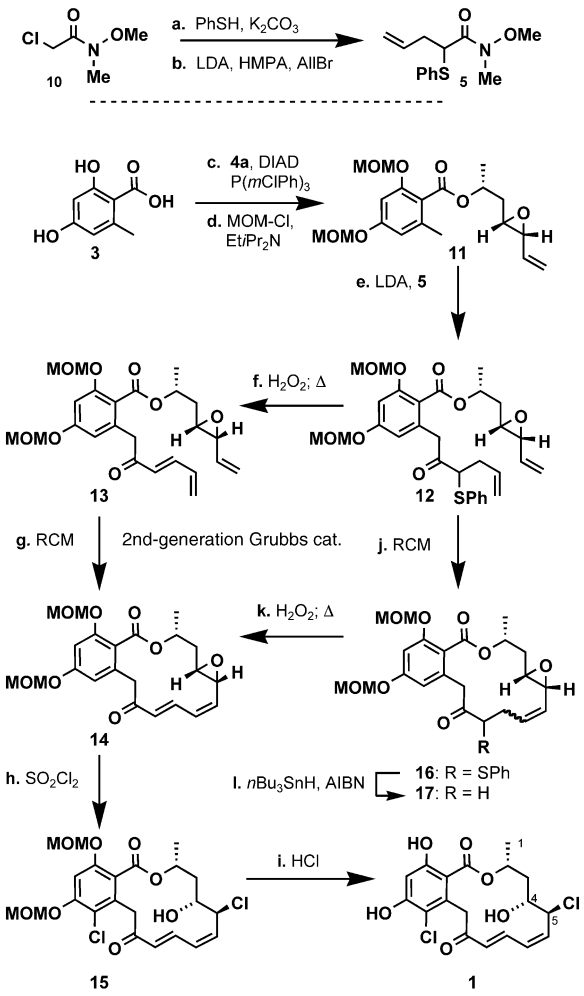
Scheme 3. Stereodivergent synthesis of alcohols **4a** and **4b**. a) TBDPSCl (1.1 equiv), imidazole (1.7 equiv), CH_2Cl_2, 23 °C, 4 h, 98%; b) O_3, CH_2Cl_2, −78 °C, 5 min; Ph_3P (1.5 equiv), 23 °C, 2 h, 94%; c) allyl chloride (2.0 equiv), LiN*c*Hex (2.0 equiv), IpcBOMe (1.5 equiv), BF_3OEt_2 (2.5 equiv), −95 °C, 4 h, 68% (93:7 d.r.); d) DBU (3.0 equiv), CH_2Cl_2, 0 °C, 8 h, 97%; e) TBAF (1.2 equiv), THF, 23 °C, 6 h, 98%; f) thiophenol (4.4 equiv), *t*BuOK (3.3 equiv), 23 °C, 1 h; then, **8** (1.0 equiv), DMF, 0→23 °C, 86%; g) Me_3OBF_4 (2.0 equiv), CH_2Cl_2, 0→23 °C, 4 h; h) DBU (3.0 equiv), CH_2Cl_2, 0 °C, 4 h, 80% (two steps); i) TBAF (1.2 equiv), THF, 23 °C, 6 h, 98%. DBU = 1,8-diazabicyclo[5.4.0]undec-7-ene, DMF = *N*,*N*-dimethylformamide, imid = imidazole, Ipc = isopinocampheyl, TBAF = tetrabutylammonium fluoride, TBDPS = *tert*-butyldiphenylsilyl.

alcohol **6**[10,11] followed by ozonolysis afforded the protected aldehyde **7** in excellent yield. Modified Brown allylation with allyl chloride[12] yielded the halohydrin **8**, which was converted directly into the *cis* epoxide **4b** by the action of DBU and subsequent TBAF-induced deprotection. The corresponding *trans* epoxide **4a** was reached by S_N2 displacement of the chlorine atom with thiophenoxide to obtain compound **9**. The oxirane was then formed by activation of the thioether through methylation of the sulfur atom; this was followed by the addition of base to yield the corresponding *trans* epoxide. Removal of the silyl protecting group with TBAF led to the desired alcohol **4a**.[13]

The Weinreb amide **5** was obtained by displacement of the chloride center from **10**[10] with thiophenol and subsequent alkylation of the resulting product with allyl bromide in the presence of HMPA (Scheme 4).

Esterification of the dihydroxytoluic acid under Mitsunobu or carbodiimide conditions was found to work best when the 2-OH group was unprotected. Rather than manipulate protecting groups to access the suitably monoprotected dihydroxytoluic acid, we opted to investigate a selective Mitsunobu esterification of the unprotected acid **3**.[10] While the use of classical conditions (Ph_3P, DIAD, CH_2Cl_2, THF, or toluene)[14] gave poor selectivity between the desired esterification and undesired alkylation of the *para*-phenol, the use of tris(3-chlorophenyl)phosphane[15] gave the desired ester with greater than 95:5 selectivity and in good yield. Subsequent protection of the two phenol groups with MOMCl afforded toluic ester **11**. Deprotonation of the benzylic position[16] with LDA at −78 °C gave a deep red solution which was quenched with the Weinreb amide **5** to yield the cyclization precursor **12**. Notably, the reaction required 2 equivalents of LDA to proceed. Treatment of intermediate **12** with the second-generation Grubbs catalyst[17] in toluene at 120 °C[18] led to rapid ring closure and the formation of macrocycle **16** as an inseparable mixture of *cis* and *trans* olefins (1:1). The high yield of the reaction was gratifying as the β-thioether could potentially form a stable complex that would shut down the catalytic cycle.[19] Chemoselective oxidation of the thioether with H_2O_2 in hexafluoropropan-2-ol[20] led to clean conversion into the thiosulfoxide with no overoxidation product or epoxide opening, as had been observed with *meta*-chloroperoxybenzoic acid or H_2O_2/$ScOTf_3$ (Tf = trifluoromethanesulfonyl).[21] Interestingly, elimination of the sulfoxide proceeded *only* for the compound leading to the desired *trans*,*cis* diene **14**. Presumably, the *trans* olefin **16** cannot adopt an adequate conformation to participate in a 1,2-*syn* elimination of the sulfoxide group. Conversely, the thioether group could be removed under free radical conditions to obtain the dihydroradicicol macrocycle **17**. The selectivity in the elimination clearly suggested that carrying out the metathesis on diene **13** should lead to the desired *trans*,*cis* diene. Indeed oxidation/elimination of thioether **12** prior to ring closure followed by RCM at 120 °C led exclusively to the desired conjugated *trans*,*cis* diene **14** (Table 1) within 10 min. It has been shown that the *cis*/*trans* selectivity of the RCM in unsubstituted 14-membered macrocycles is kinetically controlled;[22] however, the high degree of selectivity in the ring closure of **13** cannot be attributed to the short reaction time considering the lack of selectivity for the closure of **12** under the same conditions. All that remained in order to reach pochonin C was the chlorination of the aryl ring and stereoselective opening of the epoxide. After investigating several reaction-sequence permutations, it was found that both operations could be carried out in a single step by using an excess of SO_2Cl_2 (no overchlorination of the

 © 2004 Wiley-VCH Verlag GmbH & Co. KGaA, Weinheim



Scheme 4. Synthesis of pochonin C (**1**) from alcohol **4a.** a) PhSH (1.2 equiv), K_2CO_3 (1.5 equiv), DMF, 23 °C, 3 h, 98%; b) LDA (1.0 equiv), HMPA (1.0 equiv), AllBr (1.1 equiv), THF, −78→23 °C, 3 h, 82%; c) **4a** (1.0 equiv), P(*m*ClPh)$_3$ (2.0 equiv), DIAD (2.0 equiv), toluene, 23 °C, 3 h, 84%; d) MOMCl (4.0 equiv), DIPEA (4.0 equiv), TBAI (cat.), DMF, 80 °C, 3 h, 91%; e) LDA (2.0 equiv), THF, −78 °C, **5** (1.0 equiv), 81%; f) H_2O_2 (2.0 equiv), $(CF_3)_2CHOH$, 23 °C, 3 h; then, toluene, 80 °C, 1 h, 92%; g) second-generation Grubbs catalyst (5 mol%), toluene (2 mM), 120 °C, 10 min, 87%; h) SO_2Cl_2 (3.0 equiv), Et_2O, 0 °C, 68%; i) HCl (conc.; 2.5% in dioxane), 23 °C, 3 h, 74%; j) second-generation Grubbs catalyst (5 mol%), toluene (2 mM), 120 °C, 10 min, 94%; k) H_2O_2 (2.0 equiv), $(CF_3)_2CHOH$, 23 °C, 3 h; then, toluene, 80 °C, 1 h, 22% (85% based on recovered sulfoxide); l) nBu_3SnH (5.0 equiv), AIBN (cat.), toluene, microwave at 300 W, 10 min, 91%. AIBN = 2,2′-azobisisobutyronitrile, DIAD = diisopropyl-azodicarboxylate, DIPEA = diisopropylethylamine, HMPA = hexamethyl-phosphoramide, LDA = lithium diisopropylamide, MOM = methoxy-methyl, second-generation Grubbs catalyst = [ruthenium{1,3-bis-(2,4,6-trimethylphenyl)-2-imidazolidinylidene}dichloro (phenylmethylene)(tri-cyclohexylphosphane)], TBAI = tetrabutylammonium iodide.

aromatic ring was observed).[8,23] Final deprotection of the MOM groups from **15** led to compound **1** (Table 1), which was found to have identical NMR spectra to pochonin C.[24] Importantly, treatment of compound **1** with K_2CO_3 led to rapid and clean oxirane formation to yield compound **2**, which was identical to radicicol (Scheme 5).

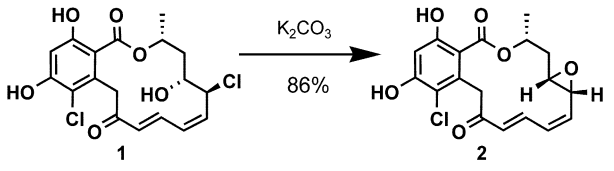
Table 1: Selected data for compounds **1**, **14**, **15**, and **19**.

1: R_f = 0.11 (SiO_2, EtOAc/cyclohexane (1:3)); ^{1}H NMR (400 MHz, $CDCl_3$, 25 °C): δ = 9.28 (s, 1H), 8.59 (s, 1H), 7.11 (dd, 1H, J = 14.7, 12.3 Hz), 6.66 (s, 1H), 6.31 (t, 1H, J = 10.4 Hz), 6.10 (d, 1H, J = 16.1 Hz), 5.91 (m, 1H), 5.78 (t, 1H, J = 9.9 Hz), 5.22 (d, 1H, J = 15.8 Hz), 4.92 (t, 1H, J = 9.1 Hz), 3.96 (d, 1H, J = 15.8 Hz), 3.95 (m, 1H), 2.48 (dd, 1H, J = 15.8, 10.7 Hz), 2.13 (m, 1H), 1.54 ppm (d, 3H, J = 6.4 Hz); ^{1}H NMR (400 MHz, [D$_6$]DMSO, 25 °C): δ = 10.58 (s, 1H), 10.13 (s, 1H), 7.12 (dd, 1H, J = 16.1, 11.3 Hz), 6.56 (s, 1H), 6.27 (t, 1H, J = 10.8 Hz), 6.04 (d, 1H, J = 16.1 Hz), 5.78 (t, 1H, J = 10.8 Hz), 5.46 (d, 1H, J = 5.4 Hz), 5.28 (m, 1H), 5.10 (dd, 1H, J = 9.9, 4.8 Hz), 4.05 (d, 1H, J = 16.1 Hz), 3.99 (m, 1H), 3.60 (d, 1H, J = 16.1 Hz), 1.90–1.84 (m, 2H), 1.37 ppm (d, 3H, J = 6.2 Hz); ^{13}C NMR (125 MHz, [D$_6$]DMSO, 25 °C): δ = 197.0, 166.5, 155.5, 139.1, 137.0, 133.2, 132.1, 129.9, 115.1, 112.2, 102.9, 71.1, 69.5, 60.8, 44.9, 37.8, 19.0 ppm; HRMS (ESI-TOF): calcd for $C_{18}H_{18}Cl_2O_6$ [M+Na$^+$]: 422.9995; found: 423.0337

14: R_f = 0.19 (SiO_2, EtOAc/cyclohexane (1:3)); ^{1}H NMR (400 MHz, $CDCl_3$, 25 °C): δ = 7.68 (dd, 1H, J = 16.1, 11.3 Hz), 6.75 (d, 1H, J = 2.1 Hz), 6.59 (d, 1H, J = 2.1 Hz), 6.26 (t, 1H, J = 11.3 Hz), 6.05 (d, 1H, J = 16.1 Hz), 5.84 (dd, 1H, J = 10.8 Hz, 4.4 Hz), 5.42–5.33 (m, 1H), 5.21–5.17 (m, 2H), 5.14 (s, 2H), 3.97 (d, 1H, J = 14.0 Hz), 3.86 (d, 1H, J = 13.4 Hz), 3.57 (m, 1H), 3.48 (s, 3H), 3.47 (s, 3H), 3.10–3.13 (ddd, 1H, J = 7.5, 3.7, 2.2 Hz), 2.47 (dt, 1H, J = 14.5, 4.8 Hz), 1.73 (ddd, 1H, J = 15.0, 7.5, 3.2 Hz), 1.59 ppm (d, 3H, J = 6.4 Hz); ^{13}C NMR (100 MHz, $CDCl_3$, 25 °C): δ = 197.9, 166.8, 159.2, 156.0, 140.2, 136.6, 134.5, 131.8, 130.2, 117.8, 108.7, 102.1, 94.6, 94.3, 69.8, 56.3, 55.8, 54.9, 42.4, 37.1, 29.7 18.9 ppm; HRMS (ESI-TOF): calcd for $C_{22}H_{26}O_8$ [M+Na$^+$]: 441.1520; found: 441.1595

15: R_f = 0.25 (SiO_2, EtOAc/cyclohexane (1:1)); ^{1}H NMR (400 MHz, $CDCl_3$, 25 °C): δ = 7.18 (dd, 1H, J = 16.2, 11.2 Hz), 7.04 (s, 1H), 6.26 (t, 1H, J = 10.9 Hz), 6.10 (d, 1H, J = 16.4 Hz), 5.81 (t, 1H, J = 10.2 Hz), 5.47 (m, 1H), 5.35–5.12 (m, 6H), 4.11 (d, 1H, J = 15.8 Hz), 3.92 (d, 1H, J = 15.8 Hz), 3.56–3.48 (m, 2H), 3.55 (s, 3H), 3.53 (s, 3H), 1.57 ppm (d, 3H, J = 6.4 Hz); ^{13}C NMR (100 MHz, $CDCl_3$, 25 °C): δ = 196.3, 166.7, 159.3, 156.0, 140.8, 137.9, 134.7, 133.2, 131.2, 117.8, 102.0, 95.2, 94.6, 71.9, 69.7, 60.4, 56.7, 56.4, 45.1, 21.0, 18.8 ppm; HRMS (ESI-TOF): calcd for $C_{22}H_{26}Cl_2O_8$ [M+Na$^+$]: 510.9994; found: 511.0002

19: R_f = 0.19 (SiO_2, EtOAc/cyclohexane (1:3)); ^{1}H NMR (400 MHz, $CDCl_3$, 25 °C): δ = 7.66 (dd, 1H, J = 15.8, 10.8 Hz), 6.75 (s, 1H), 6.58 (s, 1H), 6.25 (t, 1H, J = 9.7 Hz), 6.04 (d, 1H, J = 15.8 Hz), 5.83 (dd, 1H, J = 10.8 Hz, 4.3 Hz), 5.37 (m, 1H), 5.20–5.16 (m, 2H), 5.13 (s, 2H), 3.96 (d, 1H, J = 13.7 Hz), 3.85 (d, 1H, J = 13.7 Hz), 3.56 (br s, 1H), 3.48 (s, 3H), 3.46 (s, 3H), 3.11–3.09 (m, 1H), 2.49–2.42 (ddd, 1H, J = 15.2, 5.1, 4.3 Hz), 1.73–1.68 (ddd, 1H, J = 15.2, 7.2, 3.0 Hz), 1.58 ppm (d, 3H, J = 6.3 Hz); ^{13}C NMR (100 MHz, $CDCl_3$, 25 °C): δ = 197.8, 166.8, 159.2, 156.1, 140.1, 136.6, 132.8, 131.8, 130.2, 114.2, 108.7, 102.1, 94.6, 94.3, 69.8, 56.3, 55.7, 54.9, 42.4, 37.1, 29.7 18.8 ppm; HRMS (ESI-TOF): calcd for $C_{22}H_{26}O_8$ [M+Na$^+$]: 441.1520; found: 441.1599

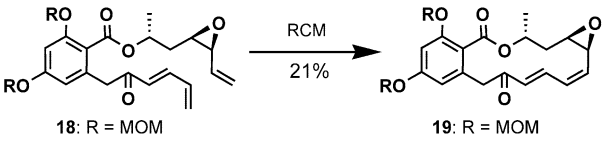


Scheme 5. Conversion of pochonin C (**1**) into radicicol (**2**). K_2CO_3 (2.0 equiv), DMF, 23 °C, 1 h, 86%.

A similar reaction sequence starting from alcohol **4b** and toluic acid **3** led to the triene **18**. Treatment of this compound with the successful metathesis conditions used for **13** afforded

 © 2004 Wiley-VCH Verlag GmbH & Co. KGaA, Weinheim

the ring-closure product **19** (Table 1) as the conjugated *trans*,*cis* diene, albeit in poor yield (Scheme 6).



18: R = MOM **19**: R = MOM

Scheme 6. Ring-closing metathesis with the *cis* epoxide stemming from alcohol **4b**. second-generation Grubbs catalyst (5 mol%), toluene (2 mM), 120°C, 10 min, 21%.

In conclusion, we have developed an expedient stereoselective synthesis of pochonin C and demonstrated the conversion of the product into radicicol, thereby assigning the stereochemistry of C5 as *S*. RCM has been used extensively for the synthesis of macrocyclic natural products,[25] but with some unpredictability in the stereochemical outcome.[26] There are, however, few examples of RCM for macrocycles with conjugated diene functionalities[27] that could potentially give rise to different modes of cyclization. The exceptionally selective RCM for the conversion of **13** into **14** testifies to the conformational restrictions of the radicicol macrocycles and adds a precedent for the feasibility of this transformation. The use of the described chemistry for the construction of combinatorial libraries is currently underway.

Received: February 26, 2004 [Z54108]

Keywords: asymmetric synthesis · conformation analysis · metathesis · natural products · total synthesis

[1] V. Hellwig, A. Mayer-Bartschmid, H. Mueller, G. Greif, G. Kleymann, W. Zitzmann, H.-V. Tichy, M. Stadler, *J. Nat. Prod.* **2003**, *66*, 829–837.
[2] P. Delmotte, J. Delmotte-Plaquee, *Nature* **1953**, *171*, 344.
[3] R. N. Mirrington, E. Ritchie, C. W. Shoppee, W. C. Taylor, S. Sternhell, *Tetrahedron Lett.* **1964**, 365–370.
[4] H. G. Cutler, R. F. Arrendale, J. P. Springer, P. D. Cole, R. G. Roberts, R. T. Hanlin, *Agric. Biol. Chem.* **1987**, *51*, 3331–3338.
[5] S. M. Roe, C. Prodromou, R. O'Brien, J. E. Ladbury, P. W. Piper, L. H. Pearl, *J. Med. Chem.* **1999**, *42*, 260–266.
[6] T. Agatsuma, H. Ogawa, K. Akasaka, A. Asai, Y. Yamashita, T. Mizukami, S. Akinaga, Y. Saitoh, *Bioorg. Med. Chem.* **2002**, *10*, 3445–3454.
[7] P. Workman, *Curr. Cancer Drug Targets* **2003**, *3*, 297–300.
[8] M. Lampilas, R. Lett, *Tetrahedron Lett.* **1992**, *33*, 773–776; I. Tichkowsky, R. Lett, *Tetrahedron Lett.* **2002**, *43*, 4003–4007.
[9] R. M. Garbaccio, S. J. Stachel, D. K. Baeschlin, S. J. Danishefsky, *J. Am. Chem. Soc.* **2001**, *123*, 10903–10908; Z.-Q. Yang, S. J. Danishefsky, *J. Am. Chem. Soc.* **2003**, *125*, 9602–9603.
[10] Commercially available.
[11] H. C. Brown, P. K. Jadhav, *J. Am. Chem. Soc.* **1983**, *105*, 2092–2093.
[12] S. Hu, S. Jayaraman, A. C. Oehlschlager, *J. Org. Chem.* **1996**, *61*, 7513–7520; C. Hertweck, W. Boland, *Tetrahedron* **1997**, *53*, 14651–14654.
[13] This compound was identical to a sample synthesized through an alternative strategy: U. Schlede, M. Nazare, H. Waldmann, *Tetrahedron Lett.* **1998**, *39*, 1143–1144.
[14] O. Mitsunobu, *Synthesis* **1981**, 1–28.
[15] D. L. Hughes, R. A. Reamer, J. J. Bergan, E. J. J. Grabowski, *J. Am. Chem. Soc.* **1988**, *110*, 6487–6491.
[16] P. L. Creger, *J. Am. Chem. Soc.* **1970**, *92*, 1396–1397.
[17] M. Scholl, S. Ding, C. W. Lee, R. H. Grubbs, *Org. Lett.* **1999**, *1*, 953–956; A. K. Chatterjee, J. P. Morgan, M. Scholl, R. H. Grubbs, *J. Am. Chem. Soc.* **2000**, *122*, 3783–3784.
[18] For a study of the effect of temperature, see: K. Yamamoto, K. Biswas, C. Gaul, S. J. Danishefsky, *Tetrahedron Lett.* **2003**, *44*, 3297–3299.
[19] S. K. Armstrong, B. A. Christie, *Tetrahedron Lett.* **1996**, *37*, 9373–9376; J. L. Mascareñas, A. Rumbo, L. Castedo, *J. Org. Chem.* **1997**, *62*, 8620–8621; A. Furstner, G. Seidel, N. Kindler, *Tetrahedron* **1999**, *55*, 8215–8230; G. Spagnol, M.-P. Heck, S. P. Nolan, C. Mioskowski, *Org. Lett.* **2002**, *4*, 1767–1770.
[20] K. S. Ravikumar, J.-P. Bégué, D. Bonnet-Delpon, *Tetrahedron Lett.* **1998**, *39*, 3141–3144; K. S. Ravikumar, Y. M. Zhang, J.-P. Bégue, D. Bonnet-Delpon, *Eur. J. Org. Chem.* **1998**, *12*, 2937–2940.
[21] M. Matteucci, G. Bhalay, M. Bradley, *Org. Lett.* **2003**, *5*, 235–237.
[22] C. W. Lee, R. H. Grubbs, *Org. Lett.* **2000**, *2*, 2145–2147.
[23] J. A. Elix, S. Norfolk, *Aust. J. Chem.* **1975**, *28*, 1113–1124.
[24] A ^{1}H NMR spectrum of pochinin C was kindly provided by Dr. Stadler (Bayer Health Care, Wuppertal, Germany).
[25] For selected examples, see: Z. Yang, Y. He, D. Vourloumis, H. Vallberg, K. C. Nicolaou, *Angew. Chem.* **1997**, *109*, 170–172; *Angew. Chem. Int. Ed. Engl.* **1997**, *36*, 166–168; D. Meng, P. Bertinato, A. Balog, D.-S. Su, T. Kamenecka, E. Sorensen, S. J. Danishefsky, *J. Am. Chem. Soc.* **1997**, *119*, 10073–10092; Y. Wu, X. Liao, R. Wang, X.-S. Xie, J. K. De Brabander, *J. Am. Chem. Soc* **2002**, *124*, 3245–3253; A. B. Smith, J. Zheng, *Tetrahedron* **2002**, *58*, 6455–6471.
[26] J. Prunet, *Angew. Chem.* **2003**, *115*, 3444–3448; *Angew. Chem. Int. Ed.* **2003**, *42*, 2826–2830.
[27] L. M. M. Cabrejas, S. Rohrbach, D. Wagner, J. Kallen, G. Zenke, J. Wagner, *Angew. Chem.* **1999**, *111*, 2595–2599; *Angew. Chem. Int. Ed.* **1999**, *38*, 2443–2446; C. A. Dvorak, W. D. Schmitz, D. J. Poon, D. C. Pryde, J. P. Lawson, R. A. Amos, A. I. Meyers, *Angew. Chem.* **2000**, *112*, 1730–1732; *Angew. Chem. Int. Ed.* **2000**, *39*, 1664–1666; K. Biswas, H. Lin, J. T. Njardarson, M. D. Chappell, T.-C. Chou, Y. Guan, W. P. Tong, L. He, S. B. Horwitz, S. J. Danishefsky, *J. Am. Chem. Soc.* **2002**, *124*, 9825–9832.

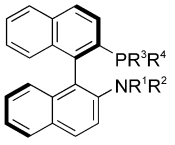
 © 2004 Wiley-VCH Verlag GmbH & Co. KGaA, Weinheim

Bidentate P,N Ligands

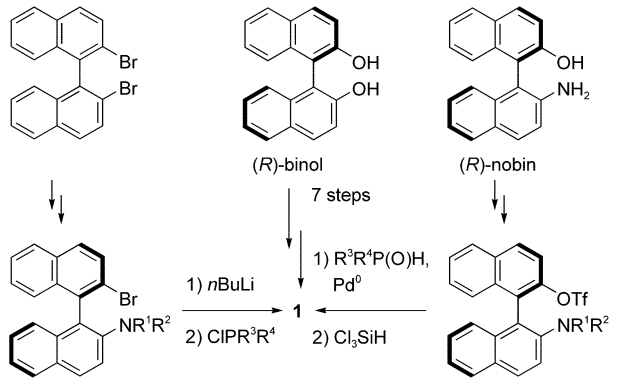
A Staudinger Approach towards Binol-Derived MAP-Type Bidentate P,N Ligands**

Peter N. M. Botman, Olivier David, Alessia Amore, Jasper Dinkelaar, Martin T. Vlaar, Kees Goubitz, Jan Fraanje, Henk Schenk, Henk Hiemstra, and Jan H. van Maarseveen**

Ligands based on nonsymmetrically 2,2′-substituted 1,1′-binaphthyl compounds find widespread use in homogeneous catalysis.[1] Within this class, the heterobidentate MAP-type ligands **1** stand out because of their high reactivities and selectivities in several transition-metal-catalyzed reactions, such as Hartwig–Buchwald amination reactions, (enantioselective) Suzuki–Miyaura coupling reactions, and the formation of aryl ethers.[2] For the synthesis of enantiopure MAP-type ligands, binol seems the most logical choice as both enantiomers are commercially available. To date, only one direct synthesis of a MAP-type ligand from binol has been reported, namely, the synthesis of **1** ($R^1 = R^2 =$ Ph, $R^3 = R^4 = H$) by Noyori and co-workers in 7 steps (Scheme 1).[3] Alternative routes towards optically pure



1: MAP-type ligand



Scheme 1. Syntheses of MAP-type ligands **1**.

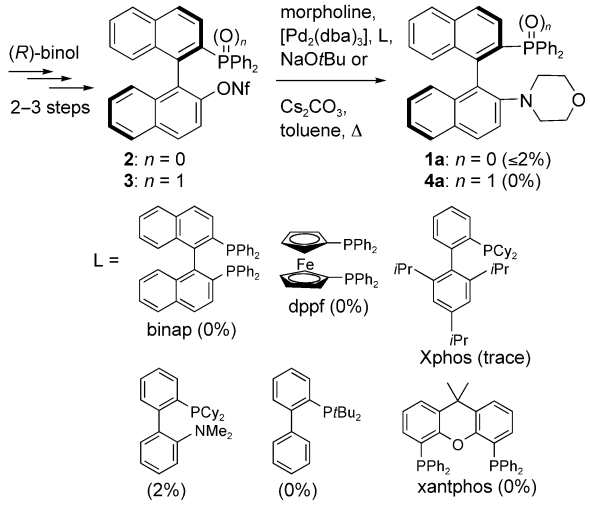
[*] P. N. M. Botman, Dr. O. David, A. Amore, J. Dinkelaar, M. T. Vlaar, K. Goubitz, J. Fraanje, Prof. Dr. H. Schenk, Prof. Dr. H. Hiemstra, Dr. J. H. van Maarseveen
Van't Hoff Institute of Molecular Sciences
University of Amsterdam
Nieuwe Achtergracht 129, 1018 WS Amsterdam (The Netherlands)
Fax: (+31) 20-525-5670
E-mail: hiemstra@science.uva.nl
jvm@science.uva.nl

[**] This research was supported by the National Research School Combination Catalysis (NRSC-C) and the Council for Chemical Sciences of the Netherlands Organization for Scientific Research (CW-NWO). MAP = 2′-dimethylamino-2-(diphenylphosphanyl)-1,1′-binaphthalene.

Supporting information for this article is available on the WWW under http://www.angewandte.org or from the author.

MAP ligands have been disclosed starting from 2,2′-dibromo-1,1′-bisnaphthalene[4] or nobin.[5,6] A common feature of these routes is that the introduction of the amino group precedes phosphane or phosphane oxide installation (Scheme 1).

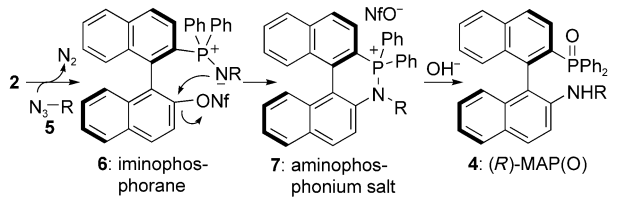
For the synthesis of a series of MAP ligands which vary in the amine substituent, we decided to start from binol and to reverse the order of reactions by introducing the phosphorus moiety first to give **2**, followed by introduction of the amino group by using the Buchwald–Hartwig amination reaction (Scheme 2). The required phosphanyl nonaflate **2** was prepared in three steps from (*R*)-binol based on literature procedures for the triflate analogue in an overall yield of 89%.[7] The feasibility of this approach is suggested by several reports describing the successful introduction of phosphane, phosphane oxide, and aryl groups into the triflate analogue of **2** by transition-metal catalysis.[8] Although we tried the most powerful ligands known to date, used sets of several conditions, started both from **2** and the oxide **3**, and used morpholine as the nucleophile, only when Xphos[9] or the P,N ligand [2′-(Dicyclohexylphosphanyl)biphenyl-2-yl]dimethylamine[10] were used as the ligand could traces (2% at maximum) of **1a** be detected by ^{1}H NMR spectroscopy.[11]



Scheme 2. Attempts towards Pd^0-catalyzed amine introduction. For each ligand L, the yield is given in brackets. Nf = nonaflate = nonafluorobutanesulfonate.

From the experience gained with our work on intramolecular Staudinger ligations for the synthesis of cyclopeptides we envisioned at this stage the possibility of amine introduction by a similar strategy—the reaction of phosphane **2** with alkyl or aryl azides.[12] In this approach intramolecular nucleophilic aromatic substitution of the nonaflate substituent by the iminophosphorane unit in **6** would yield an aminophosphonium salt **7**, thus providing, after basic hydrolysis, MAP(O)-type compounds **4** (Scheme 3).[13] Herein we show the usefulness of iminophosphorane nitrogen atoms as nucleophiles in an unprecedented intramolecular S_NAr reaction that provides efficient access to MAP ligands.

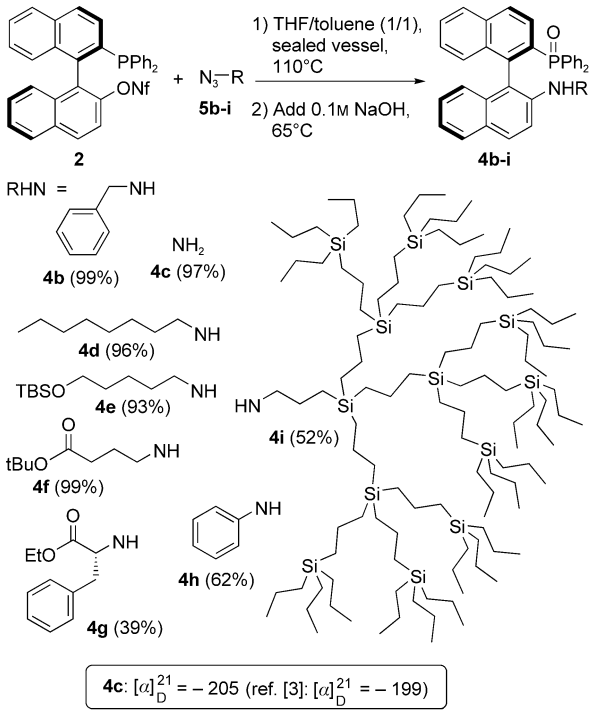
 DOI: 10.1002/anie.200454146 © 2004 Wiley-VCH Verlag GmbH & Co. KGaA, Weinheim



Scheme 3. A Staudinger approach towards P,N ligands.

In a first attempt, equimolar amounts of **2** and benzyl azide (**5b**) were heated at reflux in toluene. Much to our satisfaction, ^{31}P NMR spectroscopic analysis of the reaction mixture after 8 h revealed, besides some starting material and iminophosphorane **6b**, the anticipated aminophosphonium salt **7b** (Scheme 3, R = Bn). After heating for an additional 10 h, only aminophosphonium salt **7b** could be detected. Evaporation of the solvent yielded **7b** as an air-stable off-white viscous oil. Hydrolysis of the P–N bond was accomplished by refluxing **7b** in a mixture of EtOH/THF/aqueous 0.1M NaOH (1/1/1) to provide **4b**. Under optimized conditions (see Scheme 4) **4b** could be isolated almost quantitatively. It was observed that in the THF/toluene mixture iminophosphorane formation already proceeded at room temperature, whereas in toluene heating was required.[14]

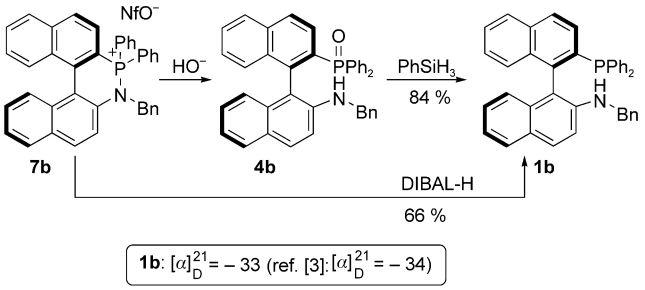
To show the broad synthetic scope of this approach towards 2-amino-2′-diphenylphosphinoyl-1,1′-binaphthyl compounds **4** we treated **2** with azides **5b–i** (Scheme 4). To introduce a primary amino group, commercially available Me_3SiN_3 (12 equiv, added in 3 portions at 12-hour intervals) was stirred with **2** in THF/toluene (1/1) to give **4c** almost quantitatively. Thus, by using this Staudinger ligation method, des-dimethyl MAP(O) (**4c**), which is an important intermediate for the synthesis of MAP-type ligands, was synthesized from binol in 4 steps in an overall yield of 87%.[3] Comparison of the optical rotation of **4c** with literature data revealed that no racemization had taken place during the reaction sequence (see Scheme 4).[3] Also, we did not observe any change in the optical rotation after heating **4c**, which bears the small NH_2 group and is thus most prone to racemization, for 10 min at 300 °C. Prolonged heating led to decomposition of the product. These experiments show that racemization under the normal reaction conditions is very unlikely.



Scheme 4. A new approach to MAP(O)-type ligands. For each amino substituent RNH, the yield is given in brackets.

Azides with benzyl, *n*-alkyl, ether, or ester functionalities all reacted readily to provide **4b**, **4d**, **4e**, and **4f** in yields of 99, 96, 93, and 99%, respectively. The phenylalanine-derived α-azido ester **5g**, which was prepared from Phe-OEt by a diazo transfer, gave **4g** in 39% yield. The diazo-transfer reactions were performed as described in ref. [19]. Despite the lower nucleophilicity of its intermediate *N*,*N*-diaryliminophosphorane nitrogen atom, phenyl azide **5h** reacted smoothly to give **4h** in 62% yield. A very bulky third-generation carbosilane dendritic wedge featuring an azide in the focal point could also be introduced to give **4i** in 52% yield.[15]

For applications of **4a–i** in catalysis, reduction to the corresponding phosphane is required. As an example **4b** was treated with phenylsilane at 114 °C for 17 h to provide **1b** (84%, Scheme 5). A more convenient method would be the direct hydride-promoted cleavage of the P–N bond of the intermediate phosphonium salts **7**. Indeed, upon treatment of **7b** with DIBAL-H clean reduction occurred to provide optically pure **1b** (66% yield, Scheme 5).[3]

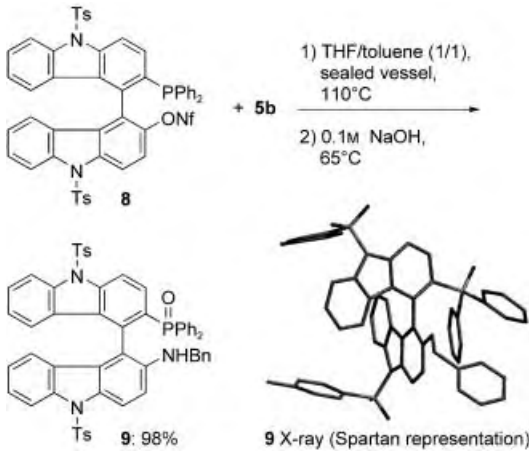


Scheme 5. Two routes to phosphanes derived from **4**. DIBAL-H = diisobutylaluminum hydride.

Finally, reaction of the racemic phosphanyl nonaflate of the structurally related bicol[16]-derived biscarbazole **8**[17] with benzyl azide (**5b**), followed by hydroxide treatment (Scheme 6) gave phosphane oxide **9** (98% yield), the structure of which was confirmed by X-ray analysis.[20]

In conclusion, we have shown that the synthetic potential of the 85-year-old Staudinger reaction[18] between phosphanes and azides is still far from being exhausted. The Staudinger reaction between 2-diphenylphosphanyl-2′-nonaflyloxy-1,1′-biaryl compounds and azides provides, through an unprecendented S_NAr reaction, a wide range of MAP(O)-type ligands in high yields and enantiomerically pure form in only 4 steps

 © 2004 Wiley-VCH Verlag GmbH & Co. KGaA, Weinheim



Scheme 6. Synthesis and structure of **9**.

from binol. This strategy is especially attractive because the phosphorus atom is an essential element in the product instead of waste as in usual Staudinger approaches. Furthermore, the required number of synthetic steps is significantly decreased compared to the current synthetic routes towards MAP-type P,N ligands. Finally, this new method provides access to analogues which until now could only be prepared with great difficulty or not at all.

Received: February 28, 2004 [Z54146]

Keywords: azides · biaryl compounds · nucleophilic aromatic substitution · P ligands

[1] R. Noyori in *Asymmetric Catalysis in Organic Synthesis*, Wiley, New York, **1994**; *Catalytic Asymmetric Synthesis* (Ed.: I. Ojima), Wiley-VCH, Weinheim, **2000**; *Comprehensive Asymmetric Catalysis* (Eds.: E. N. Jacobson, A. Pfaltz, H. Yamamoto), Springer, Heidelberg, **1999**; M. McCarthy, P. J. Guiry, *Tetrahedron* **2001**, *57*, 3809 – 3844.

[2] P. Kočovský, Š. Vyskočil, M. Smrčina, *Chem. Rev.* **2003**, *103*, 3213 – 3245; for a comprehensive review on N,P ligands in general, see: P. J. Guiry, C. P. Saunders, *Adv. Synth. Catal.* **2004**, *346*, 497 – 537.

[3] K. Sumi, T. Ikariya, R. Noyori, *Can. J. Chem.* **2000**, *78*, 697 – 703.

[4] T. Hamada, S. L. Buchwald, *Org. Lett.* **2002**, *4*, 999 – 1001.

[5] a) Š. Vyskočil, M. Smrčina, V. Hanuš, M. Polášek, P. Kočovský, *J. Org. Chem.* **1998**, *63*, 7738 – 7748; b) K. Ding, Y. Wang, H. Yun, J. Liu, Y. Wu, M Terada, Y. Okubo, K. Mikami, *Chem. Eur. J.* **1999**, *5*, 1734 – 1737.

[6] A formal synthesis of MAP-type ligands from (*R*)-binol can be envisioned as (*R*)-nobin has been prepared from (*R*)-binol in 6 steps (61 % overall yield); see: R. A. Singer, S. L. Buchwald, *Tetrahedron Lett.* **1999**, *40*, 1095 – 1098.

[7] L. Kurz, G. Lee, D. Morgans, Jr., M. J. Waldyke, T. Ward, *Tetrahedron Lett.* **1990**, *31*, 6321 – 6324.

[8] For the introduction of phosphane and phosphane oxide groups, see: I. P. Beletskaya, M. A. Kazankova, *Russ. J. Org. Chem.* **2002**, *38*, 1391 – 1430; for the introduction of aryl groups, see: T. Hayashi, J. W. Han, A. Takeda, J. Tang, K. Nohmi, K. Mukaide, H. Tsuji, Y. Uozumi, *Adv. Synth. Catal.* **2001**, *343*, 279 – 283.

[9] X. Huang, K. W. Anderson, D. Zim, L. Jiang, A. Klapars, S. L. Buchwald, *J. Am. Chem. Soc.* **2003**, *125*, 6653 – 6655.

[10] a) Š. Vyskočil, M. Smrčina, V. Hanuš, M. Polášek, P. Kočovský, *J. Org. Chem.* **1998**, *63*, 7738 – 7748; b) A. Aranyos, D. W. Old, A. Kiyomori, J. P. Wolfe, P. Sadigishi, S. L. Buchwald, *J. Am. Chem. Soc.* **1999**, *121*, 4369 – 4378; c) Š. Vyskočil, M. Smrčina, P. Kočovský, *Tetrahedron Lett.* **1998**, *39*, 9289 – 9292; d) D. W. Old, J. P. Wolfe, S. L. Buchwald, *J. Am. Chem. Soc.* **1998**, *120*, 9722 – 9723.

[11] For a recent article on Pd-catalyzed aminations starting from nonaflates, see: K. W. Anderson, M. Mendez-Perez, J. Priego, S. L. Buchwald, *J. Org. Chem.* **2003**, *68*, 9563 – 9573.

[12] a) O. David, W. J. N. Meester, H. Bieräugel, H. E. Schoemaker, H. Hiemstra, J. H. van Maarseveen, *Angew. Chem.* **2003**, *115*, 4509 – 4511; *Angew. Chem. Int. Ed.* **2003**, *42*, 4373 – 4375; for the original work on Staudinger ligations, see: b) E. Saxon, C. R. Bertozzi, *Science* **2000**, *287*, 2007 – 2010; c) E. Saxon, J. I. Armstrong, C. R. Bertozzi, *Org. Lett.* **2000**, *2*, 2141 – 2143; d) E. Saxon, S. J. Luchansky, H. C. Hang, C. Yu, S. C. Lee, C. R. Bertozzi, *J. Am. Chem. Soc.* **2002**, *124*, 14893 – 14902; e) B. L. Nilsson, L. L. Kiessling, R. T. Raines, *Org. Lett.* **2000**, *2*, 1939; f) B. L. Nilsson, L. L. Kiessling, R. T. Raines, *Org. Lett.* **2001**, *3*, 9 – 12; g) M. B. Soellner, B. L. Nilsson, R. T. Raines, *J. Org. Chem.* **2002**, *67*, 4993 – 4996.

[13] For reviews on the Staudinger reaction, see: a) Y. G. Gololobov, I. N. Zhmurova, L. F. Kasukhin, *Tetrahedron* **1981**, *37*, 437 – 472; b) Y. G. Gololobov, L. F. Kasukhin, *Tetrahedron* **1992**, *48*, 1353 – 1406.

[14] The choice for THF as cosolvent was based on the results reported by Hemming et al. and Peterson Jr. et al. concerning the reaction between PPh_3 and Me_3SiN_3: a) K. Hemming, M. J. Bevan, C. Loukou, S. D. Patel, D. Renaudeau, *Synlett* **2000**, 1565 – 1568; b) S. S. Washburne, W. R. Peterson Jr. , *J. Organomet. Chem.* **1971**, *33*, 153 – 156.

[15] For the synthesis of focal-point-functionalized carbosilane dendritic wedges, see: R. van Heerbeek, P. C. J. Kamer, J. N. H. Reek, P. W. N. M. van Leeuwen, *Tetrahedron Lett.* **1999**, *40*, 7127 – 7130.

[16] P. N. M. Botman, M. Postma, J. Fraanje, K. Goubitz, H. Schenk, J. H. van Maarseveen, H. Hiemstra, *Eur. J. Org. Chem.* **2002**, 1952 – 1955.

[17] P. N. M. Botman, J. Fraanje, K. Goubitz, R. Peschar, J. W. Verhoeven, J. H. van Maarseveen, H. Hiemstra, *Adv. Synth. Cat.*, submitted.

[18] H. Staudinger, J. Meyer, *Helv. Chim. Acta* **1919**, *2*, 635 – 646.

[19] J. T. Lundquist, J. C. Pelletier, *Org. Lett.* **2001**, *3*, 781 – 783.

[20] CCDC 239743 contains the supplementary crystallographic data for this paper. These data can be obtained free of charge via www.ccdc.cam.ac.uk/conts/retrieving.html (or from the Cambridge Crystallographic Data Centre, 12, Union Road, Cambridge CB21EZ, UK; fax: (+44) 1223-336-033; or deposit@ccdc.cam.ac.uk).

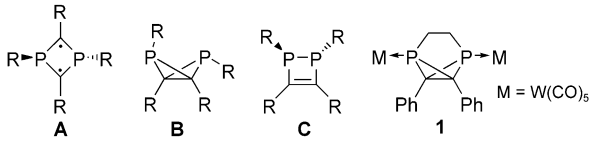
 © 2004 Wiley-VCH Verlag GmbH & Co. KGaA, Weinheim

Phosphorus Heterocycles

2-Phospha-4-silabicyclo[1.1.0]butane as a Reactive Intermediate**

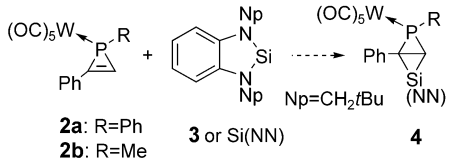
*J. Chris Slootweg, Frans J. J. de Kanter, Marius Schakel, Andreas W. Ehlers, Barbara Gehrhus, Martin Lutz, Allison M. Mills, Anthony L. Spek, and Koop Lammertsma**

Bicyclo[1.1.0]butane remains a fascinating compound. Stretching of its central C–C σ-bond culminates in a planar singlet diradical transition structure for inversion,[1] whereas stretching of the peripheral bonds leads to valence isomerization.[2] Bridging heteroatoms affect both processes. They enable the coexistence of the puckered bicyclic and planar diyl structures, and have thereby sparked intensive studies dominated by recent discoveries of diphosphorus analogues. Niecke et al. synthesized a crystalline 2,4-diphosphacyclobutane-1,3-diyl **A**[3] that isomerizes photolytically to 2,4-diphosphabicyclo[1.1.0]butane **B**[4] and thermally to 1,2-dihydro-1,2-diphosphete **C**.[5] A still more congested diyl **A** that does not isomerize was reported by Yoshifuji and co-workers.[6] The group of Bertrand obtained both stable planar diyl and puckered forms for the isoelectronic 1,3-dibora-2,4-diphosphoniocyclobutanes.[7] 2,4-Diphosphabicyclo[1.1.0]butane is puckered when the phosphorus atoms are *endo*,*endo* substituted as in dihydro diphosphabenzvalene **1**, which Mathey and co-workers obtained by an *intra*molecular phosphinidene addition to the C=C bond of a 1*H*-phosphirene.[8] Without geometrical constraints, such additions invariably lead to 1,2-diphosphetes of type **C** by isomerization or direct C–P insertion.[9]



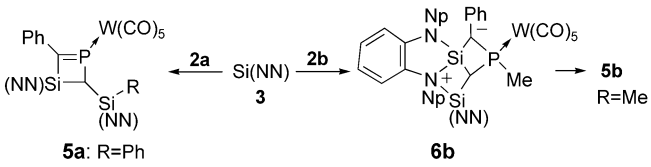
A **B** **C** **1**

Data on 2,4-disilabicyclo[1.1.0]butanes[10] is limited to two disilabenzvalenes[11] and is absent for the corresponding planar diyls. Only a single 2-silabenzvalene is known, generated by photolysis of a silabenzene.[12] For the synthesis of the 2,4-disila derivatives Ando et al. applied valence isomerization of bis(silirene) that involves an intramolecular silylene addition to the C=C bond of a silirene.[11] The use of stable silylenes might simplify this approach to a broader array of hetero derivatives, which we decided to explore for the unknown 2-phospha-4-silabicyclo[1.1.0]butanes **4**.



2a: R=Ph
2b: R=Me
3 or Si(NN)
4

Reaction of silylene Si{1,2-(NCH$_2$*t*Bu)$_2$C$_6$H$_4$} (Si(NN); **3**)[13] with 1*H*-phosphirene **2a**[14] in *n*-hexane at room temperature results in red crystalline 2,3-dihydro-1,3-phosphasilete **5a** instead of the desired **4** (Scheme 1).[15] Evidently, two silylenes are involved, one in forming the novel ring structure and the other as a substituent after transfer of a phenyl group. No intermediate was detected by ^{31}P NMR spectroscopy, either at low temperatures or with different stoichiometries of the reactants. The W(CO)$_5$-complexed phosphaalkene part of **5a** is characterized by the downfield absorptions at $\delta(^{31}P) = 278.3$ ppm ($^1J(P,W) = 254.0$ Hz) and $\delta(^{13}C) = 197.3$ ppm ($^1J(C,P) = 3.5$ Hz). A single-crystal X-ray analysis confirmed the structure of **5a** (Figure 1).[16] Its four-membered ring deviates from planarity owing to steric congestion, which is reflected in the torsion angle of 11.6(2)° for C1–P1–C2–Si1. The P1–C1 and P1–C2 bond lengths (1.689(4) and 1.835(4) Å, respectively) are normal, but the short Si1–C1 bond (1.841(5) Å) suggests some delocalization of charge.



5a: R=Ph
6b

Scheme 1. Synthesis of 2,3-dihydro-1,3-phosphasiletes **5**.

To lower the migratory aptitude of the phosphorus substituent, we replaced the phenyl for a methyl group and used 1*H*-phosphirene **2b**[14] instead of **2a** for the addition of silylene **3**. This had the desired effect, giving the crystalline zwitterion **6b** (68%), which only rearranged at elevated temperatures (75°C, 2 h) to 2,3-dihydro-1,3-phosphasilete **5b** (Scheme 1). The molecular structure of **6b** (Figure 2,[16] the crystal contains two independent molecules with similar geometries) shows a unique fused tricyclic ring structure which is retained in solution ($\delta(^{31}P) = -6.8$ ppm ($^1J(P,W) =$

[*] J. C. Slootweg, Dr. F. J. J. de Kanter, Dr. M. Schakel, Dr. A. W. Ehlers, Prof. Dr. K. Lammertsma
Department of Organic and Inorganic Chemistry
Faculty of Sciences, Vrije Universiteit
De Boelelaan 1083, 1081 HV, Amsterdam (The Netherlands)
Fax: (+31) 20-444-7488
E-mail: lammert@chem.vu.nl
Dr. B. Gehrhus
Department of Chemistry
School of Life Science, University of Sussex
Brighton, BN1 9QJ (UK)
Dr. M. Lutz, Dr. A. M. Mills, Prof. Dr. A. L. Spek
Bijvoet Center for Biomolecular Research
Crystal and Structural Chemistry, Utrecht University
Padualaan 8, 3584 CH, Utrecht (The Netherlands).

[**] The Netherlands Organization for Scientific Research (NWO/CW) is acknowledged for partial support.

Supporting information for this article is available on the WWW under http://www.angewandte.org or from the author.

 © 2004 Wiley-VCH Verlag GmbH & Co. KGaA, Weinheim DOI: 10.1002/anie.200454183

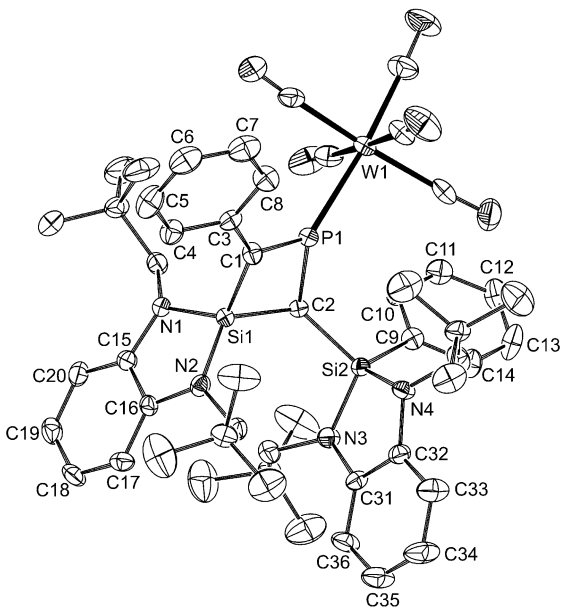


Figure 1. Structure of **5a** in the crystal (displacement ellipsoids drawn at the 50% probability level; hydrogen atoms and the hexane solvent molecule are omitted for clarity). Selected bond lengths [Å], angles [°], and torsion angles [°]: W1–P1 2.4492(11), P1–C1 1.689(4), P1–C2 1.835(4), Si1–C1 1.841(5), Si1–C2 1.908(4); C1-P1-C2 92.9(2), P1-C2-Si1 86.13(17), C1-Si1-C2 85.96(18), P1-C1-Si1 92.7(2); C1-P1-C2-Si1 11.6(2).

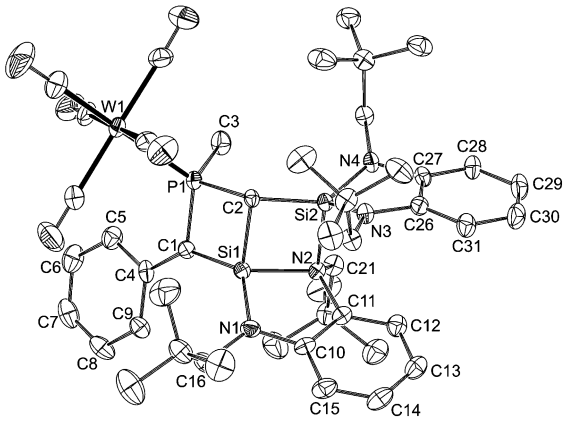
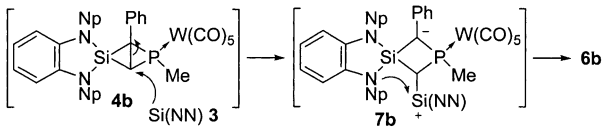


Figure 2. Structure of **6b** in the crystal, one of the two crystallographically independent molecules is shown (displacement ellipsoids drawn at the 50% probability level; hydrogen atoms omitted for clarity). Selected bond lengths [Å], angles [°], and torsion angles [°]: W1–P1 2.5363(12), P1–C1 1.793(4), P1–C2 1.863(4), Si1–N1 1.725(4), Si1–N2 1.923(4), Si1–C1 1.750(4), Si1–C2 1.906(4), Si2–N2 1.933(4), Si2–N3 1.710(4), Si2–N4 1.705(4), Si2–C2 1.828(4), N1–C10 1.409(6), N1–C16 1.471(6), N2–C11 1.471(5), N2–C21 1.510(5), C1–C4 1.455(6); C1-P1-C2 90.79(19), P1-C2-Si1 85.70(18), C1-Si1-C2 90.70(19), P1-C1-Si1 92.7(2); C2-P1-C1-Si1 −2.4(2), P1-C1-C4-C5 8.2(8).

240.0 Hz), $\delta(^{29}\mathrm{Si}) = -11.2$ ($^2J(\mathrm{Si,P}) = 17.2$ Hz, SiNN) and −33.4 ppm ($^2J(\mathrm{Si,P}) = 18.4$ Hz, $\mathrm{SiNN^+}$). The negatively charged C1 is in a planar environment and is surrounded by shortened C1–P1 (1.793(4) Å), C1–C4 (1.455(6) Å), and C1–Si1 (1.750(4) Å) bonds that can be attributed to negative hyperconjugation, which is supported by the shielding of Si1 ($\delta(^{29}\mathrm{Si}) = -33.4$ ppm).[17] Furthermore, the cationic N2 lengthens the N2–Si and N2–C bonds.[18]

We assume that the reaction starts by addition of the silylene to the C=C bond of the phosphirene to give 2-phospha-4-silabicyclo[1.1.0]butane **4b** as a transient intermediate, followed by attack of a second silylene to the bridgehead carbon atom in a manner analogous to the reaction of nucleophiles with bicyclo[1.1.0]butane (Scheme 2).[19] The resulting **7b** carries a silylium cation,



Scheme 2. Mechanism for the formation of **6b**.

which requires stabilization[20] by coordination with the lone pair of electrons of a nearby nitrogen atom.[21] This hypothesis was tested with SCS-MP2/6-311+G** energy calculations on B3LYP6-31G* optimized model structures (labeled **B**),[22] which are devoid of $W(CO)_5$, carry H instead of Np substituents, and have the nitrogen atoms linked by ethylene instead of phenyl groups. This simplification is validated by the similarity in optimized structures between **4B** and that containing the Np and $W(CO)_5$ groups. Formation of **4B** from the reactants $C_2H_4N_2Si$ and C_3H_5P is exothermic by 17.5 kcal mol^{-1} with an additional 8.5 kcal mol^{-1} for the addition of a second silylene to give **7B** (Figure 3). Lewis base stabilization

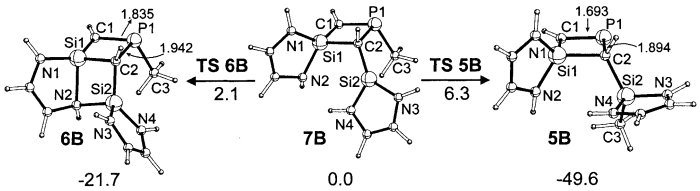
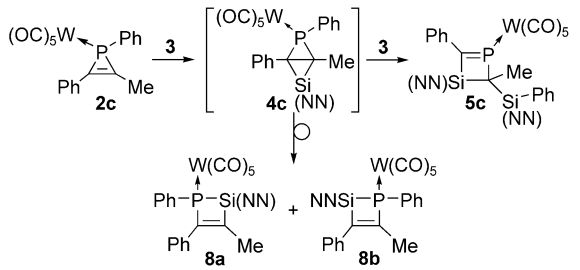


Figure 3. Relative SCS-MP2/6-311+G**//B3YLP/6-31G* energies (in kcal mol^{-1}) for the rearrangement of **6B** to the thermodynamically more stable **5B** with selected bond lengths [Å].

of the silylium cation gives the kinetically favored zwitterion **6B** ($\Delta E = 21.7$, $\Delta E^{\neq} = 2.1$ kcal mol^{-1}), whereas a 1,3-methyl shift from phosphorus to silicon results in the thermodynamically favored phosphasilete **5B** ($\Delta E = 49.6$, $\Delta E^{\neq} = 6.3$ kcal mol^{-1}). Such 1,3-shifts to an electron-deficient silicon are very rare for both the methyl and phenyl groups.[23,24]

To reduce the attractiveness of the transient 2-phospha-4-silabicyclo[1.1.0]butane for attack by a second silylene, a methyl group was introduced at the bridgehead position by treating 1*H*-phosphirene **2c**[14] with **3**. This had the desired effect, but mainly valence isomerization occurred to the isomeric 1,2-dihydro-1,2-phosphasiletes **8a** and **8b**,[25] together with the formation of some **5c** (5:2:2), because of the elevated temperatures (80 °C, 13 h) required for the reaction to take place (Scheme 3). After fractional crystallization, **8a** could be obtained as a yellow solid for which only single resonances were observed at $\delta(^{31}\mathrm{P}) = 15.2$ ppm

 © 2004 Wiley-VCH Verlag GmbH & Co. KGaA, Weinheim



Scheme 3. Isomerization of **4c**.

(^1J(P,W) = 205.0 Hz) and $\delta(^{29}\text{Si}) = -17.1$ ppm (^1J(Si,P) = 45.6 Hz) confirming the stoichiometry of the reaction. The structure of **8a** was established unequivocally by a single-crystal X-ray structural analysis (Figure 4),[16] which shows

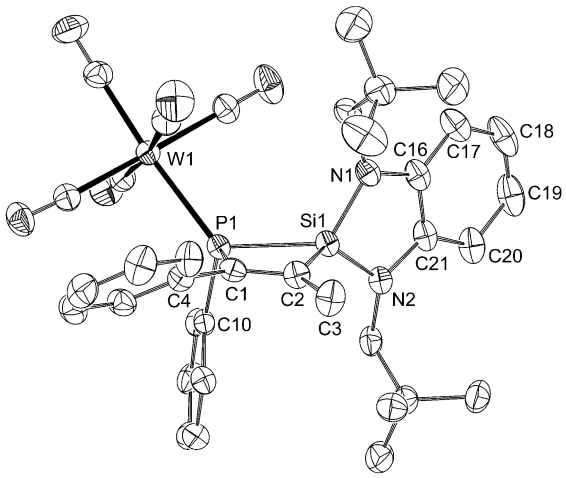


Figure 4. Structure of **8a** in the crystal (displacement ellipsoids drawn at the 50% probability level; hydrogen atoms are omitted for clarity). Selected bond lengths [Å], angles [°], and torsion angles [°]: W1–P1 2.5269(6), P1–Si1 2.3074(8), P1–C1 1.854(2), P1–C10 1.841(2), Si1–N1 1.726(2), Si1–N2 1.7249(19), Si1–C2 1.863(2), C1–C2 1.360(3), C1–C4 1.489(3), C2–C3 1.507(3); C1-P1-Si1 73.30(7), P1-Si1-C2 76.89(7); P1-C1-C2-Si1 7.46(17).

that the four-membered ring is nearly planar with a torsion angle of 7.46(17)° for P1–C1–C2–Si1 and that the P1–Si1 bond (2.3074(8) Å) is slightly elongated owing to steric congestion.

SCS-MP2/6-311+G** calculations on B3LYP/6-31G* model structures containing carbon substituents[22] show that intermediate 2-phospha-4-silabicyclo[1.1.0]butane **4C** can isomerize to the thermodynamically preferred 1,2-dihydro-1,2-phosphasiletes **8A** and **8B** with barriers of only 21.3 and 21.6 kcal mol^{-1}, respectively. This similarity in $\Delta E^{\neq}$ values is reflected in the two experimentally observed isomers. The valence isomerization of **4C** to **8** is symmetry-allowed and can be described as a [σ2s+σ2a] process.[26] Such a pathway is unprecedented for the analogous isomerization of bicyclo[1.1.0]butane, for which *s-trans*-1,3-butadiene is the favored product.

In conclusion, thermally stable silylene **3** reacts with 1*H*-phosphirenes **2** to give the first isolated 2,3-dihydro-1,3-phosphasiletes **5**, zwitterion **6b**, and 1,2-dihydro-1,2-phosphasiletes **8** with the novel 2-phospha-4-silabicyclo[1.1.0]butanes **4** being a reactive intermediate in the reaction, the course of which can be tuned by changing the substituents.

Experimental Section

5a: Complex **2a**[14] (38.6 mg, 72.3 μmol) in *n*-hexane (5 mL) was added slowly to a solution of **3**[13] (39.7 mg, 144.6 μmol) in *n*-hexane (2 mL) at −50 °C, warmed to ambient temperature, and stirred for 16 h. Filtration, concentration, and cooling at −20 °C affording red crystals of **5a** (56 mg, 66%): m.p. 245 °C (decomp.); ^{29}Si NMR (79.5 MHz, C_6D_6): $\delta = -5.1$ (d, ^2J(Si,P) = 6.9 Hz; Ph-SiNN), −13.5 ppm (d, ^2J(Si,P) = 31.8 Hz; SiNN); ^{31}P{^{1}H} NMR (101.3 MHz, $CDCl_3$): $\delta = 278.3$ ppm (^1J(P,W) = 254.0 Hz); HRMS (EI, 70 eV): *m/z* (%): 1082 (2) [M^+]; calcd for $C_{51}H_{63}O_5N_4Si_2PW$: 1082.35840; found: 1082.35376.

5b: Complex **2b**[14] (12.3 mg, 26.0 μmol) and **3** (14.3 mg, 52.1 μmol) were heated at 75 °C for 2 h in C_6D_6 (0.5 mL). Evaporation to dryness, extraction into *n*-hexane, and subsequent filtration and cooling at −20 °C gave red crystals of **5b** (15 mg, 57%): m.p. 150 °C (decomp.); ^{29}Si NMR (79.5 MHz, C_6D_6): $\delta = 4.8$ (d, ^2J(Si,P) = 4.2 Hz; Me-SiNN), −13.8 ppm (d, ^2J(Si,P) = 33.2 Hz; SiNN); ^{31}P{^{1}H} NMR (101.3 MHz, C_6D_6): $\delta = 276.6$ ppm (^1J(P,W) = 246.1 Hz); HRMS (EI, 70 eV): *m/z* (%): 1020 (5) [M^+]; calcd for $C_{46}H_{61}O_5N_4Si_2PW$: 1020.34277; found: 1020.3391.

6b: Complex **2b** (20.4 mg, 43.2 μmol) in *n*-hexane (5 mL) was added to a solution of **3** (23.7 mg, 86.3 μmol) in *n*-hexane (2 mL) at ambient temperature and stirred for 2 h. Concentration and cooling at 0 °C affording yellow crystals of **6b** (30 mg, 68%): m.p. 149 °C (decomp.); ^{29}Si NMR (79.5 MHz, C_6D_6): $\delta = -33.4$ (d, ^2J(Si,P) = 18.4 Hz; $SiNN^+$), −11.2 ppm (d, ^2J(Si,P) = 17.2 Hz; SiNN); ^{31}P{^{1}H} NMR (101.3 MHz, C_6D_6): $\delta = -6.8$ ppm (^1J(P,W) = 240.0 Hz).

8: Complex **2c**[14] (44.9 mg, 81.9 μmol) and **3** (33.7 mg, 122.8 μmol) were heated at 80 °C for 13 h in C_6D_6 (0.5 mL). ^{31}P{^{1}H} NMR (101.3 MHz, C_6D_6): $\delta = 12.0$ (^1J(P,W) = 198.5 Hz, 19% yield of **8b** by NMR spectroscopy), 15.2 (^1J(P,W) = 205.6 Hz, 50% yield of **8a** by NMR spectroscopy), 308.1 ppm (br s, 19.5% yield of **5c** by NMR spectroscopy). Evaporation to dryness, extraction into *n*-hexane, and subsequent cooling at −80 °C gave yellow crystals of **8a** (30 mg, 45%): m.p. 157 °C (decomp.); ^{29}Si NMR (79.5 MHz, C_6D_6): $\delta = -17.1$ ppm (d, ^1J(Si,P) = 45.6 Hz; SiNN); ^{31}P{^{1}H} NMR (101.3 MHz, C_6D_6): $\delta = 15.2$ ppm (^1J(P,W) = 205.0 Hz); HRMS (EI, 70 eV): *m/z* (%): 822 (80) [M^+]; calcd for $C_{36}H_{39}O_5N_2SiPW$: 822.1876; found: 822.1880. **5c**: MS (EI, 70 eV): *m/z* (%): 1096 (30) [M^+].

Received: March 4, 2004 [Z54183]

Keywords: phosphorus heterocycles · reaction mechanisms · reactive intermediates · substituent effects · valence isomerization

[1] K. A. Nguyen, M. S. Gordon, J. A. Boatz, *J. Am. Chem. Soc.* **1994**, *116*, 9241–9249.
[2] K. A. Nguyen, M. S. Gordon, *J. Am. Chem. Soc.* **1995**, *117*, 3835–3847.
[3] E. Niecke, A. Fuchs, F. Baumeister, M. Nieger, W. W. Schoeller, *Angew. Chem.* **1995**, *107*, 640–642; *Angew. Chem. Int. Ed. Engl.* **1995**, *34*, 555–557.
[4] E. Niecke, A. Fuchs, M. Nieger, *Angew. Chem.* **1999**, *111*, 3213–3216; *Angew. Chem. Int. Ed.* **1999**, *38*, 3028–3031.
[5] O. Schmidt, A. Fuchs, D. Gudat, M. Nieger, W. Hoffbauer, E. Niecke, W. W. Schoeller, *Angew. Chem.* **1998**, *110*, 995–998; *Angew. Chem. Int. Ed.* **1998**, *37*, 949–952.

 © 2004 Wiley-VCH Verlag GmbH & Co. KGaA, Weinheim

[6] H. Sugiyama, S. Ito, M. Yoshifuji, *Angew. Chem.* **2003**, *115*, 3932 – 3934; *Angew. Chem. Int. Ed.* **2003**, *42*, 3802 – 3804.

[7] a) D. Scheschkewitz, H. Amii, H. Gornitzka, W. W. Schoeller, D. Bourissou, G. Bertrand, *Science* **2002**, *295*, 1880 – 1881; b) D. Scheschkewitz, H. Amii, H. Gornitzka, W. W. Schoeller, D. Bourissou, G. Bertrand, *Angew. Chem.* **2004**, *116*, 595 – 597; *Angew. Chem. Int. Ed.* **2004**, *43*, 585 – 587.

[8] M. White, L. Ricard, F. Mathey, *Organometallics* **2003**, *22*, 4825 – 4828.

[9] a) N. H. Tran Huy, L. Ricard, F. Mathey, *Organometallics* **1997**, *16*, 4501 – 4504; b) B. Wang, K. A. Ngyen, G. N. Srinivas, C. L. Watkins, S. Menzer, A. L. Spek, K. Lammertsma, *Organometallics* **1999**, *18*, 796 – 799.

[10] Only one Si_2C_2-ring is known: G. Fritz, S. Wartenessian, E. Matern, W. Hömle, H. G. Von Schnering, *Z. Anorg. Allg. Chem.* **1981**, *475*, 87 – 108.

[11] a) W. Ando, T. Shiba, T. Hidaka, K. Morihashi, O. Kikuchi, *J. Am. Chem. Soc.* **1997**, *119*, 3629 – 3630; b) Y. Kabe, K. Ohkubo, H. Ishikawa, W. Ando, *J. Am. Chem. Soc.* **2000**, *122*, 3775 – 3776.

[12] K. Wakita, N. Tokitoh, R. Okazaki, N. Takagi, S. Nagase, *J. Am. Chem. Soc.* **2000**, *122*, 5648 – 5649.

[13] B. Gehrhus, M. F. Lappert, J. Heinicke, R. Boese, D. Bläser, *J. Chem. Soc. Chem. Commun.* **1995**, 1931 – 1932.

[14] A. Marinetti, F. Mathey, *Organometallics* **1984**, *3*, 456 – 461. Synthesis of **2b** and **2c** was performed in analogy to **2a**; see Supporting Information.

[15] So far, only one $1\lambda^3$-1,3-phosphasilete was mentioned: M. Driess, H. Pritzkow, *Phosphorus Sulfur Silicon Relat. Elem.* **1993**, *76*, 57 – 60.

[16] Crystal structure determinations: X-ray intensities were measured on a Nonius KappaCCD diffractometer with rotating anode ($\lambda = 0.71073$ Å) at a temperature of 150(2) K. The structures were refined with SHELXL97[27] against F^2 of all reflections. Illustrations, structure calculations and checking was performed with the PLATON package.[28] **5a** ($C_{51}H_{63}N_4O_5PSi_2W \cdot 0.6\,C_6H_{14}$): $M_w = 1134.76$, red block, $0.06 \times 0.18 \times 0.21$ mm^3, monoclinic, $P2_1$ (No. 4), $a = 10.5532(1)$, $b = 16.0049(2)$, $c = 17.2900(2)$ Å, $\beta = 100.5233(5)$, $V = 2871.21(6)$ Å^3, $Z = 2$, $\rho = 1.313$ g cm^{-3}; 51129 measured reflections, 13052 unique reflections ($R_{int} = 0.050$); structure solution with automated Patterson methods;[29] 643 refined parameters, 46 restraints; $R1/wR2$ [$I > 2\sigma(I)$]: 0.0338/0.0755, $R1/wR2$ (all reflections) = 0.0472/0.0794; GoF = 1.072; Flack × parameter: −0.024(4). **6b** ($C_{46}H_{61}N_4O_5PSi_2W$): $M_w = 1020.99$, yellow block, $0.18 \times 0.24 \times 0.30$ mm^3, triclinic, $P\bar{1}$ (No. 2), $a = 10.6476(3)$, $b = 21.2390(8)$, $c = 22.6862(5)$ Å, $\alpha = 74.495(2)$, $\beta = 89.5698(19)$, $\gamma = 82.814(3)°$, $V = 4903.0(3)$ Å^3, $Z = 4$, $\rho = 1.383$ g cm^{-3}. The crystal appeared to be non-merohedrally twinned with a 180° rotation about $uvw = [100]$ as twin operation. The intensity data were evaluated with EvalCCD;[30] taking this twin relation into account; 55937 measured reflections, 22336 unique reflections ($R_{int} = 0.058$); sructure solution with direct methods;[31] 1064 refined parameters, 388 restraints; bond lengths and angles of the two independent molecules were restrained to be the same; $R1/wR2$ [$I > 2\sigma(I)$]: 0.0499/0.1070, $R1/wR2$ (all reflections) = 0.0767/0.1216; GoF = 1.128; the refinement[24] of the twin fraction resulted in 0.794(1):0.206. **8a** ($C_{36}H_{39}N_2O_5PSiW$): $M_w = 822.60$, yellow plate, $0.06 \times 0.36 \times 0.42$ mm^3, monoclinic, $P2_1/c$ (No. 14), $a = 19.1665(1)$, $b = 10.6482(1)$, $c = 20.5181(1)$ Å, $\beta = 119.8343(4)°$, $V = 3632.53(5)$ Å^3, $Z = 4$, $\rho = 1.504$ g cm^{-3}; 58693 measured reflections, 8329 unique reflections ($R_{int} = 0.046$); structure solution with automated Patterson methods;[29] 422 refined parameters, no restraints; $R1/wR2$ [$I > 2\sigma(I)$]: 0.0204/0.0455, $R1/wR2$ (all reflections) = 0.0289/0.0488; GoF = 1.038. CCDC-216769 (**5a**), -216770 (**6b**), and -232111 (**8a**) contain the supplementary crystallographic data for this paper. These data can be obtained free of charge via www.ccdc.cam.ac.uk/conts/retrieving.html (or from the Cambridge Crystallographic Data Centre, 12, Union Road, Cambridge CB2 1EZ, UK; fax: (+44) 1223-336-033; or deposit@ccdc.cam.ac.uk).

[17] M. Sebastian, M. Nieger, D. Szieberth, L. Nyulászi, E. Niecke, *Angew. Chem.* **2004**, *116*, 647 – 651; *Angew. Chem. Int. Ed.* **2004**, *43*, 637 – 641.

[18] R. Bettenhausen, W. Milius, W. Schnick, *Chem. Eur. J.* **1997**, *3*, 1337 – 1341.

[19] S. Hoz in *The Chemistry of the Cyclopropyl Group*, *Part 2* (Ed.: Z. Rappoport), Wiley, New York, **1987**, Chapter 19.

[20] K. -C. Kim, C. A. Reed, D. W. Elliott, L. J. Mueller, F. Tham, L. Lin, J. B. Lambert, *Science* **2002**, *297*, 825 – 827.

[21] R. Corriu, G. Lanneau, C. Priou, *Angew. Chem.* **1991**, *103*, 1153 – 1155; *Angew. Chem. Int. Ed. Engl.* **1991**, *30*, 1130 – 1132.

[22] a) Gaussian 98 (Revision A.7), M. J. Frisch, G. W. Trucks, H. B. Schlegel, G. E. Scuseria, M. A. Robb, J. R. Cheeseman, V. G. Zakrzewski, J. A. Montgomery, R. E. Stratmann, J. C. Burant, S. Dapprich, J. M. Millam, A. D. Daniels, K. N. Kudin, M. C. Strain, O. Farkas, J. Tomasi, V. Barone, M. Cossi, R. Cammi, B. Mennucci, C. Pomelli, C. Adamo, S. Clifford, J. Ochterski, G. A. Petersson, P. Y. Ayala, Q. Cui, K. Morokuma, D. K. Malick, A. D. Rabuck, K. Raghavachari, J. B. Foresman, J. Cioslowski, J. V. Ortiz, B. B. Stefanov, G. Liu, A. Liashenko, P. Piskorz, I. Komaromi, R. Gomperts, R. L. Martin, D. J. Fox, T. Keith, M. A. Al-Laham, C. Y. Peng, A. Nanayakkara, C. Gonzalez, M. Challacombe, P. M. W. Gill, B. G. Johnson, W. Chen, M. W. Wong, J. L. Andres, M. Head-Gordon, E. S. Replogle, J. A. Pople, Gaussian, Inc., Pittsburgh, PA, **1998**; b) A. D. Becke, *Phys. Rev. A* **1988**, *38*, 3098 – 3100; c) C. Lee, W. Yang, R. G. Parr, *Phys. Rev. B* **1988**, *37*, 785 – 789; d) S. Grimme, *J. Chem. Phys*, **2003**, *118*, 9095 – 9102; see Supporting Information.

[23] a) K. Ueno, K. Nakano, H. Ogino, *Chem. Lett.* **1996**, 459 – 460, and references therein; b) K. Ueno, M. Sakai, H. Ogino, *Organometallics* **1998**, *17*, 2138 – 2140.

[24] C. Eaborn, A. Kowalewska, W. Stanczyk, *J. Organomet. Chem.* **1998**, *560*, 41 – 46, and references therein.

[25] Only one other synthesis of 1,2-dihydro-1,2-phosphasiletes was reported: a) S. Haber, R. Boese, M. Regitz, *Angew. Chem.* **1990**, *102*, 1523 – 1525; *Angew. Chem. Int. Ed. Engl.* **1990**, *29*, 1436 – 1438; b) S. Haber, M. Schmitz, U. Bergsträßer, J. Hoffmann, M. Regitz, *Chem. Eur. J.* **1999**, *5*, 1581 – 1589.

[26] J. C. Slootweg, A. W. Ehlers, K. Lammertsma, *Phosphorus Sulfur Silicon Relat. Elem.* **2004**, *179*, 803 – 807.

[27] G. M. Sheldrick, SHELXL-97, Program for crystal structure refinement, University of Göttingen, Germany, **1997**.

[28] A. L. Spek, *J. Appl. Crystallogr.* **2003**, *36*, 7 – 13.

[29] P. T. Beurskens, G. Admiraal, G. Beurskens, W. P. Bosman, S. Garcia-Granda, R. O. Gould, J. M. M. Smits, C. Smykalla, The DIRDIF99 program system, Technical Report of the Crystallography Laboratory, University of Nijmegen, The Netherlands, **1999**.

[30] A. J. M. Duisenberg, L. M. J. Kroon-Batenburg, A. M. M. Schreurs, *J. Appl. Crystallogr.* **2003**, *36*, 220 – 229.

[31] G. M. Sheldrick, SHELXS-97, Program for crystal structure solution, University of Göttingen, Germany, **1997**.

 © 2004 Wiley-VCH Verlag GmbH & Co. KGaA, Weinheim

Protein Structures

Simultaneous Assignment and Structure Determination of Protein Backbones by Using NMR Dipolar Couplings**

*Young-Sang Jung, Mukesh Sharma, and Markus Zweckstetter**

The wealth of genomic data that has recently become available with completion of the sequencing of both the human and a variety of other genomes[1] has created a need for rapid and efficient determination of three-dimensional (3D) structures of the corresponding proteins. To date, most effort in this so-called structural genomics has focused on X-ray crystallography, but NMR spectroscopy also shows considerable potential.[2,3] Conventionally, NMR spectroscopic structure determination consists of a time-consuming, mainly manually performed resonance-assignment phase followed by a phase in which the 3D structure is determined.[3] Herein we describe an automated approach where the assignment and the determination of backbone structures of medium accuracy is performed simultaneously using chemical shifts and residual dipolar couplings (RDCs). The new software, called Itas (ITerative Assignment and Structure), is applicable to proteins of up to around 125 amino acid residues and offers the opportunity to greatly accelerate NMR structure determination.

Rapid fold determination starts from a list of unassigned chemical shifts and RDCs that are grouped according to their common $^{1}H^{N}$,^{15}N chemical shifts (see Supporting Information). In the first step, assignment of backbone resonances is automatically performed by Itas using only chemical shift information and with algorithms developed from previous methods.[4] No information about the tertiary structure is available at this point. The degree of assignment that is obtained depends on the size and complexity of the protein and on the type and quality of NMR spectra available (Table 1). RDCs and chemical shifts, which were assigned, are used subsequently for a molecular-fragment search. Molecular fragments are selected from a nonredundant database of protein crystal structures of a resolution of 2 Å or better. The selection is performed on the basis of multiple sequence alignment and the fit between measured RDCs and chemical shifts and those back-calculated from the structure of each data base fragment.[5,6] Then a compact structure is assembled from these fragments using the structure-calculation program RosettaNmr.[6] 1000 low-resolution structural models are generated and are ranked according to agreement with experimental RDCs and energetically favorable nonlocal interactions which include hydrophobic burial, pairing of β-strands, and overall compactness. The 20 lowest-energy structures are used by Itas in a second iteration step to enhance the assignment of the backbone resonance signals. This time assignment no longer relies only on chemical shifts, but can be improved by comparison of experimental RDCs with values back-calculated from the low-resolution structural models. To take into account variations in the RosettaNMR structural models, assignment is performed on all 20 structures and only assignments that are consistent across all 20 structures are selected (see Supporting Information). The resulting increased number of assignments makes a larger number of chemical shifts and RDCs available for a second

Table 1: Simultaneous assignment and structure determination for proteins varying in topological complexity and size.

Protein (PDB code)	Length	Chemical shifts[a]	Assignment [%] (No. of errors)[c]		RDC type[d]	No. of RDCs	Residue range[e]	Backbone rmsd [Å][f]	
			Start	Final				Itas	Full
interleukin 1β[g] (2I1B)	153	C^{α}/C^{β}	60 (0)	98 (2)	1,2,3,4	553	2–140	2.1	1.9
calmodulin (1J7O)	148	C^{α}/C^{β}	49 (0)	99 (0)	1,2,3	396	5–75	2.0	2.3
calmodulin (1J7P)[h]							82–146	1.4	2.4
profilin[g] (1ACF)	125	C^{α}/C^{β}	82 (0)	98 (2)	1,2,3	341	2–125	1.5	1.3
KH domain (1KHM)	89	C^{α}	8 (0)	98 (3)	1,2,3	153	12–84	1.8	1.6
DinI (1GHH)	81	C^{α}	38 (0)	97 (1)	1,2,3,4	271	2–80	5.1	5.4
Ubiquitin (1UBI)	76	C^{α}	22 (0)	96 (2)	1,2,4	185	2–72	2.0	1.4
Z domain[g] (2SPZ)	71	C^{α}/C^{β}[b]	77 (0)	99 (2)	1,2,3	192	15–70	3.6	2.4
		C^{α}	15 (0)	78 (6)	1,2,3	174	15–70	5.0	2.4
protein G[i] (1PGB)	56	C^{α}	2 (0)	95 (0)	1,2,3	145	2–55	0.7	1.9

[a] Chemical shift used to establish sequential connectivity. Connectivity thresholds were 0.3 ppm for C^{α} and 0.5/0.5 ppm for C^{α}/C^{β}. [b] Connectivity thresholds were 0.3 ppm for C^{α} and 0.5 ppm for C^{β}. [c] Assignment scores were determined according to previously established methods.[4] Start: without RDCs; Final: at the end of Itas. [d] $^{1}D_{NH}$, $^{1}D_{C^{\alpha}C'}$, $^{1}D_{C^{\alpha}H^{\alpha}}$, $^{1}D_{NC'}$ are indicated by 1, 2, 3, 4, respectively. [e] Structured backbone (heavy atoms) of proteins used for rmsd calculations. [f] For the lowest energy structure relative to the native structure. "Full" indicate structures obtained from published assignments. [g] RDCs simulated using shape prediction.[9] [h] RDCs simulated for residues 77–81. [i] Alignment tensor after first assignment run was obtained by shape prediction.[9]

[*] Y.-S. Jung, M. Sharma, Dr. M. Zweckstetter
NMR Based Structural Biology
Max Planck Institute for Biophysical Chemistry
Am Fassberg 11, 37077 Göttingen (Germany)
Fax: (+49) 551-201-2202
E-mail: mzwecks@gwdg.de

[**] We thank Gaetano Montelione for the peak lists of the Z domain and Christian Griesinger for useful discussions. M.Z. is the recipient of a DFG Emmy Noether-Fellowship (ZW 71/1-3).

Supporting information for this article is available on the WWW under http://www.angewandte.org or from the author.

 DOI: 10.1002/anie.200353588 © 2004 Wiley-VCH Verlag GmbH & Co. KGaA, Weinheim

round of molecular-fragment selection and structure assembly. This iterative procedure of assignment and structure calculation is continued until the number of backbone assignments converges and a medium-resolution 3D structure of the protein is obtained. Typically four to eight iterations are required. Structural models obtained with the largest number of assigned residues are finally subjected to a short energy minimization.

Itas has been applied to eight proteins varying in length from 56 to 153 residues and covering different topologies (Table 1). At the start of Itas, using $^{13}C^{\alpha}$ chemical shifts with a tolerance of 0.3 ppm for establishing sequential connectivity, 8% of the C-terminal KH domain of heterogeneous nuclear ribonucleoprotein could be assigned. Thus, only 14 RDCs were available for the first structure calculation and the root-mean-square-deviation (rmsd) between the high-resolution NMR structure and the 20 best-scoring structural models is on average around 14.5 Å (with a minimum value of 9.3 Å). Despite the large deviation from the native structure these initial models are already useful for improving the backbone assignment. Comparison of $^{1}D_{N,H}$, $^{1}D_{C^{\alpha},C'}$ and $^{1}D_{C^{\alpha},H^{\alpha}}$ couplings that are back-calculated from these structural models with experimental values increases the assignment score to 66% (Figure 1). This big improvement is possible, as substructures of the 14.5 Å RosettaNmr models (especially secondary structure elements and partly their relative orientation) already agree well with the native structure.

For all the tested proteins the number of assigned signals significantly improves during Itas because of the continually improving structural model. On average more than 96% of residues were assigned correctly at the end of Itas. Thus, a large number of chemical shifts and RDCs were available for structure calculation. In case of KH domain, a total of 153 RDCs could be used for structure generation and the lowest-energy structure deviates by 1.8 Å from the high-resolution NMR structure (Table 1). Using all 157 experimental RDCs according to the published assignment results in a deviation of 1.6 Å. This demonstrates that the three wrong and two missing assignments, present at the end of the Itas procedure, do not significantly deteriorate the quality of the backbone structure. Similar results are obtained for seven other proteins including the 153-residue protein interleukin 1β (Figure 2 and Table 1).

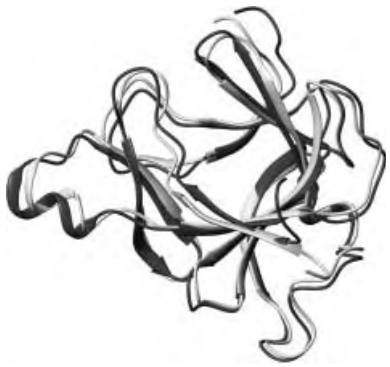


Figure 2. Comparison of the Itas structure (light gray), determined automatically without prior assignment, and the 2.0-Å X-ray crystal structure of interleukin 1β (dark gray) (PDB code: 2I1B).

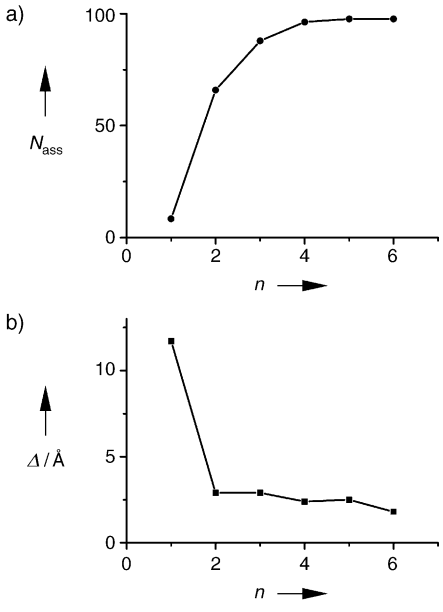


Figure 1. a) Increase in the percentage of assigned residues, N_{ass}, of the KH domain during Itas. b) Decrease in the backbone root-mean-square-deviation, Δ between the Itas fold (average of five lowest energy structures) and the high-resolution NMR spectroscopy structure of the native protein (PDB code: 1 KHM). The value *n* is the iteration number.

For KH domain chemical shifts and RDCs were taken from the BMRB (Bio Mag Res Bank) database.[7] To put Itas to a more rigorous test, we started from raw peak lists obtained from the automatic peak picking of NMR spectra recorded for the Z domain of Staphylococcal protein A.[8]. With Itas, using only C^{α} chemical shift values to determine the sequential connectivity (cutoff of 0.3 ppm) and three types of RDCs from different internuclear vector types, the signal assignment increased from 15 to 78% and the final Itas structure differs by 5.0 Å from the native structure. Using all 201 RDCs that were observed for the 71 residues of Z domain (corresponding to 100% assignment) RosettaNmr generates a structure that differs by 2.4 Å from the native one. The lower quality of the Itas structure is expected in this case, as the iterative procedure converged at a final assignment score of 78% and a significant lower number of RDCs was available for structure calculation. The six wrongly assigned residues, however, do not cause any problem as correcting the wrong assignments (thereby giving a total of 51 correct assignments) does not change the quality of the structure (data not shown). This robustness against a small number of wrong assignments is achieved by selecting 25% of fragments, which are subsequently used for assembly of the ternary structure in RosettaNmr, without chemical shifts and RDCs, that is, these fragments are selected solely on the basis of

 © 2004 Wiley-VCH Verlag GmbH & Co. KGaA, Weinheim

agreement with multiple sequence alignment and sequence-based predicted secondary structure. Finally, the Itas structure of the Z domain fold could be improved to 3.6 Å when both C^{α} and C^{β} connectivity information was employed. Only two assignment errors remain, the assignments of L58 and N65 are interchanged (both are located in helix 3 and do not have experimental C^{α} or C^{β} chemical shifts).

For some proteins, backbone structures deviating by less than 2–3 Å from the native structure can be obtained with Itas. For other proteins, such as the RecA-binding protein DinI, the deviation amounts to 5–6 Å, even when assignments were determined manually prior to structure calculation (Table 1; rmsd values labeled as "Full"). Additional information is clearly needed to determine the high-resolution structure of these proteins. Wrong folds, however, are not generated by Itas. Itas folds are only identified as reliable when more than 95% of backbone resonance signals have been assigned at the end of the procedure. Structure determination is strongly governed by experimental RDCs, the statistical energy terms employed by Rosetta play a less important role. Moreover, in cases where the quality and amount of experimental data are not sufficient, the 20 lowest energy structures, which are energy minimized at the end of Itas, will not show the same global fold. The deviation from the native fold can further be assessed by cross-validation using H^N–H^N NOEs not used during Itas (Supporting Information).

A low resolution of an Itas fold can be indicated when experimental RDCs (measured in nearly neutral bicelles and assigned during Itas), are compared with values predicted from the three-dimensional shape of the Itas structure.[9] Although, flexible loops can have a strong influence on the protein shape, a low correlation R_S between experimental and shape-predicted RDCs for small, compact proteins, points to structural errors. For example, in the native structure of DinI residues 75 to 78 form a small α-helix that is in contact with residue L21. In the 5.1-Å Itas fold the orientation of this helix is inverted and points towards S11. This error causes a R_S value of 0.55 compared to 0.84 for the 0.7-Å fold of protein G. Note, however, that a high R_S value does not rule out a low-resolution fold.

Herein we demonstrate that protein folds can be achieved rapidly and without manual intervention starting from unassigned backbone chemical shifts and RDCs. Previously, it was shown that protein folds can be determined solely using RDCs. This, however, required completion of the time-consuming backbone resonance assignment.[5,10] A first step in overcoming the requirement for assignment was recently proposed for the 54-residue protein rubredoxin: a large set of RDCs measured in two liquid-crystalline media are used for both geometric information and as a filter in the assembly of residues in a sequential manner.[11] Itas goes significantly further, allowing automatic fold determination of proteins up to approximately 125 residues with less-complete data. In addition, by removing the need for C^{β} connectivity information, Itas is applicable to small to medium-sized proteins that are not enriched above the natural abundance of ^{13}C. Medium-resolution models generated by Itas can often provide clues about biochemical function.[12] Moreover, they can serve as valuable starting points for determining high-resolution 3D structures when additional NOEs are available.

Received: December 19, 2003
Revised: February 16, 2004 [Z53588]

Keywords: automated techniques · genomics · NMR spectroscopy · protein structures

[1] a) International Human Genome Sequencing Consortium, *Nature* **2001**, *409*, 860; b) J. C. Venter et al. , *Science* **2001**, *291*, 1304.
[2] a) A. Abbott, *Nature* **2000**, *408*, 130; b) G. T. Montelione, D. Y. Zheng, Y. P. J. Huang, K. C. Gunsalus, T. Szyperski, *Nat. Struct. Biol.* **2000**, *7*, 982.
[3] K. Wüthrich, *Angew. Chem.* **2003**, *115*, 3462; *Angew. Chem. Int. Ed.* **2003**, *42*, 3340.
[4] Y. S. Jung, M. Zweckstetter, *J. Biomol. NMR*, in press.
[5] a) G. Cornilescu, F. Delaglio, A. Bax, *J. Biomol. NMR* **1999**, *13*, 289; b) F. Delaglio, G. Kontaxis, A. Bax, *J. Am. Chem. Soc.* **2000**, *122*, 2142.
[6] a) C. A. Rohl, D. Baker, *J. Am. Chem. Soc.* **2002**, *124*, 2723; b) K. T. Simons, C. Kooperberg, E. Huang, D. Baker, *J. Mol. Biol.* **1997**, *268*, 209.
[7] J. F. Doreleijers, S. Mading, D. Maziuk, K. Sojourner, L. Yin, J. Zhu, J. L. Markley, E. L. Ulrich, *J. Biomol. NMR* **2003**, *26*, 139.
[8] D. E. Zimmerman, C. A. Kulikowski, Y. P. Huang, W. Q. Feng, M. Tashiro, S. Shimotakahara, C. Y. Chien, R. Powers, G. T. Montelione, *J. Mol. Biol.* **1997**, *269*, 592.
[9] M. Zweckstetter, A. Bax, *J. Am. Chem. Soc.* **2000**, *122*, 3791.
[10] J. C. Hus, D. Marion, M. Blackledge, *J. Am. Chem. Soc.* **2001**, *123*, 1541.
[11] F. Tian, H. Valafar, J. H. Prestegard, *J. Am. Chem. Soc.* **2001**, *123*, 11791.
[12] a) M. J. Berardi, C. H. Sun, M. Zehr, F. Abildgaard, J. Peng, N. A. Speck, J. H. Bushweller, *Struct. Folding Des.* **1999**, *7*, 1247; b) K. T. Simons, C. Strauss, D. Baker, *J. Mol. Biol.* **2001**, *306*, 1191.

 © 2004 Wiley-VCH Verlag GmbH & Co. KGaA, Weinheim

Scanning Probe Techniques

Label-Free Electrochemical Recognition of DNA Hybridization by Means of Modulation of the Feedback Current in SECM**

*Florin Turcu, Albert Schulte, Gerhard Hartwich, and Wolfgang Schuhmann**

Carrying systematically ordered libraries of gene-specific nucleic acid recognition entities on solid supports, DNA microarrays ("DNA chips") are microanalytical tools for studying the activity of a variety of genes at a time. Such DNA microarrays are thus valuable for rapid gene-expression profiling, sequence mapping, and genotyping of mutations and polymorphisms or pharmacogenomics.[1] Hybridization of immobilized, single-stranded DNA capture probes with complementary DNA fragments in solution (targets) has to be efficiently transformed into a detectable analytical signal for reliable application of DNA microarrays. Electrochemical (EC) detection schemes[2] were explored and considered cost-effective alternatives to well-established fluorescence-based optical read-outs of hybridization as they offer a high sensitivity in combination with simplicity of instrumentation and compatibility with microfabrication technology. In general, EC detection schemes take advantage of inherent electrochemical properties of single stranded (ss) and double stranded (ds) DNA and/or electrochemically active hybridization indicators, intercalating compounds, and redox labels.[3]

Herein, we report an electrostatic approach for visualizing the status of surface-bound DNA probes. Detection of complementary DNA hybridization is simply achieved through coulomb interactions between a negatively charged, free-diffusing redox mediator and the phosphate groups in the backbone of the immobilized DNA strands. Electrostatic repulsion between the two ionic species is capable of modulating the transfer of mediator molecules towards the electrode surface at DNA-modified regions. A corresponding local modulation of current was used to establish a simple and sensitive assay for truly label-free electrochemical imaging of single-stranded capture probes and their aggregates with complementary targets.

[*] Dipl.-Chem. F. Turcu, Dr. A. Schulte, Prof. Dr. W. Schuhmann
Analytische Chemie—Elektroanalytik & Sensorik
Ruhr-Universität Bochum
44780 Bochum (Germany)
Fax: (+49) 234-321-4683
E-mail: wolfgang.schuhmann@rub.de
Dr. G. Hartwich
FRIZ Biochem
Staffelseestrasse 6, 81477 Munich (Germany)

[**] The authors would like to thank Dr. Thomas Kratzmüller, FRIZ Biochem, Munich (Germany) for spotting the samples and comparative fluorescence measurements as well as Dr. Herbert Wieder, FRIZ Biochem, Munich (Germany) for helpful discussion. We are grateful to the DFG for financially supporting this work (DFG Schu929/6-1). SECM = scanning electrochemical microscopy.

A DNA microarray is a sample with considerable local variations in surface redox activity, in particular when anionic electroactive species are used. For imaging these regions and for verifying the above-mentioned concept of electrostatic detection of hybridization, scanning electrochemical microscopy (SECM)[4] was the method of choice. SECM has an exceptional capability to visualize microscopically small local variations in (electro)chemical reactivity with high spatial resolution. Furthermore, SECM has demonstrated a high level of performance for studying immobilized biomolecules and biological processes at solid–liquid interfaces.[5] High-precision positioning devices are used in SECM to position a disk-shaped voltammetric ultramicroelectrode (the SECM tip) within the regime of electrochemical feedback, typically at working distances of only a few electrode radii. In the simplest mode of operation, the SECM tip is scanned in constant height above the sample, while simultaneously monitoring the tip current (I) as a function of x/y tip position. The dependence of the microelectrode response on the tip-to-sample distance (d) and on the nature of the substrate allow revealing spatially resolved information about chemical properties and the morphology of the surface.

Figure 1 shows the suggested repelling mode of SECM as used to recognize the presence, and to characterize the status

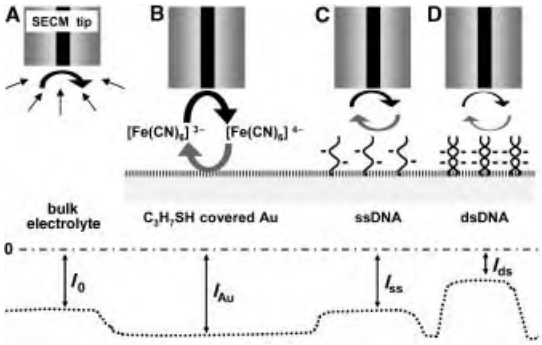


Figure 1. Schematic representation of repelling-mode SECM. A) A diffusion-limited steady-state reduction current is observed in $[Fe(CN)_6]^{3-}$-containing solutions with the tip kept at 0 mV (vs. Ag/AgCl/3 M KCl). B) Recycling of tip-generated $[Fe(CN)_6]^{4-}$ to $[Fe(CN)_6]^{3-}$ occurs with the SECM tip close to a propane thiol-modified Au surface causing an increase in tip current because of positive feedback redox cycling. C) Above a DNA spot, tip-generated $[Fe(CN)_6]^{4-}$ ions experience charge interactions with the oligonucleotide backbone causing a hindered diffusion of the mediator to the Au surface and hence a modulation of the mass-transfer rate which provokes a drop in tip current. D) Hybridization increases the density of anionic phosphate groups leading to a further drop in tip current owing to enhanced repulsion of the redox mediator molecules.

(ss/ds) of immobilized DNA. The SECM tip is kept at sufficient constant cathodic potentials to reduce $[Fe(CN)_6]^{3-}$ under diffusion control. Far above the sample surface, the amperometric tip current is controlled by the diffusion of $[Fe(CN)_6]^{3-}$ molecules towards the tip, which leads to a steady-state current (I_0, Figure 1 A). However, after approach of the SECM tip to nearfield distance to a conducting surface (propane thiol-modified Au), consumed mediator molecules can be reconverted into their initial oxidation state (electro-

 © 2004 Wiley-VCH Verlag GmbH & Co. KGaA, Weinheim DOI: 10.1002/anie.200454228

chemical recycling, positive feedback)[4] in turn leading to a distance-dependent increase in the tip current ($I_{Au} > I_0$, Figure 1B). Above a DNA spot, the anionic phosphate groups repel the tip-generated $[Fe(CN)_6]^{4-}$ molecules. This process hinders their diffusion towards the Au electrode, reduces the rate of recycling and leads to a local drop in the observed cathodic tip current ($I_{ss} < I_{Au}$, Figure 1C). The hybridization of the immobilized capture-probe strands with complementary single strands and the resulting formation of double helices multiplies the number of negative charges on the surface, which leads to a further drop in tip current ($I_{ds} < I_{ss}$, Figure 1D).

SECM measurements were performed on 150-μm diameter spots of bifunctionalized 20-base synthetic oligodeoxynucleotides using a 10-μm diameter Pt microdisk electrode as the SECM tip. The 3′ thiol-modified DNA strands with a fluorescent label attached to the 5′ end were immobilized on gold-covered glass slides through standard thiol-monolayer assisted molecular self-assembly. To avoid critical nonspecific adsorption and to increase hybridization efficiency, surfaces were treated with propane thiol after spotting with oligonucleotides. In the electrochemical cell of the SECM, DNA-modified slides were covered with an electrolyte containing 5 mM $K_3[Fe(CN)_6]$ in 3 M NaCl/0.1 M phosphate buffer (1:1 KH_2PO_4/K_2HPO_4; pH 5.7). Far away from the chip surface and operated amperometrically at a potential of 0 mV versus Ag/AgCl/3 M KCl, the Pt microelectrode typically displayed a steady-state reduction current (I_0) of about −6 nA owing to the diffusion-controlled reduction of Fe^{3+} centers to Fe^{2+} centers. Before imaging capture-probe spots, tip approach curves (I as a function of d) were recorded in the neighborhood of the spots and used to determine the vertical expansion of positive feedback and hence the chip-to-tip distance. Based on this information and theoretically derived approach curves,[6] the microelectrode tip could be positioned reproducibly and scanned across the sample at a user-defined spacing. Line scans (I as a function of traveled distance in the x direction) were acquired for the spatially resolved analysis of the DNA-modified surface.

In Figure 2, curve 1 displays a representative amperometric recording taken during a complete line scan over an individual oligonucleotide spot. The current values to the left and right of the spot are indicative for the unbiased positive feedback from the propane thiol modified gold surface. In agreement with the model, drastically lowered current values in the central part (above the DNA spot) signify reduced rates of redox recycling owing to electrostatically hindered diffusion. Note that there was almost no drop in the tip current when the negatively charged mediator was substituted by a positively charged mediator. With $[Ru(NH_3)_6]^{3+}$, only a negligible decrease in current occurs (Figure 2, curve 2) which is probably caused by the purely steric influence of the surface-bound capture probes on the mass-transfer rate. This effect is proof that when measuring in the presence of a negatively charged mediator an electrostatic repellent force really is responsible for a DNA-induced modulation of the tip current.

High-quality, 3D SECM images (I vs. x/y) of DNA spots were constructed from multiple line scans (Figure 3). The

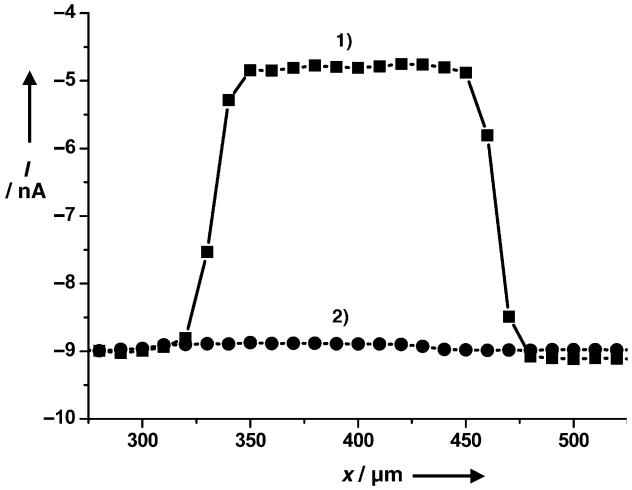


Figure 2. Line scans acquired by scanning the tip of a 10-μm-diameter Pt microelectrode at a fixed height of 10 μm across a spot of the single-stranded capture oligonucleotide. 1) $[Fe(CN)_6]^{3-}$ ions (5 mM in 3 M NaCl/0.1 M phosphate buffer (1:1 KH_2PO_4/K_2HPO_4) at pH 5.7) were used as the mediator with the SECM tip being polarized to 0 mV (vs. Ag/AgCl/3 M KCl). 2) $[Ru(NH_3)_6]^{3+}$ ions (5 mM in 3 M NaCl/0.1 M phosphate buffer; pH 5.7) were used as mediator with the SECM tip being polarized to −400 mV (vs. Ag/AgCl/3 M KCl).

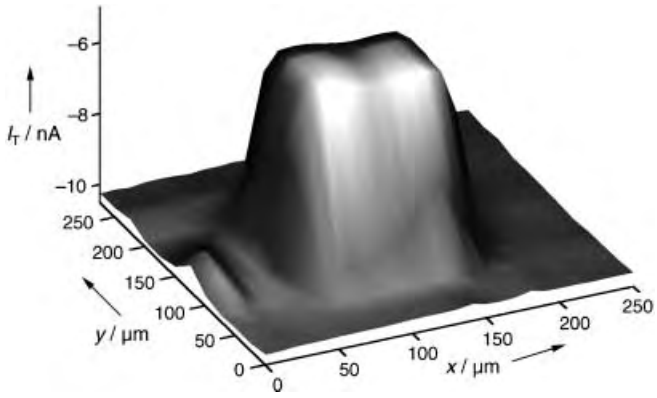


Figure 3. Three-dimensional SECM image of an individual spot of a single stranded 20-base oligonucleotide as obtained by means of repelling-mode SECM. Solution: 5 mM $[Fe(CN)_6]^{3-}$ in 3 M NaCl/0.1 M phosphate buffer (pH 5.7); tip potential: 0 mV (vs. Ag/AgCl/3 M KCl).

images demonstrate the potential of the repelling mode of SECM for imaging immobilized nucleic acids. Such images can be used for controlling the quality of the spotting process and the homogeneity of the lateral surface concentration of the DNA capture probes within the spot. To test the suitability of the approach as a hybridization assay, spots of ssDNA were subjected to hybridization experiments before SECM imaging. One of two neighboring spots was exposed to a diluted solution of the complementary target DNA while the other (control) was covered with target-free "hybridization solution". Upon completion of hybridization,[7] slides were rinsed and the two spots were examined by means of repelling-mode SECM.

Figure 4 illustrates the result obtained, and that hybridization could be clearly detected as a visible difference

 © 2004 Wiley-VCH Verlag GmbH & Co. KGaA, Weinheim

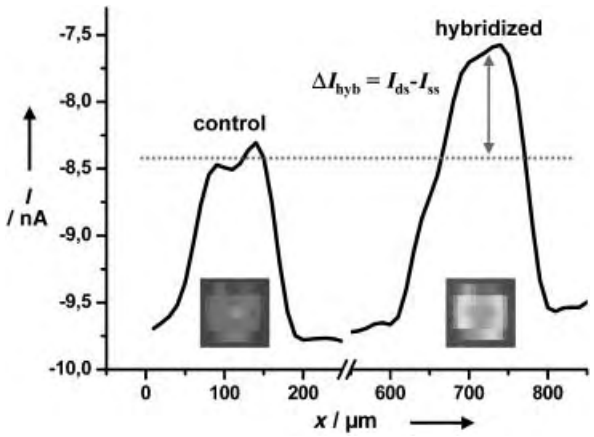


Figure 4. Detection of hybridization through electrostatic repulsion and visualization of DNA duplex formation by means of repelling-mode SECM. A selected spot of a 20-base oligonucleotide was exposed to the hybridization buffer (1 M NaCl/0.1 M phosphate buffer; pH 6.3) containing 2 µM of the complementary oligonucleotide target. A neighboring spot was subjected to target-free hybridization buffer (control). After completion of hybridization (about 2 h) and thorough rinsing with 3 M NaCl/0.1 M phosphate buffer (pH 5.7), SECM line scans were measured by operating the tip of a 10-µm-diameter Pt microelectrode (0 mV vs. Ag/AgCl/3 M KCl) in solutions of 5 mM $[Fe(CN)_6]^{3-}$ in 3 M NaCl/0.1 M phosphate buffer; pH 5.7).

between the response of the SECM tip above the control and hybridized spot. Consistent with our hypothesis, the cathodic tip current was found to be much lower at the hybridized spot since here duplex formation took place concomitantly increasing the number of repellent charges.

The detection scheme described herein was performed by taking local electrochemical measurements in a sophisticated SECM set-up that clearly is not suitable for common use in medical diagnostics. However, in principle, it should be possible to design a simplified electrochemical device that could be produced using microfabrication technology. Such a device could, for example, consist of an array of immobilized DNA capture probes in a base plate and an array of individually addressable Pt microelectrodes in a cover plate. Using specially designed spacer and alignment elements, the microelectrodes and DNA spots could be arranged on top of each other and kept at the proper working distance. The difference in the response of an individual Pt microelectrode before and after exposure to a sample would evaluate the hybridization status of the DNA capture probes in the corresponding region.

In summary, we confirmed that simple coulomb interactions between immobilized DNA and ferricyanide effectively modulates the diffusion transport properties of the dissolved mediator to the gold surface. This property has a strong impact on local amperometric feedback currents and allows the imaging of DNA-modified surface spots by SECM. The increase in the density of negative charge as a result of duplex formation made electrostatic repulsion a sensitive assay for truly label-free electrochemical recognition and visualization of hybridization. For optimization and quantification, we are currently studying the influence of a number of parameters (i.e. surface density and lengths of the DNA capture probes, length of targets, temperature, ionic strength, and pH value of the scanning solution) on the performance of the method.

Experimental Section

Spotted DNA microarrays, oligonucleotides probes, and targets were supplied by FRIZ Biochem, Munich. Probes were 3′ thiol modified 20-mer oligonucleotides ([Fluo-HN-C_{12}]-TGC GGA TAA CAC AGT-CAC CT-[C_3-S-S-C_3-OH]) while as target an unmodified oligonucleotide with the complementary sequence (ACG CCT ATT GTG T-CA GTG GA) was used. Spotting of the probe was on Au-sputtered glass slides using a microarrayer (Cartesian Technologies) equipped with a printhead (ChipMaker) and microspotting pins (120 µm diameter; Telechem International). The capture probes were arrayed in spots of 150-µm diameter in two rows with a fine scratch dividing a control area from a hybridization area. An O-ring defined the area subjected to SECM measurements.

Solutions required for the experiments were prepared with tridistilled water. KH_2PO_4, $K_2HPO_4 \cdot 3H_2O$, NaCl, $K_3[Fe(CN)_6]$, and $[Ru(NH_3)_6]Cl_3$ were purchased from Sigma. SDS (Sodium dodecylsulphate) was from Merck.

Conventional, glass-insulated Pt disk microelectrodes (∅ 10 µm, RG values 10–20) were used as SECM tips. They were polished with alumina paste (particle sizes: 3, 1, and 0.3 µm) on a soft polishing cloth and tested by cyclic voltammetry in 5 mM ferricyanide solutions. SECM experiments were performed with a home-built SECM in a one-compartment cell and with a two-electrode configuration (the SECM tip and a miniaturized Ag/AgCl 3 M KCl reference electrode). The set-up was located in a Faraday cage and a low-noise amplifier (VA10, npi electronic) was applied for the electrochemical measurements. The electrochemical cell with the sample fixed to the bottom was mounted on a two-axis translation stage driven by computer-controlled stepper motors (Owis), which allowed sample movements in the *x*, *y* direction with a nominal resolution of 0.625 µm per half step. Tip approach (*z* movement) was achieved with a third stepper motor that was mounted perpendicular to the ones moving the cell. A PC in combination with Windows software programmed in Microsoft Visual Basic 3.0 (Microsoft) was used for the control of all system parameters and for data acquisition (16 bit AD/DA card; Plug-In).

Tip approach curve measurements (z scans) helped to position the SECM tip within the nearfield of electrochemical feedback. The working distance was chosen to a value corresponding to an increase in the amperometric tip current of 50 % of the value measured in bulk solution and typically was about 10 µm. SECM imaging was achieved by moving the DNA chip at fixed tip-to-sample separation in *x*, *y* direction while simultaneously monitoring the tip current as a function of position.

Received: March 10, 2004 [Z54228]
Published Online: June 8, 2004

Keywords: DNA recognition · electrostatic interactions · scanning probe techniques · SECM · surface analysis

[1] a) R. C. McGlennen, *Clin. Chem.* **2001**, *47*, 393–402; b) S. A. Greenberg, *Neurology* **2001**, *57*, 755- 761; c) J. G. Hacia, S. C. Collins, *J. Med. Genet.* **1999**, *36*, 730–736; d) D. Gerhold, T. Rushmore, C. T. Caskey, *Trends Biochem. Sci.* **1999**, *24*, 168–173; e) M. Schena, D. Shalon, R. W. Davis, P. O. Brown, *Science* **1995**, *270*, 467–470.

[2] a) T. G. Drummond, M. G. Hill, J. K. Barton, *Nat. Biotechnol.* **2003**, *10*, 1192–1199; b) E. Palecek, F. Jelen, *Crit. Rev. Anal. Chem.* **2002**, *33*, 261–270; c) J. J. Gooding, *Electroanalysis* **2002**, *13*, 1149–1156.

 © 2004 Wiley-VCH Verlag GmbH & Co. KGaA, Weinheim

[3] a) G. Hartwich, D. J. Caruana, T. de Lumley-Woodyear, Y. B. Wu, C. N. Campbell, A. Heller, *J. Am. Chem. Soc.* **1999**, *121*, 10803 – 10812; b) R. E. Holmlin, P. J. Dandliker, J. K. Barton, *Angew. Chem.* **1997**, *109*, 2830 – 2848; *Angew. Chem. Int. Ed. Engl.* **1997**, *36*, 2714 – 2730; c) S. O. Kelly, N. M. Jackson, M. G. Hill, J. K. Barton, *Angew. Chem.* **1999**, *111*, 991 – 996; *Angew. Chem. Int. Ed.* **1999**, *38*, 941 – 945; d) K. M. Millan, S. R. Mikkelsen, *Anal. Chem.* **1993**, *65*, 2317 – 2323; e) J. Wang, G. Rivas, C. Parrado, X. H. Chai, M. N. Flair, *Talanta* **1997**, *40*, 2003 – 2010; f) M. Minunni, S. Tombelli, E. Mariotti, M. Mascini, *Fresenius J. Anal. Chem.* **2001**, *369*, 589 – 593; g) A. Erdem, K. Kerman, B. Meric, M. Ozsoz, *Electroanalysis* **2001**, *12*, 219 – 223; h) P. M. Armistead, H. H. Thorp, *Anal. Chem.* **2000**, *72*, 3764 – 3777; i) S. O. Kelly, E. M. Boon, J. K. Barton, N. M. Jackson, M. G. Hill, *Nucleic Acids Res.* **1999**, *27*, 4830 – 4837; j) D. J. Caruana, A. Heller, *J. Am. Chem. Soc.* **1999**, *121*, 769 – 774; k) J. Wang, A.-N. Kawde, *Anal. Chim. Acta* **2001**, *431*, 219 – 224; l) M. Gheorghe, A. Guiseppi-Elie, *Biosens. Bioelectron.* **2003**, *18*, 95 – 102; m) J. J. Gooding, A. Chou, F. J. Mearns, E. Wong, K. L. Jericho, *Chem. Commun.* **2003**, *15*, 1938 – 1939.

[4] a) A. J. Bard, F.-R. F. Fan, J. Kwak, O. Lev, *Anal. Chem.* **1989**, *61*, 132 – 138; b) A. J. Bard, F.-R. F. Fan, D. T. Pierce, P. R. Unwin, D. O. Wipf, F. Zhou, *Science* **1991**, *254*, 68 – 74; c) M. V. Mirkin, *Mikrochim. Acta* **1999**, *130*, 127 – 153; d) A. L. Barker, M. Gonsalves, J. V. Macpherson, C. J. Slevin, P. R. Unwin, *Anal. Chim. Acta* **1999**, *385*, 223 – 240; e) G. Nagy, L. Nagy, *Fresenius J. Anal. Chem.* **2000**, *366*, 735 – 744.

[5] a) G. Wittstock, W. Schuhmann, *Anal. Chem.* **1997**, *69*, 5059 – 5066; b) S. Gaspar, M. Mosbach, L. Wallman, T. Laurell, E. Csöregi, W. Schuhmann, *Anal. Chem.* **2001**, *73*, 4254 – 4261; c) A. Hengstenberg, A. Blöchl, I. D. Dietzel, W. Schuhmann, *Angew. Chem.* **2001**, *113*, 942 – 946; *Angew. Chem. Int. Ed.* **2001**, *40*, 905 – 908; d) W. B. Nowall, D. O. Wipf, W. G. Kuhr, *Anal. Chem.* **1998**, *70*, 2601 – 2606; e) H. Shiku, T. Matsue, I. Uchida, *Anal. Chem.* **1996**, *68*, 1276 – 1278; f) K. Yamashita, M. Takagi, K. Uchida, H. Kondo, S. Takenaka, *Analyst* **2001**, *126*, 1210 – 1211; g) J. Wang, F. Song, F. Zhou, *Langmuir* **2002**, *18*, 6653 – 6658.

[6] a) J. Kwak, A. J. Bard, *Anal. Chem.* **1989**, *61*, 1221 – 1227; b) A. J. Bard, F.-R. F. Fan, M. V. Mirkin in *Electroanalytical Chemistry*, (Ed.: A. J. Bard), Marcel Dekker, New York, **1994**, pp. 243 – 373.

[7] Efficiency of hybridization for the given experimental conditions (temperature, buffer composition, concentration of target, time of exposure) was confirmed by comparative fluorescence measurements (not shown).

 © 2004 Wiley-VCH Verlag GmbH & Co. KGaA, Weinheim

Polyoxometalates

Structural Control on the Nanomolecular Scale: Self-Assembly of the Polyoxotungstate Wheel $[\{\beta\text{-}Ti_2SiW_{10}O_{39}\}_4]^{24-}$**

*Firasat Hussain, Bassem S. Bassil, Li-Hua Bi, Markus Reicke, and Ulrich Kortz**

Polyoxometalates are metal–oxygen clusters with an enormous structural variety combined with very interesting properties.[1–6] This class of inorganic compounds has been known for a long time, but the rate of discovery of novel species is currently faster than ever before.[7,8] Nevertheless, the mechanism of formation of polyoxoanions is not well understood and commonly described as self-assembly. The search for novel polyanions is predominantly driven by the catalytic properties of many transition-metal substituted polyoxotungstate salts.[9] The catalytic activity (e.g. activation of O_2 and H_2O_2) combined with high thermal stability have led to industrial applications of these species, mostly as heterogeneous catalysts in the oxidation of organic substrates (e.g. Wacker process).[3–6]

The redox-activity of titanium in the oxidation state +4 has led to numerous catalytic studies using TiO_2 as a photocatalyst.[10] To date only a few titanium(IV)-substituted polyoxoanions have been synthesized and most of them are of the Keggin-type. Structural characterization in the solid state indicates a strong tendency towards dimer formation via Ti–O–Ti bonds as seen in $[(\alpha\text{-}Ti_3PW_9O_{38.5})_2]^{12-}$, $[(x\text{-}Ti_3SiW_9O_{38.5})_2]^{14-}$ ($x = \alpha$, β), $[(\alpha\text{-}Ti_3GeW_9O_{38.5})_2]^{14-}$, and $[(\alpha\text{-}1,2\text{-}Ti_2PW_{10}O_{39})_2]^{10-}$.[11] Nevertheless two monomeric species have also been structurally characterized.[12] Some of the above species have shown interesting catalytic (e.g. photocatalysis) as well as medicinal activity (e.g. antiviral).[13,14]

Recently we have structurally characterized some dimeric and tetrameric titanium-substituted polyoxotungstates based on the Wells–Dawson fragment.[15] Soon afterwards Nomiya et al. reported similar tetrameric species.[16]

Our group has been working extensively on the interaction of the dilacunary tungstosilicate $[\gamma\text{-}SiW_{10}O_{36}]^{8-}$ with low-valent, first-row transition metals.[17] Herein we investigate the system $Ti^{4+}/[\gamma\text{-}SiW_{10}O_{36}]^{8-}$ in some detail.

Interaction of solid $TiO(SO_4)$ with $[\gamma\text{-}SiW_{10}O_{36}]^{8-}$ in the ratio 2:1 in aqueous acidic medium (pH 2) resulted in the novel, tetrameric $[\{\beta\text{-}Ti_2SiW_{10}O_{39}\}_4]^{24-}$ (**1**; Figure 1 and Figure 2). The polyanion **1** is the first cyclic, tetrameric

[*] F. Hussain, B. S. Bassil, Dr. L.-H. Bi, M. Reicke, Prof. U. Kortz
International University Bremen
School of Engineering and Science
P.O. Box 750 561, 28725 Bremen (Germany)
Fax: (+49) 421-200-3229
E-mail: u.kortz@iu-bremen.de

[**] U.K. thanks the International University Bremen for research support. U.K. also highly appreciates that the Florida State University Chemistry Department (USA) allowed him unlimited access to the single-crystal X-ray diffractometer. Figures 1–4 were generated by Diamond Version 2.1e (copyright Crystal Impact GbR).

 DOI: 10.1002/anie.200454203 © 2004 Wiley-VCH Verlag GmbH & Co. KGaA, Weinheim

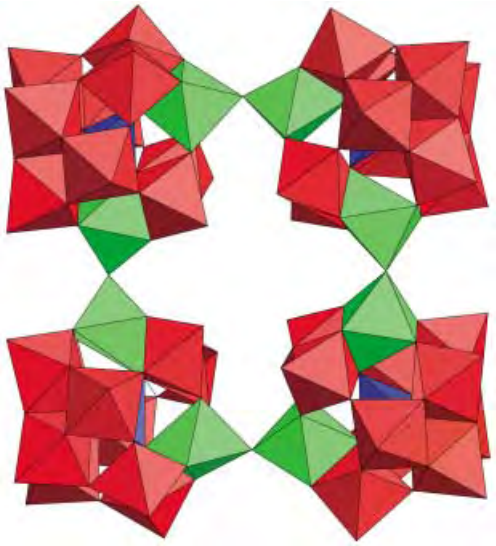


Figure 1. Polyhedral representation of $[\{\beta\text{-}Ti_2SiW_{10}O_{39}\}_4]^{24-}$ (**1**). Red = WO_6, green = TiO_6, and blue = SiO_4.

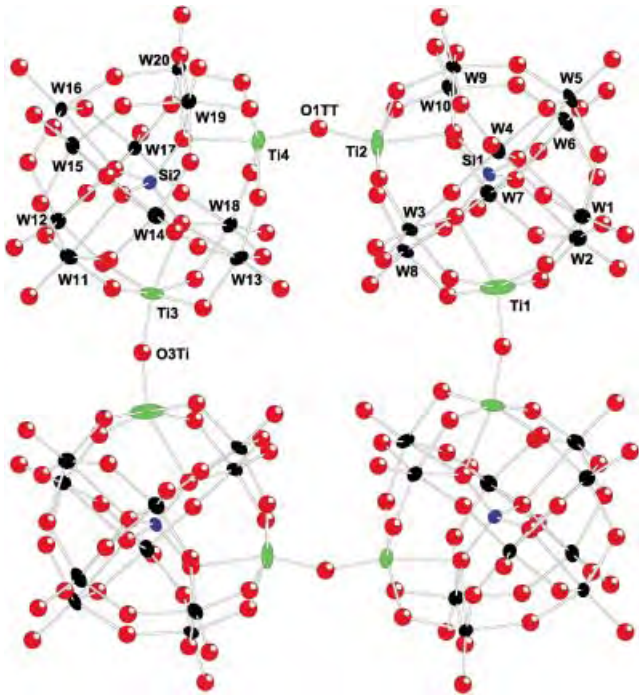


Figure 2. Ball-and-stick representation of **1** (thermal ellipsoids are set at 50% probability). All the heavy atoms of the asymmetric unit are labeled.

polyoxotungstate and it is also the largest titanium-substituted tungstosilicate known to date.[18] Bond valence sum calculations (BVS) indicate that **1** is not protonated and therefore its charge must be −24.[19] This result is fully consistent with elemental analysis, which indicated the presence of 24 potassium ions. Owing to disorder we could identify only 17 potassium counterions by X-ray diffraction.

The central cavity of the wheel-shaped **1** is occupied by a potassium ion (K8) and two additional K^+ ions (K9, K9′) act as "wheel caps" (Figure 3). The central ion K8 (which is disordered over two positions) is seven coordinate (K···O = 2.91–3.25(3) Å), namely by six oxo groups of the tungsten-oxo framework of **1** and one water molecule. The two equivalent,

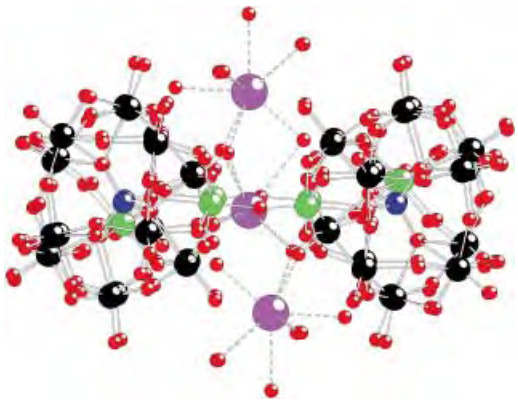


Figure 3. Side-view of **1** including the potassium ions (purple) inside the central cavity (K8) and above and below the cavity (K9, and K9′).

external cations K9 and K9′ are nine coordinate (K···O = 2.66–3.22(3) Å), by seven water molecules and two terminal oxo groups of tungsten atoms. The remaining potassium ions are distributed around **1** being coordinated to bridging and terminal oxo-groups of **1** as well as water molecules of hydration. The bond lengths of the central K8 ion (see above) are somewhat longer than expected, but we discovered that in the presence of Rb^+ and K^+ ions the title polyanion still crystallizes exclusively as a potassium salt. Therefore we believe that potassium ions exhibit a template effect during the formation of **1**. Furthermore, the selective binding of an alkali-earth ion by the macrocyclic polyanion **1** is reminiscent of crown ether properties.

The solid-state structure of $K_{24}[\{\beta\text{-}Ti_2SiW_{10}O_{39}\}_4]\cdot 50\,H_2O$ (K_{24}-**1**) is composed of polyanions **1** that have self-assembled face-by-face along the crystallographic *a* axis, which leads to a nanotube-like arrangement (Figure 4).

Polyanion **1** is composed of four $\{\beta\text{-}Ti_2SiW_{10}O_{39}\}$ Keggin fragments that are linked via Ti–O–Ti bridges leading to a cyclic assembly. Close inspection of **1** indicates that the four Keggin fragments are of the beta-type, which is rare and the first structurally characterized compound containing such a dilacunary tungstosilicate fragment was the dimeric, nickel-substituted polyanion $[\{\beta\text{-}Ni_2SiW_{10}O_{36}(OH)_2(H_2O)\}_2]^{12-}$.[17c] Therefore **1** is only the second example composed of a β-decatungstosilicate Keggin fragment and it represents the first tetrameric derivative.

The two titanium atoms of each beta-Keggin fragment are not located in the same M_3O_{13} triad. In fact they are separated by four bonds (Ti2-O-W3-O-Ti1 or Ti2-O-W8-O-Ti1, see Figure 2) and one of the two Ti atoms is located in the rotated triad (Ti2 and Ti4, see Figure 2). Based on the IUPAC nomenclature the two titanium atoms are located in positions 1 and 10 (the position 10 being in the rotated triad).[4,20] This arrangement does not allow formation of a dimeric product, which is usually favored in titanium-polyoxotungstate chemistry.[11,15] In **1**, each of the four Keggin fragments has a mirror

 © 2004 Wiley-VCH Verlag GmbH & Co. KGaA, Weinheim

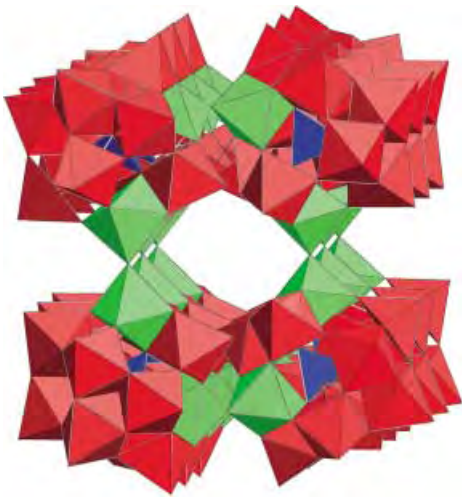


Figure 4. View along the crystallographic *a* axis showing three adjacent wheels of **1** and the resulting tunnel-like cavity. Cations and lattice water molecules are not shown for clarity.

plane and both titanium atoms are located in this plane of symmetry (see Figure 1 and Figure 2). For comparison, the nickel(II) centers in $[\{\beta\text{-}Ni_2SiW_{10}O_{36}(OH)_2(H_2O)\}_2]^{12-}$ are in the 4 and 10 positions.[17c]

The structure of polyanion **1** can be viewed as a larger titanium-derivative of the trimeric, cyclic manganese(II)-substituted tungstosilicate $[(\beta_2\text{-}SiW_{11}MnO_{38}OH)_3]^{15-}$. This product was also synthesized from $[\gamma\text{-}SiW_{10}O_{36}]^{8-}$ and it also contains β-Keggin fragments.[17a] However, the important difference to **1** is that its basic building block is a monosubstituted ($\beta\text{-}SiW_{11}O_{39}$) Keggin-unit and as a result the Keggin–Keggin connectivities are accomplished via Mn–O–W bonds.

Compound **1** is not perfectly cyclic, but somewhat ellipsoidal (see Figure 1 and Figure 2). This shape reflects the inequivalence of the two titanium centers within each Keggin fragment. In **1**, the short axis (distance between O3Ti and O3Ti′, see Figure 2) is 10.8 Å, whereas the long axis is 13.0 Å (distance between O1TT and O1TT′). The reason for this distortion is that **1** contains two pairs of inequivalent Ti-O-Ti bridges: the type which involves two Ti centers in the rotated triad (Ti2-O1TT-Ti4, Ti2′-O1TT′-Ti4′, see Figure 2) and the type which involves two Ti centers that are not in the rotated triad (Ti3-O3Ti-Ti3′, Ti1-O3Ti-Ti1′). The two types of Ti-O-Ti bond angles are only marginally different in the solid state: 152.8(12)° (Ti3-O3Ti-Ti3′) versus 153.9(12)° (Ti2-O1TT-Ti4). All of the above indicates that **1** is best described as a dimer of dimers.

Synthesis of **1** is accomplished by reaction of $TiO(SO_4)$ with $[\gamma\text{-}SiW_{10}O_{36}]^{8-}$, which means that the mechanism of formation of **1** must occur in the following sequence: a) metal insertion, b) rotational isomerization (γ-Keggin→β-Keggin), c) dimerization, and d) ring closure. Most likely, insertion of two Ti^{IV} ions into $[\gamma\text{-}SiW_{10}O_{36}]^{8-}$ leads to the monomeric species $[\gamma\text{-}Ti_2(OH)_2SiW_{10}O_{38}]^{6-}$, which isomerizes to $[\beta(1,10)\text{-}Ti_2(OH)_2SiW_{10}O_{38}]^{6-}$. This species is also unstable and dimerizes to $\{[\beta(1,10)\text{-}Ti_2(OH)SiW_{10}O_{38}]_2(O)\}^{12-}$, which is equivalent to the asymmetric unit of **1**. In most structurally characterized titanium-substituted polyoxometalates the titanium atoms do not contain terminal bonds. Therefore it is not surprising that $\{[\beta(1,10)\text{-}Ti_2(OH)SiW_{10}O_{38}]_2(O)\}^{12-}$ is a highly reactive, dimeric species which reacts with other, identical dimers leading to the formation of **1**. This "dimer-of-dimer mechanism" excludes the possibility of a gradual growth by individual Keggin units and it also implies that a trimeric intermediate is not present during formation of **1**. It is virtually impossible to prove the above hypothesis and the identity of the proposed intermediates experimentally, as formation of **1** occurs by rapid self-assembly as soon as the proper reaction conditions are present.

In the ^{183}W NMR spectrum of **1** (at 16.66 MHz on a 400 MHz JEOL ECX instrument at room temperature using D_2O as a solvent) we identified 10 signals of about equal intensity ($\delta = -111.4$, -118.0, -122.8, -125.7, -141.4, -156.2, -157.8, -170.6, -173.8, -221.0 ppm). The solid-state structure of polyanion **1** indicates C_i point-group symmetry and as a result the asymmetric unit consists of 20 tungsten atoms (see Figure 2). However, it is expected that in solution the apparent symmetry of **1** is C_2. In this case, polyanion **1** contains 10 magnetically inequivalent tungsten groups (W1/W2, W3/W8, W4/W7, W5/W6, W9/W10, W11/W12, W13/W18, W14/W17, W15/W16, W19/W20, and their symmetry equivalents, see Figure 2). Therefore 10 signals of equal intensity are expected for ^{183}W NMR spectrum of **1** in solution. Indeed, the ^{183}W NMR spectrum of redissolved K_{24}-**1** in D_2O shows a 10-line spectrum (see above), but the ^{183}W NMR spectrum of freshly synthesized **1** at very high concentration contains some additional signals of much lower intensity which we cannot assign yet. Nevertheless, any solid which precipitated or crystallized from this solution gave an IR spectrum identical to that of K_{24}-**1**.

In summary, we have synthesized a unique tetrameric and cyclic tungstosilicate assembly using mild, one-pot reaction conditions. Polyanion **1** was fully characterized in solution and in the solid state by several analytical techniques. Formation of **1** indicates that a) very large and cyclic Ti^{IV}-substituted tungstosilicates can be formed, b) it might be possible to construct even larger wheel-shaped polyoxotungstates, c) it might be possible to construct inorganic nanotubes by linking or orientating individual polyoxoanion wheels appropriately, d) the gigantic, mixed-valence polyoxomolybdate wheels have some smaller, fully oxidized polyoxotungstate analogues, e) the structural variety of supra- and supersupramolecular polyoxotungstates is just beginning to be explored, and finally that f) undoubtedly no other class of inorganic compounds allows for preparation of discrete, nanomolecular objects of similar size, structure, and function as those made with polyoxometalates.

Currently we are investigating the electro- and photochemical, electrocatalytic, and oxidation catalysis properties of **1** and this work will be published elsewhere.

Experimental Section

$K_{24}[\{\beta\text{-}Ti_2SiW_{10}O_{39}\}_4]\cdot 50H_2O$ (K_{24}-**1**): A sample of $K_8[\gamma\text{-}SiW_{10}O_{36}]$ (2.23 g, 0.75 mmol; synthesized according to ref. [21]) was added with stirring to a solution of $TiO(SO_4)$ (0.26 g, 1.65 mmol; Merck) in H_2O (40 mL). The pH value was adjusted to 2 by addition of 4 M HCl. This

 © 2004 Wiley-VCH Verlag GmbH & Co. KGaA, Weinheim

solution was heated to 80 °C for 1 h and then cooled to room temperature and filtered. Slow evaporation of the filtrate at room temperature resulted in a white, crystalline product after 2–3 weeks that was collected by filtration and air-dried. Yield: 1.39 g (61 %); IR: 1000(w), 966(m), 913(s), 803(s), 657(m), 541(w), 516(w), 487(w), 467(w) cm^{-1}; elemental analysis calcd (%) for K_{24}-**1**: K 7.7, W 60.4, Ti 3.1, Si 0.9; found: K 7.3, W 61.6, Ti 2.8, Si 1.2. Elemental analysis was performed by Kanti Labs Ltd. in Mississauga, Canada.

Received: March 6, 2004 [Z54203]

Keywords: cluster compounds · polyoxometalates · self-assembly · titanium · tungsten

[1] M. T. Pope, *Heteropoly and Isopoly Oxometalates*, Springer, Berlin, **1983**.
[2] M. T. Pope, A. Müller, *Angew. Chem.* **1991**, *103*, 56 – 70; *Angew. Chem. Int. Ed. Engl.* **1991**, *30*, 34 – 48.
[3] *Polyoxometalates: from Platonic Solids to AntiRetroviral Activity* (Eds.: M. T. Pope, A. Müller), Kluwer, Dordrecht, **1994**.
[4] *Chem. Rev.* **1998**, *98*, 1 – 389 (Special Thematic Issue on Polyoxometalates).
[5] *Polyoxometalate Chemistry: From Topology via Self-Assembly to Applications* (Eds.: M. T. Pope, A. Müller), Kluwer, Dordrecht, **2001**.
[6] *Polyoxometalate Chemistry for Nano-Composite Design* (Eds.: T. Yamase, M. T. Pope), Kluwer, Dordrecht, **2002**.
[7] J. Berzelius, *Pogg. Ann.* **1826**, *6*, 369.
[8] a) J. F. Keggin, *Nature* **1933**, *131*, 908 – 909; b) J. F. Keggin *Proc. R. Soc. London Ser. A* **1934**, *144*, 75 – 77.
[9] C. L. Hill, C. M. Prosser-McCartha, *Coord. Chem. Rev.* **1995**, *143*, 407 – 455.
[10] a) R. R. Ozer, J. L. Ferry, *Environ. Sci. Technol.* **2001**, *35*, 3242 – 3246; b) D. A. Friesen, L. Morello, J. V. Headley, C. H. Langford, *J. Photochem. Photobiol. A* **2000**, *133*, 213 – 220; c) I. Texier, C. Giannotti, S. Malato, C. Richter, J. Delaire, *Catal. Today* **1999**, *54*, 297 – 307.
[11] a) K. Nomiya, M. Takahashi, K. Ohsawa, J. A. Widegren, *J. Chem. Soc. Dalton Trans.* **2001**, 2872 – 2878; b) Y. Lin, T. J. R. Weakley, B. Rapko, R. G. Finke, *Inorg. Chem.* **1993**, *32*, 5095 – 5101; c) T. Yamase, T. Ozeki, H. Sakamoto, S. Nishiya, A. Yamamoto, *Bull. Chem. Soc. Jpn.* **1993**, *66*, 103 – 108; d) O. A. Kholdeeva, G. M. Maksimov, R. I. Maksimovskaya, L. A. Kovaleva, M. A. Fedotov, V. A. Grigoriev, C. L. Hill, *Inorg. Chem.* **2000**, *39*, 3828 – 3837; e) J. He, X. Wang, Y. Chen, J. Liu, N. Hu, H. Jia, *Inorg. Chem. Commun.* **2002**, *5*, 796 – 799.
[12] a) W. H. Knoth, P. J. Domaille, D. C. Roe, *Inorg. Chem.* **1983**, *22*, 198 – 201; b) T. Yamase, T. Ozeki, S. Motomura, *Bull. Chem. Soc. Jpn.* **1992**, *65*, 1453 – 1459; c) P. J. Domaille, W. H. Knoth, *Inorg. Chem.* **1983**, *22*, 818 – 822; d) T. Ozeki, T. Yamase, *Acta Cryst. Sect. C* **1991**, *47*, 693 – 696.
[13] a) F. X. Gao, T. Yamase, H. Suzuki, *J. Mol. Catal. A* **2002**, *180*, 97 – 108; b) E. Ishikawa, T. Yamase, *J. Mol. Catal. A* **1999**, *142*, 61 – 76; c) T. Yamase, E. Ishikawa, Y. Asai, S. Kanai, *J. Mol. Catal. A* **1996**, *114*, 237 – 245.
[14] S. Shigeta, S. Mori, E. Kodama, J. Kodama, K. Takahashi, T. Yamase, *Antiviral Res.* **2003**, *58*, 265 – 271, and references therein.
[15] U. Kortz, S. S. Hamzeh, N. A. Nasser, *Chem. Eur. J.* **2003**, *9*, 2945 – 2952.
[16] a) Y. Sakai, K. Yoza, C. N. Kato, K. Nomiya, *Chem. Eur. J.* **2003**, *9*, 4077 – 4083; b) Y. Sakai, K. Yoza, C. N. Kato, K. Nomiya, *J. Chem. Soc. Dalton Trans.* **2003**, 3581 – 3586.
[17] a) U. Kortz, S. Matta, *Inorg. Chem.* **2001**, *40*, 815 – 817; b) U. Kortz, S. Isber, M. H. Dickman, D. Ravot, *Inorg. Chem.* **2000**, *39*, 2915 – 2922; c) U. Kortz, Y. P. Jeannin, A. Tézé, G. Hervé, S. Isber, *Inorg. Chem.* **1999**, *38*, 3670 – 3675.
[18] Crystal data for $K_{24}[\{\beta\text{-}Ti_2SiW_{10}O_{39}\}_4]\cdot 50H_2O$ (K_{24}-**1**): A colorless block of K_{24}-**1** with dimensions $0.06\times0.10\times0.10\ mm^3$ was mounted on a glass fiber for indexing and intensity data collection at 173 K on a Bruker D8 SMART APEX CCD single-crystal diffractometer using $Mo_{K\alpha}$ radiation ($\lambda = 0.71073$ Å). Of the 23877 unique reflections ($2\theta_{max} = 56.64°$), 19910 reflections ($R_{int} = 0.093$) were considered observed ($I > 2\sigma(I)$). Direct methods were used to solve the structure and to locate the tungsten and titanium atoms (SHELXS97). Then the remaining atoms were found from successive difference maps (SHELXL97). The final cycle of refinement, including the atomic coordinates, anisotropic thermal parameters (W, Ti, K, and Si atoms) and isotropic thermal parameters (O atoms) converged at $R = 0.104$ and $R_w = 0.201$ ($I > 2\sigma(I)$). In the final difference map the deepest hole was $-2.501\ e\,Å^{-3}$ and the highest peak $5.731\ e\,Å^{-3}$. Routine Lorentz and polarization corrections were applied and an absorption correction was performed using the SADABS program (G. M. Sheldrick, Siemens Analytical X-ray Instrument Division, Madison, WI, **1995**). Further details of the crystal structure investigation may be obtained from the Fachinformationszentrum Karlsruhe, D-76344 Eggenstein-Leopoldshafen, Germany (Fax: (+49) 7247-808-666; E-mail: crysdata@fiz-karlsruhe.de) on quoting the depository number CSD-413815.
[19] I. D. Brown, D. Altermatt, *Acta Crystallogr. Sect. B* **1985**, *41*, 244 – 247.
[20] Y. Jeannin, M. Fournier, *Pure Appl. Chem.* **1987**, *59*, 1529 – 1548.
[21] A. Tézé, G. Hervé, *Inorganic Syntheses*, **1990**, *27*, 88 – 89.

 © 2004 Wiley-VCH Verlag GmbH & Co. KGaA, Weinheim

Cover Picture



Maarten A. C. Broeren, Joost L. J. van Dongen, Michael Pittelkow, Jørn B. Christensen, Marcel H. P. van Genderen, and E. W. Meijer*

The deconvoluted mass spectrum shown in the cover picture of a third-generation poly(propylene imine) dendrimer to which one to eight guest molecules are bound indicates that the complex with four guest molecules is the most abundant. Each of these aggregates can be selected, and the guests can be removed one by one by collision-induced dissociation (CID). The results provide new insight into the role of important secondary interactions in the gas phase. For more information, see the Communication by E. W. Meijer and co-workers on page 3557 ff.

Contents

Angewandte EarlyView

The following Communications are available online (in Wiley InterScience). You can find them, as well as forthcoming Reviews, Highlights, and Essays, at www.angewandte.org, under Early View.

M. Johnsson, S. Lidin, K. W. Törnroos, H.-B. Bürgi, P. Millet:*
Host–Guest Compounds in the Family of Tellurium–Nickel Oxohalogenides
DOI: 10.1002/anie.200460001
Published online: June 23, 2004

K. C. Nicolaou, S. Vyskocil, T. V. Koftis, Y. M. A. Yamada, T. Ling, D. Y.-K. Chen, W. Tang, G. Petrovic, M. O. Frederick, Y. Li, M. Satake*:*
Structural Revision and Total Synthesis of Azaspiracid-1, Part 1: Intelligence Gathering and Tentative Proposal
DOI: 10.1002/anie.200460695
Published online: June 25, 2004

K. C. Nicolaou, T. V. Koftis, S. Vyskocil, G. Petrovic, T. Ling, Y. M. A. Yamada, W. Tang, M. O. Frederick:*
Structural Revision and Total Synthesis of Azaspiracid-1, Part 2: Definition of the ABCD Domain and Total Synthesis
DOI: 10.1002/anie.200460696
Published online: June 29, 2004

Articles judged by the referees or the editor as being either very important or very urgent are immediately edited, proof-read, and electronically published once the manuscript has arrived in the editorial office in its final form. As long as there is no page number available these articles should be cited in the following manner:

Author(s), *Angew. Chem. Int. Ed.*, online publication date, DOI.

News

Chemical Society of Japan Awards ——— **3508 – 3509**

Books

Molecular Biology in Medicinal Chemistry ——— **3510**	Theodor Dingermann, Dieter Steinhilber, Gerd Folkers	*reviewed by R. Breinbauer*
Physics and Chemistry of Interfaces ——— **3510**	Hans-Jürgen Butt, Karlheinz Graf, Michael Kappl	*reviewed by M. Steinhart*
Nanocosm ——— **3511**	William Illsey Atkinson	*reviewed by R. N. Zare*

Highlights

Endogenous Ozone

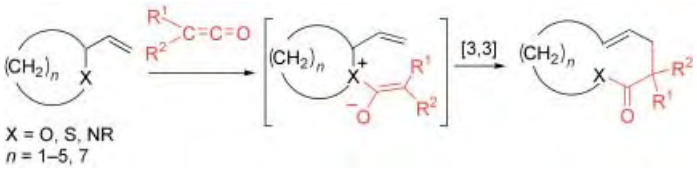
H. Sies* ——— **3514 – 3515**

Ozone in Arteriosclerotic Plaques: Searching for the "Smoking Gun"



Ozone as an endogenous compound? The discovery of 5,6-secosterol, a characteristic product of the in vitro ozonolysis of cholesterol, in atherosclerotic tissue (see picture) suggests that ozone is formed by biochemical processes. This and other typical products of oxidation may serve as indicators ("biomarkers") of endogenous ozone.

Minireviews



Now a quarter of a century since its serendipitous discovery, the Belluš–Claisen rearrangement of ketenes with allylic ethers, amines, and thioethers has been developed into a simple and reliable [3,3] bond reorganization reaction. This rearrangement, which proceeds via a zwitterionic intermediate, is especially powerful for the ring expansion of cyclic allylic substrates by four carbon atoms (see scheme). R^1, R^2 = alkyl, Cl.

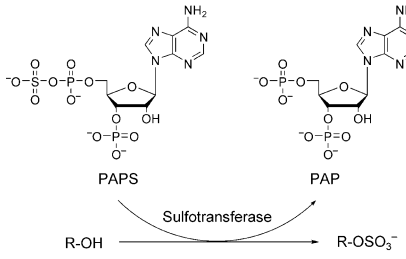
Sigmatropic Rearrangement

J. Gonda* ——— **3516 – 3524**

The Belluš–Claisen Rearrangement

Reviews

A diverse range of biomolecules, including steroids and glycosaminoglycans, are sulfonated enzymatically by the cosubstrate PAPS in the presence of sulfotransferases (see scheme). As these enzymes have been implicated in several crucial pathophysiological events (regulation of estrogen sulfate synthesis and leukocyte adhesion, viral entry) they have emerged as promising therapeutic targets.



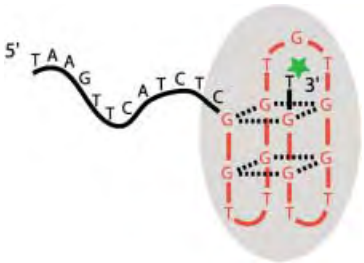
Enzyme Chemistry

E. Chapman, M. D. Best, S. R. Hanson, C.-H. Wong* ——— **3526 – 3548**

Sulfotransferases: Structure, Mechanism, Biological Activity, Inhibition, and Synthetic Utility

Communications

A DNA aptamer structure is the basis of a molecular machine that can be instructed to grab or release the human blood-clotting factor α-thrombin, depending on the operator DNA sequence addressing it. In the picture the aptamer structure, which assumes a conformation characterized by two stacked guanine quadruplex structures, is linked to thrombin (gray ellipse).



DNA Structures

W. U. Dittmer, A. Reuter, F. C. Simmel* ——— **3550 – 3553**

A DNA-Based Machine That Can Cyclically Bind and Release Thrombin

For the USA and Canada:
ANGEWANDTE CHEMIE International Edition (ISSN 1433-7851) is published weekly by Wiley-VCH PO Box 191161, D 69451 Weinheim, Germany. Air freight and mailing in the USA by Publications Expediting Inc. 200 Meacham Ave., Elmont, NY 11003. Periodicals postage paid at Jamaica NY 11431. US POSTMASTER: send address changes to *Angewandte Chemie*, Wiley-VCH, 111 River Street, Hoboken, NJ 07030. Annual subscription price for institutions: Europe € 3430.00/3118.00; outside Europe US$ 4499.00/4090.00 (valid for print and electronic/print or electronic delivery); for individuals who are personal members of a national chemical society, or whose institution already subscribes, or who are retired or self-employed consultants, print only: Europe € 248.00/outside Europe US$ 378.00. Postage and handling charges included. All Wiley-VCH prices are exclusive VAT.

 © 2004 Wiley-VCH Verlag GmbH & Co. KGaA, Weinheim

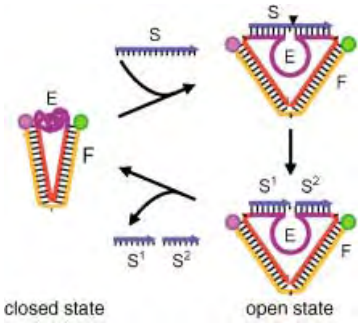
Contents

Nanotechnology

Y. Chen, M. Wang, C. Mao* . **3554 – 3557**

An Autonomous DNA Nanomotor Powered by a DNA Enzyme

The power of life: An autonomous DNA nanomotor powered by an RNA-cleaving DNA enzyme (see figure) has been constructed that works in the same way as cellular protein motors: it continuously extracts chemical energy from fuel molecules to power mechanical motions. The fuel for the DNA nanomotor is the RNA substrate of the DNA enzyme.

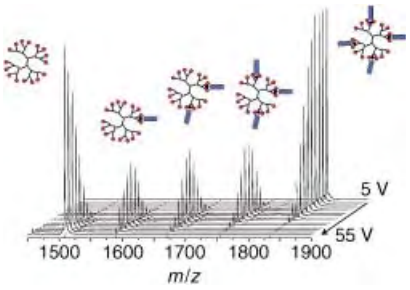


Host–Guest Chemistry

M. A. C. Broeren, J. L. J. van Dongen, M. Pittelkow, J. B. Christensen, M. H. P. van Genderen, E. W. Meijer* **3557 – 3562**

Multivalency in the Gas Phase: The Study of Dendritic Aggregates by Mass Spectrometry

Selective guest ejection: Up to eight guest molecules are assembled at the periphery of a third-generation dendrimer. Collision-induced dissociation mass spectrometry has demonstrated that the guests are removed very selectively in a one-by-one manner (see spectrum).

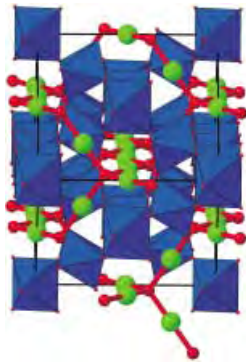


Reduced Pyrochlores

G. D. Blundred, C. A. Bridges, M. J. Rosseinsky* **3562 – 3565**

New Oxidation States and Defect Chemistry in the Pyrochlore Structure

Titanium(III) pyrochlores with Ti^{III} centers at up to 90% of the B sites of the $A_2B_2O_6O'$ pyrochlore structure (see picture; blue: BO_6, green: A, red: O′), which is well-known for supporting high oxidation states at the octahedral B sites, were obtained by the low-temperature reduction of lanthanide pyrochlores $Ln_2Ti_2O_7$ with CaH_2. This leads to significant rearrangement of the anion sublattice and introduces antisite disorder between the two distinct cation arrays.

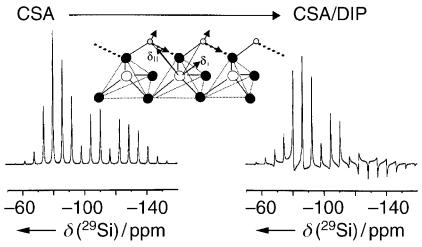


NMR Spectroscopy

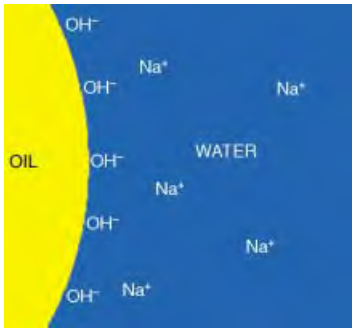
C. Gardiennet, F. Marica, X. Assfeld, P. Tekely* **3565 – 3568**

Exploiting the Joint Action of Chemical Shielding and Heteronuclear Dipolar Interactions To Probe the Geometries of Strongly Hydrogen-Bonded Silanols

Magic probes: The geometry of strongly hydrogen bonded silanols in octosilicate can be probed by exploiting the ^1H NMR distance correlations together with the joint effects of ^{29}Si chemical shielding and dipolar ^1H–^{29}Si interactions. Dipolar-modulated, slow magic-angle spinning ^{29}Si NMR spectra allow the determination of Si···H distances, the magnitude of the ^{29}Si chemical-shielding tensor, and its orientation in the molecular frame.



 © 2004 Wiley-VCH Verlag GmbH & Co. KGaA, Weinheim



Stable oil-in-water emulsions are obtained in alkaline solution in the absence of any conventional surfactant. The oil droplets are charged by hydroxide ions (see picture). The surface charge density is obtained by measuring the size of the emulsion droplets by electroacoustics and the quantity of NaOH required to keep the pH constant during homogenization.

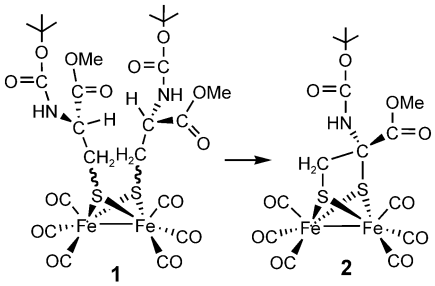
Surfactant-Free Emulsions

J. K. Beattie,*
A. M. Djerdjev ——— **3568 – 3571**

The Pristine Oil/Water Interface: Surfactant-Free Hydroxide-Charged Emulsions

---

Classical organometallic chemistry was used to prepare the dinuclear iron complex **1** with two protected cysteinyl-*S* ligands. Oxidative addition of the thiol to $[Fe_3(CO)_{12}]$ gave complex **1**, which undergoes an unusual intramolecular nucleophilic cyclization with inversion of the configuration to form the chiral carbon-bridged diiron complex **2**.

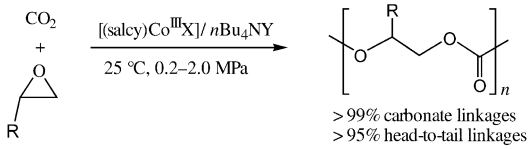


Bioinorganic Chemistry

C. He, M. Wang,* X. Zhang, Z. Wang, C. Chen, J. Liu, B. Åkermark, L. Sun* ——— **3571 – 3574**

An Unusual Cyclization in a Bis(cysteinyl-*S*) Diiron Complex Related to the Active Site of Fe-Only Hydrogenases

---



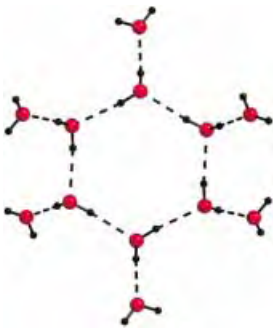
Excellent activity and selectivity in the copolymerization of CO_2 with epoxides at extremely mild temperature and pressure are observed in the presence of binary nucleophile–electrophile catalyst systems based on chiral [(salcy)Co^{III}X] complexes and quaternary ammonium salts (see scheme). Completely alternating copolymers are obtained with >95% head-to-tail linkages.

Copolymerization

X.-B. Lu,* Y. Wang ——— **3574 – 3577**

Highly Active, Binary Catalyst Systems for the Alternating Copolymerization of CO_2 and Epoxides under Mild Conditions

---



An infinite network is formed by the hydrogen bonding of a cluster of 12 hydrogen-bonded water molecules (see picture) to the secondary amino nitrogen atoms of a laterally nonsymmetric aza-cryptand. This mode of association had not previously been predicted or found experimentally.

Self-Assembly

S. K. Ghosh,
P. K. Bharadwaj* ——— **3577 – 3580**

A Dodecameric Water Cluster Built around a Cyclic Quasiplanar Hexameric Core in an Organic Supramolecular Complex of a Cryptand

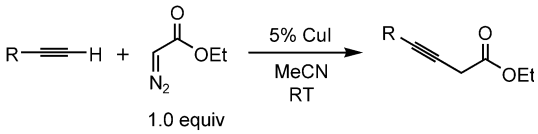
 © 2004 Wiley-VCH Verlag GmbH & Co. KGaA, Weinheim

Contents

Coupling Reactions

A. Suárez, G. C. Fu* ——— **3580 – 3582**

A Straightforward and Mild Synthesis of Functionalized 3-Alkynoates

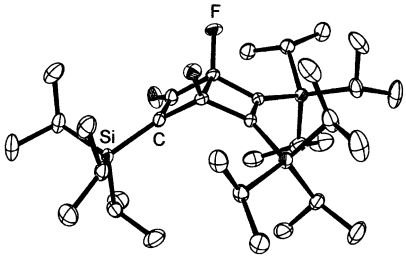


Diazoacetates in coupling reactions: CuI serves as an effective catalyst for coupling terminal alkynes with diazo compounds to generate 3-alkynoates (see scheme). This method is efficient (1:1 ratio of reactants), mild (room temperature), and simple (no additional ligand), and a range of functional groups are tolerated (e.g., C—C double bonds, heteroatoms, and hydroxy groups).

Strained Molecules

T. Hanamoto,* Y. Koga, T. Kawanami, H. Furuno, J. Inanaga ——— **3582 – 3584**

Crystal Structure of a Dewar Benzene Derivative Formed from Fluoro(triisopropylsilyl)acetylene



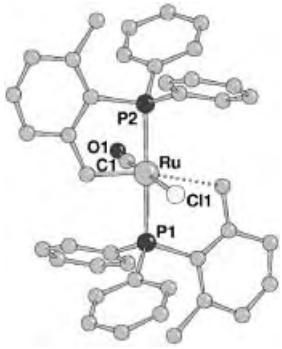
Spontaneous trimerization of fluoro(triisopropylsilyl)acetylene, prepared from 1,1-difluoroethylene in one step, gives the corresponding fluorinated Dewar benzene derivative, whose structure was determined by X-ray diffraction (see picture).

Homogeneous Catalysis

W. Baratta,* P. Da Ros, A. Del Zotto, A. Sechi, E. Zangrando, P. Rigo ——— **3584 – 3588**

Cyclometalated Ruthenium(II) Complexes as Highly Active Transfer Hydrogenation Catalysts

Quantitative conversion: Reaction of the 14-electron complex $[RuCl_2\{(2,6\text{-}Me_2C_6H_3)PPh_2\}_2]$ with CH_2O in the presence of NEt_3 gave a five-coordinate cyclometalated complex with a δ-agostic interaction of one *ortho*-methyl group (see X-ray crystal structure). Displacement of one phosphane group with 2-(aminomethyl)pyridine gave a highly active catalyst for the quantitative conversion of ketones into alcohols.



Gas-Phase Reactions

T. Giroldo, L. A. Xavier, J. M. Riveros* ——— **3588 – 3590**

An Unusually Fast Nucleophilic Aromatic Displacement Reaction: The Gas-Phase Reaction of Fluoride Ions with Nitrobenzene

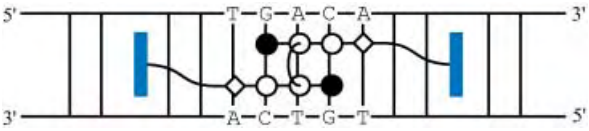


Quick reactions: The gas-phase nucleophilic displacement reaction of fluoride ions with nitrobenzene proceeds with a rate constant close to the collision limit. The calculated energy profile indicates that the reaction proceeds by an out-of-plane attack, with the Meisenheimer complex being the local transition state for the reaction (see picture).

DNA Bisintercalators

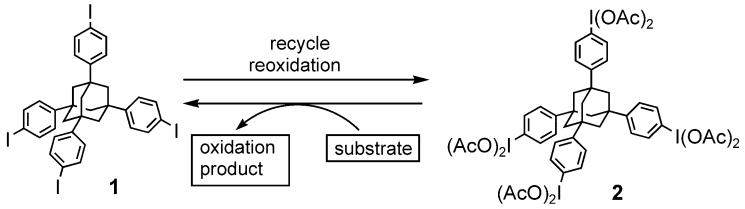
E. J. Fechter, B. Olenyuk, P. B. Dervan* ——— **3591 – 3594**

Design of a Sequence-Specific DNA Bisintercalator



Programmable bisintercalators: Symmetric synthetic DNA bisintercalators (see picture) based on the H-pin polyamide motif afford high affinity and programmable sequence specificity.

 © 2004 Wiley-VCH Verlag GmbH & Co. KGaA, Weinheim

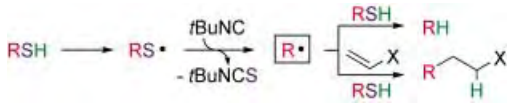


A wide range of oxidative reactions are mediated by novel, nonpolymeric, and recyclable hypervalent I^{III} reagents (e.g. **2**). In all cases, tetraiodide **1** was recovered nearly quantitatively in pure form after a simple workup. Reoxidation of **1** to **2** with *m*-chloroperbenzoic acid also proceeded quantitatively, without loss of oxidative activity.

Oxidations

H. Tohma,* A. Maruyama, A. Maeda, T. Maegawa, T. Dohi, M. Shiro, T. Morita, Y. Kita* ——— **3595 – 3598**

Preparation and Reactivity of 1,3,5,7-Tetrakis[4-(diacetoxyiodo)phenyl]-adamantane, a Recyclable Hypervalent Iodine(III) Reagent

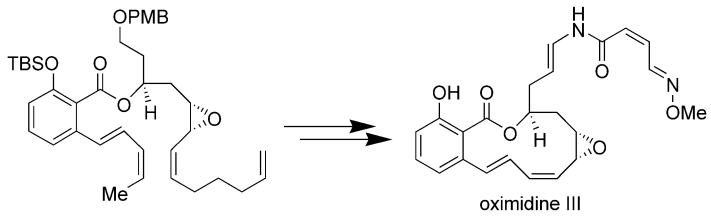


Desulfuration as a source of alkyl radicals: The addition of alkylsulfanyl radicals to isocyanides gives the corresponding alkyl radicals. This methodology can replace the usual tin-mediated radical procedures and allows for the generation of tertiary, secondary, and even nonstabilized primary radicals that can be used efficiently in reductive defunctionalizations and intermolecular additions to electron-rich olefins (see scheme).

Radical Reactions

L. Benati, R. Leardini, M. Minozzi,* D. Nanni,* R. Scialpi, P. Spagnolo, S. Strazzari, G. Zanardi ——— **3598 – 3601**

A Novel Tin-Free Procedure for Alkyl Radical Reactions

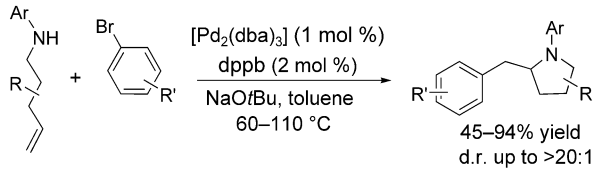


The vacuolar-type (H^+)-adenosine triphosphatase inhibitor oximidine III and its enamide and epoxide stereoisomers have been synthesized enantioselectively. A relay ring-closing metathesis (RCM) strategy was employed to facilitate the macrocyclization of a well-defined substrate possessing two differentially functionalized RCM alkene partners (see scheme).

Natural Product Synthesis

X. Wang, E. J. Bowman, B. J. Bowman, J. A. Porco, Jr.* ——— **3601 – 3605**

Total Synthesis of the Salicylate Enamide Macrolide Oximidine III: Application of Relay Ring-Closing Metathesis



The formation of a C–C and a C–N bond in a reaction between γ-(*N*-arylamino) alkenes and aryl bromides results in the stereoselective synthesis of substituted pyrrolidine derivatives (see scheme). Preliminary studies suggest these reactions proceed by intramolecular alkene insertion into the Pd–N bond of intermediate [Pd(Ar)(amido)] complexes. dba = dibenzylideneacetone, dppb = 1,3-bis(diphenylphosphanyl)butane.

Heterocycle Synthesis

J. E. Ney, J. P. Wolfe* ——— **3605 – 3608**

Palladium-Catalyzed Synthesis of *N*-Aryl Pyrrolidines from γ-(*N*-Arylamino) Alkenes: Evidence for Chemoselective Alkene Insertion into Pd–N Bonds

VIP Communications labeled with this symbol have been judged by two referees as being "very important papers".

 © 2004 Wiley-VCH Verlag GmbH & Co. KGaA, Weinheim

Looking for outstanding employees?

Do you need another expert for your excellent team?
...Chemists, PhD Students, Managers, Professors, Sales Representatives...

Place an advert in the printed version and have it made available online for 1 month, free of charge!

Angewandte Chemie International Edition
Advertising Sales Department: Marion Schulz
Phone: 0 62 01 - 60 65 65
Fax: 0 62 01 - 60 65 50
E-Mail: MSchulz@wiley-vch.de

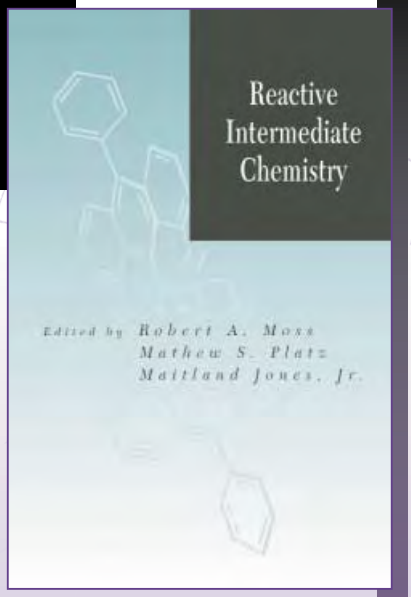
Service

Keywords ——— *3610*

Authors ——— *3611*

Preview ——— *3613*

Reactive Intermediate Chemistry



Robert A. Moss, *Rutgers University*
Matthew S. Platz, *Ohio State University*
Maitland Jones, *Princeton University*

ISBN 0-471-23324-2 • 1,080 pages • Cloth
$99.95 / £64.50 / €90.90
December 2003

Reactive Intermediate Chemistry presents a detailed and timely examination of key intermediates central to the mechanisms of numerous organic chemical transformations. Spectroscopy, kinetics, and computational studies are integrated in chapters dealing with the chemistry of carbocations, carbanions, radicals, radical ions, carbenes, nitrenes, arynes, nitrenium ions, diradicals, etc. Nanosecond, picosecond, and femtosecond kinetic realms are explored, and applications of current dynamics and electronic structure calculations are examined.

WILEY

Reactive Intermediate Chemistry provides a deeper understanding of contemporary physical organic chemistry, and will assist chemists in the design of new reactions for the efficient synthesis of pharmaceuticals, fine chemicals, and agricultural products. Among its features, this authoritative volume is:

- Edited and authored by world-renowned leaders in physical organic chemistry.
- Ideal for use as a primary or supplemental graduate textbook for courses in mechanistic organic
- Enhanced by supplemental reading lists and summary overviews in each chapter.

CONTENTS

Preface

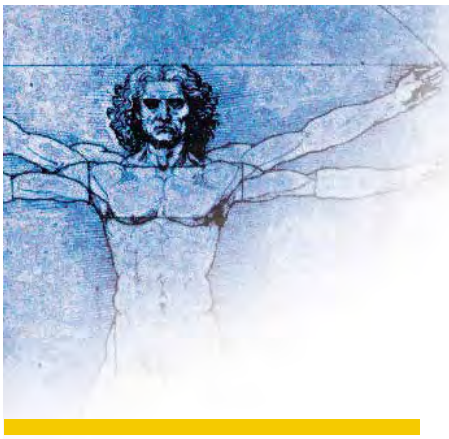
PART 1: REACTIVE INTERMEDIATES

1. Carbocations (R.A. McClelland)
2. Crossing the Borderline Between SN1 and SN2 Nucleophilic Substitution at Aliphatic Carbon (T.L. Amyes, et al.)
3. Carbanions (S. Gronert)
4. Radicals (M. Newcomb)
5. Non-Kekul Molecules as Reactive Intermediates (J.A. Berson)
6. Organic Radical Ions (H.D. Roth)
7. Singlet Carbenes (M. Jones Jr. and R.A. Moss)
8. Stable Singlet Carbenes (G. Bertrand)
9. Triplet Carbenes (H. Tomioka)
10. Atomic Carbon (P.B. Shevlin)
11. Nitrenes (M.S. Platz)
12. Synthetic Carbene and Nitrene Chemistry (M.P. Doyle)
13. Nitrenium Ions (D.E. Falvey)
14. Silylenes (W. Ando and N. Tokitoh)
15. Strained Hydrocarbons: Structures, Stability, and Reactivity (K.B. Wiberg)
16. Arynes (M. Winkler, et al.)

PART 2: METHODS AND TEMPORAL REGIMES

17. Matrix Isolation (T. Bally)
18. Nanosecond Laser Flash Photolysis: A Tool for Physical Organic Chemistry (J.C. Scaiano)
19. The Picosecond Realm (E. Hilinski)
20. Reactions on the Femtosecond Time Scale (J.E. Baldwin)
21. Potential Energy Surfaces and Reaction Dynamics (B.K. Carpenter)
22. The Partnership Between Electronic Structure Calculations and Experiments in the Study of Reactive Intermediates (W.T. Borden)

 © 2004 Wiley-VCH Verlag GmbH & Co. KGaA, Weinheim



The Chemical Society of Japan (CSJ) presents a number of awards annually, including six CSJ Awards for significant contributions to chemistry in terms of both applications and basic research. In the following we present the recipients for 2003 and their award-winning research.

Y. Iwasawa: Heterogeneous Catalysis

Yasuhiro Iwasawa is a recipient of a CSJ Award for his studies on active structures and dynamic catalysis on surfaces. His recent research includes kinetic studies on the elementary steps in the CO-induced disintegration of rhodium clusters on surfaces.[1] For the characterization of these clusters he employs a wide range of modern methods for surface analysis: EXAFS, XPEEM, ESDIAD, STM, AFM, IR, XRD, and solid-state NMR spectroscopy.



Y. Iwasawa

Iwasawa completed his chemistry studies at Tokyo University in 1973 with a PhD. He then taught and carried out research at Yokohama University until he was appointed professor at Tokyo University in 1984. He has authored books on catalysis and surfaces and is Executive Editor of the journal *The Chemical Record*.

T. Osaka: Electrochemistry

Tetsuya Osaka has been recognized with a CSJ Award for his work on the preparation of multifunctionalized materials by electrochemical processes. The work of his research group includes the development of batteries based on polymers and lithium ions, sensors, thin films, and materials for magnetic recording, as well as electrochemical separation processes. He recently described "Metallic bismuth on strontium–bismuth tantalate thin films for ferroelectric memory application".[2]



T. Osaka

Osaka completed his studies at Waseda University in Tokyo with a PhD in 1974. He carried out postdoctoral research at Georgetown University (Washington, DC) from 1976 to 1978, then returned to Waseda University, where he has been Professor of Applied Physical Chemistry since 1986. He became dean of the Graduate School of Science and Engineering at this institution in 1998. Osaka has received several awards, including the Pergamon Gold Medal of the International Society of Electrochemistry.

G. Saito: Organic Conductors

Gunzi Saito has been recognized for his contributions to the development of conductive molecular organic materials through self-assembly. The design, synthesis, and characterization of the physical properties of functional organic molecules and self-assembled systems form the central research interests of his group. Further interests include organic solids with metallic, superconductive, and magnetic properties as well as systems with neutral–ionic phase transitions or proton or charge-transfer interactions. He recently reported on "The Interaction of C_{60}, C_{70}, and $C_{60}(CN)_2$ Radical Anions with Cobalt(II) Tetraphenylporphyrin in Solid Multicomponent Complexes".[3]



G. Saito

Saito completed his PhD at Hokkaido University in Sapporo in 1972. After several years as a postdoctoral researcher with F. M. Menger (Atlanta, GA, USA), A. K. Colter (Guelph, ON, Canada), and J. P. Ferraris (Richardson, TX, USA) he returned to Japan to work as a scientist at the Institute of Molecular Science in Okazaki. In 1984, he became a professor at the Institute for Solid State Physics of Tokyo University. He has been at Kyoto University since 1989 and was a visiting professor several times in Rennes (France).

S. Shinkai: Supramolecular Chemistry

Seiji Shinkai completed his PhD in 1972 at Kyushu University in Fukuoka. After postdoctoral studies at the University of California, Santa Barbara in the research group of Thomas C. Bruice, he returned to Kyushu University in 1975 and was made a professor there in 1988. He leads several international collaborations.



S. Shinkai

The research of Shinkai and his group is focused on host–guest chemistry, molecular recognition, gels, saccharides, and nucleotides. He has received the CSJ Award in recognition of his work on functional supramolecular systems based on molecular recognition. In a recent Communication in *Angewandte Chemie* he reported a light-harvesting organogel composed of cholesterol-based perylene derivatives.[4] Shinkai has been a member of the International Advisory Board of *Angewandte Chemie* since 2000.

 © 2004 Wiley-VCH Verlag GmbH & Co. KGaA, Weinheim DOI: 10.1002/anie.200460847

H. Nakatsuji: Quantum Chemistry

A further CSJ Award goes to the quantum chemist Hiroshi Nakatsuji (Kyoto University), whose research is concentrated on the development of methods in quantum chemistry. He is interested in the calculation of excited states (SAC-CI: symmetry-adapted cluster/configuration interaction), the direct determination of the density matrix, the structure of exact wave functions, as well as electronic mechanisms and relativistic effects in the calculation of chemical shifts. He has now been recognized with this award for his contributions towards the application of quantum mechanics in chemistry. He recently described the electronic excitation of the protonated form of the GFP chromophore.[5]



H. Nakatsuji

Nakatsuji studied chemistry at Kyoto University, completed his PhD there in 1971, then took up a teaching position there. From 1973 to 1975 he undertook postdoctoral studies in New York with J. I. Musher and in Chapel Hill (North Carolina, USA) with R. G. Parr, after which he returned to Kyoto. He has been a professor at Kyoto University since 1988, and since 2004 he has also been director of the Fukui Institute for Fundamental Chemistry. Nakatsuji is one of three editors of the *Journal of Computational Chemistry*.

M. Hirama: Natural-Product Synthesis

Masahiro Hirama (Tohoku University, Sendai) is the recipient of a CSJ Award for his work on the total synthesis of ciguatoxins and bioactive natural products. His research is concerned with natural-product synthesis, including that of chromoprotein antitumor antibiotics and marine neurotoxins based on polyether structures. In this research molecular recognition and the mechanism of interactions between these molecules and biopolymers play a crucial role. He recently reported the total synthesis of the proteasome inhibitor TMC-95A in *Angewandte Chemie*.[6]



M. Hirama

Hirama completed his PhD in 1977 at Tohoku University under the guidance of S. Ito. After periods of postdoctoral research in the groups of S. Danishefsky in Pittsburgh and S. Masamune at the Massachusetts Institute of Technology he returned to Japan to work with K. Nakanishi at the Suntory Institute for Bioorganic Research. Since 1983 he has been a professor at Tohoku University.

[1] A. Suzuki, Y. Inada, A. Yamaguchi, T. Chihara, M. Yuasa, M. Nomura, Y. Iwasawa, *Angew. Chem.* **2003**, *115*, 1325; *Angew. Chem. Int. Ed.* **2003**, *42*, 4795.

[2] K. Asami, T. Osaka, T. Yamanobe, I. Koiwa, *Surf. Interf. Anal.* **2000**, *30*, 391.

[3] D. V. Konarev, S. S. Khasanov, G. Saito, R. N. Lyubovskaya, Y. Yoshida, A. Otsuka, *Chem. Eur. J.* **2003**, *9*, 3837.

[4] K. Sugiyasu, N. Fujita, S. Shinkai, *Angew. Chem.* **2004**, *116*, 1249; *Angew. Chem. Int. Ed.* **2004**, *43*, 1229.

[5] A. K. Das, J. Hasegawa, T. Miyahara, M. Ehara, H. Nakatsuji, *J. Comp. Chem.* **2003**, *24*, 1421.

[6] M. Inoue, H. Sakazaki, H. Furuyama, M. Hirama, *Angew. Chem.* **2003**, *115*, 2758; *Angew. Chem. Int. Ed.* **2003**, *42*, 2654.

 © 2004 Wiley-VCH Verlag GmbH & Co. KGaA, Weinheim

Endogenous Ozone

Ozone in Arteriosclerotic Plaques: Searching for the "Smoking Gun"

*Helmut Sies**

Keywords:
arteriosclerosis · metabolism · oxidative stress · ozone · ozonolysis

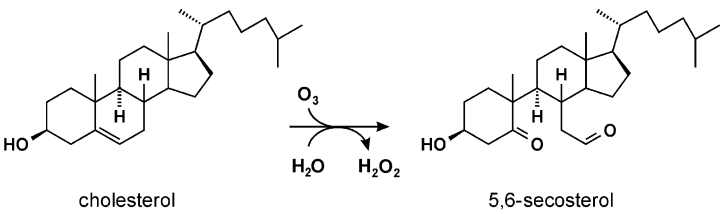
Gathering evidence for weapons of biological destruction can be a difficult proposition. Here is such a case. The notion that oxidation processes are seminal in the development of arteriosclerosis has been in the literature for more than twenty years. Steinbrecher et al.[1] reported on lipid peroxidation as a crucial modification of low-density lipoproteins by endothelial cells. However, the exact nature of the oxidant and the process of oxidant generation have been elusive. Oxidants examined in this context range from the hydroxyl radical generated by transition-metal-catalyzed oxidation through lipid hydroperoxides and peroxynitrite to oxidants generated by enzymatic catalysis, for example, by lipoxygenases and myeloperoxidase. Solid evidence for involvement of all of these intermediates in lipid peroxidation has been provided, but what is unclear to date is their actual contribution to the process of arteriosclerosis. Now, there is an additional and unexpected newcomer: ozone.

Wentworth et al.[2] reported on ozone formation in human atherosclerotic arteries. If anything, this came as a surprise, since ozone, in terms of biological reactivity, has been associated with environmental pollution and inhalatory toxicity to the lung. Formation and utilization of ozone from endogenous sources, if substantiated, provides a new twist in research on oxidative stress.

Wentworth et al.[3] themselves were the originators of the notion that the production of trioxygen species may occur during antibody-catalyzed chemical modification of antigens. Recently, in probing the process termed "antibody-catalyzed water-oxidation pathway", Zhu et al.[4a] observed structural evidence for modifications of two specific amino acid residues within murine antibody antigen-binding Fab fragments by reactive species generated during the antibody-generated water-oxidation process. Structure analyses of UV-irradiated murine Fab fragments revealed complex oxidative modifications of tryptophan 163 in the light chain and hydroxylation of the γ-C atom of glutamine 6 in the heavy chain. Zhu et al.[4a] therefore postulate that the "active site" of the water-oxidation pathway is located within the interfacial region of the constant and variable domains of these antibodies. Altogether, this highly unusual oxygen chemistry becomes a focus of interest. In recent work it was shown that dihydrogen trioxide, HOOOH, is generated during the thermochemical reaction between hydrogen peroxide and ozone. [4b]

What conclusions should we draw? First, it is noteworthy that nature apparently makes full use of the arsenal of oxygen metabolites, whether in soluble or gaseous form, for its intrinsic use in the organism for chemical warfare against perpetrators such as bacteria and virus particles. These weapons, the most reactive oxygen species known, include the hydroxyl radical, singlet oxygen, hydrogen peroxide, nitric oxide, and further derived products, and now also ozone. Ozonation is a known process for cleaning water supplies, but the generation of ozone inside the organism is still perplexing. In general, all of these oxygen metabolites occur at very low concentrations, and their existence can be inferred largely by circumstantial evidence. Thus, evidence for ozone involvement was gathered not directly but rather by identification of "signature products".

So, where is the "smoking gun" indicating that ozone was involved? Wentworth et al.[2] identified the cholesterol ozonolysis product, 5,6-secosterol [Eq. (1)], in atherosclerotic tissue, and secondly they demonstrated the oxidation of indigo carmine as a indicator reaction for ozone to yield the product isatin sulfonate when human atherosclerotic plaque material was stimulated with phorbol myristate acetate (PMA). These observations appear compelling, except for a caveat inherent in this type of study: specificity for readout. While there is no doubt that cholesterol ozonolysis leads to the product 5,6-secosterol in vitro, the generation of this product



cholesterol 5,6-secosterol (1)

[*] Prof. Dr. H. Sies
Institut für Biochemie
und Molekularbiologie I
Heinrich-Heine-Universität Düsseldorf
Postfach 101007
40001 Düsseldorf (Germany)
Fax: (+49) 211-811-3029
E-mail: sies@uni-duesseldorf.de

 © 2004 Wiley-VCH Verlag GmbH & Co. KGaA, Weinheim DOI: 10.1002/anie.200460118

in a biological matrix may not necessarily occur selectively by ozonolysis. Playing the devil's advocate: it could be that other pathways also generate 5,6-secosterol. A systematic examination of various oxidants in terms of their capability to generate the product appears warranted in order to corroborate the use of it as signature product for ozone in biological samples.

As to the formation of isatin sulfonate from indigo carmine, Kettle et al.[5] point out that this reaction is possible with the superoxide anion radical generated either enzymatically from xanthine oxidase and acetaldehyde, or from stimulated neutrophils in a superoxide dismutase inhibitable fashion. These authors[5] concluded, therefore, that the bleaching of indigo carmine cannot be used to invoke ozone production by neutrophils. Obviously, these interesting topics will now be investigated further with refined chemical and biochemical techniques. An old laboratory axiom comes to mind: specific reactions are specific until there is proof to the contrary. Nevertheless, the intervention of ozone as a novel reactive oxygen species in metabolism offers intriguing new possibilities.

What is known about ozone biology at the molecular level? There is ample literature on lipid ozonides generated upon exposure to ozone, as studied by Pryor et al.[6] and Smith et al.,[7] but the endogenous formation of ozone is a novel concept. However, the concept of the formation of the inflammatory signal transduction species generated by ozonation and/or peroxidation of tissue lipids has been known for some time. It extends not only to cholesterol but also to various classes of lipids containing C=C bonds, including phosphatidyl cholines (lecithins), leading to aldehydes, 1-hydroxy-1-hydroperoxides, together with a small yield of so-called Criegee ozonides.[8]

Examining the mutagenic fingerprint of ozone in human cells, Jorge et al.[9] observed the following molecular hallmarks from the mutational spectrum: like numerous oxidizing agents, ozone induces mutations mainly at G:C base pairs but, in contrast to other oxidants, the three classes of base substitutions are induced at a similar level, resembling the mutational spectrum for p53 mutations in nonsmall-cell lung carcinomas in nonsmokers. Another "smoking gun" for ozone, even in nonsmokers?

What are the medical implications of these findings? Starting out from arteriosclerosis (Figure 1) and the generally held concept of it as a long-term disease with a chronic inflammatory component, Wentworth and his colleagues went further into the medical arena: Zhang et al.[10] recently observed that cholesterol ozonolysis products trigger misfolding in β-amyloid as well as α-synuclein and are present in clinical brain samples. The authors go on to correlate ozonation with protein oxidation, accumulation, and plaque formation. These and more implications will rest on corroboration of ozone as a true player. As of now, many questions remain regarding the endogenous production of ozone in the vasculature.[11] The biochemistry of oxidative stress[12] enters into yet another exciting phase. A closer look at the concept of signature products, when utilized as biomarkers, will be worthwhile. The term, biomarker of oxidative stress, was adapted from molecular epidemiology to describe a molecular change in a biological molecule that has arisen from attack by reactive oxygen, nitrogen, or halogen species. A recent comprehensive presentation of current knowledge on oxidized biomarkers, including lipid peroxidation products such as malondialdehyde, lipid hydroperoxides, and F2-isoprostanes, underlines the substantial difficulties of their use in biological research.[13] Future efforts will identify the appropriate place for endogenously generated ozone—when the smoke has cleared…

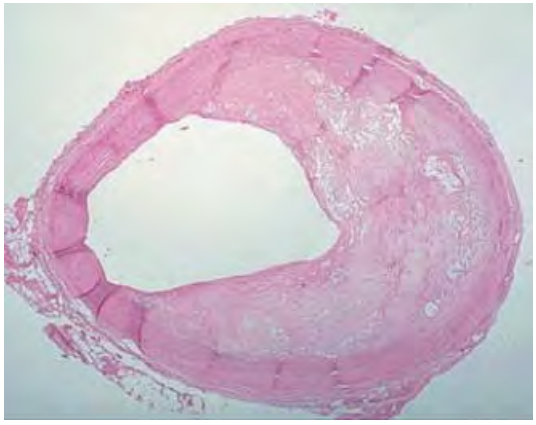


Figure 1. Cross-section of a coronary artery with atherosclerosis. An eccentric atherosclerotic plaque covers about one-third of the circumference; the remaining intima is thickened only slightly.

[1] U. P. Steinbrecher, S. Parthasarathy, D. S. Leake, J. L. Witztum, D. Steinberg, *Proc. Natl. Acad. Sci. USA* **1984**, *81*, 3883–3887.

[2] P. Wentworth, J. Nieva, C. Takeuchi, R. Galve, A. D. Wentworth, R. B. Dilley, G. A. DeLaria, A. Saven, B. M. Babior, K. D. Janda, A. Eschenmoser, R. A. Lerner, *Science* **2003**, *302*, 1053–1056.

[3] P. Wentworth, A. D. Wentworth, X. Zhu, I. A. Wilson, K. D. Janda, A. Eschenmoser, R. A. Lerner, *Proc. Natl. Acad. Sci. USA* **2003**, *100*, 1490–1493.

[4] a) X. Zhu, P. Wentworth, A. D. Wentworth, A. Eschenmoser, R. A. Lerner, I. A. Wilson, *Proc. Natl. Acad. Sci. USA* **2004**, *101*, 2247–2252; b) P. T. Nyffeler, L. Eltepu, N. A. Boyle, C.-H. Wong, A. Eschenmoser, R. A. Lerner, P. Wentworth, *Angew. Chem. Int. Ed.* **2004**, in press.

[5] A. J. Kettle, B. M. Clark, C. C. Winterbourn, *J. Biol. Chem.* **2004**, *279*, 8521–6525.

[6] W. A. Pryor, B. Das, D. F. Church, *Chem. Res. Toxicol.* **1991**, *4*, 341–348.

[7] L. L. Smith, E. L. Ezell, K. Jaworski, *Steroids* **1996**, *61*, 401–406.

[8] "Singlet Oxygen, UV-A and Ozone": G. L. Squadrito, M. G. Salgo, F. R. Fronczek, W. A. Pryor, *Methods Enzymol.* **2000**, *319*, 570–582.

[9] S. A. Jorge, C. F. Menck, H. Sies, M. R. Osborne, D. H. Phillips, A. Sarasin, A. Stary, *DNA Repair* **2002**, *1*, 369–378.

[10] Q. Zhang, E. T. Powerts, J. Nieva, M. E. Huff, M. A. Dendle, J. Bieschke, C. G. Glabe, A. Eschenmoser, P. Wentworth, R. A. Lerner, J. W. Kelly, *Proc. Natl. Acad. Sci. USA* **2004**, *101*, 4572–4575.

[11] J. Loscalzo, *N. Engl. J. Med.* **2004**, *350*, 834–835.

[12] H. Sies, *Angew. Chem.* **1986**, *98*, 1061–1075; *Angew. Chem. Int. Ed. Engl.* **1986**, *25*, 1058–1071.

[13] H. R. Griffiths, L. Moller, G. Bartosz, A. Bast, C. Bertoni-Freddari, A. Collins, M. Cooke, S. Coolen, G. Haenen, A.-M. Hoberg, S. Loft, J. Lunec, R. Olinski, J. Parry, A. Pompella, H. Poulsen, H. Verhagen, S. B. Astley, *Mol. Aspects Med.* **2002**, *23*, 101–208.

 © 2004 Wiley-VCH Verlag GmbH & Co. KGaA, Weinheim

Sigmatropic Rearrangement

The Belluš–Claisen Rearrangement

*Jozef Gonda**

Keywords:
allylic compounds · ketenes · macrocycles · ring expansion · sigmatropic rearrangement

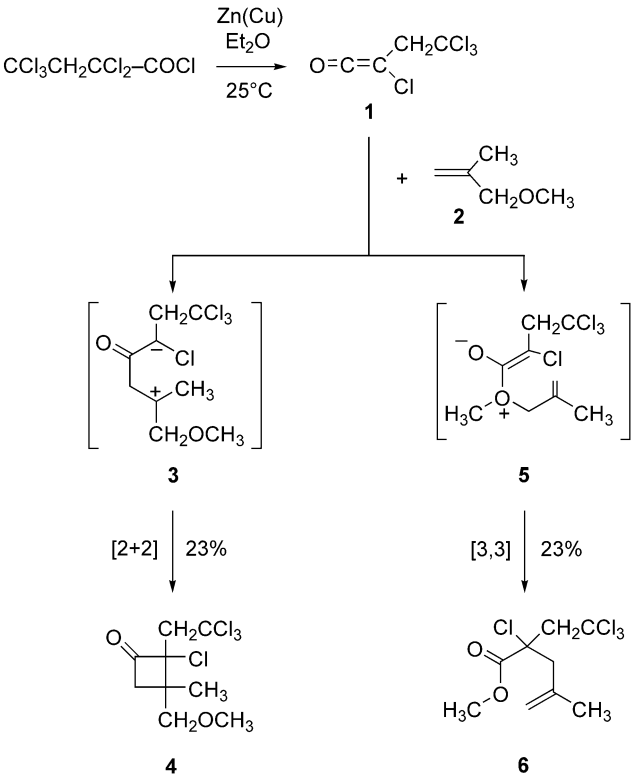
Dedicated to Professor Daniel Belluš on the occasion of his 65th birthday

***A**mong the reactions available to synthetic chemists for the construction of new C–C bonds, the Claisen rearrangement is one of the most powerful, elegant, and well-characterized methods. A genuinely new variant, the Belluš–Claisen rearrangement came to light a quarter of a century ago: The reaction of an allylic ether, thioether, or amine with a ketene leads through a [3,3] sigmatropic bond reorganization of a zwitterionic intermediate to an* E *unsaturated ester, thioester, or amide. When applied to cyclic allylic substrates, a ring-enlargement by four carbon atoms in one step provides medium-ring unsaturated* E*-configured lactones, thiolactones, and lactams. The scope of the Belluš–Claisen rearrangement and the optimum reaction conditions will be discussed in this Minireview.*

1. Introduction, Mechanism, and Scope

The synthesis of complex organic molecules from simple chemical building blocks represents an enticing and profound intellectual challenge, which lies at the heart of chemistry and has immense practical value. In this context, the discovery of a new carbon–carbon bond-forming reaction, especially a simple and reliable one, is of evident benefit. A quarter of a century ago, a serendipitous experimental result led Belluš and Malherbe to the discovery of a conceptually new intermolecular method for creating very reactive zwitterionic intermediates that are poised for a [3,3] sigmatropic Claisen-type rearrangement.[1]

In an attempt to prepare the 2-chlorocyclobutanone derivative **4** (Scheme 1), a key compound in a versatile synthesis of pyrethroid insecticides,[2] Belluš and Malherbe treated the chloro(trichloroethyl)ketene **1** (generated in situ) with the allylic ether **2** at ambient temperature. Besides the expected [2+2] cycloaddition product **4**, the γ,δ-unsaturated ester **6** was also isolated. Apparently, the nucleophilic oxygen atom of the allylic ether in **2** can compete successfully with the double bond in **2** for the electrophilic ketene. Thus, not only is the expected 1,4-dipolar intermediate **3** formed, but also the zwitterionic intermediate **5**. The zwitterion **5** is beautifully set up for a [3,3] sigmatropic rearrangement to form the unsaturated ester **6** of the Johnson–Claisen type.[3] In a seminal paper demonstrating the synthetic usefulness of the newly discovered reaction, Malherbe and Belluš[4] employed readily accessible, highly electrophilic dichloroketene,[5] which reacted with allylic ethers in a similar way to the rather exotic ketene **1**. Thus, an



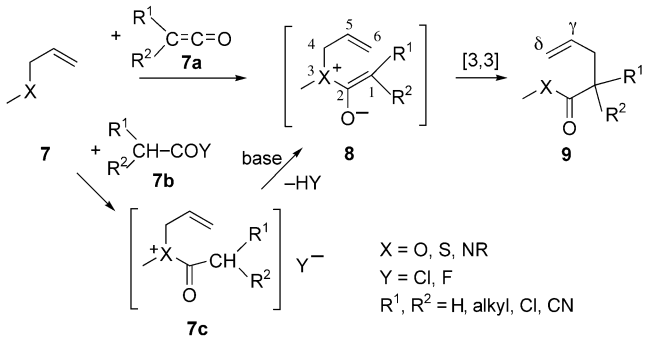
Scheme 1. First observation of the Belluš–Claisen rearrangement.

[*] Prof. Dr. J. Gonda
Institute of Chemistry, P. J. Safarik University
Moyzesova 11, 041 54 Kosice (Slovak Republic)
Fax: (+421) 556-222-124
E-mail: jgonda@kosice.upjs.sk

 © 2004 Wiley-VCH Verlag GmbH & Co. KGaA, Weinheim DOI: 10.1002/anie.200301718

unprecedented two-component Claisen-type rearrangement had been discovered, for which Belluš and Malherbe used the name "ketene-Claisen rearrangement".

It was later shown by other authors that in the case of allylic amines, the aza analogue of the zwitterion **8** (X = N-R; Scheme 2) can be formed from the allylic amine **7** (X = N-R)



Scheme 2. Mechanism of the Belluš–Claisen rearrangement.

upon reaction with a ketene **7a**. This ketene may be employed as an isolated substance,[6] or may be formed in situ either by Zn-induced dehalogenation of a 2-chloroacyl chloride,[7] photolysis of a chromium–carbene complex,[8] or dehydrohalogenation of an acyl chloride.[9] Under the latter reaction conditions the allylic amine **7** (X = N-R) may react with the acyl chloride (e.g. **7b**) to form an acyl ammonium salt **7c** (X = N-R), which, of course, is structurally unable to undergo a [3,3] sigmatropic rearrangement. Only after fast in situ dehydrohalogenation of **7c** occurs to afford the ketene-derived aza analogue **8** can the fast [3,3] bond reorganization take place.

The base-induced transformation of the adduct **7c** (X = N-R) into the zwitterion **8** (X = N-R) can be facilitated by the complexation of the acyl carbonyl group with a variety of Lewis acids, which may be added in either stoichiometric or catalytic[10] amounts. When used stoichiometrically, both achiral[11] and chiral[12] Lewis acids may be employed. Moreover, Lewis acid activation of **7c** allows the participation of ketenes that are less electrophilic than dichloroketene in the ketene Claisen rearrangement to give **9** (X = N-R). When X = O or S, direct formation of **8** is at present confined to electrophilic ketenes: dichloroketene ≈ chloro(trichloroethyl)ketene ≫ chloro(methyl)ketene > chloroketene ≈ chloro(cyano)ketene. They represent synthetic equivalents of the corresponding chloro-free ketenes, as the reductive removal of chloro groups from the position α to the carbonyl group in the rearrangement products **9** is easy to achieve preparatively. Several methods are available, for example, treatment with Zn/AcOH at elevated temperature,[4] with Zn/Ag alloy, MeOH/AcOH (5:1) at room temperature,[7] with Zn, NH_4Cl, MeOH at room temperature or above,[13] with H_2, catalytic Pt/C,[14] or with Bu_3SnH, AIBN, toluene at reflux.[15]

Alternative names, such as the "zwitterionic aza-Claisen reaction"[16] and "acyl-Claisen rearrangement"[17] have also appeared in the literature for the aza variant of the ketene-Claisen rearrangement, even though the prerequisite and at present unquestioned occurrence of **8** had already first been proposed 25 years ago in the original paper of Malherbe and Belluš.[4] Other individual names bearing at least one surname of the discoverers have been used for the underlying reaction in the literature.[18] Herein I will use the term Belluš–Claisen rearrangement (BC rearrangement), in analogy with the already established terms Eschenmoser–, Johnson–, and Ireland–Claisen rearrangements.[19]

In general, the BC rearrangement proceeds very fast at room temperature or below. This is in accordance with the well-known fact that the presence of a positively charged or chelated heteroatom in position 3[20,21] of the rearranging 1,5-hexadiene system, or a negatively charged substituent at C2,[19c,d,22] provides a significant rate acceleration of the Claisen [3,3] bond reorganization. For the first time within the Claisen family of rearrangements, the rearranging intermediate **8** contains both rate-accelerating charges in one molecule working in synergy![23]

In terms of the design of target molecules that can be prepared by using the BC rearrangement, at least one remarkable synthetic transformation deserves particular attention because of its uniqueness amongst the Claisen family of [3,3] rearrangements: If the nonparticipating alkyl substituent on the heteroatom X in **7** (X = O, S, or N-R) is connected to the adjacent sp^3 carbon atom of the allylic group to form a ring, then the BC rearrangement results in a ring enlargement by four carbon atoms in a single step, thus providing medium-sized lactones (Schemes 3–5), thiolactones (Schemes 7 and 8), or lactams (Schemes 9, 11, and 12). As a rule, the BC reaction generally affords the *E* isomer of the unsaturated rearrangement product stereoselectively. The stereoselective synthesis of these compounds is much more tedious by other routes. The yields of the ring-enlarged products are typically moderate to excellent, up to 96%.

Herein the research efforts of the first twenty-five years since the publication of the seminal paper in 1978 are summarized,[4] with a focus on the synthetic aspects of chemo-, regio-, stereo-, and enantioselective applications of the carbon–carbon bond-forming Belluš–Claisen rearrangement.



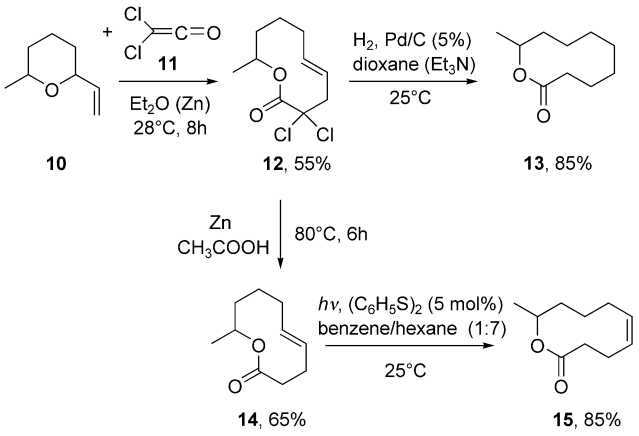
Jozef Gonda, born in 1957 in Presov (Slovakia), received his PhD in 1986 from the University of P. J. Safarik in Kosice, where he has been a full professor since 2003. From 1991 to 1995 he undertook postdoctoral research with Prof. Daniel Belluš at the University of Fribourg and Ciba-Geigy in Basel on [3,3] sigmatropic reactions. He completed his habilitation in Kosice in 1995. His main research interests include the stereoselective synthesis of natural products, in particular rare amino acids and aminosaccharides.

 © 2004 Wiley-VCH Verlag GmbH & Co. KGaA, Weinheim

2. Allylic Ethers

Shortly after the first observation of the Belluš–Claisen rearrangement with the chloro(trichloroethyl)ketene **1** (Scheme 1), a number of acyclic allylic ethers were also subjected to reaction with the well-investigated ketene[5] dichloroketene (**11**).[4,14] The ketene **11** was generated in situ from trichloroacetyl chloride by dechlorination with activated zinc in diethyl ether, and the expected α,α-dichloro-γ,δ-unsaturated esters, analogous to **6**, were formed in moderate yields (40–65%). The moderate yields suggest that competitive formation of the corresponding cyclobutanones (analogous to **4**) takes place when allylic ethers containing a nucleophilic trialkyl-substituted double bond are used. The use of 1,2-dimethoxyethane as a co-solvent capable of complexing the Lewis acid $ZnCl_2$ generated in situ favors the [2+2] cycloaddition pathway over the [3,3] sigmatropic rearrangement pathway.[24]

In spite of the limited chemoselectivity and moderate yields, Belluš and Malherbe immediately decided to further elucidate the newly discovered [3,3] sigmatropic rearrangement mode, this time with the cyclic allylic ether *cis*-2-vinyl-6-methyltetrahydro-4*H*-pyran (**10**). A successful outcome would result in a very useful synthetic methodology, that is, a conceptually new and simple one-step route to medium-sized lactones, whose synthesis is not only a challenge, because their formation is disfavored by both enthalpy and entropy, but also of practical importance, as they occur in a variety of interesting natural products.[25] In fact, the straightforward synthesis of the naturally occurring 10-membered-ring macrolides (±)-phoracantholide I (**13**) and (±)-phoracantholide J (**15**)[26] was successful on the first attempt, just as designed![4] (Scheme 3). The synthesis exemplified the unique



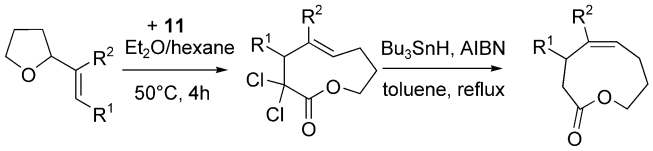
10 **12**, 55% **13**, 85%

14, 65% **15**, 85%

Scheme 3. Synthesis of the macrolides (±)-phoracantholide I (**13**) and (±)-phoracantholide J (**15**).

applicability of the new reaction to the transformation of an *n*-membered, 2-vinyl-substituted cyclic ether into an unsaturated, $(n+4)$-membered lactone. Interestingly, both 10-membered *E*-configurated lactones **12** and **14** assume two rapidly interconverting ground-state conformations, related to each other by a 180° flip of the double bond.[14] A cyclobutane by-product ($\tilde{\nu}_{max} = 1810\ cm^{-1}$) was observed in the crude reaction mixture in 10–15% yield, but did not survive chromatography on silica gel.

Along similar lines, several authors investigated the scope of the BC rearrangement in terms of the possible ring sizes of the cyclic allylic ethers used as starting materials. Taylor and co-workers[15] sought an efficient procedure for the construction of unsaturated nine-membered lactones for use in the total synthesis of diverse bioactive marine metabolites. After due consideration of the methods known at the time for cyclizations into medium-sized rings, they decided to utilize the BC rearrangement (Scheme 4) and reported: a) that this



16a, $R^1 = R^2 = H$
16b, $R^1 = H$, $R^2 = SiMe_3$
16c, $R^1 = CH_2OSiPh_2tBu$, $R^2 = H$

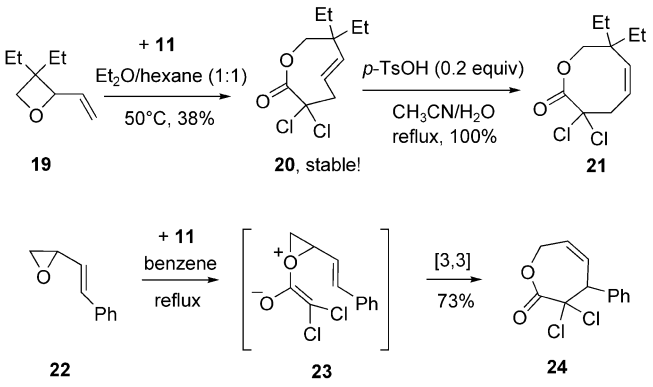
17a, 65%
17b, 64%
17c, 55%

18a, 66%
18b, 77%
18c, 75%

Scheme 4. Ring expansion to nine-membered lactones. AIBN = azobisisobutyronitrile.

chemistry is extremely useful for the preparation of lactones such as **17** and **18** from the corresponding 2-vinyltetrahydrofurans **16** and dichloroketene (**11**; generated in situ by a CCl_3COCl/Zn procedure), b) that the methodology is compatible with a bulky silyl ether substituent, for example, as in **16c**, and c) that the cyclic *E* alkenes **17** thus formed can undergo dechlorination in the presence of Bu_3SnH and AIBN with concomitant double-bond isomerization to provide the thermodynamically preferred *Z*-unsaturated lactones **18**.

An impressive result was obtained by Dean and Taylor.[27] They subjected 3,3-diethyl-2-vinyloxetane (**19**) to the usual ring expansion conditions with **11** generated from CCl_3COCl/Zn (Scheme 5). The reaction with **19** was far more rapid than with 2-vinyltetrahydrofurans, probably due to the ring-strain relief during the reaction. The remarkable unsaturated eight-membered lactone **20**, which contains an *E* double bond, was



19 **20**, stable! **21**

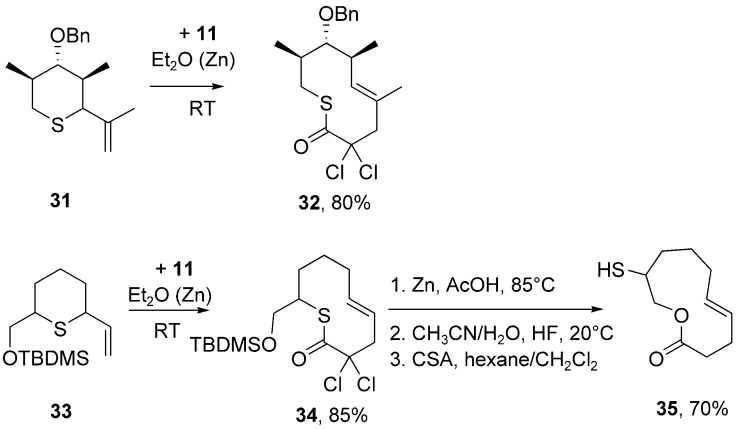
22 **23** **24**

Scheme 5. Ring-enlargement reaction of the 2-vinyloxetane **19** and the 2-vinyloxirane **22**. Ts = toluenesulfonyl.

 © 2004 Wiley-VCH Verlag GmbH & Co. KGaA, Weinheim

isolated in 38% yield. Although the double bond did not isomerize at room temperature, isomerization to the thermodynamically stable *Z* isomer **21** occurred quantitatively in the presence of a catalytic amount of *p*-TsOH in aqueous acetonitrile at reflux.

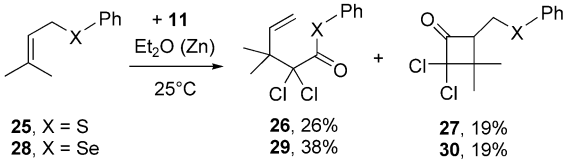
In striking contrast with unsuccessful attempts at the ring expansion of six-[1] and four-membered[27] 2-vinyl cyclic ethers by reaction with dichloroketene (**11**) generated in situ from dichloroacetyl chloride by dehydrochlorination with an organic base, these appear to be the only viable reaction conditions for the ring expansion of a series of 2-vinyloxiranes.[9] For example, 2-styryloxirane **22** reacted with **11** (from $CHCl_2COCl/Et_3N$) to furnish, presumably via the zwitterion **23**, the 3,3-dichloro-4-phenyl-2,3,4,7-tetrahydrooxepin-2-one **24** in a good 73% yield (Scheme 5). However, **24** was not formed if **11** was generated in situ from CCl_3COCl and zinc, probably because of a fast $ZnCl_2$-catalyzed polymerization of the oxirane **22**. Only the unsaturated seven-membered lactones bearing a *Z* double bond were isolated.[9]



Scheme 7. The contribution of Vedejs et al. to the synthesis of 10- and 11-membered lactones by the Belluš–Claisen rearrangement.

3. Allylic Thioethers

Given the higher nucleophilicity of sulfur versus oxygen, it is not surprising that in their first publication Malherbe and Belluš already reported the successful application of the new [3,3] bond reorganization reaction to several acyclic allylic thioethers, and, as a curiosity, also to an allylic selenoether (Scheme 6).[4,14]

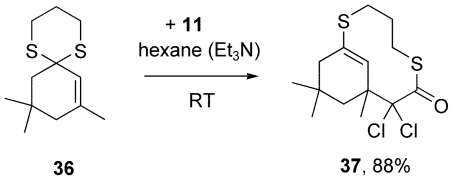


Scheme 6. Examples of rearrangements of the allylic thioether **25** and selenide **28**.

The cyclic version of this reaction was originally reported to proceed in a disappointing yield of 8%.[14] However, Vedejs et al. showed that an optimized ring-expansion procedure with dichloroketene (**11**) generated by the slow addition with a syringe pump of excess CCl_3COCl to the substrate and Zn/Cu couple in ether at reflux gave 10-membered thiolactones in consistently good yields (75–85%; Scheme 7). The double bond in the 10-membered ring is formed exclusively with the *E* configuration.[28,29]

Thiolactones such as **32** and **34** are not only interesting as final targets but can also be used as intermediates in the total synthesis of natural products. Thus, Vedejs et al. used **32** in studies towards the stereoselective synthesis of a key fragment of the natural macrolide erythronolide, and **34** was used to demonstrate a convenient transformation of the initially formed macrocyclic ω-hydroxyalkyl thiolactones into lactones such as **35** by means of an intramolecular S to O acyl shift. This elegant ring expansion by one carbon atom was catalyzed by anhydrous camphorsulfonic acid (CSA). Vedejs and Buchanan stated that "there is good reason to believe that efficient (cyclic) sulfide ring expansion with dichloroketene is a general reaction".[29]

Rossini et al.[30] found that the readily accessible five- and six-membered cyclic thioketals of α,β-unsaturated cyclopentenones and cyclohexenones, such as **36**, underwent an efficient ring enlargement to bicyclic thiolactones, such as **37**, in yields of 78–88% (Scheme 8). Interestingly, in this case **11** had to be formed in situ by dehydrohalogenation of dichloroacetyl chloride with Et_3N. No cyclobutanone products were observed.[24,30]

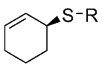
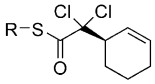
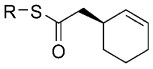
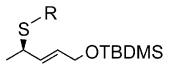
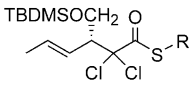
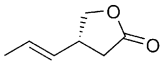
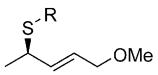
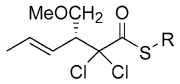
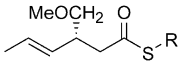
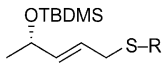
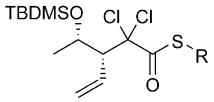
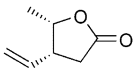
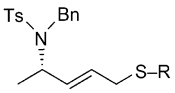
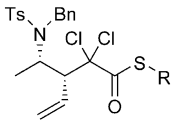
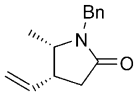


Scheme 8. An example of a four-carbon-atom ring enlargement of a cyclic thioketal.

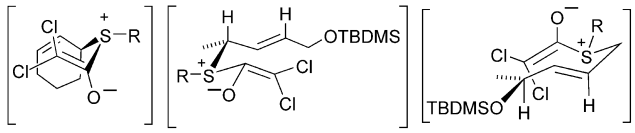
Much effort has been invested in the study of chirality transfer and chirality induction in standard Claisen [3,3] rearrangements.[19c,d,31] In a number of early publications, Belluš, Ernst, and co-workers studied the effect of chiral substituents on the BC reaction of allylic thioesters. Thus, nearly complete (> 98%) 1,3-chirality transfer occurred from the allylic C center of a C–S bond in **41** to the stereogenic allylic C center in the new C–C bond in the chiral thioester **42**, as determined by ^1H NMR spectroscopic shift experiments with (*R*)-(−)-TFAE (2,2,2-trifluoro-1-(9-anthryl)ethanol; Table 1).[32,33] Conceivably, the zwitterionic intermediate **38** (Figure 1) is involved in the suprafacial [3,3] bond reorganization step, thus leading to a new C–C bond oriented exclusively "*cis*" with respect to the original C–S bond. The stereochemical integrity of **42** was conserved during the subsequent dechlorination with Zn in AcOH at 100 °C to give the thioester **43**.

 © 2004 Wiley-VCH Verlag GmbH & Co. KGaA, Weinheim

Table 1: Selected examples of the stereo- and chemoselective BC rearrangement of allylic thioethers with dichloroketene (**11**).[a]

Allylic thioether	Dipolar intermediate (Figure 1)	Product of rearrangement (yield [%])	Product after treatment with Zn/AcOH (yield [%])
	**38**		
41, 96% *ee*[32,33]		**42**, 95% *ee* (80)	**43**, 95% *ee* (92)
	**39**		
44, 85% *ee*[32,33]		**45**, 83% *ee* (76)	**46**, 66.4% *ee* (66)
	like **39**		
47, 85% *ee*[34]		**48**, 83% *ee* (86)	**49**, 83% *ee* (98)
	**40**		
50, ≥94% *ee*[34]		**51**, d.r. ≥97:3 (82)	**52**, *cis/trans* 97:3 (82)
	like **40**		
53, ≥95% *ee*[35]		**54**, d.r. 90:10 (89)	**55**, d.r. n.d. (95)

[a] R = isopropyl, n.d. = not determined. Bn = benzyl, TBDMS = *tert*-butyldimethylsilyl.



38 R = *i*Pr **39** **40**

Figure 1. Chairlike reactive zwitterionic intermediates derived from dichloroketene (**11**) and the chiral allylic thioethers **41**, **44**, and **50** (Table 1).

The *E* allylic thioethers **44** and **47** served as models for scrutinizing the stereochemical course of the BC reaction with **11** in open-chain systems.[32–34a] Very high enantioselectivity was also observed for the 1,3-chirality transfer from **44** and **47** (85% *ee*) to the unsaturated *E* thioesters **45** and **48** (83% *ee*), as well as excellent chemical yields. A chairlike zwitterion **39** is responsible for the high level of chirality transfer. Interestingly, if both allylic S-alkyl and allylic O-alkyl groups are present in the molecule, as in **47**, dichloroketene (**11**) reacts highly chemoselectively with the more nucleophilic S atom, thus leading in this case exclusively to the thioester **48**.[34] The recently published Pd-catalyzed synthesis of chiral allylic thioethers could expand the scope of the thia-BC rearrangement by making the starting materials more readily accessible.[36]

As a result of the very mild experimental conditions, the 1,2-asymmetric induction in the BC reaction of the allylic thioether **50**, derived from (−)-L-lactic acid, with dichloroketene (**11**) is close to 100% (Table 1). The resulting diastereomer **51** has the *syn* configuration. Three subtle factors allow **11** to differentiate between the two possible diastereotopic faces of **50** in favor of the depicted intermediate **40** (Figure 1): First, the minimized 1,3-allylic strain as a stereochemical controlling factor;[37] second, the preferred equatorial position of the chiral substituent at the terminal allylic sp^2 carbon in the intermediate **40**; and third, the highly preferred *anti* quasi-nucleophilic attack of the terminal sp^2 carbon atom of the ketene with respect to the (C–O) bond on the chiral substituent, as has also been observed in the mechanistically related [2,3] sigmatropic Wittig rearrangement[38] and later in aza-BC reactions.[16,39]

In contrast to the complete diastereoselectivity observed in the BC rearrangement of **50**, only d.r. 75:25 and 57.5:43.5 were observed in the Ireland–Claisen rearrangement of structurally related silylketene acetals derived from L-lactaldehyde[40] and D-glyceraldehyde, respectively.[41] An analogous thermal (140°C) Johnson–Claisen rearrangement with triethyl orthoacetate furnished only a 1:1 mixture of diastereomeric products.[42]

In comparison to results with **50**, slightly lower 1,2-*syn*-diastereoinduction was observed in the BC reaction of *N*-toluenesulfonyl- (**53**; Table 1) and analogous *N*-Boc-protected chiral thioethers with dichloroketene (**11**).[35] As the basicity of the allylic nitrogen atom in **53** is greatly reduced by either of these protecting groups, chemoselective [3,3] rearrangement of the allylic thioester to afford *syn*-**54** was observed. An attempt was made to understand the difference between the diastereoselectivities in the rearrangements of **50** and **53** by calculating all possible (two chairlike and two boatlike) zwitterionic intermediates at a semiempirical AM1 SCF-MO level. For **50**, calculation revealed that there is an energy difference of 17.15 kJ mol^{-1} in favor of a "*syn*" chairlike intermediate **40** relative to the next-best chairlike intermediate, which would lead to an *anti* diastereomer of **51.** Thus, the calculated diastereoselectivity of d.r. > 99.9:0.1 is in perfect agreement with the experimental findings. In contrast, the calculated best chairlike zwitterionic intermediate arising from **53** and **11**, which leads to **54** as the main *syn* isomer, is favored by only 1.08 kJ mol^{-1} relative to the energetically closest (boatlike(!)) intermediate. These results are indicative of a more-complex electronic and steric interaction in the sulfonium intermediate derived from **53** and **11** than in that derived from **50**. Conceivably, electronic and steric fine-

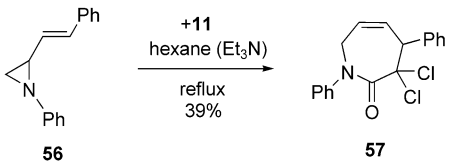
 © 2004 Wiley-VCH Verlag GmbH & Co. KGaA, Weinheim

tuning of the two substituents on the allylic nitrogen atom in compounds such as **53** would offer many synthetic opportunities for the use of BC rearrangements with differing outcomes in terms of *syn*/*anti* selectivity or even of chemoselectivity (reaction of the allylic sulfur atom versus the allylic nitrogen atom).

The reductive treatment of the rearrangement products **45**, **51**, or **54** with Zn in acetic acid at 100 °C initiates three simultaneous reactions: α,α-dechlorination, deprotection of O or N, and a ring closure to afford the novel chiral γ-butyrolactones **46** or **52**, or the lactam **55** (Table 1). These compounds possess interesting substitution patterns and retain the stereochemical integrity of their precursors.

4. Allylic Amines

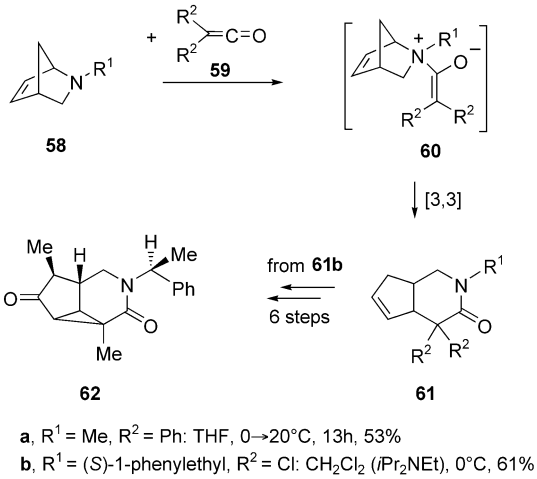
Curiously enough, the aziridine **56** was the first substrate used in a Belluš–Claisen rearrangement of a tertiary allylic amine and dichloroketene (**11**).[9] In analogy with **24**, the double bond in the resulting 2,3,4,7-tetrahydro-1*H*-azepinone **57** has the *Z* configuration. (Scheme 9). So far, this remains the only reported BC reaction of a 2-vinylaziridine.



Scheme 9. The first reported example of an aza-BC reaction.

The second reported case of an aza-BC rearrangement is also rather unconventional, as it represents the only known reaction that utilizes a stable isolated ketene. Roberts et al.[6] described an interesting skeletal rearrangement of the *N*-methylazanorbornene **58a** with isolated diphenylketene (**59a**) to form the bicyclic piperidone **61** in moderate yield (Scheme 10). For the *N*-benzyl derivative of **58**, a dramatic increase in the reaction rate was reported when the reaction was performed in an ultrasonic bath.

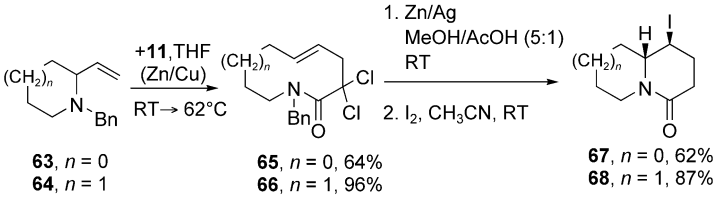
Pombo-Villar and co-workers ingeniously applied the principle of the transformation of **58** described by Roberts et al. to an enantioselective total synthesis of the three monoterpene alkaloids (−)-2-skytanthine, (+)-epidihydrotecomanine, and (−)-*N*-demethyl-δ-skytanthine, from a common enantiomerically pure tricycle **62**, which in turn was prepared in six steps from the product **61b** of the aza-BC rearrangement of **58b** with dichloroketene (**11**; Scheme 10).[13,43] The *cis* ring junction in **61** is the result of a concerted [3,3] rearrangement of a transient intermediate **60** via a boat conformation. Because of structural constraints, this system is unable to adopt a chair conformation. As a precursor for **58b**, (*S*)-1-phenylethylamine was used as the original source of chirality for the whole synthesis. For the BC reaction with **58b**, **11** had to be generated in situ from dichloroacetyl chloride by using diisopropylethylamine in CH_2Cl_2 at 0 °C.



a, R^1 = Me, R^2 = Ph: THF, 0→20 °C, 13h, 53%
b, R^1 = (*S*)-1-phenylethyl, R^2 = Cl: CH_2Cl_2 (*i*Pr_2NEt), 0 °C, 61%

Scheme 10. Preparative access to the azabicyclo[4.3.0] skeleton of monoterpene alkaloids.

A number of papers report on that highly characteristic transformation of the BC rearrangement: the ring expansion of 2-vinyl cyclic amines by four carbon atoms in one step to prepare nine and ten-membered lactams, which can be useful precursors to natural products or their subunits. However, only Edstrom[7,44] has utilized **11**, generated in situ from trichloroacetyl chloride and a Zn/Cu couple, to access the unsaturated lactams **65** and **66** (Scheme 11). Evidence for a



Scheme 11. A route to functionalized indolizidine and quinolizidine ring systems based on the aza-BC rearrangement.

zwitterionic intermediate of the type **8** (from **63**) was obtained by ^{1}H and ^{13}C NMR spectroscopy. Subsequent exposure of the lactams **65** and **66**, or their α-dechlorinated derivatives, to certain electrophiles triggered a simultaneous transannular cyclization–debenzylation. For example, the indolizidine **67** and quinolizidone **68** were formed upon treatment with iodine. Their skeletons are widespread among alkaloid natural products.

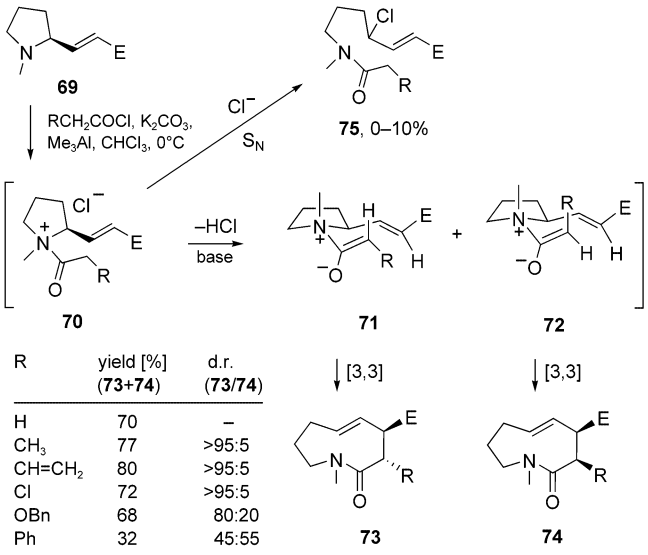
Analogous sequences that start with a BC rearrangement, which is then followed by a stereoselective transannular reaction, have been thoroughly investigated by Nubbemeyer and co-workers.[11,16,45] As a result of their pioneering expansion of the scope of the aza-BC reaction by elaboration of an alternative approach to reactive 1,5-hexadiene intermediates of the type **8** via their *N*-acyl ammonium precursors of the type **7c**, they were not confined to the use of highly electrophilic ketenes. Additional substitution patterns, intro-

 © 2004 Wiley-VCH Verlag GmbH & Co. KGaA, Weinheim

duced in the form of substituents on the acyl group thus became accessible in the products of the [3,3] rearrangement.

The experimental variant of the BC rearrangement of Nubbemeyer and co-workers will be exemplified by means of the reaction of the optically active 2-pyrrolidine acrylic ester **69** with various acyl chlorides (Scheme 12).[11,16] They found that:

1) The rearrangement is not restricted to activated ketenes.
2) Special two-phase conditions are recommended: A slurry of the allylic amine and solid K_2CO_3 in anhydrous $CHCl_3$ or CH_2Cl_2 is treated with the acyl chloride and the Lewis acid trimethylaluminum (> 20 mol %).
3) The major competing reaction is a von Braun process involving nucleophilic attack of a chloride ion on the intermediate acyl ammonium salts, for example, on **70** to give **75**.[11]
4) The use of acyl fluorides instead of acyl chlorides as in situ sources of ketenes seems to completely suppress the von Braun process, as no formation of *N*-acyl ammonium fluorides of the type **70** is observed.[45a,c]
5) Complete 1,3-chirality transfer takes place; the orientation of the C–N bond dictates that of the new C–C bond. Deprotonation of the acyl ammonium salt (e.g. **70**) generates predominantly the *Z*-enolate structure corresponding to **71** because of minimized 1,3-diaxial and other steric interactions. As a result, 3,4-*trans*-difunctionalized 2-azonines **73** are the major diastereomers produced by the reaction.
6) Because of restricted flipping of the *E* double bond with respect to the ring, in nine- and ten-membered lactams, such as **66**, **73**, and **74**, planar-chirality phenomena frequently occur.[45d] One can take advantage of these phenomena in introducing new stereogenic centers in total syntheses of bicyclic natural products, such as the pumiliotoxins.[45e]



R	yield [%] (**73**+**74**)	d.r. (**73**/**74**)
H	70	–
CH_3	77	>95:5
$CH{=}CH_2$	80	>95:5
Cl	72	>95:5
OBn	68	80:20
Ph	32	45:55

Scheme 12. The diastereoselective synthesis of nine-membered lactams via the ketene precursors **70** by Nubbemeyer and co-workers. E = CO_2Et.

Hegedus and co-workers[8] extended the aza-BC rearrangement to include photogenerated ketenes originating from the photolysis of chromium–carbene complexes, such as $[(CO)_5Cr{=}C(OR)Me]$ in THF. These ketenes can be used to install two geminal substituents α to the carbonyl carbon atom in products of the [3,3] rearrangement, for example, α-methyl,α-*n*-butoxy substitution in skeletons corresponding to **61** (R^1 = Bn; 51 % yield), **65** (66 % yield), and **77** (Table 2, 68 % yield). Whereas the strained compounds **58** (R^1 = Bn) underwent an efficient BC reaction with *n*-butoxymethylketene even in the absence of a Lewis acid, the less-strained **63** required the mild Lewis acid $ZnCl_2$, and the acyclic allylic amine **76** required the presence a strong Lewis acid, such as Me_2AlCl. More electron-rich carbene complexes, such as $CO_5Cr{=}C(NR_2)H$, were much less efficient, giving the corresponding rearranged products in only low yields (< 22 %). The results of Hegedus and co-workers are mechanistically significant for the aza-BC rearrangement, as they reveal that even with electron-rich ketenes an "acyl ammonium intermediate" of the type **7c** need not be formed, provided that the ketene part of the reacting zwitterionic 1,5-hexadiene system of the type **8** is chelated by an appropriate Lewis acid.

Nubbemeyer applied the two-phase experimental conditions described under b) above for the cyclic compound **69** to the BC rearrangement of optically active open-chain *N*-allyl pyrrolidones.[39,46] As in the case of structurally similar chiral thioethers (e.g. **50**), high 1,2-asymmetric induction was observed in the construction of a new C–C bond adjacent to the stereogenic C center bonded to O. The yields of the isolated γ,δ-unsaturated amides thus formed were 60–90 %.

A powerful feature of the aza variant of the BC rearrangement involving *N*-acyl ammonium intermediates of the type **7c**, in which both the ketene and allylic *E* or *Z* double bonds can bear electronically diverse substituents, is the capacity to build diverse functional and stereochemical arrays. This capacity was demonstrated by Nubbemeyer and co-workers (with Me_3Al as the activating Lewis acid)[11,16,45] and Yu et al. (without a Lewis acid).[47] Recently MacMillan and co-workers[10] reported the successful catalysis of a diastereoselective [3,3] rearrangement of the type **8**→**9** with a variety of Lewis acids, including $Yb(OTf)_3$, $AlCl_3$, $Ti(OiPr)_2Cl_2$, and $TiCl_4{\cdot}2$ thf. Although only the BC reactions with (*E*)-**76** and (*Z*)-**78** can be compared directly so far, Table 2 suggests the preparative superiority of the reaction conditions B of MacMillan and co-workers in terms of chemical yield and diastereoselectivity. Significant structural variation in the substituent on the double bond of the allyl group (H, aryl, or Cl instead of Me) as well as in the acyl chloride (NPht, SPh, or OBn instead of Me) is also possible without loss of yield or diastereoselectivity. If 3,3-disubstituted allylic morpholines are used, the chairlike transition state controls the π-facial discrimination, so that one can introduce elusive quarternary carbon stereocenters stereoselectively in d.r. > 97.5:2.5.

High-yielding experimental conditions enabled Dong and MacMillan[17] to design and perform a series of tandem aza-BC rearrangements that could be used to build up functional and stereochemical acyclic systems of considerable complex-

 © 2004 Wiley-VCH Verlag GmbH & Co. KGaA, Weinheim

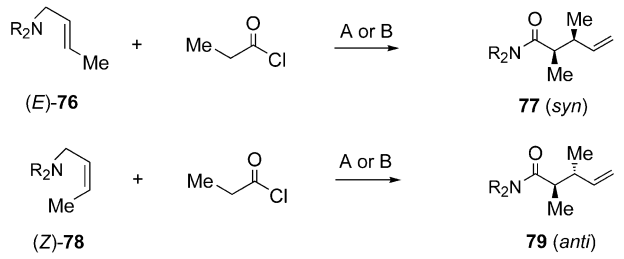
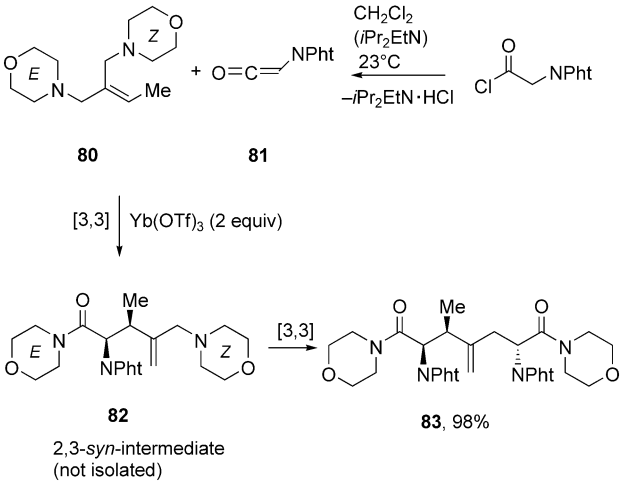


Table 2: Comparison of different experimental conditions for the generation of methylketene for the aza-BC rearrangement.

R_2N	Conditions[a]	Allylic amine	Product (yield [%])	*syn*/*anti*	Ref.
piperidyl	A	(*E*)-**76**	**77** (41)	94:6	[47]
		(*Z*)-**78**	**79** (38)	3:97	
morpholyl	B	(*E*)-**76**	**77** (92)	>99:1	[10]
		(*Z*)-**78**	**79** (74)	5:95	

[a] Conditions: A: K_2CO_3, toluene, 0 °C; B: $TiCl_4$·2thf (5 mol %), iPr_2EtN, CH_2Cl_2, 23 °C.

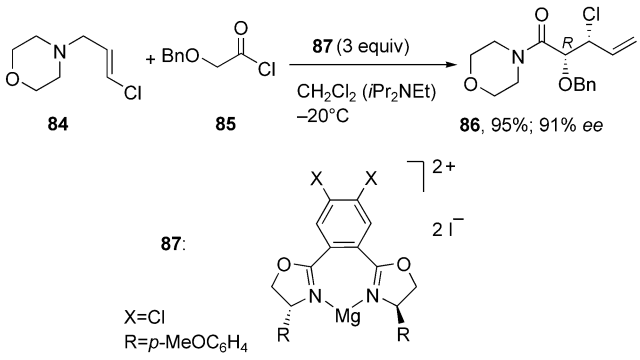
ity. These systems are not readily accessible by other synthetic methods. Thus, two consecutive [3,3] rearrangements of **80** with phthaloylglycyl chloride as a surrogate of *N*-phthaloylimidoketene **81** allowed the rapid construction of **83** with two masked α-amino acid moieties, with >95% diastereoselectivity in favor of the 2,3-*syn*-3,6-*anti* isomer and in a superb overall yield of 98% (Scheme 13). The intermediate **82** (2,3-



Scheme 13. An example of a tandem aza-Belluš–Claisen rearrangement. Pht = phthaloyl.

syn), the product of the first rearrangement involving the *E* allylic morpholine moiety, need not be isolated. Considerable variations in the substituents on the double bond in **80** and in the structure of the acyl chloride are tolerated.

Recently, Yoon and MacMillan[12] used the demonstrated utility of auxiliary-metal chelation as an organizational control element in asymmetric synthesis[48] to develop the first examples of the enantioselective BC rearrangement (Scheme 14). A survey of ligand/metal-salt combinations revealed that the (*R*,*R*)-arbox framework **87** exhibited superior levels of enantioselectivity. For example, its use as a chiral Lewis acid in the BC reaction of achiral **84** with



Scheme 14. The contribution of Yoon and MacMillan to the development of an enantioselective aza-BC rearrangement.

benzyloxyacetyl chloride (**85**) as a precursor to benzyloxyketene led to **86** in 95% yield, with *syn*/*anti* diastereoselectivity of 98:2 and, most significantly, with 91% *ee*. It seems that a strongly chelating heteroatom, such as the alkyl-substituted oxygen atom in the ketene moiety, promotes the enantiofacial discrimination of the [3,3] rearrangement process, because poorly chelating ketenes, such as acetoxyketene and *tert*-butyldimethylsilyloxyketene, exhibited only modest levels of stereoselectivity (<38% *ee*). Significant variation in the substituents on the double bond of the allylic amine was tolerated without loss of enantioselectivity.

5. Conclusions and Outlook

The Belluš–Claisen rearrangement offers abundant synthetic potential. Even with its current scope it considerably broadens the range of possible stereoselective approaches to *E* γ,δ-unsaturated esters, thioesters, and amides. At present this experimentally simple and reliable reaction is one of the most efficient and predictable methods for the synthesis of nine- and ten-membered lactones, thiolactones, and lactams containing an *E* double bond. The reactions of allylic ethers and thioethers with electrophilic ketenes, such as dichloroketene, furnish products of the BC rearrangement in good yields, whereas the reactions of allylic amines with neutral or electron-rich ketenes can be efficiently catalyzed by Lewis acids. When chiral Lewis acids were employed in equimolar amounts, remarkable enantioselectivity was reported. However, even twenty-five years after its discovery, the Belluš variant of the Claisen rearrangement is still in its infancy in comparison with the established Johnson, Eschenmoser, and Ireland variants. Further imaginative exploration of metal-chelation effects might render allylic ethers and thioethers amenable to reaction with a broader variety of ketenes. The interaction of aromatic or heteroaromatic allylic systems with ketenes has not yet been investigated, and neither has the

 © 2004 Wiley-VCH Verlag GmbH & Co. KGaA, Weinheim

reaction of allenic and propargylic O, S, and N systems by single or tandem protocols. It is to be expected that the Belluš–Claisen rearrangement will become very useful in organic synthesis in the near future.

Received: October 9, 2003 [M1718]
Published Online: May 24, 2004

[1] D. Belluš, personal communication.
[2] a) P. Martin, H. Greuter, D. Belluš, *J. Am. Chem. Soc.* **1979**, *101*, 5853; b) P. Martin, H. Greuter, D. Belluš, *Helv. Chim. Acta* **1981**, *64*, 64.
[3] W. S. Johnson, L. Werthemann, W. R. Bartlett, T. J. Brocksom, T.-T. Li, D. J. Faulkner, M. R. Petersen, *J. Am. Chem. Soc.* **1970**, *92*, 741.
[4] R. Malherbe, D. Belluš, *Helv. Chim. Acta* **1978**, *61*, 3096 – 3099.
[5] T. T. Tidwell, *Ketenes*, Wiley, New York, **1995**, pp. 336 – 3348.
[6] a) S. M. Roberts, C. Smith, R. J. Thomas, *J. Chem. Soc. Perkin Trans. 1* **1990**, 1493 – 1495; b) R. Maurya, C. A. Pittol, R. J. Pryce, S. M. Roberts, R. J. Thomas, J. O. Williams, *J. Chem. Soc. Perkin Trans. 1* **1992**, 1617 – 1621.
[7] E. D. Edstrom, *Tetrahedron Lett.* **1991**, *32*, 5709 – 5712.
[8] C. J. Deur, M. W. Miller, L. S. Hegedus, *J. Org. Chem.* **1996**, *61*, 2871 – 2876.
[9] M. Ishida, H. Muramaru, S. Kato, *Synthesis* **1989**, 562 – 564.
[10] T. P. Yoon, V. M. Dong, D. W. C. MacMillan, *J. Am. Chem. Soc.* **1999**, *121*, 9726 – 9727.
[11] M. Diederich, U. Nubbemeyer, *Chem. Eur. J.* **1996**, *2*, 894 – 900.
[12] T. P. Yoon, D. W. C. MacMillan, *J. Am. Chem. Soc.* **2001**, *123*, 2911 – 2912.
[13] M. M. Cid, E. Pombo-Villar, *Helv. Chim. Acta* **1993**, *76*, 1591 – 1607.
[14] R. Malherbe, G. Rist, D. Belluš, *J. Org. Chem.* **1983**, *48*, 860 – 869.
[15] M. R. Kling, G. A. McNaughton-Smith, R. J. K. Taylor, *Chem. Commun.* **1993**, 1593 – 1595.
[16] M. Diederich, U. Nubbemeyer, *Angew. Chem.* **1995**, *107*, 1095 – 1098; *Angew. Chem. Int. Ed. Engl.* **1995**, *34*, 1026 – 1028.
[17] V. M. Dong, D. W. C. MacMillan, *J. Am. Chem. Soc.* **2001**, *123*, 2448 – 2449.
[18] Malherbe–Belluš variant of the Claisen rearrangement,[8,15] Belluš–Claisen rearrangement,[11] Belluš–Claisen reaction,[10] Belluš ketene-Claisen reaction,[17] Belluš reaction.[12]
[19] For reviews, see: a) F. E. Ziegler, *Chem. Rev.* **1988**, *88*, 1423 – 1452; b) S. Blechert, *Synthesis* **1989**, 71 – 82; c) P. Wipf in *Comprehensive Organic Synthesis*, *Vol. 5* (Eds.: B. M. Trost, I. Fleming), Pergamon, Oxford, **1991**, pp. 827 – 873; d) H. Frauenrath, *Methods Org. Chem. (Houben-Weyl)*, *Vol.E 21d* **1995**, pp. 3300–3756; e) Y. Chai, S. Hong, H. A. Lindsay, C. McFarland, M. C. McIntosh, *Tetrahedron* **2002**, *58*, 2905 – 2926.
[20] S. Jolidon, H. J. Hansen, *Helv. Chim. Acta* **1977**, *60*, 978.
[21] For reviews, see: a) R. P. Lutz, *Chem. Rev.* **1984**, *84*, 205; b) B. Ganem, *Angew. Chem.* **1996**, *108*, 1014 – 1023; *Angew. Chem. Int. Ed. Engl.* **1996**, *35*, 936 – 945; c) M. Hiersemann, L. Abraham, *Eur. J. Org. Chem.* **2002**, 1461 – 1471.
[22] U. Kazmeier, H. Mues, A. Krebs, *Chem. Eur. J.* **2002**, *8*, 1850.
[23] For remotely related charged aza-Claisen rearrangements, see also: a) S. Mageswaran, W. D. Ollis, R. Somanathan, I. O. Sutherland, *J. Chem. Soc. Perkin Trans. 1* **1982**, 893; b) E. Vedejs, M. Gingras, *J. Am. Chem. Soc.* **1994**, *116*, 579; c) T. H. Lambert, D. W. C. MacMillan, *J. Am. Chem. Soc.* **2002**, *124*, 13646; d) A. V. Novikov, A. R. Kennedy, J. D. Rainier, *J. Org. Chem.* **2003**, *68*, 993.
[24] B. D. Johnston, E. Czyzewska, A. C. Oehlschlager, *J. Org. Chem.* **1987**, *52*, 3693 – 3697.
[25] a) G. Rousseau, *Tetrahedron* **1995**, *51*, 2777 – 2849; b) P. von-Zezschwitz, K. Voigt, M. Nottemeyer, A. de Meijere, *Synthesis* **2000**, 1327 – 1340.
[26] B. P. Moore, W. V. Brown, *Aust. J. Chem.* **1976**, *29*, 1365.
[27] J. C. Dean, MSc thesis, University of East Anglia, Norwich, **1995**; J. K. Taylor, personal communication.
[28] E. Vedejs, J. M. Dolphin, H. Mastalerz, *J. Am. Chem. Soc.* **1983**, *105*, 127 – 130.
[29] E. Vedejs, R. A. Buchanan, *J. Org. Chem.* **1984**, *49*, 1840 – 1841.
[30] G. Rossini, G. G. Spineti, E. Foresti, G. Pradella, *J. Org. Chem.* **1981**, *46*, 2228 – 2230.
[31] a) D. Enders, M. Knopp, R. Schiffers, *Tetrahedron: Asymmetry* **1996**, *7*, 1847 – 1882; b) H. Ho, T. Taguchi, *Chem. Soc. Rev.* **1999**, *28*, 43 – 50; c) B. Werschkun, J. Thiem, *Top. Curr. Chem.* **2001**, *215*, 293 – 325; d) U. Nubbemeyer, *Synthesis* **2003**, 961 – 1008.
[32] R. Oehrlein, R. Jeschke, B. Ernst, D. Belluš, *Tetrahedron Lett.* **1989**, *30*, 3517 – 3520.
[33] B. Ernst, J. Gonda, R. Jeschke, U. Nubbemeyer, R. Oehrlein, D. Belluš, *Helv. Chim. Acta* **1997**, *80*, 876 – 891.
[34] a) U. Nubbemeyer, R. Oehrlein, J. Gonda, B. Ernst, D. Belluš, *Angew. Chem.* **1991**, *103*, 1533 – 1534; *Angew. Chem. Int. Ed. Engl.* **1991**, *30*, 1465 – 1467; see also: b) V. K. Aggarwal, A. Lattanzi, D. Fuentes, *Chem. Commun.* **2002**, 2534 – 2535.
[35] J. Gonda, M. Martinkova, B. Ernst, D. Belluš, *Tetrahedron* **2001**, *57*, 5607 – 5613.
[36] H.-J. Gais, A. Böhme, *J. Org. Chem.* **2002**, *67*, 1153.
[37] R. W. Hoffmann, *Chem. Rev.* **1989**, *89*, 1841.
[38] H. Priebke, R. Brückner, *Chem. Ber.* **1990**, *123*, 153.
[39] U. Nubbemeyer, *J. Org. Chem.* **1996**, *61*, 3677 – 3686.
[40] S. Hatekayama, K. Saijo, S. Takano, *Tetrahedron Lett.* **1985**, *26*, 865.
[41] J. K. Cha, S. C. Lewis, *Tetrahedron Lett.* **1984**, *25*, 5263.
[42] S. Takano, A. Kurotaki, M. Takahashi, K. Ogasawara, *J. Chem. Soc. Perkin Trans. 1* **1987**, 91.
[43] M. M. Cid, U. Eggnauer, H. P. Weber, E. Pombo-Villar, *Tetrahedron Lett.* **1991**, *32*, 7233 – 7236.
[44] E. D. Edstrom, *J. Am. Chem. Soc.* **1991**, *113*, 6690 – 6692.
[45] a) A. Sudau, U. Nubbemeyer, *Angew. Chem.* **1998**, *110*, 1178 – 1181; *Angew. Chem. Int. Ed.* **1998**, *37*, 1140 – 1143; b) S. Laabs, A. Scherrmann, A. Sudau, M. Diederich, C. Kierig, U. Nubbemeyer, *Synlett* **1999**, 25 – 28; c) A. Sudau, W. Münch, U. Nubbemeyer, J. W. Bats, *J. Org. Chem.* **2000**, *65*, 1710 – 1720; d) U. Nubbemeyer, *Eur. J. Org. Chem.* **2001**, 1801 – 1816; e) A. Sudau, W. Münch, J. W. Bats, U. Nubbemeyer, *Eur. J. Org. Chem.* **2002**, 3304 – 3314.
[46] U. Nubbemeyer, *J. Org. Chem.* **1995**, *60*, 3773 – 3780.
[47] C.-M. Yu, H.-S. Choi, J. Lee, W.-H. Jung, H.-J. Kim, *J. Chem. Soc. Perkin Trans. 2* **1996**, 115 – 116.
[48] J. S. Johnson, D. A. Evans, *Acc. Chem. Res.* **2000**, *33*, 325.

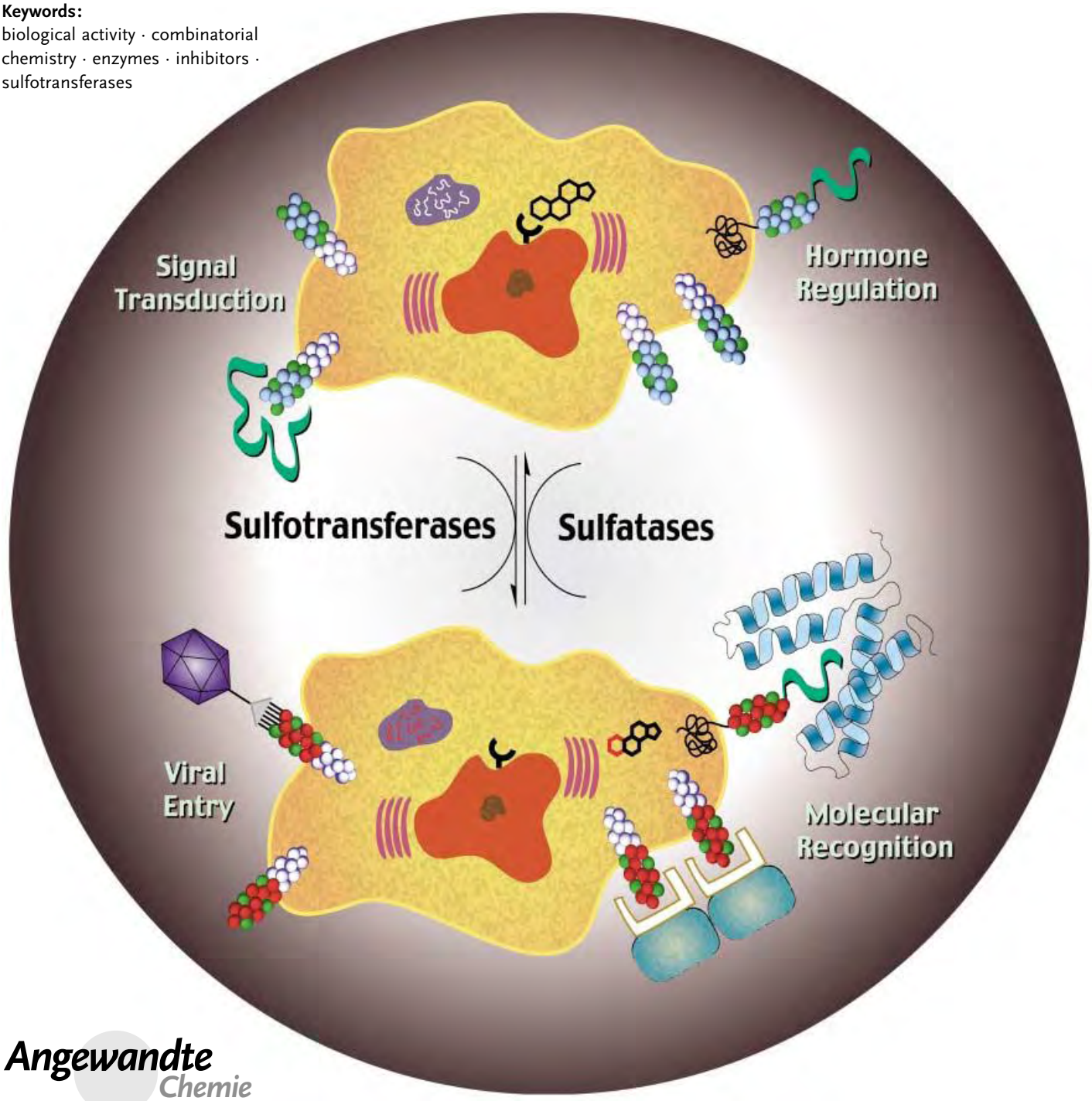
 © 2004 Wiley-VCH Verlag GmbH & Co. KGaA, Weinheim

Enzyme Chemistry

Sulfotransferases: Structure, Mechanism, Biological Activity, Inhibition, and Synthetic Utility

*Eli Chapman, Michael D. Best, Sarah R. Hanson, and Chi-Huey Wong**

Keywords:
biological activity · combinatorial chemistry · enzymes · inhibitors · sulfotransferases



© 2004 Wiley-VCH Verlag GmbH & Co. KGaA, Weinheim
DOI: 10.1002/anie.200300631

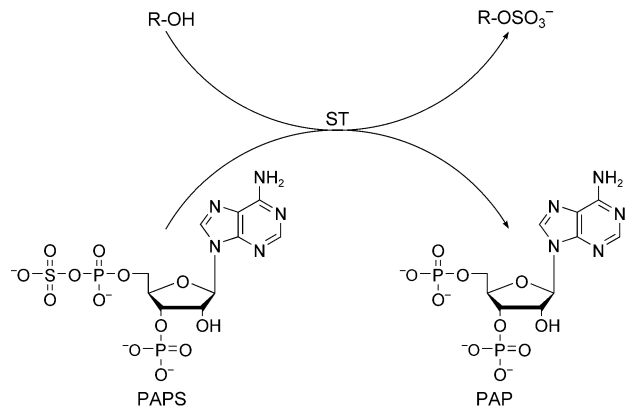
The sulfonation (also known as sulfurylation) of biomolecules has long been known to take place in a variety of organisms, from prokaryotes to multicellular species, and new biological functions continue to be uncovered in connection with this important transformation. Early studies of sulfotransferases (STs), the enzymes that catalyze sulfonation, focused primarily on the cytosolic STs, which are involved in detoxification, hormone regulation, and drug metabolism. Although known to exist, the membrane-associated STs were not studied as extensively until more recently. Involved in the sulfonation of complex carbohydrates and proteins, they have emerged as central players in a number of molecular-recognition events and biochemical signaling pathways. STs have also been implicated in many pathophysiological processes. As a result, much interest in the complex roles of STs and in their targeting for therapeutic intervention has been generated. Progress in the elucidation of the structures and mechanisms of sulfotransferases, as well as their biological activity, inhibition, and synthetic utility, are discussed in this Review.

From the Contents

1. Introduction	3527
2. Nomenclature	3528
3. Substrate Specificity	3529
4. Structure	3529
5. Mechanism	3532
6. Biological Activity of Sulfotransferases and Their Products	3535
7. Sulfotransferase Inhibition	3539
8. Synthetic Applications	3542
9. Summary and Outlook	3544

1. Introduction

As early as 1876, sulfate-containing biomolecules were known to exist.[1] However, the mechanism by which sulfonation takes place was not examined until after the isolation of the active sulfate donor, 3′-phosphoadenosine 5′-phosphosulfate (PAPS), about 80 years later.[2] Sulfotransferases (STs) catalyze the transfer of a sulfuryl group (SO_3) from a donor molecule, usually PAPS, to a variety of amine and hydroxy substrates as nucleophiles in a process originally called sulfation, but more correctly referred to as sulfonation or sulfurylation (Scheme 1). There are two classes of STs: cytosolic STs and membrane-associated STs. Cytosolic STs sulfonate small endogenous and exogenous compounds, such as hormones, bioamines, drugs, and various xenobiotic agents. Membrane-associated STs, many of which have been implicated recently in crucial biological processes, sulfonate larger biomolecules, such as carbohydrates and proteins.



Scheme 1. General ST-catalyzed reaction with PAPS as the cosubstrate.

Although cytosolic STs were initially thought to be primarily involved in detoxification, it is now clear that this is not their exclusive function. For example, they have been implicated in the activation and deactivation of hormones and carcinogens through the formation of sulfate conjugates.[3] It has been noted that certain sulfate esters of hormones are present in higher concentrations than the non-sulfated species.[4] Furthermore, the enzymes that catalyze the formation of PAPS (ATP sulfurylase and adenosine 5′-phosphosulfate kinase (APS kinase)) are highly conserved among all organisms and the deletion of these activities is lethal.[5]

Membrane-associated proteins have only recently been implicated in several biological processes of great importance, including viral entry into cells, leukocyte adhesion, and anticoagulation. More generally, enzymatic transformations of cell-surface proteoglycans by STs appear to trigger vital molecular-recognition and signal-transduction events. This suggests that the STs govern extracellular signaling events and are thus analogous to the kinases, which control signaling cascades inside the cell. If this is the case, it is likely that additional functions of STs will continue to emerge, and their prominence as targets of therapeutic interest will increase further.

Because of the biological importance and medical relevance of STs, there is intense interest in the exact functions of

[*] Dr. E. Chapman,[+] Dr. M. D. Best,[+] S. R. Hanson, Prof. C.-H. Wong
Department of Chemistry and
The Skaggs Institute for Chemical Biology
The Scripps Research Institute
10550 North Torrey Pines Road, La Jolla, CA 92037 (USA)
Fax: (+1) 858-784-2409
E-mail: Wong@scripps.edu

[+] Both authors contributed equally.

 DOI: 10.1002/anie.200300631 © 2004 Wiley-VCH Verlag GmbH & Co. KGaA, Weinheim

these enzymes. Much information is available with regard to the structure, substrate specificity, and kinetic mechanism of cytosolic STs, but less information is available on the transition-state structure and design of potent and specific inhibitors. The membrane-associated enzymes are not as well understood, particularly because their important roles in biological processes have only recently been uncovered. A number of excellent reviews on STs have been published.[6–14] Herein we discuss the current state of knowledge on their structure, chemical and kinetic mechanisms, biological activity, inhibition, and synthetic applications. We will also address the issues of substrate specificity and nomenclature.

2. Nomenclature

To date 10 or 11 human cytosolic STs have been characterized. The nomenclature of these enzymes has a long and confusing history. There is a great deal of substrate overlap among the known STs, which led to confusion in early naming schemes. Only with more rigorous biochemical, biophysical, and genetic characterization has this issue been resolved, although many different names for the same enzyme can still be encountered in the literature. Herein we use the designation SULT to indicate cytosolic STs, followed by a numerical designation to specify a particular ST (Table 1).[15] For example, we refer to the three known phenol STs as SULT1A1, SULT1A2, and SULT1A3, and to the estrogen ST as SULT1E. All SULT1 STs have higher affinities for phenolic moieties, and the SULT2 STs show a higher specificity for hydroxysteroids. The membrane-associated STs are still without a consistent, universal nomenclature scheme. STs in this class are named according to their substrate specificity, whereby we use the name most frequently encountered in the literature. For example, tyrosyl-

Table 1: Nomenclature of human cytosolic sulfotransferases.

Name	Synonyms	Substrate	Amino acid sequence identity[a]
SULT1A1	ST1A3, STP-1, P-PST, TS-PST-1, HAST-1, HAST-2, H-PST	phenols	100
SULT1A2	ST1A2, STP-2, TS-PST-2, HAST-4, HAST-4v	phenols (low affinity)	95
SULT1A3	ST1A5, STM, TL-PST, M-PST, AST-3, HAST-3	catecholamines	93
SULT1B1	HAST-1, 1B2 hydroxylamine-ST	thyroid hormones	54
SULT1C1	ST1C2	aryl hydroxylamines	37
SULT1C2	ST1C3	aryl hydroxylamines	41
SULT1E1	EST	estrogens	51
SULT2A1	DHEA-ST, DST, HSST-1, HAST, STa	hydroxysteroids	37
SULT1A1	cholesterol-ST, HSST-2, HST	hydroxysteroids	41
SULT1A1	pregnenolone-ST, HSST-3, HST	hydroxysteroids	39

[a] Relative to SULT1A1.



Chi-Huey Wong received his BS and MS degrees from the National Taiwan University, and his PhD in Chemistry from the Massachusetts Institute of Technology. After a postdoctoral year at Harvard University, he moved to Texas A&M University in 1983, and became Professor of Chemistry at The Scripps Research Institute in 1989 (Ernest W. Hahn Chair). His current research interests include bioorganic and organic methods in synthesis, as well as biocatalysis, with a specific focus on the study of carbohydrate-mediated biological recognition.



Eli Chapman received his BS from the University of California, Berkeley in 1996, with work for Prof. Peter G. Schultz on non-natural amino acid mutagenesis, and his MA from Columbia University in 1998 with work for Prof. James L. Leighton on rhodium-catalyzed silylformylation. He completed his PhD on sulfotransferases at The Scripps Research Institute under the guidance of Prof. Chi-Huey Wong. Currently he is a postdoctoral fellow with Prof. Arthur Horwich at Yale University School of Medicine, where he studies molecular chaperones.



Michael Best received his BS in chemistry from Boston College in 1997, where he worked with Prof. Lawrence T. Scott on the synthesis of fullerene derivatives. He completed his PhD in 2002 at the University of Texas at Austin under the guidance of Prof. Eric V. Anslyn on the design and synthesis of fluorescent sensors for biomolecules. He has since undertaken postdoctoral research pertaining to the development of small organic molecules which perturb biological systems in the research group of Prof. Chi-Huey Wong at The Scripps Research Institute.



Sarah R. Hanson received her BS in chemistry in 1999 from the University of California, Berkeley, where she worked on the synthesis and evaluation of antiproliferative purine derivatives with Prof. Peter G. Schultz. She also spent a summer as a NSF Undergraduate Fellow with Prof. Maria C. Linder. After graduating, she took an industrial position at Diversa, where she was involved with the development of enzyme catalysts. Since 2002 she has been studying sulfatases as a graduate student at The Scripps Research Institute under the guidance of Prof. Chi-Huey Wong.

 © 2004 Wiley-VCH Verlag GmbH & Co. KGaA, Weinheim

protein sulfotransferase is abbreviated TPST. This nomenclature is clarified as required.

3. Substrate Specificity

Membrane-associated STs tend to be quite specific in the molecules they recognize as substrates. Cytosolic STs, on the other hand, can be quite promiscuous. Many of this class recognize a variety of molecules as substrates, so that their biological function is often obscured. In early studies of STs, nonhomogeneous enzymes were used, which added further to the confusion. As can be seen in Table 2,[16–27] the enzymes more intimately connected with hormone regulation (that is, SULT1E1) show higher specificity for a given substrate than those thought to be involved in detoxification. In the next section, a structure-based explanation for differences in specificity is provided.

There have been a number of substrate-specificity studies carried out on STs. Many of these studies were conducted with β-aryl sulfotransferase IV from rats (for reviews, see reference [6,28]). One study of SULT1A1 and SULT1A2 showed a correlation between specificity and the chain length of alkyl phenols, as well as the position of substituents. Short carbon chains (one to four carbon atoms) were shown to be the best substrates, and substitution at the 2-position resulted in the best catalytic efficiency. Compounds with long carbon chains inhibited the enzyme.[29] Similar studies of SULT2A1 with benzyl alcohols substituted in the *para* position with *n*-alkyl groups showed a maximum catalytic efficiency for the *n*-pentylbenzyl alcohol. Similarly, it was shown for primary *n*-alcohols that the optimal chain length is 9–11 carbon atoms.[30]

A number of studies have also been conducted on the specificity of the PAPS-binding site by using affinity-labeling techniques and a variety of substrates.[31–34] One such study on SULT1A1 showed the enzyme to bind tightly to both ribose and adenine, as well as to other nucleotides. It was further shown that SULT1A1 can catalyze the sulfonation of adenosine 2′,3′-cyclic phosphate 5′-phosphate (2′,3′-cyclic PAP), adenosine monophosphate (AMP), and adenosine 2′,5′-bisphosphate (2′,5′-PAP). Of the cofactors studied, PAP ($K_m = 0.4$ μM) had the lowest K_m value, followed by 2′,3′-cyclic PAP ($K_m = 2.3$ μM) and 2′,5′-PAP ($K_m = 67$ μM). AMP ($K_m = 4300$ μM) had the highest K_m value.[35]

4. Structure

To date nine structures of STs have been solved on five different enzymes. Four of the five enzymes are cytosolic STs with a high degree of homology, and the other (NST-1) is found on the ST domain of human heparan sulfate *N*-deacetylase-*N*-sulfotransferase (HSNDST), a membrane-bound ST (Figure 1). The structures are highly conserved and are most similar to those of nucleotide kinases.[36] They are all approximately spherical and contain a single α/β fold with a central four- or five-stranded parallel β sheet surrounded by α helices. One minor exception is found in retinol dehydratase, a member of the ST superfamily. This enzyme

Table 2: Substrate specificity of human cytosolic sulfotransferases.

SULT	Representative substrates	K_m [μM]	K_m (PAPS) [μM]
1A1	pNP	1.1	0.98
	2-napthol	200	
	dopamine	130	
	tyramine	6483	
	minoxidol	2800	
	3,3′-T_2	0.14	
	T_3	29.1	
1A2	PNP	69 (HAST-4)	5.52 (HAST-4)
		4.1 (HAST-4v)	0.203 (HAST-4v)
	dopamine	ND	
1A3	PNP	1024	1.1
	tyramine	35	
	dopamine	3.7	
1B1	PNP	5	1.2
	T_4	23	
	T_3	ND	
	rT_3	141	
	3,3′-T_2	51	
1C1	PNP	84.07[a]	8.8[b]
	dopamine	ND	
	N-OH-2AAF	28.6	
1C2	PNP	75.3[a]	
	dopamine	ND	
	N-OH-2AAF	47.5	
1E1	estradiol	0.025	0.3
	DHEA	4.569	
	androstenediol	3.224	
	PNP	76.6	
2A1	estradiol	2.0	1.6
	DHEA	0.993	
	androstenediol	0.191	
2B1a	DHEA	2.27	0.09
	pregnenolone	0.20	
	17α-hydroxypregneno-lone	0.89	
2B1b	DHEA	4.37	0.07
	pregnenolone	0.60	
	17α-hydroxy-pregnenolone	0.97	

[a] Values given are activities (pmol min^{-1} mg^{-1}). [b] For rSULT1C1.

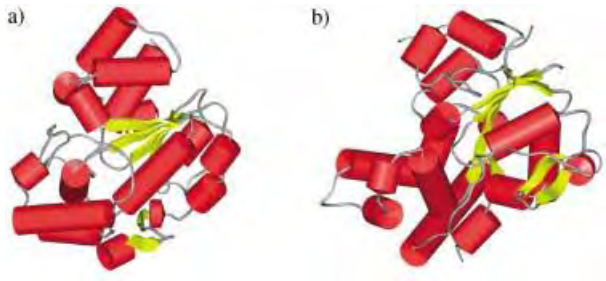


Figure 1. Crystal structures of a) estrogen ST (SULT1E1) and b) heparan sulfate N-deacetylase-N-sulfotransferase (HSNDST).

 © 2004 Wiley-VCH Verlag GmbH & Co. KGaA, Weinheim

has two domains, one consisting of a five-stranded parallel β sheet and eight α helices and one with a three-stranded antiparallel β sheet and six α helices.[37] However, the conserved active site and PAPS-binding residues are present. Just as the PAPS-binding region is conserved at the amino acid level for all STs (Figure 2), the structure of this region is also conserved. The largest variation among these STs is found in the substrate-binding region. A great deal of mechanistic insight has come from the study of structures with a bound substrate and/or cosubstrate, as well as from the investigation of a vanadate complex as a potential transition-state mimetic. Structural comparisons have shown that SULT1A3 superposes on mSULT1E1 with a root-mean-square (RMS) deviation of 0.81 Å for the C^{α} atoms,[38] and similar comparisons between the PAPS-binding region of NST-1 and mSULT1E1 showed a RMS deviation of 1.16 Å.[39] A few of the most important structural aspects are summarized in the following; the reader is referred to a number of excellent review articles for more details.[40,41]

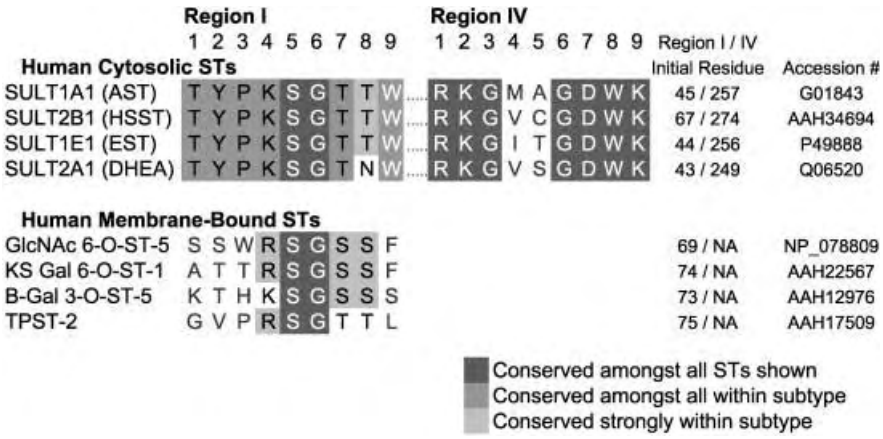
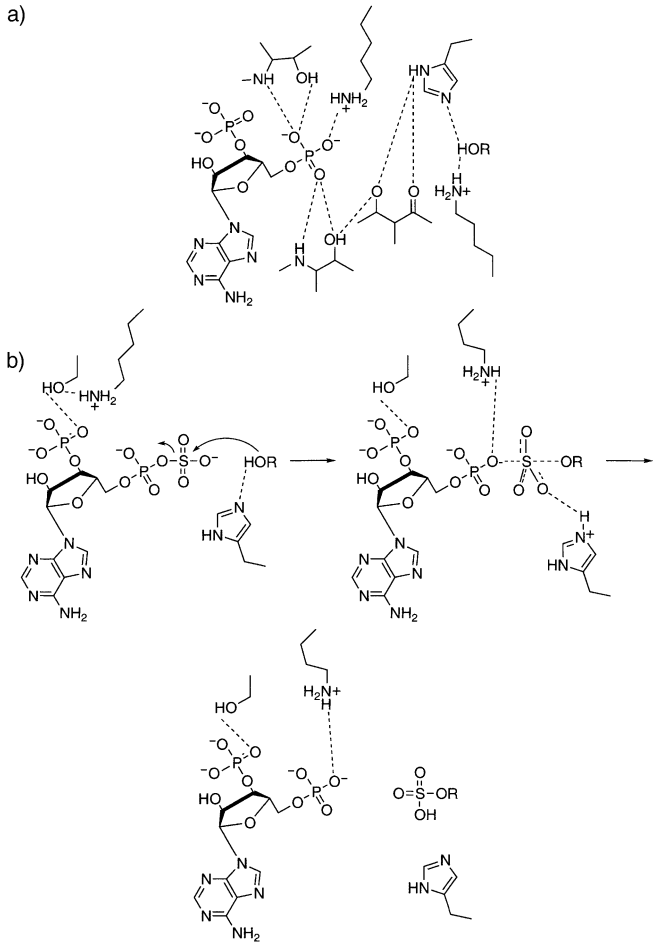


Figure 2. Sequence homologies for cytosolic and membrane-associated STs.

4.1. PAPS-Binding Region

The PAPS-binding region is highly conserved at the amino acid level. Three structural features are responsible for PAPS binding: the 5′-phosphosulfate-binding (PSB) loop, the 3′-phosphate-binding (PB) loop, and the β-strand–loop–α-helix (SLH3) motif.[42] Only one of the solved structures showed a deviation in these binding motifs; SULT1A3 was reported to show a great deal of disorder in the 3′-PB region. The authors concluded that the binding of the 3′-phosphate was less important than the binding of the 5′-phosphate.[38] However, in a structure solved in the same year for the same enzyme, this disorder was not reported.[43]

Three structures have been solved for SULT1E1: one with PAP and estradiol bound,[36] one with vanadate as a transition-state analogue,[44] and one with PAPS bound.[45] In mSULT1E1 with PAP and estradiol bound, which was the first ST structure to be solved, amino acid residues 45–51 define the PSB loop. Hydrogen bonds are formed between the 5′-phosphate and the N^{ζ} atom of Lys48 and O^{γ} atoms of Thr51 and Thr52. The PB loop is made up of residues 257–259. Hydrogen bonds are formed between the amide N atoms of Lys257 and Gly259, as well as the side chain of Arg257, and the 3′-phosphate. Gly259 marks the beginning of a GxxGxxK motif, which has been shown to be necessary for the binding of PAPS and estradiol. Mutagenesis of two of the conserved amino acid residues led to a tenfold increase in the K_m value for PAPS, and mutagenesis of all three conserved residues produced an inactive enzyme.[46] Arg130 and the O_{γ} atom of Ser138 are also within hydrogen-bonding distance. Finally, the location of Trp153 and Phe229 is such that they form a parallel stack with the adenine group of PAP. In the vanadate complex Lys48, His108, and Lys106 coordinate to the vanadate center. It became clear from the structure in which PAPS is bound that Lys48 interacts initially with Ser138 and shifts upon initiation of the reaction to interact with the leaving sulfate group (Scheme 2). Mutagenesis studies of conserved active-site residues showed that His108 is



Scheme 2. Catalytic center of a sulfotransferase. a) Interaction with the 5′-phosphate group of PAPS and with conserved catalytic residues of mSULT1E1. b) Mechanism of ST-catalyzed sulfonation as deduced from structural studies.

 © 2004 Wiley-VCH Verlag GmbH & Co. KGaA, Weinheim

necessary for catalytic activity and that if Lys48 and Lys106 are replaced by anything other than an arginine residue, complete loss of activity occurs.[44] Furthermore, mutagenesis of Ser138 showed the interaction between this residue and Lys48 to be important in protecting PAPS from autohydrolysis.[45]

4.2. Substrate-Binding Region

As expected, the largest degree of structural variation is found in the substrate-binding region. The substrate-binding region in the SULT1A family has been shown to be comprised of a number of hydrophobic residues. In a comparison study of SULT1A1 and SULT1A3, which are 93% identical but exhibit marked differences in substrate binding, two variable regions were analyzed (region I (84–89) and region II (143–148)) and shown to be responsible for the observed specificity. By generation of chimeric proteins, the substrate specificity was reversed. A chimeric construct of SULT1A1 with region I replaced with region II showed SULT1A3 specificity, and vice versa.[47] Further, it was shown that by mutating Asp86A/E89I/E146A in SULT1A3, the catalytic efficiency decreased with dopamine as the substrate and the catalytic efficiency increased to the level of SULT1A1 with *p*-nitrophenol (PNP) as the substrate. It is postulated that these negatively charged amino acids interact with the amino group of dopamine (or other monoamine substrates) to stabilize the charge and orient the substrate correctly. Similar mutations in SULT1A1 did not induce similar changes, but a small enhancement of the catalytic efficiency was observed with dopamine as the substrate.[48]

A similar, predominantly hydrophobic binding pocket is found in the steroid ST. In an interesting mutagenesis study of SULT1E1, the mutation Y81L allowed this enzyme to bind dehydroepiandrosterone (DHEA). In the wild-type enzyme, the 3β-hydroxy group of DHEA is excluded from the binding pocket because of steric interactions of Tyr81 with the methyl group at C19.[24] Structural studies of SULT2A3 showed that Trp77 and Phe133 form a gatelike structure (similar to the Tyr81 gate of SULT1E1), whose function is not yet known. It was also shown that the SULT2A3 binding pocket is highly flexible and that the substrate is rotated by 30° relative to estradiol in the SULT1E1 structure. An alternative substrate-binding mode in which DHEA is shifted 2.87 Å toward PAP was proposed as an explanation of substrate inhibition.[49,50] Deletion studies of variable N-terminal and C-terminal regions of SULT2B1a and SULT2B1b showed that the N-terminal peptide of 23 amino acids of SULT2B1b is crucial for cholesterol sulfonation, whereas the deletion of 53 amino acids from the C terminus does not affect the activity. Analogous results were not observed for SULT2B1a: neither deletion of the N terminus nor deletion of the C terminus affected the sulfonation of pregnenolone.[51] The structure of retinol dehydratase shows a number of aromatic residues surrounding retinol. These residues are thought to participate in deprotonation during the dehydration step. The conserved residues of the catalytic and PAPS-binding site are similar to those in other STs (Figure 3).[37]

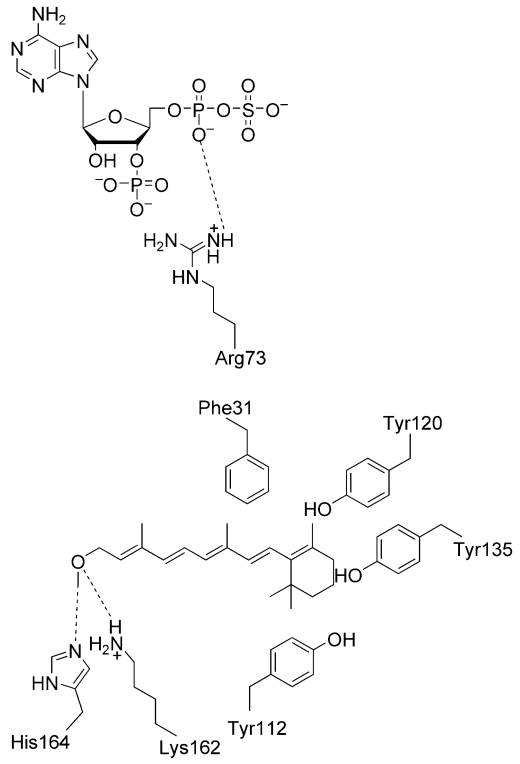


Figure 3. Binding pocket of retinol dehydratase as deduced by crystal-structure analysis.

In the membrane-associated NST-1, which sulfonates heparan sulfate (HS), the substrate-binding site is a large hydrophilic cleft.[39] Modeling studies of HS D-glucosaminyl 3-O-ST-1 also showed it to have a large open cleft with a large number of basic residues.[42] According to domain-swapping studies with 3-O-ST-1 and 3-O-ST-3, it is the ST domain that imparts specificity and not the divergent N terminus. The sulfotransferase 3-O-ST-1 generates antithrombin-binding sites, and 3-O-ST-3 creates binding sites for the gD envelope protein of herpes simplex virus 1 (HSV-1). After fusion of the N-terminal region of 3-O-ST-1 with the ST domain of 3-O-ST-3, the protein generates gD-binding sites. Similarly, upon fusion of the N-terminal region of 3-O-ST-3 with the ST domain of 3-O-ST-1, the protein generates antithrombin-binding sites.[52]

4.3. Dimerization Motif

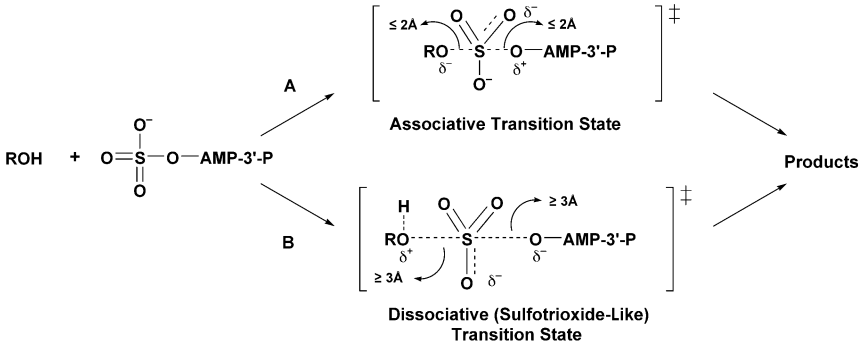
The majority of STs are homodimers in their catalytically active forms. In some of the solved structures the enzymes crystallized as dimers, but these were unlikely to be the catalytic species, as the substrate-binding site is blocked by the dimer interface. Structural comparisons and mutagenesis studies were undertaken with mSULT1E1 (a monomer) and hSULT1E1 (a dimer) in an attempt to identify a common structural motif. It was found that the mutations V269E and V260E converted the homodimers SULT1E1 and SULT2A1,

 © 2004 Wiley-VCH Verlag GmbH & Co. KGaA, Weinheim

respectively, into monomers. It was further shown that the mutations P269T and E270V in mSULT1E1 precipitated the formation of a homodimeric structure. It was concluded that the common motif KxxxTVxxxE is responsible for the dimerization of STs.[24]

4.4. Mechanistic Conclusions

A great deal of mechanistic insight has been derived from the solved structures. It is clear that the sulfonation reactions proceed by an in-line attack of the nucleophile at the sulfate group of PAPS. It seems likely that the conserved active-site histidine residue assists in this reaction by deprotonating the attacking substrate; however the possibility that this histidine residue acts as a nucleophile to form an unstable protein–sulfate complex can not be ruled out.[36] It has also not been possible to determine from structural studies whether the reaction proceeds by an associative (S_N2-like) mechanism or by a dissociative (S_N1-like) reaction (Scheme 3). Support for both was provided by a theoretical study on NST-1. In an associative mechanism, the largest change in charge would occur at the sulfuryl group, whereby the charge could be stabilized by Lys614, Lys676, and Lys833. However, if the pathway were dissociative, the largest change in charge would affect the bridging oxygen atom of the 5′-phosphate group, and this charge could be stabilized by Thr617 and Thr618.[53] This topic is covered in more detail in the next section.



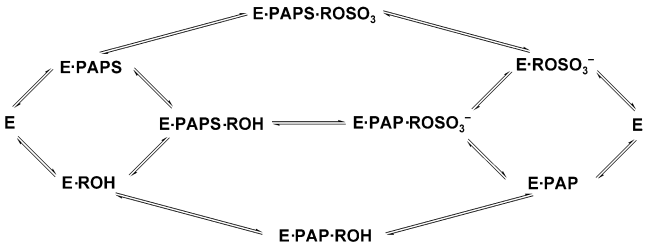
Scheme 3. Two possible transition states for ST-catalyzed sulfonation. Pathway A has an associative transition state in which the nucleophilicity of the substrate dominates. Pathway B has a dissociative transition state in which leaving-group ability dominates.

5. Mechanism

Kinetic mechanisms of ST-catalyzed reactions have a long and confusing history, but recombinant DNA technology and structural studies have helped enormously to clarify the issue. Many early studies were wrought with problems caused by impurities in the enzymes studied, multiple isoforms of various enzymes, and oxidative differences. With some early exceptions, all the reactions studied with STs from higher organisms proceed by sequential mechanisms, which are either random or ordered. For all bacterial STs that use cosubstrates other than PAPS, ping-pong kinetic mechanisms were found. The enzymatic mechanism of STs is termed "bi–bi", as the reaction involves two substrates that lead to two products.

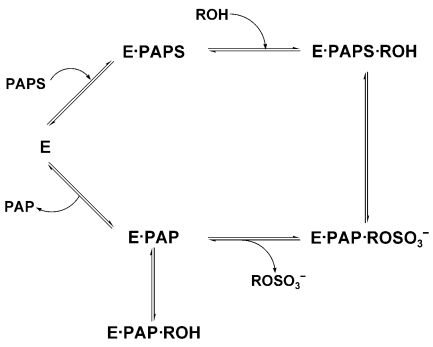
5.1. Sequential Mechanisms

In recent studies, as well as in most older studies, it could be shown that reactions of STs that utilize PAPS as a cosubstrate proceed by sequential kinetic mechanisms in which a ternary enzyme complex is formed prior to the release of products. Sequential mechanisms either proceed in a random fashion, whereby there is no obligatory order of substrate addition (Scheme 4), or in an ordered fashion, whereby one of the substrates will only bind after the first has bound (Scheme 5). A variety of techniques can be used to determine the order of substrate binding in a bireactant



Scheme 4. Random bi–bi kinetic mechanism with two dead-end inhibition complexes E·PAPS·$ROSO_3$ and E·PAP·ROH.

reaction. Binding events can be measured directly, and product-inhibition data and other inhibition data can be used. However, data can be obscured by the formation of one or more dead-end complexes or by impurities in enzyme preparations. Product-inhibition studies are among the most common methods for determining the order of substrate addition. An ordered bi–bi mechanism predicts three noncompetitive inhibition patterns and one competitive inhibition pattern (Figure 4). In the case shown in Scheme 5, PAP should inhibit PAPS competitively. In a random kinetic mechanism all inhib-



Scheme 5. Ordered bi–bi kinetic mechanism with one dead-end complex E·PAP·ROH.

 © 2004 Wiley-VCH Verlag GmbH & Co. KGaA, Weinheim

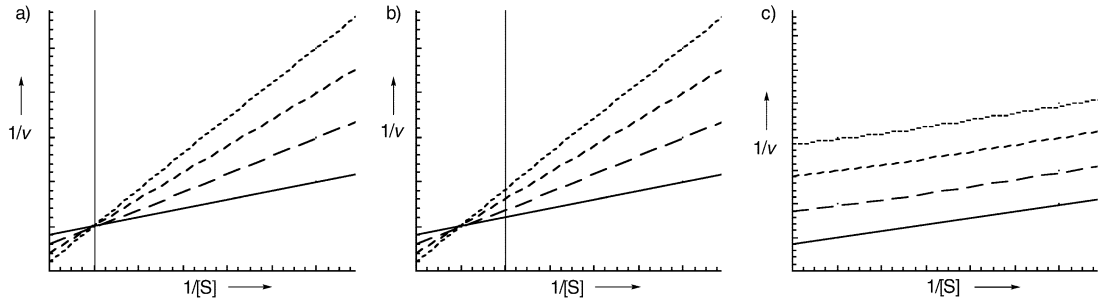


Figure 4. Product-inhibition patterns. Plots were generated by varying the amount of one of the substrates at a fixed concentration of the other substrate at four different concentrations of the inhibitor. a) Expected pattern for competitive inhibition, b) pattern observed for noncompetitive inhibition, and c) pattern for uncompetitive inhibition.

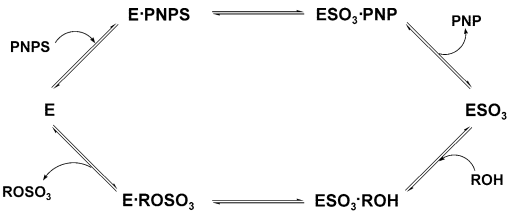
ition patterns are competitive unless dead-end complexes are formed. Such complexes show noncompetitive inhibition and can therefore complicate the interpretation of results.[54]

Initial investigations of SULT1E1 from bovine adrenal glands showed a sequential mechanism to be operative, but it was not clear whether the mechanism was ordered or random.[55] In another study of SULT1E1 isolated from bovine adrenal glands, a wavelike kinetic pattern was observed.[56] Both of these studies were performed on an enzyme that may not have been homogeneous, so the data must be interpreted with caution. Binding studies with recombinant hSULT1E1 and further data on initial reaction rates showed that a random bi–bi mechanism was involved with rapid equilibration and the participation of two dead-end complexes: E·PAPS·E_2S and E·PAP·E_2. It was further shown that the stoichiometry of E_2 binding is 2:1. It was proposed that one site is catalytic and that the other is an allosteric site, which regulates turnover. Further, it was noted that the fluorescence binding experiments might also measure the binding of nonproductive complexes, thus complicating data interpretation.[57]

Similar kinetic and binding studies on phenol-sulfonating sulfotransferases from rats and guinea pigs also showed sequential mechanisms, but the order of binding is not clear. Early studies on partially purified gpPST and rPST supported a random bi–bi mechanism with rapid equilibration.[58,59] Possibly conflicting results were obtained from studies on PST isolated from rat brain; in this case an ordered sequential mechanism with an E·PAP·ROH dead-end complex was proposed.[60] The results of the most comprehensive study to date (binding, initial reaction rates, and inhibition data), which was carried out on apparently homogeneous AST-IV (rSULT1C1) from rat liver, were in agreement with this mechanism.[26] It was later shown that there are two oxidative forms of the same sulfotransferase with different kinetic properties. It was also found that an E·PAP complex can either dissociate or bind the product PNP to form a dead-end complex. Thus, it can be concluded that the mechanism must be ordered, as the findings are inconsistent with a random mechanism under rapid equilibration.[54,61] This example illustrates potential pitfalls in other mechanistic studies and should prompt the reexamination of other systems. Both ordered and random mechanisms have been found for other STs that utilize PAPS, but in all cases the mechanisms were sequential.[62–65]

5.2. Ping-Pong Bi–Bi Mechanisms

Aryl sulfotransferases isolated from *Eubacterium A-44*, *Enterobacter amnigenus*, and *Aspergillus oryzae* have all been shown to react by ping-pong bi–bi kinetic mechanisms. These enzymes do not use PAPS as their source of activated sulfur, but instead use an activated aryl species, such as *p*-nitrophenol sulfate (PNPS). Ping-pong mechanisms follow the general pathway shown in Scheme 6. For a ping-pong



Scheme 6. General kinetic mechanism of a ping-pong bi–bi reaction.

mechanism, double reciprocal plots of 1/*v* versus 1/[substrate] give a characteristic series of parallel lines at different, fixed concentrations of the second substrate (Figure 5).[54] This pattern of double reciprocal plots along with the finding that free sulfate is not incorporated into the product led to the suggestion that the aryl sulfotransferase from *Aspergillus oryzae* reacts by a ping-pong mechanism with the formation of an enzyme–sulfate intermediate.[66] It was later shown with a similar enzyme from *Eubacterium A-44* that in the presence of ^{35}S-PNPS, in the absence of an acceptor molecule, 2 mol of ^{35}S per mol of enzyme were incorporated into a tyrosine residue in the active site. Furthermore, it was shown that the histidine-modifying reagent diethyl pyrocarbamate completely suppresses enzyme activity, but that the enzyme is protected by addition of the donor substrate. These findings led to the proposal of the mechanism shown in Scheme 7, in which the sulfate is first transferred to an active-site histidine

 © 2004 Wiley-VCH Verlag GmbH & Co. KGaA, Weinheim

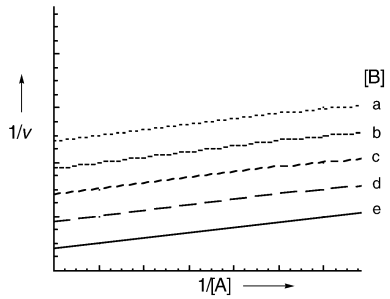
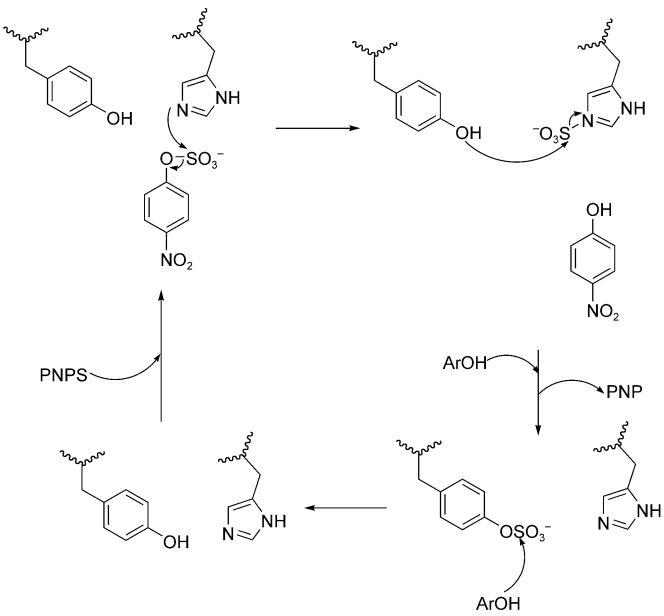
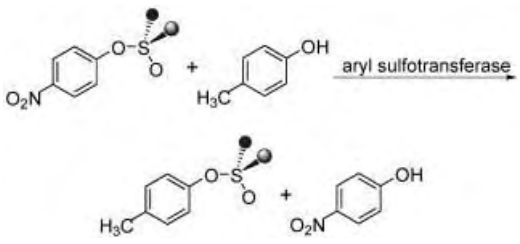


Figure 5. Pattern observed from a double reciprocal plot when a ping-pong bi–bi kinetic mechanism is operative. The rate at a fixed concentration of substrate A is measured at different concentrations of substrate B.



Scheme 7. Mechanism proposed for sulfonation by the aryl sulfotransferase from *Eubacterium A-44*.

residue and then to a tyrosine residue.[67] Later radioactive-labeling studies with the same enzyme gave similar results and also showed that a chiral sulfate group is transferred with retention of configuration (Scheme 8). Based on these studies it was also proposed that the histidine residue may not be acting as a nucleophile but as a general base.[68] Investigations with the aryl sulfotransferase from *Enterobacter amnigenus* led to the same characteristic double reciprocal pattern, as well as to the finding that PNP is a noncompetitive inhibitor of the sulfate donor PNPS and a competitive inhibitor of the acceptor 1-naphthol.[69]

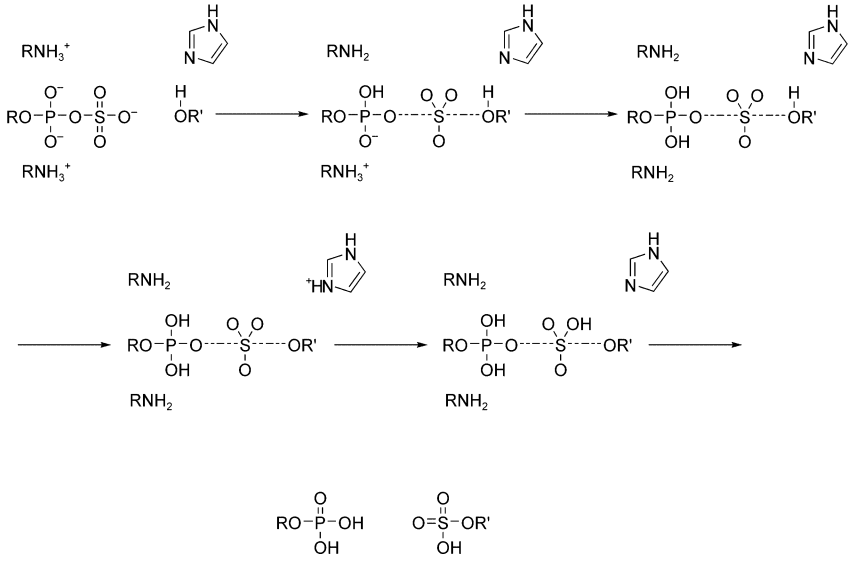


Scheme 8. Use of a chiral sulfate to probe the mechanism of the sulfonation catalyzed by the aryl sulfotransferase from *Eubacterium A-44* (black: ^{18}O, gray: ^{17}O).

5.3. Transition-State Structure

As mentioned in Section 4.4, the reaction proceeds by an in-line attack of the nucleophile at the sulfur atom. There are two possible transition states that could be operative (Scheme 3): an associative transition state in which the nucleophile dominates and a dissociative transition state in which the S–OAMP-3′-P bond of the starting sulfate is first largely broken to form a sulfotrioxide-like intermediate. In the associative case, the distances between the leaving oxygen atom of PAP and the sulfur atom, and between the incoming nucleophile and the sulfur atom, would be expected to be short (<2 Å). In the dissociative case, these two distances should be longer (≥ 3 Å; Scheme 3). As mentioned in Section 4.4, structural data appear to support either of these mechanisms. A theoretical study conducted on SULT1E1 indicated that the reaction proceeds in several steps: first the charge on PAPS is neutralized, then the O–S bond is lengthened, and finally the nucleophile is activated by deprotonation (Scheme 9).[70]

The results of studies carried out by our research group are in agreement with a dissociative mechanism. With a series of fluorinated and sulfated *p*-nitrophenols, linear free-energy relationships were calculated for the forward and reverse



Scheme 9. Sulfonation mechanism based on theoretical calculations with SULT1E1 as a model.

 © 2004 Wiley-VCH Verlag GmbH & Co. KGaA, Weinheim

reactions. The apparent second-order rate constants were plotted as a function of the pK_a values to yield the Brønsted nuleophile coefficient $\beta_{nuc} = +0.33$ and the leaving-group coefficient $\beta_{lg} = -0.45$. From these values, it is possible to calculate Leffler α values ($\alpha = \beta_{nuc}/\beta_{EQ}$; β_{EQ} = difference in effective charges for reactants and products), which indicate the amount of charge buildup in the transition state. The calculated values of 0.19 for the forward reaction and 0.61 for the reverse reaction[71] are in reasonable agreement with literature values for uncatalyzed reactions with pyridine analogues.[72] The results of this study, together with results of theoretical studies and investigations of the uncatalyzed reaction, led to the conclusion that the reaction proceeds in a more dissociative fashion with some nucleophilic participation (Figure 6).

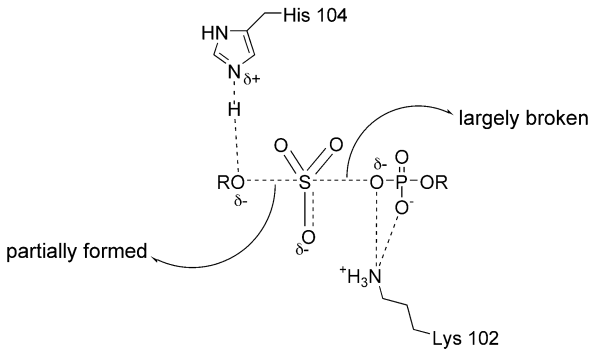


Figure 6. Proposed transition state of the catalytic sulfonation showing two of the highly conserved amino acid residues in the active site.

6. Biological Activity of Sulfotransferases and Their Products

Sulfotransferases and their products are involved in a wide array of biological processes, including hormone regulation, detoxification, molecular recognition, cell signaling, and viral entry into cells. As a result, a large field of research has developed aimed at uncovering novel functions of STs and their products and at understanding how these functions are carried out. In view of the extensive amount of literature that has been published in this area, we focus on a selection of STs that play particularly intriguing roles in crucial biological events. The reader is also directed to previous review articles.[12,73,74]

6.1. Estrogen Sulfotransferase

Estrogen ST (SULT1E1) is a cytosolic enzyme that catalyzes the sulfonation of the hormone estrogen to estrogen sulfate (**1**, Figure 7). Thus, SULT1E1 is involved in regulating the balance between these compounds in the cytosol. Studies have uncovered a correlation between increased levels of estrogen sulfotransferase[75] and estrogen sulfate,[76] and the presence of mammary tumors, thus making the enzyme a promising therapeutic target. In other studies, however, an inverse correlation was found between the immunoreactivity of this enzyme and tumor size.[77] The enzyme was also found to be absent in MCF-7 breast cancer cells[78] and its restoration led to a decrease in estrogen-dependant tumor growth.[79]

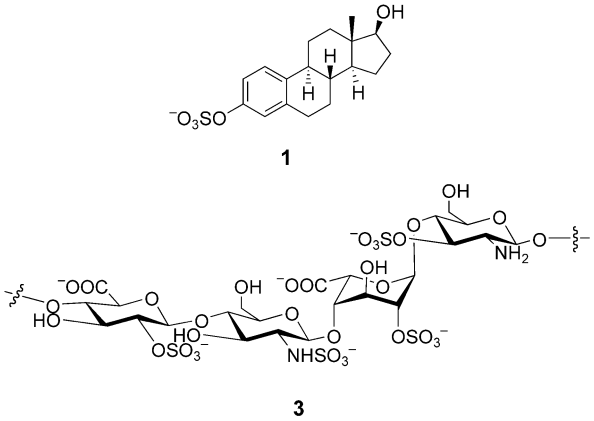


Figure 7. The regulatory biomolecules estrogen sulfate (**1**) and **3**, the HSV-1-binding epitope of HS; both were produced by enzymatic sulfonation.

6.2. Heparan Sulfotransferases

Heparan STs are a class of membrane-associated STs (Table 3) with critical biological properties.[80,81] These enzymes catalyze the sulfonation of heparan sulfate glycosaminoglycans (HSGAGs) to create complex HS sulfoforms with high structural diversity. The differences observed in their biological activity mainly result from point changes in chemical functionality. The saccharide portion of HS generally consists of alternating subunits derived from glucosamine and uronic acid. The oligosaccharide chains are derivatized with different patterns of sulfonated hydroxy, sulfonated amino, and acetylated amino groups, as well as through epimerizations. The combination of the oligosaccharide composition and the sulfonation pattern provides both the diversity in these structures and the specificity in their interactions with other proteins, with growth factors, chemokines, and viruses, which have been reviewed recently.[82]

The biosynthesis of HS occurs in such a way that diversity is introduced in the final steps, following the assembly of a more generalized oligosaccharide structure. Scheme 10 shows the biosynthesis of the AT-III-binding pentasaccharide **2** schematically.[83] The attachment of D-glucuronic acid and *N*-acetyl-D-glucosamine units is catalyzed by glucuronosyltransferases (GlcAT1) and α-*N*-acetylglucosaminyltransferases (αGlcNAcTIA and B), respectively. The resulting polymer is then modified by *N*-deacetylase-*N*-sulfotransferases (NDSTs), by 5′-uronosylepimerase (EPI), which transforms certain D-glucuronic acid residues into L-idouronic acid residues, and finally by a series of heparan STs, which sulfonate specific hydroxy groups. Heparan STs are promising targets for therapeutic intervention as a result of their involvement in the final steps of HS differentiation, which determines the specific function of the product.

 © 2004 Wiley-VCH Verlag GmbH & Co. KGaA, Weinheim

Table 3: Membrane-associated sulfotransferases.

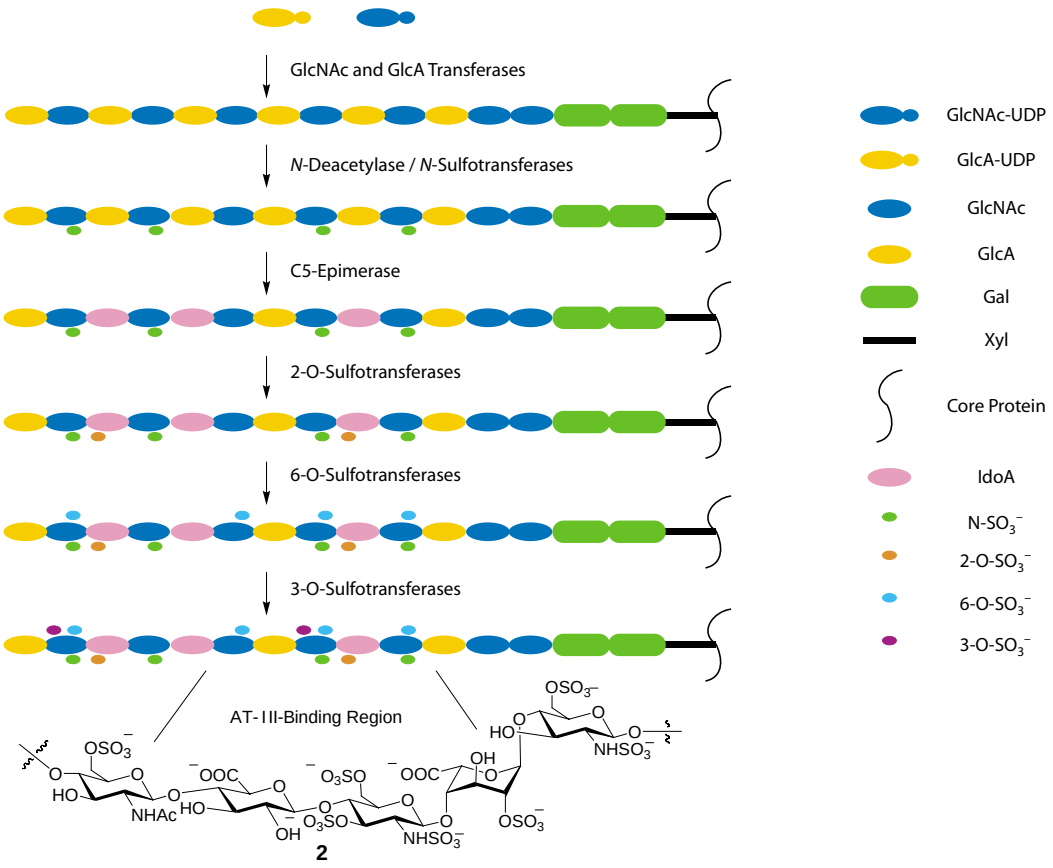
Name	Abbreviation	Substrate	Biological event
heparan sulfate D-glucosaminyl 3-O-ST-3a and b	HS-3-O-ST-3a and b	heparan sulfate	cell entry by HSV-1
heparan sulfate D-glucosaminyl 3-O-ST-1	HS-3-O-ST-1	heparan sulfate	AT-III binding, anticoagulation
heparan sulfate idouronic acid 2-O-ST	HS-2-O-ST	heparan sulfate	FGF binding, angiogenesis
heparan sulfate D-glucosaminyl 6-O-ST	HS-6-O-ST	heparan sulfate	FGF activation, angiogenesis
tyrosylprotein ST	TPST	CCR-5 PSGL-1	cell entry by HSV-1 P-selectin binding, leukocyte adhesion
N-acetylglucosamine 6-O-ST	GlcNAc-6-O-ST	sialyl Lewis^x	L-selectin binding, leukocyte adhesion
chondroitin sulfate *N*-galactosamine 4-O-ST-1, 2, and 3	CS-4-O-ST-1, 2, and 3	chondroitin sulfate	cartilage development, neuronal functions, lymphocyte binding, T-cell response
chondroitin sulfate *N*-galactosamine 6-O-ST	CS-6-O-ST	chondroitin sulfate, keratan sulfate	cartilage development, neuronal functions, lymphocyte binding, T-cell response
HNK-1 glucuronic acid 3-O-ST	HNK-1 ST	HNK-1 sulfate	expressed in nervous tissue
N-acetylgalactosamine 4-O-ST	GalNAc-4-O-ST	saccharide receptor units on lutropin, thyrotropin, and pro-opiomelanocortin	circulatory half-life control
dermatan sulfate *N*-galactosamine 4-O-ST	DS-4-O-ST	dermatan sulfate	glycolipid and glycoprotein component
keratan sulfate galactose 6-O-ST	KS-6-O-ST	keratan sulfate	corneal transparency

Heparan sulfate has been implicated in the entry of herpes simplex virus 1 (HSV-1) into cells.[84] The defined tetrasaccharide region **3** (Figure 7) provides binding sites for the gD envelope protein of HSV-1, thus leading to cell entry.[85] The heparan ST isoform 3-O-ST-3 catalyzes the key sulfonation of the 3-hydroxy group of D-glucosamine residues on HS units, which is necessary for the recognition of gD. Heparin and HS have also been shown to interact with human immunodeficiency virus 1 (HIV-1) and thus to deter the entry of the virus into the cell.[86,87] In this inhibitory interaction, HS molecules bind to the V3 loop of the viral glycoprotein gp120 and block the fusion of the virus to the CD4 receptor of the target cell.[88–90] These compounds are also known to bind to the viral Tat protein, which is required for HIV-1 replication.[91,92]

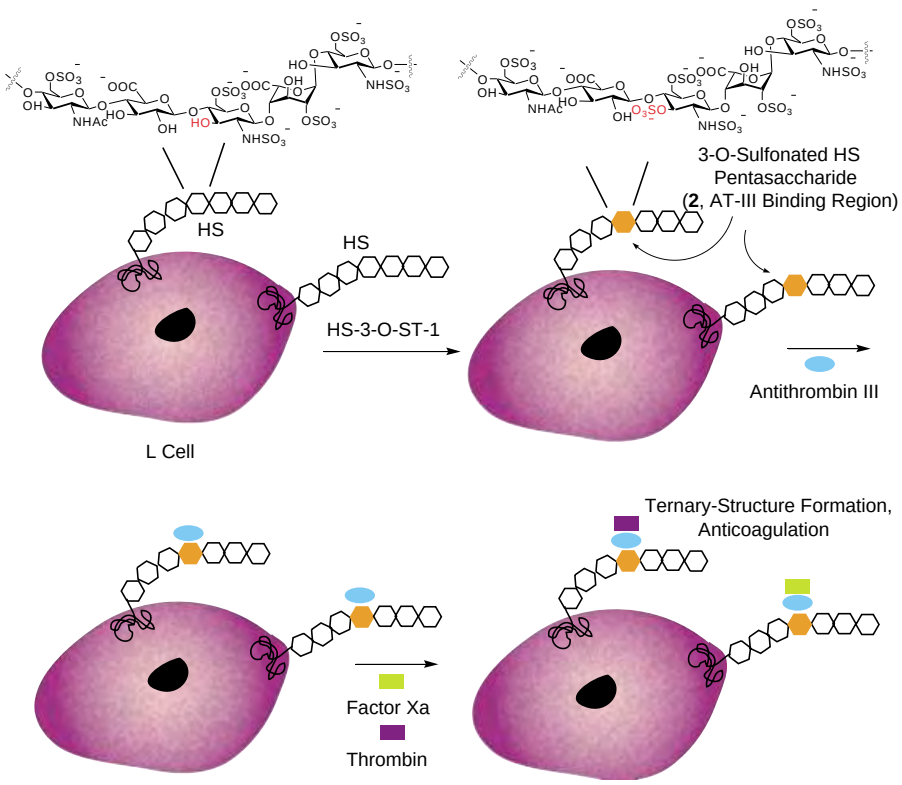
The interaction of HS with antithrombin III (AT-III) has been studied extensively (Scheme 11). The binding of HS to AT-III through the pentasaccharide region **2** enhances its inactivation of the blood-coagulation factors thrombin and Xa, thus accounting for its anticoagulation properties.[93–96] Rosenberg and co-workers determined that the HS derivative with high affinity for AT-III is the product of sulfonation of a D-glucosamine subunit by the enzyme heparin 3-O-ST-1.[97] The same research group used gel mobility shift assays to determine the critical functional groups in HS–receptor interactions.[98] Sulfonation at the 3-O and 6-O positions was found to be important for the binding of AT-III by the oligosaccharide. In a separate study, HS-6-O-ST-1 was found to be a crucial enzyme in the synthesis of HS with anticoagulation properties.[99]

The products of the enzymes HS idouronic acid 2-O-ST and HS glucosaminyl 6-O-ST bind to fibroblast growth factors (FGFs).[100–103] This interaction initiates a signal-transduction event in angiogenesis by causing dimerization of FGF followed by autophosphorylation of the FGF tyrosine

 © 2004 Wiley-VCH Verlag GmbH & Co. KGaA, Weinheim



Scheme 10. Schematic representation of the biosynthesis of heparan sulfate.



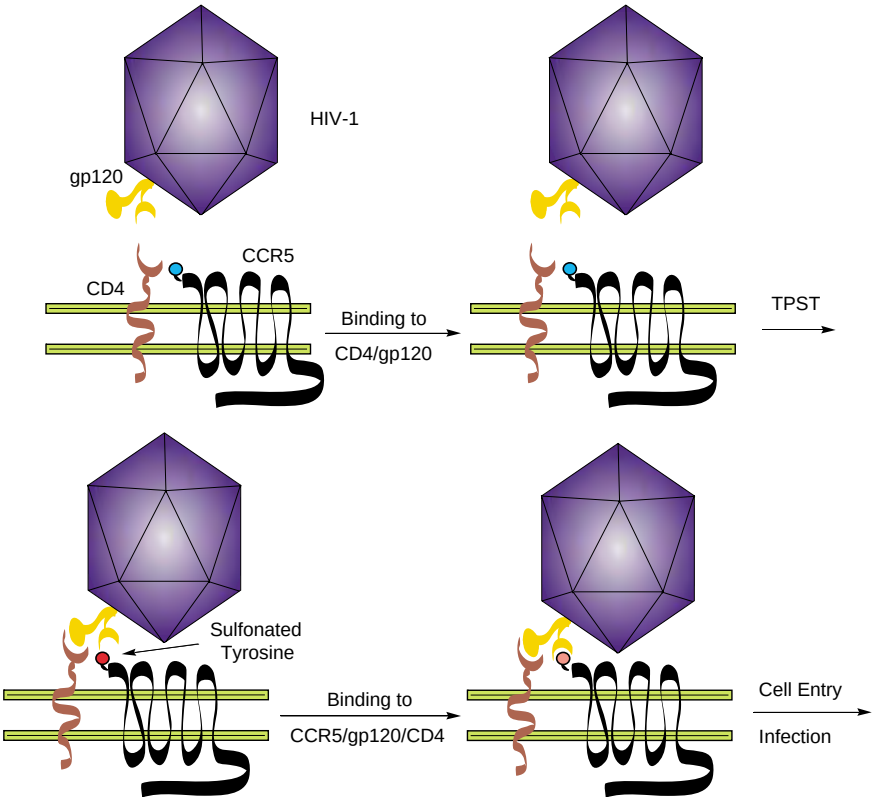
Scheme 11. Schematic representation of heparan sulfonation, which leads to a HS derivative with a high affinity for antithrombin III and anticoagulation properties.

kinase domain. Heparan sulfates are also known to interact with other cytokines and chemokines,[104–108] as well as with lipid- and membrane-binding proteins and adhesion molecules.[109–112] A total of five isoforms of HS-3-O-ST, three isoforms of HS-6-O-ST, and four isoforms of NDSTs are known,[113–116] although the functions of many have not yet been determined.

6.3. Tyrosylprotein Sulfotransferases

Tyrosylprotein sulfotransferases (TPSTs) catalyze the sulfonation of tyrosine residues within specific peptide sequences. These enzymes have also been implicated in several crucial physiological events. Recently, it was shown that one such enzyme is involved in the recognition of target cells by HIV-1,[117] whereby TPST catalyzes the sulfonation of the N-terminal tyrosine residues of the chemokine

 © 2004 Wiley-VCH Verlag GmbH & Co. KGaA, Weinheim



Scheme 12. Schematic representation of cell entry by HIV-1 following sulfonation of CCR5 by a tyrosylprotein sulfotransferase.

receptor CCR5 (Scheme 12). This transformation leads to the entry of the virus into the cell through the binding of the sulfonated CCR5 to gp120/CD4 complexes. More recently it was found that antibodies with sulfonated tyrosine residues fight infection by binding to the CCR5 region of HIV-1 gp120.[118]

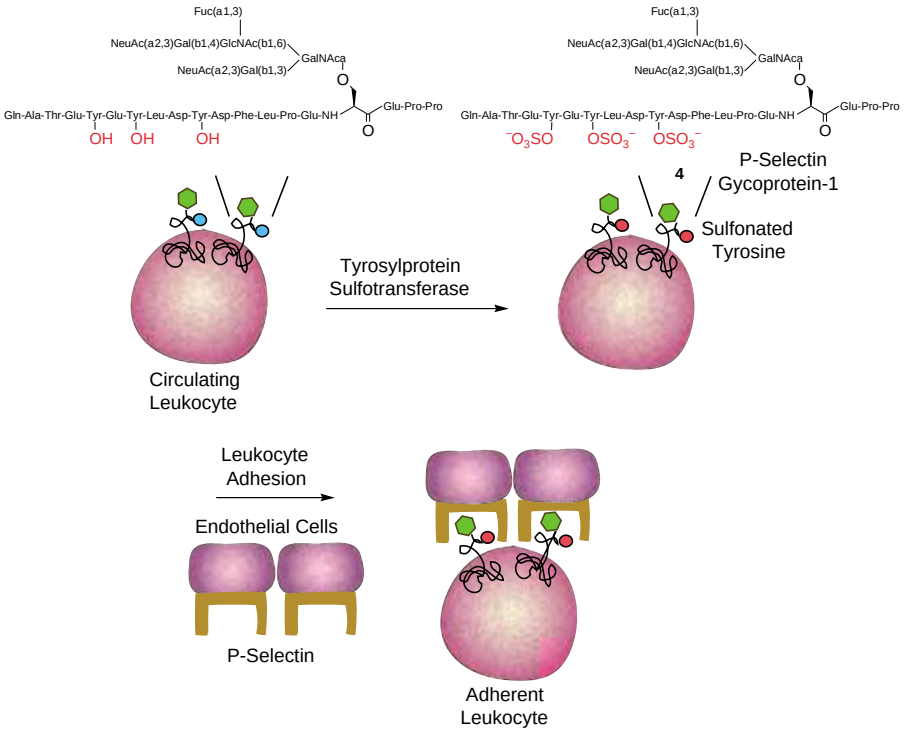
The sulfonation of tyrosine residues by TPST also has an impact on leukocyte adhesion in inflammatory responses (Scheme 13).[119] The N terminus of the primary ligand for P-selectin (P-selectin glycoprotein ligand 1 (PSGL-1)) is sulfonated by TPST to give **4**.[120,121] This sulfonation step leads to an increase in binding affinity of approximately five orders of magnitude between the receptor and the ligand.[122] As a result, TPST has become a therapeutic target for diseases caused by chronic inflammation, such as rheumatoid arthritis, inflammation of the skin, cardiac allograft rejection, and bronchial asthma.

6.4. N-Acetylglucosamine 6-O-Sulfotransferases

The sulfonation of the 6-hydroxy group of *N*-acetylglucosamine residues is another vital transformation catalyzed by STs. For example, GlcNAc-6-O-ST sulfonates *N*-acetylglucosamine subunits of carbohydrates that are located on endothelial cells and contain the sialyl Lewis^x motif **5** (Scheme 14).[123–128] This sulfonation leads to a strong interaction between the resulting carbohydrates and receptors on L-selectin cell adhesion molecules and thus provokes an anti-inflammatory response. Therefore, these enzymes have also been identified as targets for the treatment of diseases caused by chronic inflammation. As previously mentioned, heparan STs also catalyze the sulfonation of glucosamine moieties.

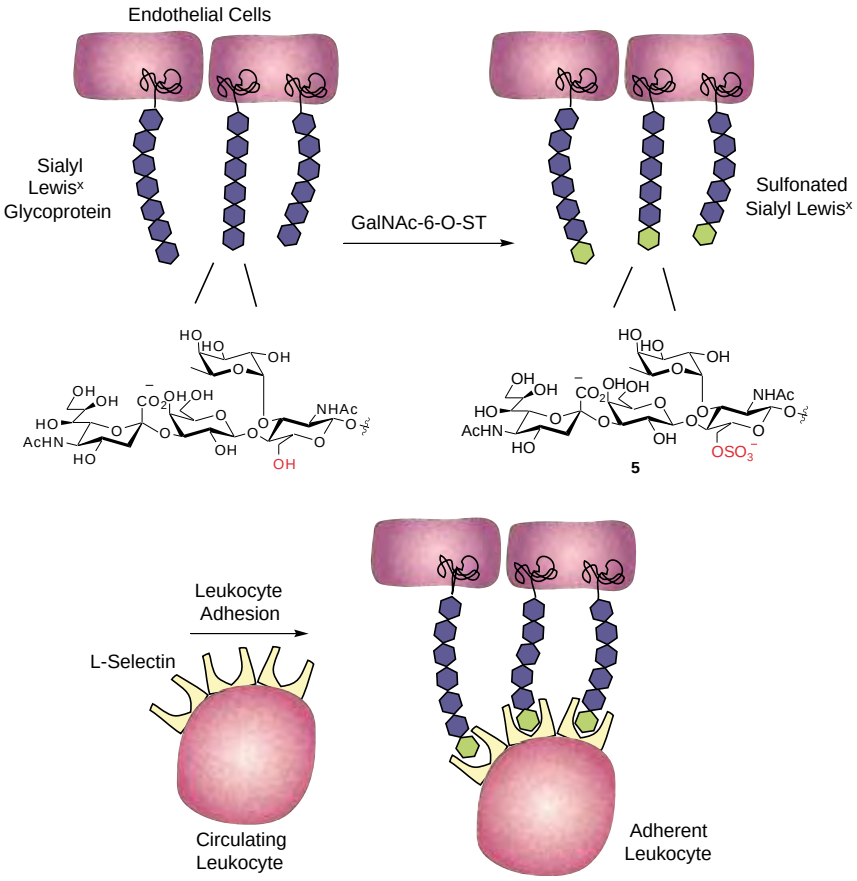
6.5. Other Carbohydrate Sulfotransferases

Another family of carbohydrate sulfotransferases catalyze the sulfonation of galactosamine derivatives within polysaccharide chains. The sulfonation of chondroitin, which is involved in cartilage development,[129] neuronal functions,[130,131] lymphocyte–endothelial-cell binding,[132] and enhancement of T-cell response,[133] is catalyzed by chondroitin 4-O-



Scheme 13. Schematic representation of the regulation of leukocyte adhesion by sulfonation of a tyrosine residue on PSGL-1.

 © 2004 Wiley-VCH Verlag GmbH & Co. KGaA, Weinheim



Scheme 14. Schematic representation of the sulfonation of sialyl Lewis^x leading to leukocyte recruitment.

STs[134] and chondroitin 6-O-ST.[135] Chrondroitin STs are also thought to sulfonate keratan sulfate.[136,137] HNK-1 ST sulfonates the HNK-1-binding carbohydrate expressed on glycolipids and glycoproteins of nervous tissue.[138,139] *N*-Acetylgalactosamine 4-O-STs (GalNAc-4-O-STs) sulfonate saccharide receptor units on the pituitary hormones lutropin, thyrotropin, and pro-opiomelanocortin, which control circulatory half-life.[140–142] Furthermore, dermatan 4-O-ST sulfonates dermatan sulfate (chondroitin sulfate B), another oligosaccharide present in glycolipids and glycoproteins.[143] The product of keratan 6-O-ST has been implicated in corneal transparency.[144]

Cell-surface glycolipids are another class of compounds that perform important biological functions after sulfonation. For example, the sulfatides, which consist of a lipid backbone attached to a sulfonated sugar moiety, are T-cell antigens presented by CD-1 proteins anchored in the cell membrane.[191,192] The interaction of these glycolipids with natural killer T (NKT) cells leads to NKT activation and the resulting immune response.

7. Sulfotransferase Inhibition

The involvement of sulfotransferases in the development of various disease states has led to a search for inhibitors of these enzymes as potential therapeutics. In this section, successful strategies for the inhibition of sulfotransferases will be discussed.

PAPS analogues form a structural class that has yielded effective inhibitors of STs.[145,146] A study of the inhibition of the M and P forms of human-brain phenol sulfotransferases (SULT1A1 and SULT1A3) revealed that PAP was the most effective inhibitor of the transformation of dopamine and phenol substrates (with an inhibition constant of $K_i = 100$ nM). The derivatization of PAP led to large increases in this value. For example, an approximately 100-fold increase was observed for 2′,5′-PAP, which only differs from the original structure in that it contains a 2′-phosphate group instead of a 3′-phosphate group. However, the sulfate group of PAPS does not affect binding, as PAPS and PAP were found to have similar affinities for the enzymes. The enzymatic reactions were monitored by using ^{35}S-PAPS, whereby the radio-labeled product was detected with a scintillation spectrophotometer following chromatographic separation.

A series of small aromatic compounds have been reported as inhibitors of STs with aryl substrates. 2,6-Dichloro-4-nitrophenol (DCNP) and pentachlorophenol (PCP) are the best studied of such compounds.[147] Initially DCNP was found to inhibit the sulfonation by rat-liver PST of harmol, a phenolic drug ($IC_{50} = 100$ nM). In this assay the desulfonation of *p*-nitrophenyl sulfate was detected through absorbance measurements at 400 nm. Elaboration of the structure of DCNP led to the development of further inhibitors. For example, hydroxylated polychlorinated biphenyl compounds were identified as inhibitors of hSULT1E1 with IC_{50} values as low as 0.10–0.19 nM.[148]

Another example of this type is *N*-hydroxy-2-acetylaminofluorene, which was found to inactivate rat hepatic aryl sulfotransferase IV (rSULT1C1 or AST-IV) irreversibly.[149] Various aryl carboxylic acids have also been studied with this enzyme.[150] 1-Naphthoic acid ($K_i = 16$ μM) was found to be more potent than 2-naphthoic acid ($K_i = 41$ μM). Furthermore, 1-naphthoic acid was 12.5 times more potent than 1-naphthylacetic acid and 17.5 times more potent than benzoic acid. The K_i values of salicylic acid and naproxen were determined to be approximately 100 μM.

In a further study with this enzyme, 1-naphthaldehyde was found to have a K_i value of 29 μM.[151] In this case, the rates of the enzymatic reaction were determined by HPLC analysis. Benzo[a]pyrene-7,8-dihydrodiols inhibited rSULT1C1 with K_i values of about 3–4 μM, whereas the corresponding hydroxybenzo[a]pyrene was found to act as a substrate.[152] This observation was attributed to a different binding mode

 © 2004 Wiley-VCH Verlag GmbH & Co. KGaA, Weinheim

for the dihydrodiols, which leads to its inactivity as a substrate.

Two studies focused on dietary chemicals and the inhibition of various STs by food additives, such as catechin, octyl gallate, tartrazine, vanillin,[153] epicatechin gallate, and epigallocatechin gallate.[154] The inhibition of STs by common drugs[155] and amines[156] has also been reported. In another study, pyridoxyl phosphate was found to inhibit bovine PST by covalent binding to the enzyme through Schiff base formation.[157] An IC_{50} value of 100 nM was determined for the inhibition of hSULT1A1 by quercetin; with other STs, such as hSULT1A3 and hSULT2A1, the IC_{50} values for quercetin are three to four times higher.[158]

Another strategy for the development of inhibitors of STs and the elucidation of the enzyme–substrate interaction focused on the derivatization of substrates through chemical synthesis. For example, from a range of estra-1,3,5(10)-trien-17β-ols the 4-nitro derivative was identified as the most effective inhibitor of porcine endometrial SULT1E1 (K_i = 2.4 μM).[159]

Bertozzi and co-workers synthesized several disaccharide analogues of GlcNAc-6-sulfotransferase substrates to ascertain which functional groups are crucial for interaction with the enzyme.[160] Thus, the functional groups on the substrates were systematically removed and the activity of the resulting derivatives was determined. The results of screening experiments with two human STs, CHST2 and HEC-GlcNAc6ST, are summarized in Figure 8.

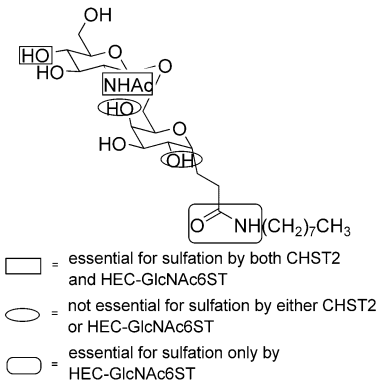


Figure 8. Functional-group analysis of disaccharide analogues of the GlcNAc-6-ST substrate.

Synthetic bisubstrate analogues have been studied in an attempt to develop molecules that inhibit both the PAPS- and the substrate-binding domains of STs simultaneously. For example, analogues of adenine and PAPS with covalently bound estrogen groups were tested (Figure 9).[161] The derivative **6**, in which an estrogen group is attached to the adenosine 5′-hydroxy group of a PAPS analogue through a diphosphate linker, showed the highest inhibition of bovine adrenal SULT1E1 (K_i = 250 nM).

Bertozzi and co-workers screened a 139-compound kinase-directed library for inhibition of GlcNAc-6-ST NodH from *Rhizobium meliloti*.[162] This approach was taken because of the similarities between the substrates of sulfotransferases and kinases. Through combinatorial synthesis[163]

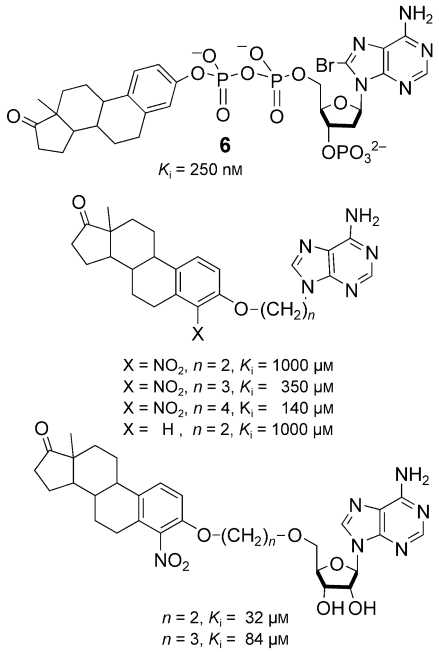
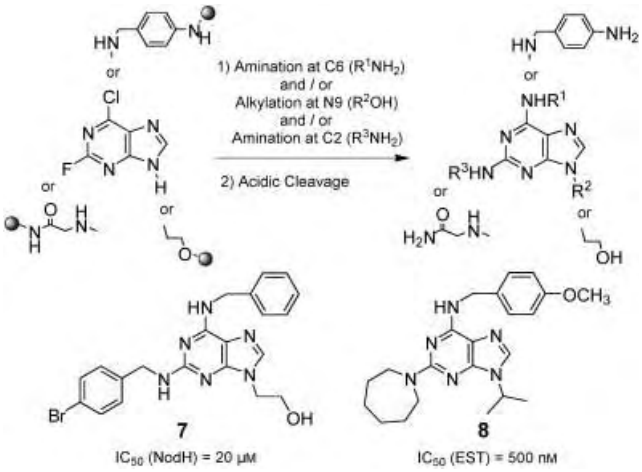


Figure 9. Estrogen-substituted PAPS and adenine analogues as inhibitors of EST. EST = estrogen sulfotransferase.

(Scheme 15) various primary and secondary amines were introduced at the 2- and 6-positions of the purine ring, and the N9-position was functionalized with a range of alcohols through Mitsunobu reactions. The syntheses were carried out on the solid phase by linking the compounds at position C2, C6, or N9 to resin beads.



Scheme 15. Top: kinase-directed synthesis of a purine library; bottom: resulting inhibitors of NodH and SULT1E1.

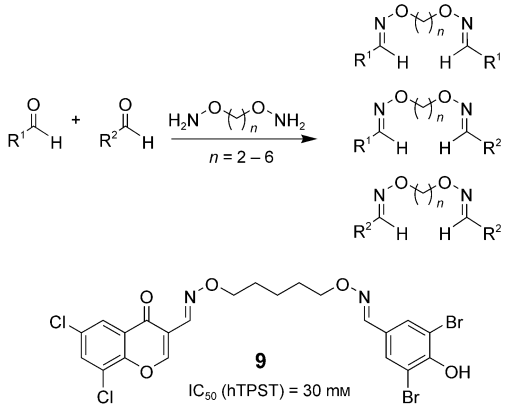
The most effective inhibitors in this study each contained a purine ring with a benzylic substituent at N6. The most potent compound **7** had an IC_{50} value of 20 μM for this enzyme. Whereas the lead compounds showed little inhibition of human high-endothelial GlcNAc-6-O-ST and keratan sulfate ST, thus indicating some selectivity for the target enzyme, cross-reactivity was observed with CDK2, as IC_{50}

 © 2004 Wiley-VCH Verlag GmbH & Co. KGaA, Weinheim

values with this enzyme ranged from 15 to 40 μM. A high-throughput assay with ^{35}S-PAPS and product analysis through phosphor imaging of the resulting TLC traces was also developed to screen the library.

In a subsequent study, 275 compounds from this purine library were screened for inhibition of mSULT1E1.[164] The most potent compound **8**, which has similar structural features to **7**, had an IC_{50} value of 500 nM. No inhibitory activity was observed for **8** with the bacterial GlcNAc-6-sulfotransferase NodH, the human GlcNAc-6-sulfotransferase HEC-GlcNAc6ST, or CHST2 at 200 μM. Both inhibitors also showed selectivity compared to CDKs, such as CDK1 ($IC_{50} = 4000$ nM). Both the previously mentioned TLC assay and a high-throughput MS assay were used to screen for inhibition.

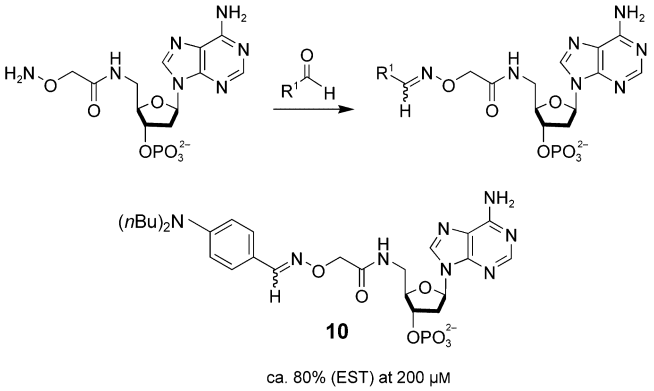
In another study Bertozzi and co-workers utilized target-guided ligand assembly[165] to develop inhibitors of human tyrosylprotein sulfotransferase 2 (hTPST-2).[166] Monomers that showed activity at 1 mM or higher were used to create a library of 171 dimers to be screened for inhibitory activity. Dimerization was performed through oxime formation between the aldehyde-functionalized monomers and *O*,*O*′-diaminoalkane diol linkers of varying lengths (Scheme 16). Each well contained two aldehydes and six linkers of varying



Scheme 16. Target-guided formation of a dimer library for the identification of inhibitors of hTPST-2.

length, and a total of fifteen compounds were obtained. The most active inhibitor **9** had an IC_{50} value of 30 μM and was much more active than the two monomers used to form this structure. The binding of **9** was shown to be reversible, although cross-reactivity was observed (NodST: $IC_{50} = 15$ μM, hEST: $IC_{50} = 250$ μM).

Another library consisted of 447 compounds with a 2′-deoxy-PAP analogue linked to different hydrophobic moieties.[167] The synthetic scheme was based on an PAP analogue with an *O*-linked hydroxylamine group, which was condensed with a range of aldehydes (Scheme 17). The resulting library was screened against hSULT1E1, and the optimal inhibition observed was around 80% at 200 μM for compounds such as **10**. Another inhibitor developed for this enzyme is **11**, which contains covalently attached PAPS and sulfate-acceptor mimetics (Figure 10).[168] It was found to have a K_i value of



Scheme 17. Library of PAP analogues for the identification of inhibitors of SULT1E1.

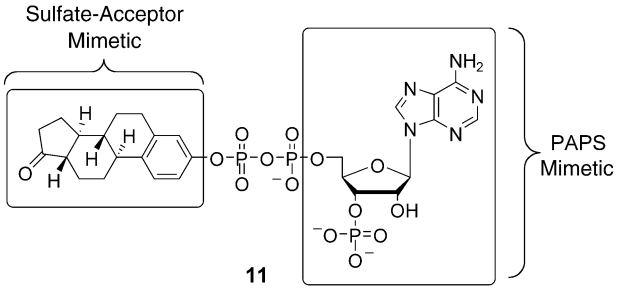
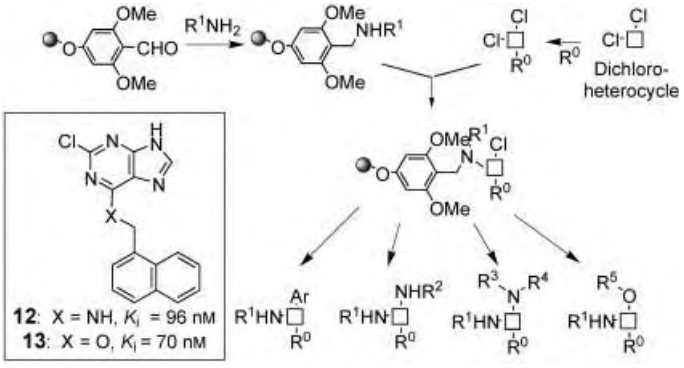


Figure 10. Inhibitor with covalently attached PAP and estrogen analogues.

2.9 nM versus PAPS, but showed noncompetitive inhibition of the steroid site, thus suggesting that it is not a true bisubstrate inhibitor.

Recently, our research group collaborated with Schultz and co-workers to screen around 35000 purine and pyrimidine analogues for activity against β-AST-IV.[169] In the synthesis of this library, dichloroheterocycles were first monofunctionalized and then coupled with an amine group attached to a resin bead to introduce the second functional group (Scheme 18).[170] The installation of the third functional group was performed on the solid phase, followed by cleavage to give the final product. The three substituents were introduced by using different combinations of reductive

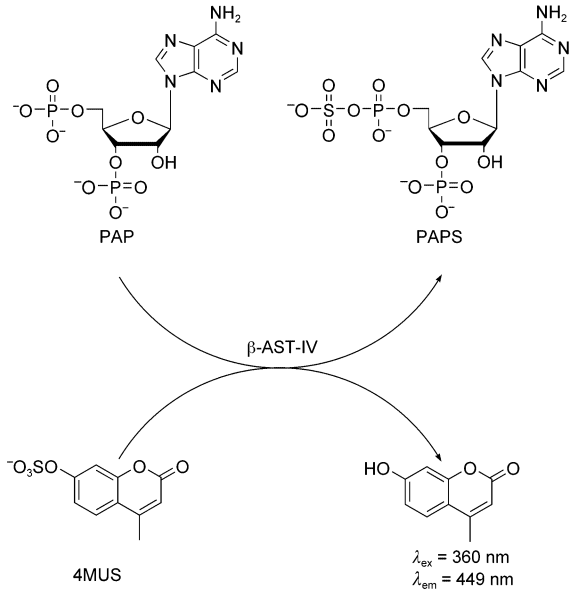


Scheme 18. Heterocycle library and resulting inhibitors of rSULT1C1 (β-AST-IV).

 © 2004 Wiley-VCH Verlag GmbH & Co. KGaA, Weinheim

amination, Mitsunobu, and palladium-catalyzed cross-coupling reactions. The advantage of this method is that it can be used for the synthesis of a variety of heterocycles, including purines, pyrimidines, quinazolines, pyrazines, phthalazines, pyridazines, and quinoxalines.

To screen the library, a fluorescence assay was developed in which the desulfonation of 4-methylumbelliferone sulfate (4MUS) is followed (Scheme 19).[171] From the screen, 11 hits



Scheme 19. Reverse enzymatic assay for the high-throughput screening of ST inhibitors.

were obtained, all of which were aryl-substituted purine derivatives; 10 of the 11 hits contained a naphthyl group at N6. Compound **12** was the most active inhibitor ($K_i = 96$ nM). The interaction was found to be reasonably specific, with modest inhibition of SULT1A1 by **12** and no inhibition of Nod factor ST, protein kinase G, hexokinase, pyruvate kinase, lactic dehydrogenase, or fucosyltransferase V (Table 4). A follow-up study produced **13**, in which linkage to the purine group through an oxygen atom leads to a K_i value of 70 nM.

We further elaborated this structure by rapid, diversity-oriented combinatorial synthesis through amide-bond formation.[172] The resulting library of compounds, which contained purine moieties linked through chains of an even number (2–12) of carbon atoms to a wide range of acids (Scheme 20), was synthesized in microplates and screened in situ for

Table 4: Specificity of compound **12**.

Enzyme	IC_{50}
SULT1A1	770 nM
Nod factor ST	no inhibition[a]
protein kinase G	no inhibition[a]
hexokinase	no inhibition[b]
pyruvate kinase	no inhibition[b]
lactic dehydrogenase	no inhibition[b]
fucosyltransferase V	no inhibition[b]

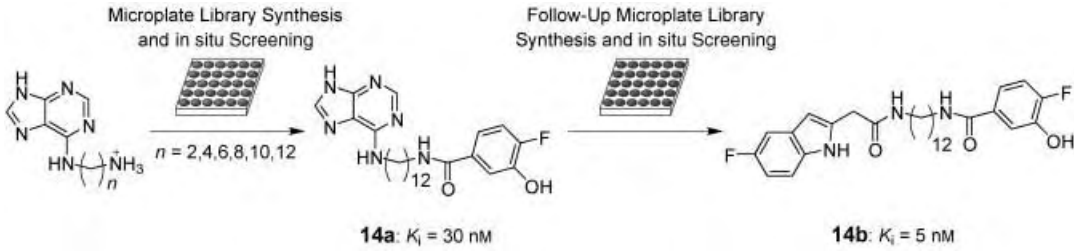
[a] At 10 μM of **12**. [b] At 100 μM of **12**.

activity against β-AST-IV. The most effective inhibition was observed for the compound derived from the coupling of 4-fluoro-3-hydroxybenzoic acid with the longest linker (**14a**, $K_i = 30$ nM). The high activity of **14a** may be due to its flexibility, which allows the molecule to adopt such a geometry as to maximize its interaction with the residues in the active site or to increase its hydrophobicity. We later improved upon **14a** through the formation of a follow-up library in which the purine group was replaced. The K_i value (5 nM) of **14b** thus obtained is over five orders of magnitude lower than the K_m value (1 mM) of the substrate whose binding site it occupies.

8. Synthetic Applications

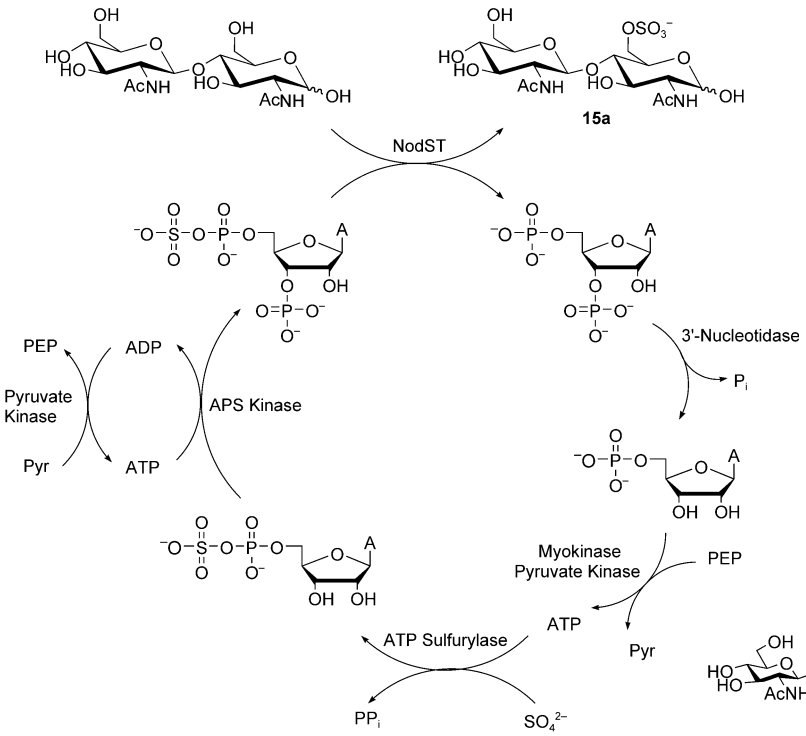
The synthesis of a number of sulfated biomolecules has been reported. For example, PAPS has been synthesized both chemically and enzymatically in several syntheses.[173–178] Furthermore, chemical syntheses of various sulfated sialyl Lewis^x (sLe^x) structures,[179] chemoenzymatic syntheses of 6′-sulfo-sLe^x[180] and chondroitin sulfate E,[181] and syntheses of glycosulfopeptides by both chemical and enzymatic reactions[122,182] have been reported. However, examples of the use of STs in synthesis are rare. In all the syntheses of sulfated biomolecules listed above, the sulfate group was installed chemically.

One of the problems associated with the use of STs as synthetic tools is product inhibition. PAP is a strong (nM to low μM) inhibitor of STs. One approach to avoid this problem is to use a regeneration pathway. Lin and co-workers used the regeneration pathway shown in Scheme 21 to synthesize *N*,*N*′-diacetylchitobiose 6-sulfate (**15a**).[183] This regeneration approach allows the reaction to be run at low concentrations of PAPS and less expensively. PAP is removed, thus minimizing inhibition. The primary drawback of this method is its



Scheme 20. Optimization of small-molecule rSULT1C1 inhibitors through rapid diversity-oriented library formation and high-throughput screening.

 © 2004 Wiley-VCH Verlag GmbH & Co. KGaA, Weinheim

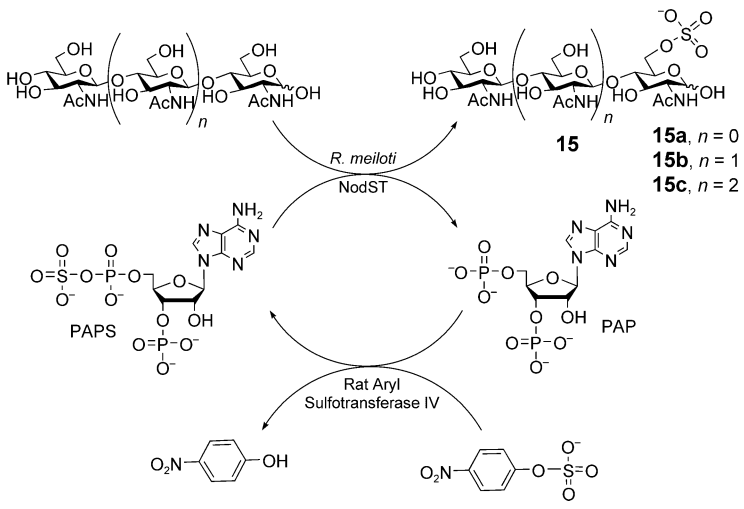


Scheme 21. NodST-catalyzed synthesis of *N*,*N*′-diacetylchitobiose 6-sulfate (**15a**) with multienzymatic regeneration of PAPS.

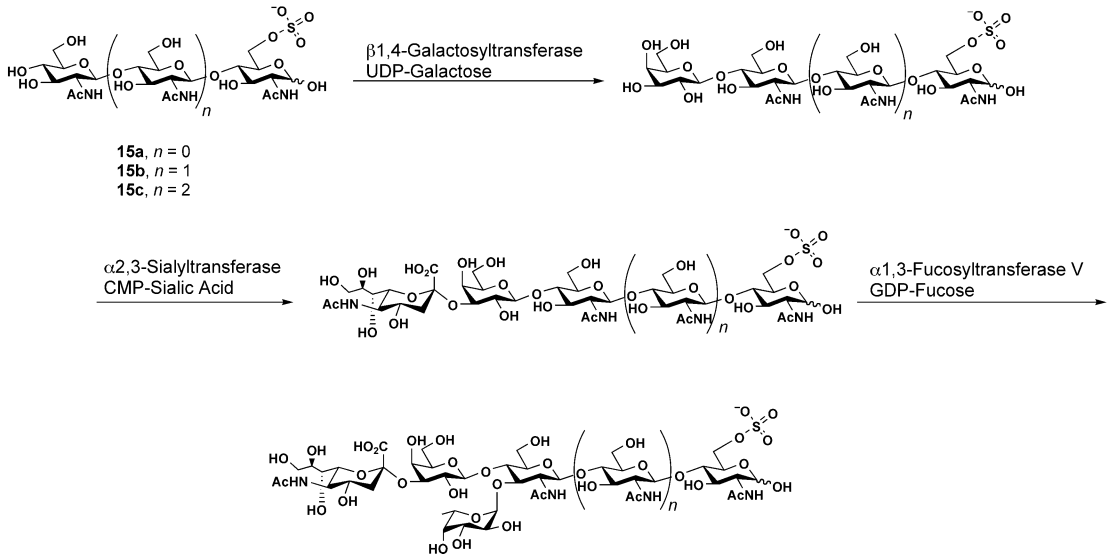
complexity, as six enzymes and their substrates are required. To address this issue, Burkart et al. developed a regeneration approach in which rSULT1C1 (β-AST-IV) is used in the reverse physiological direction to generate PAPS from *p*-nitrophenol sulfate (PNPS; Scheme 22).[184]. This coupled reaction was used to synthesize the sLe^x analogues shown in Scheme 23.

Recently, Rosenberg and co-workers reported exciting new chemoenzymatic syntheses of antithrombin III binding heparan sulfates. Compounds of this type have been prepared by conventional chemical synthesis;[185,186] however, such approaches are often tedious, as a large number of steps are required. In one example, engineered HS chains containing the antithrombin III binding domain were synthesized chemoenzymatically in a two-step process from the nonsulfated *N*-acetyl heparosan polysaccharide **16** from the *E. Coli* strain K5 (Scheme 24).[187] The aim of the study was to improve upon HS therapeutics, which are known to cause side effects. PAP^{35}S was incorporated in the final step, the sulfonation of **17**, to make it possible to evaluate AT-III affinity by using gel mobility assays. The specific activity of the product mitrin (**18**) was four to five times that of commercial HS.

In another publication, the chemoenzymatic synthesis of the antithrombin III binding HS pentasaccharide was described (Scheme 25).[188]

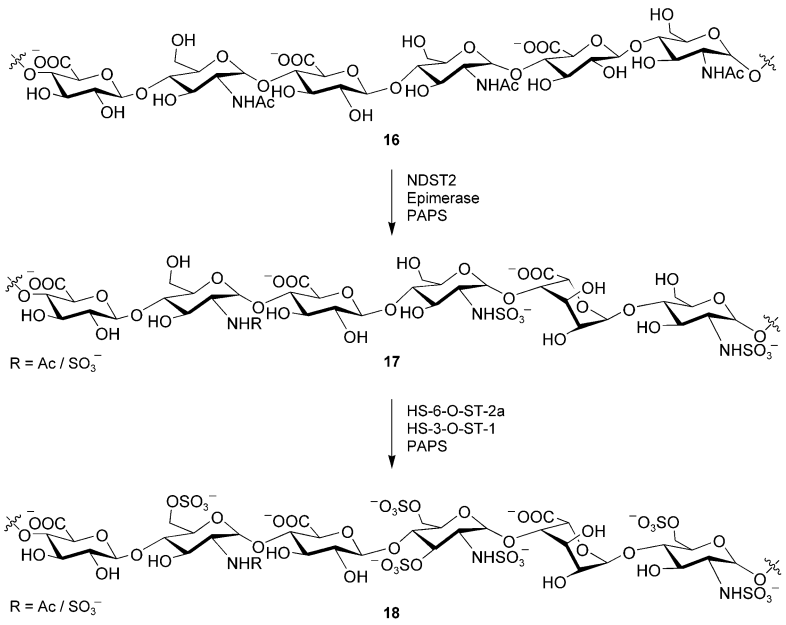


Scheme 22. Synthesis of sulfated chitooligosaccharides with AST-IV-catalyzed regeneration of PAPS



Scheme 23. Synthesis of sialyl Le^x 6-sulfate analogues.

 © 2004 Wiley-VCH Verlag GmbH & Co. KGaA, Weinheim



Scheme 24. Two-step chemoenzymatic synthesis of mitrin (**18**).

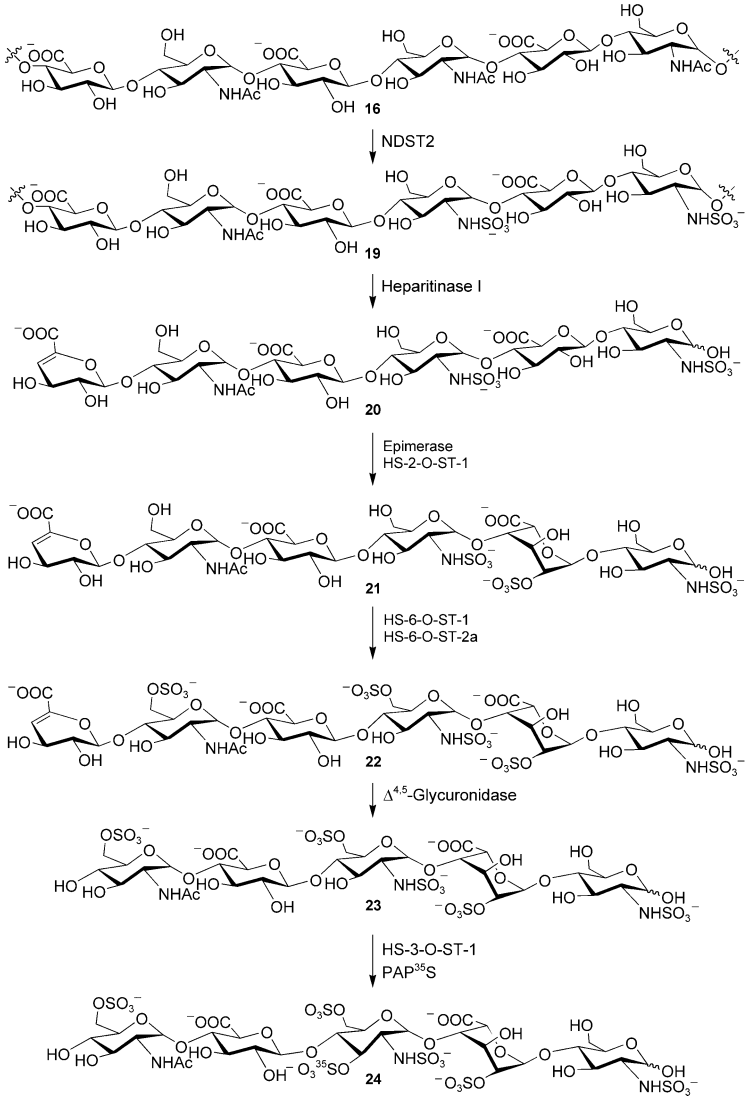
The heparosan **16** was again used as the starting material for the synthesis. NDST2 was first used to *N*-deacetylate and *N*-sulfonate glucosamine residues selectively to form **19**. Next, **19** was partially cleaved by heparitinase I into a mixture of oligosaccharides, from which the hexassacharide **20** was isolated by HPLC. In the next two steps, epimerization and sulfonation reactions were performed with C5-epimerase and HS-2-O-ST-1 to form **21**, and then with HS-6-O-ST-1 and HS-6-O-ST-2a to yield **22**. Finally, the bacterial enzyme $\Delta^{4,5}$-glycuronidase was used to remove the unsaturated uronic acid residue to give **23**, and treatment with HS-3-O-ST-1 and PAP^{35}S led to the final product **24**. Gel mobility assays confirmed that **24** is an effective binder of AT-III.

Because of the prominent roles of sulfonated glycoaminoglycans in crucial biological events, practical methods for the synthesis of these compounds are of great interest. Recent examples of the efficient application of chemoenzymatic methods show great promise. A combination of chemoenzymatic synthesis and PAPS regeneration should lead to great advances in terms of access to molecules of this type.

9. Summary and Outlook

There is increasing interest in the sulfotransferases because of the potential biomedical and regulatory importance of this class of biocatalysts. Although structural and mechanistic studies have already provided a great deal of insight, further studies are required if potent and specific inhibitors are to be designed for therapeutic use and the further characterization of STs.

The majority of the biochemical and biophysical studies were carried out on cytosolic STs, as these enzymes are more readily accessible through recombinant techniques than their membrane-associated counterparts. From the results of these studies a complete mechanistic picture is emerging, but the rational design of an inhibitor with high potency for a specific ST has not yet been demonstrated. The preparation of bisubstrate transition-state or ground-state analogues has been proposed as a possible solution to this problem; however, earlier attempts were probably hindered by the incomplete understanding of the transition-state structure. The required length of the linker between the two binding moities will be defined by this structure. Studies with the protein tyrosine kinase (Csk) confirm that the length of the linker must correspond to the dissociative transition state.[189,190]



Scheme 25. Chemoenzymatic synthesis of the AT-III-binding HS pentasaccharide.

 © 2004 Wiley-VCH Verlag GmbH & Co. KGaA, Weinheim

Another important question is whether a sulfoenzyme intermediate is involved. Based on the available structural and mechanistic data, this possibility can not be ruled out. The active-site histidine residue (or with less likelihood another residue) could be acting as a nucleophile to generate a sulfohistidine intermediate that is not stable and therefore eludes mechanistic studies. Structural analysis shows that the conserved active-site histidine residue could be in a suitable position to act as a nucleophile and not as a base.[36] Mutagenesis studies on rSULT1C1, although inconclusive, showed both H104A and H104S mutants to be inactive, and the activity could not be recovered even through the use of imidizole.[78] This finding could indicate that the histidine residue is not acting as a base. A suicide inhibitor of rSULT1C1 has also been reported, but the enzyme–inhibitor complex was not subjected to rigorous characterization.[149] Further investigations into this matter are necessary and could change the current approach to the design of ST inhibitors.

One of the limiting factors in the study of membrane-associated STs is the low availability of recombinant protein. Further work toward the cloning and over-expression of these enzymes is needed if a complete picture is to be obtained. A better understanding of the active sites and substrate-binding sites will help in the design of potent and specific inhibitors of this important class of molecules.

We acknowledge the support of the NIH. S.R.H. thanks the ARCS foundation for a fellowship. We also thank Marian Bryan for her generous assistance in generating the graphics.

Received: September 1, 2003 [A631]
Published Online: June 21, 2004

[1] E. Baumann, *Ber. Dtsch. Chem. Ges.* **1876**, 54.
[2] P. W. Robbins, F. Lipmann, *J. Am. Chem. Soc.* **1956**, *78*, 2652–2653.
[3] C. Clarke, P. Thorburn, D. McDonald, J. B. Adams, *Biochim. Biophys. Acta* **1982**, *707*, 28–37.
[4] B. J. Buirchell, R. Hahnel, *J. Steroid Biochem.* **1975**, *6*, 1489–1494.
[5] A. Superti-Furga, *Am. J. Hum. Genet.* **1994**, *55*, 1137–1145.
[6] M. W. Duffel, A. D. Marshall, P. McPhie, V. Sharma, W. B. Jakoby, *Drug Metab. Rev.* **2001**, *33*, 369–395.
[7] K. Nagata, Y. Yamazoe, *Annu. Rev. Pharmacol. Toxicol.* **2000**, *40*, 159–176.
[8] H. Glatt, *FASEB J.* **1997**, *11*, 314–321.
[9] M. Matsui, H. Homma, *Int. J. Biochem.* **1994**, *26*, 1237–1247.
[10] Y. Yamazoe, K. Nagata, S. Ozawa, R. Kato, *Chem.-Biol. Interact.* **1994**, *92*, 107–117.
[11] C. Niehrs, R. Beisswanger, W. B. Huttner, *Chem.-Biol. Interact.* **1994**, *92*, 257–271.
[12] C. A. Strott, *Endocr. Rev.* **2002**, *23*, 703–732.
[13] M. A. Runge-Morris, *FASEB J.* **1997**, *11*, 109–117.
[14] C. N. Falany, T. W. Wilborn, *Adv. Pharmacol.* **1994**, *27*, 301–329.
[15] C. Her, T. C. Wood, E. E. Eichler, H. W. Mohrenweiser, L. S. Ramagli, M. J. Siciliano, R. M. Weinshilboum, *Genomics* **1998**, *53*, 284–295.
[16] L. A. Brix, A. C. Barnett, R. G. Duggleby, B. Leggett, M. E. McManus, *Biochemistry* **1999**, *38*, 10474–10479.
[17] G. P. Chen, P. A. Rabjohn, J. L. York, C. Wooldridge, D. Q. Zhang, C. N. Falany, A. Radominska-Pandya, *Biochemistry* **2000**, *39*, 16000–16007.
[18] R. J. Anderson, P. E. Kudlacek, D. L. Clemens, *Chem.-Biol. Interact.* **1998**, *109*, 53–67.
[19] L. A. Brix, R. G. Duggleby, A. Gaedigk, M. E. McManus, *Biochem. J.* **1999**, *337*, 337–343.
[20] L. A. Brix, R. Nicoll, X. Y. Zhu, M. E. McManus, *Chem.-Biol. Interact.* **1998**, *109*, 123–127.
[21] J. Wang, J. L. Falany, C. N. Falany, *Mol. Pharmacol.* **1998**, *53*, 274–282.
[22] Y. Sakakibara, K. Yanagisawa, J. Katafuchi, D. P. Ringer, Y. Takami, T. Nakayama, M. Suiko, M. C. Liu, *J. Biol. Chem.* **1998**, *273*, 33929–33935.
[23] N. Hempel, A. C. Barnett, R. M. Bolton-Grob, N. E. Liyou, M. E. McManus, *Biochem. Biophys. Res. Commun.* **2000**, *276*, 224–230.
[24] E. V. Petrotchenko, M. E. Doerflein, Y. Kakuta, L. C. Pedersen, M. Negishi, *J. Biol. Chem.* **1999**, *274*, 30019–30022.
[25] W. J. Geese, R. B. Raftogianis, *Biochem. Biophys. Res. Commun.* **2001**, *288*, 280–289.
[26] M. W. Duffel, W. B. Jakoby, *J. Biol. Chem.* **1981**, *256*, 1123–1127.
[27] W. Honma, Y. Kamiyama, K. Yoshinari, H. Sasano, M. Shimada, K. Nagata, Y. Yamazoe, *Drug Metab. Dispos.* **2001**, *29*, 274–281.
[28] M. W. Duffel, *Chem.-Biol. Interact.* **1994**, *92*, 3–14.
[29] R. M. Harris, R. H. Waring, C. J. Kirk, P. J. Hughes, *J. Biol. Chem.* **2000**, *275*, 159–166.
[30] G. P. Chen, E. Banoglu, M. W. Duffel, *Chem. Res. Toxicol.* **1996**, *9*, 67–74.
[31] M. W. Duffel, G. P. Chen, V. Sharma, *Chem.-Biol. Interact.* **1998**, *109*, 81–92.
[32] Y. S. Yang, S. W. Tsai, E. S. Lin, *Chem.-Biol. Interact.* **1998**, *109*, 129–135.
[33] Y. Q. Zheng, A. Bergold, M. W. Duffel, *J. Biol. Chem.* **1994**, *269*, 30313–30319.
[34] D. M. Otterness, S. P. Powers, L. J. Miller, R. M. Weinshilboum, *Mol. Pharmacol.* **1991**, *39*, 34–41.
[35] E. S. Lin, Y. S. Yang, *Biochem. Biophys. Res. Commun.* **2000**, *271*, 818–822.
[36] Y. Kakuta, L. G. Pedersen, C. W. Carter, M. Negishi, L. C. Pedersen, *Nat. Struct. Biol.* **1997**, *4*, 904–908.
[37] S. Pakhomova, M. Kobayashi, J. Buck, M. E. Newcomer, *Nat. Struct. Biol.* **2001**, *8*, 447–451.
[38] R. Dajani, A. Cleasby, M. Neu, A. J. Wonacott, H. Jhoti, A. M. Hood, S. Modi, A. Hersey, J. Taskinen, R. M. Cooke, G. R. Manchee, M. W. H. Coughtrie, *J. Biol. Chem.* **1999**, *274*, 37862–37868.
[39] Y. Kakuta, T. Sueyoshi, M. Negishi, L. C. Pedersen, *J. Biol. Chem.* **1999**, *274*, 10673–10676.
[40] M. Negishi, L. G. Pedersen, E. Petrotchenko, S. Shevtsov, A. Gorokhov, Y. Kakuta, L. C. Pedersen, *Arch. Biochem. Biophys.* **2001**, *390*, 149–157.
[41] K. Yoshinari, E. V. Petrotchenko, L. C. Pedersen, M. Negishi, *J. Biochem. Mol. Toxicol.* **2001**, *15*, 67–75.
[42] R. Raman, J. Myette, G. Venkataraman, V. Sasisekharan, R. Sasisekharan, *Biochem. Biophys. Res. Commun.* **2002**, *290*, 1214–1219.
[43] L. M. Bidwell, M. E. McManus, A. Gaedigk, Y. Kakuta, M. Negishi, L. Pedersen, J. L. Martin, *J. Mol. Biol.* **1999**, *293*, 521–530.
[44] Y. Kakuta, E. V. Petrotchenko, L. C. Pedersen, M. Negishi, *J. Biol. Chem.* **1998**, *273*, 27325–27330.
[45] L. C. Pedersen, E. Petrotchenko, S. Shevtsov, M. Negishi, *J. Biol. Chem.* **2002**, *277*, 17928–17932.

 © 2004 Wiley-VCH Verlag GmbH & Co. KGaA, Weinheim

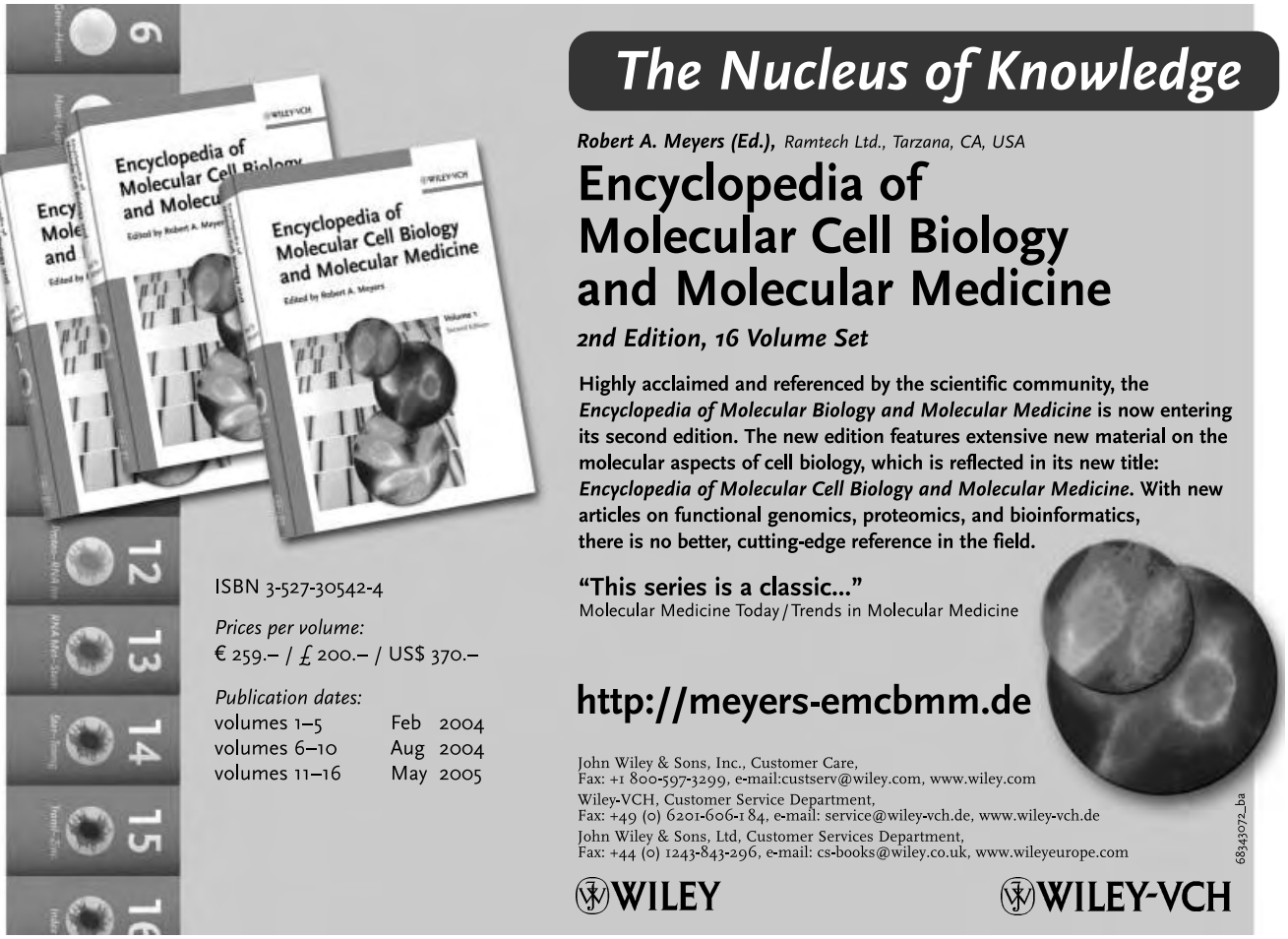
[46] W. J. Driscoll, K. Komatsu, C. A. Strott, *Proc. Natl. Acad. Sci. USA* **1995**, *92*, 12328 – 12332.
[47] Y. Sakakibara, Y. Takami, T. Nakayama, M. Suiko, M. C. Liu, *J. Biol. Chem.* **1998**, *273*, 6242 – 6247.
[48] M. C. Liu, M. Suiko, Y. Sakakibara, *J. Biol. Chem.* **2000**, *275*, 13460 – 13464.
[49] P. H. Rehse, M. Zhou, S. X. Lin, *Biochem. J.* **2002**, *364*, 165 – 171.
[50] L. C. Pedersen, E. V. Petrotchenko, M. Negishi, *FEBS Lett.* **2000**, *475*, 61 – 64.
[51] H. Fuda, Y. C. Lee, C. Shimizu, N. B. Javitt, C. A. Strott, *J. Biol. Chem.* **2002**, *277*, 36161 – 36166.
[52] T. Yabe, D. Shukla, P. G. Spear, R. D. Rosenberg, P. H. Seeberger, N. W. Shworak, *Biochem. J.* **2001**, *359*, 235 – 241.
[53] A. Gorokhov, L. Perera, T. A. Darden, M. Negishi, L. C. Pedersen, L. G. Pedersen, *Biophys. J.* **2000**, *79*, 2909 – 2917.
[54] W. W. Cleland, *Enzymes* **1967**, *2*, 1 – 65.
[55] J. B. Adams, A. Poulos, *Biochim. Biophys. Acta* **1967**, *146*, 493 – 508.
[56] J. B. Adams, R. K. Ellyard, J. Low, *Biochim. Biophys. Acta* **1974**, *370*, 160 – 188.
[57] H. P. Zhang, O. Varmalova, F. M. Vargas, C. N. Falany, T. S. Leyh, *J. Biol. Chem.* **1998**, *273*, 10888 – 10892.
[58] R. K. Banerjee, A. B. Roy, *Biochem. J.* **1966**, *100*, P59 – P60.
[59] R. K. Banerjee, A. B. Roy, *Biochim. Biophys. Acta* **1968**, *151*, 573 – 586.
[60] E. J. M. Pennings, R. Vrielink, G. M. J. Vankempen, *Biochem. J.* **1978**, *173*, 299 – 307.
[61] A. D. Marshall, P. McPhie, W. B. Jakoby, *Arch. Biochem. Biophys.* **2000**, *382*, 95 – 104.
[62] L. Varin, R. K. Ibrahim, *J. Biol. Chem.* **1992**, *267*, 1858 – 1863.
[63] E. Vakiani, J. G. Luz, J. Buck, *J. Biol. Chem.* **1998**, *273*, 35381 – 35387.
[64] Z. Tong, M. O. James, *Arch. Biochem. Biophys.* **2000**, *376*, 409 – 419.
[65] P. Mattock, D. J. Barford, J. M. Basford, J. G. Jones, *Biochem. J.* **1970**, *116*, 805 – 810.
[66] G. R. J. Burns, E. Galanopoulou, C. H. Wynn, *Biochem. J.* **1977**, *167*, 223 – 227.
[67] K. Kobashi, D. H. Kim, T. Morikawa, *J. Protein Chem.* **1987**, *6*, 237 – 244.
[68] C. L. L. Chai, G. Lowe, *Bioorg. Chem.* **1992**, *20*, 181 – 188.
[69] A. R. Kwon, H. J. Yun, E. C. Choi, *Biochem. Biophys. Res. Commun.* **2001**, *285*, 526 – 529.
[70] Y. Bartolotti, Y. Kakuta, L. Pedersen, M. Negishi, L. Pedersen, *J. Mol. Struct.* **1999**, *461–462*, 105 – 111.
[71] E. Chapman, M. C. Bryan, C. H. Wong, *Proc. Natl. Acad. Sci. USA* **2003**, *100*, 910 – 915.
[72] A. Williams, *Adv. Phys. Org. Chem.* **1992**, *27*, 1 – 55.
[73] K. G. Bowman, C. R. Bertozzi, *Chem. Biol.* **1999**, *6*, R9 – R22.
[74] S. Hemmerich, *Drug Discovery Today* **2001**, *6*, 27 – 35.
[75] J. B. Adams, T. Pewnim, D. P. Chandra, L. Archibald, M. S. Foo, *Cancer Res.* **1979**, *39*, 5124 – 5126.
[76] J. R. Pasqualini, G. Chetrite, C. Blacker, M. C. Feinstein, L. Delalonde, M. Talbi, C. Maloche, *J. Clin. Endocrinol. Metab.* **1996**, *81*, 1460 – 1464.
[77] T. Suzuki, T. Nakata, Y. Miki, C. Kaneko, T. Moriya, T. Ishida, S. Akinaga, H. Hirakawa, M. Kimura, H. Sasano, *Cancer Res.* **2003**, *63*, 2762 – 2770.
[78] J. L. Falany, C. N. Falany, *Cancer Res.* **1996**, *56*, 1551 – 1555.
[79] Y. Qian, C. Deng, W. C. Song, *J. Pharmacol. Exp. Ther.* **1998**, *286*, 555 – 560.
[80] U. Lindahl, M. Kusche-Gullberg, L. Kjellén, *J. Biol. Chem.* **1998**, *273*, 24979 – 24982.
[81] N. Razi, U. Lindahl, *J. Biol. Chem.* **1995**, *270*, 11267 – 11275.
[82] I. Capila, R. J. Linhardt, *Angew. Chem.* **2002**, *114*, 426 – 450; *Angew. Chem. Int. Ed.* **2002**, *41*, 391 – 412.
[83] J. D. Esko, S. B. Selleck, *Annu. Rev. Biochem.* **2002**, *71*, 435 – 471.
[84] D. Shukla, J. Liu, P. Blaiklock, N. W. Shworak, X. M. Bai, J. D. Esko, G. H. Cohen, R. J. Eisenberg, R. D. Rosenberg, P. G. Spear, *Cell* **1999**, *99*, 13 – 2.
[85] J. A. Liu, Z. Shriver, P. Blaiklock, K. Yoshida, R. Sasisekharan, R. D. Rosenberg, *J. Biol. Chem.* **1999**, *274*, 38155 – 38162.
[86] C. C. Rider, *Glycoconjugate J.* **1997**, *14*, 639 – 642.
[87] D. S. Newburg, R. J. Linhardt, S. A. Ampofo, R. H. Yolken, *J. Nutr.* **1995**, *125*, 419 – 424.
[88] H. A. Harrop, D. R. Coombe, C. C. Rider, *AIDS* **1994**, *8*, 183 – 192.
[89] L. N. Callahan, M. Phelan, M. Mallinson, M. A. Norcross, *J. Virol.* **1991**, *65*, 1543 – 1550.
[90] D. Batinic, F. A. Robey, *J. Biol. Chem.* **1992**, *267*, 6664 – 6671.
[91] M. Rusnati, D. Coltrini, P. Oreste, G. Zoppetti, A. Albini, D. Noonan, F. D. di Fagagna, M. Giacca, M. Presta, *J. Biol. Chem.* **1997**, *272*, 11313 – 11320.
[92] H. C. Chang, F. Samaniego, B. C. Nair, L. Buonaguro, B. Ensoli, *AIDS* **1997**, *11*, 1421 – 1431.
[93] D. H. Atha, J. C. Lormeau, M. Petitou, R. D. Rosenberg, J. Choay, *Biochemistry* **1985**, *24*, 6723 – 6729.
[94] D. H. Atha, A. W. Stephens, R. D. Rosenberg, *Proc. Natl. Acad. Sci. USA* **1984**, *81*.
[95] D. H. Atha, J. C. Lormeau, M. Petitou, R. D. Rosenberg, J. Choay, *Biochemistry* **1987**, *26*, 6454 – 6461.
[96] R. D. Rosenberg, P. S. Damus, *J. Biol. Chem.* **1973**, *248*, 6490 – 6505.
[97] J. Liu, N. W. Shworak, L. M. S. Fritze, J. M. Edelberg, R. D. Rosenberg, *J. Biol. Chem.* **1996**, *271*, 27072 – 27082.
[98] Z. L. L. Wu, L. J. Zhang, D. L. Beeler, B. Kuberan, R. D. Rosenberg, *FASEB J.* **2002**, *16*, 539 – 545.
[99] L. J. Zhang, D. L. Beeler, R. Lawrence, M. Lech, J. Liu, J. C. Davis, Z. Shriver, R. Sasisekharan, R. D. Rosenberg, *J. Biol. Chem.* **2001**, *276*, 42311 – 42321.
[100] A. C. Rapraeger, *Chem. Biol.* **1995**, *2*, 645 – 649.
[101] D. A. Pye, R. R. Vives, J. E. Turnbull, P. Hyde, J. T. Gallagher, *J. Biol. Chem.* **1998**, *273*, 22936 – 22942.
[102] S. Faham, R. E. Hileman, J. R. Fromm, R. J. Linhardt, D. C. Rees, *Science* **1996**, *271*, 1116 – 1120.
[103] Z. L. Wu, L. Zhang, T. Yabe, B. Kuberan, D. L. Beeler, A. Love, R. D. Rosenberg, *J. Biol. Chem.* **2003**, *278*, 17121 – 17129.
[104] S. E. Marshall, M. Luscombe, D. S. Pepper, J. J. Holbrook, *Biochim. Biophys. Acta* **1984**, *797*, 34 – 39.
[105] K. Ibel, G. A. Poland, J. P. Baldwin, D. S. Pepper, M. Luscombe, J. J. Holbrook, *Biochim. Biophys. Acta* **1986**, *870*, 58 – 63.
[106] E. Mbemba, J. C. Gluckman, L. Gattegno, *Glycobiology* **2000**, *10*, 21 – 29.
[107] G. S. V. Kuschert, F. Coulin, C. A. Power, A. E. I. Proudfoot, R. E. Hubbard, A. J. Hoogewerf, T. N. C. Wells, *Biochemistry* **1999**, *38*, 12959 – 12968.
[108] R. J. Lipscombe, A. M. Nakhoul, C. J. Sanderson, D. R. Coombe, *J. Leukocyte Biol.* **1998**, *63*, 342 – 350.
[109] R. Ishitsuka, K. Kojima, H. Utsumi, H. Ogawa, I. Matsumoto, *J. Biol. Chem.* **1998**, *273*, 9935 – 9941.
[110] A. D. Cardin, N. Hirose, D. T. Blankenship, R. L. Jackson, J. A. K. Harmony, D. A. Sparrow, J. T. Sparrow, *Biochem. Biophys. Res. Commun.* **1986**, *134*, 783 – 789.
[111] K. H. Weisgraber, S. C. Rall, R. W. Mahley, R. W. Milne, Y. L. Marcel, J. T. Sparrow, *J. Biol. Chem.* **1986**, *261*, 2068 – 2076.
[112] K. Fuxe, B. Tinner, W. Staines, G. David, L. F. Agnati, *Brain Res.* **1997**, *746*, 25 – 33.
[113] J. A. Liu, N. W. Shworak, P. Sinay, J. J. Schwartz, L. J. Zhang, L. M. S. Fritze, R. D. Rosenberg, *J. Biol. Chem.* **1999**, *274*, 5185 – 5192.

 © 2004 Wiley-VCH Verlag GmbH & Co. KGaA, Weinheim

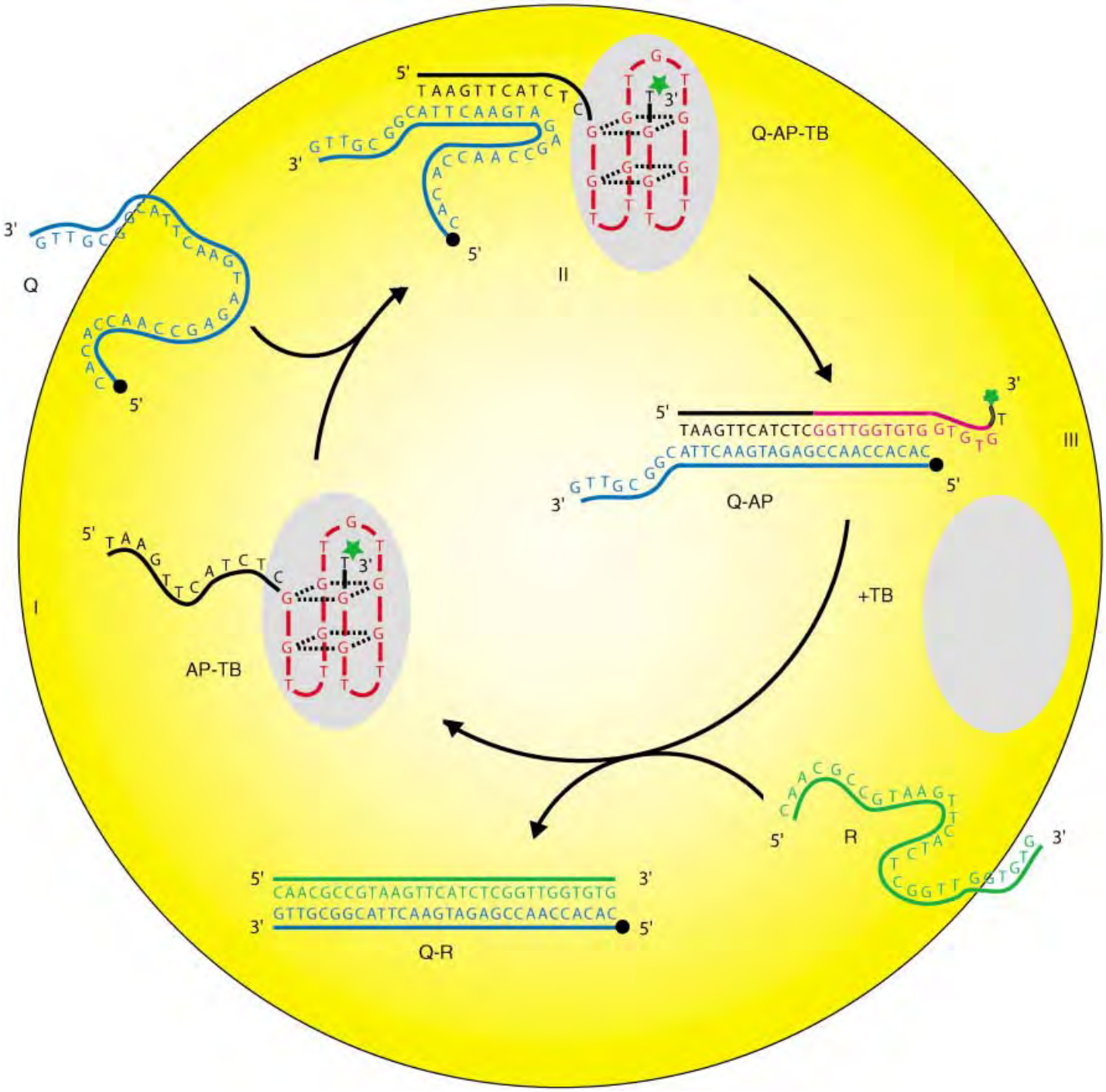
[114] N. W. Shworak, J. A. Liu, L. M. Petros, L. J. Zhang, M. Kobayashi, N. G. Copeland, N. A. Jenkins, R. D. Rosenberg, *J. Biol. Chem.* **1999**, *274*, 5170 – 5184.
[115] J. Aikawa, K. Grobe, M. Tsujimoto, J. D. Esko, *J. Biol. Chem.* **2001**, *276*, 5876 – 5882.
[116] H. Habuchi, M. Tanaka, O. Habuchi, K. Yoshida, H. Suzuki, K. Ban, K. Kimata, *J. Biol. Chem.* **2000**, *275*, 2859 – 2868.
[117] M. Farzan, T. Mirzabekov, P. Kolchinsky, R. Wyatt, M. Cayabyab, N. P. Gerard, C. Gerard, J. Sodroski, H. Choe, *Cell* **1999**, *96*, 667 – 676.
[118] H. Choe, W. Li, P. L. Wright, N. Vasilieva, M. Venturi, C.-C. Huang, C. Grundner, T. Dorfman, M. B. Zwick, L. Wang, E. S. Rosenberg, P. D. Kwong, D. R. Burton, J. E. Robinson, J. G. Sodroski, M. Farzan, *Cell* **2003**, *114*, 161 – 170.
[119] G. S. Kansas, *Blood* **1996**, *88*, 3259 – 3287.
[120] D. Sako, K. M. Comess, K. M. Barone, R. T. Camphausen, D. A. Cumming, G. D. Shaw, *Cell* **1995**, *83*, 323 – 331.
[121] T. Pouyani, B. Seed, *Cell* **1995**, *83*, 333 – 343.
[122] K. M. Koeller, M. E. B. Smith, C. H. Wong, *J. Am. Chem. Soc.* **2000**, *122*, 742 – 743.
[123] Y. Imai, L. A. Lasky, S. D. Rosen, *Nature* **1993**, *361*, 555 – 557.
[124] D. D. Manning, C. R. Bertozzi, N. L. Pohl, S. D. Rosen, L. L. Kiessling, *J. Org. Chem.* **1995**, *60*, 6254 – 6255.
[125] K. Shailubhai, P. R. Streeter, C. E. Smith, G. S. Jacob, *Glycobiology* **1997**, *7*, 305 – 314.
[126] A. Bistrup, S. Bhakta, J. K. Lee, Y. Y. Belov, M. D. Gunn, F. R. Zuo, C. C. Huang, R. Kannagi, S. D. Rosen, S. Hemmerich, *J. Cell Biol.* **1999**, *145*, 899 – 910.
[127] K. Uchimura, H. Muramatsu, K. Kadomatsu, Q. W. Fan, N. Kurosawa, C. Mitsuoka, R. Kannagi, O. Habuchi, T. Muramatsu, *J. Biol. Chem.* **1998**, *273*, 22577 – 22583.
[128] N. Hiraoka, B. Petryniak, J. Nakayama, S. Tsuboi, M. Suzuki, J. C. Yeh, D. Izawa, T. Tanaka, M. Miyasaka, J. B. Lowe, M. Fukuda, *Immunity* **1999**, *11*, 79 – 89.
[129] M. T. Bayliss, D. Osborne, S. Woodhouse, C. Davidson, *J. Biol. Chem.* **1999**, *274*, 15892 – 15900.
[130] S. J. A. Davies, D. R. Goucher, C. Doller, J. Silver, *J. Neurosci.* **1999**, *19*, 5810 – 5822.
[131] J. Garwood, O. Schnadelbach, A. Clement, K. Schutte, A. Bach, A. Faissner, *J. Neurosci.* **1999**, *19*, 3888 – 3899.
[132] C. J. Derry, C. Faveeuw, K. R. Mordsley, A. Ager, *Eur. J. Immunol.* **1999**, *29*, 419 – 430.
[133] M. F. Naujokas, M. Morin, M. S. Anderson, M. Peterson, J. Miller, *Cell* **1993**, *74*, 257 – 268.
[134] H. G. Kang, M. R. Evers, G. Q. Xia, J. U. Baenziger, M. Schachner, *J. Biol. Chem.* **2002**, *277*, 34766 – 34772.
[135] K. Uchimura, K. Kadomatsu, H. Nishimura, H. Muramatsu, E. Nakamura, N. Kurosawa, O. Habuchi, F. M. El-Fasakhany, Y. Yoshikai, T. Muramatsu, *J. Biol. Chem.* **2002**, *277*, 1443 – 1450.
[136] G. Sugumaran, M. Katsman, R. R. Drake, *J. Biol. Chem.* **1995**, *270*, 22483 – 22487.
[137] O. Habuchi, Y. Matsui, Y. Kotoya, Y. Aoyama, Y. Yasuda, M. Noda, *J. Biol. Chem.* **1993**, *268*, 21968 – 21974.
[138] H. Bakker, I. Friedmann, S. Oka, T. Kawasaki, N. Nifantev, M. Schachner, N. Mantei, *J. Biol. Chem.* **1997**, *272*, 29942 – 29946.
[139] E. Ong, J. C. Yeh, Y. L. Ding, O. Hindsgaul, M. Fukuda, *J. Biol. Chem.* **1998**, *273*, 5190 – 5195.
[140] G. Q. Xia, M. R. Evers, H. G. Kang, M. Schachner, J. U. Baenziger, *J. Biol. Chem.* **2000**, *275*, 38402 – 38409.
[141] T. Okuda, S. Mita, S. Yamauchi, N. Fukuta, H. Nakano, T. Sawada, O. Habuchi, *J. Biol. Chem.* **2000**, *275*, 40605 – 40613.
[142] H. G. Kang, M. R. Evers, G. Q. Xia, U. Baenziger, M. Schachner, *J. Biol. Chem.* **2001**, *276*, 10861 – 10869.
[143] M. R. Evers, G. Q. Xia, H. G. Kang, M. Schachner, J. U. Baenziger, *J. Biol. Chem.* **2001**, *276*, 36344 – 36353.
[144] M. Fukuta, J. Inazawa, T. Torii, K. Tsuzuki, E. Shimada, O. Habuchi, *J. Biol. Chem.* **1997**, *272*, 32321 – 32328.
[145] S. S. Rensdomiano, J. A. Roth, *J. Neurochem.* **1987**, *48*, 1411 – 1415.
[146] J. P. Horwitz, R. S. Misra, J. Rozhin, J. P. Neenan, A. Huo, V. C. Godefroi, K. D. Philips, H. L. Chung, G. Butke, S. C. Brooks, *Biochim. Biophys. Acta* **1978**, *525*, 364 – 372.
[147] G. J. Mulder, E. Scholtens, *Biochem. J.* **1977**, *165*, 553 – 559.
[148] M. H. A. Kester, S. Bulduk, D. Tibboel, W. Meinl, H. Glatt, C. N. Falany, M. W. H. Coughtrie, A. Bergman, S. H. Safe, G. Kuiper, A. G. Schuur, A. Brouwer, T. J. Visser, *Endocrinology* **2000**, *141*, 1897 – 1900.
[149] B. L. K. Mangold, J. Erickson, C. Lohr, D. J. McCann, J. B. Mangold, *Carcinogenesis* **1990**, *11*, 1563 – 1567.
[150] S. I. Rao, M. W. Duffel, *Drug Metab. Dispos.* **1991**, *19*, 543 – 545.
[151] M. W. Duffel, Y. Q. Zheng, *Drug Metab. Dispos.* **1993**, *21*, 400 – 402.
[152] S. I. Rao, M. W. Duffel, *Xenobiotica* **1992**, *22*, 247 – 255.
[153] K. J. Bamforth, A. L. Jones, R. C. Roberts, M. W. H. Coughtrie, *Biochem. Pharmacol.* **1993**, *46*, 1713 – 1720.
[154] M. W. H. Coughtrie, L. E. Johnston, *Drug Metab. Dispos.* **2001**, *29*, 522 – 528.
[155] K. J. Bamforth, K. Dalgliesh, M. W. H. Coughtrie, *Eur. J. Pharmacol. Environ. Toxicol. Pharmacol. Sec.* **1992**, *228*, 15 – 21.
[156] M. Matsui, M. Takahashi, Y. Miwa, Y. Motoyoshi, H. Homma, *Biochem. Pharmacol.* **1995**, *49*, 739 – 741.
[157] R. Bartzatt, J. D. Beckmann, *Biochem. Pharmacol.* **1994**, *47*, 2087 – 2095.
[158] T. Walle, E. A. Eaton, U. K. Walle, *Biochem. Pharmacol.* **1995**, *50*, 731 – 734.
[159] J. P. Horwitz, V. K. Iyer, H. B. Vardhan, J. Corombos, S. C. Brooks, *J. Med. Chem.* **1986**, *29*, 692 – 698.
[160] B. N. Cook, S. Bhakta, T. Biegel, K. G. Bowman, J. I. Armstrong, S. Hemmerich, C. R. Bertozzi, *J. Am. Chem. Soc.* **2000**, *122*, 8612 – 8622.
[161] V. K. Iyer, W. B. Butler, J. P. Horwitz, J. Rozhin, S. C. Brooks, J. Corombos, D. Kessel, *J. Med. Chem.* **1983**, *26*, 162 – 166.
[162] J. I. Armstrong, A. R. Portley, Y. T. Chang, D. M. Nierengarten, B. N. Cook, K. G. Bowman, A. Bishop, N. S. Gray, K. M. Shokat, P. G. Schultz, C. R. Bertozzi, *Angew. Chem.* **2000**, *112*, 1359 – 1362; *Angew. Chem. Int. Ed.* **2000**, *39*, 1303 – 1306.
[163] N. S. Gray, L. Wodicka, A. Thunnissen, T. C. Norman, S. J. Kwon, F. H. Espinoza, D. O. Morgan, G. Barnes, S. LeClerc, L. Meijer, S. H. Kim, D. J. Lockhart, P. G. Schultz, *Science* **1998**, *281*, 533 – 538.
[164] D. E. Verdugo, M. T. Cancilla, X. Ge, N. S. Gray, Y. T. Chang, P. G. Schultz, M. Negishi, J. A. Leary, C. R. Bertozzi, *J. Med. Chem.* **2001**, *44*, 2683 – 2686.
[165] D. J. Maly, I. C. Choong, J. A. Ellman, *Proc. Natl. Acad. Sci. USA* **2000**, *97*, 2419 – 2424.
[166] J. W. Kehoe, D. J. Maly, D. E. Verdugo, J. I. Armstrong, B. N. Cook, Y. B. Ouyang, K. L. Moore, J. A. Ellman, C. R. Bertozzi, *Bioorg. Med. Chem. Lett.* **2002**, *12*, 329 – 332.
[167] J. I. Armstrong, X. Ge, D. E. Verdugo, K. A. Winans, J. A. Leary, C. R. Bertozzi, *Org. Lett.* **2001**, *3*, 2657 – 2660.
[168] J. I. Armstrong, D. E. Verdugo, C. R. Bertozzi, *J. Org. Chem.* **2003**, *68*, 170 – 173.
[169] E. Chapman, S. Ding, P. G. Schultz, C. H. Wong, *J. Am. Chem. Soc.* **2002**, *124*, 14524 – 14525.
[170] S. Ding, N. S. Gray, X. Wu, Q. Ding, P. G. Schultz, *J. Am. Chem. Soc.* **2002**, *124*, 1594 – 1596.
[171] M. D. Burkart, C. H. Wong, *Anal. Biochem.* **1999**, *274*, 131 – 137.
[172] M. D. Best, A. Brik, E. Chapman, L. V. Lee, W.-C. Cheng, C.-H. Wong, *ChemBioChem* **2004**, *5*, 811 – 819.
[173] J. P. Horwitz, J. P. Neenan, R. S. Misra, J. Rozhin, A. Huo, K. D. Philips, *Biochim. Biophys. Acta* **1977**, *480*, 376 – 381.

 © 2004 Wiley-VCH Verlag GmbH & Co. KGaA, Weinheim

[174] J. Baddiley, J. G. Buchanan, R. Letters, A. R. Sanderson, *J. Chem. Soc.* **1959**, 1731 – 1734.
[175] J. I. Mukai, *Agric. Biol. Chem.* **1989**, *53*, 883 – 884.
[176] C. Satishchandran, G. D. Markham, *J. Biol. Chem.* **1989**, *264*, 15012 – 15021.
[177] P. Hiram, P. Fernando, A. Karakawa, Y. Sakakibara, H. Ibuki, H. Nakajima, M. C. Liu, M. Suiko, *Biosci. Biotechnol. Biochem.* **1993**, *57*, 1974 – 1975.
[178] R. D. Sekura, *Methods Enzymol.* **1981**, *77*, 413 – 415.
[179] K. C. Nicolaou, N. J. Bockovich, D. R. Carcanague, *J. Am. Chem. Soc.* **1993**, *115*, 8843 – 8844.
[180] P. R. Scudder, K. Shailubhai, K. L. Duffin, P. R. Streeter, G. S. Jacob, *Glycobiology* **1994**, *4*, 929 – 932.
[181] O. Habuchi, R. Moroi, S. Ohtake, *Anal. Biochem.* **2002**, *310*, 129 – 136.
[182] E. G. Cormier, M. Persuh, D. A. D. Thompson, S. W. Lin, T. P. Sakmar, W. C. Olson, T. Dragic, *Proc. Natl. Acad. Sci. USA* **2000**, *97*, 5762 – 5767.
[183] C. H. Lin, G. J. Shen, E. Garciajunceda, C. H. Wong, *J. Am. Chem. Soc.* **1995**, *117*, 8031 – 8032.
[184] M. D. Burkart, M. Izumi, E. Chapman, C. H. Lin, C. H. Wong, *J. Org. Chem.* **2000**, *65*, 5565 – 5574.
[185] M. Petitou, L. P. Herault, A. Bernat, P. A. Driguez, P. Duchaussoy, J. C. Lormeau, J. M. Herbert, *Nature* **1999**, *398*, 417 – 422.
[186] P. Sinay, J. C. Jacquinet, M. Petitou, P. Duchaussoy, I. Lederman, J. Choay, G. Torri, *Carbohydr. Res.* **1984**, *132*, C5 – C9.
[187] B. Kuberan, D. L. Beeler, R. Lawrence, M. Lech, R. D. Rosenberg, *J. Am. Chem. Soc.* **2003**, *125*, 12424 – 12425.
[188] B. Kuberan, M. Z. Lech, D. L. Beeler, Z. L. Wu, R. D. Rosenberg, *Nat. Biotechnol.* **2003**, *21*, 1343 – 1346.
[189] K. Kim, P. A. Cole, *J. Am. Chem. Soc.* **1998**, *120*, 6851 – 6858.
[190] K. Parang, J. H. Till, A. J. Ablooglu, R. A. Kohanski, S. R. Hubbard, P. A. Cole, *Nat. Struct. Biol.* **2001**, *8*, 37 – 41.
[191] D. B. Moody, S. A. Porcelli, *Nature Rev.* **2003**, *3*, 11 – 22.
[192] G. De Libero, L. Mori, *News Physiol. Sci.* **2003**, *18*, 71 – 76



Communications



In the Communication on the following pages F. C. Simmel and co-workers describe a molecular device based on a DNA aptamer which can be instructed to repeatedly bind and release the protein thrombin.

DOI: 10.1002/anie.200353537
© 2004 Wiley-VCH Verlag GmbH & Co. KGaA, Weinheim

DNA Structures

A DNA-Based Machine That Can Cyclically Bind and Release Thrombin**

*Wendy U. Dittmer, Andreas Reuter, and Friedrich C. Simmel**

Molecular machines can be used to produce controlled nanoscale movements.[1] In particular, the unique molecular recognition properties of DNA have been used to devise a number of nanomechanical devices that can be reversibly switched between several distinct conformations.[2] Although these devices display a variety of motions including rotational and stretching-type movements,[3,4] they do not perform any particular function. DNA structures with functionality can be found in DNA aptamers, which are short stretches of single-stranded DNA selected from a random pool of DNA sequences for their binding affinities to proteins or small molecules.[5] We report here on the construction of a protein-bearing molecular machine based on a DNA aptamer, which can be instructed to grab or release the human blood-clotting factor, α-thrombin, depending on an operator DNA sequence addressing it. In the operation of this DNA nanomachine, the thrombin-binding DNA aptamer is mechanically switched between a binding and a nonbinding form. The functioning of this "molecular hand" is demonstrated by gel electrophoresis, fluorescence resonance energy transfer (FRET), and fluorescence anisotropy measurements.

The machine is based on the 15-base DNA sequence 5′-GGTTGGTGTGGTTGG-3′, which has been found to bind strongly to α-thrombin[6] with a dissociation constant on the order of 3–450 nM.[7] In the presence of potassium ions, the aptamer assumes a conformation characterized by two stacked guanine quadruplex structures (see Figure 1). To construct the machine, we modified the aptamer at the 5′-end by adding a 12-base "toehold" section to address the device. The 5′-end was chosen in order not to interfere with thrombin binding sites.[8] We validated, using melting-curve experiments monitoring the absorbance, that in the presence of K^+ ions, the aptamer device (AP) indeed assumes its G quartet

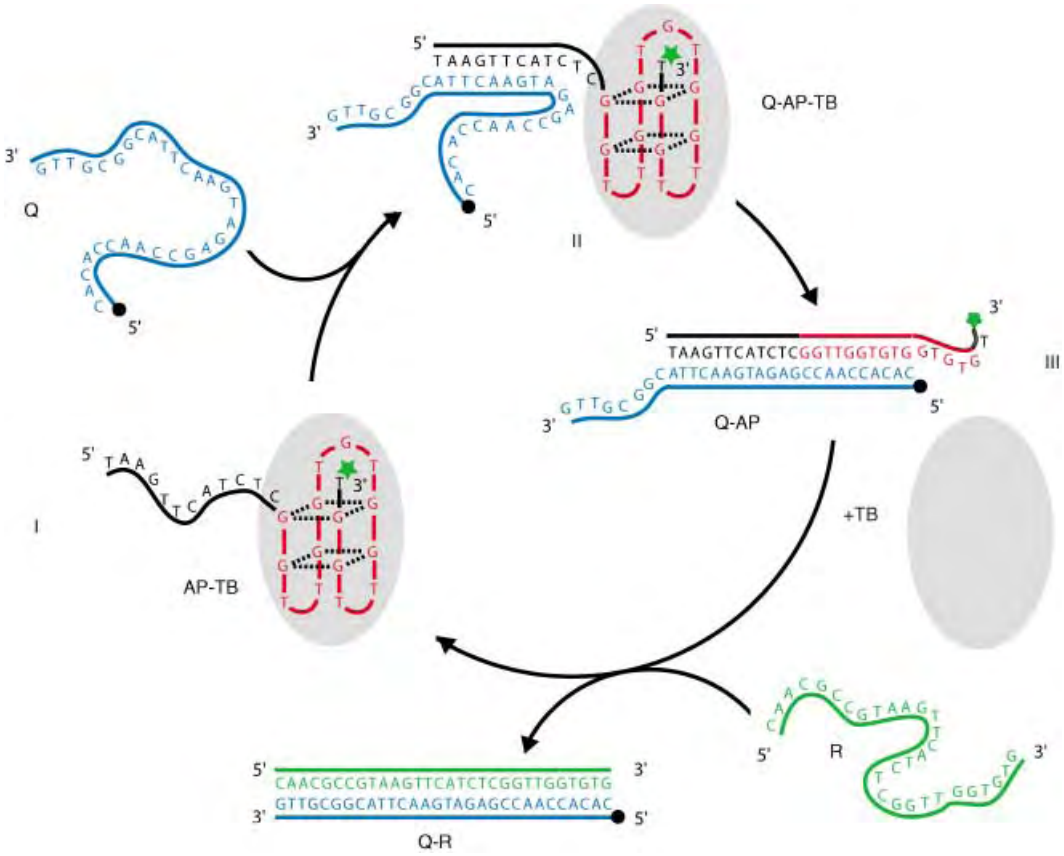


Figure 1. Representation of the operation cycle of the aptamer-based molecular machine in the presence of thrombin (for an explanation see the text). Sequences are shown for the labeled strands A3, Q5, and R.

[*] Dr. W. U. Dittmer, A. Reuter, Dr. F. C. Simmel
Sektion Physik and Center for Nanoscience
LMU Munich
Geschwister Scholl Platz 1, 80539 Munich (Germany)
Fax: (+49) 89-2180-3182
E-mail: simmel@lmu.de

[**] We thank Prof. Dr. John S. McCaskill for helpful discussions and Prof. Dr. Jörg P. Kotthaus for continuous support. This work was funded by the Deutsche Forschungsgemeinschaft, the Bavarian State Ministry of Sciences, Research, and the Arts, and the Alexander von Humboldt Foundation.

 © 2004 Wiley-VCH Verlag GmbH & Co. KGaA, Weinheim DOI: 10.1002/anie.200353537

form.[9] The operation cycle of the machine is depicted in Figure 1. Upon the addition of thrombin (TB), strand AP binds to the protein (I in Figure 1). By the addition of an "opening" strand Q, the DNA device extends to a duplex structure AP-Q, which is not capable of binding to TB (III). Q is complementary to the toehold and the first ten bases of the aptamer sequence and additionally has an eight-base-long sequence at the 3′-end which serves as a point of attachment for the fully complementary "removal" strand R. This is the fundamental operating principle used to cycle DNA machines through their various conformations.[4] Q was not chosen to be completely complementary to AP, because R would otherwise also contain the full aptamer sequence and thus could bind to thrombin. Removal of Q by R returns the device to its original conformation (I), where it binds to TB again.

We observed the operation of the machine with an electrophoretic band-shift experiment (Figure 2). Binding of

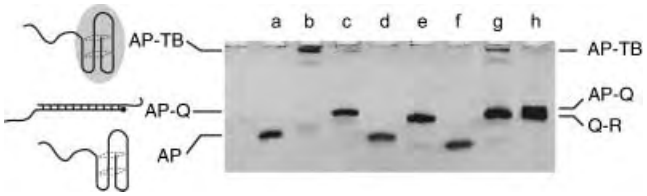


Figure 2. Gel evidence for the operation of the DNA machine. Lanes contain: a) AP, b) AP + thrombin (TB), c) (AP + TB) + Q, d) Q, e) Q + R, f) R, g) ((AP + TB) + Q) + R, h) (((AP + TB) + Q) + R) + Q. Pairs in brackets were incubated for 1 h before the addition of the next component. In the hybridization reactions the oligonucleotides each have a concentration of 1 μM. Human α-thrombin (Fluka) was added in a protein:aptamer ratio of 10:1. Due to the higher fluorescence intensity of the gel stain when bound to DNA duplexes, the total amount of DNA loaded into wells c, e, g, and h was adjusted to obtain a uniform intensity for the bands without extensive broadening or smearing. In lane g only 60% of the amount of strand AP was added relative to that in lane b, which explains the reduced intensity for the AP–TB complex in this lane.

AP (lane a) to thrombin results in a strong band shift (lane b). By the addition of Q, thrombin is released from AP and a band appears for the duplex AP–Q (lane c). Upon addition of R, AP is released and can bind to thrombin once again (lane g). This can be judged from the reappearance of the AP–TB band and a second band from the "waste" product Q–R. An additional, faint band is observed in lanes b and g just below that corresponding to AP–TB. It is found that the intensity of this band varies from one thrombin sample to another. Furthermore, it is more intense with older thrombin samples than with fresh ones. We therefore attribute this additional band to an impurity in our thrombin solution, possibly a thrombin decay product to which the aptamer can also bind. In lane h, further addition of Q releases thrombin again and two closely spaced bands appear for the duplex AP–Q and the waste product from the previous cycle. The gel experiments thus show unambiguously that the aptamer device can be switched repeatedly between its two conformations and cyclically binds and releases thrombin.

To follow the functioning of the aptamer device in real time, FRET experiments were performed. FRET is the nonradiative transfer of excitation energy from a "donor" fluorophore to an "acceptor" chromophore whose absorption spectrum overlaps with the emission spectrum of the donor. The efficiency of this process is strongly dependent on the distance between the two dyes and can be used to determine the proximity of labeled molecules.[10] Several FRET sensors based on aptamers have been constructed.[7,11] Here, FRET is used to follow the conformational changes of the DNA device accompanying the binding and release of thrombin. In Figure 3 the results of FRET experiments are shown in

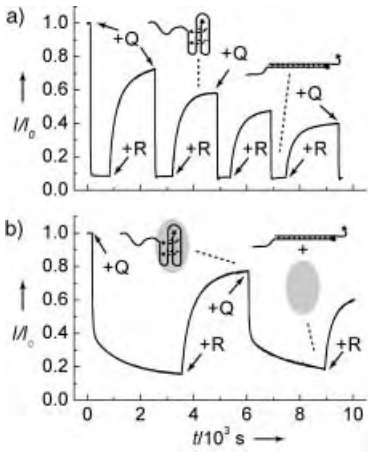


Figure 3. Normalized fluorescence intensity I/I_0 collected during the operation of the DNA device, a) without thrombin, b) in the presence of thrombin. The conformations corresponding to the different fluorescence levels are indicated by the icons.

which the strands AP3, Q5 (labeled at the 3′- and 5′-ends, respectively, see Figure 1), and R are used in the absence (Figure 3a) and presence (Figure 3b) of thrombin. Upon binding of Q5 to AP3, the fluorophore on AP3 is quenched by the FRET acceptor on Q5. AP3 is already partly quenched when Q5 attaches to the toehold (cf. II in Figure 1); full quenching occurs after complete binding of Q5 to AP3. Figure 3 indicates that the device can be switched from the G quartet to the duplex form much more rapidly in the absence of thrombin. In contrast, the removal step does not involve thrombin and displays second order kinetics with roughly the same time constants for both situations ($\tau = 220$–240 s without thrombin, $\tau = 290$–350 s with thrombin).

The operation kinetics of the machine is influenced to a great extent by the presence of the toehold section attached to the aptamer sequence. To elucidate this effect, a shorter opening strand, Q5-S, was constructed to be complementary to the original 15-base aptamer sequence but not to contain the complement of the toehold. In the absence of thrombin, the device rapidly undergoes a transition to the duplex form upon addition of either Q5 or Q5-S. The final fluorescence level for the AP3–Q5-S structure is slightly lower, since the fluorophores are closer together here than in the AP3–Q5 complex. In both cases the half-lives for the transitions are on the order of $\tau = 5$ s. The situation is very different in the presence of thrombin. The fluorescence decay induced by the opening strand Q5 is well modeled by the superposition of a

 © 2004 Wiley-VCH Verlag GmbH & Co. KGaA, Weinheim

second order and a first order process. The half-life for the second order step is $\tau = 24$ s. The half-life for the first order step is $\tau = 960$ s. The fast component is likely due to reaction of Q5 with thrombin-free AP strand and also due to its binding to and release from the toehold section (II in Figure 1). The slow first order part corresponds to the release of protein from the Q–AP–TB complex. When the short opening strand Q5-S, which does not attach to the toehold section, is used, a much slower first order step with half-life $\tau = 1740$ s is observed. The fits indicate that the toehold section increases the rate of protein release approximately twofold (Figure 4).

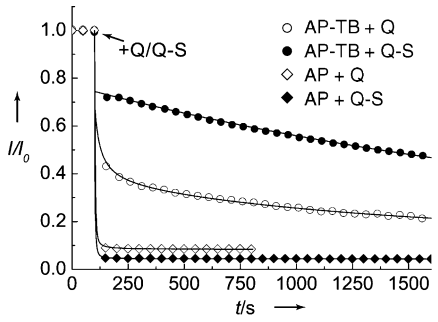


Figure 4. Fluorescence decay after the addition of a quencher sequence Q to the device in the presence of TB (circles) or without TB (squares). Every 50th data point is displayed. The continuous lines are fits to the data (see text).

In order to directly observe the binding and release of thrombin by the machine, measurements of the fluorescence anisotropy r were completed (see the Experimental Section).[12] In Figure 5 r is displayed for several operation cycles of the device. For these experiments only the aptamer strand AP3 was labeled. Fluorescence anisotropy is sensitive to the environment of a fluorophore and the presence of the protein constrains the dye's rotational degree of freedom and thus enhances the anisotropy. The change in r therefore corresponds to protein-binding or -release events. The opening step confirms the first order release kinetics with a half-life of roughly 600 s, the binding step is second order with a half-life

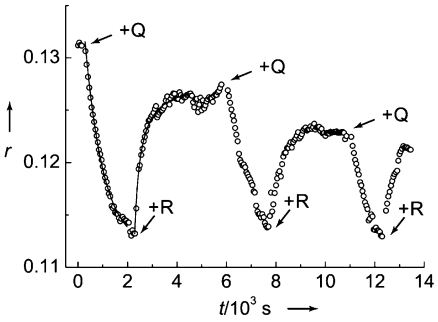


Figure 5. Fluorescence anisotropy r collected during the operation of the aptamer device in the presence of thrombin. The signal is only sensitive to the binding of the device to the protein and thus directly shows the binding and releasing of thrombin. The continuous lines are fits to the data.

$\tau = 230$ s. A thorough investigation of the kinetics of the device is in progress.

We have constructed a DNA molecular machine based on a DNA aptamer that can be instructed repeatedly to bind or release a protein. In essence, the device functions to precisely control the concentration of thrombin protein in solution between a depleted and an enriched state. The combination of the operating principles of DNA-based nanomechanical devices with the binding properties of DNA aptamers significantly opens up design possibilities for the construction of further functional DNA nanostructures. As aptamers can be selected to bind to a large variety of arbitrarily chosen compounds, DNA-based nanomachines useful for carrying, binding, and releasing molecules other than thrombin could be easily constructed from the device reported here.

Experimental Section

The DNA sequences for AP3, Q5, and R are shown in Figure 1: The 3′-label of AP3 is Oregon Green 488 (Molecular Probes, Oregon). The 5′-label of Q5 is TAMRA (5(6)-carboxytetramethylrhodamine). Strand AP is like AP3 without the thymine spacer and the label at 3′. Unlabeled Q has the same sequence as Q5. Short Q5-S is 5′-TAMRA CCAACCACACCAACC-3′; R is 5′-CAACGCCGTAAGTT-CATCTCGGTTGGTGTG-3′. All oligonucleotides were synthesized by biomers.net, Ulm, Germany. Unless stated otherwise, chemicals were obtained from Sigma-Aldrich, Germany, and used without further purification. The buffer used for all experiments, unless otherwise indicated, was a modified physiological buffer consisting of 20 mM Tris HCl, 140 mM NaCl, 10 mM $MgCl_2$, and 10 mM KCl at pH 8.5.

Polyacrylamide gel electrophoresis was performed on a 15% native gel in TB buffer (89 mM Tris HCl, 89 mM boric acid) with 10 mM KCl and run for 1.5 h with a field of 10 $V\,cm^{-1}$ at 20 °C. Gels were stained using the nucleic acid stain SYBR gold (Molecular Probes). Thrombin is not fluorescent itself and is not stained by the dye.

For FRET experiments, fluorescence was excited with an Argon ion laser ($\lambda = 488$ nm) and detected with a Si photodiode through a 10-nm bandpass filter centered at 514.5 nm using lock-in detection. The temperature was thermostated at 25 °C. The concentration of strand AP was 1 μM in all cases; other strands were added stoichiometrically. Thrombin was added at fivefold excess over AP.

In anisotropy experiments, fluorescence was excited through a Glan–Thompson (GT) polarizer. Parallel and perpendicular components $I_{\parallel}$, $I_{\perp}$ of the fluorescence intensity were collected through two GT analyzers in a T-format. Anisotropy is defined as $r = (I_{\parallel} - I_{\perp})/(I_{\parallel} + 2I_{\perp})$.

Received: December 15, 2003 [Z53537]
Published Online: April 28, 2004

Keywords: aptamers · DNA structures · DNA · molecular devices · nanostructures

[1] V. Balzani, A. Credi, F. M. Raymo, J. F. Stoddart, *Angew. Chem.* **2000**, *112*, 3484; *Angew. Chem. Int. Ed.* **2000**, *39*, 3349.
[2] C. M. Niemeyer, M. Adler, *Angew. Chem.* **2002**, *114*, 3933; *Angew. Chem. Int. Ed.* **2002**, *41*, 3779.
[3] C. D. Mao, W. Q. Sun, Z. Y. Shen, N. C. Seeman, *Nature* **1999**, *397*, 144.
[4] a) B. Yurke, A. J. Turberfield, A. P. Mills, F. C. Simmel, J. L. Neumann, *Nature* **2000**, *406*, 605; b) F. C. Simmel, B. Yurke,

 © 2004 Wiley-VCH Verlag GmbH & Co. KGaA, Weinheim

Phys. Rev. E **2001**, *6304*; c) F. C. Simmel, B. Yurke, *Appl. Phys. Lett.* **2002**, *80*, 883; d) H. Yan, X. P. Zhang, Z. Y. Shen, N. C. Seeman, *Nature* **2002**, *415*, 62; e) J. W. J. Li, W. H. Tan, *Nano Lett.* **2002**, *2*, 315; f) P. Alberti, J. L. Mergny, *Proc. Natl. Acad. Sci. USA* **2003**, *100*, 1569; g) A. J. Turberfield, J. C. Mitchell, B. Yurke, A. P. Mills, M. I. Blakey, F. C. Simmel, *Phys. Rev. Lett.* **2003**, *90*; h) L. P. Feng, S. H. Park, J. H. Reif, H. Yan, *Angew. Chem.* **2003**, *115*, 4478; *Angew. Chem. Int. Ed.* **2003**, *42*, 4342.

[5] D. S. Wilson, J. W. Szostak, *Annu. Rev. Biochem.* **1999**, *68*, 611.

[6] L. C. Bock, L. C. Griffin, J. A. Latham, E. H. Vermaas, J. J. Toole, *Nature* **1992**, *355*, 564.

[7] J. W. J. Li, X. H. Fang, W. H. Tan, *Biochem. Biophys. Res. Commun.* **2002**, *292*, 31.

[8] K. Padmanabhan, K. P. Padmanabhan, J. D. Ferrara, J. E. Sadler, A. Tulinsky, *J. Biol. Chem.* **1993**, *268*, 17651.

[9] J. L. Mergny, A. T. Phan, L. Lacroix, *FEBS Lett.* **1998**, *435*, 74.

[10] a) T. Förster, *Ann. Phys.* **1948**, *2*, 55; b) L. Stryer, R. P. Haugland, *Proc. Natl. Acad. Sci. USA* **1967**, *58*, 719.

[11] a) R. Nutiu, Y. F. Li, *J. Am. Chem. Soc.* **2003**, *125*, 4771; b) M. Rajendran, A. D. Ellington, *Nucleic Acids Res.* **2003**, *31*, 5700.

[12] a) J. R. Lakowicz, *Principles of Fluorescence Spectroscopy*, 2nd ed., Kluwer Academic/Plenum Publishers, New York, **1999**; b) R. A. Potyrailo, R. C. Conrad, A. D. Ellington, G. M. Hieftje, *Anal. Chem.* **1998**, *70*, 3419.

BE ON THE BALL!



0186_0010_vi

The new free **WILEY-VCH Alerting Service** makes time-consuming random finds a thing of the past!

Register now for the free WILEY-VCH Alerting Service

Now you can be supplied per e-mail regularly with information tailored precisely to your needs and interests. Just fill out the registration form at *www.wiley-vch.de/home/pas* for e-mails with news on the latest WILEY-VCH publications in your field. Added benefit: general info on important developments and services at WILEY-VCH.

Be on the ball so you'll be in the know!

www.wiley-vch.de

 © 2004 Wiley-VCH Verlag GmbH & Co. KGaA, Weinheim

Nanotechnology

An Autonomous DNA Nanomotor Powered by a DNA Enzyme**

*Yi Chen, Mingsheng Wang, and Chengde Mao**

Nanoscale mobile devices (nanomotors) have many potential applications, such as information processing, nanoelectronic devices, biosensors, and regulation of chemical reactions and molecular assembly.[1] Various artificial nanomotors have been reported in recent years. These motors include organic molecules,[2–5] engineered DNA constructs,[6–12] and inorganic/protein hybrids.[13] However, reports of autonomous synthetic nanomotors are very rare.[5,11,13] Autonomy is an important characteristic of cellular protein motors, which prompted us to ask whether it would be possible to design biomimetic nanomotors that continuously conduct mechanical motions powered by consumed chemical energy. Herein, we report the construction of a DNA nanomotor powered by an RNA-cleaving DNA enzyme.[14–17] The motor keeps operating as long as its fuel (the RNA substrate of the DNA enzyme) is available. This DNA motor is a biomimetic nanomotor that works in the same way as natural protein motors, that is, by continuously extracting chemical energy from covalent bonds and converting this energy into mechanical motions.[18–20]

Most protein motors,[18–22] which include myosin, kinesin, and F_0F_1 adenosine triphosphate (ATP) synthase, possess an ATPase activity. These motors can bind to and hydrolyze ATP to form ADP, which is then released. The energy released by the chemical process of ATP hydrolysis powers protein motors and enables them to change their conformation, which results in mechanical movement. The DNA motor presented herein works in a similar way. The catalytic domain of the DNA can bind to a DNA–RNA chimera substrate, cleave this substrate into two short fragments, and then release the pieces. This process leads the DNA motor to change its conformation, which generates nanoscale motions. We demonstrated the motion of the DNA motor by using fluorescence resonance energy transfer (FRET) techniques and monitored the autonomous cycling of the motor by observing substrate cleavage.

The design of the new autonomous DNA motor combines knowledge and experience of DNA nanotechnology[23–25] and DNA enzymes.[14–17] Figure 1 illustrates the molecular design and operation principle of the engineered DNA motor. The DNA motor contains two 15-base-pair helical domains, which are joined by a single-stranded 10-23 DNA enzyme[14] at one end and a single-base hinge at the other. The 10-23 DNA enzyme consists of a 15-base catalytic core and two flanking 7-base-long substrate-recognition arms. The DNA enzyme binds to its RNA substrate through Watson–Crick base pairing and cleaves the RNA into two short fragments. All the RNA residues of the substrate, except that flanking the phosphodiester bond to be cleaved, can be replaced with DNA residues. When the DNA enzyme is not bound to its substrate (a DNA–RNA chimera, S), divalent cations (for example, Mg^{2+}) cause the single-stranded DNA enzyme to collapse into a closed coil as a result of entropic forces (see ref. [26] and the Supporting Information). Under these conditions, the overall conformation of the DNA motor is quite compact ("closed state"). When the DNA enzyme binds to its DNA–RNA chimera substrate, the single-stranded DNA enzyme forms a bulged duplex with the substrate. This bulged duplex pushes the two helical domains of the DNA motor apart and leads the motor to adopt an "open state". Upon binding, the DNA enzyme cleaves its substrate into two short fragments (S_1 and S_2). The resulting fragments have a lower affinity for the DNA enzyme than the intact substrate and, therefore, dissociate from the DNA motor. Consequently, the DNA motor returns to the closed state and can undergo the next cycle of substrate binding (open state), cleavage, and dissociation (closed state). The DNA motor consumes one DNA–RNA chimera substrate in each open/

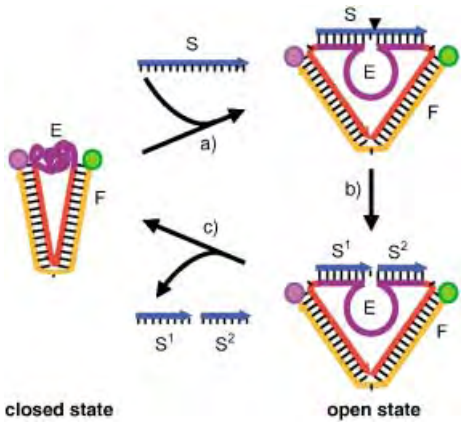


Figure 1. Structure and operation of an autonomous DNA nanomotor. The DNA motor consists of two strands (E and F). The E strand (pink-purple) contains an RNA-cleaving 10-23 DNA enzyme. The enzyme domain is colored dark purple. The F strand (gold) contains two fluorophores: fluorescein (FAM: solid green circle) and tetramethylrhodamine (TAMRA: solid pink circle). The enzyme substrate (S) is a DNA–RNA chimera (blue). a) An S strand binds to the motor and causes it to adopt an open state. b) The DNA enzyme cleaves the substrate (S). The arrowhead above the S strand indicates the cleavage site. c) The cleaved substrate fragments (S^1 and S^2) dissociate from the DNA motor, which returns to the closed state. The closed state might consist of a variety of compact conformational isomers.

[*] Y. Chen, M. Wang, Prof. C. Mao
Department of Chemistry
Purdue University
West Lafayette, IN 47907 (USA)
Fax: (+1) 765-494-0239
E-mail: mao@purdue.edu

[**] This work was supported by the National Science Foundation (grant no. EIA-0323452), the Defense Advanced Research Projects Agency/Defence Sciences Office (grant no. MDA 972-03-1-0020), and Purdue University (a start-up fund). We thank Prof. D. R. McMillin for allowing us to use a fluorometer, and M. H. Wilson for help with fluorescence measurements.

Supporting information for this article is available on the WWW under http://www.angewandte.org or from the author.

 © 2004 Wiley-VCH Verlag GmbH & Co. KGaA, Weinheim DOI: 10.1002/anie.200453779

closed cycle. The motor autonomously cycles between the open and closed states until the fuel (the enzyme substrate) runs out.

The DNA motor was formed by slowly cooling an equimolar mixture of component DNA strands. The results of polyacrylamide gel electrophoretic analysis suggest that the DNA motor behaves as expected in both the closed and open states (Figure 2). The motors migrated as clean sharp bands, which indicates that the structures are stable. We used a substrate analogue (S′) that cannot be cleaved by the enzyme to capture DNA motors in the open state. This DNA strand has the same sequence as the DNA–RNA chimera substrate (S) except that S′ contains two DNA residues instead of two of the substrate RNA residues. S and S′ have the same specificity and nearly the same affinity for the DNA enzyme domain of the DNA motor. The electrophoresis experiment also confirmed that the cleaved short fragments have a lower affinity than the whole substrate for the DNA enzyme and do not associate with the DNA motor. Even in tenfold excess, the short fragments did not bind with the DNA motor (lane 6 in Figure 2). Instead, these fragments migrated separately from the motor.

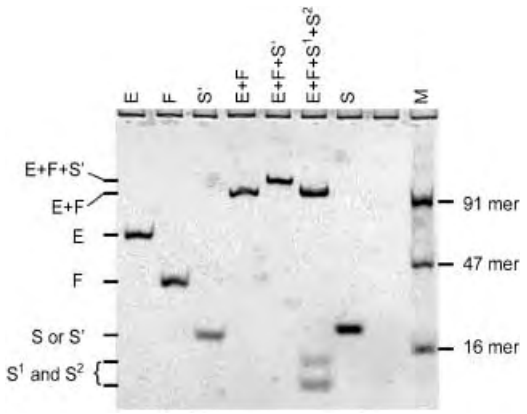


Figure 2. Native gel electrophoretic analysis of DNA motor formation. The content of each lane is indicated at the top of the gel image. A DNA motor formed in the closed state from its two component strands (E+F) was converted into the open state (E+F+S′) by the binding of an S′ strand, a DNA analogue of the substrate that cannot be cleaved by the enzyme. The mixture analyzed in lane E+F+S^1+S^2 contained a tenfold excess of (S^1+S^2) relative to (E+F). Clearly, the short fragments could not stably bind to the motors. The far right lane shows three single-stranded DNA size markers.

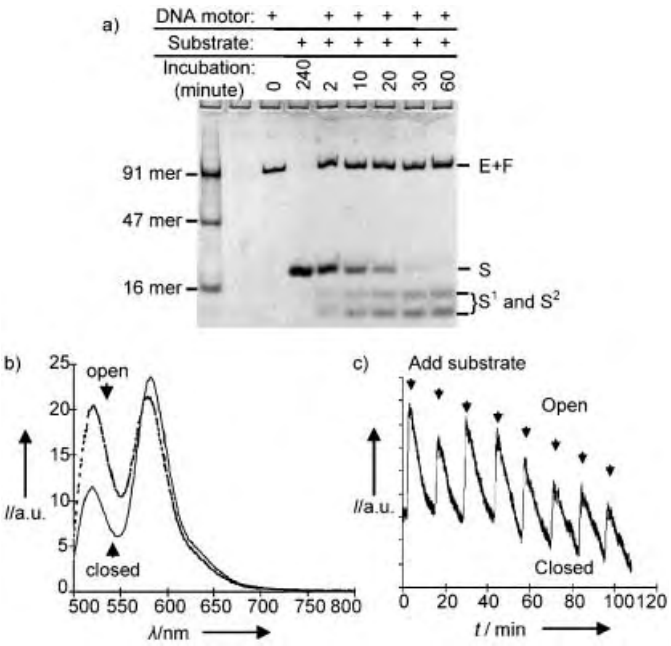


Figure 3. Motion of the DNA motor. a) The autonomous cycling of the DNA motor, as evidenced by multiple enzyme turnovers. The DNA motor (E+F) and its substrate (S) were incubated at a motor/substrate ratio of 1:20 for the indicated time periods and then resolved by polyacrylamide gel electrophoresis. The DNA motors almost completed digestion of the substrate within 30 minutes, which suggests that each motor underwent an open/closed cycle every 1.5 minutes. b) Fluorescence spectra of the DNA motor in the closed and open states. These spectra show that there was indeed a nanoscale movement upon switching between the two states. c) The DNA motor could also be cycled manually by sequential addition of equimolar amounts of enzyme substrate. Fluorescence was monitored at 520 nm, the maximum emission wavelength of FAM.

The autonomous character of the designed nanomotor is the most important achievement of this work. To demonstrate the autonomy of the DNA motor the fragmentation of the substrate was monitored while substrate molecules were consumed to power open/closed cycles of the DNA motor (Figure 3a). When the substrate and the DNA motor were incubated at room temperature, more and more substrate molecules were cleaved into two short segments with the passage of time. Under these particular experimental conditions, each DNA motor consumed an average of 20 substrate molecules in 30 minutes. In other words, each motor underwent 20 open/closed cycles in 30 minutes without any human intervention. The observed turnover speed is much greater than the cycling speeds that have been reported for human-operated systems (for example, less than 0.1 cycles per minute are reported in ref. [7]). The cycling speed could be increased to more than three cycles per minute by optimizing the working conditions.[14]

We used FRET techniques[6,7] to demonstrate that a motion does indeed accompany the chemical reaction of the DNA motor (Figure 3b). We labeled the DNA motor with two fluorophores (fluorescein (FAM) and tetramethylrhodamine (TAMRA)), one at each end of the two helical domains (Figure 1). The efficiency of the energy transfer between two fluorophores is sensitive to the distance between the fluorophores and the switching of the motor between the open and closed states could be observed readily in FRET experiments. In the closed state the two fluorophores are close to each other and energy can be transfered efficiently from FAM to TAMRA. We therefore expect the FAM signal ($\lambda_{EM} = 520$ nm) to be of low intensity and the TAMRA signal ($\lambda_{EM} = 568$ nm) to have a high intensity under these conditions. The open state should give the opposite results: the two fluorophores are far away from each other and the

 © 2004 Wiley-VCH Verlag GmbH & Co. KGaA, Weinheim

efficiency of energy transfer is low so we expect the FAM signal to increase and the TAMRA signal to decrease in intensity relative to the signals observed for the closed state. The FRET experiment confirmed this hypothesis (Figure 3b). The open state was captured by using a DNA analogue (S′ strand) of the enzyme substrate that cannot be cleaved by the enzyme. The results of this experiment show that the designed DNA motor can adopt two different conformations: closed and open. Switching between these two states requires the DNA motor to reposition its two helical domains.

The DNA motor not only operates autonomously, but can also be operated manually (Figure 3c). In the manual mode, the motor is switched between the closed and open states by sequential addition of the DNA–RNA chimera substrate. The motion of the DNA motor was observed by monitoring the fluorescence intensity at 520 nm (λ_{EM} of FAM). When the enzyme substrate was absent from the solution, the DNA motor adopted its closed state and emitted a low-intensity fluorescence signal. After addition of an equimolar amount of substrate, however, the motor bound to its substrate and changed to the open state, which resulted in an increased fluorescence signal. As time lapsed, the DNA enzyme cleaved the substrate and released the cleaved fragments. The motor returned to its closed state and the fluorescence intensity decreased as well. Each addition of an equimolar amount of substrate induced one open/closed cycle. We recorded eight open/closed cycles. The maximum fluorescence intensity decreased as the motor cycled. This decrease was presumably caused by photobleaching of the fluorescent dyes.

In summary, we have constructed an autonomous DNA nanomotor by integrating a catalytic DNA domain into a self-assembled DNA nanostructure. This work exemplifies the successful combination of structural DNA nanotechnology and catalytic DNA, which we believe could open exciting avenues to dynamic nanomaterials,[1] DNA computation,[27,28] nanorobotics, and nanodevices. The similarity between the mechanism of the DNA motor presented herein and that of cellular protein motors suggests that more complicated DNA nanomotors could conceivably be constructed by borrowing the architectures of cellular protein motors. For example, autonomous, unidirectionally translational and rotary DNA motors could be designed by mimicking myosin[20] and F_0F_1 ATP synthase,[21] respectively. It is also conceivable that a large number of different DNA motors could be designed (around 4^{14}, the pool size of the 10-23 DNA enzyme library) that are powered by different RNA substrates. Each motor could be activated individually within the same solution. Besides the potential technological applications of these motors, this work might have biological relevance. An RNA world may have existed before proteins took over most biological functions.[29] Protein motors are now involved in many essential life activities, such as DNA replication, RNA and protein synthesis, and various molecular transportation processes.[18–20] Did nucleic acids play similar functions in primitive life forms? Since the reported DNA motor could be easily translated into an RNA motor (containing a ribozyme[30]), our study might imply that nucleic acids alone could perform motor functions in primitive life forms, just as proteins do in the living systems that exist today.

Experimental Section

DNA oligonucleotides: Strand E: 5′-GGT TAG ATG GTA TGC TTC-GGC AGG CT AGC TAC AAC GAG AGT GAC TGA GCG TAA GGT CTG G-3′; strand F: 5′-FAM-GCA TAC CAT CTA ACC TCC-AGA CCT TAC GCT C-TAMRA-3′; strand S: 5′-GTC ATT CrAr-U GTC CGA-3′; strand S′: 5′-GTC ACT CAT GTC CGA-3′. All oligonucleotides were purchased from Integrated DNA Technologies, Inc. and purified by denaturing polyacrylamide gel electrophoresis.

Nanomotor formation: DNA strands (0.5 μM) were combined in a 1:1 molar ratio in a buffer (TAE/Mg^{2+}) composed of tris(hydroxymethyl)aminomethane (Tris) base (40 mM, pH 8.0), acetic acid (20 mM), ethylenediaminetetraacetate (EDTA; 2 mM), and $MgAc_2$ (12.5 mM). The nanomotor was formed by slowly cooling the DNA solution as follows: 95 °C (3 min), 65 °C (30 min), 50 °C (30 min), 37 °C (30 min), and 22 °C (30 min).

Enzyme digestion: The DNA motor (0.5 μM) and DNA–RNA chimera substrate (10 μM) were incubated in TAE/Mg^{2+} buffer at 22 °C for various time periods and then analyzed by nondenaturing polyacrylamide gel electrophoresis.

Denaturing polyacrylamide gel electrophoresis: Gels contained 20% polyacrylamide (acrylamide/bisacrylamide, 19:1) and 8.3 M urea and were run at 55 °C. Tris-borate-EDTA (TBE) was used as the separation buffer and consisted of Tris base (89 mM, pH 8.0), boric acid (89 mM), and EDTA (2 mM). Gels were run on a Hoefer SE 600 electrophoresis unit at 600 V (constant voltage).

Nondenaturing polyacrylamide gel electrophoresis: Gels contained 12% polyacrylamide (acrylamide/bisacrylamide, 19:1). The separation buffer (TAE/Mg^{+}) consisted of Tris base (40 mM, pH 8.0), acetic acid (20 mM), EDTA (2 mM), and $(CH_3COO)_2Mg$ (12.5 mM). Gels were run on a Hoefer SE 600 electrophoresis unit at 22 °C (250 V, constant voltage). After electrophoresis, the gels were stained with Stains-all dye (Sigma) and scanned.

Fluorescence spectroscopy: DNA was dissolved in TAE/Mg^{2+} buffer. Fluorescence emission spectra were recorded on a Varian Cary Eclipse fluorescence spectrophotometer. All spectra were collected at 22 °C. The samples were excited at 470 nm and the emission data were collected either between 500 and 800 nm, or at a fixed wavelength of 520 nm (for cycling of the motor). The maximal emission wavelengths of FAM and TAMRA are 520 nm and 568 nm, respectively.

Received: January 19, 2004 [Z53779]

Keywords: catalytic DNA · DNA · nanotechnology · RNA · self-assembly

[1] H. G. Craighead, *Science* **2000**, *290*, 1532 – 1535.
[2] C. P. Collier, G. Mattersteig, E. W. Wong, Y. Luo, K. Beverly, J. Sampaio, F. M. Raymo, J. F. Stoddart, J. R. Heath, *Science* **2000**, *289*, 1172 – 1175.
[3] A. M. Brouwer, C. Frochot, F. G. Gatti, D. A. Leigh, L. Mottier, F. Paolucci, S. Roffia, G. W. H. Wurpel, *Science* **2001**, *291*, 2124 – 2128.
[4] D. A. Leigh, J. K. Y. Wong, F. Dehez, F. Zerbetto, *Nature* **2003**, *424*, 174 – 179.
[5] N. Koumura, R. W. J. Zijlstra, R. A. van Delden, N. Harada, B. Feringa, *Nature* **1999**, *401*, 152 – 155.
[6] C. Mao, W. Sun, Z. Shen, N. C. Seeman, *Nature* **1999**, *397*, 144 – 146.
[7] B. Yurke, A. J. Turberfield, A. P. Mills, F. C. Simmel, J. L. Neumann, *Nature* **2000**, *406*, 605 – 608.
[8] H. Yan, X. Zhang, Z. Shen, N. C. Seeman, *Nature* **2002**, *415*, 62 – 65.
[9] J. J. Li, W. Tan, *Nano Lett.* **2002**, *2*, 315 – 318.

 © 2004 Wiley-VCH Verlag GmbH & Co. KGaA, Weinheim

[10] P. Alberti, J. Mergny, *Proc. Natl. Acad. Sci. USA* **2003**, *100*, 1569 – 1573.
[11] A. J. Turberfield, J. C. Mitchell, B. Yurke, A. P. Mills, Jr., M. I. Blakey, F. C. Simmel, *Phys. Rev. Lett.* **2003**, *90*, 118102.
[12] L. Feng, S. H. Park, J. H. Reif, H. Yan, *Angew. Chem.* **2003**, *115*, 4478 – 4482; *Angew. Chem. Int. Ed.* **2003**, *42*, 4342 – 4346.
[13] R. K. Soong, G. D. Bachand, H. P. Neves, A. G. Olkhovets, H. G. Craighead, C. D. Montemagno, *Science* **2000**, *290*, 1555 – 1558.
[14] S. W. Santoro, G. F. Joyce, *Proc. Natl. Acad. Sci. USA* **1997**, *94*, 4262 – 4266.
[15] G. M. Emilsson, R. R. Breaker, *Cell. Mol. Life Sci.* **2002**, *59*, 596 – 607.
[16] J. Liu, Y. Lu, *J. Am. Chem. Soc.* **2002**, *124*, 15208 – 15216.
[17] Y. Li, D. Sen, *Biochemistry* **1997**, *36*, 5589 – 5599.
[18] R. D. Vale, R. A. Milligan, *Science* **2000**, *288*, 88 – 95.
[19] M. Schliwa, G. Woehlke, *Nature* **2003**, *422*, 759 – 765.
[20] B. Alberts, *Cell* **1998**, *92*, 291 – 294.
[21] Y. Sambongi, Y. Iko, M. Tanabe, H. Omote, A. Iwamoto-Kihara, I. Ueda, T. Yanagida, Y. Wada, M. Futai, *Science* **1999**, *286*, 1722 – 1724.
[22] F. J. Nedelec, T. Surrey, A. C. Maggs, S. Leibler, *Nature* **1997**, *389*, 305 – 308.
[23] N. C. Seeman, *J. Theor. Biol.* **1982**, *99*, 237 – 247.
[24] N. C. Seeman, *Nature* **2003**, *421*, 427 – 431.
[25] N. C. Seeman, *Biochemistry* **2003**, *42*, 7259 – 7269.
[26] A. M. van Oijen, P. C. Blainey, D. J. Crampton, C. C. Richardson, T. Ellenberger, X. S. Xie, *Science* **2003**, *301*, 1235 – 1238.
[27] L. M. Adleman, *Science* **1994**, *266*, 1021 – 1024.
[28] C. Mao, T. LaBean, J. H. Reif, N. C. Seeman, *Nature* **2000**, *407*, 493 – 496.
[29] *The RNA World: The Nature of Modern RNA Suggests a Prebiotic RNA World* (Eds.: R. F. Gesteland, T. R. Cech, J. F. Atkins), Cold Spring Harbor Laboratory, Cold Spring Harbor, New York, **1999**.
[30] S. E. Butcher, *Curr. Opin. Struct. Biol.* **2001**, *11*, 315 – 320.

 © 2004 Wiley-VCH Verlag GmbH & Co. KGaA, Weinheim

Host–Guest Chemistry

Multivalency in the Gas Phase: The Study of Dendritic Aggregates by Mass Spectrometry**

*Maarten A. C. Broeren, Joost L. J. van Dongen, Michael Pittelkow, Jørn B. Christensen, Marcel H. P. van Genderen, and E. W. Meijer**

Insight into the strength and dynamics of noncovalent interactions in complex molecular aggregates is essential for the understanding of all forms of soft matter.[1–3] Most, if not all, studies are performed under thermodynamically controlled conditions, in which association and dissociation are in competition.[4] Exciting progress in mass spectrometry has enabled gas-phase studies of protein complexes[5–8] and organic supramolecular aggregates to be carried out.[9–11] Electrospray ionization mass spectrometry (ESI-MS) has proven to be most successful in achieving the delicate transfer of large molecules, including dendrimers,[12] from solution to the gas phase.[13–15] The stability of ions in the gas phase can be probed with collision-induced dissociation (CID), in which an ion is selected, accelerated, and subsequently collided in a cell with neutral gas atoms, for example, argon.[16,17] In the collision process a part of the ion's kinetic energy is transformed into internal energy, which eventually results in fragmentation. The extent of fragmentation depends on the internal energy of the excited ion, which in turn is related to the imposed acceleration. Despite widespread application of CID in the analysis of covalent structure,[18] it appears to be difficult to analyze the dissociation of noncovalent structures in the gas phase. Moreover, the relationship between the strength of the aggregate in solution (thermodynamically controlled) and in the gas phase (kinetically controlled) remains controversial.[19–21] Here we report on dendritic aggregates with one to eight guest molecules, which were designed to assemble at the periphery of the dendrimer. Analysis of the aggregates by collision-induced dissociation mass spectrometry shows that the guest molecules are removed one by one in a highly controlled way. The analysis presented unequivocally proves the existence of multicomponent dynamic libraries and also allows the relative stabil-

[*] M. A. C. Broeren, J. L. J. van Dongen, M. Pittelkow, Dr. J. B. Christensen, Dr. M. H. P. van Genderen, Prof. E. W. Meijer
Laboratory of Macromolecular and Organic Chemistry
Eindhoven University of Technology
P.O. Box 513, 5600 MB, Eindhoven (The Netherlands)
Fax: (+31) 40-245-1036
E-mail: e.w.meijer@tue.nl

[**] We acknowledge grants from the department of Biomedical Engineering of Eindhoven University, the Council for Chemical Science of The Netherlands Organization for Science Research (CW-NWO), and The Danish Natural Research Council (SNF). We thank Dr. U. Boas for providing us with the tripeptides, B.F.M. de Waal for his synthetic help, and Prof. N. M. M. Nibbering for useful discussions.

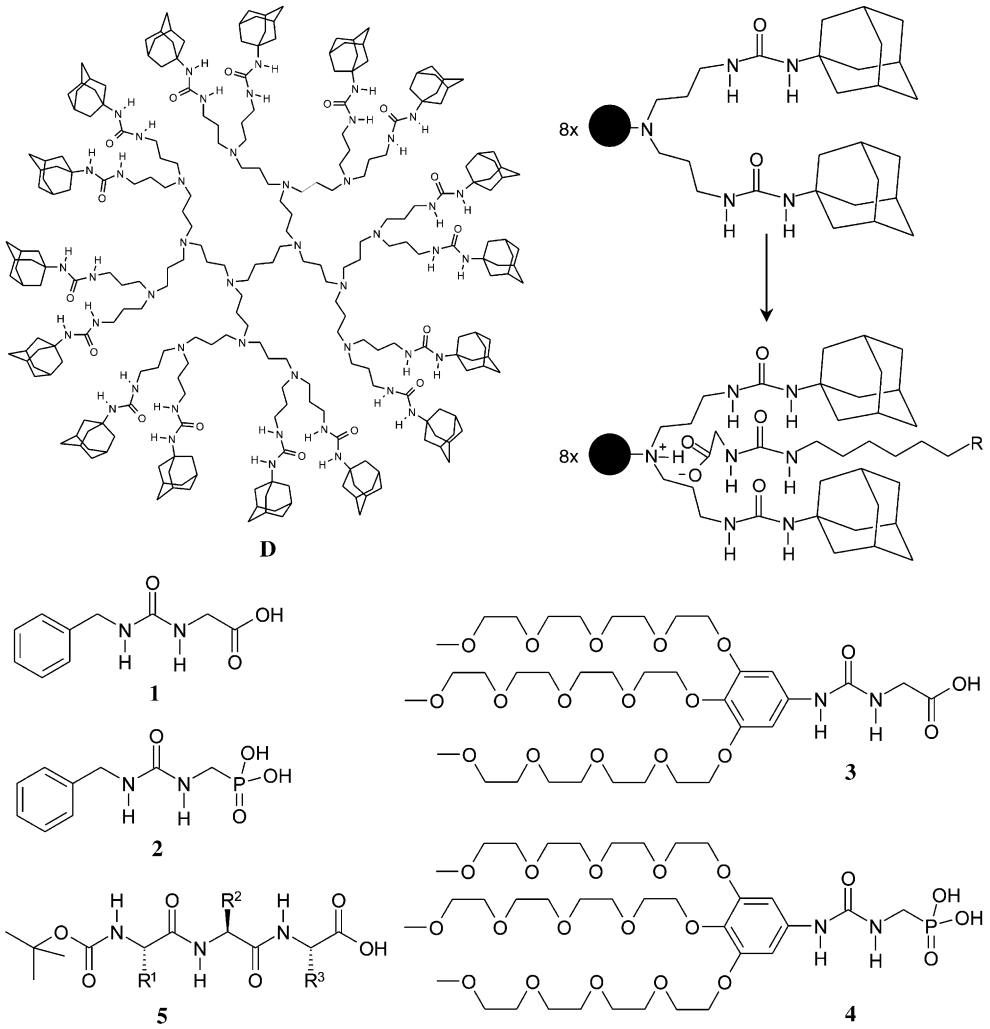
Supporting information for this article is available on the WWW under http://www.angewandte.org or from the author.

 DOI: 10.1002/anie.200453707 © 2004 Wiley-VCH Verlag GmbH & Co. KGaA, Weinheim

ities of the host–guest interactions to be determined when different guests are simultaneously anchored to the same dendrimer. The selectivity in the dissociation of the individual guests is analyzed in the molecular center of mass frame with a simple kinetic model. New insights into the behavior of multivalency in supramolecular aggregates including libraries of oligopeptides are presented here, in which mass spectrometry acts as the tool to analyze these multivalent interactions in great detail.

The compounds used in this study are based on third generation adamantylurea-substituted poly(propylene imine) dendrimers (**D**, Scheme 1), which are excellent hosts for guest molecules based on urea acids (**1**–**4**) in solvents such as chloroform. The multivalency of dendritic macromolecules[22–25] is generally seen as the way to obtain highly efficient bioactive synthetic structures.[26] An attractive methodology for dynamically modifying the periphery of dendrimers was recently disclosed, in which the end groups of the dendrimer act as the scaffold for guest molecules that assemble around the dendrimer.[27,28] If both ionic and hydrogen-bonding interactions are considered, the maximum number of guests that can be bound specifically is set by the number of end groups, thus eight guests can be bound by the third-generation dendrimer (Scheme 1). The assembly process has been studied previously with different generations of dendrimers and other guest molecules by a variety of techniques, including NOESY NMR spectroscopy.[27] Although firm experimental evidence has been presented to confirm the assignment of these supramolecular structures, definite proof of these multivalent supramolecular architectures is inherently difficult, because of the dynamic nature of the multicomponent aggregates.[29]

Electrospray ionization mass spectrometry was used to analyze mixtures containing **D** and a one- to eightfold excess of guest **2** in chloroform (10^{-6} M **D**). Triply and quadruply protonated complexes of the different aggregates were observed. Deconvolution provided the overall spectrum and, surprisingly, all possible assemblies between **D** and **2**



Scheme 1. Representation of the structures used. Third generation adamantylurea-modified poly(propylene imine) dendrimer **D** acts as a host for urea acid guests **1**–**4** which differ in size and acid strength. The Boc-protected tripeptides (**5**) also investigated are: Boc-GGG, Boc-GGA, Boc-AAA, Boc-FGG, Boc-FFF, and Boc-GVV. The symbols for the amino acids are: G = glycine (R = H), A = alanine (R = CH_3), F = phenylalanine (R = $CH_2C_6H_5$), V = valine (R = $CH(CH_3)_2$). Boc = *tert*-butoxycarbonyl.

 © 2004 Wiley-VCH Verlag GmbH & Co. KGaA, Weinheim

are observed as well as a small amount of free **D** (Figure 1a, b). The nine major peaks are separated by the mass of **2** (M_r = 244 Da) and are interpreted as the assembly of x guests **2** with **D** (notation used through the paper for the assemblies is: **D**·**2**$_x$, with x = 0–8). Selecting one of the assemblies in the quadrupole (for example, $[\mathbf{D}\cdot\mathbf{2}_4]^{3+}$; Figure 1a) and subsequently colliding the isolated ion with argon buffer gas in the collision cell resulted in dissociation of the aggregate. The products of this dissociation were analyzed by TOF-MS. Figure 1c shows a stacked plot of mass spectra obtained with increasing acceleration voltages. Dissociation of guest **2** is observed as the voltage is increased, which eventually results in empty **D**. The guests are removed as neutral species and only the tricationic dendritic aggregates are observed. This is a general observation for all aggregates (**D** with **1**–**4**) and all possible values of x. Not only do the spectra prove that the different complexes are indeed formed, ionized, and stable enough to be analyzed, the voltage needed for dissociation is a guide to the stability of the aggregate in the gas phase.

We have also analyzed complexes of **D** with **1**–**4**, and thus we now have a set of molecules that differ in acidity (**1** versus **2** and **3** versus **4**) and molecular weight (**1** versus **3** and **2** versus **4**). Importantly, the multivalency of the system makes it possible to assemble different guest molecules with the same dendrimer and perform selection and analysis of these multicomponent ions. This type of analysis is unique for comparing different guests, since the internal energy of collision is distributed over all the guests in the same aggregate. When an aggregate containing two guests of both **1** and **2** (denoted as **D**·(**1**$_2$ + **2**$_2$)) was subjected to CID, guests **1** dissociated before guests **2** started to dissociate (Figure 2a).

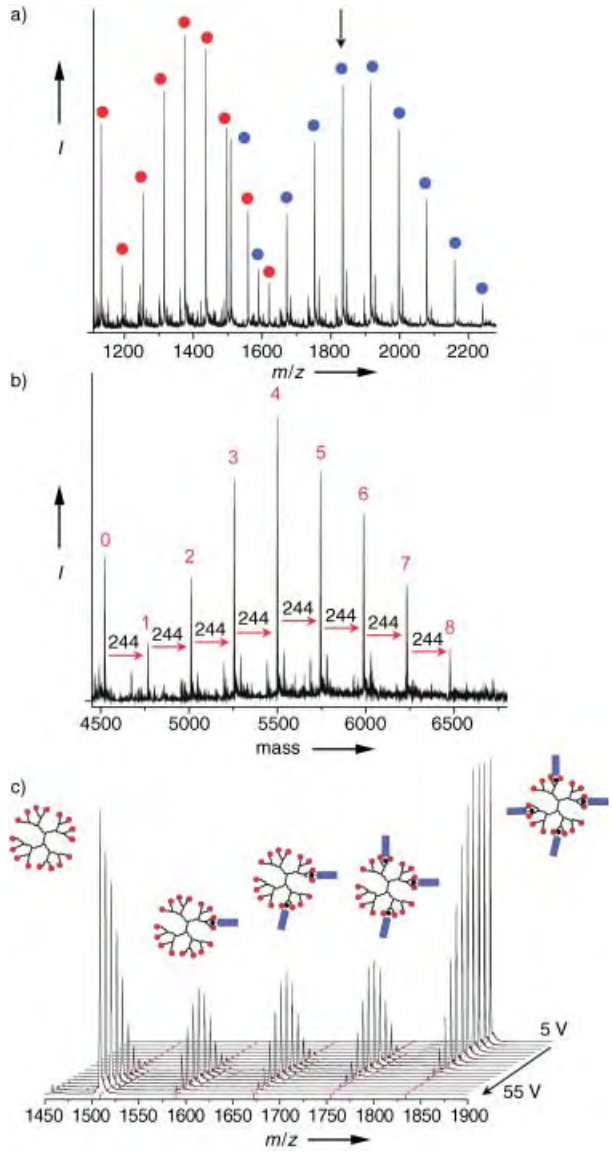


Figure 1. a) Mass spectrum of a sample of **D** with six equivalents of **2**. Two clusters of ions are observed, which consist of one to eight guests bound to the dendrimer with a 4^+ (red) or 3^+ (blue) charge. b) The mass difference between the peaks after deconvolution corresponds to the mass of **2** (244 Da). c) Selection of one ion $[\mathbf{D}\cdot\mathbf{2}_4]^{3+}$ (indicated with the arrow in (a)) followed by collision with increasing acceleration voltage in the collision cell results in sequential dissociation of the guests from the dendrimer. The charge of the complex does not change, which means that the guest dissociates as a neutral species, which is not observable by MS.

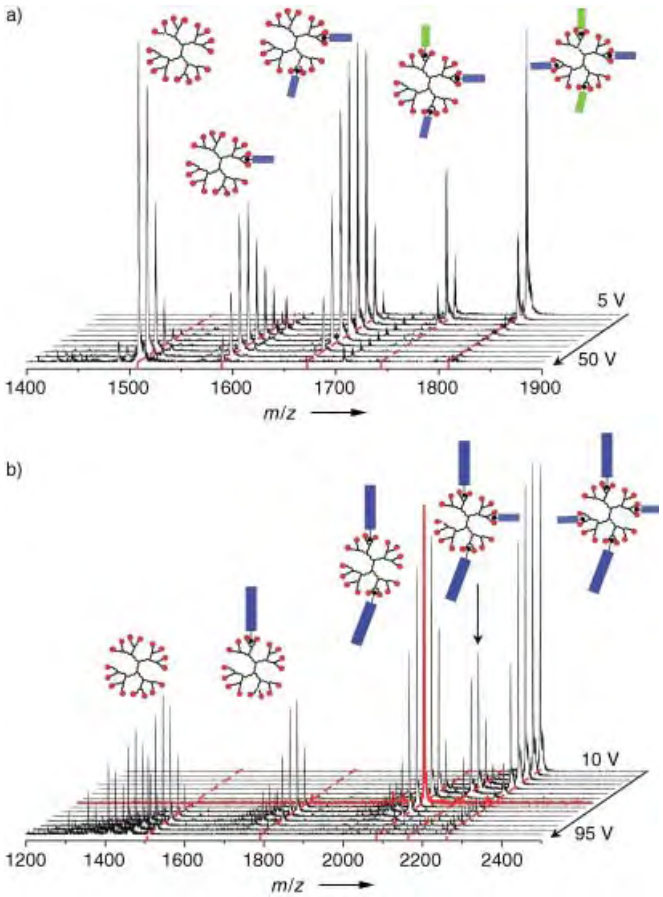


Figure 2. a) Selection of the $[\mathbf{D}\cdot(\mathbf{1}_2+\mathbf{2}_2)]^{3+}$ ion followed by CID results in selective dissociation of **1** over **2**. These differences result from the difference in the acid strengths of the guests. b) Selective dissociation also occurs for smaller guest **2** over **4** in the CID experiments of the $[\mathbf{D}\cdot(\mathbf{2}_2+\mathbf{4}_2)]^{3+}$ ion. In this case the selectivity is almost 100%: at 55 V $[\mathbf{D}\cdot\mathbf{4}_2]^{3+}$ is the only major signal (red trace). Interestingly the dendrimer itself also starts to fragment at high voltages (the adamantly groups dissociate), which indicates that covalent and noncovalent dissociation compete at that stage.

 © 2004 Wiley-VCH Verlag GmbH & Co. KGaA, Weinheim

This selective dissociation of **1** over **2** is independent of the combination of the guests attached to the dendrimer and is indicative of a difference in the binding strength in the gas phase which arises from differences in acidity. These results are in good agreement with observations of solution experiments, where a higher acidity leads to a higher association constant in chloroform. When both **2** and **4** are assembled on the same dendrimer and $\mathbf{D}\cdot(\mathbf{2}_2+\mathbf{4}_2)$ subjected to CID, the small guests are significantly less strongly anchored than the large guests (Figure 2b). Evidence for fragmentation of the covalent bonds in the dendrimer appears, even before all of **4** is removed. In contrast to the gas-phase data, the difference in the binding strength measured for **2** and **4** with **D** in chloroform is marginal. This discrepancy between the solution and gas phases is proposed to result from additional van der Waals interactions between the ethylene glycol chains of **4** and the dendrimer scaffold in the gas phase. In chloroform the chains of the guests are solvated and the association constant is then primarily determined by the urea acid motif.

To analyze the data in a more quantitative way we compared the voltage required to reach an ion survival yield of 50% of the selected ion. Dendrimers with the smaller guest **2** require significantly less voltage then dendrimers with the larger guest **4** (Figure 3a). The same trend is observed for **1** versus **3** (not depicted). However, it is important to remember when comparing different ions that the fraction of kinetic energy of an ion that can be converted into internal energy (which causes dissociation) is inversely proportional to the total mass of the complex. Therefore, the acceleration voltage has to be converted into the center of mass energy to compare the assembly of **2** with **4** in separate complexes.[16] A

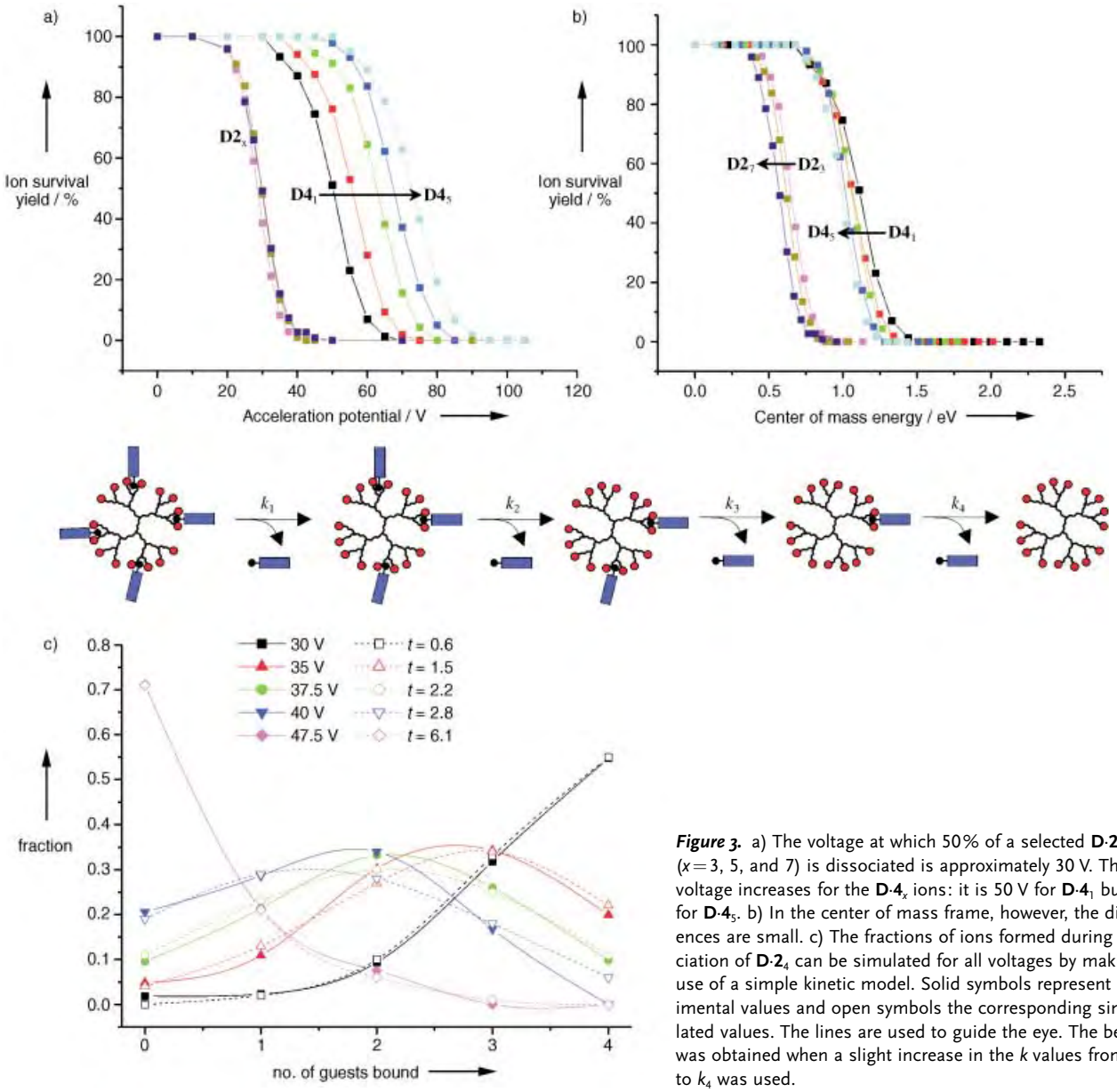


Figure 3. a) The voltage at which 50% of a selected $\mathbf{D}\cdot\mathbf{2}_x$ ion ($x = 3$, 5, and 7) is dissociated is approximately 30 V. This voltage increases for the $\mathbf{D}\cdot\mathbf{4}_x$ ions: it is 50 V for $\mathbf{D}\cdot\mathbf{4}_1$ but 75 V for $\mathbf{D}\cdot\mathbf{4}_5$. b) In the center of mass frame, however, the differences are small. c) The fractions of ions formed during dissociation of $\mathbf{D}\cdot\mathbf{2}_4$ can be simulated for all voltages by making use of a simple kinetic model. Solid symbols represent experimental values and open symbols the corresponding simulated values. The lines are used to guide the eye. The best fit was obtained when a slight increase in the k values from k_1 to k_4 was used.

 © 2004 Wiley-VCH Verlag GmbH & Co. KGaA, Weinheim

significant difference remains in the center of mass frame of $\mathbf{D}\cdot\mathbf{2}_x$ and $\mathbf{D}\cdot\mathbf{4}_x$, which indicates there is stronger binding of the larger guests (Figure 3b). The data for $\mathbf{D}\cdot\mathbf{2}_x$ and $\mathbf{D}\cdot\mathbf{4}_x$ are similar to the data of the mixed $\mathbf{D}\cdot(\mathbf{2}_2+\mathbf{4}_2)$ system (see above) if this correction is applied. The difference in dissociation energy in going from $\mathbf{D}\cdot\mathbf{2}_3$ to $\mathbf{D}\cdot\mathbf{2}_7$ and $\mathbf{D}\cdot\mathbf{4}_1$ to $\mathbf{D}\cdot\mathbf{4}_5$ (Figure 3b) is small.

We have simulated the distributions of the complexes formed during CID by a simple model to investigate the relationship between the number of guests bound to the dendrimer and the ion stability in more detail. The release of guests from a complex through collisions with argon atoms can be modeled as consecutive reaction steps that are pseudo-first order because of the constant argon concentration. We have used the $\mathbf{D}\cdot\mathbf{2}_4$ complex and defined four reaction rate constants (k_1, k_2, k_3, k_4) as parameters. After integrating the rate equations, we can calculate the fractions of the various species ($\mathbf{D}\cdot\mathbf{2}_4$, $\mathbf{D}\cdot\mathbf{2}_3$, $\mathbf{D}\cdot\mathbf{2}_2$, $\mathbf{D}\cdot\mathbf{2}_1$, and $\mathbf{D}$) as a function of time. The effect of increasing the acceleration voltage upon injection of ions into the collision cell was then simulated by taking the concentrations of the different fractions at increasing times.[30] The best fit of the model with the experimental data was achieved when the k values increase slightly in value, thus indicating that the guest molecules dissociate slightly easier when less guest molecules are bound. However, the influence of loading on the stability remains very small and is close to the statistical dissociation of the guests.

Since oligopeptides with free carboxylic acid and Boc-protected amine end groups can also be assembled at the periphery of **D** in chloroform,[28] we tested the versatility of our method by using tripeptide–dendrimer aggregates in CID-MS. A large variety of oligopeptides can be assembled in a dynamic way. Figure 4a and b show the results of two typical mass spectra for a mixture of two and three different peptides. All statistically possible structures are observed and the full dynamic library can be analyzed. By selecting a specific trication with two or three different oligopeptides it is possible to determine the different binding affinities. Remarkably, very small structural differences lead to significant changes in the dissociation. Figure 4c, for example, shows a clear preference for the dissociation of Boc-AAA over Boc-GGG, although the guests differ only by three methyl groups, which can sterically interfere with the binding motif. This effect could also explain the preference for the dissociation of Boc-GVV over Boc-FGG (not depicted), where the two isopropyl groups of Boc-GVV interfere with the binding motif. On the other hand, Boc-FFF binds more strongly than Boc-GGG, a result that is indicative of the presence of additional van der Waals interactions between the guest and host. Clearly, by now studying a large variety of peptide structures it should be possible to gain insight into protein aggregation in the gas phase.

We have shown in an unprecedented clean and simple way that collision-induced dissociation in mass spectrometry allows for detailed investigations of multicomponent supramolecular interactions. The formation of the dendritic associate in combination with the CID-MS method provides us with a wealth of information concerning important

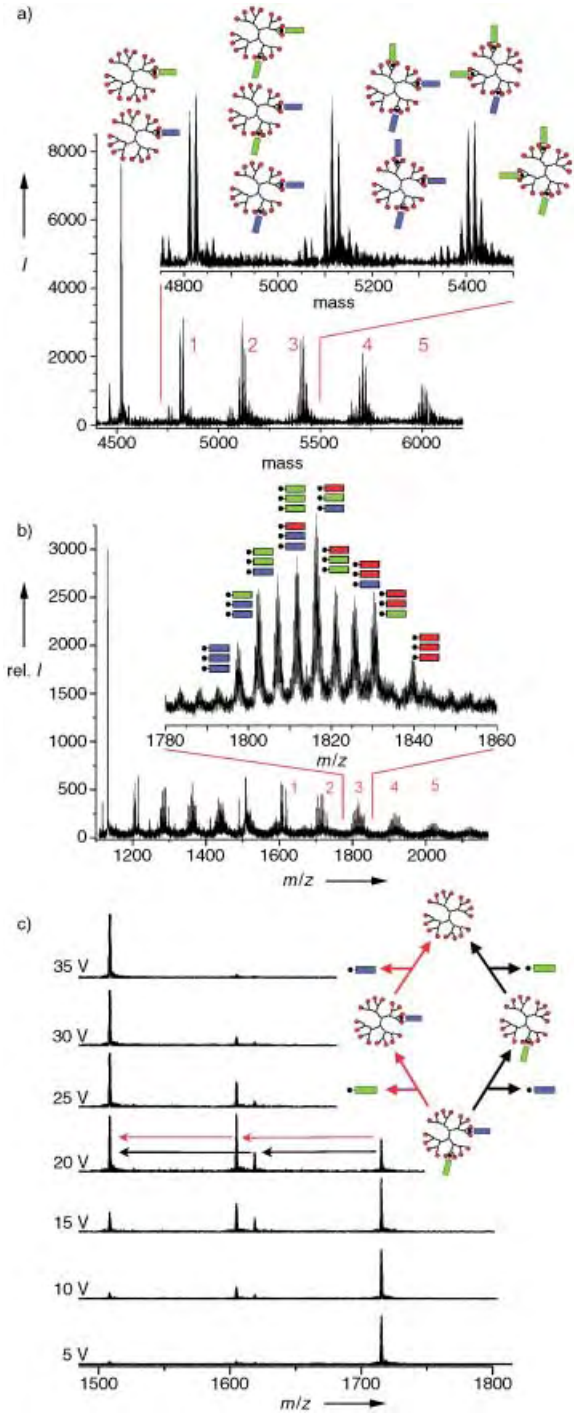


Figure 4. a) Mass spectrum after deconvolution of two tripeptides, Boc-GGG (blue) and Boc-GGA (green), bound to the dendrimer. The small difference in mass between the guests results in clusters of peaks that correspond to one to five guest molecules bound to the dendrimer (shown in red). All peaks in the clusters can be assigned to the different possible combinations of guests. b) Mass spectrum (no deconvolution) of three different tripeptides added to the dendrimer (Boc-GGG (blue), Boc-GGA (green), and Boc-AAA (red)), which results in more complicated clusters. Inspection of the cluster of signals of the dendrimer with three peptides attached to it show that ten possible combinations can be formed, all of which are visible. Two combinations result in an identical mass. c) CID-MS spectra of a dendrimer with one Boc-GGG (blue) and one Boc-AAA guest (green). Two pathways can be envisioned, of which the one indicated with the red arrow predominates.

 © 2004 Wiley-VCH Verlag GmbH & Co. KGaA, Weinheim

secondary interactions of supramolecular aggregates in the gas phase.

Received: January 9, 2004 [Z53707]
Published Online: April 5, 2004

Keywords: dendrimers · dynamic libraries · host–guest chemistry · mass spectrometry · supramolecular chemistry

[1] J.-M. Lehn, *Supramolecular Chemistry, Concepts and Perspectives*, VCH, Weinheim, Germany, **1995**.
[2] D. N. Reinhoudt, M. Crego-Calama, *Science* **2002**, *295*, 2403 – 2407.
[3] S. C. Zimmerman, L. J. Lawless, *Top. Curr. Chem.* **2001**, *217*, 95 – 120.
[4] L. J. Prins, D. N. Reinhoudt, P. Timmerman, *Chem. Eur. J.* **2001**, *7*, 2382 – 2426.
[5] J. A. Loo, *Mass Spectrom. Rev.* **1997**, *16*, 1 – 23.
[6] J. L. Beck, M. L. Colgrave, S. F. Ralph, M. M. Sheil, *Mass Spectrom. Rev.* **2001**, *20*, 61 – 87.
[7] P. Sarni-Manchado, V. Cheynier, *J. Mass Spectrom.* **2002**, *37*, 609 – 616.
[8] J. A. E. Kraunsoe, R. T. Aplin, B. Green, G. Lowe, *FEBS Lett.* **1996**, *396*, 108 – 112.
[9] C. A. Schalley, *Mass Spectrom. Rev.* **2001**, *20*, 253 – 309.
[10] C. A. Schalley, T. Müller, P. Linnartz, M. Witt, M. Schäfer, A. Lützen, *Chem. Eur. J.* **2002**, *8*, 3538 – 3551.
[11] R. R. Julian, J. A. May, B. M. Stoltz, J. L. Beauchamp, *Angew. Chem.* **2003**, *115*, 1042 – 1045; *Angew. Chem. Int. Ed.* **2003**, *42*, 1012 – 1015.
[12] J. C. Hummelen, J. L. J. Van Dongen, E. W. Meijer, *Chem. Eur. J.* **1997**, *3*, 1489 – 1493.
[13] J. B. Fenn, M. Mann, C. K. Meng, S. F. Wong, C. M. Whitehouse, *Science* **1989**, *246*, 64 – 71.
[14] B. Ganem, Y. T. Li, J. D. Henion, *J. Am. Chem. Soc.* **1991**, *113*, 6294 – 6296.
[15] W. J. H. Van Berkel, R. H. H. Van Den Heuvel, C. Versluis, A. J. R. Heck, *Protein Sci.* **2000**, *9*, 435 – 439.
[16] A. K. Shukla, J. H. Futrell, *J. Mass Spectrom.* **2000**, *35*, 1069 – 1090.
[17] P. B. Armentrout, *Top. Curr. Chem.* **2003**, *225*, 233 – 262.
[18] M. Kinter, N. E. Sherman, *Protein Sequencing and Identification Using Tandem Mass Spectrometry*, Wiley, New York, **2000**.
[19] A. Van der Kerk-Van Hoof, A. J. R. Heck, *J. Mass Spectrom.* **1999**, *34*, 813 – 819.
[20] V. J. Nesatyy, *J. Mass Spectrom.* **2001**, *36*, 950 – 959.
[21] V. J. Nesatyy, *Int. J. Mass Spectrom.* **2002**, *221*, 147 – 161.
[22] A. W. Bosman, H. M. Janssen, E. W. Meijer, *Chem. Rev.* **1999**, *99*, 1665 – 1688.
[23] S. M. Grayson, J. M. J. Fréchet, *Chem. Rev.* **2001**, *101*, 3819 – 3867.
[24] J. M. J. Fréchet, D. A. Tomalia, *Dendrimers and other dendritic polymers*, Wiley, New York, **2001**.
[25] G. R. Newkome, C. N. Moorefield, F. Vögtle, *Dendrimers and Dendrons: Concepts, Synthesis, Applications*, Wiley-VCH, Weinheim, **2001**.
[26] J. E. Gestwicki, C. W. Cairo, L. E. Strong, K. A. Oetjen, L. L. Kiessling, *J. Am. Chem. Soc.* **2002**, *124*, 14922 – 14933.
[27] M. W. P. L. Baars, A. J. Karlsson, V. Sorokin, B. F. W. De Waal, E. W. Meijer, *Angew. Chem.* **2000**, *112*, 4432 – 4435; *Angew. Chem. Int. Ed.* **2000**, *39*, 4262 – 4265.
[28] U. Boas, S. H. M. Söntjens, K. J. Jensen, J. B. Christensen, E. W. Meijer, *ChemBioChem* **2002**, *3*, 433 – 439.
[29] W. T. S. Huck, L. J. Prins, R. H. Fokkens, N. M. M. Nibbering, F. C. J. M. van Veggel, D. N. Reinhoudt, *J. Am. Chem. Soc.* **1998**, *120*, 6240 – 6246.
[30] A higher acceleration voltage in the experiment yields a higher kinetic energy for the complexes, and this in effect raises the reaction temperature for the release of the guests. As a result, the rate constants for the dissociation of the guests increase, and higher conversions are reached (more fragmentation of the initial complex). We have modeled this in a constant-temperature approach by using longer reaction times to give similarly higher conversions. In other words, we are using a temperature–time transformation, so that the fractions of the various complexes at a certain time simulate the effect of the collision cell. In the model we have assumed that the individual rate constants depend in the same way on the temperature. For a detailed description see the Supporting Information.

 © 2004 Wiley-VCH Verlag GmbH & Co. KGaA, Weinheim

Reduced Pyrochlores

New Oxidation States and Defect Chemistry in the Pyrochlore Structure**

*Giles D. Blundred, Craig A. Bridges, and Matthew J. Rosseinsky**

The introduction of anion vacancies into complex metal oxides is a powerful method of controlling structure and properties by tailoring metal coordination environment and oxidation state. The hydride anion can effect reductive transformations of oxides inaccessible to conventional metal getters or gaseous reducing agents.[1] The $A_2B_2O_7$ pyrochlore structure[2] is important for properties as diverse as anion and mixed conduction,[3] superconductivity,[4] and colossal magnetoresistance,[5] but, in contrast to ABO_3 perovskite, there is little chemistry established for the low-temperature introduction of anion vacancies and generation of associated defect structures. Pyrochlore is well known for stabilizing high oxidation states on the octahedral B site; A^{II}/B^{V} and A^{III}/B^{IV} compositions are well established, and pyrochlores with mean B site oxidation states of less than $+4$ are rare (the Y^{II}/Ti^{II} pyrochlore-related $YTiO_{2.1}$ prepared at 2800 °C is the sole example[6]). Here we report the systematic low-temperature synthesis of pyrochlore systems with up to 90% titanium(III) on the octahedral sites.

[*] Dr. G. D. Blundred, Dr. C. A. Bridges, Prof. Dr. M. J. Rosseinsky
Department of Chemistry
The University of Liverpool
Liverpool L69 7ZD (UK)
Fax: (+44) 151-794-3587
E-mail: m.j.rosseinsky@liv.ac.uk

[**] We thank the UK EPSRC and the ACS Petroleum Research Foundation for support.

Supporting information for this article is available on the WWW under http://www.angewandte.org or from the author.

 © 2004 Wiley-VCH Verlag GmbH & Co. KGaA, Weinheim DOI: 10.1002/anie.200453819

The $A_2B_2O_6O'$ pyrochlore structure (Figure 1a) is a corner-sharing network of BO_6 octahedra with large 110 tunnels intersecting at the 8b positions (space group $Fd\bar{3}m$) occupied by the O′ oxygen atoms. The A cations are eight-coordinate (2 O′ and 6 O anions). The structure can also be described as an anion-deficient, vacancy-ordered fluorite, in which the 8a anion sites at the centroids of tetrahedra of 16c B sites are vacant. This defect ordering renders the B sites octahedral, while the tetrahedral connectivity of both A and B sublattices gives rise to strong geometrical frustration[7] of antiferromagnetic ordering, manifested in the unusual magnetism of the rare earth A^{3+} sublattice in $Ln_2Ti_2O_7$[8] and of the B site cations in materials such as $NH_4Fe_2F_6$[9,10] and $Y_2Mn_2O_7$.[11] This makes the introduction of localized 3d $S = {}^1/_2$ spins on the B sublattice an important synthetic task.

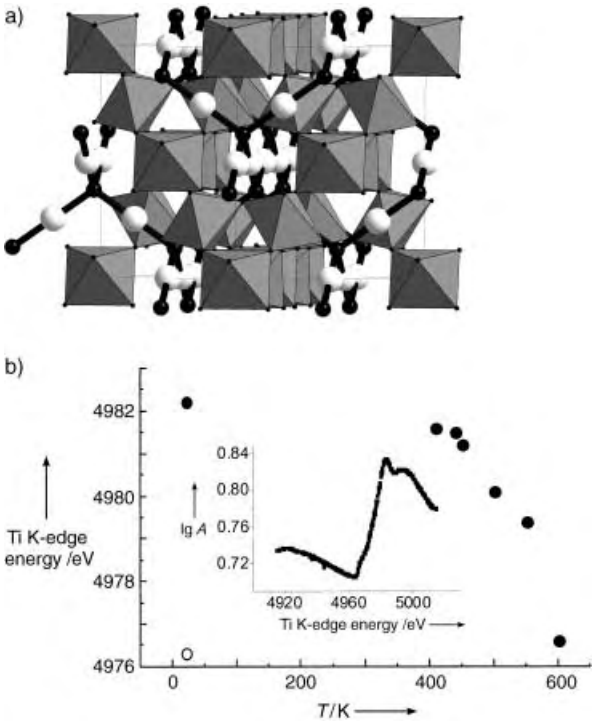


Figure 1. a) The BO_6 (gray octahedra) and A_2O' sublattices (A white spheres, O′ black spheres), showing the two independent oxygen networks in the pyrochlore structure. b) Position of the Ti X-ray absorption K-edge (black circles) in $Lu_2Ti_2O_{7-y}$ as a function of reaction temperature with CaH_2. The open circle marks the edge position in $LuTiO_3$. The inset shows data for the sample reduced at 600 °C ($y = 0.9$).

The Ti^{IV} pyrochlores $Ln_2Ti_2O_7$ are not reduced by hydrogen gas at 1200 °C. Reaction with metal hydride (LiH, CaH_2) reducing agents below 700 °C, however, affords intensely black material which retains the pyrochlore structure: the absence of $h = 4n$, $k = 4n$, $l = 2n$ reflections shows that the cations remain on the 16c and 16d sites.[12]

The reactivity of $Ln_2Ti_2O_7$ with CaH_2 is sensitively controlled by the size of the Ln^{III} cation. $Sm_2Ti_2O_7$ and $Eu_2Ti_2O_7$ form the titanium(III) perovskites $SmTiO_3$ and $EuTiO_3$ at 600 °C, but smaller lanthanides afford reduced pyrochlores. The lowest Ti oxidation states are accessible with Lu and Yb. X-ray absorption spectroscopy demonstrates reduction at the Ti rather than the lanthanide site in both $Yb_2Ti_2O_7$ and $Lu_2Ti_2O_7$, as the lanthanide L_{III} edge positions remain unchanged in the reduced materials. The extent of reduction varies with reaction temperature, and reaction at above 600 °C affords the 90 % titanium(III) phase $Lu_2Ti_2O_{6.10}$. It remains to be established whether single-phase materials with continuously varying oxygen content over the entire oxidation state range between titanium(III) and titanium(IV) can be prepared. Figure 1b shows the evolution of the Ti K-edge from 4982.2 eV in the titanium(IV) starting material to 4976.6 eV in $Lu_2Ti_2O_{6.10}$ reduced at 600 °C, comparable to the edge position in the titanium(III) phase $LuTiO_3$. Transmission electron micrographs revealed that crystallinity is retained during reaction without the formation of amorphous material, and EDX analysis demonstrated that Ca is not included into the pyrochlore crystallites during the reaction.

Reaction of $Yb_2Ti_2O_7$ with one equivalent of CaH_2 at 600 °C followed by washing with 0.1 M NH_4Cl in methanol under nitrogen to remove CaO affords $Yb_2Ti_2O_{6.45}$, which is single-phase to synchrotron X-ray powder diffraction (Figure 2b). Refinement of neutron powder diffraction data from

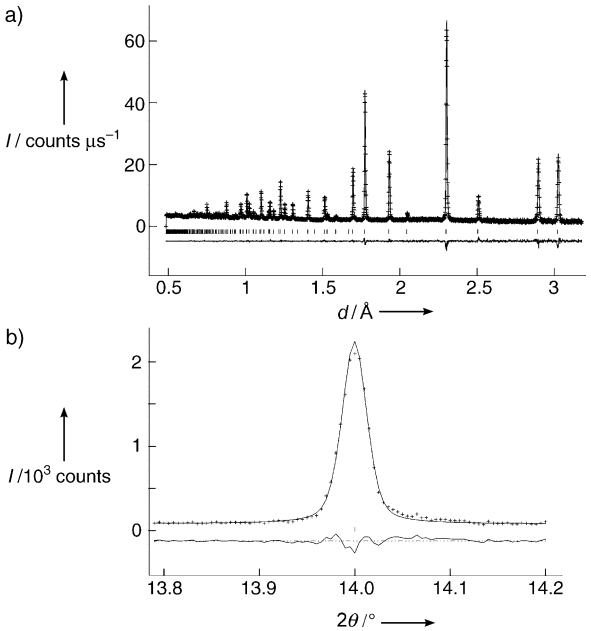


Figure 2. a) Rietveld refinement of powder neutron diffraction data from $Yb_2Ti_2O_{6.43}$ (POLARIS diffractometer, ISIS. $\chi^2 = 1.18$, $R_{wp} = 2.21$ %; $R(F^2) = 6.50$, $R(F) = 4.04$ %). b) Rietveld fit to the 222 reflection from $Yb_2Ti_2O_{6.43}$ (station 9.1, Daresbury SRS, $\chi^2 = 1.10$)

$Yb_2Ti_2O_{6.45}$ (Figure 2a) revealed preferential loss of anions from the O (83 % occupancy) rather than the O′ network and the presence of 3.3 % antisite disorder of Yb and Ti that was not present in the starting material. Electron diffraction showed that the anion vacancies remain disordered over shorter length scales than those probed by X-ray and neutron diffraction. The 8a anion site, vacant in the parent structure, is partially occupied. The extent of antisite disorder and associated structural relaxation is more pronounced in the

 © 2004 Wiley-VCH Verlag GmbH & Co. KGaA, Weinheim

$Lu_2Ti_2O_{6+x}$ phases prepared under the same conditions, and so the structure of these materials was considered in more detail.

$Lu_2Ti_2O_{6.43(1)}$ (Table 1; see Supporting Information) has 6.7(6) % antisite disorder between the two cation sublattices, 85(1) % O48f (O2 in Table 1) and 91(2) % O′ (O1) occupancy of the original oxygen positions, and two new defect anion positions. Scattering density in the vicinity of the 8a sites (equivalent to 20 % of an oxide anion) corresponds to occupancy of the 32e O3 site tetrahedrally disposed around the 8a center. The 8a site is vacant in the parent pyrochlore structure and coordinates only to the octahedral B sublattice array. The second defect O4 is 0.8 Å from the bulk 48f O2 site.

Table 1: Refined coordinates for $Lu_2Ti_2O_{6.43(1)}$.[a]

	x	y	z	U_{equiv} [Å^{-2}]	Site occupancy
Ti1/Lu2[b] 16c	0.000000	0.000000	0.000000	0.0089	0.934(6)
Lu1/Ti2[b] 16d	0.500000	0.500000	0.500000	0.023	0.934(6)
O1 8b	0.375000	0.375000	0.375000	0.014	0.912(17)
O2 48f	0.3370(2)	0.125000	0.125000	0.028	0.849(12)
O3 32e	−0.396(3)	0.1464(30)	−0.3964(30)	0.05(1)	0.045(4)
O4 48f	−0.424(6)	−0.125000	−0.125000	0.05(1)	0.041(4)

[a] $a = 10.01728(21)$ Å, space group $Fd\bar{3}m$. [b] Site occupancies were refined such that the antisite (Lu2, Ti2) and (Lu1, Ti1) main sublattice occupancies at each site summed to 1.00. The number quoted is the main sublattice occupancy. Anisotropic displacement parameters for the bulk sites are listed in the Supporting Information

The O3 oxygen defect is coordinated to Ti and locally controls occupancy of the O2 48f site. The O3 site is displaced from the 8a site towards the center of one of the triangular faces of the B_4 tetrahedron of neighboring Ti sites, creating one long and three shorter Ti–O3 contacts (Figure 3a).

The shorter Ti–O3 distance of 2.075 Å corresponds to the defect anion being located 1.94 Å from two of the bulk O2 48f sites, and this requires that in the vicinity of the 8a defect these two sites must be vacant (Figure 3b). This means that these 15 % of the Ti sites have only four O2 neighbors that produce a five-coordinate distorted trigonal-bipyramidal environment around the Ti center with a valence sum of +2.92, consistent with occupancy of this site by Ti^{III}. The mean coordination number of 5.1 of the octahedral B site by O2, determined by its refined occupancy, is then assigned as 15 % of Ti sites fourfold-coordinated by O2 in the above-mentioned trigonal bipyramids involving the O3 defect, 25 % six-coordinate (valence sum +3.9), and 60 % five-coordinate (valence sum +3.3), that is, three distinct Ti environments with a mean valence sum of +3.39 close to that expected from the TGA-derived composition.

The displacement of O3 from the center of the 8a site occurs to shorten the Ti–O distance to less than 2.168 Å. The Lu2 cations occupying the Ti sublattice due to the antisite disorder correspond to the longer (2.54(5) Å) Ti–O3 contacts. The distorted cubic environment (Figure 3c) is completed by six Lu2–O4 contacts of 2.48(5) Å to the O48f-related O4 defect anion. The calculated valence sum of +2.3 indicates underbonding and further local relaxation of the anions associated with this site. The Ti2 cations occupying the Lu sublattice correspond to absent O′ anions and are octahedrally coordinated by six O4 anions at 1.93(3) Å, with a valence sum of +4.4. The imperfect quantitative description of the bonding at both antisite cation defects can be associated with the use of only one position to describe the defect anion sites.

Removal of oxygen from $A_2B_2O_6O'$ pyrochlore poses the question of whether vacancies will be formed on the structurally distinct O or O′ sublattices. Anion-deficient pyrochlores containing lone-pair cations such as Pb^{II} lose anions from the O′ site (e.g., $Pb_2Ru_2O_{6.5}$),[13] whereas isovalent B site disorder in $Ln_2Ti_{2-x}Zr_xO_7$ favors anion transfer from the O 48f to the 8a sites,[14] consistent with modeling.[15] In $Ln_2Ti_2O_{6+x}$ oxygen vacancies are formed on the O sublattice, as reduction occurs solely at the Ti centers which are not bound to O′. The cation antisite disorder reflects the movement of O2 in response to reduction of the B cation. This

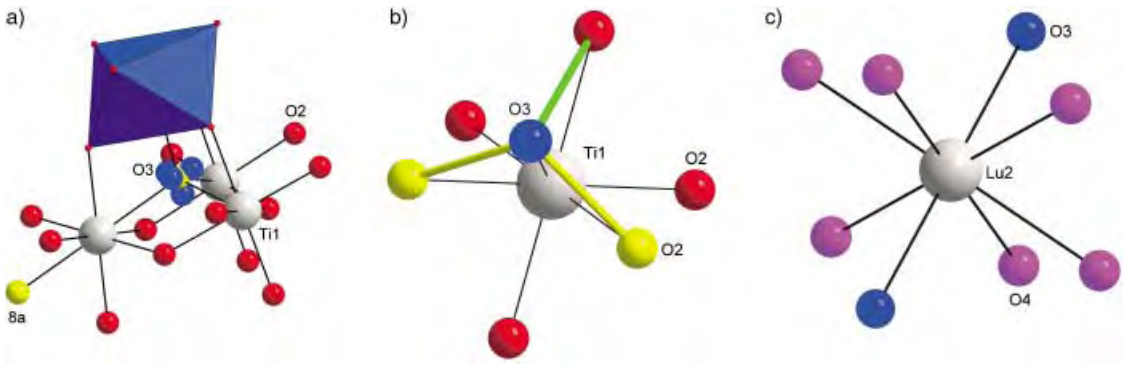


Figure 3. Anion defects and cation coordination in $Lu_2Ti_2O_{6.43}$. Distances and angles are given in the Supporting Information. a) The O3 oxygen atom on the 32e site (blue spheres) is displaced from the center of the 8a site (yellow sphere), which is vacant in the perfect parent pyrochlore structure. b) The O3 site is only occupied at Ti sites where two O2 sites (marked as yellow spheres linked by short yellow contacts of 1.94 Å; these are the 48f anion positions in the parent structure) are vacant, producing a five coordinate site. The green contact indicates the closest remaining O3–O2 distance of 2.37 Å, acceptably close to the 2.56 Å O2–O2 contacts in view of the 0.1 Å rms anion displacement ellipsoids. c) The distorted cubic arrangement of O3 (blue) and O4 anions around the Lu antisite cations on the octahedral Ti sublattice.

 © 2004 Wiley-VCH Verlag GmbH & Co. KGaA, Weinheim

lengthens the B–O2 and shortens the A–O2 bonds, and this opens up the possibility of antisite disorder of the lanthanide and titanium cations, the smaller Lu^{III} giving more extensive disorder. The occupation of the O3 defect site is a disordering of the parent pyrochlore (where differentiation between the A and B sites arises from ordering of the anion vacancies onto the 8a site that is now partially occupied) towards the fluorite structure, as observed for lanthanide zirconates which adopt both ordered (pyrochlore) and disordered (fluorite) structures.[16]

A strong motivation for preparing titanium(III) pyrochlores is to study the behavior of $S = 1/2$ centers on the geometrically frustrated B site pyrochlore lattice (synthetic procedures which minimize the antisite disorder are required if materials of this class are to be genuine model systems); the 3d electrons introduced at the Ti^{III} sites are localized, as evidenced by the persistence of the Ti–O phonons in the IR transmission spectra of the reduced materials. Magnetization measurements (Figure 4) indicate that the localized spins at

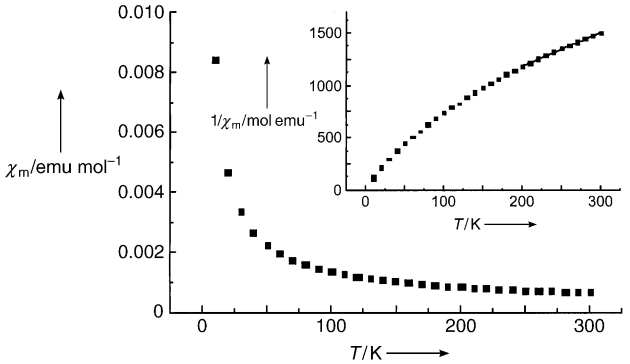


Figure 4. Magnetic susceptibility at 1.5 T and Curie–Weiss fit (inset) for $Lu_2Ti_2O_{6.10}$.

the Ti centers are strongly coupled antiferromagnetically: Curie–Weiss fits to $Lu_2Ti_2O_{6+x}$ ($x = 0.1$, 0.5) are both only valid at high temperature and give moments at the Ti sites that are lower than expected (1.12(1) μ_B per Ti ($x = 0.1$), 0.88(3) μ_B per Ti ($x = 0.5$), compared with predicted 1.64 μ_B and 1.23 μ_B) with Weiss constants of −173(6) K and −227(17) K. The moment suppression is qualitatively consistent with strong antiferromagnetic coupling between the Ti centers that is geometrically frustrated (the tetrahedral plaquette is shown in Figure 3a) against long-range order by the tetrahedral geometry of the B sublattice (no additional magnetic Bragg peaks are observed in neutron diffraction at 5 K from the Lu or Yb phases discussed above). This motivates further detailed studies of the electronic properties of this new class of defect pyrochlore by muon spin relaxation (μSR) and neutron scattering.

Received: January 21, 2004 [Z53819]

Keywords: lanthanides · magnetic properties · pyrochlore phases · reduction · titanium

[1] M. A. Hayward, E. J. Cussen, J. B. Claridge, M. Bieringer, M. J. Rosseinsky, S. J. Blundell, I. M. Marshall, F. L. Pratt, *Science* **2002**, *295*, 1882–1884.
[2] M. Subramanian, G. Aravamudan, G. C. Subba Rao, *Prog. Solid State Chem.* **1983**, *15*, 55.
[3] O. Porat, C. Heremans, H. L. Tuller, *Solid State Ionics* **1997**, *94*, 75–83.
[4] M. Hanawa, Y. Muraoka, T. Tayama, T. Sakakibara, J. Yamaura, Z. Hiroi, *Phys. Rev. Lett.* **2001**, *87*, 187001.
[5] Y. Shimakawa, Y. Kubo, T. Manako, *Nature* **1996**, *379*, 53–55.
[6] S. Mohr, H. Müller-Buschbaum, *J. Alloys Compd.* **1994**, *210*, 115–118.
[7] S. T. Bramwell, M. J. P. Gingras, *Science* **2001**, *294*, 1495–1501.
[8] A. P. Ramirez, B. S. Shastry, A. Hayashi, J. J. Krajewski, D. A. Huse, R. J. Cava, *Phys. Rev. Lett.* **2002**, *89*, 067202.
[9] G. Ferey, M. Leblanc, R. Depape, J. Pannetier, *Solid State Commun.* **1985**, *53*, 559–563.
[10] G. Ferey, R. Depape, M. Leblanc, J. Pannetier, *Rev. Chim. Miner.* **1986**, *23*, 474–484.
[11] J. N. Reimers, J. E. Greedan, R. K. Kremer, E. Gmelin, M. A. Subramanian, *Phys. Rev. B* **1991**, *43*, 3387–3394.
[12] J. L. Fourquet, H. Duroy, P. Lacorre, *J. Solid State Chem.* **1995**, *114*, 575–584.
[13] R. A. Beyerlein, H. S. Horowitz, J. M. Longo, M. Leonowicz, *J. Solid State Chem.* **1984**, *51*, 253–265.
[14] C. Heremans, B. J. Wuensch, J. K. Stalick, E. Prince, *J. Solid State Chem.* **1995**, *117*, 108–121.
[15] M. Pirzada, R. W. Grimes, L. Minervini, J. Maguire, K. E. Sickafus, *Solid State Ionics* **2001**, *140*, 201–208.
[16] J. Chen, J. Lian, L. M. Wang, R. C. Ewing, R. G. Wang, W. Pan, *Phys. Rev. Lett.* **2002**, *88*, 105901.

 © 2004 Wiley-VCH Verlag GmbH & Co. KGaA, Weinheim

NMR Spectroscopy

Exploiting the Joint Action of Chemical Shielding and Heteronuclear Dipolar Interactions To Probe the Geometries of Strongly Hydrogen-Bonded Silanols**

*Carole Gardiennet, Florea Marica, Xavier Assfeld, and Piotr Tekely**

Hydrogen bonds are the most important of all directional intermolecular interactions and play a central role in determining molecular conformation and aggregation, as well as

[*] C. Gardiennet, Prof. X. Assfeld, Dr. P. Tekely
UMR CNRS 7565
Université H. Poincaré, Nancy 1
54500 Vandoeuvre-lès-Nancy (France)
Fax: (+33) 3836-84347
E-mail: piotr.tekely@rmn.uhp-nancy.fr
Dr. F. Marica
Department of Chemistry
University of British Columbia
2036 Main Mall, Vancouver BC, V6T 1Z1 (Canada)

[**] We thank Prof. W. Schwieger, University of Erlangen-Nuremberg, for providing the sample of octosilicate and Prof. Colin A. Fyfe, University of British Columbia, for making this sample available to us and for stimulating discussions.

 DOI: 10.1002/anie.200353339 © 2004 Wiley-VCH Verlag GmbH & Co. KGaA, Weinheim

the function and dynamics of a great number of systems ranging from inorganic to biological chemistry.[1] Nuclear magnetic resonance (NMR) spectroscopy is one of the most suitable tools for studying hydrogen-bonding phenomena. Solid-state NMR spectroscopic measurements give direct access to the chemical-shift anisotropy (CSA) tensors, which by virtue of their nature, provide an improved characterization of local environments and may show significant changes of their orientation in the presence of hydrogen bonding.[2–3] Dipolar interactions provide information on internuclear distances and have also been frequently exploited in studying hydrogen bonds.[4–9]

Herein we use a new approach that takes advantage of the joint effects of chemical shielding and dipolar interactions under slow magic-angle-spinning conditions to provide detailed information on the geometry of hydrogen-bonded silanols in octosilicate[10a] (also known as ilerite[10c] or RUB-18[11]), a prominent member of the layered hydrous sodium silicates.[12] This class of material, available only in microcrystalline form, has a 2D layered structure in which the negative charge of the silicate layer is compensated by sodium ions coordinated by the oxygen atoms of the intercalated water molecules.[10–17] Hydrated sodium silicates are of rapidly growing industrial interest owing to their high ion- or proton-exchange properties and new applications in catalysis and in the synthesis of composite mesoporous materials.[13]

To understand the physical and chemical properties of this class of microporous material as well as the role of hydrogen bonds in the aggregation and ordering of silicate layers, the correlation of such contacts with the spectroscopic response is highly desired. In sodium hydrous silicates, the nature of strong hydrogen bonding with an O–O distance of less than 2.60 Å and present at room or higher temperature remains the subject of considerable controversy. Both the inter-[10b,14] and intralayer[10c,11c,15,16] characters of hydrogen bonding involving the silanol protons have been proposed. Another model involving water hydrogen atoms in a strongly hydrogen-bonded state has been suggested.[17] As the intercalation of polar molecules in layered materials can be dramatically controlled by the existence of interlayer hydrogen bonds, the appropriate recognition of the extent and the nature of hydrogen bonding present in these materials is of prime importance.

Precise geometrical information about the d(O–H···O) and d(H···O) separations can be obtained by taking advantage of their correlations with ^{1}H NMR isotropic and principal values of the shielding tensor.[18–20] In octosilicate, with the idealized formula $(Na_8\{Si_{32}O_{64}(OH)_8\}\cdot 32\,H_2O)$,[10,11] and in analogy to other sodium hydrous silicates, high-speed ^{1}H MAS spectra give a clearly resolved isotropic, downfield peak which could be assigned unambiguously to silanol protons involved in strong hydrogen bonding.[11] The isotropic chemical shift–distance relationships provide[18–19] $d(\text{O-H}\cdots\text{O}) \approx 2.5 \pm 0.05$ Å and[20] $d(\text{H}\cdots\text{O}) \approx 1.37 \pm 0.05$ Å. The chemical-shift tensor is an extremely sensitive measure of hydrogen bonding and can provide more information than the isotropic shift alone. Highly selective $^1\text{H}\rightarrow{}^{29}\text{Si}$ cross-polarization from protons involved in hydrogen bonding allowed the calculation of their principal CSA values (Table 1) from low-speed 2D shift correlation spectra (not shown). For hydrogen-bonded hydroxy protons, the proton shielding is almost axially symmetrical, with the symmetry axis almost parallel to the H···O direction.[21] For octosilicate, both the chemical-shift anisotropy $|\Delta\delta| = \delta_{\parallel} - \delta_{\perp}$ and $\delta_{\perp}$–distance relationships give[18a,b] $d(\text{O-H}\cdots\text{O}) \approx 2.46 \pm 0.05$ Å. Finally, taking advantage of the Steiner correlation between O–H and H···O bond lengths,[1] we obtain $d(\text{O-H}) \approx 1.1 \pm 0.05$ Å.

To obtain further local geometric information, we determined the internuclear Si···H distances and the orientation of the ^{29}Si chemical-shift tensor in the hydrogen-bonded Q^3-type units. For this, we exploited a simple 1D version of the local-field experiment, which is based on the cross-polarization (CP) inversion of the rare spin magnetization used as a modulation of the slow magic-angle spinning (MAS) chemical-shift spectrum.[22a] The experiment starts with the classical CP procedure followed by a period during which the contact between protons and silicon atoms is maintained but the phase of proton spin-locking irradiation is inverted. As shown in Figure 1, this leads to nonuniform dipolar modulation of the ^{29}Si CSA spinning sidebands recorded under high-power proton decoupling. Such an effect provides evidence for largely coherent magnetization transfer within the silanol groups with a pronounced inhomogeneous character of the dipolar system; the observed difference in the dipolar oscillation frequency of different spinning sidebands results from the variation of the orientation-dependent dipolar coupling. This variation allows the unambiguous visualization of the orientation dependence of spinning sidebands and is a direct consequence of the fact that in the slow-spinning regime, each particular spinning sideband represents only a narrow range of orientations owing to the destructive interference of the magnetization pathways of different crystallites.[22b] More interesting in the context of this work, the dipolar-modulated spinning sidebands contain all the desired information on the heteronuclear distance as well as the magnitude and orientation of the principal elements of the chemical-shielding tensor in the molecular frame.[22c]

To reproduce the observed dipolar-modulated envelope of Q^3 spinning sidebands in Figure 1, the presence of two different components representing two types of Q^3 sites has to

Table 1: ^{29}Si and ^{1}H NMR shift tensor parameters (in ppm from TMS) along with the geometries of hydrogen-bonded (H-B) silanols in octosilicate.

Q^3-type	^{29}Si					^{1}H					
	$\delta_{\perp}$[a]	$\delta_{\parallel}$[a]	δ_{iso}	$\beta_D(\delta_{\parallel})$[b]	$r_{Si\cdots H}$ [Å]	$\delta_{\perp}$[a]	$\delta_{\parallel}$[a]	δ_{iso}	d(O···O) [Å][c]	d(H···O) [Å][d]	d(O-H) [Å][e]
H-B silanols	−76.5	−146.1	−99.7	70.0	2.21 ± 0.05	30.75	−13.56	15.98	2.48 ± 0.05	1.37 ± 0.05	1.10 ± 0.05
				0.0	2.41 ± 0.05						
Si-O$^-$	−76.5	−146.1	−99.7								

[a] Estimated errors: ±1 ppm. [b] Polar angle of the Si···H vectors in the PAS^{CSA} (in degrees). [c] Average distance according to correlations from references [18,19]. [d] According to correlations from reference [20]. [e] According to correlations from reference [1].

 © 2004 Wiley-VCH Verlag GmbH & Co. KGaA, Weinheim

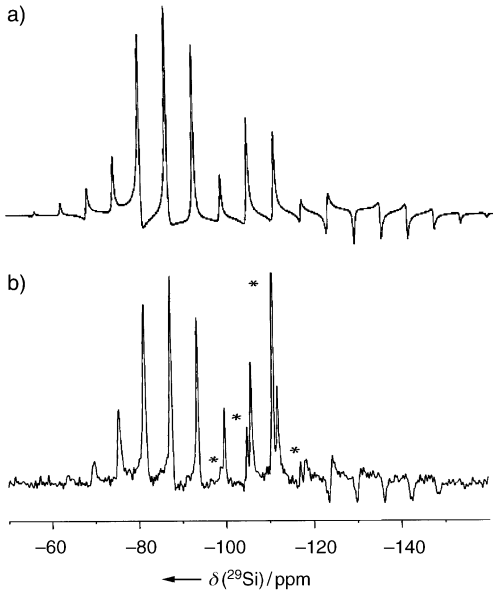


Figure 1. a) Fitted spectrum of Q^3 sites providing the internuclear Si···H distances in silanols involved in hydrogen-bonded units and their polar coordinates in the shift tensor principal axis frame (see Table 1). B) Dipolar-modulated (t_{dm} = 400 μs), natural-abundance ^{29}Si NMR spectrum of octosilicate under slow magic-angle-spinning conditions (ν_r = 357 Hz). Asterisks indicate the spinning sidebands of the Q^4 site.

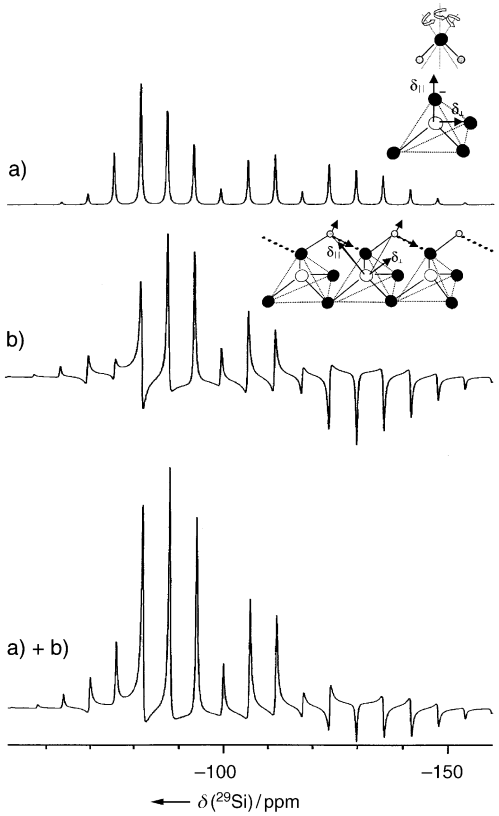


Figure 2. Fitted spectrum of Q^3 sites from Figure 1 along with its individual components. Dipolar-modulated subspectrum b represents the hydrogen-bonded tetrahedra, the subspectrum a comes from the Si-O^- type sites.

be assumed (Figure 2). Indeed, although a single isotropic Q^3 resonance signal is observed, two types of Q^3 tetrahedra, (hydrogen-bonded silanols and Si-O^--type sites) need to be distinguished by their different abilities to cross-polarize. This finding is fully confirmed by fast magic-angle spinning CP dynamic studies, which reveal that in analogy to another sodium hydrous silicate, magadiite,[15] two different types of Q^3 sites with a dramatically different ability to cross-polarize and to "feel" different mobilities of neighboring hydrous species are present. Moreover, direct and indirect proton $T_{1\rho}$ measurements provide complementary evidence that a rapidly cross-polarizing component (dipolar-modulated component a in Figure 2) relaxes as the proton signal representing hydrogen-bonded silanols, whereas the slowly cross-polarizing component (component b in Figure 2) mainly "feels" relaxing water molecules present in the interlayer space. The fitting of the dipolar-modulated spectrum included two different $r_{Si\cdots H}$ distances in hydrogen-bonded tetrahedra and their polar coordinates β_D in the principal axis system PAS^{CSA}. The principal values of the ^{29}Si CSA tensor were fitted independently from unmodulated spectra recorded at different spinning speeds and different resonance frequencies. All relevant parameters are listed in Table 1. As can be seen in Figure 1, the calculated spectrum is in excellent agreement with the experimental envelope and phase features of the Q^3 family of spinning sidebands. The simulations show that the dipolar-modulated envelope of spinning sidebands is very sensitive to small changes in $r_{Si\cdots H}$ distances and in their polar coordinates in the chemical-shielding principal axis frame. Somewhat unexpectedly, a unique set of CSA principal values characterizes both types of Q^3 tetrahedra. This means that the principal values of the axially symmetrical ^{29}Si CSA tensor in Q^3 tetrahedra from layered sodium silicates are mainly determined by the symmetry of the local site and are rather insensitive to the presence of protons in the second sphere of coordination. This would confirm the observation of Grimmer et al.[23] that the ^{29}Si shielding tensor is mainly related to the bond character of the Si–O bonds (including the lengths and interbond angle differences between terminal and bridging oxygen atoms) in the SiO_4 tetrahedron.

All the results presented in Table 1 clearly support the intralayer character of strongly hydrogen-bonded silanol groups in a bridging albeit unsymmetrical position between neighboring tetrahedra. The interlayer hydrogen bonding involving the silanols is dismissed by the d(O-H···O) distance, which is much shorter than the interlayer distance.[11a] The engagement of highly mobile water molecules (^{1}H NMR spectroscopy) in such strong contacts is incompatible with a rigid Si···H spin pair character.

The outstanding sensitivity of the dipolar-modulated CSA spectrum to the presence of slightly different $r_{Si\cdots H}$ distances in the hydrogen-bonded tetrahedra deserves special note. Apart from the $r_{H\text{-}Si}^{-6}$ dependence of the cross-polarization-transfer rate, each dipolar-modulated spinning sideband benefits under the conditions of this experiment from a particular dipole-orientation dependence of a narrow range of orientations of crystallites.[22b] In contrast to high-speed CP or REDOR-like (REDOR = rotational-echo double resonance)

 © 2004 Wiley-VCH Verlag GmbH & Co. KGaA, Weinheim

measurements of heteronuclear distances, this greatly enhances the sensitivity to dipolar modulation by avoiding the powder average damping.

In summary, we have obtained detailed information about the geometry of the hydrogen-bonded silanols in octosilicate by exploiting the ^{1}H NMR distance correlations together with the joint effect of ^{29}Si chemical shift and heteronuclear ^{1}H–^{29}Si interactions. We have shown that the dipolar-modulated slow-spinning CSA spectrum yields straightforward geometric information on the internuclear Si···H distances of hydrogen-bonded silanols as well as on the orientation of the principal elements of the ^{29}Si chemical-shielding tensor in the molecular frame. Such information is very difficult to obtain by other means. The method takes advantage of moderate proton–proton dipolar coupling networks, partially disconnected from the heteronuclear dipolar couplings within the silanol groups. This allows the use of the coherent magnetization transfer in the initial period of dipolar modulation (a few hundreds of microseconds) without applying homonuclear dipolar decoupling which in turns eliminates any uncertainty about the heteronuclear scaling factor inherently connected with homonuclear decoupling. To our knowledge, this is also the first time that the orientation of a ^{29}Si shielding tensor in the molecular frame has been obtained experimentally on a powder sample. The method presented herein is simple and robust and should be useful in obtaining similar structural information in related alkali-metal-layered polysilicates, silica gels, and other classes of microporous powder materials.

Received: November 17, 2003
Revised: April 19, 2004 [Z53339]

Keywords: hydrogen bonds · NMR spectroscopy · silicates

[1] T. Steiner, *Angew. Chem.* **2002**, *114*, 50 – 80; *Angew. Chem. Int. Ed.* **2002**, *41*, 48 – 76.
[2] G. Buntkowsky, I. Sack, H.-H. Limbach, B. Kling, J. Fuhrhop, *J. Phys. Chem. B* **1997**, *101*, 11265 – 11272.
[3] M. J. Potrzebowski, X. Assfeld, K. Ganicz, S. Olejniczak, A. Cartier, C. Gardiennet, P. Tekely, *J. Am. Chem. Soc.* **2003**, *125*, 4223 – 4232.
[4] C.-G. Hoelger, H.-H. Limbach, *J. Phys. Chem.* **1994**, *98*, 11803 – 11810.
[5] G. Wu, C. J. Freure, E. Verdurand, *J. Am. Chem. Soc.* **1998**, *120*, 13187 – 13193.
[6] G. R. Goward, I. Schnell, S. P. Brown, H. W. Spiess, H.-D. Kim, H. Ishida, *Magn. Reson. Chem.* **2001**, *39*, S5-S17.
[7] P. Lorente, I. G. Shenderovich, N. S. Golubev, G. S. Denisov, G. Buntkowsky, H.-H. Limbach, *Magn. Reson. Chem.* **2001**, *39*, S18-S29.
[8] X.-J. Song, C. M. Rienstra, A. E. McDermott, *Magn. Reson. Chem.* **2001**, *39*, S30-S36.
[9] A. Fukutani, A. Naito, S. Tuzi, H. Saito, *J. Mol. Struct.* **2002**, *602*/603, 491 – 503.
[10] a) W. Schwieger, D. Heidemann, K.-H. Bergk, *Rev. Chim. Miner.* **1985**, *22*, 639 – 650; b) Y. Huang, Z. Jiang, W. Schwieger, *Chem. Mater.* **1999**, *11*, 1210 – 1217; c) U. Brenn, H. Ernst, D. Freude, R. Herrmann, R. Jähnig, H. G. Karge, J. Kärger, T. König, B. Mädler, U.-T. Pingel, D. Prochnow, W. Schwieger, *Microporous Mesoporous Mater.* **2000**, *40*, 43 – 52.
[11] a) S. Vortmann, J. Rius, S. Siegmann, H. Gies, *J. Phys. Chem. B* **1997**, *101*, 1292 – 1297; b) I. Wolf, H. Gies, C. A. Fyfe, *J. Phys. Chem. B* **1999**, *103*, 5933 – 5938; c) M. Borowski, I. Wolf, H. Gies, *Chem. Mater.* **2002**, *14*, 38 – 43.
[12] H. P. Eugster, *Science* **1967**, *157*, 1177 – 1178.
[13] S. Inagaki, Y. Fukushima, K. Kuroda, *J. Chem. Soc. Chem. Commun.* **1993**, *8*, 680 – 682.
[14] G. G. Almond, R. K. Harris, K. R. Franklin, *J. Mater. Chem.* **1997**, *7*, 681 – 687.
[15] C. Gardiennet, P. Tekely, *J. Phys. Chem. B* **2002**, *106*, 8928 – 8936.
[16] X. Ai, F. Deng, J. Dong, L. Chen, C. Ye, *J. Phys. Chem. B* **2002**, *106*, 9237 – 9244.
[17] C. Eypert-Blaison, E. Sauzéat, M. Pelletier, L. J. Michot, F. Villéras, B. Humbert, *Chem. Mater.* **2001**, *13*, 1480 – 1486.
[18] a) B. Berglund, R. W. Vaughan, *J. Chem. Phys.* **1980**, *73*, 2037 – 2043; b) C. McMichael Rohlfing, L. C. Allen, R. Ditchfield, *J. Chem. Phys.* **1983**, *79*, 4958 – 4966.
[19] H. Eckert, J. P. Yesinowski, L. A. Silver, E. M. Stolper, *J. Phys. Chem.* **1988**, *92*, 2055 – 2064.
[20] E. Brunner, U. Sternberg, *Prog. Nucl. Magn. Reson. Spectrosc.* **1998**, *32*, 21 – 57.
[21] U. Haeberlen, *Philos. Trans. R. Soc. London Ser. A* **1981**, *299*, 497 – 504.
[22] a) P. Palmas, P. Tekely, D. Canet, *J. Magn. Reson. Ser. A* **1993**, *104*, 26 – 36; b) P. Tekely, *Solid State Nucl. Magn. Reson.* **1999**, *14*, 33 – 41; c) P. Palmas, C. Malveau, P. Tekely, D. Canet, *Solid State Nucl. Magn. Reson.* **1998**, *13*, 45 – 53.
[23] A.-R. Grimmer, R. Peter, E. Fechner, G. Molgedey, *Chem. Phys. Lett.* **1981**, *77*, 331 – 334.

 © 2004 Wiley-VCH Verlag GmbH & Co. KGaA, Weinheim

Surfactant-Free Emulsions

The Pristine Oil/Water Interface: Surfactant-Free Hydroxide-Charged Emulsions**

James K. Beattie and Alex M. Djerdjev*

Oil and water do not mix spontaneously, so the formation of a stable oil-in-water emulsion is thought to require both the input of energy to create small oil drops and the presence of a surfactant to stabilize the newly formed surface of the otherwise metastable droplets.[1,2] Amphiphilic surfactants with a polar head group and a hydrophobic tail are typically used to create a charged surface around the oil drop for electrostatic stabilization. Yet it has long been known that the oil/water interface can acquire a negative charge in the absence of surfactants.[3,4] From the pH dependence of this

[*] Prof. J. K. Beattie, Dr. A. M. Djerdjev
School of Chemistry
University of Sydney
NSW 2006 (Australia)
Fax: (+61) 2-9351-3329
E-mail: j.beattie@chem.usyd.edu.au

[**] This work was supported by the Australian Research Council. We thank Colloidal Dynamics Pty. Ltd. for the use of the AcoustoSizer, Dr Richard O'Brien for assistance with the calculation of the surface area of a polydisperse emulsion, and Robert J. Hunter, Gregory G. Warr, and a referee for helpful discussions and advice.

 © 2004 Wiley-VCH Verlag GmbH & Co. KGaA, Weinheim DOI: 10.1002/anie.200453916

charge it was inferred that hydroxide ions are responsible, but this inference was qualitative and tentative. The experiments involved only the small surface areas of dilute emulsions or plane interfaces, so the possibility of interference from trace contamination could not be excluded.[5–7] We have now used the new technique of electroacoustics to measure the increase in total surface area during homogenization of more concentrated oil-in-water emulsions and have found a linear relationship with the amount of hydroxide ion added to maintain a constant pH value. These pH-stat experiments quantitatively demonstrate that hydroxide ions do stabilize the oil/water interface; a fundamental reassessment of the perceived need for surfactants to obtain emulsion stability is thus required.

The electroacoustic technique can be used to measure the diameter d and the charge (zeta potential ζ) of emulsion droplets as they are being formed. An electroacoustic effect is created when an alternating megahertz electric field is applied to a concentrated (>1 vol%) colloidal suspension.[8] The charge on the particles causes them to "jiggle" in the field. Because of the difference between the density of the droplets and that of the surrounding fluid, this oscillatory motion creates a sound wave of the same megahertz frequency as the applied electric field. By measuring the phase and amplitude of this sound wave, the complex dynamic mobility spectrum is obtained, which can be analyzed to give the mean diameter of the emulsion droplets, their zeta potential, and the spread of a lognormal size distribution. The only input parameters required are the density and volume fraction of the oil. Because the droplets are spherical the total oil/water surface area can be immediately obtained from their diameter and the volume fraction of oil.

In a typical experiment a coarse emulsion was prepared by passing through a homogenizer a mixture of 2 vol% hexadecane in 0.2 mM NaCl solution prepared with freshly boiled water that had been cooled under a N_2 atmosphere. (The electrolyte was necessary for the electroacoustic measurements.) The pH value was then adjusted to pH 9 with NaOH solution, and the emulsion repeatedly passed through the homogenizer and the flow-through cell of a prototype of the AcoustoSizer-II, again under N_2. As the emulsification progressed the pH value would drop unless maintained at pH 9.0 ± 0.1 by the periodic addition of 20 mM NaOH solution. After each addition of alkali the dynamic mobility spectrum was measured and the droplet size d_{50}, lognormal size distribution d_{15} and d_{85}, and zeta potential were calculated (Table 1).

The surface area (SA) of a polydisperse distribution is $(6\Phi/d_{50})\exp(0.5\beta^2)$, where Φ is the volume fraction of the oil and $\beta = \ln(d_{85}/d_{15})$.[9] In this experiment, as homogenization proceeded, the droplet diameter decreased from 2.5 μm with a broad size distribution to 0.46 μm with a narrow distribution. This resulted in a threefold increase in surface area. The amount of hydroxide ion required to charge this newly formed surface is known directly from the quantity of base needed to maintain the constant pH value (Table 1). The amount of hydroxide ion added depends linearly on the new surface area created (Figure 1), which allows the surface charge density to be calculated from the slope as $-4.9\ \mu C\,cm^{-2}$ (0.31 unit charges per 100 Å^2). If the experiment is repeated at pH 7, the mixture requires more passes through the homogenizer to reduce the droplet size, but the amount of hydroxide ion added is again a linear function of the surface area created, with a slightly reduced surface charge density of $-4.5\ \mu C\,cm^{-2}$ (Figure 1).

Table 1: Quantity of hydroxide ion required to maintain pH 9.0 during emulsification of 2 vol% hexadecane (4.9 mL) in 240 mL of 0.20 mM NaCl with calculated emulsion parameters: median droplet diameter d_{50}, the 15th and 85th percentiles of the lognormal distribution d_{15} and d_{85}, and the surface area (SA).

OH^- [μmol]	Q_{surf} [C]	d_{15}–d_{50}–d_{85}[a] [μm]	SA [10^5 cm^2]
2.4	0.23	0.90–2.5–6.9	1.95
5.0	0.48	0.90–1.55–2.7	2.50
8.4	0.81	0.80–1.1–1.5	3.12
11.0	1.06	0.69–0.82–0.97	3.89
14.4	1.39	0.63–0.73–0.85	4.33
17.0	1.64	0.59–0.65–0.72	4.75
19.6	1.89	0.54–0.58–0.62	5.24
22.4	2.16	0.49–0.51–0.53	5.88
25.8	2.49	0.42–0.46–0.50	6.66

[a] A large-particle correction was applied iteratively for the larger droplets to account for the effect these have on the observed phase lags in the dynamic mobility spectra.[22]

Several alternative explanations of these results can be eliminated. For example, care was taken to eliminate carbon dioxide from the system, which otherwise would compromise the quantitative pH-stat experiments described above. Carbonate or hydrogencarbonate ions are not strongly adsorbed on the surface.[6] When 2 vol% hexadecane was homogenized in 1 mM Na_2CO_3 solution the droplet size (0.45 μm) and zeta potential (−45 mV) were found to be the same as those obtained in 1 mM NaOH solution. The purity of the hexadec-

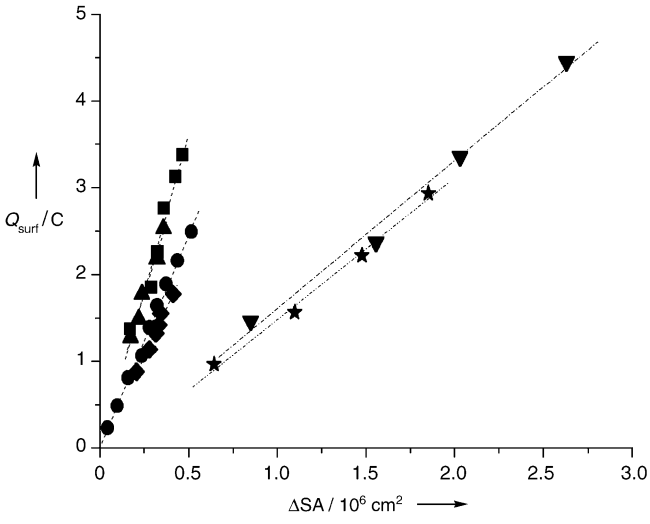


Figure 1. Surface charge density σ^o calculated from measured values of surface charge (Q_{surf}) and increase in surface area (ΔSA) for 2 vol% oils in 0.2 mM NaCl: perfluoromethyldecalin (■), pH 9.0, $-7.3\ \mu C\,cm^{-2}$; squalene (▲), pH 9.0, $-6.7\ \mu C\,cm^{-2}$; hexadecane (●), pH 9.0, $-4.9\ \mu C\,cm^{-2}$; hexadecane (◆), pH 7.0, $-4.6\ \mu C\,cm^{-2}$; hexadecane with 2 mM SDS (▼), pH 9.0; $-1.7\ \mu C\,cm^{-2}$; squalene with 2 mM SDS (*), pH 9.0, $-1.6\ \mu C\,cm^{-2}$.

 © 2004 Wiley-VCH Verlag GmbH & Co. KGaA, Weinheim

ane was not critical. Hexadecane was purified by five passages through a column of basic alumina.[10] The use of unpurified hexadecane required about 20% more hydroxide to obtain the same droplet size and zeta potential. The method of homogenization of the oil also was not a factor; emulsions were obtained whether the hexadecane was homogenized by sonication or by passage through the multivalve homogenizer.

Most importantly, hydroxide-stabilized emulsions are not confined to hexadecane, but their formation occurs generally for oils with low solubility in water. The pH-stat experiment at pH 9 gives a surface charge density of $-7.3\,\mu C\,cm^{-2}$ with perfluoromethyldecalin and $-6.7\,\mu C\,cm^{-2}$ with squalene (Figure 1). We have also prepared stable emulsions with decane, dodecane, eicosane, and squalane.

We can infer that the hydroxide ion is located at the surface of the droplet and not dispersed throughout the oil. There is insufficient water dissolved in the oil to hydrate the anion. The solubility of water in hexadecane is about $0.08\,g\,L^{-1}$.[11] For the experiment described in Table 1 this corresponds to 2×10^{-5} mol, about the same magnitude as the amount of hydroxide adsorbed. It is also unlikely that the hydroxide ions are involved in hydrogen bonding to the water dissolved in the oil, as has been suggested,[12] for this would bring all of the water to the surface of the oil drop. Furthermore, the adsorption of hydroxide depends linearly on the surface area, as illustrated in Figure 1, and not on the volume of the droplet. Most of the hydroxide ion surface charge of $-4.9\,\mu C\,cm^{-2}$ is compensated by Na^+ counterions in the Stern or stagnant layer inside the shear plane. The measured zeta potential of -105 mV at pH 9 in 0.2 mM NaCl corresponds to a diffuse layer charge of only $0.63\,\mu C\,cm^{-2}$.[13,14]

Hydroxide ions are the specific charge-generating species at the hexadecane oil/water interface. When the 0.4 mM supporting electrolyte was changed from NaCl to NaI or $NaClO_4$, the same zeta potentials were observed with the same pH dependence (Figure 2). Hence dispersion forces are not significant at these low salt concentrations.[15] Extrapolation indicates an isoelectric point between pH 3 and 4.

Such surfactant-free emulsions are remarkably stable.[16] A hexadecane emulsion prepared at pH 10.5 in 1 mM NaCl solution was slowly titrated to pH 4.5 with HCl. After measurement at pH 4.5, reversal of the pH to 10 restores the original dynamic mobility spectrum, which indicates no irreversible change in the zeta potential or droplet size. At pH 9–10 the emulsions are stable for days. They do degrade, however, if the electrolyte concentration is increased to more than about 5 mM of salt. Hence these emulsions are stabilized electrostatically by a high zeta potential with a relatively thick double layer on the order of 10 nm or more. When the double layer shrinks to a few nanometers on addition of salt, the emulsions become unstable.

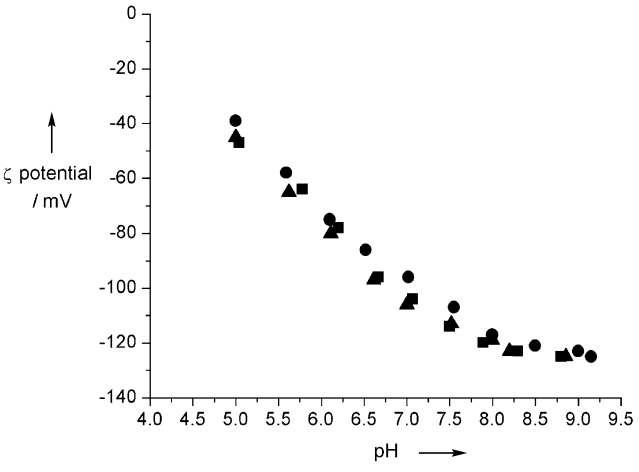


Figure 2. pH dependence of the zeta potential of 2 vol% hexadecane emulsions prepared at pH 9 in 0.4 mM $NaClO_4$ (■), NaI (●), or NaCl (▲) solutions.

When the surfactant sodium dodecylsulfate (SDS) is added to a hexadecane emulsion at pH 9 the pH rises, as SDS displaces the hydroxide ion from the surface, but the pH increase is not large enough to account for all of the adsorbed hydroxide ions. The implication is that some hydroxide ions remain on the surface in equilibrium with adsorbed SDS at pH 9–10. To test this hypothesis the pH-stat experiments were repeated in the presence of 2 mM SDS. In the presence of the surfactant the homogenization process is more efficient, and smaller droplets are produced with a consequently larger surface area (Figure 1). With both hexadecane and squalene a pH drop is still observed; the amount of base required to maintain the pH value amounts to a hydroxide surface charge density of -1.7 and $-1.6\,\mu C\,cm^{-2}$, respectively, consistent with the adsorption of some hydroxide ion on the SDS-stabilized surface.

The pH-stat experiments in the absence of surfactant demonstrate quantitatively that hydroxide ions charge and stabilize these oil-in-water emulsion droplets. This conclusion previously could only be inferred from the pH dependence of the zeta potential[6,17] and has been disputed by some authors.[12] The large surface area created by the relatively concentrated emulsion produces a measurable pH effect, and the size of this effect eliminates the possibility of contamination from trace impurities.

A similar pH dependence of the charge of the air/water interface has been observed in a number of studies and also attributed to preferential adsorption of hydroxide ion.[7,18–20] The present results require that the many experimental and theoretical studies[21] of the air/water and oil/water interfaces that have ignored this charge on the surface be re-evaluated.

Received: February 3, 2004
Revised: April 5, 2004 [Z53916]

Keywords: electroacoustics · emulsions · interfaces · zeta potential

[1] D. J. McClements, *Food Emulsions*, CRC, Boca Raton, FL, **1999**.
[2] B. P. Binks, *Modern Aspects of Emulsion Science*, The Royal Society of Chemistry, Cambridge, **1998**.
[3] J. C. Carruthers, *Trans. Faraday Soc.* **1938**, *34*, 300.
[4] W. Dickinson, *Trans. Faraday Soc.* **1941**, *37*, 140.
[5] J. Stachurski, M. Michalek, *J. Colloid Interface Sci.* **1996**, *184*, 433.
[6] K. G. Marinova, R. G. Alargova, N. D. Denkov, O. D. Velev, D. N. Petsev, I. B. Ivanov, R. P. Borwankar, *Langmuir* **1996**, *12*, 2045.
[7] C. Stubenrauch, R. von Klitzing, *J. Phys. Condens. Matter* **2003**, *15*, R1197.

 © 2004 Wiley-VCH Verlag GmbH & Co. KGaA, Weinheim

[8] R. W. O'Brien, D. W. Cannon, W. N. Rowlands, *J. Colloid Interface Sci.* **1995**, *173*, 406.
[9] T. Allen, *Particle Size Measurement*, *Vol. 1*, 5th ed., Chapman & Hall, London, **1997**.
[10] A. Goebel, K. Lunkenheimer, *Langmuir* **1997**, *13*, 369.
[11] IUPAC-NIST Solubility Database, National Institute of Standards and Technology, **1995**.
[12] E. Chibowski, A. Wiacek, *Surf. Sci. Ser.* **2002**, *106*, 893.
[13] R. J. Hunter, *Foundations of Colloid Science*, 2nd ed., Oxford University Press, Oxford, **2001**.
[14] J. Lyklema, *Fundamentals of Interface and Colloid Science*, *Vol. II*, Academic Press, London, **1995**.
[15] M. Boström, D. E. Williams, B. W. Ninham, *Phys. Rev. Lett.* **2001**, *87*, 168103.
[16] K. Kamogawa, M. Matsumoto, T. Kobayashi, T. Sakai, H. Sakai, M. Abe, *Langmuir* **1999**, *15*, 1913.
[17] B. Yang, H. Matsumura, H. Kise, K. Furusawa, *Langmuir* **2000**, *16*, 3160.
[18] D. Exerowa, *Kolloid Z. Z. Polym.* **1969**, *232*, 703.
[19] K. A. Karraker, C. J. Radke, *Adv. Colloid Interface Sci.* **2002**, *96*, 231.
[20] R. S. Schechter, A. Graciaa, J. Lachaise, *J. Colloid Interface Sci.* **1998**, *204*, 398.
[21] L. R. Pratt, A. Pohorille, *Chem. Rev.* **2002**, *102*, 2671.
[22] J. K. Beattie, A. M. Djerdjev, S. E. Gibb, *New J. Chem.* **2003**, *27*, 1433.

 © 2004 Wiley-VCH Verlag GmbH & Co. KGaA, Weinheim

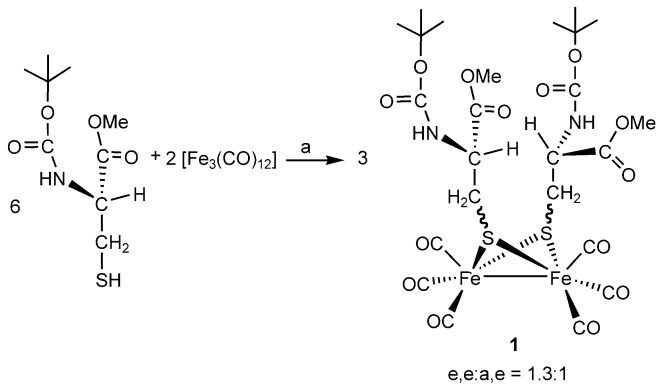
Bioinorganic Chemistry

An Unusual Cyclization in a Bis(cysteinyl-*S*) Diiron Complex Related to the Active Site of Fe-Only Hydrogenases**

Chengjiang He, Mei Wang, Xiaofeng Zhang, Zhen Wang, Changneng Chen, Jianhui Liu, Björn Åkermark, and Licheng Sun**

The recent unveiling of high-quality crystal structures of Fe-only hydrogenases isolated from *Desulfovibrio desulfuricans* and *Clostridium pasteurianum* has renewed interest in classical organometallic diiron dithiolate complexes, $[(\mu\text{-}SR)_2Fe_2(CO)_6]$ (R = Me, Et, $CH_2CH{=}CH_2$, Ph). Crystallographic studies have revealed that cysteinyl ligands exist in the active sites of [NiFe] and Fe-only hydrogenases. The active site of the [NiFe] hydrogenase from *Desulfovibrio gigas* has been established as a pyramidal $[Fe(CN)_2(CO)]$ unit with the face opposite the CN and CO ligands coordinated to two bridging cysteinyl ligands that connect the Fe and Ni moieties.[1,2] These [NiFe] dinuclear units are connected to their respective proteins by multiple cysteine residues. The H cluster of the Fe-only hydrogenase contains a single cysteinyl ligand that connects a [4Fe4S] subcluster to a dinuclear iron subcluster through a sulfur atom.[3–6] These maps of the active sites of the two major families of hydrogenase hint that the cysteinyl ligand is indispensable for H_2 production and uptake by the metal-containing hydrogenases. Although the synthesis and reactions of diverse dithiolate Fe^IFe^I hexacarbonyl compounds and their derivatives have attracted much attention,[7,8] no diiron carbonyl complex with cysteinyl ligands has been reported in the literature so far, despite the important function of the cysteinyl ligand in the H cluster. We are interested in the preparation of dinuclear iron complexes featuring one or two cysteinyl ligands with the aim of gaining an insight into the role of this amino acid in proton reduction by active-site model complexes.

The preparation of diiron dithiolate complexes by oxidative addition of thiols to iron(0) carbonyl compounds can be traced back more than half a century.[9] Many diiron complexes with the general formula $[(\mu\text{-}SR)_2Fe_2(CO)_6]$ can be obtained by using this traditional protocol.[10–13] Initial attempts to introduce two cysteinyl ligands to a dinuclear iron complex by treatment of $[Fe_3(CO)_{12}]$ with cysteine or its methyl ester were unsuccessful as the target product could not be separated from the resulting mixture by column chromatography. A protecting group (*tert*-butoxycarbonyl, Boc) was thus introduced at the amino group of the cysteine methyl ester. Treatment of the amino-protected L-cysteine ester with $[Fe_3(CO)_{12}]$ in refluxing MeOH for 1 h gave the predesigned diiron complex **1** as a dark-red crystalline product in about 30% yield (Scheme 1). The ^1H and ^{13}C NMR spectra of the product show that the bis(cysteinyl-*S*) diiron complex **1** obtained is a mixture of e,e (**1a**) and a,e (**1b**) isomers



Scheme 1. Synthesis of complex **1**. a) MeOH, reflux, 1 h, 30%.

[*] C. He, Prof. M. Wang, Z. Wang, Dr. J. Liu, Prof. L. Sun
State Key Laboratory of Fine Chemicals
Dalian University of Technology
Zhongshan Road 158-46, Dalian 116012 (P.R. China)
Fax: (+86) 411-8370-2185
E-mail: symbueno@dlut.edu.cn
X. Zhang, Prof. C. Chen
State Key Laboratory of Structural Chemistry
Fujian Institute of Research on the Structure of Matter
Fuzhou 350002 (P.R. China)
Prof. B. Åkermark, Prof. L. Sun
Department of Organic Chemistry
Arrhenius Laboratory
Stockholm University
10691 Stockholm (Sweden)
E-mail: licheng.sun@organ.su.se

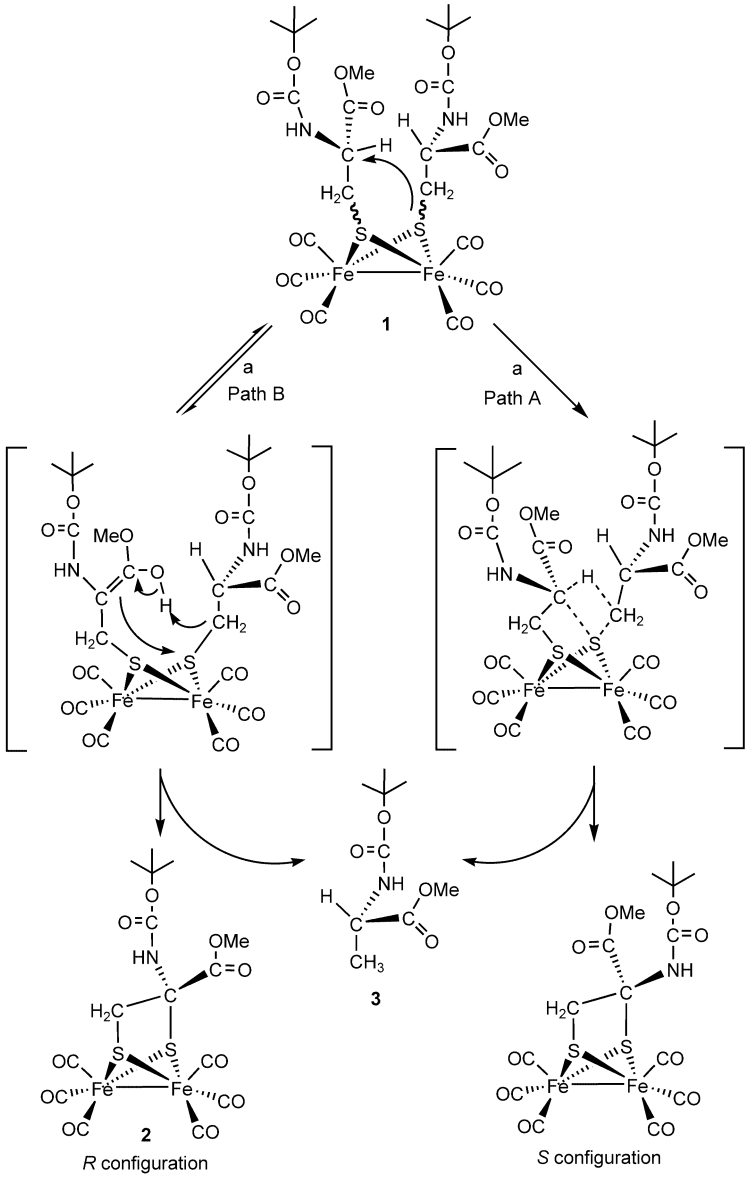
[**] Financial support for this work from the Ministry of Science and Technology of China and the Chinese National Natural Science Foundation (Grant nos. 20128005 and 20173006) is gratefully acknowledged.

 DOI: 10.1002/anie.200453961 © 2004 Wiley-VCH Verlag GmbH & Co. KGaA, Weinheim

(e, equatorial; a, axial). The e,e to a,e ratio is 1.3:1, as determined by integration of the ^{1}H NMR spectrum. This kind of geometrical isomerization, derived from the orientation of the α-C atom on the bridging thiolate, has been reported for $[(\mu\text{-}RS)_2Fe_2(CO)_6]$ complexes ($R = CH_3$, CH_2CH_3, $CH_2C_6H_5$) by King[9] and Seyferth.[14–18]

To the best of our knowledge, complex **1** is the first synthetic diiron carbonyl compound containing cysteinyl ligands. The complex is relatively stable in the solid state but is unstable in solution. When **1** was refluxed in MeOH for 30 h or in toluene and HOAc (2 equiv) for several hours, an unexpected intramolecular cyclization reaction occurred (Scheme 2). This reaction generated a two-carbon-bridged dithiolate diiron complex (**2**, yellow crystals) in about 5–12% yield by elimination of one equivalent of L-alanine methyl ester **3**, which has a Boc-protected amino group. The products were identified in solution by mass spectrometry. An uncharacterized precipitate and cysteinyl disulfide were also formed. The mechanism for this spontaneous intramolecular cyclization is not clear. One can imagine two paths for intramolecular cyclization of complex **1** in which one of the bridged sulfur atoms acts as a nucleophile (Scheme 2). The suggested nucleophilicity of the bridging sulfur atom is supported by the fact that S-alkylation of $[(\mu\text{-EDT})\{Fe(CO)_2(PMe_3)\}_2]$ (EDT = ethanedithiolato) with $EtOSO_2CF_3$ results in the formation of $[(\mu\text{-}SCH_2CH_2SEt)\{Fe(CO)_2(PMe_3)\}_2]^+[SO_3CF_3]^-$.[19] Both the paths shown in Scheme 2 lead to a chiral carbon-bridged diiron complex. In Path A, the sulfur atom attacks the stereogenic carbon atom from the side of the leaving hydrogen atom and the reaction proceeds through a transition state containing a four-membered ring. In Path B, an enolization takes place first, followed by an attack on the sulfur atom and displacement of an alanine derivative.

Although the details of the mechanism for this unprecedented intramolecular cyclization reaction are not clear, the molecular structure of the product **2** could be determined by X-ray crystallography.[20] The resulting structure is one of only a few well-characterized crystal structures of chiral carbon-bridged diiron complexes related to the active site of Fe-only hydrogenases.[21,22] Single-crystal X-ray diffraction studies of **2** show the typical butterfly framework of a 2Fe2S complex and the familiar pyramidal geometry around each iron atom (Figure 1). The Fe–Fe bond length (2.5101(8) Å) determined for **2** is comparable to the Fe–Fe bond lengths found in the structures of other SCH_2CHRS-bridged diiron hexacarbonyl complexes (Fe–Fe: R = H, 2.497(4); R = Me, 2.5196(7) Å).[22–24] The distance between the two bridging carbon atoms (C7–C8, 1.523(5) Å) is slightly longer in **2**



Scheme 2. Proposed pathway for the formation of complex **2**. a) MeOH, reflux, 30 h or HOAc (2 equiv), $CH_3C_6H_5$, reflux, 2 h; 5–12%.

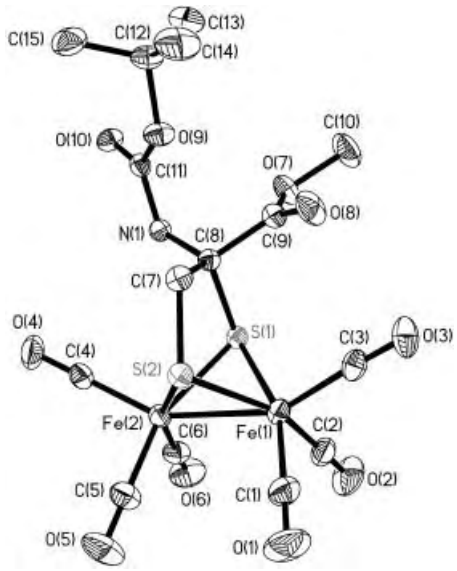


Figure 1. Molecular structure of **2** with thermal ellipsoids set at 30% probability. Selected bond lengths [Å]: Fe1–Fe2, 2.5101(8); Fe1–S1, 2.2359(10); Fe1–S2, 2.2410(11); S1–C8, 1.863(4); S2–C7, 1.823(4); C7–C8, 1.523(5); N1–C8, 1.453(4); C8–C9, 1.535(5). Selected bond angels [°]: Fe1–S1–Fe2, 68.24(3); C11–N1–C8, 122.8(3); C8–C7–S2, 113.4(3); C7–C8–S1, 110.1(2); C7–C8–C9, 111.4(3); C9–C8–S1, 104.6(2); N1–C8–C7, 113.6(3); N1–C8–C9, 111.7(3); N1–C8–S1, 105.0(2).

 © 2004 Wiley-VCH Verlag GmbH & Co. KGaA, Weinheim

than in the analogues complex $[(\mu\text{-}SCH_2CHRS)Fe_2(CO)_6]$ (bridging C–C: R = H, 1.487(6); R = Me, 1.496(6) Å). The reported mirror symmetry of $[(\mu\text{-}SCH_2CHRS)Fe_2(CO)_6]$ (R = H, Me)[22–24] in the plane defined by S1, S2, C7, and C8 is not present in **2**. The C8–C7–S2 bond angle in **2** is larger than the C7–C8–S1 angle by 3.3°. The most noteworthy characteristic of the crystal structure of **2** is that the stereogenic carbon atom in the bridge has an *R* configuration. In the light of the *R* configuration of the L-cysteine reactant, this structural result suggests that the bridging sulfur atom attacks the methine group while the C–H bond cleaves heterolytically, then the intramolecular cyclization reaction takes place with a turnover of the stereogenic carbon atom, that is, with an inversion of the configuration. An enolization mechanism (Scheme 2, Path B) would lead to a chiral carbon-bridged diiron complex mainly with the *R* configuration, while a concerted mechanism (Scheme 2, Path A) would be stereoselective for a chiral diiron product with an *S* configuration. The C11–N1 bond in the bridged-cysteinyl ligand is in an axial orientation, which avoids significant congestion of the ligands. A dimer of **2** in the solid state is formed by intermolecular H bonding of two amido groups (N(1)···O(10), 2.890(4) Å; symmetry: $-x+1, -y, -z+1$; Figure 2).

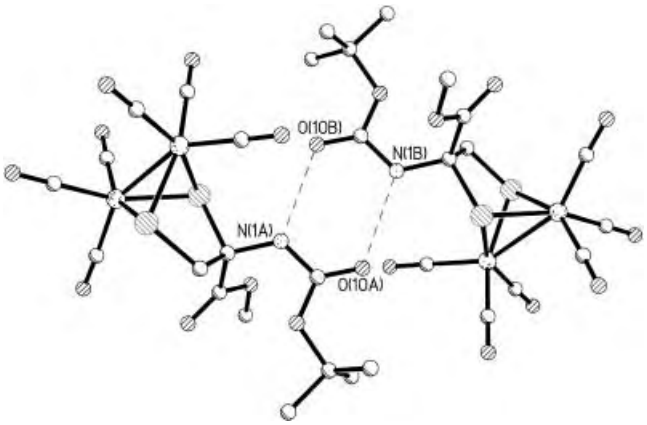


Figure 2. Plot of the unit cell of **2**. The dotted lines represent H bonds between the N1 and O10 atoms of the two molecules.

In conclusion, a dinuclear iron complex (**1**) containing two protected cysteinyl ligands was prepared by the classical oxidative addition of thiols to $[Fe_3(CO)_{12}]$. An unusual intramolecular cyclization reaction of **1** gave the chiral carbon-bridged diiron complex **2**, whose structure is related to that of the active site of Fe-only hydrogenases. The molecular structure of **2** was determined by X-ray crystallography and suggests that the unprecedented nucleophilic cyclization reaction occurs with a inversion of configuration.

Experimental Section

1: *N*-Boc-protected L-cysteine methyl ester (0.75 mL, 5.70 mmol, 7.5 M in $CHCl_3$) was added dropwise to a solution of $[Fe_3(CO)_{12}]$ (1.0 g, 1.98 mmol) in MeOH (20 mL). The mixture was refluxed for 1 h, which resulted in formation of a dark-red solution. The solvent was evaporated in vacuo and the residue was chromatographed on an Al_2O_3 column with hexane/CH_2Cl_2 (1:10) as the eluent. Recrystallization of the crude product in hexane/CH_2Cl_2 gave **1** as dark red crystals (640 mg). Yield: 30%; elemental analysis (%): calcd for $C_{24}H_{32}Fe_2N_2O_{14}S_2$: C, 38.52, H, 4.31, N, 3.74; found: C, 38.73, H, 4.48, N, 3.81; ^{1}H NMR (400 MHz, $CDCl_3$): $\delta = 1.47$ (s, 18H; *t*Bu), 2.38, 2.50, 2.83 (3 × m, 4H; SCH_2), 3.78 (s; OCH_3, a,e), 3.83 (s; OCH_3, e,e), 3.85 (s, 6H; OCH_3, 57% e,e, 43% a,e), 4.39, 4.63 (2 × m, 2H; CH), 5.17, 5.42 ppm (d, 2H; NH); ^{13}C NMR (400 MHz, $CDCl_3$): $\delta = 28.40$, 29.46 (2 × s; CH_3 of *t*Bu), 39.47, 40.88 (2 × s; SCH_2), 53.11, 54.17, 54.39 (3 × s; OCH_3), 80.56, 80.72 (2 × s; CH), 105.32 (s; C of *t*Bu), 154.92, 155.04 (2 × s; CONH), 170.15, 170.38, 170.69 (3 × s; COO), 207.86, 208.03, 208.83 ppm (3 × s; CO); IR (CH_2Cl_2): $\tilde{\nu} = 2073, 2036, 1994$ (CO), 1745, 1716 cm^{-1} (C=O); ESI MS (*m*/*z*): 770.9 (100%) $[M+Na]^+$.

2: Either a mixture of $[Fe_3(CO)_{12}]$ and *N*-Boc-protected L-cysteine methyl ester or a solution of **1** in MeOH was refluxed for 30 h to give a dark-orange solution. Complex **2** was isolated by chromatography on silica gel with MeOH/CH_2Cl_2 (2:98 v/v) as the eluent. The first yellow band was collected and the solvent was removed in vacuo. The residue was crystallized by defusing hexane into a solution of the residue in CH_2Cl_2. Yield: 5–12%; ^{1}H NMR (400 MHz, $CDCl_3$): $\delta = 1.46$ (s, 9H; *t*Bu), 2.65–3.08 (br s, 2H; SCH_2), 3.76 (s, 3H; OCH_3), 5.50 ppm (s, 1H; NH); IR (CH_2Cl_2): $\tilde{\nu} = 2085$ (w), 2075 (w), 2058 (m), 2042 (s), 1996 (s) (CO), 1743, 1718 cm^{-1} (C=O); TOF-ESI MS (*m*/*z*): calcd for $[M+Na]^+$: 567.8734; found: 567.8735 (100%).

Received: February 6, 2004
Revised: April 13, 2004 [Z53961]

Keywords:
S ligands · cyclization · enzyme models · iron hydrogenases · structure elucidation

[1] M. W. W. Adams, E. I. Stiefel, *Curr. Opin. Chem. Biol.* **2001**, *5*, 214–220.
[2] M. Frey, *ChemBioChem* **2002**, *3*, 153–160.
[3] Y. Nicolet, C. Piras, P. Legrand, C. E. Hatchikian, J. C. Fontecilla-Camps, *Structure* **1999**, *7*, 13–23.
[4] J. W. Peters, W. N. Lanzilotta, B. J. Lemon, L. C. Seefeldt, *Science* **1998**, *282*, 1853–1858.
[5] R. Cammack, *Nature* **1999**, *397*, 214–215.
[6] Y. Nicolet, B. J. Lemon, J. C. Fontecilla-Camps, J. W. Peters, *Trends Biochem. Sci.* **2000**, *25*, 138–143.
[7] M. Y. Darensbourg, E. J. Lyon, J. J. Smee, *Coord. Chem. Rev.* **2000**, *206–207*, 533–561.
[8] D. J. Evans, C. J. Pickett, *Chem. Soc. Rev.* **2003**, *32*, 268–275.
[9] R. B. King, *J. Am. Chem. Soc.* **1962**, *84*, 2460.
[10] J. A. Beer, R. J. Haines, *J. Organomet. Chem.* **1970**, *24*, 757–767.
[11] N. S. Nametkin, V. D. Tyurin, M. A. Kukina, *J. Organomet. Chem.* **1978**, *149*, 355–370.
[12] X. Zhao, Y. M. Hsiao, C. H. Lai, J. H. Reibenspies, M. Y. Darensbourg, *Inorg. Chem.* **2002**, *41*, 699–708.
[13] A. Winter, L. Zsolnai, G. Huttner, *Z. Naturforsch. B* **1982**, *37*, 1430–1436.
[14] L. F. Dahl, C. H. Wei, *Inorg. Chem.* **1963**, *2*, 328–333.
[15] G. Bor, *J. Organomet. Chem.* **1968**, *11*, 195–197.
[16] G. L. Borgne, D. Grandjean, *J. Organomet. Chem.* **1977**, *131*, 429–438.
[17] D. Seyferth, R. S. Henderson, *J. Organomet. Chem.* **1981**, *218*, C34–C36.
[18] D. Seyferth, R. S. Henderson, L. C. Song, *Organometallics* **1982**, *1*, 125–133.
[19] X. Zhao, C. Y. Chiang, M. L. Miller, M. V. Rampersad, M. Y. Darensbourg, *J. Am. Chem. Soc.* **2003**, *125*, 518–524.
[20] Crystal data for **2**: $C_{15}H_{15}Fe_2NO_{10}S_2$, $M_r = 545.10$; triclinic; space group $P\bar{1}$; $a = 7.6905(4)$, $b = 12.4367(6)$, $c = 13.3307(7)$ Å, $\alpha =$

 © 2004 Wiley-VCH Verlag GmbH & Co. KGaA, Weinheim

64.253(1), $\beta = 79.414(1)$, $\gamma = 89.292(1)°$, $V = 1125.6(1)$ Å^3; $\rho_{calcd} = 1.608$ g m^{-3}; $\mu = 1.523$ mm^{-1}; $T = 293(2)$ K; $Z = 2$; $R_1 = 0.0435$ and $wR_2 = 0.1037$ for 3373 reflections with $I > 2\sigma(I)$. CCDC-224401 (**2**) contains the supplementary crystallographic data for this paper. These data can be obtained free of charge via www.ccdc.cam.ac.uk/conts/retrieving.html (or from the Cambridge Crystallographic Data Centre, 12 Union Road, Cambridge CB21EZ, UK; fax: (+44) 1223-336-033; or deposit@ccdc.cam.ac.uk).

[21] D. Seyferth, G. B. Womack, R. S. Henderson, *Organometallics* **1986**, *5*, 1568 – 1575.

[22] Q. Q. Zhang, R. S. Dickson, G. D. Fallon, R. Mayadunne, *J. Organomet. Chem.* **2001**, *627*, 201 – 205.

[23] D. L. Hughes, G. J. Leigh, D. R. Paulson, *Inorg. Chim. Acta* **1986**, *120*, 191 – 195.

[24] J. Messelhäuser, I. Lorenz, K. Huag, W. Hiller, *Z. Naturforsch. B* **1985**, *40*, 1064 – 1067.

 © 2004 Wiley-VCH Verlag GmbH & Co. KGaA, Weinheim

Copolymerization

Highly Active, Binary Catalyst Systems for the Alternating Copolymerization of CO_2 and Epoxides under Mild Conditions**

Xiao-Bing Lu and Yi Wang*

Chemical fixation of CO_2 is of great interest with respect to the development of truly environmentally benign processes, as there are many possibilities for CO_2 to be used as a safe and cheap C_1 feedstock in organic synthesis.[1] One of the most promising reactions in this area is the alternating copolymerization of CO_2 and epoxides to polycarbonates,[2] which was first reported by Inoue et al.[3] These polycarbonates not only exhibit interesting material properties, but also have the additional environmental advantages resulting from their biodegradability.[4] In recent decades, numerous catalyst systems have been developed for this transformation.[5] Although the advances have been significant, high catalyst loading, elevated CO_2 pressure, and long reaction time are usually prerequisites for obtaining appreciable amounts of polymer, which are often not perfectly alternating and exhibit broad molecular-weight distributions. Recently, several efficient catalyst systems for the copolymerization of CO_2 and alicyclic epoxides such as cyclohexene oxide have been reported to offer significant advantages over traditional heterogeneous catalysts.[6–12] Unfortunately, these catalysts do not readily polymerize CO_2 and aliphatic epoxides such as propylene oxide (PO). Recently, Coates and co-workers[13] reported the first highly active zinc β-diiminate catalysts bearing electron-withdrawing groups for the synthesis of poly(propylene carbonate) (PPC) with carbonate linkages up to 99%, but along with the formation of cyclic propylene carbonate (PC; 7–25%). A simple decrease in temperature and increase in CO_2 pressure suppressed the formation of PC and increased the selectivity for PPC. A similar effect was reported by Darensbourg and co-workers, who used chiral salen chromium chloride, alone or in conjunction with *N*-methylimidazole as a catalyst, for this reaction.[14] Herein, we report the use of a highly active binary catalyst system, which consists of a chiral cobalt complex [(salcy)Co^{III}X] and a quaternary ammonium salt ($n$$Bu_4$NY) for completely alternating copolymerization of CO_2 and aliphatic epoxides under extremely mild conditions.

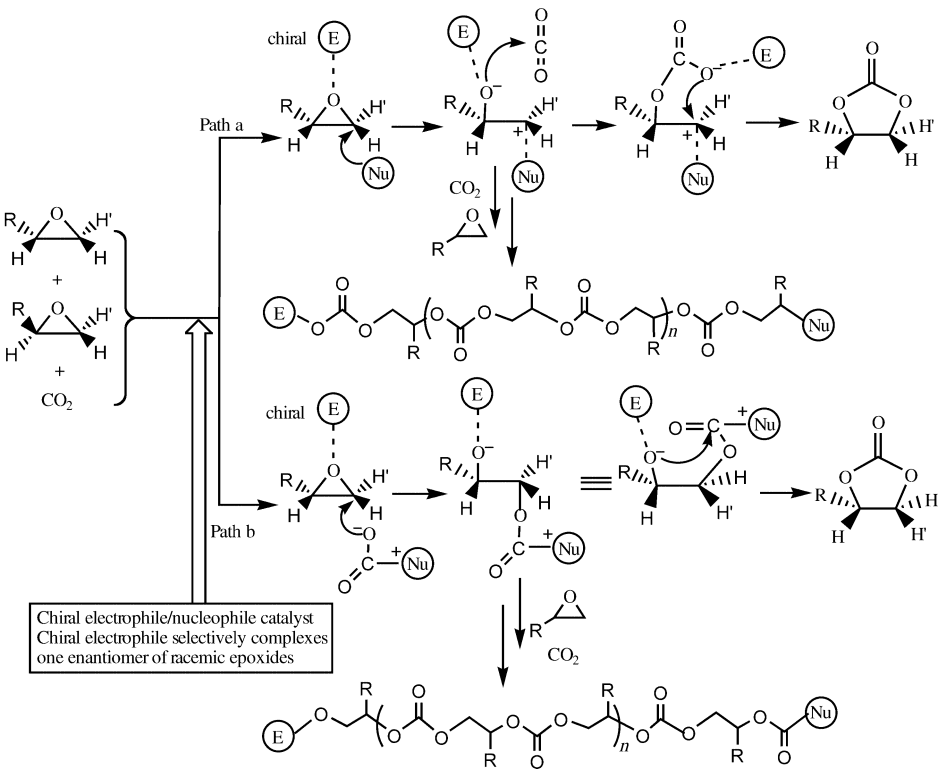
Pursuant to our own efforts toward the development of highly efficient catalysts for coupling CO_2 with epoxides under mild conditions,[15] we became interested in the possibility of developing catalyst systems for the direct synthesis of optically active cyclic carbonates from racemic epoxides, which are inexpensive or easily accessible from inexpensive commercial starting materials. Based on the fact that chiral [(salcy)Co^{III}] complexes (Jacobsen catalyst) were shown to be highly efficient and enantioselective catalysts for the hydrolytic kinetic resolution of terminal epoxides,[16] we recently designed a bifunctional nucleophile–electrophile catalyst system consisting of chiral [(salcy)Co^{III}] complexes and quaternary ammonium salts for the direct synthesis of optically active cyclic carbonates from racemic epoxides.[17] In this system, the chiral [(salcy)Co^{III}] complex was proposed to serve as an electrophile for selectively complexing one enantiomer of the racemic epoxides, and the anion of the quaternary ammonium salt serves as a nucleophile. The regioselective attack of a nucleophile or activated CO_2 at the coordinated epoxide on the less substituted carbon atom leads to enantioselective ring opening of the epoxide with subsequent formation of the chiral cyclic carbonates through intermolecular cyclic elimination (Scheme 1). We were delighted to find that the solvent-free reaction of racemic PO (0.2 mol) with CO_2 in the presence of [(salcy)-$Co^{III}(O_2CCCl_3)$] (**1b**; 0.05 mol%) as a chiral electrophile in conjunction with $n$$Bu_4$NBr (0.05 mol%) as nucleophile proceeded within 3 h at room temperature and 2.0 MPa pressure to afford a mixture of unconverted PO and PC with moderate enantioselectivity (Table 1, entry 2), along with a small quantity of PPC. To our surprise, the resulting PPC shows $>99\%$ carbonate linkage in the ^{1}H NMR spectrum. Further investigation showed that simple changes in the axial group X of chiral [(salcy)Co^{III}X] and the anion Y of $n$$Bu_4$NY drastically affect the PPC/PC selectivity (Table 1, entries 1–8). It seems that the use of a cobalt complex with an electron-withdrawing axial group X and a quaternary ammonium salt, whose anion exhibits poor leaving ability, increases the selectivity for PPC. For example, in the presence of $n$$Bu_4$NBr cocatalyst, a change in the axial group X of chiral [(salcy)Co^{III}X] from acetate to dinitrophenol resulted in an increase in the selectivity of PPC

[*] Dr. X.-B. Lu, Y. Wang
State Key Laboratory of Fine Chemicals
Dalian University of Technology
Dalian 116012 (P. R. China)
Fax: (+86) 411-8363-3080
E-mail: lxb-1999@163.com

[**] Gratitude is expressed to the National Science Foundation of China (NSFC) program (Grant 20204002) and the Science Foundation of Liaoning Province (Grant 20031074) for financial support.

Supporting information for this article (experimental procedures and characterization of polymers) is available on the WWW under http://www.angewandte.org or from the author.

 © 2004 Wiley-VCH Verlag GmbH & Co. KGaA, Weinheim DOI: 10.1002/anie.200453998



Scheme 1. A bifunctional nucleophile–electrophile catalyst system for the direct synthesis of enantiomerically pure cyclic carbonates or linear polycarbonates from racemic epoxides and CO_2.

from 3 to 78%. On the other hand, with complex **1d** as catalyst, a change in the anion of cocatalyst nBu$_4$NY from Br^- to Cl^- or CH_3COO^- resulted in an increase in the selectivity for PPC from 78 to 99%. The results may be explained in terms of greater advantages for producing linear polycarbonates by successive insertion of CO_2/epoxide towards the M–O bond as compared with the formation of cyclic carbonates by intermolecular cyclic elimination (Scheme 1) in the catalyst systems that consist of a strong electrophile in conjunction with a nucleophile with poor leaving ability. Notably, these binary catalyst systems based on chiral [{(1*R*,2*R*)-(*t*Bu)$_2$salcy}CoX] complexes all preferentially consume (*S*)-PO over (*R*)-PO with $K_{rel} = 2.8$–3.5. Notably, these cobalt complexes or quaternary ammonium salts by themselves show no (or only very low) catalytic activity under the conditions employed. Interestingly, the binary catalyst systems are inactive for the homopolymerization of PO over 1 day.

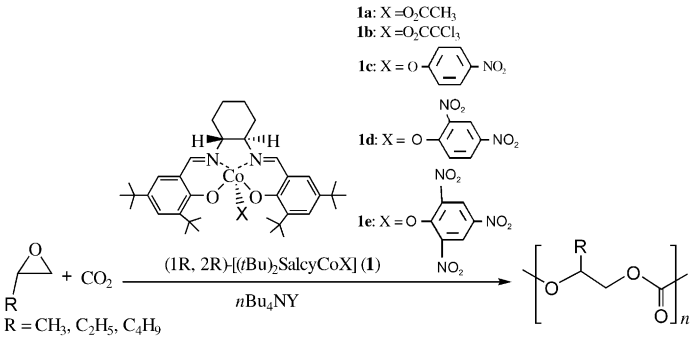
A significant drawback in the use of CO_2 as a reagent in organic synthesis is the potential danger associated with operating at high temperatures and pressures. Prior to the present work, Coates et al. reported the first discrete cobalt complexes alone as catalysts for the copolymerization of CO_2 and PO, but these complexes are inactive at low CO_2 pressures.[18] We were gratified to discover that the binary catalyst system can operate very efficiently at low temperatures and with CO_2 at atmospheric pressure. The highest activity occurs at 1.0–2.0 MPa and is maintained at 50% of the optimum TOF at only 0.2 MPa. An increase in the pressure beyond the optimal range results in a dramatic decrease in activity. Interestingly, the variation of CO_2 pressure does not lead to an observable decrease in selectivity for PPC formation. In contrast, in the presence of [(bdi)-ZnOAc] catalyst (bdi = β-diiminate),[13] an increase in the pressure of CO_2 is beneficial for suppressing PC formation and effectively increases the selectivity for polymer while moderately decreasing the catalyst activity for PPC formation. Surprisingly, a change in the reaction temperature from 25 to 40 °C, only significantly affects the activity of the catalyst, rather than the selectivity for PPC formation (Table 1, entry 16).

All the isolated polymers have narrow molecular-weight distributions, consistent with controlled polymerization; however, the M_n values are not close to the expected values, which indicates the existence of chain transfer during the reaction. The ^{1}H NMR spectra of all PPCs produced show >99% carbonate linkages, and the ^{13}C NMR spectra show that these polymers have an unprecedented head-to-tail content of >95% (Figure 1). Such a microstructure is consistent with a highly stereoselective ring opening of PO, and is in contrast to polymers prepared in the presence of zinc glutarate[19] (~60% head-to-tail linkages) and [(bdi)ZnOAc] (~54% head-to-tail linkages). Also, the catalyst system was found to be applicable to other aliphatic epoxides, providing the corresponding polycarbonates with >99% carbonate linkages (Table 1, entries 17 and 18).

In summary, chiral [(salcy)Co^{III}X] in conjunction with a quaternary ammonium salt is a highly efficient catalyst for the copolymerization of CO_2 with epoxides under extremely mild temperatures and pressures to afford the corresponding completely alternating copolymers with >95% head-to-tail

 © 2004 Wiley-VCH Verlag GmbH & Co. KGaA, Weinheim

Table 1: CO_2/Epoxides copolymerization results.[a]



Entry	1	Y	Epoxide	t [h]	P [MPa]	TOF[b] [h^{-1}]	Selectivity[c] [% PPC]	Carbonate linkages [%][c]	M_n[d] [g mol^{-1}]	PDI (M_w/M_n)	K_{rel}[e]
1	**a**	Br	PO	3	2.0	228	3	>99	–[f]	–[f]	3.9
2	**b**	Br	PO	3	2.0	264	6	>99	–[f]	–[f]	4.7
3	**d**	Br	PO	3	2.0	289	78	>99	23500	1.29	3.2
4	**d**	Cl	PO	3	2.0	257	99	>99	30400	1.36	3.4
5	**d**	I	PO	3	2.0	272	69	>99	22100	1.34	2.8
6	**d**	OAc	PO	3	2.0	167	99	>99	18200	1.23	3.1
7	**c**	Cl	PO	3	2.0	185	96	>99	21000	1.48	2.9
8	**e**	Cl	PO	3	2.0	248	99	>99	27500	1.43	3.0
9	**d**	–	PO	24	2.0	2	95	>99	–[f]	–[f]	–[f]
10	–	Cl	PO	24	2.0	<1	0	–[f]	–[f]	–[f]	–[f]
11	**d**	Cl	PO	3	0.2	130	98	>99	18200	1.29	3.2
12	**d**	Cl	PO	3	0.4	190	99	>99	28300	1.31	3.5
13	**d**	Cl	PO	3	1.0	243	99	>99	29900	1.41	3.3
14	**d**	Cl	PO	3	4.0	219	99	>99	28700	1.42	3.3
15	**d**	Cl	PO	3	6.0	173	99	>99	25500	1.33	3.4
16[g]	**d**	Cl	PO	3	4.0	371	99	>99	24000	1.37	2.8
17	**d**	Cl	1,2-BuO[h]	6	2.0	61	99	>99	11600	1.26	–[f]
18[g]	**d**	Cl	1,2-HO[i]	8	2.0	48	98	>99	7300	1.11	–[f]

[a] The reaction was carried out with neat epoxide (14 mL, 200 mmol; catalyst/co-catalyst/epoxide = 1:1:2000) at 25 °C, unless otherwise noted. [b] Turnover frequency of epoxide to products (polycarbonate and cyclic carbonate). [c] Determined by using ^{1}H NMR spectroscopy. [d] Determined by means of gel permeation chromatography in THF at 35 °C, calibrated with polystyrene standards. [e] $K_{rel} = \ln[1-c(1+ee)]/\ln[1-c(1-ee)]$; c = conversion, ee = enantiomeric excess of unconverted epoxide. [f] Not applicable. [g] 40 °C. [h] 1,2-Butene oxide. [i] 1,2-hexene oxide.

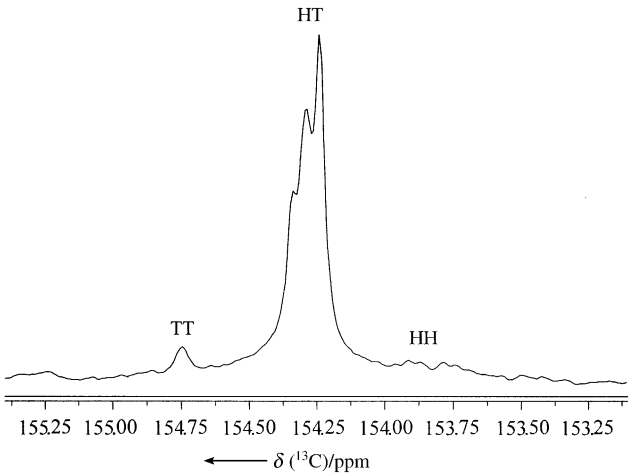


Figure 1. The carbonyl region of the ^{13}C NMR spectrum of a representative sample of poly(propylene carbonate) (PPC).

linkages. To our knowledge, these binary catalyst systems exhibit the highest reported activities for PO/CO_2 copolymerization. Furthermore, they offer unprecedented opportunities for controlling the regio- and stereochemistry of copolymerization. Further studies are focused on elucidating the catalytic mechanism and developing new bifunctional nucleophile–electrophile catalyst systems that exhibit higher regio- and stereoselectivity for epoxide ring opening in CO_2/epoxide copolymerization.

Received: February 11, 2004 [Z53998]

Keywords: carbon dioxide fixation · copolymerization · epoxides · homogeneous catalysis · polycarbonates

[1] For selected reviews, see: a) A. Behr, *Angew. Chem.* **1988**, *100*, 681–698; *Angew. Chem. Int. Ed. Engl.* **1988**, *27*, 661–678; b) W. Leitner, *Coord. Chem. Rev.* **1996**, *153*, 257–284; c) X. L. Yin, J. R. Moss. *Coord. Chem. Rev.* **1999**, *181*, 27–59; d) D. Walther, M. Ruben, S. Rau, *Coord. Chem. Rev.* **1999**, *182*, 67–100; e) H. Arakawa, M. Aresta, J. N. Armor, M. A. Barteau, E. J. Beckman, A. T. Bell, J. E. Bercaw, C. Creutz, E. Dinjus, D. A. Dixon, K. Domen, D. L. DuBois, J. Eckert, E. Fujita, D. H. Gibson,

 © 2004 Wiley-VCH Verlag GmbH & Co. KGaA, Weinheim

W. A. Goddard, D. W. Goodman, J. Keller, G. J. Kubas, H. H. Kung, J. E. Lyons, L. E. Manzer, T. J. Marks, K. Morokuma, K. M. Nicholas, R. Periana, L. Que, J. Rostrup-Nielson, W. M. H. Sachtler, L. D. Schmidt, A. Sen, G. A. Somorjai, P. C. Stair, B. R. Stults, W. Tumas, *Chem. Rev.* **2001**, *101*, 953 – 996.
[2] E. J. Beckman, *Science* **1999**, *283*, 946 – 947.
[3] S. Inoue, H. Koinuma, T. Tsuruta, *J. Polym. Sci. Polym. Lett. Ed.* **1969**, *7*, 287 – 292; b) S. Inoue, H. Koinuma, T. Tsuruta, *Makromol. Chem.* **1969**, *130*, 210 – 220.
[4] a) S. Y. Yang, X. G. Fang, L. B. Chen, *Polym. Adv. Technol.* **1996**, *7*, 605 – 608; b) M. Okada, *Prog. Polym. Sci.* **2002**, *27*, 87 – 133.
[5] For reviews on CO_2/epoxides copolymerization, see: a) A. Rokicki, W. Kuran, *J. Macromol. Sci. Rev. Macromol. Chem. Phys.* **1981**, *21*, 135 – 186; b) D. J. Darensbourg, M. W. Holtcamp, *Coord. Chem. Rev.* **1996**, *153*, 155 – 174; c) M. S. Super, E. Beckman, *Trends Polym. Sci.* **1997**, *5*, 236 – 240; d) W. Kuran, *Prog. Polym. Sci.* **1998**, *23*, 919 – 992.
[6] M. Super, E. Berluche, C. Costello, E. Beckman, *Macromolecules* **1997**, *30*, 368 – 372.
[7] M. Cheng, E. B. Lobkovsky, G. W. Coates, *J. Am. Chem. Soc.* **1998**, *120*, 11 018 – 11 019.
[8] T. Sârbu, E. J. Beckman, *Macromolecules* **1999**, *32*, 6904 – 6912.
[9] D. J. Darensbourg, J. R. Wildeson, J. C. Yarbrough, J. H. Reibenspies, *J. Am. Chem. Soc.* **2000**, *122*, 12 487 – 12 496.
[10] S. Mang, A. I. Cooper, M. E. Colclough, N. Chauhan, A. B. Holmes, *Macromolecules* **2000**, *33*, 303 – 308.
[11] M. Cheng, D. R. Moore, J. J. Reczek, B. M. Chamberlain, E. B. Lobkovsky, G. W. Coates, *J. Am. Chem. Soc.* **2001**, *123*, 8738 – 8749.
[12] D. R. Moore, M. Cheng, E. B. Lobkovsky, G. W. Coates, *Angew. Chem.* **2002**, *114*, 2711 – 2714; *Angew. Chem. Int. Ed.* **2002**, *41*, 2599 – 2602.
[13] S. D. Allen, D. R. Moore, E. B. Lobkovsky, G. W. Coates, *J. Am. Chem. Soc.* **2002**, *124*, 14 284 – 14 285.
[14] a) D. J. Darensbourg, J. C. Yarbrough, *J. Am. Chem. Soc.* **2002**, *124*, 6335 – 6342; b) D. J. Darensbourg, J. C. Yarbrough, C. Ortiz, C. C. Fang, *J. Am. Chem. Soc.* **2003**, *125*, 7586 – 7591.
[15] X. B. Lu, Y. J. Zhang, B. Liang, X. Li, H. Wang, *J. Mol. Catal. A* **2004**, *210*, 31 – 34.
[16] a) M. Tokunaga, J. F. Larrow, F. Kakiuchi, E. N. Jacobsen, *Science* **1997**, *277*, 936 – 938; b) D. A. Annis, E. N. Jacobsen, *J. Am. Chem. Soc.* **1999**, *121*, 4147 – 4154; c) S. E. Schaus, B. D. Brandes, J. F. Larrow, M. Tokunaga, K. B. Hansen, A. E. Gould, M. E. Furrow, E. N. Jacobsen, *J. Am. Chem. Soc.* **2002**, *124*, 1307 – 1315; d) E. N. Jacobsen, *Acc. Chem. Res.* **2000**, *33*, 421 – 431.
[17] X. B. Lu, B. Liang, Y. J. Zhang, Y. Z. Tian, Y. M. Wang, C. X. Bai, H. Wang, R. Zhang, *J. Am. Chem. Soc.* **2004**, *126*, 3732 – 3733.
[18] Z. Qin, C. M. Thomas, S. Lee, G. W. Coates, *Angew. Chem.* **2003**, *115*, 5642 – 5645; *Angew. Chem. Int. Ed.* **2003**, *42*, 5484 – 5487.
[19] M. H. Chisholm, D. Navarro-Llobet, Z. Zhou, *Macromolecules* **2002**, *35*, 6494 – 6504.

 © 2004 Wiley-VCH Verlag GmbH & Co. KGaA, Weinheim

Self-Assembly

A Dodecameric Water Cluster Built around a Cyclic Quasiplanar Hexameric Core in an Organic Supramolecular Complex of a Cryptand**

*Sujit K. Ghosh and Parimal K. Bharadwaj**

The fundamental importance of water in many biological, chemical, and physical processes has prompted intensive research efforts, but it is still not a fully understood liquid. Hydrogen-bonding interactions and their fluctuations are known[1] to determine the properties of water, some of which are regarded as "anomalous". However, the complexities involved in describing these interactions correctly have been a major stumbling block. Therefore, structural data of hydrogen-bonded water clusters in organic molecular crystals within inorganic–organic hybrid frameworks are very important for correctly describing the association of water molecules in different surroundings. This realization has led to theoretical[2–9] and experimental[10–22] studies of a number of small water clusters. The structural possibilities associated with the hexamer is quite extensive and theoretical calculations[23] have shown several local minima on the potential energy surface that correspond to a number of cyclic structural isomers. Out of these, the five low-energy ones, namely, "cage", "prism", "book", "boat", and "cycle" are almost isoenergetic (that is, within ca. 0.7 kcal mol^{-1}). The "cage" structure is the most stable conformation at very low temperature. The lattice of a crystalline host, on the other hand, may offer an environment for stabilizing a higher-energy hexamer. To date, chair,[15,19,24] boat,[17,19] and planar[18] forms have been characterized in crystalline hosts. The planar ring is the basic structural motif found in the ice II structure[25] under high pressure. This is also a prominent structural unit[26] in liquid water as determined by computer simulations. Recently, Nauta and Miller detected[13] the "quasiplanar" hexamer within a helium droplet.

Organic compounds with functional groups similar to those present in biological molecules can stabilize water clusters of different sizes and shapes in environments resembling living systems.[27] Herein, we report the X-ray structure of a hitherto unknown dodecameric water cluster built around a quasiplanar $(H_2O)_6$ unit in an organic supramolecular complex of a laterally nonsymmetric cryptand. A ring of twelve hydrogen-bonded water molecules was reported[28]

[*] S. K. Ghosh, Prof. Dr. P. K. Bharadwaj
Chemistry Department
Indian Institute of Technology Kanpur
Kanpur 208016 (India)
Fax: (+91) 512-259-7436
E-mail: pkb@iitk.ac.in

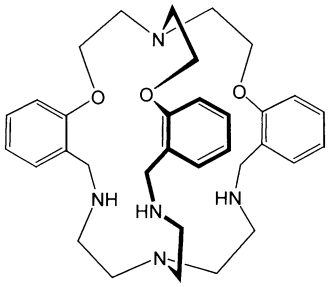
[**] Financial support from the Department of Science and Technology, New Delhi, India (grant No. SR/S5/NM-38/2003 to P.K.B.) and an SRF grant (CSIR) to S.K.G. are gratefully acknowledged.

Supporting information for this article is available on the WWW under http://www.angewandte.org or from the author.

 DOI: 10.1002/anie.200454002 © 2004 Wiley-VCH Verlag GmbH & Co. KGaA, Weinheim

earlier in an inorganic framework. Theoretical calculations on the dodecamer have revealed[29] the existence of several low-energy structures with fused cubic geometry. Other structures with slightly higher energy include cagelike structures containing four- or five-membered rings and two high-symmetry ones with two six-membered rings and six four-membered rings.

Previously, we found that the cryptand **L** (Scheme 1) crystallizes[30] from organic solvents such as acetone or acetonitrile without any association among the cryptand



L

Scheme 1. The laterally nonsymmetric azacryptand **L**.

molecules. However, it is clear that the secondary amines present in the three cryptand strands can potentially act as hydrogen-bond acceptors or donors. Compound **1** was isolated as colorless hexagonal crystals[31] from an aqueous solution of **L** in acetonitrile in the presence of pyridine vapor. Each cryptand molecule binds one H_2O molecule inside the cavity and three H_2O molecules outside (Figure 1) through hydrogen-bonding interactions. The water molecule (Ow3) inside the cavity is within hydrogen-bonding distance from the ethereal O atoms as well as the secondary amino N atoms in the three cryptand strands. The H atoms attached to Ow3 could not be located in the difference map probably because they were disordered. The H_2O molecule bonded outside

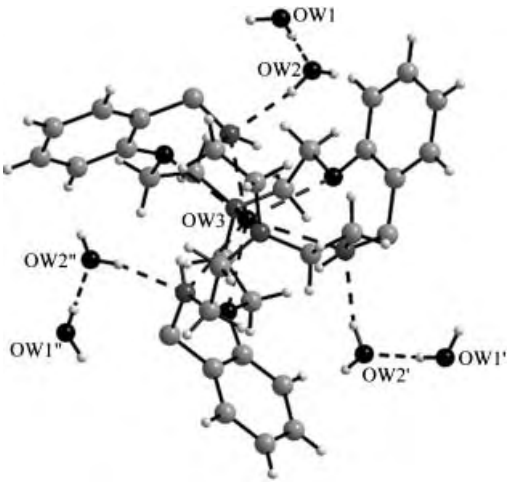


Figure 1. The mode of binding of water molecules with **L** viewed along the pseudo threefold axis of the cryptand.

(Ow2) acts as a hydrogen-bond donor to one of the secondary amino nitrogen atoms of the cryptand with a N···O distance of 2.79 Å. The Ow2 molecule also acts as a hydrogen-bond donor to Ow1, with a nonbonding distance of 2.82 Å. Six such units combine to make a quasiplanar cyclic hexameric core attached to six other water molecules at the periphery to form an overall dodecameric cluster (Figure 2). The O atoms at the

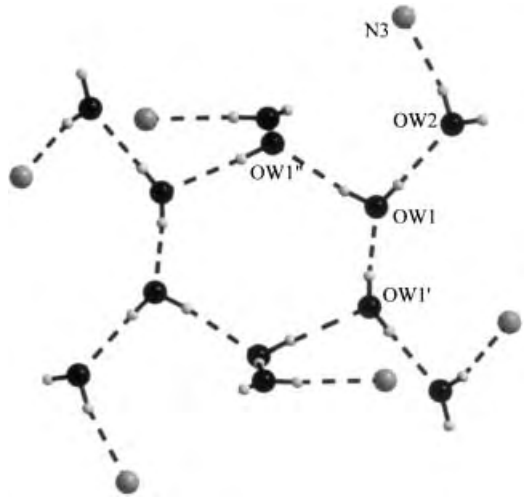


Figure 2. A simplified view of the dodecameric water cluster. Distances [Å]: OW1···OW2 2.827(6), OW1···OW1′ 2.801(6); angles [°]: OW2···H-OW1 172.26(2), OW1···H-OW′ 173.65(2), OW1′···OW1···OW1″ 119.58(1), OW2···OW1···OW1′ 109.36(2), OW2···OW1···OW1″ 104.38(2).

periphery are not coplanar with the core unit, but are situated alternately above and below the plane described by the hexamer so as to accommodate the six bulky cryptand units. These noncovalent interactions lead to a giant supramolecular unit consisting of six cryptand molecules surrounding the $(H_2O)_{12}$ cluster. Each of these units acts as a secondary building unit (SBU) and is further hydrogen bonded with H_2O molecules through the remaining secondary amines of the cryptand (Figure 3), thus resulting in propagation of the supramolecular assembly.[32] Each O atom of the dodecameric cluster is tricoordinate. Such hydrogen-bond-deficient water molecules are present[33] at the surface of liquid water and hexagonal ice. The hexameric core in the current assembly adopts a quasiplanar benzene-like cyclic structure. Although this is a higher-energy isomer, it is stabilized by the environment. The crystallographically imposed symmetry makes all the O···O distances in the hexameric core the same at 2.801 Å. This value compares[34] well with the range 2.77–2.84 Å observed in the ice II phase. Bulk water also shows[34] a short-range order in the O···O X-ray diffraction radial distribution curve of 2.85 Å. The O···O distance between the water molecule at the core and the one connected to it at the periphery is 2.827 Å.

Thermal analysis of the compound shows that onset of water loss starts at about 50 °C and complete loss of water takes place within 100 °C. The compound melts at 138 °C, which is slightly lower than that of the cryptand (145 °C).

 © 2004 Wiley-VCH Verlag GmbH & Co. KGaA, Weinheim

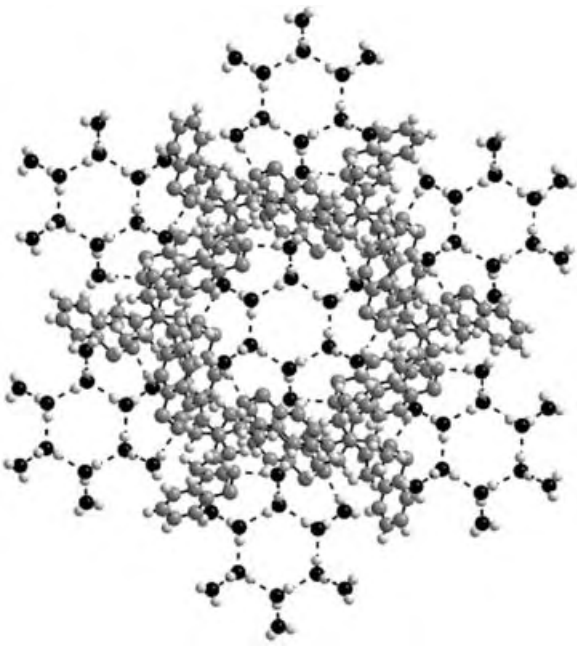


Figure 3. Building of the water clusters in **1** viewed down the crystallographic *c* axis.

The vibrational stretching frequencies of the O–H bonds pertaining to the water cluster have been characterized by FTIR spectroscopic analysis of **1**.[32] A sharp peak appears at 3635 cm^{-1} in the spectrum followed by a broad absorption centered around 3410 cm^{-1}. The IR spectrum of **1** after removal of the water is virtually superimposable on that of a standard sample of the cryptand **L**. Thus, the peak at 3635 cm^{-1} can be assigned to the $(H_2O)_{12}$ core structure. The O–H stretching vibration for the quasiplanar water hexamer appears[18] as a broad band centered around 3400 cm^{-1}; the O–H stretching vibration for the same cluster in a helium droplet appears at 3325 cm^{-1}.[13] In comparison, this vibration of the planar hexamers in ice I and II phases occur[35] at 3220 cm^{-1}. In the case of **1**, the structured band centered around 3410 cm^{-1} is attributable to the planar $(H_2O)_6$ core structure and the difference in the stretching vibration arises from its different environment.

Powder X-ray diffraction studies of the compound before and after water expulsion showed major changes[32] in the diffraction patterns which were attributable to the complete breakdown of the host lattice on exclusion of water.

In summary, we have characterized a novel dodecameric water cluster in an organic supramolecular structure. The present mode of association of twelve water molecules has not been predicted theoretically or previously found experimentally. The supramolecular self-assembly observed here is the result of hydrogen-bonding interactions between water molecules as well as between water molecules and cryptand molecules. The understanding of three-dimensional structures of water clusters has profound effects in several areas: from molecular self-assembly[36] to protein structures.[37] Attempts should thus be made to simulate water crystallization in restricted environments such as organic and inorganic host lattices. We are currently probing whether cryptands with biologically relevant functional moieties can stabilize various water clusters.

Experimental Section

Cryptand **L** was synthesized as reported previously.[30] Compound **1** was synthesized by allowing a solution of the cryptand in aqueous pyridine or aqueous acetonitrile to evaporate at room temperature. After a few days, crystals of $\mathbf{L}\cdot 7H_2O$ (**1**) appeared as colorless hexagonal plates in ca. 55% yield. Elemental analysis: calcd for $\mathbf{L}\cdot 7H_2O$ $C_{33}H_{59}N_5O_{10}$ (%): C 57.79, H 8.67, N 10.21; found: C 57.83, H 8.49, N 10.36.

Received: February 11, 2004
Revised: April 30, 2004 [Z54002]

Keywords: cryptands · hydrogen bonds · supramolecular chemistry · water chemistry · X-ray diffraction

[1] R. Ludwig, *Angew. Chem.* **2001**, *113*, 1856; *Angew. Chem. Int. Ed.* **2001**, *40*, 1808.
[2] S. S. Xantheas, T. H. Dunning, Jr, *J. Chem. Phys.* **1993**, *99*, 8774.
[3] S. D. Colson, T. H. Dunning, Jr, *Science* **1994**, *265*, 43.
[4] K. Liu, J. D. Cruzan, R. J. Saykally, *Science* **1996**, *271*, 929.
[5] R. Ludwig, *ChemPhysChem* **2000**, *1*, 53.
[6] U. Buch, F. Huisken, *Chem. Rev.* **2000**, *100*, 3863.
[7] S. Maheswary, N. Patel, N. Sathyamurthy, A. D. Kulkarni, S. R. Gadre, *J. Phys. Chem. A* **2001**, *105*, 10525.
[8] F. N. Keutsch, J. D. Cruzan, R. J. Saykally, *Chem. Rev.* **2003**, *103*, 2533.
[9] J. M. Ugalde, I. Alkorta, J. Elguero, *Angew. Chem.* **2000**, *112*, 733; *Angew. Chem. Int. Ed.* **2000**, *39*, 717.
[10] F. N. Keutsch, R. J. Saykally, *Proc. Natl. Acad. Sci. USA* **2001**, *98*, 10533.
[11] M. Matsumoto, S. Saito, I. Ohmine, *Nature* **2002**, *416*, 409.
[12] J. L. Atood, L. J. Barbour, T. J. Ness, C. L. Raston, P. L. Raston, *J. Am. Chem. Soc.* **2001**, *123*. 7129.
[13] K. Nauta, R. E. Miller, *Science* **2000**, *287,* 293.
[14] L. J. Barbour, G. W. Orr, J. L. Atwood, *Nature* **1998**, *393*, 671.
[15] R. Custelcean, C. Afloroaei, M. Vlassa, M. Polverejan, *Angew. Chem.* **2000**, *112*, 3224; *Angew. Chem. Int. Ed.* **2000**, *39*, 3094.
[16] A. Müller, E. Krickemeyer, H. Bögge, M. Schmidtmann, B. Botar, M. O. Talismanova, *Angew. Chem.* **2003**, *115*, 2131; *Angew. Chem. Int. Ed.* **2003**, *42*, 2085.
[17] K. M. Park, R. Kuroda, T. Iwamoto, *Angew. Chem.* **1993**, *105*, 939; *Angew. Chem. Int. Ed. Engl.* **1993**, *32*, 884.
[18] J. N. Moorthy, R. Natarajan, P. Venugopalan, *Angew. Chem.* **2002**, *114*, 3567; *Angew. Chem. Int. Ed.* **2002**, *41*, 3417.
[19] A. Michaelides, S. Skoulika, E. G. Bakalbassis, J. Mrozinski, *Cryst. Growth Des.* **2003**, *3*, 487.
[20] W. B. Blanton, S. W. Gordon-Wylie, G. R. Clark, K. D. Jordan, J. T. Wood, U. Geiser, T. J. Collins, *J. Am. Chem. Soc.* **1999**, *121*, 3551.
[21] K. Raghuraman, K. K. Katti, L. J. Barbour, N. Pillarsetty, C. L. Barnes, K. V. Katti, *J. Am. Chem. Soc.* **2003**, *125*, 6955.
[22] S. Pal, N. B. Sankaran, A. Samanta, *Angew. Chem.* **2003**, *115*, 1783; *Angew. Chem. Int. Ed.* **2003**, *42*, 1741.
[23] a) J. Kim, K. S. Kim, *J. Chem. Phys.* **1998**, *109*, 5886; b) K. Kim, K. D. Jordan, T. S. Zwier, *J. Am. Chem. Soc.* **1994**, *116*, 11568; c) K. Liu, M. G. Brown, C. Carter, R. J. Saykally, J. K. Gregory, D. C. Clary, *Nature* **1996**, *381*, 501.
[24] a) S. K. Ghosh, P. K. Bharadwaj, *Inorg. Chem.* **2003**, *42*, 8250; b) C. Foces-Foses, F. H. Cano, M. Martinez-Ripoli, R. Faure, C. Roussel, R. M. Claramunt, C. Lopez, D. Sanz, J. Elguero, *Tetrahedron: Asymmetry* **1999**, *10*, 65.

 © 2004 Wiley-VCH Verlag GmbH & Co. KGaA, Weinheim

[25] B. Kamb, *Acta Crystallogr.* **1964**, *20*, 1437.
[26] A. Rahaman, F. H. Stillinger, *J. Am. Chem. Soc.* **1973**, *95*, 7943.
[27] *Water and Biological Macromolecules* (Ed.: E. Westhoff), CRC, Boca Raton, FL, **1993**.
[28] S. Nishikiori, T. Iwamoto, *J. Chem. Soc. Chem. Commun.* **1993**, 1555.
[29] C. J. Tsai, K. D. Jordan, *J. Phys. Chem.* **1993**, *97*, 5208.
[30] D. K. Chand, K Ragunathan, P. K. Bharadwaj, T. C. W. Mak, *J. Org. Chem.* **1996**, *61*, 1169.
[31] Crystal data for **1**: Colorless, hexagonal, crystal dimensions $0.18\times0.16\times0.13$ mm, trigonal, space group $R\bar{3}$, $Z=3$, $a=$ 14.023(5), $b=14.023$ (5), $c=33.249(5)$ Å, $V=5662.3(2)$ Å^3, $\rho_{calcd}=0.199$ g cm^{-3}, $T=100$ K, $\mu=0.015$ mm^{-1}, $\theta_{max}=28.32^\circ$, 3139 reflections collected of which 2834 were unique. $R_1=$ 0.0684, wR2 = 0.2004 with a GOF of 1.050 for $I>2\sigma(I)$; residual electron density: 1.347 and -0.854 e Å^{-3}. The X-ray data were collected on a Bruker SMART APEX CCD diffractometer using graphite monochromated $Mo_{K\alpha}$ radiation (0.71069 Å). The following programs were used during data collection and refinement: SMART (version 5.628 to acquire frame data), SAINT (version 6.45 to determine final unit parameters and intregate frame data). The structure was solved by direct methods and refined on F^2 using SHELX-97 (G. M. Sheldrick, Program for the solution and refinement of crystal structures, University of Göttingen, Germany, **1997**) package. The hydrogen atoms connected to the OW3 could not be located in the difference Fourier maps with certainty although other H atoms could be located. The non-hydrogen atoms were refined anisotropically. H atoms were not refined. CCDC-230380 contains the supplementary crystallographic data for this paper. These data can be obtained free of charge via www.ccdc.cam.ac.uk/conts/retrieving.html (or from the Cambridge Crystallographic Data Centre, 12 Union Road, Cambridge CB21EZ, UK; fax: (+44) 1223-336-033; or deposit@ccdc.cam.ac.uk).
[32] See Supporting Information.
[33] C. J. Gruenloh, J. R. Carney, C. A. Arrington, T. S. Zwier, S. Y. Fredericks, K. D. Jordan, *Science* **1997**, *276*, 1678.
[34] G. A. Jeffrey, *An Introduction to Hydrogen Bonding I*, Oxford University Press, Oxford, **1997**.
[35] D. Eisenberg, W. Kauzmann, *The Structure and Properties of Water*, Oxford University Press, Oxford, **1969**.
[36] J. D. Joannopoulous, *Nature* **2001**, *414*, 257.
[37] P. R. ten Wolde, D. Frenkel, *Science* **1997**, *277*, 1975.

 © 2004 Wiley-VCH Verlag GmbH & Co. KGaA, Weinheim

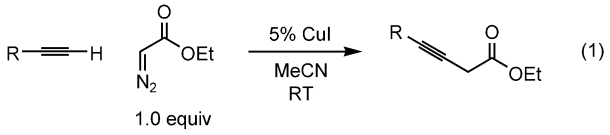
Coupling Reactions

A Straightforward and Mild Synthesis of Functionalized 3-Alkynoates**

*Andrés Suárez and Gregory C. Fu**

The methods that have been described to date for the synthesis of 3-alkynoates generally require multiple steps and/or highly basic reaction conditions.[1] One very attractive route to 3-alkynoates would be by the coupling of readily available terminal alkynes with diazoesters. Unfortunately, in the absence of a catalyst, treatment of alkynes with diazo compounds preferentially generates cyclopropenes and C_{alkyl}–H insertion products.[2] With respect to metal-catalyzed processes,[3] in the presence of rhodium complexes, reactions of terminal alkynes with diazo compounds lead not to insertion into the $C_{alkynyl}$–H bond, but typically to cyclopropenation.[4] In the case of copper, the only synthetically useful couplings that have been reported are also methods for cyclopropenation;[5] a few groups have observed the formation of a 3-alkynoate, but none of the procedures is general, elevated temperatures are employed, and the yields are modest (0–45%).[6]

In this communication we describe the development of a versatile method for coupling alkynes with diazocarbonyl compounds to produce 3-alkynoates [Eq. (1)]. Some noteworthy attributes of the system include its efficiency (1:1 ratio of reactants), mildness (room temperature), simplicity (no additional ligand), and functional-group tolerance (e.g., alkenes, heteroatoms, and hydroxy groups).



(1)

In an initial study, we explored the reaction of phenylacetylene with ethyl diazoacetate. In the presence of copper complexes such as CuCl, CuOTf, CuCN, CuSCN, Cu_2O, and CuOAc, we obtain essentially none of the target 3-alkynoate

[*] Dr. A. Suárez, Prof. Dr. G. C. Fu
Department of Chemistry
Massachusetts Institute of Technology
Cambridge, MA 02139 (USA)
Fax: (+1) 617-324-3611
E-mail: gcf@mit.edu

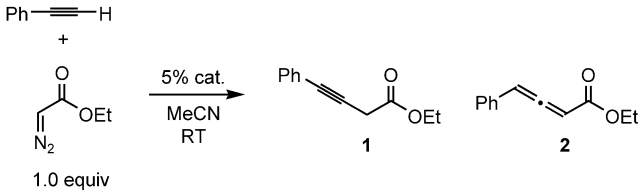
[**] Support has been provided by the National Institutes of Health (National Institute of General Medical Sciences, R01-GM066960), the Spanish Ministry of Education, Culture, and Sports (postdoctoral fellowship to A.S.), Merck Research Laboratories, and Novartis. Funding for the MIT Department of Chemistry Instrumentation Facility has been furnished in part by NSF CHE-9808061 and NSF DBI-9729592.

Supporting information for this article is available on the WWW under http://www.angewandte.org or from the author.

 © 2004 Wiley-VCH Verlag GmbH & Co. KGaA, Weinheim DOI: 10.1002/anie.200454070

(Table 1, entry 1). In contrast, CuBr and CuI are effective catalysts for the desired transformation (entries 2 and 3). The choice of solvent is critical: use of *i*PrOH, THF, dioxane, acetone, or $CHCl_3$ leads to a significantly lower yield (< 10%).[7]

Table 1: Catalysts tested for the synthesis of 3-alkynoates **1** from alkynes and diazoesters.



Entry	Catalyst	**1** [%][a]	**2** [%][a]
1	CuCl, CuOTf, CuCN, CuSCN, Cu_2O, CuOAc	< 5	< 5
2	CuBr	70	5
3	CuI	90	8

[a] Yields were determined by NMR spectroscopy vs. an internal standard (average of two runs).

Interestingly, cyclopropenation of the alkyne is not a detectable side reaction for the CuBr- or CuI-catalyzed processes (< 5%). Furthermore, the formation of fumarate and maleate side products, a complication that plagues many copper-catalyzed reactions of diazoesters, is minimal (< 5%), thereby allowing the use of a 1:1 mixture of alkyne:diazoester, without slow addition of the diazoacetate.[8] We do, however, observe a small quantity of the allene isomer (**2**) of the 3-alkynoate.[9]

We have determined that CuI-catalyzed coupling of terminal alkynes with diazoesters provides a general route to 3-alkynoates (Table 2).[10] Thus, aryl- (entry 1), alkyl- (entry 2), hindered alkyl- (entry 3), functionalized alkyl- (entry 4), and silyl-substituted (entry 5) alkynes are all suitable substrates. Formation of the desired 3-alkynoate proceeds in preference not only to cyclopropenation of an alkyne, but also to cyclopropanation of an alkene (entries 6 and 7). Furthermore, neither Lewis-basic groups such as sulfides and ethers, which could react with a copper carbene to form ylides (entries 8–10),[11] nor hydroxy groups, which could undergo O–H insertion (entry 11),[12] interfere with the reaction.

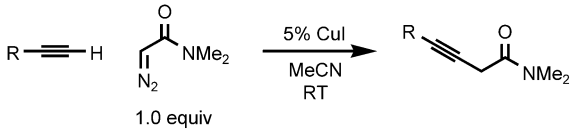
Table 2: Copper-catalyzed couplings of alkynes with a diazoester [Eq. (1)].

Entry	R	Yield [%][a]
1	Ph	76
2	CH_2Ph	74
3[b,c]	*t*Bu	98[e]
4	$CH_2CH_2CO_2Et$	87[e]
5[b]	TMS	84
6		71
7		58
8	CH_2SPh	56
9	CH_2SEt	63
10	CH_2OTHP[d]	87[e]
11	CH_2OH	75[f]

[a] Yields of isolated products (average of two runs), unless otherwise noted. [b] 10% CuI was used. [c] 1.2 equiv of alkyne was used. [d] THP = tetrahydropyranyl. [e] Contains 3–5% of the allene isomer. [f] Yield was determined by NMR spectroscopy vs. an internal standard.

In certain instances, we have experienced difficulty removing the allene side product from the target 3-alkynoate (e.g., Table 2, entries 3, 4, 10, and 11). To address this purification issue, as well as to explore the scope of the coupling with respect to other diazo compounds, we examined the reaction of alkynes with a diazoamide ($N_2CHCONMe_2$). We were pleased to observe that CuI is also an effective catalyst for these couplings (Table 3);[13] as for reactions of diazoesters, a small amount of the allene is produced, but this is readily removed by flash chromatography.

Table 3: Copper-catalyzed couplings of alkynes with a diazoamide.



Entry	R	Yield [%][a]
1[b]	*t*Bu	70
2	$CH_2CH_2CO_2Et$	71
3	CH_2OMe	57
4	CH_2OTHP	81
5	CH_2OH	54

[a] Yields of isolated products (average of two runs). [b] 1.1 equiv of alkyne was used.

In conclusion, a general, metal-catalyzed intermolecular coupling of terminal alkynes with diazo compounds has been developed, providing ready access to 3-alkynoates. It is noteworthy that this carbon–carbon bond-forming reaction proceeds efficiently under nonbasic conditions at room temperature with a simple and inexpensive catalyst, and that an array of potentially reactive functional groups are tolerated.

Received: February 21, 2004 [Z54070]

Keywords: alkynes · copper · diazo compounds · homogeneous catalysis

[1] For some examples, see: a) S.-i. Usugi, H. Yorimitsu, H. Shinokubo, K. Oshima, *Bull. Chem. Soc. Jpn.* **2002**, *75*, 2687–2690; b) R. M. Williams, D. J. Aldous, S. C. Aldous, *J. Org. Chem.* **1990**, *55*, 4657–4663; c) J. Hooz, R. B. Layton, *Can. J. Chem.* **1972**, *50*, 1105–1107.

[2] For a discussion, see: O. M. Nefedov, E. A. Shapiro, A. B. Dyatkin in *Supplement B: The Chemistry of Acid Derivatives*, *Vol. 2* (Ed.: S. Patai) Wiley, New York, **1992**, pp. 1527–1528.

 © 2004 Wiley-VCH Verlag GmbH & Co. KGaA, Weinheim

[3] M. P. Doyle, M. A. McKervey, T. Ye in *Modern Catalytic Methods for Organic Synthesis with Diazo Compounds*, Wiley, New York, **1998**.
[4] For leading references, see: a) reference [3], Chapter 4.11; b) M. N. Protopopova, E. A. Shapiro, *Russ. Chem. Rev.* **1989**, *58*, 667–681.
[5] For a discussion and leading references, see: M. M. Díaz-Requejo, M. A. Mairena, T. R. Belderrain, M. C. Nicasio, S. Trofimenko, P. J. Pérez, *Chem. Commun.* **2001**, 1804–1805.
[6] a) V. E. Baikov, L. P. Danilkina, K. A. Ogloblin, *Russ. J. Gen. Chem.* **1983**, *53*, 2172–2173; b) E. A. Shapiro, I. E. Dolgii, O. M. Nefedov, *Bull. Acad. Sci. USSR Div. Chem. Sci. (Engl. Transl.)* **1980**, *29*, 1493–1499; c) I. E. Dolgii, E. A. Shapiro, O. M. Nefedov, *Bull. Acad. Sci. USSR Div. Chem. Sci. (Engl. Transl.)* **1974**, *23*, 929; d) M. Vidal, M. Vincens, P. Arnaud, *Bull. Soc. Chim. Fr.* **1972**, 657–665; e) V. K. Jones, A. J. Deutschman Jr. , *J. Org. Chem.* **1965**, *30*, 3978–3980.
[7] The observed solvent effects may be due in part to the relative solubility of CuI.
[8] For a discussion of this problem, see p. 6 of: T. Rovis, D. A. Evans, *Prog. Inorg. Chem.* **2001**, *50*, 1–150. The typical remedy is to use a large excess of the substrate (e.g., as the solvent) and to employ slow addition of the diazo compound.
[9] The 3-alkynoate:allene ratio does not change as the reaction progresses, which suggests that the 3-alkynoate is not an intermediate in the formation of the allene.
[10] The isomeric allene is the only identifiable side product.
[11] For an early example, see: G. Pourcelot, L. Veniard, P. Cadiot, *Bull. Soc. Chim. Fr.* **1975**, 1281–1283. See also reference [3], Chapter 7.
[12] This result is particularly noteworthy in light of a recent report of selective O–H insertion upon reacting propargyl alcohol with ethyl diazoacetate in the presence of a CuTp catalyst (Tp = a homoscorpionate ligand): M. E. Morilla, M. J. Molina, M. M. Díaz-Requejo, T. R. Belderrain, M. C. Nicasio, S. Trofimenko, P. J. Pérez, *Organometallics* **2003**, *22*, 2914–2918.
[13] We have not optimized the reaction conditions for the reactions in Table 3; they are the same as those used for the reactions in Table 2.

 © 2004 Wiley-VCH Verlag GmbH & Co. KGaA, Weinheim

Strained Molecules

Crystal Structure of a Dewar Benzene Derivative Formed from Fluoro(triisopropylsilyl)acetylene**

Takeshi Hanamoto, Yukinori Koga, Toshio Kawanami, Hiroshi Furuno, and Junji Inanaga*

Halogenoacetylenes are probably one of the most intriguing classes of acetylene compounds. Although some synthetic routes to 1-haloacetylenes have been reported, there are very few reports on the syntheses of 1-fluoroacetylenes.[1] In 1959, the first synthesis of 1-fluoroacetylene itself was accomplished by Middleton and Sharkey, who used pyrolysis of fluoromaleic anhydride.[2] Five years later Viehe and et al. reported the synthesis of *tert*-butylfluoroacetylene, which trimerized spontaneously to afford the highly strained benzene valance isomers below 0 °C.[3] However, to the best of our knowledge, no fluoroacetylene derivatives aimed specifically to be synthetically useful has been examined with one exception.[4] This omission stems from the instability of fluoroacetylene compounds and their explosive nature. In connection to our ongoing research in the development of monofluorinated building blocks,[5] we have considered the corresponding fluorosilylacetylene as a promising candidate for a fluoroethynylation reagent. As the addition of silylacetylenes to carbonyl compounds catalyzed by fluoride ions has already been reported,[6] the corresponding fluorosilylacetylene should generate the fluoroethynyl anion species by means of the fluoride source. In addition, we expected that the introduction of the bulky silyl substituents should enhance the stability of fluoroacetylene. On the basis of these ideas, we chose and prepared fluoro(triisopropylsilyl)acetylene (**1**; see Scheme 1) as the first example of a silylated fluoroacetylene. Although the preparation of **1** worked well, **1** did not function as a fluoroethynyl anion towards carbonyl compounds at this stage. However, to our delight, we discovered that spontaneous trimerization of **1** generally occurred to give the corresponding 1,2,4-trifluoro-3,5,6-tris(triisopropylsilyl)bicyclo[2,2,0]hexa-2,5-dien **3** (Dewar benzene) as a stable solid.[7] Herein, we report the preparation of **1** and the crystal structure of **3**.

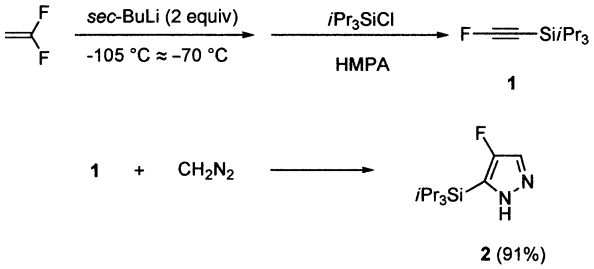
One possible procedure for the synthesis of **1** would be the silylation of metal fluoroacetylide. As a THF/ether solution

[*] Prof. Dr. T. Hanamoto, Y. Koga
Department of Chemistry and Applied Chemistry
Saga University
Honjyo-machi 1, Saga 840-8502 (Japan)
Fax: (+81) 952-28-8548
E-mail: hanamoto@cc.saga-u.ac.jp
T. Kawanami, Dr. H. Furuno, Prof. Dr. J. Inanaga
Institute for Materials Chemistry and Engineering (IMCE)
Kyushu University
Hakozaki, Higashi-ku, Fukuoka 812-8581 (Japan)

[**] We greatly thank F-Tech Co. Ltd., for a gift of 1,1-difluoroethylene and Chisso Co. Ltd., for a gift of chlorotriisopropylsilane. The Dewar benzene derivative is 1,2,4-Trifluoro-3,5,6-tris(triisopropylsilyl)bicyclo[2,2,0]hexa-2,5-dien

 © 2004 Wiley-VCH Verlag GmbH & Co. KGaA, Weinheim DOI: 10.1002/anie.200454174

that contained fluoroacetylene was prepared from 1,1-difluoroethylene by using one equivalent of *sec*-BuLi, we anticipated that the use of two equivalents of *sec*-BuLi would cause deprotonation of fluoroacetylene generated to produce the corresponding lithium fluoroacetylide. According to a slightly modified procedure reported by Sauvêtre and Normant,[8] lithium fluoroacetylide was prepared by using two equivalents of *sec*-BuLi to 1,1-difluoroethylene at −70 °C. The successive addition of chlorotriisopropylsilane and hexamethyl phosphoramide (HMPA) to the resulting lithium fluoroacetylide solution afforded the desired product **1** in high yield (Scheme 1). The GC–MS spectrometric analysis of



Scheme 1. Synthesis of fluoro(triisopropylsilyl)acetylene (**1**).

1 gave a single peak that corresponded to the molecular formula of $C_{11}H_{21}FSi$. The ^{19}F NMR spectrum showed a signal from the terminal fluorine atom at −186.8 ppm. The chemical shift of a fluorine atom bonded to an sp carbon atom is roughly comparable to the signal obtained for fluorochloroacetylene (−219 ppm).[4] Although the purification of **1** was possible by silica-gel column chromatography with hexane as eluent, evaporation of the solvent afforded the pale yellow–green oil, which soon turned brown due to decomposition. This behavior suggested to us that **1** can be safely handled only as a hexane solution for a short time at room temperature in a similar way to that of *tert*-butylfluoroacetylene.[3] Consequently, we kept the solution of **1** in the refrigerator at −20 °C to avoid decomposition. Although its accurate yield was not obtained due to its unstable nature, we estimated the yield of **1** to be at least 91 % based on its transformation to the corresponding fluoropyrazole (**2**; Scheme 1).

On the other hand, when we checked the purity of **1** by GC–MS spectrometric analysis about four months after the initial synthesis, a new major peak appeared at *m/z* 472. We attempted to separate this compound from the mixture by using silica-gel column chromatography. The compound was successfully isolated as a white solid, which was readily soluble in hexane and melted from 84.5 °C to 85.5 °C. The ^{19}F NMR spectrum displayed three signals at $\delta = -80.62$ (s), −168.31 (d, $J = 10.9$ Hz), −174.60 ppm (d, $J = 10.9$ Hz), respectively. The ^{13}C NMR spectrum showed six downfield signals at $\delta = 100.8$–175.6 ppm. The final structural determination of the compound was achieved by X-ray crystallography. The X-ray diffraction data were collected at 93 K. An ORTEP drawing of compound **3** is shown in Figure 1. The structure of **3** was 1,2,4-trifluoro-3,5,6-tris(triisopropylsilyl)-bicyclo[2,2,0]hexa-2,5-dien (Dewar Benzene). Although the molecular structures of seven Dewar benzene derivatives

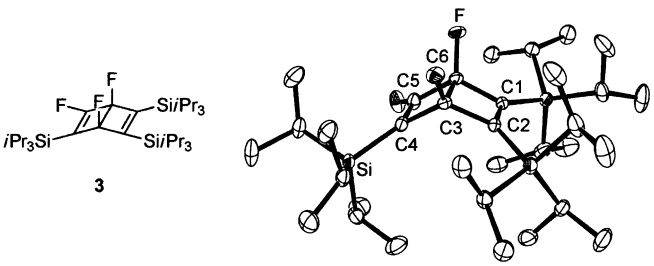


Figure 1. ORTEP drawing of the structure **3** with thermal ellipsoids shown at the 50% probability level (hydrogen atoms are omitted for clarity). Selected bond lengths [Å] and angles [°]: C1-C2 1.380(4), C2-C3 1.563(4), C3-C4 1.552(4), C4-C5 1.341(4), C5-C6 1.500(4), C1-C6 1.549(4), C3-C6 1.535(4), C1-Si2 1.902(3), C2-Si1 1.905(3), C4-Si3 1.894(3), C3-F1 1.386(3), C5 C1-F2 1.352(3), C6-F3 1.385(3), C1-C2-C3 93.0(2), C2-C1-C6 92.7(2), C3-C4-C5 88.0(2), C4-C5-C6 99.4(2), C2-C3-C4 123.0(2), C1-C6-C5 122.3(2).

have so far been determined by means of the X-ray diffraction,[9] this is the first example of a fluorinated Dewar benzene derivative to be confirmed by X-ray diffraction.[10] The following features of this fluorinated Dewar benzene derivative are noteworthy: 1) The central C3–C6 bond (1,535(4) Å) is the shortest known bond length of its type compared with the structures of other Dewar benzene derivatives. 2) The dihedral angles between the two cyclobutene rings (the folding angle) range from 123.3(2) to 123.0(2)°, thus, compound **3** has the widest dihedral angle for a Dewar benzene derivative. 3) Steric repulsive forces between neighboring triisopropylsilyl groups give rise to the lengthening of the corresponding carbon–carbon double bond (C1–C2) in the four-membered ring (1.380(4) Å) compared to the double bond on the opposite side of the molecule (C4–C5) average 1.341(4) Å). 4) Fluorine atoms occupy both bridgehead carbon atoms, which suggests that a possible precursor of **3** is 1,2-difluoro-3,4-bis(triisopropylsilyl)cyclobutadiene.[11]

In conclusion, we have demonstrated the first preparation of fluorosilylacetylene, **1**, from 1,1-difluoroethylene in one step. The spontaneous trimerization of **1** afforded not the fluorinated benzene derivative but the stable fluorinated Dewar benzene derivative **3**. Studies on the reactivity, property, and trimerization mechanism of **3** are in progress in our laboratories.

Experimental Section

General: Melting point: Yanako micro melting point apparatus MP-S3. NMR: JEOL AL-300 and Bruker DRX600. Chemical shifts were reported as δ values (ppm) relative to internal tetramethylsilane (^1H and ^{13}C) or benzotrifluoride (^{19}F) in $CDCl_3$ unless otherwise noted. GC–MS: JEOL JMS-AMII15 mass spectrometer. IR: Perkin Elmer SPECTRUM 2000 FT-IR. Elemental analysis: the Service Centre of the Elementary Analysis of Organic Compound affiliated with the Faculty of Science, Kyushu University. Analytical thin layer chromatography (TLC) and column chromatography were performed on silica gel 60 F_{254} (Merck) and silica gel 60 (40–63 mm), respectively. THF and ether were used after distillation from sodium benzophenone ketyl radical. HMPA was used after distillation from CaH_2.

A 100 mL two-neck flask equipped with a magnetic stir bar, a stopcock, and a three-way stopcock, was charged with 40 mL of THF

 © 2004 Wiley-VCH Verlag GmbH & Co. KGaA, Weinheim

under argon. *sec*-BuLi (15.0 mL, 14.4 mmol) was added dropwise by syringe at −78 °C to the stirred mixture. After this mixture had been stirred for an additional 10 min, the solution was cooled to −105 °C in a liquid N_2/ethanol bath. At this temperature, argon was replaced with 1,1-difluoroethylene (balloon). The mixture was gradually warmed to −70 °C. Chlorotriisopropylsilane (1.45 mL, 6.8 mmol) and HMPA (3 mL) were successively added to the solution by syringe. After the addition had been completed, the reaction mixture was allowed to warm to 0 °C. Hexane and aqueous sodium bicarbonate ($NaHCO_3$) was carefully added to the resulting solution. After the resultant mixture was extracted with ether, the combined ethereal solution was dried over sodium sulfate and filtered through a short silica-gel column (ether as an eluent). After the addition of 7.0 mg of phenothiazine to the solution, the solution was concentrated to half its original volume. The same concentration procedure was repeated three times after the addition of a half volume of *n*-hexane to the solution in each procedure. The solution was finally concentrated to about 3 mL, then the resulting solution was directly purified by chromatography on silica gel (hexane as an eluent) to give the desired product (**1**) as a hexane solution. Samples were routinely stored in a sample bottle at −20 °C, which showed no deterioration by GC–MS analysis over a 4 week period. After about 4 months, the solution was concentrated and the residue was purified by column chromatography on silica gel (hexane as an eluent) to give **3** as a white solid (599.5 mg, 44 %) (Not optimized for trimerization conditions).

3: $R_f = 0.82$; hexane; mp 84.5–85.5 °C; elemental analysis calcd (%) for $C_{33}H_{63}F_3Si_3$: C 65.94, H 10.56; found: C 65.82, H 10.52; $\delta_F = -80.62$ (s), −168.31 (d; $J_{FF} = 10.9$ Hz), −174.60 ppm (d; $J_{FF} = 10.9$ Hz); $\delta_C = 11.8$ (s), 13.2 (s), 13.7 (s), 18.3 (s), 18.90 (s), 18.94 (s), 19.2 (s; overlapped), 19.5 (s), 100.8 (ddd; $J_{CF} = 270.7$, 40.5, 21.7 Hz), 105.2 (ddd; $J_{CF} = 263.6$, 22.7, 20.5 Hz), 129.9 (dt; $J_{CF} = 27.8$, 4.0 Hz), 168.8 (dd; $J_{CF} = 22.9$, 2.8. Hz), 171.1 (ddd, $J_{CF} = 371.6$, 24.5, 13.9 Hz), 175.6 ppm (dd, $J_{CF} = 22.8$, 12.2 Hz); $\delta_H = 1.0$–1.3 ppm (m); $\tilde{\nu} = 2951$, 2869, 1598, 1470, 1324, 1200, 1153, 1065, 1017, 882, 692, 673 cm^{-1}.

Single crystals of **3** suitable for X-ray crystallographic analysis were grown by recrystallization from hexane. Crystal data for **3** ($C_{33}H_{63}F_3Si_3$) :$M_r = 601.10$, $T = 93(2)$ K, triclinic, space group $P\bar{1}$, $a = 8.8247(19)$, $b = 12.566(3)$, $c = 17.350(5)$ Å, $\alpha = 91.373(13)°$, $\beta = 99.892(10)°$, $\gamma = 97.728(11)°$, $V = 1875.9$ Å3, $Z = 2$, $Dx = 1.064$ $Mg\,m^{-3}$, $\mu = 0.160$ mm^{-1}, $\lambda = 0.71075$ Å, $\theta_{max} = 27.41°$, 17897 measured reflection, 8437 independent reflections, 370 refined parameters, GOF = 1.111, $R[F^2 > 2\sigma[F^2]] = 0.0576$, $wR(F^2) = 0.2106$. The intensity data were collected on a Rigaku RAXIS-RAPID diffractometer. The structure was solved by direct methods (SIR92) and the non-hydrogen atoms were refined anisotropically by full-matrix least-squares procedures on F^2 for all reductions (SHELXL97). All hydrogen atoms were positioned geometrically and refined as riding. CCDC 230758 contains the supplementary crystallographic data for this paper. These data can be obtained free of charge via www.ccdc.cam.ac.uk/conts/retrieving.html (or from the Cambridge Crystallographic Data Centre, 12 Union Road, Cambridge CB2 1EZ, UK; fax: (+44) 1223-336-033; or deposit@ccdc.cam.ac.uk).

Received: March 3, 2004 [Z54174]

Keywords: alkynes · cyclization · Dewar benzene · fluorine · silicon

[1] H. Hopf, B. Witulski in *Modern Acetylene Chemistry*, (Eds.: P. J. Stang, F. Diederich), VCH, **1995**, chap. 2.

[2] W. J. Middleton, W. H. Sharkey, *J. Am. Chem. Soc.* **1959**, *81*, 803 – 804.

[3] a) H. G. Viehe, R. Merényi, J. F. M. Oth, P. Valange, *Angew. Chem.* **1964**, *76*, 888; *Angew. Chem. Int. Ed. Engl.* **1964**, *3*, 746; b) H. G. Viehe, R. Merényi, J. F. M. Oth, J. R. Sender, P. Valange, *Angew. Chem.* **1964**, *76*, 923; *Angew. Chem. Int. Ed. Engl.* **1964**, *3*, 755 – 756.

[4] S. Y. Delavarenne, H. G. Viehe, *Chem. Ber.* **1970**, *103*, 1198 – 1208.

[5] a) T. Hanamoto, S. Harada, K. Shindo, M. Kondo, *Chem. Commun.* **1999**, 2397 – 2398; b) T. Hanamoto, T. Kobayashi, M. Kondo, *Synlett* **2001**, 281 – 283; c) T. Hanamoto, T. Kobayashi, *J. Org. Chem.* **2003**, *68*, 6354 – 6359.

[6] E. Nakamura, I Kuwajima, *Angew. Chem.* **1976**, *88*, 539; *Angew. Chem. Int. Ed. Engl.* **1976**, *15*, 498 – 499.

[7] W. Schuäfer, H. Hellmann, *Angew. Chem.* **1967**, *79*, 566 – 573; *Angew. Chem. Int. Ed. Engl.* **1967**, *6*, 518 – 525.

[8] R. Sauvêtre, J. F. Normant, *Tetrahedron Lett.* **1982**, *23*, 4325 – 4328.

[9] a) K. Weinges, W. Kasel, U. Huber-Patz, H. Rodewald, H. Irngartinger, *Chem. Ber.* **1984**, *117*, 1868 – 1876; b) K. Weinges, J. Klein, W. Sipos, P. Günther, U. Huber-Patz, H. Rodewald, J. Deuter, H. Irngartinger, *Chem. Ber.* **1986**, *119*, 1540 – 1545; c) K. Weinges, W. Sipos, J. Klein, J. Deuter, H. Irngartinger, *Chem. Ber.* **1987**, *120*, 5 – 9; d) H. Irngartinger, J. Deuter, H. Wingert, M. Regitz, *Chem. Ber.* **1990**, *123*, 345 – 350.

[10] a) G. Camaggi, F. Gozzo, *J. Chem. Soc. C* **1969**, 489 – 500; b) L. Cavalli, *J. Chem. Soc. B* **1970**, 1616 – 1623; c) W. P. Dailey, R. A. Correa, E. Harrison III, D. M. Lemal, *J. Org. Chem.* **1989**, *54*, 5502 – 5511, 5511 – 5516; d) D. M. Lemal, *J. Org. Chem.* **2004**, *69*, 1 – 11.

[11] A. Sekiguchi, M. Tanaka, T. Matsuo, H. Watanabe, *Angew. Chem.* **2001**, *113*, 1721 – 1723; *Angew. Chem. Int. Ed.* **2001**, *40*, 1675 – 1676.

 © 2004 Wiley-VCH Verlag GmbH & Co. KGaA, Weinheim

Homogeneous Catalysis

Cyclometalated Ruthenium(II) Complexes as Highly Active Transfer Hydrogenation Catalysts**

Walter Baratta, Paolo Da Ros, Alessandro Del Zotto, Alessandra Sechi, Ennio Zangrando, and Pierluigi Rigo*

Complexes of platinum group metals with PCP pincer ligands are currently being investigated in both stoichiometric and catalytic reactions.[1] Conversely, cyclometalated complexes

[*] Dr. W. Baratta, Dr. P. Da Ros, Prof. A. Del Zotto, Dr. A. Sechi, Prof. P. Rigo
Dipartimento di Scienze e Tecnologie Chimiche
Università di Udine
Via Cotonificio 108, 33100 Udine (Italy)
Fax: (+39) 0432-558-803
E-mail: inorg@dstc.uniud.it
Prof. E. Zangrando
Dipartimento di Scienze Chimiche
Università di Trieste
Via L. Giorgieri 1, 34127 Trieste (Italy)

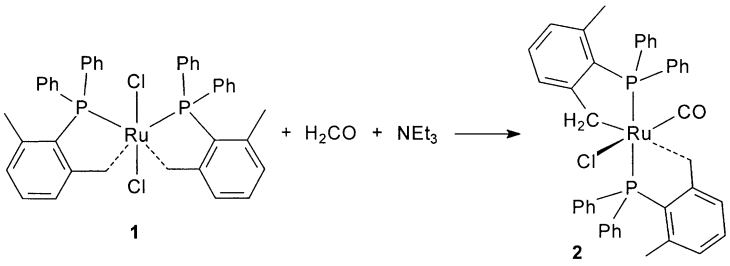
[**] This work was supported by the Ministero della Ricerca Scientifica e Tecnologica (MURST). We are very grateful to Prof. G. Esposito (Dipartimento di Scienze e Tecnologie Biomediche, Università di Udine) for ROESY experiments.

Supporting information for this article is available on the WWW under http://www.angewandte.org or from the author.

 © 2004 Wiley-VCH Verlag GmbH & Co. KGaA, Weinheim DOI: 10.1002/anie.200454199

with simple PC ligands[2] have attracted comparatively less attention in catalysis, with the exception of the palladium derivatives used for Heck-type reactions.[3] Thus, despite the large number of ruthenium compounds that have been found to be highly efficient reagents and catalysts for a variety of organic transformations,[4] very few examples of ruthenium catalysts with PC ligands have been reported.[5] In this context, the development of simple routes for the preparation of ruthenium complexes with PC ligands showing features similar to the PCP pincer derivatives would prove useful. Of the many synthetic procedures known, the cyclometalation of *ortho*-methylated aryl phosphanes offers a simple route for the preparation of stable five-membered chelate complexes.[2] Recently, we have studied the coordination chemistry of the bulky phosphanes $(2,6\text{-}Me_2C_6H_3)PR_2$ (R = Ph, cyclohexyl (Cy)) which were found to stabilize rare examples of 14-electron Ru^{II}[6] and Pt^{II}[7] complexes through δ-agostic interactions of the *ortho*-methyl groups. As expected, these ligands undergo facile cyclometalation reactions to give stable compounds in which a carbon donor atom forms a σ bond to the metal center, as found for Pt^{II}[7] and Os^{II} complexes.[8] Thus, starting from the 14-electron compound $[RuCl_2\{(2,6\text{-}Me_2C_6H_3)PPh_2\}_2]$ (**1**),[6] we report herein the synthesis of a new class of complexes containing the anionic $[(2\text{-}CH_2\text{-}6\text{-}MeC_6H_3)PPh_2]^-$ ligand and a first application of these robust metal–carbon compounds containing a σ bond in catalytic transfer hydrogenation.[9] Among the new cyclometalated complexes, the derivative bearing 2-(aminomethyl)pyridine was found to be extremely active for the reduction of a large number of ketones with turnover frequency (TOF) numbers up to 63000 h^{-1} and quantitative formation of the alcohol when using a very high substrate/catalyst ratio (up to 10000:1).

Treatment of **1** with formaldehyde in the presence of triethylamine afforded the thermally stable five-coordinate ruthenium(II) complex **2** [Eq. (1)].[10]



(1)

In this reaction one phosphorus center undergoes cyclometalation with one δ-agostic *ortho*-methyl group and the addition of formaldehyde leads to coordination of a CO ligand with extrusion of dihydrogen. The ^1H NMR spectrum of **2** shows one signal at $\delta = 1.60$ ppm (CD_2Cl_2) corresponding to two *ortho*-methyl groups. This resonance remains as a singlet even at −90 °C, which indicates there is a low energy barrier to rotation of the xylyl group, in contrast to **1**. The X-ray structure of a single crystal of **2** is shown in Figure 1.[11]

The ruthenium center is in a distorted octahedral environment with two phosphorus atoms in a *trans* arrangement, and with the chloride and the carbonyl group *cis* to the strong σ-donating alkyl ligand. The coordination sphere is completed by an *ortho*-methyl group with a Ru···C10 distance of 2.765(10) Å, which is longer than the value detected in **1** (mean value 2.651(1) Å). The hydrogen atoms of the agostic methyl group have been located by refining the torsion angle that maximizes the electron density of the group. It is noteworthy that the hydrogen atoms are "tilted" away from the metal center, which is in agreement with other complexes with δ-agostic *ortho*-methyl groups.[6,7]

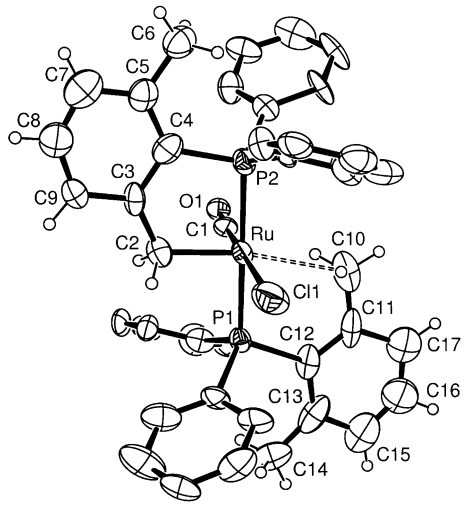
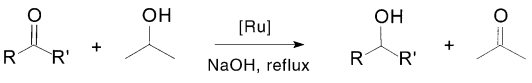


Figure 1. ORTEP representation of complex **2** in the solid state. Thermal ellipsoids are at 40% probability. The labels for the phenyl carbon atoms are omitted for clarity. Selected bond lengths [Å] and angles [°]: Ru-C(1) 1.780(9), Ru-C(2) 2.043(8), Ru···C(10) 2.765(10), Ru-Cl(1) 2.525(4), Ru-P(1) 2.351(3), Ru-P(2) 2.349(3); C(1)-Ru-C(2) 90.2(4), C(2)-Ru-P(2) 84.8(2), C(2)-Ru-P(1) 95.1(2), C(2)-Ru-Cl(1) 91.7(3), P(1)-Ru-P(2) 179.8(2), C(1)-Ru-Cl(1) 176.1(3), Ru-P(1)-C(12) 112.1(4).

Complex **2** undergoes facile displacement of the $(2,6\text{-}Me_2C_6H_3)PPh_2$ group with phosphorus or nitrogen ligands to afford a new class of cyclometalated derivatives of general formula $[RuCl(CO)\{(2\text{-}CH_2\text{-}6\text{-}MeC_6H_3)PPh_2\}L_n]$ ($n = 1$, 2). Although the corresponding five-coordinate derivative is obtained with the bulky phosphane PCy_3, reaction of **2** with two equivalents of $PMePh_2$ leads to the six-coordinate compound $[RuCl(CO)\{(2\text{-}CH_2\text{-}6\text{-}MeC_6H_3)PPh_2\}(PMePh_2)_2]$ (**3**).[12] These complexes have been proven to catalyze the reduction of acetophenone to 1-phenylethanol through hydrogen transfer using 2-propanol as the hydrogen source [Eq. (2)].



(2)

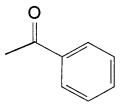
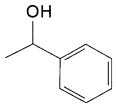
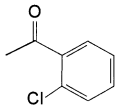
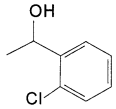
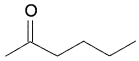
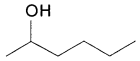
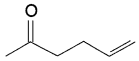
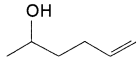
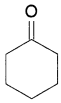
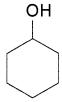
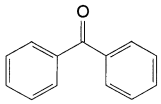
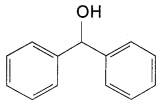
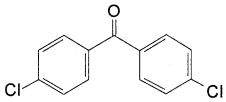
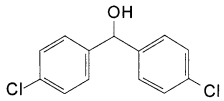
R, R' = alkyl, aryl

 © 2004 Wiley-VCH Verlag GmbH & Co. KGaA, Weinheim

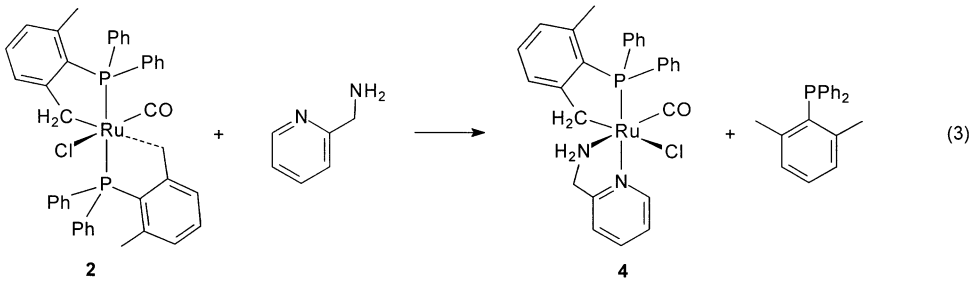
Importantly, the systems comprised of **2** and bidentate nitrogen ligands were found to be very active. Whereas complete conversion of acetophenone is achieved with **2**/ethylendiamine in 0.5 h (ketone/Ru/NaOH = 1000:1:20; TOF = 2800 h^{-1}), the reduction occurs within a few minutes with **2**/2-(aminomethyl)pyridine. Treatment of **2** with an equimolar amount of the latter ligand affords the highly efficient catalyst **4**,[13] which exhibits the same activity of the in situ prepared **2**/2-(aminomethyl)pyridine system [Eq. (3)].

Attempts to obtain suitable crystals of **4** for X-ray analysis failed. The proposed structure was supported by ^{1}H NMR and ROESY experiments; the latter showed NOE correlations between the protons of the {$RuCH_2$} moiety and those of the pyridine ligand. The carbon atoms of the pyridine ligand appear as singlets in the $^{13}C\{^1H\}$ NMR spectrum, whereas the CH_2NH_2 group *cis* to the phosphorus center appears as a doublet at $\delta = 48.8$ ppm ($^3J(C,P) = 2.9$ Hz). Furthermore, the IR spectrum of **4** shows a $\tilde{\nu}_{CO}$ band at a low wavenumber (1912 cm^{-1}), which is consistent with a strong σ-donating ligand in the *trans* position.

Table 1: Reduction of ketones (0.1 M) with **4** (0.05 mol%) and NaOH (2 mol%) in 2-propanol at 82 °C.

Ketone	Alcohol	Conversion [%][a] (min)	TOF [h^{-1}][b]
		98 (5)	60000
		99 (10)	28800
		99 (10)	63000
		95 (10)	30000
		99 (10)	33600
		99 (15)	19000
		95 (5)	36000
		98 (10)	17700

[a] The conversion was determined by GC analysis. [b] Turnover frequency (moles of ketone converted into alcohol per mole of catalyst per hour) at 50% conversion.



2 **4** (3)

A large number of alkyl aryl, dialkyl (linear and cyclic), and diaryl ketones can be converted into alcohols *quantitatively*, within a few minutes at 82 °C using catalyst **4** and a substrate/**4** ratio of 2000:1 or higher. The turnover frequencies at 50% conversion are in the range 17700–63000 h^{-1} (Table 1), depending on the stereoelectronic features of the substrate, and these values are among the highest reported in the literature.[1i,9b,14]

It is noteworthy that ketones containing an olefinic function (such as 5-hexen-2-one) can be selectively converted into the corresponding alcohol without hydrogenation or isomerization of the double bond. The high catalytic performance of **4** enables this complex to be used for preparative purposes with a substrate/catalyst ratio of up to 10000:1. Benzhydrols, which are important intermediates for the synthesis of pharmaceuticals, can now be easily prepared from diaryl ketones by transfer hydrogenation, instead of using dihydrogen.[15] Thus, starting from 3.64 g of benzophenone (0.1 M in 2-propanol) and 1.2 mg of **4** (ketone/**4**/NaOH = 10000:1:200) benzhydrol can be formed in 2 h under reflux conditions (90% yield of isolated product).

According to the mechanism proposed by Noyori and coworkers for Ru^{II}–amine complexes, it is likely that **4** reacts with the base to afford the corresponding amide compound on elimination of HCl. The subsequent reaction with 2-propanol leads to the key ruthenium hydride amine species that reduces the ketone to the alcohol with the formation of the amide, which closes the cycle.[16a] Alternatively, the active hydride catalyst may be generated from **4** through the alkoxide route.[16b] The very high catalytic performance of **4** can be ascribed to the presence of a bifunctional Ru-H/N-H motif,[17] which is associated with the stable Ru–C σ bond. It is noteworthy that the catalytically active species is not extremely sensitive to oxygen and, in addition, deactivation

 © 2004 Wiley-VCH Verlag GmbH & Co. KGaA, Weinheim

occurs slowly during catalysis, as proven by the fact that subsequently added acetophenone (up to three times) undergoes quantitative conversion. Therefore, catalyst **4** can be used in a very low amount (0.01 mol%), in contrast to the most active ruthenium catalysts which undergo rapid leaching. Since chiral ligands related to 2-(aminomethyl)pyridine have been recently employed in asymmetric hydrogen-transfer reactions with ruthenium,[18] their use with **2** holds promise for obtaining high-speed enantioselective catalysts.

In summary, the δ-agostic compound **2**, prepared from the 14-electron species **1**, gives access to the synthesis of a new class of cyclometalated derivatives. Complex **4**, prepared from **2** and 2-(aminomethyl)pyridine, is one of the most active catalysts for the reduction of ketones in 2-propanol by a hydrogen-transfer reaction. The presence of a robust cyclometalated metal–carbon bond apparently allows the formation of long-living catalytic species, which may have great potential for use in other catalytic reactions and synthetic methods.

Experimental Section

2: Triethylamine (1.90 mL, 13.6 mmol) and formaldehyde (1.00 mL, 37% solution in water, 13.4 mmol) were added to a suspension of **1** (2.00 g, 2.66 mmol) in ethanol (40 mL) under argon. The mixture was refluxed for 2 h and then concentrated to half its volume. After filtration, the product was dried under reduced pressure. Yield: 1.60 g (81%).

4: 2-(Aminomethyl)pyridine (90 μL, 0.87 mmol) and $CaCO_3$ (39 mg, 0.39 mmol) were added to a solution of **2** (535 mg, 0.72 mmol) in dichloromethane (10 mL) under argon. The suspension was heated at reflux overnight, filtered, and concentrated. The product was precipitated with diethyl ether, filtered, and dried under reduced pressure. Yield: 308 mg (76%).

Typical procedure for the catalytic hydrogen-transfer reaction: Complex **4** (2.8 mg, 5.0 μmol) was dissolved in a 0.04 M solution of NaOH in 2-propanol (5 mL). The ketone (2 mmol) was dissolved in 2-propanol (19 mL) and the solution was heated to reflux under argon. Addition of the solution of **4** (1 mL) resulted in the immediate reduction of the ketone and the yield was determined by GC analysis (ketone/**4**/NaOH = 2000:1:40; ketone 0.1 M).

Received: March 5, 2004 [Z54199]

Keywords: cyclometalation · homogeneous catalysis · noncovalent interactions · P ligands · ruthenium

[1] a) M. Albrecht, G. van Koten, *Angew. Chem.* **2001**, *113*, 3866; *Angew. Chem. Int. Ed.* **2001**, *40*, 3750; b) M. E. van der Boom, D. Milstein, *Chem. Rev.* **2003**, *103*, 1759; c) J. T. Singleton, *Tetrahedron* **2003**, *59*, 1837; d) M. Ohff, A. Ohff, M. E. van der Boom, D. Milstein, *J. Am. Chem. Soc.* **1997**, *119*, 11687; e) F. Miyazaki, K. Yamaguchi, M. Shibasaky, *Tetrahedron Lett.* **1999**, *40*, 7379; f) S. Gibson, D. F. Foster, G. R. Eastham, R. P. Tooze, D. J. Cole-Hamilton, *Chem. Commun.* **2001**, 779; g) M. Gupta, C. Hagen, W. C. Kaska, R. E. Cramer, C. M. Jensen, *J. Am. Chem. Soc.* **1997**, *119*, 840; h) F. Liu, E. B. Pak, B. Singh, C. M. Jensen, A. S. Goldman, *J. Am. Chem. Soc.* **1999**, *121*, 4086; i) P. Dani, T. Karlen, R. A. Gossage, S. Gladiali, G. van Koten, *Angew. Chem.* **2000**, *112*, 759; *Angew. Chem. Int. Ed.* **2000**, *39*, 743.

[2] a) A. D. Ryabov, *Chem. Rev.* **1990**, *90*, 403; b) I. Omae, *Coord. Chem. Rev.* **1980**, *32*, 235.

[3] a) W. A. Herrmann, C. Brossmer, C.-P. Reisinger, T. H. Riermeier, K. Öfele, M. Beller, *Chem. Eur. J.* **1997**, *3*, 1357; b) V. P. W. Böhm, W. A. Herrmann, *Chem. Eur. J.* **2001**, *7*, 4191; c) J. Dupont, M. Pfeffer, J. Spencer, *Eur. J. Inorg. Chem.* **2001**, 1917.

[4] T. Naota, H. Takaya, S.-I. Murahashi, *Chem. Rev.* **1998**, *98*, 2599.

[5] a) L. N. Lewis, *J. Am. Chem. Soc.* **1986**, *108*, 743; b) L. N. Lewis, J. F. Smith, *J. Am. Chem. Soc.* **1986**, *108*, 2728.

[6] W. Baratta, E. Herdtweck, P. Rigo, *Angew. Chem.* **1999**, *111*, 1733; *Angew. Chem. Int. Ed.* **1999**, *38*, 1629.

[7] W. Baratta, S. Stoccoro, A. Doppiu, E. Herdtweck, A. Zucca, P. Rigo, *Angew. Chem.* **2003**, *115*, 109; *Angew. Chem. Int. Ed.* **2003**, *42*, 105.

[8] W. Baratta, E. Herdtweck, P. Martinuzzi, P. Rigo, *Organometallics* **2001**, *20*, 305.

[9] a) G. Zassinovich, G. Mestroni, S. Gladiali, *Chem. Rev.* **1992**, *92*, 1051; b) R. Noyori, S. Hashiguchi, *Acc. Chem. Res.* **1997**, *30*, 97; c) J. E. Bäckvall, *J. Organomet. Chem.* **2002**, *652*, 105; d) S. Gladiali, G. Mestroni in *Transition Metals for Organic Synthesis*, *Vol. 2* (Eds.: M. Beller, C. Bolm), Wiley-VCH, Weinheim, **1998**, p. 97.

[10] **2**: ^{1}H NMR (200.1 MHz, $CDCl_3$, 20 °C, TMS): $\delta = 7.8$–6.9 (m, 26H; aromatic protons), 3.48 (d, J(H,H) = 13.4 Hz, 1H; $RuCH_2$), 3.29 (dd, J(H,H) = 13.4 Hz, J(H,P) = 5.4 Hz, 1H; CH_2), 1.76 (s, 3H; CH_3), 1.64 ppm (s, 6H; CH_3); ^{31}P{^{1}H} NMR (81.0 MHz, $CDCl_3$, 20 °C, H_3PO_4): $\delta = 53.7$ (d, J(P,P) = 301 Hz; PC), 32.8 ppm (d, J(P,P) = 301 Hz; P); IR (nujol): $\tilde{\nu}$(CO) = 1923 cm^{-1}; elemental analysis (%) calcd for $C_{41}H_{37}ClOP_2Ru$: C 66.2, H 5.0; found: C 65.9, H 5.0.

[11] Crystal structure analysis of **2**, $C_{41}H_{37}ClOP_2Ru$, $M_r = 744.17$, monoclinic, space group $P2_1$, $a = 9.502(3)$, $b = 9.974(3)$, $c = 19.771(6)$ Å, $\beta = 111.98(2)°$, $V = 1737.5(9)$ Å^3, $Z = 2$, $\rho_{calcd} = 1.422$ g cm^{-3}, $\mu(Mo_{K\alpha}) = 0.652$ mm^{-1}, $F(000) = 764$, $2.16 < \theta < 29.94°$. Final $R1 = 0.0497$, $wR2 = 0.1454$, $S = 1.045$ for 412 parameters and 9754 reflections, 9401 unique ($R_{int} = 0.0393$), max positive and negative peaks in ΔF map 0.691 and -0.821 e Å^{-3}. Data were were collected at 150(2) K on a Nonius DIP-1030H system with $Mo_{K\alpha}$ radiation ($\lambda = 0.71073$ Å).

[12] The molecular structure of **3** is related to that of **2** with two $PMePh_2$ ligands *trans* to the cyclometalated phosphane. **3**·0.5 Et_2O: $C_{49}H_{49}ClO_{1.50}P_3Ru$, $M_r = 891.31$, monoclinic, space group $C2/c$, $a = 21.735(5)$, $b = 10.385(3)$, $c = 37.589(6)$ Å, $\beta = 94.50(2)°$, $V = 8458(3)$ Å^3, $Z = 8$, $\rho_{calcd} = 1.400$ g cm^{-3}, $\mu(Mo_{K\alpha}) = 0.586$ mm^{-1}, $F(000) = 3688$, $2.17 < \theta < 27.10°$. Final $R1 = 0.0462$, $wR2 = 0.1459$, $S = 1.060$ for 506 parameters and 10511 reflections, 6096 unique (R(int) = 0.0470), residuals in ΔF map 0.680, -0.778 e Å^{-3}. Data were collected at 150(2) K on a Nonius DIP-1030H system with $Mo_{K\alpha}$ radiation ($\lambda = 0.71073$ Å). CCDC-224572 (**2**) and CCDC-224573 (**3**) contain the supplementary crystallographic data for this paper. These data can be obtained free of charge via www.ccdc.cam.ac.uk/conts/retrieving.html (or from the Cambridge Crystallographic Data Centre, 12 Union Road, Cambridge CB2 1EZ, UK; fax: (+44) 1223-336-033; or deposit@ccdc.cam.ac.uk)..

[13] **4**: ^{1}H NMR (200.1 MHz, $CDCl_3$, 20 °C, TMS): $\delta = 9.01$ (d, J(H,H) = 5.6 Hz, 1H; o-C_5H_4N), 7.92–6.88 (m, 16H; aromatic protons), 4.35 (d pseudot, J(H,H) = 16.1 Hz, J(H,H) = 4.4 Hz, 1H; CH_2N), 4.01 (d pseudot, J(H,H) = 16.2 Hz, J(H,H) = 6.4 Hz, 1H; CH_2N), 3.05 (m, 1H; NH_2), 2.95 (d, J(H,H) = 14.9 Hz, 1H; $RuCH_2$), 2.15 (d, J(H,H) = 14.8 Hz, 1H; $RuCH_2$), 1.85 (m, 1H; NH_2), 1.76 ppm (s, 3H; CH_3); ^{13}C{^{1}H} NMR (50.3 MHz, $CDCl_3$, 20 °C, TMS): $\delta = 205.4$ (d, J(C,P) = 19.1 Hz; CO), 164.1 (d, J(C,P) = 31.8 Hz; CCH_2Ru), 159.7 (s; $NCCH_2$), 152.3 (s; o-C_5H_4N), 141.3 (s, $CCCH_3$), 136.4 (s; p-C_5H_4N), 135.1–120.9 (aromatic carbon atoms), 48.8 (d, J(C,P) = 2.9 Hz; CH_2NH_2), 23.1 (d, J(C,P) = 3.6 Hz; $RuCH_2$), 22.3 ppm (d, J(C,P) = 3.8 Hz; CH_3); ^{31}P{^{1}H} NMR (81.0 MHz, $CDCl_3$, 20 °C,

 © 2004 Wiley-VCH Verlag GmbH & Co. KGaA, Weinheim

H_3PO_4): $\delta = 67.9$ ppm (s). IR (nujol): $\tilde{\nu}(CO) = 1912\ cm^{-1}$; elemental analysis (%) calcd for $C_{27}H_{26}ClN_2OPRu$: C 57.7, H 4.7, N 5.0; found: C 57.3, H 4.6, N 5.0.

[14] a) R. L. Chowdhury, J. E. Bäckvall, *J. Chem. Soc. Chem. Commun.* **1991**, 1063; b) H. Yang, M. Alvarez, N. Lugan, R. Mathieu, *J. Chem. Soc. Chem. Commun.* **1995**, 1721; c) H. Yang, M. Alvarez-Gressier, N. Lugan, R. Mathieu, *Organometallics* **1997**, *16*, 1401; d) P. Crochet, J. Gimeno, S. García-Granada, J. Borge, *Organometallics* **2001**, *20*, 4369.

[15] T. Ohkuma, M. Koizumi, H. Ikehira, T. Yokozawa, R. Noyori, *Org. Lett.* **2000**, *2*, 659.

[16] a) K.-J. Haack, S. Hashiguchi, A. Fujii, T. Ikariya, R. Noyori, *Angew. Chem.* **1997**, *109*, 297; *Angew. Chem. Int. Ed. Engl.* **1997**, *36*, 285; b) A. Aranyos, G. Csjernyik, K. J. Szabó, J. E. Bäckvall, *Chem. Commun.* **1999**, 351.

[17] a) M. Yamakawa, H. Ito, R. Noyori, *J. Am. Chem. Soc.* **2000**, *122*, 1466; b) K. Abdur-Rashid, S. E. Clapham, A. Hadzovic, J. N. Harvey, A. J. Lough, R. H. Morris, *J. Am. Chem. Soc.* **2002**, *124*, 15104; c) V. Rautenstrauch, X. Hoang-Cong, R. Churlaud, K. Abdur-Rashid, R. H. Morris, *Chem. Eur. J.* **2003**, *9*, 4954.

[18] a) E. Mizushima, H. Ohi, M. Yamaguchi, T. Yamagishi, *J. Mol. Catal. A* **1999**, *149*, 43; b) H. Brunner, M. Niemetz, *Monatsh. Chem.* **2002**, *133*, 115; c) H. Brunner, F. Henning, M. Weber, *Tetrahedron: Asymmetry* **2002**, *13*, 37.

 © 2004 Wiley-VCH Verlag GmbH & Co. KGaA, Weinheim

Gas-Phase Reactions

An Unusually Fast Nucleophilic Aromatic Displacement Reaction: The Gas-Phase Reaction of Fluoride Ions with Nitrobenzene**

*Tatiana Giroldo, Luciano A. Xavier, and José M. Riveros**

Dedicated to Professor Nicola Petragnani on the occasion of his 75th birthday

Nucleophilic displacement reactions in aromatic systems play an important role in organic chemistry and become possible when the aromatic ring is activated by electron-withdrawing substituents.[1] The most common mechanism for aromatic nucleophilic substitution (S_NAr) involves a multistep addition–elimination pathway[2] through the rate-determining formation of well-characterized σ-complex intermediates.[3] Although benzyne-type processes and electron-transfer mechanisms[4] can also mediate nucleophilic reactions in aromatic compounds, direct displacement by means of a backside attack has long been argued to be an energetically demanding pathway for monosubstituted aromatic substrates and thus regarded as very unfavorable.

Unlike S_N2 reactions, aromatic nucleophilic substitution reactions have not been well characterized in the gas phase, in which intrinsic reactivity can be assessed unequivocally.[5,6] The fact that the acidity of simple halobenzenes is comparable to that of methanol in the gas phase[7] (see Supporting Information) has precluded detailed gas-phase studies, because proton abstraction becomes the dominant reaction for some of the usual strong gas-phase nucleophiles.[8] Although multiple fluorine substitution has been shown to give rise to very diverse chemistry,[5a,c–e] the role of σ complexes in gas-phase reactions remains controversial.[9] For example, recent ab initio calculations for the symmetric $X^- + C_6H_5X$ (X = F, Cl, Br, I) gas-phase reactions led to the conclusion that σ complexes are stable intermediates for X = F, but local transition states in the other cases.[9c] Herein we report the observation of very fast gas-phase aromatic nucleophilic substitution reactions with nitrobenzene as substrate [Eq. (1)].

$$F^- + C_6H_5NO_2 \rightarrow NO_2^- + C_6H_5F \qquad (1)$$

The kinetics of this reaction were studied by FT ICR mass spectrometry[10,11] at typical pressures ($< 10^{-7}$ mbar), and the rate constants were determined from kinetic plots obtained for different partial pressures of nitrobenzene at 335 K (average temperature of the cell due to heating by the ionizing filament). These experiments lead to a bimolecular rate constant for [Eq. (1)]:

$$k_1 = (3.05 \pm 0.10) \times 10^{-9}\ \text{cm}^3\ \text{molecule}^{-1}\ \text{s}^{-1}.$$

This value, when compared with that estimated for the ADO (average dipole orientation) collision rate constant,[12] indicates that 69 % of the ion–molecule collisions are reactive and yield the products shown above. This remarkably high efficiency (fraction of collisions that yield products) is indeed surprising and several aspects should be noted:

a) Although [Eq. (1)] is exothermic by 28.7 kcal mol^{-1} at 298 K,[13] its high efficiency is unusual considering the type of reaction and the leaving group involved. This efficiency is, in fact, comparable to that of other barrier-free gas-phase ion–molecule reactions proceeding through a double-minimum potential such as gas-phase S_N2 reactions.[14]
b) The possibility of a benzyne mechanism can be discarded because the resulting neutral products, namely HF and C_6H_4, would make the displacement significantly endothermic.[13]
c) No other product ions were observed for this system under our experimental conditions.

To characterize the mechanism of [Eq. (1)], DFT calculations were carried out at the B3LYP/6-311++G(d,p)//B3LYP/6-311++G(d,p) level of theory using the Gaussian98 suite of programs.[15] Frequency calculations were carried out

[*] T. Giroldo, Dr. L. A. Xavier, Prof. J. M. Riveros
Institute of Chemistry, University of São Paulo
Caixa Postal 26077, São Paulo CEP 05513-970 (Brazil)
Fax: (+55) 11-3091-3888
E-mail: jmrnigra@iq.usp.br

[**] We thank the São Paulo Science Foundation (FAPESP), the Brazilian Research Council (CNPq), and the Millennium Institute of Complex Materials for financial support.

Supporting information for this article is available on the WWW under http://www.angewandte.org or from the author.

 © 2004 Wiley-VCH Verlag GmbH & Co. KGaA, Weinheim DOI: 10.1002/anie.200454230

for all species to establish their nature as local minima or transition states. Enthalpy changes were calculated from the energies of the optimized structures, and thermal corrections included for 298 K without any scaling of the calculated vibrational frequencies (see Supporting Information). The theoretical estimate for the $\Delta H°$ of [Eq. (1)] amounts to -28.2 kcal mol^{-1}, which is in very close agreement with the experimental value. Several stable ion–molecule intermediates were found from the interaction of F^- with nitrobenzene as a result of an extensive optimization procedure that included a search for geometries containing in-plane and out-of-plane F^-. The most stable complex, **1a**, results from an F^- ion loosely bound to the *para*-H atom of nitrobenzene, as might be expected when considering the strong ion–dipole interaction. Very stable and similar complexes were also found for F^- ions loosely bound to the *ortho*- and *meta*-H atoms of nitrobenzene. Two different types of stable complexes were also identified as resulting from the out-of-plane attack of F^- at the *para* position of **1b** and at the *ipso* carbon atom of **1c**. Figure 1 summarizes the calculated energy

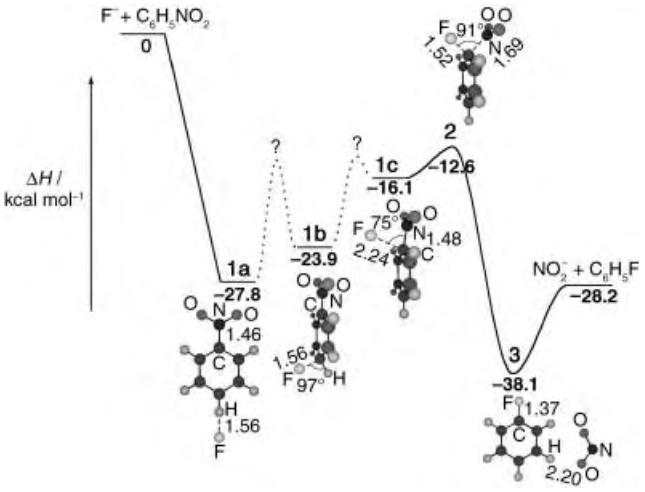


Figure 1. Calculated energy diagram for [Eq. (1)] at the B3LYP/6-311++G(d,p)//B3LYP/6-311++G(d,p) level, including the optimized structures of the different intermediates, and the local transition state for the reaction.

diagram and the important optimized structures. At this stage, we have not searched for the possible local transition states connecting **1a**, **1b**, and **1c**, as our primary interest was to characterize how **1c** evolves into the products of [Eq. (1)]. We can then envision Equation (1) as proceeding initially through the formation of a very stable complex such as **1a** (Figure 1) leading to the prereaction complex **1c**, a stable ion–molecule adduct arising from an out-of-plane attack of F^- at the *ipso* carbon atom. This species is a typical ion–molecule complex in which the calculated C–F bond length (2.24 Å) is well outside the value of covalent bonding. Complex **1c** then proceeds through the local transition state **2** that displays an imaginary frequency corresponding to the NO_2 bond breaking process, and is located only 3.5 kcal mol^{-1} above the reactant-side complex. Finally, the departing NO_2^- gives rise to a stable ion–molecule complex **3** of fluorobenzene and NO_2^-, in which

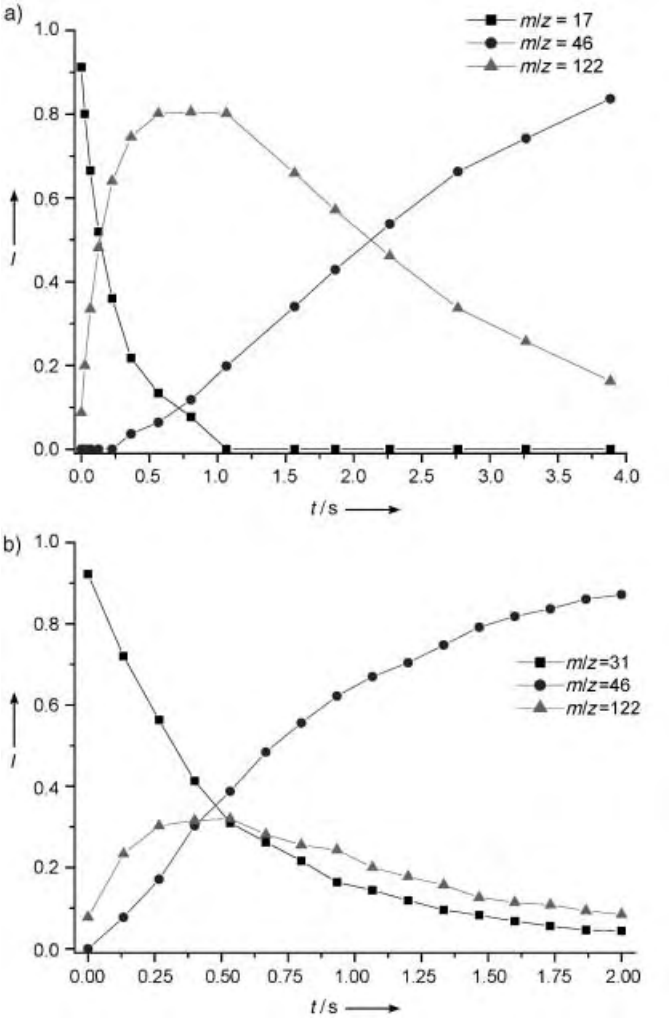


Figure 2. a) Kinetic plot of the gas-phase reaction of OH^- ($m/z=17$) with nitrobenzene reveals rapid proton transfer to yield $C_6H_4NO_2^-$ ($m/z=122$) and H_2O. The subsequent reaction of the $C_6H_4NO_2^-$ ion with neutral H_2O yields NO_2^- ($m/z=46$) and phenol. This secondary reaction is clearly observed from the delay in the appearance of the NO_2^- ion. b) A similar kinetic plot of the gas-phase reaction of MeO^- ($m/z=31$) with nitrobenzene reveals competition between proton transfer (to yield $C_6H_4NO_2^-$ ($m/z=122$) and methanol) and NO_2^- ($m/z=46$) displacement (with formation of anisole). $C_6H_4NO_2^-$ ($m/z=122$) then undergoes a subsequent reaction with neutral H_2O (used to generate MeO^- from the reaction of OH^- with MeOH) to yield NO_2^- ($m/z=46$) and phenol as in Figure 2a.

the ion has moved away from the carbon center and rotated around so that the oxygen atoms saddle the *ortho* and *meta* hydrogen atoms of the ring.[16] According to these calculations, the prototype Meisenheimer complex **2**, although below the energy of the reactants, is a *transition state* and not a *local energy minimum*. The calculated potential energy diagram is highly reminiscent of the typical energy diagram for common exothermic gas-phase ion–molecule reactions,[17] and is in agreement with the results obtained from ab initio calculations on the symmetric exchange reactions $X^- + C_6H_5X$ for X = Cl, Br, and I.[9c] Furthermore, our DFT calculations are believed to provide reasonably reliable estimates considering

 © 2004 Wiley-VCH Verlag GmbH & Co. KGaA, Weinheim

the agreement obtained in reference [9c] for the complexation energies calculated at different levels of theory. Finally, the low local energy barrier found for the nucleophilic displacement suggests that [Eq. (1)] should be fast, and its efficiency dictated by the density of states of the transition state.[18]

The displacement of NO_2^- from nitrobenzene by other nucleophiles other than F^- [19] was also observed for alkoxide ions, RO^- (R = Me, Et, *i*Pr), and OH^-. Nitrobenzene reacts rapidly with hydroxide ion by proton transfer to yield $C_6H_4NO_2^-$ at $m/z = 122$, and this product ion then undergoes secondary reactions with neutral water (used to generate the OH^- ions) to yield NO_2^- and phenol.[20] A similar behavior is observed with MeO^-, although the direct displacement becomes competitive with proton abstraction. The behavior of OH^- and MeO^- is illustrated in Figure 2. The corresponding reaction with EtO^- yields primarily NO_2^- and very little proton abstraction, whereas *i*PrO^- yields exclusively the aromatic displacement reaction. In the last two cases, the observed nucleophilic displacement reactions are not as fast as that reported for **1** but the reactions do proceed readily under our experimental conditions.

The present combined experimental and theoretical results show for the first time that direct aromatic nucleophilic displacement can, in fact, be an extremely facile process in the gas phase, and can proceed through a potential energy surface similar to those observed for other gas-phase ion-molecule reactions. Furthermore, the present observations open up a range of possibilities regarding the experimental study of these reactions and the role of σ complexes in the gas phase, as well as theoretical studies dealing with the dynamics of these reactions.

Received: March 10, 2004 [Z54230]

Keywords: ab initio calculations · aromatic substitution · gas-phase reactions · ion–molecule reactions · nucleophilic substitution

[1] a) F. Terrier, *Nucleophilic Aromatic Displacement—The Influence of the Nitro Group, Wiley, New York*, **1991**; b) F. A. Carey, R. J. Sundberg, *Advanced Organic Chemistry. Part A: Structure and Mechanisms*, 3rd ed., Plenum, New York, **1990**, p. 579.

[2] a) J. F. Bunnett, R. E. Zahler, *Chem. Rev.* **1951**, *49*, 293–412; b) J. Miller, *Aromatic Nucleophilic Substitution*, Elsevier, Amsterdam, **1968**.

[3] a) F. Terrier, *Chem. Rev.* **1982**, *82*, 78–152; b) G. A. Artamkina, M. P. Egorov, I. P. Beletskaya, *Chem. Rev.* **1982**, *82*, 427–459.

[4] See, for example: J. M. Savéant, *Tetrahedron* **1994**, *50*, 10117–10165, and references therein.

[5] a) S. M. J. Briscese, J. M. Riveros, *J. Am. Chem. Soc.* **1975**, *97*, 230–231; b) J. H. Bowie, B. J. Stapleton, *Aust. J. Chem.* **1977**, *30*, 795–800; c) S. Ingemann, N. M. M. Nibbering, *J. Org. Chem.* **1983**, *48* 183–191; d) S. Ingemann, N. M. M. Nibbering, S. A. Sullivan, C. H. DePuy, *J. Am. Chem. Soc.* **1982**, *104*, 6520–6527; e) S. Ingemann, N. M. M. Nibbering, *Nouv. J. Chim.* **1984**, *8*, 299–304; f) S. L. Van Orden, R. M. Pope, S. W. Buckner, *Org. Mass Spectrom.* **1991**, *26*, 1003–1007; g) J. M. Riveros, S. Ingemann, N. M. M. Nibbering, *J. Am. Chem. Soc.* **1991**, *113*, 1053; h) H. V. Linnert, J. M. Riveros, *Int. J. Mass Spectrom. Ion Processes* **1994**, *140*, 163–176.

[6] J. K. Laerdahl, E. Uggerud, *Int. J. Mass Spectrom.* **2002**, *214*, 277–314, and references therein.

[7] a) M. Meot-Ner (Mautner), S. A. Kafafi, *J. Am. Chem. Soc.* **1988**, *110*, 6297–6303; b) P. B. M. Andrade, J. M. Riveros, *J. Mass Spectrom.* **1996**, *31*, 767–770.

[8] a) P. G. Wenthold, R. R. Squires, *J. Am. Chem. Soc.* **1994**, *116*, 6401–6412; b) H. E. K. Matimba, S. Ingemann, N. M. M. Nibbering, *J. Am. Soc. Mass Spectrom.* **1993**, *4*, 73–81.

[9] a) B. Y. Simkin, E. B. Gluz, M. N. Glukhovtsev, V. I. Minkin, *J. Mol. Struct. (Theochem)* **1993**, *103*, 123–137; b) Y. J. Zheng, R. L. Ornstein, *J. Am. Chem. Soc.* **1997**, *119*, 648–655; c) M. N. Glukhovtsev, R. D. Bach, S. Laiter, *J. Org. Chem.* **1997**, *62*, 4036–4046.

[10] In these studies, F^- ions ($m/z = 19$) were generated inside the cell of our FT ICR spectrometer by dissociative electron attachment of NF_3 at pressures of the order of 3.7×10^{-8} mbar. In the presence of nitrobenzene (typical pressures $\approx 3.7 \times 10^{-8}$ mbar), the fluoride ions react rapidly to yield NO_2^- ions ($m/z = 46$), and these NO_2^- ions were observed to disappear completely upon pumping away NF_3. Absolute pressures were obtained from an independent calibration of the ion gauge sensitivity and position against a capacitance micromanometer by using a procedure developed in these laboratories.

[11] P. R. P. de Moraes, H. V. Linnert, M. Aschi, J. M. Riveros, *J. Am. Chem. Soc.* **2000**, *122*, 10133–10142, and references therein.

[12] T. Su, M. T. Bowers in *Gas Phase Ion Chemistry* (Ed.: M. T. Bowers), Academic Press, New York, **1979**, p. 83.

[13] See Supporting Information.

[14] C. H. DePuy, S. Gronert, A. Mullin, V. Bierbaum *J. Am. Chem. Soc.* **1990**, *112*, 8650–8655.

[15] Gaussian 98 (Revision A.7), M. J. Frisch, G. W. Trucks, H. B. Schlegel, G. E. Scuseria, M. A. Robb, J. R. Cheeseman, V. G. Zakrzewski, J. A. Montgomery, R. E. Stratmann, J. C. Burant, S. Dapprich, J. M. Millam, A. D. Daniels, K. N. Kudin, M. C. Strain, O. Farkas, J. Tomasi, V. Barone, M. Cossi, R. Cammi, B. Mennucci, C. Pomelli, C. Adamo, S. Clifford, J. Ochterski, G. A. Petersson, P. Y. Ayala, Q. Cui, K. Morokuma, D. K. Malick, A. D. Rabuck, K. Raghavachari, J. B. Foresman, J. Cioslowski, J. V. Ortiz, B. B. Stefanov, G. Liu, A. Liashenko, P. Piskorz, I. Komaromi, R. Gomperts, R. L. Martin, D. J. Fox, T. Keith, M. A. Al-Laham, C. Y. Peng, A. Nanayakkara, C. Gonzalez, M. Challacombe, P. M. W. Gill, B. G. Johnson, W. Chen, M. W. Wong, J. L. Andres, M. Head-Gordon, E. S. Replogle, J. A. Pople, Gaussian, Inc., Pittsburgh, PA, **1998**.

[16] This product side complex is identical to that found in the ab inito study of the aromatic nucleophilic substitution reaction of MeS^- with 2,4-dinitrochlorobenzene.[9b]

[17] M. L. Chabinyc, S. L. Craig, C. K. Regan, J. I. Brauman, *Science* **1998**, *279*, 1882–1886.

[18] See, for example: B. D. Wladkowski, K. F. Lim, W. D. Allen, J. I. Brauman, *J. Am. Chem. Soc.* **1992**, *114*, 9136–9153.

[19] Fluoride ions have been considered to be the most powerful nucleophiles for S_NAr reactions; see: V. M. Vlasov, *J. Fluorine Chem.* **1993**, *61*, 193–216.

[20] This behavior is similar to that observed with the halobenzenes; the halophenide ions, $C_6H_4X^-$, undergo exchange reactions with H_2O (or D_2O), and the nascent OH^- in the collision complex promotes nucleophilic substitution (see, for example, reference [5h] and references therein). In fact, reaction of $C_6H_4NO_2^-$ with D_2O yields both NO_2^- and the whole family of $C_6H_{4-n}D_nNO_2^-$ ($n = 1$–4) as product ions.

 © 2004 Wiley-VCH Verlag GmbH & Co. KGaA, Weinheim

DNA Bisintercalators

Design of a Sequence-Specific DNA Bisintercalator**

*Eric J. Fechter, Bogdan Olenyuk, and Peter B. Dervan**

The development of sequence-specific DNA bisintercalators has been an ongoing challenge in the field of bioorganic chemistry and molecular recognition. Since the first proposed model of intercalation by Lerman,[1] the disruption of transcription or replication by helix unwinding and extension has become an attractive strategy for blocking essential gene functions in the field of cancer therapy and antibiotics, but these methods have proved toxic, presumably owing to lack of specificity (Figure 1 a).[2] By the mid-1970s Waring and coworkers had reported the DNA-binding characteristics of the first known bisintercalating natural product, echinomycin[3] (Figure 1 b). This pseudosymmetrical bifuntional molecule is part of a larger class, known as quinoxaline antibiotics, and contains a cyclic octapeptide minor-groove-binding region with two linked chromophores capable of simultaneous intercalation.[4] The minor-groove-binding bicyclic depsipeptide backbone undergoes hydrogen bonding to DNA bases and was thought to impose the modest sequence specificity for poly(dG–dC) sites.[3] Similarly, the related bisintercalator triostin[5] also inhibits DNA replication and RNA synthesis,[6] yet has a slight specificity toward poly(dA–dT) sites.[7] As with other members of the quinoxaline family of antibiotics, the incorporation of modified amino acids presumably provides the relative specificities.

Synthetic bisintercalators were later constructed by linking two heterocycles, such as acridines,[8] methidium,[9] and anthracyclines,[10] with chains of varying lengths to maximize the bracketing of two (or more) base pairs between the intercalator sites (Figure 1 c). In general, these molecules have enhanced affinity for DNA but lack significant sequence specificity. To our knowledge, in the past 30 years, attempts to design bisintercalators with *programmable* sequence specificity have been largely unsuccessful.

We recently reported the synthesis of a hybrid molecule, a hairpin polyamide–acridine conjugate, which enforces two very different modes of DNA binding: groove binding and intercalation.[11] Remarkably, the pyrrole–imidazole polyamide, which prefers to bind B-form DNA, maintains its sequence specificity despite the presence of an adjacent intercalated acridine moiety which extends and unwinds the helix (unwinding angle $\phi = 14$–15°) proximal to the groove-binding ligand.[11]

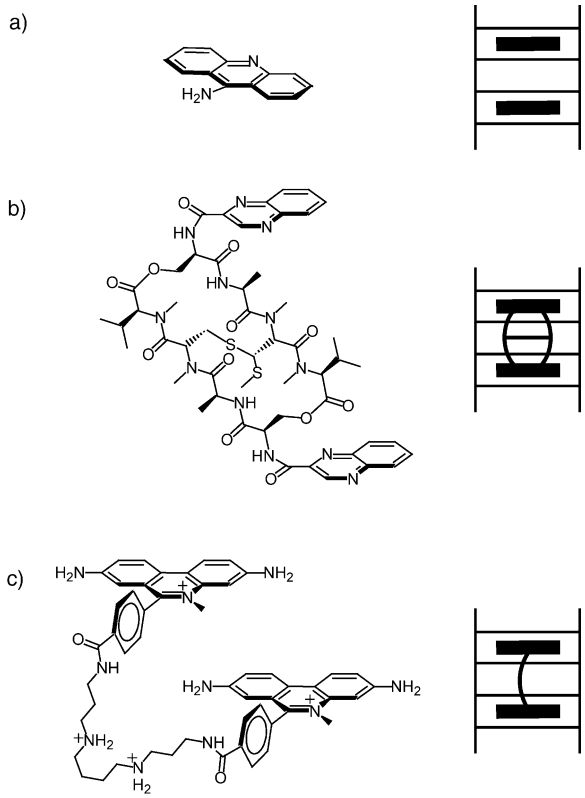


Figure 1. Intercalative models: molecular structures (left) and binding models with the shaded bars depicting the acridine intercalators (right). a) 9-Aminoacridine,[1] b) echinomycin,[3] c) bis(methidium)spermine.[9]

Based on this sequence-specific intercalator lead[12] we explored the synthesis and binding properties of *sequence-specific bisintercalators* (Figure 2). Our design is a symmetric molecule which contains a minor-groove-binding polyamide based on the H-pin motif[13] with an acridine moiety at each C terminus. According to the pairing rules[14] the H-pin core should target the sequence 5′-TGACA-3′ and, based on earlier precedent, the two acridine moieties should unwind DNA by $\geq 30^{\circ}$.

Cross-linked resin **1** was synthesized by loading β-Ala-PAM (PAM = phenylacetamido methyl) resin with activated pyrrole amino acid,[15] subsequent *tert*-butoxycarbonyl (Boc) deprotection and addition of the ring-linked dimeric building block to couple the C termini of the growing polyamide chain on the resin,[13] and final capping by using activated imidazole carboxylate (Scheme 1). Resin-bound H-pin **1** was then subjected to aminolytic cleavage with 2,2′-(ethylenedioxy)-bis(ethylamine) to form H-pin diamine **2**. Following purification, **2** was coupled with 9-chloroacridine under reported conditions[11] to produce the mono- and bisacridine–H-pin conjugates **3** ((ImPyPy-β-Do-Acr)(ImPyPy-β-Do)$(CH_2)_6$) and **4** ((ImPyPy-β-Do-Acr)$_2(CH_2)_6$), respectively.

[*] E. J. Fechter, B. Olenyuk, Prof. P. B. Dervan
Division of Chemistry and Chemical Engineering
164-30, California Institute of Technology
Pasadena, CA 91125 (USA)
Fax: (+1) 626-564-9297
E-mail: dervan@caltech.edu

[**] We thank the National Institutes of Health (GM-27681) for research support, a Research Service Award to E.J.F., and a postdoctoral fellowship to B.O. (F32 GM-19788). We also thank the Ralph M. Parsons Foundation for a predoctoral fellowship to E.J.F.

Supporting information for this article is available on the WWW under http://www.angewandte.org or from the author.

 DOI: 10.1002/anie.200454231 © 2004 Wiley-VCH Verlag GmbH & Co. KGaA, Weinheim

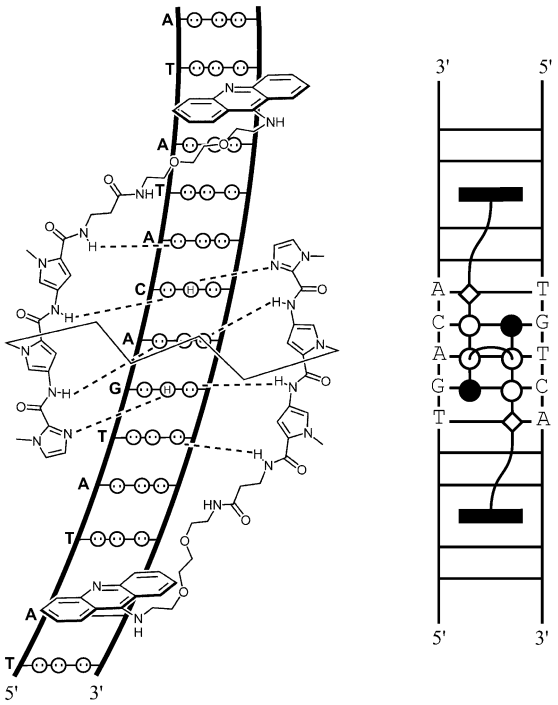
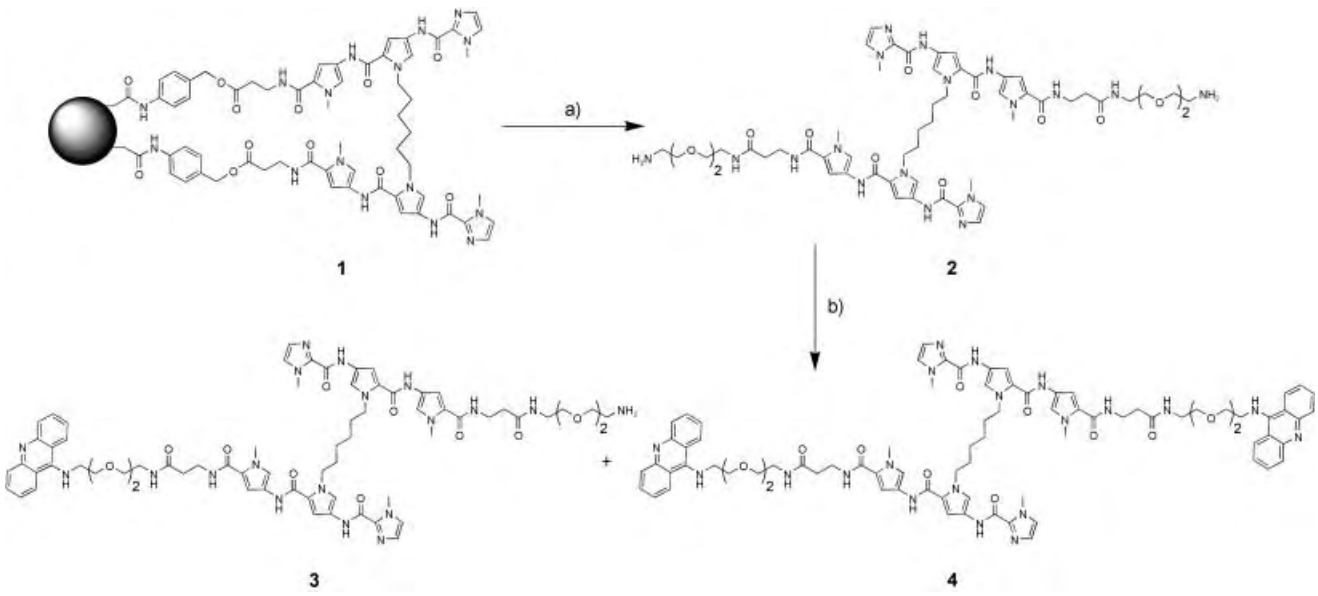


Figure 2. DNA binding model for the symmetric bisintercalating H-pin polyamide–acridine conjugate (ImPyPy-β-Do-Acr)$_2$(CH$_2$)$_6$ bound to the minor groove of 5′-TGACA-3′. Im = imidazole, Py = bridged pyrrole, Py = pyrrole, $\beta = \beta$-alanine, Do = 2,2′-(ethylenedioxy)bis(ethylamine), Acr = acridine. Left: Circles with dots represent the lone pairs of electrons of N3 of purines and O2 of pyrimidines. Circles containing an H represent the N2 hydrogen atoms of guanine. Putative hydrogen bonds are illustrated by dotted lines. Right: Solid circles represent imidazoles, open circles represent pyrroles, and diamonds denote β-alanine. According to the pairing rules, Im/Py codes for G·C, Py/Py for A·T or T·A, Py/Im for C·G, and β-alanine for A·T.

The DNA-binding properties of **2**–**4** were investigated by quantitative DNase I footprinting assays[16] (Figure 3). The 5′-^{32}P-labeled PCR-amplified fragment of pEF12 (Figure 3a) contains a match site (A) and a single-bp mismatch site (B) to study both affinity and specificity. The equilibrium binding constants of compounds **2**–**4** for match site A (5′-TGACA-3′) are compiled in Table 1 and their corresponding binding isotherms are shown in Figure 4a. Conjugation of one acridine (**3**) results in a nearly 40-fold increase in binding affinity ($K_a = 1.4 \times 10^9\,\text{M}^{-1}$) over the parent H-pin **2** ($K_a = 3.7 \times 10^7\,\text{M}^{-1}$). The conjugation of a second acridine intercalator (**4**) increases the binding affinity by an additional 10-fold ($K_a = 1.5 \times 10^{10}\,\text{M}^{-1}$), thereby resulting in the bisacridine conjugate **4** having a more than 400-times higher affinity for a DNA match site than its unconjugated counterpart **2**. It is noteworthy that polyamides conjugated to nonintercalating moieties (such as fluorescent dyes and peptides) display *decreased* binding affinities relative to their parent, unconjugated compounds.[17] The steep slopes of the isotherms for **3** and **4** in Figure 4 suggest a more complex DNA binding mode than the expected 1:1 association of parent H-pin **2**. Compounds **2** and **3** show no binding on mismatch site B (5′-TG**G**CA-3′) at concentrations as high as 1 μM. It appears that bisintercalator **4** may have a partial occupation of the mismatch site (B) at the highest concentrations (Figure 3b). Nonetheless, the affinity of H-pin **4** for mismatch site B could not be quantified at concentrations as high as 1 μM, a result indicating a high level of specificity in this series of conjugates.

The DNA-unwinding properties of compounds **3** and **4** were determined from a helical assay developed by Crothers, Zeeman, and colleagues that provides an unwinding angle (ϕ) from sequence-specific interactions.[18] A series of relaxation reactions were carried out by using topoisomerase I (Topo I) on closed-circular pUC19 DNA preequilibrated with varying concentrations of polyamides. The plasmid was then sepa-



Scheme 1. Synthetic scheme for H-pin polyamide–acridine conjugates: a) 2,2′-(ethylenedioxy)bis(ethylamine), 55 °C, 18 h; b) 9-chloroacridine (1.5 equiv), DIPEA, 100 °C (1.5 h). DIPEA = diisopropylethylamine.

 © 2004 Wiley-VCH Verlag GmbH & Co. KGaA, Weinheim

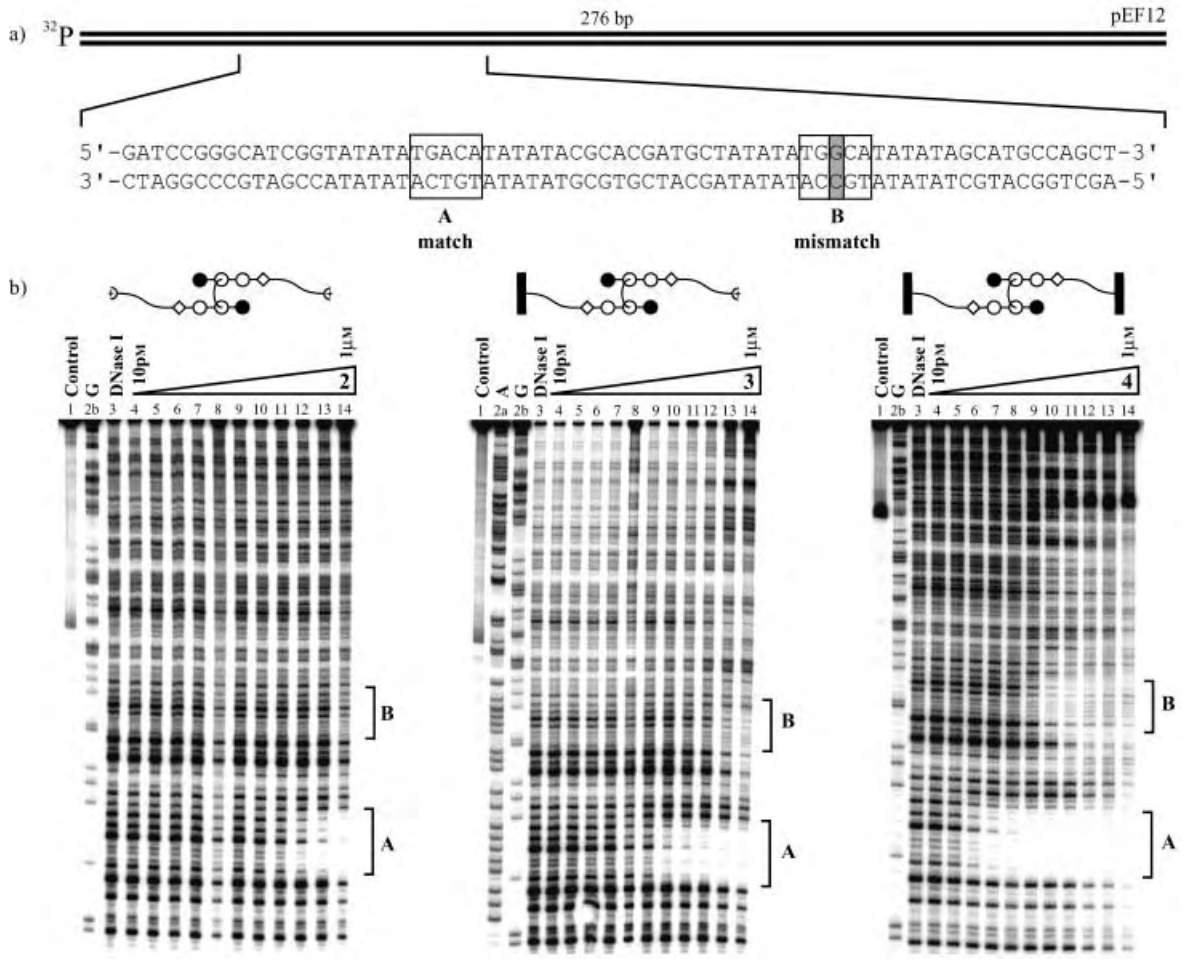


Figure 3. a) Sequence of the synthesized insert from the pEF12 plasmid containing the 5-bp target match site (A) and single-bp mismatch site (B). Target sites are shown in boxes with the mismatch site shaded. b) Quantitative DNase I footprint titration experiments with H-pins **2** (left), **3** (middle), and **4** (right) on the PCR-amplified 5′-^{32}P-labeled fragment from pEF12. Lane 1, intact DNA; lane 2a, A reaction; lane 2b, G reaction; lane 3, DNase I standard; lanes 4–14, DNase I digestion products in the presence of 10, 30, 100, 300 pM; 1, 3, 10, 30, 100, 300 nM; and 1 μM polyamide, respectively.

Table 1: Thermodynamic Data and Unwinding Angles

Polyamide	No. of acridines	K_a[a] [M^{-1}]	ϕ [°]
2	0	3.7×10^{7}	0
3	1	1.4×10^{9}	15
4	2	1.5×10^{10}	34

[a] Association constants, K_a, are the average values obtained from at least three DNase I footprint titration experiments. Assays were performed at 22 °C and pH 7.0 in the presence of tris(hydroxymethyl)-aminomethane·HCl (10 mM), KCl (10 mM), $MgCl_2$ (10 mM), and $CaCl_2$ (5 mM).

rated from the polyamide conjugate by phenol/chloroform extraction and 2D agarose-gel electrophoresis was performed to distinguish the resulting distribution of topoisomers. DNA unwinding would shift the topoisomer distribution toward a more negatively supercoiled population. Indeed, each reaction containing conjugate **4** had a more highly negative distribution of topoisomers than those containing conjugate **3** (see the Supporting Information). Control experiments lacking polyamide resulted in a primarily positive distribution of topoisomers. Mathematical analysis of the topoisomer distributions relative to the controls showed decreasing apparent unwinding angles (ϕ_{ap}) for simultaneously decreasing conjugate and plasmid concentrations (Figure 4b). The actual unwinding angles (ϕ), determined from the ordinate intercepts, are 15° and 34° for the acridine conjugate **3** and bisacridine conjugate **4**, respectively (Figure 4b).

Our results provide strong evidence that the symmetric H-pin–bisacridine conjugate **4** is a sequence-specific bisintercalator, capable of binding discrete sites at subnanomolar concentrations and unwinding DNA by more than 30°. To date, this synthetic molecule exceeds the specificity and binding affinity of any known natural or non-natural bisintercalator. Its ease of synthesis, sequence specificity, and potency of DNA distortion at discrete sites make it an attractive candidate for future biological studies, such as transcription inhibition at specific genes. The design features of combining the programmable H-pin motif with intercala-

 © 2004 Wiley-VCH Verlag GmbH & Co. KGaA, Weinheim

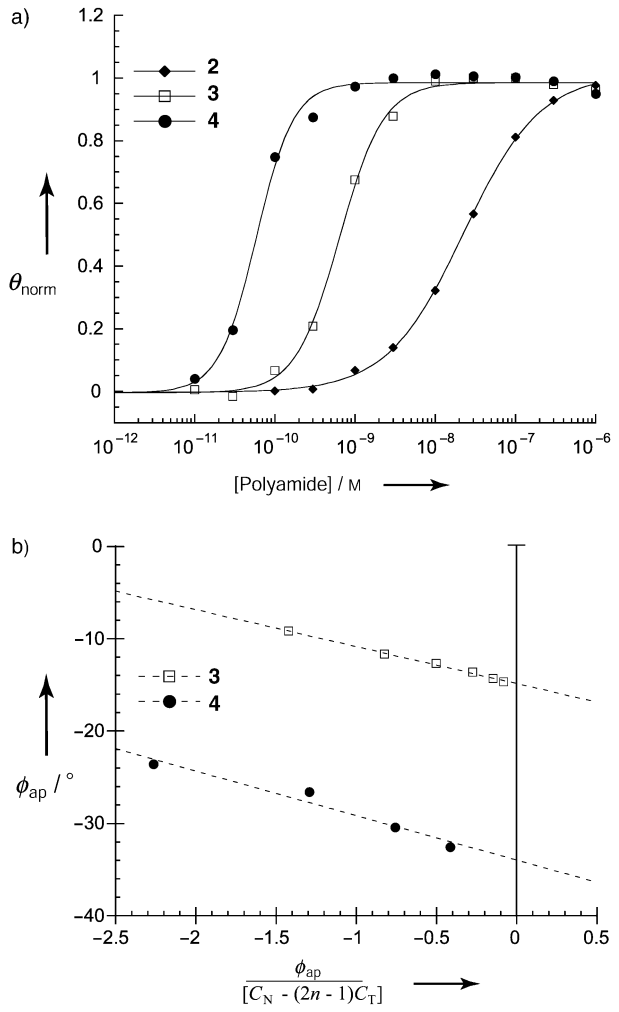


Figure 4. a) Binding isotherms at match sites for H-pins **2**, **3**, and **4**. θ_{norm} points were obtained by using storage phosphor autoradiography and processed by standard methods.[15] Each data point shows the average value obtained from three footprinting experiments. The solid curves are best-fit Langmuir binding titration isotherms obtained from a nonlinear least squares algorithm. b) Binding isotherms for polyamide–acridine conjugates **3** and **4** on pUC19. Each data point was calculated from one set of topoisomer distributions from reactions containing polyamide compared to a control distribution lacking polyamide. Interception of the ordinate yields the unwinding angle (ϕ) per polyamide–acridine conjugate.

tion should allow a large repertoire of discrete DNA sequences to be targeted.

Received: March 10, 2004 [Z54231]

Keywords: conjugation · DNA recognition · intercalation · polyamides

[1] L. S. Lerman, *J. Mol. Biol.* **1961**, *3*, 18–30.
[2] a) W. A. Denny, *Anti-Cancer Drug Des.* **1989**, *4*, 241–263; b) B. C. Baguley, *Anti-Cancer Drug Des.* **1991**, *6*, 1–35.
[3] a) M. J. Waring, L. P. G. Wakelin, *Nature* **1974**, *252*, 653–657; b) L. P. G. Wakelin, M. J. Waring, *Biochem. J.* **1976**, *157*, 721–740; c) R. H. Shafer, M. J. Waring, *Biopolymers* **1980**, *19*, 431–443; d) M. M. Van Dyke, P. B. Dervan, *Science* **1984**, *225*, 1122–1127.
[4] A. Dell, D. H. Williams, H. R. Morris, G. A. Smith, J. Feeney, G. C. K. Roberts, *J. Am. Chem. Soc.* **1975**, *97*, 2497–2502.
[5] a) A. H. J. Wang, G. Ughetto, G. J. Quigley, T. Hakoshima, G. A. van der Marel, J. H. van Boom, A. Rich, *Science* **1984**, *225*, 1115–1121; b) H. Chen, D. J. Patel, *J. Mol. Biol.* **1995**, *246*, 164–179.
[6] D. C. Ward, E. Reich, I. H. Goldberg, *Science* **1965**, *149*, 1259–1263.
[7] J. S. Lee, M. J. Waring, *Biochem. J.* **1978**, *173*, 115–128.
[8] a) J.-B. Le Pecq, M. Le Bret, J. Barbet, B. Roques, *Proc. Natl. Acad. Sci. USA* **1975**, *72*, 2915–2919. b) L. P. G. Wakelin, M. Romanos, T. K. Chen, D. Glaubiger, E. S. Canellakis, M. J. Waring, *Biochemistry* **1978**, *17*, 5057–5063.
[9] M. M. Becker, P. B. Dervan, *J. Am. Chem. Soc.* **1979**, *101*, 3664–3666.
[10] F. Leng, W. Priebe, J. B. Chaires, *Biochemistry* **1998**, *37*, 1743–1753.
[11] E. J. Fechter, P. B. Dervan, *J. Am. Chem. Soc.* **2003**, *125*, 8476–8485.
[12] For an example of a major-groove sequence-specific intercalator, see: C. L. Kielkopf, K. E. Erkkila, B. P. Hudson, J. K. Barton, D. C. Rees, *Nat. Struct. Biol.* **2000**, *7*, 117–121.
[13] B. Olenyuk, C. Jitianu, P. B. Dervan, *J. Am. Chem. Soc.* **2003**, *125*, 4741–4751.
[14] S. White, J. W. Szewczyk, J. M. Turner, E. E. Baird, P. B. Dervan, *Nature* **1998**, *391*, 468–471.
[15] E. E. Baird, P. B. Dervan, *J. Am. Chem. Soc.* **1996**, *118*, 6141–6146.
[16] J. W. Trauger, P. B. Dervan, *Methods Enzymol.* **2001**, 340, 450–466.
[17] a) T. P. Best, B. S. Edelson, P. B. Dervan, *Proc. Natl. Acad. Sci. USA* **2003**, *100*, 12063–12068; b) A. K. Mapp, A. Z. Ansari, M. Ptashne, P. B. Dervan, *Proc. Natl. Acad. Sci. USA* **2000**, *97*, 3930–3935.
[18] a) S. M. Zeeman, K. M. Depew, S. J. Danishefsky, D. M. Crothers, *Proc. Natl. Acad. Sci. USA* **1998**, *95*, 4327–4332; b) S. M. Zeeman, D. M. Crothers, *Methods Enzymol.* **2001**, 340, 51–68.

 © 2004 Wiley-VCH Verlag GmbH & Co. KGaA, Weinheim

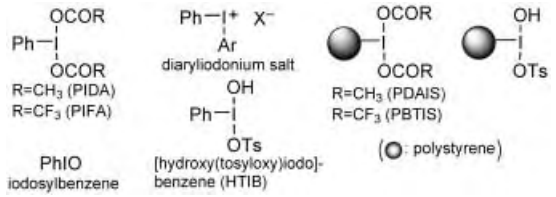
Oxidations

Preparation and Reactivity of 1,3,5,7-Tetrakis[4-(diacetoxyiodo)phenyl]adamantane, a Recyclable Hypervalent Iodine(III) Reagent**

Hirofumi Tohma, Akinobu Maruyama, Akihisa Maeda, Tomohiro Maegawa, Toshifumi Dohi, Motoo Shiro, Tetsuichiro Morita, and Yasuyuki Kita**

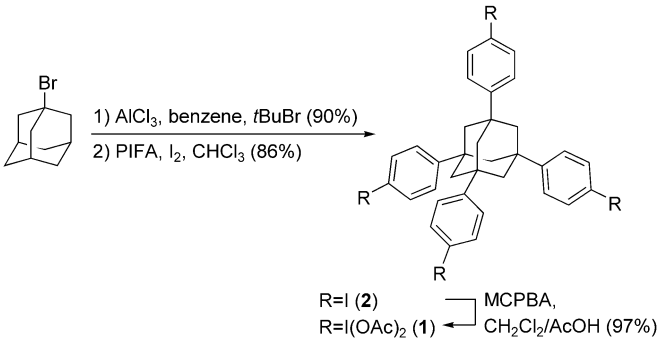
Over the past decade, the use of hypervalent iodine reagents[1] has gained importance as a safe alternative to heavy-metal reagents for performing a variety of organic transformations. In view of recent demands for ecologically friendly chemical processes in the agrochemical and pharmaceutical industries, polymer-supported hypervalent iodine reagents should be a new and useful tool as a result of their versatility, low toxicity, high yields, simple work-up procedures, and recyclability. Accordingly, Togo and co-workers,[1h,2] Ley and co-workers,[3] and we[4] demonstrated that both poly(diacetoxyiodo)styrene (PDAIS)[5] and polybis(trifluoroacetoxyiodo)styrene (PBTIS) exhibit reactivities similar to those of phenyliodine diacetate (PIDA) and phenyliodine bis(trifluoroacetate) (PIFA), respectively, and utilized them as environmentally benign replacements for I^{III} reagents such as PIDA, PIFA, and iodosyl benzene (PhIO) (Scheme 1).

Despite the utility and versatility of these polymer-supported reagents, they still have several drawbacks: 1) the loading efficiency of I^{III} sites is difficult to control, which has made the marketing of polymer-supported iodine reagents difficult; 2) the degradative loss of resin is accompanied by benzylic oxidation of the polystyrene chain after repeated use; and 3) they are much less reactive than the corresponding monomeric forms owing to steric hindrance of the reactive sites as well as their low solubility in various solvents. Therefore, slightly vigorous conditions and/or an excess amount of reagents are generally needed. Herein we report the preparation and characterization of a novel, recyclable, and nonpolymeric hypervalent iodine(III) reagent, 1,3,5,7-tetrakis[4-(diacetoxyiodo)phenyl] adamantane (**1**), and its derivatives.



Scheme 1. Hypervalent iodine(III) reagents.

As a part of our continuing research into the development of new hypervalent iodine compounds, we planned to synthesize an unprecedented tetrahedral I^{III} compound **1**, which should be a precursor to build a unique hypervalent iodine-based supramolecular structure as well as a new oxidizing agent. We prepared 1,3,5,7-tetrakis(4-iodophenyl)-adamantane (**2**) in good yield in two steps from commercially available 1-bromoadamantane according to a literature procedure.[6] Oxidation of **2** by conventional methods[7] with peracetic acid (30% H_2O_2 and acetic anhydride), sodium perborate ($NaBO_3$) in acetic acid, or sodium periodate ($NaIO_4$) unexpectedly gave **1** in low yield, accompanied by poorly soluble and unidentifiable polymeric products. After further investigations, we finally succeeded in synthesizing **1** in 97% yield by using *m*-chloroperbenzoic acid (MCPBA) in CH_2Cl_2/AcOH (1:1) under dilute conditions (Scheme 2).



Scheme 2. Preparation of 1,3,5,7-tetrakis[4-(diacetoxyiodo)phenyl]adamantane (**1**). Ts = tosyl = *p*-toluenesulfonyl.

Adamantane **1** was fully characterized by single-crystal X-ray analysis[8] as well as elemental and spectroscopic analysis. A single crystal of **1** suitable for X-ray crystallographic analysis was obtained through slow growth by the vapor diffusion from CH_2Cl_2/AcOH/hexanes. Figure 1 reveals the geometry around the iodine in **1** to be a pentagonal-planar arrangement of three strong (e.g. I1-C14, I1-O1, and I1-O3) and two weak secondary (e.g. I1-O2 and I1-O4) bonds similar to the well-known geometry of PIDA, and the unit cell consists of a tetrahedral structure.

Several I^{III} derivatives[9] such as 1,3,5,7-tetrakis[4-bis(trifluoroacetoxyiodo)phenyl]adamantane (**3**), 1,3,5,7-tetrakis[4-{hydroxy(tosyloxy)iodo}phenyl]adamantane (**4**), and 1,3,5,7-

[*] Dr. H. Tohma, A. Maruyama, A. Maeda, T. Maegawa, T. Dohi, Prof. Y. Kita
Graduate School of Pharmaceutical Sciences
Osaka University
1-6 Yamada-oka, Suita, Osaka 565-0871 (Japan)
Fax: (+81) 6-6879-8229
E-mail: kita@phs.osaka-u.ac.jp
M. Shiro
Rigaku Corporation
3-9-12 Matsubara
Akishima, Tokyo 196-8666 (Japan)
T. Morita
Group 2 Analytical Instruments Division, JEOL Ltd.
3-2-1 Musashino, Akishima, Tokyo 196-8558 (Japan)

[**] This work was financially supported by the Industrial Technology Research Grant Program from the New Energy and Industrial Technology Development Organization (NEDO) of Japan and by a Grant-in-Aid for Scientific Research (S) and for Encouragement of Young Scientists from the Ministry of Education, Science, Sports and Culture, Japan. H.T. also thanks the Takeda Science Foundation.

 DOI: 10.1002/anie.200454234 © 2004 Wiley-VCH Verlag GmbH & Co. KGaA, Weinheim

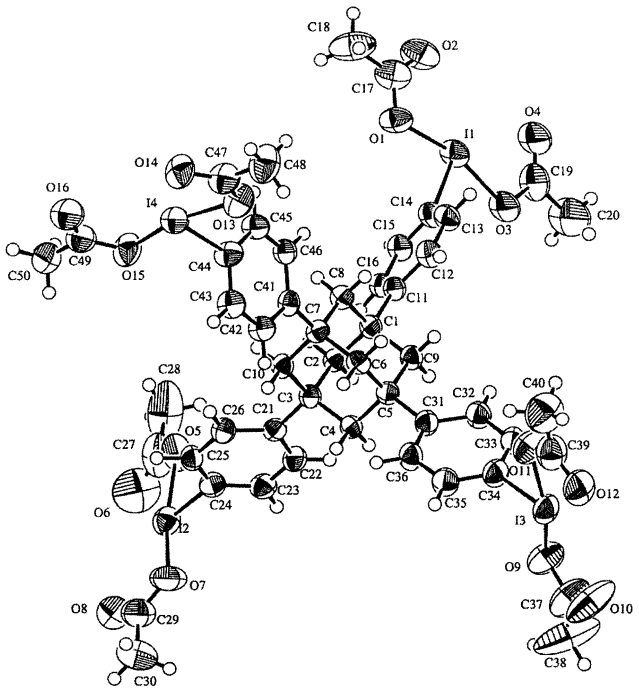
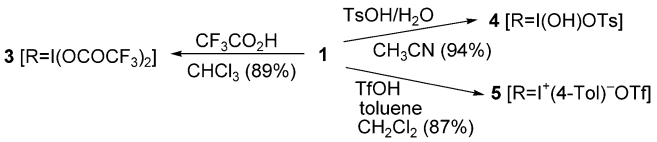


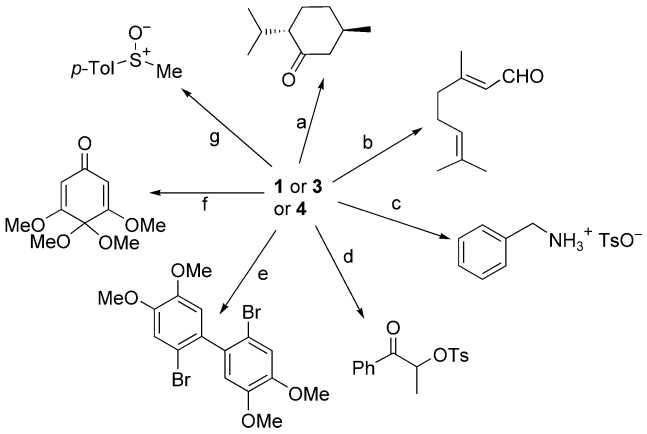
Figure 1. ORTEP drawing of **1**. Selected bond lengths [Å] and angles [°]: I1-C14 2.097(6), I1-O1 2.170(5), I1-O2 2.863(6), I1-O3 2.174(6), I1-O4 2.875(5), O1-I1-C1 80.6(2), C14-I1-O3 81.9(2), O1-I1-O3 162.4(2).

tetrakis[4-(4-tolyliodonium)phenyl]adamantane (**5**) were also prepared from **1** by conventional procedures[10] (Scheme 3).



Scheme 3. Transformation of **1** into other iodanes. Tf = trifluoromethanesulfonyl.

During the above study, we found that **2** is poorly soluble in polar protic solvents, especially in MeOH. This prompted us to develop **1** and its derivatives as new and recyclable reagents, because **2** is generated as the reduced form after oxidation reactions with **1**. Thus, we tested several oxidative transformations with **1**, **3**, and **4** to confirm the reactivity and recyclability. Consequently, all the reactions, such as phenolic oxidation,[4b,11] oxidation of alcohols,[4a,d,12] oxidation of sulfides,[2b] α-tosyloxylation of ketones,[13] and Hofmann-type rearrangement,[14] proceeded smoothly under homogeneous



Scheme 4. Reactivity of **1**, **3**, and **4**. Conditions: a) L-menthol, **1** (0.28 equiv), KBr, H_2O, room temperature, 4 h, quant. (95% recovery of **2**); b) geraniol, **1** (0.25 equiv), TEMPO (0.2 equiv), CH_2Cl_2, room temperature, 1 h, 91% (95% recovery of **2**); c) phenylacetamide, **4** (0.25 equiv), CH_3CN, reflux, 1 h, 82% (quant. recovery of **2**); d) propiophenone, **4** (0.25 equiv), CH_3CN, reflux, 3 h, 76% (98% recovery of **2**); e) 4-bromoveratrole, **3** (0.14 equiv), $BF_3{\cdot}Et_2O$, CH_2Cl_2, −40°C, 3 h, 98% (quantitative recovery of **2**); f) 3,4,5-trimethoxyphenol, **1** (0.25 equiv), MeOH, room temperature, 10 min, quant. (quant. recovery of **2**); g) methyl p-tolylsulfide, **1** (0.25 equiv), CH_2Cl_2 (1% H_2O), reflux, 2 h, 97% (quant. recovery of **2**).

conditions (except for reaction a) to afford oxidation products in excellent yields (Scheme 4).

In all cases, tetraiodide **2** was recovered nearly quantitatively in pure form after a simple work-up (i.e. quenching the reaction with MeOH followed by filtration or centrifugation), and reoxidation of **2** to **1** with MCPBA also proceeded quantitatively without loss of activity. Next, we compared the reactivity of **1** or **3** with other I^{III} reagents. As a result, reagents **1** and **3** showed high reactivities equal to those of PIDA, PIFA, and PhIO, as well as excellent recyclability (95–100%) similar to that of PDAIS (Scheme 4 and Table 1).

The high reactivity of **1** is probably caused by the tetrahedral structure, whose reactive sites do not interfere with each other. Furthermore, no degradation loss was observed in the reoxidation step to **1**, even after repeated use, because **2** has no benzylic proton. The key features of these unique I^{III} reagents are highlighted as follows: 1) high reactivity in a variety of solvents owing to their tetrahedral structure and to their improved solubility over those of conventional polymer-supported I^{III} reagents; 2) high recyclability without degradation loss; and 3) well-defined structure and convenient preparation, suitable for commercialization.

Table 1: Comparison of reactivities of **1** and **3** with PIDA, PIFA, PhIO, and PDAIS.[a]

Reaction a[b]	Reaction e[b]	Reaction g[b]
quant. (**1** (0.28 equiv), 4 h, RT)	98% (**3** (0.14 equiv), 3 h, −40°C)	97% (**1** (0.25 equiv), 2 h, reflux)
quant. (PhIO (1.1 equiv), 7 h, RT)	97% (PIFA (0.55 equiv), 1.5 h, −40°C)	97% (PIDA (1.0 equiv), 2 h, reflux)
86% (PDAIS (1.1 equiv), 20 h, RT)	58% (PDAIS (0.55 equiv), 24 h, RT)[c]	83% (PDAIS (1.0 equiv), 24 h, reflux)

[a] See Scheme 4: reaction a: oxidation of L-menthol, reaction e: biaryl coupling of 4-bromoveratrole, reaction g: oxidation of methyl *p*-tolyl sulfide. [b] Yield (reagent (equiv), time, temperature). [c] No reaction at −40°C.

 © 2004 Wiley-VCH Verlag GmbH & Co. KGaA, Weinheim

In conclusion, we have developed novel, nonpolymeric, and recyclable hypervalent iodine(III) reagents. These reagents show promise as useful and safe tools for a wide range of pharmaceutical and agrochemical research, as they are highly reactivity *and* recyclable. Application of **1** and related compounds to the construction of supramolecular structures as well as in oxidation reactions is now underway.

Experimental Section

MCPBA (3.12 g, 18 mmol) was added to a stirred solution of **2** (1.416 g, 1.5 mmol) in CH_2Cl_2 (150 mL) and AcOH (150 mL) at room temperature. The mixture was stirred for 12 h under the same reaction conditions. The resultant mixture was filtered, and CH_2Cl_2 was removed from the filtrate by using a rotary evaporator. Hexanes were added to the residue to precipitate **1**. After filtration, crude **1** was washed with hexanes several times, and was dried in vacuo to give **1** (2.07 g, 97%), colorless crystal; m.p. (decomp.) 195–196°C (from AcOH-CH_2Cl_2-hexanes by vapor diffusion method); ^{1}H NMR (300 MHz, $CDCl_3$, 25°C, TMS): $\delta = 8.09$ (d, $^3J(H,H) = 8.7$ Hz, 8H; ArH), 7.56 (d, $^3J(H,H) = 8.7$ Hz, 8H; ArH), 2.20 (s, 12H; AdH), 2.01 ppm (s, 24H; $OCOCH_3$); ^{13}C NMR (75 Hz, $CDCl_3$, 25°C, TMS): $\delta = 176.5$, 151.9, 135.2, 127.7, 119.5, 46.4, 39.6, 20.4 ppm; elemental analysis: calcd for $C_{50}H_{52}I_4O_{16}\cdot 2H_2O$: C 41.34, H 3.89, I 34.95; found: C 41.30, H 3.70, I 35.03.

Typical Oxidation Procedure: Adamantane **1** (354.2 mg, 0.25 mmol) was added to a stirred solution of 3,4,5-trimethoxyphenol (184.2 mg, 1.0 mmol) in MeOH (5 mL) at room temperature. The mixture was stirred for 10 min. MeOH (10 mL) was then added to the reaction mixture, and the mixture was filtered. The residue was washed with MeOH several times, and the residue was recovered as pure **2** quantitatively. The filtrate was then centrifuged. The supernatant liquid was evaporated in vacuo to give 3,4,4,5-tetramethoxycyclohexa-2,5-dienone[15] quantitatively.

Received: March 11, 2004 [Z54234]

Keywords: green chemistry · hypervalent compounds · iodine · oxidation · synthetic methods

[1] For recent reviews, see: a) P. J. Stang, V. V. Zhdankin, *Chem. Rev.* **1996**, *96*, 1123–1178; b) Y. Kita, T. Takada, H. Tohma, *Pure Appl. Chem.* **1996**, *68*, 627–630; c) A. Varvoglis, *Hypervalent Iodine in Organic Synthesis, Academic Press, San Diego*, **997**; d) T. Kitamura, Y. Fujiwara, *Org. Prep. Proced. Int.* **1997**, *29*, 409–458; e) M. Ochiai in *Chemistry in Hypervalent Compounds* (Ed.: K. Akiba), Wiley-VCH, New York, **1999**, chap. 12; f) T. Wirth, U. H. Hirt, *Synthesis* **1999**, 1271–1287; g) V. V. Zhdankin, P. J. Stang, *Chem. Rev.* **2002**, *102*, 2523–2584; h) H. Togo, K. Sakuratani, *Synlett* **2002**, 1966–1975; i) *Hypervalent Iodine Chemistry* (Ed.: T. Wirth), Springer, Berlin, **2003**.

[2] a) H. Togo, G. Nogami, M. Yokoyama, *Synlett* **1998**, 534–536; b) H. Togo, S. Abe, G. Nogami, M. Yokoyama, *Bull. Chem. Soc. Jpn.* **1999**, *72*, 2351–2356; c) S. Abe, K. Sakuratani, H. Togo, *J. Org. Chem.* **2001**, *66*, 6174–6177; d) H. Togo, K. Sakuratani, *Synthesis* **2003**, 21–23.

[3] a) S. V. Ley, A. W. Thomas, H. Finch, *J. Chem. Soc. Perkin Trans. 1* **1999**, 669–671; b) S. V. Ley, O. Schucht, A. W. Thomas, P. J. Murray, *J. Chem. Soc. Perkin Trans. 1* **1999**, 1251–1252; c) I. R. Baxendale, S. V. Ley, C. Piutti, *Angew. Chem.* **2002**, *114*, 2298–2301; *Angew. Chem. Int. Ed.* **2002**, *41*, 2194–2197; d) I. R. Baxendale, A.-L. Lee, S. V. Ley, *J. Chem. Soc. Perkin Trans. 1* **2002**, 1850–1857.

[4] a) H. Tohma, S. Takizawa, T. Maegawa, Y. Kita, *Angew. Chem.* **2000**, *112*, 1364–1368; *Angew. Chem. Int. Ed.* **2000**, *39*, 1306–1308; b) H. Tohma, H. Morioka, S. Takizawa, M. Arisawa, Y. Kita, *Tetrahedron* **2001**, *57*, 345–352; c) H. Tohma, H. Morioka, Y. Harayama, M. Hashizume, Y. Kita, *Tetrahedron Lett.* **2001**, *42*, 6899–6902; d) H. Tohma, T. Maegawa, S. Takizawa, Y. Kita, *Adv. Synth. Catal.* **2002**, *344*, 328–337; e) H. Tohma, T. Maegawa, Y. Kita, *ARKIVOC* **2003**, *VI*, 62–70; f) H. Tohma, T. Maegawa, Y. Kita, *Synlett* **2003**, 723–725.

[5] a) M. Okawara, K. Mizuta, *Kogyo Kagaku Zasshi* **1961**, *64*, 232–235; b) Y. Yamada, M. Okawara, *Makromol. Chem.* **1972**, *152*, 153–162; c) H. K. Livingston, J. W. Sullivan, J. I. Musher, *J. Polym. Sci. Part C* **1968**, 195–202; d) M. L. Hallensleben, *Angew. Makromol. Chem.* **1972**, *27*, 223–227.

[6] a) H. Newman, *Synthesis* **1972**, 692–693; b) E. B. Merkushev, N. D. Simakhina, G. M. Koveshnikova, *Synthesis* **1980**, 486–487; c) V. R. Reichert, L. J. Mathias, *Macromolecules* **1994**, *27*, 7015–7023; d) L. J. Mathias, V. R. Reichert, A. V. G. Muir, *Chem. Mater.* **1993**, *5*, 4–5.

[7] a) J. G. Sharefkin, H. Saltzman, *Org. Synth. Coll.* **1973**, *5*, 660–662; b) A. McKillop, D. Kemp, *Tetrahedron* **1989**, *45*, 3299–3306; c) P. Kazmierski, L. Skulski, *Synthesis* **1998**, 1721–1723.

[8] Crystal data for **1** ($C_{50}H_{56}I_4O_{18}$): $M_w = 1452.60$, monoclinic, *C*2/*c* (no. 15), $a = 24.11(1)$, $b = 17.011(9)$, $c = 33.45(2)$ Å, $\beta = 91.57(4)$, $V = 13711(11)$ Å^3, $Z = 8$, $T = 90$ K, $\rho_{calcd} = 1.407$ g cm^{-3}, $Mo_{K\alpha}$ radiation, $m = 18.74$ cm^{-1}, colorless block $0.30 \times 0.15 \times 0.05$ mm^3; 78690 measured reflections, F^2 refinement, $R_1 = 0.067$, $wR_2 = 0.183$, 19969 independent observed absorption-corrected reflections [$(I > 3.00\sigma(I))$, $2\theta = 60.1$], 700 parameters. CCDC 232058 contains the supplementary crystallographic data for this paper. These data can be obtained free of charge via www.ccdc.cam.ac.uk/conts/retrieving.html (or from the Cambridge Crystallographic Data Centre, 12, Union Road, Cambridge CB2 1EZ, UK; fax: (+44) 1223-336-033; or deposit@ccdc.cam.ac.uk).

[9] **3**: m.p. (decomp.) 196–203°C (from CH_2Cl_2/hexanes); ^{1}H NMR (300 MHz, $CDCl_3/CF_3CO_2H$ (10:1), 25°C, TMS): $\delta = 8.24$ (d, $^3J(H,H) = 8.7$ Hz, 8H; ArH), 7.73 (d, $^3J(H,H) = 8.7$ Hz, 8H; ArH), 2.30 ppm (s, 12H; AdH); ^{19}F NMR (200 MHz, $CDCl_3/CF_3CO_2H$ (10:1), 25°C, hexafluorobenzene (−162.9 ppm)): $\delta = -74.51$ ppm (s, 24F; $OCOCF_3$); elemental analysis: calcd for $C_{50}H_{28}F_{24}I_4O_{16}$: C 32.49, H 1.53; found: C 32.82, H 1.86. **4**: m.p. (decomp.) 183–190°C; ^{1}H NMR (300 MHz, $CDCl_3/CF_3CO_2H$ (10:1), 25°C, TMS): $\delta = 8.25$ (d, $^3J(H,H) = 8.9$ Hz, 8H; ArH), 7.70 (d, $^3J(H,H) = 8.9$ Hz, 8H; ArH), 7.65 (d, $^3J(H,H) = 8.4$ Hz, 8H; ArH), 7.26 (d, $^3J(H,H) = 8.1$ Hz, 8H; ArH), 2.38 (s, 12H; $ArCH_3$), 2.26 ppm (s, 12H; AdH); ^{13}C NMR (75 Hz, $CDCl_3/CF_3CO_2H$ (10:1), 25°C, TMS): $\delta = 154.2$, 144.5, 135.9, 135.1, 129.8, 129.0, 126.3, 121.1, 45.8, 39.9, 21.4 ppm; elemental analysis: calcd for $C_{62}H_{60}I_4O_{16}S_4\cdot 4H_2O$: C 42.09, H 3.87, I 28.69, S 7.25; found: C 42.03, H 3.64, I 28.32, S 7.25. **5**: m.p. (decomp.) 186–190°C; ^{1}H NMR (270 MHz, CD_3CN, 25°C, TMS): $\delta = 8.00$ (d, $^3J(H,H) = 8.6$ Hz, 8H; ArH), 7.94 (d, $^3J(H,H) = 8.4$ Hz, 8H; ArH), 7.62 (d, $^3J(H,H) = 8.6$ Hz, 8H; ArH), 7.32 (d, $^3J(H,H) = 8.1$ Hz, 8H; ArH), 2.37 (s, 12H; $ArCH_3$), 2.04 ppm (s, 12H; AdH); ^{13}C NMR (67.8 Hz, CD_3CN, 25°C, TMS): $\delta = 154.6$, 145.1, 136.2, 136.1, 133.8, 130.3, 124.0, 112.0, 110.9, 45.8, 40.6, 21.4 ppm; High-resolution cold-spray ionization (CSI-MS; CH_3CN): $m/z = 1755.88990$ ($C_{65}H_{56}F_9I_4O_9S_3^+$) [$(M-OTf)^+$].

[10] For the preparation of **3**, see: a) J. Gallos, A. Varvoglis, N. W. Alcock, *J. Chem. Soc. Perkin Trans. 1* **1985**, 757–763; for the preparation of **4**, see: b) G. F. Koser, A. G. Relenyi, A. N. Kalos, L. Rebrovic, R. H. Wettach, *J. Org. Chem.* **1982**, *47*, 2487–2489; for the preparation of **5**, see: c) T. Kitamura, J. Matsuyuki, H. Taniguchi, *Synthesis* **1994**, 147–148.

 © 2004 Wiley-VCH Verlag GmbH & Co. KGaA, Weinheim

[11] Y. Tamura, T. Yakura, J. Haruta, Y. Kita, *J. Org. Chem.* **1987**, *52*, 3927 – 3930.
[12] A. De Mico, R. Margarita, L. Parlanti, A. Vescovi, G. Piancatelli, *J. Org. Chem.* **1997**, *62*, 6974 – 6977.
[13] S. Abe, K. Sakuratani, H. Togo, *Synlett* **2001**, 22 – 24.
[14] I. M. Lazbin, G. F. Koser, *J. Org. Chem.* **1986**, *51*, 2669 – 2671.
[15] M.p. 122–123 °C (from AcOH/hexanes); ^{1}H NMR (300 MHz, $CDCl_3$, 25 °C, TMS): $\delta = 5.59$ (s, 2H; 2-H, 6-H), 3.78 (s, 6H; 3-, 5-C-OMe), 3.25 ppm (s, 6H; 4-C-$(OMe)_2$); elemental analysis: calcd for $C_{10}H_{14}O_5$: C 56.07, H 6.59; Found: C 55.74, H 6.58.

 © 2004 Wiley-VCH Verlag GmbH & Co. KGaA, Weinheim

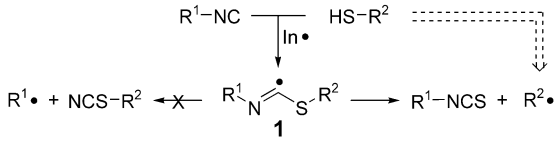
Radical Reactions

A Novel Tin-Free Procedure for Alkyl Radical Reactions**

Luisa Benati, Rino Leardini, Matteo Minozzi, Daniele Nanni,* Rosanna Scialpi, Piero Spagnolo, Samantha Strazzari, and Giuseppe Zanardi*

Radical reactions have definitely become a very powerful tool for synthetic organic chemists. Very useful defunctionalizations, formation of C–C (or even C–heteroatom) bonds, and an assortment of intra- or intermolecular cascade processes can be conducted, also with high stereoselectivity, under extremely mild conditions, and many sensitive functional groups are tolerated without any tedious protecting/deprotecting procedures.[1] This success owes much to tin reagents, and over the last four decades radical chemistry in synthesis has been literally monopolized by chain methods based on a variety of organotin derivatives. So pervasive is the presence of tin reagents in efficient radical syntheses that this dominance has been referred to as the "tyranny of tin".[2] Unfortunately, tin-based chemistry is associated with two critical drawbacks, that is, the toxicity of organotin compounds and the problems very often encountered in product purification. The quantitative removal of organotin residues from the reaction products is usually a difficult task, and this disadvantage, along with the high toxicity of those residues, can severely limit the application of tin reagents, for example for the synthesis of pharmaceuticals. It is therefore no surprise that alternative ways of carrying out radical reactions are under intensive investigation, in a search for both efficient purification protocols (special workup procedures, modified and polymer-bound tin reagents, etc.) and, above all, tin substitutes.[2,3]

The great upsurge of alternative processes to tin-based methodologies that has marked the last decade prompted us to verify whether isocyanide-based radical chemistry, which we have been studying for several years, could be also useful for performing free-radical chain reactions under reductive tin-free conditions.[4] Indeed, isocyanides are very efficient radical traps and, by addition of sulfanyl radicals, they are a valuable source of α-thioimidoyl radicals **1** (Scheme 1).[5]



Scheme 1. Fragmentation paths of thioimidoyl radicals. In• = initiator.

Although *N,S*-dialkyl-substituted thioimidoyl radicals can in principle fragment by β-scission of either the C–N or the C–S bond, giving thiocyanates and isothiocyanates, respectively, we have demonstrated that usually only fragmentation of the latter occurs.[6] This behavior is substantially independent of the relative stability of the released radicals and even primary, nonstabilized alkyl radicals can be smoothly generated at relatively low temperatures from various N-substituted thioimidoyls (Scheme 1).

As far as the precursors of thioimidoyl radicals are concerned, isocyanides are easily accessible, stable derivatives,[7] and some of them are also commercially available, for example, *tert*-butyl isocyanide. Thiols as well are very handy compounds that can be readily synthesized from haloalkanes, alcohols, or their derivatives in manifold ways.[8] Recently, treatment of halides, epoxides, or alcohols with polymer-supported hydrosulfide under very mild conditions gave the products in high yields and excellent chemoselectivity after a very easy workup.[9] This novel methodology seems to have made thiols much more easily accessible than ever.

In light of both the fast C–S β-scission of thioimidoyl radicals and the ready access to their precursors, we reasoned that thioimidoyl fragmentations could provide a clean, convenient entry to alkyl radicals from thiols. In this paper we show that this procedure can be an efficient substitute for other radical methods, mainly in defunctionalization reactions and intermolecular addition to olefins.

Trial experiments were initially performed with alkanethiols and various isocyanides to test the efficiency of the simple desulfuration reaction. The tests were carried out by adding a 0.1 M solution of the thiol in benzene (10 mL) over one hour to a solution of isocyanide (1.1 equiv) in benzene (10 mL) heated at reflux and with azobisisobutyronitrile (AIBN, 0.1 equiv) as an initiator. Under these conditions the alkyl radical generated by fragmentation of the intermediate thioimidoyl radical is smoothly reduced by the starting thiol

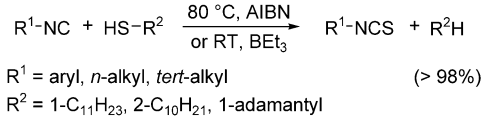
[*] Prof. L. Benati, Prof. R. Leardini, Dr. M. Minozzi, Prof. D. Nanni, Dr. R. Scialpi, Prof. P. Spagnolo, Dr. S. Strazzari, Prof. G. Zanardi
Dipartimento di Chimica Organica "A. Mangini"
Università di Bologna
Viale Risorgimento 4, 40136 Bologna (Italy)
Fax: (+39) 051-209-3654
E-mail: minus@ms.fci.unibo.it
nanni@ms.fci.unibo.it

[**] The authors gratefully acknowledge financial support from MIUR, Rome (2002–2003 Funds for "Radical Processes in Chemistry and Biology: Fundamental Aspects and Applications in Environment and Material Science"), and the University of Bologna (2001–2003 Funds for Selected Research Topics).

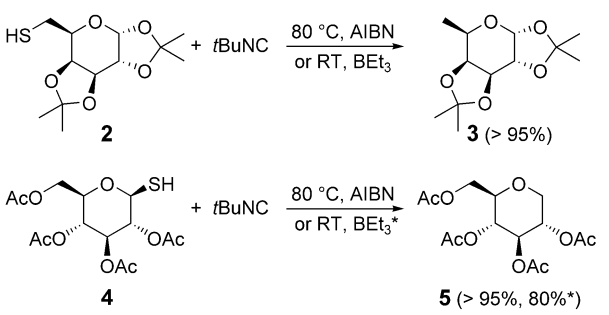
Supporting information for this article is available on the WWW under http://www.angewandte.org or from the author.

 © 2004 Wiley-VCH Verlag GmbH & Co. KGaA, Weinheim DOI: 10.1002/anie.200454245

giving the corresponding alkane in nearly quantitative yield (Scheme 2). The reactions can be also conducted in toluene solution at 80 °C and even at room temperature, when AIBN is replaced with triethylborane.[10] The reaction outcome was



Scheme 2. Defunctionalization of thiols with isocyanides.



Scheme 3. Defunctionalization of thiol-sugars (Barton–McCombie-type reaction).

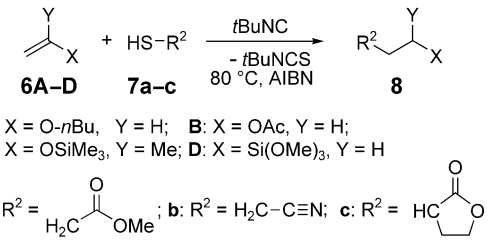
influenced neither by the thiol alkyl chain—tertiary, secondary, and even nonstabilized primary thiols were all desulfurated quantitatively—nor by the nature of the isocyanide—both aromatic and aliphatic isocyanides were used without any lowering of the reaction efficiency.

The latter point has two important consequences as far as accessibility of starting materials and workup are concerned. First, the experiments can be carried out with commercially available *tert*-butyl isocyanide without any need to synthesize suitable congeners. Second, the low boiling points of both the starting isocyanide and its by-product *tert*-butyl isothiocyanate (91 °C and 140 °C at 760 torr, respectively) allow for an extremely straightforward workup procedure: concentration of the final reaction mixture under reduced pressure results in concomitant elimination of solvent, by-product, and excess starting isocyanide, and the final desulfurated product can be recovered quantitatively in very high purity simply after rotary evaporation.[11] In light of all of these features, we think that this method can therefore be regarded as a very mild, efficient defunctionalization of thiols and, consequently, their precursors, that is, halides and alcohols.

The subsequent, logical step was to extend this procedure to Barton–McCombie-type reactions. Deoxygenation reactions are of huge importance in organic synthesis, and the Barton–McCombie reaction developed in the 1970s is a major milestone in the application of radical reactions in synthesis.[12] Although a few catalytic or tin-free deoxygenations have already been reported,[13] the Barton–McCombie realm is still strongly dominated by tin reagents. Taking into account that thiols, like xanthates, thiocarbonyl imidazolides, and dithiocarbonates, can be synthesized directly from alcohols,[9c,d,14,15] we reasoned that our isocyanide-mediated radical desulfuration of thiols could be a valid alternative to traditional Barton–McCombie procedures.

The reaction was examined on thiol-sugars **2** and **4** (Scheme 3). Under the usual conditions, at 80 °C, both compounds gave nearly quantitative yields of the corresponding desulfurated sugars **3** and **5**.[16] At room temperature, the reactions required longer times and greater amounts of initiator (BEt_3, 5 equiv) to reach completion—probably due to the presence of the oxygen atoms on the substrates—but afforded again very good yields of **3** and **5**. The result with substrate **2** is particularly noteworthy, since Barton–McCombie reactions are known to proceed quite ineffectively when primary radicals are involved.[12c,17] Our reaction proceeds instead very smoothly and without any significant side product even at room temperature. The ease of workup (see above) allows for isolation of the final sugar in very high purity without any other purification procedure (for proof of the purity of the crude product, see the ^{1}H NMR spectrum of **3** in the Supporting Information). It is worth noting that, in the case of **4**, the corresponding anomeric radical is easily produced and reduced without the 1,2-shift of the acetoxy group that is usually observed in tin-based defunctionalization procedures.[18]

In tin-based radical chemistry, the defunctionalization reactions are very often combined with intra- or intermolecular C–C bond-forming processes, in which the initial alkyl radical is trapped, for instance, by an alkene prior to hydrogen abstraction: this is undoubtedly one of the major breakthroughs of radical reactions in organic synthesis. Our isocyanide-based method does not seem suitable for Giese-type reductive additions of nucleophilic alkyl radicals to activated olefins. Indeed, hydrogen transfer from the thiol to the alkyl radical is much faster than its addition to the olefin, and the yields of adduct products are always very low, even in the presence of a large excess of alkene and very low concentrations of thiol. On the contrary, due to polar effects in the hydrogen-abstraction reaction,[19] electrophilic alkyl radicals are not easily trapped by the thiol, and they can be smoothly generated in the presence of nucleophilic olefins to give the corresponding adducts in good to almost quantitative yields. Scheme 4 and Table 1 show the results obtained at 80 °C with our standard method with four alkenes (**6A–D**, 10 equiv) and three different thiols (**7a–c**, 1 equiv). Evaporation of the final reaction mixtures removes simultaneously solvent, excess isocyanide, by-product isothiocyanate, and excess olefin giving the pure adducts **8**. Chromatography is sometimes needed to further purify compounds **8** and remove trace amounts of side products.[20]



Scheme 4. Intermolecular addition of electrophilic alkyl radicals to olefins.

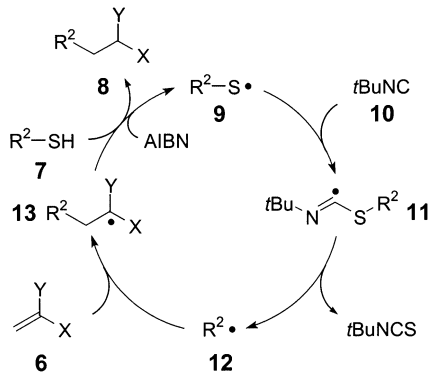
 © 2004 Wiley-VCH Verlag GmbH & Co. KGaA, Weinheim

Table 1: Yields of the adducts **8** obtained by the reaction of alkenes **6A–D** with thiols **7a–c** and *tert*-butyl isocyanide in benzene or toluene at 80 °C.

Entry	Alkene	Thiol	Adduct	Yield [%][a]
1	**6A**	**7a**	**8Aa**	66 (75)
2	**6A**	**7b**	**8Ab**	82 (91)
3	**6A**	**7c**	**8Ac**	75 (85)
4	**6B**	**7a**	**8Ba**	67 (74)
5	**6B**	**7b**	**8Bb**	75 (81)
6	**6B**	**7c**	**8Bc**[b]	79 (85)
7	**6C**	**7a**	**8Ca**	– (95)[c]
8	**6C**	**7b**	**8Cb**	– (83)[c]
9	**6C**	**7c**	**8Cc**	– (92)[c]
10	**6D**	**7a**	**8Da**	55 (64)
11	**6D**	**7b**	**8Db**	81 (92)
12	**6D**	**7c**	**8Dc**	– (70)[c]

[a] Yields are for pure products isolated by column chromatography; yields in parentheses were determined by ^{1}H NMR analysis of the crude mixtures. [b] This compound is an important intermediate for the synthesis of crop protection agents; see Supporting Information, ref. [20]. [c] Partial or total decomposition of product was observed by column chromatography.

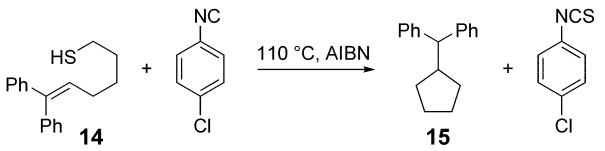
The mechanism of the efficient radical chain reaction involved in this transformation is presented in Scheme 5. Sulfanyl radical **9**, smoothly generated from thiol **7** by AIBN initiation, adds to isocyanide **10** to give the alkyl radical **12** by fast β-fragmentation of the thioimidoyl radical **11**. The



Scheme 5. Radical chain reaction of alkenes **6**, thiols **7**, and *tert*-butyl isocyanide.

electrophilic radical **12** adds to alkene **6** to generate the nucleophilic radical adduct **13**, which is eventually trapped by the starting thiol **7** to yield the final product **8** together with a new chain-propagating species **9**.

A preliminary experiment also showed that even intramolecular C–C bond formation can occur, although under slightly different conditions. Treatment of thiol **14** with 4-chlorophenyl isocyanide at 110 °C in toluene afforded the cyclization product **15** in 80 % yield after column chromatography (Scheme 6). In this case, fast 5-exo ring closure prevented premature trapping of the nucleophilic alkyl radical by the thiol and no reduction product was observed; no compounds ascribable to 6-exo cyclization of the sulfanyl radical were isolated either.



Scheme 6. Radical cyclization of thiol **14** with 4-chlorophenyl isocyanide at 110 °C.

In summary, we have shown that C–S β-scission of thioimidoyl radicals is a very effective route for the generation of alkyl radicals that can be employed in reductive defunctionalizations and intermolecular additions to electron-rich olefins. Owing to the accessibility of the starting materials, the efficient production of any kind of alkyl radical even at relatively low temperatures, and extreme ease of workup and product purification, this procedure can be an appealing substitute for many stannane/silane-mediated radical reactions. Studies are underway to find alternative ways of generation of thioimidoyl radicals not involving the thiol/isocyanide pair, with the aim of extending the method to other reactions that could suffer from the presence of a too efficient hydrogen-transfer reagent.

Received: March 12, 2004 [Z54245]

Keywords: fragmentations · isocyanides · radical reactions · synthetic methods · thiols

[1] For a comprehensive review on synthetic radical chemistry, see: *Radicals in Organic Synthesis, Vol. 1 and 2* (Eds.: P. Renaud, M. P. Sibi), Wiley-VCH, Weinheim, **2001**.
[2] P. A. Baguley, J. C. Walton, *Angew. Chem.* **1998**, *110*, 3272–3283; *Angew. Chem. Int. Ed.* **1998**, *37*, 3072–3082.
[3] For recent papers and reviews on this subject see: F. Gagosz, C. Moutrille, S. Z. Zard, *Org. Lett.* **2002**, *4*, 2707–2709; S. Kim, C. J. Lim, *Angew. Chem.* **2002**, *114*, 3399–3401; *Angew. Chem. Int. Ed.* **2002**, *41*, 3265–3267; F. Gagosz, S. Z. Zard, *Org. Lett.* **2002**, *4*, 4345–4348; S. Kim, H.-J. Song, *Synlett* **2002**, 2110–2112; A. Studer, S. Amrein, *Synthesis* **2002**, 835–849; G. Ouvry, S. Z. Zard, *Chem. Commun.* **2003**, 778–779; L. Benati, G. Calestani, R. Leardini, M. Minozzi, D. Nanni, P. Spagnolo, S. Strazzari, *Org. Lett.* **2003**, *5*, 1313–1316; J. Boivin, R. Jrad, S. Juge, V. T. Nguyen, *Org. Lett.* **2003**, *5*, 1645–1648; A.-P. Schaffner, P. Renaud, *Angew. Chem.* **2003**, *115*, 2762–2764; *Angew. Chem. Int. Ed.* **2003**, *42*, 2658–2660; Y. M. Osornio, R. Cruz-Almanza, V. Jimenez-Montano, L. D. Miranda, *Chem. Commun.* **2003**, 2316–2317; A. Studer, S. Amrein, F. Schleth, T. Schulte, J. C. Walton, *J. Am. Chem. Soc.* **2003**, *125*, 5726–5733.
[4] For a review on the use of isocyanides in radical chemistry see: D. Nanni in *Radicals in Organic Synthesis, Vol. 2* (Eds.: P. Renaud, M. P. Sibi), Wiley-VCH, Weinheim, **2001**, pp. 44–61.
[5] Thioimidoyl radicals can also be generated by radical addition to isothiocyanates, see: L. Benati, G. Calestani, R. Leardini, M. Minozzi, D. Nanni, P. Spagnolo, S. Strazzari, G. Zanardi, *J. Org. Chem.* **2003**, *68*, 3454–3464, and references therein.
[6] M. Minozzi, D. Nanni, J. C. Walton, *Org. Lett.* **2003**, *5*, 901–904; M. Minozzi, D. Nanni, J. C. Walton, *J. Org. Chem.* **2004**, *69*, 2056–2069.
[7] A. Dömling, I. Ugi, *Angew. Chem.* **2000**, *112*, 3300–3344; *Angew. Chem. Int. Ed.* **2000**, *39*, 3168–3210.

 © 2004 Wiley-VCH Verlag GmbH & Co. KGaA, Weinheim

[8] J. L. Wardell in *The Chemistry of the Thiol Group, Part 1* (Ed.: S. Patai), Wiley, London, **1974**, pp. 163 – 269.
[9] a) J. Choi, N. M. Yoon, *Synthesis* **1995**, 373 – 375; b) B. P. Bandgar, S. B. Pawar, *J. Chem. Res. Synop.* **1998**, 212 – 213; c) B. P. Bandgar, V. S. Sadavarte, *Synlett* **2000**, 908 – 910; d) B. P. Bandgar, V. S. Sadavarte, L. S. Uppalla, *Chem. Lett.* **2000**, 1304 – 1305.
[10] Trapping of the intermediate thioimidoyl radical by the thiol to give the corresponding thioimidate was never observed at these temperatures.
[11] When the reactions are conducted on a larger scale, the isothiocyanate/solvent mixture recovered in the rotary evaporator can be used to regenerate the starting isocyanide either by hydrolysis to the amine followed by the usual isocyanide syntheses, or even by one-step methods, see, for example: S. V. Lay, S. J. Taylor, *Bioorg. Med. Chem. Lett.* **2002**, *12*, 1813 – 1816; J. Fujiwara, K. Takagi, JP 05246975, **1993** [Chem. Abstr. 1994:76910]; Y. Liu, M. Bei, Z. Zhou, K. Takaki, Y. Fujiwara, *Chem. Lett.* **1992**, 1143 – 1144.
[12] a) D. H. R. Barton, S. W. McCombie, *J. Chem. Soc. Perkin Trans. 1* **1975**, 1574 – 1585; b) D. H. R. Barton, W. B. Motherwell, A. Stange, *Synthesis* **1981**, 743 – 745; c) S. Z. Zard in *Radicals in Organic Synthesis, Vol. 1* (Eds.: P. Renaud, M. P. Sibi), Wiley-VCH, Weinheim, **2001**, pp. 90 – 108.
[13] a) D. H. R. Barton, D. O. Jang, J. Cs. Jaszberenyi, *Tetrahedron Lett.* **1990**, *31*, 4681 – 4684; b) D. H. R. Barton, D. O. Jang, J. Cs. Jaszberenyi, *J. Org. Chem.* **1993**, *58*, 6838 – 6842; c) C. Chatgilialoglu, *Chem. Rev.* **1995**, *95*, 1229 – 1251; d) R. M. Lopez, D. S. Hays, G. C. Fu, *J. Am. Chem. Soc.* **1997**, *119*, 6949 – 6950; e) F. Gagosz, S. Z. Zard, *Synlett* **1999**, 1978 – 1980; f) C. Gonzales Martin, J. A. Murphy, C. R. Smith, *Tetrahedron Lett.* **2000**, *41*, 1833 – 1836; g) H. Yorimitsu, H. Shinokubo, K. Oshima, *Chem. Lett.* **2000**, 104 – 105.
[14] T. Nishio, *Chem. Commun.* **1989**, 205 – 206; T. Nishio, *J. Chem. Soc. Perkin Trans. 1* **1993**, 1113 – 1117.
[15] Thiols can also be synthesized from alcohols by prior conversion into thioesters under Mitsunobu conditions; see, for example: J. D. Park, D. H. Kim, *J. Med. Chem.* **2002**, *45*, 911 – 918.
[16] Compound **3** was obtained in 80% overall yield based on the starting galactopyranose.
[17] Sugar **5** has been obtained by Barton–McCombie-type procedures in refluxing dioxane (ref. [13b]) or even xylenes, see: D. O. Jang, D. H. Cho, D. H. R. Barton, *Synlett* **1998**, 39 – 40.
[18] B. Giese, K. S. Groninger, T. Witzel, H. -G. Korth, R. Sustmann, *Angew. Chem.* **1987**, *99*, 246 – 247; *Angew. Chem. Int. Ed. Engl.* **1987**, *26*, 233; B. Giese, S. Gilges, K. S. Groninger, C. Lamberth, T. Witzel, *Liebigs Ann. Chem.* **1988**, 615; B. Giese, K. S. Groninger, *Org. Synth.* **1990**, *69*, 66.
[19] L. Feray, N. Kuznetsov, P. Renaud in *Radicals in Organic Synthesis, Vol. 2* (Eds.: P. Renaud, M. P. Sibi), Wiley-VCH, Weinheim, **2001**, pp. 246 – 278.
[20] A common side product is the adduct of the thiol onto the alkene; however, this was produced in no more than trace amounts. Reduction of thioimidoyl radical to yield a thioimidate was observed only at very low temperatures, for example, below −40 °C (see: C. M. Camaggi, R. Leardini, D. Nanni, G. Zanardi, *Tetrahedron* **1998**, *54*, 5587 – 5598).

 © 2004 Wiley-VCH Verlag GmbH & Co. KGaA, Weinheim

Natural Product Synthesis

Total Synthesis of the Salicylate Enamide Macrolide Oximidine III: Application of Relay Ring-Closing Metathesis**

*Xiang Wang, Emma Jean Bowman, Barry J. Bowman, and John A. Porco, Jr.**

Vacuolar-type (H^+)-adenosine triphosphatases (V-ATPases) are important membrane-bound proteins that control the pH level of intracellular compartments in eukaryotic cells. These proteins affect many membrane processes, such as intracellular membrane transport, bone resorption, and tumor metastasis.[1] A number of structurally related salicylate enamide macrolides have recently been disclosed as V-ATPase inhibitors. Unlike other known V-ATPase inhibitors (for example, bafilomycins and concanamycins), salicylate enamide macrolides are selective inhibitors of mammalian V-ATPases.[2] The oximidines[3,4] (Scheme 1) are a growing subclass of the salicylate enamides and contain both macrocyclic triene and diene epoxide moieties. Oximidine III (**3**) from *Pseudomonas sp.* QN05727 was recently identified by Hayakawa et al.[4] Compound **3** is closely related to oximidines I (**1**) and II (**2**)[5] but contains an *E* enamide side chain and lacks a secondary hydroxy group at C14. Interestingly, **3** exists in two conformers at ambient temperature[4] and its activity against transformed 3Y1 cells is three to eightfold higher than that of **1**. To further evaluate the structure–activity relationships (SARs) of the oximidines, we initiated a program to synthesize **3** and the corresponding epoxide and enamide stereoisomers.

Our retrosynthetic analysis for oximidine III is shown in Scheme 1. We planned to utilize late-stage copper(I)-mediated cross-coupling[6] of *E* vinyl iodide (*E*)-**4** with amide **5**[6a] to attach the enamide side chain. Macrocyclization would then rely on ring-closing metathesis (RCM)[7] of precursors **6** and **7**, which may be prepared by base-mediated transesterification[5a,8] of 4*H*-1,3-benzodioxin-4-one **8** and alcohol **9**. Our experience with oximidine II[5a] suggested that the ability

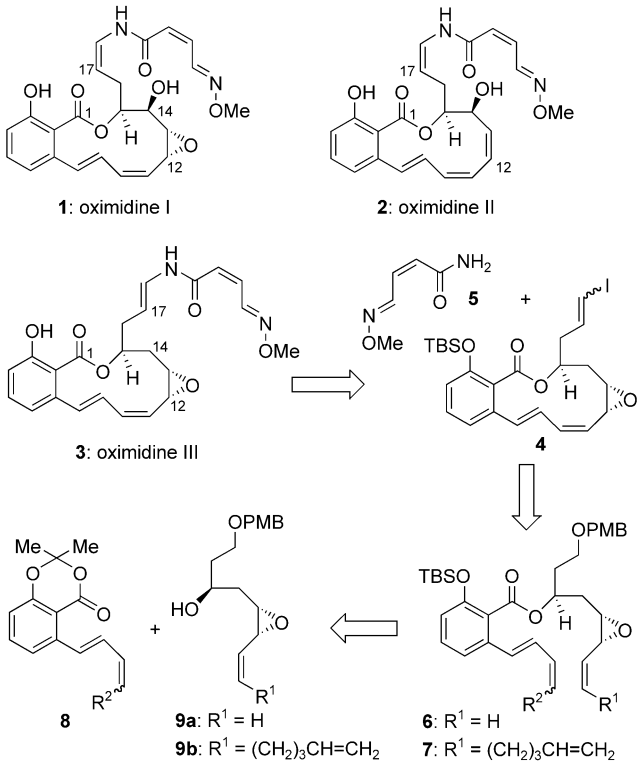
[*] X. Wang, Prof. J. A. Porco, Jr.
Department of Chemistry and
Center for Chemical Methodology and Library Development
Boston University, 590 Commonwealth Avenue
Boston, MA 02215 (USA)
Fax: (+1) 617-353-6466
E-mail: porco@chem.bu.edu

Dr. E. J. Bowman, Prof. B. J. Bowman
Department of Molecular, Cell and Developmental Biology
Sinsheimer Labs, University of California
Santa Cruz, CA 95064 (USA)

[**] We thank Prof. Y. Hayakawa (Tokyo University of Science) for kindly providing an authentic sample of oximidine III, Dr. J. Lee (Boston University) for assistance with NMR spectroscopy, and Mr. R. Shen (Boston University) for helpful suggestions. We thank the National Institutes of Health (Grant no. GM-62842) for research support.

Supporting information for this article is available on the WWW under http://www.angewandte.org or from the author.

 DOI: 10.1002/anie.200460042 © 2004 Wiley-VCH Verlag GmbH & Co. KGaA, Weinheim



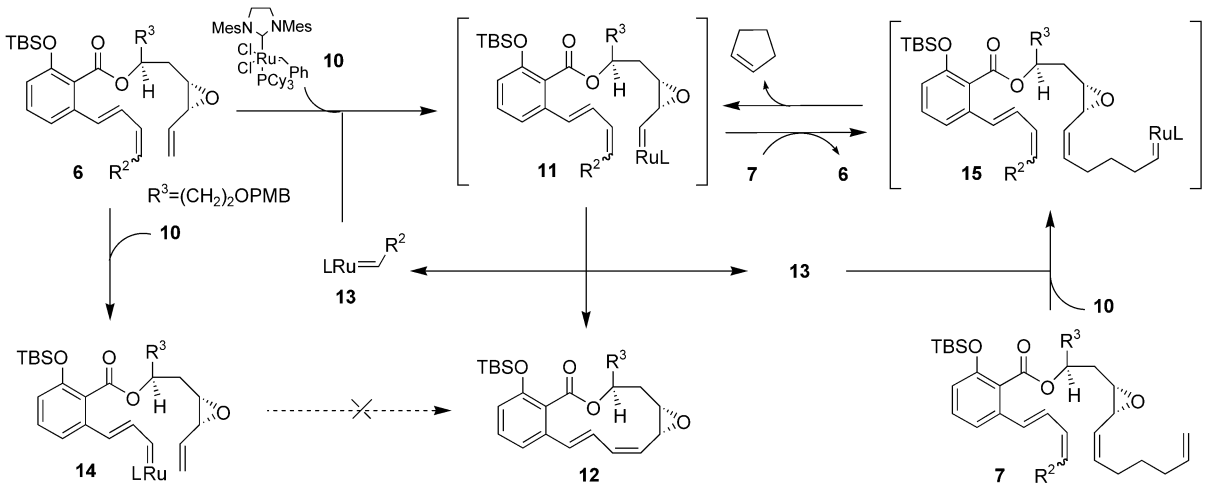
Scheme 1. Chemical structures of the oximidines and retrosynthetic analysis of oximidine III (**3**). TBS = *tert*-butyldimethylsilyl, PMB = *para*-methoxybenzyl, R^2 = Me or *i*Pr (see Table 1).

to perform RCM cleanly may be related to successful initiation of the metathesis reaction. We hoped that the ruthenium catalyst **10** (Scheme 2) would react with the epoxy alkene function of substrate **6** to form intermediate **11**, and that **11** would undergo macrocyclization to afford the desired 12-membered macrolactone **12**. Accordingly, we planned to substitute the terminus of the conjugated diene to avoid formation of stable ruthenium complex **14**. In the event that initiation of the metathesis at the vinyl epoxide site proved difficult,[9] we planned to evaluate an alternative approach to the generation of intermediate **11** involving the introduction of a relay moiety.[10] We hoped that the ruthenium catalyst would react with the least sterically hindered terminal olefin of substrate **7** to provide intermediate **15**. After release of cyclopentene as a by-product, **15** could then be converted into the desired intermediate **11** for RCM macrocyclization.

Synthesis of vinyl epoxide fragments **9a**/**9b** was initiated by adding chiral, nonracemic epoxide **16**[11] to an alkynyl lithium reagent derived from **17** to afford alkynol **18** (Scheme 3). Acetylation of **18**, followed by desilylation and Lindlar semihydrogenation, afforded allylic alcohol **19** (85%, 4 steps). Sharpless asymmetric epoxidation[12] oxidized **19** to epoxide **20** (78%, d.r. > 16:1).[13] The primary alcohol was then oxidized by treatment with Dess–Martin periodinane[14] to form an intermediate aldehyde, which was treated with either methylene or 5-hexenylidenetriphenylphosphorane to afford vinyl epoxides **9a**/**9b** after deacetylation.

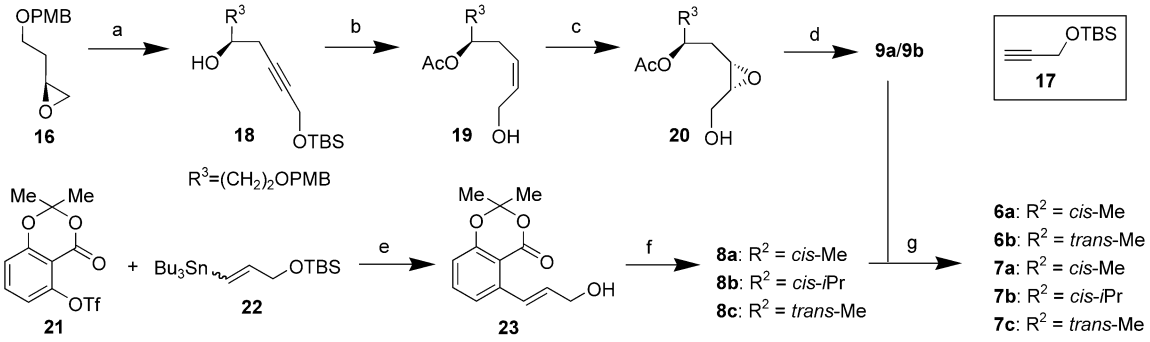
Preparation of the salicylate fragment began with Stille coupling of triflate **21**[6c] and vinyl stannane **22** (E:Z = 6:1),[15] followed by desilylation with TBAF to form E allylic alcohol **23** (82%, 2 steps). In this transformation the Z alkene isomer was converted into a lactone by-product that was easily separated from the desired product by flash chromatography. Oxidation of **23** with MnO_2 and Wittig olefination gave E,Z dienes **8a**,**b**. Treatment of **9b** with NaHMDS followed by addition of **8a**–**c**[5a] and in situ silylation afforded tetraenes **7a**–**c**, respectively. Substrates **6a** (R^2 = *cis*-Me) and **6b** (R^2 = *trans*-Me) were prepared from **8a**, **8c**, and **9a** by employing analogous procedures.

We next evaluated a number of substrates in RCM macrocyclizations (Table 1). Treatment of **6b** with the Grubbs second-generation catalyst **10** (CH_2Cl_2, reflux) afforded a low yield of the desired product **12**, accompanied by significant amounts of oligomers. Substrate **6a** reacted more slowly with catalyst **10** and also afforded a low yield of **12** (entries 1 and 2, Table 1). This result may be explained by the formation of the unreactive alkylidene **14** (Scheme 2). We next examined the relay RCM reactivity of substrates **7a**–**c**. We found that it was necessary to add the substrate to a solution of ruthenium catalyst in CH_2Cl_2 to prevent formation of by-product **6**



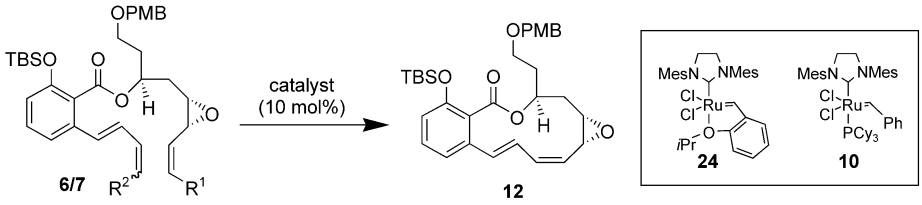
Scheme 2. Analysis of ring-closing metathesis pathways. Mes = trimethylphenyl, L = ligand.

 © 2004 Wiley-VCH Verlag GmbH & Co. KGaA, Weinheim



Scheme 3. Synthesis of RCM precursors. a) **17**, *n*BuLi, then **16**, $BF_3{\cdot}OEt_2$, THF, −78–25 °C; b) 1. Ac_2O, pyridine, cat. DMAP, CH_2Cl_2; 2. AcOH/H_2O/THF (3:1:1), 60 °C; 3. Lindlar catalyst, 1 atm H_2, Et_3N, THF, 85 % for 4 steps; c) $Ti(OiPr)_4$, D-DIPT, 4-Å molecular sieves, CH_2Cl_2, −20 °C, 76 %; d) 1. Dess–Martin periodinane, CH_2Cl_2, RT; 2. $Ph_3P^+Me{\cdot}Br^-$, NaHMDS, THF, −10 °C, 62 %; or $Ph_3P^+(CH_2)_4CH{=}CH_2{\cdot}I^-$, NaHMDS, THF, −10 °C, 70 %, *Z*:*E* > 16:1; 3. K_2CO_3, MeOH, RT, 95 %; e) 1. $[Pd_2(dba)_3]$, tri(2-furyl)phosphane, LiCl, DMF, 60 °C; 2. TBAF, THF, RT, 82 % for 2 steps; f) 1. MnO_2, CH_2Cl_2, RT; 2. $(Ph_3PEt){\cdot}Br$ or $(Ph_3PiBu){\cdot}Br$, NaHMDS, −78–25 °C, 60–62 % for 2 steps (for **8c**, see ref. [5a]); g) **9**, NaHMDS, **8**; then TBSCl, imidazole, THF, 0–25 °C, 92–96 %. THF = tetrahydrofuran, DMAP = 4-dimethylaminopyridine, DIPT = diisopropyl tartrate, HMDS = 1,1,1,3,3,3-hexamethyldisilazane, dba = *trans*,*trans*-dibenzylideneacetone, DMF = dimethylformamide, TBAF = tetrabutylammonium fluoride.

Table 1: Evaluation of substrates and conditions for RCM macrocyclization.[a]

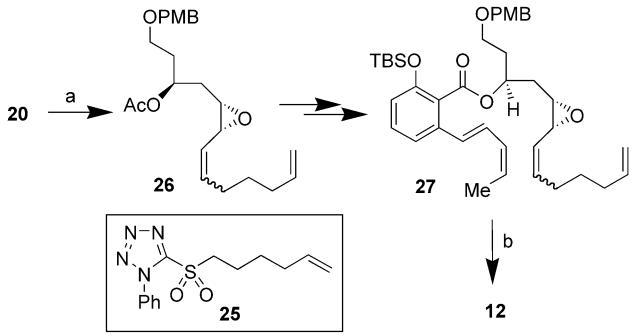


	SM[b]	R^1	R^2	Addition time [min]	Catalyst	Conversion [%][e]	Yield [%][f]
1[c]	**6a**	H	*cis*-Me	–	**10** or **24**	38	15
2[c]	**6b**	H	*trans*-Me	–	**10** or **24**	75	12
3	**7a**	$(CH_2)_3CH{=}CH_2$	*cis*-Me	120	**10**	> 90	45
4	**7b**	$(CH_2)_3CH{=}CH_2$	*cis*-*i*Pr	150	**10**	71	30
5	**7c**	$(CH_2)_3CH{=}CH_2$	*trans*-Me	240	**10**	77	30
6	**7a**	$(CH_2)_3CH{=}CH_2$	*cis*-Me	60	**10**	> 90	58
7	**7a**	$(CH_2)_3CH{=}CH_2$	*cis*-Me	60	**24**	> 90	58
8[d]	**7a**	$(CH_2)_3CH{=}CH_2$	*cis*-Me	30	**24**	> 90	71

[a] Reactions were conducted in refluxing CH_2Cl_2 unless otherwise noted; the final concentration of **6**/**7** was 2.0 mM. [b] SM = starting material. [c] Catalyst added to the starting material in refluxing CH_2Cl_2 and stirred for 2 h. [d] Reaction conducted at 50 °C in 1,2-dichloroethane. [e] Conversions based on recovered starting material. [f] Yields of isolated products; in all cases, only 12-membered cyclic *E*,*Z* diene **12** was isolated.

(Scheme 2).[16] Substrate **7a** was optimal for the RCM-RCM process; significant amounts of the corresponding by-products **6** were obtained when substrates **7b** and **7c** were used, which indicates slow reaction rates for the second RCM (entries 3–5, Table 1). Faster addition of the substrate resulted in reduced decomposition of the product (entry 6, Table 1). The recyclable ruthenium catalyst **24** described by Hoveyda and co-workers[17] showed a similar reactivity to catalyst **10** (entry 7, Table 1) and produced a colorless product. We investigated the relationship between the addition rate and temperature further in an attempt to minimize oligomer formation.[7c] We found that production of oligomers was minimized at a higher temperature than that initially used (entry 8, Table 1). Catalyst **24** was pretreated with 20 mol % *o*-isopropoxystyrene to convert the highly reactive ruthenium–alkylidene species **13** (R^2 = Me, Scheme 2) into the less reactive catalyst **24** during the reaction. A slower reaction rate was observed, but the chemical yield was not improved.

To evaluate the influence of the vinyl epoxide olefin geometry on the relay RCM process we prepared epoxy alkene **26** (*E*:*Z* = 1.3:1, Scheme 4) from **20** and phenyltetrazole sulfone **25**.[18] Compound **26** was converted into RCM precursor **27** in several steps (see Scheme 3). Relay RCM (2.0 mM, DCE, 50 °C) of substrate **27** provided only a 34 % yield of the desired product **12**. The *E* vinyl epoxide stereoisomer of **27** was purified and used in the further study of this transformation. Submission of this *E* isomer of **27** to relay RCM conditions gave neither the desired macrolactone **12** nor by-product **6a**, only oligomeric by-

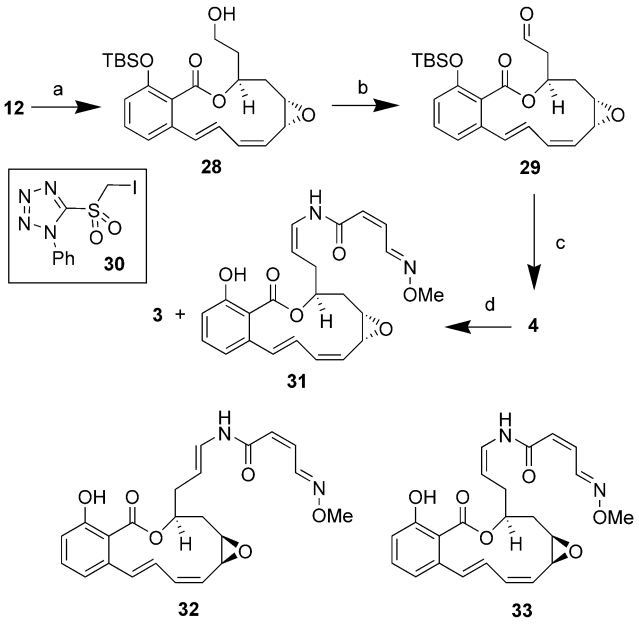


Scheme 4. Relay RCM with substrate **27**. a) 1. Dess–Martin periodinane, CH_2Cl_2, RT; 2. **25**, NaHMDS, −78–25 °C, 74 % (*E*:*Z* = 1.3:1). b) 10 mol % **24**, DCE, 2.0 mM, 50 °C, 30 min, 34 %. DCE = dichloroethane.

 © 2004 Wiley-VCH Verlag GmbH & Co. KGaA, Weinheim

products were formed, which indicates that the *Z* configuration of the epoxy alkene is required for a fast reaction rate in the first RCM step.

To advance **12** to oximidine III, the PMB protecting group was removed by treatment with DDQ and the resulting alcohol **28** was oxidized by PDC to produce aldehyde **29** (Scheme 5). Transformation of **29** into *E* vinyl iodide (*E*)-**4**



Scheme 5. Syntheses of oximidine III (**3**) and its enamide stereoisomer **31**. a) DDQ, CH_2Cl_2, pH 7 buffer, 0–25 °C, 95 %; b) PDC, 4-Å molecular sieves, CH_2Cl_2; c) **30**, NaHMDS, THF, −78–25 °C, 62 % for 2 steps (*E*:*Z* ≈ 1:1); d) TBAF (1.0 equiv), THF, 0–25 °C; concentrate, then **5**, CuTC, *N*,*N*′-dimethylethylenediamine, K_2CO_3, DMA, 50 °C, 1 h, 45 % (*E*:*Z* = 7:1). DDQ = 2,3-dichloro-5,6-dicyano-1,4-benzoquinone, PDC = pyridinium dichromate, CuTC = copper(I) thiophenecarboxylate, DMA = *N*,*N*-dimethylacetamide.

was problematic because the vinyl epoxide is sensitive to both acidic and reductive[19] conditions. Treatment of **29** with the Seyferth/Gilbert reagent[20] converted the aldehyde into a terminal alkyne. Hydrozirconation of the alkyne, followed by addition of iodine (THF, 0 °C) afforded vinyl iodide (*E*)-**4** in low yield. Direct homologation of aldehyde **29** was achieved by Kociénski–Julia olefination with the novel phenyltetrazole sulfone reagent **30**.[21] This transformation led to an inseparable mixture of vinyl iodides (*E*)-**4** and (*Z*)-**4** (62 % yield, *E*:*Z* = 1:1).[22]

We next tested the crucial late-stage Cu^I-mediated vinylic amidation reaction. The TBS protecting group of **4** was first removed by treatment with TBAF to avoid the use of excess base.[23] The deprotected compound, presumed to be the phenolate salt, was submitted directly to amidation by treatment with copper(I) thiophenecarboxylate-*N*,*N*′-dimethylethylenediamine.[5a] The vinyl iodides were consumed quickly when a stoichiometric amount of CuTC was used. Oximidine III (**3**) and the corresponding *Z* enamide stereoisomer **31** were isolated in 45 % yield (*E*:*Z* = 7:1) after 1 h (50 °C). Extended reaction times resulted in decomposition of **3** and a higher yield of *Z* enamide **31** (3 h, 21 % yield, *E*:*Z* = 1:1).[6c] The synthetic product **3** was confirmed as identical to natural oximidine III by ^1H and ^{13}C NMR spectroscopy, mass spectrometry, $[\alpha]_D^{20}$ measurement, HPLC, and TLC R_f values in three solvent systems.

After successful synthesis of oximidine III (**3**) and its enamide stereoisomer **31**, we also synthesized **32** (the C12-C13 epimer of oximidine III) and its enamide stereoisomer **33** by employing L-DIPT in the epoxidation step. Unlike oximidine III (**3**) and **31**, both **32** and **33** each exist as a single conformer, as shown by ^1H NMR spectroscopy (RT). Oximidines **3** and **31**–**33** were evaluated for activity against bovine V-ATPase and their IC_{50} values (concentration required for 50 % inhibition) were found to be 2.2, 65, 4.3, and 65 nM, respectively.[24] These initial SAR data indicate that the C17-C18 olefin geometry has a more substantial effect on V-ATPase inhibition than the C12-C13 epoxide stereochemistry.

In summary, enantioselective total syntheses of the natural product oximidine III (**3**) and stereoisomers **31**–**33** have been developed, which has allowed unambiguous assignment of the relative and absolute stereochemistry of **3**. A relay RCM strategy was employed to facilitate the crucial macrocyclization reaction, and a well-defined substrate possessing two differentially functionalized RCM alkene partners was found to be required for the RCM-RCM process. A novel phenyltetrazole sulfone reagent **30** was developed for homologation of aldehydes to form vinyl iodides under mild conditions. Further synthetic studies on the oximidines and simplified analogues of these compounds will be reported in due course.

Received: March 18, 2004 [Z460042]

Keywords: antitumor agents · enamides · natural products · ring-closing metathesis · vinyl iodides

[1] T. Nishi, M. Forgac, *Nat. Rev. Mol. Cell Biol.* **2002**, *3*, 94.
[2] a) M. R. Boyd, C. Farina, P. Belfiore, S. Gagliardi, J. W. Kim, Y. Hayakawa, J. A. Beutler, T. C. McKee, B. J. Bowman, E. J. Bowman, *J. Pharmacol. Exp. Ther.* **2001**, 297, 114; b) for a recent review of syntheses and SAR studies, see: L. Yet, *Chem. Rev.* **2003**, *103*, 4283.
[3] J. W. Kim, K. Shin-ya, K. Furihata, Y. Hayakawa, H. Seto, *J. Org. Chem.* **1999**, *64*, 153.
[4] a) Y. Hayakawa, T. Tomikawa, K. Shin-Ya, N. Arao, K. Nagai, K-I. Suzuki, *J. Antibiot.* **2003**, *56*, 899; b) Y. Hayakawa, T. Tomikawa, K. Shin-Ya, N. Arao, K. Nagai, K-I. Suzuki, K. Furihata, *J. Antibiot.* **2003**, *56*, 905.
[5] For the total synthesis of oximidine II, see: a) X. Wang, J. A. Porco, Jr, *J. Am. Chem. Soc.* **2003**, *125*, 6040; for recent studies on the synthesis of the oximidines, see: b) T. Haack, S. Kurtkaya, J. P. Snyder, G. I. Georg, *Org. Lett.* **2003**, *5*, 5019; c) J. E. Harvey, S. A. Raw, R. J. K. Taylor, *Tetrahedron Lett.* **2003**, *44*, 7209.
[6] a) R. Shen, J. A. Porco, Jr, *Org. Lett.* **2000**, *2*, 1333; b) R. Shen, C. T. Lin, E. J. Bowman, B. J. Bowman, J. A. Porco, Jr, *J. Am. Chem. Soc.* **2003**, *125*, 7889; for applications of this method, see: ref. [5a] and c) A. Fürstner, T. Dierkes, O. R. Thiel, G. Blanda, *Chem. Eur. J.* **2001**, *7*, 5286; d) R. Shen, C. T. Lin, J. A. Porco, Jr, *J. Am. Chem. Soc.* **2002**, *124*, 5650; e) K. C. Nicolaou, D. W. Kim, R. Baati, A. O'Brate, P. Giannakakou, *Chem. Eur. J.* **2003**, *9*,

 © 2004 Wiley-VCH Verlag GmbH & Co. KGaA, Weinheim

6177; f) R. S. Coleman, P.-H. Liu, *Org. Lett.* **2004**, *6*, 577; g) Q. Su, J. S. Panek, *J. Am. Chem. Soc*, **2004**, *126*, 2425.
[7] Recent reviews: a) A. Fürstner, *Angew. Chem.* **2000**, *112*, 3140; *Angew. Chem. Int. Ed.* **2000**, *39*, 3012; b) T. M. Trnka, R. H. Grubbs, *Acc. Chem. Res.* **2001**, *34*, 18; c) for RCM with a vinyl epoxide, see: K. Yamamoto, K. Biswas, C. Gaul, S. J. Danishefsky, *Tetrahedron Lett.* **2003**, *44*, 3297.
[8] Y. Wu, X. Liao, R. Wang, X.-S. Xie, J. K. De Brabander, *J. Am. Chem. Soc.* **2002**, *124*, 3245.
[9] For an example of allylic substitution effects on reaction rates of RCM, see: T. R. Hoye, H. Zhao, *Org. Lett.* **1999**, *1*, 1123.
[10] For studies regarding relay RCM, see: a) T. R. Hoye, J. Wang, *226th ACS National Meeting* (New York, NY), **2003**, ORGN-670; b) T. R. Hoye, R. Thomas, H. Zhao, *218th ACS National Meeting*, (New Orleans, LA), **1999**, ORGN-620; c) T. R. Hoye, H. Zhao, *218th ACS National Meeting* (New Orleans, LA), **1999**, ORGN-303; d) for another application of a "relay" entity in the assembly of reacting sites in RCM, see: A. Fürstner, K. Langemann, *Synthesis* **1997**, 792.
[11] The chiral nonracemic epoxide **16** was prepared by hydrolytic kinetic resolution of the racemic epoxide (48% yield, 95% *ee*): S. E. Schaus, B. D. Brandes, J. F. Larrow, M. Tokunaga, K. B. Hansen, A. E. Gould, M. E. Furrow, E. N. Jacobsen, *J. Am. Chem. Soc.* **2002**, *124*, 1307.
[12] T. Katsuki, V. S. Martin, *Org. React. (N.Y.)* **1996**, *48*, 1.
[13] Use of a sterically demanding TBS protecting group on the secondary alcohol resulted in low diastereoselectivity of the Sharpless asymmetric epoxidation (4:1).
[14] D. B. Dess, J. C. Martin, *J. Org. Chem.* **1983**, *48*, 4155.
[15] J. W. Labadie, D. Tueting, J. K. Stille, *J. Org. Chem.* **1983**, *48*, 4634.
[16] Use of the Grubbs first-generation catalyst led to the corresponding by-products **6** (Scheme 2).
[17] S. B. Garber, J. S. Kingsbury, B. L. Gray, A. H. Hoveyda, *J. Am. Chem. Soc.* **2000**, *122*, 8168.
[18] P. R. Blakemore, W. J. Cole, P. J. Kociénski, A. Morley, *Synthesis* **1996**, 285. For the preparation of **25**, see the Supporting Information.
[19] K. Takai, K. Nitta, K. Utimoto, *J. Am. Chem. Soc.* **1986**, *108*, 7408.
[20] a) D. Seyferth, R. S. Marmor, P. Hilbert, *J. Org. Chem.* **1971**, *36*, 1379; b) R. Ratcliffe, B. Christensen, *Tetrahedron Lett.* **1973**, *14*, 4645; c) J. C. Gilbert, U. Weerasooriya, *J. Org. Chem.* **1982**, *47*, 1837; d) D. G. Brown, E. J. Velthuisen, J. R. Commerford, R. G. Brisbois, T. R. Hoye, *J. Org. Chem.* **1996**, *61*, 2540.
[21] For the preparation of **30**, see the Supporting Information; a) for a related chloromethyl benzothiazole sulfone reagent, see: J. B. Baudin, G. Hareau, S. A. Julia, R. Lorne, O. Ruel, *Bull. Soc. Chim. Fr.* **1993**, *130*, 856; b) for use of iodoalkyl phenyl sulfone reagents in free radical reactions, see: P. Jankowski, M. Masnyk, J. Wicha, *Synlett* **1995**, 866.
[22] The *E*:*Z* ratio was determined by ^{1}H NMR analysis.
[23] In our synthesis of oximidine II (ref. [5a]), we utilized a silylated phenol substrate treated with base and amide (2 equiv each) in a copper-mediated coupling to effect both silyl ether deprotection and enamide formation. However, use of excess base and amide in the syntheses described herein led to significant decomposition of the sensitive vinyl epoxide moiety.
[24] V-ATPase activity was determined as described in the Supporting Information.

 © 2004 Wiley-VCH Verlag GmbH & Co. KGaA, Weinheim

Heterocycle Synthesis

Palladium-Catalyzed Synthesis of *N*-Aryl Pyrrolidines from γ-(*N*-Arylamino) Alkenes: Evidence for Chemoselective Alkene Insertion into Pd–N Bonds**

*Joshua E. Ney and John P. Wolfe**

In recent years, palladium(aryl)(amido) complexes have been shown to serve as key intermediates in the synthesis of aniline derivatives.[1] Although the propensity of these intermediates to undergo C–N bond-forming reductive elimination has been well established,[1] small molecule (alkene) insertion reactions of these complexes have been largely unexplored and have not been exploited in catalytic processes.[2] In fact, only a single example of the stoichiometric insertion of an activated alkyne into an isolated [Pd(Ar)(NR_2)] complex has been reported,[2b] and insertions of alkenes have not been demonstrated. Herein we describe a new, stereoselective, palladium-catalyzed synthesis of pyrrolidines from γ-(*N*-arylamino) alkenes and aryl bromides, and present mechanistic evidence that suggests the transformation proceeds by a chemoselective intramolecular insertion of an unactivated alkene into the Pd–N bond of an intermediate [Pd(Ar)(NRR′)] complex.[3] This reaction allows convergent access to substituted pyrrolidines, which are found in a variety of natural products.[4] In contrast to most methods available for the synthesis of substituted pyrrolidines,[5] this reaction effects intramolecular C–N bond formation with concomitant intermolecular formation of a C1′–C bond.[6]

In preliminary studies we employed γ-aminoalkene substrates with *N*-aryl substituents because of their ease of preparation and handling. After optimization of the reaction conditions we found that the reaction of *N*-phenyl-4-pentenylamine (**1a**) with 2-bromonaphthalene in the presence of NaO*t*Bu and a catalytic amount of [$Pd_2(dba)_3$]/dppb (1 mol%; dppb = 1,4-bis(diphenylphosphanyl)butane) at 60°C in toluene afforded the desired *N*-aryl 2-(β-naphthylmethyl)pyrrolidine **2a** and regioisomeric product **3a** in 94% yield and a 25:1 ratio [Eq. (1)].

As shown in Table 1, the reactions of electron-rich, electron-neutral, and electron-deficient *N*-aryl amine derivatives with a variety of aryl bromide coupling partners proceeded in good yield. A number of functional groups are

[*] J. E. Ney, Prof. J. P. Wolfe
University of Michigan
Department of Chemistry
Ann Arbor, MI 48109-1055 (USA)
Fax: (+1) 734-763-2307
E-mail: jpwolfe@umich.edu

[**] This research was supported by the University of Michigan. J.P.W. thanks The Dreyfus Foundation for a New Faculty Award and Research Corporation for an Innovation Award. J.E.N. thanks the University of Michigan for a Regents Fellowship. Additional unrestricted support was provided by Eli Lilly, 3M, and Amgen.

Supporting information for this article is available on the WWW under http://www.angewandte.org or from the author.

 DOI: 10.1002/anie.200460060 © 2004 Wiley-VCH Verlag GmbH & Co. KGaA, Weinheim

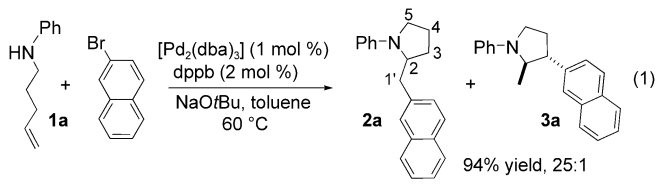
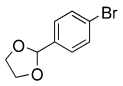
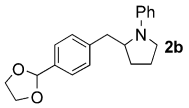
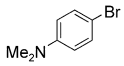
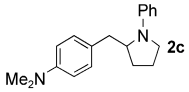
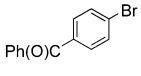
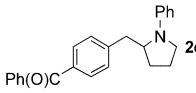
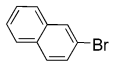
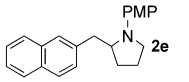
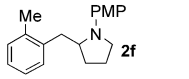
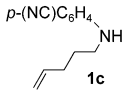
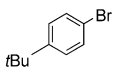
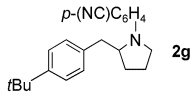
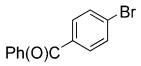
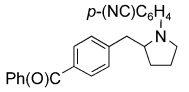
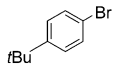
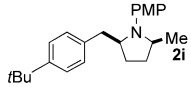
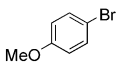
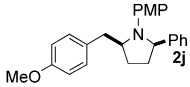
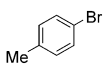
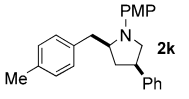
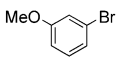
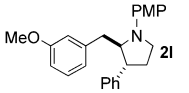


Table 1: Palladium-catalyzed synthesis of pyrrolidines.[a]

Entry	Amine	Aryl bromide	Product	2/3	Yield [%]
1				16:1	73
2	**1a**			17:1	81[b]
3	**1a**			100:1	45
4				14:1	67
5	**1b**			35:1	75
6				100:1	78
7	**1c**			>100:1	86
8				10:1	66[c] (d.r. >20:1)
9				10:1	72[c] (d.r. >20:1)
10				8:1	88[c] (d.r. 2:1)
11				10:1	68[c,d] (d.r. >20:1)

[a] Conditions: amine (1.0 equiv), ArBr (1.1–1.3 equiv), NaO*t*Bu (1.1–1.3 equiv), $[Pd_2(dba)_3]$ (1 mol%), dppb (2 mol%), toluene (0.25 M), 60 °C. [b] This material contained a second, unidentified regioisomer in approximately 3% yield. [c] Reaction conducted at 100 °C; dppe used in place of dppb. [d] This material contained *N*-(PMP)-2-(3-methoxybenzyl)-3-phenylpyrrole in approximately 8% yield. dppe = 1,4-bis(diphenylphosphanyl)ethane, PMP = 4-methoxyphenyl.

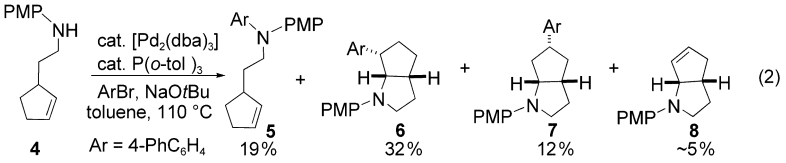
tolerated, including nitriles, nonenolizable ketones, and acetals. The main side products in these reactions are arenes that result from reduction of the aryl bromide[7] and *N*,*N*-diaryl amines that presumably form through Pd-catalyzed N-arylation of the substrate.[1] Side products resulting from Heck arylation of the alkene are generally not observed. These results contrast with those of previously described Pd-catalyzed reactions of γ-(*N*-benzylamino)alkenes with aryl iodides, which have been reported to afford exclusively products resulting from Heck arylation of the alkene.[8]

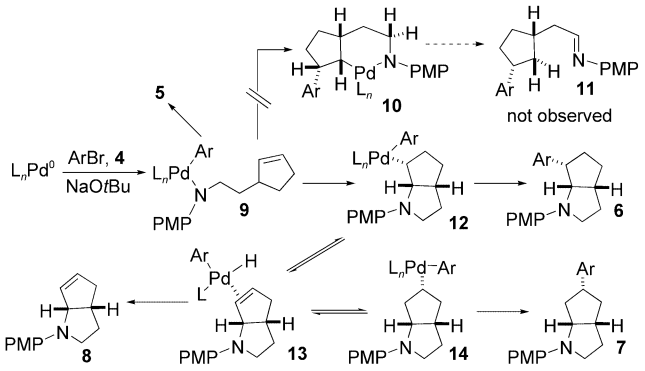
In most cases examined the cyclizations proceed with good levels of diastereoselectivity. The 3-substituted alkenyl amine **1g** underwent cyclization with >20:1 diastereoselectivity to provide the *trans*-2,3-disubstituted product **2l** (Table 1, entry 11),[9] and reactions of the 1-substituted alkenyl amines **1d** and **1e** gave the *cis*-2,5-disubstituted pyrrolidines **2i** and **2j** with d.r. >20:1 (Table 1, entries 8–9). In contrast, the C2-substituted amine **1f** reacted with only modest (2:1) *cis* stereoselectivity for the 2,4-disubstituted product **2k** (Table 1, entry 10).

The ratio of the regioisomeric products **2**/**3** of the cyclization reactions typically ranged from 10:1 to 25:1 for substrates with terminal alkenes, although in some instances selectivities of up to >100:1 were observed.[10] However, reactions of substrates with internal alkenes provided complex mixtures of regioisomeric products. Interestingly, the reaction of **4** with 4-bromobiphenyl in the presence of catalytic $[Pd_2(dba)_3]$/P(*o*-tol)$_3$ afforded a mixture of four products [Eq. (2)].[11] The desired 6-aryl pyrrolizidine product **6** was formed as the major regioisomer. A substantial amount of the 5-aryl regioisomer **7** was also isolated, along with a small amount of the unsaturated pyrrolizidine **8**. The use of dppb or dppe as a ligand led to the formation of increased amounts of **8** relative to the other products.[11,12]

Although the yield of the desired regioisomer **6** is modest, these results provide important information about the mechanism of the cyclization reaction. This transformation presumably occurs through initial oxidative addition of the aryl bromide to Pd^0 followed by reaction of the resulting complex with the substrate and base to afford **9** (Scheme 1).[1] A *syn* insertion of the alkene into the Pd–C bond of **9** would provide **10**. However, products **7** and **8** can not derive from **10**; C–C bond-forming alkene-insertion reactions are generally

 © 2004 Wiley-VCH Verlag GmbH & Co. KGaA, Weinheim





Scheme 1. Proposed mechanism.

not reversible.[13] Furthermore, if the alkene underwent insertion into the metal–carbon bond to give **10**, the use of ligands that decrease the rate of reductive elimination, such as dppe,[12] would not provide increased amounts of **8** as is observed. A *syn* β-hydride elimination[13] of the intermediate **10** would instead afford the arylated imine **11**, which is not detected.[11]

A more reasonable pathway, which would account for all products formed in the reaction, involves *syn* insertion of the alkene into the Pd–N bond in **9** to afford **12** (Scheme 1).[2] Complex **12** could either undergo C–C bond-forming reductive elimination with retention of configuration to afford the desired product **6**,[14] or could undergo reversible β-hydride elimination to give the alkene complex **13**.[13] Reinsertion of the alkene into the Pd–H bond with reversal of regiochemistry would afford **14**,[15] which would yield the regioisomeric side product **7** following reductive elimination. Dissociation of the alkene complex **13** before reinsertion would provide **8**. The *N*-arylated product **5** is presumably formed through C–N bond-forming reductive elimination of **9**.[1] This mechanistic pathway is also consistent with observed ligand effects: ligands that decrease the rate of reductive elimination afford increased amounts of products derived from the proposed intermediate **13**.

Examples of the insertion of alkenes into palladium–nitrogen bonds are rare,[2,16] and only two catalytic reactions that proceed by alkene insertion into a Pd(NRR′)X complex (X = Cl,[16a] $OC(O)C_6F_5$[16b]) have been described.[17–19] The insertion of unactivated alkenes into [Pd(Ar)(NR_2)] complexes has not been reported.

In conclusion, we have developed a new, stereoselective synthesis of pyrrolidines from γ-(*N*-arylamino) alkenes. The transformations described herein are the first examples of catalytic reactions that most likely proceed by the chemoselective intramolecular insertion of an alkene into a [Pd(Ar)(NRR′)] intermediate. Furthermore, the reaction of **4** with 4-bromobiphenyl provides the first probe of the chemoselectivity of insertion under catalytic conditions; the most plausible pathway for the conversion of **4** into **7** and **8** involves olefin insertion into a Pd–N bond. Further studies on the scope, limitations, applications, and mechanism of these reactions are currently underway.

Received: March 19, 2004 [Z460060]

Keywords: alkene insertion · aryl halides · diastereoselectivity · nitrogen heterocycles · palladium

[1] For reviews on aryl C–N bond-forming reactions that involve Pd(Ar)(NR_2) intermediates, see: a) A. R. Muci, S. L. Buchwald, *Top. Curr. Chem.* **2002**, *291*, 131–209; b) J. F. Hartwig, *Pure Appl. Chem.* **1999**, *71*, 1417–1423.

[2] a) J. M. Boncella, L. A. Villanueva, *J. Organomet. Chem.* **1994**, *465*, 297–304; b) L. A. Villanueva, K. A. Abboud, J. M. Boncella, *Organometallics* **1992**, *11*, 2963–2965.

[3] For related studies on the synthesis of tetrahydrofurans, see: J. P. Wolfe, M. A. Rossi, *J. Am. Chem. Soc.* **2004**, *126*, 1620–1621.

[4] a) D. O'Hagan, *Nat. Prod. Rep.* **2000**, *17*, 435–446; b) J. R. Lewis, *Nat. Prod. Rep.* **2001**, *18*, 95–128.

[5] a) A. Mitchinson, A. Nadin, *J. Chem. Soc. Perkin Trans. 1* **2000**, 2862–2892; b) M. Pichon, B. Figadere, *Tetrahedron: Asymmetry* **1996**, *7*, 927–964.

[6] For pyrrolidine syntheses that involve intramolecular C–N bond formation and intermolecular C–C bond formation, see: a) Y. Tamaru, M. Kimura, *Synlett* **1997**, 749–757; b) Y. Tamaru, M. Hojo, Z.-i. Yoshida, *J. Org. Chem.* **1988**, *53*, 5731–5741; c) H. Yorimitsu, K. Wakabayashi, H. Shinokubo, K. Oshima, *Bull. Chem. Soc. Jpn.* **2001**, *74*, 1963–1970; d) R. C. Larock, H. Yang, S. M. Weinreb, R. J. Herr, *J. Org. Chem.* **1994**, *59*, 4172–4178.

[7] Imine side products presumably formed through β-hydride elimination of an intermediate [Pd(Ar)(NR_2)] complex are occasionally observed; see reference [1].

[8] G. Fournet, G. Balme, J. Gore, *Tetrahedron* **1990**, *46*, 7763–7774.

[9] Diastereomeric ratios were determined by ^{1}H NMR spectroscopy and/or GC analysis of the crude reaction mixture. The stereochemistry of the products was assigned on the basis of ^{1}H NMR NOE experiments and/or by analogy with related compounds of known configuration.

[10] The reaction of 2-bromonaphthalene with *N*-(4-methoxyphenyl)-3-pentenylamine under the standard reaction conditions afforded only the product of N-arylation; no cyclized products were observed. This result suggests that the regioisomeric products are not formed through initial isomerization of the alkene substrate followed by 5-endocyclization.

[11] ^{1}H NMR spectroscopic analysis of the reaction mixture showed that the products **5**, **6**, **7**, and **8** were formed in a ratio of 6:7:2:1. The use of dppe as a ligand led to a 2:1:2:4 ratio of **5**/**6**/**7**/**8**, and the use of dppb as a ligand afforded a 2:2:2:1 mixture of **5**/**6**/**7**/**8**.

[12] The ligands dppe and dppb have been shown to decrease the rate of C–C and C–N bond-forming reductive elimination and increase the formation of side products by competing β-hydride elimination; see: a) A. Gillie, J. K. Stille, *J. Am. Chem. Soc.* **1980**, *102*, 4933–4941; b) M. S. Driver, J. F. Hartwig, *J. Am. Chem. Soc.* **1997**, *119*, 8232–8245; c) J. P. Wolfe, S. L. Buchwald, *J. Org. Chem.* **2000**, *65*, 1144–1157.

[13] I. P. Beletskaya, A. V. Cheprakov, *Chem. Rev.* **2000**, *100*, 3009–3066.

[14] D. Milstein, J. K. Stille, *J. Am. Chem. Soc.* **1979**, *101*, 4981–4991.

 © 2004 Wiley-VCH Verlag GmbH & Co. KGaA, Weinheim

[15] H. Qian, R. A. Widenhoefer, *J. Am. Chem. Soc.* **2003**, *125*, 2056 – 2057.
[16] a) J. Helaja, R. Göttlich, *Chem. Commun.* **2002**, 720 – 721; b) H. Tsutsui, K. Narasaka, *Chem. Lett.* **1999**, 45 – 46
[17] The treatment of *trans*-[PdH(NHPh)($P(C_6H_{11})_3$)$_2$] with ethylene or acrylonitrile led to reductive elimination of aniline rather than alkene insertion: A. L. Seligson, R. L. Cowan, W. C. Trogler, *Inorg. Chem.* **1991**, *30*, 3371 – 3381.
[18] For examples of insertion reactions of activated alkenes into platinum–nitrogen bonds, see: a) R. L. Cowan, W. C. Trogler, *Organometallics* **1987**, *6*, 2451 – 2453; b) R. L. Cowan, W. C. Trogler, *J. Am. Chem. Soc.* **1989**, *111*, 4750 – 4761.
[19] For an example of a catalytic reaction that proceeds through the insertion of norbornene into an iridium–nitrogen bond, see: A. L. Casalnuovo, J. C. Calabrese, D. Milstein, *J. Am. Chem. Soc.* **1988**, *110*, 6738 – 6744.

 © 2004 Wiley-VCH Verlag GmbH & Co. KGaA, Weinheim

Cover Picture



Franklin Kim, Stephen Connor, Hyunjoon Song, Tevye Kuykendall, and Peidong Yang*

Platonic shapes of gold nanocrystals are prepared by a modified polyol process in the presence of the surface-regulating polymer poly(vinyl pyrrolidone). P. Yang and co-workers describe in their Communication on page 3673 ff. how the careful regulation of the growth rate along different crystallographic directions allows exquisite shape control. The drawing in the center of the cover picture was proposed by the astronomer Johannes Kepler in the 17th century, in which one platonic solid fits between each pair of planetary spheres.

The Future of Chemistry...

...is the theme of a seminal Essay by George M. Whitesides in this issue (see page 3632 ff.). "Chemistry is the Future", "No Future without Chemistry", and similar slogans are familiar to everyone, but few chemists seriously think about where chemistry is going and what solutions it can offer for anticipated problems, and especially, what problems chemistry may eventually cause. In 1990 *Angewandte Chemie* published a Review by George M. Whitesides with the title "What Will Chemistry Do in the Next Twenty Years?"[1] and it is certainly a worthwhile exercise to look at these predictions as the end of this time frame approaches. George M. Whitesides has played a significant role in the activities of many committees that consider the future of our discipline, and he now presents his thoughts, which this time go far further into the future than just twenty years. Assumptions of this sort can set the tone for chemistry; they can also, later, be found to be far from the mark. They do however, provide highly stimulating material for discussion among colleagues, with students, and the public.



George M. Whitesides



Jean-Marie Lehn

One area that will no doubt gain further importance in the future is supramolecular chemistry, especially when broadly considered as the chemistry of molecular systems. It is thus appropriate that in this issue there is a Review by Jean-Marie Lehn and Mario Ruben which covers one aspect of this theme (see page 3644 ff.). Supramolecular chemistry is chemistry on the nanometer scale, and nano is "in". Sometimes I think that every second Communication that is sent to us is sailing under the nano flag. Apart from the overselling of bandwagon and buzzword research, nanochemistry does in fact offer a great deal that is new and original and it is developing along with nanobiology and nanophysics into nanoscience. For the many interdisciplinary papers in this not so new, but now rapidly expanding area of research, Wiley-VCH is launching a new journal in 2005: *Small* with the subtitle Micro & Nano is a sister journal to *Advanced Materials*, and as such *Small* will have a very large circulation from the very start. The Chairmen of the Editorial Advisory Board are a chemist from North America (Chad Mirkin, Northwestern University), a physicist from Europe (Harald Fuchs, Münster University and Research Center Karlsruhe), and a nanobiotechnologist from Asia (Toshio Yanagida, Osaka University). Jean-Marie Lehn and George M. Whitesides are, together with H. Gleiter, A. Heeger, H. Kroto, R. Smalley, and G. Stucky, honorary members of the Editorial Advisory Board. *Small* is all set for a big journey—great news for small science!

Jean-Marie Lehn and George M. Whitesides are also both members of the International Advisory Board of *Angewandte Chemie*, and have, for a

Table 1: Authors with the most publications in *Angewandte Chemie* between 1962–2003. Members of the Editorial Board and the International Advisory Board are marked with a star.

Name	Publications	Country
Herbert W. Roesky	142	DE
Emanuel Vogel*	141	DE
Carl Krüger	123	DE
K. C. Nicolaou*	115	US
Wolfgang A. Herrmann*	105	DE
Dieter Seebach*	103	CH
Hans Bock	101	DE
Hubert Schmidbaur*	97	DE
Horst Prinzbach	93	DE
Fritz Vögtle	92	DE
Helmut Werner	91	DE
Achim Müller	90	DE
J. Fraser Stoddart*	88	US
Gottfried Huttner	79	DE
Klaus Müllen	79	DE
Hans Pritzkow	78	DE
Roland Boese	77	DE
Hans Georg von Schnering*	77	DE
Günther Maier	75	DE
Thomas Kauffmann	74	DE
Bernt Krebs	73	DE
David J. Williams	72	UK
Dieter Fenske	72	DE
Armin de Meijere	70	DE
Konrad Seppelt	68	DE
Armin Berndt	67	DE
Hans Jürgen Bestmann	67	DE
Helmut Schwarz	67	DE
Manfred L. Ziegler	67	DE
Johann Lex	66	DE
Rolf Gleiter	66	DE
Rudolf Gompper	66	DE

Name	Publications	Country
Manfred T. Reetz*	65	DE
Werner Massa	65	DE
François Diederich*	61	CH
Otto J. Scherer	61	DE
Heinrich Nöth	60	DE
Ernst O. Fischer	59	DE
Gernot Boche	59	DE
Mathias Noltemeyer	59	DE
Samuel J. Danishefsky	59	US
Gerhard Müller	58	DE
Peter G. Jones	58	DE
Alfred Schmidpeter	57	DE
Edgar Niecke	57	DE
Henri Brunner*	56	DE
Lutz F. Tietze	56	DE
Paul von Ragué Schleyer	55	US
Ullrich Schöllkopf	55	DE
Gottfried Märkl	54	DE
Richard R. Schmidt	54	DE
George M. Sheldrick	53	DE
Klaus Hafner	53	DE
Waldemar Adam	53	DE
Dietmar Stalke	51	DE
Henning Hopf	51	DE
Horst Kunz	51	DE
Wolfgang Steglich	51	DE
Franz Effenberger	50	DE
Günther Wilke*	50	DE
Horst Kessler*	50	DE
Karl Wieghardt	50	DE
Manfred Regitz	50	DE
Martin Jansen*	50	DE

[1] G. M. Whitesides, *Angew. Chem.* **1990**, *102*, 1247-1257; *Angew. Chem. Int. Ed. Engl.* **1990**, *29*, 1209–1218.

 © 2004 Wiley-VCH Verlag GmbH & Co. KGaA, Weinheim



Emanuel Vogel



Herbert W. Roesky

long time, published many important articles in this journal. The character of a scientific journal is very much determined by its authors. What this means for *Angewandte Chemie* can be easily seen with the aid of the completely retro-digitized International Edition (see www.interscience.wiley.com/backfiles/angewandte). In Table 1 the authors who published the most articles (more than 50) in *Angewandte Chemie*, between 1962 and 2003 are listed. Table 2 covers only the last ten years (authors with more than 15 articles). With the exception of book and website reviews, all types of article are included. The list is not restricted to corresponding authors and as a consequence scientists who, for example, provided a valuable service over a long period could have made it on to the list as "non-corresponding authors"; to filter these names seemed inappropriate.) From the Tables there is a great deal that can be learnt, and they can (and will) be over-interpreted—however, one thing that is clear is the internationalization of the journal: of the top authors in Table 1 the vast majority have German names, whereas in Table 2 only half of the authors are German. Naturally many of the older authors found in Table 1 who contributed greatly to the quality of the journal in the second half of the last century, do not appear in Table 2. Instead, in this Table there are many chemists of the younger generation who shape the chemistry of today and tomorrow. Each reader can contemplate the distribution by country, city, and institution, subdiscipline, school, and whatever else for themselves. The editorial staff, the publishers Wiley-VCH, and the owners, the German Chemical Society (GDCh), are in any case particularly grateful to all these authors, who have influenced and determined the quality of the journal to a large degree.

A generally accepted measure of the quality of a journal is its Impact Factor, which has increased significantly for *Angewandte Chemie*: from 7.671 to 8.427! The widespread assumption that the Impact factor of *Angewandte Chemie* is distorted by the Reviews is a misconception: With approximately 50 Reviews and almost 1000 Communications published, the Reviews contribute



K. C. Nicolaou



Samuel J. Danishefsky

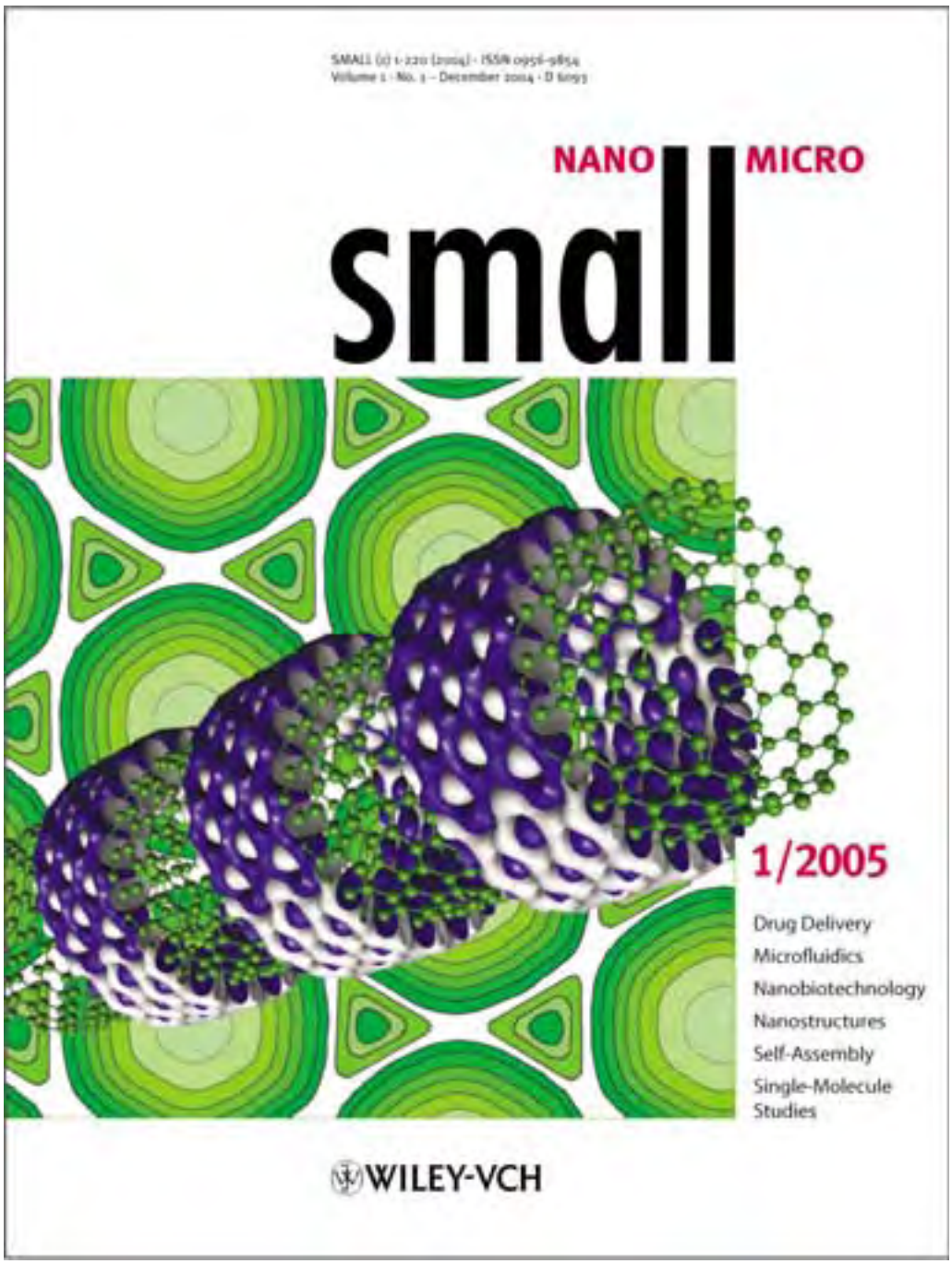
Table 2: Authors with the most publications in *Angewandte Chemie* between 1994–2003. Members of the Editorial Board and the International Advisory Board are marked with a star.

Name	Publications	Country	Name	Publications	Country
K. C. Nicolaou*	97	US	Euro Solari	19	CH
Samuel J. Danishefsky	56	US	Günther Jung	19	DE
Herbert W. Roesky	48	DE	Horst Kunz	19	DE
J. Fraser Stoddart*	42	US	Marilyn M. Olmstead	19	US
François Diederich*	39	CH	Peter R. Ashton	19	UK
Peter G. Jones	38	DE	Dieter Enders	18	DE
Herbert Waldmann	36	DE	Dieter Seebach*	18	CH
Paul von Ragué Schleyer	36	US	Edgar Niecke	18	DE
David J. Williams	35	UK	Erich Krickemeyer	18	DE
Dieter Fenske	35	DE	Frank Hampel	18	DE
Paul Knochel	31	DE	Fritz Vögtle	18	DE
Hans Pritzkow	30	DE	Itamar Willner	18	IL
Barry M. Trost	29	US	John Meurig Thomas	18	UK
Klaus Müllen	29	DE	K. Barry Sharpless	18	US
Wolfgang A. Herrmann*	29	DE	Karl Wieghardt	18	DE
Chi-Huey Wong	28	US	Robert H. Grubbs	18	US
Dietmar Stalke	28	DE	William Clegg	18	UK
Martin Nieger	28	DE	Alois Fürstner	17	DE
Achim Müller	27	DE	David A. Evans	17	US
Martin Jansen*	26	DE	Eberhardt Herdtweck	17	DE
Hansgeorg Schnöckel	25	DE	François Mathey	17	FR
Julius Rebek, Jr.	25	US	Kimoon Kim	17	KR
Roland Fröhlich	25	DE	Lutz F. Tietze	17	DE
Werner Massa	24	DE	Simon Parsons	17	UK
Heinrich Nöth	23	DE	Detlef Schröder	16	DE
Jean-Marie Lehn*	23	FR	Marc Schmidtmann	16	DE
Johann Lex	23	DE	Matthias Driess	16	DE
Mathias Noltemeyer	23	DE	Rainer Herges	16	DE
Andrew J. P. White	22	US	Siegfried Blechert	16	DE
Arnold L. Rheingold	22	US	Carsten Bolm	15	DE
Manfred T. Reetz*	22	DE	Glenn P. A. Yap	15	CA
Matthias Hofmann	22	DE	Gregory C. Fu	15	US
Paul R. Raithby	22	UK	Guy Bertrand	15	FR
Roland Boese	22	DE	Hans-Georg Schmidt	15	DE
David N. Reinhoudt	21	NL	Hansjörg Grützmacher	15	CH
Hartmut Bögge	21	DE	Helge Willner	15	DE
Helmut Schwarz	21	DE	Kenneth N. Raymond	15	US
Matthias Beller	21	DE	Kentaro Yamaguchi	15	JP
Peter B. Hitchcock	21	UK	Klaus Harms	15	DE
Anthony L. Spek	20	NL	Makoto Fujita	15	JP
Armin Berndt	20	DE	Phil S. Baran	15	US
Carlo Floriani*	20	CH	Philip P. Power	15	US
Helmut Werner	20	DE	Richard R. Schmidt	15	DE
Konrad Seppelt	20	DE	Roeland J. M. Nolte	15	NL
Yoshinori Yamamoto	20	JP	Seiji Shinkai	15	JP
Armin de Meijere	19	DE	Steven V. Ley	15	UK
Emanuel Vogel*	19	DE	Ulrich Koert	15	DE

© 2004 Wiley-VCH Verlag GmbH & Co. KGaA, Weinheim

less than one point to the Impact Factor (based on the assumption that the Review section alone would have an Impact Factor of about 20). Last but not least, the introduction of manuscriptXpress, the online system for manuscript submission, refereeing, and administration for *Angewandte Chemie* and its sister journals went quite smoothly (on March 15 for *Angewandte Chemie*). Authors and referees have immediately taken to the system. However, it is unlikely that the leap in manuscript submissions in April and May (an increase of 20%!) is a result of the arrival of manuscriptXpress. The overall increase in manuscript submission over the last several years is perhaps a result of the increased internationalization of the journal (see above) and the widened scope of manuscripts published—including those in the nano and micro arena. But please don't forget: *Small* is now accepting manuscripts as well! For more information, see: www.small-journal.com

Latest Impact Factor 8.427



Peter Gölitz

 © 2004 Wiley-VCH Verlag GmbH & Co. KGaA, Weinheim

Angewandte EarlyView

The following Communications are available online (in Wiley InterScience). You can find them, as well as forthcoming Reviews, Highlights, and Essays, at www.angewandte.org, under Early View.

U. N. Nehete, V. Chandrasekhar, G. Anantharaman, H. W. Roesky, D. Vidovic, J. Magull:*
Molecular $\{(SnO)_6\}$ Trapped by Two $\{R_2Si_2O_3\}$ Fragments: X-Ray Single-Crystal Structure of $[(SnO)_6(R_2Si_2O_3)_2]$
DOI: 10.1002/anie.200454149
Published online: June 23, 2004

M. Johnsson, S. Lidin, K. W. Törnroos, H.-B. Bürgi, P. Millet:*
Host–Guest Compounds in the Family of Tellurium–Nickel Oxohalogenides
DOI: 10.1002/anie.200460001
Published online: June 23, 2004

Articles judged by the referees or the editor as being either very important or very urgent are immediately edited, proof-read, and electronically published once the manuscript has arrived in the editorial office in its final form. As long as there is no page number available these articles should be cited in the following manner:

Author(s), *Angew. Chem. Int. Ed.*, online publication date, DOI.

Obituary

Murray Goodman (1928–2004): Peptide Chemistry — **3628** — *L. Moroder*

Books

Enzymes in Industry — **3629** — Wolfgang Aehle — *reviewed by B. Cooper*

Elemental Sulfur and Sulfur-Rich Compounds, Vols. I and II — **3629** — Ralf Steudel — *reviewed by F. Breher*

Essays

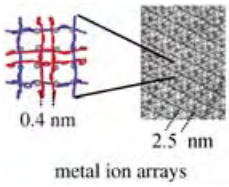
Is thinking about the future an important thing to do or just a diversion? Science periodically requires society to discard important assumptions, with profound consequences. Failed assumptions are easy to identify with hindsight, but can they be predicted? In this Essay, the author discusses assumptions society accepts, and the potential of science to disprove them.

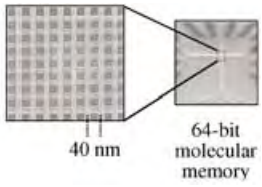
Future of Chemistry

G. M. Whitesides* — **3632 – 3641**

Assumptions: Taking Chemistry in New Directions

Reviews





Ions and information: The generation by self-assembly of metal ion arrays of grid-type architecture (left) with unique magnetic, electronic, or optical properties could provide decisive impulses for the development of molecular information storage and processing (right). Such two-dimensionally arrayed switchable elements of nanometric size display "ion dot" type features, which are of much smaller size than quantum dots arrays, and which may foreshadow multistate nano-digital information processing.

Self-Assembly

M. Ruben, J. Rojo, F. J. Romero-Salguero, L. H. Uppadine, J.-M. Lehn* — **3644 – 3662**

Grid-Type Metal Ion Architectures: Functional Metallosupramolecular Arrays

 © 2004 Wiley-VCH Verlag GmbH & Co. KGaA, Weinheim

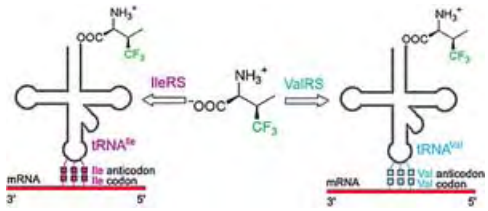
Contents

Communications

RNA Translation

P. Wang, A. Fichera, K. Kumar, D. A. Tirrell* ——— **3664 – 3666**

Alternative Translations of a Single RNA Message: An Identity Switch of (2*S*,3*R*)-4,4,4-Trifluorovaline between Valine and Isoleucine Codons

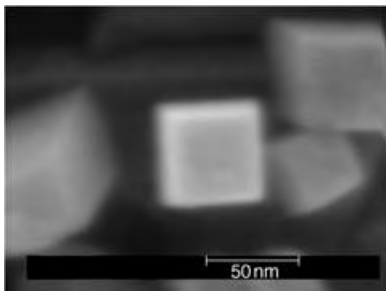


Changed in translation: Bacterial expression hosts can be engineered so that a single RNA message can be read in different ways depending on the relative rates of competing aminoacylation reactions. The (2*S*,3*R*)-4,4,4-trifluorovaline can be assigned either to isoleucine or to valine codons according to whether the bacterial host overexpresses the isoleucyl- or the valyl-tRNA synthetase (IleRS and ValRS, respectively; see scheme).

Nanotechnology

L. Vayssieres,* M. Graetzel **3666 – 3670**

Highly Ordered SnO_2 Nanorod Arrays from Controlled Aqueous Growth



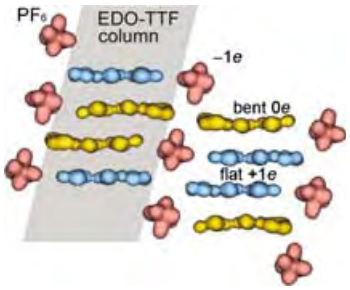
Without template, surfactant, applied field, or undercoating, well-defined and highly ordered rutile SnO_2 nanorods were grown directly onto various substrates at low temperatures from aqueous solutions. These nanorods are elongated along the *c* axis and have stable prismatic (110) faces, which results in nanorods with a square cross section (see picture).

Phase Transitions

S. Aoyagi, K. Kato, A. Ota, H. Yamochi, G. Saito, H. Suematsu, M. Sakata, M. Takata* ——— **3670 – 3673**

Direct Observation of Bonding and Charge Ordering in $(EDO\text{-}TTF)_2PF_6$

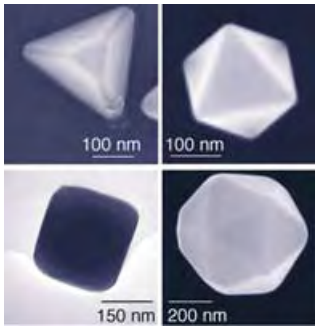
Dimers of flat $(EDO\text{-}TTF)^+$ molecules separated by bent neutral EDO-TTF (ethylenedioxytetrathiafulvalene) molecules are found in the insulator phase of $(EDO\text{-}TTF)_2PF_6$, but not in that of the metallic phase. The cooperativity of Peierls distortion, charge ordering, and anion ordering in this metal–insulator transition can be regarded as the result of a molecular displacement.



Crystal Growth

F. Kim, S. Connor, H. Song, T. Kuykendall, P. Yang* ——— **3673 – 3677**

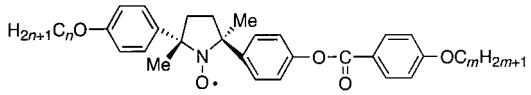
Platonic Gold Nanocrystals



Systematic shape evolution of gold nanocrystals with sizes between 100 and 300 nm was observed in a modified polyol process. By adding a surface-regulating polymer and foreign ions, one can readily access the distinct shapes of tetrahedron, cube, octahedron, and icosahedron (dubbed platonic nanocrystals, see picture) with high yield and good uniformity.

For the USA and Canada:
ANGEWANDTE CHEMIE International Edition (ISSN 1433-7851) is published weekly by Wiley-VCH PO Box 191161, D 69451 Weinheim, Germany. Air freight and mailing in the USA by Publications Expediting Inc. 200 Meacham Ave., Elmont, NY 11003. Periodicals postage paid at Jamaica NY 11431. US POSTMASTER: send address changes to *Angewandte Chemie*, Wiley-VCH, 111 River Street, Hoboken, NJ 07030. Annual subscription price for institutions: Europe € 3430.00/3118.00; outside Europe US$ 4499.00/4090.00 (valid for print and electronic/print or electronic delivery); for individuals who are personal members of a national chemical society, or whose institution already subscribes, or who are retired or self-employed consultants, print only: Europe € 248.00/outside Europe US$ 378.00. Postage and handling charges included. All Wiley-VCH prices are exclusive VAT.

© 2004 Wiley-VCH Verlag GmbH & Co. KGaA, Weinheim

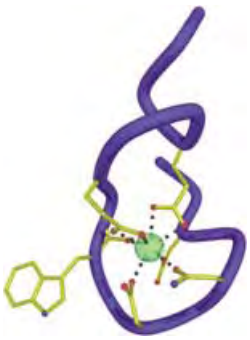


Lining them up: Purely organic paramagnetic liquid crystals (see picture) showing thermally stable nematic or cholesteric phases were successfully prepared. The molecular orientation of the bulk liquid crystals induced by weak magnetic fields was confirmed by magnetic susceptibility measurements and EPR spectroscopy.

Liquid Crystals

N. Ikuma, R. Tamura,* S. Shimono, N. Kawame, O. Tamada, N. Sakai, J. Yamauchi, Y. Yamamoto — **3677 – 3682**

Magnetic Properties of All-Organic Liquid Crystals Containing a Chiral Five-Membered Cyclic Nitroxide Unit within the Rigid Core



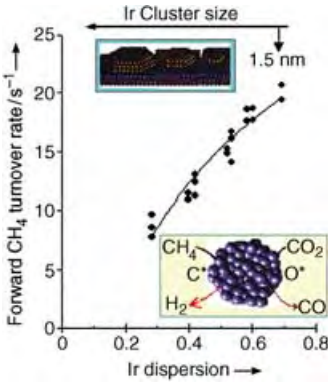
Playing tag with terbium: New hydrophobic contacts and ligating amino acids are revealed in the 2.0-Å resolution X-ray crystal structure of a chemically evolved 17-residue lanthanide-binding peptide complexed with a Tb^{3+} ion (see ribbon diagram). The crystal structure agrees well with luminescence-lifetime measurements in solution, which indicate that no first-shell-coordinating water molecules are present in the complex.

Lanthanide-Binding Peptides

M. Nitz, M. Sherawat, K. J. Franz, E. Peisach, K. N. Allen,* B. Imperiali* — **3682 – 3685**

Structural Origin of the High Affinity of a Chemically Evolved Lanthanide-Binding Peptide

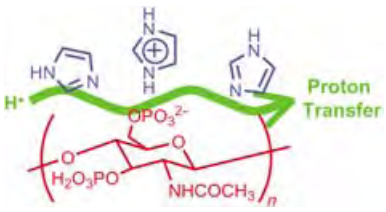
The only kinetically relevant step for catalytic CH_4 activation on Ir clusters is—according to a detailed analysis—C–H bond activation (see picture). This step is favored on surfaces of small Ir clusters supported on oxides, as also found on other noble metal catalysts. Other elementary steps remove chemisorbed carbon species rapidly and preserve essentially uncovered surfaces during catalysis.



Methane Activation

J. Wei, E. Iglesia* — **3685 – 3688**

Structural and Mechanistic Requirements for Methane Activation and Chemical Conversion on Supported Iridium Clusters



What a waste! A highly effective proton-conducting biopolymer has been prepared from imidazole and chitin phosphate, which is an environmentally benign, low-cost, and commonly discarded biopolymer (see picture). The composite material has a conductivity of 7×10^{-3} S cm^{-1} at 150 °C under anhydrous (water-free) conditions.

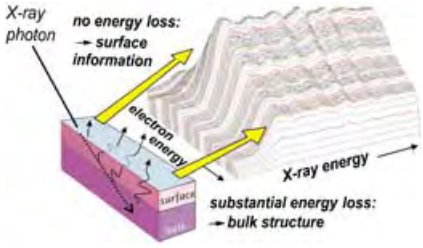
Conducting Materials

M. Yamada, I. Honma* — **3688 – 3691**

A Biopolymer Composite Material as an Anhydrous Proton-Conducting Membrane

 © 2004 Wiley-VCH Verlag GmbH & Co. KGaA, Weinheim

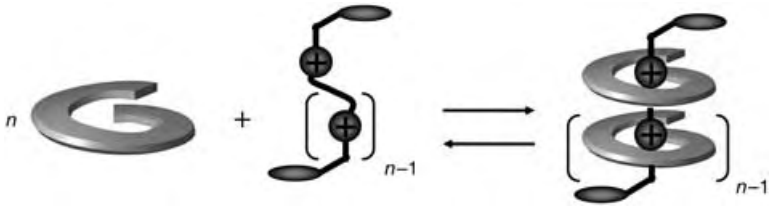
The use of a gas microstrip detector in X-ray absorption spectroscopy allows energy-resolved electron detection under ambient conditions and thereby non-destructive depth profiling or greatly improved surface sensitivity (see scheme). Results of an in situ study of a heterogeneous chemical reaction and preliminary electrochemical experiments are discussed.



Surface Characterization

A. Vollmer, J. D. Lipp, H. Weiss, R. O'Malley, T. Rayment* — **3691 – 3695**

In Situ Investigations into Chemical Processes by Electron-Energy-Resolved X-Ray Absorption Spectroscopy

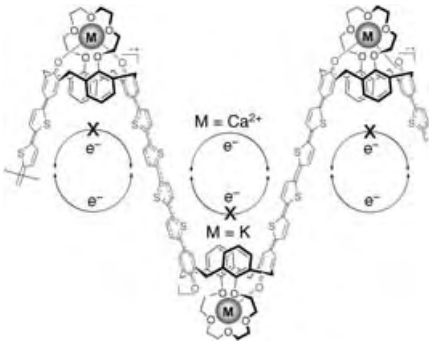


Self-assembly with a twist: Linear polyammonium threads are templates in the organization of helical heterocyclic building blocks to form stacks of helices as a model for the Tobacco Mosaic Virus. The length of the cationic substrate and the spacing of the positive charges within the thread dictate the size of the final self-organized supramolecular architecture (see picture).

Supramolecular Chemistry

A. Petitjean, H. Nierengarten, A. van Dorsselaer, J.-M. Lehn* — **3695 – 3699**

Self-Organization of Oligomeric Helical Stacks Controlled by Substrate Binding in a Tobacco Mosaic Virus Like Self-Assembly Process



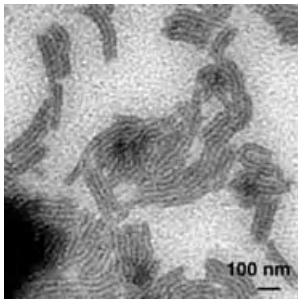
Charged with hopping: A conducting polymer containing electroactive segments interconnected by crown ether calix[4]arene units (see picture) exhibits dramatic changes in its conductivity in response to the binding of ions. There is over three orders of magnitude difference in conductivity between the incorporation of K^+ and Ca^{2+} ions. The electrical conduction is best considered to be by a hopping mechanism.

Conducting Polymers

H.-h. Yu, A. E. Pullen, M. G. Büschel, T. M. Swager* — **3700 – 3703**

Charge-Specific Interactions in Segmented Conducting Polymers: An Approach to Selective Ionoresistive Responses

Hydrosilylative crosslinking of the coronas of tubules of self-assembled poly(ferrocenyldimethylsilane-*b*-polymethylvinylsiloxane) (PFS–*b*–PVMS) formed in hexane result in shell-crosslinked organometallic nanotubes (see picture) with reversible redox behavior and tunable swellability.



Organometallic Nanotubes

X.-S. Wang, M. A. Winnik,* I. Manners* — **3703 – 3707**

Swellable, Redox-Active Shell-Crosslinked Organometallic Nanotubes

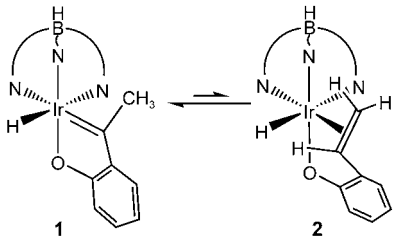
 © 2004 Wiley-VCH Verlag GmbH & Co. KGaA, Weinheim

Contents

C–H Bond Activation

M. Paneque, M. L. Poveda, L. L. Santos, E. Carmona,* A. Lledós,* G. Ujaque, K. Mereiter _____ **3708 – 3711**

A Measureable Equilibrium between Iridium Hydride Alkylidene and Iridium Hydride Alkene Isomers

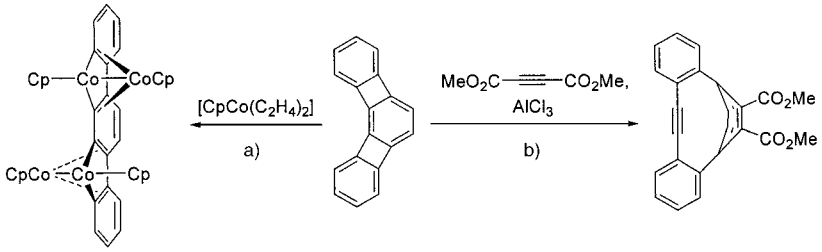


An almost thermoneutral equilibrium mixture of hydride alkylidene **1** and hydride alkene **2** (see scheme) is feasible with a $Tp^{Me_2}Ir^{III}$ system (Tp is tris(pyrazolyl)borate) through its reaction with *o*-$C_6H_4(OH)CH_2CH_3$ under activation of sp^3 C–H bonds.

Phenylenes

S. Kumaraswamy, S. S. Jalisatgi, A. J. Matzger, O. Š. Miljanić, K. P. C. Vollhardt* _____ **3711 – 3715**

Anatomy of a Cyclohexatriene: Chemical Dissection of the π and σ Frame of Angular [3]Phenylene

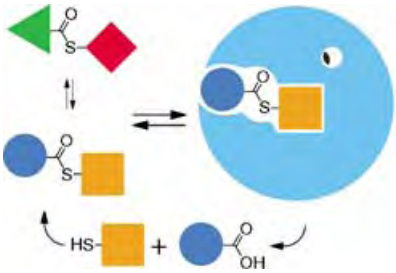


A loaded spring: Partial rupture of the central cyclohexatriene nucleus of angular [3]phenylene yields a novel tetranuclear cluster through regio- and stereospecific double C–C bond activation by cyclopentadienylcobalt (see scheme, a)). Complete rupture upon treatment with dimethyl butynedioate in b) leads to a highly strained and completely unsaturated [6]paracyclophane.

Combinatorial Chemistry

R. Larsson, Z. Pei, O. Ramström* _____ **3716 – 3718**

Catalytic Self-Screening of Cholinesterase Substrates from a Dynamic Combinatorial Thioester Library

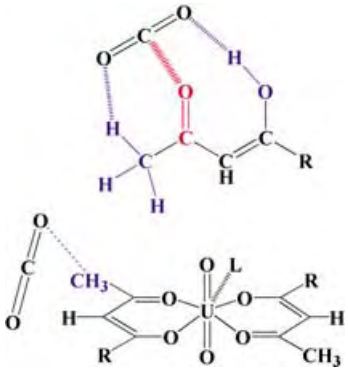


Simply the best: Dynamic combinatorial chemistry coupled to enzyme catalysis was used to identify enzyme substrates in a library constructed from a series of thioesters and thiols by transesterification. The library was directly coupled to the catalytic action of acetylcholinesterase, which selectively hydrolyzed the best substrate candidates (see schematic representation). The process allowed rapid identification of discrete substrates.

Supercritical Fluids

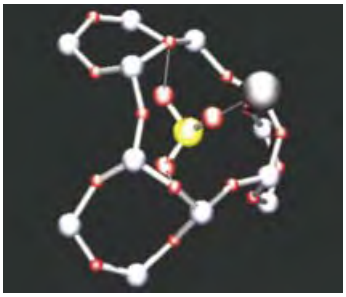
T. Tsukahara, Y. Kayaki, T. Ikariya,* Y. Ikeda* _____ **3719 – 3722**

^{13}C NMR Spectroscopic Evaluation of the Affinity of Carbonyl Compounds for Carbon Dioxide under Supercritical Conditions



CO_2-philicity: The ^{13}C NMR chemical shift (δ_C) of supercritical CO_2 containing carbonyl compounds moves to lower fields with increasing CO_2 density in parallel with the δ_C value of neat $scCO_2$. The difference in the magnitude of these shifts ($\Delta\delta_C$) is attributed to the strength of solute–CO_2 interactions (see picture, R = CH_3 or CF_3, L = DMSO) and allows determination of the CO_2-philicity of solute molecules in $scCO_2$.

 © 2004 Wiley-VCH Verlag GmbH & Co. KGaA, Weinheim

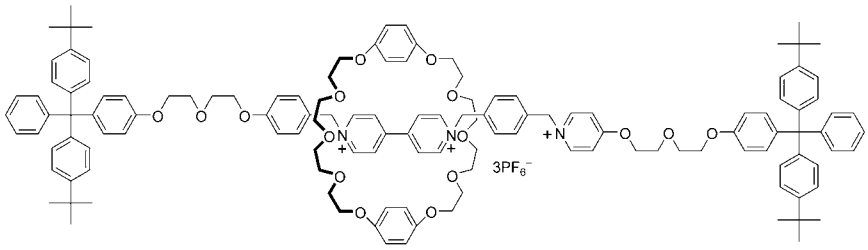


Exceptional resistance to sulfur poisoning of the Na–Y zeolite arises from the localization of adsorbed sulfur dioxide on the zeolite in the presence of water. The work shows that Rietveld refinement of guest molecules is a powerful method to determine positions and states of different molecules co-adsorbed on a zeolite (see picture; H_2SO_3 in yellow (S) and large red spheres (O); zeolite framework in small red (O) and gray (Si or Al) spheres; large gray sphere is the Na cation).

Zeolites

C. E. A. Kirschhock, A. Sultana, E. Godard, J. A. Martens* ——— **3722 – 3724**

Adsorption Chemistry of Sulfur Dioxide in Hydrated Na–Y Zeolite

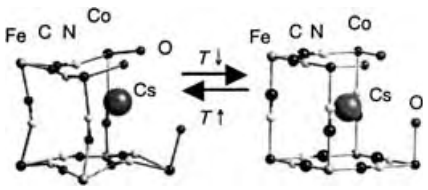


It's all in the mix: The reaction between solid reactants undergoes rate acceleration and results in an increase in yield when the reactants are premixed in solution and then concentrated to dryness. This protocol has been successfully applied to the end-capping synthesis of a [2]rotaxane (see structure).

Rotaxane Synthesis

A. Orita, J. Okano, Y. Tawa, L. Jiang, J. Otera* ——— **3724 – 3728**

Rate Acceleration of the Reaction between Solid Reactants by Premixing in Solution: Application to the Efficient Synthesis of a [2]Rotaxane



A central role for the alkali metal cation was determined in the thermally activated electron transfer $Co^{III}(LS)$-$Fe^{II}(LS) \rightleftharpoons Co^{II}(HS)$-$Fe^{III}(LS)$ in a CsCoFe Prussian blue derivative by localizing the alkali metal ion and identifying its interactions with the surrounding network in the high- and low-temperature states (see scheme).

Electron Transfer

A. Bleuzen,* V. Escax, A. Ferrier, F. Villain, M. Verdaguer, P. Münsch, J.-P. Itié ——— **3728 – 3731**

Thermally Induced Electron Transfer in a CsCoFe Prussian Blue Derivative: The Specific Role of the Alkali-Metal Ion

VIP Communications labeled with this symbol have been judged by two referees as being "very important papers".

WILEY InterScience® DISCOVER SOMETHING GREAT

"**Hot Papers**" are chosen by the Editors for their importance in a rapidly evolving field of high current interest. A preview with the graphical abstracts of these articles can be found on the *Angewandte Chemie* homepage in Wiley InterScience at www.angewandte.org.

"**VIPs**" are Communications which are identified by two referees as being very important. They are published online up to several weeks ahead of print. A preview with short summaries of these articles can also be found on the journal's homepage.

Service

Keywords ——— *3734*

Authors ——— *3735*

Angewandte's Sister Journals ——— *3732 – 3733*

Events ——— *3738*

Preview ——— *3737*

 © 2004 Wiley-VCH Verlag GmbH & Co. KGaA, Weinheim

Murray Goodman (1928–2004): Peptide Chemistry

"For he was our own! *…… Fruitful both in counsel and deed; this we experienced and appreciated."*

With the death of Murray Goodman on June 1 in Munich (Germany) after a short but severe illness during a scientific visit to Europe, we lost one of the grand pioneers of peptide chemistry. He was a generous and extremely gifted man, whose strength was to tackle essential biological problems at a molecular level with simple model systems and to draw insightful conclusions from them.



M. Goodman

Murray Goodman was born on July 6, 1928 in Brooklyn into an immigrant family from Krivoizera (Ukraine). He completed a Bachelor of Science at Brooklyn College in 1950 and his doctorate three years later at the University of California, Berkeley, where he worked with Melvin Calvin (Nobel Prize in Chemistry, 1961) on the use of isotopes as tracers to probe the mechanisms of photosynthesis. Drawn by the challenges of peptide chemistry, Goodman undertook postdoctoral research at the Massachusetts Institute of Technology with John C. Sheehan, and at Cambridge University (UK) with Lord Alexander Todd on the synthesis of natural nucleotides and peptides. In 1956, he joined the faculty of the Polytechnic Institute in Brooklyn and became director of its Polymer Research Institute. In 1970, he moved to the University of California, San Diego (UCSD) as a professor of organic chemistry. He was Chair of the Department of Chemistry there for six years and was recently honored with the establishment of an endowed professorship in his name: the Goodman Chair in Chemistry.

Goodman's exceptional scientific achievements in the field of peptide science are reflected in over 500 original research papers on peptide synthesis, optically active polymers, the stereochemistry of polymers and biopolymers, conformational studies of poly-α-amino acids and bioactive peptides, the use of peptidomimetics for drug design, and new biomaterials. His work was recognized worldwide by numerous awards and honors, including the Scoffone Medal of the University of Padua (1980), the Alexander von Humboldt Research Award (Germany, 1986), the Pierce Award of the American Peptide Society (1989), the Max Bergmann Medal (1991), and the Ralph Hirschmann Award for Peptide Chemistry of the American Chemical Society (1997).

Murray Goodman developed a stepwise synthesis of linear oligopeptides as models of protein conformations,[1] uncovered the "active monomer" mechanism of *N*-carboxyanhydride polymerization, analyzed racemization in peptide synthesis,[2] and was one of the first to use circular dichroism and NMR spectroscopic techniques to study peptide conformations.[3] He made fundamental contributions to the development of these spectroscopic methods for the analysis of secondary structures. He initiated the concept of combining synthetic challenges with structural analysis and bioassays to probe the interaction of molecules in the (patho)physiological events of life.

Despite his increased interest in chemoreception, Goodman continued to develop new synthetic methods, which are now widely used as standard procedures. To mention a few examples, he introduced urethane-protected *N*-carboxyanhydrides, triflyldiurethane-protected guanidines as guanidinylation reagents, and the very effective reagent DEBT (*N*,*N*-diethyl-*N*′-benzoylthiourea) for peptide-bond formation. During his work towards his major goal, the use of peptidomimetic structures for drug design, he developed retro-inverso peptide analogues, various peptide cyclization modes, and conformationally restricted amino acid analogues. In this context, he elaborated syntheses of novel amino acid derivatives as building blocks for peptidomimetics.[4] Cyclic lanthionine structures were produced in his laboratory as candidates for new drugs with highly selective opioid activity.[5] With his most recent studies on new scaffolds for the assembly of triple-helical structures and the expansion of this concept to dendritic collagen-like molecules he has opened the way to new biomaterials.[6]

Goodman also deserves admiration and gratitude for his extensive editorial activities. As editor-in-chief of *Biopolymers* since 1963 and founding editor of *Peptide Science* he created forums in which chemistry meets structural research and biology, and as editor-in-chief of the five-volume work *Synthesis of Peptides and Peptidomimetics* (*Methoden Org. Chem. (Houben-Weyl), 4th ed., Vol. E22*, **2002–2003**), he has left a treatise on the state of the art in the field as a legacy to the peptide community.

Those of us who knew him are saddened by his passing away and feel the great loss of a dear friend and colleague. He will always be remembered as an inspiring teacher and mentor, as an enthusiastic scientist, and as the père des peptides, the father of the peptide community, but first and foremost as a warm and sincere human being, a mensch.

Luis Moroder
Max-Planck-Institut für Biochemie, Martinsried (Germany)

[1] M. Goodman, E. E. Schmitt, D. A. Yphantis, *J. Am. Chem. Soc.* **1962**, *84*, 1283–1288.
[2] M. Goodman, W. J. McGahren, *J. Am. Chem. Soc.* **1965**, *87*, 3028–3029.
[3] M. Goodman, A. S. Verdini, C. Toniolo, W. D. Phillips, F. A. Bovey, *Proc. Natl. Acad. Sci. USA* **1969**, *64*, 444–450.
[4] J. R. Del Valle, M. Goodman, *Angew. Chem.* **2002**, *114*, 1670–1672; *Angew. Chem. Int. Ed.* **2002**, *41*, 1600–1602.
[5] Y. Rew, S. Malkmus, C. Svensson, T. L. Yaksh, N. N. Chung, P. W. Schiller, J. A. Cassel, R. N. DeHaven, M. Goodman, *J. Med. Chem.* **2002**, *45*, 3746–3754.
[6] J. Kwak, A. De Capua, E. Locardi, M. Goodman, *J. Am. Chem. Soc.* **2002**, *124*, 14085–14091.

 © 2004 Wiley-VCH Verlag GmbH & Co. KGaA, Weinheim DOI: 10.1002/anie.200460962

Future of Chemistry

Assumptions: Taking Chemistry in New Directions**

*George M. Whitesides**

Keywords:
Bioorganic chemistry · genomics · medicinal chemistry · philosophy of chemistry

> *"When a distinguished but elderly scientist states that something is possible, he is almost certainly right. When he states that something is impossible, he is very probably wrong."*
> Arthur C. Clarke

The Temptations and Hazards of Predicting the Future

Speculating about the future of science seems to be genetically encoded in scientists. We all do it. We also take it as an article of faith that serious predictions are almost always wrong. Is thinking about the future an important thing to do, or just a diversion—like daydreaming, or gardening, or playing the lottery? Why do we spend our time guessing about matters we believe we cannot predict?

There are at least five reasons. The first is utilitarian: to plan our work. Thinking about the future is a part of choosing research problems. We who make our living in science tell ourselves that we work for the satisfaction of solving problems and for the thrill of discovery; sociologists, less charitably, suggest that we do so to make a living and to get ahead professionally. The truth is probably a mixture of the two. Finding good problems—problems that polish a new facet of reality and that change the way some part of the world works—is both satisfying intellectually and rewarding professionally.

The second reason is to feed our curiosity. We wonder about the world of the future. What neat widgets will make *that* world run? Which of our fantasies will grow into our grandchildren's realities?

The third is philosophical. Science and technology are major elements of the culture of our times. They, probably more than other elements (materialism, religious fundamentalism, capitalism, …), will change the nature of individuals and of society. We wonder: What will the *big* changes be? How will science be involved?

The fourth is that society *expects* us to speculate. We are part of its early warning system for change.

The fifth is to answer an uncomfortable question: "Is there research that we should *not* do?" We scientists generally cohabit quite comfortably with an amoral curiosity. We should ask if there is research we can do now—research that is technically feasible and scientifically interesting—that we should forgo because it is ethically problematic. Are there questions we don't want to ask, because there are *no* circumstances in which we might want to know the answers?

The objective of science is to make a difference.

Science is a Mixture of the Ordinary and the Extraordinary

Surprises: Is the future of science really so unpredictable? The answer is both "no" and "yes". Science is a mixture of a lot of the relatively predictable "ordinary", and a little of the quite unpredictable "extraordinary". The part of science that is ordinary and business-as-usual—useful, important, familiar science—can often be extrapolated into the future with fair accuracy. It is the *extraordinary* science—the *surprises*—that we cannot predict, and it is this science that gives speculation about the future its well-deserved bad reputation. It is also the surprises that make science so intensely interesting, and that have the power, for better or worse, to turn the lives of our grandchildren upside down.

One of the many charms of science is that it provides an endless string of surprises. Some surprises grow slowly and incrementally, while some come, apparently, out of the blue. Each of us can make two lists of surprises: one of personal favorites, and one of surprises that have remade the world. These two lists are usually rather different. We have a particular affection for what we know, and find small quirks in familiar science endearing. Appreciation for big discoveries in unfamiliar fields requires more effort.

Since I am a chemist, I was immediately delighted—in fact, ecstatic—to learn that XeF_4 is a stable compound; because I knew less about biology, it took me years to assimilate the discovery of apoptosis, and to begin to appreciate how the cell chooses between life and death. Not all surprises are equal: xenon tetrafluoride clarified the chemical bond for chemists; apoptosis changed the understanding of "life" for all of science.

One unstated objective of science is to *make a difference*: to learn something,

[*] Prof. G. M. Whitesides
Department of Chemistry and Chemical Biology
Harvard University
12 Oxford Street
Cambridge, MA 02138-2902 (USA)
Fax: (+1) 617-495-9857
E-mail: gwhitesides@gmwgroup.harvard.edu

[**] I thank Michael Mayer, Mila Boncheva, and Barbara Whitesides for their suggestions and editorial help with this paper.

 © 2004 Wiley-VCH Verlag GmbH & Co. KGaA, Weinheim DOI: 10.1002/anie.200330076

or make something, that changes the way people think or behave. Many of the biggest discoveries—the most important scientifically, and the most consequential socially—are surprises, and their consequences are unimaginable at the time they are made. Who would have predicted the changes in society that have come from classification of the elements into the periodic table, or from quantum mechanics, or the world wide web? Who could have guessed that the first NMR spectrum of ethanol would grow into the ability to watch the brain think?

The unpredictability of these big surprises makes us timid in our speculations: it is embarrassing to be publicly wrong, and big surprises make dunces of us all. But, avoiding speculation makes science dreary, and neglects our responsibility to society to warn of change, even as we cause it.

Picking Assumptions, Not Making Predictions

In speculating about the future, we—scientists and nonscientists—are really interested in knowing what the science and technology will be that will make a *big* difference, and in knowing whether that difference will be good, or bad, or both, or a matter of context, or circumstance, or personal opinion.

The process of starting with current science, extrapolating it into the future, and then guessing how society will use or abuse this future science is so uncertain it will probably fail. I suggest that a different and perhaps more direct approach to identifying where science might reshape society is to start by identifying areas where change would *matter*, and then ask if *imaginable* science might cause this change.

How are we to identify areas where society is vulnerable to change? Or where the push of a new idea or a new technology might topple established institutions? I propose that we begin by identifying the *assumptions* that our society makes, and then ask about the vulnerability of these assumptions in the face of plausible science.

An *assumption* is an idea that is taken for granted: it tacitly separates the imaginable from the unimaginable. If an assumption is vulnerable, then the probability that it will eventually fracture—for better or worse—under the blows of science is very high. Let me give an example. We assume, as an article of faith—a deeply held assumption—that we are the most intelligent entities on the planet. We would certainly be disconcerted to discover that science and technology had generated an entity more intelligent than we: a peer competitor (or perhaps a peer partner, although, as a species, we have never been good at "sharing"). How probable, technically, is it that science will do so? The answer to this question depends on whether you believe that intelligence is an oddity characteristic of highly evolved living organisms (humans, porpoises, whales, chimpanzees), or whether it is inevitable in (or perhaps can be engineered into) any information-processing system of sufficient complexity. So, will information science produce intelligent machines? (… and what is "intelligence" in a machine, anyway?) I don't know, but I (and others more knowledgeable than I) also don't know that it is impossible. Hence it is an area that we, and society, should watch carefully.

Society changes when it discards a major assumption.

Where, in the past, has science dissolved important assumptions with profound consequences for society? Failed assumptions are easy to identify in hindsight: they are the facts of daily life that we now accept as routine, but that would, at some earlier time, have provoked a reaction of "impossible!" If one had asked Frederick the Great or Sun Tsu if it would ever be possible utterly to destroy a city on the other side of the globe in a single stroke, their answer would have been "No!" They, and their societies, assumed this limitation to the art of war. We now accept as unremarkable a world in which science and technology—born as quantum mechanics and grown to be nuclear-tipped intercontinental ballistic missiles (ICBMs; or perhaps just a rental truck containing an amateur's fully functional fission bomb)—make this single stroke distressingly possible. The failure of this assumption has changed society.

We have discarded many other assumptions, with consequences both good and bad. At one time, knowledge could be passed on only through speech: the written word and moveable type gave our society a long-term memory. At one time it was impossible to talk to or to see others over long distances; the telephone, radio, TV, and the web are now among the threads that hold society together. Controlling human fertility fundamentally changed the relation of women to society. Society changes when it discards a major assumption.

Thinking about assumptions and working backward is not necessarily less fallible than thinking about science and working forwards, but it tends to focus more on big societal problems and less on small technological evolutions. Concentrating on assumptions might, therefore, provide better advance warning about issues that the scientific community (and society) should consider carefully than extrapolating from existing science. It would also accomplish four other ends. It would: 1) show that the dreary intellectual senescence suggested by John Horgan's stimulating book "The End of Science" is wrong-headed; 2) identify directions where science would unquestionably have large impact; 3) indicate especially interesting problems on which scientists might work; and 4) suggest new ways of doing business: big problems do not have disciplinary boundaries—academic departments do.

In what follows, I list nine assumptions that, I believe, are fundamental to western society, and that, I believe, are vulnerable to disproof by science. This list is entirely personal: others would make other lists. These assumptions are different in nature: some are conceptual, some are practical, and some are sociological.

Where Does Chemistry Fit In?

Chemistry has had a wonderful period of two centuries in which it revolutionized the understanding and manipulation of the physical world: it revealed the atomic and molecular structure of matter, and provided physical things—drugs, clothing, fuels, weapons, materi-

 © 2004 Wiley-VCH Verlag GmbH & Co. KGaA, Weinheim

als—that changed society. There is still much to be learned about molecules, bonds, and reactivity, but these subjects seem of a different character than aging, machine intelligence, and privacy—more evolutionary than revolutionary. Are the *revolutionary* discoveries now elsewhere, or are there still chemical discoveries as profound as the laws of thermodynamics, the nature of the chemical bond, and the molecular basis of inheritance waiting to be made?

Any answers to this question hinge on personal opinion, and on the definition of "chemistry". Is it profound to understand the origin of life, or the nature of sentience? It is, to me. Are these subjects "chemistry"? They are, to me. Is it profound to understand complexity (whatever "complexity" means), or to develop nonliving intelligence? Yes, and both have important chemical components. Is it profound to hybridize living and nonliving systems? Of course, and chemistry offers much to the effort.

This Essay is about the assumptions that our society accepts, and the potential of science to sweep aside these assumptions. It is not specifically about chemistry. However, I am a chemist, and I believe that chemistry can be *everywhere*, if chemists so choose, or that it can contract into an invisible part of the infrastructure of technology, if they don't. Chemistry, by its culture, has been almost blindly reductionist. I am repeatedly reminded that "Chemists work on molecules", as if to do anything else were suspect. Chemists *do* and *should* work on molecules, but also on the *uses* of molecules, and on problems of which molecules may be only a part of the solution. If chemists move beyond molecules to learn the *entire* problem—from design of surfactants, to synthesis of colloids, to MRI contrast agents, to the trajectories of cells in the embryo, to the applications of regenerative medicine—then the flow of ideas, problems, and solutions between chemistry and society will animate both.

As a technology, chemistry has built the foundation from which many of the discoveries of "biology", or "microelectronics", or "brain science" (or "planetary exploration", for that matter) have grown. There would be no genomics without chemical methods for separating fragments of DNA, and for synthesizing primers and probes, and for separating restriction endonucleases into pure activities. There would be no nuclear ICBMs without methods of refining plutonium and uranium, and making explosive lenses. There would be no drugs without synthesis and mass spectrometry. There would be no interplanetary probes without fuels, and carbon/carbon rocket throat nozzles, and silicon single crystals.

Those are the past. What about the future? Chemistry is, still, everywhere: It *must* be! It is the science of the real world. But, to remain a star in the play rather than a stagehand, it must open its eyes to new problems. It is impossible that the human life span will increase dramatically without manipulation of the molecules of the human organism, but understanding this problem will require more than manipulating molecules. Communication between the living and nonliving will also require engineering a molecular interface between them, but designing this interface will require understanding the nature of "information" in organisms and in computers, and how to translate between them. A society that uses information technology to interweave all its parts requires new systems for generating, distributing, and storing power, but batteries will be only one part of these systems.

Chemistry has always been the invisible hand that builds and operates the tools, and sustains the infrastructure. It can be more. We think of ourselves as experts in quarrying blocks from granite; we have not thought it our job to build cathedrals from them. Whether we choose to focus on the molecules, materials, and tools that are at the beginnings of discovery, or bring our particular, unique understanding of the world to bear on unraveling the problems at the end, is for us to decide.

I believe that everything from methane to sentience is chemistry, and that we should reexamine our own assumptions concerning the boundaries of our field. Examining the broader assumptions that follow may provide some stimulus to do so.

Assumptions

1. We Are Mortal

We assume we are mortal: we will die. We know that from experience, albeit the experience of others. But die of what? One hundred years ago, infectious disease was a major cause of death; now, it is a relatively minor problem. Most of us now alive will die of cardiovascular disease, cancer, Alzheimer's disease, diabetes, degenerative disease. Regardless of the details, we die of old age.

We know, however, that some cells age differently than others. Transformed cells are in some sense immortal (although they are not an organism); single-celled organisms that replicate by division have a kind of immortality. There are strategies that strongly prolong life: caloric deprivation does so in mice and fruit flies, and probably also does so in man. Inheritance certainly makes a difference.

Molecular biology has begun to illuminate each of our infirmities, and to suggest remedies. Cardiovascular (CV) disease is already following the path of infectious disease: the combination of medications that control blood pressure, and others (HMGA-CoA reductase inhibitors; aspirin) that control cholesterol concentrations and the clotting of blood is decreasing mortality as a result of CV disease; these benefits will increase when treatment begins earlier in life, before the damage is done. Understanding the role of free radicals in damage to tissues can help to limit injury after blockage to a blood supply. Infectious disease may also play an important role in the damage to the intima of the blood vessels, and help to initiate plaque formation. Changes in lifestyle—eating less fat and red meat, smoking fewer cigarettes—contribute to limiting injury. Many of the causes of CV disease seem understandable, and, in principle, controllable. Minimize these causes, and when these medical strategies finally fail, replace the dysfunctional organ with one from a pig engineered immunologically to resemble a human, or regenerate the organ entirely. There seems a realistic possibility that CV disease—now the largest single cause of death—may cease to be a significant contributor to mortality.

 © 2004 Wiley-VCH Verlag GmbH & Co. KGaA, Weinheim

If CV disease were marginalized, other diseases would take center stage. Cancer is next in line, and is a much, much more difficult problem. The enormous advances in cancer biology have taught, if nothing else, how complicated cancer is. Cancer is fundamentally a cumulative derangement of the genome within a population of cells. By the time the disease is detectable, there is usually already extensive damage to genes and chromosomes. The growing, molecular-level understanding of the etiology of cancer explains why success in cancer therapy has been so halting.

While genomics has so far primarily been useful in understanding, rather than in treating, the disease, it offers many suggestions for the future. There are many genomic defects that are common among cancers: damage to the signaling pathways responsible for control of the cell cycle; breakdown in the processes that check for genetic damage, and guide the damaged cell to its own death through apoptosis; breakdown in the pathways that prevent cells from leaving their origin and colonizing other organs. Understanding the role of telomers—the chromosomal structures that count the age of cells by progressive shortening during each cell division—and resetting this internal clock may have important consequences. New approaches to cancer—especially blocking factors that are essential for metastasis; preventing vascularization of tumors; developing viruses that are specific to tumor cells—all suggest new strategies for control. Other strategies will certainly appear; some will certainly be useful. The nascent field of systems biology will help to coordinate these strategies.

For cancer (and perhaps for most diseases) prevention (or presymptomatic detection) may be more important than cure. Avoiding influences that cause genetic damage—most obviously, specific compounds in the environment or in foods (and especially in tobacco smoke) that react with DNA—and avoiding exposure to ultraviolet light or ionizing radiation may be the most cost-effective method of reducing this risk.

We certainly do not see an end to cancer, nor even, yet, a real beginning to its prevention and cure. We have, however, an enormously expanded molecular understanding of the disease, and ideas for therapies.

After cancer come the diseases of aging. The details of these diseases are even less-well understood than are those of cancer. For most, we have only hints of the importance of genetic susceptibility, infection, environmental exposure, and genomic programming. A flood of genetic information will, however, emerge from studies of multiple human and non-human genomes; we can control many infectious diseases and environmental exposures; we will be able to reset biological clocks and repair genetic dysfunction. We see the beginnings of broad *strategies* to combat the diseases of aging, although we have no idea of effective *tactics*.

These changes in the understanding of disease and aging, and of medical treatment, do not promise immortality. But, they are constructing, for the first time, a true molecular *science* of disease and of medicine. The change from empiricism to understanding, and from reaction to anticipation, forms the basis for a revolution in health care. As this revolution unfolds, it has the potential to transform society.

Immortality is not necessary to change the world; much less will do. How would our social institutions perform if the average life span were 200+ years? What would happen if the period of female fertility were 100 years? How would we behave if life expectancy could be extended by a factor of five, but only the very, very rich could afford the extension? How would the world change if the difference in life span between first and third world countries were a factor of ten?

Chemistry is at the core of changes in biomedicine. Chemistry makes drugs and vaccines. Chemistry makes the analytical systems that will enable detailed genomic analysis of individuals. Chemistry provides the understanding of the changes in molecules that accompany disease and aging. Chemistry identifies (and sometimes generates) the environmental factors that lead to biological damage. What chemistry does *not* do now is to integrate molecular-level characteristics with cellular and organismic behavior—to see the picture in the pointillist splatter of dots. Still, molecular chemistry, molecular biology, and medicine are fundamentally the same subject—the understanding of molecules important to life, and the application of that understanding to the improvement of human health.

2. Only Living Creatures Think; We Think Best

We are, at least in our own opinion, the crown of creation: the most intelligent and versatile of species, and renowned for our ability to subjugate other species. We assume that there is no threat to this position (barring the appearance of aliens, or some other incalculable improbability).

Will we continue to be unique? Is there another species that could become as intelligent as we are? It seems unlikely that other living creatures could emerge as superior intelligences: biological evolution is relatively slow, and we would probably not be kind or hospitable to a potential competitor. An alternative to the improbable emergence of another intelligent animal (or insect, or plant) species is that the next sentience on the planet might be silicon- rather than carbon-based.

Individual computers probably do not currently have the complexity necessary to be intelligent (or at least self-conscious) in the way that we are. As the global information network—the world wide web; high bandwidth communications systems; universal connectivity—is assembled (or, increasingly, as it self-assembles, to use the phrase from organic chemistry), there will be an opportunity (or perhaps even a certainty) for a complexity that rivals or exceeds that of each of us as individuals. A global, interconnected entity that operates at frequencies of petaflops will do things that we cannot begin to imagine. Why not think? Why not think about itself? Perhaps even think about us?

The probability of a new intelligence emerging by biological evolution is limited by the decades-long generational times of complex organisms, by the low rate at which new variants arise by mutation, and by the complexity and functional form of the central nervous system. Evolution and selection have taken millennia to jostle us into our

 © 2004 Wiley-VCH Verlag GmbH & Co. KGaA, Weinheim

present situation; I suspect it would require special circumstances for another to jostle us aside quickly. Our intelligence, adaptability, and self-awareness (aided by the chance development during evolution of an opposed thumb and an oddly positioned larynx) have enabled us to survive and out-reproduce many more voracious but less-intelligent and self-aware forms of life.

Computers operate by different rules, and without the constraints of biology. Computer cycles are much faster than the diffusion of neurotransmitters across synapses in the brain; change through evolutionary selection is much slower than change by adaptive reprogramming. With the Internet, computer interconnectivity will become very large, and communication among nodes very rapid.

Perhaps most importantly, the growth of complexity in the web is driven by us: a significant part of the creativity of the human race—perhaps hundreds of thousands of creative, energetic, purposeful people—is now devoted to the mission of making more competent components for the web, to enabling those components to communicate as efficiently as possible, and to encouraging the resulting systems to perform their tasks with little or no human supervision. As we develop software agents, applets, and autonomous systems, we seek local performance; what global connectivity among these local systems will bring remains for us to experience.

We could ask at least four interesting questions about the potential for sentience in computer networks. The first question concerns the connections between complexity, emergence, and intelligence. (The word "emergence" is taken to mean the appearance of properties in a complex system that we cannot predict from the properties of its individual components.) How complex must a system be to think? … to become sentient? Can we—scientists, and especially chemists, who generally are committed reductionists—predict complex behaviors based on knowledge of simple components? Understanding complexity has not been a strength of reductionist science. A second question concerns the basic requirements for "intelligence". Are complexity and density of connections enough, or is there something about the human brain that makes it uniquely capable of intelligence? I personally doubt that there is anything special about the wetware inside my skull other than its complexity, the three-dimensional density with which it is internally connected, and its ability to modify itself through experience; I doubt, but cannot disprove, that there are quantum subtleties to self-consciousness. A third question deals with the relationship between intelligence and self-awareness. Is there a correlation, or is self-awareness something different in character than intelligence? A fourth question touches on the delicate issue of the relation between life and intelligence. We speculate endlessly about evolution in living systems, and whether biological evolution leads inevitably to intelligence. What about intelligence *without* life? An intelligent web would certainly not be alive in any sense a biologist would recognize.

We have opinions about the potential of computer networks to support sentience, but not knowledge. Self-awareness is probably not unique to humans, and not all that is *Homo sapiens* is self-aware. A porpoise or a chimpanzee is probably self-aware. A human fetus is certainly not self-aware; a baby grows into self-awareness; an Alzheimer's patient grows out of it. Can we guarantee that a computer system would not grow to be self-aware? I doubt it.

Would we even know if some future version of the world wide web had developed self-awareness? I suspect that we would not, at least for a long time. Our ability to imagine existences not our own is profoundly limited. The ability of a silicon-based intelligence—one inhabiting a distributed web of cunningly doped crystals and giant magnetoresistive films, of optical fibers and satellite repeaters, and "thinking" through the flow of photons and electrons—to imagine a world of water, salt gradients, food, and sex seems equally improbable. If aqueous and silicon intelligences did become aware of one another, it is not clear what the outcome would be.

What does this have to do with chemistry? Probably everything. One of the great intellectual challenges humans face is to understand intelligence as a property that emerges from the interactions of molecules (which, whatever they are, are not intelligent). Chemistry is familiar with complexity, but has not yet embraced the task of understanding the forms of complex behavior that can emerge from large groups of molecules, or of systems (for example, cells) formed from molecules. In studying intelligence in a complex system, our own intelligence is probably the best example with which to begin. This effort is the best preparation we can presently imagine for an encounter with another intelligence, whether met on our own planet or encountered elsewhere.

Redrawing the Line between Living and Dead

3. Animals and Machines are Different

Humankind tends to categorize. Among the categories that have been separate in the past have been "living" and "nonliving", and "animal" and "machine". An animal is a biological entity made of tissue and bone. It is born of other animals, lives, and dies, and has characteristics that are what they are by virtue of evolution and genetic inheritance. In the past, we have not designed animals, although their performance may in a few cases have been optimized empirically through domestication and selective breeding to meet certain of our needs. Since we and animals are alive, we recognize various degrees of ethical responsibility toward them.

A machine is qualitatively different: an object of metal, ceramic, and plastic, which we design and build de novo. We now feel no ethical responsibilities toward machines.

This convenient distinction between animal and machine is beginning to fail at several levels. In the most biological sense, we are developing the ability to design animals. We are rapidly developing biological tools that will enable us to specify the characteristics of animals in a way similar to that in which we specify the characteristics of machines. We already use genetic engineering with animals for the same sorts of tasks as we use

 © 2004 Wiley-VCH Verlag GmbH & Co. KGaA, Weinheim

mechanical engineering with machines. We have chimeras that build components of one species into another; we can add or delete genes; we can re-engineer entire subsystems of one animal to resemble that of another. We are learning how to modify the surface antigens of one species to make its organs compatible with transfer into another species. We have taken the first steps in learning how to regenerate organs from stem cells, and perhaps to de-differentiate differentiated tissue, and then regrow it into regenerated parts. We are developing a toolkit that is making possible the machinelike design of animals using parts that can range from nucleotide sequences to whole organs.

Most of this work has, of course, been focused on objectives in biology and biomedicine. As the capabilities of biology extend, however, the idea of animals (or insects) for other uses quickly follows. Animals as sensors—that is, as "canaries"—is now plausible. Plants and microorganisms are unquestionably already alternatives to chemical reactors for carrying out some chemical transformations. We know that selective breeding can produce unusual plants and animals; applied biology can only increase our skills at "species engineering". We will ultimately consider—perhaps will *have* to consider—species-engineering for ourselves. Were we to embark on multigenerational space flight, would we be better off with artificial gravity and our current physical form, or with a physical form better adapted for low gravity, high radiation, and whatever other aspects of the environment the ship could best provide?

More radical, but much earlier in development, is work intended to fuse the world of man and machines. Current technology builds implantable sensors to control cardiac rhythm and glucose levels. Cochlear implants help the deaf to hear. The targets are becoming more ambitious: electrodes implanted in insects and rats that begin to control their motion or relay information about their environment; retinal chips to provide sight for the blind; systems that transduce thought directly into mechanical motion. For the more distant future, the goal is direct, efficient, communication between human brains and machines.

These efforts point toward an extraordinarily complex (and perhaps unachievable) future goal: the ability to connect brain and computer directly—that is, to allow information flowing in the nerves of an organism to shift directly into information flowing as electrons or photons in a computer. The technological barriers to this kind of fusion of animate and inanimate are immense, but do not violate any fundamental physical laws, and do not seem ultimately insurmountable. Progress in solving some of them—for example, in developing interfaces that are biocompatible—has been rapid; progress towards others—for example, learning how to transfer information between neural and silicon-based systems—has been slow. Given the unarguable fact that biology and information technology have been the scientific revolutions of the last half of the 20th century, it is almost certain that the 21st century will see their overlap and fusion.

What are the major technical problems? One must learn the code used in the brain and the nerves to convey, process, and interpret information; (we already know the code used in computers, since we *designed* it); one must learn how to build a physical interface between the two—perhaps between nerves and microelectrodes. One must learn how to convert between the currencies used by the neurons to transfer information—ion gradients across membranes and pulses of neurotransmitters in synapses—and the currencies used by silicon-based systems—electrons and photons. The goal of direct communication between human brain and computer also faces a serious problem of dimensional translation: computers are now intrinsically 2D in their architectures, and brains are 3D. We have no solution yet to the problem of making a sufficient number of the correct kinds of neural-to-computer connections. Perhaps growing specialized neural tissues to act as connectors—that is, genetic modification of the human to fit better to the computer—will be the final approach.

With a capability to build hybrid systems—systems containing not just two kinds of biological molecule or tissue, but systems containing some components that are biological and others that are silicon—the issue of whether computer networks might emerge as sentient entities capable of competing with humans could become moot: one could imagine wetware and silicon co-developing, and a blurring of the concepts of "animal" and "machine" and "alive" and "dead" in a way that is unimaginable now.

Many of the most important of these problems ultimately have components that are molecular. Although molecules may be only a part of the systems that transmit and interpret information in organisms, building interfaces between the living and nonliving, and designing translators to bridge the languages of ions and electrons, both depend intimately upon chemistry. The tools for genetic engineering of specialized neural tissues will require chemical manipulation of genetic materials. Biocompatibility is a molecular and materials problem.

The 21st century will almost certainly see us redraw the line between "living" and "dead," and many of the tools to do so must ultimately be molecular.

4. Human Life Is Invaluable

The idea of a long, healthy life fits neatly with the assumption of western civilizations that life is invaluable, and that prolonging it, when possible, is a moral obligation. This obligation is increasingly in conflict with the need to limit the costs of medical treatments, to balance the distribution of health benefits, and to stabilize population levels. We may be forced to confront the value of prolonging life on two fronts:

First, as we move toward the objective of a long, healthy life, we already see that there is an interval where life can be prolonged, but only at great expense, and not necessarily with high quality. If, for example, we can extend life through combinations of artificial devices (artificial joints and organs), xenotransplantation, immunosuppression, and organ regeneration, the cost to the patient may be a life of immunological crisis and constant flirtation with infection. We may be able to buy a longer life, but only an expensive and uncomfortable one. As biomedical sci-

 © 2004 Wiley-VCH Verlag GmbH & Co. KGaA, Weinheim

ence makes it possible to patch up (but not cure) many previously terminal conditions, a serious collision of interests seems inevitable.

Second, and more complicated, are the demographic consequences of reaching the technical goal of building a medical capability that greatly prolongs healthy life. Balancing prolongation of life span, birthrate, and population control requires arithmetically that something give: there must be either limitations on birthrates, or limitations on life spans. We may find that we have a choice: "New life or old?" Placing termination of life—killing a person—on the same footing as birth control—an everyday part of recreational sex—would mean a fundamental shift in values.

Sorting Humans

5. All Are Born Equal

An assumption in many western societies is equality at birth: equal rights under law, and equal access to opportunity. This assumption is respectful of the individual, and there have been no means—or no means that we have chosen to validate and adopt—of quantifying inequality. Genetics has the potential to change our convenient inability to measure innate capability; cognitive science and psychology will also contribute.

Pandora could not resist opening the box. Can we?

Genomic analysis of individuals is just dawning. The first complete maps of the human genome are still being refined, and the task of correlating and confirming the association of single genes and gene clusters with the characteristics of individuals has begun. It is the "Panama Canal" project of modern biology. Eventually there will be a highly profitable shipping trade between the genomic and phenotypic oceans, but now there is a lot of mud to move and many mosquitoes to swat. We do not know how complicated the task will be: it is possible that the characteristics that make us what we are will be determined by single proteins or relatively uncomplicated clusters of proteins, and that genomics will open a window directly onto behavior and capability; it is more probable that these characteristics reflect the behavior of complex biological systems, and will require many decades to decipher. In any event, even with dramatic improvements in the relevant technologies—both for the collection of the needed biological information and for its analysis—the task of correlating genetic constitution with the potential strengths and weaknesses of individuals will require decades (but probably not centuries) of work.

This enterprise—the mapping of genomic information onto an understanding of capabilities, weaknesses, and behaviors—has, of course, the potential for enormous good. It will be one foundation for medical science; it will help individuals to understand where they might be susceptible to damage through disease or environmental exposure; it will allow them the opportunity to identify and exercise their strongest capabilities.

It will also change society if used to *classify* individuals—especially children—according to these capabilities. If it is very *easy* to collect genomic information about individuals, will we be able to resist the temptation to use this information to understand as much about them as possible? Not just their susceptibility to emphysema from smoking, but their ability to handle the stresses of office work, combat, or marriage? Or their potential to be good parents? Or to pay traffic tickets on time? Or to have a sense of humor? We *are* incorrigibly curious and mischievous. Pandora could not resist opening the box; will we do any better?

For good or evil, chemistry is a central player in this project. The development of analytical systems that allow rapid, accurate, inexpensive analysis of the genome of individuals; the intimately linked areas of functional genomics and proteomics that will associate genes with proteins, and proteins with biological function; the correlation of environmental influences—from food components to stress, and from stress-induced chemicals to disease or dysfunction—will all depend centrally on chemistry to build the tools to study genomics, proteomics, and metabolism…

…and, eventually, to sort human beings according to their characteristics and potentials.

6. We Are Individuals, and Privacy is Important

We are accustomed to thinking of ourselves as individuals, and as such we value the accoutrements of individuality: freedom of choice, privacy, lack of control by others, self-determination. We are individuals in the sense that we choose our own paths; we keep our own secrets; we are unpredictable to others.

We are individuals partly by choice, and partly by accident: we are not able to read the thoughts of others, nor to control their thinking. Characteristic of the revolutions in information technology and in genetics is that they have the capability to provide information about individuals in such abundance and detail that privacy and unpredictability become moot. Many of us now have cellphones and other microelectronic assistants; these phones are a step toward a global technology in which everyone is able to communicate with anyone on the globe, at any time, using sound, sight, and data, by portable communications systems. The global positioning system (GPS) and related systems allow us to determine positions; with a simple transponder, it will allow others to determine our positions. Universal surveillance—by monitors inside buildings; from unpiloted, long-endurance vehicles outside buildings—will one day allow our actions to be monitored continuously. A history of our behaviors and actions can be stored in large databases. Genetic analysis has the potential to predict capabilities, susceptibilities, and patterns of behavior. Sociology and psychology, as they become sciences, will help to connect the dots between molecules and behaviors, and between individuals and crowds and societies.

It may be that it is still impossible to read our minds; but if it is possible to know our positions and circumstances, to watch and record our activities, to

 © 2004 Wiley-VCH Verlag GmbH & Co. KGaA, Weinheim

know our intrinsic capabilities, and to communicate with us at all times, it may be *unnecessary* actually to read our minds: all the information that is needed to predict our behaviors may already be available.

Many of the major technologies needed to begin to transform humankind from a society of individuals to a kind of hive-animal are, in practical fact, already available, albeit in the form of early prototypes: GPS, very high-density information storage; sensors for remote surveillance, systems for genetic testing. One essential technology that is not available is portable power. It is possible that we may develop methods of providing power wirelessly inside buildings and in cities as we now provide light; beyond enclosed spaces, devices for generation and storage of power will be required. To be in constant electronic communication requires that the individual carry devices that broadcast, but broadcasting requires power. The energy density of any battery that we can imagine will not fill this need: what is required is either a direct, low-temperature hydrocarbon fuel cell, or more exotic power sources: perhaps small nuclear power sources, or methods of extracting electrical energy from the metabolism of individuals. That extra cake for dessert might power more minutes of high-bandwidth communication!

The Democratization of Information and Expertise

7. Experts Know Best; Doctors Control the Medical System

We assume that specialized knowledge belongs to experts. I do not expect my auto mechanic—an expert in his own field—to do Diels–Alder reactions. We depend on experts, and on their ability to use their expert knowledge to our benefit.

We are, understandably, especially interested in the workings of the experts—doctors—in the medical system: we all become sick; we all age. The medical profession has been a prototypic guild—one controlled by highly trained individuals, who establish the standards that others must pass to join. Doctors also control most of the aspects of medicine: information about disease and treatment; approval of new drugs and new methods of treatment; and access to drugs. Although those who pay for medicine (in the US HMOs, or health maintenance organizations, and insurers) are challenging this system, doctors still largely run medicine. This system has many good features, and some bad ones as well.

An interesting consequence of the development of the world wide web is the ability of individuals with common interests to find and communicate with one another. There are few individuals who are as motivated as those who are sick (or who believe that they are sick) and who wish to be well. The development of web-based medicine allows these individuals to talk to one another, and to share opinion, gossip, and fact without formal medical supervision. They can often buy drugs that are not approved by the medical establishment, and they can experiment on themselves: the sales of "nontraditional" medicines is now claimed to be comparable to that of medicines that have regulatory approval. It is common for a physician to be faced with a patient carrying a thick folder of computer printouts describing the disease. In short, the medical profession is losing its control of the flow of authoritative medical information, and to an extent, of the course of medical treatment taken by patients.

Medicine is changing, and doctors must keep up with an enormous volume of information. Patients have as much access as doctors to much of the information, and often a more intense motivation to assimilate it. They may be better informed than their doctors, and collectively they can call on an extraordinary breadth of expertise. The Internet allows information—true, false, untested—to flow internationally without professional or peer supervision. Nontraditional and unapproved drugs are readily available.

The democratization of information and expertise that springs from the world wide web, and the power of groups of motivated amateurs to strike out on their own in technical subjects, is weakening the authority of "experts" in society. Travel agents are a disappearing breed—one can order tickets on the web. Accounting programs are replacing tax accountants. A free-form community of hackers and programmers developed the Linux operating system. Computers routinely land commercial airliners. The environmental and consumer advocacy groups that so bedevil technology (sometimes to excellent effect) are highly skilled in collective expertise and collective action. Doctors are losing their grip on their profession. Even universities are beginning to worry about their monopoly to certify expertise.

Of course, someone still has to hold the scalpel and the bedpan. Or some *thing*: the hand wielding the knife could well be a machine's.

The Globe

8. Earth Will Remain Habitable

Although discussions of the environment and global warming are endless, to much of the world the problems these phrases represent are still abstract. The first-world countries have not slashed their use of fossil fuels; the third-world countries continue to reduce forests to wastelands; and coal is the fuel of choice for some of the largest economies of this century.

There seems to be growing agreement that anthropogenic contributions—carbon dioxide, soot, methane, others—to the atmosphere are significant, and are increasing global temperatures relative to what they would be in the absence of these contributions. There is no agreement on the significance of this increase in temperature on society. The temperature of the Earth has gone through a set of sawtooth excursions over the last millennia: we are now in an exceptionally warm period in this normal climatic cycle in any event, and despite our mischievous efforts to achieve warming on a planetary scale, temperatures may again fall in the future.

But what happens if the assumption that the Earth will remain habitable (or at least as accommodating to mammalian life as it now is) proves wrong? Changes in the environment will probably be relatively slow; even if we melt the west Greenland ice sheet, it seems

 © 2004 Wiley-VCH Verlag GmbH & Co. KGaA, Weinheim

unlikely that we will tip the balance of the planet so that Earth becomes Venus (although we would submerge New York and Tokyo). We would adjust.

Other changes—for example, those resulting from all-out nuclear war or a large meteor strike—would probably give us much less time to adapt, and far fewer options.

How much of a technological insurance policy, and of what nature, should we have against events that might fundamentally change the habitability of earth? There are many possibilities to reduce carbon emissions significantly: replacing gasoline engines with efficient diesels, developing highly efficient fuel cells, developing solar and wind power optimally, and reintroducing nuclear power are four. Industrial solutions to pollution would proceed more rapidly if there were active investment in "green" technologies, and the rate of the investment is primarily a matter of regulation and public policy, albeit complicated by the fact that regulations apply locally within countries, but the problem is global.

Technical issues are less important than political ones in nuclear matters, and we have not begun to take the problem of a meteor strike seriously.

9. Nations Are the Most Powerful of Human Organizations

The world is now organized into nations—social and political entities with defined geographical boundaries. Nations made sense in a world in which wealth was based on natural resources, fertile land, water, and people. Wealthy nations were those that could lay claim to vast natural resources, and had access to trade routes; wealthy nations were also those that could afford to wage war.

It was easy to keep score with nations as central political entities. The ground has, however, shifted. It is more important now to be able to control and use information than to mine bauxite or diamonds. It is more important now to have a highly educated population than large reserves of coal. The fluidity of information, and the difficulty of owning and containing it, also opens opportunities for small groups of people. The Internet allows almost any group of people access to floods of useful information, and at almost no cost. The technology of information has redefined wealth—from material goods to information and services—and thus makes the centrality of nations—which control physical space but not information space—open to question.

As for war: The cold war was a period in which the two most powerful nations faced one another in a competition ostensibly organized along conventional lines: with armies and weapons. The armies were never used directly, although they were employed in surrogate conflicts in Korea, Vietnam, and Afghanistan. Ultimately, however, the conflict proved to be economic: the US won, in significant part because it outspent the Soviet Union.

As information, information systems, and people become central to wealth, large countries (especially those housing open societies) become more vulnerable to cyber attacks. The US and the Soviet Union also had a virtual monopoly on strategic nuclear systems for many years; they have no corresponding monopoly in terrorist weapons, especially those for biological weapons. Joshua Lederberg has said "biological weapons enable a single man to wage war," and biological and cyber attacks—plausibly originating in small countries or in nonstate entities such as criminal, religious, or ideological groups, or even, perhaps, corporations—now rank with nuclear attacks in the risk they hold for society.

Technology has started a shift away from nations as the central political entity to supranational entities: alliances, economic regions, multinational corporations, capitalist groupings, religions. It has posed risks to the developed countries, which value openness and capitalism, and which require relatively few barriers to the movement of people, information, and goods for efficient operation. This openness of western societies makes them difficult to defend. Developing new technologies to defend against these new threats—sensors, drugs, and defensive agents for use against biological threats; software agents and security systems to protect computer networks—are important problems, and all have central components in chemistry.

Deciding how much protection is "enough", and how much is "too much"—that is, deciding how to value security and privacy when the two are in conflict—is a broader question for society.

Not Everything is Built on Sand

Is there *nothing* that is secure, then? The answer is, of course, that we do not know, but a number of assumptions seem most unlikely to fall. We assume that it is impossible to read minds, or to teleport physical objects, or to move faster than the speed of light in vacuum. We assume that time can not be made to run in reverse, and that the major laws discovered by physical science over the last several centuries will continue to be true: water at room temperature will not spontaneously separate into steam and ice; objects will not spontaneously rise against gravity; we will not discover a source of energy for free. The second law of thermodynamics will continue to describe the world in which we live. Not everything is built on sand.

Are There Questions We Should Not Ask?

Is "big" science—science that changes the world—good for the world it changes? I am constitutionally an optimist, and would answer "Usually 'yes'". We (at least in the developed world) live longer than our forebears, devote less of our lives to personal survival; suffer less from disease; understand the world more fully; have more time to spend building society and appreciating existence. I *believe* that science has *generally* worked for the common good in the past, and will continue to do so in the future. Still, science and technology will unlock some doors we may not choose to open.

Science that changes the world inevitably brings ethical issues. Building a microfluidic system for analysis of the human genome may be no more or less challenging technically than building a better catalyst for the production of polyethylene, but it is more important for society.

 © 2004 Wiley-VCH Verlag GmbH & Co. KGaA, Weinheim

We scientists *do* have something special to contribute to discussions of the outcomes of science. We know some things that *will* be done before they are done; we know some things that cannot be done at all; we can speculate about things that *might* be done. We can alert our neighbors to the possibility of change, and be a part of discussions and decisions that encourage the good, and avoid or forestall the bad. We can try to prevent fear of new ideas from blocking beneficial technology. In choosing to work on problems with the potential to change society, we should, ideally, accept an obligation to help society understand how it might benefit, and what it might pay, for that change.

We can suggest what doors can be opened, and what might wait in the rooms behind them. Our neighbors will decide for their own reasons whether they would like to open these doors and move in.

Finally: Is there science that must not be done? There are easy cases—I can see no redeeming virtue of publicly available research that develops strains of anthrax that are resistant to multiple antibiotics—but much of research is not easily classified as "good" or "bad".

Chemistry contributes broadly to the foundations of technology, and thus it is particularly difficult to guess its future impact: a new chemical reaction might be used to make a cancer therapeutic or a chemical weapon. Some of the opportunities that seem within the reach of investigation, if not within the reach of solution—technologies that might substantially prolong life, or develop new forms of life, or lead to sentient systems that rival us in intelligence—will do both good and harm. At the very minimum, those of us who pursue these problems should accept an obligation to explain to our fellow citizens fully and clearly what we are doing, and why, and (to the limited extent we can) with what possible outcomes.

Humankind will do what it will do, but at least everyone should understand—in so far as is possible—what the choices are, and what the consequences might be. Chemistry, if it takes more interest in (and responsibility for) the full scope of programs—from molecules, to applications, and to influence on society—may be able to use the very breadth of its connections to technology to help in this explanation.

After that, the surprises take over. The last, most realistic, assumption may be that the law of unintended consequences will ultimately apply.

Published Online: June 24, 2004

J. N. Abramovitz, *Vital Signs 2002: The Trends that are Shaping the Future*, W. W. Norton, New York, NY, **2002**.
C. M. Christensen, *The Innovator's Dilemma*, Harvard Business School Press, Boston, MA, **1997**.
H. Collins, T. Pinch, *The Golem: What Everybody Should Know about Science*, Cambridge University Press, Cambridge, **1998**.
J. Diamond, *Guns, Germs, and Steel: The Fates of Human Societies*, W. W. Norton, New York, NY, **1997**.
P. Feyerabend, *Against Method*, Verso, London, **1975**.
R. P. Feynman, *Feynman Lectures on Computation*, Addison-Wesley, New York, NY, **1996**.
Y. Fukuyama, *The End of History and the Last Man*, Avon Books, New York, NY, **1993**.
J. Horgan, *The End of Science: Facing the Limits of Knowledge in the Twilight of the Scientific Age*, Broadway Books, New York, NY, **1997**.
A. Huxley, *The Brave New World*, Perennial Classics, New York, NY, **1998** (first published in **1932**).
T. S. Kuhn, *The Structure of Scientific Revolutions*, University of Chicago Press, Chicago, IL, **1970**.
R. Kurzweil, *The Age of Intelligent Machines*, MIT Press, Cambridge, MA, **1993**.
P. A. Lawrence, *The Making of a Fly*, Blackwell, London, **1992**.
H. Lodish, A. Berk, L. S. Zipursky, P. Matsudaira, D. Baltimore, J. Darnell, *Molecular Cell Biology*, Freeman, New York, **2000**.
J. R. Maddox, *What Remains to be Discovered: Mapping the Secrets of the Universe, the Origins of Life, and the Future of the Human Race*, Touchstone Books, New York, NY, **1999**.
L. McLaughlin, *The Pill, John Rock, and the Church: Biography of a Revolution*, Little and Brown, New York, NY, **1982**.
S. Pinker, *How the Mind Works*, W. W. Norton, New York, NY, **1999**.
K. Popper, *The Logic of Scientific Discovery*, Routledge, New York, NY, **2002**.
J. S. Rigden, *Hydrogen, The Essential Element*, Harvard University Press, Cambridge, MA, **2002**.
E. Schroedinger, *What is Life?*, Cambridge University Press, Cambridge, **1967**.
S. J. R. Searle, *Minds, Brains, and Science*, Harvard University Press, Cambridge, MA, **1986**.
A. M. Turing, M. Woodger, *The Automatic Computing Engine*, MIT Press, Cambridge, MA, **1986**.
H. C. von Baeyer, *Maxwell's Demon*, Random House, New York, NY, **1998**.
M. Mitchell Waldrop, *Complexity: The Emerging Science at the Edge of Order and Chaos*, Simon and Schuster, New York, NY, **1992**.
R. Weinberg, *One Renegade Cell: How Cancer Begins*, Basic Books, New York, NY, **1998**.

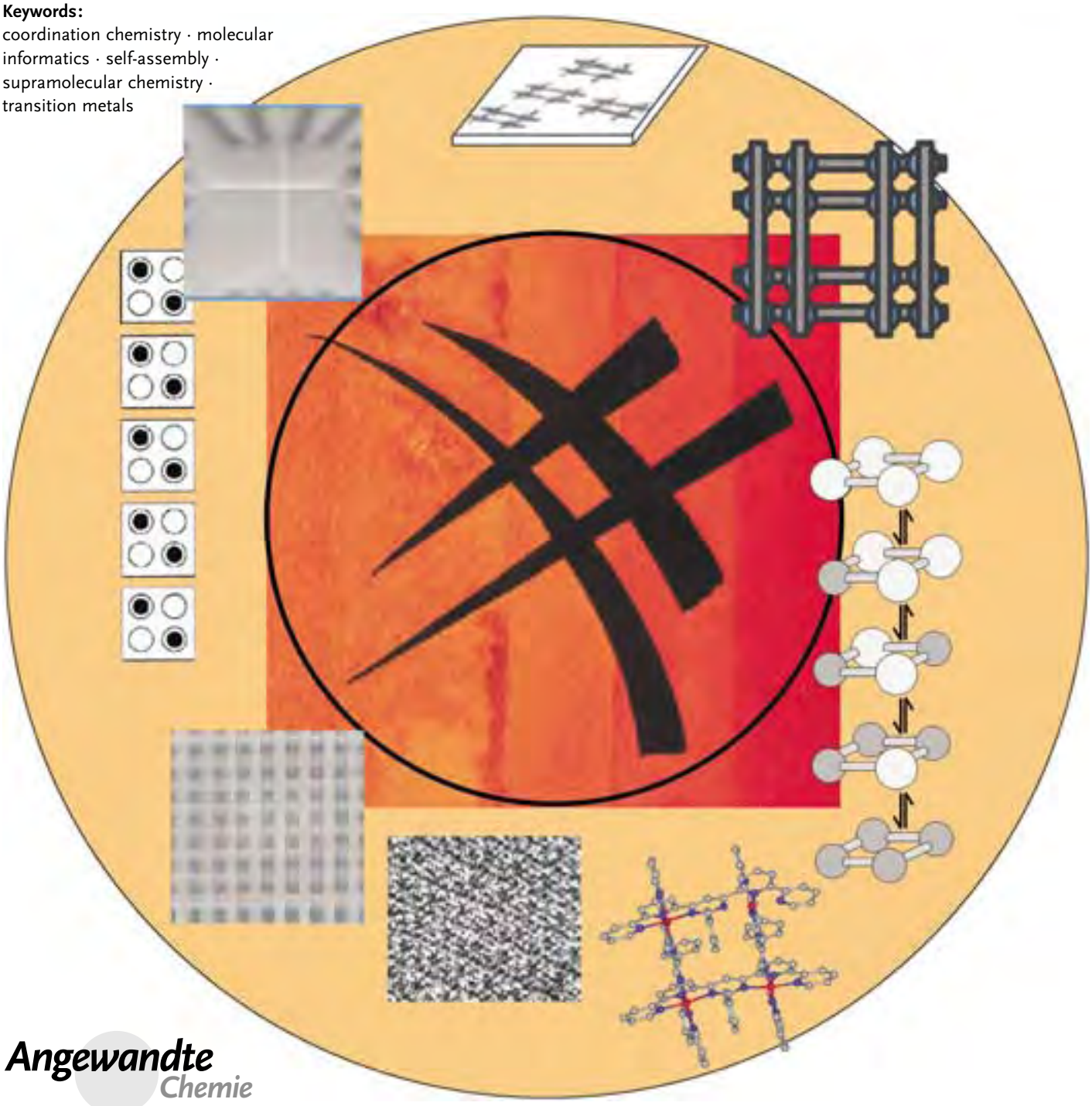
 © 2004 Wiley-VCH Verlag GmbH & Co. KGaA, Weinheim

Self-Assembly

Grid-Type Metal Ion Architectures: Functional Metallosupramolecular Arrays

*Mario Ruben, Javier Rojo, Francisco J. Romero-Salguero, Lindsay H. Uppadine, and Jean-Marie Lehn**

Keywords:
coordination chemistry · molecular informatics · self-assembly · supramolecular chemistry · transition metals



 © 2004 Wiley-VCH Verlag GmbH & Co. KGaA, Weinheim DOI: 10.1002/anie.200300636

Recent advances in supramolecular coordination chemistry allow access to transition-metal complexes of grid-type architecture comprising two-dimensional arrays of metal ions connecting a set of organic ligands in a perpendicular arrangement to generate a multiple wiring network. General design principles for these structures involve the thermodynamically driven synthesis of complex discrete objects from numerous molecular components in a single overall operation. Such supramolecular metal ion arrays combine the properties of their constituent metal ions and ligands, showing unique optical, electrochemical, and magnetic behavior. These features present potential relevance for nanotechnology, particularly in the area of supramolecular devices for information storage and processing. Thus, a dense organization of addressable units is represented by an extended "grid-of-grids" arrangement, formed by interaction of grid-type arrays with solid surfaces.

From the Contents

1. Introduction	3645
2. General Concepts	3647
3. Grid-Type Metal Ion Arrays	3649
4. Mechanistic Features of the Self-Assembly Process	3654
5. Multistability and Addressability	3655
6. Conclusion and Outlook	3660

1. Introduction

The drive to shrink electronic devices to the nano-level, has, in recent years, led to the design and investigation of molecular-scale components endowed with sensing, switching, logic, and information storage functions.[1–3] Although the implementation of information processing with such devices faces hurdles in the development of logic architecture and intermolecular hook-up schemes,[1] molecular data storage is subject to active interest, namely in view of the rapidly approaching upper limit in conventional magnetic data storage resulting from thermal erasure at the superparamagnetic limit. Species suitable for molecular data storage must 1) possess two or more physicochemically distinct states that can be conveniently switched by application of external triggers (e.g. thermodynamic parameters or electromagnetic fields) and 2) should be addressable and switchable within the nanometer regime. Toward this end, gridlike metal ion arrays, in which a set of metal ions is held in a regular network of organic ligands in a perpendicular arrangement (Figure 1), present several attractive features: 1) their redox, magnetic, and spin-state transitions are well-documented, 2) the well-defined two-dimensional (2D) arrangement of an exact number of metal ions resembles strongly the binary coded matrices and cross-bar architectures used in information storage and processing technology, and 3) they may be arranged into extended two-dimensional ensembles by deposition onto solid surfaces. The nuclearity and dimensionality of the gridlike metalloarrays are clearly based on the polytopic nature of the ligands and the ability of the metal to read and interpret the coordination options presented by the ligand in the most efficient way depending on its own coordination algorithm.



Figure 1. Molecular structures of several gridlike metal ion arrays that exhibit a regular network of perpendicular arranged organic ligands.[4a, 5a, 6]

The two-dimensional (2D) grid motif was recently the architectural base of a molecular 64-bit logic and storage device.[7a] The resulting architecture consists of two perpendicular sets of eight Pt wires (top and bottom). A bit of molecular memory (around 1000 molecules of an organic compound) is sandwiched at the crossing points between the higher and lower wire (Figure 2). The whole storage and switching units have an area of around 1 μm^2 with a wire-to-wire distance of about 40 nm. Although, the working principles of such a device are still under discussion, it is possible to "write" and to "read" the information at different voltages.[7b] Crossbar arrays based on nanowires may lead to addressable nanosystems.[7c]

Further interest in gridlike molecular architectures might arise from an alternative encoding concept called "cellular

[*] Dr. M. Ruben,[+] Dr. J. Rojo,[++] Dr. F. J. Romero-Salguero,[+++] Dr. L. H. Uppadine, Prof. Dr. J.-M. Lehn
ISIS,Université Louis Pasteur
8, Allée Gaspard Monge, BP 70028
67083 Strasbourg cedex (France)
Fax: (+33) 390-245-140
E-mail: lehn@isis.u-strasbg.fr

[+] Institut für Nanotechnologie
Forschungszentrum Karlsruhe GmbH, PF 3640
76021 Karlsruhe (Germany)

[++] Dpto. Química Bioorgánica, IIQ, CSIC
Américo Vespucio s/n
41092 Sevilla (Spain)

[+++] Dpto. Química Orgánica, Universidad de Córdoba
Campus de Rabanales, edificio "Marie-Curie"
14014 Córdoba (Spain)

DOI: 10.1002/anie.200300636

© 2004 Wiley-VCH Verlag GmbH & Co. KGaA, Weinheim

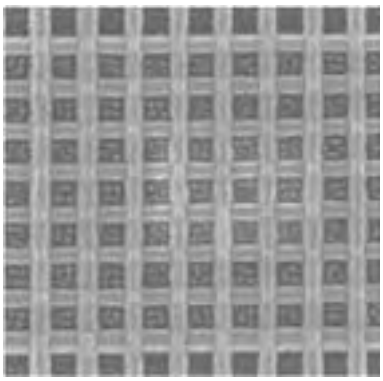


Figure 2. A 64-bit molecular storage device. The crossed-wire structure of the memory shows the eight top and the eight bottom Pt wires (wire-to-wire distance ca. 40 nm).[7a]

automata", in which molecules do not act as current switches but as structured charge containers.[8] Envisaged first for quantum dots, binary information is encoded in the charge configuration of a cell composed of a small number of differently charged redox centers, which are electronically communicating within the entity but are not completely delocalized (Robin-Day type II) (Figure 3). Each cell has two degenerate ground states, which can be interconverted by an internal electron density redistribution (e.g. by the transfer of two or more electrons within the cell). The electrostatic interaction of two neighboring cells (arranged in one, two, or three dimensions) lifts the given degeneracy and results in "1" or "0" states. Remarkably, the intercellular information exchange is purely based on Coulomb interactions and involves no current flow. If such interaction can be realized, this approach may enable a general purpose computation.[9]

From the standpoint of nanochemistry, the cells can comprise molecular or supramolecular entities. Multinuclear metal ion coordination arrays present particularly attractive features in this respect. The main interest arises from a self-organization strategy involving appropriate ligands and metal ions, which allows close control of the structural and physical properties of the resulting assemblies. Recent progress in molecular self-assembly processes has opened the way to generate extended supramolecular structures by spontaneous, but controlled build-up from their components.[3,10] Such self-fabrication techniques are of intense interest, due to the possibility of bypassing or complementing tedious (top-down) nanofabrication and nanomanipulation procedures.[3]



Jean-Marie Lehn was born in Rosheim, France in 1939. In 1970 he became Professor of Chemistry at the Université Louis Pasteur in Strasbourg and since 1979 he is Professor at the Collège de France in Paris. He received the Nobel Prize in Chemistry in 1987 for his studies on the chemical basis of "molecular recognition". Over the years his work led to the definition of a new field of chemistry, which he called "supramolecular chemistry". He is the author of more than 700 scientific publications, and member of many academies, institutions, and industrial bodies.



Francisco José Romero-Salguero was born in Baena, Spain, in 1967. He graduated both in chemistry (1990) and food science and technology (1992) from the University of Córdoba where he obtained his PhD in 1995. He then spent two years with Prof. J.-M. Lehn in Strasbourg as a postdoctoral researcher working on inorganic nanoarchitectures, before returning in 1998 to Córdoba where he is now an assistant professor in Organic Chemistry. His research interests focus on supramolecular synthesis and micro- and mesostructured catalysts for organic reactions.



Javier Rojo received his PhD degree under the supervision of Prof. J. C. Carretero at the University Autónoma, Madrid in 1995. He was a postdoctoral fellow with Prof. J.-M. Lehn at the Université Louis Pasteur in Strasbourg (1995–1998) and with Prof. L. W. McLaughlin at Boston College (1998–1999). In January 2000, he joined the Carbohydrate Group at the Spanish Research Council (CSIC) in Seville where he is now a permanent research scientist. In 2001 he was awarded a "Ramón y Cajal" fellowship. His research interests include supramolecular chemistry and molecular recognition of carbohydrates.



Mario Ruben studied Chemistry in Germany and Spain. He obtained his PhD in 1998 at the University of Jena, Germany, under the supervision of Prof. D. Walther. A DAAD postdoctoral fellowship brought him to Prof. J.-M. Lehn's research group at the ISIS-ULP in Strasbourg, France, where he worked on supramolecular coordination compounds. Since 2001 he is a group leader at the Institute of Nanotechnology, Karlsruhe. His research interests involve functional molecule-based systems and their implementation into operational nanosystems. He is the coordinator of several European networks (FUN-SMARTs; BIOMACH) dealing with molecular nanodevices.



Lindsay Uppadine obtained an M.Chem. degree from the University of Oxford in 1997. She stayed at Oxford for her doctoral research in the group of Prof. P. D. Beer, where she worked in the field of anion and ion pair recognition. She is currently a CNRS Postdoctoral Fellow in Prof. J.-M. Lehn's research group at the Université Louis Pasteur, Strasbourg.

 © 2004 Wiley-VCH Verlag GmbH & Co. KGaA, Weinheim

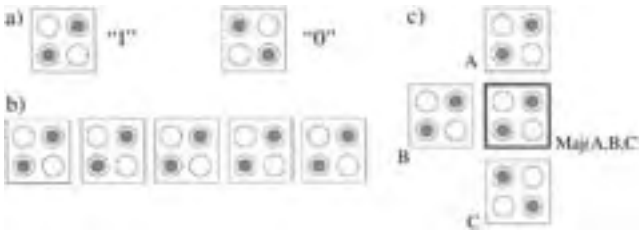


Figure 3. Schematic representation and working principle of "cellular automata". a) Coulomb repulsion keeps the electron density (dark) at antipodal sites resulting in the degenerate "1" and "0" state. b) A wire of "cellular automata" can be formed by a one-dimensional arrangement of cells. The intercellular Coulomb interactions force all units into the same state. c) Working principle of a majority logic gate consisting of three inputs (A, B, C) which converge to an output (Maj(A;B;C;)).[8]

2. General Concepts

Metallosupramolecular chemistry is an actively pursued area of research in supramolecular chemistry, which uses the interaction between organic ligands and metal ions to construct multicomponent and multinuclear coordination entities in the nanometer regime. It thus allows one to combine the properties of metal ions with those of the organic ligands in a defined structure with the potential for the generation of new properties not found in the individual components. A rich variety of metallosupramolecular architectures has been synthesized in the last few years, including helicates, rotaxanes, catenanes, and cages.[10]

The design of gridlike metal ion arrays rests on the directing coordination instructions, which are based on the coordination geometry of the metal ion and the structure of the ligand's coordination sites. It requires perpendicular arrangements of the ligand planes at each metal center. Given such a coordination environment around the metal centers, the linear and rigid extension of the ligand system from mono- to multitopicity will automatically lead to a gridlike two-dimensional coordination network with regularly arrayed metal ions. According to this general "leitmotif", metal ion arrays can be prepared in principle by careful prearrangement of the subunits using any set of metal ions and organic ligands possessing compatible coordination features. This requires ligands containing either bidentate or tridentate binding subunits in combination with metal ions possessing tetrahedral or octahedral (and in some cases bipyramidal) coordination geometry, respectively (Figure 4).

Two-dimensional gridlike coordination complexes lead to a well-defined 2D arrangement of an exact number of metal ions. A number of square $[n \times n]$ and rectangular $[n \times m]$ grids with $n,m \leq 4$ has been obtained for metal ions with tetrahedral as well as octahedral (and sometimes square-bipyramidal) coordination geometry (vide infra). Thus, a ligand with n coordination subunits is capable of forming a homoleptic $[n \times n]$ metalloarray, composed of $2n$ organic ligands and n^2 metal ions with an overall $[M_{(n^2)}L_{(2n)}]$ stoichiometry.[11] Mixtures of different ligands containing unequal numbers of coordination subunits n and m may, in addition to square arrays, yield

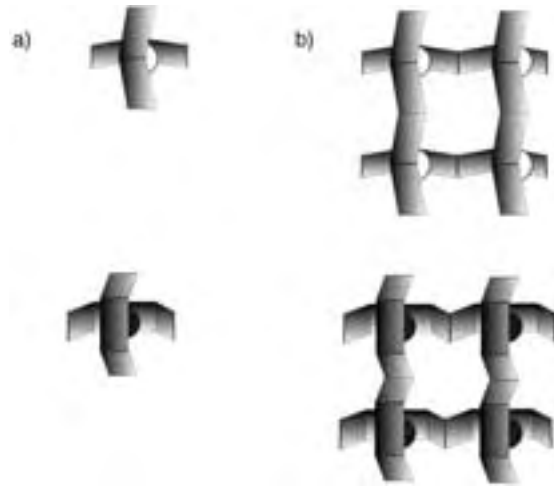


Figure 4. General principles and building blocks for perpendicular arrangement of the ligand L about a metal center M. a) $[M(L)_2]$ units are formed with monotopic ligands ($n=1$); b) gridlike metal ion arrays $[M_4(L)_4]$ are formed with multitopic ligands (here $n=2$). Coordination geometry of the metal ions: ○ tetrahedral, ● octahedral.

rectangular structures $[M_{(n\times m)}L_{(n+m)}]$ with a total of $(n + m)$ organic ligands and $(n \times m)$ metal ions. In incomplete gridlike coordination compounds, the available coordination sites are not fully occupied thus generating several *(p)* subsets of $[n \times n]$ or $[n \times m]$ arrays within the same coordination compound (Figure 5).

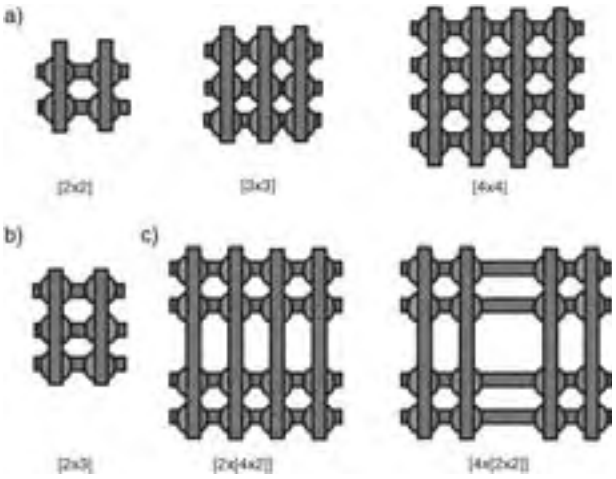


Figure 5. Different types of grid-type metal ion arrays: a) squares $[n \times n]$, b) rectangles $[n \times m]$, and c) incomplete architectures $[p \times [n \times m]]$.

In designing such metal ion arrays, the choice of organic ligands follows the coordination chemistry of the metal ions to be incorporated. In most cases, the coordination number of the metal ion is 4 or 6, with tetrahedral or octahedral coordination geometries. Appropriate design of the systems requires the choice of a ligand that presents an adequate number of binding sites in the coordination subunit to satisfy the coordination sphere of the metal ion. Most of the ligands used for the construction of grids, so far, are listed in Figure 6.

 © 2004 Wiley-VCH Verlag GmbH & Co. KGaA, Weinheim

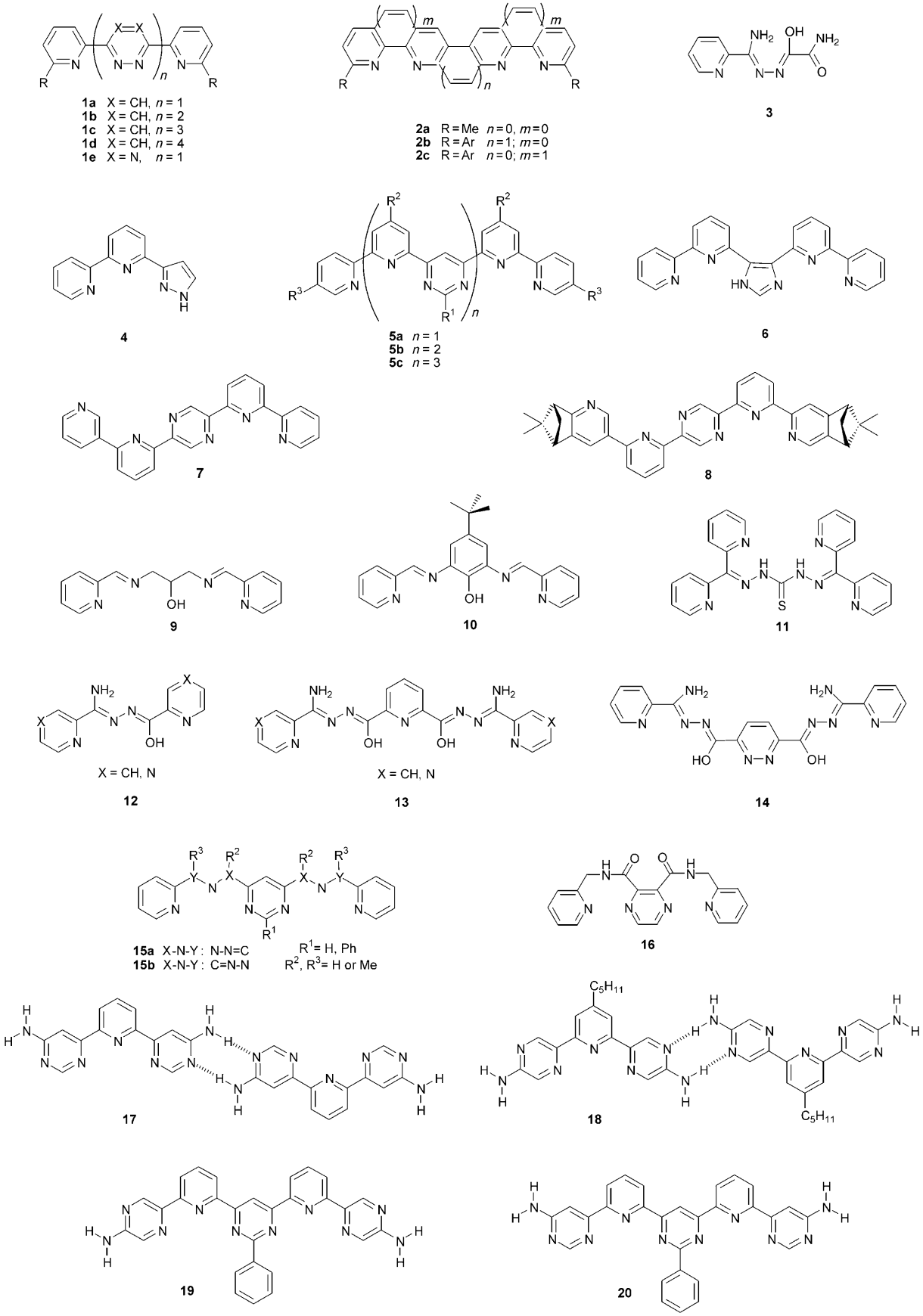


Figure 6. Ligands **1**–**20** employed in the self-assembly of gridlike metal ion arrays.

 © 2004 Wiley-VCH Verlag GmbH & Co. KGaA, Weinheim

Those based on nitrogen donor ligands (such as bipyridine or terpyridine) are the most common, but ligands with sulfur- and oxo-bridging subunits have also been used.

Although some early examples can be identified,[12] grid-type architectures have only recently experienced active and coherent development and are mainly based on tetrahedrally and octahedrally coordinated metal complexes of azaaromatic ligands containing bidentate or tridentate subunits.[4–6, 13–26a]

In general, the matching information encoded in both the metal ions (nature, number, and disposition of electronic orbitals, charge, etc.) and in the organic ligands (number and nature of the donor atoms and the geometrical disposition, molecular conformations, rigidity, etc.) is interpreted during the self-assembly process and steers it to a mutually acceptable 2D architecture. All ligands shown in Figure 6 are chelating ligands, as their increased preorganization and stronger binding may result in cooperative effects during the self-assembly process. Furthermore, all these ligands contain rigid aromatic ring systems (mostly pyridine groups), which yield kinetically labile intermediates as well as thermodynamically stable end products with many M^{I}, M^{II}, and some M^{III} ions. The rigidity of these aromatic ring systems and their ability to participate in π–π interactions are further stabilizing factors for the gridlike array formation.

Energetically, the formation of the grid-motif competes with the generation of other types of structures (e.g. finite and infinite coordination oligo- and polymers). The defined gridlike array is favored enthalpically, since it maximizes the coordination site occupancy, as well as entropically, giving rise to the largest number of discrete entities. Furthermore, intercomponent interactions (π–π stacking, H-bonding) may contribute to achieving the correct alignment of all bricks.

Thus, the generation of grid-type arrays depends on three factors, which influence the self-assembly of metallosupramolecular architectures in general: 1) a robust set of coordination instructions that impose the correct (perpendicular) geometry and drive the process on the basis of the principle of maximal, optimally full, binding site occupancy;[27] 2) internal orienting effects, such as steric factors that hinder the formation of undesired entities, or stabilizing interactions (e.g. stacking) that channel the assembly to the desired product; 3) external factors such as binding of solvent molecule(s), counterion(s), or other species present in the environment. In addition to the energetic parameters, entropy favors the formation of the largest number of products.

These different factors promote the formation of the discrete, "closed" grid architectures over polymetallic entities, which might in principle also form. In addition to entropy considerations, such polymers are disfavored energetically by the remaining free sites at the ends ("sticky ends") of the polymer chains, as well as by the marked steric crowding that would occur between ligands bound to vicinal sites.

In addition to the assembly parameters mentioned so far, ligand substitutions provide the opportunity to fine-tune inherent functional properties (e.g. electronic, optical, magnetic, etc.). It is also possible to introduce a second coordination site on the ligand backbone, to enable multistep hierarchical organization of the self-assembly process.

It is crucial to note that the binding of metal ions to polyazaheterocyclic ligands involves major structural and energetical changes. Indeed, α,α′-connected aromatic azaheterocycles present a *transoid* orientation of the nitrogen sites around the C(α)–C(α′) bond, which is more favorable than the *cisoid* orientation required for metal ion coordination by about 25–30 kJ mol^{-1}.[26b] This feature has been implemented for designing heterocyclic "folding codons", in particular "helicity codons" that determine the shape of molecular strands.[26c] Thus, the free uncoordinated ligands based on α,α′-linked bipyridine or terpyridine moieties adopt a *transoid* conformation of the nitrogen atoms relative to the interheterocyclic C–C bond. The conversion of the all-*transoid* conformer into the energetically disfavored all-*cisoid* one upon metal complexation occurs at the cost of large amounts of conformational energy, which must be overcompensated by the interaction energy resulting from metal ion binding (Figure 7). For example, the change from an all-*transoid* to an all-*cisoid* form of the bis(terpyridine) ligand **5a** costs about 100 kJ mol^{-1} per ligand (i.e. 400 kJ mol^{-1} in total on formation of the corresponding [2×2] M_4 grid complex), and energy costs in excess of 1500 kJ mol^{-1} are attained on the self-assembly of the [4×4] Pb^{II}_{16} grid (see Section 3.3)!

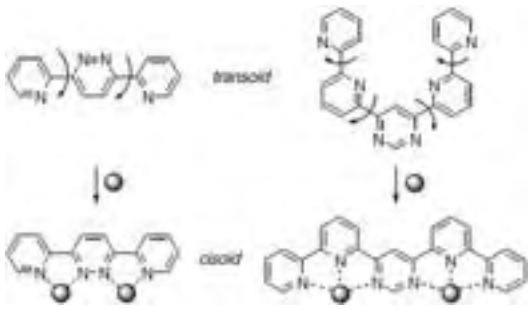


Figure 7. For the complete complexation, all binding sites of polyazaheterocyclic ligands must be present in the *cisoid* conformation. The required change in ligand conformation from all-*transoid* (uncoordinated ligand) to all-*cisoid* (coordinated ligand) is shown, for example, for the ligands **1a** (left) and **5a** (right).

In conclusion, the formation of gridlike architectures involves a subtle interplay of steric, enthalpic, and entropic effects, concerning both the ligand and the metal binding features. Thus, different metal ions and ligands can lead to the formation of different supramolecular coordination entities and self-assembly may result in several stable products partitioned under thermodynamic equilibrium. Only carefully designed systems of appropriate ligands and metal ions will lead to the self-assembly of gridlike metal ion arrays in a "programmed" fashion.

3. Grid-Type Metal Ion Arrays

3.1. [2×2] Metal Ion Arrays

The first report on the formation of [2×2] metal ion arrays based on tetrahedral coordination geometry involved

 © 2004 Wiley-VCH Verlag GmbH & Co. KGaA, Weinheim

four *ditopic* ligands **1a** of the bis(pyridyl)pyridazine type arranged around four metal ions.[13a] Both Cu_4^I and Ag_4^I ion arrays (Figure 8) assemble spontaneously when the metal and ligand components are mixed in a 1:1 stoichiometry.[13]

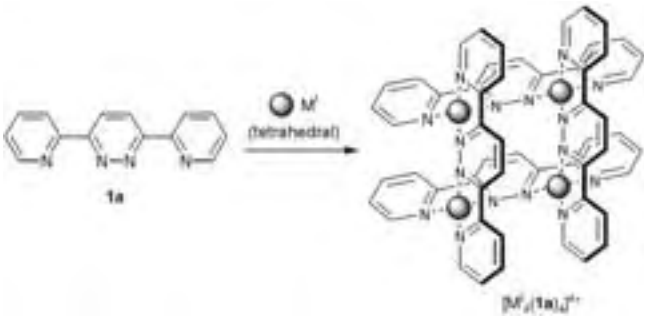


Figure 8. Schematic representation of the self-assembly process of ligand **1a** and tetrahedrally coordinating metal ions ($M = Ag^I$, Cu^I) leading to a [2×2] grid-type metalloarray $[M_4^I(\mathbf{1a})_4]^{4+}$.

The X-ray structure analysis of the $[Cu_4^I(\mathbf{1a})_4]^{4+}$ complex reveals a distorted rhombus with an almost planar arrangement of the metal ions in a distorted tetrahedral environment. The average Cu^I–N and Ag^I–N distances are about 2.0 and 2.3 Å, respectively, while the Cu^I–Cu^I distance is 3.57 Å and the Cu^I-Cu^I-Cu^I angles are approximately 79° and 101°.

An unusual self-assembled [2×2] metal ion array deviating from the general M_4L_4 stoichiometry was obtained by using the bis(phenanthroline)-based ligand **2c** and Cu^I ions. In addition to the expected $[Cu_4^I(\mathbf{2c})_4]^{4+}$ scaffold, two additional, uncoordinated "guest" ligands **2c** were sandwiched in the upper and in the lower groove of the complex by multiple C-H-N and π–π interactions.[14]

A [2×2] $Cu_4^{II}L_4$ metal ion array was obtained with the flexible ligand **3**; the two different ligand moieties are twisted by almost exactly 90° thus arranging the metal ions in a square-like fashion.[15]

Ligand systems containing terpyridine-like coordination sites enable the arrangement of octahedrally coordinating metal ions: a number of late first- and second-row transition metal ions (e.g. Mn^{II}, Co^{II}, Fe^{II}, Ni^{II}, Cu^{II}, Zn^{II}, Cd^{II}) as well as some main group metal ions (e.g. Pb^{II}) have been introduced into gridlike arrays.[4,6,16–17,24] The range of transition metals that can coordinate to ligand systems such as **5a** gives access to a wide variety of optical, electrochemical, photophysical, and magnetic properties. Furthermore, by using ligand system **5a**, these properties can be tuned by the choice of the different substituents R^1, R^2, and R^3 (Figure 9).

Ligand **5a** yields gridlike arrays of the metal ions with inter-metal distances of 6.0–6.5 Å between neighboring ions. The exchange of the central μ-pyrimidine group for an imidazole (**4**) or a pyrazole bridge (**6**) leads to only slightly shortened ion–ion distances.[18,19] However, the use of oxo- and sulfur-bridged ligands **9**–**12** (after deprotonation) resulted in more closely spaced metal ions with intermetallic distances of between 4.0 and 4.6 Å[20–22] (e.g. 4.04 Å in the phenoxo-bridged metalloarray $[Cu_4^{II}(\mathbf{10})_4]^{4+}$).

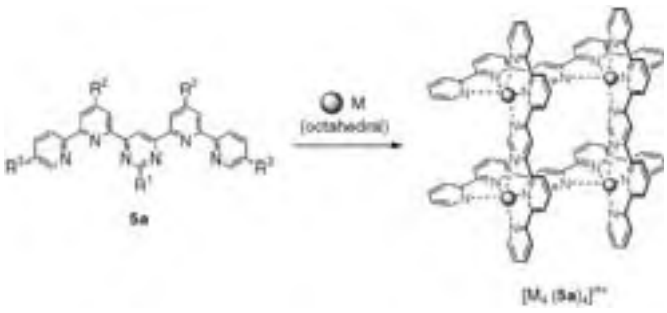


Figure 9. Schematic representation of the self-assembly of a [2×2] metal ion array from bis(terpyridine) ligands **5a** and octahedrally coordinating metal ions.

Ligand systems **15**[23] and **16** bearing acidic protons open the way to ionizable [2×2] arrays, whose self-assembly and properties can be influenced by the protonation state of the ligand (see Section 5.1.1 and 5.1.4).[24,25]

X-ray structure analyses show that anions can be located within the central cage of the [2×2] architecture, although this is not a prerequisite for the stability of the gridlike structure. On the other hand, a direct coordinative involvement of the anions was found in the [2×2] array $[Pb_4^{II}(\mathbf{5a})_4]^{8+}$, where a triflate anion is directly coordinated to each Pb^{II} center to fulfill the coordinative requirements of the large Pb^{II} ion.[17]

The controlled introduction of different metal ions at specific locations in a grid array is of great interest, because of the cross-over properties which may result from the presence of different metal ions in the same entity. Mixed ion [2×2] grid structures were obtained by a sequential synthesis protocol involving stereochemical features, for example, homochiral assembly of the intermediate *R* or *S* "corner" type intermediates (Figure 10). This self-assembly reaction is reminiscent of the "Coupe de Roi", in which an achiral object is divided into two identical homochiral components.[26a]

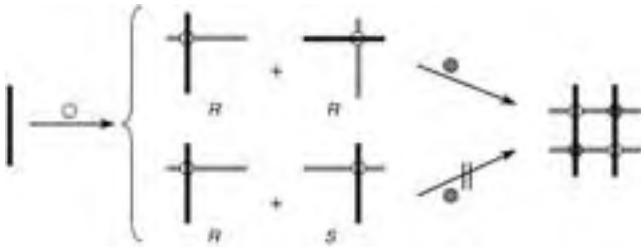


Figure 10. Self-assembly of a chiral heterobimetallic [2×2] grid from two cornerlike homochiral precursors (*R* + *R*) or (*S* + *S*).[26a] The resulting grid is achiral in the homometallic case ("Coupe de Roi" process) and chiral in the heterobimetallic case.

A [2×2] grid-type structure with two pairs of unlike metal ions may exist as either the *anti* or *syn* topoisomer. It is not possible to select a priori which form is generated by simply mixing together the components; however, the *anti* topoisomer, with diagonally located identical ions, can be obtained selectively from a precursor complex consisting of

 © 2004 Wiley-VCH Verlag GmbH & Co. KGaA, Weinheim

two terpyridine-type ligands (e.g. **5a**) and a strongly coordinating metal ion such as Ru^{II} or Os^{II} (to give for example $[M^{II}(\mathbf{5a})_2]$). They contain two vacant sites, which combine with a second metal ion M'^{II} of lower coordinative binding strength to yield a heterometallic $[2\times2]$ complex as the thermodynamic product. The combination of homochiral fragments leads to a C_2-symmetric array (e.g. $[M^{II}_2M'^{II}_2(\mathbf{5a})_4]$) in a process displaying spontaneous chiral discrimination.

Such a methodology represents sequential self-assembly and introduces different metal ions in order of increasing coordinative lability. Thus, a system containing three different metal ions was isolated from an equimolar mixture of Ru^{II} and Os^{II} "cornerlike" fragments $[Ru^{II}(\mathbf{5a})_2]$ and $[Os^{II}(\mathbf{5a})_2]$ in the presence of Fe^{II} ions.[26a]

An even more sophisticated, three-tiered synthesis, incorporating regioselective, redox, and chiroselective features, was used to construct $[Co^{III}_2M^{II}_2(\mathbf{15a})_4]$ grid-type arrays (M^{II} = Co^{II}, Zn^{II}, Fe^{II}) based on the bis(hydrazone) ligand-type **15a** (R^2 = H and Me, $R^2_{left} \neq R^2_{right}$) containing both ionizable and nonionizable compartments.[24b] As a consequence, the oxidation state of cobalt could be modified according to the charge on the hydrazone moiety.

The first stereoselective synthesis of a $[2\times2]$ metal ion array was achieved by using the chiral ligand system **8**. The "chiralization" of the parent ligand **7** was carried out by the introduction of pinene moieties, which gives access to both ligand diastereomers of **8** (only one is shown in Figure 6). The reaction of **8** with Zn^{II} ions delivers the tetranuclear (all-Δ)$[Zn_4((R,R)\text{-}\mathbf{8})_4]^{8+}$ metal ion array as the major product in good diastereomeric excess.[28]

3.2. [3×3] Metal Ion Arrays

The first $[3\times3]$ M_9 grid, $[Ag^{I}_9(\mathbf{1b})_6](OTf)_9$, was obtained in high yield by self-assembly of six equivalents of the tritopic ligand **1b** with nine equivalents of silver(I) ions.[29] Because of the deviation of the coordinated ligand planes from the ideal $\gamma = 90°$, the resulting $[3\times3]$ Ag^{I}_9 array forms a trapezoid with corners (angle Ag-Ag-Ag) of about 73° and 107°.

The self-assembly of ligand system **5b** with octahedrally coordinating metal ions gave mainly incomplete metal ion arrays (see Section 3.5).[30a] Some evidence for $[3\times3]$ gridlike species was only obtained by electroscpray mass spectrometry in solution for the very large metal ions such as Pb^{II} or Hg^{II}.[30b] The behavior of **5b** may be ascribed to ligand bending due to the pinching of the binding subunit on coordination of transition-metal ions.[30c] Conversely, large metal ions such as Pb^{II} or Hg^{II} cause less pinching so that the ligand is less distorted from a linear arrangement, resulting in a less strained grid architecture.

The aromatic polytopic ligands **13** readily self-assemble with Mn^{II}, Cu^{II}, and Zn^{II} salts to produce nonanuclear $[3\times3]$ gridlike metal ion structures, in which the ligands are arranged in parallel sets and alkoxide bridging groups are located between adjacent metal ions. Spectroscopic and other evidence indicate that similar metalloarrays are produced with Ni^{II}, Co^{II}, and Fe^{III} ions, but not with Pb^{II} ions.[5,21] The cationic structures consist of a homoleptic $[M_9(\mathbf{13})_6]^{n+}$ complex in a roughly planar square array with metal–metal distances of about 4.0–4.3 Å (Figure 11).

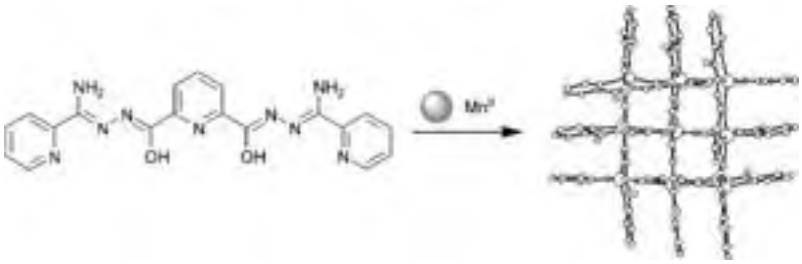


Figure 11. Self-assembly of the $[3\times3]$ metal ion array $[Mn^{II}_9(\mathbf{13})_6]^{6+}$, the molecular structure of which is depicted on the right.[5a]

3.3. [4×4] Metal Ion Arrays

The largest square grid reported to date, $[Pb^{II}_{16}(\mathbf{5c})_8](OTf)_{32}$, is formed quantitatively from eight equivalents of the tetratopic tridentate ligand **5c** and sixteen equivalents of Pb^{II} ions.[17] This remarkable species arises from the self-organization of 24 precursors and involves the formation of 96 coordination bonds. This example highlights the power of metallosupramolecular chemistry to create complex structures through self-assembly in a single operation.[6]

The final composition of the $[4\times4]$ Pb_{16} array consists of 8 molecules of ligand **5c**, 16 lead(II) ions, 16 triflate ions, and 8 coordinated water molecules; 16 further triflate ions and 1 molecule of water are located in close proximity. The eight ligands **5c** are arranged into two perpendicularly disposed sets of four outer and four inner ligands, resulting in a set of four $[2\times2]$ subgrids rather than a regular $[4\times4]$ grid (Figure 12).

The four inner ligands allow considerable overlap between the aromatic groups situated in a face-to-face stacking arrangement, with an average π–π stacking distance of 3.62 Å corresponding to the van der Waals contacts. The Pb^{II} ions form a saddle arrangement with an average Pb···Pb distance of 6.3 Å and average inner angles of 89.5°. The coordination polyhedron around the Pb^{II} ions reveals a hemidirected structure, and all of them present a distorted seven-, eight- or nine-coordinate geometry. The open faces of the metal ions are oriented towards the interior of the four $[2\times2]$ Pb^{II}_4 grid subsets and are occupied by one or two of the 16 internally coordinated triflate ions. Some of the internal triflate ions act as bridges between two adjacent Pb^{II} ions. Thus, each square of four Pb^{II} ions is linked on three sides by bridging triflate ions, whereby the remaining coordination sites at the Pb^{II} ions are filled with nonbridging triflate ions or water molecules.

 © 2004 Wiley-VCH Verlag GmbH & Co. KGaA, Weinheim

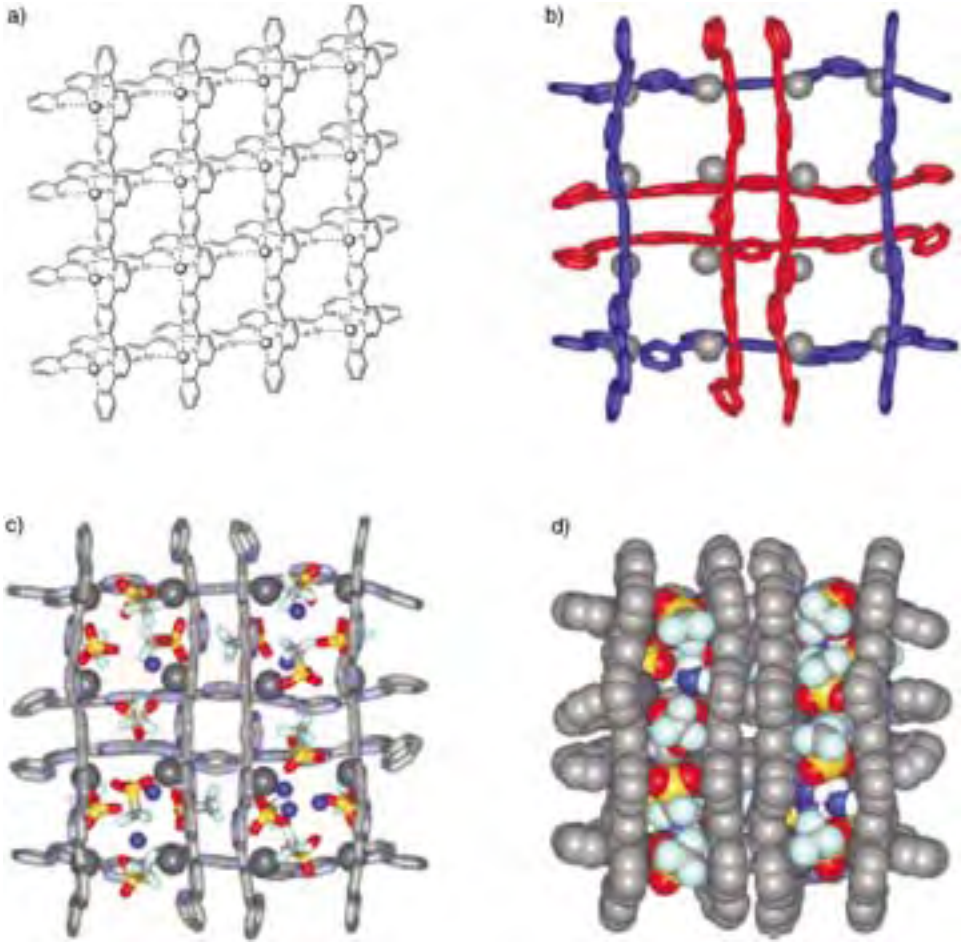


Figure 12. A [4×4] grid assembled from eight tetratopic ligands **5c** and sixteen Pb^{II} ions: structure (a) and ball-and-stick model (b) of the $[Pb^{II}_{16}(\mathbf{5c})_8]$ framework. The framework with coordinated triflate anions and water molecules as ball-and-stick model (c) and as space-filling model (d).[6]

3.4. Rectangular [n×m] Metal Ion Arrays with (n≠m)

The construction of a rectangular grid involves the self-assembly of two ligands with a different number of coordination sites. In this case, however, the reactions with different ligands could lead to mixed homo- and heteroleptic products, as described, for example, for the reaction of the di- and tritopic ligands **1a** and **1b**, respectively, and $AgCF_3SO_4$.[31a] When a 3:2:6 stoichiometric ratio of these components was used, a [2×3] grid was obtained as major compound (90%) in nitromethane solution, together with minor amounts of a [2×2] and a [3×3] grid (8% and 2%, respectively; Figure 13).

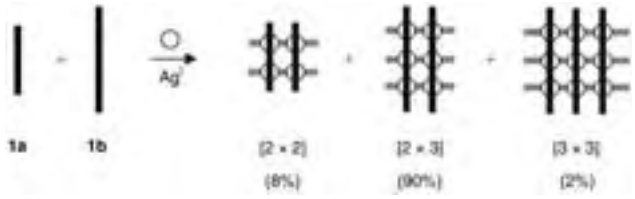


Figure 13. Synthesis of a [2×3] array from three ditopic ligands **1a**, two tritopic ligands **1b**, and six Ag^I metal ions.[31]

This preferential assembly could be due to the lower stability of the metal–ligand coordination bonds at the central coordination site of the [3×3] grid as well as from solvation and thermodynamic parameters. In the [2×3] grid structure, the silver ions are arranged on a [2×3] rhombohedrally distorted rectangular matrix with an average Ag–Ag distance of 3.75 Å.[31]

Rectangular [2×2] M^{II} arrays can be also obtained where ligands of type **12** (see Figure 6) coordinate in different conformations with different bridging groups.[21a,31b,32]

3.5. Incomplete Metal Ion Arrays [p×[n×m]]

The self-assembly of the pentatopic ligand **1d** with Ag^I ions, aimed at constructing a [5×5] grid, ultimately led to the formation of two isolable polynuclear architectures: an incomplete grid-type species (Figure 14) and a quadruple-helicate, which crystallize side-by-side from an equilibrating mixture of the complexes in solution.[33] Twisting around the central bond in the set of five parallel ligands releases a significant amount of strain so that a [2×[2×5]] species is generated rather than the complete [5×5] grid.

 © 2004 Wiley-VCH Verlag GmbH & Co. KGaA, Weinheim

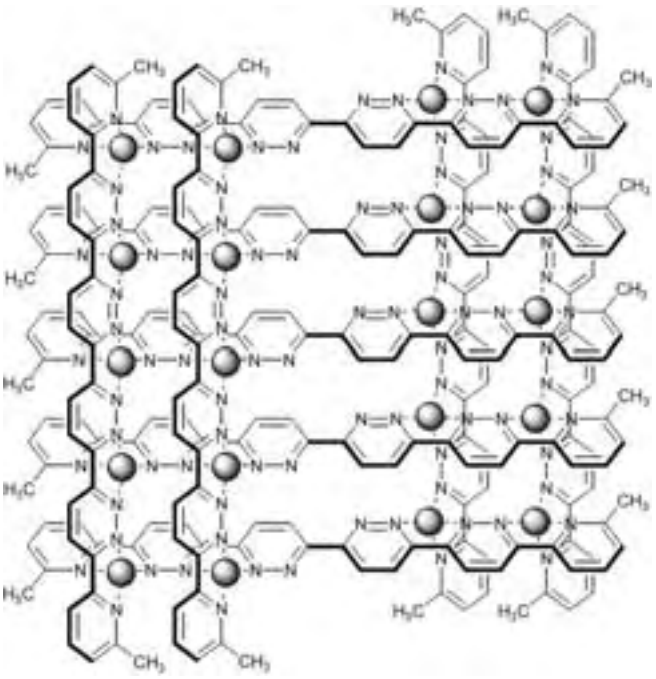


Figure 14. The $[2\times[2\times5]]$ Ag^{I}_{20} grid assembled from nine pentatopic ligands **1d** and twenty Ag^{I} ions.[33]

The X-ray structure analysis of the icosanuclear complex $[Ag^{I}_{20}(\mathbf{1d})_9]^{20+}$ reveals two $[2\times5]$ Ag^{I}_{10} rectangular subgrids located on opposite sides of an array of parallel ligands twisted into a *transoid* conformation across the central pyridazine–pyridazine bond, one above and one below the mean plane through the 20 Ag^{I} ions. This arrangement may be described as a "grid-of-grids" $[2\times[2\times5]]$ with a distorted rhombohedral geometry of 23.3×23.3 Å, where within each column the average Ag^{I}–Ag^{I} separation is 3.73 Å along each ligand and 3.93 Å between the inner Ag^{I} ion of each $[2\times5]$ column.[33]

Attempted construction of $[3\times3]$ grid-type architectures with bis(terpyridine)-type ligands **5c** revealed that in most cases only a $[2\times3]$ complex comprising five ligands and six metal ions could be obtained (Figure 15).[30a] In these $[2\times3]$ structures, all sites are occupied by metals except for a vacant central row. Although some evidence for the formation of $[3\times3]$ grid-type complexes could be obtained for large metal ions, such as Hg^{II} and Pb^{II}, the enhanced ligand distortion for metal ions with smaller ionic radii becomes a decisive factor in determining the thermodynamically most stable complex, which in this case is the intermediate $[2\times3]$ grid-type structure with only a few of the central binding sites occupied. Thus, the predominant self-assembly of $[2\times3]$ architectures is a deviation from the "maximum coordination site occupancy" principle and is caused by ligand strain. Often in these cases, various other complexes representing incompletely assembled grids and cyclic structures were detected in lesser amounts.

The X-ray structure analysis of the $[2\times3]$ Co^{II}_6 grid $[Co^{II}_6(\mathbf{5b})_5]^{12+}$ ($R^1=Ph$) consists of five ligands arranged into two sets.[30a] The first set includes three parallel ligands at a distance of 6.7 Å which are twisted into a *transoid* conformation about the two central pyrimidine-pyridine-pyrimidine C–C bonds. The central binding site of each is unoccupied. The second ligand set is composed of two units markedly warped, whose nitrogen atoms are fully coordinated and in a *cisoid* conformation. The Co^{II} ions are arranged into two rows of three ions with a Co–Co separation of 6.5 Å. The distance between two Co^{II} atoms in different rows is 13.8 Å.

A dodecanuclear metal ion array was obtained in the self-assembly of ligand **14** with Cu^{II} ions.[34a] It is based on a $[4\times4]$ grid-motif, with an exclusive occupation of the peripheral coordination sites (leaving the inner four positions empty).

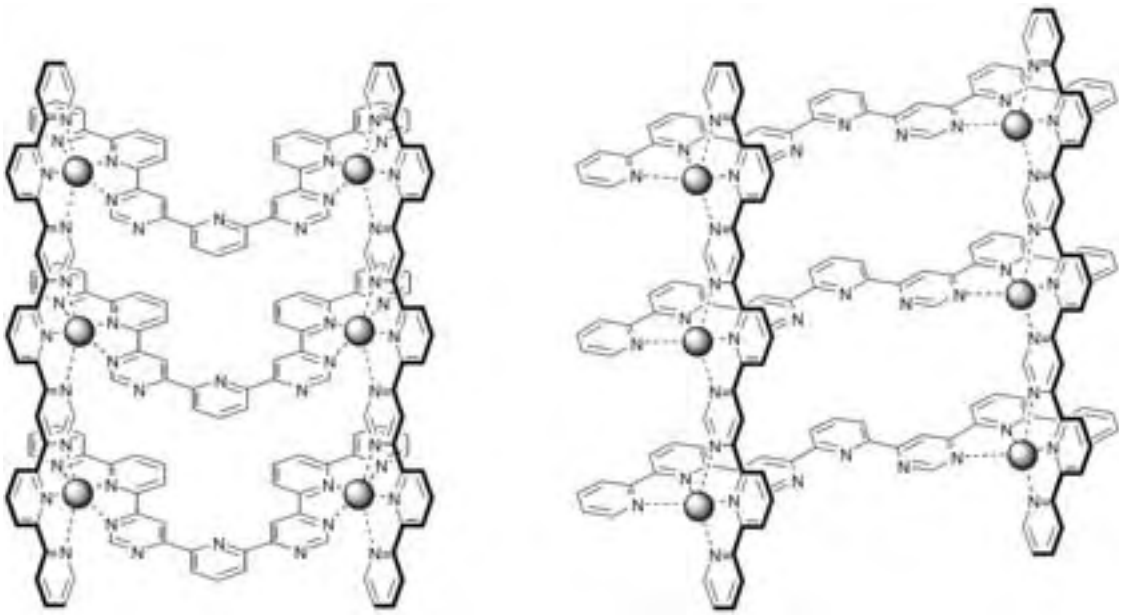


Figure 15. Two structures of the $[2\times3]$ incomplete grid architectures obtained by self-assembly of ligand **5b** and metal ions such as Co^{II}, Zn^{II} or Fe^{II}[30a]

 © 2004 Wiley-VCH Verlag GmbH & Co. KGaA, Weinheim

More recently, the same basic type of ligand system was used to generate a $[4\times[2\times2]]$ Pb^{II}_{16} array.[34b]

4. Mechanistic Features of the Self-Assembly Process

The nature of the emerging species during the self-assembly of the different grid-type complexes has been studied in solution and in the solid-state. A self-assembled collection of species is obtained upon mixing of the bis(bipyridine)-based ligand **2a** and Cu^{I} ions. Detailed analysis of the resulting equilibrium mixture indicated the presence of three major species: a double-helical architecture, a triangular complex, and square $[2\times2]$ grid complexes (Figure 16). These represent the output of a dynamic combinatorial library of supramolecular components, from which the double-helical complex could be trapped by crystallization.[35] Very similar observations were made for ligand systems **7** with Zn^{II} ions, which yielded an equilibrium mixture of triangular and tetranuclear reaction products.[28]

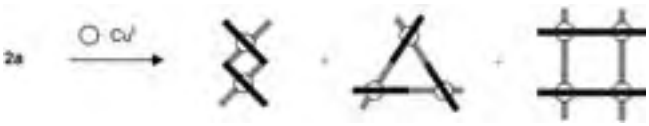


Figure 16. Self-assembly of an equilibrating mixture of the double-helical, triangular, and square $[2\times2]$ grid complexes from **2a** and Cu^{I} ions. Gray bars correspond to ligands located on the underside.[35]

The formation pathway of the $[3\times3]$ $[Ag^{I}_{9}(\mathbf{1b})_6]^{9+}$ metal ion array has been extensively studied by NMR spectroscopy.[36] This self-assembly process involves several intermediates, which are generated at different metal/ligand stoichiometries. A mixture of several unidentified species is observed at low $Ag^{I}/(\mathbf{1b})$ ratios until $Ag^{I}/(\mathbf{1b})\approx1{:}1$ is reached, when two complexes of $[Ag^{I}_{n}(\mathbf{1b})_n]^{n+}$ type are mainly present. They are characterized by an intertwined structure and a *transoid* arrangement of ligands. At $Ag^{I}/(\mathbf{1b})\approx6{:}5$ a species $[Ag^{I}_{6}(\mathbf{1b})_5]$ has been identified which has three ligands in *transoid* form and two ligands in the all-*cisoid* form. Further addition of Ag^{I} ions leads to the conversion of this intermediate into the final $[Ag^{I}_{9}(\mathbf{1b})_6]^{9+}$ grid presumably through a $[Ag^{I}_{6}(\mathbf{1b})_5]^{6+}$ entity with all five ligands in the all-*cisoid* form. These observations imply an overall positive cooperativity and a robust structure for the final $[3\times3]$ $[Ag^{I}_{9}(\mathbf{1b})_6]^{9+}$ complex (Figure 17).

The templating effect of certain anions upon the construction of metallosupramolecular nanostructures was clearly recognized for circular helicates and results from the operation of dynamic combinatorial diversity.[37] The self-assembly of Ni^{II} or Zn^{II} ions with ligand **1e** in the presence of

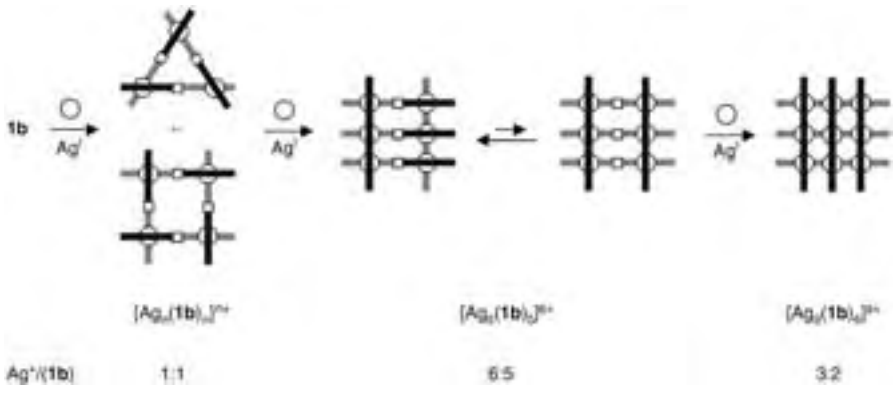


Figure 17. Self-assembly pathway for the $[3\times3]$ array $[Ag_9(\mathbf{1b})_6]^{9+}$. The uncomplexed bipyridine-type sites are noted by an open square; they are expected to adopt the more stable *transoid* arrangement.[36]

BF_4^- or ClO_4^- ions leads to the formation of the $[2\times2]$ grid complexes (Figure 18).[38] The metal ions have octahedral coordination geometry, with four of the coordination sites occupied by two ligands and the other two positions by acetonitrile and/or water molecules.

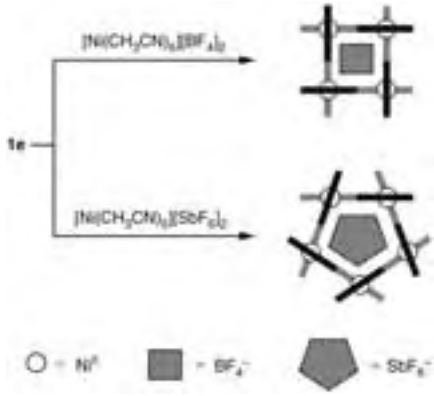


Figure 18. Templating effect of the anions BF_4^- and SbF_6^- on the formation of metallosupramolecular nanoarchitectures with the ligand **1e**.

An anion is encapsulated within the cavity of these grids. Moreover, the ligands are disposed in an interwoven manner, giving rise to a chiral grid which could be spontaneously resolved as chiral crystals.[38b] However, the self-assembly of the same ligand with Ni^{II} ions in the presence of a larger counterion such as SbF_6^- resulted in the formation of a molecular pentagon consisting of five ligands and five Ni^{II} ions (Figure 18).[39]

As it has been stressed earlier, correct self-assembly implements both maximal site occupation and pathway selection (or orientation) by the introduction of appropriate substitution. The nature of the solvent and the concentration of reagents may also affect the output of the self-assembly process. For example, ligand **2a** (R = H) in the presence of Cu^{II} ions in a 1:1 ratio in acetonitrile gives equilibrating mixtures of a $[2\times2]$ grid and a hexagonal architecture

 © 2004 Wiley-VCH Verlag GmbH & Co. KGaA, Weinheim

(Figure 19).[40] At increased concentrations in acetonitrile, the relative amount of hexamer increases. Its crystal structure revealed the presence of acetonitrile molecules and hydroxo groups bound to the Cu^{II} centers, which are therefore five-coordinate. On the other hand, only the [2 × 2] metal ion array could be detected in nitromethane. Replacement of nitromethane by acetonitrile and vice versa indicated the reversible switching between a solution containing either the grid alone or an equilibrating mixture of the grid and the hexameric ring. This process displays three remarkable features: 1) self-assembly with substrate binding, 2) dynamic combinatorial structure generation, and 3) environment-sensitive behavior resulting in a process of adaptive self-assembly.[40]

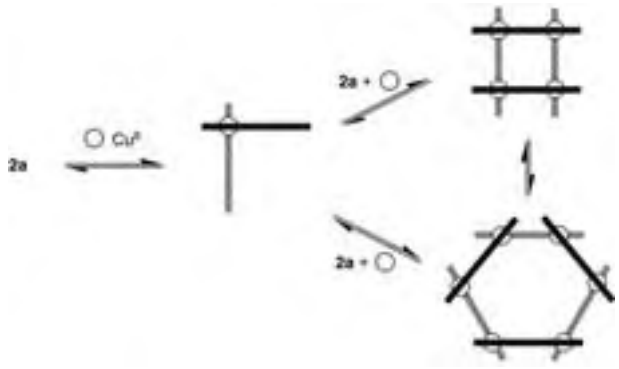


Figure 19. Adaptive self-assembly of the [2 × 2] grid $[Cu^{II}_4(\mathbf{2a})_4]^{8+}$ and the hexameric cyclic complex $[Cu^{II}_6(\mathbf{2a})_6]^{12+}$ from ditopic ligand **2a** (R = H) and Cu^{II} ions. The products exist in a solvent-dependent equilibrium.[40]

On the basis of the results obtained for many different grid self-assembly experiments, it can be stated that $[n \times n]$ grid-type complexes of high nuclearity may be disfavored by: 1) the imposition of a *cisoid* conformation for all ligands; 2) the bent, domelike shape in two perpendicular directions ("pinching-in") of the ligand; and 3) the presence of central metal ion coordination sites containing poorer donor atoms. On the other hand, they are favored by: 1) the trend towards establishing the highest number of coordination interactions and therefore towards maximum site occupancy; 2) maximization of stabilizing π–π contacts between ligands, and 3) the interaction with included anions or guest molecules. Thus, a subtle interplay between metal coordination, strain, and steric demand of the ligands as well as external factors, reaction conditions, and the nature of the counterions determines the product of the self-assembly.

5. Multistability and Addressability

High density information storage and informatics on the nanoscale may take advantage of a designed exploitation of intrinsic functional molecular properties and their modifications, such as size, multiplicity, and heteronuclearity as well as different redox, magnetic, or spin states. Planar multicenter transition-metal complexes appear to be very attractive candidates for the design of multilevel information storage devices, because they could fulfill intrinsically two important prerequisites for nanoscale memory devices: 1) multistability and 2) addressability.

5.1. Multistability

5.1.1. Redox States

The first report on the electrochemical properties of a [2 × 2] gridlike complex concerned the copper(I) complex $[Cu_4(\mathbf{1a})_4](BF_4)_4$, which exhibits seven reversible single-electron reduction waves.[13a] The electrochemical behavior of a family of tetranuclear gridlike oligopyridine complexes of the general formula $[M^{II}_4(\mathbf{5a})_4]^{8+}$ displays well-resolved multiple one-electron reductions in all complexes investigated.[41] Furthermore, the introduction of electron-donating or -attracting groups into the ligands tunes systematically the potential of the first reduction. As a consequence, one Co^{II}_4 member of this family exhibits up to twelve well-resolved reversible one-electron processes at room temperature, which appears to be the most extended redox series known for well-characterized molecular compounds.[41]

The rather low values of the redox potentials are of importance for the stability of the multielectron species generated and thus for their possible applications as devices presenting multiple electronic levels. Spectroelectrochemical experiments revealed that the reductions take place on the coordinated ligands in all cases; no reduction of the metal centers was observed in the accessible potential range. Interestingly, the Co^{II}_4 species exhibited an amazing regularity in the disposition of the reduction waves, as well as a remarkable stability and reversibility towards reduction (Figure 20). In contrast, analogous Mn^{II}_4 arrays with M^{II} = Fe^{II}, Ru^{II}, Os^{II}, Zn^{II}, and Mn^{II} were found to be more sensitive towards decomposition and to produce more complex reduction schemes. The nature of the M^{II} ions in gridlike complexes plays a very important role for mediating electronic communication within the metalloorganic supramolecular array.[41]

The oxidation of the manganese(II) [3 × 3] array $[Mn_9(\mathbf{13})_6]^{6+}$ was studied by cyclic voltammetry and coulometry.[21b] A series of $Mn^{II} \rightarrow Mn^{III}$ oxidation waves was found,

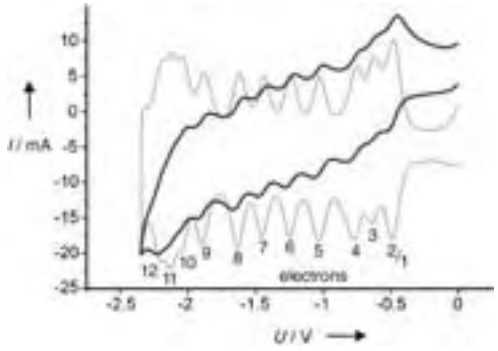


Figure 20. Plot of the sequential 12-electron reduction of the $[Co^{II}_4(\mathbf{5a})_4]^{8+}$ array in dimethylformamide (DMF) at room temperature. Black line: cyclic voltammogram (CV); gray line: deconvolution of the CV; reference: Fc^+/Fc. [41b]

 © 2004 Wiley-VCH Verlag GmbH & Co. KGaA, Weinheim

and the number of electrons per wave gave an insight into the sequence of oxidations in the array (Figure 21). A four-electron oxidation event occurs at +0.61 V, tentatively assigned to simultaneous oxidation at the grid's four equivalent corners. Four additional oxidation waves at +0.92, +1.13, +1.33, and +1.53 V were attributed to the remaining edge-located Mn atoms, but oxidation of the central ion was not observed. Spectroscopic changes were correlated to an increasing proportion of positive charge on the array.

The protonation state of the ligand can also be used to manipulate the electrochemical properties of the gridlike array. For example, protonic modulation of redox properties has been achieved for ionizable [2×2] Co_4^{II} and [2×2] Co_4^{III} grids based on ligand **15a** ($R^2 = H$).[42]

Thus, the [2×2] Co_4^{II} and [3×3] Mn_9^{II} arrays are intriguing electron reservoirs, representing multiredox state electronic systems. Future studies may uncover a system presenting the features required for investigation into nanometric devices used for data representation, and addressable either locally, at a given metal or ligand site, or through the overall redox state (see Figure 21 and ref. [3a]).

5.1.2. Magnetic States

A new type of molecular material has recently emerged based on polynuclear metal complexes called "single-molecule magnets" (SMMs). SMMs possess slowly relaxing magnetic moments, a prerequisite for use in future magnetic information storage devices. This class of molecules exhibits a unique concomitance of both macroscopic (e.g. magnetism) and quantum regime properties (e.g. quantum tunneling) within monodispersed molecular entities.[43]

The principal interest for potential use of SMMs as magnetic memory units arises from their size, undercutting the paramagnetic limit of conventional information storage materials, and from the presence of an energy barrier for the reversal of the direction of the molecular magnetization. The origin of magnetism in the SMMs is the spin(s) on individual metal ions, which couple to give rise to a high-spin ground state. The SMMs have an axial zero-field splitting, which leads to a double well potential with an energy barrier between "spin-up" and "spin-down" states. The final height U of the barrier is determined by $U = |D| S^2$, where D is the zero-field splitting parameter and S the resulting spin quantum number. Consequently, SMMs display hysteresis in their magnetic susceptibility versus external magnetic field loop (so far, only at very low temperature), which might be used in molecular data storage.[44]

In conclusion, to achieve such molecular magnetic data storage, the respective molecule has to possess 1) a high total spin quantum number S and 2) a high Ising-type anisotropy barrier arising from a negative zero-field splitting parameter D. A high spin quantum number S demands intramolecular ferromagnetic coupling of the involved metal ion spins. The commonly found antiferromagnetic coupling "destroys" the spin densities and renders completely antiferromagnetic-coupled molecules useless for magnetic information storage. Usable SMMs exhibiting AF coupling are molecular ferrimagnets, where the overall spin ground state is a result of the noncompensation of spins. A negative zero field splitting parameter D depends on the electronic nature of the metal ions involved (e.g. Mn^{III}) in combination with the low overall symmetry of the molecule.

The first and still most prominent example exhibiting SMM-like behavior was a spin cluster referred to in the literature as "Mn_{12}".[45] Later, other molecular compounds such as "Fe_8", "Fe_{19}", or "Mn_4" joined the SMM family.[46]

The ongoing search for SMMs exhibiting high anisotropy barriers (preferentially above room temperature to overcome the thermal fluctuation) is driving the increasing interest in the magnetic properties of spin bearing metal ion arrays. Thus, the [2×2] Co_4^{II} entity was shown to represent an isolated magnetic domain, a model system for studying magnetic interactions in discrete entities.[47] However, the whole series of [2×2] M_4^{II} ion arrays $[M_4^{II}(\mathbf{5a})_4]^{8+}$ (M = Mn^{II}, Co^{II}, Ni^{II}, and Cu^{II}) exhibited exclusively weak antiferromagnetic intramolecular exchange couplings. Evidently, the μ-pyrimidine unit in ligand **5a** is able to mediate antiferromagnetic but not the necessary ferromagnetic magnetic exchange couplings. The weak magnitude of the coupling parameter J can be attributed to the rather long metal–metal distances of around 6.5 Å.[48] The change to the negatively charged μ-phenoxo bridging group in the [2×2] $[Cu_4^{II}(\mathbf{10}^-)_4]^{4+}$ compound leads to even weaker antiferromagnetic couplings.[20]

Ferromagnetic exchange coupling was found in the μ-alkoxo-bridged $[Cu_4^{II}(\mathbf{12})_4]^{4+}$ grid complex, but only antiferromagnetic couplings were observed for all further spin-bearing ions assembled with the same ligand.[21] Related to this work, the tritopic ligand **13** (X = CH) gave access to a ferromagnetically coupled Cu_8^{II} pin-wheel [2×2] gridlike complex (Figure 22).[49]

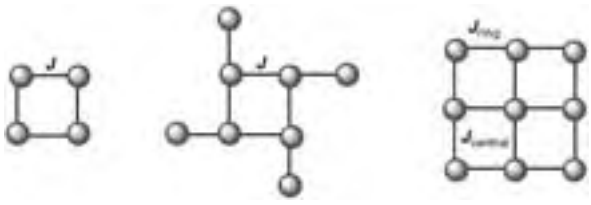


Figure 22. Definition of the coupling constants J in [2×2] arrays (left), [2×2] "pin-wheel" arrays (middle), and [3×3] arrays (right).

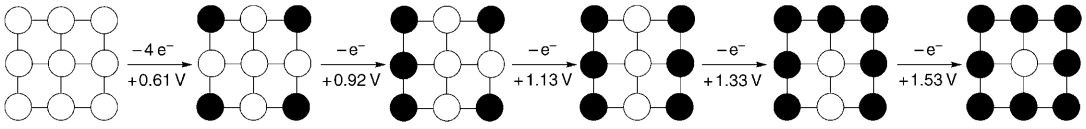


Figure 21. Proposed oxidation sequence of manganese ions in the [3×3] metal ion array $[Mn_9(\mathbf{13})_6]^{6+}$ (○ Mn^{II}, ● Mn^{III}), based on experimental data.[21b]

 © 2004 Wiley-VCH Verlag GmbH & Co. KGaA, Weinheim

The magnetic properties were thoroughly investigated for a series of nonanuclear [3×3] grid complexes incorporating doubly μ-O bridging ligands **13**.[21c] Some of the $[M_9^{II}(\mathbf{13})_6]^{n+}$ systems exhibit magnetic features which can be interpreted as a combination between ferromagnetic and antiferromagnetic exchange processes. The relative contributions of ferromagnetic and antiferromagnetic coupling vary according to the temperature (e.g. the ferromagnetic behavior is more pronounced at low temperatures because all antiferromagnetic contributions are effectively coupled to a small spin ($S=0$) ground state). To explain the combined antiferromagnetic/ferromagnetic coupling situation found in these metal ion arrays, the [3×3] grid can be considered as the sum of a ring of eight metal ions coupled to the central metal ion yielding two different exchange constants J_{ring} and $J_{central}$ (Figure 22). The $[Mn_9^{III}(\mathbf{13})_6]^{15+}$ system involves $|J_{ring}| \gg |J_{central}|$, and displays only antiferromagnetic behavior.[5b] However, the orbital based magnetic orthogonality leads to the simultaneous observation of both exchange modes in the Cu_9^{II} case, with dominant ferromagnetic exchange coupling at low temperatures.[5,50a]

There is currently no evidence for an anisotropic energy barrier in either the ferromagnetically coupled Cu_4^{II} grid arrays or the antiferromagnetically/ferromagnetically coupled Cu_9^{II} systems. However, a recent hint for magnetic anisotropy was given by the observation of metamagnetic-like behavior in antiferromagnetically coupled [3×3] Mn_9^{II} and [2×2] Co_4^{II} arrays.[50b,c]

The investigation, understanding, and manipulation of magnetic coupling between metal ions in metallogrid complexes is a first step towards the potential use of gridlike arrays in information storage devices. The discovery of ferromagnetic coupling in some Cu^{II} arrays is encouraging, although ways to introduce a magnetic anisotropy barrier have still to be explored. The choice of donor atoms, bridging groups, paramagnetic metal ions, and systematic synthetic design strategies (in contrast to the mostly serendipitous syntheses of magnetic oxo clusters) might render such supramolecular metallogrid arrays well suited for magnetic data storage at the nanometric scale.

5.1.3. Electronic Spin States

Among the physical properties that may be considered for magnetic molecular data storage systems, the spin transition (ST) phenomenon between the low-spin (LS) and the high-spin (HS) state of Fe^{II} ions is an attractive process to enable molecular memory effects.[51] Spin transition systems possess an unique concomitance of possible "write" (temperature, pressure, light) and "read" (magnetic, optical) parameters.[52] Investigations along these lines revealed ST behavior in several Fe_4^{II} gridlike [2×2] arrays (e.g. $[Fe_4^{II}(\mathbf{5a})]^{8+}$). The internal spin states of the incorporated Fe^{II} ions could be switched between the diamagnetic (LS; $S=0$) and the paramagnetic (HS; $S=2$) state by applying external field triggers (temperature, pressure, light) on macroscopic samples.[53]

The occurrence of ST in [2×2] gridlike ion arrays of the type $[Fe_4^{II}(\mathbf{5a})_4]^{8+}$ depends directly on the nature of the substituent R^1 in the 2-position of ligand **5a**. All metal ion arrays with substituents R^1 favoring relatively strong ligand fields (R^1 = H; OH) remain entirely in the diamagnetic LS state throughout all studied temperatures. Only complexes bearing substituents R^1 that attenuate the ligand field by steric (and to a lesser extent electronic) effects (R^1 = Me, Ph) exhibit temperature triggered spin transition (Figure 23). The

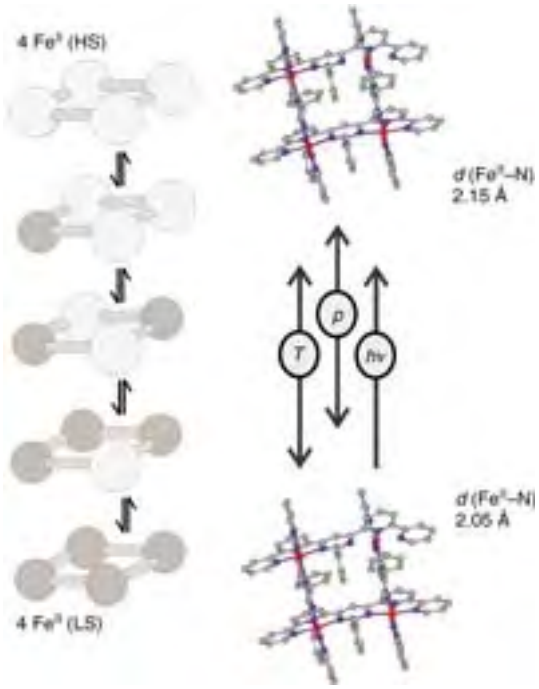


Figure 23. General switching scheme between the Fe^{II} spin states in the $[Fe_4^{II}(\mathbf{5a})_4]^{8+}$ metal ion arrays triggered by temperature, pressure, and light. The averaged Fe–N bond lengths in the 3 HS/1 LS (top) and in the 1 HS/3 LS states (bottom).[54]

magnetic switching behavior can be characterized in solution (by ^{1}H NMR and UV/Vis spectroscopy) and in the solid state (by X-ray structure analysis, magnetic susceptibility measurements, and Mössbauer spectroscopy). Very gradual and incomplete transitions without hysteresis seem to be typical for all investigated, magnetically active [2×2] Fe_4^{II} arrays. Intramolecular cooperativity between the four iron centers was revealed, and improving the intermolecular interaction between the tetranuclear centers by introduction of hydrogen bonding between the grid units increased the HS fraction over the whole temperature range, although the spin transition remained very gradual and incomplete.[54]

In a farther-reaching perspective, molecular architectures such as $[Fe_4^{II}(\mathbf{5a})_4]^{8+}$ present spin state properties that may be switched by external triggers, and may provide access to (supra)molecular spintronic devices.

5.1.4. Optical States

The UV/Vis spectra of the [2×2] metal ion arrays $[Co_4^{II}(\mathbf{15a})_4]^{8+}$ and $[Co_4^{II}(\mathbf{15b})_4]^{8+}$ both bearing acidic protons display reversible pH-modulation of the optical properties in

 © 2004 Wiley-VCH Verlag GmbH & Co. KGaA, Weinheim

solution. Due to the high accumulated charge of the complex cations, the eight N–H protons of the bis(hydrazone) ligands **15** ($R^1 = Ph$; see Figure 6) can be abstracted progressively and reversibly at relatively low pH values (below 7).[24a] The color of the solution of $[Co_4^{II}(\mathbf{15a})_4]^{8+}$ ($R^2 = H$, $R^3 = H$) changes from pale-yellow at low pH to orange and finally to deep violet above neutral pH, and repeated cycling indicates that the process is completely reversible (Figure 24).

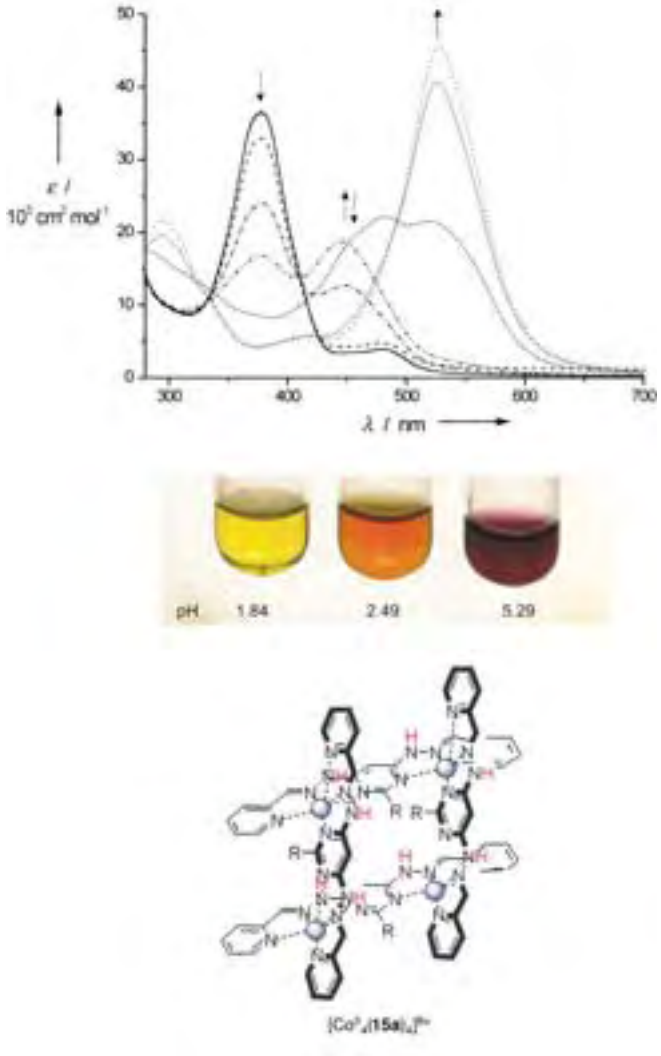


Figure 24. The color change and UV/Vis spectra of complex $[Co_4^{II}(\mathbf{15a})_4](BF_4)_8$ ($R^1 = Ph$; the abstracted acidic protons are labeled in red) depending on the pH of the acetonitrile/water solution.[24a]

Furthermore, the $[Zn_4^{II}(\mathbf{15a})_4]^{8+}$ ($R^1 = Ph$; $R^2 = R^3 = H$) complex exhibits an emission (originating from sandwich-like π–π interactions of the phenyl substituents intercalated between two ligands **15a**), which depends on the protonation state.[55]

5.2. Two-Dimensional Ordering and Addressability
5.2.1. Two-Dimensional Self-Ordering in Crystals

Simple mononuclear metal complexes bearing H-bonding-donor and -acceptor sites are able to undergo hierarchical self-assembly processes. The same approach can also be applied to [2 × 2] grids, which can be organized into a chessboard-like 2D "grid-of-grids" arrangement (Figure 25). This strategy is a powerful alternative to the more laborious stepwise construction of high nuclearity metalloarrays.

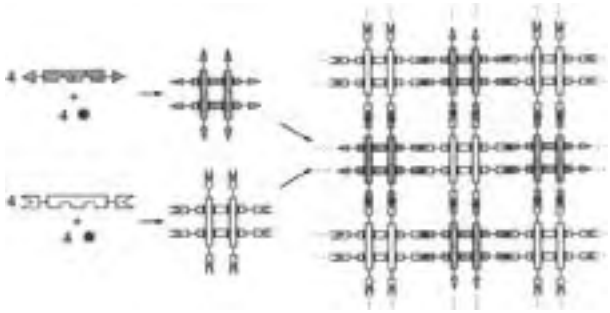


Figure 25. Schematic representation of the two-step hierarchical self-assembly sequence to generate a 2D "grid-of-grids" pattern.

Such 2D-extended supramolecular arrays of precise architecture would be of special interest for addressing the metal ions individually. However, their formation and stabilization requires control over the various noncovalent interactions, so as to make them the thermodynamically preferred products and to avoid clusterlike structures as result of undesired interactions. The hierarchical self-organization of mononuclear metal complexes with the ligands **17** or **18**, which form self-complementary hydrogen bonds, illustrates the problems. Since the energies for the formation of the double hydrogen bonds are almost the same order of magnitude as the energies of crystal packing phenomena and π–π interactions, different thermodynamic products could be observed in these experiments.

The self-complementary aminopyrimidine units of the monotopic terpyridine-type ligand **17** lead to an infinite two-dimensional gridlike structure of the corresponding $[Co^{II}(\mathbf{17})_2](PF_6)_2$ in the solid state.[56] The complexes are connected by intermolecular double hydrogen-bonds between the amino groups and the noncoordinating pyrimidine nitrogen atoms. This creates a sinusoidal arrangement of the complexes, which are interwoven into a two-dimensional network (Figure 26). However, changing the counteranion from PF_6^- to BF_4^- causes a partial breakup of this grid motif leaving one quarter of the H-bonding sites unsaturated.

The extension of this methodology towards [2 × 2] gridlike complexes afforded 2D arrays representing dual levels of organization. The complex $[Co_4^{II}(\mathbf{19})_4](BF_4)_8$ was characterized by single-crystal X-ray diffraction.[57] Although the presence of the aminopyrimidine units in the ligand should enable their metal complexes to generate hydrogen-bonded networks of grids, the hydrogen-bonding motif is only present

 © 2004 Wiley-VCH Verlag GmbH & Co. KGaA, Weinheim

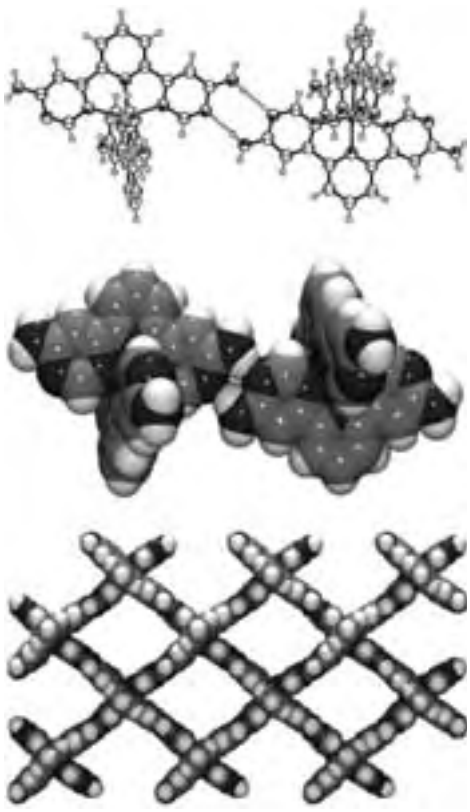


Figure 26. X-ray structure analysis of the mononuclear complex $[Co^{II}(\mathbf{17})_2](PF_6)_2$. The complex ions are arranged to give sinusoidal arrangements through the formation of double hydrogen-bonds. Top: Section with two complex ions with hydrogen boding contacts (ORTEP representation); middle: space-filling representation. Bottom: Infinite 2D gridlike metal ion array extracted from the crystal packing diagram.[56]

in one dimension, leading to the formation of infinite one-dimensional chains of grids. Neighboring complexes without hydrogen-bonding interactions show weak π-stacking between their ligands. Thus, $[Co^{II}_4(\mathbf{20})_4](BF_4)_8$ only generates a partially hydrogen-bonded network, because of the competition between hydrogen bonding and π–π stacking interactions.

The different structural outcomes of the mono- as well as the tetranuclear H-bonding approach illustrate the subtle energy interplay between H-bonding and crystal packing effects. This exemplifies a general problem found for this type of hierarchical self-assembly process.

5.2.3. *Two-Dimensional Ordering at Surfaces and Single Molecule Addressing*

One important factor in the exploitation of supramolecular architectures as components of functional devices is the ability to prepare ordered structures on solid surfaces. Recent advances in scanning probe techniques (STM, AFM) have enabled imaging and manipulation of surface-bound objects with molecular resolution.[58] Thin films of metalloorganic grid complexes have been studied by these methods with the prospect that the resulting high density of active elements could be engineered into functional surfaces, for example, memory devices.

Highly stable monolayers of the cobalt(II) [2 × 2] complex $[Co^{II}_4(\mathbf{5a})_4]^{8+}$ were prepared on an atomically flat graphite surface (highly ordered pyrolytic graphite (HOPG)) by evaporation of dilute acetone solutions, yielding defect-free areas of up to 0.5 μm^2.[59] The ordered structures form spontaneously, growing outward from single nucleation points; this process may be viewed as a two-dimensional crystallization. It was found that the orientation of the grids relative to the surface plane is controlled by the substitution pattern of ligand **5a**: the ligand with $R^1,R^2 = H$ and $R^3 = CH_3$ gave an edgewise orientation of grids with respect to the surface, while the ligand with $R^1 = CH_3$ and $R^2,R^3 = H$ resulted in flat tiles forming a superarray of [2 × 2] metallogrids. The superarray arrangement was reflected in an orthogonal 2.5 nm × 2.4 nm periodicity in the STM image (Figure 27a).

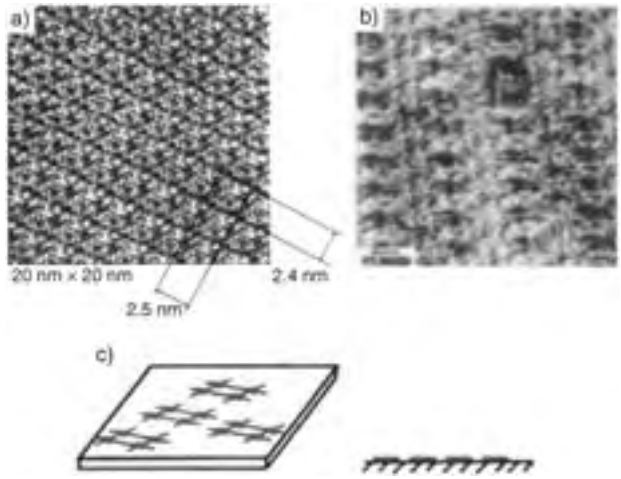


Figure 27. a) STM image of the monolayer of $[Co^{II}_4(\mathbf{5a})_4]^{8+}$ gridlike compounds on graphite. b) Hole in the monolayer produced by potential-induced lifting of a single $[Co^{II}_4(\mathbf{5a})_4]^{8+}$ molecule with the STM tip. c) Schematic representation of the disposition of the metalloarrays at the surface (top and side view).[59]

A −500 mV voltage pulse applied to the STM tip (normally operated at below −50 mV for imaging) was employed to pluck a single grid from the monolayer, resulting in a square hole with the dimensions of a single gridlike complex (Figure 27b). This represents the first indication for the possibility of controlled addressing of the [2 × 2] metalloarrays using state-of-the-art technological devices. The migration rate of the hole was measured, and found to be 200 times slower than for a monolayer of cycloalkanes, reflecting strong adsorption to the graphite surface.[60]

Analogous [2 × 2] gridlike Co^{II} complexes formed by bis(terpyridine)-derived ligands substituted with an additional *para*-pyridyl or n-propyl thia unit **5a** were adsorbed as monolayers on graphite (HOPG). They gave rise to a weaker adsorption and higher mobility compared to the corresponding parent complex.[61,62]

 © 2004 Wiley-VCH Verlag GmbH & Co. KGaA, Weinheim

Thin films of [2 × 2] Co^{II}_4 metallogrids on gold surfaces have been prepared and imaged by in situ electrochemical deposition STM. Films of pure cobalt grid are poorly conductive ($< 10^{-6}$ S cm^{-1}), but upon doping with an excess of cadmium(II) ions, conductivity rises by four orders of magnitude to 10^{-2} S cm^{-1} resulting from additional electronic states in the material's insulating bandgap. While this increase is large, conductivity is still low relative to metallic conductors such as copper (10^6–10^8 S cm^{-1}).[63] [2 × 2] Co^{II}_4 grid complexes have been included in thin films[64a] and may serve as components[64b] for metallosupramolecular polymers providing novel properties to the polymeric network.[64c] Recently, a Mn^{II}_9 grid (derived from a ligand similar to **13**; Figure 6) was similarly investigated on a Au(111) surface.[65]

A two-step process of an air–water interfacial reaction between free ligand **1a** (R = Ph) and Ag^I ions contained in the aqueous subphase led to the formation of a [2 × 2] Ag^I_4 grid complex, followed by its self-assembly into an oriented crystalline monolayer. On surface compression, the original monolayer underwent a transition to a crystalline bilayer, almost retaining the initial in-plane arrangement.[66]

A single report of thin film preparation employing grids of higher order concerns the silver(I) [3 × 3] complex $[Ag_9(\mathbf{1b})_6]^{9+}$. Self-assembly of the grids was achieved at the air–water interface by spreading uncomplexed ligand **1b** on an aqueous solution of silver(I) triflate. This gave ordered crystalline films of 13–20 Å thickness that could be transferred successfully onto quartz slides.[67] Grazing incidence X-ray diffraction (GIXD) revealed that grid orientation in the films could be controlled by varying the substituents of ligand **1b**: the grids lie parallel to the surface when R = Ph, but "stand up" normal to the air–water interface when R = CH_3. Thus, the formation of metallogrid monolayers represents a twofold self-assembly sequence; conventional synthetic techniques are only employed for preparation of the ligand.

6. Conclusion and Outlook

The synthetic accessibility by self-assembly of two-dimensionally arrayed switchable elements of nanometric size complements theoretical developments in molecular information storage and processing.[1,2] Gridlike metal ion architectures are attractive in this context for several reasons. For example, grid-type arrays can behave as multilevel electronic species, triggered by electrochemical, magnetic, and optical parameters. In addition, it has been shown that single grid units on surfaces are addressable within the nanometer regime. It is important to recognize the challenges that remain in order to combine these two main features in a working functional device by detecting, controlling, and addressing the electronic or magnetic states of individual grids or even ions, for instance in 2D monolayers. The information-representing metastable states must be sufficiently robust to permit room-temperature operation. The question of implementation and integration of possible devices with the supporting frame (wiring, pinning, powering) has yet to be addressed.

A sense for the potential of information storage using (supra)molecular memory elements can be obtained by contrasting the density of magnetic disk and CD-ROM technologies (~10^8 bits cm^{-2}) with the estimated storage capacity of DNA (10^{21} bits cm^{-3} corresponding to ~10^{10} bits cm^{-2}). The cationic metalloarrays, deposited on surfaces, have shown external dimensions in the order of 25 × 25 Å and a closely packed 2D array; with one data bit stored per [2 × 2] matrix, they would lead to a potential surface data storage density of about 10^{12} bits cm^{-2}.

Gridlike arrays display "ion dot" type features, by analogy with semiconductor quantum dot arrays.[3a] One may remark that "ion dots" are of much smaller size than quantum dots. It has been pointed out that "… such architectures may foreshadow multistate digital supramolecular chips for information storage in and retrieval from inscribed patterns that might be addressable by light or electrically. Different states could, in principle, be characterized either by different local features at a given *x*, *y* coordinate, in ion dot fashion, or by specific overall optical or oxidation levels. Inducing ± 1 redox changes at specific locations in a single unit would then correspond to a sort of single electronics at ion dots."[3a]

In conclusion, the power of self-assembly to create ordered nanostructures of intriguing technological potential has been underlined through the investigation of metalloorganic grid complexes. It has been stressed that self-organization represents a self-fabrication process, allowing in principle one to bypass tedious nanofabrication procedures.[3] Considering the panoramic properties of transition-metal compounds, and the small collection of metals and ligands that have as yet been incorporated into metallogrid or other types of architectures, there can be little doubt that a very wide set of nanosize devices and materials with a rich palette of properties will spring from novel metal–ligand combinations for the benefit of the development of supramolecular electronics, spintronics, and optotronics.[68]

The authors are very thankful to Prof. M. Krische and Dr. E. Archer, University of Texas, Austin, for initiating and stimulating the writing of this review article as well as to all the other coworkers in our group who have contributed to the work reviewed herein: Dr. C. Arana, Dr. D. M. Bassani, Dr. P. N. W. Baxter, Dr. M. Barbiou, G. Blasen, Dr. E. Breuning, Prof. K. Fromm, Dr. A. Garcia, Prof. G. Hanan, Dr. A. Marquis, Dr. V. Patrowiak, Prof. U. S. Schubert, Dr. D. Volkmer, Dr. U. Ziener. We also acknowledge very fruitful collaborations with several laboratories on different aspects of the work, as indicated by the references cited.

Received: October 16, 2003 [A636]
Published Online: June 9, 2004

[1] a) M. C. Petty, M. R. Bryce, D. Bloor, *Introduction to Molecular Electronics*, Oxford University Press, New York, **1995**; b) J. M. Tour, *Acc. Chem. Res.* **2000**, *33*, 791–804; c) A. R. Pease, J. O. Jeppesen, J. F. Stoddart, Y. Luo, C. P. Collier, J. R. Heath, *Acc. Chem. Res.* **2001**, *34*, 433–444.

[2] C. Joachim, J. K. Gimzewski, A. Aviram, *Nature* **2000**, *408*, 541–548; R. F. Service, *Science* **2001**, *293*, 782–785.

 © 2004 Wiley-VCH Verlag GmbH & Co. KGaA, Weinheim

[3] a) J.-M. Lehn, *Supramolecular Chemistry. Concepts and Perspectives*, VCH, Weinheim, **1995**, chap. 9, p. 200; b) J.-M. Lehn, *Science* **2002**, *295*, 2400 – 2403; J.-M. Lehn, *Proc. Natl. Acad. Sci. USA* **2002**, *99*, 4763 – 4768.

[4] a) J. Rojo, F. J. Romero-Salguero, J.-M. Lehn, G. Baum, D. Fenske, *Eur. J. Inorg. Chem.* **1999**, 1421 – 1428; b) V. Patroniak, P. N. W. Baxter, J.-M. Lehn, M. Kubicki, M. Nissinen, K. Rissanen, *Eur. J. Inorg. Chem.* **2003**, 4001 – 4009.

[5] a) L. Zhao, Z. Xu, L. K. Thompson, S. L. Heath, D. O. Miller. M. Ohba, *Angew. Chem.* **2000**, *112*, 3244 – 3247; *Angew. Chem. Int. Ed.* **2000**, *39*, 3114 – 3117; b) L. K. Thompson, L. Zhao, Z. Xu, D. O. Miller, W. M. Reiff, *Inorg. Chem.* **2003**, *42*, 128 – 139.

[6] M. Barbiou, J.-M. Lehn, *J. Am. Chem. Soc.* **2003**, *125*, 10257 – 10265.

[7] a) S. Williams, www.nanotechweb.org/articles/news/1/9/8/1 **2002**; b) R. F. Service, *Science* **2003**, *302*, 556 – 558; c) Z. Zhong, D. Wang, Y. Cui, M. W. Bockrath, C. M. Lieber, *Science* **2003**, *302*, 1377 – 1380.

[8] C. S. Lent, B. Isaksen, M. Lieberman, *J. Am. Chem. Soc.* **2003**, *125*, 1056 – 1063; M. Lieberman, S. Chellamma, B. Varughese, Y. Wang, C. Lent, G. H. Bernstein, G. Snider, F. C. Peiris, *Ann. N. Y. Acad. Sci.* **2002**, *960*, 225 – 239; A. O. Orlov, I. Amlani, G. H. Bernstein, C. S. Lent, G. L. Snider, *Science* **1997**, *277*, 928 – 930.

[9] C. S. Lent, P. D. Tougaw, *Proc. IEEE* **1997**, *85*, 541.

[10] P. J. Stang, B. Olenyuk, *Acc. Chem. Res.* **1997**, *30*, 502 – 518; D. L. Caulder, K. N. Raymond, *Acc. Chem. Res.* **1999**, *32*, 975 – 982; J.-M. Lehn in *Supramolecular Science: Where It Is and Where It Is Going* (Eds.: R. Ungaro, E. Dalcanale), Kluwer, Amsterdam, **1999**; G. F. Swiegers, T. J. Malefetse, *Chem. Rev.* **2000**, *100*, 3483 – 3537.

[11] P. N. W. Baxter in *Comprehensive Supramolecular Chemistry, Vol. 9* (Eds.: J.-M. Lehn, J. L. Atwood, J. E. D. Davies, D. D. MacNicol, F. Vögtle), Pergamon, Oxford, **1996**, pp. 254 – 288; G. S. Hanan, D. Volkmer, U. S. Schubert, J.-M. Lehn, G. Baum, D. Fenske, *Angew. Chem.* **1997**, *109*, 1929 – 1931; *Angew. Chem. Int. Ed. Engl.* **1997**, *36*, 1842 – 1844.

[12] A. W. Maverick, F. E. Klavetter, *Inorg. Chem.* **1984**, *23*, 4129 – 4135; R. Köhler, B. Kirmse, R. Richter, J. Sieler, E. Hoyer, L. Beyer, Z. *Anorg. Allg. Chem.* **1986**, *537*, 133 – 144.

[13] a) M. T. Youinou, N. Rahmouni, J. Fischer, J. A. Osborn, *Angew. Chem.* **1992**, *104*, 771 – 773; *Angew. Chem. Int. Ed. Engl.* **1992**, *31*, 733 – 735; b) P. N. W. Baxter, J.-M. Lehn, B. O. Kneisel, D. Fenske, *Chem. Commun.* **1997**, 2231 – 2232.

[14] S. Toyota, C. R. Woods, M. Benaglia, R. Haldimann, K. Wärnmark, K. Hardcastle, J. S. Siegel, *Angew. Chem.* **2001**, *113*, 773 – 776; *Angew. Chem. Int. Ed.* **2001**, *40*, 751 – 754.

[15] P. van Koningsbruggen, E. Müller, J. G. Haasnoot, J. Reedijk, *Inorg. Chim. Acta* **1993**, *208*, 37 – 42.

[16] G. S. Hanan, PhD thesis, Université Louis Pasteur, Strasbourg, **1995**.

[17] A. M. Garcia, F. J. Romero-Salguero, D. Bassani, J.-M. Lehn, G. Baum, D. Fenske, *Chem. Eur. J.* **1999**, *5*, 1803 – 1808.

[18] J. C. Jeffery, P. L. Jones, K. L. V. Mann, E. Psillakis, J. A. McCleverty, M. D. Ward, C. M. White, *Chem. Commun.* **1997**, 175 – 176.

[19] M. Ruben, J.-M. Lehn, unpublished results.

[20] J. Rojo, J.-M. Lehn, G. Baum, D. Fenske, O. Waldmann, P. Müller, *Eur. J. Inorg. Chem.* **1999**, 517 – 522.

[21] a) C. J. Mathews, K. Avery, Z. Xu, K. L. Thompson, L. Zhao, D. O. Miller, K. Biradha, K. Poirier, M. J. Zaworotko, C. Wilson, A. E. Goeta, J. A. K. Howard, *Inorg. Chem.* **1999**, *38*, 5266 – 5281; b) L. Zhao, C. J. Matthews, L. K. Thompson, S. L. Heath, *Chem. Commun.* **2000**, 265 – 266; c) L. Zhao, Z. Xu, L. K. Thompson, D. O. Miller, *Polyhedron* **2001**, *20*, 1359 – 1364.

[22] a) C. Duan, Z. Liu, X. You, F. Xue, T. C. W. Mak, *Chem. Commun.* **1997**, 381 – 382; b) A. Gelasco, A. Askenas, V. L. Pecoraro, *Inorg. Chem.* **1996**, *35*, 1419 – 1420.

[23] Efficient synthesis of **15a** and **15b** by hydrazone formation: K. M. Gardiner, R. G. Khoury, J.-M. Lehn, *Chem. Eur. J.* **2000**, *6*, 4124 – 4131; J.-L. Schmitt, A.-M. Stadler, N. Kyritsakas, J.-M. Lehn, *Helv. Chim. Acta* **2003**, *86*, 1598 – 1624.

[24] a) M. Ruben, J.-M. Lehn, G. Vaughan, *Chem. Commun.* **2003**, 1338 – 1339; b) L. H. Uppadine, J.-M. Lehn, *Angew. Chem.* **2004**, *116*, 242 – 245; *Angew. Chem. Int. Ed.* **2004**, *43*, 240 – 243.

[25] J. Hausmann, G. B. Jameson, S. Brooker, *Chem. Commun.* **2003**, 2992 – 2993; D. S. Cati, J. Ribas, J. Ribas-Ariño, H. Stoeckli-Evans, *Inorg. Chem.* **2004**, 43, 1021 – 1030.

[26] a) D. M. Bassani, J.-M. Lehn, K. Fromm, D. Fenske, *Angew. Chem.* **1998**, *110*, 2534 – 2537; *Angew. Chem. Int. Ed.* **1998**, *37*, 2364 – 2367; b) S. T. Howard, *J. Am. Chem. Soc.* **1996**, *118*, 10269 – 10274; c) D. M. Bassani, J.-M. Lehn, G. Baum, D. Fenske, *Angew. Chem.* **1997**, *109*, 1931 – 1933; *Angew. Chem. Int. Ed. Engl.* **1997**, *36*, 1845 – 1848; D. M. Bassani, J.-M. Lehn, *Bull. Soc. Chim. Fr.* **1997**, *134*, 897 – 906; M. Okhita, J.-M. Lehn, G. Baum, D. Fenske, *Chem. Eur. J.* **1999**, *5*, 3471 – 3478.

[27] R. Krämer, J.-M. Lehn, A. Marquis-Rigault, *Proc. Natl. Acad. Sci. USA* **1993**, *90*, 5394 – 5398.

[28] T. Bark, M. Düggeli, H. Stoeckli-Evans, A. von Zelevsky, *Angew. Chem.* **2001**, *113*, 2924 – 2927; *Angew. Chem. Int. Ed.* **2001**, *40*, 2848 – 2850.

[29] P. N. W. Baxter, J.-M. Lehn, J. Fischer, M.-T. Youinou, *Angew. Chem.* **1994**, *106*, 2432 – 2434; *Angew. Chem. Int. Ed. Engl.* **1994**, *33*, 2284 – 2287.

[30] a) E. Breuning, G. S. Hanan, F. J. Romero-Salguero, A. M. García, P. N. W. Baxter, J.-M. Lehn, E. Wegelius, K. Rissanen, H. Nierengarten, A. van Dorsselaer, *Chem. Eur. J.* **2002**, *8*, 3458 – 3466; b) H. Nierengarten, E. Leize, E. Breuning, A. García, F. Romero-Salguero, J. Rojo, J.-M. Lehn, A. van Dorsselaer, *J. Mass Spectrom.* **2002**, *37*, 56 – 62; c) G. S. Hanan, C. R. Arana, J.-M. Lehn, G. Baum, D. Fenske, *Chem. Eur. J.* **1996**, *2*, 1292 – 1299.

[31] a) P. N. W. Baxter, J.-M. Lehn, G. Baum, D. Fenske, *Angew. Chem.* **1997**, *109*, 2067 – 2070; *Angew. Chem. Int. Ed. Engl.* **1997**, *36*, 1978 – 1981; b) M. Schmittel, V. Kalsani, D. Fenske, A. Wiegrefe, *Chem. Commun.* **2004**, 490 – 491.

[32] L. K. Thompson, C. J. Matthews, L. Zhao, Z. Xu, D. O. Miller, C. Wilson, M. A. Leech, J. A. K. Howard, S. L. Heath, A. G. Whittaker, R. E. P. Winpenny, *J. Solid State Chem.* **2001**, *159*, 308 – 320.

[33] P. N. W. Baxter, J.-M. Lehn, G. Baum, D. Fenske, *Chem. Eur. J.* **2000**, *6*, 4510 – 4517.

[34] a) C. J. Matthews, S. T. Onions, G. Morata, M. Bosch Salvia, M. R. J. Elsegood, D. J. Price, *Chem. Commun.* **2003**, 320 – 321; b) S. T. Onions, A. M. Frankin, P. N. Horton, M. B. Hursthouse, C. J. Matthews, *Chem. Commun.* **2003**, 2864 – 2865; c) Z. He, C. He, Z.-M. Wang, E.-Q. Gao, Y. Lin, C.-H. Yan, *J. Chem. Soc. Dalton Trans.* **2004**, *502*–504.

[35] P. N. W. Baxter, J.-M. Lehn, K. Rissanen, *Chem. Commun.* **1997**, 1323 – 1324.

[36] A. Marquis, J.-P. Kintzinger, R. Graff, P. N. W. Baxter, J.-M. Lehn, *Angew. Chem.* **2002**, *114*, 2884 – 2888; *Angew. Chem. Int. Ed.* **2002**, *41*, 2760 – 2764; Erratum: A. Marquis, J.-P. Kintzinger, R. Graff, P. N. W. Baxter, J.-M. Lehn, *Angew. Chem.* **2002**, *114*, 3888; *Angew. Chem. Int. Ed.* **2002**, *41*, 3738.

[37] B. Hasenknopf, J.-M. Lehn, B. O. Kneisel, G. Baum, D. Fenske, *Angew. Chem.* **1996**, *108*, 1987 – 1990; *Angew. Chem. Int. Ed. Engl.* **1996**, *35*, 1838 – 1840; B. Hasenknopf, J.-M. Lehn, N. Boumediene, A. Dupont-Gervais, A. van Dorsselaer, B. O. Kneisel, D. Fenske, *J. Am. Chem. Soc.* **1997**, *119*, 10956 – 10958.

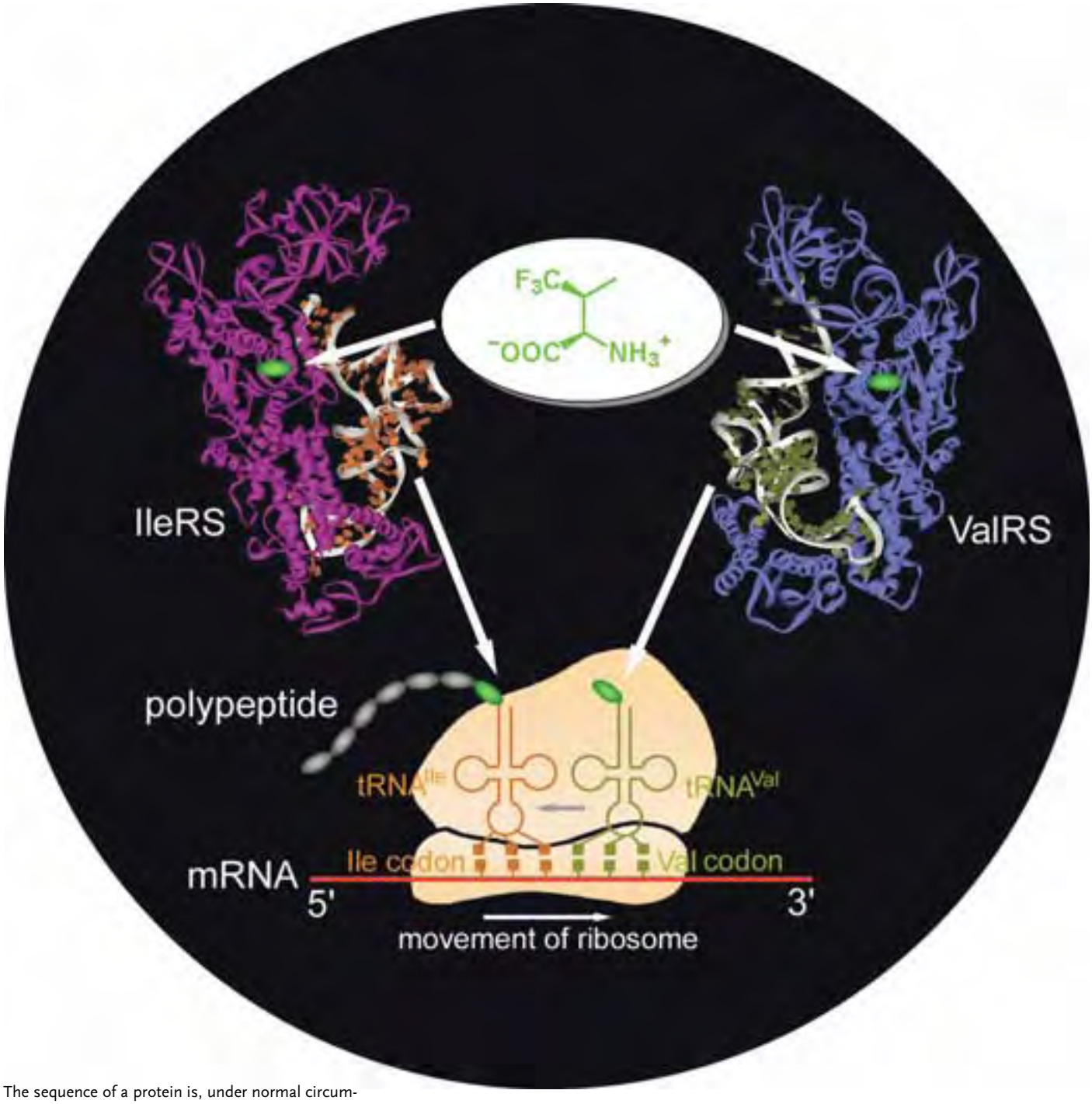
[38] a) C. S. Campos-Fernández, R. Clérac, K. R. Dunbar, *Angew. Chem.* **1999**, *111*, 3685 – 3688; *Angew. Chem. Int. Ed. Engl.* **1999**, *38*, 3477 – 3479; b) X.-H. Bu, H. Morishita, K. Tanaka, K. Biradha, S. Furusho, M. Shionoya, *Chem. Commun.* **2000**, 971 – 972.

 © 2004 Wiley-VCH Verlag GmbH & Co. KGaA, Weinheim

[39] C. S. Campos-Fernández, R. Clérac, J. M. Koomen, D. H. Russell, K. R. Dunbar, *J. Am. Chem. Soc.* **2001**, *123*, 773 – 774.
[40] P. N. W. Baxter, R. G. Khoury, J.-M. Lehn, G. Baum, D. Fenske, *Chem. Eur. J.* **2000**, *6*, 4140 – 4145.
[41] a) M. Ruben, E. Breuning, J.-P. Gisselbrecht, J.-M. Lehn, *Angew. Chem.* **2000**, *112*, 4312 – 4315; *Angew. Chem. Int. Ed.* **2000**, *39*, 4139 – 4142; b) M. Ruben, E. Breuning, M. Barboiu, J.-P. Gisselbrecht, J.-M. Lehn, *Chem. Eur. J.* **2003**, *9*, 291 – 299; D. M. Bassani, J.-M. Lehn, S. Serroni, F. Puntoriero, S. Campagna, *Chem. Eur. J.* **2003**, *9*, 5936 – 5946.
[42] L. H. Uppadine, J.-P. Gisselbrecht, J.-M. Lehn, *Chem. Commun.* **2004**, 718 – 719.
[43] B. Barbara, L. Gunther, *Phys. World* **1999**, March, 35 – 39; C. Sangregorio, T. Ohm, C. Paulsen, R. Sessoli, D. Gatteschi, *Phys. Rev. Lett.* **1997**, *78*, 4645 – 4648.
[44] O. Kahn, *Molecular Magnetism*, VCH, Weinheim, **1993**.
[45] R. Sessoli, D. Gatteschi, A. Caneschi, M. A. Novak, *Nature* **1993**, *365*, 141 – 144; D. Gatteschi, A. Caneschi, L. Pardi, R. Sessoli, *Science* **1994**, *265*, 1054 – 1057.
[46] A.-L. Barra, P. Debranner, D. Gatteschi, R. Sessoli, *Europhys. Lett.* **1996**, *35*, 133 – 138; J. C. Goodwin, R. Sessoli, D. Gatteschi, W. Wernsdorfer, A. K. Powell, S. C. Heath, *J. Chem. Commun. Dalton Trans.* **2000**, 1835 – 1841; S. M. J. Aubin, M. W. Wemple, D. M. Adams, H.-L. Tsai, G. Christou, D. N. Hendrickson, *J. Am. Chem. Soc.* **1996**, *118*, 7746 – 7753.
[47] O. Waldmann, J. Hassmann, P. Müller, G. S. Hanan, D. Volkmer, U. S. Schubert, J.-M. Lehn, *Phys. Rev. Lett.* **1997**, *78*, 3390 – 3393; O. Waldmann, J. Hassmann, P. Müller, D. Volkmer, U. S. Schubert, J.-M. Lehn, *Phys. Rev. B* **1998**, *58*, 3277 – 3285.
[48] M. Ruben, J.-M. Lehn, V. Ksenofontov, P. Gütlich, unpublished results.
[49] Z. Xu, L. K. Thompson, D. O. Miller, *Chem. Commun.* **2001**, 1170 – 1171.
[50] a) O. Waldmann, R. Koch, S. Schromm, P. Müller, L. Zhao, L. K. Thompson, *Chem. Phys. Lett.* **2000**, *332*, 73 – 79; b) O. Waldmann, L. Zhao, L. K. Thompson, *Phys. Rev. Lett.* **2002**, *88*, 066401; c) O. Waldmann, P. Müller, M. Ruben, U. Ziener, J.-M. Lehn, *Europhys. Lett.* **2004**, submitted.
[51] O. Kahn, J. C. Martinez, *Science* **1998**, *279*, 44-48.
[52] P. Gütlich, A. Hauser, H. Spiering, *Angew. Chem.* **1994**, *106*, 2109 – 2141; *Angew. Chem. Int. Ed. Engl.* **1994**, *33*, 2024 – 2054.
[53] E. Breuning, M. Ruben, J.-M. Lehn, F. Renz, Y. Garcia, V. Ksenofontov, P. Gütlich, E. Wegelius, K. Rissanen, *Angew. Chem.* **2000**, *112*, 2563 – 2566; *Angew. Chem. Int. Ed.* **2000**, *39*, 2504 – 2507.
[54] M. Ruben, E. Breuning, J.-M. Lehn, V. Ksenofontov, F. Renz, P. Gütlich, G. Vaughan, *Chem. Eur. J.* **2003**, *9*, 4422 – 4429; corrigendum: *Chem. Eur. J.* **2003**, *9*, 5176; M. Ruben, E. Breuning, J.-M. Lehn, V. Ksenofontov, P. Gütlich, G. Vaughan, *J. Magn. Magn. Mater.* **2003**, in press.
[55] M. Ruben, M. Barbiou, J.-M. Lehn, L. Prodi, unpublished results.
[56] U. Ziener, E. Breuning, J.-M. Lehn, E. Wegelius, K. Rissanen, G. Baum, D. Fenske, G. Vaughan, *Chem. Eur. J.* **2000**, *6*, 4132 – 4139.
[57] E. Breuning, U. Ziener, J.-M. Lehn, E. Wegelius, K. Rissanen, *Eur. J. Inorg. Chem.* **2001**, 1515 – 1521.
[58] a) C. A. Mirkin, *Inorg. Chem.* **2000**, *39*, 2258 – 2272; b) J. Chen, M. A. Reed, C. L. Asplund, A. M. Cassell, M. L. Myrick, A. M. Rawlett, J. M. Tour, P. G. Van Patten, *Appl. Phys. Lett.*, **1999**, *75*, 624 – 626.
[59] A. Semenov, J. P. Spatz, M. Möller, J.-M. Lehn, B. Sell, D. Schubert, C. H. Weidl, U. S. Schubert, *Angew. Chem.* **1999**, *111*, 2701 – 2705; *Angew. Chem. Int. Ed.* **1999**, *38*, 2547 – 2550.
[60] A. Semenov, J. P. Spatz, J.-M. Lehn, C. H. Weidl, U. S. Schubert, M. Möller, *Appl. Surf. Sci.* **1999**, *144–145*, 456 – 460.
[61] U. Ziener, J.-M. Lehn, A. Mourran, M. Möller, *Chem. Eur. J.* **2002**, *8*, 951 – 957.
[62] M. Ruben, J.-M. Lehn, S. Strömsdörfer, P. Müller, unpublished results.
[63] J. Hassmann, C. Y. Hahn, O. Waldmann, E. Volz, H.-J. Schleemilch, N. Hallschmid, P. Müller, G. S. Hanan, D. Volkmer, U. S. Schubert, J.-M. Lehn, H. Mauser, A. Hirsch, T. Clark, *Mater. Res. Soc. Symp. Proc.* **1998**, *488*, 447 – 452.
[64] a) T. Salditt, Q. An, A. Blech, C. Eschbaumer, U. S. Schubert, *Chem. Commun.* **1998**, 2731 – 2732; b) U. S. Schubert, C. H. Weidl, J.-M. Lehn, *Des. Monomers Polym.* **1999**, *2*, 1 – 17; U. S. Schubert, C. Eschbaumer, *Angew. Chem.* **2002**, *114*, 3016 – 3050; *Angew. Chem. Int. Ed.* **2002**, *41*, 2892 – 2926.
[65] L. Weeks, L. K. Thompson, J. G. Shapter, K. J. Pope, Z. Xu, *J. Microsc.* **2003**, *212*, 102 – 106.
[66] I. Weissbuch, P. N. W. Baxter, I. Kuzmenko, H. Cohen, S. Cohen, K. Kjaer, P. B. Howes, J. Als-Nielsen, J.-M. Lehn, L. Leiserowitz, M. Lahav, *Chem. Eur. J.* **2000**, *6*, 725 – 734.
[67] I. Weissbuch, P. N. W. Baxter, S. Cohen, H. Cohen, K. Kjaer, P. B. Howes, J. Als-Nielsen, G. S. Hanan, U. S. Schubert, J.-M. Lehn, L. Leiserowitz, M. Lahav, *J. Am. Chem. Soc.* **1998**, *120*, 4850 – 4860.
[68] Note added in proof (April 19, 2004): Since the submission of this article, the following relevant paper has appeared: J. Nitzschke, J.-M. Lehn, *Proc. Natl. Acad. Sci. USA* **2003**, *100*, 11 970 – 11 974.

 © 2004 Wiley-VCH Verlag GmbH & Co. KGaA, Weinheim

Communications



The sequence of a protein is, under normal circumstances, determined uniquely by the sequence of its mRNA. In the following Communication, Kumar, Tirrell, and their co-workers show that this need not be true: 4,4,4-trifluorovaline can be assigned either to valine codons or to isoleucine codons, depending on the levels of activity of the respective aminoacyl-tRNA synthetases in the expression host.

DOI: 10.1002/anie.200454036
© 2004 Wiley-VCH Verlag GmbH & Co. KGaA, Weinheim

RNA Translation

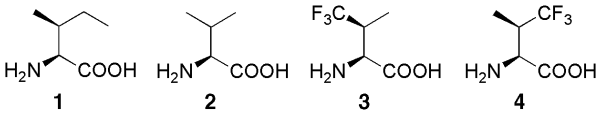
Alternative Translations of a Single RNA Message: An Identity Switch of (2*S*,3*R*)-4,4,4-Trifluorovaline between Valine and Isoleucine Codons**

*Pin Wang, Alfio Fichera, Krishna Kumar, and David A. Tirrell**

The genetic code links the sequence of a messenger RNA to the sequence of the corresponding protein. Codon assignments are established in the aminoacylation step, wherein the aminoacyl-tRNA synthetases (aaRSs) catalyze the attachment of the amino acids to their cognate tRNAs.[1,2] Here we show that engineering of bacterial expression hosts can allow a single RNA message to be translated in different ways depending on the relative rates of competing aminoacylation reactions. Specifically, we show that the identity of the noncanonical amino acid (2*S*,3*R*)-4,4,4-trifluorovaline can be changed by its assignment either to isoleucine or to valine codons according to the intracellular levels of the canonical amino acids and their cognate synthetases. It has been known for many years that relative aminoacylation rates play a critical role in determining translational fidelity.[3]

This work was motivated by previous demonstrations that fluorinated amino acids can be used to engineer the stability and dimerization specificity of coiled-coil peptides and proteins.[4–10] Trifluoroleucine and hexafluoroleucine can be introduced into recombinant proteins by using a leucine auxotroph as the bacterial expression host.[7,8] High-level incorporation of either of the fluorinated amino acids requires depletion of leucine in the culture medium prior to induction of gene expression. For hexafluoroleucine, depletion of the natural amino acid is not enough; efficient incorporation demands the use of an engineered bacterial host with enhanced leucyl-tRNA synthetase activity.[7] One of our continuing objectives is to expand the availability of novel amino acids for use in protein engineering.

There are two stereoisomeric forms of (2*S*)-4,4,4-trifluorovaline (2*S*-Tfv; Scheme 1): the 2*S*,3*S* form (**3**) and the 2*S*,3*R* form (**4**). Previously we found that both the 2*S*,4*S* and the 2*S*,4*R* forms of 5,5,5-trifluoroleucine are readily incorporated into recombinant proteins; the leucyl-tRNA synthetase of *Escherichia coli* apparently activates both isomers.[8] In evaluating 2*S*-Tfv as a substrate for protein synthesis, we considered two related questions. First, would 2*S*-Tfv function more efficiently as a surrogate for valine (**2**) or for isoleucine (**1**)? Second, would either the valyl-tRNA synthetase or the isoleucyl-tRNA synthetase discriminate between the two diastereomeric forms of 2*S*-Tfv?



Scheme 1. Amino acids used in this work: (2*S*)-isoleucine (**1**), (2*S*)-valine (**2**), (2*S*,3*S*)-4,4,4-trifluorovaline (2*S*,3*S*-Tfv, **3**), and (2*S*,3*R*)-4,4,4-trifluorovaline (2*S*,3*R*-Tfv, **4**).

Initial efforts to incorporate **3** and **4** into recombinant proteins failed. Neither **3** nor **4** supported protein synthesis in *E. coli* cultures depleted of either isoleucine or valine. We then examined the kinetics of activation of **3** and **4** by the valyl- and isoleucyl-tRNA synthetases (ValRS and IleRS, respectively). The requisite genes were obtained by PCR amplification of chromosomal DNA of *E. coli*. A hexahistidine tag was placed at the amino terminus of each enzyme, and the His-tagged variants of the wild-type IleRS and ValRS were expressed in *E. coli* and purified by immobilized-metal affinity chromatography. Amino acid activation kinetics were determined in vitro by using the adenosine triphosphate–inorganic pyrophosphate ($ATP–PP_i$) exchange assay.[11,12] The results were striking; **4** is activated by both enzymes, **3** by neither (Table 1). When we compared the rates of activation by IleRS, we found the specificity constant, k_{cat}/K_m, for **4** to be reduced approximately 600-fold with respect to the native substrate **1**; for ValRS, the k_{cat}/K_m value was reduced approximately 2500-fold with respect to **2**.

Table 1: Kinetic parameters for activation of amino acids **1**–**4** by *E. coli* IleRS and ValRS.[a]

Substrate	Enzyme	k_{cat} [S^{-1}]	K_m [M]	k_{cat}/K_m (rel.)
1	IleRS	3.00	6.8	1
3	IleRS	n.a.[b]	n.a.[b]	n.a.[b]
4	IleRS	0.21	282	1/590[c]
2	ValRS	5.96	36.6	1
3	ValRS	n.a.[b]	n.a.[b]	n.a.[b]
4	ValRS	0.36	5542	1/2490[d]

[a] Substrates **1** and **2** were used as the L isomers, **3** was the 2*S*,3*S* form, and **4** was the 2*S*,3*R* form. [b] n.a. = not activated. [c] Relative to k_{cat}/K_m for activation of **1** by IleRS. [d] Relative to k_{cat}/K_m for activation of **2** by ValRS.

In our previous work on the incorporation of methionine and leucine analogues into recombinant proteins, we found that elevation of the cellular activity of aminoacyl-tRNA synthetase could facilitate introduction of amino acids that are poor substrates for the wild-type synthetases.[7,13] The

[*] P. Wang, Prof. D. A. Tirrell
Division of Chemistry and Chemical Engineering
California Institute of Technology
Pasadena, CA 91125 (USA)
Fax: (+1) 626-568-8824
E-mail: tirrell@caltech.edu
A. Fichera, Prof. K. Kumar
Department of Chemistry
Tufts University
Medford, MA 02155 (USA)

[**] This work was supported by the National Institutes of Health (grant nos. GM65500 and GM62523), by a National Sciences Foundation CAREER award (CHE-0236846), and by the National Science Foundation Center for Science and Engineering of Materials at the California Institute of Technology.

Supporting information for this article is available on the WWW under http://www.angewandte.org or from the author.

 © 2004 Wiley-VCH Verlag GmbH & Co. KGaA, Weinheim DOI: 10.1002/anie.200454036

results shown in Table 1 encouraged us to test this approach with **4**. Expression plasmids harboring either of the synthetase genes *ileS* and *valS*, each outfitted with its endogenous promoter, were constructed from pQE15 and designated pQE15-ileS and pQE15-valS, respectively. Assays of whole-cell lysates from the corresponding transformants (designated AIV-IQ[pQE15-ileS] and AIV-IQ[pQE15-valS], respectively[14]) showed enhanced activity in the ATP-PP_i exchange assay. (For AIV-IQ[pQE15-ileS], total synthetase activity was elevated approximately eightfold; for AIV-IQ[pQE15-valS], total synthetase activity was elevated approximately sixfold.)

Murine dihydrofolate reductase (mDHFR), a marker protein encoded in pQE15, served as the test protein for experiments on in vivo incorporation of **3** and **4**. Assays were performed in *E. coli* cultures depleted in the canonical amino acid and supplemented with the analogue of interest. As shown in Figure 1, strains bearing either pQE15-ileS or pQE15-valS supported protein biosynthesis in media supplemented with **4**; cultures enriched in **3** showed only background levels of mDHFR.[15] Amino acid analysis indicated that approximately 92% of the encoded isoleucine residues were replaced by **4** in mDHFR produced by the strain outfitted with additional copies of IleRS; approximately 86% of encoded valine residues were replaced by **4** in the strain outfitted with additional copies of ValRS. "Reassignment" of the isoleucine and valine codons was confirmed by MALDI MS analysis of tryptic fragments of mDHFR (Figure 2). The fragment (**5**) corresponding to residues 124–147 contains a single residue encoded as isoleucine and four encoded as valine. When this fragment is derived from mDHFR produced in pQE15-ileS cultures supplemented with **4**, reassignment of the isoleucine codons to **4** causes the expected mass shift of +40 Da (Figure 2a). In contrast, reassignment of the valine codons causes a mass increase of 54 Da for fragment **6** (corresponding to residues 62–69) derived from mDHFR expressed in the strain bearing pQE15-valS. MALDI mass spectra of the intact proteins were consistent with the results of the amino acid analyses and analyses of tryptic peptide fragments. mDHFR contains 14 sites each for valine and for isoleucine. Quantitative replacement of valine by **4** would shift the mass of the protein by +756 Da; quantitative replacement of isoleucine would give a shift of +560 Da. The observed shifts were +690 and +569 Da, respectively, a result indicating efficient—although perhaps not quantitative—codon reassignment.

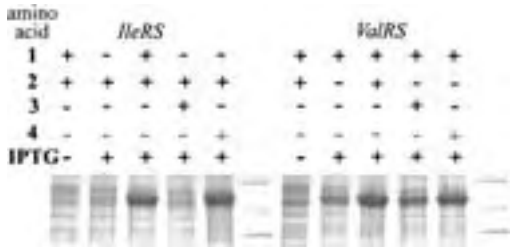


Figure 1. Sodium dodecylsulfate PAGE assay for translational incorporation of noncanonical amino acids into recombinant mDHFR. Analyses were conducted on whole-cell lysates; expression conditions are noted above each lane. IPTG = isopropyl-β,D-thiogalactoside.

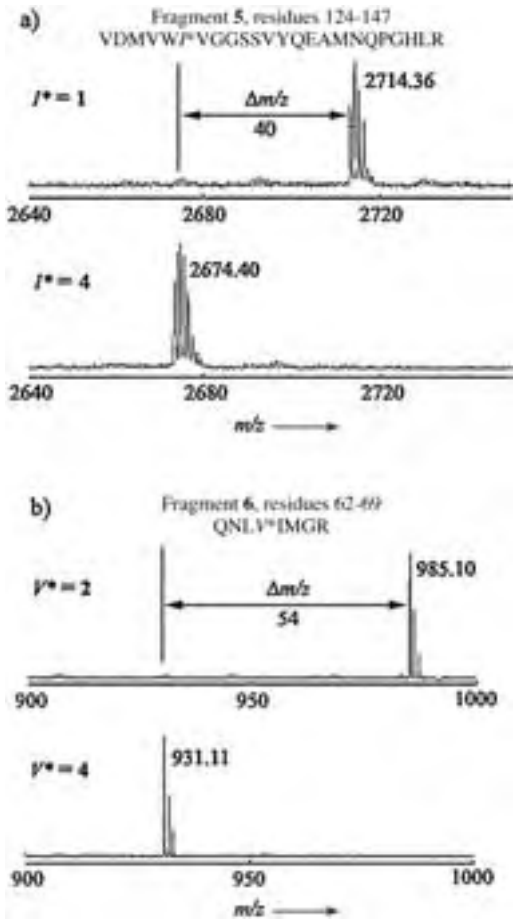


Figure 2. Reassignment of isoleucine and valine codons can be detected by MALDI MS analysis of tryptic fragments of mDHFR. a) Spectrum for fragment **5** (Val124–Arg147) from mDHFR produced by strain pQE15-ileS. The mass of this fragment is 2674.40 when the single isoleucine codon is assigned to **1** (bottom panel; mDHFR from culture supplemented with **1**). The mass shifts to 2714.36 Da when this codon is assigned to **4** (top panel; mDHFR from culture supplemented with **4**). b) Spectrum for fragment **6** (Gln62–Arg69) from mDHFR produced by strain pQE15-valS. The mass of this fragment is 931.11 Da when the single valine codon is assigned to **2** (bottom panel; mDHFR from culture supplemented with **2**). The mass shifts to 985.10 Da when this codon is assigned to **4** (top panel; mDHFR from culture supplemented with **4**).

In conclusion, these results demonstrate efficient, stereospecific introduction of 2*S*-Tfv into recombinant proteins in *E. coli*. We find that **4** can be assigned either to isoleucine codons or to valine codons depending on whether the host is engineered with enhanced IleRS or ValRS activity. Alternative translations of a single RNA message can thus be accomplished by control of the aminoacyl-tRNA synthetase activity and the amino acid pools of the expression host.

Received: February 17, 2004 [Z54036]
Published Online: June 21, 2004

Keywords: amino acids · biosynthesis · gene expression · tRNA

 © 2004 Wiley-VCH Verlag GmbH & Co. KGaA, Weinheim

[1] P. Schimmel, *Proc. Natl. Acad. Sci. USA* **1996**, *93*, 4521.
[2] L. R. de Pouplana, P. Schimmel, *Trends Biochem. Sci.* **2001**, *26*, 591.
[3] D. Soll, U. L. Rajbhandary, *tRNA: Structure, Biosynthesis, and Function*, ASM Press, Washington, DC, **1995**.
[4] B. Bilgicer, X. Xing, K. Kumar, *J. Am. Chem. Soc.* **2001**, *123*, 11815.
[5] B. Bilgicer, A. Fichera, K. Kumar, *J. Am. Chem. Soc.* **2001**, *123*, 4393.
[6] N. C. Yoder, K. Kumar, *Chem. Soc. Rev.* **2002**, *31*, 335.
[7] Y. Tang, D. A. Tirrell, *J. Am. Chem. Soc.* **2001**, *123*, 11089.
[8] Y. Tang, G. Ghirlanda, W. A. Petka, T. Nakajima, W. F. DeGrado, D. A. Tirrell, *Angew. Chem.* **2001**, *113*, 1542; *Angew. Chem. Int. Ed.* **2001**, *40*, 1494.
[9] Y. Tang, G. Ghirlanda, N. Vaidehi, J. Kua, D. T. Mainz, W. A. Goddard, W. F. DeGrado, D. A. Tirrell, *Biochemistry* **2001**, *40*, 2790.
[10] A. J. Link, M. L. Mock, D. A. Tirrell, *Curr. Opin. Biotechnol.* **2003**, *14*, 603.
[11] T. L. Hendrickson, T. K. Nomanbhoy, P. Schimmel, *Biochemistry* **2000**, *39*, 8180.
[12] Y. Tang, D. A. Tirrell, *Biochemistry* **2002**, *41*, 10635.
[13] K. L. Kiick, J. C. M. van Hest, D. A. Tirrell, *Angew. Chem.* **2000**, *112*, 2232; *Angew. Chem. Int. Ed.* **2000**, *39*, 2148.
[14] Expression strains were derived from the isoleucine and valine double-auxotrophic strain AIV-IQ (*E. coli* $BF-ompThsdS(r_B^- m_B^-)$ *gal dcm L(DE3) ilvD691*), which has been described previously (P. Wang, Y. Tang, D. A. Tirrell, *J. Am. Chem. Soc.* **2003**, *125*, 6900).
[15] Our medium-shift protocol does not completely exhaust the intracellular pool of **2**, so significant background expression was observed in the strain bearing pQE15-valS in cultures supplemented with **3**. MALDI MS analysis of tryptic peptides from these background proteins showed the valine codons in mDHFR were assigned exclusively to **2**.

 © 2004 Wiley-VCH Verlag GmbH & Co. KGaA, Weinheim

Nanotechnology

Highly Ordered SnO_2 Nanorod Arrays from Controlled Aqueous Growth**

Lionel Vayssieres and Michael Graetzel*

Besides the conventional nanorods, nanowires, and nanotubes,[1] a plethora of new 1D nanomaterials, that is, nanobelts, nanoribbons, nanodisks, nanosheets, and nanodendrites have emerged recently.[1a] Such accomplishments confirm the tremendous efforts spread worldwide to create advanced and functional building blocks for the development of innovative nanomaterials and smart nanodevices. However, the hierarchical design of well-defined and highly oriented 3D arrays of conventional 1D nanomaterials such as nanorods and nanowires in general, and their large-scale manufacturing at low cost in particular, remain crucial challenges to unfold the very promising future of nanotechnology. In addition to the economical manufacturing of nanomaterials, a better fundamental knowledge of their electronic structure, physical, interfacial, and structural properties, as well as their stability is required to fully exploit their fascinating physical and chemical potential. To fulfill such essential requirements, the creation of stable and structurally well-defined and well-ordered nanomaterials at low cost is essential.

Tin(IV) dioxide, SnO_2 (also called stannic oxide) is an insulator and an important, colorless, low-cost, large-bandgap (n-type) semiconductor material when doped with oxygen vacancies or with Sb or F ions. It is widely used as a transparent conducting oxide (TCO) substrate [2] and gas sensor[3] as well as electrode material for energy conversion[4] and storage applications.[4a] Thus, the design of SnO_2 1D nanomaterials with novel and well-defined morphologies and, in particular, as highly ordered 3D arrays, is of noteworthy importance for basic fundamental research as well as of relevance for various fields of industrial and high-tech applications.

[*] Dr. L. Vayssieres
Photonics and Interface Laboratory
Institute of Chemical Sciences and Engineering
Swiss Federal Institute of Technology (EPFL)
1015 Lausanne (Switzerland)
and
International Center for Young Scientists
National Institute for Materials Science
Namiki 1-1, Tsukuba, Ibaraki 305-0044 (Japan)
Fax: (+81) 298-604-706
E-mail: vayssieres.lionel@nims.go.jp
Prof. M. Graetzel
Photonics and Interface Laboratory
Institute of Chemical Sciences and Engineering
Swiss Federal Institute of Technology (EPFL)
1015 Lausanne (Switzerland)

[**] This work was supported by the Swiss National Science Foundation under the NRP 47 program. K. Schenk (Laboratoire de Cristallographie) as well as I. Brauer and P. Stadelman (Centre Interdisciplinaire de Microscopie Electronique) from the Ecole Polytechnique Fédérale de Lausanne are acknowledged for their assistance.

 © 2004 Wiley-VCH Verlag GmbH & Co. KGaA, Weinheim DOI: 10.1002/anie.200454000

Hitherto, several reports have described the fabrication of powders of SnO_2 nanorods by various techniques that involve a microemulsions,[5] redox reactions,[6] thermal decomposition of oxalate in air[7] or in solution,[8] vapor–liquid–solid (VLS) catalytic growth,[9] laser ablation,[10] thermal evaporation[11] or oxidation of metallic tin.[12] However, only one method has been reported for the creation of SnO_2 oriented nanorod arrays.[13] This synthesis involves conventional processing by using template techniques, that is, electrodeposition and thermal oxidation in an anodic alumina membrane. However, the morphology of the nanorods is rather ill-defined as a result of the processing technique. We report herein a simple, one-step, aqueous, low-temperature growth process for the inexpensive fabrication of large (several tens of cm^2) 3D arrays of highly ordered and crystalline SnO_2 nanorods of typically 50 nm in width and 500 nm in length with a uniquely designed architecture and without the need of template, surfactant, applied field, or undercoating on various substrates. Well-defined and perpendicularly oriented crystalline nanorods with a square cross section (elongated along the *c* axis and exhibiting (110) prismatic faces) are obtained directly on polycrystalline, single-crystalline, or amorphous substrates from the controlled heteronucleation of SnO_2 by aqueous precipitation of Tin(IV) salts at mild temperatures (i.e., below 100 °C) in the presence of urea.

The thermodynamically stable crystal structure of SnO_2 is rutile (tetragonal crystal system), which occurs in nature as the native mineral cassiterite, the principal ore of tin. Cassiterite is isostructural to rutile (TiO_2), argutite (GeO_2), paratellurite (TeO_2), plattnerite (PbO_2), stishovite (SiO_2) and pyrolusite (MnO_2) as well as VO_2, CrO_2, RuO_2, NbO_2, TaO_2, OsO_2, and IrO_2. SnO_2 crystallizes in point group symmetry $4/mmm$ and space group $P4_2/mnm$ (D_{4h}^{14}) with tin and oxygen atoms in 2a and 4f positions, respectively. The unit cell consists of two tin atoms and four oxygen atoms. Each metal atom is situated amidst six oxygen atoms, which approximately form the corners of a regular octahedron. Oxygen atoms are surrounded by three tin atoms, which approximate the corners of an equilateral triangle. Two of each twelve octahedral edges are shared with other octahedra. Edge sharing is symmetrical; the shared edges are opposite each other in the rutile structure. Thus, the octahedra form linear chains, and these chains run parallel to the *c* axis and combine by sharing two opposed edges per octahedron. Each of these chains is surrounded and cross-linked to four identical octahedral chains that twisted at 90° to the first chain. Adjacent chains are all staggered *c*/2 by the 4_2 screw axes that are oriented along tunnels that are parallel to the *c* axis. Consequently, the highest electron density as well as high polarizability and birefringence is observed along the *c* axis. Typical lattice parameters are $a = 4.737$ Å, and $c = 3.186$ Å yielding an axial ratio of $a:c = 1:0.672$. The low index (110) face is the thermodynamically most-stable bulk termination[14] and has the lowest surface energy,[14a] that is, the surface excess free energy per unit area. The sequence of surface energy per crystal face is $(110) < (100) < (101) \ll (001)$. The (110) stoichiometric surface, in which a half of the surface cations are fivefold coordinated with oxygen atoms and the other half are sixfold coordinated because of the presence of a row of bridging oxygen atoms, yields tin atoms with a formal oxidation state of +IV. Thus, surface and bulk have similar resistivity. The (110) surface has no net dipole moment in the [110] direction and is therefore a nonpolar surface. Additionally, this centrosymmetric structure of low axial ratios reduces substantially the probability of anisotropic growth of the crystal along the [001] direction, and thus reduces the generation of *c*-elongated prismatic crystals. For this reason, SnO_2 1D nanostructures seldom grow along the *c* axis but rather along the [101],[1,7,15] [301],[9,15a] [200],[10] or [11−2][5] directions. However, by allowing a slow generation of nuclei by chemical means as well as a slow nucleation and growth at low interfacial tension conditions (thermodynamic stability), stable *c*-elongated anisotropic nanocrystals exhibiting stable (110) faces may be generated. Thus, according to crystal-symmetry and surface-energy considerations, a typical crystal habit should be acicular and tabular and should exhibit a square cross section (Figure 1). In addition, if such a mechanism were operative directly at the surface of a substrate (single or polycrystalline, or amorphous), which represents a reduced surface-energy barrier compared to homogeneous nucleation, highly oriented nanorods would grow with normal incidence onto the substrate surface.

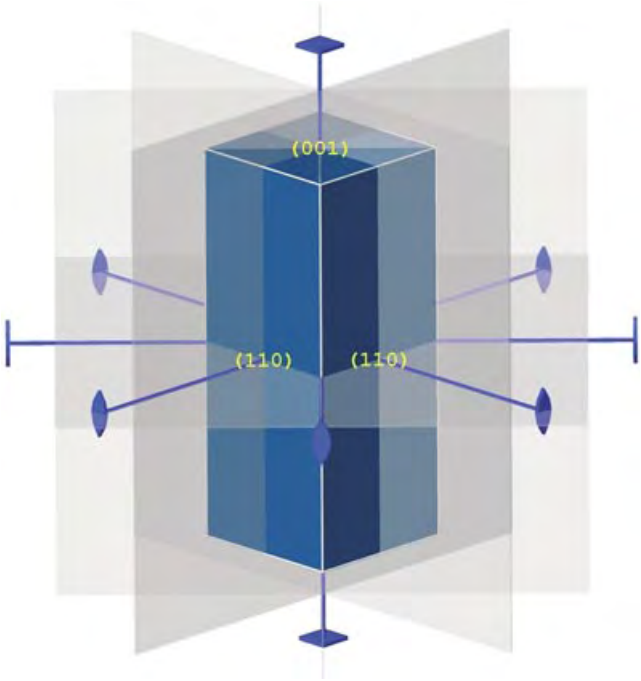


Figure 1. Crystal habit of a rutile SnO_2 (cassiterite) nanorod according to $P4_2/mnm$ symmetry elements and surface energy considerations.

Our strategy to design and control the morphology and orientation of crystallites in large 2D and 3D arrays consists of monitoring the thermodynamics and kinetics of nucleation and growth of metal-oxide materials by controlling experimentally their interfacial tension[16] through a variation of the chemical and electrostatic composition of the water–oxide interface. The synthesis conditions (pH, ionic strength, and

 © 2004 Wiley-VCH Verlag GmbH & Co. KGaA, Weinheim

aqueous precursors) are tuned to allow the system to evolve with minimum surface energy, that is, under conditions that are thermodynamically stable. The kinetics are regulated by adjusting the temperature and the concentration of precursors, thus controlling the hydrolysis rate and ratio, which in turn control the nucleation and growth processes. By conducting experiments in solutions that result from the hydrolysis–condensation of aqueous metal-ion precursors (see below), the morphology is therefore dictated by the crystal symmetry as well as by the surface energy in the aqueous environment and thus the most stable crystal habit is generated directly onto the substrates, without template, surfactant, applied field, or undercoating from molecular scale to nano-, meso- or microscale. This concept of "purpose-built nanomaterials",[17] and the thin-film aqueous-growth method[18] have been successfully applied to the fabrication of oriented arrays of basic transition-metal oxides and oxyhydroxides. For instance, the design of large arrays of 3D crystalline highly ordered α-Fe_2O_3,[19] β-FeOOH,[19a] γ-MnOOH,[19b] α-Fe[19c] nanorod arrays, as well as ZnO nanorod,[19d] microrod,[19e] and microtube[19f] arrays have been conducted successfully to illustrate the capability of such an approach.

In accordance with the above-mentioned growth concept, the synthesis was conducted by hydrolysis–condensation of hydrated metal cations by aqueous thermohydrolysis of Sn^{IV} centers in acidic medium with reagent-grade chemicals. Urea, $(NH_2)_2CO$ (also called carbamide or carbonyl diamine) is a nonionic, nontoxic, inexpensive, stable, crystalline, and water-soluble compound. It was chosen to afford simultaneously hydrolysis–condensation by olation of the tetravalent Sn^{IV} ion, most probably from the of zero-charge complex $[Sn(OH)_4(H_2O)_2]$, and the nucleation and growth of its stable dioxide form, rutile SnO_2, by oxolation (the formation of oxo bridges by the elimination of water) from the slow release of hydroxyl ions owing to the well-known thermal decomposition of urea in aqueous solutions. A typical synthesis involved the preparation of a 100 mL aqueous solution (MilliQ+, 18.2 MΩcm) consisting of 0.034 g of $SnCl_4{\cdot}5H_2O$ and 0.920 g of $(NH_2)_2CO$ in presence of 5 mL of fuming HCl (37%) in a closed pyrex bottle with autoclavable screw cap. A large, polycrystalline F–SnO_2 glass substrate (e.g., Hartford Glass Inc. TEK-8), silicon or silicon oxide wafer, or a bare piece of glass (e.g., microscope glass slide), cleaned with diluted acid, ethanol, acetone, subsequently rinsed with MilliQ water, and dried in air was placed standing against the walls of the closed bottle. Thereafter, the bottle was placed in a regular laboratory oven and heated at a constant temperature of 95°C for 2 days. Subsequently, the fully covered and homogeneous thin films were thoroughly washed with water (MilliQ) to remove any possible contamination from residual salts. Fully covered and uniform arrays of several tens of centimeters square, and potentially much larger with larger substrate and container, may be easily produced at very low cost and in a reasonable amount of time.

As expected from the thermodynamic and crystal-symmetry arguments, crystalline nanorods with square cross sections and well-defined crystallographic faces are grown directly onto the substrates. These nanorods, which are typically 50 nm in width and about 500 nm in length (aspect ratio 1:10), are generally perpendicular and arranged in very-large uniform arrays (Figure 2). According to electron and X-ray diffractions, cassiterite (SnO_2 with the rutile structure) is

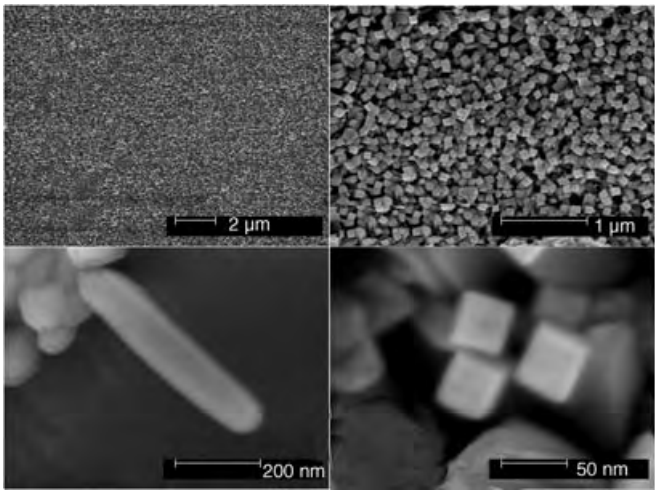


Figure 2. Field-emission gun scanning electron microscopy (FEGSEM) images of SnO_2 nanorods and oriented nanorod arrays, which have a square cross section and have been grown on a TCO glass substrate by controlled aqueous growth.

the only crystallographic phase detected, without significant shift of the lattice spacing compared to bulk SnO_2 (Figure 3). Refinements yield lattice parameters equal to 4.754 and 3.175 Å for *a* and *c*, respectively. The thin film XRD pattern, whose intensity has been normalized to the strongest reflection, shows a substantial texture effect in accordance with the crystal shape anisotropy and orientation. The relative maximum intensity sequence is no longer $(110) > (101) > (211) > (200) > (301) \approx (310) \approx (220) \gg (002) \gg (111) \gg (210)$ but $(101) > (110) > (211) \gg (002) \approx (200) \approx (112) > (301) \approx (111) \approx (220) > (310)$.

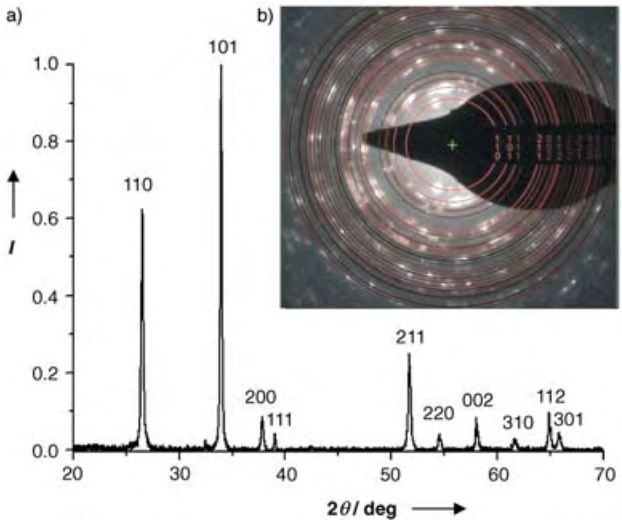


Figure 3. a) Indexed electron and b) X-ray diffraction patterns of SnO_2 nanorods and oriented nanorod-arrays, respectively. *I* is intensity.

 © 2004 Wiley-VCH Verlag GmbH & Co. KGaA, Weinheim

As-prepared nanorods are polycrystalline as illustrated by high-resolution (HR) TEM observations (Figure 4) and consist of bundles of finer nanorods of about 2–4 nm in width (aspect ratio of about 1:100). The spacing of the lattice

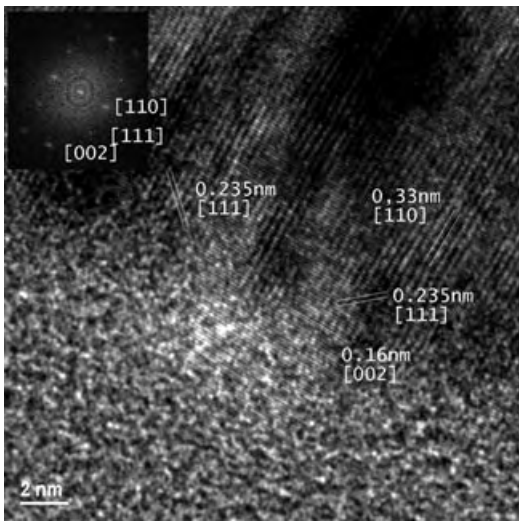


Figure 4. HRTEM and Fourier transform images of a typical SnO_2 nanorod bundle consisting of finer nanorods.

fringes was found to be 0.33, 0.235, and 0.16 nm and these planes are best indexed as (110), (111), and (002) of rutile SnO_2, respectively. Accordingly, the direction of growth of the SnO_2 nanorods is along the *c* axis and with side and top faces consisting of (110) and (001) planes, respectively.

Besides the great stability of (110) faces, it was demonstrated that this surface provides the best efficiency for the chemisorption and dissociation of oxygenated compounds at the SnO_2 interface owing to the lowest interatomic distances between tin atoms (compared to (101) and (111) faces).[20] This factor in particular is of crucial importance for the improvement of the efficiency of SnO_2 photocatalytic and sensing devices. Given that the exposed prismatic faces of the SnO_2 nanorods presented here are the most stable (110) faces, such unique architecture, that is, *c*-elongated and squared cross section with well-defined faces, confers to these arrays a great potential for the development of innovative and functional SnO_2 nanosensors. For instance, better sensitivity and selectivity is foreseen due to the optimized exposed faces as well as a fast response (lower latency time) due to the direct growth of the nanorod bundles onto various substrates, their perpendicular orientation and their anisotropy along the *c* axis, which offers a direct and very efficient electron pathway. Finally, such arrays are excellent candidates for a better fundamental understanding of the electronic-structure and quantum-confinement effects of anisotropic nanocrystals, for example, by polarization-dependent soft-X-ray spectroscopic studies[21] as well as for modeling and simulation studies of interfacial interactions and structure–reactivity relationships of 1D metal oxide nanostructures.

Received: February 11, 2004
Revised: April 22, 2004 [Z54000]

Keywords: nanostructures · nanotechnology · thin films · tin · water chemistry

[1] L. Vayssieres in *Encyclopedia of Nanoscience and Nanotechnology, Vol. 8* (Ed.: H. S. Nalwa), American Scientific Publishers, Stevenson Ranch, CA, **2004**, pp. 147–166; a) Z. R. Dai, Z. W. Pan, Z. L. Wang, *Adv. Funct. Mater.* **2003**, *13*, 9–24.
[2] T. Minami, *MRS Bull.* **2000**, *25(8)*, 38–44; E. Elangovan, K. Ramamurthi, *J. Optoelectron. Adv. Mater.* **2003**, *5*, 45–54.
[3] Y. Shimizu, T. Hyodo, M. Egashira, *J. Eur. Ceram. Soc.* **2004**, *24*, 1389–1398; C. O. M. Su, S. Li, V. P. Dravid, *J. Am. Chem. Soc.* **2003**, *125*, 9930–9931M. Law, H. Kind, B. Messer, F. Kim, P. D. Yang, *Angew. Chem.* **2002**, *114*, 2511; *Angew. Chem. Int. Ed.* **2002**, *41*, 2405; P. G. Harrison, M. J. Willet, *Nature* **1988**, *332*, 337–339.
[4] N. Park, M. G. Kang, K. S. Ryu, K. M. Kim, S. H. Chang, *J. Photochem. Photobiol. A* **2004**, *161*, 105–110; G. Benko, P. Myllyperkio, J. Pan, A. P. Yartsev, V. Sundstrom, *J. Am. Chem. Soc.* **2003**, *125*, 1118–1119; T. Hasobe, H. Imahori, P. V. Kamat, S. Fukuzumi, *J. Am. Chem. Soc.* **2003**, *125*, 14962–14963; C. Bauer, G. Boschloo, E. Mukhtar, A. Hagfeldt, *Int. J. Photoenergy* **2002**, *4*, 17–20; M. Graetzel, *Nature* **2001**, *414*, 338–344; a) P. R. Bueno, E. R. Leite, T. R. Giraldi, L. O. S. Bulhoes, E. Longo, *J. Phys. Chem. B* **2003**, *107*, 8878–8883; N. Li, C. R. Martin, B. Scrosati, *Electrochem. Solid-State Lett.* **2000**, *3*, 316–318.
[5] D.-F. Zhang, L.-D. Sun, J.-L Yin, C.-H. Yan, *Adv. Mater.* **2003**, *15*, 1022–1025; a) Y. Liu, C. Zheng, W. Wang, C. Yin, G. Wang, *Adv. Mater.* **2001**, *13*, 1883–1887.
[6] Y. Liu, C. Zheng, W. Wang, Y. Zhan, G. Wang, *J. Cryst. Growth* **2001**, *233*, 8–12.
[7] C. Xu, G. Xu, Y. Liu, X. Zhao, G. Wang, *Scr. Mater.* **2002**, *46*, 789–794.
[8] Y. Wang, X. Jiang, Y. Xia, *J. Am. Chem. Soc.* **2003**, *125*, 16176–16177.
[9] Y. Chen, X. Cui, K. Zhang, D. Pan, S. Zhang, B. Wang, J. G. Hou, *Chem. Phys. Lett.* **2003**, *369*, 16–20.
[10] Z. Liu, D. Zhang, S. Han, C. Li, T. Tang, W. Jin, X. Liu, B. Lei, C. Zhou, *Adv. Mater.* **2003**, *15*, 1754–1757.
[11] W. Wang, C. Xu, X. Wang, Y. Liu, Y. Zhan, C. Zheng, F. Song, G. Wang, *J. Mater. Chem.* **2002**, *12*, 1922–1925.
[12] A. Kolmakov, Y. Zhang, M. Moskovits, *Nano Lett.* **2003**, *3*, 1125–1129; J. K. Jian, X. L. Chen, T. Xu, Y. P. Xu, L. Dai, M. He, *Appl. Phys. A* **2002**, *75*, 695–697.
[13] A. Kolmakov, Y. Zhang, G. Sheng, M. Moskovits, *Adv. Mater.* **2003**, *15*, 997–1000; M. Zheng, G. Li, X. Zhang, S. Huang, Y. Lei, L. Zhang, *Chem. Mater.* **2001**, *13*, 3859–3861.
[14] M. Batzill, K. Katsiev, U. Diebold, *Surf. Sci.* **2003**, *529*, 295; V. A. Gercher, D. F. Cox, J.-M. Themlin, *Surf. Sci.* **1994**, *306*, 279–293; D. F. Cox, T. B. Fryberger, S. Semancik, *Phys. Rev. B* **1988**, *38*, 2072–2083; a) A. Beltran, J. Andres, E. Longo, E. R. Leite, *Appl. Phys. Lett.* **2003**, *83*, 635–637; J. Oviedo, M. J. Gillan, *Surf. Sci.* **2000**, *463*, 93–101; P. A. Mulheran, J. H. Harding, *Modell. Simul. Mater. Sci. Eng.* **1992**, *1*, 39–43.
[15] L. B. Fraigi, D. G. Lamas, N. E. W. de Reca, *Mater. Lett.* **2001**, *47*, 262; C. Xu, X. Zhao, S. Liu, G. Wang, *Solid State Commun.* **2003**, *125*, 301–304; a) J. X. Wang, D. F. Liu, X. Q. Yan, H. J. Yuan, L. J. Ci, Z. P. Zhou, Y. Gao, L. Song, L. F. Liu, W. Y. Zhou, *Solid State Commun.* **2004**, *130*, 89–94.
[16] L. Vayssieres, *Int. J. Nanotechnol.* **2004**, *1*, 1–41; L. Vayssieres, *J. Colloid Interface Sci.* **1998**, *205*, 205–212; L. Vayssieres, PhD thesis, Université Pierre et Marie Curie (Paris), **1995**.
[17] L. Vayssieres, A. Hagfeldt, S.-E. Lindquist, *Pure Appl. Chem.* **2000**, *72*, 47–52.
[18] L. Vayssieres, *Int. J. Mater. Prod. Technol.* **2003**, *18*, 313–337; L. Vayssieres, A. Hagfeldt, S.-E. Lindquist, Patent WO9935312, **1999**, pp. 1–49.

 © 2004 Wiley-VCH Verlag GmbH & Co. KGaA, Weinheim

[19] L. Vayssieres, N. Beermann, S.-E. Lindquist, A. Hagfeldt, *Chem. Mater.* **2001**, *13*, 233 – 235; a) L. Vayssieres, J.-H. Guo, J. Nordgren, *Mater. Res. Soc. Symp. Proc.* **2001**, *635*, 781 – 786; b) L. Vayssieres, A. Manthiram, *Mater. Res. Soc. Symp. Proc.* **2003**, *739*, 249 – 254; c) L. Vayssieres, L. Rabenberg, A. Manthiram, *Nano Lett.* **2002**, *2*, 1393 – 1395; d) L. Vayssieres, *Adv. Mater.* **2003**, *15*, 464 – 466; e) L. Vayssieres, K. Keis, S.-E. Lindquist, A. Hagfeldt, *J. Phys. Chem. B* **2001**, *105*, 3350 – 3352; f) L. Vayssieres, K. Keis, A. Hagfeldt, S.-E. Lindquist, *Chem. Mater.* **2001**, *13*, 4395 – 4398.

[20] V. Brinzari, G. Korotcenkov, V Golovanov, J. Schwank, V. Lantto, S. Saukko, *Thin Solid Films* **2002**, *408*, 51 – 58; D. Kohl, *Sens. Actuators* **1989**, *18*, 71; M. Egashira, T. Matsumoto, Y. Shimizu, H. Iwanaga, *Sens. Actuators* **1988**, *14*, 205; V. Brinzari, G. Korotcenkov, S. Dmitriev, *Sens. Actuators B* **1999**, *61*, 143 – 153.

[21] J.-H. Guo, L. Vayssieres, C. Persson, R. Ahuja, B. Johansson, J. Nordgren, *J. Phys. Condens. Matter* **2002**, *14*, 6969 – 6974.

 © 2004 Wiley-VCH Verlag GmbH & Co. KGaA, Weinheim

Phase Transitions

Direct Observation of Bonding and Charge Ordering in $(EDO\text{-}TTF)_2PF_6$**

*Shinobu Aoyagi, Kenichi Kato, Akira Ota, Hideki Yamochi, Gunzi Saito, Hiroyoshi Suematsu, Makoto Sakata, and Masaki Takata**

The characteristics of the metal–insulator (MI) phase transition in $[(EDO\text{-}TTF)(EDO\text{-}TTF^{+})PF_6^{-}]$ (EDO-TTF = ethylenedioxytetrathiafulvalene) have been suggested so far to be the result of cooperative phenomena: Peierls distortion, charge ordering, anion ordering, and the molecular deformation which is evident from the single-crystal X-ray analysis and the peak shifts in the Raman spectrum.[1,2] However, there has been no direct evidence of charge-ordering patterns connected with the MI transition. Herein, we present direct evidence for an ordering of $(EDO\text{-}TTF)^{+}$ and $(EDO\text{-}TTF)^{0}$ along the nesting vector visualized in the $(EDO\text{-}TTF)_2PF_6$ charge density distributions obtained by a combination of the MEM (maximum entropy method) and the Rietveld method.[3–9] The charge transfer and coulombic interactions between PF_6^{-} anions and EDO-TTF molecules as well as a hole concentration on one S atom in $(EDO\text{-}TTF)^{+}$ were also revealed by the charge densities. In addition, a bonding between the EDO-TTF molecules that suggests quasi-one-dimensional (1D) properties was found in the MEM charge density. Changes in the bonding during the MI transition that may explain the existence of the insulator singlet state also became evident.

A number of 1D organic conductors that are formed from large planar electron-donating molecules such as TTF derivatives have been studied extensively because of their attractive phase transitions and the possibility of using them in functional molecular devices.[10,11] Most of the MI transitions can be classified as Peierls transitions, charge ordering, Mott transitions, or Anderson localization.[10–15] The MI transition in the $^3/_4$-filled-band ($^1/_4$-filled in terms of holes) quasi-1D system $(EDO\text{-}TTF)_2PF_6$ ($C_{16}H_{12}S_8O_4PF_6$) ($T_{MI} \approx 280$ K), however, has been considered as the particular example which shows the cooperative action of Peierls distortion, charge ordering, and anion ordering, together with a molecular deformation.[1,2] The charge-ordering pattern of EDO-TTF donor molecules has been suggested to be [0,0,+1,+1,…] by previous studies,[1,2] despite the fact that in most $^1/_4$-filled-band 1D systems the ordering pattern [0,+1,0,+1,…] is found as a result of strong neighbor-site coulombic interactions.[13–15] Recently, ultrafast photoswitching from the insulator to the metallic phase has also been reported for this system.[16] The peculiar phase transition in $(EDO\text{-}TTF)_2PF_6$ is quite attractive for a better understanding of cooperative and coherent phenomena in organic conductors. However, the structural information was limited to the atomic parameters when conventional single-crystal X-ray analysis was applied.[1] More detailed information on the MI transition, such as intermolecular bonding and charge transfer between molecules, must be obtained by an X-ray charge-density study.[17–19]

The synchrotron-radiation (SR) powder-diffraction experiment with imaging-plate (IP) detectors was carried out with the large Debye–Scherrer camera at SPring-8 BL02B2.[20] The wavelength of the incident X-rays was 1.0 Å. Data were measured for the metallic phase at 285 K and for the insulator phase at 260 K and analyzed by the MEM/Rietveld method.[3,21,22] This method has been successfully applied, for example, in charge-density studies of fullerene compounds,[3–6] intermetallic compounds,[7] α-boron,[8] and manganite.[3,9] In the case of metallofullerenes, it has revealed charge transfer from the encapsulated metal atom to the fullerene cage.[3–6] The best-fit plots of the results of the Rietveld analyses are shown in Figure 1. The reliability

[*] K. Kato, Prof. Dr. H. Suematsu, Prof. Dr. M. Takata
SPring-8/JASRI
Kouto, Mikazuki, Sayo, Hyogo 679-5198 (Japan)
Fax: (+81) 791-58-0946
E-mail: takatama@spring8.or.jp
Dr. S. Aoyagi, Prof. Dr. M. Sakata
Department of Applied Physics
Nagoya University
Nagoya 464-8603 (Japan)
A. Ota, Prof. Dr. G. Saito
Division of Chemistry
Graduate School of Science
Kyoto University
Sakyo-ku, Kyoto 606-8502 (Japan)
Prof. Dr. H. Yamochi
Research Center for Low Temperature and Materials Sciences
Kyoto University
Sakyo-ku, Kyoto 606-8502 (Japan)

[**] We thank Dr. E. Nishibori for his help in the MEM/Rietveld analyses. The synchrotron radiation experiments were performed at SPring-8 BL02B2 with the approval of the Japan Synchrotron Radiation Research Institute (JASRI). This work was partly supported by Grants-in-Aid for scientific research and for the 21st century COE program of Kyoto University Alliance for Chemistry from the Ministry of Education, Culture, Sports, Science and Technology of Japan. This work was also supported by the Showa Shell Environmental Research Foundation.

 © 2004 Wiley-VCH Verlag GmbH & Co. KGaA, Weinheim DOI: 10.1002/anie.200454075

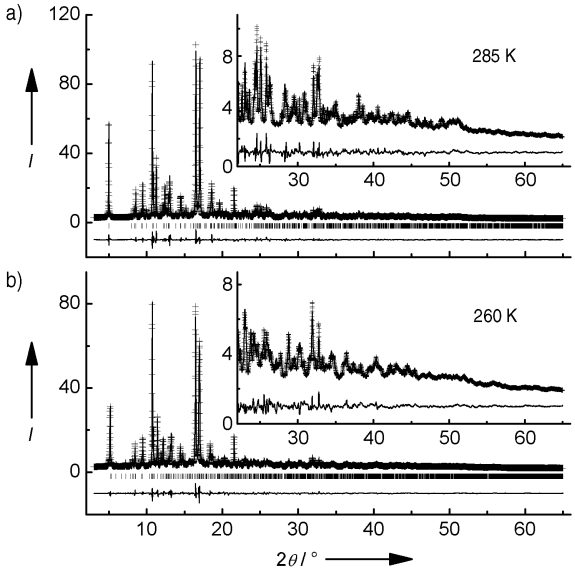


Figure 1. Best-fit plots of the results of Rietveld analysis for metallic (a) and insulating (b) $(EDO\text{-}TTF)_2PF_6$. The data up to 65° in 2θ, which corresponds to 0.93 Å in d spacing, were used in the analyses. The high-angular region is shown enlarged in the insets.

factors based on the Bragg intensities, R_I, and on the weighted profile, R_{WP}, were 0.0375 (0.0338) and 0.0447 (0.0425), respectively, for the metallic (insulator) phase. A total of 1564 (3093) independent structure factors were used in the MEM analyses, which were carried out with the unit cell divided into $64 \times 64 \times 128$ ($128 \times 128 \times 128$) pixels by using the program ENIGMA.[23] The R factor based on the structure factors, R_{MEM}, for the final MEM charge densities was 0.0285 (0.0528).

The equi-charge-density surfaces at the level of 0.7 e Å^{-3} of metallic and insulating $(EDO\text{-}TTF)_2PF_6$ are shown in Figure 2. In both the metallic and the insulator phases, layers of EDO-TTF molecules form columns by a head-to-tail stacking perpendicular to the molecular plane, which provides a donor layer parallel to the ab plane. PF_6^- anions are located at the cavities between the EDO-TTF layers. Whereas the metallic and insulator phases have the same space group $P\bar{1}$, the unit cell is doubled in the insulator phase ($Z = 2$), corresponding to a Peierls instability along the [110] direction in the cell of the metallic phase ($Z = 1$). Cell parameters were derived as $a_M = 7.1942$, $b_M = 7.3214$, $c_M = 11.9304$ Å, $\alpha_M = 93.345$, $\beta_M = 75.054$, $\gamma_M = 97.435°$ for the metallic phase, and $a_I = 10.9898$, $b_I = 9.7954$, $c_I = 11.4864$ Å, $\alpha_I = 80.734$, $\beta_I = 78.079$, $\gamma_I = 90.241°$ for the insulator phase. The averaged intermolecular distances in the insulator phase are 0.7 and 2.3 % longer along a and b and 3.7 % shorter along c than those in the metallic phase.

The PF_6^- anions are disordered in the metallic phase (overlapping of two octahedra with a tilt of about 50°), whereas they are ordered in the insulator phase. These results are slightly different from the results of reference [1], and indicate an isotropic-to-uniaxial rotational ordering of the PF_6^- anions. The reason for this discrepancy may be the poor quality of the previous diffraction data. In the insulator phase, two types of EDO-TTF molecules are present, flat and bent molecules, whereas in the metallic phase, there is only one type of EDO-TTF molecule. This molecular-shape change associated with the MI transition is in good agreement with the previously reported X-ray structure model.[1]

Since MEM charge densities reflect total electron densities, the charge states of EDO-TTF and PF_6^- can be examined by counting the number of electrons around them, as was done in the metallofullerene studies.[3–6] The results for the metallic phase (Figure 2a,c) are +0.6(1) e for EDO-TTF and −1.2(1) e for PF_6^-. For the insulator phase (Figure 2b,d), the results are +0.8(1) e for flat EDO-TTF, +0.2(1) e for bent EDO-TTF, and −1.0(1) e for PF_6^-. Thus, the bent EDO-TTF molecules are almost electrically neutral and the flat EDO-TTF molecules have an excess charge concentration close to +1 e in the insulator phase. This is the first direct evidence of a charge-ordering pattern.

The PF_6^- anions are located close to the sulfur atoms S1 (S11, S21) and S4 (S14, S24), and to the terminal hydrogen atoms of the EDO-TTF molecules (see Figure 2). The distances between the PF_6^- anions and the neighboring sulfur atoms are given in Figure 3 for both phases. The MI transition leads not only to a rotational ordering of the PF_6^- anions but also to their displacement from the inversion center by 0.26 Å. This has the biggest effect on the P–S11 distance, which is shortened from 4.32 to 4.14 Å. A particular electrostatic interaction between PF_6^- and S11 must play an important role in this shortening. To investigate the local charge concentration, the charge-density differences, $\Delta\rho$,

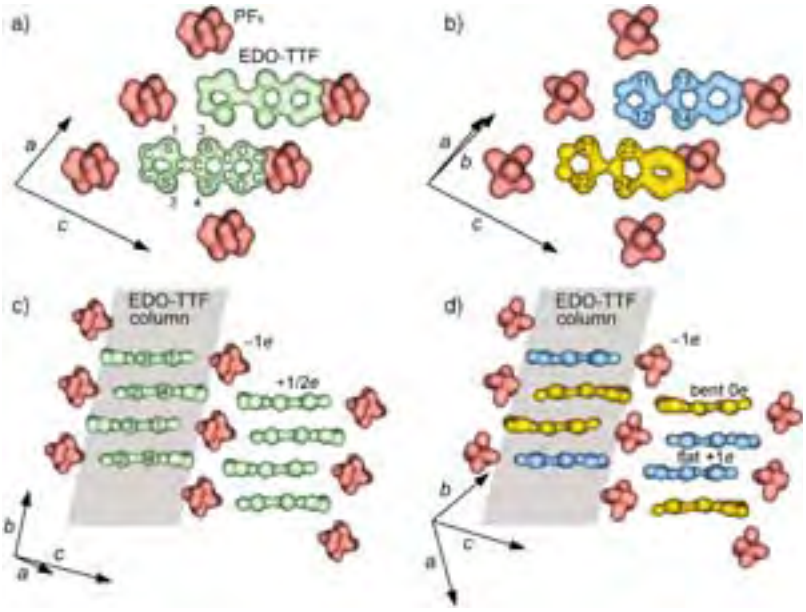


Figure 2. Equi-charge-density surfaces of metallic ((a) and (c)) and insulating ((b) and (d)) $(EDO\text{-}TTF)_2PF_6$ at the level of 0.7 e Å^{-3}. The views in (a) and (b) are along the EDO-TTF stacking direction; in (c) and (d), side views of the EDO-TTF columns are shown. The PF_6^- anion is colored in red. The EDO-TTF molecules are colored in green for the metallic phase, and in blue and yellow for the flat and bent molecules, respectively, for the insulator phase. Sulfur atoms are labeled S1–S4 for the metallic phase and S11–S14, S21–S24 for the insulator phase.

 © 2004 Wiley-VCH Verlag GmbH & Co. KGaA, Weinheim

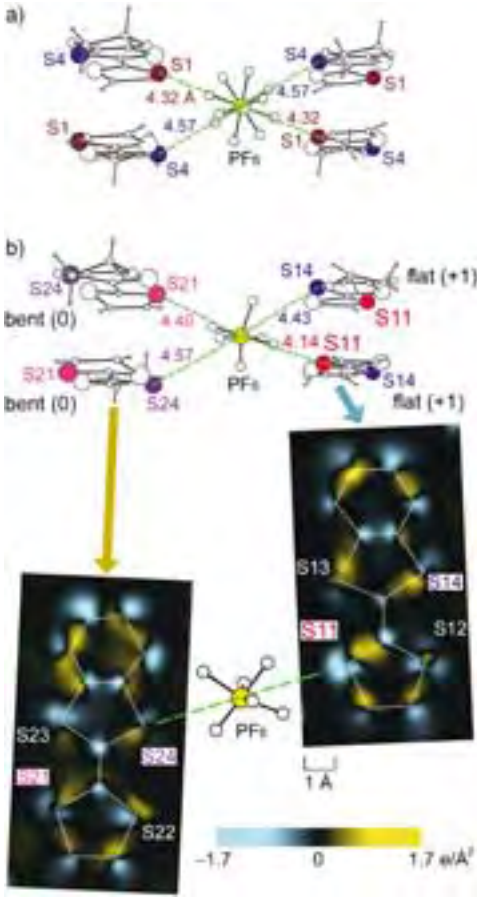


Figure 3. Structure model and interatomic distances between P and S atoms for the metallic phase (a) and for the insulator phase (b). The charge-density differences for the bent and flat EDO-TTF molecules in the insulator phase, integrated perpendicular to the molecular plane for the range of ±1.5 Å, are also shown in (b); blue: residual positive charge; yellow: residual negative charge.

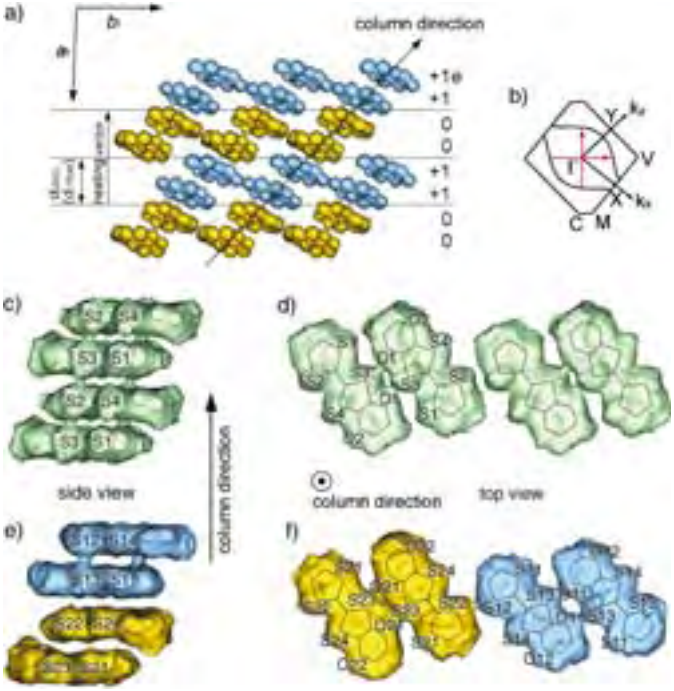


Figure 4. MEM equi-charge-density surface of an EDO-TTF layer at 0.7 e Å^{-3} and charge-ordering pattern in the insulator phase viewed along the *c* axis (a). Schematic Fermi surface in the a^*b^* plane for the metallic phase, with red arrows indicating the $2k_F$ nesting vectors (b). Side and top views of the lower MEM equi-charge-density surfaces of EDO-TTF columns in the metallic phase ((c) and (d)) and in the insulator phase ((e) and (f)). The levels of the surfaces are 0.11 for (c) and (d) and 0.13 e Å^{-3} for (e) and (f).

between the observed MEM charge density, ρ_{obs}, and the density calculated based on an arrangement of neutral free atoms, ρ_{cal}, for the bent and flat EDO-TTF molecules in the insulator phase are also shown in Figure 3b. As can be seen from Figure 3b, there is a significant positive-charge concentration around the S11 atomic site in flat EDO-TTF compared to the corresponding S21 site in bent EDO-TTF, which indicates that the conduction holes of the metallic phase are localized and trapped on the S11 atoms of the flat molecules in the insulator phase. Therefore, the local electrostatic P–S11 interaction should contribute to the hole trapping on the S11 atom. In addition, it is plausible that the suppression of the anion rotation is caused by the anion displacement that is necessary to increase the electrostatic stabilization.

The hole trapping on the EDO-TTF molecule and the displacement of the PF_6^- anion alternate in the *ab* plane with a periodicity of $2k_F$ ($2\boldsymbol{k}_F = (\boldsymbol{a}^*_M \pm \boldsymbol{b}^*_M)/2$: nesting vector of the Fermi surface). As a result, the [0,0,+1,+1,…] ordering of the charges is along the a^*_I axis ($[1\bar{1}0]_M$, Figure 4a), whereas a [0,+1,0,+1,..] ordering is expected for a $^1/_4$-filled-band system if there is no Peierls instability and if off-site Coulomb repulsions are effective.[13–15]

The side view of the lower equi-charge-density surface of an EDO-TTF column in the metallic phase at 0.11 e Å^{-3} (Figure 4c) reveals intracolumnar intermolecular overlap of charge density, thus indicating a weakly bonded S2···S3···S2···S3··· chain. This chain is considered as a 1D conducting path of holes along the EDO-TTF stacking axis. Figure 4d shows a top view of the EDO-TTF columns. In the intercolumnar region, charge-density overlap occurs between S3 and O1 atoms. It has been argued that the contribution of the external oxygen atoms to the highest occupied molecular orbital (HOMO) in BEDO-TTF complexes is less than that of the internal sulfur atoms.[24] However, it is suggested that the external O1 atoms in $(EDO\text{-}TTF)_2PF_6$ participate greatly in the intercolumnar interaction to increase the electronic dimensionality of the complex.

The lower equi-charge-density surfaces of EDO-TTF columns in the insulator phase at 0.13 e Å^{-3} are shown in Figure 4e,f. The charge-density overlaps between EDO-TTF columns in the insulator phase and in the metallic phase are very similar (Figure 4d,f). On the other hand, there is a significant change in the intracolumnar intermolecular charge density accompanying the MI transition (see Figure 4c,e). The bond between the flat molecules still exists, whereas the bonds between flat and bent molecules and between bent

 © 2004 Wiley-VCH Verlag GmbH & Co. KGaA, Weinheim

molecules vanish. In other words, the flat $(EDO\text{-}TTF)^+$ molecules in the insulator phase are dimerized to provide a singlet state, consistent with the diamagnetism observed.[1] From the viewpoint of the intermolecular orbital interactions, this dimerization stabilizes the electronic structure overcoming the neighbor-site Coulomb repulsion and thus causing the [0,0,+1,+1,…] charge-ordering pattern.

In conclusion, our study revealed that the molecular displacements observed in the metal–insulator phase transition of $(EDO\text{-}TTF)_2PF_6$ assist the anion ordering and the electrostatic and electronic stabilization of the crystal structure of the insulator phase. The cooperativity in this peculiar MI transition shall be regarded as a result of the molecular displacement that occurs along the nesting vector in the metallic phase. Along with the bistability illustrated by the thermal hysteresis of this transition, the cooperativity should contribute to our understanding of the origin of this ultrafast photo-induced phase transition.

Received: February 23, 2004 [Z54075]

Keywords: charge density · organic conductors · synchrotron radiation · tetrathiafulvalenes · X-ray diffraction

[1] A. Ota, H. Yamochi, G. Saito, *J. Mater. Chem.* **2002**, *12*, 2600–2602.
[2] O. Drozdova, K. Yakushi, A. Ota, H. Yamochi, G. Saito, *Synth. Met.* **2003**, *133–134*, 277–279.
[3] M. Takata, E. Nishibori, M. Sakata, *Z. Kristallogr.* **2001**, *216*, 71–86.
[4] E. Nishibori, M. Takata, M. Sakata, A. Taninaka, H. Shinohara, *Angew. Chem.* **2001**, *113*, 3086–3087; *Angew. Chem. Int. Ed.* **2001**, *40*, 2998–2999.
[5] C. R. Wang, T. Kai, T. Tomiyama, T. Yoshida, Y. Kobayashi, E. Nishibori, M. Takata, M. Sakata, H. Shinohara, *Nature* **2000**, *408*, 426–427.
[6] M. Takata, B. Umeda, E. Nishibori, M. Sakata, Y. Saito, M. Ohno, H. Shinohara, *Nature* **1995**, *377*, 46–49.
[7] Y. Kubota, M. Takata, M. Sakata, T. Ohba, K. Kifune, T. Tadaki, *J. Phys. Condens. Matter* **2000**, *12*, 1253–1259.
[8] M. Fujimori, T. Nakata, T. Nakayama, E. Nishibori, K. Kimura, M. Takata, M. Sakata, *Phys. Rev. Lett.* **1999**, *82*, 4452–4455.
[9] M. Takata, E. Nishibori, K. Kato, M. Sakata, Y. Moritomo, *J. Phys. Soc. Jpn.* **1999**, *68*, 2190–2193.
[10] T. Ishiguro, K. Yamaji, G. Saito, *Organic Superconductors*, Springer, New York, **1998**.
[11] N. F. Mott, *Metal–Insulator Transitions*, Taylor&Francis, London, **1990**.
[12] H. Seo, *J. Phys. Soc. Jpn.* **2000**, *69*, 805–820.
[13] K. Hiraki, K. Kanoda, *Phys. Rev. Lett.* **1998**, *80*, 4737–4740.
[14] D. S. Chow, F. Zamborszky, B. Alavi, D. J. Tantillo, A. Baur, C. A. Merlic, S. E. Brown, *Phys. Rev. Lett.* **2000**, *85*, 1698–1701.
[15] P. Monceau, F. Ya. Nad, S. Brasovskii, *Phys. Rev. Lett.* **2001**, *86*, 4080–4083.
[16] N. Uchida, S. Koshihara, T. Ishikawa, A. Ota, S. Fukaya, C. Matthieu, H. Yamochi, G. Saito, *J. Phys. IV France* **2004**, *114*, 143–145.
[17] P. Coppens, *Phys. Rev. Lett.* **1975**, *35*, 98–100.
[18] E. Espinosa, E. Molins, C. Lecomte, *Phys. Rev. B* **1997**, *56*, 1820–1833.
[19] F. Wudl, D. Nalewajek, J. M. Troup, M. W. Extine, *Science* **1983**, *222*, 415–417.
[20] E. Nishibori, M. Takata, K. Kato, M. Sakata, Y. Kubota, S. Aoyagi, Y. Kuroiwa, M. Yamakata, N. Ikeda, *Nucl. Instrum. Methods Phys. Res. Sect. A* **2001**, *467–468*, 1045–1048.
[21] M. Sakata, M. Sato, *Acta Crystallogr., Sect. A* **1990**, *46*, 263–270.
[22] H. M. Rietveld, *J. Appl. Crystallogr.* **1969**, *2*, 65–71.
[23] H. Tanaka, M. Takata, E. Nishibori, K. Kato, T. Iishi, M. Sakata, *J. Appl. Crystallogr.* **2002**, *35*, 282–286.
[24] S. Horiuchi, H. Yamochi, G. Saito, K. Sakaguchi, M. Kusunoki, *J. Am. Chem. Soc.* **1996**, *118*, 8604–8622.

 © 2004 Wiley-VCH Verlag GmbH & Co. KGaA, Weinheim

Crystal Growth

Platonic Gold Nanocrystals**

*Franklin Kim, Stephen Connor, Hyunjoon Song, Tevye Kuykendall, and Peidong Yang**

As was known by the ancient Greeks, there are five platonic solids that can be constructed by selecting a regular convex polygon and having the same number of them meet at each corner: tetrahedron, octahedron, hexahedron (cube), icosahedron, dodecahedron.[1] The beauty in their symmetry and their apparent simplicity continue to inspire generations of mathematicians and scientists. In nature, certain viruses and radiolaria also routinely take the form of these polyhedral shapes.[2] Recently, the concept of shape control has started to revitalize the centuries-old metal colloidal synthesis. Nanoparticles of various shapes[3–5] (rods,[6–9] wires,[10–12] prisms,[13–19] cubes[20,21]), particularly those of silver and platinum, have been prepared by using a variety of different methodologies. The preparation of nanoparticles of highly symmetric platonic shapes with a unified method, however, has yet to be demonstrated, and is by itself a scientific curiosity and great challenge that requires exquisite crystal growth control. Herein, we report a systematic shape evolution of gold nanocrystals with sizes of 100–300 nm in a modified polyol process. By adding surface-regulating polymer and foreign

[*] F. Kim, S. Connor, H. Song, T. Kuykendall, Prof. P. Yang
Department of Chemistry
University of California, Berkeley
Materials Science Division
Lawrence Berkeley National Laboratory
Berkeley, CA 94720 (USA)
Fax: (+1) 510-642-7301
E-mail: p_yang@uclink.berkeley.edu

[**] This work was supported by the Camille and Henry Dreyfus Foundation, Beckman Foundation, the National Science Foundation (CAREER) and Department of Energy. P.Y. is an Alfred P. Sloan Research Fellow. Work at the Lawrence Berkeley National Laboratory was supported by the Office of Science, Basic Energy Sciences, Division of Materials Science of the U.S. Department of Energy. We thank the National Center for Electron Microscopy for the use of their facilities.

Supporting information for this article is available on the WWW under http://www.angewandte.org or from the author.

 DOI: 10.1002/anie.200454216 © 2004 Wiley-VCH Verlag GmbH & Co. KGaA, Weinheim

ions, we can readily access the distinct shapes of tetrahedron, cube, octahedron, and icosahedron (dubbed platonic nanocrystals) with high yield and good uniformity. These nanocrystals have the perfect symmetry for 2D and 3D packing and therefore could enable the rational tuning of their optical, electrical, and catalytic properties.

Gold nanocrystals were produced by a modified polyol process,[22] with the presence of the surface-regulating polymer poly(vinyl pyrrolidone) (PVP). Briefly, ethylene glycol solutions of hydrogen tetrachloroaurate ($HAuCl_4 \cdot 3H_2O$) and PVP were injected simultaneously into boiling ethylene glycol. Ethylene glycol served as both solvent and reducing agent for the reaction. PVP not only stabilized the particles but also controlled the shape of the particles. The molar ratio between the PVP and the gold precursor was kept between 4.3 and 8.6. Gold particles formed within minutes, and the final diluted colloidal solution was iridescently blue.

A transmission electron microscopy (TEM) image showed that the majority ($\approx 70\,\%$) of the particles had a triangular shape (Figure 1a), and sizes of 210 ± 20 nm.

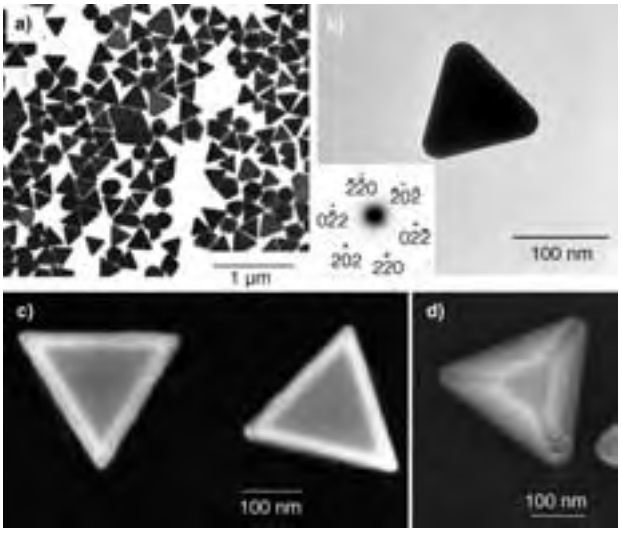


Figure 1. a,b) TEM image of truncated tetrahedral gold nanocrystals. The inset in (b) is the electron diffraction pattern taken along the [111] zone axis from the particle shown in (b). c,d) SEM images of several partially developed gold tetrahedra.

Electron diffraction of a single particle (Figure 1b, inset) shows that the particle was single crystalline, with the top and bottom covered with (111) surfaces. This initial inspection of the TEM data suggests the formation of flat nanoprisms as have been reported previously for silver.[14–16] Detailed scanning electron microscopy (SEM) studies, however, revealed otherwise. Interestingly, the sides of the particles were clearly slanted (Figure 1c,d), which indicates that rather than being flat prisms, these particles can be more accurately described as tetrahedra with a truncated corner, or as partially developed tetrahedra (hereafter we will call them tetrahedra for simplicity). The surfaces of these particles are dominated with {111} planes, which make them energetically favorable compared to prisms with other high-energy side surfaces such as $(1\bar{1}0)$ or $(11\bar{2})$. Occasionally, we were able to observe similar-sized particles with nearly fully developed tetrahedral shapes (Figure 1d), which points to the possibility of obtaining gold tetrahedra upon further growth of these triangular particles.

It was found that the nanoparticle shapes were highly sensitive to the concentration of the gold precursor used in the experiments. By slightly reducing this concentration, we were able to produce nanocrystals with icosahedral shapes. In one particular example, the gold precursor concentration was reduced to 80 % of that used for the synthesis of tetrahedra, and the final molar ratio between the PVP and the gold precursor was maintained at 8.6. Observation by TEM showed that $>90\,\%$ of the particles had a projected hexagonal shape (Figure 2a) and sizes of 230 ± 20 nm. The

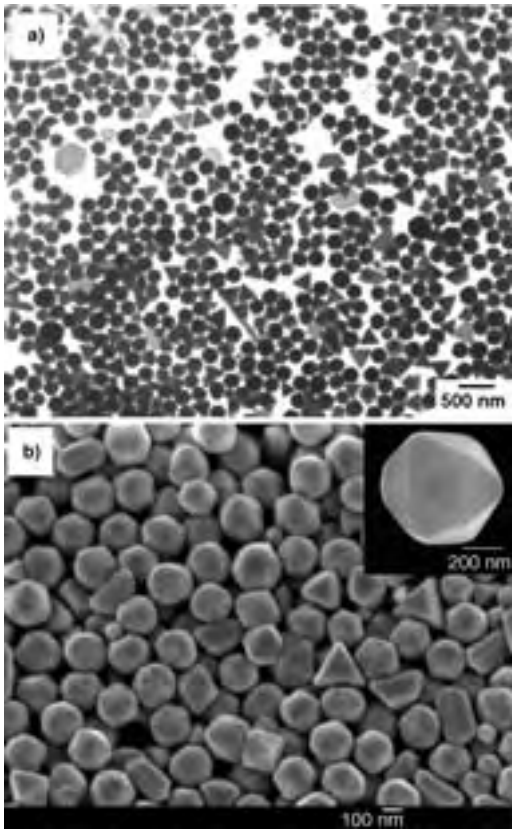


Figure 2. Icosahedral nanocrystals: a) TEM image and b) SEM image of icosahedral gold nanoparticles. Inset in (b) shows clearly all (111) facets of a typical icosahedron.

size of a particle is defined here as the distance from one edge of the hexagonal projection to the opposite side. Electron diffraction on a single particle showed a complex pattern, indicating that the particle was composed of multiple crystal domains. Further investigation by SEM showed that the particles were mostly icosahedra (Figure 2b and inset). Note that icosahedral particles of face centered cubic (fcc) metals represent one of the most investigated multiply twinned particles (MTP) in gas-phase experiments.[23,24] However, we observed for the first time the preparation in solution of uniform metal particles with such complex yet well defined structures and sizes ranging from several tens to hundreds of

 © 2004 Wiley-VCH Verlag GmbH & Co. KGaA, Weinheim

nanometers. In addition to the shapes of tetrahedron or icosahedron, which formed the majority of the product, a small portion (≈10%) of decahedra (another type of MTP) and regular octahedra were also commonly observed in the final products (see Supporting Information).

Tetrahedron and icosahedron are two of the platonic solid shapes that are covered with the {111} family of planes. Further shape control can be achieved by introducing foreign ions during the nanocrystal growth process. For example, the addition of a small amount of silver ions prior to the synthetic method normally used to obtain gold tetrahedra yields instead uniform gold nanocubes. Typically, a solution of silver nitrate (0.5 mL, 0.0059 M; 1.1% of the gold precursor) in ethylene glycol solution was injected into the boiling ethylene glycol five minutes before the injection of the gold precursor and the PVP. The final colloidal solution was iridescently bluish-purple. TEM and SEM observation showed that gold nanocubes (>95%) of average size of 150 ± 14 nm were produced (Figure 3). Electron diffraction (Figure 3c inset) on a single particle showed that the cube is a single domain, with (100) surfaces.

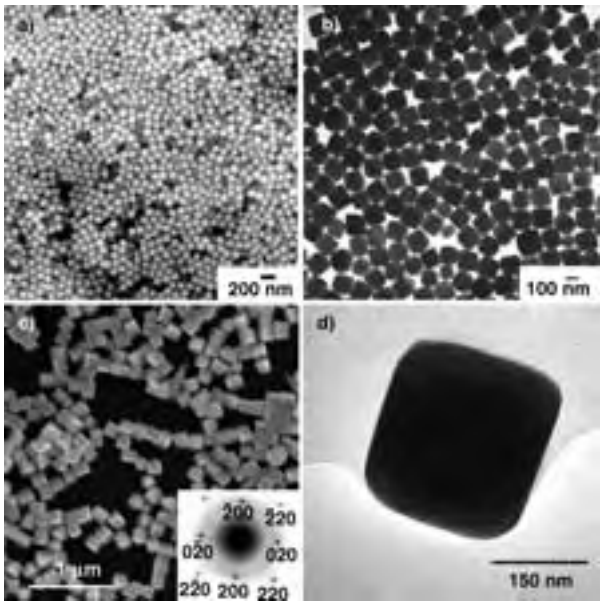


Figure 3. Gold nanocubes. (a–d). TEM and SEM images of gold nanocubes dispersed on a TEM grid and a silicon substrate. Inset in (c) shows the electron diffraction pattern recorded along the [100] axis of a gold nanocube shown in (d).

While SEM and TEM often sample only a small portion of the products, X-ray diffraction (XRD) can be used to assess the overall quality and purity of these facetted nanoparticles. Three XRD patterns recorded on three different shapes are compiled in Figure 4a. All peaks of fcc gold. A comparison of the (111) and the (200) diffraction intensities reveals very interesting features that are intrinsically related to the shapes of the particles being examined. For the gold nanocube sample, the intensity ratio between the (200) and the (111) diffractions is 1.93, which is significantly larger than the conventional bulk intensity ratio (≈0.53). This is a clear indication that the faces of these nanocubes, primarily

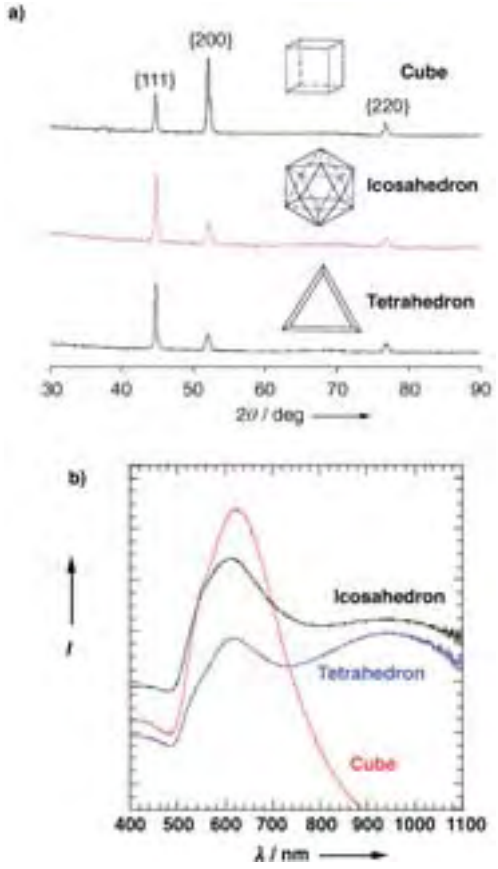


Figure 4. a) X-ray diffraction patterns and b) UV/VIS spectra for the three types of gold nanocrystals: tetrahedron, cube and icosahedron. I is intensity (arbitrary units).

composed of {100} planes, tend to preferentially orient parallel to the supporting substrates, thus giving a significantly high (200) diffraction intensity. On the other hand, the intensity ratios between the (200) and the (111) diffractions are much smaller than the bulk values for the tetrahedron and icosahedron samples, being 0.25 and 0.31, respectively. This again indicates that for tetrahedron and icosahedron samples, the {111} family of planes is dominant. This set of XRD patterns unambiguously demonstrates our capability of synthesizing with a high degree of selectivity, gold nanoparticles of different platonic shapes.

The optical properties of metal nanoparticles are highly dependent on the size and shape of the particles. This has been extensively explored both theoretically and experimentally on several systems including gold nanorods, silver nanorods, prisms, and cubes.[3–21] Several groups have theoretically simulated the optical properties of metal nanoparticles with arbitrary shapes and found distinctive shape-dependent behavior.[25–28] UV/Vis spectra collected on the ethylene glycol (EG) solutions of these three different shapes are compiled in Figure 4b. It was found that gold nanoparticles of different shapes clearly displayed different surface plasmon resonance, 621 nm for the nanocubes, 626, 950 nm for the tetrahedra and 613, 950 nm for icosahedra. The spectral features of the nanocube and tetrahedron are fairly consistent with previous theoretical simulations.[25–28] The UV/

 © 2004 Wiley-VCH Verlag GmbH & Co. KGaA, Weinheim

Vis spectrum of the icosahedral nanoparticles resembles that of spherical nanoparticles of similar size. The additional broad near-IR band is most likely to arise from co-existing triangular particles.

It is commonly accepted that the shape of an fcc nanocrystal is mainly determined by the ratio (R) of the growth rate along the [100] versus the [111] direction.[29,30] Tetrahedra and icosahedra bound by the most stable {111} planes will be formed when R is large (≈ 1.73), and perfect cubes bounded by the less stable {100} planes will result if R is reduced (≈ 0.58). The surface-regulating polymer (PVP) and the introduction of foreign ions are believed to play the key roles here. Selective interaction between PVP and the different surface planes of the gold nanocrystals could greatly enhance the growth rate along the [100] direction, reduce the growth rate along [111] direction, and ultimately result in particles with tetrahedral or icosahedral shapes. The mechanism for the selective growth of icosahedral nanoparticles versus that of tetrahedral nanoparticles is yet to be determined. The fact that lower overall gold precursor concentration (under otherwise identical synthetic conditions) results in the selective growth of icosahedra suggests that subtle differences in the gold embryonic seed formation and their subsequent growth might lead to this shape selection.

With another means of shape control, the introduction of foreign ions could greatly influence the relative growth rates along certain directions. We believe that the introduction of silver ions in the current process can significantly reduce the growth rate along the [100] direction and/or enhance the growth rate along the [111] direction, and ultimately cubic particles result. There have been previous studies in which the introduction of silver impurity during gold particle formation resulted in the control of the nanocrystal shape.[3,6,7,9] For example, silver ions were used to control the aspect ratio of the gold nanorods produced by electrochemistry and photochemistry.[3,6,7,9] It is also interesting to note that our shape-control scheme is vastly different from that reported by Xia and Sun for the silver system,[21] in which the interaction of the particles with PVP promotes the nanocube formation. The formation of nanocubes observed in our system may be due to the fact that the gold and silver systems interact differently with the polymer.

The successful preparation of gold platonic nanocrystals exemplifies the exquisite shape control that can be achieved through careful growth rate regulation along different crystallographic directions, and demonstrates a strategy that could be generally applicable to other material systems. These platonic nanocrystals have perfect symmetry for 2D and 3D packing and therefore should lead to interesting research on nanotectonics, the formation of high-order nano- or microstructures, and the rational tuning of optical, electrical, and catalytic properties.

Experimental Section

For a typical synthesis of tetrahedral particles, of ethylene glycol (5 mL) was stirred with a magnetic bar and heated to reflux in a silicone oil bath at 280 °C. Nitrogen was continuously flowed through the entire refluxing system. Solutions of PVP (0.375 M) in EG, and $HAuCl_4 \cdot 3H_2O$ (0.083 M) in EG were prepared. The PVP solution was injected to boiling EG (5 mL) by using a micropipette, then the $HAuCl_4$ solution was injected twice. This process was repeated 15 more times for every 30 seconds. The solution turned red within 8 minutes after the final injection, thus indicating formation of gold nanoparticles. The solution was aged for 45 minutes to ensure that the reaction was complete. The solution was collected, and the large aggregates and unconverted salts were removed by centrifugation. The solution was centrifuged at 1000 rpm for 5 minutes and the precipitate was removed. After repeating this three times, the solution was centrifuged at 3500 rpm for 30 minutes. The precipitate was collected and redispersed in EG (4 mL).

For the synthesis of icosahedral particles, the gold precursor concentration was reduced to 4/5 of that used in the synthesis of tetrahedral particles under otherwise similar conditions.

For the synthesis of nanocubes, a solution of $AgNO_3$ (0.0059 M) in EG (0.5 mL) was first added to the boiling EG 5 minutes before the injection of gold precursor and PVP.

Typically, for the icosahedral- and tetrahedral-particle syntheses, the solution turns from light pink–orange to strong rust red about 7 min after the final injection. When diluted, the solution becomes iridescently blue. For the cube synthesis, the reaction solution shows a similar color change around 4 min after the final injection.

Received: March 8, 2004
Revised: April 24, 2004 [Z54216]

Keywords: crystal growth · gold · nanostructures · self-assembly

[1] D. M. Davis, *The Nature and Power of Mathematics*. Princeton University Press, **1993**.
[2] A. J. Levine, *Viruses*, Scientific American Library, New York, **1991**.
[3] M. P. , Pileni, *Nat. Mater.* **2003**, *2*, 145 – 150.
[4] a) M. Brust, C. J. Kiely, *Colloids Surf. A* **2002**, *202*, 175 – 186; b) P. Y Silvert, K. Tekaia-Elhsissen, *Solid State Ionics*, **1995**, *82*, 53 – 60.
[5] S. Sun, C. B. Murray, D. Weller, L. Folks, A. Moser, *Science* **2000**, *287*, 1989 – 1992.
[6] S. S. Chang, C. W. Shih, C. D. Chen, W. C. Lai, C. R. C. Wang, *Langmuir* **1999**, *15*, 701 – 709.
[7] F. Kim, J. Song, P. Yang, *J. Am. Chem. Soc.* **2002**, *124*, 14316 – 14317.
[8] F. Dumestre, B. Chaudret, C. Amiens, M.-C. Fromen, M.-J. Casanove, P. Renaud, P. Zurcher, *Angew. Chem.* **2002**, *114*, 4462 – 4465; *Angew. Chem. Int. Ed.* **2002**, *41*, 4286 – 4289.
[9] N. R. Jana, L. Gearheart, C. J. Murphy, *J. Phys. Chem. B* **2001**, *105*, 4065 – 4067.
[10] C. J. Johnson, E. Dujardin, S. A. Davis, C. J. Murphy, S. Mann, *J. Mater. Chem.* **2002**, *12*, 1765 – 1770.
[11] Y. Sun, B. Gates, B. Mayers, Y. Xia, *Nano. Lett.* **2002**, *2*, 165 – 168.
[12] A. Tao, F. Kim, C. Hess, J. Goldberger, R. He, Y. Sun, Y. Xia, P. Yang, *Nano. Lett.* **2003**, *3*, 1229 – 1232.
[13] Y. Sun, Y. Xia, *Adv. Mater.* **2003**, *15*, 695 – 699.
[14] R. Jin, Y. Cao, C. A. Mirkin, K. L. Kelly, G. C. Schatz, J. G. Zheng, *Science* **2001**, *294*, 1901 – 1904.
[15] M. Maillard, S. Giorgio, M. P. Pileni, *Adv. Mater.* **2002**, *14*, 1084 – 1086.
[16] R. Jin, Y. Cao, E. Hao, G. S. Metraux, G. C. Schatz, C. A. Mirkin, *Nature* **2003**, *425*, 487 – 490.
[17] I. Pastoriza-Santos, L. M. Liz-Marzan, *Nano Lett.* **2002**, *2*, 903 – 905.
[18] S. H. Chen, Z. Y. Fan, D. L. Carroll, *J. Phys. Chem. B* **2002**, *106*, 10777 – 10781.
[19] V. F. Puntes, D. Zanchet, C. K. Erdonmez, A. P. Alivisatos, *J. Am. Chem. Soc.* **2002**, *124*, 12874 – 12880.
[20] T. S. Ahmadi, Z. L. Wang, T. C. Green, A. Henglein, M. A. El-Sayed, *Science* **1996**, *272*, 1924 – 1926.

 © 2004 Wiley-VCH Verlag GmbH & Co. KGaA, Weinheim

[21] Y. Sun, Y. Xia, *Science* **2002**, *298*, 2176 – 2179.
[22] F. Fievet, J. P. Lagier, M. Figlarz, *Mater. Res. Bull.* **1989**, *14*, 29 – 32.
[23] L. D. Marks, *Rep. Prog. Phys.* **1994**, *57*, 603 – 649.
[24] M. J. Yacaman, J. A. Ascencio, H. B. Liu, J. Gardea-Torresdey, *J. Vac. Sci. Technol. B* **2001**, *19*, 1091 – 1103.
[25] J. J. Mock, M. Barbic, D. R. Smith, D. A. Schultz, S. Schultz, *J. Chem. Phys.* **2002**, *116*, 6755 – 6762.
[26] K. L. Kelly, E. Coronado, L. L. Zhao, G. C. Schatz, *J. Phys. Chem. B* **2003**, *107*, 668 – 677.
[27] W. H. Yang, G. C. Schatz, R. P. Van Duyne, *J. Chem. Phys.* **1995**, *103*, 869 – 875.
[28] I. O. Sosa, C. Nogeuez, R. G. Barrera, *J. Phys. Chem. B* **2003**, *107*, 6269 – 6275.
[29] Z. L. Wang, *J. Phys. Chem. B* **2000**, *104*, 1153 – 1175.
[30] J. M. Petroski, Z. L. Wang, T. C. Green, M. A. El-Sayed, *J. Phys. Chem. B* **1998**, *102*, 3316 – 3320.

 © 2004 Wiley-VCH Verlag GmbH & Co. KGaA, Weinheim

Liquid Crystals

Magnetic Properties of All-Organic Liquid Crystals Containing a Chiral Five-Membered Cyclic Nitroxide Unit within the Rigid Core

Naohiko Ikuma, Rui Tamura, Satoshi Shimono, Naoyuki Kawame, Osamu Tamada, Naoko Sakai, Jun Yamauchi, and Yukio Yamamoto*

The orientation of liquid crystals (LCs) can generally be controlled by magnetic and electric fields owing to their molecular magnetic and dielectric anisotropies, respectively. The threshold of the magnetic fields necessary to align liquid-crystalline substances decreases with increasing magnetic susceptibility anisotropy ($|\Delta\chi|$) of the mesogens and the decreasing viscosity of the material.[1] As the orientation of a diamagnetic calamitic organic LC by external magnetic fields is ascribed to the small diamagnetic susceptibility anisotropy ($0 < |\Delta\chi_{dia}| < 60 \times 10^{-6}$ emu mol^{-1}) of the mesogen which arises from the constituent aromatic rings,[2] relatively strong magnetic fields (> 1 T) are necessary for the orientation of this type of LC. Therefore, it is quite reasonable to take advantage of a paramagnetic susceptibility anisotropy ($\Delta\chi_{para}$) for the orientation of LCs by weak magnetic fields, because χ_{para} is usually one or two orders of magnitude larger than χ_{dia}. For this reason, a number of metallomesogens with permanent spins that originate from their transition-metal centers have been prepared.[1,3] Particularly, calamitic lanthanide-containing metallomesogens have a large paramagnetic anisotropy, but the intrinsic high viscosity brought about by the ligand-coordinated metal-complex structure frequently renders their orientation by weak magnetic fields difficult.[3]

In contrast, a calamitic organic LC with a stable nitroxyl (NO) group as a spin source can benefit from a small paramagnetic susceptibility anisotropy and a low viscosity by means of an appropriate molecular design; for example, 1) a cyclic nitroxide framework is incorporated into the rigid core of the mesogen to maximize the paramagnetic anisotropy, and 2) the side chains are extended from the two quaternary carbon atoms adjacent to the nitroxyl group to reduce the viscosity. Consequently, its orientation may be controlled by weak magnetic fields.

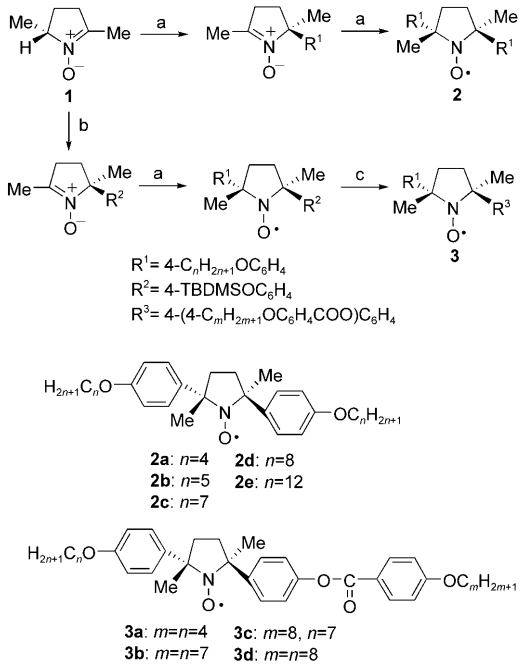
To test the above assumption, it is essential to find a prototype of the calamitic mesogen that exhibits an extremely stable paramagnetic liquid-crystalline phase. Furthermore, to obtain a series of mesogens showing the nematic and chiral-nematic (cholesteric) phases, and/or the smectic and chiral-smectic phases,[4] the prototypic molecular structure should be chiral. However, very few LCs containing the organic spin center have been prepared mainly because the geometry and bulkiness of the radical-stabilizing substituents are detrimental to the stability of liquid-crystalline phases. Their molecular structures were limited to those containing a nitroxyl group within the alkyl side chain, away from the rigid core and hence allowed the free rotation of the nitroxyl moiety inside the molecule, leading to a decrease in the paramagnetic anisotropy of the whole molecule.[5] Unfortunately, all attempts to prepare monomeric or polymeric mesogens by using the organic spin as part of the rigid core have been unsuccessful.[5,6]

With this in mind, we focused on the chiral 3,4-dihydro-2,5-dimethyl-2*H*-pyrrole 1-oxide (**1**) from which a variety of chiral derivatives can be prepared in the form of racemates or nonracemates (Scheme 1).[7] First we synthesized the C_2-symmetric *trans*-2,5-bis(alkoxyphenyl) derivatives **2a**–**e** with various alkyl side chains, but they were not liquid-crystalline—this was most likely a result of their compact molecular packing in the crystalline state as judged from the crystal structures of (±)-**2a** and (2*S*,5*S*)-**2a** (Figure 1).[8] We then modified the molecular structure to decrease the molecular symmetry and strengthen the core-to-core interactions in the liquid-crystalline state. Consequently, the C_1-symmetric *trans*-2-alkoxyphenyl-5-[4-(4-alkoxybenzenecarbonyloxy)phenyl] derivatives **3**, which have disordered alkyl side chains in the crystalline state (Figure 2), successfully exhibited enantiotropic liquid-crystalline phases over wide temperature ranges (see Table 1 and Supporting Information); the racemic samples of **3a**–**d** showed a Schlieren texture typical for a nematic phase by hot-stage polarizing microscopy (Figure 3a), whereas the corresponding nonracemic samples (94–97% *ee*) exhibited an oily-streak texture characteristic

[*] N. Ikuma, Prof. R. Tamura
Graduate School of Global Environmental Studies and
Graduate School of Human and Environmental Studies
Kyoto University, Kyoto 606-8501 (Japan)
Fax: (+81) 75-753-7915
E-mail: tamura@fischer.jinkan.kyoto-u.ac.jp
S. Shimono, N. Kawame, Prof. O. Tamada, N. Sakai,
Prof. Y. Yamamoto
Graduate School of Human and Environmental Studies
Kyoto University, Kyoto 606-8501 (Japan)
Prof. J. Yamauchi
Graduate School of Science, Kyoto University
Kyoto 606-8501 (Japan)

Supporting information for this article is available on the WWW under http://www.angewandte.org or from the author.

 DOI: 10.1002/anie.200460007 © 2004 Wiley-VCH Verlag GmbH & Co. KGaA, Weinheim



Scheme 1. Preparation of chiral nitroxides **2** and **3**. Reagents and conditions: a) 1. R^1MgBr, THF −78 °C; 2. $Cu(OAc)_2$, O_2; b) 1. R^2MgBr, −78 °C; 2. $Cu(OAc)_2$, O_2; c) TBAF, Et_3N. $C_mH_{2m+1}OC_6H_4COCl$, THF, 0 °C. TBAF = tetra-*n*-butylammonium fluoride

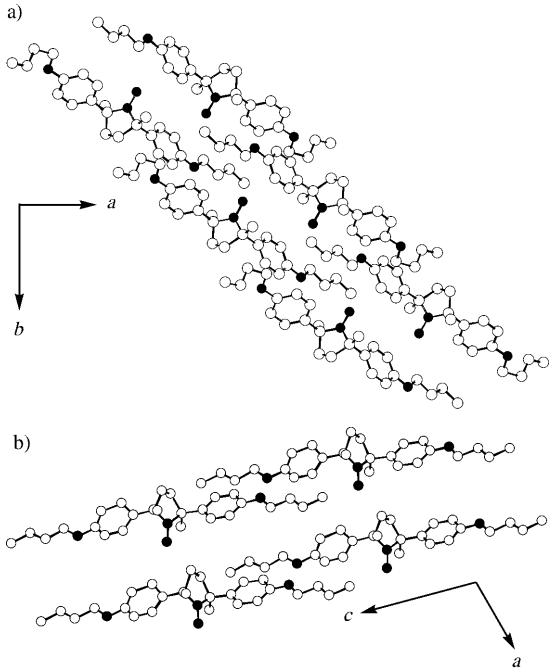


Figure 1. Crystal structures of a) (±)-**2a** and b) (2*S*,5*S*)-**2a**. The carbon, nitrogen, and oxygen atoms are represented by open, grid, and closed circles, respectively. Hydrogen atoms are omitted for clarity.

of a cholesteric phase (Figure 3b).[4] These liquid-crystalline phases are extremely thermally stable; for example, after allowing (±)-**3c** to stand at 73 °C for 24 h, there was no decrease in the purity of the material, and the racemic and nonracemic samples of **3a–d** did not decompose after several heating and cooling cycles between the individual melting and clearing points.

More interesting are the bulk magnetic properties of **3**. The magnetic susceptibilities of the racemic and nonracemic samples of **3a–d** were measured in a quartz tube (3.5 ϕ × 40 mm) on a SQUID susceptometer at a field of 0.5 T in the temperature range 2–380 K. During the first heating process starting from the crystalline phase, (±)-**3c** and (±)-**3d**

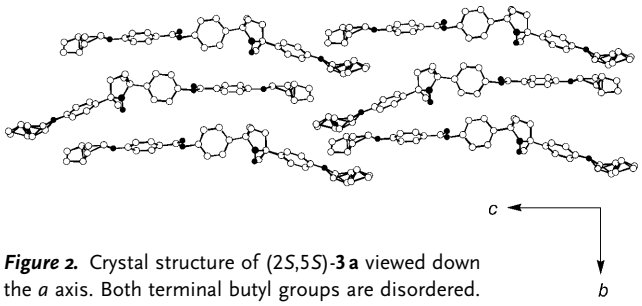


Figure 2. Crystal structure of (2*S*,5*S*)-**3a** viewed down the *a* axis. Both terminal butyl groups are disordered. The carbon, nitrogen, and oxygen atoms are represented by open, grid, and closed circles, respectively. Hydrogen atoms are omitted for clarity.

Table 1: Optical, magnetic, and thermal data of **3a–d**.

Compound	*ee* [%][a]	$[\alpha]_D^{26}$[b]	ESR[b] *g*	ESR[b] a_N [mT]	*C* [$emu^{-1}\,K\,mol^{-1}$][c]	θ [K][d]	Phase transition [°C][e]
(±)-**3a**	–	–	2.0068	1.34	0.37[f]	−0.04[f]	C 113.2 N 140.6 I
(2*S*,5*S*)-**3a**	94.5	−111.40 (*c* = 0.993)	2.0068	1.34	0.37[f], 0.38[g]	−0.01,[f] −0.40[g]	C 93.2 N* 143.8 I
(±)-**3b**	–	–	2.0070	1.33	0.38,[f] 0.38[g]	−0.21,[f] −0.28[g]	C 67.1 N 103.4 I
(2*S*,5*S*)-**3b**	94.9	−95.59 (*c* = 0.995)	2.0069	1.34	0.38,[f] 0.38[g]	−0.07,[f] −0.31 [g]	C 67.6 N* 101.7 I
(±)-**3c**	–	–	2.0073	1.37	0.36,[f] 0.37[g]	+0.38,[f] −0.40[g]	C 63.3 N 103.1 I
(2*S*,5*S*)-**3c**	96.9	−88.80 (*c* = 0.998)	2.0070	1.34	0.37,[f] 0.37[g]	−0.01,[f] −0.26[g]	C 79.3 N* 103.5 I
(±)-**3d**	–	–	2.0069	1.34	0.38,[f] 0.38[g]	+0.31,[f] −0.34[g]	C 71.5 N 103.1I
(2*S*,5*S*)-**3d**	95.8	−87.24 (*c* = 0.981)	2.0069	1.34	0.38,[f] 0.38[g]	−0.10,[f] −0.33[g]	C 71.2 N* 97.6 I

[a] Determined by HPLC analysis on a chiral stationary phase column (Daicel OD-H, 0.4 × 25 cm) and a mixture of hexane and 2-propanol (9:1) as the mobile phase. [b] Measured in THF. [c] Curie constant. [d] Weiss temperature. [e] Determined by DSC analysis upon heating. Standard notation gives the transition temperatures between the crystalline (C), liquid crystalline (N = nematic, N* = chiral nematic), and isotropic (I) states. [f] First heating process from the crystalline phase. [g] First cooling process from the isotropic phase.

 © 2004 Wiley-VCH Verlag GmbH & Co. KGaA, Weinheim

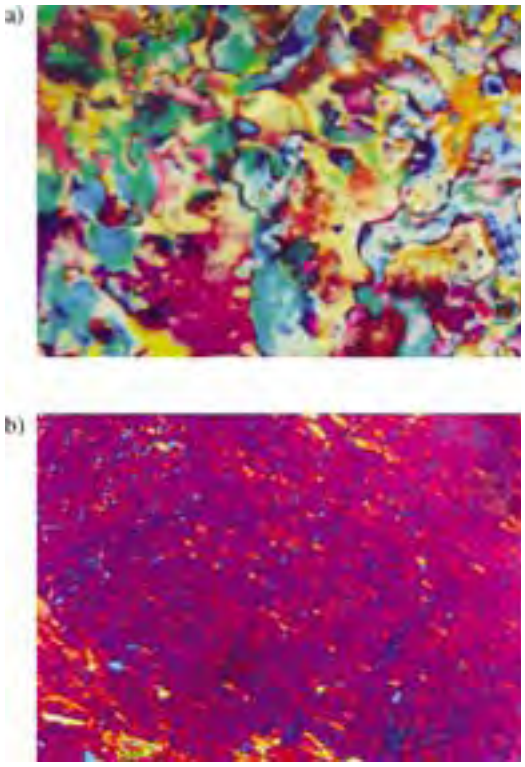


Figure 3. Optical polarized micrographs showing a) Schlieren texture of (±)-**3c** at 93.0 °C and b) oily streaks texture of (2*S*,5*S*)-**3c** at 83.0 °C.

showed weak ferromagnetic intermolecular interactions, whereas the other samples showed weak antiferromagnetic interactions. On the other hand, during the first cooling process from the isotropic phase, all of the samples except (±)-**3a** showed weak antiferromagnetic intermolecular interactions (Figure 4 and Table 1).[9] Noteworthy is the distinct change in the χ_{para} values observed at the crystal-to-LC phase transition during the first heating process; for example, (±)-**3c** showed an abrupt increase in χ_{para} at 342 K, followed by a sudden decrease at 378 K (Figure 4c). But during the cooling run from the isotropic phase, neither an appreciable decrease in χ_{para} nor the LC-to-crystal phase transition in the DSC curve were observed, owing to the considerable stability of the supercooled liquid-crystalline phase; the glassy phase was preserved for more than 24 h at 25 °C.

In contrast, for (2*S*,5*S*)-**3c** of 96.9 % *ee*, only a small increase in χ_{para} was noted upon the crystal-to-LC phase transition during the first heating process (Figure 4d). Such differences in the observed changes in χ_{para} values between the racemic and nonracemic samples can be accounted for by their molecular arrangement in the nematic and cholesteric phases, respectively; that is, the racemic nematic phase has only orientational order along the long molecular axis, whereas the nonracemic cholesteric phase has an additional helical superstructure with a twist axis perpendicular to the local director. The distinct increase in χ_{para} upon the phase change during the first heating process of (±)-**3c** is assumed to originate from the orientation of the molecules in the liquid-crystalline phase with the axis of maximum suscepti-

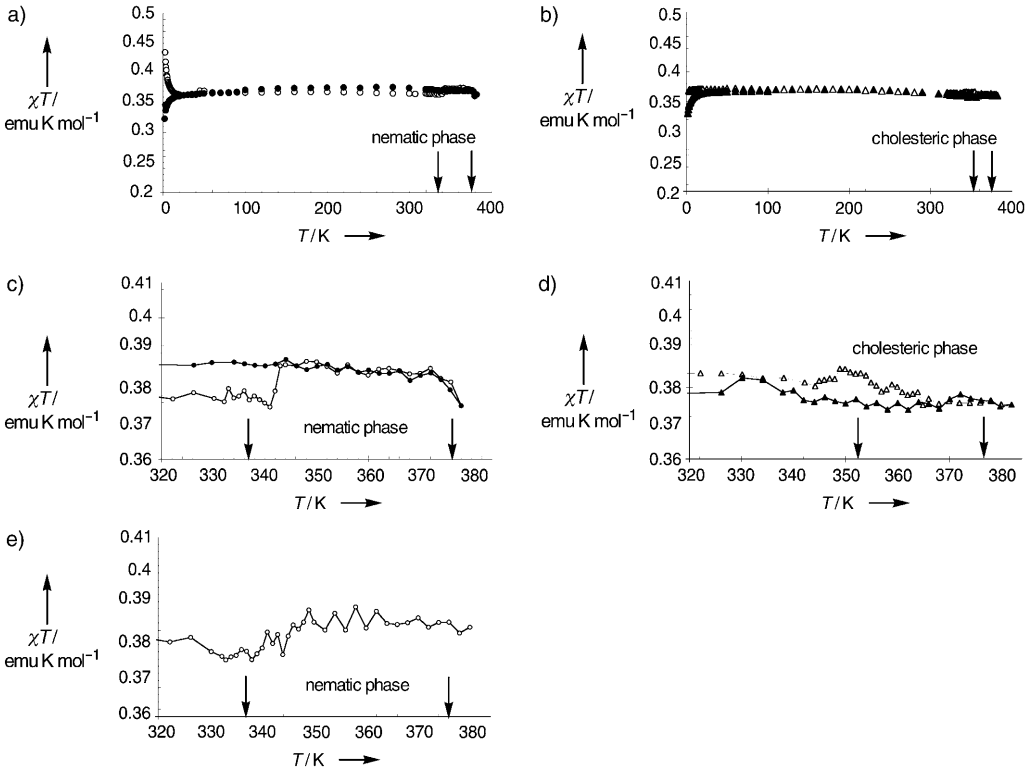


Figure 4. Temperature dependence of the magnetic susceptibility of a) (±)-**3c** and b) (2*S*,5*S*)-**3c** at the rate of 2 °C min^{-1} between 2 and 380 K at a field of 0.5 T, c) (±)-**3c** and d) (2*S*,5*S*)-**3c** at the rate of 0.5 °C min^{-1} between 320 and 380 K at a field of 0.5 T, and (e) (±)-**3c** at the rate of 0.5 °C min^{-1} between 320 and 380 K at a field of 0.05 T, measured during the first heating and cooling processes. ○ and △ represent the first heating process, ● and ▲ represent the first cooling process.

 © 2004 Wiley-VCH Verlag GmbH & Co. KGaA, Weinheim

bility parallel to the magnetic field. Such an increase in χ_{para} upon the crystal-to-LC phase transition was also observed at a field of 0.05 T or below (Figure 4e). This is a rare example in which the orientation of the mesogens can be effected by very weak magnetic fields during the heating process.[1,2]

To gain better insight into the direction of the molecular orientation in the bulk LC in the magnetic field, the temperature dependence of the *g* value for **3c** was measured by EPR spectroscopy (Figures 5 and 6). During the heating process, the *g* value of (±)-**3c** gradually decreased in the crystalline state, then decreased abruptly upon the crystal-to-LC phase transition, and then became constant in the liquid-crystalline state. However, during the cooling process *g* was constant in the liquid-crystalline state and then gradually increased in the supercooled liquid-crystalline state (Figure 6a). As the *g* value of a nitroxyl group generally shows distinct anisotropy (in which the g_{xx} value along the NO axis is 2.008–2.009, the g_{zz} value along its $2p_z$ orbital axis is less than 2.003, and the g_{yy} value perpendicular to both axes is 2.005–2.006[10]), the observed decrease in *g* from 2.0065 to 2.0052 is assumed to correspond to the increasing contribution of the g_{yy} and g_{zz} values; that is, the majority of the molecules align in such a way that the NO axis is perpendicular to the applied magnetic field (Scheme 2). Accordingly, on the basis of the molecular structure of **3a** (Figure 2), the molecular long axis as well as the director axis should be approximately oriented parallel to the direction of the magnetic field. In contrast, for (2*S*,5*S*)-**3c**, *g* did not show any temperature dependence, and the value was almost constant between 2.0060 and 2.0070, close to the mean value in solution (Figure 6b); this result seems to reflect the peculiar helical superstructure of the cholesteric phase in which a uniform molecular orientation is impossible.[4]

Furthermore, a striking increase in the intensity of the EPR signal was observed for both racemic and nonracemic

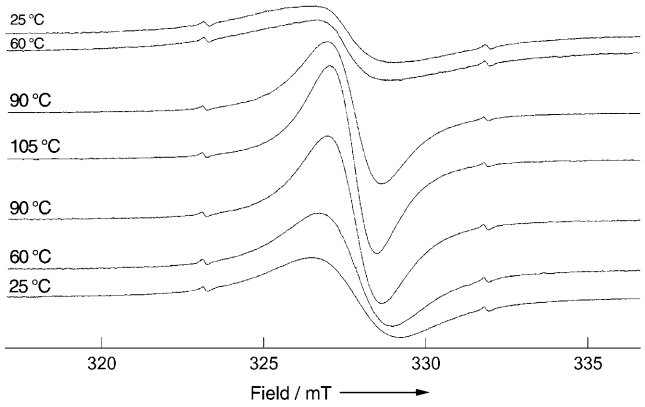


Figure 5. Selected EPR spectra of (±)-**3c** measured at various temperatures from the crystalline phase (top) through the liquid-crystalline phase to the supercooled liquid-crystalline phase (bottom).

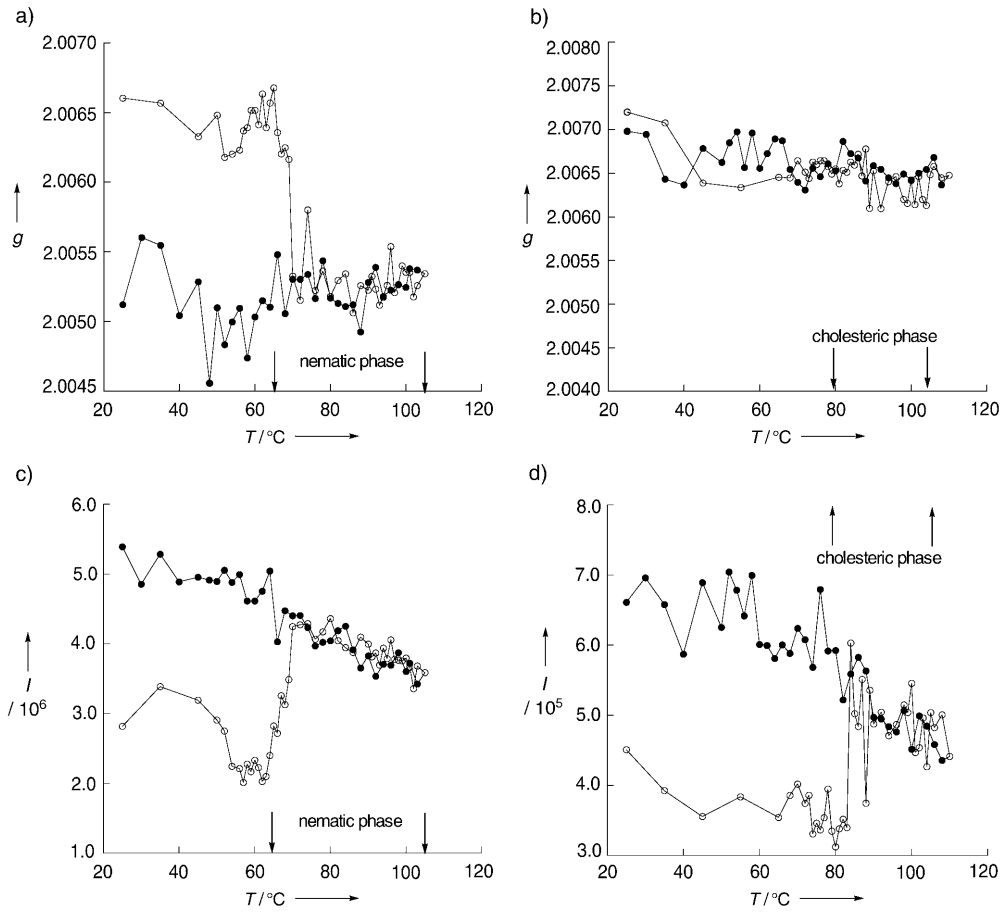
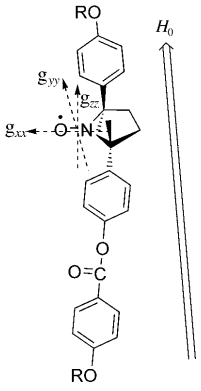


Figure 6. Variation of the *g* values of a) (±)-**3c** and b) (2*S*,5*S*)-**3c**, and the signal intensities of c) (±)-**3c** and d) (2*S*,5*S*)-**3c**, upon variation of the temperature; measured through the first heating (○) and cooling (●) processes.

 © 2004 Wiley-VCH Verlag GmbH & Co. KGaA, Weinheim



Scheme 2. Molecular orientation of **3** approximately parallel to the magnetic field (H_0).

samples of **3c** upon the phase transition observed during the heating process from the crystalline phase (Figures 6c and d). During the cooling process from the isotropic phase, the intensity gradually increased in the liquid-crystalline and the supercooled liquid-crystalline phases in both samples. In line with the intensity of the EPR signal being proportional to the χ value, a microscopic increase in the χ_{para} value was indeed observed upon the phase transition from the crystalline phase to the nematic or cholesteric phase.

We thus observed the microscopic decrease in the g value as well as the macro- and microscopic increases in the χ_{para} value upon the phase transition from the crystalline phase of (±)-**3c** to the liquid-crystalline phase during the heating process.

It is assumed that the molecular magnetic susceptibility anisotropy ($\Delta\chi$), which results from the cooperation of the paramagnetic and diamagnetic components originating from the nitroxyl group and the benzene rings, respectively, is responsible for the orientation of the bulk LC in the applied magnetic field. As $\chi_{\parallel}$ (parallel) is surely larger than $\chi_{\perp}$ (perpendicular) for (±)-**3c**, the experimental magnetic susceptibility anisotropy $\Delta\chi_{exp}$ was determined to be $+0.47\times10^{-4}$ emu mol^{-1} according to Equation (1),[2a] in which the

$$\Delta\chi_{exp}=\frac{3}{2}(\chi_{ordered}-\chi_{isotropic}) \quad (1)$$

experimental values of $\chi_{ordered}=+1.136\times10^{-3}$ emu mol^{-1} at 340 K (cooling process) and $\chi_{isotropic}=+1.105\times10^{-3}$ emu mol^{-1} at 340 K (heating process) were used.

Thus, it has been shown that a chiral racemic nematic phase is more suitable than a cholesteric phase with respect to the orientation of the bulk LC by weak magnetic fields. Alternatively, these paramagnetic LC substances may serve as dopants to align diamagnetic mesophases by weak magnetic fields, or as a real LC probe to investigate the dynamic behavior of a given diamagnetic LC material by EPR spectroscopy. Furthermore, if a paramagnetic chiral smectic (SmC*) phase is available, the orientation of the ferroelectric sample may also be controlled by application of weak magnetic fields.[11]

Received: March 16, 2004 [Z460007]

Keywords: chirality · EPR spectroscopy · liquid crystals · magnetic properties · phase transitions

[1] a) K. Griesar, W. Haase in *Magnetic Properties of Organic Molecules* (Ed.: P. M. Lahti), Marcel Dekker, New York, **1999**, pp. 325–344; b) P. Kaszynski in *Magnetic Properties of Organic Molecules* (Ed.: P. M. Lahti), Marcel Dekker, New York, **1999**, pp. 305–324; c) M. Marcos, J.-L Serrano, *Adv. Mater.* **1991**, *3*, 256–257.

[2] H. Müller, W. Haase, *J. Phys. (Paris)* **1983**, *44*, 1209–1213.

[3] a) K. Binnemans, Y. G. Galyametdinov, R. V. Deun, D. W. Bruce, S. R. Collinson, A. P. Polishchuk, I. Bikchantaev, W. Haase, A. V. Prosvirin, L. Tinchurina, I. Litvinov, A. Gubajdullin, A. Rakhmatullin, K. Uytterhoeven, L. V. Meervelt, *J. Am. Chem. Soc.* **2000**, *122*, 4335–4344; b) Y. Galyametdinov, M. A. Athanassopoulou, K. Griesar, O. Kharitonova, E. A. S. Bustamante, L. Tinchurina, I. Ovchinnikov, W. Haase, *Chem. Mater.* **1996**, *8*, 922–926; c) K. Griesar, Y. Galyametdinov, M. Athanassopoulou, I. Ovchinnikov, W. Haase, *Adv. Mater.* **1994**, *6*, 381–384.

[4] a) I. Dierking, *Texture of Liquid Crystals, Wiley-VCH, Weinheim*, **003**; b) S. T. Lagerwall, *Ferroelectric and Antiferroelectric Liquid Crystals, Wiley-VCH, Weinheim*, **999**; c) D. Demus, J. W. Goodby, G. W. Gray, H. W. Spiess, V. Vill, *Handbook of Liquid Crystals*, *Vol. 1–4*, Wiley-VCH, Weinheim, **1998**.

[5] a) S. Nakatsuji, M. Mizumoto, H. Ikemoto, H. Akutsu, J. Yamada, *Eur. J. Org. Chem.* **2002**, 1912–1918; b) J. Allgaier, H. Finkelmann, *Macromol. Chem. Phys.* **1994**, *195*, 1017–1030; c) M. Dvolaitzky, J. Billard, F. Poldy, *Tetrahedron* **1976**, *32*, 1835–1838; d) M. Dvolaitzky, J. Billard, F. Poldy, *C. R. Hebd. Seances Acad. Sci. Ser. C* **1974**, *279*, 533–535.

[6] a) S. Shimono, R. Tamura, N. Ikuma, T. Takimoto, N. Kawame, O. Tamada, N. Sakai, H. Matsuura, J. Yamauchi, *J. Org. Chem.* **2004**, *69*, 475–481; b) R. Tamura, S. Shimono, K. Fujita, K. Hirao, *Heterocycles* **2001**, *54*, 217–224; c) R. Tamura, S. Susuki, N. Azuma, A. Matsumoto, F. Toda, T. Takui, D. Shiomi, K. Itoh, *Mol. Cryst. Liq. Cryst.* **1995**, *271*, 91–96; d) R. Tamura, S. Susuki, N. Azuma, A. Matsumoto, F. Toda, Y. Ishii, *J. Org. Chem.* **1995**, *60*, 6820–6825; e) R. Tamura, S. Susuki, N. Azuma, A. Matsumoto, F. Toda, A. Kamimura, K. Hori, *Angew. Chem.* **1994**, *106*, 914–915; *Angew. Chem. Int. Ed. Engl.* **1994**, *33*, 878–880.

[7] a) N. Ikuma, R. Tamura, S. Shimono, N. Kawame, O. Tamada, N. Sakai, J. Yamauchi, Y. Yamamoto, *Mendeleev Commun.* **2003**, 109–111; b) J. Einhorn, C. Einhorn, F. Ratajczak, I. Gautier-Luneau, J.-L. Pierre, *J. Org. Chem.* **1997**, *62*, 9385–9388; c) N. Benfaremo, M. Steenbock, M. Klapper, K. Müllen, V. Enkelmann, K. Cabrera, *Liebigs Ann.* **1996**, 1413–1415; d) J. F. W. Keana, S. E. Seyedrezai, G. Gaughan, *J. Org. Chem.* **1983**, *48*, 2644–2647.

[8] The X-ray crystallographic data were collected at 298 K on an Enraf-Nonius Kappa CCD diffractometer. The crystal structure was solved by direct methods and refined by full-matrix least squares. All non-hydrogen atoms were refined anisotropically. All of the crystallographic calculations were performed by using the maXus software package.[12] Crystal data for (±)-**2a**: $C_{26}H_{36}NO_3$, $M_r=410.578$, $0.26\times0.20\times0.16$ mm^3, monoclinic, space group $C2/c$, $a=14.363(2)$, $b=15.1763(13)$, $c=22.269(4)$ Å, $\beta=99.155(7)°$, $V=4792.5(12)$ Å^3, $Z=8$, $\rho_{calcd}=1.138$ g cm^{-3}, $2\theta_{max}=50.72°$, $Mo_{K\alpha}$ ($\lambda=0.71073$ Å), $\mu=0.73$ cm^{-1}, ϕ-ω-scans, $T=298$ K, 4403 independent reflections, 2133 observed reflections ($I>2.0\sigma(I)$), 295 refined parameters, $R=0.064$, $R_w=0.166$, $\Delta\rho_{max}=0.320$ e Å^{-3}, $\Delta\rho_{min}=-0.341$ e Å^{-3}. Crystal data for (2*S*,5*S*)-**2a**: $C_{26}H_{36}NO_3$, $M_r=410.578$, $0.31\times0.21\times0.09$ mm^3, triclinic, space group $P\bar{1}$, $a=6.3786(2)$, $b=7.5419(3)$, $c=13.7089(9)$ Å, $\alpha=98.448(2)°$, $\beta=90.959(2)°$, $\gamma=114.567(4)°$, $V=591.06(5)$ Å^3, $Z=1$, $\rho_{calcd}=1.154$ gcm^{-3}, $2\theta_{max}=54.96°$, $Mo_{K\alpha}$($\lambda=0.71073$ Å), $\mu=0.74$ cm^{-1}, ϕ-ω-scans, $T=298$ K, 2611 independent reflections, 1396 observed reflections ($I>2.0\sigma(I)$), 277 refined parameters, $R=0.058$, $R_w=0.119$, $\Delta\rho_{max}=0.215$ e Å^{-3}, $\Delta\rho_{min}=-0.258$ e Å^{-3}. Crystal data for (2*S*,5*S*)-**3a**: $C_{33}H_{40}NO_5$, $M_r=530.685$, $0.36\times0.30\times0.03$ mm^3, monoclinic, space group $P2_1$, $a=7.1625(7)$, $b=9.696(2)$, $c=21.609(2)$ Å, $\beta=98.171(6)°$, $V=1485.5(4)$ Å^3, $Z=2$, $\rho_{calcd}=1.186$ g cm^{-3}, $2\theta_{max}=49.80°$, $Mo_{K\alpha}$($\lambda=0.71073$ Å), $\mu=0.79$ cm^{-1}, ϕ-ω-scans, $T=298$ K, 2733 independent reflections, 1809 observed reflections ($I>2.0\sigma(I)$), 424 refined parameters,

 © 2004 Wiley-VCH Verlag GmbH & Co. KGaA, Weinheim

$R = 0.048$, $R_w = 0.091$, $\Delta\rho_{max} = 0.191$ e Å^{-3}, $\Delta\rho_{min} = -0.201$ e Å^{-3}. CCDC-233749–233751 contain the supplementary crystallographic data for this paper. These data can be obtained free of charge via www.ccdc.cam.ac.uk/conts/retrieving.html (or from the Cambridge Crystallographic Data Centre, 12, Union Road, Cambridge CB21EZ, UK; fax: (+44) 1223-336-033; or deposit@ccdc.cam.ac.uk).

[9] For recent reviews, see: a) *Magnetism: Molecules to Materials II* (Ed.: J. S. Miller, M. Drillon), Wiley-VCH, Weinheim, **2001**; b) S. Nakatsuji, H. Anzai, *J. Mater. Chem.* **1997**, *7*, 2161–2174 c) J. Veciana, J. Cirujeda, C. Rovira, J. Vidal-Gancedo, *Adv. Mater.* **1995**, *7*, 221–225. Also see ref [1].

[10] a) O. Takizawa, J. Yamauchi, H. O. Nishiguchi, Y. Deguchi, *Bull. Chem. Soc. Jpn.* **1973**, *46*, 1991–1995; b) O. H. Griffith, D. W. Cornell, H. M. McConnell, *J. Chem. Phys.* **1965**, *43*, 2909–2910.

[11] T. Kimura, T. Goto, H. Shintani, K. Ishizaka, T. Arima, Y. Tokura, *Nature* **2003**, *426*, 55–58.

[12] S. Mackay, C. J. Gilmore, C. Edwards, M. Tremayne, N. Stuart, K. Shankland, *maXus: A Computer Program for the Solution and Refinement of Crystal Structures from Diffraction Data*, University of Glasgow, Scotland, UK, Nonius BV, Delft, The Netherlands and MacScience Co. Ltd., Yokohama, Japan, **1998**.

[13] The Supporting Information contains Figure S1, in which the DSC curves and temperature-variable XRD patterns of (±)-**3c** and (2*S*,5*S*)-**3c** are shown.

 © 2004 Wiley-VCH Verlag GmbH & Co. KGaA, Weinheim

Lanthanide-Binding Peptides

Structural Origin of the High Affinity of a Chemically Evolved Lanthanide-Binding Peptide**

Mark Nitz, Manashi Sherawat, Katherine J. Franz, Ezra Peisach, Karen N. Allen, and Barbara Imperiali**

Lanthanide-binding tags (LBTs) have been developed to enable the efficient production of fusion proteins that contain a high-affinity lanthanide-binding site.[1] These multitasking tags, which comprise only encoded amino acids, are easily incorporated, at the DNA level, into any recombinant protein. Upon complexation of a lanthanide ion, the LBT in a fusion protein provides a powerful and versatile handle to facilitate investigations involving luminescence,[1–4] NMR spectroscopy,[5–9] and X-ray crystallography.[10,11] Previously, these biophysical techniques have been implemented by binding lanthanides to the EF-hand motifs of calcium-binding proteins.[2,4,12] Ca^{2+}-binding loops are stabilized in EF-hand proteins by intraprotein interactions across the flanking helices of the helix–loop–helix motif. Achieving the nM–pM level of affinity of native calcium-binding proteins in an LBT for lanthanide ions necessitated the optimization of short peptides that bind lanthanides tightly without relying on the stabilizing forces of the native protein scaffold. Another design consideration was to build a lanthanide-binding site that satisfies the coordination chemistry solely from peptide-based ligands, thereby excluding water molecules from the primary coordination sphere, which would lead to luminescence quenching.[13,14] LBTs with these attributes were obtained through a combination of peptide design, targeted combinatorial synthesis, and a powerful screening protocol that utilized Tb^{3+}-based luminescence.[1,15]

Herein we present the 2.0-Å resolution X-ray crystal structure of a Tb^{3+}–LBT complex that achieves the design goals by using only 17 amino acids to maintain an overall structural integrity that is similar to an EF-hand motif found in calcium-binding proteins. The closed-shell coordination of the Tb^{3+} ion observed in the crystal structure is maintained in solution, as confirmed by time-resolved luminescence measurements. These studies provide insight into the origins of the enhanced luminescence of the LBT and its selectivity and high affinity for Tb^{3+} ions.

Figure 1A shows a ribbon diagram of the Tb^{3+}–LBT complex, together with the metal-binding residues. The eight-coordinate Tb^{3+} complex is formed by the monodentate oxygen ligands of Asp1, Asn3, and Asp5, bidentate carboxylate ligands from Glu9 and Glu12, and the backbone carbonyl group of Trp7, which also provides the indole group that sensitizes the Tb^{3+} luminescence. All the metal–oxygen bond lengths are within the expected range of 2.3–2.5 Å commonly found in eight-coordinate terbium complexes.[16,17] Subtle but significant differences are evident between this structure and the corresponding site (Figure 1B) from the structure of loop 3 of troponin C bound to Tb^{3+},.[18] An overlay of the backbones of the Tb^{3+}–LBT complex and Tb^{3+}-loaded troponin C gives a root-mean square deviation of only 1.18 Å over all main-chain atoms (Figure 1C) despite the *absence* of a supporting protein scaffold for the troponin C loop. Additionally, new side-chain contacts have been created both to the Tb^{3+} ion and between noncontiguous residues within the LBT. Most importantly, the chemical evolution achieved a coordination sphere for the Tb^{3+} ion that was provided exclusively by peptide-based ligands in the LBT, whereas an ordered water molecule provides one of the seven ligands in the troponin C structure (Figure 1B).

The most noticeable deviation between the structures occurs at residues 9 and 10 at the top of the loop (Figure 1C). This part of the backbone has moved closer to the metal

[*] M. Sherawat, Dr. E. Peisach, Prof. Dr. K. N. Allen
Department of Physiology and Biophysics
Boston University School of Medicine
715 Albany Street, Boston, MA 02118 (USA)
Fax: (+1) 617-638-4273
E-mail: allen@med-xtal.bu.edu
Dr. M. Nitz, Dr. K. J. Franz, Prof. Dr. B. Imperiali
Department of Chemistry
Massachusetts Institute of Technology
77 Massachusetts Avenue, Cambridge, MA 02139 (USA)
Fax: (+1) 617-452-2419
E-mail: imper@mit.edu

[**] We acknowledge the National Science Foundation Collaborative Research in Chemistry program (CHE-0304832 to B.I. and K.N.A.). The award of a National Institutes of Health/National Research Service Award fellowship to K.J.F., a Natural Science and Engineering Research Council postdoctoral fellowship to M.N., and a National Institutes of Health training grant fellowship (HL07291) to E.P. is also gratefully acknowledged.

Supporting information for this article is available on the WWW under http://www.angewandte.org or from the author.

 © 2004 Wiley-VCH Verlag GmbH & Co. KGaA, Weinheim DOI: 10.1002/anie.200460028

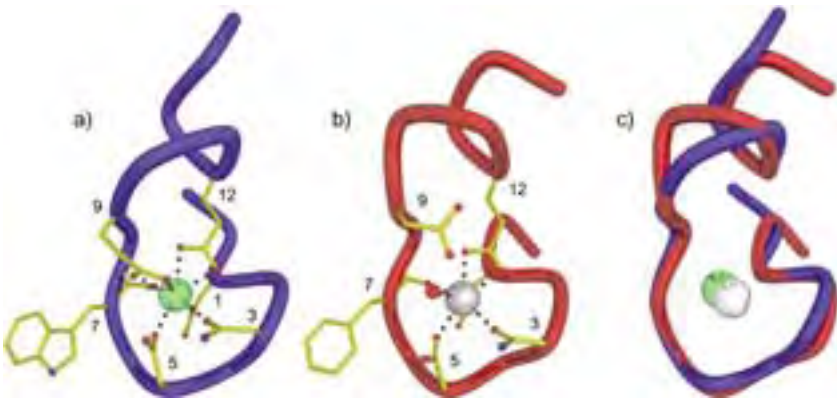


Figure 1. a) Ribbon structure of the LBT–Tb^{3+} complex showing metal-ligating residues and the terbium ion (green sphere). b) Ribbon structure of the Tb^{3+}-bound troponin C EF-hand motif (residues 104–120, PDB accession code: 1NCZ) showing metal-ligating residues, the terbium ion (gray sphere), and the ligating water molecule (red sphere). c) Overlay of the Tb^{3+} complexes of LBT (blue) and troponin C (red) complexes.

center in the LBT, thereby allowing bidentate chelation by Glu9. In fact, position 9 is the only metal-binding residue that differs between the two peptides, as shown in Table 1. In troponin C, the aspartate residue at position 9 does not coordinate the metal directly, rather it forms a hydrogen bond to a metal-ligating water molecule. So it is the Asp9Glu mutation, together with the translation of the backbone, that allows the exclusion of water from the Tb^{3+} coordination sphere. Bidentate coordination has not been observed previously at position 9 of EF-hand motifs. In the parvalbumins, a glutamate residue occupies this position, but it cannot easily adopt the correct conformation for bidentate ligation.[19] The dihedral angles of Gly10($\phi = 43.7°$, $\psi = -123.4°$) of the LBT complex are uniquely allowed for glycine residues and it is this conformation that allows translation of the peptide backbone to position the glutamate residue at position 9 so as to achieve the bidentate coordination that is key to the LBT structure.

Table 1: Sequence alignment of the LBT and the corresponding EF-hand motif of troponin C.

	Position														
	−1	1	3	5	7	9	11	13	15						
troponin C	I	F	**D**	K	**N**	A	**D**	G	**F**	I	**D**	I	E	**E**	L	G	E
LBT	Y	I	**D**	T	**N**	N	**D**	G	**W**	Y	**E**	G	D	**E**	L	L	A

Measurements of the terbium luminescence lifetime in solution were performed to correlate the crystallographic results with the solution-state biophysical properties.[14] The number of water ligands (q) to the Tb^{3+} ion can be measured by determining the luminescence lifetime of the complex in H_2O and D_2O since the lanthanide-excited state is quenched by the vibrational overtones of H_2O. The lifetimes of the LBT complex were fitted to a single exponential decay and were determined to be exceptionally long (2.6 ms in H_2O and 3.4 ms in D_2O; Figure 2). These rates lead to a q value of 0.3, thereby reinforcing the crystal-structure results indicating that there are no water ligands in the first coordination sphere of the Tb^{3+} center. Uncertainties in the q value arise from errors in the empirical proportionality constant relating the number of ligating water molecules to the luminescence decay rates and are estimated to be considerably less than 0.5 water molecules.[14] The closed-shell coordination of the Tb^{3+} ion is the major source of the improved luminescence intensities and long lifetimes, which have not previously been observed with peptide ligands.

Terbium ligation by the Trp7 backbone carbonyl group observed in the crystal structure is consistent with the early work in the Szabo research group who established that the tryptophan residue at position 7 of a calcium-binding loop is optimal for sensitizing Tb^{3+} lumines-

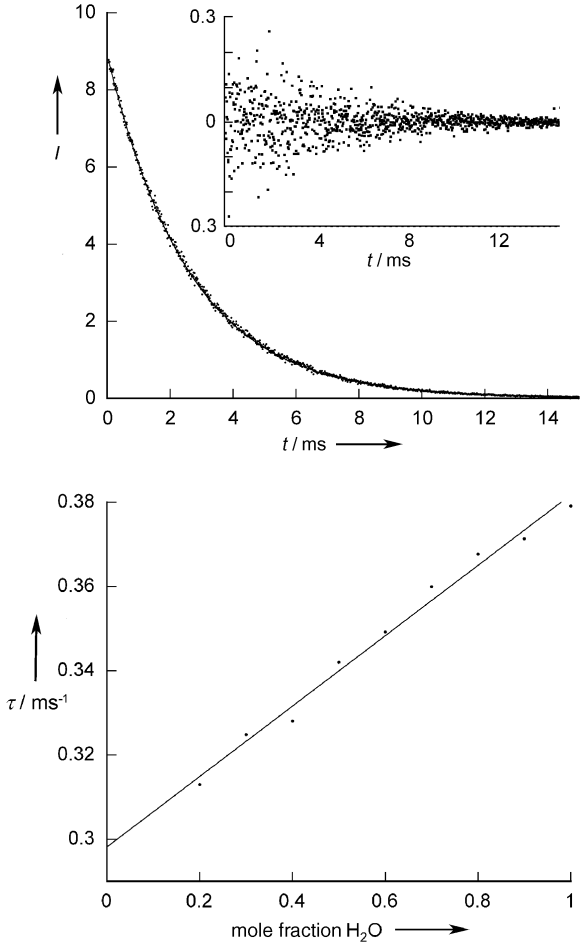


Figure 2. Top: Luminescent decay of a Tb^{3+} ion bound to the LBT. The excitation wavelength was 280 nm, and Tb^{3+}-sensitized emission was recorded at 544 nm. The line represents a single exponential curve fit of the experimentally determined intensities. Inset: Residuals (that is, deviation of the experimental intensities from the curve fit). Bottom: Luminescent decay rates with increasing H_2O concentrations. Extrapolation to an H_2O-free solution provides the rate constant in D_2O.

 © 2004 Wiley-VCH Verlag GmbH & Co. KGaA, Weinheim

cence.[20] The structure of the LBT confirms that the center of the indole is positioned 7.0 Å from the Tb^{3+} center, thereby maximizing sensitization of the terbium luminescence.[21] In the LBT structure Tyr8 is 6.0 Å from the terbium center and may also contribute to the sensitized luminescence of the complex. To determine its contribution to the luminescence intensity, a mutant LBT peptide was synthesized in which Trp7 was replaced with phenylalanine, a residue that does not sensitize Tb^{3+} luminescence. Based on the integrated intensities of the major terbium emission peak (544 nm), the Trp7Phe mutant shows approximately 15% of the luminescence of the parent LBT. Therefore, while Tyr8 makes some contribution to the energy transfer to the Tb^{3+} ion, Trp7 provides the majority of the sensitizing power.

Analysis of the electrostatic potential of the LBT shows that the motif has been optimized to shield the terbium ion from water. The surface potential of the LBT is neutral and hydrophobic, despite the positive charge of the terbium ion and the negatively charged ligands. In contrast, the surface associated with the Tb^{3+}-binding site in the troponin C is positively charged and favors water ligation (Figure 3).

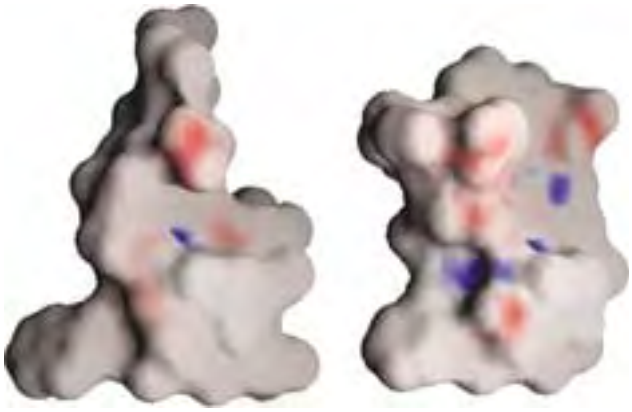


Figure 3. Electrostatic surface potential as calculated by the GRASP method.[22] The LBT–Tb^{+3} complex is shown on the left and the troponin C EF-hand motif on the right. The electrostatic surface was contoured at −15 kT (red, negative) and +15 kT (blue, positive).

In addition to improving the luminescence intensity of LBT peptides, the other goal of this study was to improve the lanthanide affinity. During the design process, hydrophobic amino acids were added at the C and N termini to promote hydrophobic interactions that would preorganize the loop for metal-ion binding. Examination of the structure reveals an N terminus with an extended conformation that allows it to pack against the C terminus. A hydrophobic cluster formed by Tyr1, Tyr8, and Leu13 (Figure 4) appears to "cinch" the loop closed, thereby creating a pseudo macrocycle that is primed for ion binding. The importance of these interactions is emphasized by the diminished affinity of LBT mutants that perturb this hydrophobic cluster for Tb^{3+} ions. Deletion of the N-terminal tyrosine residue reduces the terbium affinity 25-fold and the replacement of Tyr8 by an arginine residue reduces terbium affinity 120-fold. Replacement of Leu13 with an alanine residue reduces the affinity 36-fold. Conversely, deletion of the two C-terminal residues does not significantly



Figure 4. Ribbon structure of the LBT–Tb^{+3} complex with the interaction amongst hydrophobic residues Tyr1, Tyr8, and Leu13 emphasized (red).

reduce the affinity of the LBT for Tb^{3+} ions, a fact suggesting that these residues may have a minor role in predisposing the C terminus to a helical conformation.

The impetus for the design of the LBT sequences was to have a single tag that could take advantage of the range of useful physical properties possessed by lanthanide ions. Evaluation of the affinity of the LBT for the lanthanides across the series was carried out with competitive titrations.[23] The affinity of the LBT for lanthanides varies across the series in a harmonic relationship with the ionic radius, as previously observed for calcium-binding proteins.[23] The range in affinities varies from an apparent dissociation constant K_d of 4 μM for La^{3+} ions to 57 nM for Tb^{3+} ions. The range of affinities observed stems from the lanthanide contraction across the series, which leads to a 20% decrease in ionic radii with a concomitant increase in the Lewis acidity of the metal.[24] Thus, the size complementarity between the ion and the binding site (with bias for smaller lanthanides because of their higher Lewis acidity) is responsible for the range of affinities observed. With the minimum free energy of binding in the middle of the series, a range of useful high-affinity lanthanide complexes are readily accessed with the LBT (Figure 5).

The current crystallographic and luminescence studies indicate that the LBT binding environment for the Tb^{3+} ions has been optimized to provide a full complement of peptide-based ligands that exclude water from the first coordination sphere. In addition, the LBT has high affinity for a range of trivalent lanthanides, thereby allowing access to the varied physical properties displayed across the series. The LBT is independently folded, with the first and final residues proximal, which makes it compatible with insertion at the N terminus, at the C terminus, or within a loop of a target protein. The structure presented will facilitate the development of future generations of the LBT and provide a basis on which to model the LBT into known protein structures for

 © 2004 Wiley-VCH Verlag GmbH & Co. KGaA, Weinheim

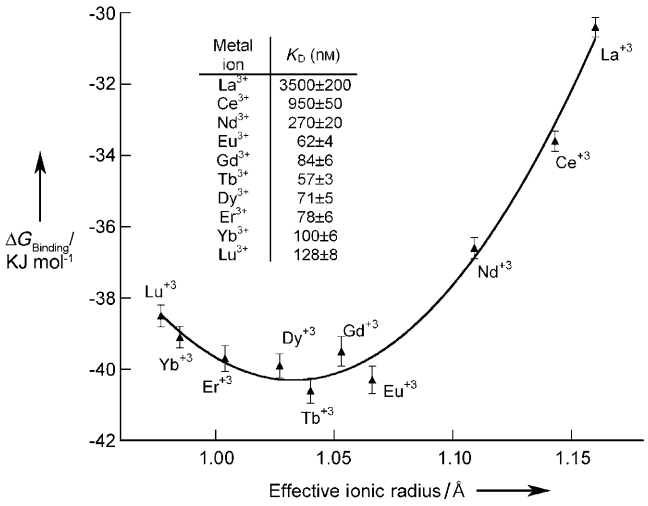


Figure 5. Dependence of binding free energy with the LBT on the effective ionic radii of rare-earth metals. The line is added to depict the trend rather than a theoretical correlation. Error bars indicate combined sources of error implicit in each competitive titration.

biophysical studies such as lanthanide-based resonance energy transfer (LRET).[12,25,26]

Received: March 17, 2004 [Z460028]

Keywords: fluorescent probes · lanthanides · peptide design · peptides · structure elucidation

[1] K. J. Franz, M. Nitz, B. Imperiali, *ChemBioChem* **2003**, *4*, 265.
[2] M. Elbanowski, B. Makowska, *J. Photochem. Photobiol. A* **1996**, *99*, 85.
[3] F. S. Richardson, *Chem. Rev.* **1982**, *82*, 541.
[4] J. C. G. Bunzli, G. R. Choppin, *Lanthanide Probes in Life, Chemical and Earth Sciences*, Elsevier, New York, **1989**.
[5] J. Wohnert, K. J. Franz, M. Nitz, B. Imperiali, H. Schwalbe, *J. Am. Chem. Soc.* **2003**, *125*, 13338.
[6] J. G. Shelling, M. E. Bjornson, R. S. Hodges, A. K. Taneja, B. D. Sykes, *J. Magn. Reson.* **1984**, *57*, 99.
[7] D. Bentrop, I. Bertini, M. A. Cremonini, S. Forsèn, C. Luchinat, A. Malmendal, *Biochemistry* **1997**, *36*, 11605.
[8] M. Allegrozzi, I. Bertini, M. B. Janik, L. Y.-M. Lee, *J. Am. Chem. Soc.* **2000**, *122*, 4154.
[9] R. Barbieri, I. Bertini, Y. M. Lee, C. Luchinat, A. H. Velders, *J. Biomol. NMR* **2002**, *22*, 365.
[10] W. I. Weis, R. Kahn, R. Fourme, K. Drickamer, W. A. Hendrickson, *Science* **1991**, *254*, 1608.
[11] M. D. Purdy, P. Ge, J. Chen, P. R. Selvin, M. R. Wiener, *Acta Crystallogr.* **2002**, *D58*, 1111.
[12] J. L. Vazquez-Ibar, A. B. Weinglass, H. R. Kaback, *Proc. Natl. Acad. Sci. USA* **2002**, *99*, 3487.
[13] W. D. Horrocks, D. R. Sudnick, *J. Am. Chem. Soc.* **1979**, *101*, 334.
[14] A. Beeby, I. M. Clarkson, R. S. Dickins, S. Faulkner, D. Parker, L. Royle, A. S. de Sousa, J. A. Gareth Williams, M. Woods, *J. Chem. Soc. Perkin Trans. 2* **1999**, 493–503.
[15] M. Nitz, K. J. Franz, R. L. Maglathlin, B. Imperiali, *ChemBioChem* **2003**, *4*, 272.
[16] D. Parker, R. S. Dickins, H. Puschmann, C. Crossland, J. A. K. Howard, *Chem. Rev.* **2002**, *102*, 1977.
[17] See the Supporting Information.
[18] S. T. Rao, K. A. Satyshur, M. L. Greaser, M. Sundaralingam, *Acta Crystallogr.* **1996**, *D52*, 916.
[19] C. Evrard, V. Lamzin, J. Parello, *Protein Sci.* **1999**, *8*, 2194.
[20] J. P. MacManus, C. W. Hogue, B. J. Marsden, M. Sikorska, A. Szabo, *J. Biol. Chem.* **1990**, *265*, 10358.
[21] W. E. Collier, W. D. J. Horrocks, *J. Am. Chem. Soc.* **1981**, *103*, 2856.
[22] A. Nicholls, K. Sharp, B. Honig, *Proteins*: *Struct. Funct. Genet.* **1991**, *11*, 281.
[23] E. E. Snyder, B. W. Buoscio, J. J. Falke, *Biochemistry* **1990**, *29*, 3937.
[24] R. D. Shannon, *Acta. Cryst.* **1976**, *A32*, 751.
[25] P. R. Selvin, *Annu. Rev. Biophys. Biomol. Struct.* **2002**, *31*, 275.
[26] Details regarding peptide synthesis, crystallization, data collection and refinement, and luminescence spectroscopy are available in the Supporting Information.

 © 2004 Wiley-VCH Verlag GmbH & Co. KGaA, Weinheim

Methane Activation

Structural and Mechanistic Requirements for Methane Activation and Chemical Conversion on Supported Iridium Clusters**

*Junmei Wei and Enrique Iglesia**

Chemical conversion of CH_4 into larger molecules is practiced by initially forming H_2–CO mixtures over metal catalysts. These reactions use CO_2 or H_2O as co-reactants in processes which also produce H_2, that is then used in refining and petrochemical processes and in fuel cells. The strong bonds in CH_4 (439 kJ mol^{-1} [1]) and the endothermic nature of re-forming reactions call for high temperatures and stable catalysts.[2–4] Supported Ir clusters catalyze CO_2–CH_4 reactions without detectable carbon formation,[5–7] with turnover rates higher than those found with other Group VIII metals, except Pt.[2]

Experimental and theoretical studies on model surfaces[8,9] have suggested that C–H bond activation is sensitive to surface structure and requires coordinatively unsaturated sites.[10,11] The effects of cluster size and of concomitant changes in surface coordination on re-forming turnover rates remain unexplored for Ir catalysts. Contradictory conclusions about the kinetic relevance of C–H activation steps within catalytic sequences remain, and catalytic supports have often been claimed to be required for the activation of CO_2 or H_2O co-reactants.[6,7]

[*] Dr. J. Wei, Prof. Dr. E. Iglesia
Department of Chemical Engineering
University of California at Berkeley
Berkeley, CA 94720 (USA)
Fax: (+1) 510-642-4778
E-mail: iglesia@cchem.berkeley.edu

[**] This study was supported by BP as part of the Methane Conversion Cooperative Research Program at the University of California. Helpful technical discussions with Dr. John Collins and Dr. Theo Fleisch (BP) throughout these studies are gratefully acknowledged.

 DOI: 10.1002/anie.200352703 © 2004 Wiley-VCH Verlag GmbH & Co. KGaA, Weinheim

C–H bond dissociation controls CH_4 conversion rates on many metal clusters,[2–4] but CH_4 re-forming kinetics and support and cluster-size effects have not been examined with respect to Ir catalysts. Herein we report evidence for the pathways involved in CH_4–CO_2, CH_4–H_2O, and CH_4-decomposition reactions on Ir.

CH_4 reaction rates are solely limited by C–H bond cleavage on Ir surfaces that remain essentially uncovered during catalysis. Turnover rates do not depend on the concentration or identity of the co-reactant; in these cases, turnover rates increase with increasing Ir dispersion, but they do not depend on the identity of the support (Al_2O_3, ZrO_2).

CH_4 reaction rates were measured on Ir catalysts (5 mg; 0.2, 0.4, 0.8, 1.6 wt% of Ir) diluted as pellets (25 mg inert support; pellet size 250–425 μm) and within the bed (500 mg ground quartz) to avoid temperature and concentration gradients; rates were unaffected by dilution, confirming the absence of these artifacts. Kinetic effects of CH_4, H_2O, and CO_2 pressures on reaction rates were measured at 823–1023 K and 100–1000 kPa for reactant ratios (CO_2, H_2O)/CH_4 of 0.5–4 by correcting measured rates for approach to equilibrium to obtain rates for forward re-forming reactions.[2]

Figure 1 shows that turnover rates increase linearly with increasing CH_4 pressure at 873 K on 0.8 wt% Ir/ZrO_2; they were not influenced by CO_2 pressures (10–300 kPa) for CH_4–CO_2 reactions. Similar CH_4 and H_2O dependences were observed in CH_4–H_2O reactions. In both re-forming reactions, CO or H_2 addition influenced net turnover rates because of higher reverse rates as expected from thermodynamic considerations, but forward turnover rates were unaffected by CO or H_2 pressures. These data indicate that Ir surfaces remain essentially uncovered by CH_4-derived intermediates or by reaction products, because co-reactant or product concentrations would have otherwise influenced forward rates. H_2 and CO desorb from Ir (111) at 380 K (0.5-L exposure) and 510 K (1-L exposure), respectively.[12,13] CO adsorption enthalpies (150 kJ mol^{-1}) would lead to CO coverages below 0.1% at 873 K, even at equilibrium CH_4 conversions (for equimolar CH_4–CO_2 reactants, 100 kPa); thus, no inhibition by chemisorbed CO is expected or, indeed, detected.

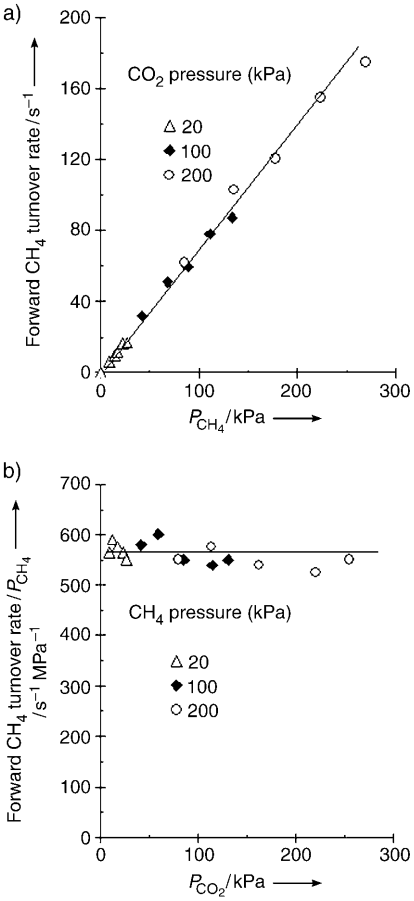


Figure 1. Effects of CH_4 (a) and CO_2 (b) pressure on forward CH_4 turnover rates for CH_4–CO_2 reactions on 0.8 wt% Ir/ZrO_2 (873 K, balance He, average pressure is the average of inlet and outlet pressures within the reactor; The unit for turnover rate is molecules/surface atom measured by H_2 chemisorption per second).

Table 1: Forward CH_4 turnover rates, rate constants, activation energies, and pre-exponential factors for CH_4 reactions on 0.8 wt% Ir/ZrO_2 (873 K, 20 kPa CH_4, 25 kPa CO_2 or H_2O, balance Ar).

Co-reactant	Turnover rate [s^{-1}]	Rate constant [$s^{-1}kPa^{-1}$]	Activation energy [kJ mol^{-1}]	Pre-exponential factor [$s^{-1}kPa^{-1}$]
CO_2	13.0	0.65	86	9.1×10^4
H_2O	12.4	0.62	87	9.9×10^4
None	11.2[a]	0.56	81	3.9×10^4

[a] Initial CH_4 rate.

The sole kinetic relevance of C–H bond activation on uncovered Ir surfaces leads to similar turnover rates for CH_4–CO_2 and CH_4–H_2O reactions at a given CH_4 pressure (Table 1). Thus, the identity of the co-reactants, with the consequent implications for their reactivity, does not influence rates because both H_2O and CO_2 react with CH_4-derived intermediates rapidly relative to C–H activation steps. These re-forming rates are also similar to initial rates for CH_4 decomposition, a stoichiometric noncatalytic reaction that forms carbon and H_2(g) on Ir catalysts (Table 1). These similarities in rate constants and turnover rates remain throughout a wide temperature range (823–1023 K), and as such the activation energies are also similar for these reactions (Table 1). Measured preexponential factors (Table 1) are about 10 times larger than those predicted from transition state theory (5.5×10^3 $s^{-1}kPa^{-1}$) assuming immobile activated complexes, but they approach experimental values when activated complexes are allowed modest two-dimensional mobility.

The kinetic relevance of C–H bond activation was confirmed by similar kinetic isotopic effects (1.70–1.81) measured for CO_2 re-forming, H_2O re-forming, and decomposition reactions (0.8 wt% Ir/ZrO_2; 873 K). The fast and quasi-equilibrated nature of co-reactant activation was dem-

 © 2004 Wiley-VCH Verlag GmbH & Co. KGaA, Weinheim

onstrated by the identical ^{13}C content in the CO and CO_2 leaving a catalyst bed used to react $CO_2/CH_4/^{13}CO$ (1:1:0.4) mixtures.[14]

The uncovered nature of Ir surfaces and the persistence and catalytic relevance of Ir dispersions measured before reaction were confirmed by measuring rates of CO oxidation, a structure-insensitive reaction,[15] before and after re-forming reactions. CO turnover rates at 363 K on 1.6 wt% Ir/ZrO_2 were similar before and after CH_4–CO_2 or CH_4–H_2O reactions (Figure 2). Thus, Ir atoms are not covered by unreactive

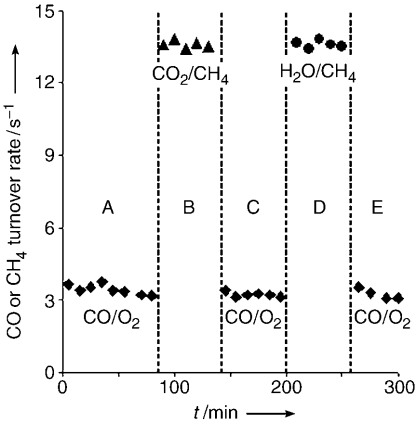


Figure 2. CO oxidation and forward CH_4 re-forming turnover rates on 1.6 wt% Ir/ZrO_2 (A, C, E, CO oxidation turnover rates, 363 K, 0.19 kPa CO and O_2; B, D, forward CH_4 turnover rates for CH_4–CO_2 and CH_4–H_2O reactions, 873 K, 25 kPa CH_4 and 25 kPa CO_2 or H_2O; The unit for turnover rate is molecules/surface atom measured by H_2 chemisorption per second).

carbon residues or lost by sintering during CH_4 re-forming at 873 K. Re-forming and CO oxidation rates did not change with time, indicating that Ir surfaces are stable for extended periods of time under CH_4 re-forming conditions.

The simple kinetic equation $r_f = kP_{CH_4}$ accurately describes measured CH_4 re-forming and decomposition kinetics on Ir. CO_2 and H_2O co-reactants and H_2 and CO products do not influence rates. This expression is accurate for all catalysts throughout the temperature range examined (823–1023 K). These conclusions and the dispersion effects discussed below appear to be generally applicable to Pt,[2] Ru,[16] and Rh[17] clusters.

CH_4 re-forming and decomposition turnover rates increased with increasing Ir dispersion (Figure 3), as it varied with metal content (0.2–1.6 wt%) or support. These data contradict the lack of dispersion effects reported for CO_2–CH_4 reactions on Ir/Al_2O_3,[5] but they are consistent with coordinative unsaturation requirements inferred from theoretical and experimental studies on model surfaces.[4,18–24] Density functional theory showed that CH_4 binds 18–22 kJ mol^{-1} more strongly on kink sites than on Ir (111).[21] C_2H_6 dissociates with ~20 kJ mol^{-1} lower activation energies on Ir (110)-(1 × 2) than on Ir (111).[22,23] Ir (110)-(1 × 2) activates C_2–C_7 alkanes, whereas Ir (111) does not.[22,23] Similar trends are apparent from the reactivity of defect sites on Ir (111)[24] and of Ir (110) relative to Ir (111).[4,20]

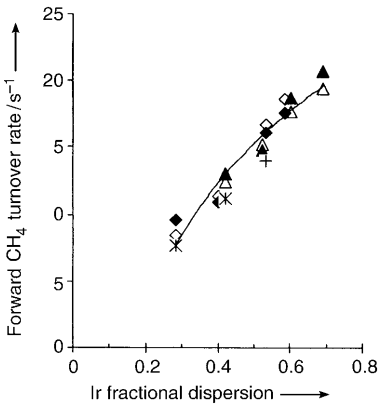


Figure 3. Forward CH_4 turnover rates for CH_4–CO_2 (solid symbol), CH_4–H_2O (open symbol), and CH_4 decomposition reactions as a function of Ir dispersion (873 K, 20 kPa CH_4, (◇◆) Ir/ZrO_2, (▲△) Ir/Al_2O_3, (*) CH_4 decomposition on Ir/ZrO_2, (+) CH_4 decomposition on Ir/Al_2O_3). (The unit for turnover rate is molecules/surface atom measured by H_2 chemisorption per second).

We note that activation energies on model surfaces are much lower than those measured on Ir clusters in this study. Very active sites could form unreactive carbon, leaving less reactive sites to catalyze CH_4 conversion turnovers. Figure 2 shows unequivocally that CH_4 re-forming reactions do not change the number of exposed Ir atoms. We cannot rule out the presence of minority sites (< 5% of exposed Ir atoms) with remarkable reactivity for activation of C–H bonds. We can conclude, however, that such sites do not react and are thus not relevant to catalysis. These issues illustrate the essential requirement that experiment and theory rigorously address catalytic cycles, and not merely the stoichiometric steps presumably involved in such cycles.

Support effects have been attributed to co-reactant activation sites, without rigorous assessment of the concomitant effects of the support on metal dispersion or transport artifacts.[25] We measured similar turnover rates on Ir/Al_2O_3 and Ir/ZrO_2 (Figure 3), as also found for other metals with a wider range of supports.[2,16,17] Co-reactant activation on supports, even if it occurred, could not influence CH_4 turnover rates, because such steps are not kinetically relevant. Thus, previously reported support effects[25] cannot be compared with our data or with our mechanistic conclusions. The absence of support effects agrees with a previous study of re-forming reactions catalyzed by Ir,[26] whose kinetic character is, however, equivocal, because of near-equilibrium conversions.

In summary, C–H bond activation is the only kinetically relevant step in CH_4 activation on supported Ir clusters, the reactivity of which increases with increasing dispersion. Kinetically relevant C–H bond activation steps and consequently, overall CH_4 re-forming rates are unaffected by the chemical identity of the support.

Experimental Section

Ir/Al_2O_3 and Ir/ZrO_2 were prepared by incipient wetness impregnation of Al_2O_3 or ZrO_2 with aqueous $IrCl_3 \cdot 3H_2O$. Ir dispersions were

 © 2004 Wiley-VCH Verlag GmbH & Co. KGaA, Weinheim

measured by using volumetric methods to determine uptakes of strongly chemisorbed H_2 at 313 K. The high-pressure reactor system was described elsewhere.[2] Reactant and product concentrations were measured with a HP 6890 gas chromatograph. Catalysts (20 mg) diluted with quartz powder (500 mg) were used in CH_4 decomposition kinetic measurements. Chemical composition was measured by on-line mass spectrometry. Ir/ZrO_2 (1.6 wt %; 5 mg) was used to measure CO oxidation reaction rates at 363 K and 0.19 kPa CO and O_2 pressures.

Received: August 22, 2003
Revised: March 23, 2004 [Z52703]

Keywords: C–H activation · heterogeneous catalysis · iridium · kinetics · supported catalysts

[1] S. J. Blanksby, G. B. Ellison, *Acc. Chem. Res.* **2003**, *36*, 255.
[2] J. Wei, E. Iglesia, *J. Phys. Chem. B* **2004**, *108*, 4094.
[3] T. A. Jachimowski, C. J. Hagedorn, W. H. Weinberg, *Surf. Sci.* **1997**, *393*, 126.
[4] D. C. Seets, C. T. Reeves, B. A. Ferguson, M. C. Wheeler, C. B. Mullins, *J. Chem. Phys.* **1997**, *107*, 10229.
[5] M. F. Mark, W. F. Maier, *J. Catal.* **1996**, *164*, 122.
[6] J. R. Rostrup-Nielsen, J. H. Bak Hansen, *J. Catal.* **1993**, *144*, 38.
[7] A. T. Ashcroft, A. K. Cheetham, M. L. H. Green, P. D. F. Vernon, *Nature* **1991**, *352*, 225.
[8] M. Boudart, *Adv. Catal.* **1969**, *20*, 153.
[9] H. Burghgraef, A. P. Jansen, R. A. van Santen, *Faraday Discuss.* **1993**, *96*, 337.
[10] M. C. McMaster, R. J. Madix, *J. Chem. Phys.* **1993**, *98*, 15.
[11] K. Klier, J. S. Hess, R. G. Herman, *J. Chem. Phys.* **1997**, *107*, 4033.
[12] J. R. Engstrom, W. Tsai, W. H. Weinberg, *J. Chem. Phys.* **1987**, *87*, 3104.
[13] J. Lauterbach, R. W. Boyle, M. Schick, W. J. Mitchell, B. Meng, W. H. Weinberg, *Surf. Sci.* **1996**, *350*, 32.
[14] J. Wei, E. Iglesia, *Phys. Chem. Chem. Phys.*, in press.
[15] M. Boudart, F. Rumpf, *Surf. Sci.* **1987**, *35*, 95.
[16] J. Wei, E. Iglesia, *J. Phys. Chem. B* **2004**, *108*, 2253.
[17] J. Wei, E. Iglesia, *J. Catal.* **2004**, *225*, 116.
[18] P. D. Szuromi, J. R. Engstrom, W. H. Weinberg, *J. Phys. Chem.* **1985**, *89*, 2497.
[19] Z. Liu, P. Hu, *J. Am. Chem. Soc.* **2003**, *125*, 1958.
[20] C. T. Reeves, D. C. Seets, C. B. Mullins, *J. Mol. Catal. A* **2001**, *167*, 207.
[21] G. Henkelman, H. Jonsson, *Phys. Rev. Lett.* **2001**, *86*, 664.
[22] D. F. Johnson, H. Weinberg, *Science* **1993**, *261*, 5117.
[23] D. F. Johnson, H. Weinberg, *J. Chem. Phys.* **1995**, *103*, 5833.
[24] D. F. Johnson, H. Weinberg, *J. Chem. Phys.* **1994**, *101*, 6289.
[25] A. Erdohelyi, K. Fodor, F. Solymosi, *Stud. Surf. Sci. Catal.* **1997**, *107*, 525.
[26] K. Nakagawa, K. Anzai, N. Matsui, N. Ikenaga, T. Suzuki, Y. Teng, T. Kobayashi, M. Haruta, *Catal. Lett.* **1998**, *51*, 163.

 © 2004 Wiley-VCH Verlag GmbH & Co. KGaA, Weinheim

Conducting Materials

A Biopolymer Composite Material as an Anhydrous Proton-Conducting Membrane**

*Masanori Yamada and Itaru Honma**

Chitin is a biopolymer famous as a natural mucopolysaccharide resource and is present in the exoskeleton of crustaceans and insects, as well as in chitin-enriched materials, such as crab and shrimp shells. These are generally discarded as industrial waste around the world,[1] and so chitin can be considered to be an extremely low-cost, nonhazardous, and environmentally benign polymer. The use of chitin and its derivatives as biomedical materials has been reported, for example as tissue engineering materials, surgical tape, and artificial skin.[2,3] However, their use in electronically or optically active materials has not been reported. Application of these biopolymers in electrical devices would be attractive not only in terms of product cost and environmental safety but also from a materials science point of view.

Recently, polymer electrolyte membrane fuel cells (PEMFCs) that operate under anhydrous conditions (or extreme low humidity) and intermediate temperature (100–200 °C) have attracted much attention as clean, advanced energy conversion systems with high efficiencies.[4] The operation of the PEMFCs at higher temperatures improves the tolerance of the Pt electrode for carbon monoxide and provides higher energy efficiency, simplified heat management, and co-generation.[4] However, the customary perfluorinated sulfonic acid membranes that are used, such as nafion, are unstable at higher temperatures, which result in proton conductivity abruptly decreasing as a result of the evaporation of water from the electrolyte membrane and destruction of the polymer structure. Additionally, the production cost of perfluorinated membranes is extremely high, which makes industrialization of the PEMFCs difficult. Therefore, highly conducting proton membranes composed of inexpensive materials that conduct at intermediate temperatures are necessary for advanced PEMFC technology. In particular, composite materials of strong acids and basic polymers have been proposed as novel polymer electrolytes of single proton conductors under anhydrous and intermediate temperature conditions.[4–8]

In this study we prepared an anhydrous proton-conducting membrane using a composite of chitin phosphate (CP;

[*] Dr. M. Yamada, Dr. I. Honma
Energy Materials Group, Energy Electronic Institute
National Institute of Advanced Industrial Science and Technology (AIST)
Umezono 1-1-1, Tsukuba, Ibaraki 305-8568 (Japan)
Fax: (+81) 29-861-5829
E-mail: i.homma@aist.go.jp

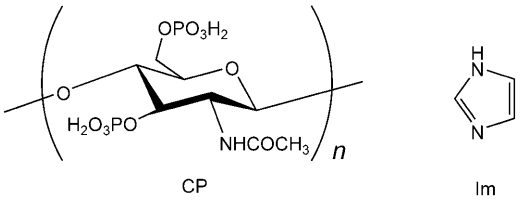
[**] This work was supported by the R&D program of PEMFC of the New Energy and Industrial Technology Development Organization (NEDO), Japan.

Supporting information for this article is available on the WWW under http://www.angewandte.org or from the author.

 © 2004 Wiley-VCH Verlag GmbH & Co. KGaA, Weinheim DOI: 10.1002/anie.200353176

chitin modified with a phosphonic acid group) and the basic heterocycle imidazole (Im). A composite material of CP and 200 wt% Im showed a high proton conductivity of 7×10^{-3} S cm^{-1} at 150 °C under anhydrous (water-free) conditions. Additionally, the thermal stability of CP/Im composite material was found to increase with the doping ratio of the imidazole.

Chitin phosphate (CP) was synthesized by a previously reported procedure.[9] The CP/heterocycle composite materials were prepared as follows: a mixed aqueous solution of CP/Im was cast onto a teflon plate and dried at room temperature or 70 °C for 1–3 days. The dried-membrane was then stripped from the teflon plate.[10] The molecular structures of CP and imidazole are shown in Scheme 1. Figure 1a and b show the



Scheme 1. Molecular structures of chitin phosphate (CP) and imidazole (Im).

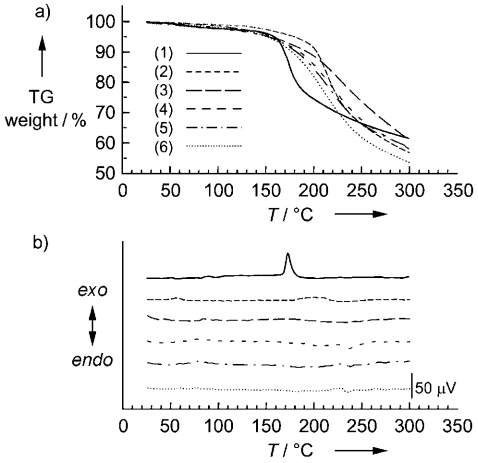


Figure 1. a) Thermogravimetric (TG) and b) differential thermal analyses (DTA) curves of CP/Im composite materials. (1) pure CP, (2) CP/20 wt% Im, (3) CP/50 wt% Im, (4) CP/100 wt% Im, (5) CP/200 wt% Im, and (6) CP/500 wt% Im composite materials.

thermogravimetric (TG) and differential thermal analyses (DTA) of pure chitin phosphate (**1**), CP/20 wt% Im (**2**), CP/50 wt% Im (**3**), CP/100 wt% Im (**4**), CP/200 wt% Im (**5**), and CP/500 wt% Im (**6**) composite materials, respectively, measured at the heating rate of 10 °C min^{-1} under a dry nitrogen flow. The pure CP and composite materials showed a TG weight loss of a few percent at 160 °C. This TG weight loss is due to the evaporation of solvent or imidazole from the material (Figure 1a) and dehydration of the phosphate group. An exothermic peak at 167.9 °C corresponding to thermal decomposition was evident in the DTA analysis of the pure chitin phosphate (line (1) in Figure 1b). Surprisingly, this exothermic peak disappeared on doping with imidazole (lines (2)–(4), Figure 1b). It is indicated from these results that the CP/Im composite material formed an acid/base complex through electrostatic interactions in the composite membrane. As a result, the composite becomes more stable than the pure CP. The large TG weight loss of the CP/Im composite material above 200 °C is because of evaporation of imidazole from the membrane or thermal decomposition.

The molecular structure of the acid/base complex in the CP/Im composite material was characterized by infrared (IR) spectroscopic analysis with a diamond attenuated total reflection prism with a resolution of 4 cm^{-1}. Figure 2 shows

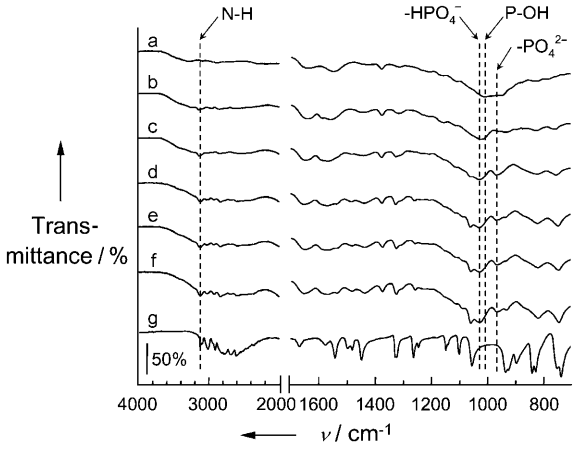
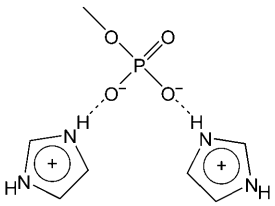


Figure 2. IR spectra of CP/Im composite materials with different doping ratios of imidazole. a) pure CP, b) CP/20 wt% Im, c) CP/50 wt% Im, d) CP/100 wt% Im, e) CP/200 wt% Im, f) CP/500 wt%Im, and g) pure Im materials.

the IR spectra of the CP/Im composite materials of a) pure CP, b) CP/20 wt% Im, c) CP/50 wt% Im, d) CP/100 wt% Im, e) CP/200 wt% Im, f) CP/500 wt% Im, and g) pure imidazole, respectively. The absorption band at 1011 cm^{-1}, attributed to the asymmetric stretching vibration of the P–OH group (dashed line in Figure 2),[11,12] decreased when imidazole was mixed in the CP. In addition, two new absorption bands appeared at 1028 and 967 cm^{-1}, the stretching vibration bands of $-HPO_4^-$ and $-PO_4^{2-}$ (dashed line in Figure 2),[13] respectively. These results indicated that the P–OH group of CP is deprotonated on doping of imidazole and forms the P–O$^-$ group. Alternatively, the absorption band at approximately 3100 cm^{-1} in the composite materials, which corresponding to the stretching band of the N–H group,[11] moderately increased in comparison with the spectrum of pure imidazole. These results suggest that the P–OH groups of CP are deprotonated on doping with imidazole and form P–O$^-$ groups. This free proton strongly interacts with the nonprotonated imidazole –N= atom. Therefore, the composite material of CP and imidazole is an acid/base salt (Scheme 2).

The proton conductivity measurements of the CP/Im composite materials were demonstrated by the a.c. impedance method over the frequency range 1 Hz–1 MHz under a

 © 2004 Wiley-VCH Verlag GmbH & Co. KGaA, Weinheim



Scheme 2. Acid–base composite material.

dry nitrogen flow. Thus, the measured impedance response indicates the anhydrous proton conductivity. A typical impedance response, as shown by Cole–Cole plots, of the CP/Im composite materials was similar to that of highly conducting proton membranes, such as humidified nafion, organic/inorganic hybrid membranes mixed with heteropolyacids,[14] monododecylphosphate (MDP)/benzimidazole,[5] 2-undecylimidazole (UI)/MDP,[6] uracil (U)/MDP,[7] and poly(vinylphosphonic acid) (PVPA)/heterocycle[8] composite materials (Figure 3a). The proton conductivity measurements

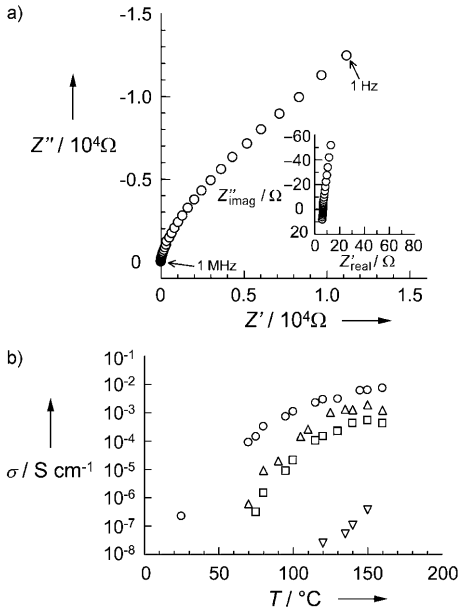


Figure 3. a) Typical impedance response (Cole–Cole plots) of CP/200 wt% Im composite material under anhydrous conditions. The frequency range is 1 Hz–1 MHz. The insert indicates the impedance response at the frequency range of 2 kHz–1 MHz. b) Proton conductivities of CP/Im composite materials with different imidazole doping ratios under anhydrous conditions. The doping ratios of Im are: ▽: 20 wt% Im, □: 50 wt% Im, ○: 200 wt% Im, and △: 500 wt% Im, respectively.

were carried out on the same sample four times under anhydrous conditions, with the temperature being varied from ambient to 160 °C. The conductivity decreased slightly on repeated measurements and reached a steady state after three. The anhydrous, steady-state proton conductivities of the CP/Im composite materials and their variation with the imidazole doping level and temperature are shown in Figure 3b. The anhydrous proton conductivity of the CP/Im composite materials increased with temperature and reached a maximum at 150 °C. Additionally, the conductivity of the composite material became larger as the imidazole doping ratio increased. The CP/200 wt% Im composite material indicated the largest anhydrous proton conductivity of 7×10^{-3} S cm^{-1} at 150 °C, while the pure CP membrane did not show any measurable proton conductivity ($< 10^{-8}$ S cm^{-1} at 150 °C). Additionally, the anhydrous proton conductivity of pure imidazole could not be measured by melting and evaporation at intermediate temperatures.[15] These results indicate that the biopolymer/heterocycle composite material becomes proton-conductive by forming acid/base ionic pairs and constructs a proton-conductive pathway with fast proton transfer.

Previously, we reported a acid/base composite material with a heterocycle that acted as a proton-conducting membrane under anhydrous conditions.[5–8] In this case, a Grotthuss-type mechanism was proposed, in which proton transport by basic heterocycles can occur by movement from protonated molecules to nonprotonated neighbor molecules with a small activation energy of approximately 0.5 eV.[5,6,8] Namely, the protonated and nonprotonated nitrogen atoms in the heterocycle can act as donors and acceptors in proton-transfer reactions, respectively. In our investigations, the calculated activation energy (E_a) from the Arrhenius plots of the conductivities is approximately 0.6–0.4 eV (see the Supporting Information). This value is almost the same as other materials reported as anhydrous single proton conductors of UI/MDP composite materials[6] and PVPA/heterocycle composite materials.[8] These results suggest that proton conductivity in the CP/Im composite materials is based on proton transport by a Grotthuss-type mechanism[16,17] between imidazole groups. Therefore, the proton-conducting mechanism was proposed to be as follows: protonated imidazole centers are formed by proton transfer from the phosphonic acid group of the CP. These acid/base complexes composed of imidazole and the phosphonic acid groups can be confirmed by the IR spectroscopic analysis (see Figures 2 and Scheme 2). The phosphonic acid groups in CP appears to act as proton donors[16,17] to the imidazole centers, and the proton conductivity occurs between the imidazole centers by a Grotthuss-type mechanism. As a result, the CP/Im composite material gives a high proton conductivity of 7×10^{-3} S cm^{-1} at 150 °C under anhydrous conditions. These biocomposite proton-conducting materials without the presence of water molecules are novel and could be applicable as an advanced electrolyte membrane for PEMFCs operated above 100 °C.

In summary, we have prepared an anhydrous proton conductor consisting of a commonly discarded biopolymer, chitin phosphate, and imidazole. The CP/200 wt% Im composite material showed a large proton conductivity of 7×10^{-3} S cm^{-1} at 150 °C under anhydrous conditions. The utilization of a biopolymer such as CP for PEMFC technologies is novel and challenging as it is inexpensive, nonhazardous, and environmentally benign. Besides its superior ion-conducting properties under anhydrous or extremely low-humidity conditions, this biopolymer composite material may

 © 2004 Wiley-VCH Verlag GmbH & Co. KGaA, Weinheim

have the potential for application in bioelectrochemical devices, including implantable batteries and biosensors.

Received: October 28, 2003
Revised: April 13, 2004 [Z53176]

Keywords: conducting materials · heterocycles · membranes · polymers · proton transfer

[1] M. N. V. R. Kumar, *React. Funct. Polym.* **2000**, *46*, 1.
[2] a) M. Mochizuki, Y. Kadoya, Y. Wakabayashi, K. Kato, I. Okazaki, M. Yamada, T. Sato, N. Sakairi, N. Nishi, M. Nomizu, *FASEB J.* **2003**, *17*, 875; b) K. Kato, A. Utani, N. Suzuki, M. Mochizuki, M. Yamada, N. Nishi, H. Matsuura, H. Shinkai, M. Nomizu, *Biochemistry* **2002**, *41*, 10747.
[3] a) J. K. F. Suh, H. W. T. Matthew, *Biomaterials* **2000**, *21*, 2589; b) T. Chandy, C. P. Sharma, *Biomater. Artif. Cells Artif. Organs* **1990**, *18*, 1; c) I. V. Yannas, J. F. Burke, D. P. Orgill, E. M. Skrabut, *Science* **1982**, *215*, 174.
[4] a) Q. Li, R. He, J. O. Jensen, N. J. Bjerrum, *Chem. Mater.* **2003**, *15*, 4896; b) K. D. Kruer, *ChemPhysChem* **2002**, *3*, 771; c) J. A. Kerres, *J. Membr. Sci.* **2001**, *185*, 3; d) K. D. Kreuer, *J. Membr. Sci.* **2001**, *185*, 29; e) M. Rikukawa, K. Sanui, *Prog. Polym. Sci.* **2000**, *25*, 1463.
[5] M. Yamada, I. Honma, *Electrochim. Acta* **2003**, *48*, 2411.
[6] M. Yamada, I. Honma, *J. Phys. Chem. B*, in press.
[7] M. Yamada, I. Honma, *ChemPhysChem*, in press.
[8] M. Yamada, I. Honma, unpublished results.
[9] a) N. Nishi, S.-I. Nishimura, A. Ebina, A. Tsutsumi, S. Tokura, *Int. J. Biol. Macromol.* **1984**, *6*, 53; b) N. Nishi, A. Ebina, S.-I. Nishimura, A. Tsutsumi, O. Hasegawa, S. Tokura, *Int. J. Biol. Macromol.* **1986**, *8*, 311; c) N. Nishi, Y. Maekita, S.-I. Nishimura, O. Hasegawa, S. Tokura, *Int. J. Biol. Macromol.* **1987**, *9*, 109. The phosphorylation of chitin was confirmed by the infrared spectroscopic analysis with a diamond attenuated total reflection prism. The degree of phosphorylation (DS) of chitin was determined by elemental analysis and by inductivity coupled plasma atomic emission spectrophotometry for phosphorus. Elemental analysis (%) calcd for $C_8H_{15}NO_{11}P_2 \cdot 0.33\,H_2O$: C 26.03, H 4.28, N 3.79, P 16.78, found: C 26.05, H 4.65, N 3.79, P 16.99. The chitin used was fully phosphorylated (DS = 2.0, 100 % phosphorylated).
[10] The doping ratio of imidazole:CP was determined by: (doping ratio of imidazole) = 100 × (weight of imidazole)/(weight of CP).
[11] R. M. Silverstein, F. X. Webster in *Spectrometric Identification of Organic Compounds*, Wiley, New York, **1998**.
[12] D. E. C. Corbridge in *Topics* in *Phosphorus Chemistry* (Eds.: M. Grayson, E. J. Griffith), Wiley, New York, **1969.**
[13] M. Kawahara, J. Morita, M. Rikukawa, K. Sanui, N. Ogata, *Electrochim. Acta* **2000**, *45*, 1395.
[14] a) I. Honma, H. Nakajima, O. Nishikawa, T. Sugimoto, S. Nomura, *J. Electrochem. Soc.* **2003**, *150*, A616; b) I. Honma, H. Nakajima, O. Nishikawa, T. Sugimoto, S. Nomura, *Solid State Ionics* **2003**, *162–163*, 237; c) I. Honma, H. Nakajima, O. Nishikawa, T. Sugimoto, S. Nomura, *J. Electrochem. Soc.* **2002**, ***149***, A1389.
[15] The melting point of pure imidazole is 90–91 °C. Namely, imidazole is in the liquid state at the intermediate temperature. In our experiments, the proton conductive measurements were performed by the sandwich of two Pt electrodes. Therefore, the conductivity of imidazole at the intermediate temperature could not be measured.
[16] K. D. Kreuer, *Chem. Mater.* **1996**, ***8***, 610.
[17] T. Dippel, K. D. Kreuer, J. C. Lassègues, D. Rodriguez, *Solid State Ionics* **1993**, ***61***, 41.

 © 2004 Wiley-VCH Verlag GmbH & Co. KGaA, Weinheim

Surface Characterization

In Situ Investigations into Chemical Processes by Electron-Energy-Resolved X-Ray Absorption Spectroscopy**

*Antje Vollmer, John D. Lipp, Helmut Weiss, Rachel O'Malley, and Trevor Rayment**

Over the last 200 years industrial catalysis has become increasingly important so that currently more than 90% of the world's chemical manufacturing processes are controlled by catalysis.[1] Catalytic converters used in exhaust detoxication and for atom-economic processes are of comparable importance,[2,3] and yet the elementary steps and in particular the role of the support material are frequently unclear.[4,5]

Surface-sensitive analytical probes are highly desirable, but most of those in common use rely upon the low mean free path of electrons in materials and operate under ultrahigh-vacuum (UHV) conditions that are far from those under which the material functions. X-ray absorption spectroscopy (XAS) is an invaluable tool for the study of catalysts because it yields interatomic distances, coordination numbers, the identities of neighboring atoms, and details of electronic structure in the presence of short-range order.[6] It is also ideal for studies under normal operating conditions because X-rays will readily pass through the reactive gas atmospheres used in catalysis. Yet in this advantage lies also the greatest challenge to the use of X-rays in the study of catalysts: the penetrating nature of X-rays means that the surface sensitivity of XAS is low. Most XAS experiments provide no surface information. However, there is an alternative method for detecting XAS signals that offers some surface sensitivity. If the Auger emission arising from relaxation of the core hole is measured instead of the photon transmission or fluorescence emission, then only the region lying within the escape depth of the elastically and inelastically scattered Auger electrons contributes to the signal.[7] It has been shown that electron detection is possible in most gases, at elevated pressures and temperature.[8] Unfortunately, the total escape depth for Auger electrons in these circumstances is substantial: typically between 100 and a few 1000 Å.[9–11]

[*] Dr. A. Vollmer, R. O'Malley, Dr. T. Rayment
Department of Chemistry, University of Cambridge
Lensfield Road, Cambridge CB21EW (UK)
Fax: (+44) 1223-336-362
E-mail: tr22@cam.ac.uk
J. D. Lipp
CCLRC Rutherford Appleton Laboratory
Prof. H. Weiss
Otto-von-Guericke-Universität Magdeburg (Germany)

[**] We thank the staff of the synchrotron radiation facility, Daresbury for their help and support and EPSRC for generous funding. H.W. thanks the DFG for financial support.

Supporting information for this article is available on the WWW under http://www.angewandte.org or from the author.

 DOI: 10.1002/anie.200353235 © 2004 Wiley-VCH Verlag GmbH & Co. KGaA, Weinheim

Auger electrons lose energy as they move to the surface and the elastic mean free path is typically an order of magnitude smaller than the escape depth. Thus energy-selective detection radically improves the surface sensitivity that can be achieved by use of electrons. This fact is well known for UHV experiments, but it is only recently that a practical scheme for energy-resolved electron detection has been presented for use at ambient pressure.[12] This scheme uses a gas microstrip detector (GMSD) that functions as a very robust proportional counter. The key component shown in Figure 1a is a pattern of interleaved metallic strips

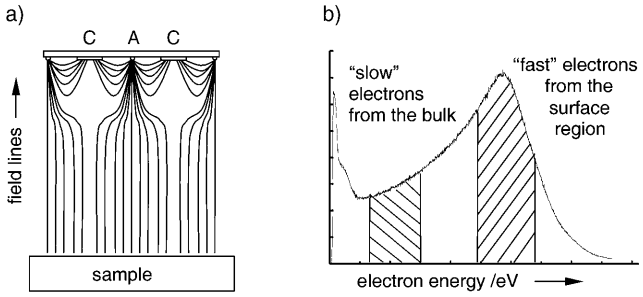


Figure 1. a) Schematic diagram of the GMSD detection showing the characteristic field line geometry. The sample is biased to high negative potentials creating a drift field to the detector plate that supports interleaved cathode (C) and anode (A) strips. An electron cascade caused by impact ionisation of the detector gas only micrometers away from the detector plate allows pulse-counting measurements. b) A typical pulse height distribution for a GMSD showing the relationship between electron energy and the depth of origin in the solid. (The vertical axis shows the number of events in a given energy range.)

deposited onto a semiconducting glass plate. In a suitable gas atmosphere, these strips function as the anodes, and the sample as the cathode, of an avalanching gas counter. The amplification is such that an Auger electron gives a measurable pulse, the amplitude of which is proportional to the initial energy of the electron. A typical pulse height distribution (PHD) is shown in Figure 1b in which the height of the pulse has been converted into electron energy. Since the depth from which an Auger electron originates increases as the energy of the emerging electron decreases, the PHD contains information about this depth.

The feasibility of nondestructive depth profiling at ambient pressure with energy-selective XAS had been demonstrated for a model system in a previous publication.[12] This system comprised overlayers of NiO on a polished nickel plate and the use of a standard detector gas mixture of isobutane and helium. In these experiments, X-ray spectra could be collected with just two electron-energy-detection windows: a high-energy window for electrons emerging close to the surface and a low-energy window for electrons that originated deep within the bulk as shown in Figure 1b. It is clear that the measurement of a full electron-energy spectrum at each incident photon energy would yield the maximum information on surface composition. Improved instrumentation now makes the collection of two-dimensional datasets a practical proposition: data for copper powder reduced in a hydrogen atmosphere are shown in Figure 2.

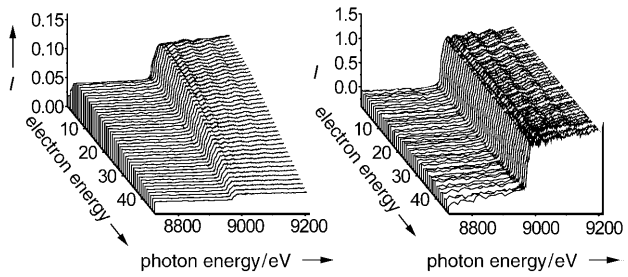


Figure 2. Typical data derived from powdered copper. a) A two-dimensional matrix of raw data showing a PHD at every photon energy step of the EXAFS scan. The labeling of the electron energy axis (pulse heights) corresponds to the pulse counting channels of the MCA electronics (see Supporting Information). b) Data normalized to a constant edge step.

Figure 2a shows raw data in which for each value of incident X-ray energy, the typical PHD can be seen. Consideration of the normalized data in Figure 2b indicates that the X-ray spectra display little dependence upon electron energy. The most simple (and correct) interpretation of these data is that the structure of this sample shows little depth dependence. Though not obvious, it is worth noting that constancy of these data also shows that the detection scheme is immune to the nonlinearities present in the use of fluorescent detection for concentrated samples.[8]

Despite this progress, if the technique is to move beyond from being a curiosity to become a useful tool for a wider community, it has to demonstrate three capabilities: operation with useful (reactive) gas mixtures, independence of sample form, and operation at non-ambient temperatures. Each of these criteria has now been satisfied. Gas microstrip detectors are not restricted to the standard gas mixture used in proportional counters (typically a mixture of a noble gas and a hydrocarbon) but will operate in reducing and oxidizing gas mixtures that are wet or dry and that may or may not contain hydrocarbons. Details of these investigations can be found elsewhere.[13] Fulfillment of the second and third criterion is described below. Results are presented herein upon a metal, semiconductor, and insulator in powdered form (data have also been collected for oils and liquids). The first results of a variable-temperature GMSD study of an in situ reduction process are described below, followed by preliminary results for an electrochemical system.

Experiments were carried out for temperatures up to 300 °C.[14] Copper oxide provides an ideal test system for variable-temperature GMSD studies, since it is readily reduced at modest temperatures, and since copper is both a key component of catalysts for methanol synthesis and is widely used in the purification of gases. The sequence of the experiment is best illustrated by considering the total electron-yield spectra (Figure 3) that give the structure averaged over a sampling depth of about 600 Å.

Three spectra (A) were collected at room temperature in a H_2/He gas mixture, during which time there was no discernable change. These spectra show a sharp feature at 8996 eV, which is highly characteristic of oxides (called the "white line" for historical reasons). After the third spectrum had been completed the temperature was raised to 170 °C

 © 2004 Wiley-VCH Verlag GmbH & Co. KGaA, Weinheim

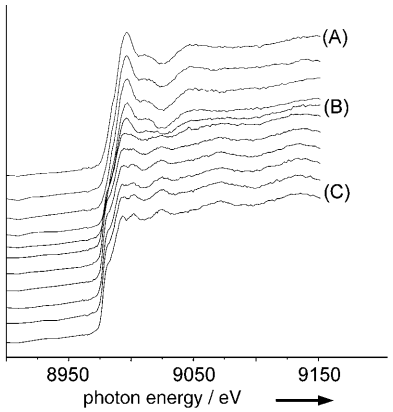


Figure 3. A time sequence of total electron yield spectra for the in situ reduction of copper oxide. A) Spectra 1–3, room temperature; spectrum 4, during heating to 170 °C. B) Spectra 5–10, 170 °C. C) Spectrum 11, 170 °C following complete reduction.

over the course of a single scan (11 min). It can be seen that during the next six scans (B) the intensity of the white line diminishes and the spectra gradually evolve to that characteristic of copper metal. After this time, no more changes in the spectra were seen (C).

The extent of the reaction in each spectrum was determined by fitting a linear combination of the spectra for pure Cu and CuO to it. Figure 4 shows zero-order reaction kinetics up to 80% conversion. This result suggests that reduction does not occur according to a core–shell model for which $\sqrt{t}$ dependence is predicted. Analysis of the structure as a function of depth from the surface as the reaction proceeds provides direct confirmation as shown in Figure 5.

The X-ray spectra for both the starting material and the product are independent of the electron-energy depth, which indicates a uniform structure throughout the sampling depth. However, during the process of reduction, a substantial core–shell structure might have been expected. The middle plot of Figure 5 shows the energy-resolved spectra for datasets in which the total electron yield (or average composition) spectra could be fitted by the spectrum of an about 50:50 mixture of CuO and Cu. To a first approximation, all spectra have the same shape in the vicinity of the edge, irrespective of the depth from which they originate. Pattern matching shows that the fraction of metallic Cu in each sample is in the range of 45 to 55%. Thus there is only a very small variation of composition throughout the outermost 60 nm of the material and certainly no discrete copper–copper oxide shell structure. This result is in agreement with the above conclusion that the progression of the reduction is not dominated by diffusion.

GMSDs function exceedingly well in the presence of water vapor.[13] This offers the possibility of conducting studies on wet surfaces. Figure 6 shows a schematic drawing of the simple three-electrode electrochemical cell that fits in place of the normal sample holder for investigations under ambient conditions. The key feature of the cell is the ability to flood the sample with electrolyte to undertake an electrochemical modification. The electrolyte is then drained away leaving a thin layer covering the sample that allows potential control to be maintained at all times.

Nickel oxides and hydroxides have been extensively studied previously by a range of spectroelectrochemical techniques because of their applications in batteries, capacitors, and electrochromic devices. The useful electrochemical

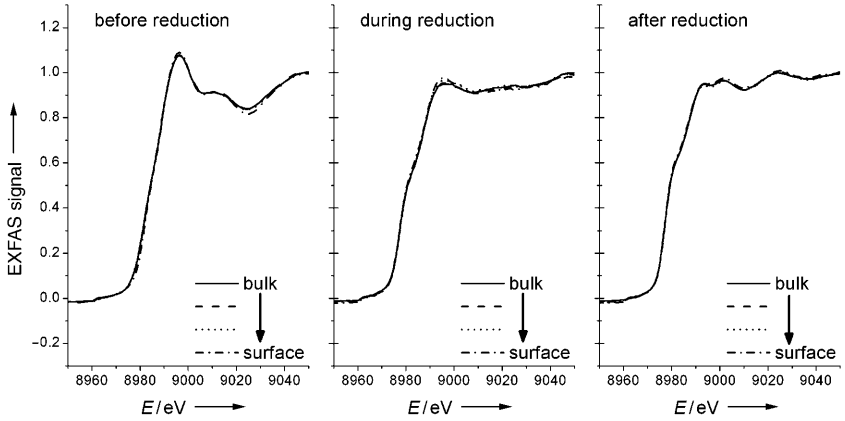


Figure 5. Energy-resolved EXAFS spectra of the initial CuO (left), a sample in the course of the reduction (middle) and the metallic copper product (right). Data have been summed within four electron energy ranges to improve statistics.

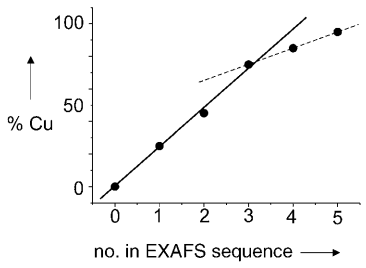


Figure 4. Dependence of the extent of reaction as a function of reduction time (expressed as number in the EXAFS sequence).

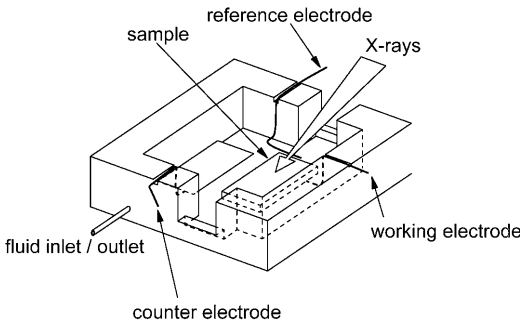


Figure 6. Schematic drawing of the in situ PTFE electrochemical cell. The grounded stainless steel frame of the cell to prevent its surface from charging when exposed to X-rays is not shown. The cell is made leak tight by two mylar windows clamped over its front and rear apertures (omitted for clarity). The sample acts as the working electrode, the counter electrode is a platinum foil of comparable area, and the reference electrode is a silver wire.

 © 2004 Wiley-VCH Verlag GmbH & Co. KGaA, Weinheim

properties of nickel hydroxides arise from the facile and reversible oxidative conversion of $Ni(OH)_2$ to NiOOH. Both materials can exist in two phases, and the mechanism for the conversion is very complex, involving cation, anion, and solvent transfer both within the electrode and also between the electrode and the solution electrolyte.[15] The purpose of the experiments described here is to establish that it will be possible in future to investigate the evolution of structure and oxidation state of thin films under potential control, in the presence of a thin film of electrolyte.

It was convenient to deposit a nickel hydroxide film onto a nickel electrode. Figure 7 shows a set of electron-energy resolved extended X-ray absorption fine structure (EXAFS) spectra for the starting material. The spectra arising from low-energy electrons are identical to those obtained for nickel metal, but under ambient conditions polished nickel has a native oxide/hydroxide overlayer of about 2–5 nm thickness. In the spectra arising from the surface region, the intensity of the white line is substantially increased, thus confirming the presence of oxide species.[12]

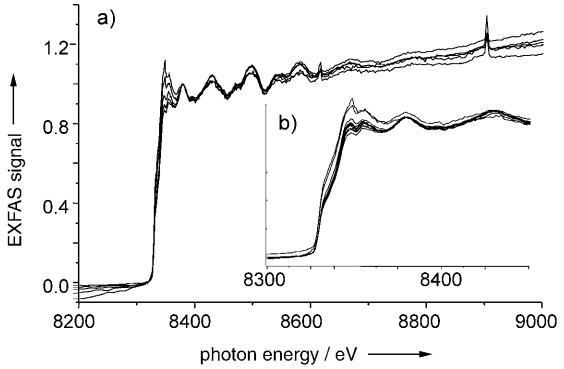


Figure 7. a) Depth-dependent EXAFS spectra of a Ni plate exposed to water vapor at room temperature in the detector cell. b) Zoom into the XANES region. The spectra are arranged vertically in order of increasing electron energy window. Thus the lowest and the uppermost spectra correspond to signals arising from the bulk and surface, respectively.

Figure 8 gives the spectra collected from a thick layer of electrochemically deposited nickel hydroxide and these show that there are marked differences in the X-ray absorption near-edge structure (XANES) region between signals emerging from the surface and the bulk of the electrode. A comparison of these data with the most recent data obtained by Hillman's group suggests that the outermost surface has retained the structure of Ni^{II} hydroxide but the deeper layers have been electrochemically charged to form NiOOH.[16] This proposal is somewhat speculative, but it does show that in future it will be possible to study electrochemical oxidations in conditions that are very close those found in situ and to be able to determine depth profiles of oxidation state without recourse to the use of invasive analytical tools of surface science.

The development of gas microstrip detectors has made it possible to perform energy-resolved Auger electron detection

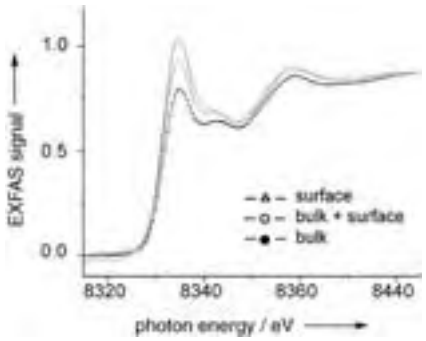


Figure 8. Electron-energy-resolved XANES spectra of $Ni(OH)_2$, electrochemically deposited onto a nickel plate from $Ni(NO_3)_2$.

under ambient conditions. The work described here shows that this technique is suitable for in situ studies in the field of heterogeneous catalysis and electrochemically modified surfaces. It could be argued that this technique represents a significant step forward in bridging the materials and pressure gap in analytical science. In these challenging experiments, the statistical quality has not yet reached the level at which a full EXAFS data analysis is possible at each electron energy, but improvements to the design of GMSD plates and the addition of more data channels will bring this about. A program of study is underway to build a suite of software tools that will permit quantitative deconvolution of the depth profile information contained in these data; the results of which will be reported elsewhere.

Received: November 3, 2003
Revised: April 13, 2004 [Z53235]

Keywords: EXAFS spectroscopy · heterogeneous catalysis · surface analysis · surface chemistry · X-ray absorption spectroscopy

[1] P. L. Gai, E. D. Boyes in *Electron Microscopy in Heterogenous Catalysis*, IOP, Bristol, **2003**, 1.
[2] P. T. Anastas, J. C. Warner in *Green Chemistry: Theory and Practice*, Oxford University Press, Oxford, **1998**.
[3] G. Ertl, H. Knözinger, H. Weitkamp in *Handbook of Heterogeneous Catalysis*, Wiley-VCH, Weinheim, **1997**.
[4] M. Haruta, *Catal. Surv. Jpn.* **1997**, *1*, 61.
[5] Z.-M. Liu, M. A. Vannice, *Catal. Lett.* **1997**, *43*, 51 – 54.
[6] Y. Iwasawa in *X-ray Absorption Fine-Structure for Catalysts and Surfaces*, World Scientific, Singapore, **1996**.
[7] A. Erbil, C. S. Cargill III, R. Frahm, R. F. Boehme, *Phys. Rev. B* **1988**, *37*, 2450 – 2464.
[8] S. L. M. Schroeder, G. D. Moggridge, R. M. Lambert, T. Rayment in *Advances in Spectroscopy*, *Vol. 26* (Eds.: R. J. E. Clark, R. E. Hester), Wiley, New York, **1998**, pp. 1 – 29, .
[9] S. L. M. Schroeder, G. D. Moggridge, R. M. Ormerod, T. Rayment, R. M. Lambert, *Surf. Sci.* **1995**, *324*, L371 – L377.
[10] S. L. M. Schroeder, *Solid State Commun.* **1996**, *98*, 405 – 409.
[11] S. L. M. Schroeder, *J. Phys. IV* **1997**, *7*, 153 – 154.
[12] T. Rayment, S. L. M. Schroeder, G. D. Moggridge, J. E. Bateman, G. E. Derbyshire, R. Stephenson, *Rev. Sci. Instrum.* **2000**, *71*, 3640 – 3645.

 © 2004 Wiley-VCH Verlag GmbH & Co. KGaA, Weinheim

[13] A. Vollmer, J. D. Lipp, J. R. I. Lee, G. E. Derbyshire, T. Rayment, *Anal. Chem.* **2003**, *75*, 6571 – 6575.
[14] Details of experimental procedures are provided as Supporting Information.
[15] H. M. French, M. J. Henderson, A. R. Hillman, E. Vieil, *Solid State Ionics* **2002**, *150*, 27 – 37.
[16] N. R. S. Farley, S. J. Gurman, A. R. Hillman, *Electrochim. Acta* **2001**, *46*, 3119 – 3127.

 © 2004 Wiley-VCH Verlag GmbH & Co. KGaA, Weinheim

Supramolecular Chemistry

Self-Organization of Oligomeric Helical Stacks Controlled by Substrate Binding in a Tobacco Mosaic Virus Like Self-Assembly Process**

*Anne Petitjean, Hélène Nierengarten, Alain van Dorsselaer, and Jean-Marie Lehn**

A major line of investigation in supramolecular chemistry is to understand the processes underlying the self-organization of matter[1,2] and to implement them in artificial systems.[3] Synthetic models that reproduce the recognition properties of nucleic acids,[4,5] proteins,[6] and carbohydrates,[7] as well as the organization of membranes,[8] are useful tools for the study of naturally occurring processes. The self-assembly of viruses represents a biological touchstone for the elaboration of complex architectures on the basis of molecular information. The Tobacco Mosaic Virus (TMV), one of the best-characterized viral systems,[9] is composed of 2130 identical protein subunits, which self-assemble around the viral RNA into a helical supramolecular polymer to define a tower whose height is determined by the polynucleotide substrate. Herein we describe the self-organization of synthetic helical subunits around a molecular cationic strand as a model for the self-assembly of the TMV.

The individual protein building blocks of the TMV self-assemble to yield cylindrical or lock-washer-type helical oligomers of different lengths depending on the pH and ionic strength of the medium. The specific recognition between the protein units and their nucleic acid substrate leads to the exclusive formation of a complex in which the RNA fits inside the nanotube-type helical assembly and dictates its length.

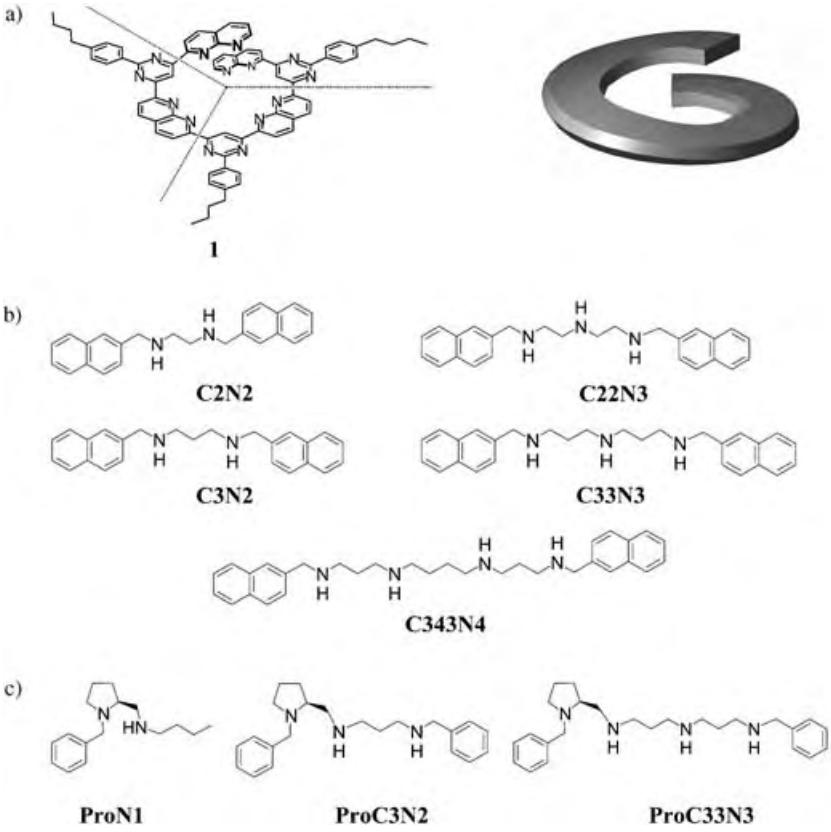


Figure 1. Structures of the compounds: a) helical strand **1**, in which the 3.5 identical motifs encoding for the global helical conformation are highlighted; b) achiral oligoamine substrates; c) chiral oligoamine substrates.

[*] Dr. A. Petitjean,[+] Prof. Dr. J.-M. Lehn
Laboratoire de Chimie Supramoléculaire
ISIS, 8 allée Gaspard Monge, BP 70028,
67083 Strasbourg Cedex (France)
Fax: (+33) 3-9024-5140
E-mail: lehn@isis.u-strasbg.fr
Dr. H. Nierengarten, Prof. Dr. A. van Dorsselaer
Laboratoire de Spectrométrie de Masse Bioorganique
ECPM, 25 rue Becquerel,
67088 Strasbourg Cedex (France)
[+] Present address:
Department of Chemistry M/C 127-72, Caltech,
1200 E. California Blvd., Pasadena, CA 91125 (USA)

[**] A.P. is grateful to the French Ministère de L'Éducation Nationale, de la Recherche et de la Technologie for financial support, to Dr. J.-A. Bousquet for assistance with the CD measurements, and to Dr. André Matthis (Institut Charles Sadron, Strasbourg) for his kind help with powder diffraction studies.

The naphthyridine-based helical oligomer **1**[10] (Figure 1 a) may be considered as a structural analogue of the one-turn, lock-washer-type protein oligomers occuring in the assembly of TMV. Whereas the latter helical species are based on the *noncovalent* interaction of individual proteins (16.3 per turn), **1** is preorganized into a helix through *covalent* linkage of helicity-enforcing motifs (3.5 per turn) that are based on the *transoid* conformational preference of *ortho*-linked aromatic azaheterocycles.[11] The convergence of several strong electric dipoles of the naphthyridine groups ($\mu = 4.1$ D in benzene, 25 °C)[12] towards the center of the helix creates a polar internal void of ≈ 3.5 Å diameter within **1** which is well-suited to accommodate small cationic guests such as alkali or guanidinium ions. These, in turn, promote the interaction with a free helix through ion–dipole and van der Waals interactions to result in the formation of polymolecular assemblies of

 DOI: 10.1002/anie.200353492 © 2004 Wiley-VCH Verlag GmbH & Co. KGaA, Weinheim

helices **1**.[10] The pH- and ionic strength (salt)-induced polymerization of TMV proteins into helical supramolecular architectures in aqueous solutions is thus mirrored by the cation-promoted polyassociation of helix **1** in organic solvents (Figure 2).

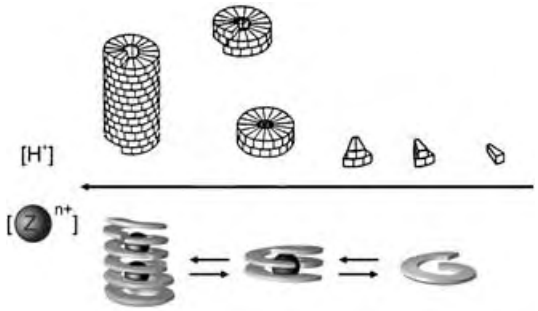


Figure 2. Schematic illustration of the parallel between the pH- and ionic-strength-dependent self-assembly of the TMV protein units and the cation-promoted aggregation of helical components **1** which may involve inorganic (alkali, lead(II)) or small organic (guanidinium) ions.[10]

As single cations are able to induce the aggregation of helices, we anticipated that a "string of cations" could serve as a template for the controlled oligomerization of helices, with the size of the overall architecture possibly dictated by the number of positive charges within the string. Therefore, two families of linear oligoammonium cations were synthesized by standard procedures (Figure 1b and c) and were characterized by ^{1}H and ^{13}C NMR spectroscopy, electrospray mass spectrometry (ESMS),[13] and elemental analysis. The symmetrical oligoammonium ions of the first family (Figure 1b) were obtained from primary diamines and contain internal secondary amines separated by two to four methylene groups. They are designated by **C*m*N*n***, in which ***n*** stands for the number of amine sites and ***m*** denotes the sequence of the number of methylene groups in all the spacers linking the successive N sites. The naphthyl end groups were introduced to allow easy identification of the complexes with **1**.[13b] The second family consists of proline-appended chiral oligoamines in which the protonation sites are separated by propylene spacers (Figure 1c).

The interaction of the symmetrical oligoamines **C*m*N*n*** with the helix **1** was monitored by means of ESMS analysis[13] of a freshly prepared mixture of **1** (500 μL of a 1.3×10^{-4} M stock solution in $CHCl_3$), trifluoroacetic acid (92 μL of a 7.0×10^{-4} M stock solution in $CHCl_3$; 1.0 equiv relative to **1**), and the amine in various proportions. Figure 3 shows the ES mass spectra of **1** in combination with the different oligoamines. The spectrum of **1** alone (data not shown) displays very weak signals of different oligomers in which one to three residual cations (H^+, K^+, Na^+) form complexes with 1—4 equivalents of **1** (see Figure 5 left, for a graphical illustration).

When **1** was mixed with 0.5 equivalents of the diamines **C2N2** and **C3N2** (**1**/diammonium = 2:1) in the presence of 1 equivalent of protons, only those complexes in which all the interaction sites (ammonium groups) are occupied were detected by means of ESMS. In the case of **C2N2**, a small peak at $m/z = 1487.0$ was detected that corresponds to the monoadduct $(\mathbf{1}\text{–}\mathbf{C2N2}H)^+$ but accounted at most for 7% of the overall signal. The two triamines **C*mm*N3** exhibit different behavior. In the case of **C33N3**, the nature of the major adduct depends on the relative proportions of the triammonium species and **1** in the mixture. Introduction of a stoichiometric amount of **1** with respect to N sites (**1**/**C33N3** = 3:1) leads to incomplete complexation of the receptor (Figure 3d bottom), with the fully saturated adduct (m/z 1283.7) present as the major species ($(\mathbf{1}_3\text{–}\mathbf{C33N3}H_3)^{3+}$/$(\mathbf{1}_2\text{–}\mathbf{C33N3}H_2)^{2+} = 1.5$). In the presence of an excess of **1** (**1**/**C33N3** = 5:1 and 10:1), the unsaturated complex almost completely disappears to the benefit of the fully saturated complex. With **C22N3** however, even a large excess of receptor (10:1) only yields minor amounts of the fully saturated species (Figure 3c). One explanation for this discrepancy may arise from the lower pK_a value of **C22N3** relative to that of **C33N3** since the third positive charge has to be accommodated closer to the two peripheral charges in **C22N3**. Nevertheless, as protonation of **1** is not observed, **C22N3** must be fully protonated as no other accessible base is present in the medium ($CHCl_3$).

Another factor arises from the steric requirements for the formation of the trimeric complex, if the van der Waals thickness of aromatic groups (3.4–3.5 Å) and the distance between two consecutive ammonium sites are taken into account. In the $-NH_2^+CH_2CH_2NH_2^+-$ fragment, the largest distance between two consecutive ammonium groups is about 3.8 Å when they adopt an *anti* conformation (based on molecular-modeling studies). Stacking two strictly planar aromatic surfaces on top of each other requires a minimal distance of 3.4–3.5 Å between the terminal ammonium sites. The helical units **1** are not planar and therefore need more room to fit. In the adduct with **C2N2**, the shorter distance between the two consecutive binding sites can be compensated by a shift of the two units of **1** towards the end groups. However, in the saturated adduct of **C22N3,** the proximity of the N sites could hinder the insertion of the central unit of **1** which would result in a smaller binding constant of this third receptor and hence a lower proportion of the saturated adduct. On the other hand, with two consecutive ammonium binding sites separated by about 5 Å in **C3N2** and **C33N3** there is enough room for the binding of a receptor unit to each ammonium site such that a ratio of 5:1 between **1** and **C33N3** allows quasi-complete saturation of the triammonium substrate (Figure 3d, middle).

To investigate this length-regulation process, spermine was functionalized with the same end groups to give the longer tetrammonium chain **C343N4** (Figure 1b) in which consecutive ammonium binding sites are separated by spacers containing three or four methylene groups. Upon mixing **C343N4** and **1** in a 1:7 ratio under acidic conditions (1 equivalent of acid relative to **1**), the ESMS spectrum (not shown) showed the coexistence of two species in equal quantities: the expected $(\mathbf{1}_4\text{–}\mathbf{C343N4}H_4)^{4+}$ adduct was accompanied by the lesser-charged $(\mathbf{1}_4\text{–}\mathbf{C343N4}H_3)^{3+}$ species, but four ligands were bound in both cases. The presence of the latter species, which accommodates four ligands with one

 © 2004 Wiley-VCH Verlag GmbH & Co. KGaA, Weinheim

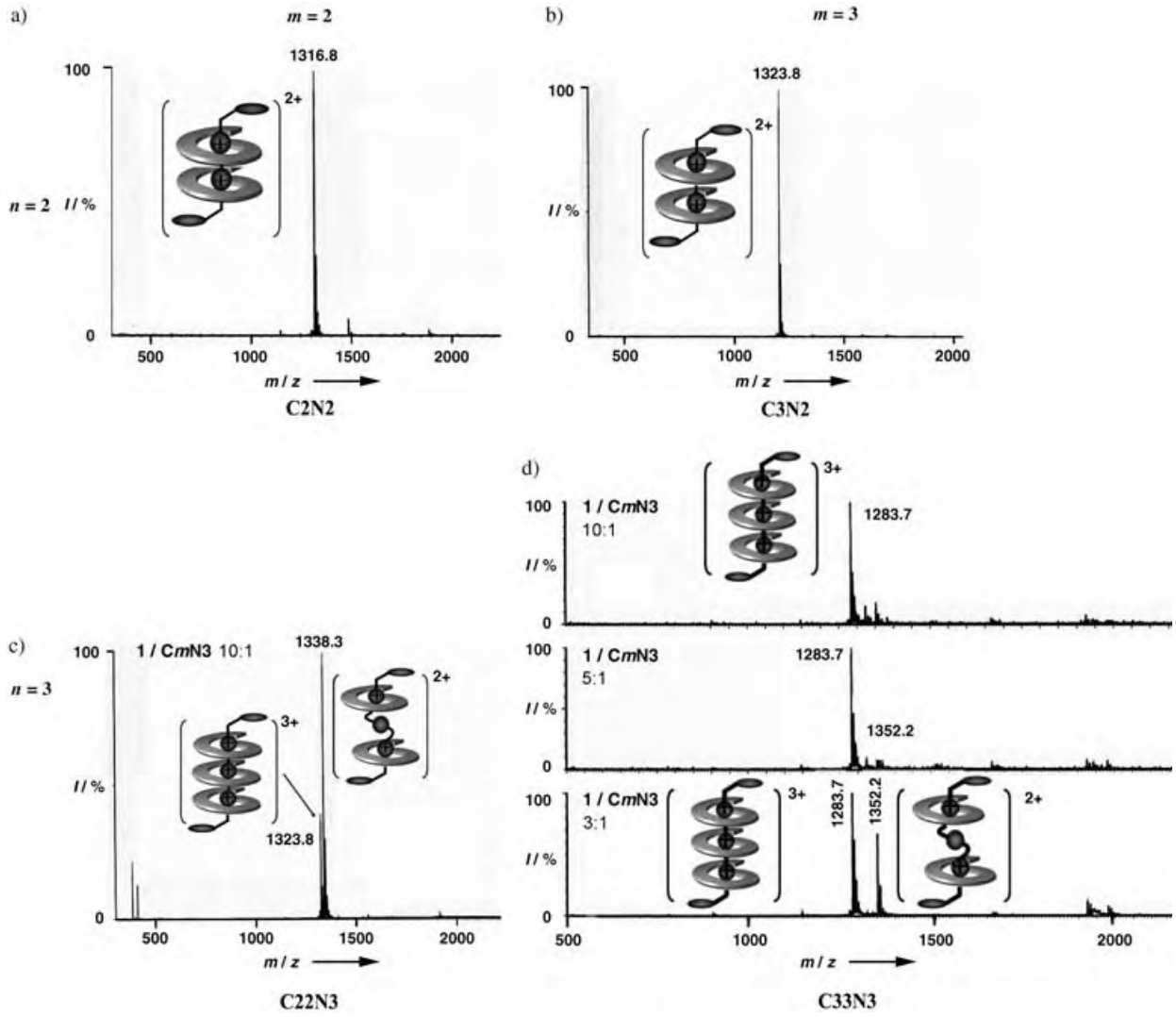


Figure 3. ESMS spectra obtained by mixing **1**, TFA (1 equiv) and the oligoamines **C*m*N*n*** (1/*n* equiv) in $CHCl_3$. In the case of **C*m*N3**, different **1**/**C*m*N3** ratios were investigated and are indicated. For experimental details see reference [13].

tricationic substrate, indicates that the ion–dipole and van der Waals interactions within the complex are strong enough to hold one of the ligands around an unprotonated nitrogen site.

Self-organization by selection[3] involves the selective assembly of a mixture of those components that are required for generating the final entity. This is the case in the formation of the "correct" double and triple inorganic double helices (helicates) from a mixture of ligand strands and metal ions,[14] and in the assembly of inorganic grid-type architectures.[15] To test for such selection in the present dynamic system of equilibrating species, competition experiments were carried out with mixtures of the **C*m*N*n*** substrates (***m***, ***n*** = 2 or 3). The selectivity of the self-assembly of units of **1** around the oligoammonium substrates bears relation to the specificity of the protein-coating process in the TMV to the exact viral RNA.

When **1** was mixed with TFA (1 equiv), **C2N2** (0.5 equiv), **C3N2** (0.5 equiv), **C22N3** (0.33 equiv), and **C33N3** (0.33 equiv), the only species observed were (in decreasing abundance): $[\mathbf{1}_2\text{–}\mathbf{C3N2}H_2]^{2+}$ (56%), $(\mathbf{1}_2\text{–}\mathbf{C33N3}H_2)^{2+}$ (26%), $(\mathbf{1}_3\text{–}\mathbf{C33N3}H_3)^{3+}$ (11%), and $(\mathbf{1}_2\text{–}\mathbf{C22N3}H_2)^{2+}$ (7%). It appears therefore that the **C3N2** and **C33N3** strands are strongly selected with the latter being present under both fully and partially complexed forms. On the contrary, **C2N2** and **C22N3** are markedly under-represented in this selection in agreement with the results above. Interestingly, the fully assembled complex with **C33N3** is present in significant proportions despite the required 3:1 stoichiometry, the competition with the other species, and the entropic cost of its full assembly—a noteworthy sign of its stability.

The poorer binding of oligoammonium chains containing short internal spacers between successive charges is a first indication that the helical conformation of the neutral ligand **1** is conserved in the oligoammonium complexes, in agreement with powder diffraction measurements on the K^+, Cs^+, and guanidinium complexes.[10] Related to this, we investigated chirality induction in the self-assembled oligomers through complexation of **1** with chiral oligoammoniums derived from L-proline (Figure 1c). A short C2 spacer between the first two ammonium binding sites was intention-

 © 2004 Wiley-VCH Verlag GmbH & Co. KGaA, Weinheim

ally chosen instead of a C3 spacer so that the first interaction site would be closer to the stereogenic center. The receptor that interacts with the first secondary amine may then also experience a positive attraction towards the protonated appended proline, and thus be brought closer to the chiral inducer. Benzyl end groups, instead of naphthyl groups, were selected because of their lower spectroscopic absorption in the region of interest.

The circular dichroism (CD) signals of a mixture of **1** (0.5 mM), TFA (1 equiv), and **ProC3N2** ($n = 2$; $1/n$ equiv) or **ProC33N3** ($n = 3$) in $CHCl_3$ were monitored in a region where only receptor **1** absorbs light energy (350–400 nm) and the proline substrates show no absorption. Hence any CD signal detected in this region should result from a transfer of chirality from the proline substrate to ligand **1**. Figure 4 shows

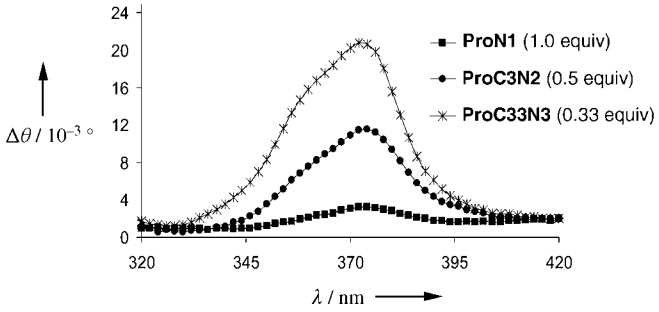


Figure 4. Circular dichroism spectra of a mixture of **1** (0.5 mM), TFA (1 equiv), and the proline-derived oligoamines ($1/n$ equiv) in $CHCl_3$ as a function of wavelength, in a region where only the naphthyridine groups of **1** absorb (the ellipticity $\Delta\theta$ is measured in millidegrees).

the CD curves of the three complexes in the naphthyridine absorption region. The shape of the signals is the same in all three cases with primary and secondary maxima at 372 and 362 nm, respectively.

The appearance of a CD signal indicates that the interaction between **1** and the substrates gives rise to a supramolecular chiral assembly in which the chirality originates from the noncovalently bound substrate. The interaction of **1** with **ProN1** (■, Figure 4) gives only a weak signal, which suggests that the complex does not have a strong chiral organization (ESMS studies suggest that monoammonium cations such as dibenzylammonium are complexed under these conditions). Although introduced in smaller concentrations, **ProC3N2** and **ProC33N3** give much stronger signals, which are a sign that the ligands absorbing in this region are chirally organized. Moreover, the number of interacting sites is increased which may also correspond to a better-defined geometry (the data are reported in ellipticity units, that is, relative to the same number of absorbing molecules **1**).

The CD data therefore indicate that the ligands **1** in the oligomeric species organize in accordance with a chiral pattern that is imposed by the proline-derivatized oligoammonium assembling agents; the similarity of the shape of the signals reflects a similar environment for the different complexes. Combined with the powder diffraction measurements on single cations[10] and the poor complexing ability of sterically hindered substrates, these data support a helical organization of the ligand **1** around the oligoammonium substrate. They indicate that the interaction of **1** with oligoammonium strands leads to the self-assembly of oligomeric chiral stacks of helical units **1** by the optically active polycationic scaffold, and that the size of the supramolecular architectures thus formed is dictated by the number of interaction sites present in the substrate (Figure 5). As stacking is expected to be better for helices **1** of the same chirality, the formation of homochiral stacks involves chiral selection of molecules **1** of the same helicity. On the other hand, diastereomeric stacks may, in principle, form between the optically active polycationic thread and enantiomeric stacks of **1** such that the CD effects represent an overall result for the population of all assemblies.

Taken together, the present ESMS and CD results are in agreement with the model of $(\mathbf{1}_x\text{–}\mathbf{C}m\mathbf{N}n\mathrm{H}_p)^{p+}$ stacks as outlined although they do not provide precise geometrical information. In particular, the ESMS data provide compelling evidence in favor of the structural model proposed.[16] Such stacks also represent rotaxanes[17] based on helical components. Their mechanism of formation may involve partial unwrapping of the helical unit **1** followed by insertion of the substrate chain into the opened cavity, in line with the process of dynamic helicity interconversion of related strands.[11] An alternative mechanism may be slippage, one of the processes that leads to the formation of rotaxanes.[17] Notably, the control of the polyrotaxane assembly[18] by the length of the thread is a process related to that described herein.

The length selection in these synthetic models reproduces the regulation process in the self-assembly of the TMV.

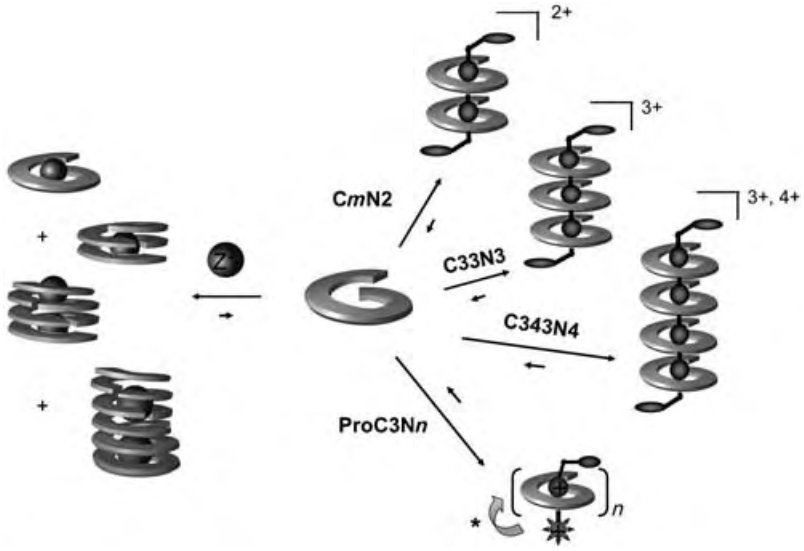


Figure 5. Graphical summary of the supramolecular oligomerization control directed by oligoammoniums substrates versus free oligomerization promoted by monocations (the curved arrow indicates chirality transfer).

 © 2004 Wiley-VCH Verlag GmbH & Co. KGaA, Weinheim

However, unlike the viral coat which results from lateral interactions between more than 16 individual proteins assembling into the basic lock-washer entity through non-covalent interactions, helices **1** are covalently preorganized (Figure 2). In both cases, assembly occurs around a central scaffold that imposes supramolecular control of the final architecture. Organization mediated by lateral interactions has been described for systems that exhibit liquid-crystal properties.[19] Overall, the process described herein involves a first level of molecular self-organization to generate a helical building block followed by a further two levels of supramolecular self-organization, namely, the stacking of the helical units and the control of the stack by endo-recognition. It represents a higher level of self-organization[3] along a hierarchical three-stage sequence.

Received: December 10, 2003
Revised: April 30, 2004 [Z53492]

Keywords: amines · helical structures · N ligands · self-assembly · supramolecular chemistry

[1] M. Eigen, *Naturwissenschaften* **1971**, *58*, 465 – 523.
[2] *Self Organizing Systems, The Emergence of Order* (Eds.: F. E. Yates, A. Garfinkel, D. O. Walter, G. B.Yates), Plenum, New York, **1987**.
[3] J.-M. Lehn, *Proc. Natl. Acad. Sci. USA* **2002**, *99*, 4763 – 4768.
[4] M. J. Han, J. Y. Chang, *Adv. Polym. Sci.* **2000**, *153*, 1 – 36.
[5] C. Leumann, *Bioorg. Med. Chem.* **2002**, *10*, 841 – 854.
[6] A. G. Cochran, *Curr. Opin. Chem. Biol.* **2001**, *5*, 654 – 659.
[7] C. A. Bertozzi, L. L. Kiessling, *Science* **2001**, *291*, 2353 – 2364.
[8] T. Kunitake in *Physical Chemistry of Biological Interfaces* (Eds.: A. Baskin, W. Norde), Marcel Dekker, New York, **2000**, pp. 283 – 305.
[9] A. Klug, *Angew. Chem.* **1983**, *95*, 579 – 596; *Angew. Chem. Int. Ed. Engl.* **1983**, *22*, 565 – 582.
[10] A. Petitjean, L. A. Cuccia, J.-M. Lehn, H. Nierengarten, M. Schmutz, *Angew. Chem.* **2002**, *114*, 1243 – 1246; *Angew. Chem. Int. Ed.* **2002**, *41*, 1195 – 1198.
[11] M. Ohkita, J.-M. Lehn, G. Baum, D. Fenske, *Chem. Eur. J.* **1999**, *5*, 3471 – 3481, and references therein.
[12] J. H. Markgraf, J. F. Skinner, G. T. Marshall, *J. Chem. Eng. Data* **1988**, *33*, 9 – 10.
[13] a) ESMS measurements were performed on a triple-quadrupole mass spectrometer Quattro II (Micromass, Altrincham, UK). The ES source was heated to 60 °C. The sampling cone voltage (Vc) was set at 70 V to avoid any fragmentation processes. The appropriate volume of oligoamine ($6–8\times10^{-4}$ M in $CHCl_3$) and TFA (7×10^{-4} M solution in $CHCl_3$, 1 equiv) were successively added to solutions of ligand **1** (1.3×10^{-4} M in $CHCl_3$). After 10 min, sample solutions were introduced into the mass spectrometer source with a syringe pump (Harvard type 55 1111: Harvard Apparatus Inc., South Natick, MA, USA) at a flow rate of 5 μL min^{-1}. Calibration was performed with protonated horse myoglobin. Scanning was performed in the MCA (multichannel analyzer) mode, and several scans were combined to obtain the final spectrum. b) MS signals of the different adducts with the parent oligoammonium chains that bear free primary amines at both ends, are very close and almost equal to the value for a 1:1 complex between **1** and a potassium ion. c) ESMS is not an exact quantitative method. One may assume that the intensities of the peaks of species of the same charge can be compared more accurately than when the charges are different. Species of higher charge usually 'fly' less well so they may be underestimated in this case, further favoring our interpretation.
[14] R. Krämer, J.-M. Lehn, A. Marquis-Rigault, *Proc. Natl. Acad. Sci. USA* **1993**, *90*, 5394 – 5398.
[15] J. Nitschke, J.-M. Lehn, *Proc. Natl. Acad. Sci. USA* **2003**, *100*, 11 970 – 11 974.
[16] The NMR spectra of the assemblies presented very broad signals displaced to lower chemical shifts; these features support the formation of stacked assemblies. Crystals suitable for X-ray crystallographic studies could not be obtained. UV/Vis and fluorescence spectrophotometric measurements require solutions of much lower concentrations at which aggregates do not form. Other methods of structural characterization are sought. A very approximate binding constant of 1000 M^{-1} was estimated for the interaction of **1** with the cesium cation. The broadness of the NMR signals may indicate nonspecific aggregation, as was observed when **1** was treated with protons in the presence of water.[10] However, the combination of helix **1** with the four oligoammonium chains studied clearly shows the formation of only those complexes that correspond to the number of ammonium sites (ESMS and CD). Still these defined entities may coexist with nonspecific aggregates. Nevertheless, if the entities observed by ESMS were simply undefined aggregates, one would expect the formation of the same mixture irrespective of the oligoammonium compound used. The structural assignment is therefore validated but other types of assemblies may coexist depending on the concentration (the concentration used in the NMR spectroscopic studies is 14-fold higher than that used in the ESMS experiments). A few features of the ESMS measurements deserve to be highlighted in this regard: In contrast to alkaline cations, the introduction of oligoammonium chains leads to very 'clean' ESMS spectra in which no small aggregates, excluding the ammonium substrates, are observed (even the protonated ligand is not detected). Additionally, nonspecific aggregates of specific assemblies (e.g., $(\mathbf{1}_n\text{–}\mathbf{C}_m\mathbf{N}_n)_x$) are not seen either, although one may expect a range of nonspecific products to form; it would therefore be surprising not to find any small assemblies contaminating the ESMS spectra.
[17] D. B. Amabilino, J. F. Stoddart, *Chem. Rev.* **1995**, *95*, 2725 – 2828; see, in particular, oligoamine-threaded cucurbituril pseudorotaxanes: K. Kim, *Chem. Soc. Rev.* **2002**, *31*, 96 – 107.
[18] A. Harada, *Acc. Chem. Res.* **2001**, *34*, 456 – 464; T. Dünnwald, R. Jäger, F. Vögtle, *Chem. Eur. J.* **1997**, *3*, 2043 – 2051; S. Anderson, H. L. Anderson, *Angew. Chem.* **1996**, *108*, 2075 – 2078; *Angew. Chem. Int. Ed. Engl.* **1996**, *35*, 1956 – 1959; H. W. Gibson, S. Liu, P. Lecavalier, C. Wu, Y. X. Shen, *J. Am. Chem. Soc.* **1995**, *117*, 852 – 874; G. Wenz, *Angew. Chem.* **1994**, *106*, 851 – 870; *Angew. Chem. Int. Ed. Engl.* **1994**, *33*, 803 – 822.
[19] V. Percec, *J. Macromol. Sci. Pure Appl. Chem.* **1996**, *33*, 1479 – 1496; M. Suarez, J.-M. Lehn, S. C. Zimmerman, A. Skoulias, B. Heinrich, *J. Am. Chem. Soc.* **1998**, *120*, 9526 – 9532.

 © 2004 Wiley-VCH Verlag GmbH & Co. KGaA, Weinheim

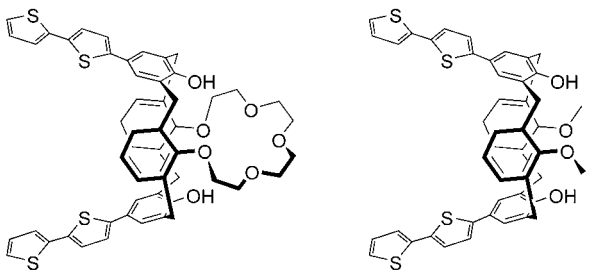
Conducting Polymers

Charge-Specific Interactions in Segmented Conducting Polymers: An Approach to Selective Ionoresistive Responses**

*Hsiao-hua Yu, Anthony E. Pullen, Michael G. Büschel, and Timothy M. Swager**

Conductivity-based sensory devices built on electrically conductive polymers have proved to offer great promise towards the detection of a wide variety of analytes.[1] Selective chemoresistive responses have been demonstrated with charge localization,[2] planarization/twist of the polymer backbone to modify conjugation length,[3] and segmental energy matching/mismatching of the polymer backbone.[4] We have been interested in developing new chemoresistive methods to determine blood electrolyte levels that are diagnostic in determining the physiological condition of individuals. In particular, the determination of Ca^{2+} ion concentration has attracted interest as a growing number of ionochromic sensors for this ion have been developed.[5] However, in view of the importance of this analyte new systems with enhanced specificity, better signal/noise ratios, and alternative sensory platforms remain a topic of interest. Herein, we report a new approach to produce a selective ionoresistivity resulting from a charge-specific interaction between the segmented conducting-polymer backbone and the bound metal ion.

We have previously reported a proton-doped calix[4]arene-based conducting polymer, formed by oxidative polymerization of monomer **2**.[6] The conductivity of the polymer film relies on rapid self-exchange between the discrete electroactive units attached to the upper (wider) rim of the calix[4]arene. To have this process be sufficiently fast, a condition for high conductivity, all of the phenolic oxygen atoms need to be maintained in their protonated state to ensure that the redox centers have equivalent energy levels and chemical structures. The high sensitivity of the resistivity to the chemical state of lower-rim phenolic oxygen atoms suggested to us that new sensory materials could be produced by designing specific cationic interactions with these centers. Herein we report our investigation of related polymers derived from monomer **1** (Scheme 1) which integrate a recognition site through the calix[4]arenecrown-5 moiety, a motif that has been demonstrated to provide differential



Scheme 1. Structures of calix[4]arene-based monomers **1** and **2**.

binding of metal cations.[7–10] Monomer **1** was synthesized by a pathway similar to that we reported for **2** by using palladium-catalyzed cross-coupling methodology.[6,11,12] To determine the binding of various metal ions, we treated monomer **1** with 10 equivalents of the respective salts, and the proton NMR spectra of the solutions revealed significant changes, as summarized in Table 1. To assert that these effects are the result of metal-ion binding, we confirmed that there was no change to the proton NMR spectra of **1** on the addition of $(n\text{Bu})_4\text{NPF}_6$, a non-binding electrolyte. In addition, we observed that solutions of **2** displayed no spectroscopic differences with these metal-ion salts, which indicates that the difference in the NMR shifts is not simply due to an enhanced ionic strength.

Table 1: Proton NMR signals from bridge -CH_2- of the calix[4]arene moiety and free O-H of monomer **1** in the presence of different Group 1 and Group 2 metal salts.[a]

Metal Ions	Bridge Ar-CH_2-Ar [ppm] chemical shifts	$\Delta\delta$[b]	O-H [ppm]
none[c]	3.50, 4.43	0.93	8.42
Li^+	3.60, 4.32	0.72	8.28
Na^+	3.65,[d] 4.22	0.57	7.86
K^+	3.65, 4.25[d]	0.60	none[e]
Mg^{2+}	3.51, 4.39	0.88	8.16
Ca^{2+}	3.67, 4.34	0.67	7.96

[a] The spectra were obtained in the presence of 10 equivalents of the corresponding PF_6^- or ClO_4^- salt. [b] The difference between the pairs of high and low resonance signals. [c] Addition of the electrolyte, $(n\text{Bu})_4\text{NPF}_6$, resulted in no difference in the NMR spectrum. [d] The resonance signals overlap with the signals assigned to the ethylene-oxo bridge (-OCH_2CH_2O-). [e] No NMR signal associated with free OH is observed.

The resonances assigned to the -CH_2- bridge (Ar-CH_2-Ar) of the calix[4]arene remain a pair of doublets in the presence of alkali-metal ions, but their relative chemical shifts ($\Delta\delta$) changes. The initial $\Delta\delta$ for the ion-free calix[4]arenecrown is 0.93 ppm. When metal ions are introduced, we observed a diagnostic decrease in $\Delta\delta$ ranging from 0.57 to 0.88 ppm, suggestive of a "flattened-cone" conformation.[13] The characteristic shifts of the ethylene-oxo bridge resonances (-OCH_2CH_2O-) between $\delta = 3.50$ and 4.50 ppm confirm that the alkali-metal ions bind to the crown moiety at the lower rim. This is further supported by the fact that there are no significant changes of the upper-rim aromatic-ring resonance

[*] H.-h. Yu, Dr. A. E. Pullen, Dr. M. G. Büschel, Prof. T. M. Swager
Department of Chemistry and Institute for Soldier Nanotechnologies
Massachusetts Institute of Technology
Cambridge, Massachusetts 02139 (USA)
Fax: (+1) 617-253-7929
E-mail: tswager@mit.edu

[**] This research was supported by the U.S. Army through the Institute for Soldier Nanotechnologies under Contract DAAD-19-02-D-0002 with the U.S. Army Research Office.

Supporting information for this article is available on the WWW under http://www.angewandte.org or from the author.

 © 2004 Wiley-VCH Verlag GmbH & Co. KGaA, Weinheim DOI: 10.1002/anie.200453896

signals on ion binding. In contrast, we found that for free phenol the $\delta = 8.42$ ppm ^{1}H NMR signal shifts upfield and decreases in intensity or completely disappears in the case of K^+, indicating rapid proton exchange.

Monomers **1** and **2** were subjected to anodic electropolymerization to form films of Poly(**1**) and Poly(**2**) on the surface of the electrode.[14] Both films display a quasireversible two-electron wave with a half-wave potential ($E_{1/2}$) around 0.55 V (E^1 and E^2 in Figure 1a).[15,16] While nonbonding Poly(**2**) films are completely insensitive to the presence of metal ions, the voltammetric responses of Poly(**1**) films in solution containing the different metal ions (PF_6^- or ClO_4^- salts) display significant differences. Smaller ions (Na^+, Li^+) only produced minor shifts of the cathodic peak potentials ($E_{p,c}$) and this limited response is attributed to the low binding constant between these ions and the calix[4]arenecrown-5 system.[7] In contrast, cycling in an electrolyte containing K^+ ions transforms the voltammogram from a single two-electron wave to two new waves with $E_{1/2}^{1\prime,K} = 0.28$ V and $E_{1/2}^{2\prime,K} = -0.26$ V (Figure 1a). The steady-state voltammogram evolves with continued cycling (Figure 1b). The development of electroactivity at more negative potentials is probably the result of proton loss from the oxidized phenol units to give an extended *p*-diquinone-like redox system.[17,18] We had previously observed small amounts of proton loss in Poly(**2**) in CH_3CN, however it appears that in the case of Poly(**1**) the deprotonation is driven to completion by the presence of K^+ ions under oxidizing potentials and the resulting dianions are stabilized by the binding of the metal ions. Therefore the evolution of the voltammograms not only can be explained by the coupling between electrochemical process and proton–metal-ion exchange but also suggests that the exchange is accelerated by the applied potential (Scheme 2). This explanation is also consistent with the

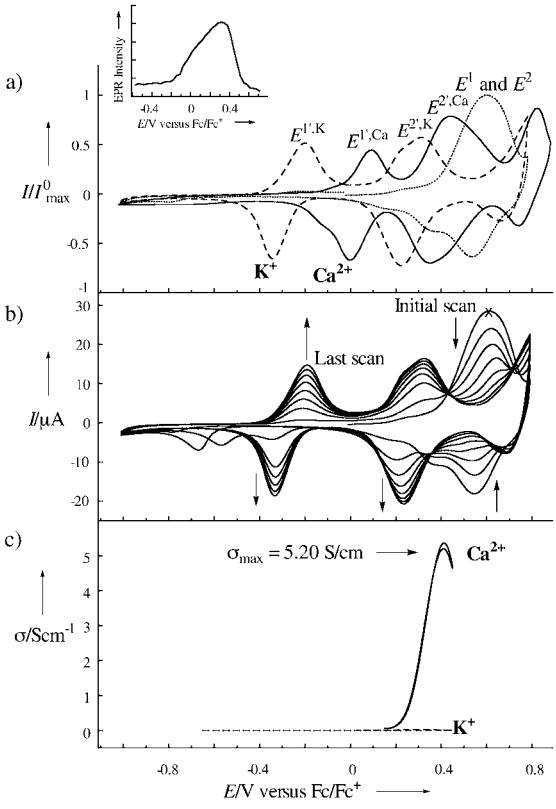
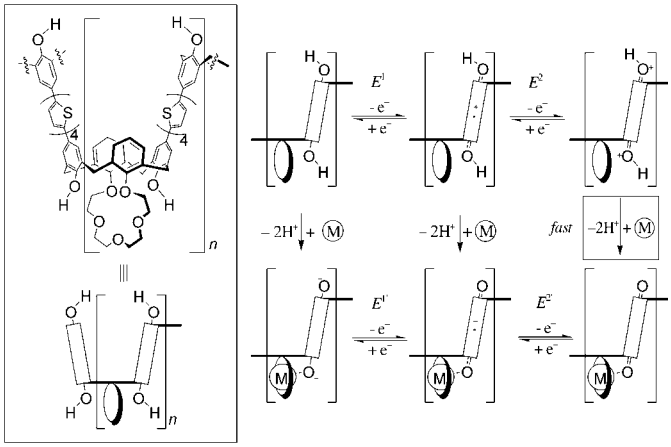


Figure 1. Cyclic voltammograms and in situ conductivity measurement of Poly(**1**) film in 0.1 M $(n\text{Bu})_4NPF_6/CH_3CN$ containing 10 mM K^+ or Ca^{2+} ions at a scan rate of 50 mVs^{-1}. a) Comparison of the original cyclic voltammogram (dotted line) and voltammetric responses toward K^+ (dashed line), and Ca^{2+} (solid line) ions. I^0_{max} is the maximum current obtained in the initial scan (e.g. marked with an X in Figure 1b). Inset: In situ EPR spectroscopy of Poly(**1**) after the film is saturated with K^+ ions. b) Scan-by-scan transformation of Poly(**1**) film on Pt button electrode (2 mm^2 surface area) as the K^+ ions diffuse into the binding sites of the polymer film; X marks the initial scan. c) In situ conductivity measurements for Poly(**1**) films with K^+ and Ca^{2+} ions. Measurements made on a 5 μm interdigitated microelectrode at a sweep rate of 5 mVs^{-1} with a 40 mV offset potential between adjacent electrodes.



Scheme 2. Coupling equilibria between electrochemical process and proton–ion exchange of Poly(**1**) and Poly(**2**). The exchange occurs fastest once the complex has undergone a two-electron oxidation.

transient more negative reduction wave at −0.67 V ($E_{p,c}$) that is present in the initial cycles before shifting to a less negative potential at −0.33 V. The −0.67 V wave in the initial scans is attributed to an incomplete distribution of K^+ ions throughout all of the receptor sites, which leads to the formation of higher energy anions. When Poly(**1**) films are immersed in electrolyte solution containing Ca^{2+}, we see a similar behavior, however, both waves ($E_{1/2}^{1\prime,Ca} = 0.06$ V and $E_{1/2}^{2\prime,Ca} = 0.41$ V) are shifted to values that are positive relative to the K^+ complex, consistent with the higher charge of the Ca^{2+} ion.

In situ EPR spectroscopy revealed a maximum signal ($g = 2.005$ and constant peak-to-peak width of ca. 5 G) at $E = 0.11$ V, which is positioned midway between the two principle redox waves (Figure 1a, inset). This profile is consistent with weakly interacting electroactive segments that undergo single-electron redox processes. A similar profile is observed for material complexed with Ca^{2+} ion. To find further support the proton–metal-ion exchange mechanism, a small amount of methylviolet was added to the solution.[19] After cycling in electrolyte solution containing K^+ or Ca^{2+} ions, an increase of absorption intensity from the indicator's acid form ($\lambda_{max} = 442$ nm) was displayed (see Supporting Information), identi-

 © 2004 Wiley-VCH Verlag GmbH & Co. KGaA, Weinheim

fying the release of protons from the polymer to the solution. In addition, K^+-ion recognition of Poly(**1**) film is also examined in the presence of trifluoroacetic acid, which hinders the deprotonation of the calixarene. In contrast to the negative shift observed without the acid (Figure 1a), the incorporation of metal ion results in a positive shift of the oxidation potential of the extended *p*-dihydroquinone ($E_{1/2} =$ 0.77 V, see Supporting Information), which is due to the positively charged ion bound to the protonated phenol unit.

Given the localized behavior of the redox segments of Poly(**1**) in the presence of K^+ and Ca^{2+} ions, it is clear that electrical conduction is best considered to be by a hopping (self-exchange) mechanism. The hopping rate will be optimal when each segment has the same environment to ensure isoenergetic character. The maximum conductivity (σ_{max}) of Poly(**1**) is 0.6 $S\,cm^{-1}$ (not shown) when oxidized in CH_2Cl_2 or acidic CH_3CN solutions,[20] however, upon addition of K^+ ions, the conductivity is reduced to $<1\%$ of its original value (Figure 1c). In contrast, subjecting Poly(**1**) films to similar conditions but in the presence of Ca^{2+} ions gives very different results. The maximum conductivity raises to 5.2 $S\,cm^{-1}$, almost an order of magnitude increase over the as-synthesized film.

There are several ways in which Ca^{2+}-ion complexation can influence the rate of electron transfer (conductivity). The conductivity maximum at 0.41 V ($E_{1/2}^{2\prime,Ca}$) for the Ca^{2+}–Poly(**1**) complex corresponds to a state where there is an equal amount radical anion segments and neutral *p*-diquinone segments (Figure 2, boxed section). As is the case with bound protons in the conductive Poly(**2**) film, bound Ca^{2+} ions located near the *p*-diquinone units enhance the electron delocalization of these electroactive segments. Therefore a lower energy barrier for electron hopping results. However, in the case of the K^+ ions, the fact that the calix[4]arenecrown receptor can only precisely bind one monovalent cation creates a situation wherein there are net negative charges on the polymer backbone (Figure 3). To compensate the charges, there are unbound K^+ and/or small numbers of protons in the K^+–Poly(**1**) film. The presence of disordered unbound ions results in nondegenerate energy levels of individual electroactive segments. In addition, the dissociation of unbound K^+ ions with partial oxidation results in even greater inequivalence and hopping becomes a more activated process. It is also possible that the interaction of the receptor with ions can produce a geometry change in the calix[4]arene that places the redox-active segments closer to each other and thereby increases the intersegment electron-transfer rate. As was mentioned above, solution ^1H NMR spectroscopy measurements suggest a flattened-cone conformation that potentially reduces the interchain distance between redoxactive segments.

Of all the potential mechanisms by which Ca^{2+} ions can enhance the conductivity of Poly(**1**), we believe that charge balance between the polymer backbone and the bound metal ion is dominant. Our rationale for this statement is supported by the general trends observed when Poly(**1**) is exposed to different monovalent and divalent metal ions. Specifically, treatment of Poly(**1**) films with solutions containing monovalent cations Na^+ and Li^+, similar to K^+, resulted in insulating films, even though NMR spectroscopic measurements suggest similar perturbations to the calixarene's conformation. To further support our charge-balancing model we found that treatment with 10 mM of divalent Mg^{2+} and Ba^{2+} also provide high conductivity films ($\sigma_{max} = 0.48\ S\,cm^{-1}$ for Mg^{2+} and 1.71 $S\,cm^{-1}$ for Ba^{2+}).

In summary, we have demonstrated a new conceptual approach to selective ionoresistive sensing. Although the binding of monovalent K^+ and divalent Ca^{2+} ions to the calixarenecrown produces extremely similar NMR spectroscopic and cyclic voltammetric behaviors, the conductivities show more than three orders of magnitude difference. We propose that this profound sensitivity to the charge state of

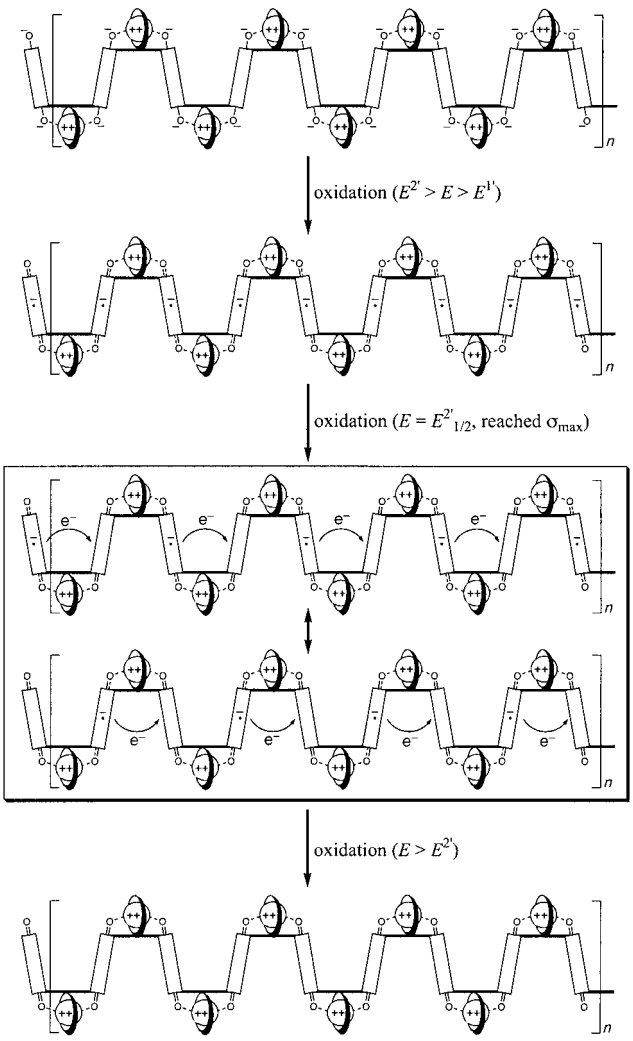


Figure 2. Schematic representation of the conducting mechanism of Ca^{2+}–Poly(**1**) film.

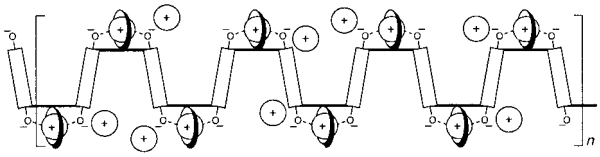


Figure 3. Schematic representation of K^+–Poly(**1**) film at fully reduced state.

 © 2004 Wiley-VCH Verlag GmbH & Co. KGaA, Weinheim

the metal ion is related to the need for charge balancing between the redox segments and the metal ions, which is essential for efficient hopping conductivity. This charge-balancing principle is general and will be applied to other sensor designs.

Received: January 30, 2004
Revised: April 16, 2004 [Z53896]

Keywords: calixarenes · conducting materials · crown compounds · polymers · sensors

[1] a) D. T. McQuade, A. E. Pullen, T. M. Swager, *Chem. Rev.* **2000**, *100*, 2537; b) T. M. Swager, *Acc. Chem. Res.* **1998**, *31*, 201.
[2] M. J. Marsella, P. J. Carroll, T. M. Swager, *J. Am. Chem. Soc.* **1994**, *116*, 9347.
[3] a) M. J. Marsella, T. M. Swager, *J. Am. Chem. Soc.* **1993**, *115*, 12214; b) M. J. Marsella, R. J. Newland, P. J. Carroll, T. M. Swager, *J. Am. Chem. Soc.* **1995**, *117*, 9842.
[4] a) S. S. Zhu, T. M. Swager, *J. Am. Chem. Soc.* **1997**, *119*, 12568; b) R. P. Kingsborough, T. M. Swager, *Adv. Mater.* **1998**, *10*, 1100; c) T. Shioya, T. M. Swager, *Chem. Commun.* **2002**, 1364.
[5] a) Y. H. Kim, N. R. Cha, S.-K. Chang, *Tetrahedron Lett.* **2002**, *43*, 3883; b) Y. Kubo, S. Tokita, Y. Kojima, Y. T. Osano, T. Matsuzaki, *J. Org. Chem.* **1996**, *61*, 3758; c) Y. Kubo, S. Obara, S. Tokita, *Chem. Commun.* **1999**, 2399.
[6] H.-h. Yu, B. Xu, T. M. Swager, *J. Am. Chem. Soc.* **2003**, *125*, 1142.
[7] Similar compounds with calix[4]arenecrown-5 moiety have been found with the binding free energy: $K^+ > Na^+ > Li^+$, see A. Casnati, A. Pochini, R. Ungaro, C. Bocchi, F. Ugozzoli, R. J. M. Egberink, H. Struijk, R. Lugtenberg, F. deJong, D. N. Reinhoudt, *Chem. Eur. J.* **1996**, *2*, 436.
[8] Other compounds with calix[4]arenecrown-5 moiety have also been found binding Ca^{2+} and Ba^{2+} ions, respectively, see reference [5a] and R. Cacciapaglia, A. Casnati, L. Mandolini, R. Ungaro, *J. Am. Chem. Soc.* **1992**, *114*, 10956.
[9] a) P. J. Dijkstra, J. A. J. Brunink, K. E. Bugge, D. N. Reinhoudt, S. Harkema, R. Ungaro, F. Ugozzoli, E. Ghidini, *J. Am. Chem. Soc.* **1989**, *111*, 7567; b) E. Ghidini, F. Ugozzoli, R. Ungaro, S. Harkema, A. A. El-Fadl, D. N. Reinhoudt, *J. Am. Chem. Soc.* **1990**, *112*, 6979; c) K. Takahashi, A. Gunji, D. Guillaumont, F. Pichierri, S. Nakamura, *Angew. Chem.* **2000**, *112*, 3047; *Angew. Chem. Int. Ed.* **2000**, *39*, 2925.
[10] For reports of cyclic voltammetric studies of polythiophene with pendant crown ether moieties see: a) J. Roncali, R. Garreau, M. Lemaire, *J. Electroanal. Chem.* **1990**, *278*, 373; b) P. Bäuerle, S. Scheib, *Acta Polym.* **1995**, *46*, 124; c) H. K. Youssoufi, M. Hmyene, F. Garnier, D. Delabouglise, *J. Chem. Soc. Chem. Commun.* **1993**, 1550.
[11] Detailed experimental conditions and material preparations are available in the Supporting Information. Monomer **1**: m.p. 181–182 °C; ^{1}H NMR (500 MHz, $CDCl_3$): $\delta = 7.93$ (s, 2H), 7.33 (s, 4H), 7.19 (dd, 2H, $J = 5.0$, 1.0 Hz), 7.17 (dd, 2H, $J = 3.5$, 1.0 Hz), 7.12 (d, 2H, $J = 3.5$ Hz), 7.09 (d, 2H, $J = 3.5$ Hz), 7.01 (dd, 2H, $J = 5.0$, 3.5 Hz), 6.93 (d, 4H, $J = 8.0$ Hz), 6.77 (t, 2H, $J = 8.0$ Hz), 4.46 (d, 4H, $J = 13.5$ Hz), 4.12 (bm, 8H), 3.96 (t, 4H, $J = 5.5$ Hz), 3.85 (t, 4H, $J = 5.5$ Hz), 3.42 ppm (d, 4H, $J = 13.5$ Hz); ^{13}C NMR (125 MHz, $CDCl_3$): $\delta = 153.6$, 152.0, 143.9, 137.8, 135.0, 132.7, 129.1, 128.5, 127.8, 126.0, 125.4, 125.1, 124.5, 123.9, 123.1, 122.1, 76.8, 71.1, 71.0, 70.2, 31.1 ppm. FT-IR (KBr): $\tilde{\nu} = 3500$–3100 (broad, OH), 2919, 2361, 2339, 1484, 1456, 1250, 1202, 1136, 1081, 1051, 796, 694 cm^{-1}. HR-MS (ESI): calcd for $C_{52}H_{46}O_7S_4 + NH_4^+$ 928.2464 [$(M+NH_4)^+$]; found 928.2461.
[12] A. F. Littke, G. C. Fu, *Angew. Chem.* **2002**, *114*, 4350; *Angew. Chem. Int. Ed.* **2002**, *41*, 4176.
[13] C. D. Gutsche, *Calixarenes, Monographs in Supramolecular Chemistry* (Ed.: J. F. Stoddart), The Royal Society of Chemistry, Cambridge, UK, **1989**.
[14] Electropolymerizations were performed in CH_2Cl_2 containing 1 mM of monomer **1** or **2** and 0.1 M $(n\text{Bu})_4NPF_6$ by repeated cycling of the electrode between −0.4 V and 0.8 V at a scan rate of 100 mV s^{-1}.
[15] All potentials are referenced to Fc/Fc^+ (Fc = ferrocene). A standard three-electrode setup was used for all electrochemical studies: Pt button working electrode, Pt coil counter electrode, and Ag/Ag^+ reference electrode. Ferrocene is used as an external standard.
[16] In situ EPR experiments confirm the redox wave as a two-electron transition. A build up of intensity ($g = 2.002$) was displayed as the polymer oxidized and reached a maximum at anodic peak potential ($E_{p,a} = 0.58$ V), indicating the formation of a state with unpaired electrons. The spin density decreased as the film was further oxidized. This is evidence of the formation of another spinless state. This build up and decay is consistent with a two-electron transition.
[17] The coupling equilibria of electroactivity and proton–ion exchange from the repeating unit is similar to what was reported by Echegoyan and co-workers, see a) D. A. Gustowski, M. Delgado, V. J. Gatto, L. Echegoyen, G. W. Gokel, *J. Am. Chem. Soc.* **1986**, *108*, 7553; b) M. Delgado, D. A. Gustowski, H. K. Yoo, V. J. Gatto, G. W. Gokel, L. Echegoyen, *J. Am. Chem. Soc.* **1988**, *110*, 119.
[18] Electrochemical properties of thiophene-extended *p*-diquinone have been studied, see K. Takahashi, T. Suzuki, *J. Am. Chem. Soc.* **1989**, *111*, 5483.
[19] M. Lapkowski, E. M. Genies, *J. Electroanal. Chem.* **1990**, *284*, 127.
[20] A method originally designed by Wrighton and co-workers (G. P. Kittlesen, H. S. White, M. S. Wrighton, *J. Am. Chem. Soc.* **1984**, *106*, 7389) was used for the measurement.

 © 2004 Wiley-VCH Verlag GmbH & Co. KGaA, Weinheim

Organometallic Nanotubes

Swellable, Redox-Active Shell-Crosslinked Organometallic Nanotubes

Xiao-Song Wang, Mitchell A. Winnik, and Ian Manners**

Carbon nanotubes have a range of remarkable properties and these fascinating structures now represent a key building block in nanoscience and technology.[1] Since their discovery,[2] the synthesis of analogous structures with other

[*] X.-S. Wang, M. A. Winnik, I. Manners
Department of Chemistry
University of Toronto
80 St. George Street, Toronto, Ontario, M5S 3H6 (Canada)
Fax: (+1) 416-978-6157
E-mail: mwinnik@chem.utoronto.ca
imanners@utoronto.ca

Supporting information for this article is available on the WWW under http://www.angewandte.org or from the author.

 DOI: 10.1002/anie.200453969 © 2004 Wiley-VCH Verlag GmbH & Co. KGaA, Weinheim

compositions has attracted much attention and a variety of inorganic nanotubes have also been described.[3] Organic and organometallic nanotubes[4] would further complement the available structures. However, relatively few successes have been reported in this area.

Block copolymers comprise chemically distinct but individually homogeneous polymer chains joined together end-to-end by covalent bonds. These molecules self-assemble in block-selective solvents into core–corona micellar nanostructures, in which the solvent-insoluble block forms the core and the solvent-soluble block forms the shell.[5] Although a range of micellar morphology, including spheres, cylinders, vesicles, have been identified,[6] nanotubes are rare.[4g–i] We recently found that PFS–*b*–PDMS (PFS: polyferrocenylsilane, PDMS: polydimethylsilane) with a block ratio of 1:12 self-assembles either in hexane or in decane (solvents which are selective for PDMS) to form organometallic nanotubes with PFS as the inner wall and PDMS as the corona. From the fact that these tubes in hexane were able to entrap tetrabutyl lead, we imagine that the tube ends are open to solvent.[7] However, the further exploration and utility of these fascinating nanomaterials, which should have interesting physical properties by virtue of the metal-containing PFS block,[8,9] has been impeded by the instability of these self-assembled structures, which dissociate in solvent that is not selective for PDMS or at elevated temperature.

Core- and shell-crosslinking reactions have been developed as a technique to endow permanence to block copolymer micelles and to create additional opportunities for applications.[10,11] For example, nanocages have been created from shell-crosslinked spherical micelles.[12] We recently reported the self-assembly of PI–PFS (PI: polyisoprene) cylindrical micelles, which could be shell-crosslinked by metal-catalyzed hydrosilylation.[13] The resulting permanent organometallic cylinders served as a precursor for ceramic nanolines upon pyrolysis and could be aligned on a flat substrate through a microfluidic template, thus providing an opportunity for the fabrication of nanopatterned arrays. Herein, we report the synthesis, self-assembly, and shell-crosslinking of PFS–PMVS (PMVS: polymethylvinylsiloxane), which leads to stable organometallic nanotubes that have redox activity and tunable swellability (Scheme 1).

The organometallic–inorganic block copolymer PFS_{48}-$PMVS_{300}$ (number average molecular weight ($\bar{M}_n$) = 40700; polydispersity index (PDI) = 1.10, PFS:PMVS = 1:6) was synthesized through sequential anionic polymerization in THF. The polymers self-assemble in hexane, a selective solvent for PMVS, to form nanotubes. As shown in Figure 1a, the nanotubes appear as stiff hollow structures, with a mean

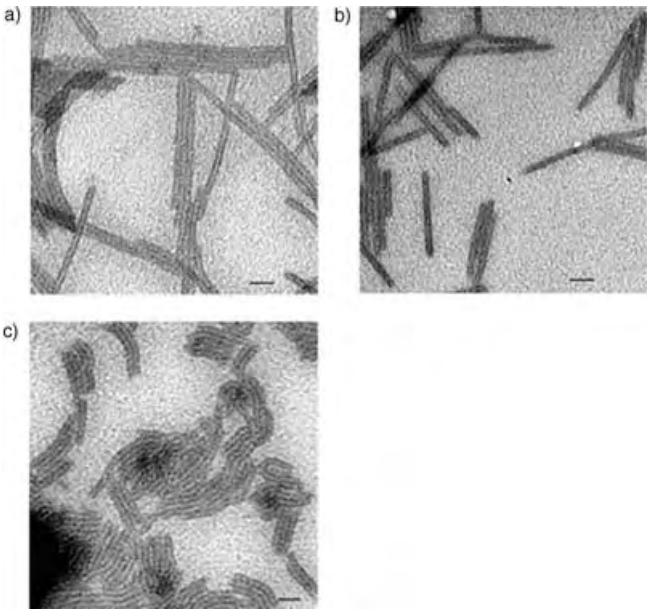
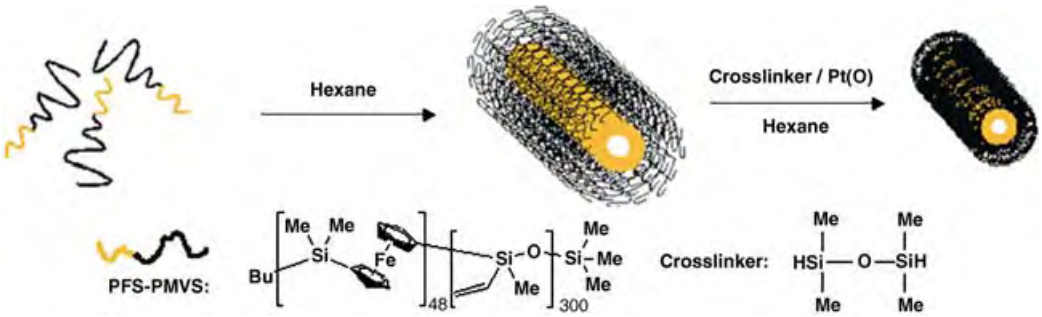


Figure 1. TEM images for the samples prepared from a) self-assembled PFS–PMVS nanotubes in hexane, b) shell-crosslinked nanotubes in hexane and c) in THF. Scale bar: 100 nm.

length of about 400 nm, and they have a cavity diameter of 8 nm and a PFS wall thickness of 8 nm.[7,14]

Taking advantage of pendant vinyl groups in PMVS,[13] we were able to crosslink the corona by using a metal-catalyzed hydrosilylation reaction with tetramethyldisiloxane. For example, a solution of PFS–PMVS nanotubes in hexane (1 mg mL^{-1}) was treated at room temperature for 3 days with tetramethyldisiloxane (0.5 equiv per vinyl group) in the presence of Karstedt's catalyst. Dynamic light scattering (DLS) measurements are useful for monitoring changes in micelle size. These measurements showed that the apparent hydrodynamic radius, R_h, of 85 nm for uncrosslinked micelles was reduced to 69 nm for the crosslinked micelles. The reduction in R_h indicates that the micelle corona is less swollen by solvent at this level of crosslinking. In the TEM



Scheme 1. Synthesis of stable organometallic nanotubes.

 © 2004 Wiley-VCH Verlag GmbH & Co. KGaA, Weinheim

images, however (see Figure 1b) the structures appear to be very similar.[15]

A more important test of the influence of crosslinking is to examine the consequences of exposing the nanotubular structures shown in Figure 1b to a common solvent for both blocks such as benzene, toluene, or tetrahydrofuran (THF). For the uncrosslinked PFS–b–PMVS nanotubes (Figure 1a), exposure to these solvents led to a solution of unimers. In contrast, the crosslinked nanotubes maintained their size. DLS measurements on this sample in THF gave an R_h value of 67 nm, similar to the value of 69 nm for the value in hexane. ^{1}H NMR spectroscopic analysis in C_6D_6 allowed the reaction of the pendant vinyl groups of the PMVS chains to be monitored. After shell-crosslinking, it become barely possibly to observe the signals due to vinyl groups, which suggests that most were consumed and that a high degree of crosslinking occurred.

A droplet of the crosslinked micelle solution in THF was placed on a TEM grid and, after solvent evaporation, gave images such as that shown in Figure 1c. The structures formed are similar in contour length to those seen in Figure 1b. They appear to be hollow, but much more flexible. The overall width of the core of the tubes is expanded slightly from a value of 25 nm for tubes formed in hexane to 30 nm for the sample formed as the THF evaporates on the TEM grid. Another difference between this structure and that of the initially crosslinked nanotubes in hexane is the nature of the PFS domains. Films formed from the nanotubes in hexane, both before and after the crosslinking reaction, exhibit a strong peak in the wide-angle X-ray scattering (WAXS) spectrum with a d spacing of 6.3 Å, characteristic of the distance between adjacent planes in crystalline PFS.[16,17] In contrast, no peaks were seen in the WAXS spectrum of films formed from a THF solution of the crosslinked structures.[17] These films yielded only an amorphous halo. The flexibility of the structures seen in Figure 1c may be related to the amorphous nature of the PFS domains, as amorphous structures have a lower degree of rigidity than crystalline analogues.

Another test of the stability of a self-assembled structure is its stability upon exposure to ultrasound. We previously reported that the cylindrical micelles formed from PFS_{50}–$PDMS_{300}$ underwent irreversible fragmentation to form shorter, stubbier cylinders of similar width when a hexane solution of the micelles was place in a 60 w ultrasonic cleaning bath.[18] The process was followed by DLS. Here we found similar results. A solution of the uncrosslinked nanotubes in hexane underwent eventual degradation when placed in a 60 w ultrasonic bath. Over 25 min of sonication, R_h decreased from about 85 nm to less than 50 nm. Shorter tubelike structures were observed by TEM, and the smaller structures did not grow in size (DLS, TEM) when the hexane solution was allowed to stand undisturbed for 3 days at 23 °C. In contrast, the R_h of the crosslinked structures, under the same set of sonication conditions, remained constant at 67 nm (Figure 2).

The success of the crosslinking reaction opens the way for new experiments in which the nature and the extent of crosslinking can be varied. For example, one can choose a

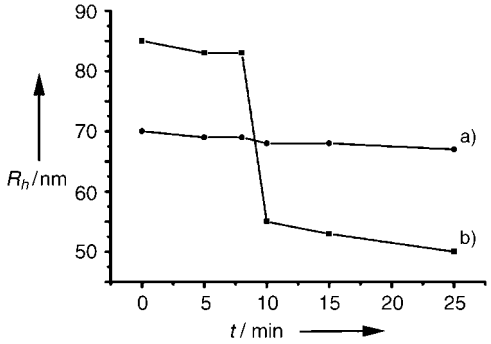


Figure 2. R_h as a function of sonication time for a) crosslinked micelles and b) uncrosslinked micelles.

different siloxane-based crosslinker with a longer spacer between the reactive Si–H groups. We carried out a series of reactions with hydride-terminated polydimethylsiloxane (H–PDMS–H, $\bar{M}_n = 400$–500, 0.5 wt % H). The TEM images of the resulting shell-crosslinked micelles deposited from hexane (Figure 3a) appear identical to those crosslinked by

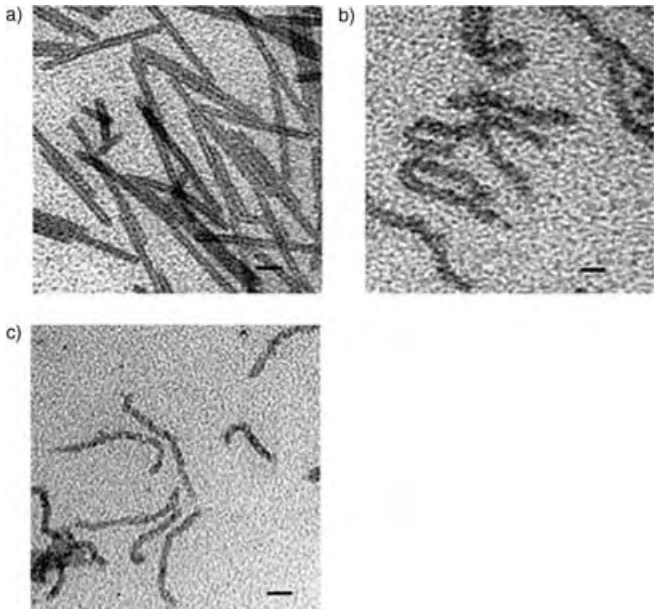


Figure 3. TEM images for shell crosslinked micelles with hydride-terminated polydimethyl siloxane, $\bar{M}_n = 400$, as crosslinker. a) Sample prepared from crosslinked micelles in hexane, b) from crosslinked micelles in toluene, and c) from crosslinked micelles in toluene/hexane mixture (1:3 by volume). Scale bar: 100 nm.

tetramethyldisiloxane (see Figure 1b). Differences appear in the TEM images of these structures when they are spread on the TEM grid from toluene, a common solvent in which both blocks are soluble. As seen in Figure 3b, the structures are not only less rigid but also wider. Their width is about 55 nm, which is more than twice that of original micelles formed in hexane (25 nm).

To help us understand the origin of this increase in tube diameter for structures seen in the TEM images, we carried

 © 2004 Wiley-VCH Verlag GmbH & Co. KGaA, Weinheim

out additional experiments in which we slowly added hexane to the toluene solution of the nanotubes crosslinked with H–PDMS–H. Remarkably, the "swollen" shell-crosslinked tubes seen in Figure 3b gradually decreased in thickness back towards their original size. As shown in Figure 3c, TEM samples prepared from a solution containing a 3:1 mixture by volume of hexane to toluene had a PFS core width of 27 nm. In addition, these structures no longer appear to be hollow. They more closely resemble dense cylinders. Thus, the TEM images of these structures are sensitive to the state of the crosslinked structures in solution. In samples formed in pure toluene, both polymer blocks are swollen by the common solvent, and phase separation probably occurs on the TEM grid as the solvent evaporates. When hexane is added to the solution, it promotes selective precipitation of the PFS chains to form domains of nanometer dimensions, whose size is limited by the connectivity of the PFS to the crosslinked PMVS corona. Hexane evaporates more rapidly than toluene, and the final structures seen in Figure 3c are likely to be related in a complex way to the composition of the medium as the sample dried.

Crosslinked structures of nanometer dimensions swollen by solvent are often referred to as "microgel" particles. The crosslinked nanotubes "dissolved" in a common suitable solvent are two-component microgels, in which the PFS chains dangle from the network of PMVS chains. The stability of these structures in a common solvent for both blocks makes it possible to characterize their electrochemical behavior by cyclic voltammetry (CV). The experiments, on samples crosslinked with tetramethyldisiloxane, were carried out in a mixture of dichloromethane and benzonitrile (2:1 by volume) that contained 0.1 M $[NBu_4][PF_6]$ as the supporting electrolyte. For comparison, CV experiments were also carried out on the uncrosslinked block copolymers. Under these conditions, the polymers exist as unimers as characterized by DLS. As shown in Figure 4a, the PMVS network of the microgel particles does not prevent electron transfer involving the redox-active PFS component. Two reversible oxidation waves for the PFS chains were observed which, based on studies of PFS homopolymer, is characteristic of the presence of interacting metal centers.[19] In fact, the protection afforded by the PMVS network appears to prevent the deposition of oxidized micelles on the electrode surface, as suggested by the presence of a relative smooth reduction curve. In contrast, the uncrosslinked block copolymers exhibit a sharp peak upon reduction (Figure 4b), characteristic of the precipitation of oxidized PFS chains on the electrode surface.[19]

In summary, PFS–*b*–PMVS block copolymers, synthesized by anionic polymerization, underwent self-assembly in hexane to form organometallic nanotubes. The PMVS shell could be crosslinked in hexane, thus preserving the structure but leading to a contraction of the corona dimensions. These crosslinked micelles formed stable redox-active microgel particles in a common suitable solvent, and these particles swell or shrink depending on the solvent composition. The degree of swelling was dictated by the molecular weight of the crosslinker. These properties may render these nanotubes useful building blocks for a variety of applications.

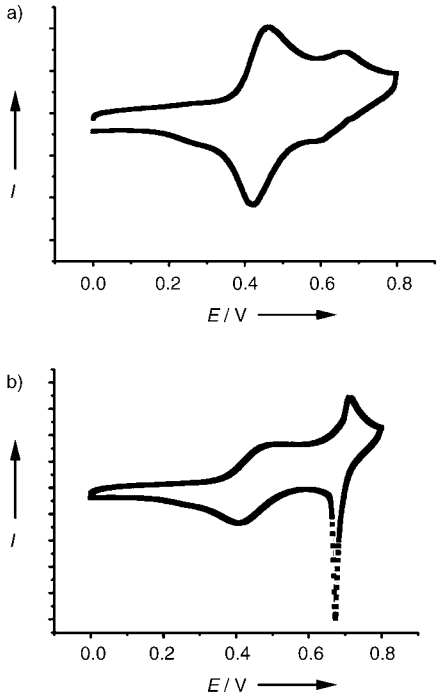


Figure 4. Cyclic voltammetry of a) crosslinked nanotubes and b) PFS–PMVS block copolymer in dichloromethane/benzonitrile (2:1) with 0.1 M $[Bu_4N][PF_6]$ as supporting electrolyte.

Experimental Section

Synthesis of PFS–PMVS: In an N_2-filled glovebox at room temperature, *n*BuLi (1.6 M; 60 μL, 9.6×10^{-5} mol) in hexanes was added quickly to a stirred solution of [1]silaferrocenophane (1.18 g, 4.8×10^{-3} mol) in THF (10 mL). After 40 min, the solution changed from a red to a deep amber color, and then 1,3,5-trivinyl-1,3,5-trimethylcyclotrisiloxane (2.90 g, 11.60×10^{-3} mol) was added to the solution of living polymer along with a few drops of [12]crown-4. The reaction flask was immediately removed from the glovebox and placed on a Schlenk line under prepurified Ar and cooled to 0 °C. The reaction proceeded for 20 h at 0 °C and was terminated by the addition of a few drops of Me_3SiCl. The block copolymer was precipitated into methanol (ca. 500 mL) in the presence of triethylamine (ca. 10 mL), isolated, and washed with hexane to remove side products, followed by drying under vacuum for 24 h, yielding 3.8 g of the amber gummy product (yield = 93 %). ^{1}H NMR (300 MHz, C_6D_6) data: $\delta = 0.50$ (s, $[(\eta\text{-}C_5H_4)_2FeSiMe_2]_x$), 4.10 (s, Cp), 4.26 (s, Cp), and 0.28 (s, $[MeSiO]_{3y}$), 5.80–6.40 ppm (m, $[CH_2{=}CH{-}SiO]_{3y}$). GPC: M_n (PDI): 11700 (1.02) for the PFS block, and 40700 (1.10) for the PFS-PMVS diblock copolymer.

Self-Assembly of PFS-PMVS and Shell-crosslinking Reactions:Instrumentation and characterization: Molecular weight and molecular-weight distribution was characterized by gel permeation chromatography (GPC) by using a Waters Associates 2690 Separations Module equipped with Ultrastyragel columns with pore sizes of 10^3–10^5 Å, in-line degasser, and a differential refractometer. The ^{1}H NMR spectra were recorded on a Varian Gemini 300 spectrometer with deuterated benzene as solvent. DLS experiments were carried out by using AVL-5000 operating in the dynamic mode. Cumulant fitting of autocorrection functions provide hydrodynamic radii with an error of ± 0.1 nm and no model was used. WAXS samples were prepared by casting a film from PFS–PVMS hexane solution on an aluminum substrate. Transmission electron microscopy (TEM) measurements were carried out with an Hitachi model 600 electron microscope operating at 75 kV. The samples were prepared by drying a drop of

 © 2004 Wiley-VCH Verlag GmbH & Co. KGaA, Weinheim

the micelle solution on a carbon-coated copper grid. Iron-containing PFS chains provide electron-rich domains, which furnished the contrast for imaging self-assembled nanostructures.

Micellization: Tubelike micelles were prepared by mixing PFS–PMVS with hexane at 50–60 °C with stirring for 1 hour before cooling to room temperature. An aliquot was taken for light scattering and TEM experiments.

Shell crosslinking: A typical hydrosilylation shell-crosslinking reaction was performed as follows: Tetramethylsiloxane (7 μL, 1.2×10^{-4} mmol) and Karstedt's catalyst (7 μL) were added to a PFS–PVMS hexane micelle solution (10 mg/10 mL; vinyl group content: 2.4×10^{-4} mmol) at room temperature with stirring. At the end of the reaction, the solution was passed through an aluminum oxide column to remove the metal catalyst to yield a clear yellow solution of micelles. An aliquot of the hexane solution was used for DLS and TEM analysis. Then the hexane was removed by a flow of air to recover solid crosslinked micelles, which were redispersed in THF. DLS and TEM analyses of the shell crosslinked micelles in THF solution were carried out as described above directly without filtration.

Received: February 9, 2004 [Z53969]

Keywords: block copolymers · micelles · nanotubes · redox chemistry · shell-crosslinking

[1] R. C. Haddon, *Acc. Chem. Res.* **2002**, *35*, a special issue on nanotube science.
[2] S. Iijima, *Nature* **1991**, *354*, 56–58.
[3] C. N. R. Rao, M. Nath, *Dalton Trans.* **2003**, 1–24.
[4] a) D. T. Bong, T. D. Clark, J. R. Granja, M. R. Ghadiri, *Angew. Chem.* **2001**, *113*, 1016–1041; *Angew. Chem. Int. Ed.* **2001**, *40*, 988–1011; b) M. R. Ghadiri, J. R. Granja, R. A. Milligan, D. E. Mcree, N. Khazanovich, *Nature* **1993**, *366*, 324–327; c) M. Reches, E. Gazit, *Science* **2003**, *300*, 625–627; d) S. F. Ai, G. Lu, Q. He, J. B. Li, *J. Am. Chem. Soc.* **2003**, *125*, 11140–11141; e) Y. Kim, M. F. Mayer, S. C. Zimmerman, *Angew. Chem.* **2003**, *115*, 1153–1158; *Angew. Chem. Int. Ed.* **2003**, *42*, 1121–1126; For macroscopic tubes see: f) D. Y. Yan, Y. F. Zhou, J. Hou, *Science* **2004**, *303*, 65–67; Nanotubes from block copolymers: g) S. Stewart, G. Liu, *Angew. Chem.* **2000**, *112*, 348–352; *Angew. Chem. Int. Ed.* **2000**, *39*, 340–344; h) R. Mäki-Ontto, K. de Moel, W. de Odorico, J. Ruokolainen, M. Stamm, G. ten Brinke, O. Ikkala, *Adv. Mater.* **2001**, *13*, 117–121; i) K. Yu, A. Eisenberg, *Macromolecules* **1998**, *31*, 3509–3518; j) S. Rosselli, A.-D. Ramminger, T. Wagner, B. Silier, S. Wiegand, W. Häußler, G. Lieser, V. Scheumann, S. Höger, *Angew. Chem.* **2001**, *113*, 3233–3237; *Angew. Chem. Int. Ed.* **2001**, *40*, 3137–3141.
[5] a) A. Halperin, M. Tirrell, T. P. Lodge, *Adv. Polym. Sci.* **1992**, *100*, 31–71; b) S. Förster, M. Antonietti, *Adv. Mater.* **1998**, *10*, 195–217; c) A. Choucair, A. Eisenberg, *Eur. Phys. J. E* **2003**, *10*, 37–44.
[6] a) L. Zhang, A. Eisenberg, *Science* **1995**, *268*, 1728–1731; b) S. Jain, F. S. Bates, *Science* **2003**, *300*, 460–464; c) D. E. Discher, A. Eisenberg, *Science* **2002**, *297*, 967–973; d) S. A. Jenekhe, X. L. Chen, *Science* **1998**, *279*, 1903–1907; e) Z. L. Zhou, Z. B. Li, Y. Ren, M. A. Hillmyer, T. P. Lodge, *J. Am. Chem. Soc.* **2003**, *125*, 10182–10183; f) J. F. Gohy, N. Willet, S. Varshney, J. X. Zhang, R. Jerome, *Angew. Chem.* **2001**, *113*, 3314–3316; *Angew. Chem. Int. Ed.* **2001**, *40*, 3214–3216; j) Y. F. Liu, V. Abetz, A. H. E. Müller, M *acromolecules* **2003**, *36*, 7894–7898.
[7] For detailed characterization of PFS block copolymer nanotubes see: J. Raez, I. Manners, M. A. Winnik, *J. Am. Chem. Soc.* **2002**, *124*, 10381–10395.
[8] a) I. Manners, *Science* **2001**, *294*, 1664–1666; b) J. A. Massey, M. A. Winnik, I. Manners, Z. H. V. Chan, J. M. Ostermann, R. Enchelmaier, J. P. Spatz, M. Möller, *J. Am. Chem. Soc.* **2001**, *123*, 3147–3148; c) K. Kulbaba, I. Manners, *Macromol. Rapid Commun.* **2001**, *22*, 711–724.
[9] For recent work on the solution self-assembly of metal-containing block copolymers see: a) J.-F. Gohy, B. G. G. Lohmeijer, S. K. Varshney, U. S. Schubert, *Macromolecules* **2002**, *35*, 7427–7435; b) S. Hou, K. Y. K. Man, W. K. Chan, *Langmuir* **2003**, *19*, 2485–2490.
[10] For core crosslinking reactions: a) A. Guo, G. Liu, J. Tao, *Macromolecules* **1996**, *29*, 2487–2493; b) F. Henselwood, G. Liu, *Macromolecules* **1998**, *31*, 4213–4217; c) Y. Won, H. T. Davis, F. S. Bates, *Science* **1999**, *283*, 960–963.
[11] For shell-crosslinking reactions: a) K. B. Thurmond, T. Kowalewski, K. L. Wooley, *J. Am. Chem. Soc.* **1996**, *118*, 7239–7240; b) K. B. Thurmond, T. Kowalewski, K. L. Wooley, *J. Am. Chem. Soc.* **1997**, *119*, 6656–6665; c) J. Ding, G. Liu, *Macromolecules* **1998**, *31*, 6554–6558; d) V. Bütün, A. B. Lowe, N. C. Billingham, S. P. Armes, *J. Am. Chem. Soc.* **1999**, *121*, 4288–4289.
[12] a) G. J. Liu, *Curr. Opin. Colloid Interface Sci.* **1998**, *3*, 200–208; b) K. L. Wooley, *Chem. Eur. J.* **1997**, *3*, 1397–1399.
[13] X. S. Wang, A. Arsenault, G. A. Ozin, M. A. Winnik, I. Manners, *J. Am. Chem. Soc.* **2003**, *125*, 12686–12687.
[14] The block ratio appears to have little effect on the morphologies of the micelles. For example, PFS–PMVS block copolymers with block ratio of 1:10 also self-assemble into nanotubes. X. S. Wang, M. A. Winnik, I. Manners, unpublished results.
[15] Only the PFS inner wall is visible in TEM, corona chains are invisible due to their comparatively low electron density.
[16] J. A. Massey, K. Temple, L. Cao, Y. Rharbi, J. Raez, M. A. Winnik, I. Manners, *J. Am. Chem. Soc.* **2000**, *122*, 11577–11584; b) V. S. Papkov, M. V. Gerasimov, I. I. Dubovik, S. Sharma, V. V. Dementiev, K. H. Pannell, *Macromolecules* **2000**, *33*, 7107–7115.
[17] see supporting information for further details.
[18] J. Massey, K. N. Power, I. Manners, M. A. Winnik, *J. Am. Chem. Soc.* **1998**, *120*, 9533–9540.
[19] a) D. A. Foucher, J. M. Nelson, C. Honeyman, B. Z. Tang, I. Manners, *Angew. Chem.* **1993**, *105*, 1843–1845; *Angew. Chem. Int. Ed. Engl.* **1993**, *32*, 1709–1711; b) R. Rulkens, A. J. Lough, I. Manners, S. R. Lovelace, C. Grant, W. E. Geiger, *J. Am. Chem. Soc.* **1996**, *118*, 12683–12695.

 © 2004 Wiley-VCH Verlag GmbH & Co. KGaA, Weinheim

C–H Bond Activation

A Measureable Equilibrium between Iridium Hydride Alkylidene and Iridium Hydride Alkene Isomers**

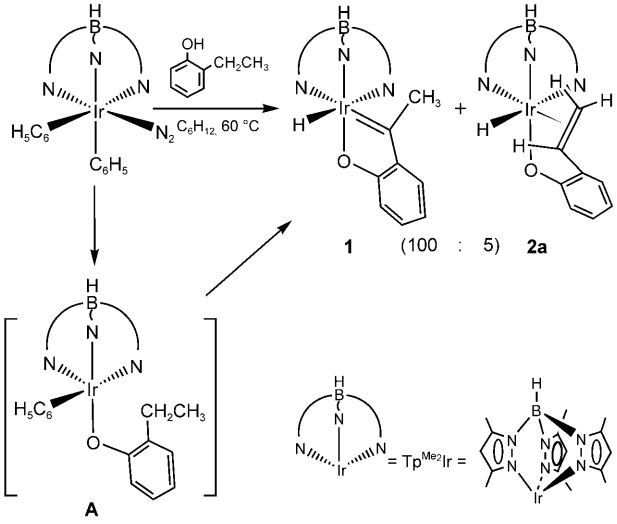
Margarita Paneque, Manuel L. Poveda, Laura L. Santos, Ernesto Carmona, Agustí Lledós,* Gregori Ujaque, and Kurt Mereiter*

Dedicated to Professor H. Werner on his 70th birthday

Rearrangement between isomeric M–olefin and M–alkylidene units (in which M is a transition-metal atom) is a fundamental transformation key to many homogeneous and heterogeneous catalytic processes.[1] However, whereas conversion of a metal alkylidene into the corresponding metal alkene has been known for some time, particularly for cationic electrophilic metal alkylidenes,[2,3] the reverse transformation is a rarely observed process, known only for a few transition-metal complexes that have few d electrons.[4] Moreover, detection of a thermoneutral (or almost thermoneutral) redistribution of this kind, that is, a process whereby the alkene and the alkylidene isomers exist in equilibrium, finds little precedent and appears to be limited to some complexes of the early transition metals.[5] We report herein that a d^6 $Tp^{Me_2}Ir^{III}$ fragment allows attainment of an equilibrium mixture of the hydride alkylidene and hydride alkene structures **1** and **2a** (Scheme 1), through a reaction that implies the activation of sp^3 C–H bonds of *o*-$C_6H_4(OH)CH_2CH_3$.

[*] Dr. M. Paneque, Dr. M. L. Poveda, L. L. Santos, Prof. Dr. E. Carmona
Instituto de Investigaciones Químicas
Departamento de Química Inorgánica
Consejo Superior de Investigaciones Científicas
Universidad de Sevilla
Avda. Américo Vespucio s/n, Isla de la Cartuja, 41092 Sevilla (Spain)
Fax: (+34) 95–446–0565
E-mail: guzman@us.es
Prof. Dr. A. Lledós, Dr. G. Ujaque
Unitat de Química Física
Departament de Química, Edifici Cn
Universitat Autònoma de Barcelona
08193 Bellaterra, Barcelona (Spain)
Fax: (+34) 93–581–2920
E-mail: agusti@klingon.uab.es
Dr. K. Mereiter
Department of Chemistry
Vienna University of Technology
Getreidemarkt 9/164SC, 1060 Vienna (Austria)
Fax: (+43)1–558801–17199
E-mail: kurt.mereiter@tuwien.ac.at

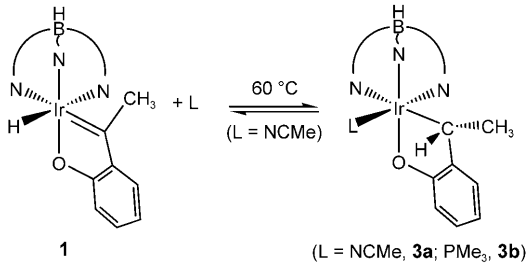
[**] Financial support from the DGESIC (Projects BQU2001-1995, COST support, and BQU2002-04110-C02-02), and from the Junta de Andalucía, and EU COST Action WG-D17–003 are gratefully acknowledged. L.L.S. thanks the Spanish Ministry of Education for a grant. G.U. thanks the Spanish MCyT for funding through the "Ramón y Cajal" program. We thank a reviewer for bringing reference 5 to our attention.



Scheme 1. Double sp^3 C–H bond activation of *o*-$C_6H_4(OH)C_2H_5$.

The thermal reaction of $Tp^{Me_2}Ir(C_6H_5)_2(N_2)$[6a] and 2-ethylphenol (ca. 1:2.5 molar ratio, cyclohexane solvent, 60 °C) produces the hydride alkylidene **1** (Scheme 1) as the main product (95% conversion into products as determined by NMR spectroscopy; 90% yield of isolated **1**). Presumably, the reaction starts with alcoholysis of one of the Ir–C_6H_5 bonds (structure **A**, Scheme 1), and this is then followed by a facile, double activation[6,7] of the methylenic C–H bonds of the *ortho* ethyl substituent. The C–H bond cleavage is highly regioselective. Monitoring by ^{1}H NMR spectroscopy reveals that under kinetic control, the alternative reaction product, namely the hydride alkene isomer **2a** that derives from β- as opposed to α-hydride elimination in the last C–H activation step, amounts to only about 5% of the total reaction product (Ir–H signals at $\delta = -20.40$ for **1** and −17.49 ppm for **2a**, with intensity ratio of ca. 100:5).

Characterization of **1** from the analytical and spectroscopic data is unequivocal (see Experimental Section). Lewis bases, such as NCMe or PMe_3, induce a stereospecific 1,2-hydrogen shift to yield the corresponding adducts, **3a** and **3b**, respectively (Scheme 2); the latter has been characterized by X-ray crystallography (Figure 1).[8] The 1,2-hydrogen shift is reversible;[7,9,10] heating the acetonitrile adduct **3a** in C_6H_{12} at 100 °C for 1 h cleanly restores the hydride alkylidene structure (only trace amounts of compound **2a** are detected under these conditions). It seems clear, therefore, that an α-agostic intermediate of type **B** (Scheme 3) can be reached from **1**



Scheme 2. Reversible 1,2-hydrogen shift of hydride alkylidene **1**.

 © 2004 Wiley-VCH Verlag GmbH & Co. KGaA, Weinheim DOI: 10.1002/anie.200454040

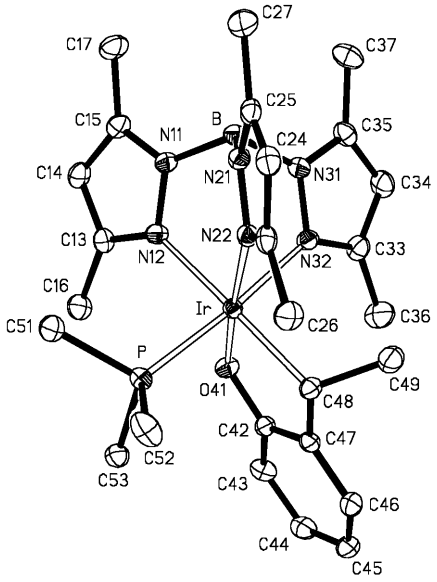
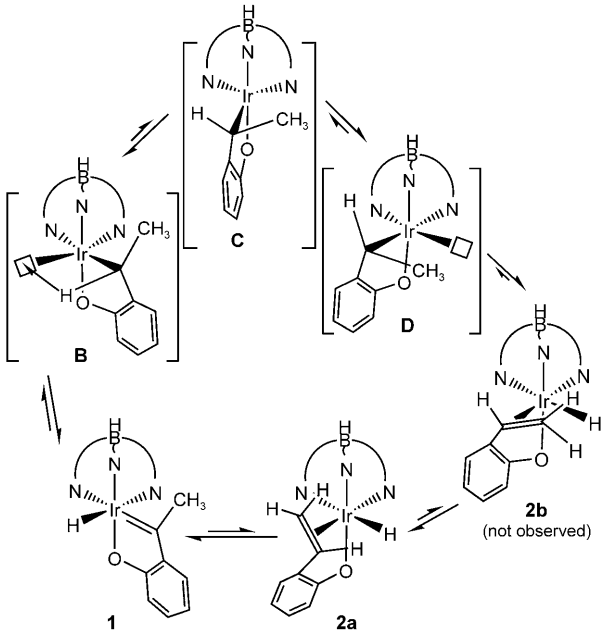


Figure 1. Molecular structure of **3b** in **3b**·CH_2Cl_2 (50% ellipsoids, H atoms and CH_2Cl_2 omitted for clarity). Selected bond lengths [Å] and angles [°]: Ir-P 2.2526(7), Ir-N(12) 2.205(2), Ir-N(22) 2.106(2), Ir-N(32) 2.159(2), Ir-O(41) 2.035(2), Ir-C(48) 2.091(2), O(41)-C(42) 1.343(3), C(47)-C(48) 1.515(3), C(48)-C(49) 1.544(3); O(41)-Ir-C(48) 84.02(8), O(41)-Ir-P 89.61(5), C(48)-Ir-P 89.28(7), N(22)-Ir-P 95.62(5).



Scheme 3. Thermal equilibration of compounds **1** and **2a**.

under mild conditions.[11] Access to structure **D** (that would precede β-hydride elimination[11,12] to generate the hydride alkene isomer **2b**) requires, assuming chiral integrity of the alkyl carbon, metal inversion through a five-coordinate structure such as **C**. This is expected to be energetically costly,[13] and accordingly, the **1**–**2a** isomerization requires prolonged heating at temperatures around 100 °C. The equilibrium constant shows little temperature dependence ($K_{eq} \approx 8$ in C_6D_{12}, temperature range 90–130 °C) and favors the hydride alkylidene **1**.

Despite its low equilibrium concentration, the hydride alkene **2** can be isolated, although only diastereomer **2a** can be detected. Coordination of the other enantiotopic face of the alkene,[2c,14] **2b**, appears to be sterically hindered, although it is accessible upon heating (Scheme 3). A strong correlation signal between the olefinic *H*C= resonance ($\delta =$ 6.88 ppm, dd, 8.3 and 11.2 Hz; see Experimental section) and the hydride signal ($\delta = -17.53$ ppm) found in the NOESY spectrum supports the coordination mode shown in **2a** for the olefin.

Pure samples of **2a**, namely, the minor component of the **1**–**2a** equilibrium, equilibrate upon heating (measurements between 90 and 130 °C, with intervals of 10 °C) to provide K_{eq} values identical to those obtained when the equilibrium is approached starting from **1**. The equilibration rates follow first-order kinetics (^{1}H NMR spectroscopic monitoring in C_6D_{12}) through about 75% conversion. From the gradient of the slopes obtained by plotting $\ln(c\text{-}c_e/c_o\text{-}c_e)$ versus time[15] and from the value of K_{eq} at each temperature, the forward (k_1, **2a**→**1**) and reverse (k_{-1}) rate constants have been determined (at 100 °C, $k_1 = 4.5 \times 10^{-5}$, $k_{-1} = 4.7 \times 10^{-6}\ s^{-1}$). An Eyring plot gives $\Delta H^{\neq} = 21.3$ kcal mol^{-1} and $\Delta S^{\neq} = -21$ cal mol^{-1} K^{-1}.

The mechanistic hypothesis outlined in Scheme 3 has been analysed by means of theoretical calculations (see Experimental Section). The relative energies of alkylidene **1** and alkene **2a** are 0.0 and 1.8 kcal mol^{-1}, respectively, therefore providing a theoretical justification for the almost thermoneutral character of the **1**–**2a** equilibrium. Calculations show that the detected alkene diastereoisomer, **2a**, is 8.2 kcal mol^{-1} more stable than **2b**, which is in full agreement with the experimental results. Alkene **2a** has the double bond slightly closer to the metal center, with Ir–C bond lengths of 2.185 Å and 2.253 Å for **2a**, and 2.252 Å and 2.243 Å for **2b**.

The other postulated intermediates for the isomeric interconversion reaction (Scheme 3) are located as minima in the potential-energy surface. Structure **B** is 19.6 kcal mol^{-1} above the alkylidene, and contains a clear α-agostic interaction, with a C–H bond length of 1.191 Å and an Ir-C-H angle of 76.1°. The energy of intermediate **D** is 21.5 kcal mol^{-1}. Its structure shows neither an α- nor a β-agostic interaction, the three C–H bond lengths range from 1.090 Å to 1.098 Å. The calculated energies for these intermediates are within the expected range given the experimental value of the activation enthalpy, therefore supporting the proposed mechanism. Moreover, the accuracy of energies obtained by density functional theory (DFT) has been checked by MP2 single-point calculations. MP2 energies were similar to DFT energies for all the determined structures. Their values are 0.0 kcal mol^{-1} for **1**, −0.6 kcal mol^{-1} for **2a**, 5.2 kcal mol^{-1} for **2b**, 19.5 kcal mol^{-1} for **B**, and 20.8 kcal mol^{-1} for **D**.

In conclusion, we have presented an example of an unusual double activation of sp^3 C–H bonds that gives rise to a kinetic mixture of a hydride alkylidene, **1**, and the isomeric hydride alkene **2a** of about 20:1. The kinetic predominance of the alkylidene product **1** may result from the preferential

 © 2004 Wiley-VCH Verlag GmbH & Co. KGaA, Weinheim

activation of the methylene hydrogen atom of the presumed structure **A** (Scheme 1) that leads to the α-agostic intermediate **B**. Interestingly, the hydride alkylidene **1** is thermodynamically somewhat more stable than the hydride alkene compound **2a**, possibly as a result of the combination of a favorable alkylidene conformation within the five-membered chelate ring in **1**, with a strained olefin coordination in **2a**. Isolated samples of either of these complexes convert into equilibrium mixtures of the two, therefore demonstrating that alkene and alkylidene functionalities can be readily interconverted by d^6, $Tp^{Me_2}Ir^{III}$ fragments.

Experimental Section

1: A suspension of $[Tp^{Me_2}Ir(C_6H_5)_2(N_2)]$ (0.10 g, 0.15 mmol) and 2-ethylphenol (0.023 mL, 0.194 mmol) in C_6H_{12} (6 mL) was heated at 60 °C for 14 h. The solvent was then removed in vacuo, to leave a dark green residue, which was dissolved in 10 mL of CH_2Cl_2. Excess of the phenol was eliminated by successive washings with aquous solutions of NaOH (10%), NH_4OH (saturated), and brine. The CH_2Cl_2 solution was dried over Na_2SO_4, the solvent removed in vacuo, and the resulting solid material (ca. 95%) was subjected to chromatography through silica (hexane:Et_2O mixtures, from 5:1 to 1:5) to yield pure **1** as a dark-green solid (ca. 90% yield of isolated product). IR (Nujol): $\tilde{\nu} = 2519$ (B-H), 2146 cm^{-1} (Ir-H); ^1H NMR ($CDCl_3$, 25 °C): $\delta = 7.50$, 7.27, 7.17, 6.56 (dd, ddd, d, ddd, 1H each, $^3J(H,H) \approx 8$, $^4J(H,H) \approx 1$ Hz, 4 CH_{ar}), 5.88, 5.87, 5.57 (s, 1H each, 3 CH_{pz}), 2.87 (s, 3H, Ir=CCH_3), 2.58, 2.44, 2.39, 2.37, 2.09, 1.27 (s, 3H each, 6 Me_{pz}), −20.42 ppm (s, 1H, IrH); $^{13}C\{^1H\}$ NMR ($CDCl_3$, 25 °C): $\delta = 274.2$ (Ir=C), 189.6, 151.9 (C_qO and C_qC=Ir resp.), 152.9, 152.5, 152.2, 144.7, 144.3, 143.3 (C_{qpz}), 137.4, 123.0, 117.5, 114.1 (CH_{ar}), 106.8, 106.7, 106.6 (CH_{pz}), 35.3 (Ir=CCH_3, $^1J(C,H) = 126$ Hz), 16.9, 14.4, 13.4, 12.6, 12.5, 11.8 ppm (Me_{pz}); elemental analysis calcd (%) for $C_{23}H_{30}BN_6OIr \cdot 1/2\,Et_2O$: C 46.4, H 5.4, N 13.0; found: C 46.8, H 5.6, N 13.0.

2a: A solution of **1** in C_6H_{12} (0.54 g, 0.90 mmol; 20 mL) was heated at 90 °C for 22 h. The volatile products were removed in vacuo and the resulting **1**:**2a** mixture (ca. 88:12) was subjected to chromatography (silica gel, hexane:Et_2O eluent) to give **2a** (0.060 g, 11%) and 0.45 g of **1** (83%). Compound **2a** was isolated as a pale-green microcrystalline solid by crystallization from a 3:1 mixture of pentane:CH_2Cl_2 at −20 °C. IR (Nujol): $\tilde{\nu} = 2528$ (B-H), 2180 cm^{-1} (Ir-H); ^1H NMR ($CDCl_3$, 25 °C): $\delta = 7.20$, 6.84, 6.50, 6.47 (d, t, d, t, respectively, 1H each, $^3J(H,H) \approx 8$ Hz, 4 CH_{ar}), 6.89 (dd, 1H, $^3J(A,C) = 11.2$, $^3J(A,B) = 8.3$ Hz, CH_A=CH_BH_C), 5.90, 5.83, 5.64 (s, 1H each, 3 CH_{pz}), 4.28 (d, 1H, H_C), 3.29 (d, 1H, H_B), 2.44, 2.38, 2.35, 2.29, 1.95 (s, 1:2:1:1:1:1, 6 Me_{pz}), −17.53 ppm (s, 1H, IrH); $^{13}C\{^1H\}$ NMR ($CDCl_3$, 25 °C): $\delta = 173.6$, 131.3 (C_qO and C_qC=H resp.), 152.4, 150.8, 144.1, 143.8, 143.4 (1:2:1:1:1, C_{qpz}), 127.9, 125.9, 115.7, 114.4 (CH_{ar}), 108.2, 107.2, 106.9 (CH_{pz}), 77.0 (CH_A, $^1J(C,H) = 165$ Hz), 46.2 (CH_BH_C, $^1J(C,H) = 162$ Hz), 14.0, 13.8, 12.9, 12.4, 12.3, 12.2 ppm (Me_{pz}); elemental analysis calcd for $C_{23}H_{30}BN_6OIr$: C 45.3, H 4.9, N 13.8; found: C 45.6, H 4.9, N 13.7.

Calculations: The calculations were performed by using the Gaussian 98 program.[16] All geometries were fully optimized at the ONIOM(BHandH:UFF) level.[17] The Ir, 2-ethylphenolate, and three NH=CH_2 groups that represent the Tp^{Me_2} ligand were described at the DFT by level using the BHandH functional,[16] whereas the rest of the Tp^{Me_2} ligand was described at the molecular-mechanics level by using the UFF force field[18]. For the Ir atom, the lanl2dz[19] effective core potential was used to replace the inner electrons, whereas its associated double-ζ basis set[16,19] was employed to describe the 15 outer electrons. The 6-31g(d) basis set was used for the others.[20] The energies presented in the text were obtained by full quantum mechanics at both BHandH and MP2 levels on the real molecules by using the ONIOM(BHandH:UFF) optimized geometries.

Received: February 17, 2004 [Z54040]

Keywords: alkene ligands · C–H activation · carbene ligands · hydrides · iridium

[1] a) *Catalysis: An Integrated Approach to Homogeneous, Heterogeneous, and Industrial Catalysis* (Ed.: J. A. Moulijn, P. W. N. M. van Leeuwen, R. A. van Santen), Elsevier, Amsterdam, **1993**; b) J. M. Thomas, W. J. Thomas, *Principles and Practice of Heterogeneous Catalysis*, VCH, Weinheim, **1997**; c) F. Zaera, *Chem. Rev.* **1995**, *95*, 2651; d) R. R. Schrock, *Chem. Rev.* **2002**, *102*, 145; e) R. H. Grubbs, G. W. Coates, *Acc. Chem. Res.* **1996**, *29*, 85.

[2] See for example: a) M. Brookhart, J. R. Tucker, G. R. Husk, *J. Am. Chem. Soc.* **1981**, *103*, 979; b) C. P. Casey, W. H. Miles, H. Tukada, *J. Am. Chem. Soc.* **1985**, *107*, 2924; c) C. Roger, G. S. Bodner, W. G. Hatton, J. A. Gladysz, *Organometallics* **1991**, *10*, 3266; d) F. M. Alías, M. L. Poveda, M. Sellin, E. Carmona, *J. Am. Chem. Soc.* **1998**, *120*, 5816.

[3] R. H. Crabtree, *The Organometallic Chemistry of the Transition Metals*, 3rd ed., Wiley, New York, **2001**.

[4] a) O. V. Ozerov, L. A. Watson, M. Pink, K. G. Caulton, *J. Am. Chem. Soc.* **2003**, *125*, 9604; b) A. S. Veige, P. T. Wolczanski, E. B. Lobkovsky, *Angew. Chem.* **2001**, *113*, 3741; *Angew. Chem. Int. Ed.* **2001**, *40*, 3629; c) L. Giannini, G. Guillemot, E. Solari, C. Floriani, N. Re, A. Chiesi-Villa, C. Rizzoli, *J. Am. Chem. Soc.* **1999**, *121*, 2797; d) R. P. Hughes, S. M. Maddock, A. L. Rheingold, I. A. Guzei, *Polyhedron* **1998**, *17*, 1037; e) J. S. Freundlich, R. R. Schrock, W. M. Davis, *J. Am. Chem. Soc.* **1996**, *118*, 3643; f) G. A. Miller, N. J. Cooper, *J. Am. Chem. Soc.* **1985**, *107*, 709.

[5] a) J. D. Fellmann, R. R. Schrock, D. D. Traficante, *Organometallics* **1982**, *1*, 481; b) G. Parkin, E. Bunel, B. J. Burger, M. S. Trimmer, A. van Asselt, J. E. Bercaw, *J. Mol. Catal.* **1987**, *41*, 29.

[6] a) E. Gutiérrez-Puebla, A. Monge, M. C. Nicasio, P. J. Peréz, M. L. Poveda, E. Carmona, *Chem. Eur. J.* **1998**, *4*, 2225; b) H. Werner, B. Weker, O. Nürnberg, J. Wolf, *Angew. Chem.* **1992**, *104*, 1105; *Angew. Chem. Int. Ed. Engl.* **1992**, *31*, 1025; c) J. N. Coalter III, J. C. Huffman, K. G. Caulton, *Chem. Commun.* **2001**, 1158.

[7] For an account of our work on double C–H bond activation reactions, including reversible 1,2-hydrogen shifts see: E. Carmona, M. Paneque, M. L. Poveda, *Dalton Trans.* **2003**, 4022.

[8] Crystal data of **3b**·CH_2Cl_2($C_{27}H_{41}BCl_2IrN_6OP$): triclinic, space group $P\bar{1}$ (no. 2); $a = 8.4368(11)$, $b = 10.2709(13)$, $c = 18.197(2)$ Å, $\alpha = 84.326(2)$, $\beta = 77.630(2)$, $\gamma = 88.211(2)$°, $V = 1532.6(3)$ Å^3, $Z = 2$, $T = 123(2)$ K, $\rho_{calc} = 1.670$ g cm^{-3}, $\mu = 4.61$ mm^{-1}, $R1 = 0.029$, $wR2 = 0.047$ (all data); Bruker AXS Smart CCD system with $Mo_{K\alpha}$ radiation ($\lambda = 0.71073$ Å), 22402 measured reflections, of which 8720 were unique ($R_{int} = 0.028$). Correction for absorption by multiscan method and program SADABS. Structure solved by Patterson method and refined on F^2 by using the SHELXL97 program. CCDC-231190 contains the supplementary crystallographic data for this paper. These data can be obtained free of charge via www.ccdc.cam.ac.uk/conts/retrieving.html (or from the Cambridge Crystallographic Data Centre, 12 Union Road, Cambridge CB2 1EZ, UK; fax: (+44) 1223-336-033; or deposit@ccdc.cam.ac.uk).

[9] D.-H. Lee, J. Chen, J. W. Faller, R. H. Crabtree, *Chem. Commun.* **2001**, 213.

[10] R. R. Schrock, S. W. Seidel, N. C. Mösch-Zanetti, K-Y. Shih, M. B. O'Donoghue, W. M. Davis, W. M. Reiff, *J. Am. Chem. Soc.* **1997**, *119*, 11876.

 © 2004 Wiley-VCH Verlag GmbH & Co. KGaA, Weinheim

[11] a) M. Brookhart, M. L. H. Green, L. L. Wong, *Prog. Inorg. Chem.* **1988**, *36*, 1; b) Y. Han, L. Deng, T. Ziegler, *J. Am. Chem. Soc.* **1997**, *119*, 5939.
[12] a) J. N. Coalter III, J. C. Bollinger, J. C. Huffman, U. Werner-Zwanziger, K. G. Caulton, E. R. Davidson, H. Gerard, E. Clot, O. Eisenstein, *New J. Chem.* **2000**, *24*, 9b) J. Jaffart, M. Etienne, F. Maseras, J. E. McGrady, O. Eisenstein, *J. Am. Chem. Soc.* **2001**, *123*, 6000.
[13] a) J. A. Gladysz, B. J. Boone, *Angew. Chem.* **1997**, *109*, 566; *Angew. Chem. Int. Ed. Engl.* **1997**, *36*, 550; b) M. A. Dewey, Y. Zhou, Y. Liu, J. A. Gladysz, *Organometallics* **1993**, *12*, 3924; c) P. A. Deck, T. J. Marks, *J. Am. Chem. Soc.* **1995**, *117*, 6128; d) C. P. Casey, M. A. Fagan, S. L. Hallenbeck, *Organometallics* **1998**, *17*, 287.
[14] T-S. Peng, J. A. Gladysz, *J. Am. Chem. Soc.* **1992**, *114*, 4174.
[15] K. A. Connors, *Chemical Kinetics: the study of reaction rates in solution*, VCH, New York, **1990**.
[16] Gaussian 98 (Revision A.7), M. J. Frisch, G. W. Trucks, H. B. Schlegel, G. E. Scuseria, M. A. Robb, J. R. Cheeseman, V. G. Zakrzewski, J. A. Montgomery, R. E. Stratmann, J. C. Burant, S. Dapprich, J. M. Millam, A. D. Daniels, K. N. Kudin, M. C. Strain, O. Farkas, J. Tomasi, V. Barone, M. Cossi, R. Cammi, B. Mennucci, C. Pomelli, C. Adamo, S. Clifford, J. Ochterski, G. A. Petersson, P. Y. Ayala, Q. Cui, K. Morokuma, D. K. Malick, A. D. Rabuck, K. Raghavachari, J. B. Foresman, J. Cioslowski, J. V. Ortiz, B. B. Stefanov, G. Liu, A. Liashenko, P. Piskorz, I. Komaromi, R. Gomperts, R. L. Martin, D. J. Fox, T. Keith, M. A. Al-Laham, C. Y. Peng, A. Nanayakkara, C. Gonzalez, M. Challacombe, P. M. W. Gill, B. G. Johnson, W. Chen, M. W. Wong, J. L. Andres, M. Head-Gordon, E. S. Replogle, J. A. Pople, Gaussian, Inc., Pittsburgh, PA, **1998**.
[17] a) F. Maseras, K. Morokuma, *J. Comput. Chem.* **1995**, *16*, 1170; b) M. Svensson, S. Humbel, R. D. Froese, T. Matsubara, S. Sieber, K. Morokuma, *J. Phys. Chem.* **1996**, *100*, 19357; c) S. Dapprich, I. Komáromi, K. S. Byun, K. Morokuma, M. J. Frisch, *J. Mol. Struct.* **1999**, *461–462*, 1.
[18] A. K. Rappe, C. J. Casewit, K. S. Colwell, W. A. Goddard III, W. M. Skiff, *J. Am. Chem. Soc.* **1992**, *114*, 10024.
[19] P. J. Hay, W. R. Wadt, *J. Chem. Phys.* **1985**, *82*, 299.
[20] W. J. Hehre, R. Ditchfield, J. A. Pople, *J. Phys. Chem.* **1972**, *76*, 2257.

 © 2004 Wiley-VCH Verlag GmbH & Co. KGaA, Weinheim

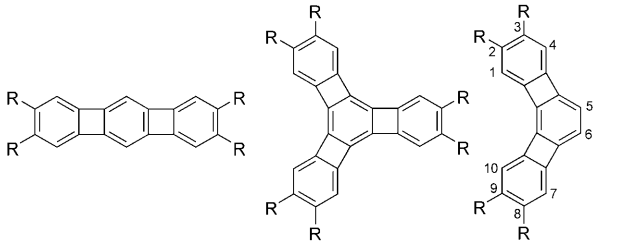
Phenylenes

Anatomy of a Cyclohexatriene: Chemical Dissection of the π and σ Frame of Angular [3]Phenylene**

*Sriram Kumaraswamy, Satish S. Jalisatgi, Adam J. Matzger, Ognjen Š. Miljanić, and K. Peter C. Vollhardt**

The syntheses of several topological forms of the phenylenes have been reported,[1] but an exploration of their chemical behavior has been limited mainly to the parent system [2]phenylene (biphenylene),[2] the linear frame (e.g. the linear [3]phenylene **1**),[3] and the triangular variety (e.g. the C_3-symmetric [4]phenylene **2**).[4] Noticeably absent from these investigations is the behavior of angular [3]phenylene (**3**), for which only hydrogenation of the central ring[4a,5] and flash-pyrolytic isomerization have been recorded.[6]

In **3**, angular fusion minimizes cyclobutadienoid antiaromaticity by rendering the central ring extensively (62%)



1a: R = H
1b: R = $SiMe_3$

2a: R = H
2b: R = $SiMe_3$

3a: R = H
3b: R = $SiMe_3$

bond-localized and thus comparatively less diatropic,[4a,7] while leaving one double bond exposed. In contrast, and besides its distinct topology, **1** is qualitatively very different[1a,3] with a distorted but relatively more diatropic center, flanked by relatively paratropic neighbors.[7] On the other hand, **2** differs quantitatively in the degree of central cyclohexatriene character (100%) and exhibits lower steric

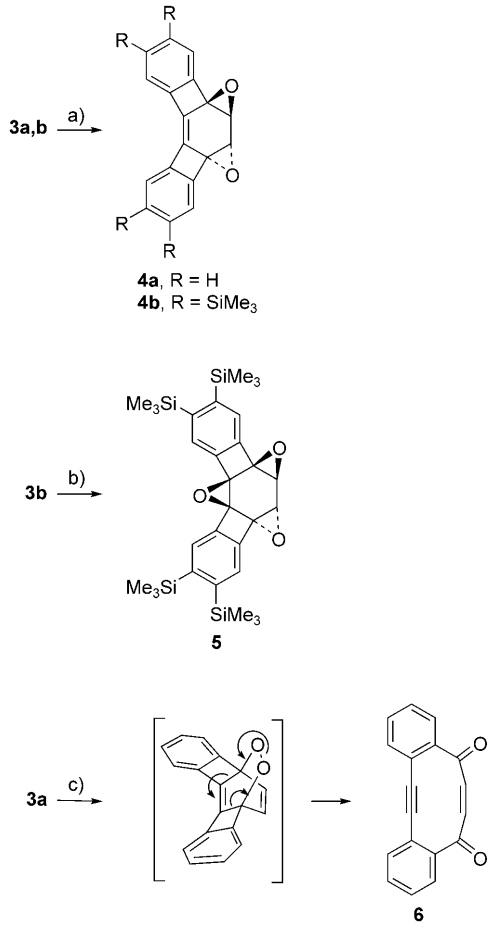
[*] Dr. S. Kumaraswamy, Dr. S. S. Jalisatgi, Dr. A. J. Matzger, O. Š. Miljanić, Prof. K. P. C. Vollhardt
Center for New Directions in Organic Synthesis
Department of Chemistry, University of California at Berkeley
and
Chemical Sciences Division
Lawrence Berkeley National Laboratory
Berkeley, CA 94720-1460 (USA)
Fax: (+1) 510-643-5208
E-mail: kpcv@berkeley.edu

[**] This work was supported by the NSF (CHE 0071887). A.J.M. was an ACS Division of Organic Chemistry Graduate Fellow (made possible by Rohm and Haas Co.). The Center for New Directions in Organic Synthesis is supported by Bristol-Myers Squibb and Novartis. We are grateful to Professor Yoshito Tobe for enlightening correspondence.

 DOI: 10.1002/anie.200454126 © 2004 Wiley-VCH Verlag GmbH & Co. KGaA, Weinheim

accessibility. The motif of **3** is important as the repeating structural unit of the heliphene[8] and zigzag phenylene oligomers[9] and polymers,[10] *anti*-kekulene,[11] and archimedene.[1b] Herein we compare the reactivity of **3** with that of **1** and **2** and reveal some unprecedented transformations and their novel products.

Initial experiments were directed at the reactivity of the π system, particularly the central cyclohexatriene moiety. Indeed, under conditions that convert biphenylene, albeit sluggishly,[12] and **2a** rapidly[4b] into the corresponding trisoxacyclopropanes (*trans* and *cis*, respectively), **3a** and **3b** underwent oxidation within 30 min to yield the heat-and moisture-sensitive bisoxacyclopropanated products **4a** and **4b**, respectively (Scheme 1, see Experimental Section).[13]

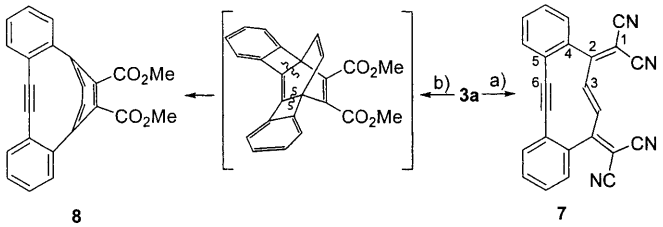


Scheme 1. a) 3,3-Dimethyl-1,2-dioxacyclopropane, acetone, 23 °C, 30 min (**3a**), 100%; 60 min (**3b**), 100%; b) as for a) 6 h, 26%; c) methylene blue (0.09 equiv), O_2, CH_2Cl_2, *hv*, 23 °C, 70%.

Only **4b** could be isolated cleanly and its stereochemistry was ascertained through its conversion into the similarly sensitive, fully desymmetrized trisoxacyclopropanated product **5**. Attempts at triscyclopropanation of **3a**, as effected for **2a** and **b**,[4b] with a variety of reagents left the system intact, demonstrating its relatively lower reactivity. However, addition of singlet oxygen[14] to **3a** proceeded efficiently to furnish the (*Z*)-dione **6**, in a similar fashion to both biphenylene[12] and **1b** (whose reaction proceeded in the absence of a sensitizer),[3a] but unlike **2a** or **b**, which are inert. The unreactivity of **2** may be explained by a cycloaddition–retrocyclization sequence, analogous to that shown in Scheme 1 for **3**, which would lead to an unfavorable benzocyclobutadiene substructure.

The structure of **6** was confirmed by the spectral data (see Experimental Section), which highlight its component functional groups and symmetry, and also through comparison with a serendipitous oxidation product in the zigzag phenylene series for which an X-ray crystal structure was obtained.[9] The molecule **6** constitutes a promising entry into the elusive class of benzodehydro[10]annulenes.[15]

Having established the feasibility of cycloadditions to **3**, we then turned our attention to carbon-based dienophiles, which led to the unprecedented chemistry shown in Scheme 2.[13] When **3a** and tetracyanoethylene (TCNE) were mixed in CH_3CN, a green solution of a charge-transfer (CT) complex resulted instantly ($\lambda_{max} = 562$ nm).[16] Upon heating, the green solution gradually turned brown and was found to contain the adduct **7** in which the initial C–C bond connectivities at the center of **3a** as well as in the dienophile had been completely disrupted. As crystals suitable for X-ray crystallographic studies could not be obtained, the structural assignment was based on spectral data, particularly IR and NMR spectroscopic measurements, which point to a symmetrical structure containing the functional groups depicted in Scheme 2. Moreover, a combination of DEPT experiments



Scheme 2. a) TCNE (1 equiv), CH_3CN, $\triangle$, 8 h, 78%; b) dimethyl butynedioate (1.6. equiv), $AlCl_3$ (0.1 equiv), toluene, 23 °C, 1 h, 74%.

on **7** and comparisons with model systems[17] allowed a complete assignment of the most important carbon signals C1–C6 (see Experimental Section).

TCNE is known to undergo cycloaddition to double bonds, including those in activated arenes, in both a [2+2] and [4+2] manner and either with or without subsequent tetranitrile C–C bond cleavage.[18] Addition of TCNE to **3a** is envisaged to proceed along the lines depicted for singlet-oxygen addition to **3** in Scheme 1, namely [4+2] cycloaddition–[2+2+2] cycloreversal followed by double bond isomerization, with the latter perhaps facilitated by the relief of strain of the sterically encumbered nitrile groups located *cis* to the phenyl moieties.

The mechanism that gives rise to **7** suggests that employment of an alkyne as a dienophile might allow the isolation of the initial addition product. Indeed, biphenylene and other arenes have been reported to be converted into the corresponding bicyclo[2.2.2]octatrienes in the presence of reactive

 © 2004 Wiley-VCH Verlag GmbH & Co. KGaA, Weinheim

triple bonds such as those in arynes, dicyanoacetylene, and bis(fluoroalkyl)alkynes.[2,18b,19] Remarkably, dimethyl butynedioate in the presence of catalytic $AlCl_3$ smoothly converted **3a** into the cyclophane **8**. This indicates not only that the desired cycloaddition had occurred, but also that the initial adduct underwent unusually facile alkyne extrusion (Scheme 2).[19,20]

X-ray crystallographic analysis of **8** secures the structural assignment and heralds the molecule as the most distorted, completely unsaturated [6]paracyclophane (Figure 1).[18b,21,22]

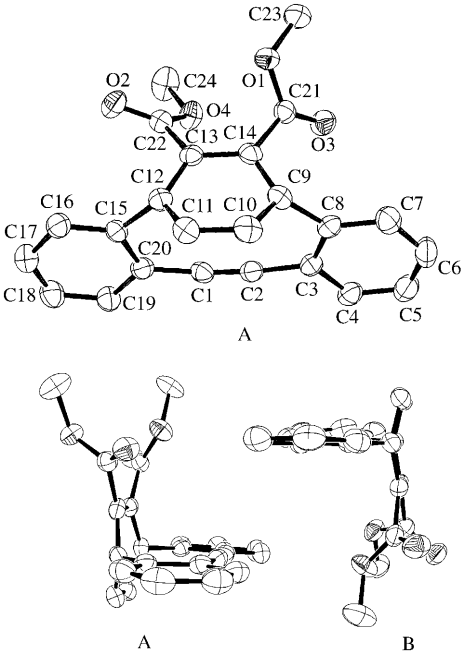
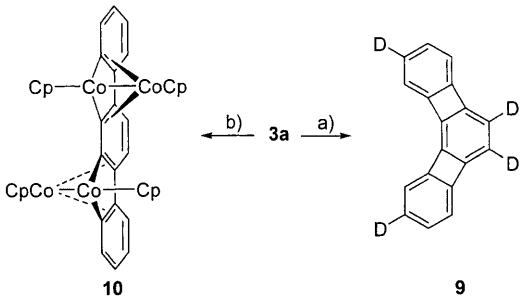


Figure 1. X-ray crystal structure of **8**. Views from above (A, top) and the side (two non-equivalent molecules A and B in the unit cell; bottom). Selected bond lengths [Å] and angles [°] for A; [average of all corresponding equivalent values in A and B in square brackets]: C1-C2 1.202(4) [1.200], C2-C3 1.461(4) [1.457], C3-C8 1.429(4) [1.427], [C1-C2 (centroid)]-[C10-C11-C13-C14 (centroid)] 2.80 [2.80]; C1-C2-C3 172.3(1) [170.3], C2-C3-C8 118.1(1) [118.49], C3-C8-C9 112.0(1) [112.28].

The bow-shaped diarenoalkyne bridges are twisted and bent with noticeable elongation of the C2–C3 and C3–C8 bonds (and their equivalents in both A and B in the unit cell).[23] Most instructive is the pronounced boat conformation of the central arene moiety, characterized by the relatively high α (16.6–18.7°) and β values (21.9–25.4°), with an average for $\alpha+\beta=41.4°$.[24] POAV2 analysis[25] reflects the degree of pyramidalization of the arene carbon atoms (average pyramidalization angles: C9 7.62°, C12 7.31°, C13 3.39°, C14 5.23°). The NMR and UV/Vis spectral data do not reveal any unusual bridge conjugation or transannular interactions.[18b,21,24,26] The molecule is thermally robust, melts without decomposition, and is also photoinert. The strain in **8** is estimated to be 37.2 kcal mol^{-1} from the calculated (B3LYP6-31G*) heat of the (homodesmotic) cycloaddition involved in its formation ($\Delta H°=-62.5$ kcal mol^{-1}), and the measured σ/π ring strain in **3a** (99.7 kcal mol^{-1}).[4a] Similarly, the hypothetical reaction **8** + 2 C_6H_6 → dimethyl 3,6-diphenylbenzene-1,2-dicarboxylate + diphenylethyne has a calculated $\Delta H°=-35.6$ kcal mol^{-1}, reflecting the energy gain of opening the cyclophane bridge.

In view of the behavior of **3** towards electrophilic reagents, the question arose as to how **3** would behave upon simple protonation (deuteration). Biphenylene[2] and **2a** undergo H/D exchange with D^+ exclusively at C2 (β positions), whereas **1a** decomposes in the presence of acid.[3b] There are five potential sites for D incorporation in **3a** of which the relative reactivity of the cyclohexatrienic "α" positions, C5 and C6, was of special interest. Emulating the approach taken by Maksić and co-workers for biphenylene,[27] calculations (HF/6-31G*) of the five protonated species reveal extensively delocalized systems, the energy ranking of which is largely controlled by the avoidance of cyclobutadienoid resonance forms. Thus, attack at C5 should be most favored (relative energy 0 kcal mol^{-1}), followed by that at C2 (+2.27 kcal mol^{-1}), C3 (+5.10 kcal mol^{-1}), C4 (+11.55 kcal mol^{-1}), and C1 (+14.70 kcal mol^{-1}). This order of reactivity is also indicated by the decrease in the corresponding HOMO coefficients of **3a** (HF/STO-3G): 0.31, 0.25, 0.17, −0.17, −0.01. Experimental results conformed partly with these expectations (Scheme 3), in as much as deuteration of **3a** at C5 and C6 occurred before deuteration at C2 and C9 in a clearly stepwise manner to yield **9**, as observed by NMR[1a] and mass spectral analysis. Unfortunately, more stringent conditions caused decomposition.



Scheme 3. a) CF_3CO_2D (0.5 mL), $CDCl_3$ (3 mL), 60 °C, 8 h (C5,6-deuteration), 80%; then CF_3CO_2D (0.5 mL), $CDCl_3$ (3 mL), 100 °C, 8 h (C2,9-deuteration), 82%; b) [$CpCo(C_2H_4)_2$] (10 equiv), C_6H_6, 70 °C, 6 h, 71%.

Finally, in a similar fashion to biphenylene[28] and **1b**,[3b] it was thought that **3a** would be subject to C–C bond activation in the presence of electrophilic metal fragments. Treatment of **3a** with excess [$CpCo(C_2H_4)_2$] (Scheme 3) gave rise to **10**, the result of double regio- and stereoselective dinuclear cobalt insertion. The spectral data confirm its overall connectivity,[28] with more details obtained by X-ray crystallographic studies (Figure 2).[22] Four-membered-ring-opening thus occurs at adjacent sites and the two η^4-coordinated cobalt atoms are located *anti* with respect to the terphenyl ligand plane; both observations are probably of steric origin. The terphenyl ligand is notably planar, but shows considerable bond alternation. Fluxionality around the dinuclear moiety is not detectable as there is no observed coalescence of the ^{1}H NMR signals for the Cp groups upon heating to 100 °C.[28] The generation of **10** suggests interesting extensions to higher

 © 2004 Wiley-VCH Verlag GmbH & Co. KGaA, Weinheim

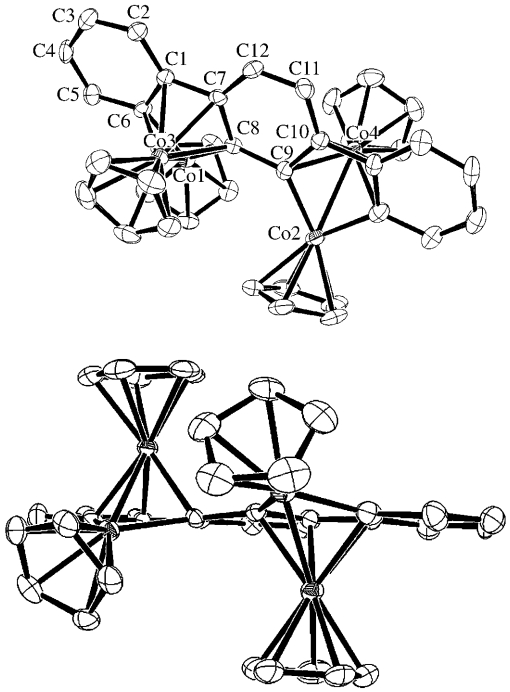


Figure 2. X-ray crystal structure of **10**·C_6H_6 (solvent molecule omitted). Views from above (top) and the side (bottom). Selected bond lengths [Å]: Co1-Co3 2.4498(6), Co2-Co4 2.4800(7), Co1-C6 1.886(30, Co1-C8 1.937(3), Co3-C6 2.054(3), Co3-C1 2.067(3), Co3-C7 2.081(3), Co3-C8 2.070(3), C1-C2 1.434(4), C1-C6 1.428(5), C1-C7 1.453(5), C2-C3 1.354(5), C3-C4 1.415(5), C4-C5 1.366(5), C5-C6 1.437(5), C7-C8 1.454(4), C7-C12 1.435(5), C8-C9 1.491(5), C9-C10 1.449(5), C10-C11 1.440(5), Co_n-Cp(centroid) 1.66, 1.71, 1.68, 1.72.

phenylenes for the construction of novel organometallic oligomers.[29]

In summary, although the central ring in the angular [3]phenylene (**3**) may stay intact on exposure to electrophilic reagents, it mostly behaves as a "loaded spring" ready to unravel into a remarkable array of products. The chemistry reported herein, which places the reactivity of angular phenylene between those of its linear and triangular relatives, significantly expands the potential of the angular motif to give rise to a plethora of novel structures.

Experimental Section

4a: sensitive, colorless oil ($t_{1/2}\sim 2$ min); ^{1}H NMR (500 MHz, $CDCl_3$): $\delta = 7.36$ (dt, $J = 7.9$, 0.9 Hz, 2H), 7.08 (td, $J = 7.9$, 0.9 Hz, 2H), 7.00 (td, $J = 7.9$, 0.9 Hz, 2H), 6.86 (dt, $J = 7.9$, 0.9 Hz, 2H), 3.68 ppm (s, 2H); MS (70 eV): *m*/*z* (%): 258 (6) [M^+], 226 (100).

4b: sensitive, light-orange wax; ^{1}H NMR (500 MHz, CD_2Cl_2): $\delta =$ 7.77 (s, 2H), 7.64 (s, 2H), 4.49 (s, 2H), 0.42 (s, 18H), 0.38 ppm (s, 18H); $^{13}C\{^1H\}$ NMR (125 MHz, CD_2Cl_2): $\delta = 150.6$, 150.0, 146.6, 146.3, 129.4, 128.5, 126.7, 69.3, 56.4, 1.84, 1.80 ppm; IR (film): $\tilde{\nu} =$ 2953, 2922, 2853, 1251, 1083, 840, 757 cm^{-1}; MS (70 eV): *m*/*z* (%): 546 (41) [M^+], 531 (18), 514 (54), 73 (100); HRMS: calcd for $C_{30}H_{42}O_2Si_4$: 546.2262; found: 546.2241.

5: sensitive, light-yellow solid; ^{1}H NMR (500 MHz, $CDCl_3$): $\delta =$ 7.84 (d, $J = 0.9$ Hz, 1H), 7.79 (d, $J = 0.9$ Hz, 1H), 7.65 (d, $J = 0.9$ Hz, 1H), 7.56 (d, $J = 0.9$ Hz, 1H), 4.48 (d, $J = 1.4$ Hz, 1H), 4.36 (d, $J =$ 1.4 Hz, 1H), 0.42 (s, 18H), 0.42 (s, 9H), 0.39 (s, 9H), 0.39 ppm (s, 18H); $^{13}C\{^1H\}$ NMR (100 MHz, CD_2Cl_2): $\delta = 150.8$, 150.2, 149.54, 148.4, 147.0, 145.8, 143.5, 141.9, 128.8, 128.7, 128.6, 128.4, 72.2, 71.7, 70.9, 70.4, 58.2, 58.0, 1.95, 1.88, 1.86, 1.76 ppm; MS (70 eV): *m*/*z* (%): 562 (34) [M^+], 547 (26), 531 (12), 199 (75), 73 (100); HRMS: calcd for $C_{30}H_{42}O_3Si_4$: 562.2211; found: 562.2219.

6: colorless crystals (from ethyl acetate); m.p. 160–162 °C (decomp); ^{1}H NMR (500 MHz, $CDCl_3$): $\delta = 7.45$–7.39 (m, 8H), 6.59 (s, $^{H-H}J = 12$ Hz (from the ^{13}C satellites), 2H); $^{13}C\{^1H\}$ NMR (100 MHz, $CDCl_3$): $\delta = 196.8$, 142.3, 136.1, 131.1, 129.6, 129.5, 127.2, 120.5, 95.6 ppm; UV/Vis (hexane): λ_{max} (logε) = 238 (3.34), 254 (3.28), 293 (3.09), 312 (3.04), 324 nm (3.04); IR (KBr): $\tilde{\nu} = 3061$, 3020, 1687, 1589, 1479, 1449, 1274, 1260, 1213, 1007, 996, 755 cm^{-1}; MS (70 eV): *m*/*z* (%): 258 (25) [M^+], 230 (100), 202 (57); HRMS: calcd for $C_{18}H_{10}O_2$: 258.0681; found: 258.0684.

7: green crystals (from CH_2Cl_2); m.p. 185–187 °C (decomp); ^{1}H NMR (500 MHz, $CDCl_3$): $\delta = 7.81$–7.76 (m, 2H), 7.66–7.56 (m, 6H), 6.90 (s, $^{H-H}J = 16$ Hz (from the ^{13}C satellites), 2H); $^{13}C\{^1H\}$ NMR (100 MHz, CD_3CN): $\delta = 168.1$ (C2), 138.2 (C3), 134.3 (C4), 133.4, 133.2, 131.12, 130.4, 123.2 (C5), 112.8 (CN), 112.7 (CN), 98.0 (C6), 86.3 ppm (C1); UV/Vis (hexane): λ_{max} (logε) = 264 (4.59), 283 (4.45), 325 (4.34), 398 (3.83), 486 nm (3.19); IR (KBr): $\tilde{\nu} = 3062$, 2917, 2849, 2231, 1589, 1563, 1478, 1267, 1182, 969, 762, 736 cm^{-1}; MS (70 eV): *m*/*z* (%): 354 (100) [M^+], 327 (50), 300 (22), 289 (35), 150 (18), 137 (16); HRMS: calcd for $C_{24}H_{10}N_4$: 354.0905; found: 354.0906.

8: colorless crystals (from ethyl acetate); m.p. 165–167 °C; ^{1}H NMR (300 MHz, $CDCl_3$): $\delta = 7.59$ (br d, $J = 7.2$ Hz, 2H), 7.55 (s, 2H), 7.36 (td, $J = 7.2$, 1.3 Hz, 2H), 7.22 (td, $J = 7.2$, 1.3 Hz, 2H), 7.10 (br d, $J = 7.2$ Hz, 2H), 3.60 ppm (s, 6H); $^{13}C\{^1H\}$ NMR (100 MHz, $CDCl_3$): $\delta = 168.8$, 144.5, 144.4, 135.7, 135.7, 129.6, 128.1, 127.8, 127.5, 125.1, 93.9, 52.2 ppm; UV/Vis (methanol): λ_{max} (logε) 278 (5.16), 295 (5.32), 301 (5.26), 313 nm (5.31); IR (KBr): $\tilde{\nu} = 3065$, 2990, 2945, 1723, 1460, 1428, 1362, 1288, 1260, 1193, 1152, 1120, 1041, 749 cm^{-1}; MS (70 eV): *m*/*z* (%): 368 (100) [M^+], 337 (35), 224 (48), 212 (28), 59 (16); elemental analysis: calcd for $C_{24}H_{16}O_4$: C 78.25, H 4.38; found: C 78.10, H 4.54.

10: black-brown crystals (from benzene/pentane, 4:1); m.p. 178–179 °C; ^{1}H NMR (400 MHz, [D_8]THF): $\delta = 8.69$ (d, $J = 8.4$ Hz, 2H), 7.72 (d, $J = 8.7$ Hz, 2H), 7.58 (s, 2H), 7.12 (ddd, $J = 8.7$, 8.4, 0.7 Hz, 2H), 6.91 (ddd, $J = 8.7$, 8.4, 0.7 Hz, 2H), 5.10 (s, 10H), 4.37 ppm (s, 10H); $^{13}C\{^1H\}$ NMR (100 MHz, [D_8]THF): $\delta = 155.2$, 129.2, 127.6, 126.9, 121.5, 117.1, 108.2, 81.4, 81.3 ppm; MS (70 eV): *m*/*z* (%): 722 (45) [M^+], 189 (100).

Received: February 27, 2004 [Z54126]

Keywords: aromaticity · C—C activation · cleavage reactions · cycloaddition · cyclophanes

[1] a) D. L. Mohler, K. P. C. Vollhardt in *Advances in Strain in Organic Chemistry, Vol. 5* (Ed.: B. Halton), JAI, London, **1996**, p. 121; for recent references, see: b) D. Bruns, H. Miura, K. P. C. Vollhardt, *Org. Lett.* **2003**, *5*, 549; c) C. Dosche, M. U. Kumke, F. Ariese, A. N. Bader, C. Gooijer, P. I. Dosa, S. Han, O. Š. Miljanić, K. P. C. Vollhardt, R. Puchta, N. J. R. van Eikema - Hommes, *Phys. Chem. Chem. Phys.* **2003**, *5*, 4563.

[2] M. K. Shepherd, *Cyclobutarenes. The Chemistry of Benzocyclobutene, Biphenylene, and Related Compounds*, Elsevier, Amsterdam, **1991**.

[3] a) H. Mestdagh, K. P. C. Vollhardt, *J. Chem. Soc. Chem. Commun.* **1986**, 281; b) B. C. Berris, G. H. Hovakeemian, Y.-H. Lai, H. Mestdagh, K. P. C. Vollhardt, *J. Am. Chem. Soc.* **1985**, *107*, 5670.

[4] a) H.-D. Beckhaus, R. Faust, A. J. Matzger, D. L. Mohler, D. W. Rogers, C. Rüchardt, A. K. Sawhney, S. P. Verevkin, K. P. C. Vollhardt, S. Wolff, *J. Am. Chem. Soc.* **2000**, *122*, 7819; b) D. L. Mohler, K. P. C. Vollhardt, S. Wolff, *Angew. Chem.* **1995**, *107*, 601; *Angew. Chem. Int. Ed. Engl.* **1995**, *34*, 563; c) D. L. Mohler,

 © 2004 Wiley-VCH Verlag GmbH & Co. KGaA, Weinheim

K. P. C. Vollhardt, S. Wolff, *Angew. Chem.* **1990**, *102*, 1200; *Angew. Chem. Int. Ed. Engl.* **1990**, *29*, 1151; d) R. Diercks, K. P. C. Vollhardt, *J. Am. Chem. Soc.* **1986**, *108*, 3150.

[5] R. Diercks, K. P. C. Vollhardt, *Angew. Chem.* **1986**, *98*, 268; *Angew. Chem. Int. Ed. Engl* **1986**, *25*, 266.

[6] P. I. Dosa, A. Schleifenbaum, K. P. C. Vollhardt, *Org. Lett.* **2001**, *3*, 1017.

[7] J. M. Schulman, R. L. Disch, H. Jiao, P. von R. Schleyer, *J. Phys. Chem. A* **1998**, *102*, 8051.

[8] a) S. Han, D. R. Anderson, A. D. Bond, H. V. Chu, R. L. Disch, D. Holmes, J. M. Schulman, S. J. Teat, K. P. C. Vollhardt, G. D. Whitener, *Angew. Chem.* **2002**, *114*, 3361; *Angew. Chem. Int. Ed.* **2002**, *41*, 3227; b) S. Han, A. D. Bond, R. L. Disch, D. Holmes, J. M. Schulman, S. J. Teat, K. P. C. Vollhardt, G. D. Whitener, *Angew. Chem.* **2002**, *114*, 3357; *Angew. Chem. Int. Ed.* **2002**, *41*, 3223.

[9] C. Eickmeier, D. Holmes, H. Junga, A. J. Matzger, F. Scherhag, M. Shim, K. P. C. Vollhardt, *Angew. Chem.* **1999**, *111*, 856; *Angew. Chem. Int. Ed.* **1999**, *38*, 800.

[10] a) J. M. Schulman, R. L. Disch, *J. Phys. Chem. A* **2003**, *107*, 5223; b) A. Rajca, A. Safronov, S. Rajca, C. R. Ross II, J. J. Stezowski, *J. Am. Chem. Soc.* **1996**, *118*, 7272; c) M. Baumgarten, F. Dietz, K. Müllen, S. Karabunarliev, N. Tyutyulkov, *Chem. Phys. Lett.* **1994**, *221*, 71; d) N. Trinajstić, T. G. Schmalz, T. P. Živković, S. Nikolić, G. E. Hite, D. J. Klein, W. A. Seitz, *New J. Chem.* **1991**, *15*, 27; e) J. L. Brédas, R. H. Baughman, *J. Polym. Sci. Polym. Lett. Ed.* **1983**, *21*, 475.

[11] C. Eickmeier, H. Junga, A. J. Matzger, F. Scherhag, M. Shim, K. P. C. Vollhardt, *Angew. Chem.* **1997**, *109*, 2194; *Angew. Chem. Int. Ed. Engl.* **1997**, *36*, 2103.

[12] W. Adam, M. Balci, H. Kiliç, *J. Org. Chem.* **1998**, *63*, 8544. The *trans* stereochemistry of this trioxide was assigned on mechanistic grounds, but an *all-cis* array could not be ruled out: M. Balci, personal communication.

[13] All new compounds gave satisfactory analytical and/or spectral data, unless mentioned otherwise.

[14] F. Sevin, M. L. McKee, *J. Am. Chem. Soc.* **2001**, *123*, 4591, and references therein.

[15] A. T. Balaban, M. Banciu, V. Ciorba, *Annulenes, Benzo-, Hetero-, Homo-Derivatives and Their Valence Isomers*, *Vol. 2*, CRC, Boca Raton, FL, **1987**, p. 146.

[16] For comparison, biphenylene–TCNE has a CT band at 620 nm in CH_2Cl_2: a) B. Uno, N. Okumura, K. Seto, *J. Phys. Chem. A* **2000**, *104*, 3064; similarly **2a**–TCNE absorbs at 664 nm in CH_2Cl_2: b) D. L. Mohler, K. P. C. Vollhardt, unpublished results; neither complex proceeds to cycloadducts.

[17] a) H.-O. Kalinowski, S. Berger, S. Braun, *^{13}C NMR-Spektroskopie*, Thieme, Stuttgart, **1984**; b) L. Knothe, H. Prinzbach, *Justus Liebigs Ann. Chem.* **1977**, 687; c) W. W. Zajac, Jr., T. R. Walters, J. Buzby, J. Gagnon, M. Labroli, *Synth. Commun.* **1994**, *24*, 427.

[18] a) For cyclobutarenes, see, for example: F. Toda, P. J. Garratt, *Chem. Rev.* **1992**, *92*, 1685; b) for cyclophanes, see, for example: F. Vögtle, *Cyclophane Chemistry*, Wiley, Chichester, **1993**.

[19] See: a) M. A. Battiste, J.-X. Duan, Y.-A. Zhai, I. Ghiviriga, K. A. Abboud, A. Roitberg, G. R. Shelton, W. R. Dolbier, Jr., *Tetrahedron Lett.* **2002**, *43*, 7047; b) F.-G. Klärner, R. Ehrhardt, H. Bandmann, R. Boese, D. Bläser, K. N. Houk, B. R. Beno, *Chem. Eur. J.* **1999**, *5*, 2119; c) H. Hopf, B. Witulski in *Modern Acetylene Chemistry* (Eds.: P. J. Stang, F. Diederich), VCH, Weinheim, **1995**, p. 33; d) E. Ciganek, *Org. React.* **1984**, *32*, 1; e) I. Tabushi, H. Yamada, Z. Yoshida, R. Oda, *Bull. Chem. Soc. Jpn.* **1977**, *50*, 285; f) R. S. H. Liu, C. G. Krespan, *J. Org. Chem.* **1969**, *34*, 1271, and references therein.

[20] The E_a for the extrusion of ethyne from bicyclo[2.2.2]octatriene is 41.7 kcal mol^{-1}: H.-D. Martin, T. Urganek, R. Braun, R. Walsh, *Int. J. Chem. Kinet.* **1984**, *16*, 117; see also: M.-C. Lasne, J.-L. Ripoll, *Synthesis* **1985**, 121.

[21] a) G. J. Bodwell, T. Satou, *Angew. Chem.* **2002**, *114*, 4175; *Angew. Chem. Int. Ed.* **2002**, *41*, 4003, and references therein; b) for the closest ethynologous analogues of **8**, see: S. K. Collins, G. P. A. Yap, A. G. Fallis, *Angew. Chem.* **2000**, *112*, 393; *Angew. Chem. Int. Ed.* **2000**, *39*, 385.

[22] **8**: Crystal size $0.32\times0.15\times0.14$ mm^3, space group $P2_12_12_1$ (no. 19), scan range $4.00<2\theta<45°$, $a=9.9102(2)$, $b=15.7845(4)$, $c=23.5844(6)$, $V=3689.3(1)$ Å^3, $Z=8$, $\rho_{calcd}=1.326$ g cm^{-3}, $\mu(Mo_{K\alpha})=0.90$ cm^{-1}, 3720 unique reflections, of which 3133 were taken as observed $[F_o>3.00\sigma(F_o)]$, $R=0.043$, $R_w=0.052$. **10**: Crystal size $0.35\times0.32\times0.03$ mm^3, space group $P2_1/c$ (no. 14), scan range $3.00<2\theta<52.2°$, $a=11.5888(3)$, $b=17.2456(5)$, $c=16.6625(5)$, $\beta=100.140(1)$ Å, $V=3278.1(1)$ Å^3, $Z=4$, $\rho_{calcd}=1.630$ g cm^{-3}, $\mu(Mo_{K\alpha})=20.23$ cm^{-1}, 5982 unique reflections, of which 3772 were taken as observed $[F_o>3.00\sigma(F_o)]$, $R=0.027$, $R_w=0.030$. CCDC-232267 (**8**) and CCDC-232268 (**10**) contain the supplementary crystallographic data for this paper. These data can be obtained free of charge via www.ccdc.cam.ac.uk/conts/retrieving.html (or from the Cambridge Crystallographic Data Centre, 12, Union Road, Cambridge CB21EZ, UK; fax: (+44) 1223-336-033; or deposit@ccdc.cam.ac.uk).

[23] See the structure of diphenylethyne: A. A. Espiritu, J. G. White, *Z. Kristallogr.* **1978**, *147*, 177.

[24] a) There appears to be only one other [6]paracyclophane structure with a higher value (44.6°): Y. Tobe, K. Ueda, T. Kaneda, K. Kakiuchi, Y. Odaira, Y. Kai, N. Kasai, *J. Am. Chem. Soc.* **1987**, *109*, 1136; see also: J. Liebe, C. Wolff, C. Krieger, J. Weiss, W. Tochtermann, *Chem. Ber.* **1985**, *118*, 4144; b) a [1.1]paracyclophane, formally a [6]paracyclophane, is even more distorted (49.8°): T. Tsuji, M. Ohkita, H. Kawai, *Bull. Chem. Soc. Jpn.* **2002**, *75*, 415, and references therein.

[25] a) R. C. Haddon, *J. Am. Chem. Soc.* **1986**, *108*, 2837; b) L. W. Jenneskens, E. N. van Eenige, J. N. Louwen, *New J. Chem.* **1992**, *16*, 775.

[26] a) Y. Tobe, *Top. Curr. Chem.* **1994**, *172*, 1; b) H. Meier in *Advances in Strain in Organic Chemistry*, *Vol. 1* (Ed.: B. Halton), JAI, London, **1991**, p. 216.

[27] M. Eckert-Maksić, W. M. F. Fabian, R. Janoschek, Z. B. Maksić, *J. Mol. Struct.* (*THEOCHEM*) **1995**, *338*, 1.

[28] See, for example: a) C. Perthuisot, B. L. Edelbach, D. L. Zubris, W. D. Jones, *Organometallics* **1997**, *16*, 2016; for a review, see: M. Oh, K. Yu, H. Li, E. J. Watson, G. B. Carpenter, D. A. Sweigart, *Adv. Synth. Catal.* **2003**, *345*, 1053.

[29] M. Kurashina, M. Murata, T. Watanabe, H. Nishihara, *J. Am. Chem. Soc.* **2003**, *125*, 12420, and references therein.

 © 2004 Wiley-VCH Verlag GmbH & Co. KGaA, Weinheim

Combinatorial Chemistry

Catalytic Self-Screening of Cholinesterase Substrates from a Dynamic Combinatorial Thioester Library**

*Rikard Larsson, Zhichao Pei, and Olof Ramström**

Dynamic combinatorial chemistry (DCC) has proven to be a useful tool in the rapid identification of ligands and inhibitors for receptors and enzymes, as well as receptors for certain ligands.[1–6] The technique relies on reversible interconnections between building elements, assembled into discrete entities of interacting species, which constitute libraries of dynamically interchanging species. Different formats of the technique have been developed, including the adaptive approach,[7–11] the pre-equilibrated approach,[12,13] the iterative approach,[14] and the deletion approach,[15] all of which address specific challenges. The concept has also been demonstrated for a range of applications: from model systems to biological applications.

One major advantage with dynamic combinatorial libraries (DCLs) over their static counterparts is their potential susceptibility to change in response to an external selection pressure. Under such conditions the DCLs will reconstitute to adopt the best overall arrangement. For example, in the presence of a selective receptor, certain constituents of a DCL of potential ligands will be bound by the receptor, thereby forcing the remaining building blocks to establish a new equilibrium with more of the bound ligand being generated in the process. Thus, one or more of the DCL constituents may be favored and amplified—increased concentrations generated at the expense of other constituents—from binding to the receptor. This whole process is highly dependent on the binding constants, and high amplification is mainly achieved with strong binding of single constituents. If the binding event can be coupled to a secondary process, the selection can be enhanced by allowing the bound species to be removed from the equilibrating pool; this process generates more of this species by re-equilibration of the DCL. If, for example, the bound species is transformed in a catalytic process and expelled from the binding site, the site is free to host more of the DCL constituent and the dynamic system is thus forced to run to completion. An additional advantage with this approach is that only catalytic amounts of the target species need to be present.

An important challenge with DCC is the need for new means to generate reversible reactions. Until now, mainly imines,[7,10,16] acyl hydrazones,[12,17,18] and disulfides[9,13,19,20] have been used for DCLs since these formats have proven to be the most efficient in the systems studied. This is especially the case when biological systems are targeted, since these require reactions that are stable under mild conditions in the aqueous phase. New methods are needed to advance the technique, and new reaction types are necessary for rapid, yet sufficiently stable DCL generation and screening. In this respect, transthioesterification appears to be highly useful. The reaction type is reversible under mild conditions and relatively compatible with common target protein molecules since side reactions are considerably slower. In addition, thioester DCLs can be rapidly extended by simple means to larger libraries.

In the present study transthioesterification has been used to produce prototype DCLs, and it has further been demonstrated that an enzyme catalyst may be used to assist the dynamic self-screening of its substrates (Figure 1). Thus,

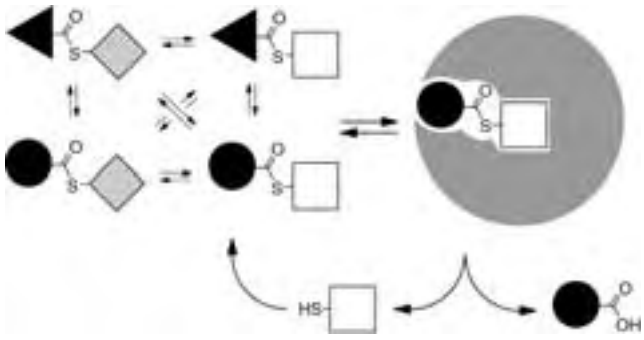


Figure 1. Schematic representation of the DCL catalytic self-screening process with thioesters.

acetylcholinesterase (AChE; see refs. [21,22] and references cited therein) in conjunction with transthioesterification allowed rapid generation and screening of the DCL, a process which results in an apparently complete amplification of the best substrates.

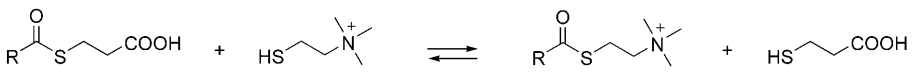
The dynamic combinatorial libraries were generated from a series of thioesters and thiols, respectively (Scheme 1; for further details see the Supporting Information). A homologous series of five different acyl groups was used, ranging from acetyl to hexanoyl and chosen for their resemblance to the native substrate of the enzyme, acetylcholine. The thioesters were all prepared from the same 3-sulfanylpropionic acid in order to keep all components soluble at neutral pH values. Two different thiol groups were also employed, sulfanylpropionic acid and thiocholine. During formation of the dynamic libraries these components may potentially form ten different thioesters, all of which are in exchange with the others during the whole process. If the process was started with equimolar amounts of all acyl components and five equivalents of thiocholine, the resulting concentrations of the formed constituents were relatively comparable and the libraries showed close to isoenergetic behavior, with the sulfanylpropionic acid derivatives formed in slightly higher amounts than their thiocholine counterparts (0.6:0.4).

[*] R. Larsson, Z. Pei, Dr. O. Ramström
Royal Institute of Technology
Department of Chemistry
Teknikringen 36, 10044 Stockholm (Sweden)
Fax: (+46) 8-7912333
E-mail: ramstrom@kth.se

[**] This work was supported by the Swedish Research Council.

Supporting information for this article is available on the WWW under http://www.angewandte.org or from the author.

 © 2004 Wiley-VCH Verlag GmbH & Co. KGaA, Weinheim DOI: 10.1002/anie.200454165



R = Me, Et, *n*Pr, *n*Bu, *n*Pe

Scheme 1. DCL generation by transthioesterification.

The transthioesterification reaction took place effectively under very mild conditions in aqueous media by simple mixing all the components. The ^{1}H NMR spectrum of a mixture of the five original acyl components is displayed in Figure 2a and the spectrum after formation of the full library is shown in Figure 2b. A pD value of 7.0 and room temperature (298 K) were used for all measurements; under these conditions, the libraries were generated with a $t_{1/2}$ value of about 50 minutes. The catalytic action of the enzyme acetylcholinesterase was relatively slow under the same set of conditions. This lower rate was chosen to ensure pseudoequilibrium conditions of the libraries during the enzymatic action, with scrambling being faster than enzyme catalysis.

Treatment of the thioester library with acetylcholinesterase resulted in the best substrate being immediately recognized by the enzyme and hydrolyzed. This resulted in loss of the acyl component from the library, which forced the library to reconstitute to accommodate the increasing amounts of free thiol and to generate more of the hydrolyzed species. Over time, two of the acyl functionalities, the acetyl and propionyl groups, proved to be mainly acted upon by the enzyme, with the acetyl species being more rapidly hydrolyzed than the propionyl counterpart (Figure 2c). The overall rate of formation of acetic acid ($t_{1/2} = 210$ min) proved to be around 20% faster than the rate of formation of propionic acid ($t_{1/2} = 270$ min, Figure 3). Only after substantial hydrolysis of the two main substrates (> 600 min) did the enzyme start hydrolyzing the butyrate ester, and even then, the reaction was considerably less efficient ($t_{1/2} =$ ca. 1100 min). This long lag phase may be caused by inhibitory activities of the present esters.[23] All the other acyl groups remained untouched by the enzyme, a result which is in accordance with the known specificity of acetylcholinesterase. Addition of the enzyme after complete equilibration of the library, as compared to addition of enzyme from the beginning, did not result in any major differences and the same distribution of compounds was recorded, as had been anticipated. In both cases, the combined library interchange and catalytic processes resulted in the complete hydrolysis of

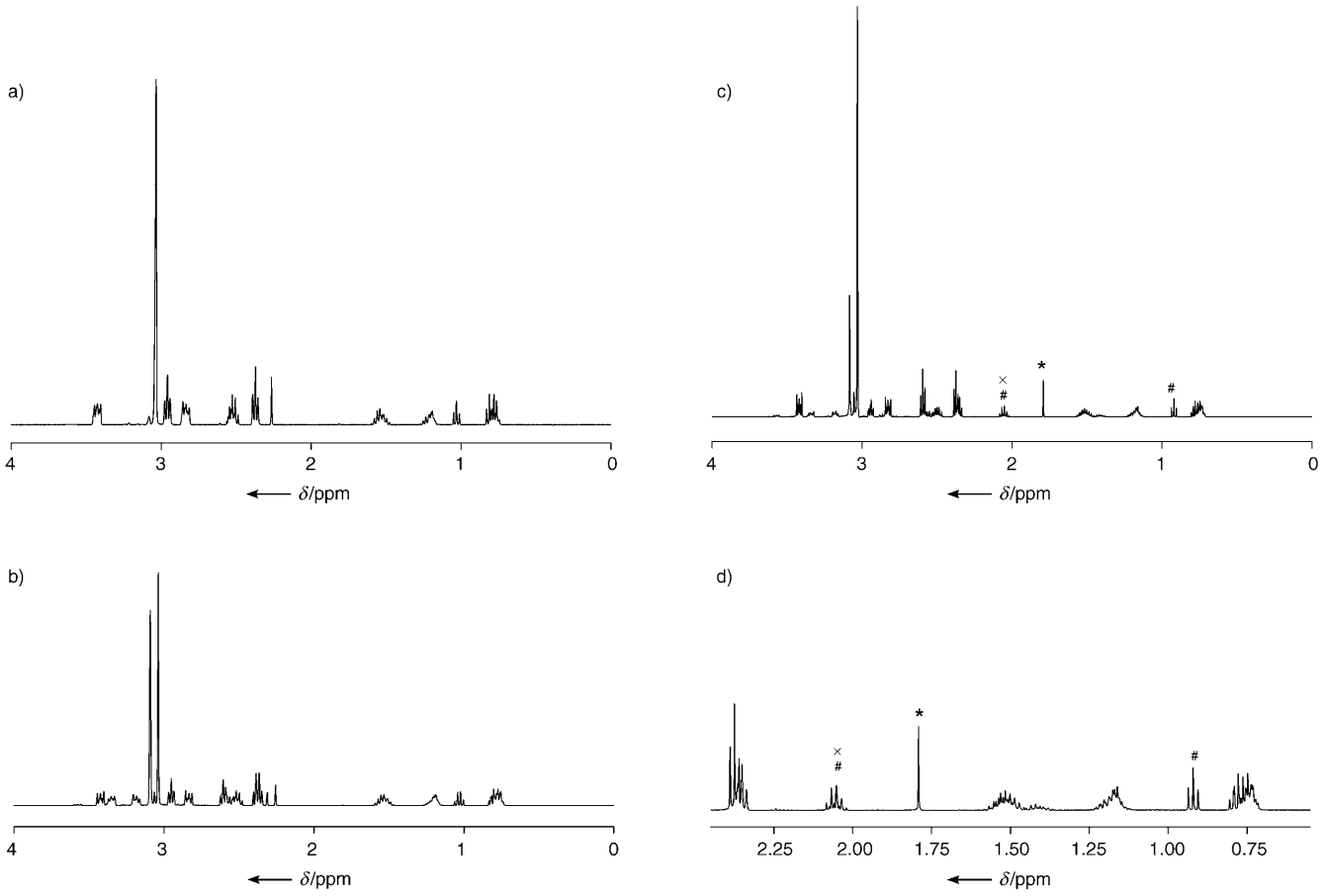


Figure 2. ^{1}H NMR spectra of library components/constituents: a) Before library generation, b) DCL in the absence of AChE, c) DCL in the presence of AChE, d) enlarged section of (c). ⋆, #, and × indicate the signals for acetate, propionate, and butyrate groups, respectively.

 © 2004 Wiley-VCH Verlag GmbH & Co. KGaA, Weinheim

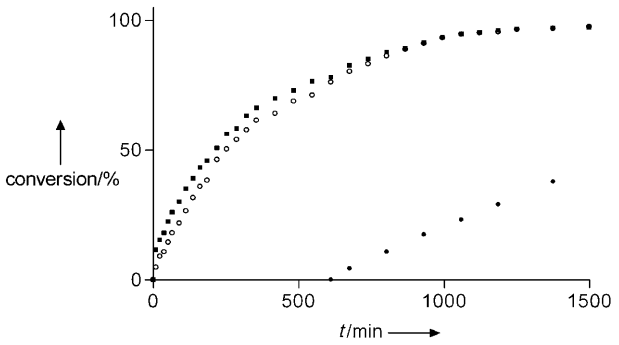


Figure 3. Formation of acetate (■), propionate (○), and butyrate (●) hydrolysis products.

certain acyl thioesters to form the corresponding acids and thiols. Thus, this catalysis assistance could be used to fully amplify the selected acyl groups. It was rapidly shown for the thiol components that removal of thiocholine failed to generate any hydrolytic products under the same conditions, thus demonstrating that thiocholine was essential for the reaction to occur. The screening of the DCL thus proved straightforward, and the selection effect of the combined process can be estimated as the ratio of the amount of hydrolytic products formed versus the amount of substrate fragment added. In the present case, 100% selection/amplification was achieved for the acetate and propionate groups, respectively.

The present study has demonstrated that catalysis can be used as a means to self-screen substrates from a dynamic combinatorial library. Acetylcholinesterase could thus be targeted to allow rapid identification of the most efficient substrate in the library. This system is however not restrained to enzyme catalysis; it may be extended to any catalytic system, including organic and inorganic catalysts, and may be employed to rapidly screen reactions of catalysts for new substrates. In particular, catalysts of unknown specificity may be easily mapped with such systems, for example, in proteomics and catalyst-development campaigns. This approach also enables screening of complex DCLs without the necessity of using equimolar amounts of targets. In addition, it has been shown that transthioesterification can be readily employed to generate DCLs that are compatible with mild conditions in aqueous media.

Received: March 2, 2004 [Z54165]

Keywords: combinatorial chemistry · enzyme catalysis · hydrolysis · proteomics · transesterification

[1] O. Ramström, J.-M. Lehn, *Nat. Rev. Drug Discovery* **2002**, *1*, 26–36.
[2] I. Huc, R. Nguyen, *Comb. Chem. High Throughput Screening* **2001**, *4*, 53–74.
[3] G. R. L. Cousins, S. A. Poulsen, J. K. M. Sanders, *Curr. Opin. Chem. Biol.* **2000**, *4*, 270–279.
[4] J.-M. Lehn, *Chem. Eur. J.* **1999**, *5*, 2455–2463.
[5] B. Klekota, B. L. Miller, *Trends Biotechnol.* **1999**, *17*, 205–209.
[6] A. Ganesan, *Angew. Chem.* **1998**, *110*, 2989–2992; *Angew. Chem. Int. Ed.* **1998**, *37*, 2828–2831.
[7] M. Hochgürtel, H. Kroth, D. Piecha, M. W. Hofmann, C. Nicolau, S. Krause, O. Schaaf, G. Sonnenmoser, A. V. Eliseev, *Proc. Natl. Acad. Sci. USA* **2002**, *99*, 3382–3387.
[8] S. Otto, R. L. Furlan, J. K. M. Sanders, *Science* **2002**, *297*, 590–593.
[9] S. Otto, R. L. E. Furlan, J. K. M. Sanders, *J. Am. Chem. Soc.* **2000**, *122*, 12063–12064.
[10] I. Huc, J.-M. Lehn, *Proc. Natl. Acad. Sci. USA* **1997**, *94*, 2106–2110.
[11] B. Hasenknopf, J.-M. Lehn, B. O. Kneisel, G. Baum, D. Fenske, *Angew. Chem.* **1996**, *108*, 1987–1990; *Angew. Chem. Int. Ed. Engl.* **1996**, *35*, 1838–1840.
[12] T. Bunyapaiboonsri, O. Ramström, S. Lohmann, J.-M. Lehn, L. Peng, M. Goeldner, *ChemBioChem* **2001**, *2*, 438–444.
[13] O. Ramström, J.-M. Lehn, *ChemBioChem* **2000**, *1*, 41–47.
[14] A. Eliseev, M. Nelen, *J. Am. Chem. Soc.* **1997**, *119*, 1147–1148.
[15] J. D. Cheeseman, A. D. Corbett, R. Shu, J. Croteau, J. L. Gleason, R. J. Kazlauskas, *J. Am. Chem. Soc.* **2002**, *124*, 5692–5701.
[16] M. Hochgurtel, R. Biesinger, H. Kroth, D. Piecha, M. W. Hofmann, S. Krause, O. Schaaf, C. Nicolau, A. V. Eliseev, *J. Med. Chem.* **2003**, *46*, 356–358.
[17] O. Ramström, S. Lohmann, T. Bunyapaiboonsri, J.-M. Lehn, *Chem. Eur. J.* **2004**, *10*, 1711–1715.
[18] T. Bunyapaiboonsri, H. Ramström, O. Ramström, J. Haiech, J.-M. Lehn, *J. Med. Chem.* **2003**, *46*, 5803–5811.
[19] D. A. Erlanson, J. W. Lam, C. Wiesmann, T. N. Luong, R. L. Simmons, W. L. DeLano, I. C. Choong, M. T. Burdett, W. M. Flanagan, D. Lee, E. M. Gordon, T. O'Brien, *Nat. Biotechnol.* **2003**, *21*, 308–314.
[20] H. Hioki, W. C. Still, *J. Org. Chem.* **1998**, *63*, 904–905.
[21] P. Taylor, Z. Radic, *Annu. Rev. Pharmacol. Toxicol.* **1994**, *34*, 281–320.
[22] D. M. Quinn, *Chem. Rev.* **1987**, *87*, 955–979.
[23] S. J. Cho, M. L. Garsia, J. Bier, A. Tropsha, *J. Med. Chem.* **1996**, *39*, 5064–5071.

 © 2004 Wiley-VCH Verlag GmbH & Co. KGaA, Weinheim

Supercritical Fluids

^{13}C NMR Spectroscopic Evaluation of the Affinity of Carbonyl Compounds for Carbon Dioxide under Supercritical Conditions**

Takehiko Tsukahara, Yoshihito Kayaki, Takao Ikariya, and Yasuhisa Ikeda**

Supercritical carbon dioxide ($scCO_2$) has received much attention as a green alternative to organic solvents for chemical reactions, separations, and extractions because of its pressure-tunable physicochemical properties and economic advantages.[1] A variety of these applications can be realized by controlling the formation of molecular clusters produced by solvation around a solute molecule in $scCO_2$, as well as the mobility of the solute's solvation sphere.[2] The relationships between the solubility and intermolecular interactions of solute molecules in $scCO_2$ have been extensively investigated from the viewpoint of identifying CO_2-philic molecules with a strong affinity for $scCO_2$.[3] It was demonstrated that the solubility of fluorocarbons in $scCO_2$ is exceptionally enhanced by specific interactions of CO_2 with fluorine and/or highly repulsive fluorine–fluorine interactions.[4] Additionally, carbonyl compounds have recently become of interest as inexpensive and easily available CO_2-philes compared to fluorocarbons.[5] For example, spectroscopic and theoretical studies on the interaction of aldehydes, ketones, or acetates in the CO_2 medium suggested that the Lewis acid–Lewis base (LA–LB) interactions between the CO_2 carbon atom and the carbonyl oxygen atoms of these carbonyl compounds play a significant role in the enhancement of CO_2-philicity.[6] In addition to the LA–LB interactions (C=O···C), a relatively weak C–H···O hydrogen-bonding interaction between hydrogen atoms attached to the carbonyl carbon atoms or to the α-carbon atoms and the CO_2 oxygen atoms may also act cooperatively. Most physicochemical studies concerning solute–solvent interactions in $scCO_2$ have focused on the behavior of solute molecules,[3–7] and limited information is available on how the local interactions of CO_2 with solute molecules dissolved in $scCO_2$ affect the bulk properties of the CO_2 solvent. Herein, we discuss the density dependence of the ^{13}C NMR chemical shift (δ_C) of neat CO_2 and CO_2 containing carbonyl compounds under supercritical conditions, and demonstrate the usefulness of the δ_C values of the CO_2 solvent as a reliable criterion for predicting the affinity of solute molecules for $scCO_2$.

The chemical shift δ_C is generally related to the nuclear shielding (σ) arising from intermolecular interactions, and is expressed as a function of the density of the medium ρ (g cm^{-3}): $-\delta_C \cong \rho\sigma$.[4b,c] We first determined the δ_C values of neat $scCO_2$ in the pressure range 7 to 25 MPa at 40 °C ($0.2 < \rho < 0.9$) using high-pressure NMR spectroscopy as a powerful tool for studying solute–solvent interactions.[8] Figure 1 shows

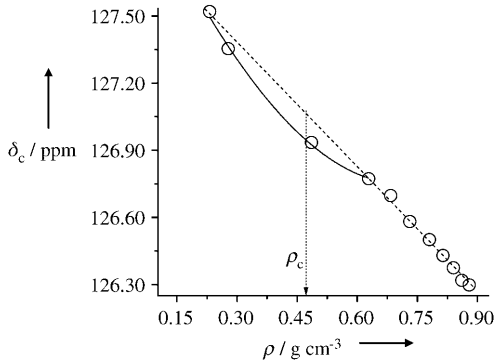


Figure 1. Plot of the δ_C value of neat $scCO_2$ (○) versus the density of CO_2 ($0.2 < \rho < 0.9$). The broken and solid lines are the slope expected from the bulk susceptibility of CO_2 (-1.98×10^{-6}) and experimental data, respectively.

a plot of the δ_C values of neat $scCO_2$ against the density of CO_2. In the higher-density regions ($0.6 < \rho < 0.9$) corresponding to the pressure range 10 to 25 MPa, the δ_C value moves linearly to a higher field with increasing density of CO_2. The slope in Figure 1 is -1.93×10^{-6} cm^3 g^{-1}, which agrees with the value (-1.98×10^{-6} cm^3 g^{-1}) expected from a change of only the bulk susceptibility of CO_2. However, the deviation from the linear slope toward the higher field (solid line in Figure 1) was observed in lower-density regions ($0.2 < \rho \leq 0.6$). The appreciable deviation is possibly attributable to the local density enhancement of CO_2, as a result of specific CO_2–CO_2 interactions in the vicinity of the critical density ($\rho_c = 0.469$ g cm^{-3}), as previously published.[9]

To determine relative CO_2-philicities on the basis of the specific solute–CO_2 interactions, a series of ^{13}C NMR spectra of $scCO_2$ in the presence of β-diketones including acetylacetone (Hacac), 1,1,1-trifluoroacetylacetone (Htfacac), and 1,1,1,5,5,5-hexafluoroacetylacetone (Hhfacac) was measured in the higher-density region above 0.6 g cm^{-1}. These β-diketones are well-known CO_2-philes for extracting metal ions in $scCO_2$ from industrial radioactive wastes.[2b,10] Figure 2 shows the δ_C values for neat $scCO_2$ and $scCO_2$ containing β-diketones at a concentration of 2.13×10^{-2} M as functions of CO_2 density. The slopes of the linear plots for $scCO_2$ containing Hacac, Htfacac, and Hhfacac were -1.97×10^{-6}, -1.87×10^{-6}, and -1.92×10^{-6} cm^3 g^{-1}, respectively, which

[*] Dr. Y. Kayaki, Prof. T. Ikariya
Graduate School of Science and Engineering and
Frontier Collaborative Research Center
Tokyo Institute of Technology and PRESTO
Japan Science and Technology Agency
2-12-1 O-Okayama, Meguro-ku, Tokyo 152-8552 (Japan)
Fax: (+81) 3-5734-2637
E-mail: tikariya@apc.titech.ac.jp
Dr. T. Tsukahara, Prof. Y. Ikeda
Research Laboratory for Nuclear Reactors
Tokyo Institute of Technology
2-12-1 O-Okayama, Meguro-ku, Tokyo 152-8550 (Japan)
Fax: (+81) 3-5734-3061
E-mail: yikeda@nr.titech.ac.jp

[**] This work was financially supported by a Grant-in-Aid from the Ministry of Education, Science, Sports, and Culture of Japan (No. 14078209, Reaction Control of Dynamic Complexes). This work was partly supported by the 21st Century COE program.

 DOI: 10.1002/anie.200454190 © 2004 Wiley-VCH Verlag GmbH & Co. KGaA, Weinheim

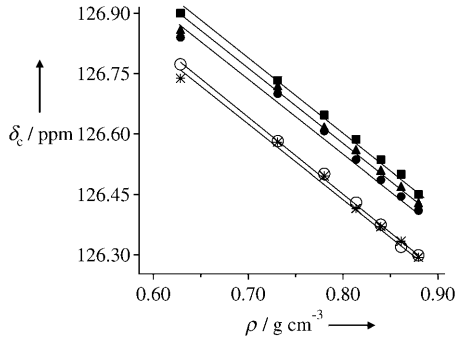
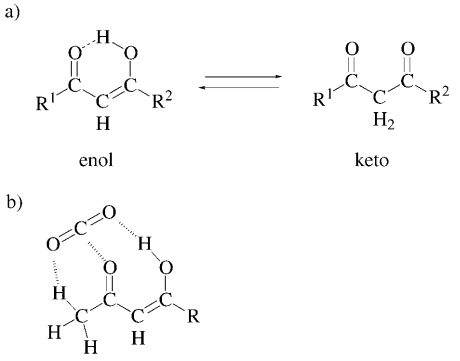


Figure 2. Plots of the δ_c value of neat $scCO_2$ (○) and $scCO_2$ containing Hacac (●), Htfacac (■), Hhfacac (▲), and the $[UO_2(tfacac)_2]$·DMSO complex (*) versus the density of CO_2. The sample concentrations were 2.13×10^{-2} M .

indicates that the δ_C values of these $scCO_2$ systems are also dominated mainly by the bulk susceptibility of CO_2.

It is worth noting that the δ_C values of $scCO_2$ containing β-diketones move to lower fields in parallel with the δ_C values of neat $scCO_2$. The magnitude of the parallel shifts ($\Delta\delta_C$) of $scCO_2$ containing these β-diketones decreased in the order Htfacac > Hhfacac > Hacac. The ^{1}H NMR spectra of the β-diketones in $scCO_2$ showed that the enol–keto equilibrium (Scheme 1a) shifts in favor of enol formation. However, the



Scheme 1. a) Tautomeric equilibrium between the enol and keto forms of β-diketones (Hacac: $R^1=CH_3$, $R^2=CH_3$; Htfacac: $R^1=CH_3$, $R^2=CF_3$; Hfacac: $R^1=CF_3$, $R^2=CF_3$). b) Schematic structures showing LA–LB interactions and hydrogen bonding between CO_2 and β-diketones.

fraction of the enol isomer of Hacac in $scCO_2$ is about 30%, which is less than that of Htfacac and Hhfacac in $scCO_2$ (25 MPa, 40 °C).[11,12] Consequently, favorable enol formation should cause an increase in the O–H···O hydrogen-bonding interaction between enolic protons on the β-diketones and the oxygen atoms of CO_2.

The generation of enhanced electron deficiency at the central carbon atoms of CO_2, possibly as a consequence of O–H···O hydrogen bonding, could result in parallel shifts of the δ_C values for $scCO_2$ to a lower-field direction. In addition, the parallel shift might partly arise from the LA–LB interactions between electronically positive carbon atoms of the CO_2 molecules and negative carbonyl oxygen atoms of the β-diketones as well as C–H···O hydrogen bonding between terminal CH_3 protons of the β-diketones and the CO_2 oxygen atoms, as previously proposed by Wallen and co-workers(see Scheme 1b).[6] The decrease in $\Delta\delta_C$ values induced by Hhfacac is attributable to the lack of protons participating in the C–H···O interactions. As shown in Figure 3, the $\Delta\delta_C$ value of

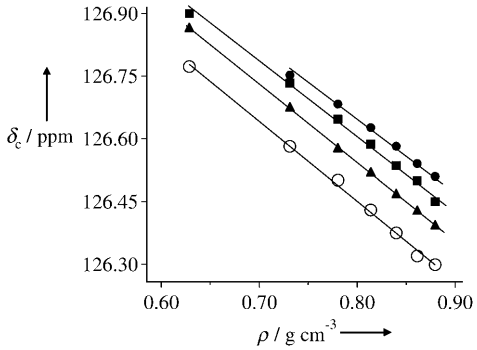
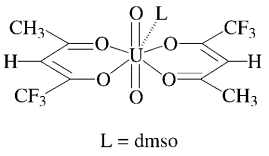


Figure 3. Plots of the δ_C values of neat $scCO_2$ (○) and $scCO_2$ containing Htfacac versus the density of CO_2, and the dependence of the δ_c values on the concentration of Hfacac. The sample concentrations were 2.00×10^{-3} M (▲), 2.13×10^{-2} M (■), and 1.20×10^{-1} M (●).

$scCO_2$ containing Htfacac in the lower-field direction was markedly increased with increasing concentration of Htfacac.[13] Thus, an enhancement of the CO_2–solute interactions through the LA–LB and/or hydrogen-bonding interactions reflects an appreciable gain of the parallel shifts of the δ_C values of CO_2.

The validity of the parallel shifts of the δ_C values based on the CO_2–solute interactions can be demonstrated by a separate experiment using the $[UO_2(tfacac)_2]$·DMSO complex[14] (tfacac = 1,1,1-trifluoroacetylacetonato, DMSO = dimethyl sulfoxide) in $scCO_2$ (Scheme 2). Figure 2 shows



Scheme 2. Schematic structure of the $[UO_2(tfacac)_2]$·DMSO complex.

that the $[UO_2(tfacac)_2]$·DMSO complex does not provide any significant parallel shifts from the result obtained with neat CO_2, because the absence of free carbonyl and OH groups in the coordinating tfacac moiety prevents it from strongly affecting the CO_2 solvent properties.

The $\Delta\delta_C$ values of CO_2 containing organic compounds can be used for assessment of the relative CO_2-philicities of solute molecules in $scCO_2$. Table 1 shows the $\Delta\delta_C$ values of $scCO_2$ containing CH_3OH, $(CH_3)_2CO$, $HCON(CH_3)_2$, CH_3CHO, and $(CH_3)_2SO$ (2.25×10^{-2} M), estimated from the density dependence of the δ_C values in a similar manner as $scCO_2$ containing β-diketones. The $\Delta\delta_C$ values for CO_2 doped with these compounds are apparently smaller than those of β-diketones

 © 2004 Wiley-VCH Verlag GmbH & Co. KGaA, Weinheim

Table 1: Slopes of the linear plots (σ) and the parallel shift ($\Delta\delta_C$) values of neat $scCO_2$ and $scCO_2$ containing organic solute molecules.[a]

Solute	σ ($cm^3\,g^{-1}$)	δ' (at 0.6 $g\,cm^{-3}$)	$\Delta\delta_C$
neat $scCO_2$	-1.93×10^{-6}	126.828	–
Htfacac[b]	-1.87×10^{-6}	126.988	0.160
CH_3OH	-1.89×10^{-6}	126.926	0.098
$(CH_3)_2CO$	-1.92×10^{-6}	126.918	0.090
$HCON(CH_3)_2$	-1.87×10^{-6}	126.898	0.070
CH_3CHO	-1.91×10^{-6}	126.884	0.056
$(CH_3)_2SO$	-1.84×10^{-6}	126.906	0.078

[a] The δ' values are the chemical shifts of CO_2 at 0.6 $g\,cm^{-3}$ calculated from experimental data using the least-squares method, and the $\Delta\delta_C$ values are the differences of the δ' values between the neat $scCO_2$ and $scCO_2$ containing organic solutes. [b] For comparison, the $\Delta\delta_C$ value of $scCO_2$ containing Htfacac (*, Figure 2) is also shown.

and decrease in the order $CH_3OH > (CH_3)_2CO > (CH_3)_2SO > HCON(CH_3)_2 > CH_3CHO$. Thus, the CO_2 solvent properties might be strongly perturbed by alcoholic protons through the O–H···O hydrogen-bonding interaction, rather than by carbonyl oxygen atoms and neighboring hydrogen atoms through the LA–LB interaction (C=O···C) and the cooperative C–H···O hydrogen-bonding interaction. The latter effect should give rise to increasing $\Delta\delta_C$ values in $(CH_3)_2CO$ and $HCON(CH_3)_2$ compared with that in CH_3CHO, because of an increase in the number of C–H···O hydrogen bonding sites. The difference in the $\Delta\delta_C$ values between $(CH_3)_2CO$ and $HCON(CH_3)_2$ could be interpreted as resulting from the symmetrical structure of acetone, which leads to less steric hindrance and allows the CH_3 protons to move closer to the CO_2 oxygen atoms. Moreover, the sulfinyl moiety is also available as a CO_2-philic functional group, possibly as a result of an LA–LB interaction (S=O···C) of the sulfinyl groups[6a] as well as the C–H···O hydrogen-bonding interaction.

In summary, we have demonstrated the density dependence of δ_C values of neat $scCO_2$ and $scCO_2$ containing solute molecules, which clearly provide a useful and reliable criterion for evaluating the CO_2-philicity of solutes in $scCO_2$. A marked correlation between the parallel shifts, $\Delta\delta_C$, of $scCO_2$ and the structures of the solute molecules is attributed to LA–LB interactions and/or hydrogen-bonding interactions between the solute and CO_2 molecules. Such reproducible parallel shifts are based on the fact that the local CO_2–solute interactions influence a large number of CO_2 molecules under supercritical conditions. The use of ^{13}C NMR spectroscopy to obtain novel information about $scCO_2$ could be a viable approach to designing CO_2-philic materials and could lead to the development of polymers, cosolvents, catalysts, surfactants, and chelating agents.

Experimental Section

^{13}C NMR spectra were measured using a JEOL JNM-LA300 spectrometer at 75.5 MHz and 40 °C in the pressure range 7 or 10 to 25 MPa without spinning. A zirconia cell (inner diameter 5.4 mm, outer diameter 9.0 mm, length 152.0 mm) was used as a high-pressure NMR cell, which enabled measurements at up to approximately 50 MPa. A glass capillary containing C_6D_6 as an internal lock was inserted into the high-pressure cell. This tube was effective for easily adjusting the shim coil and for minimizing the sample's convection. The reproducibility of all chemical shifts was better than ±0.005 ppm, and the susceptibility of the C_6D_6 in the capillary was constant. The δ_C values were referenced to the carbon atoms at 128.0 ppm in the C_6D_6. The effective sample volume was 0.8 cm^3. The zirconia cell was mounted in a stainless-steel sample holder and sealed with a stainless-steel valve and an O-ring. Pressure was exerted on the NMR cell with an ISCO syringe pump by charging it with CO_2 gas, and monitored by a back-pressure regulator (JASCO, 880-81). Impurities and air in the stainless-steel tube, which was connected to the high-pressure NMR cell, were removed by evacuating the cell several times. The temperature of the samples was controlled by supplying heated air with a temperature control unit in the NMR spectrometer. The high-pressure NMR apparatus used in the present study was described in more detail previously.[15]

Received: March 5, 2004 [Z54190]

Keywords: carbon dioxide · carbonyl compounds · NMR spectroscopy · solvolysis · supercritical fluids

[1] P. G. Jessop, T. Ikariya, R. Noyori, *Chem. Rev.* **1999**, *99*, 475–493.
[2] a) O. Kajimoto, *Chem. Rev.* **1999**, *99*, 355–389; b) J. A. Darr, M. Poliakoff, *Chem. Rev.* **1999**, *99*, 495–541.
[3] a) J. C. Meredith, K. P. Johnston, J. M. Seminario, S. G. Kazarian, C. A. Eckert, *J. Phys. Chem.* **1996**, *100*, 10837–10848; b) F. Rindfleisch, T. P. DiNoia, M. A. McHugh, *J. Phys. Chem.* **1996**, *100*, 15581–15587; c) A. Cece, S. H. Jureller, J. L. Kerschner, K. F. Moschner, *J. Phys. Chem.* **1996**, *100*, 7435–7439; d) P. Diep, K. D. Johnson, E. J. Beckman, *J. Phys. Chem. A* **1998**, *102*, 2231–2236; e) J. F. Kauffman, *J. Phys. Chem. A* **2001**, *105*, 3433–3442.
[4] a) G. G. Yee, J. L. Fulton, R. D. Smith, *J. Phys. Chem.* **1992**, *96*, 6172–6181; b) A. Dardin, J. M. DeSimone, E. T. Samulski, *J. Phys. Chem. B* **1998**, *102*, 1775–1780; c) C. R. Yonker, B. J. Palmer, *J. Phys. Chem. A* **2001**, *105*, 308–314.
[5] a) S. G. Kazarian, M. F. Vincent, F. V. Bight, C. L. Liotta, C. A. Eckert, *J. Am. Chem. Soc.* **1996**, *118*, 1729–1736; b) T. Sarbu, T. Styranec, E. J. Beckman, *Nature* **2000**, *405*, 165–168; c) X. Zhang, B. Han, Z. Hou, J. Zhang, Z. Liu, T. Jiang, J. He, H. Li, *Chem. Eur. J.* **2002**, *8*, 5107–5111; d) P. Raveendran, S. L. Wallen, *J. Am. Chem. Soc.* **2002**, *124*, 7274–7275; e) O. Ihata, Y. Kayaki, T. Ikariya, *Angew. Chem.* **2004**, *116*, 735–737; *Angew. Chem. Int. Ed.* **2004**, *43*, 717–719.
[6] a) P. Raveendran, S. L. Wallen, *J. Am. Chem. Soc.* **2002**, *124*, 12590–12599; b) M. A. Blatchford, P. Raveendran, S. L. Wallen, *J. Am. Chem. Soc.* **2002**, *124*, 14818–14819; c) P. Raveendran, S. L. Wallen, *J. Phys. Chem. B* **2003**, *107*, 1473–1477; d) M. A. Blatchford, P. Raveendran, S. L. Wallen, *J. Phys. Chem. A* **2003**, *107*, 10311–10323; e) M. R. Nelson, R. F. Borkman *J. Phys. Chem. A* **1998**, *102*, 7860–7863.
[7] a) M. Kanakubo, T. Aizawa, T. Kawakami, O. Sato, Y. Ikushima, K. Hatakeda, N Saito, *J. Phys. Chem. B* **2000**, *104*, 2749–2758; b) T. Umecky, M. Kanakubo, Y. Ikushima, *J. Phys. Chem. B* **2002**, *106*, 11114–11119.
[8] a) S. Gaemers, C. J. Elsevier, *Chem. Soc. Rev.* **1999**, *28*, 135–141; b) S. L. Wallen, L. K. Schoenbachler, E. D. Dawson, M. A. Blatchford, *Anal. Chem.* **2000**, *72*, 4230–4234; c) J. W. Rathke, R. J. Klingler, R. E. Gerald II, K. W. Kramarz, K. Woelk, *Prog. Nucl. Magn. Reson. Spectrosc.* **1997**, *30*, 209–253.
[9] a) R. Ishii, S. Okazaki, I. Okada, M. Furusaka, N. Watanabe, M. Misawa, T. Fukunage, *J. Chem. Phys.* **1996**, *105*, 7011–7021; b) J. E. Adams, A. S. Haghighi, *J. Phys. Chem. B* **2002**, *106*, 7973–7980.
[10] a) Y. Lin, R. D. Brauer, K. E. Laintz, C. M. Wai, *Anal. Chem.* **1993**, *65*, 2549–2551; b) M. J. Carrott, C. M. Wai, *Anal. Chem.*

 © 2004 Wiley-VCH Verlag GmbH & Co. KGaA, Weinheim

1998, *70*, 2421 – 2425; c) C. M. Wai, S. Wang, *J. Chromatogr. A* **1997**, *785*, 369 – 383.

[11] The ^{1}H NMR data for Hacac, Htfacac, and Hhfacac in $scCO_2$ (25 MPa, 40 °C) are as follows. The peak area ratio for $-CH_3$ (enol) and $-CH_3$ (keto) of Hacac was 6:1, whereas the enol forms of Htfacac and Hhfacac were observed solely under the present experimental conditions. Hacac: $\delta = 15.94$ (−OH/enol), 5.72 (−CH/enol), 3.73 ($-CH_2$/keto), 2.41 ($-CH_3$/keto), 2.27 ppm ($-CH_3$/enol). Htfacac: $\delta = 14.68$ (−OH), 6.22 (−CH), 2.44 ppm ($-CH_3$). Hhfacac: $\delta = 12.85$(−OH), 6.66 ppm (−CH).

[12] S. L. Wallen, C. R. Yonker, C. L. Phelps, C. M. Wai, *J. Chem. Soc. Faraday Trans.* **1997**, 2391 – 2394.

[13] In Figure 3, the δ_C values of $scCO_2$ containing 1.20×10^{-1} M Htfacac at around 0.60 g cm^{-3} were not plotted because of insufficient solubility of Htfacac in $scCO_2$.

[14] This complex was synthesized according to the procedure described previously: K. Mizuguchi, S.-H. Lee, Y. Ikeda, H. Tomiyasu, *J. Alloys Compd.* **1998**, *271–273*, 163 – 167.

[15] Y. Kayaki, T. Suzuki, Y. Noguchi, S. Sakurai, M. Imanari, T. Ikariya, *Chem. Lett.* **2002**, 424 – 425.

 © 2004 Wiley-VCH Verlag GmbH & Co. KGaA, Weinheim

Zeolites

Adsorption Chemistry of Sulfur Dioxide in Hydrated Na–Y Zeolite**

*Christine E. A. Kirschhock, Asima Sultana, Eric Godard, and Johan A. Martens**

Na–Y is one of the oldest known synthetic zeolite materials. Like zeolite X, it has the faujasite framework topology. The framework structure of zeolites Na–X and Na–Y extensively was studied by diffraction methods[1a,b] and the positions of exchangeable cations in dehydrated faujasites are well documented.[1c] Positions and occupation numbers of sodium cations in Na–Y dehydrated by evacuation[2a,b] and drying in gas streams[2c] were derived by solid-state NMR spectroscopy. Neutron- and X-ray-diffraction techniques revealed the presence of guest molecules interacting with the sodium ions, which results in a reorganization of the cation distribution.[1a,3a,3b] The presence of water molecules in the structure has a strong impact on position and occupation numbers of sodium atoms.[5,4a,b,c] Exposure of Na–Y zeolite to a gas mixture containing 5–10% water at 250°C results in a water content of 50–60 water molecules per unit cell.[5] These water molecules interact with the sodium ions of the host to form a complex water–cation structure. The water–sodium arrangement consists of chains of alternating SV and SIII cations, bridged by water molecules. Additional water molecules associated with cations on SII positions stabilize this structure. When nitrogen oxides are present, these can reversibly be inserted into the water–cation net as N_2O_3 (Figure 1), which characterizes Na–Y as an exceptional NO_x storage compound.[5] On Na–Y the NO_x is physisorbed as N_2O_3 that can be conveniently released in a pressure-swing process by using hydrated, inert gas.[5,6] Adsorbents and catalysts for environmental applications have to withstand sulfur oxides. SO_2 is the main sulfur compound in exhaust gas. Even with the stringent regulations on the maximum tolerated sulfur content of diesel and gasoline fuels, the minute concentrations of SO_2 in the exhaust gas still pose problems of poisoning the catalyst within the required lifetimes.[7] When operated in a pressure-swing process for NO_x removal from engine exhaust, Na–Y zeolite is exceptionally resistant to SO_2.[5,6b] The reason for this behavior was not known. Literature on SO_2 adsorption in zeolites is mostly related to the adsorption of pure SO_2.[8] Studies that dealt with SO_2 adsorption in the presence of other relevant gases such as water, carbon dioxide, and NO_x[9] did not provide decisive conclusions as to the position of adsorbed SO_2 molecules in a Na–Y zeolite that had been exposed to exhaust gas. The data suggested a strong dependence on hydration level.

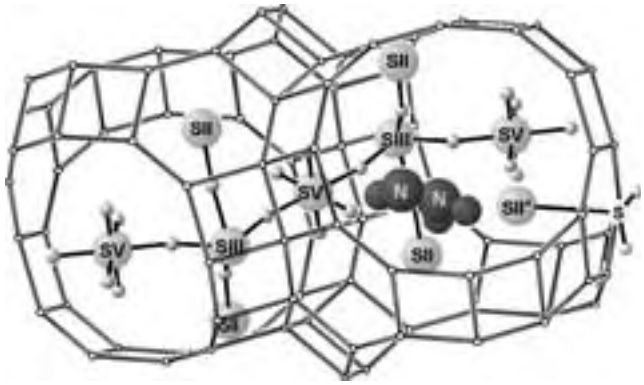


Figure 1. Illustration of the refined structure of SO_2 in Na–Y zeolite in the presence of water and NO_x. For clarity, oxygen atoms of the zeolite framework have been omitted. Sodium cations are labeled SII, SII*, SIII, and SV according to their position. The small spheres are oxygen atoms of water molecules that bridge sodium cations or are from the refined H_2SO_3 molecule. The darkly shaded N_2O_3 molecule has not been refined but has been inserted based on a previous refinement.[5] The figure shows that the presence of H_2SO_3 in the structure does not sterically encumber NO_x adsorption when NO_x is N_2O_3.

We brought an Na–Y zeolite (silicon/aluminum ratio of 2.6) into contact with a gas mixture at 250°C, quenched it to room temperature, and transferred a small amount into a sealed capillary for transmission XRD studies. Contact of the sample with the atmosphere was carefully avoided. When the zeolite was brought into contact with SO_2 in the absence of water, no strict localization of sulfur dioxide was observed.

[*] Dr. C. E. A. Kirschhock, Dr. A. Sultana, Dr. E. Godard, Prof. J. A. Martens
Center for Surface Chemistry and Catalysis
Catholic University of Leuven
Kasteelpark Arenberg 23, 3001 Leuven (Belgium)
Fax: (+32) 16-32-1998
E-mail: johan.martens@agr.kuleuven.ac.be

[**] The work was supported by the European Union through the fifth framework project AHEDAT. J.A.M. acknowledges the Flemish government for a GOA grant on the understanding of the active site in catalysis. C.E.A.K. acknowledges the Flemish FWO for a postdoctoral fellowship.

 © 2004 Wiley-VCH Verlag GmbH & Co. KGaA, Weinheim DOI: 10.1002/anie.200454266

Rietveld refinement of the XRD of this sample resulted in a satisfactory profile fit; only the host framework and the sodium cations were considered. However, an elevated residual electron density in the supercages in front of the six-ring windows was detected. This was in agreement with previous studies of the position of SO_2 in dehydrated faujasite zeolites, in which the preferred occupation of SII* sites by sulfur dioxide was reported.[4c] In the work presented herein, we encountered a different situation when water was present; the refined structure of Na–Y saturated with SO_2 revealed that the sulfur was now located in the six rings of the sodalite cages flanking supercages (Figure 2).[10] A close inspection of

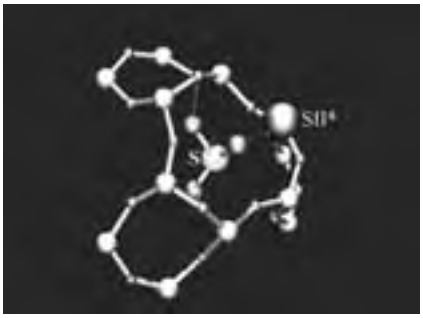


Figure 2. Refined position of the sulfite group in the six ring of hydrated Na–Y. One sulfite O atom is in interaction distance with a sodium ion on the SII* position. The distance from the other two sulfite O atoms to framework oxygen atoms suggest hydrogen bonding.

the observed and refined electron density in the vicinity of this position revealed two symmetrically independent electron-density maxima within bonding distance to the sulfur atom (Figure 3). One of the two maxima is tripled by the threefold symmetry of the cubic space group of the host. Examination of bond length and angles and the refined occupation numbers led to the identification of this entity as



Figure 3. Observed electron density map (mapsize: 10 Å) before last-cycle refinement. Shown is a side-view of the six rings that containing the sulfite group (marked in grey). Water molecules are labeled W, cation sites are labeled SII and SIII* according to their position. Electron density between framework oxygen O4 and oxygen atoms of the sulfite group suggest hydrogen bonding.

sulfite. One oxygen atom of the sulfite molecule points straight into the supercage, and interacts with a sodium cation on SII*. Of the three symmetrically equivalent positions, only two are occupied and point to O4 atoms of the faujasite six ring. The distance between O4 and the oxygen atoms of the sulfurous acid of 1.93 ± 0.04 Å, and observed electron density between the oxygen atoms indicate hydrogen bonding of both hydroxy groups. In this arrangement the sulfurous acid molecules are not dissociated. Free sulfurous acid is known as an unstable molecule. Its presence in the zeolite can only be explained by its strong interaction with, and stabilization by, the host. The coincidence of observed and theoretical bond lengths and angles of free H_2SO_3 is surprisingly good.[11] The distance from the sulfur atom to the doubly bonded oxygen atom O31, which points into the supercage was determined to be 1.493 Å compared to the theoretical value of 1.496 Å. The distance between hydroxy oxygen atoms (O32 and O33) and sulfur was observed to be 1.93 ± 0.02 Å compared to theoretical values of 1.690 and 1.695 Å. The bond angles between O33-S-O31 and O32-S-O31 of $103 \pm 3°$ are close to the theoretical value of 107°. The angle between the hydroxyl groups, however, was observed to be larger than calculated, namely, 116° compared to 107°. This discrepancy may be caused by the hydrogen bonding to framework oxygen atom O4, which results in increased negative charge on O32 and O33 and the presence of a repulsive force between these two atoms. In this structure sulfur assumes a typical cation position (SII) in the zeolite framework. In sulfurous acid, the sulfur atom is indeed positively charged, which supports the experimental observations. Another strong support for the identification of H_2SO_3 within the Na–Y structure is the previous observation of the UV adsorption band at 205 nm usually assigned to a hydrogen sulfite species in the investigated sample.[6b,9a,12]

The position of the sulfurous acid molecule in the six-ring window of the supercage has only slight influence on the cation and water distribution in the host. The SII* cation, which interacts with the nonprotonated oxygen atom of the sulfurous acid, is shifted by 1.2 Å into the supercage. For the stabilization of the SV–SIII chain of interlinked sodium ions and water molecules, only two of the four possible SII sites per supercage are necessary, which means that theoretically up to two SO_2 molecules per supercage can be adsorbed as H_2SO_3 on the observed site without disturbing the water–cation chain necessary for reversible NO_x adsorption. This theoretical value translates to 80 mg of SO_2 per gram of adsorbent. The shift of the SII cations into the supercage should have, if any, a beneficial influence on the adsorption of N_2O_3, which itself is known to shift the SII cation into the supercage to a position close to the cation position observed in the presence of H_2SO_3. These results show that SO_2 can be adsorbed independently of the water–cation structure, whereas N_2O_3 is incorporated into the water–cation network by replacing three water molecules. Too high loadings of sulfur-dioxides, however, break down the water–cation net either by replacing the two necessary SII cations or by assuming a new position. In any case the adsorption capacity for NO_x should drastically decrease as has been observed previously.[7] This observation explains the experimentally

 © 2004 Wiley-VCH Verlag GmbH & Co. KGaA, Weinheim

proven advantage of using short adsorption–regeneration cycles to prevent deactivation by sulfur oxides of Na–Y zeolite as a NO_x storage material.[7]

In summary, Na–Y zeolite was brought into contact with sulfur dioxide and water vapor at 250 °C. Rietveld refinement of the XRD patterns of the zeolite revealed the formation of sulfurous acid molecules at a specific site of the Na–Y zeolite cage. This discovery is particularly relevant to environmental catalytic applications that involve faujasite-type zeolites. Na–Y zeolite was recently identified as an effective DeNOx catalyst for exhaust gas after-treatment systems[13] and as a sulfur-tolerant NO_x trap.[5] The sulfur resistance of Na–Y zeolite can now be explained by the reversible formation of sulfurous acid molecules at locations in the zeolite cages remote from the NO_x adsorption sites. This study shows that Rietveld refinement of guest molecules in zeolites can be a powerful tool to elucidate complex molecular interactions inside porous crystalline host materials on an atomic level.

Received: March 15, 2004
Revised: May 10, 2004 [Z54266]

Keywords: environmental chemistry · nitrogen oxides · sulfur · X-ray diffraction · zeolites

[1] a) A. N. Fitch, H. Jobic, A. Renouprez, *J. Phys. Chem.* **1986**, *90*, 1311; b) D. Olson, *Zeolites* **1995**, *15*, 439; c) W. J. Mortier, *Compilation of Extra Framework Sites in Zeolites*, Butterworth, London, **1982**.

[2] a) M. Feuerstein, M. Hunger, G. Engelhardt, J. P. Amoureux, *Solid State Nucl. Magn. Reson.* **1996**, *7*, 95–103; b) G. Engelhardt, *Microporous Mater.* **1997**, *12*, 369–373; c) H. A. M. Verhulst, W. J. J. Welters, G. Vorbeck, L. J. M. van de Ven, V. H. J. De Beer, R. A. Van Santen, J. W. De Haan, *J. Phys. Chem.* **1994**, *98*, 7056–7062.

[3] a) H. Klein, C. Kirschhock, H. Fuess, *J. Phys. Chem.* **1994**, *98*, 12345–12360; b) J. Döbler, H. Förster, H. Fues, E. Geidel, B. Hunger, C. Kirschhock, O. Klepel, E. Poschnar, *Phys. Chem. Chem. Phys.* **1999**, *1*, 3183–3192.

[4] a) B. Hunger, O. Klepel, C. Kirschhock, M. Heuchel, H. Toufar, H. Fues, *Langmuir* **1999**, *15*, 5937–5941; b) C. Kirschhock, B. Hunger, J. A. Martens, P. A. Jacobs, *J. Phys. Chem. B.* **2000**, *104*, 439–448; c) K.-H. Hu, L.-P. Hwang, *Solid State Nucl. Magn. Reson.* **1998**, *12*, 211–220.

[5] A. Sultana, R. Loenders, O. Monticelli, C. Kirschhock, P. A. Jacobs, J. A. Martens, *Angew. Chem.* **2000**, *112*, 3062–3066; *Angew. Chem. Int. Ed.* **2000**, *39*, 2934–2937.

[6] a) J. F. Brilhac, A. Sultana, P. Gilot, J. A. Martens, *Environ. Sci. Technol.* **2002**, *36*, 1136–1140; b) A. Sultana, D. D. Habermacher, C. E. A. Kirschhock, J. A. Martens, *Appl. Catal. B* **2004**, *48*, 65–76.

[7] P. Engstrom, A. Amberntsson, M. Skoglundh, E. Fridell, G. Smedler, *Appl. Catal. B* **1999**, *22*, 241–248.

[8] a) H. G. Karge, M. Laniecki, M. Ziolek, *Stud. Surf. Sci. Catal.* **1986**, *28,* 617; b) M. Laniecki, M. Ziolek, H. G. Karge, *J. Phys. Chem.* **1987**, *91*, 4–6; c) S. D. Kirik, A. A. Dubkov, S. A. Dubkova, O. M. Sharonova, A. G. Anshits, *Zeolites* **1992**, *12*, 292–298; d) A. M. Shor, A. I. Rubaylo, *J. Mol. Struct.* **1997**, *410*, 133–136; e) M. Mello, M. Eic, *Stud. Surf. Sci. Catal.* **1999**, *125*, 657–666.

[9] a) S. V. Gollakota, C. D. Chriswell, *Ind. Eng. Chem. Res.* **1988**, *27*, 139–143; b) A. Srinivasan, M. W. Grutzeck, *Environ. Sci. Technol.* **1999**, *33*, 1464–1469; c) H. G. Stenger Jr. , K. Hu, D. R. Simpson, *Gas. Sep. Purif.* **1993**, *7*, 19–25.

[10] The powder-diffraction pattern was recorded at room temperature on a D5000 diffractometer in Debye–Scherrer geometry. As the X-ray source served a rotating anode with a Cu target, a Goebel mirror was used to obtain a parallel beam. Residual β-radiation was removed with a Ni filter. A scintillation detector was used to record the data set (4–70° 2Θ, 0.02° steps). The sample was sealed in a capillary (inner diameter 0.7 mm). Rietveld refinement was performed with GSAS (Rp = 1.6 %, Rwp = 2.5 %). Further details on the crystal-structure investigation may be obtained from the Fachinformationszentrum Karlsruhe, 76344 Eggenstein-Leopoldshafen, Germany (fax: (+49) 7247-808-666; email: crysdata@fiz-karlsruhe.de), on quoting the depository number CSD-413809.

[11] M. W. Schmidt, K. K. Baldridge, J. A. Boatz, S. T. Elbert, M. S. Gordon, J. H. Jensen, S. Koseki, N. Matsunaga, K. A. Nguyen, S. J. Su, T. L. Windus, M. Dupuis, J. A. Montgomery, *J. Comput. Chem.* **1993**, *14*, 1347–1363.

[12] A. Huss Jr, C. A. Eckert, *J. Phys. Chem.* **1977**, *81*, 2268–2270.

[13] a) S. Yoon, A. G. Panov, R. G. Tonkyn, A. C. Ebeling, S. E. Barlow, M. L. Balmer, *Catal. Today* **2002**, *72*, 251–257; b) S. J. Schmieg, B. Y. Cho, S. H. Oh, *Appl. Catal. B* **2004**, *49*, 113–125; c) J.-H. Lee, J.-G. Kim, J.-K. Lee, J.-H. Kim, *Catal. Today* **2003**, *87*, 35–42.

 © 2004 Wiley-VCH Verlag GmbH & Co. KGaA, Weinheim

Rotaxane Synthesis

Rate Acceleration of the Reaction between Solid Reactants by Premixing in Solution: Application to the Efficient Synthesis of a [2]Rotaxane

*Akihiro Orita, Junji Okano, Yoshiki Tawa, Lasheng Jiang, and Junzo Otera**

Solventless reactions are currently a subject of extensive interest in both inorganic and organic chemistry.[1] In particular, organic synthesis may benefit from avoiding the use of organic solvents, yet this is valid only if a whole process, including work-up operations, is free from organic solvents. The higher efficiencies and selectivities frequently encountered under solventless conditions are of prime significance in terms of organic synthesis and process chemistry. Many common organic reactions are accelerated under solventless conditions, and we also previously disclosed dramatic rate enhancement for supramolecular self-assembly.[2,3] Most reactions between solid reactants demand mechanical forces such as grinding in a mortar with a pestle or compounding in a ball mill.[4] The reaction generally proceeds through formation of a liquid or melt phase containing an intimate mixture

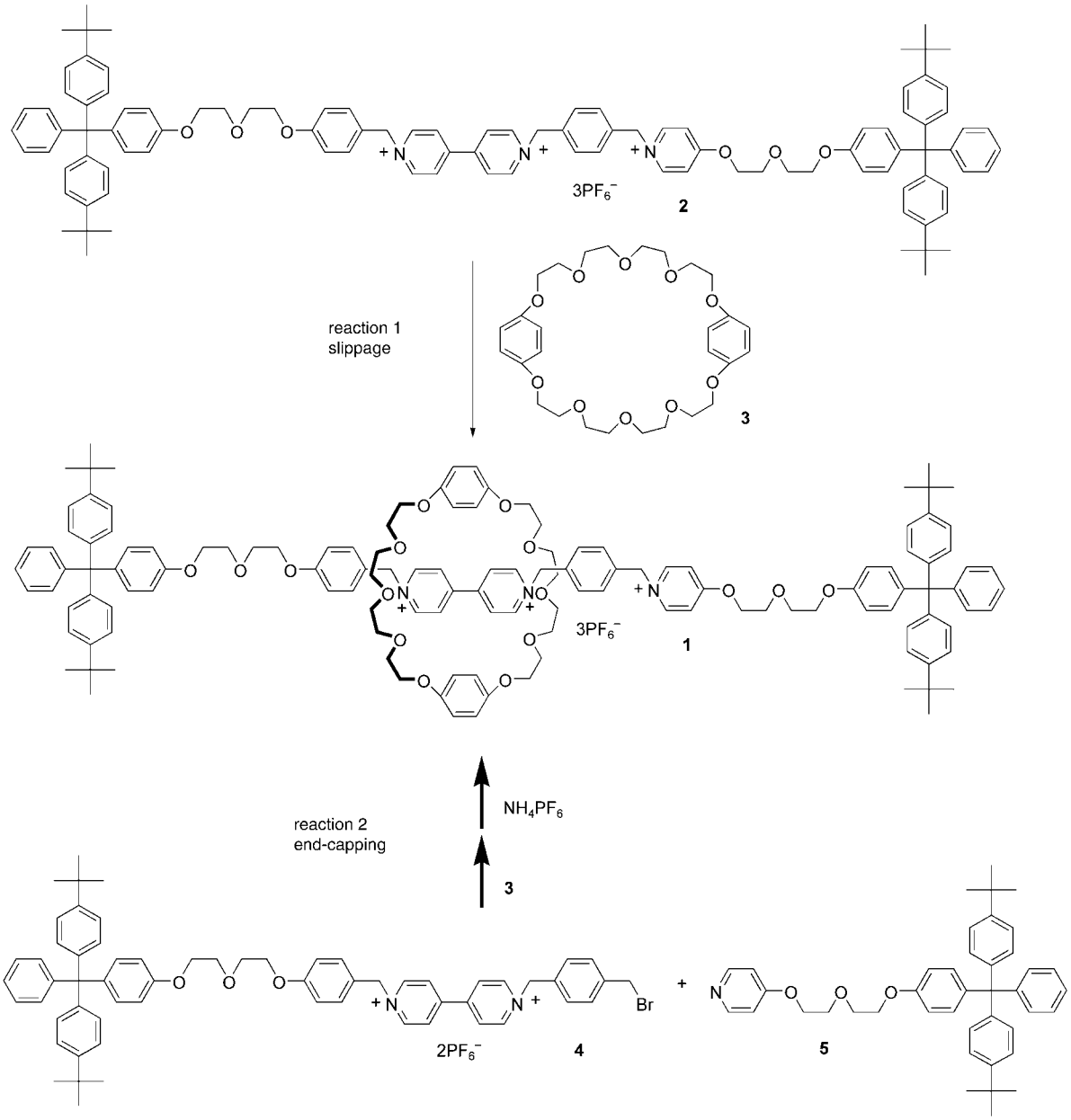
[*] Prof. Dr. A. Orita, J. Okano, Y. Tawa, Dr. L. Jiang, Prof. Dr. J. Otera
Department of Applied Chemistry
Okayama University of Science
Ridai-cho, Okayama 700-0005 (Japan)
Fax: (+81) 86-256-4292
E-mail: otera@high.ous.ac.jp

 © 2004 Wiley-VCH Verlag GmbH & Co. KGaA, Weinheim DOI: 10.1002/anie.200460062

of macroscopic solid reactant particles, so that the molecules of the solid particles are sufficiently mobile for frequent molecular collisions to occur.[5] It was observed in a few cases that solid, powdered reactants liquefy simply on contact with each other. Once the melt has been formed, the reaction occurs very quickly. High mobility was also obtained in the formation of a co-crystal by adding a small amount of an appropriate solvent (2 drops (ca. 0.05 mL) of an organic solvent per ca. 200 mg of the solid mixture).[6]

Bearing in mind the importance of the mixing effect on the reaction between the solid reactants, we postulated that the mixing of reactants in solution followed by evaporation should give rise to a more favorable amalgam for a solventless reaction because the reactant molecules in the solid thus formed should be brought into contact. We demonstrate here that such a molecular-level mixing is, in fact, much more effective than the mixing of solid particles, as shown by the example of the efficient synthesis of [2]rotaxane **1**.

The present study stemmed from the synthesis of **1** (Scheme 1, reaction 1) by the incomplete slippage method.[7] A poor yield (38%) was obtained after heating the thread **2** with four equivalents of crown ether **3** in CH_3CN at 55°C for three days. Consequently, we utilized an end-capping method (reaction 2),[8] which involves reaction between *p*-substituted benzyl bromide **4** and *p*-substituted pyridine **5** as a key step to provide **2** [Eq. (1)]. The simple solventless protocol was not so effective: When solid **4** and **5** were ground at ambient temperature in a mortar with a pestle for 1.5 h **2** was produced in 60% yield and a substantial amount of the starting materials remained. The reactant mixture stayed powdery



Scheme 1. Synthesis of the [2]rotaxane **1**.

 © 2004 Wiley-VCH Verlag GmbH & Co. KGaA, Weinheim

and no melt was formed on grinding. However, a remarkable improvement was made by using the premixing method. Both reactants were dissolved in acetone in a mortar, and then the solvent was evaporated in vacuo for 5 min. The film that had formed on the surface of the mortar was then ground. The starting materials disappeared within 50 min, as evident from thin-layer chromatography, and an 85% yield of **2**[9] was obtained even though no melt was formed during the manipulation. More interestingly, when the film was merely kept on the mortar or more conveniently on an inner surface of a flask without grinding, the reaction also proceeded to afford **2** in 80% yield after 2 h. No change was observed in the appearance of the film, except a slight deepening of the yellow color.

$$\mathbf{4} + \mathbf{5} \rightarrow \overset{NH_4PF_6}{\longrightarrow} \mathbf{2} \qquad (1)$$

An NMR investigation was then carried out on the shorter thread **8** synthesized in an analogous manner to confirm that the reaction actually proceeded in the solid film without grinding (Table 1, entry 1). Grinding of the film composed of **6** and **7** for 30 minutes afforded **8** in 79% yield, while standing for 2 h afforded **8** in 85% yield. The reaction was monitored by ^{1}H NMR spectroscopy (Figure 1). The reaction proceeded to some extent in a fresh film which was obtained by mixing **6** and **7** in solution and subsequent evaporation (5 min after the start of mixing) as shown by the 75% recovery of **6** (Figure 1a).[10] The reaction then progressed to leave 2% of **6** after 2 h (Figure 1c). The reaction could apparently be driven without external mechanical forces, probably because of the effective contacts between the reactants molecules. For comparison, the same reaction was conducted in solution. The high concentration method was recently found to be useful for the end-capping synthesis of rotaxanes.[11] This protocol furnished **2** in 85% yield (by NMR) after standing a solution (0.2 mL) of **4** (0.03 mmol) and **5** (0.06 mmol)[12] in acetone at ambient temperature. Unfortunately, however, it took two days to reach the maximum yield. Similarly, **8** was obtained in 83% yield after two days.

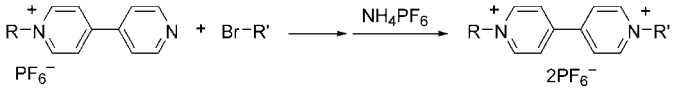
Similar but more enhanced reactivity was observed with a simpler case (Table 1, entry 2). Grinding a solid mixture of neat **9** and **10** for 1.5 h resulted in the *N*-alkylation product **11**[9] in 63% yield (by NMR). However, grinding a film produced from a solution of **9** and **10** in acetone afforded an 82% yield (by NMR) of **11** after 15 minutes, while an 80% yield (by NMR) was obtained after the film had stood for 40 minutes. The freshly prepared film was extracted with $CDCl_3$ and the ^{1}H NMR spectrum recorded to ascertain if the acetone solvent remained in the film. No signal attributable to the acetone was observed in this solution, which implied the acetone played no role in the interactions between the reactant molecules in the film. In contrast, two days were necessary for the high concentration solution method to provide an 86% yield (by NMR) of **11**.

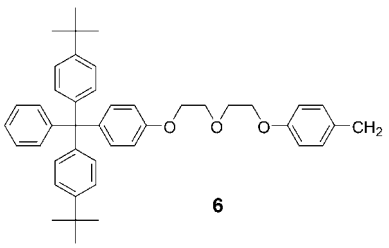
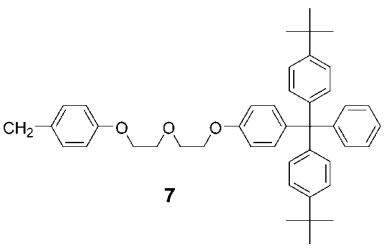
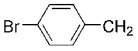
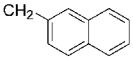
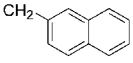
The use of *N*-methyl derivative **12** instead of **9** led to unsatisfactory results (Table 1, entry 3). Evaporation of a solution of **12** and **10** in acetone did not give a film, but instead gave a white solid. No reaction occurred upon grinding or on standing of this solid, while the reaction gave a quantitative yield of the *N*-alkylation product[9] in two days in acetone. This result implies that formation of the film is crucial for the smooth reaction in the solid state.

The importance of the molecular-level mixing was proved as follows. A well-shaken powdery mixture composed of **3**/**4**, **6**/**7**, or **9**/**10** was pressed (40 kg cm^{-2}) for 1 h. No reaction occurred in all cases, thus indicating that molecule-to-molecule contacts are crucial for the reaction to occur: mixing in solution is the best while mechanical forces are somewhat useful. The grinding helps to change relatively compatible solid reactants into a molten state. The formation of voids and cracks[13] may be facilitated by mechanical forces in the cases of the solid reactants where no molten mixtures are formed.

Finally, the premixing protocol also proved to be effective for the synthesis of [2]rotaxane **1**[9] (Scheme 1, reaction 2).

Table 1: Solventless N-alkylation by the premixing method.



Entry	R	R′	Product	Yield [%]/*t* [min] grinding	standing
1	 **6**	 **7**	**8**	79/30	85/120
2	 **9**	 **10**	**11**	82/15	80/40
3	 **12**	 **10**		no reaction	

 © 2004 Wiley-VCH Verlag GmbH & Co. KGaA, Weinheim

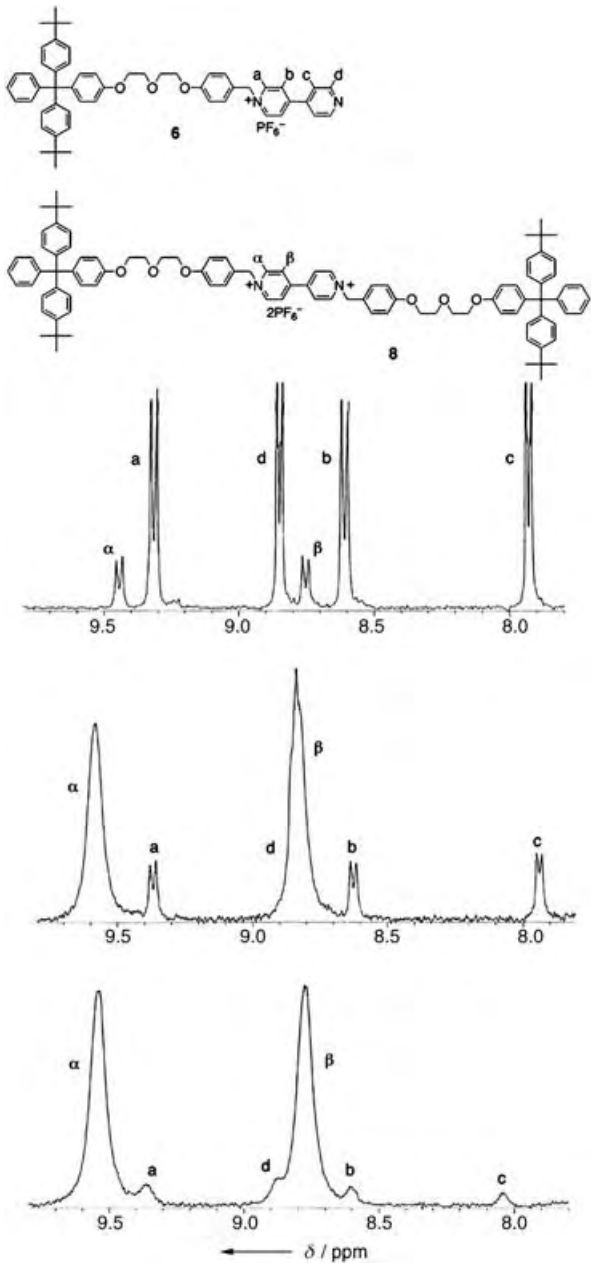


Figure 1. NMR spectra of a portion of the film consisting of **6** and **7** in $CDCl_3$: a) after 5 min (see text): 75% of **6** remaining; b) after 1 h: 43% of **6** remaining; c) after 2 h: 2% of **6** remaining.

The film was obtained by mixing **3** (0.06 mmol), **4** (0.03 mmol), and **5** (0.06 mmol) in a binary solvent of acetone (0.1 mL) and dichloromethane (0.1 mL) followed by evaporation. The mixed solvent was used because crown ether **3** is not soluble in acetone. Rotaxane **1** was formed in 85% yield along with 8% of **2** after the film had stood for four hours at ambient temperature. It should be noted that the yield of **1** was only 11%, with 12% of **2** and 57% of **4**, when a powdery mixture of **3**, **4**, and **5** was ground directly. The high concentration solution method required three days in anisole at 25°C to afford **1** and **2** in yields of 78% and 11%, respectively.

In conclusion, the reaction between solid reactants is accelerated by premixing the reactants in solution. The acceleration is accessible only when a film is formed after evaporation. It seems that the reactants must be compatibile for the formation of the film, which results in molecular-level amalgamation. The longer reaction time in solution offsets the essential features of the solventless reaction, in particular, of the molecule-to-molecule contacts. The reaction is accelerated by the high concentration effect under solventless conditions and, more importantly, the de-solvation energy, which is inevitable in a solution reaction, is saved.

This protocol might not be categorized as a solventless reaction in a strict sense if the premixing step is counted, yet the reaction itself proceeds under solventless conditions. In a practical sense, however, reactants can be charged into a reactor much more conveniently in solution than can solid reactants. We have so far demonstrated the validity of the new protocol with simple N-alkylation. Further applications to other reactions are now in progress.

Experimental Section

2: Compounds **4** (37 mg, 0.03 mmol) and **5** (36 mg, 0.06 mmol) were dissolved in acetone (0.2 mL) in a mortar. The acetone solution turned into a yellow film after 5 min on standing in open air followed by evaporation in vacuo. The film was ground with a pestle for 50 min. The mixture was dissolved in a mixture of acetone (5 mL), $CHCl_3$ (2 mL), and H_2O (1 mL). NH_4PF_6 (146 mg, 0.9 mmol) was then added to the resulting solution. The acetone was evaporated from this solution, and the resulting H_2O suspension was filtered. The solid product thus obtained was dried in vacuo. The ^{1}H NMR spectrum of this crude mixture indicated formation of **2** in 85% yield. Column chromatography of this mixture on silica gel (70:16:11:3 CH_3OH/CH_2Cl_2/CH_3NO_2/NH_4Cl(2N)) furnished **2** (42 mg, 76%): ^{1}H NMR (300 MHz, CD_3COCD_3): $\delta = 9.46$ (d, $J = 5.1$ Hz, 4H), 8.93 (d, $J = 7.2$ Hz, 2H), 8.80–8.75 (m, 4H), 7.79–7.61 (m, 8H), 7.34–7.05, (m, 34H), 6.87–6.80 (m, 4H), 6.20 (s, 2H), 6.10 (s, 2H), 5.88 (s, 2H), 4.64–4.62 (m, 2H), 4.20–4.12 (m, 6H), 4.01–3.99 (m, 2H), 3.90–3.88 (m, 6H) 1.30 ppm (s, 36H); ^{13}C NMR (75.5 MHz, CD_3COCD_3) $\delta = 172.0$, 161.1, 157.8, 157.7, 151.4, 151.1, 149.2, 149.1, 148.2, 146.8, 146.7, 146.4, 145.0, 140.1, 140.0, 136.6, 135.3, 132.8, 132.7, 132.1, 131.6, 131.3, 131.1, 130.7, 128.5, 128.3, 128.2, 128.1, 126.6, 126.5, 125.8, 125.1, 125.0, 116.2, 115.2, 114.1, 114.0, 71.5, 70.4, 70.2, 69.4, 68.5, 68.1, 68.0, 65.3, 65.0, 64.2, 62.7, 34.8, 31.6 ppm; MS (MALDI-TOF) found: *m/z* 1643.76 $[M-2PF_6]^+$, calcd for $C_{104}H_{112}F_6N_3O_6P$: *m/z* 1643.82.

The film prepared as above in a mortar or in a flask was kept standing in open air at ambient temperature for 2 h to provide **2** in 80% yield based on ^{1}H NMR spectroscopy and isolated in 72% yield.

1: A mixture of **3** (32 mg, 0.06 mmol), **4** (37 mg, 0.03 mmol), and **5** (36 mg, 0.06 mmol) were dissolved in acetone (0.1 mL) and dichloromethane (0.1 mL) in a 50-mL flask. The resulting red solution was evaporated in vacuo, whereupon a film developed on the surface of the flask. After 5 min, the evaporation was stopped and the film was left standing in the open air at ambient temperature for 4 h. The mixture was dissolved in acetone (10 mL) and H_2O (2 mL). NH_4PF_6 (98 mg, 0.6 mmol) was added to the resulting solution. The acetone was evaporated from this solution, and the resulting H_2O suspension was filtered. The solid product thus obtained was dried in vacuo. The ^{1}H NMR spectrum of this crude product indicated formation of **1** in 85% yield together with **2** in 8% yield. Column chromatography of this mixture on silica gel (70:16:11:3 CH_3OH/CH_2Cl_2/CH_3NO_2/NH_4Cl(2N)) furnished **1** (56 mg, 79%): ^{1}H NMR (300 MHz, CD_3COCD_3): $\delta = 9.23$ (d, $J = 6.6$ Hz, 2H), 9.18 (d, $J = 6.6$ Hz, 2H), 8.93 (d, $J = 7.3$ Hz, 2H), 8.30–8.25 (m, 4H), 7.89 (d, $J = 8.4$ Hz, 2H),

 © 2004 Wiley-VCH Verlag GmbH & Co. KGaA, Weinheim

7.79–7.72 (m, 4H), 7.61 (d, $J = 7.5$ Hz, 2H), 7.33–7.06 (m, 34H), 6.85–6.80 (m, 4H), 6.17 (s, 2H), 6.05 (s, 8H), 5.90 (s, 2H), 4.54–4.52 (m, 2H), 4.22–4.20 (m, 2H), 4.14–4.08 (m, 4H), 3.96–3.65 (m, 40H), 1.29 ppm (s, 36H); ^{13}C NMR (75.5 MHz, CD_3COCD_3): $\delta = 171.9$, 161.1, 157.8, 157.7, 152.9, 149.2, 149.1, 148.2, 146.8, 146.7, 146.4, 145.0, 140.2, 140.1, 136.6, 135.3, 132.9, 132.8, 132.3, 131.6, 131.5, 131.4, 130.7, 128.2, 128.1, 126.6, 126.5, 126.3, 126.1, 125.1, 125.0, 116.1, 115.5, 115.1, 114.1, 114.0, 71.5, 71.3, 71.0, 70.7, 70.5, 70.4, 70.3, 69.4, 68.6, 68.3, 68.1, 68.0, 65.3, 65.0, 64.2, 62.7, 34.8, 31.6 ppm; MS (MALDI-TOF) found: m/z 2180.78 $[M-2PF_6]^+$, calcd for $C_{132}H_{152}F_6N_3O_{16}P$: m/z 2180.08.

Received: March 20, 2004 [Z460062]

Keywords: alkylation · rotaxanes · solvent effects · supramolecular chemistry

[1] a) F. Toda, *Synlett* **1993**, 303; b) F. Toda, *Acc. Chem. Res.* **1995**, *28*, 480; c) K. Tanaka, F. Toda, *Chem. Rev.* **2000**, *100*, 1025; d) G. W. V. Cave, C. L. Raston, J. L. Scott, *Chem. Commun.* **2001**, 2159; e) K. Tanaka in *Solvent-free Organic Synthesis*, Wiley-VCH, Weinheim, **2003**.

[2] A. Orita, L. Jiang, T. Nakano, N. Ma, J. Otera, *Chem. Commun.* **2002**, 1362.

[3] For other reports on self-assembly by solventless reactions, see a) D. Braga, L. Maini, M. Polito, L. Mirolo, F. Grepioni, *Chem. Eur. J.* **2003**, *9*, 4362; b) V. Chandrasekhar, V. Baskar, R. Boomishankar, K. Gopal, S. Zacchini, J. F. Bickley, A. Steiner, *Organometallics* **2003**, *22*, 3710; c) S. Mann, *Chem. Commun.* **2004**, 1.

[4] a) K. Komatsu, G.-W. Wong, Y. Murata, T. Tanaka, K. Fujiwara, *J. Org. Chem.* **1998**, *63*, 9358; b) V. P. Balema, J. W. Wiench, M. Pruski, V. K. Pecharsky, *Chem. Commun.* **2002**, 724.

[5] G. Rothenberg, A. P. Downie, C. L. Raston, J. L. Scott, *J. Am. Chem. Soc.* **2001**, *123*, 8701.

[6] N. Shan, F. Toda, W. Jones, *Chem. Commun.* **2002**, 2372.

[7] For the slippage method, see E. W. Wong, C. P. Collier, M. Belohradsky, F. M. Raymo, J. F. Stoddart, J. R. Heath, *J. Am. Chem. Soc.* **2000**, *122*, 5831.

[8] For the end-capping method, see Y. Furusho, H. Sasabe, D. Natsui, K.-i. Murakawa, T. Takata, T. Harada, *Bull. Chem. Soc. Jpn.* **2004**, *77*, 179, and references therein.

[9] The mixed Br^-/PF_6^- salt is sparingly soluble in organic solvents, and thus the product was converted into a simple PF_6^- salt.

[10] As described in reference [9], it is not possible to determine the yield of the primary product because of the poor solubility of the mixed salt. The reaction was, therefore, monitored by consumption of **6**.

[11] a) K. Nikitin, B. Long, D. Fitzmaurice, *Chem. Commun.* **2003**, 282; b) the high concentration effect for asymmetric catalysis has also been reported: Y. Yuan, X. Zhang, K. Ding *Angew. Chem. Int. Ed.* **2003**, *42*, 5478.

[12] The concentration of the substrates was set to nearly the same as that reported in reference [11].

[13] R. P. Rastogi, N. B. Singh, R. R. Singh, *J. Solid State Chem.* **1977**, *20*, 191.

 © 2004 Wiley-VCH Verlag GmbH & Co. KGaA, Weinheim

Amplification of Local Interactions

Thermally Induced Electron Transfer in a CsCoFe Prussian Blue Derivative: The Specific Role of the Alkali-Metal Ion**

Anne Bleuzen, Virginie Escax, Alban Ferrier, Françoise Villain, Michel Verdaguer, Pascal Münsch, and Jean-Paul Itié*

Prussian blue was described for the first time in 1704. Since then, spectacular electrochemical,[1,2] magnetic,[3,4] and photomagnetic[5] properties have been revealed in Prussian blue analogues, all of which revived interest in their study. These compounds crystallize in face-centered cubic (fcc) structures. Insertion of alkali metal ions in the tetrahedral sites (Td) is accompanied by a change in stoichiometry.[6,7] Several recent studies pointed out the role played by the inserted alkali metal ions for the properties of the Prussian blue analogues.[2,7,8] Here we focus on the role of cesium in the thermally activated electron transfer Co^{II}(high spin)-$Fe^{III} \rightarrow Co^{III}$(low spin)-$Fe^{II}$ in the derivative $Cs_{0.7}Co_4[Fe(CN)_6]_{2.9}\square_{1.1}\cdot 16H_2O$ (**$Cs_{0.7}$**; $\square$ represents the intrinsic $[Fe(CN)_6]$ vacancies). We chose this specific stoichiometry since its most probable Td-site environment is $Co_4Fe_3\square_1$. The electron transfer occurs over the temperature range 280–180 K.[7] In **$Cs_{0.7}$**, the Co^{III}/Co^{II} ratio is 9:1 at room temperature and 3:2 at 20 K.[7,9] The study of the local environment of the metal ions (by X-ray absorption spectroscopy) and of the long-range order (by powder energy-dispersive X-ray diffraction) made it possible for the first time to localize the alkali metal cations in the structure, to demonstrate specific interactions between them and the bimetallic network, and to determine a displacement of them in the cavities between room and low temperatures.

Extended X-ray absorption fine structure (EXAFS) measurements were performed at the Fe and Co K-edges at 300 and 20 K. The $[Fe(CN)_6]$ entity is stable and rigid. The EXAFS signals at the Fe K-edge at 300 and 20 K are therefore very close to each other.[10] In contrast, at the Co K-edge, the EXAFS signals are very different at 300 and 20 K (Figure 1).

[*] Dr. A. Bleuzen, Dr. V. Escax, A. Ferrier, Dr. F. Villain, Prof. Dr. M. Verdaguer
Laboratoire de Chimie Inorganique et Matériaux Moléculaires
UMR CNRS 7071, Université Pierre et Marie Curie
Bat F, 4, place Jussieu, 75252 Paris Cedex 05 (France)
Fax: (+33) 144-273-841
E-mail: bleuzen@ccr.jussieu.fr
Dr. P. Münsch, Dr. J.-P. Itié
Laboratoire pour L'Utilisation du Rayonnement Electromagnétique
UMR CNRS 130-CEA-MENRS
Bat 209d, Université Paris Sud
BP34, 91898 Orsay Cedex (France)

[**] This research was supported by the DFG (Schwerpunktprogramm 1137: Molekularer Magnetismus), the European Community (TMR Programme), and MENESR (grant for V.E.).

Supporting information for this article is available on the WWW under http://www.angewandte.org or from the author.

 © 2004 Wiley-VCH Verlag GmbH & Co. KGaA, Weinheim DOI: 10.1002/anie.200460086

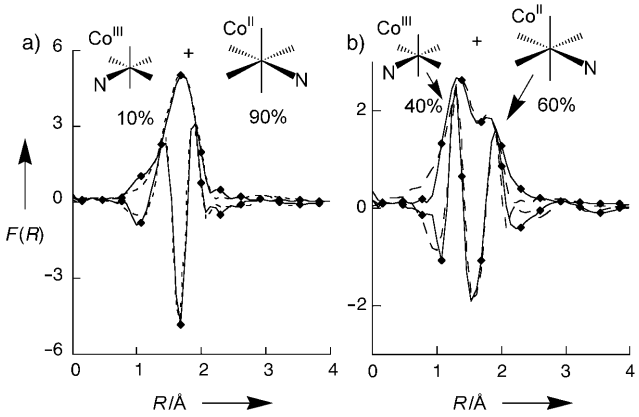


Figure 1. Experimental (——) and calculated (– – –) modulus and imaginary parts of the first-neighbor contributions to the Fourier transform of the EXAFS signal at the Co K-edge of $\mathbf{Cs_{0.7}}$ a) at 300 K and b) at 20 K.

The data analysis at 300 K shows the presence of 5.4 N or O at 2.09(3) Å (corresponding to 90% octahedrally coordinated Co^{II}(HS)) and 0.6 N or O at 1.90(3) Å (corresponding to 10% Co^{III}(LS)). At 20 K, we find 3.6 N or O at 2.08(3) Å (60% Co^{II}(HS)) and 2.4 N or O at 1.89(3) Å (40% Co^{III}(LS)).[7,9]

Powder energy-dispersive X-ray diffraction (EDX) spectra of $\mathbf{Cs_{0.7}}$ were recorded as a function of temperature on cooling from 300 to 140 K. At 300 K, the diffraction pattern of $\mathbf{Cs_{0.7}}$ can be indexed to a fcc unit cell. On cooling, the area and the linewidth of the peaks do not vary significantly (Figure 2), whereas all the diffraction lines shift progressively towards higher energy, corresponding to a progressive decrease of the cell parameter from 10.30(5) Å at 300 K to 10.08(5) Å at 140 K. This cell contraction is due to the shortening of the Co–ligand bond accompanying the Co^{II}(HS)→Co^{III}(LS) transformation. These observations correspond to a second-order transformation which starts locally and spreads homogeneously in the solid without loss of crystallinity.[11]

EXAFS measurements were also performed at the Cs L_3-edge at 300 and 20 K (Figure 3). At 300 K, the Fourier transform of the EXAFS signal of $\mathbf{Cs_{0.7}}$ exhibits well-defined contributions: the Cs ion has rather strong interactions with its neighbors. The first contribution to the Fourier transform is well simulated by three O and six N atoms situated 3.46(5) Å from the Cs ion. A coordination number of nine is sensible for a cation of this size and charge.[12] The second shell is well simulated by 6 C atoms situated at 3.72(5) Å, while the third and fourth ones are well simulated by three Co and three Fe atoms situated at 4.37(5) Å and 5.05(5) Å, respectively. The four well-resolved shells and the distances obtained clearly indicate that the Cs ion is not situated at the center of the Td site. The vacancy □, the center of the Td site, and—for symmetry reasons—the Cs ion are situated on a threefold axis (see Figure 3a).

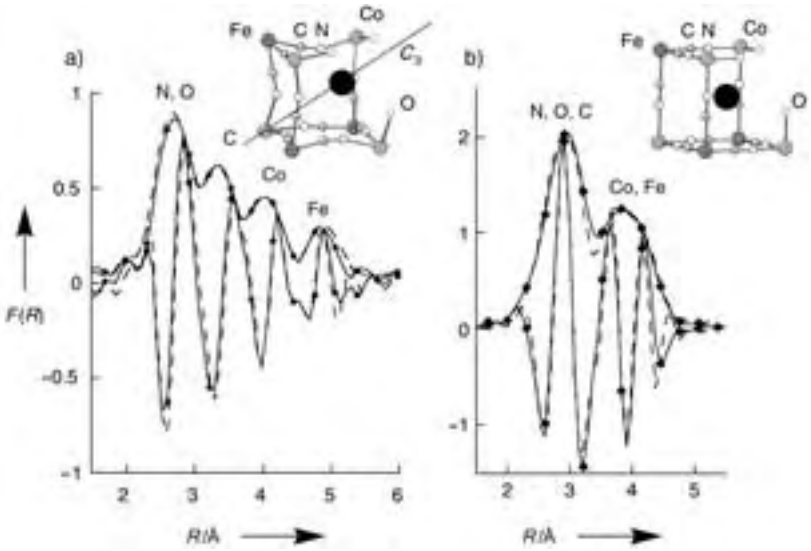


Figure 3. Experimental (——) and calculated (– – –) modulus and imaginary parts of the first-neighbor contributions to the Fourier transform of the EXAFS signal at the Cs L_3-edge of $\mathbf{Cs_{0.7}}$ and schematic presentation of the Cs environment a) at 300 K and b) at 20 K.

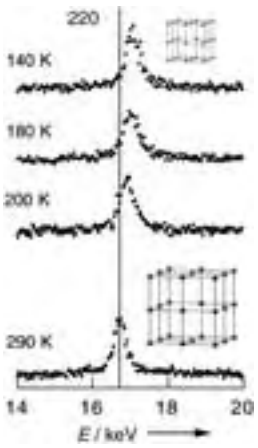


Figure 2. EDX spectra of $\mathbf{Cs_{0.7}}$ between 14 and 20 keV [(220) diffraction line] as a function of temperature.

From the Cs–Fe and Cs–Co distances and from the cell parameters, it is easy to localize the Cs ion on the threefold axis at about 1 Å from the center of the Td site towards the vacancy. Taking an Fe–C distance as 1.93 Å,[10] it is possible to calculate from X-ray diffraction and absorption data the coordinates of the Cs, C, N, Co, and Fe atoms in the plane containing the Co, Fe, and Cs metal ions and the CN bridge interacting with them (CoFeCs plane). The positions of the atoms are shown in Figure 4.[13] The Co–NC entity is bent.[14,15] A schematic drawing of the environment of the Cs ion is given Figure 3a.

At 20 K, only two shells of neighboring atoms can be extracted from the Fourier transform of the EXAFS signal of $\mathbf{Cs_{0.7}}$. The first one is well simulated by 21 O, N, or C atoms situated at 3.55(5) Å and the second one by 7 Co or Fe atoms located 4.30(5) Å from the Cs ion. The Cs ion is located at the center of the Td site at equal distances from the Co and Fe

 © 2004 Wiley-VCH Verlag GmbH & Co. KGaA, Weinheim

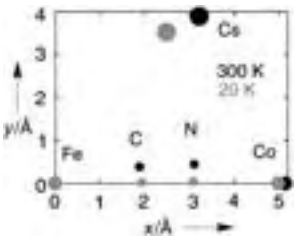


Figure 4. Position of the Co, Fe, C, N, and Cs atoms in the CoFeCs plane at 300 K (black circles), and at 20 K (gray circles).

ions.[16] Taking an Fe–C distance of 1.93 Å,[10] we calculated the coordinates of the different atoms in the CoFeCs plane from the 20-K EXAFS data. A schematic drawing of the environment of the Cs ion and the calculated positions for a Co^{III}–N distance of 1.89 Å are shown in Figure 3b and 4, respectively.[13] There is no sensible solution for the coordinates of the N atom with a Co^{II}–N distance of 2.08 Å. The EXAFS data at the Cs L_3-edge are not compatible with a structure in which Co^{II}(HS) would be the closest Co neighbors.[17] At 20 K, the Cs ions are surrounded exclusively by Co^{III}(LS) ions and linear Co-NC-Fe entities. Furthermore, since the number of Co ions undergoing an oxidation-state change on cooling (30%) corresponds exactly to the number of Co ions surrounding the Cs ion,[18] one might conclude that only these Co ions are involved in the electron transfer. Thus, the presence of the Cs ion appears as a condition for the electron transfer.

This structural investigation shows that in $\mathbf{Cs_{0.7}}$ the electron transfer occurs only around the Td sites containing a Cs ion. At 300 K, the Cs ion is surrounded by Co^{II} and Fe^{III} ions (see Figure 3a). It is displaced from the center of the Td site and interacts with the O atoms of three H_2O molecules, which are bound to the three Co ions neighboring the vacancy, and with the six nearest CN bridges. The Co^{II}-NC-Fe^{III} entities are bent. The orbital interactions between Co and NC are weak (compared to those in the linear conformation). The ligand field of Co is weak, the Co ions are HS at the oxidation state +II. $\mathbf{Cs_{0.7}}$ is essentially composed of Co^{II} and Fe^{III} ions. The Cs ion fits into the CoFe bimetallic network to complete its coordination sphere with nine neighbors. The crystal and electronic structures of $\mathbf{Cs_{0.7}}$ are close to those of the CoFe Prussian blue analogue free of the alkali metal ion.

At low temperature, the alkali metal ions move to the center of the Td sites and interact with all the ligands surrounding this site (nine CN bridges and three H_2O molecules). The Co^{III}-NC-Fe entities become linear. The orbital interactions between Co and NC are stronger and so is the Co ligand field. The Co ions around the alkali metal ion are LS at the oxidation state +III. $\mathbf{Cs_{0.7}}$ is still mainly composed of Co^{II} ions (60%) except around the alkali metal ion. The cell parameters are shortened due to the formation of linear Co^{III}-NC-Fe entities around the alkali metal ions. As shown by the absence of loss of crystallinity in the sample, the structural change spreads in a cooperative way in the whole solid, made possible by the flexibility of the Co-NC angle in the Co^{II}-NC-Fe entities and by the swing of the Co and Fe coordination polyhedra.

The high- and low-temperature states of $\mathbf{Cs_{0.7}}$ are close in energy, with a lower entropy in the more rigid low-temperature state. The switching process is reversible, thermally (and entropy-) driven in line with the observations by Sorai and Seki about the coupling between electronic states and phonons.[21] It is accompanied by a move of the alkali metal ion and by an electron transfer. Our finding is related to the very peculiar structural role of the alkali metal ion in the process: it fits into the CoFe bimetallic network at 300 K, moves to the center of the Td site, and modifies the structure around it at low temperature. Such geometry changes were already observed in perovskite oxides, where they were imposed by interactions between lanthanide ions and oxo bridges and associated with changes in some properties.[19] What is spectacular in the CoFe Prussian blue analogues is the macroscopic influence of local interactions on the network as a consequence of their amplification by electron transfer and Co-spin change. Work is in progress on other Prussian blue analogues, at both structural and electronic levels (in particular to determine the ligand field of the cobalt ions), to check the general existence of such interactions in these analogues.

Experimental Section

The synthesis of $\mathbf{Cs_{0.7}}$ is described in ref. [7].

The EXAFS measurements were carried out in transmission mode on the XAS 13 beamline at LURE (Orsay) and the signals were calculated in the single-scattering approximation.[20]

EDX patterns were recorded on the DW-11A energy-dispersive X-ray beamline at LURE (Orsay).[11] The photoexcitation of the sample under the X-ray beam prevented us from recording EDX spectra at temperatures below 140 K. XAS data parameters of the calculated spectra and calculation of the atomic coordinates are available in the Supporting Information.

Received: March 22, 2004 [Z460086]

Keywords: electron transfer · Prussian blue analogues · spin crossover · X-ray absorption spectroscopy · X-ray diffraction

[1] K. Honda, J. Ochiachi, H. Hayashi, *Chem. Commun.* **1986**, 168–170.
[2] D. R. Rosseinsky, H. Lim, X. Zhang, H. Jiang, J. Wei Chai, *Chem. Commun.* **2002**, 2988–2989.
[3] T. Mallah, S. Thiébault, M. Verdaguer, P. Veillet, *Science* **1993**, *262*, 1554–1557.
[4] a) S. Ferlay, T. Mallah, R. Ouhaès, P. Veillet, M. Verdaguer, *Nature* **1995**, *378*, 701–703; b) S. M. Holmes, G. S. Girolami, *J. Am. Chem. Soc.* **1999**, *121*, 5593–5594; c) N. Shimamoto, O. Ohkoshi, O. Sato, K. Hashimoto, *Inorg. Chem.* **2002**, *41*, 678–684.
[5] O. Sato, T. Iyoda, A. Fujishima, K. Hashimoto, *Science* **1996**, *272*, 704–705.
[6] A. Lüdi, H. U. Güdel, *Structure and Bonding*, Springer, Berlin, **1973**, pp. 1–21.
[7] V. Escax, A. Bleuzen, C. Cartier dit Moulin, F. Villain, A. Goujon, F. Varret, M. Verdaguer, *J. Am. Chem. Soc.* **2001**, *123*, 12536–12543.
[8] a) J. J. Garcia-Jareno, A. Sanmatias, J. Navarro-Laboulais, F. Vicente, *Electrochim. Acta* **1998**, *43*, 395–405; b) J. J. Garcia-

 © 2004 Wiley-VCH Verlag GmbH & Co. KGaA, Weinheim

Jareno, J. Navarro-Laboulais, A. Sanmatias, F. Vicente, *Electrochim. Acta* **1998**, *43*, 1045 – 1052.
[9] A. Bleuzen, V. Escax, J.-P. Itié, P. Münsch, M. Verdaguer, *C. R. Chim.* **2003**, *6*, 343 – 352.
[10] T. Yokoyama, T. Ohta, O. Sato, K. Hashimoto, *Phys. Rev. B* **1998**, *58*, 8257 – 8266.
[11] V. Escax, A. Bleuzen, J. P. Itié, P. Münsch, F. Varret, M. Verdaguer, *J. Phys. Chem. B* **2003**, *107*, 4763 – 4767.
[12] H. Ohtaki, T. Radnai, *Chem. Rev.* **1993**, *93*, 1157 – 1204.
[13] The C–N distance in the CN bridge calculated from the calculated coordinates is 1.2(1) Å at 300 K and 1.1(1) Å at 20 K, and thus of the expected order of magnitude (1.14 Å).
[14] K. H. Hallmeier, S. Sauter, R. Szargan, *Inorg. Chem. Commun.* **2001**, *4*, 153 – 156.
[15] R. Garde, F. Villain, M. Verdaguer, *J. Am. Chem. Soc.* **2002**, *124*, 10531 – 10538.
[16] T. Yokoyama, H. Tokoro, S.-I. Ohkoshi, K. Hashimoto, K. Okamoto, T. Ohta, *Phys. Rev. B* **2002**, *66*, 184111 – 184111-20.
[17] Furthermore, for a Co^{II} ion and a necessarily bent Co^{II}-NC-Fe entity around the Cs ion, or for a mixture of this environment and the linear Co^{III}-NC-Fe entity, the calculated EXAFS signal is completely different from the experimental one.
[18] The number of Co atoms per unit cell surrounding one Td site is $(1+{}^{3}/_{4})$. As the Cs ions are diluted in the structure (0.7 per unit cell), the number of Co atoms surrounding one Cs ion is given by $0.7\times(1+{}^{3}/_{4})$, which corresponds to 30% of the Co ions.
[19] P. Lacorre, J. B. Torrance, J. Pannetier, A. Nazzal, P. W. Wang, T. C. Huang, *J. Solid State Chem.* **1991**, *91*, 225 – 237.
[20] C. Cartier dit Moulin, F. Villain, A. Bleuzen, M.-A. Arrio, P. Sainctavit, C. Lomenech, V. Escax, F. Baudelet, E. Dartyge, J. J. Gallet, M. Verdaguer, *J. Am. Chem. Soc.* **2000**, *122*, 6653 – 6658.
[21] M. Sorai, S. Seki, *J. Phys. Chem. Solids* **1974**, *35*, 555 – 570.

 © 2004 Wiley-VCH Verlag GmbH & Co. KGaA, Weinheim

Cover Picture



Andrey Gutnov,* Barbara Heller,* Christine Fischer, Hans-Joachim Drexler, Anke Spannenberg, Bernd Sundermann, and Corinna Sundermann

Nature decided in favor of the left-handed helical isomer for the hop vine shown in the cover picture. In contrast, the [2+2+2] cycloaddition yielding biaryl nitrogen heterocycles gives access to both enantiomers. In their Communication on p. 3795 ff. A. Gutnov, B. Heller et al. describe this photochemical reaction which is conducted with a chiral cobalt catalyst. (The picture of the hop plant is taken from the book by H. Brunner, *Rechts oder Links. In der Natur und anderswo*, Wiley-VCH, **1999**.)

Contents

Angewandte EarlyView

The following Communications are available online (in Wiley InterScience). You can find them, as well as forthcoming Reviews, Highlights, and Essays, at www.angewandte.org, under Early View.

P. Wu, A. K. Feldman, A. K. Nugent, C. J. Hawker, A. Scheel, B. Voit, J. Pyun, J. M. J. Fréchet, K. B. Sharpless,* V. V. Fokin*:*
Efficiency and Fidelity in a Click-Chemistry Route to Triazole Dendrimers by the Copper(I)-Catalyzed Ligation of Azides and Alkynes
DOI: 10.1002/anie.200454078
Published online: June 30, 2004

K. C. Nicolaou, S. Vyskocil, T. V. Koftis, Y. M. A. Yamada, T. Ling, D. Y.-K. Chen, W. Tang, G. Petrovic, M. O. Frederick, Y. Li, M. Satake*:*
Structural Revision and Total Synthesis of Azaspiracid-1, Part 1: Intelligence Gathering and Tentative Proposal
DOI: 10.1002/anie.200460695
Published online: June 25, 2004

K. C. Nicolaou, T. V. Koftis, S. Vyskocil, G. Petrovic, T. Ling, Y. M. A. Yamada, W. Tang, M. O. Frederick:*
Structural Revision and Total Synthesis of Azaspiracid-1, Part 2: Definition of the ABCD Domain and Total Synthesis
DOI: 10.1002/anie.200460696
Published online: June 29, 2004

Articles judged by the referees or the editor as being either very important or very urgent are immediately edited, proof-read, and electronically published once the manuscript has arrived in the editorial office in its final form. As long as there is no page number available these articles should be cited in the following manner:

Author(s), *Angew. Chem. Int. Ed.*, online publication date, DOI.

Meeting Reviews

When Chemistry Met Biology ——— **3750 – 3751** *T. Berg*

Books

Inorganic Electrochemistry ——— **3752** Piero Zanello *reviewed by D. Astruc*

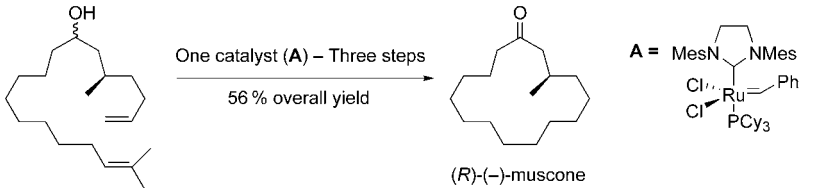
Organotin Chemistry ——— **3753** Alwyn G. Davies *reviewed by M. Weidenbruch*

Minireviews

Multifunctional Catalysis

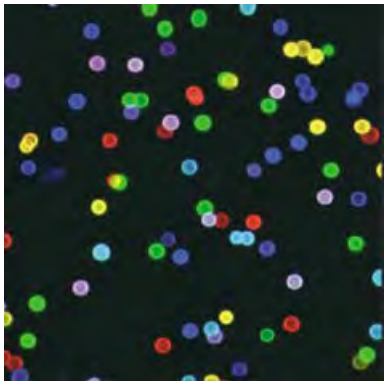
A. Ajamian, J. L. Gleason* — **3754 – 3760**

Two Birds with One Metallic Stone: Single-Pot Catalysis of Fundamentally Different Transformations



Multitasking catalysts: Metal catalysis has been pushed to a new level with the development of methods that use a single catalyst for several fundamentally different transformations in a single reaction flask (see example). Several examples from the recent literature are highlighted, including methods in which a single catalyst mediates two reactions simultaneously. Mes = 2,4,6-trimethylphenyl, Cy = cyclohexyl.

Reviews



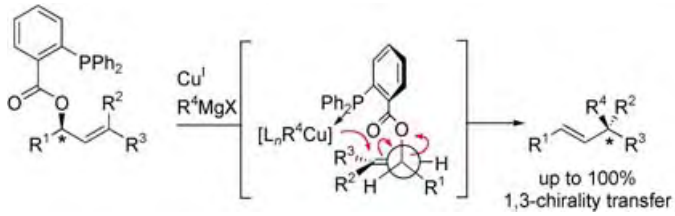
Wrap artists: Hollow polyelectrolyte microcapsules have promising perspectives in numerous applications, such as engineering, biotechnology, and medicine. In this Review, the recent advances in this field are presented, with a focus on the permeability properties of the capsules as well as on their application as microreactors. The picture shows a library of 15 dye-modified capsules of poly(allylamine)/poly(styrene sulfonate).

Materials Science

C. S. Peyratout, L. Dähne* _ **3762 – 3783**

Tailor-Made Polyelectrolyte Microcapsules: From Multilayers to Smart Containers

Communications

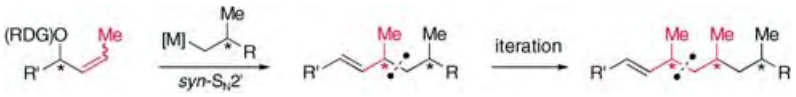


Selectivity at the flick of a switch: Through 1,3-chirality transfer, a directing/nondirecting leaving group facilitates the stereospecific and stereodivergent construction of quaternary carbon centers by copper-mediated allylic substitution with Grignard and organozinc reagents (see scheme; the use of the corresponding phosphane oxide leads to selective *anti* substitution).

Asymmetric Synthesis

B. Breit,* P. Demel, C. Studte _ **3786 – 3789**

Stereospecific and Stereodivergent Construction of Quaternary Carbon Centers through Switchable Directed/Nondirected Allylic Substitution



Can't have too much of a good thing: A flexible, iterative strategy based on a highly selective copper-mediated allylic substitution makes the preparation of any desired oligo(deoxypropionate) stereoisomer possible (see scheme; RDG = reagent-directing group). This approach differs from the established enolate-alkylation methodology through the reversed polarity of the reaction partners and avoids several problems associated with the latter method.

Polyketides

B. Breit,* C. Herber _ **3790 – 3792**

Iterative Deoxypropionate Synthesis Based on a Copper-Mediated Directed Allylic Substitution

For the USA and Canada:
ANGEWANDTE CHEMIE International Edition (ISSN 1433-7851) is published weekly by Wiley-VCH PO Box 191161, D 69451 Weinheim, Germany. Air freight and mailing in the USA by Publications Expediting Inc. 200 Meacham Ave., Elmont, NY 11003. Periodicals postage paid at Jamaica NY 11431. US POSTMASTER: send address changes to *Angewandte Chemie*, Wiley-VCH, 111 River Street, Hoboken, NJ 07030. Annual subscription price for institutions: Europe € 3430.00/3118.00; outside Europe US$ 4499.00/4090.00 (valid for print and electronic/print or electronic delivery); for individuals who are personal members of a national chemical society, or whose institution already subscribes, or who are retired or self-employed consultants, print only: Europe € 248.00/outside Europe US$ 378.00. Postage and handling charges included. All Wiley-VCH prices are exclusive VAT.

 © 2004 Wiley-VCH Verlag GmbH & Co. KGaA, Weinheim

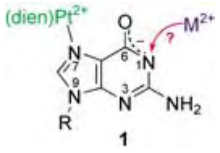
Contents

Stability Constants

B. Knobloch, R. K. O. Sigel,* B. Lippert, H. Sigel ——— **3793 – 3795**

Two Metal Ions Coordinated to a Purine Residue Tolerate Each Other Well

The catalytic sites of ribozymes generally contain two or more metal ions. Guanine is the nucleobase most often involved in binding to metal ions. The repulsion between two M^{2+} ions simultaneously coordinated to guanine in aqueous solution was investigated by using complex **1** (see picture; dien = diethylenetriamine, R = C_2H_5) as a model, for which the

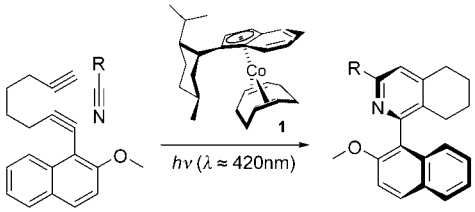


stability constants for the binding of Mg^{2+} and Cu^{2+} were determined.

Asymmetric Catalysis

A. Gutnov,* B. Heller,* C. Fischer, H.-J. Drexler, A. Spannenberg, B. Sundermann, C. Sundermann ——— **3795 – 3797**

Cobalt(I)-Catalyzed Asymmetric [2+2+2] Cycloaddition of Alkynes and Nitriles: Synthesis of Enantiomerically Enriched Atropoisomers of 2-Arylpyridines



82–93 % *ee*

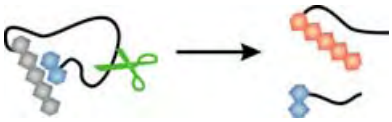
A new flavor of chiral induction in the [2+2+2] cycloaddition yielding pyridines: Atropoisomers were prepared in the reaction of alkynes and nitriles in the presence of 1 mol% chiral Co^{I} catalysts such as **1** with high yields and up to 93% *ee*.

Biosensors

N. Marmé, J.-P. Knemeyer, J. Wolfrum, M. Sauer* ——— **3798 – 3801**

Highly Sensitive Protease Assay Using Fluorescence Quenching of Peptide Probes Based on Photoinduced Electron Transfer

Making the cut and then detecting it: Short fluorophore-labeled peptide substrates (see scheme) show strong fluorescence quenching due to electron transfer from a tryptophan residue (blue) to the dye (gray, red). Upon specific cleavage of the peptide by proteolytic enzymes, quenching is prevented and the fluorescence intensity increases. The

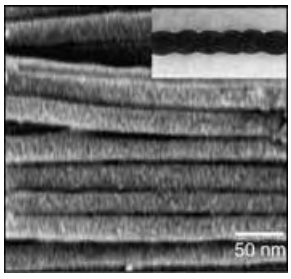


method can be used to assay proteolytic enzymes with detection limits in the picomolar range.

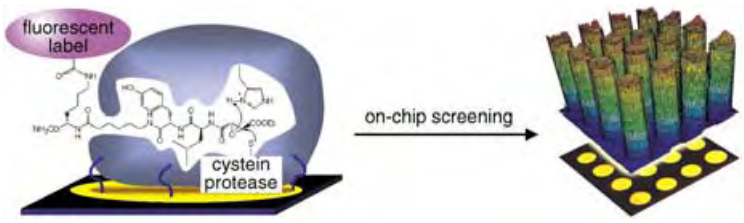
Conducting Materials

J. Jang,* J. Bae ——— **3803 – 3806**

Fabrication of Polymer Nanofibers and Carbon Nanofibers by Using a Salt-Assisted Microemulsion Polymerization



Salt-assisted sphere-to-cylinder micelle conversion in the microemulsion polymerization process is the crucial step for the formation of polyacrylonitrile nanofibers (see picture). Iron(III) chloride is used as a structure-directing agent and is coordinated by polyacrylonitrile nanoparticles, which is essential for the formation of the nanofibers.



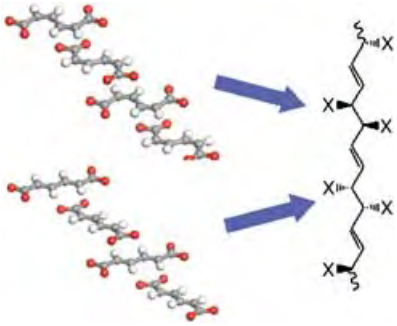
High-throughput screening of libraries of potential inhibitors is possible by using an enzyme microarray method that combines low sample consumption with accuracy and speed. Information about enzyme inhibition can be obtained "on-chip" by the addition of a fluorescently tagged affinity label to a microarray of functional enzymes (see picture).

Microarray Technology

J. Eppinger,* D. P. Funeriu,* M. Miyake, L. Denizot, J. Miyake ——— **3806 – 3810**

Enzyme Microarrays: On-Chip Determination of Inhibition Constants Based on Affinity-Label Detection of Enzymatic Activity

---



The intermolecular interactions that lead to translational and alternate molecular stacking of 1,3-diene monomers in the solid state (see example, $X = CO_2CH_2$-$C_6H_4OCH_3$) as well as the molecular symmetry of muconic acid derivatives have been utilized in controlling the stereoregularity of polymers. This crystal engineering approach has enabled the four kinds of stereoregular diene polymers to be synthesized in a solid-state polymerization.

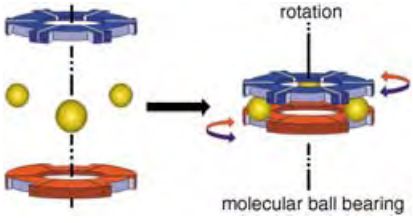
Topochemistry

S. Nagahama, T. Tanaka, A. Matsumoto* ——— **3811 – 3814**

Supramolecular Control over the Stereochemistry of Diene Polymers

---

A thrust in the right direction: Two different disk-shaped ligands (a tris-monodentate and a hexa-monodentate ligand) and three Ag^+ ions have been used as bearings and balls, respectively, in the construction of a molecular thrust ball bearing (see schematic representation). Rotation occurs through a combination of intramolecular, reversible multipoint ligand exchange and flip motions that act in concert.

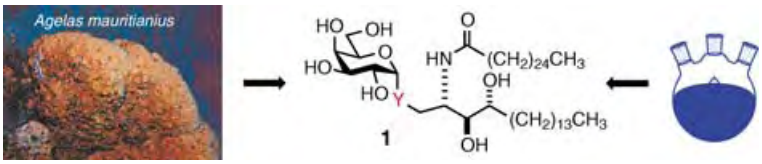


Molecular Devices

S. Hiraoka, K. Hirata, M. Shionoya* ——— **3814 – 3818**

A Molecular Ball Bearing Mediated by Multiligand Exchange in Concert

---



Which source provides the better drug? The fully synthetic C-glycoside **1** ($Y = CH_2$) is about 1000 times more potent against malaria in mice than the corresponding O-glycoside ($Y = O$), which is derived from a natural product and itself known to show remarkable activity against a wide range of diseases. The results of comparative biological assays emphasize the potential of C-glycosides as therapeutic agents.

Biologically Active Compounds

G. Yang, J. Schmieg, M. Tsuji, R. W. Franck* ——— **3818 – 3822**

The C-Glycoside Analogue of the Immunostimulant α-Galactosylceramide (KRN7000): Synthesis and Striking Enhancement of Activity

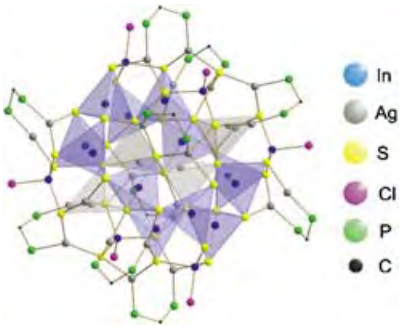
 © 2004 Wiley-VCH Verlag GmbH & Co. KGaA, Weinheim

Contents

Cluster Compounds

R. Ahlrichs, A. Eichhöfer, D. Fenske,* O. Hampe, M. M. Kappes, P. Nava, J. Olkowska-Oetzel _____ **3823 – 3827**

Synthesis and Structure of $[Ag_{26}In_{18}S_{36}Cl_6(dppm)_{10}(thf)_4][InCl_4(thf)]_2$ —A Combined Approach of Theory and Experiment

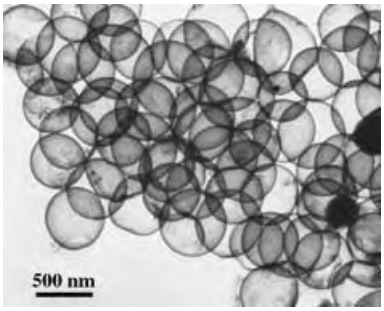


Difficult to determine, the molecular structure of the ionic cluster $[Ag_{26}In_{18}S_{36}Cl_6(dppm)_{10}(thf)_4]^{2+}$-$[InCl_4(thf)^-]_2$ (see picture, dppm = bis-(diphenylphosphanyl)methane) was independently resolved by theoretical (density functional theory) and experimental (single-crystal XRD, FTMS) methods. The cluster was synthesized by the reaction of AgOOCPh and $InCl_3$ with $S(SiMe_3)_2$ in the presence of the bidentate phosphane dppm.

Microspheres

X. Sun, Y. Li* _____ **3827 – 3831**

Ga_2O_3 and GaN Semiconductor Hollow Spheres

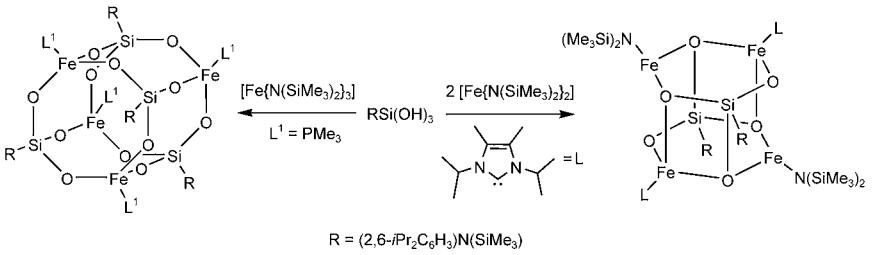


Carbon spheres are used as templates to prepare semiconductor hollow spheres of Ga_2O_3 (depicted) and GaN. The thickness and uniformity of the final products are predetermined by the thickness of the active layer of the carbon spheres. The diameter of the spheres can be adjusted in the range of 100 nm to 1.5 μm, which covers the band gaps in the spectral regime from UV to near infrared.

Cage Compounds

U. N. Nehete, G. Anantharaman, V. Chandrasekhar, R. Murugavel, M. G. Walawalkar, H. W. Roesky,* D. Vidovic, J. Magull, K. Samwer, B. Sass _____ **3832 – 3835**

Polyhedral Ferrous and Ferric Siloxanes



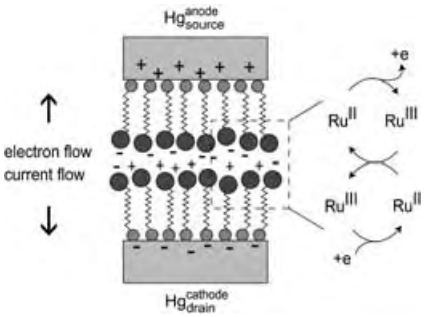
The synthesis, isolation, and single-crystal X-ray structures of the first polyhedral ferrous and ferric siloxanes (see scheme) suggest that similar synthetic strategies will allow the preparation of other transition-metal siloxane frameworks.

Molecular Electronics

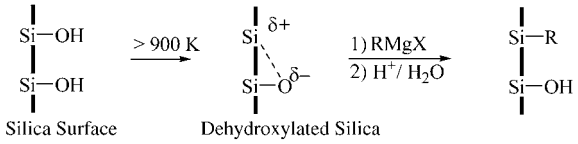
E. Tran, M. A. Rampi,* G. M. Whitesides* _____ **3835 – 3839**

Electron Transfer in a Hg-SAM//SAM-Hg Junction Mediated by Redox Centers

Current affairs: The electron-transport properties of a metal–molecule–metal junction based on two contacting redox-active self-assembled monolayers of $[Ru(NH_3)_5(NC_5H_4\text{-}4\text{-}CH_2NHCO(CH_2)_{10}\text{-}SH](PF_6)_2$ (see picture) is described. The junction becomes conductive when the electrode potentials are adjusted to the formal potential of the redox centers and shows diode- and transistor-like characteristics analogous to those of solid-state devices.



 © 2004 Wiley-VCH Verlag GmbH & Co. KGaA, Weinheim



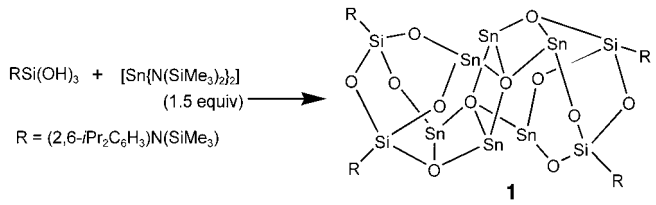
Electron-deficient silicon atoms, which are generated on a silica surface by evacuation above 900 K, are attacked by Grignard reagents (see picture). This reactivity provides a novel route for the surface modification of mesoporous silicas as the organic groups are strongly bound to the surface through the formation of Si–C bonds. The pore structures of the mesoporous silicas are not destroyed by the modification.

Mesoporous Materials

J. E. Lim, C. B. Shim, J. M. Kim,* B. Y. Lee,* J. E. Yie ——— **3839 – 3842**

Dehydroxylation Route to Surface Modification of Mesoporous Silicas by Using Grignard Reagents

---

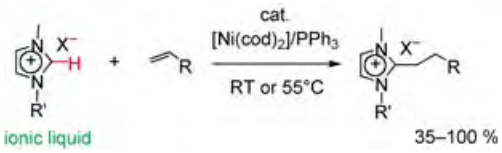


The hexatin(II) cage containing siloxane ligands is obtained by the addition of $Sn[N(SiMe_3)_2]_2$ to a suspension of $RSi(OH)_3$ in a hexane/THF mixture (see scheme). The X-ray crystal structure analysis of compound **1** reveals a central $\{(SnO)_6\}$ motif enclosed by two outer $\{R_2Si_2O_3\}$ siloxane ligands.

Main-Group-Metal Clusters

U. N. Nehete, V. Chandrasekhar, G. Anantharaman, H. W. Roesky,* D. Vidovic, J. Magull ——— **3842 – 3844**

Molecular $\{(SnO)_6\}$ Trapped by Two $\{R_2Si_2O_3\}$ Fragments: X-ray Single-Crystal Structure of $[(SnO)_6(R_2Si_2O_3)_2]$



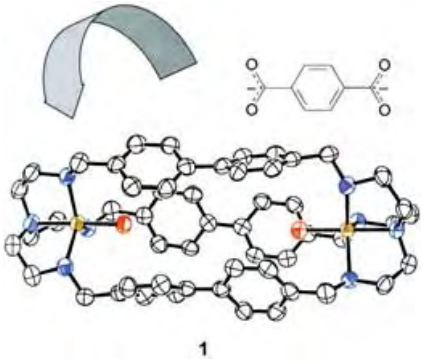
Reactive Couples: Imidazolium salts react with alkenes under mild conditions in the presence of a Ni^0-based catalyst to produce 2-alkyl imidazolium salts (see scheme, cod = 1,5-cyclooctadiene). The mechanism involves oxidative addition of an imidazolium C–H bond to M^0 to give a (carbene)M–H intermediate and finally bond formation between the carbene and an alkyl ligand through reductive elimination.

Ionic Liquids

N. D. Clement, K. J. Cavell* . **3845 – 3847**

Transition-Metal-Catalyzed Reactions Involving Imidazolium Salt/N-Heterocyclic Carbene Couples as Substrates

---



Fits like a glove! The dicopper(II) complex **1** of a bistren cage containing ditolyl spacers binds dicarboxylate anions in aqueous solutions. The inclusion is highly selective on the basis of the distance between the COO^- groups. For example, terephthalate (see picture) is discriminated from isophthalate and phthalate.

Anion Sensors

M. Boiocchi, M. Bonizzoni, L. Fabbrizzi,* G. Piovani, A. Taglietti ——— **3847 – 3852**

A Dimetallic Cage with a Long Ellipsoidal Cavity for the Fluorescent Detection of Dicarboxylate Anions in Water

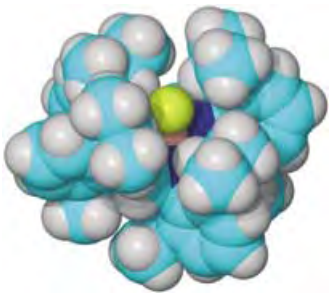
 © 2004 Wiley-VCH Verlag GmbH & Co. KGaA, Weinheim

Contents

Metal Hydride Complexes

R. J. Baker, C. Jones,* P. C. Junk, M. Kloth ——— **3852 – 3855**

Kinetic Control over the Thermal Stability of the In–H Bond: Synthesis and Characterization of Amido Indium Hydride Complexes



High thermal stability is a characteristic feature of the depicted amido indium hydride complex (In red; hydride yellow), which is amongst the first to be synthesized and characterized. The stability arises from steric shielding of the In–H bond, which frustrates the formation of the intermolecular In–H–In bridges.

VIP Communications labeled with this symbol have been judged by two referees as being "very important papers".

Sources

Product and Company Directory

You can start the entry for your company in "Sources" in any issue of *Angewandte Chemie*.

If you would like more information, please do not hesitate to contact us.

Wiley-VCH Verlag – Advertising Department
Tel.: 0 62 01 - 60 65 65
Fax: 0 62 01 - 60 65 50
E-Mail: MSchulz@wiley-vch.de

Service

Keywords ——— *3856*

Authors ——— *3857*

Angewandte's Sister Journals ——— *3858 – 3859*

Preview ——— *3861*

Corrigenda

In the Communication "Continuous Glucose Sensing with a Fluorescent Thin-Film Hydrogel" by B. Singaram et al. (*Angew. Chem. Int. Ed.* **2003**, *42*, 5857–5859, DOI 10.1002/anie.200352405) on page 5859, the top right paragraph says "operate under physiological conditions (37 °C, 0.1 μM ionic strength, pH 7.4)". Instead it should read "operate under physiological conditions (37 °C, 0.1 M ionic strength, pH 7.4)".

In the Communication "The Circumambulation of a Phosphirane: Taking 9-Phenyl-9-phosphabicyclo[6.1.0]nona-2,4,6-triene for a 'Walk'" by K. Lammertsma et al. (*Angew. Chem. Int. Ed.* **2004**, *43*, 714 – 717, DOI 10.1002/anie.200351855), the ^{1}H NMR chemical shift of compound **3P** of 3.65 ppm should be 2.65 ppm and the ^{31}P NMR chemical shift at 179 ppm should be reversed in sign. The first reference reporting the conversion of **3P** to **7P** should also have been cited: T. J. Katz, C. R. Nicholson, C. A. Reilly, *J. Am. Chem. Soc.* **1966**, *88*, 3832 – 3842.

Apologies

In the Communication "Diffusion-Limited, Aggregation-Based, Mesoscopic Assembly of Roughened Core-Shell Bimetallic Nanoparticles into Fractal Networks at the Air–Water Interface" by Y. Jin and S. Dong (*Angew. Chem. Int. Ed.* **2002**, *41*, 1040–1044), the title is incorrect. The correct title is: "Diffusion-Limited, Aggregation-Based, Mesoscopic Assembly of Surface-Roughened Shell-Type Bimetallic Nanoparticles into Fractal Networks at the Air–Water Interface". The interior-hollowed structure of the unit bimetallic nanoparticles was clearly revealed in a related publication (Y. D. Jin, S. J. Dong, *J. Phys. Chem. B* **2003**, *107*, 12902–12905). The authors apologize for this oversight.

In the Communication "Size-dependent Magnetic Properties of Colloidal Mn_3O_4 and MnO Nanoparticles" by J. T. Park et al. (*Angew. Chem. Int. Ed.* **2004**, *43*, 1115 – 1117, DOI 10.1002/anie.200352400), the following important reference for the preparation of soluble, monodisperse MnO and Mn_3O_4 is missing: M. Yin, S. O'Brien, *J. Am. Chem. Soc.* **2003**, *125*, 10180 – 10181. This work appeared online (August 5, 2003) during the review process and eluded the authors' attention.

Vacancies

GEORG-AUGUST-UNIVERSITÄT GÖTTINGEN

At the Faculty of Chemistry at the University of Goettingen a vacancy for a

W3 (C 4)-Professor in Organic and Biomolecular Chemistry (succeeding Prof. Zeeck)

has to be filled starting October 1st, 2005.

The chair is intended to strengthen the research areas which already exist at the Institute for Organic and Biomolecular Chemistry. The faculty is looking for a chemist with a strong background in biomolecular chemistry and molecular biology. A cooperation with the Goettingen Center for Molecular Biosciences (GZMB), the SFB 416 and the interdisciplinary graduate college is desired.

The chair holder will be responsible for teaching "Biomolecular Chemistry" in the course of diploma studies in chemistry. Apart from that a participation in the education of "Chemistry for Medical Students" as well as teaching chemistry in the international program "Molecular Biology" is expected.

Participation in academic examinations (Vordiplom, Bachelor, Diplom, Master, Staatsexamen, Promotion) and in academic administration is expected as well as the willingness to accept academic positions.

The requirements for the appointment as a professor are mentioned in § 26 Niedersaech-sisches Hochschulgesetz (Nds. GVBI S. 286 2002). Candidates are asked to provide a proof of their specific academic qualification, normally a "Habilitation" or an equivalent scientific qualification. Details will be given upon request.

The University of Goettingen aims at increasing the number of women among the scientific staff and therefore encourages applications of qualified women. Given an equivalent level of qualification women will receive preferential attention.

Provided there are applicants with equal qualifications disabled persons will be preferred.

It will not be possible to work part-time.

Applications including CV, a detailed account of the academic career including teaching activities and a list of publications, reprints of the five most important publications as well as a short outline of the planned research activities should be sent before September 30, 2004 to **Dekan der Fakultaet fuer Chemie, der Georg-August-Universitaet Goettingen, Herrn Prof. Dr. G. Eckold, Tammannstraße 4, D-37077 Goettingen, Germany**

BOKU - University of Natural Resources & Applied Life Sciences

Professorship of Wood-, Pulp- and Fiber Chemistry

The University of Natural Resources & Applied Life Sciences, Boku, Vienna, is currently inviting applications for a Professorship of Wood-, Pulp- and Fiber Chemistry at the Department of Chemistry, starting in November, 2004. The position is initially limited to 5 years, with the possibility for unlimited extension upon positive evaluation.

The main teaching activities of the candidate should cover the fields of wood chemistry, pulp- and fiber chemistry as well as chemistry and technology of renewable resources.

The research focus is on the non-energetic utilization of plant-based renewable materials, particularly in the topics:

Chemistry and technology of cellulose preparation and by-product utilization; pulp- and cellulose chemistry comprising also structural and physicochemical aspects; chemistry and technology of cellulose processing and –derivatization, structure and chemistry of regenerated fibers and paper.

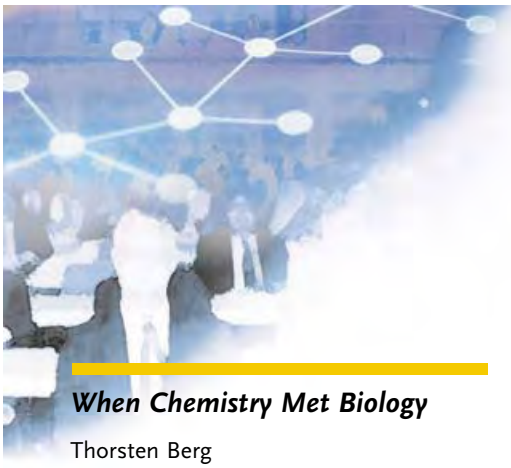
The deadline for applications is the 3st September 2004 (date of receipt at the address above).

The University of Natural Resources & Applied Life Sciences, Boku, Vienna, tends to increase its proportion of female staff. Qualified female scientists are therefore encouraged to apply. In the case of candidates with comparable qualifications, women will be given preference.

For detailed information see the website of the BOKU-University of Natural Resources an Applied Life Sciences, Vienna: http://www.boku.ac.at/chemie/announcements.htm

The Rector
Dipl.-Fw.Dr. Hubert Dürrstein

 © 2004 Wiley-VCH Verlag GmbH & Co. KGaA, Weinheim



When Chemistry Met Biology

Thorsten Berg

"Chemistry meets Biology" was the title of the second symposium held by the Young Investigator Programme of the European Molecular Biology Organization (EMBO) in Heidelberg (Germany) on June 5 and 6, 2004. The meeting was attended by internationally renowned scientists with a broad range of backgrounds in both chemistry and biology, and demonstrated how the interface between chemistry and the biological sciences has established itself as a research field of its own.

In the introductory lecture to the first session, which was entitled "Chemical Tools for Cell Biology", Tim Mitchison (Harvard Medical School, USA) gave an overview of the use of automated microscopy for the discovery of small-molecule inhibitors of cell division in phenotypic screens. He outlined how the mechanism of action of a compound can be elucidated by using a panel of antibodies and assessing various microscopic markers. Kai Johnsson (EPFL, Switzerland) then presented a versatile method for tagging proteins in living cells, based on the expression of fusion proteins with the human DNA repair protein O6-alkylguanine-DNA alkyltransferase (hAGT) and the reaction of hAGT with O6-benzylguanine derivatives. Steve Adams (University of California, San Diego) discussed an alternative system for the tagging of proteins with a rainbow of synthetic fluorophores containing arsenic(III). These fluorophores bind to a tetracysteine motif fused to a protein of interest. Philippe Bastiaens (EMBL Heidelberg) introduced approaches for sampling the spatial organization of signal transduction via the different isoforms of the GTPase Ras. The last talk of the first session was given by Craig Crews (Yale University, New Haven, USA), who demonstrated the use of small-molecule probes for the analysis of cellular signaling networks. He discussed the identification of protein targets of the natural product fumagillin and presented a new chemical strategy by which a desired protein can be targeted for selective degradation.

The second session was titled "Signal Transduction and Cell Division" and began with an introductory lecture by Herbert Waldmann (MPI Dortmund, Germany) on the chemical biology of protein lipidation. Waldmann discussed the synthesis of Ras variants with chemically modified farnesyl or palmitoyl groups and the application of these modified proteins to the analysis of the role of farnesyl and palmitoyl groups in Ras-mediated signal transduction. He also pointed out the advantages of using natural products for studies in chemical biology and for drug development. Thomas Mayer (MPI Martinsried, Germany) then presented his work on the identification of small-molecule inhibitors of molecular motor proteins (kinesins) and the use of these small molecules as tools for analyzing the biological functions of kinesins (Figure 1). Jan-Michael Peters (IMP, Vienna, Austria) discussed the use of low-molecular-weight organic molecules for the analysis of chromosome segregation in mitosis. Carsten Schultz (EMBL Heidelberg) presented the synthesis of fluorescent small-molecule probes that can be used for intracellular fluorescence resonance energy transfer (FRET), and their application to the spatial and temporal analysis of enzyme activity in living cells. In the last talk of the day, Theodorus Gadella (Amsterdam University, The Netherlands) presented his work on the imaging and manipulation of biochemical reactions at the plasma membrane in single living cells.

After these two stimulating sessions, roundtable discussions took place on the topics of protein-labeling techniques, drug design, chemical genomics, and fluorophores, and provided ample opportunity for exchanging opinions and discussing relevant topics with experts in the respective areas.

The second day of the meeting began with presentations on the "Control of RNA and DNA". The introductory lecture by Peter Nielsen (The Panum Institute, Copenhagen, Denmark) covered the control of gene expression by peptide nucleic acids (PNAs), which can bind to DNA and RNA in a sequence-specific manner. He introduced a peptide nucleic acid which inhibits the protein Mdm2 and thereby restores the function of the tumor suppressor p53. Orlando Schärer (Universität Zürich, Switzerland) presented chemical tools for the investigation of complex mammalian DNA-repair pathways. Peter Seeberger (ETH Zürich) described the automated solid-phase synthesis of complex carbohydrates and the immobilization of carbohydrates on a solid surface (carbohydrate arrays). These arrays allow the rapid analysis of the interactions between carbohydrates and their binding partners (Figure 2). He also highlighted the potential of synthetic carbohydrates as vaccines. Oliver Seitz (Humboldt Universität, Berlin, Germany)

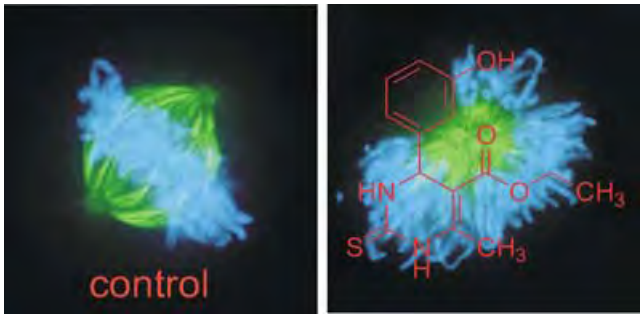


Figure 1. Mitotic cells in the absence (left) and presence (right) of monastrol. The DNA is stained blue, the microtubules green. (Kindly provided by T. U. Mayer, MPI Martinsried).

[*] T. Berg
Max Planck Institute of Biochemistry
Martinsried (Germany)
E-mail: berg@biochem.mpg.de

 © 2004 Wiley-VCH Verlag GmbH & Co. KGaA, Weinheim DOI: 10.1002/anie.200460998

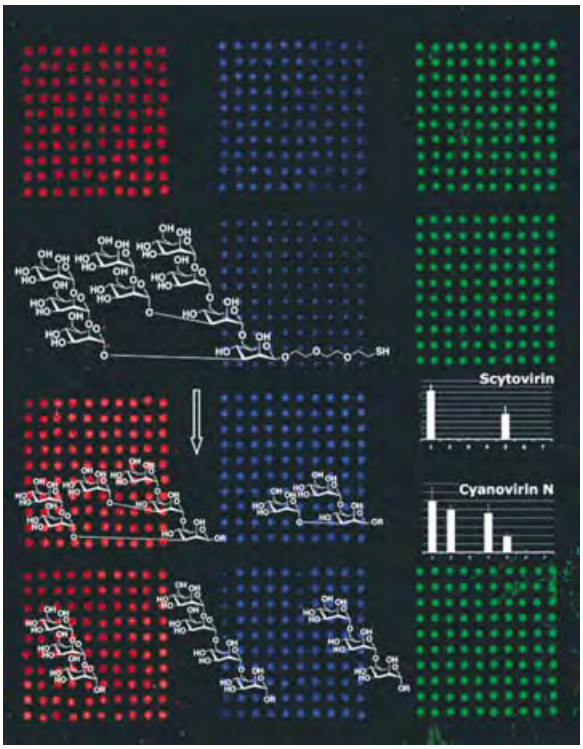


Figure 2. Carbohydrate arrays. (Kindly provided by P. H. Seeberger, ETH Zürich).

presented an approach for detecting single-base mutations in DNA by forcing a dye whose fluorescence intensity is sensitive to its environment to intercalate adjacent to the expected mutation site. He also outlined a system for the study of methyl transferases involving the stabilization of "base-flipped" sites. Michael Famulok (Universität Bonn, Germany) discussed the generation of aptamers, which are functional RNA molecules with high affinity for their protein targets. This concept was extended to intracellularly expressed RNA aptamers (intramers) and their application for the screening of small-molecule inhibitors of macromolecules.

Greg Petsko (Brandeis University, Waltham, USA) started the last session, titled "Structural Biology and Drug Design", with a discussion of the shortcomings of the current drug-discovery process, and introduced his approach to structure-guided drug discovery. He was followed by Louis Serrano (EMBL Heidelberg), who introduced a computational method for protein design, and its application to the prediction of protein–protein interactions. Ilme Schlichting (MPI Heidelberg) discussed the challenges involved in the design of selective inhibitors for individual members of the highly conserved family of nitric oxide synthases (NOS), and the progress achieved to date. Annette Beck-Sickinger (Universität Leipzig, Germany) reported on the role of neuropeptide Y in breast cancer, the development of selective tools for neuropeptide Y receptor subtypes, and the prerequisites for the application of these tools in tumor reversion. In the last talk of the meeting, A. Ganesan (University of Southampton, UK) discussed the synthesis of natural products, such as spiruchostatin A and petromindole, and their application to the study of biological processes.

Key to the success of the meeting was the ability of the speakers to adapt their talks to a heterogeneous audience. The science presented was of a very high quality and illustrated how close chemistry and biology have become in recent years. It would be great to see more such interdisciplinary meetings in the future.

 © 2004 Wiley-VCH Verlag GmbH & Co. KGaA, Weinheim

Multifunctional Catalysis

Two Birds with One Metallic Stone: Single-Pot Catalysis of Fundamentally Different Transformations

*Alain Ajamian and James L. Gleason**

Keywords:
Pauson–Khand reaction · catalysis · domino reactions · metathesis · transition metals

Advances in metal catalysis have revolutionized organic synthesis, with the scope of metal-catalyzed reactions now covering nearly all areas of carbon–carbon, carbon–hydrogen, and carbon–heteroatom bond formation. For years, the goal was to develop catalysts that were highly selective for a single transformation. However, a promising current area of research is the use of a single catalyst to mediate more than one transformation in a selective manner. Whereas much early work was focused on using a catalyst for several similar transformations, recent investigations have shown that it is also possible to employ a single catalyst for several very different transformations in a single reaction sequence. This Minireview focuses on methods in which the mechanisms of the transformations are fundamentally very different.

1. Introduction

Advances in the field of transition-metal catalysis have revolutionized organic synthesis. When R. B. Woodward and co-workers published the total synthesis of strychnine 50 years ago,[1] the use of transition metals in the synthesis of complex molecules was usually limited to simple oxidation and reduction chemistry. Today, it is nearly inconceivable to undertake a synthesis of a complex natural product without at least considering the use of one or a number of modern transition-metal-mediated reactions. Although many transition-metal catalysts often employ expensive metals or ligands, the fact that they can be used in catalytic amounts, combined with their often high chemo- and stereoselectivity, outweighs their high unit costs. One common goal in catalyst development is high catalyst efficiency, which becomes important as reaction scale or catalyst cost increases. A quantum leap in efficiency can potentially be obtained by using a single catalyst to conduct more than one chemical transformation in a single synthetic operation. There are numerous examples in which a catalyst is used to conduct two or more mechanistically similar reactions. These include cascade/domino reactions as well as those which are sequenced by either a specific order of reagent addition or by differing reactivity of functional groups (e.g. two cross-coupling reactions, the first with a vinyl triflate and the second with a vinyl bromide).[2]

A new area of research seeks to use a single catalyst to mediate two or more reactions that are fundamentally different in nature (e.g. carbon–carbon bond formation followed by alkene hydrogenation). This research area has great potential, as there are many different reactions susceptible to catalysis which might be linked in sequence. Numerous examples have been reported over the past two or three years under labels such as tandem, dual, or multifunctional catalysis. For the purposes of this Minireview, we can divide published examples into two categories: sequential catalysis and concurrent catalysis.[3] In the first category, a single catalyst is used for several sequential transformations in a single pot. Each new reaction is initiated by a change in conditions (e.g. change in temperature) or by the addition of a new reagent. In some cases, the nature of the catalyst will change, such that it can no longer mediate the first reaction. In the second class, concurrent catalysis, two different transformations are catalyzed simultaneously by the same catalyst. With regard to a specific substrate, the individual reactions may be sequential processes, the second reaction keying on an intermediate formed in the first. Alternatively, a true simultaneous process may be involved, in which two reactions occur at equal rates, either at two different locations within a single substrate or on completely different substrates. Importantly, for concurrent catalysis all reagents are added at the beginning, the same reaction conditions are maintained

[*] A. Ajamian, Prof. J. L. Gleason
Department of Chemistry, McGill University
801 Sherbrooke Street West, Montreal, QC H3A 2K6 (Canada)
Fax: (+1) 514-398-3797
E-mail: jim.gleason@mcgill.ca

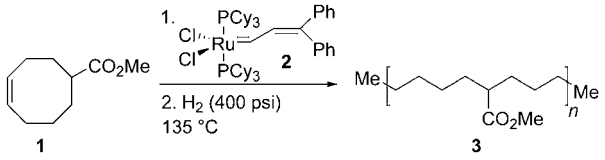
 © 2004 Wiley-VCH Verlag GmbH & Co. KGaA, Weinheim DOI: 10.1002/anie.200301727

throughout, and a single catalyst is responsible for all transformations. Regardless of the definitions used herein, highly practical methods have been developed within both categories, several of which have been put into practice in the synthesis of natural products.

2. Sequential Catalysis

Of the two categories, sequential-catalysis systems are probably the easier to develop and thus far have generally proved broader in scope. To develop a sequential catalytic process, knowledge is required of the types of reactions that metal catalysts are capable of mediating and of the changes in conditions or reagents that are most likely to produce a successful sequential event.

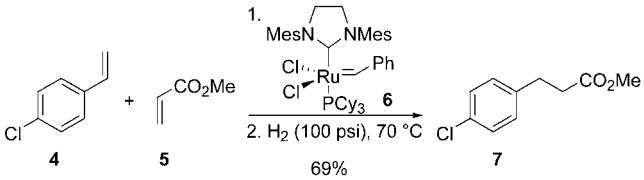
The largest category of sequential reactions features the ruthenium metathesis catalysts developed by Grubbs and co-workers.[4] These catalysts have been used extensively for ring-opening metathesis polymerization (ROMP), ring-closing metathesis (RCM), cross metathesis, and acyclic diene metathesis (ADMET). Their first use in a sequential process was reported by McLain et al., who showed that an ethylene/methyl acrylate copolymer formed by a ROMP process with $[(PCy_3)_2Cl_2Ru{=}CHCH{=}CPh_2]$ (**2**) could be hydrogenated by placing the product of the polymerization reaction under high pressures (400 psi, 1 psi = 6894.8 Pa) of hydrogen (Scheme 1).[5] This process led to >99% hydrogenation of



Scheme 1. Ruthenium alkylidene catalyzed ring-opening metathesis polymerization and hydrogenation.[5] Cy = cyclohexyl.

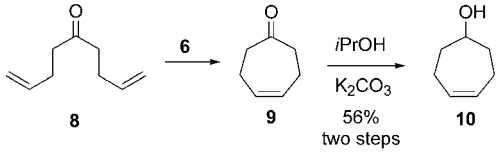
the polymer. In this instance, it was presumed that the addition of hydrogen transformed the metathesis catalyst into $[(PCy_3)_2RuHCl]$, an active hydrogenation catalyst. Similar effects were observed by Dias and Grubbs with a bimetallic ruthenium reagent, which could be used to reduce polybutadiene, obtained from the ROMP of cyclooctadiene, under lower pressures of hydrogen (60 psi) with >95% conversion.[6] Subsequently, Watson and Wagener showed that the hydrogenation could be carried out by adding a silica-gel support,[7] with the advantage that the ruthenium catalyst could be removed by simple filtration after the hydrogenation was complete. More recently, Fogg and co-workers have shown that the metathesis activity may be regenerated by adding 3-chloro-3-methyl-1-butyne to the hydrogenation catalyst.[8]

Grubbs and co-workers were the first to demonstrate this methodology in small-molecule synthesis.[9] They showed that it was possible to use either their first-generation or second-generation catalysts to mediate either RCM or cross-metathesis followed by hydrogenation (Scheme 2). The process



Scheme 2. Ruthenium alkylidene catalyzed cross-metathesis and hydrogenation.[9] Mes = 2,4,6-trimethylphenyl.

was tolerant of many functional groups, including aryl halides, and in one case high selectivity was observed for the hydrogenation of the less-substituted alkene in dienes. In an important extension of this chemistry, it was shown that the catalyst could also be used for the oxidation of alcohols and the reduction of ketones through transfer hydrogenation (Scheme 3). These steps could be initiated by the addition of a base and either isopropyl alcohol (for reduction) or 3-pentanone (for oxidation). The utility of this method was



Scheme 3. Ruthenium alkylidene catalyzed ring-closing metathesis and ketone reduction.[9]



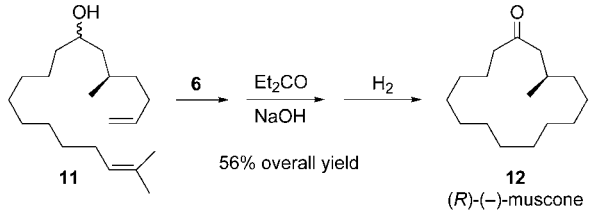
Jim Gleason was born in Montreal (Canada) in 1967 and received his BSc from McGill University (Montreal) in 1989. He completed his PhD in 1994 under the guidance of Robert E. Ireland at the University of Virginia (USA) on the total synthesis of FK-506. After a period as an NIH postdoctoral fellow with Andrew G. Myers at Caltech, he took a faculty position at McGill in 1996 and was promoted to associate professor in 2002. His research interests include the asymmetric formation of quaternary carbon centers and receptor-assisted dynamic combinatorial chemistry.



Alain Ajamian received his BSc degree in biochemistry from Concordia University (Montreal, Canada) in 1998. He then joined the research group of Prof. Stephen Hanessian at the University of Montreal, where he was a research associate from 1998–1999. Currently, he is completing his PhD under the supervision of Prof. James L. Gleason at McGill University. His PhD research has focused on a novel cobalt-catalyzed cycloisomerization reaction and its application to natural product synthesis.

© 2004 Wiley-VCH Verlag GmbH & Co. KGaA, Weinheim

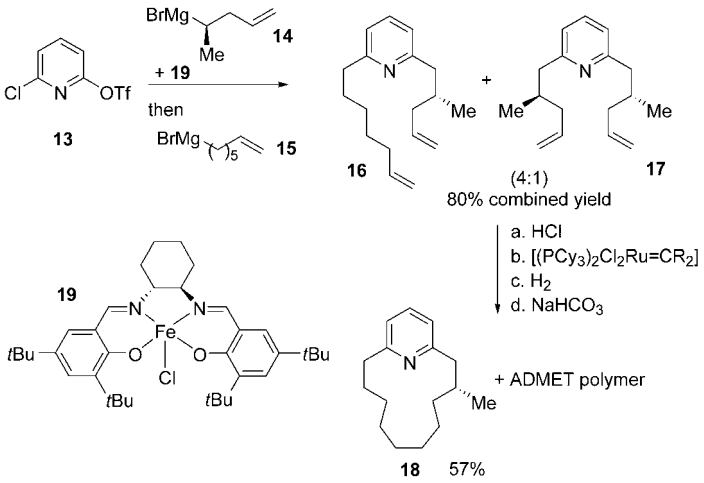
highlighted by a one-pot synthesis of (*R*)-(−)-muscone (**12**) through a RCM/oxidation/hydrogenation process (Scheme 4). The acyclic diene **11**, which is available in a single step from (*R*)-citronellal, underwent RCM to form the expected 15-membered cycloalkene ring in good yield.



Scheme 4. Synthesis of (*R*)-(−)-muscone (**12**) by a ruthenium-catalyzed RCM/oxidation/hydrogenation process.[9]

Subsequent addition of 3-pentanone and NaOH initiated oxidation of the secondary alcohol. Finally, the reaction mixture was placed under a hydrogen atmosphere, which led to the formation of (*R*)-(−)-muscone (**12**) in 56% yield from **11**.

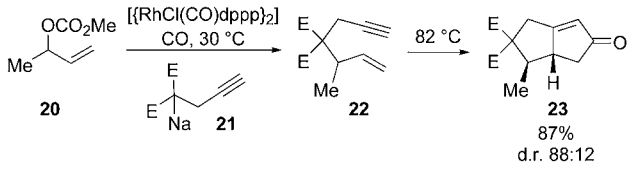
The RCM/hydrogenation process was also used effectively in a recent synthesis of muscopyridine (**18**) by Fürstner and Leitner (Scheme 5).[10] The substrate for RCM was prepared



Scheme 5. Synthesis of muscopyridine (**18**) featuring a ruthenium alkylidene catalyzed ring-closing-metathesis/hydrogenation process.[10] Tf = trifluoromethanesulfonyl.

by the sequential iron(III)–salen-catalyzed cross-coupling of the pyridine **13** with two different Grignard reagents to form an inseparable 4:1 mixture of the unsymmetrical diene **16** and the symmetrical diene **17**. This is an example of a sequential process with a single catalyst, but of a process that does not involve significantly different reactions. Protonation of the pyridine nitrogen atoms in **16** and **17**, followed by the addition of a ruthenium metathesis catalyst, initiated the RCM of **16** and an advantageous ADMET polymerization of **17**. The subsequent addition of hydrogen effected reduction of the alkenes to complete the sequential process. Simple filtration removed the ADMET polymer derived from **17** to yield pure muscopyridine (**13**) in 57% yield.

Several methods based on sequential catalysis in the presence of rhodium catalysts have been developed. For example, in one of the first examples of the sequential catalysis of a reaction sequence in which no metathesis was involved, Evans and Robinson combined the known ability of Rh^I complexes to effect both allylic alkylation and Pauson–Khand annulations in a one-pot process (Scheme 6).[11] The

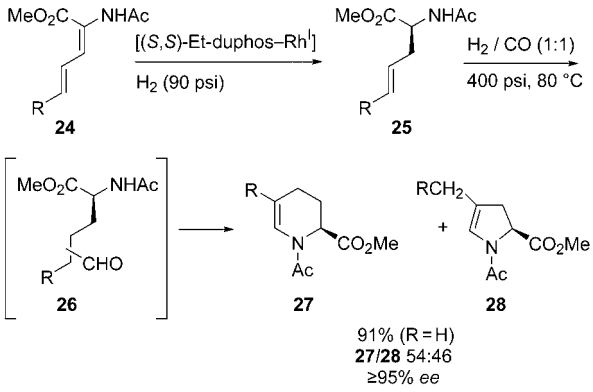


Scheme 6. Rhodium-catalyzed allylic alkylation and Pauson–Khand reaction.[11] E = ester group, dppp = 1,3-bis(diphenylphosphanyl)propane.

treatment of the methyl carbonate of 3-buten-2-ol with a malonate anion in the presence of $[\{RhCl(CO)(dppp)\}_2]$ and CO (1 atm) at 30 °C in acetonitrile afforded the corresponding allylic substitution product **22**. Warming the reaction mixture to reflux then induced a Pauson–Khand cycloaddition to form a bicyclic cyclopentenone such as **23** in excellent yield.

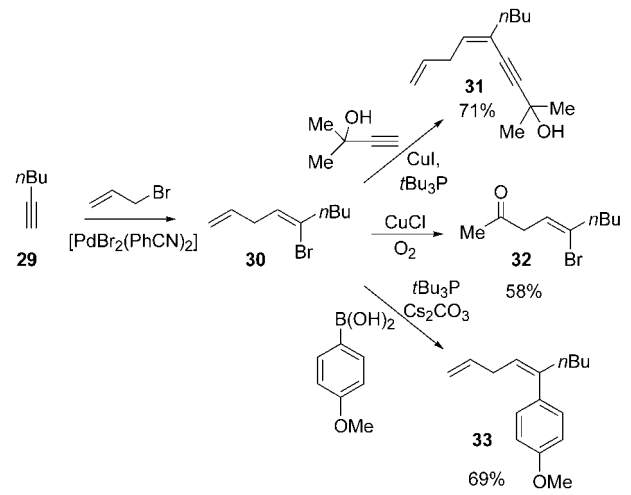
Robinson and co-workers have developed a sequential hydrogenation/hydroformylation reaction in the presence of a Rh^I complex.[12] The hydrogenation of dienamide esters, such as **24**, with [(*S*,*S*)-Et-duphos–Rh^I] afforded allyl glycines (**25**) with high enantioselectivity. The reaction vessel was charged subsequently with a mixture of H_2 and CO (1:1 ratio, 400 psi) and heated at 80 °C, which led to the formation of a 1:1 mixture of the tetrahydropyridine **27** and the dihydropyrrolidine **28** from the corresponding intermediate aldehyde (Scheme 7). The selectivity for the formation of **27** could be improved by incorporating a methyl group in the starting material (R = Me).

Thadani and Rawal have shown that it is possible to conduct palladium-catalyzed haloallylations of alkynes, which may be followed immediately by one of several reactions (Scheme 8).[13] The treatment of an allylic bromide with an



Scheme 7. Rhodium-catalyzed hydrogenation and hydrocarbonylation.[12]

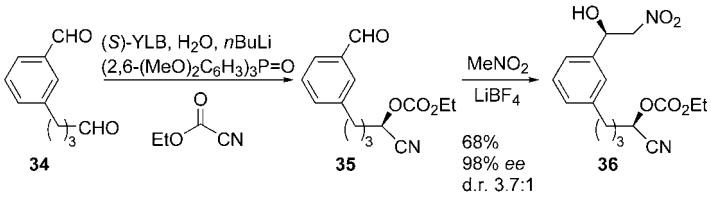
 © 2004 Wiley-VCH Verlag GmbH & Co. KGaA, Weinheim



Scheme 8. Palladium-catalyzed haloallylation followed by cross-coupling or Wacker–Tsuji oxidation.[13]

acetylene (e.g. **29**) in the presence of $[PdBr_2(PhCN)_2]$ in dimethoxyethane leads to the formation of the corresponding vinyl bromide (e.g. **30**). The subsequent addition of an alkyne, CuI, and tri-*tert*-butylphosphane intiates a Sonogashira cross-coupling reaction. Suzuki cross-coupling reactions may also be carried out by adding a vinyl or aryl boronic acid, cesium carbonate, and tri-*tert*-butylphosphane. As well as cross-coupling reactions, it is also possible to carry out a Wacker–Tsuji oxidation of the terminal vinyl group simply by adding CuCl and placing the reaction mixture under an oxygen atmosphere. All three types of sequential reactions are high yielding and take place with both terminal and internal alkynes.

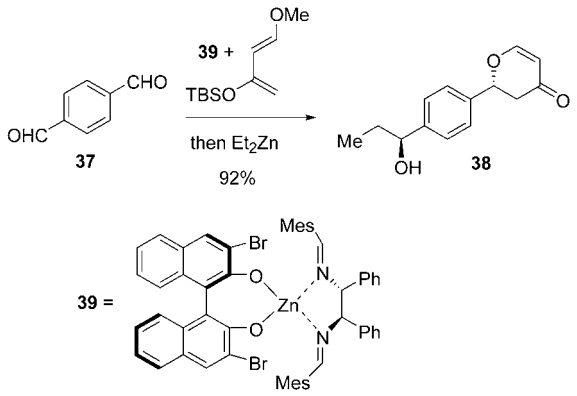
Two reports have shown that it is also possible to conduct sequential reactions with catalysts that have harder transition-metal centers. For example, Shibasaki and co-workers showed that with careful catalyst tuning it was possible to subject a dialdehyde to a sequential cyanation–nitroaldol sequence (Scheme 9).[14] The addition of the Mander reagent and the



Scheme 9. Yttrium-catalyzed cyanation and nitroaldol addition.[14]

YLi_3[tris(binaphthoxide)] (YLB) catalyst of Shibasaki to the dialdehyde **34** in the presence of H_2O (30 mol%), *n*BuLi (10 mol%), and $(2,6\text{-}(MeO)_2C_2H_3)_3P{=}O$ (10%) led to a chemoselective and enantioselective cyanation of the aliphatic aldehyde. To conduct a subsequent nitroaldol reaction of the remaining aromatic aldehyde, it was necessary to add $LiBF_4$ to dissociate the phosphane oxide from the catalyst. When $LiBF_4$ was omitted, the reaction still proceeded, but the enantioselectivity was lower (25% *ee*) than when $LiBF_4$ was included (up to 68% *ee*).

Du and Ding also examined a sequential reaction of a dialdehyde (Scheme 10).[15] In this case, they used the binol-



Scheme 10. Zinc-catalyzed hetero-Diels–Alder and diethylzinc addition.[15]

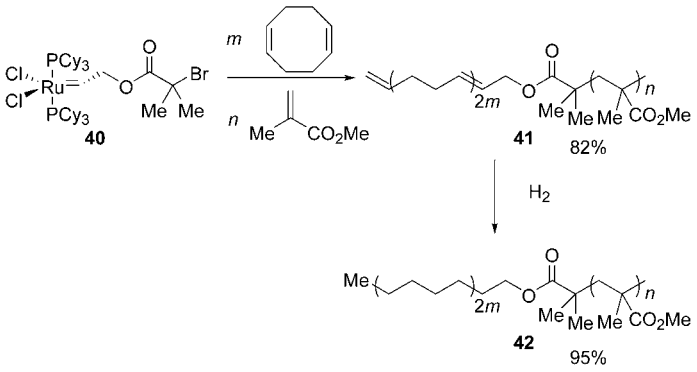
based zinc reagent **39** as a Lewis acid to catalyze a hetero-Diels–Alder reaction between the Danishefsky diene and either terphthalaldehyde (**37**) or isophthalaldehyde. The reaction proceeded with good chemoselectivity, as the intermediate product is less prone to undergo cycloaddition than the starting dialdehyde. Diethylzinc was then added to the reaction mixture, which resulted in the addition of an ethyl unit to the remaining aldehyde. Analysis showed that the initial cycloaddition had occurred with $\geq 97\%$ *ee* and the diethylzinc addition with d.r. > 97:3.

3. Concurrent Catalysis

The development of methods based on concurrent catalysis is more difficult than the development of sequential processes. In a sequential process, a change in reaction conditions or reagents initiates a new catalytic cycle, and in many cases the nature of the catalyst is altered such that it is either temporarily or permanently incapable of mediating the first transformation. Concurrent catalysis requires a delicate balancing act to ensure that a single catalyst can mediate two transformations, that the catalytic processes run at comparable rates and, perhaps most importantly, that they do not interfere with each other.

One of the first examples of concurrent catalysis was demonstrated by Grubbs and co-workers. Ruthenium carbenes were shown by Noels and co-workers to be efficient mediators of atom-transfer radical polymerization (ATRP).[16] Grubbs and co-workers showed that ROMP and ATRP could be carried out simultaneously starting from the ruthenium carbene **40**, which contains both the metal precatalyst and the cornerstone unit for a block copolymer (Scheme 11).[17] The addition of cyclooctadiene and methyl

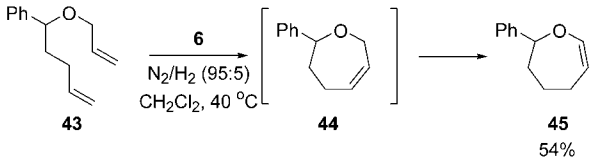
 © 2004 Wiley-VCH Verlag GmbH & Co. KGaA, Weinheim



Scheme 11. Ruthenium alkylidene catalyzed ring-opening metathesis polymerization and atom-transfer polymerization.[17]

methacrylate (MMA) to **40** resulted in the formation of a well-defined cyclobutadiene/MMA diblock copolymer **41**. Analysis of the reaction rates indicated that this was a sequential process when only **40** was used, with the ROMP occurring prior to ATRP. However, the addition of excess PCy_3 (10 equiv) slowed the rate of ROMP to the extent that the polymerizations took place simultaneously. Finally, the process could be linked in a sequence with hydrogenation by adding hydrogen to the crude block-copolymer mixture, which still contained the ruthenium catalyst, to afford the saturated polymer **42**.

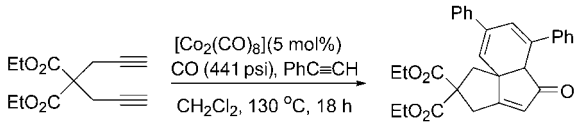
The Grubbs metathesis reagent has also been used in concurrent metathesis/alkene isomerization processes. Alkene isomerization has been a sporadically observed and unpredictable phenomenon in alkene metathesis. Its capricious nature had prevented it from being harnessed for synthetic use until Snapper and co-workers found that the reaction could be induced in an RCM process by adding small quantities of hydrogen to the reaction mixture.[18] This resulted in the formation of enol ethers with excellent control of the final regiochemistry, in all cases favoring the less-substituted enol ether (Scheme 12). Schmidt and Pohler



Scheme 12. Ruthenium alkylidene catalyzed ring-closing metathesis and alkene isomerization.[18]

observed similar results when they treated the metathesis catalyst with hydride sources (NaH or $NaBH_4$).[19] Snapper and co-workers noted that neither purified **6**, nor a new species formed by pretreatment with H_2, were effective isomerization catalysts, and it remains to be clarified whether or not this is a true case of concurrent catalysis as defined herein (i.e. one in which the isomerization catalyst and the metathesis catalyst are one and the same).

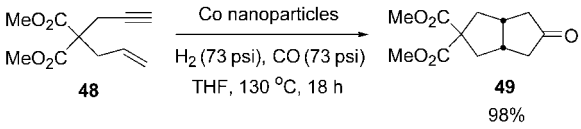
Two methods of concurrent catalysis based on cobalt-catalyzed [2+2+1] cyclizations have been reported by Chung and co-workers.[20a] In the first example, 1,6-diynes underwent a cyclocarbonylation reaction to form cyclopentadienones. This process is similar to the Pauson–Khand cyclization, but has not been used because of the instability of the products. In this instance, the highly reactive cyclopentadienone is trapped through a further cobalt-catalyzed [2+2+2] cycloaddition with phenylacetylene (Scheme 13). When the starting diyne is



Scheme 13. Cobalt-catalyzed sequential alkyne annulations.[20a]

derived from a malonate anion, the resulting tricyclic products are generally obtained in high yields and with excellent regioselectivities. Diynes lacking gem-dialkyl substitution at the 4-position also undergo this reaction, but give mixtures of cross- and homodimerization products.

Chung and co-workers also reported a reductive Pauson–Khand method in which 1,6-enynes were treated with charcoal-supported cobalt nanoparticles under a CO/H_2 (1:1) atmosphere.[20b] Under these conditions, the enynes underwent a Pauson–Khand cyclization to form bicyclic cyclopentenones, which were subsequently hydrogenated to give cyclopentanones (Scheme 14). The reaction proceeded in



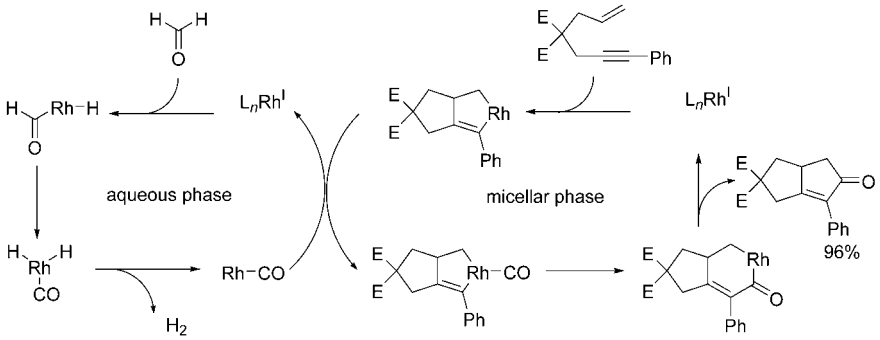
Scheme 14. Cobalt-nanoparticle-catalyzed Pauson–Khand reaction and hydrogenation.[20b]

high yield for a series of enynes and could even be used for intermolecular Pauson–Khand reactions if norbornene was used as the alkene component.

A classic example of simultaneous catalysis is catalytic transfer hydrogenation, whereby formic acid or another hydrogen source is dehydrogenated to provide the H_2 necessary for alkene hydrogenation. Several research groups have recently reported a conceptually similar variant of the Pauson–Khand reaction. These examples utilize the well-known ability of rhodium(I) catalysts to catalyze the decarbonylation of aldehydes to generate the CO necessary for the [2+2+1] process. For instance, Morimoto et al. showed that pentafluorobenzaldehyde could be used as a CO source in the Pauson–Khand reaction in the presence of $[\{RhCl(cod)\}_2]$/dppp (1:2).[21] Subsequent work showed that cinnamaldehyde could also be used as a CO source with either $[RhCl(dppp)_2]$

 © 2004 Wiley-VCH Verlag GmbH & Co. KGaA, Weinheim

or [{RhCl(cod)}$_2$]/tol-binap (1:2).[22] In these cases, *ee* values of up to 81% were observed for the reactions of aryl acetylenes. A disadvantage of using aldehydes is the low atom economy of the reaction. To address this problem, Morimoto, Kakiuchi, and co-workers investigated the use formaldehyde as the CO source.[23] The use of [{RhCl(cod)}$_2$]/dppp/TPPTS (1:2:2) under micellar conditions (with SDS as the surfactant) provided the best results. The use of two phosphane sources, one soluble in an organic solvent and one soluble in water, was found to accelerate the reaction relative to the use of a single ligand. From this observation and from the solubilities of the enyne substrates and formaldehyde, it was proposed that the decarbonylation of formaldehyde takes place in the aqueous phase, whereas the Pauson–Khand cycloaddition occurs in the micelle (Scheme 15).



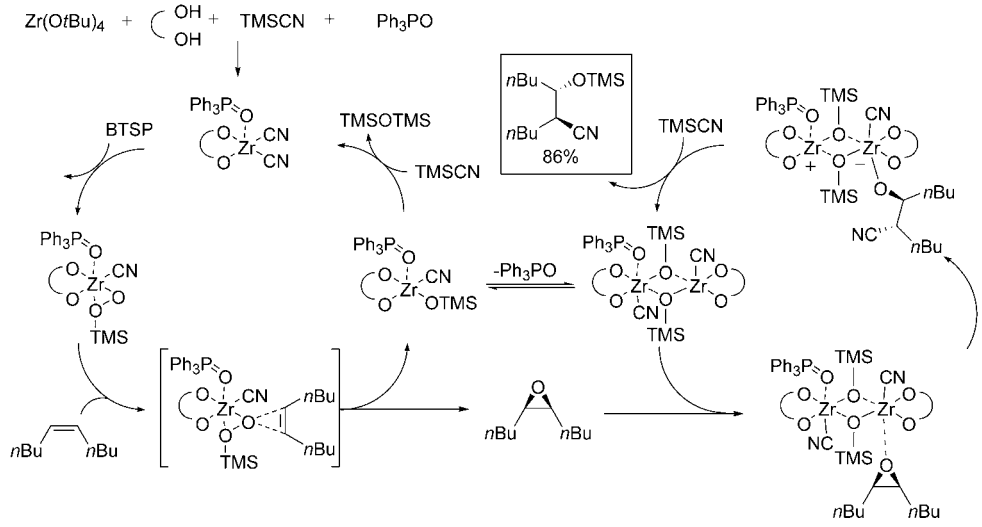
Scheme 15. Rhodium-catalyzed decarbonylation/Pauson–Khand reaction.[23]

Finally, Shibasaki and co-workers have shown that it is possible to conduct concurrent catalytic reactions with zirconium alkoxide catalysts.[24] It was found that zirconium tetraisopropoxide could catalyze the epoxidation of unfunctionalized alkenes by bis(trimethylsilyl)peroxide (BTSP) if the reaction was carried out in the presence of trimethylsilyl acetate or trimethylsilyl cyanide. The epoxide intermediate then underwent zirconium-mediated ring opening to form either a hydroxy acetate or a β-cyanohydrin, depending on the silyl reagent used. In the latter case, it was found that the use of a bidentate ligand and the addition of triphenylphosphane oxide had a beneficial effect on the reaction rate. Mechanistic studies suggested that a mononuclear zirconium complex was probably responsible for the epoxidation, whereas a binuclear complex was involved in the ring opening (Scheme 16). Finally, moderate enantioselectivity was observed when taddol was used as the bidentate ligand.

4. Prospects

The wealth of knowledge regarding mechanisms of transition-metal-catalyzed reactions bodes well for the future development of methods for sequential and concurrent catalysis. There will always be limits on the molecular complexity that can be gained in a single reaction. The ability to use a single catalyst for multiple processes opens the door to higher levels of complexity, while at the same time streamlining the overall synthetic process. One can easily foresee benefits for both academic research and industrial-scale processes, particularly when these methods are combined with efficient catalyst recycling. The challenge remains to find catalysts that can mediate multiple reactions in either a sequential or a concurrent fashion. In particular, areas such as Lewis acid catalysis, and potentially even organocatalysis, seem ripe for the development of such methods.

Received: October 21, 2003 [M1727]
Published Online: June 15, 2004



Scheme 16. Zirconium-catalyzed epoxidation and cyanide addition.[24] TMS = trimethylsilyl.

 © 2004 Wiley-VCH Verlag GmbH & Co. KGaA, Weinheim

[1] R. B. Woodward, M. P. Cav, W. D. Ollis, A. Hunger, H. U. Daeniker, K. Schenker, *J. Am. Chem. Soc.* **1954**, *76*, 4749.
[2] For reviews of metal-catalyzed and metal-mediated domino and sequenced reactions, see: a) M. Malacria, *Chem. Rev.* **1996**, *96*, 289; b) G. A. Molander, C. R. Harris, *Chem. Rev.* **1996**, *96*, 307; c) A. de Meijere, S. Bräse, *J. Organomet. Chem.* **1999**, *576*, 88; d) R. Grigg, V. Sridharan, *J. Organomet. Chem.* **1999**, *576*, 65; e) G. Poli, G. Giambastiani, A. Heumann, *Tetrahedron* **2000**, *56*, 5959; f) A. de Meijere, M. Schelper, *Actual. Chim.* **2003**, 51.
[3] These definitions are analogous to "consecutive" and "domino" reactions as defined by Tietze; see: L. F. Tietze, U. Beifuss, *Angew. Chem.* **1993**, *105*, 137; *Angew. Chem. Int. Ed. Engl.* **1993**, *32*, 131; L. F. Tietze, *Chem. Rev.* **1996**, *96*, 115.
[4] T. M. Trnka, R. H. Grubbs, *Acc. Chem. Res.* **2001**, *34*, 18.
[5] S. J. McLain, S. D. Arthur, E. Hauptman, J. Feldman, W. A. Nugent, L. K. Johnson, S. Mecking, M. Brookhart, *Polym. Mater. Sci. Eng.* **1997**, *76*, 246.
[6] E. L. Dias, R. H. Grubbs, *Organometallics* **1998**, *17*, 2767.
[7] M. D. Watson, K. B. Wagener, *Macromolecules* **2000**, *33*, 3196.
[8] S. D. Drouin, F. Zamanian, D. E. Fogg, *Organometallics* **2001**, *20*, 5495.
[9] J. Louie, C. W. Bielawski, R. H. Grubbs, *J. Am. Chem. Soc.* **2001**, *123*, 11312.
[10] A. Fürstner, A. Leitner, *Angew. Chem.* **2003**, *115*, 320; *Angew. Chem. Int. Ed.* **2003**, *42*, 308.
[11] P. A. Evans, J. E. Robinson, *J. Am. Chem. Soc.* **2001**, *123*, 4609.
[12] E. Teoh, E. M. Campi, W. R. Jackson, A. J. Robinson, *Chem. Commun.* **2002**, 978.
[13] a) A. N. Thadani, V. H. Rawal, *Org. Lett.* **2002**, *4*, 4317; b) A. N. Thadani, V. H. Rawal, *Org. Lett.* **2002**, *4*, 4321.
[14] J. Tian, N. Yamagiwa, S. Matsunaga, M. Shibasaki, *Angew. Chem.* **2002**, *114*, 3788; *Angew. Chem. Int. Ed.* **2002**, *41*, 3636.
[15] H. Du, K. Ding, *Org. Lett.* **2003**, *5*, 1091.
[16] F. Simal, A. Demonceau, A. F. Noels, *Angew. Chem.* **1999**, *111*, 559; *Angew. Chem. Int. Ed.* **1999**, *38*, 538.
[17] C. W. Bielawski, J. Louie, R. H. Grubbs, *J. Am. Chem. Soc.* **2000**, *122*, 12872.
[18] A. E. Sutton, B. A. Seigal, D. F. Finnegan, M. L. Snapper, *J. Am. Chem. Soc.* **2002**, *124*, 13390.
[19] B. Schmidt, M. Pohler, *Org. Biomol. Chem.* **2003**, *1*, 2512; b) B. Schmidt, *Eur. J. Org. Chem.* **2003**, 816.
[20] a) S. U. Son, D. S. Choi, Y. K. Chung, S.-G. Lee, *Org. Lett.* **2000**, *2*, 2097; b) S. U. Son, K. H. Park, Y. K. Chung, *Org. Lett.* **2002**, *4*, 3983.
[21] T. Morimoto, K. Fuji, K. Tsutsumi, K. Kakiuchi, *J. Am. Chem. Soc.* **2002**, *124*, 3806.
[22] T. Shibata, N. Toshida, K. Takagi, *Org. Lett.* **2002**, *4*, 1619; b) T. Shibata, N. Toshida, K. Takagi, *J. Org. Chem.* **2002**, *67*, 7446; tol-binap = (−)-2,2′-bis(di-p-tolylphosphanyl)-1,1′-binaphthyl.
[23] K. Fuji, T. Morimoto, K. Tsutsumi, K. Kakiuchi, *Angew. Chem.* **2003**, *115*, 2511; *Angew. Chem. Int. Ed.* **2003**, *42*, 2409; SDS = sodium dodecylsulfate, TPPTS = triphenylphosphane-(3,3′,3″)-trisulfonic acid trisodium salt.
[24] I. Sakurada, S. Yamasaki, R. Göttlich, T. Iida, M. Kanai, M. Shibasaki, *J. Am. Chem. Soc.* **2000**, *122*, 1245; b) S. Yamasaki, M. Kanai, M. Shibasaki, *J. Am. Chem. Soc.* **2001**, *123*, 1256.

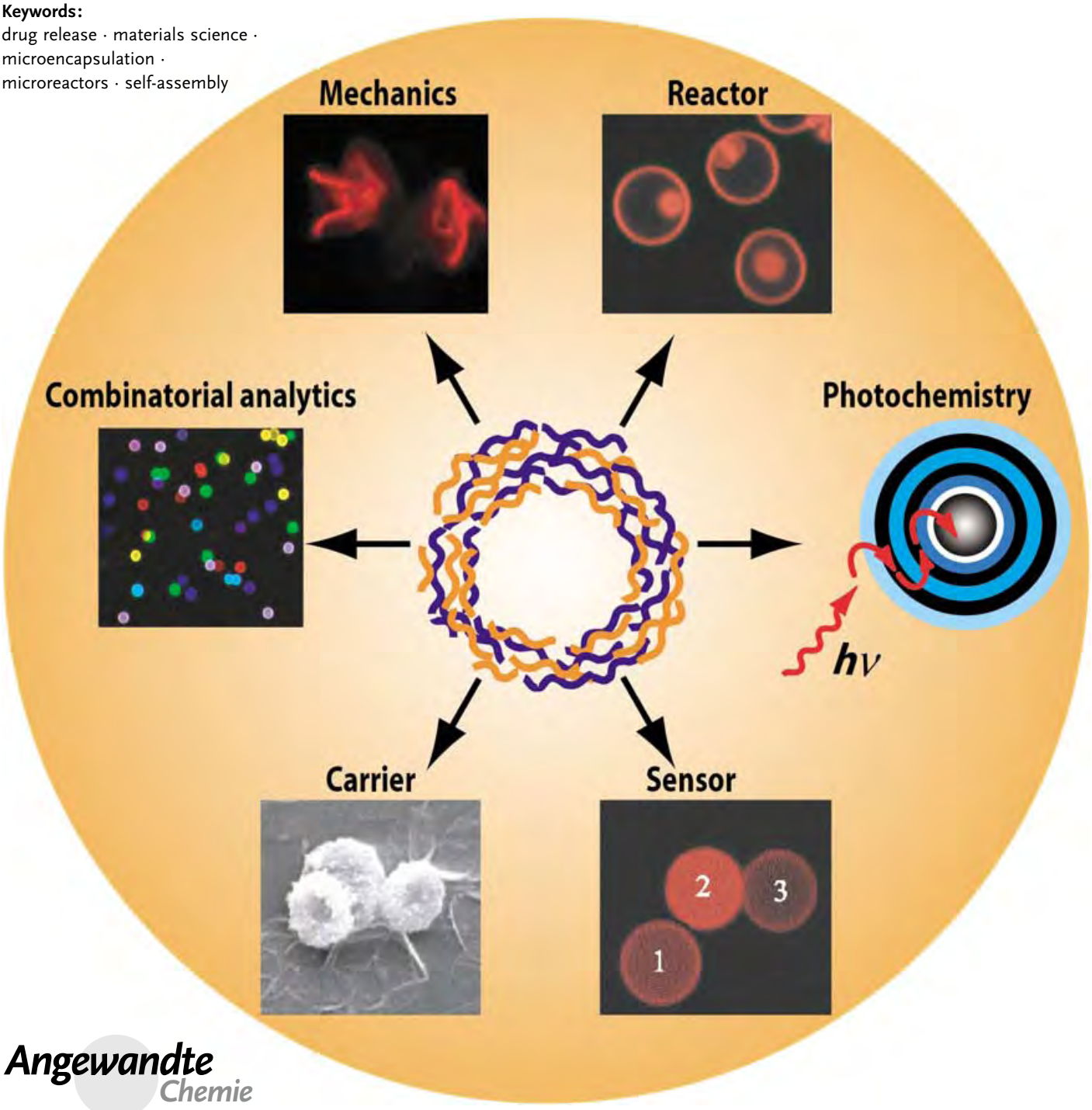
 © 2004 Wiley-VCH Verlag GmbH & Co. KGaA, Weinheim

Materials Science

Tailor-Made Polyelectrolyte Microcapsules: From Multilayers to Smart Containers

*Claire S. Peyratout and Lars Dähne**

Keywords:
drug release · materials science · microencapsulation · microreactors · self-assembly



© 2004 Wiley-VCH Verlag GmbH & Co. KGaA, Weinheim
DOI: 10.1002/anie.200300568

This review addresses the fabrication and properties of novel polyelectrolyte microcapsules, with an emphasis on their mechanical and permeability properties. Ease of preparation through layer-by-layer self assembly, accurate control over wall thickness as well as flexibility in the choice of constituents make these capsules very promising for numerous applications in materials and life science. Moreover, by engineering the inner and outer interfaces, these capsules can be used as microreactors for precipitation, crystallization, and polymerization reactions, as well as enzymatic, and heterogeneous catalysis.

From the Contents

1. Introduction 3763

2. Preparation of Polyelectrolyte Capsules 3764

3. Properties of the Capsules 3773

4. Filling of the Capsules: Properties and Potential Applications 3777

5. Conclusions and Outlook 3779

1. Introduction

The encapsulation of materials at the macroscopic scale has long been used to store different solids or liquids and to protect them from environmental influences. One simple archaic example is the storing of wine in tubes of leather or in bottles as a protection from oxygen. Nature offers also many examples of encapsulation in the macroscopic scale, for example, seeds or bird eggs, but one can find infinite examples of encapsulation in the microscopic world as well.[1] Every cell and its interior is an example of encapsulation. In this case, a further capsule function is employed, namely the use of permeability behavior of the capsule wall for the selective release or uptake of materials out or into the capsule.

The functionality of such "capsules" in nature goes far beyond the artificial man-made capsules prepared up to now. In this review, it will be demonstrated that progress in the field of encapsulation at the micron scale is moving towards the fabrication of artificial cells, particularly in terms of structure and semipermeability, even though the first techniques of microencapsulation were developed only approximately 30 years ago.

Nowadays, microcapsules are used in many applications in the pharmaceutical, cosmetic, food, textile, adhesive, and agricultural industries.[2–4] One of the oldest examples of an industrial application of microencapsulation can be found in the printing industry. Capsules made by coacervation of gelatin and Arabic gum containing several dyes have been intercalated in paper for reproduction processes, where they replaced carbon paper. Applying mechanical pressure onto the impermeable capsules destroys them and the dyes are released.[5]

Today, microcapsule systems have the highest potential in the pharmaceutical industry since many different requirements have to be fulfilled to deliver a drug at the right moment, in the right place, and at an adequate concentration. One of the simplest examples is the protection of orally applied drugs from the attack of acids in the stomach before they can be adsorbed in the intestine. This problem is solved in many cases by the use of gelatin microcapsules, which are insoluble at the low pH values found in the stomach allowing the desired release later in the intestinal tract.[6]

A more difficult task is the sustained release of drug in the body. It takes usually 20 to 30 min after the oral uptake of an analgesic to reach the maximum drug concentration needed to ease the pain. However, after this spike, the desired effect decreases fast. In this case, encapsulation techniques that allow a controlled and continuous release of the drug during its stay in the intestinal tract are necessary. Modern drug-delivery systems based on drugs encapsulated in alginate or poly(lactic-co-glycolic acid) (PLGA)[+] beads allows a relatively constant release owing to a tunable slow decomposition of the polymer.[7]

A further task, not yet solved, is a triggered drug release. The drug should be transported to the target organ without any loss and then released by a specific internal or external stimulus. Although several systems based on microwaves, laser light, or magnetic fields are being developed this problem is up to now not really solved for microcapsules.

Several approaches have been used to fabricate nanocapsules[8] One approach is to use systems that self-assemble into capsules at given conditions, such as the aggregation of lipid molecules into spherically closed bilayer structures at low concentration, so-called vesicles or liposomes.[9,10] These relatively unstable structures can be in turn used as precursors for the preparation of more stable nanocapsules by cross-linking the lipid molecules. The required chemical functionalization of the lipids results in a limited applicability in vivo. In an analogous fashion, amphiphilic block copolymers can also aggregate in aqueous solution to vesicular structures.[11]

A second approach to prepare capsules involves suspension and emulsion polymerization around latex particles. Harsh conditions, such as prolonged alkali and acid treat-

[*] Dr. L. Dähne
Capsulution Nanoscience AG
Volmerstrasse 7b
12489 Berlin (Germany)
Fax: (+49) 306-392-3601
E-mail: lars.daehne@capsulution.com
Dr. C. S. Peyratout
Max Planck Institute of Colloids and Interfaces
14424 Potsdam (Germany)

[+] A list of abbreviations used is given at the end of this review.

 DOI: 10.1002/anie.200300568 © 2004 Wiley-VCH Verlag GmbH & Co. KGaA, Weinheim

ments at high temperature are required to remove the latex cores.[12,13]

A third method is to use dendrimers or hyperbranched polymers for nanoencapsulation.[14,15] However, the particle preparation requires a rather costly and tedious procedure, which clearly presents a limiting factor for possible applications.

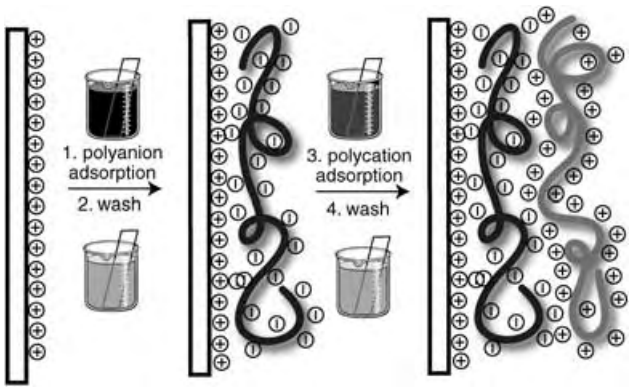
Another method involves the covering of a sacrificial template core with a membrane, which is permeable for the products of subsequent core dissolution. For this approach, semipermeable polyelectrolyte complex membranes are well-suited. Polyelectrolyte capsules were first prepared by dropping a polyelectrolyte solution of a polycation into a solution of a polyanion. At the interface, an insoluble complex forms a capsule wall. Control over the properties of such polyelectrolyte capsules is effected by the concentration of the solutions, the polymeric substances, and the drop size. The size of the resulting capsules is limited to diameters above 20 μm and for mechanical reasons, the wall thickness has to be above 100 nm.[16,17]

Advanced polyelectrolyte capsules with smaller dimensions were developed five years ago by the use of layer-by-layer (LbL) technology.[18] These capsules are the subject of this article. After a short introduction of the LbL technique, we will describe methods and materials used to fabricate the microcapsules, and discuss the key properties of these capsules, namely their permeability, the various loading technologies, and their mechanical stability.

2. Preparation of Polyelectrolyte Capsules

2.1. Polyelectrolyte Films on Planar Surfaces

An influential domain in the use of noncovalent interactions in polymer thin-films research, is electrostatic LbL assembly (for reviews, see ref. [19–22]). This 13-year-old technique is based on the alternating absorption of multiply charged cationic and anionic species. The popularity of the method is due to the ability to create highly tailored polymer thin films with a nearly unlimited range of functional groups incorporated in the film structure. This flexibility is achieved through the use of a simple, highly inexpensive, and readily accessible adsorption process. Electrostatic interactions between polyions in solution and an oppositely charged interface are the key to the final structure of the polyion layered thin film (Scheme 1). During the self-assembly



Scheme 1. Schematic diagram of the buildup of multilayer assemblies by the consecutive adsorption of anionic and cationic polyelectrolytes (multiple repetition of both steps). This diagram is highly idealized. In reality, the layers are well interpenetrated. Adapted from ref. [20]

process, the polymer adsorption proceeds until the surface charge is reversed. This allows in a next step, the adsorption of a counterpolyion. The alternating adsorption of polycations and polyanions can be repeated at will. Fabrication and properties of electrostatic multilayer thin-film assemblies have been recently and exhaustively reviewed,[23–25] and we will just briefly cite the various charged components that have been integrated in LbL films.

2.1.1. Multilayer Materials

Most diverse charged polymers have been successfully assembled into thin films by the LbL technique. The most used polyelectrolytes are commercially available ones, such as poly(ethyleneimine) (PEI), poly(allylamine) (PAH), poly(diallyldimethylammonium chloride) (PDADMAC), poly(styrenesulfonate) (PSS), poly(vinylsulfate) (PVS), and poly(acrylic acid) (PAA; for structures, see Table 2).



Claire S. Peyratout received her degree in chemical engineering from ESCOM (Paris, France) in 1990. One year before, she joined the Ph.D. program of Purdue University, Indiana (USA) where she worked on the role and influence of metals in and on biological systems under the supervision of Prof. David R. McMillin. In 1994, after obtaining her Ph.D. degree, she went to Strasbourg (France) where she taught physics and chemistry. Since 1997, she has been a research assistant at the Max Planck Institute of Colloids and Interfaces, in the department led by Prof. Möhwald, where she is currently investigating the interactions of polyelectrolytes with dyes and biological molecules.



Lars S. Dähne was born 1959 in Berlin, Germany. He studied chemistry at the Humboldt-University Berlin. In 1991 he received the Ph.D. in Organic Chemistry (Prof. J. Bendig). After post-doc positions at the Nagoya-University in Japan (Prof. J. Tanaka) and the Technical University Braunschweig (Prof. W. Grahn), he moved in 1994 to the Institute of Physical Chemistry of the Free University Berlin (Prof. H. Baumgärtel). For his work there obtained his habilitation and the Otto-Röhm Memorial prize in 1998. In 1999 he moved to the Max Planck Institute of Colloids and Interfaces and started research on polyelectrolyte capsules in the group of Prof. H. Möhwald/Prof. E. Donath. In 2001 he co-founded the company Capsulution.

 © 2004 Wiley-VCH Verlag GmbH & Co. KGaA, Weinheim

The scope of functional polymers studied is vast and comprises conducting and light-emitting polymers, nonconjugated redox-active polymers, polymeric complexes, reactive polymers, polymers bearing nonlinear optically active dyes, liquid-crystalline polyelectrolyte, temperature-sensitive and switchable polymers, and dendrimers. In addition, a number of standard polyelectrolytes modified with a small number of functional units has been used, for example, for labeling or for molecular recognition studies.

Incorporation of nanoparticles in LbL films is a particularly extensive and fast developing area of research, since the variety of colloidal objects that may be placed in multilayer films is immense. To date, stable colloidal dispersions of charged silica, metal oxides, polyoxometalates, semiconductors, and fullerenes, as well as metal colloids, metallosupramolecular complexes, charged latex spheres, microcrystallites, clay platelets, or charged inorganic sheets have been successfully employed to prepare LbL coatings. In addition, natural polyelectrolytes have been used for LbL, such as nucleic acids, proteins, polysaccharides, as well as certain charged supramolecular biological assemblies, such as viruses or membrane fragments. The investigations were mostly motivated by their biological functions and biomimicking applications, for example, for biocompatibilization of surfaces, enzymatic activity, sensing purposes, or molecular recognition.

2.1.2. *Substrates*

A wide variety of substrate has been used as well. The substrates have to carry a minimal surface charge so that the polyion can adhere to it. This charge can be inherent or created by surface treatment. We will just mention substrates having application in capsules, such as silicium dioxide and polystyrene (PS). Some biological templates were also used. Multilayers have been assembled onto highly cell-adherent biological surfaces, such as extracellular matrix and type I collagen, making such surfaces bioinert, thus preventing cell and protein adhesion.[26,27]

2.1.3. *Permeability*

Permeability of the LbL wall is one of the key properties of polyelectrolyte capsules. Hence, we will cite some studies conducted on the permeability of planar polyelectrolyte thin films, which are partly exploited for capsule systems. Rubner and co-workers studied the influence of pH value on thin films of weak polyelectrolytes, such as PAA and PAH.[28] In these systems, the charge density along the chain can be readily controlled by adjusting the pH value of the polyelectrolyte solution during the assembly process. Depending on the pH value, the thickness of a layer of an adsorbed weak polycation or polyanion can be varied from 5 to 80 Å. Immersion of such multilayers after assembly in a medium of different pH provokes a substantial and irreversible transformation of the film morphology. For example, with layers of weak polyacids (e.g. PAA) a lower pH-value environment cleaves interchain ionic bonds by protonation of carboxylate groups and induces charge imbalance in the LbL film. The microporous structures formed exhibiting 2–3 times the thickness of the original films and pores of up to 100 nm.[29]

Recently, loading capabilities and release behavior of PAA/PAH films were studied using methylene blue as an indicator. PAA/PAH films which were assembled at pH 2.5 loaded the dye at higher pH values because of the presence of available binding sites and a permeable structure throughout the multilayers. A pH-sensitive loading and release mechanism of the dye from the LbL film was demonstrated.[30,31]

The influence of salt concentration on the stability, permeability, and film thickness of multilayers made from a weak polyacid and a strongly dissociated polycation was investigated. Preformed multilayers decompose rapidly and, for polyelectrolytes with high molecular weights, completely when exposed to concentrated salt solutions. The dissolution of the LbL films is caused by the competition between polymer-to-polymer interactions which hold the film together and polymer interactions with external salt ions. This result was determined from electrochemical studies on polyelectrolyte-coated electrodes.[32]

Permeability of ions, gases, and solutes through LbL films was the subject of several investigations: ions permeability was studied using conductivity measurements.[33] The multibipolar structure of the polyelectrolyte membranes favors the separation of mono- and divalent ions as a result of the Donnan potential. Various factors, such as salt concentration, pH value, and polymer charge density, influence the rate of ion permeation and selectivity. The dependence of these effects on charge density and concentration of excess charges in the polyelectrolyte membrane was investigated.[34]

The excellent tunable and selective permeability of LbL films has already found an application in hydrogen peroxide sensors, which can be used in the presence of possible interference-inducing substances, such as ascorbic acid, uric acid, and acetaminophen. Hydrogen peroxide can diffuse smoothly through the polyelectrolyte membrane film to a platinum electrode while ascorbic acid, uric acid, and acetaminophen are size excluded.[35]

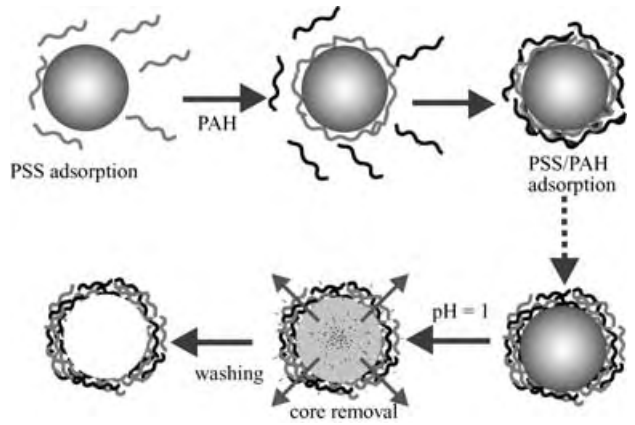
2.2. Coating Colloidal Particles with Polyelectrolytes

Techniques to fabricate hollow polyelectrolyte shells have been individually reviewed[36–40] and will only be summarized and compared in the following paragraph. Problems in transferring the LbL technique from macroscopic flat substrates to the surface of colloidal particles lie in the separation of the coated colloids from free, excess polyelectrolyte prior to the next deposition cycle. In addition, flocculation instead of layer growth is often induced by the added polyelectrolyte. To prevent these undesirable effects, the initial colloidal substrate as well as each of the employed polyelectrolyte species has to be sufficiently charged. Moreover, it has to be ensured that the particle is added to the polyelectrolyte solution and that the amount of the adsorbing polyelectrolyte used is large enough to provide complete coverage. If this requirement is not met, incomplete layer growth and aggregation arising from the coexistence of particles having different charge density occur. Typical adsorption conditions

 © 2004 Wiley-VCH Verlag GmbH & Co. KGaA, Weinheim

used to form polyelectrolyte layers on colloidal particles are taken from the planar films assembly. Generally, a polyelectrolyte solution (1 mg mL^{-1}) in 0.5 M NaCl aqueous solution is adsorbed for at least 20 minutes. Since an excess of polyelectrolyte is needed, the total particle surface in the batch must be evaluated from the colloid concentration and diameter. The drying process often applied in planar film assembly between the deposition of two subsequent layers cannot be performed with particles.

LbL assembly of polyelectrolyte onto colloidal particles (Scheme 2) can be performed in two different ways: either the



Scheme 2. Schematic illustration of the polyelectrolyte deposition process for PSS/PAH capsules and of the subsequent MF-core decomposition. The initial steps involve stepwise film formation by repeated exposure of the colloid MF template to alternatively charged polylelectrolytes. The excess polyelectrolyte is removed by cycles of centrifugation and washing before the next layer is deposited. After the desired number of layers has been deposited, the coated particles are exposed to HCl pH 1. The MF core immediately decomposes. Finally, after washing, a suspension of polyelectrolyte hollow shells is obtained.

concentration of polyelectrolyte added at each step is just sufficient to form a saturated layer, or the adsorption is carried in an excess of polyelectrolyte. In the latter case, the excess polyelectrolyte molecules must be removed before adding the next polyelectrolyte to avoid formation of complexes in solution. This separation can be achieved either by centrifugation or filtration.[41] These approaches provide sequential layer growth of multilayers on colloidal particles.[41–43] Polyelectrolytes can also be deposited on a colloidal-template surface in a one-step procedure by the so-called controlled precipitation.[44] In the following, we will compare the advantages and drawbacks of the techniques.

Sequential adding of polyelectrolyte at the exactly required concentrations required to form complete layers can be performed in a short time because the polyelectrolytes are adsorbed in few minutes and no washing cycles are needed. Furthermore, there is no loss of polyelectrolyte.[45] However, the probability of forming free polyelectrolyte complexes in solution and particle aggregates is rather high. This problem can be bypassed by using a highly diluted particle suspension or determining accurately the exact amount of polyelectrolyte needed for fully covering the particles. In spite of this, particles aggregation, especially in case of submicron size colloids, cannot be avoided by this method. Therefore, the most widely used method is the addition of an excess of polyelectrolyte to the particles. After adsorption of each polyelectrolyte layer, excess polyelectrolyte has to be removed from the solution before adding oppositely charged polyelectrolyte to the particles. The excess is removed by performing at least three washing cycles either with pure water or with 0.1 M NaCl solution. Separation of the particles from the solution can be by centrifugation but this often results in problems with resuspension, difficulties for smaller particles of low density to settle, loss of materials, and the length of time required.

An alternative separation method is filtration, the particles are filtered from the excess polyelectrolyte through size-matched filters.[41] The particles are not stressed, since they are only subjected to a slow and adjustable stirring. The liquid level above the filter can be easily controlled by the interplay between the inflow of the reagents and the pressure applied to facilitate the filtration, and the filtrate can be easily recovered. To date the filtration method is the only method that can be scaled-up practically and in principle automated. However, for small colloids, the particle-size-matched filters are readily clogged, increasing the particle loss and the fabrication time.

In the one-step approach, slow heterocoagulation of polymers presence of a colloidal-particle suspension is used. This so-called controlled precipitation (CP) method can be applied for systems which form an insoluble complex between polyelectrolyte and multivalent ions. The polymer solubility can be decreased by using an appropriate solvent.[46] It is a fast method for the preparation of polyelectrolyte capsules, but the controlled layered structure is lost. The proper choice of the concentration ratio between polymers, particles, and speed of coagulation provide coverage with a defined amount of precipitated polymer on each particle.[44]

Several methods have been applied to check the layer growth of polyelectrolytes onto colloidal suspensions. For polyelectrolytes electrophoresis yields a complete charge reversal at each step as measured by the ζ potential. For ampholytes or weakly charged molecules, the charge can alternate between a weak and strong positive (or negative) ζ potential. With single particle light scattering (SPLS) the adsorption of each polyelectrolyte layer can be detected separately. In addition this method can discriminate between single particles and aggregates.[40]

Recently, small-angle neutron scattering measurements of PAH/PSS multilayers adsorbed on deuterated latex particles allowed the direct determination of the thickness of the polyelectrolyte multilayer on coated colloids in water. A mean thickness of 16.6 Å per layer, independent of the curvature of the colloid surface and weakly dependent on the number of the adsorbed polyelectrolyte layers was evaluated.[47] Transmission electron microscopy (TEM) was applied to follow the polyelectrolyte layer growth especially for very small particles.[48,49] After removal of the core, atomic force microscopy (AFM) enables the determination of the surface profile, the layer thickness of dried and collapsed capsules, as well as their diameter, shape, and filling.[50–52]

 © 2004 Wiley-VCH Verlag GmbH & Co. KGaA, Weinheim

2.3. Templates

The decomposition of the encapsulated template is a key step for capsule fabrication. Suitable templates have to fulfill three requirements:

1. They have to be stable under the LbL process.
2. The conditions required for template dissolution should not affect the structure and stability of the multilayer.
3. The dissolved template molecules have to leave the capsule easily and completely.

In addition, for most purposes, monodispersity and a spherical shape are desired.

Several templates have been used for the capsule preparation, such as weakly cross-linked melamine–formaldehyde (MF) latices,[18] organic[53–56] and inorganic crystals,[57] silica particles,[163] polystyrene latices,[58] metal nanoparticles and nanorods,[48,49,59] and biological templates.[50,60,61] None of them met all requirements. Hence, research is still needed to find alternatives. The most widely used templates and their properties are listed in Table 1.

The majority of capsules have been prepared to date with MF templates. Weakly cross-linked, monodisperse MF templates are produced in the size range 500–5000 nm (Microparticle GmbH, Germany). They are stable at pH values above 5 allowing the assembly of the polyelectrolyte shell at neutral pH. In 0.1 M HCl the template can be dissolved within seconds into protonated MF oligomers.[62] The online observation of the MF core decomposition process under confocal laser scanning microscopy revealed that the capsules swell as a result of the decomposition of the MF core (Figure 1 a). The oligomers are too large to diffuse easily out of the capsules. The temporarily high concentration of the dissolved MF oligomers in the interior generates an osmotic pressure. This situation leads to swelling of the capsules and exerts a high mechanical stress on the polyelectrolyte film. This effect increases strongly with layer numbers and template diameter. Capsules of 5 μm with 8–12 layers shrink back slowly after the dissolution process but higher layer numbers leads to a complete breach of the capsule wall. The size of the oligomers produced on template dissolution depends on the quality and age of the MF batch and differs between 5000 g mol^{-1} and 12000 g mol^{-1}. Therefore, the capsule properties depend strongly on the MF template batch which makes general statements to the permeability and further properties of MF capsules difficult. One should keep in mind that the reproducibility of the reported studies concerning MF capsules is limited.

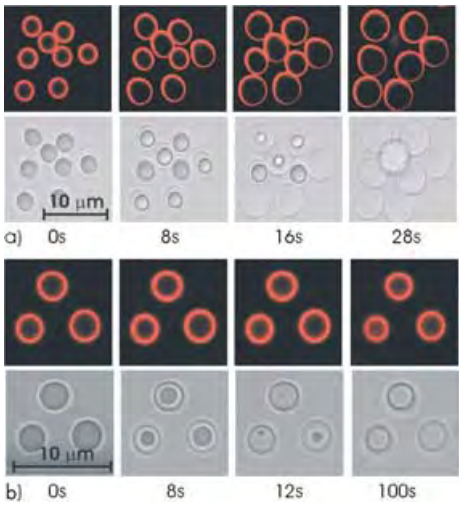


Figure 1. Online observation of the core dissolution using CLSM, the upper, colored, part shows the fluorescent-labeled wall (fluorescence channel) and the lower part the core (transmission channel). a) Dissolution of MF particles (3.5 μm) covered by 12 layers of PAH/PSS in 0.1 M HCl, b) dissolution of SiO_2 particles (2.8 μm) covered by 16 layers of PAH/PSS in 1 M HF.

The capsule integrity depends on the pH value of the dissolution medium. Optimization of the dissolution requires a pH value of 1. Higher proton concentration accelerates the core decomposition process, but generates a larger MF oligomer gradient and induces a higher osmotic pressure. Lower proton concentration promotes cross-linking of the MF oligomers and generates larger residues, which also increase the osmotic pressure, as a result of the lower diffusion rate through the wall.[62]

Owing to these mechanisms, between 5 and 20 % of MF capsules are generally broken. The remaining capsules show a remarkably higher permeability than the planar and unstressed polyelectrolyte films of the same material and thickness. As already discussed, the permeability of planar polyelectrolyte films for small ions, dyes, or even gases is rather small.[63,64] In contrast, compounds of molecular weights up to 10000 g mol^{-1} penetrate the wall of MF capsules

Table 1: Templates used for the preparation of hollow polyelectrolyte capsules.

Parameter	Melamine formaldehyde[18]	Polystyrene latex[58]	Silica[163]	Erythrocytes[162]	$CdCO_3$, $MnCO_3$, $CaCO_3$	PLA/PLGA[160]
Size (μm)	0.3–10	0.1–5	0.03–100	5.5–7.5	3–8	0.2–20
shape	spherical	spherical	spherical	discocytes	crystalline, porous	spherical
monodispersity	excellent	excellent	good–excellent	good	medium	low
commercial availability	+	+	+	+	–	+/–
price	very high	medium	low	low	–	low
problems upon dissolution	mechanical stress; residues	mechanical stress; residues	aggregation	chemical stress; wall destruction	no stress	residues

© 2004 Wiley-VCH Verlag GmbH & Co. KGaA, Weinheim

easily whereas larger molecules are partly excluded (Figure 2b,c). Presumably, the high mechanical pressure during the dissolution process leads to pores or weak parts in the capsule wall that determine the permeability more than the intrinsic

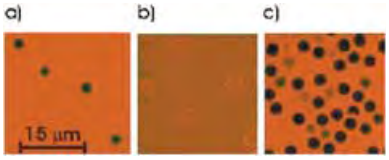


Figure 2. Permeability of capsules at neutral pH for different probe molecules a) Silica capsules (2.8 µm) in 10^{-4} M rhodamine 6G, b) MF capsules (4.1 µm) in 10^{-4} M rhodamine 6G, c) MF capsules in rhodamine-labeled PAH (2×10^{-2} M; 70000 g mol^{-1}).

diffusion properties of the polyelectrolyte films do. This assumption is strongly supported by observation of pores in the capsules after acid treatment.[65]

To reduce the permeability of MF capsules, further polyelectrolyte layers can be assembled after the dissolution of the core, this results in a closing of the pores and a remarkable decrease of the permeability even for small dye molecules.[66]

A further disadvantage of MF capsules is the presence of MF residues in the capsule interior, which remain there owing to their large size or interactions with the inner PSS layer. It has been determined that these residues amount to 20–50% of the overall mass of the capsules.[51] The presence of MF oligomers and the subsequent formation of a negatively charged complex with PSS molecules from the capsule wall can be exploited for the trapping of water-soluble substances, such as albumin and peroxidase.[67,68] However, because of the accidental amount of oligomer in the capsule interior, this encapsulation method is not controlled enough for viable applications.

In a few cases, colloidal PS latices have been used as core, which can be dissolved in THF.[69] The swelling of PS in THF leads to a large volume increase that is directly responsible for capsules fractures. The prevention of high amounts of broken capsules is therefore very dependent on the PS solubilization procedure.

Red blood cells present an alternative to MF particles. Erythrocytes, although seemingly rather exotic substrates, presents several advantages over "conventional" templates: they are available in nonspherical shapes, are quasi monodisperse and are very inexpensive. One drawback of using biological cells as a template is their limited membrane stability. To prevent breakage upon polyelectrolyte coating, human erythrocytes are stabilized by glutaraldehyde.[50] The decomposition of the biological templates can be achieved by using a pH 12 sodium hypochlorite solution. However, it was discovered that, under these harsh conditions, the polyelectrolyte wall is also oxidized. This oxidation causes the loss of all the positive charges and of some polyelectrolyte material, in addition it results in a cross-linking of the wall materials.[51] The extent of these changes is a function of the length of exposure to, the temperature, and the concentration of the sodium hypochlorite solution during the dissolution process. The choice is thus to either keeps the wall almost intact and have remarkable residues of the erythrocytes in the capsules or to accept an almost complete chemical change of the wall.[51]

As a promising alternative, silicon dioxide particles have been used recently as templates and subsequently dissolved in hydrofluoric acid.[163] These particles are available over a broad size range and often with a high monodispersity. The core is decomposed in 1M HF within few seconds into $[SiF_6]^{2-}$ ions, which can leave the capsule wall during the dissolution without problems. This process was observed online with the confocal microscope on 3-µm silica particles encapsulated in 16 layers of PAH/PSS (Figure 1b). Although the dissolution process is as fast as for the MF templates, the capsules do not swell. Hence, the mechanical stress applied to the wall during the dissolution is negligibly small and the polyelectrolyte layer structure is kept almost unchanged. Investigations of the permeability confirmed this assumption. The permeability of these capsules is very low. In contrast to MF capsules, small dye molecules do not permeate silica capsules and even small salt ions penetrate only slowly into their interior (Figure 2a). Disadvantages of these systems are the danger in handling HF and problems with aggregation of the capsules during dissolution.

A current development is the use of inorganic crystals, such as $CdCO_3$, $CaCO_3$, or $MnCO_3$, as templates, which can be prepared with low dispersity in the range 2–8 µm. The dissolution can be performed under mild conditions and the products can leave the capsule interior without problem. However, these templates are often porous, and the first polyelectrolyte layer can penetrate into them and form complexes.

2.4. Wall Materials

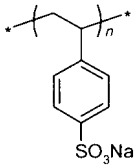
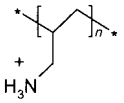
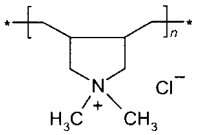
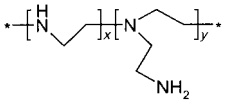
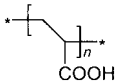
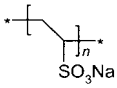
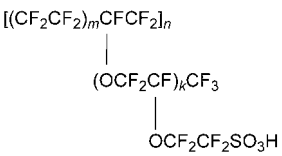
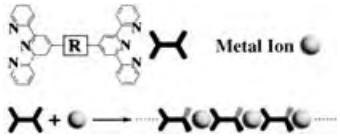
A prerequisite for potential wall materials is the presence of a number of charged groups. For polyelectrolytes at least 50% of the monomer units should carry a charge.[70] The LbL approach employed for planar films is generally transferable to colloidal surfaces, which makes all materials used for the planar films potentially suitable for the preparation of capsules. However, some limitations exist for capsules owing to the mechanical stability of the resulting free-standing polyelectrolyte films and the aggregation problem in colloidal systems. However, the large number of "construction" materials available allows a broad variability of the chemical and physical capsule properties.

2.4.1. Functionalized Polyelectrolytes

Similarly to planar polyelectrolyte multilayer films, the most used polymers are commercially available synthetic polyelectrolytes such as PSS, PAH,[18] and PDADMAC (Table 2).[71] To date, the most studied capsules are of PAH/PSS. Nevertheless, shells based on other synthetic polyelectrolytes such as poly(ethyleneimine) or Nafion (Table 2) have been synthesized.[72,73] Owing to the potential applicability of

 © 2004 Wiley-VCH Verlag GmbH & Co. KGaA, Weinheim

Table 2: Some polyelectrolytes used in the fabrication of hollow capsules.

poly(styrene sulfonate), sodium salt (PSS)	
poly(allylammine) (PAH)	
poly(diallyldimethylammonium chloride) (PDADMAC)	
poly(ethyleneimine) (PEI)	
poly(acrylic acid) (PAA)	
poly(vinylsulfonate) (PVS)	
Nafion	
metallosupramolecular polyelectrolyte (MEPE)	

capsules in the pharmaceutical industry, there is increasing interest in the area of naturally occurring polyelectrolytes, such as polysaccharides. Recently, LbL capsules containing carrageenan,[74] dextran sulfate,[75] chitosan/chitosan sulfate,[76] sodium alginate, carboxymethyl cellulose,[77] and protamine[78] were reported.

The next challenge is the introduction of properties, such as color or surface structures of biological or technical relevance, into the wall or at the surface of capsules. To improve the observation and detection of the empty shells by confocal fluorescence microscopy, polymers with covalently bound fluorescent probes or copolymers of dyes and polyelectrolytes have been incorporated in the capsule walls. For in vitro diagnostics, tagging of capsules with different fluorescent dyes opens a wide field of applications. In contrast to well-established particle assays, the interior of the capsules can be used for immobilization of antibodies, nucleotides, or other biologically relevant materials. For such combinatorial applications, PAH was labeled with four dyes (pyrene, fluorescein, rhodamine 6G, bisindolenylpentamethine (Cy5)) selected for their well-separated excitation wavelengths and emission spectra. A luminescent library of 15 $(PAH/PSS)_5$ capsules were prepared by assembling the dyes in different combinations (Figure 3).[164] The order of

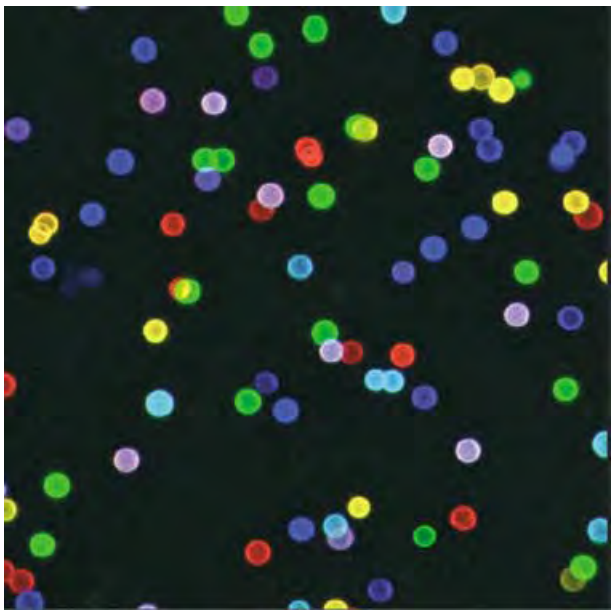


Figure 3. Library of 15 dye-modified capsules with $(PAH/PSS)_5$ layers, prepared by layering different dye combinations. Adapted from ref. [164]

assembling was selected in such a way that intermediate unmarked polyelectrolyte layers suppress undesirable interactions between dyes. Although all capsules have the same size and properties, they can easily be distinguished by multichannel confocal fluorescence microscopy or by flow cytometry. Tagged capsules have several advantages over similar commercial colored-particle libraries:

1. Owing to their low mass, they sediment slowly.
2. There is little interaction between the various dyes.
3. The interior of the tagged capsules as well as the surface can be used for chemical reactions.
4. The covalent linkage of the dyes to the wall materials prevents leakage.
5. Capsules are stable in most organic solvents.
6. All dye molecules can be located close to the outer surface, allowing efficient Förster resonance energy transfer (FRET) in modern separation-free particle assays.[79]

Capsules with other important functions and increased stability have been prepared by the cross-linking of water-soluble ionene precursor polymers containing fluorene units in the multilayer shell, to yield luminescent conjugated oligofluorenes.[69]

A copolymer of poly(aniline) and PSS was introduced to obtain walls with reducing properties for use in the preparation of metal nanoparticles.[80]

By using diazoresins, that is, polymers with photoreactive diazo groups, the ionic bonds between the negative PSS and

 © 2004 Wiley-VCH Verlag GmbH & Co. KGaA, Weinheim

the positive diazoresin (assembled using the LbL technique), which initially hold the layers together, are converted into covalent cross-links. Cross-linked hollow capsules are mechanically more stable in various chemical environments than their ionically linked counterparts.[81] Photochromic hollow shells using an azobenzene polyene were produced. The thermal *E*/*Z* relaxation of the photochemically generated *cis* isomers is slower in the constrained geometry of the LbL film than in solution.[74] Several ion- and oxygen-sensitive fluorophores were also incorporated, although it was not determined if the probes are adsorbed on the surface, trapped in the wall or immobilized in the capsule interior.[82–84]

2.4.2. *Incorporation of Small Molecules*

There is a limited absorption of low-molecular-weight, water-insoluble species onto monodisperse templates. One interesting possibility is the incorporation of low-charge, low-molecular-weight compounds as building blocks in LbL self-assembly process.

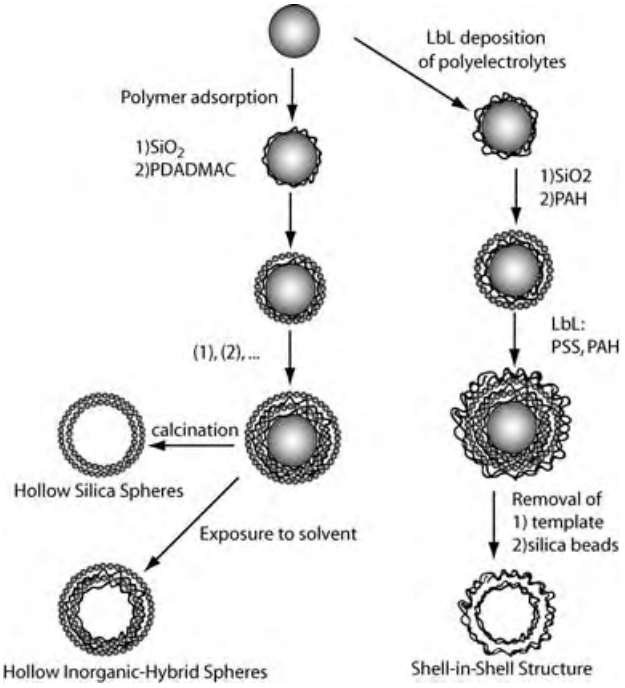
The adsorption of the trivalent ions Tb^{3+} or Y^{3+} in combination with PSS was obtained by Radtchenko et al.[85] However, the multilayers obtained are not very stable. They dissociate under physiological salt concentration or under increasing temperature. This property and the subsequent coating of these less stable capsules however, yielded a method to encapsulate macromolecules in polyelectrolyte shells (which will be discussed in Section 4).

A general aspect is the integration of water-insoluble compounds in LbL films. Dai et al. introduced several water-insoluble organic dyes in capsule walls by depositing them in non-aqueous solution alternatively with polyelectrolytes in aqueous solution.[86] The spectroscopic evidence obtained indicated the formation of dye aggregates upon adsorption on polyelectrolytes. Clearly, for neutral or weakly charged molecules, further interactions, such as hydrophobic and van der Waals interactions can be exploited for the preparation of LbL films. In a next step, we constructed a two-step energy-transfer cascade in the wall of hollow microcapsules by the defined assembly of three cyanine dyes, working respectively as antenna, intermediate, and receiver.[87,88] The dyes are assembled in two different ways, which allows the FRET mechanism to occur within one layer or through all the layers from the outside to the inside.

Functional polyelectrolytes from metallosupramolecular chemistry have also been used for capsule preparation. Alternate deposition of negatively charged macromolecules and of the positively charged coordination polyelectrolyte Fe^{II}-MEPE (Table 2) on weakly cross-linked MF particles, followed by MF particle decomposition and removal, resulted in hollow Fe^{II}-MEPE/PSS shells. Surprisingly, in contrast to the free Fe^{II}-MEPE polymer, the Fe^{II}-MEPE/PSS hollow shells were found to be stable upon exposure to acidic solutions or chelating agents.[89,90]

2.4.3 *Composite Organic–Inorganic Nanoparticles*

Several inorganic materials can be prepared as charged nanoparticles, which are also useful as layer components in the LbL process. SiO_2, TiO_2, laponite,[91] and CdTe nanoparticles have been used for the preparation of capsules (for a review on core-shell particles, see refs. [92–94]). Incorporation of a stable colloidal dispersion of charged silica nanobeads as one of the wall components led to composite organic–inorganic colloidal materials with a regular coating and a nanometer-scale control over the thickness.[95–97] The multilayers were constructed by consecutively depositing nanoparticles and polyelectrolyte onto colloidal templates, utilizing the electrostatic attraction between particles and polymer for layer build-up. Depending on the method chosen to remove the core, either a hollow inorganic–organic hybrid wall (by dissolution of the MF core in HCl) or a hollow silica sphere (by thermal decomposition (calcination) of the organic compounds), is obtained (Scheme 3).[98,99]



Scheme 3. Procedures for preparing inorganic, hybrid hollow-spheres and shell-in-shell structures. Adapted from refs. [98, 100]

Advanced capsule architectures, such as nanoporous capsule walls or shell-in-shell structures have been constructed by consecutive alternating adsorption of polyelectrolytes and SiO_2 on MF particles, followed by removal of MF the cores with HCl acid and of the SiO_2 particle layers sandwiched between indestructible PAH/PSS walls with HF. By labeling the inner shell with fluorescein and the outer shell with rhodamine B it was possible to distinguished the inner and outer shell by spectral resolution enhancement of confocal laser scanning microscopy although the distance between the shells was only 50 nm (Figure 4).[100]

 © 2004 Wiley-VCH Verlag GmbH & Co. KGaA, Weinheim

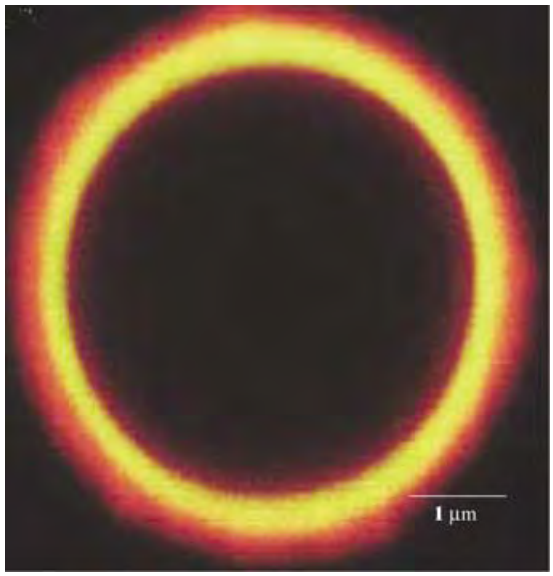


Figure 4. CLSM fluorescence image of a capsule of (PSS/PAH/PSS/PAH-FITC)(SiO_2/PAH/SiO_2)(PAH-TRITC/PSS/PAH/PSS/PAH) after removal of the silica layers. Red emission results from the rhodamine in the outer layers and yellow emission from the fluorescein emission in the inner layer. Adapted from ref. [100].

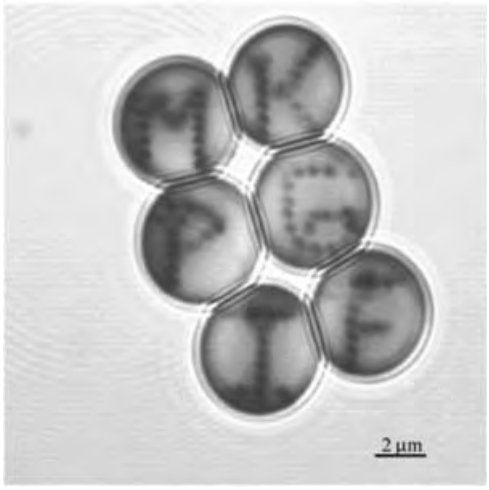


Figure 5. Silver nanopainting: Each silver dot on the capsule surface is reduced by a laser beam. From ref. [80].

2.4.5. *Nanoparticles with Magnetic, Fluorescent, or Catalytic Activity*

Functional nanoparticles were incorporated into capsules to introduce magnetic, fluorescent, or catalytic properties. Iron oxide particles with superparamagnetic properties have applications in drug delivery systems and in diagnostics, where the particles can be directed by application of an external magnetic field. Furthermore, it is possible to imagine a triggered release of the content of a magnetic capsule by applying an external alternating magnetic field. Superparamagnetic magnetite (Fe_3O_4) was mounted as a component of the shell wall[101–104] or as a part of the capsule interior.[105] Owing to the dissolution of the magnetic particles at pH 1, magnetic capsules could not be directly prepared by the sequential adsorption of magnetite nanoparticles and polyelectrolyte on MF templates. Either they were produced on PS templates, which were dissolved in THF, or by deposition of additional magnetite layers on hollow MF capsules.[104] Calcination of the core–shell magnetite particles at elevated temperature also produced intact magnetic spheres.[103]

Other core–shell systems, based on titanium[106,107] or luminescent semiconductor nanocrystals of CdTe[108,109] have been constructed. However, from these systems, no hollow shells have been fabricated up to now. Calcination of a composite between a PDADMAC and silica–gold nanoparticle (Au@SiO_2) core–shell system deposited onto polymer spheres gave rise to hollow spheres of Au@SiO_2.[103] To develop novel catalytic systems, noble metals, such as silver, were incorporated either inside the capsule or in the capsule wall. Three approaches have been described:

1. Entrapment of Ag^+ ions in polyelectrolyte multilayers, followed by the reduction of the ion by laser irradiation at 480 nm (Figure 5).
2. Entrapment of the silver ions inside a shell containing a PSS-polyaniline copolymer.
3. Chemical (i.e. silver mirror reaction) reduction deposition of metal onto the colloidal surface.[80]

2.4.6. *Towards Biochemical Functionality*

The LbL strategy permits the preparation of functional films on colloids with a high density of biomacromolecules, which can find applications as multienzyme biocatalysts. While the incorporation of biomolecules in flat films has been often demonstrated, only a few attempts have been made with colloids. Biocolloid particles with tailored enzymatic activities can be produced by means of protein multilayer architectures on colloidal particles. Multilayer films of bovine serum albumine,[110] immunoglobulin alone[110] or in combination with a fluorescent label,[111] β-glucosidase,[112] glucose oxidase,[113–116] horseradish peroxidase,[113] and urease[117] have been assembled on polystyrene microspheres by the alternate deposition of the protein and oppositely charged polymer. The protein multilayer shell could be varied from several nanometers in thickness to hundreds of nanometers.

The preparation of hollow capsules from bioactive molecules is limited owing to the harsh conditions used for the dissolution of the core. Decomposable hollow capsules based on deoxyribonucleic acid (DNA) and a low-molecular-weight organic molecule, a naturally occurring tris(amine), spermidine (SP), were formed by assembling DNA/SP multilayers on colloids and subsequently removing the core (Figure 6). The hollow DNA/SP capsules displayed a high sensitivity to salt. Exposure to 5 M NaCl solution for 12 h decomposes the capsules completely.[58] The decomposition is due to the trivalent charge of spermidine and can be varied using molecules with different numbers of charges. Such capsules might be attractive for encapsulation and controlled release of various substances, for example, the release of encapsulated compounds, such as dyes, drugs, or DNA can occur when loaded biocompatible DNA/SP capsules are exposed to environmental conditions that decompose them,

 © 2004 Wiley-VCH Verlag GmbH & Co. KGaA, Weinheim

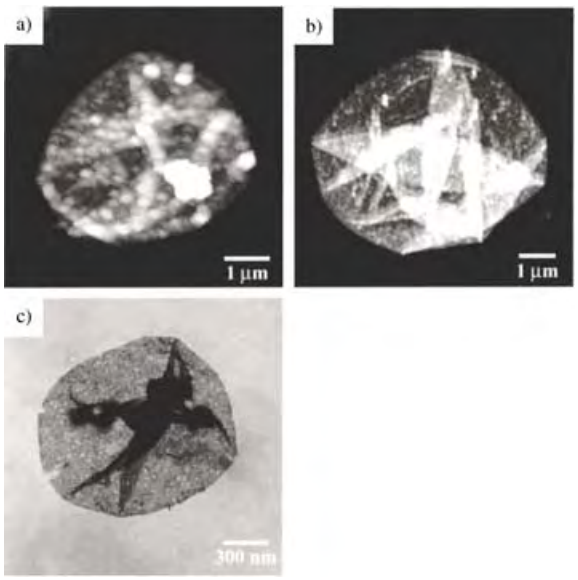


Figure 6. AFM images of biocompatible hollow capsules consisting of a) $(DNA/SP)_2/DNA$ and b) $(ALG/PL)_2/ALG$. The *z* axis ranges (maximum height) for the AFM images are 250 nm (a) and 150 nm (b). The hollow capsules were prepared by assembling the respective multilayers on 5.7-μm diameter MF colloid particles and subsequently removing the core by exposure to an HCl solution of pH 1.5–1.6. c) TEM micrograph of hollow $(DNA/SP)_2/DNA$ capsules, prepared from DNA/SP multilayer-coated 1.8-μm diameter MF particles. Adapted from ref. [58].

for example, in the blood or in the intracellular region. However, there are several problems to be solved for the preparation of such sensitive capsules: on the one hand, assembly has to be performed in a very low salt concentration and on the other hand, capsules must remain stable during the dissolution process.

Lipid vesicles and planar bilayers have been widely used as models for biological membranes. One shortcoming of liposomes is that they have a rather low stability and exhibit structural fluctuations. In nature, biomembranes are supported by a polymer network, the cell cytoskeleton. The combination of lipids and poolyelectrolyte capsules creates a similar artificial system, mimicking biological membranes. Hence, study of the composite lipid-layer–polyelectrolyte shell could contribute to the understanding of the interaction principles between membranes and biopolymers. Dipalmitoyldiphosphatidic acid (DPPA), dipalmitoyldiphosphatidylcholine (DPPC), and sphingosine were attached either by adsorption of preformed vesicles onto the capsule surface or by a solvent-exchange method onto polyelectrolyte capsules. Confocal microscopy images of capsules coated with fluorescent lipids demonstrated, within the resolution of the instrument, a homogeneous coverage of the capsule surface by DPPA/DPPC bi- or multilayers.[118] The electrical properties of lipid–polyelectrolyte composite capsules were studied by means of electrorotation. Measured conductivities of lipid–polyelectrolyte composite capsules (in the range 10^{-4}–10^{-1} $mS\,m^{-1}$) were higher than for simple lipid membranes. The conductivity increased with the bulk electrolyte concentration, which was attributed to the presence of pores or defects in the lipid film, estimated at 0.01 % of the total capsule surface area.[119]

2.4.7. *Dendrimers*

For planar LbL films on glass substrates, a basis layer of hyperbranched polyethylene imine is usually used. This polymer allows assembly of a high charge-density per volume owing to its dendrimer-like structure. Hence, the incorporation of dendrimer-like structures in the walls of capsules should also be possible. This was demonstrated recently by means of the 4th generation dendrimer poly(amidoamine) (4G PAMAM). Core–shell particles coated with multilayers containing PAMAM adsorb and retain negatively charged dyes as a result of strong electrostatic interactions with inner dendrimer charges, which are not used for the LbL interaction. The dyes can be released in salt-concentration-dependent manner by means of competing salt ions.[120]

To produce hollow shells, multilayers of PSS/(4G PAMAM) were deposited onto MF colloidal particles. Thin and highly porous fragile capsules were obtained in low yields. The yield could be improved by means of compensating the electrostatically unsaturated negative charges of PSS within the multilayer with a cationic compound that results in the formation of an insoluble complex. Before removal of the core, the fluorescent cationic anthracycline doxorubicin (DOX) was added to MF particles covered by multilayers of PSS/4G PAMAM. This yielded stabilized capsules.[121]

2.4.8. *Stability of Polyelectrolyte Shells*

Standard PAH/PSS capsules are stable at high ionic strength in aqueous solution between pH 0–13. The stability at high pH value is larger for the LbL PAH/PSS capsules than for a random PAH/PSS complex formed in solution. The pH range of stability for combinations of weaker polyelectrolytes can be remarkably smaller. As described in Section 2.4.6, high ionic strength can lead to the dissolution of capsules consisting of materials of low charge. But even PAH/PSS capsules exhibit a strong increase of permeability with increasing ionic strength, which points to a weakening of the bond strength between polyelectrolytes as a result of competition with the salt ions.[150]

PAH/PSS capsules could be suspended in various organic media by a gradual solvent exchange whereby the shell stability and integrity was preserved.[122] However, a strong increase in permeability in organic solvents is also reported, which points to changes in the wall structure.[123] The stability in organic solvents makes possible the preparation of oil-in-water (illustrated by Figure 7) or water-in-oil emulsions without employing any surfactants. Particularly in the field of drug delivery, it might be desirable to avoid the addition of emulsifiers. Moreover, microdrops are highly stable and have a high degree of monodispersity. The presence of two different, immiscible solvents, one inside the capsule and one outside, could also be useful for phase-transfer catalysis processes through a nanosized insoluble meshwork of polymers.

 © 2004 Wiley-VCH Verlag GmbH & Co. KGaA, Weinheim

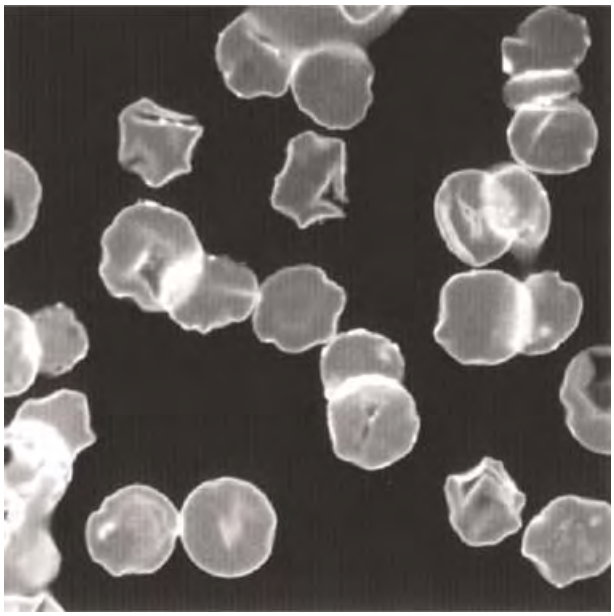


Figure 7. Oil-in-water suspension. Confocal micrograph of polyelectrolyte capsules $(PSS/PAH)_{10}$ templated on erythrocyte cells filled by a solvent-exchange process with rhodamine B-labeled octanol and resuspended in water. The size of the image is 50 μm × 50 μm. Adapted from ref. [122].

3. Properties of the Capsules

3.1. Permeability

Permeability of polyelectrolyte microcapsules is a key factor in achieving the controlled release of encapsulated materials. Permeability studies on capsules have been tackled by two approaches. One approach consists of encapsulating soluble materials and measuring their release from the capsule interior. This method has the disadvantage that capsules are prepared and observed under different equilibrium conditions (pH value, solvent), particularly as variations in environmental conditions can remarkably affect the permeability. Furthermore, the dissolution of the core results in osmotic pressure in the capsule interior especially for materials of high saturation concentration. A high pressure difference leads to increased release rates.

Another approach consists of adding a fluorescent-labeled permeating substance to the outer solution of a hollow capsules suspension and in monitoring the penetration into the capsules by confocal microscopy. This method allows the investigation of the permeability of individual capsules. However, as a result of a broad distribution of capsule permeability, a statistical analysis of many capsules is necessary before general conclusions can be drawn.

The latter method was used in the first capsule permeability experiments. Using fluorescent-labeled PAH molecules, first rough estimations gave a cutoff of 5000 $g\,mol^{-1}$ for capsules prepared from $(PSS/PAH)_4$ on MF cores.[18] Later, it was found that other factors, such as ionic strength, pH value, capsule age, and solvent influence the permeability. In addition, the permeability differs from batch to batch as a function of the core dissolution, which, as discussed in Section 2.3, is itself regulated by the core diameter and the size of dissolved MF oligomers.

3.1.1. Permeability as a Function of the Ionic Strength

The structure of multilayers and therefore the permeability strongly depends on the ionic strength as well as the pH value during adsorption and washing processes. These effects have already been investigated in detail for planar films.[32,64,124–129] The salt concentration of the polyelectrolyte solution is an essential parameter in the LbL process.[32,126,127] In particular, von Klitzing and co-workers found a linear increase of PAH/PSS film thickness with the square root of the salt concentration but noted no additional influence of the salt after completion of the adsorption process.[126] However, Fery et al., using AFM, spotted considerable structural changes to the surface of the prepared PAH/PAA film upon altering the ionic strength: washing with pure water after deposition of each layer produces films with considerable surface roughness (effective roughness of approximately 17 nm for a 10-layer film). In contrast, relatively smooth (effective roughness 1 nm) and homogeneous PAH/PAA multilayer films are formed when the salt concentration is kept constant, both during the assembly process and the washing steps. For such smooth films, subsequent exposure to pure water leads to the introduction of regular, discrete, nanometer-sized pores.[128]

Standard $(PSS/PAH)_4$ capsules templated on MF cores exhibit a semipermeable behavior. In pure water, they are impermeable for labeled PAH with a molecular weight above 15000 $g\,mol^{-1}$, whereas dyes such as fluorescein or rhodamine permeate instantly (Figure 2b,c). We observed that capsules became permeable even for the polymer PAH with a molecular weight of 70000 $g\,mol^{-1}$ when the salt concentration is increased above 10^{-2} M.[150] We concluded that increasing salt concentration results in a weakening of the electrostatic interactions between the polyelectrolytes as a result of the competing salt ions. The intercalation of salt ions promotes a swelling of the capsule wall caused by the osmotic storage of water. The wall structure is then loosely connected and the mesh widths become larger which induces an increased diffusion rate for the probe polymer. The opening of the wall is reversible. After removing the salt, capsules are again impermeable to polymers. A method was thus developed for loading capsules with polymers by using salt to switch the capsule permeability.[150]

Similar investigations have been performed on capsules templated on erythrocytes.[75] The results show a similar trend but are explained in a different way. As a result of the strong oxidizing agent used to remove the template, there are large pores or defects present in the capsule wall, which are responsible for the penetration of macromolecules. At low salt concentration, electrostatic repulsions between the permeating molecules (human serum albumin) and the charged surface of the capsule prevent penetration. High ionic strength shields the charges and results in a penetration through the pores. This hypothesis is supported by the fact that neutral molecules, such as dextrane, permeate regardless

 © 2004 Wiley-VCH Verlag GmbH & Co. KGaA, Weinheim

of the ionic strength. Purely electrostatic effects are suggested as a reason for the ionic-strength dependence of adsorption and permeability of polymers observed in investigations on chitosan/chitosansulfate capsules.[76] This explanation, however, is inconsistent with other results, where a strong dependency of the permeability on the number of deposited layers has been found.

In agreement with the different conclusions derived from the diffusion of molecules into the capsules, Antipov et al. observed that the release of encapsulated fluorescein microcrystals from PSS/PAH capsules is also strongly enhanced by increasing salt concentration.[130] Additional measurements at lower salt concentrations and in different salts have shown that this effect can not be described by pure electrostatic effects but depends on additional specific interactions of the salts with the capsule wall as well. Diffusion independent of the salt concentration has been reported for the drug ibuprofen encapsulated with various types of polyelectrolyte multilayer.[73] However, these measurements have been performed in the range 0.25 M to 1 M, which is far outside the range studied before.[150]

3.1.2. Permeability as a Function of the Film Thickness

Several fluorescent dyes, such as pyrene and fluorescein microparticles, were used as models and coated with various numbers of PSS/PAH multilayers under conditions of low solubility of the dyes.[54,57,131] By adding ethanol to the coated pyrene or changing the pH value of the fluorescein dispersion, the cores were dissolved and the fluorescent dyes were released from the microcapsules into the solution. The dependence of the release profile as a function of the multilayer thickness was quantified by fluorescence spectroscopy. The crystalline portions of the fluorescein and pyrene did not perturb the fluorescence signal, because of the self-quenching of fluorescence in the solid state. Results on PSS/PAH encapsulated fluorescein reveal an increase of the release rate with increasing pH value and ionic strength and a decrease with layer numbers.[57] Encapsulation in up to six layers had almost no influence on the dye dissolution. However the presence of more layers resulted in a remarkable decrease of the release time. The diffusion coefficient per layer decreased up to ten layers where it reached a constant value of approximately $10^{-16}\,m^2 s^{-1}$. In contrast, for planar films of PAH/PSS, diffusion coefficients of 10^{-18} to $10^{-20}\,m^2 s^{-1}$ have been measured.[132] This difference was explained by deviations in the preparation process and by neglecting pores in the measuring principle on planar films. However, the release rates of for the fluorescein particle were measured in a buffer solution which was added to keep a constant high pH value. The resulting high ionic strengths could also be the reason for the high permeability. In addition, osmotic pressure, caused by the saturated fluorescein solution in the capsule interior and the almost pure water in the outer solution can also raise the release rate. Measurements at low ionic strength yielded two orders of magnitude smaller diffusion coefficients and showed an odd-even effect depending on the charge of the outer layer which decreases with layer number (Figure 8).

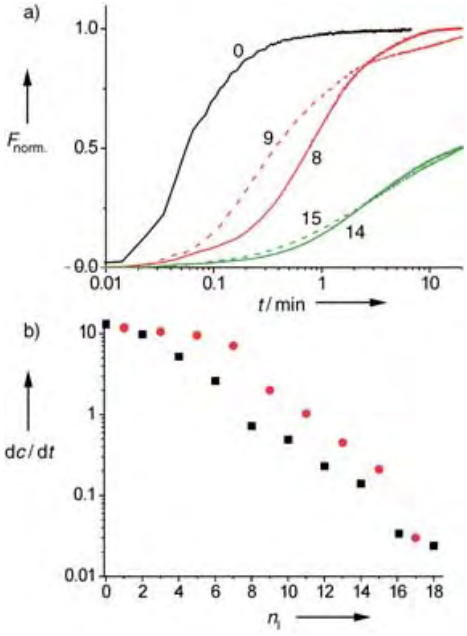


Figure 8. a) Release curves of fluorescein crystals (diameter 4–6 μm), encapsulated with 0, 8, 9, 14, and 15 layers of polyelectrolytes; dashed curves mark a positive surface charge; release in sodium tetraborate buffer ($c = 6\times10^{-4}$ mol L^{-1}, pH 9.16, $c_{Fl(100\%\,release)} = 1.4\times10^{-6}$ mol L^{-1}). b) Dependence of the maximum release rate dc/dt on the layer number (n_l) and the surface charge, squares mark PSS as the outer layer and circles PAH as the outer layer. The odd–even effect for the average layer thickness can be clearly seen, but it decreases with increasing layer thickness.

Donath and co-workers used a similar approach where ibuprofen (IB) was chosen as a model drug.[73,77] They exploited the pH-dependent solubility of IB to vary the concentration gradient. The release rate of IB increases with the solubility of IB, which in turn is governed by the pH value in bulk solution. At pH 7.4, the solubility of the drug is very high and IB is released very fast. At pH 1.4, where the IB solubility is very low, the release of the drug takes hours and is proportional to the wall thickness. This result supports the model of two release channels, one by diffusion at pH 1.4 and one by pressure through pore-like structures at pH 7.4. As mentioned above, such pores were observed for thin flat PAA/PAH films. At a molecular scale, polyelectrolyte films are not smooth but may have nanoscopic pores that can be influenced by outside conditions, such as pH value or salt content.[28,29,133]

We investigated the permeability of dyes into hollow capsules by assembling additional multilayers onto capsules after release of the MF core.[66] The addition of just a few more layers seal the wall against the penetration of macromolecules. Adding eight further layers to the capsules gave a strongly reduced permeability even for small dye molecules. This finding presents a novel way to load the capsules with a polymer and to ensure its complete immobilization in the interior by additional adsorption of few extra layers.

 © 2004 Wiley-VCH Verlag GmbH & Co. KGaA, Weinheim

3.1.3. Permeability as a Function of pH Value

Antipov et al. used the previously cited pH influence on weak polyelectrolytes to control the permeability of the PSS/PAH capsule walls and to encapsulate macromolecules.[123] PAH/PSS capsules were prepared at neutral pH. Capsules could be switched between an open and a closed state by tuning the pH value. Macromolecules can then penetrate into the capsules at low pH values but are excluded at a pH values higher than 7. This reversible transition provides the opportunity to encapsulate different substances under mild conditions within several minutes. The switching behavior was explained by means of the protonization/deprotonization of the weak polybase PAH. Variations in the pH value influence the interactions in the PAH/PSS wall and create locally charges and defects in the film. Unfortunately, this behavior could not be systematically reproduced. Some independent attempts to open PSS/PAH capsules by means of low pH value failed.

3.1.4. Permeability as a Function of the Wall Materials

Donath and co-workers studied the permeability of ibuprofen through various polyelectrolyte multilayer capsule walls.[73] Factors controlling the permeability are the charge density of the polymer forming the capsule wall and the hydrophobicity of the substance that diffuses through the wall. An explanation for this behavior was based on studies of ion permeability through planar polyelectrolyte multilayers by Tieke and co-workers.[33,63] It was proposed that two types of cavities are available for permeation within polyelectrolyte multilayers membranes, that is, small, strongly hydrophobic cavities and large, less hydrophobic cavities. High-charge-density polyelectrolyte multilayers tend to form small, hydrophobic cavities while a low-charge-density polyelectrolyte multilayers give large cavities. The model drug chosen, ibuprofen, is a rather hydrophobic molecule and is expected to transport through the large less hydrophobic cavities. It is most probable that only polyelectrolyte multilayers constructed with high charge density and well-matched charge distances can form small hydrophobic cavities. Otherwise, polyelectrolyte multilayers will generally have large cavities. Studying the permeability of much larger molecules could test this latter hypothesis.

PAH/PSS capsules formed on MF are less permeable than PDADMAC/PSS capsules, which are permeable to polymers with molecular weights of up to 2×10^6 g mol^{-1}. Although both polyelectrolytes PSS and PDADMAC have a large charge density they clearly form especially large pores (see Section 3.2.5. on wall structure).

3.2. Mechanical Properties

The mechanical properties of polyelectrolyte capsules in aqueous solution, but also as dried materials play an important role in many applications. Despite of this importance, only few systematic investigations of the mechanical properties have been conducted. In general, a higher mechanical stability can be achieved for LbL films than for fluid membranes or liposomes. Moreover, the mechanical properties can be varied over a wide range by using different compositions of polyelectrolytes and by increasing the number of deposited layers. Cross-linking of the noncovalently bound polyelectrolytes can improve the capsule stability and causes a transition from a viscous to an elastic response. The mechanical properties of hollow capsules were investigated by the methods described in the following sections.

3.2.1. Application of an External Osmotic Pressure

Owing to the impermeability of the capsules to large molecules, high osmotic pressure from the outside can be applied by addition of charged polymers to the outer solution. The osmotic pressure arising is determined mainly by the concentration of the counterions. Solutions of sodium PSS with a molecular weight of 70000 g mol^{-1} were added to spherical capsules of PAH/PSS. Above a specific concentration of PSS or a critical pressure (P_c), a shape transition from a spherical to a sickle shape was observed (see Figure 9). A theoretical model was developed, which describes the dependence of the critical osmotic pressure P_c on the elasticity modulus of the multilayer, the layer number, and the geometric parameters of the capsules. Because the wall thickness and dimensions could be varied in a defined way, the model could be verified and elasticity moduli between 500 and 700 Mpa, depending on the system, have been determined. These values are comparable to results obtained with macroscopic plastic materials and reflect a high degree of local interactions between the polyanion and the polycation.[134]

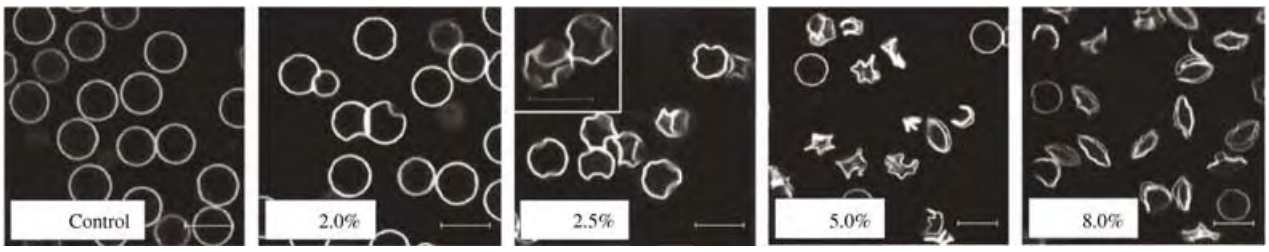


Figure 9. Outside osmotic pressure induces deformation of polyelectrolyte capsules: CLSM images of capsules consisting of 10 layers of PSS/PDADMAC as a function of the PSS (M_r = 70000 g mol^{-1}) bulk concentration. PSS concentrations, in wt%, are indicated. Scale bars equal 5 μm. Adapted from ref. [71].

 © 2004 Wiley-VCH Verlag GmbH & Co. KGaA, Weinheim

Investigations on different polyelectrolyte materials showed that the elasticity depends on the material. For example, PSS/PDADMAC capsules have a remarkably smaller elasticity than PSS/PAH capsules.[71]

An increase in the pressure stability was found for the shell-in-shell capsules described in Section 2.4.3. For these capsules, no collapse was observed under the layer number and PSS concentration conditions that collapsed the normal capsules. In this system, two shell walls are separated by an intermediate PAH solution with a layer thickness around 50 nm, which acts as an osmotic-pressure buffer and yields higher stability against pressure from outside.[100]

3.2.2. Application of an Internal Osmotic Pressure

The mechanical properties of capsules could be investigated by loading microcapsules with polyelectrolytes and by varying the polyelectrolyte concentration outside (different methods of loading macromolecules are described in Section 4). When capsules are filled with a 1 M PSS solution by a "ship-in-a-bottle" synthesis, results, in aqueous solution, in an enlargement of the capsule diameter by factor of 3 (Figure 10). Higher pressure led to breakage of the capsules.

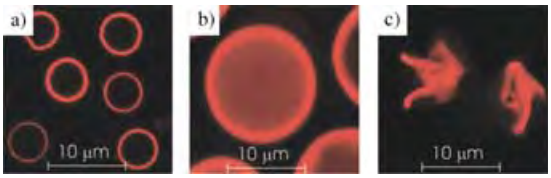


Figure 10. Effect of inner osmotic pressure on PSS/PAH capsules. CLSM images of the same capsules a) before and b) after they were filled by polymerization of a 1 M styrene sulfonate solution, and c) shrinking of the capsules in (b) caused by the osmotic pressure of a 2 M PDADMAC solution in the exterior. From ref. [52].

Deformations of such extent are not reversible. Reduction of the osmotic pressure after swelling by adding salt or polyelectrolytes to the outer solution does not result in a shrinking of the spherical capsules but in a collapse of the wall (Figure 10 b,c),[52] pointing to a non-elastic deformation.

In contrast, at lower swelling, a partly reversible elastic behavior was reported. Capsules which were filled using the precipitation method shrank back, after swelling to an certain extent, once the external osmotic pressure was increased again.[85] A further indication of some elastic behavior is given by the investigation of the MF-core dissolution (see Figure 1), where a swelling of the capsule as a result of the presence of MF oligomers was observed. After the MF oligomers diffused out of the capsules, the shells shrank back to their original size having expanded from 4 to 6 μm during the dissolution.[62,135]

3.2.3. Investigations with a Micropipette

The deformability and osmotic properties of hollow PSS/PAH microcapsules assembled on the decomposable template MF were studied by means of the micropipette video microscopic technique.[136] The polyelectrolyte microcapsules reacted to micropipette suction with plastic deformation. The upper-limit value of the plastic modulus *Dp* was evaluated at roughly 5 kPa. Addition of lipids to the polyelectrolyte layers resulted in a remarkable change of the mechanical properties: after stress application in the micropipette, the capsules regained their original shape completely. It was concluded that covering with lipids yields a high degree of plasticity, at least in the range of the applied mechanical forces.[136]

3.2.4. Capsule Nanostructure: An Indirect Method to Evaluate the Mechanical Properties

The nanostructure of capsules on mica was investigated by atomic force microscopy (AFM). Although measurements are performed on dried samples, and the observed morphology is then different to that in solution, indirect conclusions onto the capsule stability were drawn.[137,138] Polyelectrolyte capsules prepared on MF particles and biological cell templates exhibit a grainy structure at high resolution. These nanometer grains are attributed to segregated polyelectrolyte complexes. For PSS/PDADMAC capsules significantly larger grains (124 ± 10 nm) were observed than for PSS/PAH capsules (50–100 nm).[71] As described in the previous section, the elasticity of PSS/PDADMAC capsules is smaller than that of PSS/PAH capsules. It was concluded that the size of the grains correlates with the capsule-wall stability and elasticity.

3.2.5. Influence of Annealing on the Wall Structure

The influence of temperature on the shell structure was studied by AFM for PSS/PAH capsules.[139] Annealing at 70 °C produces a temperature-induced shrinking. The wall thickness increases parallel to decrease of the capsule diameter. These size changes were explained by a transition towards a more coiled arrangement of the individual polyelectrolyte molecules in multilayers. This rearrangement is a result of breaking and re-forming ion pairs to yield a more bulky configuration of the polymers. However, the experimental base for this assumption is weak. For example, annealing of other polyelectrolyte combinations, such as PDADMAC/PSS, led to an increase of the capsule diameter even at 40 °C,[140] and heating the capsules at 70 °C destroyed them. Clearly, the electrostatic coupling of PDADMAC and PSS is much weaker than the coupling of PAH and PSS. This result confirms the higher permeability of PDADMAC/PSS capsules (see Section 3.2,1). This weaker interaction was attributed to topological restrictions between the two stiff and bulky polymers.[140]

We showed using fluorescence recovery after photobleaching (FRAP) that the rate of penetration of fluorescein in PSS/PAH capsules was reduced by three orders of magnitude after annealing at 80 °C. The rearrangement of the polymers chains was also invoked as the reason for the resealing of the pores formed during the core-dissolution process.[141]

 © 2004 Wiley-VCH Verlag GmbH & Co. KGaA, Weinheim

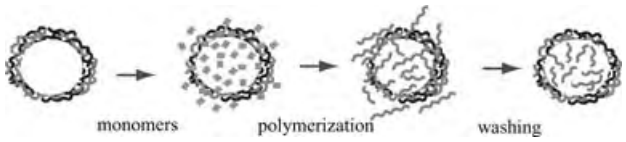
4. Filling of the Capsules: Properties and Potential Applications

4.1. Encapsulation of Macromolecules and Crystals

The simplest method of encapsulation consists in using the core itself as substance to be encapsulated. The problem is to obtain colloidal crystals of low dispersity in the desired size range and with a voluminous shape. Long needles or amorphous materials are not suited as templates. Furthermore, the materials should have a low solubility under the polyelectrolyte assembling conditions. For water-soluble substances, the material saturated polyelectrolyte and wash solutions are used to avoid the dissolution of the core. If the colloidal materials fulfill these conditions, they can be covered by polyelectrolyte multilayers. For instance, protein aggregates and dye crystals have been encapsulated using this method. For colloids with a low surface charge, a basic layer of tensides or block-copolymers is necessary to increase the surface charge.[56,131]

In producing monodisperse encapsulated materials, the filling of preformed shells is a big challenge. In the presence of capsules, low-molecular-weight materials precipitate, in most cases, on the wall surface or in the bulk solution but not in the interior of capsules.[143,144] A solution to this problem is offered by the immobilization of functional macromolecules in the capsules interior. They can change the physical properties in the capsule interior (pH, ion strength, hydrophobicity) from those of the bulk solution which can lead to a preferred precipitation inside the capsules. Three approaches have been followed to immobilize macromolecules permanently in the capsule interior:

An elegant encapsulation technique for synthetic macromolecules exploits the semipermeable property of the polyelectrolyte capsule for a polymer synthesis in the presence of empty capsules (Scheme 4).[52] In this "ship-in-a-bottle" approach, monomers are incubated together with empty preformed shells. Small monomers and the initiator, potassium peroxodisulfate, diffuse inside the shell. The polymerization is then started inside and outside the capsule by increasing the temperature. The resulting polymers are trapped and after subsequent washing, capsules filled with high concentrations of polymers are isolated (see Figure 10). The captured polymers modify the properties of the capsule interior and enable the selective control of ionic strength, charge density, pH value, and dielectric constant in the capsules interior. Although this method has been applied to several polymers, some problems were observed. Depending on the surface charge of the capsule wall, an unequal distribution of the initiator is produced, which leads to increased polymer synthesis in the wall or on the surface of the wall, which in turn modifies the properties of the capsule wall. For example, high concentration of PSS in the wall leads, after adding an organic cation, to wall destruction and the release of the entrapped macromolecules.[52]



Scheme 4. Filling polyelectrolyte microcapsules with polymers by a "ship-in-a-bottle" synthesis.

A second encapsulation method has two stages. First, polymers are precipitated onto a sacrificial core. This can be done by complexation of the polyelectrolyte with multivalent ions since multilayers of polymer and multiple-charge metal ions, such as Tb^{3+} and Y^{3+}, are not stable and will decompose, leaving the large polymer filling the capsule interior while the small multivalent ions diffuse away in the aqueous solution.[85] Second, stable classical LbL polyelectrolyte multilayers are assembled. The core is removed, the initial multiion–polymer layers decompose spontaneously, and the inside of the capsule is filled with the polymer.[145] Dextrane, PSS, and PAH have been encapsulated by this technique.

Another approach for encapsulation consists of loading preformed capsules by switching the shell-wall permeability through variation of environmental conditions, such as pH value[65,121,149] and ionic strength (see also Sections 3.1.1 and 3.1.3).[150] However, these methods allow only the encapsulation of small amounts.

Physicochemical differences between the polymer solution in the capsules and the outer medium can be used for selective preparation or accumulation of small molecules or nanoparticles inside the capsules. Polymer-filled shells have been used to trap semiconductor nanocrystals, iron oxide, or nanosized magnetic ferrite particles.[105,146,147] Fluorescent CdTe nanoparticles with different sizes and emission wavelengths can be immobilized within polymers through electrostatic interaction with them. The surface charge of the nanoparticles used can be easily tuned by employing various thiols that carry either a positive or negative charge. When nanoparticles were incubated with the polymer-filled shells, they diffused inside the capsule and were retained inside through electrostatic attraction with the oppositely charged polymer (see Figure 11).[146] Two parameters govern the amount of nanoparticles encapsulated: the concentration of the nanoparticle suspension and the concentration of free polyelectrolyte molecules inside the capsules. However, it is to be expected that in pure water or in the presence of a higher salt concentration or of compounds having higher affinity to the immobilized polymer, the nanoparticles will slowly diffuse out of the capsule, a problem that reduces the practicality of proposed uses in combinatorial libraries.

A gradient of polarity between the bulk and the polymer-filled shells was exploited for the encapsulation of hydrophobic materials, for example, the dye Disperse Red 1.[148] The polarity gradient arises from the hydrated polyelectrolyte charges. Hence, in a mixture of a water-miscible organic solvent and water, the water concentration in the interior of the capsules is higher than the surrounding solution. Thus the hydrophobic material is less soluble inside the capsules than outside.

Several dyes and inorganic salts, such as fluorescein, rhodamine, pseudoisocyanine, calcium carbonate, and barium carbonate were precipitated inside polyelectrolyte capsules

 © 2004 Wiley-VCH Verlag GmbH & Co. KGaA, Weinheim

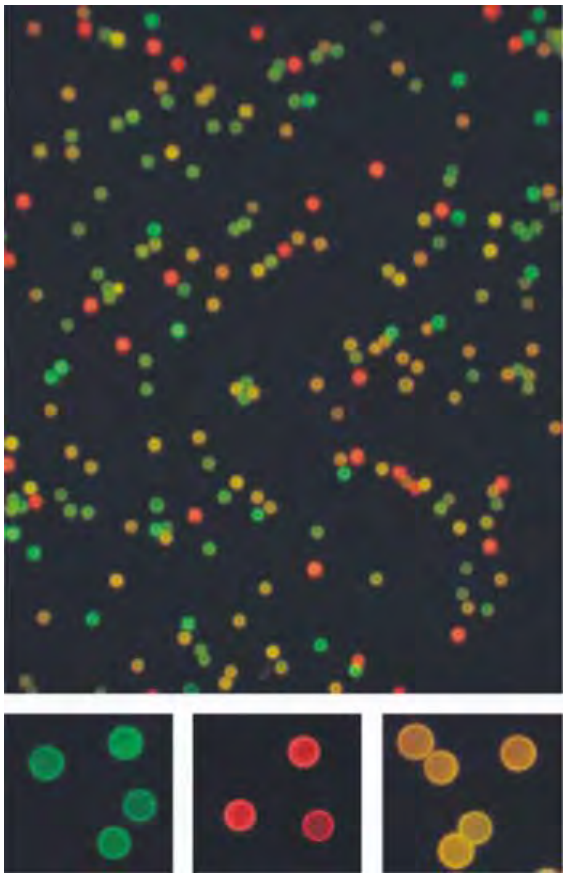


Figure 11. Top: Fluorescence image of a mixture of polymer microspheres loaded with CdTe nanocrystals of different sizes. Both single-color (emission wavelength 548, 558, 581, 615, and 633 nm) and multicolor (mixture of the five mentioned wavelengths) tagged spheres are present in the mixture. Bottom: enlarged view of the microspheres encoded green, red, and orange (five-color tagging). From ref. [146].

by exchanging the solvent, the counterion,[10] or by varying the pH value, thus modifying the dye solubility. For example, 6-carboxyfluorescein (6-CF) was precipitated from a basic solution in the presence of empty and PSS filled (pH gradient) capsules until supersaturation took place at pH 6. SEM characterization of the resulting 6-CF precipitates showed that the polyelectrolyte capsules are selectively filled with spherical 6-CF solids.[143,144] By means of electrostatic interactions with PSS, J-aggregates of the cationic dye pseudoisocyanine could be prepared inside the capsules. In a second step the aggregates were transformed into fluorescent nanocrystals by addition of tetraphenylborate counterions.[10]

4.2. Encapsulation of Biomolecules

Encapsulation of active biomolecules, such as enzymes, could have several purposes. Polyelectrolyte capsules have the ability to protect encapsulated proteins from high-molecular-weight denaturing agents or bacteria. Furthermore, they allow regulation of the permeability towards small substrates, which can enter and leave the capsules to react with the biomolecules in the interior. Such loaded capsules find use as microenzymereactors, in biosensing, cell transfection,[151] and the polymerase chain reaction (PCR) of DNA.

One method to encapsulate enzymes is to coat enzyme crystals or aggregates with the LbL technique.[152,153] The size of the protein primary aggregates, the aggregate morphology, and their hierarchical arrangement into secondary aggregates are determined by preparation parameters, such as protein concentration, ionic strength, salt exposure time, and nature of the polyelectrolyte used for shell formation. Hence, the use of enzyme crystal templates presents several challenges.

Caruso et al. coated catalase crystals using the LbL method (Figure 12).[152] The activity of the encapsulated

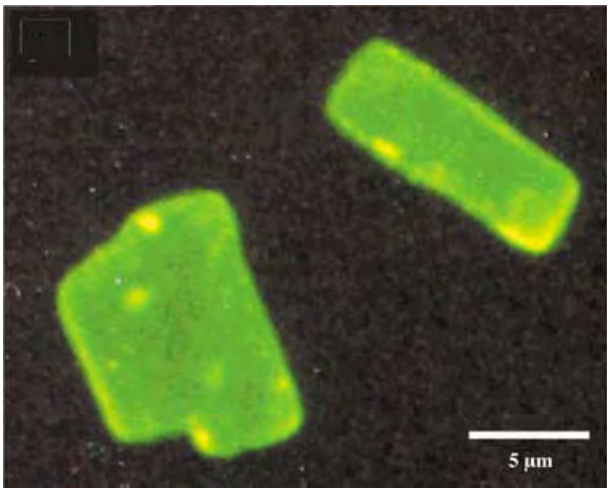


Figure 12. Fluorescence optical micrograph of catalase crystals coated with eight $(PSS/FITC\text{-}PAH)_4$ polyelectrolyte multilayers. Adapted from ref. [152].

enzyme was fully retained after 24 h of exposure to protease. Thus, a thin polymer film (thickness of about 8 nm) is sufficient to prevent proteolysis of the polymer-encapsulated catalase.

Using chymotrypsin as a model enzyme, the selective permeability of the capsule wall was demonstrated for substrates and inhibitors of different molecular weight and solubility: when a low-molecular-weight inhibitor (phenylmethylsulfonyl fluoride (PMSF) $M_r = 174\ g\,mol^{-1}$) was added to a suspension of capsule containing chymotrypsin, the encapsulated chymotrypsin was deactivated by 70%. However, when a high-molecular-weight inhibitor was used (the protein BPTI, $M_r = 6500\ g\,mol^{-1}$), the degree of deactivation sinks to 13%. This results again points to the semipermeable character of the capsule wall.[154]

Lactate dehydrogenase was also encapsulated in polyelectrolyte multilayers by this method. The encapsulation of the enzyme did not influence its affinity for the substrate pyruvate. Compared with the free-enzyme form, the encapsulated lactate dehydrogenase exhibits an increased lifetime in diluted solutions (from 30 min to 1–2 days) and presents a higher stability against basic denaturation. The changes in the catalytic characteristics of encapsulated lactate dehydrogen-

 © 2004 Wiley-VCH Verlag GmbH & Co. KGaA, Weinheim

ase are probably caused by an increase in effective p*K* values of the amino acids, which is caused by the polyelectrolyte coating of the enzyme.[155]

The use of enzyme aggregates and crystals has the disadvantage that the size and shape of the obtained particles depends strongly on the prepared enzyme templates. It is not possible to obtain monodisperse, spherical particles by this method. Therefore, to load monodisperse capsules with enzyme the concept of macromolecule encapsulation through the opening and closing the capsule pores can be used (see Section 4.1). The size distribution and the shape of the capsules can be easily predetermined. In addition, the sometimes harsh procedures of enzyme precipitation can be avoided.

Tiourina et al. encapsulated a proteolytic enzyme, α-chymotrypsin, in hollow PSS/PAH shells. The encapsulation of the enzyme was carried out at pH 4.0, where pores are present in the capsules walls, then subsequent washing at pH 8.0 which closes the shell wall. The protein in the capsules retained a high activity (50 to 60%) and storage stability. The enzyme functionality was preserved for more than one week at room temperature. The polyelectrolyte shell protected the proteinase α-chymotrypsin from high-molecular-weight inhibitors, such as the enzyme BPTI, whereas small molecules can readily reach the enzyme in the capsules.[156]

Urease was also encapsulated into PSS/PAH shell using a similar approach: the pore-controlling factor was in this case the solvent.[142] Lvov et al. exploited the fact that polyelectrolyte interactions depend on the solvent polarity. When ethanol is added to a urease/microcapsule suspension, pores opens in the polyelectrolyte walls and urease can penetrate the capsules (Figure 13). Upon resuspension of the filled

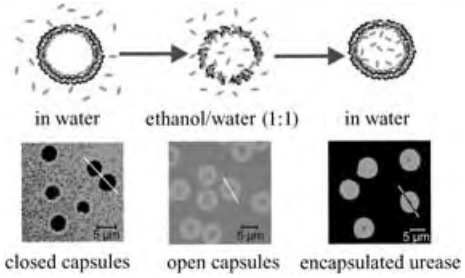


Figure 13. Permeation and encapsulation of urease-FITC into polyion multilayer capsules. Left: in water, fluorescence is observed only in the supernatant; middle: in water/ethanol mixture 1:1, fluorescent material is inside as well as outside of the capsule; right: capsule with encapsulated urease resuspended in water, the fluorescent material is inside of the capsules. Top: Scheme and bottom: confocal fluorescence micrographs. Adapted from ref. [142].

capsules in pure water, the pores will close and the enzyme is then encapsulated (Figure 13, right). In this example the encapsulated enzyme urease preserved only 13% of its activity compared with the free enzyme in ethanol. This decrease is probably due to the difficulties encountered by the substrate in penetrating the capsules. The problem that only a small fraction of enzyme in solution is encapsulated can be circumvented by having in addition polyelectrolytes inside the capsules that favor binding and precipitation. Thus, encapsulation efficiencies of up to 90% were reached.[67,68]

Using these urease-loaded PAH/PSS polyelectrolyte capsules, the biomimetic synthesis of calcium carbonate exclusively inside of the capsules was achieved. The carbonate anions were generated inside of the capsules by a urease-catalyzed urea decomposition. Addition of calcium ions caused precipitation of calcium carbonate, which completely filled the capsule volume. Owing to the easiness in varying experimental parameters, such as the wall thickness, internal composition, and diffusion rate, these polyelectrolyte capsule-based systems can be used to study fundamental aspects of biomineralization processes.[157]

5. Conclusions and Outlook

Since the development of the electrostatic LbL self-assembly of polyelectrolyte thin films about 10 years ago,[158] lots of progresses have been made towards the understanding of the theoretical principles underlying this method as well as towards the development of successful applications, many of which have been patented, such as coatings for contact lenses.[159] One milestone was the use of such films in 1998 for the preparation of hollow capsules. This opened new avenues in the encapsulation business. The prime advantages of the new polyelectrolyte capsules are their large versatility and modularity as regards materials and properties. This led in the last few years to a fast development of the technology in widespread research and application areas, as demonstrated by the selected examples in this review. However, owing to the short development time of this technology and the almost infinite possibilities to vary parameters in the preparation process, there are still many open questions. Although a lot of interesting developments have been demonstrated in principle, many more studies are necessary to optimize the experiments and to improve results reproducibility. It is today not clear if all of the potential uses given herein can be really fulfilled by the LbL capsules. For example, the permeability to small molecules is still too high for a controlled long-term release from the capsule interior. In addition, owing to a wide distribution of permeability per capsule within one batch, only a rough cutoff the molecular-weight discrimination can be achieved.

In terms of the new development of LbL capsules, one domain that will be strongly addressed in the future concerns biological applications. To improve the biocompatibility, efforts concerning the synthesis of biodegradable, biocompatible monodisperse, and shape-controlled cores are under way.[160] The use of capsules as biomimetic systems for investigating the physical principles underlying cell-adhesion processes is planned. Another important development is the modification of the capsule surface to recognize specific materials or interfaces. For this purpose, the surface can be simply positively or negatively charged but can also incorporate biochemical functions, such as proteins, receptors, or DNA sequences. This opens the way for creating shells with specific adhesion properties that are of great potential for drug-delivery applications as well as in diagnostics.

 © 2004 Wiley-VCH Verlag GmbH & Co. KGaA, Weinheim

Another interesting development is the combination of capsules with liposomes to combine the stability of capsules with the permeability of liposomes. Capsules can be coated by lipid bilayers and vice versa leading to lipid-bilayer/polymer-layer composite systems which resemble lipid-bilayer/cytoskeleton composite systems of biological cells. The next step in the biomimicry process could be the incorporation of ion channels and receptors in such capsule-liposomes.[161] Encapsulation of DNA for non-viral gene therapy is also a future development, as well as the use of microcapsules as novel cages for compartmentalization of materials, and thus as templates for biomineralization processes.

To keep the potential of the new capsules technology in mind, we will finish this review with a list of drawbacks and advantages of the LbL capsules compared to other applied capsules:

Drawbacks:

- High permeability to small molecules.
- Aggregation, particularly of small capsules (< 1 μm in diameter).
- Reproducibility of results is low.
- Long-term stability unknown.
- Time-consuming preparation process.

Advantages:

- Tunable semipermeability.
- High chemical stability.
- Large size range (from 15 μm to 100 nm).
- Monodispersity.
- Low ratio between wall material and interior volume.
- Multifunctionalization of the capsule wall and wall surfaces in nanometer resolution possible.
- Modification of the physicochemical properties of the capsule interior is possible.
- Preparation of capsules from biodegradable and FDA (Food and Drug Administration) approved materials is possible.

The list of advantages and disadvantages could be elongated by more specific reasons. However, the above mentioned points show clearly that LbL capsules will not substitute all other encapsulation technologies but that they can contribute to new applications especially in high technology fields. However, the investigation of LbL polyelectrolyte capsules is almost at the beginning and many new developments and surprises can be expected in the future of this highly fascinating research field, which could help to overcome the mentioned drawbacks.

Abbreviations

4G PAMAM	4th generation poly(amidoamine)
ALG	Alginate
BPTI	Bovine Pancreatic Trypsin Inhibitor
FRET	Förster Resonance Energy Transfer
IB	Ibuprofen
LbL	Layer-by-Layer
LSCM	Light Scanning Confocal Microscopy
MB	Methylene blue
MEPE	Metallosupramolecular coordination polyelectrolyte
MF	Melamine Formaldehyde
PAA	Poly(acrylic acid)
PAH	Poly(allylamine)
PDADMAC	Poly(diallyldimethylammonium chloride)
PEI	Poly(ethyleneimine)
PL	polylysine
PLA	Poly(DL-lactic acid)
PLGA	Poly(DL-lactic-co-glycolic acid)
PS	Polystyrene
PSS	Poly(styrene sulfonate)
PVS	Poly(vinylsulfate)
SP	Spermidine
THF	tetrahydrofurane

The authors thank Prof. Dr. Helmut Möhwald, Prof. Edwin Donath, and Dr. Gleb B. Sukhorukov for stimulating discussion and comments during the preparation of the manuscript, and C.S.P. thanks the Max Planck Society for a fellowship. We thank Alexei Antipov for his help with graphics and illustrations and the Fonds der chemischen Industrie for financial support.

Received: December 27, 2002
Revised: December 12, 2003
Published Online: June 15, 2004

[1] A. R. Hemsley, P. C. Griffiths, *Philos. Trans. R. Soc. London Ser. A* **2000**, *358*, 547–564.
[2] L. Brannonpeppas, *ACS Symp. Ser.* **1993**, *520*, 42–52.
[3] J. Jung, M. Perrut, *J. Supercrit. Fluids* **2001**, *20*, 179–219.
[4] G. Rafler, *Spektrum der Wissenschaft* **1994**, 122–124.
[5] L. Schleicher, B. K. Green, US Patent 2730456, **1956**.
[6] K. M. Wasan, *Drug Dev. Ind. Pharm.* **2001**, *27*, 267–276.
[7] A. Prokop, D. Hunkeler, A. C. Powers, R. R. Whitesell, T. G. Wang, *Adv. Polym. Sci.* **1998**, *136*, 53–73 (*Microencapsulation/Microgels/Iniferters*).
[8] W. Meier, *Chem. Soc. Rev.* **2000**, *29*, 295–303.
[9] S. Lutz, F. Essler, S. Panzner in *Controlled Release Society 29th Annual Meeting*, **2002**, p 271.
[10] C. Peyratout, H. Möhwald, L. Dähne, *Adv. Mater.* **2003**, *15*, 1722–1726
[11] S. Förster, T. Plantenberg, *Angew. Chem.* **2002**, *114*, 712–739; *Angew. Chem. Int. Ed.* **2002**, *41*, 689–714.
[12] A. Renken, D. Hunkeler, *Polimery* **1998**, *43*, 530–539.
[13] D. Hunkeler, *Trends Polym. Sci.* **1997**, *5*, 286–293.
[14] A. Manna, T. Imae, K. Aoi, M. Okada, T. Yogo, *Chem. Mater.* **2001**, *13*, 1674–1681.
[15] A. Sunder, M. Krämer, R. Hanselmann, R. Mühlaupt, H. Frey, *Angew. Chem.* **1999**, *111*, 3758–3761; *Angew. Chem. Int. Ed.* **1999**, *38*, 3552–3555.
[16] H. Dautzenberg, U. Schuldt, G. Grasnick, P. Karle, P. Müller, M. Löhr, M. Pelegrin, M. Piechaczyk, K. V. Rombs, W. H. Günzburg, B. Salmons, R. M. Saller, *Ann. N. Y. Acad. Sci.* **1999**, *875*, 46–63 (*Bioartificial Organs II: Technology, Medicine, and Materials*).
[17] H. Dautzenberg, U. Schuldt, D. Lerche, H. Woehlecke, R. Ehwald, *J. Membr. Sci.* **1999**, *162*, 165–171.

 © 2004 Wiley-VCH Verlag GmbH & Co. KGaA, Weinheim

[18] E. Donath, G. B. Sukhorukov, F. Caruso, S. A. Davis, H. Möhwald, *Angew. Chem.* **1998**, *110*, 2324 – 2327; *Angew. Chem. Int. Ed.* **1998**, *37*, 2202 – 2205.
[19] G. Decher, *Compr. Supramol. Chem.* **1996**, *9*, 507 – 552.
[20] G. Decher, *Science* **1997**, *277*, 1232 – 1237.
[21] G. Decher, M. Eckle, J. Schmitt, B. Struth, *Curr. Opin. Colloid Interface Sci.* **1998**, *3*, 32 – 39.
[22] W. Knoll, *Curr. Opin. Colloid Interface Sci.* **1996**, *1*, 137 – 143.
[23] P. Bertrand, A. Jonas, A. Laschewsky, R. Legras, *Macromol. Rapid Commun.* **2000**, *21*, 319 – 348, and references therein.
[24] X. Arys, A. Jonas, A. Laschewsky, R. Legras in *Supramolecular Polymers*, Marcel Dekker, New York, **2000**, pp. 505 – 563, and references therein.
[25] P. T. Hammond, *Curr. Opin. Colloid Interface Sci.* **1999**, *4*, 430 – 442, and references therein.
[26] D. L. Elbert, C. B. Herbert, J. A. Hubbell, *Langmuir* **1999**, *15*, 5355 – 5362.
[27] P. Schwinte, J. C. Voegel, C. Picart, Y. Haikel, P. Schaaf, B. Szalontai, *J. Phys. Chem. B* **2001**, *105*, 11 906 – 11 916.
[28] J. D. Mendelsohn, C. J. Barrett, V. V. Chan, A. J. Pal, A. M. Mayes, M. F. Rubner, *Langmuir* **2000**, *16*, 5017 – 5023.
[29] S. S. Shiratori, M. F. Rubner, *Macromolecules* **2000**, *33*, 4213 – 4219.
[30] A. J. Chung, M. F. Rubner, *Langmuir* **2002**, *18*, 1176 – 1183.
[31] M. F. Rubner in *Multilayer Thin Films* (Eds.: G. Decher, J. B. Schlenoff), Wiley-VCH, **2003**, pp 133 – 154.
[32] S. T. Dubas, J. B. Schlenoff, *Macromolecules* **2001**, *34*, 3736 – 3740.
[33] L. Krasemann, B. Tieke, *Langmuir* **2000**, *16*, 287 – 290.
[34] B. Tieke, F. van Ackern, L. Krasemann, A. Toutianoush, *Eur. Phys. J. E* **2001**, *5*, 29 – 39.
[35] T. Hoshi, H. Saiki, S. Kuwazawa, C. Tsuchiya, Q. Chen, J. Anzai, *Anal. Chem.* **2001**, *73*, 5310 – 5315.
[36] H. Möhwald, H. Lichtenfeld, S. Moya, A. Voigt, H. Bäumler, G. Sukhorukov, F. Caruso, E. Donath, *Macromol. Symp.* **1999**, *145*, 75 – 81.
[37] H. Möhwald, *Colloids Surf. A* **2000**, *171*, 25 – 31.
[38] H. Möhwald, E. Donath, G. B. Sukhorukov in *Multilayer Thin Films*, Wiley-VCH, New York, **2003**, pp 363 – 392.
[39] G. B. Sukhorukov, *Stud. Interface Sci.* **2001**, *11*, 384 – 414 (*Novel Methods to Study Interfacial Layers*).
[40] G. B. Sukhorukov, *MML Series* **2002**, *5*, 111 – 147.
[41] A. Voigt, H. Lichtenfeld, G. B. Sukhorukov, H. Zastrow, E. Donath, H. Bäumler, H. Möhwald, *Ind. Eng. Chem. Res.* **1999**, *38*, 4037 – 4043.
[42] E. Donath, G. B. Sukhorukov, H. Möhwald, *Nachr. Chem. Tech. Lab.* **1999**, *47*, 400 – 403.
[43] G. B. Sukhorukov, E. Donath, H. Lichtenfeld, E. Knippel, M. Knippel, A. Budde, H. Möhwald, *Colloids Surf. A* **1998**, *137*, 253 – 266.
[44] V. Dudnik, G. B. Sukhorukov, I. L. Radtchenko, H. Möhwald, *Macromolecules* **2001**, *34*, 2329 – 2334.
[45] G. B. Sukhorukov, E. Donath, S. Davis, H. Lichtenfeld, F. Caruso, V. I. Popov, H. Möhwald, *Polym. Adv. Technol.* **1998**, *9*, 759 – 767.
[46] A. Voigt, E. Donath, H. Möhwald, *Macromol. Mater. Eng.* **2000**, *282*, 13 – 16.
[47] I. Estrela-Lopis, S. Leporatti, S. Moya, A. Brandt, E. Donath, H. Möhwald, *Langmuir* **2002**, *18*, 7861 – 7866.
[48] D. I. Gittins, F. Caruso, *J. Phys. Chem. B* **2001**, *105*, 6846 – 6852.
[49] K. S. Mayya, D. I. Gittins, A. M. Dibaj, F. Caruso, *Nano Lett.* **2001**, *1*, 727 – 730.
[50] B. Neu, A. Voigt, R. Mitlöhner, S. Leporatti, C. Y. Gao, E. Donath, H. Kiesewetter, H. Möhwald, H. J. Meiselman, H. Bäumler, *J. Microencapsulation* **2001**, *18*, 385 – 395.
[51] S. Moya, L. Dähne, A. Voigt, S. Leporatti, E. Donath, H. Möhwald, *Colloids Surf. A* **2001**, *183*, 27 – 40.
[52] L. Dähne, S. Leporatti, E. Donath, H. Möhwald, *J. Am. Chem. Soc.* **2001**, *123*, 5431 – 5436.
[53] F. Caruso, W. J. Yang, D. Trau, R. Renneberg, *Langmuir* **2000**, *16*, 8932 – 8936.
[54] A. A. Antipov, G. B. Sukhorukov, E. Donath, H. Möhwald, *J. Phys. Chem. B* **2001**, *105*, 2281 – 2284.
[55] D. Trau, W. J. Yang, M. Seydack, F. Caruso, N. T. Yu, R. Renneberg, *Anal. Chem.* **2002**, *74*, 5480 – 5486.
[56] Z. F. Dai, A. Voigt, E. Donath, H. Möhwald, *Macromol. Rapid Commun.* **2001**, *22*, 756 – 762.
[57] A. I. Petrov, A. V. Gavryushkin, G. B. Sukhorukov, *J. Phys. Chem. B* **2003**, *107*, 868 – 875.
[58] C. Schüler, F. Caruso, *Biomacromolecules* **2001**, *2*, 921 – 926.
[59] D. I. Gittins, F. Caruso, *Adv. Mater.* **2000**, *12*, 1947 – 1948.
[60] A. Diaspro, D. Silvano, S. Krol, O. Cavalleri, A. Gliozzi, *Langmuir* **2002**, *18*, 5047 – 5050.
[61] E. Donath, S. Moya, B. Neu, G. B. Sukhorukov, R. Georgieva, A. Voigt, H. Bäumler, H. Kiesewetter, H. Möhwald, *Chem. Eur. J.* **2002**, *8*, 5481 – 5485.
[62] C. Y. Gao, S. Moya, H. Lichtenfeld, A. Casoli, H. Fiedler, E. Donath, H. Möhwald, *Macromol. Mater. Eng.* **2001**, *286*, 355 – 361.
[63] L. Krasemann, A. Toutianoush, B. Tieke, *J. Membr. Sci.* **2001**, *181*, 221 – 228.
[64] S. T. Dubas, J. B. Schlenoff, *Langmuir* **2001**, *17*, 7725 – 7727.
[65] G. B. Sukhorukov, A. A. Antipov, A. Voigt, E. Donath, H. Möhwald, *Macromol. Rapid Commun.* **2001**, *22*, 44 – 46.
[66] G. Ibarz, L. Dähne, E. Donath, H. Möhwald, *Macromol. Rapid Commun.* **2002**, *23*, 474 – 478.
[67] C. Y. Gao, X. G. Liu, J. C. Shen, H. Möhwald, *Chem. Commun.* **2002**, 1928 – 1929.
[68] C. Y. Gao, E. Donath, H. Möhwald, J. C. Shen, *Angew. Chem.* **2002**, *114*, 3943 – 3947; *Angew. Chem. Int. Ed.* **2002**, *41*, 3789 – 3793.
[69] M. K. Park, C. J. Xia, R. C. Advincula, P. Schütz, F. Caruso, *Langmuir* **2001**, *17*, 7670 – 7674.
[70] K. Glinel, A. Moussa, A. Jonas, A. Laschewsky, *Langmuir* **2002**, *18*, 1408 – 1412.
[71] C. Y. Gao, S. Leporatti, S. Moya, E. Donath, H. Möhwald, *Langmuir* **2001**, *17*, 3491 – 3495.
[72] Z. F. Dai, H. Möhwald, *Chem. Eur. J.* **2002**, *8*, 4751 – 4755.
[73] X. P. Qiu, E. Donath, H. Möhwald, *Macromol. Mater. Eng.* **2001**, *286*, 591 – 597.
[74] B. D. Jung, J. D. Hong, A. Voigt, S. Leporatti, L. Dähne, E. Donath, H. Möhwald, *Colloids Surf. A* **2002**, *198*, 483 – 489.
[75] R. Georgieva, S. Moya, M. Hin, R. Mitlöhner, E. Donath, H. Kiesewetter, H. Möhwald, H. Bäumler, *Biomacromolecules* **2002**, *3*, 517 – 524.
[76] G. Berth, A. Voigt, H. Dautzenberg, E. Donath, H. Möhwald, *Biomacromolecules* **2002**, *3*, 579 – 590.
[77] X. P. Qiu, S. Leporatti, E. Donath, H. Möhwald, *Langmuir* **2001**, *17*, 5375 – 5380.
[78] O. P. Tiourina, G. B. Sukhorukov, *Int. J. Pharm.* **2002**, *242*, 155 – 161.
[79] H. Härmä, *Technol. Rev.* **2002**, *126*, 1 – 30.
[80] A. A. Antipov, G. B. Sukhorukov, Y. A. Fedutik, J. Hartmann, M. Giersig, H. Möhwald, *Langmuir* **2002**, *18*, 6687 – 6693.
[81] I. Pastoriza-Santos, B. Schöler, F. Caruso, *Adv. Funct. Mater.* **2001**, *11*, 122 – 128.
[82] T. A. Duchesne, J. Q. Brown, K. B. Guice, S. R. Nayak, Y. M. Lvov, M. J. McShan in *Proceedings of SPIE*, *Vol. 4624*, **2002**, S. 66 – 75.
[83] T. A. Duchesne, J. Q. Brown, K. B. Guice, Y. M. Lvov, M. J. McShane, *Sens. Mater.* **2002**, *14*, 293 – 308.
[84] M. J. McShane, J. Q. Brown, K. B. Guice, Y. M. Lvov, *J. Nanosci. Nanotechnol.* **2002**, *2*, 411 – 416.

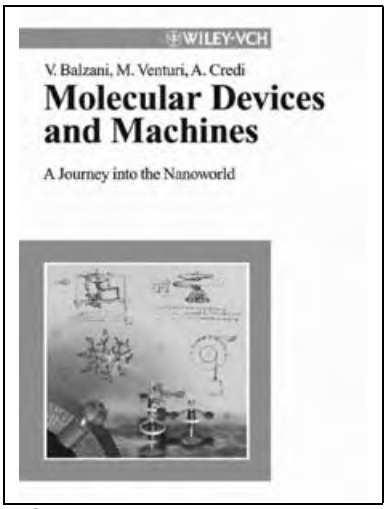
 © 2004 Wiley-VCH Verlag GmbH & Co. KGaA, Weinheim

[85] I. L. Radtchenko, G. B. Sukhorukov, S. Leporatti, G. B. Khomutov, E. Donath, H. Möhwald, *J. Colloid Interface Sci.* **2000**, *230*, 272 – 280.
[86] Z. F. Dai, A. Voigt, S. Leporatti, E. Donath, L. Dähne, H. Möhwald, *Adv. Mater.* **2001**, *13*, 1339 – 1342.
[87] Z. F. Dai, L. Dähne, E. Donath, H. Möhwald, *Langmuir* **2002**, *18*, 4553 – 4555.
[88] Z. F. Dai, L. Dähne, E. Donath, H. Möhwald, *J. Phys. Chem. B* **2002**, *106*, 11501 – 11508.
[89] F. Caruso, C. Schüler, D. G. Kurth, *Chem. Mater.* **1999**, *11*, 3394 – 3399.
[90] D. G. Kurth, F. Caruso, C. Schüler, *Chem. Commun.* **1999**, 1579 – 1580.
[91] R. A. Caruso, A. Susha, F. Caruso, *Chem. Mater.* **2001**, *13*, 400 – 409.
[92] F. Caruso, *Adv. Mater.* **2001**, *13*, 11 – 22.
[93] F. Caruso, *Aust. J. Chem.* **2001**, *54*, 349 – 353.
[94] F. Caruso in *Nano-Surface Chemistry* (Ed.: M. Rosoff), Marcel Dekker, New York, **2002**, pp. 505 – 526.
[95] F. Caruso, H. Lichtenfeld, M. Giersig, H. Möhwald, *J. Am. Chem. Soc.* **1998**, *120*, 8523 – 8524.
[96] F. Caruso, H. Möhwald, *Langmuir* **1999**, *15*, 8276 – 8281.
[97] F. Caruso, *Chem. Eur. J.* **2000**, *6*, 413 – 419.
[98] F. Caruso, R. A. Caruso, H. Möhwald, *Science* **1998**, *282*, 1111 – 1114.
[99] F. Caruso, R. A. Caruso, H. Möhwald, *Chem. Mater.* **1999**, *11*, 3309 – 3314.
[100] Z. F. Dai, L. Dähne, H. Möhwald, B. Tiersch, *Angew. Chem.* **2002**, *114*, 4191 – 4194; *Angew. Chem. Int. Ed.* **2002**, *41*, 4019 – 4022.
[101] G. B. Sukhorukov, E. Donath, S. Moya, A. S. Susha, A. Voigt, J. Hartmann, H. Möhwald, *J. Microencapsulation* **2000**, *17*, 177 – 185.
[102] A. Voigt, N. Buske, G. B. Sukhorukov, A. A. Antipov, S. Leporatti, H. Lichtenfeld, H. Bäumler, E. Donath, H. Möhwald, *J. Magn. Magn. Mater.* **2001**, *225*, 59 – 66.
[103] F. Caruso, M. Spasova, A. Susha, M. Giersig, R. A. Caruso, *Chem. Mater.* **2001**, *13*, 109 – 116.
[104] F. Caruso, A. S. Susha, M. Giersig, H. Möhwald, *Adv. Mater.* **1999**, *11*, 950 – 953.
[105] D. G. Shchukin, I. L. Radtchenko, G. B. Sukhorukov, *J. Phys. Chem. B* **2003**, *107*, 86 – 90.
[106] K. S. Mayya, D. I. Gittins, F. Caruso, *Chem. Mater.* **2001**, *13*, 3833 – 3836.
[107] X. Y. Shi, T. Cassagneau, F. Caruso, *Langmuir* **2002**, *18*, 904 – 910.
[108] A. Rogach, A. Susha, F. Caruso, G. Sukhorukov, A. Kornowski, S. Kershaw, H. Möhwald, A. Eychmüller, H. Weller, *Adv. Mater.* **2000**, *12*, 333 – 336.
[109] I. L. Radtchenko, G. B. Sukhorukov, N. Gaponik, A. Kornowski, A. L. Rogach, H. Möhwald, *Adv. Mater.* **2001**, *13*, 1684 – 1687.
[110] F. Caruso, H. Möhwald, *J. Am. Chem. Soc.* **1999**, *121*, 6039 – 6046.
[111] W. J. Yang, D. Trau, R. Renneberg, N. T. Yu, F. Caruso, *J. Colloid Interface Sci.* **2001**, *234*, 356 – 362.
[112] F. Caruso, H. Fiedler, K. Haage, *Colloids Surf. A* **2000**, *169*, 287 – 293.
[113] F. Caruso, C. Schüler, *Langmuir* **2000**, *16*, 9595 – 9603.
[114] C. Schüler, F. Caruso, *Macromol. Rapid Commun.* **2000**, *21*, 750 – 753.
[115] M. Fang, P. S. Grant, M. J. McShane, G. B. Sukhorukov, V. O. Golub, Y. M. Lvov, *Langmuir* **2002**, *18*, 6338 – 6344.
[116] P. S. Grant, M. Fang, Y. M. Lvov, M. J. McShane in *Proceedings of SPIE*, *Vol. 4624*, **2002**, pp. 47–54.
[117] Y. Lvov, F. Caruso, *Anal. Chem.* **2001**, *73*, 4212 – 4217.
[118] S. Moya, E. Donath, G. B. Sukhorukov, M. Auch, H. Bäumler, H. Lichtenfeld, H. Möhwald, *Macromolecules* **2000**, *33*, 4538 – 4544.
[119] R. Georgieva, S. Moya, S. Leporatti, B. Neu, H. Bäumler, C. Reichle, E. Donath, H. Möhwald, *Langmuir* **2000**, *16*, 7075 – 7081.
[120] A. J. Khopade, F. Caruso, *Nano Lett.* **2002**, *2*, 415 – 418.
[121] A. J. Khopade, F. Caruso, *Biomacromolecules* **2002**, *3*, 1154 – 1162.
[122] S. Moya, G. B. Sukhorukov, M. Auch, E. Donath, H. Möhwald, *J. Colloid Interface Sci.* **1999**, *216*, 297 – 302.
[123] A. A. Antipov, G. B. Sukhorukov, S. Leporatti, I. L. Radtchenko, E. Donath, H. Möhwald, *Colloids Surf. A* **2002**, *198*, 535 – 541.
[124] J. J. Harris, J. L. Stair, M. L. Bruening, *Chem. Mater.* **2000**, *12*, 1941 – 1946.
[125] J. J. Harris, M. L. Bruening, *Langmuir* **2000**, *16*, 2006 – 2013.
[126] R. Steitz, V. Leiner, R. Siebrecht, R. von Klitzing, *Colloids Surf. A* **2000**, *163*, 63 – 70.
[127] Y. Lvov, G. Decher, H. Möhwald, *Langmuir* **1993**, *9*, 481 – 486.
[128] A. Fery, B. Schöler, T. Cassagneau, F. Caruso, *Langmuir* **2001**, *17*, 3779 – 3783.
[129] T. R. Farhat, J. B. Schlenoff, *Langmuir* **2001**, *17*, 1184 – 1192.
[130] A. A. Antipov, G. B. Sukhorukov, H. Möhwald, *Langmuir* **2003**, *19*, 2444 – 2448.
[131] X. Y. Shi, F. Caruso, *Langmuir* **2001**, *17*, 2036 – 2042.
[132] R. von Klitzing, H. Möhwald, *Macromolecules* **1996**, *29*, 6901 – 6906.
[133] J. Hiller, J. D. Mendelsohn, M. F. Rubner, *Nat. Mater.* **2002**, *1*, 59 – 63.
[134] C. Gao, E. Donath, S. Moya, V. Dudnik, H. Möhwald, *Eur. Phys. J. E* **2001**, *5*, 21 – 27.
[135] C. Y. Gao, S. Moya, E. Donath, H. Möhwald, *Macromol. Chem. Phys.* **2002**, *203*, 953 – 960.
[136] H. Bäumler, G. Artmann, A. Voigt, R. Mitlöhner, B. Neu, H. Kiesewetter, *J. Microencapsulation* **2000**, *17*, 651 – 655.
[137] S. Leporatti, A. Voigt, R. Mitlöhner, G. Sukhorukov, E. Donath, H. Möhwald, *Langmuir* **2000**, *16*, 4059 – 4063.
[138] C. Y. Gao, S. Leporatti, E. Donath, H. Möhwald, *J. Phys. Chem. B* **2000**, *104*, 7144 – 7149.
[139] S. Leporatti, C. Gao, A. Voigt, E. Donath, H. Möhwald, *Eur. Phys. J. E* **2001**, *5*, 13 – 20.
[140] C. Y. Gao, S. Leporatti, S. Moya, E. Donath, H. Möhwald, *Chem. Eur. J.* **2003**, *9*, 915 – 920.
[141] G. Ibarz, L. Dähne, E. Donath, H. Möhwald, *Chem. Mater.* **2002**, *14*, 4059 – 4062.
[142] Y. Lvov, A. A. Antipov, A. Mamedov, H. Möhwald, G. B. Sukhorukov, *Nano Lett.* **2001**, *1*, 125 – 128.
[143] G. Sukhorukov, L. Dähne, J. Hartmann, E. Donath, H. Möhwald, *Adv. Mater.* **2000**, *12*, 112 – 115.
[144] G. B. Sukhorukov, A. S. Susha, S. Davis, S. Leporatti, E. Donath, J. Hartmann, H. Möhwald, *J. Colloid Interface Sci.* **2002**, *247*, 251 – 254.
[145] I. L. Radtchenko, G. B. Sukhorukov, H. Möhwald, *Colloids Surf. A* **2002**, *202*, 127 – 133.
[146] N. Gaponik, I. L. Radtchenko, G. B. Sukhorukov, H. Weller, A. L. Rogach, *Adv. Mater.* **2002**, *14*, 879 – 882.
[147] I. L. Radchenko, M. Giersig, G. B. Sukhorukov, *Langmuir* **2002**, *18*, 8204 – 8208.
[148] I. L. Radtchenko, G. B. Sukhorukov, H. Möhwald, *Int. J. Pharm.* **2002**, *242*, 219 – 223.
[149] G. B. Sukhorukov, M. Brumen, E. Donath, H. Möhwald, *J. Phys. Chem. B* **1999**, *103*, 6434 – 6440.
[150] G. Ibarz, L. Dähne, E. Donath, H. Möhwald, *Adv. Mater.* **2001**, *13*, 1324 – 1327.

 © 2004 Wiley-VCH Verlag GmbH & Co. KGaA, Weinheim

[151] R. Dallüge, A. Haberland, S. Zaitsev, M. Schneider, H. Zastrow, G. Sukhorukov, M. Böttger, *Biochim. Biophys. Acta* **2002**, *1576*, 45 – 52.
[152] F. Caruso, D. Trau, H. Möhwald, R. Renneberg, *Langmuir* **2000**, *16*, 1485 – 1488.
[153] W. Jin, X. Y. Shi, F. Caruso, *J. Am. Chem. Soc.* **2001**, *123*, 8121 – 8122.
[154] N. G. Balabushevitch, G. B. Sukhorukov, N. A. Moroz, D. V. Volodkin, N. I. Larionova, E. Donath, H. Möhwald, *Biotechnol. Bioeng.* **2001**, *76*, 207 – 213.
[155] M. E. Bobreshova, G. B. Sukhorukov, E. A. Saburova, L. I. Elfimova, L. I. Shabarchina, B. I. Sukhorukov, *Biofizika* **1999**, *44*, 813 – 820.
[156] O. P. Tiourina, A. A. Antipov, G. B. Sukhorukov, N. L. Larionova, Y. Lvov, H. Möhwald, *Macromol. Biosci.* **2001**, *1*, 209 – 214.
[157] A. A. Antipov, D. G. Shchukin, Y. A. Fedutik, I. Zanaveskina, V. Klechkovskaya, G. B. Sukhorukov, H. Möhwald, *Macromol. Rapid Commun.* **2003**, *24*, 274 – 277.
[158] The principle of electrostatic LbL deposition was first described in R. K. Iler, *J. Colloid Interface Sci.* **1966**, *21*, 569 – 594.
[159] G. Decher in *Multilayer Thin Films* (Eds.: G. Decher, J. B. Schlenoff), Wiley-VCH, New York, **2003**, pp. 1 – 46.
[160] D. B. Shenoy, G. B. Sukhorukov, H. Möhwald, *Biomacromolecules* **2003**, *4*, 265 – 272.
[161] O. P. Tiourina, I. Radtchenko, G. B. Sukhorukov, H. Möhwald, *J. Membr. Biol.* **2002**, *190*, 9 – 16.
[162] E. Donath, S. Moya, B. Neu, G. B. Sukhorukov, R. Georgieva, A. Voigt, H. Baumler, H. Kiesewetter, H. Möhwald, *Chem. Eur. J.* **2002**, *8*, 5481 – 5485.
[163] L. Dähne, B. Baude, Patent Application Az102004013637.8, **2004**.
[164] L. Dähne, B. Baude, A. Voigt, Patent WO 2004/014540 A1, **2003**.

Key-Technologies of the Future



ISBN 3-527-30506-8
€ 99,- / sFr 146,-*

**The Euro price is only valid for Germany.*

VINCENZO BALZANI, Italy, ALBERTO CREDI, and MARGHERITA VENTURI, all of University of Bologna, Italy

Molecular Devices and Machines
A Journey into the Nanoworld
2003. XVII, 494 pp Hbk

The miniaturization of bulky devices and machines is a process that confronts us on a daily basis. However, nanoscale machines with varied and novel characteristics may also result from the enlargement of extremely small building blocks, namely individual molecules. This bottom-up approach to nanotechnology is already being pursued in information technology, with many other branches about to follow.
Written by Vincenzo Balzani and his team of co-authors, this book provides a comprehensive overview of this fascinating and multifarious topic, offering newcomers and experts alike a wealth of information.

- Most important new technologies for a broad audience
- Unifying, critical, and stimulating overview of red-hot topics

Wiley-VCH Verlag
Fax: +49 (0)6201 606 184
e-Mail: service@wiley-vch.de
www.wiley-vch.de

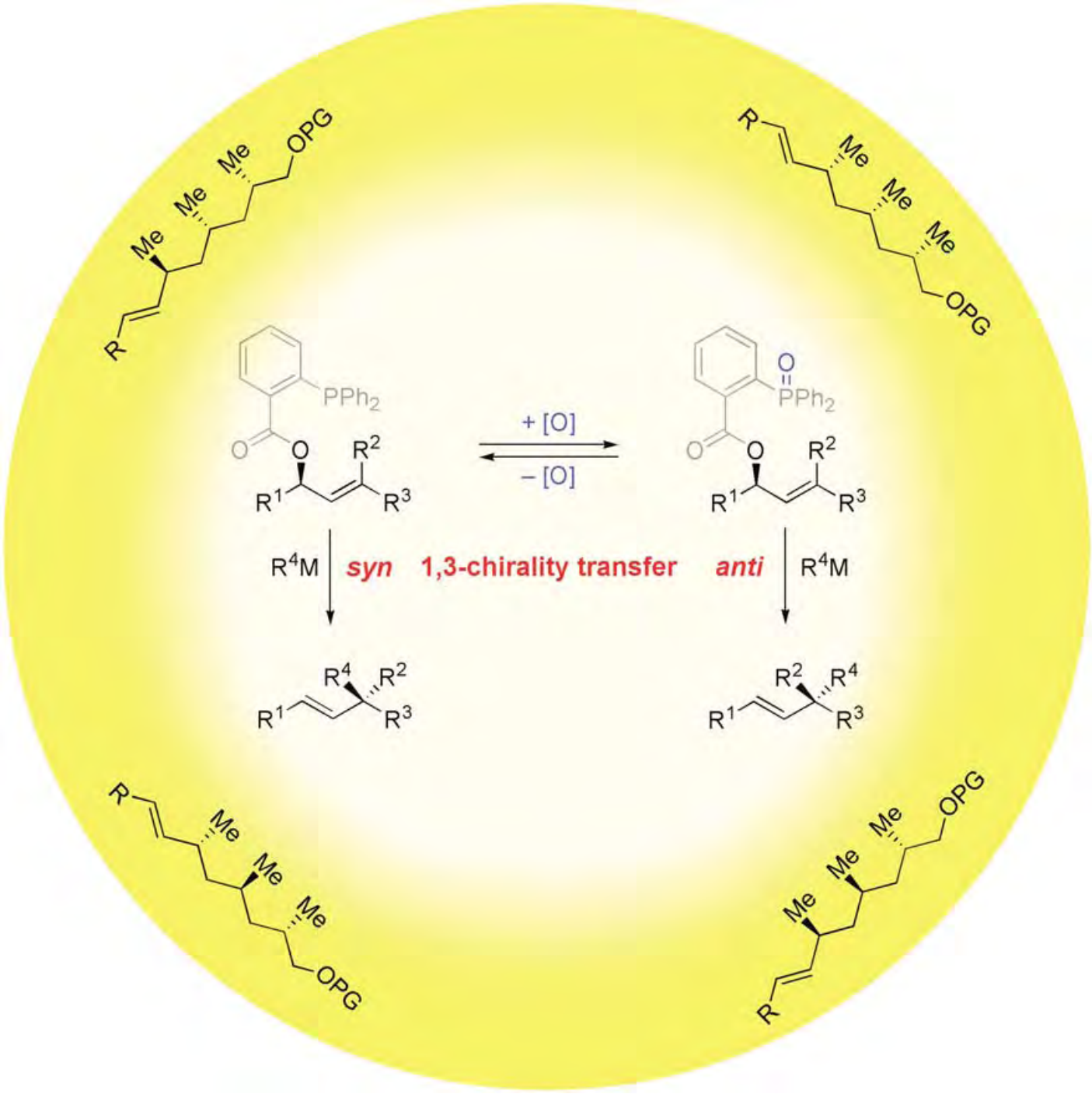
Register now for the free
WILEY-VCH Newsletter!
www.wiley-vch.de/home/pas

WILEY-VCH

50313032_kn

 © 2004 Wiley-VCH Verlag GmbH & Co. KGaA, Weinheim

Communications



Oxidation of the directing leaving group in an S_N2' reaction with Grignard reagents causes a switch in the sense of the 1,3-chirality transfer from *syn* to *anti* substitution. The *syn*-directing effect is used for building up oligo(deoxypropionate)s diastereoselectively. For more information, see the Communications by B. Breit and co-workers on the following pages.

DOI: 10.1002/anie.200453991
© 2004 Wiley-VCH Verlag GmbH & Co. KGaA, Weinheim

Asymmetric Synthesis

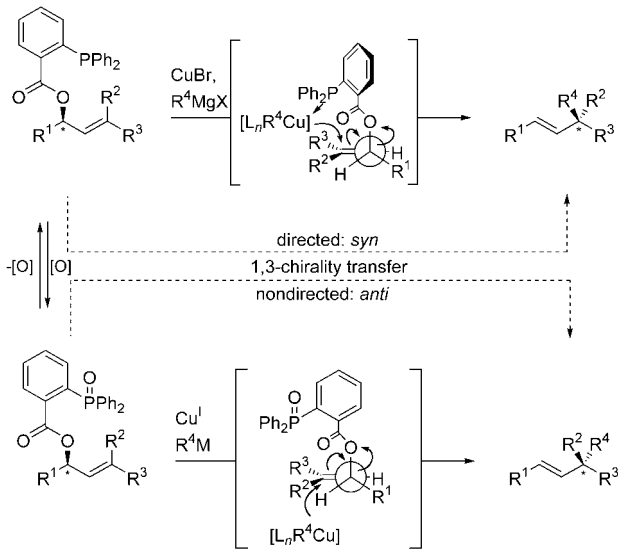
Stereospecific and Stereodivergent Construction of Quaternary Carbon Centers through Switchable Directed/Nondirected Allylic Substitution**

Bernhard Breit, Peter Demel, and Christopher Studte*

The enantioselective construction of quaternary stereogenic carbon centers is a challenge in organic synthesis. Much progress has been made with enantioselective catalytic methods, but still no general solution to this synthetic problem exists.[1] A reliable alternative strategy for the predictable installation of a quaternary stereocenter is 1,3-chirality transfer from a more readily accessible stereogenic center by a sigmatropic process, such as the Claisen rearrangement.[2] However, the nature of the sigmatropic process sets structural limitations on the type of carbon nucleophile that can be transferred. Allylic substitution with organometallic carbon nucleophiles could provide a more general solution if all aspects of selectivity could be controlled. Of particular interest is copper-mediated allylic substitution, as it allows the introduction of hard nucleophiles, such as alkyl, alkenyl, and aryl groups, into an existing carbon skeleton.[3] These reactions generally proceed by *anti* attack of the nucleophile with respect to the leaving group.[3,4] However, the simultaneous control of regio- and stereochemistry is a difficult problem to solve, and only a few successful examples are known.[5]

Progress has been made in this area with substrate-directed reactions in which reagent-directing leaving groups, such as carbamates[6] and benzothiazoles,[7] are used. However, control over the geometry of the double bond in the product is often unsatisfactory, so that the chirality transfer is incomplete.[3] Furthermore, in many cases an excess of the organometallic reagent is required, which is particularly undesirable if valuable organic residues are to be transferred. We recently found a solution to these problems by employing the *ortho*-diphenylphosphanylbenzoate group (*o*-DPPB) as a new reagent-directing leaving group. Copper-mediated and copper-catalyzed allylic substitution with only a stoichiometric amount of a Grignard reagent could be carried out with excellent chemo-, regio-, and stereoselectivity and with recovery of the directing group.[8]

We report herein on the regioselective, stereospecific, and stereodivergent construction of quaternary carbon stereocenters through *o*-DPPB-directed, copper-mediated allylic substitution with Grignard reagents. Furthermore, we show that the stereochemical outcome of the title reaction can be reversed through an oxidative on/off switch with regard to the directing power of the *o*-DPPB group. Thus, both enantiomers of the substitution product can be prepared from a single enantiomer of the substrate (Scheme 1).



Scheme 1. Concept of stereodivergent allylic substitution with organocopper reagents for the stereospecific construction of quaternary carbon centers by employing a switchable directing/nondirecting leaving group.

In a first series of experiments we studied the regioselectivity of the directed allylic substitution with respect to the formation of a quaternary carbon center. Thus, treatment of the secondary trisubstituted allylic *o*-DPPB derivative **1**[9] with $CuBr{\cdot}SMe_2$ (0.5 equiv)[10] and a methyl or *n*-butyl Grignard reagent (1.1 equiv)[11] provided the S_N2' substitution products **2** and **3**, respectively, with complete control of regioselectivity and double-bond geometry (Table 1, entries 1 and 2). Furthermore, the *o*-DPPB esters (*E*)-**4** and (*Z*)-**4**, derived from the primary trisubstituted allylic alcohols geraniol and nerol, respectively, underwent analogous transformations to give the products **5**–**7** of S_N2' substitution in excellent yields and with perfect regioselectivity, independent of the double-bond geometry in the starting material (Table 1, entries 3–6).

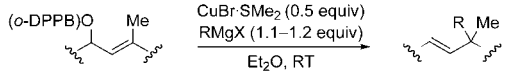
To study chirality transfer we chose the *o*-DPPB esters (−)-**8a** and (−)-**8b**, which are readily available from D-mannitol. The corresponding products of allylic substitution are equipped with appropriate functionalities for the flexible incorporation of the quaternary stereocenter into a desired carbon skeleton. The reaction of the *p*-methoxybenzyl (PMB) ether derivative (−)-**8a** with a range of Grignard reagents in the presence of $CuBr{\cdot}SMe_2$ (0.5 equiv) proceeded smoothly with excellent regio- and stereoselectivity (Scheme 2; Table 2,

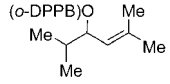
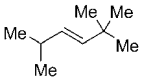
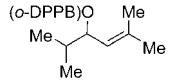
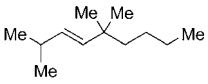
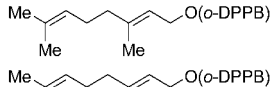
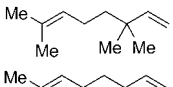
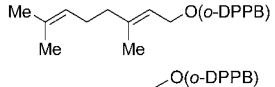
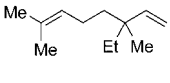
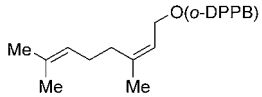
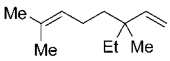
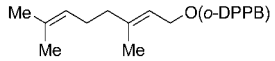
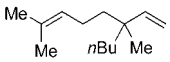
[*] Prof. Dr. B. Breit, Dr. P. Demel, Dipl.-Chem. C. Studte
Institut für Organische Chemie und Biochemie
Albert-Ludwigs-Universität Freiburg
Albertstrasse 21, 79104 Freiburg (Germany)
Fax: (+49) 761-203-8715
E-mail: bernhard.breit@orgmail.chemie.uni-freiburg.de

[**] This work was supported by the DFG, the Fonds der Chemischen Industrie, and the Krupp Foundation (Alfried Krupp Award for Young Professors to B.B.).

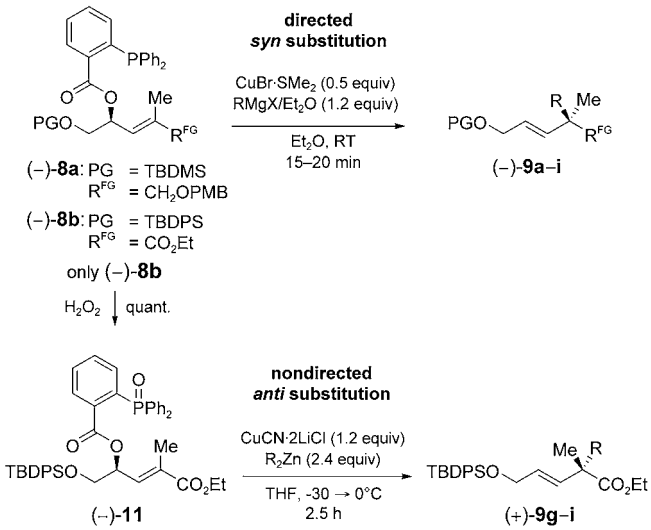
 © 2004 Wiley-VCH Verlag GmbH & Co. KGaA, Weinheim DOI: 10.1002/anie.200453991

Table 1: Regioselective formation of quaternary carbon centers through *o*-DPPB-directed allylic substitution.[a]



Entry	*o*-DPPB ester[b]		RMgX (equiv)	Product		S_N2'/S_N2[c]	Yield [%][d]
1		**1**	MeMgI (1.1)		**2**	>99:1	68[e]
2		**1**	*n*BuMgBr (1.1)		**3**	99:1	99
3		(*E*)-**4**	MeMgI (1.2)		**5**	95:5	91
4		(*E*)-**4**	EtMgBr (1.2)		**6**	>98:2	80
5		(*Z*)-**4**	EtMgBr (1.2)		**6**	>98:2	95
6		(*E*)-**4**	*n*BuMgBr (1.2)		**7**	>99:1	87

[a] Reactions were performed in diethyl ether, c(*o*-DPPB ester) = 0.05 M. The Grignard reagent (0.51–1.23 M in diethyl ether) was added to the reaction mixture with a syringe pump over a period of 30 min. [b] Prepared from the corresponding allylic alcohol by an esterification protocol reported previously.[9] [c] Determined by GC (CPSil5CB, 30 m, 0.32 mm ID, Chrompack). [d] Yield of isolated product after distillation (entry 1) or chromatographic purification (entries 2–6). [e] The low yield is due to the volatility of the product.



Scheme 2. Stereospecific and stereodivergent construction of quaternary carbon centers through the switchable directed/nondirected allylic substitution of the acyclic substrates (−)-**8a**/**b** and (−)-**11** (see Table 2). PG = protecting group, PMB = *p*-methoxybenzyl, TBDMS = *tert*-butyldimethylsilyl, TBDPS = *tert*-butyldiphenylsilyl.

entries 1–4). Perfect 1,3-chirality transfer was observed in the construction of quaternary carbon centers (Table 2, entries 2–4). However, when a benzyl Grignard reagent was used the degree of chirality transfer was slightly lower (91%; Table 2, entry 5). The absolute configuration of the substitution products was determined upon the conversion of (−)-**9b** into the known ester (−)-**10** [Eq. (1); (DDQ = 2,3-dichloro-5,6-dicyano-1,4-benzoquinone)].[5b]

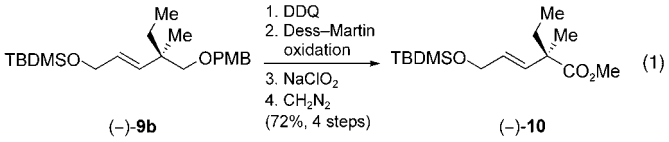
Table 2: Stereospecific and stereodivergent formation of quaternary carbon centers: acyclic substrates.[a]

Entry	Substrate[b] (*ee* [%])	R^2	S_N2'/S_N2[c]	E/Z[c]	Product (*ee* [%])[c]	CT[d] [%]	Yield[e] [%]
1	**8a** (94)	Me	>95:5	>95:5	**9a**	–	72
2	**8a** (94)	Et	>99:1	>99:1	(−)-**9b** (94)	100	86
3	**8a** (93)	*n*Bu	>99:1	>99:1	(−)-**9c** (93)	100	99
4	**8a** (93)	*i*Pr	>99:1	>99:1	(−)-**9d** (93)	100	89
5[f]	**8a** (93)	Bn	>99:1	>99:1	(−)-**9e** (85)	91	53
6	**8a** (92)	*t*Bu	14:86[g]	80:20[g]	**9f** (n.d.[h])	n.d.[h]	90
7	**8b** (>99)	Et	>99:1	>99:1	(−)-**9g** (98)	98	84
8	**8b** (>99)	*n*Bu	>99:1	>99:1	(−)-**9h** (97)	98	87
9	**8b** (>99)	*i*Pr	>99:1	>99:1	(−)-**9i** (97)	98	84
10	**11** (>99)	Et	>99:1	>99:1	(+)-**9g** (99)	100	85
11	**11** (>99)	*n*Bu	>98:2	>98:2	(+)-**9h** (99)	100	87
12[i]	**11** (>99)	*i*Pr	97:3[g]	>95:5	(+)-**9i** (>99)	100	94

[a] All reactions were performed in diethyl ether, c(*o*-DPPB ester) = 0.05 M. The Grignard reagent (0.76–1.23 M in diethyl ether) was added to the reaction mixture with a syringe pump over a period of 15–20 min. [b] Prepared from the corresponding allylic alcohol[12] by an esterification protocol reported previously.[9] The enantiomeric excess was determined by HPLC analysis of the corresponding allylic alcohol (Chiralpak AD (**8a**), Chiralcel OD-H (**8b**)). [c] Determined by ^{1}H NMR spectroscopy (entry 1) or HPLC analysis (entries 2, 3, 5, 7, 9: Chiralcel OD-H; entry 4: Chiralpak AD after removal of the TBDMS group; entries 9, 12: Chiralcel OD-H after removal of the TBDPS group). [d] The chirality transfer (CT) was calculated as CT = (*ee*(**9**)/*ee*(**8** or **11**)) × 100. [e] Yield of isolated product after chromatographic purification. [f] c(**8a**) = 0.01 M in diethyl ether; the Grignard reagent (0.07 M in diethyl ether) was added over a period of 90 min. [g] Product ratios were determined by ^{1}H NMR spectroscopy. [h] n.d. = not determined. [i] With 1-methyl-2-pyrrolidinone (NMP) as a cosolvent (one third of the total solvent volume).

Thus, as expected, the reaction proceeds through a *syn* substitution pathway with respect to the leaving group. The *o*-DPPB group acts as a directing leaving group through

 © 2004 Wiley-VCH Verlag GmbH & Co. KGaA, Weinheim



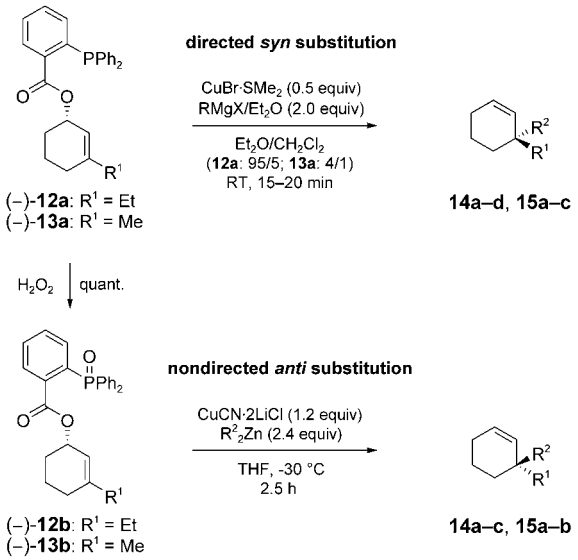
phosphane coordination of the organocopper reagent. A transition state that accounts for the observed stereochemistry is depicted in Scheme 1.

Next, allylic substitution of the enoate (−)-**8b** was examined. In this case the problem of thermodynamically unfavorable enoate deconjugation combines with a chemoselectivity issue arising from reactivity of the ethyl ester functionality toward the nucleophilic Grignard reagent.[3,5a,b] Interestingly, even in this case the directed allylic substitution of occurred with complete chemo-, regio-, and stereoselectivity and with excellent chirality transfer to give the substitution products (−)-**9g–i** (Table 2, entries 7–9).

To access the opposite enantiomers of the substitution products of the same allylic *o*-DPPB ester substrates the stereochemical course of the allylic substitution must be reversed. Instead of proceeding through a directed *syn* substitution pathway, the reaction should proceed through the nondirected *anti* attack of the nucleophile with respect to the leaving group. Thus, the directing power of the *o*-DPPB functionality would have to be turned off, for example, by oxidation of the phosphane group of the *o*-DPPB enoate (−)-**8b** to give the phosphane oxide (−)-**11**. The ability of the *o*-DPPB group to coordinate the copper reagent should thus be suppressed and the leaving-group ability of the benzoate group increased significantly.

Treatment of the allylic *o*-DPPB oxide ester (−)-**11** with dialkyl zinc reagents in the presence of CuCN·2 LiCl in THF furnished the *anti* S_N2' substitution products (+)-**9g–i** in good yields with perfect regioselectivity and excellent 1,3-*anti* chirality transfer.[13] However, when the *o*-DPPB ester (−)-**8b** was subjected to reaction conditions identical to those used in entries 10–12 of Table 2, allylic substitution did not occur even after warming the reaction mixture to room temperature and prolonged reaction time (24 h). Evidently the oxidation of the phosphane functionality to the phosphane oxide serves two purposes. First, it switches off the directing power of the phosphane group and thus suppresses the directed *syn* substitution pathway. Second, it enhances the leaving-group ability of the benzoate group to make nondirected *anti* substitution possible. This methodology is also applicable to cyclic substrates with similar efficiency. For example, stereodivergent directed/nondirected substitution of the six-membered-ring systems **12a**,**b** and **13a**,**b** is possible (Scheme 3; Table 3).

In conclusion, we have shown that the *o*-DPPB/*o*-DPPB oxide system can be used as a switchable directing/nondirecting leaving group in a copper-mediated allylic substitution reaction with Grignard and organozinc reagents for the regioselective, stereospecific, and stereodivergent construction of quaternary carbon centers. Thus, both enantiomers of the substitution product are readily available from one enantiomer of the substrate.



Scheme 3. Stereospecific and stereodivergent construction of quaternary carbon centers through the switchable directed/nondirected allylic substitution of the cyclic substrates (−)-**12a/b** and (−)-**13a/b** (see Table 3).

Table 3: Stereospecific and stereodivergent formation of quaternary carbon centers: cyclic substrates.

Entry	Substrate[a] (*ee* [%])	R	S_N2'/S_N2[b]	Product (*ee* [%])[b]	CT[c] [%]	Yield[d] [%]
1[e]	**12a** (97)	Me	99:1	(+)-**14a** (96)	99	>95
2[e]	**12a** (97)	*n*Bu	>99:1	(+)-**14b** (96)	99	>95
3[e]	**12a** (97)	*i*Pr	98:2	(−)-**14c** (96)	99	>95
4[e]	**12a** (97)	Ph	40:60	(+)-**14d** (92)	95	>95
5[f]	**13a** (94)	Et	96:4	(−)-**14a** (91)	97	>95
6[f]	**13a** (94)	*n*Bu	98:2	(+)-**15a** (94)	100	>95
7[f]	**13a** (94)	*i*Pr	96:4	(−)-**15b** (91)	97	>95
8[f]	**13a** (94)	Ph	41:59	(+)-**15c** (82)	87	>95
9[g]	**12b** (97)	Me	99:1	(−)-**14a** (93)	96	>95
10[g]	**12b** (97)	*n*Bu	>99:1	(−)-**14b** (96)	99	>95
11[g]	**12b** (97)	*i*Pr	97:3	(+)-**14c** (94)	97	>95
12[g]	**13b** (94)	Et	>99:1	(+)-**14a** (93)	99	>95
13[g]	**13b** (94)	*n*Bu	99:1	(−)-**15a** (94)	100	>95
14[g]	**13b** (94)	*i*Pr	99:1	(+)-**15b** (93)	99	>95

[a] Prepared from the corresponding allylic alcohol following an esterification protocol reported previously.[9] The enantiomeric excess was determined by HPLC analysis (Chiralpak AD-H (**12a**), Chiralcel OD-H (**13a**)). [b] Determined by ^{1}H NMR spectroscopy and GC analysis (Supelco Beta Dex 110 (**14a**,**14d**,**15c**), C.E.I. G-TA (**14b**,**14c**,**15a**,**15b**)). [c] The chirality transfer (CT) was calculated as CT = (*ee*(**14**)/*ee*(**12**)) × 100. [d] Yield was determined by GC. [e] The Cu-complexed *o*-DPPB esters were added in diethyl ether/dichloromethane (95:5, c = 0.01 M) to the Grignard reagent (0.05 M in diethyl ether) by using a syringe pump (6 mL h^{-1}). [f] As for [e], but diethyl ether/dichloromethane (4:1, *c* = 0.01 M). [g] The oxidized *o*-DPPB esters (*c* = 0.07 M in THF) were added to the zinc–copper reagents (*c* = 1.00 M in THF) at a rate of 12 mL h^{-1}.

Experimental Section

Synthesis of (−)-**9h** (*syn* substitution): $CuBr{\cdot}SMe_2$ (11.9 mg, 0.058 mmol) was added to a solution of freshly purified (−)-**8b** (82 mg, 0.117 mmol, >99% *ee*) in diethyl ether (2.3 mL), and the mixture was stirred for a further 5 min at room temperature. *n*BuMgBr (0.11 mL, 0.140 mmol, 1.23 M solution in diethyl ether)

 © 2004 Wiley-VCH Verlag GmbH & Co. KGaA, Weinheim

was added to the resulting yellow solution over a period of 20 min by using a syringe pump. When the addition of the Grignard reagent was complete, the reaction mixture was quenched by adding a saturated aqueous solution of NH_4Cl (2.5 mL), followed by diethyl ether (10 mL) and an aqueous solution of NH_3 (12.5%, 1 mL). This mixture was extracted with diethyl ether (3 × 20 mL). The combined ethereal phases were washed with water (10 mL), then brine (10 mL), and dried ($MgSO_4$). The solvent was then removed in vacuo. Flash chromatography of the residue on silica with petroleum ether (60–70)/diethyl ether (95:5) yielded analytically pure (−)-**9h** (45 mg, 85%, $S_N2'/S_N2 > 99:1$, $E/Z > 99:1$, >97% *ee*) as a colorless oil. HPLC (Chiralcel OD-H, 15°C, *n*-heptane, 0.8 mL min^{-1}, 227 nm): t_R ((−)-**9h**): 20.01 min (98.7%), t_R ((+)-**9h**): 21.90 min (1.3%); $[\alpha]_D^{22} = -3.7$ ($c = 1.75$, $CHCl_3$); ^{1}H NMR (400.136 MHz, $CDCl_3$, TMS): $\delta = 0.89$ (t, 3H, $J = 7.3$ Hz, CH_3), 1.06 (s, 9H, 3 × CH_3), 1.23 (t, 3H, $J = 7.3$ Hz, CH_3), 1.24 (s, 3H, CH_3), 1.28 (m, 4H, 2 × CH_2), 1.53 (m, 1H, CH_2), 1.67 (m, 1H, CH_2), 4.10 (m, 1H, CH_2), 4.13 (m, 1H, CH_2), 4.22 (dd, 2H, $J = 5.5$, 1.7 Hz, CH_2), 5.58 (m, 1H, CH), 5.90 (dt, 1H, $J = 15.9$, 1.7 Hz, CH), 7.39 (m, 6H, Ar-H), 7.68 ppm (m, 4H, Ar-H); ^{13}C NMR (100.624 MHz, $CDCl_3$): $\delta = 14.0$, 14.2, 19.2, 21.0, 23.1, 26.8 (3 × C), 26.8, 39.2, 47.6, 60.5, 64.5, 127.6 (4 × C), 127.6, 129.6 (2 × C), 133.9, 134.2 (2 × C), 135.6 (4 × C), 176.0 ppm; elemental analysis (%) calcd for $C_{28}H_{40}O_3Si$ (452.70): C 74.29, H 9.01; found: C 74.38, H 8.91.

Synthesis of (+)-**9h** (*anti* substitution): A freshly prepared solution of CuCN·2 LiCl in THF (52 μL, 0.052 mmol, 1M; a mixture of the two salts was dried for 2 h at 120°C in vacuo (oil pump) prior to use) was cooled to −30°C and diluted with additional THF (0.5 mL). A solution of nBu$_2$Zn in heptane (0.1 mL, 0.1 mmol, 1.0M) was added dropwise, and the resulting colorless solution was stirred for a further 10 min at −30°C. A solution of (−)-**11** (31 mg, 0.043 mmol, >99% *ee*) in THF (1 mL) was added over a period of 5 min. The resulting colorless solution was warmed to 0°C over 2.5 h, during which time a beige suspension formed (quantitative conversion by TLC). The reaction was quenched by adding a saturated aqueous solution of NH_4Cl (2 mL), followed by diethyl ether (20 mL) and an aqueous solution of NH_3 (12.5%, 0.5 mL). This mixture was extracted with diethyl ether (3 × 10 mL). The combined ethereal phases were washed with water (10 mL), then brine (10 mL), and dried ($MgSO_4$). The solvent was removed in vacuo. Flash chromatography of the residue on silica with petroleum ether (60–70)/ethyl acetate (95:5) yielded pure (+)-**9h** (17 mg, 87%, $S_N2'/S_N2 > 99:1$, $E/Z > 98:2$, >99% *ee*) as a colorless oil. HPLC (Chiralcel OD-H, 15°C, *n*-heptane, 0.5 mL min^{-1}, 227 nm): t_R ((−)-**9h**): 20.01 min (0.5%), t_R ((+)-**9h**): 21.90 min (99.5%); $[\alpha]_D^{20} = +9.1$ ($c = 0.87$, $CHCl_3$).

Received: February 11, 2004 [Z53991]
Published Online: May 26, 2004

Keywords: allylation · asymmetric synthesis · enantioselectivity · Grignard reaction · organocopper reagents

[1] a) S. F. Martin, *Tetrahedron* **1980**, *36*, 419–460; b) K. Fuji, *Chem. Rev.* **1993**, *93*, 2037–2066; c) E. J. Corey, A. Guzman-Perez, *Angew. Chem.* **1998**, *110*, 402–415; *Angew. Chem. Int. Ed.* **1998**, *37*, 388–401; d) C. Spino, C. Beaulieu, *Angew. Chem.* **2000**, *112*, 2006–2008; *Angew. Chem. Int. Ed.* **2000**, *39*, 1930–1932; e) J. Christoffers, A. Mann, *Angew. Chem.* **2001**, *113*, 4725–4732; *Angew. Chem. Int. Ed.* **2001**, *40*, 4591–4597; f) J. Christoffers, A. Baro, *Angew. Chem.* **2003**, *115*, 1726–1728; *Angew. Chem. Int. Ed.* **2003**, *42*, 1688–1690.

[2] a) For [3,3′] sigmatropic processes, see: H. Frauenrath, *Methods of Organic Chemistry (Houben-Weyl), Vol. E21*, Thieme, Stuttgart, **1995**, pp. 3301–3756; b) for [2,3′] sigmatropic processes, see: J. Kallmerten, *Methods of Organic Chemistry (Houben-Weyl), Vol. E21*, Thieme, Stuttgart, **1995**, pp. 3757–3809; c) for the Wittig rearrangement, see: T. Nakai, K. Mikami, *Chem. Rev.* **1986**, *86*, 885–902.

[3] Y. Yamamoto, *Methods of Organic Chemistry (Houben-Weyl), Vol. E21*, Thieme, Stuttgart, **1995**, pp. 2011–2040; b) B. Breit, P. Demel in *Modern Organocopper Chemistry* (Ed.: N. Krause), Wiley-VCH, Weinheim, **2002**, pp. 188–223.

[4] E. J. Corey, N. W. Boaz, *Tetrahedron Lett.* **1984**, *25*, 3063–3066.

[5] a) T. Ibuka, M. Tanaka, S. Nishii, Y. Yamamoto, *J. Chem. Soc. Chem. Commun.* **1987**, 1596–1598; b) T. Ibuka, N. Akimoto, M. Tanaka, S. Nishii, Y. Yamamoto, *J. Org. Chem.* **1989**, *54*, 4055–4061; c) N. Harrington-Frost, H. Leuser, M. I. Calaza, F. F. Kneisel, P. Knochel, *Org. Lett.* **2003**, *5*, 2111–2114.

[6] a) C. Gallina, *Tetrahedron Lett.* **1982**, *23*, 3094–3096; b) H. L. Goering, S. S. Kantner, C. C. Tseng, *J. Org. Chem.* **1983**, *48*, 715–721; c) J. H. Smitrovich, K. A. Woerpel, *J. Am. Chem. Soc.* **1998**, *120*, 12998–12999; d) J. H. Smitrovich, K. A. Woerpel, *J. Org. Chem.* **2000**, *65*, 1601–1614.

[7] a) P. Barsanti, V. Calò, L. Lopez, G. Marchese, F. Naso, G. Pesce, *J. Chem. Soc. Chem. Commun.* **1978**, 1085–1086; b) V. Calò, L. Lopez, W. F. Carlucci, *J. Chem. Soc. Perkin Trans. 1* **1983**, 2953–2956; c) S. Valverde, M. Bernabé, S. Garcia-Ochoa, A. M. Gómez, *J. Org. Chem.* **1990**, *55*, 2294–2298.

[8] B. Breit, P. Demel, *Adv. Synth. Catal.* **2001**, *343*, 429–432.

[9] The *o*-DPPB esters described in this work were prepared according to methodology described previously: B. Breit, G. Heckmann, S. K. Zahn, *Chem. Eur. J.* **2003**, *9*, 425–434.

[10] $CuBr{\cdot}SMe_2$ (99% purity) was purchased from Aldrich and used without further purification.

[11] All Grignard reagents were freshly prepared under standard conditions by using activated magnesium turnings in diethyl ether according to the dry-stir activation protocol: K. V. Baker, J. M. Brown, N. Hughes, A. J. Skarmilis, A. Sexton, *J. Org. Chem.* **1991**, *56*, 698–703.

[12] J. H. Hong, M.-Y. Gao, Y. Choi, Y.-C. Cheng, R. F. Schinazi, C. K. Chu, *Carbohydr. Res.* **2000**, *328*, 37–48.

[13] Experiments with magnesium cuprates also lead to excellent 1,3-chirality transfer through *anti* substitution. However, the regioselectivity for the S_N2' substitution product was incomplete. An excess of the zinc reagent was required for quantitative conversion.

 © 2004 Wiley-VCH Verlag GmbH & Co. KGaA, Weinheim

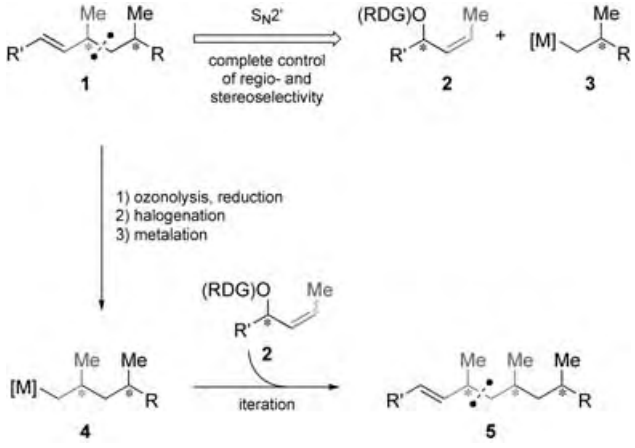
Polyketides

Iterative Deoxypropionate Synthesis Based on a Copper-Mediated Directed Allylic Substitution**

Bernhard Breit and Christian Herber*

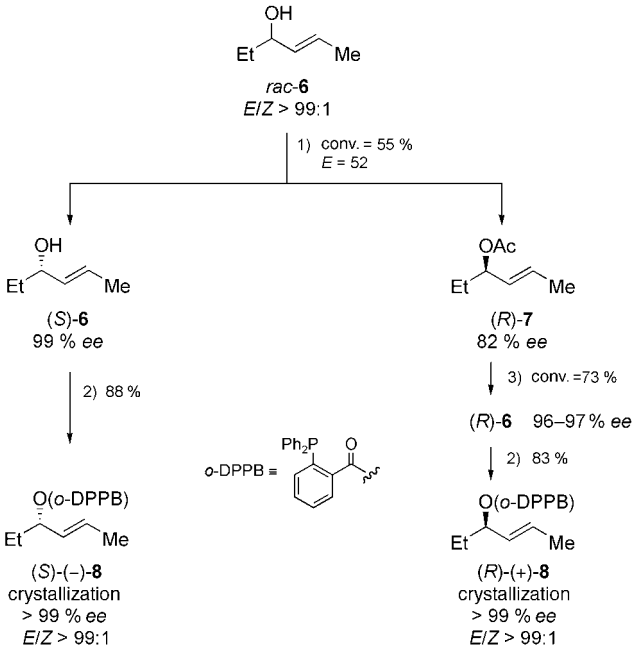
Many biologically relevant natural products of polyketide origin contain a fully reduced 1,3,5,*n*("skip")-polymethyl-substituted carbon chain.[1] Such structures, referred to as "deoxypropionate oligomers", are usually constructed through an iterative asymmetric enolate alkylation of the type introduced by Evans et al.[2] Although the use of amide enolates based on pseudoephedrine[3] and azaenolates derived from (*R*)-1-amino-2-(methoxymethyl)pyrrolidine (RAMP) hydrazones[4] have led to significant improvements in this methodology, disadvantages still include the often low reactivity of the enolate intermediate towards the alkylating agent, and the cost and removability of the chiral auxiliary. These drawbacks prohibit large-scale applications. We report herein an alternative iterative strategy based on a stereospecific copper-mediated directed allylic substitution. This flexible approach allows the preparation of any desired oligo(deoxypropionate) stereoisomer. The strategy is outlined in Scheme 1.

The key step of our strategy is an S_N2' reaction of the organometallic reagent **3** with the electrophile **2** derived from an allylic alcohol, to furnish the bis(deoxypropionate) building block **1**. Oxidative cleavage of the alkene in the bis(deoxypropionate) **1** followed by conversion of the product into a new organometallic nucleophile should then make it possible to carry out an iterative process. This approach is complementary to the known enolate-alkylation strategy, as the growing propionate chain is introduced as a nucleophile and not as an electrophile ("Umpolung"). Key to the success of this strategy is the availability of an allylic substitution reaction that occurs in acyclic systems with complete chemo-, regio-, and stereoselectivity, as well as complete 1,3-chirality transfer. Our recently developed "directed" copper-mediated allylic substitution reaction with *o*-diphenylphosphanylbenzoate (*o*-DPPB) as the reagent-directing leaving group meets these requirements.[5] However, its compatibility with enantiomerically pure Grignard reagents **3** that are branched in the β position remained untested. Furthermore, it was necessary to develop a practical route to enantiomerically pure building blocks **2** and **3**.



Scheme 1. Iterative strategy for the enantioselective construction of deoxypropionate structures based on a directed copper-mediated allylic substitution (RDG = reagent-directing group).

Enzyme catalysis was selected as a suitable method for the preparation of large quantities of both enantiomers of allylic electrophiles **2**. Thus, the allylic alcohol *rac*-**6** was subjected to enzymatic resolution with Novozym 435 (Scheme 2).[6] Enantiomerically pure (*S*)-**6** was obtained at 55% conversion (enantioselectivity factor $E = 52$). The acetate (*R*)-**7** (82% *ee*) formed in the reaction underwent hydrolysis (also catalyzed by Novozym 435) to furnish (*R*)-**6** (96–97% *ee*). Both enantiomers of **6** were transformed into the corresponding *o*-diphenylphosphanylbenzoate compounds **8**, which were purified by crystallization. In this way, gram quantities of both enantiomers of **8** could be prepared in enantiomerically pure form. The crystalline allylic *o*-DPPB esters **8** could be stored



Scheme 2. Preparation of the enantiomerically pure *o*-DPPB allylic esters **8**: 1) Novozym 435, vinyl acetate, 30°C; 2) *o*-diphenylphosphanylbenzoic acid, DCC, DMAP, CH_2Cl_2; 3) Novozym 435, buffer (pH 7), 5°C. DCC = *N*,*N*′-dicyclohexylcarbodiimide, DMAP = 4-dimethylaminopyridine.

[*] Prof. Dr. B. Breit, Dipl.-Chem. C. Herber
Institut für Organische Chemie und Biochemie
Albert-Ludwigs-Universität Freiburg
Albertstrasse 21, 79104 Freiburg (Germany)
Fax: (+49) 761-203-8715
E-mail: bernhard.breit@orgmail.chemie.uni-freiburg.de

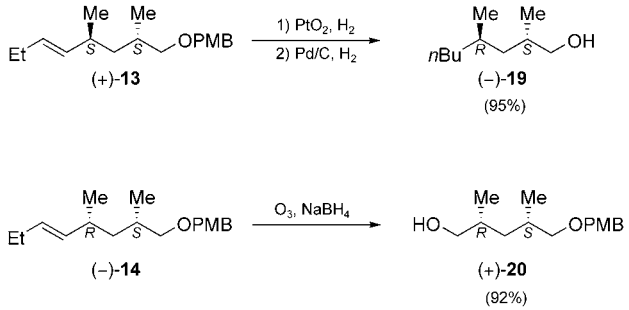
[**] This work was supported by the DFG, the Fonds der Chemischen Industrie, and the Krupp Foundation (Alfried Krupp Award for Young Professors to B.B.).

 © 2004 Wiley-VCH Verlag GmbH & Co. KGaA, Weinheim DOI: 10.1002/anie.200453990

for several months without detectable decomposition (e.g. oxidation to the corresponding phosphane oxide).

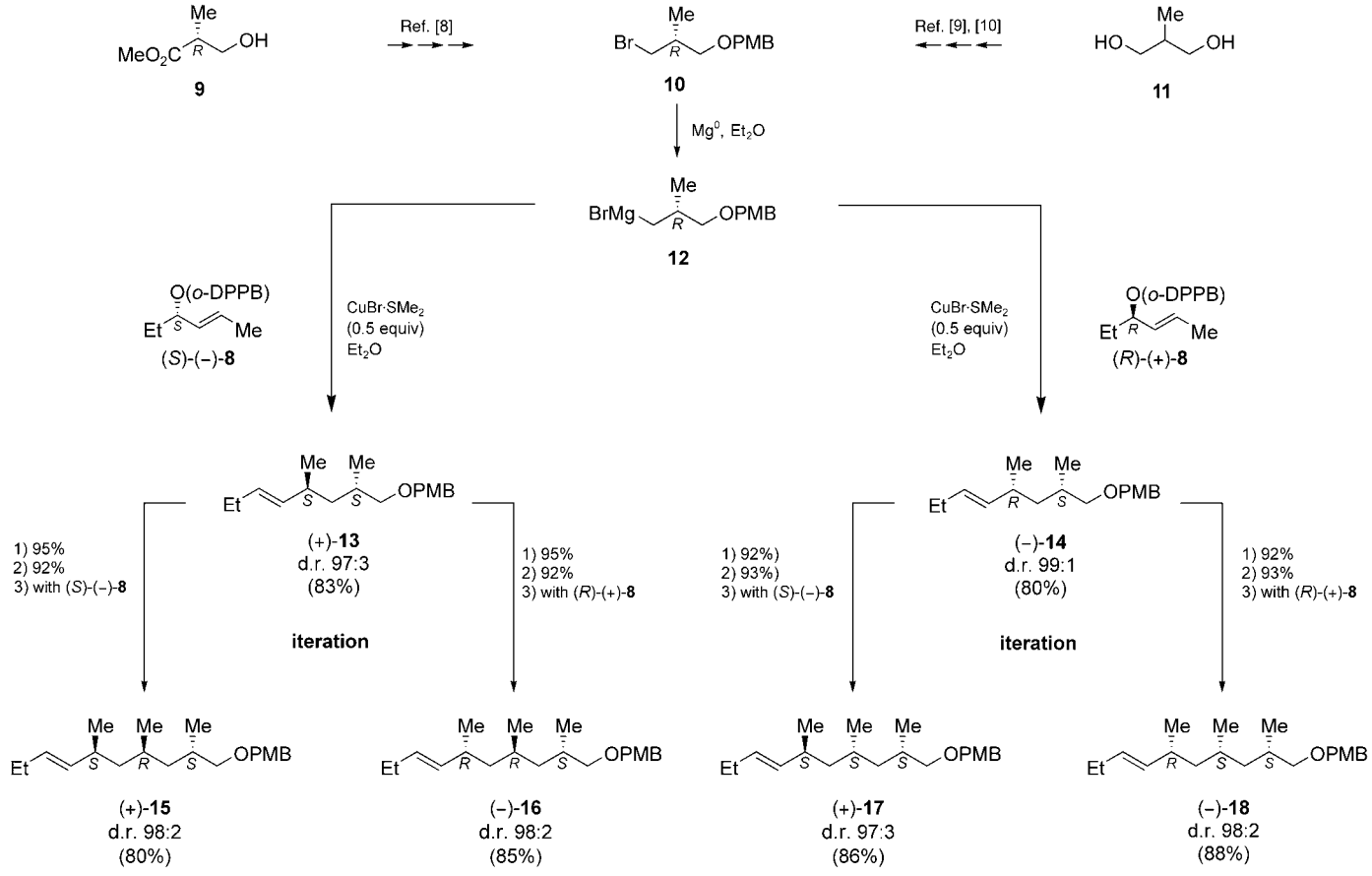
We believed that the Grignard reagent **12** derived from the known bromide **10** would be a suitable organometallic building block of the type **3** (Scheme 3).[7] Both enantiomers of **10** are readily accessible from the commercially available Roche esters **9**[8] or through enzymatic esterification processes starting from 2-methylpropane-1,3-diol (**11**)[9] or a derivative thereof.[10]

To demonstrate the practicability and flexibility of our strategy, we decided to prepare all possible diastereomers of a series of bis- and tris(deoxypropionate)s. First the bromide **10** was converted into the corresponding Grignard reagent **12**. It proved essential to activate the magnesium by the dry-stir method.[11,12] The addition of **12** (1 equiv) as a freshly prepared solution in diethyl ether to the allylic ester (*S*)-(−)-**8** in the presence of $CuBr{\cdot}SMe_2$ (0.5 equiv) initiated a clean allylic substitution to give the bis(deoxypropionate) (+)-**13** in good yield with perfect regioselectivity (> 99:1) and excellent stereoselectivity (d.r. 97:3). Even better stereoselectivity was observed in the reaction of **12** with the *R* allylic ester (+)-**8** (d.r. 99:1). Thus, the reaction that leads to the 1,3-*syn* relative configuration (in (−)-**14**) appears to represent a matched case, whereas the reaction that leads to the 1,3-*anti* configuration (in (+)-**13**) represents a mismatched case. The relative and absolute configurations of the bis(deoxypropionate)s (+)-**13** and (−)-**14** were verified upon conversion into the known alcohols (−)-**19**[13] and (+)-**20**,[14] respectively (Scheme 4).



Scheme 4. Determination of the relative and absolute configuration of (+)-**13** and (−)-**14**.

The iteration of this sequence, starting from (+)-**13** and (−)-**14**, began with oxidative cleavage of the alkene by ozonolysis and reductive workup to give the corresponding alcohols in excellent yields (Scheme 3, step 1). At this stage we decided to explore an alternative method for the generation of the Grignard reagent based on a halogen–metal exchange. This procedure turned out to be operation-



Scheme 3. Enantioselective construction of bis- and tris(deoxypropionate) building blocks based on an iterative *o*-DPPB-directed copper-mediated allylic substitution: 1) O_3, $NaBH_4$; 2) I_2, Im, PPh_3; 3) *t*BuLi (2 equiv), $MgBr_2{\cdot}OEt_2$, then (*S*)-(−)-**8**, $CuBr{\cdot}SMe_2$, Et_2O. Im = imidazole, PMB = *p*-methoxybenzyl.

 © 2004 Wiley-VCH Verlag GmbH & Co. KGaA, Weinheim

ally more convenient for small-scale reactions. The primary alcohols formed in the first step were therefore converted into the corresponding iodides (Scheme 3, step 2). The halogen–metal exchange proceeded cleanly upon treatment with *tert*-butyllithium and was followed by transmetalation with $MgBr_2{\cdot}OEt_2$. The directed allylic substitution of the resulting Grignard reagents with (*S*)-(−)-**8** and (*R*)-(+)-**8** in the presence of $CuBr{\cdot}SMe_2$ (0.5 equiv) proceeded cleanly to give all four possible diastereomeric tris(deoxypropionate) building blocks **15**–**18** in good yield, with perfect regioselectivity and excellent stereoselectivity.

In conclusion, a new flexible iterative strategy has been developed for the preparation of any desired oligo(deoxypropionate) stereoisomer. The key step, which allows perfect control of all aspects of selectivity, is an *o*-DPPB-directed copper-mediated allylic substitution with an enantiomerically pure Grignard reagent. This fragment-coupling step features reversed polarity relative to established methodology involving enolate alkylation. Problems associated with strategies based on enolate alkylation, such as low enolate reactivity and the cost of the chiral auxiliary, which is also often difficult to remove, can thus be avoided.

Experimental Section

Synthesis of (+)-**13**: $CuBr{\cdot}SMe_2$ (20.6 mg, 0.10 mmol) was added to a solution of (−)-**8** (77.7 mg, 0.20 mmol) in diethyl ether (4 mL) at room temperature, and the reaction mixture was stirred for a further 5 min. The Grignard reagent **12** (2.4 mL, 0.24 mmol, 0.1 M solution in diethyl ether) was added dropwise at room temperature to the resulting yellow solution, and the mixture was stirred for a further 2 h. A saturated aqueous solution of NH_4Cl (2 mL) was then added to the reaction mixture, the phases were separated, and the aqueous phase was extracted with dichloromethane (3 × 5 mL). The combined organic phases were dried (Na_2SO_4) and the solvents were removed in vacuo. Flash chromatography of the residue (petroleum ether/*tert*-butyl methyl ether 50:1) yielded (+)-**13** as a colorless oil (45.9 mg, 83 %, d.r. 97:3). HPLC (Macherey-Nagel EC 250/4 Nucleosil 100-5, 0.4 × 25 cm, 25 °C, *n*-heptane/ethyl acetate (200:0.3), 0.8 mL min^{-1}, 275 nm): t_R ((−)-**13**): 52.4 min (2.8 %), t_R ((+)-**13**): 55.0 min (97.2 %); $[\alpha]_D^{20} = +18.2$ ($c = 0.68$, $CHCl_3$); ^{1}H NMR (499.873 MHz, $CDCl_3$, 27 °C, TMS): $\delta = 0.91$ (d, $^3J = 6.8$ Hz, 3H, CH_3), 0.92 (d, $^3J = 6.8$ Hz, 3H, CH_3), 0.95 (t, $^3J = 7.5$ Hz, 3H, CH_3), 1.08 (dt, $^2J = 13.5$ Hz, $^3J = 7.5$ Hz, 1H, CH_2), 1.29 (m_c, 1H, CH_2), 1.81 (m_c, 1H, CH), 1.98 (m_c, 2H, CH_2), 2.14 (mc, 1H, CH), 3.18 (dd, $^2J = 9.1$ Hz, $^3J = 7.1$ Hz, 1H, CH_2), 3.32 (dd, $^2J = 9.1$ Hz, $^3J = 5.4$ Hz, 1H, CH_2), 3.80 (s, 3H, O-CH_3), 4.41 (d, $^2J = 11.7$ Hz, 1H, CH_2Ar), 4.44 (d, $^2J = 11.7$ Hz, 1H, CH_2Ar), 5.25 (ddt, $^3J = 15.3$, 7.6 Hz, $^4J = 1.4$ Hz, 1H, CH), 5.38 (dtd, $^3J = 15.3$, 6.2 Hz, $^4J = 0.9$ Hz, 1H, CH), 6.87 (m, 2H, ArH), 7.26 ppm (m, 2H, ArH); ^{13}C NMR (125.709 MHz, $CDCl_3$, 27 °C, TMS): $\delta =$ 14.0, 17.7, 20.7, 25.5, 31.0, 34.0, 41.2, 55.3, 72.6, 75.6, 113.7 (2 × C), 129.1 (2 × C), 129.9, 131.0, 135.6, 159.0 ppm; elemental analysis (%) calcd for $C_{18}H_{28}O_2$ (276.41): C 78.21, H 10.21; found: C 77.90, H 10.32.

Received: February 11, 2004 [Z53990]
Published Online: May 26, 2004

Keywords: allylation · asymmetric synthesis · diastereoselectivity · organocopper reagents · polyketides

[1] For ionomycin, see: W.-C. Liu, D. Smith-Slusarchyk, G. Astle, W. H. Trejo, W. E. Brown, E. J. Meyers, *J. Antibiot.* **1978**, *31*, 815–819; for borrelidin, see: J. Berger, L. M. Jampolsky, M. W. Goldberg, *Arch. Biochem.* **1949**, *22*, 476–478; for pectinatone, see: J. E. Biskupiak, C. M. Ireland, *Tetrahedron Lett.* **1983**, *24*, 3055–3058.

[2] D. A. Evans, R. L. Dow, T. L. Shih, J. M. Takacs, R. Zahler, *J. Am. Chem. Soc.* **1990**, *112*, 5290–5313.

[3] A. G. Myers, B. H. Yang, H. Chen, D. J. Kopecky, *Synlett* **1997**, 457–459.

[4] A. A. Birkbeck, D. Enders, *Tetrahedron Lett.* **1998**, *39*, 7823–7826.

[5] B. Breit, P. Demel, C. Studte, *Angew. Chem.* **2004**, *116*, 3874–3877; *Angew. Chem. Int. Ed.* **2004**, *43*, 3786–3789; B. Breit, P. Demel, *Adv. Synth. Catal.* **2001**, *343*, 429–432.

[6] a) Novozym 435 is a lipase from *Candida antarctica* (*Candida antarctica* lipase B, CAL-B); for more details, see: www.novozymes.com; b) for selected examples of 2-alkanols that have been resolved with CAL-B, see: U. T. Bornscheuer, R. J. Kazlauskas in *Hydrolases in Organic Synthesis*, Wiley-VCH, Weinheim, **1999**, pp. 70–72.

[7] D. Sawada, M. Kanai, M. Shibasaki, *J. Am. Chem. Soc.* **2000**, *122*, 10521–10532.

[8] For the synthesis of (*S*)-**10**, see: S. D. Meyer, T. Miwa, M. Nakatsuka, S. L. Schreiber, *J. Org. Chem.* **1992**, *57*, 5058–5060.

[9] a) E. Santaniello, P. Ferraboschi, P. Grisenti, *Tetrahedron Lett.* **1990**, *31*, 5657–5660; b) C. Bertucci, A. Petri, G. Felix, B. Perini, P. Salvadori, *Tetrahedron: Asymmetry* **1999**, *10*, 4455–4462; c) P. Grisenti, P. Ferraboschi, A. Manzocchi, E. Santaniello, *Tetrahedron* **1992**, *48*, 3827–3834; d) Z.-F. Xie, H. Suemune, K. Sakai, *Tetrahedron: Asymmetry* **1993**, *4*, 973–980.

[10] T. Akeboshi, Y. Ohtsuka, T. Ishihara, T. Sugai, *Adv. Synth. Catal.* **2001**, *343*, 624–637.

[11] P. M. Smith, E. J. Thomas, *J. Chem. Soc. Perkin Trans. 1* **1998**, 3541–3556.

[12] K. V. Baker, J. M. Brown, N. Hughes, A. J. Skarnulis, A. Sexton, *J. Org. Chem.* **1991**, *56*, 698–703.

[13] S. Karlsson, E. Hedenström, *Acta Chem. Scand.* **1999**, *53*, 620–630.

[14] For (−)-**20**, see: P. J. Kocienski, R. C. D. Brown, A. Pommier, M. Procter, B. Schmidt, *J. Chem. Soc. Perkin Trans. 1* **1998**, 9–40.

 © 2004 Wiley-VCH Verlag GmbH & Co. KGaA, Weinheim

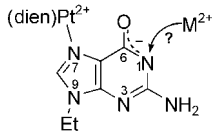
Stability Constants

Two Metal Ions Coordinated to a Purine Residue Tolerate Each Other Well**

Bernd Knobloch, Roland K. O. Sigel, Bernhard Lippert, and Helmut Sigel*

In biological systems two (or more) metal ions are often located relatively close to one another.[1] For example, in the active-site cavity of Cu,Zn superoxide dismutase the two metal ions are linked by the imidazolate of a histidine residue, and in certain iron clusters the metal centers may be bridged by sulfide ions or cysteine residues. Not only proteins, but also RNA molecules require monovalent and divalent metal ions (usually Mg^{2+}) for folding and activity.[2a–f] Several examples are known in which up to five Mg^{2+} ions are located close to one another,[2g–m] either to stabilize local structures and tertiary contacts[2g–j] or to participate directly in catalysis.[2k–m] The binding of Mg^{2+} (sometimes outersphere through water molecules)[2c,i] often occurs at N7 and/or C(6)O of a guanine residue.[2h,i,l] However, recently it was also proposed that the deprotonated N1 position participates directly in catalysis by the hairpin ribozyme.[2n] In proteins and RNA molecules metal ions are held in place through binding to further ligation sites located within the molecules. What happens in the absence of such additional supporting binding sites? From studies with kinetically inert metal ions, such as Pt^{II}, it is known that two metal ions can bind simultaneously to N1 and N7 sites of adenine[3a,b] and guanine.[3c,d] Except for the results of one study with Pd^{2+},[4] no equilibrium data are available on the simultaneous binding of two biologically relevant or kinetically labile metal ions to a nucleobase in solution. However, such information would be of high relevance with regard to understanding the structure and function of ribozymes.

To quantify the effect that two metal ions coordinated to the same purine moiety exert on one another with respect to their binding stability, we studied the metal-ion-binding properties of a guanine residue with a metal ion already coordinated at N7. The cationic complex $[(dien)Pt(9EtG\text{-}N7)]^{2+}$ (Scheme 1), which consists of 9-ethylguanine (9EtG) with a kinetically inert $(dien)Pt^{2+}$ unit at N7, is suitable for this purpose, as after deprotonation of the H(N1) site, the coordination of an additional metal ion can occur. Therefore, by potentiometric pH titrations (25 °C; $I = 0.1$ M, $NaNO_3$)[5a,b] we determined first the acidity constant $K^{H}_{(dien)Pt(9EtG\text{-}N7)}$ for the equilibrium (1a):



Scheme 1. What is the effect of metalation at N7 on the binding of M^{2+} to N1 in the cationic complex $[(dien)Pt(9EtG\text{-}N7{-}HN1)]^{+}$? (dien = diethylenetriamine = 1,4,7-triazaheptane; 9-EtG = 9-ethylguanine)

$$[(dien)Pt(9EtG\text{-}N7)]^{2+} \rightleftharpoons [(dien)Pt(9EtG\text{-}N7{-}HN1)]^{+} + H^{+} \quad (1a)$$

$$K^{H}_{(dien)Pt(9EtG\text{-}N7)} = \frac{[[(dien)Pt(9EtG\text{-}N7{-}HN1)]^{+}]\,[H^{+}]}{[[(dien)Pt(9EtG\text{-}N7)]^{2+}]} \quad (1b)$$

We obtained the result $pK^{H}_{(dien)Pt(9EtG\text{-}N7)} = 8.17 \pm 0.03$, which agrees perfectly with the value 8.14 ± 0.06 previously determined by NMR spectroscopy.[5c] Comparison with the value for free 9EtG ($pK^{H}_{9EtG} = 9.57 \pm 0.05$)[5a] shows that coordination of a $(dien)Pt^{2+}$ unit at N7 of the guanine residue increases the acidity of the proton at N1 by $\Delta pK_{a/Pt,H} = 1.40 \pm 0.06$.

The coordination properties of the deprotonated N1 site of $[(dien)Pt(9EtG\text{-}N7{-}HN1)]^{+}$ were investigated with Cu^{2+} and Mg^{2+} according to the equilibrium (2a), in which $^{2+}Pt\mathit{N7}{\cdot}G{\cdot}N1^{-}$ represents the complex $[(dien)Pt(9EtG\text{-}N7{-}HN1)]^{+}$ and $(Pt\mathit{N7}{\cdot}G{\cdot}\mathit{N1}M)^{3+}$ the bimetallic species formed between $[(dien)Pt(9EtG\text{-}N7{-}HN1)]^{+}$ and M^{2+}:

$$^{2+}Pt\mathit{N7}\cdot G\cdot \mathit{N1}^{-} + M^{2+} \rightleftharpoons (Pt\mathit{N7}\cdot G\cdot \mathit{N1}M)^{3+} \quad (2a)$$

$$K^{M}_{Pt\mathit{N7}\cdot G\cdot \mathit{N1}M} = \frac{[(Pt\mathit{N7}\cdot G\cdot \mathit{N1}M)^{3+}]}{[^{2+}Pt\mathit{N7}\cdot G\cdot N1^{-}]\,[M^{2+}]} \quad (2b)$$

Cu^{2+} was used because of its high affinity for nitrogen ligands[6] and Mg^{2+} because of its biologically important role in ribozymes.[2] The following stability constants as defined by Equation (2b) were determined: $\lg K^{Cu}_{Pt\mathit{N7}\cdot G\cdot \mathit{N1}Cu} = 3.45 \pm 0.25$ and $\lg K^{Mg}_{Pt\mathit{N7}\cdot G\cdot \mathit{N1}Mg} = 0.65 \pm 0.3$. These results become meaningful if compared with the affinity of these metal ions for the N1 position of deprotonated 9EtG, that is, $\lg K^{Cu}_{Cu(9EtG-HN1)} = 4.45 \pm 0.25$ for $[Cu(9EtG{-}HN1)]^{+}$[7a] and $\lg K^{Mg}_{Mg(9EtG-HN1)} = 1.0 \pm 0.2$ for $[Mg(9EtG{-}HN1)]^{+}$:[7b] The stability differences due to $(dien)Pt^{2+}$ coordination at N7 are $\Delta\lg K_{Pt,Cu} = (4.45 \pm 0.25) - (3.45 \pm 0.25) = 1.0 \pm 0.35\,(3\sigma)$ and $\Delta\lg K_{Pt,Mg} = (1.0 \pm 0.2) - (0.65 \pm 0.3) = 0.35 \pm 0.35\,(3\sigma)$ for the Cu^{2+} and Mg^{2+} systems, respectively. Clearly there is a repulsive interaction between the two divalent metal ions coordinated at N1 and N7, but surprisingly this repulsion is relatively small. As expected, the repulsive effect upon the coordination of Mg^{2+} is smaller, as this metal ion commonly interacts with N sites of this type in an outersphere manner.[7c–e] Thus repulsion is reduced in accord with theoretical calculations.[8] However,

[*] Dr. B. Knobloch, Prof. Dr. R. K. O. Sigel
Institute of Inorganic Chemistry
Universität Zürich
Winterthurerstrasse 190, 8057 Zürich (Switzerland)
Fax: (+41) 1-635-6802
E-mail: roland.sigel@aci.unizh.ch
Prof. Dr. B. Lippert
Department of Chemistry
Universität Dortmund
Otto-Hahn-Strasse 6, 44227 Dortmund (Germany)
Dr. B. Knobloch, Prof. Dr. H. Sigel
Department of Chemistry, Inorganic Chemistry
Universität Basel
Spitalstrasse 51, 4056 Basel (Switzerland)

[**] This study was supported by the Swiss National Science Foundation under grant numbers PP002-68733/1 (R.K.O.S., Förderungsprofessur) and 20-66647.01 (H.S.), the Deutsche Forschungsgemeinschaft (B.L.), and the Fonds der Chemischen Industrie (B.L.), as well as by the Swiss Federal Office for Education and Science within the COST D20 programme (H.S.).

 DOI: 10.1002/anie.200453987 © 2004 Wiley-VCH Verlag GmbH & Co. KGaA, Weinheim

the apparently low stability constant of the Mg^{2+} complex should not be underestimated. In an RNA structure the water molecules of the relatively stable hydration sphere of a Mg^{2+} ion are strongly linked through hydrogen bonds to a number of other sites, including nucleobases,[2g–j,m] thus compensating for the intrinsic low stability of the Mg^{2+} coordination.

How do the metal–metal and metal–proton interactions compare to the proton–proton interaction between the N7 and N1 positions? The micro acidity constant[9a] $pk^{H\cdot N7-N1}_{H\cdot N7-N1\cdot H} = 7.22 \pm 0.01$ describes the deprotonation of the H(N1) site of an *N7*-protonated H(9EtG)$^+$ to give the zwitterionic tautomer $(^+H\mathit{N7}\cdot 9EtG-H\mathit{N1}^-)^{\pm}$. Therefore, the proton–proton interaction amounts to $\Delta pK_{a/H,H} = (9.57 \pm 0.05) - (7.22 \pm 0.01) = 2.35 \pm 0.05\,(3\sigma)$. This repulsion is considerably larger than the Pt^{2+}–proton ($\Delta pK_{a/Pt,H} = 1.40 \pm 0.06$) and the Pt^{2+}–M^{2+} interactions ($\Delta \lg K_{Pt,Cu} = 1.0 \pm 0.35\,(3\sigma)$ and $\Delta \lg K_{Pt,Mg} = 0.35 \pm 0.35\,(3\sigma)$; see above). Thus, it follows that the clustering of metal ions in RNA, especially of Mg^{2+}, can occur surprisingly easily, and we therefore expect that more metal-ion clusters will be identified in RNA structures. Such clusters are able to stabilize certain folds in the tertiary structure or to serve as tools to promote catalysis. Indeed, it has been proposed that several metal ions cooperate with one another in ribozymes such as RNase P.[2f]

The results presented show that for divalent metal ions the metal–metal repulsive interaction is smaller than the metal–proton repulsion,[9b] which is in turn much smaller than the proton–proton interaction. These findings are in agreement with observations[4a] based on equilibrium studies of Pd^{2+}–purine systems by ^1H NMR spectroscopic shift experiments.[4b] The effects of charges located at N7 and N1 of purine residues are reciprocal and equal. That is, the effect of a charge at N1 on that at N7 is equal to the effect of a charge at N7 on that at N1; this equivalence has been shown for M^{2+}–H^+ interactions.[9b]

The acidity constant $pK^H_{(dien)Pt(9EtG-\mathit{N7})} = 8.17$ is close to the physiological pH range. For guanosine and 2′-deoxyguanosine residues pK_a values are even lower by about 0.3 pK units.[5a,b] In addition to the increase in acidity of H(N1) through coordination of a metal ion at N7, the coordination of a second metal ion at N1 further facilitates the simultaneous deprotonation of H(N1) because of competition between the metal ion and the proton for the binding site. Therefore, at a physiological pH value of about 7.5, purine residues in ribozymes may well coordinate two metal ions simultaneously at N7 and N1.

Experimental Section

9-Ethylguanine was purchased from Sigma Chemical Co., St. Louis, MO (USA). The complex $[(dien)Pt(9EtG-\mathit{N7})](ClO_4)_2\cdot 2H_2O$ was prepared via the intermediate [(dien)PtI]I.[3c,10a] For the other reagents, see reference [5a,b]. The potentiometric pH titrations in aqueous solution were carried out and evaluated as described previously.[5b] For the determination of the acidity constant $pK^H_{(dien)Pt(9EtG-\mathit{N7})}$ [Eq. (1b)], aqueous HNO_3 (0.2 mM, 25 mL, 25 °C; $I = 0.1$ M, $NaNO_3$) was titrated both in the presence and in the absence of $[(dien)Pt(9EtG-\mathit{N7})]^{2+}$ (0.29 to 0.41 mM) with NaOH (0.03 M, 0.8 mL) under N_2. The stability constants $K^M_{Pt\mathit{N7}\cdot G\cdot \mathit{N1}M}$ [Eq. (2b)] of the Mg^{2+} and Cu^{2+} complexes were determined under the same conditions,[10b] but with $NaNO_3$ partly or fully replaced by $M(NO_3)_2$. The ratios $[(dien)Pt(9EtG-\mathit{N7})]^{2+}/M^{2+}$ were 1:90 for Mg^{2+} and 1:58, 1:45, or 1:36 for Cu^{2+}. The error limits of the measured stability constants are relatively large because the buffer depression (which is the difference between the pK_a value of the ligand and the apparent acidity constant, pK_a', measured in the presence of M^{2+})[10b] in the Mg^{2+} system is small and the experiments with the Cu^{2+} system were hampered by the formation of hydroxo complexes. The value for $K^H_{(dien)Pt(9EtG-\mathit{N7})}$ [Eq. (1b)] was calculated as the average of five independent pairs of titrations; the stability constants [Eq. (2b)] for the Cu^{2+} and Mg^{2+} systems are the average of three and four independent pairs of titrations, respectively. The error limits indicated correspond to three times the standard error of the mean value (3σ) or the sum of the probable systematic errors, whichever value is larger.

Received: February 10, 2004 [Z53987]

Keywords: magnesium · metal–metal interactions · ribozymes · RNA · stability constants

[1] *Handbook on Metalloproteins* (Eds.: I. Bertini, A. Sigel, H. Sigel), Dekker, New York, **2001**, pp. 1–1182.

[2] a) R. K. O. Sigel, A. M. Pyle, *Met. Ions Biol. Syst.* **2003**, *40*, 477–512; b) A. M. Pyle, *J. Biol. Inorg. Chem.* **2002**, *7*, 679–690; c) S. E. Butcher, *Curr. Opin. Struct. Biol.* **2001**, *11*, 315–320; d) R. K. O. Sigel, D. G. Sashital, D. L. Abramovitz, A. G. Palmer III, S. E. Butcher, A. M. Pyle, *Nat. Struct. Mol. Biol.* **2004**, *11*, 187–192; e) R. K. O. Sigel, A. Vaidya, A. M. Pyle, *Nat. Struct. Biol.* **2000**, *7*, 1111–1116; f) M. Bränvall, L. A. Kirsebom, *Proc. Natl. Acad. Sci. USA* **2001**, *98*, 12943–12947; g) C. C. Correll, B. Freeborn, P. B. Moore, J. A. Steitz, *Cell* **1997**, *91*, 705–712; h) P. Auffinger, L. Bielecki, E. Westhof, *Chem. Biol.* **2003**, *10*, 551–561; i) J. H. Cate, R. L. Hanna, J. A. Doudna, *Nat. Struct. Biol.* **1997**, *4*, 553–558; j) L. Jovine, S. Djordjevic, D. Rhodes, *J. Mol. Biol.* **2000**, *301*, 401–414; k) L. B. Weinstein, B. C. N. M. Jones, R. Cosstick, T. R. Cech, *Nature* **1997**, *388*, 805–808; l) S.-O. Shan, A. Yoshida, S. Sun, J. A. Piccirilli, D. Herschlag, *Proc. Natl. Acad. Sci. USA* **1999**, *96*, 12299–12304; m) S.-O. Shan, A. V. Kravchuk, J. A. Piccirilli, D. Herschlag, *Biochemistry* **2001**, *40*, 5161–5171; n) P. C. Bevilacqua, *Biochemistry* **2003**, *42*, 2259–2265.

[3] a) R. K. O. Sigel, S. M. Thompson, E. Freisinger, B. Lippert, *Chem. Eur. J.* **2001**, *7*, 1968–1980; b) R. K. O. Sigel, S. M. Thompson, E. Freisinger, B. Lippert, *Chem. Commun.* **1999**, 19–20; c) G. Frommer, H. Schoellhorn, U. Thewalt, B. Lippert, *Inorg. Chem.* **1990**, *29*, 1417–1422; d) B. Longato, G. Bandoli, G. Trovo, E. Marasciulo, G. Valle, *Inorg. Chem.* **1995**, *34*, 1745–1750.

[4] a) R. B. Martin, *Met. Ions Biol. Syst.* **1996**, *32*, 61–89, see page 84; b) K. H. Scheller, V. Scheller-Krattiger, R. B. Martin, *J. Am. Chem. Soc.* **1981**, *103*, 6833–6839.

[5] a) B. Song, J. Zhao, R. Griesser, C. Meiser, H. Sigel, B. Lippert, *Chem. Eur. J.* **1999**, *5*, 2374–2387; b) C. P. Da Costa, H. Sigel, *Inorg. Chem.* **2003**, *42*, 3475–3482; c) R. K. O. Sigel, E. Freisinger, B. Lippert, *J. Biol. Inorg. Chem.* **2000**, *5*, 287–299.

[6] a) R. B. Martin, *Inorg. Chim. Acta* **2002**, *339*, 27–33; b) H. Sigel, D. B. McCormick, *Acc. Chem. Res.* **1970**, *3*, 201–208.

[7] a) As the acidity constants $pK^H_{9EtG} = 9.57 \pm 0.05$ and $pK^H_{9MeG} = 9.56 \pm 0.02$ (9MeG = 9-methylguanine) are identical, the averaged value of the stability constants of the corresponding Cu^{2+} complexes[5a] was used for comparison; b) the stability constant of the Mg^{2+} complex of $(dGuo-H\mathit{N1})^-$ (N1-deprotonated 2′-deoxyguanosine) is $\lg K^{Mg}_{Mg(dGuo-H\mathit{N1})} = 0.94 \pm 0.14$;[5b] as the acidity constant $pK^H_{dGuo} = 9.25 \pm 0.02$[5b] is only slightly smaller than that of 9EtG ($pK^H_{9EtG} = 9.57 \pm 0.05$)[5a] and the stability of Mg^{2+}

complexes formed with N donor ligands is practically independent of the basicity of the N atom involved,[7c–e] the stability constant for the [Mg(9EtG–H*N1*)]$^+$ complex is probably very close to $\lg K^{Mg}_{Mg(9EtG-HN1)} = 1.0 \pm 0.2$ and well within the error limits indicated; c) L. E. Kapinos, H. Sigel, *Inorg. Chim. Acta* **2002**, *337*, 131 – 142; d) L. E. Kapinos, B. Song, H. Sigel, *Chem. Eur. J.* **1999**, *5*, 1794 – 1802; e) L. E. Kapinos, B. Song, H. Sigel, *Inorg. Chim. Acta* **1998**, *280*, 50 – 56.

[8] a) J. Šponer, M. Sabat, L. Gorb, J. Leszczynski, B. Lippert, P. Hobza, *J. Phys. Chem. B* **2000**, *104*, 7535 – 7544; b) J. E. Šponer, J. Leszczynski, F. Glahé, B. Lippert, J. Šponer, *Inorg. Chem.* **2001**, *40*, 3269 – 3278.

[9] a) G. Kampf, L. E. Kapinos, R. Griesser, B. Lippert, H. Sigel, *J. Chem. Soc. Perkin Trans. 2* **2002**, 1320 – 1327; b) R. Griesser, G. Kampf, L. E. Kapinos, S. Komeda, B. Lippert, J. Reedijk, H. Sigel, *Inorg. Chem.* **2003**, *42*, 32 – 41.

[10] a) G. W. Watt, W. A. Cude, *Inorg. Chem.* **1968**, *7*, 335 – 338; b) R. K. O. Sigel, B. Song, H. Sigel, *J. Am. Chem. Soc.* **1997**, *119*, 744 – 755.

 © 2004 Wiley-VCH Verlag GmbH & Co. KGaA, Weinheim

Asymmetric Catalysis

Cobalt(I)-Catalyzed Asymmetric [2+2+2] Cycloaddition of Alkynes and Nitriles: Synthesis of Enantiomerically Enriched Atropoisomers of 2-Arylpyridines**

Andrey Gutnov, Barbara Heller,* Christine Fischer, Hans-Joachim Drexler, Anke Spannenberg, Bernd Sundermann, and Corinna Sundermann*

In memory of Oleg Okhlobystin

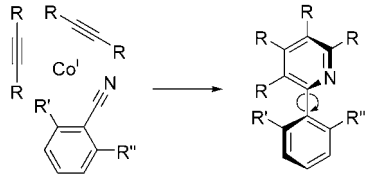
The [2+2+2] cycloaddition of alkynes and nitriles is a useful tool in organic synthesis, allowing easy access to a broad variety of benzene and pyridine derivatives in one step. Although achiral reactions of this type are well documented,[1] there are only two examples of catalytic asymmetric [2+2+2] homocyclizations yielding benzene derivatives with simultaneous introduction of an element of chirality.[2,3]

[*] Dr. A. Gutnov, Dr. B. Heller, Dr. C. Fischer, Dr. H.-J. Drexler, Dr. A. Spannenberg
Leibniz-Institut für Organische Katalyse
Universität Rostock e.V.
Buchbinderstrasse 5–6, 18055 Rostock (Germany)
Fax: (+49) 381-46693-24
E-mail: andrey.gutnov@ifok.uni-rostock.de
barbara.heller@ifok.uni-rostock.de
Dr. B. Sundermann, Dr. C. Sundermann
Grünenthal GmbH, Center of Research
52099 Aachen (Germany)

[**] This work was supported by Deutsche Forschungsgemeinschaft (He 3330/1-1; He 3330/1-3) and Grünenthal GmbH. We are grateful to Professor Uwe Rosenthal for helpful critical discussions, Beate Friedrich for technical assistance, and Hannelore Baudisch for analytical measurements.

Supporting information for this article is available on the WWW under http://www.angewandte.org or from the author.

Our recent studies on the Co^{I}-catalyzed [2+2+2] cycloaddition of alkynes and nitriles to give pyridines have shown that the photochemical variant provides a valuable extension of existing syntheses.[4] By irradiation of the reaction mixture with visible light ($\lambda = 350$–500 nm), or, alternatively, with sunlight as the energy source for catalyst activation, the reaction could be carried out under very mild conditions: ambient temperature and pressure, possibility of using water as the reaction medium, and, after optimization, substrate-to-catalyst ratios of up to 10000:1. To take full advantage of such mild conditions, we set out to develop a new kind of asymmetric [2+2+2] cycloaddition of nitriles and alkynes in the presence of modified chiral cobalt(I) complexes of the type $[Cp^{R}Co(cod)]$ (Cp^{R} = substituted cyclopentadienyl, cod = cycloocta-1,5-diene) as catalysts (Scheme 1). Bulky substituents R′ and R″ attached at the *ortho* positions of the 2-arylpyridine derivatives should prevent the internal rotation, thus leading to the formation of two stable atropoisomers. A chiral ligand in the cobalt catalyst would be responsible for preferential formation of only one of them.

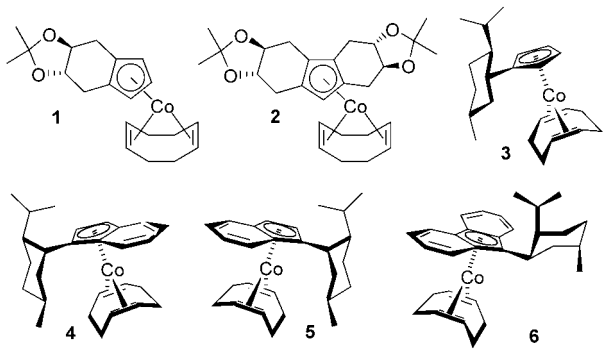


Scheme 1. [2+2+2] Cycloaddition giving axially chiral 2-arylpyridines.

A short survey of the literature showed that a reasonable number of chiral pyridines of this type have been synthesized, resolved, and applied successfully as ligands in numerous asymmetric transformations.[5] However, in many cases multistep procedures are necessary, and optical resolutions are often troublesome. Therefore the direct asymmetric synthesis of the compounds is highly desired.

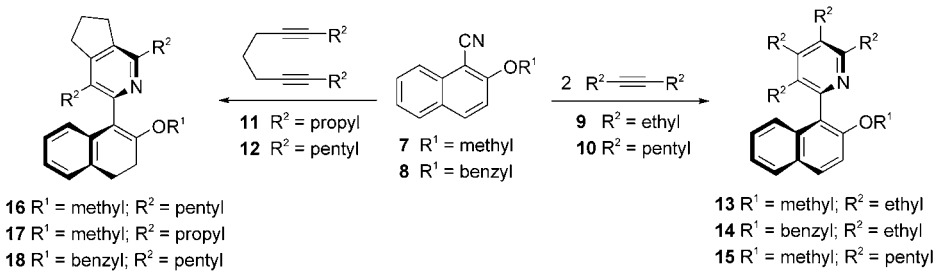
With the synthesis of axially chiral pyridine derivatives in mind, we screened the reaction of 2-substituted 1-naphthonitriles with several alkynes using chiral cobalt(I) complexes as catalysts (Schemes 2 and 3). The tartrate-derived cobalt complexes **1** and **2** as well as the four menthyl-derived complexes **3**–**6**[6] were tested in this reaction as catalysts. The results are summarized in Table 1.

Fortunately our preliminary analyses of the racemic pyridines with dynamic HPLC on a chiral stationary phase



Scheme 2. Chiral cobalt(I) complexes employed.

 DOI: 10.1002/anie.200454164 © 2004 Wiley-VCH Verlag GmbH & Co. KGaA, Weinheim



Scheme 3. Asymmetric cocycloaddition of internal alkynes and 1-naphthonitriles.

Table 1: [2+2+2] Cycloaddition of 2-alkoxy-1-naphthonitriles and substituted alkynes.

Run[a]	Cat.	Prod.	Yield [%][b]	Sel. [% *ee*][c]
1	**1**	**13**	14	45 (+)
2	**2**	**13**	traces	–
3	**3**[d]	**13**	34	19 (+)
4	**4**	**13**	11	63 (+)
5	**5**	**13**	10	64 (−)
6[e]	**5**	**13**	2	71 (−)
7	**6**	**13**	traces	–
8	**1**	**16**	81	32 (+)
9	**1**	**15**	11	40 (−)
10	**4**	**14**	3	59 (+)
11	**4**	**18**	7	39 (+)
12	**4**	**16**	32	37 (+)
13	**4**	**17**	8	31 (+)
14	**5**	**16**	33	38 (−)
15	**5**	**17**	8	32 (−)
16	**5**	**15**	2	63 (+)

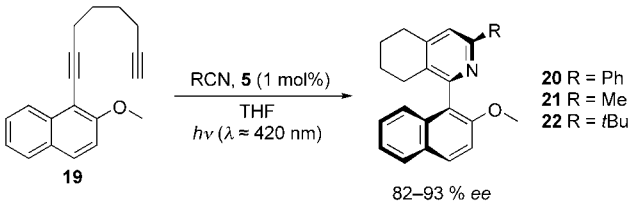
[a] The reaction was carried out in THF at 20 °C for 9 h and irradiated with visible light; molar ratio: [nitrile]/[alkyne]/[catalyst] = 1:2.2:0.1 unless indicated otherwise; analytical data and synthetic procedures for the new compounds are given in Supporting Information. [b] Yields of isolated products. [c] Determined by HPLC on a chiral stationary phase (see the Supporting Information for details); direction of optical rotation given in parentheses: $c = 0.1$, toluene, 25 °C. [d] 5 mol% catalyst. [f] Reaction temperature 3 °C.

at different temperatures showed that the barriers to internal rotation are high enough (> 110 kJ mol^{-1}) for secure handling of the enantiomerically enriched products at ambient conditions.

The enantioselectivity of the reaction does not depend on the solvent; hexane, toluene, dioxane and THF lead to comparable results. The duration of irradiation and the amount of catalyst also have no influence on the enantiomeric excess of the reaction. An attempt to increase the enantiomeric excess of the pyridine **13** in the reaction with catalyst **5** by decreasing the reaction temperature from 20 to 3 °C led indeed to the highest *ee* (71% *ee*); however, the yield dropped dramatically from 10 to 2% (Table 1, runs 5 and 6).

It is noteworthy that yields of the racemic 2-arylpyridines obtained from the reactions catalyzed by the unsubstituted [CpCo(cod)] complex (5 mol%) were substantially higher in all cases: **13** (71%), **14** (67%), **15** (45%), **16** (71%), **17** (46%), and **18** (47%). In reactions with the enantioselective catalysts **4** and **5** neither extended longer periods of irradiation nor higher temperatures—at the cost of enantioselectivity—resulted in improved yields.

To obtain better results we chose bulkier substrates for the reaction. For this purpose 2-methoxy-1-(1,7-octadiynyl)naphthalene (**19**) was prepared by coupling 1-iodo-2-methoxynaphthalene and 1,7-octadiyne, and the compound was reacted with several nitriles in the presence of catalyst **5** (Scheme 4). The reaction with benzonitrile proceeded smoothly at 20 °C over 24 h to give pyridine **20** in high yield (75%) relative to the starting diyne **19**, and the enantiomeric excess of the product was 82% *ee*. A single recrystallization furnished the pure product **20** with 49% yield and more than 98% *ee*. No traces of a regioisomeric pyridine were found, and the total yield of homocyclization products did not exceed 5% (GC-MS).



Scheme 4. Asymmetric cycloaddition giving optically enriched 1-aryl-5,6,7,8-tetrahydroisoquinolines.

Surprisingly, the temperature had only little effect on the yield of the reaction (Table 2). The yield was usually high after a reaction time of 24 h in the temperature range between 3 and 20 °C. On the other hand, the enantioselectivity increased from 82% *ee* at 20 °C to 89% *ee* at 3 °C. Lowering the temperature further (−20 °C) led to a selectivity of 93% *ee*; however, the reaction became sluggish and required three days to reach a yield of 86%.

Table 2: Enantioselectivities and yields in the syntheses of isoquinolines **20**–**22**.

Run	Prod.	*T* [°C]	Yield [%]	Sel. [% *ee*]
1	**20**	20	79[a] (49[b])	82[c] (>98[b])
2	**20**	3	86[a] (57[b])	89[c] (>98[b])
3	**20**	−20	86[a] (56[b])	93[c] (>98[b])
4	**21**	3	88[a] (54[b])	88[c] (>98[b])
5	**22**	3	74[a] (46[b])	88[c] (>98[b])

[a] Yield after chromatography. [b] Determined after recrystallization. [c] Measured in reaction mixture.

The analogous reaction of **19** with acetonitrile for 24 h at 3 °C led to the corresponding methyl derivative **21** in 88% yield and 88% *ee* (54% yield and >98% *ee* after recrystallization). When pivalonitrile was employed, the *tert*-butyl derivative **22** was prepared with 74% yield and 88% *ee* (46% yield and >98% *ee* after recrystallization). The optically pure compounds **20**–**22** could be stored in toluene solution for six months at room temperature without degradation of the optical rotation. An X-ray analysis revealed *R* configuration for the compound **20** obtained with catalyst **5** (Figure 1).[7] As expected, catalyst **4** furnished opposite enantiomers for the compounds **20**–**22** with identical yields and enantioselectivities.

The origin of enantioselectivity in this reaction is supposed to be the intermediate formation of a diastereomeric

 © 2004 Wiley-VCH Verlag GmbH & Co. KGaA, Weinheim

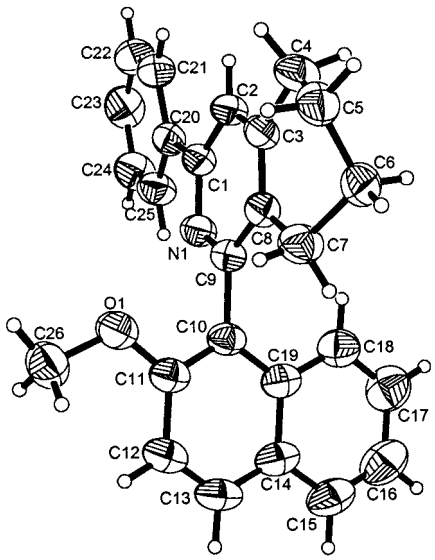
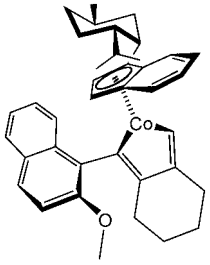


Figure 1. X-ray crystal structure of (+)-(*R*)-1-(2-methoxy-1-naphthyl)-3-phenyl-5,6,7,8-tetrahydroisoquinoline **20** (ellipsoids set at 50% probability level). The best planes of the ten atoms of the naphthyl moiety (C10–C19) and the six atoms of the pyridine ring (N1, C1–C3, C8, C9) intersect at the angle of 84.46(3)°.



Scheme 5. The intermediate cobaltacyclopentadiene.

cobaltacyclopentadiene (Scheme 5). This species is then attacked by a nitrile to form the pyridine ring, retaining configuration in the act. This explains in particular the lack of influence of sterically and electronically different nitriles on the stereochemical course of the reaction, as the compounds **20**–**22** were formed with nearly identical enantioselectivities.

In conclusion, we have discovered the first asymmetric approach to biaryl atropoisomers by [2+2+2] cycloaddition of alkynes and nitriles using chiral cobalt(I) complexes, which led to a practical preparation of homochiral 2-arylpyridines.

Experimental Section

Representative example (synthesis of **20**): A thermostated (3°C) reaction vessel was loaded with diyne **19** (524 mg, 2 mmol), catalyst **5** (8.4 mg, 0.02 mmol), THF (20 mL), and benzonitrile (412 μL, 4 mmol) under argon atmosphere. The mixture was stirred and irradiated by two 460-W lamps ($\lambda \approx 420$ nm) for 24 h. The reaction was quenched by switching off the lamps and simultaneously letting in air. The extent of reaction, i.e. conversion of the starting diyne **19**, was determined by GC. The reaction mixture was filtered through a thin pad of silica gel, eluting with THF. The solvent was removed in vacuo to give an oily residue, which was further dissolved in Et_2O (10 mL). Colorless crystals of **20** (413 mg, 57% yield) were filtered off and washed with Et_2O. The optical purity was determined to be >98% *ee* by HPLC.

HPLC: Chiralpak AD-H, hexane/ethanol 99:1, 1.0 mL min^{-1}, t_1 = 6.67 min, t_2 = 8.31 min. M.p. = 200–201°C; $[\alpha]_D^{25} = +202.5°$ (c = 0.1, toluene); ^{1}H NMR (400 MHz, $CDCl_3$, 25°C): δ = 2.11–1.86 (m, 4H, CH_2), 2.51–2.44 (m, 1H; CH_2), 2.81–2.73 (m, 1H; CH_2), 3.18 (m, 2H, CH_2), 4.11 (s, 3H, OCH_3), 7.69–7.55 (m, 7H, ArH), 7.78 (s, 1H, PyH), 8.12–8.08 (m, 1H, ArH), 8.17 (d, 1H, J = 9.1 Hz, ArH), 8.28–8.26 ppm (m, 2H, ArH); ^{13}C NMR (100 MHz, $CDCl_3$, 25°C): δ = 156.29, 154.57, 154.42, 147.38, 140.59, 133.78, 132.46, 130.16, 129.81, 128.99, 128.65, 128.44, 127.57, 127.02, 125.23, 124.3, 124.04, 120.69, 114.31, 57.2, 30.21, 25.97, 23.46, 22.92 ppm; MS (70 eV): m/z (%): 365 (72) [M^+], 364 (100), 346 (40), 334 (27), 321 (18), 306 (6).

Received: March 2, 2004 [Z54164]
Published Online: May 26, 2004

Keywords: asymmetric catalysis · atropoisomerism · cobalt · cyclotrimerization · nitrogen heterocycles

[1] a) K. P. C. Vollhardt, *Angew. Chem.* **1984**, *96*, 525–628; *Angew. Chem. Int. Ed. Engl.* **1984**, *23*, 539–556; b) H. Bönnemann, *Angew. Chem.* **1985**, *97*, 264–279; *Angew. Chem. Int. Ed. Engl.* **1985**, *24*, 248; c) N. E. Schore, *Chem. Rev.* **1988**, *88*, 1081–1119; d) N. E. Schore in *Comprehensive Organic Synthesis, Vol. 5* (Eds.: B. M. Trost, I. Fleming), Pergamon, Oxford, **1991**, pp. 1129–1162; e) D. B. Grotjahn in *Comprehensive Organometallic Chemistry II, Vol. 12* (Ed.: L. S. Hegedus), Pergamon, Oxford, **1995**, pp. 741–770; f) M. Lautens, W. Klute, W. Tam, *Chem. Rev.* **1996**, *96*, 49–92; g) S. Saito, Y. Yamamoto, *Chem. Rev.* **2000**, *100*, 2901–2915; h) J. A. Varela, C. Saá, *Chem. Rev.* **2003**, *103*, 3787–3801.

[2] Y. Sato, T. Nishimata, M. Mori, *J. Org. Chem.* **1994**, *59*, 6133–6135.

[3] a) I. G. Stará, I. Starý, A. Kollárovič, F. Teplý, Š. Vyskočil, D. Šaman, *Tetrahedron Lett.* **1999**, *40*, 1993–1996; b) F. Teplý, I. G. Stará, I. Starý, A. Kollárovič, D. Šaman, Š. Vyskočil, P. Fiedler, *J. Org. Chem.* **2003**, *68*, 5193–5197.

[4] a) B. Heller, G. Oehme, *J. Chem. Soc. Chem. Commun.* **1995**, 179–180; b) B. Heller, D. Heller, G. Oehme, *J. Mol. Catal. A* **1996**, *110*, 211–219; c) B. Heller, B. Sundermann, H. Buschmann, H.-J. Drexler, J. You, U. Holzgrabe, E. Heller, G. Oehme, *J. Org. Chem.* **2002**, *67*, 4414–4422; d) B. Heller, B. Sundermann, C. Fischer, J. You, W. Chen, H.-J. Drexler, P. Knochel, W. Bonrath, A. Gutnov, *J. Org. Chem.* **2003**, *68*, 9221–9225.

[5] a) N. W. Alcock, J. M. Brown, D. I. Hulmes, *Tetrahedron: Asymmetry* **1993**, *4*, 743–756; b) R. W. Baker, S. O. Rea, M. V. Sargent, E. M. C. Schenkelaars, B. W. Skelton, A. H. White, *Tetrahedron: Asymmetry* **1994**, *5*, 45–48; c) X. C. Wang, H. N. C. Wong, *Tetrahedron* **1995**, *51*, 6941–6960; d) G. Chelucci, M. A. Cabras, A. Saba, A. Sechi, *Tetrahedron: Asymmetry* **1996**, *7*, 1027–1032; e) H. Zhang, F. Xue, T. C. W. Mak, K. C. Chan, *J. Org. Chem.* **1996**, *61*, 8002–8003; f) G. Chelucci, A. Bacchi, D. Fabbri, A. Saba, F. Ulgheri, *Tetrahedron Lett.* **1999**, *40*, 553–556; g) H. Brunner, G. Olschewski, B. Nuber, *Synthesis* **1999**, *3*, 429–434; h) H. L. Wong, Y. Tian, K. S. Chan, *Tetrahedron Lett.* **2000**, *41*, 7723–7726; i) S. C. Tucker, J. M. Brown, J. Oakes, D. Thornthwaite, *Tetrahedron* **2001**, *57*, 2545–2554; j) T. Shimada, A. Kina, S. Ikeda, T. Hayashi, *Org. Lett.* **2002**, *4*, 2799–2801; k) A. V. Malkov, L. Dufková, L. Farrugia, P. Kočovský, *Angew. Chem.* **2003**, *115*, 3802–3805; *Angew. Chem. Int. Ed.* **2003**, *42*, 3674–3677.

[6] a) A. Gutnov, B. Heller, H.-J. Drexler, A. Spannenberg, G. Oehme, *Organometallics* **2003**, *22*, 1550–1553; b) A. Gutnov, H.-J. Drexler, A. Spannenberg, G. Oehme, B. Heller, *Organometallics* **2004**, *23*, 1002–1009.

[7] X-ray data and experimental procedures are given in Supporting Information. CCDC-232659 (**20**) contains the supplementary crystallographic data for this paper. These data can be obtained free of charge via www.ccdc.cam.ac.uk/conts/retrieving.html (or from the Cambridge Crystallographic Data Centre, 12, Union Road, Cambridge CB2 1EZ, UK; fax: (+44) 1223-336-033; or deposit@ccdc.cam.ac.uk).

 © 2004 Wiley-VCH Verlag GmbH & Co. KGaA, Weinheim

Biosensors

Highly Sensitive Protease Assay Using Fluorescence Quenching of Peptide Probes Based on Photoinduced Electron Transfer**

*Nicole Marmé, Jens-Peter Knemeyer, Jürgen Wolfrum, and Markus Sauer**

The interest in fast and sensitive assays for proteases, that is, enzymes that specifically cleave peptide bonds, has increased considerably in the last few years. Two medically important facts in particular have accelerated the development of proteolytic assays. One is that proteases are implicated in more and more diseases. Because of their involvement in tumor progression and metastasis, for example, matrix metalloproteinases, urokinase plasminogen activator (uPA), and cathepsins such as cathepsin B and cathepsin D, proteases play a central role in cancer diagnosis and follow-up of malignant diseases.[1–6] In addition, viral infections such as HIV could be detected directly by detection and monitoring of their own specific proteases. This underscores the need for new highly sensitive and fast assays for the specific detection of proteolytic enzymes.[7–11]

To date, several different fluorescence-based assays have been developed to prove the presence of a specific protease in a sample using labeled enzyme substrates. Typically, enzyme substrates, for example, a specific peptide sequence, are doubly labeled with a donor and an acceptor fluorophore in a way that ensures efficient fluorescence resonance energy transfer (FRET).[12,13] Upon cleavage of the peptide substrate by a protease the interaction between the donor and acceptor fluorophore is lost. This enables the direct monitoring of protease activity by measuring the increase in donor fluorescence intensity. Alternatively, a peptide substrate might be doubly labeled with the same fluorophore. In aqueous solution hydrophobic interactions of the fluorophores might force the peptide into a conformation in which the fluorophores can form non- or only weakly fluorescent dimers.[14–17] Nevertheless, chemical modifications of peptide substrates reduce the affinity of the resulting probe to the target molecule and hence the detection sensitivity of the assay. Thus, a minimum of chemical modification is favorable for the design of high-affinity molecular probes for proteases. In addition, doubly labeled peptide probes require site-specific labeling with two extrinsic fluorophores, and synthesis of such compounds is still relatively complicated and expensive. Furthermore, incomplete labeling of peptide probes with only one extrinsic fluorophore, which is not quenched, complicates highly sensitive assays because of the stronger background signal. A method that takes advantage of properties of naturally occurring amino acids instead of a second extrinsic fluorophore would be more useful.

Here we describe a novel fluorescence assay for the ultrasensitive and specific detection of proteolytic enzymes in homogeneous solution using singly labeled peptide probes, the fluorescence of which is quenched by the substrate itself. The basic idea of the experiment is that the fluorescence of suitable fluorophores is efficiently quenched by the amino acid tryptophan by means of photoinduced electron transfer (Figure 1).[18–23] All other amino acids are much less efficient at fluorescence quenching.[18–21]

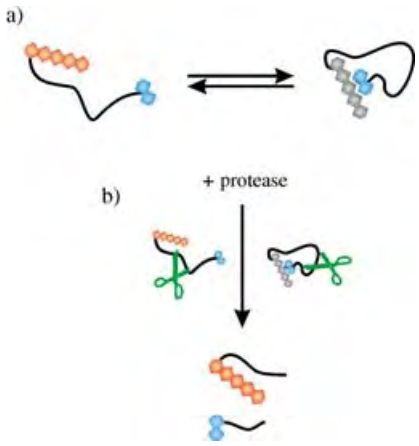


Figure 1. General principle behind using selective fluorescence quenching of fluorophores by tryptophan residues to monitor the presence of specific proteases. a) The fluorophore (gray/red) is coupled to one end of the peptide in close proximity to a tryptophan residue (blue) located, for example, at the other end of the peptide. The flexibility of the peptide backbone will lead to conformations in which the fluorophore and the tryptophan residue come into contact. This contact formation results in efficient fluorescence quenching by photoinduced electron transfer. b) In the presence of a protease that specifically recognizes the peptide sequence located between the fluorophore and tryptophan residue, contact formation and subsequent fluorescence quenching is prevented due to specific cleavage. Thus, the fluorescence intensity of the fluorophore increases.

In the first step a suitable fluorescent dye and a tryptophan residue are incorporated into a peptide. Equilibrium fluctuations of the backbone lead to conformations in which the fluorophore and the tryptophan residue come into contact. After excitation of the fluorophore, it either emits a fluorescence photon (dependent on the fluorescence quantum yield) or the fluorescence is quenched due to an electron transfer reaction with the tryptophan residue. Therefore, the fluorescence quantum yield of the peptide conjugate is reduced depending on the conformational flexibility and the

[*] Prof. Dr. M. Sauer
Fakultät für Physik
Angewandte Laserphysik und Laserspektroskopie
Universität Bielefeld
Universitätsstrasse 25, 33615 Bielefeld (Germany)
Fax: (+49) 521-106-2958
E-mail: sauer@physik.uni-bielefeld.de
Dr. N. Marmé, Dr. J.-P. Knemeyer, Prof. Dr. J. Wolfrum
Physikalisch-Chemisches Institut
Universität Heidelberg
Im Neuenheimer Feld 253, 69120 Heidelberg (Germany)

[**] The authors thank K. H. Drexhage for the oxazine derivative MR121. Financial support by the Bundesministerium für Bildung, Wissenschaft, Forschung und Technologie is gratefully acknowledged.

 © 2004 Wiley-VCH Verlag GmbH & Co. KGaA, Weinheim DOI: 10.1002/anie.200453835

number of amino acids separating the fluorophore and the tryptophan residue.

Recently,[20] selective fluorescence quenching of a red-absorbing oxazine derivative by tryptophan residues was used to measure association (contact formation) and dissociation rates in the range of a few hundred nanoseconds in flexible peptides at the single-molecule level. The rates determined are consistent with previously published data on the dynamics of unstructured peptides obtained with a different ensemble methodology.[24] The advantage of this fluorescence-quenching-based technique over the previously discussed comprises the ease of experimental monitoring in water under air with single-molecule sensitivity. If, however, contact formation between the fluorophore and tryptophan residue is prevented because of specific binding of the peptide to a target protein, for example, binding to an antibody in the case of a peptide epitope, or cleavage of the peptide by a protease enzyme (Figure 1), the fluorescence intensity of the fluorophore increases. This can be used advantageously, for example, to monitor the presence of p53 autoantibodies in sera of cancer patients. Two flexible fluorescently labeled peptide epitopes of the amino terminal transactivation domain of human p53 both carrying a single tryptophan residue can be used, and the presence of p53 autoantibodies can be detected by an increase in fluorescence intensity.[19]

To demonstrate the potential of the method for the development of a fast and highly sensitive protease assay, we monitored the increase in fluorescence intensity of a simple dipeptide, lysine–tryptophan, with different fluorescence labels after addition of carboxypeptidase A (CPA) (Figure 2).[25,26] All peptide conjugates investigated so far were substrates for CPA. In agreement with the constants for intermolecular quenching,[21] the oxazine-labeled conjugates MR121-Lys-Trp and ATTO655-Lys-Trp show the most pronounced increase in fluorescence intensity (Figure 2a). The fluorescence intensity of a 10^{-7} M peptide solution increases roughly tenfold upon addition of 10^{-9} M CPA within four minutes. The Bodipy-FL conjugate shows a sixfold increase (Figure 2b), whereas the fluorescence intensity of the Cy5 conjugate increases only slightly. This is consistent with previous studies which demonstrated that the fluorescence of Cy5 is only slightly quenched by tryptophan residues.[21] In addition, the digestion rate differs significantly and is highest for the two conjugates MR121-Lys-Trp and ATTO655-Lys-Trp (Figure 2a).

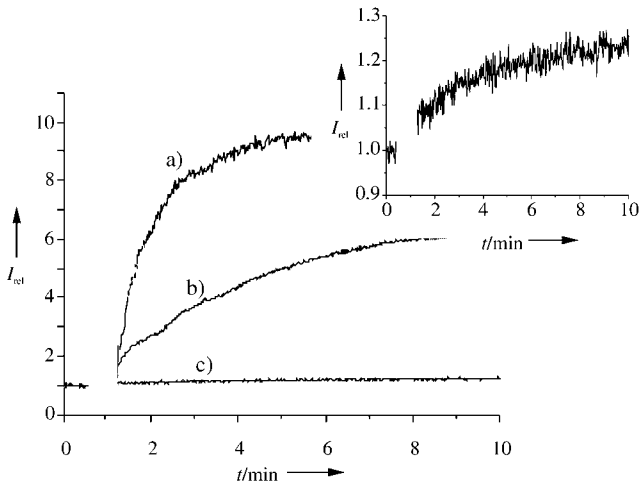


Figure 2. Relative fluorescence intensities (I_{rel}) of solutions of differently labeled dipeptides Lys-Trp (10^{-7} M) versus time (t) in phosphate-buffered saline (PBS, pH 7.4, 25 °C) after addition of 10^{-9} M carboxypeptidase A (CPA). a) MR121-Lys-Trp (almost identical results were obtained with ATTO655-Lys-Trp), b) Bodipy-FL-Lys-Trp, and c) Cy5-Lys-Trp. The inset shows an expanded view of the curve recorded for Cy5-Lys-Trp. Excitation was performed at the absorption maximum of each fluorophore (λ_{ex} = 667, 650, and 490 nm, respectively). Fluorescence intensities were recorded at the emission maximum of each fluorophore (λ_{em} = 690, 670, and 515 nm, respectively). Control experiments without CPA show a stable fluorescence signal for several hours.

The influence of the fluorophore structure on enzyme activity is unknown and difficult to estimate, but a direct interaction between the fluorophore and enzyme could indeed strongly influence enzyme activity. Our results prove that the contact-induced interactions between MR121 or ATTO655 and tryptophan enable the fast and reliable detection of nanomolar concentrations of CPA in aqueous solutions. Therefore, we chose MR121 as the reporter fluorophore in the following experiments.

When MR121 is coupled directly to tryptophan, the relative fluorescence quantum yield is 0.02.[21] For the dipeptide MR121-Lys-Trp, the fluorescence quantum yield increases to 0.10. Therefore, it is expected that the quenching efficiency will decrease with increasing distance between the fluorophore and the tryptophan residue in longer peptides due to less frequent contact formation. However, when nine amino acids separate MR121 and a tryptophan residue, relative quantum yields of $\approx$0.30 have been measured.[19,20]

At the same time, the peptide length and structure can influence enzyme activity. Figure 3 shows the time-dependent fluorescence intensity of three MR121 peptide conjugates with an increasing number of glycine residues separating the fluorophore and tryptophan residue after addition of 10^{-7} M CPA. Although the relative fluorescence quantum yields of

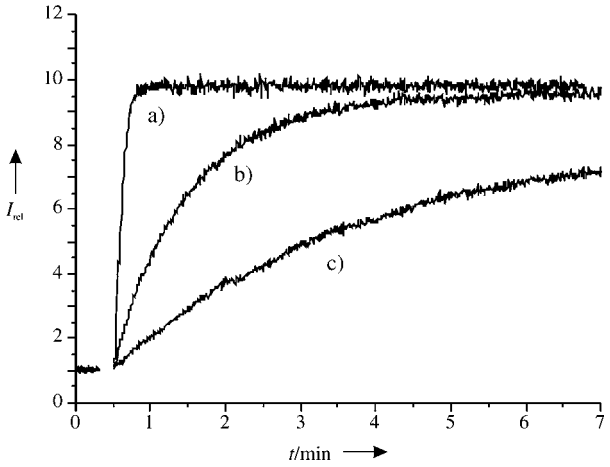


Figure 3. Relative fluorescence intensities (I_{rel}) versus time (t) (λ_{ex} = 640 nm, λ_{em} = 690 nm) of different MR121-labeled peptides (10^{-7} M in PBS, pH 7.4 at 25 °C) after addition of 10^{-7} M CPA. a) MR121-Lys-Gly-Trp, b) MR121-Lys-Gly_2-Trp, c) MR121-Lys-Gly_3-Trp.

 © 2004 Wiley-VCH Verlag GmbH & Co. KGaA, Weinheim

the three labeled peptides are similar due to the high flexibility of the glycine residues, the enzyme activity (digestion rate) differs significantly. With an increasing number of glycine residues the digestion rate of CPA decreases (Figure 3).

To evaluate the sensitivity of this assay, we measured the fluorescence intensity of an aqueous solution of MR121-Lys-Trp in the presence of different concentrations of CPA (Figure 4). The measurements were performed in pure water

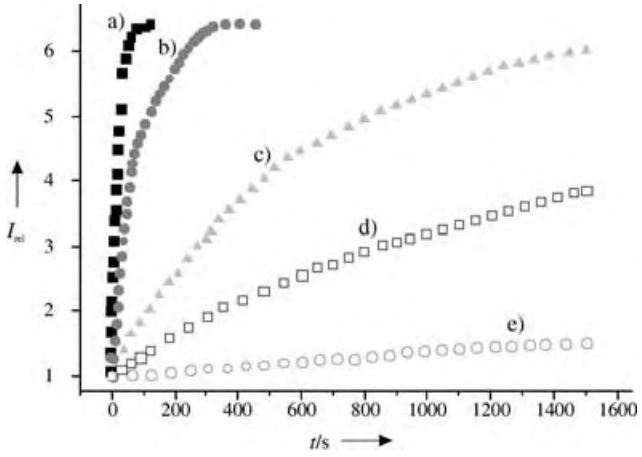


Figure 4. Relative fluorescence intensities (I_{rel}) measured for the peptide MR121-Lys-Trp (10^{-7} M) versus time (t) after addition of various amounts of CPA: a) 10^{-6} M, b) 10^{-9} M, c) 10^{-11} M, d) 10^{-13} M, and e) 10^{-15} M. Measurements were performed in pure water at 25 °C ($\lambda_{ex} = 640$ nm, $\lambda_{em} = 690$ nm). Data points were measured every 5–20 s depending on the sample.

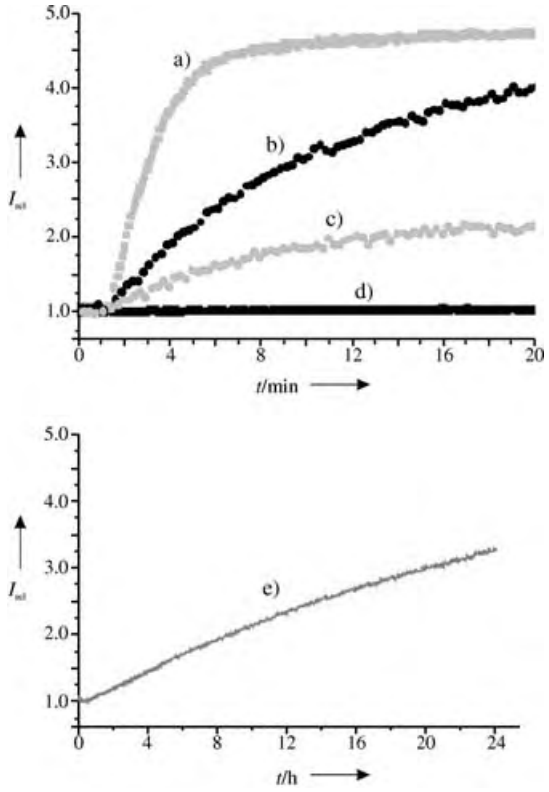


Figure 5. Relative fluorescence intensities (I_{rel}) of the peptide MR121-Lys-Arg_3-Trp (10^{-7} M) versus time (t) after addition of various amounts of trypsin: a) 10^{-9} M, b) 10^{-10} M, c) 10^{-11} M, and d) 10^{-12} M. e) Fluorescence increase upon addition of 10^{-12} M trypsin monitored on a longer time scale. Measurements were performed in 50 mM Tris-HCl buffer (pH 7.0) with 1 mM calcium chloride, at 25 °C ($\lambda_{ex} = 640$ nm, $\lambda_{em} = 690$ nm).

to reduce the salt-induced nonspecific adsorption of CPA molecules on the glass walls of the cuvette. In pure water, a maximum increase in fluorescence intensity of about 6.5-fold was achieved after addition of an excess of CPA. At a concentration of 10^{-6} M CPA (tenfold excess) the maximum increase is reached within seconds (Figure 4a). Even a CPA concentration of 10^{-13} M, which correlates to one enzyme molecule per 10^6 substrate molecules, effects a 2.5-fold increase in fluorescence intensity in only ten minutes (Figure 4d). For a further increase of detection sensitivity longer measurement times have presently to be accepted. However, our data demonstrate that even a CPA concentration of 10^{-15} M can be detected by a 1.5-fold increase in fluorescence intensity in approximately 25 minutes (Figure 4e).

To demonstrate the general applicability of the new assay we designed a peptide substrate for an endopeptidase. Trypsin was chosen as the model protease because it is readily available and often used as a standard in other protease assays. Trypsin cleaves peptide bonds on the carboxyl side of lysine and arginine residues.[27] We used MR121-Lys-Arg_3-Trp as the peptide substrate, which has a relative fluorescence quantum yield of 0.20 in 50 mM Tris-HCl buffer (pH 7.0) containing 1 mM calcium chloride. As Figure 5 demonstrates, trypsin concentrations down to 10^{-11} M can be detected easily within minutes owing to the increase in fluorescence intensity. For lower concentrations, the fluorescence signal has to be monitored for several hours (Figure 5e).

This approach for assaying proteolytic enzymes using fluorescent-labeled peptide probes, in which fluorescence is quenched by photoinduced electron transfer between fluorophores and tryptophan residues upon contact formation offers several advantages. First, the synthesis of large quantities of singly labelled peptide probes is uncomplicated and inexpensive compared to the use of doubly labeled peptide probes. Second, modification of the peptide substrate is reduced to the minimum, that is, a single reporter fluorophore, which potentially enables more accurate monitoring of enzyme activity. By monitoring the time-dependent fluorescence intensity, the presented technique permits real-time analysis of proteolysis. Third, our new protease assay enables fast, specific, and highly sensitive detection of proteolytic enzymes with a broad dynamic range (more than six orders of magnitude) and detection limits below the picomolar range. Our results raise our hopes that singly labeled peptide probes can be used advantageously for the development of new fast and highly sensitive fluorescence

 © 2004 Wiley-VCH Verlag GmbH & Co. KGaA, Weinheim

assays for cancer diagnosis and follow-up of malignant diseases through the detection of specific proteases.

Experimental Section

N-terminal labeling of the peptides with the fluorescent dye was performed by classical *N*-hydroxysuccinimidyl ester (NHS ester) chemistry using standard solvents purchased from Merck (Darmstadt, Germany). The oxazine derivative MR121 was kindly provided by the group of Prof. K. H. Drexhage (Universität-Gesamthochschule, Siegen). ATTO655 (ATTO-TEC, Siegen, Germany), Bodipy-FL (Molecular Probes, Göttingen, Germany) and Cy5 (Amersham Pharmacia Biotec, Freiburg, Germany) were purchased as NHS esters. Fluorophores (1 μmol mL^{-1}) and the synthetic peptides (1 μmol mL^{-1}) were dissolved in dimethylformamide (DMF). A 10-μL (10 nmol) portion of the dye solution was added to 100 μL (100 nmol, tenfold excess) of peptide and 2 μL diisopropylethylamine (DIPEA). The solution was incubated for 3 h at room temperature in the dark. The N-terminal conjugate was purified by reversed-phase (Hypersil-ODS column) HPLC (Agilent Technologies, Waldbronn, Germany) using a linear gradient of 0–75% acetonitrile in 0.1M aqueous triethylammonium acetate. Molecular weights were determined by mass spectrometry. The labeled peptides are stable for several months when stored at −20°C.

Absorption measurements were recorded with a Cary 500 UV/Vis-NIR spectrometer (Varian, Darmstadt, Germany) at room temperature. Steady-state emission spectra were measured with a Cary Eclipse fluorescence spectrometer. All measurements were conducted in PEG-coated standard quartz cuvettes. In all measurements the concentration was kept strictly below 1 μM to avoid reabsorption and reemission effects. Relative fluorescence quantum yields were measured with respect to the fluorescence intensity of the free dye.

Carboxypeptidase A (CPA) is a zinc-containing exopeptidase secreted by the pancreas. It acts preferentially, but not exclusively, on peptide bonds adjacent to the C-terminus of amino acid residues with aromatic or branched side chains at pH 7–8. Peptide bonds involving glycine, aspartic acid, and glutamic acid are hydrolyzed slowly, while those involving arginine, proline, and hydroxyproline are not hydrolyzed.[25,26]

Trypsin is a digestive enzyme, which has a serine residue in the active center. This endopeptidase hydrolyzes peptide bonds in which the carbonyl group is connected to the basic amino acids lysine or arginine. The optimum pH is in the range of 7–9.[27] As storage buffer 0.046M Tris-HCl buffer, pH 8.0 with 0.0115M calcium chloride was used. For digestion experiments, 1 μL of the respective enzyme was mixed with 600 μL of a 10^{-7}M solution of the peptide substrates in PBS buffer (phosphate-buffered saline, pH 7.4).

Received: January 23, 2004 [Z53835]

Keywords: analytical methods · electron transfer · enzymes · fluorescence spectroscopy · proteases

[1] O. Simonetti, G. Lucarini, D. Brancorsini, P. Nita, M. L. Bernardini, G. Biagini, A. Offidani, *Cancer* **2002**, *95*, 1963–1970.
[2] A. Franchi, M. Santucci, E. Masini, I. Sardi, M. Paglierani, O. Gallo, *Cancer* **2002**, *95*, 1902–1910.
[3] A. Kugler, *Anticancer Res.* **1999**, *19*, 1589–1592.
[4] Y. Mochizuki, S. Tsuda, H. Kanetake, S. Kanda, *Oncogene* **2002**, *21*, 7027–7033.
[5] N. Harbeck, R. E. Kates, M. P. Look, M. E. Meijer-Van Gelder, J. G. Klijn, A. Kruger, M. Kiechle, F. Janicke, M. Schmitt, J. A. Foekens, *Cancer* **2002**, *15*, 4617–4622.
[6] K. Bajou, J. M. Lewalle, C. R. Martinez, C. Soria, H. Lu, A. Noel, J. M. Foidart, *Int. J. Cancer* **2002**, *100*, 501–506.
[7] C. Jumper, E. Cobos, C. Lox, *Anticancer Res.* **2002**, *22*, 2073–2076.
[8] O. D. Liang, T. Chavakis, S. M. Kanse, K. T. Preissner, *J. Biol. Chem.* **2001**, *276*, 28946–28953.
[9] M. R. Gyetko, S. Sud, G. H. Chen, J. A. Fuller, S. W. Chensue, G. B. Toews, *J. Immunol.* **2002**, *168*, 801–809.
[10] J. E. Koblinski, M. Ahram, B. F. Sloane, *Clin. Chim. Acta* **2000**, *291*, 113–135.
[11] G. Berchem, M. Glondu, M. Gleizes, J. P. Brouillet, F. Vignon, M. Garcia, E. Liaudet-Coopman, *Oncogene* **2002**, *21*, 5951–5955.
[12] E. D. Matayoshi, G. T. Wang, G. A. Krafft, J. Erickson, *Science* **1990**, *247*, 954–958.
[13] M. Cavrois, C. de Noronah, W. C. Greene, *Nat. Biotechnol.* **2002**, *20*, 1151–1154.
[14] M. J. Blackman, J. E. Corrie, J. C. Croney, G. Kelly, J. F. Eccleston, D. M. Jameson, *Biochemistry* **2002**, *41*, 12244–12252.
[15] B. Z. Packard, A. Komoriya, V. Nanda, L. Brand, *J. Phys. Chem.* **1998**, *102*, 1820–1827.
[16] B. Z. Packard, D. D. Toptygin, A. Komoriya, L. Brand, *Proc. Natl. Acad. Sci. USA* **1996**, *93*, 11640–11645.
[17] B. Z. Packard, D. D. Toptygin, A. Komoriya, L. Brand, *Methods Enzymol.* **1997**, *278*, 15–23.
[18] R. M. Watt, E. W. Voss, *Immunochemistry* **1977**, *14*, 533–541.
[19] H. Neuweiler, A. Schulz, A. C. Vaiana, J. C. Smith, S. Kaul, J. Wolfrum, M. Sauer, *Angew. Chem.* **2002**, *114*, 4964–4068; *Angew. Chem. Int. Ed.* **2002**, *41*, 4769–4773.
[20] H. Neuweiler, A. Schulz, M. Böhmer, J. Enderlein, M. Sauer, *J. Am. Chem. Soc.* **2003**, *125*, 5324–5330.
[21] N. Marmé, J. P. Knemeyer, M. Sauer, J. Wolfrum, *Bioconjugate Chem.* **2003**, *14*, 1133–1139.
[22] M. Sauer, *Angew. Chem.* **2003**, *115*, 1834–1837; *Angew. Chem. Int. Ed.* **2003**, *42*, 1790–1793.
[23] A. Vaiana, H. Neuweiler, A. Schulz, J. Wolfrum, M. Sauer, J. C. Smith, *J. Am. Chem. Soc.* **2003**, *125*, 14564–14572.
[24] L. J. Lapidus, W. A. Eaton, J. Hofrichter, *Proc. Natl. Acad. Sci. USA* **2000**, *97*, 7220–7225.
[25] W. Lipscomb, *Proc. Natl. Acad. Sci. USA* **1973**, *70*, 3797–3801.
[26] R. H. Bradshaw, L. H. Ericsson, K. A. Walsh, H. Neurath, *Proc. Natl. Acad. Sci. USA* **1969**, *63*, 1389–1394.
[27] W. Brown, F. Wold, *Biochemistry* **1973**, *12*, 835–840.

 © 2004 Wiley-VCH Verlag GmbH & Co. KGaA, Weinheim

Conducting Materials

Fabrication of Polymer Nanofibers and Carbon Nanofibers by Using a Salt-Assisted Microemulsion Polymerization**

Jyongsik Jang and Joonwon Bae*

Among various types of nanomaterials, nanofibers have attracted much attention because of their intriguing chemical and physical properties.[1] The most widely used method for nanofiber preparation is template synthesis. This method involves the introduction of organic, inorganic, and metallic materials within channels of templates, such as silica,[2] anodic aluminum oxide,[3] zeolites,[4] and track-etched polycarbonates.[5] To date, microemulsion polymerization has been considered to be a facile process to produce polymer nanomaterials as reviewed by Antonietti and co-workers.[6] While nanoparticles,[7] hollow nanospheres,[8] and nanotubes[9] of several polymers were fabricated by using microemulsion polymerization, the synthesis of polymer nanofibers has not yet been performed. Herein, we report that novel polyacrylonitrile (PAN) nanofibers and carbon nanofibers with a high aspect ratio were fabricated by using a salt-assisted microemulsion polymerization. In this work, iron(III) chloride ($FeCl_3$) was employed as a structure-directing agent, it forms a coordination-complex with PAN nanoparticles during polymer nanofiber formation, and it acts as a catalyst for the conversion of the polymer into the carbon nanofibers. Salt-assisted sphere-to-cylinder micelle transformation is the crucial step for nanofiber formation. To the best of our knowledge, this is the first experimental evidence for the fabrication of carbon nanofibers derived from polymer nanofibers by using a salt-assisted microemulsion polymerization.

The overall fabrication procedure is presented in Figure 1. In a typical procedure, a variable amount of dodecyltrimethylammonium bromide (DoTAB) was magnetically stirred in 40 mL of distilled water at room temperature. Monomeric acrylonitrile (AN) was added dropwise to the micelle solution and monomers inside micelles were polymerized by using redox initiators, cerium sulfate and nitrilotriacetic acid (NTA). After 30 min of polymerization, iron(III) chloride was introduced and the polymerization proceeded for an additional 4 h with magnetic stirring. The product was precipitated in methanol to remove surfactants and initiators.

When surfactants are dissolved in water, spherical micelles form between CMC (CMC = critical micelle concentration, 0.016 m for DoTAB) and the concentration of transformation of sphere to cylinder (0.32 m for DoTAB).[10] After 30 min of polymerization, the size of PAN nanoparticles were approximately 20 nm (Figure 2 a). It was reported that

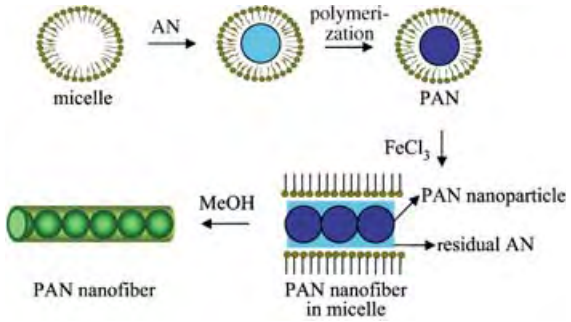


Figure 1. The overall fabrication scheme for PAN nanofibers by using a salt-assisted microemulsion polymerization.

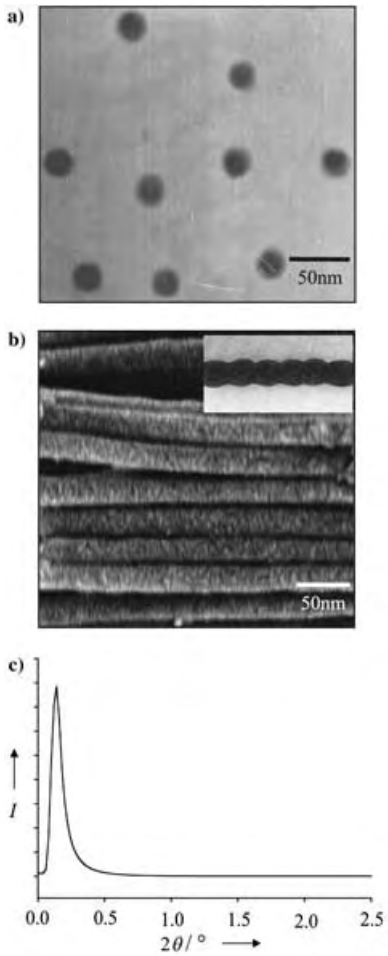


Figure 2. a) TEM image of fabricated PAN nanoparticles. A surfactant, DoTAB was used for micelle formation and acrylonitrile monomer (1 g, 0.02 mol) was polymerized with initiators, cerium sulfate, and nitrilotriacetic acid; b) SEM image of fabricated PAN nanofibers. PAN nanofibers were obtained by addition of iron(III) chloride (1.0 g, 6.2 mmol) in the middle of polymerization reaction. The inset shows the TEM image of the noded nanofiber structure; c) SAXS pattern of the PAN nanofiber.

[*] Prof. Dr. J. Jang, J. Bae
Hyperstructured Organic Materials Research Center and
School of Chemical Engineering
Seoul National University
Shinlimdong 56-1, Seoul 151-742 (Korea)
Fax: (+82) 2-888-7295
E-mail: jsjang@plaza.snu.ac.kr

[**] This work was supported by the Brain-Korea 21 Program of the Korea Ministry of Education, by the Korea Science and Engineering Foundation, and by the Hyperstructured Organic Materials Research Center in Seoul National University.

 DOI: 10.1002/anie.200353580 © 2004 Wiley-VCH Verlag GmbH & Co. KGaA, Weinheim

the concentration required for the transformation of sphere to cylinder drops significantly with the addition of salt into microemulsion systems.[11] Spherical micelles that contain presynthesized PAN nanoparticles transform into cylindrical micelles after the addition of iron(III) chloride. This salt-assisted sphere-to-cylinder micelle conversion is the crucial step for PAN nanowire formation. Consequently, the self-assembled PAN nanoparticles generated the nodated nanofiber structure (inset in Figure 2b) and the additional polymerization of the residual monomer inside the cylindrical micelles produced the smooth surface of PAN nanofiber (Figure 2b). The average diameter of a PAN nanofiber was about 25 nm and reasonably monodisperse. According to energy dispersive X-ray spectroscopy (EDX) analysis, the PAN nanofiber consisted of carbon (65.2%), nitrogen (19.5%) and iron (3.6%). The atomic ratio of carbon/nitrogen (approximately 3.3) was in good agreement with the theoretical atomic composition of PAN. The presence of Fe atoms demonstrates that iron(III) chloride was embedded in the PAN nanofiber. Control experiments were also performed without $FeCl_3$, consequently, PAN nanoparticles were exclusively synthesized. No polymer nanofibers were formed when the added amount of $FeCl_3$ was below 0.3 g, 1.8 mmol. This means that the cylindrical transformation from spherical micelles does not occur without the presence of salt such as iron(III) chloride under these experimental conditions. In addition, coordination between cyano group in the PAN nanoparticles and iron(III) chloride seems to be a prerequisite for PAN nanofiber formation. FTIR spectra showed that the vibrational band for C≡N stretching that is normally observed at 2244 cm^{-1} for PAN nanoparticles shifted down to 2236 cm^{-1} in the case of PAN nanofiber. This shift is because the vibrational motion of the CN group is restricted by its coordination with embedded iron. EDX and FTIR provide evidence to support the presence of coordination between iron and cyano group in PAN. To verify the coordination complex formation between iron and cyano group, additional experiments were also performed by using 3-ethoxy acrylonitrile, methacrylonitrile, methyl methacrylate, and styrene. CN coordination was substantiated by using AN derivatives, which contained the cyano (C≡N) functional group. In the case of 3-ethoxy acrylonitrile, polymer nanofibers with an average diameter of 30 nm were obtained along with poly(methacrylonitrile) nanofibers (approximately 25 nm in diameter). In contrast, polymer nanospheres were selectively fabricated with methyl methacrylate (approximately 20 nm in diameter) and styrene (approximately 25 nm in diameter), which do not have the cyano functional group. From these results, it is evident that coordination between the cyano group and iron(III) chloride is a prerequisite for the formation of polymer nanofibers. In Figure 2c), the structure of PAN nanofiber was investigated by small angle X-ray scattering (SAXS). A characteristic peak in the SAXS pattern indicated that PAN nanofibers had long-range order. The calculated lattice parameter for PAN nanofibers was approximately 21.5 nm, which was consistent with the average size of PAN nanoparticles. This result revealed that PAN nanoparticles act as lattice crystals for polymer nanofiber formation.[12]

To obtain carbon nanofiber (CNF), the PAN nanofibers were heated up to 900 °C. The diameter of the carbonized PAN nanofiber was approximately 20 nm, which is smaller than PAN nanofiber; the reduction in size is due to mass transfer during carbonization (Figure 3a).[7] Raman spectrum of CNF is displayed in Figure 3b. The band at 1580 cm^{-1}, assigned to the E_{2g} vibration of the infinite crystal, is associated with graphitic carbon atoms with sp^2 electronic configuration. Polycrystalline graphite has a distinct peak in its Raman spectrum at 1360 cm^{-1} arising from the A_{1g} mode, which is attributed to diamondlike carbon atoms with sp^3 configuration.[13] The integrated intensity ratio of A_{sp^2}/A_{sp^3} for carbonized PAN nanofibers is 0.80, which indicates a higher degree of graphitization compared with pristine PAN carbon (approximately 0.30). It was reported that the presence of transition metal atoms boost the formation of graphite during the carbonization process.[14] The powder XRD pattern of CNF also confirmed the presence of characteristic 002 and 110

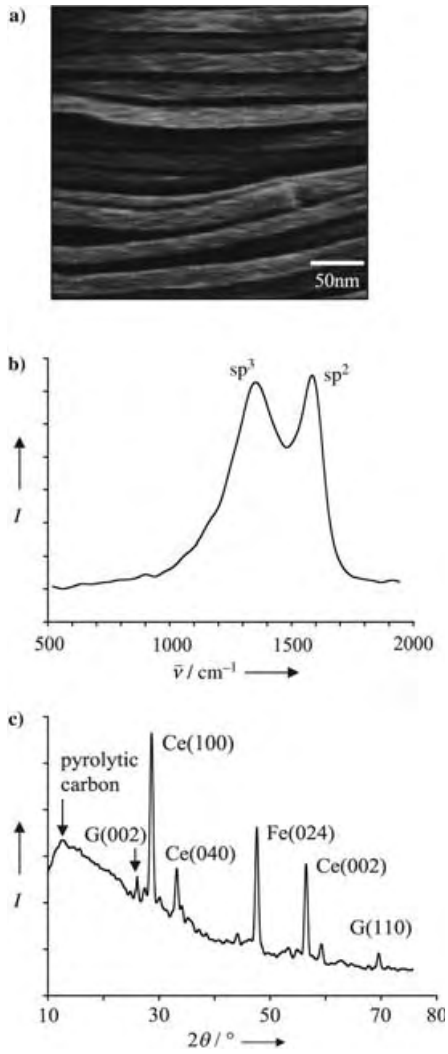


Figure 3. a) SEM image of carbon nanofibers obtained by heating the PAN nanofibers at a heating ratio of 1 °C min^{-1} to 300 °C then continuously 3 °C min^{-1} to 900 °C, and holding it at that temperature for 4 h under an N_2 atmosphere; b) Raman spectrum; and c) X-ray diffraction pattern of the carbon nanofibers.

 © 2004 Wiley-VCH Verlag GmbH & Co. KGaA, Weinheim

Bragg reflections of graphite(Figure 3c). The weight ratios of the Ce and Fe atoms within the carbon nanofiber increased after carbonization process compared with pristine PAN nanofiber due to degradation and loss of PAN during cyclization, dehydrogenation, and decomposition.[15] The residual cerium-based products originated from the presence of initiators. Iron centers embedded in the PAN nanofiber catalyze the carbonization. Therefore, strong peaks associated with Ce and Fe atoms were observed at 28° and 48°, respectively.

Liquid-crystalline epoxy (LCE, diglycidyl ether of 4,4′-dihydroxy α-methyl stilbene[16]) is a typical matrix for display media, adhesives, antistatic coatings, and highly conductive composites. A typical LCE is composed of an aromatic mesogenic unit and a reactive oxirane ring, which takes part in the crosslinking reaction with an amine. The balanced properties between a liquid-crystalline polymer and a cured epoxy indicate that LCE can be used as a matrix for high performance polymer composites. To fabricate the conducting polymer composite, carbonized PAN nanofibers were used as a conducting filler and blended with LCE matrix. Figure 4 displays the electrical conductivity of LCE/CNF

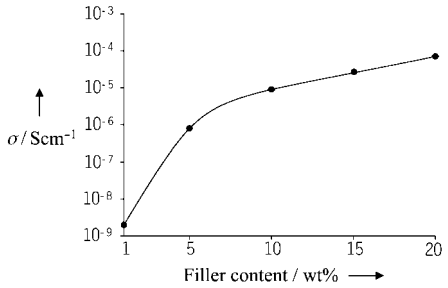


Figure 4. The electrical conductivity of LCE/CNF composite as a function of CNF content. The LCE/CNF sample was cured at 150 °C for 4 h and postcured at 175 °C for 1 h. The electrical conductivity of LCE/CNF sample was measured by a standard four-probe method.

composites as a function of filler content. The electrical conductivity of CNF filled LCE composite was measured by a standard four-probe method.[17] As the amount of CNF increased, the electrical conductivity of CNF/LCE composite increased drastically. The conductivity pattern represented that the CNF/LCE composite shows percolation threshold behavior, which means that more electrical paths are generated with an increasing number of carbonized PAN nanofibers. Besides, LCE/CNF composites have enhanced electrical conductivity (ca. 10^{-4} S cm^{-1}) compared with conventional epoxy composites.[18]

In summary, we have demonstrated a salt-assisted microemulsion polymerization for the novel synthesis of polymer and carbon nanofibers. Salt-assisted sphere-to-cylinder micelle transformation is the crucial step for nanofiber formation. Iron(III) chloride is coordinated by PAN nanoparticles, it acts as a structure-directing agent for the formation of polymer nanofibers, and it is the catalyst for the production of carbon nanofibers. The carbonized PAN nanofibers can be applied as a conducting filler for polymer composites and has enhanced conductivity in liquid-crystalline epoxy medium.

Experimental Section

General procedure: Variable quantities of cationic surfactants (DoTAB, 3–6 g, 0.01–0.02 mol; docyltrimethylammonium bromide (DeTAB), 3–6 g, 0.011–0.022 mol) were dissolved in distilled water (40 mL) and AN monomer (1–2 g, 0.02–0.04 mol) was added dropwise to the surfactant solution and stirred for 2 h. The initiators, cerium(IV) sulfate (0.4 g, 1.2 mmol) and nitrilotriacetic acid (0.1 g, 0.5 mmol), were added for the polymerization of AN. After AN was polymerized for 30 min, iron(III) chloride (0.3–1.5 g, 1.8–9.2 mmol) was added into the polymer solution consecutively and the resulting solution was stirred for additional 4 h at ambient condition. The product was precipitated in methanol to remove surfactants and initiators. The carbonization process was performed by heating the PAN nanofibers at a heating rate of 1 °C min^{-1} to 300 °C then continuously at 3 °C min^{-1} to 900 °C, and holding it at that temperature for 4 h under an N_2 atmosphere. The LCE/CNF composites were cured at 150 °C for 4 h and postcured at 175 °C for 1 h. Sulfanilamide was used as curing agent. The electrical conductivity of LCE/CNF composite was measured by standard four-probe method.[17]

FTIR spectra were recorded on a Bomem MB 100 spectroscope (Quebec, Canada) in the absorption mode. The EDX was carried out on a JEOL JSM 5410 LV. Photographs of SEM were taken with a JEOL 6700. TEM analysis was performed with a JEOL JEM-200CX. Raman spectrum was obtained on a Jobin-Yvon T64000 spectrometer. XRD patterns were recorded on a Rigaku D-max/3C X-ray diffractometer. SAXS pattern was obtained with a Bruker AXS Nanostar small angle X-ray scattering spectrometer with a generator voltage of 40 KV and a current of 35 mA.

Received: December 19, 2003
Revised: May 17, 2004 [Z53580]

Keywords: conducting materials · iron · micelles · nanomaterials · polymerization

[1] a) J. F. Wang, M. S. Gudiksen, X. F. Duan, Y. Cui, C. M. Lieber, *Science* **2001**, *293*, 1455–1457; b) J. D. Holmes, K. P. Johnston, R. C. Doty, B. A. Korgel, *Science* **2000**, *287*, 1471–1473; c) Y. Wu, P. Yang, *J. Am. Chem. Soc.* **2001**, *123*, 3165–3166; d) H. Kind, H. Yan, B. Messer, M. Law, P. D. Yang, *Adv. Mater.* **2002**, *14*, 158–161.

[2] a) C. R. Martin, *Chem. Mater.* **1996**, *8*, 1739–1746; b) J. Jang, B. Lim, J. Lee, T. Hyeon, *Chem. Commun.* **2001**, 83–84; c) Y. J. Han, J. M. Kim, G. D. Stucky, *Chem. Mater.* **2000**, *12*, 2068–2069.

[3] a) D. Xu, D. Chen, G. Guo, L, Gui, Y. Tang, *Adv. Mater.* **2000**, *12*, 520–523; b) S. H. Jeong, O. J. Lee, K. H. Lee, S. H. Oh, C. G. Park, *Chem. Mater.* **2002**, *14*, 4003–4005.

[4] J. Lee, S. Yoon, S. M. Oh, C. H. Shin, T. Hyeon, *Adv. Mater.* **2001**, *13*, 359–362.

[5] a) K. Kim, J. Jin, *Nano. Lett.* **2001**, *1*, 631–636; b) S. J. Choi, S. M. Park, *Adv. Mater.* **2000**, *12*, 1547–1550; c) C. R. Martin, *Acc. Chem. Res.* **1995**, *28*, 61–66.

[6] a) U. Yildiz, K. Landfester, M. Antonietti, *Macromol. Chem. Phys.* **2003**, *204*, 1966–1970; b) C. M. Roland, P. G. Santangelo, M. Antonietti, M. Neese, *Macromolecules* **1999**, *32*, 2283–2287; c) M. Antonietti, R. A. Caruso, C. G. Goltner, M. C. Weissenberger, *Macromolecules* **1999**, *32*, 1383–1389; d) M. Antonietti, H. P. Hentze, *Adv. Mater.* **1996**, *8*, 840–843; e) G. Liu, X. Yan, S. Duncan, *Macromolecules* **2002**, *35*, 9783–9788; f) J. Huang, S. Virji, B. H. Weiller, R. B. Kaner, *J. Am. Chem. Soc.* **2003**, *125*,

 © 2004 Wiley-VCH Verlag GmbH & Co. KGaA, Weinheim

314 – 315; g) K. de Moel, G. O. R. Alberda van Ekenstein, H. Nijland, E. Polushkin, G. Brinke, R. Maeki-Ontto, O. Ikkala, *Chem. Mater.* **2001**, *13*, 4580 – 4583; h) C. S. Yang, D. D. Awschalom, G. D. Stucky, *Chem. Mater.* **2002**, *14*, 1277 – 1284; i) M. Kahlweit, *Angew. Chem.* **1985**, *97*, 655 – 669; *Angew. Chem. Int. Ed. Engl.* **1985**, *24*, 654 – 668; j) B. J. Holliday, C. A. Mirkin, *Angew. Chem.* **2001**, *113*, 2076 – 2097; *Angew. Chem. Int. Ed.* **2001**, *40*, 2022 – 2043.

[7] a) F. M. Pavel, R. A. Mackay, *Langmuir* **2000**, *16*, 8568 – 8574; b) J. Jang, J. H. Oh, G. D. Stucky, *Angew. Chem.* **2002**, *114*, 4188 – 4191; *Angew. Chem. Int. Ed.* **2002**, *41*, 4016 – 4019; c) F. Reynolds, K. Jun, Y. Li, *Macromolecules* **2001**, *34*, 167 – 170; d) S. A. Johnson, P. J. Ollivier, T. E. Mallouk, *Science* **1999**, *283*, 963 – 965.

[8] a) D. Walsh, S. Mann, *Nature* **1995**, *377*, 320 – 323; b) J. Jang, K. Lee, *Chem. Commun.* **2002**, 1098 – 1099; c) F. Caruso, *Adv. Mater.* **2001**, *13*, 11 – 22; d) J. Jang, H. Ha, *Chem. Mater.* **2003**, *15*, 2109 – 2111; e) L. J. Zhang, M. X. Wan, *Adv. Funct. Mater.* **2003**, *13*, 815 – 820.

[9] a) X. Duan, Y. Huang, Y. Cui, J. Wang, C. M. Lieber, *Nature* **2001**, *409*, 66 – 69; b) J. Jang, H. S. Yoon, *Chem. Commun.* **2003**, 720 – 721.

[10] a) S. Zhou, F. Yeh, C. Burger, B. Chu, *J. Phys. Chem. B* **1999**, *103*, 2107 – 2112; b) J. M. DeSimone, *Angew. Chem.* **2001**, *113*, 534 – 544; *Angew. Chem. Int. Ed.* **2001**, *40*, 518 – 527.

[11] a) R. J. Meagher, T. A. Hatton, A. Bose, *Langmuir* **1998**, *14*, 4081 – 4088; b) B. Jonsson, B. Lindman, K. Holmberg, B. Kronberg, *Surfactants and Polymers in Aqueous Solution*, Wiley, NY, **1998**, p. 34.

[12] J. Jang, J. H. Oh, *Chem. Commun.* **2002**, 2200 – 2201.

[13] G. T. Fey, Y. C. Kao, *Mater. Chem. Phys.* **2002**, *73*, 37 – 43.

[14] C. R. Park, Y. J. Kim, *Abstr. Pap. Am. Chem. Soc.* **2000**, *219*, 476-POLYM. Part 2.

[15] E. Fitzer, D. J. Muller, *Carbon* **1975**, *13*, 63 – 70.

[16] H. -J. Sue, J. D. Earls, R. E. Hefner, *J. Mater. Sci.* **1997**, *32*, 4031 – 4038.

[17] J. Jang, J. Bae, S.-H. Yoon, *J. Mater. Chem.* **2003**, *13*, 676 – 681.

[18] J. Sandler, M. S. P. Shaffer, T. Prasse, W. Bauhofer, K. Schulte, A. H. Windle, *Polymer* **1999**, *40*, 5967 – 5972.

 © 2004 Wiley-VCH Verlag GmbH & Co. KGaA, Weinheim

Microarray Technology

Enzyme Microarrays: On-Chip Determination of Inhibition Constants Based on Affinity-Label Detection of Enzymatic Activity**

Jörg Eppinger, Daniel P. Funeriu,* Masato Miyake, Lucile Denizot, and Jun Miyake*

The completion of the human genome's deciphering is opening previously unforeseeable opportunities. This major step towards the understanding and control of living bodies lays a fertile ground for proteomic science and, in particular, for the identification of novel enzymatic therapeutic targets. The understanding of the biochemical complexity is paralleled, in the chemical sciences, by an ever-increasing ability to generate large numbers of vastly diverse chemical structures.[1] For the evaluation of the activity of these compounds as enzyme-activity modulators, a plethora of high throughput screening (HTS) assays are currently explored. In particular, protein chips have been proposed to bring high throughput assays into the picoscale range.[2] It was thought that just as DNA chips are a pivotal contributor to genomic science, protein chips would become a major tool for proteomics, including HTS. However, protein-chip technology until recently has failed to provide information about the most crucial property of microarrayed enzymes:[3,4] the state of their catalytic activity. Herein we report a kinetic approach to on-chip enzyme-activity determination and its detailed demonstration for papain, a member of the cystein protease family. This method, due to the data quality that it provides, its automation potential and its demonstrated robustness should soon find applications in large scale HTS.

The developed method uses, as its key step, the intrinsic property of tagged affinity labels[5,6] to react with enzymes in an activity-dependent manner. The methodology (Figure 1) involves the covalent immobilization of the enzyme of interest on a functionalized glass slide. The remaining,

[*] Dr. J. Eppinger[+]
ForschungsDozentur Molekulare Katalyse Lehrstuhl für Anorganische Chemie
Technische Universität München
Lichtenbergstr. 4, 85748, Garching (Germany)
Fax: (+49) 89289-13473
E-mail: joerg.eppinger@ch.tum.de

Dr. D. P. Funeriu,[+] Dr. M. Miyake, L. Denizot, Dr. J. Miyake
Tissue Engineering Research Center
National Institute of Advanced Industrial Science and Technology
3-11-46 Nakouji, Amagasaki, Hyogo, 661-0974 (Japan)
Fax: (+81) 6-6494-7863
E-mail: danielpetru-funeriu@aist.go.jp

[+] These authors contributed equally to this work.

[**] This work was supported by the Stifterverband für die Deutsche Wissenschaft (Projekt-Nr. 11047: ForschungsDozentur Molekulare Katalyse) and by AIST. We thank Dr. Chikashi Nakamura and Dr. Nicolas Giuseppone for assistance at various stages.

Supporting information for this article is available on the WWW under http://www.angewandte.org or from the author.

 © 2004 Wiley-VCH Verlag GmbH & Co. KGaA, Weinheim DOI: 10.1002/anie.200353623

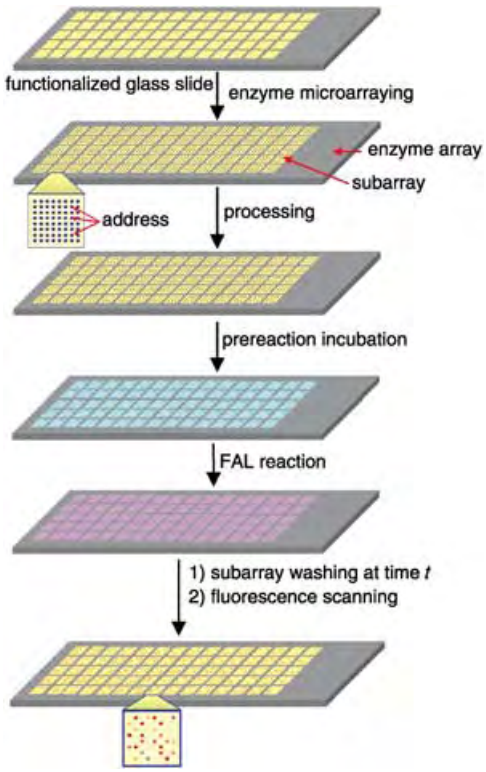
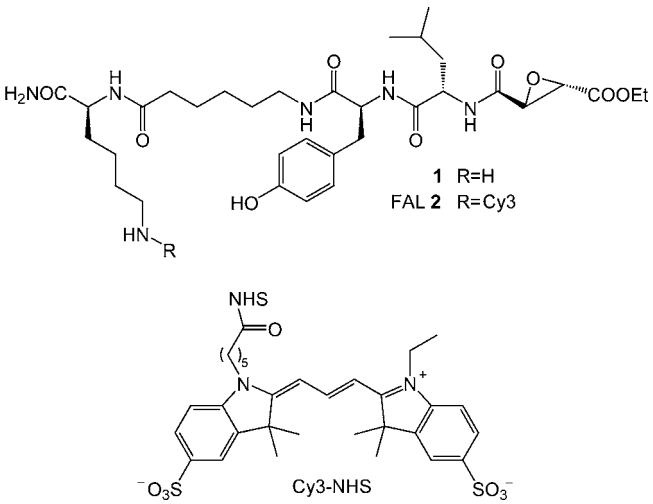


Figure 1. General methodology for the affinity label on-chip enzyme inhibitor screening (ALCEIS). At the final stage, the fluorescence of each address correlates with the amount of reacted enzyme at time *t*.

unconverted surface functionalities are blocked with a surface-reactive compound. After a series of washings, an appropriate fluorescently tagged affinity label (FAL) is incubated on the top of the enzyme-immobilized area for the desired time (in absence or presence of a potential inhibitor). The amount of reacted enzyme microarrayed at a given address can then be correlated with the fluorescence measured at that address. Based on this correlation, kinetic parameters of an immobilized enzyme can be readily obtained.

The successful realization of such a system requires, as the key components, a surface-immobilization chemistry that maintains the activity of the studied enzyme and a FAL that efficiently and specifically reacts with the active enzyme(s) of interest and has very low reactivity towards other surface-immobilized molecules. To prove the principle of such a system, we synthesized a cystein protease FAL derived from the work of Barett et al.[7] and Bogyo and co-workers,[5] by the conjugation of N-hydroxysuccinimide functionalized Cy3 dye to the amino terminal group of compound **1** (see Scheme 1).[8] The obtained compound was purified by reverse phase (RP) HPLC and characterized by ESMS. Its capacity to efficiently and specifically label papain but not trypsin, bovine serum albumin or E-64 inhibited papain was demonstrated by gel-electrophoresis.

Furthermore, we evaluated the on-chip reactivity of FAL **2** towards papain that was microarrayed on a hydrogel–NHS-functionalized glass slide that contained squares of $3 \times 3\,mm^2$ each (subarrays), separated by a 20 μm-thick teflon coating.



Scheme 1. Structure of the FAL **2** used in this study.

Such an array design allows each subarray to be addressed both individually and collectively.

Incubation of the subarrays for different periods of time with different concentrations of **2** followed by washing with hot SDS buffer reveals that significant fluorescence is associated with papain-containing areas (spots) within each subarray (Figure 2a) and that the level of fluorescence is time-dependent, with a saturation time dependent on the concentration of **2** used. The washing conditions employed prove that **2** is covalently bound to the microarrayed enzyme. Indeed, when identical washing conditions were used for an array on which biotinilated albumin was immobilized and subsequently detected by a noncovalent biotin-streptavidin interaction with streptavidin-phycoerythrin (SAPE), no significant signal was observed. After the array had been washed, the background fluorescence level was very low (signal:noise ratio > 50), thus demonstrating the specific reaction of **2** with papain. Moreover, the reaction in the absence of dithiothreitol (DTT) or with microarrayed heat-denatured papain or other, non-cystein protease enzymes (such as trypsin or chymotrypsin) resulted in no significant fluorescence signal. The quality of the data obtained with this method is very high: the typical standard deviation between spots within a 4×4 array is less than 7% (Figure 2d, e) and less than 10% between different, identically treated subarrays. These data all strongly support the fact that **2** is an excellent candidate for the on-chip determination of microarrayed cystein proteases.

To obtain a quantitative model for the kinetics of the reaction between the immobilized cystein protease and **2**, the fluorescence data was quantified by comparing these data with a calibration microarray and fitted to several models.[9] The best fit was obtained (Figure 2b) for a reaction sequence derived from a Michaelis–Menten kinetic model. A slow side reaction ($k_{side} = 0.53(4)\,M^{-1}s^{-1}$) had to be taken into account, which presumably can be attributed to the attack by free thiol groups from inactive, immobilized protein on the epoxide moiety of **2**. Correspondingly, analysis of the initial velocities v_0 versus the concentration of **2** (Figure 2c) obeys to what is

 © 2004 Wiley-VCH Verlag GmbH & Co. KGaA, Weinheim

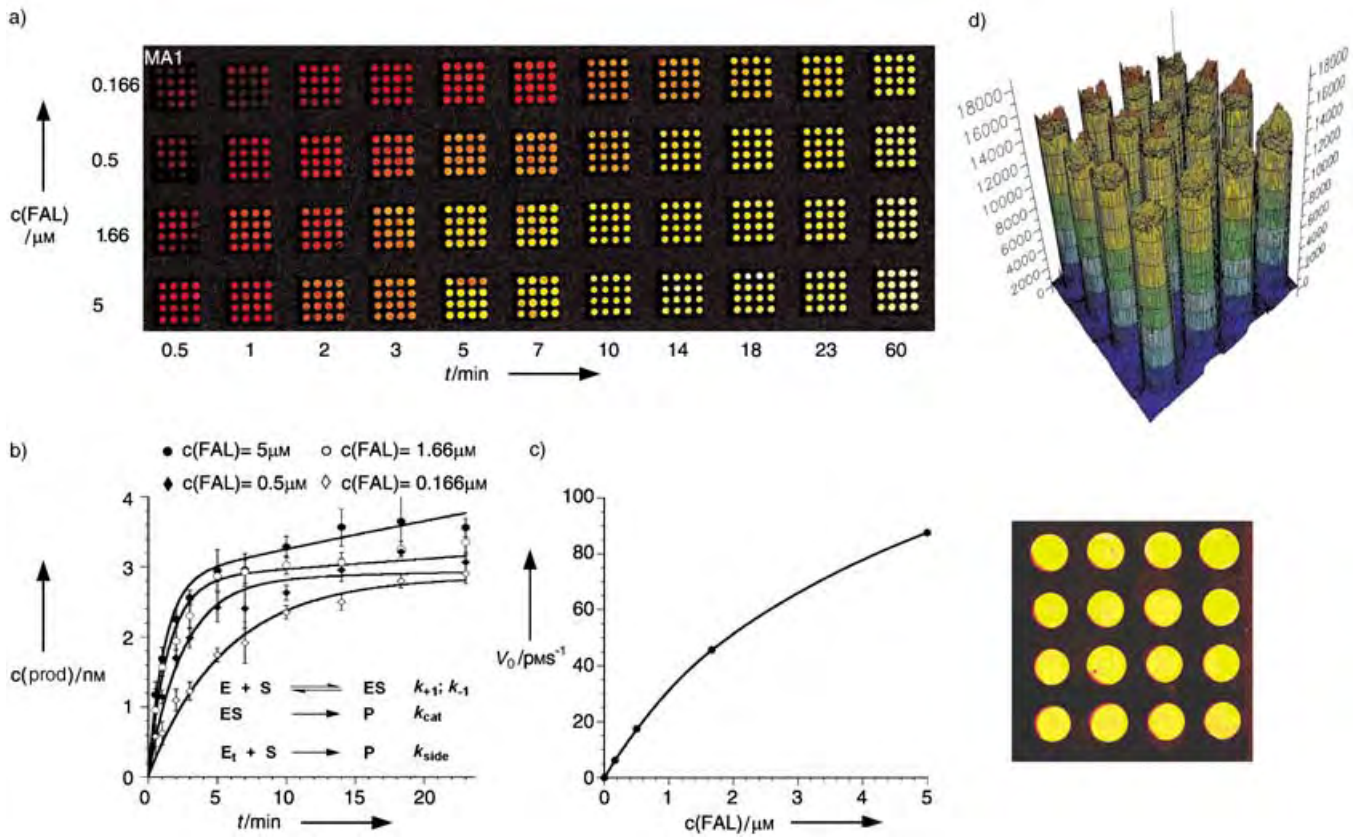


Figure 2. a) Image of a microarray (MA1) composed of 44 subarrays of 4×4 papain spots each, treated for 11 different reaction times with four different concentrations of **2**. b) Quantified data corresponding to the microarray MA1 and best-fit reaction model, derived from a Michaelis–Menten kinetic. c) Plot of initial velocities (v_0) versus concentration of FAL **2**, c(FAL). d) Spot-to-spot reproducibility within a subarray for the presented method. e) Typical fluorescence image of a sub array.

expected for an enzyme-catalyzed reaction with $K_M^{app} = 3.9(5)$ μM and $v_{max} = 0.152(11)$ nM s^{-1} ($c_{papain} = 2.8(3)$ nM), though no turn over is completed (see Supporting Information for detailed discussion). Simplification of the model did not lead to a good agreement of the theoretical progress curve with the experimental data, while including diffusion or further pre-equillibria did not improve the goodness of fit. However, comparison of on-chip kinetics with the corresponding rate constants, that were established by an independent solution experiment, revealed a tenfold decreased rate constant for the binding of **2** to papain (k_{+1}) on the surface. This result supports the argument in favor of a diffusion limitation of the fast binding processes. Therefore, for all models that involve the binding of a small molecule, a pre-equilibrium was implemented to account for this diffusion limitation. Consequently, the difference of the pseudosecond-order rate constants k_{2nd} determined for the reaction of **2** with papain on chip and in solution falls below the error range of the constants (Table 1).

To demonstrate that this method can be used for the discovery and characterization of inhibitors—both reversible and irreversible—we preincubated microarrays with four different concentrations of leupeptin (competitive papain inhibitor; MA2) or E-64 (irreversible inhibitor for cystein proteases; MA3), before **2** was added and incubated for various times. The obtained time curves (Figure 3b, d) clearly indicate that addition of leupeptin slows down the reaction between **2** and the active enzyme in a concentration-dependent manner, but does not influence the saturation level reached after a long reaction time. Typically for reversible inhibition, the saturation level corresponds to the concentration of the active microarrayed papain (Figure 3b). However when E-64 is used as an inhibitor, the saturation level

Table 1: Characteristic kinetic constants of tested inhibitors

Array	k_{2nd} (**2**) [μM^{-1} s^{-1}]	k_{2nd} (E-64) [μM^{-1} s^{-1}]	K_i (Leu) [nM]
MA1	0.14(3)	–	–
MA2	0.14(3)[a]	–	120(12)
MA3	0.14(3)[a]	0.32 (18)	–
MA4[b]	0.14(3)[a]	0.53 (9)	150(5)
MA4[c]	–	0.12 (16)	100(21)
solution	0.16 (3)[d]	0.37–0.64[e]	160(49)[f]

[a] Determined on MA1 and not refined for this experiment. [b] Preincubation with inhibitor for 1 h before addition of **2**. [c] Simultaneous addition of inhibitor and **2**. [d] Quantification of solution experiment analogous to [8]. [e] Literature values.[2] [f] Quantification of solution experiment analogous to reference [8]. The value determined at pH 5.8 with a fluorogenic substrate is 2.5.[11]

 © 2004 Wiley-VCH Verlag GmbH & Co. KGaA, Weinheim

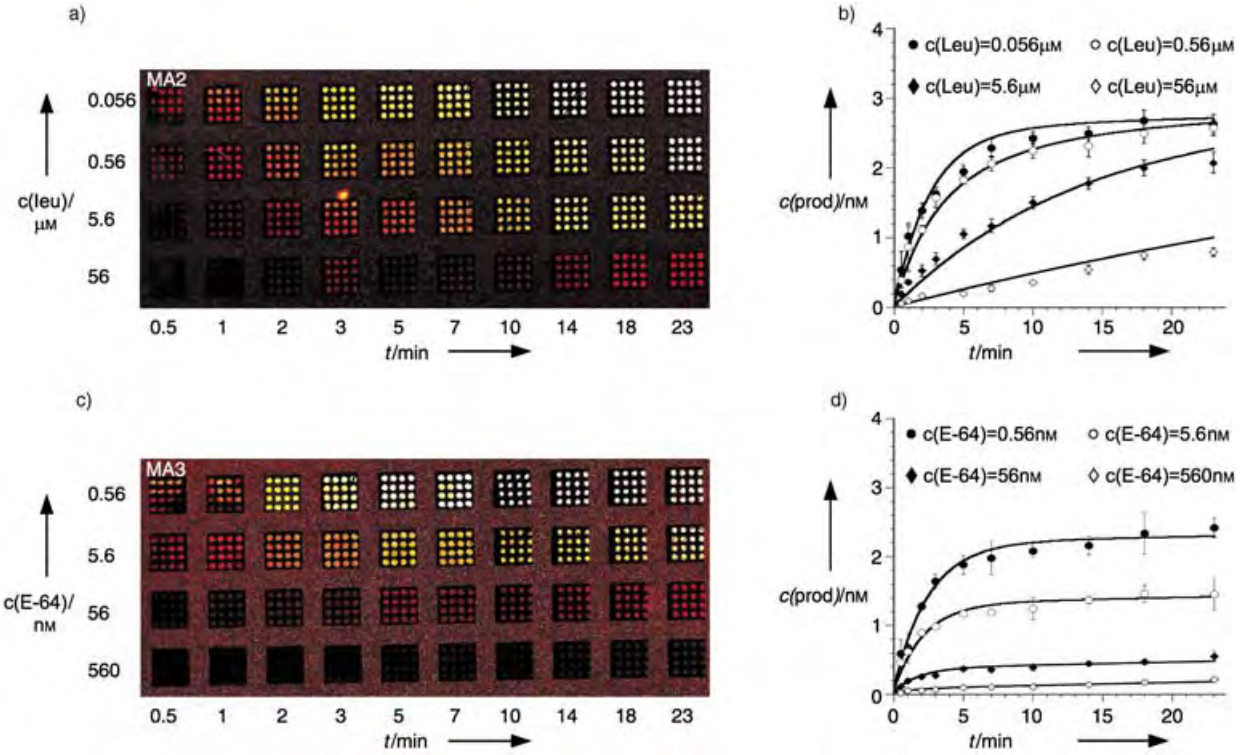


Figure 3. a, c) Image of two microarrays (MA2 and MA3) composed of 40 subarrays each preincubated for 1 h with four different concentrations of leupeptin (respectively E-64) before reaction with **2** at 0.5 μM for ten different times. b) Quantified data corresponding to the microarray MA2. The data corresponding to one sub-array (3 min, c(Leu) = 56 μM) of MA2 was excluded from the analysis due to experimental error. d) Quantified data corresponding to the microarray MA3.

reached is correlated with the E-64 concentration, as it is expected for irreversible inhibition (Figure 3d).

These facts show that the presented method allows one to distinguish between reversible and irreversible inhibition, provided that a minimum of two time points are measured at relevant times. Based on the model and the kinetic constants derived from MA1, we could determine characteristic on-chip inhibition constants for leupeptin and E-64 (Table 1). While for E-64 the pseudosecond-order rate constant of $k_{2nd} = 0.32(18)\ \mu M^{-1} s^{-1}$ corresponds well to the known value,[10] the reversible inhibition constant for leupeptin of $K_i = 115(12)$ nM is about 50 times higher than previously reported values.[11] This difference can partly be attributed to the influence of DTT (present at much higher concentrations on the chip) on the complex equilibria that take place in an aqueous solution of leupeptin.[11] A determination of K_i in solution under similar conditions (see Supporting Information) as they were applied on the chip resulted in a value of 150(5) nM.

After having established the measurement of on-chip kinetic constants, we set out to demonstrate that our method is well suited to derive quantitative inhibition constants from only one time point, an important asset for the use of this method in HTS. Thus, two experimental setups were envisioned: in the first case, 11 subarrays were preincubated for 1 hour with decreasing concentrations of inhibitor. Subsequently each subarray was treated with **2** for 2 minutes (Figure 4a, MA4, bottom 2 rows). Alternatively, in a direct competition experiment, each subarray was incubated with a DTT activation buffer, followed by 2 minutes treatment with a mixture of **2** and decreasing concentrations of inhibitor (Figure 4a, MA4, top 2 rows).

Extraction of the inhibition constants is straightforward from the preincubation experiment. K_i values for leupeptin can be obtained from the ratios of the initial velocities v_i/v_0 at a given inhibitor concentration,[12] since the measurement takes place prior to a substantial inactivation of the enzyme by the FAL and the FAL is applied in a concentration below its reversible binding constant. The K_i values, derived from any of the points satisfying the condition $0.1 < v_i/v_0 < 0.9$, were within the same order of magnitude, which is suitable for high throughput screening. To retrieve k_{2nd} values for E-64, the v_i/v_0 ratio can be used to calculate the amount of active enzyme after a certain preincubation time, which is directly correlated to the pseudosecond order velocity of reaction of **2** with papain.

In the co-incubation situation, the inhibition constants can only be derived with a full understanding of the underlying kinetic model and the kinetic constants from MA1. Thus, this method is based on a faster experiment, but needs a predetermination of the kinetic parameters of the process. The kinetic parameters derived are listed in Table 1. Overall, they correspond well with the constants determined in solution. Whereas for irreversible inhibition, the preincubation methodology provides superior results, for competitive inhibition both methods are acceptable.

 © 2004 Wiley-VCH Verlag GmbH & Co. KGaA, Weinheim

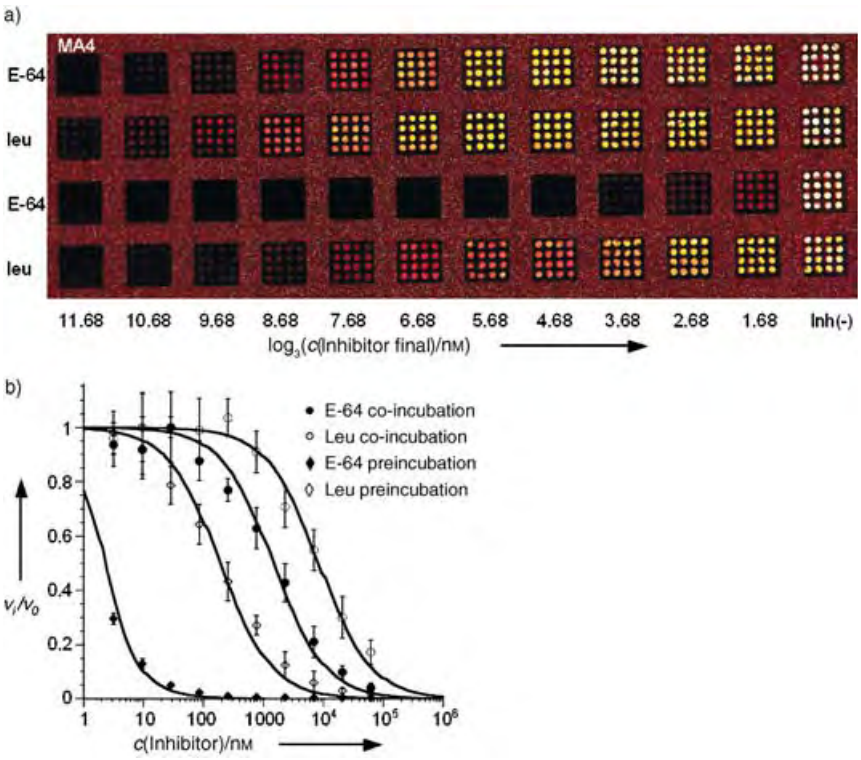


Figure 4. a) Image of MA4 composed of 48 subarrays. Top two rows were co-incubated with **2** and different concentrations of E-64 (leupeptin) for 2 minutes. Bottom rows were preincubated with different concentrations of E-64 (respectively leupeptin) for 1 h before **2** was added for 2 min. b) Evolution of the ratio between the initial velocities (v_i/v_0) as a function of the inhibitor concentration (c(Inhibitor)) derived from the quantified data of MA4.

Placed in the context of other on-chip methods that use mainly binding events for detection,[2] this method has several noticeable advantages: first, it clearly differentiates between the capacity of an arrayed enzyme to catalyze a chemical reaction rather than only bind a chemical partner. The second important advantage is the independence of the obtained result on the postprocessing washing step. Indeed, it usually is difficult to ensure consistent washing conditions for two different batches for example, whereas, as this method involves covalent binding of the activity-reporter molecule, very drastic washing conditions can be used with little variation in the observed fluorescence of the active enzymes. This adds to the enzyme chip technology an additional robustness, which is an important fact for their reliable exploitation. The practical possibilities to reliably use ALCEIS with many classes of enzymes require optimization of the immobilization chemistry as well as a full kinetic characterization of each of the immobilized enzyme. Since this latter aspect, including reaction modeling, must be determined only once for a given set of enzymes, the method described can be used in a high-throughput system. By using such an assay, as well as appropriate automation it appears realistic to run more than a million enzymatic tests a day with a single working station and a significantly reduced amount of material consumption with respect to current techniques. The method presented herein complements well the recently demonstrated use of FALs for the determination of inhibitor's specificity profile in tissue proteomes.[13,14] Different in nature, our method requires at this stage purified enzymes, yet has the advantage of a higher throughput. Considering the recent spectacular progress made in this field,[15] one can expect a rapid broadening of the method presented herein.

In conclusion, we have proven the possibility of quantitatively and reliably measuring on a chip the activity level of reversible and irreversible inhibitors by taking advantage of the specific reaction between a class of enzymes and fluorescently tagged affinity labels. We do provide both the theoretical and practical basis for further developments in the promising field of enzyme(s) microarrays.

Received: December 29, 2003
Revised: April 14, 2004 [Z53623]

Keywords: enzymes · fluorescent probes · high-throughput screening · inhibitors · microarrays · on-chip kinetics

[1] see for example M. D. Burke, S. L. Schreiber, *Angew. Chem.* **2004**, *116*, 48; *Angew. Chem. Int. Ed.* **2004**, *43*, 46, and references therein.
[2] For reviews see: G. McBeath, *Nat. Genet.* **2002**, *32*, 526; the state of the art in this field is comprehensively reviewed in the recent issue dedicated to protein microarrays of *Proteomics* **2003**, *3*, 2077–2270.
[3] This technique effectively solves the on-chip diffusion problem; however it does not measure the activity of immobilized enzymes and has inherent advantages as well as disadvantages over the method presented herein. D. N. Gosalia, S. L. Diamond, *Proc. Natl. Acad. Sci. USA* **2003**, *100*, 8721.
[4] Chen et al. have shown that affinity labels can be used to label microarrayed enzymes. G. Y. J. Chen, M. Uttamchandani, Q. Zhu, G. Wang, S. Q. Yao, *ChemBioChem* **2003**, *4*, 336.
[5] D. C. Greenbaum, W. D. Arnold, F. Lu, L. Hayrapetian, A. Baruch, J. Krumrine, S. Toba, K. Chehade, D. Brömme, I. D. Kuntz, M. Bogyo, *Chem. Biol.* **2002**, *9*, 1085.
[6] G. C. Adam, E. J. Sorensen, B. F. Cravatt, *Nat. Biotechnol.* **2002**, *20*, 805.
[7] A. J. Barett, A. A. Kembhavi, M. A. Brown, H. Kirschke, C. G. Knight, M. Tamai, K. Handa, *Biochem. J.* **1982**, *201*, 189.
[8] D. Greenbaum, K. F. Medzihradszky, A. Burlingame, M. Bogyo, *Chem. Biol.* **2000**, *7*, 569.
[9] Kinetic Parameters were extracted by best fit analysis by using the Program DYNAFIT: P. Kuzmic, *Anal. Biochem.* **1996**, *237*, 260–273.
[10] H.-H. Otto, T. Schirrmeister, *Chem. Rev.* **1997**, *97*, 133.
[11] R. M. Schultz, P. Varma-Nelson, R. Oritz, K. A. Kozlowski, A. T. Orawski, P. Pagast, A. Frankfater, *J. Biol. Chem.* **1989**, *264*, 1497.
[12] P. Kuzmic, S. Sideris, L. M. Cregar, K. C. Elrod, K. D. Rice, J. W. Janc, *Anal. Biochem.* **2000**, *281*, 62.
[13] M. P. Patricelli, D. K. Giang, L. M. Stamp, J. J. Burbaum, *Proteomics* **2001**, *1*, 1067–1071.
[14] D. Leung, C. Hardouin, D. L. Boger, B. F. Cravatt, *Nat. Biotechnol.* **2003**, *21*, 687.
[15] D. A. Jeffery, M. Bogyo, *Curr. Opin. Biotechnol.* **2003**, *14*, 87.

 © 2004 Wiley-VCH Verlag GmbH & Co. KGaA, Weinheim

Topochemistry

Supramolecular Control over the Stereochemistry of Diene Polymers**

*Sadamu Nagahama, Toshihiro Tanaka, and Akikazu Matsumoto**

Polymers with different properties can be derived from the same starting monomers by changing the way the repeating units are connected during formation of the polymer. For example, although cellulose, starch, and glycogen consist of glucose as the repeating unit and have a similar repeating structure, and natural rubber and guttapercha are *cis*- and *trans*-1,4-polyisoprenes, respectively, they have different physical and other properties because of their stereochemical structure. Thus, the stereochemistry of polymers, namely, the tacticity, is one of the most important factors for determining the properties of polymeric materials, as well as the repeating unit structure, molecular weight, and molecular-weight distribution. Various catalytic polymerization techniques have been developed since the first discovery of the stereospecific polymerization by Natta and co-workers.[1] As a result, polymer tacticity can now be precisely controlled by the coordination and anionic polymerization of olefins, dienes, and several polar vinyl monomers,[2] as well as by a radical polymerization process.[3,4]

Topochemical polymerization in the crystalline state is the most promising method for controlling the stereochemistry of polymers.[5,6] The structure of polymer chains as well as the polymerization rate are determined by the molecular packing of the monomers in the crystals. Recent amazing developments in supramolecular assembly and crystal engineering now enable us to design and fabricate crystals with a molecular stacking for any function and reaction.[7–10] The rational design of organic crystals has changed topochemical polymerization from a trial-and-error approach to a credible molecular and materials design.[11–13] Here, we report the control that can be achieved over the stereochemical structure of polymers during the solid-state polymerization of 1,3-diene monomers by a novel approach based on crystal engineering. Molecular alignment in the monomer crystals is controlled by several intermolecular interactions, such as strong and weak hydrogen bonds, which leads to the formation of various types of stereoregular polymers through a topochemical polymerization process. This approach to the stereocontrol of polymers differs from other conventional ways of controlling the propagating chain end using catalysts or additives during solution polymerization.

The 1,3-diene dicarboxylic acid derivative muconic acid has three isomers with *Z*,*Z*, *E*,*E*, and *E*,*Z* configurations.[14] 1-Naphthylmethylammonium (*Z*,*Z*)- and (*E*,*E*)-muconates ((*Z*,*Z*)-**1** and (*E*,*E*)-**1**, respectively) with C_2 symmetry favor a translational molecular packing in the crystals. The reacting diene moieties stack in a columnar structure with the aid of two-dimensional (2D) hydrogen-bonding networks at the interface of the muconate anion and countercation layers in the lamella crystals. Topochemical polymerization of (*Z*,*Z*)-**1** and (*E*,*E*)-**1** by UV irradiation in the crystalline state produces the same stereoregular polymer with a *meso*-diisotactic structure.[15] On the other hand, the *Z*,*Z* and *E*,*E* 4-methoxybenzyl muconates (*Z*,*Z*)-**2** and (*E*,*E*)-**2**, respectively, stack alternately in a column through a CH/π interaction between the methoxy protons and the π electrons of the phenyl group, which results in the formation of a *racemo*-disyndiotactic polymer upon photoirradiation.[16]

Topochemical polymerization of the corresponding *E*,*Z* monomers with a different symmetrical structure produced a new type of stereoregular polymer (Scheme 1). The translational molecular packing of 1-naphthylmethylammonium (*E*,*Z*)-muconate ((*E*,*Z*)-**1**) by the interaction of 2D hydrogen-bonding networks gives a *racemo*-diisotactic polymer. Similarly, the alternate stacking of 4-methoxybenzyl (*E*,*Z*)-muconate ((*E*,*Z*)-**2**) results in the formation of a *meso*-disyndiotactic polymer.[17]

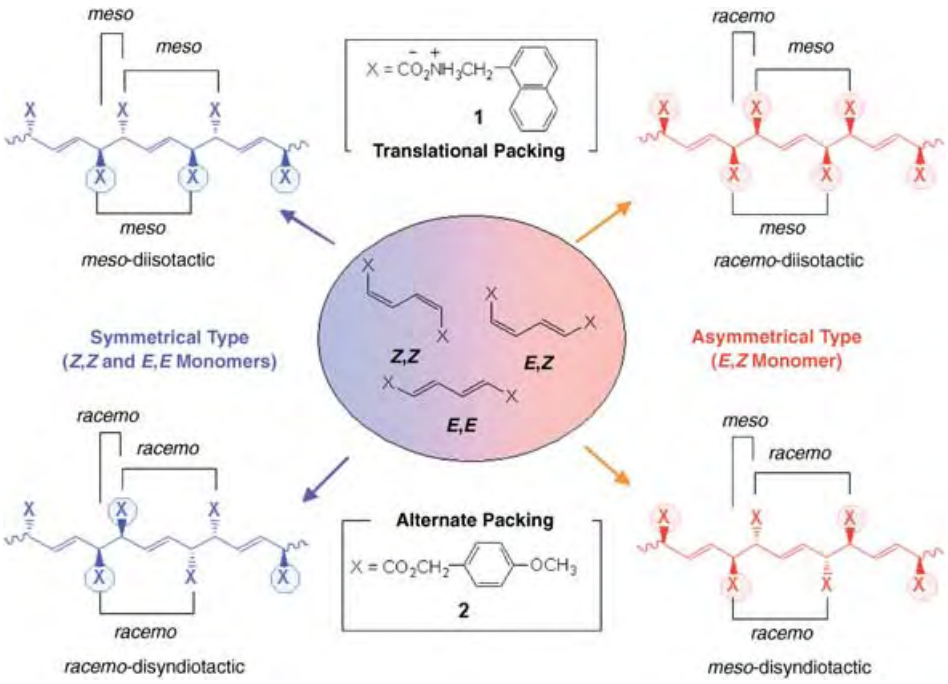
Irradiation of the crystals of (*E*,*Z*)-**1** with UV light afforded an atactic polymer as a result of the simultaneous occurrence of isomerization and polymerization, while no reaction occurred with (*E*,*Z*)-**2** (Table 1). However, polymerization of (*E*,*Z*)-**1** and (*E*,*Z*)-**2** with γ-radiation at 200 kGy provided polymers in yields of 61 and 96%, respectively, without any isomerization to form the *E*,*E* isomers. The powder X-ray diffraction profiles of the monomers and the polymers showed that the polymerizations proceed by a topochemical reaction process in which a similar and highly crystalline structure is maintained (see the Supporting Information). The structure of the *racemo*-diisotactic polymer obtained from (*E*,*Z*)-**1** was confirmed by the solid-state hydrolysis of the corresponding poly(muconic acid) derived from the ammonium polymers. A pair of adjacent carboxy groups of the *racemo*-diisotactic poly(muconic acid) are located in the same direction along the main chain, while the carboxy groups of the *meso*-diisotactic polymer are on opposite sides of the polymer chain. Heating the *racemo* polymer at 250 °C resulted in a weight loss as a consequence of the formation of the five-membered ring acid anhydride; in contrast no weight loss was observed for the *meso* polymers at the same temperature. The stereospecific dehydration was also confirmed by IR spectroscopy by the appearance of new peaks at 1864, 1777, and 921 cm^{-1}.

[*] Dr. T. Tanaka, Prof. Dr. A. Matsumoto
Department of Applied Chemistry
Graduate School of Engineering
Osaka City University and PRESTO-JST
Sugimoto, Sumiyoshi-ku, Osaka 558-8585 (Japan)
Fax: (+81) 6-6605-2981
E-mail: matsumoto@a-chem.eng.osaka-cu.ac.jp
Dr. S. Nagahama
Department of Applied Chemistry
Graduate School of Engineering
Osaka City University
Sugimoto, Sumiyoshi-ku, Osaka 558-8585 (Japan)

[**] The authors acknowledge Dr. Kunio Oka (Research Institute for Advanced Science and Technology, Osaka Prefecture University) for performing the γ-radiation experiment.

Supporting information for this article is available on the WWW under http://www.angewandte.org or from the author.

 DOI: 10.1002/anie.200453738 © 2004 Wiley-VCH Verlag GmbH & Co. KGaA, Weinheim



Scheme 1. Stereoregular polymer sequences for *trans*-1,4-polymers obtained from 1,3-diene dicarboxylic acid derivatives.

Table 1: Radiation polymerization of muconates in the crystalline state.[a]

Monomer	UV irradiation		γ-radiation	
	Polymer structure	Yield [%]	Polymer structure	Yield [%]
(*Z*,*Z*)-**1**	*meso*-diisotactic	90	*meso*-diisotactic	96
(*E*,*E*)-**1**	*meso*-diisotactic	71	*meso*-diisotactic	99
(*E*,*Z*)-**1**	atactic	8[b]	*racemo*-diisotactic	61
(*Z*,*Z*)-**2**	*racemo*-disyndio-tactic	93	*racemo*-disyndio-tactic	ca. 100
(*E*,*E*)-**2**	*racemo*-disyndio-tactic	81	*racemo*-disyndio-tactic	ca. 100
(*E*,*Z*)-**2**	no reaction	0	*meso*-disyndiotac-tic	96

[a] UV irradiation was carried out using a high-pressure mercury lamp for 8 h at room temperature. γ-Radiation was carried out using ^{60}Co at a dose of 200 kGy. [b] UV irradiation for 40 h. An atactic polymer was formed by the *E*,*Z* isomerization of (*E*,*Z*)-**1** and the subsequent copolymerization of the *E*,*Z* and *E*,*E* isomers.

The polymer obtained from the γ radiation of (*E*,*Z*)-**2** was soluble in chloroform despite its high crystallinity. As shown in the molecular stacking structures of (*Z*,*Z*)-**2**, (*E*,*E*)-**2**, and (*E*,*Z*)-**2** in Figure 1, the reactive section of these monomers has an alternate stacking, which leads to formation of the stereoregular polymer with a disyndiotactic structure. The *racemo* and *meso* structures of poly((*Z*,*Z*)-**2**) or poly((*E*,*E*)-**2**) and poly((*E*,*Z*)-**2**), respectively, were confirmed by ^{13}C NMR spectroscopy. Poly((*Z*,*Z*)-**2**) as well as poly((*E*,*E*)-**2**) were insoluble in organic solvents in the highly crystalline forms in which they are obtained by polymerization, but they can be isolated as amorphous and readily soluble solids after the bulk material is heated above their melting points (199 and 195 °C for poly((*Z*,*Z*)-**2**) and poly((*E*,*E*)-**2**), respectively), or from a polar solvent at a high temperature. X-ray diffraction and DSC analyses confirmed the amorphous structure of the polymers recovered after cooling or reprecipitation. A comparison of the NMR data of the related polymers concludes that the chemical shifts for a series of the polymers show they are predominantly determined by the difference in the *meso*-*racemo* structure rather than that in the diisotactic-disyndiotactic one (see the Supporting Information).

Poly(**2**) compounds in which the benzyl ester groups were substituted by an electron-donating 4-methoxy group were readily converted into poly(muconic acid) by acid-catalyzed hydrolysis. Although diisotactic poly((*Z*,*Z*)-**2**) and poly((*E*,*E*)-**2**) dissolved and then underwent hydrolysis in concentrated sulfuric acid, the disyndiotactic poly((*E*,*Z*)-**2**) underwent heterogeneous hydrolysis in the reaction. Surprisingly, the conversion was quantitative even under mild conditions; completely hydrolyzed poly(muconic acid) was formed within 1 h at room temperature in concentrated sulfuric acid. We previously reported that poly(muconic acid) acts as an organic host compound for an organic intercalating system.[18] Disyndiotactic poly(muconic acid) was also examined as a host polymer for the intercalation of alkyl amines. The repeated intercalation behavior depended on the tacticity and hydrogen-bonding network structure of the polymers: the difference in the tacticity of the host polymer seriously affects the host–guest interactions. We are further investigating the details of the intercalation behavior as well as the physical properties of the polymers with a different stereochemical structure.

In conclusion, we have succeeded in synthesizing all four kinds of stereoregular polymers by controlling the stacking of symmetrical and asymmetrical monomers. This approach contrasts with the difficulty seen in the stereocontrol of diene polymers by catalytic routes.[19]

Experimental Section

(*Z*,*Z*)-Muconic acid was obtained from Mitsubishi Chemical Co., Ltd., Tokyo. Heating and photoirradiation of the *Z*,*Z* acid in solution provided the (*E*,*Z*)- and (*E*,*E*)-muconic acids, respectively. All ammonium monomers were prepared from the corresponding isomer of muconic acid with an amine in quantitative yield. All ester monomers were prepared by the reaction of the muconic acid and corresponding benzyl halides with potassium carbonate in hexamethylphosphoramide. The structures of all the monomers were determined by NMR, IR, and UV spectroscopies.

 © 2004 Wiley-VCH Verlag GmbH & Co. KGaA, Weinheim

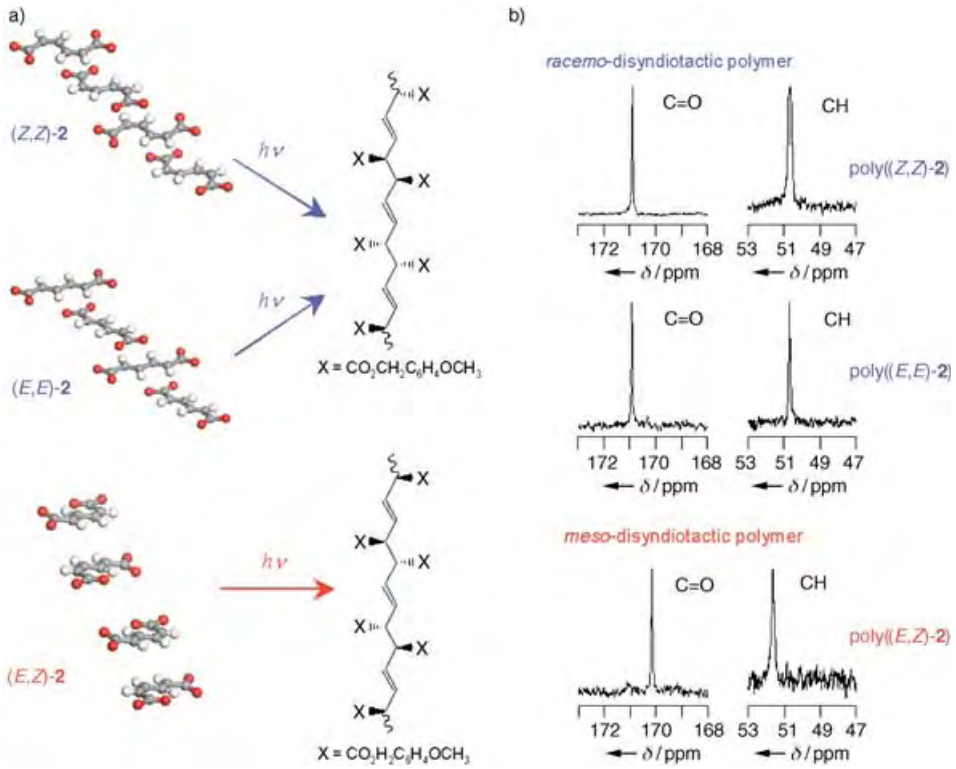


Figure 1. a) Alternate molecular stacking of (*Z*,*Z*)-**2**, (*E*,*E*)-**2**, and (*E*,*Z*)-**2** in a columnar structure in the crystals. The benzyl groups are omitted here for clarity. (*Z*,*Z*)-**2** and (*E*,*E*)-**2** produce the same stereoregular polymer, that is, the *racemo*-disyndiotactic-2,5-*trans* polymer, through the topochemical polymerization, while (*E*,*Z*)-**2** provides a *meso*-disyndiotactic-2,5-*trans* polymer. b) ^{13}C NMR spectra of *racemo*-disyndiotactic poly((*Z*,*Z*)-**2**) and poly((*E*,*E*)-**2**) as well as *meso*-disyndiotactic poly((*E*,*Z*)-**2**).

The monomer crystals were placed in a pyrex tube, which was then degassed and sealed. γ-Radiation was carried out with ^{60}Co at the Research Institute for Advanced Science and Technology, Osaka Prefecture University, Japan. The irradiation dose was 200 kGy at a dose rate of 48.6 kGy h^{-1}. After irradiation, the polymer was isolated by removal of any remaining monomer with methanol. The polymer yield was determined by gravimetric analysis.

NMR, IR, and UV spectra were recorded on a JEOL JMN A-400, JASCO Herschel FT-IR-430, and JASCO V-550 spectrometer, respectively. The powder X-ray diffraction data were collected with a Rigaku RINT-2100 diffractometer with monochromated $Cu_{K\alpha}$ radiation ($\lambda = 1.5418$ Å, 30 kV, 20 mA, scan speed 1 deg min^{-1}). The thermogravimetric/differential thermal analysis measurements were carried out using a Seiko TG/DTA 6200 in a nitrogen stream at a heating rate of 10 °C min^{-1}.

Received: January 12, 2004 [Z53738]

Keywords: crystal engineering · polymerization · solid-state reactions · supramolecular chemistry · topochemistry

[1] *Stereoregular Polymers and Stereospecific Polymerization: The Contribution of Gulio Natta and his School to Polymer Chemistry*, *Vols. 1 and 2* (Eds.: G. Natta, F. Danusso), Pergamon, Oxford, **1967**.

[2] a) M. Farina, *Top. Stereochem.* **1987**, *17*, 1; b) P. Pino, U. W. Suter, *Polymer* **1976**, *17*, 977; c) H. H. Brintzinger, D. Fischer, R. Mulhaupt, B. Rieger, R. M. Waymouth, *Angew. Chem.* **1995**, *107*, 1255; *Angew. Chem. Int. Ed. Engl.* **1995**, *34*, 1143; d) W. Kaminsky, M. Arndt, *Adv. Polym. Sci.* **1997**, *127*, 143; e) H. Yasuda, E. Ihara, *Bull. Chem. Soc. Jpn.* **1997**, *70*, 1745; f) K. Soga, T. Shiono, *Prog. Polym. Sci.* **1997**, *22*, 1503; g) G. W. Coates, *Chem. Rev.* **2000**, *100*, 1223; h) K. Hatada, T. Kitayama, *Polym. Int.* **2000**, *49*, 11.

[3] A. Matsumoto, *Handbook of Radical Polymerization* (Eds.: K. Matyjaszewski, T. P. Davis), Wiley, New York, **2002**, p. 691.

[4] a) T. Nakano, Y. Okamoto, *Chem. Rev.* **2001**, *101*, 4013; b) Y. Okamoto, S. Habaue, Y. Isobe, *ACS Symp. Ser.* **2003**, *854*, 59; c) N. A. Porter, C. L. Mero, *Radicals in Organic Synthesis*, *Vol. 1* (Eds.: P. Renaud, M. P. Sibi), Wiley-VCH, Weinheim, **2001**, p. 489; d) T. Serizawa, K. Hamada, M. Adashi, *Nature* **2004**, *429*, 52..

[5] G. M. J. Schmidt, *Pure Appl. Chem.* **1971**, *27*, 647.

[6] a) A. Matsumoto, *Polym. J.* **2003**, *35*, 93; b) A. Matsumoto, T. Odani, *Macromol. Rapid Commun.* **2001**, *22*, 1195.

[7] G. R. Desiraju, *Crystal Engineering: The Design of Organic Solids*, Elsevier, Amsterdam, **1989**.

[8] "Solid-State Supramolecular Chemistry: Crystal Engineering": *Comprehensive Supramolecular Chemistry*, *Vol. 6* (Eds.: D. D. MacNicol, F. Toda, R. Bishop), Pergamon, Oxford, **1996**.

[9] J. W. Steed, J. L. Atwood, *Supramolecular Chemistry*, Wiley, Chichester, **2000**, p. 389.

[10] a) M. D. Hollingsworth, *Science* **2002**, *295*, 2410; b) B. Moulton, M. J. Zaworotko, *Chem. Rev.* **2001**, *101*, 1629; c) K. T. Holman, A. M. Pivovar, M. D. Ward, *Science* **2001**, *294*, 1907; d) T. Kato, *Science* **2002**, *295*, 2414; e) S. I. Stupp, V. LeBonheur, K. Walker, L. S. Li, K. E. Huggins, M. Keser, A. Amstutz, *Science* **1997**, *276*, 384; f) V. Percec, C. H. Ahn, G. Ungar, D. J. P. Yeardley, M. Moller, S. S. Seiko, *Nature* **1998**, *391*, 161; g) H. Engelkamp, S. Middelbeek, R. J. M. Nolte, *Science* **1999**, *284*, 785.

[11] J. Xiao, M. Yang, J. W. Lauher, F. W. Fowler, *Angew. Chem.* **2000**, *112*, 2216; *Angew. Chem. Int. Ed.* **2000**, *39*, 2132.

[12] A. Matsumoto, K. Sada, K. Tashiro, M. Miyata, T. Tsubouchi, T. Tanaka, T. Odani, S. Nagahama, T. Tanaka, K. Inoue, S. Saragai, S. Nakamoto, *Angew. Chem.* **2002**, *114*, 2612; *Angew. Chem. Int. Ed.* **2002**, *41*, 2502.

[13] A. Matsumoto, T. Tanaka, T. Tsubouchi, K. Tashiro, S. Saragai, S. Nakamoto, *J. Am. Chem. Soc.* **2002**, *124*, 8891.

[14] J. A. Elvidge, R. P. Linstead, P. Sims, B. A. Orkin, *J. Chem. Soc.* **1950**, 2235.

[15] a) A. Matsumoto, S. Nagahama, T. Odani, *J. Am. Chem. Soc.* **2000**, *122*, 9109; b) S. Nagahama, K. Inoue, K. Sada, M. Miyata, A. Matsumoto, *Cryst. Growth Des.* **2003**, *3*, 247.

[16] T. Tanaka, A. Matsumoto, *J. Am. Chem. Soc.* **2002**, *124*, 9676.

[17] The stereochemistry of these polymers is represented by the following two kinds of relationships: 1) the relative configuration between the two repeating monomer units: when all the

 © 2004 Wiley-VCH Verlag GmbH & Co. KGaA, Weinheim

repeating units are in a *meso* arrangement the polymer is diisotactic, and when they are *racemo* it is disyndiotactic; 2) the relative configuration between the vicinal carbon centers (also represented by the same term, *meso* and *racemo*): when monomer molecules stack in a translational manner in a column in the crystals, both *Z*,*Z* and *E*,*E* isomers provide an identical *meso*-diisotactic polymer, and the *E*,*Z* isomer provides a *racemo*-diisotactic polymer. On the other hand, both the *Z*,*Z* and *E*,*E* monomers result in the formation of a *racemo*-disyndiotactic polymer when the monomers alternately stack in a column, and the *E*,*Z* monomer produces a *meso*-disyndiotactic polymer. See also refs. [2a] and [15a].

[18] a) A. Matsumoto, T. Odani, K. Sada, M. Miyata, K. Tashiro, *Nature* **2000**, *405*, 328; b) A. Matsumoto, S. Oshita, D. Fujioka, *J. Am. Chem. Soc.* **2002**, *124*, 13749.

[19] a) G. Natta, M. Farina, M. Donati, *Makromol. Chem.* **1961**, *43*, 251; b) M. Donati, G. Perego, M. Farina, *Makromol. Chem.* **1965**, *85*, 301; c) A. Takasu, M. Ishii, Y. Inai, T. Hirabayashi, K. Inomata, *Macromolecules* **2003**, *36*, 7055.

 © 2004 Wiley-VCH Verlag GmbH & Co. KGaA, Weinheim

Molecular Devices

A Molecular Ball Bearing Mediated by Multiligand Exchange in Concert**

*Shuichi Hiraoka, Kaori Hirata, and Mitsuhiko Shionoya**

There is much interest in the development of devices based on molecular motion similar to that seen in living organisms.[1–3] A variety of chemical bonding patterns have been extensively utilized so far for the realization of such molecular devices at the molecular level: for example, covalent bonding for a controlled rotation through single bonds[4,5] and photoisomerized double bonds[6] as well as noncovalent bonding for the formation of interlocked architectures such as rotaxanes[1,7] and catenanes.[8,9] Among the possible modes of noncovalent bonding, metal coordinative bonding shows particular promise for the fabrication of rotational devices, as evidenced by recent excellent reports on mononuclear bisporphyrinate double-decker complexes[10,11] and a functionalized ferrocene derivative.[12] Herein we present a novel rotational device, a molecular ball bearing mediated by metal ions, which is quantitatively formed as a thermodynamically favorable product from three Ag^+ ions and disk-shaped tris-monodentate and hexa-monodentate ligands through a heterotopic, self-assembly process. In the device the three Ag^+ ions serve as the balls for the relative rotational motion of the two disk-shaped ligands by allowing their efficient rotation through a combination of intramolecular, reversible multipoint ligand exchange and flip motions that act in concert.

In a preliminary study we recently constructed a sandwich-type trinuclear Ag^+ complex $[Ag_3(\mathbf{2})_2]$ using two disk-shaped, tris-monodentate thiazolyl ligands **2**. In this complex, each Ag^+ ion is bound by the two thiazolyl nitrogen donors of the two ligands, and all the monodentate ligand rings attached to **2** tilt toward the same direction to form a helical structure. This arrangement is further accompanied by a 120° flipping rotation of the ligands as a result of the *P* versus *M* equilibrium.[13] This system was further advanced to a heterogeneous Ag^+-mediated association of a hexa-monodentate and a tris-monodentate thiazolyl ligands, **1** and **2**, respectively, to form a heterotopic trinuclear complex $[Ag_3(\mathbf{1})(\mathbf{2})]$.[14] In this complex all three nitrogen donors of the tris(thiazolyl) ligand **2** and every alternate nitrogen donor atoms of the hexa(thiazolyl) ligand **1** participate in the complexation with the three Ag^+ ions in a linear coordination geometry (Figure 1b). This heterotopic complex is quantitatively formed by a simple mixing of **1** and **2** in a 1:1 ratio in the presence of three equivalents of Ag^+ ions in CD_3OD. Moreover, the variable-temperature (VT) ^{1}H NMR spectroscopic studies strongly suggested that the intramolecular three-point ligand exchange occurred in concert between the two disk-shaped ligands (namely, $\boldsymbol{M} \rightleftharpoons \boldsymbol{P}$ in Figure 2).[15] In an $\boldsymbol{M} \rightarrow \boldsymbol{P}$ conversion, for example, alternate coordinatively free ligand rings of **1** (rings B, D, and F) in $\boldsymbol{M}$ (with *M* configuration) rotates clockwise and then comes close to the neighboring Ag^+ ion and ligand exchange finally leads to $\boldsymbol{P}$ (with *P* configuration), presumably through formation of a three-coordinate transition state. The thiazolyl rings B, D, and F independently coordinate to each Ag^+ ion in the structure $\boldsymbol{P}$. The $\boldsymbol{M} \rightarrow \boldsymbol{P}$ metal–ligand exchange converts an Ag^+-mediated pair of ligands from a ring 1-Ag-A, 3-Ag-E, and 5-Ag-C in $\boldsymbol{M}$ into a ring 1-Ag-B, 3-Ag-F, and 5-Ag-D in $\boldsymbol{P}$. A 60° rotation from $\boldsymbol{M}$ to $\boldsymbol{M}'$ is realized if a subsequent rewinding of complex $\boldsymbol{P}$ by the flip motion that maintains the linked three pairs take place (Figure 2). Further motions in the clockwise direction as well as in the reverse direction ($\boldsymbol{M}' \rightarrow \boldsymbol{P}$ and $\boldsymbol{P} \rightarrow \boldsymbol{M}$) should occur with equal probability. Therefore, sequential metal–ligand exchanges and flip motions occurring in concert finally give rise to the full relative rotation between the two disk-shaped ligands **1** and **2**.

The previous VT ^{1}H NMR study of the $[Ag_3(\mathbf{1})(\mathbf{2})]$ complex revealed the 60° relative rotational oscillation of the two disk-shaped ligands mediated by multipoint metal–ligand exchanges ($\boldsymbol{M} \rightleftharpoons \boldsymbol{P}$ in Figure 2).[15] We thus examined the dynamic behavior of a similar heterotopic $[Ag_3(\mathbf{1})(\mathbf{5})]$ complex formed from **1** and a tris(thiazolyl) ligand **5** with a C_{2v} symmetry (Figure 3) to obtain evidence for the free

[*] Dr. S. Hiraoka, K. Hirata, Prof. M. Shionoya
Department of Chemistry
Graduate School of Science
The University of Tokyo
Hongo, Bunkyo-ku, Tokyo 113-0033 (Japan)
Fax: (+81) 3-5841-8061
E-mail: shionoya@chem.s.u-tokyo.ac.jp

[**] This study was supported by a Grant-in-Aid for Scientific Research on Priority Area "Dynamic Complex" (No. 15036216), a Grant-in-Aid for Encouragement of Young Scientists (B) (No. 1474036), and a Grant-in-Aid for The 21st Century COE Program for Frontiers in Fundamental Chemistry from the Ministry of Education, Culture, Sports, Science, and Technology of Japan.

Supporting information for this article is available on the WWW under http://www.angewandte.org or from the author.

 © 2004 Wiley-VCH Verlag GmbH & Co. KGaA, Weinheim DOI: 10.1002/anie.200453753

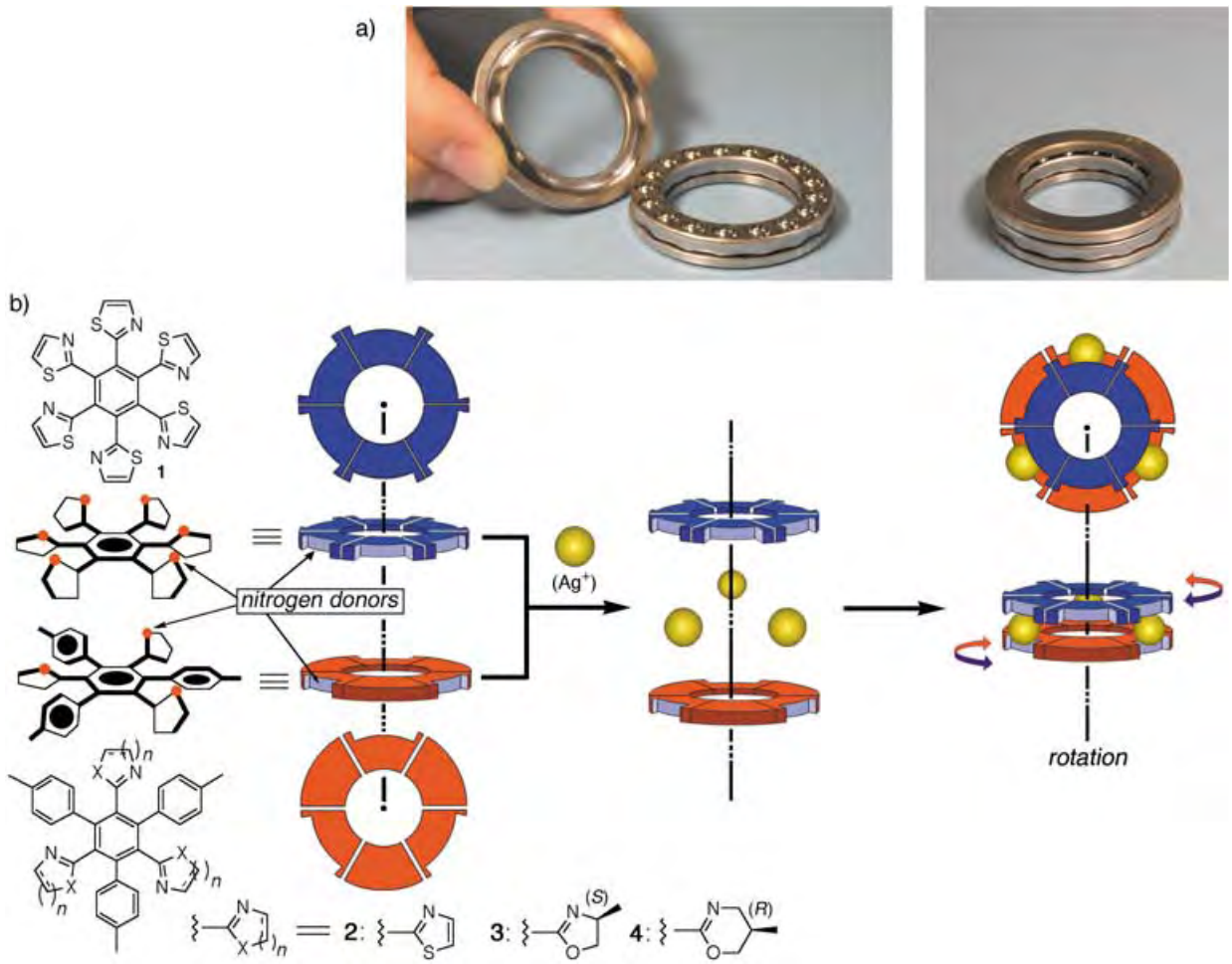


Figure 1. a) A thrust ball bearing, b) the envisioned scheme of the rotation with molecular ball bearings and the disk-shaped ligands used in this study.

rotation of the two disks by the mechanism shown in Figure 2. If the relative rotation between the two disk-shaped ligands **1** and **5** is faster than the NMR timescale, the symmetry of the signals for **1** would not be affected by the less-symmetrical **5** and, as a result, only one set of thiazolyl proton signals should be observed in the spectrum. In the case of slower or no relative rotation, on the other hand, four sets of inequivalent thiazolyl proton signals for rings I–IV should appear for **1**. The quantitative formation of the $[Ag_3(\mathbf{1})(\mathbf{5})]$ complex was unambiguously evidenced by ^{1}H NMR spectroscopy (Figure 3c) and ESI-TOF mass spectrometric measurements in CD_3OD (*m*/*z* 529.9, 842.4, 1779.9: dideuterated $[Ag_3(\mathbf{1})(\mathbf{5})]^{3+}$, $[Ag_3(\mathbf{1})(\mathbf{5})(CH_3SO_3)]^{2+}$, and $[Ag_3(\mathbf{1})(\mathbf{5})(CH_3SO_3)_2]^{+}$, respectively).[16] Upon complexation, the aromatic H^g, H^h, H^i, and H^j protons of **5** were divided into two sets as a consequence of the formation of a sandwich complex in which the inner and outer aromatic protons are inequivalent. This result indicates that the intermolecular ligand exchanges between Ag^+ complexes are slower than the NMR timescale at 293 K,[17] and that the following dynamic spectral changes should, therefore, arise from intramolecular motions. At 293 K, the H^a and H^b protons of **1** were observed as one set of signals at $\delta = 7.90$ and 7.67 ppm, respectively (Figure 3c), which indicates that the six thiazolyl rings of **1** in the $[Ag_3(\mathbf{1})(\mathbf{5})]$ complex are equivalent. This result reveals that the two disk-shaped ligands connected by three Ag^+ ions rotate freely and faster than the NMR timescale at 293 K. In contrast, cooling the sample to 213 K resulted in the H^a resonances dividing into three distinct signals in a 1:2:3(1:2) ratio (Figure 3g), thus showing that the thiazolyl rings of **1** are inequivalent as a consequence of the slower relative rotation of the opposite ring **5**. These results taken together lead us to conclude that the intramolecular relative rotation between the two disk-shaped ligands in $[Ag_3(\mathbf{1})(\mathbf{2})]$ and $[Ag_3(\mathbf{1})(\mathbf{5})]$ takes place in concert, and that the three Ag^+ ions positioned between the tris- and hexa-monodentate ligands can act as both couplers and mediators for the rotational motion.[18]

To investigate the rotation mechanism in detail, optically active tris-monodentate nitrogen ligands (*S*)-**3** and (*R*)-**4** were used in the VT ^{1}H NMR study, in the expectation that the *P*- and *M*-helical isomers could be distinguished as diastereomers at low temperatures. The tris(oxazolyl) and tris(oxazinyl) ligands **3** and **4**, respectively, were found to heterogeneously associate with **1** in the presence of three equivalents of Ag^+ ions, as observed with **2**. The quantitative formation of $[Ag_3(\mathbf{1})(\mathbf{3})]$ and $[Ag_3(\mathbf{1})(\mathbf{4})]$ were similarly confirmed by the

 © 2004 Wiley-VCH Verlag GmbH & Co. KGaA, Weinheim

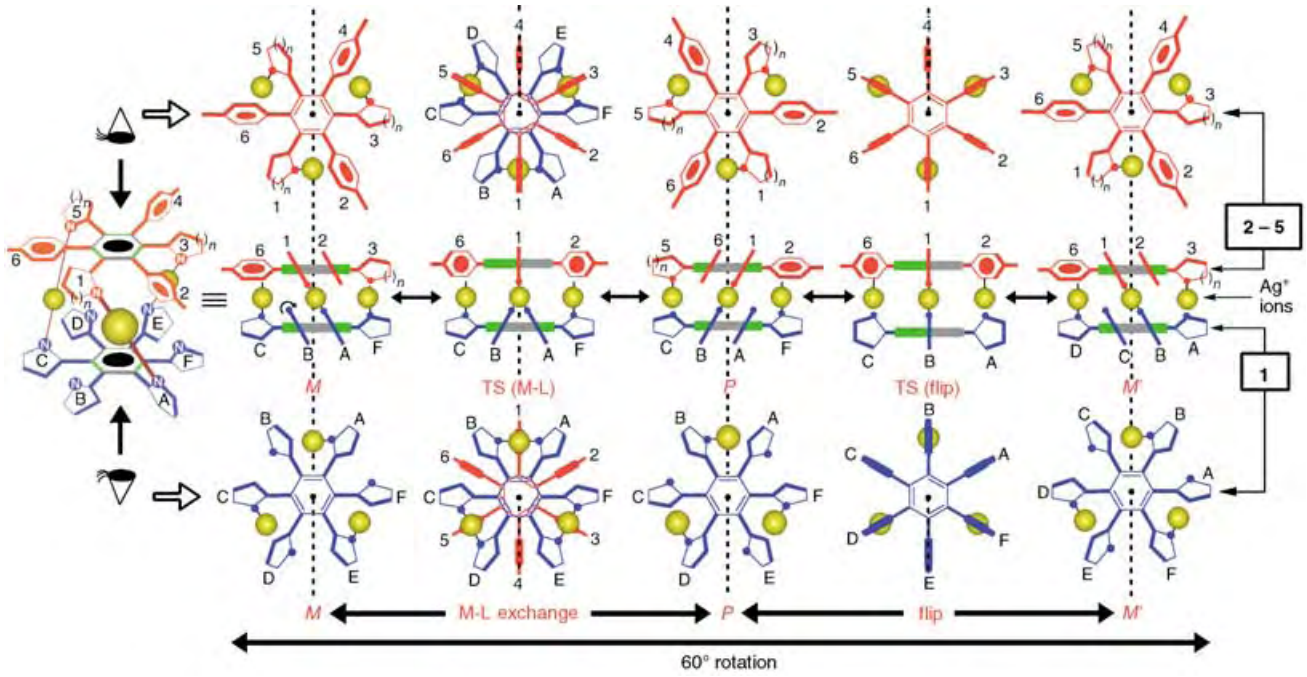


Figure 2. A plausible rotation mechanism of the Ag^+ sandwich complex with the aid of the metal–ligand (M-L) exchange and flip motion. In the M-L exchange from ***M*** to ***P***, the binding pairs of the rings between the two ligands through Ag^+ ions change from 1-A, 3-E, and 5-C in ***M*** to 1-B, 3-F, and 5-D in ***P*** with a conversion of the helicity from *P* into *M*. The subsequent flip motion maintaining the binding pairs converts the chirality of the structure from ***P*** into ***M***′. A combination of concerted M-L exchange at the three Ag^+ centers (***M*** ⇌ ***P***) and a flip motion (***P*** ⇌ ***M***′) finally allows a 60° rotational motion. Sequential M-L exchanges and flip motions results in the relative free rotation between the two disk-shaped ligands.

^{1}H NMR spectroscopic and ESI mass spectrometric measurements.[16] The proton signals for the six thiazolyl rings of **1** were equivalent in both [Ag_3(**1**)(**3**)] and [Ag_3(**1**)(**4**)] complexes at 293 K, thus indicating their faster rotation relative to the NMR timescale (Figure 4a, f). Cooling the sample of [Ag_3(**1**)(**3**)] to 213 K resulted in the thiazolyl proton signals for H^a and H^b being divided into two sets ($\delta = 7.85$, 7.76 (overlapped), and 7.59 ppm), while the signals of the tris-monodentate ligand **3** did not show any changes, probably because the metal–ligand exchange becomes slower than the NMR timescale while the flip motion is still faster (Figure 4e). These results suggest that the energy barrier of the metal–ligand exchange $\Delta G^{\ddagger}_{M\text{-}L}$ is greater than that of the flip motion $\Delta G^{\ddagger}_{flip}$.[19] In contrast, each signal of both the thiazolyl protons of **1** and the aromatic protons of **4** were divided into two sets at temperatures around 223 K in the case of the [Ag_3(**1**)(**4**)] complex (Figure 4i). Four sets of signals for the thiazolyl protons of **1** and two sets of signals for **4** were observed at 203 K (Figure 4k),[20] which indicates that the coordinating and uncoordinating thiazolyl rings of the hexa-monodentate ligand **1** are distinguishable in both the *P* and *M* diastereomers of the [Ag_3(**1**)(**4**)] complex because both the metal–ligand exchange and the flip processes are slower. From these spectral changes we concluded that $\Delta G^{\ddagger}_{flip}$ is equal to or greater than $\Delta G^{\ddagger}_{M\text{-}L}$ in [Ag_3(**1**)(**4**)] ($\Delta G^{\ddagger}_{flip} \geq \Delta G^{\ddagger}_{M\text{-}L}$). In such a case, at temperatures at which the flip motion becomes slower than the NMR timescale but the metal–ligand exchange is still faster, the *P* and *M* isomers can not be observed separately because of the rapid intraconversion through the metal–ligand exchange process (***M*** ⇌ ***P*** in Figure 2). Therefore, the NMR signals do not show any significant changes. Furthermore, cooling down the solutions to temperatures at which the metal–ligand exchange becomes slower than the NMR timescale should result in the signals for the hexa-monodentate ligand **1** and the tris-monodentate ligand **4** being divided simultaneously. In fact, the energy difference between the metal–ligand exchange and the flip motion was affected by the nature of the monodentate ligand rings bound to the Ag^+ ions. The destabilization of the transition state in the flip motion was particularly noticeable for the [Ag_3(**1**)(**4**)] complex containing the six-membered ligand rings of **4**. Such a marked tendency is consistent with our previous findings.[13] These results suggest that the rate or frequency of their rotation is controllable through the effect of the size of the tris-monodentate ligands on the flip processes.

In summary, we have established a quantitative formation of a novel molecular thrust ball bearing consisting of three Ag^+ ions as balls and two disk-shaped multi-monodentate ligands as nanosized bearings. This molecular ball bearing allows the relatively free rotation of two ligands connected by three Ag^+ ions that is mediated by sequential, multiligand exchanges and flip motions occurring in concert. Finally, a rotational rate (approximately 8000 rotations per second at 298 K) was obtained for [Ag_3(**1**)(**2**)] from the VT ^{1}H NMR study.[20] Furthermore, the energy barriers between the $P \rightarrow M$ and the $M \rightarrow P$ processes in ball bearings using chiral ligands could be differentiated from each other as a result of the difference in stability between the *P* and *M* diastereomers. Such ball bearings could work as parts of chiral molecular

 © 2004 Wiley-VCH Verlag GmbH & Co. KGaA, Weinheim

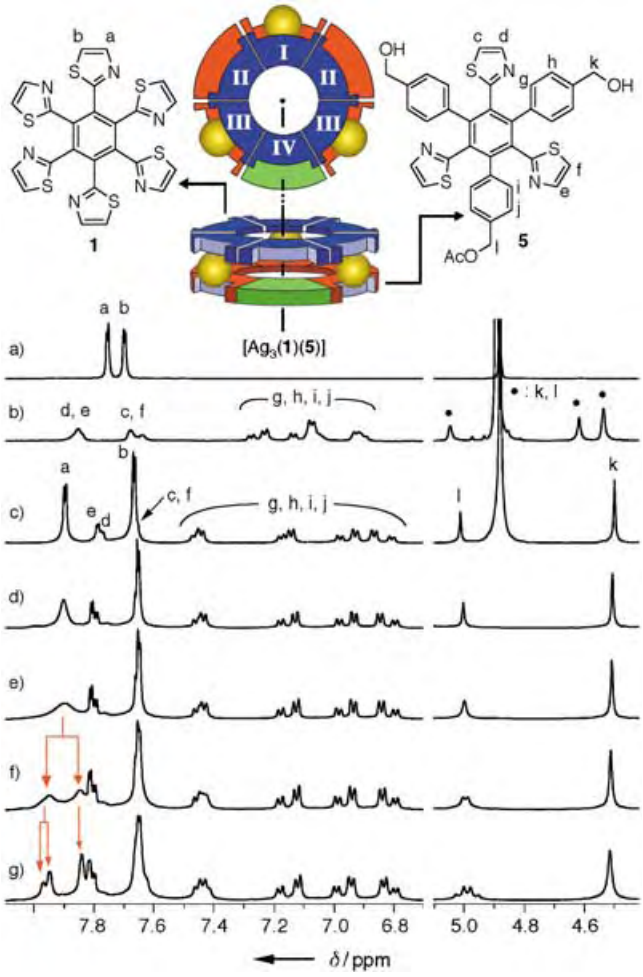


Figure 3. ^{1}H NMR spectra (500 MHz, CD_3OD): a) **1** + 3 equiv of $AgCH_3SO_3$,b) $[Ag_3(\mathbf{5})_2]$ at 293 K, c) $[Ag_3(\mathbf{1})(\mathbf{5})]$ at 293 K, d) $[Ag_3(\mathbf{1})(\mathbf{5})]$ at 243 K, e) $[Ag_3(\mathbf{1})(\mathbf{5})]$ at 233 K, f) $[Ag_3(\mathbf{1})(\mathbf{5})]$ at 223 K, g) $[Ag_3(\mathbf{1})(\mathbf{5})]$ at 213 K.

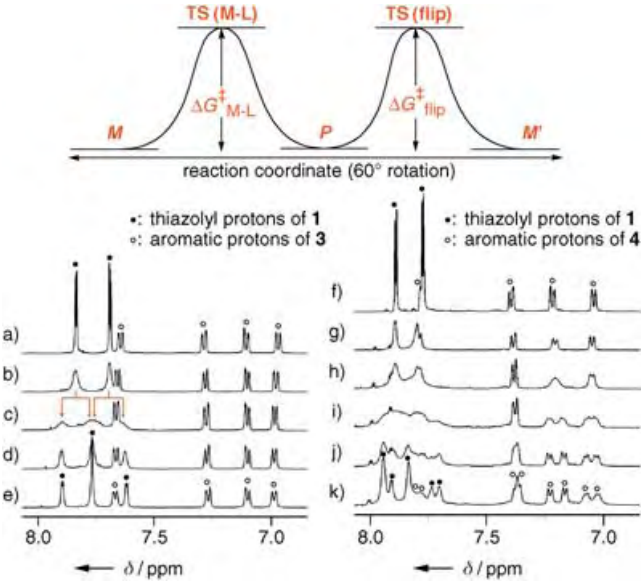


Figure 4. Schematic representation of a reaction coordinate for 60° rotation, and partial ^{1}H NMR spectra (500 MHz, CD_3OD) of $[Ag_3(\mathbf{1})(\mathbf{3})]$ (a)–(e) and $[Ag_3(\mathbf{1})(\mathbf{4})]$ (f)–(k). a) 293 K, b) 253 K, c) 233 K, d) 223 K, e) 213 K, f) 293 K, g) 243 K, h) 233 K, i) 223 K, j) 213 K, k) 203 K.

motors which make unidirectional rotation feasible in a controlled manner with the aid of external energy sources.

Received: January 14, 2004
Revised: April 28, 2004 [Z53753]

Keywords: ligand exchange · molecular recognition · self-assembly · silver · supramolecular chemistry

[1] V. Balzani, *Molecular Devices and Machines: A Journey into the Nano World*, Wiley-VCH, Weinheim, **2003**.
[2] L. Raehm, J.-P. Sauvage, *Structure and Bonding*, Springer, Berlin, **2001**, pp. 99–78.
[3] Special issue on molecular machines: *Acc. Chem. Res.* **2001**, *34*, 409–522.
[4] T. R. Kelly, H. De Silva, R. A. Silva, *Nature* **1999**, *401*, 150–152.
[5] T. C. Bedard, J. S. Moore, *J. Am. Chem. Soc.* **1995**, *117*, 10662–10671.
[6] N. Koumura, R. W. J. Zijistra, R. A. Van Delden, N. Harada, B. L. Feringa, *Nature* **1999**, *401*, 152–155.
[7] C. A. Schalley, K. Beizal, F. Vögtle, *Acc. Chem. Res.* **2001**, *34*, 465–476.
[8] M. C. Jimenez-Molero, C. Dietrich-Buchecker, J.-P. Sauvage, *Chem. Commun.* **2003**, 1613–1616.
[9] D. A. Leigh, J. K. Y. Wong, F. Dehez, F. Zerbetto, *Nature* **2003**, *424*, 174–179.
[10] M. Ikeda, M. Takeuchi, S. Shinkai, F. Tani, Y. Naruta, S. Sakamoto, K. Yamaguchi, *Chem. Eur. J.* **2003**, *9*, 5542–5550.
[11] K. Tashiro, K. Konishi, T. Aida, *J. Am. Chem. Soc.* **2000**, *122*, 7921–7926.
[12] T. Muraoka, K. Kinbara, Y. Kobayashi, T. Aida, *J. Am. Chem. Soc.* **2003**, *125*, 5612–5613.
[13] S. Hiraoka, K. Harano, T. Tanaka, M. Shiro, M. Shionoya, *Angew. Chem.* **2003**, *115*, 5340–5343; *Angew. Chem. Int. Ed.* **2003**, *42*, 5182–5185; for a recent report on the molecular motion of multinuclear metal complexes and a detailed discussion on the NMR spectroscopic study, see: R. W. Saalfrank, C. Deutsher, H. Maid, A. M. Ako, S. Sperner, T. Nakajima, W. Bauer, F. Hampel, B. A. Heß, N. J. R. van Eikema Hommes, R. Puchta, E. W. Heinemann, *Chem. Eur. J.* **2004**, *10*, 1899–1905.
[14] S. Hiraoka, M. Shiro, M. Shionoya, *J. Am. Chem. Soc.* **2004**, *126*, 1214–1218.
[15] The ^{1}H NMR spectrum of $[Ag_3(\mathbf{1})(\mathbf{2})]$ showed only one set of the thiazolyl protons of **1** ($\delta = 7.90$ (d, $J = 3.3$ Hz, 6H), 7.64 ppm (d, $J = 3.3$ Hz, 6H)) above 263 K. Upon cooling the sample down to 213 K the thiazolyl signals were divided into two sets ($\delta = 7.96$ (d, $J = 3.3$ Hz, 3H), 7.83 (d, $J = 3.3$ Hz, 3H), 7.64 (d, $J = 3.3$ Hz, 3H), 7.62 ppm (d, $J = 3.3$ Hz, 3H)), whereas the signals of **2** did not show any changes. The VT ^{1}H NMR results of the $[Ag_3(\mathbf{1})(\mathbf{2})]$ and the discussion on the energy barrier of the metal–ligand exchange are described in detail in ref. [14].
[16] See Supporting Information.
[17] In the ^{1}H NMR titration studies using **1** and **5**, the signals of $[Ag_3(\mathbf{1})(\mathbf{5})]$ and $[Ag_3(\mathbf{5})_2]$ ($[\mathbf{5}] > [\mathbf{1}]$) or those of $[Ag_3(\mathbf{1})(\mathbf{5})]$ and unidentified Ag^+ complexes with **1** ($[\mathbf{5}] < [\mathbf{1}]$) were independently observed. These results also support the relatively slow intermolecular ligand exchanges in the Ag^+ complexes.
[18] The relatively free rotation of the two disks in the ball bearings contains every rotational motion produced by the combination of the metal–ligand exchange and the flip motion between the *P* and *M* isomers, such as a 360° full rotation and a back and forth movement.
[19] In the chiral $[Ag_3(\mathbf{1})(\mathbf{3})]$ and $[Ag_3(\mathbf{1})(\mathbf{4})]$ complexes, the stabilities of the *P* and *M* isomers would be different from each other for each case, and therefore the energy barriers of both the

 © 2004 Wiley-VCH Verlag GmbH & Co. KGaA, Weinheim

metal–ligand exchange and the flip motion from *P* to *M* ($\Delta G^{\ddagger}_{\text{M-L}(P\rightarrow M)}$ and $\Delta G^{\ddagger}_{\text{flip}(P\rightarrow M)}$) should be different from those of *M* to *P* ($\Delta G^{\ddagger}_{\text{M-L}(M\rightarrow P)}$ and $\Delta G^{\ddagger}_{\text{flip}(M\rightarrow P)}$, respectively; namely, $\Delta G^{\ddagger}_{\text{M-L}(P\rightarrow M)} \neq \Delta G^{\ddagger}_{\text{M-L}(M\rightarrow P)}$ and $\Delta G^{\ddagger}_{\text{flip}(P\rightarrow M)} \neq \Delta G^{\ddagger}_{\text{flip}(M\rightarrow P)}$). Here we discuss the relative energy differences between the energy barriers of the ligand exchanges and the flip motions using the greater one in each motion.

[20] Four sets of thiazolyl signals for the [Ag_3(**1**)(**4**)] complex at 203 K were confirmed by its H-H COSY spectrum, as shown in the Supporting Information.

[21] From the VT ^{1}H NMR studies for the molecular motion of the [Ag_3(**1**)(**2**)] complex, in which the metal–ligand exchange is the rate-determining step ($\Delta G^{\ddagger}_{\text{M-L}} \gg \Delta G^{\ddagger}_{\text{flip}}$), the rate constant of the intramolecular ligand exchange at 298 K can be calculated to be approximately 49000 s^{-1}.[14] The rate of a single 360° rotation is at least six times greater than the rate of metal–ligand exchange, and hence the maximum rotation rate can be estimated to be about 8000 rps.

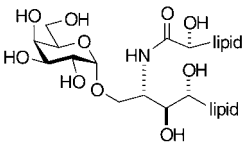
 © 2004 Wiley-VCH Verlag GmbH & Co. KGaA, Weinheim

Biologically Active Compounds

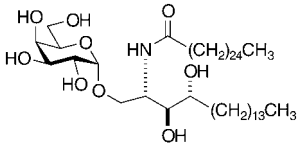
The C-Glycoside Analogue of the Immunostimulant α-Galactosylceramide (KRN7000): Synthesis and Striking Enhancement of Activity**

*Guangli Yang, John Schmieg, Moriya Tsuji, and Richard W. Franck**

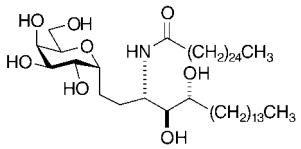
In the early 1990s a research group at Kirin Pharmaceuticals reported their results from screening lipophilic extracts from the Okinawan sponge *Agelas mauritianus*. When their extracts were tested in mice, but not in cell culture, they observed potent antitumor activity by glycolipids that they named the agelasphins (**1**).[1] Structure–activity studies of compounds available through synthesis revealed that a slightly simpler analogue of the natural agelasphins, an α-galactosyl ceramide named KRN7000 (**2**), had the best activity of the compounds tested, and that the functional groups and configuration of **2** were optimal. The only acceptable variables are the lengths of the lipid chains, the insertion of "taggants" at the terminus of the fatty amide chain through amide linkages, substitution at C6 of the galactose residue, the removal of the hydroxy group at C4 of the phytosphingosine moiety, and the presence or absence of an α hydroxy group in the fatty amide.[2]



1: agelasphins



2: KRN7000



3: C-glycoside analogue

Since the initial disclosures by the Kirin group, a multifaceted exploration of the biological effects of KRN7000 has unveiled its remarkable activity against a disparate group of diseases, such as cancer, including melanoma,[3] hepatic metastases of pancreatic cancer,[4] hepatic metastases of colon cancer,[5] and primary tumor formation in three different models,[6] as well as malaria,[7] juvenile diabetes,[8] hepatitis B,[9] and autoimmune encephalomyelitis,[10] in murine/whole animal versions of all the diseases. Although no activity against cell-culture versions of the diseases is ever detected, in vitro activity can be measured by incubating the glycolipid with antigen-presenting dendritic cells or their isolated CD1d receptors and then challenging NKT-cell hybridomas with the resulting complex.[11] This explosion of research has led to that finding that the unifying mechanism of action of KRN7000 is its remarkable ability to induce a potent expansion of Vα24+NKT cells. The sequence of events is: 1) the galactosyl ceramide binds to the CD1d receptor of antigen-presenting cells, then 2) the ceramide receptor complex binds to NKT cells, which stimulate a cascade of cytokines: signals for the processes that result in the suppression of the disease.[12] It is not yet known why an α-galactosyl ceramide of marine origin should be recognized by a mammalian receptor and elicit a spectacular immune response. It has also not been established whether an endogenous mammalian substance exists as the "natural" ligand for the CD1d receptor. Suffice to say that KRN7000 is a potent lead compound for the development of immunostimulant drugs.[13]

In our search for challenging targets that might showcase our application of the Ramberg–Bäcklund reaction for C-

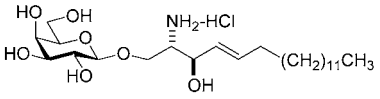
[*] Dr. G. Yang, Prof. Dr. R. W. Franck
Department of Chemistry
Hunter College of CUNY
New York, NY 10021 (USA)
Fax: (+1) 212-772-5332
E-mail: rfranck@hunter.cuny.edu
J. Schmieg
Department of Medical and Molecular Parasitology
New York University School of Medicine
New York, NY (USA)
Prof. Dr. M. Tsuji
Department of Medical and Molecular Parasitology
New York University School of Medicine
New York and Aaron Diamond AIDS Research Center
The Rockefeller University
New York, NY (USA)

[**] The synthesis research at Hunter College was supported by grants from the NIH (GM 60271) to R.W.F. and NIH-RCMI (RR03037) to the college for chemistry department infrastructure. The bioassay research at NYU Medical School was supported by grants from the NIH (AI 45606, AI 01682, and AI 47840) to M.T.

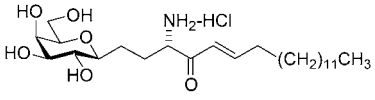
Supporting information for this article is available on the WWW under http://www.angewandte.org or from the author.

 © 2004 Wiley-VCH Verlag GmbH & Co. KGaA, Weinheim DOI: 10.1002/anie.200454215

glycoside synthesis, we chose to prepare **3**, the nearest C-glycoside analogue of **2**, on the basis of the well-known rationale for the study of C-glycosides, namely that the O-glycoside may be susceptible to enzymatic degradation, whereas the corresponding C-glycoside is not. That the lability of **2** may be a problem is conjecture by the present authors, as little has been published about the metabolism of KRN7000 in mammals.[14] The C-glycoside concept has existed for many years and has been thoroughly reviewed.[15] It is fair to conclude that comparisons of bioactivities of synthetic C-glycosides with those of their O-glyco parents have uncovered some examples of similar activity,[16] many of diminished activity,[17] and none of significant improvement. The most apposite data for our ceramide project are those of Bertozzi et al., who compared the binding of the closely matched, but not identical β-O- and β-C-glycosides **4** and **5** to



4: 96% inhibition of binding of β-GalCer with gp120 at 1 mg mL^{-1}; IC_{50} = 160 μm



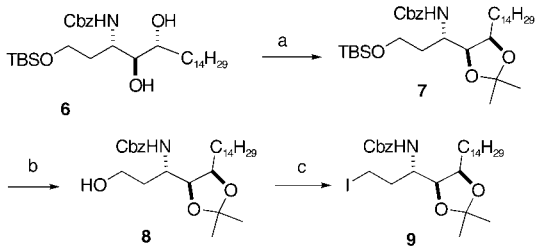
5: 86% inhibition of binding of β-GalCer with gp120 at 1 mg mL^{-1}; IC_{50} = 120 μm

a gp120 receptor. The binding constants of the two compounds were similar, and no kinetic data was presented to show that the longer lifetime of the C-glycoside had any effect.[18] There are a few examples of C-glycoside constructs that are not analogous to any specific O-glycoside. For example, Schmidt and co-workers recently described a C-glycoside mimetic of a complex proposed to be important in galactosyl transfer.[19] Although syntheses of C-glycosyl sphingosine substances somewhat related to **3** have been reported by two other research groups,[20] these groups have not reported the synthesis of the same analogue of KRN7000 prepared by us.

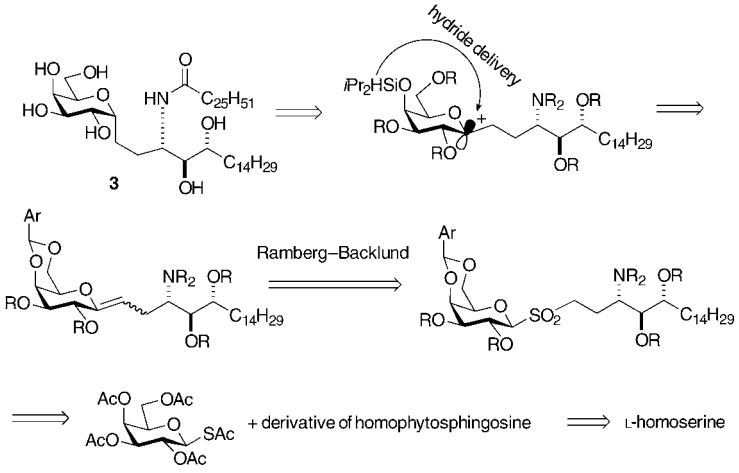
In our first approach to **3**, outlined retrosynthetically in Scheme 1, we embarked on a route with a Ramberg–Bäcklund (RB) reaction to "stitch" a homophytosphingosine side chain to galactose as the key feature, as our group had had previous success with this method for C-glycoside synthesis.[21] A second component of our plan was to establish the desired anomeric configuration through an intramolecular hydride transfer from a silyl group to an intermediate carbocation center.

The six-step synthetic route from commercially available L-homoserine to the homophytosphingosine component **6** is described in the Supporting Information. The sequence mimics a synthesis of phytosphingosine reported by Nakanishi and co-workers in which L-serine was used as the starting material.[22] The Cbz-substituted homophytosphingosine **6** was then converted into the iodo derivative **9** in anticipation of the ensuing S-glycoside formation (Scheme 2).[23]

The synthesis was continued by treatment of the galactose thioacetate **10** with hydrazinium acetate in DMF under nitrogen to deprotect the thiol,[24] which was subsequently treated with the electrophile **9** and triethylamine to provide the β-D-thiogalactoside **11** in 90% overall yield (Scheme 3). Treatment of **11** with NaOMe in MeOH to cleave the remaining four acetate groups followed by protection of the 4- and 6-hydroxy groups with *p*-methoxybenzaldehyde dimethyl acetal and *p*-toluenesulfonic acid produced the 4,6-*O*-(4-methoxybenzylidene)-β-D-1-thiogalactoside **12** in 86% yield.[25] Sodium hydride promoted benzylation of the remaining hydroxy groups of **12**,



Scheme 2. Synthesis of an iodo derivative of homophytosphingosine: a) $(CH_3)_2C(OMe)_2$, PPTS, CH_2Cl_2, 95%; b) nBu_4NF, AcOH, THF, 86%; c) I_2, PPh_3, THF, reflux, 85%. Cbz = benzyloxycarbonyl, PPTS = pyridinium *p*-toluenesulfonate.

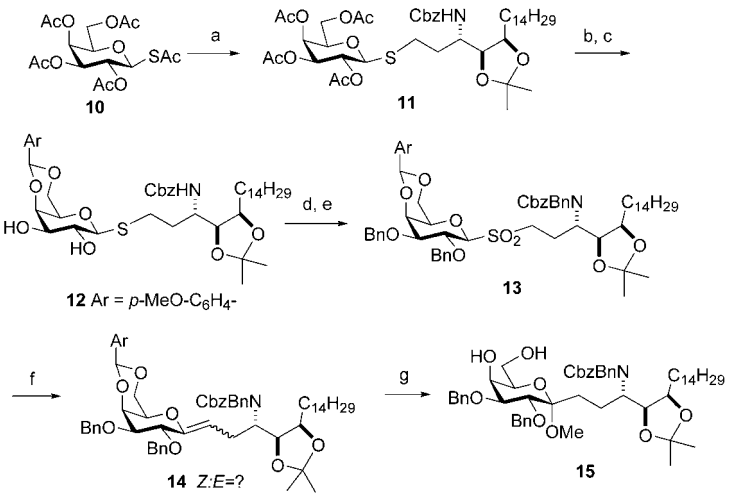


Scheme 1. Retrosynthesis of a C-glycoside analogue of KRN7000.

followed by oxidation of the thiogalactoside with MMPP, gave the sulfonyl galactoside **13** in good yield. We could not avoid *N*-benzylation in this step.

The RB reaction of **13** in the presence of $C_2F_4Br_2$, *t*BuOH, and KOH–Al_2O_3 at reflux afforded the product **14**. The *Z*:*E* ratio of alkene isomers was not determined because of the peak broadening in the NMR spectra. The 1-*O*-methyl-2,3-*O*-dibenzyl-β-galactoside **15** was prepared in one step from **14** by using chlorotrimethylsilane in methanol. At this stage, preliminary experiments with BF_3-catalyzed hydride transfer revealed that the isopropylidene protecting group was not sufficiently robust. It was therefore exchanged for a carbonate group. However, this carbonate protecting group would not be suitable for the RB step, in which KOH is required.

 © 2004 Wiley-VCH Verlag GmbH & Co. KGaA, Weinheim

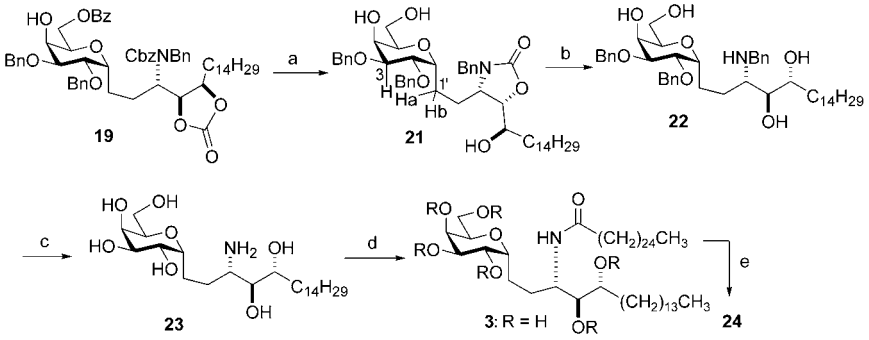


Scheme 3. Formation of the C-glycoside linkage: a) 1. NH_2NH_2, AcOH, DMF; 2. **9**, Et_3N, 90%; b) NaOMe, MeOH; c) *p*-$(MeO)C_6H_4CH(OMe)_2$, *p*-TsOH, DMF, CH_2Cl_2, 86% (2 steps); d) NaH, BnBr, THF, 83%; e) MMPP, THF, H_2O, EtOH, 60°C, 93%; f) $C_2F_4Br_2$, *t*BuOH, KOH, Al_2O_3, reflux, 70%; g) TMSCl, MeOH, 0°C, 66%. Bn = benzyl, DMF = *N*,*N*-dimethylformamide, MMPP = magnesium monoperoxyphthalate, TMS = trimethylsilyl, Ts = toluenesulfonyl.

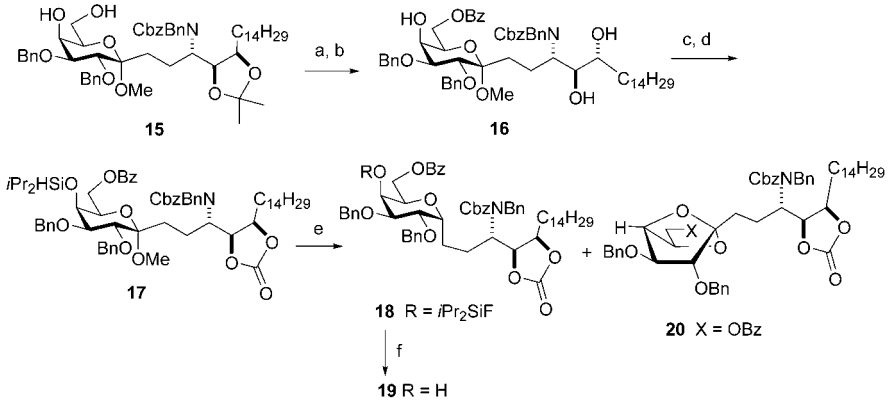
Our protecting-group manipulations began with **15**, whereby esterification of the primary hydroxy group at C6 and cleavage of the acetonide group afforded the corresponding diol **16** in good yield (Scheme 4). Cyclic carbonation of the diol in the presence of triphosgene followed by silylation of the axial hydroxy group at C4 then afforded the silyl ether **17**.[26] The controlled addition with a syringe pump of **17** as a solution in CH_2Cl_2 (0.01M) to $BF_3{\cdot}Et_2O$ (5 equiv) in CH_2Cl_2 afforded the α-C-galactosides **18** and **19**, as well as the 1,4-anhydro compound **20** (15%).[27] Treatment of the silyl ether **18** with Bu_4NF (1N) in THF afforded the product **19** (combined yield of 76%), which was identified by ^{1}H NMR spectroscopy (δ(anomeric H) = 3.95 ppm, J_{12} = 4.6 Hz).

The final deprotection steps prior to the ultimate amidation to form the target compound **3** were more challenging than anticipated. The total debenzylation of compound **19** failed under a variety of conditions, including with the Pearlman catalyst (H_2, 20% $Pd(OH)_2$, 30 psi), Birch reduction (Na/liquid NH_3), with 10% Pd/C, and with 4.4% formic acid in methanol. We therefore elected to remove the carbonyl protecting groups before the hydrogenolytic debenzylation process (Scheme 5).

Compound **19** was treated with NaOH at reflux in a mixture of dioxane and H_2O (1:1) to afford the oxazolidinone **21**, which was fully characterized. NOE effects were observed between 3-H and 1′-Ha or b, and between 5-H and 1′-Ha or b, which confirmed that the configuration of compound **21** (and hence **19**) was correctly assigned (α isomer). Hydrolysis of **21** (at reflux in KOH/EtOH) gave the *N*-benzylamine **22**, which was fully debenzylated by transfer hydrogenolysis (10% Pd/C, cyclohexene, reflux) to afford crude **23** in 80% overall yield.[28] The fatty amide chain was then introduced by using *p*-nitrophenyl hexadecanoate as the acylating agent[2a] to afford the target **3** in 60% yield. Final purification was carried out by flash chromatography on silica gel (eluant: $CHCl_3$/MeOH 4:1). The ^{1}H and ^{13}C NMR spectra, optical rotation value ($[\alpha]_D^{25} = +40.8$ (c = 0.13, pyridine)), m.p. (175–178°C), and high resolution MS (FAB) spectrum: m/z = 856.7601 ($C_{51}H_{101}O_8N+H^+$ requires 856.7605) served to fully characterize a sample of **3**. The mass spectrum and ^{1}H NMR spectrum of fully acylated **24** further confirmed the structure of **3**. Interestingly, the optical rotation value and NMR data for the O- and C-glycosides showed



Scheme 5. Removal of protecting groups followed by ceramidation: a) 1,4-dioxane, H_2O, NaOH, reflux, >90%; b) KOH, EtOH, reflux, 80%; c) 10% Pd/C, cyclohexene, HCl (1N), MeOH, reflux, >90%; d) *p*-nitrophenyl hexadecanoate, THF, DMAP, 48 h, room temperature, 60%; e) Ac_2O, DMAP, 80%. DMAP = 4-dimethylaminopyridine.



Scheme 4. Introduction of the α-C-glycoside linkage: a) BzCl, Et_3N, CH_2Cl_2, 88%; b) HCl (1N), Et_2O, MeOH, 80%, c) triphosgene, pyridine, CH_2Cl_2, 83%; d) iPr_2SiHCl, imidazole, DMF, 96%; e) $BF_3{\cdot}OEt_2$ (5 equiv), CH_2Cl_2, 0°C; f) TBAF, THF. Bz = benzoyl, TBAF = tetrabutylammonium fluoride.

 © 2004 Wiley-VCH Verlag GmbH & Co. KGaA, Weinheim

a remarkable congruence, except for the chemical shifts of C1, C1′, and C2′.[29]

The coupling constant of 8.8 Hz between 2-H and 3-H of the galactose unit of **3** suggests that the $^4C_1$ chair (as drawn) is the principal conformer. Whereas the anomeric effect of the O-glycoside serves to compensate for the steric repulsions of the axial ceramide moiety, there is no such compensation in the C-glycoside analogue, so its actual conformation can not be assumed to be a chair. For example, Veyrières and co-workers reported two examples of α-C-galactosides for which the coupling constants clearly show that the standard chair can not be the principal conformer.[30]

A range of assays were carried out in which **3** was found to show outstanding activity, even in comparison with the very active O-glycoside **2**. In the following we summarize the results of these assays, which clearly demonstrate the excellent potential of C-glycoside analogues as therapeutic agents.

One assay that was carried out was a mouse malaria model, whereby mice were treated with galactosyl ceramide and then, after an interval, were challenged with malaria (*P. yoeli*).[31] After a further interval, the animals were sacrificed, and their livers were assayed for the sporozoite stage of malaria. Both the O- and the C-glycoside **2** and **3** were very effective at reducing sporozoite levels at a dosage level of 1 μg per mouse relative to the control. However, the C-glycoside **3** continued to show excellent activity at the 1-ng level. Thus, **3** is approximately 1000 times more protective than the O-glycoside (Figure 1).

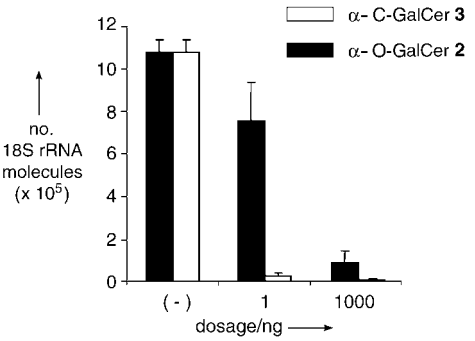


Figure 1. Assay for sporozoites in mouse liver with 1) no glycolipid, 2) 1 ng of **2** or **3**, and 3) 1 μg of **2** or **3**. Number of *P. Yoelii* specific 18S rRNA molecules (determined 42 h after challenge with 10000 viable sporozites) is plotted against dosage of **2** or **3**.

The results of this experiment do not show explicitly that the lifetime of the glycoside is a factor in the activity difference observed between **2** and **3**. Therefore, a "kinetics" experiment was carried out. The interval between the administration of the glycolipid and sporozoite challenge was varied. These experiments showed that the C-glycoside is effective with intervals of up to four days between drug dosage and challenge, whereas the O-glycoside is effective with only a one-day interval. One interpretation of these results is that the C-glycoside is not degraded by endogenous α-galactosidases, whereas the O-glycoside is; thus, the C-glycoside can remain active in the mouse for a longer period of time. Another argument could be that different forms of binding to the important receptors takes place, with the C-glycoside analogue favoring more effective signaling cascades in the immune system. Even though the former explanation is most consistent with the prevalent hypothesis of the merit of C-glycosides, we believe that our detailed bioassay data, presented elsewhere, favor the latter.[32]

A second assay carried out was a melanoma challenge in C57BL/6 mice. The animals were treated with either the C-glycoside or the O-glycoside 2 days before the challenge with B16 melanoma cells. In these mice, the melanoma attacks the lungs. The mice were sacrificed after two weeks and their lungs were examined visually for melanomas (black spots). Figure 2 hardly needs an explanation. It is clear that the C-glycoside at the 10-ng dosage level is far more effective than the O-glycoside at the same dose. In fact, detailed dose–response experiments showed that the C-glycoside **3** was 100 times more effective than the O-glycoside **2** in this assay.



Figure 2. Melanoma appearance (black spots) on mouse lung after two weeks: untreated or treated with 10 ng of **2** or **3**.

These very promising initial results leave many important questions unanswered. More studies are required to extend these findings, including the preparation of more analogues in the search for compounds with greater potency, extensive bioassays to determine the effectiveness of these materials in other disease models, and modelling and biophysical studies to find an explanation for the dramatic difference between C- and O-glycosides in this series.

The experiments with animals were carried out with the permission of the Institutional Animal Care and Use Committee at New York University School of Medicine. The Laboratory Animal Protocol number is #4627-02 in the context of NIH/GM60271.

Received: March 8, 2004 [Z54215]
Published Online: June 30, 2004

Keywords: biological activity · C-glycosides · drug design · immunostimulants · Ramberg–Bäcklund reaction

[1] a) T. Natori, M. Morita, K. Akimoto, Y. Koezuka, *Tetrahedron* **1994**, *50*, 2771–2784; b) similar substances have been isolated from *Agelas Clathrodes* by the Mangoni research group: V. Costantino, E. Fattorusso, C. Imperatore, A. Mangoni, *J. Org. Chem.* **2004**, *69*, 1174–1179, and references therein.

 © 2004 Wiley-VCH Verlag GmbH & Co. KGaA, Weinheim

[2] a) M. Morita, K. Motoki, K. Akimoto, T. Natori, T. Sakai, E. Sawa, K. Yamaji, Y. Koezuka, E. Kobayashi, H. Fukushima, *J. Med. Chem.* **1995**, *38*, 2176 – 2187; b) Y. Vo-Hoang, L. Micouin, C. Ronet, G. Gachelin, M. Bonin, *ChemBioChem* **2003**, *4*, 27 – 33; c) T. Sakai, O. Naidenko, H. Iijima, M. Kronenberg, Y. Koezuka, *J. Med. Chem.* **1999**, *42*, 1836 – 1841; d) T. Sakai, H. Ehara, Y. Koezuka, *Org. Lett.* **1999**, *1*, 359 – 361; e) X. T. Zhou, C. Forestier, R. D. Goff, C. Li, L. Teyton, A. Bendelac, P. B. Savage, *Org. Lett.* **2002**, *4*, 1267 – 1270; f) T. Sakai, M. Morita, N. Matsunaga, K. Akimoto, T. Yokoyama, H. Iijima, Y. Koezuka, *Bioorg. Med. Chem. Lett.* **1999**, *9*, 697 – 702.

[3] A. Kikuchi, M. Nieda, C. Schmidt, Y. Koezuka, S. Ishihara, Y. Ishikawa, K. Tadokoro, S. Durrant, A. Boyd, T. Juji, A. Nicol, *Br. J. Cancer* **2001**, *85*, 741 – 746.

[4] G. Matsumoto, S. Nagai, M. Toi, S. Ishiyama, K. Kuroi, K. Turuta, A. Okamoto, T. Takahashi, *Nippon Geka Gakkai Zasshi* **2001**, *102*, 421.

[5] R. Nakagawa, K. Motoki, H. Ueno, H. Iijima, H. Nakamura, E. Kobayashi, A. Shimosaka, Y. Koezuka, *Cancer Res.* **1998**, *58*, 1202 – 1207.

[6] Y. Hayakawa, S. Rovero, G. Forni, M. J. Smyth, *Proc. Natl. Acad. Sci. USA* **2003**, *100*, 9464 – 9469.

[7] G. Gonzalez-Aseguinolaza, C. de Oliveira, M. Tomaska, S. Hong, O. Bruna-Romero, T. Nakayama, M. Taniguchi, A. Bendelac, L. Van Kaer, Y. Koezuka, M. Tsuji, *Proc. Natl. Acad. Sci. USA* **2000**, *97*, 8461 – 8466.

[8] a) S. Hong, M. T. Wilson, I. Serizawa, L. Wu, N. Singh, O. V. Naidenko, T. Miura, T. Haba, D. C. Scherer, J. Wei, M. Kronenberg, Y. Koezuka, L. Van Kaer, *Nat. Med.* **2001**, *7*, 1052 – 1056; b) S. Sharif, G. A. Arreaza, P. Zucker, Q. S. Mi, J. Sondhi, O. V. Naidenko, M. Kronenberg , Y. Koezuka, T. L. Delovitch, J. M. Gombert, M. Leite-De-Moraes, C. Gouarin, R. Zhu, A. Hameg, T. Nakayama, M. Taniguchi, F. Lepault, A. Lehuen, J. F. Bach, A. Herbelin, *Nat. Med.* **2001**, *7*, 1057 – 1062.

[9] K. Kakimi, L. G. Guidotti, Y. Koezuka, F. V. Chisari, *J. Exp. Med.* **2000**, *192*, 921 – 930.

[10] K. Miyamoto, S. Miyake, T. Yamamura, *Nature* **2001**, *413*, 531 – 534.

[11] a) L. Brossay, O. Naidenko, N. Burdin, J. Matsuda, T. Sakai, M. Kronenberg, *J. Immunol.* **1998**, *161*, 5124 – 5128; b) K. Benlagha, A. Weiss, A. Beavis, L. Teyton, A. Bendelac, *J. Exp. Med.* **2000**, *191*, 1895.

[12] a) D. B. Moody, G. S. Besra, I. A. Wilson, S. A. Porcelli, *Immunol. Rev.* **1999**, *172*, 285 – 296; b) M. T. Wilson, A. K. Singh, L. Van Kaer, *Trends Mol. Med.* **2002**, *8*, 225 – 231.

[13] a) For an overview of current research on glycosphingolipids in medicine, see: "Glycolipids in cell biology and medicine": *Philos. Trans. Biol. Sci.* **2003**, *358*, 845 – 983, organized and edited by R. A. Dwek, T. D. Butters, F. M. Platt, T. M. Cox; b) for a review of marine glycolipids, see: E. Fattorusso, A. Mangoni, *Fortschr. Chem. Org. Naturst.* **1997**, *72*, 215 – 301.

[14] M. Crul, R. A. Mathot, G. Giaccone, C. A. Punt, H. Rosing, M. X. Hillebrand, Y. Ando, N. Nishi, H. Tanaka, J. M. Schellens, J. H. Beijnen, *Cancer Chemother. Pharmacol.* **2002**, *49*, 287 – 293.

[15] "Synthesis of C-Glycosides: Stable Mimics of O-Glycosidic Linkages": a) C. R. Bertozzi, M. D. Bednarski in *Modern Methods in Carbohydrate Synthesis*, Harwood Academic Publishers, Reading, **1996**, pp. 316 – 351; b) Y. Du, R. J. Linhardt, I. R. Vlahov, *Tetrahedron* **1998**, *54*, 9913 – 9959; c) "C-Oligosaccharide Synthesis": T. Skrydstrup, B. Vauzailles, J.-M. Beau in *Glycoscience: Chemistry and Chemical Biology, Vol. 3* (Eds.: B. Fraser Reid, K. Tatsuta, J. Thiem), Springer, Heidelberg, **2001**, p. 2679.

[16] For a C-trisaccharide with lectin-binding behavior similar to that of the parent O-trisaccharide, see: L. M. Mikkelsen, M. J. Hernaiz, M. Martin-Pastor, T. Skrydstrup, J. Jimenez-Barbero, *J. Am. Chem. Soc.* **2002**, *124*, 14940 – 14951.

[17] a) For a C-glycoside with a tenfold loss of activity relative to phlorizin in an SGLT-inhibition assay, see: J. T. Link, B. K. Sorensen, *Tetrahedron Lett.* **2000**, *41*, 9213 – 9217; b) for a C-glycoside with a 500-fold reduction in antileukemia activity relative to the parent daunomycin, see: E. M. Acton, K. J. Ryan, M. Tracy, S. K. Arora, *Tetrahedron Lett.* **1986**, *27*, 4245 – 4248.

[18] C. R. Bertozzi, D. G. Cook, W. R. Kobertz, F. Gonzalez-Scarano, M. D. Bednarski, *J. Am. Chem. Soc.* **1992**, *114*, 10639 – 10641.

[19] B. Waldscheck, M. Streiff, W. Notz, W. Kinzy, R. R. Schmidt, *Angew. Chem.* **2001**, *113*, 4120 – 4124; *Angew. Chem. Int. Ed.* **2001**, *40*, 4007 – 4011.

[20] a) A. Dondoni, D. Perrone, E. Turturici, *J. Org. Chem.* **1999**, *64*, 5557 – 5564; b) M. K. Gurjar, R. Reddy, *Carbohydr. Lett.* **1997**, *2*, 293 – 298.

[21] For recent applications of the Ramberg–Bäcklund reaction to the synthesis of C-glycosides, see: a) D. E. Paterson, F. K. Griffin, M.-L. Alcaraz, R. J. K. Taylor, *Eur. J. Org. Chem.* **2002**, 1323; b) Y. Ohnishi, Y. Ichikawa, *Bioorg. Med. Chem. Lett.* **2002**, *12*, 997; c) P. Pasetto, R. W. Franck, *J. Org. Chem.* **2003**, *68*, 8042 – 8060.

[22] O. Shirota, K. Nakanishi, N. Berova, *Tetrahedron* **1999**, *55*, 13643 – 13658.

[23] S. J. Spak, O. R. Martin, *Tetrahedron* **2000**, *56*, 217 – 224.

[24] W. K. Park, S. S. J. Meunier, D. Zanini, R. Roy, *Carbohydr. Lett.* **1995**, *1*, 179 – 184.

[25] R. Johansson, B. Samuelsson, *J. Chem. Soc. Perkin Trans. 1* **1984**, *1*, 2371 – 2374.

[26] R. M. Burk, M. B. Roof, *Tetrahedron Lett.* **1993**, *34*, 395 – 398.

[27] M. Yu, B. L. Pagenkopf, *J. Org. Chem.* **2002**, *67*, 4553 – 4558.

[28] W. R. Roush, M. A. Adam, *J. Org. Chem.* **1985**, *50*, 3752 – 3757.

[29] This synthesis of the C-glycoside **3** has been disclosed at ACS meetings and is the subject of a patent application: R. W. Franck, G. Yang, J. Schmeig, M. Tsuji, ACS Meeting, Boston, August **2002**, ABS O-862; R. W. Franck, G. Yang, J. Schmeig, M. Tsuji, ACS Meeting, New Orleans, March **2003**, ABS Carbo-26; "Synthetic *C*-glycolipid and its use for treating cancer, infectious diseases and autoimmune diseases": M. Tsuji, R. W. Franck, G. Yang, G. Chen, US Patent Provisional App. June, **2002**, Full App. June **2003**.

[30] A. Jégou, C. Pacheco, A. Veyrières, *Tetrahedron* **1998**, *54*, 14779 – 14790.

[31] G. Gonzalez-Aseguinolaza, C. de Oliveira, M. Tomaska, S. Hong, O. Bruan-Romero, T. Nakayama, M. Taniguchi, A. Bendela, L. Van Kaer, Y. Koezuka, M. Tsuji, *Proc. Natl. Acad. Sci. USA* **2000**, *97*, 8461 – 8466.

[32] J. Schmieg, G. Yang, R. W. Franck, M. Tsuji, *J. Exp. Med.* **2003**, *198*, 1631 – 1641.

 © 2004 Wiley-VCH Verlag GmbH & Co. KGaA, Weinheim

Cluster Compounds

Synthesis and Structure of $[Ag_{26}In_{18}S_{36}Cl_6(dppm)_{10}(thf)_4][InCl_4(thf)]_2$—A Combined Approach of Theory and Experiment**

Reinhart Ahlrichs, Andreas Eichhöfer, Dieter Fenske, Oliver Hampe, Manfred M. Kappes, Paola Nava, and Jolanta Olkowska-Oetzel*

Dedicated to Professor Martin Jansen on the occasion of his 60th birthday

The synthesis, structure, and physical properties of nanosized metal and semiconductor cluster molecules is of topical interest.[1] For the synthesis of metal chalcogenide cluster compounds, we have used the reaction of metal salts MX (M = Cu, Ag, Au; X = Cl, $OOCCH_3$) with bis- or monosilylated main-group element derivates $E(SiMe_3)_2$ or $RESiMe_3$ (E = S, Se, Te; R = organic group) in the presence of tertiary phosphanes PR_3.[2] The driving force of this reaction is the formation of $XSiMe_3$. In this way, a large number of cluster compounds have been synthesized and structurally characterized, for example, $[Cu_{146}Se_{72}(PPh_3)_{30}]$,[3] $[Ag_{172}Se_{40}(Se\mathit{n}Bu)_{92}dppp]$ (dppp = bis(diphenylphosphanyl)propane),[4] $[Ag_{188}S_{94}(PR_3)_{30}]$ (R = *n*Pr, *n*Bu)[5] and $[Ag_{262}S_{100}(S\mathit{t}Bu)_{62}(dppb)_6]$ (dppb = bis(diphenylphosphanyl)butane).[6] Calculations reveal that the PR_3-stabilized cluster complexes are metastable intermediates on the way to forming the corresponding binary phases.[7] Ternary compounds, however, offer a broader spectrum of tunable properties and are viable candidates for technical use, for example, $CuInSe_2$ is one of the most promising materials for thin-film technology in solar cells,[8] and conversion efficiencies of up to 18.8% have been achieved with $Cu(In,Ga)Se_2$ under laboratory conditions;[9] $AgInS_2$, $AgIn_5S_8$, and $AgGaS_2$ are of interest as materials for non-linear optical devices.[10] This prompted us to investigate the synthesis of ternary cluster compounds composed of elements of Group 11, 13, and 16. Similar to the synthetic approach for binary clusters outlined above, the reaction of mixtures of the metal halides with $E(SiMe_3)_2$ (E = Se, S) yielded cluster compounds such as $[Cu_{11}In_{15}Se_{16}(SePh)_{24}(PPh_3)_4]$,[11] $[Cu_{20}Ga_{10}Cl_4Se_{23}(PEt_2Ph)_{12}]$[12] and $[M_6M'_8Cl_4E_{13}(PPh_3)_6]$, (M = Cu, Ag; M′ = Ga, In; E = S, Se).[11,13] Interestingly, the stoichiometric composition and structure of the cluster molecules differ from the corresponding bulk material. We report herein the synthesis, structural characterization, and theoretical investigation of $[Ag_{26}In_{18}S_{36}Cl_6(dppm)_{10}(thf)_4][InCl_4(thf)]_2$ (**1**).

Compound **1** has been prepared by treating a suspension of silver benzoate, dppm and $InCl_3$ with $S(SiMe_3)_2$ in tetrahydrofuran at −50 °C. The reaction mixture was stirred at room temperature giving an orange solution. After several days, yellow crystals of **1** formed [Eq. (1)]

$$1.26\,PhCO_2Ag + 0.5\,dppm + InCl_3 + 1.8\,S(SiMe_3)_2 \xrightarrow{THF} [Ag_{26}In_{18}S_{36}Cl_6(dppm)_{10}(thf)_4][InCl_4(thf)]_2\ \mathbf{1} \quad (1)$$

The molecular structure of **1** has been determined by single-crystal X-ray structural analysis.[14] The assignment of the atom positions solely on the basis of the X-ray analysis is virtually impossible due to similar scattering factors of the atom pairs silver/indium and sulfur/chlorine. However, the final structure description was independently obtained by chemical intuition and quantum chemical calculations, and the chemical composition was confirmed by Fourier transfer mass spectrometry (FTMS) as detailed below.

The ionic compound **1** crystallizes in the space group $P\bar{1}$, with the cluster cation $[Ag_{26}In_{18}Cl_6(dppm)_{10}(thf)_4]^{2+}$ residing on a crystallographic inversion center (Figure 1a). The two anions $[InCl_4(thf)]^-$ are formed by trigonalbipyramidally coordinated indium atoms (In–Cl: 235.0(4)–241.9(4) pm; Cl-In-Cl: 96.41(12)–119.80(15)°; In–O: 245.7 pm). The indium atoms in the cation display mostly a distorted tetrahedral coordination environment: In4–In9 and symmetry equivalent atoms are coordinated by four sulfur atoms (S-In-S: 97.92(8)° to 116.88(7)°), while the remaining six indium atoms (In1–In3 and symmetry equivalent atoms) are each surrounded by three sulfur and one chlorine ligand (S-In-S: 103.63(8)° to 123.48(8)°; Cl-In-S: 93.94(11)° to 113.5(10)°) with In–S bond lengths ranging from 240.6(3) (In3-S17′) to 252.4(2) pm (In7-S2). Additional weak coordination of In3 and In3′ by a THF molecule (In-O: 272.5 pm) causes a distortion of the tetrahedral symmetry leading to a distorted trigonalbipyramidal coordination.

The 26 silver atoms display a larger variety of coordination geometries: distorted linear, trigonal, and tetrahedral. Eight of the silver atoms exhibit distorted tetrahedral coordination by either four sulfur atoms (Ag12, Ag12′, Ag13, Ag13′) or one phosphorus and three sulfur atoms (Ag9, Ag9′, Ag10, Ag10′). Twelve of the silver atoms have distorted trigonal environments (Ag1-Ag3, Ag6-Ag8 and symmetry equivalent atoms), which are bonded to two sulfur atoms and one phosphorus atom of the bidentate phosphane ligand (dppm). For these atoms, the values of the angular sum

[*] Prof. Dr. D. Fenske, Dr. J. Olkowska-Oetzel
Institut für Anorganische Chemie, Universität Karlsruhe
Engesserstrasse, Geb. 30.45, 76128 Karlsruhe (Germany)
Fax: (+49) 721-608-8440
E-mail: dieter.fenske@chemie.uni-karlsruhe.de
Prof. Dr. R. Ahlrichs, P. Nava
Institut für Physikalische Chemie
Lehrstuhl für Theoretische Chemie
Universität Karlsruhe, Kaiserstrasse 12
76128 Karlsruhe (Germany)
Prof. Dr. M. M. Kappes
Institut für Physikalische Chemie
Universität Karlsruhe, Kaiserstrasse 12
76128 Karlsruhe (Germany)
Dr. A. Eichhöfer, Dr. O. Hampe
Institut für Nanotechnologie
Forschungszentrum Karlsruhe
Postfach 3640, 76021 Karlsruhe (Germany)

[**] This work was supported by the Deutsche Forschungsgemeinschaft (Research Center for Functional Nanostructures) and the Fond der Chemischen Industrie. dppm = bis(diphenylphosphanyl)methane.

 DOI: 10.1002/anie.200460052 © 2004 Wiley-VCH Verlag GmbH & Co. KGaA, Weinheim

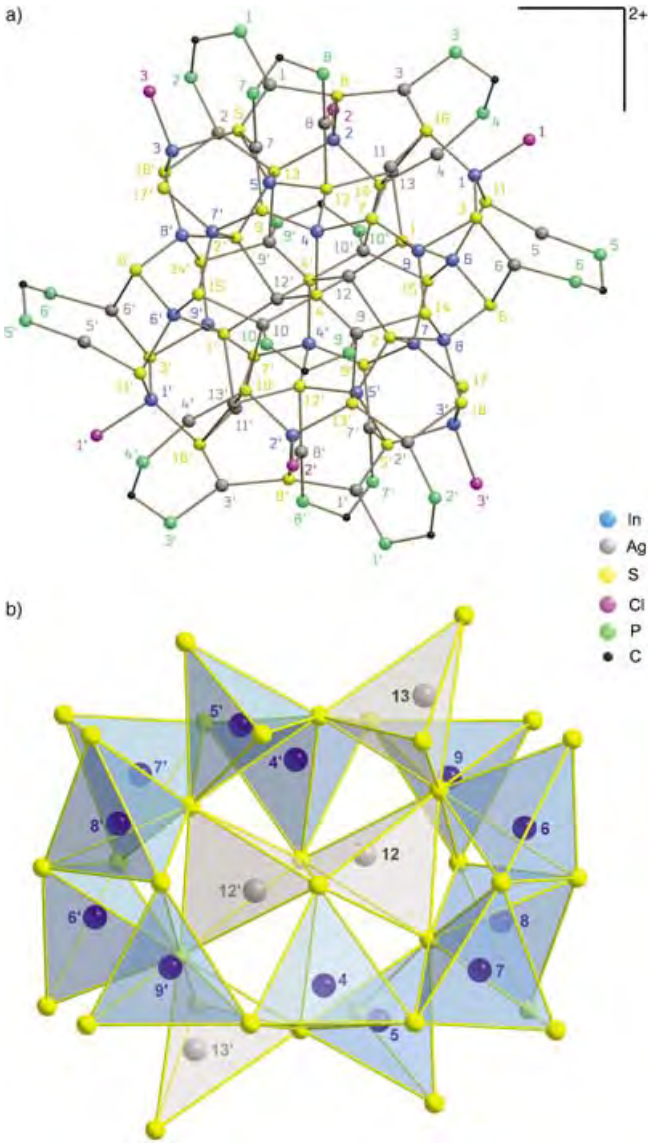


Figure 1. a) Molecular structure of the cluster cation $[Ag_{26}In_{18}S_{36}Cl_6(dppm)_{10}(thf)_4]^{2+}$ in **1** (phenyl rings of the phosphane (dppm) and coordinating THF molecules are omitted for clarity). Atoms are labeled with numbers only. b) Inner section of **1**, which displays similar indium and silver positions that are tetrahedrally coordinated by four sulfur atoms, nonbonding S–S separations range from 345.5 pm (S1-S2) to 479.2 pm (S10-S16).

range from 358.35° for Ag3 to 359.92° for Ag6. The remaining six silver atoms have a distorted linear coordination of either two sulfur atoms (Ag11, Ag11′) or one sulfur atom and one phosphorus atom (Ag4, Ag4′, Ag5, Ag5′) with angles: S-Ag-S 159.24(8)° and P-Ag-S 170.45(8), whereas Ag5 und Ag5′ are also weakly coordinated by a THF molecule (Ag–O: 261.8 pm). In contrast to the In–S bond lengths, the Ag–S separations cover a broader range from 238.3(2) (Ag4–S10) to 281.7(2) (Ag12–S4). The shortest separation of silver atoms in **1** is found to be 282.3 pm (Ag12-Ag12′), which is comparable with metal–metal distances in other silver sulfide complexes and clusters considered to be nonbonding.[5,6,15] Common values were also found for the Ag–P bond lengths, which range from 237.5(3) pm to 250.0(3) pm.

If we assume a maximum M–S distance of 281.7(2) pm for M = Ag and 256.5(2) pm for M = In, we find four different bridging modes for the S^{2-} ligands. S17 binds as μ_2-ligand and S4 is coordinated to five metal atoms. The atoms S1, S3, S6, S7, S9, S11, S14, S15, and S18 act as μ_3-bridging ligands, whereas S2, S5, S8, S10, S12, S13, and S16 are μ_4-bridging ligands.

Although the $\{Ag_4In_{12}S_{34}\}$ cluster core of **1** (Figure 1b) consists of corner-sharing tetrahedra of sulfur atoms with a central metal atom, their arrangement does not result in an ordered and layered structure, as in the related bulk material. $AgInS_2$ crystallizes at normal pressure and room temperature in the chalcopyrite structure, which is closely related to the cubic zincblende structure.[16] The sulfur atoms form a cubic network with ABC layering and the metal atoms occupy $^1/_2$ of the tetrahedral holes with the silver and indium atoms perfectly distributed over these sites.

A mass-spectrometric analysis was performed to determine charge state and stoichiometry of the two ions constituting **1**. We employed a modified electrospray/ionization source interfaced to a high-resolution Fourier transform ion cyclotron resonance (FTICR) mass spectrometer.[17] The source had been modified by introducing an ion funnel to improve ion sensitivity while keeping collisional fragmentation of ions to a minimum.

Figure 2 displays a mass spectrum of an electrosprayed yellow solution of **1** in 1,2-dichloroethane. The positive-ion mass spectrum is dominated by a single peak centered at $m/z = 5040.7$. Mass differences between silver and indium as well as between sulfur and chlorine are substantial and allow an unequivocal assignment of this peak to the doubly charged ion of $[Ag_{26}In_{18}S_{36}Cl_6(dppm)_{10}]^{2+}$. The THF solvent molecules present in the single crystal of **1** are lost upon redissolving/

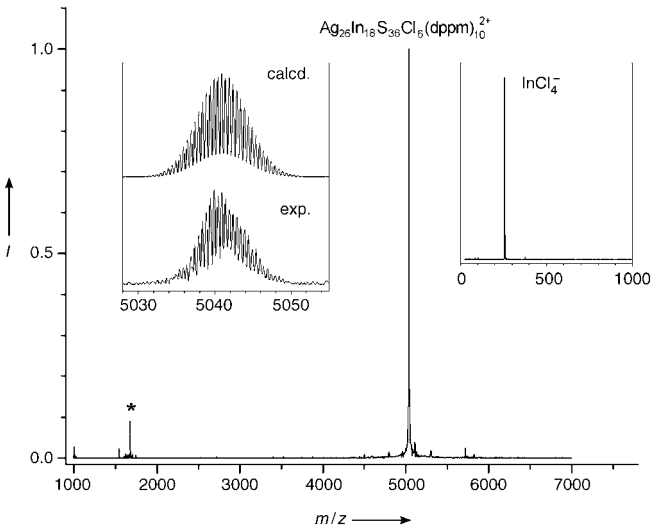


Figure 2. Electrospray mass spectra of **1** in $C_2H_4Cl_2$. Left inset: Comparison between experimentally observed high-resolution parent-cation peak around $m/z = 5040.7$ and isotopomer simulation. Right inset: Corresponding negative-ion mass spectrum. (Peak marked with an asterisk is due to an electronic artefact)

 © 2004 Wiley-VCH Verlag GmbH & Co. KGaA, Weinheim

spraying, which indicates the very weak interaction of THF with the stable cluster ion. The highly resolved parent-ion peak is compared to the calculated isotope distribution in the left inset of Figure 2. Note that the charge state of the parent-ion peak is evidenced by the isotopomer splitting of 0.5 mass units. As a second inset in Figure 2 a negative-ion mass spectrum is shown that depicts a single peak at $m/z = 256.8$ that can be attributed to $InCl_4^-$. Again the isotopomer splitting is in excellent agreement with the simulated one (not shown).

Assignment of atoms: The XRD yields the location of atoms in space but it is almost impossible to assign atoms to crystallographic sites for two reasons: the silver and indium atoms have virtually identical X-ray structure factors and bond lengths for Ag–S and In–S are also very similar, around 250 pm.[18] Therefore molecular electronic-structure calculations have been performed to tackle this problem at the density functional theory (DFT) level.[19] The calculations were carried out for the model compound in which the phenyl groups were replaced by hydrogen atoms, thus leading to $[Ag_{26}In_{18}S_{36}Cl_6(H_2PCH_2PH_2)_{10}]^{2+}$ **2**, with 176 atoms. Since it is impossible to consider all possible distributions of silver and indium atoms on the sites in question, we made the following assumptions in the interpretation of the XRD and in the calculations, which have been tested in preliminary treatments:

1) terminal M–X is identified as In–Cl, since this guarantees local charge neutrality;[20]
2) the bidentate dppm binds to silver atoms;
3) the central metal pair must be silver atoms: Ag12,Ag12′ (replacement by indium atoms yields a computed interatomic distance of 385 pm instead of 283 pm);
4) the position Ag11 must be occupied by silver atoms as it is coordinated by only two sulfur atoms with short bond lengths.[21]

We are thus left with only six additional alternatives besides the one shown in Figure 1 a (in C_i symmetry): Ag13 can be swapped with In4 to In9 (Figure 1 b). All seven cases have been structurally optimized with the relatively small SV(P)[22] basis. The energies obtained are compared in Table 1. Next we checked results by the larger TZVP and TZVPP[22] bases, including structure optimization, which confirmed the energetic ordering for the most stable isomers.

Table 1: Computed relative DFT energies (kJ mol^{-1}) of isomers of **2**, with basis sets SV(P) and TZVPP.[a]

In	SV(P)	TZVPP
	0	0
6	45	15
5	94	95
9	177	
8	197	
4	257	
7	271	

[a] The column In indicates the indium center to be interchanged with Ag13 according to Figure 1 a.

The atom assignment given in Figure 1 a corresponds to the structure which is calculated to be the most stable one.

A comparison of calculated and experimental bond lengths is shown in Figure 3. Figure 3 a,b,c demonstrate a good convergence towards experiment on basis set expansion. TZVP and TZVPP differ mainly in the set of f functions for all atoms except hydrogen. The improvement obtained from TZVP to TZVPP is somewhat unexpected but can be rationalized as follows. Some atoms, especially sulfur and silver, have a "nonisotropic" surrounding of counterions leading to appreciable electric fields and an ensuing polarization of electron distributions, which require f functions for a proper description. All directly bonded In–S and In–Cl are calculated (TZVPP) with errors of less than 6 pm. Ag–S and Ag–P distances up to 270 pm show larger variations in experiment, which indicates less uniform bonding characteristics. This is in line with larger deviations between calculated and measured distances. There is only a single Ag–S distance with a deviation larger than 12 pm, which is at the cluster surface (Ag10–S10, deviation of 21 pm). Ag–X distances in the range from 270 to 360 pm include X = Ag, In, and S; the corresponding atoms are never directly bonded. Errors go up to 43 pm (Ag9–Ag10) for silver atoms connected by dppm. This deficiency is partly due to the replacement of phenyl groups with a hydrogen atom.[23]

The good agreement shown in Figure 3 c is exceptional as in neutral compounds Ag–P is typically calculated to be too large, by about 10–15 pm, mainly because DFT does not properly describe dispersion interactions that tend to shorten bond lengths. However, **2** is a dication and the positive charge of the cluster core enhances Ag–P bonding, thus decreasing the deficiency of DFT. Figure 3 d shows the errors in interatomic distances for the second best structure in energy, which is only 15 kJ mol^{-1} higher (TZVPP). In this case, In6 has been interchanged with Ag13 according to Figure 1 a. This causes a large rearrangement of the neighborhood of In6, Ag13, and Ag11, with deviations in bond lengths up to 220 pm (In6-S11, Figure 3). It is obvious that experiment and calculation cannot be reconciled. Even In–X bond lengths (up to 270 pm) show too large deviations. It is gratifying that energetic ordering and distance statistics lead to the same conclusion: only the assignment in Figure 1 a agrees with the calculations.

The combination of various investigative approaches employed in this work opens new perspectives for similar cases in which a single method alone would not allow one to reach conclusions with confidence.

Experimental Section

$[Ag_{26}In_{18}S_{36}Cl_6(dppm)_{10}(thf)_4][InCl_4(thf)]_2$ **1.** $PhCO_2Ag$ (silver benzoate; 65 mg, 0.284 mmol) and dppm (43 mg, 0.112 mmol) were added to a solution of $InCl_3$ (50 mg, 0.226 mmol) in THF (20 mL). After the addition of $S(SiMe_3)_2$ (0.085 mL, 0.407 mmol) at −50 °C the suspension was allowed to warm up to room temperature while stirring, the precipitate dissolved, and the solution became orange. The solution was left to stand for several days, which resulted in the formation of yellow single crystals suitable for X-ray diffraction analysis. Yield: 50 %.

 © 2004 Wiley-VCH Verlag GmbH & Co. KGaA, Weinheim

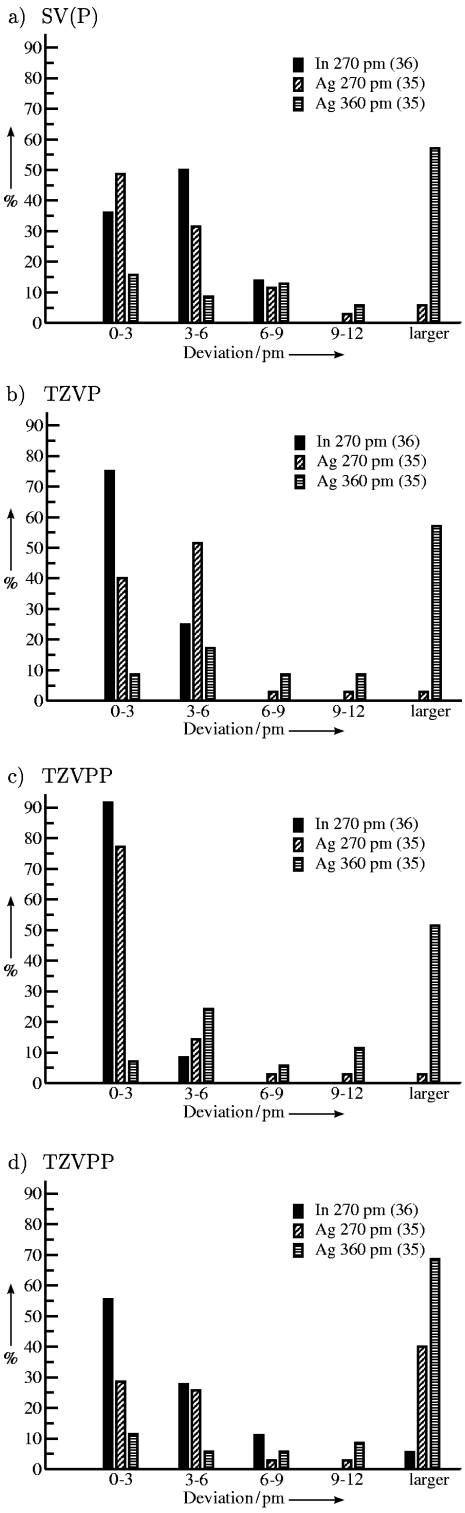


Figure 3. Histograms showing statistics of deviations (pm) between experimental and computed interatomic distances. The column height gives the percentage of cases with deviations indicated on the abscissa. Three classes are considered: In–X up to 270 pm, Ag–X up to 270 pm, and Ag–X between 271 and 360 pm, X = P, S, Cl, Ag, In. The number of cases in each class is indicated in parentheses as an inset. a), b), and c) refer to the most stable structure computed with SV(P), TZVP, and TZVPP respectively. d) refers to the second most stable structure (TZVPP) in which In6 was interchanged with Ag13, labeling of Figure 1 a.

ESFTMS: Mass spectra were recorded on a Fourier transform ion cyclotron resonance mass spectrometer (Bruker Daltonics, APEX II) equipped with an electrospray ion source modified by a home-built ion funnel for improved sensitivity.

Received: March 19, 2004 [Z460052]

Keywords: cluster compounds · density functional calculations · mass spectrometry · X-ray diffraction

[1] *Cluster and colloids. From theory to Applications* (Ed.: G. Schmid), VCH, Weinheim, **1994**; *Physics and chemistry of Metal Cluster Compounds* (Ed.: L. J. de Jongh), Kluwer, Dordrecht, **1994**.

[2] S. Dehnen, A. Eichhöfer, D. Fenske, *Eur. J. Inorg. Chem.* **2002**, 279 – 317.

[3] H. Krautscheid, D. Fenske, G. Baum, M. Semmelmann, *Angew. Chem.* **1993**, *105*, 1364 – 1367; *Angew. Chem. Int. Ed. Engl.* **1993**, *32*, 1303 – 1306.

[4] D. Fenske, N. Zhu, T. Langetepe, *Angew. Chem.* **1998**, *110*, 2783 – 2788; *Angew. Chem. Int. Ed. Engl.* **1998**, *37*, 2639 – 2644.

[5] J. Wang, T. Langetepe, C. Persau, B. S. Kang, G. S. Sheldrick, D. Fenske, *Angew. Chem.* **2002**, *114*, 3972 – 3977; *Angew. Chem. Int. Ed. Engl.* **2002**, *41*, 3818 – 3822.

[6] D. Fenske, C. Persau, S. Dehnen, C. A. Anson, *Angew. Chem.* **2004**, *116*, 308 – 313; *Angew. Chem. Int. Ed. Engl.* **2004**, *43*, 305 – 309.

[7] S. Dehnen, A. Schäfer, D. Fenske, R. Ahlrichs, *Angew. Chem.* **1994**, *106*, 786 – 790; *Angew. Chem. Int. Ed. Engl.* **1994**, *33*, 746 – 748; A. Schäfer, R. Ahlrichs, *J. Am. Chem. Soc.* **1994**, *116*, 10686 – 10692; S. Dehnen, A. Schäfer, R. Ahlrichs, D. Fenske, *Chem. Eur. J.* **1996**, *2*, 429 – 435.

[8] K. Mitchell in *Solar Cells and Their Applications* (Ed.: L. Partain), John, New York, **1995**, pp. 185 – 210.

[9] M. A. Contreras, B. Egaas, K. Ramanathan, J. Hiltner, A. Swartzlander, F. Hasoon, R. Noufi, *Prog. Photovoltaics* **1999**, *7*, 311 – 316.

[10] S. C. Abrahams, J. L. Bernstein, *J. Chem. Phys.* **1973**, *59*, 1625 – 1629; I. Yonenga, K. Sumino, E. Niwa, K. Masumoto, *J. Cryst. Growth* **1996**, *167*, 616 – 620.

[11] A. Eichhöfer, D. Fenske, *J. Chem. Soc. Dalton Trans.* **2000**, 941 – 944.

[12] A. Eichhöfer, D. Fenske, J. Olkowska-Oetzel, *Z. Anorg. Allg. Chem.* **2004**, *630*, 247 – 251.

[13] J. Olkowska-Oetzel, D. Fenske, P. Scheer, A. Eichhöfer, *Z. Anorg. Allg. Chem.* **2003**, *629*, 415 – 420.

[14] X-ray analysis: STOE-IPDS II on a SCHNEIDER rotating anode ($Mo_{K\alpha}$-radiation; data collection and refinement (SHELX97, SHELXL93); numerical absorption correction. CCDC-233798 contains the supplementary crystallographic data for this paper. These data can be obtained free of charge via www.ccdc.cam.ac.uk/conts/retrieving.html (or from the Cambridge Crystallographic Data Centre, 12 Union Road, Cambridge CB2 1EZ, UK; fax: (+44) 1223-336-033; or deposit@ccdc.cam.ac.uk). **1**: $C_{250}H_{220}Ag_{26}Cl_{14}In_{20}P_{20}S_{36}\cdot 18\,C_4H_8O$, triclinic, space group $P\bar{1}$ (Nr. 2), $Z = 1$, lattice constants (190 K): $a =$ 2002.2(4), $b = 2361.6(5)$, $c = 2624.3(5)$ pm, $\alpha = 104.54(3)$, $\beta =$ 104.78(3), $\gamma = 111.62(3)°$, $V = 10299 \times 10^6$ pm^3, $\mu(Mo_{K\alpha}) =$ 2.697 mm^{-1}, $2\theta_{max} = 55°$, 66322 reflections of which 33751 are unique (R(int) = 0.070) and 27994 with $I > 2\sigma(I)$, 1832 parameters (Ag, In, Cl, S, P and C anisotrope, H atoms of the dppm ligands included in calculated positions. O and C of THF isotrope). Residual electron density 2.4 e Å^{-3}, $R1(I > 2\sigma(I)) =$ 0.0480; $wR2$ (all data) = 0.1847.

 © 2004 Wiley-VCH Verlag GmbH & Co. KGaA, Weinheim

[15] I. G. Dance, L. J. Fitzpatrick, A. D. Rae, A. L. Scudder, *Inorg. Chem.* **1983**, *22*, 3785 – 3788; T. C. Deivaraj, J. J. Vittal, *J. Chem. Soc. Dalton Trans.* **2001**, 329 – 335.
[16] H. Hahn, G. Frank, W. Klinger, A. Meyer, G. Störger, *Z. Anorg. Allg. Chem.* **1953**, *271*, 153.
[17] D. Fenske, T, Langetepe, M. M. Kappes, O. Hampe, P. Weis, *Angew. Chem.* **2000**, *112*, 1925 – 1928; *Angew. Chem. Int. Ed. Engl.* **2000**, *39*, 1857 – 1860; A. Eichhöfer, O. Hampe, M. Blom, *Eur. J. Inorg. Chem.* **2003**, 1307 – 1314.
[18] An interchange of tetrahedrally coordinated indium atoms with Ag13 (Figure 1b) has only small influences on the resulting *R*-values in comparison to the values for the proposed structure[14] in Figure 1a (In6: $R1 = 0.0486$, $wR2 = 0.1867$; In5: $R1 = 0.0484$, $wR2 = 0.1857$).
[19] All calculations were performed with the TURBOMOLE program. a) R. Ahlrichs, M. Bär, M. Häser, H. Horn, C. Kölmel, *Chem. Phys. Lett.* **1989**, *162*, 165 – 169; b) O. Treutler, R. Ahlrichs, *J. Chem. Phys.* **1995**, *102*, 346 – 354. We employed the Becke–Perdew (BP86) exchange-correlation functional and the very efficient MARIJ technique. c) A. D. Becke, *Phys. Rev. A* **1988**, *38*, 3098 – 3100; d) S. H. Vosko, L. Wilk, M. Nusair, *Can. J. Phys.* **1980**, *58*, 1200 – 1211; e) J. P. Perdew, *Phys. Rev. B* **1986** *33*, 8822 – 8824; erratum: J. P. Perdew, *Phys. Rev. B* **1986**, *34*, 7406; f) K. Eichkorn, O. Treutler, H. Öhm, M. Häser, R. Ahlrichs, *Chem. Phys. Lett.* **1995**, *242*, 652 – 660. g) M. Sierka, A. Hogekamp, R. Ahlrichs, *J. Chem. Phys.* **2003**, *118*, 9136 – 9148. We used RECP (relativistic effective core potential) for In and Ag. h) D. Andrae, U. Häussermann, M. Dolg, H. Stoll, H. Preuss, *Theor. Chim. Acta* **1990**, *77*, 123 – 141.
[20] The possibility of terminal Ag–Cl was tested by interchanging Ag13 with In1, Figure 1b. After corresponding geometry optimization, the energy is 137 kJ mol^{-1} above the ground state, connected with a drastic change in the local coordination pattern.
[21] By interchanging Ag11 with In atoms from various other positions, energies increase by more than 250 kJ mol^{-1}.
[22] The basis and the auxiliary basis sets were a SV(P) (split valence with a set of polarization functions for each atom with the exception of H), a TZVP (triple-valence basis with a set of polarization functions), and a TZVPP, taken from the standard TURBOMOLE basis set file. TZVPP includes for example, (2d1f) polarization functions for p-block elements. a) A. Schäfer, H. Horn, R. Ahlrichs, *J. Chem. Phys.* **1992**, *97*, 2571 – 2577; b) A. Schäfer, C. Huber, R. Ahlrichs, *J. Chem. Phys.* **1994**, *100*, 5829 – 5835; c) K. Eichkorn, F. Weigend, O. Treutler, R. Ahlrichs, *Theor. Chem. Acc.* **1997**, *97*, 119 – 124; d) ftp://ftp.chemie.uni-karlsruhe.de/pub/.
[23] We could not afford calculations that included either Ph or Me (instead of H) for dppm in connection with a TZVPP basis for the cluster core. However, putting Ph or Me on selected dppm reduced the Ag–Ag distance by about 20 pm, thus reducing deviations to the experiment by 50%.

 © 2004 Wiley-VCH Verlag GmbH & Co. KGaA, Weinheim

Microspheres

Ga_2O_3 and GaN Semiconductor Hollow Spheres**

*Xiaoming Sun and Yadong Li**

Both monoclinic Ga_2O_3 and Wurtzite-structured GaN are wide-band-gap semiconductors (energy gap, $E_g = 4.9$ eV and 3.39 eV, respectively) that exhibit luminescence and conduction properties, thus, they have potential applications in optoelectronic devices,[1–8] high-temperature stable gas sensors,[9] and high-temperature/high-power electronic devices.[10,11] The future of full-colored, flat panel displays, blue lasers, and optical communication is likely to be based on GaN.[5,12] Nanostructured Ga_2O_3 and GaN with varied morphology, for instance, nanoparticles,[13] nanorods,[14] nanowires,[3,15] nanobelts,[4,16] and nanotubes[5–6,17–18] have been prepared. However, monodispersed spherical structures of the two semiconductor compounds have not been prepared up to now.

Monodispersed micro- or nanospheres, as a kind of competitive building blocks for future nanodevices, have become a new focus of research. This interest has arisen because it is now relatively easy to synthesize uniform spheres and to control their size, and these spheres can self-assemble into 2D or 3D colloidal arrays or photonic band gap crystals.[19–23] The preparation of uniform micro- or nanospheres of semiconducting materials would enable their use as building blocks for new photonic crystals or as model systems for light scattering, which are of both theoretical and practical significance. New approaches to semiconductor hollow spheres have been made in the last five years.[24–33] Semiconducting oxide ceramic hollow spheres (e.g., TiO_2, SnO_2) have been prepared by templating the sol–gel precursor solutions with monodispersed latex beads.[24] By alternating the shape and structure of the templates, the morphology of hollow structures can also be changed.[25,26] The II–VI family of semiconductor luminescent nanoparticles, such as CdTe, CdS, ZnS, have been assembled on spherical templates to form luminescent shells by using a layer-by-layer self-assembly strategy,[27–29] sonochemical deposition,[30] or chemical-bath deposition.[31–32] Very recently, our group has developed a solution-based template-free route to ZnSe semiconducting hollow spheres by condensing ZnSe nanoparticles on a liquid–gas interface.[33] Herein, we report the application

[*] X. Sun, Prof. Dr. Y. Li
Department of Chemistry
The Key Laboratory of Atomic and Molecular Nanosciences
(Ministry of Education)
Tsinghua University
Beijing, 100084 (China)
Fax: (+86) 10-6278-8765
E-mail: ydli@mail.tsinghua.edu.cn

[**] This work was supported by the NSFC (20025102, 50028201, 20151001), the Foundation for the Author of National Excellent Doctoral Dissertation of P.R. China, and the State Key Project of Fundamental Research for nanomaterials and nanostructures.

 DOI: 10.1002/anie.200353212 © 2004 Wiley-VCH Verlag GmbH & Co. KGaA, Weinheim

of a facile surface-layer-absorption (SLA) templating technique to obtain monodispersed Ga_2O_3 and GaN hollow spheres.

The strategy used to obtain monodispersed hollow Ga_2O_3 and GaN spheres can be divided into three steps (Figure 1):

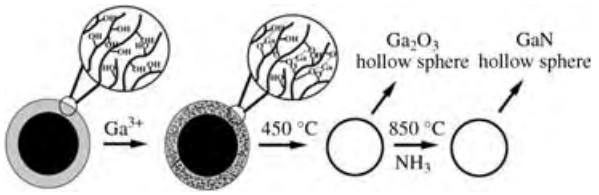


Figure 1. Schematic mechanism for the formation of GaN hollow spheres using carbon spheres as templates.

1) the adsorption of gallium ions from solution into surface layer; 2) calcination of the composite spheres in air to remove the carbon core, which results in oxide hollow spheres; 3) in situ conversion of the as-prepared oxide hollow spheres into nitride hollow spheres in an ammonia atmosphere at 700–900 °C. There are some essential differences between the current strategy and traditional strategies.[21–32,34,35] In traditional templating processes, which use latex or silica as templates, a coating is deposited on the sacrificial core by controlled surface precipitation/absorption of the inorganic precursors from a solution/suspension. These processes usually require alkoxides as a starting material (e.g., in sol–gel methods), or use nanoparticles as "building units" and polyelectrolytes as "glue".[34] The core is then subsequently removed by thermal or chemical means, thus leaving behind hollow spheres.[35] During the process, surface modification is usually required for efficient adsorption and the experimental parameters must be precisely controlled to avoid heterogeneous agglomeration. In most cases, the growth is outward from the template surface,[21–25,34,35] and the void formed is approximately equal to the original size of the template. However, in our method, the templates used were carbon spheres prepared by dehydrating glucose or sucrose under hydrothermal conditions.[36] The surface of the spheres is hydrophilic and has a distribution of -OH and -C=O groups similar to that of polysaccharide in,[36] which makes surface modification unnecessary. When the carbon spheres are dispersed in solutions of metal salts, the cations are adsorbed into the surface. Agglomeration is naturally avoided because cations are absorbed into the surface layer to form a composite shell rather than form a heterogeneous coating. In the following calcination process, the metal atoms in the shell become denser, the spheres contract and cross-link to form metal-oxide hollow spheres, which are a smaller replica of the carbon spheres (≈40 %). The salts (e.g., chlorides) can thus be used as the starting material instead of alkoxides, which reduces the preparation cost. The use of transition-metal salts should lead to hollow spheres of different compositions. We believe that this is a general, simple, and cheap approach to hollow spheres. Moreover, since the thickness of the functional "surface layer" is predetermined by hydrothermal synthesis, the integrity and uniformity of the shell of final products can be ensured in this way. Herein, we demonstrate that gallium ions can be adsorbed into the surface layer and then transformed into oxide and nitride under the right conditions.

Carbon spheres were prepared according to a reported procedure.[36] A typical image obtained by scanning electronic microscopy (SEM) is shown in Figure 2a. Zeta potential analysis on the spheres indicated that the surfaces of the spheres were negatively charged in water (pH 7, $\zeta = -47$ eV). However, this value changed to -18 eV when the spheres were ultrasonicated in a solution of $GaCl_3$ (0.5 M) for 10 min, washed (centrifugation and redispersion in water, five cycles) and suspension aged for 24 h before analysis. This result implies that Ga^{3+} ions were adsorbed into the surface layer of the carbon spheres.

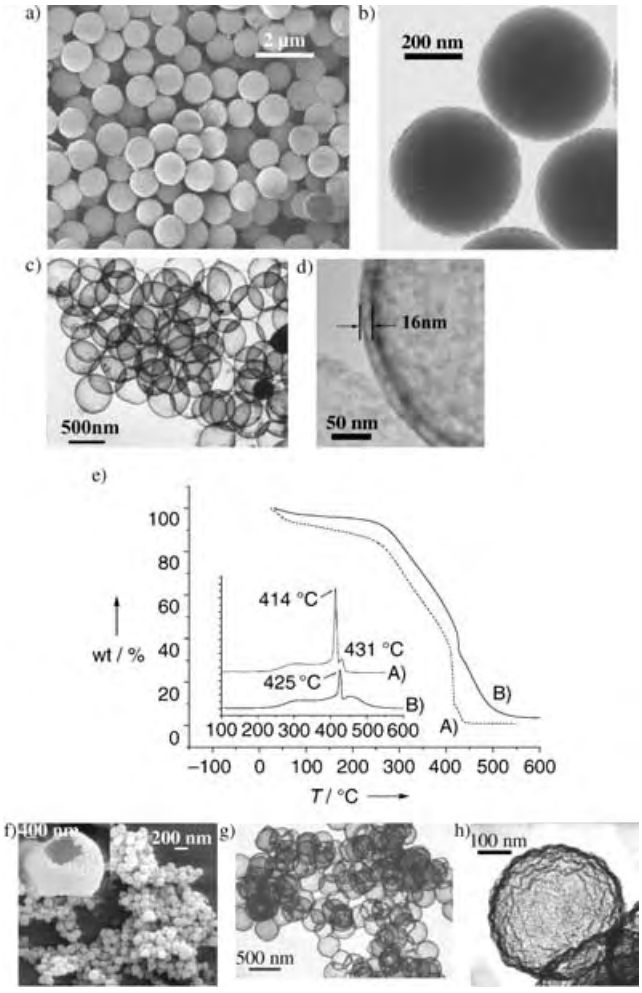


Figure 2. a) Typical SEM image of carbon spheres; b) typical TEM image of carbon spheres; c,d) typical TEM image of Ga_2O_3 hollow spheres; e) TGA plots of A) templating carbon spheres and B) Ga-adsorbed carbon spheres (inset: their differential curves); f) SEM image of intact Ga_2O_3 hollow spheres 100 nm in diameter (inset: SEM image of large hollow spheres 1500 nm in diameter, which were deliberately broken by crushing in a mortar to show the hollow interior); g,h) typical TEM images of Ga_2O_3 hollow spheres prepared by using templating carbon spheres from sucrose rather than glucose solutions.

 © 2004 Wiley-VCH Verlag GmbH & Co. KGaA, Weinheim

Images of the spheres obtained by transmission electron microscopy (TEM) indicate that the gallium ions were adsorbed into the surface layer rather than grafted onto the surface (Figure 2b). No amorphous layer or aggregations of gallium compounds, such as hydroxides, were observed, though energy dispersive X-ray (EDX) analysis on the spheres clearly revealed the existence of elemental Ga and an atomic ratio of Ga to Cl greater than 10:1. This result indicates that cationic Ga^{3+} ions were selectively absorbed in the surface layer and anionic Cl^- ions were excluded since the ratio of Ga^{3+} to Cl^- in bulk solution was 1:3, while that of adsorbed ions was greater than 10:1 after washing cycles. We propose that the polysaccharide-like layer at the surface of carbon spheres serves as an adsorbent, which can chelate Ga^{3+} ions and protect them from heterogeneous coagulation or being washed off. It is noteworthy that the size of carbon spheres can be manipulated in the range from 200 nm to 4000 nm, or even larger, by adjusting experimental parameters. Smaller spheres (about 400 nm in diameter) were chosen to show the surface morphology more clearly.

The gallium-adsorbed carbon spheres were calcined in air to remove the carbon component, resulting in Ga_2O_3 hollow spheres. TEM micrographs reveal the hollow structure of the calcined samples (Figure 2c). A selected-area electron-diffraction pattern shows that the spheres are polycrystalline. XRD characterization indicate that the as-prepared sample is Ga_2O_3 (JCPDS 060509, shown in Figure 3a). The average crystalline size was about 4 nm, as calculated from the broaden peaks by using the Scherrer equation. The hollow spheres prepared from carbon spheres of 1000 ± 50 nm in diameter (shown in Figure 2a) had diameters of 370 ± 20 nm, about 60% smaller than the starting spheres and had a shell thickness of about 16 nm as measured by using a TEM image that had been further magnified (Figure 2d). The large shrinkage ratio is essentially different to that obtained by using traditional sacrificial-core methods. In these methods, the prepared hollow spheres were nearly the same size or slightly smaller than the template.[21–26,34,35] We believe that the large shrinkage is caused by further dehydration of the loosely cross-linked structure of the carbon spheres, which leads to densification of Ga^{3+} ions in surface layer. Consequently, cross-linking and crystallization of gallium oxide take places when the carbon is removed in air during the calcination process, thus resulting in metal-oxide hollow spheres.

This hypothesis was partly evidenced by thermal gravimetric analysis (TGA) of Ga-loaded templates and templating carbon spheres. The similarity of the two curves (shown in Figure 2e) revealed that the two microspheres experience similar oxidation procedures: first (< 400 °C), a slow loss of weight attributed to the further dehydration and densification of carbon spheres; second, sharp weight-loss peak at 414 or 425 °C (Figure 2e, inset), which are attributed to burning of the carbon spheres. The weight-loss peak from the Ga-absorbed spheres shifts to a higher temperature; it is considered that Ga absorption might inhibit the inner oxidation. After the sharp weight loss, there is still a process of weight loss (430–550 °C), which might be caused by oxidation of carbon found deep within the core. The final weight of Ga-absorbed spheres was measured to be 3.3%.

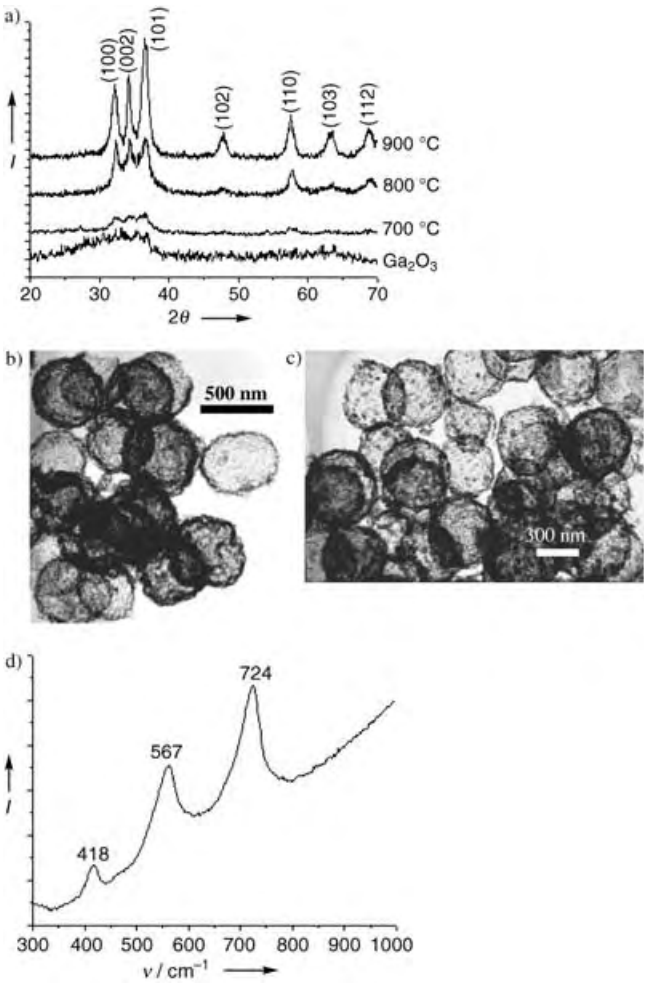


Figure 3. a) XRD patterns of Ga_2O_3 and GaN hollow spheres prepared at 700 °C, 800 °C, and 900 °C; b,c) typical TEM image of GaN hollow spheres prepared at 700 °C and 900 °C, respectively. d) Raman spectrum of GaN hollow spheres prepared at 900 °C. *I* = intensity, arbitrary units.

By alternating the size of templates from 200 nm to 4 μm, the average size of hollow spheres can be manipulated in the range from 100 nm to 1.5 μm with an almost constant shrinkage ratio about 40%. Figure 2f and the inset show the SEM of some intact and individual broken hollow spheres with diameters of 100 ± 5 nm and 1500 nm, respectively. Though the diameter of the hollow spheres may vary considerably, the thickness of the shell changes little (16 nm) even when the concentration of $GaCl_3$ is reduced from 0.5 M to 0.1 M or the adsorption temperature is increased from room temperature to 90 °C. However, when the templating carbon spheres (1000 ± 50 nm) were prepared from sucrose rather than glucose solution, the hollow Ga_2O_3 spheres had a rippled thinner shell (≈ 10 nm) and particle size 330 ± 15 nm were fabricated (Figure 2g, h). Such effects are attributed to the predetermined thickness of the "reactive-surface layer" of the carbon spheres. During the hydrothermal synthesis, there is a "growing layer" surrounding the carbon spheres, which moves outward as the size of the carbon spheres increases. As the growth process is stopped by

 © 2004 Wiley-VCH Verlag GmbH & Co. KGaA, Weinheim

terminating the hydrothermal treatment, the growing layer solidifies at the surface of carbon spheres and serves as a reactive-surface layer for the adsorption of cations. The thickness of the growing layer and the subsequent reactive-surface layer should remain unchanged despite the diameters of the carbon spheres increasing with increasing hydrothermal time. When sucrose rather than glucose was used for preparation of carbon spheres, the thickness of growing layer changed, resulting in different shell structures. This synthetic aspect is also different from previous inorganic-coating sacrificial-core methods, in which the relative ratios of the reactants (e.g., alkoxide, organic solvent, and water) in the sol–gel coating process considerably influence the quality and thickness of the coating.[34] The structure of the spheres would make it a promising material for catalysis and light advanced ceramic materials.

When the Ga_2O_3 hollow spheres were heated in an ammonia atmosphere at 700 °C, GaN hollow spheres were formed. The wide-angle XRD patterns shown in Figure 3 clearly indicate the presence of the wurtzite structure of GaN (JCPDS 760703, space group P6mc). Lattice parameters calculated from the patterns ($a = 3.191(1)$, and $c = 5.187(6)$ Å), agree well with the standard data ($a = 3.190$, and $c = 5.189$ Å). The crystallinity of final products obtained at 700, 800, and 900 °C were compared through XRD characterization (Figure 3a). The average crystalline sizes of samples obtained at these temperatures were 4 nm (700 °C), 7 nm (800 °C), and 14 nm (900 °C), according to the Scherrer equation. These results indicate that the GaN nanoparticles recrystallize and grow at a high temperature. Figures 3b, c show the TEM images of the samples obtained at 700 °C and 900 °C, respectively. The shell of the former was uniform, whereas the latter was decorated randomly with nanoparticles of 20 nm in diameter. The room-temperature Raman spectrum of the hollow spheres (Figure 3d) shows three broad symmetric peaks at 418, 567, and 724 cm^{-1}. The second and third peaks were assigned to first-order phonon frequencies of E_2(high) and A_1(LO) modes, which have been measured at 570 and 730 cm^{-1} for GaN nanorods.[7] The lower-frequency shift of the E_2(high) peak implies that the spheres experience some strain in structure since the shift is significantly influenced by compressive or tensile strains.[37–38] The peak positioned at 418 nm^{-1} is close to an acoustic overtone peak found in the spectrum of a wurtzite GaN crystal.[39]

The tunable size range of GaN hollow spheres from 100 nm to 1.5 μm is especially attractive for optical applications because this range covers the band gaps in the spectral regime from the ultraviolet (100–400 nm), visible (400–800 nm), to near infrared (800–1500 nm), while the intrinsic emission band of GaN is also in this range (370 nm). Former studies indicate that the emission properties of semiconductor nanoparticles are affected by the way in which they pack and embed into the voids of the colloidal crystals.[40,41] Hollow GaN spheres with average outside diameter of 370 nm (shown in Figure 3c) were chosen for photoluminescence study since they were expected to show specific interaction with the emission of GaN. One can see that the GaN hollow spheres showed two major emission bands (Figure 4a): one centered at 371 nm and the other comprising several emissions

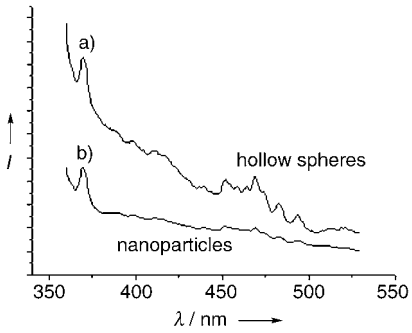


Figure 4. The photoluminescence spectrum of a) GaN hollow spheres and b) GaN nanoparticles.

positioned at 452, 470, 475, 483, and 494 nm. The band at 371 nm is related to band-edge emission, which could be attributed to the recombination of excitons bound at neutral donor sites.[9,42] But the latter is difficult to identify.[42–45] The band positioned between the yellow luminescence (2.2 eV, 563 nm) caused by deeply trap states[43,18] and the donor–acceptor pair emission (3.2 eV, 380 nm) [44] may be caused by impurities.[44–45] When the used reagent ($GaCl_3$) was directly precipitated from solution with ammonia, dehydrated in air, and converted to GaN in NH_3 at 900 °C, the as-formed GaN nanoparticles exhibited only band-edge photoluminescence (Figure 4b). So the emission around 470 nm may be morphologically related. The shell of hollow spheres is composed of GaN nanoparticles, while the structure of GaN quantum dots at the electronic level has not yet been clearly determined,[42] which further complicates the assignment of the observed peaks to specific transitions at the present time. Further detailed optical studies, such as absorbance, reflectance, and photoluminescence, on GaN hollow spheres with different sizes and crystallinities will be reported elsewhere.

In summary, size-tunable Ga_2O_3 and GaN semiconductor hollow spheres with uniform shells were prepared by using carbon spheres as templates. The size of the hollow spheres could be adjusted in the range from 100 nm to 1.5 μm by selecting different sized templating carbon spheres. This approach provides a general, simple, and cheap method to uniform hollow spheres. Surface modification and agglomeration is naturally avoided. Hollow spheres of other metal oxides may be prepared by using this method.

Experimental Section

Carbon template spheres: In a typical procedure, glucose or sucrose (4–8 g, analytic purity, Beijing Chemical Reagent Factory) was dissolved in water (40 mL) to form a clear solution. The solution was then sealed in a 40 ml teflon-lined autoclave and maintained at 160–180 °C for 4–20 h. The black or puce products were isolated after centrifugation at 5000 rpm for 20 min. The products were centrifuged, washed, and redispersed in water, and this cycle was repeated five times. Next, the products were centrifuged, washed, and redispersed in alcohol, and this cycle was repeated five times. The spheres were then oven-dried at 80 °C for 4–8 h.[36]

GaN spheres: The as-prepared carbon spheres were washed, redispersed in 0.5 M $GaCl_3$ solution, and ultrosonicated for 10 minutes. The resulting suspension was aged for 12 h before being subjected to

 © 2004 Wiley-VCH Verlag GmbH & Co. KGaA, Weinheim

five cycles of centrifugation/wash/redispersion in water. The oven-dried sample was heated to 450 °C in a tube furnace in air and maintained at the temperature for one hour. Ammonia (> 99.5 %, 30 sccm) was introduced and the temperature to 800 °C at a rate of 3 °C per minute. Argon was flowed into the reaction vessel at a rate of 200 sccm while maintaining the temperature at 800 °C for 3 h. Slightly yellow powders were obtained as the sample was allowed to cool to room temperature. Products were characterized with XRD (Bruker D8 advance), TEM (Hitachi H800, Jeol 2010F, both operated at 200 kV), and SEM (Leo-1530). Fluorescent spectra were recorded with a Hitachi F-4500 fluorescence spectrophotometer. The quantity of Ga adsorbed onto the carbon spheres were determined by thermal gravimmetric analysis (TA instruments, TGA2050) in air at a heating rate of 10 °C min^{-1} from room temperature to 600 °C.

Received: October 31, 2003
Revised: April 1, 2004 [Z53212]

Keywords: gallium · microspheres · nanostructures · semiconductors · template synthesis

[1] T. Harwig, F. Kellendonk, *J. Solid State Chem.* **1978**, *24*, 255 – 263.
[2] L. Dai, X. L. Chen, X. N. Zhang, A. Z. Jin, T. Zhou, B. Q. Hu, Z. Zhang, *J. Appl. Phys.* **2002**, *92*, 1062.
[3] B. Cheng, E. T. Samulski, *J. Mater. Chem.* **2001**, *11*, 2901 – 2902.
[4] S. Shama, M. K. Sunkara, *J. Am. Chem. Soc.* **2002**, *124*, 12288.
[5] F. A. Ponce, D. P. Bour, *Nature* **1997**, *386*, 351.
[6] T. Someya, R. Werner, A. Forchel, M. Catalano, R. Cingolani, Y. Arakawa, *Science* **1999**, *285*, 1905.
[7] S. Y. Bae, H. W. Seo, J. Park, H. Yang, H. Kim, S. Kim, *Appl. Phys. Lett.* **2003**, *82*, 4564.
[8] C. H. Liang G. W. Meng, G. Z. Wang, Y. W. Wang, L. D. Zhang, S. Y. Zhang, *Appl. Phys. Lett.* **2001**, *78*, 3202.
[9] Y. X. Li, A. Trinchi, W. Wlodarski, K. Galatsis, K. Kalantar-zadeh, *Sens. Actuators B* **2003**, *93*, 431.
[10] G. Fasol, *Science* **1996**, *272*, 1751.
[11] H. M. Kim, T. W. Kang, K. S. Chung, *Adv. M*ater. **2003**, *15*, 567.
[12] S. Nakamura, *Science* **1998**, *281*, 956.
[13] C. H. Wallace, S. H. Kim, G. A. Rose, L. Rao, J. R. Heath, M. Nicol, and R. B. Kaner, *Appl. Phys. Lett.* **1998**, *72*, 596 – 598.
[14] W. Q. Han, S. S. Fan, Q. Q. Li, Y. D. Hu, *Science* **1997**, *277*, 1287.
[15] X. F. Duan, C. M. Lieber, *J. Am. Chem. Soc.* **2000**, *122*, 188 – 189.
[16] S. Y. Bae, H. W. Seo, J. Park, H. Yang, J. C. Park, S. Y. Lee, *Appl. Phys. Lett.* **2002**, *81*, 126 – 128.
[17] J. Goldberger, R. R. He, Y. F. Zhang, S. K. Lee, H. Q. Yan, H-. J. Choi, P. D. Yang, *Nature* **2003**, *422*, 599.
[18] J. Q. Hu, Y. Bando, D. Golberg, Q. L. Liu, *Angew. Chem.* **2003**, *115*, 3617 – 3621; *Angew. Chem. Int. Ed.* **2003**, *42*, 3493 – 3497.
[19] Y. N. Xia, B. Gates, Y. D. Yin, Y. Lu, *Adv. Mater.* **2000**, *12*, 693 – 713.
[20] W. Schärtl, *Adv. Mater.* **2000**, *12*, 1899 – 1908.
[21] F. Caruso, *Top. Curr. Chem.* **2003**, *227*, 145 – 168, and references therein.
[22] Y. N. Xia, B. Gates, Z. Y. Li, *Adv. Mater.* **2001**, *13*, 409, and references therein.
[23] H. Fudouzi, Y. N. Xia, *Adv. Mater.* **2003**, *15*, 892.
[24] Z. Y. Zhong, Y. D. Yin, B. Gates, Y. N. Xia, *Adv. Mater.* **2002**, *14*, 206 – 209.
[25] Y. Lu, Y. D. Yin, Y. N. Xia, *Adv. Mater.* **2001**, *13*, 267 – 271.
[26] Z. Z. Yang, Z. W. Niu, Y. F. Lu, Z. B. Hu, C. C. Han, *Angew. Chem.* **2003**, *115*, 1987 – 1989; *Angew. Chem. Int. Ed.* **2003**, *42*, 1943.
[27] A. Rogach, A. Susha, F. Caruso, G. Sukhorukov, A. Kornowski, S. Kershaw, Möhwald, A. Eychmüller, H. Weller, *Adv. Mater.* **2000**, *12*, 333 – 337.
[28] I. L. Radtchenko, G. B. Sukhorukov, N. Gaponik, A. Kornowski, A. L. Rogach, H. Möhwald, *Adv. Mater.* **2001**, *13*, 1684 – 1687.
[29] D. Y. Wang, A. L. Rogach, F. Caruso, *Chem. Mater.* **2003**, *15*, 2724.
[30] M. L. Breen, A. D. Dingsmore, R. H. Pink, S. B. Qadri, and B. R. Ratna, *Langmuir* **2001**, *17*, 903 – 907.
[31] C. X. Song, G. H. Gu, Y. S. Lin, H. Wang, Y. Guo, X. Fu, Z. S. Hu, *Mater. Res. Bull.* **2003**, *38*, 917 – 924.
[32] K. P. Velikov, A. van Blaaderen, *Langmuir* **2001**, *17*, 4779 – 4786.
[33] Q. Peng, Y. J. Dong, Y. D. Li, *Angew. Chem.* **2003**, *115*, 3135 – 3138; *Angew. Chem. Int. Ed.* **2003**, *42*, 3027 – 3030.
[34] F. Caruso, *Chem. Eur. J.* **2000**, *6*, 413 – 419.
[35] Y. D. Yin, Y. Lu, B. Gates, Y. N. Xia, *Chem. Mater.* **2001**, *13*, 1146.
[36] X. M. Sun, Y. D. Li, *Angew. Chem.* **2004**, *116*, 607 – 611; *Angew. Chem. Int. Ed.* **2004**, *43*, 597 – 601.
[37] H. W. Seo, S. Y. Bae, J. Park, H. Yang, K. S. Park, S. Kim, *J. Chem. Phys.* **2002**, *116*, 9492.
[38] M. Klose, N. Wieser, G. C. Rohr, R. Dassow, F. Scholz, J. Off, *J. Cryst. Growth* **1998**, *189*/190, 634.
[39] C.-C. Chen, C.-C. Yeh, C.-H. Chen, M.-Y. Yu, H.-L. Liu, J.-J. Wu, K.-H. Chen, L.-C. Chen, J.-Y. Peng, Y.-F. Chen, *J. Am. Chem. Soc.* **2001**, *123*, 2791.
[40] A. S. Susha, F. Caruso, A. L. Rogach, G. B. Sukhorukov, A. Kornowski H. Möhwald, M. Giersig, A. Eychmüller, H. Weller, *Colloids Surf. A* **2000**, *163*, 39.
[41] Y. A. Vlasov, K. Luterova, I. Pelant, B. N. Hönerlage, V. N. Astratov, *Appl. Phys. Lett.* **1997**, *71*, 1616.
[42] O. I. Mićić, S. P. Ahrenkiel, D. Bertram, and A. J. Nozik, *Appl. Phys. Lett.* **1999**, *75*, 478 – 480.
[43] E. R. Glaser, T. A. Kennedy, K. Doverspike, L. B. Rowland, D. K. Gaskill, J. A. Freitas, Jr., M. Asif Khan, J. N. Kuzina, D. K. Wickenden, *Phys. Rev. B* **1995**, *51*, 13326.
[44] J. Y. Leem, C. R. Lee, J. I. Lee, S. K. Noh, Y. S. Kwon, Y. H. Ryu, S. J. Son, *J. Cryst. Growth* **1998**, *193*, 491 – 495.
[45] H. J. Lozykowski, W. M. Jadwisienczak, I. Brown, *Appl. Phys. Lett.* **1999**, *74*, 1129.

 © 2004 Wiley-VCH Verlag GmbH & Co. KGaA, Weinheim

Cage Compounds

Polyhedral Ferrous and Ferric Siloxanes**

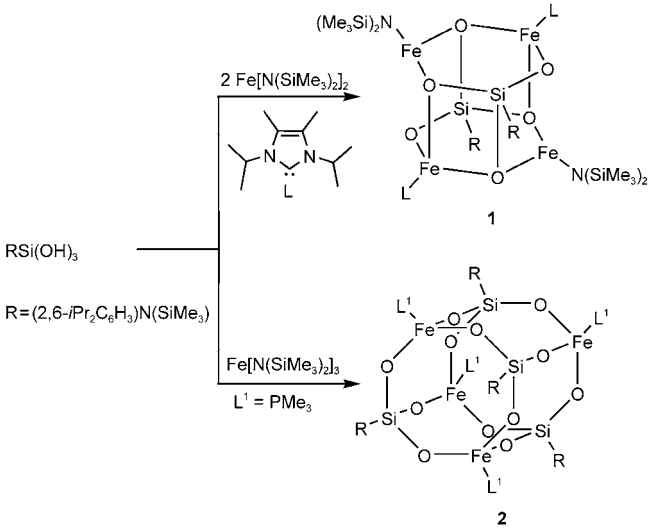
Umesh N. Nehete, Ganapathi Anantharaman, Vadapalli Chandrasekhar, Ramaswamy Murugavel, Mrinalini G. Walawalkar, Herbert W. Roesky, Denis Vidovic, Jörg Magull, Konrad Samwer, and Björn Sass*

Dedicated to Professor Michael Veith on the occasion of his 60th birthday

Iron is the fourth most abundant element in the earth's crust after oxygen, silicon, and aluminum. Although iron atoms are present in the ore hematite (Fe_2O_3) in the formal oxidation state +III, in magnetite (Fe_3O_4) they exhibit both the +II and +III oxidation states. In the naturally occurring olivine, $MgFeSiO_4$, iron atoms are present in the +II oxidation state while in garnets, $[M^{2+}_3 M^{3+}_2(SiO_4)_3]$ (M^{2+} = Co, Mg, Fe; M^{3+} = Al, Cr, Fe) they are found in both oxidation states.[1,2] Other examples of iron-containing silicate frameworks include zeolites such as iron-modified ZSM-5, which have been shown to be important as catalysts, as for example in the synthesis of phenol from benzene and N_2O.[3] Moreover the Lewis acidity of the iron centers in iron-modified ZSM-5 enables its use as an acid catalyst in the benzylation reaction of benzene by using benzyl chloride[4] and also in the esterification of *tert*-butanol by acetic anhydride.[5]

We have a long-standing interest in molecular assemblies that contain the {Si-O-M} motif.[6] Firstly, this is in view of the importance of such compounds as models for naturally occurring minerals.[7] Secondly, these compounds are also quite valuable in understanding the mechanism of many catalytic processes particularly those involving silica-supported transition-metal catalysts.[8] A case in point are the molecular cubic titanosiloxanes $[\{Ti(OR^1)O_3SiR\}_4]$ [R^1 = *t*Bu, *t*BuO, *t*BuCH$_2$; R = (2,6-*i*Pr$_2$C$_6$H$_3$)N(SiMe$_3$)], which have not only helped in the elucidation of the Si-O-Ti stretching frequency observed in TS-1 and TS-2 catalysts (TS is titanium silicate) but have also themselves been quite effective in catalytic reactions that involve the epoxidation of 1-hexene and 1-octene.[9,10] In view of this success, it was of interest to build analogous molecular iron siloxane frameworks. Previous work on iron siloxanes centered around the use of R_3SiO[11] or silsesquioxane ligands.[12] However, polyhedral iron siloxanes have remained elusive and the preparation of such compounds is a synthetic challenge in view of the instability of iron alkyls. We have overcome this synthetic hurdle by choosing bis- and trisamido derivatives of iron[13,14] as the starting precursor and have been able to assemble two different iron siloxanes that contain iron atoms in the formal oxidation states of +II and +III, respectively. Accordingly, herein we report the synthesis and single-crystal molecular structures of ferrous $[\{(Me_3Si)_2NFe\}_2\{LFe\}_2\{O_3SiR\}_2]$ (L = 1,3-diisopropyl-4,5-dimethylimidazol-2-ylidene) **1** and ferric siloxanes $[\{(L^1Fe)(O_3SiR)\}_4]$ [L^1 = PMe_3; R = (2,6-*i*Pr$_2$C$_6$H$_3$)N(SiMe$_3$)] **2** (Scheme 1).

The addition of two equivalents of $Fe[N(SiMe_3)_2]_2 \cdot THF$[13] to a suspension of $RSi(OH)_3$ in hexane/toluene mixture at room temperature in the presence of the N-heterocyclic carbene L (L = 1,3-diisopropyl-4,5-dimethylimidazol-2-ylidene) affords **1** in moderate yield (Scheme 1). The use of the auxiliary coordinating ligand L allowed the isolation of the ferrous siloxane **1** as a crystalline product. Single crystals of **1**, thus obtained, were found to be soluble in many common organic solvents. The IR spectrum of **1** shows characteristic absorptions for the {Fe-O-Si} groups in the range of 900 to 1000 cm^{-1}. However no peak attributable to the molecular ion of **1** can be observed in the EI or other mass spectrometric methods.



Scheme 1. Synthesis of ferrous **1** and ferric siloxanes **2**.

[*] U. N. Nehete, G. Anantharaman, Prof. Dr. H. W. Roesky, D. Vidovic, J. Magull
Institut für Anorganische Chemie
Universität Göttingen
Tammannstrasse 4, 37077 Göttingen (Germany)
Fax: (+49) 551-39-3373
E-mail: hroesky@gwdg.de
Prof. Dr. K. Samwer, B. Sass
I. Physikalisches Institut
Universität Göttingen
Tammannstrasse 1, 37077 Göttingen (Germany)
Prof. Dr. V. Chandrasekhar
Department of Chemistry
IIT-Kanpur
Kanpur-208 016 (India)
Prof. Dr. R. Murugavel, Dr. M. G. Walawalkar
Department of Chemistry
IIT-Bombay
Powai, Mumbai, 400 076 (India)

[**] This work was supported by the Deutsche Forschungsgemeinschaft (Graduiertenkolleg: Spektroskopie und Dynamik molekularer Aggregate, Ketten, Knäuel und Netzwerke) and the Göttinger Akademie der Wissenschaften. V.C. thanks the Alexander von Humboldt Foundation, Bonn (Germany), for the Friedrich Wilhelm Bessel-Research award. M.G.W. and R.M. thank the Alexander von Humboldt Foundation, Bonn (Germany), for a research fellowship.

 © 2004 Wiley-VCH Verlag GmbH & Co. KGaA, Weinheim DOI: 10.1002/anie.200453740

The molecular structure of **1** has been determined by single-crystal X-ray diffraction experiments[15a] and it consists of an $\{Fe_4O_6Si_2\}$ core (Figure 1a). The structure of **1** exhibits two $\{Fe_2O_3Si\}$ rings that are fused to each other, which results in the formation of a drumlike architecture with a pseudoinversion center. The sides of the drum are defined by two four-membered $\{FeO_2Si\}$ and two six-membered $\{Fe_2O_3Si\}$ rings. Two types of iron centers are present in the structure of **1**. While Fe1 and Fe4 have a coordination environment comprising one N and two O atoms with one intact $N(SiMe_3)_2$ ligand, Fe2 and Fe3 have a coordination environment of one C and three O atoms, in which the N-heterocyclic carbene takes up the fourth coordination side. The tricoordinate iron centers (Fe1 and Fe4) are in a trigonal planar geometry while the tetracoordinate iron centers, (Fe2 and Fe3) have an approximate tetrahedral geometry. Another view of the structure of **1** (Figure 1b) shows that the four iron centers are nearly in one plane and are held together by two essentially bicapping $RSiO_3$ units. This mode of interaction of the $RSiO_3$ ligand is similar to that of the RPO_3 ligand as found in molecular metal phosphonate and phosphate structures.[16–18]

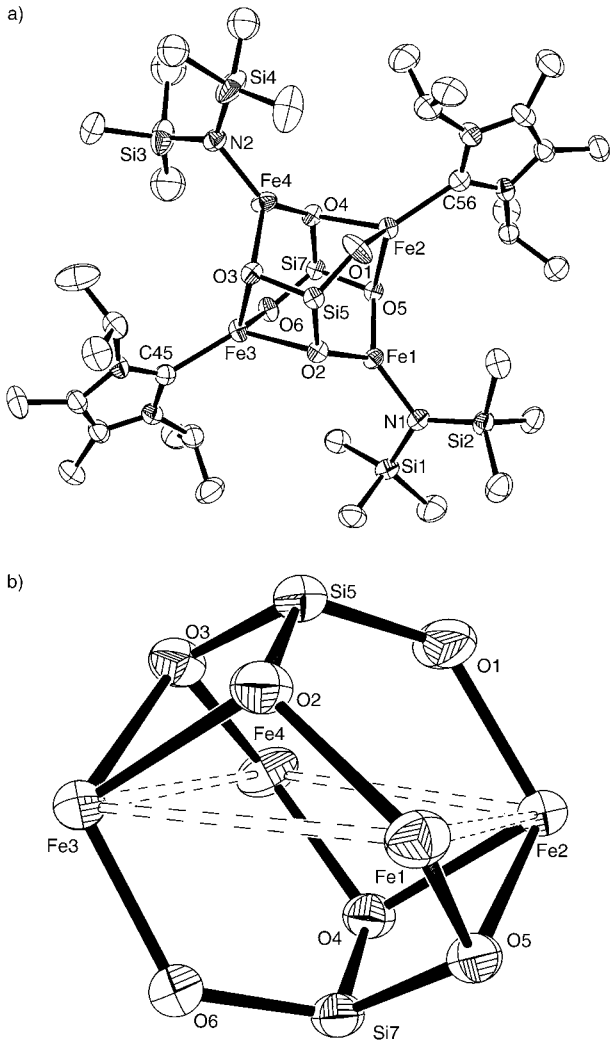


Figure 1. Molecular structure of **1**. a) The substituents on silanetriol have been removed for the sake of clarity. Selected bond lengths [Å] and angles [°]: Fe(1)-O(2) 1.940(2), Fe(1)-O(5) 1.945(2), Fe(2)-O(1) 1.891(2), Fe(2)-O(4) 2.143(2), Fe(2)-O(5) 2.098(2), Fe(1)-N(1) 1.938(3), Fe(2)-C(56) 2.123(4), Si(5)-O(1) 1.605(3), Si(5)-O(2) 1.641(3), Si(5)-O(3) 1.653 (2); O(2)-Fe(1)-O(5) 105.15(10), O(2)-Fe(1)-N(1) 128.58(12), O(5)-Fe(1)-N(1) 126.27(11), O(1)-Fe(2)-O(5) 106.00(10), C(56)-Fe(2)-O(1) 118.92(12), C(56)-Fe(2)-O(5) 124.35(11), O(1)-Si(5)-O(2) 115.01(14), O(1)-Si(5)-O(3) 105.84 (15), O(2)-Si(5)-O(3) 100.78(12), Fe(1)-O(2)-Fe(3) 112.67(10), Fe(3)-O(2)-Si(5) 90.79(11), Fe(1)-O(2)-Si(5) 123.09(14), Fe(2)-O(1)-Si(5) 131.19(15). b) Core structure of **1**. Imaginary lines are drawn between iron atoms to show its planar arrangement.

One of the three oxygen atoms (O1, O6) of each silanetriol in **1** is involved in a μ-bridging mode (Fe-O-Si), while the other two oxygen atoms (O2, O3, O4, O5) are involved in a μ_3-bridging mode that links two iron centers and one silicon. In general, the bond lengths that involve the μ_3-oxygen centers are found to be longer (av. Si–O, 1.651 Å; Fe–O, 2.055 Å) than the corresponding distances that involve the μ-oxygen atom (av. Si–O, 1.605 Å; Fe–O, 1.892 Å).

The reaction of the silanetriol with the ferric amide $[Fe\{N(SiMe_3)_2\}_3]$[14] proceeds with complete elimination of $HN(SiMe_3)_2$ to afford the ferric siloxane **2** which was crystallized in the presence of trimethyl phosphane L[1] (Scheme 1). Compound **2**, like **1** discussed above is highly lipophilic and is soluble in common organic solvents including hexane. The ferric siloxane **2** is thermally stable up to its melting point (242–244 °C). The ESIMS of **2** shows the base peak for $[M^+-PMe_3]$, which suggest a remarkable stability of the core structure of **2** under these conditions. Compound **2** exhibits broad resonances in its NMR spectra, thus indicating that it is paramagnetic.

The molecular structure of **2** (Figure 2) is made up of a $\{Fe_4O_{12}Si_4\}$ cuboid core at which the corners of the cube are alternately occupied by iron and silicon atoms.[15b] Each of the twelve edges of the cube contain the bridging oxygen atoms. Thus, the overall core structure of the ferric siloxane contains six $\{Fe_2O_4Si_2\}$ eight-membered rings as the faces of the cube. Unlike in the ferrous siloxane **1**, in compound **2** all the oxygen atoms are involved in a μ-bridging mode that interconnects a silicon and an iron atom. Each iron is tetracoordinate with a coordination environment of one P and three O atoms. The coordination geometry around both iron and silicon centers is nearly tetrahedral. The average Fe–O distance (1.824 Å) found in the ferric siloxane **2** is much shorter due to the smaller ionic radius of an Fe^{III} center compared to that of an Fe^{II} in **1**. In contrast the Si–O distance in **2** is similar (av. 1.618 Å) to that found in **1** (μ-O).

Magnetic-susceptibility measurements[19] were carried out in the temperature range from 300 K to 5 K for compounds **1** and **2**. A plot of $1/\chi$ (Oe emu^{-1}; χ is magnetic susceptibility) versus T (K) is shown in Figure 3. The plots indicate an antiferromagnetic behavior for both compounds.

In conclusion we report the first examples of polyhedral ferrous and ferric siloxanes. The isolation of these compounds suggests that similar synthetic strategies will allow the preparation of other transition-metal siloxane frameworks. These perspectives will lead to interesting new systems.

 © 2004 Wiley-VCH Verlag GmbH & Co. KGaA, Weinheim

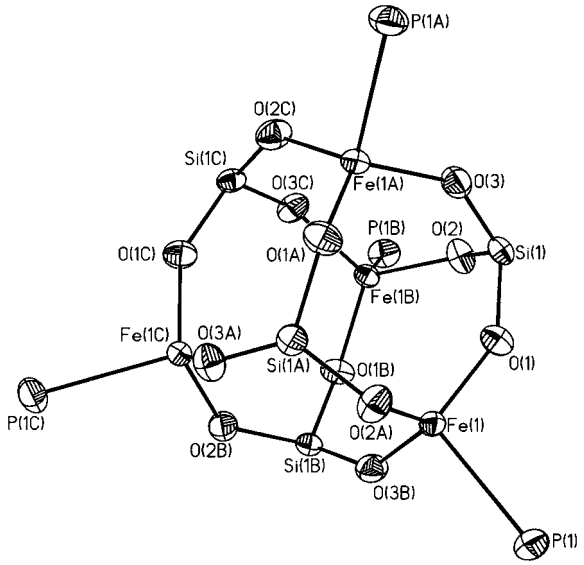


Figure 2. Core structure of **2**. The substituents on silanetriol and the phosphane have been omitted for the sake of clarity. Selected bond lengths [Å] and angles [°]: Fe(1)-O(1) 1.802(3), Fe(1)-O(3B) 1.829(3), Fe(1)-O(2A) 1.831(3), Fe(1)-P(1) 2.468(1), Si(1)-O(1) 1.628(3), Si(1)-O(2) 1.616(3), Si(1)-O(3) 1.612(3); Si(1)-O(1)-Fe(1) 147.60(19), O(1)-Fe(1)-O(3B) 114.61(14), O(3)-Si(1)-O(2) 111.40(16), O(2)-Si(1)-O(1) 108.73(17).

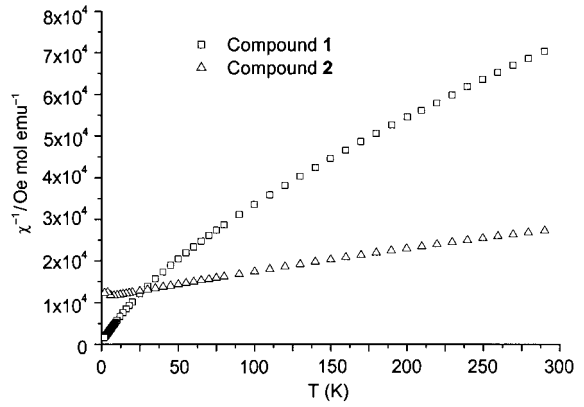


Figure 3. Plot of $1/\chi$ (Oe mol emu^{-1}) versus T (K) for compounds **1** and **2**.

Experimental Section

1: $[Fe\{N(SiMe_3)_2\}_2]$·THF (3.5 g, 9.17 mmol) was slowly added to a suspension of $RSi(OH)_3$ (**1**) (1.5 g, 4.59 mmol) in THF/hexane (10 mL, 40 mL) at room temperature. The solution turned from green to dark brown. This solution was stirred for further 16 h at room temperature. A solution of N-heterocyclic carbene L (2 g, 11.47 mmol) in toluene (10 mL) was added and the stirring was continued for one more day. The volatile components were removed to obtain a brown solid. To this a mixture of toluene (10 mL) and THF (1 mL) was added. Colorless crystals of **1** were obtained after several days at 0 °C: (0.50 g, 13 % of single crystals); mp >220 °C; IR (nujol): $\tilde{\nu}$ = 1260, 1245, 1221, 1186, 1100, 1043, 1019, 983, 964, 945, 927, 885, 836, 820, 801, 752, 723, 680, 607, 567, 544, 491 cm^{-1}; elemental analysis (%) calcd (toluene molecules were removed by drying under vacuum) for $C_{64}H_{128}Fe_4N_8O_6Si_8$ (1407.44): C 49.47, H 8.30, N 7.21; found: C 47.7, H 8.0, N 6.2.

2: $[Fe\{N(SiMe_3)_2\}_3]$ (2.3 g, 4.28 mmol) in hexane (25 mL) was slowly added to a suspension of silanetriol (1.4 g, 4.28 mmol) in the same solvent (40 mL). After the addition was complete, the reaction mixture was stirred for 72 h at room temperature. The green solution slowly turned to greenish brown. The solvents and hexamethyldisilazane were removed in vacuo to give a brownish-green product. This was recrystallized from a mixture of toluene and THF (1:0.05) in the presence of PMe_3 as the auxiliary coordinating ligand at room temperature over a period of two weeks (0.29 g, 14 %; it was observed that the yield of compound **2** was improved to about 25 % of single crystals by the use of a mixture of hexane and THF (1:0.25) along with PMe_3 for crystallization); mp 242–244 °C; ESIMS (CH_3CN): m/z (%) 1750 (100) [$M^+ - PMe_3$]; IR (nujol): $\tilde{\nu}$ = 1585, 1576, 1440, 1420, 1321, 1308, 1290, 1245, 1190, 1107, 1096, 1054, 1033, 967, 956, 923, 836, 800, 757, 749, 726, 682, 642, 613, 599, 549, 534, 489, 462, 434 cm^{-1}; elemental analysis (%) calcd (toluene molecules were removed by drying under vacuum) $C_{72}H_{140}Fe_4N_4O_{12}P_4Si_8$ (1825.89): C 47.36, H 7.73, N 3.07; found: C 46.68, H 7.17, N 3.24.

Received: January 13, 2004 [Z53740]

Keywords: cage compounds · iron · N ligands · silicon · siloxanes

[1] A. F. Holleman, E. Wiberg, *Lehrbuch der Anorganischen Chemie*, 81st-90th ed., Walter de Gruyter, Berlin, **1976**.
[2] a) N. N. Greenwood, A. Earnshaw, *Chemistry of the Elements*, 1st ed., Pergamon, Oxford, **1984**; b) A. F. Wells, *Structural Inorganic Chemistry*, 5th ed., Clarendon, Oxford, **1984**, p. 329.
[3] a) A. A. Ivanov, V. S. Chernyavsky, M. J. Gross, A. S. Kharitonov, A. K. Uriarte, G. I. Panov, *Appl. Catal. A* **2003**, *249*, 327–343; b) D. P. Ivanov, V. I. Sobolev, L. V. Pirutko, G. I. Panov, *Adv. Synth. Catal.* **2002**, *344*, 986–995; c) D. P. Ivanov, M. A. Rodkin, K. A. Dubkov, A. S. Kharitonov, G. I. Panov, *Kinet. Catal.* **2000**, *41*, 771–775.
[4] a) V. R. Choudhary, S. K. Jana, A. S. Mamman, *Microporous Mesoporous Mater.* **2002**, *56*, 65–71; b) V. R. Choudhary, S. K. Jana, *J. Mol. Catal. A* **2002**, *180*, 267–276.
[5] V. R. Choudhary, K. Mantri, S. K. Jana, *Microporous Mesoporous Mater.* **2001**, *47*, 179–183.
[6] a) R. Murugavel, A. Voigt, M. G. Walawalkar, H. W. Roesky, *Chem. Rev.* **1996**, *96*, 2205–2236; b) R. Murugavel, V. Chandrasekhar, H. W. Roesky, *Acc. Chem. Res.* **1996**, *29*, 183–189; c) H. J. Gosink, H. W. Roesky, H.-G. Schmidt, M. Noltemeyer, E. Irmer, R. Herbst-Irmer, *Organometallics* **1994**, *13*, 3420–3426.
[7] a) M. L. Montero, A. Voigt, M. Teichert, I. Usón, H. W. Roesky, *Angew. Chem.* **1995**, *107*, 2761–2763; *Angew. Chem. Int. Ed. Engl.* **1995**, *34*, 2504–2506; b) A. Voigt, R. Murugavel, E. Parisini, H. W. Roesky, *Angew. Chem.* **1996**, *108*, 823–825; *Angew. Chem. Int. Ed. Engl.* **1996**, *35*, 748–750; c) A. Voigt, M. G. Walawalkar, R. Murugavel, H. W. Roesky, E. Parisini, P. Lubini, *Angew. Chem.* **1997**, *109*, 2313–2315; *Angew. Chem. Int. Ed. Engl.* **1997**, *36*, 2203–2205; d) G. Anantharaman, H. W. Roesky, H.-G. Schmidt, M. Noltemeyer, J. Pinkas, *Inorg. Chem.* **2003**, *42*, 970–973; e) G. Anantharaman, N. D. Reddy, H. W. Roesky, J. Magull, *Organometallics* **2001**, *20*, 5777–5779; f) G. Anantharaman, H. W. Roesky, J. Magull, *Angew. Chem.* **2002**, *114*, 1274–1277; *Angew. Chem. Int. Ed.* **2002**, *41*, 1226–1229.
[8] a) N. Winkhofer, H. W. Roesky, M. Noltemeyer, W. T. Robinson, *Angew. Chem.* **1992**, *104*, 670–671; *Angew. Chem. Int. Ed. Engl.* **1992**, *31*, 599–601; b) A. I. Gouzyr, H. Wessel, C. E. Barnes, H. W. Roesky, M. Teichert, I. Usón, *Inorg. Chem.* **1997**, *36*, 3392–3393.

 © 2004 Wiley-VCH Verlag GmbH & Co. KGaA, Weinheim

[9] M. Fujiwara, H. Wessel, H.-S. Park, H. W. Roesky, *Tetrahedron* **2002**, *58*, 239 – 243.
[10] M. Fujiwara, H. Wessel, H.-S. Park, H. W. Roesky, *Chem. Mater.* **2002**, *14*, 49 – 75.
[11] a) H. Schmidbaur, M. Schmidt, *J. Am. Chem. Soc.* **1962**, *84*, 3600 – 3601; b) A. N. Kornev, T. A. Chesnokova, V. V. Semenov, E. V. Zhezlova, L. N. Zakharov, L. G. Klapshina, G. A. Domrachev, V. S. Rusakov, *J. Organomet. Chem.* **1997**, *547*, 113 – 119; c) C. Nozaki, C. G. Lugmair, A. T. Bell, T. D. Tilley, *J. Am. Chem. Soc.* **2002**, *124*, 13194 – 13203; d) T. A. Chesnokova, E. V. Zhezlova, A. N. Kornev, Y. V. Fedotova, L. N. Zakharov, G. K. Fukin, Y. A. Kursky, T. G. Mushtina, G. A. Domrachev, *J. Organomet. Chem.* **2002**, *642*, 20 – 31.
[12] a) F. C. Liu, K. D. John, B. L. Scott, R. T. Baker, K. C. Ott, W. Tumas, *Angew. Chem.* **2000**, *112*, 3257 – 3260; *Angew. Chem. Int. Ed.* **2000**, *39*, 3127 – 3130; b) P. A. Shapley, W. S. Bigham, M. T. Hay, *Inorg. Chim. Acta* **2003**, *345*, 255 – 260; c) M. T. Hay, B. J. Hainaut, S. J. Geib, *Inorg. Chem. Commun.* **2003**, *6*, 431 – 434.
[13] M. M. Olmstead, P. P. Power, S. C. Shoner, *Inorg. Chem.* **1991**, *30*, 2547 – 2551.
[14] E. C. Alyea, D. C. Bradley, R. G. Copperthwaite, *J. Chem. Soc. Dalton Trans.* **1972**, 1580 – 1584.
[15] Crystal data for compounds: a) The single crystals suitable for X-ray diffraction studies of compound **1**·1.5 C_7H_8 were obtained from toluene at 0 °C. $C_{74.50}H_{140}Fe_4N_8O_6Si_8$, $M_r = 1692.06$, triclinic, space group $P\bar{1}$, $a = 12.6202(5)$ Å, $b = 14.7837(6)$ Å, $c = 27.2205(12)$ Å, $\alpha = 93.949(4)^\circ$, $\beta = 97.850(3)^\circ$, $\gamma = 109.689(3)^\circ$, $V = 4700.8(3)$ Å^3, $Z = 2$, $\rho_{calcd} = 1.195$ mg m^{-3}, $F(000) = 1814$, $\lambda = 0.71073$ Å, $T = 133(2)$ K, $\mu(Mo_{K\alpha}) = 0.755$ mm^{-1}. The data were collected using the ω scan mode in the range of $1.47 \le \theta \le 24.84$, $-14 \le h \le 14$, $-17 \le k \le 17$, $-32 \le l \le 27$. Of 45117 reflections collected, 16133 were unique. Final $R1$ ($I > 2\sigma(I)$) = 0.0497; $wR2$ (all data) = 0.1452. Maximum and minimum heights in the final Fourier-difference map were 1.031 and −1.016 e·A^{-3}; b) **2**·2 C_7H_8: $C_{86}H_{156}Fe_4N_4O_{12}P_4Si_8$, $M_r = 2010.15$, tetragonal, space group $P42_1c$, $a = b = 19.7056(11)$ Å, $c = 15.1916(11)$ Å, $\alpha = \beta = \gamma = 90^\circ$, $V = 5899.1(6)$ Å^3, $Z = 2$, $\rho_{calcd} = 1.132$ mg m^{-3}, $F(000) = 2144$, $\lambda = 0.71073$ Å, $T = 133(2)$ K, $\mu(Mo_{K\alpha}) = 0.666$ mm^{-1}. The data were collected by using the ω scan mode in the range of $1.69 \le \theta \le 24.81$, $-23 \le h \le 20$, $-23 \le k \le 19$, $-17 \le l \le 11$. Of 12247 reflections collected, 4732 were unique. Final $R1$ ($I > 2\sigma(I)$) = 0.0431; $wR2$ (all data) = 0.1309. Maximum and minimum heights in the final Fourier difference map were 0.752 and −0.249 e·A^{-3}. The single crystals suitable for X-ray diffraction studies of compound **2**·2 C_7H_8 were obtained from a mixture of toluene and THF in the presence of PMe_3 at room temperature. Diffraction data were collected on a IPDS II Stoe image-plate diffractometer with graphite-monochromated Mo Kα radiation ($\lambda = 0.71073$ Å). The structure was solved by direct methods (SHELX-97)[20] and refined against F^2 on all data by full-matrix least squares with SHELX-97.[21] The heavy atoms were refined anisotropically. Hydrogen atoms were included by using the riding model with U_{iso} tied to U_{iso} of the parent atoms. CCDC-225526 (**1**) and CCDC-225525 (**2**) contain the supplementary crystallographic data (excluding structure factors) for this paper. These data can be obtained free of charge via www.ccdc.cam.ac.uk/conts/retrieving.html (or from the Cambridge Crystallographic Data Centre, 12, Union Road, Cambridge CB2 1EZ, UK; fax: (+44) 1223-336-033; or deposit@ccdc.cam.ac.uk).
[16] V. Chandrasekhar, S. Kingsley, B. Rhatigan, M. K. Lam, A. L. Rheingold, *Inorg. Chem.* **2002**, *41*, 1030 – 1032.
[17] G. Anantharaman, V. Chandrasekhar, M. G. Walawalkar, H. W. Roesky, D. Vidovic, J. Magull, M. Noltemeyer, *J. Chem. Soc. Dalton Trans.* **2004**, 1271 – 1275.
[18] A. Clearfield, G. D. Smith, *Inorg. Chem.* **1969**, *8*, 431 – 436.
[19] Variable-temperature magnetic measurements were recorded using a SQUID magnetometer (Quantum Design). Crushed single crystals were restrained between the two halves of a gelatine capsule by inverting the top half.
[20] G. M. Sheldrick, *Acta Crystallogr. Sect. A* **1990**, *46*, 467 – 473.
[21] G. M. Sheldrick, SHELX-97, Program for Crystal Structure Refinement, University of Göttingen, Göttingen (Germany), **1997**.

 © 2004 Wiley-VCH Verlag GmbH & Co. KGaA, Weinheim

Molecular Electronics

Electron Transfer in a Hg-SAM//SAM-Hg Junction Mediated by Redox Centers**

Elizabeth Tran, Maria A. Rampi, and George M. Whitesides**

Studies of electron transport through molecules using metal–molecule–metal junctions[1–3] or scanning probe devices[2,4–6] suggest principles that may be useful in designing systems for organic/organometallic electronics. Molecules are, in general, poor conductors of electrons, and "conduct" by tunneling. For some molecules, however, applying a potential across the electrodes of a metal–molecule–metal junction can cause an orbital (usually the HOMO or LUMO) of the molecule to fall between the Fermi levels of the electrodes and thus increase conductivity.[7,8] Molecules with well-defined and readily accessible redox states are, thus, attractive candidates for use in testing theories of electron transport (and perhaps for electronic devices),[4,9–18] and a few examples are now known in which two or more metal redox centers organized in space and energy with respect to one another display electronic functions such as rectification and switching.[19,20] Here we report the first example of a metal–molecule–metal junction comprising two closely spaced alkane thiolate monolayers,

[*] Prof. M. A. Rampi
Dipartimento di Chimica, Università di Ferrara
via L. Borsari 46, 44100 Ferrara (Italy)
Fax: (+39) 053-229-1162
E-mail: rmp@unife.it
Dr. E. Tran, Prof. G. M. Whitesides
Department of Chemistry and Chemical Biology
Harvard University, Cambridge, MA 02138 (USA)
Fax: (+1) 617-495-9857
E-mail: gwhitesides@gmwgroup.harvard.edu

[**] The support of DARPA, NSEC (award no. NSF-PHY-0117795), EC (award no. G5RD-CT-2002-00776 MWFM), and NSERC (in the form of a postdoctoral fellowship to E.T.) is gratefully acknowledged. We thank Prof. Royce Murray, Prof. Wolfgang Schmickler, Mandar Deshmukh, Mark Gudiksen, Amy Prieto, Babak Parviz, Logan McCarty, Rosaria Ferrigno, and Sam Sia for helpful discussions, and Prof. Harry Finklea for providing a procedure for the synthesis of the ruthenium-containing thiol.

Supporting information for this article is available on the WWW under http://www.angewandte.org or from the author.

 DOI: 10.1002/anie.200453945 © 2004 Wiley-VCH Verlag GmbH & Co. KGaA, Weinheim

each presenting redox centers at their surface.[21] Standard electrochemical techniques demonstrate that this junction becomes conductive when the electrode potentials are adjusted to the formal potential of the redox centers, and that it shows diode- and transistor-like characteristics analogous to those of solid-state devices.

Figure 1a shows a schematic illustration of the junction[22–30] and the associated electrochemical system. The junction consists of two mercury-drop electrodes, both of which support a self-assembled monolayer (SAM) of the thiol terminated with the ruthenium peta-amine pyridine-terminated thiol $[Ru(NH_3)_5(NC_5H_4\text{-}4\text{-}CH_2NHCO(CH_2)_{10}SH](PF_6)_2$ (henceforth abbreviated as HS-C_{10}-Ru).[31,32] The thiol HS-C_{10}-Ru readily adsorbs from 1 mM acetonitrile solutions onto mercury electrodes and gives electroactive monolayers.[33] Cyclic voltammetry of a monolayer in contact with 0.2 M aqueous Na_2SO_4 at pH 4 (Figure 1c) shows a redox wave corresponding to the $Ru^{II} \rightleftarrows Ru^{III}$ interconversion at $E^{o'}_{SAM} = -0.01$ V versus Ag/AgCl, a value that is close to that of a related compound dissolved in the same medium ($E^{o'}_{soln} = +0.04$ V versus the saturated calomel electrode[31]). At scan rates < 100 mV s^{-1}, the oxidation and reduction peaks are stable to electrochemical cycling over at least 16 scans, and essentially symmetric, with a peak separation of < 10 mV and a full-width at half-maximum of about 90 mV. This ideal behavior indicates that the ruthenium moieties are uniform in their redox behavior. We infer that these moieties are located at the external surface of the monolayer.

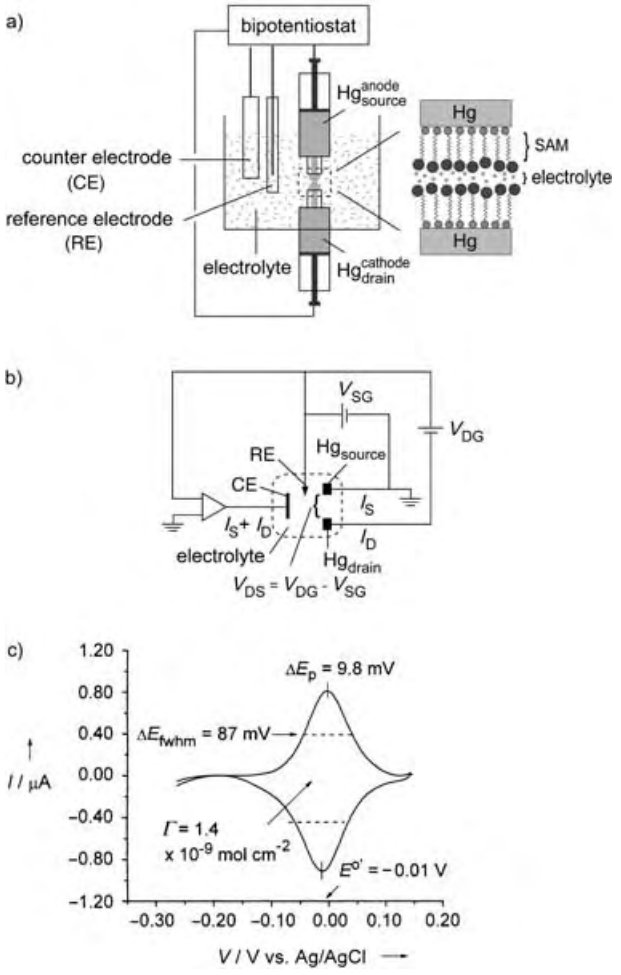


Figure 1. Schematic representations of a) the Hg-SAM//SAM-Hg junction and the electrochemical system used to characterize it, and b) the electrical circuit for the experimental setup in (a). V_{SG} and V_{DG} are the potentials of the source and drain electrodes with respect to the reference electrode, respectively. The electrolyte is the gate whose potential is established by the voltage applied to the reference electrode relative to ground. I_D and I_S are the currents at the drain and source electrodes. c) Cyclic voltammogram (corrected for charging current) for a mercury-drop electrode supporting a SAM of HS-C_{10}-Ru in contact with 0.2 M aqueous Na_2SO_4 at pH 4. The scan rate was 50 mV s^{-1}.

We studied electron transport across the Hg-SAM//SAM-Hg junction by placing the junction, together with an Ag/AgCl reference electrode and a platinum counter electrode, in a Na_2SO_4 electrolyte solution at pH 4, and by using a bipotentiostat that allowed the potentials of the mercury electrodes to be controlled independently with respect to the reference electrode (Figure 1a). The potentials of the mercury electrodes were controlled such that one (cathode) acted as an electron donor and the other (anode) as an electron acceptor. We designated the cathode and anode as the drain and source electrodes, respectively, by analogy to the convention used in semiconductor devices, where current is considered to flow from a more positive region to a more negative region.[34] We measured the conductance through the junction as a function of the potentials of the drain and source electrodes with respect to the reference electrode (that is, V_{DG} and V_{SG}, respectively) and as a function of the potential between the source and drain (V_{DS}) using the electrolyte solution as a gate.[35] We controlled the potential of the gate by controlling the potential applied to the reference electrode relative to the ground potential. Since the source electrode is at ground potential, this voltage is V_{SG}.

Figure 2a shows the drain/source currents when V_{DG} is fixed at -0.20 V, whereby the attached ruthenium is in its $+2$ oxidation state, and V_{SG} is varied. The currents are negligible and the junction is nonconducting for $V_{SG} \leq V_{DG}$. Increasing V_{SG} to values more positive than -0.14 V results in an anodic current flow corresponding to the oxidation of Ru^{II} to Ru^{III} at the source and a cathodic current flow corresponding to the reduction of Ru^{III} to Ru^{II} at the drain. The anodic and cathodic currents are equal and increase to a plateau with a half-wave (half-maximum) potential (-0.04 V) that is near the formal potential $E^{o'}$ of the Ru^{II}/Ru^{III} couple. The maximum current passing through the electrodes with an electrode contact area of about 0.20 mm^2 is typically about 1.3 mA mm^{-2} (or 1000 electrons per second per molecule), a value that is approximately 600-fold higher than that observed when only one of the mercury electrodes is electrically connected to the bipotentiostat.

The observation that the current depends on the $E^{o'}$ value of the redox couple is evidence that charge transport in the junction is related to the presence of the surface-bound redox centers. To determine whether charge transport requires redox centers on both electrodes, we replaced the drain electrode with a bare mercury electrode in one experiment and with a mercury electrode modified with the non-electro-

 © 2004 Wiley-VCH Verlag GmbH & Co. KGaA, Weinheim

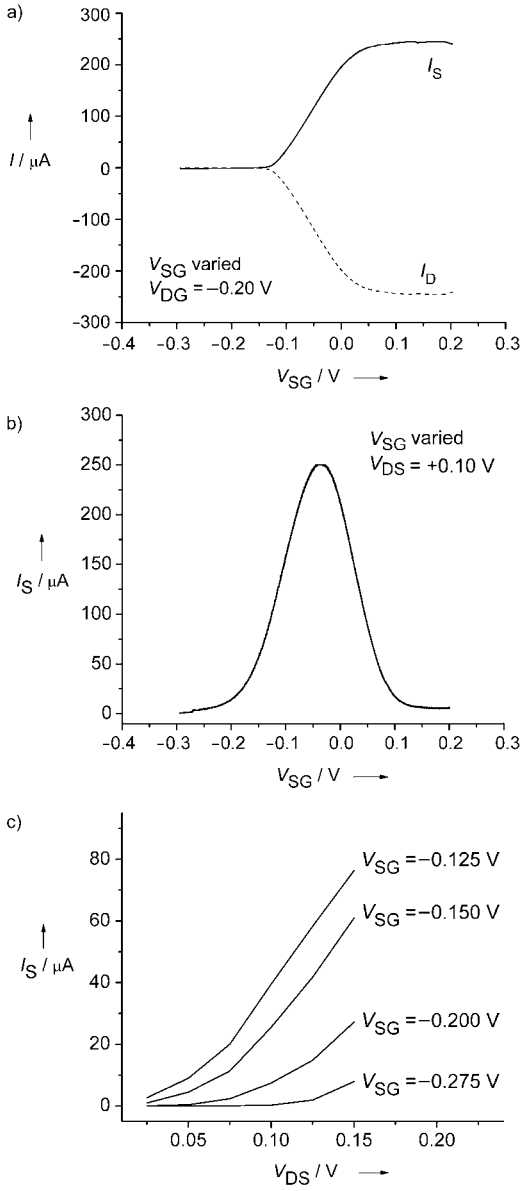


Figure 2. Current–voltage characteristics of the Hg-SAM//SAM-Hg junction showing diodelike and transistor-like behavior. All experiments were carried out in 0.2 M aqueous Na_2SO_4 at pH 4. a) I_D and I_S as a function of V_{SG}. V_{DG} was fixed at −0.20 V and the scan rate was 50 mV s^{-1}. b) I_S as a function of V_{SG} for the same junction as in (a). V_{DS} was fixed at +0.10 V. c) I_S as a function of V_{DS} at different values of V_{SG}. For (b) and (c), I_D (not shown) is equal in magnitude but opposite in sign to I_S; the scan rate was 10 mV s^{-1}.

active thiol $HS(CH_2)_{10}COOH$ in another. In both experiments, we observed negligible current at the drain and a peak-shaped voltammetric wave consistent with reversible oxidation of Ru^{II} to Ru^{III} at the source. The current level at the source was in the range (< 10% difference) of that observed in the cyclic voltammogram and suggested that electron transfer between an electrode and its redox-active SAM is faster than electron transfer between an electrode and the redox centers on the neighboring electrode. The presence of redox centers on both electrodes is therefore needed for current to pass from one electrode to another.

Based on these observations, we propose that charge transport through the junction occurs as a result of oxidation of Ru^{II} to Ru^{III} at the source, electron exchange between Ru^{III} at the source and Ru^{II} at the drain, and reduction of Ru^{III} at the drain back to Ru^{II} as key steps (Figure 3).[36] Similar

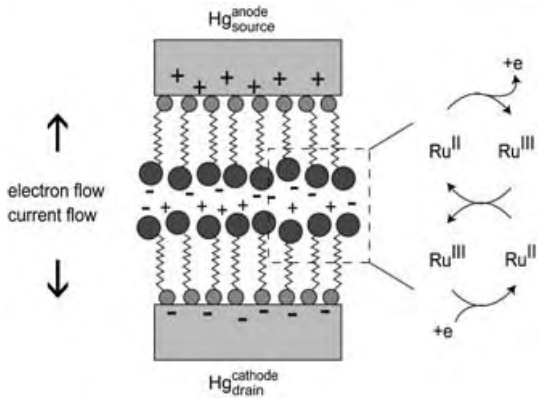


Figure 3. Schematic diagram of the proposed mechanism of charge transport through the Hg-SAM//SAM-Hg junction when V_{SG} is more positive than −0.14 V and $V_{DG} = -0.14$ V.

surface-to-surface charge-transport mechanisms have been reported previously for a variety of interfaces including polymer/polymer[37,38] and polymer/electrolyte solutions;[39] such electron-transport processes, however, have not been reported for molecular monolayers. The work reported here thus shows that the magnitude of current flow can be controlled by controlling the potential of the two electrodes with respect to the $E^{o'}$ value of the redox couple. Significantly, the current can be made to flow unidirectionally, in a diodelike sense, depending on the applied potential.

The conductance of the Hg-SAM//SAM-Hg junction operating at fixed drain-source potentials is shown in Figure 2b and c. Figure 2b shows that at a fixed V_{DS} value of +0.10 V, the source current is negligible for a V_{SG} value of less than −0.25 V and greater than +0.15 V. Scanning V_{SG} from −0.25 to +0.15 V results in the current increasing from zero to a maximum near the $E^{o'}$ value of the redox couple and then decreasing again to zero. Charge therefore passes from one electrode to another only when the value of V_{SG} is at or close to the Ru^{II}/Ru^{III} redox potential. Figure 2c shows that when the V_{SG} value is below the threshold value required for the oxidation of Ru^{II} to Ru^{III} to occur, the source current is essentially zero at all values of V_{DS}. Upon changing V_{SG} to potentials more positive than the threshold value, the current increases with increasing V_{DS} as V_{SG} approaches $E^{o'}$. The observation that the current scales with V_{SG} (the gate potential) is indicative of transistor-like behavior. Unlike conventional solid-state devices which exhibit linear and saturation regions for a given applied gate bias, however, the current passing through the Hg-SAM//SAM-Hg junction described here increases nonlinearly with increasing V_{DS} values. Similar current–potential curves have been reported for a number of systems,[40,41] where charge transport has also been proposed to occur by an electron hopping mechanism. Such

 © 2004 Wiley-VCH Verlag GmbH & Co. KGaA, Weinheim

behavior has been attributed to field-dependent charge mobility.

The observation that current passing from one electrode to another depends on the values of both V_{SG} and V_{DS} can also be explained in terms of an energy diagram relating the potential of the mercury electrodes on the Ag/AgCl scale to a vacuum and to the corresponding Fermi energy. The potential of the mercury electrodes with respect to Ag/AgCl is related to the absolute potential (V_{vacuum}) and the Fermi energy (U_F) by the equations: $V_{vacuum} = V_{Ag/AgCl} + 4.63\,V$ and $U_F = -4.63\,eV - eV_{Ag/AgCl}$, respectively.[42] Figure 4 indicates that

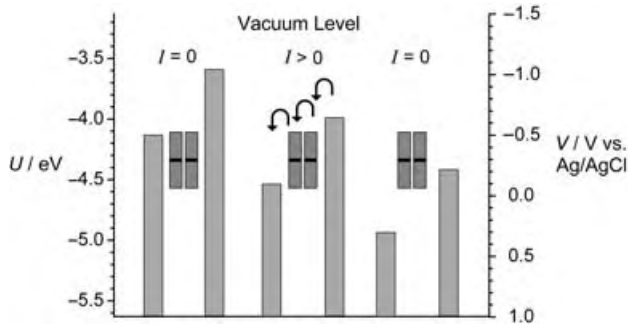


Figure 4. Relationship between the electrochemical potential of the Ru^{II}/Ru^{III} couple measured on the Ag/AgCl scale and the position of the Fermi energy of the mercury electrodes. More negative potentials on the Ag/AgCl scale are closer to vacuum. The small boxes represent the potential limits for the $Ru^{II} \leftrightarrows Ru^{III}$ interconversion.

when both the drain and source electrodes are at potentials very negative or very positive relative to $E^{o'}$, no current flows and the junction is nonconducting. The only time the current flows is when the electronic states of the Ru^{II}/Ru^{III} couple fall between the Fermi energies of the source and the drain. This situation can be achieved by changing the value of V_{DS} and/or V_{SG}.

In conclusion, a system based on a Hg-SAM//SAM-Hg junction is described that allows the incorporation of two monolayers of redox-active centers between the mercury electrodes and the potentials of the two mercury electrodes to be controlled independently with respect to the formal potential of the redox centers. In this system, electron transport through the molecules can be controlled readily by tuning the Fermi energy of the mercury electrodes relative to the energy of the redox centers; this potential control not only determines the direction but also the magnitude of current flow through the junction. The junction switches from *off* to *on* when the electronic states of the redox centers on the two monolayers fall between the Fermi levels of the electrodes. Only when the junction has Ru^{II}/Ru^{III} centers on both electrodes does it conduct electrons (under appropriate conditions); this conduction depends on the number of redox centers trapped in the area in which the two compliant mercury electrodes are in contact, and on the rates of a) electron tunneling between the mercury electrodes and the surface-bound Ru^{II}/Ru^{III} centers and b) electron hopping between adjacent Ru^{II} and Ru^{III} centers.

The junction shows electrical behavior similar to that of a solid-state transistor when the electrolyte is used as the gate. The channel length in this case is defined essentially by the thickness of the SAMs between the two mercury electrodes. Although the system is mechanically less stable than conventional field-effect transistors (FETs) and is limited in value for studying the influence of temperature on electron-transfer rates (because of the liquid mercury electrodes), the system described here is easy to assemble and makes it easy to modify both the area and electrical properties of the metal–metal junction. The area can be modified by changing the pressure applied to the mercury electrodes, while tuning of the electrical properties may be achieved by changing the nature of the redox centers, and the length and structure of the hydrocarbon chains anchoring these centers. Finally, the junction is well-characterized and yields reproducible data, and thus it is well-suited for collecting fundamental information relevant to the fabrication of molecular switches and field-effect transistors.

Received: February 5, 2004 [Z53945]

Keywords: electron transfer · mercury · molecular electronics · monolayers · redox chemistry

[1] W. Wang, T. Lee, M. A. Reed, *Phys. Rev. B* **2003**, *68*, 035416.
[2] L. A. Bumm, J. J. Arnold, M. T. Cygan, T. D. Dunbar, T. P. Burgin, L. Jones II, D. L. Allara, J. M. Tour, P. S. Weiss, *Science* **1996**, *271*, 1705.
[3] J. G. Kushmerick, D. B. Holt, J. C. Yang, J. Naciri, M. H. Moore, R. Shashidhar, *Phys. Rev. Lett.* **2002**, *89*, 086802.
[4] W. Han, E. N. Durantini, A. L. Moore, D. Gust, P. Rez, G. Leatherman, G. R. Sealey, N. J. Tao, S. M. Lindsay, *J. Phys. Chem. B* **1997**, *101*, 10719.
[5] Z. J. Donhauser, B. A. Mantooth, K. F. Kelly, L. A. Bumm, J. D. Monnell, J. J. Stapleton, D. W. Price, Jr., A. M. Rawlett, D. L. Allara, J. M. Tour, P. S. Weiss, *Science* **2001**, *292*, 2303.
[6] X. D. Cui, A. Primak, X. Zarate, J. Tomfohr, O. F. Sankey, A. L. Moore, T. A. Moore, D. Gust, G. Harris, S. M. Lindsay, *Science* **2001**, *294*, 571.
[7] A. Nitzan, M. A. Ratner, *Science* **2003**, *300*, 1384.
[8] D. Cahen, G. Hodes, *Adv. Mater.* **2002**, *14*, 789.
[9] D. I. Gittins, D. Bethell, D. J. Schiffrin, R. J. Nichols, *Nature* **2000**, *408*, 67.
[10] J. Park, A. N. Pasupathy, J. I. Goldsmith, C. Chang, Y. Yaish, J. R. Petta, M. Rinkoski, J. P. Sethna, H. D. Abruna, P. L. McEuen, D. C. Ralph, *Nature* **2002**, *417*, 722.
[11] W. Liang, M. P. Shores, M. Bockrath, J. R. Long, H. Park, *Nature* **2002**, *417*, 725.
[12] J. Chen, M. A. Reed, A. M. Rawlett, J. M. Tour, *Science* **1999**, *286*, 1550.
[13] N. J. Tao, *Phys. Rev. Lett.* **1996**, *76*, 4066.
[14] D. L. Feldheim, C. D. Keating, *Chem. Soc. Rev.* **1998**, *27*, 1.
[15] U. Mazur, K. W. Hipps, *J. Phys. Chem. B* **1999**, *103*, 9721.
[16] R. A. Wassel, G. M. Credo, R. R. Fuierer, D. L. Feldheim, C. B. Gorman, *J. Am. Chem. Soc.* **2004**, *126*, 295.
[17] W. Haiss, H. van Zalinge, S. J. Higgins, D. Bethell, H. Höbenreich, D. J. Schiffrin, R. J. Nichols, *J. Am. Chem. Soc.* **2003**, *125*, 15294.
[18] R. Rinaldi, A. Biasco, G. Maruccio, R. Cingolani, D. Alliata, L. Andolfi, P. Facci, F. De Rienzo, R. Di Felice, E. Molinari, *Adv. Mater.* **2002**, *14*, 1449.
[19] C. Patoux, C. Coudret, J.-P. Launay, C. Joachim, A. Gourdon, *Inorg. Chem.* **1997**, *36*, 5037.
[20] R. M. Metzger, B. Chen, U. Hopfner, M. V. Lakshmikantham, D. Vuillaume, T. Kawai, X. Wu, H. Tachibana, T. V. Hughes, H.

 © 2004 Wiley-VCH Verlag GmbH & Co. KGaA, Weinheim

Sakurai, J. W. Baldwin, C. Hosch, M. P. Cava, L. Brehmer, G. J. Ashwell, *J. Am. Chem. Soc.* **1997**, *119*, 10455.
[21] For analysis of the electron transport properties of this system, see W. Schmickler, M. A. Rampi, E. Tran, G. M. Whitesides, *Faraday Discuss.* **2004**, *125*, 171.
[22] K. Slowinski, H. K. Y. Fong, M. Majda, *J. Am. Chem. Soc.* **1999**, *121*, 7257.
[23] R. E. Holmlin, R. Haag, M. L. Chabinyc, R. F. Ismagilov, A. E. Cohen, A. Terfort, M. A. Rampi, G. M. Whitesides, *J. Am. Chem. Soc.* **2001**, *123*, 5075.
[24] R. E. Holmlin, R. F. Ismagilov, R. Haag, V. Mujica, M. A. Ratner, M. A. Rampi, G. M. Whitesides, *Angew. Chem.* **2001**, *113*, 2378; *Angew. Chem. Int. Ed.* **2001**, *40*, 2316.
[25] R. L. Young, P. T. Nguyen, K. Slowinski, *J. Am. Chem. Soc.* **2003**, *125*, 5948.
[26] Y. Selzer, A. Salomon, D. Cahen, *J. Phys. Chem. B* **2002**, *106*, 10432.
[27] Y. Selzer, A. Salomon, D. Cahen, *J. Am. Chem. Soc.* **2002**, *124*, 2886.
[28] R. Haag, M. A. Rampi, R. E. Holmlin, G. M. Whitesides, *J. Am. Chem. Soc.* **1999**, *121*, 7895.
[29] R. L. York, P. T. Nguyen, K. Slowinski, *J. Am. Chem. Soc.* **2003**, *125*, 5948.
[30] H.-Z. Yu, Y.-J. Liu, *ChemPhysChem* **2003**, *4*, 335.
[31] H. O. Finklea, D. D. Hanshew, *J. Am. Chem. Soc.* **1992**, *114*, 3173.
[32] H. O. Finklea, D. D. Hanshew, *J. Electroanal. Chem.* **1993**, *347*, 327.
[33] The Supporting Information provided with this paper includes details of the experimental protocols and a cyclic voltammogram (uncorrected for charging current) of a mercury electrode coated with a monolayer of $[Ru(NH_3)_5(NC_5H_4\text{-}4\text{-}CH_2NHCO\text{-}(CH_2)_{10}SH](PF_6)_2$
[34] P. Horowitz, H. Winfield, *The Art of Electronics*, Cambridge University Press, New York, **1995**.
[35] The use of an electrolyte as a gate electrode and the reference electrode to establish the gate potential is called electrochemical gating. The operating principle of this technique is that the Fermi energy of the source and drain electrodes can be raised or lowered by controlling their potentials with respect to the reference electrode. For example, driving the source electrode to more positive potentials (with respect to the reference) lowers the Fermi energy and hence the energy of the electrons within the electrode. The positive charge on the source electrode is balanced by anions in the electrolyte. The presence of excess electrolyte anions, in turn, raises the orbital energy of the surface-bound redox species. Oxidation of the redox species ensues when the potential of the source electrode reaches a level positive enough to accept an electron from the redox species.
[36] A referee has asked how we excluded interpenetration of the monolayers. Although we cannot rule out the possibility that the two opposing SAMs interpenetrate, the fact that negligible electron transfer occurs between an electrode and the redox centers on the neighboring electrode is consistent with the mechanism proposed in Figure 3.
[37] G. P. Kittlesen, H. S. White, M. S. Wrighton, *J. Am. Chem. Soc.* **1985**, *107*, 7373.
[38] P. G. Pickup, W. Kutner, C. R. Leidner, R. W. Murray, *J. Am. Chem. Soc.* **1984**, *106*, 1991.
[39] T. Ikeda, C. R. Leidner, R. W. Murray, *J. Am. Chem. Soc.* **1981**, *103*, 7422.
[40] X. L. Chen, Z. Bao, J. H. Schön, A. J. Lovinger, Y.-Y. Lin, B. Crone, A. Dodabalapur, B. Batlogg, *Appl. Phys. Lett.* **2001**, *78*, 228.
[41] B. H. Hamadani, D. Natelson, *J. Appl. Phys.* **2004**, *95*, 1227.
[42] H. Reiss, A. Heller, *J. Phys. Chem.* **1985**, *89*, 4207.

 © 2004 Wiley-VCH Verlag GmbH & Co. KGaA, Weinheim

Mesoporous Materials

Dehydroxylation Route to Surface Modification of Mesoporous Silicas by Using Grignard Reagents**

Jung Eun Lim, Chang Bo Shim, Ji Man Kim, Bun Yeoul Lee,* and Jae Eui Yie*

Since researchers at the Mobil company reported the syntheses of mesoporous silicas such as MCM-41 and MCM-48,[1] there have been a lot of development in their synthesis, structural characterization, and applications due to their large-pore diameters compared with those of conventional microporous zeolites.[2] The modification of silica materials with various organic functional groups[3] is desirable for applications such as catalysts, adsorbents, use in reversed-phase chromatography, and advanced materials.[2–4] Organic modification has been conventionally conducted by the reaction of organoalkoxysilane or organosilyl chloride with surface silanols (SiOH) to form SiO–SiR bond.[3] However, the attached organic group leaches out under harsh conditions through cleavage of the Si–O bonds.[4c] Moreover, some unwanted side reactions, for example, self-polymerization of organoalkoxysilane, may occur on the surface during the modification.[5]

A strained siloxane bridge is generated on the silica surface when the silica is subjected to vacuum degassing at temperatures above 900 K, and it was suggested that the silicon atom of the strained siloxane bridge is electron deficient, thereby acting as a Lewis acid center.[6] As the strained siloxane is reactive to the organoalkoxysilane, or acid-labile acetal or ketal groups, the moiety has been successfully used to modify the surface or to anchor organo-

[*] J. E. Lim, Prof. Dr. J. M. Kim
Functional Materials Laboratory
Department of Molecular Science and Technology
Ajou University
Suwon, 442-749 (Korea)
Fax: (+82) 31-219-2394
E-mail: jimankim@ajou.ac.kr

C. B. Shim, Prof. Dr. B. Y. Lee
Polymer Synthesis Laboratory
Department of Molecular Science and Technology
Ajou University
Suwon, 442-749 (Korea)
Fax: (+82) 31-219-2394
E-mail: bunyeoul@ajou.ac.kr

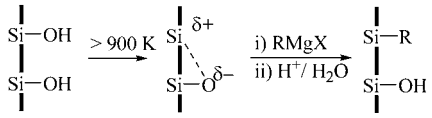
Prof. Dr. J. E. Yie
Catalyst and Surface Laboratory
Department of Applied Chemistry
Ajou University
Suwon, 442-749 (Korea)

[**] J.M.K would like to thank the Korea Science and Engineering Foundation (R01-2002-000-00164-0(2003)) for financial support. B.Y.L. is also grateful to the Research Center for Nanocatalysis, one of the National Science Programs for Key Nanotechnology.

Supporting information for this article is available on the WWW under http://www.angewandte.org or from the author.

 DOI: 10.1002/anie.200454076 © 2004 Wiley-VCH Verlag GmbH & Co. KGaA, Weinheim

metallic catalysts.[7] However, these modification methods also result in the formation of the Si–O bond, which is susceptible to cleavage under certain harsh conditions. Herein, we propose a novel strategy for the modification of mesoporous silica surface through a dehydroxylation route by using a Grignard reagent as shown in Equation (1). The route gives not only the formation of a direct Si–C bond, which is much more resistant to hydrolytic cleavage, but also preclusion of the formation of both surface-bound oligomers and variable modes of attachment.



(1)

Treatment of the MCM-41 that had been dehydroxylated by evacuation at 1123 K for 15 h with excess *n*BuLi in hexane, subsequent quenching, and washing with water furnished modified MCM-41 that contained 12% carbon (2.5 mmol butyl g^{-1}). However, the X-ray diffraction (XRD) pattern reveals that the mesoscopically ordered structures are somewhat destroyed by the treatment, which is probably due to the high reactivity of *n*BuLi. When relatively less reactive *n*BuMgCl in diethyl ether is used for the modification, the modified MCM-41 (*n*Bu-MCM-41) thus obtained exhibits relatively low carbon content (9.6%, 2.0 mmol butyl g^{-1}). Thermogravimetric analysis (TGA) shows slight weight loss up to 773 K but rapid decrease of weight is observed at 773–873 K. The total weight losses obtained from the TGA curve (11% butyl) are in agreement with the elemental analysis datum of 9.6% carbon content. When the surface modification is conducted by the conventional method, that it, the reaction of calcined MCM-41 with trimethoxypropylsilane in ethanol at room temperature for 24 h, only 2.4% carbon content ($\approx$0.7 mmol propyl g^{-1}) is observed.

The N_2 adsorption–desorption isotherm obtained at liquid-N_2 temperature (−196 °C) for the modified MCM-41 is type-IV with a well-defined step in the adsorption and desorption curves. The pore size and the pore volume are reduced by the modification while the surface area and wall thickness increase. Surface area, pore size, pore volume, and wall thickness are measured to be 1340 m^2g^{-1}, 2.3 nm, 0.79 cm^3g^{-1}, and 2.2 nm, respectively, for the *n*Bu-MCM-41, and 1200 m^2g^{-1}, 2.9 nm, 1.24 cm^3g^{-1}, and 1.7 nm, respectively, for the unmodified MCM-41. When the surface area and elemental analysis datum are taken into consideration, the carbon content (9.6%) is calculated to be equivalent to the coverage of 0.90 butyl nm^{-2}. When SBA-15 is modified by the dehydroxylation route with *n*BuMgCl, the material has 5.4% carbon content (1.1 mmol g^{-1}). The relatively low carbon content compared with that observed for the *n*Bu-MCM-41 may be attributed to the relatively low surface area of the SBA-15 ($\approx$700 m^2g^{-1}).

XRD patterns for MCM-41 and SBA-15 before and after modification with *n*BuMgCl are shown in Figure 1. All

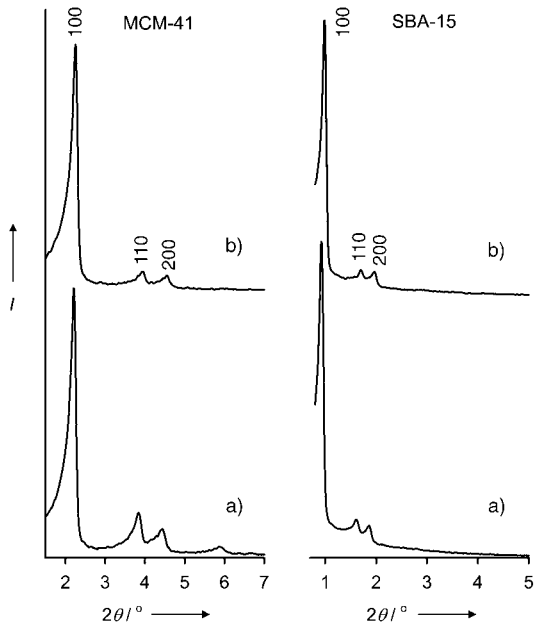


Figure 1. XRD patterns for MCM-41 and SBA-15: a) before and b) after modification with *n*BuMgCl. *I* is intensity (arbitrary units).

materials exhibit XRD patterns with a very intense diffraction peak and two or more weak peaks, which are characteristic of a 2D hexagonal (*P6mm*) structure.[1,2] There are no significant changes upon surface modification, except the expected slight decreases in lattice parameters due to the thermal treatment, which indicates that the mesoscopically ordered structures are retained after modification with *n*BuMgCl. The TEM image also confirms that the highly ordered 2D hexagonal structures are preserved during the modification.

There are only Q^3 ($\delta = -102$ ppm) and Q^4 ($\delta = -110$ ppm) resonances in the ^{29}Si MAS NMR spectrum (MAS is magic-angle spinning) before the modification, but a new peak around $\delta = -60$ ppm (T^n,) appears after the treatment, which is attributed to the Si species directly bonded to carbon (Figure 2). The intensity of Q^3 band corresponding to the surface silanol group is also reduced after the modification. This is clear evidence of direct formation of Si–C bond as depicted in Equation (1). Two signals are observed at 12.8 ppm and 25.1 ppm in the ^{13}C CP–MAS NMR spectrum (CP is cross polarization) with almost the same intensity (Figure 2). The former signal can be assigned to the $-CH_3$ and the $-CH_2-Si$ carbon atoms and the latter to the other two $-CH_2-$ carbon atoms.[8]

Figure 3 shows the TGA curves for the samples obtained by treatment with *n*BuMgCl of the MCM-41 dehydroxylated at temperatures in the range of 473–1273 K. The samples dehydroxylated at 473, 573, 673, and 773 K and modified with butyl groups show almost same curves. However, the weight loses increases rapidly by increasing the dehydroxylation temperature above 873 K. The loading amount reaches a maximum at 1123 K and decreases when the temperature is increased to 1173 K, which is attributed to the collapse of the pore structures above 1123 K.[9a,b] It was reported that an electron-deficient siloxane group is generated by evacuating

 © 2004 Wiley-VCH Verlag GmbH & Co. KGaA, Weinheim

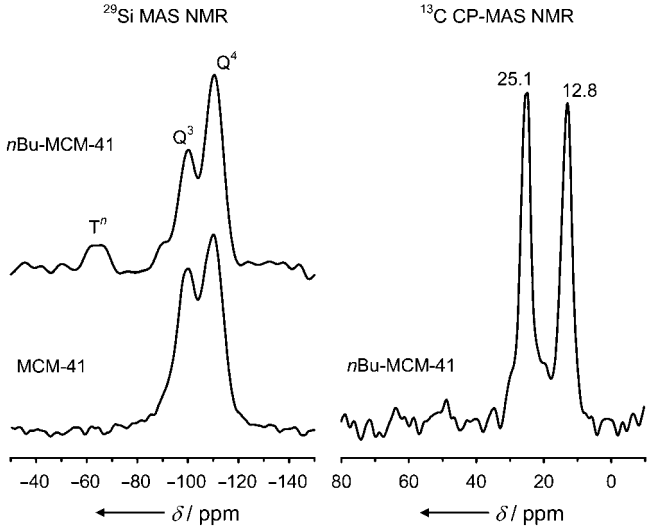


Figure 2. ^{29}Si and ^{13}C MAS NMR spectra for calcined MCM-41 and *n*Bu-MCM-41 obtained by treatment with *n*BuMgCl after dehydroxylation at 1123 K.

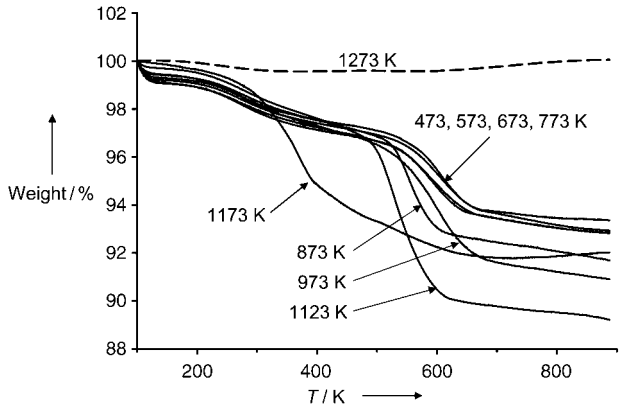
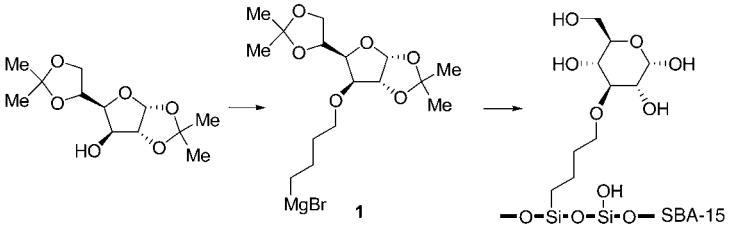


Figure 3. TGA curves for the samples obtained by treatment with *n*BuMgCl on MCM-41 dehydroxylated at temperatures in the range of 473–1273 K.

silica above 900 K, and the number of such strained siloxane group increases as the temperature increases.[6] The TGA curves in Figure 3 support the argument that the electron-deficient siloxane group, formed on the surface of mesoporous silica by evacuation above 900 K, mainly participates in the reaction with *n*BuMgCl as shown in Equation (1).

Hydrothermal stability of the mesoporous material is an important issue in many potential applications because structural disintegration is frequently observed.[9] The main feature of the XRD pattern is preserved when the *n*Bu-MCM-41 is heated to 373 K in water for five days under static conditions, whereas in the case of the unmodified MCM-41 or MCM-41 modified by the conventional method (by the reaction of trimethoxypropylsilane onto the surface silanol group) the mesostructures are completely destroyed within two days. Moreover, the TGA curve for the *n*Bu-MCM-41 is not altered by the five-day treatment in water, which supports argument that the butyl group is not cleaved. However, the MCM-41 modified by the conventional method loses most of the attached organic groups after two days.

Other functional groups can be attached on the silica surface by this novel method. Treatment with benzylmagnesium chloride or phenylmagnesium bromide on the MCM-41 dehydroxylated at 1123 K provides modified silicas that contain 9.9 % (1.2 mmol g^{-1}) or 8.1 % (1.1 mmol g^{-1}) carbon, respectively. The mesostructures of these modified MCM-41 materials are not affected by the treatments. Highly functionalized molecules, such as a glucose derivative, have also been attached (Scheme 1). Grignard reagent **1** that contains



Scheme 1. Attachment of a glucose derivative on the surface of the dehydroxylated SBA-15.

acetonide-protected glucose unit is easily synthesized from commercially available diacetone-D-glucose. The addition of the Grignard reagent **1** to the SBA-15 dehydroxylated at 1123 K, subsequent treatment with aqueous acidic water (2 N HCl), thus removing the acetonide protection groups to furnish diols, and finally Sohxlet extraction with methanol afforded a D-glucose modified SBA-15 that contained 4.6 % carbon (0.38 mmol g^{-1}).

In conclusion, a novel surface-modification strategy has been developed by treating dehydroxylated silica with Grignard reagents. High loading of organic groups can be achieved and the mesoporous structures are not destroyed by the modification. The modified materials thus obtained exhibit excellent hydrothermal stability by forming direct ≡Si−C bonds. Since highly functionalized Grignard reagents are now available,[10] we believe that the present synthesis strategy can be applied to the surface modification of various silica nanostructures in addition to mesoporous silica materials to obtain robust organic functional groups.

Experimental Section

Mesoporous silicas, MCM-41 and SBA-15, were synthesized following the procedures described elsewhere,[11] by using cetyltrimethylammonium bromide and triblock copolymer P123, respectively, as the templates. Typical procedure for surface modification: The MCM-48 and SBA-15 were dehydroxylated by evacuation at 1123 K for 15 h. A Grignard reagent (4.0 mmol) was added to a slurry of the dehydroxylated silica (1.0 g) in diethyl ether (10 mL) at room temperature and the mixture was stirred for 15 h. An aqueous HCl solution (2.5 M, 25 mL) was added and the two phase mixture was stirred for 3 h. The silica was isolated by filtration and washed successively with water, methanol, and diethyl ether. The silica was dried under vacuum. In the case of **1**, 2.0 mmol of **1** per gram of silica and THF solvent were used instead, and the Sohxlet extraction was

 © 2004 Wiley-VCH Verlag GmbH & Co. KGaA, Weinheim

conducted with methanol for 24 h to remove any physisorbed organics.

Received: February 23, 2004
Revised: April 24, 2004 [Z54076]

Keywords: Grignard reaction · mesoporous materials · silica · surface chemistry

[1] a) C. T. Kresge, M. E. Leonowicz, W. J. Roth, J. C. Vartuli, J. S. Beck, *Nature* **1992**, *359*, 710; b) J. S. Beck, J. C. Vartuli, W. J. Roth, M. E. Leonowicx, C. T. Kresge, K. D. Schmitt, C. T.-W. Chu, D. H. Olson, E. W. Sheppard, S. B. McCullen, J. B. Higgins, J. L. Schlenger, *J. Am. Chem. Soc.* **1992**, *114*, 10834.

[2] a) U. Ciesla, F. Schüth, *Microporous Mesoporous Mater.* **1999**, *27*, 131; b) J. Y. Ying, C. P. Mehnert, M. S. Wong, *Angew. Chem.* **1999**, *111*, 58; *Angew. Chem. Int. Ed.* **1999**, *38*, 56; c) A. Corma, *Chem. Rev.* **1997**, *97*, 2373; d) M. Linden, S. Schacht, F. Schüth, A. Steel, K. K. Unger, *J. Porous Mater.* **1998**, *5*, 177.

[3] a) A. Sayari, S. Hamoudi, *Chem. Mater.* **2001**, *13*, 3151; b) A. P. Wight, M. E. Davis, *Chem. Rev.* **2002**, *102*, 3589; c) D. Brunel, A. C. Blanc, A. Galarneau, F. Fajula, *Catal. Today* **2003**, *78*, 139; d) P. M. Price, J. H. Clark, D. J. Macquarrie, *J. Chem. Soc. Dalton Trans.* **2000**, 101; e) D. Margolese, J. A. Melero, S. C. Christiansen, B. F. Chmelka, G. D. Stucky, *Chem. Mater.* **2002**, *14*, 2448.

[4] a) X. Feng, G. E. Fryxell, L. Q. Wang, A. Y. Kim, J. Liu, K. M. Kemner, *Science* **1997**, *276*, 923; b) B. C. Trammell, L. Ma, H. Luo, M. A. Hillmyer, P. W. Car, *J. Am. Chem. Soc.* **2003**, *125*, 10504; c) X. Yuan, H. I. Lee, J. W. Kim, J. E. Yie, J. M. Kim, *Chem. Lett.* **2003**, *32*, 650; d) Y.-J. Han, G. D. Stucky, A. Butler, *J. Am. Chem. Soc.* **1999**, *121*, 9897; e) J. H. Clark, S. J. Tavener, S. J. Barlow, *Chem. Commun.* **1996**, 2429; f) C. Copéret, M. Chabanas, R. P. Saint-Arroman, J. -M. Basset, *Angew. Chem.* **2003**, *115*, 164; *Angew. Chem. Int. Ed.* **2003**, *42*, 156.

[5] a) J. H. Clark, D. J. Macquarrie, *Chem. Commun.* **1998**, 853; b) S. Ek, E. I. Iiskola, L. Niinistoe, T. T. Pakkanen, A. Root, *Chem. Commun.* **2003**, 2032.

[6] B. A. Morrow, I. A. Cody, *J. Phys. Chem.* **1976**, *80*, 1995.

[7] a) J. Blümel, *J. Am. Chem. Soc.* **1995**, *117*, 2112; b) B. Y. Lee, J. S. Oh, *Macromolecules* **2000**, *33*, 3194.

[8] E. Bayer, K. Albert, J. Reiners, M. Nieder, D. Müller, *J. Chromatogr.* **1983**, *264*, 197.

[9] a) J. M. Kim, R. Ryoo, *Bull. Korean Chem. Soc.* **1996**, *17*, 66; b) J. M. Kim, J. H. Kwak, S. Jun, R. Ryoo, *J. Phys. Chem.* **1995**, *99*, 16742; c) J. M. Kisler, M. L. Gee, G. W. Stevens, A. J. O'Connor, *Chem. Mater.* **2003**, *15*, 619.

[10] P. Knochel, W. Dohle, N. Gommermann, F. F. Kneisel, F. Kopp, T. Korn, I. Sapountzis, V. A. Vu, *Angew. Chem.* **2003**, *115*, 4438; *Angew. Chem. Int. Ed.* **2003**, *42*, 4302.

[11] a) R. Ryoo, J. M. Kim, *J. Chem. Soc. Chem. Commun.* **1995**, 711; b) J. M. Kim, G. D. Stucky, *Chem. Commun.* **2000**, 1159.

 © 2004 Wiley-VCH Verlag GmbH & Co. KGaA, Weinheim

Main-Group-Metal Clusters

Molecular $\{(SnO)_6\}$ Trapped by Two $\{R_2Si_2O_3\}$ Fragments: X-ray Single-Crystal Structure of $[(SnO)_6(R_2Si_2O_3)_2]$**

Umesh N. Nehete, Vadapalli Chandrasekhar, Ganapathi Anantharaman, Herbert W. Roesky, Denis Vidovic, and Jörg Magull*

Dedicated to Professor Oskar Glemser on the occasion of his 93rd birthday

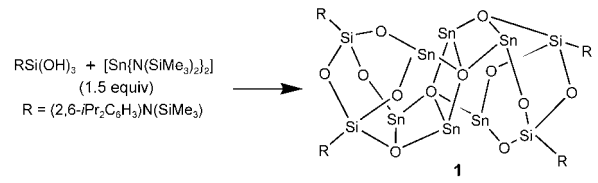
We have a long-standing interest in the design and synthesis of molecular assemblies that contain the {Si-O-M} motif.[1] This interest is motivated, in part, by the possibility of these soluble metallasiloxanes functioning as structural models for the more-complex naturally occurring metallasilicates or synthetic metal-modified zeolites.[2] Another reason for our interest stems from the opportunity provided by molecular metallasiloxane structural frameworks for incorporating basic structural motifs of inorganic oxides as part of the larger cage or ring structures.[3] Such systems can be viewed as organic-soluble solids that contain the inorganic oxide core enveloped by a sheath of lipophilic organic exterior.[3] Although tin(II) alkoxide cage structures have been known for some time, there is a relative paucity of the corresponding tin(II) siloxane cages.[4] In contrast molecular stannasiloxanes that contain tin(IV) have been widely studied.[5] Herein, we describe the synthesis and structural characterization of $[(SnO)_6(R_2Si_2O_3)_2]$ $[R = (2,6\text{-}i\text{Pr}_2C_6H_3)N(SiMe_3)]$ **1.** This compound represents the first example of a hexatin(II) cage that contains siloxane ligands. Interestingly compound **1** contains a central embedded tin oxide, in the form of a molecular $\{(SnO)_6\}$ motif between two $\{R_2Si_2O_3\}$ fragments. To the best of our knowledge, there has been no previous report on the isolation and structural characterization of any molecular tin(II) oxide.

The reaction of the tin amide[6] $[Sn\{N(SiMe_3)_2\}_2]$ with the N-bonded silanetriol[7] $RSi(OH)_3$ $[R = (2,6\text{-}i\text{Pr}_2C_6H_3)N(SiMe_3)]$ in a 1.5:1 stoichiometric ratio afforded **1** in about 65% yield (Scheme 1). The reaction proceeds under elimination of $HN(SiMe_3)_2$ with a concomitant Si-O-Sn bond formation. Colorless crystals of **1** were obtained after four

[*] U. N. Nehete, Dr. G. Anantharaman, Prof. Dr. H. W. Roesky, D. Vidovic, Prof. Dr. J. Magull
Institut für Anorganische Chemie
Universität Göttingen
Tammannstrasse 4, D-37077 Göttingen (Germany)
Fax: (+49) 551-393-373
E-mail: hroesky@gwdg.de
Prof. Dr. V. Chandrasekhar
Department of Chemistry
IIT-Kanpur, Kanpur-208 016 (India)

[**] This work was supported by the Deutsche Forschungsgemeinschaft and the Göttinger Akademie der Wissenschaften. V.C. thanks the Alexander von Humboldt Foundation, Bonn (Germany), for the Friedrich Wilhelm Bessel-Research Award. $R = (2,6\text{-}i\text{Pr}_2C_6H_3)N(SiMe_3)$

 © 2004 Wiley-VCH Verlag GmbH & Co. KGaA, Weinheim DOI: 10.1002/anie.200454149



Scheme 1. Synthesis of compound **1**.

days at room temperature. Compound **1** is highly lipophilic and is soluble in a large number of common organic solvents, including hydrocarbons such as hexane. Compound **1** has been fully characterized by means of analytical, spectroscopic, and single-crystal X-ray diffraction studies.[8] A remarkable feature of the stannasiloxane **1** is its high thermal stability. It is stable up to 307 °C, at which point the compound turns black brown. The EI-mass spectrum of **1** shows a highly intense peak at 1740 (100%) $[M^+-18\,CH_3]$ thus indicating that the $\{Sn_6Si_4O_{12}\}$ core is stable under these conditions. The corresponding ^{29}Si NMR spectrum shows the presence of two resonances at $\delta = 7.3$ and -70.2 ppm. The latter corresponds to δ SiO_3N while the former is assigned to δ $SiMe_3N$. The ^{119}Sn NMR of **1** shows three signals ($\delta = -138.6$, -290.5 and -393.1 ppm), which correspond to the three types of tin centers present in **1**.

Compound **1** is formed as a result of the reaction of the in situ generated disiloxanetetrol $[RSi(OH)_2]_2O$ with $[Sn\{N(SiMe_3)_2\}_2]$. Such self-condensation of silanetriols has been previously reported by us.[9] Furthermore, the water liberated from the condensation of the two silanetriol molecules assists in the formation of SnO from $[Sn\{N(SiMe_3)_2\}_2]$.

Compound **1** crystallizes in the monoclinic space group $P2_1/c$ along with two molecules of THF and one molecule of hexane in the asymmetric unit. The molecular structure of **1** is shown in Figure 1. The core structure of **1** along with selected metric parameters are given in Figure 2.

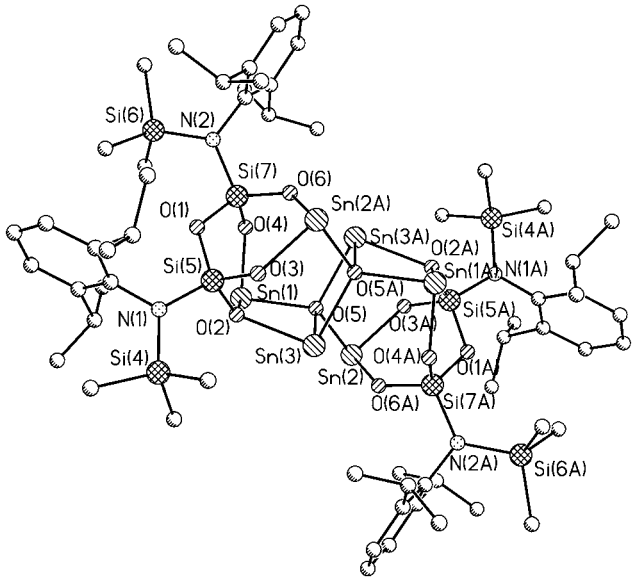


Figure 1. Molecular structure of **1** in the crystal.

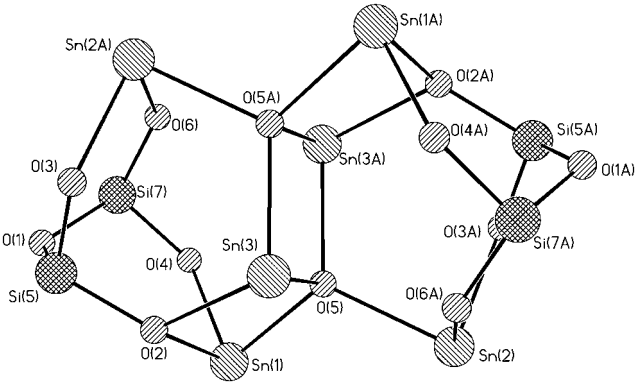


Figure 2. Core structure of **1**. The substituents on silicon have been omitted for the sake of clarity. Selected bond lengths [Å] and angles [°]: Sn(1)-O(5) 2.190(2), Sn(1)-O(2) 2.141(2), Sn(1)-O(4) 2.025(2), Sn(2)-O(5) 2.184(2), Sn(2A)-O(6) 2.095(2), Sn(2A)-O(3) 2.060(2), Sn(3)-O(2) 2.288(2), Sn(3)-O(5) 2.190(2), Sn(3)-O(5A) 2.287(2), Sn(3A)-O(5) 2.287(2); Sn(1)-O(2)-Sn(3) 102.42(6), Sn(2)-O(5)-Sn(1) 112.66(7), Sn(2)-O(5)-Sn(3) 107.34(6), Sn(1)-O(5)-Sn(3) 104.08(6), Sn(2)-O(5)-Sn(3A) 115.21(6), Sn(1)-O(5)-Sn(3A) 112.82(7), Sn(3)-O(5)-Sn(3A) 103.47(6), Sn(7)-O(6)-Sn(2A) 132.46(9), O(2)-Sn(3)-O(5A) 98.77(6), O(2)-Sn(3)-O(5) 73.40(6), O(2)-Sn(1)-O(5) 76.36(6), O(3A)-Sn(2)-O(5) 87.34(6), O(4)-Sn(1)-O(2) 92.17(6), O(4)-Sn(1)-O(5) 91.39(6), O(5)-Sn(3)-O(5A) 76.53(6), O(6A)-Sn(2)-O(3A) 92.49(6), O(6A)-Sn(2)-O(5) 81.30(6).

The structure of **1** contains two centrosymmetrically related siloxane ligands that bind a central hexatin motif (Figure 2). The tin core consists of three mutually perpendicular $\{Sn_2O_2\}$ four-membered rings. The two oxygen atoms of the central distannoxane are linked further to two other tin centers (Sn 2 and Sn 2A). It is important to note that none of the tin atoms have any other ligands in their coordination environment except oxygen. Thus, the $\{(SnO)_6\}$ motif may be considered as representing a trapped molecular form of tin(II) oxide. All six tin centers in **1** are tricoordinate. It is noteworthy that in the solid-state structure of tin(II) oxide, the coordination environment of the tin atom is four, and the tin atom is positioned in the apex of a square pyramid.[10] The shortest Sn–O distances in **1** are for the Sn(1)–O(4) [2.025(2) Å] and Sn(2A)–O(3) bonds [2.060(2) Å] while the longest distances are found for the Sn(3)–O(5A) [2.287(2) Å] and Sn(3)–O(2) bonds [2.288(2) Å]. It is interesting to compare these distances with those observed in other tin(II) siloxanes. Thus, in $[\{Sn\text{-}(\mu\text{-}OtBu)(OSiPh_3)\}_2]$, which contains a four-membered $\{Sn_2O_2\}$ ring with an Sn–O distance of 2.084(4) Å.[5g] In the case of $[Ca\{Sn(\mu\text{-}OSiMe_2tBu)_3\}_2]$, which contains two $\{SnO_3\}$ motifs binding to a central calcium atom, the average Sn–O distance is 2.106(7) Å.[5i] However, in tin(II) oxide itself, the Sn–O distance was reported as 2.21 Å.[10]

The bond angles around Sn(3) in **1** add up to 249° while those at Sn(1) and Sn(2) add up to 260° and 263°, respectively. There are three different kinds of oxygen environments in the structure of **1**. Thus, there are four dicoordinate oxygen atoms that bridge Si and Sn atoms [O(3), O(4), O(6)] or Si and Si atoms [O(1)]. The angles at all these oxygen atoms are much less than 180°, the largest being at O(6) (132.42°) and the smallest at O(1) (121.20°). There is only one tricoordinate

 © 2004 Wiley-VCH Verlag GmbH & Co. KGaA, Weinheim

oxygen atom, O(2), that caps one silicon and two tin atoms. The other oxygen atom, O(5), is tetracoordinate and bridges four tin centers.

In conclusion, we report a novel hexameric stannasiloxane **1** that contains a tin atom in a formal oxidation state of +2. The structure of **1** contains a central $\{(SnO)_6\}$ motif enclosed by two outer $R_2Si_2O_3$ siloxane ligands.

Experimental Section

1: $[Sn\{N(SiMe_3)_2\}_2]$ (2.02 g, 4.59 mmol) was slowly added to a stirred suspension of the silanetriol (1.0 g, 3.06 mmol) in hexane (25 mL) and THF (10 mL). After the addition was complete, the reaction mixture was stirred for 1 h at room temperature. Subsequently, the reaction mixture was refluxed for 1 h. The volatile components were removed to obtain a white solid. To this solid, a mixture of hexane (10 mL) and THF (1 mL) was added. Colorless crystals of **1** were obtained after four days at room temperature (1.12 g, 65.4%); mp 307 °C (dec); ^{1}H NMR (500 MHz, C_6D_6, TMS): $\delta = 0.20$ (s, 36H, $Si(CH_3)_3$), 1.40, 1.42 (d, 48H, $CH(CH_3)_2$), 3.70 (sept, 8H, $CH(CH_3)_2$), 7.05–7.12 ppm (m, 12H, aromatic); ^{29}Si NMR (99 MHz, C_6D_6, TMS): $\delta = 7.3$ ($SiMe_3$), −70.2 ppm (SiO_3); ^{119}Sn NMR (186 MHz, C_6D_6, TMS): $\delta = -138.6$, −290.5, −393.1 ppm; IR (Nujol): $\tilde{\nu} = 1316$ (w), 1259 (s), 1247 (s), 1179 (m), 1104 (m), 1073 (w), 1042 (s), 1007 (m), 969 (s), 954 (s), 907 (m), 876 (m), 836 (s), 801 (s), 752 (w), 721 (w), 685 (w), 641 (w), 603 (w), 543 (w), 521 (m), 501 (w), 466 (m) cm^{-1}; MS (70 eV): *m*/*z* (%): 1740 (100) $[M^+ - 18\,CH_3]$; Elemental analysis calcd (%) for $C_{60}H_{104}N_4O_{12}Si_8Sn_6$ (2010.43): C 35.85, H 5.21, N 2.79; found: C 36.94, H 5.57, N 2.79.

Received: March 1, 2004 [Z54149]
Published Online: June 23, 2004

Keywords: cluster compounds · O ligands · silanes · structure elucidation · tin

[1] a) V. Chandrasekhar, R. Murugavel, A. Voigt, H. W. Roesky, *Organometallics* **1996**, *15*, 918–922; b) R. Murugavel, A. Voigt, M. G. Walawalkar, H. W. Roesky, *Chem. Rev.* **1996**, *96*, 2205–2236; c) R. Murugavel, V. Chandrasekhar, H. W. Roesky, *Acc. Chem. Res.* **1996**, *29*, 183–189; d) H. J. Gosink, H. W. Roesky, H. G. Schmidt, M. Noltemeyer, E. Irmer, R. Herbst-Irmer, *Organometallics* **1994**, *13*, 3420–3426.

[2] a) M. L. Montero, A. Voigt, M. Teichert, I. Usón, H. W. Roesky, *Angew. Chem.* **1995**, *107*, 2761–2763; *Angew. Chem. Int. Ed. Engl.* **1995**, *34*, 2504–2506; b) A. Voigt, R. Murugavel, E. Parisini, H. W. Roesky, *Angew. Chem.* **1996**, *108*, 823–825; *Angew. Chem. Int. Ed. Engl.* **1996**, *35*, 748–750; c) A. Voigt, M. G. Walawalkar, R. Murugavel, H. W. Roesky, E. Parisini, P. Lubini, *Angew. Chem.* **1997**, *109*, 2313–2315; *Angew. Chem. Int. Ed. Engl.* **1997**, *36*, 2203–2205; d) G. Anantharaman, H. W. Roesky, H.-G. Schmidt, M. Noltemeyer, J. Pinkas, *Inorg. Chem.* **2003**, *42*, 970–973.

[3] H. W. Roesky, *Solid State Sci.* **2001**, *3*, 777–782.

[4] a) M. Veith, *Chem. Ber.* **1978**, *111*, 2536–2546; b) P. Kircher, G. Huttner, L. Zsolnai, A. Driess, *Angew. Chem.* **1998**, *110*, 1756–1758; *Angew. Chem. Int. Ed.* **1998**, *37*, 1666–1668; c) P. G. Harrison, B. J. Haylett, T. J. King, *J. Chem. Soc. Chem. Commun.* **1978**, 112–113; d) T. J. Boyle, T. M. Alam, M. A. Rodriguez, C. A. Zechmann, *Inorg. Chem.* **2002**, *41*, 2574–2582; e) W.-W. du Mont, M. Grenz, *Z. Naturforsch. B* **1983**, *38*, 113–114; f) M. J. McGeary, R. H. Cayton, K. Folting, J. C. Huffman, K. G. Caulton, *Polyhedron* **1992**, *11*, 1369–1382; g) M. Veith, C. Mathur, V. Huch, *J. Chem. Soc. Dalton Trans.* **1997**, 995–999; h) C. Eaborn, P. B. Hitchcock, J. D. Smith, S. E. Sözerli, *Organometallics* **1997**, *16*, 5653–5658; i) G. M. de Lima, D. J. Duncalf, *Main Group Met. Chem.* **2000**, *23*, 395–400; j) L. R. Sita, R. M. Xi, G. P. A. Yap, L. M. Liable-Sands, A. L. Rheingold, *J. Am. Chem. Soc.* **1997**, *119*, 756–760.

[5] a) J. Beckmann, K. Jurkschat, *Coord. Chem. Rev.* **2001**, *215*, 267–300; b) J. Beckmann, K. Jurkschat, D. Müller, S. Rabe, M. Schürmann, *Organometallics* **1999**, *18*, 2326–2330; c) J. Beckmann, B. Mahieu, W. Nigge, D. Schollmeyer, M. Schürmann, K. Jurkschat, *Organometallics* **1998**, *17*, 5697–5712; d) J. Beckmann, K. Jurkschat, B. Mahieu, M. Schürmann, *Main Group Met. Chem.* **1998**, *21*, 113–122; e) M. Veith, S. Mathur, V. Huch, *J. Chem. Soc. Dalton Trans.* **1996**, 2485–2490.

[6] M. J. S. Gynane, D. H. Harris, M. F. Lappert, P. P. Power, P. Riviere, M. Riviere-Baudet, *J. Chem. Soc. Dalton* **1977**, *20*, 2004–2009.

[7] N. Winkhofer, A. Voigt, H. Dorn, H. W. Roesky, A. Steiner, D. Stalke, A. Reller, *Angew. Chem.* **1994**, *106*, 1414–1416; *Angew. Chem. Int. Ed. Engl.* **1994**, *33*, 1352–1354.

[8] Crystal data for compound $\mathbf{1}\cdot 2\,C_4H_8O\cdot C_6H_{14}$: $C_{74}H_{134}N_4O_{14}Si_8Sn_6$, $M_r = 2240.71$, monoclinic, space group $P2(1)/c$, $a = 14.5130(7)$ Å, $b = 17.3237(9)$ Å, $c = 19.8882(10)$ Å, $\alpha = 90°$, $\beta = 105.986(4)°$, $\gamma = 90°$, $V = 4806.9(4)$ Å^3, $Z = 2$, $\rho_{calcd} = 1.548$ mg m^{-3}, $F(000) = 2260$, $T = 133(2)$ K, μ ($Mo_{K\alpha}$) = 1.690 mm^{-1}. The data were collected using the ω scan mode in the range of $1.59 \le \theta \le 24.81$, $-17 \le h \le 17$, $-20 \le k \le 20$, $-23 \le l \le 23$. Of 47029 reflections collected, 8260 were unique. Final $R1$ ($I > 2\sigma(I)$) = 0.0195; $wR2$ (all data) = 0.0498. Maximum and minimum heights in the final Fourier difference map were 0.583 and −0.411 e A^{-3}. Colorless single crystals of compound $\mathbf{1}\cdot 2\,C_4H_8O\cdot C_6H_{14}$ suitable for X-ray diffraction studies were obtained from hexane/THF at room temperature. Diffraction data were collected on an IPDS II Stoe image-plate diffractometer with graphite-monochromated $Mo_{K\alpha}$ radiation ($\lambda = 0.71073$ Å). The structure was solved by direct methods (SHELX-97)[11] and refined against F^2 on all data by full-matrix least squares with SHELX-97.[12] The heavy atoms were refined anisotropically. Hydrogen atoms were included by using the riding model with U_{iso} tied to the U_{iso} of the parent atoms. CCDC 232378 contains the supplementary crystallographic data for this paper. These data can be obtained free of charge via www.ccdc.cam.ac.uk/conts/retrieving.html (or from the Cambridge Crystallographic Data Centre, 12 Union Road, Cambridge CB2 1EZ, UK; fax: (+44) 1223-336-033; or deposit@ccdc.cam.ac.uk).

[9] R. Murugavel, P. Böttcher, A. Voigt, M. G. Walawalkar, H. W. Roesky, E. Parisini, M. Teichert, M. Noltemeyer, *Chem. Commun.* **1996**, 2417–2418.

[10] N. N. Greenwood, A. Earnshaw, *Chemistry of the Elements*, 1st ed., Pergamon, Oxford, **1984**.

[11] G. M. Sheldrick, *Acta Crystallogr. Sect. A* **1990**, *46*, 467–473.

[12] G. M. Sheldrick, SHELX-97, *Program for Crystal Structure Refinement*, University of Göttingen, Göttingen (Germany), **1997**.

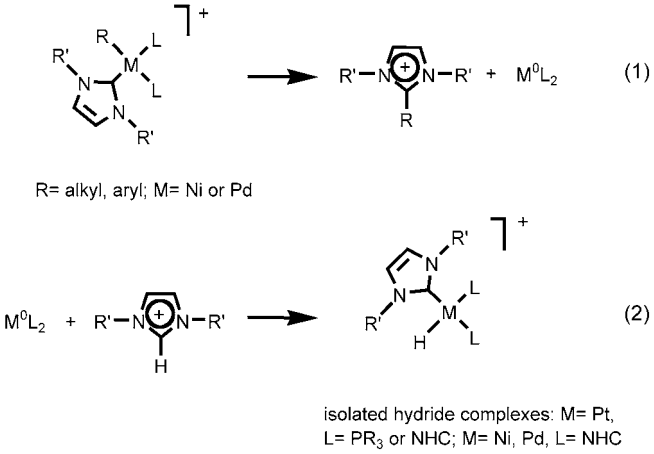
 © 2004 Wiley-VCH Verlag GmbH & Co. KGaA, Weinheim

Ionic Liquids

Transition-Metal-Catalyzed Reactions Involving Imidazolium Salt/N-Heterocyclic Carbene Couples as Substrates**

*Nicolas D. Clement and Kingsley J. Cavell**

In previous studies we demonstrated that hydrocarbyl–M–carbene complexes (M = Group 10 metal) readily undergo reductive elimination to give M^0 and C2-substituted imidazolium salts (Scheme 1, Equation (1)).[1] As this presents a



(1)

(2)

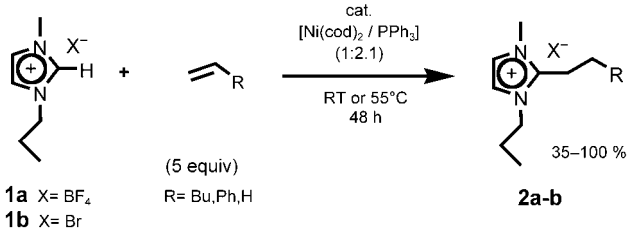
Scheme 1. Redox processes undergone by the carbene/imidazolium couple.

potential impediment for the use of N-heterocyclic carbene (NHC) complexes in catalysis, we investigated methods for controlling or restricting the reaction. Subsequently, we were able to show that this reductive elimination reaction could be "reversed". Reaction of imidazolium salts with Pt^0 species gave carbene–Pt–hydride complexes,[2] and very recently we reported that the reaction of imidazolium salts (ionic liquids) with low-valent M^0 (M = Pd, Ni) bearing strong σ-donor ligands can be a facile process for the generation of surprisingly stable carbene–M–hydride complexes (Scheme 1, Equation (2)).[3] One notable feature of this study is that direct formation of a carbene-—M–H provides an atom-efficient, in situ route to an active catalytic species. NHCs have found application in a wide range of catalytic reactions (such as the Heck, Kumada, Stille, Suzuki-Miyaura, and Sonogashira coupling reactions, amination reactions, hydrosilylation, olefin metathesis, hydroformylation, polymerization, etc.),[4] and metal hydrides are implicated in a number of these catalytic processes.

Furthermore, 1,3-dialkyl imidazolium salts have been extensively employed as ionic-liquid solvents, potentially valuable alternatives to non-aqueous solvents for biphasic catalysis.[5] Although commonly considered as inert solvents, a number of reports have suggested their possible participation during catalysis, forming strong σ-donor carbene ligands with the metal center under basic conditions, and the generation of carbene complexes from imidazolium salts has frequently been observed in the presence of base.[6] Our studies demonstrate that basic conditions are unnecessary and that imidazolium-based ionic liquids can react with low-valent metal complexes of Group 10 through C2–H oxidative addition.[2,3]

Herein we report on the continuation of our studies in which the unusual chemical reactivity of imidazolium salts/NHC couples with transition metals is examined, and the potential applications of this chemistry are explored. We describe a C–C coupling reaction in which imidazolium salts act as substrates in a novel catalytic reaction that proceeds through a redox process involving a carbene intermediate. Combining the two "half-reactions" described in Equations (1) and (2) (Scheme 1) in the presence of an alkene establishes a unique catalytic process.

On stirring a solution of imidazolium salts **1a**,**b** in acetone/thf with various alkenes in the presence of a Ni^0 catalyst, the salts are progressively converted into the C2-alkylated products **2a**,**b** (Scheme 2; Table 1).



Scheme 2. Imidazolium C–H/alkene coupling reaction.

Compounds **2a**,**b** were isolated and characterized by NMR spectroscopy. The imidazolium C–H/alkene coupling reaction occurs under very mild conditions in the presence of the commonly employed $Ni(cod)_2/PPh_3$ (cod = 1,5-cyclooctadiene) catalyst system. The addition of 2 equivalents of PPh_3 is essential for the effective catalytic performance of the system. Use of $Ni(cod)_2$ on its own quickly leads to decomposition of the catalyst, resulting in poor reaction yields (Table 1, entry 1). Increasing or decreasing the PPh_3/Ni ratio gives lower conversions. We found that the addition of 2.1 equivalents of PPh_3/Ni gives the best overall catalytic results. The reactions could also be conducted in the ionic liquid itself, although conversions were considerably lower

[*] N. D. Clement, Prof. K. J. Cavell
Department of Chemistry
Cardiff University
PO Box 912, Cardiff CF10 3TB, Wales (UK)
Fax: (+44) 29-2087-5899
E-mail: cavellkj@cf.ac.uk

[**] We are grateful to the Engineering and Physical Sciences Research Council (EPSRC) for financial support and a stipend for N.D.C.

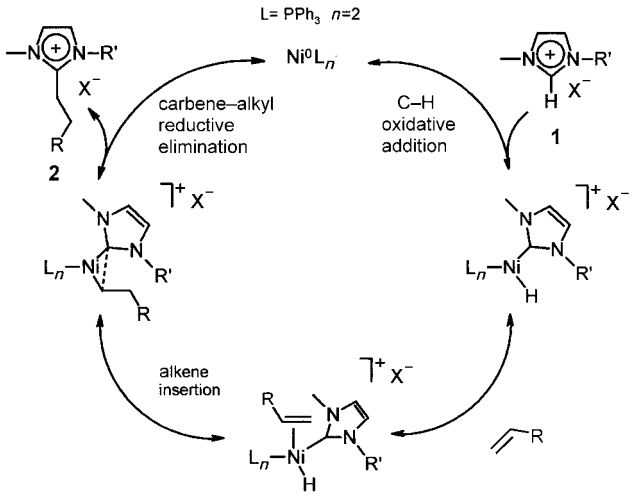
Supporting information for this article (catalytic procedure, separation method and spectroscopic data for compounds **2a**,**b**) is available on the WWW under http://www.angewandte.org or from the author.

 DOI: 10.1002/anie.200454166 © 2004 Wiley-VCH Verlag GmbH & Co. KGaA, Weinheim

Table 1: Catalytic coupling results.[a]

Entry	Ionic Liquid	Alkene	*T* [°C]	Yield [%][b]
1	**1a**,**b**		55, RT	<15[c]
2	**1a**		55	56
3	**1b**		55	51
4	**1b**		RT	64
5	**1b**	Ph	55	39[d]
6	**1a**	[e]	55	100;[a] 72[f]
7	**1b**	[e]	55	100;[a] 95[g]
8	**1b**	[e]	RT	35

[a] Conditions: Catalyst [$Ni(cod)_2$/PPh_3 (1:2.1)] (10 mol%); acetone/THF (3:1); reaction stopped after 48 h. [b] Determined by ^{1}H NMR spectroscopy, average of two runs or more. [c] Catalytic [$Ni(cod)_2$] only. [d] Mixture of linear and branched product (4:1). [e] Pressure: 1 bar. [f] Catalyst (5 mol%). [g] Catalyst (3 mol%).



Scheme 3. Proposed catalytic cycle for imidazolium/alkene coupling reaction.

(yields $<10\%$). The various 1-alkenes (1-hexene, ethylene) and styrene undergo coupling with the imidazolium salts to varying extents (Table 1).

Not surprisingly, ethylene (1 bar) couples more readily with imidazolium salts than does 1-hexene (Table 1, entries 6,7 and 2,3). This follows the expected reactivity pattern for alkenes (ethylene > propylene > butene ~ higher alkenes). Styrene gives lower conversions than either of the aliphatic alkenes (Table 1, entries 5 and 2–4/6–7); steric elements may be a factor in this observed behavior. Interestingly, styrene uniquely gives rise to linear and branched isomers — the branched isomer has a chiral center linking the imidazolium ring to the benzene ring. Both the tetrafluoroborate **1a** and bromide **1b** salts react with the different alkenes tested, especially with ethylene for which complete or nearly complete conversions were observed (Table 1, entries 6–7). With ionic liquid **1b** at 55 °C, almost complete conversion was observed even with a lower catalyst loading of 3%. (Table 1, entry 7).

Based on previous detailed theoretical and experimental studies on the mechanism of individual reaction steps,[1–3] the following catalytic cycle is proposed (Scheme 3) and described below.

Imidazolium salts **1a**,**b** oxidatively add to low-valent, [$Ni(PPh_3)_n$] generated in situ to form a carbene–Ni–hydrido species. C–H oxidative addition of imidazolium salts has been shown to be facile with low-valent Ni complexes, in particular with coordinatively unsaturated complexes bearing σ-donor ligands.[3] Alkene insertion into the ensuing M–H bond produces an alkyl–Ni intermediate that subsequently undergoes reductive elimination with the carbene ligand to produce 2-alkyl imidazolium salts **2a**,**b** and re-form M^0L_n. Kinetic and density functional studies have shown that reductive elimination from NHC–alkyl complexes proceeds in a concerted fashion.[1] The reductive elimination effectively involves orbital overlap between the carbene carbon p(π) orbital, the alkyl sp^3 orbital, and the metal d orbital, which occurs with concurrent opening of the angle between the two nonparticipating ligands L (Figure 1).

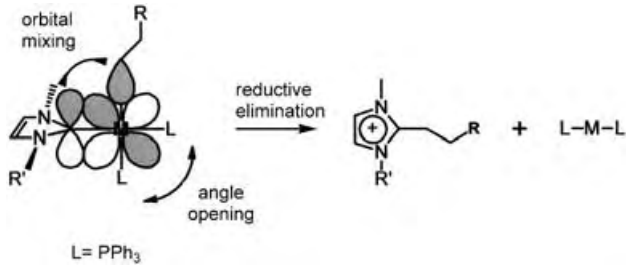


Figure 1. Proposed mechanism for carbene–alkyl reductive elimination.

For the alkenes studied, only the monoinsertion product is observed (i.e. for ethylene, only the 2-ethyl product is formed), which suggests that under the conditions employed the rate of carbene–alkyl reductive elimination is faster than the rate of alkene insertion into the Ni–alkyl bond. Consistent with this proposal, in earlier studies with Ni–carbene complexes as catalysts for alkene dimerization, effective catalysis was only observed in ionic liquid solvents.[7] In toluene the predominant reaction was reductive elimination to give imidazolium salts and Ni^0. In studies pertinent to our investigations, Bergman, Ellman, and co-workers have recently used a Rh^I complex to catalyze the conversion of benzimidazoles, thiazoles, and oxazoles into 2-substituted azole rings and also into fused azole-based heterocyclic compounds.[8] Rh–carbene complexes have been isolated from the reaction mixture, indicating that these may be intermediates in the catalytic reaction. On first consideration the reaction appears similar to that reported herein. However, the mechanism proposed by Bergman, Ullman and co-workers consists of an initial H-atom shift on the imidazole substrate to generate a Rh^I-NHC complex. This is then followed by the insertion of the coordinated alkene into the Rh–carbene bond to form a zwitterionic intermediate and generate the C–C bond. An intramolecular proton transfer, C–H reductive elimination, and product displacement complete the catalytic cycle.[8b]

 © 2004 Wiley-VCH Verlag GmbH & Co. KGaA, Weinheim

Our study represents the first example in which the imidazolium oxidative addition and carbene reductive elimination processes have been combined into the same catalytic cycle, and the first demonstration that the imidazolium C–H activation step can be used to generate an active catalyst. These results also illustrate the ease with which interconversion between imidazolium salts and NHC–transition-metal complexes occur even under very mild conditions, particularly under conditions where low-valent, unsaturated metal species are generated.

These results have important catalytic implications. First, this reaction represents a unique example of Ni^0-catalyzed C–H activation/C–C bond-formation reactions under mild conditions.[9] Second, the results also provide a catalytic methodology for producing 2-alkyl imidazolium-type salts through a coupling reaction. Third and most importantly, these results have direct ramifications for the use of imidazolium-based ionic liquids as solvents in transition-metal catalysis. It is clear that imidazolium salts can form carbene–hydrido species in the presence of a M^0 source, or when M^0 species are generated in situ during a reaction. Generation of carbene—-M–hydrido species would have a major impact on catalysis reactions in ionic-liquid media. This study, when considered in conjunction with our earlier investigations on imidazolium-based ionic-liquid solvents in catalysis,[7] demonstrates the unique potential for employing ionic liquids concomitantly as solvent and activator, generating long-lived (stabilized) active catalyst sites for a range of catalytic processes.

In conclusion we have demonstrated a new type of Ni^0-catalyzed C–H activation/C–C bond-forming reaction to produce 2-alkyl imidazolium-type salts under mild conditions. These results illustrate the facile redox processes associated with these salts, commonly used as ionic liquids. Of significance is the generation of (carbene)metal-hydride species in situ that may be employed in catalytic processes using the ionic liquid as both solvent and activator. The optimization and extension of the methodology described herein is currently under investigation.

Received: March 2, 2004 [Z54166]

Keywords: C–C coupling · C–H activation · carbene ligands · ionic liquids · nickel

[1] D. S. McGuinness, N. Saendig, B. F. Yates, K. J. Cavell, *J. Am. Chem. Soc.* **2001**, *123*, 4029.

[2] D. S. McGuinness, K. J. Cavell, B. F. Yates, *Chem. Commun.* **2001**, 355; D. S. McGuinness, K. J. Cavell, B. F. Yates, B. W. Skelton, A. H. White, *J. Am. Chem. Soc.* **2001**, *123*, 8317; M. A. Duin, N. D. Clement, K. J. Cavell, C. J. Elsevier, *Chem. Commun.* **2003**, 400.

[3] N. D. Clement, K. J. Cavell, C. Jones, C. J. Elsevier, *Angew. Chem.* **2004**, *116*, 1297; *Angew. Chem. Int. Ed.* **2004**, *43*, 1277.

[4] D. Bourissou, O. Guerret, F. P. Gabbaï, G. Bertrand, *Chem. Rev.* **2000**, *100*, 39; W. A. Herrmann, *Angew. Chem.* **2002**, *114*, 1342; *Angew. Chem. Int. Ed.* **2002**, *41*, 1290.

[5] T. Welton, *Chem. Rev.* **1999**, *99*, 2071; P. Wasserscheid, W. Keim, *Angew. Chem.* **2000**, *112*, 3926; *Angew. Chem. Int. Ed.* **2000**, *39*, 3772; R. Sheldon, *Chem. Commun.* **2001**, 2399; D. Zhao, M. Wu, Y. Kou, E. Min, *Catal. Today* **2002**, *74*, 157; J. Dupont, R. F. de Souza, P. A. Z. Suarez, *Chem. Rev.* **2002**, *102*, 3667.

[6] L. Xu, W. Chen, J. Xiao, *Organometallics* **2000**, *19*, 1123; C. J. Mathews, P. J. Smith, T. Welton, A. J. P. White, D. J. Williams, *Organometallics* **2001**, *20*, 3848.

[7] D. S. McGuinness, W. Mueller, P. Wasserscheid, K. J. Cavell, B. W. Skelton, A. H. White, U. Englert, *Organometallics* **2002**, *21*, 175.

[8] a) K. L. Tan, R. G. Bergman, J. A. Ellman, *J. Am. Chem. Soc.* **2001**, *123*, 2685; b) K. L. Tan, R. G. Bergman, J. A. Ellman, *J. Am. Chem. Soc.* **2002**, *124*, 3202; c) K. L. Tan, R. G. Bergman, J. A. Ellman, *J. Am. Chem. Soc.* **2002**, *124*, 13964; d) K. L. Tan, A. Vasudevan, R. G. Bergman, J. A. Ellman, A. J. Souers, *Org. Lett.* **2003**, *5*, 2131; e) J. C. Lewis, S. H. Wiedemann, R. G. Bergman, J. A. Ellman, *Org. Lett.* **2004**, *6*, 35.

[9] For reviews on catalytic C–H activation/C–C bond formation reactions see: Y. Guari, S. Sabo-Etienne, B. Chaudret, *Eur. J. Inorg. Chem.* **1999**, 1047; G. Dyker, *Angew. Chem.* **1999**, *111*, 1808; *Angew. Chem. Int. Ed.* **1999**, *38*, 1698; C. Jia, T. Kitamura, Y. Fujiwara, *Acc. Chem. Res.* **2001**, *34*, 633; V. Ritleng, C. Sirlin, M. Pfeffer, *Chem. Rev.* **2002**, *102*, 1731; F. Kakiuchi, S. Murai, *Acc. Chem. Res.* **2002**, *35*, 826.

 © 2004 Wiley-VCH Verlag GmbH & Co. KGaA, Weinheim

Anion Sensors

A Dimetallic Cage with a Long Ellipsoidal Cavity for the Fluorescent Detection of Dicarboxylate Anions in Water**

Massimo Boiocchi, Marco Bonizzoni, Luigi Fabbrizzi, Giulio Piovani, and Angelo Taglietti*

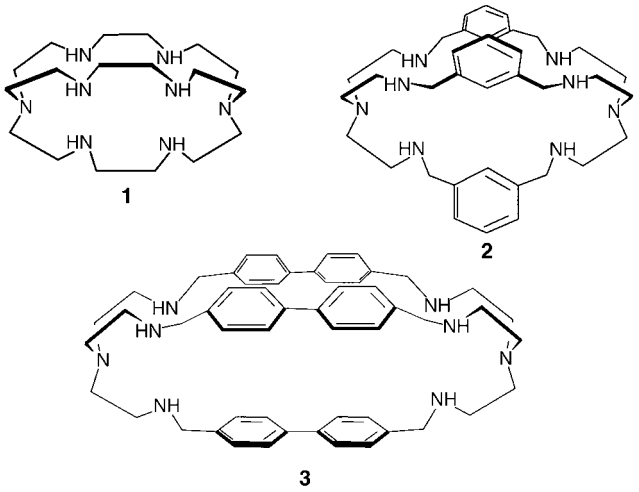
Host–guest chemistry is governed by the principle of size and shape complementarity: given a particular guest, a concave host must be designed whose cavity presents geometrical features complementary to those of the guest.[1] Moreover, the cavity must offer groups capable of establishing strong yet reversible interactions with the guest. A classical example is provided by octamine cages such as **1** and **2**, in which two tren subunits (tren = tris(2-aminoethyl)amine) are linked by either aliphatic (-CH_2CH_2-, **1**) or aromatic (1,3-xylyl, **2**) spacers. In aqueous acidic solution, the six secondary amine

[*] Dr. M. Bonizzoni, Prof. L. Fabbrizzi, G. Piovani, Dr. A. Taglietti
Dipartimento di Chimica Generale, Università di Pavia
viale Taramelli 12, 27100 Pavia (Italy)
Fax: (+39) 0382-528544
E-mail: luigi.fabbrizzi@unipv.it
Dr. M. Boiocchi
Centro Grandi Strumenti, Università di Pavia
via Bassi 21, 27100 Pavia (Italy)

[**] This work was financially supported by the European Union (RT Network Molecular Level Devices and Machines—Contract HPRN-CT-2000-00029), and by MIUR (COFIN—Progetto "Dispositivi Supramolecolari" and FIRB—Project RBNE019H9K).

Supporting information for this article is available on the WWW under http://www.angewandte.org or from the author.

 DOI: 10.1002/anie.200460036 © 2004 Wiley-VCH Verlag GmbH & Co. KGaA, Weinheim



nitrogen atoms of each cage are protonated and the positively charged cavity is suitable for the inclusion of an inorganic anion.[2] The length of the spacer defines the shape and the size of the cavity and the selectivity towards the anion. The hexammonium cage **1** provides a spherical cavity and selectively includes the spherical F^- ion.[3] The hexammonium cage **2** offers an ellipsoidal cavity suitable for the inclusion of the rodlike ion N_3^-.[4] However, other positively charged species, namely transition metal ions, can be placed within a bistren cage for interaction with an included anion. In particular, the dicopper(II) complex with the all-amine cryptand **2** incorporates ambidentate anions such as N_3^-,[5] NCO^-,[5] and HCO_3^-[6] to give stable inclusion complexes: Each metal center is coordinated by a tren subunit in a trigonal bipyramidal arrangement, and an axial position is available for interaction with a further ligand. Thus, an ambidentate anion such as N_3^- can place its terminal donor atoms in the two available axial sites to bridge the two Cu^{II} centers. Equilibrium investigations in water at pH 7 have shown that the dicopper(II) cryptate of **2** selectively incorporates N_3^- to give a very stable inclusion complex[7] in which the Cu^{II}–Cu^{II} distance is 6.10 Å. Anions with either a shorter (e.g. NO_3^-) or a larger (e.g. NCS^-) "bite" ("bite" indicates the distance between two consecutive donor atoms) show a distinctly lower affinity towards inclusion.

Herein we describe the inclusion properties of the dicopper(II) cryptate complex with the polycyclic octamine ligand **3**, whose tren subunits are linked by 4,4′-ditolyl spacers to provide an unusually long ellipsoidal cavity. Such a cavity is suitable for inclusion of ambidentate anions whose donor groups are well separated, as may be the case with either aromatic or aliphatic dicarboxylates. Dicarboxylate anions are among the most attractive targets for molecular recognition and sensing since several -COO^- functional groups are present in a variety of biomolecules such as amino acids and proteins. As an example, the glutamate ion, an amino acid containing two -COO^- groups, is a major excitatory transmitter in the central nervous system and its determination both temporally and spatially is required by neurophysiologists.[8]

Cryptand **3** was obtained in good yield through a modification of a reported procedure,[9] followed by the slow evaporation of an aqueous solution containing **3** and copper(II) nitrate (1:2) to yield crystals of a complex of formula $[Cu^{II}_2(\mathbf{3})(H_2O)_2](NO_3)_4{\cdot}2H_2O$ of suitable quality for X-ray diffraction studies.[10] The structure of the dimetallic complex is shown as an ORTEP plot in Figure 1. Both

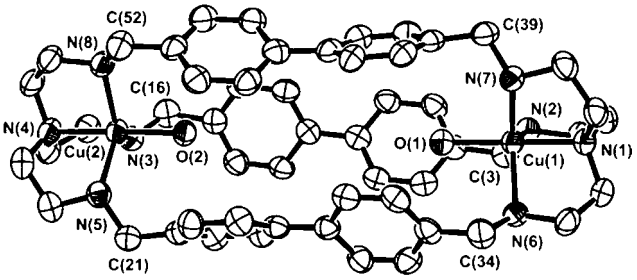


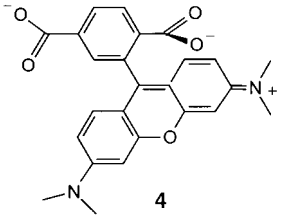
Figure 1. An ORTEP view of the $[Cu^{II}_2(\mathbf{3})(H_2O)_2](NO_3)_4{\cdot}2H_2O$ complex. Thermal ellipsoids are drawn at the 30% probability level. Hydrogen atoms, four nitrate counterions, and two isolated water molecules have been omitted for clarity. Element symbols are reported only for atoms bonded to metal centers and for carbon atoms that define the three ditolyl spacers. Selected bond lengths [Å] and angles [°] around the two Cu^{II} metal centers: Cu(1)-N(1) 2.001(3); Cu(2)-N(4) 2.000(3); Cu(1)-N(2) 2.140(4); Cu(2)-N(3) 2.152(4); Cu(1)-N(6) 2.131(3); Cu(2)-N(5) 2.160(4); Cu(1)-N(7) 2.134(3); Cu(2)-N(8) 2.124(4); Cu(1)-O(1) 1.982(3); Cu(2)-O(2) 1.971(3); N(1)-Cu(1)-N(2) 85.91(13); N(4)-Cu(2)-N(3) 86.25(16); N(1)-Cu(1)-N(6) 85.19(14); N(4)-Cu(2)-N(5) 84.80(15); N(1)-Cu(1)-N(7) 85.43(14); N(4)-Cu(2)-N(8) 85.27(14); N(1)-Cu(1)-O(1) 179.86(14); N(4)-Cu(2)-O(2) 178.42(15); N(2)-Cu(1)-N(6) 119.80(14); N(3)-Cu(2)-N(5) 118.82(14); N(2)-Cu(1)-N(7) 115.82(14); N(3)-Cu(2)-N(8) 120.72(15); N(2)-Cu(1)-O(1) 94.06(13); N(3)-Cu(2)-O(2) 92.54(15); N(6)-Cu(1)-N(7) 122.55(14); N(5)-Cu(2)-N(8) 118.58(15); N(6)-Cu(1)-O(1) 94.95(12); N(5)-Cu(2)-O(2) 94.90(13); N(7)-Cu(1)-O(1) 94.45(12); N(8)-Cu(2)-O(2) 96.24(14).

copper(II) ions are included within the cage and are coordinatively bound to the tren subunits. In particular, each Cu^{II} ion shows a trigonal bipyramidal coordination and, as usually observed with Cu^{II} complexes of tren derivatives, the equatorial Cu–N bond lengths (mean values of 2.135(4) Å for Cu(1), and 2.145(4) Å for Cu(2)) are longer than the axial Cu–N bond lengths of 2.001(3) and 2.000(3) Å, respectively. The other axial site is occupied by a water molecule. In particular, the Cu–O bond lengths (1.982(3) and 1.971(3) Å) are similar to that observed in the mononuclear precursor complex $[Cu^{II}(tren)(H_2O)]^{2+}$ (1.975(6) Å).[15] The three ditolyl spacers show dihedral angles between the phenyl planes of 32.8(2), 34.3(2), and 36.8(2)°. Similar values have been observed in the crystalline 4,4′-ditolyl compound (36 and 40° for the two molecules present in the asymmetric unit).[16] This suggests the absence of any steric constraints in the carbon backbone of the cage. The presence of especially long spacers results in a Cu–Cu separation of 11.305(6) Å, which is the longest distance ever observed for dimetallic bistren cryptate complexes.

The inclusion tendencies of the $[Cu_2^{II}(\mathbf{3})(H_2O)_2]^{4+}$ complex towards dicarboxylates were investigated in neutral aqueous solution following the "fluorescent indicator dis-

 © 2004 Wiley-VCH Verlag GmbH & Co. KGaA, Weinheim

placement" approach.[17] According to this approach, a receptor **R** (e.g. the cryptate complex $[Cu_2^{II}(\mathbf{3})(H_2O)_2]^{4+}$) first binds and quenches a fluorescent indicator **I**. Then, the envisaged substrate **S** (e.g. a dicarboxylate ion) displaces **I** from the receptor cavity and allows **I** to fluoresce again, thus signalling the binding of **S**. We chose carboxy-rhodamine (**4**) as the fluorescent indicator; **4** contains two carboxylate groups and emits at 571 nm (orange fluorescence) upon excitation at 496 nm (isosbestic point).



4

First, we investigated the interaction of rhodamine with the receptor $[Cu_2^{II}(\mathbf{3})(H_2O)_2]^{4+}$. An aqueous HEPES-buffered solution (pH 7) of the fluorescent indicator (2.5×10^{-7} M), was titrated with a standard solution of the cryptate complex. Addition of the dicopper complex induced a gradual decrease of the fluorescence intensity I_F of **4** until complete quenching occurred as shown in Figure 2. Least-squares nonlinear fitting of the titration profile (Figure 2, inset)[18] indicates the formation of a 1:1 adduct between the cryptate and **4** with an association constant $\log K_I = 7.0 \pm 0.2$. This suggests that the benzene-1,4-dicarboxylate moiety of **4** is included within the cryptate and the two -COO^- groups coordinate the two Cu^{II} centers. In this situation, the transition metal centers could effectively quench the fluorophore through either an electron transfer or an electronic energy transfer process.

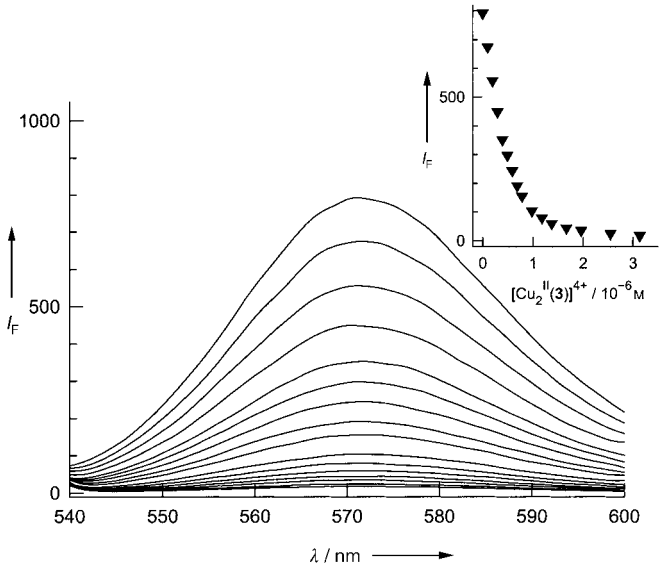


Figure 2. Emission spectra of an aqueous solution of the rhodamine indicator **4** (2.5×10^{-7} M) when titrated with the complex $[Cu_2^{II}(\mathbf{3})]^{4+}$. Inset: titration profile (I_F versus the concentration of $[Cu_2^{II}(\mathbf{3})]^{4+}$).

We then prepared an aqueous solution containing the cryptate complex $[Cu_2^{II}(\mathbf{3})]^{4+}$ (2.5×10^{-6} M) and the indicator **4** (2.5×10^{-7} M) whose fluorescence was thereby completely quenched through its incorporation into the complex. Then, the solution was adjusted to pH 7 and was titrated with a selection of dicarboxylate substrates.

Initially, we considered the family of positional phthalate isomers. We observed that titration with benzene-1,2-dicarboxylate (phthalate) and benzene-1,3-dicarboxylate (isophthalate) derivatives led to no (1,2-) or only minor (1,3-) rhodamine fluorescence emission (see Figure 3). However,

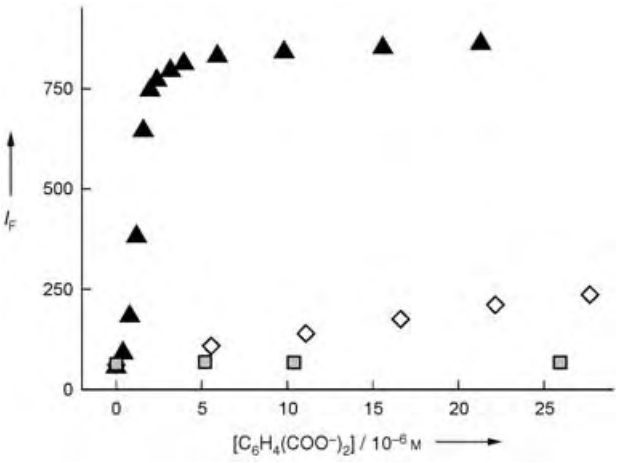


Figure 3. Titration of a solution of $[Cu_2^{II}(\mathbf{3})]^{4+}$ (2.5×10^{-6} M) and **4** (2.5×10^{-7} M) with *m*,*n*-benzenedicarboxylates in an aqueous solution buffered at pH 7. ▲ 1,4-, ◇ 1,3-, □ **1,2-benzenedicarboxylate.**

addition of the 1,4-derivative (terephthalate) fully restored rhodamine fluorescence. Thus, receptor $[Cu^{II}{}_2(\mathbf{3})]^{4+}$ clearly discriminates terephthalate from the other isomeric dicarboxylates. Through nonlinear fitting of the titration profiles in Figure 3, the binding constants K_S for the 1:1 adducts of the dicopper(II) cryptate and the three dicarboxylates were calculated,[19] and their values are reported in Figure 4. Importantly, to determine K_S values for 1,2- and 1,3-derivatives, anion concentrations up to 10^{-3} M had to be employed.

In Figure 4, the association constant K_I for the cryptate with the indicator is reported as a horizontal line. The diagram shows that only the 1,4-derivative has a higher affinity towards the cryptate than the rhodamine indicator, resulting in the displacement of the latter. On the other hand, 1,2- and 1,3-derivatives exhibit distinctly lower K_S values and cannot displace the indicator (in the concentration range considered in Figure 3). This highly selective behavior can be explained on the basis of geometrical considerations.

The molecular structure in Figure 1 shows that the distance between the oxygen atoms of the two coordinated water molecules is 7.355(4) Å, whereas the distance between two opposite oxygen atoms in the terephthalate ion is 7.39 Å, as observed from the X-ray crystal structure of its ammonium salt.[20] It follows that the terephthalate ion has an almost

 © 2004 Wiley-VCH Verlag GmbH & Co. KGaA, Weinheim

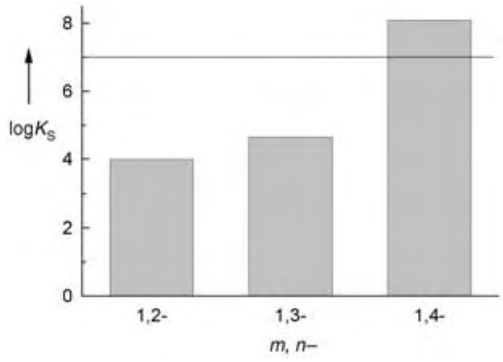


Figure 4. Equilibrium constants for the interaction of the receptor $[Cu_2^{II}(\mathbf{3})]^{4+}$ with *m*,*n*-benzenedicarboxylates (bars) and the fluorescent indicator **4** (horizontal line). The position of the horizontal line with respect to the bars determines the selectivity of the chemosensor ensemble $\{\mathbf{4}+[Cu_2^{II}(\mathbf{3})]^{4+}\}$ towards the chosen dicarboxylate.

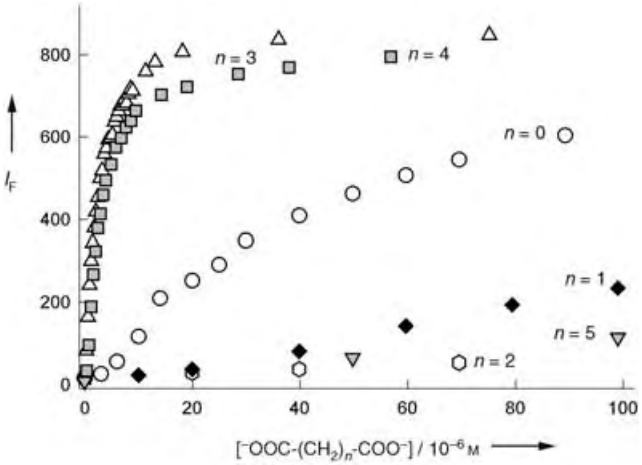


Figure 5. Titration of a solution of $[Cu_2^{II}(\mathbf{3})]^{4+}$ (2.5×10^{-6} M) and **4** (2.5×10^{-7} M) with aliphatic dicarboxylates of formula $^-OOC\text{-}(CH_2)_n\text{-}COO^-$ in an aqueous solution buffered at pH 7.

perfect O–O bite and displaces the two water molecules to bridge the two Cu^{II} centers without inducing any endoergonic rearrangement of the cage. On the other hand, an unfavorable rearrangement is expected to occur with the inclusion of isophthalate and phthalate ions, whose O–O distances are distinctly smaller (4.98 Å,[21] and 3.16 Å,[22] respectively). This therefore suggests that the terephthalate fragment has the correct length to place an oxygen atom from each -COO^- group in the available coordination site (the axial position of a trigonal bipyramid) of each of the two Cu^{II} ions, thus maintaining the cage framework in its more relaxed arrangement. Rhodamine **4** itself also contains the benzene-1,4-dicarboxylate fragment, which ensures the most favorable fit. Its association constant is one order of magnitude lower than that of the terephthalate anion probably owing to repulsive effects exerted by the appended fluorogenic fragment (steric) and by the positive charge on the fluorophore (electrostatic). A colorimetric method based on an anion-induced reaction has recently been reported to discriminate the 1,2-derivative with respect to the 1,3- and 1,4-isomers in solution in dioxane–water (70:30 v/v).[23]

We next considered the family of aliphatic dicarboxylates $^-OOC\text{-}(CH_2)_n\text{-}COO^-$ with $n=0$–5. Figure 5 displays the profiles obtained upon titration of the dicopper(II) cryptate–rhodamine solution with the envisaged dicarboxylate in a solution buffered at pH 7. High selectivity was also observed in this case. In particular, glutarate ($n=3$) and adipate ($n=4$) both displaced the indicator from the receptor as observed from the rhodamine fluorescence emission. However, upon contraction (succinate, $n=2$) and expansion (pimelate, $n=5$) of the aliphatic chain joining the -COO^- groups, no displacement of the indicator occured and the fluorescence remained almost quenched.

The association constants for the varying dicarboxylates ($n=2$–5), shown in the bar diagram in Figure 6 and calculated through nonlinear fitting of titration profiles account for the described behaviour. Even though glutarate and adipate exhibit association constants similar to that of rhodamine (Figure 6, horizontal line), they compete successfully for the

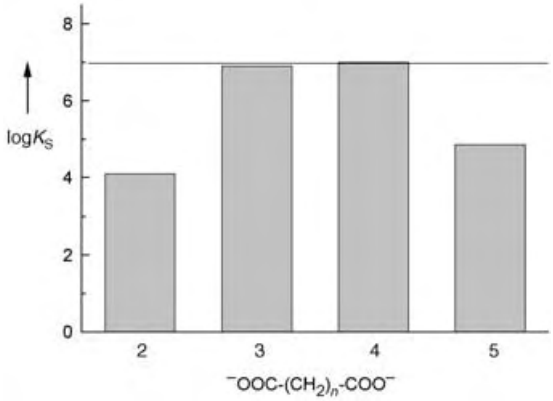


Figure 6. Equilibrium constants for the interaction of the receptor $[Cu_2^{II}(\mathbf{3})]^{4+}$ with $^-OOC\text{-}(CH_2)_n\text{-}COO^-$ dicarboxylates (bars) and the fluorescent indicator **4** (horizontal line). In the abscissa, $n=$ number of methylene groups in the spacer.

receptor when they are present in a much higher concentration than the indicator. Succinate and pimelate exhibit association constants well below that of the indicator and therefore cannot displace rhodamine from the receptor. The highest inclusion affinity is exhibited by glutarate and adipate whose crystallographically determined O–O distances (7.20[24] and 7.83 Å,[25] respectively) are the closest to that observed between the oxygen atoms of the coordinated water molecules in the $[Cu_2^{II}(\mathbf{3})(H_2O)_2]^{4+}$ complex. Dicarboxylates exhibiting smaller (succinate, 6.04 Å)[26] or larger (pimelate, 9.67 Å)[27] O–O distances give much less stable inclusion complexes.

The oxalate anion ($n=0$, see Figure 5) also exhibits competitive behavior. However, least-squares treatment of titration data shows that the dicopper(II) cryptate undergoes stepwise inclusion of *two* oxalate ions, with $\log K_{S1}=6.1\pm0.3$ and $\log K_{S2}=3.2\pm0.3$. The inclusion of two distinct molecules

 © 2004 Wiley-VCH Verlag GmbH & Co. KGaA, Weinheim

was also observed in the case of malonate ($\log K_{S1} = 4.8 \pm 0.3$; $\log K_{S2} = 3.2 \pm 0.3$). This behavior is explained by the relatively small size of the two anions which is insufficient to encompass the distance between the two metal centers so that they prefer individual coordination to each Cu^{II} ion. Despite this observation, the dicopper(II) cryptate $[Cu^{II}_2(\mathbf{3})]^{4+}$ still clearly discriminates glutarate and adipate anions from oxalate anions.

Recognition of aromatic and aliphatic dicarboxylates by a hexammonium cage in which the two tren subunits are linked by long carbon spacers (i.e. -CH_2-C_6H_4-CH_2-C_6H_4-CH_2-; -C_6H_4- = 1,4-phenyl) has been investigated through ^{1}H NMR titrations conducted in solution in D_2O adjusted to pH 6. The highest inclusion affinity was observed for terephthalate ($\log K = 4.4$) whereas no particular selectivity was noted in the case of $^-$OOC-$(CH_2)_n$-COO^- anions, for which log$K$ values ranged from 3.1 to 3.4 upon moving from $n = 2$ to $n = 7$.[28] This lack of selectivity may be attributed to the higher flexibility of the spacers (an sp^3 carbon atom joins the two phenyl rings) and to the nondirectional character of the electrostatic interactions.

In conclusion, this work has demonstrated that the dicopper(II) complex of a rigid bistren cryptand such as **3** is an ideal receptor for difunctional anions which are neatly discriminated on the basis of the distance between their functional groups. In particular, the investigated cryptate performs chain-length recognition of aliphatic dicarboxylates. The strong metal–ligand interactions established between the receptor and the anion easily compensate for unfavorable dehydration effects and allow recognition in pure water at pH 7— a rare occurrence when anion recognition is based on electrostatic interactions such as hydrogen bonding.[29] Most of the studies on carboxylate recognition to date have been carried out in non-aqueous solvents.[30]

Moreover, the use of a fluorescent indicator in an "indicator displacement" approach provides sharp signalling of the recognition event. The transition metals present in the receptor cavity quench the included fluorophore until it is displaced by the substrate to provide a valuable OFF–ON switching of the signal.[31] Finally, changing the length of the spacer allows the selective recognition of $^-$OOC-$(CH_2)_n$-COO^- dicarboxylates of different n values: in such a case an appropriate bidentate indicator that fits the Cu^{II}–Cu^{II} distance within the receptor is required.

Received: March 18, 2004 [Z460036]

Keywords: copper · cryptands · fluorescent probes · molecular recognition · sensors

[1] D. J. Cram, J. M. Cram, *Container Molecules and Their Guests*, Royal Society of Chemistry, Cambridge, UK, **1997**.
[2] J.-M. Lehn, *Supramolecular Chemistry, Concepts and Perspectives*, VCH, Weinheim, **1995**.
[3] B. Dietrich, J.-M. Lehn, J. Guilhem, C. Pascard, *Tetrahedron Lett.* **1989**, *30*, 4125.
[4] B. Dietrich, J. Guilhem, J.-M. Lehn, C. Pascard, E. Sonveaux, *Helv. Chim. Acta* **1984**, *67*, 91.
[5] C. J. Harding, F. E. Mabbs, E. J. L. MacInnes, V. McKee, J. Nelson, *J. Chem. Soc. Dalton Trans.* **1996**, 3227.
[6] R. Menif, J. Reibenspies, A. E. Martell, *Inorg. Chem.* **1991**, *30*, 3446.
[7] L. Fabbrizzi, A. Leone, A. Taglietti, *Angew. Chem.* **2001**, *113*, 3156; *Angew. Chem. Int. Ed.* **2001**, *40*, 3066.
[8] G. J. Siegel, B. W. Agranoff, R. W. Albers, P. B. Molinoff, *Basic Neurochemistry: Molecular, Cellular and Medical Aspects*, *5th ed.*, Raven, New York, **1994**.
[9] D. Chen, A. E. Martell, *Tetrahedron*, **1991**, *47*, 6895.
[10] Crystal data for $[Cu^{II}_2(\mathbf{3})(H_2O)_2](NO_3)_4 \cdot 2H_2O$ ($C_{54}H_{74}Cu_2N_{12}O_{16}$): $M_r = 1274.35$, $T = 293$ K, crystal dimensions $0.55 \times 0.30 \times 0.15$ mm^3, orthorhombic, $Pna2_1$ (No. 33), $a = 34.0372(20)$, $b = 11.2959(6)$, $c = 15.6098(10)$ Å, $V = 6001.6(6)$ Å, $Z = 4$, $\rho_{calcd} = 1.410$, $F(000) = 2672$, $\mu = 0.785$ mm^{-1}, $Mo_{K\alpha}$ radiation ($\lambda = 0.7107$ Å), $2\theta_{max} = 52°$, 44805 measured , 11535 independent ($R_{int} = 0.0334$), 9813 strong reflections [$I_o > 2\sigma(I_o)$], 773 refined parameters, $R1 = 0.0526$ (strong data) and 0.0620 (all data), $wR2 = 0.1400$ (strong data) and 0.1476 (all data), GOF = 1.053, 0.98/−0.35 max./min. residual electron density. Diffraction data were collected on a Bruker-Axs Smart-Apex CCD based diffractometer. Omega rotation frames (scan width 0.3°, scan time 20 s, sample-to-detector distance 8 cm) were processed with the SAINT software (Bruker-Axs Inc.) and corrected for Lorentz and polarization effects. Absorption effects were analytically evaluated by the SADABS software[11] and correction was applied to the data (0.75 and 0.89 min. and max. transmission factor). The structure was solved by direct methods (SIR-97)[12] and refined by full-matrix least-square procedures on F^2 using all reflections (SHELXL-97).[13] Calculations were performed with the WinGx package.[14] All non-hydrogen atoms were refined with anisotropic temperature factors, except for those of the N(12) nitro group, that showed the three O atoms disordered over two alternative positions with the same statistical probability. Hydrogen atoms were placed using the appropriate AFIX instructions. CCDC 233940 contains the supplementary crystallographic data for this paper. These data can be obtained free of charge via www.ccdc.cam.ac.uk/conts/retrieving.html (or from the Cambridge Crystallographic Data Centre, 12, Union Road, Cambridge CB21EZ, UK; fax: (+44) 1223-336-033; or deposit@ccdc.cam.ac.uk).
[11] G. M. Sheldrick, SADABS, Siemens Area Detector Absorption Correction Program, University of Göttingen, Germany, **1996**.
[12] A. Altomare, M. C. Burla, M. Cavalli, G. L. Cascarano, C. Giacovazzo, A. Guagliardi, A. G. G. Moliterni, G. Polidori, R. Spagna, *J. Appl. Crystallogr.* **1999**, *32*, 115.
[13] G. M. Sheldrick, Institut für Anorganische Chemie der Universität, Göttingen, Germany, **1997**.
[14] L. J. Farrugia, *J. Appl. Crystallogr.* **1999**, *32*, 837.
[15] D. K. Chand, P. K. Bharadwaj, *Inorg. Chem.* **1998**, *37*, 5050.
[16] G. Casalone, C. Mariani, A. Mugnoli, M. Simonetta, *Acta Crystallogr.* **1969**, *B25*, 1741.
[17] S. L. Wiskur, H. Ait-Haddou, J. J. Lavigne, E. V. Anslyn, *Acc. Chem. Res.* **2001**, *34*, 963.
[18] P. Gans, A. Sabatini, A. Vacca, *Talanta* **1996**, *43*, 1739.
[19] K. A. Connors, *Binding Constants, the Measurements of Molecular Complex Stability*, Wiley, New York, **1987**.
[20] J. A. Kaduk, *Acta Crystallogr.* **2000**, *B56*, 474.
[21] E. Cadot, J. Marrot, F. Sécheresse, *Angew. Chem.* **2001**, *113*, 796; *Angew. Chem. Int. Ed.* **2001**, *40*, 774;
[22] R. A. Smith, *Acta Crystallogr.* **1975**, *B31*, 1773.
[23] F. Sancenón, R. Martínez-Máñez, M. A. Miranda, M.-J. Seguí, J. Soto, *Angew. Chem.* **2003**, *115*, 671; *Angew. Chem. Int. Ed.* **2003**, *42*, 647.
[24] M. Vanire, F. Brisse, *Acta Crystallogr.* **1982**, *B38*, 3060.
[25] I. A. Teslya, A. I. Tursina, L. D. Iskhakova, L. M. Avdonina, V. V. Marugin, *Zh. Strukt. Khim.* **1990**, *31*, 123.

 © 2004 Wiley-VCH Verlag GmbH & Co. KGaA, Weinheim

[26] H. Kutzke, L. Wiehl, H. Klapper, *Z. Kristallogr.* **1994**, *209*, 256.
[27] N. T. Saraswathi, S. Roy, M. Vijayan, *Acta Crystallogr.* **2003**, *B59*, 641.
[28] J. M. Lehn, R. Méric, J. P. Vigneron, I. Bkouche-Waksman, C. Pascard, *Chem. Commun.* **1991**, 62.
[29] F. P. Schmidtchen, M. Berger, *Chem. Rev.* **1997**, *97*, 1609.
[30] R. J. Fitzmaurice, G. M. Kyne, D. Douheret, J. D. Kilburn, *J. Chem. Soc. Perkin Trans. 1* **2002**, 841.
[31] L. Fabbrizzi, M. Licchelli, A. Taglietti, *Dalton Trans.* **2003**, 3471.

 © 2004 Wiley-VCH Verlag GmbH & Co. KGaA, Weinheim

Metal Hydride Complexes

Kinetic Control over the Thermal Stability of the In–H Bond: Synthesis and Characterization of Amido Indium Hydride Complexes**

Robert J. Baker, Cameron Jones, Peter C. Junk, and Marc Kloth*

In memory of Colin Eaborn

Aluminium and gallium hydride chemistry is now well developed and complexes that incorporate Al–H and Ga–H bonds have found a wide variety of applications in organic transformations, inorganic synthesis, and materials chemistry.[1] Until recently, this situation was not mirrored by indium hydride complexes as it was generally accepted that the relative weakness of the In–H bond led to their observed thermal instability. In this respect, Downs and co-workers have rightly pointed out that the In–H bond is stronger than the In–C bond and given the thermal stability of indium alkyls, the instability of indium (and gallium) hydride compounds is partly kinetic in origin.[2] It is likely that this instability is derived from the propensity of the metal hydrides to associate through M-H-M bridges, which lower the energy barrier to homolytic decomposition processes that involve dihydrogen elimination. This proposal is in line with the recent first observation of solid $[(InH_3)_n]$, which decomposes above 180 K.[3]

[*] Dr. R. J. Baker, Prof. C. Jones, Dipl.-Eng. M. Kloth
School of Chemistry, Cardiff University
Cardiff, P.O. Box 912, Park Place, Cardiff, CF10 3TB (UK)
Fax: (+44) 2920-874030
E-mail: jonesca6@cardiff.ac.uk
Assoc. Prof. P. C. Junk
School of Chemistry, Monash University
PO Box 23, Victoria 3800 (Australia)

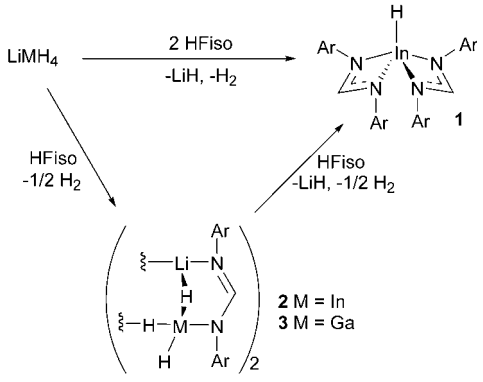
[**] This work was supported by the Engineering and Physical Sciences Research Council and the Leverhulme Trust (UK).

Supporting information for this article is available on the WWW under http://www.angewandte.org or from the author.

In contrast, we have prepared the first InH_3 complexes that have moderate thermal stability given the right choice of ligand.[4] Most success has been had with highly nucleophilic N-heterocyclic carbenes (NHCs), which form strong C–In dative bonds and discourage the formation of intermolecular In-H-In bridges by providing a degree of steric shielding to the InH_3 fragment.[5] A number of alkyl, halogen, phosphido and gallyl indium hydride complexes[4,6] have also been prepared and are finding applications in inorganic[4] and organic synthesis.[7] For these applications to expand, greater control over the thermal stability of indium hydride complexes is required.

Bulky amide ligands have been widely used to stabilize aluminium and gallium hydride complexes,[8] though amido indium hydride complexes are unknown, except for several matrix-isolated examples, for example, $[H_2InNH_2]$.[9] We wished to prepare such complexes and saw the amidinate class of ligand, $[RNC(R')NR]^-$, as being appropriate to this cause. The stabilizing features this class of ligand offers include an ability to chelate metal centers and the potential to incorporate bulky substituents on the N atom and on the C backbone of the ligand. Both stabilizing features have been previously exploited in a range of Group 13 halide and alkyl complexes.[10] In this preliminary study, we have specifically chosen the bulky formamidinate ligand, $[ArNC(H)NAr]^-$ $Ar = C_6H_3iPr_2$-2,6 (Fiso),[11] which has been utilized to prepare the first amido indium hydride complexes, one of which displays unprecedented thermal stability.

Treatment of an ethereal solution of $LiInH_4$[4] with two equivalents of HFiso led to H_2 and LiH elimination and a moderate yield of **1** after recrystallization from diethyl ether (Scheme 1). In the solid state, **1** does not show any decomposition in air after one week and under argon does not begin to decompose until 160 °C (compare with $[AlH(Fiso)_2]$, decomp 231–233 °C).[12] In toluene solutions it can be heated in a sealed tube at 125 °C for 3 h before complete decomposition occurs. This does not afford indium metal but HFiso and an insoluble, brown organo-indium material, the exact identity of which could not be determined. The decomposition process is presumably intramolecular and involves hydrogen transfer to one Fiso ligand and metallation of the other (compare with NHC metallation in the decomposition of $[InH_3\{C[N(iPr)CH]_2\}]$).[4] The ^1H NMR spectrum of **1** does



Scheme 1. Synthesis of compounds **1**–**3**.

 © 2004 Wiley-VCH Verlag GmbH & Co. KGaA, Weinheim DOI: 10.1002/anie.200460304

not exhibit an observable In–H resonance signal, which can be explained by quadrupolar broadening of this signal by the ^{113}In and ^{115}In isotopes ($I = 9/2$). Its infrared spectrum does, however, show a sharp In–H stretching absorption, as would be expected for a terminal hydride ligand. This occurs at significantly higher frequency (1748 cm^{-1}, compared with 1823 cm^{-1} for $[AlH(Fiso)_2]$[12]) than the In–H stretching modes of InH_3 complexes (1640–1660 cm^{-1})[4] due to a negative inductive effect from the two anionic Fiso ligands, which decreases the relative polarity of the In–H bond. Consequently, this decrease should lead to a decrease in the predisposition of the indium hydride fragment to be involved in intermolecular hydride bridges. The deuteride analogue of **1**, namely, **1**–D (decomp 165–170 °C), was prepared from $LiInD_4$ and HFiso and its infrared spectrum is essentially identical to that of **1**, though no absorption at 1748 cm^{-1} is present. A corresponding In–D stretch was not discernable at the expected wavenumber (ca. 1240 cm^{-1}) due to strong masking from the fingerprint region.

The molecular structure of **1** (Figure 1a)[13] shows that the complex is monomeric and has a heavily distorted trigonal bipyramidal indium coordination environment with N(2) and N(4) in axial positions. The hydride ligand was located from difference maps and refined isotropically; the In–H bond length is 1.71(6) Å (av 1.68 Å in $[InH_3(PCy_3)]$, Cy = cyclohexyl[4]). The geometry of **1** is similar to that of the related indium chloride complex, $[InCl\{CyNC(tBu)NCy\}_2]$,[14] and the only other example of a structurally characterized amidinate Group 13 hydride complex, $[AlH\{(Me_3Si)NC(Ph)N(SiMe_3)\}_2]$,[15] though the bulk of the Ar substituents in **1** cause it to be significantly more distorted. We believe that these groups also lead to the remarkable thermal stability of the complex by forming a heavily protected "pocket" in which the hydride ligand sits (Figure 1b). This pocket prevents the formation of intermolecular In-H-In bridges and hinders chemical attack of the InH moiety.

To examine the mechanism of formation of **1**, the reaction of $LiInH_4$ with HFiso was carried out in a 1:1 stoichiometry, which led to the formation of the amidotrihydrido indate complex, **2**, in moderate yield. The corresponding gallium complex, **3**, was prepared by an analogous procedure. Further treatment of **2** with HFiso led to the formation of **1**, H_2, and LiH, thus confirming that **2** is an intermediate in the aforementioned 2:1 reaction. In contrast, **3** did not react with HFiso, which can be explained by the less hydridic nature of Ga–H compared with In–H bonds[4] and the fact that gallium hydride complexes disfavor coordination numbers greater than 4.[1b] In the solid state, **2** begins to decompose at 42 °C (compare with **3**, m.p. 84–86 °C) and in solution it is unstable above 0 °C deposits indium metal, evolves H_2 gas, and generates a solution of [Li(Fiso)], as determined by ^{7}Li and ^{1}H NMR studies.

The infrared spectrum (Nujol mull) of **2** displays In–H stretching absorptions for the terminal (1719 cm^{-1}; compare with that in **3** 1879 cm^{-1}) and bridging (1632 cm^{-1}; **3** 1769 cm^{-1}) hydride ligands, the assignment of which was confirmed by their absence in the spectrum of the corresponding trideuteride complex, **2**–D_3 (1161 cm^{-1} In–D bridging, In–D terminal-masked). Because of the thermal instability of **2**, solution NMR spectroscopic studies of this compound were carried out at ≤ -30 °C and in the case of the ^{1}H NMR spectrum, a broad In–H resonance was observed at $\delta = 6.02$ ppm (**3**, Ga–H $\delta = 4.68$ ppm) in the normal region.[4] The ^{1}H-coupled and decoupled ^{6}Li and ^{7}Li spectra comprise only singlet resonances in the temperature range, −30 to −80 °C. In contrast, the ^{6}Li NMR spectrum of **3** exhibits a sharp doublet resonance signal at 25 °C ($^1J_{LiH} = 1.2$ Hz), which suggests that this compound exists as a monomer in solution with the intramolecular Li-H-Ga bridge remaining intact.[16] Cooling solutions of **3** led only to loss of resolution of the doublet at about −15 °C and the resultant broad singlet did not resolve to a doublet of doublets, as expected for a hydride bridged dimeric structure, down to −80 °C.

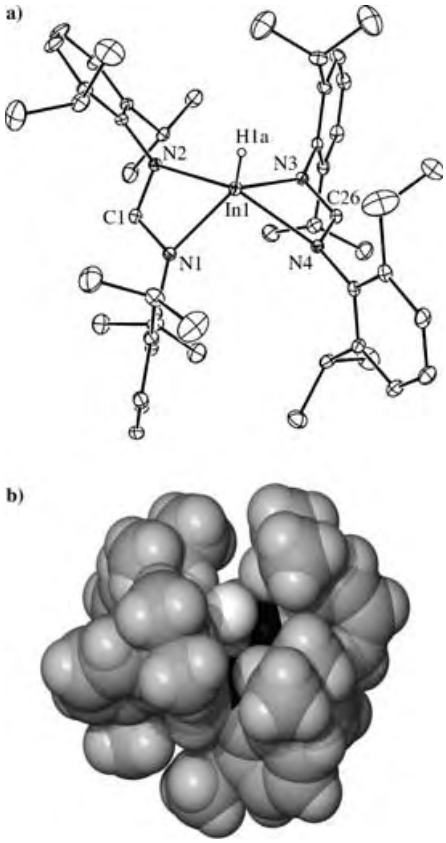


Figure 1. a) Molecular structure of **1** (ORTEP, thermal ellipsoids set at 20 % probability). Selected bond lengths [Å] and angles [°]: In(1)-N(3) 2.177(3), In(1)-N(1) 2.196(3), In(1)-N(2) 2.289(3), In(1)-N(4) 2.301(3), In(1)-H(1a) 1.71(6), N(1)-C(1) 1.320(4), N(2)-C(1) 1.310(4), N(3)-C(26) 1.305(4), N(4)-C(26) 1.307(4); N(1)-In(1)-N(2) 59.64(10), N(3)-In(1)-N(4) 59.38(10), N(2)-In(1)-N(4) 146.08(10), N(1)-In(1)-N(3) 116.26(10), N(1)-In(1)-(H1a) 123.9(17), N(2)-In(1)-(H1a) 113.8(19), N(3)-In(1)-(H1a) 119.1(17), N(4)-In(1)-(H1a) 100.0(19), N(2)-C(1)-N(1) 116.1(3), N(3)-C(26)-N(4) 116.4(3). b) Space filling model of **1**. The hydride ligand is shown in white (at the center).

The solid-state structure of **2** is depicted in Figure 2[13] and represents the first structural characterization of a trihydrido indate complex. The location and isotropic refinement of the hydride ligands confirmed that the complex dimerizes through intermolecular hydride bridges to give a $\{Li_2In_2H_4\}$

 © 2004 Wiley-VCH Verlag GmbH & Co. KGaA, Weinheim

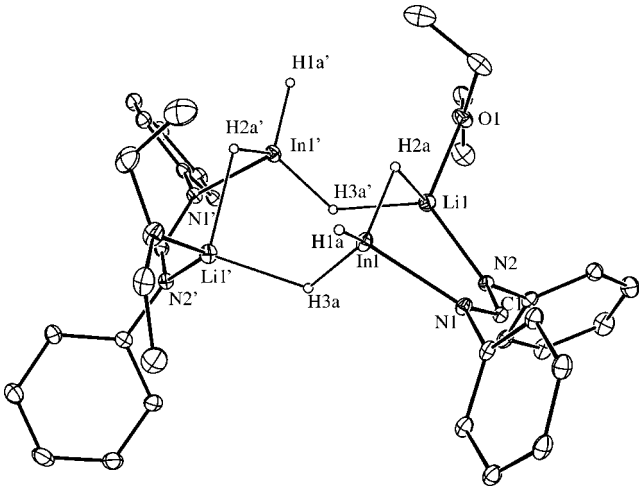


Figure 2. Molecular structure of **2** (isopropyl groups omitted for clarity). Selected bond lengths [Å] and angles [°]: In(1)-N(1) 2.178(3), In(1)-H(1a) 1.64(4), In(1)-H(2a) 1.71(4), In(1)-H(3a) 1.66(4), Li(1)-H(2a) 2.14(5), Li(1)-H(3a′) 2.10(5), N(2)-Li(1) 2.002(6), N(1)–C(1) 1.329(4), N(2)–C(1) 1.308(4); N(1)-In(1)-H(1a) 106.9(15), N(1)-In(1)-H(2a) 99.7(15), N(1)-In(1)-H(3a) 104.8(13), H(1a)-In(1)-H(2a) 114.6(19), H(1a)-In(1)-H(3a) 115.3(19), H(2a)-In(1)-H(3a) 113(2), In(1)-H(2a)-Li(1) 106(2), Li(1′)-H(3a)-In(1) 124(2), N(1)-C(1)-N(2) 124.8(3). Symmetry transformation: ′ $-x, y, -z+1/2$.

ring, which adopts what could be described as a boat conformation with the intramolecular hydride bridges, H(2) and H(2′), *cis* to each other. It is noteworthy that the gallium analogue, **3**, has a similar structure[13,16] though these hydride bridges are *trans*, thus giving a pseudochair conformation to the corresponding $\{Li_2Ga_2H_4\}$ ring. There is no difference in the bridging and terminal In–H bond lengths, within experimental error, as is the case for both crystallographically independent Li–H bonds. Not surprisingly, the bridging formamidinate ligand backbones in **2** are more open [N(1)-C(1)-N(2) 124.8(3)°] and significantly more localized than the chelating ligands in **1** [N-C-N, 116.3° av].

In summary, we have prepared and structurally characterized the first examples of amido indium hydride complexes, one of which, **1**, has unprecedented thermal stability. We believe this arises largely from steric shielding of the In–H fragment, which not only protects it from chemical attack but also circumvents the formation of M-H-M bridges, a proposed pathway to Group 13 hydride decomposition. We are currently examining the preparation and reactivity of other amidinate Group 13 hydride complexes. In addition, the characteristics of bulky amidinates may lend them to the eventual stabilization of thallium hydride complexes, a goal we are pursuing.

Experimental Section

1: A solution of HFiso (1.03 g, 2.82 mmol) in Et_2O (40 cm^3) was added over 5 min to an in situ generated solution of $LiInH_4$ (1.41 mmol) in Et_2O (50 cm^3) at −78 °C. The resultant suspension was warmed to 25 °C, concentrated to about 35 cm^3 and filtered. Slow cooling of the filtrate to −35 °C yielded colorless crystals of **1** (0.34 g, 29 %); m.p.: 160–170 °C (decomp); ^{1}H NMR (250 MHz, C_6D_6, 298 K): $\delta = 1.18$ (d, 24 H, ^3J(H,H) = 6.7 Hz, CH_3), 1.26 (d, 24 H, ^3J(H,H) = 6.7 Hz, CH_3), 3.55 (sept, 8 H, ^3J(H,H) = 6.7 Hz, CH), 7.22–7.35 (m, 12 H, Ar-H), 7.77 ppm (s, 2 H, NC(H)N); ^{13}C{^{1}H} NMR (250 MHz, C_6D_6, 298 K): $\delta = 23.7$ (CH_3), 24.4 (CH_3), 28.5 (CH), 123.6 (*p*-ArC), 125.4 (*m*-ArC), 140.9 (*o*-ArC), 143.7 (*ipso*-ArC), 164.3 ppm (NCN); IR (Nujol): $\tilde{\nu}$ = 1748 cm^{-1} (s, In-H); MS/APCI *m*/*z* (%): 366 [HFiso]$^+$ (100), 844 [*M*H]$^+$ (18); Elemental analysis cald (%) for $C_{50}H_{71}InN_4$: C 71.24, H 8.49, N 6.64 %; found: C 71.12, H 8.57, N 6.94 %.

2: A solution of HFiso (0.51 g, 1.41 mmol) in Et_2O (20 cm^3) was added to an in situ generated solution of $LiInH_4$ (1.41 mmol) in Et_2O (50 cm^3) at −78 °C over 5 min. The resultant suspension was warmed to −20 °C whereupon the volatile products were removed in vacuo. The residue was extracted into hexane (20 cm^3) and the extract cooled to −35 °C yielding colorless crystals of **2** (0.43 g, 27 %); m.p.: 42–44 °C (decomp); ^{1}H NMR (300 MHz, [D_8]toluene, 243 K): $\delta = 0.79$ (br, 12 H, OCH_2CH_3), 1.21–1.46 (br overlapping m, 48 H, CH_3), 2.91 (br, 8 H, OCH_2), 3.54 (br, 4 H, CH), 3.72 (br, 4 H, CH), 6.02 (br, 6 H, InH), 7.10–7.25 (br, 12 H, Ar-H), 7.29 ppm (br, 2 H, NC(H)N); ^{13}C{^{1}H} NMR (300 MHz, [D_8]toluene, 243 K): $\delta = 14.3$ (OCH_2CH_3), 23.5 (CH_3), 25.2 (CH_3), 28.1 (CH_3), 32.1 (CH), 34.6 (CH), 65.2 (OCH_2), 123.6 (*p*-ArC), 124.2 (*m*-ArC), 143.0 (*o*-ArC), 147.4 (*ipso*-ArC), 167.9 ppm (NCN), all signals broad; ^{7}Li{^{1}H} NMR (300 MHz, [D_8]toluene, 243 K): $\delta = 1.45$; ^{6}Li{^{1}H} NMR (300 MHz, [D_8]toluene, 243 K): $\delta = 1.51$ ppm; IR (Nujol): $\tilde{\nu} = 1719$ cm^{-1} (s, terminal In-H), 1632 (br s, bridging In-H); MSAPCI *m*/*z* (%): 366 [HFiso]$^+$ (100). The thermal instability of **2** precluded its elemental analysis.

Received: April 13, 2004 [Z460304]

Keywords: amides · gallium · hydrides · indium · structure elucidation

[1] for example, a) *Chemistry of Aluminium, Gallium, Indium and Thallium* (Ed.: A. J. Downs), Blackie Academic, Glasgow, **1993**, b) M. G. Gardiner, C. L. Raston, *Coord. Chem. Rev.* **1997**, *166*, 1–34, c) J. A. Jegier, W. L. Gladfelter, *Coord. Chem. Rev.* **2000**, *206–207*, 631–650, and references therein.
[2] a) A. J. Downs, C. R. Pulham, *Chem. Soc. Rev.* **1994**, 175–184, b) S. Aldridge, A. J. Downs, *Chem. Rev.* **2001**, *101*, 3305–3365.
[3] L. Andrews, X. Wang, *Angew. Chem.* **2004**, *116*, 1738–1741; *Angew. Chem. Int. Ed.* **2004**, *43*, 1706–1709; .
[4] C. Jones, *Chem. Commun.* **2001**, 2293–2298, and references therein.
[5] C. D. Abernethy, M. L. Cole, C. Jones, *Organometallics* **2000**, *19*, 4852–4857.
[6] R. J. Baker, C. Jones, M. Kloth, J. A. Platts, *Angew. Chem.* **2003**, *115*, 2764–2767; *Angew. Chem. Int. Ed.* **2003**, *42*, 2660–2663.
[7] For example, a) I. Shibata, H. Kato, T. Ishida, M. Yasuda, A. Baba, *Angew. Chem.* **2004**, *116*, 729–732; *Angew. Chem. Int. Ed.* **2004**, *43*, 711–714; b) C. D. Abernethy, M. L. Cole, A. J. Davies, C. Jones, *Tetrahedron Lett.* **2000**, *41*, 7567–7570, and references therein.
[8] For example, a) H. Zhu, J. Chai, H. W. Roesky, M. Noltemeyer, H.-G. Schmidt, D. Vidovic, J. Magull, *Eur. J. Inorg. Chem.* **2003**, 3113–3119; b) B. Luo, V. G. Young, W. L. Gladfelter, *Inorg. Chem.* **2000**, *39*, 1705–1709, and references therein.
[9] H.-J. Himmel, A. J. Downs, T. M. Greene, *J. Am. Chem. Soc.* **2000**, *122*, 9793–9807.
[10] For example, a) S. Dagorne, I. A. Guzei, M. P. Coles, R. F. Jordan, *J. Am. Chem. Soc.* **2000**, *122*, 274–289; b) J. A. R. Schmidt, J. Arnold, *Organometallics*, **2002**, *21*, 2306–2313; c) D. Abeysekera, K. N. Robertson, T. S. Cameron, J. A. C. Clyburne, *Organometallics* **2001**, *20*, 5532–5536, and references therein.
[11] M. L. Cole, P. C. Junk, *J. Organomet. Chem.* **2003**, *666*, 55–62.
[12] M. L. Cole, C. Jones, P. C. Junk, M. Kloth, unpublished results.

 © 2004 Wiley-VCH Verlag GmbH & Co. KGaA, Weinheim

[13] Crystal data for **1**: $C_{50}H_{71}InN_4$ $M_r = 842.93$, monoclinic, space group $P2_1/n$, $a = 14.774(3)$, $b = 16.317(3)$, $c = 20.936(4)$ Å, $\beta = 110.24(3)°$, $V = 4735.3(17)$ Å^3, $Z = 4$, $\rho_{calcd.} = 1.182$ g cm^{-3}, $F(000) = 1792$, $\mu(Mo_{K\alpha}) = 0.535$ mm^{-1}, 150(2) K, 9211 unique reflections [R_{int} 0.0707], R (on F) 0.0463, wR (on F^2) 0.1159 ($I > 2\sigma(I)$); **2**.$(Et_2O)_{0.5}$: $C_{60}H_{102}In_2Li_2N_4O_{2.5}$, $M = 1161.97$, monoclinic, space group $C2/c$, $a = 23.916(5)$, $b = 15.999(3)$, $c = 21.368(4)$ Å, $\beta = 111.49(3)°$, $V = 7608(3)$ Å^3, $Z = 4$, $\rho_{calcd.} = 1.014$ g cm^{-3}, $F(000) = 2452$, $\mu(Mo_{K\alpha}) = 0.640$ mm^{-1}, 150(2) K, 8676 unique reflections [R_{int} 0.0679], R (on F) 0.0474, wR (on F^2) 0.1234 ($I > 2\sigma(I)$); **3**: $C_{58}H_{96}Ga_2Li_2N_4O_2$ $M = 1034.71$, triclinic, space group $P\bar{1}$, $a = 11.103(2)$, $b = 13.166(3)$, $c = 21.211(4)$ Å, $\alpha = 92.95(3)$, $\beta = 91.12(3)$, $\gamma = 93.83(3)°$, $V = 3088.8(11)$ Å^3, $Z = 2$, $\rho_{calcd.} = 1.113$ g cm^{-3}, $F(000) = 1112$, $\mu(Mo_{K\alpha}) = 0.911$ mm^{-1}, 150(2) K, 12440 unique reflections [R_{int} 0.0482], R (on F) 0.0434, wR (on F^2) 0.0950 ($I > 2\sigma(I)$). CCDC-235631–235633 (**1**–**3**) contain the supplementary crystallographic data for this paper. These data can be obtained free of charge via www.ccdc.cam.ac.uk/conts/retrieving.html (or from the Cambridge Crystallographic Data Centre, 12 Union Road, Cambridge CB21EZ, UK; fax: (+44) 1223-336-033; or deposit@ccdc.cam.ac.uk).

[14] Y. Zhou, D. S. Richeson, *Inorg. Chem.* **1996**, *35*, 2448–2451.

[15] R. Duchateau, A. Meetsma, J. H. Teuben, *Chem. Commun.* **1996**, 223–224.

[16] Selected spectroscopic and structural data for **3** have been submitted as Supporting Information.

BE ON THE BALL!



0186_0010_vi

The new free **WILEY-VCH Alerting Service** makes time-consuming random finds a thing of the past!

Register now for the free WILEY-VCH Alerting Service

Now you can be supplied per e-mail regularly with information tailored precisely to your needs and interests. Just fill out the registration form at *www.wiley-vch.de/home/pas* for e-mails with news on the latest WILEY-VCH publications in your field. Added benefit: general info on important developments and services at WILEY-VCH.

Be on the ball so you'll be in the know!

www.wiley-vch.de

 © 2004 Wiley-VCH Verlag GmbH & Co. KGaA, Weinheim

Cover Picture

Peng Wu, Alina K. Feldman, Anne K. Nugent, Craig J. Hawker,* Arnulf Scheel, Brigitte Voit, Jeffrey Pyun, Jean M. J. Fréchet, K. Barry Sharpless,* and Valery V. Fokin*



Structural diversity is possible in dendrimer syntheses based on the highly efficient construction of triazoles from functionalized azides and alkynes. In their Communication on page 3928 ff., V. V. Fokin et al. describe the application of this Cu^{I}-catalyzed transformation, which proceeds in near-quantitative yields even to the third and fourth generation.

Contents

Angewandte EarlyView

The following Communications are available online (in Wiley InterScience). You can find them, as well as forthcoming Reviews, Highlights, and Essays, at www.angewandte.org, under Early View.

I. Paterson, R. Britton, O. Delgado, A. Meyer, K. G. Poullennec:*
Total Synthesis and Configurational Assignment of (−)-Dictyostatin, a Microtubule-Stabilizing Macrolide of Marine Sponge Origin
DOI: 10.1002/anie.200460589
Published online: July 1, 2004

Y. Shin, J.-H. Fournier, Y. Fukui, A. M. Brückner, D. P. Curran:*
Total Synthesis of (−)-Dictyostatin: Confirmation of Relative and Absolute Configurations
DOI: 10.1002/anie.200460593
Published online: July 1, 2004

Articles judged by the referees or the editor as being either very important or very urgent are immediately edited, proof-read, and electronically published once the manuscript has arrived in the editorial office in its final form. As long as there is no page number available these articles should be cited in the following manner:

Author(s), *Angew. Chem. Int. Ed.*, online publication date, DOI.

News

H. B. Gray Receives Prestigious Awards ——— **3874**

Recognition for M. Jansen ——— **3874**

Distinctions for M. T. Reetz ——— **3874**

Books

Comprehensive Coordination Chemistry II ——— **3875**
Jon A. McCleverty, Thomas J. Meyer — *reviewed by K. Heinze*

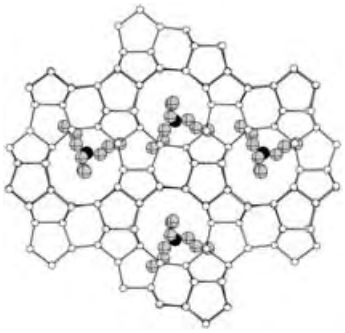
The Chemistry of Heterocycles ——— **3876**
Theophil Eicher, Siegfried Hauptmann — *reviewed by A. Nadin*

Highlights

Porous Materials

J. Patarin* ——— **3878 – 3880**

Mild Methods for Removing Organic Templates from Inorganic Host Materials



Getting the guests to leave without destroying them and potentially damaging the templated inorganic host (see structure) is crucial to the preparation of completely porous materials. Alternatives to calcining, such as extraction and chemical cleavage of the template, are being developed.

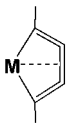
Minireviews

Metallacycles

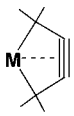
U. Rosenthal* ——— **3882 – 3887**

Stable Cyclopentynes—Made by Metals!?

The rather exotic and uncommon structures formed by the complexation of zirconocene fragments with butadiynes and butatrienes were described to be five-membered zirconacyclocumulenes **A** and zirconacyclopentynes **B**—made by metals! Nevertheless, the description of these interesting molecules by theoretical calculations becomes much more complicated by resonance and internal interactions of the metals with the multiple bonds. This leads to the question: Really made by metals?



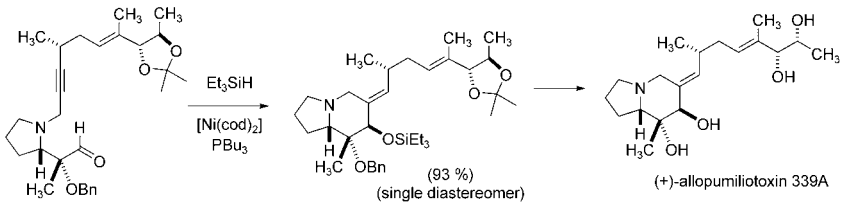
A



B

© 2004 Wiley-VCH Verlag GmbH & Co. KGaA, Weinheim

Reviews



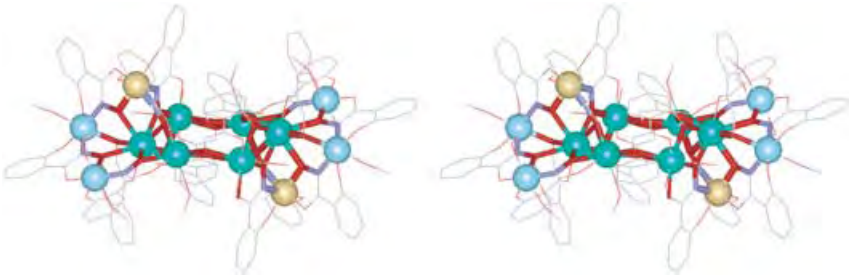
New opportunities: Nickel catalysis opens the door for a broad array of multicomponent coupling processes. Fundamentally new entries to useful building blocks are allowed, and complex molecule syntheses may be designed using the new processes. An example is the total synthesis of (+)-allopumiliotoxin 339A (see scheme; cod = 1,5-cyclooctadiene).

Multicomponent Coupling Reactions

J. Montgomery* _____ 3890 – 3908

Nickel-Catalyzed Reductive Cyclizations and Couplings

Communications

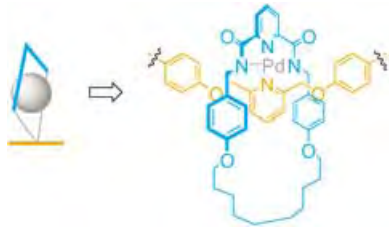


The largest known Dy–Mn complex is $[Dy^{III}_6Mn^{III}_4Mn^{IV}_2(H_2shi)_4(Hshi)_2(shi)_{10}]$ (H_3shi is salicylhydroxamic acid; see stereopicture). The Dy ions are arranged in a nearly planar hexagonal ring and are capped on opposite sides by a $Mn^{III}_2Mn^{IV}$ trimer. This mixed-metal topology provides a new structure class for the examination of interesting magnetic phenomena of individual molecules.

Single-Molecule Magnets

C. M. Zaleski, E. C. Depperman, J. W. Kampf, M. L. Kirk,* V. L. Pecoraro* _____ 3912 – 3914

Synthesis, Structure, and Magnetic Properties of a Large Lanthanide–Transition-Metal Single-Molecule Magnet



One step beyond: The synthesis of a three-dimensional interlocked molecular architecture (a rotaxane) from a two-dimensional square-planar metal template (see scheme) has been achieved. A combination of steric and electronic factors direct the synthesis in the third dimension, either by promoting or preventing interlocking.

Rotaxane Synthesis

A.-M. Fuller, D. A. Leigh,* P. J. Lusby, I. D. H. Oswald, S. Parsons, D. B. Walker _____ 3914 – 3918

A 3D Interlocked Structure from a 2D Template: Structural Requirements for the Assembly of a Square-Planar Metal-Coordinated [2]Rotaxane

For the USA and Canada:
ANGEWANDTE CHEMIE International Edition (ISSN 1433-7851) is published weekly by Wiley-VCH PO Box 191161, D 69451 Weinheim, Germany. Air freight and mailing in the USA by Publications Expediting Inc. 200 Meacham Ave., Elmont, NY 11003. Periodicals postage paid at Jamaica NY 11431. US POSTMASTER: send address changes to *Angewandte Chemie*, Wiley-VCH, 111 River Street, Hoboken, NJ 07030. Annual subscription price for institutions: Europe € 3430.00/3118.00; outside Europe US$ 4499.00/4090.00 (valid for print and electronic/print or electronic delivery); for individuals who are personal members of a national chemical society, or whose institution already subscribes, or who are retired or self-employed consultants, print only: Europe € 248.00/outside Europe US$ 378.00. Postage and handling charges included. All Wiley-VCH prices are exclusive VAT.

 © 2004 Wiley-VCH Verlag GmbH & Co. KGaA, Weinheim

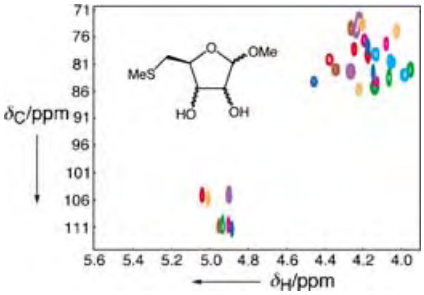
Contents

Cell-Wall Glycolipids

W. B. Turnbull, K. H. Shimizu, D. Chatterjee, S. W. Homans, A. Treumann* ——— **3918 – 3922**

Identification of the 5-Methylthiopentosyl Substituent in *Mycobacterium tuberculosis* Lipoarabinomannan

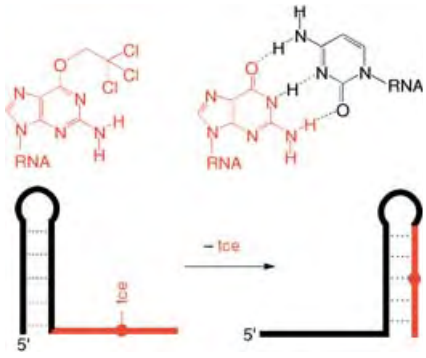
An unexpected configuration of a novel carbohydrate structure in the cell wall of *Mycobacterium tuberculosis* was revealed by synthesizing the isomers of 5-deoxy-5-methylthio-D-pentofuranose as α- and β-methyl glycosides and analyzing their NMR spectra (see picture). Cell-wall glycolipids are crucial factors for the pathogenesis of infectious diseases, and the results presented might open new research avenues into host–pathogen interactions.



RNA Structural Rearrangements

C. Höbartner, H. Mittendorfer, K. Breuker, R. Micura* ——— **3922 – 3925**

Triggering of RNA Secondary Structures by a Functionalized Nucleobase

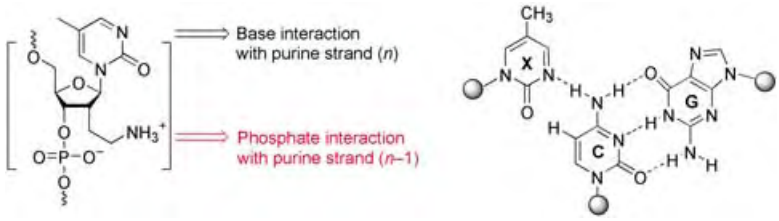


Rearranging RNA: Defined RNA secondary-structure rearrangements can be controlled by chemically functionalized nucleobases. The proof of principle for this previously unrecognized concept for manipulating secondary structures is based on a novel type of functionalized guanosine residue that provides an easily cleavable trichloroethyl (tce) moiety at the Watson–Crick base-pairing site (see scheme).

DNA Recognition

S. Buchini, C. J. Leumann* ——— **3925 – 3928**

Stable and Selective Recognition of Three Base Pairs in the Parallel Triple-Helical DNA Binding Motif



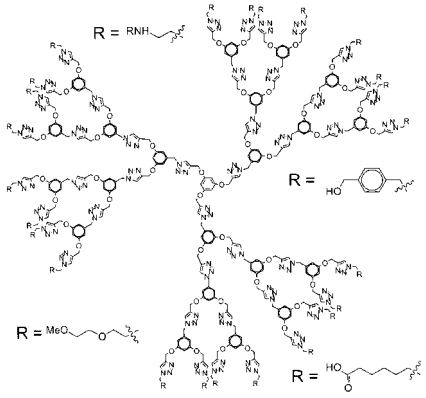
Modifying bases in parallel-triplex-forming oligonucleotides with a 2′-*O*-aminoethyl backbone enabled an extended DNA triplex recognition code to be developed for use in the control of gene expression. Removal of the oxygen atom at C4 of thymine transforms a donor/acceptor base into a double acceptor base and redirects recognition from A–T to strong and highly selective C–G recognition (see scheme).

VIP

Dendrimers

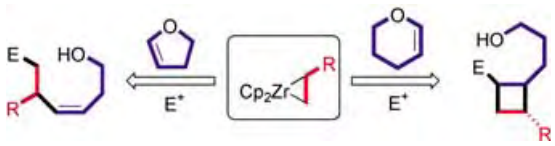
P. Wu, A. K. Feldman, A. K. Nugent, C. J. Hawker,* A. Scheel, B. Voit, J. Pyun, J. M. J. Fréchet, K. B. Sharpless,* V. V. Fokin* ——— **3928 – 3932**

Efficiency and Fidelity in a Click-Chemistry Route to Triazole Dendrimers by the Copper(I)-Catalyzed Ligation of Azides and Alkynes



Components that click: A large number of diverse dendrimers (see scheme) was prepared in almost quantitative yield by the click-chemistry transformation described in the title. In some cases filtration or solvent extraction was the only method required for purification in this highly efficient construction of the triazole units of the dendrimers.

 © 2004 Wiley-VCH Verlag GmbH & Co. KGaA, Weinheim

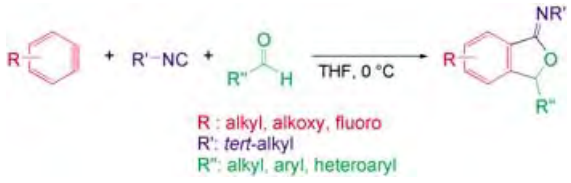


Unexpected results are obtained on treatment of alkene–zirconocene complexes with cyclic enol ethers. The ring size of the enol ether makes the reaction proceed through different mechanisms allowing *Z* alkenols to be prepared from furan derivatives and cyclobutanes from pyran derivatives (see scheme).

Synthetic Methods

J. Barluenga,* L. Álvarez-Rodrigo, F. Rodríguez, F. J. Fañanás _ **3932 – 3935**

Reaction of Alkene–Zirconocene Complexes and Cyclic Enol Ethers through New Reaction Pathways

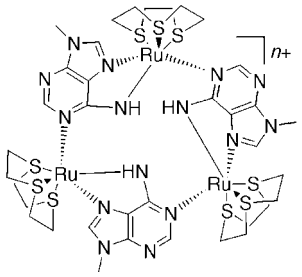


Mix the components, stir, and ... voilà! A variety of benzoannulated iminofurans can be obtained in this straightforward manner from an aryne, an isocyanide, and an aldehyde in modest to high yields (see scheme). Perfect regioselectivity was observed with a 3-substituted aryne and 4-fluorobenzyne, whereas 4-methylbenzyne gave a mixture of regioisomers.

Multicomponent Reactions

H. Yoshida,* H. Fukushima, J. Ohshita, A. Kunai* _____ **3935 – 3938**

Arynes in a Three-Component Coupling Reaction: Straightforward Synthesis of Benzoannulated Iminofurans



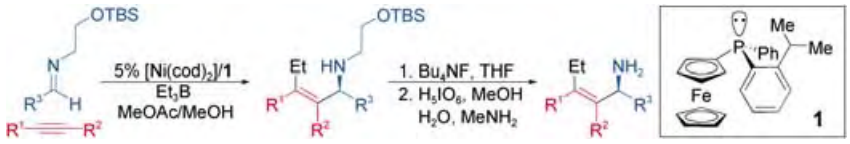
1: $n = 3$–6

A valence-mixing bowl: A kinetically locked, trinuclear Ru^{II} metallamacrocycle **1** has been synthesized (see picture). Electrochemical and photophysical studies reveal that this complex undergoes three separate, fully reversible oxidations. Of the four accessible redox states, two are mixed-valence (one of which is valence-localized, whereas the other is valence-delocalized).

Metallamacrocycles

N. Shan, S. J. Vickers, H. Adams, M. D. Ward, J. A. Thomas* _ **3938 – 3941**

Switchable Electron-Transfer Processes in a Mixed-Valence, Kinetically Locked, Trinuclear Ru^{II} Metallamacrocycle



The aryl substituent on the catalyst is central to the success of the title reaction (see scheme) which affords allylic amines in up to 89% *ee* and 91% yield with a catalyst derived from $[Ni(cod)_2]$ and a P-chiral ferrocenyl phosphane (e.g. **1**). The coupling products are easily deprotected to enantiomerically enriched, tetrasubstituted primary allylic amines, which can be recrystallized to optical purity.

Imine Chemistry

S. J. Patel, T. F. Jamison* ___ **3941 – 3944**

Asymmetric Catalytic Coupling of Organoboranes, Alkynes, and Imines with a Removable (Trialkylsilyloxy)ethyl Group—Direct Access to Enantiomerically Pure Primary Allylic Amines

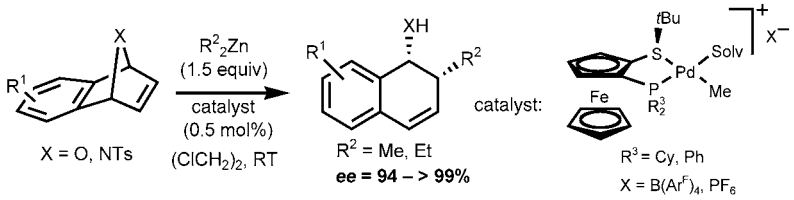
 © 2004 Wiley-VCH Verlag GmbH & Co. KGaA, Weinheim

Contents

Ring-Opening Catalysts

S. Cabrera, R. Gómez Arrayás, J. C. Carretero* ——— 3944 – 3947

Cationic Planar Chiral Palladium P,S Complexes as Highly Efficient Catalysts in the Enantioselective Ring Opening of Oxa- and Azabicyclic Alkenes



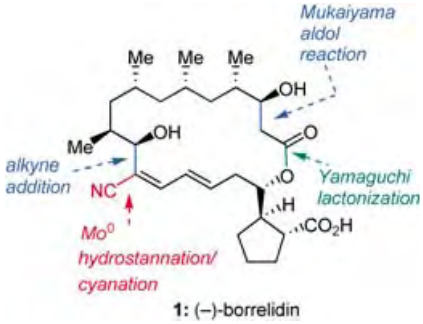
Open plan: Cationic methylpalladium(II) complexes of planar chiral Fesulphos ligands (Fesulphos = 1-phosphanyl-2-sulfenylferrocene) show excellent performance in the alkylative ring opening of oxa- and azabicyclic alkenes with dialkyl zinc reagents (see scheme, Cy = cyclohexyl, Ar^F = 3,5-bis(trifluoromethyl)phenyl). Catalyst loadings as low as 0.5 mol% are normally sufficient to achieve high enantioselectivities (94–>99% *ee*).

Natural Product Synthesis

B. G. Vong, S. H. Kim, S. Abraham, E. A. Theodorakis* ——— 3947 – 3951

Stereoselective Total Synthesis of (−)-Borrelidin

A convergent synthesis of (−)-borrelidin (**1**) is reported based on the retrosynthetic disconnections indicated in the picture. Highlights of the strategy include the construction of a strained enynone-containing macrolide and the installation of a cyano group in a regioselective manner by a novel molybdenum-catalyzed hydrostannation of the alkyne.

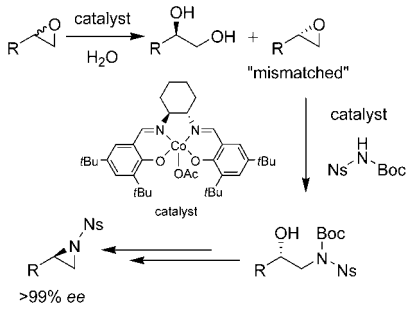


Asymmetric Catalysis

S. K. Kim, E. N. Jacobsen* ——— 3952 – 3954

General Catalytic Synthesis of Highly Enantiomerically Enriched Terminal Aziridines from Racemic Epoxides

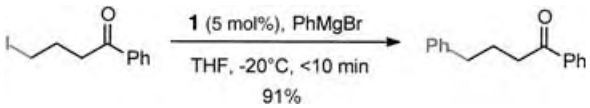
If life deals you a lemon ...: Low selectivity in the [Co(salen)]-catalyzed kinetic resolution of terminal epoxides with *N*-Boc sulfonamides is parlayed into an efficient one-pot synthesis of enantiopure amino alcohol derivatives. This provides the foundation for a general route to the title compounds (see scheme; Boc = *tert*-butoxycarbonyl; Ns = 2-nitrobenzenesulfonyl).



Reversal of Reactivity

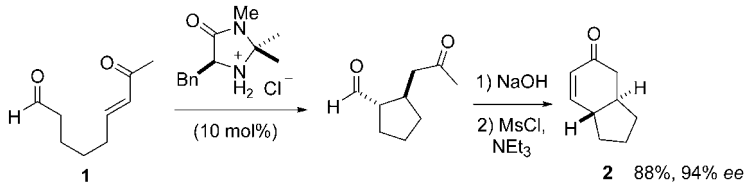
R. Martin, A. Fürstner* ——— 3955 – 3957

Cross-Coupling of Alkyl Halides with Aryl Grignard Reagents Catalyzed by a Low-Valent Iron Complex



A striking reversal of the usual reactivity pattern of aryl Grignard reagents is observed for reactions in the presence of catalytic amounts of the "bare" ferrate complex $[Li(tmeda)]_2[Fe(C_2H_4)_4]$ (**1**). Highly reduced iron–magnesium clusters may play a decisive role in the exceptionally facile and chemoselective cross-coupling reaction with alkyl halides (see scheme).

 © 2004 Wiley-VCH Verlag GmbH & Co. KGaA, Weinheim



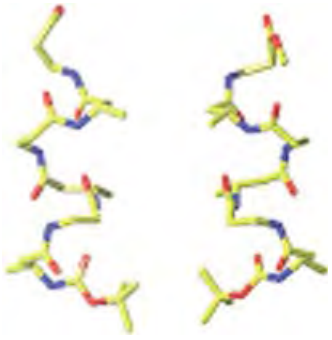
Efficient organocatalysis of the intramolecular Michael reaction of formyl enones, such as **1**, by an imidazolidinone catalyst leads to the corresponding ketoaldehydes in excellent yields and with high enantioselectivities (see scheme). This reaction can be included as part of a tandem process, as the ketoaldehyde products undergo aldolization readily to give hydrindenones, such as **2**. Bn = benzyl, Ms = methanesulfonyl.

Asymmetric Catalysis

M. T. Hechavarria Fonseca, B. List* ——— 3958 – 3960

Catalytic Asymmetric Intramolecular Michael Reaction of Aldehydes

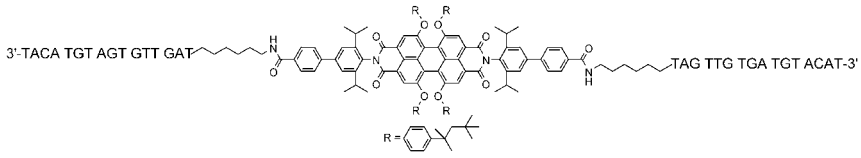
Ambidextrous peptides: Novel mixed β-peptides were synthesized from alternating C-linked carbo-β^3-amino acid and β-homoglycine residues. The peptides form unprecedented left-handed 10/12 and 12/10 helices (see picture) in addition to the corresponding right-handed helices.



Peptide Structures

G. V. M. Sharma,* K. R. Reddy, P. R. Krishna, A. R. Sankar, P. Jayaprakash, B. Jagannadh,* A. C. Kunwar* ——— 3961 – 3965

Left-Handed Helical Twists in "Mixed β-Peptides" Derived From Alternating C-Linked Carbo-β^3-Amino Acids and β-hGly Units

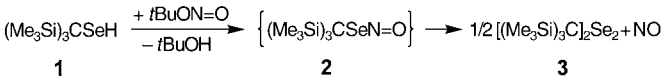


DNA–dye polymer: Two complementary perylenediimide–bis(oligonucleotide) conjugates (see picture) were synthesized that are soluble in water and can be transferred into nonpolar solvents, such as *n*-decane, by means of detergents. Self-assembled DNA–dye polymers formed when solutions of these conjugates are mixed.

DNA–Dye Conjugates

M. A. Abdalla, J. Bayer, J. O. Rädler,* K. Müllen* ——— 3967 – 3970

Synthesis and Self-Assembly of Perylenediimide–Oligonucleotide Conjugates



The nitrosation of selenol 1 with an alkyl nitrite (see scheme) at −78 °C generated the first *Se*-nitrososelenol **2**, which was identified by IR spectroscopy and further proven by its 1,4-addition to dimethylbutadiene. Compound **2** decomposes rapidly to give **3**. The experiments may give insight into the interactions of selenoproteins with NO in vivo.

Bioinorganic Chemistry

C. Wismach, W.-W. du Mont,* P. G. Jones, L. Ernst, U. Papke, G. Mugesh, W. Kaim, M. Wanner, K. D. Becker ——— 3970 – 3974

Selenol Nitrosation and *Se*-Nitrososelenol Homolysis: A Reaction Path with Possible Biochemical Implications

 © 2004 Wiley-VCH Verlag GmbH & Co. KGaA, Weinheim

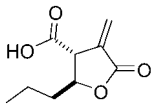
Contents

Epigenetics

M. Biel, A. Kretsovali,* E. Karatzali, J. Papamatheakis, A. Giannis* _____ **3974 – 3976**

Design, Synthesis, and Biological Evaluation of a Small-Molecule Inhibitor of the Histone Acetyltransferase Gcn5

HATs off! The development of the first cell-permeable small-molecule inhibitor of the human histone acetyltransferase (HAT) Gcn5 opens up new possibilities for understanding the histone code. Based on kinetic data and the proposed mechanism of the acetylation by Gcn5,



the relatively simple butyrolactone structure of the inhibitor was identified.

VIP Communications labeled with this symbol have been judged by two referees as being "very important papers".

The issues for July 2004 appeared online on the following dates
Issue 25: June 16. · Issue 26: June 22. · Issue 27: June 29. · Issue 28: July 16

Deadline for recruitment adverts

35/2004	August 20	Publication date:	September 6
36/2004	August 27	Publication date:	September 13

Angewandte Chemie International Edition
Advertising Sales Department:
Marion Schulz
Phone: 0 62 01 – 60 65 65
Fax: 0 62 01 – 60 65 50
E-Mail: MSchulz@wiley-vch.de

Place an advert in the printed version and have it made available online for 1 month, free of charge!

Service

Keywords _____ *3978*

Authors _____ *3979*

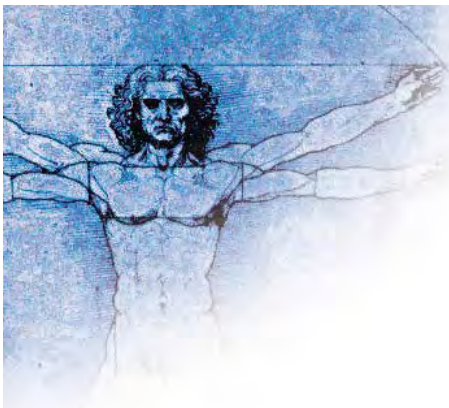
Preview _____ *3981*

Corrigendum

In the Communication "Homolytic C_α–C_β Bond Cleavage in a Chiral Alkylarene Radical Cation: Effects of Asymmetric Microsolvation" by M. Speranza et al. (*Angew. Chem. Int. Ed.* **2004**, *43*, 1868–1871 [DOI: 10.1002/anie.200353462]) on page 1870, second paragraph, the sentences "In particular, the heterochiral complex exhibits shorter O–H···O–H and O–H···α hydrogen-bond distances than the homochiral adduct. This implies that BD_{SS} is a better H-bond acceptor than BD_{RR} when associated with the chiral $(BZC_2H_5)_R$ moiety." should be replaced by "In particular, the homochiral complex exhibits a shorter O–H···O–H distance (2.006 Å) than the heterochiral adduct (2.021 Å). This implies that BD_{RR} is a better H-bond acceptor than BD_{SS} when associated with the chiral $(BZC_2H_5)_R$ moiety."

On page 1871, first paragraph, the last sentence "This difference may be attributed to structural factors that make solv in the former adduct a better H-bond acceptor than in the latter, although other hypotheses, such as that involving the interaction of the solvent molecule with the C_α center of $[(BZC_2H_5)_R]^+$ cannot be excluded." should be replaced by "This difference may be attributed to structural factors that make solv in the latter adduct a better H-bond acceptor than in the former, although other hypotheses, such as that involving the interaction of the solvent molecule with the C_α center of $[(BZC_2H_5)_R]^+$ cannot be excluded."

In the Table of Contents, the sentence "The difference is ascribed to structural factors that make BD_{SS} a better H-bond acceptor than BD_{RR} in their adducts with $[(BZC_2H_5)_R]^+$." should be replaced by "The difference is ascribed to structural factors that make BD_{RR} a better H-bond acceptor than BD_{SS} in their adducts with $[(BZC_2H_5)_R]^+$."



H. B. Gray Receives Prestigious Awards

The two distinctions recently bestowed on Harry B. Gray (California Institute of Technology, Pasadena) are regarded as the "Nobel Prizes" of the countries concerned: the Benjamin Franklin Medal (USA) and the Wolf Prize (Israel). The prizes are awarded annually in several categories and presented at the Franklin Institute (Philadelphia) and the Knesset (Israeli parliament), respectively. Gray has been honored for his work in the field of bioinorganic chemistry. The focus of his research is electron transfer in (metallo)proteins (Fe, Mg). The fact that synthetic work is also involved in these studies is shown in a recent publication in *Angewandte Chemie* on high-valent manganese complexes with corrole ligands and a review on metallocorrole-catalyzed oxidations.[1]



H. B. Gray

After completing his PhD in 1960 at Northwestern University near Chicago (USA) under the supervision of F. Basolo and R. Pearson, Gray carried out postdoctoral research in Copenhagen (Denmark) with C. Ballhausen. At that time his research focused on ligand-field theory. After a few years at Columbia University in New York (USA), he became interested in bioinorganic chemistry in 1966 at the California Institute of Technology, where he currently holds the Arnold O. Beckman Chair of Chemistry.

Recognition for M. Jansen

Martin Jansen (Max-Planck-Institut für Festkörperforschung, Stuttgart, Germany) has received several distinctions for his work in the field of solid-state chemistry and materials research: He is the recipient of the Science Prize of the Stifterverband der Deutschen Wissenschaft (German Donors' Association for the Promotion of the Sciences and the Humanities) for his studies on amorphous high-performance ceramics. This prize is awarded annually based on the recommendation of the Max-Planck-Gesellschaft and is worth € 50000. Jansen also gave the C. N. R. Rao Lecture at the conference "Emerging Directions in Chemical Sciences" in Bangalore (India) to honor the 70th birthday of C. N. R. Rao, and the Egon Wiberg Lecture at Ludwig-Maximilians-Universität (München, Germany). The topic of the latter, planning syntheses in solid-state chemistry, was also the topic of his recent Review in *Angewandte Chemie*.[2]



M. Jansen

Jansen studied chemistry and completed his PhD in 1973 with R. Hoppe at the Universität Giessen (Germany), where he went on to complete his habilitation. He took up a position at the Universität Hannover in 1981 and moved to the Universität Bonn in 1987. In 1998 he left Bonn to become director of the Max-Planck-Institut in Stuttgart. His work has been recognized by a number of awards, including the Leibniz Prize (German Research Foundation), the Otto Bayer Prize (Bayer AG), and the Alfred Stock Memorial Prize (Gesellschaft Deutscher Chemiker). Martin Jansen has been a member of the Editorial Board of *Angewandte Chemie* since 2001.

Distinctions for M. T. Reetz

Manfred T. Reetz (Max-Planck-Institut für Kohlenforschung, Mülheim/Ruhr, Germany) has also been honored with several awards. The Technische Universität Braunschweig and the Gesellschaft für Biotechnologische Forschung (German Research Centre for Biotechnology) awarded him the Hans Herloff Inhoffen Prize, which is cofunded by Schering AG and which was presented within the context of the Inhoffen Lecture. He has been recognized for his work on enantioselective enzyme catalysis. The required enzymes were obtained through the mutation of *Pseudomonas* bacteria. He also gave the Novartis Chemistry Lecture in Basel (Switzerland), Vienna (Austria), and Horsham (Sussex, UK), and the Bruno Wedelmann Lecture at the Universität Duisburg–Essen (Germany). Besides "evolution in the test tube", chiral ligands for asymmetric transition-metal catalysis and supramolecular transition-metal catalysis are focus areas of his research. He recently presented "Combinatorial and Evolution-Based Methods in the Creation of Enantioselective Catalysts" in a Review in *Angewandte Chemie*.[3]



M. T. Reetz

Reetz studied chemistry at Washington University in St. Louis (MO, USA) and at the University of Michigan in Ann Arbor (USA). He completed his PhD in 1969 under the guidance of U. Schöllkopf at the Universität Göttingen and his habilitation in 1974 with R. W. Hoffmann at the Universität Marburg, then took up positions first at the Universität Bonn, then at the Universität Marburg. In 1991 he moved to the Max-Planck-Institut für Kohlenforschung in Mülheim an der Ruhr, where he became director two years later. Manfred Reetz has been a member of the Editorial Board of *Angewandte Chemie* since 2002.

[1] a) G. Golubkov, J. Bendix, H. B. Gray, A. Mahammed, I. Goldberg, A. J. DiBilio, Z. Gross, *Angew. Chem.* **2001**, *113*, 2190; *Angew. Chem. Int. Ed.* **2001**, *40*, 2132; b) Z. Gross, H. B. Gray, *Adv. Synth. Catal.* **2004**, *346*, 165.

[2] M. Jansen, *Angew. Chem.* **2002**, *114*, 3896; *Angew. Chem. Int. Ed.* **2002**, *41*, 3746.

[3] M. T. Reetz, *Angew. Chem.* **2001**, *113*, 292; *Angew. Chem. Int. Ed.* **2001**, *40*, 284.

 © 2004 Wiley-VCH Verlag GmbH & Co. KGaA, Weinheim DOI: 10.1002/anie.200461115

Porous Materials

Mild Methods for Removing Organic Templates from Inorganic Host Materials

*Joël Patarin**

Keywords:
host–guest systems · solid-state structures · template removal · zeolites

Inorganic porous materials with controlled pore-size distribution are very attractive for a wide range of applications such as catalysis, adsorption, and separation.[1–3] Two main families have been reported: crystalline microporous solids and organized mesoporous materials.[4] In the former, zeolites and related materials (e.g., aluminophosphates and gallophosphates) are the most representative solids. The second family comprises the so-called M41S materials[5] and related solids (e.g., SBA type[6,7] and MSU type[8]). Most of these solids are prepared by hydrothermal or solvothermal treatment of an inorganic mixture in the presence of an organic template around which the inorganic framework forms. After synthesis, the resulting material is in fact a nonporous organic–inorganic hybrid since the organic agent is usually trapped in the cavities of the solid (Figure 1). Depending on the type of porous solid, different templating agents have been introduced in the starting mixtures: molecules such as amines, ammonium ions, or crown ethers for the preparation of crystalline microporous solids, and surfactants or more generally amphiphilic molecules for the synthesis of organized mesoporous solids. To obtain a completely porous solid, it is necessary to remove the organic species from the as-made material. The most common method consists of calcining the materials in a flow of oxygen or air. Under these conditions the template, which is the high-cost reactant, is destroyed. Such a procedure may also damage the porous material. Indeed during the calcination high local temperatures and water formation may occur, and therefore extra-framework species may be formed. This is the case for some aluminosilicates, for instance, where extra-framework aluminum species can be detected after removal of the template by calcination. The procedure can be optimized by first heating the sample under an inert atmosphere with a slow heating rate, and then introducing air or oxygen to remove the carbon residues. However, pore shrinkage is generally observed. One way to decrease the cost of synthesis of the porous inorganic materials is to develop methods for the nondestructive removal of the organic template, which would allow the recovery and reuse of these expensive organic species.

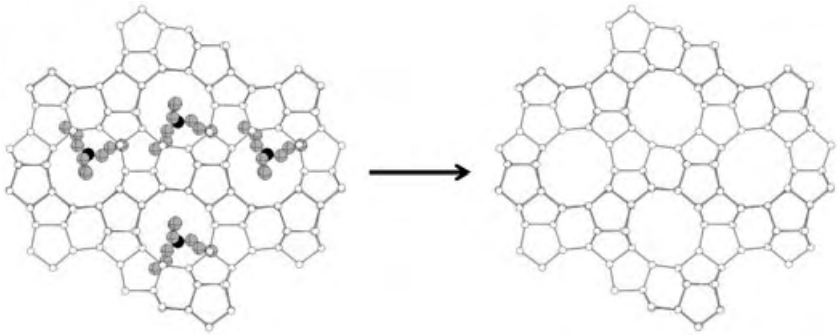


Figure 1. Removal of the organic template (black and gray spheres) from an as-made material to obtain a porous solid.

Such alternative methods have been developed in particular for mesoporous materials. In these solids, the framework–surfactant interactions are weak (electrostatic, van der Waals or hydrogen-bonding interactions), and the pore size is larger than that observed for microporous solids. Therefore, the extraction of the template can be carried out by mild treatments such as liquid extraction using acidic solutions, neutral salt solutions, alcohols, or mixture of these.[9,10] For instance, about 70% of the hexadecyltrimethylammonium ions used as templates in the synthesis of Al-MCM-41 could be removed by extraction with acidic ethanol ($EtOH/H_2SO_4$, 1 h, 78 °C, procedure repeated twice).[9] Under these acidic conditions, exchange of the sodium ions for protons is achieved simultaneously. For HMS-type materials prepared with nonionic surfactants, the removal of the template by solvent extraction is more effective, which is probably due to the fact that the framework–surfactant interactions are weaker.[10] Similar behavior was observed for the SBA-15 silica material prepared in the presence of a nonionic triblock copolymer.

In zeolites the removal of the template, which is also referred to as a

[*] Dr. J. Patarin
Laboratoire de Matériaux Minéraux
ENSCMu
Université de Haute-Alsace
UMR CNRS 7016
3 rue Alfred Werner
68093 Mulhouse Cedex (France)
Fax: (+33) 3-8933-6885
E-mail: j.patarin@uha.fr

 © 2004 Wiley-VCH Verlag GmbH & Co. KGaA, Weinheim DOI: 10.1002/anie.200301740

"structure-directing agent" (SDA), by solvent extraction is more difficult. Attempts were reported on MFI and BEA structure types by Jones et al.[11] For both molecular-sieve topologies, the amount of SDA that could be removed by extraction was found to be dependent on the size of the SDA and the strength of its interaction with the molecular-sieve framework. These authors showed that for different BEA-type materials (zincosilicate, aluminosilicate, and borosilicate) the ease of liberation of the organic template (tetraethylammonium ions (TEA)) is in the order Zn > B > Al and follows the reverse trend of the known Brønsted acidity of the various types of sites. However, in these materials, the SDA is only partly extracted. Moreover, for the boron-containing samples, in particular, solvent extraction (aqueous acetic acid, 80 °C) results in the removal of 60 % of the boron from the framework.[11] It is worth noting that under these experimental conditions complete removal of the TEA ions from a pure silica β-zeolite is possible.

Other mild procedures have been tested for the removal of organic species from mesoporous inorganic frameworks. Microwave-assisted template removal was performed on organized SBA-15 silica materials in the presence of nitric acid and H_2O_2 as solvents (0.1–0.2 g SBA-15, 1.5 mL of 15 M HNO_3, 1 mL of 9.3 M H_2O_2).[12] In this procedure the maximum temperature was close to 200 °C and the template (triblock copolymer, Pluronic P123, $EO_{20}PO_{70}EO_{20}$) can be removed completely within minutes. Compared to the ordinary calcined samples, these materials have more highly ordered frameworks with higher surface areas, larger pore volumes, lower structural shrinkage, and a higher silanol-group density. Such a procedure was also successfully applied to mesoporous films and macromesoporous membranes.

Extraction with supercritical CO_2 was used by Kawi et al.[13] and subsequently by van Grieken et al.[14] for removing organic templates from MCM-41 and SBA-15 silica materials, respectively. It appears that under similar experimental conditions no surfactant removal is observed for MCM-41 materials in the absence of alcohol as cosolvent, whereas the solvating strength of pure CO_2 is sufficient to extract the nonionic surfactant from the SBA-15 samples. However, the highest extraction efficiency was achieved in the presence of ethanol. According to Kawi et al.,[13] for a pure siliceous MCM-41 material, 93.2 % of the template (hexadecyltrimethylammonium ions) could be removed from the as-made solid after 3 h under the following experimental conditions: extraction temperature 85 °C, extraction pressure 350 bar, CO_2 flow rate of 1 mL min^{-1}, and methanol flow rate of 0.2 mL min^{-1}. This method allowed the recovery and reuse of organic templates.

Ozone treatments[15,16] have been used to eliminate the organic template from as-synthesized MCM-41 silica materials. In an initial study, ozone was generated by using a UV lamp (estimated temperature close to 250 °C) operating at a wavelength that created ozone from atmospheric oxygen, and in a second study, ozone was produced directly by an ozone generator. In the former study, after 24 h of treatment, complete removal of the organic species was observed (the ozone-treated sample showed 1 % weight loss by thermogravimetric analysis at 1000 °C). In the second study, the treatment was performed on dry samples and on as-made MCM-41 samples resuspended in water or in their mother liquors. The best results were obtained for the resuspended samples. Thus, after 14 h, 82 % of the organic species was removed from the ozone-treated sample in water. However, when the treatment time was too long (up to 26 h) the pore structure collapsed. Compared to the calcined samples, ozone-treated samples displayed higher surface areas, larger pore sizes, narrower pore-size distributions, and a higher silanol-group density.

Recently Schüth and co-workers[17] used ether cleavage by an acid to partly remove the triblock copolymer template (Pluronic P123) from an as-synthesized SBA-15 silica material. The SBA-15 material prepared at low temperature displays micropores and mesopores, and it was proposed that the poly(ethylene oxide) chains (EO) of the surfactant are occluded in the silica walls, whereas the more hydrophobic poly(propylene oxide) chains (PO) are located in the mesopores of the SBA-15 material.[18–20] The authors clearly showed that the ether cleavage by sulfuric acid at quite a low temperature (95 °C under reflux) generated mesopores by the removal of the PO groups. The EO chains, which are less accessible to the acid, could be decomposed by a subsequent thermal treatment in air at 200 °C to create micropores. Such acid and low-temperature treatments led to a SBA-15 material with better characteristics than those of the classical calcined SBA-15 material (larger mesopore size, larger micropore volume).

A similar approach was used by Lee et al. for removing the structure-directing agents in as-synthesized zeolites.[21] The strategy developed by these authors is summarized in Figure 2. It is based on an SDA that can be cleaved easily into fragments (A and B in Figure 2) without

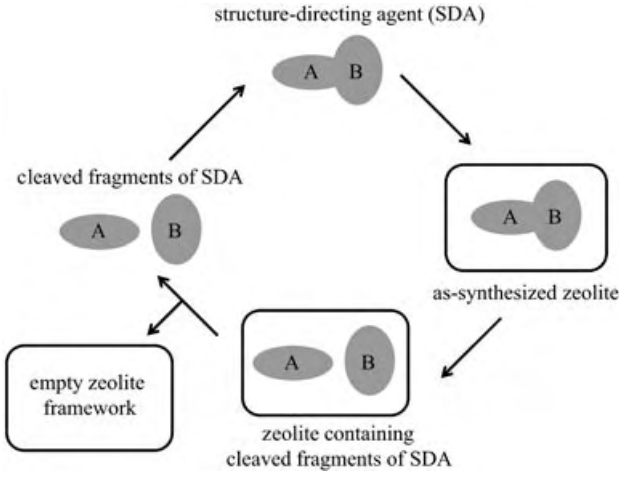


Figure 2. Strategy proposed by Lee et al. for synthesizing zeolites (figure adapted from ref. [21]).

 © 2004 Wiley-VCH Verlag GmbH & Co. KGaA, Weinheim

affecting the zeolite structure. The fragements are removed from the zeolite structure, and then recombined to regenerate the SDA.

This strategy was successfully applied to the synthesis of the zeolite ZSM-5. The SDA, a derivative of 1,4-dioxa-8-azaspiro[4,5]decane which contains a cyclic ketal, was found occluded intact in the as-synthesized zeolite. It was then cleaved into ethylene glycol and a ketone by treatment of the zeolite in acidic solution (HCl 1M, 80°C, 20 h). After this treatment the ketone was still present in the structure, and it was removed by a subsequent treatment with a NaOH/NaCl solution (100°C, 72 h). Under these conditions the structure of the empty zeolite was not affected. The two components of the SDA can then be recombined for a subsequent synthesis. This strategy was also applied to the synthesis of the zeolites ZSM-11 and ZSM-12 and might be extended to SDAs having acetals and ortho-ester functionalities.

In conclusion, numerous studies have been performed to remove the organic species from inorganic frameworks. For mesoporous organized materials, most of the mild routes developed allow the reuse of the organic templates for a subsequent synthesis and lead to an inorganic solid with better characteristics (higher surface area, larger pore volume, less structural shrinkage, and higher silanol-group density). For zeolites and related materials, the strategy proposed by Lee and coworkers[21] opens new perspectives in this field.

Published Online: July 7, 2004

[1] M. E. Davis, *Nature* **2002**, *417*, 813 – 821.
[2] Y. Wang, Y. Tang, A. Dong, X. Wang, N. Ren, W. Shan, Z. Gao, *Adv. Mater.* **2002**, *14*, 994 – 997.
[3] C. Marcilly in *Zeolites and Mesoporous Materials at the Dawn of the 21st Century*, *Vol. 135* (Eds.: A. Galarneau, F. Di Renzo, F. Fajula, J. Védrine), Elsevier, Amsterdam, **2001**, pp. 37 – 60.
[4] For recent advances on these solids see: *Handbook of Porous Solids*, *Vol. 1–5* (Eds.: F. Schüth, K. S. W. Sing, J. Weitkamp), Wiley-VCH, Weinheim, **2002**.
[5] C. T. Kresge, M. E. Leonowicz, W. J. Roth, J. C. Vartuli, J. S. Beck, *Nature* **1992**, *359*, 710 – 712.
[6] Q. Huo, D. I. Margolèse, U. Ciesla, D. G. Demuth, P. Feng, T. E. Gier, P. Sieger, A. Firouzi, B. F. Chmelka, F. Schüth, G. D. Stucky, *Chem. Mater.* **1994**, *6*,1176 – 1191.
[7] D. Zhao, J. Feng, Q. Huo, N. Melosh, G. H. Fredrickson, B. F. Chmeka, G. D. Stucky, *Science* **1998**, *279*, 548 – 552.
[8] S. A. Bagshaw, E. Prouzet, T. J. Pinnavaia, *Science* **1995**, *269*, 1242 – 1244.
[9] S. Hitz, R. Prins, *J. Catal.* **1997**, *168*, 194 – 206.
[10] P. T. Tanev, T. J. Pinnavaia, *Chem. Mater.* **1996**, *8*, 2068 – 2079.
[11] C. W. Jones, K. Tsuji, T. Takewaki, L. W. Beck, M. E. Davis, *Microporous Mesoporous Mater.* **2001**, *48*, 57 – 64.
[12] B. Tian, X. Liu, C. Yu, F. Gao, Q. Luo, S. Xie, B. Tu, D. Zhao, *Chem. Commun.* **2002**, 1186 – 1187.
[13] S. Kawi, M. W. Lai, *Chem. Commun.* **1998**, 1407 – 1408.
[14] R.van Grieken, G. Calleja, G. D. Stucky, J. A. Melero, R. A. Garcia, J. Iglesias, *Langmuir* **2003**, *19*, 3966 – 3973.
[15] M. T. J. Keene, R. Denoyel, P. L. Llewellyn, *Chem. Commun.* **1998**, 2203 – 2204.
[16] G. Büchel, R. Denoyel, P. L. Llewellyn, J. Rouquerol, *J. Mater. Chem.* **2001**, *11*, 589 – 593.
[17] C. M. Yang, B. Zibrowius, W. Schmidt, F. Schüth, *Chem. Mater.* **2003**, *15*, 3739 – 3741.
[18] M. Kruk, M. Jaroniec, C. H. Ko, R. Ryoo, *Chem. Mater.* **2000**, *12*, 1961 – 1968.
[19] M. Impéror-Clerc, P. Davidson, A. Davidson, *J. Am. Chem. Soc.* **2000**, *122*, 11 925 – 11 933.
[20] A. Galarneau, H. Cambon, F. Di Renzo, F. Fajula, *Langmuir* **2001**, *17*, 8328 – 8335.
[21] H. Lee, S. I. Zones, M. E. Davis, *Nature* **2003**, *425*, 385 – 388.

 © 2004 Wiley-VCH Verlag GmbH & Co. KGaA, Weinheim

Metallacycles

Stable Cyclopentynes—Made by Metals!?**

*Uwe Rosenthal**

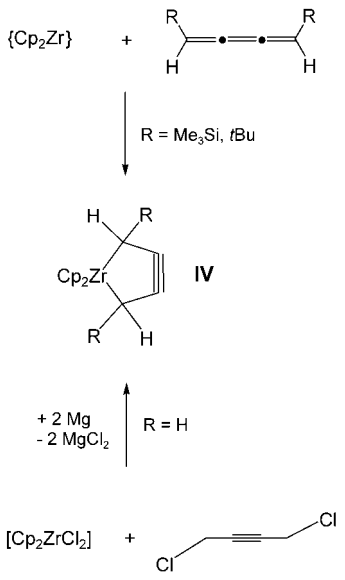
Keywords:
cycloalkynes · metallacycles · small ring systems · strained molecules · zirconium

Dedicated to Professor Eluvathingal D. Jemmis

Structural limitations in small cyclic hydrocarbons are a longstanding challenge to chemistry, leading to molecules with unusual geometric parameters and reactivity. For example, incorporation of C=C=C=C or C−C≡C−C arrangements, which are normally linear in open-chain compounds, into small carbocyclic rings results in enormous ring strain as a result of the angle deformation. Nevertheless, such uncommon structures have been realized by complexation of zirconocene fragments with butadiynes and butatrienes, giving five-membered metallacyclocumulenes and metallacyclopentynes. The metal atom is essential for these molecules but complicates the simplified description because of internal interactions of the metals with the multiple bonds.

1. Introduction

Small cyclic alkynes are usually unstable because of the nonlinear triple bond and the resulting ring strain. They are often detected only in kinetic investigations, by matrix spectroscopy, in isotope labeling experiments, or in trapping reactions.[1] The smallest unsubstituted cycloalkyne isolated so far is cyclooctyne.[2] Generally, stabilization is achieved by substituents on the ring or by heteroatoms in the ring.[1] An outstanding example for this are the 1-zirconacyclopent-3-ynes, recently obtained by N. Suzuki and co-workers.[3a,b] The first synthesis started with the Negishi reagent ($[Cp_2ZrCl_2]$ and two equivalents of *n*BuLi), giving a divalent zirconocene equivalent $\{Cp_2Zr\}$, which reacted with 1,4-disubstituted *Z* butatrienes RHC=C=C=CHR. In the second synthesis, the reaction mixture consisting of $[Cp_2ZrCl_2]$, 1,4-dichloro-but-2-yne, and two equivalents of magnesium led to the formal generation of an unsubstituted butatriene $H_2C=C=C=CH_2$, and its coordination with $\{Cp_2Zr\}$ also formed provided the 1-zirconacyclopent-3-yne. This was described to be the first "unsubstituted" metallacyclopentyne (Scheme 1). Though the complexation of butatrienes has been described a number of times,[3c] the compounds prepared by Suzuki et al. display a special coordination mode.[3a,b] In principle, these interactions had been suggested by Maercker et al. for products from $Me_2C=C=C=CMe_2$ and $\{Cp_2Ti\}$, but these particular structures turned out to be stabilized by CH activation.[4]



Scheme 1. Preparation of 1-zirconacyclopent-3-ynes **IV**.

[*] Prof. Dr. U. Rosenthal
Leibniz-Institut für Organische Katalyse
an der Universität Rostock e.V
Buchbinderstrasse 5–6, 18055 Rostock (Germany)
Fax: (49) 381-466-9376
E-mail: uwe.rosenthal@ifok.uni-rostock.de

[**] I thank my group members Drs. P. Arndt, W. Baumann, B. Heller, and A. Spannenberg as well our guest Dr. V. V. Burlakov for many fruitful discussions.

 © 2004 Wiley-VCH Verlag GmbH & Co. KGaA, Weinheim DOI: 10.1002/anie.200401761

2. General

To understand the bonding in the novel 1-zirconacyclopent-3-ynes one should discuss it in the context of other five-membered metallacycles, which are important intermediates in the stoichiometric and catalytic C–C coupling and cleavage reactions of unsaturated molecules.[5] Symmetrically substituted titanocene and zirconocene complexes of this type include the five-membered metallacycles summarized in Scheme 2.

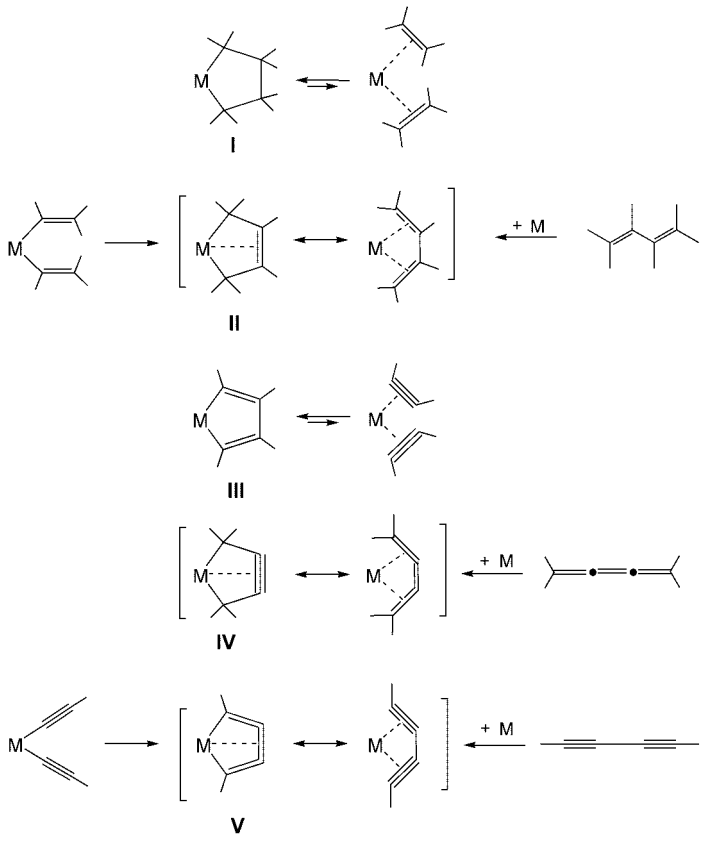
I 1-metallacyclopentanes (eight substituents) formed by oxidative coupling of two olefins[5,6]

II 1-metallacyclopent-3-enes (six substituents) prepared by complexation of 1,3-butadienes[5,7] or reductive elimination of two anionic vinyl groups[8]

III 1-metallacyclopenta-2,4-dienes (four substituents) obtained by oxidative coupling of two alkynes[5,9]

IV 1-metallacyclopent-3-ynes (four substituents) prepared by complexation of butatrienes[3a,b]

V 1-metallacyclopenta-2,3,4-trienes (two substituents) formed by complexation of 1,3-butadiynes[10] or reductive elimination of two anionic acetylide groups[11]



Scheme 2. Preparation of the symmetrically substituted five-membered metallacycles **I**–**V**.

Only structure **I** is an example of a saturated ring system. Whereas complexes **I**, **II**, and **III** have been known for a long time, the more unusual examples **IV**[3a,b] and **V**[10,11] were found more recently. Interesting is the formation of 1-metallacyclopent-3-enes (1,3-butadiene complexes) **II** by reductive elimination of two anionic vinyl groups and of the 1-metallacyclopenta-2,3,4-trienes (1,3-butadiyne complexes) **V** by the coupling of two anionic acetylides. Also the mixed reductive elimination of one acetylide and one vinyl group to give but-1-en-3-ynes has been observed (see below).[12] The 1-metallacyclopent-3-enes **II** and 1-metallacyclopenta-2,3,4-trienes **V**, both formed by the coupling of two anions, were calculated to be thermodynamically more stable than the corresponding starting materials $[Cp_2M(CH{=}CHR)_2]$[13] and $[Cp_2M(C{\equiv}CR)_2]$.[14c] The reverse C–C cleavage reaction was found only for **V** with the help of another metal center.[11,14]

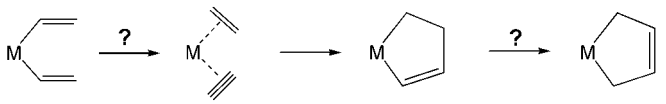


Uwe Rosenthal, born in 1950 in the Altmark, Germany, studied chemistry (1968–1972), received his Ph.D. under the supervision of Erhard Kurras (1976), and completed his habilitation (1991) at the University of Rostock. He pursued postdoctoral work at the A. N. Nesmeyanov Institute of Organoelement Compounds of the Russian Academy of Sciences in Moscow with Mark E. Vol'pin and Vladimir B. Shur (1988) and became a visiting research scientist at the Max-Planck-Institut für Kohlenforschung in Mülheim/Ruhr with Günther Wilke and Klaus Pörschke (1990–1991). He headed the Max Planck Research group "Complex Catalysis" (1992–1996) and became Professor of Inorganic Chemistry at the University of Rostock (1993). Today he is Vice Director of the Leibniz Institute of Organic Catalysis at the University of Rostock, a member of the Advisory Editorial Board of Organometallics, and member of the reviewing board for "The Chemistry of Inorganic Molecules" of the Deutsche Forschungsgemeinschaft.

The metallacyclopentanes **I** and metallacyclopentadienes **III**, which result from the oxidative coupling of two neutral olefins and two alkynes, respectively, can give typical cycloreversion reactions through cleavage of the C2–C3 bond even under very mild conditions.[5,15] The driving force for this reaction is the formation of neutral olefins and alkynes (or their complexes), and this is the reason that **I** and **III** are less stable than **II** and **V**. The interconversion of σ-dianionic structures into structures with π interactions seems to be important for all of the metallacycles mentioned. This interconversion is possible for **I** and **III** by dissociation and for **II**, **IV**, and **V** by resonance. Also the mixed oxidative coupling of an alkyne and an olefin to give 1-metallacyclopent-2-enes is a typical reaction in metallocene chemistry.[9,16,17]

As mentioned above, five-membered metallacycles are important because of their relevance to the C–C coupling and cleavage reactions of anionic groups (σ-acetylide, σ-vinyl) and unsaturated molecules (alkynes, olefins). A bridge between charged and neutral ligands may be spanned by considering the reductive elimination of two vinyl groups to give either symmetrical or unsymmetrical metallacyclopentenes (Scheme 3). Interestingly, the formation of ethylene and acetylene was detected during this reaction.[8b] Thus one can

 © 2004 Wiley-VCH Verlag GmbH & Co. KGaA, Weinheim

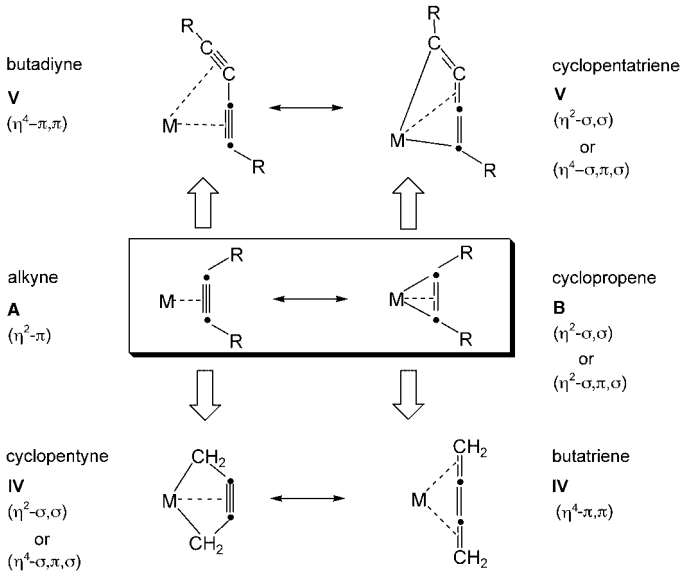


Scheme 3. Mechanistic suggestions for the formation of 1-metallacyclopent-3-enes **II**.

assume that reaction proceeds by a hydrogen transfer, formation of complexes with the neutral molecules ethylene and acetylene, and then oxidative coupling to give an unsymmetrical 1-metallacyclopent-2-ene. A subsequent isomerization would yield complexes **II**.

3. Bonding Description

It is difficult to decide whether anionic or π-bonded species exist in metallacycles of types **II**, **IV**, and **V**, and whether the new metallacycles **IV** and **V** are best described by the extreme resonance form with a dianionic interaction (with additional π bonding of the unsaturated unit in the 3-position) or alternatively by a bis-π complexation of the butatriene and 1,3-butadiyne. The real bonding situation and the reactivity of the five-membered metallacycles **IV** and **V** can be deduced from the complexation behavior of simple embedded building blocks (Scheme 4). The interaction of an alkyne with the



Scheme 4. Formal similarities of alkyne complexes and metallacyclopropenes with metallacyclopentynes **IV** and metallacyclocumulenes **V**.

electronically and coordinatively unsaturated titanocene or zirconocene center can be described as intermediate between the metal(II) η^2-π complex **A** and the 1,2-dianionic metallacyclopropene **B**, which has a metal(IV) center,[5] and for which an additional interaction of the double bond to give a η^2-σ,π,σ-metallacyclopropene complex has been discussed.[5,18] Formal modification of **A** and **B** leads to metallacycles of types **II**, **IV**, and **V**. The insertion of methylene groups CH_2 into **B** gives complexes **II** stepwise (via metallacyclobutenes[5,18]). If R represents CH_2 groups in **A** and **B**, 1-metallacyclo-3-pentynes and buta-1,2,3-trienes **IV** are formed[3a,b] (via σ-propargyl and π-allenyl complexes, respectively).[19] In an analogous formal consideration, when complexes **A** and **B** include an acetylide RC≡C unit, 1,3-butadiyne complexes and 1-metallacyclopenta-2,3,4-trienes **V** result.[10,11] In summary, the known alkyne, metallacyclopropene, σ-propargyl, and π-allenyl complexes form basic structural units for understanding the bonding situation in Suzuki's complexes as 1-zirconacyclopent-3-ynes of type **IV** or bis-π-butatriene complexes of type **V**.

4. Calculations

The unusual bonding situation of the related five-membered metallacycles **IV** and **V** prompted several theoretical groups to calculate these structures, and different orbital schemes have been published.[14f,20a] Jemmis et al. did a lot of pioneering work in this area.[14] The systems were first compared by Lin et al.[20a] Detailed studies of the electronic structure of substituted complexes **IV** $[Cp_2ZrCHRCCCHR]$ ($R = Me_3Si$) suggest that the zirconocene complex should be described by a resonance hybrid between a metallacyclopentyne and a butatriene complex. An approach based on isodesmic reactions suggested that the butatriene complex contributes significantly to the stability of the zirconocene complex. Alone, the metallacyclopentyne structure proposed by Suzuki et al. cannot describe the structural behavior and the stability of the complex. In a parallel study on a related complex of type **V**, $[Cp^*_2ZrC(R)CCC(R)]$ ($R = Me_3Si$), Lin et al. found that a resonance hybrid between a metallacyclocumulene and a butadiyne complex is also required to adequately describe its structure and stability.[20a]

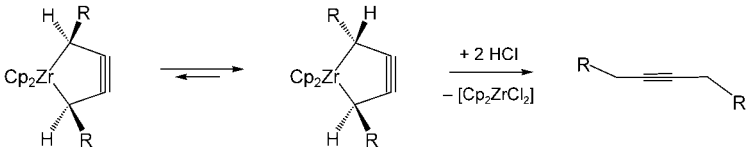
A more systematic comparison of the structure and bonding of the metallacycles **I**–**V** by Jemmis et al. and by Jiao et al. showed that there are considerable metal–π interactions in **II**, **IV**, and **V**.[14f] The analysis of geometric and magnetic properties showed the presence of strong delocalization in these systems, including the metallacyclopentynes **IV**. Additionally, the metallacyclopentenes **II** and the metallacyclopentynes **IV** were found to be "neutral bishomoaromatic", while the metallacyclocumulene **V** is "in-plane aromatic". A comparison of the hydrogenation energies of the parent carbocycles and metallacycles showed that the strain present in cyclopentynes and cyclopentatrienes is practically released when the CH_2 group is replaced by a $\{Cp_2M\}$ fragment with M = Ti or Zr.[14f]

The delocalization of electron density in the σ plane of the bent metallocene seems to be essential for the stabilization of complexes of type **IV**. This is the reason why the first description of a 1-zirconacyclopenta-3-yne was far too simplified[3a] and was later qualified.[3b] The particular ability of bent metallocenes to act as orientated σ-acceptors is typical and stabilizes these metallacycles.[20b]

 © 2004 Wiley-VCH Verlag GmbH & Co. KGaA, Weinheim

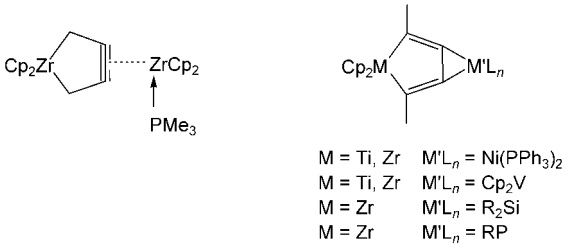
5. Reactions

Whereas reactions of the metallacyclocumulenes **V** were investigated in detail, corresponding data on the 1-zirconacyclopent-3-ynes **IV** are limited. Hydrolysis of the substituted 1-zirconacyclopent-3-ynes with HCl gave the corresponding 1,4-disubstituted 2-butynes $RCH_2C{\equiv}CCH_2R$ in nearly quantitative yield without any other isomers.[3a] Additionally, the substituted 1-zirconacyclopent-3-ynes were found to undergo isomerization (Scheme 5).[3a]



Scheme 5. *cis–trans* Isomerization and hydrolysis of 1-zirconacyclopent-3-ynes **IV**.

Interestingly, owing to the multiple-bond character of the C2–C3 bond complexes, **IV** and **V** coordinate to other metal complexes to form heterobimetallic complexes.[3b,10d] 1-Zirconacyclopent-3-yne (type **IV**) reacts with $\{Cp_2Zr(PMe_3)\}$ to form a cycloalkyne complex containing a planar C_4 unit between the metals, which was described as a "flat" 1-zirconacyclopent-3-ene (type **II**).[3b] A similar reaction was found earlier in the complexation of 1-metallacyclo-penta-2,3,4-trienes **V** with $\{Ni(PPh_3)_2\}$.[10d] The cyclotriene complexes that formed also had a planar C4 unit between the metals and were considered to be 1-metallacyclo-penta-2,4-dienes **III**.[11b] These complexes are intermediates in the cleavage of the C–C single bond of butadiynes. Interestingly, similar structures with $\{Cp_2V\}$,[21a,b] $\{RP\}$,[21c] and $\{R_2Si\}$[21d,e] have been assumed to be intermediates in some other reactions (Scheme 6).



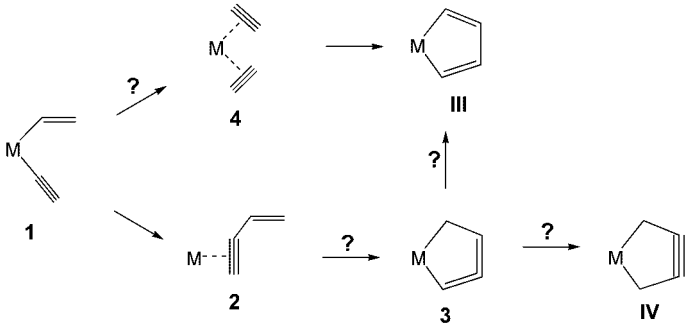
Scheme 6. Complexation of metallacyclopentynes **IV** and metallacyclocumulenes **V**.

6. Outlook

The new method of preparation and the existence of complexes of type **IV** give some perspectives for extremely interesting investigations:

a) Are 1-metallacyclopent-3-ynes formed also in the reductive elimation of anionic groups?
b) Can 1-metallacyclopent-3-ynes be prepared with other metals?
c) Which other metal complexes of 1-metallacyclopent-3-ynes exist?
d) It is possible to oligomerize 1-metallacyclopent-3-ynes?
e) Can the elegant synthetic procedure be used for other systems?

Concerning question (a), the mixed reductive elimination of anionic σ-acetylide and σ-vinyl groups should also give in principle the 1-metallacyclopent-3-ynes described by Suzuki et al. (Scheme 7). In the sequence starting from $[Cp_2M(-CH{=}CH_2)(-C{\equiv}CH)]$ (**1**), the but-1-en-3-ynes formed would probably give not only the simple η^2-π alkyne complexes **2**, as found for titanocene;[12] for zirconocene, η^4-π,π complexation (as found for butatrienes and butadiynes) and the formation of unsymmetrical 1-zirconacyclopenta-2,3-dienes **3** are expected. Some 1,3-diynes, which react with permethyltitanocene to give η^2-π-alkyne complexes, react with the larger permethylzirconocene to give



Scheme 7. Preparation of 1-zirconacyclopent-3-ynes **IV** by reductive elimination.

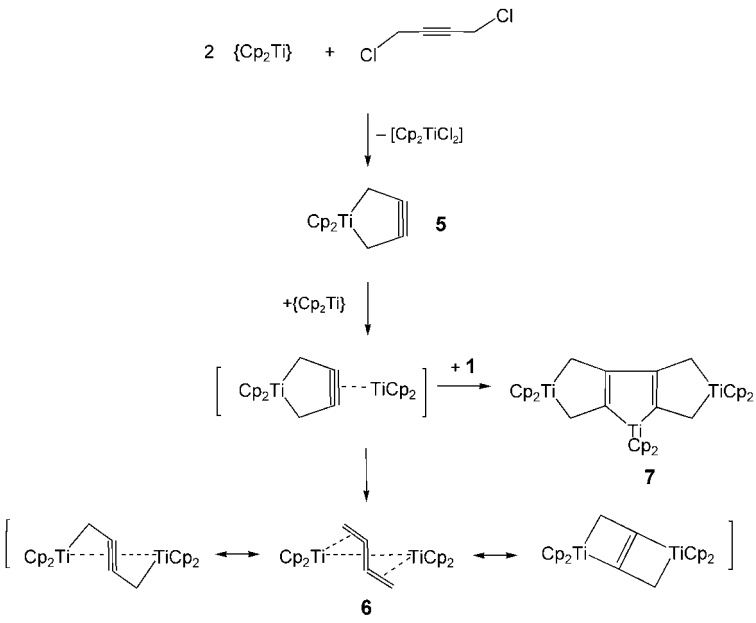
η^4-π,π complexes (1-zirconacyclopenta-2,3,4-trienes, **V**). It is questionable whether the above postulated (so far not isolated) unsymmetrical 1-zirconacyclopenta-2,3-dienes (but-1-en-3-yne complexes) should have the potential to isomerize to either symmetrical 1-zirconacyclopenta-2,4-dienes **III**[9] or 1-zirconacyclo-3-pentynes **IV**.[3a,b] In principle the symmetrical 1-zirconacyclopenta-2,4-dienes **III** should also be formed from complex **1** by a hydrogen shift to the bisacetylene complex $[Cp_2M(HC{\equiv}CH)(HC{\equiv}CH)]$ (**4**) and subsequent oxidative coupling of the two alkyne units.

Answers to questions (b)–(d) are available in yet unpublished results of the reaction of the titanocene source $[Cp_2Ti(\eta^2\text{-}Me_3SiC_2SiMe_3)]$[22] with 1,4-dichlorobut-3-yne, from which the products **5** and **6** have been isolated so far (Scheme 8).[23] In analogy to μ-*trans*-butadiyne complexes[10] the structure of **6**[23] as a μ-*trans*-butatriene complex is better described as a dititanabicycle and not a σ-propargyl or π-allenyl complex.[19] It is also different from "bridged allylic"[24a,b] and μ-butyne-1,4-diyl[24b] structures and from special μ-butadiyne complexes.[24c]

The dimerization of **1** with $\{Cp_2Ti\}$ should give the titanacyclopentadiene **7**, and trimerization of **5** by Ni^0 catalysts, the product **4**, which is expected also from the

© 2004 Wiley-VCH Verlag GmbH & Co. KGaA, Weinheim

reaction of hexakis(bromomethyl)benzene with $[Cp_2TiCl_2]$ and magnesium or alternatively from hexakis(bromomethyl)-benzene and $[Cp_2Ti(\eta^2\text{-}Me_3SiC_2SiMe_3)]$ in a modified application of Suzuki's elegant synthetic procedure [question (e)] (Scheme 8, (Scheme 9). Both reactions are under investigation[23] and should give product **8** with very interesting bonding modes as "*ortho*-quinodimethane" or radialene derivatives.[7a]



Scheme 8. Preparation and reactions of the 1-titanacyclopent-3-yne (**5**).

7. Conclusion

As an extension of the classical butadiene chemistry described by Erker et al.[7a] and Nakamura et al.,[7b] and following investigations with butadiynes,[10] Suzuki et al. has found that reactions of butatrienes with zirconocene fragments generate the surprising and uncommon zirconacyclopentynes.[3a,b] Extensive theoretical studies were initiated by this experimental work. Interesting novel stoichiometric and catalytic reactions of these compounds are expected. Repeatedly it has been proven that the combination of organometallic complexes with suitable substrates very often leads to novel bond types and reactivities: *Made by Metals!* Nevertheless, the description of these molecules becomes much more complicated by the influence of the metals according to theoretical calculations: *Zirconacyclopentynes—Really Made by Metals?*

Published Online: June 15, 2004

[1] a) A. Krebs, J. Wilke, *Top. Curr. Chem.* **1983**, *109*, 189–233; b) R. Gleiter, R. Merger in *Modern Acetylene Chemistry* (Eds.: P. J. Stang, F. Diederich), Wiley-VCH, Weinheim, **1995**, pp. 284–319; c) W. M. Jones, J. Klosin, *Adv. Organomet. Chem.* **1998**, *42*, 147–221.

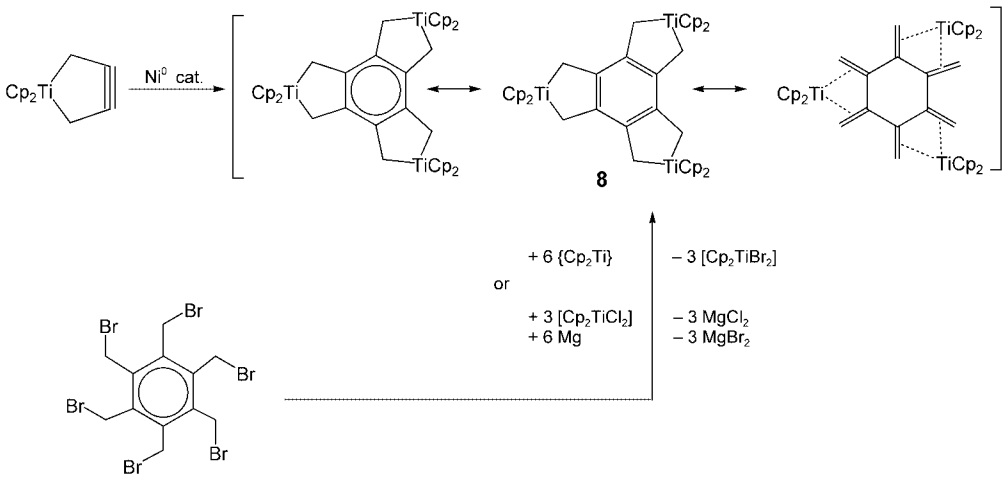
[2] A. T. Blomquist, L. H. Liu, *J. Am. Chem. Soc.* **1953**, *75*, 2153–2154.

[3] a) N. Suzuki, M. Nishiura, Y. Wakatsuki, *Science* **2002**, *295*, 660–663; b) N. Suzuki, N. Ahihara, H. Takahara, T. Watanabe, M. Iwasaki, M. Saburi, D. Hashizume, T. Chihara, *J. Am. Chem. Soc.* **2004**, *126*, 60–61; c) N. Suzuki, Y. Fukuda, C. E. Kim, H. Takahara, M. Iwasaki, M. Saburi, M. Nishiura, Y. Wakatsuki, *Chem. Lett.* **2003**, *295*, 16–17, and references therein.

[4] A. Maercker, A. Groos, *Angew. Chem.* **1996**, *108*, 216–218; *Angew. Chem. Int. Ed. Engl.* **1996**, *35*, 210–212.

[5] a) E. Negishi, T. Takahashi, *Bull. Chem. Soc. Jpn.* **1998**, *71*, 755–769; b) "Zirconocenes": E. Negishi, J.-L. Montchamp in *Metallocenes*, *Synthesis*, *Reactivity*, *Applications*, *Vol. 1* (Eds.: A. Togni, R. L. Halterman), Wiley-VCH, Weinheim, **1998**, pp. 241–319; c) "Titanocenes": R. Beckhaus in *Metallocenes*, *Synthesis*, *Reactivity*, *Applications*, *Vol. 1* (Eds.: A. Togni, R. L. Halterman), Wiley-VCH, Weinheim, **1998**, pp. 153–239.

[6] a) T. Takahashi, R. Fischer, Z. Xi, K. Nakajima, *Chem. Lett.* **1996**, *241*, 357–358.



Scheme 9. Expected trimerization of 1-titanacyclopent-3-yne (**5**).

 © 2004 Wiley-VCH Verlag GmbH & Co. KGaA, Weinheim

[7] a) G. Erker, C. Krüger, G. Müller, *Adv. Organomet. Chem.* **1985**, *24*, 1–39; b) H. Yasuda, A. Nakamura, *Angew. Chem.* **1987**, *99*, 745–764; *Angew. Chem. Int. Ed. Engl.* **1987**, *26*, 723-, and references therein.

[8] a) R. Beckhaus, K.-H. Thiele, *J. Organomet. Chem.* **1984**, *268*, C7-C8; b) R. Beckhaus, K.-H. Thiele, *Z. Anorg. Allg. Chem.* **1989**, *573*, 195–198; c) U. Böhme, K.-H. Thiele, A. Rufinska, *Z. Anorg. Allg. Chem.* **1994**, *620*, 1455–1462.

[9] a) K. Sato, Y. Nishihara, S. Huo, Z. Xi, T. Takahashi, *J. Organomet. Chem.* **2001**, *633*, 18–26; b) T. Takahashi, M. Ishikawa, S. Q. Huo, *J. Am. Chem. Soc.* **2001**, *123*, 388–389, and references therein.

[10] a) U. Rosenthal, A. Ohff, W. Baumann, R. Kempe, A. Tillack, V. V. Burlakov, *Angew. Chem.* **1994**, *106*, 1678–1680; *Angew. Chem. Int. Ed. Engl.* **1994**, *33*, 1605–1607; b) V. V. Burlakov, A. Ohff, C. Lefeber, A. Tillack, W. Baumann, R. Kempe, U. Rosenthal, *Chem. Ber.* **1995**, *128*, 967–971; c) U. Rosenthal, S. Pulst, P. Arndt, A. Ohff, A. Tillack, W. Baumann, R. Kempe, V. V. Burlakov, *Organometallics* **1995**, *14*, 2961–2968. d) U. Rosenthal, P.-M. Pellny, F. G. Kirchbauer, V. V. Burlakov, *Acc. Chem. Res.* **2000**, *33*, 119–129.

[11] a) W. Frömberg, PhD Thesis, Univ. Bochum **1986**; b) S. Pulst, P. Arndt, B. Heller, W. Baumann, R. Kempe, U. Rosenthal, *Angew. Chem.* **1996**, *108*, 1175–1178; *Angew. Chem. Int. Ed. Engl.* **1996**, *35*, 1112–1114; c) B. Temme, G. Erker, R. Fröhlich, M. Grehl, *Angew. Chem.* **1994**, *106*, 1570–1573; *Angew. Chem. Int. Ed. Engl.* **1994**, *33*, 1480–1482; d) P.-M. Pellny, F. G. Kirchbauer, V. V. Burlakov, W. Baumann, A. Spannenberg, U. Rosenthal, *J. Am. Chem. Soc.* **1999**, *121*, 8313–8323; e) F. G. Kirchbauer, P.-M. Pellny, V. V. Burlakov, W. Baumann, A. Spannenberg, R. Kempe, U. Rosenthal, *Chem. Eur. J.* **2000**, *6*, 81–90.

[12] P. Stepnicka, R. Gyepes, I. Cisarova, M. Horacek, J. Kubista, K. Mach, *Organometallics* **1999**, *18*, 4869–4880.

[13] R. Beckhaus, *Angew. Chem.* **1997**, *109*, 694–722; *Angew. Chem. Int. Ed. Engl.* **1997**, *36*, 686–713.

[14] a) P. N. V. Pavankumar, E. D. Jemmis, *J. Am. Chem. Soc.* **1988**, *110*, 125; b) E. D. Jemmis, K. T. Giju, *Angew. Chem.* **1997**, *109*, 633–635; *Angew. Chem. Int. Ed. Engl.* **1997**, *36*, 606–608; c) E. D. Jemmis, K. T. Giju, *J. Am. Chem. Soc.* **1998**, *120*, 6952–6964; d) E. D. Jemmis, A. K. Phukan, U. Rosenthal, *J. Organomet. Chem.* **2001**, *635*, 204–211; e) E. D. Jemmis, A. K. Phukan, A. T. Giju, *Organometallics* **2002**, *21*, 2254–2261; f) E. D. Jemmis, A. K. Phukan, H. Jiao, U. Rosenthal, *Organometallics* **2003**, *22*, 4958–4965.

[15] For metallacyclopentanes, see: a) S. Mansel, D. Thomas, C. Lefeber, D. Heller, R. Kempe, W. Baumann, U. Rosenthal, *Organometallics* **1997**, *16*, 2886–2890; For metallacyclopentadienes, see: b) G. Erker, R. Zwettler, *J. Organomet. Chem.* **1991**, *409*, 179–188; c) C. Lefeber, A. Ohff, A. Tillack, W. Baumann, R. Kempe, V. V. Burlakov, U. Rosenthal, H. Görls, *J. Organomet. Chem.* **1995**, *501*, 179–188.

[16] C. Mc Date, J. E. Bercaw, *J. Organomet. Chem.* **1985**, *279*, 281–315.

[17] J. W. Lauher, R. Hoffmann, *J. Am. Chem. Soc.* **1976**, *98*, 1729–1742.

[18] a) F. N. Tebbe, R. L. Harlow, *J. Am. Chem. Soc.* **1980**, *102*, 6149–6151; b) F. N. Tebbe, R. L. Harlow, *J. Am. Chem. Soc.* **1980**, *102*, 6149–6151.

[19] a) P. W. Blosser, J. C. Galucci, A. Wojcicki, *J. Am. Chem. Soc.* **1993**, *115*, 2994–2995; b) P. W. Blosser, J. C. Galucci, A. Wojcicki, *J. Organomet. Chem.* **2000**, *597*, 125–132.

[20] a) K. C. Lam, Z. Lin, *Organometallics* **2003**, *22*, 3466–3470; b) J. W. Lauher, R. Hoffmann, *J. Am. Chem. Soc.* **1976**, *98*, 1729–1742.

[21] a) R. Choukroun, B. Donnadieu, J. Zhao, P. Cassoux, C. Lepitit, B. Silvi, *Organometallics* **2000**, *19*, 1901–1911; b) C. Danjoy, J. Zhao, B. Donnadieu, J.-P. Legros, L. Valade, R. Choukroun, A. Zwick, P. Cassoux, *Chem. Eur. J.* **1998**, *4*, 1100–1105; c) A. Mahiheu, Y. Miquel, A. Igau, J.-P. Majoral, *Organometallics* **1997**, *16*, 3086–3088; d) T. Takahashi, Z. Xi, Y. Obora, N. Suzuki, *J. Am. Chem. Soc.* **1995**, *117*, 2665–2666; e) Z. Xi, R. Fischer, R. Hara, W.-H. Sun, Y. Obora, N. Suzuki, K. Nakajima, T. Takahashi, *J. Am. Chem. Soc.* **1997**, *119*, 12842–12848.

[22] a) "Organometallic Chemistry of Titanocene and Zirconocene Complexes with Bis(trimethylsilyl)acetylene as the Basis for Applications in Organic Synthesis": U. Rosenthal, V. V. Burlakov in *Titanium and Zirconium in Organic Synthesis* (Ed.: I. Marek), Wiley-VCH, Weinheim, **2002**, pp. 355–389; b) U. Rosenthal, V. V. Burlakov, P. Arndt, W. Baumann, A. Spannenberg, *Organometallics* **2003**, *22*, 884–900.

[23] V. V. Burlakov, U. Rosenthal, *Chem. Commun.* **2004**, submitted.

[24] a) J. N. Gerlach, R. M. Wing, P. C. Ellgen, *Inorg. Chem.* **1976**, *15*, 2959–2964; b) T. Matsuo, M. Tanaka, A. Sekiguchi, *Chem. Commun.* **2001**, 503–504, and references therein; c) Y. Wang, H. Wang, H. Wang, H.-S. Chan, Z. Xie, *J. Organomet. Chem.* **2003**, *683*, 39–43.

 © 2004 Wiley-VCH Verlag GmbH & Co. KGaA, Weinheim

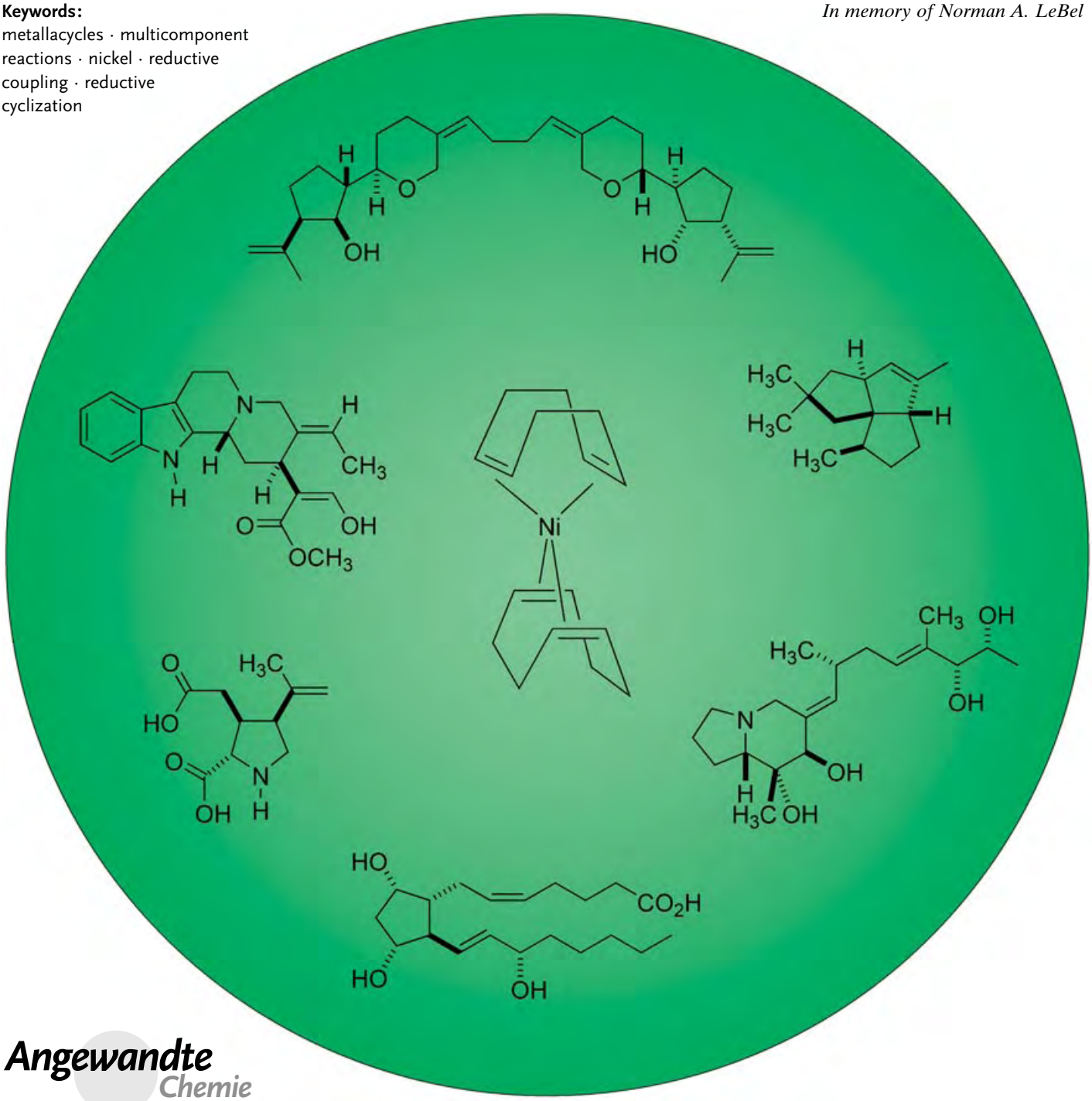
Multicomponent Coupling Reactions

Nickel-Catalyzed Reductive Cyclizations and Couplings

*John Montgomery**

Keywords:
metallacycles · multicomponent reactions · nickel · reductive coupling · reductive cyclization

In memory of Norman A. LeBel



© 2004 Wiley-VCH Verlag GmbH & Co. KGaA, Weinheim
DOI: 10.1002/anie.200300634

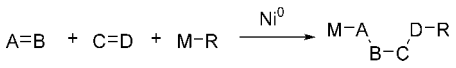
For over 50 years, nickel catalysis has been applied in cycloaddition processes. Nickel-catalyzed reductive couplings and cyclizations, however, have only recently attracted a high level of interest. This group of new reactions allows a broad range of multicomponent couplings involving two or more π components with a main-group or transition-metal reagent. These processes allow the assembly of important organic substructures from widely available reaction components. Multiple contiguous stereocenters, polycyclic ring systems, and novel arrays of complex functionality may often be prepared from simple, achiral, acyclic precursors. With three or more reactive functional groups participating in the catalytic processes, many mechanistic questions abound, including the precise timing of bond constructions and the nature of reactive intermediates. This Review is thus aimed at providing a critical evaluation of recent progress in this rapidly developing field.

From the Contents

1. Introduction	3891
2. General Mechanistic Considerations	3891
3. Choice of Catalysts	3892
4. Three-Component Couplings	3892
5. Applications in the Synthesis of Complex Molecules	3903
6. Summary and Outlook	3906

1. Introduction

Oligomerizations of acetylene and butadiene were among the earliest reports of synthetically useful nickel-catalyzed reactions, and contemporary applications of these processes have resulted in methodological advances of substantial importance.[1] For instance, nickel-catalyzed [4+4],[2] [4+2],[3] and [2+2+2][4] cycloadditions have received considerable attention. Other important nickel-catalyzed processes include olefin polymerizations,[2b,5] dimerizations,[1a,6] hydrocyanations,[7] and hydrometallations.[8] One particular grouping of nickel-catalyzed reactions that has received substantial attention recently is the reductive coupling of two π components with one main-group organometallic reagent or metal hydride (Scheme 1).[9] Within this grouping of contemporary



Scheme 1. Intermolecular nickel-catalyzed coupling of π components in the presence of a main-group organometallic complex.

studies, many fundamental advances in reaction discovery and complex synthetic applications have been presented. The purpose of this Review is to highlight recent discoveries and applications in nickel-catalyzed reductive couplings and cyclizations as well as mechanistic hypotheses that have grown from studies in this area.

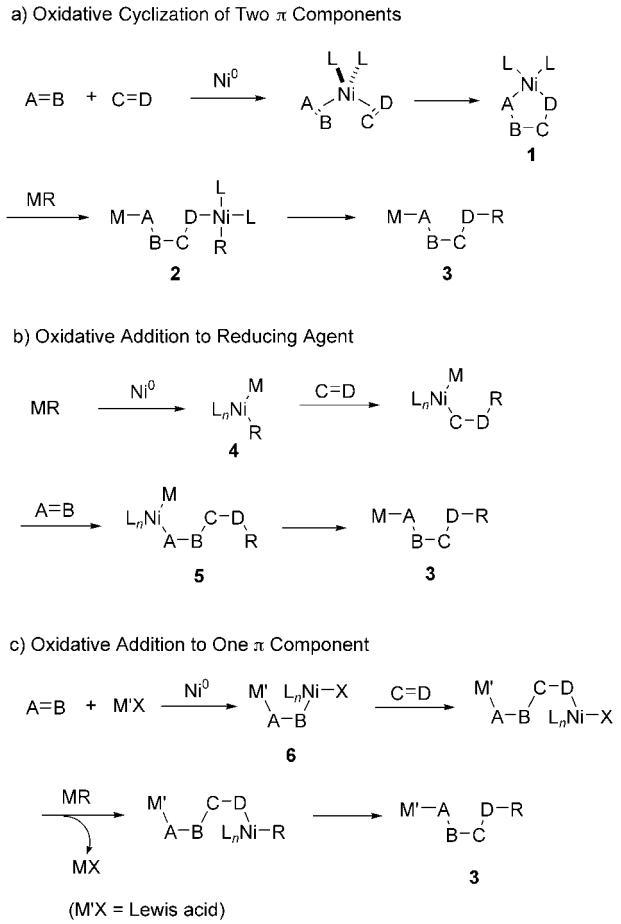
2. General Mechanistic Considerations

Despite the considerable attention that has been devoted to three-component couplings of two π components and a main-group organometallic reagent or metal hydride, many interesting mechanistic questions still remain. Of the various mechanistic pathways that have been advanced, most fall into three general groupings. These three groupings can be characterized according to the oxidative transformation that initiates the overall coupling process (Scheme 2). The first general mechanism is initiated by oxidative cyclization of nickel(0) with two π components A=B and C=D to form a metallacycle **1**. Transmetallation of a metal alkyl MR to afford **2** followed by reductive elimination affords product **3**. The second general mechanism is initiated by oxidative addition of nickel(0) to MR (a metal hydride or metal alkyl) to form a reactive nickel hydride or nickel alkyl **4**. Sequential migratory insertions of the two π components C=D and A=B, followed by reductive elimination of **5**, affords product **3**. The third general mechanism is initiated by oxidative addition of nickel (0) to one of the π components A=B, often facilitated by a Lewis acid (M′X), to form a reactive nickel alkyl **6** (most often a π-allyl complex). Migratory insertion of the second π component C=D, followed by transmetallation of MR, and finally reductive elimination affords product **3**.

These are undoubtedly oversimplified descriptions, and many variations on the three mechanism classes summarized above are possible. Issues such as metal coordination number, prior association of reactive components, and changes in the hapticity of unsaturated reactive ligands provide many reasonable variations in the mechanisms highlighted above. Furthermore, electron-transfer processes are certainly possible and have been well documented and thoroughly studied in other classes of nickel-catalyzed reactions.[10] The involvement of electron-transfer pathways could be important in the individual steps of the three mechanism classes described above. Alternatively, entirely distinct mechanisms that involve cyclizations of free radicals, radical anions, or paramagnetic nickel intermediates are also possible. This Review

[*] Prof. J. Montgomery
Department of Chemistry
Wayne State University
Detroit, MI 48202-3489 (USA)
Fax (+1) 313-577-2554
E-mail: jwm@chem.wayne.edu

 DOI: 10.1002/anie.200300634 © 2004 Wiley-VCH Verlag GmbH & Co. KGaA, Weinheim



Scheme 2. Possible mechanisms for the three-component coupling of two π components with a main-group organometallic complex or a main-group-metal hydride: a) oxidative cyclization of two π components; b) oxidative addition to a reducing agent and subsequent insertion of the π components; c) oxidative addition to one π component and subsequent insertion of the second component.

primarily presents the mechanistic descriptions provided by the authors who initially reported the work, but readers should be aware that most mechanistic proposals in this area are largely speculative. Further study may involve revision of many of the mechanistic proposals summarized in this report.



John Montgomery was born in 1965 in Concord, NC. He studied chemistry at the University of North Carolina with Prof. Joe Templeton and Prof. Maurice Brookhart (1987). He received his PhD at Colorado State University with Prof. Louis Hegedus (1991). He was an American Cancer Society Postdoctoral Fellow at the University of California at Irvine (1991–1993) with Prof. Larry Overman. In 1993, he moved to Wayne State University where he is now Professor of Chemistry. His work is focused on transition metals in reaction discovery, synthetic methodology development, mechanistic chemistry, and complex molecule synthesis.

3. Choice of Catalysts

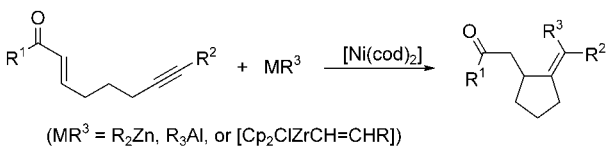
The vast majority of reactions developed that fall within the scope of this Review utilize either $[Ni(cod)_2]$ (cod = 1,5-cyclooctadiene) or $[Ni(acac)_2]$ (acac = acetyl acetonate) as the commercially available source of the active catalyst. It has generally been proposed that the active oxidation state of nickel in the catalytic processes is 0, and thus $[Ni(cod)_2]$ requires no prior activation for catalysis to occur. Whereas various complexes of nickel(0) with phosphanes and amines (and related derivatives) may be prepared, the typical strategy involves preparation of various catalysts in situ simply by premixing $[Ni(cod)_2]$ with the appropriate ligand. A description of the relative reactivities of various ligands will be provided throughout this Review.

$[Ni(acac)_2]$ may often be used as the catalyst source, although this nickel(II) species typically requires reduction for catalysis to occur. Some of the more nucleophilic reducing agents such as dialkyl zinc reagents can reduce $[Ni(acac)_2]$ to a lower oxidation state, but a reliable procedure that is often employed involves prior reduction of $[Ni(acac)_2]$ with DIBAL-H (diisobutyl aluminum hydride). This procedure was studied by Schwartz and co-workers in the context of nickel-catalyzed conjugate additions, and those original studies included electrochemical evidence that DIBAL-H promotes the formation of a paramagnetic nickel(I) species when $[Ni(acac)_2]$ and DIBAL-H in THF are employed in a 1:1 ratio.[10a–b] Later studies by Mackenzie and Krysan demonstrated that a 1:2 ratio of $[Ni(acac)_2]$:DIBAL-H in THF in the presence of cod provides a convenient preparation of $[Ni(cod)_2]$,[11] so it appears that there is little doubt that a nickel(0) species may be produced under the appropriate conditions. The advantages of $[Ni(acac)_2]$ over of $[Ni(cod)_2]$ include the lower cost and air stability of $[Ni(acac)_2]$ ($[Ni(cod)_2]$ requires storage and handling under inert atmosphere). In addition to the stability and cost issues, it was shown by Mori that DIBAL(acac), which is produced by reduction of $[Ni(acac)_2]$ with DIBAL-H, can have a substantial impact on some reactions. Hence $[Ni(acac)_2]$/DIBAL-H should not be viewed as rigorously equivalent to $[Ni(cod)_2]$.[12]

4. Three-Component Couplings

4.1. Couplings of Alkenes with Alkynes

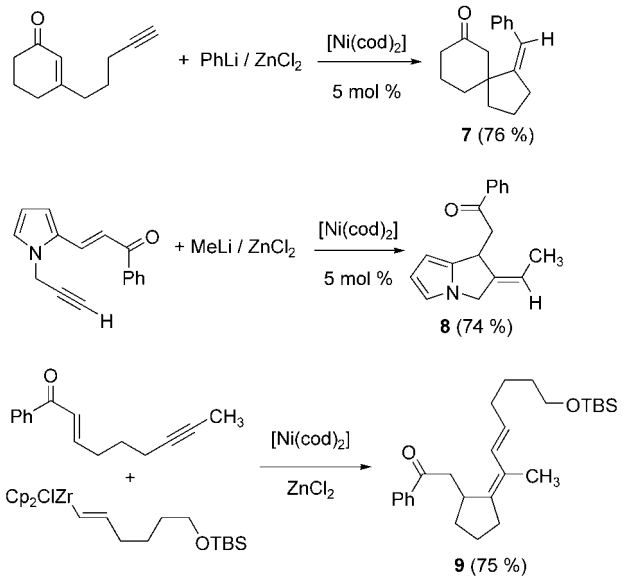
The nickel-catalyzed coupling of an alkene, an alkyne, and a main-group organometallic reagent has been studied intensively in a variety of contexts (Scheme 3). This process provides an excellent way to control the stereochemistry of



Scheme 3. Intramolecular coupling of enynes with main-group organometallic reagents.

 © 2004 Wiley-VCH Verlag GmbH & Co. KGaA, Weinheim

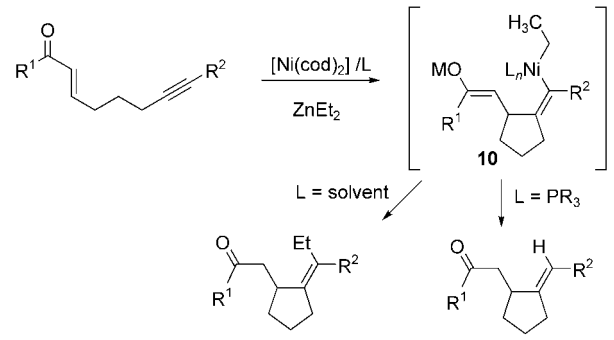
challenging tri- and tetrasubstituted alkenes. An apparent requirement for the coupling or cyclization to proceed effectively is that the alkene unit must be electron deficient. Intramolecular versions of this process, largely developed in our laboratories, have been demonstrated with organozinc reagents (as in the production of **7** and **8**),[13] organoaluminum reagents,[14] and alkenyl zirconium reagents (as in the production of **9**, Scheme 4).[15] Both internal and terminal



Scheme 4. Examples for syntheses through coupling of enynes and main-group organometallic reagents. TBS = *tert*-butyldimethylsilyl.

alkynes are cleanly tolerated as the acetylenic component, and enones, alkylidene malonates, nitroalkenes, and unsaturated imides are tolerated as the electron-deficient alkene component. The scope of the reaction is very broad (Scheme 4). Several total synthesis applications of this reaction class have been demonstrated (Sections 5.1 and 5.2).

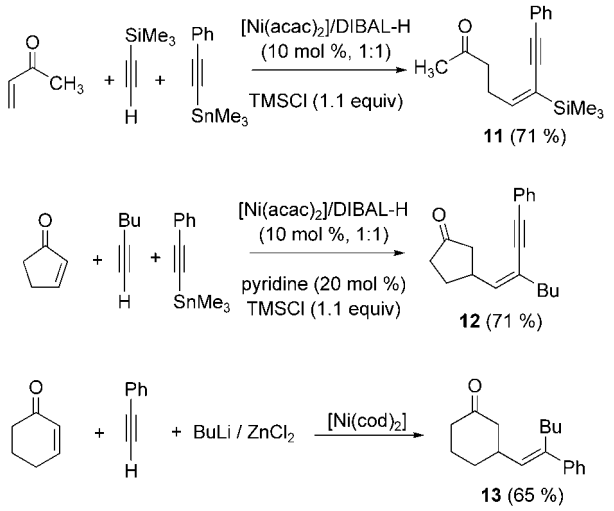
Organozinc reagents that bear β-hydrogen atoms are tolerated in the process, although ligand effects become important (Scheme 5). In the absence of phosphanes, alkyl-group transfer is observed, but when the nickel(0) catalyst is pretreated with triphenylphosphane, selective hydrogen-atom



Scheme 5. Effect of phosphane additives on the reactivity of organozinc reagents that bear β-hydrogen atoms.

incorporation occurs. This feature adds considerable flexibility to the method. It was proposed that nickel species **10** is an intermediate for both alkylative and reductive manifolds, and that the σ-donating ability of the ligands controls the reaction outcome.[13a,b]

The corresponding intermolecular couplings of enones, alkynes, and main-group organometallic reagents also proceed efficiently to generate acyclic structures, which may be further elaborated by a variety of procedures. The first reported examples of couplings of this type from Ikeda et al. involved acetylenic tin reagents to generate conjugated enynes such as **11** and **12** (Scheme 6).[16] Both internal and



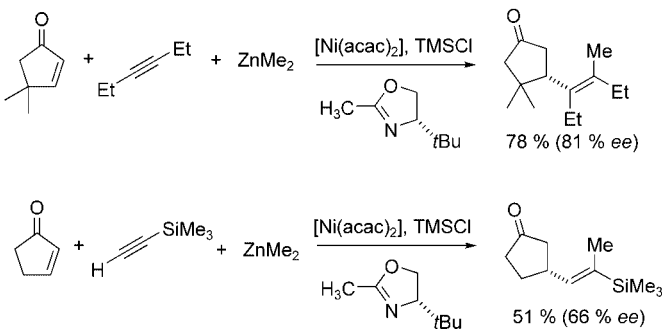
Scheme 6. Examples of the first intermolecular couplings of enones, alkynes, and main-group organometallic reagents.

terminal alkynes participate in the couplings, and regioselectivities are very high with terminal alkynes to generate products derived from coupling of the enone with the unsubstituted alkyne terminus. Acetylenic zinc reagents participate in the couplings, although yields and regioselectivities of alkyne insertion are lower than in the corresponding alkynyl tin reagent couplings.[17] Alkyl zinc reagents, either in pure form or generated from the corresponding organolithium and zinc chloride, also participate cleanly in the three-component couplings, as demonstrated by the production of **13**.[18]

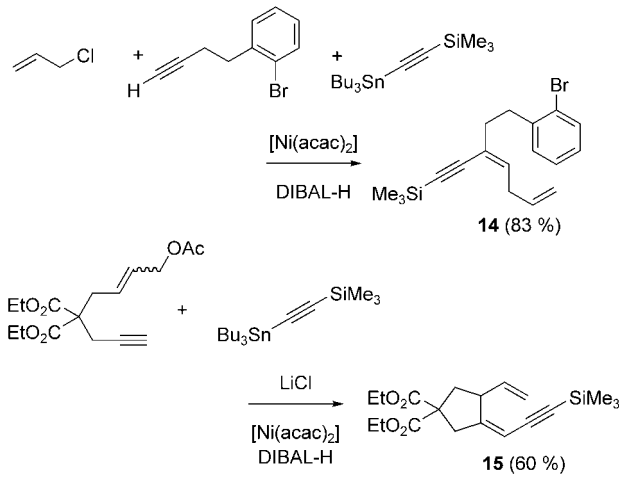
An asymmetric version of the intermolecular couplings was developed by Ikeda et al., who used a nickel catalyst modified with a chiral monodentate oxazoline (Scheme 7).[19] Yields and enantioselectivities ranged from good to modest in this procedure. A variety of bidentate ligands including bisphosphanes, bisoxazolines, phospanyloxazolines, and pyridinyloxazolines afforded poorer results both in efficiency and enantioselectivity.

A related process developed by Ikeda et al. involves couplings of allylic halides and acetates with alkynes in the presence of acetylenic stannanes (Scheme 8).[20] This procedure provides a very attractive entry to conjugated enynes. The reactions can be entirely intermolecular (→**14**) or partially intramolecular (→**15**). Although the process was

 © 2004 Wiley-VCH Verlag GmbH & Co. KGaA, Weinheim



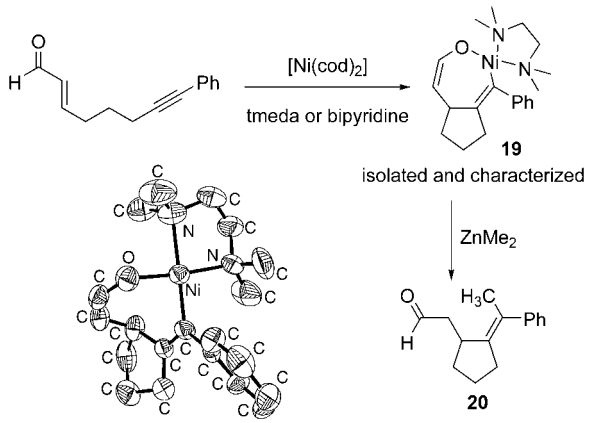
Scheme 7. Asymmetric variants of intermolecular coupling.



Scheme 8. Coupling of allyl halides or acetates with alkynes in the presence of alkynyl stannanes.

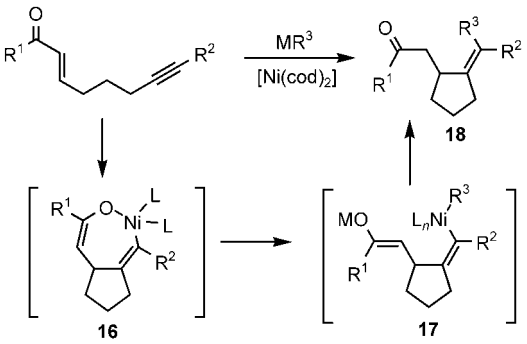
most extensively developed with acetylenic stannanes, organozinc and organoaluminum reagents are also effective participants.[21]

The mechanistic proposals for the enone/alkyne couplings have largely focused on the involvement of nickel metallacycles derived from the oxidative cyclization of an enone and an alkyne with nickel(0) (Scheme 9).[9] Once the initial oxidative cyclization occurs to produce metallacycle **16**, transmetallation of the main-group organometallic reagent occurs to generate intermediate **17**. Direct reductive elimination of **17** provides the observed product **18**, whereas β-H elimination occurs when phosphanes are used (Scheme 5). By omitting the organozinc reagent, metallacycle **19** was isolated and fully characterized as the η^1, O-bound enolate (Scheme 10).[22] Treatment of metallacycle **19** with dimethylzinc affords the same product **20**, which may be obtained from the catalytic reaction of an alkynyl enal and dimethyl zinc. This observation in no way proves that catalytic reactions proceed by this mechanism, but the sequence does provide direct precedent for each of the key individual steps of the metallacycle mechanism. Studies in our laboratory are aimed at directly investigating the kinetic competence of **19** in catalytic reactions, and a detailed full report of that study involving both experimental and computational chemistry is forthcoming. Further synthetic applications of the proposed nickel metallacycle and related metallacycles that are beyond the scope of this Review have also been reported.[23]

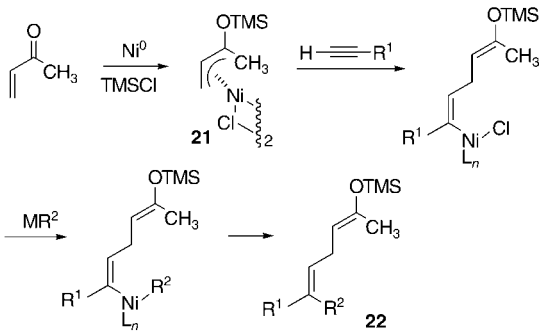


Scheme 10. Intramolecular enone–alkyne coupling without organozinc reagents. tmeda = *N*,*N*,*N*′,*N*′-tetramethylethylenediamine.

An alternate mechanism for this class of transformations has been discussed. If the reaction is initiated by Lewis acid promoted oxidative addition of nickel(0) to the enone, then π-allyl intermediate **21** would result (Scheme 11). Alkyne insertion, transmetallation of the organozinc reagent, and finally reductive elimination would afford the observed



Scheme 9. Proposed mechanism for intramolecular enone–alkyne coupling.



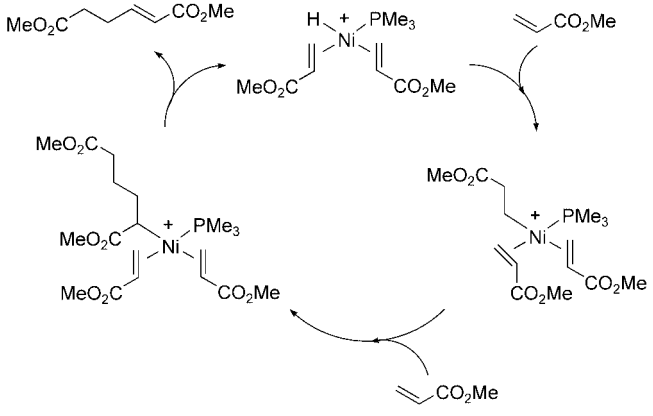
Scheme 11. Alternative mechanism for enone–alkyne coupling in the presence of Ni^0.

product **22**. The formation of π-allyl complexes from enones, nickel(0), and trimethylsilyl chloride is well precedented,[24] but direct precedent for the conversion of π-allyl complex **21** into products such as **22** has not been obtained. Furthermore, trimethylsilyl chloride is not a required additive in most variants. Therefore, the metallacycle-based mechanism is probably more reasonable based on data currently available. The allyl chloride couplings by Ikeda et al. (Scheme 8) were reported to proceed through a similar π-allyl-based pathway, although a metallacycle-based mechanism may be operative with that group of reactions as well.

Additional mechanistic pathways, including alkyne carbometallation pathways with organozinc or organonickel as well as radical cyclization pathways, have been considered.[25] Various probe substrates were examined and provided data that appeared to be most consistent with the metallacycle or π-allyl mechanisms described above.

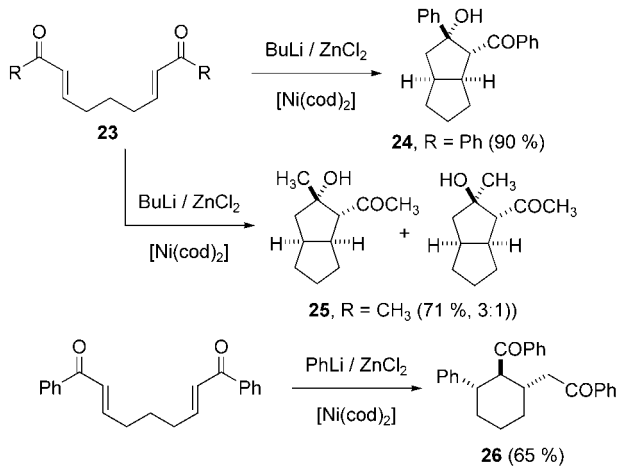
4.2. Coupling of Two Alkenes

The nickel-catalyzed dimerization of olefins has a rich history dating back to the elegant early studies of Wilke[1a] into the dimerization of simple α-olefins such as propylene as well as activated olefins such as methyl acrylate. A general theme of these early studies was that electrophilic nickel(II) catalysts were employed. For instance, η^3-allyl nickel(II) halide catalysts were activated by Lewis acids to generate a cationic nickel(II) species (which can also be viewed as a Lewis acid activated neutral species), which catalyzes the dimerization of propylene. Similarly, treatment of $[Ni(cod)_2]$ with HBF_4 or an η^3-allyl nickel(II) halide species with $AgBF_4$ generates a cationic nickel(II) tetrafluoroborate species that catalyzes the dimerization of methyl acrylate. These highly active species almost certainly operate by formation of a catalytically active nickel hydride that undergoes sequential olefin insertions prior to β-hydride elimination to produce the dimeric product and regenerate the active nickel hydride (Scheme 12). This general mode of reactivity has been further illustrated in the nickel-catalyzed cyclization of α,ω-dienes,[6b] in the heterodimerization of ethylene and styrenes,[6a] and in the polymerization of ethylene with highly active catalysts under similar conditions.[5]



Scheme 12. Catalytic cycle of olefin dimerization in the presence of a Ni^{II} complex.

In contrast to the well-studied dimerization and cycloisomerization of olefins by highly active cationic nickel hydrides, much less is known about the corresponding nickel-catalyzed *reductive* cyclization of dienes catalyzed by electron-rich nickel(0) catalysts. The cyclization of bis-enones has been developed in our laboratories by using $[Ni(cod)_2]$ as catalyst and an organozinc complex as the reducing agent (Scheme 13).[13b,26] For instance, bis-enones undergo efficient



Scheme 13. Reductive cyclization of bis-enones with $[Ni(cod)_2]$ catalyst.

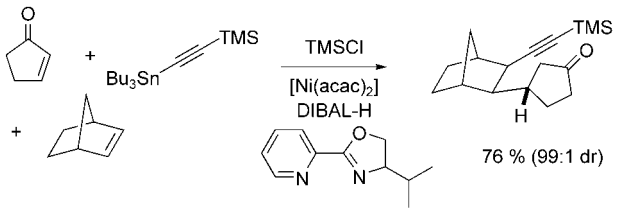
cyclization with $BuLi/ZnCl_2$ to afford [3.3.0]bicyclooctanol products. Bis-enone **23** (R = Ph) undergoes efficient cyclization to afford a single isomer of bicycloctanol **24** in 90% yield, whereas **23** (R = Me) provides **25** (3:1 ratio of diastereomers) in 71% combined yield. The organozinc structure plays a critical role, since more reactive sp^2-hybridized organozinc reagents undergo direct conjugate addition to provide products derived from tandem conjugate additions, as illustrated by the formation of **26** with $PhLi/ZnCl_2$ (Scheme 13).

Little is known about the mechanism of the potentially interesting bis-enone cyclization, which involves a reductive cyclization/aldol addition sequence. The original report of this reaction suggested that the cyclization is initiated by oxidative addition of nickel(0) to a single enone (in analogy to Scheme 11),[26] although organozinc-promoted formation of a metallacycle is also possible. In contrast to alkynyl enones, which cleanly afford metallacycles upon treatment with $[Ni(cod)_2]$ and tmeda, treatment of a bis-enone with a stoichiometric quantity of nickel(0) leads to simple coordination of the alkenes to nickel without cyclization. Thus, if metallacycles are involved in the catalytic cyclization of bis-enones, they are either generated in a small equilibrium concentration, or their formation is promoted by the organozinc reagent. Bis-enones are good substrates for free radical cyclizations, and the process could be initiated by electron transfer from a low-valent Ni species, although this apparently does not happen in the absence of an organozinc reagent or another Lewis acidic reducing agent. Free radical cyclizations

 © 2004 Wiley-VCH Verlag GmbH & Co. KGaA, Weinheim

of bis-enones to afford [3.3.0]bicyclooctanols are well documented.[27]

Whereas the intramolecular couplings of two enones described above require that both alkenes bear activating substituents, an intermolecular process was developed by Ikeda et al. that involves coupling of an electron-deficient olefin with a strained olefin (Scheme 14).[28] Upon treatment



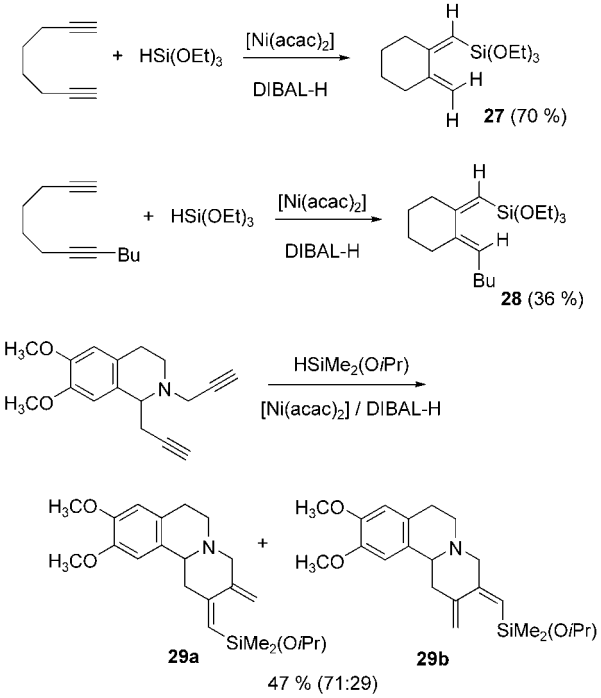
Scheme 14. Intermolecular coupling of an electron-deficient olefin with a strained olefin.

of an enone with norbornene or norbornadiene and an acetylenic stannane in the presence of $[Ni(acac)_2]$/DIBAL-H/TMSCl and a pyridinyloxazoline ligand, efficient coupling occurs to generate products with up to five contiguous stereocenters in a highly diastereoselective sense. Both acyclic and cyclic enones participate in the process. This particular variant was proposed to proceed by the mechanism described in Section 4.1 for related alkyne couplings.

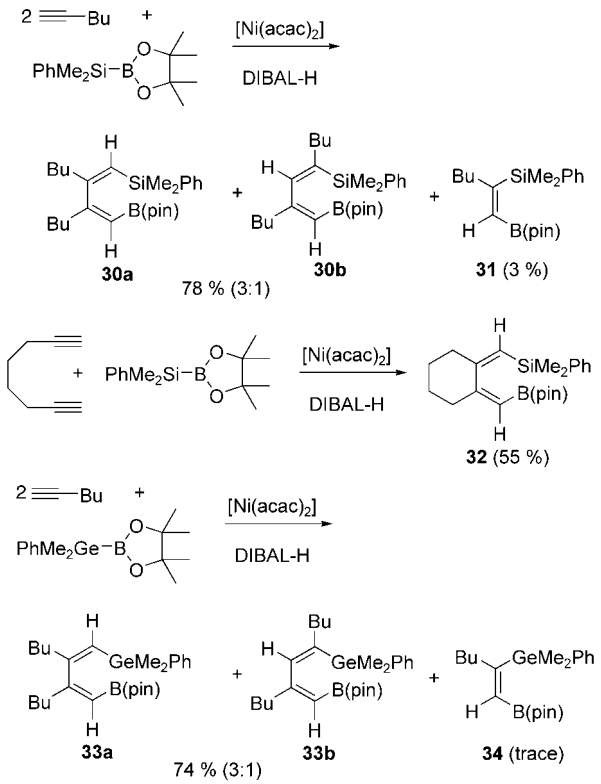
4.3. Coupling of Two Alkynes

The coupling of two alkynes with silyl hydrides is among the earliest examples of the general reactivity mode covered in this Review. In the original reports of this process, Lappert et al. discussed the fully intermolecular variant, but the scope and stereoselectivity of the process was not studied.[29] The real synthetic utility was not realized until the intramolecular variant with diynes was examined by Tamao, Ito, and coworkers.[30] The coupling of 1,7-diynes with a variety of silanes proceeds cleanly to produce six-membered ring products with a *Z*-configured vinyl silane moiety, as illustrated by the production of **27** (Scheme 15). With mixed terminal/internal diyne substrates, the silyl unit was chemoselectively introduced at the terminal alkyne to give product **28**, and yields with tethered internal alkynes were poor. Cyclizations of unsymmetrical diynes with basic nitrogen atoms in the tether chain proceeded with modest regioselectivity to afford products **29a** and **29b** (71:29).

Both inter- and intramolecular couplings involving silylboranes provide a useful entry to interesting 1-silyl-4-boryl-1,3-dienes (Scheme 16).[31] Intermolecular couplings are moderately selective, with regioisomers **30a** and **30b** being produced in a 3:1 ratio in couplings of 1-hexyne. A small amount of product **31**, derived from silylboration of a single alkyne, was also obtained. Yields were best when a large excess (6 equiv) of alkyne was used. The corresponding intramolecular coupling of 1,7-octadiyne proceeded in 55% yield to generate product **32**. Attempts to effect intermolecular cross-dimerizations were modestly successful, and formation of the homodimeric products was difficult to suppress. Related "germaboration" couplings of 1-hexyne proceeded smoothly to generate dimeric products **33a** and **33b**, whereas



Scheme 15. Intramolecular coupling of 1,7-diynes with silanes.

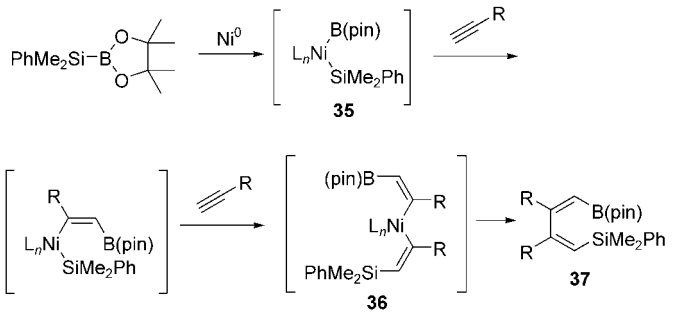


Scheme 16. Inter and intramolecular coupling of alkynes with silylboranes. pin = pinacolyl.

 © 2004 Wiley-VCH Verlag GmbH & Co. KGaA, Weinheim

Pd and Pt catalysts produced substantial amounts of the simple germaborated product **34.**

The authors proposed mechanisms that involve initial oxidative addition of the Si–H, Si–B, or Ge–B bond to nickel(0) to afford intermediates such as **35** (Scheme 17).[31]

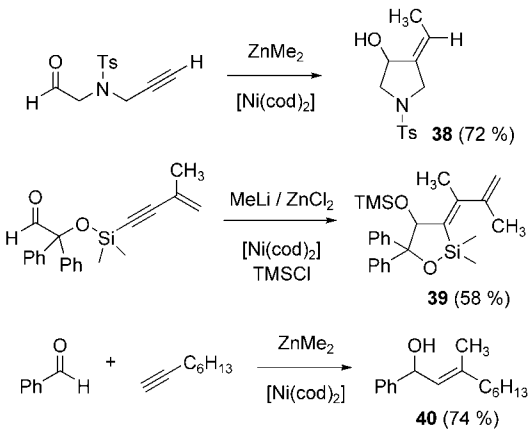


Scheme 17. Proposed mechanism for the intermolecular coupling of alkynes with silylboranes.

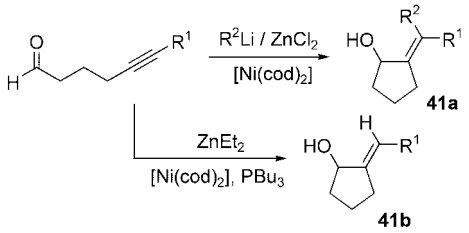
Several different options were considered for the timing of the following insertions, but the proposal for the intermolecular silylborative couplings is representative. An initial insertion of one alkyne into the Ni–B bond and the second alkyne into the Ni–Si bond of **35** would afford the divinyl nickel species **36**. Direct reductive elimination of this species would afford the observed product **37**. The analogous mechanism that involves insertion of the second alkyne into the initially formed vinyl nickel species is deemed unlikely in intermolecular couplings on the basis of regiochemical considerations. The authors also argue against the potential involvement of metallacycles since there is little precedent for the cleavage of a nickel metallacyclopentadiene with silanes or silylboranes. (Most metallacycle-based mechanistic proposals described herein involve metallacycles that bear a ligand activated for displacement, such as an alkoxide or enolate, whereas the metallacyclopentadiene derived from nickel(0) and two alkynes would likely have a much higher activation barrier towards cleavage by a reducing agent.)

4.4. Coupling of Carbonyl Compounds or Imines with Alkynes

The coupling of aldehydes with alkynes has been extensively developed in both reductive and alkylative processes in our laboratory. Couplings of this type provide access to structurally diverse and synthetically useful allylic alcohols. Alkylative couplings with organozinc reagents were established as both intra- (e.g., **38** and **39**) and intermolecular (e.g., **40**) processes (Scheme 18).[32] In a similar fashion to that described with enone/alkyne cyclizations, a strong ligand dependence was noted (Scheme 19): $[Ni(cod)_2]$ alone catalyzes alkylative cyclizations effectively with a variety of organozinc reagents to give product **41a**, and $[Ni(cod)_2]/PBu_3$ catalyzes reductive cyclizations with diethylzinc to give product **41b**.

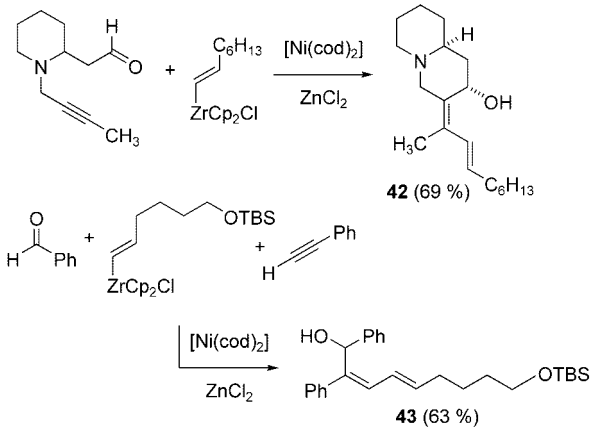


Scheme 18. Intra and intermolecular alkylative alkyne–aldehyde couplings. TMS = trimethylsilyl, Ts = *p*-toluenesulfonyl.



Scheme 19. Ligand dependence of the intramolecular alkylative alkyne–aldehyde coupling.

Although alkylative cyclizations could be accessed with a variety of organozinc reagents, undesired 1,2-addition to the aldehyde is problematic with alkenyl zinc reagents. To avoid this limitation and to expand the scope of readily available alkenyl units, we examined the addition of alkenyl zirconium reagents in both intra- (e.g., **42**) and intermolecular (e.g., **43**) additions (Scheme 20).[15] Both processes proceed efficiently and avoid many of the limitations derived from the high reactivity of alkenyl zinc reagents. However, a surprising observation in the intermolecular couplings is that a regio-

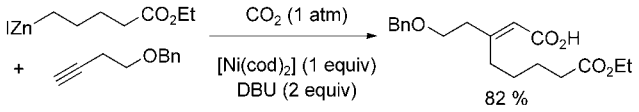


Scheme 20. Intra and intermolecular addition of alkenyl zirconium complexes to aldehydes and alkynes.

 © 2004 Wiley-VCH Verlag GmbH & Co. KGaA, Weinheim

chemical reversal of the mode of terminal alkyne insertion occurs with alkenyl zirconium reagents compared with our earlier observations with alkyl zinc reagents.

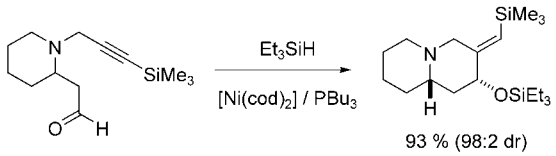
Recent developments from Mori and co-workers illustrated that couplings employing CO_2 instead of an aldehyde directly provide trisubstituted acrylic acid derivatives (Scheme 21).[33] Although couplings involving CO_2 were



Scheme 21. Reductive coupling of alkynes and organozinc reagents with CO_2. DBU = 1,8-diazabicyclo[5.4.0]undec-7-ene.

restricted to the stoichiometric use of $[Ni(cod)_2]$, functionalized organozinc reagents derived from active zinc insertion to alkyl and aryl halides were efficient participants in the process.

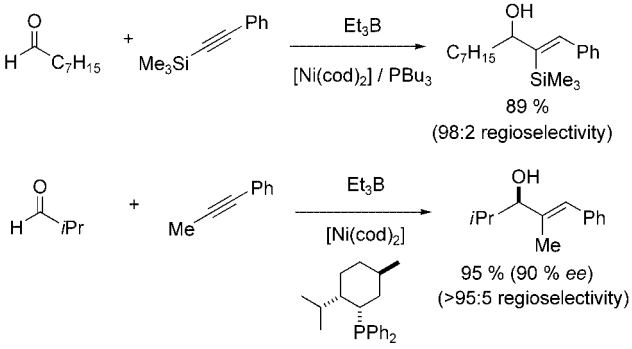
Although simple reductive cyclizations of aldehydes and alkynes were effective with diethylzinc, we noted two problems with more complex substrates. First, selectivity between hydrogen-atom and ethyl-group incorporation eroded with substrate complexity. Second, as the cyclizations become more demanding, direct 1,2-addition of diethylzinc to the aldehyde became a significant problem. To avoid these complexities, a very efficient procedure employing triethylsilane as the reducing agent and tributylphosphane as ligand was developed (Scheme 22).[34] These simple changes avoid



Scheme 22. Reductive intramolecular coupling of alkynes and carbonyl groups with triethylsilane as the reducing agent and tributylphosphane as ligand.

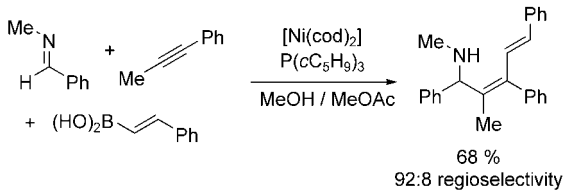
the need for selectivity for H vs. ethyl incorporation, as a hydrogen atom is directly transferred, and undesired aldehyde reduction does not occur. The scope of reductive cyclizations that proceed under this set of conditions is very broad, and the process has been used in several applications in complex molecule synthesis (Section 5.4).

Despite the efficiency of a broad range of cyclizations that proceed with $[Ni(cod)_2]/PBu_3/Et_3SiH$, the corresponding intermolecular process is not effective under these conditions. Jamison, however, found that using the same catalyst/ligand combination, but changing the reducing agent to Et_3B, allows the intermolecular process to proceed efficiently (Scheme 23).[35] A range of intermolecular couplings was thus developed, and couplings of enynes were recently found to be particularly regioselective.[32d,35d] Additionally, a very attractive asymmetric variant employing a menthyl-based monodentate phosphane proceeded with excellent enantioselectivities.[36]



Scheme 23. Top: reductive coupling of alkynes to aldehydes with Et_3B as the reducing agent and tributylphosphane as ligand; bottom: asymmetric variant with a menthylphosphane derivative as ligand.

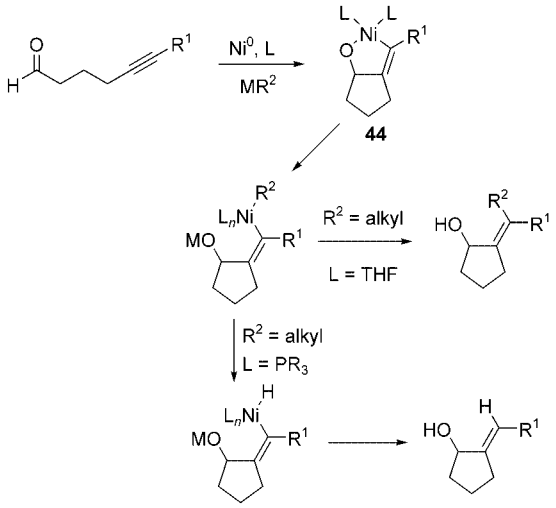
The corresponding alkylative intermolecular couplings of imines and alkynes was also developed by Jamison and Patel (Scheme 24).[37] Interestingly, a similar set of conditions that



Scheme 24. Alkylative intermolecular coupling of imines with alkynes and alkenyl boronic acids.

led to reductive couplings with aldehydes predominantly led to the alkylative manifold with imines, although methanol is a required cosolvent in imine couplings. Aryl and alkenyl boronic acids were used to prepare a broad range of 1,3 dienes and styrene derivatives.

The fundamental mechanistic theme that we originally suggested for this set of transformations involves oxidative coupling of an alkyne and aldehyde with nickel(0) to afford oxametallacycle **44**, followed by a transmetallation/reductive elimination sequence (Scheme 25).[32a] The initial oxidative cyclization is clearly promoted by the reducing agent. The structures of the ligand, substrate, and reducing agent all play a role in controlling the β-hydride elimination/reductive elimination selectivity. Subsequent reports by our group and others on related processes suggested the same fundamental mechanism or similar variations. A number of issues have not been explained, including the regiochemical reversal of alkyne insertions with organozinc reagents versus alkenyl zirconium reagents, and the crossover from reductive to alkylative manifolds based on subtle changes in substrate structure, reducing agent, or reaction conditions. In addition to the oxidative cyclization mechanism depicted (Scheme 25), hydrometallation or silylation mechanisms may be operative in some instances. Indeed, it is very likely that the different variants of aldehyde/alkyne couplings proceed by different mechanisms. In recent developments from our group, a crossover deuterium-labeling study unambiguously demonstrated that two fundamentally different mechanisms are

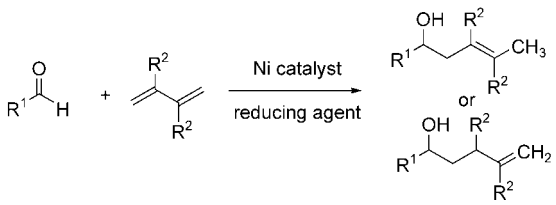


Scheme 25. Proposed mechanism for alkyne–aldehyde coupling with a nickel(0) complex.

operative in reductive couplings of aldehydes and alkynes involving triethylsilane, and that the change in mechanism is ligand-dependent. This insight is likely applicable to other related processes described in this Review.[32d]

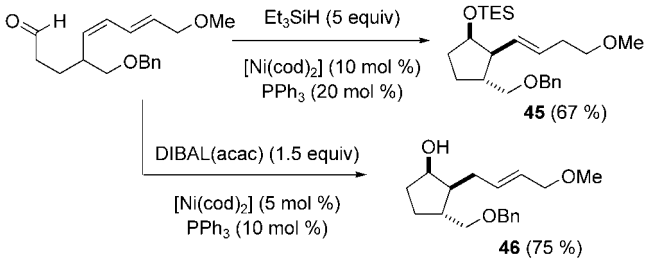
4.5. Couplings of Carbonyls with Dienes

The reductive coupling of aldehydes with 1,3-dienes, largely developed by Mori and co-workers and by Tamaru, Kimura, and co-workers has been one of the most thoroughly developed reaction classes covered within this Review. Reactions of this type may proceed in either the 1,4 or 1,2 sense to afford either homoallylic or bis-homoallylic alcohols (Scheme 26). A variety of reducing agents have been employed, with triethylsilane, triethylborane, diethylzinc, or DIBAL(acac) being most common.



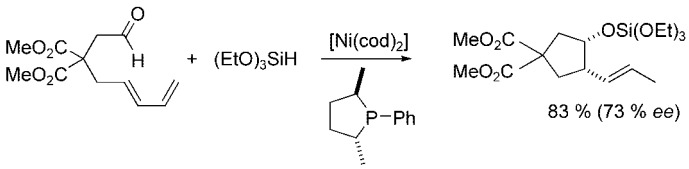
Scheme 26. Reductive coupling of aldehydes with 1,3-dienes.

Catalytic intramolecular variants developed by Mori and co-workers employ either triethylsilane or DIBAL(acac) as the reducing agent, although earlier examples employed stoichiometric quantities of $[Ni(acac)_2]$ and DIBAL-H.[12,38] Alternatively, cyclizations developed by Tamaru and co-workers involved either diethylzinc or triethylborane as the reducing agent.[39] In the studies by Mori and co-workers, the selectivity for formation of homoallylic alcohols **45** or bis-homoallylic alcohols **46** completely switches between experiments that employ triethylsilane and DIBAL(acac) as the reducing agent (Scheme 27). A broad range of cyclizations



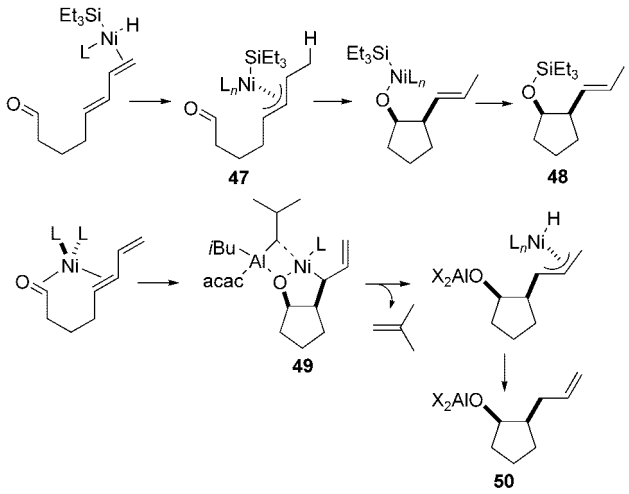
Scheme 27. Selective intramolecular coupling of aldehydes with 1,3-dienes: The selectivity of the reaction depends on the reducing agent.

was demonstrated, and related couplings involving $Me_3SiSnBu_3$ were reported.[40] Further applications of these processes in complex synthetic applications are described in Sections 5.4 and 5.5. An attractive asymmetric version was developed with a chiral monodentate phosphane ligand (Scheme 28).[41]



Scheme 28. Asymmetric variant of the intramolecular coupling of aldehydes with 1,3-dienes.

A proposal was advanced by Mori and co-workers that two mechanisms are operative in reductive cyclizations of diene aldehydes to produce internal and terminal alkene isomers **48** and **50** (Scheme 29).[12] With triethylsilane as reducing agent, the reaction is initiated by oxidative addition of nickel(0) to the silane. Hydrometallation of the diene gives π-allyl intermediate **47**, and subsequent carbonyl insertion and O–Si reductive elimination affords internal alkene **48**. Alternatively, with DIBAL(acac) as the reducing agent, oxidative cyclization to metallacycle **49** is followed by a

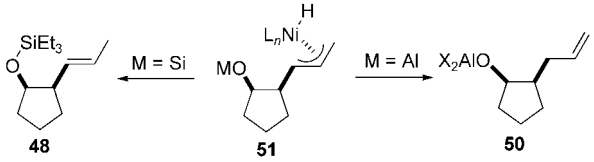


Scheme 29. Different mechanisms for the reductive cyclization of diene aldehydes lead to internal or terminal alkenes.

 © 2004 Wiley-VCH Verlag GmbH & Co. KGaA, Weinheim

transmetallation/reductive elimination sequence to afford terminal alkene product **50**.

It was proposed that the metallacycle mechanism was probably not operative in the formation of internal alkene product **48**, largely on the basis that treatment of a diene/aldehyde substrate with stoichiometric amounts of $[Ni(cod)_2]$ did not generate substantial quantities of cyclized product. However, the catalytic generation of a reactive equilibrium quantity of a metallacycle or the promotion of metallacycle formation by the reducing agent (triethylsilane) are both fully consistent with this observation. Given that ligand substitutions and other modifications of reaction conditions are known to alter regioselectivities substantially in reductive eliminations of metal–allyl complexes,[42] a unified mechanism involving reductive elimination from either allyl terminus of π-allyl **51** (derived from metallacycle **49**) is an alternative that should be considered (Scheme 30). However, in the studies of

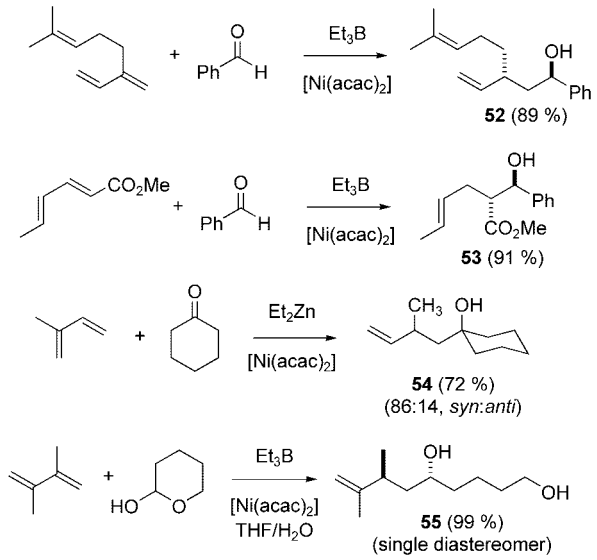


Scheme 30. Proposed mechanism for the reductive elimination through a common intermediate.

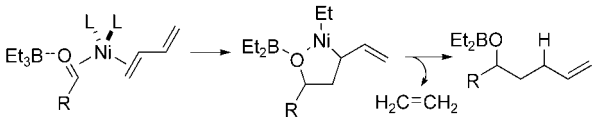
asymmetric catalysis described above (Scheme 28), the internal and terminal alkene isomers of an asymmetric dienal cyclization were obtained with different *ee* values, thus providing evidence that a common intermediate after the enantioselectivity-determining step is likely not involved. Additional mechanisms analogous to those recently proposed in ynal cyclizations are also possible.[32d]

Tamaru, Kimura and co-workers developed the intermolecular version of this process through the use of triethylborane and diethylzinc as reducing agents (Scheme 31).[43] The scope of both variants is broad, and of particular interest is that triethylborane-mediated couplings work best for couplings of aromatic and unsaturated aldehydes, as demonstrated in the production of **52** and **53**, whereas diethylzinc-promoted couplings work best for aliphatic aldehydes and ketones, as shown by the synthesis of **54**. These studies provided the first clear illustration of the complementary behavior of these two reducing agents. The process works very nicely for solving problems in 1,2- and 1,3-acyclic stereocontrol, as the examples illustrate. Remarkably, the process was illustrated to be effective in water and alcohols, thus allowing aqueous solutions of glutaraldehyde and cyclic hemiacetals to participate in the couplings, as illustrated by the production of **55** (Scheme 31).[44] The mechanism proposed for this class of reactions involves metallacycle formation and transmetallation of Et_3B, followed by a β-hydride elimination/reductive elimination sequence (Scheme 32). Related intermolecular procedures were developed by Mori and co-workers[45] and Loh et al.[46]

The corresponding alkylative cyclizations and couplings of carbonyls and dienes have been less well-developed

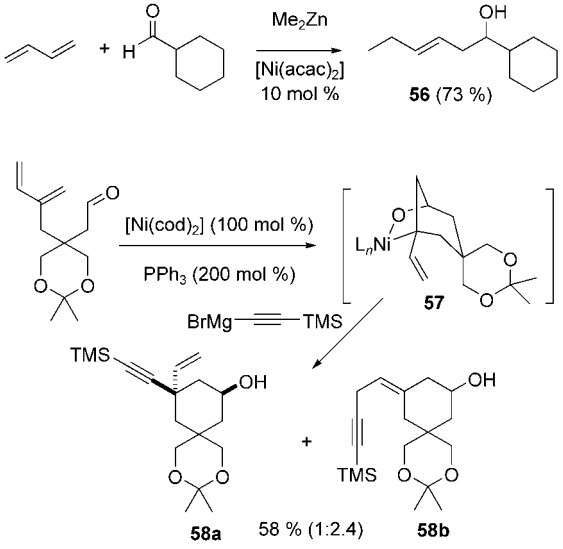


Scheme 31. Intermolecular diene–aldehyde coupling with triethylborane or diethylzinc.



Scheme 32. Proposed mechanism for the intermolecular diene–aldehyde coupling with triethylborane.

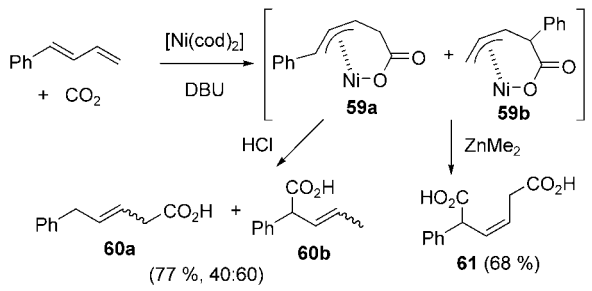
(Scheme 33).[47,48] Several transmetallating agents that lack β-hydrogen atoms (e.g., dimethylzinc and diphenylzinc) are effective participants in catalytic reactions, as demonstrated in the production of **56**, and Grignard reagents are participants in stoichiometric reactions in which metallacycle **57** is preformed prior to the introduction of the reducing agent, as illustrated in the formation of **58a** and **58b**.



Scheme 33. Examples of alkylative cyclizations and coupling reactions of carbonyl compounds with dienes.

 © 2004 Wiley-VCH Verlag GmbH & Co. KGaA, Weinheim

Surprisingly, attempts by Mori and co-workers to develop the analogous stoichiometric procedure with CO_2 in place of the aldehyde component led to the discovery of a double carboxylation of dienes (Scheme 34).[49] Treatment of a diene

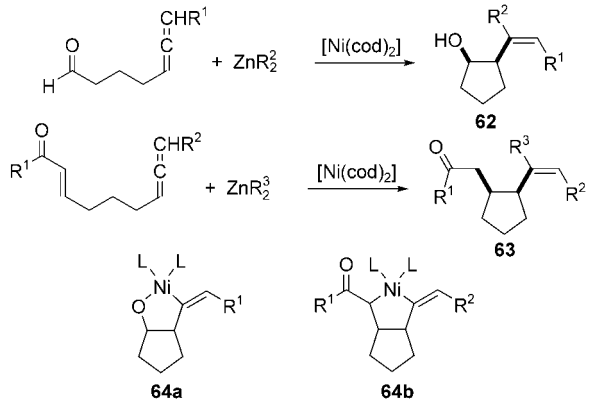


Scheme 34. Diene–CO_2 coupling with double carboxylation.

and CO_2 in the presence of $[Ni(cod)_2]$ and DBU afforded a solution of metallacycles **59a** and **59b**, and the subsequent addition of acid affords carboxylic acids **60a** and **60b**. However, treatment of **59a** and **59b** with dimethylzinc led to the incorporation of a second equivalent of CO_2 to afford product **61**. Although the mechanism of this latter process is unclear, it was shown that the 2 equivalents of CO_2 add in an *anti* sense across cyclic dienes.

4.6. Coupling of Alkenes or Carbonyl Compounds with Allenes

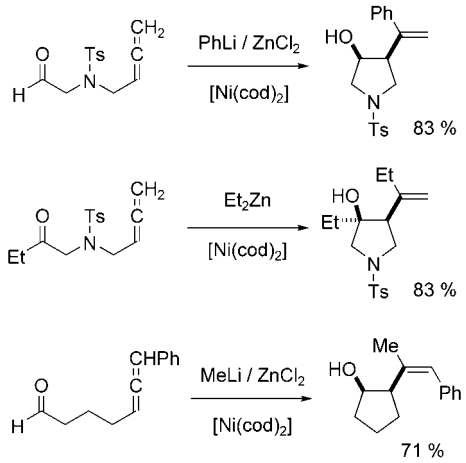
Alkylative coupling reactions of allenes with either aldehydes or electron-deficient alkenes have been developed as an approach to prepare homoallylic alcohols **62** and δ,ε-unsaturated carbonyl compounds **63** (Scheme 35). A metallacycle-based mechanism involving intermediates **64a** and **64b** was proposed for these processes in direct analogy to the proposals made in the corresponding enone/alkyne and aldehyde/alkyne couplings (Sections 4.1 and 4.4). These processes were first reported by our group in the total syntheses of kainic acid (Section 5.1)[50] and testudinariol A (Section 5.6),[51] and more extensive methodology studies of



Scheme 35. Syntheses of homoallylic alcohols and δ,ε-unsaturated carbonyl compounds through alkylative coupling of allenes with aldehydes or alkenes.

the allene/aldehyde cyclization process were concurrently developed by Kang and Yoon[52] and by us.[53]

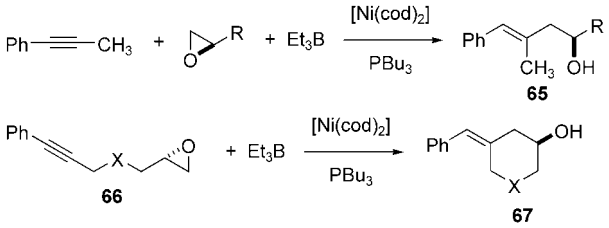
It was demonstrated that both aldehydes and ketones participate in the cyclization process as do monosubstituted and 1,3-disubstituted allenes (Scheme 36). In most cases, the substituted cyclopentane rings were formed with high *cis* selectivities, and good selectivities in favor of the *Z* alkene were typically observed.



Scheme 36. Cyclization through coupling of aldehydes and ketones with monosubstituted and 1,3-disubstituted allene groups

4.7. Coupling of Aldehydes with Epoxides

A very recent development by Jamison and Molinaro was the inter- and intramolecular reductive coupling of epoxides and alkynes with triethylborane as the reducing agent (Scheme 37).[54] Intermolecular coupling, as illustrated by



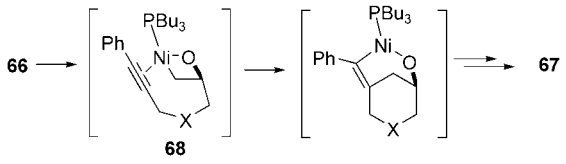
Scheme 37. Examples of alkyne–epoxide coupling reactions

the production of **65**, is effective with internal alkynes, with most examples involving aryl alkynes or enynes. A variety of cyclizations to form five- and six-membered rings were observed. All examples involved monosubstituted epoxides, and addition always occurred at the unsubstituted epoxide position (e.g., →**67**).

The regioselectivity of the addition to the unsubstituted position of the epoxide in intramolecular versions has interesting mechanistic implications, as a metallacycle-based mechanism would likely require addition at the substituted position. The mechanism thus likely falls within the classification involving oxidative addition to one of the reaction

 © 2004 Wiley-VCH Verlag GmbH & Co. KGaA, Weinheim

components. As suggested by Jamison and Molinaro, direct oxidative addition to the epoxide would afford a four-membered oxametallacycle **68** (Scheme 38). Alkyne insertion, followed by reduction of the C–Ni bond by ethyl transfer from boron to nickel, and then a β-hydride elimination/reductive elimination sequence would afford the observed product **67**. The formulation of a mechanism that differs from that of most processes covered in this Review is reasonable because the epoxide opening involves the cleavage of a single bond during the catalytic process, unlike the other reactions covered herein.



Scheme 38. Proposed mechanism for the alkyne–epoxide coupling.

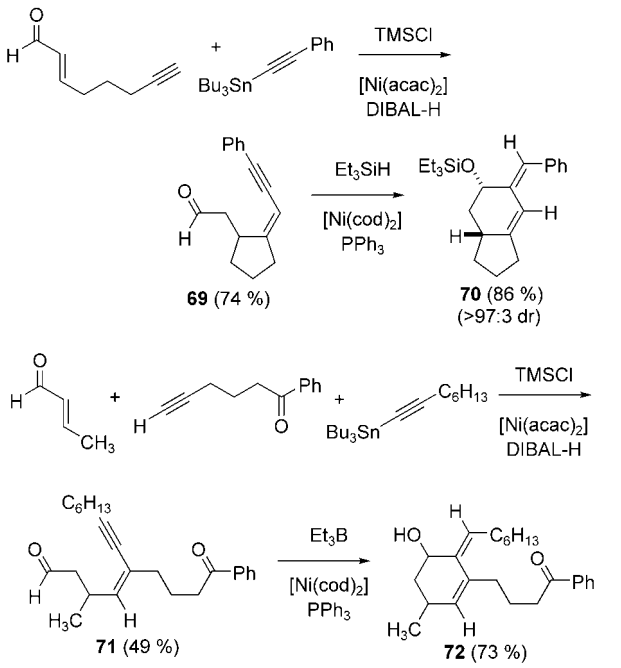
4.8. Combinations and Domino Reactions

Whereas the previous sections largely focused on three-component couplings involving two π systems and a main-group organometallic reagent or metal hydride, several processes have been developed that involve four or more components through combinations of the previously reported methods.

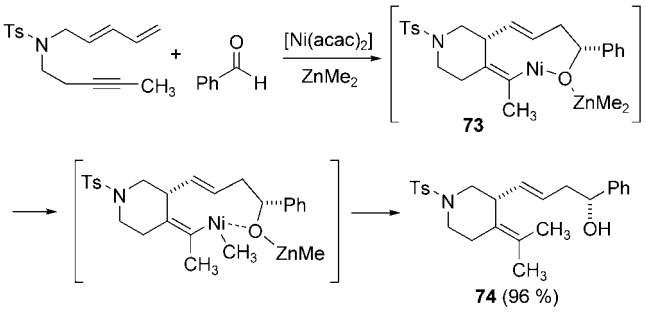
In one example, our group recognized that strong similarities exist between the ynal cyclizations and alkynyl enone cyclizations developed in our laboratories.[55] Thus, we examined the reactivity of enals with the idea that both the C=C and C=O bonds could participate in sequential couplings or cyclizations (Scheme 39). Coupling of an enal with an alkyne and acetylenic stannane affords conjugated enynes such as **69** and **71** with a tethered aldehyde, with the observed reaction taking place by addition to the C=C bond of the enal. Further treatment of the initial products **69** and **71** under similar conditions then results in cyclization of the aldehyde and alkyne units to afford products such as **70** and **72**. In the second coupling event, organozinc reagents lead exclusively to the introduction of carbon substituents, whereas triethylborane leads exclusively to the introduction of a hydrogen atom. Fully intermolecular four-component couplings and partially intramolecular variants are possible.

Tamaru and co-workers developed a one-pot combination sequence involving a 1,3-diene, an alkyne, an organozinc reagent, and an aldehyde (Scheme 40).[56] Impressive chemoselectivity is illustrated in this process, which allows the rapid assembly of complex structures such as **74**. It was proposed that the diene, alkyne, and aldehyde form metallacycle **73** prior to the transmetallation event.

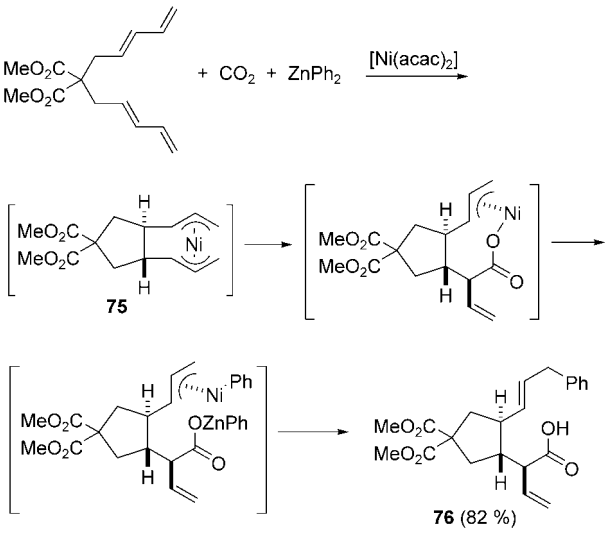
Mori and Takimoto developed a different four-component coupling of two 1,3-dienes, CO_2, and an organozinc reagent (Scheme 41).[57] The catalytic process allows densely functionalized ring systems such as **76** to be assembled in a



Scheme 39. Sequential coupling and cyclization of an alkynyl enal with an acetylenic stannane.



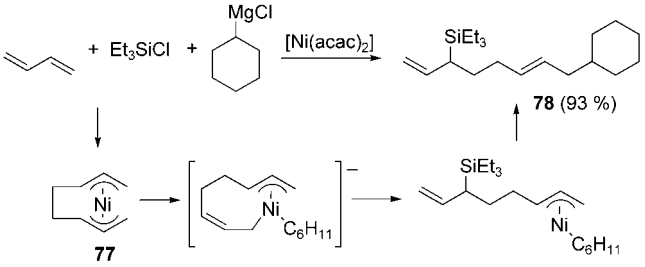
Scheme 40. Chemoselective one-pot synthesis of **74**.



Scheme 41. Example of a four-component reaction for the preparation of highly functionalized rings.

 © 2004 Wiley-VCH Verlag GmbH & Co. KGaA, Weinheim

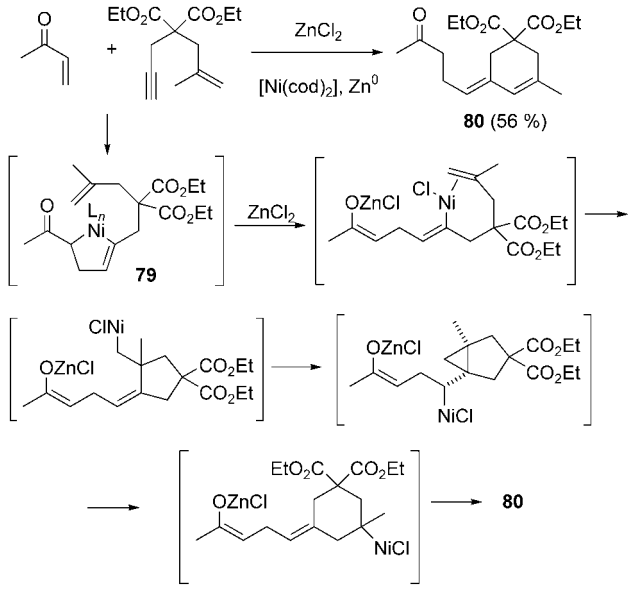
straightforward fashion from simple precursors. A very recent report describes asymmetric variants of this process.[57b] A related multicomponent coupling of two dienes, a silyl chloride, and a Grignard reagent was developed by Kambe and co-workers to afford products such as **78** (Scheme 42).[58]



Scheme 42. Example of a multicomponent coupling reaction with a Grignard reagent.

The mechanism of these processes likely involves the formation of metallacycle **75** or **77** by oxidative cyclization of two dienes, followed by alkylation and transmetallation/reductive-elimination steps. Kambe and co-workers demonstrated that transmetallation likely precedes alkylation.

Ikeda et al. also developed a multicomponent coupling that involves an enone, an alkyne, an alkene, $ZnCl_2$, and Zn dust as the reducing agent (Scheme 43).[59] This interesting



Scheme 43. Proposed mechanism for the multicomponent coupling reaction to form **80**.

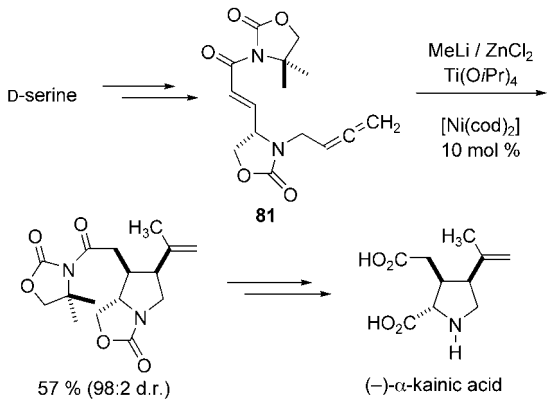
process was proposed to involve the formation of metallacycle **79**, followed by $ZnCl_2$-mediated metallacycle cleavage, 5-*exo* and 3-*exo* cyclization, β-C–C cleavage, and β-hydride elimination to afford product **80**. The latter portion of this mechanism explains the stereochemistry reversal that would have occurred if the process proceeded by a simpler 6-*endo* pathway. A similar effect was elucidated by Negishi and co-workers in apparent 6-*endo* Heck cyclizations.[60]

5. Applications in the Synthesis of Complex Molecules

As many of the methods described above constitute very recent developments, application of these methods in the synthesis of complex molecules are just beginning to appear. In several examples below, the Ni-catalyzed process is critical to the complete synthetic plan. The overall synthetic plans will only be described briefly, and the discussion that follows will focus on how a key nickel-catalyzed step is critical in the assembly of important structural features of the target molecules. Additionally, the reader is directed to the important advances that appeared since submission of this Review.[35b,c]

5.1. Kainoid Amino Acids

The kainoid amino acids comprise a large class of natural products ranging from the simplest members, kainic acid and allokainic acid, up to more complex members such as isodomoic acid G (Schemes 44–46). Through the use of

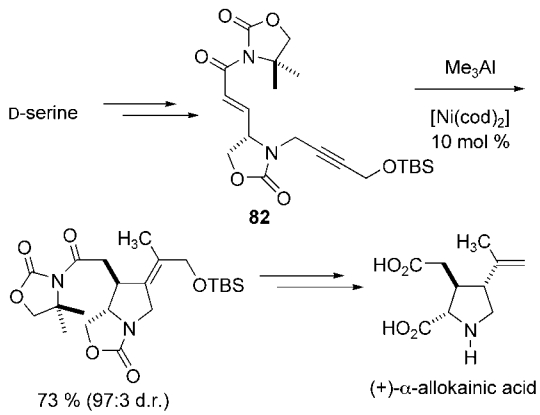


Scheme 44. Key step in the total synthesis of kainic acid.

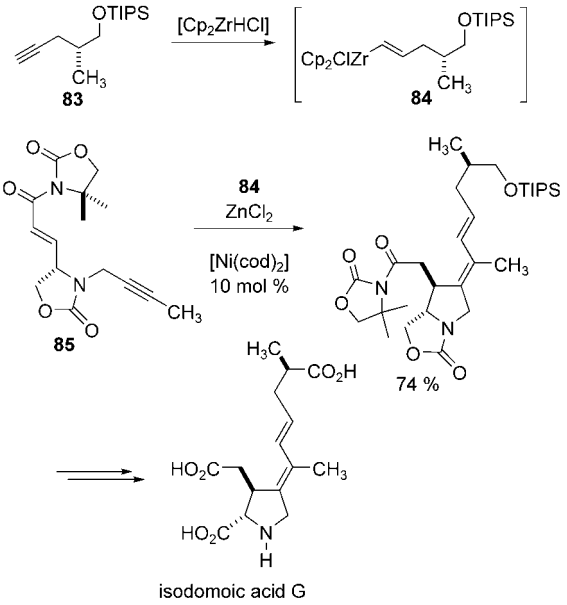
nickel-catalyzed unsaturated imide/alkyne and unsaturated imide/allene cyclizations, our group recently completed the total syntheses of each of these three natural products. Kainic acid was prepared by the nickel-catalyzed cyclization of allene **81** with dimethylzinc (Scheme 44).[50] This key cyclization directly assembled the pyrrolidine nucleus and set the relative stereochemistry about the five-membered ring. The epimeric structure allokainic acid was prepared by the nickel-catalyzed cyclization of alkyne **82** with dimethylzinc, followed by a Tsuji rearrangement to install the C4 stereocenter (Scheme 45).[14] This complementary sequence allows allene cyclizations and alkyne cyclizations to provide a stereodivergent strategy for the preparation of these two epimeric natural products.

Isodomoic acid G contains an exocyclic alkene at C4 which is more structurally complex than the corresponding

 © 2004 Wiley-VCH Verlag GmbH & Co. KGaA, Weinheim



Scheme 45. Key step in the total synthesis of allokainic acid.

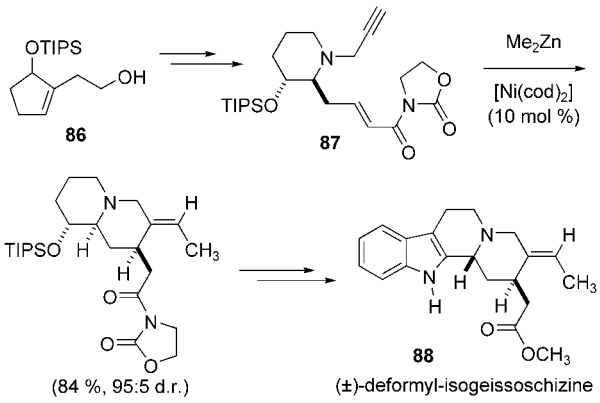


Scheme 46. Key step in the total synthesis of isodomoic acid G. TIPS = triisopropylsilyl.

side chain of kainic and allokainic acids (Scheme 46). The nickel-catalyzed cyclization of alkyne **85** with the vinyl zirconium reagent **84** derived from alkyne **83** was used to prepare directly the isodomoic acid G core structure.[61] Notably, the pyrrolidine unit, the C2/C3 relative stereochemistry, and the complete densely functionalized 1,3-diene were assembled in a single operation in a completely selective fashion to allow an efficient total synthesis of this natural product.

5.2. Indole Alkaloids

Geissoschizine, which has been isolated from a variety of plant species, is an important biosynthetic precursor to a large number of polycyclic indole alkaloids. Through the use of a nickel-catalyzed unsaturated imide/alkyne cyclization, our group recently prepared the isogeissoschizoid skeleton (Scheme 47).[62] Cyclization of substrate **87**, which was

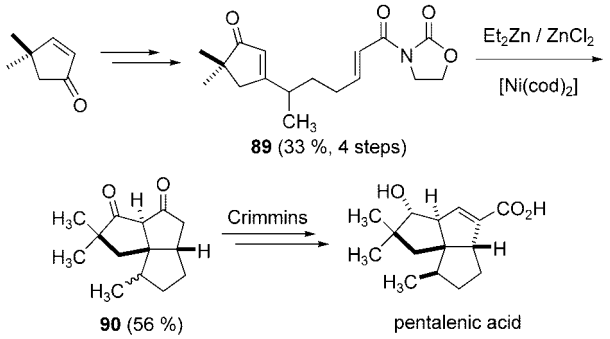


Scheme 47. Construction of the framework of isogeissoschizine.

prepared by ozonolysis and double reductive amination of cyclopentene precursor **86**, was cleanly effected in 84 % yield with dimethylzinc and $[Ni(cod)_2]$ (10 mol %). A sequence involving a Fischer indole synthesis proceeded with epimerization to allow the preparation of the isogeissoschizine framework **88**. This sequence allowed the construction of the alkaloid D-ring and the installation of the exocyclic ethylidene in a single step.

5.3. Pentalenene Triquinanes

The angularly-fused triquinane unit is a common structural motif in a variety of naturally occurring terpenes, including pentalenene, pentalenic acid, and deoxypentalenic acid. Through the use of a nickel-catalyzed bis-enone cyclization, our group prepared a triquinane structure by sequential reductive cyclization and Dieckmann condensation (Scheme 48).[63] 1,2-Addition of an alkyllithium to



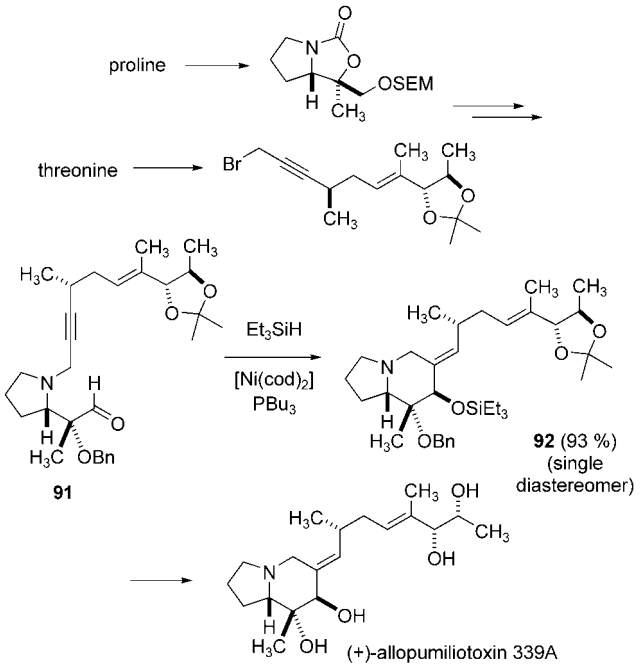
Scheme 48. Triquinane synthesis through nickel-catalyzed bis-enone cyclization.

dimethylcyclopentenone, followed by oxidative transposition with pyridinium chlorochromate allowed efficient preparation of cyclization substrate **89**. Treatment of **89** with $ZnEt_2$/$ZnCl_2$ and $[Ni(cod)_2]$ (10 mol %) afforded triquinane **90** in 56 % yield as a mixture of epimers. Compound **90**, which was thus prepared in only five steps from dimethylcyclopentenone, had previously been converted into each of the triquinane natural products noted above.[64]

 © 2004 Wiley-VCH Verlag GmbH & Co. KGaA, Weinheim

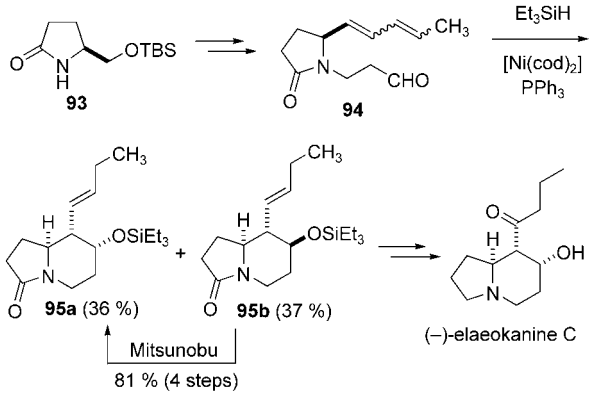
5.4. Indolizidine Alkaloids

The indolizidine skeleton is present in a diverse range of alkaloids. Through the use of a nickel-catalyzed ynal cyclization, our group completed the total syntheses of three members of the pumiliotoxin family.[34] In a representative example, (+)-allopumiliotoxin 339A was prepared from structurally complex ynal **91**, which was assembled from proline and threonine (Scheme 49). Cyclization of ynal **91**



Scheme 49. Total synthesis of (+)-allopumiliotoxin 339A. SEM = trimethylsilylethoxymethyl.

with triethylsilane and a catalytic quantity of $[Ni(cod)_2]/PBu_3$ proceeded in a remarkably efficient manner, furnishing bicycle **92** as a single diastereomer in 93%. This single step assembles the six-membered ring of the indolizidine core, controls the relative stereochemistry adjacent to a quaternary center, and assembles the alkylidene unit, with each of these features being controlled in a completely selective manner. Simple deprotection of the nickel-mediated cyclization product allowed completion of the synthesis.

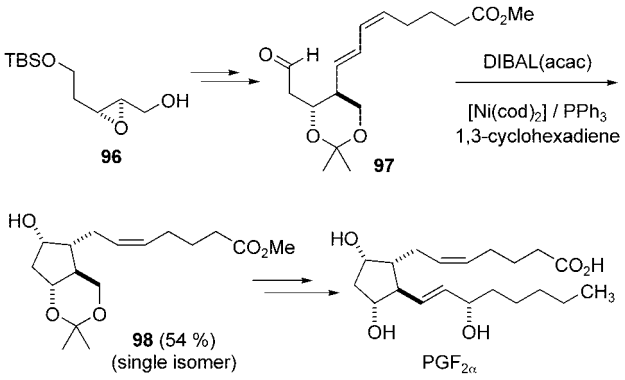


Scheme 50. Total synthesis of (−)-elaeokanine C through nickel-catalyzed aldehyde–diene cyclization.

The indolizidine alkaloid (−)-elaeokanine C was prepared by Mori and co-workers through a nickel-catalyzed aldehyde–diene cyclization (Scheme 50).[65] Cyclization precursor **94**, which was prepared from compound **93**, was treated with triethylsilane and catalytic quantities of $[Ni(cod)_2]/PPh_3$. Although a nearly 1:1 ratio of diastereomers was obtained, the undesired isomer **95b** was recycled by a Mitsunobu reaction to **95a**, which was then converted into an advanced intermediate, thus completing the formal synthesis of elaeokanine C.

5.5. Prostaglandins

The prostaglandins comprise a very large class of natural products with diverse biological activities. Through the use of a nickel-catalyzed aldehyde/diene cyclization, Mori and co-workers synthesized a representative member of this class of natural products, prostaglandin $F_{2\alpha}$ (Scheme 51).[66] Substrate



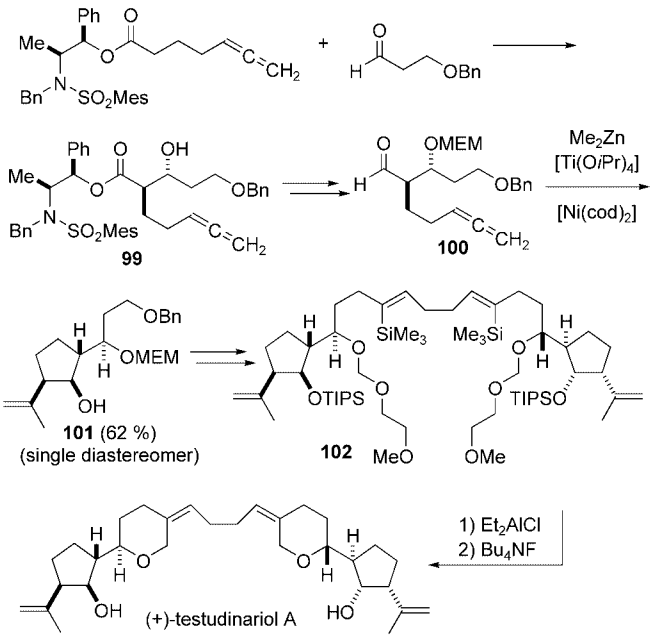
Scheme 51. Total synthesis of prostaglandin $F_{2\alpha}$ (PGF2) through aldehyde–diene cyclization.

97 was efficiently prepared by a sequence involving the addition of vinylmagnesium bromide to enantioenriched epoxide **96**. Treatment of **97** with DIBAL(acac), catalytic $[Ni(cod)_2]/PPh_3$, and 1,3-cyclohexadiene (as a critical additive to control the position and stereochemistry of the desired *Z* alkene) resulted in the selective formation of product **98**, with complete control of the contiguous stereocenters and alkene stereochemistry. Compound **98** was then converted into prostaglandin $F_{2\alpha}$ in a straightforward fashion to complete a very attractive synthesis of this natural product.

5.6. Testudinariol A

Testudinariol A is a member of a small family of C_2-symmetric natural products with an internal butylene core. Through the use of a nickel-catalyzed aldehyde/allene cyclization, our group recently completed an asymmetric total synthesis of this natural product (Scheme 52).[51] The

 © 2004 Wiley-VCH Verlag GmbH & Co. KGaA, Weinheim



Scheme 52. Asymmetric total synthesis of testudinariol A through nickel-catalyzed aldehyde–allene cyclization. Mes = 2,4,6-trimethylphenyl, MEM = methoxyethoxymethyl.

synthesis began with an Abiko–Masamune asymmetric *anti* aldol reaction to assemble compound **99**, which was converted into cyclization precursor **100**. Treatment of **100** with dimethylzinc and catalytic $[Ni(cod)_2]/PBu_3$, with $Ti(OiPr)_4$ as a coadditive, resulted in the selective production of **101** as a single diastereomer in 62% yield. Conversion of **101** into **102** followed by a two-directional oxocarbenium ion cyclization resulted in a very direct and efficient synthesis of (+)-testudinariol A. Notably, the nickel-catalyzed cyclization allowed the stereoselective introduction of four contiguous stereocenters and directly assembled the requisite functionality needed to complete the synthesis.

6. Summary and Outlook

Over the past decade, nickel-catalyzed reductive cyclizations and couplings have evolved into a broadly useful strategy for assembling synthetically versatile substructures as well as complex molecules. The three-component nature of the processes lends itself very well to the rapid generation of molecular complexity from simple π components and main-group organometallic reagents. Although many different classes of reaction components have been demonstrated to participate in the processes, new variants are rapidly being discovered, and that trend will likely continue for some time. Furthermore, useful asymmetric versions are just beginning to emerge. Many complex mechanistic questions surrounding these processes exist, and future work will likely clarify many of these questions. The complexity of problems that will be addressed by these methods, as well as the frequency with which these methods are utilized, will also undoubtedly continue to increase. Nickel maintains a unique place among the transition metals in terms of reactivity trends, functional-group tolerance, and catalytic activity. The reductive cyclizations and couplings described in this Review provide a clear illustration of this unique position.

I thank the National Institutes of Health, National Science Foundation, Petroleum Research Fund, Arthur C. Cope Foundation, Camille and Henry Dreyfus Foundation, Johnson and Johnson, Pfizer, and 3M Pharmaceuticals for support of our research in the area of developing nickel-catalyzed reactions.

Received: September 9, 2003 [A634]
Published Online: June 17, 2004

[1] a) G. Wilke, *Angew. Chem.* **1988**, *100*, 189; *Angew. Chem. Int. Ed. Engl.* **1988**, *27*, 185; b) P. W. Jolly, *Comprehensive Organometallic Chemistry, Vol. 8* (Ed.: G. Wilkinson), Pergamon, Oxford, **1982**, p. 615; c) "Organometallic Complexes of Nickel": J. Montgomery in *Science of Synthesis (Houben-Weyl Methods of Molecular Transformations), Vol. 1* (Eds.: B. M. Trost, M. Lautens), Thieme, Stuttgart, **2001**, p. 11.

[2] a) R. Benn, B. Büssemeier, S. Holle, P. W. Jolly, R. Mynott, I. Tkatchenko, G. Wilke, *J. Organomet. Chem.* **1985**, *279*, 63; b) W. Keim, *Angew. Chem.* **1990**, *102*, 251; *Angew. Chem. Int. Ed. Engl.* **1990**, *29*, 235; c) P. A. Wender, N. C. Ihle, *Tetrahedron Lett.* **1987**, *28*, 2451; d) P. A. Wender, M. L. Snapper, *Tetrahedron Lett.* **1987**, *28*, 2221; e) P. A. Wender, N. C. Ihle, C. R. D. Correia, *J. Am. Chem. Soc.* **1988**, *110*, 5904; f) P. A. Wender, M. J. Tebbe, *Synthesis* **1991**, 1089; g) P. A. Wender, J. M. Nuss, D. B. Smith, A. Suárez-Sobrino, J. Vagberg, D. Decosta, J. Bordner, *J. Org. Chem.* **1997**, *62*, 4908; h) P. A. Wender, N. C. Ihle, *J. Am. Chem. Soc.* **1986**, *108*, 4678.

[3] a) P. A. Wender, T. E. Jenkins, *J. Am. Chem. Soc.* **1989**, *111*, 6432; b) P. A. Wender, T. E. Smith, *J. Org. Chem.* **1995**, *60*, 2962; c) P. A. Wender, T. E. Jenkins, S. Suzuki, *J. Am. Chem. Soc.* **1995**, *117*, 1843; d) P. A. Wender, T. E. Smith, *J. Org. Chem.* **1996**, *61*, 824; e) P. A. Wender, T. E. Smith, *Tetrahedron* **1998**, *54*, 1255.

[4] a) M. Lautens, W. Klute, W. Tam, *Chem. Rev.* **1996**, *96*, 49; b) P. Bhatarah, E. H. Smith, *J. Chem. Soc. Perkin Trans. 1* **1992**, 2163; c) Y. Sato, T. Nishimata, M. Mori, *J. Org. Chem.* **1994**, *59*, 6133; d) S. Ikeda, H. Watanabe, Y. Sato, *J. Org. Chem.* **1998**, *63*, 7026; e) M. Shanmugasundaram, M. S. Wu, M. Jeganmohan, C.-W. Huang, C.-H. Cheng, *J. Org. Chem.* **2002**, *67*, 7724; f) J. Louie, J. E. Gibby, M. V. Farnworth, T. N. Tekavec, *J. Am. Chem. Soc.* **2002**, *124*, 15188.

[5] a) L. K. Johnson, C. M. Killian, M. Brookhart, *J. Am. Chem. Soc.* **1995**, *117*, 6414; b) C. M. Killian, D. J. Tempel, L. K. Johnson, M. Brookhart, *J. Am. Chem. Soc.* **1996**, *118*, 11664; c) C. M. Killian, L. K. Johnson, M. Brookhart, *Organometallics* **1997**, *16*, 2005; d) S. A. Svejda, M. Brookhart, *Organometallics* **1999**, *18*, 65.

[6] a) N. Nomura, J. Jin, H. Park, T. V. RajanBabu, *J. Am. Chem. Soc.* **1998**, *120*, 459; b) B. Radetich, T. V. RajanBabu, *J. Am. Chem. Soc.* **1998**, *120*, 8007.

[7] a) R. J. McKinney, W. A. Nugent, *Organometallics* **1989**, *8*, 2871; b) A. L. Casalnuovo, T. V. RajanBabu, T. A. Ayers, T. H. Warren, *J. Am. Chem. Soc.* **1994**, *116*, 9869; c) T. Horiuchi, E. Shirakawa, K. Nozaki, H. Takaya, *Tetrahedron: Asymmetry* **1997**, *8*, 57.

[8] a) Y. Kiso, M. Kumada, K. Tamao, M. Umeno, *J. Organomet. Chem.* **1973**, *50*, 297; b) M. Lautens, P. Chiu, S. Ma, T. Rovis, *J. Am. Chem. Soc.* **1995**, *117*, 532; c) M. Lautens, T. Rovis, *J. Am. Chem. Soc.* **1997**, *119*, 11090; d) M. Lautens, S. Ma, P. Chiu, *J. Am. Chem. Soc.* **1997**, *119*, 6478; e) S. Vettel, A. Vaupel, P.

 © 2004 Wiley-VCH Verlag GmbH & Co. KGaA, Weinheim

Knochel, *Tetrahedron Lett.* **1995**, *36*, 1023; f) S. Vettel, A. Vaupel, P. Knochel, *J. Org. Chem.* **1996**, *61*, 7473.

[9] For reviews of segments of this area, see: a) J. Montgomery, *Acc. Chem. Res.* **2000**, *33*, 467; b) J. Montgomery, K. K. D. Amarasinghe, S. K. Chowdhury, E. Oblinger, J. Seo, A. V. Savchenko, *Pure Appl. Chem.* **2002**, *74*, 129; c) S. Ikeda, *Acc. Chem. Res.* **2000**, *33*, 511; d) S. Ikeda, *Angew. Chem.* **2003**, *115*, 5276; *Angew. Chem. Int. Ed.* **2003**, *42*, 5120; e) K. M. Miller, C. Molinaro, T. F. Jamison, *Tetrahedron: Asymmetry* **2003**, *14*, 3619.

[10] a) F. M. Dayrit, D. E. Gladkowski, J. Schwartz, *J. Am. Chem. Soc.* **1980**, *102*, 3976; b) F. M. Dayrit, J. Schwartz, *J. Am. Chem. Soc.* **1981**, *103*, 4466; c) D. G. Morrell, J. K. Kochi, *J. Am. Chem. Soc.* **1975**, *97*, 7262; d) C. Amatore, A. Jutand, *Acta. Chem. Scand.* **1990**, *44*, 755.

[11] D. J. Krysan, P. B. Mackenzie, *J. Org. Chem.* **1990**, *55*, 4229.

[12] Y. Sato, M. Takimoto, M. Mori, *J. Am. Chem. Soc.* **2000**, *122*, 1624.

[13] a) J. Montgomery, A. V. Savchenko, *J. Am. Chem. Soc.* **1996**, *118*, 2099; b) J. Montgomery, E. Oblinger, A. V. Savchenko, *J. Am. Chem. Soc.* **1997**, *119*, 4911; c) J. Montgomery, M. V. Chevliakov, H. L. Brielmann, *Tetrahedron* **1997**, *53*, 16449.

[14] M. V. Chevliakov, J. Montgomery, *Angew. Chem.* **1998**, *110*, 3346; *Angew. Chem. Int. Ed.* **1998**, *37*, 3144.

[15] Y. Ni, K. K. D. Amarasinghe, J. Montgomery, *Org. Lett.* **2002**, *4*, 1743.

[16] a) S. Ikeda, Y. Sato, *J. Am. Chem. Soc.* **1994**, *116*, 5975; b) S. Ikeda, K. Kondo, Y. Sato, *J. Org. Chem.* **1996**, *61*, 8248.

[17] S. Ikeda, K. Kondo, Y. Sato, *Chem. Lett.* **1999**, 1227.

[18] a) S. Ikeda, H. Yamamoto, K. Kondo, Y. Sato, *Organometallics* **1995**, *14*, 5015; b) J. Montgomery, J. Seo, H. M. P. Chui, *Tetrahedron Lett.* **1996**, *37*, 6839.

[19] S. Ikeda, D.-M. Cui, Y. Sato, *J. Am. Chem. Soc.* **1999**, *121*, 4712.

[20] a) S. Ikeda, D.-M. Cui, Y. Sato, *J. Org. Chem.* **1994**, *59*, 6877; b) D.-M. Cui, T. Tsuzuki, K. Miyake, S. Ikeda, Y. Sato, *Tetrahedron* **1998**, *54*, 1063.

[21] S. Ikeda, H. Miyashita, Y. Sato, *Organometallics* **1998**, *17*, 4316.

[22] K. K. D. Amarasinghe, S. K. Chowdhury, M. J. Heeg, J. Montgomery, *Organometallics* **2001**, *20*, 370.

[23] a) G. M. Mahandru, A. R. L. Skauge, S. K. Chowdhury, K. K. D. Amarasinghe, M. J. Heeg, J. Montgomery, *J. Am. Chem. Soc.* **2003**, *125*, 13481; b) S. K. Chowdhury, K. K. D. Amarasinghe, M. J. Heeg, J. Montgomery, *J. Am. Chem. Soc.* **2000**, *122*, 6775.

[24] a) J. R. Johnson, P. S. Tully, P. B. Mackenzie, M. Sabat, *J. Am. Chem. Soc.* **1991**, *113*, 6172; b) B. A. Grisso, J. R. Johnson, P. B. Mackenzie, *J. Am. Chem. Soc.* **1992**, *114*, 5160.

[25] J. Montgomery, J. Seo, *Tetrahedron* **1998**, *54*, 1131.

[26] A. V. Savchenko, J. Montgomery, *J. Org. Chem.* **1996**, *61*, 1562.

[27] a) E. J. Enholm, K. S. Kinter, *J. Org. Chem.* **1995**, *60*, 4850; b) E. J. Enholm, K. S. Kinter, *J. Am. Chem. Soc.* **1991**, *113*, 7784; c) D. S. Hays, G. C. Fu, *J. Org. Chem.* **1996**, *61*, 4.

[28] D.-M. Cui, H. Yamamoto, S. Ikeda, K. Hatano, Y. Sato, *J. Org. Chem.* **1998**, *63*, 2782.

[29] a) M. F. Lappert, S. Takahashi, *J. Chem. Soc. Chem. Commun.* **1972**, 1272; b) M. F. Lappert, T. A. Nile, S. Takahashi, *J. Organomet. Chem.* **1974**, *72*, 425.

[30] a) K. Tamao, K. Kobayashi, Y. Ito, *J. Am. Chem. Soc.* **1989**, *111*, 6478; b) K. Tamao, K. Kobayashi, Y. Ito, *Synlett* **1992**, 539.

[31] M. Suginome, T. Matsuda, Y. Ito, *Organometallics* **1998**, *17*, 5233.

[32] a) E. Oblinger, J. Montgomery, *J. Am. Chem. Soc.* **1997**, *119*, 9065; b) M. Lozanov, J. Montgomery, *Tetrahedron Lett.* **2001**, *42*, 3259; c) X. Qi, J. Montgomery, *J. Org. Chem.* **1999**, *64*, 9310; d) G. M. Mahandru, G. Liu, J. Montgomery, *J. Am. Chem. Soc*, **2004**, *126*, 3698.

[33] a) M. Takimoto, K. Shimizu, M. Mori, *Org. Lett.* **2001**, *3*, 3345; b) K. Shimizu, M. Takimoto, M. Mori, *Org. Lett.* **2003**, *5*, 2323.

[34] a) X.-Q. Tang, J. Montgomery, *J. Am. Chem. Soc.* **1999**, *121*, 6098; b) X.-Q. Tang, J. Montgomery, *J. Am. Chem. Soc.* **2000**, *122*, 6950.

[35] a) W.-S. Huang, J. Chan, T. F. Jamison, *Org. Lett.* **2000**, *2*, 4221. New reports are frequently appearing in this very active field, and many developments have been published since submission of this Review. Of particular note, two reports in total synthesis from the Jamison group on the methods described in Sections 4.4 and 4.7 greatly expand the scope of the processes and demonstrate significant applications in complex molecule synthesis: b) J. Chan, T. F. Jamison, *J. Am. Chem. Soc.* **2003**, *125*, 11514; c) E. A. Colby, K. C. O'Brien, T. F. Jamison, *J. Am. Chem. Soc.* **2004**, *126*, 998; d) K. M. Miller, T. Luanphaisarnnont, C. Molinaro, T. F. Jamison, *J. Am. Chem. Soc.* **2004**, *126*, 4130.

[36] a) K. M. Miller, W.-S. Huang, T. F. Jamison, *J. Am. Chem. Soc.* **2003**, *125*, 3442; b) E. A. Colby, T. F. Jamison, *J. Org. Chem.* **2003**, *68*, 156.

[37] S. J. Patel, T. F. Jamison, *Angew. Chem.* **2003**, *115*, 1402; *Angew. Chem. Int. Ed.* **2003**, *42*, 1364.

[38] a) Y. Sato, M. Takimoto, K. Hayashi, T. Katsuhara, K. Takagi, M. Mori, *J. Am. Chem. Soc.* **1994**, *116*, 9771; b) Y. Sato, M. Takimoto, M. Mori, *Tetrahedron Lett.* **1996**, *37*, 887; c) Y. Sato, T. Takanashi, M. Hoshiba, M. Mori, *Tetrahedron Lett.* **1998**, *39*, 5579; d) Y. Sato, R. Sawaki, M. Mori, *Organometallics* **2001**, *20*, 5510.

[39] K. Shibata, M. Kimura, M. Shimizu, Y. Tamaru, *Org. Lett.* **2001**, *3*, 2181.

[40] Y. Sato, N. Saito, M. Mori, *Chem. Lett.* **2002**, 18.

[41] a) Y. Sato, N. Saito, M. Mori, *J. Am. Chem. Soc.* **2000**, *122*, 2371; b) Y. Sato, N. Saito, M. Mori, *J. Org. Chem.* **2002**, *67*, 9310.

[42] a) J. S. Temple, J. Schwartz, *J. Am. Chem. Soc.* **1980**, *102*, 7381; b) Y. Hayasi, M. Riediker, J. S. Temple, J. Schwartz, *Tetrahedron Lett.* **1981**, *22*, 2629; c) J. S. Temple, M. Riediker, J. Schwartz, *J. Am. Chem. Soc.* **1982**, *104*, 1310.

[43] a) M. Kimura, A. Ezoe, K. Shibata, Y. Tamaru, *J. Am. Chem. Soc.* **1998**, *120*, 4033; b) M. Kimura, H. Fujimatsu, A. Ezoe, K. Shibata, M. Shimizu, S. Matsumoto, Y. Tamaru, *Angew. Chem.* **1999**, *111*, 410; *Angew. Chem. Int. Ed.* **1999**, *38*, 397.

[44] M. Kimura, A. Ezoe, S. Tanaka, Y. Tamaru, *Angew. Chem.* **2001**, *113*, 3712; *Angew. Chem. Int. Ed.* **2001**, *40*, 3600.

[45] a) M. Takimoto, Y. Hiraga, Y. Sato, M. Mori, *Tetrahedron Lett.* **1998**, *39*, 4543; b) Y. Sato, R. Sawaki, N. Saito, M. Mori, *J. Org. Chem.* **2002**, *67*, 656.

[46] T.-P. Loh, H.-Y. Song, Y. Zhou, *Org. Lett.* **2002**, *4*, 2715.

[47] a) M. Kimura, S. Matsuo, K. Shibata, Y. Tamaru, *Angew. Chem.* **1999**, *111*, 3586; *Angew. Chem. Int. Ed.* **1999**, *38*, 3386; b) M. Kimura, K. Shibata, Y. Koudahashi, Y. Tamaru, *Tetrahedron Lett.* **2000**, *41*, 6789; c) K. Shibata, M. Kimura, K. Kojima, S. Tanaka, Y. Tamaru, *J. Organomet. Chem.* **2001**, *624*, 348.

[48] Y. Sato, T. Takanashi, M. Mori, *Organometallics* **1999**, *18*, 4891.

[49] M. Takimoto, M. Mori, *J. Am. Chem. Soc.* **2001**, *123*, 2895.

[50] M. V. Chevliakov, J. Montgomery, *J. Am. Chem. Soc.* **1999**, *121*, 11139.

[51] K. K. D. Amarasinghe, J. Montgomery, *J. Am. Chem. Soc.* **2002**, *124*, 9366.

[52] S.-K. Kang, S.-K. Yoon, *Chem. Commun.* **2002**, 2634.

[53] J. Montgomery, M. Song, *Org. Lett.* **2002**, *4*, 4009.

[54] C. Molinaro, T. F. Jamison, *J. Am. Chem. Soc.* **2003**, *125*, 8076; see also references [35c,d].

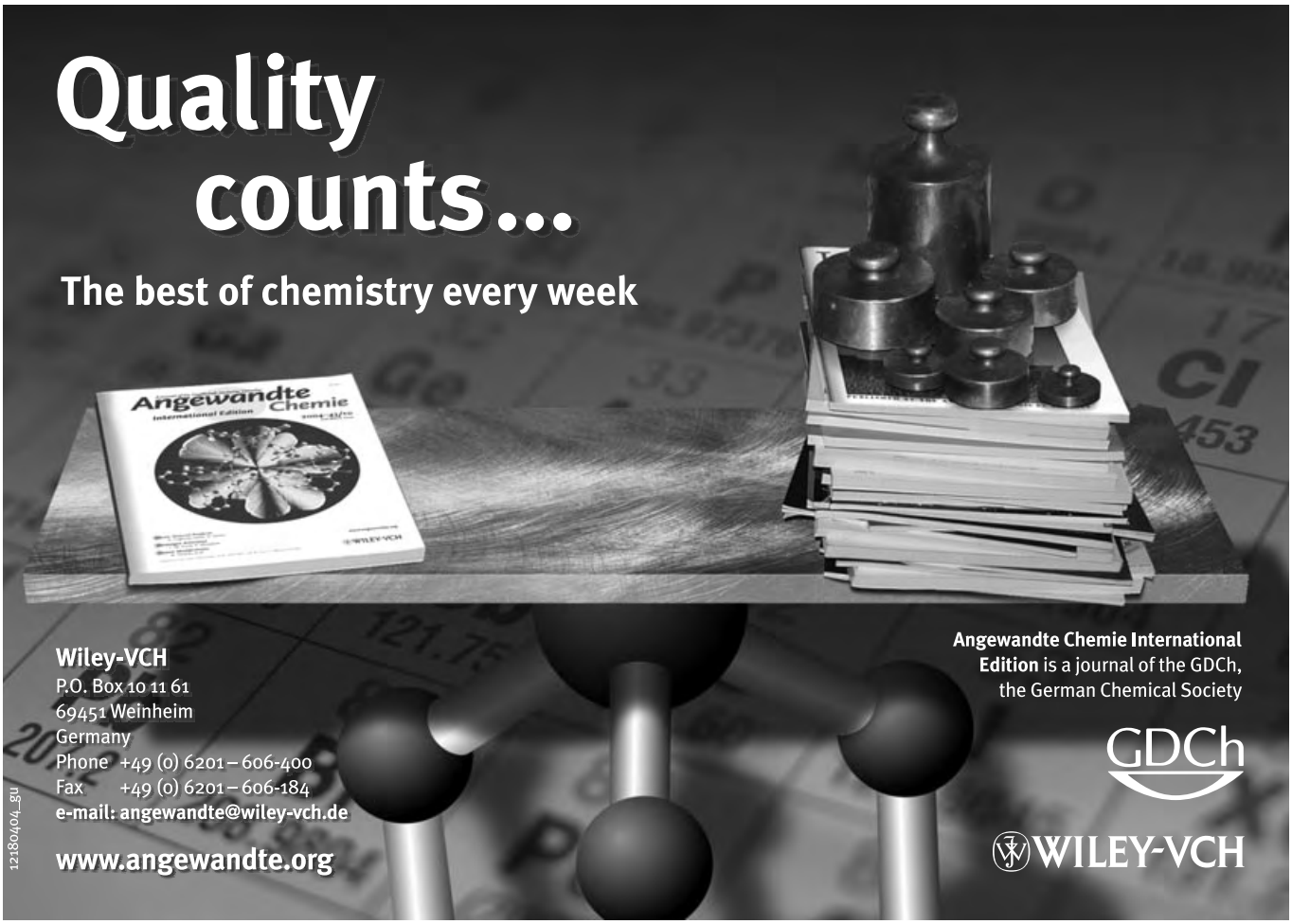
[55] M. Lozanov, J. Montgomery, *J. Am. Chem. Soc.* **2002**, *124*, 2106.

[56] A. Ezoe, M. Kimura, T. Inoue, M. Mori, Y. Tamaru, *Angew. Chem.* **2002**, *114*, 2908; *Angew. Chem. Int. Ed.* **2002**, *41*, 2784.

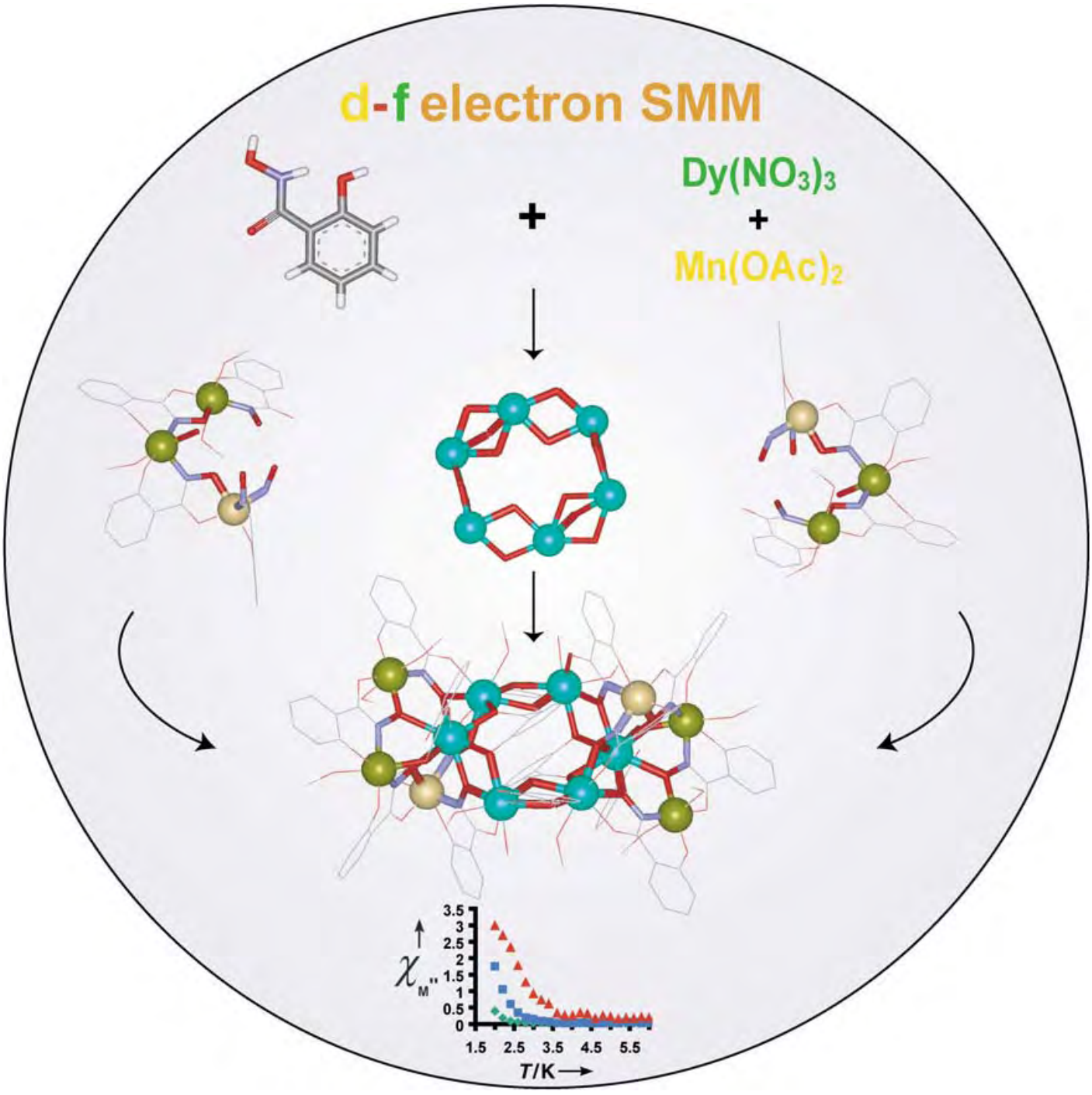
[57] a) M. Takimoto, M. Mori, *J. Am. Chem. Soc.* **2002**, *124*, 10008; b) M. Takimoto, Y. Nakamura, K. Kimura, M. Mori, *J. Am. Chem. Soc.* **2004**, *126*, 5956.

 © 2004 Wiley-VCH Verlag GmbH & Co. KGaA, Weinheim

[58] J. Terao, A. Oda, A. Ikumi, A. Nakamura, H. Kuniyasu, N. Kambe, *Angew. Chem.* **2003**, *115*, 3534; *Angew. Chem. Int. Ed.* **2003**, *42*, 3412.
[59] S. Ikeda, H. Miyashita, M. Taniguchi, H. Kondo, M. Okano, Y. Sato, K. Odashima, *J. Am. Chem. Soc.* **2002**, *124*, 12060.
[60] Z. Owczarczyk, F. Lamaty, E. J. Vawter, E. Negishi, *J. Am. Chem. Soc.* **1992**, *114*, 10091.
[61] Y. Ni, K. K. D. Amarasinghe, B. Ksebati, J. Montgomery, *Org. Lett.* **2003**, *5*, 3771.
[62] R. S. Fornicola, K. Subburaj, J. Montgomery, *Org. Lett.* **2002**, *4*, 615.
[63] J. Seo, H. Fain, J.-B. Blanc, J. Montgomery, *J. Org. Chem.* **1999**, *64*, 6060.
[64] M. T. Crimmins, J. A. DeLoach, *J. Am. Chem. Soc.* **1986**, *108*, 800.
[65] a) Y. Sato, N. Saito, M. Mori, *Tetrahedron Lett.* **1997**, *38*, 3931; b) Y. Sato, N. Saito, M. Mori, *Tetrahedron* **1998**, *54*, 1153.
[66] a) Y. Sato, M. Takimoto, M. Mori, *Synlett* **1997**, 734; b) Y. Sato, M. Takimoto, M. Mori, *Chem. Pharm. Bull.* **2000**, *48*, 1753.



Communications



The Dy–Mn cluster depicted is the first to behave as a single-molecule magnet. The trimeric $Mn^{III}_2Mn^{IV}$ "wings" combine with the hexagonal dysprosium ring to from the cluster, which displays an out of phase magnetic susceptibility signal in ac SQUID experiments. For more information, see the Communication by M. L. Kirk, V. L. Pecoraro, and co-workers on the following pages.

DOI: 10.1002/anie.200454013
© 2004 Wiley-VCH Verlag GmbH & Co. KGaA, Weinheim

Single-Molecule Magnets

Synthesis, Structure, and Magnetic Properties of a Large Lanthanide–Transition-Metal Single-Molecule Magnet**

Curtis M. Zaleski, Ezra C. Depperman, Jeff W. Kampf, Martin L. Kirk, and Vincent L. Pecoraro**

The chemistry of large lanthanide clusters has long been a focus of coordination chemists due to the unique properties conferred upon molecules that have f electrons. Recently, large cluster and ring compounds have been prepared with the goal of controlling the synthesis of lanthanide clusters, creating magnetic resonance imaging (MRI) contrast agents and luminescent sensors, and understanding the magnetic exchange interactions between lanthanide ions.[1] However, most of this research has been directed solely towards lanthanide clusters and not hybrid lanthanide–transition-metal clusters. Lanthanide–transition-metal cluster chemistry has primarily focused on Gd^{III}–Cu^{II} cluster systems, most notably by Kahn and co-workers, in the hope of understanding the magnetic interactions between the two different metal ions.[2a] Although subsequent work has firmly established that the Gd^{III} and Cu^{II} ions are ferromagnetically exchange coupled in the cluster,[2] few examples of lanthanide clusters with other transition metals have been realized and these tend to be small in size.[3] Recently, a $\{Cu_2Tb_2\}$ complex was reported that exhibits an out-of-phase ac magnetic susceptibility component that is consistent with it being a single-molecule magnet (SMM).[4] Previous work performed by our group has focused on the class of metallamacrocycles known as metallacrowns[5] which have interesting magnetic properties as they combine numerous metal ions in close proximity. [2d,6] Recently, we decided to return to one of the original metallacrown ligands to synthesize large complexes that contain both paramagnetic lanthanide ions and manganese ions.[5] We believed that such complexes could yield complex and interesting magnetic properties due to the large single-ion anisotropy inherent to these ions. Herein we report the largest lanthanide–manganese cluster synthesized to date, $[Dy_6Mn_6(H_2shi)_4(Hshi)_2(shi)_{10}(CH_3OH)_{10}(H_2O)_2]\cdot 9\,CH_3OH\cdot 8\,H_2O$ (H_3shi = salicylhydroxamic acid) **1**, and only the second example of a lanthanide–transition-metal complex that behaves as an SMM.[7]

The structure of **1** (Figure 1) is centered about a nearly planar hexagonal ring of Dy^{III} ions that is capped on either end by a $Mn^{III}_2Mn^{IV}$ trimer. The three pairs of symmetry equivalent Dy^{III} ions are interlinked by one- or two-atom bridges (Figure 2), and the Dy^{III} ions are also connected to the manganese ions by one or two-atom bridges. Dy1 and Dy2 are eight coordinate while Dy3 is nine coordinate. In addition, to two solvent oxygen atoms, Dy1 is coordinated by six ligand-derived oxygen atoms. Of particular note are two μ_2-hydroxylimino oxygen atoms that form a bridge to Dy2 (3.88 Å), and the one μ_2-phenolato oxygen atom that bridges with another μ_2-hydroxylimino oxygen atom to Dy3A (3.94 Å). Other μ_2-hydroxylimino oxygen atoms bridge Dy1 to Dy2. Remarkably, eight of the nine ligands to Dy3A form either one- or two-atom bridges to Dy or Mn atoms. The oxime that links Dy1 and Dy3A also serves to couple Dy1 and Dy3A to Mn1 (an Mn^{IV} ion) through a Dy-O-N-Mn connectivity pattern. Dy3A, which has only oxygen donors from ligands, exhibits three single-atom bridges (two from oxime oxygen atoms and one from a carbonyl oxygen atom) to Dy2A (Dy2A–Dy3A = 3.68 Å). The Dy2A ion is bound by seven ligand derived oxygen atoms and one solvent oxygen atom. Dy3A also forms either one- or two-atom bridges to all three Mn atoms (Dy3A to: Mn1, 3.70 Å; Mn2, 3.84 Å; Mn3, 3.95 Å). The Dy2A forms two atom oxime bridges to Mn1 and Mn3 (Dy2A to: Mn1, 5.01 Å; Mn3, 5.00 Å). The three Mn ions are all six coordinate with average Mn–(O,N) bond lengths of 1.91 Å for Mn1 and 2.04 Å and 2.05 Å for Mn2 and Mn3, respectively. The longer average bond lengths and the obvious Jahn–Teller axes support assignment of Mn2 and Mn3 as Mn^{III} ions. The Mn2 has a two-atom oxime bridge to Mn1 and an identical bridge to Mn3. There is no direct interaction between Mn1 and Mn3. The Mn separations are Mn1–Mn2, 4.75 Å; Mn1–Mn3, 5.98 Å and Mn2–Mn3, 4.68 Å. The three Mn ions are interconnected through the shi^{3-} ligand in a manner that is similar, but not identical, to that previously described.[5]

Due to the magnetic interactions that should arise as a result of the multiple short distances between the metal ions in the cluster, dc magnetic-susceptibility measurements were performed on a powdered sample mulled in eicosane. These data were collected on a Quantum Design dc superconducting quantum interference device (SQUID) magnetometer in the 5–300 K temperature range. The χT value decreases from 105 $cm^3\,K\,mol^{-1}$ at 300 K to 47.4 $cm^3\,K\,mol^{-1}$ at 2 K (see Supporting Information), which is indicative of dominant intramolecular antiferromagnetic exchange interactions in the cluster, depopulation of dysprosium single-ion sublevels, or a combination of both. Variable-temperature, variable-field magnetization measurements were collected on a Quantum Design physical properties measurement system

[*] E. C. Depperman, Prof. M. L. Kirk
Department of Chemistry
The University of New Mexico
MSC03 2060, 1 University of New Mexico
Albuquerque, NM 87131-0001 (USA)
Fax: (+1) 505-277-2609
E-mail: mkirk@unm.edu
C. M. Zaleski, Dr. J. W. Kampf, Prof. V. L. Pecoraro
Department of Chemistry
Willard H. Dow Laboratories
The University of Michigan
Ann Arbor, MI 48109-1055 (USA)
Fax: (+1) 734-936-7628
E-mail: vlpec@umich.edu

[**] This work was supported by NSF (NSF CHE-0111428); M.L.K. acknowledges the Petroleum Research Fund ACS PRF 38086-AC3 for financial support. The authors wish to thank Dr. Joe Thompson at Los Alamos National Laboratory (MST-10) and the National High Magnetic Field Laboratory at Los Alamos National Laboratory for use of their magnetometers.

Supporting information for this article is available on the WWW under http://www.angewandte.org or from the author.

 © 2004 Wiley-VCH Verlag GmbH & Co. KGaA, Weinheim DOI: 10.1002/anie.200454013

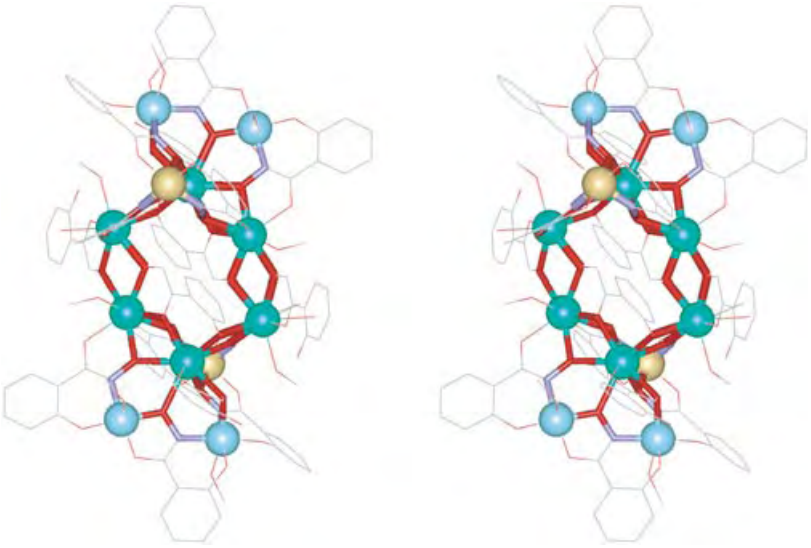


Figure 1. X-ray crystal structure of **1**. Color scheme: Green spheres Dy^{III}; blue spheres Mn^{III}; gold spheres Mn^{IV}.

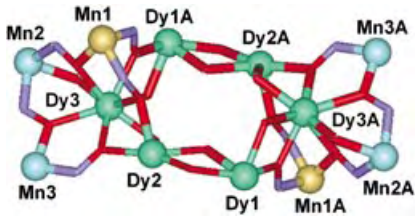


Figure 2. Highlight of one- and two-atom bridging motifs in **1**. Color scheme: See Figure 1.

(PPMS) at five different temperatures (2 K, 2.5 K, 3.33 K, 5 K, and 10 K) over an applied field range of 0.5–14 T (see Supporting Information). The magnetization values slightly decrease at low fields (< 9 T) upon increasing the temperature from 2 K to 5 K, followed by a large drop in the magnitude of the magnetization at 10 K. At higher fields (> 9 T) the magnetization increase linearly with the applied field and the magnetization data converge for all temperatures. The magnetization values never saturate at high fields, which indicates that either an energetically isolated spin state is never achieved even at the highest fields due to field induced level crossings and a high density of states, or there is a sizable temperature independent paramagnetism. The latter results from field-induced mixing of specific excited spin states with the ground spin state. Regardless of the reason for the observed magnetization behavior, the ground spin state for **1** can not be determined at this time.

As **1** had such a high χT value at low temperatures and contained a large number of anisotropic paramagnetic metal ions, we viewed **1** as a potential member of the relatively new SMM subclass that comprises lanthanide ion complexes.[4,8,9] Variable-temperature powder ac SQUID measurements were performed on a Quantum Design instrument from 2–100 K at frequencies of 10 Hz, 100 Hz, and 1000 Hz with a 3.5 G oscillating ac magnetic field and no applied dc magnetic field. Near 4.0 K the in-phase ac susceptibility ($\chi' T$) signal begins to decrease and the out-of-phase component (χ'') increases dramatically at all frequencies (Figure 3), with the magnitude of χ'' being frequency dependent. Due to the 2 K temperature limit of the instrument, a maximum in χ'' was not observed at frequencies as high as 1000 Hz. Nevertheless, these data support the assignment of **1** as a new member of the SMM family, expanding upon the recent report of the first f--d type SMM.[4] Unfortunately, as a result of the low blocking temperature ($T_B <$ 2 K) we did not observe hysteretic behavior in the magnetization of this sample. Additionally, two isostructural lanthanide analogues of this complex have been prepared and structurally characterized. Importantly, neither the Tb^{III} nor the Gd^{III} analogue exhibit an out-of-phase component in the ac experiment even though they retain high χT values at low temperatures (see Supporting Information). The lack of an out-of-phase ac magnetic

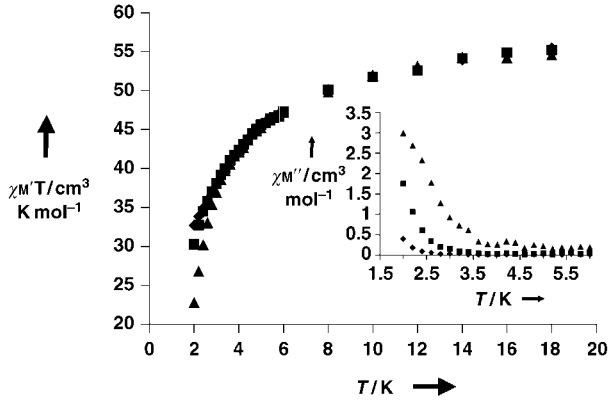


Figure 3. In-phase magnetic susceptibility of **1**. Inset: Out-of-phase magnetic susceptibility of **1**. (◆ 10 Hz; ■ 100 Hz; ▲ 1000 Hz).

susceptibility signal indicates that the SMM behavior is not solely a function of the manganese ions, nor can it be simply explained by invoking a magnetic phase transition or glassy magnetic behavior. Clearly, the molecular structure and the identity of the lanthanide ion are critical to the observed magnetic properties of these complexes.

In summary, we have synthesized a new lanthanide–transition-metal cluster complex with a high nuclearity of both types of metal ions, and initial magnetic measurements indicate that **1** is a member of the SMM family. Further studies at lower temperatures are required to understand more fully the interesting magnetic behavior of this complex. The results of these experiments and those of the various lanthanide analogues of **1** will be communicated in a future report.

Experimental Section

Complex **1** was prepared by the reaction of $Dy(NO_3)_3 \cdot 5H_2O$ (0.125 mmol), $Mn(O_2CCH_3)_2 \cdot 4H_2O$ (1 mmol), and salicylhydroxamic

 © 2004 Wiley-VCH Verlag GmbH & Co. KGaA, Weinheim

acid (1 mmol) in wet methanol (30 mL). The mixture was stirred overnight with a resulting brown solution and white precipitate. The precipitate was filtered, and the brown filtrate was allowed to slowly evaporate. Within three weeks, X-ray quality brown, needle crystals of **1** were obtained. We have repeated this synthesis with other lanthanide metal salts and obtained similar results.

Received: February 12, 2004
Revised: May 21, 2004 [Z54013]

Keywords: cluster compounds · dysprosium · lanthanides · magnetic properties · manganese

[1] a) D. Freedman, T. J. Emge, J. G. Brennan, *J. Am. Chem. Soc.* **1997**, *119*, 11112 – 11113; b) R. Wang, Z. Zheng, T. Jin, R. J. Staples, *Angew. Chem.* **1999**, *111*, 1929 – 1932; *Angew. Chem. Int. Ed.* **1999**, *38*, 1813 – 1815; c) M. R. Bürgstein, P. W. Roesky, *Angew. Chem.* **2000**, *112*, 559 – 562; *Angew. Chem. Int. Ed.* **2000**, *39*, 549 – 551; d) J. Xu, K. N. Raymond, *Angew. Chem.* **2000**, *112*, 2857 – 2859; *Angew. Chem. Int. Ed.* **2000**, *39*, 2745 – 2747; e) Y. Bretonnière, M. Mazzanti, J. Pécaut, M. M. Olmstead, *J. Am. Chem. Soc.* **2002**, *124*, 9012 – 9013; f) N. Fatin-Rouge, É. Tóth, D. Perret, R. H. Backer, A. Merbach, J.-C. G. Bünzli, *J. Am. Chem. Soc.* **2000**, *122*, 10810 – 10820; g) L. G. Westin, M. Kritikos, A. Caneschi, *Chem. Commun.* **2002**, 1012 – 1013.

[2] a) M. Andruh, I. Ramade, E. Codjovi, O. Guillou, O. Kahn, J. C. Trombe, *J. Am. Chem. Soc.* **1993**, *115*, 1822 – 1829; b) X.-M. Chen, S. M. J. Aubin, Y.-L. Wu, Y.-S. Yang, T. C. W. Mak, D. N. Hendrickson, *J. Am. Chem. Soc.* **1995**, *117*, 9600 – 9601; c) R. E. P. Winpenny, *Chem. Soc. Rev.* **1998**, *27*, 447 – 452; d) A. J. Stemmler, J. W. Kampf, M. L. Kirk, B. H. Atasi, V. L. Pecoraro, *Inorg. Chem.* **1999**, *38*, 2807 – 2817; e) C. Benelli, D. Gatteschi, *Chem. Rev.* **2002**, *102*, 2369 – 2387.

[3] a) R. A. Reyonlds III, D. Coucouvanis, *J. Am. Chem. Soc.* **1998**, *120*, 209 – 210; b) C. Benelli, M. Murrie, S. Parsons, R. E. P. Winpenny, *J. Chem. Soc. Dalton Trans.* **1999**, 4125 – 4126; c) B.-Q. Ma, S. Gao, O. Bai, H.-L. Sun, G.-X. Xu, *J. Chem. Soc. Dalton Trans.* **2000**, 1003 – 1004; d) B. Yan, Z. Chen, S. Wang, S. Gao, *Chem. Lett.* **2001**, 350 – 351; e) A. J. Tasiopoulos, T. A. O'Brien, K. A. Abboud, G. Christou, *Angew. Chem.* **2004**, *116*, 349 – 353; *Angew. Chem. Int. Ed.* **2004**, *43*, 345 – 349.

[4] S. Osa, T. Kido, N. Matsumoto, N. Re, A. Pochaba, J. Mrozinski, *J. Am. Chem. Soc.* **2004**, *126*, 420 – 421.

[5] M. S. Lah, V. L. Pecoraro, *J. Am. Chem. Soc.* **1989**, *111*, 7258 – 7259.

[6] C. Dendrinou-Samara, M. Alexiou, C. M. Zaleski, J. W. Kampf, M. L. Kirk, D. P. Kessissoglou, V. L. Pecoraro, *Angew. Chem.* **2003**, *115*, 3893 – 3896; *Angew. Chem. Int. Ed.* **2003**, *42*, 3763 – 3766.

[7] Crystals of **1** have been structurally characterized with the formula $[Dy_6Mn_6(H_2shi)_4(Hshi)_2(shi)_{10}(CH_3OH)_{10}(H_2O)_2]\cdot(CH_3OH)_9(H_2O)_8$. Elemental Analysis calcd (%) for **1**: $C_{131}H_{170}N_{16}O_{77}Mn_6Dy_6$ (Fw = 4505.44) C 34.92; H 3.80; N 4.97; Found: C 34.82, H 3.69, N 4.92. Yield 15%. Crystal data for **1**: $M_r = 4505.44$, monoclinic, space group $C2/c$ (no. 15), $a = 34.292(5)$ Å, $b = 19.508(3)$ Å, $c = 27.666(4)$ Å, $\alpha = 90°$, $\beta = 102.475(5)°$, $\gamma = 90°$, $V = 18071(5)$ Å^{-3}, $Z = 4$; $\rho_{calc} = 1.655$ mg m^{-3}; $2.98° < \theta < 26.70°$; crystal dimensions (mm), $0.50 \times 0.18 \times 0.16$; $\mu = 2.943$ mm^{-1}; $T = 118(2)$ K; 18715 unique of 76992 reflections collected. 18715 reflections and 1083 parameters were used for the full matrix, least-squares refinement on F^2, $R1 = 0.0564$ $[I > 2\sigma(I)]$, $R1 = 0.0958$ (all data); $wR2 = 0.1576$ $[I > 2\sigma(I)]$, $wR2 = 0.1771$ (all data). Further details are given in the Supporting Information. CCDC-231260 (**1**) contains the supplementary crystallographic data for this paper. These data can be obtained free of charge via www.ccdc.cam.ac.uk/conts/retrieving.html (or from the Cambridge Crystallographic Data Centre, 12 Union Road, Cambridge CB21EZ, UK; fax: (+44) 1223-336-033; or deposit@ccdc.cam.ac.uk).

[8] a) R. Sessoli, H.-L. Tsai, A. R. Schake, S. Wang, J. B. Vincent, K. Folting, D. Gatteschi, G. Christou, D. N. Hendrickson, *J. Am. Chem. Soc.* **1993**, *115*, 1804 – 1816; b) G. Christou, D. Gatteschi, D. N. Hendrickson, R. Sessoli, *MRS Bull.* **2000**, *25*, 66 – 71; c) D. Gatteschi, R. Sessoli, *Angew. Chem.* **2003**, *115*, 278 – 309; *Angew. Chem. Int. Ed.* **2003**, *42*, 268 – 297.

[9] N. Ishikawa, M. Sugita, T. Ishikawa, S.-Y. Koshihara, Y. Kaizu, *J. Am. Chem. Soc.* **2003**, *125*, 8694 – 8695.

 © 2004 Wiley-VCH Verlag GmbH & Co. KGaA, Weinheim

Rotaxane Synthesis

A 3D Interlocked Structure from a 2D Template: Structural Requirements for the Assembly of a Square-Planar Metal-Coordinated [2]Rotaxane**

Anne-Marie Fuller, David A. Leigh, Paul J. Lusby, Iain D. H. Oswald, Simon Parsons, and D. Barney Walker*

The starting point for the revolution in catenane and rotaxane synthesis that occurred during the last part of the 20th century was the realization by Sauvage and co-workers that metal–ligand coordination geometries could fix molecular fragments in three-dimensional space such that they were predisposed to form mechanically interlocked architectures through macrocyclization or "stoppering" reactions.[1] Efficient synthetic methods to rotaxanes were subsequently developed based on four- (tetrahedral)[2], five- (trigonal bipyramidal and square pyramidal)[3] and, most recently, six-coordinate (octahedral)[4] metal templates (Figure 1).[5] One of the benefits of using specific coordination motifs for such assemblies is that the resulting interlocked ligands often do not permit other metal geometries in their binding site, which can consequently be exploited either to lock a metal in an unusual geometry for its oxidation state[6] or to bring about large-amplitude "shuttling" of the ligand components.[3,7] Here we show that three-dimensional interlocked architectures can also be assembled from two-dimensional coordination templates by using steric and electronic restrictions to direct the synthesis in the third

[*] A.-M. Fuller, Prof. D. A. Leigh, Dr. P. J. Lusby, I. D. H. Oswald, Dr. S. Parsons, D. B. Walker
School of Chemistry, University of Edinburgh
The King's Buildings, West Mains Road, Edinburgh EH9 3JJ (UK)
Fax: (+44) 131-667-9085
E-mail: David.Leigh@ed.ac.uk

[**] We thank E. R. Kay for assistance with the graphics and crystallography data. This work was supported by the European Union Future and Emerging Technology Program MechMol and the EPSRC.

Supporting information for this article is available on the WWW under http://www.angewandte.org or from the author.

 © 2004 Wiley-VCH Verlag GmbH & Co. KGaA, Weinheim DOI: 10.1002/anie.200353622

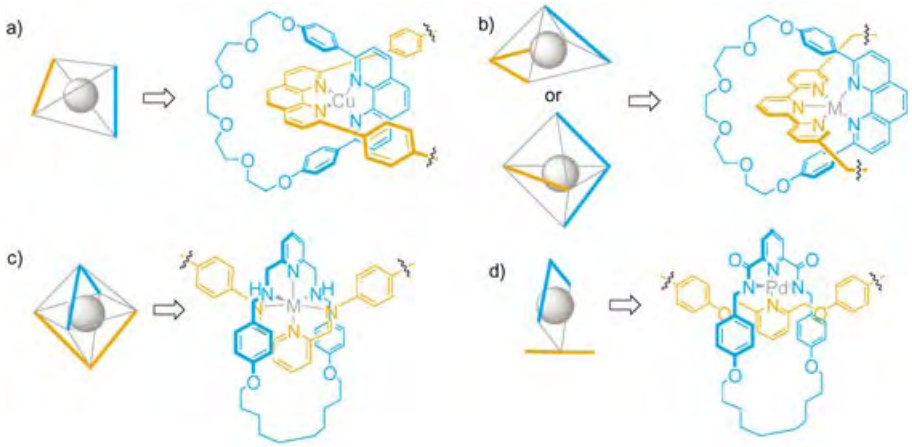
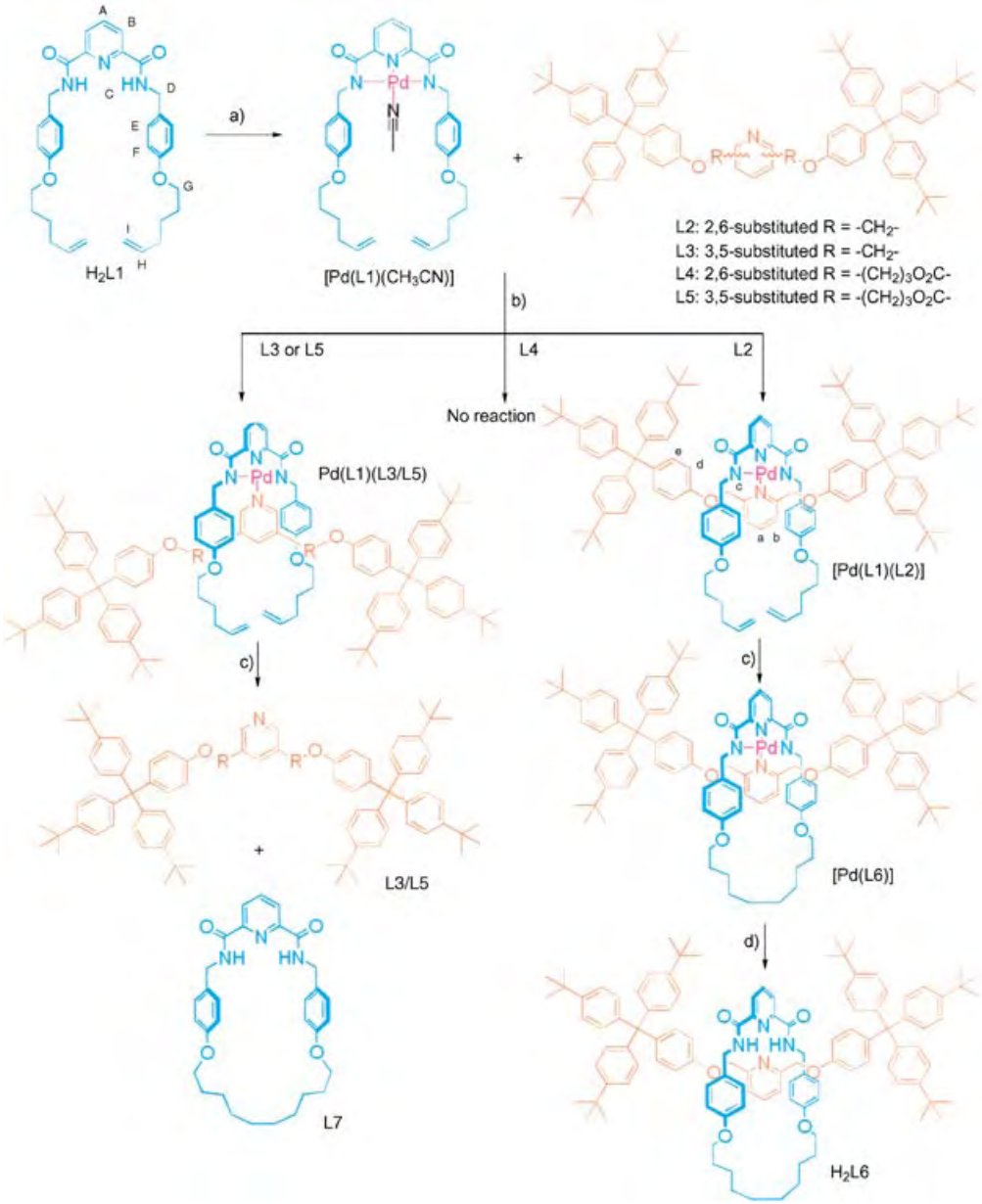


Figure 1. Exploiting transition-metal–ligand geometries in the synthesis of mechanically interlocked architectures: a) tetrahedral, b) square pyramidal and trigonal bipyrimidal, c) octahedral, and d) square-planar coordination motifs.



Scheme 1. Reagents and conditions: a) $Pd(OAc)_2$, CH_3CN, 76%; b) $CHCl_3$, 50 °C; L2: 63%, L3: 96%, L4: 0%, L5: 97%; c) 1. Grubbs catalyst (0.1 equiv), CH_2Cl_2; 2. H_2, Pd/C, THF, H_2L6: 98%, L3 + L7: 63%, L5 + L7: 69% (over 2 steps); d) KCN, MeOH, CH_2Cl_2, 20 °C, 1 h and then 40 °C, 0.5 h, 97%.

 © 2004 Wiley-VCH Verlag GmbH & Co. KGaA, Weinheim

dimension. The resulting [2]rotaxane is the first example of a mechanically interlocked ligand that forms a four-coordinate square-planar metal complex.[8]

The square-planar [2]rotaxane ligand design consists of a tridentate benzylic amide macrocycle and a monodentate thread (Figure 1d). The macrocycle incorporates a 2,6-dicarboxyamidopyridine unit to exploit the palladium chemistry recently developed[9] by Hirao and co-workers. The thread contains a pyridine donor group substituted with appropriately bulky stoppers in either the 2,6- or 3,5-positions. It was envisioned that in the key intermediate, [Pd(L1)(L2–L5)] (see Scheme 1), the geometry of the precursor to the macrocycle (previously used to direct hydrogen bond assembly processes[10]) would promote intercomponent π-π stacking, thus encouraging the pyridine donor of the thread to bind the metal ion orthogonally to the N_3 ligand (complimenting the normally preferred orientation[11]) and directing the asssembly in the third dimension. A series of readily available threads L2–L5 was investigated during the study.

The rotaxane synthesis was carried out according to Scheme 1. Treatment of H_2L1 with $Pd(OAc)_2$ in acetonitrile smoothly generated a complex [Pd(L1)(CH_3CN)] in which the fourth coordination site of the metal is occupied by a normally labile acetonitrile molecule. Nevertheless, displacement of the acetonitrile by bis-ester pyridine ligand L4 was unsuccessful (see below). However, simple combination of L5 or either of the bis-ether pyridine threads (L2 and L3) with [Pd(L1)(CH_3CN)] in either dichloromethane or chloroform gave the desired complexes [Pd(L1)(L5/L2/L3)] in 97, 63 and 96% yields, respectively. The ^{1}H NMR spectrum of [Pd(L1)(L2)] is shown in Figure 2c. Comparison with the spectra of [Pd(L1)(CH_3CN)] and H_2L1 (Figure 2b and 2a, respectively) shows features clearly indicative of metal coordination (the absence of H_C and shifts in H_A and H_B) and the anticipated aromatic stacking between the tridentate and monodentate ligands (particularly H_E and H_F). Similar chemical shift differences were observed for [Pd(L1)(L3)] and [Pd(L1)(L5)], however, ring closing olefin metathesis (RCM) followed by hydrogenation (Scheme 1, step c) of the three complexes produced very different results. Whilst cyclization of [Pd(L1)(L2)] gave the corresponding [2]rotaxane [Pd(L6)] in 77% yield following hydrogenation of the olefin, no [2]rotaxane was produced from RCM of either [Pd(L1)(L3)] or [Pd(L1)(L5)], the only products in each case being the free macrocycle and thread. Why does only one of the four threads direct rotaxane synthesis in the desired manner?

The ^{1}H NMR spectra of the [2]rotaxane ([Pd(L6)], Figure 2d), mass spectrometric analysis, and the preserved association of the organic fragments upon demetalation, unambiguously confirmed the interlocked structure. In addition to the loss of the terminal alkene protons, some subtle differences in the ^{1}H NMR spectrum of [Pd(L6)] compared to [Pd(L1)(L2)] (Figure 2c) indicates that some rearrangement of the ligands does occur on formation of the rotaxane. Single crystals of [Pd(L6)] suitable for X-ray crystallography[12] were grown by slow cooling of a warm, saturated solution of the [2]rotaxane in acetonitrile. The solid-state structure (Figure 3) shows the interlocked architecture and the

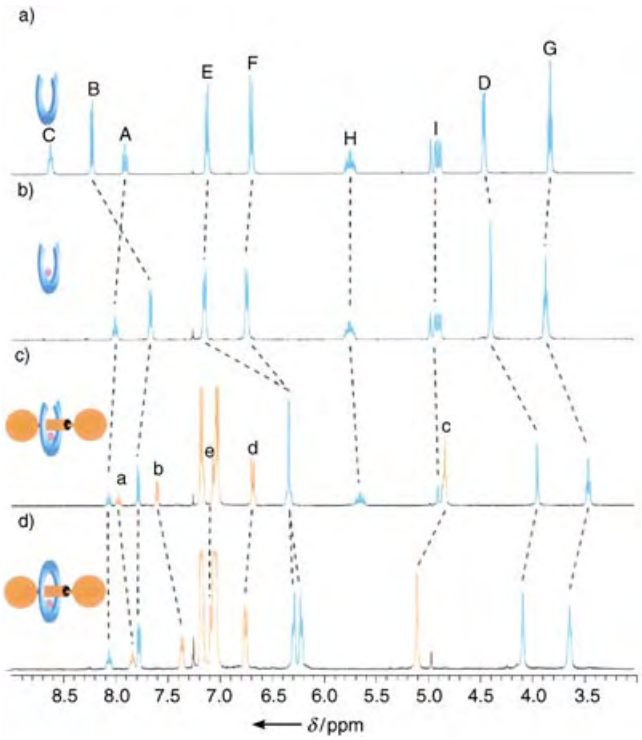


Figure 2. ^{1}H NMR spectra (400 MHz, 9:1 $CDCl_3$:CD_3CN, 298 K) of a) H_2L1; b) [Pd(L1)(CH_3CN)]; c) [Pd(L1)(L2)]; d) [2]rotaxane [Pd(L6)]. The lettering refers to the assignments in Scheme 1.

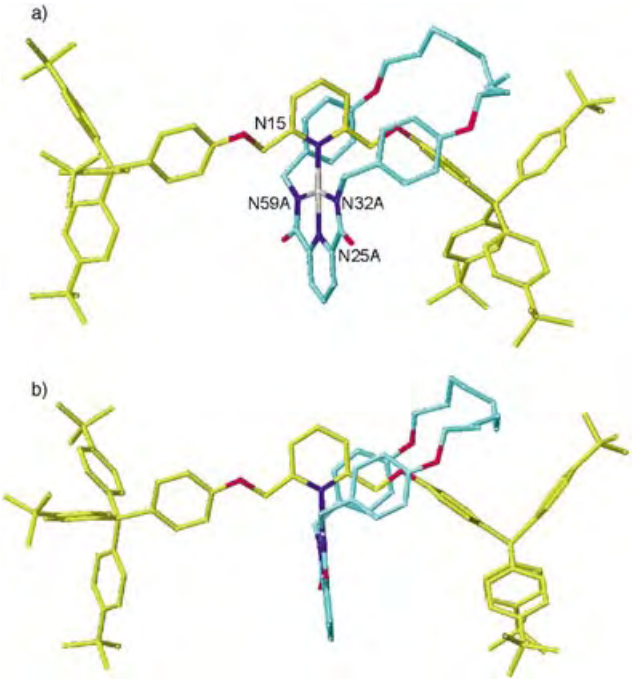


Figure 3. X-ray crystal structure of rotaxane [Pd(L6)] showing a) staggered and b) side-on views.[12] Carbon atoms of the macrocycle are shown in light blue and those of the thread in yellow; oxygen atoms are red, nitrogen dark blue, palladium gray. Selected bond lengths [Å]: Pd-N15 1.95, Pd-N25 1.86, Pd-N32 2.04, Pd-N59 2.02; other selected distance [Å]: N15-N25 3.81; macrocycle bite angle [°]: N59-Pd-N32 160.0. The macrocycle is disordered over two similar sites (50:50), but one is omitted for clarity together with the hydrogen atoms.

 © 2004 Wiley-VCH Verlag GmbH & Co. KGaA, Weinheim

pseudo-square-planar geometry (the N_3 bite angle is 160.0°) around the palladium center. The π stacking between the macrocycle and the pyridine ring of the thread so apparent in solution from the ^{1}H NMR shifts is significantly offset in the solid state (see the side-on view, Figure 3b). The co-conformation adopted by the macrocycle and thread in the crystal structure of the rotaxane clearly illustrates why RCM of the complexes formed with the 3,5-disubstituted threads ([Pd(L1)(L3)] and [Pd(L1)(L5)]) can lead to uninterlocked products; even with both fragments attached to the metal, cyclization of L1 can readily occur without encircling a 3,5-substituted pyridine thread. Similarly, the conformation of the thread suggests a possible reason for the lack of reactivity of the 2,6-bis-ester thread L4 towards [Pd(L1)(CH_3CN)]. In the crystal structure the electron density of the ether oxygen atoms of the thread is directed away from the occupied d_{z^2} orbital lobes which lie above and below the plane of the square-planar geometry at the d^8 palladium center. Chelation of L4 to [Pd(L1)] has to occur orthogonally for steric reasons. Such an arrangement would force electron density from the ester carbonyl groups into this high-energy space.

Demetalation of [Pd(L6)] with potassium cyanide (Scheme 1, step d) generates the free [2]rotaxane H_2(L6) in 97% yield, thus confiming that the coordination bonds are not required to stabilize the interlocked architecture once it is formed. The ^{1}H NMR spectrum of H_2(L6) and its uninterlocked components in $CDCl_3$ are shown in Figure 4. The shielding of the benzyl groups in the rotaxane relative to the free macrocycle, together with the large ($\delta = 1.7$ ppm) downfield shift of the amide protons (H_C), indicate that specific hydrogen-bonding interactions between the thread and the macrocycle are "switched on" by the demetalation/protonation procedure. It appears that the amide groups of H_2L6 simultaneously hydrogen bond to the pyridine groups in both the macrocycle and thread.

In conclusion, we have described methodology for assembling a three-dimensional interlocked molecular architecture from a two-dimensional metal template. A combination of steric and electronic factors direct the synthesis in the third dimension, either promoting or preventing interlocking. The resulting [2]rotaxane is the first example derived from a square-planar-coordinated metal center and completes the series of mechanically interlocked ligands for common transition-metal geometries initiated by Sauvage and co-workers in 1983.

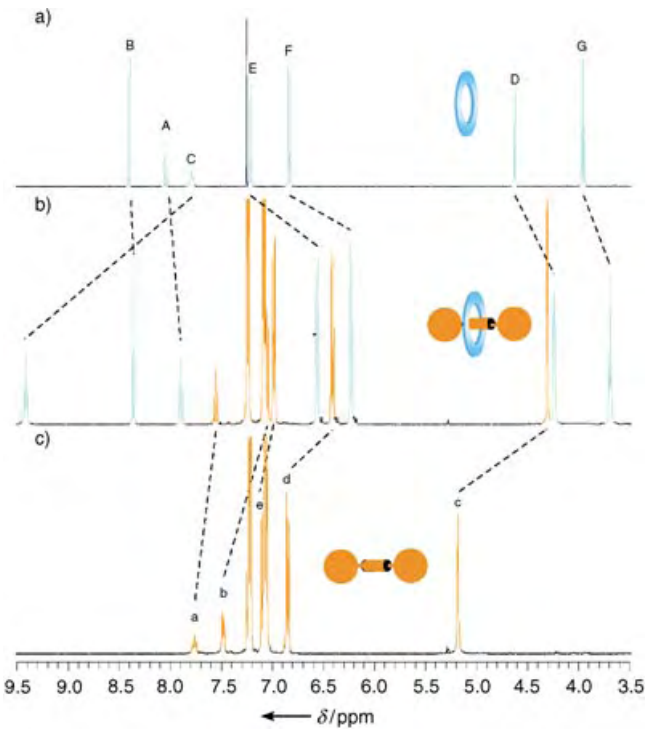


Figure 4. ^{1}H NMR spectra (400 MHz, $CDCl_3$, 298 K) of a) macrocycle; b) demetalated [2]rotaxane H_2L6; c) thread L2. The lettering refers to the assignments in Scheme 1.

Received: December 29, 2003 [Z53622]

Keywords: coordination modes · palladium · rotaxanes · template synthesis

[1] C. O. Dietrich-Buchecker, J.-P. Sauvage, J.-P. Kintzinger, *Tetrahedron Lett.* **1983**, *24*, 5095–5098.

[2] a) J.-P. Sauvage, C. Dietrich-Buchecker, G. Rapenne in *Molecular Catenanes, Rotaxanes and Knots* (Eds.: J.-P. Sauvage, C. Dietrich-Buchecker), Wiley-VCH, Weinheim, **1999**; b) J.-P. Collin, C. Dietrich-Buchecker, P. Gaviña, M. C. Jimenez-Molero, J.-P. Sauvage, *Acc. Chem. Res.* **2001**, *34*, 477–487.

[3] a) N. Armaroli, V. Balzani, J.-P. Collin, P. Gaviña, J.-P. Sauvage, B. Ventura, *J. Am. Chem. Soc.* **1999**, *121*, 4397–4408; b) L. Raehm, J.-M. Kern, J.-P. Sauvage, *Chem. Eur. J.* **1999**, *5*, 3310–3317.

[4] a) D. Pomeranc, D. Jouvenot, J.-C. Chambron, J.-P. Collin, V. Heitz, J.-P. Sauvage, *Chem. Eur. J.*, **2003**, *9*, 4247–4254; b) L. Hogg, D. A. Leigh, P. J. Lusby, A. Morelli, S. Parsons, J. K. Y. Wong, *Angew. Chem.* **2004**, *116*, 1238–1241; *Angew. Chem. Int. Ed.* **2004**, *43*, 1218–1221.

[5] For complexes in which metal coordination forms part of the macrocycle in a rotaxane, see a) K.-S. Jeong, J. S. Choi, S.-Y. Chang, H.-Y. Chang, *Angew. Chem.* **2000**, *112*, 1758–1761; *Angew. Chem. Int. Ed.* **2000**, *39*, 1692–1695; b) S.-Y. Chang, J. S. Choi, K.-S. Jeong, *Chem. Eur. J.* **2001**, *7*, 2687–2697; c) S.-Y. Chang, K.-S. Jeong, *J. Org. Chem.* **2003**, *68*, 4014–4019; d) S.-Y. Chang, H.-Y. Jang, K.-S. Jeong, *Chem. Eur. J.* **2003**, *9*, 1535–1541; for complexes in which metal coordination forms part of the thread in a rotaxane, see e) K.-M. Park, D. Whang, E. Lee, J. Heo, K. Kim, *Chem. Eur. J.* **2002**, *8*, 498–508; for complexes in which metal coordination forms the stoppers in a rotaxane, see f) R. B. Hannak, G. Färber, R. Konrat, B. Kräutler, *J. Am. Chem. Soc.* **1997**, *119*, 2313–2314; g) J.-C. Chambron, J.-P. Collin, J.-O. Dalbavie, C. O. Dietrich-Buchecker, V. Heitz, F. Odobel, N. Solladié, J.-P. Sauvage, *Coord. Chem. Rev.* **1998**, *178–180*, 1299–1312; h) A. J. Baer, D. H. Macartney, *Inorg. Chem.* **2000**, *39*, 1410–1417; i) G. J. E. Davidson, S. J. Loeb, N. A. Parekh, J. A. Wisner, *J. Chem. Soc. Dalton Trans.* **2001**, 3135–3136; for polyrotaxanes based on metal-coordination polymers, see j) S. R. Batten, R. Robson, *Angew. Chem.* **1998**, *110*, 1558–1595; *Angew. Chem. Int. Ed.* **1998**, *37*, 1460–1494; k) A. J. Blake, N. R. Champness, P. Hubberstey, W.-S. Li, M. A. Withersby, M. Schröder, *Coord. Chem. Rev.* **1999**, *183*, 117–138; l) K. Kim, *Chem. Soc. Rev.* **2002**, *31*, 96–107.

 © 2004 Wiley-VCH Verlag GmbH & Co. KGaA, Weinheim

[6] N. Armaroli, L. De Cola, V. Balzani, J.-P. Sauvage, C. O. Dietrich-Buchecker, J.-M. Kern, A. Bailal, *J. Chem. Soc. Dalton Trans.* **1993**, 3241 – 3247.
[7] M. Consuelo Jiménez, C. Dietrich-Buchecker, J.-P. Sauvage, *Angew. Chem.* **2000**, *112*, 3422 – 3425; *Angew. Chem. Int. Ed.* **2000**, *39*, 3284 – 3287.
[8] For a rotaxane which utilizes square-planar metal complexes as the stoppers, see S. J. Loeb, J. A. Wisner, *Chem. Commun.* **1998**, 2757 – 2758; for a pseudo-rotaxane based on a square-planar metal geometry, see C. Hamann, J.-M. Kern, J.-P. Sauvage, *Dalton Trans.* **2003**, 3770 – 3775.
[9] T. Moriuchi, S. Bandoh, M. Miyaishi, T. Hirao, *Eur. J. Inorg. Chem.* **2001**, 651 – 657.
[10] a) T. J. Kidd, D. A. Leigh, A. J. Wilson, *J. Am. Chem. Soc.* **1999**, *121*, 1599 – 1600; b) J. S. Hannam, T. J. Kidd, D. A. Leigh, A. J. Wilson, *Org. Lett.* **2003**, *5*, 1907 – 1910.
[11] a) J. E. Kickham, S. J. Loeb, *Inorg. Chem.* **1994**, *33*, 4351 – 4359; b) G. R. Newkome, T. Kawato, D. K. Kohli, W. E. Puckett, B. D. Olivier, G. Chiari, F. R. Fronczek, W. A. Deutsch, *J. Am. Chem. Soc.* **1981**, *103*, 3423 – 3429; c) this particular combination of metal coordination and π stacking to control the interaction of tridentate and monodentate ligands is very reminiscent of a series of metalloreceptors for DNA bases [J. E. Kickham, S. J. Loeb, S. L. Murphy, *Chem. Eur. J.* **1997**, *3*, 1203 – 1213].
[12] [Pd(L6)]: $C_{121}H_{141.5}N_{8.5}O_6Pd$, $M_r = 1917.33$, yellow block, crystal size $0.47 \times 0.31 \times 0.27\ mm^3$, triclinic, space group $P\bar{1}$, $a = 15.7840(10)$, $b = 15.9967(10)$, $c = 22.8029(14)$ Å, $\alpha = 84.9850(10)$, $\beta = 71.8430(10)$, $\gamma = 80.5460(10)°$, $V = 5392.5(6)$ Å^3, $Z = 2$, $\rho_{calcd} = 1.193\ Mg\,m^{-3}$; $Mo_{K\alpha}$ radiation (graphite monochromator, $\lambda = 0.71073$ Å), $\mu = 0.231\ mm^{-1}$, $T = 150(2)$ K. 34043 data (15412 unique, $R_{int} = 0.0331$, $2.06 < \theta < 23.26°$), were collected on a Brucker SMART CCD diffractometer using narrow frames (0.5° in ω), and were corrected semiempirically for absorption and incident beam decay. Data beyond 0.9 Å were weak and were not used for refinement. The structure was solved by direct methods (SIR92)[13] and refined by full-matrix least-squares against F^2.[14] Phenyl groups were constrained to be rigid hexagons and hydrogen atoms were placed in calculated positions. The whole macrocyclic component, inclusive of the Pd atom, is disordered (50:50) over two positions. The alkyl chain is further disordered and the refinement of this portion of the structure was controlled by application of restraints to both 1,2 and 1,3 distances and use of a common isotropic displacement parameter for all C atoms forming the chain. The only disorder present in the thread is in two of the *tert*-butyl groups. That based on C244 is rotationally disordered (70:30) with the central carbon atom (C244) fully occupied and the two alternative sets of methyl positions related by a 60° rotation about the C244–C243 bond. All atoms in the groups were refined with anisotropic displacement parameters (adps), those of "opposite" C atoms being constrained to be equal. The *tert*-butyl group attached to C263 is disordered (70:30) over two positions and was refined isotropically. Similarity restraints were applied to chemically equivalent 1,2 and 1,3 distances in both disordered *tert*-butyl groups. In the latter stages of refinement there was still significant unassigned electron density associated with diffuse solvent. This density was modeled by using the procedure of van der Sluis and Spek,[15] comprising 199 electrons per unit cell, and corresponds to approximately 4.5 MeCN solvent molecules per asymmetric unit; values of M_r, $F(000)$, μ etc. have been calculated on this assumption. $wR = \{\Sigma[w(F_o^2 - F_c^2)^2]/\Sigma[w(F_o^2)^2]\}^{1/2} = 0.2527$, conventional $R = 0.0806$ for F values of 15412 reflections with $F_o^2 > 2\sigma F_o^2$), $S = 1.115$ for 885 parameters. Residual electron density extremes were 1.03 and -0.94 e Å^{-3}. CCDC-229418 contains the supplementary crystallographic data for this paper. These data can be obtained free of charge via www.ccdc.cam.ac.uk/conts/retrieving.html (or from the Cambridge Crystallographic Data Centre, 12 Union Road, Cambridge CB21EZ, UK; fax: (+44) 1223-336-033; or deposit@ccdc.cam.ac.uk).
[13] A. Altomare, G. Cascarano, C. Giacovazzo, A. Guagliardi, *J. Appl. Crystallogr.* **1993**, *26*, 343 – 350.
[14] G. M. Sheldrick, University of Göttingen, Germany, **1997**.
[15] P. van der Sluis, A. L. Spek, *Acta. Crystallogr. Sect. A* **1990**, *46*, 194 – 201.

 © 2004 Wiley-VCH Verlag GmbH & Co. KGaA, Weinheim

Cell-Wall Glycolipids

Identification of the 5-Methylthiopentosyl Substituent in *Mycobacterium tuberculosis* Lipoarabinomannan**

*W. Bruce Turnbull, Kazumi Hiruma Shimizu, Delphi Chatterjee, Steve W. Homans, and Achim Treumann**

The search for new and improved drugs against tuberculosis continues to focus on the biosynthesis of the *Mycobacterium tuberculosis* (Mtb) cell wall.[1] Lipoarabinomannan (LAM)[2] is a major component of this cell wall and facilitates entry of Mtb into macrophages. Furthermore, LAM promotes the intracellular survival of Mtb by down-regulating the immune response and providing antioxidative protection.[2] LAM is a lipid-anchored polysaccharide comprising dendritic arabinan chains which emanate from a poly-α(1→6)-mannosyl core bearing α(1→2)-mannosyl substituents (Figure 1). In Mtb, the arabinan chains are capped with several further mannosyl residues, which form the nonreducing termini. We recently discovered[3] a novel substituent of these mannosyl caps, which, through a combination of NMR spectroscopic and

[*] Dr. W. B. Turnbull,[++] Dr. K. H. Shimizu, Prof. S. W. Homans, Dr. A. Treumann[+]
Astbury Centre for Structural Molecular Biology
School of Biochemistry and Microbiology
University of Leeds
Leeds, LS2 9JT (UK)
E-mail: atreumann@rcsi.ie
Prof. D. Chatterjee
Department of Microbiology, Immunology, and Pathology
Colorado State University
Fort Collins, CO 80523-1682 (USA)
[+] Present address:
Royal College of Surgeons in Ireland
123 St Stephen's Green, Dublin 2 (Ireland)
Fax: (+353) 1-402-2274
[++] Present Address:
School of Chemistry
University of Leeds
Leeds, LS2 9JT (UK)

[**] This work was supported in the UK by the Wellcome Trust and in the USA by grants from the National Institutes of Health (NIAID AI 37139 and AI 47197).

 © 2004 Wiley-VCH Verlag GmbH & Co. KGaA, Weinheim DOI: 10.1002/anie.200454119

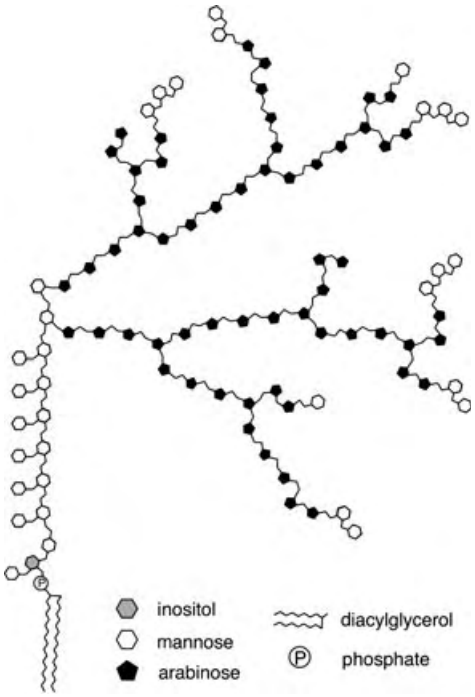
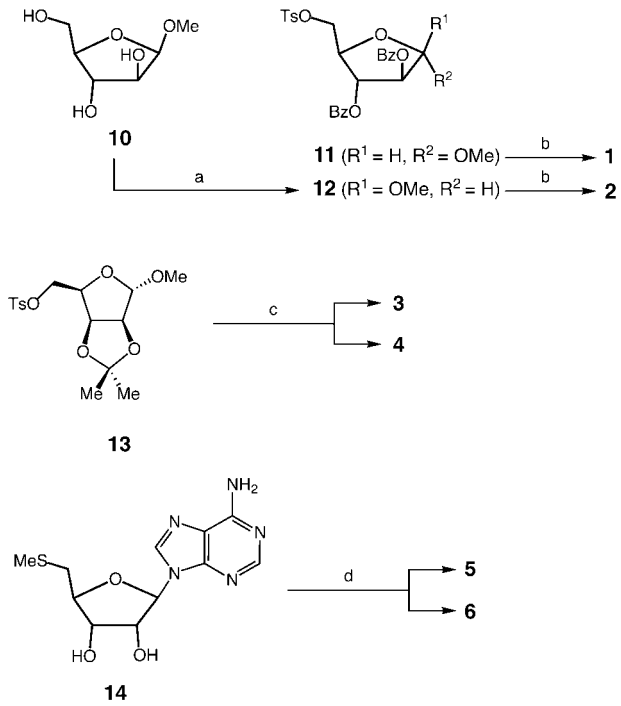


Figure 1. Cartoon representation of LAM, a phosphatidylinositol-anchored polysaccharide from *Mycobacterium tuberculosis*. It is not known how many arabinan side chains are attached to the branched mannan core of LAM. The novel 5-deoxy-5-methylthiopentofuranosyl residue was found to be attached to one of the short oligomannosyl chains capping the arabinan side chains.



Scheme 1. Reagents: a) 1. $TrCl/C_5H_5N$; 2. $BzCl/C_5H_5N$; 3. 80% AcOH (aq)/△; 4. $TsCl/C_5H_5N$ (48%); b) 1. MeSNa/[18]crown-6/DMF; 2. NaOMe/MeOH (**1**: 94%, **2**: 90%); c) 1. MeSNa/[18]crown-6/DMF; 2. $SrCl_2$/MeOH/TFA/△ (**3**: 7%, **4**: 41%); d) MeOH/TFA/△ (**5**: 15%, **6**: 40%). Tr = triphenylmethyl, Bz = benzoyl, Ts = 4-toluenesulfonyl, TFA = trifluoroacetic acid.

mass spectrometric techniques, was identified as having a 5-deoxy-5-methylthiopentofuranosyl (MTP) structure. The presence of an oxidized form of this residue, 5-deoxy-5-methylsulfoxypentofuranosyl (MSP), was also observed. Such monosaccharide residues have never previously been identified in an oligosaccharide. Herein, we use a combination of chemical synthesis and NMR spectroscopy to reveal the configuration of this novel component of the Mtb cell wall.

The fluctional conformations of furanose rings[4] make the identification of their relative configuration from ^3J coupling constants more difficult than for pyranose sugars. Consequently, we chose to synthesize all four isomers of 5-deoxy-5-methylthio-D-pentofuranose, each as their α- and β-methyl glycosides (see Figure 2, compounds **1**–**8**). Only the *xylo*-configured sugars **7** and **8** have been reported previously, albeit as a mixture of α- and β-anomers.[5] Although it is not possible to distinguish compounds **7** and **8** by thin layer chromatography, they were separated readily by using an anion exchange chromatography column (Dowex 1-X2, OH^- form) and eluting with water. The α-*arabino* isomer **1** was synthesized (Scheme 1) from the known[6] tosylate **11** by reaction with MeSNa and subsequent removal of the benzoyl groups under Zemplén conditions. The analogous β isomer **2** was prepared in a similar fashion from methyl glycoside **10**[7] via tosylate **12**.

Whereas the synthesis of α-lyxofuranose derivatives is relatively straightforward, the β anomers are notoriously difficult to prepare as a consequence of having all four substituents pointing toward the same face of the furanose ring.[8] However, Angyal et al. discovered that the proportion of the β-furanose isomer increased from trace quantities to about 30% when the acid-catalyzed preparation of methyl glycosides of lyxose was conducted in the presence of strontium chloride.[9] Consequently, following the displacement of the Ts group in compound **13**[10] with MeSNa, the acetonide protecting group was removed by acid-catalyzed methanolysis in the presence of anhydrous $SrCl_2$, with concomitant anomerization. Isomers **3** and **4** were thus obtained in 7 and 41% yield, respectively, after chromatography on a Sr^{2+} ion exchange column (Dowex 50WX2-400)[9] and eluting with water. Finally, the *ribo*-configured derivatives **5** and **6** were prepared by methanolysis of 5′-methylthioadenosine (**14**), which is commercially available. In this case, the two isomers were found to be separable by careful silica-gel chromatography. Analytical data for compounds **1**–**8** are presented in Table 1.

The HSQC spectra for compounds **1**–**8** are shown in Figure 2.[11] The signals of the anomeric proton (Figure 2a) are grouped together in two main clusters with ^{13}C chemical shifts of about $\delta = 105$ ppm for the 1,2-*cis* glycosides and about $\delta = 110$ ppm for the 1,2-*trans* glycosides. These groups are further divided into pairs of C3 epimers, with the β anomers located upfield of the α anomers in the ^1H dimension. The remaining signals for the ring atoms are more randomly spread, providing a fingerprint region for comparison with the spectra of MTP-containing LAM.

 © 2004 Wiley-VCH Verlag GmbH & Co. KGaA, Weinheim

Table 1: Chemical shifts[a] and optical rotations[b] for compounds **1**–**9** and MTP/MSP-LAM.

Compound	**1**	**2**	**3**	**4**	**5**	**6**	**7**	**8**	**9**	MTP[c]	MSP[c]
H-1	4.93	4.89	4.95	4.90	5.00	4.90	**5.03**	4.88	5.06	**5.40**	5.44
									5.06		5.45
H-2	4.06	4.13	4.17	4.23	4.20	4.08	**4.17**	4.14	4.18	**4.21**	4.20
									4.18		4.22
H-3	3.95	4.05	4.26	4.22	4.02	4.19	**4.24**	4.17	4.31	**4.26**	4.34
									4.31		4.34
H-4	4.14	3.98	4.34	4.26	4.22	4.13	**4.37**	4.45	4.62	**4.38**	4.65
									4.60		4.61
H-5	2.80	2.77	2.74	2.74	2.73	2.74	**2.69**	2.76	3.29	**2.68**	3.28
									3.13		3.12
H-5′	2.88	2.86	2.82	2.86	2.83	2.88	**2.79**	2.85	3.11	**2.80**	3.08
									3.13		3.12
OCH_3	3.41	3.42	3.46	3.40	3.44	3.41	3.46	3.40	3.46	n.a.[d]	n.a.
									3.46		
SCH_3	2.18	2.17	2.17	2.18	2.17	2.19	**2.17**	2.19	2.80	**2.21**	2.84
									2.79		2.83
C-1	110.5	104.8	110.5	104.9	105.8	110.5	**105.0**	111.4	105.0	**105.2**	105.4
									105.0		105.4
C-2	83.5	79.5	79.6	74.7	73.9	77.2	**79.6**	82.5	79.6	**79.4**	79.4
									79.6		79.3
C-3	82.4	80.6	74.2	72.8	75.0	76.8	**78.4**	77.8	78.7	**78.3**	78.5
									78.7		78.5
C-4	85.3	83.1	82.1	82.4	85.6	84.3	**80.4**	84.3	76.0	**80.5**	76.5
									75.5		75.6
C-5	38.6	40.6	35.0	36.7	39.1	40.5	**35.8**	35.9	55.4	**35.8**	55.6
									57.0		57.1
OCH_3	57.7	58.2	59.2	58.3	58.3	58.2	58.7	58.3	58.4	n.a.	n.a.
									58.4		
SCH_3	17.6	17.4	17.3	17.3	17.6	17.4	**17.4**	17.4	40.2	**17.4**	39.9
									40.5		40.2
$[\alpha]_D$	102.3	−60.1	56.7	−72.1	113.6	−5.4	119.6	−38.2	n.d.[e]	n.a.	n.a.

[a] Chemical shifts [ppm] relative to 3-trimethylsilylpropionate in D_2O. [b] Optical rotations recorded at the sodium D line at 22 °C in H_2O have units of $deg\,cm^3\,g^{-1}\,dm^{-1}$. [c] Values for MTP-LAM and MSP-LAM are taken from reference [3]; values in bold to aid comparison between **7** and MTP. [d] Not applicable. [e] Not determined, as **9** is a mixture of diastereomers.

Similarly, the upfield region (Figure 2b) shows that the methyl-group resonances have near identical chemical shifts and that those for the methylene group attached to the methylthio moiety are somewhat more dispersed.

Comparison of these spectra with TOCSY (Figure 2c) and HSQC (Figure 2d and e) spectra for LAM clearly demonstrates that only the resonances for the α-*xylo* compound **7** are comparable to those for MTP. Indeed, the ^{13}C resonances all agree within $\Delta\delta = 0.2$ ppm with those of MTP and the ^1H resonances within $\Delta\delta = 0.04$ ppm, with the exception of that for the anomeric proton. It is perhaps not surprising that there is disagreement between the anomeric signals when one considers that MTP is attached in LAM to an underlying mannosyl residue and not to a methyl group as in compounds **1**–**8**. The extent of the downfield shift for the anomeric proton ($\Delta\delta = 0.4$ ppm) is nevertheless significant and might indicate steric effects constraining the conformation of the MTP–mannosyl linkage. To seek further confirmation for the α-*xylo* configuration, an aqueous solution of compound **7** was treated with hydrogen peroxide to convert the thioether into a 1:1 diastereomeric mixture of sulfoxides **9**. The HSQC spectrum of compound **9** compares extremely well with that for MSP-LAM (Figure 2d, e), again with the sole exception of the anomeric proton resonance. Furthermore, the distinct downfield shift for the atoms adjacent to the sulfur atom, following oxidation to **9**, demonstrates that compounds **1**–**8** are free from oxidation products.

The discovery of a 5-deoxy-5-methylthio-α-xylofuranosyl (MTX) structure in LAM is remarkable for two reasons. Firstly, there is no precedent, to our knowledge, for a methylthio sugar incorporated into an oligosaccharide. Secondly, there are very few other examples of *xylo*-configured sugars outside the plant kingdom[12] and only one prior example in a bacterial polysaccharide.[12c] Nevertheless, MTX is widespread in strains of Mtb including the well-characterized laboratory strains H37Rv and H37Ra[3] and the clinical isolates CSU20[3] and MT103.[13] Recently MTX was also found in a clinical strain of the nontuberculous opportunistic pathogen *Mycobacterium kansasii*,[14] in which it is attached to the core mannan domain of the related lipomannan and of LAM. This is distinct from LAM of Mtb wherein MTX is attached to the mannosyl caps.

It would be reasonable to predict that MTX is derived biosynthetically from **14**, which is a ubiquitous by-product of polyamine biosynthesis. We would thus tentatively assign the D configuration to MTX, as this would require epimerization of only one stereocenter in **14** (Scheme 2). Indeed, this hypothesis is supported by the remarkable discovery of *xylo*-

 © 2004 Wiley-VCH Verlag GmbH & Co. KGaA, Weinheim

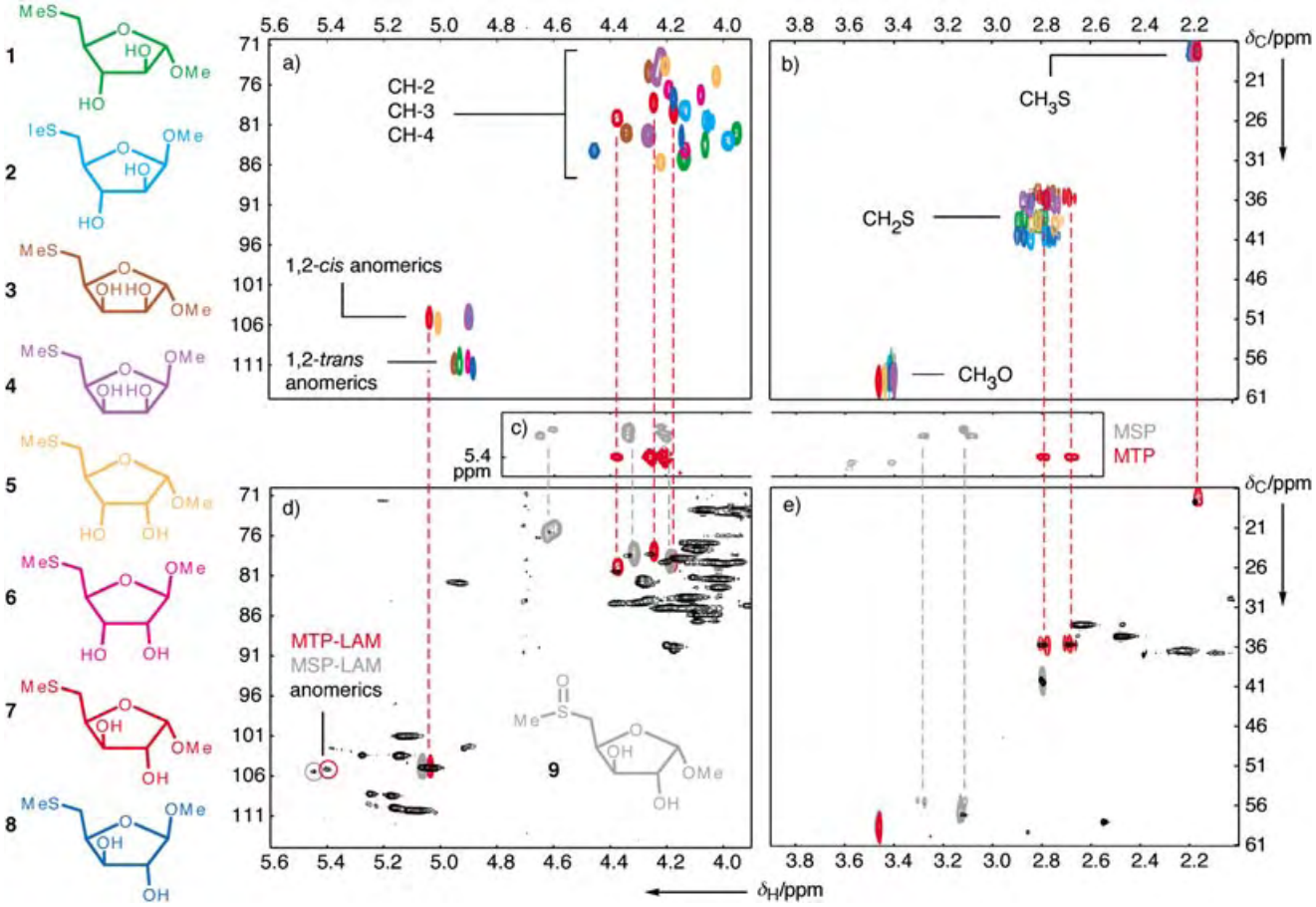
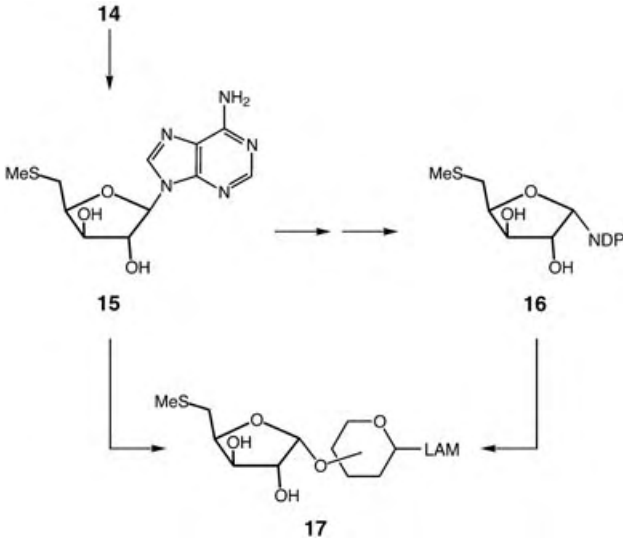


Figure 2. Structural formulas of the eight possible methyl glycosides of MTP (compounds **1**–**8**) and their NMR spectra. a) Low- and b) high-field regions of the HSQC spectra. c) A strip from the TOCSY spectrum of MTP-LAM showing resonances of nuclei correlating with the anomeric protons for MTP and MSP (red and gray, respectively). d) Low- and e) high-field regions of the HSQC spectrum of MTP-LAM (in black) are presented for comparison with those of α-*xylo*-configured compounds **7** and **9** (red and gray, respectively).

configured methylthioadenosine **15** in the mediterranean nudibranch mollusc *Doris verrucosa*,[12d] wherein compound **15** is produced by epimerization at C3′.[15] Whether biosynthesis of MTX-LAM (**17**) proceeds through direct glycosylation with **15**, or, more likely, via a nucleoside diphosphate activated sugar **16** remains to be demonstrated.



Scheme 2. Proposed biosynthesis of MTX-LAM (**17**).

Although no biological activity has yet been observed for **15**,[16] the extra biosynthetic effort that mycobacteria must expend to make MTX-LAM and also its widespread occurrence[3,13,14] would suggest that MTX provides some biological advantage to these pathogens. The relative stability of compounds **1**–**8** would imply that the nonstereoselective oxidation of MTX in LAM might occur as the result of exposure to reactive oxygen species which would be found within macrophage cells in vivo. Although the low concentration of MTX in LAM detracts from the argument that sulfide oxidation may give rise to the antioxidative properties of LAM,[2] it is difficult to imagine how else a polysaccharide could accomplish such protection chemically. Nevertheless, the identification of an unusual *xylo*-configured sugar residue in LAM opens new avenues for research into the role played by LAM in Mtb pathogenesis. If enzymes involved in MTX-LAM biosynthesis turn out to be essential for Mtb, they may be potential novel targets for the future development of antituberculosis drugs.

Received: February 26, 2004 [Z54119]

 © 2004 Wiley-VCH Verlag GmbH & Co. KGaA, Weinheim

Keywords: carbohydrates · cell wall · NMR spectroscopy · structure elucidation · xylofuranose

[1] a) K. F. M. Pasqualoto, E. I. Ferreira, *Curr. Drug Targets* **2001**, *2*, 427 – 437; b) Y. Zhang, L. M. Amzel, *Curr. Drug Targets* **2002**, *3*, 131 – 154; c) L. Kremer, G. S. Besra, *Expert Opin. Invest. Drugs* **2002**, *11*, 1033 – 1049; d) P. Chopra, L. S. Meena, Y. Singh, *Indian J. Med. Res.* **2003**, *117*, 1 – 9.
[2] a) D. Chatterjee, K.-H. Khoo, *Glycobiology* **1998**, *8*, 113 – 120; b) G. R. Strohmeier, M. J. Fenton, *Microbes Infect.* **1999**, *1*, 709 – 717; c) M. Nigou, M. Gilleron, G. Puzo, *Biochimie* **2003**, *85*, 153 – 166.
[3] A. Treumann, F. Xidong, L. McDonnell, P. J. Derrick, A. E. Ashcroft, D. Chatterjee, S. W. Homans, *J. Mol. Biol.* **2002**, *316*, 89 – 100.
[4] J. F. Stoddart, *Stereochemistry of Carbohydrates*, Wiley-Interscience, New York, **1971**, pp. 97 – 102.
[5] B. Nestadt, T. Van Es, *Tetrahedron* **1968**, *24*, 1973 – 1980.
[6] R. J. Ferrier, S. R. Haines, *J. Chem. Soc. Perkin Trans. 1* **1984**, *8*, 1689 – 1692.
[7] I. Augestad, E. Berner, *Acta Chem. Scand.* **1954**, *8*, 251 – 256.
[8] C. T. Bishop, F. P. Cooper, *Can. J. Chem.* **1963**, *41*, 2743 – 2758.
[9] S. J. Angyal, C. L. Bodkin, F. W. Parrish, *Aust. J. Chem.* **1975**, *28*, 1541 – 1549.
[10] D. A. Berges, N. Zhang, L. Hong, *Tetrahedron* **1999**, *55*, 14251 – 14260.
[11] NMR spectra were acquired on a Varian Unity Inova 500 MHz spectrometer in D_2O at 25 °C and referenced to 3-trimethylsilylpropionate as an internal standard. HSQC datasets contained $256\,t_1 \times 1024\,t_2$ complex points with spectral widths of 4000 Hz and 30000 Hz in ^{1}H and ^{13}C dimensions, respectively. TOCSY spectra were recorded as described in reference [3].
[12] We are aware of only four examples: a) M. Iorizzi, L. Minale, R. Riccio, H. Kamiya, *J. Nat. Prod.* **1990**, *53*, 1225 – 1233; b) K. Kenji, Y. Mimura, T. Tamamura, S. Yatagai, Y. Sato, A. Takahashi, K. Sato, H. Naganawa, H. Nakamura, *J. Antibiot.* **1992**, *45*, 458 – 464; c) N. A. Kocharova, Y. A. Knirel, A. S. Shashkov, N. K. Kochetkov, E. V. Kholodkova, E. S. Stanislavsky, *Carbohydr. Res.* **1994**, *263*, 327 – 331; d) G. Cimino, A. Crispino, S. De Stefano, M. Gavagnin, G. Sodano, *Experientia* **1986**, *42*, 1301 – 1302.
[13] P. Ludwiczak, M. Gilleron, Y. Bordat, C. Martin, B. Gicquel, G. Puzo, *Microbiology* **2002**, *148*, 3029 – 3037.
[14] Y. Guérardel, E. Maes, V. Briken, F. Chirat, Y. Leroy, C. Locht, G. Strecker, L. Kremer, *J. Biol. Chem.* **2003**, *278*, 36637 – 36651.
[15] M. Porcelli, G. Cacciapuoti, G. Cimino, M. Gavagnin, G. Sodano, V. Zappia, *Biochem. J.* **1989**, *263*, 635 – 640.
[16] A. Pani, M. E. Marongiu, P. Obino, M. Gavagnin, P. La Colla, *Experientia* **1991**, *47*, 1228 – 1229.

 © 2004 Wiley-VCH Verlag GmbH & Co. KGaA, Weinheim

RNA Structural Rearrangements

Triggering of RNA Secondary Structures by a Functionalized Nucleobase**

*Claudia Höbartner, Harald Mittendorfer, Kathrin Breuker, and Ronald Micura**

The ability of nucleic acids to undergo conformational changes is a prerequisite for their immense functional repertoire. The definition of nucleic acid conformational changes is rather broad and ranges from local structural transformations, such as base flipping, to complex reorganizations of the secondary and tertiary structure.[1] The most prominent examples of the latter are metabolite-binding riboswitches, which have been recognized as a general means for gene regulation in many organisms.[2] Other examples concern ligand-responsive aptamer–ribozyme constructs with the ribozyme activity directed by allosteric effects upon binding of the ligand to a receptor domain.[3] The modular nature of these molecular sensors makes them highly flexible with respect to the rational design of diagnostic tools, such as the recently introduced target-assisted signal-amplifying ribozymes for the detection of single nucleotide polymorphism (SNP) or of microRNAs.[4,5]

A crucial feature of the above examples is that an effector molecule, either a small ligand or another oligonucleotide, induces the nucleic acid conformational change. As for natural riboswitches, the conformational changes in the designed molecules also occur at the secondary-structure level and lead, for example, to the formation of defined, mutually dependent stem–loop motifs (terminator–antiterminator) that are responsible for an on/off signal for transcription or translation.[6,7]

With the present work we introduce a novel concept for the manipulation of nucleic acid secondary structures. The idea relies on chemically functionalized nucleotides that play the role of an effector and that have potential as a previously unrecognized tool for designable secondary-structure modulation.

The underlying basic concept is depicted in Figure 1. A natural nucleoside is modified by a functional group at the Watson–Crick base-pairing site. When incorporated into an oligoribonucleotide this functionalized nucleoside is responsible for the selection of a distinct, defined secondary structure due to its deficiency of base pairing. However,

[*] Dipl.-Ing. C. Höbartner, Mag. H. Mittendorfer, Dr. K. Breuker, Prof. Dr. R. Micura
Leopold Franzens Universität
Institut für Organische Chemie
Innrain 52a, 6020 Innsbruck (Austria)
Fax: (+43) 512-507-2892
E-mail: ronald.micura@uibk.ac.at

[**] Financial support from the Austrian Science Fund (Grants P15042 to R.M. and P15767 to K.B.) is gratefully acknowledged.

Supporting information for this article is available on the WWW under http://www.angewandte.org or from the author.

 © 2004 Wiley-VCH Verlag GmbH & Co. KGaA, Weinheim DOI: 10.1002/anie.200460068

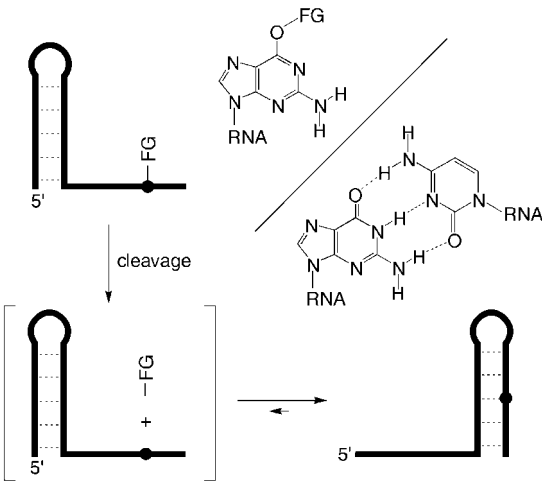
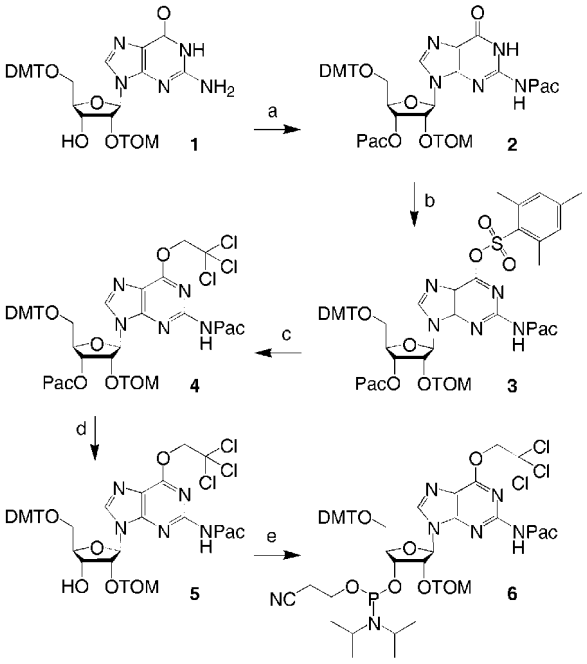


Figure 1. Novel concept for the modulation of nucleic acid secondary structures. A nucleobase, for example, guanine, is chemically functionalized at the Watson–Crick base-pairing site. Upon release of the functional group (FG) the base-pairing properties of the nucleobase are restored; the fold then becomes metastable and reorganizes into a thermodynamically favorable one.



Scheme 1. Synthesis of O^6-(2,2,2-trichloroethyl)guanosine phosphoramidite **6**. a) Phenoxyacetyl chloride (5.5 equiv), pyridine/CH_2Cl_2, 0 °C, 2 h, 74%; b) mesitylenesulfonyl chloride (1.2 equiv), triethylamine (5.0 equiv), DMAP (0.1 equiv), CH_2Cl_2, RT, 1 h; c) 2,2,2-trichloroethanol (2.5 equiv), ethyldimethylamine (5.0 equiv), DBU (1.0 equiv), CH_2Cl_2, RT, 2 h, 58% over two steps; d) 0.05 M NaOH, THF/methanol/H_2O, 4 °C, 3 min, 97%; e) 2-cyanoethyl-*N*,*N*-diisopropylchlorophosphoramidite (1.5 equiv), ethyldimethylamine (10 equiv), CH_2Cl_2, RT, 2 h, 90%. DBU = 1,8-diazabicyclo[5.4.0]undec-7-ene, DMAP = 4-dimethylaminopyridine, DMT = 4,4′-dimethoxytrityl, Pac = phenoxyacetyl, THF = tetrahydrofuran, TOM = triisopropylsilyloxymethyl.[9]

upon release of the functional moiety the capability for Watson–Crick base pairing is restored and the secondary structure becomes metastable and reorganizes into a thermodynamically favorable one.

To prove this concept, we considered O^6-(2,2,2-trichloroethyl)-modified guanosine (^{tce}G) to be appropriately functionalized. On the one hand, the O^6-tce group alters the donor–acceptor pattern of the guanosine Watson–Crick base-pairing site and is therefore expected to significantly lower the residue's base-pairing probability. On the other hand, release of this group should be easily achieved in aqueous solution by zinc, thereby restoring the guanosine as a potential base-pairing candidate that then represents the driving force for a secondary-structure rearrangement.

The synthesis of the O^6-tce-guanosine phosphoramidite **6** used in our studies is shown in Scheme 1. The 2′-*O*-TOM-guanosine derivative **1**[8] was treated with phenoxyacetyl chloride in pyridine to give compound **2**. Then, mesitylation of the O^6 atom of the lactam moiety and substitution of the corresponding mesitylenesulfonyl ester **3** with 2,2,2-trichloroethanol in the presence of DBU and ethyldimethylamine yielded **4**. Selective cleavage of the 3′-*O*-phenoxyacetyl group with aqueous NaOH in THF/methanol resulted in compound **5**, which was readily transformed into the O^6-tce-guanosine cyanoethyl phosphoramidite **6**.[9]

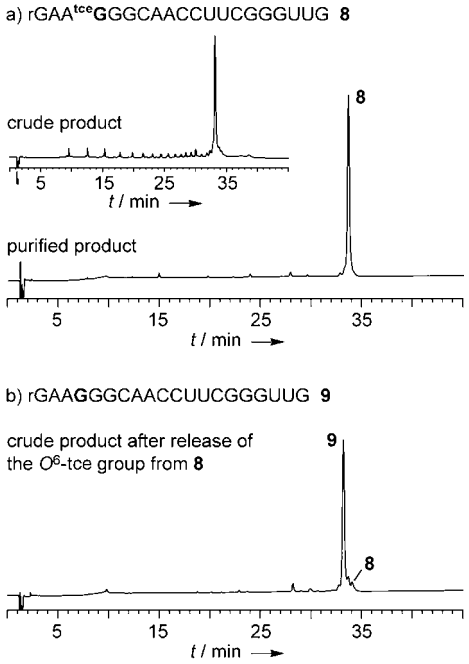


Figure 2. a) Representative example for the deprotection and purification of an O^6-tce-containing RNA sequence. HPLC trace of the product **8**, after treatment with aqueous NH_3/ethanol (1:1) at 55 °C for 5 h, treatment with 0.9 M TBAF in THF/H_2O (9:1) at 25 °C for 14 h, and purification by anion-exchange chromatography; MALDI-TOF MS: *m*/*z* calcd for $[M+H]^+$: 6594.3; found: 6597.5 ± 5. The inset shows the crude product before purification. b) Representative example for the release of the functional group, the O^6-tce group from **8**. HPLC trace of the crude product **9**, after treatment with zinc dust and 1 M NH_4OAc at pH 7 and 25 °C; $t_{1/2}$ = 5 min; MALDI-TOF MS: *m*/*z* calcd for $[M+H]^+$: 6462.9; found: 6466.3 ± 5. Anion-exchange HPLC: Dionex DNAPac column (4 × 250 mm), 80 °C, 1 mL min^{-1}, 0→60% B in 45 min (A: 25 mM tris(hydroxymethyl)aminomethane/HCl, 6 M urea, pH 8.0; B: same as A with addition of 0.5 M $NaClO_4$).

 © 2004 Wiley-VCH Verlag GmbH & Co. KGaA, Weinheim

The incorporation of phosphoramidite **6** into oligoribonucleotides was achieved with coupling yields higher than 99% by using standard DNA/RNA protocols and 2′-*O*-triisopropylsilyloxymethyl-protected nucleoside phosphoramidites.[10–12] For capping, phenoxyacetic anhydride was used instead of acetic anhydride. The deprotection of the synthesized O^6-tce-guanosine-containing oligoribonucleotides was optimized thoroughly, as the 2,2,2-trichloroethyl moiety was unstable under standard RNA-deprotection conditions based on methylamine. We finally found that treatment with aqueous ammonia in ethanol (1/1) at 55 °C for 5–10 hours followed by treatment with 0.9 M tetrabutylammonium fluoride (TBAF) in THF/water (9/1) at 25 °C for 14 hours resulted in complete deprotection without strand degradation (Figure 2). A prerequisite for this procedure was the use of either N^2-methoxyacetylated or N^2-unprotected 2′-*O*-TOM-guanosine phosphoramidites instead of the commonly used N^2-acetylated counterparts. Otherwise, cleavage of the guanosine N^2-acetyl groups was incomplete under the conditions tolerated by the O^6-tce group.[13]

Release of the O^6-tce group from the oligoribonucleotides as suggested in our concept (Figure 1) was optimized experimentally and proceeded smoothly in aqueous ammonium acetate buffer at pH 7 in the presence of zinc dust. Clean and complete cleavage was achieved at room temperature and under slight agitation. The half lives of the O^6-tce groups depended on the length of the oligoribonucleotide and ranged from 0.5 minutes for a pentamer to 5 minutes for the 20-mer oligoribonucleotides (see the Supporting Information and Figure 2).[14]

The sequence set in Figure 3 documents the feasibility of our proposed concept for the modulation of nucleic acid secondary structures. The RNA 20-mer 5′-rGAAGG-(GCAA)CC(UUCG)GGUUG (**9**) is a rationally designed sequence that exists in a monomolecular equilibrium of two equally populated secondary structures.[15,16] However, upon replacement of a single guanosine by O^6-tce-guanosine in strand positions 4 or 17, respectively, only one of the two folds is selected. The functionalized 20-mer 5′-rGAA^{tce}GGG-CAACC(UUCG)GGUUG (**8**) exclusively adopts a UUCG hairpin conformation, whereas the 20-mer 5′-rGAAGG-(GCAA)CCUUCGG^{tce}GUUG (**7**) solely forms the alternative hairpin with a GCAA tetraloop. Cleavage of the O^6-tce group in **7** or **8** results in sequence **9** and restores the secondary-structure equilibrium.

The second sequence example was designed to satisfy the requirements for a complete transformation of the secondary structure and is represented by the RNA sequence of 5′-rUGUCUCCG(GACA)CGGAGAC (**12**). This oligonucleotide forms a highly stable GACA hairpin with a seven-base-pair stem. However, when a tandem of O^6-tce labels is introduced into this sequence, 5′-rUGUC(UCCG)GACAC ^{tce}G^{tce}GAGAC (**11**) selects the UCCG hairpin with a four-base-pair stem as the exclusive conformation. Upon release of the labels, the secondary structure switches to the thermodynamically favorable one, **12**. All secondary structures discussed above were ascertained by comparative imino proton NMR spectroscopy, a simple approach that we have introduced recently for the reliable probing of secondary structures of small RNAs (see Figure 3 and the Supporting Information).[16,17]

We have demonstrated here that chemical functionalization of the Watson–Crick base-pairing site is an efficient tool for inducing defined rearrangements of RNA secondary

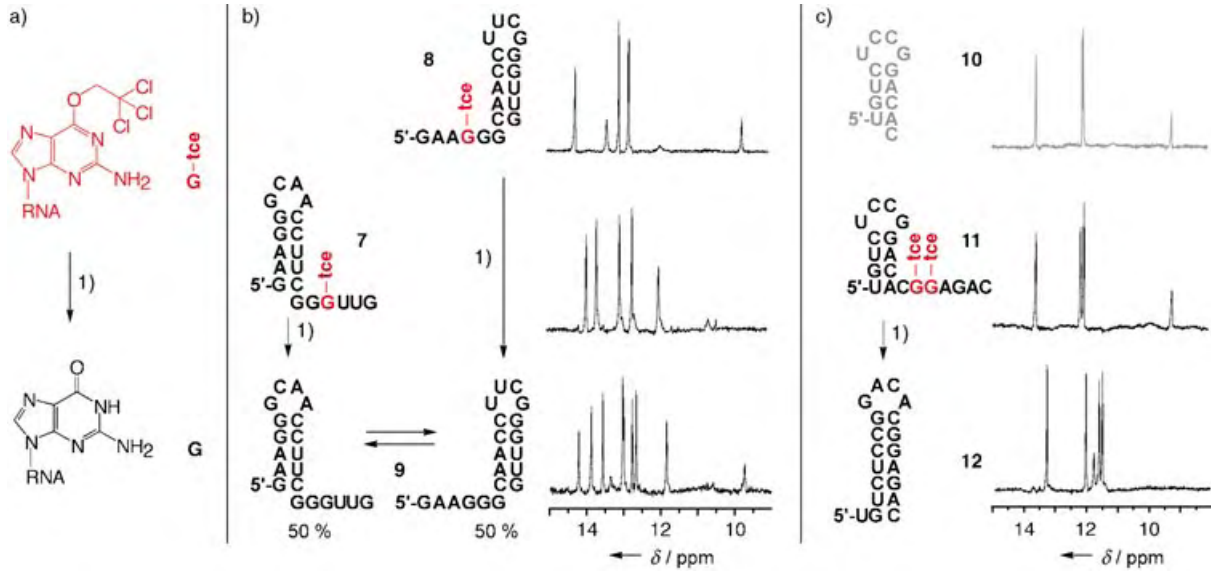


Figure 3. Secondary-structure modulation of short RNAs containing functionalized nucleosides. a) O^6-(2,2,2-trichloroethyl)guanosine (^{tce}G). b) Incorporation of ^{tce}G at positions 17 or 4 of the sequence rGAA(G^4)GGCAACCUUCGG(G^{17})UUG results in conformation selection of either the GCAA hairpin, **7**, or the UUCG hairpin, **8**. Release of the O^6-tce groups restores the conformational equilibrium of **9** (see also Figure 2). c) rUGU-C(UCCG)GACAC^{tce}G^{tce}GAGAC (**11**) forms a stable hairpin with a UCCG tetraloop corresponding to reference sequence **10**. Upon release of the O^6-tce groups this RNA sequence converts into the thermodynamically favorable GACA hairpin, **12**. 1) Zn^0, 1 M NH_4OAc, pH 7, 25 °C. Structural probing of the RNA secondary structures by comparative imino proton NMR spectroscopy (500 MHz): 0.2–0.3 mM strand concentration, H_2O/D_2O (9:1), 25 mM sodium arsenate buffer, pH 7.4, 26 °C (see also the Supporting Information).

 © 2004 Wiley-VCH Verlag GmbH & Co. KGaA, Weinheim

structures. The requirements for the functional labels are quite stringent. With respect to their incorporation into RNAs, they have to be orthogonal to the protecting groups used throughout the solid-phase synthesis. This is effectively achieved by use of the trichloroethyl group. In the late sixties, this group was introduced into oligonucleotide chemistry in the context of phosphate protection.[18] With respect to the applications of the trichloroethyl group for secondary-structure manipulation, we had to consider that the Zn^{2+} ions generated during the cleavage of the O^6-tce group may affect the secondary structure.[19–21] However, for the relatively small RNAs investigated so far we have no evidence for a structure-determining influence of the Zn^{2+} ions. In extending our approach towards larger RNAs, nucleobase functionalization by other chemical groups is conceivable; highly promising candidates are photolabile groups.

The control of conformational changes of nucleic acid structures is an important issue in RNA biotechnology. In particular, great efforts have been made in the development of allosterically triggered ribozymes for gene therapy and for nucleic acid diagnostics.[22–24] With the present concept for secondary-structure manipulation by functionalized nucleobases, a potential tool for applications in these fields has been created.

Received: March 21, 2004 [Z460068]

Keywords: conformational switches · nucleobase modifications · oligonucleotides · RNA structures

[1] D. M. Crothers in *RNA* (Eds.: D. Söll, S. Nishimura, P. B. Moore), Pergamon Elsevier Science, Oxford, **2001**, pp. 61–70.
[2] W. C. Winkler, R. R. Breaker, *ChemBioChem* **2003**, *4*, 1024–1032.
[3] R. R. Breaker, *Curr. Opin. Biotechnol.* **2002**, *13*, 31–39.
[4] S. Sando, T. Sasaki, K. Kanatani, Y. Aoyama, *J. Am. Chem. Soc.* **2003**, *125*, 15720–15721.
[5] J. S. Hartig, I. Grüne, S. H. Najafi-Shoushtari, M. Famulok, *J. Am. Chem. Soc.* **2004**, *126*, 722–723.
[6] A. S. Mironov, I. Gusarov, R. Rafikov, L. E. Lopez, K. Shatalin, R. A. Kreneva, D. A. Perumov, E. Nudler, *Cell* **2002**, *111*, 747–757.
[7] M. Mandal, R. Breaker, *Nat. Struct. Biol.* **2004**, *11*, 29–35.
[8] A. Stutz, C. Höbartner, S. Pitsch, *Helv. Chim. Acta* **2000**, *83*, 2477–2503.
[9] For detailed experimental procedures, see the Supporting Information.
[10] R. Micura, *Angew. Chem.* **2002**, *114*, 2269–2373; *Angew. Chem. Int. Ed.* **2002**, *41*, 2265–2267.
[11] S. Pitsch, P. A. Weiss, L. Jenny, A. Stutz, X. Wu, *Helv. Chim. Acta* **2001**, *84*, 3773–3795.
[12] C. Höbartner, C. Kreutz, E. Flecker, E. Ottenschläger, W. Pils, K. Grubmayr, R. Micura, *Monatsh. Chem.* **2003**, *134*, 851–873.
[13] Oligoribonucleotide synthesis and deprotection protocols were first elaborated for the sequence rCG^{tce}GUA by using N^2-acetyl-, N^2-methoxyacetyl-, or N^2-unprotected 2′-*O*-TOM-guanosine phosphoramidites in various combinations with N^2-acetyl-, N^2-methoxyacetyl-, or N^2-phenoxyacetyl-protected O^6-tce-2′-*O*-TOM-guanosine phosphoramidites. These experiments and the synthesis of the corresponding building blocks will be described elsewhere.
[14] Deprotection of the O^6-tce groups was first evaluated for the sequence rCG^{tce}GUA under conditions with various pH values, strand concentrations, and buffer compositions, as well as different metals (Zn, Cd). For details, see the Supporting Information.
[15] For other examples of short bistable RNAs, see: C. Höbartner, M.-O. Ebert, B. Jaun, R. Micura, *Angew. Chem.* **2002**, *114*, 619–623; *Angew. Chem. Int. Ed.* **2002**, *41*, 605–609.
[16] C. Höbartner, R. Micura, *J. Mol. Biol.* **2003**, *325*, 421–431.
[17] R. Micura, C. Höbartner, *ChemBioChem* **2003**, *4*, 984–990.
[18] F. Eckstein, I. Rizk, *Angew. Chem.* **1967**, *79*, 939; *Angew. Chem. Int. Ed. Engl.* **1967**, *6*, 949.
[19] E. Ennifar, P. Walter, P. Dumas, *Nucleic Acids Res.* **2003**, *31*, 2671–2682.
[20] E. B. Khomyakova, H. Gousset, J. Liquier, T. Huynh-Dinh, C. Gouyette, M. Takahashi, V. L. Florentiev, E. Taillandier, *Nucleic Acids Res.* **2000**, *28*, 3511–3516.
[21] M. Wu, I. Tinoco, Jr., *Proc. Natl. Acad. Sci. USA* **1998**, *95*, 11555–11560.
[22] M. Warashina, T. Kuwabara, H. Kawasaki, J. Ohkawa, K. Taira in *RNA* (Eds.: D. Söll, S. Nishimura, P. B. Moore), Pergamon Elsevier Science, Oxford, **2001**, pp. 277–308.
[23] B. A. Sullenger, E. Gilboa, *Nature* **2002**, *418*, 252–258.
[24] M. B. Long, J. P. Jones III, B. A. Sullenger, J. Byun, *J. Clin. Invest.* **2003**, *112*, 312–318.

 © 2004 Wiley-VCH Verlag GmbH & Co. KGaA, Weinheim

DNA Recognition

Stable and Selective Recognition of Three Base Pairs in the Parallel Triple-Helical DNA Binding Motif**

*Sabrina Buchini and Christian J. Leumann**

Selective artificial control of gene expression is a longstanding dream of researchers in biotechnology and human therapy. Oligonucleotides seem perfectly suited to this purpose because of their unique base–base recognition properties. The triplex approach uses oligonucleotides that sequence-selectively bind genomic, double-stranded DNA and interfere with transcription and the DNA processing machinery through formation of a triple helix. This approach allows not only transcriptional activation and deactivation but also gene knock-out, targeted mutagenesis, targeted recombina-

[*] Dipl.-Chem. S. Buchini, Prof. C. J. Leumann
Department of Chemistry and Biochemistry
University of Bern, Freiestrasse 3
3012 Bern (Switzerland)
Fax: (+41) 31-631-4355
E-mail: leumann@ioc.unibe.ch

[**] The authors thank Christine Brotschi, Alain Mayer, and Dorte Renneberg for advice on experimental procedures. Financial support from the Swiss National Science Foundation (Grant no. 200020-100178) is gratefully acknowledged.

 DOI: 10.1002/anie.200460159 © 2004 Wiley-VCH Verlag GmbH & Co. KGaA, Weinheim

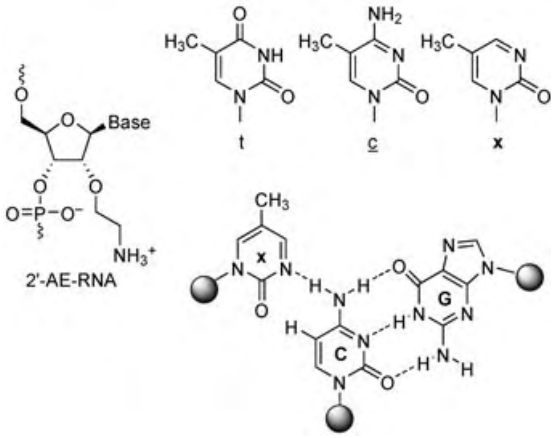
tion, and sequence-selective manipulation of genomic DNA.[1–3]

In the parallel or pyrimidine binding motif a homopyrimidine triplex-forming oligonucleotide (TFO) oriented parallel to the purine strand of a DNA molecule binds to the major groove of the target duplex by forming Hoogsteen C^+·G–C and T·A–T base triples. However, formation of the C^+·G–C base triple is pH sensitive and disfavored at neutral pH. Furthermore, recognition of duplex DNA is constrained to homopurine/homopyrimidine sequence tracts, and the third-strand affinities of the oligonucleotides to their targets are generally low. These factors severely restrict the applicability of TFOs in vitro and in vivo.

Numerous attempts have been made to chemically modify TFOs to remove these constraints, but with limited success.[4] Conformationally constrained locked nucleic acids (LNAs)[5–7] and 2′-aminoethyl-oligoribonucleotides (2′AE-RNAs)[8,9] are milestones in this field. The latter molecules recognize duplex DNA not only through base–base contacts but also by formation of a salt bridge between the protonated amino function of the oligonucleotide and a phosphodiester unit of the target purine strand (dual recognition). Both modifications proved to dramatically increase TFO affinity for duplex targets.

It seems plausible that a combination of general-affinity-enhancing modifications of the TFO sugar units or backbone and inclusion of new base analogues that selectively recognize pyrimidine bases could alleviate restriction of the target sequence. This idea has been explored with remarkable success by Imanishi and co-workers, who used LNAs containing a 2-pyridone base designed to selectively recognize a C–G base pair.[10,11] We recently investigated selective C–G recognition by oligodeoxynucleotides containing single 2′-aminoethylribonucleosides with a 5-methyl-2-pyrimidinone base (Scheme 1, **x**).[12] Herein we present experimental evidence that such a nucleoside within the context of a fully modified 2′AE-RNA is able to recognize up to five C–G inversions in a 15-mer DNA target duplex (33% pyrimidine content) with high selectivity and a third-strand affinity matching or even excelling the affinity of the two strands of the target duplex for one another.

The synthesis of the modified nucleoside **x**[12] and the corresponding fully modified AE-TFOs by standard phosphoramidite chemistry will be described in detail elsewhere. All TFOs contained a deoxynucleoside unit at their 3′ end for synthetic ease. All TFOs were analyzed by ESI-MS and found to have masses corresponding to the expected values. To analyze the effect of up to five 5-methyl-2-pyrimidinone (**x**) substitutions in a 15-mer we prepared the TFOs and duplex targets listed in Table 1 and measured the corresponding T_m values by standard UV/melting-curve techniques. The melting curves corresponding to entry 1 are shown in Figure 1 as a representative example.



Scheme 1. Top: Chemical structure of a 2′-aminoethylribonucleotide unit and the bases thymine (t), 5-methylcytosine (c), and 5-methyl-2-pyrimidone (**x**). Bottom: Anticipated **x**·C–G base triplet.

Table 1: T_m data for third-strand melting, taken from UV/melting curves ($\lambda = 260$ nm).[a] T_m values for duplex melting are indicated in parentheses.

Entry	Triplex sequence	T_m value of the third strand (duplex) [°C]			
		Y/Z: C/G	G/C	A/T	T/A
1	5′-GCTAAAAAGA**Y**AGAGAGATCG-3′ 3′-CGATTTTTCT**Z**TCTCTCTAGC-3′ 5′-ttttt**c**t**x**t**c**t**c**t**c**T-3′	77 (63)	66 (62)	66 (61)	65 (61)
2	5′-GCTAAAAA**Y**A**Y**A**Y**AGAGATCG-3′ 3′-CGATTTTT**Z**T**Z**T**Z**TCTCTAGC-3′ 5′-ttttt**x**t**x**t**x**t**c**t**c**T-3′	67 (64)	26 (62)	26 (60)	<10 (58)
3	5′-GCTAA**Y**AA**Y**A**Y**A**Y**AGA**Y**ATCG-3′ 3′-CGATT**Z**TT**Z**T**Z**T**Z**TCT**Z**TAGC-3′ 5′-tt**x**tt**x**t**x**t**x**t**c**t**x**T-3′	67 (67)	n.d.[b] (63)	n.d.[b] (59)	n.d.[b] (55)

[a] $c = 1.6$ μM in 10 mM sodium cacodylate, 100 mM NaCl, 0.25 mM spermine, pH 6.75 ± 0.25. [b] No T_m value could be determined for third-strand melting.

As can be seen from the T_m data in Table 1, triplex formation occurs preferentially at the C–G inversion site of the DNA duplex. In the case of a single substitution (entry 1), all other arrangements are less stable and have T_m values at least 11 °C lower than that observed with a C–G inversion site. All the triplexes containing one **x** unit melt at higher temperatures than the underlying Watson–Crick duplexes. Triple substitution of the target duplex (entry 2) results in increased destabilization at non-C–G sites, as characterized by a difference in the T_m value of more than 40 °C between molecules with C–G sites and those without. Again, the thermal stability of the triplex formed by third (Hoogsteen)-strand binding to the purine C–G target at neutral pH is higher than that of the Watson–Crick duplex. The melting curves of the triplexes with five substitutions (Table 1, entry 3) revealed only one transition in each case, with T_m values in the same range as those of the underlying duplexes. It was difficult to conclude from this T_m analysis alone whether triplex formation occurred at all in the presence of five substitutions. Clarification came from a gel

 © 2004 Wiley-VCH Verlag GmbH & Co. KGaA, Weinheim

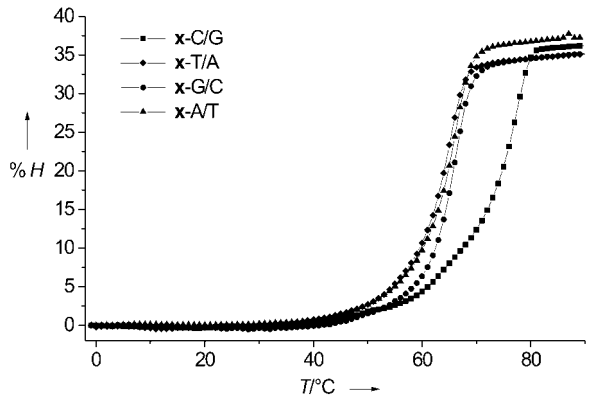


Figure 1. UV/melting curves (260 nm) of the triplexes listed in Table 1, entry 1. Experimental conditions are described in Table 1.

shift assay (Figure 2), which clearly indicated the presence of a triplex containing a C–G inversion site and the absence of triplex formation by all other duplexes. We thus conclude that

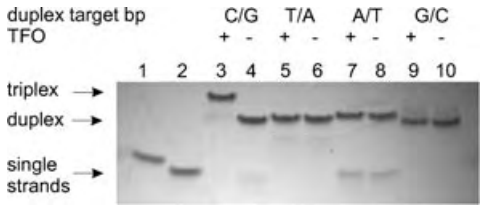


Figure 2. Nondenaturing 20% polyacrylamide gel of triplexes with five **x** substitutions (Table 1, entry 3). Lanes 1 and 2: single-strand controls (the strands correspond to those present in the target duplexes); lanes 3–10: stoichiometric mixtures (0.8 nmol) of the strands of the target duplexes, with and without TFO (2 equiv). Buffer: tris(hydroxymethyl)aminomethane borate (90 mM), $MgCl_2$ (10 mM), pH 7.0, 4 °C. Visualization by exposure to UV light.

the transitions observed in the melting curves correspond to triplex-to-single-strand melting in the case of the C–G target duplex and duplex-to-single-strand transitions in all other cases. The higher hyperchromicity of the transition with the C–G target duplex compared to the hyperchromicities of the transitions involving the other targets corroborates this interpretation. The same gel experiment was also conducted with the triplexes given in entry 2 of Table 1 (data not shown). Again, triplex formation was only observed with the C–G duplex target.

The next step was to explore different sequences. We prepared a further series of TFOs and target duplexes with the sequences given in Table 2 and determined the corresponding T_m values for the melting of the triplex. In the first sequence context investigated (Table 2, entry 1), three **x** units interrupt a stretch of six contiguous methylcytidine units in the TFO. Use of this sequence, rich in contiguous c nucleotides, leads to triplexes with a lower stability than the target duplex. When the **x** units are placed between thymidine and methylcytidine residues and contiguous c residues are avoided (Table 2, entry 2), the third strand affinity is similar to that observed when **x** is located between two thymidine residues (for example, Table 1, entry 2). The reason for the decreased affinity in the first case seems to be local repulsion of the accumulated positive charges in the pile of protonated c residues rather than the effect of the modification **x**. Sequence effects on AE-RNA/DNA interactions within the context of canonical base recognition (t·A-T, c^+·G-C) have not been addressed so far. However, it is well-known that contiguous cytosine units in a TFO decrease the affinity for the third strand,[13] both for RNA and for DNA TFOs. Three contiguous **x** residues in an AE-TFO (Table 2, entry 3) lead to a strongly bound triplex, which corroborates the view that not the modification **x** but the contiguous protonated cytosine sequence is mostly responsible for the observed reduction in stability.

The triplex stabilities found for the systems described herein are remarkable given that **x** recognizes the cytosine base by forming only one hydrogen bond, possibly assisted by a favorable electrostatic C–H···O interaction (Scheme 1). These stabilities suggest that the dual recognition scheme, in which the protonated ammonium function on the 2′-side chain of the third strand unselectively recognizes a phosphate oxygen atom on the purine strand of the target duplex, can energetically replace the loss of a hydrogen bond at the base interface without a loss of overall selectivity. This hypothesis seems plausible since formation of a salt bridge is strongly distance-dependent and would not tolerate the structural isomorphism expected in base mismatching. Indeed, we have previously found that the presence of an **x** unit in a TFO with a DNA backbone does not lead to an increase in stability such as that observed in the context of the fully modified AE-TFOs, which points to an energetically less significant contribution of the implied salt bridge to triplex stability.[12] The lack of impact made by formation of a salt bridge on stability is probably the result of differences in third-strand conformation (DNA versus RNA) and thus differences in the distance between the relevant phosphodiester backbones in the triplex.

Within the context of 2′-*O*-aminoethyl-oligoribonucleotides, the unit **x** fulfills the criteria of selectivity and high affinity for C–G inversion sites and expands the recognition

Table 2: T_m data for third-strand melting, taken from UV/melting curves ($\lambda = 260$ nm).[a]

Entry	Triplex sequence	T_m duplex [°C]	T_m value of third strand [°C]
1	5′-GCTAAAG**C**GG**C**GG**C**GAAATCG-3′ 3′-CGATTTC**G**CC**G**CC**G**CTTTAGC-3′ 5′-ttt**c**x**c**c**x**c**x**c**ttT-3′	73	20[b]
2	5′-GCTGGAG**C**AG**C**AG**C**AGAATCG-3′ 3′-CGACCTC**G**TC**G**TC**G**TCTTAGC-3′ 5′-**c**c**t**c**x**t**c**x**t**c**x**t**c**t**T-3′	72	ca. 60[c]
3	5′-GCTGAAGA**CCC**GAGGAGATCG-3′ 3′-CGACTTCT**GGG**CTCCTCTAGC-3′ 5′-**c**ttc**t**t**xxx**c**t**cc**t**c**T-3′	71	ca. 62[c]

[a] $c = 1.6$ μM in 10 mM sodium cacodylate, 100 mM NaCl, 0.25 mM spermine, pH 6.5. [b] pH 6.0. [c] Third strand and duplex melting partially overlaid.

 © 2004 Wiley-VCH Verlag GmbH & Co. KGaA, Weinheim

scheme in the parallel triplex binding motif from two to three duplex base pairs. It now remains to define the limitations of the binding of **x** to target DNA and to show whether **x** can be used productively for selective recognition and manipulation of cellular targets, for example in applications such as targeted gene knock-out.[14,15] It will be a challenge for future research to find new bases that, within the context of AE-TFOs, selectively recognize T–A inversion sites.

Received: March 30, 2004 [Z460159]

Keywords: antigenes · DNA recognition · DNA triplex · intercalation · oligonucleotides

[1] R. V. Guntaka, B. R. Varma, K. T. Weber, *Int. J. Biochem. Cell Biol.* **2003**, *35*, 22 – 31.
[2] M. M. Seidman, P. M. Glazer, *J. Clin. Invest.* **2003**, *112*, 487 – 494.
[3] S. Buchini, C. J. Leumann, *Curr. Opin. Chem. Biol.* **2003**, *7*, 717 – 726.
[4] J. Robles, A. Grandas, E. Pedroso, F. J. Luque, R. Eritja, M. Orozco, *Curr. Org. Chem.* **2002**, *6*, 1333 – 1368.
[5] S. Obika, Y. Hari, T. Sugimoto, M. Sekiguchi, T. Imanishi, *Tetrahedron Lett.* **2000**, *41*, 8923 – 8927.
[6] S. Obika, T. Uneda, T. Sugimoto, D. Nanbu, T. Minami, T. Doi, T. Imanishi, *Bioorg. Med. Chem.* **2001**, *9*, 1001 – 1011.
[7] H. Torigoe, Y. Hari, M. Sekiguchi, S. Obika, T. Imanishi, *J. Biol. Chem.* **2001**, *276*, 2354 – 2360.
[8] M. J. J. Blommers, F. Natt, W. Jahnke, B. Cuenoud, *Biochemistry* **1998**, *37*, 17714 – 17725.
[9] B. Cuenoud, F. Casset, D. Hüsken, F. Natt, R. M. Wolf, K.-H. Altmann, P. Martin, H. E. Moser, *Angew. Chem.* **1998**, *110*, 1350 – 1353; *Angew. Chem. Int. Ed.* **1998**, *37*, 1288 – 1291.
[10] S. Obika, Y. Hari, M. Sekiguchi, T. Imanishi, *Angew. Chem.* **2001**, *113*, 2149 – 2151; *Angew. Chem. Int. Ed.* **2001**, *40*, 2079 – 2081.
[11] S. Obika, Y. Hari, M. Sekiguchi, T. Imanishi, *Chem. Eur. J.* **2002**, *8*, 4796 – 4802.
[12] S. Buchini, C. J. Leumann, *Tetrahedron Lett.* **2003**, *44*, 5065 – 5068.
[13] S. Hildbrand, A. Blaser, S. P. Parel, C. J. Leumann, *J. Am. Chem. Soc.* **1997**, *119*, 5499 – 5511.
[14] N. Puri, A. Majumdar, B. Cuenoud, F. Natt, P. Martin, A. Boyd, P. S. Miller, M. M. Seidman, *J. Biol. Chem.* **2001**, *276*, 28991 – 28998.
[15] N. Puri, A. Majumdar, B. Cuenoud, F. Natt, P. Martin, A. Boyd, P. S. Miller, M. M. Seidman, *Biochemistry* **2002**, *41*, 7716 – 7724.

 © 2004 Wiley-VCH Verlag GmbH & Co. KGaA, Weinheim

Dendrimers

Efficiency and Fidelity in a Click-Chemistry Route to Triazole Dendrimers by the Copper(I)-Catalyzed Ligation of Azides and Alkynes**

Peng Wu, Alina K. Feldman, Anne K. Nugent, Craig J. Hawker, Arnulf Scheel, Brigitte Voit, Jeffrey Pyun, Jean M. J. Fréchet, K. Barry Sharpless,* and Valery V. Fokin**

Unique properties of dendrimers, which are a direct consequence of their regular structure, have sparked significant interest in recent years.[1] A large number of dendritic structures varying in size, solubility, and function have been prepared. However, most dendrimer syntheses, particularly at later generations, require high monomer loading, rely on tedious and lengthy chromatographic separations, and generate considerable waste.[2] For example, the synthesis of polyether dendrimers,[3] based on a sequence of Williamson etherifications and halogenations, suffers from its incompatibility with various functional groups and complicated purifications.[4]

Herein, we report on an efficient and preparatively simple approach for the generation of diverse dendritic structures of high purity and in excellent yield. The unique aspects of this route arise from the near-perfect reliability of the Cu^{I}-

[*] A. K. Nugent, Dr. C. J. Hawker, A. Scheel, Dr. J. Pyun
IBM Almaden Research Center
650 Harry Road, San Jose, CA 95120 (USA)
Fax: (+1) 408-927-3310
E-mail: hawker@almaden.ibm.com

P. Wu, A. K. Feldman, Prof. K. B. Sharpless, Prof. V. V. Fokin
Department of Chemistry and
The Skaggs Institute for Chemical Biology
The Scripps Research Institute
10550 North Torrey Pines Road, La Jolla, CA 92037 (USA)
Fax: (+1) 858-784-7562
E-mail: sharples@scripps.edu
fokin@scripps.edu

A. Scheel, Prof. B. Voit
Institut für Polymerforschung Dresden e.V.
Hohe Strasse 6, 01069 Dresden (Germany)

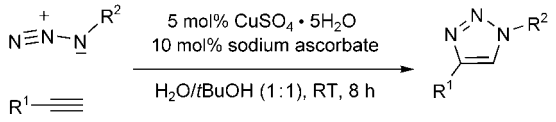
Dr. J. Pyun, J. M. J. Fréchet
University of California
Department of Chemistry and Materials Sciences Division
Lawrence Berkeley National Laboratory
Berkeley, CA 94720 (USA)

[**] We thank the National Institute of General Medical Sciences, the National Institutes of Health (GM 28284), the National Science Foundation (CHE-9985553), the W. M. Keck Foundation, the Skaggs Institute for Chemical Biology, the MRSEC Program of the National Science Foundation (award no. DMR-0213618 for the Center for Polymeric Interfaces and Macromolecular Assemblies), the NIRT Program of the National Science Foundation (grant no. 0210247), IBM Corporation, DOE-BES, and NSF International/DAAD for financial support. We are also grateful to Prof. M. G. Finn for helpful discussions.

Supporting information for this article is available on the WWW under http://www.angewandte.org or from the author.

 © 2004 Wiley-VCH Verlag GmbH & Co. KGaA, Weinheim DOI: 10.1002/anie.200454078

catalyzed synthesis of 1,2,3-triazoles from azides and alkynes (Scheme 1).[5] The reaction is experimentally simple—proceeding well in aqueous solutions without protection from



Scheme 1. Copper(I)-catalyzed synthesis of 1,4-disubstituted 1,2,3-triazoles.

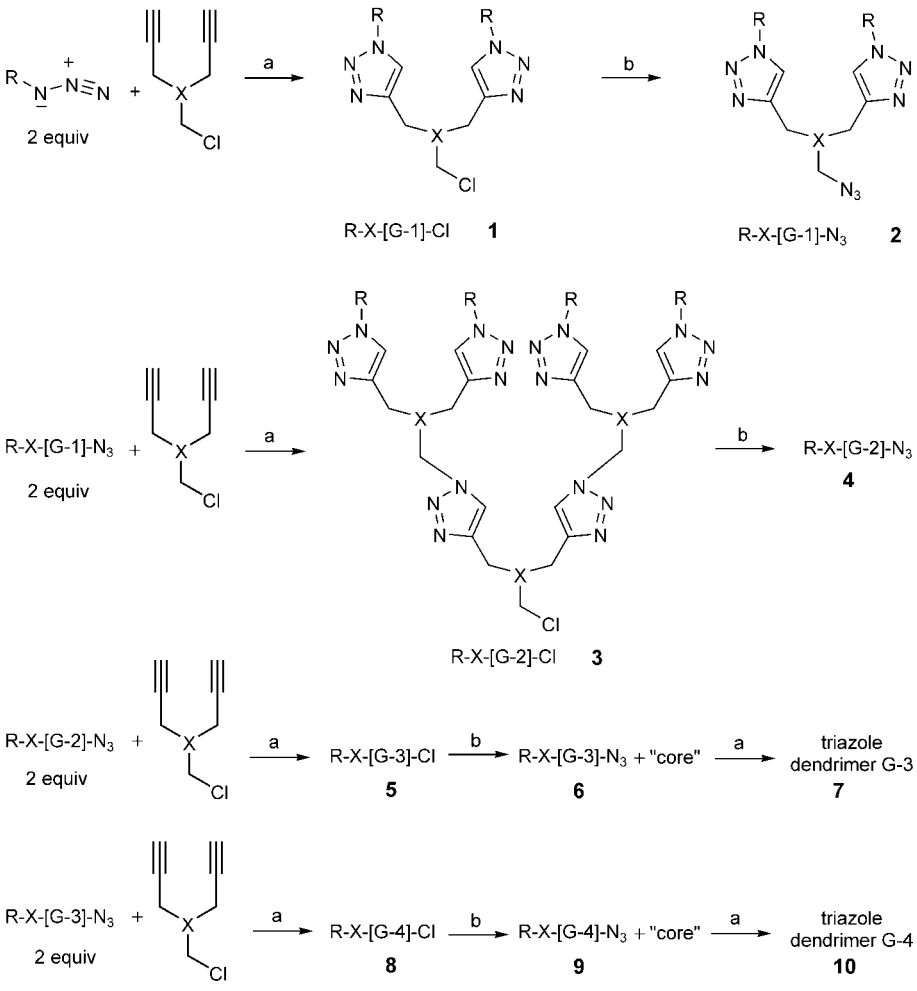
oxygen, requiring only stoichiometric amounts of starting materials, and generating virtually no by-products. Equally important is the wide scope, high selectivity, and nearly quantitative yields of this transformation. In our procedure for the best click reaction to date,[6] the components and catalyst are simply mixed and stirred, whereupon pure products are isolated by filtration or simple extraction.

Fréchet's convergent approach was utilized in our dendrimer synthesis.[7] Thus, the individual branches or dendrons were built sequentially, starting on the "outside" of the molecule. They were then coupled to a multivalent centerpiece ("core") in the last step, as outlined in Scheme 2, which led to a variety of dendrimers with different chain-end groups (R) and internal repeat units (X).

In exploiting Cu^I-catalyzed reaction for dendrimer construction, we envisaged a variety of AB_2 monomers based on terminal alkynes and alkyl halide functionalities. Readily available starting materials and simple synthetic strategies for the introduction of alkynyl groups lead to significant structural diversity (Figure 1). However, one structural feature was common to monomers **11**–**13**, namely the presence of a single chloromethyl group. This was specifically incorporated into our synthetic strategy to allow facile activation of the focal-point group during dendrimer construction by the convergent-growth approach. We envisaged that reaction of dendritic fragments containing a single chloromethyl group with sodium azide would lead to quantitative formation of the desired azidomethyl group, which could then be coupled with **11**, **12**, or **13** to give the next-generation dendron (Scheme 2). As with AB_2 monomer units, a variety of the chain ends with reactive functional groups ranging from carboxylic acid to alcohol could be employed in the construction of diverse triazole dendrimers (Figure 2).

Copper(I)-catalyzed reactions of AB_2 monomers and the chain-end units were carried out in the presence of $CuSO_4$ (2–5 mol%) and sodium ascorbate (5–10 mol%) in a 1:1 mixture of water and *tert*-butyl alcohol at room temperature to generate the desired bistriazoles in near-quantitative yields. Trace amounts of copper salts in the products were easily removed by washing with an ammonium hydroxide/citrate aqueous buffer. Owing to the high degree of efficiency, the reaction could be conducted with a stoichiometric amount (2.0 equiv) of the azides. Purifications were greatly simplified due to the absence of side products. This is in direct contrast with the classical synthesis of polyether dendrimers by the convergent-growth approach, where an excess of dendron (2.05–2.20 equiv) is typically used to increase yields of the next-generation dendritic fragment. Furthermore, purification by flash chromatography is usually required at each step.[7]

In the next step, the primary chlorides were converted into the corresponding azides by reaction with 1.5 equiv sodium azide in acetone/water.[9] This transformation was equally facile and typically resulted in yields of more than 95% with NaCl as the only by-product. The dendrons were then "grown" by the reaction of the



Scheme 2. Convergent approach toward triazole dendrimers. a) $CuSO_4$ (5 mol%), sodium ascorbate (10 mol%), H_2O/*t*BuOH (1:1); b) 1.5 equiv NaN_3, CH_3COCH_3/H_2O (4:1), 60°C, 1–3 h.[8]

 © 2004 Wiley-VCH Verlag GmbH & Co. KGaA, Weinheim

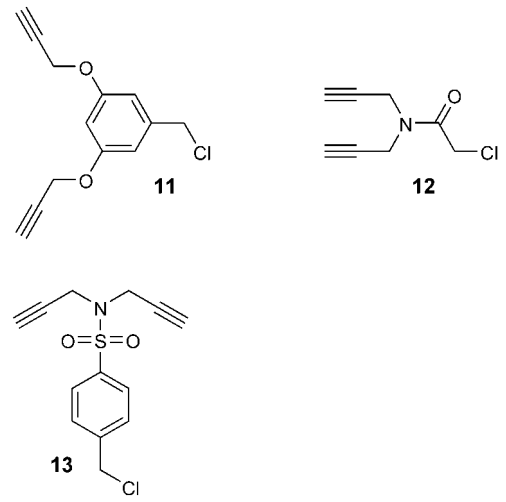


Figure 1. Structures of the AB_2 monomers **11**–**13** used in the synthesis of dendrimers based on click chemistry.

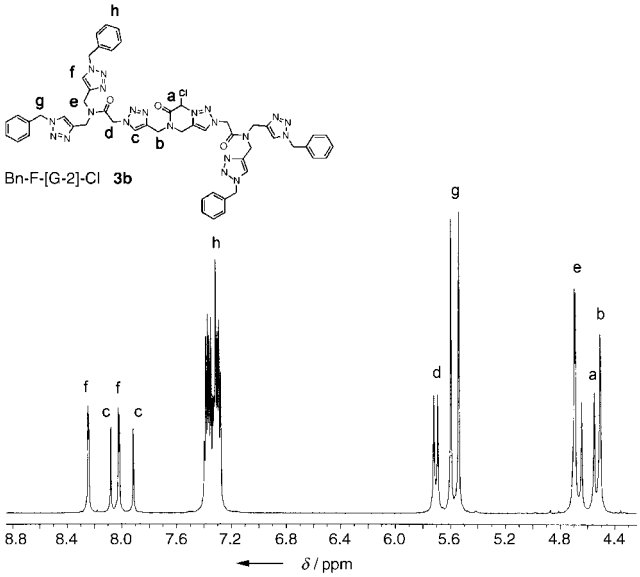


Figure 3. ^{1}H NMR spectrum of the crude reaction mixture containing dendron **3b**.

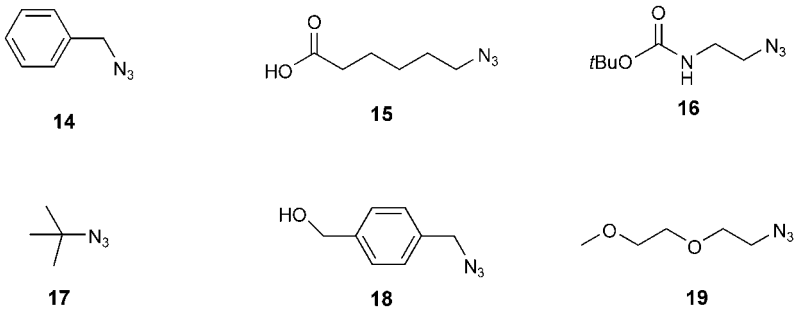


Figure 2. Azides **14**–**19** used in the synthesis of chain-end-functionalized dendrimers based on click chemistry.

resulting azides with the original monomers **11, 12**, or **13**. All second-generation dendrons were isolated as pure white solids by simple filtration or aqueous workup in yields exceeding 90% for the isolated products. As seen in the crude ^{1}H NMR spectrum of dendron Bn-F-[G-2]-Cl **3b** (Figure 3), the integration ratio for protons f and c is 2:1 which, in comparison with the spectrum of the mixture obtained from a purely thermal process, indicates 100% regioselectivity in its construction.

Following the same procedure, dendrons based on amide monomer **12** with *tert*-butyl azide **17** at the periphery as well as the benzyl ether monomer **11** with azide **19** were propagated to the fourth generation. Dendrons constructed from monomer **12** with the azides **16** and **19** at the periphery were propagated to the third generation. When the dendrimers were not soluble in aqueous mixtures, slight modification of the reaction conditions led to the same degree of efficiency and near-quantitative yields. For example, benzyl-terminated dendrons prepared from **14** and **11** were insoluble in 1:1 H_2O/THF solutions at the second generation and led to incomplete conversions. Similarly, conversion of the chloromethyl group to the azide group was unsuccessful with aqueous sodium azide. To overcome this difficulty, the copper-catalyzed reaction was performed in THF with an organosoluble Cu^I species, $[(PPh_3)_3CuBr]$, under microwave irradiation, leading to quantitative yields of the next-generation dendritic fragment. Similar results for azide formation were obtained when the displacement was performed with sodium azide in dimethylformamide or dimethyl sulfoxide. Analysis of the dendrons by MALDI-TOF mass spectrometry as well as by gel-permeation chromatography (GPC) provides no signs of products with defects that would arise from incomplete branches (Figure 4).

Works by Tomalia, Fréchet, and others demonstrate that the solubility properties of dendritic molecules are dominated by their periphery.[2] As expected, our observations largely follow these trends. A unique property of

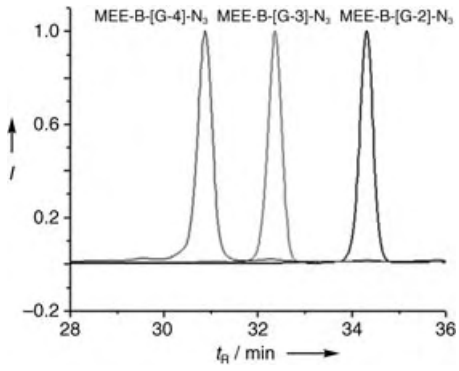


Figure 4. GPC traces for the crude reaction products MEE-B-[G-4]-N_3 **9d**, MEE-B-[G-3]-N_3 **6d**, and MEE-B-[G-2]-N_3 **4d**, obtained by dendritic growth from the benzyl ether monomer **11** and the azido di(ethylene glycol) derivative **19**.

 © 2004 Wiley-VCH Verlag GmbH & Co. KGaA, Weinheim

these triazole-based dendrons is, as the molecules reach higher generations, they become less soluble in ethyl acetate and slightly more soluble in dichloromethane, chloroform, alcohols and, surprisingly, aqueous mixtures.[10]

Finally, several third- and fourth-generation triazole dendrimers were constructed by anchoring these dendrons to a variety of polyacetylene cores (Figure 5). A representative example is shown in Scheme 3, where the third-generation dendron *t*Bu-F-[G-3]-N_3 **6a** was coupled directly with 2,4,6-tris(prop-2-ynyloxy)-1,3,5-triazine (**23**) in the presence of the Cu^I catalyst generated in situ. It is noteworthy that even at these low concentrations (0.06 M in alkyne and azide), the reaction proceeded rapidly enough at room temperature and reached completion in less than 30 h as indicated by LC-MS analysis. Dendrimer **7a**, with 24 periphery units (M_w = 6322 Da), was isolated as a white solid in 92% yield. All dendrimers were characterized by ^1H and ^{13}C NMR spectroscopy, and the structure and purity were confirmed further by GPC and MALDI-TOF mass spectrometry (Figure 6). High polarity, good solubility in alcohol/water mixtures, and strong UV absorptions at $\lambda = 210$ and 229 nm are unique features of this new class of triazole dendrimers.

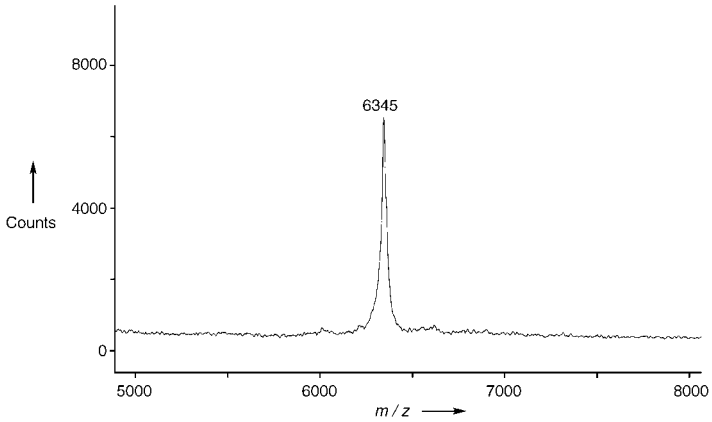


Figure 6. MALDI-TOF mass spectrum of **7a** (M+Na^+, resolution ± 0.1%).

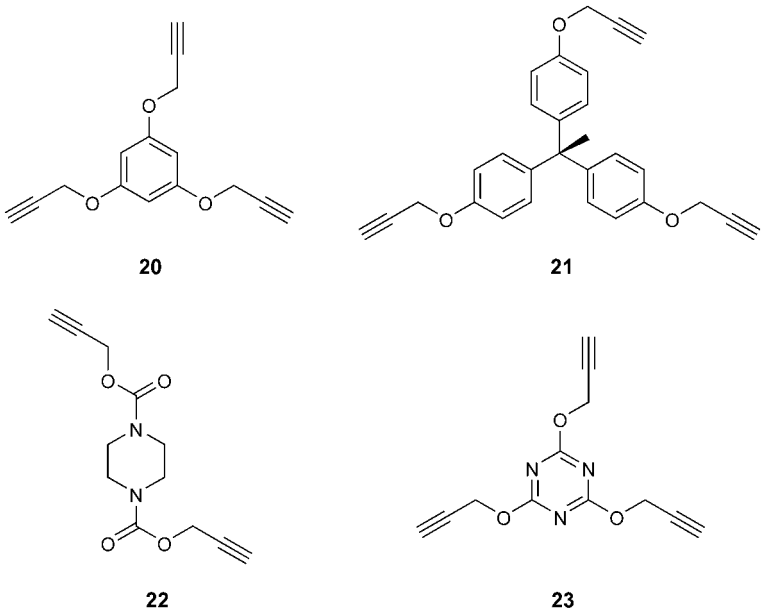
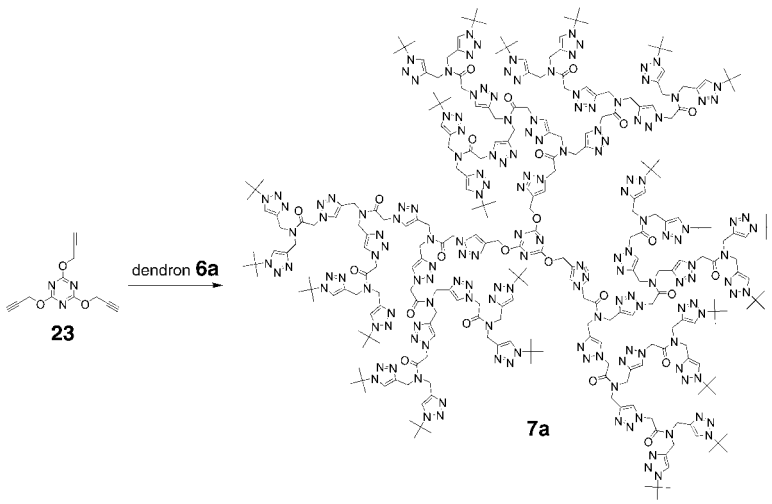


Figure 5. Polyacetylene cores used in the synthesis of chain-end-functionalized dendrimers based on click chemistry.



Scheme 3. Synthesis of dendrimer **7a**.

In summary, a highly efficient route to triazole-based dendrimers is now available thanks to the unprecedented reliability of the Cu^I-catalyzed ligation of terminal alkynes and azides. This chemistry is highly regioselective, resulting in 1,4-disubstituted triazoles. A variety of functional groups are compatible with the process, and the only major by-product formed in the reaction is NaCl. All second-generation and some third-generation dendrons were isolated directly as pure solids (i.e. without chromatographic separations), meeting the requirements for large-scale applications.

The recently discovered ability of polydentate 1,4-disubstituted 1,2,3-triazole ligands to stabilize Cu^I species even under aqueous aerobic conditions,[11] has already proven crucial in biological applications.[12] Exploration of the copper-binding ability of this new class of dendrimers and their ligand properties in homogeneous catalysis is underway.

Received: February 23, 2004 [Z54078]
Published Online: June 30, 2004

Keywords: alkynes · azides · click chemistry · copper · dendrimers

[1] For reviews, see: a) D. A. Tomalia, A. M. Naylor, W. A. Goddard III, *Angew. Chem.* **1990**, *102*, 119–157; *Angew. Chem. Int. Ed. Engl.* **1990**, *29*, 138; b) D. A. Tomalia, H. D. Durst in *Topics in Current Chemistry*, *Vol. 165* (Ed.: E. Weber), Springer,

 © 2004 Wiley-VCH Verlag GmbH & Co. KGaA, Weinheim

Berlin, **1993**, pp. 193 – 313; c) F. Zeng, S. C. Zimmerman, *Chem. Rev.* **1997**, *97*, 1681 – 1712; d) C. J. Hawker in *Advances in Polymer Science*, *Vol. 147*, Springer, Berlin, **1999**, pp. 113 – 160; e) M. Fischer, F. Vögtle, *Angew. Chem.* **1999**, *111*, 934 – 955; *Angew. Chem. Int. Ed.* **1999**, *38*, 884 – 905; f) A. W. Bosman, H. M. Janssen, E. W. Meijer, *Chem. Rev.* **1999**, *99*, 1665 – 1688; g) J.-P. Majoral, A.-M. Caminade, *Chem. Rev.* **1999**, *99*, 845 – 880; h) L. J. Twyman, A. S. H. King, I. K. Martin, *Chem. Soc. Rev.* **2002**, *31*, 69 – 82; i) J. M. J. Fréchet, *Proc. Natl. Acad. Sci. USA* **2002**, *99*, 4782 – 4787.

[2] a) S. M. Grayson, J. M. J. Fréchet, *Chem. Rev.* **2001**, *101*, 3919 – 3967; b) J. M. J. Fréchet, *J. Polym. Sci. Part A* **2003**, *41*, 3713 – 3725.

[3] a) S. C. Zimmerman, I. Zharov, M. S. Wendland, N. A. Rakow, K. S. Suslick, *J. Am. Chem. Soc.* **2003**, *125*, 13504 – 13518; b) S. Kimata, D. L. Jiang, T. Aida, *J. Polym. Sci. Part A* **2003**, *41*, 3524 – 3530; c) A. Dahan, M. Portnoy, *Macromolecules* **2003**, *36*, 1034 – 1038; d) E. M. Harth, S. Hecht, B. Helms, E. E. Malmstrom, J. M. J. Fréchet, C. J. Hawker, *J. Am. Chem. Soc.* **2002**, *124*, 3926 – 3938; e) F. S. Precup-Blaga, G. C. Garcia-Martinez, A. P. H. J. Schenning, E. W. Meier, *J. Am. Chem. Soc.* **2003**, *125*, 12953 – 12960.

[4] Protic functional groups at the periphery, such as OH, COOH, and NH_2, are not compatible with Williamson etherifications and halogenations.

[5] V. V. Rostovtsev, L. G. Green, V. V. Fokin, K. B. Sharpless, *Angew. Chem.* **2002**, *114*, 2708 – 2711; *Angew. Chem. Int. Ed.* **2002**, *41*, 2596 – 2599; C. W. Tornøe, C. Christensen, M. Meldal, *J. Org. Chem.* **2002**, *67*, 3057.

[6] H. C. Kolb, M. G. Finn, K. B. Sharpless, *Angew. Chem.* **2001**, *113*, 2056 – 2075; *Angew. Chem. Int. Ed.* **2001**, *40*, 2004 – 2021.

[7] C. J. Hawker, J. M. J. Fréchet, *J. Am. Chem. Soc.* **1990**, *112*, 7638 – 7647.

[8] The nomenclature used for the dendritic framework is as follows: R-X-[G-*n*]-Y, where R describes the functional groups at periphery, Bn for benzyl, Boc for *tert*-butyl carbamate, MEE for (2-methoxyethoxy)ethane; X describes internal repeat units, B for 3,5-dioxybenzyl, F for formamide, S for benzenesulfonamide; *n* is the number for generations; Y describes functional group at the focal point, either chloride, Cl, or azide, N_3.

[9] Monochloride dendrons generated from benzenesulfonamide **13** were converted into the corresponding azides in wet DMF.

[10] In general, dendrons generated from benzenesulfonamide **13** are less soluble than dendrons made from acetamide **12** in all solvents tested, while the incorporation of **19** as a chain end increases the solubility substantially.

[11] T. R. Chan, R. Hilgraf, K. B. Sharpless, V. V. Fokin, *Org. Lett.*, in press.

[12] a) Q. Wang, T. R. Chan, R. Hilgraf, V. V. Fokin, K. B. Sharpless, M. G. Finn, *J. Am. Chem. Soc.* **2003**, *125*, 3192 – 3193; b) A. E. Speers, G. C. Adam, B. F. Cravatt, *J. Am. Chem. Soc.* **2003**, *125*, 4686 – 4687; c) A. J. Link, D. A. Tirrell, *J. Am. Chem. Soc.* **2003**, *125*, 11164 – 11165; d) A. Deiters, T. A. Cropp, M. Mukherji, J. W. Chin, J. C. Anderson, P. G. Schultz, *J. Am. Chem. Soc.* **2003**, *125*, 11782 – 11783.

 © 2004 Wiley-VCH Verlag GmbH & Co. KGaA, Weinheim

Synthetic Methods

Reaction of Alkene–Zirconocene Complexes and Cyclic Enol Ethers through New Reaction Pathways**

José Barluenga, Lucía Álvarez-Rodrigo, Félix Rodríguez, and Francisco J. Fañanás*

In recent years there has been increasing interest in the use of organozirconocene complexes in organic and organometallic chemistry because of their unique ability to promote uncommon transformations.[1] In this context, the discovery by Negishi et al. of a convenient method for the generation of low-valent zirconocene species was considered to be a crucial achievement.[2] Thus, the butene–zirconocene complex **1** (Negishi reagent) has been shown to be an excellent reagent for carbon–carbon coupling reactions involving different unsaturated substrates.[3] Some years ago, we initiated a program for developing new reactions using organozirconocene complexes[4] and became interested in the reaction of alkyne– and imine–zirconocene[5,6] complexes with enol ethers. In closely related work, Marek and co-workers reported the generation of vinyl–zirconium derivatives from the reaction of acyclic enol ethers and the Negishi reagent.[7] Initially, this transformation was thought to proceed through a formal exchange of the olefinic ligand to generate a new alkene–zirconocene complex followed by β-elimination of the alkoxide.[7] Further investigations by Marek and co-workers seem to indicate that this reaction occurs through a carbometalative ring-expansion that generates the zirconacyclopentane intermediate **I** followed by an elimination reaction (Scheme 1).[8] Unfortunately, the intermediate **I** could not be trapped. Herein, we report our preliminary results on the reaction of cyclic enol ethers and alkene–zirconocene complexes to yield new functionalized molecules arising from unprecedented reaction pathways that involve the coupling of enol ethers and alkene–zirconocene complexes.

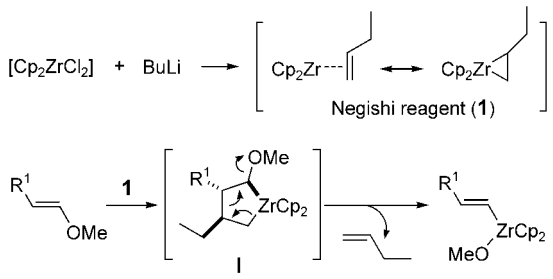
Our investigations began by studying the reaction of several alkene–zirconocene complexes **2** and five-membered cyclic enol ethers **3**. Thus, $[Cp_2ZrCl_2]$ was treated with two equivalents of an organolithium compound **4** in THF at −78 °C to generate the corresponding alkene–zirconocene complex **2**. In situ treatment of **2** with the corresponding cyclic enol ether **3** was followed by heating to room temperature

[*] Prof. Dr. J. Barluenga, L. Álvarez-Rodrigo, Dr. F. Rodríguez, Dr. F. J. Fañanás
Instituto Universitario de Química Organometálica "Enrique Moles"
Unidad Asociada al C.S.I.C., Universidad de Oviedo
Julián Clavería, 8, 33006 Oviedo (Spain)
Fax: (+34) 985-103-450
E-mail: barluenga@uniovi.es

[**] We gratefully acknowledge financial support from the DGICYT (BQU-2001-3853), MEC for their grant to L.A.-R., and MCYT for the "Ramón y Cajal" grant to F.R.

Supporting information for this article is available on the WWW under http://www.angewandte.org or from the author.

 © 2004 Wiley-VCH Verlag GmbH & Co. KGaA, Weinheim DOI: 10.1002/anie.200454151



Scheme 1. Negishi reagent **1** and Marek's synthesis of vinyl–zirconocene complexes from acyclic enol ethers. Cp = cyclopentadienyl.

and further treatment with an electrophile. After hydrolysis, the new alcohol or phenol derivatives **5** was formed in high yield and as single *Z* diastereoisomers in all cases (Scheme 2 and Table 1). Of particular interest are compounds functionalized with carbon electrophiles (**5d** and **5e**) and assembled in a one-pot, three-component coupling reaction. To our surprise, none of the expected compounds arising from a mechanism analogous to that described by Marek and co-workers[7] for acyclic enol ethers were formed.

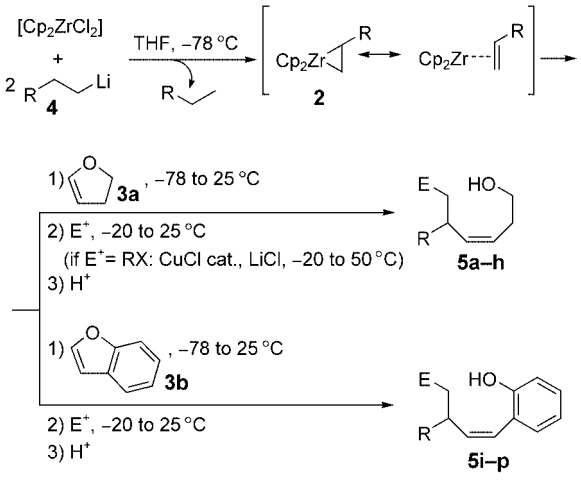
The unusual insertion process described above prompted us to investigate the reaction of alkene–zirconocene complexes **2** and the six-membered cyclic enol ether **6**. When these experiments were performed under the same conditions as those previously described, we obtained cyclobutane derivatives **7** in high yields and as single diastereoisomers in all cases (Scheme 3 and Table 2).[9] Surprisingly, the expected olefins analogous to **5** were not observed. It was also possible in this case that the resulting cyclobutane derivative had been functionalized by carbon electrophiles (**7c**) in a one-pot, three-component coupling reaction. Moreover, these unexpected results indicate that, as far as we know, it is the first time a six-membered enol ether participates in a coupling reaction with zirconocene complexes.[10]

We propose the mechanism depicted in Scheme 4 to explain the formation of compounds **5** and **7**. Initially, the double bond of the enol ether **3a** is inserted between the secondary carbon atom and the zirconium center of zirconacyclopropane (**2**) to generate the bicyclic intermediate **9**. β-Elimination of the alkoxy group from **9** results in the formation of oxazirconacyclooctene derivative **10**. After the hydrolysis step, the final addition of the electrophile leads to the *Z*-alkene derivative **5**. It is important to note that this process is doubly regioselective. On one hand, the insertion only occurs at the Zr–C bond of **2**, which implies the more substituted carbon atom is attacked,[3d] while conversely, the reaction is also regioselective with respect to the enol ether **3a**: the double bond is orientated during the insertion step so that the oxygen atom is far away from the zirconocene moiety. Moreover, we believe that the *Z* stereochemistry of **5** is fixed by the *cis* geometry of the bicyclic derivative **9** and the subsequent *anti*-periplanar elimination. The formation of

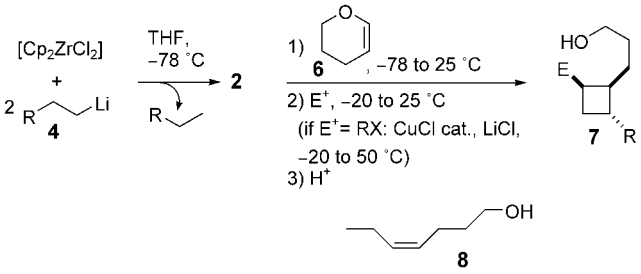
Table 1: Alkenol derivatives **5** from the zirconium-mediated reaction of alkyllithium derivatives **4** and enol ether **3**.

Alkyllithium	R[a]	Enol ether	E^+	E	Product	Yield [%][b]
4a	Et	**3a**	H_2O	H	**5a**	80
4a	Et	**3a**	D_2O	D	**5b**	81
4a	Et	**3a**	I_2	I	**5c**	75
4a	Et	**3a**	$CH_2{=}CHCH_2Cl$[c]	allyl	**5d**	82
4a	Et	**3a**	$PhCH_2Br$[d]	Bn	**5e**	68
4b	Pent	**3a**	H_2O	H	**5f**	78
4b	Pent	**3a**	I_2	I	**5g**	76
4c	Me	**3a**	I_2	I	**5h**	70
4a	Et	**3b**	H_2O	H	**5i**	85
4a	Et	**3b**	D_2O	D	**5j**	81
4a	Et	**3b**	I_2	I	**5k**	72
4b	Pent	**3b**	D_2O	D	**5l**	82
4b	Pent	**3b**	I_2	I	**5m**	73
4c	Me	**3b**	I_2	I	**5n**	78
4d	H	**3b**	H_2O	H	**5o**	82
4d	H	**3b**	I_2	I	**5p**	70

[a] Pent = pentyl. [b] Based on starting enol ether **3**. [c] CuCl (5 mol%) and LiCl (1 equiv) are also added. After 1 h at 25 °C, the reaction was stirred at 50 °C for 6 h. [d] CuCl (10 mol%) and LiCl (1 equiv) are also added. After 1 h at 25 °C, the reaction was stirred at 50 °C for 6 h.



Scheme 2. Zirconium-mediated reaction of alkyllithium compounds **4** and five-membered cyclic enol ethers **3** to give alkenol derivatives **5**.



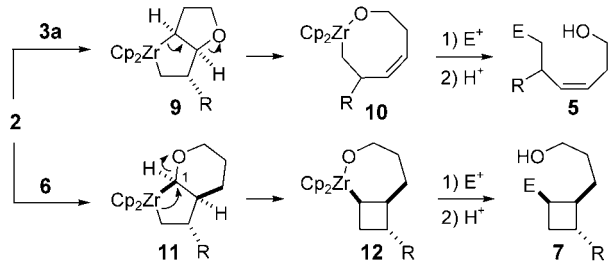
Scheme 3. Zirconium-mediated reaction of alkyllithium compounds **4** and six-membered cyclic enol ether **6** to give cyclobutane derivatives **7**.

 © 2004 Wiley-VCH Verlag GmbH & Co. KGaA, Weinheim

Table 2: Cyclobutane derivatives **7** from the zirconium-mediated reaction of alkyllithium derivatives **4** and enol ethers **6**.

Alkyllithium	R	E^+	E	Product	Yield [%][a]
4a	Et	H_2O	H	**7a**	69
4a	Et	D_2O	D	**7b**	63
4a	Et	$CH_2{=}CHCH_2Cl$[b]	allyl	**7c**	53
4b	Pent	H_2O	H	**7d**	70
4c	Me	D_2O	D	**7e**	60
4d	H	H_2O	H	**7f**	66[c]

[a] Based on the amount of starting $[Cp_2ZrCl_2]$. Very small amounts (< 5%) of the corresponding compounds analogous to **8** were detected in the crude pruduct of the reactions. [b] CuCl (5 mol%) and LiCl (1 equiv) are also added. After 1 h at 25 °C, the reaction was stirred at 50 °C for 6 h. [c] The total yield corresponded to an approximately 1:1 inseparable mixture of **7f** and alkenol **8**. Pure **7f** (33% yield) was obtained after treating the mixture of **7f** and **8** with bromine and further purification.



Scheme 4. Proposed mechanism for the formation of compounds **5** and **7**.

phenol derivatives **5i–p** from enol ether **3b** follows a similar pathway.

Moreover, the generation of cyclobutane derivatives **7** from the six-membered enol ether **6** can be explained by insertion of the double bond of this enol ether into **2** to produce the bicyclic intermediate **11**. An intramolecular migratory insertion process[11] generates intermediate **12**, which after reaction with an electrophile and hydrolysis affords cyclobutane derivatives **7**.[9] As before, this insertion process is regioselective with respect to **2**, with the reaction occurring at the more substituted Zr–C bond.[3d] The reaction is also regioselective with respect to the enol ether **6** since the double bond of this enol ether is oriented so that the oxygen atom is close to the zirconocene moiety.

The coupling products obtained firmly support the carbometalative ring-expansion mechanism tentatively formulated by Marek and co-workers for the reaction of the Negishi reagent and acyclic enol ethers to give vinyl–zirconocene complexes.[7,8] In fact, intermediate **11** is analogous to **I** (see Scheme 1). However, in our case the elimination reaction leading to the vinyl–zirconocene complexes (see Scheme 1) does not proceed and instead an intramolecular migratory insertion process furnishes the cyclobutane derivatives **7**. According to model proposed by Marek and co-workers for the formation of (*E*)-vinylzirconocenes,[8] an isomerization at C1 in **11** should occur before the elimination step. We believe that in our case this process is not favored because of the rigidity of the bicyclic intermediate **11**, and hence the intramolecular migratory insertion process is preferred.

Another surprising feature of these reactions is that the orientation adopted by the enol ether during the insertion process depends on the size of the enol ether ring. Although a more detailed study is required, we believe that the orientation adopted by the five-membered enol ether **3** is governed by electronic effects.[12] However, steric effects probably play an important role in the opposite orientation adopted by the pyran derivatives **6** during the insertion process. In fact, it has been observed that the reaction of **6** and the sterically less-demanding zirconacyclopropane **2** (R = H) (derived from the reaction of EtLi and zirconocene dichloride) leads to an approximately 1:1 mixture of the cyclobutyl derivative **7f** and the alkene derivative **8** (Scheme 3 and Table 2). The formation of compound **8** could be explained by a mechanism analogous to that described for the formation of **5** (Scheme 4) where pyran **6** is oriented during the insertion step in a way that is analogous to that adopted by the furans **3**.

In summary, we have described the first coupling reaction of cyclic enol ethers and alkene–zirconocene complexes. The reactions described here follow different pathways compared to previously reported results for acyclic enol ethers. The reaction has been shown to be dependent on the ring size of the enol ether, and thus, for five-membered enol ethers, the reaction leads to alcohols or phenols containing a *Z* double bond through an insertion/β-elimination process, while the reaction with six-membered enol ethers generates cyclobutane derivatives through an unprecedented insertion/intramolecular migratory insertion reaction. Moreover, these results firmly support the carbometalative ring-expansion mechanism tentatively proposed by Marek and co-workers for related reactions.

Besides the important mechanistic aspects described, this work is expected to have wide application in synthetic organic chemistry since highly functionalized compounds can be readily obtained from simple starting materials. Further detailed investigations into the synthetic and mechanistic aspects of these reactions, including experimental and theoretical calculations, are underway.[13]

Received: March 1, 2004 [Z54151]

Keywords: insertion · organometallic reagents · small ring systems · synthetic methods · zirconium

[1] *Titanium and Zirconium in Organic Synthesis* (Ed.: I. Marek), Wiley–VCH, Weinheim, **2002**.
[2] E. Negishi, F. E. Cederbaum, T. Takahashi, *Tetrahedron Lett.* **1986**, *27*, 2829.
[3] For some leading reviews, see: a) T. Takahashi, M. Kotora, R. Hara, Z. Xi, *Bull. Chem. Soc. Jpn.* **1999**, *72*, 2591; b) E. Negishi, T. Takahashi, *Bull. Chem. Soc. Jpn.* **1998**, *71*, 755; c) E. Negishi, D. Y. Kondakov, *Chem. Soc. Rev.* **1996**, *25*, 417; d) E. Negishi, T. Takahashi, *Acc. Chem. Res.* **1994**, *27*, 124.
[4] a) J. Barluenga, R. Sanz, F. J. Fañanás, *Chem. Eur. J.* **1997**, *3*, 1324; b) J. Barluenga, R. Sanz, F. J. Fañanás, *J. Org. Chem.* **1997**, *62*, 5953; c) J. Barluenga, R. Sanz, F. J. Fañanás, *J. Chem. Soc. Chem. Commun.* **1995**, 1009; d) J. Barluenga, R. Sanz, R.

 © 2004 Wiley-VCH Verlag GmbH & Co. KGaA, Weinheim

González, F. J. Fañanás, *J. Chem. Soc. Chem. Commun.* **1994**, 989.

[5] a) J. Barluenga, F. Rodríguez, L. Álvarez-Rodrigo, F. J. Fañanás, *Chem. Eur. J.* **2004**, *10*, 101; b) J. Barluenga, R. Sanz, F. J. Fañanás, *Z. Naturforsch. B* **1995**, *50*, 312; see also: c) T. Takahashi, D. I. Kondakov, Z. Xi, N. Suzuki, *J. Am. Chem. Soc.* **1995**, *117*, 5871.

[6] J. Barluenga, F. Rodríguez, L. Álvarez-Rodrigo, J. M. Zapico, F. J. Fañanás, *Chem. Eur. J.* **2004**, *10*, 109.

[7] a) A. Liard, J. Kaftanov, H. Chechik, S. Farhat, N. Morlender-Vais, C. Averbuj, I. Marek, *J. Organomet. Chem.* **2001**, *624*, 26; b) A. Liard, I. Marek, *J. Org. Chem.* **2000**, *65*, 7218; c) for related studies, see also: N. Chinkov, S. Majumdar, I. Marek, *J. Am. Chem. Soc.* **2003**, *125*, 13258; d) N. Chinkov, S. Majumdar, I. Marek, *J. Am. Chem. Soc.* **2002**, *124*, 10282.

[8] a) S. Farhat, I. Zouev, I. Marek, *Tetrahedron* **2004**, *60*, 1329; b) S. Farhat, I. Marek, *Angew. Chem.* **2002**, *114*, 1468; *Angew. Chem. Int. Ed.* **2002**, *41*, 1410; c) N. Chinkov, H. Chechik, S. Majumdar, A. Liard, I. Marek, *Synthesis* **2002**, 2473.

[9] The relative configuration of the chiral centers has been unequivocally ascertained by NMR spectroscopic analysis (including HMQC, HMBC, COSY, and NOESY experiments).

[10] 3,4-Dihydro-2*H*-pyran (**6**) does not react with alkyne–zirconocene complexes; see ref. [5c].

[11] For an excellent account on zirconium-mediated migratory insertion processes, see: S. Dixon, R. J. Whitby in *Titanium and Zirconium in Organic Synthesis* (Ed.: I. Marek), Wiley–VCH, Weinheim, **2002**, p. 86.

[12] The polarization of the carbon–zirconium bond of the zirconacyclopropane **2** and the carbon–carbon double bond of the enol ethers clearly support the formation of intermediate **9**; see refs. [5b and 6].

[13] Iodo derivatives, such as **5n**, could be precursors of interesting 1-benzoxepin derivatives (for example the fungal metabolite pterulone). Also the cyclobutane derivatives **7** have pleasant odor properties with potential application.

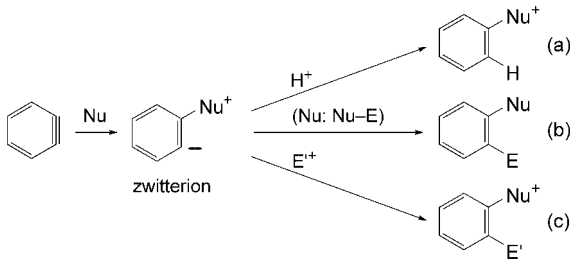
 © 2004 Wiley-VCH Verlag GmbH & Co. KGaA, Weinheim

Multicomponent Reactions

Arynes in a Three-Component Coupling Reaction: Straightforward Synthesis of Benzoannulated Iminofurans**

Hiroto Yoshida, Hiroyuki Fukushima, Joji Ohshita, and Atsutaka Kunai**

Arynes are highly strained and kinetically unstable molecules that have been recognized as useful reactive intermediates in organic synthesis.[1] Owing to their low-lying LUMO, arynes exhibit salient electrophilicity, and even neutral nucleophiles, which are inert towards alkynes, readily add to arynes. Hence, considerable attention has been paid to nucleophilic coupling reactions with arynes, and these reactions have been exploited in the construction of complex organic molecules.[2] The coupling reactions proceed through an initially formed zwitterion and can be divided into three categories (Scheme 1): a) formation of a monosubstituted arene by



Scheme 1. The reaction of arynes with neutral nucleophiles.

proton abstraction, b) insertion into a nucleophilic–electrophilic σ bond (Nu–E) by intramolecular nucleophilic substitution,[3] and c) three-component coupling by trapping the zwitterion with an electrophile. Although the three-component coupling would be the most attractive approach from a synthetic standpoint for generating molecular complexity and diversity, examples are limited, probably because of the difficulty associated with regulating the reactivity of arynes.[4]

We recently reported novel coupling reactions of arynes with neutral nucleophiles: the synthesis of *N*-alkyl *N*′-aryl imidazolium salts through the addition of imidazoles to arynes (reaction type a, Scheme 1)[5a] and the insertion of arynes into N–CO σ bonds of ureas (reaction type b).[5b,6] Herein we disclose that arynes undergo an unprecedented three-component coupling with isocyanides and aldehydes, thus offering a straightforward method for the synthesis of diverse benzoannulated iminofurans.[7–9]

First, we investigated the reaction of benzyne, generated in situ from 2-(trimethylsilyl)phenyl triflate (**1a**)[10] in the presence of KF and [18]crown-6, with 1,1,3,3-tetramethylbutyl isocyanide (**2a**) and benzaldehyde (**3a**) in THF at 0 °C for 7 h, and observed that the three-component coupling product *N*-(3-phenyl-1(3*H*)-isobenzofuranylidene)-1,1,3,3-tetramethylbutylamine (**4a**) was formed in 65 % yield (Table 1, entry 1).[11] The aromatic aldehydes **3b**, which contains an electron-donating substituent, and **3c**, with an electron-withdrawing substituent, also underwent the reaction efficiently to give the expected products in good yields (Table 1, entries 2 and 3). Furthermore, reactions of the *meta*-substituted aromatic aldehyde **3d** and the sterically congested aldehydes **3e** and **3f** proceeded smoothly to provide the corresponding iminofurans **4d**–**4f** in good yields (Table 1, entries 4–6). The thienyl group in **3g** was compatible with the reaction conditions (Table 1, entry 7),[12] and the aliphatic aldehydes **3h** and **3i** could also be used (Table 1, entries 8 and 9). Besides **2a**, *tert*-butyl (**2b**) and 1-adamantyl isocyanide (**2c**)

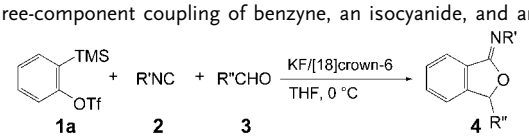
[*] Dr. H. Yoshida, H. Fukushima, Prof. J. Ohshita, Prof. A. Kunai
Department of Applied Chemistry
Graduate School of Engineering, Hiroshima University
Higashi-Hiroshima 739-8527 (Japan)
Fax: (+81) 82-424-5494
E-mail: yhiroto@hiroshima-u.ac.jp
akunai@hiroshima-u.ac.jp

[**] We thank Central Glass Co. Ltd. for a generous gift of trifluoromethanesulfonic anhydride.

Supporting information for this article is available on the WWW under http://www.angewandte.org or from the author.

 DOI: 10.1002/anie.200460009 © 2004 Wiley-VCH Verlag GmbH & Co. KGaA, Weinheim

Table 1: Three-component coupling of benzyne, an isocyanide, and an aldehyde.

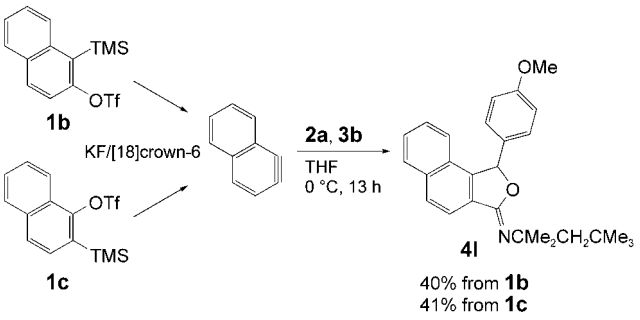


Entry	Isocyanide	R″		*t* [h]	Yield[a] [%]	Product
1	**2a** (R′ = $CMe_2CH_2CMe_3$)	Ph	**3a**	7	65	**4a**
2	**2a**	4-(MeO)C_6H_4	**3b**	7	73	**4b**
3	**2a**	4-(CF_3)C_6H_4	**3c**	7	69	**4c**
4	**2a**	3-(MeO)C_6H_4	**3d**	5	65	**4d**
5	**2a**	2,4-$Me_2C_6H_3$	**3e**	5	61	**4e**
6	**2a**	1-naphthyl	**3f**	5	73	**4f**
7	**2a**	2-thienyl	**3g**	7	50	**4g**
8	**2a**	Et	**3h**	5	50	**4h**
9	**2a**	*t*Bu	**3i**	7	40	**4i**
10	**2b** (R′ = *t*Bu)	1-naphthyl	**3f**	5	49	**4j**
11	**2c** (R′ = 1-Ad)	4-(MeO)C_6H_4	**3b**	24	77	**4k**

[a] Yield of isolated product based on the isocyanide. Tf = trifluoromethanesulfonyl, TMS = trimethylsilyl.

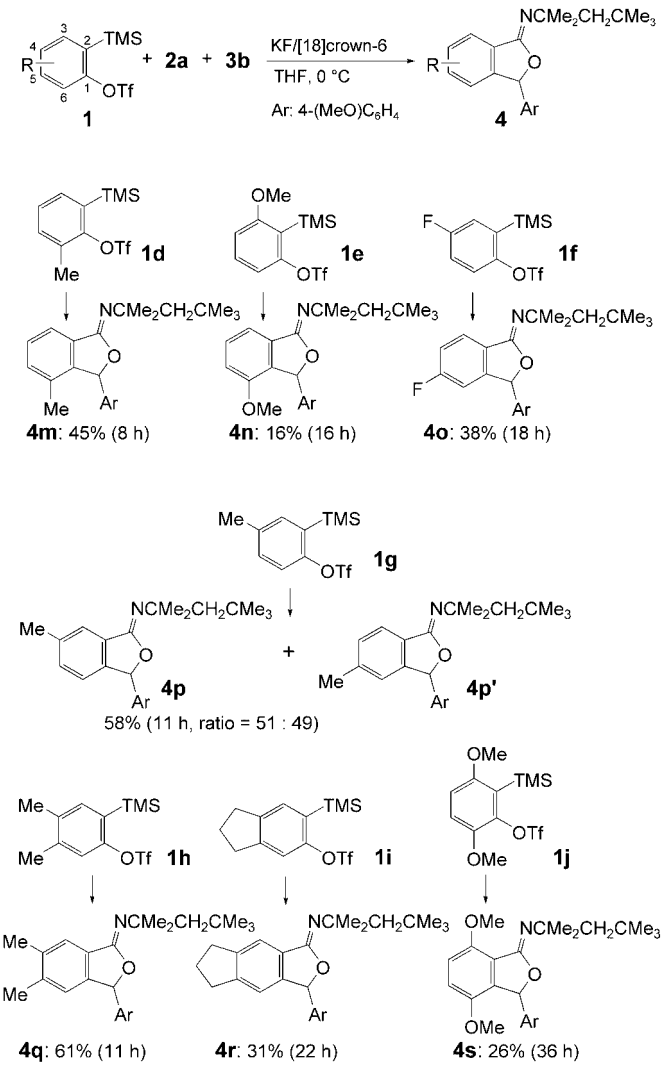
participated in the reaction to afford the desired product in 49% and 77% yield, respectively (Table 1, entries 10 and 11). In contrast, the reaction of sterically less congested cyclohexyl or *n*-octyl isocyanide resulted in the formation of a complex mixture of products.

As well as unsubstituted benzyne, variously substituted arynes could be used in the reaction. When 1-(trimethylsilyl)-2-naphthyl triflate (**1b**), a 1,2-naphthalyne precursor, was treated with **2a** and **3b**, **4l** was formed as the sole product (Scheme 2). Exclusive formation of **4l** was also observed in



Scheme 2. Three-component coupling of 1,2-naphthalyne, 1,1,3,3-tetramethylbutyl isocyanide, and *p*-anisaldehyde.

the reaction of 2-(trimethylsilyl)-1-naphthyl triflate (**1c**), which confirms the intermediacy of an aryne in the three-component coupling. The reactions of 3-substituted arynes (from **1d** or **1e**) also took place with perfect regioselectivity, whereby the imino moiety was introduced at the sterically less hindered position of the aryne (Scheme 3). The reaction of the aryne derived from **1f**, with a fluoro substituent at position 4, occurred regioselectively to afford **4o** exclusively, whereas the reaction of 4-methylbenzyne (from **1g**) furnished almost equal amounts of the regioisomeric products **4p** and **4p′**. The 4,5-disubstituted arynes derived from **1h** and **1i**, as



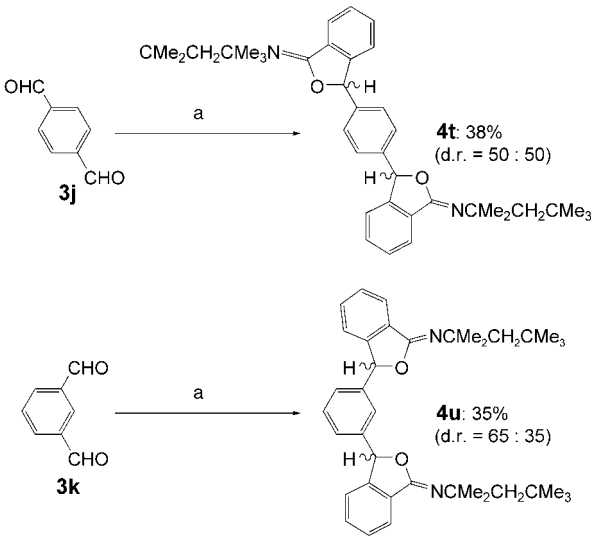
Scheme 3. Three-component coupling with variously substituted arynes.

well as sterically congested 3,6-dimethoxybenzyne (from **1j**), also participated in the reaction to give the corresponding iminofurans **4q**, **4r**, and **4s**.[13]

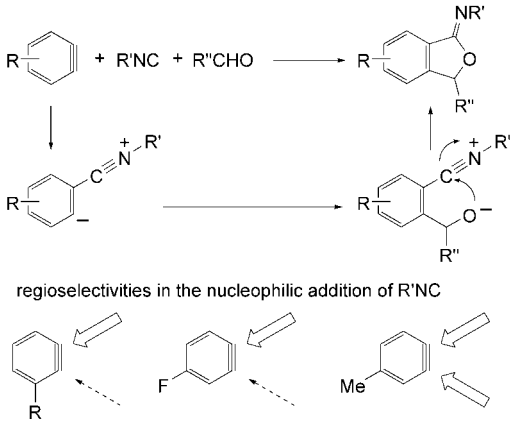
The reaction was also found to be applicable to an aldehyde with two reactive sites. As depicted in Scheme 4, terephthalaldehyde (**3j**) reacted with benzyne and **2a** to afford **4t** in 38% yield and with a diastereomeric ratio (d.r.) of 50:50. The equivalent reaction of isophthalaldehyde (**3k**) gave the product **4u** with d.r. 65:35.

We propose the nucleophilic attack of the carbon atom of the isocyanide group to the aryne as the initiation step of the three-component coupling (Scheme 5).[14] The resulting zwitterion is then trapped by the aldehyde, and a subsequent intramolecular cyclization affords the product.[15] The observed perfect regioselectivities in the reactions of 1,2-naphthalyne and 3-substituted arynes can be explained rationally as being due to a steric effect, which favors nucleophilic attack at the *meta* position of the substituent.[2a,16] Owing to the strong electron-withdrawing effect of a fluoro substituent, developing negative charge at the *meta*

 © 2004 Wiley-VCH Verlag GmbH & Co. KGaA, Weinheim



Scheme 4. Three-component coupling of benzyne, 1,1,3,3-tetramethylbutyl isocyanide, and a phthalaldehyde: a) **1a** (5 equiv), **2a** (2.5 equiv), KF (10 equiv), [18]crown-6 (10 equiv), THF, 0°C, 7 h.



Scheme 5. Proposed reaction mechanism for the three-component coupling.

position would be stabilized to a greater extent than at the *para* position in the transition state for the addition of an isocyanide to 4-fluorobenzyne, thus resulting in the regioselective formation of **4o**.[17] In contrast, steric and electronic effects around the triple bond would be negligible in the reaction of 4-methylbenzyne, and the isocyanide therefore adds to both ends of the triple bond equally.

In conclusion, we have demonstrated that a variety of arynes, despite their transient nature, can be utilized in a selective three-component coupling reaction with a suitable combination of nucleophile and electrophile. Based upon the present three-component coupling with isocyanides and aldehydes, diverse benzoannulated iminofurans, which are difficult to obtain by conventional methods, can be prepared readily. Further studies on the multicomponent coupling of arynes in the presence of a different combination of reagents are in progress.

Experimental Section

4a: Compound **1a** (0.090 g, 0.30 mmol) was added to a solution in THF (1.0 mL) of KF (0.035 g, 0.60 mmol), [18]crown-6 (0.16 g, 0.60 mmol), **2a** (0.021 g, 0.15 mmol), and **3a** (0.032 g, 0.30 mmol), and the resulting mixture was stirred at 0°C for 7 h. The reaction mixture was then diluted with ethyl acetate, filtered through a plug of celite, and concentrated. Column chromatography on alumina (eluent: 25% ethyl acetate/hexane) followed by gel-permeation chromatography (eluent: benzene) gave **4a** as a white powder (0.031 g, 65%). ^{1}H NMR (400 MHz, $CDCl_3$): $\delta = 1.03$ (s, 9H), 1.47 (s, 6H), 1.77 (s, 2H), 6.37 (s, 1H), 7.13–7.17 (m, 1H), 7.27–7.41 (m, 7H), 7.78–7.82 ppm (m, 1H); ^{13}C NMR (100 MHz, [D_8]THF): $\delta =$ 30.9, 32.4, 32.7, 56.2, 57.9, 85.6, 122.9, 124.2, 127.4, 129.2, 129.5, 129.7, 131.8, 133.0, 140.7, 147.1, 152.5 ppm; HRMS calcd for $C_{22}H_{27}NO$ (M^+): 321.2093; found: m/z 321.2100.

Received: March 16, 2004 [Z460009]

Keywords: arynes · isocyanides · multicomponent reactions · oxygen heterocycles · regioselectivity

[1] For reviews, see: a) R. W. Hoffmann, *Dehydrobenzene and Cycloalkynes*, Academic Press, New York, **1967**; b) H. Hart in *The Chemistry of Triple-Bonded Functional Groups*, *Supplement C2* (Ed.: S. Patai), Wiley, Chichester, **1994**, chap. 18; c) H. Pellissier, M. Santelli, *Tetrahedron* **2003**, *59*, 701.

[2] a) S. V. Kessar in *Comprehensive Organic Synthesis*, *Vol. 4* (Eds.: B. M. Trost, I. Fleming), Pergamon, Oxford, **1991**, pp. 483–515; b) E. R. Biehl, S. P. Khanapure, *Acc. Chem. Res.* **1989**, *22*, 275.

[3] For Te–Te, see: a) N. Petragnani, V. G. Toscano, *Chem. Ber.* **1970**, *103*, 1652; for S–S, see: b) J. Nakayama, T. Tajiri, M. Hoshino, *Bull. Chem. Soc. Jpn.* **1986**, *59*, 2907; for C–Si, see: c) Y. Sato, Y. Kobayashi, M. Sugiura, H. Shirai, *J. Org. Chem.* **1978**, *43*, 199.

[4] Three-component coupling reactions of arynes have been carried out previously with anionic nucleophiles: a) A. I. Meyers, P. D. Pansegrau, *Tetrahedron Lett.* **1983**, *24*, 4935; b) A. I. Meyers, P. D. Pansegrau, *J. Chem. Soc. Chem. Commun.* **1985**, 690; c) S. Tripathy, R. LeBlanc, T. Durst, *Org. Lett.* **1999**, *1*, 1973.

[5] a) H. Yoshida, S. Sugiura, A. Kunai, *Org. Lett.* **2002**, *4*, 2767; b) H. Yoshida, E. Shirakawa, Y. Honda, T. Hiyama, *Angew. Chem.* **2002**, *114*, 3381; *Angew. Chem. Int. Ed.* **2002**, *41*, 3247.

[6] We also reported palladium-catalyzed insertion reactions of arynes into element–element σ bonds; for carbostannylation (C–Sn), see: a) H. Yoshida, Y. Honda, E. Shirakawa, T. Hiyama, *Chem. Commun.* **2001**, 1880; for bissilylation (Si–Si), see: b) H. Yoshida, J. Ikadai, M. Shudo, J. Ohshita, A. Kunai, *J. Am. Chem. Soc.* **2003**, *125*, 6638.

[7] For previous reports on the synthesis of benzoannulated iminofurans, see: a) A. I. Meyers, M. A. Hanagan, L. M. Trefonas, R. J. Baker, *Tetrahedron* **1983**, *39*, 1991; b) W. Meise, B. Suedkamp, *Arch. Pharm.* **1987**, *320*, 1210.

[8] For the Lewis acid mediated synthesis of iminofurans with isocyanides, see: a) Y. Ito, H. Kato, T. Saegusa, *J. Org. Chem.* **1982**, *47*, 741; b) N. Chatani, M. Oshita, M. Tobisu, Y. Ishii, S. Murai, *J. Am. Chem. Soc.* **2003**, *125*, 7812.

[9] For the three-component coupling of alkynes, isocyanides, and aldehydes to give 2-aminofuran derivatives, see: a) V. Nair, A. U. Vinod, *Chem. Commun.* **2000**, 1019; b) A. Fayol, J. Zhu, *Angew. Chem.* **2002**, *114*, 3785; *Angew. Chem. Int. Ed.* **2002**, *41*, 3633; c) A. Fayol, J. Zhu, *Org. Lett.* **2004**, *6*, 115.

[10] Y. Himeshima, T. Sonoda, H. Kobayashi, *Chem. Lett.* **1983**, 1211.

[11] Although structural elucidation of the product of the three-component coupling by NMR spectroscopy showed it to be a

 © 2004 Wiley-VCH Verlag GmbH & Co. KGaA, Weinheim

single isomer, we could not determine the exact stereochemistry (*E* or *Z*) of the imine unit.
[12] For the Diels–Alder reaction of thiophene with an aryne, see: D. D. Callander, P. L. Coe, J. C. Tatlow, *J. Chem. Soc. Chem. Commun.* **1966**, 143.
[13] Owing to the complexity of the reaction mixtures, we did not pursue the identification of by-products of low-yielding reactions. At present, the reasons for which the desired products formed in low yields in the reactions of **1e**, **1i**, and **1j** are unclear.
[14] R. Knorr, *Chem. Ber.* **1965**, *98*, 4038.
[15] A referee suggested another mechanism, in which the isocyanide acts as an electrophile: Nucleophilic attack of the oxygen atom of the carbonyl group of the aldehyde at the carbon atom of the isocyanide group produces a 1,3-dipole, which then undergoes 1,3-dipolar cycloaddition with an aryne to afford the product. Although this alternative mechanism can not be ruled out entirely, the mechanism proposed by us appears more likely, as the electrophilic coupling of an isocyanide with a neutral nucleophile is generally known to be sluggish, except in special cases. Furthermore, if the oxygen atom of the carbonyl group acted as a nucleophile, it would first interact with the highly electrophilic aryne, rather than the isocyanide, to provide a different product to those described herein. For the electrophilic coupling of an isocyanide with a neutral nucleophile, see: a) M. Suginome, T. Fukuda, Y. Ito, *Org. Lett.* **1999**, *1*, 1977; for the nucleophilic coupling of a carbonyl compound with an aryne, see: b) H. Heaney, C. T. McCarty, *J. Chem. Soc. Chem. Commun.* **1970**, 123.
[16] Because of the electron-donating nature of the methyl substituent, the regioselectivity of the reaction of 3-methylbenzyne seems to be unfavorable electronically. However, such regioselectivity is often observed in nucleophilic coupling reactions with 3-methylbenzyne; see: T. K. Vinod, H. Hart, *Tetrahedron Lett.* **1988**, *29*, 885.
[17] Similar regioselectivity was observed in nucleophilic coupling reactions with 4-chlorobenzyne: a) J. F. Bunnett, C. Pyun, *J. Org. Chem.* **1969**, *34*, 2035; b) J. F. Bunnett, J. K. Kim, *J. Am. Chem. Soc.* **1973**, *95*, 2254.

 © 2004 Wiley-VCH Verlag GmbH & Co. KGaA, Weinheim

Metallamacrocycles

Switchable Electron-Transfer Processes in a Mixed-Valence, Kinetically Locked, Trinuclear Ru^{II} Metallamacrocycle**

*Naz Shan, Steven J. Vickers, Harry Adams, Michael D. Ward, and Jim A. Thomas**

The use of metal ions to template the self-assembly of discrete molecular structures has attracted a great deal of attention,[1] and an area of particular recent interest has been the assembly of metallamacrocyclic complexes, which, in addition to their appealing structures, can act as highly specific hosts and sensors for neutral molecules, cations and anions.[2] Bowl-shaped metallamacrocyclic complexes such as **1** were first described by Fish and co-workers; these contain adenine-based units as bridging ligands and cationic [Cp^*Rh^{III}] units as vertices and act as effective hosts for guests such as aromatic amino acids.[3]

Consequent work by Yamanari et al. resulted in higher order macrocycles,[4] and Sheldrick and co-workers reported the structures of related [(arene)Ru^{II}] and [(arene)Ir^{III}] systems.[5] Using Ir^{III}, Rh^{III}, and Ru^{II} metal centers and pyridyl-based ligands, Severin and co-workers prepared analogous neutral metallamacrocycles, such as **2**, which function as highly specific hosts and sensors for cations and anions.[6]

Apart from their host–guest chemistry, triangular complexes such as these are appealing targets for the study of redox properties and metal–metal interactions because of their unusual topology. The triangular arrangement of the redox centers means that two different mixed-valence states can, in principle, be generated. However, solution studies on previously reported Ru macrocycles reveal that they are in equilibrium with their monomeric building blocks[5] and that they are unstable towards substitution reactions.[7] These observations are reflected in reports of their electrochemistry, in which the metal-based redox couples exhibit poor reversibility.[6]

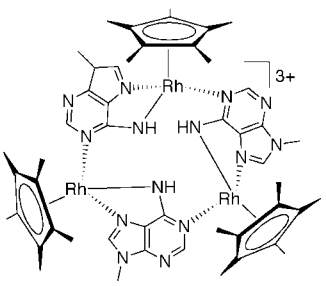
Herein we describe the synthesis of a *kinetically inert* triangular electroactive bowl, which displays well-behaved reversible electrochemical behavior and demonstrates two mixed-valence states with substantially different characters. The [([9]-ane-S_3)Ru^{II}] moiety was selected as a precursor for the corner units; previous work has demonstrated that this fragment exhibits suitable electronic and electrochemical properties,[8] and that self-assembly at high temperatures

[*] N. Shan, S. J. Vickers, H. Adams, Prof. M. D. Ward, Dr. J. A. Thomas
Department of Chemistry
University of Sheffield, Sheffield S3 7HF (UK)
Fax: (+44) 114-273-8673
E-mail: james.thomas@sheffield.ac.uk

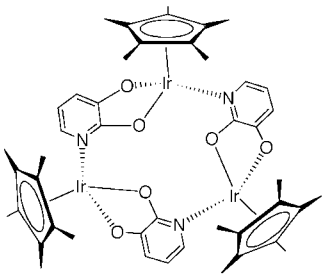
[**] We gratefully acknowledge the support of The Royal Society (J.A.T), EPSRC (N.Z, S.J.V) and the Leverhulme Trust (S.J.V).

Supporting information for this article is available on the WWW under http://www.angewandte.org or from the author.

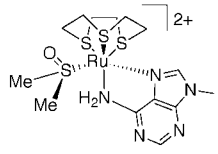
 © 2004 Wiley-VCH Verlag GmbH & Co. KGaA, Weinheim DOI: 10.1002/anie.200460022



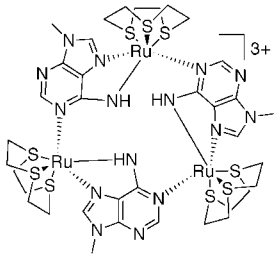
1



2



3



4

allows the thermodynamic assembly of species that become "kinetically locked" at room temperature,[9] thereby avoiding the kinetic lability of previously reported systems.

Reaction of the readily available starting material $[RuCl_2(dmso)([9]\text{-ane-S3})]$[10] with 9-methyladenine (9-MA) in an aqueous buffered solution (pH 7) heated at reflux for several hours afforded a single product, which was isolated as a hexafluorophosphate salt. ^{1}H NMR spectroscopy and FAB-MS studies revealed that the new compound was the mononuclear dicationic complex $\mathbf{3}(PF_6)_2$ The structure of the cation was confirmed by X-ray crystallographic analysis of its triflate salt (Figure 1).

An analysis of this structure reveals why the anticipated self-assembly into a metallamacrocycle is inhibited: the exocyclic NH_2 group in complex **3** is still intact and has not been deprotonated. In contrast to the $[Cp^*Rh^{III}]$ center, the coordinated $[Ru([9]\text{-ane-S3})]^{2+}$ moiety is not a strong enough Lewis acid to initiate deprotonation of N6. Consequently, the N1 position of 9-MA is not a sufficiently good donor to compete for the metal-coordination site occupied by dmso in **3**.

To deprotonate the exocyclic NH_2 site and attain bridged polynuclear structures, we repeated the reaction under more basic conditions. In the presence of the sterically hindered base pentamethylpiperidine (PMP), which is a very strong Brønsted base but a weak nucleophile, reaction of $[RuCl_2(DMSO)([9]\text{-ane-S3})]$ with 9-MA afforded (as the hexafluorophosphate salt) a single product whose ^{1}H NMR, FAB-MS, and high-resolution mass spectra as well as elemental analysis were all consistent with the metallamacrocycle of formula $\mathbf{4}(PF_6)_3$. Although attempts at growing crystals suitable for X-ray crystallographic studies were unsuccessful, the *m*/*z* values and isotope-distribution models of the FAB-MS and ES-MS peaks corresponding to the fragments obtained for both the hexafluorophosphate and triflate salts of **4** confirm the trinuclear formulation.

The redox properties of $\mathbf{4}(PF_6)_3$ were investigated by means of cyclic voltammetry (CV). Between 0.6–1.6 V (versus the Ag/AgCl couple) the new complex undrgoes three metal-based $Ru^{III/II}$ oxidation processes (Figure 2). In contrast to previously reported Ru^{II} species[6] and **3** (which displays a single irreversible oxidation), each of these couples is reversible with $\Delta E = 100$ mV and $|I_{Pa}/I_{Pc}| = 1$. Interestingly, although $\Delta E_{1/2}(1,2)$ is 175 mV, $\Delta E_{1/2}(2,3)$ is much larger with a value close to 380 mV. Comproportionation constants (K_c) derived from these figures indicate that the $[Ru^{II}/Ru^{III}/Ru^{III}]$ $\mathbf{4}^{5+}$ state has a stronger intermetallic interaction ($K_c = 2.8 \times 10^6$) than the $[Ru^{III}/Ru^{II}/Ru^{II}]$ $\mathbf{4}^{4+}$ state ($K_c = 760$). This observation is in contrast to other redox-active triangular complexes in which the spacings are approximately constant, as would be expected if there was no variation in the individual pairwise metal–metal interactions across the redox series. This implies that on moving from $\mathbf{4}^{4+}$ to $\mathbf{4}^{5+}$, there is a much greater delocalization of the positive charges which render the final oxidation more difficult than it would otherwise be.

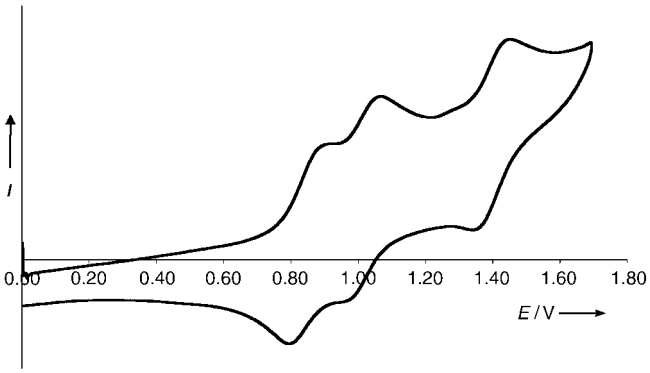


Figure 2. Cyclic voltammogram of oxidative processes for $\mathbf{4}(PF_6)_3$ in $MeCN/Bu_4NPF_6$ (0.1 M) (versus Ag/AgCl).

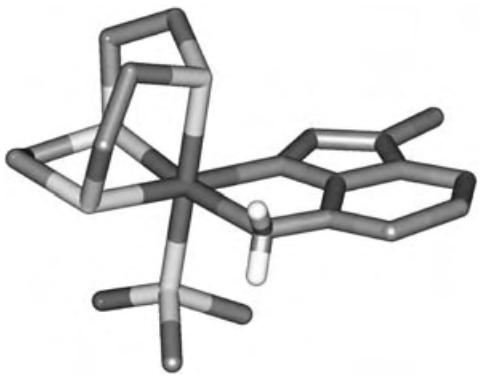


Figure 1. X-ray crystal structure of cation **3**, determined from $\mathbf{3}(CF_3SO_3)_2$, showing the coordinating NH_2 group. All other hydrogen atoms and lone pairs have been removed for clarity.

 © 2004 Wiley-VCH Verlag GmbH & Co. KGaA, Weinheim

On their own, K_c values are not always a true indication of the strengths of metal–metal electronic couplings; more accurate information can be obtained from the intensity, position, and shape of any observable intervalence charge-transfer (IVCT) bands. Therefore, the optical properties of the two mixed-valence and isovalent Ru^{III} states were investigated by UV/Vis/NIR spectroelectrochemistry in an OTTLE cell.

The evolution of electronic spectra through the redox series $\mathbf{4}^{3+}$ to $\mathbf{4}^{6+}$ is shown in Figure 3. In all cases, clean isosbestic points were observed, and at the end of the

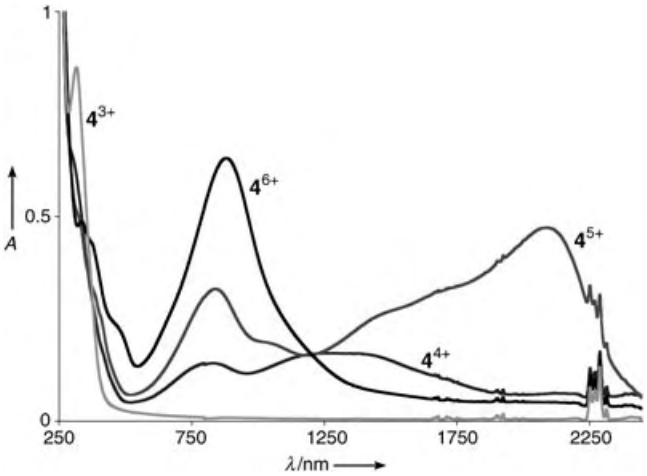


Figure 3. UV/Vis/NIR spectra of $\mathbf{4}^{3+}$, $\mathbf{4}^{4+}$,$\mathbf{4}^{5+}$, and $\mathbf{4}^{6+}$.

experiment the spectrum of $\mathbf{4}^{3+}$ was regenerated to confirm the full chemical reversibility of all the processes. The spectrum of $\mathbf{4}^{3+}$ shows only a Ru(d)→L(π*) metal-to-ligand charge-transfer (MLCT) band (313 nm) involving the adenine ligands. On one-electron oxidation to $\mathbf{4}^{4+}$ this MLCT band, whose origin is Ru^{II}, diminishes in intensity. A lower energy band centered at 800 nm was assigned to a thiacrown(S)→Ru^{III} ligand-to-metal charge transfer (LMCT). Furthermore, the spectrum of $\mathbf{4}^{4+}$ above 950 nm is dominated by a broad, low intensity absorption ($\varepsilon = 2950\ mol^{-1}\,dm^3\,cm^{-1}$), which we assign as an IVCT band.

Further oxidation to $\mathbf{4}^{5+}$ results in the further collapse of the Ru^{II}→adenine MLCT band accompanied by the simultaneous growth of the S→Ru^{III} LMCT band. However, the most notable feature of the $\mathbf{4}^{5+}$ absorption spectrum is an intense, structured band in the NIR region with an absorbance maximum at 2085 nm ($\varepsilon = 8400\ mol^{-1}\,dm^3\,cm^{-1}$). The final oxidation to give $\mathbf{4}^{6+}$ results in the collapse of all bands in the NIR region (which confirms their assignment as IVCT processes) and further growth of the S→Ru^{III} LMCT band.

The energies of the bands in the NIR region observed for the mixed-valence [Ru^{II}/Ru^{II}/Ru^{III}] $\mathbf{4}^{4+}$ and [Ru^{II}/Ru^{III}/Ru^{III}] $\mathbf{4}^{5+}$ states are consistent with previous reports of IVCT that indicate electron transfer between Ru^{II} and Ru^{III} sites.[11] However, the differing intensities and structures of these bands imply very different electron-transfer properties. The NIR spectral region for $\mathbf{4}^{4+}$ contains a structured, low-intensity, and extremely broad band that seems to be comprised of several overlapping transitions. Similar structured IVCTs were previously observed in oligonuclear Ru- and Os-based mixed-valence systems[12] and arise as a result of a combination of low-symmetry, extensive orbital mixing and spin–orbit coupling, which split the $d\pi^5$ states into Kramer doublets. The relatively low intensity of these transitions and the low K_c value of 760 indicate that $\mathbf{4}^{4+}$ is a valence-localized structure. In contrast, the band for $\mathbf{4}^{5+}$ in the NIR region is intense and clearly consists of at least three overlapping transitions. The intensity of these transitions and their sharpness suggest that the $\mathbf{4}^{5+}$ state is a valence-delocalized system.

Further evidence for these conclusions can be drawn from the application of the Hush theory[13] to the lowest energy IVCTs of the $\mathbf{4}^{4+}$ and $\mathbf{4}^{5+}$ states. If the bands are assumed to be Gaussian-shaped, the low-energy shoulder for the IVCT of $\mathbf{4}^{4+}$ can be used to estimate $\Delta\tilde{\nu}_{1/2}$ for this transition.[12c] In this case, $\Delta\tilde{\nu}_{1/2} \approx 3500\ cm^{-1}$, which is relatively close to $\Delta\tilde{\nu}_{1/2}(\text{calcd}) = 4100\ cm^{-1}$. Taken together, the data for $\mathbf{4}^{4+}$ indicates that it is a Robin and Day[14] class II (valence-localized/solvent-coupled) system, or perhaps a class II/III (valence-localized/solvent-decoupled) system.[12c,15]

In contrast, the same calculation carried out on the lowest energy band for $\mathbf{4}^{5+}$ reveals that $\Delta\tilde{\nu}_{1/2}(\text{experimental}) = 900\ cm^{-1}$ is much narrower than $\Delta\tilde{\nu}_{1/2}(\text{calcd}) = 3325\ cm^{-1}$. Given this very narrow bandwidth, the large K_c, and the exceptionally high intensity of this IVCT ($\varepsilon_{max} = 8500\ mol^{-1}\,dm^3\,cm^{-1}$), it is clear that $\mathbf{4}^{5+}$ is a fully valence-delocalized, solvent-decoupled class III system.

In summary, the triangular metallamacrocyclic complex $\mathbf{4}^{6+}$ is kinetically stable in all oxidation states and takes part in a reversible four-membered redox chain in which, remarkably, one mixed-valence state is a class II and the second is a class III system. Further investigations of this phenomenon and the host–guest chemistry of the complex in its different oxidation states are in progress.

Experimental Section

3$(CF_3SO_3)_2$: Crystal data for $C_{16}H_{25}F_6N_5O_7RuS_6$ ($M = 806.84$); which crystallizes from ethanol as yellow blocks, were measured on a Bruker Smart CCD area detector with an Oxford Cryosystems low-temperature system. Cell parameters were refined from the setting angles of 2900 reflections (θ range $1.66 < 28.29°$). Crystal dimensions $0.21 \times 0.10 \times 0.10\ mm^3$, triclinic, $a = 10.9018(15)$, $b = 11.9162(16)$, $c = 12.8948(18)$ Å, $\alpha = 73.636(3)°$, $\beta = 81.112(3)°$, $\gamma = 83.179(3)°$, $U = 1583.0(4)$ $Å^3$, $Z = 2$, $\rho_{calcd} = 1.693\ Mg\,m^{-3}$, space group $P\bar{1}$ ($C^{1,i}$, no. 2), $Mo_{K\alpha}$ radiation ($\lambda,^- = 0.71073$ Å), $\mu(Mo_{K\alpha}) = 0.969\ mm^{-1}$, $F(000) = 812$. Of the 10213 reflections measured, all of which were corrected for Lorentz and polarization effects and for absorption by semiempirical methods based on symmetry-equivalent and repeated reflections (minimum and maximum transmission coefficients 0.8225 and 0.9094), 3878 independent reflections exceeded the significance level $|F|/\sigma(|F|) > 4.0$. Refinement converged at a final $R = 0.0744$ ($WR_2 = 0.2049$, for all 7221 data, 369 parameters, mean and maximum $\delta/\sigma 0.000$) with allowance for the thermal anisotropy of all non-hydrogen atoms.CCDC 233715 contains the supplementary crystallographic data for this paper. These data (excluding structure factors) can be obtained free of charge via www.ccdc.cam.ac.uk/conts/retrieving.html (or from the Cambridge Crystallographic Data

Centre, 12, Union Road, Cambridge CB21EZ, UK; fax: (+44) 1223-336-033; or deposit@ccdc.cam.ac.uk).

Received: March 17, 2004 [Z460022]

Keywords: electrochemistry · electron transfer · mixed-valent compounds · ruthenium · self-assembly

[1] a) G. F. Swiegers, T. J. Malefetse, *Chem. Rev.* **2000**, *100*, 3483; b) G. F. Swiegers, T. J. Malefetse, *Coord. Chem. Rev.* **2002**, *225*, 91; c) M. Fujita, *Chem. Soc. Rev.* **1998**, *27*, 417; d) S. Leninger, B. Olenyuk, P. J. Stang, *Chem. Rev.* **2000**, *100*, 853; e) M. Fujita, K. Umemoto, M. Yoshizawa, N. Fujita, T. Kusukawa, K. Biradha, *Chem. Commun.* **2002**, 509; f) S. R. Seidel, P. J. Stang, *Acc. Chem. Res.* **2002**, *35*, 972.

[2] a) P. H. Dinolfo, J. T. Hupp, *Chem. Mater.* **2001**, *13*, 3113; b) M. H. Keefe, K. D. Benkstein, J. T. Hupp, *Coord. Chem. Rev.* **2002**, *225*, 91.

[3] a) D. P. Smith, E. Baralt, B. Morales, M. M. Olmstead, M. F. Maestre, R. H. Fish, *J. Am. Chem. Soc.* **1992**, *114*, 10647; b) H. Chen, S. Ogo, R. H. Fish, *J. Am. Chem. Soc.* **1995**, *117*, 3631; c) H. Chen, S. Ogo, R. H. Fish, *J. Am. Chem. Soc.* **1996**, *118*, 4993; d) R. H. Fish, *Coord. Chem. Rev.* **1999**, *185–186*, 569.

[4] a) K. Yamanari, S. Yamamoto, R. Ito, Y. Kushi, A. Fuyuhiro, N. Kubota, T. Fukuo, R. Arakawa, *Angew. Chem.* **2001**, *113*, 2328; *Angew. Chem. Int. Ed.* **2001**, *40*, 2268; b) K. Yamanari, R. Ito, S. Yamamoto, T. Konno, A. Fuyuhiro, K. Fujioka, R. Arakawa, *Inorg. Chem.* **2002**, *41*, 6824.

[5] a) S. Korn, W. S. Sheldrick, *J. Chem. Soc. Dalton Trans.* **1997**, 2191; b) P. Annen, S. Schildberg, W. S. Sheldrick, *Inorg. Chim. Acta* **2000**, *307*, 115.

[6] a) T. Habereder, M. Warchhold, H. Nöth, K. Severin, *Angew. Chem.* **1999**, *111*, 3422; *Angew. Chem. Int. Ed.* **1999**, *38*, 3225; b) H. Piotrowski, K. Polborn, G. Hilt, K. Severin, *J. Am. Chem. Soc.* **2001**, *123*, 2699; c) H. Piotrowski, G. Hilt, A. Schulz, P. Mayer, K. Polborn, K. Severin, *Chem. Eur. J.* **2001**, *7*, 3196; d) K. Severin, *Coord. Chem. Rev.* **2003**, *245*, 3.

[7] Z. Grote, R. Scopelliti, K. Severin, *Angew. Chem.* **2003**, *115*, 3951; *Angew. Chem. Int. Ed.* **2003**, *42*, 3821.

[8] a) S. Roche, L. J. Yellowlees, J. A. Thomas, *Chem. Commun.* **1998**, 1429; b) C. S. Araújo, M. G. B. Drew, V. Félix, L. Jack, J. Madureira, M. Newell, S. Roche, T. M. Santos, J. A. Thomas, L. Yellowlees, *Inorg. Chem.* **2002**, *41*, 2260.

[9] S. Roche, C. Haslam, H. Adams, S. L. Heath, J. A. Thomas, *Chem. Commun.* **1998**, 1429.

[10] C. Landgrafe, W. S. Sheldrick, *J. Chem. Soc. Dalton Trans.* **1994**, 1885.

[11] a) C. Creutz, *Prog. Inorg. Chem.* **1983**, *30*, 1; b) R. J. Crutchley, *Adv. Inorg. Chem.* **1994**, *41*, 273.

[12] a) V. Kasack, W. Kaim, J. H. Binder, J. Jordanov, E. Rothl, *Inorg. Chem.* **1995**, *34*, 1924; b) M. Moscherosch, E. Waldhör, H. Binder, W. Kaim, J. Fiedler, *Inorg. Chem.* **1995**, *34*, 4326; c) K. D. Demadis, C. M. Hartshorn, T. J. Meyer, *Chem. Rev.* **2001**, *101*, 2655, and references therein.

[13] a) N. S. Hush, *Prog. Inorg. Chem.* **1967**, *8*, 391; b) N. S. Hush, *Electrochim. Acta* **1968**, *13*, 1005.

[14] M. B. Robin, P. Day, *Adv. Inorg. Chem. Radiochem.* **1967**, *10*, 247.

[15] B. S. Brunschwig, C. Creutz, N. Sutin, *Chem. Soc. Rev.* **2002**, *31*, 168.

 © 2004 Wiley-VCH Verlag GmbH & Co. KGaA, Weinheim

Imine Chemistry

Asymmetric Catalytic Coupling of Organoboranes, Alkynes, and Imines with a Removable (Trialkylsilyloxy)ethyl Group—Direct Access to Enantiomerically Pure Primary Allylic Amines**

*Sejal J. Patel and Timothy F. Jamison**

Enantiomerically enriched allylic amines are frequently used as synthetic intermediates, auxiliaries, and resolving agents in the synthesis of both natural and nonnatural compounds.[1] Herein we report the first highly enantioselective catalytic synthesis of allylic amines from alkynes, imines, and organoboranes. Catalyzed by a complex derived from $[Ni(cod)_2]$ and a P-chiral ferrocenyl phosphane, this three-component process provides enantiomerically enriched, tetrasubstituted allylic amines in a single operation. A (*tert*-butyldimethylsilyloxy)ethyl ($TBSOCH_2CH_2$) group on the imine nitrogen not only maximizes reactivity and selectivity in these transformations, but also is easily removed after the coupling reaction, thus providing direct access to versatile primary allylic amines that can be recrystallized to optical purity.[2]

Several catalytic asymmetric syntheses of allylic alcohols from alkynes and aldehydes in high enantioselectivities have been reported,[3] but comparable success has not been achieved for the corresponding synthesis of allylic amines from imines.[4,5] Buchwald and co-workers have reported that stoichiometric reactions of chiral *ansa*-zirconocene imine complexes and alkynes provide trisubstituted allylic amines in high enantiomeric excess.[6] Bisoxazolines and (−)-sparteine promote enantioselective additions of organolithium reagents to imines (69–91% *ee*); however, reactions catalytic in the ligand result in lower selectivity (51–82% *ee*).[7] A complementary strategy was recently reported by Hayashi and Ishigedani involving the rhodium-catalyzed asymmetric addition of aryl stannanes to α,β-unsaturated imines.[8]

We recently reported a nickel-catalyzed three-component coupling reaction of alkynes, imines, and organoboron reagents (boronic acids and organoboranes), which affords

[*] S. J. Patel, Prof. Dr. T. F. Jamison
Department of Chemistry
Massachusetts Institute of Technology
Cambridge, MA 02139 (USA)
Fax: (+1) 617-324-0253
E-mail: tfj@mit.edu

[**] This work was supported by the National Institute of General Medical Sciences (GM-063755). We also thank the NSF (CAREER CHE-0134704), Merck Research Laboratories, Pfizer, Amgen, Boehringer-Ingelheim, Johnson & Johnson, GlaxoSmithKline, 3M, and MIT for generous financial support. NSF grants CHE-9809061 and DBI-9729592 and NIH grant 1S10RR13886-01 provided partial support for the MIT Department of Chemistry Instrumentation Facility (DCIF). We thank Elizabeth A. Colby and Johann Chan for assistance with the preparation of phosphane ligands.

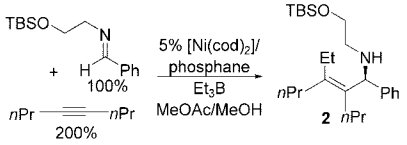
Supporting information for this article is available on the WWW under http://www.angewandte.org or from the author.

 DOI: 10.1002/anie.200460044 © 2004 Wiley-VCH Verlag GmbH & Co. KGaA, Weinheim

tetrasubstituted allylic amines.[9] Good to excellent yields, high regioselectivity, and complete *E*/*Z* selectivity (*cis* addition to the alkyne) are observed when electron-rich tri(*sec*-alkyl) phosphane ligands were employed. Although our research group has recently reported that nickel-catalyzed coupling reactions of certain alkynes and aldehydes in the presence of neomenthyldiphenylphosphane afford allylic alcohols in excellent enantioselectivities and yields,[3a] this ligand is ineffective in analogous reactions of imines.[10]

An extensive evaluation of a large number and variety of chiral monophosphanes[11] demonstrated that P-chiral ferrocenyl phosphanes afforded the desired allylic amines in good yields and enantioselectivities, as long as the group on nitrogen was aliphatic in nature (Table 1).[12] These ligands,

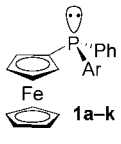
Table 1: Evaluation of P-chiral ferrocenyl phosphanes in the catalytic three-component assembly of allylic amines.[a]



Entry	Phosphane	Yield [%]	*ee*[b]
1	**1a**	88	75
2	**1b**	90	80
3	**1c**	60	75
4	**1d**	**85**	**89**
5	**1e**	19	45
6	**1f**	85	75
7	**1g**	25	77
8	**1h**	20	45
9	**1i**	64	54
10	**1j**	41	41
11	**1k**	73	51

[a] See Experimental Section for details. [b] Determined by HPLC (Chiralcel OD, results with **1d** are highlighted in bold).

1a–**k**, were synthesized in enantiomerically pure form by a modification of Jugé's ephedrine-based method.[3b,13] A notable feature of this ligand family is that, in contrast to trialkyl phosphane ligands, reductive coupling by-products are not observed (transfer of H instead of Et from Et_3B).[9]

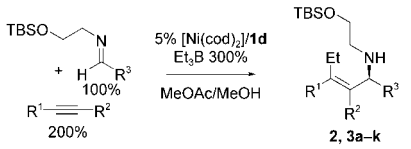


	Ar		Ar
a	*o*-tolyl	**g**	2-*i*Pr-5-MeC_6H_3
b	2-EtC_6H_4	**h**	3,5-*t*Bu$_2C_6H_3$
c	2-*n*BuC_6H_4	**i**	*o*-anisyl
d	2-*i*PrC_6H_4	**j**	2-EtOC_6H_4
e	*o*-biphenylyl	**k**	2-*i*PrOC_6H_4
f	2,5-Me$_2C_6H_3$		

Remarkably, desymmetrization of $FcPPh_2$ by replacing H with Me at the *ortho* position of one of the phenyl groups (i.e. **1a**) provided allylic amine **2** in 75% *ee* and very good yield (Table 1, entry 1). We further observed that enantioselectivity tended to increase as the steric bulk in this *ortho* position increased (Table 1, entries 2–4), up to a point. A phenyl substituent in the *ortho* position (i.e. Ar = *o*-biphenylyl (**1e**), entry 5) led to a severely diminished yield (19%) and enantioselectivity (45%). Unfortunately, all efforts to synthesize more sterically demanding phosphanes (for example Ar = 2-*t*BuC_6H_4, 2,6-Me$_2C_6H_3$) were unsuccessful.[14] Furthermore, lower yields and enantioselectivities were obtained with other substitution patterns (Table 1, entries 6–8) and with ligands possessing alkoxy groups in the *ortho* position (Table 1, entries 9–11). Modifications of ligand/metal stoichiometry, solvent composition, and modes of reagent addition decreased efficacy and/or selectivity. The highest yields and enantioselectivities were observed with the portionwise addition of the alkyne and Et_3B (as a solution in MeOAc; see Experimental Section for details).

Ligand **1d** proved to be the most selective phosphane in these studies, and it also allowed the preparation of allylic amines from a variety of substrate combinations in moderate to very good enantioselectivities (Table 2). Both symmetrical

Table 2: Enantiomerically enriched allylic amines prepared through catalytic intermolecular coupling of an alkyne, an imine, and triethylborane.[a]



Entry	R^1	R^2	R^3	Product	Yield [%] (regio)[b]	*ee* [%][c]
1	*n*Pr	*n*Pr	Ph	**2**	85	89
2	*n*Bu	*n*Bu	Ph	**3a**	83	89
3	Et	Et	Ph	**3b**	89	83
4	*n*Pr	*n*Pr	*o*-tolyl	**3c**	74	85
5	*n*Pr	*n*Pr	*p*-anisyl	**3d**	75	82
6	*n*Pr	*n*Pr	*p*-$CF_3C_6H_4$	**3e**	91	85
7	*n*Pr	*n*Pr	2-naphthyl	**3f**	90	73
8	nPr	*n*Pr		**3g**	95	73
9	Et	Et	*c*-C_6H_{11}	**3h**	53	51
10	Ph	Me	Ph	**3i**	45 (80:20)	84
11	Ph	Et	Ph	**3j**	62 (>98:2)	71
12	2-naphthyl	Me	Ph	**3k**	42 (85:15)	70

[a] See Experimental Section for details. [b] Determined by ^{1}H NMR. [c] Enantiomeric excess of the major product determined by HPLC or GC.

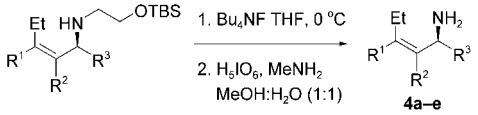
dialkyl acetylenes (entries 1–9) and unsymmetrical alkynes of the general form Ar–C≡C–Alkyl (entries 10–12) are effective in these reactions, the latter allowing the preparation of enantiomerically enriched tetrasubstituted allylic amines with four different substituents on the alkene with good to complete control of olefin geometry and regioselectivity. Furthermore, several aromatic imines undergo this three-component coupling reaction to give the products in both high enantiomeric excess and yield (Table 2, entries 4–8). No significant difference in enantioselectivity was observed with electron-donating (Table 2, entries 4 and 5) or elec-

 © 2004 Wiley-VCH Verlag GmbH & Co. KGaA, Weinheim

tron-withdrawing (entry 6) substituents on the phenyl group; however, imines derived from 2-naphthaldehyde or piperonal were less selective (entries 7 and 8). Notably, even an enolizable aliphatic imine undergoes catalytic asymmetric three-component coupling in moderate enantioselectivity and yield (Table 2, entry 9).[15]

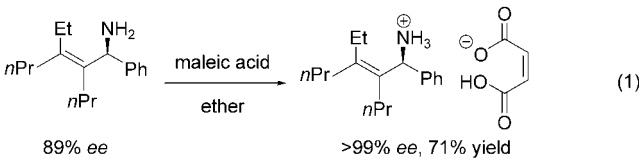
The $TBSOCH_2CH_2$-protected allylic amines are readily deprotected by a two-step protocol: deprotection of the TBS ether with Bu_4NF, followed by oxidative cleavage of the resulting 2-amino alcohol (Table 3).[16] Since the optical purity is conserved in this reaction sequence, enantiomerically enriched tetrasubstituted primary allylic amines are obtained in good overall yield and good enantiomeric excess. Several chiral 2-amino alcohols (mostly derived from amino acids) have been used as auxiliaries for diastereoselective imine addition reactions,[17] but this is the first example of a catalytic, enantioselective addition to imines derived from an *achiral* 2-amino alcohol. These primary allylic amines can be recrystallized to optical purity as maleic acid salts [Eq. (1)].

Table 3: Deprotection of $TBSOCH_2CH_2$-protected allylic amines.



Entry	R^1	R^2	R^3	Product	Yield [%]	*ee* [%]
1	*n*Pr	*n*Pr	Ph	**4a**	73	89
2	*n*Pr	*n*Pr	o-tolyl	**4b**	66	85
3	*n*Pr	*n*Pr	2-naphthyl	**4c**	59	76
4	*n*Pr	*n*Pr		**4d**	68	73
5	Ph	Me	Ph	**4e**	63	84

[a] Enantiomeric excess of the major product, determined by HPLC.



(1)

In conclusion, the above catalytic asymmetric transformation provides enantiomerically enriched tetrasubstituted allylic amines in a single step, and high reaction yields (up to 95%) and good enantioselectivities (up to 89% *ee*) are observed in many cases. Furthermore, removal of the (*tert*-butyldimethylsilyloxy)ethyl protecting group provides direct access to versatile primary allylic amines that can be further recrystallized to >99% *ee*.

Experimental Section

General procedure: The imine (0.5 mmol) and alkyne (0.20 mmol) were added to a solution of Et_3B (0.30 mmol, 3 M in MeOAc), $[Ni(cod)_2]$ (0.025 mmol), phosphane ligand (0.025 mmol), and MeOH (2.5 mL) under Ar. Four equal portions of additional Et_3B (4 × 0.30 mmol) and alkyne (4 × 0.20 mmol) were added every 10 min, and the reaction was stirred an additional 12 h. Concentration in vacuo and purification over silica gel (hexanes/EtOAc) afforded the allylic amines. Enantioselectivities were measured by HPLC (Chiralcel OD or AD columns) or GC (Chiraldex B-PH, B-DA, and G-TA capillary columns).

Received: March 18, 2004 [Z460044]

Keywords: alkynes · allylic amines · asymmetric catalysis · imines · nickel

[1] a) M. Hagihara, N. J. Anthony, T. J. Stout, J. Clardy, S. L. Schreiber, *J. Am. Chem. Soc.* **1992**, *114*, 6568; b) Takasago process: R. Noyori, *Asymmetric Catalysis in Organic Synthesis*, Wiley, New York, **1994**; c) M. Johannsen, K. A. Jørgensen, *Chem. Rev.* **1998**, *98*, 1689.

[2] *N*-Diphenylphosphinoylimines and *N*-tosylimines do not undergo three-component coupling. *N*-Aryl imines and *N*-benzylimines afforded low yields and selectivities.

[3] a) K. M. Miller, W.-S. Huang, T. F. Jamison, *J. Am. Chem. Soc.* **2003**, *125*, 3442; b) E. A. Colby, T. F. Jamison, *J. Org. Chem.* **2003**, *68*, 156; c) for catalytic, asymmetric Nozaki–Hiyama–Kishi reactions, see: H. W. Choi, K. Nakajima, D. Demeke, F. A. Kang, H. S. Jun, Z. K. Wan, Y. Kishi, *Org. Lett.* **2002**, *4*, 4435; for reactions that are catalytic in a chiral ligand, see: d) W. Oppolzer, R. N. Radinov, *Helv. Chim. Acta* **1992**, *75*, 170; e) P. Wipf, S. Ribe, *J. Org. Chem.* **1998**, *63*, 6454.

[4] For diastereoselective additions to chiral imines, see: a) J. A. Ellman, T. D. Owens, T. P. Tang, *Acc. Chem. Res.* **2002**, *35*, 984; b) R. Bloch, *Chem. Rev.* **1998**, *98*, 1407; c) D. Enders, U. Reinhold, *Tetrahedron: Asymmetry* **1997**, *8*, 1895; for diastereoselective additions to chiral iminium ions, see: d) N. A. Petasis, I. A. Zavialov, *J. Am. Chem. Soc.* **1997**, *119*, 445; e) N. A. Petasis, I. A. Zavialov, *J. Am. Chem. Soc.* **1998**, *120*, 11798; f) R. A. Batey, D. B. MacKay, V. Santhakumar, *J. Am. Chem. Soc.* **1999**, *121*, 5075; g) for a review of catalytic, enantioselective additions to imines, see: a) S. Kobayashi, H. Ishitani, *Chem. Rev.* **1999**, *99*, 1069.

[5] For catalytic, asymmetric rearrangements of prochiral allylic imidates to allylic amines, see: a) M. Calter, T. K. Hollis, L. E. Overman, J. Ziller, G. G. Zipp, *J. Org. Chem.* **1997**, *62*, 1449; b) C. E. Anderson, L. E. Overman, *J. Am. Chem. Soc.* **2003**, *125*, 12412; c) for the rearrangement of chiral allylic alcohols to trichloroacetimidates, see: L. E. Overman, *J. Am. Chem. Soc.* **1974**, *96*, 597; d) for a recent application of ref. [3d] and [5c], see: A. E. Lurain, P. J. Walsh, *J. Am. Chem. Soc.* **2003**, *125*, 10677.

[6] a) R. B. Grossman, W. M. Davis, S. L. Buchwald, *J. Am. Chem. Soc.* **1991**, *113*, 2321; b) for the synthesis of enantiomerically enriched allylic alcohols by using chiral titanium–alkyne complexes, see: Y. Takayanagi, K. Yamashita, Y. Yoshida, F. Sato, *Chem. Commun.* **1996**, 1725.

[7] a) S. E. Denmark, N. Nakajima, O. J.-C. Nicaise, *J. Am. Chem. Soc.* **1994**, *116*, 8797; b) S. E. Denmark, C. M. Stiff, *J. Org. Chem.* **2000**, *65*, 5875.

[8] a) T. Hayashi, M. Ishigedani, *J. Am. Chem. Soc.* **2000**, *122*, 976; b) T. Hayashi, M. , Ishigedani, *Tetrahedron* **2001**, *57*, 2589.

[9] S. J. Patel, T. F. Jamison, *Angew. Chem.* **2003**, *115*, 1402; *Angew. Chem. Int. Ed.* **2003**, *42*, 1364.

[10] A maximum of 41% *ee* and 36% yield was observed; see reference [9].

[11] P,N ligands, (*R*)-MOP (2-(diphenylphosphanyl)-2′-methoxy-1,1′-binaphthyl), PPF-OMe ((*R*)-1-[(*S*)-2-(diphenylphosphanyl)ferrocenyl]ethyl methyl ether), imidazolium carbenes, and men-

 © 2004 Wiley-VCH Verlag GmbH & Co. KGaA, Weinheim

thol-derived phosphanes are examples of monophosphane ligands tested.
[12] Replacement of the aliphatic group on nitrogen with *p*-anisyl resulted in lower enantioselectivity (35% *ee*) with ligand **1d** under otherwise identical reaction conditions.
[13] S. Jugé, M. Stephan, J. A. Laffitte, J. P. Genêt, *Tetrahedron Lett.* **1990**, *31*, 6357.
[14] 2-*tert*-Butylphenyllithium and 2,6-dimethylphenyllithium did not undergo addition to the oxazaphospholidine–borane complex. Other research groups have reported similar difficulties with mesityllithium, 9-anthryllithium, and 2,4,6-trimethoxyphenyllithium: a) F. Maienza, F. Spindler, M. Thommen, B. Pugin, C. Malan, A. Mezzetti, *J. Org. Chem.* **2002**, *67*, 5239.
[15] In general, additions to imines derived from enolizable aldehydes suffer from deprotonation and decomposition. For recent references, see: a) K. Yamada, S. J. Harwood, H. Groger, M. Shibasaki, *Angew. Chem.* **1999**, *111*, 3713; *Angew. Chem. Int. Ed.* **1999**, *38*, 3504; b) A. Boezio, J. Pytkowicz, A. Côté, A. B. Charette, *J. Am. Chem. Soc.* **2003**, *125*, 14260; c) ref. [4].
[16] a) D. M. Spero, S. R. Kapadia, *J. Org. Chem.* **1997**, *62*, 5537; b) Z.-Y. Chang, R. M. Coates, *J. Org. Chem.* **1990**, *55*, 3475.
[17] a) Reference [4b,c] and references therein; b) G. Alvaro, D. Savoia, *Synlett* **2002**, *5*, 651.

 © 2004 Wiley-VCH Verlag GmbH & Co. KGaA, Weinheim

Ring-Opening Catalysts

Cationic Planar Chiral Palladium P,S Complexes as Highly Efficient Catalysts in the Enantioselective Ring Opening of Oxa- and Azabicyclic Alkenes**

*Silvia Cabrera, Ramón Gómez Arrayás, and Juan C. Carretero**

A huge effort has been devoted to the development of highly efficient asymmetric transition-metal-catalyzed reactions using chiral ligands based on P,P, P,N or N,N coordination modes,[1] some of which have reached the status of privileged ligands.[2] In sharp contrast, thioether-based chiral ligands[3] have received much less attention, despite a key structural feature that makes them very attractive in asymmetric catalysis: the sulfur atom becomes stereogenic upon coordination to the metal, thus imposing a unique asymmetric environment next to the reactive metal center. In this context, we recently reported that the planar chiral Fesulphos ligands **1** (1-phosphanyl-2-sulfenylferrocenes) behave as very efficient P,S ligands in Pd-catalyzed allylic substitutions and in Cu-catalyzed additions to imines.[4]

Among recently described new Pd-catalyzed enantioselective reactions, the ring opening of *meso* oxabicyclic alkenes with dialkyl zinc reagents in the presence of chiral P,P and P,N ligands reported by Lautens et al. constitutes a synthetically outstanding C–C bond forming desymmetrization reaction.[5] According to mechanistic evidence[5b] this alkylative ring-opening reaction proceeds by coordination and subsequent enantioselective carbopalladation of the alkene, with a cationic alkyl palladium intermediate $[L_2PdR]^+$ formed in situ under the reaction conditions employed.[6] Inspired by this work, we envisaged that the cationic methylpalladium complexes of Fesulphos ligands $[(\mathbf{1})PdMe]^+$ could act as very active catalysts in this type of reaction. Herein, we report that this robust and readily available catalyst system combines low catalyst loading, high enantioselectivity, easy fine-tuning, mild reaction conditions, and broad structural scope.

Treatment of ligands **1** with $[PdCl_2(CH_3CN)_2]$[7] afforded in very high yield the corresponding complexes $[(\mathbf{1})PdCl_2]$ as single epimers at the sulfur atom.[4b] Interestingly, the transmetalation reaction of these complexes with Me_2Zn was completely stereoselective, affording a single complex [(**1**)Pd(Cl)(Me)] in 70–95% yield (Scheme 1). The *cis* arrangement of the methyl group and the phosphane moiety was established by analysis of their ^1H, ^{13}C, and ^{31}P NMR spectra; the low coupling constants $^2J_{P,C(Me)}$ (< 1.0 Hz) and $^3J_{P,H(Me)}$ (2.4 Hz) were of great diagnostic value.[8] This stereochemical assignment was unequivocally confirmed by X-ray crystal diffraction analysis[9] of [(**1a**)Pd(Cl)(Me)] (Figure 1). Additional relevant structural information includes the preservation of the *anti* arrangement of the *tert*-butyl group with respect to the iron atom ($R_P R_S$ configuration), and the elongation of the Pd–S bond (2.444 Å) compared to that of the starting dichloro complex (2.314 Å)[4b] as result of the strong *trans* effect of the highly σ-donating methyl group. The removal of the chloride ion in [(**1a**)Pd(Cl)(Me)] by treatment with $AgPF_6$ (CH_2Cl_2, room temperature) or $NaB(Ar^F)_4$ [Ar^F = 3,5-bis(trifluoromethyl)phenyl][10] in the presence of benzonitrile afforded a single cationic benzonitrile-coordinated palladium species $[(\mathbf{1a})Pd(Me)(PhCN)]^+X^-$. The crystal structure of this complex[11] (Figure 1) is very similar to that of its precursor [**1a**·Pd(Cl)(Me)] although, as expected, the Pd–Me bond is even shorter (2.011 versus 2.048 Å) and the Pd–S bond is longer (2.461 versus 2.444 Å) as a result of the enhanced σ donation of the methyl group to the cationic Pd atom.

Table 1 summarizes the most significant results obtained with this set of potential P,S catalysts in the model reaction of 7-oxabenzonorbornadiene with Me_2Zn.

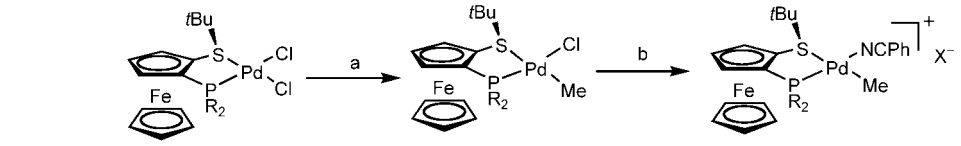
As the starting point we used similar experimental conditions to those previously described: 5 mol% of catalyst in toluene or 1,2-dichloroethane (DCE) at room temperature

[*] S. Cabrera, Dr. R. Gómez Arrayás, Prof. Dr. J. C. Carretero
Departamento de Química Orgánica
Facultad de Ciencias, Universidad Autónoma de Madrid
Cantoblanco 28049 Madrid (Spain)
Fax: (+34) 914-973-966
E-mail: juancarlos.carretero@uam.es

[**] This work was supported by the MCyT (project BQU2000-0226 and BQU2003-0508). S.C. thanks the UAM for a predoctoral fellowship. R.G.A. thanks the MCyT for a Ramón y Cajal contract. We acknowledge the skilled assistance of Prof. Jaime Rodríguez González in solving the X-ray crystal structure of the cationic palladium complex. Prof. José L. García-Ruano is gratefully acknowledged for unrestricted access to the HPLC equipment of his group. We thank Johnson Matthey PLC for a generous loan of $PdCl_2$.

Supporting information for this article is available on the WWW under http://www.angewandte.org or from the author.

 © 2004 Wiley-VCH Verlag GmbH & Co. KGaA, Weinheim DOI: 10.1002/anie.200460087



R = Ph, [(**1a**)PdCl$_2$], 86% — [(**1a**) Pd(Cl)(Me)], 93% — [(**1a**) Pd(Me)(NCPh)]$^+$X$^-$

R = (*p*-F)C$_6$H$_4$, [(**1b**)PdCl$_2$], 99% — [(**1b**) Pd(Cl)(Me)], 95%

R = *o*-Tol, [(**1c**)PdCl$_2$], 99% — [(**1c**) Pd(Cl)(Me)], 87%

R = 1-Naph, [(**1d**)PdCl$_2$], 78% — [(**1d**) Pd(Cl)(Me)], 70%

R = Cy, [(**1e**)PdCl$_2$], 99% — [(**1e**) Pd(Cl)(Me)], 95%

X$^-$ = PF$_6^-$, 81%

X$^-$ = BAr$^F{}_4^-$, 71%

Scheme 1. Synthesis of Fesulphos palladium complexes. a) Me_2Zn (1.5 equiv), CH_2Cl_2, RT; b) $AgPF_6$ or $NaBAr^F{}_4$, PhCN, CH_2Cl_2, RT. Cy = cyclohexyl.

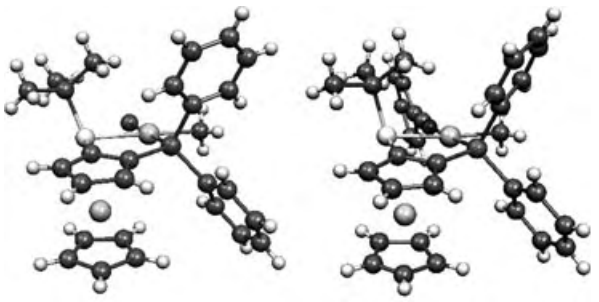


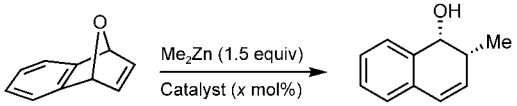
Figure 1. X-Ray crystal structures of [(**1a**)Pd(Cl)(Me)] and [(**1a**)Pd(Me)(PhCN)]B(Ar^F)$_4$ (the B(Ar^F)$_4^-$ anion has been omitted for clarity).

(RT).[5] Catalyst [(**1a**)PdCl$_2$] led to 80% conversion in 24 hours (entry 1) to give the *cis* alcohol (*R*,*R*)-**2a**[12] with a remarkable 81% *ee*. A similar result was achieved using the methyl complex [(**1a**)Pd(Cl)(Me)] (entry 2), which supports the proposal that both complexes evolve to the same active catalyst under the reaction conditions used. A significant increase in the reaction rate occurred when a catalytic amount of $AgPF_6$ was added to dissociate the chloride ligand (entry 3). However, the greatest acceleration effect was produced by adding NaB(Ar^F)$_4$ (entry 4). A complete conversion was observed within 10 minutes with this noncoordinating counterion. This outstanding reactivity allowed a dramatic decrease of the catalyst loading: 0.5 mol% of catalyst drove the reaction to completion in 30 minutes (entry 5). As expected, a similar result was obtained using 0.5 mol% of the isolated air-stable cationic complex (entry 6) instead of catalyst generated in situ.

To fine-tune the reactivity and enantioselectivity of the process, we next studied the effect of the substitution at the phosphorus atom (complexes of ligands **1b–e**). With the exception of the complex containing the bulky naphthylphosphane ligand **1d** (entry 9), the reactions were complete in 10–30 minutes, with the electronically rich phosphane **1e** providing the best enantioselectivity (entry 10). The combination [(**1e**)Pd(Cl)(Me)]+NaB(Ar^F)$_4$ proved to be so effective that the reaction could be performed with severely decreased catalyst loading and temperature, which resulted in an enhancement of the enantioselectivity. Thus, 0.2 mol% of catalyst was sufficient to reach quantitative conversion within 5 h at −25 °C, which afforded alcohol **2a** in 88% yield with 97% *ee* (entry 11).

With these optimized P,S catalysts in hand, we turned our attention toward the substrate generality of the process. The use of 0.5 mol% [(**1e**)Pd(Cl)(Me)][13] in combination with NaB(Ar^F)$_4$ (0.5 mol%) as a halogen scavenger catalyzed the enantioselective opening of a variety of substituted *meso* oxabenzonorbornadienes with both Me_2Zn and Et_2Zn in DCE[14] at room temperature. As shown in Scheme 2, complete conversions within 10–30 minutes, good chemical yields (61–98%), and excellent enantioselectivities (94–>99% *ee*, HPLC) were obtained for all products **2–5**.

Table 1: Ring opening of 7-oxabenzonorbornadiene with Me_2Zn catalyzed by palladium complexes of ligands **1**.

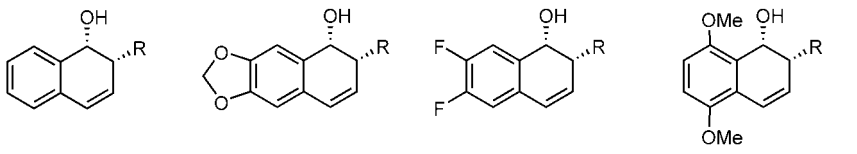


(*R*, *R*)-**2a**

Entry	Catalyst (*x* mol%)	Additive (*x* mol%)	*t* (min)	Yield [%][a]	*ee* [%][b]
1	[(**1a**)PdCl$_2$] (5)	–	1440	80[c]	81
2	[(**1a**)Pd(Cl)(Me)] (5)	–	2880	75[c]	85
3	[(**1a**)Pd(Cl)(Me)] (5)	$AgPF_6$ (5)	420	83	83
4	[(**1a**)Pd(Cl)(Me)] (5)	NaBAr$^F{}_4$ (5)	10	86	78
5	[(**1a**)Pd(Cl)(Me)] (0.5)	NaBAr$^F{}_4$ (0.5)	30	78	78
6	[(**1a**)Pd(Me)(PhCN)]$^+$(BAr$^F{}_4$)$^-$ (0.5)	–	30	82	72
7	[(**1b**)Pd(Cl)(Me)] (5)	NaBAr$^F{}_4$ (5)	15	71	69
8	[(**1c**)Pd(Cl)(Me)] (5)	NaBAr$^F{}_4$ (5)	30	74	64
9	[(**1d**)Pd(Cl)(Me)] (5)	NaBAr$^F{}_4$ (5)	360	80	46
10	[(**1e**)Pd(Cl)(Me)] (5)	NaBAr$^F{}_4$ (5)	10	77	83
11[d]	[(**1e**)Pd(Cl)(Me)] (0.2)	NaBAr$^F{}_4$ (0.2)	300	88	97

[a] In pure product. [b] HPLC (Chiralpak AD column). [c] Conversion yield. [d] In 1,2-dichloroethane at −25 °C.

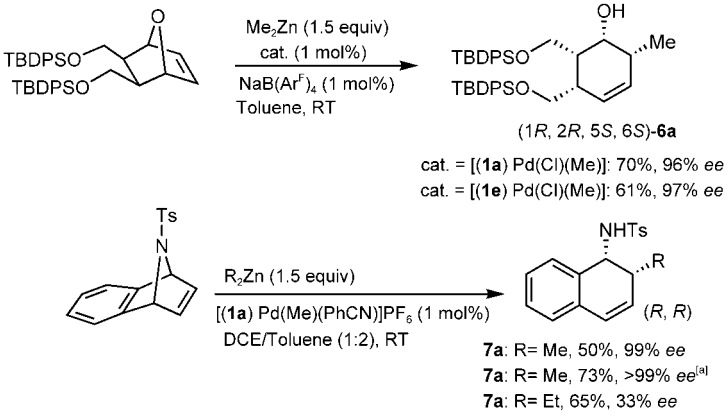
 © 2004 Wiley-VCH Verlag GmbH & Co. KGaA, Weinheim



2a: R = Me, 88%, 97% *ee*[a] **3a**: R = Me, 71%, >99% *ee* **4a**: R = Me, 95%, 95% *ee* **5a**: R = Me, 98%, 97% *ee*
2b: R = Et, 81%, 95% *ee* **3b**: R = Et, 61%, 94% *ee* **4b**: R = Et, 79%, 96% *ee* **5b**: R = Et, 85%, 94% *ee*

Scheme 2. Alcohols **2**–**5** resulting from the reaction of substituted oxabenzonorbornadienes with Me_2Zn and Et_2Zn catalyzed with $[(\mathbf{1e})PdMe]^+$. [a] The reaction was carried out at −25 °C.

Finally, to test the efficiency of these highly active catalysts toward much less reactive bicyclic substrates, we studied the opening reaction of nonaromatic [2.2.1]oxabicyclic alkenes and azabenzonorbornadienes, which usually require harsher reaction conditions.[5c] Notably, $[(\mathbf{1a})PdMe]^+$ and $[(\mathbf{1e})PdMe]^+$ (1 mol%) induced the ring opening of the [2.2.1]oxabicyclic alkene with Me_2Zn within three hours at room temperature, which led to cyclohexenol **6a**[12] in 96–97% *ee* (Scheme 3).

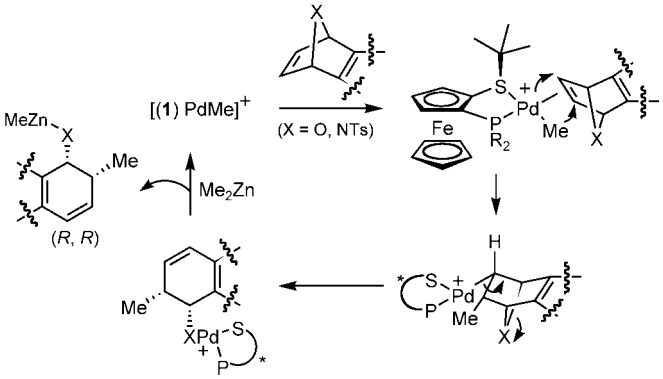


Scheme 3. Ring opening of less reactive *meso* substrates. TBDPS = *tert*-butyldiphenylsilyl, Ts = toluene-4-sulfonyl. [a] The reaction was carried out with 5 mol% of catalyst.

The most reactive catalyst for the opening of the azabenzonorbornadiene derivative was the complex $[(\mathbf{1a})Pd(Me)(PhCN)]^+(PF_6)^-$. In the reaction with Me_2Zn the ring-opened product (*R*,*R*)-**7a** was obtained within 30 minutes (73% yield) with virtually complete enantiocontrol (> 99% *ee*) by using 5 mol% of catalyst. The use of 1 mol% of catalyst resulted in a much slower reaction (60% conversion after 48 h). The reaction with Et_2Zn was faster, but surprisingly much less enantioselective, and gave **7b** in 33% *ee*.

According to the X-ray structures shown in Figure 1, the high enantioselectivity displayed by these P,S-palladium species could be explained by assuming a combination of electronic and steric factors: a) coordination of the bicyclic alkene *trans* to the phosphorus atom on the palladium center; and b) coordination of the alkene from its less hindered *exo* face, with orientation of the oxygen (or nitrogen) bridge to the opposite side of the very bulky *tert*-butyl group. Thus, the synergetic effect derived from the strong electronic *trans* effect of the phosphorus moiety and the great steric control exerted by the close, bulky stereogenic sulfur substituent would be responsible for the high asymmetric induction in the key carbopalladation step (Scheme 4).

In summary, the cationic methylpalladium species derived from the readily available planar chiral P,S ligands **1** display an excellent profile as catalysts for the enantioselective alkylative ring opening of oxa- and azabicyclic alkenes with dialkyl zinc reagents. The structure of these catalysts suggests that the high asymmetric induction relies on the strong *trans* effect of the phosphane moiety that acts in combination with the sterically demanding environment imposed by the stereogenic sulfur atom directly bonded to the palladium atom.



Scheme 4. Mechanistic proposal.

Received: March 22, 2004 [Z460087]

Keywords: alkenes · asymmetric catalysis · ferrocenyl ligands · palladium · S ligands

[1] a) *Comprehensive Asymmetric Catalysis* (Eds.: E. N. Jacobsen, A. Pfaltz, H. Yamamoto), Springer, Berlin, **1999**; b) *Catalytic Asymmetric Synthesis* (Ed.: I. Ojima), Wiley, New York, **2000**.
[2] T. P. Yoon, E. N. Jacobsen, *Science* **2003**, *299*, 1691–1693.
[3] For leading recent references on P,S ligands in enantioselective catalysis, see: *sulfenyl phosphinites*: a) D. A. Evans, F. E. Michael, J. S. Tedrow, K. R. Campos, *J. Am. Chem. Soc.* **2003**, *125*, 3534–3543; b) T. Kanayama, K. Yoshida, H. Miyabe, Y. Takemoto, *Angew. Chem.* **2003**, *115*, 2100–2102; *Angew. Chem. Int. Ed.* **2003**, *42*, 2054–2056; c) D. A. Evans, K. R. Campos, J. S. Tedrow, F. E. Michael, M. R. Gagne, *J. Am. Chem. Soc.* **2000**, *122*, 7905–7920; *sulfenyl phosphines*: d) T. Tu, Y.-G. Zhou, X.-L. Hou, L.-X. Dai, X.-C. Dong, Y.-H. Yu, J. Sun, *Organometallics* **2003**, *22*, 1255–1265; e) H. Nakano, Y. Suzuki, C. Kabuto, R. Jujita, H. Hongo, *J. Org. Chem.* **2002**, *67*, 5011–5014; f) D. Enders, R. Peters, R. Lochtman, G. Raabe, J. Runsik, J. W. Bats, *Eur. J. Org. Chem.* **2000**, 3399–3426; g) X. Verdaguer, A. Moyano, M. A. Pericàs, A. Riera, M. A. Maestro, J. Mahía, *J. Am. Chem. Soc.* **2000**, *122*, 10242–10243.
[4] a) O. García Mancheño, R. Gómez Arrayás, J. C. Carretero, *J. Am. Chem. Soc.* **2004**, *126*, 456–457; b) O. García Mancheño, J. Priego, S. Cabrera, R. Gómez Arrayás, T. Llamas, J. C. Carre-

 © 2004 Wiley-VCH Verlag GmbH & Co. KGaA, Weinheim

tero, *J. Org. Chem.* **2003**, *68*, 3679 – 3686; c) J. Priego, O. García Mancheño, S. Cabrera, R. Gómez Arrayás, T. Llamas, J. C. Carretero, *Chem. Commun.* **2002**, 2512 – 2513.

[5] a) M. Lautens, S. Hiebert, *J. Am. Chem. Soc.* **2004**, *126*, 1437 – 1447; b) M. Lautens, S. Hiebert, J.-L. Renaud, *J. Am. Chem. Soc.* **2001**, *123*, 6834 – 6839; c) M. Lautens, S. Hiebert, J.-L. Renaud, *Org. Lett.* **2000**, *2*, 1971 – 1973; d) M. Lautens, J.-L. Renaud, S. Hiebert, *J. Am. Chem. Soc.* **2000**, *122*, 1804 – 1805. For a review on enantioselective metal-catalyzed opening reactions of oxabicyclic alkenes, see: M. Lautens, K. Fagnou, S. Hiebert, *Acc. Chem. Res.* **2003**, *36*, 48 – 58.

[6] According to the participation of cationic palladium species, it has been recently reported that the cationic μ-hydroxo complex $[\{Pd((R)\text{-binap})\text{-}(\mu\text{-}OH)\}_2]^{2+}(OTf^-)_2$ is much more effective than the currently used dichloro complex, see reference [5a] (binap = 2,2′-bis(diphenylphosphanyl)-1,1′-binaphthyl, Tf = trifluoromethanesulfonyl).

[7] For the use of the parent ligands **1** in the Pd-catalyzed desymmetrization of oxabenzonorbornadiene, see reference [4c].

[8] For achiral cationic methyl P,S-palladium complexes, see: a) O. Daugulis, M. Brookhart, P. S. White, *Organometallics* **2002**, *21*, 5935 – 5943; b) G. P. Suranna, P. Mastrorilli, C. F. Nobile, W. Keim, *Inorg. Chim. Acta* **2000**, *305*, 151 – 156.

[9] Crystal structure for $C_{27}H_{30}ClFePPdS$ [(**1a**)Pd(Cl)(Me)]: crystal size $0.35 \times 0.34 \times 0.32$ mm, hexagonal, space group $P6_1$, $a = 18.3144(2)$, $b = 18.3144(2)$, $c = 15.7573(2)$ Å, $\gamma = 120°$, $V = 4577.18(9)$ Å^3, $Z = 6$, $\rho_{calcd} = 1.339$ Mg m^{-3}, $\mu = 10.583$ mm^{-1}, $2\theta_{max} = 70.25°$, $Cu_{K\alpha}$ radiation, $\lambda = 1.54178$ Å, $2\theta/\omega$ scans, $T = 296(2)$ K, absorption correction: none, 29638 reflections collected, 5709 independent. Refinement on F^2 for 5709 reflections and 293 parameters gave GOF = 0.996, $R1 = 0.0334$, $wR2 = 0.0992$ for $I > 2\sigma(I)$. Residual electron density $-0.391 < \Delta\rho < 0.775$ e Å^{-3}. Absolute structure parameter −0.008(5).

[10] M. Brookhart, M. Wagner, *J. Am. Chem. Soc.* **1994**, *116*, 3641 – 3642.

[11] Crystal structure for $C_{66}H_{47}BF_{24}FeNPPdS$ {[(**1a**)Pd(Me)(NCPh)]$^+$[$(Ar^F{}_4)B$]$^-$}: crystal size $0.23 \times 0.14 \times 0.10$ mm, monoclinic, space group $P2_1$, $a = 17.372(3)$, $b = 23.423(4)$, $c = 18.140(3)$ Å, $\beta = 110.615(3)°$, $V = 6909(2)$ Å^3, $Z = 4$, $\rho_{calcd} = 1.487$ Mg m^{-3}, $\mu = 0.628$ mm^{-1}, $2\theta_{max} = 56.56°$, $Mo_{K\alpha}$ radiation, $\lambda = 0.71073$ Å, $2\theta/\omega$ scans, $T = 293$ K, absorption correction: none, 24303 reflections collected, 10937 independent. Refinement on F^2 for 24303 reflections and 1739 parameters gave GOF = 1.002, $R1 = 0.0895$, $wR2 = 0.2353$ for $I > 2\sigma(I)$. Residual electron density $-1.655 < \Delta\rho < 0.944$ e Å^{-3}. Absolute structure parameter −0.01(3). CCDC-231878 and CCDC-229828 contain the supplementary crystallographic data for this paper. These data can be obtained free of charge via www.ccdc.cam.ac.uk/conts/retrieving.html (or from the Cambridge Crystallographic Data Centre, 12 Union Road, Cambridge CB2 1EZ, UK; fax: (+44) 1223-336-033; or deposit@ccdc.cam.ac.uk).

[12] The absolute configuration of the alcohols **2**–**4** and **6a** was established by comparison with the data obtained by HPLC using a chiral stationary phase for both enantiomers of these compounds (see references [5c] and [5d]).

[13] In all these reactions the enantioselectivity achieved from [(**1e**)Pd(Cl)(Me)] was significantly higher than that from the parent diphenylphosphanyl catalyst [(**1a**)Pd(Cl)(Me)].

[14] A higher reactivity was found in DCE than in toluene, probably as a result of the increased solubility of the cationic Pd complex in the former.

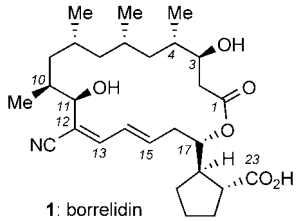
 © 2004 Wiley-VCH Verlag GmbH & Co. KGaA, Weinheim

Natural Product Synthesis

Stereoselective Total Synthesis of (−)-Borrelidin**

*Binh G. Vong, Sun Hee Kim, Sunny Abraham, and Emmanuel A. Theodorakis**

Borrelidin (treponemycin, **1**) is a biologically intriguing and structurally unique macrolide, first isolated by Berger et al. from a soil sample of *Streptomyces rochei* and subsequently



1: borrelidin

identified in other related *Streptomyces* species.[1] Initial biological screening indicated that **1** exhibits broad antiviral[2] and antibacterial[3] activity, which presumably arises from its inhibition of threonyl-tRNA synthetase and protein synthesis.[4] More recently, borrelidin was found to inhibit cyclin-dependent kinase (CDK) and thus display potent antimitotic properties at low μM concentrations.[5] Equally impressive are reports that **1** inhibits angiogenesis in rat aorta models at subnanomolar concentrations ($IC_{50} = 0.4\ ng\,mL^{-1}$) through a yet unknown mechanism of action.[6] These results underline the significant potential of borrelidin as a lead compound for the development of novel antiangiogenesis drugs.

Chemical degradation[7] and crystallographic studies[8] revealed that borrelidin is an 18-membered macrolide with an unprecedented structure, composed of a repeated isopropyl subunit (C4–C10),[9] a conjugated cyanodiene fragment (C12–C15), and a cyclopentane carboxylic acid substituent (C18–C23).[10] The unique structure of **1** has spurred the development of several synthetic routes,[11] which recently led to two elegant syntheses by the Morken[12] and Hanessian[13] research groups. Inspired by the structural and biological uniqueness of borrelidin, we devised a strategy toward its

[*] B. G. Vong, S. H. Kim, S. Abraham, Prof. E. A. Theodorakis
Department of Chemistry and Biochemistry
University of California, San Diego
9500 Gilman Drive, MC: 0358, La Jolla, CA 92093-0358 (USA)
Fax: (+1) 858-822-0386
E-mail: etheodor@chem.ucsd.edu

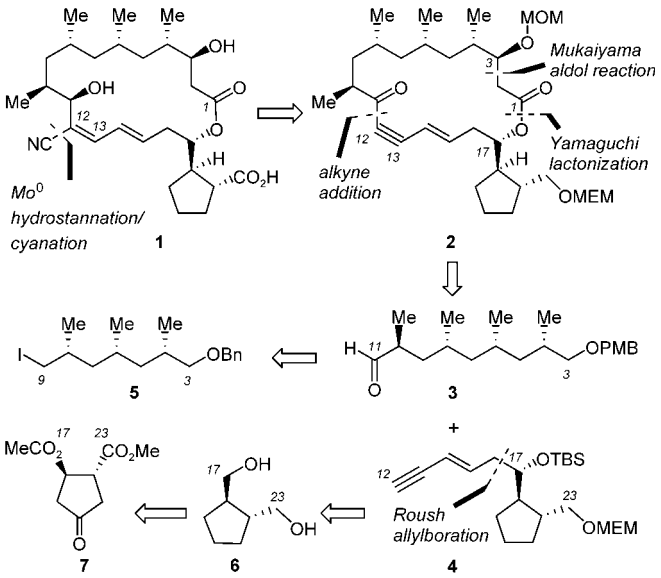
[**] In honor of Professor E. J. Corey, recipient of the 2004 Priestley Medal. Financial support from the NIH (CA 086079) is gratefully acknowledged. We also thank Dr. L. N. Zakharov and Dr. P. Gantzel (UCSD, X-ray Facility) for the reported crystallographic studies and Professor D. B. Ball, California State University, Chico, for a sample of natural borrelidin.

Supporting information for this article is available on the WWW under http://www.angewandte.org or from the author.

 DOI: 10.1002/anie.200460203 © 2004 Wiley-VCH Verlag GmbH & Co. KGaA, Weinheim

synthesis. Crucial to our approach was the installation of the cyano group after the construction of the macrocyclic ring of **1**. The installation of the cyano group occurred with excellent regioselectivity by a novel Mo^0-catalyzed hydrostannation of an enynone (at C11–C15).[14] Herein we present the results of our study.

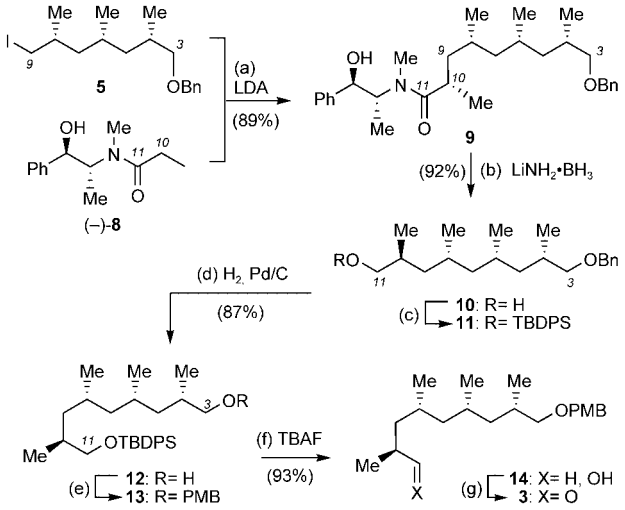
Our retrosynthetic strategy towards borrelidin (**1**) is illustrated in Scheme 1. We hypothesized that the *Z*,*E* cyanodiene motif of **1** could be constructed by the *syn*



Scheme 1. Strategic bond disconnections in the retrosynthesis of borrelidin (**1**). Bn = benzyl, MEM = (2-methoxyethoxy)methyl, MOM = methoxymethyl, PMB = *p*-methoxybenzyl, TBS = *tert*-butyldimethylsilyl.

addition of an H–CN unit across a C12–C13 triple bond, thus suggesting the use of macrolide **2**, which contains an enyne conjugated system, as a viable synthetic precursor. This disconnection raised two major challenges related to the overall construction of such a strained macrocycle and the regioselectivity of the HCN addition. Despite this risk we were intrigued by the possibilities offered by the macrolide **2** as a test case for the hydrocyanation reaction and as a scaffold for the synthesis of analogues to help in the evaluation of structure–activity relationships of the natural product. An additional advantage of this approach is that compound **2** could be disconnected into two major fragments **3** and **4**, thus adding to the convergence of our strategy. The postulated key bond-forming reactions would include the coupling of **4** with aldehyde **3**, extension of the northern fragment by using a Mukaiyama aldol reaction, and subsequent macrolactonization. Aldehyde **3** could be formed by the extension of alkyl iodide **5**,[11d] whereas the cyclopentane subunit of **4** can be traced back to diol **6**, which is available from diester **7**.

The synthesis of aldehyde **3** is shown in Scheme 2. The Myers alkylation[15] of iodide **5** with the lithium enolate of (−)-pseudoephedrine propionamide ((−)-**8**), followed by reduction of the resulting amide **9** with $LiNH_2{\cdot}BH_3$, produced alcohol **10** as a single diastereomer (d.r. > 98:2) in 82%



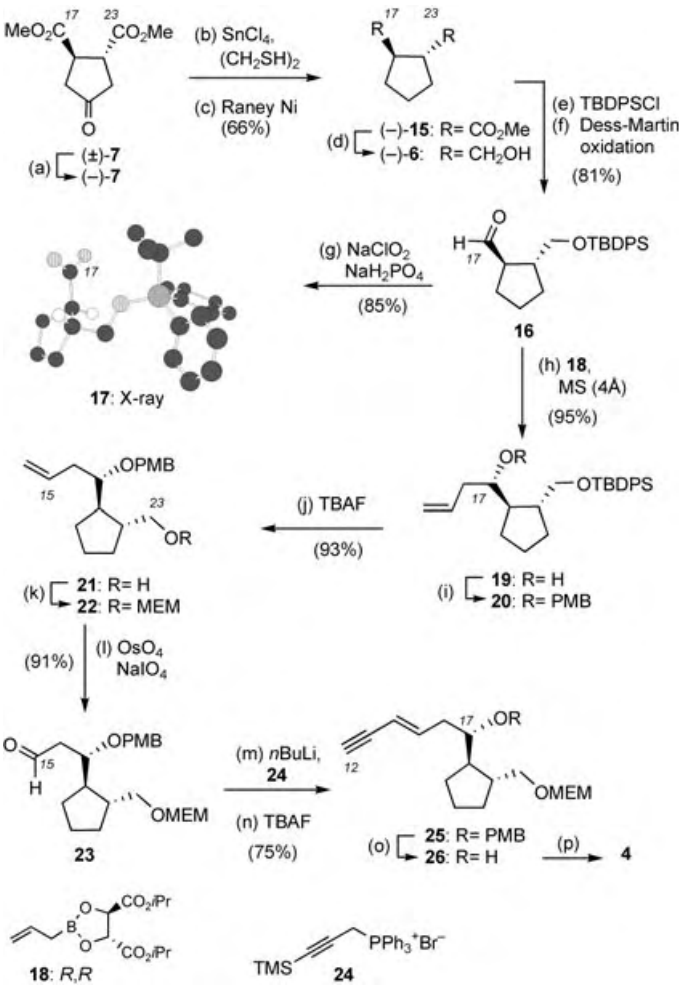
Scheme 2. Reagents and conditions: a) (−)-**8** (2.1 equiv), LDA (4.0 equiv), LiCl (12.2 equiv), THF, 0 °C, 18 h, 89%; b) $LiNH_2{\cdot}BH_3$ (4.0 equiv), CH_2Cl_2, −78→0 °C, 3 h, 92%; c) TBDPSCl (2.0 equiv), imidazole (3.0 equiv), DMAP (0.1 equiv), 25 °C, 8 h, 95%; d) H_2, Pd/C, EtOH, 25 °C, 12 h, 87%; e) NaH (3.0 equiv), THF, 0 °C, 1 h; then PMBBr (2.0 equiv), TBAI (0.1 equiv), 25 °C, 12 h, 85%; f) TBAF (1.5 equiv), THF, 25 °C, 12 h, 93%; g) Dess–Martin periodinane (1.2 equiv), CH_2Cl_2, 25 °C, 1 h, 94%. DMAP = *N*,*N*-dimethylaminopyridine, LDA = lithium diisopropylamide, TBDPS = *tert*-butyldiphenylsilyl, TBAF = tetrabutylammonium fluoride, TBAI = tetrabutylammonium iodide.

overall yield.[16] Adjustment of the protecting groups and oxidation of the hydroxy group at C11 produced the desired aldehyde **3** in 61% yield from **10**.

The synthesis of the southern fragment **4** of borrelidin is illustrated in Scheme 3. The cyclopentane diester subunit **7** was first prepared in an enantioselective manner by enzymatic resolution of racemic **7** with pig liver esterase (PLE) under conditions reported previously.[17] During this reaction (+)-**7** was selectively hydrolyzed to the corresponding monoacid, thus allowing facile separation of the desired *R*,*R* ester (−)-**7** in excellent yield and with > 97% *ee*. This compound was converted into the corresponding dithioketal, which underwent reductive desulfurization with Raney Ni to produce diester **15** in 66% yield from (−)-**7**. The reduction of both ester functionalities of **15**, followed by monosilylation by using the bulky reagent TBDPSCl and oxidation of the available hydroxy group with Dess–Martin periodinane produced aldehyde **16** (three steps, 75% yield). Single-crystal X-ray analysis of carboxylic acid **17**, obtained by oxidation of aldehyde **16**, confirmed the depicted relative stereochemistry of the cyclopentane ring in **16** unambiguously.[18]

Aldehyde **16** underwent allylation with boronate ester **18** under the conditions of Roush and co-workers[19] to give homoallylic alcohol **19** as an 8:1 mixture of isomers at the C17 center in favor of the desired compound and in 95% combined yield. Model studies towards esterification of the C17 hydroxy group of **19** under a variety of conditions led to the corresponding ester in low yields, presumably because of the bulkiness of the neighboring TBDPS group. To overcome this problem we decided to protect the alcohol at C23 with a

 © 2004 Wiley-VCH Verlag GmbH & Co. KGaA, Weinheim



Scheme 3. Reagents and conditions: a) PLE (3.0 equiv), H_2O, phosphate buffer (pH 7.0), 1 h, 49% (from 50% maximum yield), >97% *ee*; b) $SnCl_4$ (5.0 equiv), 1,2-ethanedithiol (1.8 equiv), CH_2Cl_2, 0→25 °C, 8 h, 72%; c) Raney Ni, MeOH, reflux, 3 h, 92%; d) $LiAlH_4$ (5.0 equiv), Et_2O, 25 °C, 12 h, 92%; e) TBDPSCl (2.1 equiv), imidazole (2.1 equiv), DMAP (0.1 equiv), CH_2Cl_2, 25 °C, 8 h, 84% (+8% recovered **6**); f) Dess–Martin periodinane (1.2 equiv), CH_2Cl_2, 25 °C, 1 h, 89%; g) $NaClO_2$ (3.0 equiv), NaH_2PO_4 (3.0 equiv), 2-methyl-2-butene, *t*BuOH/H_2O (2:1), 25 °C, 0.5 h, 85%; h) **18** (1.4 equiv), MS (4 Å), toluene, −78 °C, 1 h, 95% (8:1 ratio at C17); i) NaH (3.5 equiv), THF, 0 °C, 1 h; then PMBBr (3.5 equiv), TBAI (0.1 equiv), 12 h, 25 °C, 94%; j) TBAF (2.0 equiv), THF, 25 °C, 12 h, 93%; k) MEMCl (3.0 equiv), *i*Pr_2NEt (5.0 equiv), CH_2Cl_2, 0→25 °C, 8 h, 93%; l) OsO_4 (3 mol%), NMO (1.2 equiv), pyridine (0.1 equiv), acetone/H_2O (10:1), 25 °C, 12 h; then $NaIO_4$ (1.4 equiv), THF/H_2O (5:4), 25 °C, 2 h, 91%; m) **24** (3.0 equiv), *n*BuLi (3.0 equiv), THF, −78 °C, 1 h; then **23**, THF, −78 °C, 2 h, 77% (5:1 *trans*/*cis*); n) TBAF (1.2 equiv), THF, 25 °C, 0.5 h, 98%; o) DDQ (1.5 equiv), buffer (pH 7.0, 10 equiv), CH_2Cl_2, 25 °C, 1 h, 91%; p) TBSOTf (2.0 equiv), imidazole (3.1 equiv), DMAP (0.1 equiv), 40 °C, 8 h, 93%. DDQ = 2,3-dichloro-5,6-dicyano-1,4-benzoquinone, NMO = 4-methylmorpholine *N*-oxide, PLE = pig liver esterase, Tf = trifluoromethanesulfonyl.

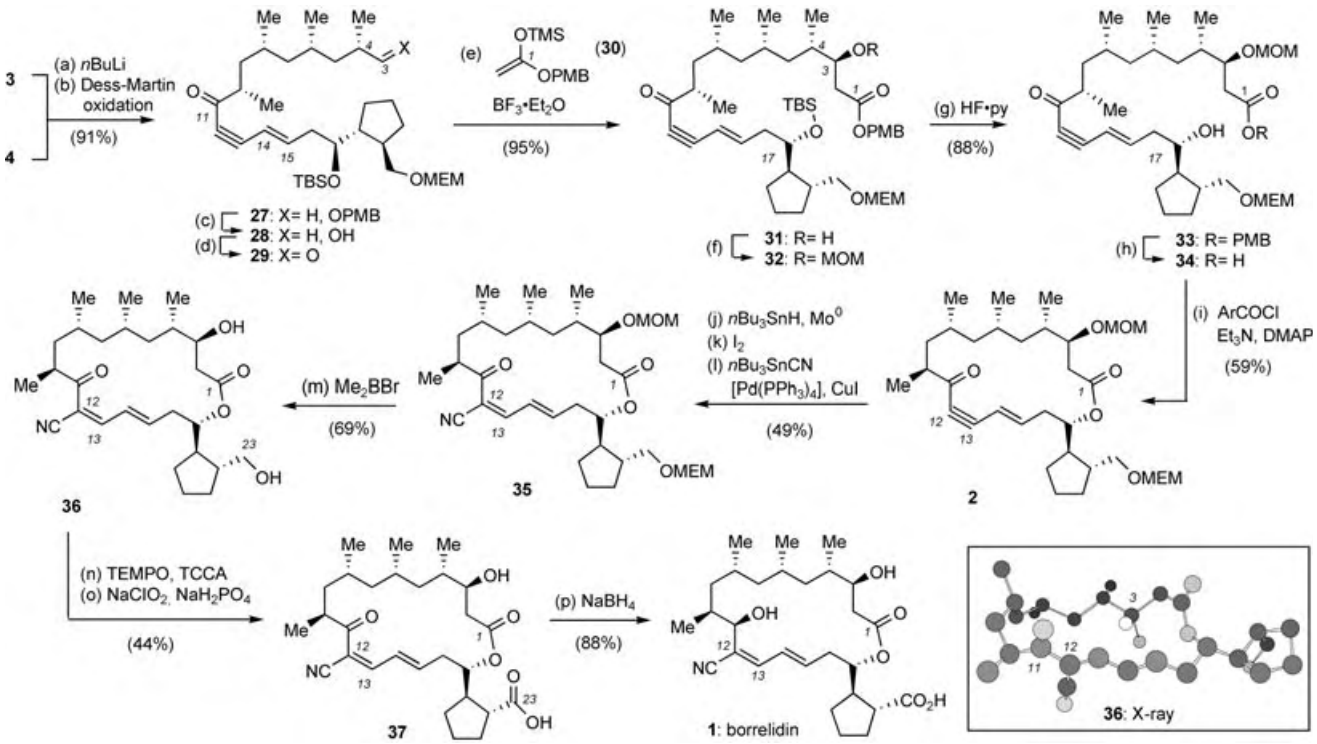
sterically less imposing group, such as MEM. Compound **19** was therefore converted into its PMB ether **20**, which underwent fluoride-induced desilylation and alkylation of the alcohol group at C23 with MEMCl to give **22** in three steps and 81% yield.

Exposure of the protected homoallylic alcohol **22** to osmium tetroxide and sodium periodate furnished aldehyde **23**, which was treated immediately with deprotonated **24** as its lithium salt. Desilylation of the C12 center then gave enyne **25** (*trans*/*cis* 5:1) in 68% combined yield.[20] Final adjustment of the protecting groups afforded enyne **4**, which represents the southern fragment of borrelidin (Scheme 3).

With the two major fragments **3** and **4** in hand, the stage was now set for the completion of the synthesis of borrelidin (Scheme 4). To this end, the lithiation of **4** followed by the addition of aldehyde **3** produced the coupled product as a 3:1 mixture of isomers at the C11 center (93% combined yield). During optimization attempts it was found that the use of a 1:1 solvent mixture of THF and DME together with molecular sieves led to an increase in the reactivity of the enyne nucleophile and a decrease in side reactions.[21] At this step, the *trans* and *cis* isomers of the alkene functionality (C14–C15) became separable; the *cis* isomer was separated from the *trans* and was subjected to radical isomerization with sunlight in the presence of catalytic diphenyl sulfide to give a mixture of *cis* and *trans* alkenes in a ratio of 1:1.[22] Oxidation of the alcohol functionality with Dess–Martin periodinane afforded ketone **27**, which was converted uneventfully into aldehyde **29** (84% yield).[23] An aldol reaction with the silyl ketene acetal **30** under Mukaiyama conditions[24] produced a 4:1 mixture of isomers at the C3 center in favor of the desired ester **31** and in 95% combined yield. The stereochemical outcome of this addition was efficiently controlled by the chirality of the neighboring C4 center. The protection of **31** with MOMCl, followed by a two-step unmasking of the C17 hydroxy group and the C1 carboxylic acid, furnished hydroxy acid **34** in 63% overall yield. The macrolactonization of **34** under the Yamaguchi conditions[25] then afforded macrolide **2** in 59% yield. Similar yields were observed for the Mukaiyama macrolactonization procedure.[26]

Several catalysts and conditions, such as $[Ni\{P(OPh)_3\}_4]$ and HCN or acetone cyanohydrin,[27] were evaluated for the regioselective installation of the nitrile functionality at the C12 center. As this direct metal-catalyzed hydrocyanation was found to be unsuccessful,[28] we attempted an alternative sequence involving the regioselective hydrostannation of the C12–C13 alkyne, followed by conversion of the vinyl stannane into the corresponding vinyl iodide, which was then subjected to palladium-based cyanation. The problem with this sequence arose from the complete loss of regioselectivity observed during the initial hydrostannation reaction under the known Pd-based catalytic conditions.[29] In an effort to improve this reaction, we attempted a molybdenum-based hydrostannation with $[Mo(CO)_3(t\text{BuNC})_3]$ as the catalyst.[14,30] We were delighted to observe that under these conditions the tributylstannane residue was installed exclusively at the C12 center. The regioselectivity of this addition was influenced by the presence of the C11 carbonyl group; in a related experiment with a macrolide containing an enyne–alcohol motif the hydrostannation was much less regioselective. To the best of our knowledge, this is the first example of the use of a Mo^0-catalyzed hydrostannation in the context of complex natural product synthesis, and it clearly demonstrates the scope of this reaction. After iodination of the vinyl

 © 2004 Wiley-VCH Verlag GmbH & Co. KGaA, Weinheim



Scheme 4. Reagents and conditions: a) **4** (1.3 equiv), **3** (1.0 equiv), *n*BuLi (1.3 equiv), THF/DME (1:1), MS (4 Å), −78 °C, 1 h, 93%; b) Dess–Martin periodinane (1.2 equiv), CH_2Cl_2, 25 °C, 0.5 h, 98%; c) DDQ (1.5 equiv), H_2O (pH 7), CH_2Cl_2, 25 °C, 0.5 h, 89%; d) TEMPO (0.1 equiv), BAIB (1.5 equiv), CH_2Cl_2, 25 °C, 2 h, 94%; e) **30** (5.0 equiv), $BF_3{\cdot}OEt_2$ (3.0 equiv), MS (4 Å), THF, −78 °C, 1 h, 95%; f) iPr_2NEt (20 equiv), MOMCl (10 equiv), CH_2Cl_2, 25 °C, 12 h, 86%; g) HF·pyridine (20%), THF, 25 °C, 12 h, 88%; h) TFA (3%), CH_2Cl_2, 0 °C, 8 h, 83%; i) 2,4,6-trichlorobenzoyl chloride (10 equiv), Et_3N (20 equiv), THF, 25 °C, 3 h; then DMAP (10 equiv), toluene, 25 °C, 12 h, 59%; j) hydroquinone (2.0 equiv), $[Mo(CO)_3(t\text{BuNC})_3]$ (0.5 equiv), $n\text{Bu}_3\text{SnH}$ (5.0 equiv), THF, 55 °C, 12 h; k) I_2 (1.1 equiv), CH_2Cl_2, 25 °C, 54% (over two steps); l) $n\text{Bu}_3\text{SnCN}$ (2.3 equiv), $[Pd(PPh_3)_4]$ (0.6 equiv), CuI (0.4 equiv), toluene, 80 °C, 12 h, 90%; m) Me_2BBr (3.0 equiv), CH_2Cl_2, −78 °C, 1 h, 69%; n) TEMPO (0.01 equiv), TCCA (1.1 equiv), CH_2Cl_2, 25 °C, 1 h, 85%; o) $NaClO_2$ (3.0 equiv), NaH_2PO_4 (3.0 equiv), *t*BuOH/H_2O (2:1), 25 °C, 0.5 h, 52%; p) $NaBH_4$ (1.2 equiv), $CeCl_3$ (cat.), 0 °C, 0.5 h, 88%, 10:1 ratio of epimers at C11. BAIB = bis(acetoxy)iodobenzene, DME = dimethoxyethane, TCCA = trichlorocyanuric acid, TEMPO = 2,2,6,6-tetramethylpiperidine *N*-oxide, TCCA = trichlorocyanuric acid, TFA = trifluoroacetic acid.

stannane, a Pd-catalyzed cyanation produced macrolide **35** in 49% yield from **2**.

Further elaboration of **35** included the simultaneous removal of both the MOM and MEM groups to give diol **36**. Gratifyingly, **36** was found to be a crystalline solid, and single-crystal X-ray analysis confirmed the stereochemistry of the macrolide core (Scheme 4).[18] The primary alcohol at C23 of diol **36** was oxidized selectively by using TEMPO/TCCA,[31] and the resulting aldehyde was converted into carboxylic acid **37** upon treatment with $NaClO_2$ (44% yield from **36**). Reduction of acid **37** under Luche conditions with $NaBH_4$ and $CeCl_3$[32] produced synthetic borrelidin in 10:1 diastereoselectivity with respect to the C11 center and in 88% yield. Spectroscopic and analytical data for synthetic borrelidin were in full agreement with those reported for the natural product.

In conclusion, a stereoselective total synthesis of borrelidin (**1**) has been reported. The strategy developed is distinguished by the construction of a strained enynone-containing macrocycle **2**, and the regioselective introduction of a cyano group by implementing a novel molybdenum-catalyzed hydrostannation reaction. The late installation of the nitrile unit in a fully functionalized macrocyclic scaffold paves the way for the preparation of analogues of borrelidin that could be used to evaluate structure–activity relationships of this natural product.

Received: April 2, 2004 [Z460203]

Keywords: hydrostannation · macrolactonization · natural products · synthetic methods · total synthesis

[1] J. Berger, L. M. Jampolsky, M. W. Goldberg, *Arch. Biochem.* **1949**, *22*, 476–478; for the subsequent isolation of **1** from related *Streptomyces* strains, see: S. K. Singh, S. Gurusiddaiah, J. W. Whalen, *Antimicrob. Agents Chemother.* **1985**, *27*, 239–245; H. Maher, R. H. Evans, *J. Antibiot.* **1987**, *40*, 1455–1456.

[2] M. Lumb, P. E. Macey, J. Spyvee, J. M. Whitmarsh, R. D. Wright, *Nature* **1965**, *206*, 263–265; L. Dickinson, A. J. Griffiths, C. G. Mason, R. F. N. Mills, *Nature* **1965**, *206*, 265–268.

[3] M. Buck, A. C. Farr, R. J. Schnitzer, *Trans. N. Y. Acad. Sci. Ser. 2* **1949**, *11*, 207–209; E. Grunberg, D. Eldrige, G. Soo-Hoo, D. R. Kelly, *Trans. N. Y. Acad. Sci. Ser. 2* **1949**, *11*, 210–212; T. C. Schüz, H. Zähner, *FEMS Microbiol. Lett.* **1993**, *114*, 41–46; K.

 © 2004 Wiley-VCH Verlag GmbH & Co. KGaA, Weinheim

Otoguro, H. Ui, A. Ishiyama, M. Kobayashi, H. Togashi, Y. Takahashi, R. Masuma, H. Tanaka, H. Tomoda, H. Yamada, S. Omura, *J. Antibiot.* **2003**, *56*, 727 – 729.

[4] J. S. Cantt, C. A. Bennett, S. M. Arfin, *Proc. Natl. Acad. Sci. USA* **1981**, *78*, 5367 – 5370; T. Hirakawa, H. Morinaga, K. Watanabe, *Agric. Biol. Chem.* **1974**, *38*, 85 – 89; W. Paetz, G. Nass, *Eur. J. Biochem.* **1973**, *35*, 331 – 337; G. Nass, K. Poralla, H. Zähner, *Naturwissenschaften* **1971**, *58*, 603 – 610; K. Poralla, H. Zähner, *Arch. Microbiol.* **1968**, *61*, 143 – 153; for a review on threonyl-tRNA synthetase, see: W. Friest, D. H. Gauss, *Biol. Chem. Hoppe-Seyler* **1995**, *376*, 213 – 224.

[5] E. Tsuchiya, M. Yukawa, T. Miyakawa, K. Kimura, H. Takahashi, *J. Antibiot.* **2001**, *54*, 84 – 90; K. Poralla in *Mechanism of Action of Antimicrobial and Antitumor Agents* (Eds.: J. W. Corcoran, F. E. Hahn), Springer, Berlin, **1975**, pp. 365 – 388.

[6] T. Wakabayashi, R. Kageyama, N. Naruse, N. Tsukahara, Y. Funahashi, K. Kitoh, Y. Watanabe, *J. Antibiot.* **1997**, *50*, 671 – 676; E. L. Eastwood, S. E. Schaus, *Bioorg. Med. Chem. Lett.* **2003**, *13*, 2235 – 2237.

[7] K. Anderton, R. W. Rickards, *Nature* **1965**, *206*, 269; M. S. Kuo, D. A. Yurek, D. A. Kloosterman, *J. Antibiot.* **1989**, *42*, 1006 – 1007; W. Keller-Schierlein, *Experientia* **1966**, *22*, 355 – 359; W. Keller-Schierlein, *Helv. Chim. Acta* **1967**, *50*, 731 – 753.

[8] The absolute stereochemistry of **1** was determined by incorporating a chiral solvent in the crystal lattice: B. F. Anderson, A. J. Herlt, R. W. Rickards, G. B. Robertson, *Aust. J. Chem.* **1989**, *42*, 717 – 730.

[9] The repeated isopropyl motif constitutes a common structural element in many natural products of polyketide origin, including ionomycin, rapamycin, and related macrolides; for a recent monograph on macrolides, see: *Macrolide Antibiotics Chemistry, Biology, and Practice*, 2nd ed. (Ed.: S. Omura), Academic Press, London, **2002**, pp. 1 – 637.

[10] For recent studies on the biosynthesis of this natural product, see: C. Olano, B. Wilkinson, C. Sanchez, S. J. Moss, R. Sheridan, V. Math, A. J. Weston, A. F. Brana, C. J. Martin, M. Oliynyk, C. Mendez, P. F. Leadlay, J. A. Salas, *Chem. Biol.* **2004**, *11*, 87 – 97; C. Olano, B. Wilkinson, C. Sanchez, S. J. Moss, A. F. Brana, C. Mendez, P. F. Leadlay, J. A. Salas, *Chem. Commun.* **2003**, 2780 – 2782.

[11] a) N. Haddad, M. Grishko, A. Brik, *Tetrahedron Lett.* **1997**, *38*, 6075 – 6078; b) N. Haddad, A. Brik, M. Grishko, *Tetrahedron Lett.* **1997**, *38*, 6079 – 6082; c) C.-X. Zhao, M. O. Duffey, S. J. Taylor, J. P. Morken, *Org. Lett.* **2001**, *3*, 1829 – 1831; d) B. G. Vong, S. Abraham, A. X. Xiang, E. A. Theodorakis, *Org. Lett.* **2003**, *5*, 1617 – 1620; e) D. B. Ball, B. R. Taft, *Abstracts of Papers, CHED-933*, 227th ACS National Meeting, Anaheim, CA, **2004**; f) D. B. Ball, B. R. Taft, M. Mahoney, *Abstracts of Papers, CHED-597*, 225th ACS National Meeting, New Orleans, LA, **2003**.

[12] M. O. Duffey, A. LeTiran, J. P. Morken, *J. Am. Chem. Soc.* **2003**, *125*, 1458 – 1459.

[13] S. Hanessian, Y. Yang, S. Giroux, V. Mascitti, J. Ma, F. Raeppel, *J. Am. Chem. Soc.* **2003**, *125*, 13784 – 13792.

[14] U. Kazmaier, D. Schauss, M. Pohlman, *Org. Lett.* **1999**, *1*, 1017 – 1019; U. Kazmaier, M. Pohlman, D. Schauss, *Eur. J. Org. Chem.* **2000**, *15*, 2761 – 2766; S. Braune, U. Kazmaier, *J. Organomet. Chem.* **2002**, *641*, 26 – 29.

[15] A. G. Myers, B. H. Yang, H. Chen, J. L. Gleason, *J. Am. Chem. Soc.* **1994**, *116*, 9361 – 9362; A. G. Myers, B. H. Yang, H. Chen, L. McKinstry, D. J. Kopecky, J. L. Gleason, *J. Am. Chem. Soc.* **1997**, *119*, 6496 – 6511.

[16] The use of other chiral auxiliaries in conjunction with β-branched iodides leads to low yields as a result of the reduced reactivity of the electrophile. However, such reduced reactivity is not observed in the pseudoephedrine-based alkylation reported by Myers and co-workers;[15] see also: A. G. Myers, B. H. Yang, H. Chen, D. J. Kopecky, *Synlett* **1997**, 457 – 459.

[17] A. Rosenquist, I. Kvarnström, S. C. T. Svensson, B. Classon, B. Samuelsson, *Acta Chem. Scand.* **1992**, *46*, 1127 – 1129; F. C. Acher, F. J. Tellier, R. Azerard, I. N. Brabet, L. Fagni, J.-P. R. Pin, *J. Med. Chem.* **1997**, *40*, 3119 – 3129; D. Nöteberg, J. Brånalt, I. Kvarnström, M. Linschoten, D. Musil, J.-E. Nyström, G. Zuccarello, B. Samuelsson, *J. Med. Chem.* **2000**, *43*, 1705 – 1713.

[18] CCDC-234162 (**17**) and CCDC-234484 (**36**) contain the supplementary crystallographic data for this paper. These data can be obtained free of charge via www.ccdc.cam.ac.uk/conts/retrieving.html (or from the Cambridge Crystallographic Data Centre, 12, Union Road, Cambridge CB2 1EZ, UK; fax: (+44) 1223-336-033; or deposit@ccdc.cam.ac.uk).

[19] L. K. Hoong, M. A. Palmer, J. C. Park, W. R. Roush, *J. Org. Chem.* **1990**, *55*, 4109 – 4117; L. K. Hoong, M. A. Palmer, J. C. Park, A. D. Palkowitz, W. R. Roush, *J. Org. Chem.* **1990**, *55*, 4117 – 4126.

[20] The *cis*/*trans* isomers were easily separated by column chromatography after the coupling between **3** and **4**.

[21] For a discussion on the activation of organolithium reagents, see: M. Schlosser, *J. Organomet. Chem.* **1967**, *8*, 9 – 16.

[22] P. E. Sonnet, *Tetrahedron* **1980**, *36*, 557 – 604.

[23] A. DeMico, R. Margarita, L. Parlanti, A. Vescovi, G. Piancarelli, *J. Org. Chem.* **1997**, *62*, 6974 – 6977.

[24] T. Mukaiyama, K. Banno, K. Narasaka, *J. Am. Chem. Soc.* **1974**, *96*, 7503 – 7509.

[25] J. Inanaga, K. Hirata, H. Saeki, T. Katsuki, M. Yamaguchi, *Bull. Chem. Soc. Jpn.* **1979**, *52*, 1989 – 1993.

[26] T. Mukaiyama, M. Usui, K. Saigo, *Chem. Lett.* **1976**, 49 – 50.

[27] W. R. Jackson, C. G. Lowel, *Aust. J. Chem.* **1983**, *36*, 1975 – 1982; W. R. Jackson, P. Perlmutter, A. J. Smallridge, *Aust. J. Chem.* **1988**, *41*, 251 – 261.

[28] In our hands, direct hydrocyanation in the presence of $[Ni\{P(OPh)_3\}_4]$ did not yield any addition product.

[29] For selected reports on this issue, see: N. D. Smith, J. Mancuso, M. Lautens, *Chem. Rev.* **2000**, *100*, 3257 – 3282; M. B. Rice, S. L. Whitehead, C. M. Horvath, J. A. Muchnij, R. E. Maleczka, Jr., *Synthesis* **2001**, *10*, 1495 – 1504.

[30] For recent applications of this reaction, see: S. Braune, M. Pohlman, U. Kazmaier, *J. Org. Chem.* **2004**, *69*, 468 – 474; U. Kazmaier, D. Schauss, M. Pohlman, S. Raddatz, *Synthesis* **2000**, 914 – 916.

[31] L. DeLuca, G. Giacomelli, A. Porcheddu, *Org. Lett.* **2001**, *3*, 3041 – 3043.

[32] J. L. Luche, L. Rodriguez-Hahn, P. Crabbe, *J. Chem. Soc. Chem. Commun.* **1978**, *14*, 601 – 602.

 © 2004 Wiley-VCH Verlag GmbH & Co. KGaA, Weinheim

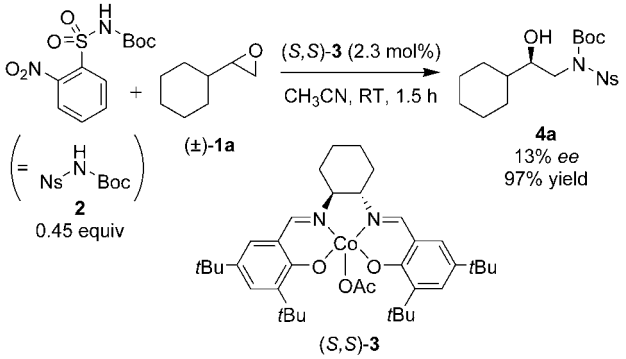
Asymmetric Catalysis

General Catalytic Synthesis of Highly Enantiomerically Enriched Terminal Aziridines from Racemic Epoxides**

*Sang Kyun Kim and Eric N. Jacobsen**

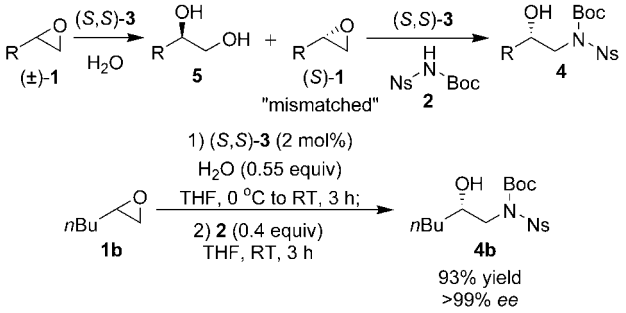
Exploitation of terminal aziridines in organic synthesis has been constrained to a significant extent by the lack of useful methods for their preparation in suitably protected and enantiopure form.[1] Direct enantioselective aziridination of alkene or imine substrates represents a most straightforward approach to these chiral building blocks. However, despite recent advances in the development of effective asymmetric aziridination catalysts,[1a,b,e–j] these have not proven generally useful in the context of terminal aziridine synthesis.[2] At this stage, indirect routes involving preparation and cyclization of 1,2-amino alcohols stand as the most viable alternatives.[1b] We report here a new and practical route to highly enantioenriched (>99% *ee*) 1,2-amino alcohol derivatives from racemic epoxides,[3] and the efficient conversion of these products to terminal aziridines bearing labile *N*-sulfonyl protecting groups. The utility of these aziridines in representative nucleophilic ring-opening reactions is also described.

Enantiomerically enriched 1-azido-2-ols are accessible by the [(salen)Cr]-catalyzed kinetic resolution of terminal epoxides by using trimethylsilyl azide ($TMSN_3$).[4] However, practical concerns associated with the use of azides[5] limit the application of this reaction, and we have sought to identify alternative ammonia equivalents capable of participating in enantioselective epoxide ring-opening reactions. Unfortunately, an extensive screen of nucleophiles led only to modest results in the best cases (e.g. kinetic resolution of vinylcyclohexane oxide (**1a**) with phthalimide is catalyzed by [(salen)Co] complex with $k_{rel} = 10$). However, an intriguing result was obtained in attempted kinetic resolutions of terminal epoxides using *N*-Boc-2-nitrobenzenesulfonamide (**2**)[6] as the nucleophilic component (Scheme 1). The reaction of (±)-vinylcyclohexane oxide (**1a**) with 0.45 equivalents of sulfonamide **2** in the presence of [(salen)Co–OAc] complex (*S*,*S*)-**3** provided adduct **4a** in high yield (97% based on **2**) but only 13% *ee*. No reaction was observed in the absence of catalyst, indicating that (*S*,*S*)-**3** promoted addition to both enantiomers of **1a** with very similar rates ($k_{rel} < 1.5$). Given that complex **3** is a highly effective catalyst for the hydrolytic kinetic resolution (HKR) of terminal epoxides,[7] this result suggested the possibility of an *indirect* kinetic resolution



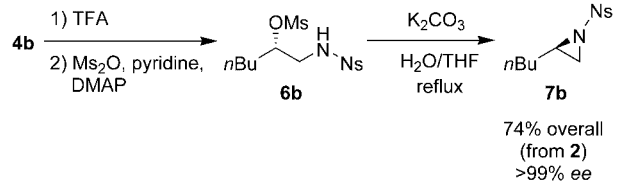
Scheme 1. Kinetic resolution with sulfonamide **2**. Boc = *tert*-butoxycarbonyl, Ns = 2-nitrobenzenesulfonyl.

process with sulfonamide **2**, wherein a highly selective HKR would be followed by ring-opening of the "mismatched", unreacted enantiomer of the epoxide by **2** promoted by the same catalyst (Scheme 2). A one-pot reaction sequence to generate enantiopure adduct **4** could be envisioned, as long as the diol by-product **5** of the HKR did not interfere with the second step. In this manner, the only practical deviation from the original goal of direct kinetic resolution with **2** would be inclusion of water as a co-reagent.



Scheme 2. Indirect kinetic resolution with sulfonamide **2**.

Proof-of-principle was provided through the sequential addition of water (0.55 equiv) and sulfonamide **2** (0.4 equiv) to a solution of (±)-1,2-epoxyhexane (**1b**) and catalyst (*S*,*S*)-**3** in THF, which afforded **4b** in >99% *ee* and 93% yield based on **2** (Scheme 2).[8] Product isolation was effected simply by filtration of the crude reaction mixture through a pad of silica gel. Compound **4b** was then transformed to the corresponding *N*-nosylaziridine by removal of the Boc group, conversion to the *O*-mesylate, and cyclization with K_2CO_3 (Scheme 3).[9]



Scheme 3. Synthesis of *N*-Ns-butylaziridine (**7b**). TFA = trifluoroacetic acid, DMAP = 4-dimethylaminopyridine, Ms = methanesulfonyl.

[*] S. K. Kim, Prof. E. N. Jacobsen
Department of Chemistry and Chemical Biology
Harvard University
12 Oxford St., Cambridge, MA 02138 (USA)
Fax: (+1) 617-496-1880
E-mail: jacobsen@chemistry.harvard.edu

[**] This work was supported by the NIH (GM-43214).

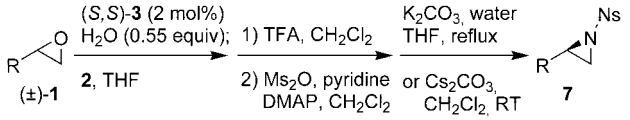
Supporting information for this article is available on the WWW under http://www.angewandte.org or from the author.

 © 2004 Wiley-VCH Verlag GmbH & Co. KGaA, Weinheim DOI: 10.1002/anie.200460369

The overall process afforded analytically pure aziridine **7b** in >99% *ee* and 74% yield based on **2** as limiting reagent, with only one chromatographic purification in the sequence.

The scope of the aziridine synthesis is summarized in Table 1. A range of terminal aziridines bearing aliphatic substituents of varying steric demand (**7a**–**7c**) was accessed in high enantiomeruc excess. The synthesis of the methyl glycidate derived aziridine **7d** required a modified procedure (Cs_2CO_3/CH_2Cl_2/room temperature) to prevent ester hydrolysis in the aziridine ring-closure. Successful preparation of highly enantioenriched chloromethylaziridine **7e** also relied on these modified conditions, because elevated reaction temperatures in the cyclization resulted in partial racemization by the reversible formation of the achiral dichloride derivative. The intermediate mesylate **6e** was recrystallized from EtOAc, and **7e** was isolated in pure form simply by filtration through a silica pad. Aziridine **7e** was thus synthesized on an 8.4 mmol (2.3 g) scale without recourse to column chromatography. This constitutes the first synthesis of this very interesting building block in enantiopure form (vide infra).[10]

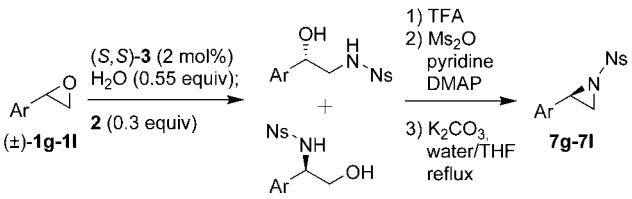
Table 1: Syntheses of nosyl-protected terminal aziridines.[a]



Aziridine	R	Yield [%][b]	*ee* [%][c]	Method[d]
7a	*c*Hex	86	>99	A
7b	*n*Bu	79	>99	A
7c	*t*Bu	67	99.8	A
7d	CO_2Me	69	>99	B
7e	CH_2Cl	75	>99	B
7f	1-butene	58	>99	A
7g	Ph	81	98.9	C
7h	3-ClPh	82	99.9	C
7i	2-ClPh	81	99.8	C
7j	4-ClPh	85	99.5	C
7k	3-MeOPh	80	99.4	C
7l	3-NO_2Ph	72	99.7	C

[a] Reactions were carried out with 2.5 mmol of epoxide. [b] Yield of isolated product based on **2**. [c] The enantioselectivities were determined by HPLC by using a commercially available chiral stationary phase. For details, see Supporting Information. [d] Method A: 0.4 equivalents of **2** and saturated aqueous K_2CO_3/THF (1/9), reflux in the last step. Method B: 0.4 equivalents of **2** and 1.1 equivalents of Cs_2CO_3, CH_2Cl_2, RT in the last step. Method C: 0.3 equivalents of **2** and O_2 atmosphere in the first step, column chromatography performed after the second step and saturated aqueous K_2CO_3/THF (1/9), reflux in the last step.

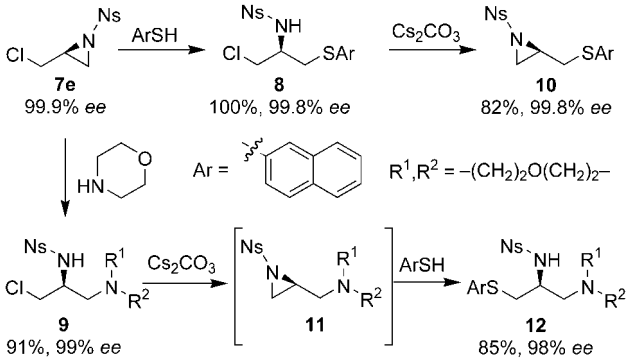
Arylaziridine derivatives (**7g**–**7l**) were also synthesized in high enantiomeric excess, with consistent results obtained for a variety of aryl substituents. Ring-opening of styrene oxide derivatives with sulfonamide **2** occurred with modest regioselectivity to afford mixtures of isomeric amino alcohol adducts. However, separation of these products proved unnecessary, as both isomers were transformed to the same aziridine enantiomer by using the deprotection/mesylation/cyclization protocol (Scheme 4).



Scheme 4. Synthesis of *N*-Ns-arylaziridines.

The *N*-nosyl protecting group imparts several useful properties to the terminal aziridine derivatives. For example, nosylaziridines are 50–60 times more reactive toward nucleophilic addition than the corresponding tosylaziridines;[11] in addition, *N*-nosyl amines obtained after aziridine ring-opening are alkylated and/or deprotected selectively under mild conditions.[12]

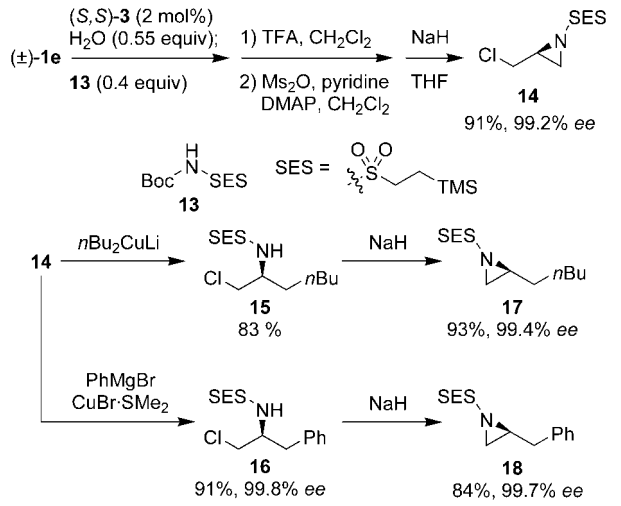
Compound **7e**, an aziridine analogue of epichlorohydrin, displays a range of useful reactivity reminiscent of its epoxide counterpart.[13] For example, it may be elaborated to other *N*-nosylaziridine derivatives through a simple two-step nucleophilic ring-opening/base-induced cyclization sequence (Scheme 5). This methodology affords convenient access to aziridines in cases in which the corresponding racemic epoxides are either poor substrates for the HKR (due to the presence of strongly Lewis basic functionality) or too precious to be used practically in a resolution process.



Scheme 5. Representative transformations of *N*-Ns-chloromethylaziridine (**7e**).

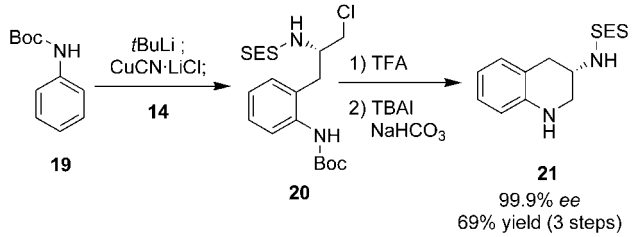
Nitro groups are not compatible with strongly basic carbon nucleophiles,[14] and this imposes a significant limitation on the utility of *N*-nosylaziridines in ring-opening reactions. In contrast, the 2-(trimethylsilyl)ethanesulfonyl-(SES-) protecting group is compatible with anionic carbon nucleophiles and is easily removed by treatment with fluoride ion.[15] *N*-SES-protected chloromethylaziridine **14** was synthesized in 91% yield and 99.2% *ee* from **13**[16] by using a method similar to that applied in the synthesis of **7e** (Scheme 6).[17] Aziridine **14** underwent clean reaction with both alkyl and aryl cuprates to afford the corresponding ring-opening products **15** and **16**. These were converted smoothly to the highly enantioenriched aziridines **17** and **18** with NaH. Aziridine **14** was also used in the asymmetric synthesis of 3-

 © 2004 Wiley-VCH Verlag GmbH & Co. KGaA, Weinheim



Scheme 6. Synthesis of *N*-SES-chloromethylaziridine (**14**) and its applications. SES = 2-(trimethylsilyl)ethanesulfonyl.

aminotetrahydroquinoline[18] (Scheme 7). The cuprate generated from the dianion of **19** and CuCN·LiCl underwent reaction with **14** to afford the ring-opening product **20**. Deprotection followed by cyclization in the presence of added iodide afforded 3-aminotetrahydroquinoline **21**.



Scheme 7. Synthesis of 3-aminotetrahydroquinoline **21**. TBAI = tetrabutylammonium iodide.

In summary, a general asymmetric catalytic method for the preparation of highly enantiomerically enriched *N*-sulfonylated terminal aziridines has been devised. Enantiopure chloromethylaziridines **7e** and **14** were synthesized for the first time, and the synthetic utility of these difunctional building blocks was demonstrated. Current efforts are directed toward elucidation of the mechanism of the reaction between epoxides and **2** and toward synthetic extensions and applications of this methodology.

Received: April 20, 2004 [Z460369]

Keywords: asymmetric catalysis · aziridines · nitrogen heterocycles · small ring systems · sulfonamides

[1] For reviews on the preparation and reactions of aziridines, see: a) J. B. Sweeney, *Chem. Soc. Rev.* **2002**, *31*, 247–258; b) V. H. Dahanukar, I. A. Zavialov, *Curr. Opin. Drug Discovery Dev.* **2002**, *5*, 918–927; c) W. McCoull, F. A. Davis, *Synthesis* **2000**, 1347–1365; d) H. Stamm, *J. Prakt. Chem.* **1999**, *341*, 319–331; e) D. Tanner, *Angew. Chem.* **1994**, *106*, 625–646; *Angew. Chem. Int. Ed. Engl.* **1994**, *33*, 599–619; f) P. Müller, C. Fruit, *Chem. Rev.* **2003**, *103*, 2905–2919; g) E. N. Jacobsen in *Comprehensive Asymmetric Catalysis, Vol. 2* (Eds.: E. N. Jacobsen, A. Pfaltz, H. Yamamoto), Springer, Berlin, **1999**, pp. 607–618; h) R. S. Atkinson, *Tetrahedron* **1999**, *55*, 1519–1559; i) H. M. I. Osborn, J. Sweeney, *Tetrahedron: Asymmetry* **1997**, *8*, 1693–1715.

[2] Moderate-to-high *ee* values have been reported only in the direct aziridination of styrene: a) H. Nishikori, T. Katsuki, *Tetrahedron Lett.* **1996**, *37*, 9245–9248; b) Z. Li, K. R. Conser, E. N. Jacobsen, *J. Am. Chem. Soc.* **1993**, *115*, 5326–5327; c) D. A. Evans, M. M. Faul, M. T. Bilodeau, B. A. Anderson, D. M. Barnes, *J. Am. Chem. Soc.* **1993**, *115*, 5328–5329.

[3] For a review of the synthesis of 1,2-amino alcohols, see: S. C. Bergmeier, *Tetrahedron* **2000**, *56*, 2561–2576.

[4] J. F. Larrow, S. E. Schaus, E. N. Jacobsen, *J. Am. Chem. Soc.* **1996**, *118*, 7420–7421.

[5] C. Moberg, H. Adolfsson in *Science of Synthesis, Vol. 4* (Ed.: I. Fleming), Thieme, Stuttgart, **2002**, pp. 435–449.

[6] T. Fukuyama, M. Cheung, T. Kan, *Synlett* **1999**, 1301–1303.

[7] a) M. Tokunaga, J. F. Larrow, F. Kakiuchi, E. N. Jacobsen, *Science* **1997**, *277*, 936–938; b) L. P. C. Nielsen, C. P. Stevenson, D. G. Blackmond, E. N. Jacobsen, *J. Am. Chem. Soc.* **2004**, *126*, 1360–1362; c) S. E. Schaus, B. D. Brandes, J. F. Larrow, M. Tokunaga, K. B. Hansen, A. E. Gould, M. E. Furrow, E. N. Jacobsen, *J. Am. Chem. Soc.* **2002**, *124*, 1307–1315, and references therein.

[8] Simultaneous addition of the two reagents led to inferior results, consistent with the observation that the rates of epoxide hydrolysis and ring-opening with **2** are competitive.

[9] Synthesis of **7b** under Mitsunobu conditions proceeded in low yield (44%) as a result of the instability of the nosylaziridine to the reaction conditions.

[10] For racemic syntheses, see: a) R. S. Atkinson, E. Barker, S. Ulukanli, *J. Chem. Soc. Perkin Trans. 1* **1998**, 583–589; b) R. S. Atkinson, M. P. Coogan, C. L. Cornell, *J. Chem. Soc. Perkin Trans. 1* **1996**, 157–166; c) R. S. Atkinson, B. J. Kelly, *J. Chem. Soc. Perkin Trans. 1* **1989**, 1627–1630.

[11] P. E. Maligres, M. M. See, D. Askin, P. J. Reider, *Tetrahedron Lett.* **1997**, *38*, 5253–5256.

[12] a) T. Fukuyama, C.-K. Jow, M. Cheung, *Tetrahedron Lett.* **1995**, *36*, 6373–6374; b) W. Kurosawa, T. Kan, T. Fukuyama, *Org. Synth.* **2002**, *79*, 186–195.

[13] Compound **7e** undergoes decomposition upon storage as a neat liquid, but was stored safely for prolonged periods as a frozen 0.78 M solution in benzene at −30 °C.

[14] a) A. Ricci, M. Fochi, *Angew. Chem.* **2003**, *115*, 1482–1484; *Angew. Chem. Int. Ed.* **2003**, *42*, 1444–1446; b) G. Köbrich, P. Buck, *Angew. Chem.* **1966**, *78*, 1062–1063; *Angew. Chem. Int. Ed. Engl.* **1966**, *5*, 1044.

[15] a) S. M. Weinreb, D. M. Demko, T. A. Lessen, J. P. Demers, *Tetrahedron Lett.* **1986**, *27*, 2099–2102; b) S. M. Weinreb, C. E. Chase, P. Wipf, S. Venkatraman, *Org. Synth.* **1997**, *75*, 161–169.

[16] a) J. A. Campbell, D. J. Hart, *J. Org. Chem.* **1993**, *58*, 2900–2903; b) B. R. Neustadt, *Tetrahedron Lett.* **1994**, *35*, 379–380.

[17] NaH was employed in the final cyclization step because the corresponding reaction with Cs_2CO_3 proved much slower. Thus, the NaH reaction was completed in 30 min, whereas the Cs_2CO_3 reaction required 23 h.

[18] 3-Aminotetrahydroquinoline is the core structure of sumanirole, a drug candidate for the treatment of Parkinson's disease. a) P. G. M. Wuts, R. L. Gu, J. M. Northuis, T. A. Kwan, D. M. Beck, M. J. White, *Pure Appl. Chem.* **2002**, *74*, 1359–1368; b) P. G. M. Wuts, *Curr. Opin. Drug Discovery Dev.* **1999**, *2*, 557–564.

 © 2004 Wiley-VCH Verlag GmbH & Co. KGaA, Weinheim

Reversal of Reactivity

Cross-Coupling of Alkyl Halides with Aryl Grignard Reagents Catalyzed by a Low-Valent Iron Complex**

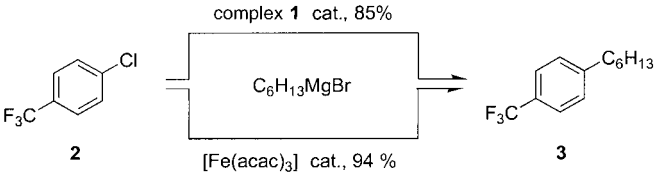
*Rubén Martin and Alois Fürstner**

While palladium- and nickel-catalyzed cross-coupling reactions of aryl and vinyl halides have evolved over decades into mature tools for advanced organic synthesis,[1] it was only recently that extensions of this chemistry to *alkyl* halides as the substrates have been possible.[2–7] The use of special ligands and additives as well as careful optimization of the reaction conditions were necessary to overcome the reluctance of alkyl halides to undergo oxidative addition and to suppress the proclivity of the resulting alkyl metal reagents for destructive β-hydride elimination.[2–7] Therefore it may come as a surprise that bare, low-valent iron species under "ligand-free" conditions offer a simple and powerful alternative. Prompted by recent reports in the literature,[8] we disclose our results on the remarkable efficiency and excellent selectivity profile of alkyl–aryl cross-coupling reactions catalyzed by a well-defined Fe^{-II} complex.

Encouraged by early reports of Kochi et al.,[9] our group has launched a program to explore in more detail the potential of iron catalysts as substitutes for palladium and nickel. Various types of substrates were found to undergo effective cross-coupling reactions with Grignard reagents in the presence of FeX_n ($n = 2, 3$; X = Cl, acac (acac = acetylacetonate)) as precatalysts.[10–17] These applications are distinguished by the low cost, ready availability, and benign character of the required iron salts as well as by exceptionally high reaction rates and notably mild conditions. Although the mechanisms are far from clear, it was speculated that highly reduced iron–magnesium clusters of the formal composition $[Fe(MgX)_2]_n$[18] generated in situ may play a decisive role in the catalytic cycle.[10,12]

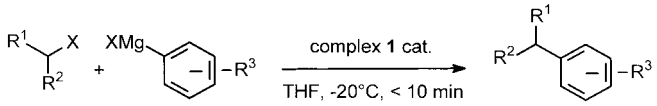
To probe this hypothesis, we investigated whether the reactivity of these presumed clusters can be emulated by structurally well-defined complexes containing an Fe^{-II} center. Of these, the tetrakis(ethylene)ferrate complex $[Li(tmeda)]_2[Fe(C_2H_4)_4]$ (**1**) (tmeda = *N*,*N*,*N*′,*N*′-tetramethylethylenediamine) described by Jonas et al.[19] seemed to be most promising. Its highly reduced metal center is only weakly ligated by four ethylene molecules, and strong ion-pair interactions between the ferrate unit and the peripheral lithium cations are observed in the solid state. Since these structural features are somewhat reminiscent of the assumed bonding situation in the intermetallic cluster $[Fe(MgX)_2]_n$, complex **1** could qualify as a catalyst for similar purposes.

As can be seen from Scheme 1, this is indeed the case. Thus, reaction of chloride **2** with hexylmagnesium bromide in THF/NMP (NMP = N-methylpyrrolidone) at 0 °C proceeded within minutes, delivering the desired product **3** in 85 % yield. This outcome compares well to the result obtained under "in situ" conditions.[10]



Scheme 1.

Even more gratifying is the fact that complex **1** also catalyzes the cross-coupling of alkyl halides and various aryl Grignard reagents or phenyllithium with exceptional ease (Scheme 2). Primary alkyl iodides and secondary alkyl bromides, as well as propargyl and allyl halides react smoothly, affording the desired arylated products in virtually quantitative yields in most cases; only tertiary halides and alkyl chlorides were found to be inert. Since these reactions usually proceed within minutes even at −20 °C, they compare favorably to the palladium- and nickel-based procedures for alkyl–aryl cross-coupling known to date[2–7] and are clearly more effective than related arylations employing stoichiometric amounts of organocopper reagents.[20]



Scheme 2.

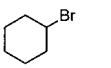
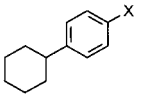
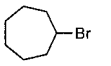
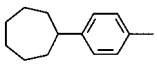
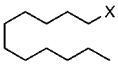
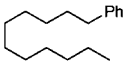
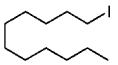
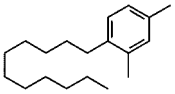
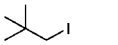
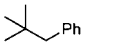
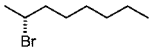
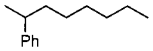
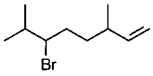
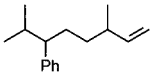
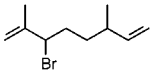
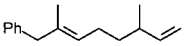
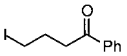
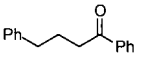
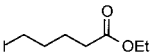
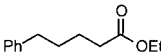
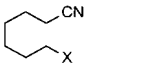
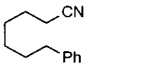
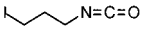
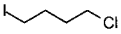
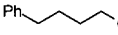
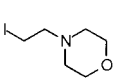
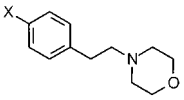
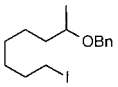
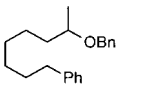
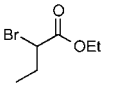
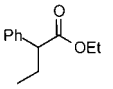
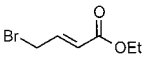
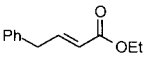
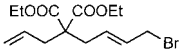
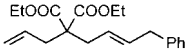
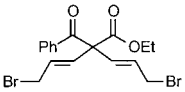
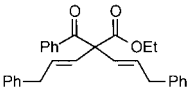
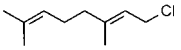
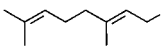
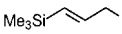
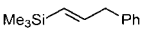
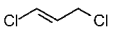
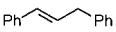
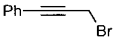
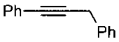
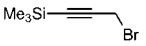
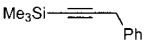
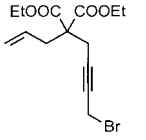
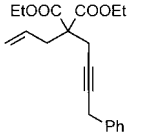
The unprecedented rate of productive cross-coupling of alkyl halides in the presence of complex **1** translates into an excellent chemoselectivity profile. Although one might assume that the use of organomagnesium reagents as the nucleophiles inherently restricts the functional-group tolerance of the method, the results compiled in Table 1 show that this is not the case. The iron-catalyzed activation of the alkyl halide turned out to be significantly faster than the uncatalyzed attack of the Grignard reagent to various other polar groups in the substrates, thus leaving ketones, esters, enoates, chlorides, nitriles, isocyanates, ethers, acetals, and trimethylsilyl groups intact. Moreover, tertiary amines do not interfere with productive C–C bond formation. This remarkable tolerance allowed us, for example, to convert even ethyl α-

[*] Dr. R. Martin, Prof. A. Fürstner
Max-Planck-Institut für Kohlenforschung
45470 Mülheim an der Ruhr (Germany)
Fax: (+49) 208-306-2994
E-mail: fuerstner@mpi-muelheim.mpg.de

[**] Generous financial support from the Deutsche Forschungsgemeinschaft (Leibniz Award Program) and the Fonds der Chemischen Industrie is gratefully acknowledged. R.M. thanks the Alexander-von-Humboldt Foundation for a postdoctoral fellowship. We express our gratitude to Prof. K. Jonas, Mülheim, for valuable discussions and for providing a generous sample of the iron complex **1**, as well as to Dr. A. Leitner for performing preliminary experiments.

 DOI: 10.1002/anie.200460504 © 2004 Wiley-VCH Verlag GmbH & Co. KGaA, Weinheim

Table 1: Cross-coupling reactions of alkyl halides catalyzed by $[Li(tmeda)]_2[Fe(C_2H_4)_4]$ (**1**) (5 mol%). All reactions were performed in THF at −20°C unless stated otherwise.

Entry	Substrate	RMgX/RLi	Product	Yield [%]
1		PhMgBr		94/89[a] (X = H)
2		PhLi		92 (X = H)
3		*p*-$MeOC_6H_4MgBr$		95 (X = OMe)
4		*p*-ClC_6H_4MgBr		67 (X = Cl)[b]
5		*p*-PhC_6H_4MgBr		93 (X = Ph)[b]
6		*m*-$(Me_3Si)_2NC_6H_4MgBr$		88 ($X = NH_2$)[b,c]
7		*p*-MeC_6H_4MgBr		95
8		PhMgBr		96 (X = I)
9		PhMgBr		61 (X = Br)
10		2,4-$(CH_3)_2C_6H_3MgBr$		94
11		PhMgBr		74[b]
12		PhMgBr		93
13		PhMgBr		89
14		PhMgBr		84
15		PhMgBr		91
16		PhMgBr		88
17		PhMgBr		83 (X = I)
18		PhMgBr		90
19		PhMgBr		86
20		PhMgBr		87 (X = H)
21		*p*-PhC_6H_4MgBr		85 (X = Ph)[b]
22		PhMgBr		95
23		PhMgBr		87
24		PhMgBr		94
25		PhMgBr		93
26		PhMgBr[d]		96
27		PhMgBr		87
28		PhMgBr		97
29		PhMgBr[d]		98
30		PhMgBr		93[e]
31		PhMgBr		96[f]
32		PhMgBr		87[g]

bromobutyrate into ethyl 2-phenylbutyrate in excellent yield within minutes (entry 23).[21] Substrates bearing more than one halide function are subject to exhaustive arylation (entries 26, 29; for an exception see entry 19).

Despite previous reports in the literature on iron-catalyzed transformations of allylic phosphates,[22] effective cross-coupling of the more abundant allylic halides have not yet been described. Entries 14 and 24–29, however, show that complex **1** is highly adequate for this purpose. In all cases investigated, the aryl group is introduced regioselectively at the least hindered site of the allylic system. Propargyl bromides behave equally well; only minor amounts, if any, of allenic by-products are formed under the chosen conditions (entries 30–32).

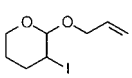
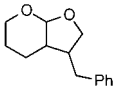
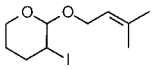
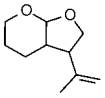
Although the development of this method was driven by the assumption that the ferrate complex **1** might mimic the behavior of the alleged iron clusters that supposedly operate under "in situ" conditions,[8,10] a concise mechanistic interpretation of the results outlined above is not yet possible. While the complete loss of optical purity in the reaction of (*R*)-2-bromooctane (98% *ee*) with PhMgBr (entry 12) could be explained by either an organometallic or by a radical pathway, the fact that the 2-iodoacetal derivative shown in entry 33 undergoes ring-closure prior to cross-coupling seems to indicate radical intermediates in this particular case.[23] Care, however, must be taken in generalizing this, because several other compounds set up for analogous 5-*exo*-trig pathways do not cyclize under otherwise identical conditions (cf. entries 13, 14, 25, 32). Moreover, tertiary halides remain unchanged, although they would afford the most stabilized alkyl radicals. In further studies we aim to unravel the mechanistic basis of this versatile iron-catalyzed alkyl–aryl coupling process and fully explore its preparative scope.

Experimental Section

Representative example: Table 1, entry 26: A solution of 2-benzoyl-6-bromo-2-(4-bromo-but-2-enyl)-hex-4-enoic acid ethyl ester (228 mg, 0.5 mmol) in THF (1 mL) was added to a solution of $[Li(tmeda)]_2[Fe(C_2H_4)_4]$ (**1**) (9 mg, 5 mol%) in THF (3 mL) at −20°C under argon, causing an immediate color change from green to red. At that point, PhMgBr (1M in THF, 1.2 mL, 1.2 mmol) was added dropwise, and the resulting mixture was stirred at −20°C for 5 min. Quenching of the reaction with saturated aq NH_4Cl followed by a

 © 2004 Wiley-VCH Verlag GmbH & Co. KGaA, Weinheim

Table 1: (Continued)

Entry	Substrate	RMgX/RLi	Product	Yield [%]
33		PhMgBr		85[b]
34		PhMgBr		77[h]

[a] Only 1 mol% of complex **1** was used. [b] The reaction was performed at 0°C. [c] After hydrolytic work-up. [d] Using 2 equiv of PhMgBr. [e] 15:1 mixture with 1,1-diphenylallene. [f] 5:1 mixture with 1-phenyl-1-trimethylsilylallene. [g] No allene by-product detected in the crude mixture. [h] No incorporation of the phenyl group was observed.

standard extractive work-up and flash chromatography (hexanes/ethyl acetate 4:1) of the crude product afforded 2-benzoyl-6-phenyl-2-(4-phenyl-but-2-enyl)-hex-4-enoic acid ethyl ester as a colorless solid (217 mg, 96%). ^{1}H NMR ($CDCl_3$, 400 MHz): $\delta = 0.92$ (t, $J =$ 6.8 Hz, 3H), 1.98 (m, 2H), 2.37 (m, 2H), 3.44 (m, 2H), 3.89 (m, 4H), 4.61 (d, $J = 6.2$ Hz, 2H), 5.23 (m, 2H), 7.31 ppm (m, 15H); ^{13}C NMR ($CDCl_3$, 100 MHz): $\delta = 13.6$, 30.8, 30.9, 52.8, 52.9, 60.3, 60.4, 77.8, 77.9, 124.86, 124.9, 125.0, 126.3, 126.6, 127.8, 127.9, 128.7, 128.8, 143.6, 143.7, 146.7, 175.8, 175.8 ppm; IR (film): $\tilde{\nu} = 3066$, 2941, 1771, 1743, 1646, 1617, 1448, 1265, 1150, 1048, 906, 791 cm^{-1}; elemental analysis calcd for $C_{31}H_{32}O_3$: C 82.27, H 7.13; found: C 82.35, H 7.30.

Received: April 29, 2004 [Z460504]
Published Online: July 7, 2004

Keywords: alkyl halides · cross-coupling · Grignard reagents · iron

[1] *Metal-Catalyzed Cross-Coupling Reactions* (Eds.: F. Diederich, P. J. Stang), Wiley-VCH, Weinheim, **1998**.
[2] For pertinent discussions see: a) D. J. Cárdenas, *Angew. Chem.* **2003**, *115*, 398–401; *Angew. Chem. Int. Ed.* **2003**, *42*, 384–387; b) T.-Y. Luh, M. Leung, K.-T. Wong, *Chem. Rev.* **2000**, *100*, 3187–3204.
[3] T. Ishiyama, S. Abe, N. Miyaura, A. Suzuki, *Chem. Lett.* **1992**, 691–694.
[4] a) A. Devasagayaraj, T. Stüdemann, P. Knochel, *Angew. Chem.* **1995**, *107*, 2952–2954; Angew . *Chem. Int. Ed. Engl.* **1995**, *34*, 2723–2725; b) R. Giovannini, P. Knochel, *J. Am. Chem. Soc.* **1998**, *120*, 11186–11187; c) R. Giovannini, T. Stüdemann, A. Devasagayaraj, G. Dussin, P. Knochel, *J. Org. Chem.* **1999**, *64*, 3544–3553; d) M. Piber, A. E. Jensen, M. Rottländer, P. Knochel, *Org. Lett.* **1999**, *1*, 1323–1326; e) A. E. Jensen, P. Knochel, *J. Org. Chem.* **2002**, *67*, 79–85.
[5] a) J. Zhou, G. C. Fu, *J. Am. Chem. Soc.* **2004**, *126*, 1340–1341; b) M. R. Netherton, C. Dai, K. Neuschütz, G. C. Fu, *J. Am. Chem. Soc.* **2001**, *123*, 10099–10100; c) J. H. Kirchhoff, M. R. Netherton, I. D. Hills, G. C. Fu, *J. Am. Chem. Soc.* **2002**, *124*, 13662–13663; d) M. R. Netherton, G. C. Fu, *Angew. Chem.* **2002**, *114*, 4066–4068; *Angew. Chem. Int. Ed.* **2002**, *41*, 3910–3912; e) J. Zhou, G. C. Fu, *J. Am. Chem. Soc.* **2003**, *125*, 12527–12530; f) J. Zhou, G. C. Fu, *J. Am. Chem. Soc.* **2003**, *125*, 14726–14727; g) H. Tang, K. Menzel, G. C. Fu, *Angew. Chem.* **2003**, *115*, 5233–5236; *Angew. Chem. Int. Ed.* **2003**, *42*, 5079–5082.
[6] a) J. Terao, H. Watanabe, A. Ikumi, H. Kuniyasu, N. Kambe, *J. Am. Chem. Soc.* **2002**, *124*, 4222–4223; b) J. Terao, Y. Naitoh, H. Kuniyasu, N. Kambe, *Chem. Lett.* **2003**, *32*, 890–891; c) J. Terao, A. Ikumi, H. Kuniyasu, N. Kambe, *J. Am. Chem. Soc.* **2003**, *125*, 5646–5647.
[7] A. C. Frisch, N. Shaikh, A. Zapf, M. Beller, *Angew. Chem.* **2002**, *114*, 4218–4221; *Angew. Chem. Int. Ed.* **2002**, *41*, 4056–4059.
[8] The following recent publications report iron-catalyzed arylations of alkyl halides using structurally undefined catalysts formed "in situ": a) M. Nakamura, K. Matsuo, S. Ito, E. Nakamura, *J. Am. Chem. Soc.* **2004**, *126*, 3686–3687; b) T. Nagano, T. Hayashi, *Org. Lett.* **2004**, *6*, 1297–1299.
[9] J. K. Kochi, *Acc. Chem. Res.* **1974**, *7*, 351–360.
[10] a) A. Fürstner, A. Leitner, M. Méndez, H. Krause, *J. Am. Chem. Soc.* **2002**, *124*, 13856–13863; b) A. Fürstner, A. Leitner, *Angew. Chem.* **2002**, *114*, 632–635; *Angew. Chem. Int. Ed.* **2002**, *41*, 609–612; c) A. Fürstner, A. Leitner, G. Seidel, *Org. Synth.*, in press.
[11] a) A. Fürstner, A. Leitner, *Angew. Chem.* **2003**, *115*, 320–323; *Angew. Chem. Int. Ed.* **2003**, *42*, 308–311; b) G. Seidel, D. Laurich, A. Fürstner, *J. Org. Chem.* **2004**, *69*, 3950–3952.
[12] B. Scheiper, M. Bonnekessel, H. Krause, A. Fürstner, *J. Org. Chem.* **2004**, *69*, 3943–3949.
[13] A. Fürstner, D. De Souza, L. Parra-Rapado, J. T. Jensen, *Angew. Chem.* **2003**, *115*, 5516–5518; *Angew. Chem. Int. Ed.* **2003**, *42*, 5358–5360.
[14] B. Scheiper, F. Glorius, A. Leitner, A. Fürstner, *Proc. Natl. Acad. Sci. USA*, in press.
[15] A. Fürstner, M. Méndez, *Angew. Chem.* **2003**, *115*, 5513–5515; *Angew. Chem. Int. Ed.* **2003**, *42*, 5355–5357.
[16] A. Fürstner, H. Brunner, *Tetrahedron Lett.* **1996**, *37*, 7009–7012.
[17] See the following for leading references on iron-catalyzed cross-coupling reactions from other laboratories: a) G. Cahiez, H. Avedissian, *Synthesis* **1998**, 1199–1205; b) H. Shinokubo, K. Oshima, *Eur. J. Org. Chem.* **2004**, 2081–2091; c) M. A. Fakhfakh, X. Franck, R. Hocquemiller, B. Figadère, *J. Organomet. Chem.* **2001**, *624*, 131–135; d) M. Hocek, H. Dvoráková, *J. Org. Chem.* **2003**, *68*, 5773–5776; e) B. Hölzer, R. W. Hoffmann, *Chem. Commun.* **2003**, 732–733; f) W. Dohle, F. Kopp, G. Cahiez, P. Knochel, *Synlett* **2001**, 1901–1904; g) M. Hojo, Y. Murakami, H. Aihara, R. Sakuragi, Y. Baba, A. Hosomi, *Angew. Chem.* **2001**, *113*, 641–643; *Angew. Chem. Int. Ed.* **2001**, *40*, 621–623; h) M. Nakamura, A. Hirai, E. Nakamura, *J. Am. Chem. Soc.* **2000**, *122*, 978–979; i) E. Alvarez, T. Cuvigny, C. Hervé du Penhoat, M. Julia, *Tetrahedron* **1988**, *44*, 119–126; j) V. Fiandanese, G. Marchese, V. Martina, L. Ronzini, *Tetrahedron Lett.* **1984**, *25*, 4805–4808, and references therein.
[18] B. Bogdanović, M. Schwickardi, *Angew. Chem.* **2000**, *112*, 4788–4790; *Angew. Chem. Int. Ed.* **2000**, *39*, 4610–4612.
[19] a) K. Jonas, L. Schieferstein, C. Krüger, Y.-H. Tsay, *Angew. Chem.* **1979**, *91*, 590–591; *Angew. Chem. Int. Ed. Engl.* **1979**, *18*, 550–551; b) see also: K. Jonas, L. Schieferstein, *Angew. Chem.* **1979**, *91*, 590; *Angew. Chem. Int. Ed. Engl.* **1979**, *18*, 549–550.
[20] B. H. Lipshutz, S. Sengupta, *Org. React.* **1992**, *41*, 135–631.
[21] For a recent Pd-based method for the arylation of α-bromoacetate see: L. J. Gooßen, *Chem. Commun.* **2001**, 669–670.
[22] a) A. Yanagisawa, N. Nomura, H. Yamamoto, *Tetrahedron* **1994**, *50*, 6017–6028; b) A. Yanagisawa, N. Nomura, H. Yamamoto, *Synlett* **1991**, 513–514.
[23] a) Y. Hayashi, H. Shinokubo, K. Oshima, *Tetrahedron Lett.* **1998**, *39*, 63–66; b) see also: K. Wakabayashi, H. Yorimitsu, K. Oshima, *J. Am. Chem. Soc.* **2001**, *123*, 5374–5375.

 © 2004 Wiley-VCH Verlag GmbH & Co. KGaA, Weinheim

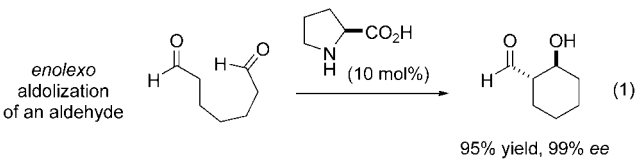
Asymmetric Catalysis

Catalytic Asymmetric Intramolecular Michael Reaction of Aldehydes**

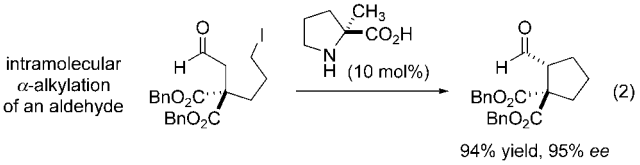
*Maria T. Hechavarria Fonseca and Benjamin List**

Dedicated to Professor Johann Mulzer on the occasion of his 60th birthday

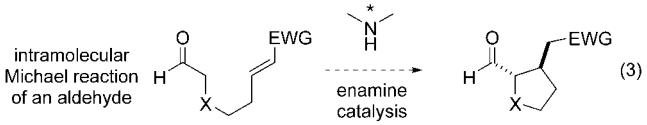
In the last few years the profound efficiency and applicability of asymmetric aminocatalysis in organic synthesis has been firmly established.[1] After discovering the first direct asymmetric enamine catalytic intermolecular aldol,[2] Mannich,[3] Michael,[4] and α-amination reactions,[5] our research group became interested in using this powerful organocatalytic strategy in the design of novel intramolecular reactions in which aldehydes are used as nucleophiles. These efforts led to the first catalytic asymmetric intramolecular *enolexo* aldolization [Eq. (1)][6] and α-alkylation reactions [Eq. (2); Bn = benzyl] of aldehydes.[7] In this context we realized that although there are a number of reports on elegant catalytic enantioselective intermolecular Michael reactions,[8] *intramolecular* catalytic asymmetric Michael reactions of aldehydes are unknown [Eq. (3); EWG = electron-withdrawing group].[9] We felt that such a process would be of great value, particularly if included in strategic reaction sequences, such as the Robinson annulation. Herein we report an efficient enantioselective cyclization of formyl enones in a process that constitutes the first catalytic asymmetric intramolecular Michael reaction of aldehydes.

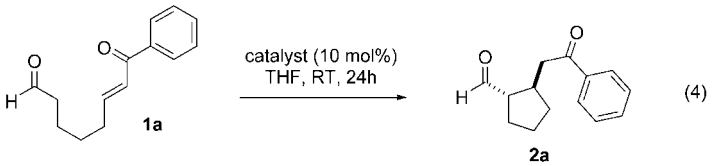


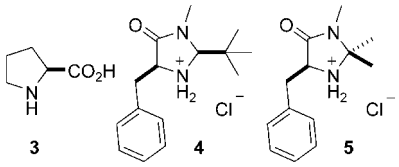
95% yield, 99% *ee*



94% yield, 95% *ee*







Cat.	Yield	d.r. (*anti*/*syn*)	*ee* (*anti*)
3	85%	2:1	15%
4	99%	19:1	39%
5	99%	24:1	97%

Remarkable progress has been made recently in the asymmetric catalysis of intermolecular Michael reactions. Both highly effective catalytic enantioselective conjugate addition reactions of stabilized and nonstabilized carbanions[10] and indirect Mukaiyama-type intermolecular Michael reactions have been developed.[11] In addition to these metal-mediated processes, highly enantioselective organocatalytic Michael reactions,[12] including variants based on iminium and enamine catalysis,[13] have been reported. However, intramolecular catalytic asymmetric Michael reactions are extremely rare.[14] We were particularly attracted to the asymmetric aminocatalysis of intramolecular Michael reactions of formyl enones. The ketoaldehydes produced should be good substrates for a subsequent aldol condensation in an overall intramolecular Robinson annulation to yield bicyclic enones of potential use in natural product synthesis. Furthermore, such aminocatalytic Michael cyclizations are mechanistically interesting as they may proceed by either enamine or iminium catalysis, or both simultaneously.

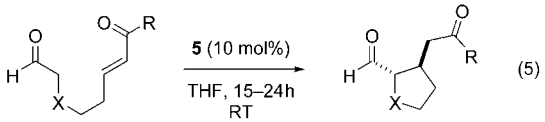
As a model reaction we studied the amine-catalyzed Michael cyclization of formyl enone **1a** to give ketoaldehyde **2a** [Eq. (4)]. This reaction was catalyzed by (*S*)-proline (**3**; 10 mol%, room temperature, DMF (*N*,*N*-dimethylformamide), 3 days), but as expected, both the diastereoselectivity and enantioselectivity were low. Next, we studied the commercial imidazolidinone catalysts **4** and **5** of MacMillan and co-workers.[15] Although these catalysts have not been used previously in enamine catalysis,[16] we found them to catalyze the cyclization reaction effectively. Interestingly, whereas the more reactive catalyst **4** provided the product in very high yield (99%) but with only 39% *ee*, catalyst **5** gave the product in the same yield and with an excellent 97% *ee*. The enantioselectivity and diastereoselectivity were determined by using an assay based on a Horner–Wadsworth–Emmons (HWE) reaction that we had developed earlier for the HPLC analysis of nonchromogenic or sensitive aldehydes.[6]

Fortunately, our results proved quite general; various other formyl enones reacted to give the desired products in excellent yields and with high *ee* values [Eq. (5), Table 1].[17] Thus, both aromatic enones (**1a** and **1b**) and aliphatic enones (**1c** and **1d**) could be used with excellent efficiency and enantioselectivity. Remarkably, even an enal could be

[*] Dr. M. T. Hechavarria Fonseca, Prof. Dr. B. List
Max-Planck-Institut für Kohlenforschung
Kaiser-Wilhelm-Platz 1, 45470 Mülheim an der Ruhr (Germany)
Fax: (+49) 208-306-2999
E-mail: list@mpi-muelheim.mpg.de

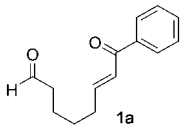
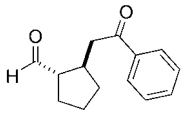
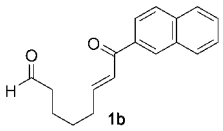
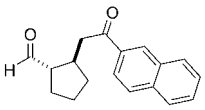
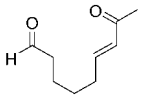
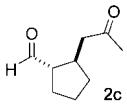
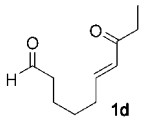
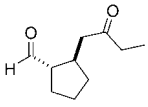
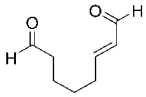
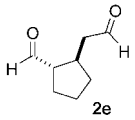
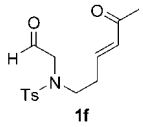
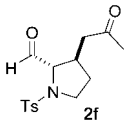
[**] We thank Linh Hoang for early experiments, Degussa for donating chemicals, and the excellent GC, HPLC, and X-ray departments of the Max-Planck-Institut für Kohlenforschung.

 © 2004 Wiley-VCH Verlag GmbH & Co. KGaA, Weinheim DOI: 10.1002/anie.200460578



(5)

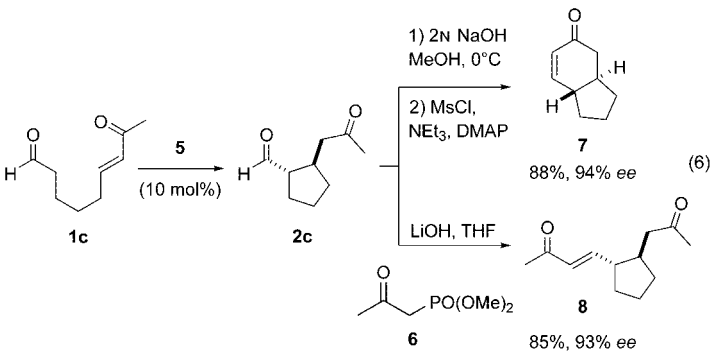
Table 1: Catalytic asymmetric intramolecular Michael reaction of aldehydes.

Starting material[a]	Yield [%]	Product	*ee* [%]	*anti*/*syn*
 1a	99	 2a	97	24:1
 1b	99	 2b	97	17:1
 1c	99	 2c	93	20:1
 1d	99	 2d	94	21:1
 1e	85	 2e	80	49:1
 1f	90	 2f	93	8:1

[a] Ts = *p*-toluenesulfonyl.

employed as the Michael acceptor to furnish a dialdehyde (**1e**→**2e**), although in somewhat reduced yield and enantioselectivity. To our delight, we were able to extend our asymmetric intramolecular Michael reaction to the synthesis of heterocyclic products. Thus, the reaction of aldehyde **1f** gave the corresponding pyrrolidine **2f** with excellent enantioselectivity and in good yield.

Having established an efficient process for the synthesis of ketoaldehydes **2**, we next investigated their application in two tandem sequences. Thus, the treatment of formyl enone **1c** with catalyst **5** and subjection of the product **2c** to an in situ intramolecular aldolization or HWE reaction with dimethyl (2-oxopropyl)phosphonate (**6**) gave enones **7** and **8**, respectively, in high yields and enantiomeric purity [Eq. (6); DMAP = 4-dimethylaminopyridine, Ms = methanesulfonyl]. Hydrindenone **7** has been described previously as the racemate, but this is the first enantioselective synthesis of **7**.[18] Both the bicyclic enone **7** and diketone **8** should be useful



(6)

additions to the chiral pool and valuable precursors in natural product synthesis.

We assume the Michael reaction described herein to proceed through an enamine mechanism. However, the observation that only enones react to give the desired products with very high enantioselectivity may be interpreted as evidence for an intriguing dual-activation mechanism involving both enamine and iminium catalysis. Furthermore, an inverse-electron-demand hetero-Diels–Alder mechanism, reminiscent of the intramolecular enamine/enal cycloaddition of Schreiber et al.[19] and the organocatalytic hetero-Diels–Alder reaction of Juhl and Jørgensen,[20] should be considered.

In summary, we have disclosed the first catalytic asymmetric intramolecular Michael reaction of aldehydes. Our process furnishes cyclic ketoaldehydes in excellent yields, with high enantioselectivities, and under very mild and convenient reaction conditions. This reaction is therefore expected to find use in organic synthesis. Further studies towards expanding the scope of this reaction and developing a more detailed mechanistic understanding are well underway in our laboratory.

Experimental Section

Typical procedure: Ketoaldehyde **1c** (123 mg, 0.8 mmol) was dissolved in dry THF (8 mL) and treated with **5** (20.4 mg, 0.08 mmol, 10%). The resulting mixture was stirred under argon at room temperature until the starting material had disappeared (15 h). The solution was then concentrated and filtered through silica. The product **2c** was dissolved in methanol (4 mL), cooled to 0°C, and treated with NaOH (2N, 4 mL).[21] After 5 min, TLC analysis indicated completion of the reaction. The mixture was poured into saturated aqueous ammonium chloride solution, the resulting mixture was extracted with ether, and the extracts were dried, filtered, and concentrated to give the crude aldol product. This material was dissolved in CH_2Cl_2 (5.2 mL) and stirred with methanesulfonyl chloride (0.16 mL), DMAP (35.6 mg), and triethylamine (0.39 mL) under argon for 30 min. After an aqueous workup and purification by chromatography on silica gel (20% ether/pentane), enone **7** was obtained as a colorless oil (95.2 mg, 0.7 mmol, 88%).[22]

Received: May 7, 2004 [Z460578]
Published Online: July 7, 2004

Keywords: asymmetric catalysis · cyclization · enamines · Michael reactions · organocatalysis

 © 2004 Wiley-VCH Verlag GmbH & Co. KGaA, Weinheim

[1] For selected reviews, see: a) B. List, *Synlett* **2001**, 1675 – 1686; b) H. Gröger, J. Wilken, *Angew. Chem.* **2001**, *113*, 545 – 548; *Angew. Chem. Int. Ed.* **2001**, *40*, 529 – 532; c) P. I. Dalko, L. Moisan, *Angew. Chem.* **2001**, *113*, 3840 – 3864; *Angew. Chem. Int. Ed.* **2001**, *40*, 3726 – 3748; d) S. Borman, *Chem. Eng. News* **2002**, *80*(50), 35; e) E. R. Jarvo, S. J. Miller, *Tetrahedron* **2002**, *58*, 2481 – 2495; f) B. List, *Tetrahedron* **2002**, *58*, 5572 – 5590; g) M. Movassaghi, E. N. Jacobsen, *Science* **2002**, 298, 1904 – 1905; h) B. List, *Acc. Chem. Res.* **2004**, in press.

[2] a) B. List, R. A. Lerner, C. F. Barbas III, *J. Am. Chem. Soc.* **2000**, *122*, 2395 – 2396; b) W. Notz, B. List, *J. Am. Chem. Soc.* **2000**, *122*, 7386 – 7387; c) B. List, P. Pojarliev, C. Castello, *Org. Lett.* **2001**, *3*, 573 – 575.

[3] B. List, *J. Am. Chem. Soc.* **2000**, *122*, 9336 – 9337; b) B. List, P. Pojarliev, W. T. Biller, H. J. Martin, *J. Am. Chem. Soc.* **2002**, *124*, 827 – 833; c) P. Pojarliev, W. T. Biller, H. J. Martin, B. List, *Synlett* **2003**, 1903 – 1904.

[4] B. List, P. Pojarliev, H. J. Martin, *Org. Lett.* **2001**, *3*, 2423 – 2425.

[5] B. List, *J. Am. Chem. Soc.* **2002**, *124*, 5656 – 5657.

[6] C. Pidathala, L. Hoang, N. Vignola, B. List, *Angew. Chem.* **2003**, *115*, 2891 – 2894; *Angew. Chem. Int. Ed.* **2003**, *42*, 2785 – 2788.

[7] N. Vignola, B. List, *J. Am. Chem. Soc.* **2004**, *126*, 450 – 451.

[8] For important recent reviews, see: a) N. Krause, A. Hoffmann-Röder, *Synthesis* **2001**, 171 – 196; b) J. Christoffers in *Encyclopedia of Catalysis*, *Vol. 5* (Ed. I. Horvath), Wiley, New York, **2002**, pp. 99 – 118; c) J. Christoffers, A. Baro, *Angew. Chem.* **2003**, *115*, 1726 – 1728; *Angew. Chem. Int. Ed.* **2003**, *42*, 1688 – 1690.

[9] For non-asymmetric catalytic intramolecular Michael reactions of aldehydes via enamine intermediates, see, for example: a) S. D. Burke, C. W. Murtiashaw, J. O. Saunders, M. S. Dike, *J. Am. Chem. Soc.* **1982**, *104*, 872 – 874; b) H. Hagiwara, N. Komatsubara, H. Ono, T. Okabe, T. Hoshi, T. Suzuki, M. Ando, M. Kato, *J. Chem. Soc. Perkin Trans. 1* **2001**, 316 – 322; c) for an elegant cobalt-catalyzed Michael cycloreduction, see: T.-G. Baik, A. L. Luis, L.-C. Wang, M. J. Krische, *J. Am. Chem. Soc.* **2001**, *123*, 5112 – 5113; d) for the base-catalyzed intramolecular Michael reaction/aldol condensation of aldehydes in the synthesis of hydrindenones, see: G. Stork, C. S. Shiner, J. D. Winkler, *J. Am. Chem. Soc.* **1982**, *104*, 310 – 312.

[10] See, for example: a) B. L. Feringa, *Acc. Chem. Res.* **2000**, *33*, 346 – 353; b) M. T. Reetz, A. Gosberg, D. Moulin, *Tetrahedron Lett.* **2002**, *43*, 1189 – 1191; c) Y. Takaya, M. Ogasawara, T. Hayashi, *J. Am. Chem. Soc.* **1998**, *120*, 5579 – 5580; d) Y. S. Kim, S. Matsunaga, J. Das, A. Sekine, T. Ohshima, M. Shibasaki, *J. Am. Chem. Soc.* **2000**, *122*, 6506 – 6507.

[11] For a catalytic asymmetric Mukaiyama–Michael reaction, see: D. A. Evans, K. A. Scheidt, J. N. Johnston, M. C. Willis, *J. Am. Chem. Soc.* **2001**, *123*, 4480 – 4491.

[12] For selected Brønsted base catalyzed intermolecular asymmetric Michael reactions, see: a) K. Hermann, H. Wynberg, *J. Org. Chem.* **1979**, *44*, 2238 – 2244; b) T. Ishikawa, Y. Araki, T. Kumamoto, H. Seki, K. Fukuda, T. Isobe, *Chem. Commun.* **2001**, 245 – 246; for selected intermolecular asymmetric Michael reactions under phase-transfer catalysis, see: c) R. S. E. Conn, A. V. Lovell, S. Karady, L. M. Weinstock, *J. Org. Chem.* **1986**, *51*, 4710 – 4711; d) E. J. Corey, F.-Y. Zang, *Org. Lett.* **2000**, *2*, 4257 – 4259.

[13] For selected iminium catalytic intermolecular asymmetric Michael reactions, see: a) M. Yamaguchi, T. Shiraishi, M. Hirama, *J. Org. Chem.* **1996**, *61*, 3520; b) A. Kawara, T. Taguchi, *Tetrahedron Lett.* **1994**, *35*, 8805; c) S. Hanessian, V. Pham, *Org. Lett.* **2000**, *2*, 2975; d) N. A. Paras, D. W. C. MacMillan, *J. Am. Chem. Soc.* **2001**, *123*, 4370; e) N. A. Paras, D. W. C. MacMillan, *J. Am. Chem. Soc.* **2002**, *124*, 7894 – 7895; f) S. P. Brown, N. C. Goodwin, D. W. C. MacMillan, *J. Am. Chem. Soc.* **2003**, *125*, 1192 – 1194; g) N. Halland, R. G. Hazell, K. A. Jørgensen, *J. Org. Chem.* **2002**, *67*, 8331 – 8338; h) N. Halland, P. S. Aburel, K. A. Jørgensen, *Angew. Chem.* **2003**, *115*, 685 – 689; *Angew. Chem. Int. Ed.* **2003**, *42*, 661 – 665; i) N. Halland, T. Hansen, K. A. Jørgensen, *Angew. Chem.* **2003**, *115*, 5105 – 5107; *Angew. Chem. Int. Ed.* **2003**, *42*, 4955 – 4957; for enamine catalytic intermolecular asymmetric Michael reactions, see: reference [4]; j) J. M. Betancort, K. Sakthivel, R. Thayumanavan, C. F. Barbas III, *Tetrahedron Lett.* **2001**, *42*, 4441 – 4444; k) D. Enders, A. Seki, *Synlett* **2002**, 26 – 28; l) P. Melchiorre, K. A. Jørgensen, *J. Org. Chem.* **2003**, *68*, 4151 – 4157; m) O. Andrey, A. Alexakis, G. Bernardinelli, *Org. Lett.* **2003**, *5*, 2559 – 2561.

[14] a) A. P. Kozikowski, B. B. Mugrage, *J. Org. Chem.* **1989**, *54*, 2275 – 2277; b) Y. Hirai, T. Terada, T. Yamazaki, T. Momose, *J. Chem. Soc. Perkin Trans. 1* **1992**, 509 – 516; c) M. G. Banwell, D. A. S. Beck, J. A. Smith, *Org. Biomol. Chem.* **2004**, *2*, 157 – 159; for auxiliary-mediated asymmetric intramolecular Michael reactions, see, for example: d) D. A. Evans, M. T. Bilodeau, T. C. Somers, J. Clardy, D. Cherry, Y. Kato, *J. Org. Chem.* **1991**, *56*, 5750 – 5752; e) F. Dumas, J. d'Angelo, *Tetrahedron: Asymmetry* **1990**, *1*, 167.

[15] a) K. A. Ahrendt, C. J. Borts, D. W. C. MacMillan, *J. Am. Chem. Soc.* **2000**, *122*, 4243 – 4244; b) J. F. Austin, D. W. C. MacMillan, *J. Am. Chem. Soc.* **2002**, *124*, 1172 – 1173.

[16] During the preparation of this manuscript, MacMillan and co-workers disclosed an enamine-catalytic α-chlorination reaction of aldehydes with catalyst **5**: M. P. Brochu, S. P. Brown, D. W. C. MacMillan, *J. Am. Chem. Soc.* **2004**, *126*, 4108 – 4109.

[17] Other Michael acceptors were either unreactive ($X = CH_2$, $EWG = CO_2Et$ or COSEt [Eq. (3)]) or less stereoselective ($EWG = NO_2$, 96% yield, *anti*/*syn* = 26:1, 51% *ee*.)

[18] S. W. Baldwin, H. R. Blomquist, Jr., *J. Am. Chem. Soc.* **1982**, *104*, 4990 – 4992.

[19] S. L. Schreiber, H. V. Meyers, K. B. Wiberg, *J. Am. Chem. Soc.* **1986**, *108*, 8274 – 8277.

[20] K. Juhl, K. A. Jørgensen, *Angew. Chem.* **2003**, *115*, 1498 – 1501; *Angew. Chem. Int. Ed.* **2003**, *42*, 1536 – 1539.

[21] J. H. Hutchinson, T. Money, *Can. J. Chem.* **1987**, *65*, 1 – 6.

[22] The absolute and relative configuration of enone **7** was determined after hydrogenation to the known saturated derivative; see: A. R. Krawczyk, J. B. Jones, *J. Org. Chem.* **1989**, *54*, 1795 – 1801.

 © 2004 Wiley-VCH Verlag GmbH & Co. KGaA, Weinheim

Peptide Structures

Left-Handed Helical Twists in "Mixed β-Peptides" Derived From Alternating C-Linked Carbo-β^3-Amino Acids and β-hGly Units**

*Gangavaram V. M. Sharma,**
Kondreddi Ravinder Reddy, Palakodety Radha Krishna, Ampapathi Ravi Sankar, Pagadala Jayaprakash, Bulusu Jagannadh, and Ajit C. Kunwar**

Synthetic oligomers of β-amino acids, that is, β-peptides,[1] are amongst the most studied class of molecules in foldamer chemistry. Changes in their substitution pattern generate a variety of interesting structural features in these molecules,[2–5] which have thus begun to prove immensely useful in bioactive peptide mimicry.[6] Amongst the various peptide secondary structures, mixed helices are unique to β-peptides. These structures contain intertwined 12 and 10-membered H-bonded rings and are unprecedented in α-proteins. Seebach et al.[4a] were the first to demonstrate the existence of right-handed 12/10 mixed helical structures in β-peptides with alternating β^2 and β^3 residues. Kessler and co-workers[4b] have reported such structures in mixed peptides containing constrained f-sugar amino acid and β-hGly repeats. We recently reported[7] the formation of both 10/12 and 12/10 right-handed helices by β-peptides derived from C-linked carbo-β^3-amino acids (Caa) with "alternating chirality." Although a variety of helical structures have been discovered in β-peptides, no reports have been published in this active area of research that describe left-handed mixed helices. Several natural proteins[8] have been found to contain small fragments of left-handed helices, most of which occur in or near an active or binding site and are thus likely to be of functional importance. Herein, we report the design, synthesis, and structural study of "mixed β-peptides" with right-handed and novel left-handed mixed (10/12 and 12/10) helical structures. These peptides are derived from alternating epimeric C-linked carbo-β^3-amino acids[9] (**1** or **2**; Scheme 1) and β-hGly units.

Our previous study revealed that Caa **1** occupies an energetically unfavorable position in the carbo-β-peptides **3** and **4**,[7] although robust mixed helical structures were formed by these peptides. We envisaged a new design intended to provide more conformational freedom and relieve steric strain[10,11] through the inclusion of alternating Caa (**1** or **2**) and β-hGly residues. Mixed β-peptides **5**–**12** (**5**/**6** and **7**/**8** with Caa **2** and **1** at the N terminus, respectively; **9**/**10** and **11**/**12** with β-hGly at the N terminus) were prepared by conventional procedures (1-ethyl-3(3-dimethylaminopropyl)carbodiimide, 1-hydroxy-1*H*-benzotriazole) and differences in the conformational behavior of the various peptides were studied. We anticipated that Caas **1** and **2** would define the conformational behavior of β-hGly in **5**–**12** (Scheme 1).

Structural studies on these peptides were carried out by using NMR and CD spectroscopic techniques. The ^{1}H NMR spectra of **5** and **6** in $CDCl_3$ show well-resolved backbone proton signals, as well as low-field NH resonances (NH(2)-NH(3) for **5**; NH(2)-NH(5) for **6**), which indicate the involvement of these NH groups in H bonding. This bonding was further confirmed by solvent titration studies.[12] The coupling constants $^3J_{C\alpha H/C\beta H}$ of the peptides (>10 Hz or <5 Hz) clearly demonstrate the predominance of a single conformation about the Cα–Cβ bond (single θ value), except in the N-terminal residue. The $^3J_{C\alpha H/C\beta H}$ values, along with various CαH/CβH and strong sequential NOE correlations (between the NH group of β-hGly or Caa **2** and the preceding $C\alpha H_{(pro\text{-}R)}$ or $C\alpha H_{(pro\text{-}S)}$ atom, respectively), confirm a θ value of around 60° for these peptides. The ROESY spectrum of **5** revealed the presence of long-range NOE correlations (CβH(1)/NH(3), $C\beta H(1)/C\alpha H_{(pro\text{-}R)}(3)$) unique to the signature of a 12-membered ring connected by an H bond involving *tert*-butoxycarbonyl (Boc)-CO and NH(3). A weak NH(2)/NH(3) NOE was observed, which supports the existence of a 10-membered ring with an H bond between NH(2) and CO(3), and confirms that **5** has a right-handed 12/10 helical structure. Similarly, the strong long-range backbone NOE interactions CβH(1)/NH(3), $C\beta H(1)/C\alpha H_{(pro\text{-}R)}(3)$, CβH(3)/NH(5), and $C\beta H(3)/C\alpha H_{(pro\text{-}R)}(5)$, and weak NH(2)/NH(3) and NH(4)/NH(5) NOE correlations observed in the ROSEY spectrum of **6** (Figure 1 A) provide ample evidence of a propagated right-handed 12/10/12/10 helical structure for this peptide. The coupling constants of both **5** and **6** ($^3J_{NH/C\beta H} > 8.9$ Hz for Caa **2**, $^3J_{NH/C\beta H} > 8.9$ Hz and < 3.3 Hz for β-hGly except in the C-terminal residue) correspond to $|\phi| \approx 100°$, which is consistent with a mixed helical structure. The first Caa residue has a $^3J_{C\beta H/C4H}$ value of 6.8 Hz, which indicates averaging of the conformation about CβH–Cβ–C4–C4H (χ^1). The other Caa residues have coupling constants $^3J_{C\beta H/C4H} > 9.5$ Hz; this value implies the preponderance of a structure with $\chi^1 \approx 180°$. The presence of several conforma-

[*] Dr. G. V. M. Sharma, K. R. Reddy, P. R. Krishna
D-211, Discovery Laboratory
Organic Chemistry Division III
Indian Institute of Chemical Technology
Hyderabad 500 007 (India)
Fax: (+91) 40-2716-0387 or 2716-0757
E-mail: esmvee@iict.res.in

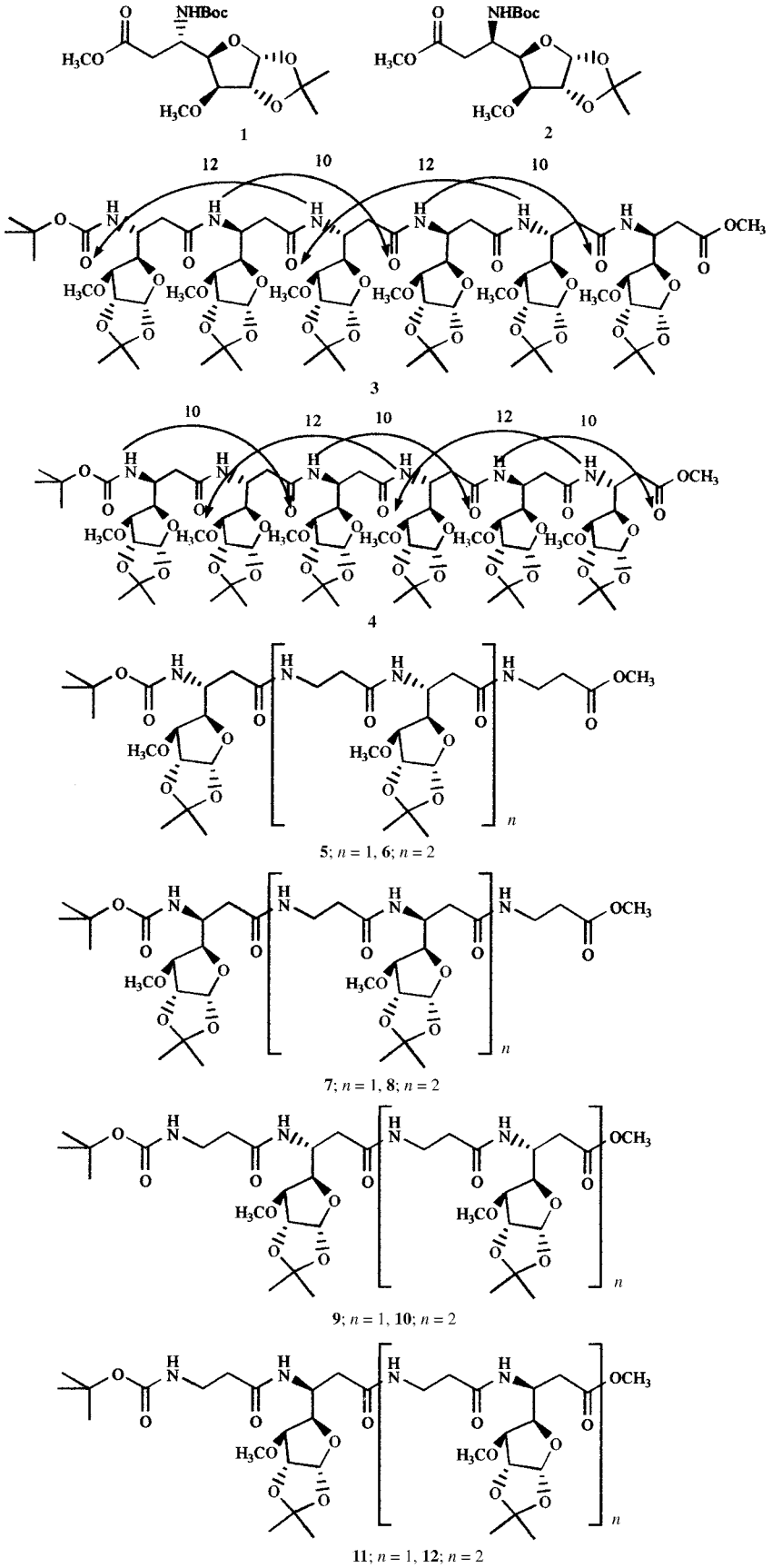
P. Jayaprakash, Dr. B. Jagannadh
Molecular Modelling Unit
Indian Institute of Chemical Technology
Hyderabad 500 007 (India)
Fax: (+91) 40-2716-0512
E-mail: jagan@iict.res.in

A. R. Sankar, Dr. A. C. Kunwar
Centre for Nuclear Magnetic Resonance
Indian Institute of Chemical Technology
Hyderabad 500 007 (India)
Fax: (+91) 40-2719-3108
E-mail: kunwar@iict.res.in

[**] Indian Institute of Chemical Technology Communication No. 031115. K.R.R. and A.R.S. are thankful to the Council of Scientific and Industrial Research, New Delhi, for financial support.

Supporting information for this article (details of NMR experiments, solvent titration plots, and the distance constraints used in MD calculations) is available on the WWW under http://www.angewandte.org or from the author.

 DOI: 10.1002/anie.200353467 © 2004 Wiley-VCH Verlag GmbH & Co. KGaA, Weinheim



Scheme 1. Structures of monomers **1** and **2**, carbo-β-peptides **3** and **4** (with H bonding indicated by arrows), and mixed β-peptides **5**–**12**.

tions as a result of fraying at the C-terminal residue is reflected by an averaging of the coupling constants.

The CD spectra (Figure 2) of **5** and **6** in methanol (0.1 mM), have maxima at about 203 nM,[4a] which is a very similar value to that observed for **3**[7] and corresponds to the signature of a mixed helical conformation. In spite of the insertion of β-hGly[10] and the resulting increase in conformational freedom, mixed helices were the intrinsically favored structures of **5** and **6**. In both peptides, the amide group of Caa **2** participates in an H bond connecting a 12-membered ring, whilst that of the β-hGly residue is effectively induced to participate in an H bond in a 10-membered ring; the result is a robust right-handed 12/10 helix.

^{1}H NMR and CD studies on **7** and **8** gave interesting results. The appearance of NH(2) and NH(3) signals at $\delta > 7$ ppm in the NMR spectrum of **7**, as well as the presence of weak NOE correlations (for example, CβH(1)/NH(3) and CβH(1)/CαH$_{(pro\text{-}S)}$(3)), suggests that the NH(3) proton of **7** participates in an H bond that results in formation of a 12-membered ring and indicates the nucleation of a structure. Definitive information about this structure could not be obtained because of averaging of the coupling constants owing to several conformations. In contrast, peptide **8** has a well-defined structure. The observation of low-field amide δ values and the results of solvent titration studies[12] confirmed that H bonding occurs from NH(2) to NH(5) in **8**. The $^3J_{C\alpha H/C\beta H}$ values (> 10 Hz or < 5 Hz) for residues (1)–(5) indicate the predominance of a single conformer (single θ value). The presence of CβH(1)/NH(3), CβH(1)/CαH$_{(pro\text{-}S)}$(3), CβH(3)/NH(5), and CβH(3)/CαH$_{(pro\text{-}S)}$(5) NOE correlations (Figure 1B) suggests the existence of 12-membered rings involving H bonds from NH(3) to CO(Boc) and NH(5) to CO(2), whilst weak NH(2)/NH(3) and NH(4)/NH(5) NOE correlations indicate the presence of 10-membered rings with H bonds from NH(2) to CO(3) and NH(4) to CO(5). These results imply a 12/10/12/10 helical structure for **8**. In contrast to the situation in previously studied peptides,[7] the amide protons of the Caa **1** residues in **8** participate in H bonds to form 12-membered instead of 10-membered rings. Moreover, NOE interactions CβH(i) and CαH$_{(pro\text{-}S)}$($i+2$) ($i = 1$ and 3) were detected for **8**. These NOE correlations verify the existence of a 12-membered ring but differ from those observed for right-handed mixed helices, which show CβH(i)/CαH$_{(pro\text{-}R)}$($i+2$) NOE correlations. The strong sequential NOE correlations observed for **8** between the NH proton of the β-hGly residue and the preceding CαH$_{(pro\text{-}S)}$ proton, and between the NH group of Caa **1** and the preceding

 © 2004 Wiley-VCH Verlag GmbH & Co. KGaA, Weinheim

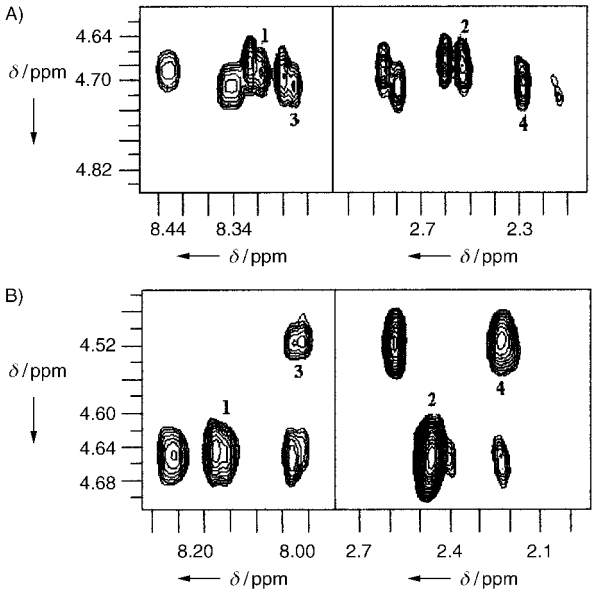


Figure 1. A) ROESY spectrum of **6**. The NOE correlations CβH(3)/NH(5), CβH(3)/CαH$_{(pro\text{-}R)}$(5), CβH(1)/NH(3), and CβH(1)/CαH$_{(pro\text{-}R)}$(3) are marked 1, 2, 3, and 4, respectively. B) ROESY spectrum of **8**. The NOE correlations CβH(3)/NH(5), CβH(3)/CαH$_{(pro\text{-}S)}$(5), CβH(1)/NH(3), and CβH(1)/CαH$_{(pro\text{-}S)}$(3) are marked 1, 2, 3, and 4, respectively.

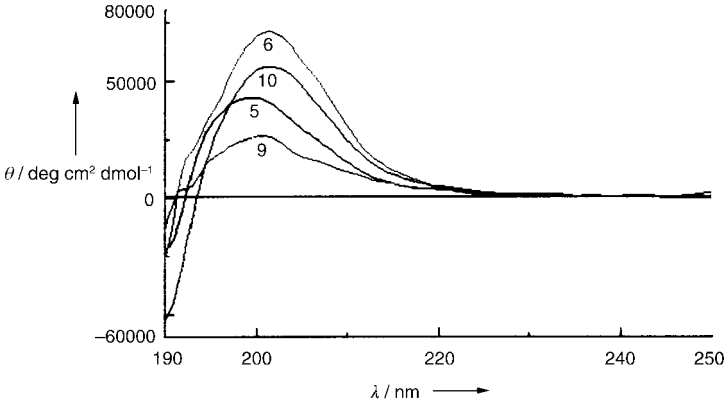


Figure 2. CD spectra of **5**, **6**, **9**, and **10**.

CαH$_{(pro\text{-}R)}$ proton are in agreement with the well-defined $^3J_{C\alpha/C\beta H}$ values recorded and imply a predominant conformation with $\theta \approx -60°$ for all these residues. Comparison of this result with the θ value of around $+60°$ determined for peptides **3**–**6** unequivocally demonstrates the occurrence of a "switch" in the sense of the helical twist in **8** relative to that in **3**–**6**. This twist leads to the formation of an unprecedented left-handed 12/10/12/10 helix. The $^3J_{NH/C\beta H}$ values ($^3J_{NH/C\beta H} >$ 9.6 Hz for Caa **1**; $^3J_{NH\text{-}C\beta H} > 9.0$ Hz and < 2.1 Hz for β-hGly) of **8** correspond to $|\phi| \approx 100°$, which is consistent with a mixed helical structure. A $^3J_{C\beta H/C4H}$ value of 6.4 Hz for the first Caa residue indicated an averaging about χ^1. The other Caa residues had large coupling constants, $^3J_{C\beta H/C4H} \approx 9$ Hz, which implies the preponderance of a structure with $\chi^1 \approx 180°$. The left-handed helical twist in **8** was further confirmed by the CD spectrum of the peptide. A minimum was observed at 205 nm (Figure 3) and the molar ellipticity of about -12000 deg cm^2 dmol^{-1} per residue is lower than the values recorded for **5** and **6**.

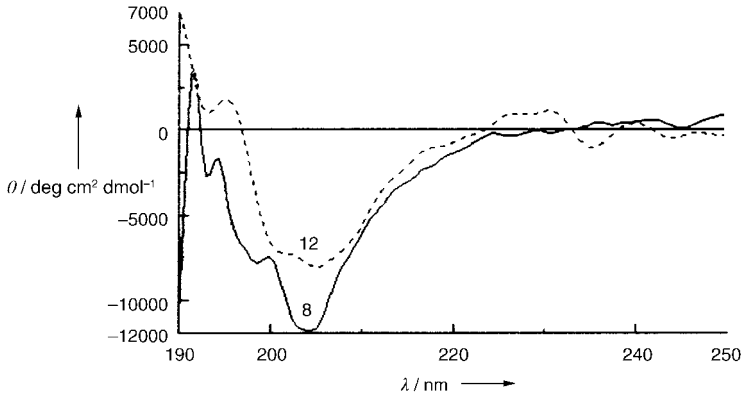


Figure 3. CD spectra of **8** and **12**.

The switch in handedness observed in **8** can be rationalized by applying energy considerations, as shown by the Newman projections about Cα–Cβ presented in Figure 4. An *anti*-periplanar arrangement of the amide carbonyl group and the sugar moiety ($\theta = 60°$) in Caa **2** (Figure 4a) is energetically favored and leads to a right-handed helix. Under similar conditions, the amide carbonyl group and sugar moiety of "epimeric" Caa **1** are in an energetically less favored (−) *syn*-clinical arrangement, as indicated in Figure 4b. However, Figure 4c shows that these groups adopt a favorable *anti*-periplanar low-energy conformation in a left-handed helical structure with $\theta = -60°$. The results of theoretical studies[10,11] are consistent with these observations. The structure depicted in Figure 4b leads to a sterically less favored axial arrangement of the Cβ–Cγ bond connecting the sugar moiety to the backbone in **1**, whereas the left-handed helical structure in Figure 4c places the Cβ–Cγ bond in a more favorable lateral arrangement with respect to the helix axis.

The study described above revealed the helical structures of mixed β-peptides **5**–**8** and clearly shows that β-hGly participates in an H bond to form a 10-membered ring under the influence of Caas **1** and **2**. By analogy, we expected the mixed β-peptides **9**–**12**, in which N-terminal β-hGly units alternate with **2** or **1**, to generate right and left-handed 10/12 helices, respectively.

The results of studies on **9** and **10** were found to be in agreement with results we reported previously for 10/12 helices.[7] Low-field amide proton resonances (NH(1), NH(3), NH(4)) and solvent titration studies[12] confirmed the presence of H bonds in **9**. The specific NOE values showed the predominance of a single conformation with $\theta \approx 60°$ for all the β-hGly and Caa **1** residues. The CβH(2)/NH(4) and CβH(2)/CαH$_{(pro\text{-}R)}$(4) NOE correlations and weak NH(1)/NH(2) and NH(3)/NH(4) NOE correlations present in the

 © 2004 Wiley-VCH Verlag GmbH & Co. KGaA, Weinheim

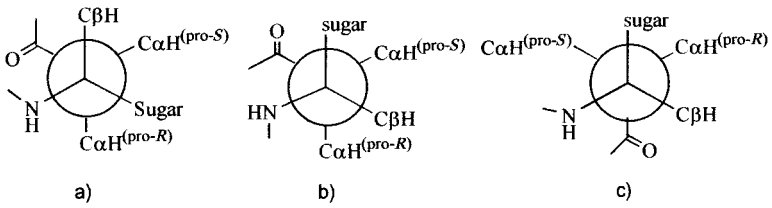


Figure 4. Newman projections about three bond axes illustrating the stereochemistries of **1** and **2** in left-handed and right-handed mixed helical arrangements.

ROESY spectrum of **9** form the distinctive signature of a right-handed 10/12/10 helix. Similarly, all the amide protons in hexapeptide **10**, except those in the second residue, participate in H bonding. Characteristic NOE correlations and coupling constants indicated an extended right-handed 10/12/10/12/10 helix conformation for **10**.

The structure of **11** could not be determined conclusively because the NOE correlations are too weak, but the signatures of helix nucleation were observed. The appearance of five amide proton signals (not NH(2)) at low field in the spectrum of **12**, along with the results of solvent titration studies,[12] confirmed the participation of these protons in H bonding. The $^{3}J_{C\alpha H/C\beta H}$ values (>10 Hz or <5 Hz) for residues (2)–(6) and the presence of strong characteristic sequential NOEs similar to those observed for **8** indicated a θ value of around $-60°$ and a single predominant conformation for all the residues. Distinctive backbone NOEs (CβH(2)/NH(4), CβH(2)/C$\alpha H_{(pro\text{-}S)}$(4), CβH(4)/NH(6), CβH(4)/C$\alpha H_{(pro\text{-}S)}$(6); weak signals: NH(1)/NH(2), NH(3)/NH(4), and NH(5)/NH(6)) confirmed an unprecedented left-handed 10/12/10/12/10 helix conformation for **12**. The CD spectra of **9**, **10** (Figure 2), and **12** (Figure 3) confirm the above-mentioned results. The incorporation of β-hGly at the N terminus resulted in the successful synthesis of peptides **9**/**10** and **12** with right and left-handed 10/12 helical structures, respectively.

NOE-restrained[13] molecular dynamics (MD) calculations for **5**, **6**, **8**–**10**, and **12** gave results that are in agreement with the structures discussed above. A large number of long-range NOE constraints were derived from the volume integrals of the ROESY spectra by using the two-spin approximation and these values were used quantitatively. Figure 5 depicts a superposition of the 10 lowest-energy structures calculated for **6** and **8**, which have right and left-handed helical structures, respectively. The backbone is well-defined, especially for the middle residues, and there is fraying at the C terminus. The calculations converge well; the maximum violations are 0.32 and 0.31 Å for **6** and **8**, and the average pair-wise heavy-atom and backbone root-mean-square deviations are 0.48 and 0.46 Å for **6** and 0.46 and 0.30 Å for **8**.

In conclusion, we have shown that the "chirality" of "epimeric" Caas **1** and **2** residues in mixed β-peptides derived from alternating β-Caa and β-hGly units induces β-hGly to participate in H bonding, which results in novel helices. In addition, the β-hGly residues provided the requisite conformational freedom for a facile "switch" in handedness leading to the formation of unprecedented left-handed 10/12 and 12/10 helices. The design and synthesis of peptides that form left-handed helices provides an opportunity to understand the active role of these secondary structures in biological functions and to create novel tertiary structures with far-reaching implications for peptide chemistry. Efficient "design control" leading to the successful formation of left and right-handed mixed helices should open up new routes towards the development of artificial tertiary structures through incorporation of the various above-mentioned secondary structural elements into new complex structures with useful functions.



Figure 5. MD structures. A) Side view of **6**; B) side view of **8**. Hydrogen atoms are omitted and sugar moieties are replaced by methyl groups after calculations.

Received: December 5, 2003
Revised: April 20, 2004 [Z53467]

Keywords: β-peptides · amino acids · helical structures · hydrogen bonds · peptides

[1] a) D. Seebach, J. L. Matthews, *Chem. Commun.* **1997**, 2015–2022; b) S. H. Gellman, *Acc. Chem. Res.* **1998**, *31*, 173–180; c) K. Gademann, T. Hintermann, J. V. Schreiber, *Curr. Med. Chem.* **1999**, *6*, 905–925; d) W. F. DeGrado, J. P. Schneider, Y. Hamuro, *J. Pept. Res.* **1999**, *54*, 206–217; e) R. P. Cheng, S. H. Gellman, W. F. DeGrado, *Chem. Rev.* **2001**, *101*, 3219–3232.

[2] a) D. Seebach, M. Overhand, F. N. M. Kuhnle, B. Martinoni, L. Oberer, U. Hommel, H. Widmer, *Helv. Chim. Acta* **1996**, *79*, 913–941; b) D. H. Appella, L. A. Christianson, I. L. Karle, D. R. Powell, S. H. Gellman, *J. Am. Chem. Soc.* **1996**, *118*, 13071–13072.

[3] D. H. Appella, L. A. Christianson, D. A. Klein, D. R. Powell, X. Huang, J. J. Barchi, Jr., S. H. Gellman, *Nature* **1997**, *387*, 381–384.

[4] a) D. Seebach, K. Gademann, J. V. Schreiber, J. L. Matthews, T. Hintermann, B. Jaun, L. Oberer, U. Hommel, H. Widmer, *Helv. Chim. Acta* **1997**, *80*, 2033–2038; b) S. A. W. Gruner, V. Truffault, G. Voll, E. Locardi, M. Stockle, H. Kessler, *Chem. Eur. J.* **2002**, *8*, 4366–4376.

[5] a) T. D. W. Claridge, J. M. Goodman, A. Moreno, D. Angus, S. F. Barker, C. Taillefumier, M. P. Watterson, G. W. J. Fleet, *Tetrahedron Lett.* **2001**, *42*, 4251–4255; b) K. Gademann, A. Hane,

 © 2004 Wiley-VCH Verlag GmbH & Co. KGaA, Weinheim

M. Rueping, B. Jaun, D. Seebach, *Angew. Chem.* **2003**, *115*, 1573 – 1575; *Angew. Chem. Int. Ed.* **2003**, *42*, 1534 – 1537.
[6] J. A. Patch, A. E. Barron, *Curr. Opin. Chem. Biol.* **2002**, *6*, 872 – 877.
[7] G. V. M. Sharma, K. Ravinder Reddy, P. Radha Krishna, A. Ravi Sankar, K. Narsimulu, S. Kiran Kumar, P. Jayaprakash, B. Jagannadh, A. C. Kunwar, *J. Am. Chem. Soc.* **2003**, *125*, 13670 – 13671.
[8] a) A. A. Adzhubei, M. J. E. Sternberg, *J. Mol. Biol.* **1993**, *229*, 472 – 493; b) P. K. Vlasov, G. T. Kilosanidze, D. L. Ukrainskii, A. V. Kuzmin, V. G. Tumanyan, N. G. Esipova, *Biophysics*, **2001**, *3*, 546 – 550; c) F. Jourdan, S. Lazzaroni, B. L. Mendez, P. Lo Cantore, M. de Julio, P. Amodeo, N. S. Iacobellis, A. Evidente, A. Motta, *Proteins* **2003**, *52*, 534 – 543.
[9] G. V. M. Sharma, V. Goverdhan Reddy, A. Subhash Chander, K. Ravinder Reddy, *Tetrahedron: Asymmetry* **2002**, *13*, 21 – 24.
[10] D. Seebach, P. E. Ciceri, M. Overhand, B. Jaun, D. Rigo, L. Oberer, U. Hommel, R. Amstutz, H. Widmer, *Helv. Chim. Acta* **1996**, *79*, 2043 – 2066.
[11] a) Y.-D. Wu, D.-P. Wang, *J. Am. Chem. Soc.* **1999**, *121*, 9352 – 9362; b) Y.-D. Wu, J.-Q. Lin, Y.-L. Zhao, *Helv. Chim. Acta* **2002**, *85*, 3144 – 3160; c) R. Gunther, H.-J. Hoffman, K. Kuczera, *J. Phys. Chem. B* **2001**, *105*, 5559 – 5567.
[12] Solvent titration was carried out by adding [D_6]dimethylsulfoxide (DMSO) stepwise to $CDCl_3$ solutions of the peptides to give a final [D_6]DMSO level of 33%.
[13] For details, see the Supporting Information.

 © 2004 Wiley-VCH Verlag GmbH & Co. KGaA, Weinheim

DNA–Dye Conjugates

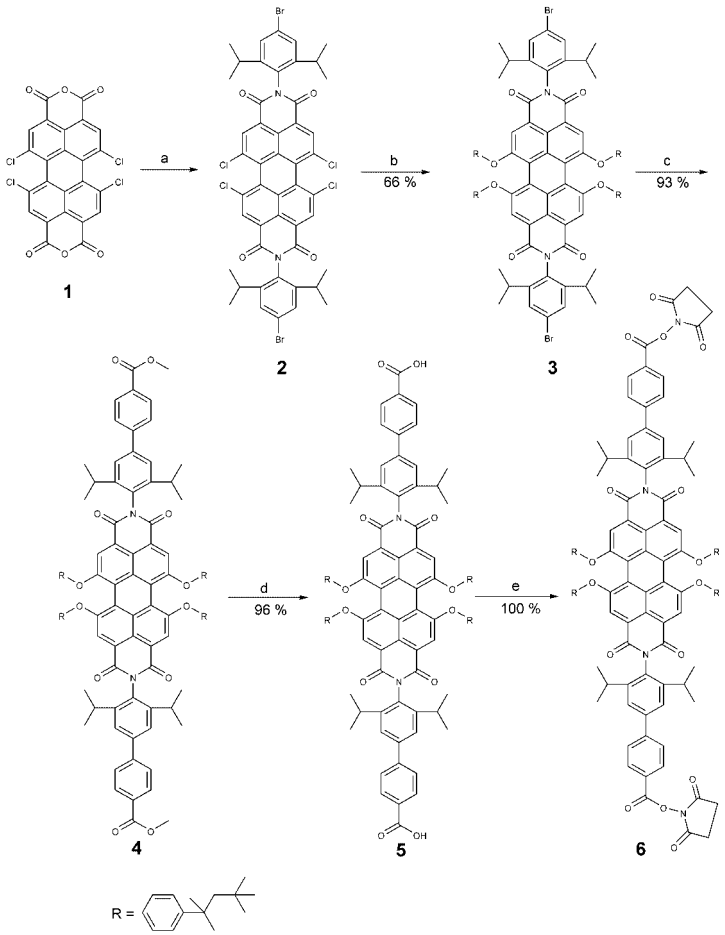
Synthesis and Self-Assembly of Perylenediimide–Oligonucleotide Conjugates**

Moustafa A. Abdalla, Johannes Bayer, Joachim O. Rädler, and Klaus Müllen**

In recent years the oligonucleotide-directed assembly of nanoscale objects like gold particles,[1] carbon nanotubes,[2] and DNA-based structures[3] has attracted much attention. Oligodeoxyribonucleotide (ODN) modified organic compounds such as ODN–cyclobutadiene[4] and trisoligonucleotidyls[5] have been synthesized and their self-assembly studied. Conjugates of ODN and dyes are particularly challenging in view of recent progress in single-molecule spectroscopy (SMS).[6] Fluorescence resonance energy transfer between donor and acceptor chromophores linked by a short DNA molecule has been investigated by SMS.[7] In this type of research it is important to arrange organic chromophores into supramolecular structures and to be able to direct and immobilize these to specific points of interest on solid devices.[8]

Here we report on the solution-phase synthesis and characterization of perylenediimide–bis(oligonucleotide) (PON) conjugates consisting of a chromophore unit covalently linked at the imide ends of the perylenediimide to single-stranded (ss) ODNs composed of 16 bases (see Scheme 1 and Figure 1). Perylenediimides are known to be excellent fluorescent dyes because of their high photostability, chemical resistance, and high fluorescence quantum yield.[8] The novel bioorganic conjugates are soluble in water and capable of hybridization with a complementary 16mer ss-ODN.

We demonstrate for the first time the reversible, DNA-directed conjugation of complementary PONs into linear chains of dyes. The physico-chemical properties of the linear dye–DNA polymers were characterized by fluorescence correlation spectroscopy (FCS), UV/Vis spectroscopy, and gel electrophoresis. The ODNs were synthesized by standard solid-phase chemistry using the phosphoramidite method on a polystyrene/divinylbenzene support. The resulting ODNs were purified by ion-exchange HPLC. Two ODNs were synthesized: ODN1 (5′-H_2N-$(CH_2)_6$-*p*-TAG TTG TGA TGT ACA T-3′) and the complementary ODN2 (5′-H_2N-$(CH_2)_6$-*p*-ATG TAC ATC ACA ACT A-3′). MALDI-TOF mass spectra of the compounds show single peaks that corresponds to the calculated molecular weights of the synthesized ODN1 (5106 g mol^{-1}) and ODN2 (5013 g mol^{-1}) sequences. The activitated carboxylic acid derivative **6** was synthesized according to Scheme 1 (for further details see the Supplementary Information).



Scheme 1. Reagents and conditions: a) 4-Bromo-2,6-diisopropylphenylamine, propionic acid, reflux, 20 h; b) 4-(1,1,3,3-tetramethylbutyl)phenol, K_2CO_3, *N*-methyl-2-pyrrolidinone (NMP) 90 °C, 12 h, 66 % yield; c) 4-methoxycarbonylphenylboronic acid, Pd cat., K_2CO_3, toluene, methanol, 75 °C, 15 h, 93 % yield; d) KOH, THF, 80 °C, 24 h, 96 % yield; e) *N*-hydroxysuccinimide, dicyclohexylcarbodiimide (DCC), DMF, RT, 48 h, 100 % yield.

Compound **6** was coupled to ODN1 and ODN2 in sodium tetraborate buffer (pH 8.5) to give PON1 and PON2, respectively (Figure 1). The PONs were purified by preparative polyacrylamide gel electrophoresis (PAGE) using TBE buffer (Tris-HCl, boric acid, ethylenediaminetetraacetate (EDTA), pH 8.3), then excised from the gel and extracted in water.

[*] J. Bayer, Prof. Dr. J. O. Rädler
Center for NanoScience, Sektion Physik
Ludwig-Maximilians-Universität München
Geschwister-Scholl-Platz 1, 80539 München (Germany)
Fax: (+49) 89-2180-3182
E-mail: joachim.raedler@physik.uni.muenchen.de
M. A. Abdalla, Prof. Dr. K. Müllen
Synthetic Chemistry Group
Max Planck Institute for Polymer Research
Ackermannweg 10, 55128 Mainz (Germany)
Fax: (+49) 6131-379-350
E-mail: muellen@mpip-mainz.mpg.de

[**] This research was supported by the European Research Foundation through the Bionics project (Eurocore) and the German National Science Foundation (DFG). We gratefully acknowledge financial support by the Bavarian States Ministry of Sciences, Research and the Arts within the program "Neue Werkstoffe". J.B. thanks the Bischöfliche Studienförderung Cusanuswerk for financial support.

Supporting information for this article is available on the WWW under http://www.angewandte.org or from the author.

 DOI: 10.1002/anie.200353621 © 2004 Wiley-VCH Verlag GmbH & Co. KGaA, Weinheim

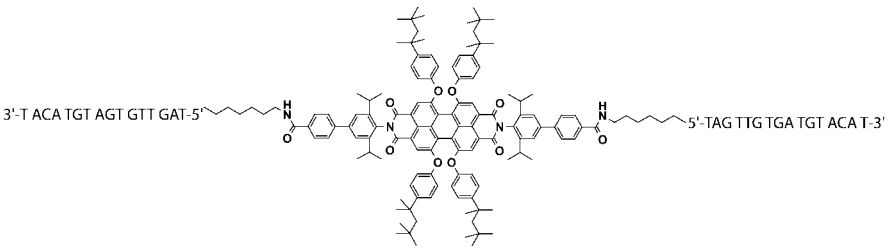


Figure 1. The perylenediimide–bis(oligonucleotide) conjugate PON1 consists of a chromophoric core flanked by two covalently linked oligonucleotides. This structure suggests PON1 may have amphiphilic character.

The fluorescence absorption and emission spectra of PON1 and PON2 in water and of compound **6** in THF indicate that they have maintained their chromophoric characteristics. Moreover, we observe a strong bathochromic shift of the absorption maximum of PON1 ($\lambda_{max} = 595$ nm) relative to that of perylene **6** to due to the functionalization of the PONs (Figure 2).

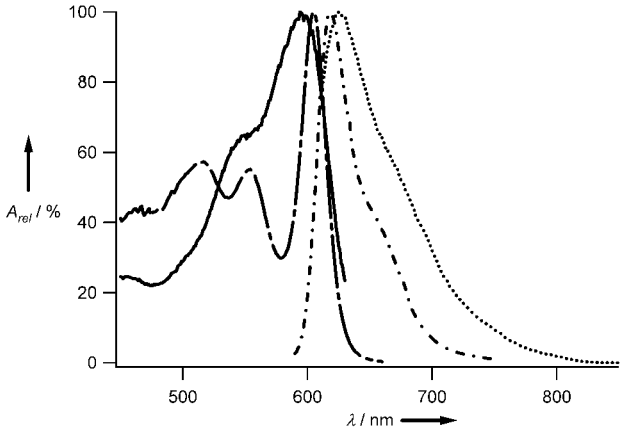


Figure 2. UV/Vis absorbance and fluorescence emission spectra ($\lambda_{ex} = 590$ nm) of PON1 and compound **6**. PON1 (in phosphate buffer, pH 7.0): UV/Vis ——, fluorescence •••••, compound **6** (in THF): UV/Vis —·—·, fluorescence –•–•.

Fluorescence correlation spectroscopy (FCS) was used to characterize the solubility and aggregation behavior of the PONs in water. In this analysis the fluorescence intensity fluctuations arising from the diffusion of chromophore molecules are examined in the small confocal volume (< 1 fl) of a laser (for more details on the FCS method, see the Supplementary Information).[9] The time autocorrelation functions of PON1 (≈ 1 μM) were measured in doubly distilled water (ddH_2O). Best fits show that the data is well described by the theoretical correlation function for diffusing monodisperse particles (the plot is shown in the Supplementary Information). We determined an average diffusion time τ_D of 41.4 ± 5.0 μs corresponding to a diffusion coefficient D_t of 257 ± 35 μm^2 s^{-1}. Assuming the PON1 to form spherical particles, one calculates a mean hydrodynamic radius of 0.85 ± 0.12 nm, which is well within the expected range for a monomeric species. Our data exhibit no indication for larger aggregates.

In order to transfer PON into *n*-decane, we used a mixture of cationic 1,2-dioleoyl-3-trimethylammoniumpropane (DOTAP) and neutral 1,2-dioleoyl-*sn*-glycero-3-phosphocholine (DOPC) lipids (m(DOPC)/[m(DOPC)+m(DOTAP)] = 0.86). The charge ratio of the PON phosphate groups and cationic lipids was chosen as 1:1. Lipids and PON1 were mixed in water before *n*-decane was added and shaken gently overnight. The transfer of PON1–lipid complexes from the polar phase into the nonpolar one was visible to the eye as the aqueous part became clear after mixing. The FCS time autocorrelation curves measured in *n*-decane correspond well to a one-component fit with an average diffusion time of 270 ± 29 μs (for the plot see the Supplementary Information). Theoretical calculations of diffusion coefficients for rodlike particles,[10] which approximate the PON1–lipid complex by a cylinder 18 nm in length and 6 nm in diameter (Figure 3) suggest a diffusion coefficient of 41.9 μm^2 s^{-1} in nonpolar solvents. This is consistent with the experimental mean diffusion coefficient of 39.0 ± 5.1 μm^2 s^{-1}.

A second method for transferring PON1 in *n*-decane was also studied. We dissolved the detergent in *n*-decane and then added it to the PON1 in aqueous solution. FCS measurements show no significant difference in the numbers of particles in the nonpolar phase in the various samples. Experiments performed on a Cy5-functionalized 30mer ss-ODN (Cy5-GCCGTCTCTGACTGCTGACTACTATCG) indicate a transfer efficiency of around 80% from water into *n*-decane.

Hybridization experiments were performed in different aqueous solutions: ddH_2O, TE buffer (10 mM Tris-HCl, 1 mM EDTA, pH 7.5), TE+0.1M NaCl, TE+0.8M NaCl, and 0.1M NaCl. PON1 and the complementary ODN2 were mixed with a molar ratio of 1:2 and a PON1 concentration in the μM range. UV-absorbance experiments at 260 nm show proof of hybridization in all buffer solutions but not for ddH_2O (data not shown). A more detailed view on the hybridization was obtained by temperature-dependent absorbance measurements in TE+60 mM NaCl. Immediately after PON1 and ODN2 were mixed, absorbance spectra were measured at 90°C as well as at 0°C. Comparing the spectrum at 0°C to the one at the higher temperature, we observe a strong decrease

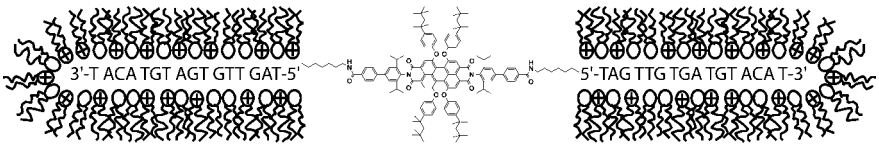


Figure 3. Schematic drawing of the PON1–lipid complex in *n*-decane; the lipid heads are oriented towards the hydrophilic ODN, whereas the tails are in contact with the nonpolar decane.

 © 2004 Wiley-VCH Verlag GmbH & Co. KGaA, Weinheim

and a small red-shift of the absorbance peak. The melting curve at 260 nm confirmed the results described above, indicating a single sharp transition which corresponds to a melting temperature of 45 °C.

As PON1 and PON2 are functionalized on both binding sides symmetrically with complementary ODNs, a mixture of these two PONs should hybridize into supramolecular chainlike structures. In order to prove this concept identical temperature-dependant experiments were executed using PON1 and the complementary PON2. The molar ratio was adjusted to 1:1. The results of the melting-curve experiments with the mixture of the PONS are similar to those with the PON/ODN mixture. The melting temperature is slightly shifted to 47 °C (Figure 4). Considering this result the perylenediimide core does not hinder hybridization of the attached ODNs.

PAGE was performed in order to distinguish between single hybridization of PONs and complementary ODNs (Figure 5a) on the one hand, and polymeric chain assembly between PON1 and PON2 (Figure 5b) on the other. The samples were dissolved in TE+60 mM NaCl, mixed, heated at 70 °C, and cooled slowly overnight to a final temperature of 4 °C. The products were then analyzed by gel electrophoresis. SYBR Gold was used as a marker for the direct visual detection of PON1–PON2 hybrids.

In comparison to samples consisting of PON and the same ODN (Ia, IVa), mixtures of PON and the complementary ODN with a molar ratio of 1:2 (IIa, IIIa) show clearly two additional bands of higher molecular weight and the disappearance of the ODN band (IIa, IIIa) and of the PON band (IIa). The new bands correspond to the mono- and dihybridzed PONs. The molar ratio of the PON to the complementary ODN influences the genesis of these hybridization products. When the PON:ODN ratio is changed from 1:2 (IIa, IIIa) to 1:1 (VIa, VIIIa), the band for the dihybridized band weakens in favor of that of the monohybridized.

In contrast, samples consisting of PON1 and PON2 show a clear ladder of higher molecular weight bands that can be attributed to polymeric chainlike structures of different lengths (IIIb–VIIb). The gel shows evidence for the genesis of PON dimers, trimers, tetramers, and pentamers. The highest band at around 800 bp might correspond to a ringlike structure. Chain formation is not evident when the PON is mixed with the complementary ODN. Changing the PON1:PON2 molar ratio does not significantly affect the tendency towards specific chain lengths, which is also due to the symmetric character of PON. When mixing both PONs with both ODNs one can observe bands corresponding to ODN1–ODN2 hybrids, PON, PON–ODN hybrids, and PON chains of different length (VIIIb). This suggests that the perylenediimide core does not hinder the hybridization properties of the attached ODNs. Further experiments

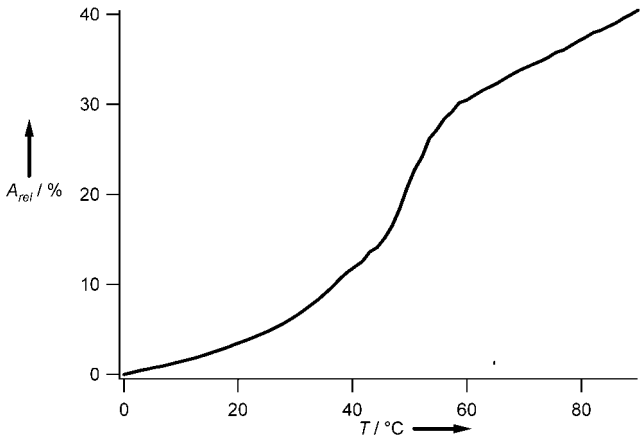


Figure 4. Melting curve of a 1:1 mixture of PON1 and PON2. The corresponding melting temperature is 47 °C.

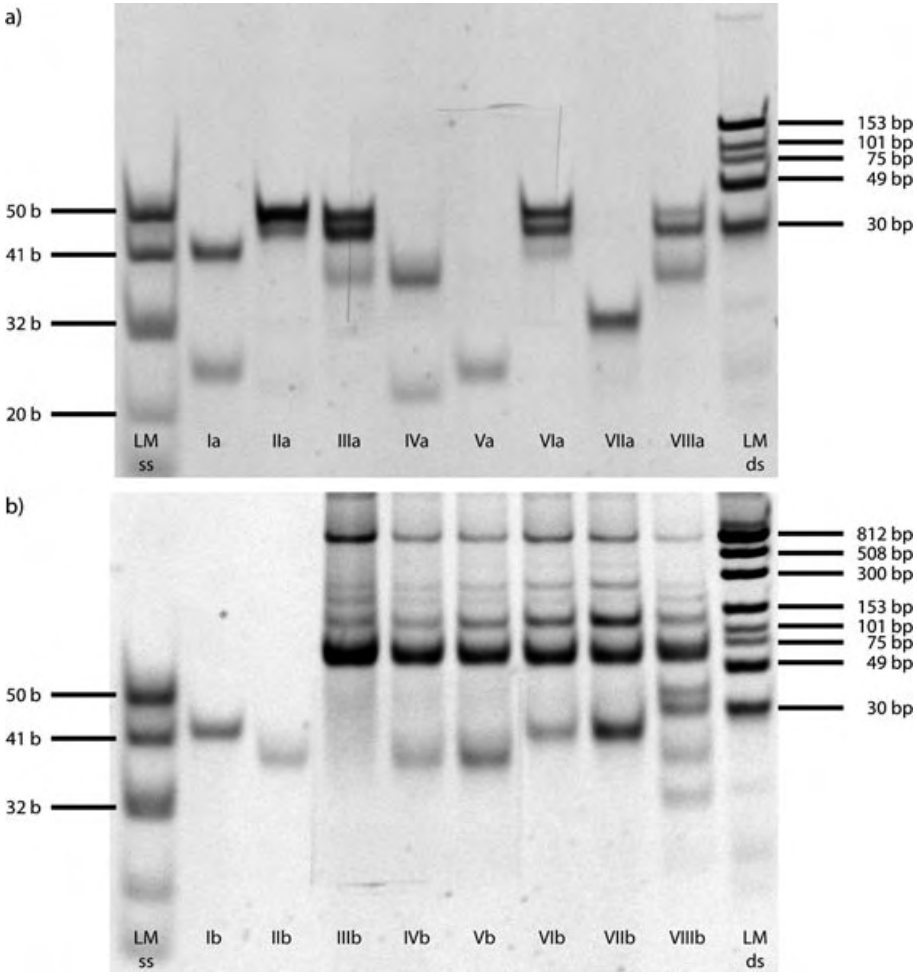


Figure 5. a) PAGE (TBE buffer, pH 8.3): lanes: Ia PON1/ODN1, IIa PON1/ODN2 (1:2), IIIa PON2/ODN1 (1:2), IVa PON2/ODN2, Va ODN1, VIa PON1/ODN2 (1:1), VIIa ODN1/ODN2 (1:1), VIIIa PON2/ODN1 (1:1). b) Polyacrylamide gel of PON1/PON2 hybrids: lanes: Ib PON1, IIb PON2, IIIb PON1/PON2 (1:1), IVb PON1/PON2 (1:2), Vb PON1/PON2 (1:3), VIb PON1/PON2 (2:1), VIIb PON1/PON2 (3:1), VIIIb PON1/PON2/ODN1/ODN2 (1:1:1:1).

 © 2004 Wiley-VCH Verlag GmbH & Co. KGaA, Weinheim

indicate that the chain assembly is not significantly influenced by ionic strength.

In conclusion, we have reported on the synthesis of a perylenediimide–bis(oligonucleotide) (PON) and demonstrated the DNA directed assembly of polyperylenediimides. We have used building blocks with two complementary sequences and formed structures of the type ABAB… . In principle, arbitrary sequences can be used as building blocks for such polymer structures, and site-specific positioning on solid surfaces may be achieved. This remarkable possibility and the fact that perylenediimide has very favorable, tailorable chromophoric properties may make PONs potential components in molecular electronic devices. The construction of supramolecular energy transfer systems in a rational bottom-up approach should be feasible. In this context, terrylenediimide, a higher linear homologue of perylenediimide, can be used as acceptor for energy transfer from perylenediimide.[11]

In the present work we have also demonstrated that the solubility of oligonucleotide-functionalized chromophores in organic solvents can be regained by using detergents, in particular cationic lipids. Hybridization of PONs was performed in aqueous phase and the product transferred into an organic solvent, which suggests further opportunities for combining DNA-based structures with non-water-soluble organic macromolecules.

Received: December 29, 2003
Revised: April 21, 2004 [Z53621]

Keywords: fluorescence spectroscopy · molecular recognition · nanostructures · perylenediimides · self-assembly

[1] a) C. A. Mirkin, R. L. Letsinger, R. C. Mucic, J. J. Storrhoff, *Nature* **1996**, *382*, 607 – 609; b) R. Elighanian, J. J. Storhoff, R. C. Mucic, R. L. Letsinger, C. A. Mirkin, *Science* **1997**, *277*, 1078 – 1081; c) J. J. Storhoff, R. Elighanian, R. C. Mucic, C. A. Mirkin, R. L. Letsinger, *J. Am. Chem. Soc.* **1998**, *120*, 1959 – 1964; d) R. C. Mucic, J. J. Storhoff, C. A. Mirkin, R. L. Letsinger, *J. Am. Chem. Soc.* **1998**, *120*, 12674 – 12675.

[2] K. A. Williams, P. T. M. Veenhuizen, B. G. de la Torre, R. Eritja, C. Dekker, *Nature* **2002**, *420*, 761.

[3] a) J. Chen, N. C. Seeman, *Nature* **1991**, *350*, 631 – 633; b) Y. Zhang, N. C. Seeman, *J. Am. Chem. Soc.* **1994**, *116*, 1661 – 1669; c) J. Shi, D. E. Linkers, *Angew. Chem.* **1997**, *109*, 70 – 72; *Angew. Chem. Int. Ed. Engl.* **1997**, *36*, 111 – 113; d) C. M. Niemeyer, B. Ceyhan, M. Noyong, U. Simon, *Biochem. Biophys. Res. Commun.* **2003**, *311*, 995 – 999; e) C. M. Niemeyer, M. Adler, S. Gao, L. F. Chi, *J. Biomol. Struct. Dyn.* **2002**, *20*, 223 – 230; f) C. M. Niemeyer, M. Adler, *Angew. Chem.* **2002**, *114*, 3933 – 3937; *Angew. Chem. Int. Ed.* **2002**, *41*, 3779 – 3783; g) C. M. Niemeyer, *Science* **2002**, *297*, 62 – 63.

[4] a) S. M. Waybright, C. P. Singleton, J. M. Tour, C. J. Murphy, U. H. F. Bunz, *Organometallics* **2000**, *19*, 368 – 370; b) S. M. Waybright, C. P. Singleton, K. Wachter, C. J. Murphy, U. H. F. Bunz, *J. Am. Chem. Soc.* **2001**, *123*, 1828 – 1833.

[5] a) M. Scheffler, A. Dorenbeck, S. Jordan, M. Wüstefeld, G. v. Kiedrowski, *Angew. Chem.* **1999**, *111*, 3514 – 3518; *Angew. Chem. Int. Ed.* **1999**, *38*, 3312 – 3315; b) L. H. Eckardt, K. Naumann, W. M. Pankau, M. Rein, M. Schweitzer, N. Windhab, G. v. Kiedrowski, *Nature* **2002**, *420*, 286 – 286; c) L. H. Eckardt, K. Nauman, W. M. Pankau, M. Reimold, M. Rein, G. v. Kiedrowski, *Pure Appl. Chem.* **2003**, *75*, 609 – 619.

[6] a) S. Weiss, *Science* **1999**, *283*, 1676 – 1683; b) L. Q. Li, L. M. Davis, *Appl. Opt.* **1995**, *34*, 3208 – 3217; c) S. Nie, R. N. Zare, *Annu. Rev. Biophys. Biomol. Struct.* **1997**, *26*, 567 – 596; d) J. Hofkens, T. Vosch, S. De Feyter, F. C. De Schryver, *Macromol. Symp.* **2002**, *178*, 1 – 10; e) G. Jung, J. Wiehler, B. Steipe, C. Bräuchle, A. Zumbusch, *ChemPhysChem* **2001**, *2*, 392 – 396.

[7] T. Ha, T. Enderle, D. F. Ogletree, D. S. Chemla, P. R. Selvin, S. Weiss, *Proc. Natl. Acad. Sci. USA* **1996**, *93*, 6264 – 6268.

[8] F. Würthner, C. Thalacker, A. Sautter, W. Schärtl, W. Ibach, O. Hollricher, *Chem. -Eur. J.* **2000**, *6*, 3871 – 3886.

[9] a) D. Magde, E. L. Elson, W. W. Webb, *Phys. Rev. Lett.* **1972**, *29*, 705 – 708; b) R. Rigler, U. Mets, J. Widengren, P. Kask, *Eur. Biophys. J.* **1993**, *22*, 169 – 175; c) O. Krichevsky, G. Bonnet, *Rep. Prog. Phys.* **2002**, *65*, 251 – 297; d) D. Magde, E. L. Elson, W. W. Webb, *Biopolymers* **1974**, *13*, 29 – 61.

[10] J. Garcia de la Torre, M. C. Lopez Martinez, M. M. Tirado, *Biopolymers* **1984**, *23*, 611 – 615.

[11] G. Schweitzer , R. Gronheid , S. Jordens, M. Lor, G. De Belder, T. Weil, E. Reuther, K. Müllen , F. C. De Schryver, *J. Phys. Chem. A* **2003**, *107*, 3199 – 3207.

 © 2004 Wiley-VCH Verlag GmbH & Co. KGaA, Weinheim

Bioinorganic Chemistry

Selenol Nitrosation and *Se*-Nitrososelenol Homolysis: A Reaction Path with Possible Biochemical Implications

Cathleen Wismach, Wolf-Walther du Mont, Peter G. Jones, Ludger Ernst, Ulrich Papke, Govindasamy Mugesh, Wolfgang Kaim, Matthias Wanner, and Klaus D. Becker*

Dedicated to Professor Reinhard Schmutzler on the occasion of his 70th birthday

The biological role of nitric oxide (NO) as a secondary messenger, for instance in the cardiovascular system, has been known for more than a decade. Nitrosation of the cysteine

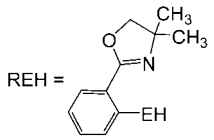
[*] Dipl.-Chem. C. Wismach, Prof. Dr. W.-W. du Mont, Prof. Dr. P. G. Jones, Prof. Dr. L. Ernst, Dr. U. Papke, Prof. Dr. K. D. Becker
Fachbereich Chemie und Pharmazie
Technische Universität Braunschweig
Postfach 3329, 38023 Braunschweig (Germany)
Fax: (+49) 531-391-5387
E-mail: w.du-mont@tu-bs.de
Prof. Dr. W. Kaim, Dr. M. Wanner
Institut für Anorganische Chemie der Universität Stuttgart
Pfaffenwaldring 55, 70569 Stuttgart (Germany)
Prof. Dr. G. Mugesh
Department of Inorganic & Physical Chemistry
Indian Institute of Science
Bangalore 560 012 (India)

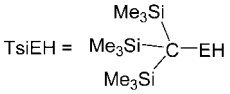
 © 2004 Wiley-VCH Verlag GmbH & Co. KGaA, Weinheim DOI: 10.1002/anie.200453872

residues of oxyhemoglobin leading to *S*-nitrosothiol functions (RSNO) supports the active transport of NO, which can be liberated enzymatically from RSNO. Accordingly, *S*-nitrosothiols are efficient vasodilators, as is NO, but also intrinsically toxic.[1–3] *Se*-nitrososelenols (RSeNO) are unknown; however, there may be factors common to the biological cycles of NO and those of selenoproteins.[4] For example, selenoproteins are efficient reagents for peroxynitrite reduction,[5] and *S*-nitrosothiols can be substrates of mammalian selenoenzymes such as GPx (glutathione peroxidases) and TrxR (thioredoxin reductases).[6–10] Whether the selenocysteine moieties (Sec) in the active centers of TrxR and GPx play a particular role in the course of the enzymatic NO liberation from *S*-nitrosothiols is still unknown. Wang et al. proposed recently that in course of the in vitro cleavage of *S*-nitrosoglutathione (GSNO), catalyzed by GPx or by bis(4-chlorophenyl)diselenide, selenols could play a crucial role.[10] In our opinion the key steps of this kind of catalysis may be selenol nitrosation with subsequent *Se*-nitrososelenol homolysis, a yet-unknown type of reaction in selenoprotein chemistry. To test this hypothesis, we studied model reactions for the nitrosation of various selenols and thiols.

Our intention was to generate *Se*-nitrososelenols that would be as stable as possible. This led us to choose selenols with organic substituents that had helped previously in stabilizing (typically labile) compounds with covalent selenium–iodine bonds: compounds that are designed for intramolecular coordination,[11,12] and compounds with extremely bulky alkyl substituents.[13,14]

A thiol designed for intramolecular coordination at the N atom of the heterocyclic ring, 2-(4,4-dimethyl-2-oxazolinyl)-phenylthiol (**1a**), reacted with *tert*-butylnitrite at temperatures above about −20 °C furnishing the red nitrosothiol **1b**, which was characterized in solution by NMR spectroscopy. At room temperature the compound decomposes forming NO and the parent disulfide **2c** [Eq. (1)]. The related selenol **2a**,





$$\mathrm{REH} + t\mathrm{BuON{=}O} \xrightarrow{-t\mathrm{BuOH}} \{\mathrm{REN{=}O}\} \rightarrow {}^{1}/_{2}\mathrm{R_2E_2} + \mathrm{NO} \quad (1)$$

E = S: **1a** **1b** **1c**

E = Se: **2a** **2b** **2c**

however, reacted immediately with *tert*-butylnitrite or with NOCl even at −78 °C furnishing deep-red solutions that become brownish within 1–2 h at −78 °C or within a few minutes at room temperature; this decomposition led to diselenide **2c.** It turns out that nitrosation products **3b** and **4b** carrying the extremely bulky trisyl substituents are significantly more stable than **1b** and **2b** [Eqs. (2) and (3), Tsi = $(Me_3Si)_3C$].

$$\underset{\mathbf{3a}}{\mathrm{TsiSH}} + t\mathrm{BuON{=}O} \xrightarrow{-t\mathrm{BuOH}} \underset{\mathbf{3b}}{\mathrm{TsiSN{=}O}} \quad (2)$$

$$\underset{\mathbf{4a}}{\mathrm{TsiSeH}} + t\mathrm{BuON{=}O} \xrightarrow{-t\mathrm{BuOH}} \underset{\mathbf{4b}}{\{\mathrm{TsiSeN{=}O}\}} \rightarrow {}^{1}/_{2}\underset{\mathbf{4c}}{\mathrm{Tsi_2Se_2}} + \mathrm{NO} + \underset{\mathbf{4d}}{\mathrm{Tsi_2Se_3}} \quad (3)$$

Selenol **4a** reacted with *tert*-butylnitrite immediately even at −78 °C.[15,16] The deep-red nitrosation product is persistent at −78 °C, and its IR spectrum displays the band (ν(N=O) = 1459 cm^{-1}) expected for the *Se*-nitrososelenol **4b**. The lithium derivative LiSeTsi was nitrosated in a similar way at −78 °C, and even $NaNO_2$ attacked selenol **4a** immediately giving a red solution (THF, 20 °C). Decomposition of the red reaction product at temperatures above −78 °C was followed by GC-MS (static headspace-MS), which confirmed release of of NO from the mixture.[16] During this decomposition ^{77}Se NMR signals could not be observed and ^{1}H NMR peaks appeared broadened, which can be explained by the presence of paramagnetic species in solution. EPR spectra recorded a few minutes after **4a** was mixed with *tert*-butylnitrite showed the intense signal of an apparently selenium-centered radical **5**.

The splitting pattern (Figure 1) can be simulated reasonably well if coupling to selenium ($a(^{77}\mathrm{Se}) = 30$ G) and to two nitrogen atoms ($a(^{14}\mathrm{N}) = 7.6$ G) is assumed.[16,17] The valency of selenium in **5** may be compared to that in $[C_6H_4N_2SeW(CO)_5]^{\bullet-}$,[18] the $\{W(CO)_5\}$ complex of the cyclic radical anion $C_6H_4N_2Se^{\bullet-}$ (Figure 2) After about 20 min at room temper-

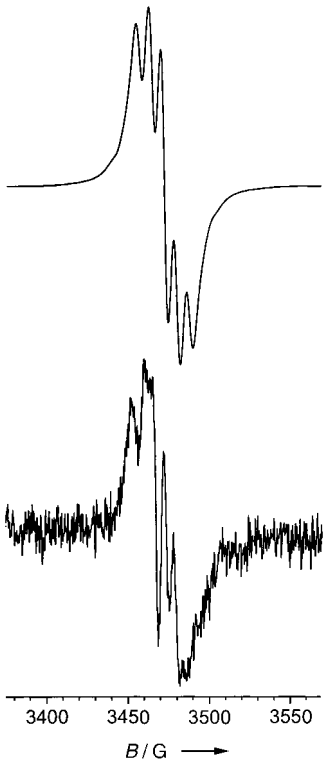
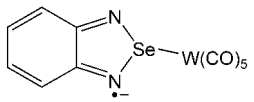


Figure 1. EPR spectra of species **5**; simulation (above) and experimental spectrum (below).

 © 2004 Wiley-VCH Verlag GmbH & Co. KGaA, Weinheim



ESR: $g = 2.005$
$a(N) = 6.4$ G (ref. [18a])

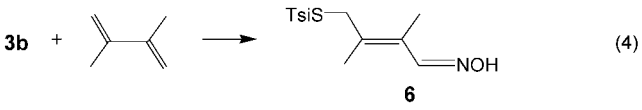
Figure 2. Structure and EPR data of a radical with N–Se–N connectivity.[18a]

ature the EPR signal of **5** vanished and a broad long-lived signal appeared consisting of a quintet (4H) of triplets (1N) and arising from a dialkylnitroxide $(RCH_2)_2NO^{\bullet}$ ($a(^{14}N) = 15.2$ G, $a(^{1}H) = 10.5$ G). For comparison, the values for diethylnitroxide are $a(^{14}N) = 16.7$ G and $a(^{1}H) = 11.2$ G.[18b] When isopentylnitrite was used in place of *tert*-butylnitrite, a similar secondary radical was observed. The final products from the nitrosation of **4a** are diselenide **4c**, the related triselenide **4d**, trisylmethane (TsiH), and small amounts of an insoluble solid that contains (according to elemental analysis) C, H, N, and Se.

In contrast to selenol **4a**, trisylthiol **3a** was not attacked by *tert*-butylnitrite or by isopentylnitrite at −78 °C. Nitrosation at 5–10 °C led to relatively stable *S*-nitrosothiol **3b** [Eq. (3)].

In a competition experiment selenol **4a** was found to be much more reactive towards *tert*-butylnitrite than thiol **3a** is. *tert*-Butylnitrite was added to an equimolar mixture of **3a**, **4a**, and diselenide **4c** (^{77}Se NMR signals of equal strength). The reaction mixture immediately turned an intense red, and ^{77}Se NMR signals could not be detected. Only after a while at room temperature were the ^{77}Se NMR resonances for diselenide **4c** and later for small amounts of **4d** detected. The typical decomposition products of **3b** were not detected. A control experiment showed that no reaction can be observed between *tert*-butylnitrite and pure diselenide **4c** (unchanged ^{77}Se NMR signal of **4c**).

These results suggest that formation of nitrososelenol **4b** is followed by homolytic cleavage of the Se–N bond. Formation of the unusual Se-centered radical **5** with the probable composition $TsiSe(NO)_2^{\bullet}$ can be understood as the reversible addition of released NO to the remaining nitrososelenol **4b** or as the addition of two NO molecules to a selenyl readical. Since attempts to isolate pure **4b** were unsuccessful, it was desirable to find a suitable trapping reaction characteristic for *Se*-nitrososelenols. Such a reaction is obviously the 1,4-addition to 2,3-dimethylbutadiene. The related nitrosothiol **3b** adds to 2,3-dimethylbutadiene with formation of an α,β-unsaturated oxime **6**, in which the

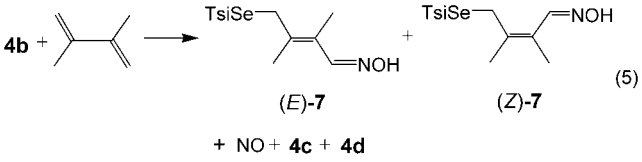


(4)

trisythio group is in the δ-position [Eq. (4)].

When Motherwell and co-workers carried out the related reaction with Ph_3CSNO, they isolated a mixture of *E*/*Z* isomers in which the *E* isomer was the major product.[19] In our work the NMR spectrum of **6** indicates that only one isomer is present, and the X-ray crystal structure determination confirms the *E* configuration (Figure 3).[20] Compound **6** crystallizes in the $P\bar{1}$ space group with two independent, but similar molecules (s-*trans* at C11-C12-C13-C14-N) that are connected by hydrogen bonds.

The very characteristic ^{13}C NMR resonance of the oxime function of **6** ($\delta = 149$ ppm) should be especially helpful for the detection of the related selenium compound **7**, even when only small amounts are present in reaction mixtures. Addition of excess dimethylbutadiene to red solutions from the nitrosation of **4a** led to reaction mixtures from which very small amounts of δ-selenooxime **7** were obtained [Eq. (5)]. The



(5)

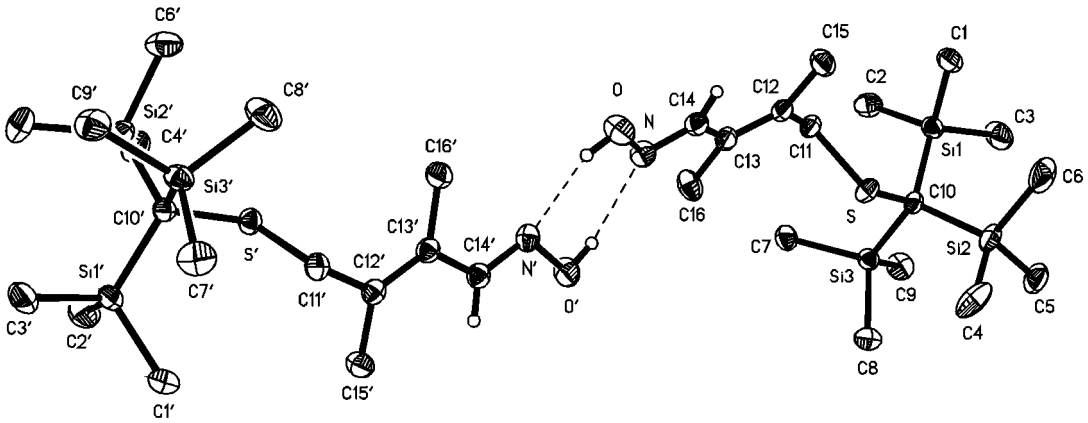


Figure 3. X-ray crystal structure of **6**. Selected distances [Å] and angles [°] (values of both independent molecules): S-C11 1.8321(12), 1.8337(12), S-C10 1.8541(12), 1.8577(12), O-N 1.4086(14), 1.4117(13), N-C14 1.2794(16), 1.2800(16), C11-C12 1.5075(17), 1.5094(17), C12-C13 1.3505(17), 1.3513(17), C13-C14 1.4561(17), 1.4570(17); C11-S-C10 109.30(6), 108.44(6), C13-C12-C11 121.19(11), 121.73(11), C13-C12-C15 125.01(12), 125.29(11), C12-C13-C16 122.87(12), 123.68(11), C14-N-O 111.21(10), 111.25(10).

 © 2004 Wiley-VCH Verlag GmbH & Co. KGaA, Weinheim

mass spectrum of δ-selenooxime **7** is analogous to that the sulfur compound **6**. NMR spectra (complete assignment through 2D $^{1}H/^{13}C$ experiments) indicate that **7** is a mixture of isomers (*E*/*Z* ca. 1:1) composition.

In summary, nitrosation of selenols **2a**, and **4a** occurs significantly faster than that of the related thiols **1a** and **3a**. The nitrosated selenium species are thermally much less stable than the related *S*-nitrosothiols and release NO much more readily.[22] We expect that the reaction sequence selenol nitrosation followed by Se–NO homolysis will give instigate further studies on the possible interactions of selenoproteins[4] with nitrosation agents.[1–3,22]

Experimental Section

1b: To a solution of **1a** (0.3 g, 1.46 mmol) in *n*-pentane (5 mL) was added *tert*-butylnitrite (1.5 mL, 14.6 mmol) at −20 °C. In the ^{13}C NMR spectrum all signals except that of a quarternary C atom (which was covered by a solvent peak) were observed. IR and UV data were obtained from the reaction mixture. **1b**: ^{1}H NMR (C_6D_6): $\delta = 1.19$ (s, CH_3), 3.63 (s, OCH_2); 6.84–6.79 (m, $2H_{Ar}$), 7.94–8.00 ppm (m, $2H_{Ar}$), ^{13}C NMR (C_6D_6): $\delta = 28.5$ (s, CCH_3), 69.0 (s, CCH_3), 78.4 (s, OCH_2), 125.3 (s, CH), 126.2 (s, CH), 126.4 (s, q), 130.1 (s, CH), 131.3 (s, CH), 160.5 ppm (s, C=N); UV/Vis (*n*-pentane, 20 °C) λ ($\lg\varepsilon$): 218 (2.89), 304 (2.28); IR (film, *n*-pentane): $\tilde{\nu} = 1648$ (st), 1467 (m), 1364 (m), 1353 (m), 1314 (m), 1189 (m,), 1135 (m), 1080 (m), 1042 (m), 1033 (st), 965 (st), 770 (m), 736 (m), 698 (m), 683 (m), 651 cm^{-1} (m).

2b: *tert*-Butylnitrite (0.11 mL, 1.06 mmol) was added to a solution of **2a** (0.27, 1.06 mmol) in THF (5 mL) at −78 °C, and the solution turned deep red instantaneously. ^{77}Se NMR measurements at −78 °C were unsuccessful. At room temperature, the signal of diselenide **2c**[11a] was detected. ^{77}Se NMR (THF/[D_8]THF): $\delta = 434$ [ref. [11a]: $\delta = 454.8$ ($CDCl_3$)]. In order to record EPR spectra the reaction was carried out in *n*-pentane and the spectra of the reaction mixture were measure at room temperature immediately. EPR (*n*-pentane): $g = 2.005$, $a(N) = 15.4$ G (1 N), $a(H\beta) = 10.1$ G (4 H, the same quintet-of-triplets pattern as that for the secondary radical obtained by nitrosation of **4a**).

3b: A solution of the freshly sublimed thiol **3a** (1 g, 3.79 mmol) in *n*-pentane (5 mL) at room temperature was treated with *tert*-butylnitrite (0.64 mL, 35.87 mmol). The resulting red–green solution was stirred for 30 min, and subsequently all volatiles were removed under reduced pressure to furnish **3b** as green solid (0.99 g, 89 %), m.p. 81–82 °C. ^{1}H NMR (C_6D_6): $\delta = 0.14$ ppm (s, CH_3); ^{13}C NMR (C_6D_6): $\delta = 1.5$ [Si($(CH_3)_3$)], 3.4 ppm (CSi_3); $^{29}Si\{^{1}H\}$ NMR (C_6D_6): $\delta = 3.1$ ppm; MS (CI/isobutane): $m/z = 294$ $[M+H]^+$; UV/Vis (*n*-pentane, 20 °C) λ ($\lg\varepsilon$): 210 (3.74); 236 (3.41); 264 (3.00); 364 (2.84); 564 (1.14); 608 (1.09). IR (KBr): $\tilde{\nu} = 612$ (st), 621 (st), 652 (m), 677 (m), 720 (m), 803 (m), 821 (m), 853 (m), 1021 (m), 1098 (m), 1261 (m), 1412 (st), 2902 (m), 2961 cm^{-1} (m). Elemental analysis (%) calcd for $C_{10}H_{27}NOSSi_3$ (293): C 40.96, H 9.22, N 4.78, S 10.92; found: C 40.83, H 8.94, N 4.26, S 10.67.

4b: *t*BuONO (0.29 mL, 2.0 mmol) was added to a solution of selenol **4a** (0.62 g, 2.0 mmol) in *n*-pentane (5 mL) at −78 °C. The solution turned red immediately. No signals could be detected by ^{77}Se NMR spectroscopy. Removal of the volatiles after 30 min gave a red oil. IR: $\tilde{\nu} = 1621$ (s), 1459 (st), 1368 (st), 1255 (st), 1099 (m), 1024 (m), 954 (s), 836 (st), 680 (m), 615 cm^{-1} (s).

MS: The reaction mixture was transferred into an argon-filled headspace tube. The sample was kept at room temperature for 1 h before a gaseous sample was removed. GC/MS [$m/z = 28$ (100), 30 (45), 32 (15)] indicated NO accompanied by some air.

EPR (*n*-pentane): The reaction mixture was transferred into an EPR tube at room temperature under N_2. First radical species **5**: $g = 2.011$ (quintet, simulation with $a(N) = 7.6$ G (2 N) and $a(Se) = 30$ G); second radical species : $g = 2.005$ (quintet of triplets, $a(N) = 15.2$ G (1 N), $a(H\beta) = 10.5$ G (4 H)).

^{77}Se NMR (C_6D_6) after decomposition of **4b**: $\delta = 635$ (**4d**), 552 (**4d**), 482, 396 (**4a**), 332 ppm; ^{1}H NMR (C_6D_6): $\delta = 0.37$, 0.32, 0.29, 0.13 ppm; IR (KBr): $\tilde{\nu} = 1259$ (st), 1098 (s), 1014 (s), 849 (st), 678 (s), 651 (2), 602 cm^{-1}(s).

6: A mixture of **3b** (1.1 g, 3.8 mmol) and 2,3-dimethylbuta-1,3-diene (2 mL) was stirred for 3 d. The volatiles were removed to give a yellow oil. On addition of *n*-pentane a colorless solid (1 g, 72 %) separated, which was recrystallized from *n*-pentane (m.p. 145 °C (decomp)). ^{1}H NMR (C_6D_6): $\delta = 0.24$ (s, $SiCH_3$), 1.67 (s, CH_3), 2.10 (s, CH_3), 3.30 (s, CH_2), 8.08 (br s, OH), 8.24 ppm (s, CH); ^{13}C NMR (C_6D_6): $\delta = 2.78$ ($SiCH_3$), 11.44 (s, Si_3CS), 13.68 (s, CH_3), 18.10 (s, CH_3), 39.15 (s, CH_2), 136 (s, q), 149.80 ppm (s, CH); MS (CI/isobutane): $m/z = 376$ $[M+H]^+$.

7: To a solution of **4a** (1.2 g, 3.8 mmol) in *n*-pentane (10 mL) at −78 °C was added *tert*-butylnitrite (1.3 mL, 38 mmol). After 5 min 2,3-dimethylbuta-1,3-diene (1 mL) was added to the red solution. The solution was stirred at −50 °C for 5 d and then warmed to room temperature. Removal of all volatiles gave a red oil, to which *n*-pentane (5 mL) was added. An insoluble white solid was removed and the pentane-soluble fraction subjected to column chromatography (SiO_2, pentane/ethylacetate 95:5). ^{13}C NMR spectra indicate that the second fraction contained **7** (a few mg).

Important NMR data of **7** in C_6D_6: (*E*)-oxime: ^{1}H NMR: $\delta = 8.20$ ppm (s, 1 H, N=C*H*); ^{13}C NMR: $\delta = 149.9$ ppm (CH, $^{1}J(C, H) = 163$ Hz, N=*C*H); (*Z*)-oxime: ^{1}H NMR: $\delta = 8.51$ ppm (s, 1 H, N=C*H*); ^{13}C NMR: $\delta = 149.8$ ppm (CH, $^{1}J(C, H) = 161$ Hz, N=*C*H). ^{77}Se NMR: $\delta = 223$, 240 ppm. MS(CI/isobutane): $m/z = 424$ $[M+H]^+$.

Received: January 28, 2004
Revised: May 6, 2004 [Z53872]

Keywords: bioinorganic chemistry · nitrogen oxides · nitrosation · oximes · selenium

[1] a) F. Murad, *Angew. Chem.* **1999**, *111*, 1976–1989; *Angew. Chem. Int. Ed.* **1999**, *38*, 1856–1868; b) L. J. Ignarro, *Angew. Chem.* **1999**, *111*, 2003–2013; *Angew. Chem. Int. Ed.* **1999**, *38*, 1882–1892.

[2] a) D. L. H. Williams, *Chem. Commun.* **1996**, 1085–1091; b) D. L. H. Williams, *Acc. Chem. Res.* **1999**, *32*, 869–876; c) N. Arulsamy, D. S. Bohle, J. A. Butt, J. Irvine, P. A. Jordan, E. J. Sagan, *J. Am. Chem. Soc.* **1999**, *121*, 7115–7123; d) A. A. Romeo, J. A. Capobianco, A. M. English, *J. Am. Chem. Soc.* **2003**, *125*, 14370–14378; e) H. Al-Sa'Doni, A. Ferro, *Clin. Sci.* **2000**, *98*, 507–520; f) D. Vorländer, E. Mittag, *Ber. Dtsch. Chem. Ges.* **1919**, *52*, 413–423.

[3] K. Wang, W. Zhang, M. Xian, Y.-C. Hou, X.-C. Chen, J.-P. Cheng, P. G. Wang, *Curr. Med. Chem.* **2000**, *7*, 821.

[4] H. Sies, L. Packer, *Methods Enzymol.* **2002**, *347*, 121–125.

[5] a) H. Sies, V. S. Sharov, L.-O. Klotz, K. Briviba, *J. Biol. Chem.* **1997**, *272*, 27812–27817; b) H. Sies, G. E. Arteel, *Free Radical Biol. Med.* **2000**, *28*, 1451–1455.

[6] M. Asahi, J. Fujii, T. Takao, T. Kuzuya, M. Hori, Y. Shimonishi, N. Taniguchi, *J. Biol. Chem.* **1997**, *272*, 19152–19157.

[7] J. E. Freedman, B. Frei, G. N. Welch, J. Loscalzo, *Am. Soc. Clin. Inv.* **1995**, *96*, 394–400.

[8] D. Nikitovic, A. Holmgren, *J. Biol. Chem.* **1996**, *271*, 19180–19185.

[9] GSNO can also be substrate of selenium-free Trx systems: S. M. Kanzok, S. Rahlfs, K. Becker, R. H. Schirmer, *Methods Enzymol.* **2002**, *347*, 370–381.

[10] Y. C. Hou, Z. M. Guo, J. Li, X. Zhu, Z. Yin, P. G. Wang, *Biochem. Biophys. Res. Commun.* **1996**, *228*, 88–93.

 © 2004 Wiley-VCH Verlag GmbH & Co. KGaA, Weinheim

[11] a) G. Mugesh, A. Panda, H. B. Singh, R. J. Butcher, *Chem. Eur. J.* **1999**, *5*, 1411 – 1421; b) G. Mugesh, H. B. Singh, R. J. Butcher, *Tetrahedron: Asymmetry* **1999**, *10*, 237 – 242.
[12] Z. Majeed, W. R. McWhinnie, P. R. Lowe, *Acta Crystallogr. Sect. C* **2000**, *56*, 105 – 106.
[13] a) I. Wagner, W.-W. du Mont, S. Pohl, W. Saak, *Chem. Ber.* **1990**, *123*, 2325 – 2357; b) W.-W. du Mont, I. Wagner, *Chem. Ber.* **1988**, *121*, 2109 – 2110; c) M. Ostrowski, I. Wagner, P. G. Jones, J. Jeske, *Z. Anorg. Allg. Chem.* **1993**, *619*, 1693 – 1698.
[14] W.-W. du Mont, G. Mugesh, C. Wismach, P. G. Jones, *Angew. Chem.* **2001**, *113*, 2547 – 2550; *Angew. Chem. Int. Ed.* **2001**, *40*, 2486 – 2489.
[15] Another IR absorption at 1621 cm^{-1} is apparently due to remaining nitrosation agent (see ref. [16]).
[16] C. Wismach, W.-W. du Mont, *7. Int. Conf. on Selenium in Biology and Medicine*, Venice, 2000, Abstract P-188; C. Wismach, Dissertation, TU Braunschweig, **2004**.
[17] The simulation of EPR spectra is often hampered by anisotropy-related asymmetries in the experimental spectrum, which cannot be averaged by rotation in solution due to the large mass of Se and the resulting high moments of inertia of the molecules: W. Kaim, *Z. Naturforsch. B* **1981**, *36*, 150 – 156.
[18] a) W. Kaim, V. Kasack, *Angew. Chem.* **1982**, *94*, 712 – 713; *Angew. Chem. Int. Ed. Engl.* **1982**, *12*, 700 – 701; b) F. Gerson, W. Huber, *Electron Spin Resonance Spectroscopy of Organic Radicals*, Wiley-VCH, Weinheim, **2003**, p. 201.
[19] M. Cavero, W. B. Motherwell, P. Potier, *Tetrahedron Lett.* **2001**, *42*, 4377 – 4379.
[20] X-ray structure determination of **6** ($C_{16}H_{37}NOSSi_3$): $M_r = 375.80$, triclinic, space group $P\bar{1}$, $a = 8.9455(6)$, $b = 15.5786(10)$, $c = 17.1565(10)$ Å, $\alpha = 94.117(3)°$, $\beta = 91.435(3)$, $\gamma = 106.193(3)°$, $V = 2287.6(3)$ $Å^3$, $Z = 4$, $\rho_{calcd} = 1.091$ $Mg\,m^{-3}$, $Mo_{K\alpha}$ radiation ($\lambda = 0.71073$ $Å^3$), $T = 133$ K; the crystal ($0.45 \times 0.28 \times 0.08$ mm^3) was mounted in inert oil on a Bruker Smart 1000 CCD area detector. Intensities were collected in the 2θ-range 4–60°. From a total of 32682 reflections, 11270 were independent ($R_{int} = 0.0322$). All non-hydrogen atoms were refined anisotropically versus F^2 with the full matrix least squares procedure: $R1 = 0.0301$, $wR2 = 0.0896$ (all data).[21] Methyl hydrogens were refined as rigid groups, OH hydrogens freely, and the other hydrogens with the riding model. CCDC-241350 contains the supplementary crystallographic data for this paper. These data can be obtained free of charge via www.ccdc.cam.ac.uk/conts/retrieving.html (or from the Cambridge Crystallographic Data Centre, 12, Union Road, Cambridge CB21EZ, UK; fax: (+44) 1223-336-033; or deposit@ccdc.cam.ac.uk).
[21] G. M. Sheldrick, SHELXL-97, *A Program for Crystal Structure Refinement*, Göttingen, **1997**.
[22] Comment added after submission: The full characterization of a stable aromatic *Se*-nitrososelenol was recently reported by K. Goto, K. Shimada, and T. Kawashima at the *11th International Conference on the Chemistry of Selenium and Tellurium*, IIT Bombay, February 23 – 27, 2004, Abstract IL-3.

 © 2004 Wiley-VCH Verlag GmbH & Co. KGaA, Weinheim

Epigenetics

Design, Synthesis, and Biological Evaluation of a Small-Molecule Inhibitor of the Histone Acetyltransferase Gcn5**

Markus Biel, Androniki Kretsovali, Efthymia Karatzali, Joseph Papamatheakis, and Athanassios Giannis**

Histone proteins are basic components of the eukaryotic chromatin.[1] They contain a DNA-interacting globular domain and a more flexible N-terminal region,[2] which is a target for several posttranslational modifications. These include the acetylation of lysine residues and the methylation of lysine and arginine residues as well as the phosphorylation of serine hydroxyl functions and the attachment of an ubiquitin group.[3] The "histone-code hypothesis"[4] is based on the assumption that these modifications create a specific substitution pattern on the histone tails. This pattern is readable by regulatory proteins, which connect the histone code with fundamental cellular processes like activation or repression of transcription. To date, acetylation is the best-studied histone modification. It has been shown that the adjustment of a specific acetylation balance on the histone N-termini within a particular gene region is the result of a highly regulated interplay of selective histone acetyltransferases (HATs) and histone deacetylases (HDACs).[5]

For decoding the histone code a carefully directed influence on fine-tuning these processes through the development of low-molecular-weight and cell-permeable inhibitors is of extraordinary importance. Furthermore new inhibitors may open up new possibilities for treatment of pathological diseases like cancer.[5,6] In contrast to the HATs, several small-molecule inhibitors of the HDACs are known, and some of them are in clinical trials.[7] Recently, anacardic acid was identified in a broad screening of plant extracts with antitumor activity as the first small-molecule inhibitor of the HAT p300.[8]

To date, many of the transcription factors described have intrinsic HAT activity.[9] In agreement with their biological function and based on sequence homologies, HATs can be

[*] Dr. A. Kretsovali, E. Karatzali, Prof. Dr. J. Papamatheakis
Institute of Molecular Biology and Biotechnology
FORTH, Vassilika Vouton
P.O. Box 1527, 71110 Heraklion, Crete (Greece)
Fax: (+30) 2810-391-101
E-mail: kretsova@imbb.forth.gr
Dipl.-Chem. M. Biel, Prof. Dr. A. Giannis
University of Leipzig
Institute of Organic Chemistry
Johannisallee 29, 04103 Leipzig (Germany)
Fax: (+49)-341-973-6599
E-mail: giannis@chemie.uni-leipzig.de

[**] This work was supported by the Fonds der Chemischen Industrie. A.K. and J.P. are grateful for funding GSRT/PENED 2002.

Supporting information for this article is available on the WWW under http://www.angewandte.org or from the author.

 © 2004 Wiley-VCH Verlag GmbH & Co. KGaA, Weinheim DOI: 10.1002/anie.200453879

divided into three families: the GNAT, CBP/p300, and MYST families.[9] In vivo, histone acetyltransferases are always associated with large multiprotein complexes. In yeast, for example, the histone acetyltransferase yGcn5 is part of the multiprotein complexes Ada and SAGA, the substrate selectivities of which differ from those of the free enzyme.[9]

Here, we describe the development and biological evaluation of the first small-molecule inhibitor of the human histone acetyltransferase Gcn5, a prominent member of the GNAT family with high preference for histone H3 as a substrate. Moreover, we present our approach, from the first working hypothesis, based on published kinetic studies and mechanistic proposals,[9,10] to the establishment of the structural class of α-methylene-γ-butyrolactones as inhibitors.

The γ-butyrolactone scaffold is a recurrent structural motif in many natural products.[11] Considering the wide sphere of biological activity, the γ-butyrolactone scaffold can be designated as a privileged structure in nature. For this reason we envisaged the development of completely new HAT inhibitors using the class of γ-butyrolactones (Figure 1b). The inspiration for choosing appropriate substituents

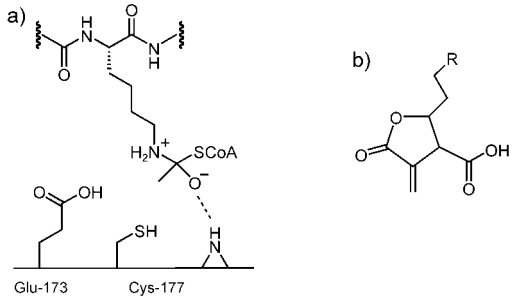
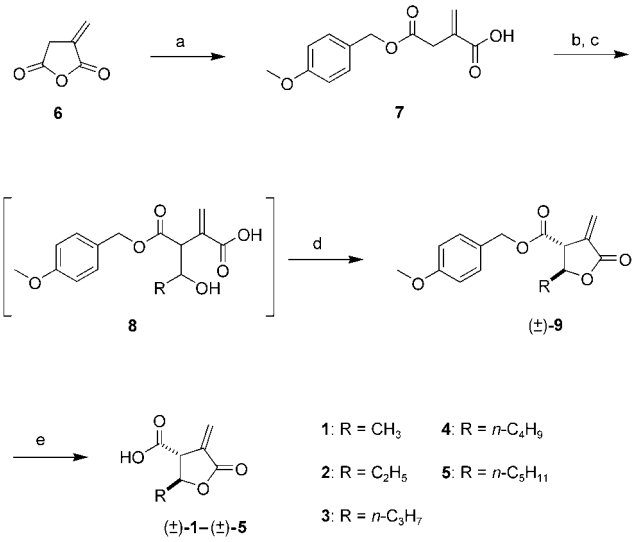


Figure 1. a) Tetrahedral intermediate in the postulated catalytic mechanism of Gcn5, and b) general structure of the inhibitors with the butyrolactone framework (for more details see text). R = alkyl chain.

at the positions 2 to 4 of the butyrolactone scaffold derived from the requirements of the postulated catalytic mechanism to the substrate.[10] According to the model of the induced fit, it is assumed that only after the binding of acetyl-CoA to Gcn5 is the binding pocket accessible for the histone protein, and a ternary complex of enzyme, acetyl-CoA, and histone can be formed. The highly conserved general base Glu173, which is surrounded by several unpolar amino acids to increase its pK_a, deprotonates the ε-amino function of the histone lysine side chain and enables a nucleophilic attack on the neighboring thioester function of acetyl-CoA (Figure 1a). The resulting tetrahedral intermediate is stabilized by a hydrogen bond to the backbone amide of Cys177 and decomposes giving the general base Glu173, acetylated histone, and CoASH.

We translated these facts into a simple working hypothesis for the development of new HAT inhibitors: the desired structure should present a possible hydrogen-bond acceptor for the backbone amide of Cys177 and a polar group for interaction with Glu173. Moreover, the molecule should possess an aliphatic side chain analogous to that of lysine.

The synthesis of the γ-butyrolactones **1**–**5**[12] started with the regioselective ring-opening of itaconic anhydride **6** with 4-methoxybenzyl alcohol to give **7**. Treatment with lithium bis(trimethylsilyl)amide converted **7** into the corresponding ester enolate, which reacted with an aliphatic aldehyde to give the hydroxycarboxlic acid **8**. Compound **8** was not isolated, and the ring-closing reaction was performed in a mixture of chloroform and ethanol. The cleavage of the 4-methoxybenzyl ester to give the final product was achieved under mild conditions by heating with acetic acid in molten phenol (Scheme 1).[17]



Scheme 1. Synthesis of the γ-butyrolactones **1**–**5**: a) 4-methoxybenzylic alcohol, *n*-hexane, toluene, 60 °C, 36 h, 88%; b) LiHMDS, THF, −78 °C, 1 h; c) RCHO, THF, −78 °C, 12 h; d) $CHCl_3$, EtOH, RT, 72 h; e) phenol, HOAc, 60 °C, 3 h. LiHMDS = lithium hexamethyldisilazide.

Butyrolactones **1**–**5** were tested in an in vitro HAT assay, using recombinant Gcn5[13] or CBP[14] and commercially available core histone proteins. As shown in Figure 2, compounds **3**–**5** lead to an inhibition of CBP, whereas only

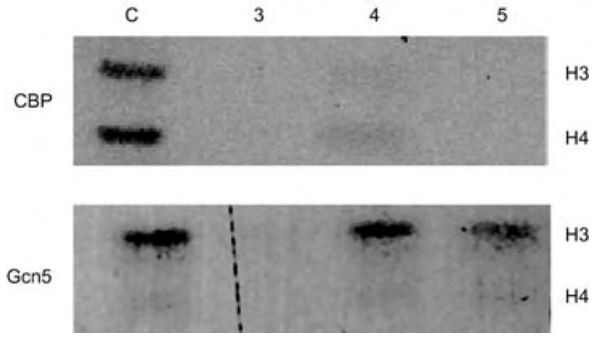


Figure 2. Inhibition of the HATs CBP and Gcn5 by compounds **3**–**5**. While butyrolactones **3**–**5** inhibit the HAT CBP, only compound **3** displays an inhibition against Gcn5. The control C contains 10 μg core histone protein, 0.05 μCi [^{3}H]-acetyl-CoA, and either 10 ng CBP or 100 ng GST-Gcn5. The inhibitor concentration for each experiment was 5 mM. After separation of the histone proteins by SDS gel electrophoresis (12% SDS), the amount of acylated histones was quantified by phosphor image analysis. H3: histone 3; H4: histone 4.

 © 2004 Wiley-VCH Verlag GmbH & Co. KGaA, Weinheim

butyrolactone **3** inhibits the HAT Gcn5. For determination of the IC_{50} values, the amount of enzymatically acetylated histone protein was determined as a function of the inhibitor concentration. As a result, compounds **3**–**5** show only a weak inhibition of CBP (IC_{50} values: **3** = 0.5 mM, **4** and **5** = 1.7–2 mM, data not shown), whereas butyrolactone **3** leads to an inhibition of Gcn5 with an IC_{50} value of 100 μM (Figure 3). In this context it is important to note that in the presence of acetyl-CoA the K_d value for binding of histone H3 to Gcn5 or PCAF is approximately 100 μM.[9a,15,16] The affinity of inhibitor **3** to the Gcn5 enzyme is comparable to that of the natural substrate H3 and provides an excellent starting point for the study of structure–activity relationships.

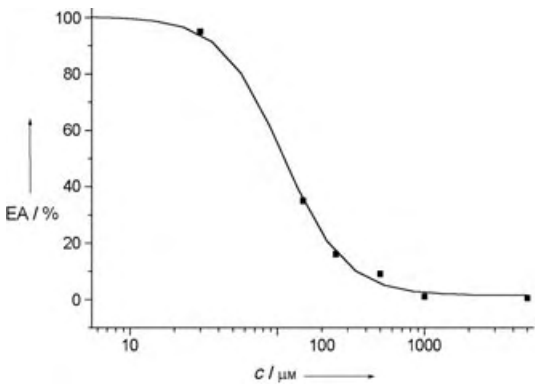


Figure 3. For determination of the IC_{50} value, butyrolactone **3** was incubated in different concentrations (*c*) together with 100 ng Gcn5, 3 μg core histone protein (Sigma), and 0.05 μCi [^{14}C]-acetyl-CoA (Amersham). After separation by SDS gel electrophoresis (12% SDS), the amount of acetylated histone proteins was quantified. Each data point represents the average of two independent measurements. EA = enzyme activity.

The length of the aliphatic side chain at position 4 of the γ-butyrolactone seems to be decisive for the biological activity. In following enzymatic experiments we could determine that the inhibition shows no time dependence. This result speaks for a nonirreversible inhibition of the enzyme, and variation of the substitution pattern at position 2 may lead to further optimization of compound **3**.

The identification of small-molecule inhibitors of the histone acetyltransferases is absolutely necessary for the evaluation of biological processes connected with the model of the histone code. On the basis of published kinetic studies and postulated catalytic mechanisms we were able to develop and identify the Gcn5 inhibitor **3**. Furthermore, we could determine a nonirreversible inhibition of Gcn5, and therefore a Michael addition of nucleophilic groups of the enzyme's active side is unlikely. As a result, derivatization of γ-butyrolactone **3**[17] at position 2 is a promising starting point for future structure–activity relationship studies.

Received: January 29, 2004
Revised: April 18, 2004 [Z53879]

Keywords: biological activity · epigenetics · histone acetyltransferase · histone code · inhibitors

[1] R. D. Kornberg, J. O. Thomas, *Science* **1974**, *184*, 865–868.
[2] K. Luger, A. W. Mader, R. K. Richmond, D. F. Sargent, T. J. Richmond, *Nature* **1997**, *389*, 251–260.
[3] S. L. Berger, *Curr. Opin. Genet. Dev.* **2002**, *12*, 142–148.
[4] a) B. D. Strahl, C. D. Allis, *Nature* **2000**, *403*, 41–45; b) M. Izuka, M. M. Smith, *Curr. Opin. Genet. Dev.* **2003**, *13*, 154–160.
[5] D. Chung, *Trends Mol. Med.* **2002**, *8*, S10–S11.
[6] a) S. L. Schreiber, B. E. Bernstein, *Cell* **2002**, *111*, 771–778; b) P. Workman, *Curr. Opin. Pharmacol.* **2001**, *1*, 342–352.
[7] T. A. Miller, D. J. Witter, S. Belvedere, *J. Med. Chem.* **2003**, *46*, 5097–5116.
[8] K. Balasubramanyam, V. Swaminathan, A. Ranganathan, T. K. Kundu, *J. Biol. Chem.* **2003**, *278*, 19134–19140.
[9] a) S. Y. Roth, J. M. Denu, C. D. Allis, *Annu. Rev. Biochem.* **2001**, *70*, 81–120; b) R. Marmorstein, *J. Mol. Biol.* **2001**, *311*, 433–444; c) M. J. Carrozza, R. T. Utley, J. L. Workman, J. Côté, *Trends Genet.* **2003**, *19*, 321–329.
[10] R. C. Trievel, J. R. Rojas, D. E. Sterner, R. N. Venkataramani, L. Wang, J. Zhou, C. D. Allis, S. L. Berger, R. Marmorstein, *Proc. Natl. Acad. Sci. USA* **1999**, *96*, 8931–8936.
[11] a) H. M. R. Hoffmann, J. Rabe, *Angew. Chem.* **1985**, *97*, 96–112; *Angew. Chem. Int. Ed. Engl.* **1985**, *24*, 94–110; b) A. G. González, M. H. Silva, J. I. Padrón, F. Léon, E. Reyes, M. Álvarez-Mon, J. P. Pivel, J. Quintana, F. Estévez, J. Bermejo, *J. Med. Chem.* **2002**, *45*, 2358–2361; c) F. P. Kuhajda, E. S. Pizer, J. N. Li, N. S. Mani, G. L. Frehywot, C. A. Townsend, *Proc. Natl. Acad. Sci. USA* **2000**, *97*, 3450–3454; d) H. M. Ogmundsdottir, G. M. Zoega, S. R. Gissurarson, K. Ingolfsdottir, *J. Pharm. Pharmacol.* **1998**, *50*, 107–115; e) A. Randazzo, C. Debitus, L. Minale, P. P. Garcia, M. J. Alcaraz, M. Paya, L. Gomez-Paloma, *J. Nat. Prod.* **1998**, *61*, 571–575; f) A. E. Mitchell, J. Zheng, B. D. Hammcock, M. Lo Bello, A. D. Jones, *Biochemistry* **1998**, *37*, 6752–6759; g) A. Huwe, R. Mazitschek, A. Giannis, *Angew. Chem.* **2003**, *115*, 2170–2187; *Angew. Chem. Int. Ed.* **2003**, *42*, 2122–2138.
[12] R. M. Carlson, A. R. Oyler, *J. Org. Chem.* **1976**, *41*, 4065–4069.
[13] E. Smith, J. Belote, R. Schlitz, X. Yang, P. Morre, S. Berger, Y. Nakatani, C. Allis, *Nucleic Acids Res.* **1998**, *26*, 2948–2954.
[14] J. Chrivia, R. Kwok, N. Lamb, M. Hagiwara, M. Montminty, R. Goodman, *Nature* **1993**, *365*, 855–859.
[15] K. G. Tanner, M. R. Langer, Y. Kim, J. M. Denu, *Biochemistry* **2000**, *39*, 11961–11969.
[16] K. G. Tanner, M. R. Langer, Y. Kim, J. M. Denu, *J. Biol. Chem.* **2000**, *275*, 22048–22055.
[17] The structure of compounds **1**–**5** was determined by NOE experiments.

 © 2004 Wiley-VCH Verlag GmbH & Co. KGaA, Weinheim